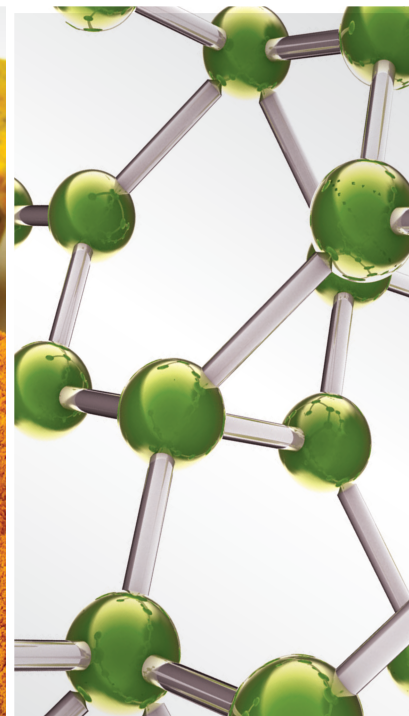


# Medicinal Plants and Natural Products in Health Promotion and Disease Prevention

Lead Guest Editor: Ruchika Garg

Guest Editors: Jelena Zivkovic and Sekar Vijayakumar







---

# **Medicinal Plants and Natural Products in Health Promotion and Disease Prevention**

Evidence-Based Complementary and Alternative Medicine

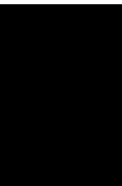
---

**Medicinal Plants and Natural Products  
in Health Promotion and Disease  
Prevention**

Lead Guest Editor: Ruchika Garg

Guest Editors: Jelena Zivkovic and Sekar  
Vijayakumar





---

Copyright © 2022 Hindawi Limited. All rights reserved.

This is a special issue published in "Evidence-Based Complementary and Alternative Medicine." All articles are open access articles distributed under the Creative Commons Attribution License, which permits unrestricted use, distribution, and reproduction in any medium, provided the original work is properly cited.

# Chief Editor

Jian-Li Gao , China

## Associate Editors







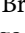

Hyunsu Bae , Republic of Korea  
Raffaele Capasso , Italy  
Jae Youl Cho , Republic of Korea  
Caigan Du , Canada  
Yuewen Gong , Canada  
Hai-dong Guo , China  
Kuzhuvelil B. Harikumar , India  
Ching-Liang Hsieh , Taiwan  
Cheorl-Ho Kim , Republic of Korea  
Victor Kuete , Cameroon  
Hajime Nakae , Japan  
Yoshiji Ohta , Japan  
Olumayokun A. Olajide , United Kingdom  
Chang G. Son , Republic of Korea  
Shan-Yu Su , Taiwan  
Michał Tomczyk , Poland  
Jenny M. Wilkinson , Australia

## Academic Editors

Eman A. Mahmoud , Egypt  
Ammar AL-Farga , Saudi Arabia  
Smail Aazza , Morocco  
Nahla S. Abdel-Azim, Egypt  
Ana Lúcia Abreu-Silva , Brazil  
Gustavo J. Acevedo-Hernández , Mexico  
Mohd Adnan , Saudi Arabia  
Jose C Adsuar , Spain  
Sayeed Ahmad, India  
Touqeer Ahmed , Pakistan  
Basiru Ajiboye , Nigeria  
Bushra Akhtar , Pakistan  
Fahmida Alam , Malaysia  
Mohammad Jahoor Alam, Saudi Arabia  
Clara Albani, Argentina  
Ulysses Paulino Albuquerque , Brazil  
Mohammed S. Ali-Shtayeh , Palestinian Authority  
Ekram Alias, Malaysia  
Terje Alraek , Norway  
Adolfo Andrade-Cetto , Mexico  
Letizia Angiolella , Italy  
Makoto Arai , Japan

Daniel Dias Rufino Arcanjo , Brazil  
Duygu AĞAGÜNDÜZ , Turkey  
Neda Baghban , Iran  
Samra Bashir , Pakistan  
Rusliza Basir , Malaysia  
Jairo Kenupp Bastos , Brazil  
Arpita Basu , USA  
Mateus R. Beguelini , Brazil  
Juana Benedí, Spain  
Samira Boulbaroud, Morocco  
Mohammed Bourhia , Morocco  
Abdelhakim Bouyahya, Morocco  
Nunzio Antonio Cacciola , Italy  
Francesco Cardini , Italy  
María C. Carpinella , Argentina  
Harish Chandra , India  
Guang Chen, China  
Jianping Chen , China  
Kevin Chen, USA  
Mei-Chih Chen, Taiwan  
Xiaojia Chen , Macau  
Evan P. Cherniack , USA  
Giuseppina Chianese , Italy  
Kok-Yong Chin , Malaysia  
Lin China, China  
Salvatore Chirumbolo , Italy  
Hwi-Young Cho , Republic of Korea  
Jeong June Choi , Republic of Korea  
Jun-Yong Choi, Republic of Korea  
Kathrine Bisgaard Christensen , Denmark  
Shuang-En Chuang, Taiwan  
Ying-Chien Chung , Taiwan  
Francisco José Cidral-Filho, Brazil  
Daniel Collado-Mateo , Spain  
Lisa A. Conboy , USA  
Kieran Cooley , Canada  
Edwin L. Cooper , USA  
José Otávio do Amaral Corrêa , Brazil  
Maria T. Cruz , Portugal  
Huantian Cui , China  
Giuseppe D'Antona , Italy  
Ademar A. Da Silva Filho , Brazil  
Chongshan Dai, China  
Laura De Martino , Italy  
Josué De Moraes , Brazil



Arthur De Sá Ferreira , Brazil  
Nunziatina De Tommasi , Italy  
Marinella De leo , Italy  
Gourav Dey , India  
Dinesh Dhamecha, USA  
Claudia Di Giacomo , Italy  
Antonella Di Sotto , Italy  
Mario Dioguardi, Italy  
Jeng-Ren Duann , USA  
Thomas Effërth , Germany  
Abir El-Alfy, USA  
Mohamed Ahmed El-Esawi , Egypt  
Mohd Ramli Elvy Suhana, Malaysia  
Talha Bin Emran, Japan  
Roger Engel , Australia  
Karim Ennouri , Tunisia  
Giuseppe Esposito , Italy  
Tahereh Eteraf-Oskouei, Iran  
Robson Xavier Faria , Brazil  
Mohammad Fattahi , Iran  
Keturah R. Faurot , USA  
Piergiorgio Fedeli , Italy  
Laura Ferraro , Italy  
Antonella Fioravanti , Italy  
Carmen Formisano , Italy  
Hua-Lin Fu , China  
Liz G Müller , Brazil  
Gabino Garrido , Chile  
Safoora Gharibzadeh, Iran  
Muhammad N. Ghayur , USA  
Angelica Gomes , Brazil  
Elena González-Burgos, Spain  
Susana Gorzalczany , Argentina  
Jiangyong Gu , China  
Maruti Ram Gudavalli , USA  
Jian-You Guo , China  
Shanshan Guo, China  
Narcís Gusi , Spain  
Svein Haavik, Norway  
Fernando Hallwass, Brazil  
Gajin Han , Republic of Korea  
Ihsan Ul Haq, Pakistan  
Hicham Harhar , Morocco  
Mohammad Hashem Hashempur , Iran  
Muhammad Ali Hashmi , Pakistan

Waseem Hassan , Pakistan  
Sandrina A. Heleno , Portugal  
Pablo Herrero , Spain  
Soon S. Hong , Republic of Korea  
Md. Akil Hossain , Republic of Korea  
Muhammad Jahangir Hossen , Bangladesh  
Shih-Min Hsia , Taiwan  
Changmin Hu , China  
Tao Hu , China  
Weicheng Hu , China  
Wen-Long Hu, Taiwan  
Xiao-Yang (Mio) Hu, United Kingdom  
Sheng-Teng Huang , Taiwan  
Ciara Hughes , Ireland  
Attila Hunyadi , Hungary  
Liaqat Hussain , Pakistan  
Maria-Carmen Iglesias-Osma , Spain  
Amjad Iqbal , Pakistan  
Chie Ishikawa , Japan  
Angelo A. Izzo, Italy  
Satveer Jagwani , USA  
Rana Jamous , Palestinian Authority  
Muhammad Saeed Jan , Pakistan  
G. K. Jayaprakasha, USA  
Kyu Shik Jeong, Republic of Korea  
Leopold Jirovetz , Austria  
Jeeyoun Jung , Republic of Korea  
Nurkhalida Kamal , Saint Vincent and the  
Grenadines  
Atsushi Kameyama , Japan  
Kyungsu Kang, Republic of Korea  
Wenyi Kang , China  
Shao-Hsuan Kao , Taiwan  
Nasiara Karim , Pakistan  
Morimasa Kato , Japan  
Kumar Katragunta , USA  
Deborah A. Kennedy , Canada  
Washim Khan, USA  
Bonglee Kim , Republic of Korea  
Dong Hyun Kim , Republic of Korea  
Junghyun Kim , Republic of Korea  
Kyungho Kim, Republic of Korea  
Yun Jin Kim , Malaysia  
Yoshiyuki Kimura , Japan

Nebojša Kladar , Serbia  
Mi Mi Ko , Republic of Korea  
Toshiaki Kogure , Japan  
Malcolm Koo , Taiwan  
Yu-Hsiang Kuan , Taiwan  
Robert Kubina , Poland  
Chan-Yen Kuo , Taiwan  
Kuang C. Lai , Taiwan  
King Hei Stanley Lam, Hong Kong  
Fanuel Lampiao, Malawi  
Ilaria Lampronti , Italy  
Mario Ledda , Italy  
Harry Lee , China  
Jeong-Sang Lee , Republic of Korea  
Ju Ah Lee , Republic of Korea  
Kyu Pil Lee , Republic of Korea  
Namhun Lee , Republic of Korea  
Sang Yeoup Lee , Republic of Korea  
Ankita Leekha , USA  
Christian Lehmann , Canada  
George B. Lenon , Australia  
Marco Leonti, Italy  
Hua Li , China  
Min Li , China  
Xing Li , China  
Xuqi Li , China  
Yi-Rong Li , Taiwan  
Vuanghao Lim , Malaysia  
Bi-Fong Lin, Taiwan  
Ho Lin , Taiwan  
Shuibin Lin, China  
Kuo-Tong Liou , Taiwan  
I-Min Liu, Taiwan  
Suhuan Liu , China  
Xiaosong Liu , Australia  
Yujun Liu , China  
Emilio Lizarraga , Argentina  
Monica Loizzo , Italy  
Nguyen Phuoc Long, Republic of Korea  
Zaira López, Mexico  
Chunhua Lu , China  
Ângelo Luís , Portugal  
Anderson Luiz-Ferreira , Brazil  
Ivan Luzardo Luzardo-Ocampo, Mexico

Michel Mansur Machado , Brazil  
Filippo Maggi , Italy  
Juraj Majtan , Slovakia  
Toshiaki Makino , Japan  
Nicola Malafrente, Italy  
Giuseppe Malfa , Italy  
Francesca Mancianti , Italy  
Carmen Mannucci , Italy  
Juan M. Manzanque , Spain  
Fatima Martel , Portugal  
Carlos H. G. Martins , Brazil  
Maulidiani Maulidiani, Malaysia  
Andrea Maxia , Italy  
Avijit Mazumder , India  
Isac Medeiros , Brazil  
Ahmed Mediani , Malaysia  
Lewis Mehl-Madrona, USA  
Ayikoé Guy Mensah-Nyagan , France  
Oliver Micke , Germany  
Maria G. Miguel , Portugal  
Luigi Milella , Italy  
Roberto Miniero , Italy  
Letteria Minutoli, Italy  
Prashant Modi , India  
Daniel Kam-Wah Mok, Hong Kong  
Changjong Moon , Republic of Korea  
Albert Moraska, USA  
Mark Moss , United Kingdom  
Yoshiharu Motoo , Japan  
Yoshiki Mukudai , Japan  
Sakthivel Muniyan , USA  
Saima Muzammil , Pakistan  
Benoit Banga N'guessan , Ghana  
Massimo Nabissi , Italy  
Siddavaram Nagini, India  
Takao Namiki , Japan  
Srinivas Nammi , Australia  
Krishnadas Nandakumar , India  
Vitaly Napadow , USA  
Edoardo Napoli , Italy  
Jorddy Neves Cruz , Brazil  
Marcello Nicoletti , Italy  
Eliud Nyaga Mwaniki Njagi , Kenya  
Cristina Nogueira , Brazil



Sakineh Kazemi Noureini , Iran  
Rômulo Dias Novaes, Brazil  
Martin Offenbaecher , Germany  
Oluwafemi Adeleke Ojo , Nigeria  
Olufunmiso Olusola Olajuyigbe , Nigeria  
Luís Flávio Oliveira, Brazil  
Mozaniel Oliveira , Brazil  
Atolani Olubunmi , Nigeria  
Abimbola Peter Oluyori , Nigeria  
Timothy Omara, Austria  
Chiagoziem Anariochi Otuechere , Nigeria  
Sokcheon Pak , Australia  
Antônio Palumbo Jr, Brazil  
Zongfu Pan , China  
Siyaram Pandey , Canada  
Niranjan Parajuli , Nepal  
Gunhyuk Park , Republic of Korea  
Wansu Park , Republic of Korea  
Rodolfo Parreira , Brazil  
Mohammad Mahdi Parvizi , Iran  
Luiz Felipe Passero , Brazil  
Mitesh Patel, India  
Claudia Helena Pellizzon , Brazil  
Cheng Peng, Australia  
Weijun Peng , China  
Sonia Piacente, Italy  
Andrea Pieroni , Italy  
Haifa Qiao , USA  
Cláudia Quintino Rocha , Brazil  
DANIELA RUSSO , Italy  
Muralidharan Arumugam Ramachandran,  
Singapore  
Manzoor Rather , India  
Miguel Rebollo-Hernanz , Spain  
Gauhar Rehman, Pakistan  
Daniela Rigano , Italy  
José L. Rios, Spain  
Francisca Rius Diaz, Spain  
Eliana Rodrigues , Brazil  
Maan Bahadur Rokaya , Czech Republic  
Mariangela Rondanelli , Italy  
Antonietta Rossi , Italy  
Mi Heon Ryu , Republic of Korea  
Bashar Saad , Palestinian Authority  
Sabi Saheed, South Africa

Mohamed Z.M. Salem , Egypt  
Avni Sali, Australia  
Andreas Sandner-Kiesling, Austria  
Manel Santafe , Spain  
José Roberto Santin , Brazil  
Tadaaki Satou , Japan  
Roland Schoop, Switzerland  
Sindy Seara-Paz, Spain  
Veronique Seidel , United Kingdom  
Vijayakumar Sekar , China  
Terry Selfe , USA  
Arham Shabbir , Pakistan  
Suzana Shahar, Malaysia  
Wen-Bin Shang , China  
Xiaofei Shang , China  
Ali Sharif , Pakistan  
Karen J. Sherman , USA  
San-Jun Shi , China  
Insop Shim , Republic of Korea  
Maria Im Hee Shin, China  
Yukihiro Shoyama, Japan  
Morry Silberstein , Australia  
Samuel Martins Silvestre , Portugal  
Preet Amol Singh, India  
Rajeev K Singla , China  
Kuttulebbai N. S. Sirajudeen , Malaysia  
Slim Smaoui , Tunisia  
Eun Jung Sohn , Republic of Korea  
Maxim A. Solovchuk , Taiwan  
Young-Jin Son , Republic of Korea  
Chengwu Song , China  
Vanessa Steenkamp , South Africa  
Annarita Stringaro , Italy  
Keiichiro Sugimoto , Japan  
Valeria Sulsen , Argentina  
Zewei Sun , China  
Sharifah S. Syed Alwi , United Kingdom  
Orazio Tagliatalata-Scafati , Italy  
Takashi Takeda , Japan  
Gianluca Tamagno , Ireland  
Hongxun Tao, China  
Jun-Yan Tao , China  
Lay Kek Teh , Malaysia  
Norman Temple , Canada




Kamani H. Tennekoon , Sri Lanka  
Seong Lin Teoh, Malaysia  
Menaka Thounaojam , USA  
Jinhui Tian, China  
Zipora Tietel, Israel  
Loren Toussaint , USA  
Riaz Ullah , Saudi Arabia  
Philip F. Uzor , Nigeria  
Luca Vanella , Italy  
Antonio Vassallo , Italy  
Cristian Vergallo, Italy  
Miguel Vilas-Boas , Portugal  
Aristo Vojdani , USA  
Yun WANG , China  
QIBIAO WU , Macau  
Abraham Wall-Medrano , Mexico  
Chong-Zhi Wang , USA  
Guang-Jun Wang , China  
Jinan Wang , China  
Qi-Rui Wang , China  
Ru-Feng Wang , China  
Shu-Ming Wang , USA  
Ting-Yu Wang , China  
Xue-Rui Wang , China  
Youhua Wang , China  
Kenji Watanabe , Japan  
Jintanaporn Wattanathorn , Thailand  
Silvia Wein , Germany  
Katarzyna Winska , Poland  
Sok Kuan Wong , Malaysia  
Christopher Worsnop, Australia  
Jih-Huah Wu , Taiwan  
Sijin Wu , China  
Xian Wu, USA  
Zuoqi Xiao , China  
Rafael M. Ximenes , Brazil  
Guoqiang Xing , USA  
JiaTuo Xu , China  
Mei Xue , China  
Yong-Bo Xue , China  
Haruki Yamada , Japan  
Nobuo Yamaguchi, Japan  
Junqing Yang, China  
Longfei Yang , China

Mingxiao Yang , Hong Kong  
Qin Yang , China  
Wei-Hsiung Yang, USA  
Swee Keong Yeap , Malaysia  
Albert S. Yeung , USA  
Ebrahim M. Yimer , Ethiopia  
Yoke Keong Yong , Malaysia  
Fadia S. Youssef , Egypt  
Zhilong Yu, Canada  
RONGJIE ZHAO , China  
Sultan Zahiruddin , USA  
Armando Zarrelli , Italy  
Xiaobin Zeng , China  
Y Zeng , China  
Fangbo Zhang , China  
Jianliang Zhang , China  
Jiu-Liang Zhang , China  
Mingbo Zhang , China  
Jing Zhao , China  
Zhangfeng Zhong , Macau  
Guoqi Zhu , China  
Yan Zhu , USA  
Suzanna M. Zick , USA  
Stephane Zingue , Cameroon






## Contents

### ***Zingiber officinale* and *Vernonia amygdalina* Infusions Improve Redox Status in Rat Brain**

Damilare Emmanuel Rotimi , Goodnews Mavoghenegbero Ben-Goru, Ikponmwosa Owen Evbuomwan, Tobiloba Christiana Elebiyo, Mohammed Alorabi, Abdullah Farasani, Gaber El-Saber Batiha , and Oluoyomi Stephen Adeyemi 


Research Article (9 pages), Article ID 9470178, Volume 2022 (2022)

### **Ethnobotanical Study of Medicinal Plants Used against COVID-19**

Mohamed Chebaibi , Dalila Boust, Mohammed Bourhia , Soukayna Baammi, Ahmad Mohammad Salamatullah , Hiba-Allah Nafidi, Hasnae Hoummani, and Sanae Achour





Research Article (6 pages), Article ID 2085297, Volume 2022 (2022)

### **The Clinical Effect and Mechanism of Prostant on Urinary Retention and Anal Pain**

Wei-Min Luo, Han Du, Hong-Liang Jiang , Ying-Jun Deng, Xue Liang, Ping Qiu, and Yao Cheng



Research Article (13 pages), Article ID 2570169, Volume 2022 (2022)

### **Ethnomedicinal Use, Phytochemistry, and Other Potential Application of Aquatic and Semiaquatic Medicinal Plants**

Ashish Kumar Arya , Medha Durgapal , Arachna Bachheti , Deepti , Kamal Kant Joshi , Yilma H. Gonfa , Rakesh Kumar Bachheti , and Azamal Husen 

Review Article (19 pages), Article ID 4931556, Volume 2022 (2022)

### **Inhibitory Effects of Rhein on Renal Interstitial Fibrosis via the SHH-Gli1 Signal Pathway**

Yan Luo, Juan Jiang, Junxiong Cheng, Chen Xuan, Yu Xiong, Weijian Xiong , Wenfu Cao, and Ying Li 





Research Article (10 pages), Article ID 4398265, Volume 2022 (2022)

### **Effect and Mechanism of Flavored Tongxie Yaofang Decoction for Diarrheal Irritable Bowel Syndrome under Intestinal Microecology**

Shunyong He, Qiong Lin, Jianfeng Huang, Lin Zheng, Jinmei Lai, and Chaoyuan Chen 

Research Article (7 pages), Article ID 3904571, Volume 2022 (2022)

### **Sulfated Polysaccharides Derived from *Hypnea valentiae* and Their Potential of Antioxidant, Antimicrobial, and Anticoagulant Activities with *In Silico* Docking**

Kokila Palani, Balamuralikrishnan Balasubramanian , Arunkumar Malaisamy, Viji Maluventhen, Vijaya Anand Arumugam , Naif Abdullah Al-Dhabi, Mariadhas Valan Arasu, Karthika Pushparaj, Wen-Chao Liu , and Maruthupandian Arumugam 



Research Article (15 pages), Article ID 3715806, Volume 2022 (2022)

### **Deciphering the Metabolomics-Based Intervention of Yanghe Decoction on Hashimoto's Thyroiditis**

Xing Zhang , Dexuan Chen , Kun Xu , and Zhaoqun Ma 


Research Article (29 pages), Article ID 6215573, Volume 2022 (2022)

### **Synovitis Ointment Improved Knee Osteoarthritis by Suppressing SDF-1/CXCR4 Signaling Pathway**

Jin Zhang, Min Zhao, Jing Liu, Ke Wang, Xiang Cai, Wei Xiao, Le Wang, Mang Wang, Lei Zhang , and Chi Zhang 














Research Article (8 pages), Article ID 7719301, Volume 2022 (2022)

**Loquat Leaf Extract Enhances Muscle Contraction-Induced Activation of Protein Synthesis Signaling in Rat Skeletal Muscle**

Yung-Li Hung, Riki Kosugi, Toshiharu Natsume, and Shuichi Machida 


Research Article (6 pages), Article ID 2234118, Volume 2022 (2022)

**Bioactive Natural Products against Systemic Arterial Hypertension: A Past 20-Year Systematic and Prospective Review**

Maisa Gomes da Silva , Sara Léa Fortes Barbosa , Diego Santos Silva , Isadora Basílio Meneses Bezerra , Érika Alves Bezerra , Angélica Gomes Coelho , Ilmara Cecília Pinheiro da Silva Morais , Luis Mário Rezende-Júnior , Iolanda Souza do Carmo , José de Sousa Lima-Neto , Simón Gabriel Comerma-Steffensen , Antônia Maria das Graças Lopes Citó , and Daniel Dias Rufino Arcanjo 



Review Article (21 pages), Article ID 8499625, Volume 2022 (2022)

***Reineckia carnea* Alleviates the Production of Inflammatory Cytokines and MUC5AC in Rats with Chronic Obstructive Pulmonary Disease**

Wei Liu , Jiang Li, Tongyao Li, Youliang Xie, and Caihong Luo


Research Article (8 pages), Article ID 2135487, Volume 2022 (2022)

**Network Pharmacology and Pharmacological Mechanism of CV-3 in Atrial Fibrillation**

Zundong Wang , Zhen Zeng, Yongsheng Hu, Hengcan Sun, Ying Tang, and Weiqin Liu 






Research Article (9 pages), Article ID 5496299, Volume 2022 (2022)

**Phillyrin Prevents Ovariectomy-Induced Osteolysis by Inhibiting Osteoclast Differentiation**

Geng Zhang, Ying Zhang, Cong Wang, Chenhe Zhou, and Shigui Yan 

Research Article (6 pages), Article ID 6065494, Volume 2022 (2022)

**Profile of Medicinal Plants Traditionally Used for the Treatment of Skin Burns**

Hanae Naceiri Mrabti , Latifa Doudach, Mouna Mekkaoui, Zineb Khalil, Khoulood Harraqui, Fozia Fozia , Nidal Naceiri Mrabti, Mohamed El-Shazly, Amal Alotaibi , Riaz Ullah , Moulay El Abbes Faouzi, and Abdelhakim Bouyahya 







Research Article (10 pages), Article ID 3436665, Volume 2022 (2022)

**Phytochemical Profiling, Antioxidant Activity, and *In Silico* Analyses of *Sterculia villosa* and *Vernonia patula***

Chadni Lyzu, Saikat Mitra, Kahkashan Perveen, Zidan Khan, Abu Montakim Tareq , Najat A. Bukhari, Fohad Mabood Husain, Evenar Parvin Lipy, Dipa Islam, Mahmuda Hakim, Talha Bin Emran , and Marjan Ganjali Dashti

Research Article (18 pages), Article ID 3190496, Volume 2022 (2022)



**Bioassay's Directed Isolation-Structure Elucidation and Molecular Docking of Triterpenes from *Persea duthiei* against Biologically Important Microbial Proteins**

Najeeb Ullah , Shan Zeb, Fozia , Shah Rukh, Shafuallah Khan , Ijaz Ahmad , Shakeel Ahmad, Nisar Ahmad, Amal Alotaibi , and Riaz Ullah 

Research Article (12 pages), Article ID 3839271, Volume 2022 (2022)


## Contents

### **Protective Effect of Salvianolic Acid A against N-Methyl-N-Nitrosourea-Induced Retinal Degeneration**

Yumei Zhou, Weiwei Xu, Anqi Liu, Ye Tao, Qun Wang, Yanfeng Yang, Liqiang Wang , and Yifei Huang 

Research Article (10 pages), Article ID 1219789, Volume 2022 (2022)

### **Ameliorative Potential of Resveratrol in Dry Eye Disease by Restoring Mitochondrial Function**

Jingyao Chen, Weijia Zhang, Yixin Zheng, and Yanze Xu 







Research Article (10 pages), Article ID 1013444, Volume 2022 (2022)

### **Inhibitory Effects of Mongolian Medicine Yihe-Tang on Continuous Darkness Induced Liver Steatosis in Zebrafish**

Rigaiqiqige Sa, Chi Feng, Hongxia Bai, Xiaoyu Yin, Lei Song, Xiaodong Hu, Rui Xu, Xinshan Li, Wu Dong , and Jingfeng Yang 


Research Article (11 pages), Article ID 5794655, Volume 2022 (2022)

### **Phytochemical Analysis, Antioxidant, Antimicrobial, and Anti-Swarming Properties of *Hibiscus sabdariffa* L. Calyx Extracts: *In Vitro* and *In Silico* Modelling Approaches**

Bechr Hamrita , Noumi Emira , Adele Papetti , Riadh Badraoui , Lamjed Bouslama , Mohamed-Iheb Ben Tekfa, Assia Hamdi , Mitesh Patel , Abdelbaset Mohamed Elsbali , Mohd Adnan , Syed Amir Ashraf , and Mejdi Snoussi 



Research Article (14 pages), Article ID 1252672, Volume 2022 (2022)

### **Study on the Mechanism of Shenjing Guben Prescription Regulating PI3K and NRF2 Signaling Pathway in the Treatment of Immune Infertility**

Handu Liu , Jianguo Xue, and Hui Mo



Research Article (9 pages), Article ID 8754188, Volume 2022 (2022)

### **Gambogic Acid and Piperine Synergistically Induce Apoptosis in Human Cholangiocarcinoma Cell via Caspase and Mitochondria-Mediated Pathway**

Rittibet Yapasert , and Ratana Banjerdpongchai 


Research Article (12 pages), Article ID 6288742, Volume 2022 (2022)

### **Orientin Enhances Colistin-Mediated Bacterial Lethality through Oxidative Stress Involvement**

Madonsela Khumbulani, Kazeem Adekunle Alayande , and Saheed Sabiu 

Research Article (9 pages), Article ID 3809232, Volume 2022 (2022)








### **Zhuye Shigao Decoction Combined with Qingqi Huatan Pills in Alleviating the Acute Exacerbation of Chronic Obstructive Pulmonary Disease (Phlegm-Heat Stagnating in the Lungs) via the IL-6-Mediated JAK1/STAT3 Signaling Pathway**

Yunkun Chen and Wenbin Zhang 

Research Article (12 pages), Article ID 7942623, Volume 2022 (2022)


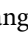



**Efficiency of *Coriandrum sativum* (Linn.) and *Petroselinum crispum* (Mill.) in Enhancing Iron**

**Absorption: An *In Silico* and *In Vitro* Approach**

T. Sangeetha , K. Syed Ibrahim , S. Deepa , B. Balamuralikrishnan , M. Arun, S. Velayuthaprabhu ,  
K. M. Saradhadevi , and A. Vijaya Anand 

Research Article (8 pages), Article ID 7359081, Volume 2022 (2022)

**The Multiple Pharmacologic Functions and Mechanisms of Action of Guizhi Fuling Formulation**

Jie Gao , Jianmei Yang , Zhiyuan Lu , Xianwen Dong , and Ying Xu 


Review Article (14 pages), Article ID 6813421, Volume 2022 (2022)

**Naringin Alleviates H<sub>2</sub>O<sub>2</sub>-Inhibited Osteogenic Differentiation of Human Adipose-Derived Stromal Cells via Wnt/ $\beta$ -Catenin Signaling**

Xufang Yang , Jianjiang Dong , Yankun Hao , Yucheng Qi , Jun Liang , Lei Yan , and Wenting Wang 


Research Article (5 pages), Article ID 3126094, Volume 2022 (2022)

**Efficacy and Mechanism of *Mallotus furetianus* Müll. Arg. Extract on Nonalcoholic Fatty Liver Disease**

Daobin Lin, Yi Ding, Yabo Cheng, Yubin Chen, Yunting Tang, Xiaowen Wu, and Yawei Cheng 



Research Article (12 pages), Article ID 4897463, Volume 2022 (2022)

**Deciphering the Molecular Mechanism of Red Raspberry in Apoptosis of Liver Cancer Cells**

Linlin Song, Qi Li, Hui Shi, and Hui Yue 

Research Article (7 pages), Article ID 2026865, Volume 2022 (2022)

**Photoprotective Potential, Cytotoxicity, and UPLC-QTOF/MS Analysis on Bioactive Solvent Fractions of *Moringa concanensis* Nimmo Bark**

Rameshkumar Santhanam , Thiruventhan Karunakaran , Kandhasamy Sowndhararajan, Muhammad Faiz Zulkifli, Mouriya Govindan Kothandaraman, Veerasamy Aravindhan, and Wan Iryani Wan Ismail

Research Article (10 pages), Article ID 3781189, Volume 2022 (2022)

**Systematic Elaboration of the Pharmacological Targets and Potential Mechanisms of ZhiKe GanCao Decoction for Preventing and Delaying Intervertebral Disc Degeneration**

Wanqing Sun , Yuan Chen , and Miao Li 







Research Article (11 pages), Article ID 8786052, Volume 2022 (2022)

**Effect of Licochalcone-A Combined with *Rab23* Gene on Proliferation of Glioma U251 Cells**

Yindong Mu , Jianjiang Dong , Hong Cui , Jiangping Hu , Jun Liang , and Lei Yan 

Research Article (8 pages), Article ID 9299442, Volume 2022 (2022)


**Fucoxanthin, a Marine Carotenoid, Suppresses *Mycoplasma pneumoniae*-Triggered Inflammatory Cytokine Production and Promotes Bacterial Clearance in a Murine Model**

Hongbo Wu , Shu Li , Linlin Wang , Jun Liang , Lei Yan , and Jianjiang Dong 






Research Article (5 pages), Article ID 6238162, Volume 2022 (2022)

## Contents



### **Effect of Zhujingqiaoyun Receptivity of Infertility with Kidney Deficiency Based on Ultrasonic Evaluation**

Xiaoli Mao, WeiMao, Ling Zhong, Zhun Qu, Huimin Chen, Qiaomin Wang, and Jingjing He   
Research Article (6 pages), Article ID 3675689, Volume 2022 (2022)


### **Topical Application of *Premna integrifolia* Linn on Skin Wound Injury in Rats Accelerates the Wound Healing Process: Evidence from *In Vitro* and *In Vivo* Experimental Models**

Saeed Ali Alsareii , Nasser A. N. Alzerwi , Mansour Yousef AlAsmari, Abdulrahman Manaa Alamri , Mater H. Mahnashi , and Ibrahim Ahmed Shaikh   
Research Article (14 pages), Article ID 6449550, Volume 2022 (2022)

### **Efficacy and Safety of Zuojin Pill for the Treatment of Chronic Nonatrophic Gastritis: A Randomized Active-Controlled Clinical Trial**

Ruilin Wang, Yanling Wang, Zheng Lu, Jing Jing, Zhongxia Wang, Tingting He, Miao Tian, Zongyang Yuan, Yanfei Cui, Wenya Rong, Xiao Ma , and Yanling Zhao   
Research Article (9 pages), Article ID 2266023, Volume 2022 (2022)


### **Artemisinin Alleviates Cerebral Ischemia/Reperfusion Injury via Regulation of the Forkhead Transcription Factor O1 Signaling Pathway**

Xiaogang Yang and Ke Wu   
Research Article (7 pages), Article ID 7824436, Volume 2022 (2022)


### **Antiosteoporosis Studies of 20 Medicine Food Homology Plants Containing Quercetin, Rutin, and Kaempferol: TCM Characteristics, *In Vivo* and *In Vitro* Activities, Potential Mechanisms, and Food Functions**

Dayue Shen , Yating Feng , Xilan Zhang , Le Gong , Jing Liu , Yuanping Li , and Hui Liao   
Review Article (20 pages), Article ID 5902293, Volume 2022 (2022)




### **Inhibitory Potential of Shen-Shuai-Ling Formulation on Renal Interstitial Fibrosis via Upregulation of PLZF**

Na Song, Haitao Tu, Ying Li , Weijian Xiong, Ling Zhang, Hong Liu, Weisen Ding, Mei Long, Dewei Ren, and Jin Zhong  
Research Article (9 pages), Article ID 5967804, Volume 2022 (2022)



### **GC-MS Analysis and Various *In Vitro* and *In Vivo* Pharmacological Potential of *Habenaria plantaginea* Lindl.**

Mater H. Mahnashi, Yahya S. Alqahtani, Bandar A. Alyami, Ali O. Alqarni, Mohammad Ahmed Alshrahili, Mahrous A. Abou-Salim, Mohammed N. Alqahtani, Sadaf Mushtaq, Abdul Sadiq, and Muhammad Saeed Jan   
Research Article (13 pages), Article ID 7921408, Volume 2022 (2022)





### **Wenyang Huazhuo Tuihuang Formula Inhibits the Th17/Treg Cell Imbalance and Protects against Acute-on-Chronic Liver Failure**

Xiufeng Wang, Yunqing Zhong, Rongzhen Zhang , Yueqiao Chen, Minggang Wang , Chao Lv, and Dewen Mao   
Research Article (11 pages), Article ID 5652172, Volume 2022 (2022)


**Acetyl-11-Keto- $\beta$ -Boswellic Acid (AKBA) Prevents Lipopolysaccharide-Induced Inflammation and Cytotoxicity on H9C2 Cells**

Danial Taherzadeh, Vafa Baradaran Rahimi, Hamed Amiri, Sajjad Ehtiati, Roghayeh Yahyazadeh, Seyed Isaac Hashemy , and Vahid Reza Askari   
Research Article (10 pages), Article ID 2620710, Volume 2022 (2022)


**Folecitin Isolated from *Hypericum oblongifolium* Exerts Neuroprotection against Lipopolysaccharide-Induced Neuronal Synapse and Memory Dysfunction via p-AKT/Nrf-2/HO-1 Signalling Pathway**

Umar Farooq, Muhammad Umar Khayam Sahibzada, Taous Khan , Rahim Ullah, Muhammad Shahid, Ameer Khusro , Veronique Seidel, Magda H. Abdellattif , and Talha Bin Emran   
Research Article (10 pages), Article ID 9419918, Volume 2022 (2022)







**Identification of Key Drug Targets and Molecular Mechanisms of Curcuma Rhizoma Acting on HBV-Related HCC: Weighted Correlation Network and Network Pharmacological Analyses**

Mengyuan Zhao, Yun Fu, Lili Liu, Yong Hou, Mei Shi, Hao Zhou, and Guoliang Zhang   
Research Article (15 pages), Article ID 5399766, Volume 2022 (2022)

**GC-MS Analysis, Heavy Metals, Biological, and Toxicological Evaluation of *Reseda muricata* and *Marrubium vulgare* Methanol Extracts**

Riaz Ullah  and Ali S. Alqahtani  
Research Article (9 pages), Article ID 2284328, Volume 2022 (2022)



















**Cytoprotective Antioxidant, Anti-Inflammatory, and Antifibrotic Impact of Celery Seed Oil and Manuka Honey Against Cyclophosphamide-Induced Cystitis in Rabbits**

Ayman M. Mousa , Khaled S. Allemailem , Fahad A. Alhumaydhi , Faris Alrumaihi, Ahmad Almatroudi , Mohammad Aljasir , Ameen S. S. Alwashmi, Osamah Al Rugaie, Khaled E. A. Soliman, Abdullah S. M. Aljohani , Waleed Al Abdulmonem, Ahmed A. Ahmed, Arif Khan, Masood A. Khan, Naif AlSuhaymi, Mahdi H. Alsugoor, Wafa Abdullah Al-Megrin, and Abulmaaty M. Elsayed  
Research Article (11 pages), Article ID 2863023, Volume 2022 (2022)

**Mechanism of Zhen Wu Decoction in the Treatment of Heart Failure Based on Network Pharmacology and Molecular Docking**








Chen-Yu Ma, Yu-Qian Ma, and Min Deng   
Research Article (10 pages), Article ID 4877920, Volume 2022 (2022)

**Traditional Uses, Phytochemistry, and Bioactivities of *Mesosphaerum suaveolens* (L.) Kuntze**

José Weverton Almeida-Bezerra , Felicidade Caroline Rodrigues , José Jailson Lima Bezerra , Anderson Angel Vieira Pinheiro , Saulo Almeida de Menezes , Aline Belém Tavares , Adrielle Rodrigues Costa , Priscilla Augusta de Sousa Fernandes , Viviane Bezerra da Silva , José Galberto Martins da Costa , Rafael Pereira da Cruz , Maria Flaviana Bezerra Morais-Braga , Henrique Douglas Melo Coutinho , Edward Teixeira de Albergaria , Marcos Vinicius Meiado , Abolghasem Siyadatpanah , Bonglee Kim , and Antônio Fernando Morais de Oliveira   
Review Article (28 pages), Article ID 3829180, Volume 2022 (2022)

## Contents


### **Harnessing the Natural Toxic Metabolites in COVID-19**

Ali Bahrami , Mohammad Taheri , Mohammad Reza Arabestani , Meysam Soleimani ,  
Mojdeh Mohammadi , Fatemeh Golabchi, Maryam Banitorfi, Seyed Mostafa Hosseini , Sodabe  
Khodabandehlou, and Fatemeh Nouri   
Review Article (7 pages), Article ID 3954944, Volume 2022 (2022)




### **Mechanism of Huoluo Xiaoling Dan in the Treatment of Psoriasis Based on Network Pharmacology and Molecular Docking**

Ke Gong , Wen Guo, Kaiqing Du, Fang Wang, Mengli Li, and Jianhui Guo   
Research Article (12 pages), Article ID 7053613, Volume 2022 (2022)




### **Molecular Mechanism Investigation on Monomer Kaempferol of the Traditional Medicine Dingqing Tablet in Promoting Apoptosis of Acute Myeloid Leukemia HL-60 Cells**

Dandan Zheng, Yongming Zhou, Yong Liu, Lihai Ma, and Lingzhan Meng   
Research Article (11 pages), Article ID 8383315, Volume 2022 (2022)




### **Ethnopharmacological-Based Validation of *Polyalthia suberosa* Leaf Extract in Neurological, Hyperalgesic, and Hyperactive Gut Disorders Using Animal Models**

Ruhul Amin , Cristina Quispe, Jesús Herrera-Bravo , Md. Mizanur Rahman, Radmila Novakovic,  
Sevgi Durna Daştan, Atul Kabra, and Javad Sharifi-Rad   
Research Article (9 pages), Article ID 1345006, Volume 2022 (2022)


### **Ethnobotanical Study of Medicinal Plants Used as Therapeutic Agents to Manage Diseases of Humans**

Sanae Achour, Mohamed Chebaibi , Hanane Essabouni, Mohammed Bourhia , Lahcen Ouahmane,  
Ahmad Mohammad Salamatullah , Mourad A M Aboul-Soud, and John P. Giesy  
Research Article (8 pages), Article ID 4104772, Volume 2022 (2022)



### **Evaluation of Antioxidant, Cytotoxic, Anti-Inflammatory, Antiarthritic, Thrombolytic, and Anthelmintic Activity of Methanol Extract of *Lepidagathis hyalina* Nees Root**

Shafiqul Islam, Fowzul Islam Fahad, Arifa Sultana, Syed Al Jawad Sayem, Shawon Baran Roy, Mohammad  
Nazmul Islam , Arpita Roy , and Mohammed Abu Sayeed   
Research Article (10 pages), Article ID 2515260, Volume 2022 (2022)

### **Shen-Shuai-Ling Formulation Attenuates Renal Interstitial Fibrosis in Chronic Kidney Disease by Regulating SHH-Gli1 Signaling Pathway**







Ying Li, Haitao Tu, Yan Luo , Weijian Xiong , Hong Liu, Yanying Xiong, Qin Zhang, Huihui Li, and  
Xuan Gao  
Research Article (10 pages), Article ID 3754985, Volume 2022 (2022)

### ***Camelina sativa* Oil Treatment Alleviates Castor Oil-Induced Diarrhea in ICR Mice by Regulating Intestinal Flora Composition**



Jie Zhu , Liqin Yu, Yi Fan , Huanan Zhang, Feifei Li, Xiao Li, Yue Wei, and Zhiyao Wang  
Research Article (12 pages), Article ID 5394514, Volume 2022 (2022)







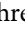






**Network Pharmacology- and Molecular Docking-Based Identification of Potential Phytochemicals from *Argyrea capitiformis* in the Treatment of Inflammation**

Ahmad J. Obaidullah , Mohammed M. Alanazi , Nawaf A. Alsaif, Ashwag S. Alanazi, Hussam Albassam , Alanazi AZ , Osama I. Alwassil , Ali M. Alqahtani , and Abu Montakim Tareq  
Research Article (22 pages), Article ID 8037488, Volume 2022 (2022)




**Insecticidal, Antimalarial, and Antileishmanial Effects of Royal Jelly and Its Three Main Fatty Acids, *trans*-10-Hydroxy-2-decenoic Acid, 10-Hydroxydecanoic Acid, and Sebacic Acid**

Abeer Mousa Alkhaibari  and Abdullah D. Alanazi   
Research Article (9 pages), Article ID 7425322, Volume 2022 (2022)



**Phytochemical Analysis,  $\alpha$ -Glucosidase and Amylase Inhibitory, and Molecular Docking Studies on *Persicaria hydropiper* L. Leaves Essential Oils**

Mater H. Mahnashi , Yahya S. Alqahtani , Bandar A. Alyami , Ali O. Alqarni, Muhammad Ayaz , Mehreen Ghufuran , Farhat Ullah , Abdul Sadiq , Ihsan Ullah , Ikram Ul Haq , Mohammad Khalid , and H. C. Ananda Murthy   
Research Article (11 pages), Article ID 7924171, Volume 2022 (2022)

***Allium cepa*: A Treasure of Bioactive Phytochemicals with Prospective Health Benefits**

Arka Jyoti Chakraborty, Tanvir Mahtab Uddin, B. M. Redwan Matin Zidan, Saikat Mitra, Rajib Das, Firzan Nainu, Kuldeep Dhama, Arpita Roy , Md. Jamal Hossain , Ameer Khusro, and Talha Bin Emran   
Review Article (27 pages), Article ID 4586318, Volume 2022 (2022)


**Caffeic Acid Prevents Vascular Oxidative Stress and Atherosclerosis against Atherosclerogenic Diet in Rats**

Ying Wang , Gurpreet Kaur , Manish Kumar , Ajay Singh Kushwah , Atul Kabra , and Ritu Kainth   
Research Article (8 pages), Article ID 8913926, Volume 2022 (2022)

**Distribution of Therapeutic Efficacy of Ranunculales Plants Used by Ethnic Minorities on the Phylogenetic Tree of Chinese Species**

Da-Cheng Hao , Yulu Zhang , Chun-Nian He , and Pei-Gen Xiao   
Research Article (10 pages), Article ID 9027727, Volume 2022 (2022)

**Quanzhenyiqitang Reverses LPS-Induced Inflammation via Inhibiting PYK2/p38MAPK/HDAC2/CK2 Signaling Pathway in Rat Alveolar Macrophage**

Ke-Qiang Chen, Da-zhi Li, Zhi-bin Chen, Chuan-lin Zhang, Bin-can Wang, and Chun-e Wang   
Research Article (11 pages), Article ID 7857022, Volume 2022 (2022)










**Structure-Based In Silico Investigation of Agonists for Proteins Involved in Breast Cancer**

Arpita Roy , Ashutosh Anand, Saksham Garg , Mohd Shahnawaz Khan, Sidharth Bhasin , Muhammad Nadeem Asghar, and Talha Bin Emran   
Research Article (12 pages), Article ID 7278731, Volume 2022 (2022)





## Contents

---

**Hepatoprotective Effects of (-) Epicatechin in CCl<sub>4</sub>-Induced Toxicity Model Are Mediated via Modulation of Oxidative Stress Markers in Rats**

Khadijah B. Alkinani , Ehab M. M. Ali , Turki M. Al-Shaikh , Jalaluddin A. Awlia Khan , Tahani M. Al-naomasi , Soad S. Ali , Asaad A. Abduljawad , Osama F. Mosa , and Tariq A. Zafar   
Research Article (12 pages), Article ID 4655150, Volume 2021 (2021)

**The Effect of Terpenoid Natural Chinese Medicine Molecular Compound on Lung Cancer Treatment**

Heng Sun , Lijia Zhang , Bowen Sui , Yu Li , Jun Yan, Peng Wang, Ye Wang, and Songjiang Liu   
Review Article (13 pages), Article ID 3730963, Volume 2021 (2021)

## Research Article

# Zingiber officinale and Vernonia amygdalina Infusions Improve Redox Status in Rat Brain

**Damilare Emmanuel Rotimi** <sup>1,2</sup>, **Goodnews Mavoghenegbero Ben-Goru**<sup>1,2</sup>,  
**Ikponmwoa Owen Evbuomwan**<sup>3</sup>, **Tobiloba Christiana Elebiyo**<sup>1,2</sup>, **Mohammed Alorabi**<sup>4</sup>,  
**Abdullah Farasani**<sup>5</sup>, **Gaber El-Saber Batiha** <sup>6</sup>, and **Oluyomi Stephen Adeyemi** <sup>1,2,7</sup>

<sup>1</sup>SDG 03 Group-Good Health & Well-Being, Landmark University, Omu-Aran 251101, Kwara State, Nigeria

<sup>2</sup>Department of Biochemistry, Medicinal Biochemistry, Nanomedicine & Toxicology Laboratory, Landmark University, PMB 1001, Omu-Aran 251101, Nigeria

<sup>3</sup>Department of Microbiology, Cellular Parasitology Unit, College of Pure and Applied Sciences, Landmark University, PMB 1001, Omu-Aran 251101, Nigeria

<sup>4</sup>Department of Biotechnology, College of Sciences, Taif University, P.O. Box 11099, Taif 21944, Saudi Arabia

<sup>5</sup>Department of Medical Laboratory Technology, Biomedical Research Unit, Medical Research Center, College of Applied Medical Sciences, Jazan University, Jazan 45142, Saudi Arabia

<sup>6</sup>Department of Pharmacology and Therapeutics, Faculty of Veterinary Medicine, Damanshour University, Damanshour 22511, AlBeheira, Egypt

<sup>7</sup>Laboratory of Sustainable Animal Environment, Graduate School of Agricultural Science, Tohoku University, 232-3 Yomogida, Naruko-Onsen, Osaki, Miyagi 989-6711, Sendai, Japan

Correspondence should be addressed to Oluyomi Stephen Adeyemi; yomibowa@yahoo.com

Received 14 February 2022; Accepted 6 September 2022; Published 26 September 2022

Academic Editor: Ruchika Garg

Copyright © 2022 Damilare Emmanuel Rotimi et al. This is an open access article distributed under the Creative Commons Attribution License, which permits unrestricted use, distribution, and reproduction in any medium, provided the original work is properly cited.

The study investigated the effects of *Zingiber officinale* root and *Vernonia amygdalina* leaf on the brain redox status of Wistar rats. Twenty-four (24) rats weighing  $160 \pm 20$  g were randomly assigned into four (4) groups, each with six (6) rats. Animals in Group 1 (control) were orally administered distilled water (1 mL), while the test groups were orally administered 5 mg/mL of either *Z. officinale*, *V. amygdalina* infusion, or a combination of both, respectively, for 7 days. The rats were sacrificed at the end of treatments and blood and tissue were harvested and prepared for biochemical assays. Results showed that administration of *V. amygdalina* and *Z. officinale*, as well as their coadministration, reduced the levels of malondialdehyde (MDA), nitric oxide (NO), acetylcholinesterase (AChE), and myeloperoxidase (MPO) in rat brain tissue compared with the control group. Conversely, coadministration of *V. amygdalina* and *Z. officinale* increased the levels of reduced glutathione (GSH) in rat brain tissue compared with the control group. However, the administration of the infusions singly, as well as the combination of both infusions, did not have any effect on the rat brain levels of glutathione peroxidase (GPx) and catalase (CAT) antioxidant enzymes compared to the control. Taken together, the findings indicate that the *V. amygdalina* and *Z. officinale* tea infusions have favorable antioxidant properties in the rat brain. The findings are confirmatory and contribute to deepening our understanding of the health-promoting effects of *V. amygdalina* and *Z. officinale* tea infusions.

## 1. Introduction

Over time, man has gradually gained knowledge and application of plants as sources of food and medicine through trial and error, and he has become able to source for his

needs from his immediate environment. The application of these plants is being refined bit by bit due to technological and scientific advances. In many regions of the world, medicinal plants contribute to primary health care delivery especially in their use as vital sources of pharmaceutical and

therapeutic products, with approximately 80% of the human population globally depending on natural products for primary health care [1, 2]. Medicinal plants are used singly or in combination with other substances (to increase treatment efficacy for several therapies) in the preparation of traditional or alternative medicines [3, 4].

Ginger (*Zingiber officinale*), belonging to the family Zingiberaceae, is a popular spice and herb used as a delicacy. *Z. officinale* has long been in use therapeutically and is currently validated as a potent medicinal spice to manage numerous diseases such as diabetes, hypertension, cancer, ulcer, diarrhea, cold, cough, spasms, and vomiting [5]. It is an effective spasmolytic, antipyretic, antiemetic, antioxidant, antiulcer, analgesic, hypotensive, antidiabetic, and anti-inflammatory agent containing scented essential oils and spicy oleoresins. The phenolic compounds (gingerols, shogaols, paradol, and gingerdiones) in *Z. officinale* have been discovered to be the source of their pharmacological benefits [5]. On the other hand, bitter leaf (*Vernonia amygdalina*) is a shrub or small tree belonging to the family Asteraceae that grows predominantly in tropical regions in Africa and Asia with the leaves having a characteristic bitter taste. For hundreds of years, bitter leaf serves as fodder, food, and herbal medicine [6]. *V. amygdalina* is rich in minerals such as potassium, magnesium, zinc, iron, and vitamins A, C, and E [7]. The shrub has been known to exhibit profound pharmacological properties such as antimalarial, antioxidant, antimicrobial anticancer, neuroprotective, anti-inflammatory, and anthelmintic properties [8–12]. The pharmacological properties of the bitter leaf have been reported to be connected to its phytochemical constituents which include flavonoids, steroidal saponins, alkaloids, sesquiterpene lactones, anthraquinones, polyphenolics, and coumarins [3, 13]. Interestingly, *Z. officinale* and *V. amygdalina* are useful components in traditional medical systems like Ayurveda to manage neurodegenerative conditions [14, 15].

Oxidative phosphorylation leads to the production of oxidants and free radicals including reactive oxygen species (ROS) and reactive nitrogen species (RNS), the two most important signaling molecules that help to sustain cellular proliferation and differentiation, trigger stress-responsive survival mechanisms, and maintain cellular homeostasis [16–18]. Under normal physiological conditions at redox equilibrium, harmful effects of the production of ROS and other free radicals during aerobic metabolism are counterbalanced by the antioxidant system, and in this way, the organs in the body including the brain efficiently regulate their oxygen consumption and redox generation capacity [19, 20]. However, when the production of ROS, other free radicals, and radical reactive species surpasses the scavenging ability of the antioxidant response system, a situation referred to as redox imbalance ensues [21]. The redox imbalance could cause oxidative cellular damage because of lipid peroxidation as well as protein and nucleic acid oxidation. The resulting oxidative stress could mediate the pathogenesis and pathophysiology of several diseases including neurodegenerative disorders and cardiovascular diseases [22–26].

The brain is one of the most metabolically active organs in the body and its oxygen consumption and redox generation capacity is under strict control. Although the brain of an adult human being weighs about 1.4 kg, it consumes approximately 20% of the total basal oxygen to power its high metabolic activity [27]. In addition, the low endogenous antioxidant defense mechanism of the brain makes it highly sensitive to oxidative damage. Therefore, ischemic/hypoxic or hyperoxic condition raises the levels of free radicals and disrupts redox homeostasis in the brain which could lead to cellular death [28, 29]. Various types of antioxidants play significant roles in redox homeostasis. These antioxidants comprise vitamins A, C, and E; glutathione, coenzyme Q, bilirubin, and ferritin; and endogenous antioxidant enzymes such as glutathione peroxidase (GPx), catalase (CAT), superoxide dismutase (SOD), glutathione reductase (GR), and heme oxygenase (HO) [30, 31]. Furthermore, many medicinal plants and their products have been shown to possess antioxidant defense capacity that helps protect against oxidative damage and maintain redox homeostasis [32–34]. Therefore, the present study aimed to determine the effect of *Z. officinale* and *V. amygdalina* infusions on rat brain redox status.

## 2. Materials and Methods

### 2.1. Identification and Authentication of the Sample.

*Z. officinale* roots were obtained from Omu-Aran market, Kwara state, while *V. amygdalina* leaves were acquired from Landmark University, Omu-Aran. Both plants were identified and authenticated at the Department of Plant Biology, University of Ilorin, Kwara State with voucher numbers; UILH|001|1023|2021 for *Z. officinale* and UILH|002|1083|2021 for *V. amygdalina*.

#### 2.1.1. Preparation of *Z. officinale* and *V. amygdalina* Infusion.

The *Z. officinale* root was washed with water, peeled, sun-dried, and pulverized into powder. The *V. amygdalina* leaf was washed, sun-dried, and the stalk was removed from the leaf before it was pulverized into powder. To make the infusion, the plant powder in the tea bag was steeped in hot water (5 mg/mL, 100°C) for 3–5 minutes [35]. The infusion was allowed to cool at room temperature (25°C) before use.

### 2.2. Phytochemical Analysis

#### 2.2.1. Qualitative Phytochemical Screening.

Qualitative screening for phytoconstituents of ginger and bitter leaf tea infusions was performed as previously described [13]. The phytochemicals assayed included saponin, phenolic compounds, water-soluble phenol, water-insoluble phenol, free and combined anthraquinones, flavonoids, poly steroid, cardiac glycosides, terpenoids, alkaloids, and tannins.

#### 2.2.2. Animal Grouping and Treatments.

The animals (24 rats) were obtained from the Department of Biochemistry, University of Ilorin, Nigeria. They were housed in a clean cage, allowed to acclimatize for 14 days, and administered

pelletized feed and water. The rats were assigned randomly into four (4) groups, consisting of six (6) rats each. Animals in Group 1 were orally administered distilled water (1 mL). Groups 2, 3, and 4 were orally administered 5 mg/mL of *Z. officinale*, *V. amygdalina*, and an oral combination of *Z. officinale* and *V. amygdalina* infusion, respectively. The treatments lasted for 7 days.

The animals received humane care in compliance with the institution's guidelines and criteria as outlined in the National Institute of Health (NIH) Guidelines for the care and use of laboratory animals, and this work had approval from the ethical committee of the Department of Biochemistry at Landmark University, reference number: LUAC/2021/003A.

After the last treatments, the animals were fasted overnight and sacrificed under mild anesthesia of diethyl ether. The brain was harvested, weighed, and homogenized in an isotonic medium (0.25 M sucrose solution). The homogenate was centrifuged at 5000 rpm for 10 min to obtain supernatants, which were used for biochemical analysis. A section of the brain was also preserved in 10% buffered neutral formalin (BNF) for a histopathology examination.

**2.2.3. Biochemical Assays.** The brain homogenates collected were used in the biochemical determination of redox markers. Total protein content in the rat brain homogenate was determined according to Gornall et al. [36]. Superoxide dismutase (SOD) and glutathione peroxidase (GPx) activities were assayed as previously reported by Misra and Fridovich [37] and Rotruck et al. [38], respectively. The procedures described by Beers and Sizer [39] and Pulli et al. [40] were used to assay for catalase (CAT) and myeloperoxidase (MPO), respectively. For the determination of reduced glutathione (GSH) and malondialdehyde (MDA) levels, the methods described by Beutler and Yeh [41] and Varshney and Kale [42] were used, respectively. Nitric oxide (NO) level and acetylcholinesterase (AChE) activity were determined using Adeyemi et al. [43] and Ellman et al. [44], respectively. DNA fragmentation was carried out following the procedure described by Perandones et al. [45].

**2.2.4. Histopathology Examination.** After the rat brain was excised from the animal, it was fixed in 10% BNF and subsequently processed for histopathology examinations as described by Adeyemi and Akanji [46]. Photomicrograph capture and scoring for morphological changes were done at the Pathology Unit, University of Ilorin Teaching Hospital, Ilorin, Nigeria.

**2.2.5. Statistical Evaluation.** The data were analyzed on GraphPad Prism Software (San Diego, CA, USA), using one-way ANOVA. Data are presented as the mean value of six replicates plus or minus the standard error of the mean (SEM). At *p* value of 0.05, mean values were considered significant.

### 3. Results

**3.1. Qualitative Phytochemical Analysis.** The qualitative phytochemical screening revealed the presence of saponin,

TABLE 1: Qualitative Phytochemical tests of the infusion of ginger, bitter leaf, and a combination of Ginger + Bitterleaf.

Phytochemical compounds	Ginger	Bitter leaf	Ginger + bitter leaf
Saponin	+	+	+
Phenolic compounds	+	+	+
Water insoluble phenol	+	+	+
Flavonoids	+	+	+
Free anthraquinones	+	+	+
Tannins	-	+	+
Alkaloids	+	+	+

+: Detected -: Not detected.

phenolics, flavonoids, alkaloids, and anthraquinones in the tea infusions of ginger and bitter leaf. However, tannins were not detected in ginger infusion but were present in bitter leaf (Table 1).

The administration of *Z. officinale* and *V. amygdalina* infusions separately had no significant effect on the rat brain superoxide dismutase (SOD) activity relative to control. In contrast, the coadministration of both infusions significantly increased the rat brain SOD activity in comparison with control (Figure 1(a)). As shown in Figure 1(d), the separate administration of *Z. officinale* and *V. amygdalina* infusions as well as the coadministration of both infusions did not significantly change the rat brain catalase (CAT) activity in relation to control (Figure 1(b)). As represented in Figure 1(c), there were no significant changes in the rat brain glutathione peroxidase activity in relation to control when *Z. officinale* and *V. amygdalina* infusions were administered separately. In addition, the coadministration of both infusions had a negligible effect on the rat brain glutathione peroxidase activity in relation to control. Glutathione level in the rat brain was reduced when *Z. officinale* infusion only was administered, as well as the coadministration of both infusions, when compared with the control (Figure 1(d)).

An appreciable decrease in the rat brain MDA level in comparison with the control was observed when the infusions were administered separately as well as coadministration of the infusions together (Figure 2(a)). In the same vein, the administration of the tea infusions separately or as a combination significantly decreased the level of the rat brain DNA fragmentation when compared with the control (Figure 2(b)).

Furthermore, the administration of the infusions separately, as well as in a combination, did not significantly affect the rat brain protein concentration when compared to control (Figure 3(a)). However, the administration of the infusions separately or as a combination significantly decreased the level of the rat brain nitric oxide (NO) in relation to control (Figure 3(b)). Figure 3(c) shows a substantial decrease in rat brain AChE activity in comparison with the control when the infusions were administered singly or in combination. Similarly, the rat brain MPO activity decreased when the infusions were administered separately or as a combination (Figure 3(d)).

For all the treatment groups, the histopathology examination revealed normal brain tissue composed of

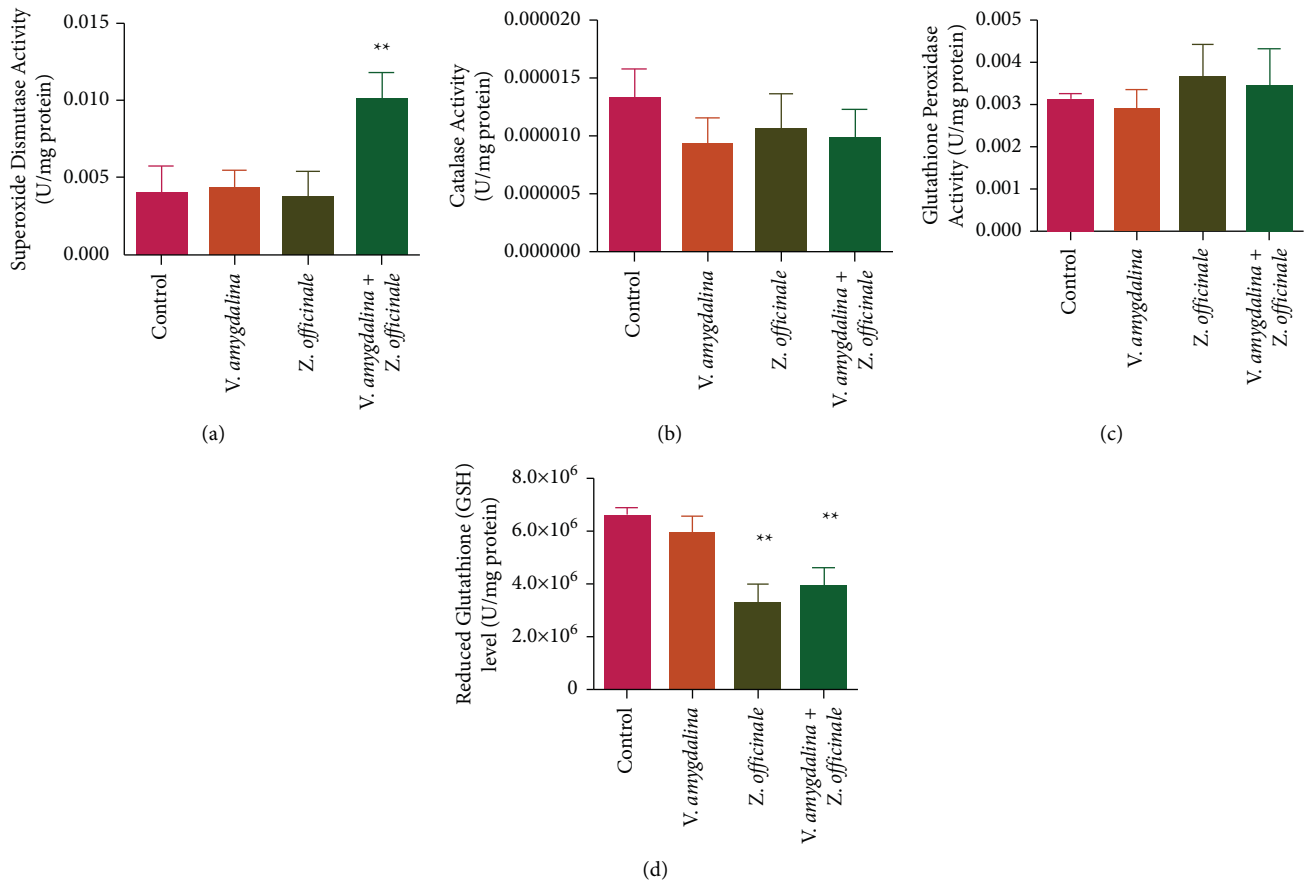


FIGURE 1: The effect of *Zingiber officinale* and *Vernonia amygdalina* on the levels of rat brain antioxidant molecules: (a) superoxide dismutase, (b) Catalase, (c) glutathione peroxidase, and (d) reduced glutathione. Each value is a mean of six replicates  $\pm$  SEM. Values bearing the asterisk are significantly different compared to the control at  $p < 0.05$ .

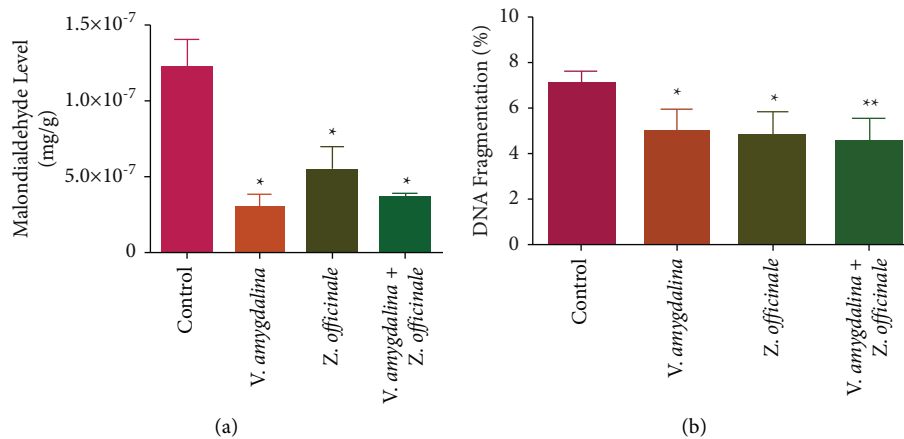


FIGURE 2: The effect of *Zingiber officinale* and *Vernonia amygdalina* on the level of rat brain oxidative stress markers: (a) malondialdehyde and (b) DNA fragmentation. Values are the mean of six replicates  $\pm$  SEM. Bars with the asterisk are significantly different from the control at  $p < 0.05$ .

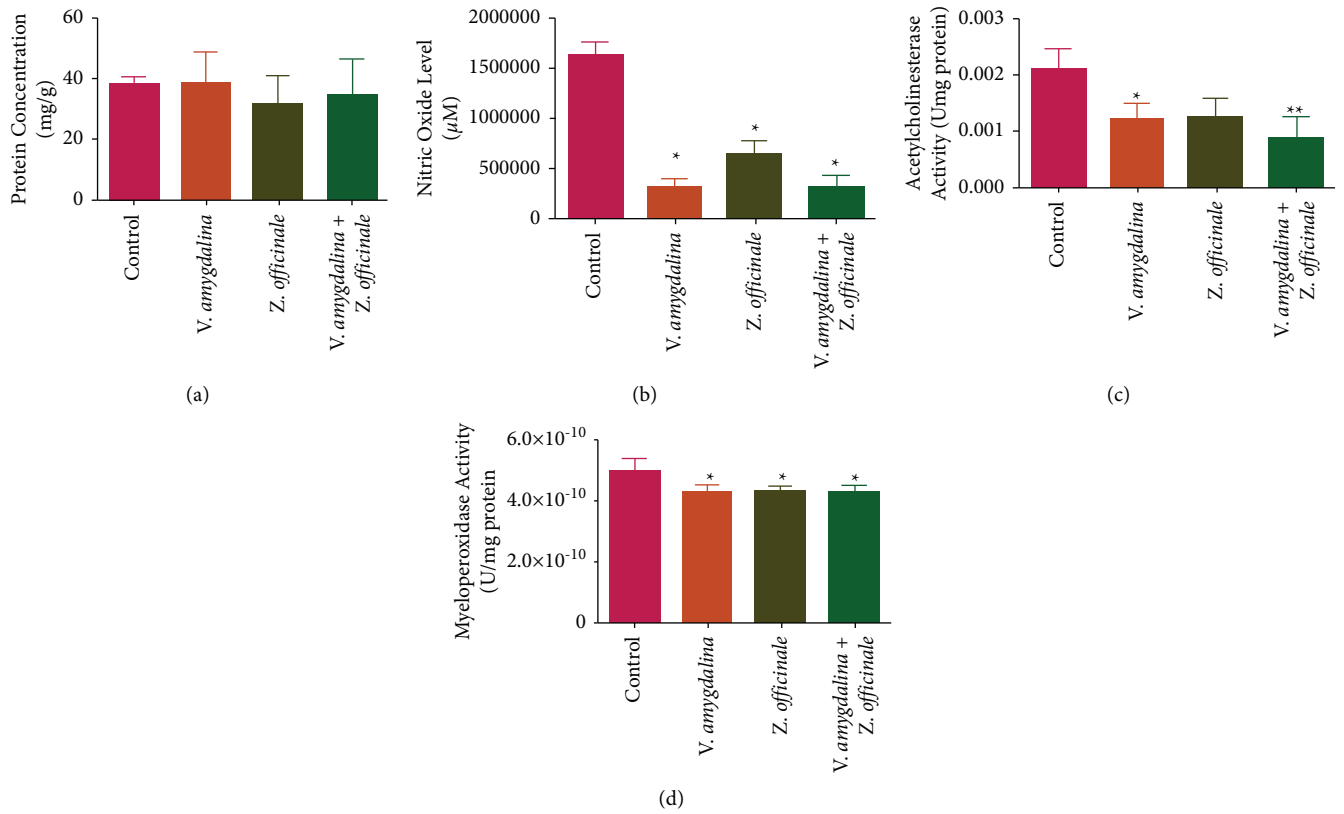


FIGURE 3: The effect of *Zingiber officinale* and *Vernonia amygdalina* on the level of rat brain biochemical parameters: (a) protein concentration, (b) nitric oxide, (c) acetylcholine esterase, and (d) myeloperoxidase. Values are the mean of six replicates  $\pm$  SEM. Bars with the asterisk are significantly different from the control at  $p < 0.05$ .

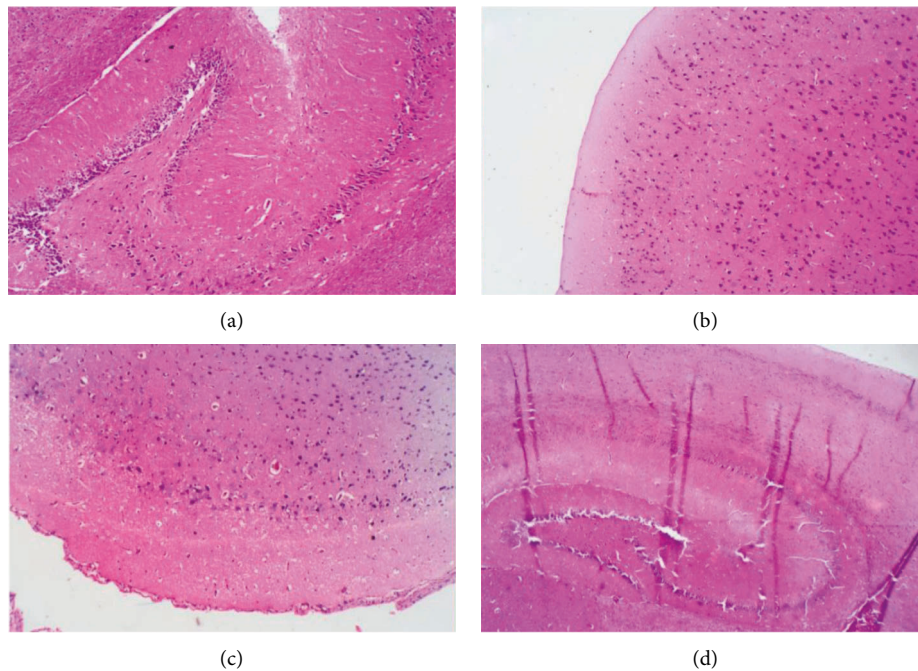


FIGURE 4: The effect of *Zingiber officinale* and *Vernonia amygdalina* on rat brain morphology: (a) control, (b) *Vernonia amygdalina*, (c) *Zingiber officinale*, and (d) combination of *Zingiber officinale* and *Vernonia amygdalina*. H&E staining (x100). The sections show normal brain tissue composed of preserved neuronal bodies surrounded by a fibrillary glial matrix (cerebral and hippocampal).



preserved neuronal bodies surrounded by a fibrillary glial matrix (cerebral and hippocampal). No observation of degenerative changes or significant inflammation (Figure 4).

#### 4. Discussion

This work investigated the effect of *Z. officinale* root and *V. amygdalina* leaf infusion on the redox status of the brain of rats to provide more understanding of the health-promoting effects of these commonly consumed medicinal plants. The phytochemical screening showed the presence of saponin, phenolics, flavonoids, free anthraquinones, and alkaloids. However, tannins were not detected in ginger but only in the tea infusions of bitter leaf and that of the combination of bitter leaf and ginger.

We found that the combined mixture of *V. amygdalina* and *Z. officinale* infusions led to a significant increase in SOD activity and an insignificant increase in GPx activity across all experimental groups when compared with the control. This finding could mean that the infusions enhanced the rat brain's oxidative defense status by improving the activities of SOD [47]. In addition, our study revealed that the combined administration of the infusions caused an insignificant increase in CAT activity but a significant decrease in reduced glutathione (GSH). GSH is an antioxidant molecule that quenches  $O_2^{\bullet-}$ ,  $HO^{\bullet}$ , and peroxynitrite anions (ONOO<sup>-</sup>) by the action of its thiol group, which donates a reducing equivalent to unstable radicals and anions that may have arisen due to respiratory processes and other metabolic activities in the body cells. In contrast to the increased antioxidant activity of SOD, CAT, and GPx, there was a significant decrease in the level of malondialdehyde (MDA), an end-product of lipid peroxidation during oxidative degradation of lipids usually caused by free radicals [48]. The coordinated function of enzymatic antioxidant systems including CAT, SOD, and GPx, and nonenzymatic antioxidants such as glutathione (GSH) and vitamin E play a significant role in the prevention of oxidative damage by ROS such as  $O_2^{\bullet-}$ ,  $HO^{\bullet}$  and  $H_2O_2$  [49, 50]. A significant decrease in the level of nitric oxide (NO), a proinflammatory agent, may indicate the anti-inflammatory action of the tea infusions. Nitric oxide (NO) participates in several physiological processes and is considered a free radical as it could accumulate and react with superoxide anion to form poisonous nitrite anion, thereby leading to nitrosative stress [51]. The decrease in the levels of both MDA and NO across all experimental groups in comparison with the control may be due to the antioxidant properties of *V. amygdalina* and *Z. officinale*. This implies that the tea infusions can suppress oxidative stress by inhibiting the production of MDA and NO in support of earlier reports [14, 52–54]. The tea infusions can limit the production of MDA and NO, and thereby prevent oxidative stress probably by enhancing the activities of the inherent enzymatic antioxidants in the rat brain. Myeloperoxidase (MPO) is a heme-containing peroxidase mainly expressed in neutrophils and, to a lesser extent, in monocytes. In the presence of  $H_2O_2$  and halides (HOCl), MPO catalyzes the formation of reactive oxygen intermediates such as hypochlorous acid. Microbial death by

neutrophils relies heavily on the MPO/HOCl system. In addition, MPO acts as a local mediator of tissue injury through inflammation [55]. The observed decrease in MPO activity due to the separate or combined administration of the tea infusions is consistent with the findings of Hussein et al. [56] and Erukainure et al. [57]. A decrease in MPO activity impedes neutrophil infiltration [58], supporting the anti-inflammatory effect of tea infusions. Furthermore, results showed a decrease in DNA fragmentation following the separate or combined administration of the tea infusions, corroborating an earlier report [57]. This fact further reinforces not only the antioxidant but also the anti-inflammatory potential of the tea infusions of *Z. officinale* and *V. amygdalina* and their capacity to protect against oxidative-induced DNA damage.

Acetylcholinesterase (AChE) is a serine hydrolase primarily responsible for the termination of signal transmission in the cholinergic system. Its substrate, acetylcholine (ACh), is a cholinergic neurotransmitter that has a strong effect on motor neurons involved in memory formation [59]. Therefore, the observed decrease in the activity of this AChE after a separate and combined administration of the tea infusions is similar to the findings reported in earlier studies [11, 59–61]. The present finding suggests that the tea infusions possess bioactive compounds that could decrease neurodegeneration or treat neurodegenerative diseases by modulating the activity of AChE. Protein is an important structural component of cells as well as a source of energy and one of the building blocks of human tissues. Extracellular and intracellular enzymes, as well as other proteins, contribute to the total protein concentrations [62]. The separate and the combined administration of the tea infusions of *V. amygdalina* and *Z. officinale* caused a negligible rise in total protein concentration, attributable to their capacity to boost the production of antioxidant proteins as reflected in the elevated levels of SOD and CAT. Furthermore, morphological examination of the rat brain revealed normal histological architectures of the cerebral and hippocampal in all the treatment groups. There are no features of degenerative changes or inflammation, thus corroborating the biochemical data and further underscoring the medicinal value of *V. amygdalina* and *Z. officinale* tea infusions in rat brains.

#### 5. Conclusions

The data from this work showed that *V. amygdalina* and *Z. officinale* infusions improved brain antioxidants and reduced oxidative stress after a 7-day separate or combined oral administration. The results support the efficacy of the tea infusions in maintaining redox status/homeostasis in rat brains. Taken together, the findings support the health-promoting effects of *V. amygdalina* and *Z. officinale*. Future studies may focus on the long-term effects of the tea infusions separately or as a combination to gain a better understanding of the therapeutic benefits of the medicinal plants.

#### Data Availability

The raw data are available from the corresponding author upon request.



## Additional Points

*Institutional Review Board Statement:* The protocol used in handling the animals was approved by the ethical committee of the Department of Biochemistry at Landmark University and assigned the reference number: LUAC/2021/003A.

## Conflicts of Interest

The authors declare that they have no conflicts of interest.

## Authors' Contributions

O.S.A. and A.T.A. conceptualized the data; O.S.A., H.F.H., and S.A.-R. curated the data; O.S.A., A.T.A., H.F.H., S.A.-R., D.R., and G.E.-S.B. formally analyzed the data; O.S.A. investigated the data; O.S.A., D.R., and G.E.-S.B. created methodology; H.H. and S.A.-R. found resources; O.S.A., A.T.A., D.R., and G.E.-S.B. wrote the original draft; O.S.A., A.T.A., H.F.H., S.A.-R., D.R., T.C.E., and G.E.-S.B. wrote, reviewed, and edited the draft. All authors have read and agreed to the published version of the manuscript.

## Acknowledgments

The authors appreciate the support of Taif University Researchers Supporting Project (number: TURSP-2020/310), Taif University, Taif, Saudi Arabia. In addition, the authors appreciation goes to Landmark University Nigeria.

## References

- [1] F. Jamshidi-Kia, Z. Lorigooini, and H. Amini-Khoei, "Medicinal plants: past history and future perspective," *Journal of Herbméd Pharmacology*, vol. 7, no. 1, p. 1, 2018.
- [2] S. Mlilo and S. Sibanda, "An ethnobotanical survey of the medicinal plants used in the treatment of cancer in some parts of Matebeleland, Zimbabwe," *South African Journal of Botany*, vol. 146, pp. 401–408, 2022, <https://doi.org/10.1016/j.sajb.2021.11.022>.
- [3] X. Liu, W. Tian, G. Wang et al., "Stigmastane-type steroids with unique conjugated  $\Delta^7$ , 9(11) diene and highly oxygenated side chains from the twigs of *Vernonia amygdalina*," *Phytochemistry*, vol. 158, pp. 67–76, 2019.
- [4] M. M. Matotoka and P. Masoko, "Phytochemical screening and pharmacological evaluation of herbal concoctions sold at Ga Maja Limpopo Province," *South African Journal of Botany*, vol. 117, pp. 1–10, 2018, <https://doi.org/10.1016/j.sajb.2018.04.013>.
- [5] F. O. Balogun, E. T. AdeyeOluwa, and A. O. T. Ashafa, "Pharmacological potentials of ginger," *Ginger Cultivation and its Antimicrobial and Pharmacological Potentials*, 2019.
- [6] O. Alara, N. Abdurahman, and O. Olalere, "Ethanol extraction of flavonoids, phenolics and antioxidants from *Vernonia amygdalina* leaf using two-level factorial design," *Journal of King Saud University-Science*, vol. 32, no. 1, pp. 7–16, 2020.
- [7] M. Johnson, O. S. Kolawole, and L. A. Olufunmilayo, "Phytochemical analysis, in vitro evaluation of antioxidant and antimicrobial activity of methanolic leaf extract of *Vernonia amygdalina* (bitter leaf) against *Staphylococcus aureus* and *Pseudomonas aeruginosa*," *Int. J. Curr. Microbiol. App. Sci*, vol. 4, pp. 411–426, 2015.
- [8] O. B. Akpor, J. Ndakotsu, I. O. Evbuomwan, T. D. Olaolu, and O. O. Osemwegie, "Bacterial growth inhibition and antioxidant potentials of leaf infusions of (*Moringa oleifera*), locust beans (*Parkia biglobosa*) and bitter leaf (*Vernonia amygdalina*)," *Scientific African*, vol. 14, 2021.
- [9] G. Oboh, B. C. Adedayo, M. B. Adetola, I. S. Oyeleye, and O. B. Ogunsuyi, "Characterization and neuroprotective properties of alkaloid extract of *Vernonia amygdalina* Delile in experimental models of Alzheimer's disease," *Drug and Chemical Toxicology*, vol. 45, no. 2, pp. 731–740, 2020.
- [10] J. O. Oladele, O. M. Oyeleke, O. T. Oladele, and A. T. Oladiji, "Covid-19 treatment: Investigation on the phytochemical constituents of *Vernonia amygdalina* as potential Coronavirus-2 inhibitors," *Computational Toxicology*, vol. 18, p. 100161, 2021.
- [11] J. O. Oladele, O. M. Oyeleke, O. T. Oladele, and M. Olaniyan, "Neuroprotective mechanism of *Vernonia amygdalina* in a rat model of neurodegenerative diseases," *Toxicology Reports*, vol. 7, pp. 1223–1232, 2020, <https://doi.org/10.1016/j.toxrep.2020.09.005>.
- [12] C. G. Yedjou, A. T. Mbemi, F. Noubissi et al., "Prostate cancer disparity, chemoprevention, and treatment by specific medicinal plants," *Nutrients*, vol. 11, no. 2, p. 336, 2019.
- [13] G. El-Saber Batiha, A. Magdy Beshbishy, O. Stephen Adeyemi et al., "Phytochemical screening and antiprotozoal effects of the methanolic berberis vulgaris and acetic rhus coriaria extracts," *Molecules*, vol. 25, no. 3, p. 550, 2020, <https://doi.org/10.3390/molecules25030550>.
- [14] R. Sharma, K. Kuca, E. Nepovimova, A. Kabra, M. M. Rao, and P. K. Prajapati, "Traditional Ayurvedic and herbal remedies for Alzheimer's disease: from bench to bedside," *Expert Review of Neurotherapeutics*, vol. 19, no. 5, pp. 359–374, 2019, <https://doi.org/10.1080/14737175.2019.1596803>.
- [15] R. Sharma, A. Kabra, M. M. Rao, and P. K. Prajapati, "Herbal and holistic solutions for neurodegenerative and depressive disorders: leads from Ayurveda," *Current Pharmaceutical Design*, vol. 24, no. 22, pp. 2597–2608, 2018.
- [16] M. Jelinek, M. Jurajda, and K. Duris, "Oxidative stress in the brain: basic concepts and treatment strategies in stroke," *Antioxidants*, vol. 10, no. 12, p. 1886, 2021.
- [17] A. Nugud, D. Sandeep, and A. T. El-Serafi, "Two faces of the coin: minireview for dissecting the role of reactive oxygen species in stem cell potency and lineage commitment," *Journal of Advanced Research*, vol. 14, pp. 73–79, 2018, <https://doi.org/10.1016/j.jare.2018.05.012>.
- [18] R. Radi, "Oxygen radicals, nitric oxide, and peroxynitrite: redox pathways in molecular medicine," *Proc Natl Acad Sci U S A*, vol. 115, no. 23, pp. 5839–5848, 2018.
- [19] P. Poprac, K. Jomova, M. Simunkova, V. Kollar, C. J. Rhodes, and M. Valko, "Targeting free radicals in oxidative stress-related human diseases," *Trends in Pharmacological Sciences*, vol. 38, no. 7, pp. 592–607, 2017.
- [20] S. Salim, "Oxidative stress and the central nervous system," *J Pharmacol Exp Ther*, vol. 360, no. 1, pp. 201–205, 2017.
- [21] H. Sies, "Biochemie des oxidativen Stress," *Angewandte Chemie*, vol. 98, no. 12, pp. 1061–1075, 1986.
- [22] X. Ba and I. Boldogh, "8-Oxoguanine DNA glycosylase 1: beyond repair of the oxidatively modified base lesions," *Redox Biology*, vol. 14, pp. 669–678, 2018.
- [23] J. Banerjee, A. Das, M. Sinha, and S. Saha, *Biological efficacy of medicinal plant extracts in preventing oxidative damage*, vol. 2018, 2018.

- [24] D. A. Butterfield and B. Halliwell, "Oxidative stress, dysfunctional glucose metabolism and Alzheimer disease," *Nature Reviews Neuroscience*, vol. 20, no. 3, pp. 148–160, 2019.
- [25] B. Matter, C. L. Seiler, K. Murphy et al., "Mapping three guanine oxidation products along DNA following exposure to three types of reactive oxygen species," *Free Radical Biology and Medicine*, vol. 121, pp. 180–189, 2018.
- [26] C. Peña-Bautista, M. Baquero, M. Vento, and C. Cháfer-Pericás, "Free radicals in Alzheimer's disease: lipid peroxidation biomarkers," *Clinica Chimica Acta*, vol. 491, pp. 85–90, 2019.
- [27] P. J. Magistretti and I. Allaman, "A cellular perspective on brain energy metabolism and functional imaging," *Neuron*, vol. 86, no. 4, pp. 883–901, 2015.
- [28] J. N. Copley, M. L. Fiorello, and D. M. Bailey, "13 reasons why the brain is susceptible to oxidative stress," *Redox Biology*, vol. 15, pp. 490–503, 2018.
- [29] I. Torres-Cuevas, M. Corral-Debrinski, and P. Gressens, "Brain oxidative damage in murine models of neonatal hypoxia/ischemia and reoxygenation," *Free Radical Biology and Medicine*, vol. 142, pp. 3–15, 2019, <https://doi.org/10.1016/j.freeradbiomed.2019.06.011>.
- [30] B. Marengo, M. Nitti, A. L. Furfaro et al., "Redox homeostasis and cellular antioxidant systems: crucial players in cancer growth and therapy," *Oxidative Medicine and Cellular Longevity*, vol. 2016, pp. 6235641–16, 2016.
- [31] J. Taile, A. Arcambal, P. Clerc, A. Gauvin-Bialecki, and M. P. Gonthier, "Medicinal plant polyphenols attenuate oxidative stress and improve inflammatory and vasoactive markers in cerebral endothelial cells during hyperglycemic condition," *Antioxidants (Basel)*, vol. 9, no. 7, p. 573, 2020.
- [32] J. Namukobe, P. Sekandi, R. Byamukama et al., "Antibacterial, antioxidant, and sun protection potential of selected ethno medicinal plants used for skin infections in Uganda," *Trop Med Health*, vol. 49, no. 1, p. 49, 2021.
- [33] C. O. Nwonuma, O. O. Osemwegie, O. O. Alejlowo et al., "Antioxidant and the ameliorating effect of *Allium cepa* (Onion) fortified feed against potassium bromate induced oxidative damage in Wistar rats," *Toxicology Reports*, vol. 8, pp. 759–766, 2021.
- [34] A. Septembre-Malaterre, G. Stanislas, E. Douraguia, and M. P. Gonthier, "Evaluation of nutritional and antioxidant properties of the tropical fruits banana, litchi, mango, papaya, passion fruit and pineapple cultivated in Reunion French Island," *Food Chemistry*, vol. 212, pp. 225–233, 2016.
- [35] A. Zachara, D. Gałkowska, and L. Juszczak, "Contamination of tea and tea infusion with polycyclic aromatic hydrocarbons," *International Journal of Environmental Research and Public Health*, vol. 15, no. 1, p. 45, 2017.
- [36] A. G. Gornall, C. J. Bardawill, and M. M. David, "Determination of serum proteins by means of the biuret reaction," *Journal of Biological Chemistry*, vol. 177, no. 2, pp. 751–766, 1949.
- [37] H. P. Misra and I. Fridovich, "The role of superoxide anion in the autoxidation of epinephrine and a simple assay for superoxide dismutase," *Journal of Biological Chemistry*, vol. 247, no. 10, pp. 3170–3175, 1972.
- [38] J. T. Rotruck, A. L. Pope, H. E. Ganther, A. B. Swanson, D. G. Hafeman, and W. G. Hoekstra, "Selenium: biochemical role as a component of glutathione peroxidase," *Science*, vol. 179, no. 4073, pp. 588–590, 1973.
- [39] R. F. Beers and I. W. Sizer, "A spectrophotometric method for measuring the breakdown of hydrogen peroxide by catalase," *Journal of Biological Chemistry*, vol. 195, no. 1, pp. 133–140, 1952.
- [40] B. Pulli, M. Ali, R. Forghani et al., "Measuring myeloperoxidase activity in biological samples," *PLoS One*, vol. 8, no. 7, p. e67976, 2013.
- [41] E. Beutler and M. K. Y. Yeh, "Erythrocyte glutathione reductase," *Blood*, vol. 21, no. 5, pp. 573–585, 1963.
- [42] R. Varshney and R. K. Kale, "Effects of calmodulin antagonists on radiation-induced lipid peroxidation in microsomes," *International Journal of Radiation Biology*, vol. 58, no. 5, pp. 733–743, 2009.
- [43] O. S. Adeyemi, O. Atolani, P. Banerjee et al., "Computational and experimental validation of antioxidant properties of synthesized bioactive ferulic acid derivatives," *International Journal of Food Properties*, vol. 21, no. 1, pp. 86–98, 2018.
- [44] G. L. Ellman, K. D. Courtney, V. Andres Jr, and R. M. Featherstone, "A new and rapid colorimetric determination of acetylcholinesterase activity," *Biochemical Pharmacology*, vol. 7, no. 2, pp. 88–95, 1961.
- [45] C. E. Perandones, V. A. Illera, D. Peckham, L. L. Stunz, and R. F. Ashman, "Regulation of apoptosis in vitro in mature murine spleen T cells," *Journal of Immunology (Baltimore, Md, 1950)*, vol. 151, no. 7, pp. 3521–3529, 1993.
- [46] O. S. Adeyemi and M. A. Akanji, "Psidium guajava leaf extract: effects on rat serum homeostasis and tissue morphology," *Comparative Clinical Pathology*, vol. 21, no. 4, pp. 401–407, 2010.
- [47] K. Ji, L. Fang, H. Zhao et al., "Ginger oleoresin alleviated  $\gamma$ -ray irradiation-induced reactive oxygen species via the Nrf2 protective response in human mesenchymal stem cells," *Oxidative Medicine and Cellular Longevity*, vol. 2017, pp. 1–12, 2017.
- [48] S. B. Nimse and D. Pal, "Free radicals, natural antioxidants, and their reaction mechanisms," *RSC Advances*, vol. 5, no. 35, pp. 27986–28006, 2015.
- [49] S. Demirci-Çekiç, G. Özkan, A. N. Avan, S. Uzunboy, E. Çapanoğlu, and R. Apak, "Biomarkers of oxidative stress and antioxidant defense," *Journal of Pharmaceutical and Biomedical Analysis*, vol. 209, 2022.
- [50] K. Ferro, D. Ferro, F. Corrà, R. Bakiu, G. Santovito, and J. Kurtz, "Cu, Zn superoxide dismutase genes in *Tribolium castaneum*: evolution, molecular characterisation, and gene expression during immune priming," *Frontiers in Immunology*, vol. 8, p. 1811, 2017.
- [51] J. C. Toledo Jr. and O. Augusto, "Connecting the chemical and biological properties of nitric oxide," *Chem Res Toxicol*, vol. 25, no. 5, pp. 975–989, 2012.
- [52] K. Danwilai, J. Konmun, B.-o. Sripanidkulchai, and S. Subongkot, "Antioxidant activity of ginger extract as a daily supplement in cancer patients receiving adjuvant chemotherapy: a pilot study," *Cancer Management and Research*, vol. 9, pp. 11–18, 2017.
- [53] I. Mustafa, N. L. Chin, S. Fakurazi, and A. Palanisamy, "Comparison of phytochemicals, antioxidant and anti-inflammatory properties of sun-oven- and freeze-dried ginger extracts," *Foods*, vol. 8, no. 10, p. 456, 2019.
- [54] Z. Naderi, H. Mozaffari-Khosravi, A. Dehghan, A. Nadjarzadeh, and H. F. Huseini, "Effect of ginger powder supplementation on nitric oxide and C-reactive protein in elderly knee osteoarthritis patients: a 12-week double-blind randomized placebo-controlled clinical trial," *Journal of Traditional and Complementary Medicine*, vol. 6, no. 3, pp. 199–203, 2016.

- [55] Y. Aratani, "Myeloperoxidase: its role for host defense, inflammation, and neutrophil function," *Archives of Biochemistry and Biophysics*, vol. 640, pp. 47–52, 2018.
- [56] S. A. Hussein, Y. A. El Senosi, M. K. Mansour, and M. F. Hassan, "Role of antioxidant and anti-inflammatory of Ginger (*Zingiber officinale* Roscoe) against metalaxyl induced oxidative stress in rats," *Benha Veterinary Medical Journal*, vol. 33, no. 2, pp. 504–516, 2017.
- [57] O. L. Erukainure, C. I. Chukwuma, O. Sanni, M. G. Matsabisa, and M. S. Islam, "Histochemistry, phenolic content, antioxidant, and anti-diabetic activities of *Vernonia amygdalina* leaf extract," *Journal of Food Biochemistry*, vol. 43, no. 2, 2019.
- [58] W. Q. Liu, Y. Z. Zhang, Y. Wu et al., "Myeloperoxidase-derived hypochlorous acid promotes ox-LDL-induced senescence of endothelial cells through a mechanism involving beta-catenin signaling in hyperlipidemia," *Biochemical and Biophysical Research Communications*, vol. 467, no. 4, pp. 859–865, 2015.
- [59] H. Khan, S. Amin, M. A. Kamal, and S. Patel, "Flavonoids as acetylcholinesterase inhibitors: current therapeutic standing and future prospects," *Biomedicine & Pharmacotherapy*, vol. 101, pp. 860–870, 2018.
- [60] L. Czernicka, A. Ludwiczuk, E. Rój, Z. Marzec, A. Jarzab, and W. Kukula-Koch, "Acetylcholinesterase inhibitors among *Zingiber officinale* terpenes—extraction conditions and thin layer chromatography-based bioautography studies," *Molecules*, vol. 25, no. 7, p. 1643, 2020.
- [61] B. T. Tung, D. K. Thu, N. T. K. Thu, and N. T. Hai, "Antioxidant and acetylcholinesterase inhibitory activities of ginger root (*Zingiber officinale* Roscoe) extract," *Journal of Complementary & Integrative Medicine*, vol. 14, no. 4, 2017.
- [62] F. Laddomada, M. M. Miyachiro, and A. Dessen, "Structural insights into protein-protein interactions involved in bacterial cell wall biogenesis," *Antibiotics (Basel)*, vol. 5, no. 2, p. 14, 2016.

## Research Article

# Ethnobotanical Study of Medicinal Plants Used against COVID-19

**Mohamed Chebaibi** <sup>1</sup>, **Dalila Bousta**,<sup>2</sup> **Mohammed Bourhia** <sup>3</sup>, **Soukayna Baammi**,<sup>4</sup>  
**Ahmad Mohammad Salamatullah** <sup>5</sup>, **Hiba-Allah Nafidi**,<sup>6</sup> **Hasnae Hoummani**,<sup>1,7</sup>  
**and Sanae Achour**<sup>1,7</sup>

<sup>1</sup>Biomedical and Translational Research Laboratory, Faculty of Medicine and Pharmacy of the Fez, University of Sidi Mohamed Ben Abdellah, BP 1893, Km 22, Road of Sidi Harazem, Fez, Morocco

<sup>2</sup>Laboratory of Biotechnology, Environment, Agri-Food, and Health (LBEAS), Faculty of Sciences, University Sidi-Mohamed-Ben-Abdellah (USMBA), Fez 30050, Morocco

<sup>3</sup>Higher Institute of Nursing Professions and Technical Health, Laayoune 70000, Morocco

<sup>4</sup>African Genome Centre (AGC), Mohammed VI Polytechnic University, Benguerir, Morocco

<sup>5</sup>Department of Food Science & Nutrition, College of Food and Agricultural Sciences, King Saud University, 11 P.O. Box 2460, Riyadh 11451, Saudi Arabia

<sup>6</sup>Department of Food Science, Faculty of Agricultural and Food Sciences, Laval University, Quebec 2325, QC G1V 0A6, Canada

<sup>7</sup>Laboratory of Pharmacology and Toxicology, University Hospital Hassan II-Fez, Fez, Morocco

Correspondence should be addressed to Mohamed Chebaibi; mohamed.chebaibi@usmba.ac.ma

Received 23 February 2022; Revised 23 July 2022; Accepted 17 August 2022; Published 15 September 2022

Academic Editor: Vijaya Anand

Copyright © 2022 Mohamed Chebaibi et al. This is an open access article distributed under the Creative Commons Attribution License, which permits unrestricted use, distribution, and reproduction in any medium, provided the original work is properly cited.

During the COVID-19 pandemic, the Moroccan population, like the entire population of the world, used medicinal plants to treat or cure symptoms of SARS-CoV-2. The present work was designed to identify the medicinal plants used by the Moroccan population in the prevention or treatment of COVID-19. To achieve this goal, a survey was conducted to collect data on plants along with the sociodemographic parameters of users. The outcome of this work showed that 1,263 people were interviewed with 63.5% male, aged between 18 and 82 years. Most plant users were between 20 and 40 years, which constituted 80.1% of the study population. The level of education of participants was 70.9% university and 27.6% secondary. The most useful plants were eucalyptus, cloves, lemon, and garlic. Notably, 61.9% of interviewed people used plants for preventing or treating COVID-19: 30.6% of them declared one-time use from the beginning of the pandemic, and 47.8% declared frequent daily use until recovery, while 17.4% declared single daily use. Five out of twenty-one plants used in the treatment are known for their potential toxicity, including *Artemisia herba-alba* and oleander (*Nerium oleander*). The findings of the present work could serve society by providing potential medicinal plants to control COVID-19.

## 1. Introduction

On May 27, 2020, the World Health Organization (WHO) declared the severe acute respiratory syndrome (SARS) of the current coronavirus disease 19 (COVID-19) outbreak, emerging in China at the end of 2019, as a pandemic. Since then, more than 585,568,206 confirmed cases of COVID-19,

including 6,428,220 deaths across the world have been recorded, according to the website <https://www.worldometers.info/coronavirus/>, accessed on August 4th, 2022 [1]. Alpha, Beta, Gamma, and Delta-coronaviruses are the four genera that make up the *Coronaviridae* family, with Alpha and Beta-coronaviruses being the human pathogens. The virus that causes COVID-19, SARS-CoV-2, also known

as 2019-nCoV, and severe acute respiratory syndrome (SARS) coronavirus (CoV)-2 virus, belongs to the genus Beta-coronavirus of the *Coronaviridae* family [2].

All the populations of the world were oriented towards natural products to prevent or treat infection caused by COVID-19 [3–5]. The Moroccan population is closely linked to phototherapy, which is back to several reasons, such as the richness of the country by medicinal plants (5,200 species and subspecies, and 600 species are medicinal plants), the economic situation of the Moroccan population, the illiterate and the inaccessibility of modern medicine) [6].

According to the Moroccan Ministry of Health, 1,261,816 confirmed cases of COVID-19 and 1618, 9 deaths have been recorded since the beginning of the pandemic. As a consequence, the Moroccan population has used plants for preventing or treating this causative agent of the severe acute respiratory syndrome [7, 8].

In this context, our study aimed to collect information on medicinal plants used by the Moroccan population in the prevention or treatment of COVID-19.

## 2. Materials and Methods

**2.1. Type and Study Area.** The present work was a prospective longitudinal cohort study, which aimed to collect data by use of a structured questionnaire via Google Forms, conducted in different regions of Morocco.

**2.2. Information Gathering.** All information was collected from 10 regions in Morocco: Marrakech-Safi, Béni Mellal-Khenifra, Fez-Meknes, Casablanca-Settat, Dakhla-Oued Ed-Dahab, Drâa-Tafilalet, Laâyoune-Sakia El Hamra, Oriental, Tanger-Tetouan-Al Hoceima, and Rabat-Salé-Kénitra (Table 1).

Each questionnaire was focused on two parts; socio-demographic characteristics and ethnomedicinal data.

**2.3. Statistical Analyses.** Variables were described by use of descriptive statistics; qualitative variables were described in terms of percentage, while quantitative variables were described in terms of mean, extreme values, and standard deviation. Data entry and statistical analysis were performed by use of IBM SPSS Statistics for Windows, version 21 (IBM Corp., Armonk, NY, USA).

## 3. Results and Discussion

**3.1. Sociodemographic Characteristics.** One thousand two hundred sixty-three people were interviewed in this study (63% men vs 37% women) whose age was between 18 and 82 years. 70.9% of them have a higher education level, followed by secondary level (27.6%) and then primary level (1.5%). 41.6% of plant users had a lower monthly income of 100 USD, 24.5% between 100 and 500 USD, 24.5% between 500 and 1000 USD, and 10.5% had more than 1000 USD. 80% are located in rural areas and 27% are without medical recovery (RAMED) (Table 2).

TABLE 1: Distribution of the population by region.

Region	Effective
Fez-Meknes	642
Casablanca-Settat	156
Rabat-Salé-Kénitra	126
Béni Mellal-Khenifra	96
Dakhla-Oued Ed-Dahab	69
Marrakech-Safi	60
Drâa-Tafilalet	60
Laâyoune-Sakia El Hamra	54

The coronavirus responsible for COVID-19, which was identified in December 2019 in China, has infected more than 574,157,623 people worldwide and caused more than 6,401,683 deaths at the date of revising the present article. Morocco is one of the most affected countries with a high circulating potency of SARS-CoV-2.

Moroccan population has used medicinal plants for therapeutic purposes for thousands of years. Moroccans have inherited the phytotherapy knowledge from the previous generation either verbally or written, recorded history [6, 9]. Moroccan population has used plants to treat symptoms of COVID-19 as reported in earlier work [5].

Unlike several ethnobotanical studies in which illiterates and women are the majority of users of plants [10–12], in our study, mostly, educated men were the users of plants in the prevention or treatment of COVID-19.

Furthermore, the economic conditions and the low income of people influence the use of plants; people with a low income were the majority of users of plants in the treatment [10, 11, 13]. Notably, people with a low income (less than 100 USD) were the most active consumers of plants during the COVID-19 pandemic.

Plants are largely used in rural than urban areas, which can be explained by the fact that people in rural areas have more accessibility to herbal products [14]. This result is in agreement with our study, wherein 80% of our population are living in rural areas.

### 3.2. Ethnobotanical Data

**3.2.1. Plants Used.** In total, 21 plants belonging to twelve botanical families have been used to treat or prevent COVID-19. The mostly used plants are eucalyptus, cloves (*Syzygium aromaticum*), lemon (*Citrus limon*), and garlic (*Allium sativum*) (Table 3).

To achieve herd immunity through mass immunization programs and the pressing demand to develop effective anti-COVID-19 treatments, several pharmaceutical drugs have been repurposed to treat COVID-19 including hydroxychloroquine, lopinavir/ritonavir/darunavir/umifenovir, remdesivir, and favipiravir [15]. Recently, Pfizer's Paxlovid, made up of both nirmatrelvir and ritonavir and oral tablets, has been granted an emergency use authorization (EUA), by the U.S. Food and Drug Administration (USFDA), for the treatment of COVID-19 in both adults and children (USFDA, 2022). However, to be effective, these compounds would need to be taken at relatively great continuous doses.

TABLE 2: Sociodemographic characteristics.

Sociodemographic characteristics		Percentage
Gender	Men	63
	Women	37
Age (years)	<20	8.22
	20–40	77.37
	40–60	10.82
	60–80	0.77
Level of education	Primary	1.5
	Secondary	27.6
	University	70.9
Monthly income	<100 USD	41.6
	100–500 USD	24.5
	500–1000 USD	23.4
	1000–2000 USD	7.3
	>2000 USD	3.2
Locality	Urban	20
	Rural	80
Medical assistance regime (RAMED)	Yes	73
	No	27

USD: United States dollar.

TABLE 3: Ethnobotanical data.

Name of plant	Families	Vernacular name	Part of plant	Use mode	NTC
<i>Eucalyptus</i>	Myrtaceae	Eucalyptus	Leaves	Fumigation	495
<i>Syzygium aromaticum</i>	Myrtaceae	Krenfel	Cloves	Fumigation Infusion	369
<i>Allium sativum</i>	Amaryllidaceae	Touma	Garlic	Raw	225
<i>Citrus limon</i>	Rutaceae	Limon	Fruit	Juice	270
<i>Lavandula officinalis</i>	Lamiaceae	Khzama	Aerial part	Infusion Fumigation	72
<i>Trigonella foenum-graecum</i>	Fabaceae	Helba	Seeds	Infusion	54
<i>Mentha pulegium</i>	Lamiaceae	Flio	Aerial part	Infusion Fumigation	63
<i>Rosmarinus officinalis</i>	Lamiaceae	Azir	Aerial part	Infusion Fumigation	45
<i>Artemisia herba-alba</i>	Asteraceae	Chih	Aerial part	Infusion Fumigation	117
<i>Cinnamomum verum</i>	Lauraceae	Karfa	Dried bark	Infusion	72
<i>Juniperus thurifera</i>	Cupressaceae	Arar	Aerial part	Fumigation	45
<i>Nerium oleander</i>	Apocynaceae	Defla	Leaves	Fumigation	27
<i>Pistacia lentiscus</i>	Anacardiaceae	Drou	Leaves	Fumigation	9
<i>Aloysia triphylla</i>	Verbenaceae	Lwiza	Leaves	Infusion	9
<i>Mentha rotundifolia</i>	Lamiaceae	Marsita	Aerial part	Infusion	9
<i>Laurus nobilis</i>	Lauraceae	Moussa	Leaves	Fumigation Infusion	18 9
<i>Ocimum basilicum</i>	Lamiaceae	Ri7an	Aerial part	Fumigation	
<i>Thymus vulgaris</i>	Lamiaceae	Zaater	Aerial part	Infusion	126
<i>Zingiber officinale</i>	Zingiberaceae	Zanajbil	Rhizome	Infusion	45
<i>Olea europaea</i>	Oleaceae	Zitoun	Leaves	Fumigation	46

NTC: total number of citations.

Therefore, they could have inherent toxic potencies. For this reason, natural products from medicinal plants hold promise [2, 16, 17].

Since the beginning of the COVID-19 outbreak, traditional herbal remedies have been employed. Of note, 90% of 214 patients treated in China recovered after using some of

these traditional treatments. Moreover, natural remedies, based on honey, seed oil of black cummin (*Nigella sativa*), and flowers and buds of chamomile (*Anthemis hyaline*) have been reported to be effective against COVID-19 treatment in the Middle Eastern countries Egypt and Saudi Arabia [16]. In Africa, represented by the Democratic Republic of Congo, a

TABLE 4: Antiviral activity of the most cited plants in our survey against different types of viruses.

	Herpes simplex virus 1	Herpes simplex virus 2	Rotavirus Wa strain	Adenovirus type 7	SARS-CoV-2	Influenza A and B	HIV
<i>Eucalyptus</i>	+	+	+	+	+*	-	-
<i>Allium sativum</i>	+	+	-	-	-	+	+
<i>Citrus limon</i>	+	+	-	-	-	-	-

+: effective against virus; -: no effect of plant against the virus; \*study carried out by molecular docking. HIV: human immunodeficiency virus.

remedy made up of clove (*Syzygium aromaticum*), blue gum (*Eucalyptus globulus*), lemon grass (*Cymbopogon citratus*), and ginger (*Zingiber officinale*) has been used to fight against COVID-19.

Regarding the antiviral activity of the most cited plants in our survey, Table 4 summarizes some studies of these plants against different types of viruses. By use of molecular docking, the antiviral activity of eucalyptus was determined against herpes simplex virus 1, herpes simplex virus 2 [18], rotavirus Wa strain, adenovirus type 7 [19], and SARS-CoV-2 [20, 21]. Moreover, garlic has been used for centuries in the treatment of diseases such as viral diseases. Antiviral activity of *Allium sativum* has been confirmed against several viruses such as influenza A and B [22], herpes simplex virus 1, herpes simplex virus 2 rhinovirus, and human immunodeficiency virus (HIV) [23, 24]. *Citrus limon*, which is used by the Moroccan population to treat COVID-19, is rich in flavonoids like diosmin, eriocitrin, and hesperidin, which possessed biological activities including antiviral power [25]. Antiviral activity of eugenin extracted from the *Allium sativum* and clove has been reported to be effective against herpes by inhibiting the viral DNA polymerase, which in turn affects DNA synthesis [26]. Moreover, eugenol showed antiviral activity against human herpes simplex [27].

**3.2.2. Mode of Use of Plants.** Results showed that 70% of the population use the leaves or aerial parts of plants in the treatment (Figure 1). This can be explained by the easy harvesting of aerial parts and the accessibility facilities [6]. Fumigation represents the most used method to prepare natural preparation against COVID-19, followed by infusion (Figure 2). Generally, fumigation was used in traditional medicine to treat pulmonary and neurological diseases [28]. Since the SARS-CoV-2 virus infects the respiratory system, people prefer using fumigation for treatment. Another reason why fumigation is used is that vapors can play a role in disinfection.

Regarding the treatment period, Figure 3 shows that 30.6% of the population used plants at least one time from the beginning of the pandemic up to the date of investigation, 23.1% once a week, 13.9% once a day, and 9.3% every day during the outbreak.

**3.3. Toxic Plants.** The empiric use of plants for medication is always linked to risks of toxicity [29]. Our results showed that 5 out of 21 plants used by the Moroccan population for treating or preventing COVID-19 were listed to be toxic (Table 5).

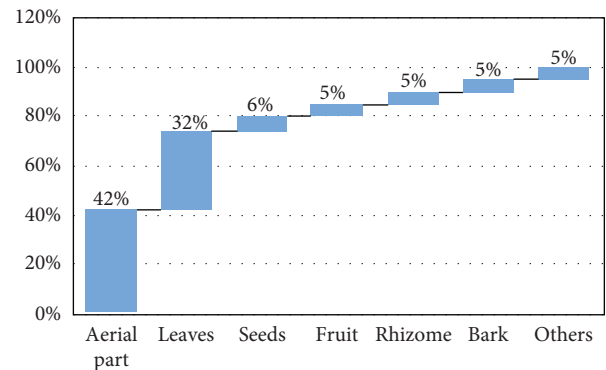


FIGURE 1: Part of plants used by the Moroccan population to prevent or treat COVID-19.

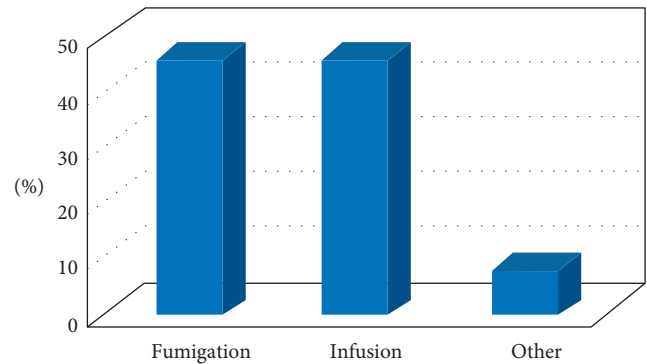


FIGURE 2: Preparation mode of plants used by the Moroccan population to prevent or treat COVID-19.

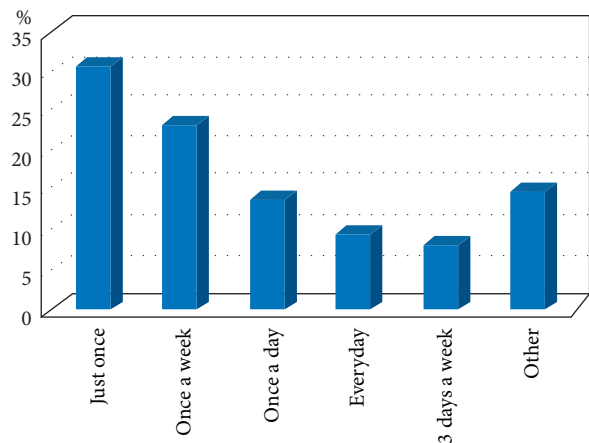


FIGURE 3: Duration of plant use by the Moroccan population during the COVID-19 pandemic.

TABLE 5: Toxic plants used by the Moroccan population in the prevention or treatment of COVID-19.

Scientific name	Families	Vernacular name	Part used
<i>Artemisia herba-alba</i>	Asteraceae	Chih	Aerial part
<i>Nerium oleander</i>	Apocynaceae	Defla	Leaves
<i>Pistacia lentiscus</i>	Anacardiaceae	Drou	Leaves
<i>Olea europaea</i>	Oleaceae	Zitoun	Leaves
<i>Juniperus thurifera</i>	Cupressaceae	Arar	Aerial part

Concerning the toxicity of *Artemisia herba-alba*, a study by Abderrahman and Shbailat showed harmful effects on the division of bone marrow cells and the induction of chromatid exchanges at doses of 375 and 500  $\mu\text{g ml}^{-1}$  [30], while another study mentioned the potential renal toxicity of this plant [31]. *N. oleander* is known for its toxicity due to the presence of cardiac glycosides in all plant parts. Cardiac glycosides inhibit  $\text{Na}^+/\text{K}^+$  ATPase pumps in cardiac cells, which lead to hyperkalemia [32–34].

*Pistacia lentiscus* is also a toxic plant whose oils cause a decrease in hepatic cytochrome P450 activity. Subacute administration of *P. lentiscus* extract in rats results in hepatic fibrosis and mild cholestasis [35–37]. Little research mentions the toxicity of *Olea europaea*. However, administration of the leaf extract of this plant for a longer period may lead to liver and kidney damage as reported in previous works [38, 39]. Furthermore, *Juniperus thurifera* oils can cause severe gastrointestinal irritation and intense congestion of the genitourinary system and intestines [40].

#### 4. Conclusion

The present study documented medicinal plants used by the Moroccan population against COVID-19. The results showed that many plants used to fight the causative agents of the severe acute respiratory syndrome, including *Artemisia herba-alba* and *Nerium oleander*. Notably, antiviral activity of most reported plants has been confirmed against some viruses elsewhere, but no activity has been yet approved in in vivo studies. Some toxic plants were included in natural preparations used by the Moroccans to control SARS-CoV-2, and hence people should pay more attention to the non-approved natural products.

#### Data Availability

The data used to support the findings of this study are included within the article.

#### Conflicts of Interest

The authors declare that they have no conflicts of interest.

#### Acknowledgments

This study was supported by the Researchers Supporting Project (RSP-2022R437), King Saud University, Riyadh, Saudi Arabia. The authors are grateful for the support.

#### References

- [1] D. Mercatelli, A. N. Holding, and F. M. Giorgi, “Web tools to fight pandemics: the COVID-19 experience,” *Briefings in Bioinformatics*, vol. 22, no. 2, pp. 690–700, 2021.
- [2] M. Bourhia, F. E.-Z. Amrati, R. Ullah et al., “Coronavirus treatments: what drugs might work against COVID-19?” *Natural Product Communications*, vol. 15, no. 7, p. 1934578X2094544, 2020.
- [3] C. A. Taylor, C. Boulos, and D. Almond, “Livestock plants and COVID-19 transmission,” *Proceedings of the National Academy of Sciences*, vol. 117, no. 50, pp. 31706–31715, 2020.
- [4] J. Middleton, R. Reintjes, and H. Lopes, “Meat plants—a new front line in the COVID-19 pandemic,” *BMJ*, vol. 370, 2020.
- [5] X. Y. Lim, B. P. Teh, and T. Y. C. Tan, “Medicinal plants in COVID-19: potential and limitations,” *Frontiers in Pharmacology*, vol. 12, p. 611408, 2021.
- [6] M. Chebaibi, D. Bousta, I. Iken et al., “Ethnopharmacological survey of medicinal plants used in traditional treatment of kidney diseases in fez-meknes region, Morocco,” *Phytothérapie*, vol. 18, no. 2, pp. 99–114, 2020.
- [7] <https://www.covidmaroc.ma/pages/Accueilfr.aspx>.
- [8] <https://www.sante.gov.ma/Pages/Accueil.aspx>.
- [9] M. Chebaibi, D. Bousta, L. Chbani, Y. Ez zoubi, N. Touiti, and S. Achour, “Acute toxicity of plants mixture used in traditional treatment of edema and colic renal in Morocco,” *Scientific African*, vol. 6, 2019.
- [10] M. Eddouks, M. Ajebli, and M. Hebi, “Ethnopharmacological survey of medicinal plants used in Daraa-Tafilalet region (Province of Errachidia), Morocco,” *Journal of Ethnopharmacology*, vol. 198, pp. 516–530, 2017.
- [11] F. Kabbaj, B. Meddah, Y. Cherrah, and E. Faouzi, “Ethnopharmacological profile of traditional plants used in Morocco by cancer patients as herbal therapeutics,” *Phytopharmacology*, vol. 2, no. 2, pp. 243–256, 2012.
- [12] A. Telli, M.-A. Esnault, and A. Ould El Hadj Khelil, “An ethnopharmacological survey of plants used in traditional diabetes treatment in south-eastern Algeria (Ouargla province),” *Journal of Arid Environments*, vol. 127, pp. 82–92, 2016.
- [13] Y. Samouh, A. Lemrani, H. Hajar, J. Mohamad, and A. A. H. Said, “Ethnopharmacological study of herbal medicines used to treat Cancer in Morocco,” *The Journal of Phytopharmacology*, vol. 8, no. 3, pp. 135–141, 2019.
- [14] D. Bousta, S. Boukhira, A. Aafi, M. Ghanmi, and L. El-Mansouri, “Ethnopharmacological Study of anti-diabetic medicinal plants used in the Middle-Atlas region of Morocco (Sefrou region),” *International Journal of Pharma Research and Health Sciences*, vol. 2, no. 1, pp. 75–79, 2014.
- [15] M. Costanzo, M. A. R. De Giglio, and G. N. Roviello, “SARS-CoV-2: recent reports on antiviral therapies based on lopinavir/ritonavir, darunavir/umifenovir, hydroxychloroquine, remdesivir, favipiravir and other drugs for the treatment of the new coronavirus,” *Current Medicinal Chemistry*, vol. 27, no. 27, pp. 4536–4541, 2020.
- [16] S. M. El Sayed, M. S. Aboonq, A. G. El Rashedy et al., “Promising preventive and therapeutic effects of TaibUV1D nutritional supplements for COVID-19 pandemic: towards



- better public prophylaxis and treatment (A retrospective study),” *American Journal of Blood Research*, vol. 10, no. 5, pp. 266–282, 2020.
- [17] C. Vicidomini, V. Roviello, and G. N. Roviello, “Molecular basis of the therapeutical potential of clove (*Syzygium aromaticum* L.) and clues to its anti-COVID-19 utility,” *Molecules*, vol. 26, no. 7, p. 1880, 2021.
- [18] M. Huleihel and M. Huleihel, “Antiviral activity of *Eucalyptus camaldulensis* leaves ethanolic extract on herpes viruses infection,” *International Journal of Computer Vision*, vol. 1, pp. 001–009, 2017.
- [19] F. K. El-Baz, K. Mahmoud, W. M. El-Senousy, O. Darwesh, and A. El Gohary, “Antiviral–antimicrobial and schistosomicidal activities of *Eucalyptus camaldulensis* essential oils,” *International Journal of Pharmaceutical Sciences Review and Research*, vol. 31, no. 1, pp. 262–268, 2015.
- [20] A. D. Sharma and I. Kaur, “Molecular docking studies on jensenone from eucalyptus essential oil as a potential inhibitor of covid 19 corona virus infection,” arXiv:2004.00217, 2020.
- [21] A. D. Sharma, “Eucalyptol (1, 8 cineole) from eucalyptus essential oil a potential inhibitor of covid 19 corona virus infection by molecular docking studies,” *Biology*, 2020.
- [22] G. Fenwick and A. Hanley, “Allium species poisoning,” *The Veterinary Record*, vol. 116, no. 1, p. 28, 1985.
- [23] N. D. Weber, D. O. Andersen, J. A. North, B. K. Murray, L. D. Lawson, and B. G. Hughes, “In vitro virucidal effects of *Allium sativum* (garlic) extract and compounds,” *Planta Medica*, vol. 58, no. 05, pp. 417–423, 1992.
- [24] Y. Tsai, L. L. Cole, L. E. Davis, S. J. Lockwood, V. Simmons, and G. C. Wild, “Antiviral properties of garlic: in vitro effects on influenza B, herpes simplex and coxsackie viruses,” *Planta Medica*, vol. 51, no. 05, pp. 460–461, 1985.
- [25] J. Del Rio, M. Fuster, P. Gómez, I. Porras, A. Garcia-Lidón, and A. Ortuño, “Citrus limon: a source of flavonoids of pharmaceutical interest,” *Food Chemistry*, vol. 84, no. 3, pp. 457–461, 2004.
- [26] D. F. Cortés-Rojas, C. R. F. de Souza, and W. P. Oliveira, “Clove (*Syzygium aromaticum*): a precious spice,” *Asian Pacific Journal of Tropical Biomedicine*, vol. 4, no. 2, pp. 90–96, 2014.
- [27] H. A. Aboubakr, A. Nauertz, N. T. Luong et al., “In vitro antiviral activity of clove and ginger aqueous extracts against feline calicivirus, a surrogate for human norovirus,” *Journal of Food Protection*, vol. 79, no. 6, pp. 1001–1012, 2016.
- [28] R. Singh, “Can ancient science and wisdom of yagya therapy ‘with herbs having immune boosting and antiviral properties’ aid in the fight against COVID19?” *Dev Sanskriti Interdisciplinary International Journal*, vol. 16, pp. 61–68, 2020.
- [29] M. Chebaibi, D. Bousta, L. Chbani et al., “*Leucotrichus, chamaemelum nobile, petroselinum crispum, and lavandula officinalis* used traditionally,” *International Journal of Pharmaceutical Research*, vol. 13, no. 2, 2021.
- [30] S. M. Abderrahman and S. Jamal Shbailat, “Genotoxic and cytotoxic effects of *Artemisia herba-alba* on mammalian cells,” *Caryologia*, vol. 67, no. 4, pp. 265–272, 2014.
- [31] A. C. Brown, “Kidney toxicity related to herbs and dietary supplements: online table of case reports. Part 3 of 5 series,” *Food and Chemical Toxicology*, vol. 107, pp. 502–519, 2017.
- [32] V. Bandara, S. A. Weinstein, J. White, and M. Eddleston, “A review of the natural history, toxinology, diagnosis and clinical management of *Nerium oleander* (common oleander) and *Thevetia peruviana* (yellow oleander) poisoning,” *Toxicology*, vol. 56, no. 3, pp. 273–281, 2010.
- [33] T. Farkhondeh, M. Kianmehr, T. Kazemi, S. Samarghandian, and M. Khazdair, “Toxicity effects of *Nerium oleander*, basic and clinical evidence: a comprehensive review,” *Human & Experimental Toxicology*, vol. 39, no. 6, pp. 773–784, 2020.
- [34] S. D. Langford and P. J. Boor, “Oleander toxicity: an examination of human and animal toxic exposures,” *Toxicology*, vol. 109, no. 1, pp. 1–13, 1996.
- [35] A. Boukeloua, A. Belkhiri, Z. Djerrou, L. Bahri, N. Boulebda, and Y. Hamdi Pacha, “Acute toxicity of *Opuntia ficus indica* and *Pistacia lentiscus* seed oils in mice,” *African Journal of Traditional, Complementary and Alternative Medicines: AJTCAM*, vol. 9, no. 4, pp. 607–611, 2012.
- [36] Z. Djerrou, H. Djaalab, F. Riachi et al., “Irritantcy potential and sub acute dermal toxicity study of *Pistacia lentiscus* fatty oil as a topical traditional remedy,” *African Journal of Traditional, Complementary and Alternative Medicines*, vol. 10, no. 3, pp. 480–489, 2013.
- [37] M. A. Gacem, A. Ould El Hadj-Khelil, B. Boudjemaa, and H. Gacem, “Phytochemistry, toxicity and pharmacology of *pistacia lentiscus, Artemisia herba-alba* and *Citrullus colocynthis*,” in *Sustainable Agriculture Reviews* vol. 39, , pp. 57–93, Springer, 2020.
- [38] C. G. Guex, F. Z. Reginato, K. C. Figueredo et al., “Safety assessment of ethanolic extract of *Olea europaea* L. leaves after acute and subacute administration to Wistar rats,” *Regulatory Toxicology and Pharmacology*, vol. 95, pp. 395–399, 2018.
- [39] S. A. Omer, M. Elobeid, M. Elamin et al., “Toxicity of olive leaves (*Olea europaea* L.) in Wistar albino rats,” *Asian Journal of Animal and Veterinary Advances*, vol. 7, no. 11, pp. 1175–1182, 2012.
- [40] D. Corrigan, “*Juniperus* species,” in *Adverse Effects of Herbal Drugs 2*, pp. 217–229, Springer, Berlin, Germany, 1993.

## Research Article

# The Clinical Effect and Mechanism of Prostant on Urinary Retention and Anal Pain

Wei-Min Luo,<sup>1</sup> Han Du,<sup>2</sup> Hong-Liang Jiang ,<sup>3</sup> Ying-Jun Deng,<sup>4</sup> Xue Liang,<sup>5</sup> Ping Qiu,<sup>3</sup> and Yao Cheng<sup>3</sup>

<sup>1</sup>Department of Colorectal Surgery, The First Affiliated Hospital of Guangzhou University of Chinese Medicine, Guangzhou 510405, China

<sup>2</sup>Department of Dermatology, Gaozhou Hospital of Traditional Chinese Medicine Affiliated to Guangzhou University of Chinese Medicine, Gaozhou 525025, China

<sup>3</sup>Department of Anorectal Medicine, Gaozhou Hospital of Traditional Chinese Medicine Affiliated to Guangzhou University of Chinese Medicine, Gaozhou 525025, China

<sup>4</sup>Graduate School of China Academy of Chinese Medical Sciences, Beijing 100091, China

<sup>5</sup>Department of Prevention and Health Care, Gaozhou Hospital of Traditional Chinese Medicine, Guangzhou University of Chinese Medicine, Gaozhou 525025, China

Correspondence should be addressed to Hong-Liang Jiang; [jiangdumirong@163.com](mailto:jiangdumirong@163.com)

Received 22 April 2022; Revised 20 July 2022; Accepted 2 August 2022; Published 6 September 2022

Academic Editor: Ruchika Garg

Copyright © 2022 Wei-Min Luo et al. This is an open access article distributed under the Creative Commons Attribution License, which permits unrestricted use, distribution, and reproduction in any medium, provided the original work is properly cited.

Anal pain and urinary retention are the two most outstanding complications of the procedure for prolapse and hemorrhoids (PPH) surgery. This study intended to assess the clinical effect and mechanism of Prostant on urinary retention and anal pain after the PPH. Here, 30 patients received PPH surgery. The role and mechanism of Prostant in patients and mice with urinary retention and anal pain were evaluated. ANOVA tests were executed and differences between groups were regarded as statistically significant when  $p < 0.05$ . Prostant effectively improved the urination status, lower abdomen symptoms, time to urinate and score of VAS, and the reduction of TNF- $\alpha$  and IL-6. Similarly, Prostant can ameliorate the outcome of urodynamics in urinary retention mice. Mechanically, Prostant reversed the urinary retention-elevated the serum level of hs-CRP and TNF- $\alpha$ , reduction of IL-2, imbalance of Treg/Th17, and level of JAK2 and phosphorylated STAT3. Besides, Prostant ameliorated the pain as shown by the reduction of writhing response, and the elevation of threshold of pain and degree of swelling. Moreover, Prostant antagonized the pain-induced dysregulation of Treg/Th17. Therefore, Prostant can treat patients and mice with anal pain and urinary retention by modulating the balance of Th17/Treg to regulate the secretion and production of inflammatory factors. We hope our results can establish a scientific treatment approach for solving anal pain and urinary retention after PPH surgery of mixed hemorrhoids.

## 1. Introduction

Hemorrhoids are one of the remarkable diseases manifested as the anal mucosa prominences that are generated by loose connective tissue, venous and arterial vessels, and smooth muscle [1]. In the clinic, hemorrhoids represent a variety of symptoms, including bleeding, pain, soiling, and itching, which had seriously affected patients' health and life [2].

Moreover, it has been reported that hemorrhoids in adults are prevalent all over the world, especially in elderly adults and pregnant women [2]. Although pharmacotherapy is an effective nonsurgical therapy for patients with mild hemorrhoids, patients with hemorrhoids generally develop a severe course owing to their insufficient perception and shame to seek medical treatment [1, 3]. Thus, surgical procedures have been a necessary therapy for patients with severe hemorrhoids.

The procedure for prolapse and hemorrhoids (PPH) surgery was first mentioned in 1998 by Longo, which then has been widely utilized in the therapy of hemorrhoids [4]. However, clinical studies have revealed that there is a series of complications after PPH. Therein, anal pain and urinary retention are the two most outstanding complications. The incidence of urinary retention in mixed hemorrhoids after surgery is 20% to 52% [5], while moderate to severe anal pain also occurs in more than 60% of postoperative patients [6]. Furthermore, anal pain and urinary retention promote each other to form a vicious circle, which causes severe pain to patients and hinders the healing of postoperative wounds. Therefore, it is urgently and crucial to effectively reduce the incidence of urinary retention and anal pain after hemorrhoid surgery.

“Treating different diseases with the same treatment” is an important fundamental theory of traditional Chinese medicine (TCM), which indicates that the same approach of treatment can be used to treat diverse diseases with analogical pathological alteration during various stages of the progression [7]. TCM theories believe that the pathological mechanism of complications such as urinary retention and anal pain after PPH surgery of damp-heat mixed hemorrhoids is damp-heat stasis, which is similar to the pathogenesis of the damp-heat stasis type lower scorch disease such as chronic prostatitis [8–11]. Prostant is a traditional Chinese patent medicine generally applied in China for the treatment of chronic prostatitis, which mainly comprises *Cortex Phellodendri* (Huang Bai), *Rhizoma Polygoni Cuspidati* (Hu Zhang), *Fructus Gardeniae* (Zhi Zi), and *Radix et Rhizoma Rhei* (Da Huang) [12]. The main active ingredient of Prostant is berberine isolated from Huang Bai that can clear away heat, and remove dampness and blood stasis. Modern medicine has proved that berberine can reduce the local inflammatory response, decline inflammatory stimulation to the local area, and relieve the convulsions of the bladder neck, and urethral sphincter by inhibiting the release of local inflammatory factors [13, 14]. In addition, Prostant also has antibacterial effects and regulates mental emotions that have been demonstrated the safety in clinical application [12]. Prostant takes the prostate, bladder neck, and rectum as the main targets, therefore, it should be put 3 to 4 cm inside the opening of the rectum based on the instruction. Thus, Prostant may be used to treat urinary retention and anal pain after PPH surgery of damp-heat mixed hemorrhoids following the “Treating different diseases with the same treatment” theory.

Here, the clinical effects of Prostant on anal pain and urinary retention after PPH surgery of damp-heat mixed hemorrhoids were evaluated based on the “Treating different diseases with the same treatment” theory combined with the “precision medicine” theory. Moreover, the mechanism of action of Prostant was investigated in animal models. We hope our results can enrich the TCM theory of “Treating different diseases with the same treatment,” as well as provide a scientific treatment method for solving anal pain and urinary retention after PPH surgery of mixed hemorrhoids.

## 2. Materials and Methods

**2.1. Survey Object.** Data of the present study were from 30 patients who were diagnosed with damp-heat mixed hemorrhoids admitted to our hospital. The diagnostic criteria were according to the “Guidelines for the Clinical Diagnosis and Treatment of Hemorrhoids” jointly stipulated by the Colorectal and Anal Surgery Group of the Chinese Medical Association Surgery Branch, the Anorectal Branch of the Chinese Society of Chinese Medicine, and the Anorectal Branch of the Chinese Society of Integrative Medicine in 2006. The diagnostic criteria for the damp-heat mixed hemorrhoids were as follows: bright red and thick blood in the stool followed by discharge or swelling of the abscess, feeling of burn pain or nourishing water, dry and loose excrement, yellow or small urine, dry mouth and tongue, yellow and dark fur, and stringy or floating pulse. A total of 30 patients with damp-heat mixed hemorrhoids were allotted into control group and treatment group ( $n=15$ ) through the randomized single-blind control method. Both patients in two groups obtained PPH surgery. Patients in the treatment group received Prostant before the end of the operation and placed 4 cm inside the opening of the rectum. Then, patients obtained Prostant treatment at 4 cm inside the opening of the rectum in the morning and evening after the operation for consecutive 7 days. Patients in control group did not receive any treatment. All subjects accredited the written informed consent. The study was approved by the Board and Ethics Committee of our Hospital.

**2.1.1. Inclusion Criteria.** ① Patients were in accord with the diagnostic criteria for hemorrhoids in the “Guidelines for the Clinical Diagnosis and Treatment of Hemorrhoids,” and meet the diagnostic criteria for damp-heat mixed hemorrhoids in TCM syndrome; ② The gender of the patients is not limited, and the age of the patients is between 18–70 years old; ③ The patients have obvious surgical indications and no surgical contraindications; and ④ The subjects were approved by the ethics committee of Gaozhou Hospital of Traditional Chinese Medicine affiliated to Guangzhou University of Chinese Medicine and the subjects’ informed consent was obtained.

**2.1.2. Exclusion Criteria.** ① Patients were with end-stage malignant tumors or cachexia; ② Patients participated or were participating in other clinical studies during the three-month period of this study; ③ Patients were of childbearing age and have a pregnancy requirement within 3 months; ④ Patients were breastfeeding or pregnant; ⑤ Patients were with severe liver and kidney problems and malignant primary diseases such as cardiovascular and cerebrovascular defects, hematopoietic system defects, lung, and nervous system defects; ⑥ Patients were with a history of mental illness; ⑦ Patients were with inflammatory bowel disease or acute diarrhea in the past week; ⑧ Patients were with a history of urethral injury; and ⑨ Patients had other diseases that were not suitable for the present clinical trials evaluated by the investigators.

*2.2. Diagnostic Criteria of Urinary Retention.* The diagnostic criteria of urinary retention were based on the modern medical standards related to postoperative urinary retention and the diagnostic criteria of TCM obstruction.

*2.2.1. The Diagnostic Criteria of TCM Obstruction.* The diagnostic criteria of TCM obstruction were based on the diagnostic criteria of Guiding Principles for Clinical Research of New Chinese Medicines for Treatment of Obstruction in the “Guiding Principles for Clinical Research of New Chinese Medicines” formulated and issued by the Ministry of Health of the People’s Republic of China in 1993. The details were as follows:

- ① The patient frequently wanted to urinate, and the urine was difficult to discharge or even harder to come out at all;
- ② The lower abdomen accumulated more urine and felt pain;
- ③ It was difficult to urinate, but there was no feeling of sore urethra;
- ④ It was detected that there was more urine left in the bladder.

*2.2.2. The Diagnostic Criteria of Postoperative Urinary Retention in Modern Medicine.* The diagnostic criteria of postoperative urinary retention in modern medicine were based on the clinical manifestations and diagnostic criteria of postoperative urinary retention in “surgical Complications.” The details were as follows:

- ① Patients did not urinate 6–8 hours after surgery;
- ② Patient had the following symptoms: desire to urinate, soreness, no pressure, urgency;
- ③ Clinical examination found bulging above the pubic joint, sore pressure, muddy sound on percussion, and palpable swollen bladder.

*2.3. Scoring Criteria for Evaluation of Symptoms of Urinary Retention.* The scoring criteria were based on the scoring criteria of “Guiding Principles for Clinical Research of New Chinese Medicines for Treatment of Obstruction.” The details were as follows:

*2.3.1. Urination Status.* 0 point, normal; 1 point, urine was as thin as a thread; 2 points, intermittent urine flow could still be thin; 3 points, urinating dripped companies with failing to form a urinary line.

*2.3.2. Lower Abdomen Symptoms.* 0 point, asymptomatic; 1 point, full of stuffiness in the lower abdomen; 2 points, discomfort in the lower abdomen; 3 points, abdominal distension with pain.

*2.3.3. Time to Urinate.* 0 point, urination time was less than 40 seconds; 1 point, urination time was between 40 and 50

seconds; 2 points, urination time was between 51 and 60 seconds; 3 points, urination time was greater than 60 seconds.

*2.4. Scoring Criteria for Pain Assessment.* Pain assessment criteria were based on the visual analog scale (VAS) (0–10 points) to directly record the score with 0 point indicating no pain and 10 points indicating maximal pain.

*2.5. Evaluation Index.* The degree of dysuria and pain of patients in the two groups was scored and analyzed. Three times were recorded at 3 h, 6 h, and 12 h after operation. After that, it was recorded again every morning and evening for 7 days. If the patient was discharged early, follow-up records would be given by telephone. In addition, the serum level of TNF- $\alpha$  and IL-6 was also measured through the enzyme-linked immunosorbent assay (ELISA) assay.

*2.6. Animals.* SPF male BALB/C mice (18–22 g) were obtained from Guangdong Medical Experimental Animal Center. All mice were bred in the SPF environment of the Animal Experiment Center of our hospital and acclimated for 3 days before experiments. Mice were offered a 12 hour/12 hour light-dark cycle and provided with water ad libitum and a standard diet at  $(21 \pm 2)^{\circ}\text{C}$ . All experiments were authorized by the Animal Ethics Committee of our hospital. The experimental operations and materials were conducted following the Guiding Opinions on the Treatment of Experimental Animals, Laboratory Animal Management Regulations, and Laboratory Animal Licensing Management Measures, and were consistent with the guidelines of the National Institutes of Health and Health.

*2.7. Animals Models and Drug Administration*

*2.7.1. Construction of a Mouse Model of Hemorrhoids.* After perianal disinfection of the mice, 0.05 mL of 75% glacial acetic acid was injected into the skin around the anus. Ulcers were formed after 24 hours. Then, 2–3 mice were randomly selected and scored the perianal area based on the local symptom scoring criteria (Table 1) to evaluate the success of the model (More than 4 points indicated successful model building). In addition, hemorrhoids model was also assessed by the pathological changes of the perianal ulcer tissues.

*2.7.2. Construction of a Mouse Model of Hemorrhoids Combined with Urinary Retention.* Mice were intraperitoneally received with 40 mg/kg sodium pentobarbital. The mouse lies in the supine position on the dissection table with a hole at the bottom. After anesthesia, the bladder is opened from the middle, and the indwelling needle is punctured and used for bladder perfusion. One end of the indwelling needle is connected to the 50 mL syringe on the micro syringe pump through a three-way valve, and the other end is connected to an amplifier through a pressure sensor. Then, the urodynamic indexes including the urination interval, maximum



TABLE 1: Local symptoms scale.

Scores	0	1	2	3
Degree of swelling	None	Barely visible	Edge higher than skin	Markedly swollen
Ulcer area	None	< 0.2 cm <sup>2</sup>	< 0.3 cm <sup>2</sup>	> 0.3 cm <sup>2</sup>

urination pressure, basal bladder pressure, and urination threshold pressure were recorded via the LabChart software in real-time. Next, the bladder was perfused with saline at 6 mL/h for 60 minutes to determine the urodynamic data of the bladder under normal conditions. After the last urination, the external urethra was ligated to result in obstruction and perfused with saline at 12 mL/h for two urination cycles. The acute urinary retention model was built 2 hours later.

Mice were randomly divided into control group, hemorrhoids combined with urinary retention model group (H&UR model group), hemorrhoids combined with urinary retention model treated with low-concentration of Prostant (H&UR + Prostant-low), and hemorrhoids combined with urinary retention model treated with high-concentration of Prostant (H&UR + Prostant-high) ( $n = 6$ ). H&UR mice models were established as described above, while mice in control group obtained no stimulation. Mice in H&UR + Prostant-low and H&UR + Prostant-high groups were administered with 0.5 g/kg and 1.0 g/kg Prostant, respectively. Therapeutic effect indexes were recorded and analyzed, including the basal pressure of the bladder during urinary retention, the time of first bladder contraction urination, the base pressure of the bladder after the first contractile urination, urination pressure, and urination threshold pressure for the first contraction of bladder urination, the base pressure of the bladder within 30 minutes after the first bladder contractile urination, urination pressure and urination threshold pressure within 30 minutes after the first bladder contraction, urination pressure during the first contraction of bladder urination, urination pressure 30 minutes after the first urinary bladder contraction and the number of unstable contractions after urination. In addition, the expression level of serum inflammatory factors, the function of T cell, the protein expression level, and the expression of VEGF in mucosa were determined by ELISA, flow cytometry, western blot, and immunohistochemistry assays.

### 2.7.3. Construction of a Mouse Model of Hemorrhoids Combined with Urinary Retention and Pain

(1) *A mouse Model of hemorrhoids Combined with Urinary Retention and Pain was Induced by Glacial Acetic Acid.* Mice were randomly divided into control group, H&UR&P-GAA model group, H&UR&P-GAA + Prostant-low group (0.5 g/kg), and H&UR&P-GAA + Prostant-high group (1.0 g/kg) ( $n = 6$ ). 0.6% glacial acetic acid was injected into the abdominal cavity of the hemorrhoids combined with urinary retention model mice, and then mice received chemical stimulation for 15 minutes to obtain the hemorrhoids combined with urinary retention and pain (H&UR&P-

GAA) model mice. After Prostant was placed into the rectum for 20 minutes, the number of writhing reactions in the mice was recorded to indirectly evaluate the analgesic effect of Prostant.

(2) *A Mouse Model of Hemorrhoids Combined with Urinary Retention and Pain was Induced by Pressure.* Mice were randomly divided into control group, H&UR&P-pressure model group, H&UR&P-pressure + Prostant-low group (0.5 g/kg), and H&UR&P-pressure + Prostant-high group (1.0 g/kg) ( $n = 6$ ). The tails of hemorrhoids combined with urinary retention model mice were depilated, and then the mice were placed in a fixed tube with the tail exposed. The tails were marked at 1 cm from the base of the tail, and the tail retraction was indicated as the pain response gradually increased the pressure. The pain response of mice at 0.5 h, 1 h, and 2 h after administration was measured 5 times in total, and the analgesic effect was evaluated by calculating the percentage increase in pain threshold.

(3) *A Mouse Model of Hemorrhoids Combined with Urinary Retention and Pain was Induced by fresh Egg Whites.* Mice were randomly divided into control group, H&UR&P-egg whites model group, H&UR&P-egg whites + Prostant-low group (0.5 g/kg) and H&UR&P-egg whites + Prostant-high group (1.0 g/kg) ( $n = 6$ ). A mark was made on the right hind foot joint of the mouse, and 0.1 mL of 1% fresh egg white was injected into the foot plantar aponeurosis to cause inflammation. After 30 min, Prostant intervention was carried out and measured at 1, 2, 3, 4, and 5 hours after inflammation. The volume of the feet, the degree of swelling, and the inhibition rate of inflammation were calculated.

In addition, cytokines secreted by Th cells in serum including IL-4, IL-10, IL-17A, and IFN- $\gamma$ , and transcriptional expression level of T-bet, ROR $\gamma$ t, GATA3, and Foxp3 was detected by ELISA and reverse transcription-quantitative polymerase chain reaction (RT-qPCR), severally.

2.8. *ELISA.* The human serum levels of TNF- $\alpha$  and IL-6 were measured via Human IL-6 ELISA Kit (EK0410) and Human TNF $\alpha$  ELISA Kit (EK0525), and the mouse serum levels of IL-2, TNF- $\alpha$ , hs-CRP, IFN- $\gamma$ , IL-4, IL-17A, and IL-10 were determined by Mouse IL-2 ELISA Kit (EK0398), Mouse TNF $\alpha$  ELISA Kit (EK0527), Mouse IFN gamma/IFNG ELISA Kit (EK0375), Mouse IL-4 ELISA Kit (EK0405), Mouse IL-17A ELISA Kit (EK0431), and Mouse IL-10 ELISA Kit (EK0417, BOSTER, Wuhan, China) in line with the manufacturer's protocol. The mouse serum levels of hs-CRP were analyzed through Mouse C Reactive Protein ELISA Kit (ab222511, Abcam, Cambridge, UK) based on the working instructions. The absorbance at 450 nm was measured using a microplate reader (SpectraMAX Plus384, America).

2.9. *Flow Cytometry Assay.* Mouse peripheral blood was collected and prepared into lymph node single cell suspension for flow cytometry assay. Cells were harvested and stained with anti-CD4 antibodies (all from BD Biosciences, USA). FoxP3 staining was performed using Foxp3/

Transcription Factor Fixation/Permeabilization Concentrate and Diluent Kit (eBioscience, USA) according to manufacturer's instruction. Then, cells were stained with anti-FoxP3 antibody (eBioscience). Regarding intracellular cytokine staining, spleen cells were cultured in media containing PMA (50 ng/ml) and Ionomycin (1  $\mu$ g/ml) plus protein transport inhibitor (BD Biosciences) for 5 hours. Cells were then fixed, permeabilized, and stained with anti-IL-17A (all from eBioscience, USA). Finally, cells were analyzed using a flow cytometer (FACSCalibur, BD Biosciences). Fluorescence minus one (FMO) samples and unstained samples were used as internal controls to set positive and negative gating. Cell gating and data collection were performed in a blinded manner.

**2.10. Western Blot Analysis.** Perianal tissues were separated and lysed using RIPA lysis buffer (BOSTER). Protein concentration was determined by a Pierce<sup>®</sup> BCA Protein Assay Kit (Thermo Fisher). Subsequently, protein samples were dissolved using 10% SDS-PAGE and then transferred onto PVDF membranes (EMD Millipore, Billerica, MA, USA). The membranes were sealed in 5% skimmed milk powder at room temperature for 2 h and then hatched with primary antibodies overnight at 4°C, followed by introduction with the corresponding secondary antibody (BOSTER) for 1 h at room temperature. An ECL chemiluminescence kit (EMD Millipore) was used to visualize the bands, and Image-ProPlus software (Media Cybernetics, Inc., Rockville, MD, USA) was utilized for the analysis of the gray value. Protein levels were calculated relative to GAPDH. The primary antibodies used in this study were as follows: GAPDH (ab181602, Abcam), JAK2 (74987, Cell Signaling Technology, Inc., Danvers, MA, USA), and phospho-STAT3 (Tyr705) (9145, CST) at 1:1,000 dilutions.

**2.11. Immunohistochemistry (IHC).** Internal hemorrhoid-damaged mucosal tissues were immobilized with 4% paraformaldehyde *f* at room temperature for 24 h. After dehydrated, embedded, and cut, the sections (5  $\mu$ m) were obtained for IHC experiment. Sections were stained with anti-VEGF antibody (A00623, BOSTER). Subsequently, the slices were assessed with a light microscope (Olympus, Tokyo, Japan) and Image-Pro Plus 6.0 (Media Cybernetics).

**2.12. RT-qPCR Analysis.** Total RNA from perianal tissues was enriched through TRIzol reagent (TaKaRa Biotechnology Co., Ltd., Dalian, China) and then reversely transcribed into cDNA by PrimeScript<sup>™</sup> RT reagent Kit with gDNA Eraser (Perfect Real Time) (TaKaRa) following the operating instruction. RT-qPCR was performed in a 25  $\mu$ l quantum involving 2  $\mu$ l of the cDNA, 12.5  $\mu$ l 2 $\times$ SYBR<sup>®</sup> Premix Ex Taq<sup>™</sup> II (Tli RNaseH Plus) (TaKaRa), 2  $\mu$ l of the 10- $\mu$ M upstream and downstream primers as well as 8.5  $\mu$ l ddH<sub>2</sub>O, using the ABI Prism<sup>™</sup> 7500 (Thermo Fisher). The RT-qPCR conditions were as follows: 30 s at 95°C, followed by 40 cycles between 95°C for 5 s and 60°C for 30 s, 95°C for 10 s, and 65°C for 5 s. The relative expressions of T-bet,

TABLE 2: Primer sequences included in the present study.

Primer name	Sequence (5'-3')
GAPDH-F	GGAGAGTGTTTCCTCGTCCC
GAPDH-R	ACTGTGCCGTTGAATTTGCC
T-bet F	AAGTTCAACCAGCACCAGACAGAG
T-bet R	GCCACGGTGAAGGACAGGAATG
ROR $\gamma$ t F	AAGGCAAATACGGTGGTGTG
ROR $\gamma$ t R	GAAAAGGGTGAAGGAGTCCG
GATA3 F	CCAAGGCACGATCCAGCACAG
GATA3 R	TTATGGTAGAGTCCCGAGGCATTG
Foxp3 F	AAGAATGCCATCCGCCACAACC
Foxp3 R	GGCGTTGGCTCCTCTCTTTC

ROR $\gamma$ t, GATA3, and Foxp3 were calculated using the  $2^{-\Delta\Delta CT}$  method and normalized to the GAPDH. All the primers used in the present study were listed in Table 2.

**2.13. Statistical Analysis.** Data in the present study were determined using SPSS 25.0 statistical software (IBM, Armonk, New York, USA). Data were first analyzed using Shapiro–Wilk test. All the measurement data were presented as means  $\pm$  SD when measurement data conformed to normal distribution. Data were tested by a rank sum test or student's *t*-test with only two groups, whereas differences were determined via one-way analysis of variance and Duncan's test among various groups. All the count data were displayed as a percentage and detected by the chi-square test. The differences were regarded as statistically significant when  $p < 0.05$ . Figures were generated using Graphpad Prism 8.0 software.

### 3. Results

**3.1. General Information.** 30 patients who accorded with the inclusion and exclusion criteria were included and allocated into control and treatment groups. As shown in Table 3, 15 patients contained 9 males and 6 females aged 23–69 years ( $41.0 \pm 13.2$  years) with medical history 0.5–10 years ( $4.1 \pm 3.1$  years) in control group. In the treatment group, 15 patients included 10 males and 5 females aged 24–69 years ( $45.5 \pm 15.1$  years) with medical history 1–30 years ( $7.3 \pm 7.9$  years). Data of the two groups showed no statistical difference ( $p > 0.05$ ).

**3.2. The Clinical Effect of Prostant on Urinary Retention and Pain.** Patients with the damp-heat mixed hemorrhoids received PPH surgery and then treated with or without Prostant. Clinical data revealed that Prostant treatment significantly ameliorated the symptoms of urinary retention including urination status (Figure 1(a)), lower abdomen symptoms (Figure 1(b)), and time to urinate (Figure 1(c)). In addition, patients treated with Prostant notably suffered less pain as indicated by a prominently lower score of VAS (Figure 1(d)). Moreover, ELISA results exhibited that the serum level of IL-6 and TNF- $\alpha$  of the two groups was no statistical difference before operation, while IL-6 and TNF- $\alpha$  levels in patients administrated with Prostant were

TABLE 3: Comparison of general information between control group and treatment group.

	Control ( <i>n</i> )	Treatment ( <i>n</i> )	$\chi^2$	<i>p</i>
Gender				
Male	9	10	0.000	1.000
Female	6	5		
Age				
< 35(year)	6	6	3.333	0.343
35–50(year)	4	3		
> 50(year)	5	6		
Medical history				
< 3.0(year)	5	4	0.000	1.000
3.0–5.0(year)	6	5		
> 5.0(year)	4	6		

observably reduced on the first day and the second day after the operation (Figures 1(e) and 1(f)). In summary, these outcomes indicated that Prostant could effectively relieve urinary retention, pain, and inflammation.

**3.3. Prostant Ameliorated the Urinary Retention in Mice Model.** To reveal the underlying mechanism of the effect of Prostant on urinary retention and pain, we built a mice model of hemorrhoids combined with urinary retention. Urodynamics results revealed that both low-dose and high-dose Prostant significantly attenuated the H&UR-induced enhancement of the basal pressure of the bladder during urinary retention (Figure 2(a)), the time of first bladder contraction urination (Figure 2(d)), the base pressure of the bladder after the first contractile urination (Figure 2(e)), and the base pressure of the bladder within 30 minutes after the first bladder contractile urination (Figure 2(f)). However, only high-dose Prostant prominently declined the H&UR-induced increase of the urination pressure and urination threshold pressure for the first contraction of bladder urination (Figure 2(c)), urination pressure 30 minutes after the first urinary bladder contraction (Figure 2(g)), urination pressure and urination threshold pressure within 30 minutes after the first bladder contraction (Figure 2(h)), and the number of unstable contractions after urination (Figure 2(i)). Besides, both low-dose and high-dose Prostant had no effect on the H&UR-induced augmentation of the urination pressure during the first contraction of bladder urination (Figure 2(b)). In brief, these data suggested that Prostant could improve urinary retention in the mice model.

**3.4. Prostant Regulated Inflammatory Factors Expression through Modulating Th17/Treg Balance with Inhibiting JAK/STAT Signaling Pathway.** The serum level of inflammatory factors including hs-CRP, IL-6, and TNF- $\alpha$  was notably increased in H&UR model mice, which was markedly reversed with high-dose Prostant treatment (Figure 3(a)). On the contrary, high-dose Prostant introduction notably promoted the H&UR-induced decrease of the serum level of IL-2 (Figure 3(a)). IHC analysis revealed that the H&UR-induced elevation of VEGF expression was dramatically reduced by both low-dose and high-dose Prostant treatment

(Figures 3(b) and 3(c)). Additionally, flow cytometry results revealed that both low-dose and high-dose Prostant prominently downregulated the H&UR-induced increase of Th17 expression, but upregulated the H&UR-induced decrease of Treg expression (Figures 3(d) and 3(e)). The relative protein levels of JAK2, STAT3, and p-STAT3 were notably enhanced in H&UR model mice, which was observably antagonized with both low-dose and high-dose Prostant treatment (Figures 3(f) and 3(g)). Based on these results, we demonstrated that Prostant regulated Th17/Treg balance in urinary retention mice by suppressing the expression of JAK/STAT axis, thereby modulating the expression of inflammatory factors, and finally improving urinary retention.

**3.5. Prostant Exerted Analgesic Effect on Mice.** Next, three pain mice models were built to assess the effect of Prostant on the pain. After H&UR model mice were administered with 0.6% glacial acetic acid, the number of writhing reactions was significantly increased, which was notably inverted with both low-dose and high-dose Prostant treatment (Figure 4(a)). Thus, the inhibition ratio of writhing response between low-dose and high-dose Prostant treatment was no statistical difference (Figure 4(b)). Besides, H&UR model mice were pressed and analyzed at 0.5 h, 1 h, and 2 h after administration. The results revealed that both low-dose and high-dose Prostant treatment prominently elevated the threshold of pain of H&UR model mice at 0.5 h, 1 h, and 2 h compared with that at 0 h (Figure 4(c)). Moreover, high-dose Prostant treatment further significantly increased the threshold of pain of H&UR model mice compared with low-dose Prostant treatment at 0.5 h, 1 h, and 2 h (Figure 4(c)). Therefore, high-dose Prostant treatment observably enhanced the increased ratio threshold of pain compared with low-dose Prostant treatment (Figure 4(d)). Similarly, the foot plantar aponeurosis of H&UR model mice was injected with 1% fresh egg white to cause inflammation. The degree of swelling of H&UR model mice was memorably enhanced relative to that in control mice at 1, 2, 3, 4, and 5 h after inflammation. However, both low-dose and high-dose Prostant treatment notably attenuated the degree of swelling of H&UR model mice at 1, 2, and 3 h, while only high-dose Prostant treatment prominently reduced the degree of swelling of H&UR model mice at 4 and 5 h (Figure 4(e)). Hence, high-dose Prostant treatment significantly elevated the inhibition rate of inflammation compared with low-dose Prostant treatment at 1, 2, 3, 4, and 5 h (Figure 4(f)). Altogether, we concluded that Prostant had an analgesic effect on mice.

**3.6. Prostant Exerted Analgesic Effect via Regulating the Balance between T Cell Subpopulations.** Based on the above-mentioned results, the balance between T cell subpopulations may exert a crucial role in urinary retention and pain. Thus, the serum level of IFN- $\gamma$ , IL-4, IL-10, IL-17A, and IL-17C was detected. ELISA results exhibited that both low-dose and high-dose Prostant treatment notably reduced H&UR&P-induced elevation of the serum level of IFN- $\gamma$ , IL-

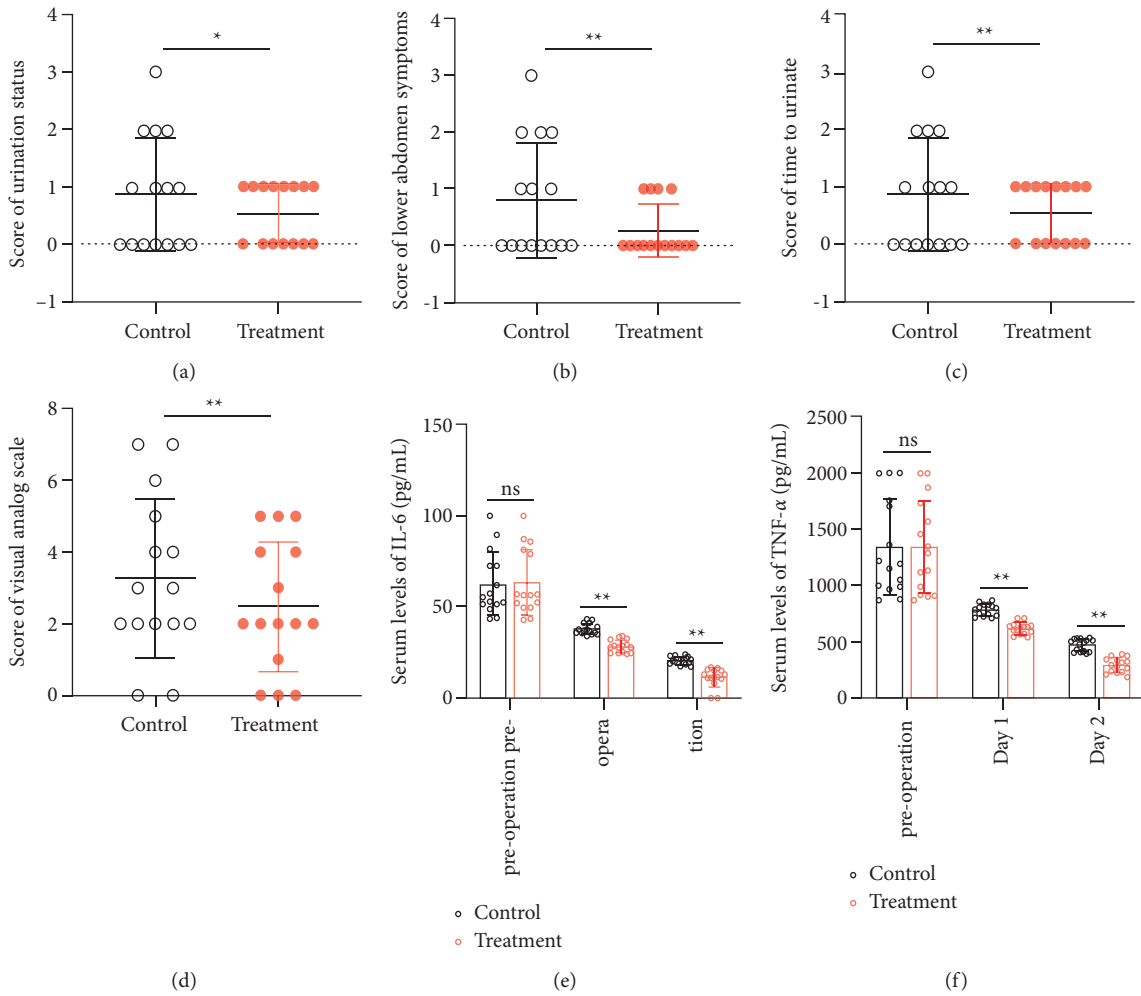


FIGURE 1: Prostant effectively alleviated urinary retention, pain, and inflammation. The symptoms of urinary retention including urination status (a), lower abdomen symptoms (b) and time to urinate (c) were scored, and the score of VAS (d) was also quantified to evaluate the pain. In addition, the serum level of IL-6 (e) and TNF- $\alpha$  (f) was determined by ELISA before operation and on the first day, and the second day after the operation. Data in (a)–(d) were evaluated by the rank sum test, while data in (e) and (f) were examined by the student's *t*-test. The means  $\pm$  SD of 15 independent samples were presented. \* $p < 0.05$  and \*\* $p < 0.01$ .

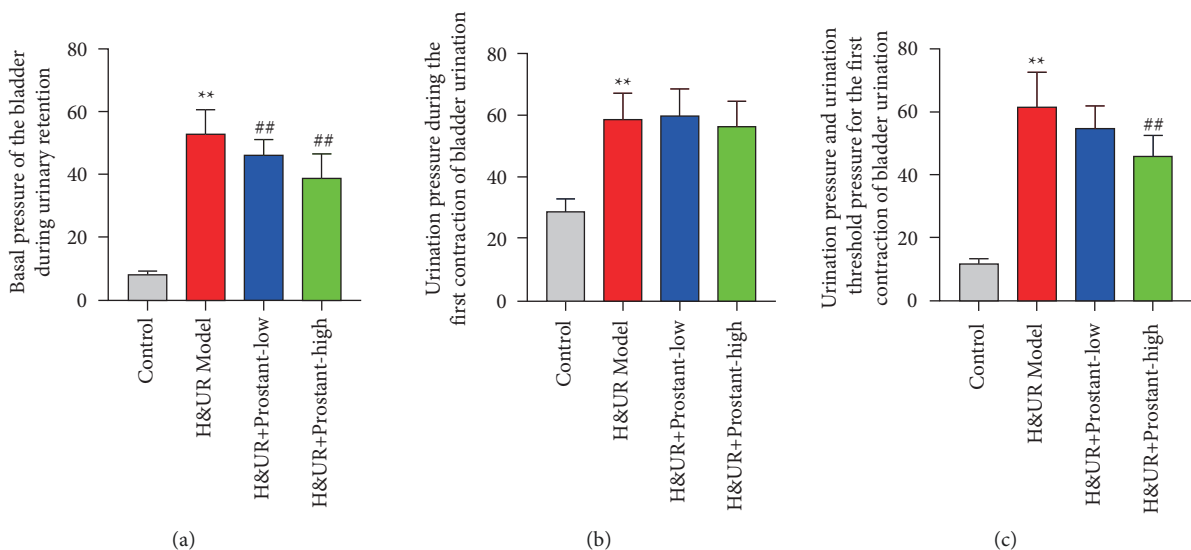


FIGURE 2: Continued.



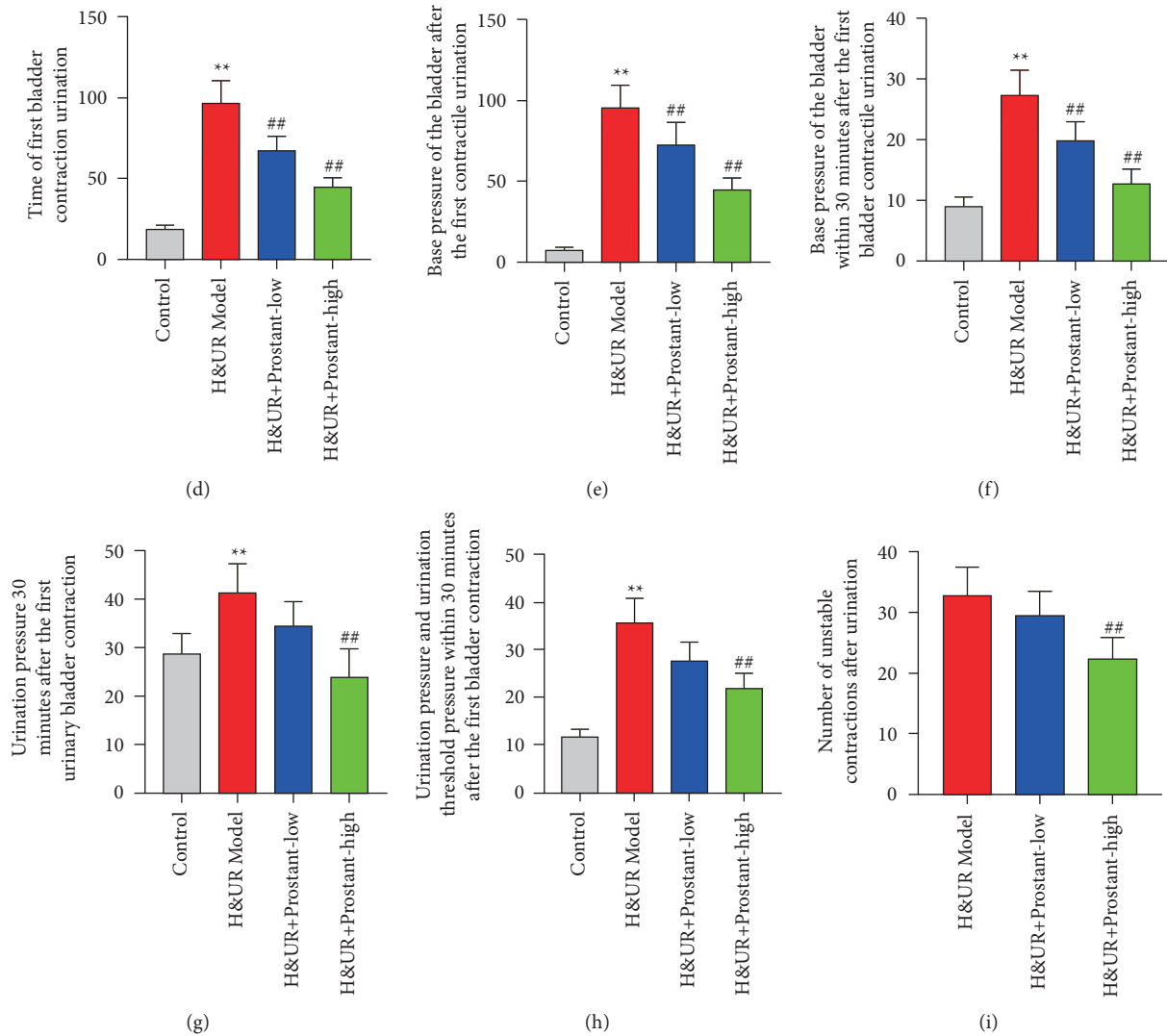


FIGURE 2: Prostant improved the urinary retention in mice model. Mice with hemorrhoids combined with urinary retention were treated with or without Prostant. Urodynamics, including the basal pressure of the bladder during urinary retention (a), the urination pressure during the first contraction of bladder urination (b), the urination pressure and urination threshold pressure for the first contraction of bladder urination (c), the time of first bladder contraction urination (d), the base pressure of the bladder after the first contractile urination (e), the base pressure of the bladder within 30 minutes after the first bladder contractile urination (f), the urination pressure 30 minutes after the first urinary bladder contraction (g), the urination pressure and urination threshold pressure within 30 minutes after the first bladder contraction (h), and the number of unstable contractions after urination (i). The means  $\pm$  SD of six independent samples were shown. \*\* $p < 0.01$  v.s control group. ## $p < 0.01$  v.s H&UR model group.

17A, and IL-17C, while both low-dose and high-dose Prostant treatment observably enhanced H&UR&P-induced reduction of the serum level of IL-10 (Figure 5(a)). However, the serum level of IL-4 was no statistical difference among the four groups (Figure 5(a)). Furthermore, qRT-PCR results uncovered that the transcriptional level of T-bet and ROR $\gamma$ t was observably increased, which was significantly reversed with both low-dose and high-dose Prostant treatment (Figure 5(b)). The mRNA expression level of GATA3 and Foxp3 was markedly reduced, which was notably rescued with high-dose Prostant treatment (Figure 5(b)). Therefore, these data indicated that Prostant mainly exerted an analgesic effect via modulating the balance of Th17/Treg.

#### 4. Discussion

In the current study, we explored the clinical effects of as well as the potential molecular mechanism of Prostant on urinary retention and anal pain based on the “Treating different diseases with the same treatment” theory combined with “precision medicine” theory. We found that Prostant could treat patients and mice with urinary retention and anal pain. Mechanically, Prostant may modulate the balance of Th17/Treg to regulate the secretion and production of inflammatory factors, which ameliorated urinary retention and anal pain.

Prostant has been demonstrated to be effective and safe in the treatment of chronic prostatitis [15]. The pathological mechanism of chronic prostatitis according to TCM theories

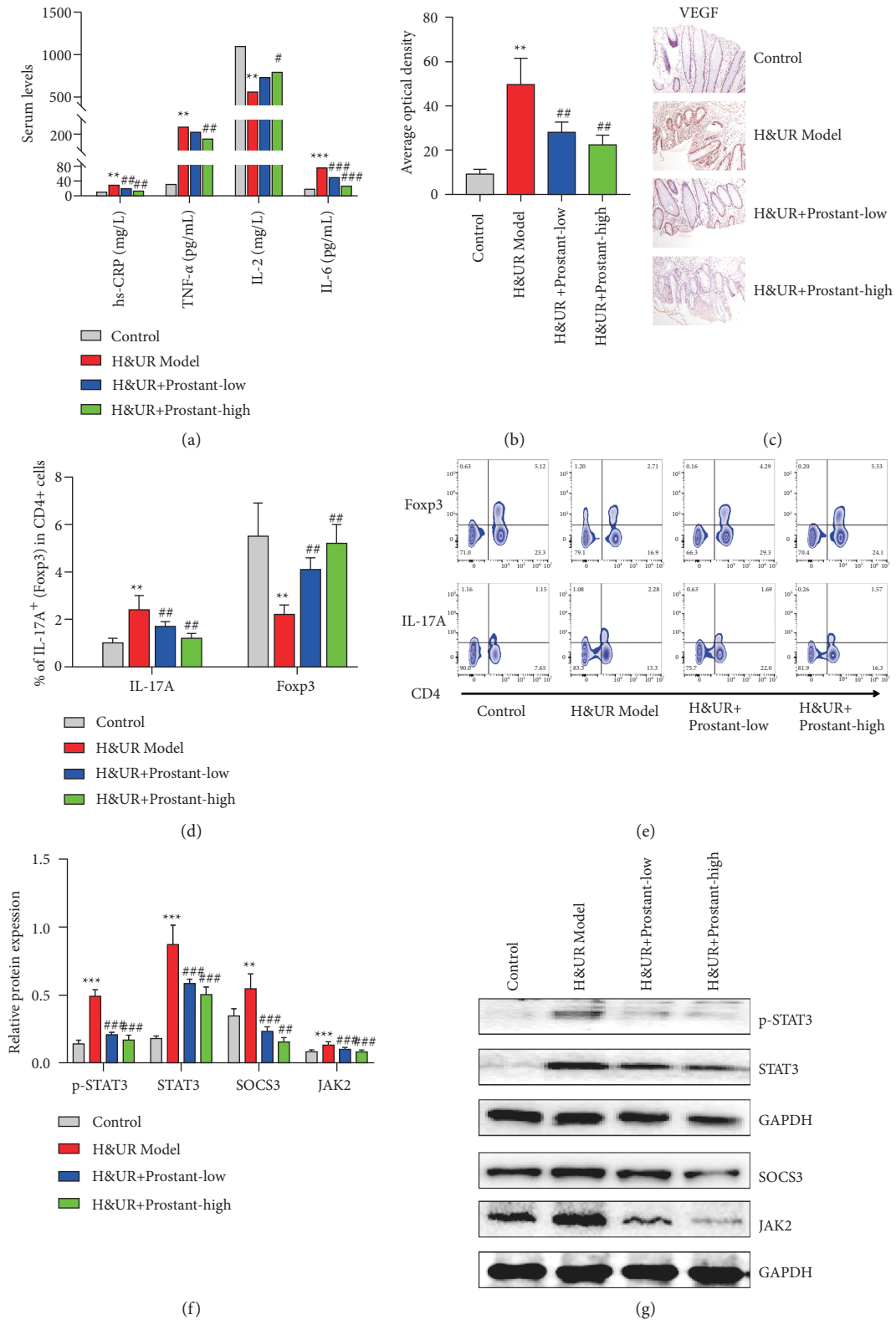


FIGURE 3: Prostant regulated inflammatory factors expression through modulating Th17/Treg balance with inhibiting JAK/STAT axis. (a) The serum level of hs-CRP, TNF- $\alpha$ , IL-2, and IL-6 was examined via ELISA. (b) and (c) The level of VEGF in mucosal tissues was determined by IHC. (d) and (e) The expression of Th17 and Treg was assessed by flow cytometry assay. (f) and (g) The protein expression of STAT3, phosphorylated STAT3, SOCS3, and JAK2 was evaluated by western blot. Data were exhibited following being normalized to GAPDH. The means  $\pm$  SD of six independent samples were displayed. \*\* $p < 0.01$  and \*\*\* $p < 0.001$  v.s control group. #  $p < 0.05$ , ##  $p < 0.01$  and ###  $p < 0.001$  v.s H&UR model group.

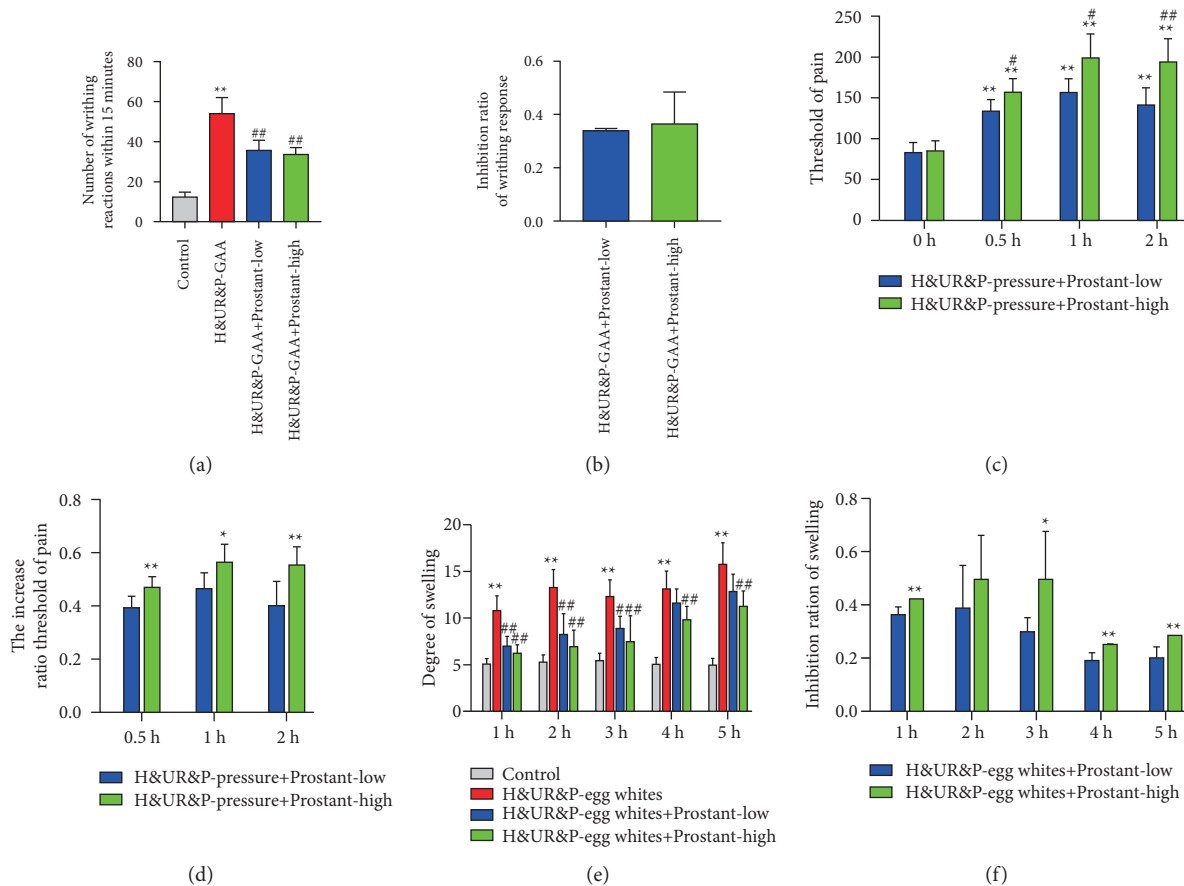


FIGURE 4: Prostant exerted analgesic effect on mice. H&UR model mice were introduced with 0.6% glacial acetic acid, and then the number of writhing reactions (a) and the inhibition ratio of writhing response (b) were detected. In addition, H&UR model mice were pressed and analyzed at 0.5 h, 1 h, and 2 h after administration. The threshold of pain (c) and the increased ratio threshold of pain (d) were determined. Besides, the foot plantar aponeurosis of H&UR model mice was injected with 1% fresh egg white to cause inflammation. The degree of swelling (e) and the inhibition rate of inflammation (f) were assessed. The means  $\pm$  SD of six independent samples were displayed. In Figures (a) and (e),  $**p < 0.01$  v.s control group, and  $##p < 0.01$  v.s H&UR model group. In Figure (c),  $**p < 0.01$  v.s that at 0 h,  $#p < 0.05$  and  $##p < 0.01$  v.s low-dose prostant at the same time point, respectively. In Figures (d) and (f),  $*p < 0.05$  and  $**p < 0.01$  v.s low-dose prostant at the same time point, respectively.

is damp-heat stasis, which is similar to that of urinary retention after PPH surgery of damp-heat mixed hemorrhoids. Thus, Prostant was used to treat the patients with urinary retention after PPH surgery in the present study based on the “treating different diseases with the same treatment” theory. Satisfactorily, Prostant was also effective for the patients with urinary retention after PPH surgery as indicated by the improvement of urination status, lower abdomen symptoms, and time to urinate. During the surgery, the traction, sharp cutting, or thermal damage around the anorectum and perineum can damage the muscles, blood vessels, and nerves, which results in the release of inflammatory factors, local inflammation, pain, local bleeding, and hematoma formation. These stimuli can reflexively cause muscle spasms and wound inflammation in the perineum, prostate, and bladder neck, which can lead to dysuria and urinary retention [16]. Thus, a previous study has highlighted that the risk of urinary retention is tightly associated with inflammation [17]. Wu et al. [18] have exhibited that the serum concentration of IL-6 was notably enhanced in patients with acute urinary retention. Our ELISA results revealed that

Prostant treatment notably diminished the serum level of proinflammatory cytokines including TNF- $\alpha$  and IL-6 both on the first and second day after the operation. TNF- $\alpha$ , a core modulator of inflammatory responses, has been identified to be relevant to the pathogenesis of inflammatory [19]. IL-6 exerts a significant role in a variety of signs of progress, such as inflammation, immune regulation, hematopoiesis, and oncogenesis [20]. In addition, the degree of pain was also markedly alleviated with Prostant treatment as shown by the reduction of score of VAS. Therefore, we concluded that Prostant might attenuate the secretion of inflammatory mediators to exert anti-inflammatory function, which slowed down the course of the disease, thereby reducing the pain after the operation.

Then, a urinary retention model was built, and urodynamics results revealed that Prostant treatment observably improved urinary retention in mice. CRP is an acute phase protein secreted by IL-6 that is upregulated during various inflammatory processes, tissue necrosis, and tissue damage (such as after surgery) [21]. Thus, serum CRP has been demonstrated to be a predictor due to an increase of its

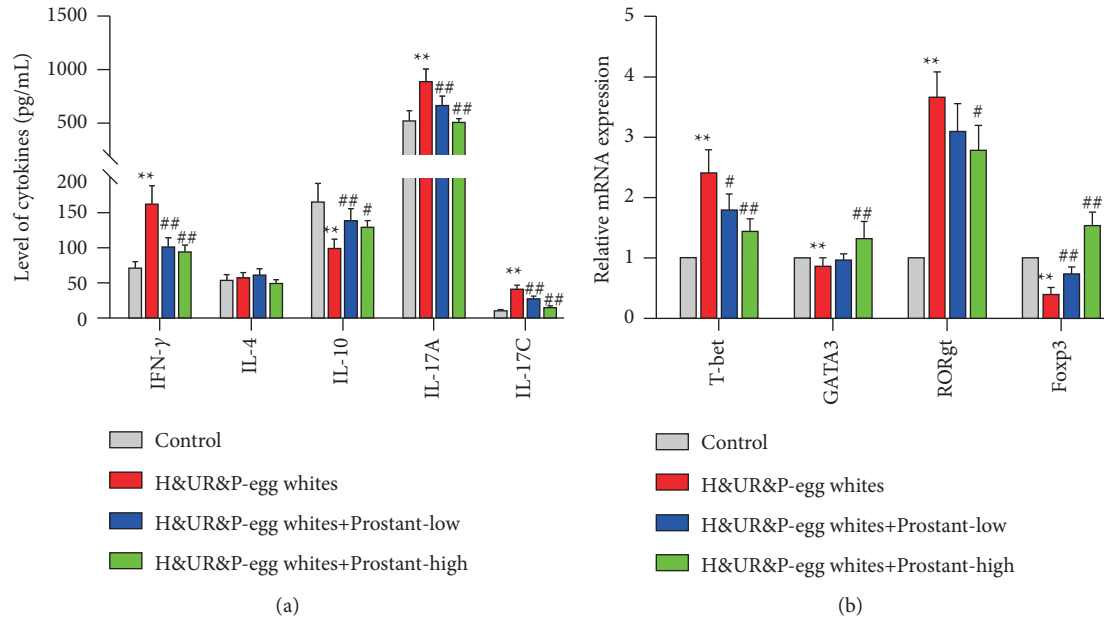


FIGURE 5: Prostant exerted analgesic effect via regulating the balance between T cell subpopulations. (a) The serum level of IFN- $\gamma$ , IL-4, IL-10, IL-17A, and IL-17C was detected by ELISA. (b) The mRNA expression level of T-bet, ROR $\gamma$ t, GATA3, and Foxp3 was measured by qRT-PCR. Data were exhibited following being normalized to GAPDH. The means  $\pm$  SD of six independent samples were displayed. \*\* $p < 0.01$  and \*\*\* $p < 0.001$  v.s control group. # $p < 0.05$ , ## $p < 0.01$  and ### $p < 0.001$  v.s H&UR&P model group.

serum level in acute urinary retention, [22] acute prostatitis [23], and liver cirrhosis [24]. IL-2 regulates the cellular activity of white blood cells in the immune system [25]. Similarly, ELISA results revealed that Prostant administration significantly declined the H&UR-induced enhancement of the serum level of hs-CRP and TNF- $\alpha$ , while enhancing the H&UR-induced reduction of the serum level of IL-2. It has been elucidated that the balance of Treg/Th17 is correlative with inflammation in various diseases, such as colon inflammation, [26] experimental autoimmune encephalomyelitis, [27] rheumatoid arthritis [28], and chronic obstructive pulmonary disease [29]. In line with these previous studies, our results also showed the unbalance of Treg/Th17 in the mice with urinary retention. However, Prostant treatment prominently rescued the dysregulation of Treg/Th17. Furthermore, Prostant treatment observably antagonized the H&UR-induced enhancement of JAK2 and phosphorylated STAT3. JAK/STAT signal pathway is a core pathway for intracellular signal transduction, which has been introduced to be essential for the differentiation of CD4<sup>+</sup> T cells into effector or regulatory phenotypes [30, 31]. Taken together, we concluded that Prostant can modulate Th17/Treg balance in urinary retention mice by inhibiting JAK/STAT signaling pathway, which regulates the generation of inflammatory cytokines to improve urinary retention.

In addition, the balance of Th17/Treg has also been demonstrated to be associated with pain, such as neuropathic pain, [32] bone cancer pain [33], and chronic low back pain [34]. Similarly, serum level of IL-17A was notably elevated in H&UR&P mice model, which could be reversed with Prostant treatment. Furthermore, Prostant treatment

prominently antagonized the H&UR&P-induced increase of ROR $\gamma$ t, and reduction of Foxp3. ROR $\gamma$ t is a pivotal transcription factor for Th17 cells differentiation, and it also regulates the expression and secretion of IL-17, [35] while Foxp3 is a representative transcription factor of Treg cells [36]. Moreover, Th1 cells can promote the occurrence of pain according to the production of proinflammatory cytokines TNF and IFN- $\gamma$ , while Th2 cells can relieve pain based on the generation of anti-inflammatory cytokines IL-4, IL-5, IL-10, and IL-13 [37]. T-bet and GATA-3 can mediate the differentiation of T cells into Th1 and Th2, respectively [38]. Thus, in the present study, Prostant treatment prominently antagonized the H&UR&P-induced increase of IFN- $\gamma$  and T-bet, and reduction of IL-10 and GATA-3. In brief, combined with the improvement of pain with Prostant treatment as indicated by the reduction of writhing response, and the elevation of threshold of pain and degree of swelling, we concluded that Prostant can alleviate urinary retention and pain through regulating the balance between T cell subpopulations in mice. Nevertheless, no statistical difference was detected in the serum level of IL-4 relative to that in the control, which might suggest that Prostant mainly alleviated urinary retention and pain through regulating the balance of Th17/Treg.

In conclusion, Prostant can treat patients and mice with anal pain and urinary retention. Mechanically, Prostant may regulate the balance of Th17/Treg to modulate the secretion and production of inflammatory factors, which ameliorated anal pain and urinary retention. However, our study still has a few limitations. First, the clinical sample size of this study is small, thus more sample numbers are needed in subsequent observations. Next, the potential and further molecular

mechanisms (such as some relevant signaling pathways) involved in pain need to be inquired about in further study. Additionally, the lack of validation of jak2/stat3 inhibitors and/or agonists is indeed another shortcoming of our study, which need to be supplemented in the following experiments. Briefly, we hope the results can establish a foundation for therapeutic drugs to treat anal pain and urinary retention after surgery.

### Data Availability

The data analyzed and used during the present study are available from the corresponding author on reasonable request.

### Disclosure

Wei-Min Luo and Han Du are cofirst authors.

### Conflicts of Interest

The authors declare that there are no conflicts of interest.

### Authors' Contributions

Wei-Min Luo and Han Du contributed equally to this work.

### Acknowledgments

The present study was supported by the Guangdong Administration of Traditional Chinese Medicine (grant no. 20202255).

### References








- [1] V. Lohsiriwat, "Treatment of hemorrhoids: a coloproctologist's view," *World Journal of Gastroenterology*, vol. 21, no. 31, pp. 9245–9252, 2015.
- [2] Y. Shi, D. Yang, S. Chen et al., "Factors influencing patient delay in individuals with haemorrhoids: a study based on theory of planned behavior and common sense model," *Journal of Advanced Nursing*, vol. 75, no. 5, pp. 1018–1028, 2019.
- [3] D. F. Altomare and S. Giuratrabocchetta, "Conservative and surgical treatment of haemorrhoids," *Nature Reviews Gastroenterology & Hepatology*, vol. 10, no. 9, pp. 513–521, 2013.
- [4] G. Zhang, R. Liang, J. Wang et al., "Network meta-analysis of randomized controlled trials comparing the procedure for prolapse and hemorrhoids, milligan-morgan hemorrhoidectomy and tissue-selecting therapy stapler in the treatment of grade iii and iv internal hemorrhoids (meta-analysis)," *International Journal of Surgery*, vol. 74, pp. 53–60, 2020.
- [5] M. Lu, B. Yang, Y. Liu, Q. Liu, and H. Wen, "Procedure for prolapse and hemorrhoids vs traditional surgery for outlet obstructive constipation," *World Journal of Gastroenterology*, vol. 21, no. 26, pp. 8178–8183, 2015.
- [6] A. Habr-Gama, A. H. e Sous Jr., and J. M. Roveló, "Stapled hemorrhoidectomy: initial experience of a Latin American group," *Journal of Gastrointestinal Surgery*, vol. 7, no. 6, pp. 809–813, 2003.
- [7] X. Zhai, X. Wang, L. Wang, L. Xiu, W. Wang, and X. Pang, "Treating different diseases with the same method-A traditional Chinese medicine concept analyzed for its biological basis," *Frontiers in Pharmacology*, vol. 11, pp. 946–2020, 2020.
- [8] C. Huang, "Clinical observation on 40 cases of chronic prostatitis treated by self-made Qingzhuo Huayu decoction," *Chinese Medicine Herald*, pp. 39-40, 2008, in Chinese.
- [9] Q. Duan, "External application of modified Kushen decoction in treating 100 cases of external hemorrhoids with damp heat and blood stasis," *Bright Chinese Medicine*, vol. 30, pp. 2015–2017, 2015, in Chinese.
- [10] L. Lu, "Study on Kang'er Xiaoyan suppository in the treatment of chronic prostatitis with damp heat and blood stasis syndrome," *Chinese Journal of Traditional Chinese Medicine*, vol. 28, pp. 1495-1496, 2010, in Chinese.
- [11] Q. Chen and H. Liu, "Observation on the curative effect of Qianlie Qingyu decoction in the treatment of 65 cases of chronic prostatitis with damp heat and blood stasis," *China Traditional Chinese Medicine Technology*, vol. 19, pp. 532-533, 2012, in Chinese.
- [12] C. Hui-Juan, L. Shi-Bing, L. Jian-Ping et al., "Qian lie an suppository (prostant) for chronic prostatitis: a systematic review and meta-analysis of randomized controlled trials," *Medicine (Baltimore)*, vol. 98, no. 14, Article ID e15072, 2019.
- [13] K. Fukuda, Y. Hibiya, M. Mutoh, M. Koshiji, S. Akao, and H. Fujiwara, "Inhibition by berberine of cyclooxygenase-2 transcriptional activity in human colon cancer cells," *Journal of Ethnopharmacology*, vol. 66, no. 2, pp. 227–233, 1999.
- [14] Y. K. Hong, H. T. Wu, T. Ma, W. J. Liu, and X. J. He, "Effects of Glycyrrhiza glabra polysaccharides on immune and anti-oxidant activities in high-fat mice," *International Journal of Biological Macromolecules*, vol. 45, no. 1, pp. 61–64, 2009.
- [15] G. Xu, Y. F. Zhang, and Q. Ding, "Efficacy of Prostant on chronic prostatitis in 119 patients," *Acta Pharmaceutica Sinica*, vol. 24, no. 6, pp. 615–618, 2003.
- [16] M. S. De Robles and C. J. Young, "Surgical technique is the main predictor of recurrence in the management of haemorrhoids," *ANZ Journal of Surgery*, vol. 91, no. 9, pp. 1854–1858, 2021.
- [17] G. L. Lloyd, J. M. Marks, and W. A. Ricke, "Benign prostatic hyperplasia and lower urinary tract symptoms: what is the role and significance of inflammation?" *Current Urology Reports*, vol. 20, no. 9, 2019.
- [18] D. Wu, Z. E. Shi, D. Xu, Y. Wu, S. B. Qian, and J. Qi, "Serum interleukin 6 and acute urinary retention in elderly men with benign prostatic hyperplasia in China: a cross-sectional study," *Translational Andrology and Urology*, vol. 10, no. 1, pp. 455–465, 2021.
- [19] D. I. Jang, A. H. Lee, H. Y. Shin et al., "The role of tumor necrosis factor Alpha (TNF- $\alpha$ ) in autoimmune disease and current TNF- $\alpha$  inhibitors in therapeutics," *International Journal of Molecular Sciences*, vol. 22, no. 5, p. 2719, 2021.
- [20] S. Kaur, Y. Bansal, R. Kumar, and G. Bansal, "A panoramic review of IL-6: structure, pathophysiological roles and inhibitors," *Bioorganic & Medicinal Chemistry*, vol. 28, no. 5, Article ID 115327, 2020.
- [21] M. Del Giudice and S. W. Gangestad, "Rethinking IL-6 and CRP: why they are more than inflammatory biomarkers, and why it matters," *Brain, Behavior, and Immunity*, vol. 70, pp. 61–75, 2018.
- [22] M. Vella, A. Abrate, A. Costanzo, F. D'Amato, M. L. Tarantino, and A. Simonato, "Predictive variables of spontaneous micturition recovery after acute urinary retention in men with benign prostatic enlargement: an



- observational prospective study,” *LUTS: Lower Urinary Tract Symptoms*, vol. 11, no. 3, pp. 104–108, 2019.
- [23] H. K. Ahn, K. C. Koo, B. H. Chung, and K. S. Lee, “Comparison of the delta neutrophil index with procalcitonin, erythrocyte sedimentation rate, and C-reactive protein as predictors of sepsis in patients with acute prostatitis,” *Prostate International*, vol. 6, no. 4, pp. 157–161, 2018.
- [24] M. Nakai, K. Ogawa, R. Takeda et al., “Increased serum C-reactive protein and decreased urinary aquaporin 2 levels are predictive of the efficacy of tolvaptan in patients with liver cirrhosis,” *Hepatology Research*, vol. 48, no. 3, pp. E311–e319, 2018.
- [25] A. K. Abbas, E. Trotta, D. R. Simeonov, A. Marson, and J. A. Bluestone, “Revisiting IL-2: biology and therapeutic prospects,” *Science Immunology*, vol. 3, no. 25, Article ID eaat1482, 2018.
- [26] Y. J. Liu, B. Tang, F. C. Wang et al., “Parthenolide ameliorates colon inflammation through regulating Treg/Th17 balance in a gut microbiota-dependent manner,” *Theranostics*, vol. 10, no. 12, pp. 5225–5241, 2020.
- [27] Z. Li, L. Nie, L. Chen, Y. Sun, and G. Li, “Rapamycin relieves inflammation of experimental autoimmune encephalomyelitis by altering the balance of Treg/Th17 in a mouse model,” *Neuroscience Letters*, vol. 705, pp. 39–45, 2019.
- [28] S. Jin, H. Chen, Y. Li et al., “Maresin 1 improves the Treg/Th17 imbalance in rheumatoid arthritis through miR-21,” *Annals of the Rheumatic Diseases*, vol. 77, no. 11, pp. 1644–1652, 2018.
- [29] Y. Q. Xu, W. Lv, H. J. Wu, and S. F. Shi, “Ginsenoside regulates Treg/Th17 cell ratio and inhibits inflammation to treat COPD,” *Pharmazie*, vol. 75, no. 11, pp. 590–594, 2020.
- [30] J. Yi, Z. Chen, F. Xu et al., “IL-27 promotes human placenta-derived mesenchymal stromal cell ability to induce the generation of CD4(+)IL-10(+)IFN- $\gamma$ (+) T cells via the JAK/STAT pathway in the treatment of experimental graft-versus-host disease,” *The Journal of Immunology*, vol. 202, no. 4, pp. 1124–1136, 2019.
- [31] M. G. Dela Peña-Ponce, J. Rodriguez-Nieves, J. Bernhardt et al., “Increasing JAK/STAT signaling function of infant CD4(+) T cells during the first year of life,” *Frontiers in Pediatrics*, vol. 5, 2017.
- [32] C. F. Wan, L. L. Zheng, Y. Liu, and X. Yu, “Houttuynia cordata Thunb reverses oxaliplatin-induced neuropathic pain in rat by regulating Th17/Treg balance,” *American Journal of Translational Research*, vol. 8, no. 3, pp. 1609–1614, 2016.
- [33] W. Huo, Y. Liu, Y. Lei et al., “Imbalanced spinal infiltration of Th17/Treg cells contributes to bone cancer pain via promoting microglial activation,” *Brain, Behavior, and Immunity*, vol. 79, pp. 139–151, 2019.
- [34] B. Luchting, B. Rachinger-Adam, J. Zeidler et al., “Disrupted TH17/Treg balance in patients with chronic low back pain,” *PLoS One*, vol. 9, no. 8, Article ID e104883, 2014.
- [35] S. Romagnani, E. Maggi, F. Liotta, L. Cosmi, and F. Annunziato, “Properties and origin of human Th17 cells,” *Molecular Immunology*, vol. 47, no. 1, pp. 3–7, 2009.
- [36] G. Deng, X. Song, S. Fujimoto, C. A. Piccirillo, Y. Nagai, and M. I. Greene, “Foxp3 post-translational modifications and Treg suppressive activity,” *Frontiers in Immunology*, vol. 10, p. 2486, 2019.
- [37] I. Kaufmann, C. Eisner, P. Richter et al., “Lymphocyte subsets and the role of TH1/TH2 balance in stressed chronic pain patients,” *Neuroimmunomodulation*, vol. 14, no. 5, pp. 272–280, 2007.
- [38] M. J. Butcher and J. Zhu, “Recent advances in understanding the Th1/Th2 effector choice,” *Fac Rev*, vol. 10, 2021.

## Review Article

# Ethnomedicinal Use, Phytochemistry, and Other Potential Application of Aquatic and Semiaquatic Medicinal Plants

Ashish Kumar Arya <sup>1</sup>, Medha Durgapal <sup>2</sup>, Arachna Bachheti <sup>1</sup>, Deepti <sup>1</sup>,  
Kamal Kant Joshi <sup>3</sup>, Yilma H. Gonfa <sup>4,5</sup>, Rakesh Kumar Bachheti <sup>4,5</sup>,  
and Azamal Husen <sup>6</sup>

<sup>1</sup>Department of Environment Science, Graphic Era (Deemed to be University), Dehradun, Uttarakhand, India

<sup>2</sup>Department of Botany and Microbiology, Gurukula Kangri (Deemed to be University), Haridwar, India

<sup>3</sup>Department of Environmental Science Graphic Era Hill University, Dehradun, Uttarakhand, India

<sup>4</sup>Department of Industrial Chemistry, College of Applied Science, Addis Ababa Science and Technology University, Addis Ababa, P.O. Box-16417, Ethiopia

<sup>5</sup>Centre of Excellence in Nanotechnology, Addis Ababa Science and Technology University, Addis Ababa, P.O. Box-16417, Ethiopia

<sup>6</sup>Wolaita Sodo University, P.O. Box-138, Wolaita, Ethiopia

Correspondence should be addressed to Azamal Husen; [adroot92@gmail.com](mailto:adroot92@gmail.com)

Received 16 February 2022; Revised 28 June 2022; Accepted 13 July 2022; Published 10 August 2022

Academic Editor: Talha Bin Emran

Copyright © 2022 Ashish Kumar Arya et al. This is an open access article distributed under the Creative Commons Attribution License, which permits unrestricted use, distribution, and reproduction in any medium, provided the original work is properly cited.

Medicinal plants have been treating various ailments and diseases since ancient times. Aquatic and semiaquatic medicinal plants play an essential role in human welfare to fulfill their daily needs. They have shown biological, pharmacological, nutraceutical, and commercial applications. This review aims to collect and update all recent information on ethnomedicinal, phytochemistry, pharmacological activities, and nanoparticle synthesis and their uses in aquatic and semiaquatic medicinal plants. Original research papers, review papers, short communications, and book chapters on aquatic and semiaquatic plants have been retrieved from PubMed, Web of Science, Scopus, and Google Scholar. Keywords, ethnomedicinal studies, phytochemistry, pharmacological activities, and nanoparticle synthesis from aquatic and semiaquatic medicinal plants are used for the search. Different aquatic and semiaquatic medicinal plants belonging to the families Acanthaceae, Alismataceae, Amaranthaceae, Apiaceae, Araceae, Asteraceae, Boraginaceae, Ceratophyllaceae, Cyperaceae, Fabaceae, Hydrocharitaceae, Lythraceae, Marsileaceae, Menyanthaceae, Nelumbonaceae, Nymphaeaceae, Onagraceae, Plantaginaceae, Poaceae, Polygonaceae, Pontederiaceae, Primulaceae, Scrophulariaceae, and Zingiberaceae have been studied. They are rich in alkaloids, flavonoids, terpenoids, phenolics, saponins, tannins, dietary fiber, glycosidic derivatives, carbohydrates, and proteins. These phytochemicals have been used for their antimicrobial, antioxidant, hepatoprotective, sedative, anticonvulsant, cytotoxic, antiparasitic, and antidiabetic activities. Besides this, various parts of the plants are used as dietary supplements and green nanoparticle synthesis. These plants are also known for their commercial value and are used as an ingredient in some pharmaceutical industries.

## 1. Introduction

Natural products from medicinal plants are known for their various uses, such as treating infectious diseases, biological applications in the industry as ingredients, food additives, and green synthesis of nanomaterials [1, 2]. About 500,000 plants worldwide have a promising potential for their medical activities [3–6]. Great civilizations such as Mesopotamian, Roman, Greek, Inca, Indus valley, Sindhu, Ghati,

and Mohanjordo indicated that humans always preferred to live near plants, streams, lakes, and different types of water bodies to get their foods and shelters. For example, various plant species and their parts have been reported to be used as human and animal diets and sources of medicine [1, 7, 8]. Aquatic and semiaquatic plants are found in all ecological zones; however, most are distributed in subtropical and tropical regions. Aquatic medicinal plants can be divided into two categories based on their habitat. They are aquatic

plants and semiaquatic plants. Aquatic plants grow mainly in water bodies or floating on water bodies like algae, whereas semiaquatic plants/amphibian plants prefer to grow in submerged water bodies. Aquatic plants can be classified into two categories based on their ethnomedicinal applications and physicochemical effects. Major aquatic medicinal plants have very high medicinal and economic values and are readily available for commercial purposes for different human welfare. Minor aquatic plants are those plants that still contain therapeutic qualities against multiple diseases and disorders, but either lack availability or have little knowledge regarding their pharmacological properties. This is due to the lack of availability of these plant materials, regional applications of plants, and the economic value of plants, unnoticed or overlooked or neglected by the researchers. However, these plants are highly rich in diversified secondary metabolites due to their association with water bodies and weather conditions [9]. Medicinal plants from the wetland ecosystems have played a vital role in the development of the world since the beginning of human civilization [10]. Aquatic and semiaquatic plants have also been reported with significant prospects for commercial and environmental protection by exploring their hidden riches of medicinal properties [11]. These plants are highly diversified in structural adaptations, distribution, and phytochemical compound syntheses, enabling them to thrive in the diet and numerous applications [12] (Table 1). Aquatic and semiaquatic medicinal plants have multifunctional bioactive compounds widely used to protect against human and livestock health disorders [41].

Aquatic and semiaquatic medicinal plants and their phytochemicals have been widely practiced as traditional medicines worldwide. For instance, 50–60% of people in India live closer to aquatic bodies and use these plants for various practices such as medicinal, ornamental, and religious offspring [10, 41]. Recently, the research interest in aquatic and semiaquatic plants has grown tremendously, increasing the screening of new possible phytoconstituents and the usage of bioactive compounds in approved pharmaceutical drugs. Various literature reports also demonstrated that plants possess high nutritional values, medicinal uses, and several biological and pharmacological activities due to their production of potentially bioactive compounds [46]. Despite the wide range of published documents on aquatic and semiaquatic medicinal plants, the information is scattered and unavailable in one place. Therefore, this review aims to bring all the published documents in one place in the form of a review paper.

## 2. Some Significant Aquatic and Semiaquatic Medicinal Plants

**2.1. *Acorus calamus* (Sweet Flag).** Sweet flag is an important aquatic medicinal plant belonging to the Araceae family, as shown in Figure 1. It is distributed in marshy areas, shallow lands, and ponds of tropical and subtropical areas such as Asia, Europe, and America [47, 48]. This herb has been used in the Indian Ayurvedic medical systems from earlier civilizations. Many parts of this plant, such as rhizomes, roots,

and leaves, are used for their medicinal properties. Sweet flag has been used to treat skin disorders, epilepsy, asthma, diarrhea, hysteria, insanity, insomnia, melancholia, neurasthenia, heart disease, and lung cancer [10]. It contains medicinally essential alkaloids such as choline, acorin, calamine A, bitter glycosides, caramel, gum, resin, and starch tannins [47, 49]. The primary chemical constituents such as  $\beta$ -asarone (27.4–45.5%), acorenone (20.86%), and isocalamendiol (12.75%) are reported from its leaves and rhizomes, respectively [50, 51].

**2.2. *Ageratum conyzoides* (White Weed).** This semiaquatic plant species belong to the Asteraceae family (Figure 2), distributed in tropical and subtropical regions, including Brazil [52]. It is common in Asia, West Africa, and South America. Its leaves and shoots treat fresh cuts and injuries and are used in preparing traditional hair lotion. It also treats pneumonia, wound healing, and skin diseases. Some secondary metabolites also found in the plant are rutin, quercitrin, avicularin hypsocide, and catechin [53].

**2.3. *Ammannia baccifera* (Monarch Redstem).** This semiaquatic medicinal plant belongs to the Lythraceae family (Figure 2), distributed commonly throughout India [54]. The plant treats fever, hepatoprotective activities, rheumatic pains, ringworm, scabies, skin diseases, skin itching, and typhoid fever and possesses antioxidant, larvicidal, and antisteroidogenic properties [55]. The plant has secondary metabolites such as 4-hydroxy- $\alpha$ -tetralone, tetralin-4O- $\beta$ -D-glucopyranoside, and ammaniol [56].

**2.4. *Amomum aromaticum* (Namra).** This aquatic medicinal plant belongs to the Zingiberaceae family (Figure 1), distributed in Bhutan, North East India, and Nepal [57]. It is a common spice and food flavoring agent in Vietnam and other Asian countries [58]. Seeds of the plant exhibit medicinal value for controlling blood pressure. The stem of this plant is consumed in a vegetable diet in Manipur [57]. The plant contains secondary metabolites such as 1,8-cineole,  $\beta$ -myrcene,  $\alpha$ -terpineol, terpinene-4-ol,  $\alpha$ -pinene, and  $\beta$ -pinene [59].

**2.5. *Bacopa monnieri* (Water Hyssop).** This aquatic plant species belong to the Plantaginaceae family and is native to India, the United States, East Asia, and Australia, as shown in Figure 1. This aquatic plant's leaves and flowers treat asthma, bronchitis, Alzheimer's disease, hypoglycemia, leprosy, ringworms, stomach diseases, blood pressure, and anxiety [60]. The plant contains secondary metabolites, including bacopa saponins such as bacopasaponin F, bacopasaponin E, bacopaside III, bacopaside IV, bacopaside N1, and bacopaside V. Additionally, the plant species has been reported to contain phytoconstituents like monnierenin, brahmin, herpestine,  $\beta$ -sitosterol, betulinic acid, luteolin, apigenin, D-mannitol, hersaponin, and stigmasterol [61].



TABLE 1: Some aquatic and semiaquatic medicinal plants with potential phytoconstituents and their applications.

Plant name	Family	Plant part used	Major phytochemicals	Type of extracts	Uses	References
<i>Aeschynomene aspera</i>	Fabaceae	Shoots	Glycosides, tannins, alkaloids, steroids, gums, and flavonoids	Crude extracts	(i) Treat cold, fever, and cough (ii) Increase semen consistency	[13]
<i>Ageratum conyzoides</i>	Asteraceae	Leaves and shoot	Rutin, quercitrin, avicularin, hyperoside, and catechin	Pure compounds	Used to treat fresh cuts and injuries and prepare traditional hair lotion	[14]
<i>Alternanthera philoxeroides</i>	Amaranthaceae	Shoot	$\alpha$ -Ionone and triglyceride	Pure compounds	Used to cure dysentery	[15]
<i>Ammannia auriculata</i>	Lythraceae	Leaf	Hydroxy-1-tetralone and $\beta$ -sitosterol	Pure compounds	(i) Decrease fevers and rheumatic pains Relieves cold, cough, dysentery, malaria, nasal congestion	[16]
<i>Caesulia axillaris</i>	Asteraceae	Whole plant part	4-Methyl-5-ergosta	Pure compound	(ii) Healing wounds (i) Relieves inflammatory effects, dysentery, epistaxis, fever, haematemesis, hemorrhoids, piles, hyperdipsia, intrinsic, scorpion sting, and ulcer	[13, 17]
<i>Ceratophyllum demersum</i>	Ceratophyllaceae	Leaves	Apigenin-7-O-glucoside, benzyl acetate, and sesquiterpene	Pure compounds	(ii) Healing wounds Decrease the urination and menstrual complaints effects	[18, 19]
<i>Coix aquatica</i>	Poaceae	Roots	Kaempferol and rutin	Pure compounds	Treats antiemetic, boils, burns, and vomiting during pregnancy	[13]
<i>Cryptocoryne retorspiralis</i>	Araceae	Fresh tubers	Triterpene	Pure compound	Treat fever and cough	[20, 21]
<i>Cyperus haspan</i>	Cyperaceae	Rhizome	$\alpha$ -Ionone and triglyceride	Pure compounds	Decreases abdominal pain, amenorrhea, cardiac risks, liver problems, nausea	[15, 22]
<i>Eleocharis dulcis</i>	Cyperaceae	Roots	Triglyceride and $\beta$ -sitosterol	Pure compounds	Used to treat the diabetic patient	[23]
<i>Fagopyrum esculentum</i>	Polygonaceae	Shoot	—	—	Decreases the anuria, blennorrhoea, catarrh, crawl-crawl, diuretic, hydropsy, menstruation, and stomach ache effects	[15, 24]
<i>Hygrophila auriculata</i>	Acanthaceae	Whole plant part	$\beta$ -Cadinene	Pure compound	Treat facial paralysis, hemiplegia, ear noise with headache, and stiff neck	[25, 26]
<i>Hygrophila polysperma</i>	Acanthaceae	Leaves and seeds	Terpinene-4-ol	Pure compound	(i) Relieves cardiac ailments (ii) Healing kidney disorders, skin problems, and swelling	[27]
<i>Lagenandra ovata</i>	Araceae	—	Sabinene and terpinen-4-ol	Pure compounds	(i) Used as antimutagenic, mucus removal, antitumor, and pain killer (ii) Treats dysentery, elephantiasis, fever, indigestion, intestinal worms, and menstrual problems	[28]
<i>Limnophila aromatica</i>	Plantaginaceae	—	Hyperoside, quercitrin, avicularin, and catechin	Pure compounds	Treats anthelmintic, antiseptic, dysentery, and elephantiasis	[29]
<i>Limnophila indica</i>	Scrophulariaceae	Aerial parts	Triterpenoids and saponins	Crude extracts		[13, 30]

TABLE 1: Continued.

Plant name	Family	Plant part used	Major phytochemicals	Type of extracts	Uses	References
<i>Lindernia Anagallis</i>	Scrophulariaceae	Whole plant	Acacetin and luteolin	Pure compounds	Treats asthma and gonorrhoea	[13]
<i>Ludwigia adscendens</i>	Onagraceae	Whole plant	$\alpha$ -Terpineol	Pure compound	(i) Used as antimicrobial and anti-inflammatory (ii) Treats dysentery, skin diseases, and ulcers	[31, 32]
<i>Ludwigia octovalvis</i>	Onagraceae	Whole plant	Geraldone and acacetin	Pure compounds	Treats body ache, boil, diarrhea, fever, flatulence, heal dermatitis, toxemia, and ulcer	[33]
<i>Lysimachia nummularia</i>	Primulaceae	—	$\beta$ -Asarone and $\alpha$ -asarone	Pure compounds	Treat cancer, stone lin syndrome, and wounds Relief biliousness, cough, headache, hypertension, insomnia, sleeping disorder, and spastic condition of leg muscles	[34]
<i>Marsilea minuta</i>	Marsileaceae	Leaves and root	Hyperoside, quercitrin, and avicularin	Pure compounds	Used as anti-inflammatory agents	[35]
<i>Monochoria hastata</i>	Pontederiaceae	Leaves	Rutin, protocatecheic acid, vanillic acid, and ferulic acid	Pure compounds	(i) Used as antioxidant, anti-inflammatory (ii) Treats asthma, coughs, stomach, toothache, swelling, and liver disorder	[36]
<i>Monochoria vaginalis</i>	Pontederiaceae	Leaves and flowers	$\beta$ -Transocimenone, kaempferol, and solanin	Pure compounds	Treats abortion, blood dysentery, dyspepsia, jaundice, leucorrhoea, menorrhagia, and piles disorders	[37]
<i>Nymphaea pubescens</i>	Nymphaeaceae	Rhizome, roots	Orientin, $\beta$ -D-glucopyranosyl	Pure compounds	Treats stomach disorders	[38]
<i>Nymphaea stellata</i>	Nymphaeaceae	Leaf	p-Cymene, $\alpha$ -selinene, and beta-gurjunene	Pure compounds	Treats eye diseases, fevers, insect bites, jaundice, scorpion sting, snakebite, and ulcer	[39]
<i>Nymphoides hydrophylla</i>	Menyanthaceae	Leaves and seeds	Kaempferol and allantoin	Pure compounds	Decreases fever, headache, rheumatism, and scabies disorders	[40]
<i>Nymphoides indica</i>	Menyanthaceae	Whole plant part	Kaempferol and allantoin	Pure compounds	Treats bleeding from wounds, colic pain, cooling agent, and ulcers	[13]
<i>Polygonum barbatum</i>	Polygonaceae	Leaf, roots, and seeds	Kaempferol, baicalin, quercetin derivatives, and myricetin	Pure compounds	Treats migraine, respiratory diseases, and stomach disorder	[41]
<i>Rotala indica</i>	Lythraceae	Flower and leaves	$\alpha$ -Pinene and $\beta$ -pinene	Pure compounds	(i) Used as antipyretic and antismelling (ii) Treats cold, fever, cough, detoxication, diuresis, gonorrhoea, menstrual cramps, piles, production in HepA2 cells, and suppression of HBV surface antigen (HBsAg)	[33, 42]
<i>Rotala rotundifolia</i>	Lythraceae	Whole plant	Methoxycinnamaldehyde and $\alpha$ -terpinene	Pure compounds	(i) Treats leucorrhoea and stomachache	[27, 43, 44]
<i>Vallisneria spiralis</i>	Hydrocharitaceae	Leaves	$\beta$ -Vetispirene, vetiselinol, husimol, $\beta$ -vetinene, and $\alpha$ -vetivone	Pure compounds		[45]

2.6. *Centella asiatica* (Indian Pennywort). This aquatic medicinal plant belongs to the Apiaceae family (Figure 1), found in most tropical and subtropical countries, including India, Pakistan, Sri Lanka, Madagascar, South Africa, South Pacific, and Eastern Europe [62]. Leaves, flowers, and fruits of the plant have many medicinal uses and are used to treat various skin diseases, fever, strangury, and brain health [63–65]. The active phytoconstituents found in this plant include triterpenes hydrocarbons [66].

2.7. *Centipeda minima* (Spreading Sneezeweed). This aquatic medicinal plant belongs to the Asteraceae family (Figure 1). It is found in wet places and the rice fields of most Asian countries [67]. The leaves and roots of the plant are used to treat various diseases. It is widely used for antibacterial, antioxidant, anti-angiogenic, and anticancer activities [68, 69]. It contains secondary metabolites such as lactones, sesquiterpenes, and triterpenes [70].

2.8. *Ceratophyllum demersum* (Coontail). This semiaquatic medicinal plant belongs to the *Ceratophyllaceae* family (Figure 2). The plant is found in ponds, ditches, lakes, and quiet streams. Leaves treat diarrhea, fever, dysentery, ulcer, wounds, burning sensation, hemorrhoids, piles, intrinsic hemorrhages, epistaxis, hyperdipsia, and haematemesis. It also cures scorpion stings and bile secretion [18]. The plant contains various secondary metabolites such as alkaloids, cardiac glycosides, tannins, and flavonoids [71].

2.9. *Coix lacryma-jobi* (Job's Tears). This aquatic medicinal plant belongs to the Poaceae family (Figure 1). It is distributed throughout Asian countries and is a native plant of Southeast Asia. Leaves, flowers, and fruits are used as a diet supplement to treat chicken pox, stomachache, and menstrual disorders [33]. It is also reported to possess analgesic and antispasmodic properties [72]. The plant contains triglyceride,  $\beta$ -sitosterol, stigmaterol, and phytol fatty acid ester [73].

2.10. *Eclipta prostrata* (False Daisy). This semiaquatic plant belongs to the family of Asteraceae (Figure 2). It is a native plant of Asia and is also distributed in tropical, subtropical, and warm temperate regions of the world [74]. The plant is used to cure eczema, headache, jaundice, mental disorders, scorpion sting, skin diseases, snakebite, spleen enlargements, and toothache. It also showed antiulcer properties. Secondary metabolites present in this plant are triterpenoids, thiophenes, coumestans, flavonoids, and steroids [75].

2.11. *Eleocharis dulcis* (Water Chestnut). This semiaquatic medicinal plant is commonly known as the Chinese water chestnut and belongs to the Cyperaceae family (Figure 2). The plant is commonly grown as a vegetable in Japan, China, India, and other Asian countries [76]. The plant contains phytochemicals such as carbohydrates, flavonoids, proteins,

and minerals [77]. The plant treats amenorrhoea, hernia, nausea, abdominal pain, cardiac risks, liver problems, constipation, pharyngitis, laryngitis, hypertension, and chronic nephritis [74, 78].

2.12. *Enhydra fluctuans* (Water Cress). This aquatic medicinal plant belongs to the Asteraceae family (Figure 1). The plant grows in the marshy areas of tropical and subtropical regions of Asia and Africa [79]. This plant species prefers to grow along with ponds, waterways, ditches, and rice fields [80]. Leaves of the plant are a rich source of protein and are used to treat diseases such as nervous diseases [81], skin diseases, and smallpox [82]. The plant leaves possess antioxidant properties [83]. The plant consists of various secondary metabolites: ethyl acetate, n-butanol, baicalein-7-O-glucoside, and baicalein 7-O-diglucoside [84].

2.13. *Hedychium coronarium* (White Ginger Lily). This aquatic medicinal plant belongs to the Zingiberaceae family (Figure 1). It is a medicinal plant of tropics and subtropics that grows closer to the rivers, streams, or shallow water systems [53]. The plant consists of active constituents such as  $\beta$ -transocimene, linalool, 1,8-cineole,  $\alpha$ -terpineol, 10-epi- $\gamma$ -eudesmol, sabinene, terpinene-4-ol, 2,8-diene, and  $\gamma$ -terpinene [85]. Leaves and flowers have a high potential for fatty acids and are used to treat hair, skin, headache, lancinating pain, inflammatory, intense pain, cough, fever, and cancer [15, 86].

2.14. *Heliotropium indicum* (Indian Heliotrope). This semiaquatic medicinal plant belongs to the Boraginaceae family (Figure 2). The plant is known as Indian heliotrope, distributed in tropical, subtropical, and warm temperate zones [87]. Flowers, shoots, and whole plant parts exhibit medicinal properties and treat asthma, boils, bronchitis, cataract, dysentery, menstrual blood loss, redness and conjunctivitis of the eyes, antiseptic, scorpion sting, and ulcers [88]. The plant possesses phytochemicals such as alkaloids, carbohydrates, proteins, flavonoids, phenolics, glycosidic derivatives, saponins, and phytosterols [89].

2.15. *Hydrocotyle sibthorpioides* (Lei/Lai-Peruk). This aquatic medicinal plant belongs to the Apiaceae family (Figure 1). It is distributed in Southeast Asia and shows various adaptations in different habitats, from terrestrial land to submerging underwater [10]. Leaves of this plant have medicinal values; the juice of fresh leaves is used to treat cough, fever, jaundice, and throat pain [90, 91]. The plant species contains some secondary metabolites such as methyl-ester-3-nitro-propanoic acid, 5-ethyl-4-methyl-5-hepten-3-one, 1-cyclohexyl-2-methyl-2-propanol, and 2-methyl-5-(1-adamantyl) pentan-2-ol [92].

2.16. *Hygrophila schulli* (Marsh Barbel). This semiaquatic medicinal plant belongs to the Acanthaceae family (Figure 2), distributed in Sri Lanka, Myanmar, Indonesia,

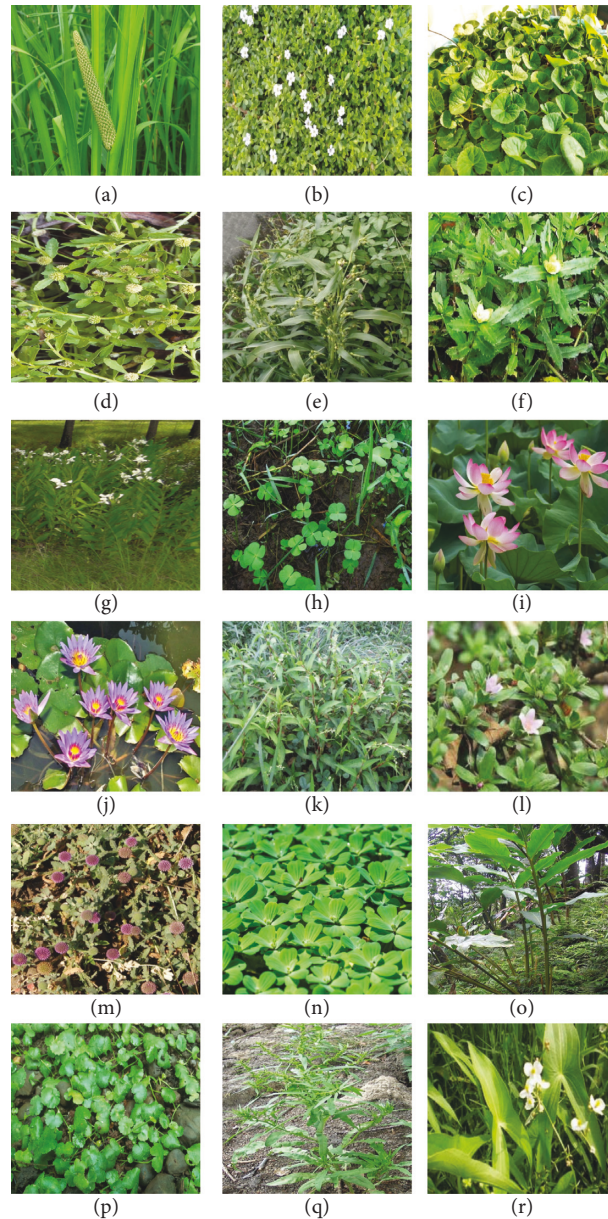


FIGURE 1: Some of the important aquatic medicinal plants. (a): *Acorus calamus*. (b): *Bacopa monnieri*. (c): *Centella asiatica*. (e): *Coix lacryma-jobi*. (f): *Enhydra fluctuans*. (d): *Centipeda minima*. (h): *Marsilea minuta*. (i): *Nelumbo nucifera*. (g): *Hedychium coronarium*. (j): *Nymphaea nouchali*. (l): *Rotula aquatic*. (k): *Persicaria hydropiper*. (n): *Pistia stratiotes*. (o): *Ammomum aromaticum*. (m): *Sphaeranthus indicus*. (r): *Sagittaria sagittifolia*. (p): *Hydrocotyle sibthorpioides*. (q): *Rumex maritimus*.

Malaysia, and the plains of India [93]. Leaves, roots, seeds, and whole plants have many medicinal values. They treat anemia, blood pressure, kidney stone, jaundice, gout, hepatic obstruction, impotence, inflammation, pain, rheumatism, spermatorrhoea, and urinary infections. The secondary metabolites present in the plant are quercetin, apigenin-7-O-glucuronide, apigenin-7-O-glucoside, luteolin, luteolin-7-O-rutinosides, and gallic acid [94, 95].

**2.17. *Limnophila aromatica* (Rice Paddy Herb).** This semi-aquatic medicinal plant is known as the rice paddy herb and belongs to the family Plantaginaceae, as shown in Figure 2. It is widely used in Southeast Asia, including Vietnam,

Malaysia, and Thailand [96]. It treats various diseases such as dysentery, elephantiasis, fever, indigestion, intestinal worms, menstrual problems, and mucus removal. The plant also has antimutagenic and antitumor properties. It contains starch, dietary fiber, protein, polysaccharides, and lignin [97].

**2.18. *Ludwigia adscendens* (Water Primrose).** This semi-aquatic medicinal plant belongs to the *Onagraceae* family (Figure 2). The plant species cure dysentery, skin diseases, and ulcers. The whole plant has been reported for its emetic, laxative, anthelmintic, antidiarrhetic, anti-inflammatory, antioxidant, and antimicrobial properties [82]. Phytochemicals such as squalene, betulonic acid, betulin, betulinic



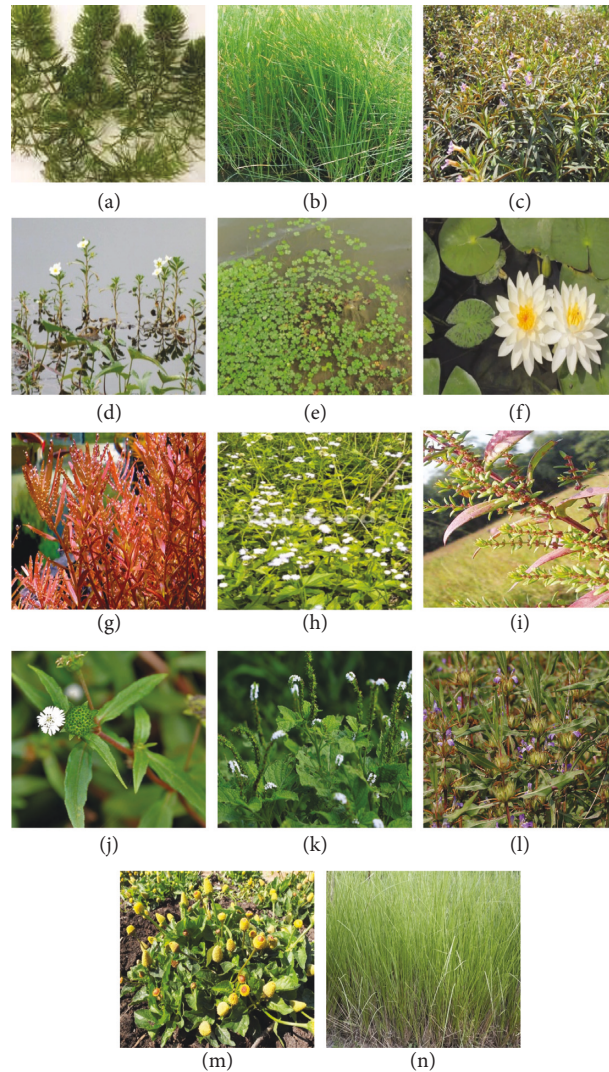


FIGURE 2: Some important semiaquatic medicinal plants. (a): *Ceratophyllum demersum*. (b): *Eleocharis dulcis*. (c): *Limnophila aromatica*. (e): *Marsilea minuta*. (d): *Ludwigia adscendens*. (f): *Nymphaea pubescens*. (g): *Rotala rotundifolia*. (h): *Ageratum conyzoides*. (i): *Ammannia baccifera*. (j): *Eclipta prostrata*. (l): *Hygrophila schulli*. (k): *Heliotropium indicum*. (m): *Spilanthes calva* Candolle. (n): *Vetiveria zizanioides*.

acid, and quercetin derivatives are some constituents reported from the plant extract [98].

**2.19. *Marsilea minuta* (Water Clover).** This aquatic medicinal plant belongs to the Marsileaceae family (Figure 1). It is popularly known as water clover and is distributed worldwide [99, 100]. Leaves of the plant are used to treat headaches, migraine, respiratory diseases, hypertension, muscle tension, and sleeping disorders [101–103]. They also treat chronic cancer and cardiovascular diseases [104]. The leaves and roots of this plant have medicinal values to treat indigestion, kidney infection, nose bleeding, diarrhoeal, cough, hepatitis, headache, hypertension, insomnia, sleeping disorder, and skin diseases [105]. The plant species is also known for its potent antioxidant and antibacterial activity [106]. It consists of many secondary metabolites such as carotenoids, flavonoids, cinnamic acids, benzoic acids, folic acids, ascorbic acids, tocopherols, and tocotrienols [107, 108].

**2.20. *Nelumbo nucifera* (Indian Lotus).** This aquatic medicinal plant belongs to the Nelumbonaceae family (Figure 1). The plant species are cultivated due to their high commercial value for their medicinal property [109] and as ornamental plants in China, Korea, Japan, India, and Australia [110]. Stems and leaves of the plant have high medicinal values. They are used for the treatment of many diseases such as cough, hypertension [111], urinary problems [13, 41], blood vomiting, piles, and eye vision [15]. Secondary metabolites found in the plant include kaempferol-3-robinobioside, quercetin-3-neohesperidose, nelumborines A, higenamine, quercetin-3-O-glucuronide, syringetin-3-O-glucoside, and 4'-O- $\beta$ -d-glucoside [112].

**2.21. *Nymphaea nouchali* (Blue Water-Lily).** This aquatic medicinal plant belongs to the Nymphaeaceae family, as shown in Figure 1. Plant parts such as leaves, roots, rhizomes, fruits, flowers, and tubers treat liver, kidney, and heart diseases. It is also known for antimicrobial, antidiabetic, and

antioxidant activities [113, 114]. It is widely distributed in South Asian countries, Australia, and Africa [115]. Plant extracts are reported to contain rutin, catechin, myricetin, ellagic acid, gallic acid, vanillic acid, rosmarinic acid, p-coumaric acid, quercetin, and ascorbic acid [116, 117].

2.22. *Nymphaea pubescens* (Pink Water-Lily). This semi-aquatic plant belongs to the Nymphaeaceae family (Figure 2). The plant species are distributed in tropical and temperate regions [118]. Rhizome and plant roots cure many diseases and ailments such as abortion, blood dysentery, dyspepsia, jaundice, blood purifier, cystitis, nephritis, fever, insomnia, hemorrhoids, leucorrhoea, menorrhagia, and piles [119]. It contains secondary metabolites such as flavonoid and phenolic compounds [120].

2.23. *Persicaria hydropiper* (Water Pepper). This aquatic medicinal plant belongs to the Polygonaceae family (Figure 1). It shows wide distribution worldwide [121] and grows in marshes, wet areas, and agricultural fields [122]. Leaves and roots of the plant species are used to cure many diseases such as uterine disorders [123], menstrual irregularities, and headaches. The plant contains various secondary metabolites such as (+)-catechin, (–)-epicatechin, hyperin, isoquercitrin, kaempferol, quercetin, rhamnazin, rutin, sesquiterpenes, 3- $\beta$ -angeloyloxy-7-epifutrone, apigenin-7-O-glucoside, galloyl kaempferol-3-O-glucoside,  $\alpha$ -pinene,  $\beta$ -pinene, 1,4-cineol, fenchone,  $\alpha$ -humulene,  $\beta$ -caryophyllene, and trans- $\beta$ -bergamotene [121].

2.24. *Pistia stratiotes* (Water Lettuce). This aquatic medicinal plant belongs to the Araceae family (Figure 1). The plant species are commonly found in stagnant water (lakes and rivers) throughout Asia and subtropical Asia, Africa, and America [124]. The leaves and roots of the plant have very high medicinal values and are used for curing many diseases such as kidney disorders, leprosy, dysentery, eczema, and ulcers. Its extracts contain secondary metabolites such as phenolics and tannins [125].

2.25. *Rotula aquatica* (Aquatic Rotala). This aquatic medicinal plant belongs to the Boraginaceae family (Figure 1). The plant species is native to India, China, and Malaysia and is also found in Africa and South America [126]. The plant species is a remedy for blood disorders, coughs, dysuria, fever, and heart diseases. The plant's leaves and flowers can be used to treat diabetes, bladder and kidney stones, piles, and venereal diseases. [41]. The plant extracts contain secondary metabolites such as allantoin, baurenol, and kaempferol [126].

2.26. *Rotala rotundifolia* (Roundleaf Tooth Cup). This semiaquatic medicinal plant belongs to the Lythraceae family, Figure 2. The plant species are found in South and Southeast Asia, Japan, Africa, Australia, China, India, and North America [127]. The plant extracts are used as antipyretic and anti-swelling. The plant species are also used in treating cold,

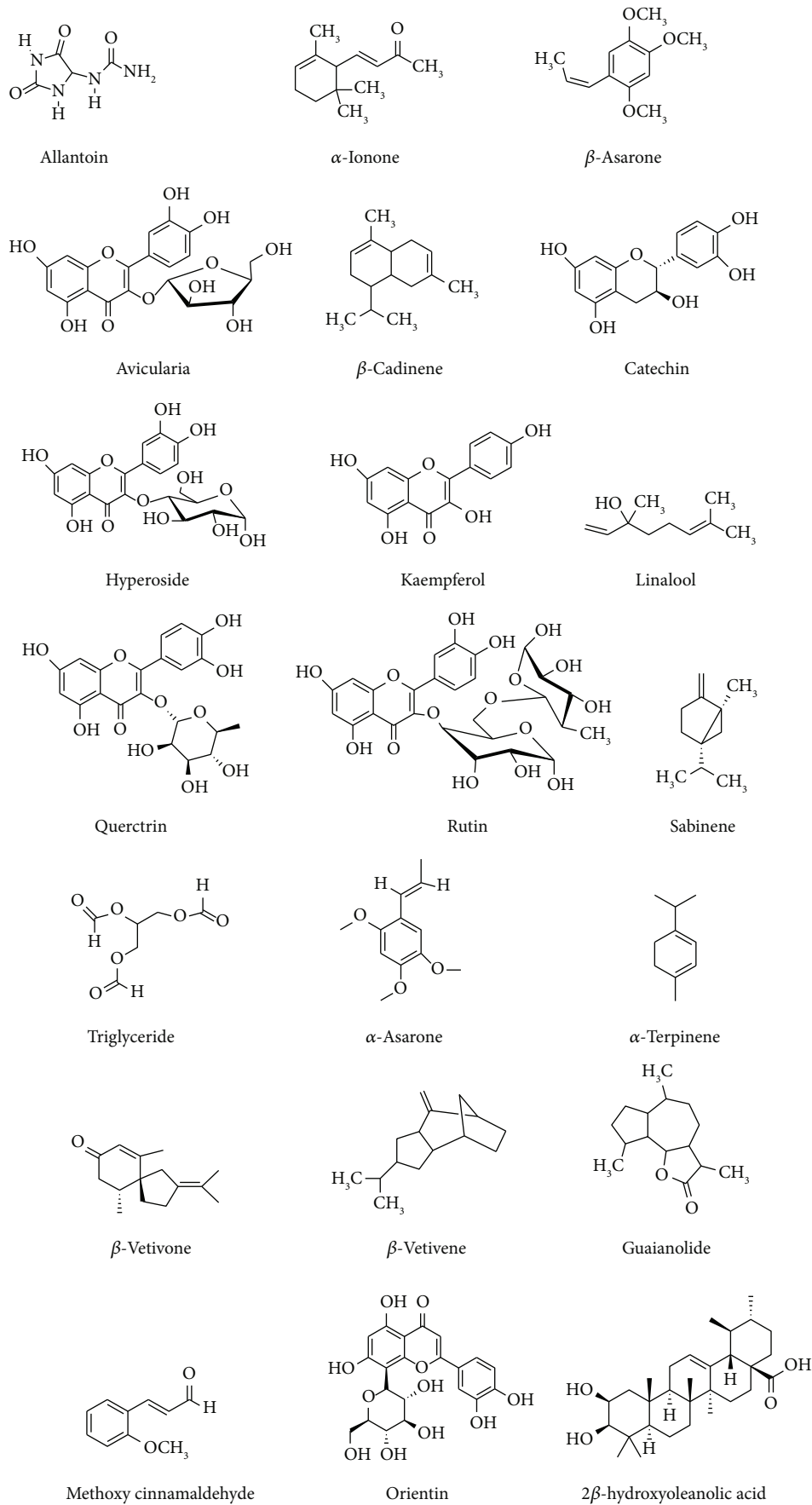
fever, cough, detoxication, diuresis, gonorrhoea, menstrual cramps, piles, production in HepA2 cells, and suppression of HBV surface antigen (HBsAg) [43]. The secondary metabolites reported from some extracts of the plant are quercetin 3-O- $\beta$ -D-2''-acetylglucuronide methyl-ester, kaempferol, quercetin, quercetin 3-O- $\beta$ -D-glucuronide methyl-ester, quercetin 3-O- $\beta$ -D-glucuronide, and apigenin [44].

2.27. *Rumex maritimus* (Torong-Khongchak). This aquatic medicinal plant belongs to the Polygonaceae family (Figure 1). It is widely distributed throughout Bangladesh, India, North Africa, and America [128]. The leaves, roots, and stems of the plant have medicinal values. Leaves paste of the plant is applied to cure leucoderma, burns, and injuries [15], and the roots are used to treat diarrhoea [128]. 2-Methoxystypane is the commonly reported secondary metabolite present in the plant [129].

2.28. *Sagittaria sagittifolia* (Koukha). This aquatic medicinal plant belongs to the Alismataceae family (Figure 1). It is the only native species of the genus *Sagittaria* in Czechoslovakia. The remaining species of this genus occur mainly in tropical and subtropical regions. It predominates in North America, Europe, and Asia [130]. It is mainly found in Asian countries, including China, Bangladesh, Indonesia, Malaysia, Nepal, Sri Lanka, Philippines, Thailand, Vietnam, Cambodia, and India. Root past showed medicinal uses to treat cough and fever. The plant species contain polysaccharides as the main phytochemical components [131].

2.29. *Sphaeranthus indicus* (East Indian Globe Thistle). This aquatic medicinal plant belongs to the Asteraceae family (Figure 1). The plant is widely distributed in India, Sri Lanka, and other continents like Australia and Africa [132]. It prefers to grow in dry or wet places. Various parts of this plant, including seeds, leaves, flowers, and roots, have many medicinal properties widely used to treat disorders like asthma, chest pains, chronic skin diseases, cough, and mental disorders [41]. Triterpenoids, resin, saponins, tannins, and steroids are the primary reported secondary metabolites present in the plant species [133].

2.30. *Spilanthes calva* (Toothache Plant). This semiaquatic plant species belong to the Asteraceae family (Figure 2). The plant species are distributed in some parts of India [134]. Flower head, roots, and whole plant part have medicinal values that cure dysentery, psoriasis, purgative, rheumatism, scabies, stammering in children, tongue paralysis, and toothache. The plant extracts have antioxidant and cytotoxic properties [135]. Saturated and unsaturated alkyl ketones, alkamides, hydrocarbons, acetylenes, lactones, alkaloids, terpenoids, flavonoids, and coumarins are the main phytochemicals present in the extract of the plant species [136].



(a)

FIGURE 3: Continued.

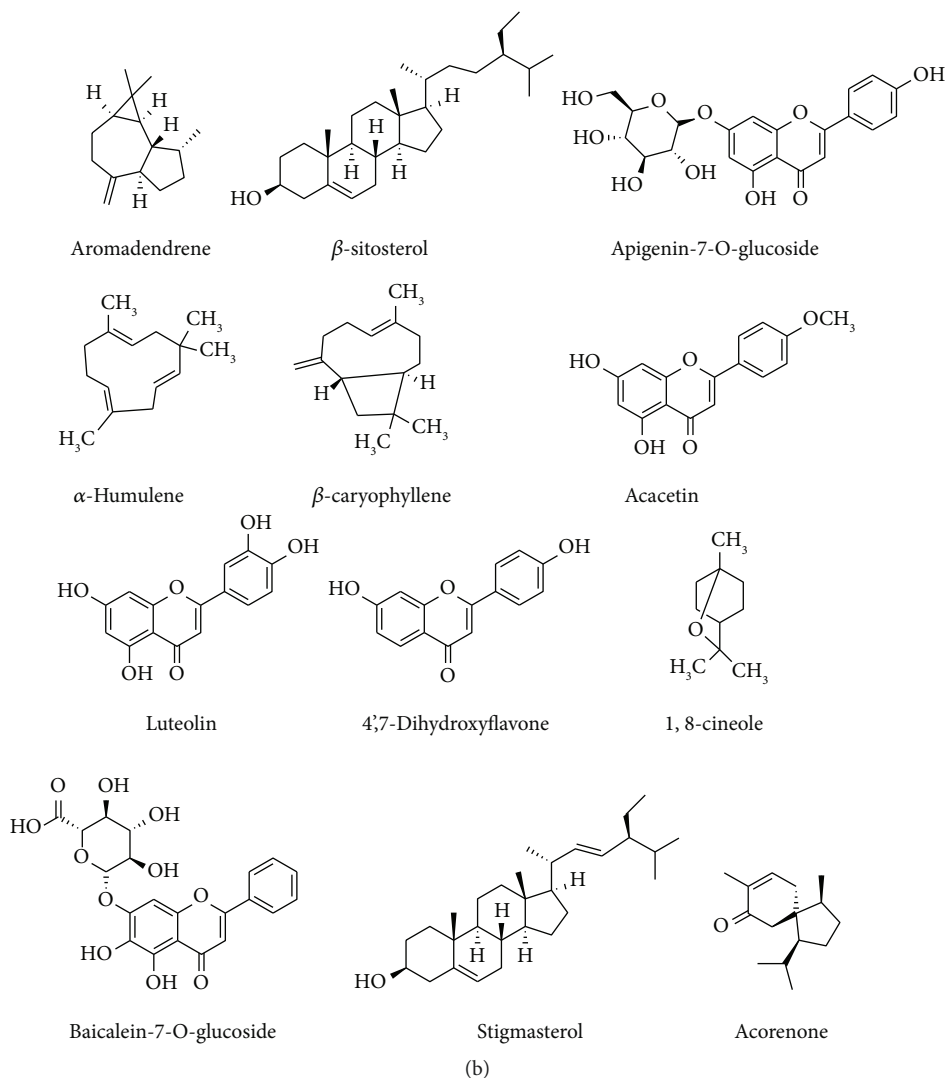


FIGURE 3: Chemical structures of some important phytochemical compounds obtained from various aquatic and semiaquatic plants: allantoin  $\alpha$ -ionone  $\beta$ -asarone; avicularia  $\beta$ -cadinene catechin; hyperoside kaempferol linalool; querctrin rutin sabinene; triglyceride  $\alpha$ -asarone  $\alpha$ -terpinene;  $\beta$ -vetivone  $\beta$ -vetivene guaianolide; methoxy-cinnamaldehyde orientin  $2\beta$ -hydroxyoleanolic acid; aromadendrene  $\beta$ -sitosterol apigenin-7-o-glucoside;  $\alpha$ -humulene  $\beta$ -caryophyllene acacetin; luteolin  $4',7$ -dihydroxyflavone  $1,8$ -cineole; baicalein-7-o-glucoside stigmasterol acorenone.

2.31. *Vetiveria zizanoides* (*Vetivergrass*). This semiaquatic medicinal plant belongs to the *Poaceae* family (Figure 2). This plant species is cultivated globally in tropical and subtropical regions [137]. The roots and rhizomes of the plant have medicinal properties. They treat burns, colic, obstinate vomiting, diaphoretic, epilepsy, febrifuge, fever, flatulence, headache, mouth ulcer, refrigerant, rheumatism, scorpion sting, and snakebite. [45]. The plant extracts have been reported to possess various secondary metabolites such as  $\beta$ -vetispirene, vetiselinol, khusimol,  $\beta$ -vetinene, and  $\alpha$ -vetivone [138].

2.32. *Phytochemistry of Aquatic and Semiaquatic Plants*. Aquatic and semiaquatic plants contain many phytochemical compounds responsible for their multifunctional properties [139]. Due to their wide-spectrum chemical properties, these plants possess potential medicinal,

biological, pharmacological, and other applications [16, 140]. Phytochemical studies on some aquatic and semiaquatic plants revealed various organic compounds with various chemical structures and functional groups. Some phytochemical compounds reported from the extracts of aquatic and semiaquatic plants are given in Figure 3.

### 3. Uses of Aquatic and Semiaquatic Medicinal Plants

Natural products produced by aquatic and semiaquatic medicinal plants are known for their potential biological applications and diet supplements. Aquatic and semiaquatic plants are often used as medicines for many health disorders and diet supplements due to their nutritional values and medicinal uses, and in pharmaceutical industries for producing herbal-based cosmetic products [10]. These plants



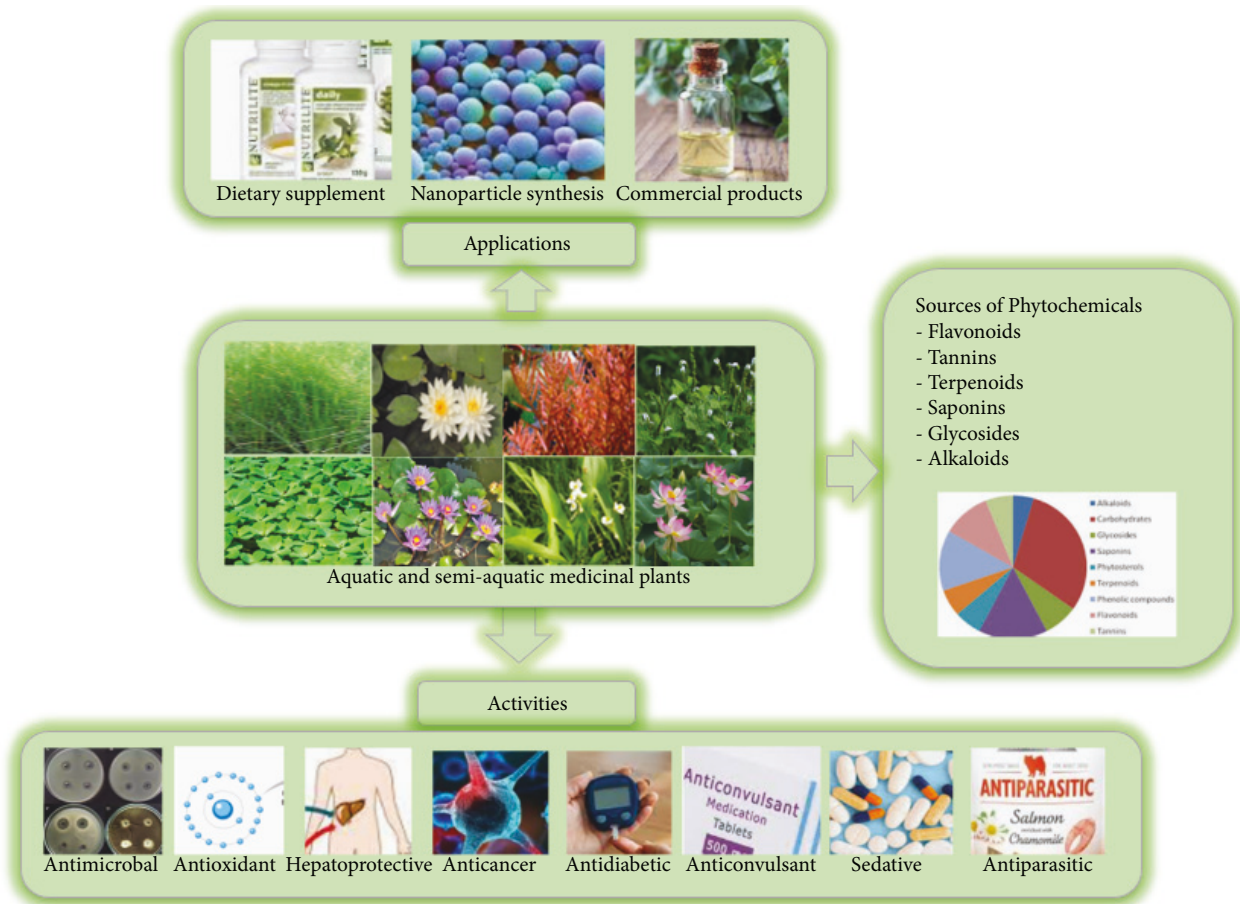


FIGURE 4: Phytochemical, biological, and some other applications of aquatic and semiaquatic medicinal plants.

diversified chemical and biological properties make them medicinally valuable and increase their demand globally. Some previous studies regarding the importance of aquatic and semiaquatic medicinal plants for biological, industrial, and other applications are discussed and presented in Figure 4.

**3.1. Antimicrobial Activity.** Phytochemicals of aquatic and semiaquatic medicinal plants have been reported to possess many antimicrobial properties. The chemical constituents of essential oil from rhizomes of *Hedychium coronarium* have shown a potential antimicrobial activity [85]. *Nymphaea nouchali* flowers effectively against bacteria strains like *Pseudomonas aeruginosa*, *Bacillus cereus*, and *Staphylococcus aureus* [16]. The extracts of *Pistia stratiotes* also displayed a wide range of antibacterial activity against *Escherichia coli* and *Staphylococcus aureus* [141]. The organic solvent extracts of *Sphaeranthus indicus* showed significant antimicrobial activity [142]. The leaves, rootstock, seeds, and stems of *Polygonum glabrum* possess antimicrobial activity [10]. Secondary metabolites from extracts of aquatic and semiaquatic medicinal plants such as *Acorus calamus*, *Centella asiatica*, *Heliotropium indicum*, *Marsilea minuta*, *Sphaeranthus indicus*, *Andrographis peniculata*, and *Clerodendrum viscosum* have been reported by different scholars for their

promising antimicrobial activities [60, 64, 85, 88, 106, 142–146].

**3.2. Antioxidant Activity.** Aquatic and semiaquatic medicinal plants are known for their potential antioxidant properties. Earlier reports showed that the reducing power of essential oil of *Hedychium coronarium* might be strongly correlated with their antioxidative activities [85]. Some literature reported that the phytoconstituents of *Bacopa monnieri* showed good antioxidant properties [147]. Epifano and his coworkers (2015) reported that the *Nymphaea nouchali* is a rich source of antioxidants. Potential antioxidant compounds are identified from the extracts of *Centella asiatica*, *Ipomea aquatic*, *Nelumbo nucifera*, *Nasturtium officinale*, and *Ludwigia adscendens*. Phytochemical compounds with antioxidant properties were found in aquatic and semiaquatic plant species such as *Persicaria hydropiper*, *Rotula aquatic*, *Sphaeranthus indicus*, *Polygonum glabrum*, *Ammannia baccifera*, *Ipomea aquatic*, *Nymphaea nouchali*, *Acorus calamus*, *Hedychium coronarium*, *Heliotropium indicum*, *Marsilea minuta*, and *Vetiveria zizanioides* [107, 148–151].

**3.3. Hepatoprotective Activity.** *Sphaeranthus amaranthoides* methanolic extracts demonstrated significantly higher

hepatoprotective activity than control groups [152]. The ethyl acetate extract of *Enhydra fluctuans* was found to have more potent hepatoprotective effects due to its potential flavonoid compounds. Phytoconstituents from *Marsilea minuta* plant species displayed significant hepatoprotective effects [108]. The protective effect of a methanolic extract of *S. indicus* against  $\text{CCl}_4$ -induced hepatotoxicity was reported [153]. The ethanolic extract of *Nymphoides hydrophylla* was checked against  $\text{CCl}_4$ -induced liver injury in albino rats and demonstrated impressive hepatoprotective activity [154]. Hepatoprotective studies of extracts of *Hygrophila auriculata* checked against HepG2 cells and paracetamol-induced hepatotoxicity and found that it improved hepatoprotective effects. [94]. The ethanolic extract of *Ipomoea aquatic* has been reported to effectively prevent thioacetamide-induced hepatic damage in animal models [155].

**3.4. Sedative Activity.** The natural products from *Marsilea minuta* [108], rhizome extract of *Acorus calamus* [149], and petroleum-ether extract of root parts of *Hygrophila schullii* [95] showed promising sedative activity. *Bacopa monnieri* and *Enhydra fluctuans* plant species have potential sedative actions [156, 157]. The alcoholic extract of *Sphaeranthus indicus* has been reported with significant sedative activity compared to standard sedative pentobarbitone and diazepam in the Swiss albino rat model [142, 153]. In the Ayurvedic system, the *Acorus calamus* plant is known as a magic root due to its sedative effect [158]. Various literature findings displayed that *Cyperus tegetum* has been used by tribal people for the treatment of mental disorders such as epilepsy [159, 160].

**3.5. Anticonvulsant Activity.** Sharma and coworkers (2020) displayed that extracts and compounds from the *Acorus calamus* demonstrated anticonvulsant activity with significant signaling pathways. For instance, methanolic and acetone extracts of *Acorus calamus* leaves have shown promising anticonvulsant activity [161]. The roots and rhizomes of the *Acorus calamus* also possess significant anticonvulsant activity [158]. Several pieces of the literature indicated that *Cyperus tegetum* plant has anticonvulsant activity [159, 160]. The aqueous and alcoholic extracts of roots and rhizomes of *Nymphoide indica* exhibited effective anticonvulsant activity [154]. Hydroalcoholic extract of *Sphaeranthus indicus* plant species showed anticonvulsant effects in the earlier studies [142].

**3.6. Cytotoxic Activity.** Samanta and coworkers (2020) reported that extract from the aerial part of *Ipomoea aquatic* showed a cytoprotective role in the liver and other organs [162]. Methanolic and aqueous extracts of the *Acorus calamus* have been known for their cytotoxicity effects [158, 163]. The methanol extract of *Mollugo cerviana*, *Trichosanthes cucumerina*, and *Vetiveria zizanioides* plants have been reported for their cytotoxicity against cancer cells such as HeLa and MCF-7 cell lines [151]. Alcoholic extracts

of *Enhydra fluctuations*, *Andrographis peniculata*, and *Clerodendrum viscosum* exhibited potent cytotoxicity against brine shrimp compared to ampicillin trihydrate as a positive control [164, 165]. The ethanolic extract of *Centella asiatica* exhibited weak cytotoxicity effects compared to the standard drugs [64].

**3.7. Antiparasitic Activity.** Several studies on aquatic and semiaquatic medicinal plants show their antiparasitic properties. *Nymphoides* plant species possess antiprotozoal, antimalarial, and anthelmintic properties [154]. Organic solvent extracts of various parts of the genus *Spilanthes*, such as dichloromethane extract of flowers, methanol extract of flowers, and cold dichloromethane extract of plant stems, have been shown to have significant activity against malaria and sleeping sickness diseases [136].

**3.8. Antidiabetic Activity.** Different plant extracts treat diabetes mellitus [166–168]. *Centella asiatica*, *Hedychium coronarium*, *Ipomea aquatic*, *Pistia stratiotes*, *Spergularia marina*, and *Nymphaea nouchali* have been reported as medicinal plants with effective antidiabetic properties due to their potency in the wide range of bioactive compounds [41, 169]. Ethyl acetate extracts and pure compounds obtained from *Acorus calamus* plant species have been reported for their strong antidiabetic effects [170]. The shoots and roots of *Ipomea aquatic* are also used to treat diabetes [171].

**3.9. As a Dietary Supplement.** Several aquatic and semiaquatic plant species are available as food using their various parts, such as stems, leaves, roots, rhizomes, flowers, flower heads, and fruits. For example, the edible part of *Oryza sativa* (rice) is its grain. In contrast, the leaves of *Nasturtium officinale* (Watercress), *Neptunia oleracea* (Water mimosa), and *Oenanthe javanica* (Japanese parsley) are used as human food [117]. Some previous studies revealed that *Enhydra fluctuation*, an edible semiaquatic herbaceous vegetable, is a rich source of phytochemicals such as  $\beta$ -carotene and ascorbic acid, which are required in diet supplements [172]. *Ipomea aquatic* is commonly used as a leafy vegetable or salad, which contains medicinally important flavonoids, alkaloids, and carotenes [10]. The leaves, roots, fruits, flowers, rhizomes, and tubers of *Nymphaea nouchali* plant species have been eaten in times of food scarcity [10, 41]. *Ludwigia adscendens* plant has been known to be consumed in the vegetable diet in China [173]. Leaves and tender shoots of the underutilized *Alternanthera sessilis* plant species are used in the vegetable diet for their potential nutritional and medicinal values [174]. Chia and coworkers (2015) reported that the leaves of the *Alternanthera sessilis* plant had been consumed raw or cooked as a food supplement [173]. Seaweeds are used for making a variety of foods. For instance, major aquatic and semiaquatic plant species that have been reported as human food includes *Acorus calamus*, *Aeschynomene aspera*, *Alternanthera philoxeroides*, *Centella asiatica*, *Colocasia esculent*, *Cyperus rotundus*, *Eleocharis dulcis*, *Hydrolea zeylanica*, *Hygroyza aristata*, *Nymphoides*

*hydrophylla*, *Oryza sativa*, *Pistia stratiotes*, *Polygonum plebeium*, *Trapa natans*, *Vallisneria spiralis*, and *Spilanthes calva* [41].

**3.10. As Industrial/Commercial Products.** The use of macroalgae in pharmaceutical industries showed their importance for humans as they were applied as antibiotic, antifouling, antiviral, anti-inflammatory, cytotoxic, and antimetabolic agents. The flour of fruits of *Trapa bispinosa* is reported to have important commercial uses in the milk industry and as a filler in the pharmaceutical industry [169]. Similarly, the rhizome extract and essential oils of the *Acorus calamus* are widely used in the flavoring industry and for commercial purposes [149, 175].

**3.11. In the Green Synthesis of Metallic Nanoparticles.** Nanoparticles have more advanced properties than bulk materials due to their superior behavior with defined shape and size [176]. The increased surface-to-volume ratio and quantum size effect properties of metal/metal oxide nanoparticles are the main reason for their chemical activity, strength, and other novel characteristics [177]. The synthesis of green metal/metal oxide nanoparticles is less likely to produce environmentally hazardous byproducts. This is primarily due to the plant-derived mediated reducing, capping, and stabilizing agents. [178]. Currently, many researchers have inclined their interests toward the secondary metabolites from various parts of plants as a route of synthesis of metal/metal oxide nanoparticles [179]. Green metal/metal oxide nanoparticles are highly used in various applications such as antibacterial, antioxidant, anti-inflammatory, catalytic, and cytotoxic activities [180]. Even though few studies have been carried out on the green synthesis using aquatic and semiaquatic plant extracts, some earlier studies revealed that these plants are rich sources of stronger bioreductants for synthesizing metallic nanoparticles. Aquatic and semiaquatic plants mediated green synthesis of metallic nanoparticles showed a faster reaction process than other plants [181]. Mathur et al. described the synthesis of silver nanoparticles (AgNPs) using extracts of *Alternanthera sessilis* and *Withania somnifera* for their applications in the assays of cytotoxicity effects and antibacterial activities with promising results [182]. The phytochemicals from the stem, fruit, seeds, leaves, and flowers of *Alternanthera sessilis* have been used for the biosynthesis of gold nanoparticles (AuNPs) and AgNPs. These synthesized nanoparticles have antibacterial, antifungicidal, antiplasmodial, anti-inflammatory, anticancer, antidiabetic, antiviral, and antioxidant activities [183]. Other studies also displayed that AgNPs synthesized from extracts of *Alternanthera sessilis* demonstrated significant cytotoxicity effects on the breast cancer cells [184].

#### 4. Conclusions and Future Prospectives

Aquatic and semiaquatic medicinal plant products have remarkable biological, pharmacological, agricultural, green materials synthesis, and industrial applications. They are also

used as nutraceuticals, food, and medicine. These plants contain diverse natural compounds with numerous biological and chemical properties. Crude extracts or pure compounds from various parts of aquatic and semiaquatic plants possess potential nutritional and medicinal values. Phytochemicals are widely used to treat various infectious and noninfectious health ailments. Further, several aquatic and semiaquatic plants are used for the green synthesis of metal and metal oxide nanomaterials, which have shown many potential applications. Moreover, they are also helpful for various commercial product preparations. Even though these plant species have a wide range of phytochemicals with potential bioactive properties, enough research work is missing. Thus, this review article was designed. However, in the future, more extensive and specific research is required to investigate the natural phytochemicals from these aquatic and semiaquatic medicinal plants for various commercial uses.

#### Data Availability

No data were used to support this study.

#### Conflicts of Interest

The authors declare that there are no conflicts of interest regarding the publication of this review article.

#### Authors' Contributions

AKA, MD, D, KKJ, and AB originated the idea, drafted, and wrote the review. YHG prepared different figures and tables and revised the manuscript. RKB and AH guided the development of the idea and revised the manuscript. All the authors read and approved the final manuscript.

#### Acknowledgments

The authors thank the Department of Environmental Science, Graphic Era University, Dehradun, for providing the required facilities while writing this review article.

#### References

- [1] T. B. Islam, F. Akter, A. Mimi et al., "Neuropharmacological effects of *Chassalia curviflora* (Rubiaceae) leaves in swiss albino mice model," *Archives of Razi Institute*, vol. 77, no. 2, pp. 881–890, 2022.
- [2] S. Mitra, M. S. Lami, T. M. Uddin et al., "Prospective multifunctional roles and pharmacological potential of dietary flavonoid narirutin," *Biomedicine & Pharmacotherapy*, vol. 150, pp. 112932–113020, 2022.
- [3] R. K. Bachheti, B. Archana, and S. S. Ramachandran, "Chemical composition of the essential oil from *Schinus molle L.* (Peruvian pepper)," *Der Pharma Chemica*, vol. 10, pp. 139–147, 2018.
- [4] F. Beshah, Y. Hunde, M. Getachew, R. K. Bachheti, A. Husen, and A. Bachheti, "Ethnopharmacological, phytochemistry and other potential applications of *Dodonaea* genus: a comprehensive review," *Current Research in Biotechnology*, vol. 2, pp. 103–119, 2020.



- [5] Y. H. Gonfa, F. Beshah, M. G. Tadesse, A. Bachheti, and R. K. Bachheti, "Phytochemical investigation and potential pharmacologically active compounds of *Rumex nepalensis*: an appraisal," *Beni-Suef University Journal of Basic and Applied Sciences*, vol. 10, no. 1, p. 18, 2021.
- [6] L. Abate, M. G. Tadesse, A. Bachheti, and R. K. Bachheti, "Traditional and phytochemical bases of herbs, shrubs, climbers, and trees from Ethiopia for their anticancer response," *BioMed Research International*, vol. 2022, Article ID 1589877, 27 pages, 2022.
- [7] G. Ganchev, V. Kuneva, and A. Stoyanova, "Nutritional and energy value of two wheat varieties," *Bulgarian Journal of Agricultural Science*, vol. 25, no. 3, pp. 47–52, 2019.
- [8] P. Tagde, P. Tagde, F. Islam et al., "The multifaceted role of curcumin in advanced nanocurcumin form in the treatment and management of chronic disorders," *Molecules*, vol. 26, no. 23, pp. 7109–7133, 2021.
- [9] U. Deka, T. Dutta, and S. Talukdar, "Aquatic/semi-aquatic macrophytes used in herbal remedies from the wetlands of western Assam, north-east India," *Asian Journal of Pharmaceutical and Clinical Research*, vol. 12, no. 8, pp. 93–96, 2019.
- [10] M. Aasim, K. M. Khawar, and S. I. Ahmed, "Multiple uses of some important aquatic and semiaquatic medicinal plants," *Plant and Human Health*, vol. 2, 2019.
- [11] V. D. Heidi and L. Smith-Adao, *National Biodiversity Assessment: Progress on the Inland Aquatic Component*, National-Biodiversity-Assessment-Freshwater-component-Heidi, Pretoria, South Africa, 2018.
- [12] J. K. Cronk and M. S. Fennessy, *Wetland Plants: Biology and Ecology*, CRC Press, Boca Raton, Florida, USA, 2016.
- [13] A. Panda and M. K. Misra, "Ethnomedicinal survey of some wetland plants of south Orissa and their conservation," *Indian Journal of traditional knowledge*, vol. 10, no. 2, pp. 296–303, 2011.
- [14] R. Chahal, A. Nanda, E. K. Akkol et al., "*Ageratumconyzoides* L. and its secondary metabolites in the management of different fungal pathogens," *Molecules*, vol. 26, no. 10, p. 2933, 2021.
- [15] A. Jain, S. Roshnibala, P. B. Kanjilal, R. S. Singh, and H. B. Singh, "Aquatic/semi-aquatic plants used in herbal remedies in the wetlands of Manipur, Northeastern India," *Indian Journal of Traditional Knowledge*, vol. 6, no. 2, pp. 346–351, 2014.
- [16] F. Epifano, M. C. Specchiulli, V. A. Taddeo, S. Fiorito, and S. Genovese, "Phytochemistry and pharmacology of the genus *Nymphaea*," *Natural Product Communications*, vol. 10, no. 6, 2015.
- [17] S. A. Punjabi, "Some less known herbal remedies against wounds from Jamkhed Tahasil areas in Ahmednagar District (MS) India," *Journal of Pharmaceutical Research and Opinion*, vol. 2, pp. 58–62, 2012.
- [18] A. D. Taranhalli, A. M. Kadam, S. S. Karale, and B. W. Yashodhan, "Evaluation of antidiarrhoeal and wound healing potentials of *Ceratophyllum demersum* Linn. whole plant in rats," *Latin American Journal of Pharmacy*, vol. 30, 2011.
- [19] L. H. Shankar and P. K. Mishra, "Study of aquatic medicinal plants of Hazaribag district of Jharkhand, India," *International Research Journal of Pharmacy*, vol. 3, no. 4, pp. 405–409, 2012.
- [20] S. Y. Kamble, S. R. Patil, P. S. Sawant, S. Sawant, S. G. Pawar, and E. A. Singh, "Studies on plants used in traditional medicine by Bhilla tribe of Maharashtra," *Indian Journal of Traditional Knowledge*, vol. 9, no. 3, pp. 591–598, 2010.
- [21] A. K. Gupta, "Cryptocoryne retrospiralis," 2011, <https://www.iucn.org/resources/conservation-tool/iucn-red-list-threatened-species>.
- [22] D. A. Simpson and C. A. Inglis, "Cyperaceae of economic, ethnobotanical and horticultural importance: a checklist," *Kew Bulletin*, vol. 56, pp. 257–360, 2001.
- [23] J. A. Duke and E. S. Ayensu, *Medicinal Plants of China*, Reference Publications, Algonac, USA, 1985.
- [24] S. Prakash and S. Deshwal, "Alpha and beta amylase activity of *Fagopyrum esculentum* (Buckwheat): a medicinal plant," *Janaki Medical College Journal of Medical Science*, vol. 1, pp. 53–58, 2013.
- [25] C. K. Ruffo, A. Birnie, and B. Tengnäs, *Edible Wild Plants of Tanzania*, Regional Land Management Unit, Nairobi, Africa, 2002.
- [26] H. M. Burkill, *The Useful Plants of West Tropical Africa*, Royal Botanic Gardens, Richmond, UK, 2004.
- [27] M. Karataş, M. Aasim, and M. Çiftçioğlu, "Adventitious shoot regeneration of roundleaf toothcup-*Rotala rotundifolia*," *The Journal of Animal & Plant Sciences*, vol. 24, 2014.
- [28] P. Selvakumari and A. Britto, "Bactericidal activity of *Lagenandra ovata* (Linn.) Thw. rhizome oil," *Indian Journal of Natural Products and Resources*, vol. 6, no. 5, pp. 382–385, 2007.
- [29] B. M. N. Islam, F. Akter, J. U. Chowdhury, and J. Begum, "Chemical constituents of essential oils from aerial parts of *Adenosma capitatum* and *Limnophila aromatic*," *Bangladesh Journal of Pharmacology*, vol. 5, no. 1, pp. 13–16, 2010.
- [30] Z. U. Ahmed, *Encyclopedia of Flora and Fauna of Bangladesh: Angiosperms: Dicotyledons: Ranunculaceae-Zygophyllaceae*, Asiatic Society of Bangladesh, Dhaka, Bangladesh, 2009.
- [31] A. Ghani, *Medicinal Plants of Bangladesh*, Asiatic Society of Bangladesh, Dhaka, Bangladesh, 2003.
- [32] F. Ahmed, M. S. T. Selim, and J. A. Shilpi, "Antibacterial activity of *Ludwigia adscendens*," *Fitoterapia*, vol. 76, no. 5, pp. 473–475, 2005.
- [33] K. Santosh and N. Satya, "Herbal remedies of wetlands macrophytes in India," *International Journal of Pharmaceutical and Biological Sciences*, vol. 1, no. 2, pp. 1–5, 2010.
- [34] I. Podolak, P. Koczurkiewicz, M. Michalik, A. Galanty, P. Zajdel, and Z. Janeczko, "A new cytotoxic triterpene saponin from *Lysimachia nummularia* L.," *Carbohydrate Research*, vol. 375, pp. 16–20, 2013.
- [35] S. Mani, "Marsilea Minuta: the IUCN red list of threatened species," 2016, <https://indiabiodiversity.org/species/show/227674>.
- [36] M. M. Haq, M. A. R. Chowdhury, H. Tayara et al., "A report on multi-target anti-inflammatory properties of phytoconstituents from *Monochoria hastata* (Family: Pontederiaceae)," *Molecules*, vol. 26, no. 23, p. 7397, 2021.
- [37] R. V. Lansdown, "Monochoria Vaginalis: The IUCN red list of threatened species," 2011, <https://indiabiodiversity.org/species/show/227674>.
- [38] N. R. Krishna, Y. N. R. Varma, and C. Saidulu, "Ethnobotanical studies of Adilabad district, Andhra Pradesh, India," *Journal of Pharmacognosy and Phytochemistry*, vol. 3, no. 1, 2014.
- [39] M. Maruga Raja, N. K. Sethiya, and S. H. Mishra, "A comprehensive review on *Nymphaea stellata*: a traditionally used bitter," *Journal of Advanced Pharmaceutical Technology & Research*, vol. 1, no. 3, p. 311, 2010.

- [40] C. D. K. Cook, *Aquatic and Wetland Plants of India*, Oxford University Press, Oxford, UK, 1996.
- [41] M. M. Swapna, R. Prakashkumar, K. P. Anoop, C. N. Manju, and N. P. Rajith, "A review on the medicinal and edible aspects of aquatic and wetland plants of India," *Journal of Medicinal Plants Research*, vol. 5, no. 33, pp. 7163–7176, 2011.
- [42] A. L. K. Gupta and V. N. Pandey, "Herbal remedies of aquatic macrophytes of Gorakhpur district, Uttar Pradesh (India)," *International Journal of Pharmaceutical and Biological Sciences*, vol. 5, no. 1, pp. 300–308, 2014.
- [43] L. J. Zhang, S. F. Yeh, Y. T. Yu, L. M. Y. Kuo, and Y. H. Kuo, "Antioxidative flavonol glucuronides and anti-hbsagflavonol from *Rotala rotundifolia*," *Journal of Traditional and Complementary Medicine*, vol. 1, pp. 57–63, 2011.
- [44] L. Zuo, J. Chen, X. Ji, and X. Zhang, "Advances in study on chemical constituents of *Lythraceae* plants in China," *Hans Journal of Medicinal Chemistry*, vol. 06, no. 02, pp. 42–53, 2018.
- [45] F. Gebashe, A. O. Aremu, J. F. Finnie, and J. Van Staden, "Grasses in South African traditional medicine: a review of their biological activities and phytochemical content," *South African Journal of Botany*, vol. 122, pp. 301–329, 2019.
- [46] K. M. Szuman, A. b van Staden, B. Madikizela, and N. Lall, *An Introduction to Aquatic Plants*, CRC Press, Boca Raton, Florida, USA, 2020.
- [47] S. Verma and N. Singh, "In vitro mass multiplication of *Acorus calamus* L.-an endangered medicinal plant," *Am Eurasian Journal of Agriculture and Environmental Sciences*, vol. 12, pp. 1514–1521, 2012.
- [48] P. S. Babar, V. D. Anuradha, S. S. Supriya, and J. J. Chavan, "Micropropagation, polyphenol content and biological properties of sweet flag (*Acorus calamus*): a potent medicinal and aromatic herb," *An International Journal of Plant Research and Biotechnology*, vol. 33, pp. 1–8, 2020.
- [49] M. B. Ahmed, S. Ahmed, M. Salahin et al., "Standardization of a suitable protocol for in vitro clonal propagation of *Acorus calamus* L. an important medicinal plant in Bangladesh," *American-urasian Journal of Scientific Research*, vol. 2, no. 2, pp. 136–140, 2007.
- [50] D. Chandra and K. Prasad, "Phytochemicals of *Acorus calamus* (sweet flag)," *Journal of Medicinal Plants Studies*, vol. 5, pp. 277–281, 2017.
- [51] W. S. Rita, R. Kawuri, and I. M. D. Swantara, "The essential oil contents of Jeringau (*Acorus calamus* L.) Rhizomes and their antifungal activity against *Candida albicans*," *Journal of Health Sciences and Medicine*, vol. 1, pp. 33–38, 2017.
- [52] M. P. Corrêa, *Dicionário das plantas úteis do Brasil e das exóticas cultivadas:HL*, Ministério da Agricultura, Instituto Brasileiro de Desenvolvimento Florestal, Federal, Brazil, 1984.
- [53] N. Yadav, S. A. Ganie, B. Singh, A. K. Chhillar, and S. S. Yadav, "Phytochemical constituents and ethnopharmacological properties of *Ageratum conyzoides* L.," *Phytotherapy Research*, vol. 33, no. 9, pp. 2163–2178, 2019.
- [54] N. Loganayaki, P. Siddhuraju, and S. Manian, "Antioxidant, anti-inflammatory and anti-nociceptive effects of *Ammannia baccifera* L. (*Lythraceae*), a folklore medicinal plant," *Journal of Ethnopharmacology*, vol. 140, no. 2, pp. 230–233, 2012.
- [55] T. Y. Suman, D. Elumalai, A. Vignesh, P. K. Kaleena, and K. Murugesan, "Evaluation of larvicidal activity of the aerial extracts of a medicinal plant, *Ammannia baccifera* (Linn) against two important species of mosquitoes, *Aedes aegypti* and *Culex quinquefasciatus*," *Asian Pacific Journal of Tropical Disease*, vol. 2, no. 1, pp. S352–S355, 2012.
- [56] H. C. Upadhyay, B. S. Sisodia, J. Agrawal, A. Pal, M. P. Darokar, and S. K. Srivastava, "Antimalarial potential of extracts and isolated compounds from four species of genus *Ammannia*," *Medicinal Chemistry Research*, vol. 23, no. 2, pp. 870–876, 2014.
- [57] G. J. Sharma, P. Chirangini, and R. Kishor, "Gingers of Manipur: diversity and potentials as bioresources," *Genetic Resources and Crop Evolution*, vol. 58, no. 5, pp. 753–767, 2011.
- [58] N. H. Dang, L. T. V. Anh, and N. T. Dat, "Anti-inflammatory effects of essential oils of *Amomum aromaticum* fruits in lipopolysaccharide-stimulated RAW264 7 cells," *Journal of Food Quality*, vol. 2020, Article ID 8831187, 5 pages, 2020.
- [59] A. Alam, M. Pharma, and V. Singh, "Composition and pharmacological activity of essential oils from two imported *Amomum Subulatum* fruit samples," *Journal of Taibah University Medical Sciences*, vol. 16, pp. 1–9, 2020.
- [60] M. K. K. Fazlul, S. P. Deepthi, M. Irfan, Y. Farzana, B. Munira, and Nazmulmhm, "Antibacterial and antifungal activity of various extracts of *Bacopa monnieri*," *International Journal of Pharmaceutical Research*, vol. 11, no. 1, pp. 1698–1702, 2019.
- [61] A. Russo and F. Borrelli, "*Bacopa monniera* a reputed nootropic plant: an overview," *Phytomedicine*, vol. 12, no. 4, pp. 305–317, 2005.
- [62] K. J. Gohil, J. Patel, and A. Gajjar, "Pharmacological review on *Centella asiatica*: a potential herbal cure-all," *Indian Journal of Pharmaceutical Sciences*, vol. 72, no. 5, p. 546, 2010.
- [63] B. M. L. Brinkhaus, M. Lindner, D. Schuppan, and E. Hahn, "Chemical, pharmacological and clinical profile of the east Asian medical plant *Centella asiatica*," *Phytomedicine*, vol. 7, no. 5, pp. 427–448, 2000.
- [64] F. N. Idris and M. Mohd Nadzir, "Comparative studies on different extraction methods of *Centella asiatica* and extracts bioactive compounds effects on antimicrobial activities," *Antibiotics*, vol. 10, no. 4, p. 457, 2021.
- [65] Y. Tanaka and V. K. Nguyen, *Edible Wild Plants of Vietnam*, Orchid Press, Bangkok, Thailand, 2007.
- [66] M. Raghavendra, R. Maiti, S. Kumar, A. Trigunayat, S. Mitra, and S. Acharya, "Role of *Centella asiatica* on cerebral post-ischemic reperfusion and long-term hypoperfusion in rats," *International Journal of Green Pharmacy*, vol. 3, no. 2, p. 88, 2009.
- [67] Y. q. Guo, H. y. Sun, C. o. Chan et al., "*Centipeda minima* (Ebushicao) extract inhibits PI3K-Akt-mTOR signaling in nasopharyngeal carcinoma CNE-1 cells," *Chinese Medicine*, vol. 10, no. 1, pp. 26–29, 2015.
- [68] S. S. Huang, C. S. Chiu, T. H. Lin et al., "Antioxidant and anti-inflammatory activities of aqueous extract of *Centipeda minima*," *Journal of Ethnopharmacology*, vol. 147, no. 2, pp. 395–405, 2013.
- [69] W. Huang, X. Yu, N. Liang et al., "Anti-angiogenic activity and mechanism of sesquiterpene lactones from *Centipeda minima*," *Natural Product Communications*, vol. 11, no. 4, 2016.
- [70] X. Zhang, J. He, W. Huang et al., "Antiviral activity of the sesquiterpene lactones from *Centipeda minima* against influenza A virus in vitro," *Natural Product Communications*, vol. 13, no. 2, 2018.
- [71] T. Abu, "Aquatic Macrophyte *Ceratophyllum demersum* L. (*Ceratophyllaceae*): plant profile, phytochemistry, and

- medicinal properties-a review," *International Journal of Science and Research*, vol. 6, no. 7, pp. 394–399, 2017.
- [72] A. Manosroi, M. Sainakham, C. Chankhampan, W. Manosroi, and J. Manosroi, "In vitro anticancer activities of Job's tears (*Coix lacryma-jobi*) extracts on human colon adenocarcinoma," *Saudi Journal of Biological Sciences*, vol. 23, no. 2, pp. 248–256, 2016.
- [73] D. S. Diningrat, M. Risfandi, N. S. Harahap, A. N. Sari, H. K. Siregar, and H. K. Siregar, "Phytochemical screening and antibacterial activity *Coix lacryma-jobi* oil," *Journal of Plant Biotechnology*, vol. 47, no. 1, pp. 100–106, 2020.
- [74] Q. M. Liu, H. Y. Zhao, X. K. Zhong, and J. G. Jiang, "Eclipta prostrata L. phytochemicals: isolation, structure elucidation, and their antitumor activity," *Food and Chemical Toxicology*, vol. 50, no. 11, pp. 4016–4022, 2012.
- [75] L. Feng, Y. Y. Zhai, J. Xu et al., "A review on traditional uses, phytochemistry and pharmacology of *Eclipta prostrata* L.," *Journal of Ethnopharmacology*, vol. 245, pp. 112109–112114, 2019.
- [76] F. Islam, F. F. N. Fyrose, T. A. Trina, and I. J. Mishu, "Evaluation of antioxidant, antimicrobial and thrombolytic activity of *Eleocharis dulcis* (Cyperaceae) fruits of methanol Extract," *Evaluation*, vol. 2, pp. 39–49, 2019.
- [77] Y. Zhang, H. Xu, Z. Hu et al., "Eleocharis dulcis corm: phytochemicals, health benefits, processing and food products," *Journal of the Science of Food and Agriculture*, vol. 102, no. 1, pp. 19–40, 2022.
- [78] Y. You, X. Duan, X. Wei et al., "Identification of major phenolic compounds of Chinese water chestnut and their antioxidant activity," *Molecules*, vol. 12, no. 4, pp. 842–852, 2007.
- [79] K. Gupta, *Enhydra Fluctuations*, IUCN Red List of Threatened Species, Gland, Switzerland, 2012.
- [80] R. Ali, M. Billah, M. Hassan, and S. M. R. Dewan, "Enhydra fluctuans Lour: a review," *Research Journal of Pharmacy and Technology*, vol. 6, no. 9, pp. 927–929, 2013.
- [81] M. Yusuf, J. Begum, M. N. Hoque, and J. U. Chowdhury, *Medicinal Plants of Bangladesh*, BCSIR Laboratories, Dhaka, Chittagong, 2nd edition, 2009.
- [82] K. R. Kirtikar and B. D. Basu, *Indian Medicinal Plants*, Vol. VIII, Sri Satguru Publications, New Delhi, India, 2002.
- [83] P. K. Swain, S. C. Dinda, D. P. Nayak, B. Kar, and V. J. Patro, "Antioxidant activity of *Enhydra fluctuans* Lour. aerial parts," *Journal of Phytotherapy and Pharmacology*, vol. 1, no. 2, pp. 23–34, 2012.
- [84] A. Barua, M. S. Alam, M. D. Junaid et al., "Phytochemistry, traditional uses and pharmacological properties of *Enhydra fluctuans* Lour: a comprehensive review," *Current Pharmaceutical Biotechnology*, vol. 22, no. 8, pp. 1061–1068, 2021.
- [85] A. Ray, S. Jena, B. Dash et al., "Chemical diversity, antioxidant and antimicrobial activities of the essential oils from Indian populations of *Hedychium coronarium* Koen.," *Industrial Crops and Products*, vol. 112, pp. 353–362, 2018.
- [86] N. Chimnoi, C. Sarasuk, N. Khunnawutmanotham et al., "Phytochemical reinvestigation of labdane-type diterpenes and their cytotoxicity from the rhizomes of *H. coronarium*," *Phytochemistry Letters*, vol. 2, no. 4, pp. 184–187, 2009.
- [87] A. Roy, "Pharmacological activities of Indian Heliotrope (*Heliotropium indicum* L.): a review," *Journal of Pharmacognosy and Phytochemistry*, vol. 4, no. 3, pp. 101–104, 2015.
- [88] P. A. Wani, A. M. Tolu, and S. Wahid, "Antioxidant, antimicrobial and antibiotic resistance modifying effect of *Heliotropium indicum*," *Biocatalysis and Agricultural Biotechnology*, vol. 15, pp. 113–118, 2018.
- [89] M. Basak and B. K. Dey, "Phytochemical and antipyretic potential of ethanolic leaf extract of *Heliotropium indicum* L.," *Journal of Applied Pharmaceutical Research*, vol. 4, no. 2, pp. 6–10, 2016.
- [90] H. C. Huang, C. C. Liaw, L. J. Zhang et al., "Triterpenoidal saponins from *Hydrocotyle sibthorpioides*," *Phytochemistry*, vol. 69, no. 7, pp. 1597–1603, 2008.
- [91] Q. Huang, S. Zhang, R. Huang et al., "Isolation and identification of an anti-hepatitis B virus compound from *Hydrocotyle sibthorpioides* Lam.," *Journal of Ethnopharmacology*, vol. 150, no. 2, pp. 568–575, 2013.
- [92] A. Swargiary and M. Daimari, "GC-MS analysis of phytochemicals and antihyperglycemic property of *Hydrocotyle sibthorpioides* Lam.," *SN Applied Sciences*, vol. 3, no. 1, pp. 36–11, 2021.
- [93] L. Sarvananda and A. D. Premarathna, "Ethnopharmacological potential and medicinal uses of *H. auriculata*," *Journal of Ayurveda and Holistic Medicine*, vol. 4, no. 4, pp. 185–188, 2018.
- [94] NK. Sethiya, N. M. Ahmed, R. M. Shekh, V. Kumar, P. Kumar Singh, and V. Kumar, "Ethnomedicinal, phytochemical and pharmacological updates on *H. auriculata* (Schum.) Heine: an overview," *Journal of Integrative Medicine*, vol. 16, no. 5, pp. 299–311, 2018.
- [95] B. Ghule, P. Agrawal, P. Lal, D. Kothari, and N. Kotagale, "Separation and quantification of lupeol in *Hygrophila schulli* by high-performance thin-layer chromatography," *JPC-Journal of Planar Chromatography-Modern TLC*, vol. 34, no. 1, pp. 79–87, 2021.
- [96] P. Thanatuskitti, V. Siripornpanich, W. Sayorwan, and N. Ruangrunsi, "The Effects of inhaled *Limnophila aromatica* essential oil on brain wave activities and emotional states in healthy volunteers: a randomized crossover study," *Research Journal of Pharmacognosy*, vol. 7, no. 4, pp. 1–9, 2020.
- [97] C. Wijaya, Q. D. Do, Y. H. Ju et al., "Isolation and characterization of starch from *Limnophilaaromatic*," *Heliyon*, vol. 5, 2019.
- [98] J. A. Shilpi, A. I. Gray, and V. Seidel, "Chemical constituents from *Ludwigia adscendens*," *Biochemical Systematics and Ecology*, vol. 38, no. 1, pp. 106–109, 2010.
- [99] R. Chakraborty, B. De, N. Devanna, and S. Sen, "Antitussive, expectorant activity of *Marsilea minuta* L., an Indian vegetable," *Journal of Advanced Pharmaceutical Technology & Research*, vol. 4, no. 1, p. 61, 2013.
- [100] A. J. De Britto, D. H. S. Gracelin, and P. B. J. R. Kumar, "Qualitative and quantitative analysis of phytochemicals in *Marsilea minuta* L.," *International Journal of Pharmaceutical and Biological Sciences*, vol. 4, no. 1, pp. 800–805, 2013.
- [101] K. Upreti, S. J. Jeewan, M. T. Lalit, G. C. Joshi, Y. P. S. Pangtey, and G. Tewari, "Ethnomedicinal uses of pteridophytes of *Kumaun himalaya*, Uttarakhand, India," *Journal of American Sciences*, vol. 5, no. 4, pp. 167–170, 2009.
- [102] M. Rahmatullah, A. A. B. T. Kabir, M. M. Rahman et al., "Ethnomedicinal practices among a minority group of christians residing in Mirzapur village of Dinajpur District, Bangladesh," *Advances in Natural and Applied Sciences*, vol. 4, no. 1, pp. 45–51, 2010.
- [103] S. Sen, R. Chakraborty, B. De, and N. Devanna, "An ethnobotanical survey of medicinal plants used by ethnic people in west and south district of Tripura, India," *Journal of Forestry Research*, vol. 22, no. 3, pp. 417–426, 2011.
- [104] O. Kaisoon, S. Siriamornpun, N. Weerapreeyakul, and N. Meeso, "Phenolic compounds and antioxidant activities



- of edible flowers from Thailand,” *Journal of Functional Foods*, vol. 3, no. 2, pp. 88–99, 2011.
- [105] G. Sabithira and R. Udayakumar, “GC-MS analysis of methanolic extracts of leaf and stem of *Marsilea minuta* (Linn.),” *Journal of Complementary and Alternative Medical Research*, vol. 3, no. 1, pp. 1–13, 2017.
- [106] S. Arokiyaraj, R. Bharanidharan, P. Agastian, and H. Shin, “Chemical composition, antioxidant activity and antibacterial mechanism of action from *Marsilea minuta* leaf hexane: methanol extract,” *Chemistry Central Journal*, vol. 12, no. 1, pp. 105–111, 2018.
- [107] M. Dwiti, “Pharmacognostic evaluation, phytochemical investigation and antioxidant activity on leaves of *Marsilea minuta* Linn. (*Marsileaceae*),” *Journal of Pharmacognosy and Phytochemistry*, vol. 5, no. 2, pp. 134–140, 2016.
- [108] R. J. Sajini, S. Prema, and K. Chitra, “Phytoconstituents, pharmacological activities of *Marsilea Minuta* L. (*Marsileaceae*)-an overview,” *International Journal of Pharmaceutical Sciences and Research*, vol. 10, no. 4, p. 1582, 2020.
- [109] N. R. Mehta, E. P. Patel, P. V. Patani, and B. Shah, “*Nelumbo nucifera* (Lotus): a review on ethanobotany, phytochemistry and pharmacology,” *Indian Journal of Pharmaceutical and Biological Research*, vol. 1, no. 04, pp. 152–167, 2013.
- [110] K. R. Paudel and N. Panth, “Phytochemical profile and biological activity of *Nelumbo nucifera*,” *Evidence-Based Complementary and Alternative Medicine*, vol. 2015, Article ID 789124, 16 pages, 2015.
- [111] K. R. Sridhar and R. Bhat, “Lotus-A potential nutraceutical source,” *Journal of Agricultural Technology*, vol. 3, no. 1, pp. 143–155, 2007.
- [112] D. Tungmunthum, D. Pinthong, and C. Hano, “Flavonoids from *Nelumbo nucifera* Gaertn, a medicinal plant: uses in traditional medicine, phytochemistry and pharmacological activities,” *Medicine (Basel)*, vol. 5, no. 4, pp. 1–13, 2018.
- [113] V. Nagavani and T. R. Rao, “Evaluation of antioxidant potential and qualitative analysis of major polyphenols by RP-HPLC in *Nymphaea nouchali* Burm flowers,” *International Journal of Pharmacy and Pharmaceutical Sciences*, vol. 2, no. 4, pp. 98–104, 2010.
- [114] G. N. Lakshmi, S. V. Smitha, C. L. Ammu, and K. V. B. Rao, “Phytochemical profile, in vitro antioxidant and hemolytic activities of various leaf extract of *Nymphaea nouchali* Linn: an in vitro study,” *International Journal of Pharmacy and Pharmaceutical Sciences*, vol. 6, no. 6, pp. 548–552, 2014.
- [115] C. Wiart, *Medicinal Plants of the Asia-Pacific: Drugs for the Future?*, World Scientific, Chennai, India, 2006.
- [116] M. A. A. Sikder, H. R. Jisha, M. R. Kuddus, F. Rumi, M. A. Kaiser, and M. A. Rashid, “Evaluation of Bioactivities of *Nymphaea Nouchali* (Burm. f)-the national flower of Bangladesh,” *Bangladesh Pharmaceutical Journal*, vol. 15, no. 1, pp. 1–5, 2012.
- [117] M. N. Uddin, M. A. Samad, M. Zubair et al., “Potential bioactive phytochemicals, antioxidant properties and anti-cancer pathways of *Nymphaea nouchali*,” *Asian Pacific Journal of Tropical Biomedicine*, vol. 10, no. 12, pp. 555–562, 2020.
- [118] E. Selvakumari, S. Shantha, P. T. Purushoth, and C. Sreenathkumar, “Antiproliferative activity of ethanolic flower extract from *Nymphaea pubescens* wild against human cervical and breast carcinoma *in vitro*,” *International Research Journal of Pharmacy*, vol. 3, no. 1, pp. 124–125, 2012.
- [119] K. Rajagopal and K. Sasikala, “Antihyperglycaemic and antihyperlipidaemic effects of *Nymphaea stellata* in alloxan-induced diabetic rats,” *Singapore Medical Journal*, vol. 49, no. 2, pp. 137–141, 2008.
- [120] E. Selvakumari, A. Shantha, C. S. Kumar, and P. T. Prabhu, “Phytochemistry and pharmacology of the genus *Nymphaea*,” *Journal of Academia and Industrial Research*, vol. 5, no. 7, pp. 98–108, 2016.
- [121] A. K. M. M. Huq, J. A. Jamal, and J. Stanislas, “Ethnobotanical, phytochemical, pharmacological, and toxicological aspects of *Persicaria hydropiper* (L.) Delarbre,” *Evidence-Based Complementary and Alternative Medicine*, vol. 2014, Article ID 782830, 12 pages, 2014.
- [122] M. Miyazawa and N. Tamura, “Inhibitory compound of tyrosinase activity from the sprout of *Polygonum hydropiper* L. (Benitade),” *Biological and Pharmaceutical Bulletin*, vol. 30, no. 3, pp. 595–597, 2007.
- [123] R. K. Choudhary, O. Sungrae, and L. Joongku, “An ethnomedicinal inventory of knotweeds of Indian Himalaya,” *Journal of Medicinal Plants Research*, vol. 5, no. 10, pp. 2095–2103, 2011.
- [124] R. Gupta, P. Tripathi, R. Kumar, A. Sharma, and A. Mishra, “*Pistia stratiotes* (Jalkumbhi),” *Pharmacognosy Reviews*, vol. 4, no. 8, p. 153, 2010.
- [125] S. Sudirman, H. Herpandi, R. Nopianti, S. Dwita Lestari, W. Wasahla, and H. Mareta, “Isolation and characterization of phenolic contents, tannin, vitamin C and E from water lettuce (*Pistia stratiotes*),” *Oriental Journal of Chemistry*, vol. 33, no. 6, pp. 3173–3176, 2017.
- [126] A. Vysakh, R. J. Nair, M. S. Latha, and M. Jyothis, “Traditional and therapeutic importance of *Rotula aquatica* Lour: an overview,” *International Journal of Pharmacy and Pharmaceutical Research*, vol. 7, pp. 97–107, 2016.
- [127] S. Bhowmik, M. Saha, and B. K. Datta, “Extended distribution of *Rotala rotundifolia* (Buch.-Ham. Ex roxb.) Koehne (*lythraceae*) from India,” *An International Journal of Environment and Biodiversity*, vol. 3, pp. 48–50, 2012.
- [128] S. D. Rout, T. Panda, and N. Mishra, “Ethnomedicinal studies on some pteridophytes of similipal biosphere reserve, Orissa, India,” *International Journal of Medicine and Medical Sciences*, vol. 1, no. 5, pp. 192–197, 2009.
- [129] M. S. Islam, A. Iwasaki, K. Suenaga, and H. Kato-Noguchi, “2-Methoxystypandrone, a potent phytochemical substance in *Rumex maritimus* L,” *Theoretical and Experimental Plant Physiology*, vol. 29, no. 4, pp. 195–202, 2017.
- [130] R. R. Haynes, D. H. Les, L. B. Holm-Nielsen, and Alismataceae, *Flowering Plants: Monocotyledons*, Springer, Berlin, Heidelberg, 1998.
- [131] J. Gu, H. Zhang, C. Wen et al., “Purification, characterization, antioxidant and immunological activity of polysaccharide from *Sagittaria sagittifolia* L,” *Food Research International*, vol. 136, pp. 109345–109436, 2020.
- [132] A. Chatterjee and S. C. Pakrashi, *The Treatise on Indian Medicinal Plants*, National Institute of Science Communication and Information Resources, New Delhi, 1st edition, 2003.
- [133] M. Garg and N. Dwivedi, “Physicochemical and phytochemical studies on *Sphaeranthus indicus* Linn. With HPTLC finger printing,” *Journal of Drug Delivery and Therapeutics*, vol. 11, no. 2, pp. 100–107, 2021.
- [134] K. K. Das, “A new distributional record of *Acmella ciliata* (Kunth) cassini [*Asteraceae*] from Assam, India,” *Pleione*, vol. 7, no. 1, pp. 258–261, 2013.
- [135] P. Pati and S. Bhatnagar, “Phytochemical, cytotoxic and antioxidant activity of solvent extracts of *Spilanthes calva*,”





- World Journal of Pharmaceutical Research*, vol. 10, no. 9, pp. 1131–1142, 2018.
- [136] J. Paulraj, R. Govindarajan, and P. Palpu, “The Genus *Splianthes* ethnopharmacology, phytochemistry, and pharmacological pharmacological properties: a review,” *Advances in Pharmacological and Pharmaceutical Sciences*, vol. 2013, Article ID 510298, 22 pages, 2013.
- [137] R. Banerjee, P. Goswami, K. Pathak, and A. Mukherjee, “Vetiver grass: an environment clean-up tool for heavy metal contaminated iron ore mine-soil,” *Ecological Engineering*, vol. 90, pp. 25–34, 2016.
- [138] S. Muthukrishnan and P. Manogaran, “Phytochemical analysis and free radical scavenging potential activity of *Vetiveria zizanioides* Linn.,” *Journal of Pharmacognosy and Phytochemistry*, vol. 7, no. 2, pp. 1955–1960, 2018.
- [139] S. Pathania, S. M. Ramakrishnan, and G. Bagler, “Phytochemica: a platform to explore phytochemicals of medicinal plants,” *Database*, vol. 2015, Article ID bav075, 8 pages, 2015.
- [140] T. Bhaigybati, J. Gurumayum, L. R. Singh, G. C. Bag, S. Sanasam, and P. G. Devi, “Phytochemical profiling, antioxidant activity, antimicrobial activity and GC-MS analysis of *Ipomoea aquatica* Forsk collected from EMA market, Manipur,” *Journal of Pharmacognosy and Phytochemistry*, vol. 9, no. 1, pp. 2335–2342, 2020.
- [141] R. G. W. D. B. Rajapaksha<sup>1</sup>, A. R. N. Silva, W. D. Ratnasooriya, B. A. R. Fernando, T. M. A. B. Thennakoon, and S. Singhabahu, “Evaluation of *in vitro* antibacterial activity of extract of semi-aquatic plants growing in the polluted water of Sri Lanka,” *International Journal of Pharmacognosy and Life Science*, vol. 1, no. 1, pp. 42–50, 2020.
- [142] D. Tandon and A. K. Gupta, “Comparative assessment of antimicrobial and antioxidant activity between whole plant and parts of *Sphaeranthus indicus* Linn. (Asteraceae),” *Clinical Phytoscience*, vol. 6, no. 1, pp. 23–15, 2020.
- [143] K. Vinod, R. Singh, and V. Joshi, “Antimicrobial activity of rhizome extract of *Acorus calamus* against different microorganisms,” *Octa Journal of Biosciences*, vol. 2, p. 3663, 2014.
- [144] P. Khatri, P. Jamdagni, A. Sindhu, and J. S. Rana, “Antimicrobial potential of important medicinal plants of India,” *International Journal of Microbial Resource Technology Accepted*, vol. 3, no. 1, pp. 1–9, 2016.
- [145] H. Sharanagouda and S. H. Shreelaxmi, “Antimicrobial activity of supercritical fluid extracted *Acorus calamus* oil against different microbes,” *Journal of Pharmacognosy and Phytochemistry*, vol. 7, no. 3, pp. 2836–2840, 2018.
- [146] R. Vakayil, S. Muruganantham, N. Kabeerdass et al., “*Acorus calamus*-zinc oxide nanoparticle coated cotton fabrics shows antimicrobial and cytotoxic activities against skin cancer cells,” *Process Biochemistry*, vol. 111, pp. 1–8, 2021.
- [147] R. G. Bhushan, A. P. Wrushali, J. Manwar, M. G. Nimbawar, N. A. Badukale, and R. L. Bakal, “Pharmacognosy, phytochemistry and clinical applications of traditional medicinal plants as memory booster,” *GSC Advanced Research and Reviews*, vol. 8, no. 2, pp. 019–029, 2021.
- [148] E. Y. Hafeez, N. Karimova, and O. Ilinskaya, “Antioxidant activity and total phenolic compound content of certain medicinal plants,” *International Journal of Biosciences*, vol. 5, no. 9, pp. 213–222, 2014.
- [149] P. Chaubey, P. Archana, O. Prakash, K. Rai, R. Kumar, and A. Pant, “*In vitro* antioxidant activity and total phenolic content of rhizome extracts from *Acorus calamus* Linn.,” *Asian Journal of Chemistry*, vol. 29, no. 11, pp. 2357–2360, 2017.
- [150] S. Pipriya, N. Kundu, and U. Tiwari, “Green Synthesis, characterization and antioxidant activity of silver nanoparticles in extracts of *Acorus calamus* and *Agaricus bisporus*,” *International Journal of Biochemistry Research & Review*, vol. 21, no. 4, pp. 1–15, 2018.
- [151] V. Devanathadesikan Seshadri, P. Vijayaraghavan, Y. O. Kim et al., “*In vitro* antioxidant and cytotoxic activities of polyherbal extracts from *Vetiveria zizanioides*, *Trichosanthes cucumerina*, and *Mollugo cerviana* on HeLa and MCF-7 cell lines,” *Saudi Journal of Biological Sciences*, vol. 27, no. 6, pp. 1475–1481, 2020.
- [152] M. R. Vinayakamurthi, J. A. J. Sunilson, A. V. A. G. Kumari, and U. Aathilakshmi, “*In-vivo* hepatoprotective and antioxidant activities of *Sphaeranthus amaranthoides* Burm.f. against anti-tubercular drugs induced hepatotoxicity in rats,” *Journal of Pharmaceutical Research International*, vol. 33, pp. 15–23, 2021.
- [153] M. George, L. Joseph, K. Sujith, and N. M. Paul, “*Sphaeranthus indicus* Linn: a pharmacological update,” *The Pharma Innovation*, vol. 6, no. 2-B, pp. 77–84, 2017.
- [154] M. H. Sohrab, Z. Khan, N. Chowdhury, and S. Sharmin, “Medicinal values of aquatic plant genus *Nymphoides* grown in Asia: a review,” *Asian Pacific Journal of Tropical Biomedicine*, vol. 8, no. 2, pp. 113–119, 2018.
- [155] S. S. Alkiyumi, M. A. Abdullah, A. S. Alrashdi, S. M. Salama, S. I. Abdelwahab, and A. H. A. Hadi, “*Ipomoea Aquatica* extract shows protective action against thioacetamide-induced hepatotoxicity,” *Molecules*, vol. 17, no. 5, pp. 6146–6155, 2012.
- [156] P. Srivastava and K. Shanker, “*Pluchea lanceolata* (Rasana): chemical and biological potential of Rasayana herb used in traditional system of medicine,” *Fitoterapia*, vol. 83, no. 8, pp. 1371–1385, 2012.
- [157] S. Halder, U. Anand, S. Nandy et al., “Herbal drugs and natural bioactive products as potential therapeutics: a review on pro-cognitives and brain boosters perspectives,” *Saudi Pharmaceutical Journal*, vol. 29, no. 8, pp. 879–907, 2021.
- [158] R. Singh, P. K. Sharma, and R. Malviya, “Pharmacological properties and ayurvedic value of Indian buch plant (*Acorus calamus*): a short review,” *Advances in Biological Research*, vol. 5, no. 3, pp. 145–154, 2011.
- [159] N. C. Chaulya, P. K. Haldar, and A. Mukherjee, “Anti-diarrhoeal activity of methanol extract of the rhizomes of *Cyperus tegetum* Roxb.,” *International Journal of Pharmacy and Pharmaceutical Sciences*, vol. 3, no. 1, pp. 133–135, 2011.
- [160] C. T. Roxb, N. C. Chaulya, P. K. Haldar, and A. Mukherjee, “Sedative properties of methanol extract of rhizome of *Cyperus Tegetum* Roxb.,” *International Journal of Pharmacognosy and Phytochemistry and Research*, vol. 2, no. 3, pp. 40–43, 2010.
- [161] A. S. Bisht, M. Chauhan, A. Dimri, A. Joshi, and M. Ali, “Pharmacognostical evaluation of leaves of *Acorus calamus* Linn.,” *International Journal of Pharmacognosy and Phytochemical Research*, vol. 5, no. 4, pp. 278–281, 2014.
- [162] J. Samanta, A. Mondal, S. Saha, S. Chakraborty, and A. Sengupta, “Oleic acid protects from arsenic-induced cardiac hypertrophy via AMPK/FoxO/NFATc3 pathway,” *Cardiovascular Toxicology*, vol. 20, no. 3, pp. 261–280, 2020.
- [163] R. Loying, R. Gogoi, N. Sarma et al., “Chemical Compositions, *in-vitro* antioxidant, antimicrobial, anti-inflammatory and cytotoxic activities of essential oil of *Acorus calamus*”

- L. Rhizome from north-east India,” *Journal of Essential Oil-Bearing Plants*, vol. 22, no. 5, pp. 1299–1312, 2019.
- [164] R. Akter, M. A. Satter, M. S. Khan, M. S. Rahman, and N. U. Ahmed, “Cytotoxic effect of five medicinal plants extracts using brine shrimp (*Artemia salina*) TEST,” *Bangladesh Journal of Scientific & Industrial Research*, vol. 47, no. 1, pp. 133–136, 2012.
- [165] M. R. Amin, R. Mondol, M. R. Habib, and M. T. Hossain, “Antimicrobial and cytotoxic activity of three bitter plants-*Enhydra fluctuans*, *Andrographis peniculata*, and *Clerodendrum viscosum*,” *Advanced Pharmaceutical Bulletin*, vol. 2, pp. 207–211, 2012.
- [166] M. Rahman, P. Sutro, F. Anika, and L. Ahmed, “Exploring the plant-derived bioactive substances as antidiabetic agent: an extensive review,” *Biomedicine & Pharmacotherapy*, vol. 152, Article ID 113217, 2022.
- [167] M. M. Rahman, M. R. Islam, S. Shohag et al., “The multifunctional role of herbal products in the management of diabetes and obesity: a comprehensive review,” *Molecules*, vol. 27, no. 5, pp. 1713–1737, 2022.
- [168] S. Mitra, F. Islam, R. Das et al., “Pharmacological potential of *Avicennia alba* leaf extract: an experimental analysis focusing on antidiabetic, anti-inflammatory, analgesic, and antidiarrheal activity,” *BioMed Research International*, vol. 2022, Article ID 7624189, 10 pages, 2022.
- [169] A. A. Sardar, Z. Khan, A. Perveen, and A. Zereen, “Appraisal of ethnobotanical uses of the wetland plants of Punjab, Pakistan,” *African Journal of Traditional, Complementary and Alternative Medicines*, vol. 12, no. 4, pp. 9–13, 2015.
- [170] V. Sharma, R. Sharma, D. N. S. Gautam, K. Kuca, E. Nepovimova, and N. Martins, “Role of Vacha (*Acorus calamus* Linn.) in neurological and metabolic disorders: evidence from ethnopharmacology, phytochemistry, pharmacology and clinical study,” *Journal of Clinical Medicine*, vol. 9, no. 4, p. 1176, 2020.
- [171] T. Z. Mazumder, “Phytochemical study of some traditional medicinal plants of north-east India,” *Agriculture and Environment*, vol. 2, no. 11, pp. 59–66, 2021.
- [172] T. K. Dua, S. Dewanjee, and R. Khanra, “Prophylactic role of *Enhydra fluctuans* against arsenic-induced hepatotoxicity via anti-apoptotic and antioxidant mechanisms,” *Redox Report*, vol. 21, no. 4, pp. 147–154, 2016.
- [173] T. T. Chai, K. F. Ooh, Y. Quah, and F. C. Wong, “Edible freshwater macrophytes: a source of anticancer and antioxidative natural products—a mini-review,” *Phytochemistry Reviews*, vol. 14, no. 3, pp. 443–457, 2015.
- [174] N. Buragohain, “Nutritional and medicinal value of some underutilized vegetable crops of north east India—a review,” *Indian Journal of Pure & Applied Biosciences*, vol. 8, no. 5, pp. 493–502, 2020.
- [175] R. M. B. D. Shanthakumari, “Determination of bioactive compounds from the extracts of *Acorus Calamus*,” *European Journal of Molecular and Clinical Medicine*, vol. 7, no. 11, 2021.
- [176] A. Bachheti, R. K. Bachheti, L. Abate, and A. Husen, “Current status of aloe-based nanoparticle fabrication, characterization and their application in some cutting-edge areas,” *South African Journal of Botany*, vol. 147, pp. 1058–1069, 2022.
- [177] A. Joshi, S. Ashutosh, R. K. Bachheti, A. Husen, and V. K. Mishra, “Plant-mediated synthesis of copper oxide nanoparticles and their biological applications book chapter,” *Nanomaterials and Plant Potential*, Springer, Cham, Switzerland, 2019.
- [178] R. K. Bachheti, A. Sharma, A. Bachheti, A. Husen, G. M. Shanka, and D. P. Pandey, “Nanomaterials from various forest tree species and their biomedical applications,” *Nanomaterials for Agriculture and Forestry Applications*, Elsevier, Amsterdam, Netherlands, 2020.
- [179] R. Kumar Bachheti, A. Fikadu, A. Bachheti, and A. Husen, “Biogenic fabrication of nanomaterials from flower-based chemical compounds, characterization and their various applications—a review,” *Saudi Journal of Biological Sciences*, vol. 27, no. 10, pp. 2551–2562, 2020.
- [180] R. K. Bachheti, Y. Godebo, A. Bachheti, M. O. Yassin, and A. Husen, “Root-based fabrication of metal/metal-oxide nanomaterials and their various applications,” *Nanomaterials for Agriculture and Forestry Applications*, Elsevier, Amsterdam, Netherlands, 2020.
- [181] P. Traiwacharanon, K. Timsorn, and C. Wongchoosuk, “Flexible room-temperature resistive humidity sensor based on silver nanoparticles,” *Materials Research Express*, vol. 4, 2017.
- [182] P. Mathur, S. Jha, S. Ramteke, and N. K. Jain, “Pharmaceutical aspects of silver nanoparticles,” *Artificial Cells, Nanomedicine, and Biotechnology*, vol. 46, no. sup1, pp. 115–126, 2018.
- [183] P. Kuppusamy, M. M. Yusoff, G. P. Maniam, and N. Govindan, “Biosynthesis of metallic nanoparticles using plant derivatives and their new avenues in pharmacological applications—an updated report,” *Saudi Pharmaceutical Journal*, vol. 24, no. 4, pp. 473–484, 2016.
- [184] A. A. Alfuraydi, S. Devanesan, M. Al-Ansari, M. S. AlSalhi, and A. J. Ranjitsingh, “Eco-friendly green synthesis of silver nanoparticles from the sesame oil cake and its potential anticancer and antimicrobial activities,” *Journal of Photochemistry and Photobiology B: Biology*, vol. 192, pp. 83–89, 2019.

## Research Article

# Inhibitory Effects of Rhein on Renal Interstitial Fibrosis via the SHH-Gli1 Signal Pathway

Yan Luo,<sup>1,2,3</sup> Juan Jiang,<sup>4</sup> Junxiong Cheng,<sup>2,3</sup> Chen Xuan,<sup>2,3</sup> Yu Xiong,<sup>2,3</sup> Weijian Xiong ,<sup>1</sup>  
Wenfu Cao,<sup>2,3</sup> and Ying Li <sup>1</sup>

<sup>1</sup>Chongqing Traditional Chinese Medicine Hospital, Chongqing 400021, China

<sup>2</sup>Chongqing Key Laboratory of Traditional Chinese Medicine for Prevention and Cure of Metabolic Diseases, Chongqing 400016, China

<sup>3</sup>College of Traditional Chinese Medicine, Chongqing Medical University, Chongqing 400016, China

<sup>4</sup>Chongqing University Cancer Hospital, Chongqing, China

Correspondence should be addressed to Weijian Xiong; [xiongfei086228@163.com](mailto:xiongfei086228@163.com) and Ying Li; [sabrina\\_pipi@163.com](mailto:sabrina_pipi@163.com)

Received 18 January 2022; Revised 21 March 2022; Accepted 11 April 2022; Published 5 August 2022

Academic Editor: Ruchika Garg

Copyright © 2022 Yan Luo et al. This is an open access article distributed under the Creative Commons Attribution License, which permits unrestricted use, distribution, and reproduction in any medium, provided the original work is properly cited.

**Background.** Rhein is the main extract of *Rheum palmatum* L., which has been proved to improve the renal function of chronic kidney disease, but its mechanism is not clear. Therefore, this experiment explored the potential pharmacological effect of rhein on renal interstitial fibrosis rats. **Methods.** This study explores the potential pharmacological action of rhein. In this work, we investigate the potential pharmacological action of rhein in unilateral urethral obstruction (UUO) rats. Thirty Sprague Dawley rats were randomly divided into three groups: sham, UUO, and rhein (rhein-treated UUO rats) groups. The left ureters of the UUO group rats were exposed and bluntly dissected. The rhein group rats were administered an intragastric gavage of rhein ( $2 \text{ mg}\cdot\text{kg}^{-1}\cdot\text{d}^{-1}$ ) for 14 d. Kidney function-related indicators were monitored in these rats, while indexes of pathologic aspects were determined histologically. The expression of  $\alpha$ -SMA, TGF- $\beta$ 1, SHH, Gli1, and Snail was quantified using real-time polymerase chain reaction and western blotting. The NRK-49F cells were incubated with and without SHH ( $100 \text{ ng}\cdot\text{ml}^{-1}$ ) for 48 hours. The SHH-activated NRK-49F cells were incubated with cyclopamine (CNP,  $20 \text{ }\mu\text{mol L}^{-1}$ ) or rhein ( $1 \text{ ng}\cdot\text{ml}^{-1}$ ). The Gli1 and Snail mRNA and protein level were detected. **Results.** In the in vivo experiment, the results exhibited that UUO caused renal pathological damages. However, these changes could be significantly reversed by the administration of rhein. Compared with the untreated UUO group, the rhein group showed reduced kidney tubular atrophy and necrosis, interstitial fibrosis, hyperplasia, and abnormal deposition of extracellular matrix. Rhein reduced the RNA and protein expression of SHH, Gli1, and Snail of the UUO rats. In the in vitro experiment, CNP or rhein treatment decreased the expression of Gli1 and Snail on mRNA and protein levels in SHH-induced NRK-49F cells, suggesting that CNP or rhein suppresses SHH-induced NRK-49F activation. Taken together, these results demonstrated that rhein suppresses SHH-Gli1-Snail signal pathway activation, with potential implications for the treatment of renal fibrosis. **Conclusions.** Treatment with rhein remarkably ameliorated renal interstitial fibrosis in UUO rats by regulating the SHH-Gli1-Snail signal pathway.

## 1. Introduction

Currently, chronic kidney disease (CKD) is the 16<sup>th</sup> cause of death worldwide. It has become a prominent public health issue in the world, with a global incidence of approximately 10–15% [1]. Once developed in irreversible end-stage kidney disease (ESRD), they can only be treated with dialysis and kidney transplants. Kidney fibrosis is the buildup of scar

within the parenchyma, and it represents the common final pathway of nearly all chronic and progressive nephropathies [2]. It has been proved that transforming growth factor  $\beta$ 1 (TGF- $\beta$ 1) secreted by renal tubular cells. TGF- $\beta$ 1 was identified to be the grandmaster that elicits numerous signals, which culminate in fibrosis and renal parenchymal loss. Importantly, TGF- $\beta$ 1 can induce activated renal interstitial fibroblasts, myofibroblasts, which are characterized by

$\alpha$ -smooth muscle actin ( $\alpha$ -SMA) expression [3]. The increased expression of TGF- $\beta$ 1 and  $\alpha$ -SMA is a manifestation of epithelial-to-mesenchymal transition (EMT). In the formation of renal interstitial fibrosis (RIF), EMT is believed to play an important role in organ fibrosis [4], chronic inflammation [5], tissue reconstruction [6], and various fibrotic diseases [7].

In recent years, SHH signal pathway has been proved to be closely related to tissue fibrosis, which involves liver, bile, lung, kidney, and other organs. It was found that SHH was almost not expressed in normal adult kidneys, while the expression of SHH in renal tubular epithelial cells was significantly upregulated in patients with CKD caused by various causes. This result has also been confirmed in various rat renal fibrosis models such as unilateral ureteral obstruction (UUO) [8]. These results suggest that SHH signal pathway activation is a common pathological result of various renal diseases. Consequently, inhibition of myofibroblast activation and SHH signal pathway may be an effective strategy to prevent renal fibrosis.

*Rheum palmatum* L., a type of traditional Chinese herb defecation-promoting purgative medicinal, has bitter and cold medicinal properties [9]. Rhein is a main bioactive component of *Rheum palmatum* L., which has been widely used for the treatment of chronic kidney-related diseases in the clinic [10]. Recent studies have shown that rhein has potent anti-autophagy [11], anti-apoptosis [12], and anti-fibrosis [13]. Rhein can remarkably improve renal interstitial fibrosis in vivo whether its potential mechanism may be related to the inhibition of SHH-Gli1-Snail signal pathway.

To investigate the mechanism of rhein and understand its potential antifibrosis effect on renal, the UUO model was used to simulate renal interstitial fibrosis in rats. Here, UUO causes subacute renal injury characterized by tubular cell injury, interstitial inflammation, and fibrosis, a well-known model to induce renal fibrosis in vivo [14]. The in vivo study aimed to investigate the pathological changes of renal fibrosis, and the effects of rhein on the expression of SHH, Gli1, and Snail proteins were analyzed. And the in vitro study aimed to investigate rhein on the expression of Gli1 and Snail on mRNA and protein levels, which activated with human SHH protein and rat NRK-49F cells. The activated renal fibrosis by SHH signal pathway and the protective mechanism antifibrosis of rhein were discussed in this study.

## 2. Materials and Methods

**2.1. Animals and Cells.** Seven-week-old thirty clean-grade male SD rats ( $200 \pm 20$ ) g were approved by the Animal Experimental Ethics Committee of Chongqing Medical University (Chongqing, China; Animal license No. SCXK: 2018-0003) and performed by the Guidelines of the Animal Care Committee of Chongqing Medical University. Normal rat kidney interstitial fibroblasts (NRK-49F) were purchased from the American Type Culture Collection (ATCC, Manassas, VA).

**2.2. Reagents and Instruments.** Reagents and instruments used for this study are as follows: rhein (Rhawn, Shanghai, China); cyclopamine (Selleck Chemicals, Houston, USA); human SHH protein (StemRD Inc, USA); antibodies against TGF- $\beta$ 1 and  $\alpha$ -SMA (Servicebio, Wuhan, China); antibodies against SHH, Gli1, Snail, and GAPDH (Affinity Biosciences, Jiangsu, China); PVDF membrane, BCA Protein Assay Kit, BeyoECL Moon kit (Beyotime Biotechnology, Shanghai, China); TRIzol (Takara Bio, Shiga, Japan); primers for qPCR (Servicebio, Wuhan, China); AU400 automatic biochemical analyzer (OLYMPUS, Tokyo, Japan); BX51T-PHD-J11 microscope (OLYMPUS Company, Tokyo, Japan); image acquisition system CMOS (OLYMPUS Company, Tokyo, Japan); Image-Pro Plus (National Institutes of Health, Bethesda, USA); and TEM (JEM1400PLUS, JEOL, Tokyo, Japan).

**2.3. Animal Experiments.** After one week of adaptive breeding, thirty male SD rats were randomly divided into three groups: sham group (sham operation rats), UUO group, and rhein group (rhein-treated UUO rats) with 10 rats in each group. Besides the sham group, the other two groups underwent the same surgical procedures to establish UUO model rats: after anesthesia with 2% sodium pentobarbital, the kidneys of rats were exposed, and then, the left ureter was double-ligated. Rats in the sham group were performed with sham operations without being ligated on left ureter. The rhein group rats were administered at  $2 \text{ mg} \cdot \text{kg}^{-1} \cdot \text{d}^{-1}$ , and rhein was dissolved in 0.5% carboxymethyl cellulose sodium (CMC-Na+) in H<sub>2</sub>O, through intragastric gavage for 14 d. The rats in the sham and model groups received intragastric administration of 0.5% CMC-Na+ ( $2 \text{ mg} \cdot \text{kg}^{-1} \cdot \text{d}^{-1}$ ) for 14 d. After 2 weeks, all rats were sacrificed. Blood and tissues were harvested from rats that were fasted for 12 h.

**2.4. In Vitro Experiments.** The NRK-49F cells were treated with 10% fetal bovine serum, 100 U/mL penicillin, 100 mg/L streptomycin, and 37°C in 5% CO<sub>2</sub> in the DMEM medium. Rhein was dissolved by dimethyl sulfoxide (DMSO). The cells were divided into four groups: the control group without any treatment, the SHH group (100 ng/L human SHH protein), the SHH + Rhein group (100 ng/L human SHH protein + 1 ng/ml rhein), and the SHH + CPN group (100 ng/L human SHH protein + 20  $\mu\text{mol/L}$  cyclopamine). When the cells grew to 80% ~ 90% fusion, the activation of cells was induced for 48 hours by 100 ng/L human SHH protein. The culture medium was discarded, the corresponding serum and reagents were added in each group, and the cells were collected 24 hours later. The expression of Gli1 and Snail in vitro was evaluated by western blot analysis or RT-PCR.

**2.5. Histopathological Analysis of Renal Tissue.** Rat renal tissue was first fixed in 4% paraformaldehyde for 48 h, embedded in paraffin, and further sectioned. The 3- $\mu\text{m}$ -thick sections obtained were dewaxed, treated with gradient

ethanol, and stained with hematoxylin-eosin (HE), Masson, and periodic acid-Schiff (PAS) stains. Pathological analysis of glomeruli and tubules was performed using a light microscope.

The interstitial score of the renal tubules was analyzed at a 200× magnification; ten tubules per visual field were observed. According to the range of renal tubular atrophy, tubular type, stromal cell infiltration, and fibrosis, scores from 0 to 3 were assigned: 0 for none; 1 for less than 25%; 2 for 25–50%; and 3 for 50–75% [15]. Photo images from each cortex were screened, and scores were added based on tubulointerstitial injury: tubular atrophy, tubular necrosis, and interstitial fibrosis [16, 17].

**2.6. Electron Microscopy.** The morphological and microstructural structures of kidneys, such as the glomerular basement membrane, mesangial cells, podocytes, endothelial cells, and collagen fibers in the interstitial tissue, were examined using transmission electron microscopy (TEM). The renal tissues from the rats were fixed in 2.5% glutaraldehyde and embedded in paraffin. The 70-nm-thick tissue sections were stained and observed by TEM.

**2.7. Immunohistochemistry.** The 3- $\mu\text{m}$ -thick renal tissue sections were incubated with citrate antigen retrieval solution for 20 min at 95°C. Thereafter, the sections were stained with a monoclonal antibody against transforming growth factor  $\beta$  (TGF- $\beta$ 1; dilution 1:500) and  $\alpha$ -smooth muscle actin ( $\alpha$ -SMA; dilution 1:500). The sections were incubated with goat anti-rabbit antibodies overnight and further, with a secondary antibody for 50 min. The positive areas were visualized using the DAB Kit. The integrated optical density of protein expression was calculated using the ImageJ software.

**2.8. Real-Time PCR.** According to the manufacturers' protocols, total RNA was extracted from renal tissue using TRIzol reagent, according to the manufacturer's instructions. Furthermore, RNA was reverse-transcribed into cDNA. The PCR cycling conditions were as follows: 94°C for 5 min, followed by 95°C for 30 s and 57°C for 30 s, and then 32 cycles of 72°C for 10 min. Gene expression levels were calculated from the standard curve using the expression of the glyceraldehyde 3-phosphate dehydrogenase (GAPDH) gene as a reference.

**2.9. Western Blotting.** Renal tissue proteins were extracted, quantified, and visualized by western blotting through electrophoresis, membrane transfer, and antibody incubation. Primary antibodies (1:1,000 dilution) against SHH, Gli1, and Snail were used, and the membranes were incubated overnight at 4°C on a shaking bed. Furthermore, the secondary antibody (1:2,000 dilution) was added and incubated at 37°C for 120 min. After applying the ECL color reagent and performing dark chamber exposure imaging, the gray value of the images was analyzed using ImageJ software (National Institutes of Health, Bethesda, MD).

**2.10. Statistical Analysis.** Data analysis was carried out using SPSS 17.0 software (SPSS Inc., Chicago, United States). Data are presented as mean  $\pm$  standard deviation. Variables in each group were tested to determine whether they were normally distributed. The statistical analyses were performed by one-way analysis of variance followed by a least significant difference test or Dunnett's multiple comparison test.  $p < 0.05$  was considered statistically significant.

### 3. Results

**3.1. Effects of Rhein Improves Histopathological Changes.** Renal fibrosis is characterized by glomerulosclerosis, renal tubulointerstitial fibrosis, renal vascular fiber sclerosis, and excessive accumulation and deposition of extracellular matrix (ECM). The pathological manifestations were renal tubular dilatation with atrophy (green arrow); renal tubular epithelial cell edema (blue arrow); cytoplasmic loose staining, lymphocyte proliferation, and infiltration (yellow arrow); endothelial cell proliferation, ECM component proliferation, renal interstitial matrix proliferation, and mesangial area expansion (orange arrow); thickening of the basement membrane (red arrow); and foot process fusion loss (brown arrow). In this research, we evaluated the pathological changes of the kidney from different perspectives by renal appearance, HE or PAS staining, and transmission electron microscopy. The positive parts of the lesions are marked with arrows in the UUO group and the rhein group. Compared with the UUO group, rhein ameliorates these pathological injuries (Figure 1).

**3.2. The Effect of Rhein in Alleviate Renal Fibrosis.** Renal fibroplasia was evaluated by Masson staining. The main components of the ECM examined the expression of TGF- $\beta$ 1 and  $\alpha$ -SMA by immunohistochemistry. In Masson staining, collagen fibers are shown in blue (purple arrow). Compared with the sham group, there was a significant accumulation of collagen fibers in the kidney tissue of the UUO group. Compared with the sham group, the ECM of TGF- $\beta$ 1 and  $\alpha$ -SMA expression shown in yellow was significant accumulation. These results confirm that our experimental model was successful and indicates that rhein delivery alleviates the pathological changes and renal fibroplasia observed in UUO rats (Figure 2).

**3.3. The Effects of Rhein on SHH-Gli1-Snail Signal Pathway.** The SHH signal pathway is an important pathway regulating fibrosis. Inhibition of the SHH signal pathway is associated with the inhibition of renal fibrosis. We examined the expression of SHH, Gli1, and Snail downstream in the renal. In comparison with the sham group, the expression of SHH, Gli1, and Snail of the UUO group was increased significantly ( $p < 0.01$ ). In comparison with the UUO group, the expression of SHH, Gli1, and Snail of the rhein group was decreased significantly ( $p < 0.05$ ). The result suggests that rhein can inhibit activation of the SHH signal pathway (Figure 3).



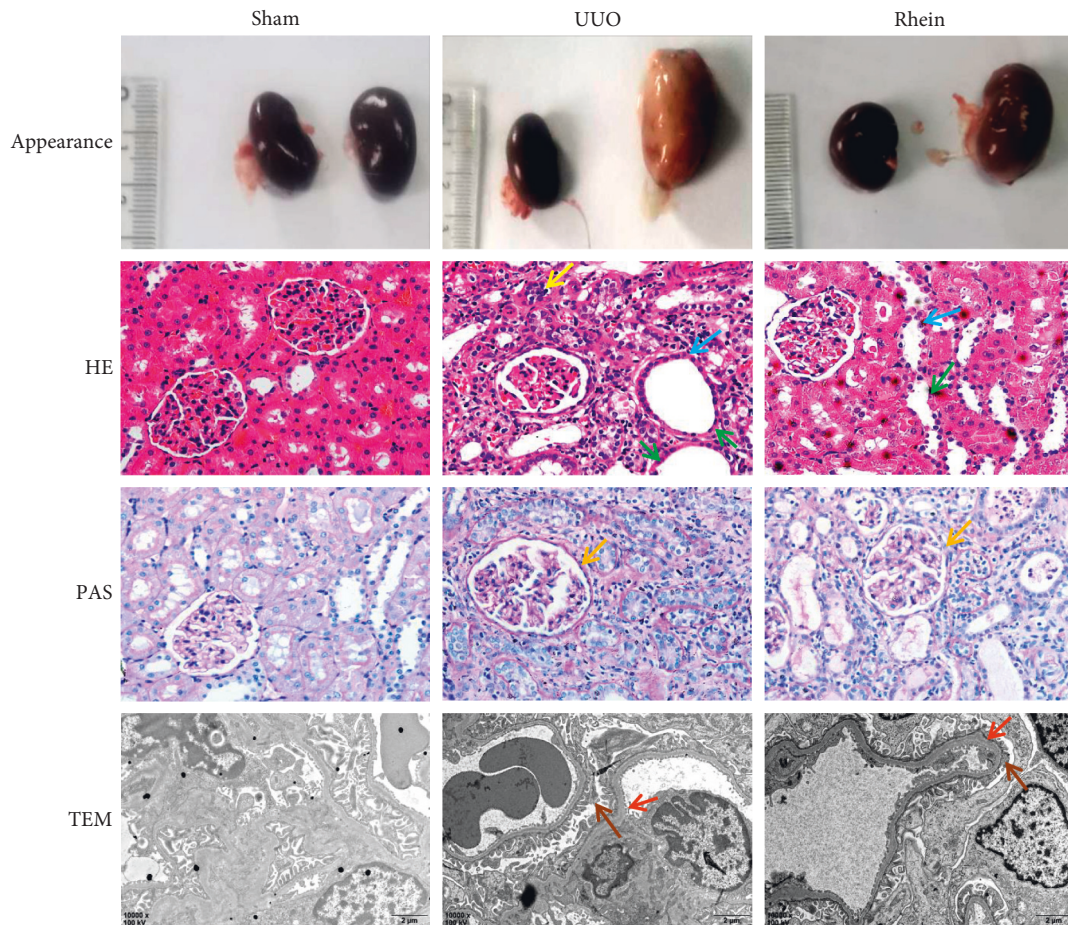


FIGURE 1: Rhein attenuated renal histological damage. Pathological changes in the renal tissues were analyzed using renal appearance, hematoxylin-eosin (HE,  $\times 200$ ), periodic acid-Schiff (PAS,  $\times 200$ ) staining, and transmission electron microscopy (TEM,  $\times 10,000$ ). The pathological manifestations of renal fibrosis include renal tubular dilatation with atrophy (green arrow), renal tubular epithelial cell edema (blue arrow), lymphocyte proliferation and infiltration (yellow arrow), mesangial area expansion (orange arrow), thickening of the basement membrane (red arrow), and loss of foot process fusion (brown arrow).

**3.4. The Effects of Rhein on SHH Pathway In Vitro Experimental Results.** Compared with the sham group, the expression of Gli1 and Snail in NRK-49F cells stimulated by SHH (100 ng/ml) was significantly increased. SHH markedly induced de novo Gli1 and Snail expression in renal interstitial fibroblast NRK-49F cells. The results showed that simultaneous incubation with cyclopamine (CNP, 20  $\mu\text{mol/L}$ ) repressed SHH-initiated Gli1 and Snail expression of NRK-49F cells ( $p < 0.05$ ). And incubation with rhein (1 ng/ml) also had the same effect as CNP ( $p < 0.05$ ). (Figure 4).

#### 4. Discussion

Rhein is one of the anthraquinone active components in *Rheum palmatum* L. *Rheum palmatum* L. is widely used in TCM as an indispensable and specific treatment for curing CKD stages 1–5 and shows good curative effects. Rhein possesses multiple pharmacological activities, including antioxidation, anticancer, antiviral, anti-inflammatory, antifibrosis, anti-hyperuricemic, and purgative effects [18, 19]. Rhein could attenuate kidney damage in diabetic rats by improving glucose metabolism abnormality,

reversing insulin resistance and dyslipidemia, and effectively preventing diabetic nephropathy [20]. Numerous research suggests that rhein protected kidney through various signal pathways involvement [11, 21, 22].

Renal fibrosis is a common pathological pathway leading to end-stage renal disease. UUO surgery can cause renal pathological changes, involving periglomerular fibrosis, rupture of glomerular capillary wall in renal capsule, blood flowing into renal capsule and coagulation, resulting in proliferation of epithelial cells, proliferation of podocytes, infiltration of monocytes, production of a variety of fibrogenic cytokines, proliferation and fibrosis of fibroblasts, and inward compression of capillaries, or the fusion of glomerular capillaries and renal capsule basement membrane is called balloon adhesion, which pulls the capillaries to the renal capsule basement membrane to form glomerulosclerosis. The basement membrane of renal vesicles was thickened, renal vesicles were dilated, and capillary loops were squeezed [23]. During glomerular ischemia, the early manifestation is ischemic shrinkage, and in the late stage, due to ischemia, the capillary wall is hypoxic, resulting in increased permeability, plasma protein leakage and

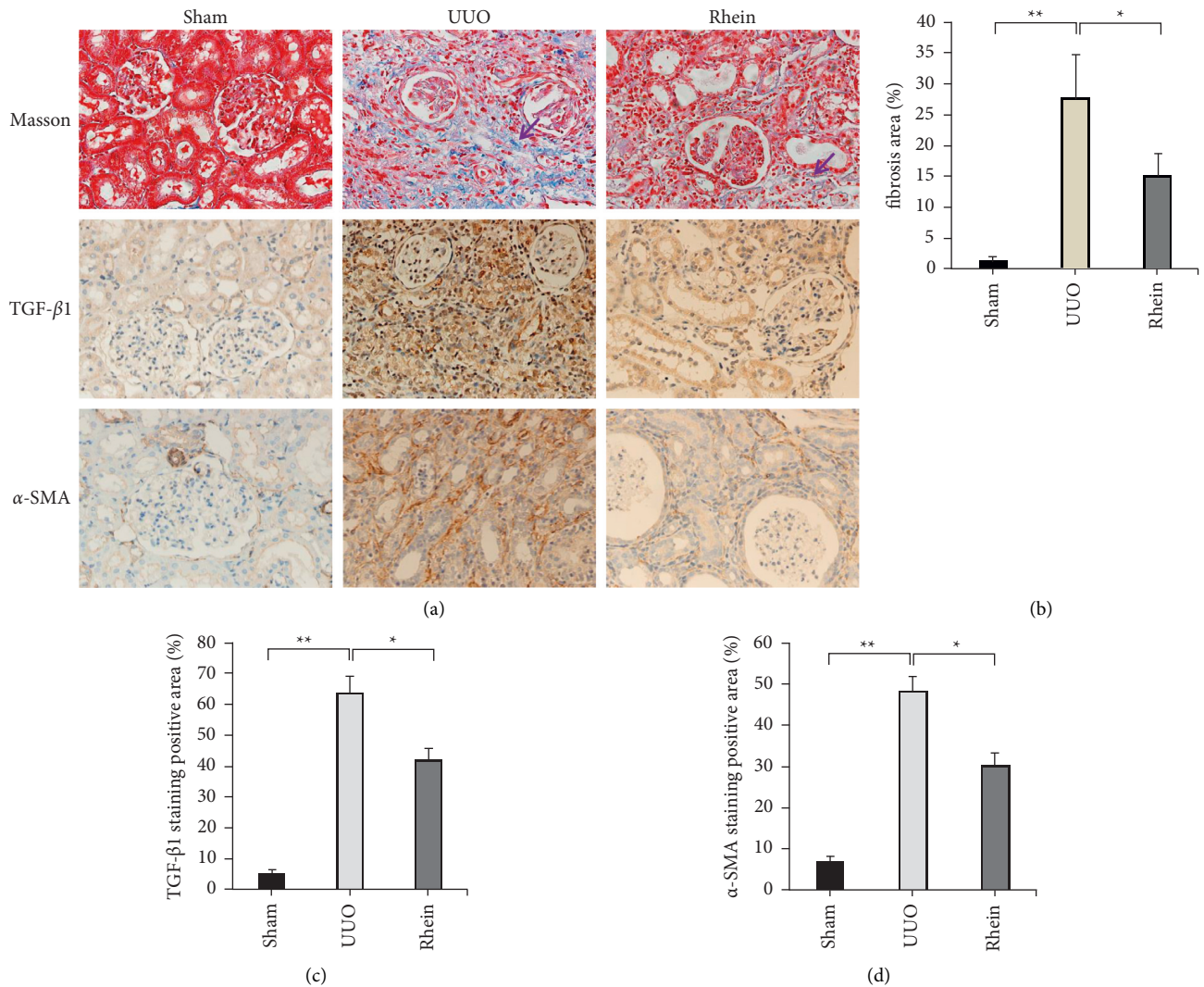


FIGURE 2: Rhein improves renal fibrosis. Collagen fiber deposition (purple arrow) was observed in Masson staining. (b) ImageJ software was used to calculate the degree of renal fibrosis. ((c), (d)) Image-pro plus software was used to statistically analyze immunohistochemical staining results of TGF- $\beta$ 1 and  $\alpha$ -SMA, respectively. \*  $p < 0.05$ , \*\*  $p < 0.01$ .

condensation in the renal capsule, and finally hardening. The blood supply of renal tubules comes from glomerulus, so renal tubules are more vulnerable to ischemic injury, cytoplasmic turbidity and swelling, renal interstitial edema, inflammatory cell infiltration, and renal interstitial fibrosis (RIF) [14].

Renal interstitial fibrosis (RIF) is the main pathological change of multiple chronic kidney disease (CKD). It is a common pathway that ultimately leads to end-stage renal disease (ESRD) [2, 24]. The extent and severity of RIF are highly correlated with the degree of renal dysfunction [25]. Therefore, improving RIF is of great significance to slow down and reverse the progression of CKD. The occurrence and development process of RIF mainly includes the following four links: regulation of cytokine expression, inflammatory cell infiltration, cell proliferation and epithelial-mesenchymal transition (EMT), and abnormal accumulation of extracellular matrix (ECM) [26]. EMT is a critical process of kidney fibrosis by which epithelial cells lose their

epithelial characteristics and acquire the mesenchymal features, and the transformation of renal tubule epithelial cells, fibroblasts and other cells into myofibroblasts, and the formation of ECM. In the formation of RIF, EMT is believed to play an important role in organ fibrosis [4]. Renal EMT consists of four key steps: loss of adhesion between epithelial cells; newly synthesized  $\alpha$ -smooth muscle actin ( $\alpha$ -SMA) expression and actin recombination; rupture of basement membrane of renal tubules; and the ability of cells to migrate and invade.  $\alpha$ -SMA is a specific marker of interstitial cells, which is expressed at a low level in normal tissues and organs but upregulated in tissues or cells during interstitial trans-differentiation. Studies have shown that the level of  $\alpha$ -SMA-positive expression is positively correlated with the degree of tissue fibrosis, and a large amount of  $\alpha$ -SMA expression is a marker of epithelial and mesenchymal cell transformation [27].

EMT in renal tubule has been demonstrated in various animal models of renal interstitial fibrosis, such as unilateral



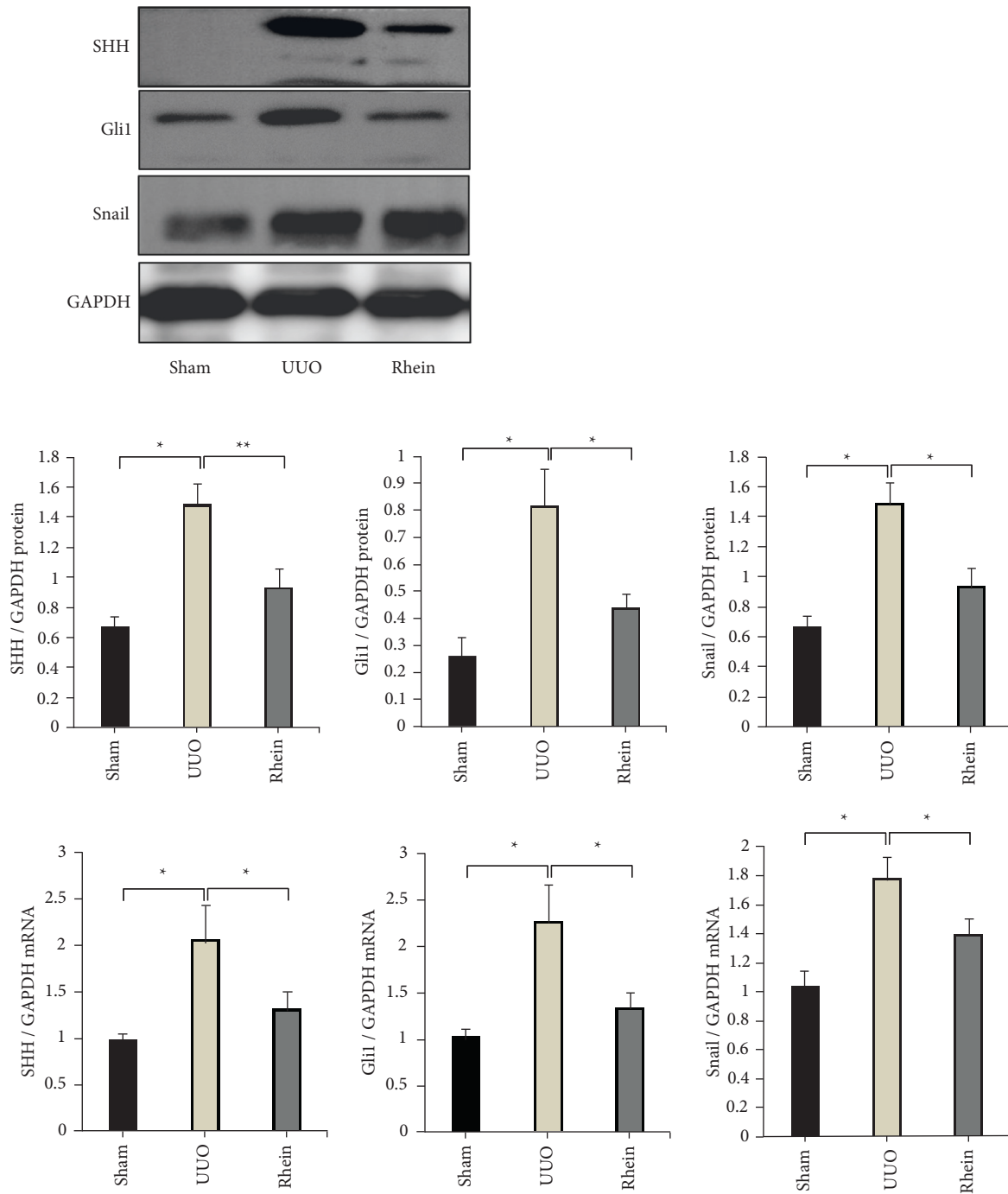


FIGURE 3: Inhibitory effect of rhein on SHH signaling pathway in UUO rats. Rhein group rats were administered rhein  $2 \text{ mg}\cdot\text{kg}^{-1}\cdot\text{d}^{-1}$  by oral gavage for 14-d sham group, and UUO group rats were administered equal volumes of water. SHH, Gli1, and Snail protein and mRNA expression levels were determined by western blotting and RT-PCR. Data are presented as mean  $\pm$  SEM. \*  $p < 0.05$ , \*\*  $p < 0.01$ .

ureteral obstructive (UUO), nephropathy, and diabetic nephropathy [28]. Transforming growth factor  $\beta 1$  (TGF- $\beta 1$ ) is a key player in the development of fibrosis. TGF- $\beta 1$  is expressed in all mammalian cells and is an important cytokine to induce EMT [29]. TGF- $\beta$  is a secretory stimulating protein, which can affect autocrine and paracrine of cells. In some cultured epithelial cells, EMT can be induced by TGF-

$\beta 1$  stimulation alone. TGF- $\beta$  mainly includes three types, namely, TGF- $\beta 1$ , TGF- $\beta 2$ , and TGF- $\beta 3$ . TGF- $\beta 1$  plays an important regulatory role in the occurrence and development of pathological processes, including tumor and fibrosis [30]. The present study demonstrated the fibrotic tissue and extracellular matrix were significantly increased in the UUO group. After administration of rhein, the expression of renal

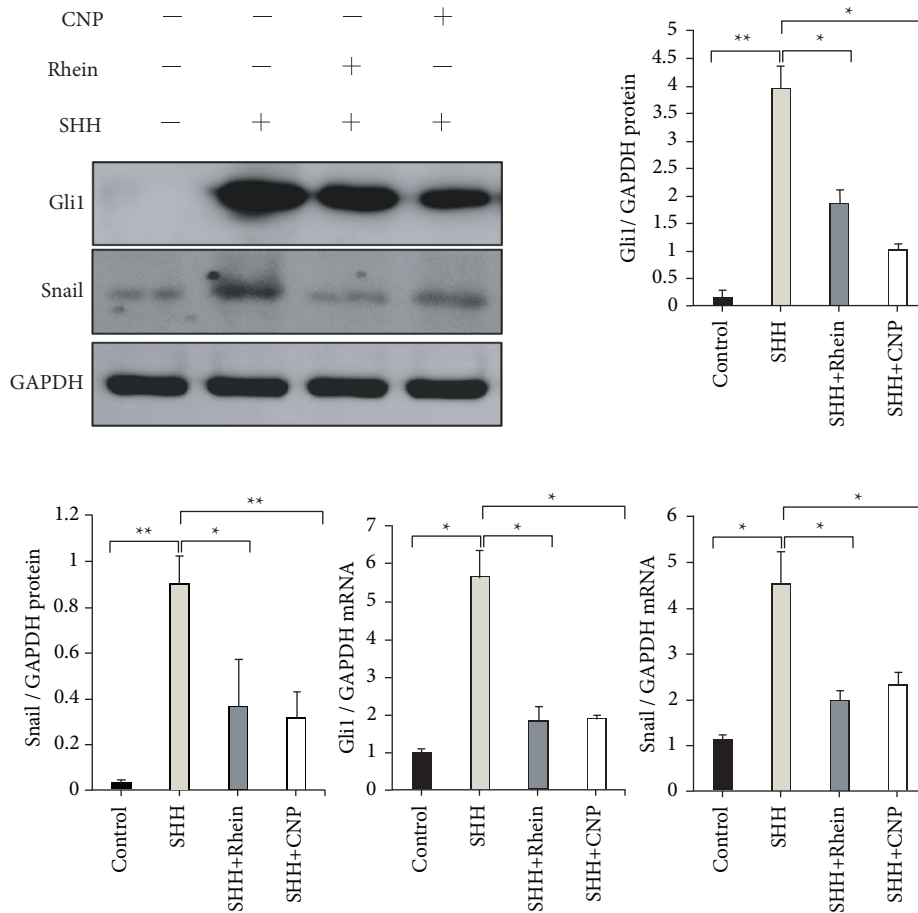


FIGURE 4: Rhein inhibits SHH signaling pathway in NRK-49F cells activated by SHH. Western blot and qPCR analysis show the expression of Gli1 and Snail increased in NRK-49F cells induced by SHH ( $100 \text{ ng}\cdot\text{ml}^{-1}$ ) for 48 hours. The NRK-49F cells were incubated with SHH in the presence of rhein ( $1 \text{ ng}\cdot\text{ml}^{-1}$ ) or CNP ( $1 \text{ ng}\cdot\text{ml}^{-1}$ ), and the expression of Gli1 and Snail mRNA and protein decreased. Data are presented as mean  $\pm$  SEM. \* $p < 0.05$ , \*\* $p < 0.01$ .

fibrin TGF- $\beta$ 1 and  $\alpha$ -SMA decreased significantly, and the thickening of basement membrane was suppressed than that in the model group.

Activation of SHH signal pathway can induce the transformation of rat renal fibroblasts into myofibroblast phenotype. Studies have shown that sonic hedgehog (Shh) signal pathway is closely related to various organ fibroses [31]. The pathway is composed of patched SHH ligands, cell membrane receptors (Ptc), smoothened (SMO) protein, and Gli1 (Gli1, Gli2 and Gli3) downstream transcription factors. SHH can hardly be detected in normal people. When fibrosis occurs, the expression of SHH is increased, which can bind to Ptc and remove the inhibitory effect of Pct on SMO. Increased SMO expression stimulates increased downstream Gli1 expression, which enters the nucleus in full-length form and initiates transcription of target genes. Gli1 is a transcription target of hedgehog signal transduction pathway, and its activation is a reliable indicator of SHH signal activity. The SHH-Gli1 pathway participates in the process of RIF by promoting cell proliferation [32]. Studies in Gli1 knockout rats have shown that the SHH-Gli1 pathway is essential in organ fibrosis [33]. Recent studies have found that the SHH-Gli1 pathway can induce the expression of the

transcription factor Snail [34], thereby activating intracellular signal transduction pathways that upregulate selected zinc finger (e.g., Snail) transcription factors and induce EMT. Studies have confirmed that Snail is an important signal molecule that triggers EMT and directly participates in the occurrence and development of RIF [32]. Study showed that TGF- $\beta$  activated crosstalk among divergent signal pathways to Gli1 that initializes and maintains Snail expression. And Snail functions as a critical integrator of information from TGF- $\beta$ 1 signal distributed through upstream pathways [35]. TGF- $\beta$ 1 promotes the process of EMT by inducing the expression of Snail, thus promoting renal fibrosis. In the process of EMT, multiple signal pathways play a role, upregulating transcription factors and promoting mesenchymal transformation of epithelial cells. Among them, the nuclear transcription factor Snail participates in the signal transduction process of multiple signal pathways including TGF- $\beta$ 1 pathway and can induce EMT in epithelial cells, which plays an important role in the activation process of myofibroblast [36]. Lovisa [37] found that in the mouse renal fibrosis model, Snail expression was abundant in renal tubular epithelial cells within the fibrosis lesion. After the deletion of Snail gene in renal tubular

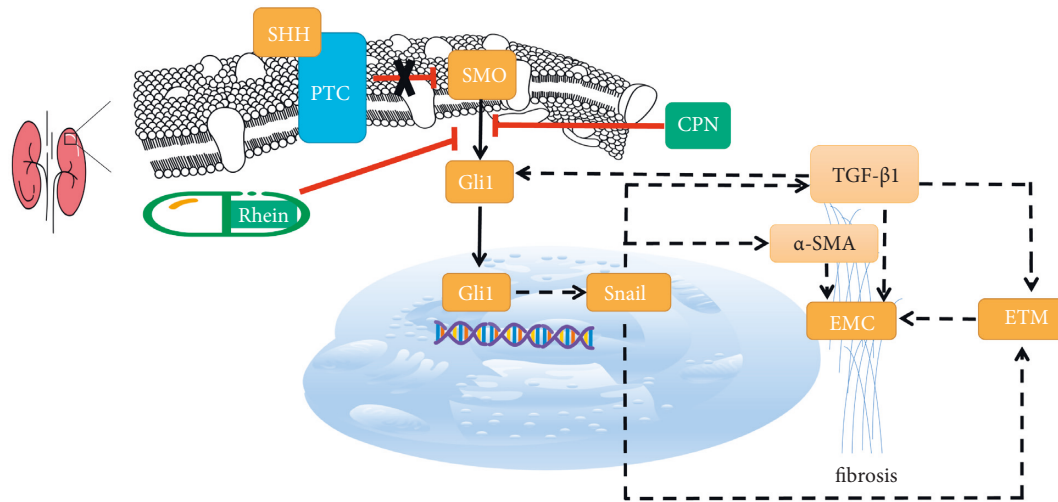


FIGURE 5: Schematic diagram of SHH signal pathway on renal fibrosis process.

epithelial cells, EMT of renal tubular epithelial cells was inhibited and renal fibrosis was alleviated (Figure 5).

The Snail family is a zinc finger transcription factor, which was first discovered in *Drosophila* gene in 1984. There are more than 50 members of the family. The vertebrate Snail family consists of two members: Snail (Snail1) and Slug (Snail2). Recently, it has been found that in addition to preventing expression of mesodermal and ectodermal genes in the mesoderm anlage, Snail also take party in cellular metabolism functions, just as regulating cell differentiation, motility and apoptosis. Studies have shown that Snail can promote EMT. Snail can upregulate the expression of marker proteins  $\alpha$ -SMA, myofilin, and fibronectin in mesenchymal cells. A large number of studies have confirmed that Snail is an important signal molecule that triggers EMT and directly participates in the occurrence and development of RIF. In the *in vivo* study, the expression of SHH, Gli1, and Snail was significantly increased in the UUO group, and the expression of SHH, Gli1, and Snail mRNA or protein was decreased after rhein treatment. The results suggest that rhein can reduce the expression of Gli1 and Snail by inhibiting SHH signal pathway, thus reducing the EMT and fibrosis in renal. The *in vitro* experiment showed that the activation of SHH signal pathway could significantly induce the expression of Gli1 and Snail in NRK-49F ( $p < 0.05$ ). Adding CPN to block the SHH pathway could inhibit the upregulation of Gli1 and Snail in rat renal fibroblasts induced by SHH protein. The addition of rhein also inhibited the upregulation of Gli1 and Snail. Therefore, we hypothesized that the SHH signal pathway may promote the phenotypic transformation of NRK-49F by inducing upregulation of Gli1 and Snail expression. The antifibrosis effect of rhein may be related to the inhibition of SHH-Gli1-Snail signal pathway.

## 5. Conclusion

Our experimental data demonstrated that ingestion of rhein can modulate the pathological changes observed in UUO

rats. Rhein was found to inhibit the SHH-Gli1-Snail signal pathway, which alleviated renal fibrosis in rhein-treated UUO rats. Hence, our findings reveal potential therapeutic targets for RIF and provide new perspectives on the pharmacological action of rhein during RIF treatment.

## Abbreviations

CKD:	Chronic kidney disease
RIF:	Renal interstitial fibrosis
UUO:	Unilateral urethral obstruction
TGF- $\beta$ 1:	Transforming growth factor $\beta$ 1
$\alpha$ -SMA:	$\alpha$ -Smooth muscle actin
EMT:	Epithelial-to-mesenchymal transition
ECM:	Extracellular matrix
ESRD:	End-stage kidney disease
SHH:	Sonic hedgehog
NRK-49F:	Normal rat kidney interstitial fibroblasts
Gli1:	Glioma-related cancer gene homologous proteins 1
Snail:	Transcriptional factor Snail.

## Data Availability

The datasets generated and/or analyzed during this study are available from the corresponding author upon reasonable request.

## Ethical Approval

All animal experiments were approved by the Animal Experimental Ethics Committee of Chongqing Medical University (Chongqing, China) (animal license no. SCXK:2018-0003) and performed by the Guidelines of the Animal Care Committee of Chongqing Medical University.

## Conflicts of Interest

The authors declared that they have no conflicts of interests.

## Acknowledgments

This research was supported by grants from the National Natural Science Foundation of China (Grant nos. 81573860 and 81904012) and the Chongqing Province Natural Scientific Foundation (Grant nos. cstc2021jxjlAX0003, cstc2019jxjl130022, and cstc2018jcyjAX0818).

## References

- [1] A. Levin, M. Tonelli, J. Bonventre et al., "Global kidney health 2017 and beyond: a roadmap for closing gaps in care," *Research and Policy*, vol. 390, no. 10105, pp. 1888–1917, 2017.
- [2] B. D. Humphreys, "Mechanisms of Renal Fibrosis," *Annual Review of Physiology*, vol. 80, pp. 309–326, 2018.
- [3] J. Zhang, H. Chen, X. Weng et al., "RCAN1.4 attenuates renal fibrosis through inhibiting calcineurin mediated nuclear translocation of NFAT2," *Cell Death Discovery*, vol. 7, no. 1, p. 317, 2021.
- [4] Y. Zhang, K. Li, Y. Li et al., "Profibrotic mechanisms of DPP8 and DPP9 highly expressed in the proximal renal tubule epithelial cells," *Pharmacological Research*, vol. 169, Article ID 105630, 2021.
- [5] Z. Gui, C. Suo, Z. Wang et al., "Impaired atg16l-dependent autophagy promotes renal interstitial fibrosis in chronic renal graft dysfunction through inducing end MT by NF- $\kappa$ B signal pathway," *Frontiers in Immunology*, vol. 12, Article ID 650424, 2021.
- [6] M. Zhao, L. Kong, Y. Liu, and H. Qu, "dbEMT: an epithelial-mesenchymal transition associated gene resource," *Scientific Reports*, vol. 5, no. 1, Article ID 11459, 2015.
- [7] T. Weng, D. Yan, D. Shi et al., "The MSP RON pathway regulates liver fibrosis through transforming growth factor beta dependent epithelial mesenchymal transition," *Liver International*, vol. 41, no. 8, pp. 1956–1968, 2021.
- [8] M. Edeling, G. Ragi, S. Huang, H. Pavenstädt, and K. Susztak, "Developmental signalling pathways in renal fibrosis: the roles of Notch, Wnt and Hedgehog," *Nature Reviews Nephrology*, vol. 12, no. 7, pp. 426–439, 2016.
- [9] K. Takayama, S. Maehara, N. Tabuchi, and N. Okamura, "Anthraquinone containing compound in rhubarb prevents indole production via functional changes in gut microbiota," *Journal of Natural Medicines*, vol. 75, no. 1, pp. 116–128, 2021.
- [10] W. Yu, W. Yang, M. Y. Zhao, and X. L. Meng, "Functional metabolomics analysis elucidating the metabolic biomarker and key pathway change associated with the chronic glomerulonephritis and revealing action mechanism of rhein," *Frontiers in Pharmacology*, vol. 11, Article ID 554783, 2020.
- [11] Y. Tu, L. Gu, D. Chen et al., "Rhein inhibits autophagy in rat renal tubular cells by regulation of AMPK/mTOR signaling," *Scientific Reports*, vol. 7, no. 1, Article ID 43790, 2017.
- [12] Y. Chen, L. Mu, L. Xing, S. Li, and S. Fu, "Rhein alleviates renal interstitial fibrosis by inhibiting tubular cell apoptosis in rats," *Biological Research*, vol. 52, no. 1, p. 50, 2019.
- [13] Q. Zhang, S. Yin, L. Liu, Z. Liu, and W. Cao, "Rhein reversal of DNA hypermethylation-associated Klotho suppression ameliorates renal fibrosis in mice," *Scientific Reports*, vol. 6, no. 1, Article ID 34597, 2016.
- [14] A. Ucerro, A. Benito-Martin, M. Izquierdo et al., "Unilateral ureteral obstruction: beyond obstruction," *Nephrology, Unilateral Ureteral Obstruction: Beyond Obstruction*, vol. 46, no. 4, pp. 765–776, 2014.
- [15] L. Yang, T. Y. Besschetnova, C. R. Brooks, J. V. Shah, and J. V. Bonventre, "Epithelial cell cycle arrest in G2/M mediates kidney fibrosis after injury," *Nature Medicine*, vol. 16, no. 5, pp. 535–543, 2010.
- [16] H. Cheng, X. Fan, W. E. Lawson, P. Pauksakon, and R. C. Harris, "Telomerase deficiency delays renal recovery in mice after ischemia-reperfusion injury by impairing autophagy," *Kidney International*, vol. 88, no. 1, pp. 85–94, 2015.
- [17] X. Wan, L. Hou, L. Zhang et al., "IKK $\alpha$  is involved in kidney recovery and regeneration of acute ischemia/reperfusion injury in mice through IL10-producing regulatory T cells," *Disease Models and Mechanisms*, vol. 8, no. 7, pp. 733–742, 2015.
- [18] C. Shen, Z. Zhang, T. Xie et al., "Rhein suppresses lung inflammatory injury induced by human respiratory syncytial virus through inhibiting NLRP3 inflammasome activation via NF- $\kappa$ B pathway in mice," *Frontiers in Pharmacology*, vol. 10, p. 1600, 2019.
- [19] Z. Meng, Y. Yan, Z. Tang et al., "Anti-hyperuricemic and nephroprotective effects of rhein in hyperuricemic mice," *Planta Medica*, vol. 81, no. 04, pp. 279–285, 2015.
- [20] W. Chen, B. Chang, Y. Zhang, P. Yang, and L. Liu, "Rhein promotes the expression of SIRT1 in kidney tissues of type 2 diabetic rat," *Chinese Journal of Cellular and Molecular Immunology*, vol. 31, no. 5, pp. 615–619, 2015.
- [21] J. Hu, Z. Yang, H. Wu, and D. Wang, "Rhein attenuates renal inflammatory injury of uric acid nephropathy via lincRNA-Cox2/miR-150-5p/STAT1 axis," *International Immunopharmacology*, vol. 85, Article ID 106620, 2020.
- [22] X. Wu, M. Liu, G. Wei et al., "Renal protection of rhein against 5/6 nephrectomied-induced chronic kidney disease: role of SIRT3-FOXO3 $\alpha$  signalling pathway," *Journal of Pharmacy and Pharmacology*, vol. 72, no. 5, pp. 699–708, 2020.
- [23] I. Sörensen, N. Susnik, T. Inhester et al., "Fibrinogen, acting as a mitogen for tubulointerstitial fibroblasts, promotes renal fibrosis," *Kidney International*, vol. 80, no. 10, pp. 1035–1044, 2011.
- [24] S. Djudjaj and P. Boor, "Cellular and molecular mechanisms of kidney fibrosis," *Molecular Aspects of Medicine*, vol. 65, pp. 16–36, 2019.
- [25] B. C. Liu, T. T. Tang, and H. Y. Lan, "Renal tubule injury: a driving force toward chronic kidney disease," *Kidney International*, vol. 93, no. 3, pp. 568–579, 2018.
- [26] M. C. Kuo, W. A. Chang, L. Y. Wu, Y. C. Tsai, and Y. L. Hsu, "Hypoxia-induced epithelial-to-mesenchymal transition in proximal tubular epithelial cells through miR-545-3p-TNFSF10," *Biomolecules*, vol. 11, no. 7, Article ID 1032, 2021.
- [27] J. Zeng and X. Bao, "Tanshinone IIA attenuates high glucose-induced epithelial-to-mesenchymal transition in HK-2 cells through VDR/Wnt/ $\beta$ -catenin signaling pathway," *Folia Histochemica et Cytobiologica*, vol. 59, no. 4, pp. 259–270, 2021.
- [28] H. Zhang, J. Xing, and L. J. H. Zhao, "Lysine-specific demethylase 1 induced epithelial-mesenchymal transition and promoted renal fibrosis through jagged-1/notch signaling pathway," *Human and Experimental Toxicology*, vol. 40, pp. S203–S214, 2021.
- [29] V. Cernaro, A. Lacquaniti, V. Donato, M. R. Fazio, A. Buemi, and M. J. N. Buemi, "Association, fibrosis, regeneration and cancer: what is the link?" *Nephrology Dialysis Transplantation*, vol. 27, no. 1, pp. 21–27, 2012.
- [30] D. M. Gonzalez and D. Medici, "Signaling mechanisms of the epithelial-mesenchymal transition," *Science Signaling*, vol. 7, no. 344, p. re8, 2014.
- [31] D. Zhou, R. J. Tan, and Y. Liu, "Sonic hedgehog signaling in kidney fibrosis: a master communicator," *Science China Life Sciences*, vol. 59, no. 9, pp. 920–929, 2016.

- [32] Y. Bai, H. Lu, C. Lin et al., “Sonic hedgehog-mediated epithelial-mesenchymal transition in renal tubulointerstitial fibrosis,” *International Journal of Molecular Medicine*, vol. 37, no. 5, pp. 1317–1327, 2016.
- [33] M. Zhang, L. Gao, Y. Ye, and X. Li, “Advances in glioma-associated oncogene (GLI) inhibitors for cancer therapy,” *Investigational New Drugs*, vol. 40, pp. 370–388, 2021.
- [34] K. B. Heiden, A. J. Williamson, M. E. Doscas et al., “The sonic hedgehog signaling pathway maintains the cancer stem cell self-renewal of anaplastic thyroid cancer by inducing Snail expression,” *Journal of Clinical Endocrinology and Metabolism*, vol. 99, no. 11, pp. E2178–E2187, 2014.
- [35] J. Zhang, X. J. Tian, Y. J. Chen, W. Wang, S. Watkins, and J. Xing, “Pathway crosstalk enables cells to interpret TGF- $\beta$  duration,” *Npj Systems Biology and Applications*, vol. 4, no. 1, p. 18, 2018.
- [36] J. Su, S. M. Morgani, C. J. David et al., “TGF- $\beta$  orchestrates fibrogenic and developmental EMTs via the RAS effector RREB1,” *Nature*, vol. 577, no. 7791, pp. 566–571, 2020.
- [37] S. Lovisa, E. Fletcher-Sananikone, H. Sugimoto et al., “Endothelial to mesenchymal transition compromises vascular integrity to induce Myc-mediated metabolic reprogramming in kidney fibrosis,” *Science Signaling*, vol. 13, no. 635, Article ID eaaz2597, 2020.

## Research Article

# Effect and Mechanism of Flavored Tongxie Yaofang Decoction for Diarrheal Irritable Bowel Syndrome under Intestinal Microecology

Shunyong He, Qiong Lin, Jianfeng Huang, Lin Zheng, Jinmei Lai, and Chaoyuan Chen 

The Affiliated People's Hospital of Fujian University of Traditional Chinese Medicine, Fuzhou 350004, Fujian, China

Correspondence should be addressed to Chaoyuan Chen; zhenbaya483484@163.com

Received 7 March 2022; Revised 16 June 2022; Accepted 8 July 2022; Published 2 August 2022

Academic Editor: Ruchika Garg

Copyright © 2022 Shunyong He et al. This is an open access article distributed under the Creative Commons Attribution License, which permits unrestricted use, distribution, and reproduction in any medium, provided the original work is properly cited.

This research was to analyze the effect of flavored Tongxie Yaofang on diarrheal irritable bowel syndrome (IBS) by the situation of intestinal microecology. The treatment mechanism was analyzed, so as to provide a more effective treatment method for patients clinically. 60 IBS patients were selected as the research objects and were divided according to the different treatment methods. For the control group ( $n = 20$  cases), oral pinaverium bromide tablets were given. For the treatment group ( $n = 40$  cases), the flavored Tongxie Yaofang decoction was given in addition to conventional treatment. The curative effects on the two groups of patients were evaluated in combination with the changes in intestinal microecology. With the syndrome score, the total effective rate of the treatment group (92.5%) was obviously superior to the control group (80%) ( $P < 0.05$ ). The clinical symptoms such as abdominal pain, abdominal distension, and diarrhea in the treatment group were significantly relieved after treatment in contrast to the control group ( $P < 0.05$ ). Intestinal Bifidobacterium, *Escherichia coli*, and Bifidobacterium/*Escherichia coli* (B/E) ratio were all greatly higher than those in the control group ( $P < 0.05$ ). In summary, flavored Tongxie Yaofang had a good effect in improving the symptoms of patients with diarrheal IBS and improved the microflora of Bifidobacterium and *Escherichia coli* in the intestinal tract of patients.

## 1. Introduction

Irritable bowel syndrome (IBS) is a functional disorder of the gastrointestinal tract, with the main clinical manifestations of gastrointestinal dysfunction accompanied by abdominal pain or discomfort, which are usually relieved after defecation [1]. According to clinical manifestations, it can be classified into diarrheal, constipated, mixed, and untyped IBS [2]. Diarrheal IBS refers to patients who had pasty/watery stools of more than 24% and lumpy/hard stools of less than 24%; it has a high incidence and a wide range of effects and is more common in young and middle-aged people [3]. It brings different degrees of negative impact on the work and life of patients [4]. The treatment of this disease in Western medicine relies on symptomatic treatment. But because the etiology and pathogenesis are not fully understood, patients are not satisfied with the current control of clinical curative effect and recurrence rate [5]. In contrast,

traditional Chinese medicine (TCM) has particular advantages in improving symptoms [6]. Fan et al. (2017) [7] proposed that Tongxie Yaofang could significantly reduce symptoms, increase stool consistency, and reduce bowel movements in 4 weeks compared to Western medicine in the treatment of IBS [7]. Chen et al. (2018) [8] and Wang et al. (2020) [9] drew the same conclusion. However, the flavored Tongxie Yaofang refers to the addition and subtraction of drugs to the original prescription according to the clinical symptoms of patients. Its clinical effect is significant in the treatment of diarrheal IBS, and the curative effect is obviously better than that of Western medicine. However, there are fewer clinical research studies about flavored Tongxie Yaofang in the treatment of diarrheal IBS, and further study is needed.

The role of microecological changes in the pathogenesis of IBS has attracted the attention of experts in recent years. A study has revealed that the intestinal microbiome is



important for normal gastrointestinal function and functions of other organs. Changes in the normal intestinal microbiome, dysbiosis, and changes in gut motility will lead to microbial overgrowth and altered gut permeability [10]. He et al. (2018) [11] propose that the gut is more susceptible to dysfunction and dysbiosis due to its contact with the external environment and gut microbes, which leads to intestinal inflammations, including IBS. It is of great significance of microecology in the pathogenesis of diarrheal IBS and to evaluate microecology to guide treatment. However, whether TCM can improve intestinal microecological changes in the treatment of diarrheal IBS needs to be explored.

This research was intended to provide more effective treatment methods for diarrheal IBS patients clinically. The curative effect of flavored Tongxie Yaofang decoction in diarrheal IBS was studied through intestinal microecological changes. Stool samples from patients were collected in both the control and treatment groups. The real-time fluorescent quantitative polymerase chain reaction (PCR) was adopted for detecting the intestinal *Bifidobacterium* and *Escherichia coli* in stool samples, as well as the logarithmic expression of paired and replicated deoxyribonucleic acid (DNA) in wet stools per g. *Bifidobacterium* and *Escherichia coli* in the intestinal tract were compared before and after treatment [12]. It was expected to improve the cure rate of diarrheal IBS patients clinically and reduce the recurrence rate.

## 2. Materials and Methods

**2.1. Research Objects.** Among patients admitted to The Affiliated People's Hospital of Fujian University of Traditional Chinese Medicine from February to December 2020, 60 patients with diarrheal IBS were included in this study. According to the different treatment methods, the patients were divided into a treatment group and a control group. The 20 patients in the control group were all treated with conventional Western medicine, and oral pinaverium bromide tablets were given. The 40 patients in the treatment group received the flavored Tongxie Yaofang decoction apart from conventional treatment through years of clinical experience. Combined with intestinal microecological changes, the curative effects of the two groups of patients were evaluated.

With the inclusion criteria, the included patients met the Western medicine diagnostic criteria of diarrheal IBS as well as the standards of TCM syndromes. They were 17–71 years old, having a course of disease of more than 1 year. They signed informed consent forms and were willing to receive the treatment. All the above criteria must be satisfied simultaneously. The exclusion criteria were formulated as follows. Patients did not meet the diagnostic criteria or the inclusion criteria. They took drugs that affect gastrointestinal motility, other antidiarrheal drugs, and antibiotics within 30 days before the treatment, or they were taking other drugs with stable efficacy. Pregnant women and lactating women were not included. Patients suffered from other organic diseases, tumors, or inflammatory bowel diseases of the

digestive system, they had other organic diseases confirmed by colonoscopy or barium enema, or their diarrhea was caused by systemic diseases, such as lactase deficiency and hyperthyroidism. Patients had fever, anemia, and hematochezia, or they had severe metabolic disorders of heart, liver, kidney, or endocrine, hematopoietic disorders, malignant tumors, mental disorders, and other diseases in the acute phase. Patients disagreed to participate in this study, because they cannot tolerate the treatment for adverse reactions, or they cannot complete the treatment as required due to other reasons. Those that met any one of the above conditions were excluded. The following criteria were laid down for discontinuing clinical tests. Patients failed to stick with the treatment. Patients got serious adverse reactions or severe complications during the treatment. This study had been approved by the Medical Ethics Committee of The Affiliated People's Hospital of Fujian University of Traditional Chinese Medicine, and the family members of the patients included signed the consent forms.

**2.2. Reagents and Instruments.** Nucleic acid extraction reagents were purchased from Zhengzhou Zhijie Biotechnology Co., Ltd. *Thermus aquaticus* (Taq) enzymes were generated from a kit. Common chemical reagents were purely made in China. Table 1 shows the main instruments used in this study.

**2.3. Bacterial DNA Extraction from the Stools.** The specimen was thawed and frozen at room temperature. 0.3 g stool was taken, and 1.1 mL phosphate buffer solution (0.06 mol/L, pH:7.5) was added to mix thoroughly for 6 minutes. The mixture was centrifuged at 1000 rpm for 1 min, and the supernatant was taken. The centrifugation and extraction were repeated 4 times. All the supernatants were collected and centrifuged at 14000 rpm for 1 min. The supernatant was removed, and the precipitation was retained. 1 mL phosphate buffer solution was added to mix the precipitation, and then it was centrifuged at 14000 rpm for 6 min. The supernatant was discarded, and the precipitation was washed 5 times with phosphate buffer solution. DNA purification was performed as follows. The bacterial fluid was centrifuged at 14000 rpm for 16 s, and a 200  $\mu$ L supernatant was taken as the isolate. 200  $\mu$ L DNA was extracted into a 0.6 mL centrifuge tube, and 51  $\mu$ L of the bacterial solution was added to the tube, reversed several times, and mixed well. It was placed for 4 min at room temperature. 25 pL DNA was added to extraction liquid B, reversed several times, and mixed thoroughly. It was centrifuged at 13000 rpm for 11 min, and the supernatant was still removed. 200 pL DNA was added to extraction liquid C, reversed repeatedly, and mixed well. It was centrifuged at 13000 rpm for 6 min, the supernatant was discarded, and the remains were put at room temperature or 56°C for 3–6 min to dry. 18 pL sample diluent was added to the suspension and centrifuged for a short time, and the liquid was dropped to the bottom of the tube. The supernatant was taken to generate the PCR.

TABLE 1: Major instruments used in this study.

Instruments	Production place
Table-top and high-speed refrigerated centrifuge	The United States
Fluorescent quantometer	Germany
Ultra-low temperature freezer	The United Kingdom
Biosafety cabinet	Japan

**2.4. Treatment Methods.** The patients in the control group were given pinaverium bromide tablets (Abbott Laboratories Trading (Shanghai) Co., Ltd.) for symptomatic western medicine treatment, oral administration at 50 mg/time, 3 times/day. The patients in the treatment group were treated with years of clinical experience combined with flavored Tongxie Yaofang in addition to the symptomatic Western medicine treatment. The patients were conditioned by restricting the liver, strengthening the spleen, and correcting and activating blood circulation. The basic prescription of flavored Tongxie Yaofang was prescribed with the following medicine materials. It included 13 g *Saposhnikovia divaricata*, 16 g *Atractylodes macrocephala* koidz, 11 g dried tangerine peels, 16 g white paeony root, 16 g turmeric, 16 g *Rhizoma corydalis*, 1 g *Costustoot*, 1 g *Lindera*, and 31 g *Jiubi*. For patients with spleen deficiency, 16–31 g *Codonopsis* was added. For patients with abdominal murmur, 61 g dried ginger was added. For those with mucus in the stool, 1 g *coptis* was added. For those who had constipation with fewer defecations, 1 g betel nut was supplemented. For those with abdominal distension, 16 g dried green tangerine peels and 16 g *Fructus aurantii* were supplemented. For those who were often tired, 31 g *Hairyvein agrimonia* and 31 g root of *Ficus hirta* Vahl were supplemented. The decoction was given one dose per day for three consecutive weeks. The stool samples of all patients in the treatment group were taken before and after treatment, and their symptoms were recorded and scored before and after treatment. Patients in both groups were treated for 4 weeks.

**2.5. Observation Indicators.** The number of defecations per day of patients was recorded. It was in a severe grade if the patients had more than 6 defecations every day. It was moderate with 4–5 defecations, it was mild with 2–3 defecations, and it was normal with 1 defecation each day. For the stool characteristics, it was recorded as severe grade with mucus in stool and watery stool; it was moderate with mushy or a small amount of mucus. It was mild with soft or a small amount of mucus, and it was normal with striped stool. For abdominal pain, it was assessed as normal grade with no abdominal pain, and it was mild with mild or occasional pain. It was moderate with several times of pain a day, and it was severe with recurrent severe pain or colic. In terms of abdominal distension, it was assessed as normal, mild, moderate, and severe with no abdominal distension, occasional abdominal distension or that after eating, severe abdominal distension of up to 6.2 hours a day, and abdominal distension with bulge all the day, respectively.

With the scoring criteria, 0, 1, 2, and 3 points were recorded for normal, mild, moderate, and severe grades, respectively.

In clinical practice, a patient was cured as the symptoms and physical signs disappeared or basically disappeared, and the syndrome score decreased by greater than or equal to 95%. The curative effect was assessed as remarkably effective, as the symptoms and physical signs of the patient were obviously improved, and the syndrome score was reduced by greater than or equal to 70%. It was effective as the symptoms and physical signs were improved, and the syndrome score was reduced by greater than or equal to 30%. It was ineffective as the symptoms and physical signs were not improved or even worsened, and the syndrome score was reduced by less than 30%.

The calculation equation was expressed as follows: total effective rate = ((syndrome score before treatment – the score after treatment)/the score before treatment) x 100%.

**2.6. Statistical Analysis.** SPSS16 was used to complete statistics. The contents of intestinal *Bifidobacterium* and *Escherichia coli* were expressed by logarithmic values. The independent sample *T* test was adopted to compare the microecology before and after treatment in the treatment group and the control group. Paired *T*-test was used to compare the contents of *Bifidobacterium* and *Escherichia coli* and the syndrome scores of patients in the treatment group before and after treatment. The chi-square test was adopted for enumeration data.

### 3. Results

**3.1. Comparison of General Data of the Patients.** 80 cases in total were selected for this study, and 20 patients who did not meet the requirements were excluded according to the exclusion criteria. Finally, 60 patients were included in this study and were divided into the treatment group and the control group with different treatment methods. As shown in Table 2, there was no significant difference in age and sex ratios of patients between the two groups ( $P > 0.05$ ), showing the two groups were comparable in age and gender.

**3.2. Improvement of Clinical Symptoms before and after Treatment.** The evaluation results of abdominal pain, abdominal distension, and diarrhea in the patients in the two groups before and after treatment are shown in Tables 3–5. It was observed that the abdominal pain, abdominal distension, and diarrhea were significantly improved in patients in the treatment group, with statistically significant differences compared with those before treatment ( $P < 0.05$ ). For patients in the control group, the abdominal pain and diarrhea were significantly improved compared with those before treatment, and the difference was statistically significant ( $P < 0.05$ ) while the abdominal distension did not change significantly ( $P > 0.05$ ) in patients in the control group. Compared with those in the control group, the clinical symptoms of patients in the treatment group were higher improved significantly, with statistically significant differences ( $P < 0.05$ ).

TABLE 2: General data of the patients.

Groups	Sample size	Average age (years)	Male (cases)	Female (cases)
Treatment group	40	42.13 ± 11.12	28	12
Control group	20	33.76 ± 6.34	14	6
Statistic value	—	0.443		-0.325
<i>P</i>	—	0.268		0.488

TABLE 3: The severity of abdominal pain before and after treatment.

	Treatment group ( <i>n</i> = 40)				Control group ( <i>n</i> = 20)			
	Normal	Mild	Moderate	Severe	Normal	Mild	Moderate	Severe
Before treatment	6	26	4	4	1	15	3	1
After treatment	22*	18	0	0	3	15	2	0
Statistic value			4.557				1.135	
<i>P</i>			0.000				0.043	

Note: \* suggested  $P < 0.05$ .

TABLE 4: The severity of abdominal distension before and after treatment.

	Treatment group ( <i>n</i> = 40)				Control group ( <i>n</i> = 20)			
	Normal	Mild	Moderate	Severe	Normal	Mild	Moderate	Severe
Before treatment	16	22	2	0	8	10	1	1
After treatment	30*	10	0	0	8	12	0	0
Statistic value			3.289				0.097	
<i>P</i>			0.000				0.553	

Note: \* indicated  $P < 0.05$ .

TABLE 5: The severity of diarrhea before and after treatment.

	Treatment group ( <i>n</i> = 40)				Control group ( <i>n</i> = 20)			
	Normal	Mild	Moderate	Severe	Normal	Mild	Moderate	Severe
Before treatment	4	26	10	0 <sup>#</sup>	2	13	5	0
After treatment	32*	6	2	0	5	12	2	1
Statistic value			5.569				1.436	
<i>P</i>			0.000				0.038	

Note: \* indicated  $P < 0.05$ .

3.3. *Comparative Analysis of Clinical Curative Effects on Patients.* Figure 1 shows the curative effect analysis of 40 patients in the treatment group. According to syndrome scores, it was cured, remarkably effective, effective, and ineffective in 10, 14, 13, and 3 cases. The total effective rate reached 92.5%. In the control group, it was cured in 2 cases, remarkably effective in 6 cases, effective in 8 cases, and ineffective in 4 cases, with a total effective rate of 80.0%. It suggested that flavored Tongxie Yaofang had a good clinical effect in treating diarrheal IBS.

3.4. *Comparison of Intestinal Microecology before and after Treatment.* The intestinal microbes of Bifidobacterium, *Escherichia coli*, and Bifidobacterium/*Escherichia coli* (B/E) of patients were compared before and after treatment between the two groups, and the results are shown in Figure 2. It was observed that there was no significant difference among Bifidobacterium, *Escherichia coli*, and B/E of patients between the control group and the treatment group before treatment ( $P > 0.05$ ). Bifidobacterium,

*Escherichia coli*, and B/E of patients in both groups increased significantly after treatment, suggesting the differences were statistically significant ( $P < 0.05$ ). Compared with those in the control group, Bifidobacterium, *Escherichia coli*, and B/E of patients in the treatment group increased obviously, and the differences were also statistically significant ( $P < 0.05$ ).

## 4. Discussion

Western medicine believes that diarrheal IBS is the result of a combination of multiple factors, which is related to abnormal gastrointestinal motion, visceral paresthesia, and psychological factors [13]. The clinical treatment of diarrheal IBS mainly depends on symptomatic treatment of western medicine, but the symptoms not the disease are cured, and the patients are prone to recurrence with a poor effect [14]. Clinical studies have discovered that the symptoms in most patients with diarrheal IBS cannot be relieved well [15]. Therefore, TCM treatment has attracted people's attention. TCM syndrome differentiation and

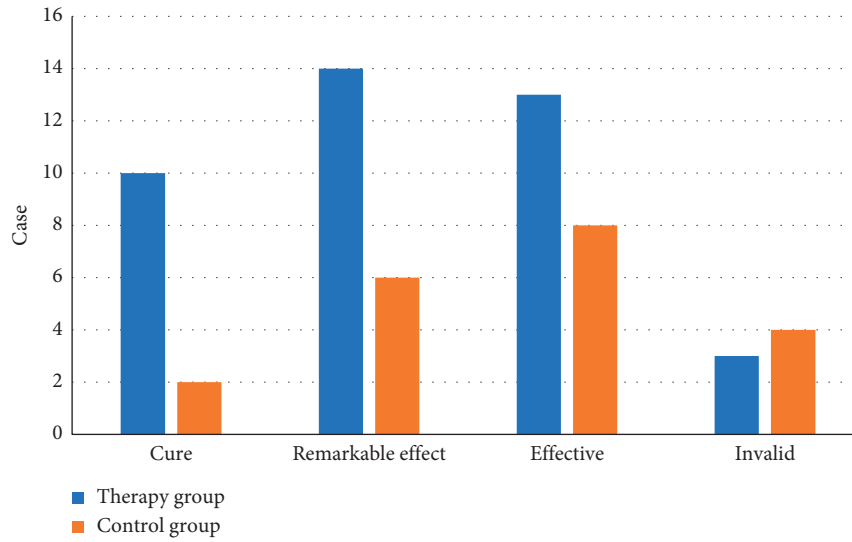


FIGURE 1: Comparison of clinical curative effects between the two groups after treatment.

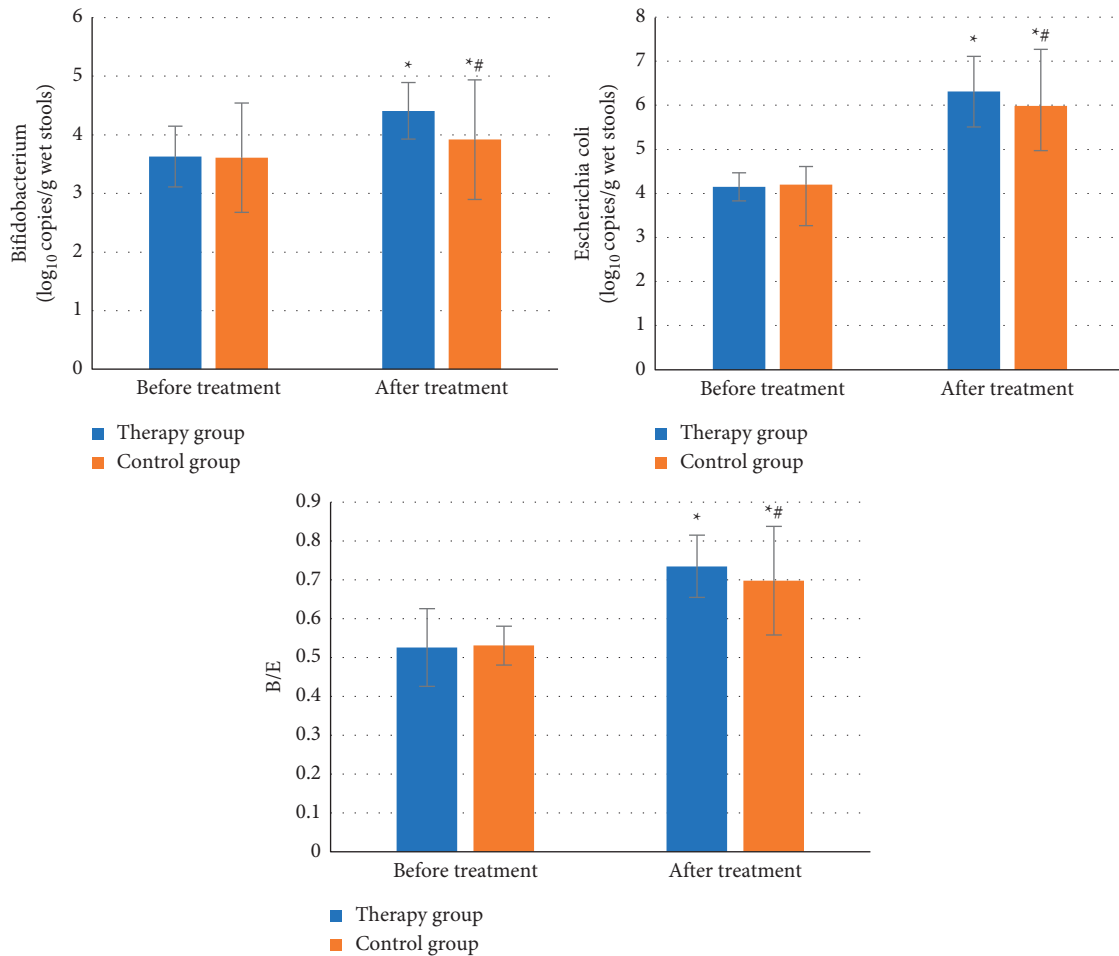


FIGURE 2: Changes in the intestinal microflora of patients before and after treatment. \* means  $P < 0.05$  compared with those before treatment, while # means  $P < 0.05$  compared with those in the treatment group.

treatment can not only improve symptoms but also shorten the course of diseases and relieve patients' suffering. It also has a notable effect on reducing the frequency of IBS [13]. Furthermore, some medical staff have

found in the process of serving patients with diarrheal IBS that the Bifidobacterium and *Escherichia coli* in the intestinal tract of these patients are prominently increased [16]. The ratio of B/E can simply reflect the general

situation of intestinal colonization resistance. However, diminished colonization resistance in the intestinal tract may also inhibit the growth and reproduction abilities of potential pathogens, such as Bifidobacterium, and maintain the function of the local immune system. This will result in local inflammations and erroneous release of chemical mediators and neurotransmitters [17, 18].

To learn the curative effect of flavored Tongxie Yaofang in the treatment of diarrheal IBS and the regulation of gastrointestinal microecological stability, this research was conducted. The total effective rate (92.5%) of the patients in the treatment group was greatly higher than that of the control group (80%) ( $P < 0.05$ ). This suggested that the flavored Tongxie Yaofang through clinical syndrome differentiation could improve the curative effect in the symptomatic treatment. It had a good clinical effect on treating diarrheal IBS. Moreover, the relief of clinical symptoms such as abdominal pain, abdominal distension, and diarrhea in the treatment group was remarkably better in contrast to the control group ( $P < 0.05$ ). This was consistent with the research results of Dai et al. (2018) [19]. The clinical curative effect of flavored Tongxie Yaofang was significantly greater than that of conventional drug therapy. In contrast, it could highly reduce abdominal pain scores, abdominal distension, diarrhea, defecation frequency, etc. This also indicated the great application prospect of TCM in treating diarrheal IBS. The research studies of Li et al. (2020) [20] and Yan et al. (2019) [21] also provided some support for this research, as immunohistochemistry was adopted to study the role of flavored Tongxie Yaofang in intestinal microecology in diarrheal IBS. The results showed that intestinal Bifidobacterium, *Escherichia coli*, and B/E ratios were observably higher in comparison with the control group ( $P < 0.05$ ). It was revealed that the flavored Tongxie Yaofang could better improve gastrointestinal flora. However, the current related research studies are relatively lacking; thus, in-depth exploration is needed to verify the accuracy and representativeness of the results.

## 5. Conclusion

In this research, the curative effect of flavored Tongxie Yaofang in treating diarrheal IBS and the regulation of gastrointestinal microecological stability were explored. Thereout, it was concluded that the flavored Tongxie Yaofang had a better effect on relieving the symptoms of diarrheal IBS patients. It could also better regulate the microbial communities of Bifidobacterium and *Escherichia coli* in the patients' intestinal tract. However, the specific mechanism of Bifidobacterium and *Escherichia coli* in the pathogenesis of diarrheal IBS remained unclear. Therefore, it was necessary to prepare corresponding animal models for further exploration in the future. The sample size in this research was too small, and more experimental samples should be included. Clinical trials should be carried out in multicenter hospitals with larger samples, rather than in a single or small area. Anyhow, the application prospect of TCM in the clinical treatment of diseases was very impressive, and it was worthwhile for clinical workers to explore.

## Data Availability

All data generated or analyzed during this study are included in this article.

## Conflicts of Interest

The authors declare no conflicts of interest.

## References





- [1] A. Llanos-Chea and A. Fasano, "Gluten and functional abdominal pain disorders in children," *Nutrients*, vol. 10, no. 10, p. 1491, 2018.
- [2] I. Aziz, O. S. Palsson, H. Törnblom, A. D. Sperber, W. E. Whitehead, and M. Simrén, "Epidemiology, clinical characteristics, and associations for symptom-based Rome IV functional dyspepsia in adults in the USA, Canada, and the UK: a cross-sectional population-based study," *Lancet Gastroenterol Hepatol*, vol. 3, no. 4, pp. 252–262, 2018.
- [3] P. Usai-Satta, G. Bassotti, M. Bellini, F. Oppia, M. Lai, and F. Cabras, "Irritable bowel syndrome and gluten-related disorders," *Nutrients*, vol. 12, no. 4, p. 1117, 2020.
- [4] L. S. Xiong, M. H. Chen, W. A. Wang, H. X. Chen, A. G. Xu, and P. J. Hu, "[Evaluation of the quality of life of patients with irritable bowel syndrome]," *Zhonghua Nei Ke Za Zhi*, vol. 43, no. 5, pp. 356–359, 2004.
- [5] A. C. Ford, B. E. Lacy, and N. J. Talley, "Irritable bowel syndrome," *New England Journal of Medicine*, vol. 376, no. 26, pp. 2566–2578, 2017.
- [6] G. J. Holtmann, A. C. Ford, and N. J. Talley, "Pathophysiology of irritable bowel syndrome," *The Lancet Gastroenterology & Hepatology*, vol. 1, no. 2, pp. 133–146, 2016.
- [7] H. Fan, L. Zheng, Y. Lai et al., "Tongxie formula reduces symptoms of irritable bowel syndrome," *Clinical Gastroenterology and Hepatology*, vol. 15, no. 11, pp. 1724–1732, 2017.
- [8] M. Chen, T. C. Tang, Y. Wang et al., "Randomised clinical trial: tong-Xie-Yao-Fang granules versus placebo for patients with diarrhoea-predominant irritable bowel syndrome," *Alimentary Pharmacology & Therapeutics*, vol. 48, no. 2, pp. 160–168, 2018.
- [9] S. S. Wang, X. R. Wang, R. Y. Yang, Y. Xu, and M. Y. Li, "[Efficacy and mechanism of acupuncture combined with Tongxieyaofang for diarrhea-type irritable bowel syndrome of liver depression and spleen deficiency]," *Zhongguo Zhen Jiu*, vol. 40, no. 6, pp. 605–609, 2020.
- [10] H. M. Staudacher and K. Whelan, "The low FODMAP diet: recent advances in understanding its mechanisms and efficacy in IBS," *Gut*, vol. 66, no. 8, pp. 1517–1527, 2017.
- [11] F. He, C. Wu, P. Li et al., "Functions and signaling pathways of amino acids in intestinal inflammation," *BioMed Research International*, vol. 2018, Article ID 9171905, 13 pages, 2018.
- [12] R. M. Lovell and A. C. Ford, "Global prevalence of and risk factors for irritable bowel syndrome: a meta-analysis," *Clinical Gastroenterology and Hepatology*, vol. 10, no. 7, 2012.
- [13] C. C. Herndon, Y. P. Wang, and C. L. Lu, "Targeting the gut microbiota for the treatment of irritable bowel syndrome," *The Kaohsiung Journal of Medical Sciences*, vol. 36, no. 3, pp. 160–170, 2020.
- [14] I. Aziz, H. Törnblom, and M. Simrén, "Small intestinal bacterial overgrowth as a cause for irritable bowel syndrome: guilty or not guilty?" *Current Opinion in Gastroenterology*, vol. 33, no. 3, pp. 196–202, 2017.



- [15] L. Saha, "Irritable bowel syndrome: pathogenesis, diagnosis, treatment, and evidence-based medicine," *World Journal of Gastroenterology*, vol. 20, no. 22, pp. 6759–6773, 2014.
- [16] M. Batten, J. Li, S. Yi et al., "Interleukin 27 limits autoimmune encephalomyelitis by suppressing the development of interleukin 17-producing T cells," *Nature Immunology*, vol. 7, no. 9, pp. 929–936, 2006.
- [17] A. C. Adejumo, T. O. Ajayi, O. M. Adegbala, and T. N. Bukong, "Higher odds of irritable bowel syndrome among hospitalized patients using cannabis: a propensity-matched analysis," *European Journal of Gastroenterology and Hepatology*, vol. 31, no. 7, pp. 756–765, 2019.
- [18] S. W. Tsang, K. K. Auyeung, Z. X. Bian, and J. K. Ko, "Pathogenesis, experimental models and contemporary pharmacotherapy of irritable bowel syndrome: story about the brain-gut Axis," *Current Neuropharmacology*, vol. 14, no. 8, pp. 842–856, 2016.
- [19] Y. K. Dai, D. Y. Li, Y. Z. Zhang et al., "Efficacy and safety of Modified Tongxie Yaofang in diarrhea-predominant irritable bowel syndrome management: a meta-analysis of randomized, positive medicine-controlled trials," *PLoS One*, vol. 13, no. 2, Article ID e0192319, 2018.
- [20] Y. L. Li, C. J. Yao, R. Lei et al., "Acupuncture combined with Tongxieyaofang for diarrhea-type irritable bowel syndrome: a protocol for meta-analysis," *Medicine (Baltimore)*, vol. 99, no. 48, Article ID e23457, 2020.
- [21] J. Yan, Z. W. Miao, J. Lu et al., "Acupuncture plus Chinese herbal medicine for irritable bowel syndrome with diarrhea: a systematic review and meta-analysis," *Evid Based Complementary and Alternative Medicine*, vol. 2019, Article ID 7680963, 16 pages, 2019.

## Research Article

# Sulfated Polysaccharides Derived from *Hypnea valentiae* and Their Potential of Antioxidant, Antimicrobial, and Anticoagulant Activities with *In Silico* Docking

Kokila Palani,<sup>1</sup> Balamuralikrishnan Balasubramanian ,<sup>2</sup> Arunkumar Malaisamy,<sup>3</sup> Viji Maluventhen,<sup>4</sup> Vijaya Anand Arumugam ,<sup>5</sup> Naif Abdullah Al-Dhabi,<sup>6</sup> Mariadhas Valan Arasu,<sup>6</sup> Karthika Pushparaj,<sup>7</sup> Wen-Chao Liu ,<sup>8</sup> and Maruthupandian Arumugam <sup>1</sup>

<sup>1</sup>Ethnopharmacology and Algal Biotechnology Division, Department of Botany, School of Life Sciences, Periyar University, Salem 636011, Tamil Nadu, India

<sup>2</sup>Department of Food Science and Biotechnology, College of Life Science, Sejong University, Seoul 05006, Republic of Korea

<sup>3</sup>Integrative Biology Division, International Centre for Genetic Engineering and Biotechnology (ICGEB), New Delhi, India

<sup>4</sup>Department of Botany, Thiagarajar College, Madurai 625009, Tamil Nadu, India

<sup>5</sup>Department of Human Genetics and Molecular Biology, Bharathiar University, Coimbatore 641046, Tamil Nadu, India

<sup>6</sup>Department of Botany and Microbiology, College of Science, King Saud University, P.O. Box 2455, Riyadh 11451, Saudi Arabia

<sup>7</sup>Department of Zoology, School of Biosciences, Avinashilingam Institute for Home Science and Higher Education for Women, Coimbatore, Tamil Nadu 641043, India

<sup>8</sup>College of Coastal Agricultural Sciences, Guangdong Ocean University, Zhanjiang 524088, China

Correspondence should be addressed to Wen-Chao Liu; [liuwc@gdou.edu.cn](mailto:liuwc@gdou.edu.cn) and Maruthupandian Arumugam; [maruthumdu82@gmail.com](mailto:maruthumdu82@gmail.com)

Received 10 March 2022; Accepted 28 May 2022; Published 20 July 2022

Academic Editor: Sekar Vijayakumar

Copyright © 2022 Kokila Palani et al. This is an open access article distributed under the Creative Commons Attribution License, which permits unrestricted use, distribution, and reproduction in any medium, provided the original work is properly cited.

Carrageenan, a sulfated polysaccharide, was produced by certain species of marine red seaweeds, which have been used as a significant source of food, feed, and antibiotic agent throughout history due to their alleged human health benefits. The present study aimed to derive the polysaccharides from *Hypnea valentiae* and describe the biological applications. Carrageenan was characterized by FT-IR, C-NMR, AFM, and their antimicrobial, antioxidant, and anticoagulant capabilities; furthermore, the larvicidal effect of methanol extract was generated from the seaweed against *Aedes aegypti* larvae at various concentrations. The molecular docking experiments were carried out computationally for finding the molecular insight of the macromolecules and small molecules' interaction using GLIDE docking by using Schrodinger software. Antibacterial zones of inhibition in different concentrations are compared with the 40 mg/mL higher activity against bacterial pathogens. Carrageenan is strong in all antioxidant activities, with the overall antioxidant (70.1 ± 0.61%) of radical at 250 µg/mL concentration being exhibited. The DPPH scavenging is effective in the inhibition of (65.74 ± 0.58%) radical at a concentration of 160 µg/mL and the hydroxyl scavenging (65.72 ± 0.60%) of activity at a concentration of 125 µg/mL being exhibited. Anticoagulant activities (APPT and PT) of carrageenan fraction were tested. *H. valentiae* and heparin sulphate shows higher activity of APTT (106.50 IU at 25 µg/mL) in comparison with the PT test (57.86 IU at 25 µg/mL) and the methanol extraction of higher larvicidal activity on *A. aegypti* (LC<sub>50</sub> = 99.675 µg/mL). In this study, the carrageenan was exploited through *in vitro* and *in silico* molecular docking studies against antimicrobial, antioxidant, and anticoagulant properties. The results were establishing the potentiality of the carrageenan which is an alternative source to control the mosquitocidal property in the future. Moreover, molecular docking of carrageenan against multiple targets results in -7 to -6 Kcal/mol binding score. Findings of carrageenan from *in vitro* to *in silico* studies are needed for further validation of clinical pieces of evidence.

## 1. Introduction

Marine macroorganisms are a rich source of functionally diversified bioactive compounds that play an active role in human nutrition and health. Seaweeds are a major source of sulfated polysaccharides, particles which are widely employed in food, feed, and medicine due to their rheological qualities as gelling and stabilizing agents [1, 2]. Sulfated polysaccharides have numerous biological and physiological activities, including antithrombotic [3], anticoagulant [4], antioxidant [5], antidiabetic [6], antibacterial [7], immunomodulatory [8, 9], antiviral [10], antiinflammatory [11], antinociceptive [12, 13], antitumor [14], and proinflammatory effects [15, 16]. Sulfated polysaccharides including agarans, galactans, and carrageenans are also available abundantly. Among these, carrageenan is a generic deviation of linear, sulfated galactans derived from species of red seaweeds [17]. Various investigations on the antioxidant and anticoagulant properties of seaweeds or their extracts have been published [18, 19]. Algal polysaccharides must be shown to serve a significant role as free-radical scavengers and antioxidants in the protection of oxidative damage in living organisms in current administration, and anticoagulants have long been used to treat blood during dialysis and surgery, as well as to treat disseminated intravascular coagulation and thrombosis in a variety of disorders and for *in vitro* blood testing [20, 21]. Mosquitoes, such as *Aedes aegypti*, are the deadliest since they act as a vector for a variety of diseases, including dengue fever, malaria, yellow fever, filariasis, and other types of chikungunya as well as Zika virus [22–25]. Furthermore, seaweed sulfated polysaccharide extracts contain primary and secondary metabolites including bioactive chemicals which are biodegradable into harmless products; it may be effective in mosquito larval control [26, 27].

The standard new therapeutic approach is complicated, exhausting, expensive, time-consuming, and laborious. Computational methods such as molecular docking have played a critical role in rationalizing the road to drug discovery in order to overcome these obstacles. A molecular docking feature becomes a promising pharmaceutical research tool for screening candidates from drug libraries effectively [28]. In such studies, the ultimate goal was to find effective therapeutics for the carrageenan molecule extracted from marine algae. It is evaluated against antimicrobial, anticoagulant, and antioxidant activity using GLIDE docking in the maestro platform of Schrodinger software (Schrödinger Release 2021-2: Maestro, Schrödinger, LLC, New York, NY, 2021). Furthermore, the efficiency of the carrageenan compound was exploited with *in vitro* validation against the foresaid targets. Carrageenan is a sulfated polysaccharide, which is obtained by extraction from red seaweed species. It has been widely utilized in the food industry, agricultural, drug delivery, tissue engineering, and biosensor applications. Therefore, the present study investigated the isolation and biofunctional activities of carrageenan extracted from *H. valentiae*, characterization of structural properties using Fourier transform infrared (FT-

IR) spectroscopy,  $^{13}\text{C}$  nuclear magnetic resonance (NMR), and atomic force microscopy (AFM) spectroscopy and evaluation of the biological properties such as antioxidant, antimicrobial, and anticoagulant activities with *in silico* molecular docking analysis.

## 2. Materials and Methods

**2.1. Collection and Extraction of Sample.** The red seaweed, *H. valentiae* (Turnur), was collected from Mandapam (Lat.  $09^{\circ}28'177\text{N}$ , Long.  $79^{\circ}18'536\text{E}$ ) located on the southeast coastline of Ramanathapuram, Tamil Nadu, India. The seaweed specimen identification number was 1759. The sample was properly cleaned with seawater to remove all undesired pollutants such as sand particles and epiphytes and then thoroughly cleaned with tap water to discard all salt on the surface. The water was drained away, and the seaweed was laid out on the blotting paper to absorb any remaining moisture before being shade-dried at room temperature for 3 days and crushed into a fine powder. Following the completion of the sulfated polysaccharide extraction, the procedure was evaluated for 100 g of seaweed powder, which was soaked separately in acetone and methanol solvent in 7:3 for two days in a shaker at 200 rpm for 10 min. The process was repeated twice to ensure the dry biomass. This biomass was dried into a powder and dispersed in 1 L of 0.1 M HCL for 24 h with constant stirring at room temperature. The pellet was reextracted as above, and the supernatants were pooled. The supernatant was kept at  $4^{\circ}\text{C}$  overnight and precipitated with two volumes of absolute 1:1 and stirred continuously for 15 min, and then the precipitate was collected to separate carrageenan gel and distilled water. Carrageenan gel was then completely soaked in 96% alcohol for 1 h and stirred continuously. The carrageenan gel was separated from alcohol and distilled water by filtration. Subsequently, the mixture was centrifuged at 5000 rpm for 10 min, and the supernatant was neutralized with 1.0 M NaOH and poured in 100 mL of methanol. The carrageenan was freeze-dried by using a membrane at  $70^{\circ}\text{C}$  for a 24 h duration which was performed for further processing [29].

**2.2. Structural Analysis.** Using an alpha FT-IR spectrophotometer and its technique, FT-IR was used to determine the functional groups of the carrageenan polysaccharides [30]. The characterization has been complemented by the  $^{13}\text{C}$ -NMR spectrum. The  $^{13}\text{C}$ -NMR spectrum of 10 mg of the carrageenan was dissolved in 0.5 mL solution in  $\text{D}_2\text{O}$  which was recorded at  $27^{\circ}\text{C}$  on an NMR spectra Bruker model MHz 400 spectrometer. The proton chemical shift was expressed in parts per million (ppm). The substance was diluted in distilled water before being mixed with a solution of  $200\ \mu\text{g}/\text{mL}$  carrageenan in 0.2 M NaOH. The carrageenan solutions were allowed to equilibrate for 1 h with NaOH prior to neutralization with HCl (pH~6-7). Solutions were then passed through a  $0.22\ \mu\text{m}$  filter and deposited onto 1 cm of a freshly cleaned glass plate surface (sample volume  $\sim 60\ \mu\text{L}$ ). Samples were dried for approximately 16 h in ambient

conditions. Imaging of AFM was performed within 24 h of carrageenan deposition to avoid sample contamination.

**2.3. Antibacterial Activity.** Antibacterial studies were carried out on two Gram-positive bacteria (*Enterococcus faecalis* (MTCC 439) and *Staphylococcus aureus* (MTCC 96)) and Gram-negative bacteria (*Escherichia coli* (MTCC 443) and *Pseudomonas aeruginosa* (MTCC 741)). All the bacteria were obtained from the Research Laboratory, Microbiology Department, Periyar University, India. Positive control includes streptomycin. All bacterial cultures were incubated at 35°C for 24 h [31].

**2.4. Antibiofilm Activity.** To determine the effect of seaweed methanol extracts against antibiofilm activity, about 3.5 mL of nutrient broth and 1.5 mL of bacterial culture were added into sterile test tubes. 10 mg of sample was added to different concentrations of methanol extract (10, 20, 30, 40, and 50 µg/mL) and additionally given into each tube. All tubes were incubated in a shaking incubator at 37°C for 24 h. After incubation, all tubes were washed with distilled water. All the tubes were breeze-dried for a few minutes and added 5 mL of crystal violet and then incubated at 37°C for 1 h. After incubation, we discarded the crystal violet from all the tubes and washed them with distilled water. About 5 mL of 95.0% ethanol was added into all test tubes and taken OD at 595 nm by UV-visible spectrophotometer [32], respectively. The antibiofilm activity was calculated using the formula of percentage:

$$\% \text{ of biofilm inhibition} = \frac{\text{control OD} - \text{treatment OD}}{\text{control OD}} \times 100. \quad (1)$$

## 2.5. Antioxidant Activity Measurement

**2.5.1. Total Antioxidant Property.** The antioxidant activities of samples were evaluated by phosphomolybdenum complex formation according to the method [33]. About 0.5 mL sample extracts were added with 3 mL of reagent solution (0.6 M sulphuric acid, 28 mM sodium phosphate, and 4 mM ammonium molybdate). The test tubes were covered with foil and incubated in a water bath at 95°C for 90 min. After the samples had cooled to room temperature, the absorbance of the mixture was measured at 695 nm against the reagent blank. The reported results were mean values expressed as mg AAE/g sample.

## 2.6. Assay for Radical Scavenging In Vitro

**2.6.1. Scavenging Activity of DPPH (2,2-Diphenyl-1-picryl Hydrazyl).** Purified polysaccharides' DPPH-free radical-scavenging activity was assessed using Q-sepharose anion-exchange chromatography, as previously described by the technique [29, 34] with slight modifications. A solution of 3 mL of 0.1 mM methanolic solution DPPH was prepared. A respective blank sample of BHA and L-ascorbic acid was

prepared by adding 100 µg/mL. The discoloration of the sample was measured with a proper blank at 517 nm after incubation for 30 min at 30°C in the dark using a UV-Vis spectrophotometer. The samples' free radical scavenging activity was calculated using the following equation:

$$\% \text{ inhibition} = \left[ \frac{(A1 - A2)}{A1} \right] \times 100, \quad (2)$$

where A1 is the absorption of the control and A2 is the absorption of the sample.

**2.6.2. Hydroxyl Radical Scavenging Assay.** The capacity of the seaweed polysaccharides against the scavenging hydroxyl radical was evaluated using Fenton's reaction ( $\text{Fe}^{2+} + \text{H}_2\text{O}_2 \rightarrow \text{Fe}^{3+} + \text{OH}^- + \text{OH}$ ) according to the modification method described [35]. The extracts of methanol were evaporated in vials. The reaction mixture contained 1 mL of (EDTA) solution, 0.5 mL of EDTA (0.018%), and 1 mL of DMSO (0.85% v/v in 0.1 M phosphate buffer, pH 7.4), and 0.5 mL of ascorbic acid (0.22%) was added to each tube. The solution was incubated at 37°C for 15 min, and the presence of yellow color was measured spectrophotometrically at 510 nm against the blank sample. The mixture without the sample was treated as a control. The scavenging activity was calculated by the following equation:

$$\% \text{ inhibition} = \left\{ 1 - \left[ \frac{(A1 - A2)}{A0} \right] \right\} \times 100, \quad (3)$$

where A0 is the control, A1 is the absorption of the sample, and A2 is absorption without sodium salicylate.

## 2.7. Anticoagulant Activity

**2.7.1. Activated Partial Thromboplastin Time (APTT).** For carrageenan fractions, APTT was calculated using a modified version of the methodology reported [36]. The positive and negative controls were heparin at a concentration of 5 g/mL and 0.9 percent w/v NaCl, respectively.

**2.7.2. Prothrombin Time (PT).** The methodology of [37] was also used to determine PT, with some modifications. The device was also programmed to perform the same procedure in APTT determination. Each poor-platelet plasma and carrageenan solution mixture was incubated for 3 min at 37°C. Then, 0.6 mL of prewarmed PT reagent was added, and the time for clot formation was also observed and repeated three times. For positive and negative control, heparin and NaCl were utilized, respectively.

**2.8. Molecular Docking.** Ligand preparation: for molecular docking studies, carrageenan structure was retrieved from the PubChem database (71597331) in a three-dimensional structure file (SDF) format, and furthermore, the structure was refined using the LigPrep module in Schrodinger's Maestro (v 12.8). The OPLS4 force field was applied, and 32 different states of stereoisomerism were derived

(Schrödinger Release 2021-2: LigPrep, Schrödinger, LLC, New York, NY, 2021).

Protein preparation: we need to evaluate the antioxidant (2C0D & 5B6M), antimicrobial (1JIJ & 2XCT), and anti-coagulant (5E8E) activity against sulfated polysaccharide computationally. The three-dimensional structure of proteins was retrieved from the database of Protein Data Bank (PDB). The X-ray crystallographic structures were imported into Maestro using the protein preparation wizard, and this module helps to solve the missing hydrogen bonds, create the disulfide bonds, and optimize (Schrödinger Release 2021-2: Protein Preparation Wizard; Epik, Schrödinger, LLC, New York, NY, 2021; Impact, Schrödinger, LLC, New York, NY; Prime, Schrödinger, LLC, New York, NY, 2021).

The molecular docking was performed using the Glide package (ligand docking) in the Schrodinger suite. The standard precision docking method was applied and performed postdocking minimization and analyzed the results in pose viewer Schrödinger Release 2021-2: Glide, Schrödinger, LLC, New York, NY, 2021.

**2.9. Mosquito Culture and Larvicidal Activity.** *A. aegypti* mosquito larvae were collected from the Indian Council of Medical Research—Vector Control Research Centre, Madurai, Tamil Nadu, India. The mosquito larvae were fed a finely powdered mixture containing a 3:1 ratio of dog biscuits and Brewer's yeast for repeated generations at 25–30°C. According to the procedure used, adult mosquitoes were kept under standard environmental conditions as larvae [38]. Following this procedure, a mortality assay was carried out on fourth instar larvae [22, 39]. The test for the larvae effect of methanol extract derived from seaweed against mosquito larvae *A. aegypti* involved 10 mg of the sample in different concentrations for 50, 100, 200, and 500  $\mu$ L. Twenty larvae were added to 250 mL distilled water in triplicates, with 1 mL DMSO serving as a negative control H<sub>2</sub>O. Dead larvae were counted, and the proportion of dead larvae was estimated for the replicates after 24 and 48 h of exposure. Profit analysis was utilized to calculate average LC<sub>50</sub> and LC<sub>90</sub> (lethal concentration) values from the duplicates.

$$\% \text{ of mortality} = \frac{\text{number of dead larvae}}{\text{number of larvae introduced}} \times 100. \quad (4)$$

**2.10. Statistical Analysis.** The results were examined using one-way analysis to calculate LC<sub>50</sub>, LC<sub>90</sub>, and 95% fiducial limits of upper confidence and lower confidence of variance and standard values presented as the mean SD (ANOVA). The asterisk (\*, \*\*, and \*\*\*) denotes a significant difference from the control ( $p < 0.01$ , ( $p < 0.05$ , and  $p < 0.001$ ).

### 3. Results

The FT-IR spectra of the carrageenan were isolated from the red seaweed *H. valentiae* and the absorption bands typical of carrageenan between the wave numbers 1000 and 3500  $\text{cm}^{-1}$  clearly highlighted the functional groups in all of the analyzed

samples (Figure 1, Table 1). The peaks at 3457.74  $\text{cm}^{-1}$  correlate with O-H stretching H-bonding vibrations which indicated alcohols and phenols. The existence of alkanes was revealed by the similarity of the peaks found at 2349.36  $\text{cm}^{-1}$ . Furthermore, the peaks observed at 1687.22  $\text{cm}^{-1}$  were attributed to alkenes. The aliphatic amines had an absorption peak position at 1187.22  $\text{cm}^{-1}$  confirming the  $-\text{C}=\text{C}-$  stretch. The spectral observations at 1222.18  $\text{cm}^{-1}$  indicated asymmetric stretching of S-O, revealing the presence of sulfate [40]. The band at 1222.18–1030.72  $\text{cm}^{-1}$  stretching of C-O was attributed to alcohols, carboxylic acids, esters, and ethers. C-H stretching vibrations indicated the existence of alkanes in the band between 1444.61  $\text{cm}^{-1}$ . The C-O-C of 3, 6-anhydro-L-galactose vibrations has been assigned to the peak at 920.72  $\text{cm}^{-1}$ . Aromatic group C-H stretching vibrations were as described to the peak 845.44  $\text{cm}^{-1}$ . The last peak which appears to be 650.30  $\text{cm}^{-1}$  was related to  $-\text{C}\equiv\text{C}-\text{H}$ : C-H bending the presence of alkanes. The NMR spectra of the carrageenan provided more structural characterization, which is shown in Figure 2, respectively, and band assignment for a sample of *H. valentiae* polysaccharide. The NMR can be used to demonstrate the existence of different carrageenan units. The NMR spectrum was also a complex polymer signal from the anomeric proton at (78.30 ppm), and ring carbons (70.16 ppm) were assigned to 3,6- $\alpha$ -L-anhydrogalactose. The signal was assigned from the 75.02 ppm which was assigned to H-1 of  $\beta$ -D-galactose linked to  $\alpha$ -L-galactose-6-sulfate. The signal at 102.86 ppm was attributed to carboxyl  $\beta$ -D-galactose.

The surface topography of the carrageenan was studied with the help of AFM measurements in a contact mode. The AFM images of the carrageenan soft template and bright spot are shown in (Figure 3(a)). Moreover, the topography of the carrageenan can be observed with peaks and valleys distributed across the surface. Apart from this, huge numbers of deformed shapes with larger sizes can also be seen in the AFM image of the carrageenan (Figure 3(b)). The AFM is a significant source for detecting the morphology and size of the carrageenan macromolecules originating from 0.0 to 0.7  $\mu\text{m}$ . The carrageenan particles' average height which ranged from 0.00 to 0.72  $\mu\text{m}$  was also noted.

The antibacterial activity of the methanol extract was evaluated for the resistance to pathogenic bacteria which may cause infection in human beings. The methanol extract of *H. valentiae* inhibitory activity against *E. faecalis*, *S. aureus*, *E. coli*, and *P. aeruginosa* was identified. The pathogenic bacterial zone of inhibition in various concentrations of the methanol extract was compared to the 40 mg/mL higher inhibitory activity against four bacterial pathogens obtained in the results shown in (Figure 4) and Table 2, respectively. The antibacterial potential of methanol extracts depends upon the ability of permeation to the bacterial cell through the cell wall of bacteria. Moreover, the methanol extract had a minimum inhibitory bacterial effect against the Gram +ve strain rather than the Gram -ve strain. Therefore, the present study focused that both extracts demonstrated high significant antibacterial inhibition activity against Gram-negative bacteria rather than Gram-positive bacteria.

The antibiofilm activity of methanol extract of *H. valentiae* has been investigated with bacterial potential against stains



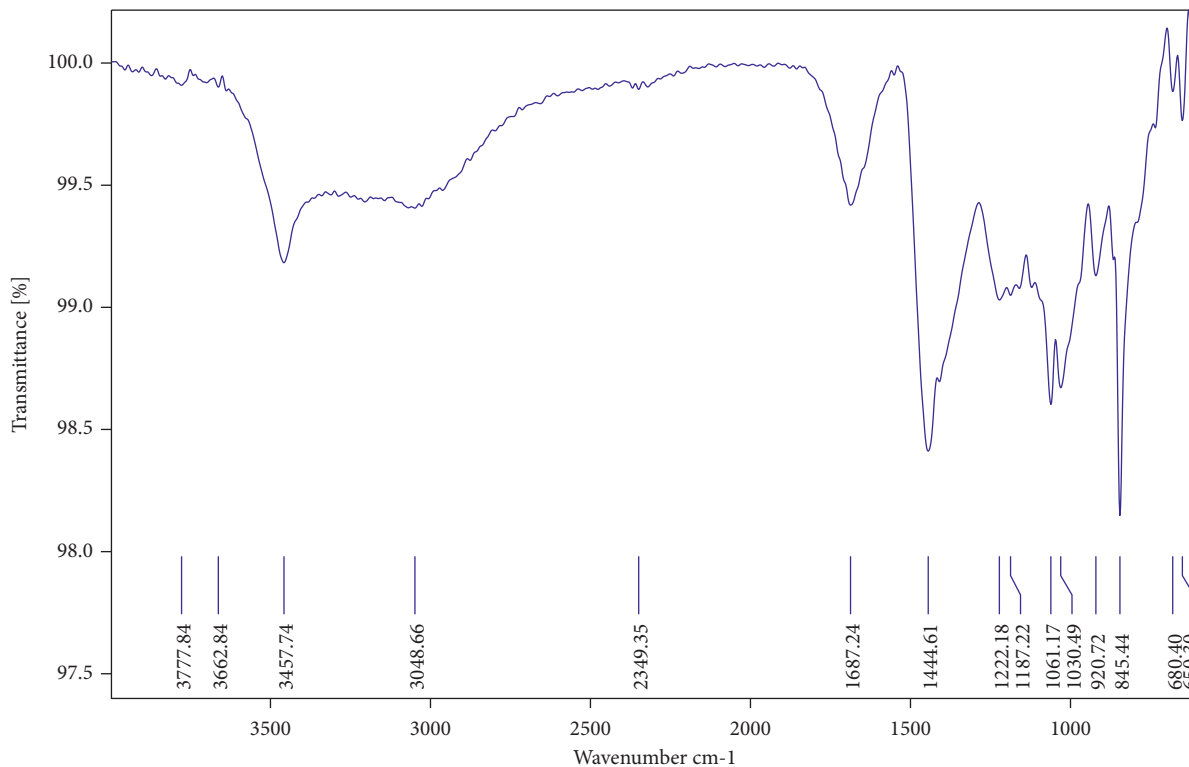


FIGURE 1: FT-IR spectrum of the carrageenan from *Hypnea valentiae*.

TABLE 1: Interpretation of functional groups in the carrageenan using FT-IR.

Peak position (wave number $\text{cm}^{-1}$ )	Spectroscopic assignments	Functional groups
$3457.74 \text{ cm}^{-1}$	O-H stretch, H-bonding	Alcohol, phenol
$2349.36 \text{ cm}^{-1}$	C-H stretch	Alkanes
$1687.22 \text{ cm}^{-1}$	-C≡C- stretch	Alkenes
$1187.22 \text{ cm}^{-1}$	C-N stretch	Aliphatic amines
$1222.18-1030.72$	C-O stretch	Alcohols, carboxylic acids, esters, and ethers
$1444.61 \text{ cm}^{-1}$	C-H bend	Alkanes
$920.72 \text{ cm}^{-1}$	C-O-C stretch	3, 6-anhydro-L-galactose
$845.44 \text{ cm}^{-1}$	C-H stretch	Aromatics
$650.30 \text{ cm}^{-1}$	-C≡C-H: C-H bend	Alkynes

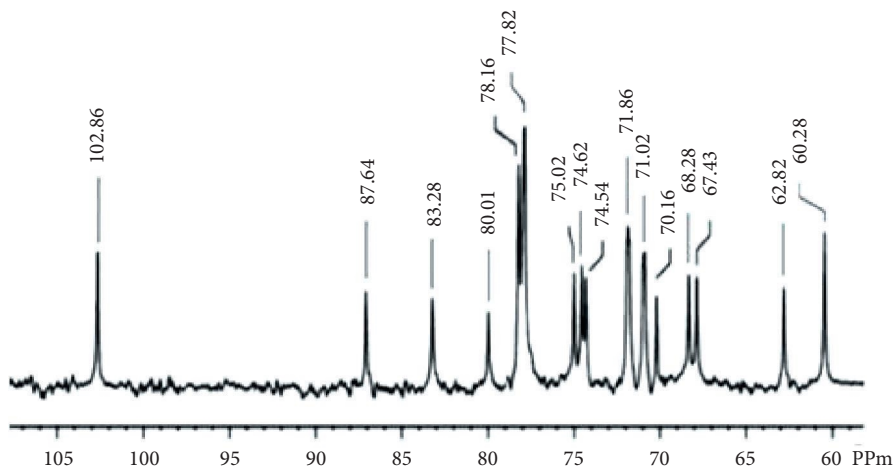


FIGURE 2:  $^{13}\text{C}$ -NMR spectrum of the carrageenan from *Hypnea valentiae*.

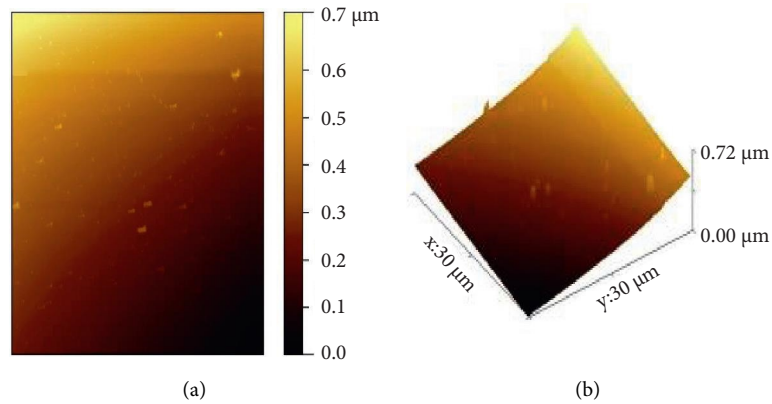


FIGURE 3: AFM of the carrageenan from *Hypnea valentiae*.

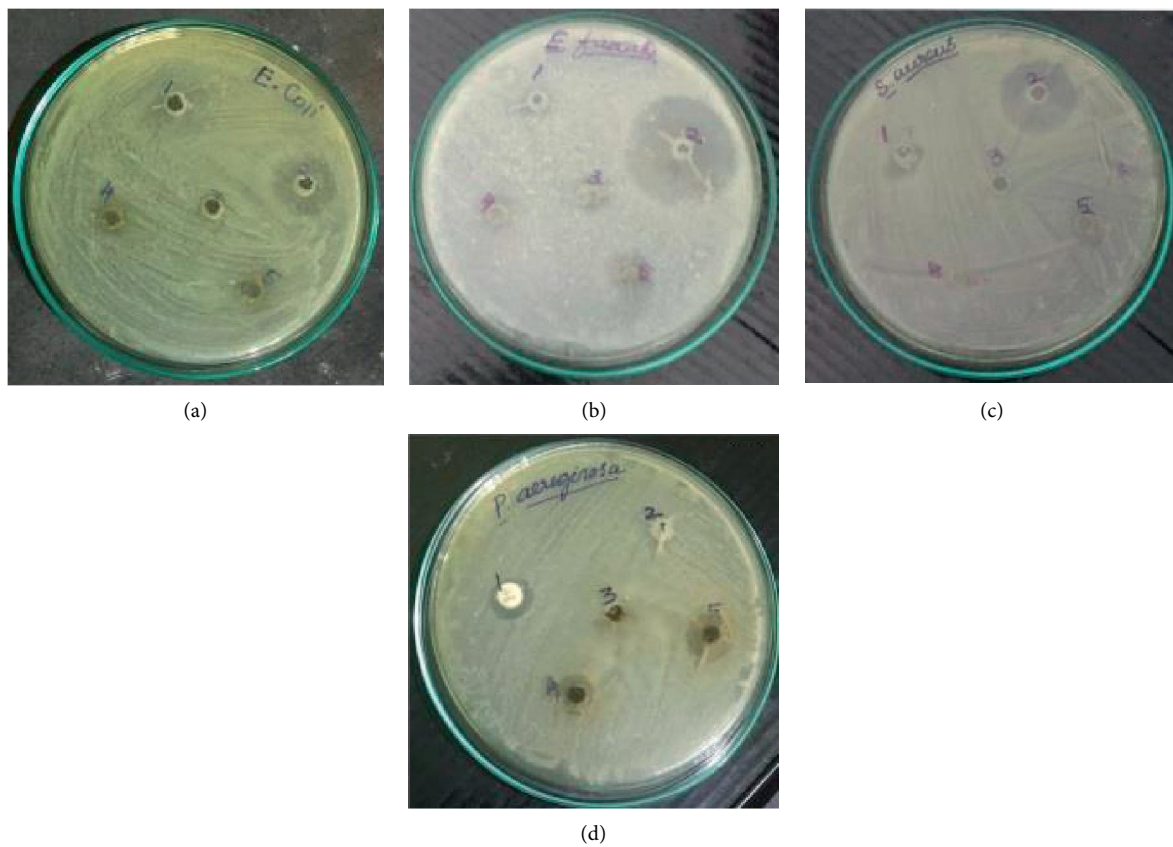


FIGURE 4: The zone of inhibition for methanol extracts of *Hypnea valentiae* activity against (a) *E. coli*, (b) *E. faecalis*, (c) *P. aeruginosa*, and (d) *S. aureus*. 1—methanol, 2—antibiotic *streptomycin*, 3—methanol extract 10 mg/mL, 4—methanol extract 20 mg/mL, and 5—methanol extract 40 mg/mL.

TABLE 2: The zone of inhibition for methanol extracts of *Hypnea valentiae* activity against bacterial species.

Bacteria	Zone of inhibition (mm)				
	1	2	3	4	5
<i>E. coli</i>	$3.0 \pm 0.577$	$5.0 \pm 0.577$	0	$1.0 \pm 0.577$	$1.0 \pm 0.274$
<i>E. faecalis</i>	$1.0 \pm 0.577$	$9.0 \pm 1.155$	0.00	$1.0 \pm 0.288$	$2.0 \pm 0.577$
<i>P. aeruginosa</i>	$2.0 \pm 0.320$	$0.0 \pm 0.000$	0.00	$3.0 \pm 0.111$	$5.0 \pm 0.412$
<i>S. aureus</i>	$1.0 \pm 0.000$	$8.0 \pm 1.155$	0	$0.0 \pm 0.000$	$0.0 \pm 0.000$

\*Data are mean=SE ( $n=3$ ). 1—methanol, 2—antibiotic *Streptomycin*, 3—methanol extract 10 mg/mL, 4—methanol extract 20 mg/mL, and 5—methanol extract 40 mg/mL.

TABLE 3: The effect of *Hypnea valentiae* methanol extracts on antibiofilm activity *E. faecalis* and *P. aeruginosa*.

Pathogens	Concentrations of methanol extracts of <i>H. valentiae</i> ( $\mu\text{g/mL}$ )				
	10	20	30	40	50
<i>E. faecalis</i>	$1.0 \pm 0.211$	$4.2 \pm 0.392$	$7.5 \pm 0.555$	$10.0 \pm 0.709$	$11.1 \pm 0.885$
<i>P. aeruginosa</i>	$4.0 \pm 0.380$	$7.0 \pm 0.885$	$9.1 \pm 0.692$	$12.0 \pm 0.883$	$14.3 \pm 0.979$

\*Data are mean $\pm$ SE ( $n=3$ ).

TABLE 4: Antioxidant activity of *Hypnea valentiae* methanol extract.

Extract/positive control	Antioxidant activity, %		
	DPPH, $\mu\text{g/mL}$	OH, $\mu\text{g/mL}$	Total antioxidant, $\mu\text{g/mL}$
Carrageenan	$65.74 \pm 0.58$	$65.72 \pm 0.60$	$70.1 \pm 0.61$
BHA	$79.01 \pm 0.70$	$77.93 \pm 0.70$	$81.99 \pm 0.75$
L-ascorbic acid	$82.05 \pm 0.73$	$81.14 \pm 0.73$	$87.22 \pm 0.80$

based on *E. faecalis* Gram +ve and *P. aeruginosa* Gram -ve bacterial activity obtained in the results shown in Table 3, respectively. The different concentrations of methanol extract (10, 20, 30, 40, and 50  $\mu\text{g/mL}$ ) were tested. The highest activity against antibiofilm activity ( $11.1 \pm 0.885$  at 50  $\mu\text{g/mL}$ ) methanol extract was recorded for *E. faecalis*. In *P. aeruginosa*, the inhibition of the biofilm activity rate as  $14.3 \pm 0.979$  at 50  $\mu\text{g/mL}$  concentration of methanol extract was found. The percentage of inhibition in *E. faecalis* activity effect methanol extract was significantly higher than that in *P. aeruginosa*. The current study investigates the antibiofilm activity of *H. valentiae* extracts bacterial activity against two different bacterial strains.

Total antioxidant activity was measured to evaluate the antioxidant capacity of sulfated polysaccharides from *H. valentiae* extracts. The carrageenan extract was shown to reduce the total antioxidant scavenging activity of radicals ( $70.1 \pm 0.61\%$ ) at 250  $\mu\text{g/mL}$  concentration rather than at the other concentrations of 50–250  $\mu\text{g/mL}$  of the displayed activities. Based on the findings visualized (Table 4) and noticed, the carrageenan was found to have significantly higher total antioxidant activities as compared with L-ascorbic acid ( $87.22 \pm 0.80\%$ ) and BHA ( $81.99 \pm 0.75\%$ ). The antiradical assay was determined by measuring the absorbance of the inhibition of DPPH radicals. The seaweed extract of sulfated polysaccharide showed that higher inhibition activity of these radicals ( $65.74 \pm 0.58\%$ ) values for DPPH scavenging at 160  $\mu\text{g/mL}$  concentration rather than at the other concentrations. According to the results shown in (Table 4), carrageenan has the potential for radical scavenging activity when compared to the compounds of L-ascorbic acid ( $82.05 \pm 0.73\%$ ) and BHA ( $79.01 \pm 0.70\%$ ) that demonstrated effective DPPH neutralizing activity.

The hydrogen radical scavenging assay was used to determine the inhibition of hydroxyl (OH) radical formation, and the results showed that the scavenging activity of sulfated polysaccharide was significant with increasing concentrations. The extract of carrageenan inhibited the hydrogen peroxide scavenging activity of the OH radical ( $65.72 \pm 0.60\%$ ) at 125  $\mu\text{g/mL}$  concentration rather than at the other concentrations of 25–125  $\mu\text{g/mL}$  of the exhibited

TABLE 5: Anticoagulant activity of *Hypnea valentiae*.

Extraction/control	Clotting time	
	APTT, 25 $\mu\text{g/mL}$	PT, 25 $\mu\text{g/mL}$
Carrageenan	$106.4 \pm 0.65$	$57.3 \pm 0.70$
Heparin-sulfate	$175.2 \pm 0.85$	$126.5 \pm 0.88$

activities. Furthermore, as shown in Table 4, carrageenan exhibited significantly higher hydroxyl radical activities when compared to L-ascorbic acid ( $81.140.73\%$ ) and BHA ( $77.930.70\%$ ).

The study of anticoagulant activity was analyzed by the APTT and PT assays which demonstrated that the anticoagulant mechanism of carrageenan inhibits plasma coagulation release during the regular phase of the coagulation process blood clotting time (Table 5). The anticoagulant activity of carrageenan was exhibited higher in APTT ( $106.50$  IU at 25  $\mu\text{g/mL}$ ) when compared with the PT test ( $57.86$  IU at 25  $\mu\text{g/mL}$ ) indicating the pathway to inhibition.

The carrageenan molecule was subjected to small molecular (ligand) docking, the antioxidant targets chosen as mitochondrial 2-cys peroxiredoxin (2C0D) from *Plasmodium falciparum* and crystal structure of human peroxiredoxin 6 (5B6M). The docking score results of  $-7$  Kcal/mol indicate strong affinity among the complex molecules, and the interaction diagrams of 3D and 2D are represented in Figure 5. The antimicrobial target protein chosen as *S. aureus* tyrosyl-t RNA synthetase (1J1J) and *S. aureus* gyrase topoisomerase II (2XCT) against the small molecule showed a strong affinity in their complex molecule with the least binding score of  $-6.894$  Kcal/mol and with their interactive sites represented (Figure 6). The phytochemical exploited against antioxidant activity using auto dock tool results in  $-3.3$  to  $-6$  Kcal/mol binding score with *in vitro* validation, wherein in our case, it was shown as  $-7$  Kcal/mol using Glide docking, Schrodinger [41]. The anticoagulant target protein was chosen as the crystal structure of thrombin (5E8E) from humans against carrageenan, showing the amino acid interaction as SER546 forms a hydrogen bond with the NH-group, and PO4 forms a hydrogen bond with the O-group with a docking score of  $-6.639$ . The structure was illustrated

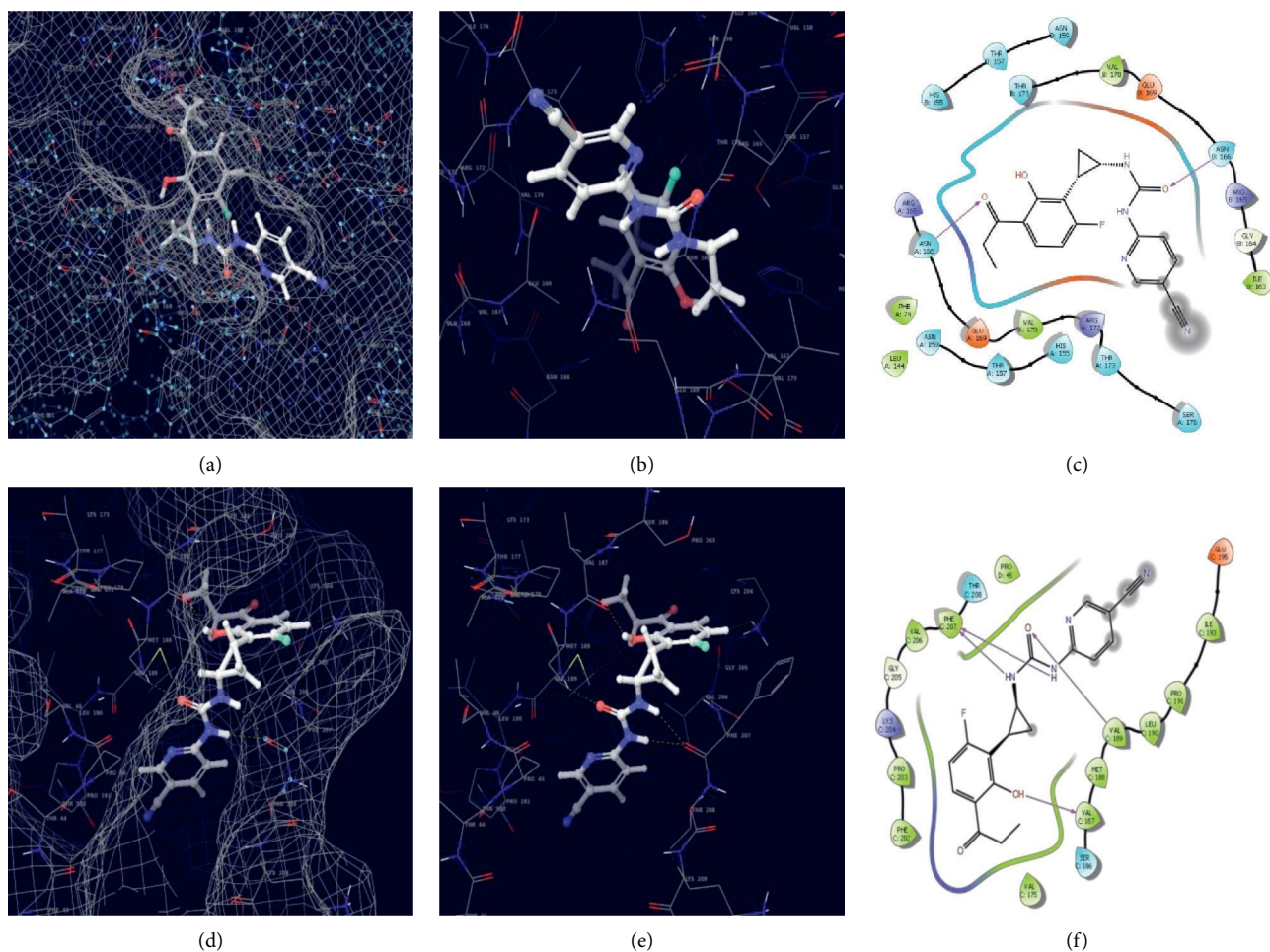


FIGURE 5: Molecular docking of the carrageenan against antioxidant targets (i) 2COD protein. (a) 3D surface mess map interaction site. (b) 3D complex interaction. (c) 2D complex interaction. (ii) 5B6M. (d) 3D surface mess map interaction site. (e) 3D complex interaction. (f) 2D complex interaction.

with 2D and 3D interaction maps with a pocket binding site (Figure 7, Table 6). Carrageenan extracted from *H. valentiae* was found to have the highest larvicidal activity against *A. aegypti* ( $LC_{50} = 99.675 \mu\text{g/mL}$ ;  $LC_{90} = 491.453 \text{ mg/L}$ ) shown (Figure 8, Table 7). The larvicidal activity of seaweeds to the larvae of *A. aegypti* was determined to the inhibition effect of seaweed mortality larvae. Seaweed is a natural product, and particularly, halogenated terpenes might be exploited for the improvement of new larvicidal compounds and its prototype insecticidal agents.

#### 4. Discussion

The present study on methanol extract of *H. valentiae* was tested for yield, antioxidant, antimicrobial, anticoagulant with *in-silico* molecular docking, and larvicidal activity properties. The extract effect is an important parameter for the chemical compounds which have been used in the screening of bioactive substances from red seaweeds enriched with secondary metabolites and have potential antioxidant, antimicrobial, and anticoagulant activities [42].

The FT-IR spectrum is one of the most important tools for polysaccharides and their spectroscopic assignments of functional groups. The O-H stretching of alcohol and phenol vibration from the intramolecular hydrogen bond corresponded to the absorption peak position at  $3457.74 \text{ cm}^{-1}$  [43]. The absorption peaks at  $2349.36\text{--}1687.22 \text{ cm}^{-1}$  is attributable to C-H stretch and  $\text{--C}\equiv\text{C--}$  stretch alkane functional groups, which probably confirmed the polymer-bound water which is a characteristic feature of red seaweed polysaccharides [44]. These absorption bands were described as enhancing the activation of molecular chain movements. Furthermore, the absorption peaks at  $1222.18\text{--}1030.72 \text{ cm}^{-1}$  correspond to assignments of functional groups. C-O stretches alcohols, carboxylic acids, esters, and ethers from lipid triglycerides and fatty acids [45]. The absorption peak position at  $1444.61 \text{ cm}^{-1}$  is attributable to C-H symmetric stretching alkanes. Another characteristic peak  $920.72 \text{ cm}^{-1}$  is attributable to C-O-C stretch 3,6-anhydro-L-galactose in the presence of high sulfated polysaccharides [42]. The absorption peak  $650.30 \text{ cm}^{-1}$  is attributed to  $\text{--C}\equiv\text{C--H}$ : C-H sulfate group alkynes.  $1030.72 \text{ cm}^{-1}$  corresponds to the high



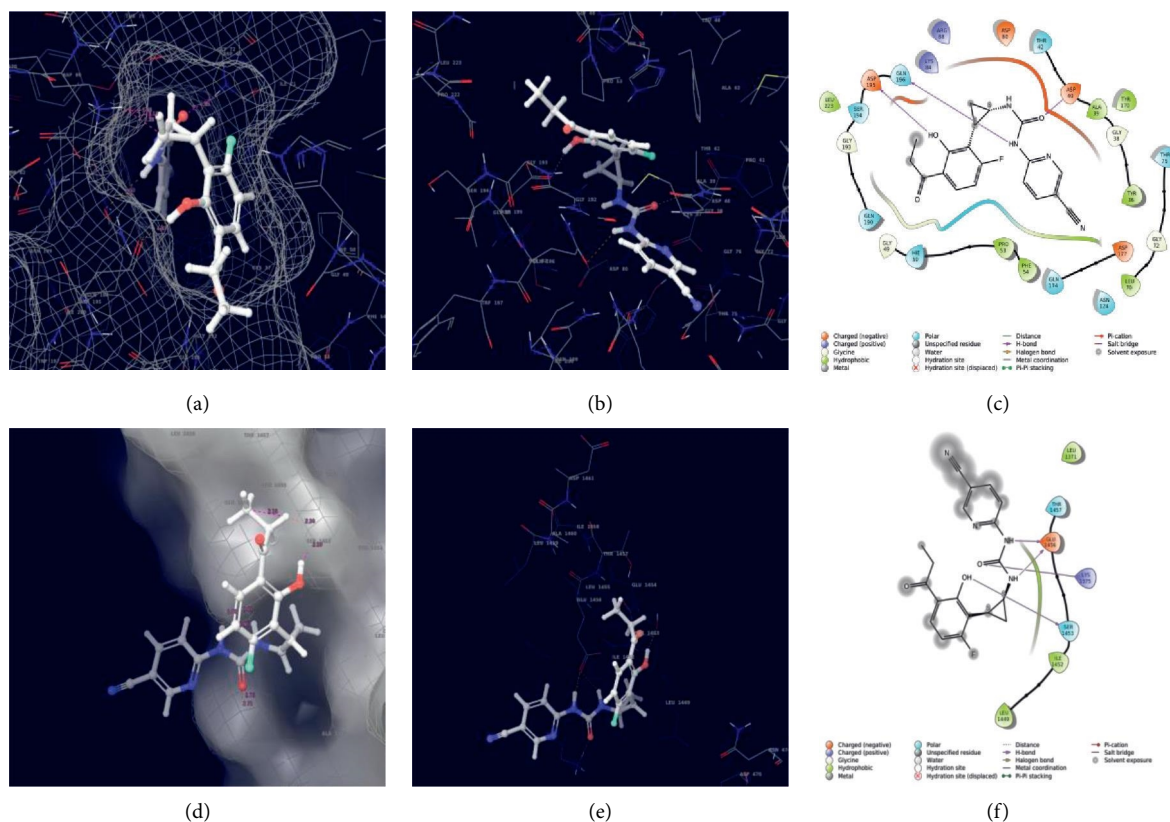


FIGURE 6: *Staphylococcus aureus* tyrosyl-tRNA synthetase docked with carrageenan. (a) 3D surface mesh map interaction site. (b) 3D interaction site. (c) 2D interaction map. *S. aureus* gyrase topoisomerase II docked with carrageenan. (d) 3D surface mesh map interaction site. (e) 3D interaction site. (f) 2D interaction map.

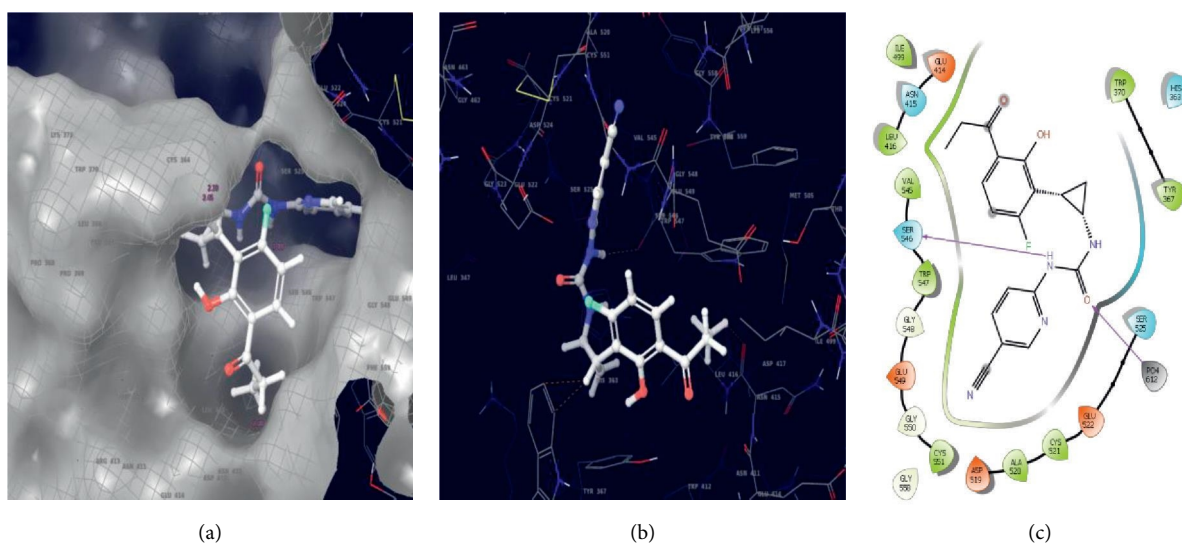


FIGURE 7: Molecular docking of the carrageenan against anticoagulant target proteins of 5EBE. (a) pocket 3D interaction site. (b) 3D complex interaction. (c) 2D complex interaction.

molecular weight skeleton of sulfated D-galactans and carrageenan bands found in *H. valentiae* [46]. These absorption bounds of oxygen, nitrogen, and biofunctional groups confirmed the presence of polyphenol compounds, polysaccharides, and protein, primary, and secondary metabolites.

The NMR spectroscopy is one of the efficient techniques for determining the structural characters of seaweed polysaccharides [47]. Recently, the report has demonstrated that the NMR spectrum used in the presence of different carrageenan components was observed to indicate the conversion of 3,6- $\alpha$ -L-anhydrogalactose units into its alditol



TABLE 6: Molecular docking of the carrageenan molecule against three different activities of 5 multiple targets, the bond length in which the range below 3 Å is hydrogen bond interaction.

S No	PDB	Target activity	Amino acid interaction site	Bond length, Å	Docking score
1	2C0D	Antioxidant	GLY164, ASN166, ASN165	2.22, (2.07, 2.67), 2.50	-7.465
2	5B6M	Antioxidant	VAL189, PHE207, LYS204, VAL187, PHE202	(2.54, 2.25), (2.32, 2.25), 2.13, 1.97, (2.58, 2.45)	-6.227
3	5E8E	Anticoagulant	ASN415, SER546, TRP370	2.38, 2.28, (2.42, 2.39)	-6.639
4	1IJJ	Antimicrobial	GLN196, ASP40, LYS84, ASP195	2.53, 1.95, (1.66 and 2.38) and 1.82	-6.894
5	2XCT	Antimicrobial	GLU1456, LYS1375, SER1453	(1.60, 2.01), (1.78, 2.21) and (2.34, 2.10)	-4.363

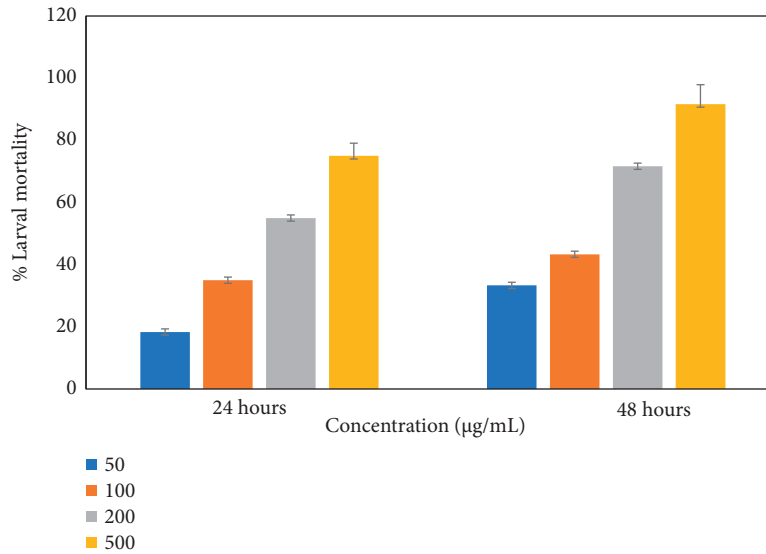


FIGURE 8: Larvicidal activity of *Hypnea valentiae*.

TABLE 7: The effect of aqueous and methanol extract of the *Hypnea valentiae* against *Aedes aegypti* larvae.

Mosquito species	Extract	Hours	LC <sub>50</sub> (µg/mL)	95% confidence limit		LC <sub>90</sub> (µg/mL)	95% confidence limit		x <sup>2</sup>	df
				Lower	Upper		Lower	Upper		
<i>Aedes aegypti</i>	Control (H <sub>2</sub> O)	24	316.083	236.821	488.167	2322.664	1171.696	8645.237	2.823	10
		48	289.440	208.435	486.467	3219.817	1359.596	20753.085	2.514	10
	Methanol (40 µg/250 mL)	24	171.464	134.073	224.234	1081.894	657.746	2603.426	3.415	10
		48	99.675	76.920	123.824	491.453	345.703	876.642	6.845	10

derivatives anomeric protons containing  $\mu$  and  $\nu$  carrageenan [48]. Previous studies illustrate the occurrence of  $\beta$ -D-galactospectroscopic functional group of sulphated polysaccharides in the sugar residues, which are in conform that the trisaccharide branches on bacterial polysaccharide [49, 50]. Collectively, the literature has reported that *Gracilaria caudata* analyzes the structural features of  $\beta$ -D-galactos linked to  $\alpha$ -L-galactose-6-sulfate, and methyl or pyruvate molecules are substituted by carrageenan polysaccharide [47, 51]. These reports indicated that the  $\alpha$ -glycosidic peaks in the carrageenan backbone were partially broken [52]. NMR spectroscopy is also useful for recognizing the conformations of polysaccharides.

The AFM is single molecular spectroscopic technology to detect the conformation of morphological structures of

polysaccharides in AFM images which provides a perfect observation of molecular assembling. The AFM provides visualization of the different types of sulfated polysaccharides such as curdlan [53], xanthan [54], carrageenan [55], xyloglucan [56], pectin [57], arabinoxylan [58], and starch [59]. The previous literature has functionalized the AFM based on the purpose of many fundamental food systems of carrageenan polysaccharides [48]. Similar reports have identified the height range in the structure of the food particles [49]. Based on the findings, the fibrous height of carrageenan was topographically similar to sulfated polysaccharides derived from the red seaweed [44]. The majority of the results from AFM analysis have reviewed the macromolecules of functional food polymers [60]. Therefore, AFM is nanostructure characteristics of polysaccharides

from different food products. The conformation of polymers to identify numerous environmental conditions controlled the temperature [61].

The potential antibacterial activity of carrageenan polysaccharides from *H. valentiae* derivatives was evaluated to affect microbial pathogens of (*E. faecalis* and *S. aureus* (Gram +ve) and *E. coli* and *P. aeruginosa* (Gram -ve) organisms. The antibacterial activity was revealed to be strong against biologically multidrug-resistant pathogens *S. aureus* and *E. faecalis* [52]. In addition, numerous reports have described the antibacterial potential using algae extracts' strong effect on various bacterial pathogens such as *E. coli*, *S. aureus*, and *E. faecalis*. These pathogenic bacterial activities to enhancing the biostimulants of medicinal properties valuable for enhancing the mint and basil antimicrobial activity against bacteria [62]. Previous reports have analyzed the antibacterial activity against bacteria *Spatoglossum asperum* biological and pharmaceutical useful for valuable drugs [50]. The antibacterial activities of highly potential biomedical applications such as drug delivery, wound healing, and tissue engineering. The antibacterial capabilities could improve rapid healing by making a barrier against microbial contamination [63].

In the present study, *H. valentiae* were tested for anti-biofilm activity potential against pathogenic strains that the reports revealed the methanol extract inhibited biofilm formation. Based on the reports, we have identified the biofilm activity inhibition of *Sargassum wightii* and *Halimeda gracillis* seaweed activity against antimicrobial pathogens and antibiofilm activity against various clinically significant pathogenic microorganisms [64]. The previous literature reported that the biofilm activities could be applied in different medical treatments to the prevention of various biofilm-related infections [65]. The biofilm pathogens are eco-friendly to presently used metal-based antifouling agents [66]. Collectively, the results have indicated the significant antibiofilm potential of the *Ulva lactuca* microbicidal effect of different microorganisms that lead to the formation of cariogenic biofilm against the environment. It has been useful to the need for clinical studies to completely enhance the antibiofilm and mechanical properties of the new product [67].

The antioxidant potential of polysaccharides for various free radical scavenging ability of higher polyphenol and flavonoids content was extracted, and they could have excellent antioxidant activity [68]. The antioxidant activity having higher polyphenol content in soluble fraction is observed to precipitate. The highly effective of polyphenol and flavonoids compounds with their hydroxyl group for scavenging free radicals [64]. The antioxidant activity of polysaccharides could protect the human system from reactive oxygen species which affect such macromolecules as membrane lipids, proteins, and DNA and lead to many functional disorders of the human body. In the current study, phenolic content was higher in methanol extract from *H. valentiae* which were screened for total antioxidant activity at 250  $\mu\text{g/ml}$  concentration. The highest total antioxidant activity is present in the methanol precipitate from *H. valentiae* ( $70.1 \pm 0.61\%$ ). Previous literature reports have

indicated the highest total antioxidant activity in the fractionated polysaccharides from *Turbinaria conoides* (246.6 mg AscAE/g) *Gracilaria filiformis* (353.3 AscAE mg/g), and *Enteromorpha compressa* (326.6 mg AscAE/g) [27]. Similar results have reported the highest total antioxidant activity occurred in extract sulfated polysaccharides *Sargassum tenerrimum* ( $22.0 \pm 06$ ) [69]. Similarly, the study reported the total antioxidant activity in aqueous extract of *codium* sp which showed the activity of  $85.53 \pm 0.25\%$  [70]. The results revealed that the polysaccharides conformed that the total antioxidant activity which was the highest inhibition in the methanol extract from the red seaweed. The potential antioxidant activity screened for DPPH radical scavenging was due to their hydrogen donating ability. The free radical scavenging activity indicated a higher value in methanol extract from *H. valentiae* ( $65.74 \pm 0.58\%$ ). Based on the results, the highest scavenging ability was present in the ethanolic precipitate of *S. wightii* ( $78.3 \pm 0.25\%$ ) [64]. The antioxidant activity of polysaccharides extracted from *Undaria pinnatifida* showed that the highest inhibition of hydrogen peroxide screening ability [71]. In our study, the occurrence of the sulfate group to activate the hydrogen atom of the anomeric carbon through the sulfate content to adsorb the antioxidant exhibited the scavenging ability of *Sargassum thunbergii* [72]. The same other results demonstrated that the sulfated polysaccharide effect on inhibiting the formation of these radicals was higher in the extract from *Laminaria japonica* [73].

The results showed that the exhibited hydroxyl radical formations determine the scavenging activity of sulfated polysaccharides was significantly higher than the extract from *H. valentiae* ( $65.72 \pm 0.60\%$ ). The hydroxyl radical result reveals the damage to the biomolecules including protein, deoxyribonucleic acid, and polyunsaturated fatty acids in the human cell membrane. These costs must lead to the expansion of various infections including cancer (*Undaria pinnatifida*) [71]. Previous literature reports have demonstrated that sulfate groups of algal polysaccharides are various kinds of biological activities as antioxidant activity in radicals scavenging (*Sargassum thunbergii*) [72]. These results indicate the antioxidant activity of sulfate content had a significant source of hydroxyl radical scavenging ability [20].

The present investigation continues to the methanol extract screening anticoagulant activity. Anticoagulant activity has evaluated the APTT and PT assay that showed higher inhibition of the coagulant in the soluble fraction. The APTT and PT assay demonstrate the anticoagulant mechanism of the carrageenan as blood coagulation. The methanol precipitate of *H. valentiae* inhibited higher APTT (106.50 IU at 25  $\mu\text{g/ml}$ ) and PT (57.86 IU at 25  $\mu\text{g/ml}$ ). The anticoagulant property of the carrageenan was assessed using human plasma from healthy donors. The results found in the APTT assay showed that the carrageenan had higher coagulation properties. The main source of the anticoagulant property of the carrageenan appears could be antithrombic activity [16]. The anticoagulant pathway indicated the potentiality of the sulfated polysaccharides in spreading the coagulation time that paves the technique for more possibility for their application in pharmaceutical industry for drugs [74]. The ray

skin dermatan sulfated DS showed higher anticoagulant activity of the skin DS as shown by APTT and PT anticoagulant drug of interest potentially useful in therapy. The report suggested the higher content of the sulfate group which presented higher coagulant property [75].

Sulfated polysaccharides are heterogeneous natural polymers found in massive quantities in marine algae with a wide range of therapeutic applications due to their chemical structure and composition. The identification of chemicals that reduce inflammation is of importance because inflammation plays a role in illnesses. Antiinflammation activity has been determined using a variety of approaches. With results of *in vitro* assays, several derivatives of carrageenan oligosaccharides had better antioxidant activity than carrageenan oligosaccharides, indicating that chemical modification of carrageenan oligosaccharides could improve their antioxidant activity [76]. The investigations of these studies showed noticeable significance, and the resultant complex molecules amino acid interaction with bond length are depicted in Table 7. Carrageenan had been exploited with antimicrobial, antiviral, and anticancer activity. The current research observed a significant interaction of the carrageenan with multiple targets resulting majorly around  $-7$  to  $-6$  Kcal/mol binding score [28, 77].

The mosquito larvicidal activity of methanol extract from *H. valentiae* has been found in the highest larvicidal activity than the control *A. aegypti* ( $LC_{50} = 99.675 \mu\text{g/mL}$ ;  $LC_{90} = 491.453 \text{ mg/L}$ ). The present investigation focused on the larvicidal efficacy of the potential effect on the development of *H. valentiae* against *A. aegypti*. Based on the results observed in *Padina australis* ( $LC_{50} = 82.55 \text{ mg/mL}$ ), *Sargassum binderi* ( $LC_{50} = 160.07 \text{ mg/mL}$ ), *Bryopsis pennata* ( $LC_{50} = 192.43 \text{ mg/mL}$ ), the methanol extract was much effective on *A. aegypti* larvicidal activities. The report provided information on numerous effects using different seaweed extracts of *A. aegypti* [78]. *Gracilaria filiformis* has been reviewed in the literature larvicidal activity against the larvae *Anopheles stephensi* in which the higher inhibition is  $LC_{50} = 0.255867$  and  $LC_{90} = 3.434589 \text{ mg/L}$  [27]. The mosquito activity of the current research reported damage and shrinkage of cells from the midgut epithelium of the seaweed treated larvae *Anopheles stephensi* and *A. aegypti* which is ( $LC_{50} = 58.34$ ;  $LC_{90} = 114.91$ ). The application of the seaweed extracts is derived from terrestrial aromatic and medicinal values [64]. *Halimeda macroloba* has been reported in the literature in the past ( $LC_{50} = 1119.0$ ;  $LC_{90} = 1890.3$ ) and similarly *Ulva lactuca* ( $LC_{50} = 952.9$ ;  $LC_{90} = 1830.4$ ) and *Caulerpa racemosa* ( $LC_{50} = 886.0$ ;  $LC_{90} = 1790.1$ ) [79]. The same was reported to show the activity against the larvicidal activity of *Hypnea muciformis* and *Padina gymnospora* [80]. Based on the results responsible for the larvicidal action, demonstrating the use of seaweed extracts has high potential as a mosquito control strategy.

## 5. Conclusion

The findings of this study suggested that the natural carrageenan derivatives with high sulfate content have greater radical scavenging antioxidant and antibacterial properties.

Carrageenan from red seaweeds has also been shown to have *in vitro* anticoagulant functions, confirming its explicit role in the coagulation pathway. However, more research is needed to confirm that seaweeds have high mosquitocidal activity in the future. In addition, the carrageenan was evaluated computationally using glide ligand—molecular docking with multiple targets of antimicrobial, antioxidant, and anticoagulant activity. The minimal binding score explicits the strong affinity among the complex molecules. However, our potential candidate needs to further validate the *in vivo* model and extend it to clinical trials.

## Data Availability

The data presented in this study are available on request from the corresponding authors.

## Conflicts of Interest

The authors hereby declare that they have no conflicts of interest.

## Authors' Contributions

This research article is done with the help of collaboration among the authors. Conceptualization was carried out by A.M., W.C., and B.B.; writing of the original manuscript was conducted by K.P and B.B.; methodology, data curation, and formal analysis were performed by K.P., K.P., and V.M.; molecular docking, software, and revision were conducted by M.A.; review and editing were carried out by V.A.M., N.A.A., and V.A.A.; organization of the working groups was conducted by B.B.; interpretation and review/revision were conducted by W.C., V.A.A., B.B., and A.M. All authors revised and approved the final article. Balamuralikrishnan Balasubramanian contributed equally to this work.

## Acknowledgments

The authors are thankful to their respective institutes for their support. Also, the authors were grateful to the authority of the International Centre for Genetic Engineering and Biotechnology (ICGEB), New Delhi, for computation analysis.

## References

- [1] W. Liang, X. Mao, X. Peng, and S. Tang, "Effects of sulfate group in red seaweed polysaccharides on anticoagulant activity and cytotoxicity," *Carbohydrate Polymers*, vol. 101, pp. 776–785, 2014.
- [2] A. Radjasegarin and A. Perumal, "Synergetic effects of seaweed extract and rhizobium on cowpea," *Natura Resource for Human Health*, vol. 1, no. 1, pp. 43–50, 2021.
- [3] C. M. P. G. Dore, M. G. d. C. Faustino Alves, L. S. E. Pofirio Will et al., "A sulfated polysaccharide, fucans, isolated from brown algae *Sargassum vulgare* with anticoagulant, antithrombotic, antioxidant and anti-inflammatory effects," *Carbohydrate Polymers*, vol. 91, no. 1, pp. 467–475, 2013.
- [4] M. B. Mansour, M. Dhahri, M. Hassine et al., "Highly sulfated dermatan sulfate from the skin of the ray *Raja montagui*:

- anticoagulant activity and mechanism of action," *Comparative Biochemistry and Physiology Part B: Biochemistry and Molecular Biology*, vol. 156, no. 3, pp. 206–215, 2010.
- [5] S. Sellimi, I. Younes, H. B. Ayed et al., "Structural, physicochemical and antioxidant properties of sodium alginate isolated from a tunisian brown seaweed," *International Journal of Biological Macromolecules*, vol. 72, pp. 1358–1367, 2015.
  - [6] A. Ben Gara, R. Ben Abdallah Kolsi, N. Jardak et al., "Inhibitory activities of *Cystoseira crinita* sulfated polysaccharide on key enzymes related to diabetes and hypertension: *in vitro* and animal study," *Archives of Physiology and Biochemistry*, vol. 123, no. 1, pp. 31–42, 2016.
  - [7] M. Jin, K. Zhao, Q. Huang, C. Xu, and P. Shang, "Isolation, structure and bioactivities of the polysaccharides from *Angelica sinensis* (oliv.) diels: a review," *Carbohydrate Polymers*, vol. 89, no. 3, pp. 713–722, 2012.
  - [8] K. Senthilkumar, P. Manivasagan, J. Venkatesan, and S. K. Kim, "Brown seaweed fucoidan: biological activity and apoptosis, growth signaling mechanism in cancer," *International Journal of Biological Macromolecules*, vol. 60, pp. 366–374, 2013.
  - [9] L. Wu, J. Sun, X. Su, Q. L. Yu, Q. Y. Yu, and P. Zhang, "A review about the development of fucoidan in antitumor activity: progress and challenges," *Carbohydrate Polymers*, vol. 154, pp. 96–111, 2016.
  - [10] H. A. Bhatti, R. Rubina, F. Rashid, S. Zaib, J. Iqbal, and A. Hameed, "Synthesis and antitumor activities of novel mannich base derivatives derived from natural flavonoids," *Natural Resources for Human Health*, vol. 2, no. 2, pp. 100–106, 2022.
  - [11] C. O. Coura, I. W. F. de Araujo, E. S. O. Vanderlei et al., "Antinociceptive and anti-inflammatory activities of sulphated polysaccharides from the red seaweed *Gracilaria cornea*," *Basic and Clinical Pharmacology and Toxicology*, vol. 110, no. 4, pp. 335–341, 2012.
  - [12] A. M. S. Assreuy, D. M. Gomes, M. S. J. da Silva et al., "Biological effects of a sulfated-polysaccharide isolated from the marine red algae *Champia feldmannii*," *Biological and Pharmaceutical Bulletin*, vol. 31, no. 4, pp. 691–695, 2008.
  - [13] G. S. Viana, A. L. P. Freitas, M. M. Lima, L. Vieira, M. C. Andrade, and N. M. B. Benevides, "Antinociceptive activity of sulfated carbohydrates from the red algae *Bryothamnion seaforthii* (turner) kutz and *B. triquetrum* (S.G. gmel.) M. howe," *Brazilian Journal of Medical and Biological Research*, vol. 35, no. 6, pp. 713–722, 2002.
  - [14] K. O. A. L. Lins, D. P. Bezerra, A. P. N. N. Alves et al., "Antitumor properties of a sulfated polysaccharide from the red seaweed *Champia feldmannii* (diaz-pifferer)," *Journal of Applied Toxicology*, vol. 29, no. 1, pp. 20–26, 2009.
  - [15] A. M. S. Assreuy, G. C. Pontes, N. V. F. C. Rodrigues et al., "Vascular effects of a sulfated polysaccharide from the red marine alga *Solieria filiformis*," *Natural Product Communications*, vol. 5, no. 8, Article ID 1934578X1000500, 2010.
  - [16] F. R. F. Silva, C. M. P. G. Dore, C. T. Marques et al., "Anticoagulant activity, paw edema and pleurisy induced carrageenan: action of major types of commercial carrageenans," *Carbohydrate Polymers*, vol. 79, no. 1, pp. 26–33, 2010.
  - [17] I. W. F. de Araújo, E. D. S. O. Vanderlei, J. A. G. Rodrigues et al., "Effects of a sulfated polysaccharide isolated from the red seaweed *Solieria filiformis* on models of nociception and inflammation," *Carbohydrate Polymers*, vol. 86, no. 3, pp. 1207–1215, 2011.
  - [18] J. Y. Je, P. J. Park, E. K. Kim et al., "Antioxidant activity of enzymatic extracts from the brown seaweed *Undaria pinnatifida* by electron spin resonance spectroscopy," *Lebensmittel-Wissenschaft und -Technologie- Food Science and Technology*, vol. 42, no. 4, pp. 874–878, 2009.
  - [19] S. K. Chandini, P. Ganesan, and N. Bhaskar, "In vitro antioxidant activities of three selected brown seaweeds of India," *Food Chemistry*, vol. 107, no. 2, pp. 707–713, 2008.
  - [20] W. S. Bartolomeu, A. Miguel, I. Ana et al., "Chemical characterization and antioxidant activity of sulfated polysaccharide from the red seaweed," *Gracilaria birdiae*. *Food Hydrocolloids*, vol. 27, pp. 287–292, 2012.
  - [21] J. Wang, Q. Zhang, Z. Zhang, H. Song, and P. Li, "Potential antioxidant and anticoagulant capacity of low molecular weight fucoidan fractions extracted from laminaria japonica," *International Journal of Biological Macromolecules*, vol. 46, no. 1, pp. 6–12, 2010.
  - [22] World Health Organization, *Dengue and Severe Dengue*, WHO, Geneva, Switzerland, 2013.
  - [23] S. A. Al-Shami, J. A. Mahyoub, M. Hatabbi, A. H. Ahmad, and C. S. M. Rawi, "An update on the incidence of dengue gaining strength in Saudi Arabia and current control approaches for its vector mosquito," *Journal of Parasites & Vectors*, vol. 7, 2014.
  - [24] M. M. Thiboutot, S. Kannan, O. U. Kawalekar et al., "Chikungunya: A Potentially Emerging Epidemic," *Neglected Tropical Diseases*, vol. 4, p. e623, 2010.
  - [25] O. Salvador-Neto, S. A. Gomes, A. R. Soares et al., "Larvicidal potential of the halogenated sesquiterpene (+)-obtusol, isolated from the alga *Laurencia dendroidea* J. agardh (Ceramiales: rhodomelaceae), against the dengue vector mosquito *Aedes aegypti* (Linnaeus)(diptera: culicidae)," *Marine Drugs*, vol. 14, no. 2, p. 20, 2016.
  - [26] K. X. Yu, I. Jantan, R. Ahmad, and CL. Wong, "The major bioactive components of seaweeds and their mosquitocidal potential," *Parasitology Research*, vol. 113, no. 9, pp. 3121–3141, 2014.
  - [27] M. Venkatesan, V. Arumugam, R. Pugalendi et al., "Antioxidant, anticoagulant and mosquitocidal properties of water soluble polysaccharides (WSPs) from Indian seaweeds," *Process Biochemistry*, vol. 84, pp. 196–204, 2019.
  - [28] M. Arunkumar, S. Gunaseelan, M. Kubendran Aravind et al., "Marine algal antagonists targeting 3CL protease and spike glycoprotein of SARS-CoV-2: a computational approach for anti-COVID-19 drug discovery," *Journal of Biomolecular Structure and Dynamics*, pp. 1–28, 2021.
  - [29] V. Suresh, N. Senthilkumar, R. Thangam et al., "Separation, purification and preliminary characterization of sulfated polysaccharides from *sargassum plagiophyllum* and its *in vitro* anticancer and antioxidant activity," *Process Biochemistry*, vol. 48, no. 2, pp. 364–373, 2013.
  - [30] X. Li, L. Wang, Y. Wang, and Z. Xiong, "Effect of drying method on physicochemical properties and antioxidant activities of *Hohenbuehelia serotina* polysaccharides," *Process Biochemistry*, vol. 51, no. 8, pp. 1100–1108, 2016.
  - [31] C. Vetrivel, B. Balamuralikrishnan, K. Durairaj et al., "Fabrication and characterization of noble crystalline silver nanoparticles from ceropogia bulbosa roxb root tuber extract for antibacterial, larvicidal and histopathology applications," *Nanoscience and Nanotechnology Letters*, vol. 11, pp. 11–21, 2019.
  - [32] P. Balaraman, B. Balasubramanian, D. Kaliannan et al., "Phyco-synthesis of silver nanoparticles mediated from marine alga *sargassum myriocystum* and its potential biological

- and environmental applications,” *Waste and Biomass Valorization*, vol. 11, no. 10, pp. 5255–5271, 2020.
- [33] P. Prieto, M. Pineda, and M. Aguilar, “Spectrophotometric quantitation of antioxidant capacity through the formation of a phosphomolybdenum complex: specific application to the determination of vitamin E,” *Analytical Biochemistry*, vol. 269, no. 2, pp. 337–341, 1999.
- [34] D. L. Spector, R. D. Goldman, and L. A. Leinwand, *Cells: A Laboratory Manual*, Cold Spring Harbor Laboratory Press, New York, NY, USA, 1998.
- [35] E. C. Leong, L. He, and H. Rahardjo, “Factors affecting the filter paper method for total and matric suction measurements,” *Geotechnical Testing Journal*, vol. 25, no. 3, pp. 322–332, 2002.
- [36] L.-O. Andersson, T. W. Barrowcliffe, E. Holmer, E. A. Johnson, and G. E. C. Sims, “Anticoagulant properties of heparin fractionated by affinity chromatography on matrix-bound antithrombin III and by gel filtration,” *Thrombosis Research*, vol. 9, no. 6, pp. 575–583, 1976.
- [37] A. J. Quick, “The clinical application of the hippuric acid and the prothrombin tests,” *American Journal of Clinical Pathology*, vol. 10, no. 3, pp. 222–233, 1940.
- [38] V. Cittrarasu, D. Kaliannan, K. Dharman et al., “Green synthesis of selenium nanoparticles mediated from *Ceropegia bulbosa* roxb extract and its cytotoxicity, antimicrobial, mosquitocidal and photocatalytic activities,” *Scientific Reports*, vol. 11, no. 1, 2021.
- [39] D. Elumalai, P. Hemalatha, and P. Kaleena, “Larvicidal activity and GC-MS analysis of *Leucas aspera* against *Aedes aegypti*, *Anopheles stephensi* and *Culex quinquefasciatus*,” *Journal of the Saudi Society of Agricultural Sciences*, vol. 16, no. 4, pp. 306–313, 2017.
- [40] A. F. Hifney, M. A. Fawzy, K. M. Abdel-Gawad, and M. Gomaa, “Industrial optimization of fucoidan extraction from *Sargassum sp.* and its potential antioxidant and emulsifying activities,” *Food Hydrocolloids*, vol. 54, pp. 77–88, 2016.
- [41] D. Salaria, R. Rolta, N. Sharma et al., “*In vitro* and *in silico* antioxidant and anti-inflammatory potential of essential oil of cymbopogon citratus (DC.) stapf. of north-western Himalaya,” *Journal of Biomolecular Structure and Dynamics*, pp. 1–15, 2021.
- [42] A. Arulkumar, T. Rosemary, S. Paramasivam, and R. B. Rajendran, “Phytochemical composition, *in vitro* antioxidant, antibacterial potential and GC-MS analysis of red seaweeds *Gracilaria corticata* and *Gracilaria edulis* from palk bay,” *Indian, Biocatalysis and agricultural Biotechnology*, vol. 15, pp. 63–71, 2018.
- [43] F. N. Baleta, J. M. Bolaños, O. C. Ruma, A. N. Baleta, and J. D. Cairel, “Phytochemicals screening and antimicrobial properties of *Sargassum oligocystum* and *Sargassum crassifolium* extracts,” *Journal of Medicinal Plants Studies*, vol. 5, no. 1, pp. 382–387, 2017.
- [44] B. M. Khan, H. M. Qiu, S. Y. Xu, Y. Liu, and K. L. Cheong, “Physicochemical characterization and antioxidant activity of sulphated polysaccharides derived from *Porphyra haitanensis*,” *International Journal of Biological Macromolecules*, vol. 145, pp. 1155–1161, 2020.
- [45] A. C. Leri, M. R. Dunigan, R. L. Wenrich, and B. Ravel, “Particulate organohalogens in edible brown seaweeds,” *Food Chemistry*, vol. 272, pp. 126–132, 2019.
- [46] L. Cunha and A. Grenha, “Sulfated seaweed polysaccharides as multifunctional materials in drug delivery applications,” *Marine Drugs*, vol. 14, pp. 14–42, 2016.
- [47] F. C. Barros, D. C. da Silva, V. G. Sombra et al., “Structural characterization of polysaccharide obtained from red seaweed *Gracilaria caudata* (J Agardh),” *Carbohydrate polymers*, vol. 92, no. 1, pp. 598–603, 2013.
- [48] D. Yang and H. Yang, “The temperature dependent extraction of polysaccharides from eucheuma and the rheological synergistic effect in their mixtures with kappa carrageenan,” *Lebensmittel-Wissenschaft & Technologie*, vol. 129, Article ID 109515, 2020.
- [49] L. Yang and L. M. Zhang, “Chemical structural and chain conformational characterization of some bioactive polysaccharides isolated from natural sources,” *Carbohydrate Polymers*, vol. 76, no. 3, pp. 349–361, 2009.
- [50] S. Palanisamy, M. Vinosha, T. Marudhupandi, P. Rajasekar, and N. M. Prabhu, “*In vitro* antioxidant and antibacterial activity of sulfated polysaccharides isolated from *spatoglossum asperum*,” *Carbohydrate Polymers*, vol. 170, pp. 296–304, 2017.
- [51] M. Tabarsa, S. J. Lee, and S. You, “Structural analysis of immunostimulating sulfated polysaccharides from *Ulva pertusa*,” *Carbohydrate Research*, vol. 361, pp. 141–147, 2012.
- [52] E. H. Junior, A. G. Gonçalves, M. D. Nosedá, M. E. R. Duarte, F. S. Murakami, and D. R. Ducatti, “Semi-synthesis of N-alkyl-kappa-carrageenan derivatives and evaluation of their antibacterial activity,” *Carbohydrate Research*, vol. 499, Article ID 108234, 2021.
- [53] M. Xiao, M. Jiang, K. Wu et al., “Investigation on curdlan dissociation by heating in water,” *Food Hydrocolloids*, vol. 70, pp. 57–64, 2017.
- [54] S. K. Gulrez, S. Al-Assaf, Y. Fang, G. O. Phillips, and A. P. Gunning, “Revisiting the conformation of xanthan and the effect of industrially relevant treatments,” *Carbohydrate Polymers*, vol. 90, no. 3, pp. 1235–1243, 2012.
- [55] J. Necas and L. Bartosikova, “Carrageenan: a review,” *Veterinarni Medicina*, vol. 58, no. 4, pp. 187–205, 2013.
- [56] N. Lucyszyn, A. F. Lubambo, L. Ono, T. A. Jo, C. F. De Souza, and M. R. Sierakowski, “Chemical, physico-chemical and cytotoxicity characterisation of xyloglucan from *Guibourtia hymenifolia* (Moric.) J. leonard seeds,” *Food Hydrocolloids*, vol. 25, no. 5, pp. 1242–1250, 2011.
- [57] W. G. Willats, J. P. Knox, and J. D. Mikkelsen, “Pectin: new insights into an old polymer are starting to gel,” *Trends in Food Science & Technology*, vol. 17, no. 3, pp. 97–104, 2006.
- [58] A. P. Gunning, A. R. Mackie, A. R. Kirby, P. Kroon, G. Williamson, and V. J. Morris, “Motion of a cell wall polysaccharide observed by atomic force microscopy,” *Macromolecules*, vol. 33, no. 15, pp. 5680–5685, 2000.
- [59] J. Maley, E. K. Asare, M. Bága, B. G. Rossnagel, R. N. Chibbar, and R. Sammynaiken, “Application of aerosol-spray deposition for determination of fine structure of barley starch using atomic force microscopy,” *Starch Staerke*, vol. 62, no. 12, pp. 676–685, 2010.
- [60] B. M. Khan, L. X. Zheng, W. Khan, A. A. Shah, Y. Liu, and K. L. Cheong, “Antioxidant potential of physicochemically characterized *Gracilaria blodgettii* sulfated polysaccharides,” *Polymers*, vol. 13, no. 3, p. 442, 2021.
- [61] J. Wang and S. Nie, “Application of atomic force microscopy in microscopic analysis of polysaccharide,” *Trends in Food Science & Technology*, vol. 87, pp. 35–46, 2019.
- [62] H. O. Elansary, K. Yessoufou, S. Shokralla, E. A. Mahmoud, and K. Skalicka-Woźniak, “Enhancing mint and basil oil composition and antibacterial activity using seaweed extracts,” *Industrial Crops and Products*, vol. 92, pp. 50–56, 2016.



- [63] S. Sellimi, H. Maalej, D. M. Rekik et al., "Antioxidant, anti-bacterial and in vivo wound healing properties of laminaran purified from *Cystoseira barbata* seaweed," *International Journal of Biological Macromolecules*, vol. 119, pp. 633–644, 2018.
- [64] S. Suganya, R. Ishwarya, R. Jayakumar et al., "New insecticides and antimicrobial derived from *Sargassum wightii* and *Halimeda gracillis* seaweeds; toxicity against mosquito vectors and anti-biofilm activity against microbial pathogens," *South African Journal of Botany*, vol. 125, pp. 466–480, 2019.
- [65] D. Viszwapriya, U. Prithika, S. Deebika, K. Balamurugan, and S. K. Pandian, "In vitro and in vivo antibiofilm potential of 2, 4-Di-tert-butylphenol from seaweed surface associated bacterium *Bacillus subtilis* against group A," *Microbiological Research*, vol. 191, pp. 19–31, 2016.
- [66] D. M. Salem, M. M. Ismail, and H. R. Tadros, "Evaluation of the anti-biofilm activity of three seaweed species and their biosynthesized iron oxide nanoparticles ( $\text{Fe}_3\text{O}_4$ -NPs)," *Egyptian Journal of Aquatic Research*, vol. 46, no. 4, pp. 333–339, 2020.
- [67] M. Pourhajibagher, A. Salehi-Vaziri, M. Noroozian et al., "An orthodontic acrylic resin containing seaweed ulva lactuca as a photoactive phytochemical in antimicrobial photodynamic therapy: assessment of anti-biofilm activities and mechanical properties," *Photodiagnosis and Photodynamic Therapy*, vol. 35, pp. 102–295, 2021.
- [68] G. N. Rajivgandhi, C. C. Kanisha, G. Ramachandran et al., "Phytochemical screening and anti-oxidant activity of *Sargassum wightii* enhances the anti-bacterial activity against *Pseudomonas aeruginosa*," *Saudi Journal of Biological Sciences*, vol. 28, no. 3, pp. 1763–1769, 2021.
- [69] M. S. G. Mohan, A. Achary, V. Mani, E. Cicinskas, A. A. Kalitnik, and M. Khotimchenko, "Purification and characterization of fucose-containing sulphated polysaccharides from *Sargassum tenerrimum* and their biological activity," *Journal of Applied Phycology*, vol. 31, no. 5, pp. 3101–3113, 2019.
- [70] G. Kallswari, S. Mahendran, P. Subalakshmi, T. Shankar, and P. Ponmanickam, "Purification, characterization and antioxidant activity of green seaweed *Codium sp.*," *Advances in Pharmacology and Pharmacy*, vol. 4, no. 2, pp. 16–21, 2016.
- [71] H. S. A. Koh, J. Lu, and W. Zhou, "Structure characterization and antioxidant activity of fucoidan isolated from *Undaria pinnatifida* grown in New Zealand," *Carbohydrate Polymers*, vol. 212, pp. 178–185, 2019.
- [72] M. C. Kang, H. Lee, H. D. Choi, and Y. J. Jeon, "Antioxidant properties of a sulfated polysaccharide isolated from an enzymatic digest of *Sargassum thunbergii*," *International Journal of Biological Macromolecules*, vol. 132, pp. 142–149, 2019.
- [73] Z. Duan, W. Duan, F. Li, Y. Li, P. Luo, and H. Liu, "Effect of carboxymethylation on properties of fucoidan from *Laminaria japonica*: antioxidant activity and preservative effect on strawberry during cold storage," *Postharvest Biology and Technology*, vol. 151, pp. 127–133, 2019.
- [74] P. Shobharani, V. H. Nanishankar, P. M. Halami, and N. M. Sachindra, "Antioxidant and anticoagulant activity of polyphenol and polysaccharides from fermented *Sargassum sp.*," *International Journal of Biological Macromolecules*, vol. 65, pp. 542–548, 2014.
- [75] M. Ben Mansour, R. Balti, V. Ollivier, H. Ben Jannet, F. Chaubet, and R. M. Maaroufi, "Characterization and anticoagulant activity of a fucosylated chondroitin sulfate with unusually procoagulant effect from sea cucumber," *Carbohydrate Polymers*, vol. 174, pp. 760–771, 2017.
- [76] H. Yuan, J. Song, W. Zhang, X. Li, N. Li, and X. Gao, "Antioxidant activity and cytoprotective effect of  $\kappa$ -carrageenan oligosaccharides and their different derivatives," *Bioorganic & Medicinal Chemistry Letters*, vol. 16, no. 5, pp. 1329–1334, 2006.
- [77] T. V. Pham, H. N. T. Hoang, H. T. Nguyen et al., "Anti-inflammatory and antimicrobial activities of compounds isolated from *Distichochlamys benenica*," *BioMed Research International*, vol. 2021, Article ID 6624347, 10 pages, 2021.
- [78] K. X. Yu, C. L. Wong, R. Ahmad, and I. Jantan, "Larvicidal activity, inhibition effect on development, histopathological alteration and morphological aberration induced by seaweed extracts in *Aedes aegypti* (Diptera: Culicidae)," *Asian Pacific Journal of Tropical Medicine*, vol. 8, no. 12, pp. 1006–1012, 2015.
- [79] G. Adaikala Raj, M. Jayaraman, S. Krishnamoorthy, M. Chandrasekaran, and V. Venkatesalu, "Screening of different extracts of marine macro algae for larvicidal activity against dengue fever mosquito, *Aedes aegypti* (diptera: culiadae)," *International Letters of Natural Sciences*, vol. 62, pp. 44–51, 2017.
- [80] E. A. C. Guedes, C. M. D. Carvalho, K. A. L. Ribeiro Junior et al., "Larvicidal activity against *Aedes aegypti* and molluscicidal activity against *Biomphalaria glabrata* of Brazilian marine algae," *Journal of Parasitology Research*, vol. 2014, pp. 1–6, 2014.

## Research Article

# Deciphering the Metabolomics-Based Intervention of Yanghe Decoction on Hashimoto's Thyroiditis

Xing Zhang , Dexuan Chen , Kun Xu , and Zhaoqun Ma 

Surgery of Chinese Medicine, Nanjing University of Chinese Medicine Affiliated Yancheng Chinese Medicine Hospital, No. 56 Renmin Road, Yancheng 224000, China

Correspondence should be addressed to Zhaoqun Ma; zhaqunma00@outlook.com

Received 17 February 2022; Revised 5 May 2022; Accepted 7 May 2022; Published 15 July 2022

Academic Editor: Ruchika Garg

Copyright © 2022 Xing Zhang et al. This is an open access article distributed under the Creative Commons Attribution License, which permits unrestricted use, distribution, and reproduction in any medium, provided the original work is properly cited.

**Background.** Yanghe decoction is a famous formula consisting of *Rehmannia*, deer horn gum, cinnamon, rue, *Ephedra*, ginger charcoal, and licorice. However, few studies have explored the role of the potential mechanism of Yanghe decoction in the treatment of Hashimoto's thyroiditis by metabolomics. **Methods.** Nine mice were randomly divided into three groups: control group (group C), model group (group M), and drug administration group (group T), with three mice in each group. Mice in groups M and T were established as models of Hashimoto's thyroiditis, and group T was treated with Yanghe decoction. The metabolome of plasma samples from each group of mice was determined using mass spectrometry coupled with high-performance liquid and gas phases, and nuclear magnetic resonance. Based on the three assays, principal component analysis was performed on all samples, as well as orthogonal partial least squares-discriminant analysis and differential metabolite molecules for groups M and T. Subsequently, pathway enrichment analysis was performed, and the intersection was taken for the differential metabolites screened in the M and T groups. The levels of inflammatory factors IL-35 and IL-6 within the serum of each group of mice were detected. **Results.** The difference analysis showed that a total of 38 differential metabolites were screened based on mass spectrometry coupled with the high-performance liquid phase, 120 differential metabolites were screened based on mass spectrometry coupled with gas phase, and a total of  $\alpha$ -glucose and  $\beta$ -glucose were the differential metabolites analyzed based on NMR test results. The pathways enriched by the differential metabolites in the M and T groups were intersected, and a total of 5 common pathways were obtained (amino acid tRNA biosynthesis, D-glutamine, D-glutamate metabolism, tryptophan metabolism, nitrogen metabolism, and arginine and proline metabolism). The results also showed a significant decrease in the serum inflammatory factor IL-35 and a significant increase in IL-6 in mice from group M compared with group C, while a significant increase in the serum inflammatory factor IL-35 and a significant decrease in IL-6 in mice from group T compared with group M. **Conclusion.** Our study reveals the metabolites as well as a metabolic network that can be altered by Yanghe decoction treatment of Hashimoto's thyroiditis and shows that Yanghe decoction can effectively reduce the level of inflammatory factors in Hashimoto's thyroid.

## 1. Introduction

Hashimoto's thyroiditis, also known as chronic lymphocytic or autoimmune thyroiditis, is an autoimmune thyroid disease that causes the immune system to attack and destroy the thyroid gland [1]. It is characterized by an enlarged thyroid gland, parenchymal lymphocytic infiltration, and the presence of thyroid antigen-specific antibodies [2]. Hashimoto's thyroiditis causes chronic inflammation of the

thyroid tissue and may result in hypothyroidism in 20–30% of patients [3]. The incidence is approximately 3 to 6 cases per 10,000 people per year, with a prevalence of at least 2% in women. The glands involved in thyroiditis often lose the ability to store iodine, produce and secrete thyroid proteins that circulate in the plasma, and fail to make hormones efficiently [4,5]. At present, methylprednisolone is often used in clinical practice for Hashimoto's thyroiditis treatment, which could inhibit the synthesis of the thyroid gland and alleviate the

patient's clinical symptoms. However, research has shown that the use of methimazole alone in patients with Hashimoto's thyroiditis for long term often have poor prognosis.

Traditional Chinese medicine is remarkably effective in the adjuvant treatment of the disease, especially in improving clinical symptoms, prolonging patient survival, and modulating immune function. As an effective method for preventing and treating diseases, TCM has been increasingly used worldwide in the past decades [6]. Yanghe decoction is a famous formula consisting of *Rehmannia*, deer horn gum, cinnamon, rue, *Ephedra*, ginger charcoal, and licorice [7]. It has the effect of warming yang and nourishing blood and dispersing cold and moving stagnation. For centuries, Yang He Tang has been proven to be used to treat a variety of noninfectious inflammatory conditions [8].

Yanghe decoction can be combined with modern therapies, which have a combination of "multicomponent, multitarget, and multipathway" regulatory mechanisms and have fewer toxic side effects [9]. In one study, Yang He Tang was shown to have a high mean cure rate (defined as complete regression or significant improvement of lumps and pain for at least two months) in patients with chronic breast fibrosis and palpable lumps [10]. Fewer studies have clinically investigated the effect of Yanghe decoction in the treatment of Hashimoto's thyroiditis. Therefore, the present study was conducted to investigate the potential mechanism of Yanghe decoction in the treatment of Hashimoto's thyroiditis through a metabolomic approach.

## 2. Material and Methods

**2.1. Animal Grouping and Model Construction.** Nine NOD mice (4 weeks old) were purchased from the Nanjing Biomedical Research Institute of Nanjing University. NOD mice were randomly divided into three groups: control group (group C), model group (group M), and drug administration group (group T), with three mice in each group. The mice in the model group and the drug administration group were treated with porcine thyroglobulin and high iodine water to establish the mouse model of autoimmune thyroiditis. After successful modeling, Yanghe decoction formula granule (Xuyang Pharmaceutical Co., LTD., China) was prepared into 0.5 g/mL liquid medicine; the drug-administered group was given 0.5 g/ml Yanghe decoction formula 1 ml/100 g by gavage for 1 h, and the model group and normal group were given the same amount of saline by gavage once a day for 10 weeks. The serum and plasma samples were collected and stored at  $-20^{\circ}\text{C}$  for serum and  $-80^{\circ}\text{C}$  for plasma. The study protocols were approved by the Institutional Animal Care and Use Committee of Nanjing University of Chinese Medicine Affiliated Yancheng.

**2.2. Enzyme-Linked Immunosorbent Assay.** The serum collected was assayed for IL-35 (interleukin-35) and IL-6 (interleukin-6) inflammatory factors using enzyme-linked immunosorbent assay (ELISA) kits. The experiment was performed according to the instructions.

**2.3. Mass Spectrometry Coupled with Ultra-High Performance Liquid-Phase Detection.** Metabolite extraction was performed in strict accordance with the operating instructions, followed by onboard detection.

**On-Board Detection.** The target compounds were chromatographed on a Waters ACQUITY UPLCBEH Amide ( $2.1\text{ mm} \times 100\text{ mm}$ ,  $1.7\text{ }\mu\text{m}$ ) column using a Vanquish (Thermo Fisher Scientific) ultra-performance liquid chromatography. The A phase of the liquid chromatography was aqueous containing 25 mmol/L ammonium acetate and 25 mmol/L ammonia, and the B phase was acetonitrile. The sample tray temperature is  $4^{\circ}\text{C}$ , and injection volume is  $2\text{ }\mu\text{L}$ .

The Thermo Q Exactive HFX mass spectrometer was capable of primary and secondary mass spectrometry data acquisition under the control of the control software Xcalibur (Thermo). Detailed parameters were as follows: sheath gas flow rate, 30 Arb; Aux gas flow rate, 25 Arb; capillary temperature:  $350^{\circ}\text{C}$ ; full ms resolution, 60000; MS/MS resolution, 7500; collision energy, 10/30/60 in NCE mode; and spray voltage: 3.6 kV (positive) or  $-3.2\text{ kV}$  (negative).

**Data Processing.** The raw data were converted to mzXML format by ProteoWizard software, and then the peak identification, peak extraction, peak alignment, and integration were performed using the R package (kernel XCMS) written by ourselves and then matched with the BiotreeDB (V2.1) self-built secondary mass spectrometry database for substance annotation.

**2.4. Mass Spectrometry Coupled with Gas Chromatography Detection.** Metabolite extraction was performed strictly according to the operating instructions, and then all samples were analyzed by gas chromatography and time-of-flight mass spectrometry.

**On-Board Detection.** GC-TOF-MS analysis was performed using an Agilent 7890 gas chromatograph and a time-of-flight mass spectrometer. The system used a DB-5MS capillary column.  $1\text{ }\mu\text{L}$  aliquots were injected in a nonsplit mode. Helium was used as the carrier gas with a front inlet purge flow rate of  $3\text{ mL min}^{-1}$  and a gas flow rate through the column of  $1\text{ mL min}^{-1}$ . The initial temperature was held at  $50^{\circ}\text{C}$  for 1 min, then increased to  $310^{\circ}\text{C}$  at a rate of  $20^{\circ}\text{C}$ , and then held at  $310^{\circ}\text{C}$  for 6 min. The injection, transmission line, and ion source temperatures were 280, 280, and  $250^{\circ}\text{C}$ , respectively. The energy in electron collision mode was  $-70\text{ eV}$ . After a solvent delay of 4.83 min, mass spectral data were acquired in full-scan mode in the  $m/z$  range of 50–500 at a rate of 12.5 spectra per second.

**Data Processing.** The mass spectral data were analyzed for peak extraction, baseline correction, deconvolution, peak integration, and peak alignment using ChromaTOF software (V 4.3x, LECO). For the substance characterization work, the LECO-Fiehn Rtx5 database was used, including mass spectrometry matching and retention time index matching.

**2.5. Nuclear Magnetic Resonance Detection.** The experimental testing equipment was Varian Inova 600M Agilent.

**Description of the Spectral Processing.** The integration interval of the serum NMR spectra was 0.5–8.5 ppm with an integration spacing of 0.002 ppm, and a section of 4.60–4.80 ppm containing the residual water peak and the urea peak at 5.20–5.25 ppm and the region of its influence was removed. Among them, the demonstration of mouse serum spectra for groups C, M, and T were chosen: 1, 9, and 17, respectively.

**2.6. Principal Component Analysis (PCA).** Data were formatted for logarithmic (LOG) transformation plus centralization (CTR) using SIMCA software (V16.0.2; Sartorius Stedim Data Analytics AB, Umea, Sweden), followed by automated modeling analysis.

**2.7. Orthogonal Partial Least Squares-Discriminant Analysis (OPLS-DA).** The data were UV-formatted using SIMCA software (V14.1; MKS Data Analytics Solutions, Umea, Sweden), and OPLS-DA modeling analysis was first performed on the first principal component, and the quality of the model was tested with 7-fold cross-validation (7-fold cross-validation). Then, R2Y (interpretability of the model for the categorical variable Y) and Q2 (predictability of the model) were used to judge the validity of the model; finally, the validity of the model was further tested by a permutation test, which randomly changed the order of the categorical variable Y several times to obtain different random Q2 values.

**2.8. Pathway Enrichment Analysis.** The metabolic pathways of differentially expressed metabolites were analyzed by searching the relevant metabolic pathways of differentially expressed metabolites using authoritative metabolite databases such as Kyoto Encyclopedia of Genes and Genomes (KEGG) and PubChem.

### 3. Results

**3.1. Principal Component Analysis.** First, we performed PCA on the results of the three assays to observe the overall metabolic levels and species differences between the groups. The results of principal component analysis (positive ions) of the mass spectrometry coupled with gas and high-performance liquid phases showed that the samples of groups M and T were more closely distributed and both groups were distant from the samples of group C. The results of the NMR principal component analysis showed that the samples of groups M and T were distributed more into and partitioned from the samples of group C. This can all indicate that the more similar the type and content of metabolites in groups M and T, the more different the overall metabolic levels in groups M and T from group C. The samples were all in the 95% confidence interval. See Figure 1.

**3.2. Orthogonal Partial Least Squares-Discriminant Analysis (OPLS-DA) and Differential Metabolite Analysis.** We then modeled OPLS-DA for the M and T groups and screened for differential metabolites. The scatter plots of OPLS-DA model scores for the three assays showed that the horizontal distance between samples was farther for group M versus group T, which could indicate the greater the difference between the two groups, and the samples were very clearly differentiated. The samples were all in the 95% confidence interval. The results of the differential metabolite analysis showed that a total of 38 differential metabolites were screened for the mass spectrometry coupled with high-performance liquid phase (Table 1); a total of 120 differential metabolites were screened for the mass spectrometry coupled with gas phase (Table 2), and the conditions for this metabolite screening were VIP value (the projected importance of the variable obtained from the OPLS-DA model for the comparison of the substance in this group) > 1 and  $P < 0.05$ . NMR analysis showed that  $\alpha$ -glucose and  $\beta$ -glucose were significant differentiating metabolites (see Figure 2).

**3.3. Enrichment Analysis of Metabolic Pathways of Differential Metabolites.** We further analyzed the effect of differential metabolites on their pathways. The analysis based on the mass spectrometry combined with high-performance liquid phase detection results showed that the differential metabolites in the M and T groups were enriched to 11 pathways (Table 3), among which the pathways with higher enrichment were histidine metabolism, amino acid tRNA biosynthesis, phenylalanine, tyrosine and tryptophan biosynthesis, tryptophan metabolism, phenylalanine metabolism, cysteine, and methionine metabolism. The analysis based on the results of mass spectrometry combined with gas-phase detection showed that the differential metabolites of the M and T groups were enriched to 28 pathways (Table 4), among which the pathways with higher enrichment were pyrimidine metabolism, biosynthesis of pantothenic acid and CoA, metabolism of  $\beta$ -alanine, sulfur metabolism, glycerolipid metabolism, and metabolism of glycine, serine, and threonine. Subsequently, we took the intersection of the pathways enriched by the differential metabolites in the M and T groups for both high-performance liquid- and gas-phase methods coupled to mass spectrometry and obtained a total of five common pathways (biosynthesis of amino acid tRNA, metabolism of D-glutamine and D-glutamate, metabolism of tryptophan, metabolism of nitrogen, and metabolism of arginine and proline). See Figure 3

**3.4. Comparison of Serum Inflammatory Factor Levels in Three Groups of Mice.** Finally, we observed the serum inflammatory factor levels in the three groups of mice to determine the effect of Yanghe decoction on inflammatory factors in mice with Hashimoto's thyroiditis. The results showed that the serum inflammatory factor IL-35 was significantly lower and IL-6 was significantly higher in mice of group M than group C, while the serum inflammatory factor IL-35 was

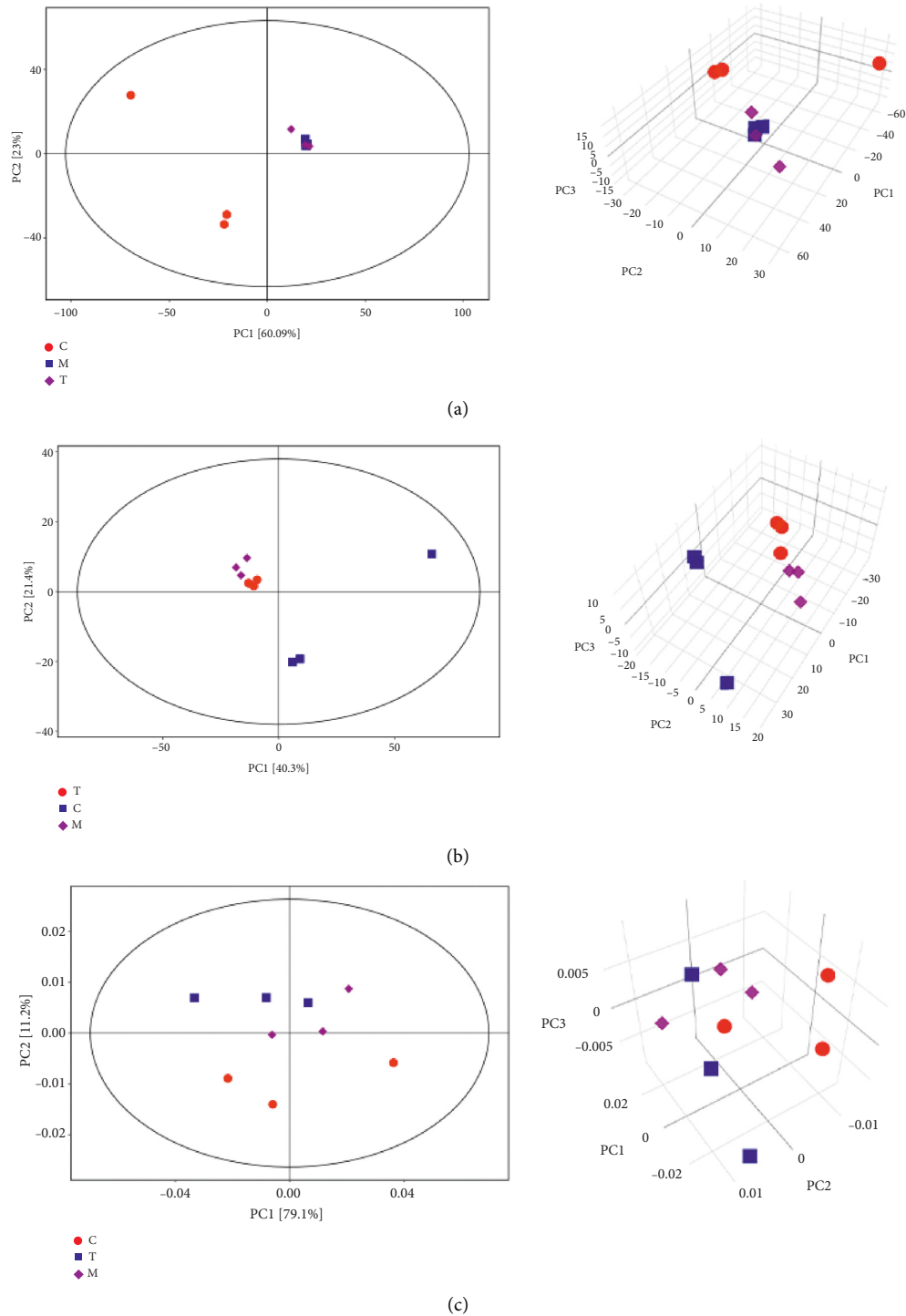


FIGURE 1: Principal component analysis. (a) Scatter plot and 3D plot of PCA scores for all samples detected by mass spectrometry coupled with the high-performance liquid phase. (b) Scatter plot and 3D plot of PCA scores for all samples detected by mass spectrometry coupled with the gas phase. (c) Scatter plot and 3D plot of PCA scores of all samples detected by NMR.

significantly higher and IL-6 was significantly lower in mice of group T than group M. The results showed that the serum inflammatory factor IL-35 was significantly lower and IL-6 was significantly lower in mice of group T than group C. See Figure 4.

#### 4. Discussion

Metabolism plays a central role as a signaling molecule, immunomodulator, endogenous toxin, and environmental sensor in all areas of biology, from ecology to bioengineering to cancer. Each of these fields is now increasingly being



TABLE 1: Differential metabolites detected by mass spectrometry and high-performance liquid chromatography.

ID	MS2 name	MS2 score	rt	mz	SuperClass	Type	MEAN T	MEAN M	VIP	P-value	Q-value	FOLD CHANGE	LOG <sub>2</sub> FOLDCHANGE
22	D-Glutamine	0.999291	389.5485	147.0759376	Organic acids and derivatives	Forward	3.746183952	3.446653347	1.931664281	0.014765644	1	1.086904767	0.120225539
47	Trigonelline	0.995484	301.0875	138.0543287	Alkaloids and derivatives	Forward	1.024957601	0.838952133	2.022165048	0.046051103	1	1.221711658	0.288903828
54	N-Acetylhistamine	0.994856	147.787	154.0968957	Organic acids and derivatives	Forward	0.073990814	0.110698454	1.829180635	0.025585478	1	0.668399709	-0.58121699
56	Kanzonol K	0.994656	35.0689	437.1927582	Phenylpropanoids and polyketides	Forward	0.051954891	0.031048015	2.101281275	0.001974289	1	1.673372393	0.742758539
69	L-Methionine	0.991602	301.415	150.0577251	Organic acids and derivatives	Forward	0.616919645	0.468069797	1.939910681	0.019678144	1	1.318007803	0.398358912
99	Egonine	0.981134	350.546	186.1120848	Alkaloids and derivatives	Forward	0.027347509	0.030654513	1.926689881	0.031693069	1	0.892120183	-0.164690017
101	L-histidine	0.979726	408.5865	156.0761942	Organic acids and derivatives	Forward	0.49405337	0.223894139	2.08197046	0.008582433	1	2.206638244	1.141850134
107	L-phenylalanine	0.977905	275.944	166.0854692	Organic acids and derivatives	Forward	4.763771466	3.828460241	1.897216209	0.034322892	1	1.244304803	0.315339929
112	L-alanine	0.975801	363.879	90.05507238	Organic acids and derivatives	Forward	0.437920469	0.363410363	1.912131498	0.031994707	1	1.205030219	0.269069326
138	Phytosphingosine	0.965381	57.8408	318.299383	Organic nitrogen compounds	forward	1.743529266	1.126406912	1.948385533	0.021992696	1	1.547868047	0.630282489
141	Pentanenitrile	0.962912	266.604	84.08082795	Organonitrogen compounds	Forward	0.264520137	0.226518588	2.005800964	0.018824486	1	1.167763487	0.223748107
153	Imidazoleacetic acid riboside	0.954489	370.1495	259.0919389	Nucleosides, nucleotides, and analogues	Forward	0.014965502	0.019469476	2.040287972	0.006044593	1	0.768664826	-0.379573442
156	3beta.6beta-Dihydroxynortropine	0.948011	52.1612	144.1012842	Alkaloids and derivatives	Forward	0.118818145	0.086495728	2.050482112	0.004431311	1	1.373688018	0.458054387
158	L- kynurenine	0.944886	280.281	209.0914398	Organic oxygen compounds	Forward	0.10372474	0.082802841	1.987721923	0.013173077	1	1.252671263	0.32500786
160	Arecaidine	0.944798	282.167	142.0858524	Alkaloids and derivatives	Forward	0.080085294	0.053014131	2.016796656	0.022004872	1	1.510640518	0.595160389
161	Carnosine	0.942805	434.3945	227.113435	Organic acids and derivatives	Forward	0.048044936	0.066372136	1.819056239	0.031112771	1	0.723872074	-0.466193334
169	Thelephoric acid	0.935613	407.237	353.0278188	Organoheterocyclic compounds	Forward	0.002605381	0.003775405	1.806140708	0.033212017	1	0.690093214	-0.535136849
180	L-acetylcarnitine	0.92253	320.788	204.1225337	Lipids and lipid-like molecules	Forward	3.698529842	2.839908003	1.877147018	0.024898946	1	1.302341427	0.381107721
204	Alpha-methylstyrene	0.898642	35.2889	119.0850948	Benzenoids	Forward	0.188441473	0.131632093	2.159887496	0.001577729	1	1.431576978	0.517605248
228	Glycerophosphocholine	0.86945	400.206	258.1089005	Lipids and lipid-like molecules	Forward	0.615951963	0.925741511	1.864643532	0.035821933	1	0.665360638	-0.587791573
230	1-(beta-D-ribofuranosyl)-1,4-dihydronicotinamide	0.865109	171.668	257.1128126	Organic oxygen compounds	Forward	0.117325608	0.138566581	2.138035911	0.004789509	1	0.846709269	-0.240061413
238	D-bioterin	0.853104	272.631	238.0928999	Organoheterocyclic compounds	Forward	0.026486036	0.021446249	1.82825674	0.040439888	1	1.234996232	0.304506664
240	N-(3-methylbutyl)acetamide	0.850798	268.9475	130.1221116	Organic acids and derivatives	Forward	0.058209581	0.049743365	2.142098263	0.00620136	1	1.170197912	0.226752549
254	N-acetylmethine	0.829892	374.192	175.1070165	Organic acids and derivatives	Forward	0.056279893	0.047008306	1.830587028	0.035370672	1	1.197232943	0.259703882
259	1-(Hydroxymethyl)-5,5-dimethyl-2,4-imidazolinedione	0.818992	407.131	159.0757679	Organoheterocyclic compounds	Forward	0.182086983	0.155835556	1.945664927	0.01442075	1	1.168455928	0.224603319
291	Biochanin A	0.769766	39.59165	285.07362	Phenylpropanoids and polyketides	forward	0.031721703	0.041732531	1.920254712	0.018257478	1	0.760119332	-0.395702167
295	Heptadecanoyl carnitine	0.756939	194.733	414.3571643	Lipids and lipid-like molecules	Forward	0.017403164	0.022118651	2.137696573	0.00072227	1	0.786809469	-0.345913775
315	3-[(3-Methylbutyl)nitrosoamino]-2-butanone	0.715231	36.73805	187.1434871	Organoxygen compounds	Forward	0.339965307	0.457120856	2.061300025	0.008977331	1	0.743709903	-0.427188112
320	2-Acetylpyrazine	0.710279	330.908	123.0549956	Organoxygen compounds	Forward	0.013123324	0.008784152	1.970470389	0.02020786	1	1.493977369	0.579158294
328	Sedoheptulose 1-phosphate	0.700854	40.022	291.0477486	Organic oxygen compounds	Forward	0.051097691	0.069345806	2.046508406	0.007069591	1	0.736853377	-0.4440550522

TABLE 1: Continued.

ID	MS2 name	MS2 score	rt	mz	SuperClass	Type	MEAN T	MEAN M	VIP	P-value	Q-value	FOLD CHANGE	LOG-FOLDCHANGE
360	Glechomaturan	0.646208	224.3045	231.1407859	Lipids and lipid-like molecules	Forward	0.010033971	0.014750196	2.095991059	0.002844627	1	0.680260196	-0.55584142
384	LysoPC(17:0)	0.611195	214.164	510.3549507	Lipids and lipid-like molecules	Forward	0.772031639	1.046868823	1.889934534	0.045513658	1	0.73746741	-0.4393488
410	Acetyl-N-formyl-5-methoxytryptamine	0.577916	24.7427	265.1210007	Organic oxygen compounds	Forward	0.010452578	0.006475994	2.18949614	9.71037E-05	1	1.614049998	0.690685269
430	Cysteinyl-serine	0.560691	25.0757	209.0581161	Organic acids and derivatives	Forward	0.542806005	0.285681699	1.941743744	0.041010554	1	1.900037726	0.926028064
435	L-octanoylcarnitine	0.556023	224.21	288.2159451	Lipids and lipid-like molecules	Forward	0.064410974	0.089677252	2.106970841	0.002284565	1	0.718253205	-0.47743557
442	S-methylmethionine	0.553207	336.697	164.0731609	Benzenoids	Forward	0.032573318	0.044869274	1.846945723	0.032907818	1	0.725960445	-0.462037152
471	4-Aminohippuric acid	0.488799	315.061	184.0895643	Lipids and lipid-like molecules	Forward	0.009328513	0.023072876	1.911670897	0.010251036	1	0.404306452	-1.306478867
477	PE(16:0/18:3(9Z,12Z,15Z))	0.471196	164.6285	714.5059277	Lipids and lipid-like molecules	Forward	0.043175276	0.027338873	1.838157839	0.032662642	1	1.579271456	0.659259173
ID	The unique data number of the substance in this qualitative analysis												
MS2 name	The substance name obtained by qualitative matching analysis of secondary mass spectrometry												
MS2 score	The score of the second-level match, with the value [0, 1]												
rt	Chromatographic retention time of the substance												
mz	Material characteristics mass charge ratio of ions												
SuperClass	Classification information of the substance in the HMDB database												
Type	The matching mode includes MS2 forward/reverse matching (MS2 forward/reverse), first-order average molecular weight/single isotope molecular weight matching and no matching												
MEAN OO	The mean of the relative quantitative value of the substance in one of the experimental groups within the group comparison												
MEAN XX	The mean of the relative quantitative value of the substance in the other experimental group within the group comparison												
VIP	The substance in the group was compared to the OPLS-DA model obtained by the variable projection significance												
P-value	The P-value obtained by the t-test of this substance in the group comparison, P-value = probability of hypothesis being correct but rejected = number of negative results/total number of results, is a test probability against the sample data												
Q-value	The hypothesis test statistic (p-value) is the result after the correction of multiple hypothesis test. Q value = the probability of being rejected but correct = the number of false-positive results/the number of presumed positive results. It is a test probability of the inference obtained from statistical test and the re-statistics of p-value												
FOLD CHANGE	The substance in this group was compared with the multiple relationship between the two groups of experiments												
LOG_FOLDCHANGE	FOLD CHANGE takes the logarithm base 2												

TABLE 2: Differential metabolites detected by mass spectrometry combined with gas phase.

ID	Peak2	Similarity	rt	Count	Mass	MEAN T	MEAN M	VIP	P-value	Q-value	FOLD CHANGE	LOG <sub>2</sub> FOLDCHANGE
69	2-Hydroxybutanoic acid	923	5.90393,0	9	131	1.272515066	1.829157	1.299843399	0.030824766	0.054717746	0.695683796	-0.523496376
87	3-Hydroxybutyric acid	917	6.15207,0	9	147	25.48762597	38.1509	1.435772881	0.006906593	0.031058352	0.668074026	-0.581920125
228	L-malic acid	910	8.38126,0	9	73	15.02098304	24.18815	1.206850204	0.045844599	0.064707169	0.621005853	-0.68732123
407	Palmitoleic acid	903	11.4327,0	9	55	4.427715453	6.258029	1.236645983	0.049653209	0.067078325	0.707525543	-0.499145861
410	Palmitic acid	878	11.5306,0	9	117	20.90998716	28.73753	1.309850706	0.025056075	0.05026023	0.727619379	-0.458744127
68	Glycine 1	876	5.88319,0	9	102	3.920530889	5.969469	1.437149115	0.003623146	0.031058352	0.656763806	-0.606553473
144	glycerol	855	6.94956,0	9	205	14.73609113	22.11935	1.316507776	0.030374647	0.054407164	0.666620819	-0.585955005
234	Threitol	852	8.47978,0	9	217	3.320598289	0.534807	1.439750027	0.003284907	0.031058352	0.599465913	-0.738250374
273	Alpha-ketoglutaric acid	826	8.93667,0	9	73	4.392760756	7.040861	1.19046366	0.04958074	0.067078325	0.623895417	-0.680623882
172	Uracil	822	7.43667,0	9	241	0.382125402	0.661469	1.353053457	0.022060725	0.047455437	0.577691894	-0.791627843
184	Pelargonic acid	794	7.60111,0	9	215	0.046390864	0.07566	1.23255862	0.043826199	0.063362351	0.613151594	-0.705684289
222	Aminomalonic acid	791	8.28837,0	9	218	0.413476931	0.584889	1.244433147	0.031388031	0.055098631	0.706932665	-0.50035529
206	2-Deoxytetronic acid	780	8.01104,0	9	73	4.28775664	6.992805	1.380659529	0.007758549	0.031058352	0.613169609	-0.705641901
85	3-Hydroxypyridine	778	6.0817,0	9	152	0.233075193	0.349579	1.473437449	0.004190223	0.031058352	0.666731544	-0.584822111
769	4-Hydroxybutyrate	769	6.69919,0	9	233	0.018386599	0.032341	1.34064562	0.025110742	0.050307906	0.568527482	-0.814698006
427	heptadecanoic acid	745	11.985,0	9	117	0.110508121	0.168502	1.336703207	0.032082258	0.055556587	0.655828223	-0.608610108
197	Thymine	677	7.85356,0	9	270	0.043778381	0.066104	1.371605211	0.012906566	0.037801216	0.662263926	-0.59452182
110	Malonic acid 1	674	6.46348,0	9	141	0.120153186	0.212515	1.480974611	0.001576369	0.031058352	0.56538798	-0.822686883
99	Methyl phosphate	665	6.28585,0	9	241	0.115662474	0.211687	1.463936501	0.002727024	0.031058352	0.5463833	-0.872014707
207	Beta-alanine 2	643	8.03652,0	9	248	0.054056527	0.101364	1.421035491	0.014950627	0.039659996	0.533289189	-0.907010013
162	2,3-Dihydroxypyridine	633	7.28778,0	9	240	0.086432291	0.12972	1.393394351	0.006663844	0.031058352	0.666297891	-0.585760767
463	N-acetyl-5-hydroxytryptamine 1	590	13.2097,0	9	290	160.0062516	231.7193	1.303021085	0.041478731	0.061714361	0.690517501	-0.534250115
113	3-Aminoisobutyric acid 2	520	6.51726,0	9	57	0.32200107	0.496484	1.338967469	0.015637714	0.04020852	0.648562563	-0.624682345
307	1,2-Cyclohexanedione 4	517	9.492,0	8	205	0.101748813	0.181678	1.387571447	0.026616559	0.051576505	0.560051285	-0.836369152
216	Erythrose 1	514	8.18007,0	9	350	0.689931679	1.092036	1.272409468	0.028301472	0.052900868	0.631784782	-0.662494907
219	Capric acid	508	8.24689,0	9	117	0.161212023	0.274597	1.358543235	0.010727066	0.035339822	0.587086555	-0.768354878
146	2-Deoxyuridine	503	7.01356,0	3	81	0.000258002	0.659853	1.539040505	0.016123039	0.040576096	0.000390999	-11.32054852
377	D-altrose 2	487	10.8282,0	3	257	0.000258002	0.138383	1.541803731	0.000279156	0.031058352	0.0018644	-9.067072758
111	Methylmalonic acid	481	6.46941,0	9	226	0.210469269	0.423913	1.496235451	0.002203188	0.031058352	0.496491996	-1.010157634
285	Digitoxose 1	452	9.08156,0	3	73	0.000258002	0.000388	1.382297717	0.007898488	0.031058352	0.664566179	-0.589515221
246	trans-4-Hydroxy-L-proline 2	449	8.64244,0	3	186	0.000258002	0.000388	1.382297717	0.007898488	0.031058352	0.664566179	-0.589515221
88	Sulfuric acid	419	6.16896,0	9	281	0.759582216	1.140343	1.321189491	0.030078726	0.054199895	0.666099824	-0.586189695
218	2,4-Diaminobutyric acid 3	416	8.2337,0	9	103	0.177346978	0.279941	1.370608087	0.009107719	0.030374562	0.633516577	-0.658545725
425	d-Glucose 1	412	11.9031,0	7	319	0.012258146	0.021077	1.315429516	0.039316399	0.060377704	0.581574962	-0.781962934
501	Isomaltose 2	410	15.118,0	7	73	0.21680148	0.330811	1.462708603	0.005347921	0.031058352	0.655363457	-0.609632863
211	N-acetyl-L-leucine 2	406	8.12433,0	8	86	0.058678762	0.087162	1.447579125	0.011125631	0.030384826	0.673218373	-0.570853545
309	L-homoserine 3	396	9.52289,0	6	290	0.052160115	0.075824	1.481796159	0.00209498	0.031058352	0.687909761	-0.539708769
77	2-Ketovaleric acid 2	393	5.97089,0	9	89	0.148017445	0.248358	1.44720369	0.004315057	0.031058352	0.595983832	-0.746654902
238	4-Acetamidobutyric acid 2	387	8.55919,0	9	174	0.262681494	0.414491	1.304395218	0.023923344	0.049245254	0.633744092	-0.658027703
343	Biuret 2	385	10.0571,0	6	171	0.131112438	0.111193	1.298491114	0.038783781	0.060035166	1.171379459	0.228208501
149	O-acetylserine 2	384	7.08467,0	3	116	0.000258002	0.000388	1.382297717	0.007898488	0.031058352	0.664566179	-0.589515221
170	Oxamide	382	7.37756,0	9	116	0.638063028	0.963743	1.375059784	0.010946865	0.035615566	0.66206751	-0.594949762

TABLE 2: Continued.

ID	Peak2	Similarity	rt	Count	Mass	MEAN T	MEAN M	VIP	P-value	Q-value	FOLD CHANGE	LOG <sub>2</sub> FOLDCHANGE
193	Resorcinol	364	7.74837,0	9	240	0.1893703	0.270561	1.422135343	0.028840031	0.053304636	0.699917794	-0.514742608
34	2-Ketobutyric acid 2	359	5.37696,0	9	174	3.895398713	6.310969	1.452753771	0.003819666	0.031058352	0.617242587	-0.69609049
495	Maltose	344	14.4673,0	3	204	0.000258002	0.000388	1.382297717	0.007898488	0.031058352	0.664566179	-0.589515221
506	Ergosterol	339	17.6037,0	7	129	0.038142477	0.170062	1.152056064	0.040476247	0.061105175	0.224285234	-2.156593449
290	D-erythronolactone 2	338	9.18748,0	9	244	0.233520567	0.335404	1.338741737	0.015238113	0.03989368	0.696237385	-0.522348811
417	Sinapyl alcohol 1	331	11.7691,0	3	241	0.000258002	0.000388	1.382297717	0.007898488	0.031058352	0.664566179	-0.589515221
416	N-acetyl-D-galactosamine 1	329	11.7478,0	3	202	0.000258002	0.000388	1.382297717	0.007898488	0.031058352	0.664566179	-0.589515221
114	3-Methylamino-1,2-propanediol 1	327	6.52733,0	9	116	0.145928713	0.251951	1.487710076	0.000575224	0.031058352	0.579194579	-0.787879996
92	4-Hydroxypyridine	326	6.20052,0	9	141	0.489927793	0.795927	1.451323971	0.002465951	0.031058352	0.615543839	-0.700066486
251	Cytosine	322	8.68941,0	9	314	2.509840552	4.082056	1.283159978	0.021963317	0.047357392	0.614847194	-0.701700187
507	Cholestane-3,5,6-triol, (3?5?6?)	321	18.7661,0	9	57	0.885146653	2.002186	1.387564892	0.006905578	0.031058352	0.442090187	-1.177587384
295	2-Carboxybenzaldehyde	318	9.29889,0	3	448	0.000258002	0.040566	1.54194144	0.001888566	0.031058352	0.006360115	-7.296731326
486	Alizarin	296	13.9349,0	3	192	0.000258002	0.000388	1.382297717	0.007898488	0.031058352	0.664566179	-0.589515221
255	Maleamate 2	272	8.72638,0	7	244	0.017984542	0.083238	1.133918922	0.023097427	0.048471018	0.216061427	-2.210486564
169	4-Acetylbutyric acid 2	265	7.37059,0	9	71	0.880439414	1.444854	1.436770641	0.018764895	0.043859407	0.60936233	-0.714627777
1	Analyte 1	0	4.85415,0	9	220	0.143627588	0.206994	1.412512528	0.009375416	0.03347991	0.693874841	-0.527252637
2	Analyte 2	0	4.86659,0	9	221	0.939179789	1.482562	1.223187422	0.048539846	0.066406466	0.633484237	-0.658619373
4	Analyte 4	0	4.906,0	9	127	25.04838891	40.41622	1.427277713	0.024022642	0.049336351	0.619760853	-0.690216464
9	Analyte 9	0	4.95133,0	9	56	0.076008724	0.130549	1.387105878	0.006481408	0.031058352	0.582225673	-0.780349639
13	Analyte 13	0	5.01281,0	9	281	0.519158543	0.88159	1.415956277	0.00432766	0.031058352	0.588889971	-0.763932441
14	Analyte 15	0	5.05415,0	9	89	0.126686366	0.194385	1.370732385	0.011314269	0.036061485	0.651727984	-0.617658153
15	Analyte 16	0	5.06096,0	9	71	0.14247583	0.254596	1.382415691	0.025128313	0.050323204	0.559614273	-0.837495336
16	Analyte 17	0	5.10467,0	9	248	0.189236239	0.277412	1.185862123	0.046349455	0.065033621	0.682149873	-0.551839351
17	Analyte 18	0	5.1217,0	9	71	0.23537597	0.369089	1.285237347	0.028223069	0.052841325	0.63772183	-0.649000828
21	Analyte 22	0	5.17593,0	9	160	0.117336438	0.227376	1.396764148	0.014713146	0.039462234	0.516045471	-0.954429902
26	Analyte 27	0	5.21607,0	9	207	1.534123014	2.442395	1.406790033	0.005116932	0.031058352	0.628122392	-0.670882394
28	Analyte 29	0	5.28378,0	9	318	0.490583082	0.81612	1.436795045	0.003319147	0.031058352	0.601116114	-0.7342844
29	Analyte 30	0	5.28985,0	9	141	0.424192495	0.699525	1.423841019	0.023362325	0.048722604	0.606400455	-0.72165726
31	Analyte 32	0	5.306,0	9	82	0.113890123	0.158043	1.300767064	0.041070167	0.061468223	0.720626315	-0.472676759
35	Analyte 36	0	5.38238,0	7	265	0.096659841	0.140997	1.323588558	0.026344832	0.051353772	0.685547745	-0.544670949
42	Analyte 43	0	5.50956,0	6	318	0.053147962	0.116636	1.389043774	0.004972626	0.031058352	0.45567417	-1.133925502
43	Analyte 44	0	5.53119,0	9	83	1.092646683	1.899617	1.374864683	0.014404096	0.039198218	0.575193161	-0.797881572
45	Analyte 46	0	5.57133,0	9	173	0.040681195	0.061956	1.280531443	0.032539528	0.055851534	0.656616292	-0.606877547
53	Analyte 54	0	5.69844,0	3	72	0.000258002	0.000388	1.382297717	0.007898488	0.031058352	0.664566179	-0.589515221
60	Analyte 61	0	5.77652,0	9	187	0.411739097	0.640732	1.381876488	0.034261264	0.056916913	0.642607665	-0.637989906
61	Analyte 62	0	5.78067,0	9	89	0.196207665	0.280779	1.249714074	0.032407158	0.055766689	0.698796716	-0.517055267
65	Analyte 66	0	5.85193,0	9	258	1.102739869	1.898571	1.45940324	0.002841114	0.031058352	0.58082638	-0.783821116
66	Analyte 67	0	5.86748,0	9	245	0.75141187	1.042003	1.340855538	0.014720908	0.039468767	0.721122764	-0.471683209
70	Analyte 71	0	5.91167,0	8	83	0.124600132	0.21066	1.46018003	0.005923432	0.031058352	0.5914747	-0.757611636
71	Analyte 72	0	5.917,0	8	206	0.109884171	0.15268	1.26573403	0.041287114	0.061599284	0.719702949	-0.474526526
79	Analyte 80	0	5.97948,0	9	130	0.06545618	0.103826	1.457571818	0.002601319	0.031058352	0.630443919	-0.665560052

TABLE 2: Continued.

ID	Peak2	Similarity	rt	Count	Mass	MEAN T	MEAN M	VIP	P-value	Q-value	FOLD CHANGE	LOG <sub>2</sub> FOLDCHANGE
83	Analyte 84	0	6.06822,0	9	89	0.629883615	0.857153	1.348964908	0.02146227	0.046845666	0.734855621	-0.444467266
86	Analyte 87	0	6.1057,0	9	355	0.013100601	0.023343	1.464859492	0.002920262	0.031058352	0.561219926	-0.833361863
94	Analyte 95	0	6.23356,0	9	322	0.091050422	0.141299	1.335935817	0.013050372	0.037944549	0.644383212	-0.634009188
96	Analyte 97	0	6.25607,0	9	221	0.273334486	0.505144	1.382718281	0.018461158	0.043496426	0.541101922	-0.88602773
97	Analyte 98	0	6.26304,0	9	267	0.052183801	0.081353	1.339044648	0.021887851	0.047281114	0.641446738	-0.640598617
98	Analyte 99	0	6.28007,0	9	152	1.243281284	1.731247	1.362450345	0.018110888	0.04307052	0.718142143	-0.477658667
100	Analyte 101	0	6.35356,0	9	211	0.149975112	0.243234	1.269434425	0.034442556	0.057025121	0.6165884	-0.697620347
101	Analyte 102	0	6.37207,0	9	221	0.126068615	0.229719	1.369812092	0.014918915	0.039633839	0.548793895	-0.865663663
112	Analyte 114	0	6.51,0	3	207	0.000258002	0.000388	1.382297717	0.007898488	0.031058352	0.664566179	-0.589515221
124	Analyte 126	0	6.667,0	4	159	0.005980118	0.035398	1.206743852	0.007595819	0.031058352	0.168941731	-2.565402355
132	Analyte 134	0	6.76096,0	9	102	0.087156126	0.13135	1.424413383	0.004694475	0.031058352	0.663543315	-0.591737451
135	Analyte 137	0	6.83089,0	9	108	0.197475333	0.322281	1.394014594	0.009483719	0.033640096	0.612743258	-0.70664539
138	Analyte 140	0	6.86778,0	9	319	1.873157639	3.114122	1.418362299	0.007847303	0.031058352	0.601504164	-0.733533337
147	Analyte 149	0	7.02956,0	9	299	230.5117654	328.7347	1.368501132	0.014450612	0.039238447	0.70120909	-0.512083397
150	Analyte 152	0	7.08911,0	3	108	0.000258002	0.000388	1.382297717	0.007898488	0.031058352	0.664566179	-0.589515221
168	Analyte 170	0	7.36319,0	9	221	0.038675613	0.064306	1.425299204	0.003779737	0.031058352	0.601426746	-0.733539068
174	Analyte 176	0	7.44822,0	3	174	0.000258002	0.000388	1.382297717	0.007898488	0.031058352	0.664566179	-0.589515221
176	Analyte 178	0	7.4663,0	9	300	0.14066929	0.25431	1.397799484	0.009390264	0.033501999	0.553141309	-0.854280007
183	Analyte 185	0	7.57178,0	9	241	0.034659852	0.05353	1.278909492	0.022639121	0.048028239	0.647485316	-0.62708062
188	Analyte 190	0	7.65457,0	7	152	0.007184055	0.027339	1.117506793	0.048028223	0.066091974	0.262776377	-1.92809251
210	Analyte 212	0	8.07785,0	9	327	0.058009466	0.101589	1.381321063	0.008796901	0.032586355	0.571020535	-0.808385465
213	Analyte 215	0	8.15637,0	9	302	0.064257101	0.098722	1.246277713	0.028098654	0.052746433	0.650889175	-0.619516174
215	Analyte 217	0	8.16556,0	9	281	0.039345122	0.080491	1.374905261	0.003686217	0.031058352	0.48881664	-1.032634697
227	Analyte 229	0	8.36156,0	9	341	0.052448759	0.086946	1.325218816	0.017092886	0.041786174	0.603232561	-0.72921379
229	Analyte 231	0	8.40367,0	8	100	0.203180031	0.32939	1.341979958	0.013693148	0.038560536	0.616837794	-0.697036932
237	Analyte 240	0	8.54081,0	9	337	0.25036522	0.455655	1.366777246	0.036832395	0.058732065	0.549461995	-0.863908397
253	Analyte 256	0	8.70644,0	9	292	0.35728929	0.515931	1.21938121	0.048453083	0.066353391	0.692978537	-0.529117425
256	Analyte 259	0	8.74333,0	8	245	0.048845708	0.090829	1.326629434	0.009723922	0.033987829	0.537777275	-0.894919303
259	Analyte 262	0	8.78319,0	9	263	0.13088251	0.231069	1.344860566	0.044434442	0.063774445	0.566422421	-0.820049721
267	Analyte 270	0	8.88467,0	9	71	0.11227297	0.204138	1.433063266	0.00608667	0.031058352	0.549984911	-0.862536055
345	Analyte 350	0	10.0673,0	5	292	0.000258002	0.063722	1.539628212	0.004952684	0.031058352	0.004048846	-7.948273624
364	Analyte 369	0	10.4758,0	3	55	0.000258002	0.063552	1.542224923	0.016254112	0.040672706	0.004059669	-7.94442022
393	Analyte 400	0	11.1802,0	6	217	0.061713649	0.161587	1.405655109	0.013522845	0.03840138	0.38192255	-1.38864799
435	Analyte 442	0	12.219,0	4	67	0.005692675	0.030499	1.184547207	0.039424771	0.060446736	0.186653558	-2.421565088
455	Analyte 463	0	12.8955,0	9	232	3.442379815	4.609231	1.359547429	0.025385868	0.050546071	0.746844736	-0.421119747
487	Analyte 495	0	13.9389,0	6	259	0.013690852	0.027019	1.401570503	0.023138199	0.048509945	0.506703381	-0.98078664
503	Analyte 511	0	15.8464,0	9	357	0.080572597	0.145165	1.270859236	0.035617861	0.057880623	0.555041297	-0.849332977
ID												
Peak												
Similarity												
rt												
Count												
Mass												
MEAN OO												

The unique data number of the substance in this qualitative analysis  
 The name of the substance obtained by qualitative analysis  
 The matching degree between the substance and the substance in the standard library in qualitative analysis, and the value is [0, 1000]

Chromatographic retention time of the substance  
 The number of times the substance was detected in all experimental groups  
 Material characteristics Mass charge ratio of ions

The mean of the relative quantitative value of the substance in one of the experimental groups within the group comparison





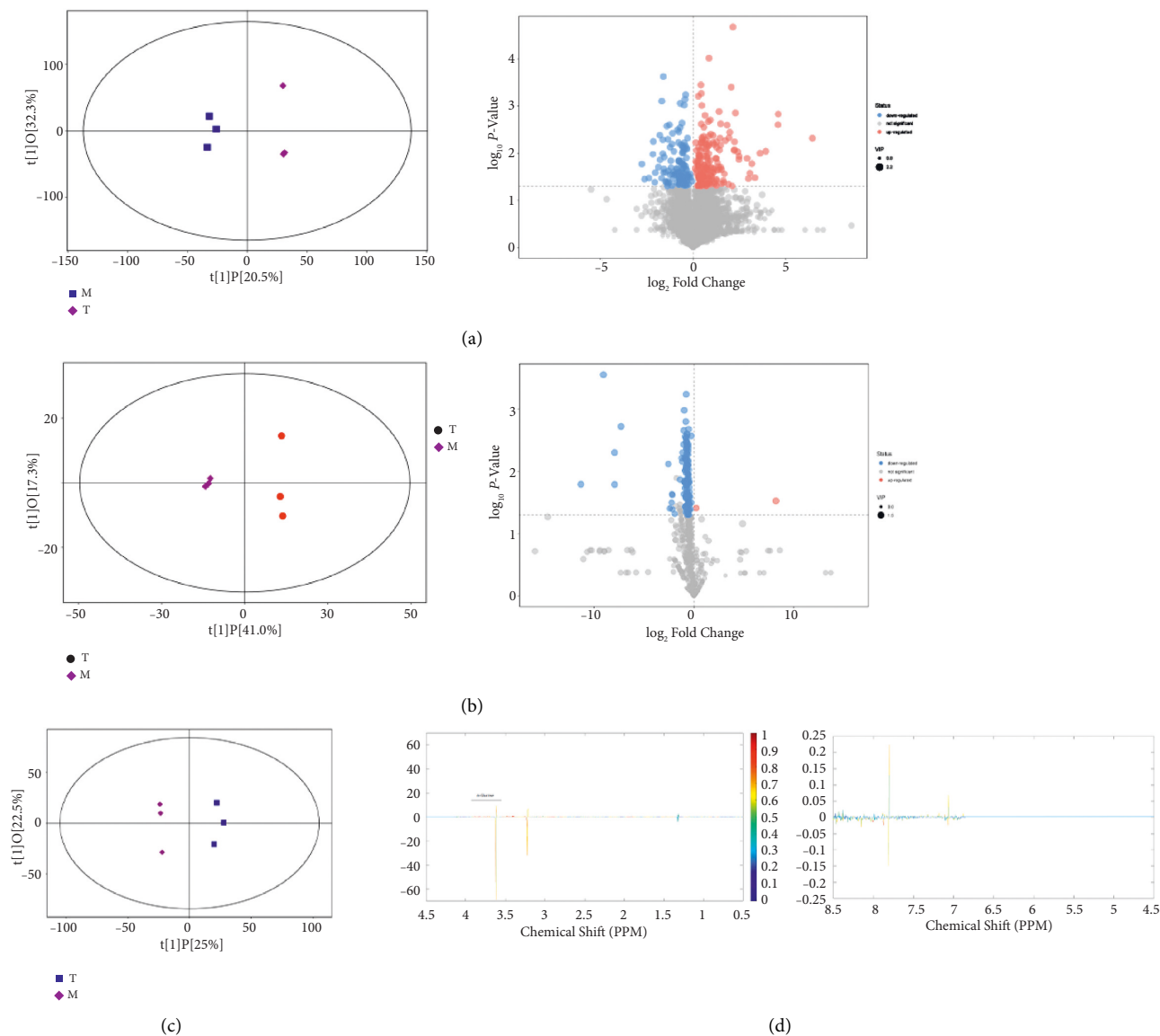


FIGURE 2: OPLS-DA model score scatter plot and differential metabolite analysis. (a) Scatter plot of OPLS-DA model score and volcano plot of differential metabolites for group M versus group T detected by mass spectrometry coupled with the high-performance liquid phase. (b) Scatter plot of OPLS-DA model score and volcano plot of differential metabolites for group M versus group T detected by mass spectrometry coupled with gas phase. The size of scattering in the volcano plot represents the VIP value of OPLS-DA model, the larger the scatter the larger the VIP value. Significantly up-regulated metabolites are shown in red, significantly down-regulated metabolites are shown in blue, and nonsignificantly different metabolites are shown in gray. (c) Scatter plot of OPLS-DA model scores for group M versus group T detected by NMR. (d) OPLS-DA loadings plot for group M versus group (T). The horizontal coordinates in the plot indicate the magnitude of chemical shifts, from right to left, with increasing values of chemical shifts; the vertical coordinates indicate the magnitude of loadings after back conversion, where the shades of color indicate the magnitude of correlation coefficients, red indicates a positive correlation, and blue indicates negative correlation. The marked substances in the figure are the differential metabolites that passed the critical value test of the correlation coefficient.

studied from a metabolic perspective. And these studies are valuable from a big picture perspective [11]. The metabolome is a collection of small-molecule chemical entities involved in metabolism and has traditionally been studied to identify biomarkers for the diagnosis and prediction of disease. Nowadays, the value of metabolomic analysis has been redefined from a simple biomarker identification tool to a technique for discovering active drivers of biological processes [12]. Metabolomics is the high-throughput

characterization of metabolites from cells, organs, tissues, or biofluids using advanced analytical chemistry techniques [13]. NMR and mass spectrometry are commonly used in metabolomics; NMR is highly reproducible and quantitative, has a simple sample preparation protocol, and is capable of measuring analytes in a variety of solvent conditions, but it has low sensitivity. In contrast, the high sensitivity and low detection limits of mass spectrometry enable the detection of subtle metabolic changes that are not visible with NMR [14].

TABLE 3: Enrichment analysis results based on mass spectrometry combined with HPLC.

Pathway	Total Hits	Raw $p$	$-\ln(p)$	Holm adjust	FDR	Impact	Hits cpd	Total cpd
Histidine metabolism	15	2	0.011526	4.4632	0.95	0.94512	0.24194	<p>L-glutamic acid cpd: C00025; 4-imidazole-5-propionic acid cpd: C03680; urocanic acid cpd: C00785; L-histidine cpd: C00135; imidazole-4-acetaldehyde cpd: C05130; 1-methylhistamine cpd: C05127; methylimidazole acetaldehyde cpd: C05827; histamine cpd: C00388; carnosine cpd: C00386; N-formyl-L-aspartate cpd: C01044; formiminoglutamic acid cpd: C00439; imidazoleacetic acid cpd: C02835; methylimidazoleacetic acid cpd: C05828; L-aspartic acid cpd: C00049; L-methylhistidine cpd: C01152</p> <p>L-asparagine cpd: C00152; tRNA(Asn) cpd: C01637; L-histidine cpd: C00135; tRNA(His) cpd: C01643; L-phenylalanine cpd: C00079; tRNA(Phe) cpd: C01648; L-arginine cpd: C00062; tRNA(Arg) cpd: C01636; L-glutamine cpd: C00064; tRNA(Gln) cpd: C01640; L-cysteine cpd: C00097; tRNA(Cys) cpd: C01639; glycine cpd: C00037; tRNA(Gly) cpd: C01642; tRNA(Asp) cpd: C01638; L-aspartic acid cpd: C00049; L-serine cpd: C00065; tRNA(Ser) cpd: C01650; L-methionine cpd: C00073; tRNA(Met) cpd: C01647; L-valine cpd: C00183; tRNA(Val) cpd: C01653; L-alanine cpd: C00041; tRNA(Ala) cpd: C01635; L-lysine cpd: C00047; tRNA(Lys) cpd: C01646; L-isoleucine cpd: C00407; tRNA(Ile) cpd: C01644; tRNA(Leu) cpd: C01645; L-leucine cpd: C00123; L-threonine cpd: C00188; tRNA(Thr) cpd: C01651; tRNA(Trp) cpd: C01652; L-tryptophan cpd: C00078; N10-formyl-thf cpd: C00234; L-methionyl-tRNA cpd: C02430; L-tyrosine cpd: C00082; tRNA(Tyr) cpd: C00787; L-proline cpd: C00148; tRNA(Pro) cpd: C01649; L-glutamic acid cpd: C00025; tRNA(Glu) cpd: C01641; glutamyl-tRNA cpd: C02282; L-asparaginyl-tRNA(Asn) cpd: C03402; tRNA(Sec) cpd: C16636; L-seryl-tRNA(Sec) cpd: C06481; O-phosphoseryl-tRNA(Sec) cpd: C16638; L-histidyl-tRNA(His) cpd: C02988; L-phenylalanyl-tRNA(Phe) cpd: C03511; L-arginyl-tRNA(Arg) cpd: C02163; L-cysteinyl-tRNA(Cys) cpd: C03125; glycyl-tRNA(Gly) cpd: C02412; L-aspartyl-tRNA(Asp) cpd: C02984; L-seryl-tRNA(Ser) cpd: C02553; L-valyl-tRNA(Val) cpd: C02554; L-alanyl-tRNA cpd: C00886; L-lysyl-tRNA cpd: C01931; L-isoleucyl-tRNA(Ile) cpd: C03127; L-leucyl-tRNA cpd: C02047; L-threonyl-tRNA(Thr) cpd: C02992; L-tryptophanyl-tRNA(Trp) cpd: C03512; tetrahydrofolic acid cpd: C00101; N-formylmethionyl-tRNA cpd: C03294; L-tyrosyl-tRNA(Tyr) cpd: C02839; L-prolyl-tRNA(Pro) cpd: C02702; L-glutamyl-tRNA(Glu) cpd: C02987; L-glutamyl-tRNA(Gln) cpd: C06112; L-aspartyl-tRNA(Asn) cpd: C06113; L-selenocysteinyl-tRNA(Sec) cpd: C06482</p> <p>Phenylpyruvic acid cpd: C00166; L-phenylalanine cpd: C00079; L-tyrosine cpd: C00082; 4-hydroxyphenylpyruvic acid cpd: C01179</p> <p>L-glutamic acid cpd: C00025; D-glutamine cpd: C00819; L-glutamine cpd: C00064; oxoglutaric acid cpd: C00026; D-glutamic acid cpd: C00217</p>
Aminoacyl-tRNA biosynthesis	69	3	0.039232	3.2383	1	1	0	<p>L-histidine cpd: C00135; L-phenylalanine cpd: C00079; L-methionine cpd: C00073</p>
Phenylalanine, tyrosine, and tryptophan biosynthesis	4	1	0.044453	3.1133	1	1	0.5	L-phenylalanine cpd: C00079
D-glutamine and D-glutamate metabolism	5	1	0.055273	2.8955	1	1	0	D-glutamine cpd: C00819

TABLE 3: Continued.

Pathway	Total Hits	Raw $P$	$-\ln(p)$	Holm adjust	FDR	Impact	Hits cpd	Total cpd
Tryptophan metabolism	40	2 0.072666	2.6219	1	1	0.10987	L-tryptophan cpd: C00078; melatonin cpd: C01598; serotonin cpd: C00780; 5-hydroxytryptamine cpd: C05638; 5-hydroxytryptamine cpd: C05651; 5-hydroxy-L-tryptophan cpd: C00643; L-formyltryptamine cpd: C02700; acetoacetyl-CoA cpd: C00332; (S)-3-hydroxybutanoyl-CoA cpd: C01144; crotonoyl-CoA cpd: C00877; glutaryl-CoA cpd: C00527; oxoadipic acid cpd: C00322; 2-amino-3-carboxymuconic acid semialdehyde cpd: C04409; 3-hydroxyanthranilic acid cpd: C00632; L-tryptamine cpd: C00328; formylanthranilic acid cpd: C05653; L-3-hydroxytryptamine cpd: C03227; 3-hydroxytryptamine cpd: C05636; indoleacetaldehyde cpd: C00637; 5-hydroxy-N-formyltryptamine cpd: C05648; 5-hydroxyindoleacetaldehyde cpd: C05634; tryptamine cpd: C00398; indoleacrylic acid cpd: C00331; acetyl-N-formyl-5-methoxytryptamine cpd: C05642; 6-hydroxymelatonin cpd: C05643; N-acetylserotonin cpd: C00978; formyl-5-hydroxytryptamine cpd: C05647; 4,6-dihydroxyquinoline cpd: C05639; acetyl-CoA cpd: C00024; 2-aminomuconic acid semialdehyde cpd: C03824; 2-aminobenzoic acid cpd: C00108; L-tryptophanyl-tRNA(Trp) cpd: C03512; cinnalminate cpd: C05640; 4-(2-amino-3-hydroxyphenyl)-2,4-dioxobutanoic acid cpd: C05645; 4-(2-aminophenyl)-2,4-dioxobutanoic acid cpd: C01252; 4,8-dihydroxyquinoline cpd: C05637; indoleacetic acid cpd: C00954; 5-hydroxyindoleacetic acid cpd: C05635; N-methylserotonin cpd: C06212; N-methyltryptamine cpd: C06213	
Nitrogen metabolism	9	1 0.097415	2.3288	1	1	0	L-histidine cpd: C00135	Ammonia cpd: C00014; carbon dioxide cpd: C00011; L-glutamic acid cpd: C00025; L-glutamine cpd: C00064; L-cystathionine cpd: C02291; L-Histidine cpd: C00135; carbamoylphosphate cpd: C00169; carbonic acid cpd: C01353; glycine cpd: C00037
Phenylalanine metabolism	11	1 0.11782	2.1386	1	1	0.40741	L-phenylalanine cpd: C00079	Phenylacetaldehyde cpd: C00601; phenylacetyl-CoA cpd: C00582; L-phenylalanine cpd: C00079; phenylethylamine cpd: C05332; phenylpyruvic acid cpd: C00166; phenylacetic acid cpd: C07086; phenylacetylglutamine cpd: C05598; ortho-hydroxyphenylacetic acid cpd: C05852; enol-phenylpyruvate cpd: C02763; 2-phenylacetamide cpd: C02505; L-tyrosine cpd: C00082
Sphingolipid metabolism	21	1 0.21351	1.5441	1	1	0	Phytosphingosine cpd: C12144	Sphinganine cpd: C00836; ceramide 1-phosphate cpd: C02960; sphingosine 1-phosphate cpd: C06124; sphinganine 1-phosphate cpd: C01120; dihydroceramide cpd: C12126; phytoceramide cpd: C12145; SM cpd: C00550; ceramide cpd: C00195; Palmitoyl-CoA cpd: C00154; L-Serine cpd: C00065; 3-dehydroshinganine cpd: C02934; galabiosylceramide cpd: C06126; galactosylceramide cpd: C02686; GM4 cpd: C06128; lactosylceramide cpd: C01290; glucosylceramide cpd: C01190; sphingosine cpd: C00319; 3-O-Sulfogalactosylceramide (d18 : : 1/24 : : 0) cpd: C06125; phytosphingosine cpd: C12144; digalactosylceramidesulfate cpd: C06127; O-phosphoethanolamine cpd: C00346

TABLE 3: Continued.

Pathway	Total Hits	Raw <i>p</i>	$-\ln(p)$	Holm adjust	FDR	Impact	Hits	Total cpd
Cysteine and methionine metabolism	27	0.26616	1.3236	1	1	0.08685	L-methionine cpd: C00073	2-Oxo-4-methylthiobutanoic acid cpd: C01180; 1,2-dihydroxy-3-keto-5-methylthiopentene cpd: C15606; 5'-methylthioadenosine cpd: C00170; S-adenosylmethionine cpd: C01137; S-adenosylmethionine cpd: C00019; L-cystathionine cpd: C02291; L-homocysteine cpd: C00155; L-serine cpd: C00065; L-methionine cpd: C00073; S-adenosylhomocysteine cpd: C00021; 2,3-diketo-5-methylthiopentyl-1-phosphate cpd: C15650; cysteic acid cpd: C00506; L-cystine cpd: C00491; L-cysteine cpd: C00097; 3-sulfinoalanine cpd: C00606; sulfite cpd: C00094; 3-mercaptopyruvic acid cpd: C00957; 3-methylthiopropionic acid cpd: C08276; 5-methylthioribose 1-phosphate cpd: C04188; 2-ketobutyric acid cpd: C00109; 2-aminoacrylic acid cpd: C02218; 3-sulfoxyruvic acid cpd: C05528; thiocysteine cpd: C01962; 3-sulfinyruvic acid cpd: C05527; pyruvic acid cpd: C00022; thiosulfate cpd: C00320; 3-mercaptolactic acid cpd: C05823 Phosphatidylethanolamine cpd: C00350; phosphatidylcholine cpd: C00157; dihydroxyacetone phosphate cpd: C00111; LysoPC (18:1(9Z)) cpd: C04230; 1,2-diacyl-sn-glycerol cpd: C00641; citicoline cpd: C00307; phosphorylcholine cpd: C00588; choline cpd: C00114; acetylcholine cpd: C01996; O-phosphoethanolamine cpd: C00346; ethanolamine cpd: C00189; PA (16:0/16:0) cpd: C00416; acyl-CoA cpd: C00040; 1-acyl-sn-glycerol 3-phosphate cpd: C00681; CDP-diacylglycerol cpd: C00269; glycerol 3-phosphate cpd: C00093; 1-acyl-sn-glycero-3-phosphoethanolamine cpd: C04438; 2-acyl-sn-glycero-3-phosphoethanolamine cpd: C05973; 2-acyl-sn-glycero-3-phosphocholine cpd: C04233; CDP-glycerol cpd: C00513; PS (16:0/16:0) cpd: C02737; phosphatidylglycerol cpd: C00344; dihydroxyacetone phosphate acyl ester cpd: C03372; CDP-ethanolamine cpd: C00570; 1-phosphatidyl-D-myo-inositol cpd: C01194; glycerylphosphorylethanolamine cpd: C01233; glycerophosphocholine cpd: C00670; phosphatidyl-N-methylethanolamine cpd: C01241; phosphatidylglycerophosphate cpd: C03892; cardiolipin cpd: C05980
Glycerophospholipid metabolism	30	0.29123	1.2336	1	1	0.02315	Glycerophosphocholine cpd: C00670	

TABLE 3: Continued.

Pathway	Total Hits	Raw <i>p</i>	-ln( <i>p</i> )	Holm adjust	FDR	Impact	Hits cpd	Total cpd
Arginine and proline metabolism	44	0.39796	0.9214	1	1	0	N-acetylmethionine cpd: C00437	L-glutamine cpd: C00064; ammonia cpd: C00014; carbamoylphosphate cpd: C00169; ornithine cpd: C00077; citrulline cpd: C00327; L-aspartic acid cpd: C00049; argininosuccinic acid cpd: C03406; L-arginine cpd: C00062; L-glutamic acid cpd: C00025; N-acetylmethionine cpd: C00437; L-proline cpd: C00148; peptide cpd: C00012; D-proline cpd: C00763; hydroxyproline cpd: C01157; pyrroline hydroxycarboxylic acid cpd: C04281; L-4-hydroxyglutamate semialdehyde cpd: C05938; L-erythro-4-hydroxyglutamate cpd: C05947; N-(o)-hydroxyarginine cpd: C05933; guanidinoacetic acid cpd: C00581; creatine cpd: C00300; gamma-aminobutyric acid cpd: C00334; agmatine cpd: C00179; L-glutamic-gamma-semialdehyde cpd: C01165; L-glutamic acid 5-phosphate cpd: C03287; (S)-1-pyrroline-5-carboxylate cpd: C03912; putrescine cpd: C00134; 4-aminobutyraldehyde cpd: C00555; S-adenosylmethionine cpd: C01137; S-adenosylmethionine cpd: C00019; spermidine cpd: C00315; N-acetylputrescine cpd: C02714; N4-acetylaminoethanol cpd: C05936; cis-4-hydroxy-D-proline cpd: C03440; fumaric acid cpd: C00122; urea cpd: C00086; N-acetyl-L-alanine cpd: C00624; 1-pyrroline-2-carboxylic acid cpd: C03564; D-4-hydroxy-2-oxoglutarate cpd: C05946; nitric oxide cpd: C00533; phosphocreatine cpd: C02305; 4-guanidinobutanoic acid cpd: C01035; spermine cpd: C00750; 4-acetamidobutanoic acid cpd: C02946; 1-pyrroline-4-hydroxy-2-carboxylate cpd: C04282
Pathway	Metabolic pathway name							
Total	The number of metabolites in this pathway							
Hits	The number of differential metabolites hit this pathway							
Raw <i>p</i>	<i>P</i> value of metabolic pathway enrichment analysis							
-ln( <i>p</i> )	Minus log base E of <i>P</i>							
Holm adjust	<i>P</i> values corrected by Holm-Bonferroni method for multiple hypothesis testing							
FDR	<i>P</i> value corrected by false discovery rate (FDR) method for multiple hypothesis testing							
Impact	Impact value of metabolic pathway topology analysis							
Hits cpd	The names and KEGG IDs of differential metabolites hit the pathway							
Total cpd	All metabolite names and KEGG IDs contained in this pathway							

TABLE 4: Enrichment analysis results based on mass spectrometry combined with gas phase.

Pathway	Total Hits	Raw $p$	$-\ln(p)$	Holm adjust	FDR	Impact	Hits cpd	Total cpd						
							Thioredoxin cpd: C00342; uridine 5'-diphosphate cpd: C00015; L-glutamine cpd: C00064; carbamoylphosphate cpd: C00169; 4,5-dihydrorotic acid cpd: C00337; orotidyllic acid cpd: C01103; RNA cpd: C00046; uridine triphosphate cpd: C00075; uridine 5'-monophosphate cpd: C00105; uridine cpd: C00299; dihydrouracil cpd: C00429; ureidopropionic acid cpd: C02642; cytidine triphosphate cpd: C00063; CDP cpd: C00112; cytidine monophosphate cpd: C00055; cytidine cpd: C00475; thioredoxin disulfide cpd: C00343; dCDP cpd: C00705; dCTP cpd: C00458; dCMP cpd: C00239; deoxycytidine cpd: C00881; deoxyuridine triphosphate cpd: C00460; dUDP cpd: C01346; dUMP cpd: C00365; deoxyuridine cpd: C00526; thymidine 5'-triphosphate cpd: C00459; dTDP cpd: C00363; 5-thymidyllic acid cpd: C00364; thymidine cpd: C00214; dihydrothymine cpd: C00906; ureidoisobutyric acid cpd: C05100; P1,P4-bis(5'-uridylyl) tetraphosphate cpd: C06198; ureidosuccinic acid cpd: C00438; phosphoribosyl pyrophosphate cpd: C00119; orotic acid cpd: C00295; uracil cpd: C00106; beta-alanine cpd: C00099; DNA cpd: C00039; deoxyribose 1-phosphate cpd: C00672; thymine cpd: C00178; 3-aminoisobutanoic acid cpd: C05145							
Pyrimidine metabolism	41	5	0.0013	6.6293	0.11	0.108	0.09731	Deoxyuridine cpd: C00526; uracil cpd: C00106; beta-alanine cpd: C00099; thymine cpd: C00178; 3-aminoisobutanoic acid cpd: C05145						
							Beta-alanine cpd: C00099; uracil cpd: C00106							
Pantothenate and CoA biosynthesis	15	2	0.0384	3.2608	1	1	0	Dephospho-CoA cpd: C00882; pantotheine 4'-phosphate cpd: C01134; pantotheine cpd: C00831; 4-phosphopantothenoylcysteine cpd: C04352; D-pantothenoyl-L-cysteine cpd: C04079; d-4'-phosphopantothenate cpd: C03492; L-cysteine cpd: C00097; pantothenic acid cpd: C00864; ureidopropionic acid cpd: C02642; dihydrouracil cpd: C00429; L-valine cpd: C00183; coenzyme a cpd: C00010; beta-alanine cpd: C00099; uracil cpd: C00106; alpha-ketoisovaleric acid cpd: C00141						
							Beta-alanine cpd: C00099; uracil cpd: C00106							
Beta-alanine metabolism	17	2	0.0484	3.0283	1	1	0.44444	Acrylyl-CoA cpd: C00894; 3-hydroxypropionyl-CoA cpd: C05668; hydroxypropionic acid cpd: C01013; malonyl-CoA cpd: C00083; beta-alanine cpd: C00099; L-aspartic acid cpd: C00049; spermine cpd: C00750; 1,3-diaminopropane cpd: C00986; 3-aminopropionaldehyde cpd: C05665; ureidopropionic acid cpd: C02642; dihydrouracil cpd: C00429; anserine cpd: C01262; propionyl-CoA cpd: C00100; Acetyl-CoA cpd: C00024; malonic semialdehyde cpd: C00222; spermidine cpd: C00315; uracil cpd: C00106						
							Beta-alanine cpd: C00099; uracil cpd: C00106							
Starch and sucrose metabolism	19	2	0.0593	2.8253	1	1	0.07451	beta-D-fructose cpd: C02336; sucrose cpd: C00089; uridine diphosphate glucuronic acid cpd: C00167; uridine diphosphate glucose cpd: C00029; glucose 1-phosphate cpd: C00103; 3-methoxy-4-hydroxyphenylglycol glucuronide cpd: C03033; glucose 6-phosphate cpd: C00668; alpha-D-glucose cpd: C00267; starch cpd: C00369; amylose cpd: C00718; trehalose cpd: C01083; D-maltose cpd: C00208; D-glucose cpd: C00031; dextrin cpd: C00721; isomaltose cpd: C00252; beta-D-fructose 6-phosphate cpd: C05345; UDP-D-xylose cpd: C00190; alpha-D-glucose 1,6-bisphosphate cpd: C01231; D-glucuronic acid cpd: C00191						
							D-maltose cpd: C00208; isomaltose cpd: C00252							



TABLE 4: Continued.

Pathway	Total Hits	Raw $p$	$-\ln(p)$	Holm adjust	FDR	Impact	Hits cpd	Total cpd
Propanoate metabolism	20	0.065	2.733	1	1	0	Beta-alanine cpd: C00099; 2-hydroxybutyric acid cpd: C05984	(S)-methylmalonic acid semialdehyde cpd: C06002; methylmalonyl-CoA cpd: C00683; propionyl-CoA cpd: C00100; propionyl adenylate cpd: C05983; R-methylmalonyl-CoA cpd: C01213; succinic acid cpd: C00042; hydroxypropionic acid cpd: C01013; beta-alanine cpd: C00099; 2-propyn-1-ol cpd: C05985; acetyl-CoA cpd: C00024; malonyl-CoA cpd: C00083; 2-hydroxybutyric acid cpd: C05984; acrylyl-CoA cpd: C00894; propionic acid cpd: C00163; succinyl-CoA cpd: C00091; 3-hydroxypropionyl-CoA cpd: C05668; malonic semialdehyde cpd: C00222; propynoic acid cpd: C00804; acetoacetyl-CoA cpd: C00332; 2-ketobutyric acid cpd: C00109
D-glutamine and D-glutamate metabolism	5	0.1016	2.2866	1	1	0	Oxoglutaric acid cpd: C00026	L-glutamic acid cpd: C00025; D-glutamine cpd: C00819; L-glutamine cpd: C00064; oxoglutaric acid cpd: C00026; D-glutamic acid cpd: C00217
Sulfur metabolism	5	0.1016	2.2866	1	1	0.3	Sulfate cpd: C00059	Phosphoadenosine phosphosulfate cpd: C00053; adenosine phosphosulfate cpd: C00224; sulfite cpd: C00094; sulfate cpd: C00059; adenosine 3',5'-diphosphate cpd: C00054
Cyanoamino acid metabolism	6	0.1207	2.1145	1	1	0	Glycine cpd: C00037	3-Cyano-L-alanine cpd: C02512; beta-aminopropionitrile cpd: C05670; glycine cpd: C00037; gamma-glutamyl-beta-cyanoalanine cpd: C05711; gamma-glutamyl-beta-aminopropionitrile cpd: C06114; L-serine cpd: C00065
Methane metabolism	9	0.1756	1.7394	1	1	0	Glycine cpd: C00037	S-formylglutathione cpd: C01031; glycine cpd: C00037; 5,10-methylene-THF cpd: C00143; S-(Hydroxymethyl)glutathione cpd: C14180; methanol cpd: C00132; formic acid cpd: C00058; L-serine cpd: C00065; formaldehyde cpd: C00067; 5-methyltetrahydrofolic acid cpd: C00440
Nitrogen metabolism	9	0.1756	1.7394	1	1	0	Glycine cpd: C00037	Ammonia cpd: C00014; carbon dioxide cpd: C00011; L-glutamic acid cpd: C00025; L-glutamine cpd: C00064; L-cystathionine cpd: C02291; L-histidine cpd: C00135; carbamoylphosphate cpd: C00169; carbonic acid cpd: C01353; glycine cpd: C00037

TABLE 4: Continued.

Pathway	Total Hits	Raw $p$	$-\ln(p)$	Holm adjust	FDR	Impact	Hits	Total cpd
Arginine and proline metabolism	44	2	0.2382	1	1	0.04414	Hydroxyproline cpd: C01157; 4-acetamidobutanoic acid cpd: C02946	L-glutamine cpd: C00064; ammonia cpd: C00014; carbamoylphosphate cpd: C00169; ornithine cpd: C00077; citrulline cpd: C00327; L-aspartic acid cpd: C00049; arginosuccinic acid cpd: C03406; L-arginine cpd: C00062; L-glutamic acid cpd: C00025; N-acetylmethionine cpd: C00437; L-proline cpd: C00148; peptide cpd: C00012; D-proline cpd: C00763; hydroxyproline cpd: C01157; pyrroline hydroxycarboxylic acid cpd: C04281; L-4-hydroxyglutamate semialdehyde cpd: C05938; L-erythro-4-hydroxyglutamate cpd: C05947; N-(o)-hydroxyarginine cpd: C05933; guanidinoacetic acid cpd: C00581; creatine cpd: C00300; gamma-aminobutyric acid cpd: C00334; agmatine cpd: C00179; L-glutamic-gamma-semialdehyde cpd: C01165; L-glutamic acid 5-phosphate cpd: C03287; (S)-1-pyrroline-5-carboxylate cpd: C03912; putrescine cpd: C00134; 4-aminobutyraldehyde cpd: C00555; S-adenosylmethionine cpd: C01137; S-adenosylmethionine cpd: C00019; spermidine cpd: C00315; N-Acetylputrescine cpd: C02714; N-Acetylmethionine cpd: C05936; cis-4-hydroxy-D-proline cpd: C03440; Fumaric acid cpd: C00122; urea cpd: C00086; N-Acetyl-L-alanine cpd: C00624; 1-pyrroline-2-carboxylic acid cpd: C03564; D-4-hydroxy-2-oxoglutarate cpd: C05946; nitric oxide cpd: C00533; phosphocreatine cpd: C02305; 4-guanidinobutanoic acid cpd: C01035; spermine cpd: C00750; 4-acetamidobutanoic acid cpd: C02946; 1-pyrroline-4-hydroxy-2-carboxylate cpd: C04282 Triacylglycerol cpd: C00422; acyl-CoA cpd: C00040; 1,2-diacyl-sn-glycerol cpd: C00641; PA(16 : 0/16 : 0) cpd: C00416; 1-acyl-sn-glycerol 3-phosphate cpd: C00681; 1-acylglycerol cpd: C01885; glycerol 3-phosphate cpd: C00093; dihydroxyacetone cpd: C00184; glycerol cpd: C00116; lactaldehyde cpd: C05999; D-glyceraldehyde cpd: C00577; glyceric acid cpd: C00258; digalactosyl-diacylglycerol cpd: C06037; fatty acid cpd: C00162; dihydroxyacetone phosphate cpd: C00111; propylene glycol cpd: C00583; 3-phospho-D-glycerate cpd: C00197; 1,2-diacyl-3-beta-D-galactosyl-sn-glycerol cpd: C03692 Enzyme N6-(dihydrolyl)lysine cpd: C15973; oxoglutaric acid cpd: C00026; thiamine pyrophosphate cpd: C00068; Enzyme N6-(lipoyl)lysine cpd: C15972; 3-carboxy-1-hydroxypropylthiamine diphosphate cpd: C05381; Succinyl-CoA cpd: C00091; succinic acid cpd: C00042; oxalosuccinic acid cpd: C05379; isocitric acid cpd: C00311; oxalacetic acid cpd: C00036; Acetyl-CoA cpd: C00024; L-malic acid cpd: C00149; cis-acornitic acid cpd: C00417; citric acid cpd: C00158; pyruvic acid cpd: C00022; 2-(a-hydroxyethyl)thiamine diphosphate cpd: C05125; [dihydrolyl)lysine-residue succinyltransferase] S-succinyl)dihydrolyl)lysine cpd: C16254; Fumaric acid cpd: C00122; S-acetyl)dihydrolyl)amide-E cpd: C16255; phosphoenolpyruvic acid cpd: C00074
Glycerolipid metabolism	18	1	0.3213	1	1	0.28098	Glycerol cpd: C00116	
Citrate cycle (TCA cycle)	20	1	0.3501	1	1	0.06799	Oxoglutaric acid cpd: C00026	

TABLE 4: Continued.

Pathway	Total Hits	Raw $p$	$-\ln(p)$	Holm adjust	FDR	Impact	Hits cpd	Total cpd	
Butanoate metabolism	22	1	0.3777	0.97365	1	1	0	0	Oxoglutaric acid cpd: C00026
Alanine, aspartate, and glutamate metabolism	24	1	0.4042	0.90587	1	1	0.06329	0	3-Butyn-1-ol cpd: C06145; (R)-3-hydroxybutyric acid cpd: C01089; acetoacetic acid cpd: C00164; 3-hydroxy-3-methylglutaryl-CoA cpd: C00356; Acetyl-CoA cpd: C00024; Acetoacetyl-CoA cpd: C00332; (S)-3-hydroxybutanoyl-CoA cpd: C01144; Crotonoyl-CoA cpd: C00877; gamma-aminobutyric acid cpd: C00334; L-glutamic acid cpd: C00025; Butanoyl-CoA cpd: C00136; butanal cpd: C01412; succinic acid semialdehyde cpd: C00232; butyric acid cpd: C00246; oxoglutaric acid cpd: C00026; thiamine pyrophosphate cpd: C00068; pyruvic acid cpd: C00022; 3-butyrate cpd: C06144; 1-butanol cpd: C06142; succinic acid cpd: C00042; 2-hydroxyglutarate cpd: C02630; 2-(alpha-hydroxyethyl)thiamine diphosphate cpd: C05125 N-Acetyl-L-aspartic acid cpd: C01042; 2-oxosuccinamate cpd: C02362; L-aspartic acid cpd: C00049; D-aspartic acid cpd: C00402; argininosuccinic acid cpd: C03406; adenylosuccinic acid cpd: C03794; L-Alanine cpd: C00041; succinic acid semialdehyde cpd: C00232; L-glutamic acid cpd: C00025; gamma-aminobutyric acid cpd: C00334; L-Glutamine cpd: C00064; ammonia cpd: C00014; 2-keto-glutaric acid cpd: C00940; (S)-1-pyrroline-5-carboxylate cpd: C03912; oxalacetic acid cpd: C00036; L-Asparagine cpd: C00152; Fumaric acid cpd: C00122; pyruvic acid cpd: C00022; ureidosuccinic acid cpd: C00438; succinic acid cpd: C00042; oxoglutaric acid cpd: C00026; carbamoylphosphate cpd: C00169; glucosamine 6-phosphate cpd: C00352; 5-phosphoribosylamine cpd: C03090 Stachyose cpd: C01613; D-tagatose 6-phosphate cpd: C01097; D-gal alpha 1->6d-gal alpha 1->6d-glucose cpd: C05404; sucrose cpd: C00089; raffinose cpd: C00492; melibiose cpd: C05402; D-galactose cpd: C00124; galactosylglycerol cpd: C05401; epimelbiose cpd: C05400; melibititol cpd: C05399; galactinol cpd: C01235; Alpha-D-Glucose cpd: C00267; alpha-lactose cpd: C00243; glucose 1-phosphate cpd: C00103; uridine diphosphategalactose cpd: C00052; uridine diphosphate glucose cpd: C00029; galactose 1-phosphate cpd: C00446; glucose 6-phosphate cpd: C00668; D-tagatose 1,6-bisphosphate cpd: C03785; D-Fructose cpd: C00095; D-glucose cpd: C00031; galactitol cpd: C01697; glycerol cpd: C00116; D-Mannose cpd: C00159; sorbitol cpd: C00794; myoinositol cpd: C00137
Galactose metabolism	26	1	0.4296	0.84494	1	1	0	0	Glycerol cpd: C00116

TABLE 4: Continued.

Pathway	Total Hits	Raw $p$	$-\ln(p)$	Holm adjust	FDR	Impact	Hits	Total cpd
Glutathione metabolism	26	1	0.4296	0.84494	1	1	0.00573	Glycine cpd: C00037
Fatty acid elongation in mitochondria	27	1	0.4419	0.8167	1	1	0	Palmitic acid cpd: C00249
Porphyrin and chlorophyll metabolism	27	1	0.4419	0.8167	1	1	0	Glycine cpd: C00037

R-S-cysteinylglycine cpd: C05729; R-S-glutathione cpd: C02320; glutathione cpd: C00051; NADP cpd: C00006; NADPH cpd: C00005; oxidized glutathione cpd: C00127; gamma-glutamylcysteine cpd: C00669; glycine cpd: C00037; L-cysteine cpd: C00097; L-glutamic acid cpd: C00025; cysteinylglycine cpd: C01419; pyroglutamic acid cpd: C01879; L-amino acid cpd: C00151; 5-L-glutamyl-L-alanine cpd: C03740; RX cpd: C01322; ornithine cpd: C00077; putrescine cpd: C00134; spermidine cpd: C00315; cadaverine cpd: C01672; tryptaredoxin cpd: C16663; trypanothione cpd: C02090; S-substituted L-cysteine cpd: C05726; spermine cpd: C00750; aminopropylcadaverine cpd: C16565; tryptaredoxin disulfide cpd: C16664; trypanothione disulfide cpd: C03170

Palmitoyl-CoA cpd: C00154; (2e)-hexadecenoyl-CoA cpd: C05272; (S)-3-hydroxyhexadecenoyl-CoA cpd: C05258; 3-oxohexadecenoyl-CoA cpd: C05259; Acetyl-CoA cpd: C00024; Tetradecenoyl-CoA cpd: C02593; (2e)-tetradecenoyl-CoA cpd: C05273; (S)-3-hydroxytetradecenoyl-CoA cpd: C05260; 3-oxotetradecenoyl-CoA cpd: C05261; Lauroyl-CoA cpd: C01832; (2e)-dodecenoyl-CoA cpd: C03221; (S)-3-hydroxydodecenoyl-CoA cpd: C05262; 3-oxododecenoyl-CoA cpd: C05263; Decanoyl-CoA (n-C10: 0CoA) cpd: C05274; (2e)-dodecenoyl-CoA cpd: C05275; (S)-hydroxydodecanoyl-CoA cpd: C05264; 3-oxododecanoyl-CoA cpd: C05265; Octanoyl-CoA cpd: C01944; (2e)-octenoyl-CoA cpd: C05276; (S)-hydroxyoctanoyl-CoA cpd: C05266; 3-oxooctanoyl-CoA cpd: C05267; Hexanoyl-CoA cpd: C05270; trans-2-hexenoyl-CoA cpd: C05271; (S)-hydroxyhexanoyl-CoA cpd: C05268; 3-oxohexanoyl-CoA cpd: C05269; Butanoyl-CoA cpd: C00136; palmitic acid cpd: C00249

Cobinamide cpd: C05774; heme O cpd: C15672; heme cpd: C00032; glycine cpd: C00037; bilirubin diglucuronide cpd: C05787; Cob(I)yrinate a,c diamide cpd: C06505; Fe2 + cpd: C14818; hemoglobin cpd: C01708; biliverdin cpd: C00500; protoporphyrinogen IX cpd: C01079; coproporphyrin III cpd: C03263; uroporphyrinogen III cpd: C01051; hydroxymethylbilane cpd: C01024; porphobilinogen cpd: C00931; 5-aminolevulinic acid cpd: C00430; uroporphyrinogen I cpd: C05766; L-Glutamic acid cpd: C00025; bilirubin cpd: C00486; protoporphyrin IX cpd: C02191; adenosyl cobinamide cpd: C06508; heme a cpd: C15670; D-Urobilinogen cpd: C05791; adenosyl cobyrimic acid a,c diamide cpd: C06506; Fe3+ cpd: C14819; coproporphyrinogen I cpd: C05768; l-glutamyl-tRNA(Glu) cpd: C02987; cytochrome c cpd: C00524

TABLE 4: Continued.

Pathway	Total Hits	Raw $p$	$-\ln(p)$	Holm adjust	FDR	Impact	Hits cpd	Total cpd
Glycine, serine, and threonine metabolism	31	0.4886	0.71625	1	1	0.26884	Glycine cpd: C00037	L-Serine cpd: C00065; choline cpd: C00114; glyceric acid cpd: C00258; betaine cpd: C00719; guanidinoacetic acid cpd: C00581; 3-phospho-D-glycerate cpd: C00197; dimethylglycine cpd: C01026; L-cystathionine cpd: C02291; glycine cpd: C00037; phosphoserine cpd: C01005; sarcosine cpd: C00213; 5,10-methylene-THF cpd: C00143; L-threonine cpd: C00188; lipoylprotein cpd: C02051; aminoacetone cpd: C01888; tetrahydrofolic acid cpd: C00101; S-aminomethyl-dihydrolipoylprotein cpd: C01242; dihydrolipoylprotein cpd: C02972; D-serine cpd: C00740; betaine aldehyde cpd: C00576; hydroxy-pyruvic acid cpd: C00168; creatine cpd: C00300; phosphohydroxy-pyruvic acid cpd: C03232; L-cysteine cpd: C00097; glyoxylic acid cpd: C00048; L-2-amino-3-oxobutanoic acid cpd: C03508; pyruvic acid cpd: C00022; carbon dioxide cpd: C00011; 5-aminolevulinic acid cpd: C00430; pyruvaldehyde cpd: C00546; ammonia cpd: C00014 Enzyme N6-(lipoyl)lysine cpd: C15972; 2-methyl-1-hydroxybutyl-ThPP cpd: C15978; enzyme N6-(dihydrolipoyl)lysine cpd: C15973; 2-methyl-1-hydroxypropyl-ThPP cpd: C15976; 3-methyl-1-hydroxybutyl-ThPP cpd: C15974; acetyl-CoA cpd: C00024; acetoacetyl-CoA cpd: C00332; acetoacetic acid cpd: C00164; 3-hydroxy-3-methylglutaryl-CoA cpd: C00356; 3-methylcrotonyl-CoA cpd: C03069; 3-hydroxyisovaleryl-CoA cpd: C05998; isovaleryl-CoA cpd: C02939; 3-methyl-2-oxovaleric acid cpd: C00671; thiamine pyrophosphate cpd: C00068; L-valine cpd: C00183; 2-methylacetoacetyl-CoA cpd: C03344; (S)-3-hydroxyisobutyrate cpd: C06001; tiglyl-CoA cpd: C03345; butyryl-CoA cpd: C00630; S-(2-methylbutanoyl)-dihydrolipamide cpd: C15979; alpha-ketoisovaleric acid cpd: C00141; L-isoleucine cpd: C00407; R-methylmalonyl-CoA cpd: C01213; methylmalonyl-CoA cpd: C00683; propionyl-CoA cpd: C00100; (S)-methylmalonic acid semialdehyde cpd: C06002; (S)-b-aminoisobutyric acid cpd: C03284; 2-methyl-3-hydroxybutyryl-CoA cpd: C04405; (S)-3-hydroxyisobutyryl-CoA cpd: C06000; methacrylyl-CoA cpd: C03460; (S)-2-methylbutanoyl-CoA cpd: C15980; S-(2-methylpropionyl)-dihydrolipamide-E cpd: C15977; 4-methyl-2-oxopentanoate cpd: C00233; S-(3-methylbutanoyl)-dihydrolipamide-E cpd: C15975; L-leucine cpd: C00123; 3-methylglutaconyl-CoA cpd: C03231; succinyl-CoA cpd: C00091; methylmalonic acid cpd: C02170
Valine, leucine, and isoleucine degradation	38	0.5614	0.57739	1	1	0	Methylmalonic acid cpd: C02170	

TABLE 4: Continued.

Pathway	Total Hits	Raw $p$	$-\ln(p)$	Holm adjust	FDR	Impact	Hits	Total cpd
Fatty acid metabolism	39	1	0.5709	0.56053	1	1	0	Palmitic acid cpd: C00249 Palmitoyl-CoA cpd: C00154; hexanoyl-CoA cpd: C05270; butanoyl-CoA cpd: C00136; acetyl-CoA cpd: C00024; (S)-3-hydroxybutanoyl-CoA cpd: C01144; cis,cis-3,6-dodecadienoyl-CoA cpd: C05280; (S)- hydroxyhexanoyl-CoA cpd: C05268; (S)-hydroxyoctanoyl-CoA cpd: C05266; octanoyl-CoA cpd: C01944; (S)-hydroxydecanoyl-CoA cpd: C05264; decanoyl-CoA (n-C10: 0CoA) cpd: C05274; (S)-3- hydroxydodecanoyl-CoA cpd: C05262; lauroyl-CoA cpd: C01832; primary alcohol cpd: C00226; glutaryl-CoA cpd: C00527; (S)-3- hydroxytetradecanoyl-CoA cpd: C05260; tetradecanoyl-CoA cpd: C02593; fatty acid cpd: C00162; (S)-3-hydroxyhexadecanoyl-CoA cpd: C05258; palmitic acid cpd: C00249; (2E)-hexadecenoyl-CoA cpd: C05272; trans-2-hexenoyl-CoA cpd: C05271; crotonoyl-CoA cpd: C00877; acetoacetyl-CoA cpd: C00332; trans,cis-Lauro-2,6-dienoyl- CoA cpd: C05279; coenzyme A cpd: C00010; 3-oxohexanoyl-CoA cpd: C05269; 3-oxooctanoyl-CoA cpd: C05267; (2E)-octenoyl-CoA cpd: C05276; 3-oxodecanoyl-CoA cpd: C05265; (2E)-decanoyl-CoA cpd: C05275; 3-oxododecanoyl-CoA cpd: C05263; (2E)-dodecenoyl-CoA cpd: C03221; aldehyde cpd: C00071; 3-oxotetradecanoyl-CoA cpd: C05261; (2E)-tetradecenoyl-CoA cpd: C05273; omega-hydroxy fatty acid cpd: C03547; 3-oxohexadecanoyl-CoA cpd: C05259; L- palmitoylcarnitine cpd: C02990 L-tryptophan cpd: C00078; melatonin cpd: C01598; serotonin cpd: C00780; 5-hydroxytryptamine cpd: C05638; 5-hydroxytryptamine cpd: C05651; 5-hydroxy-L-tryptophan cpd: C00643; L- formyltryptamine cpd: C02700; acetoacetyl-CoA cpd: C00332; (S)-3- hydroxybutanoyl-CoA cpd: C01144; crotonoyl-CoA cpd: C00877; glutaryl-CoA cpd: C00527; oxoadipic acid cpd: C00322; 2-amino-3- carboxymuconic acid semialdehyde cpd: C04409; 3-hydroxyanthranilic acid cpd: C00632; L-tryptamine cpd: C00328; formylanthranilic acid cpd: C05653; L-3-hydroxytryptamine cpd: C03227; 3- hydroxytryptamine cpd: C05636; indoleacetaldehyde cpd: C00637; 5-hydroxy-N-formyltryptamine cpd: C05648; 5- hydroxyindoleacetaldehyde cpd: C05634; tryptamine cpd: C00398; indoleacrylic acid cpd: C00331; acetyl-N-formyl-5- methoxytryptamine cpd: C05642; 6-hydroxymelatonin cpd: C05643; N-acetylserotonin cpd: C00978; formyl-5- hydroxytryptamine cpd: C05647; 4,6-dihydroxyquinoline cpd: C05639; acetyl-CoA cpd: C00024; 2-aminomuconic acid semialdehyde cpd: C03824; 2-aminobenzoic acid cpd: C00108; L-tryptophanyl- tRNA(Trp) cpd: C03512; cinnavalinate cpd: C05640; 4-(2-amino-3- hydroxyphenyl)-2,4-dioxobutanoic acid cpd: C05645; 4-(2- aminophenyl)-2,4-dioxobutanoic acid cpd: C01252; 4,8- dihydroxyquinoline cpd: C05637; indoleacetic acid cpd: C00954; 5- hydroxyindoleacetic acid cpd: C05635; N-methylserotonin cpd: C06212; N-methyltryptamine cpd: C06213
Tryptophan metabolism	40	1	0.5803	0.5443	1	1	0	N-acetylserotonin cpd: C00978



TABLE 4: Continued.

Pathway	Total Hits	Raw $p$	$-\ln(p)$	Holm adjust	FDR	Impact	Hits cpd	Total cpd
								(13Z,16Z)-docosadi-13,16-enoyl-CoA cpd: C16645; tetracosenoyl-CoA cpd: C16532; docosenoyl-CoA cpd: C16531; icosenoyl-CoA cpd: C16530; tetracosanoyl-CoA cpd: C16529; docosanoyl-CoA cpd: C16528; (7Z,10Z,13Z,16Z)-docosatetraenoyl-CoA cpd: C16170; (11Z,14Z)-icosadienoyl-CoA cpd: C16180; (7Z,10Z,13Z,16Z,19Z)-docosapentaenoyl-CoA cpd: C16166; (11Z,14Z,17Z)-icosatrienoyl-CoA cpd: C16179; palmityl-CoA cpd: C00154; stearoyl-CoA cpd: C00412; eicosanoyl-CoA cpd: C02041; oleoyl-CoA cpd: C00510; linoleoyl-CoA cpd: C02050; arachidonyl-CoA cpd: C02249; 8,11,14-eicosatrienoyl-CoA cpd: C03595; gamma-linolenoyl-CoA cpd: C03035; (4Z,7Z,10Z,13Z,16Z,19Z)-docosahexaenoyl-CoA cpd: C16169; (5Z,8Z,11Z,14Z,17Z)-icosapentaenoyl-CoA cpd: C16165; alpha-linolenoyl-CoA cpd: C16162; 13,16-docosadienoic acid cpd: C16533; nervonic acid cpd: C08323; erucic acid cpd: C08316; icosenoic acid cpd: C16526; tetracosanoic acid cpd: C08320; behenic acid cpd: C08281; 7,10,13,16-docosatetraenoic acid cpd: C16527; icosadienoic acid cpd: C16525; clupanodonic acid cpd: C16513; icosatrienoic acid cpd: C16522; palmitic acid cpd: C00249; stearic acid cpd: C01530; arachidic acid cpd: C06425; oleic acid cpd: C00712; linoleic acid cpd: C01595; arachidonic acid cpd: C00219; 8,11,14-eicosatrienoic acid cpd: C03242; gamma-linolenic acid cpd: C06426; (4Z,7Z,10Z,13Z,16Z,19Z)-docosahexaenoic acid cpd: C06429; eicosapentaenoic acid cpd: C06428; alpha-linolenic acid cpd: C06427
Biosynthesis of unsaturated fatty acids	42	1	0.5983	0.51359	1	1	0	Palmitic acid cpd: C00249
Fatty acid biosynthesis	43	1	0.6071	0.49905	1	1	0	Palmitic acid cpd: C00249
								Tetradecanoyl-[acp] cpd: C05761; malonyl-[acyl-carrier protein] cpd: C01209; hexadecanoyl-[acp] cpd: C05764; octadecanoyl-[acyl-carrier protein] cpd: C04088; oleoyl-[acyl-carrier protein] cpd: C01203; dodecanoyl-[acyl-carrier protein] cpd: C05223; decanoyl-[acp] cpd: C05755; octanoyl-[acp] cpd: C05752; Hexanoyl-[acp] cpd: C05749; butyryl-[acp] cpd: C05745; trans-hexadec-2-enoyl-[acp] cpd: C05763; (3R)-3-hydroxypalmitoyl-[acyl-carrier protein] cpd: C04633; 3-oxohexadecanoyl-[acp] cpd: C05762; trans-tetradec-2-enoyl-[acp] cpd: C05760; (3R)-3-hydroxytetradecanoyl-[acyl-carrier protein] cpd: C04688; 3-oxotetradecanoyl-[acp] cpd: C05759; trans-dodec-2-enoyl-[acp] cpd: C05758; (R)-3-hydroxydodecanoyl-[acp] cpd: C05757; 3-oxododecanoyl-[acp] cpd: C05756; trans-Dec-2-enoyl-[acp] cpd: C05754; (3R)-3-hydroxydecanoyl-[acyl-carrier protein] cpd: C04619; 3-oxodecanoyl-[acp] cpd: C05753; trans-Oct-2-enoyl-[acp] cpd: C05751; (3R)-3-hydroxyoctanoyl-[acyl-carrier protein] cpd: C04620; 3-oxooctanoyl-[acp] cpd: C05750; trans-Hex-2-enoyl-[acp] cpd: C05748; (R)-3-hydroxyhexanoyl-[acp] cpd: C05747; 3-oxohexanoyl-[acp] cpd: C05746; but-2-enoyl-[acyl-carrier protein] cpd: C04246; (3R)-3-hydroxybutanoyl-[acyl-carrier protein] cpd: C04618; acetyl-[acyl-carrier protein] cpd: C03939; Malonyl-CoA cpd: C00083; acetyl-CoA cpd: C00024; acyl-carrier protein cpd: C00229; Holo-[carboxylase] cpd: C06250; carboxybiotin-carboxyl-carrier protein cpd: C04419; myristic acid cpd: C06424; 3-oxostearoyl-[acp] cpd: C16219; stearic acid cpd: C01530; oleic acid cpd: C00712; dodecanoic acid cpd: C02679; palmitic acid cpd: C00249; acetoacetyl-[acp] cpd: C05744

TABLE 4: Continued.

Pathway	Total Hits	Raw $p$	$-\ln(p)$	Holm adjust	FDR	Impact	Hits cpd	Total cpd
Primary bile acid biosynthesis	46	1	0.6323	0.45839	1	1	0.02976	Glycine cpd: C00037
								Cholesterol cpd: C00187; cholest-5-ene-3beta,26-diol cpd: C15610; 25-hydroxycholesterol cpd: C15519; 7 alpha,26-dihydroxy-4-cholesten-3-one cpd: C17336; 4-cholesten-7alpha,12alpha-diol-3-one cpd: C17339; 7a-hydroxy-cholestene-3-one cpd: C05455; 5-b-cholestane-3a,7a,12a-triol cpd: C05454; (25R)-3alpha,7alpha,12alpha-trihydroxy-5beta-cholestan-26-oyl-CoA cpd: C15613; (25S)-3alpha,7alpha,12alpha-trihydroxy-5beta-cholestan-26-oyl-CoA cpd: C17343; 3a,7a,12a-trihydroxy-5b-cholest-24-enoyl-CoA cpd: C05460; 3a,7a,12a-trihydroxy-5b-24-oxocholestanoyl-CoA cpd: C05467; 3a,7a-dihydroxy-5b-24-oxocholestanoyl-CoA cpd: C05449; chenodeoxycholoyl-CoA cpd: C05337; glycine cpd: C00037; taurine cpd: C00245; 3alpha,7alpha,12alpha,26-tetrahydroxy-5beta-cholestane cpd: C05446; 3a,7a,12a-trihydroxy-5b-cholestan-26-al cpd: C01301; 3 beta,7 alpha-dihydroxy-5-cholestenoate cpd: C17335; 7-a,27-dihydroxycholesterol cpd: C06341; 7a-Hydroxycholesterol cpd: C03594; 7-a,25-dihydroxycholesterol cpd: C15520; Choloyl-CoA cpd: C01794; 24-hydroxycholesterol cpd: C13550; 3alpha,7alpha-dihydroxy-5beta-cholestanate cpd: C04554; 3a,7a-dihydroxy-5b-cholestane cpd: C05452; 3 alpha,7 alpha,26-trihydroxy-5beta-cholestane cpd: C05444; 3a,7a-dihydroxy-5b-cholestan-26-al cpd: C05445; (25R)-3alpha,7alpha-dihydroxy-5beta-cholestanoyl-CoA cpd: C17345; (25S)-3alpha,7alpha-dihydroxy-5beta-cholestanoyl-CoA cpd: C17346; 3a,7a-dihydroxy-5b-cholest-24-enoyl-CoA cpd: C05447; 3a,7a,12a-trihydroxy-5b-cholestanoyl-CoA cpd: C04722; 3a,7a,12a-trihydroxy-5b-cholestanoyl-CoA cpd: C05448; 3a,7a,12a,24-tetrahydroxy-5b-cholestanoyl-CoA cpd: C05450; 3 beta-hydroxy-5-cholestenoate cpd: C17333; (24S)-cholest-5-ene-3beta,7alpha,24-triol cpd: C15518; 7 alpha-hydroxy-3-oxo-4-cholestenoate cpd: C17337; 7a,12a-dihydroxy-5b-cholestan-3-one cpd: C05453; 7a-hydroxy-5b-cholestan-3-one cpd: C05451; chenodeoxycholic acid cpd: C02528; chenodeoxycholic acid glycine conjugate cpd: C05466; taurochenodesoxycholic acid cpd: C05465; 7alpha,25-dihydroxy-4-cholesten-3-one cpd: C17332; cholic acid cpd: C00695; glycocholic acid cpd: C01921; taurocholic acid cpd: C05122; 7 alpha,24-dihydroxy-4-cholesten-3-one cpd: C17331

TABLE 4. Continued.

Pathway	Total Hits	Raw <i>p</i>	$-\ln(p)$	Holm adjust	FDR	Impact	Hits cpd	Total cpd
								Guanosine diphosphate cpd: C00035; xanthine cpd: C00385; D-ribose 5-phosphate cpd: C00117; phosphoribosyl pyrophosphate cpd: C00119; L-glutamine cpd: C00064; 5-phosphoribosylamine cpd: C03090; glycineamidribotide cpd: C03838; phosphoribosylformylglycineamide cpd: C04640; AICAR cpd: C04677; SAICAR cpd: C04823; 5-amino-1-(5-phospho-D-ribosyl)imidazole-4-carboxylate cpd: C04751; RNA cpd: C00046; cyclic AMP cpd: C00575; adenosine triphosphate cpd: C00002; dATP cpd: C00131; ADP cpd: C00008; dADP cpd: C00206; adenosine monophosphate cpd: C00020; adenylysuccinic acid cpd: C03794; inosinic acid cpd: C00130; adenosine cpd: C00212; deoxyadenosine monophosphate cpd: C00360; deoxyadenosine cpd: C00559; deoxyinosine cpd: C05512; xanthosine cpd: C01762; IDP cpd: C00104; guanosine monophosphate cpd: C00144; xanthylic acid cpd: C00655; hypoxanthine cpd: C00262; inosine cpd: C00294; guanine cpd: C00499; uric acid cpd: C00366; 5-C00330; allantoinic acid cpd: C00499; uric acid cpd: C00366; 5-hydroxyisourate cpd: C11821; guanosine 3'-diphosphate 5'-triphosphate cpd: C04494; guanosine triphosphate cpd: C00044; 2'-deoxyguanosine 5'-monophosphate cpd: C00362; dGDP cpd: C00361; guanosine cpd: C00387; dGTP cpd: C00286; cyclic GMP cpd: C00942; sulfate cpd: C00059; adenosine phosphosulfate cpd: C00224; phosphoadenosine phosphosulfate cpd: C00053; 5'-Phosphoribosyl-N-formylglycinamide cpd: C04376; inosine triphosphate cpd: C00081; xanthosine 5-triphosphate cpd: C00700; diadenosine tetraphosphate cpd: C01260; P1,P4-bis(5'-xanthosyl) tetraphosphate cpd: C04392; adenosine diphosphate ribose cpd: C00301; adenine cpd: C00147; dIDP cpd: C01344; 2'-deoxyinosine triphosphate cpd: C01345; diadenosine triphosphate cpd: C06197; phosphoribosyl formamidocarboxamide cpd: C04734; 5-hydroxy-2-oxo-4-ureido-2,5-dihydro-1H-imidazole-5-carboxylate cpd: C12248; 5-aminoimidazole ribonucleotide cpd: C03373; DNA cpd: C00039; ammonia cpd: C00014; urea cpd: C00086; (S)-ureidoglycolic acid cpd: C00603; guanosine 3',5'-bis(diphosphate) cpd: C01228; adenosine 3',5'-diphosphate cpd: C00054; diguanosine tetraphosphate cpd: C01261; dIMP cpd: C06196; 5-amino-4-imidazolecarboxamide cpd: C04051; (S) (+)-allantoin cpd: C02350
Purine metabolism	68	1	0.7749	0.25507	1	1	0	Sulfate cpd: C00059

TABLE 4: Continued.

Pathway	Total Hits	Raw $p$	$-\ln(p)$	Holm adjust	FDR	Impact	Hits cpd	Total cpd
Aminoacyl-tRNA biosynthesis	69	1	0.7799	0.24863	1	1	0	Glycine cpd: C00037
								L-asparagine cpd: C00152; tRNA(Asn) cpd: C01637; L-histidine cpd: C00135; tRNA(His) cpd: C01643; L-phenylalanine cpd: C00079; tRNA(Phe) cpd: C01648; L-arginine cpd: C00062; tRNA(Arg) cpd: C01636; L-glutamine cpd: C00064; tRNA(Gln) cpd: C01640; L-cysteine cpd: C00097; tRNA(Cys) cpd: C01639; glycine cpd: C00037; tRNA(Gly) cpd: C01642; tRNA(Asp) cpd: C01638; L-aspartic acid cpd: C00049; L-serine cpd: C00065; tRNA(Ser) cpd: C01650; L-methionine cpd: C00073; tRNA(Met) cpd: C01647; L-valine cpd: C00183; tRNA(Val) cpd: C01653; L-alanine cpd: C00041; tRNA(Ala) cpd: C01635; L-lysine cpd: C00047; tRNA(Lys) cpd: C01646; L-isoleucine cpd: C00407; tRNA(Ile) cpd: C01644; tRNA(Leu) cpd: C01645; L-leucine cpd: C00123; L-threonine cpd: C00188; tRNA(Thr) cpd: C01651; tRNA(Trp) cpd: C01652; L-tryptophan cpd: C00078; N10-formyl-THF cpd: C00234; L-methionyl-tRNA cpd: C02430; L-tyrosine cpd: C00082; tRNA(Tyr) cpd: C00787; L-proline cpd: C00148; tRNA(Pro) cpd: C01649; L-glutamic acid cpd: C00025; tRNA(Glu) cpd: C01641; glutamyl-tRNA cpd: C02282; L-asparaginyl-tRNA(Asn) cpd: C03402; tRNA(Sec) cpd: C16636; L-seryl-tRNA(Sec) cpd: C06481; O-phosphoseryl-tRNA(Sec) cpd: C16638; L-histidyl-tRNA(His) cpd: C02988; L-phenylalanyl-tRNA(Phe) cpd: C03511; L-arginyl-tRNA(Arg) cpd: C02163; L-cysteinyl-tRNA(Cys) cpd: C03125; Glycyl-tRNA(Gly) cpd: C02412; L-aspartyl-tRNA(Asp) cpd: C02984; L-seryl-tRNA(Ser) cpd: C02553; L-valyl-tRNA(Val) cpd: C02554; L-alanyl-tRNA cpd: C00886; L-lysyl-tRNA cpd: C01931; L-isoleucyl-tRNA(Ile) cpd: C03127; L-leucyl-tRNA cpd: C02047; L-threonyl-tRNA(Thr) cpd: C02992; L-tryptophanyl-tRNA(Trp) cpd: C03512; tetrahydrofolic acid cpd: C00101; N-formylmethionyl-tRNA cpd: C03294; L-tyrosyl-tRNA(Tyr) cpd: C02839; L-prolyl-tRNA(Pro) cpd: C02702; L-glutamyl-tRNA(Glu) cpd: C02987; L-glutamyl-tRNA(Gln) cpd: C06112; L-aspartyl-tRNA(Asn) cpd: C06113; L-selenocysteinyl-tRNA(Sec) cpd: C06482
Pathway								Metabolic pathway name
Total								The number of metabolites in this pathway
Hits								The number of differential metabolites hit this pathway
Raw $p$								$P$ value of metabolic pathway enrichment analysis
$-\ln(p)$								Minus log base E of P
Holm adjust								$P$ values corrected by Holm-Bonferroni method for multiple hypothesis testing
FDR								$P$ value corrected by false discovery rate (FDR) method for multiple hypothesis testing
Impact								Impact value of metabolic pathway topology analysis
Hits cpd								The names and KEGG IDs of differential metabolites hit the pathway
Total cpd								All metabolite names and KEGG IDs contained in this pathway

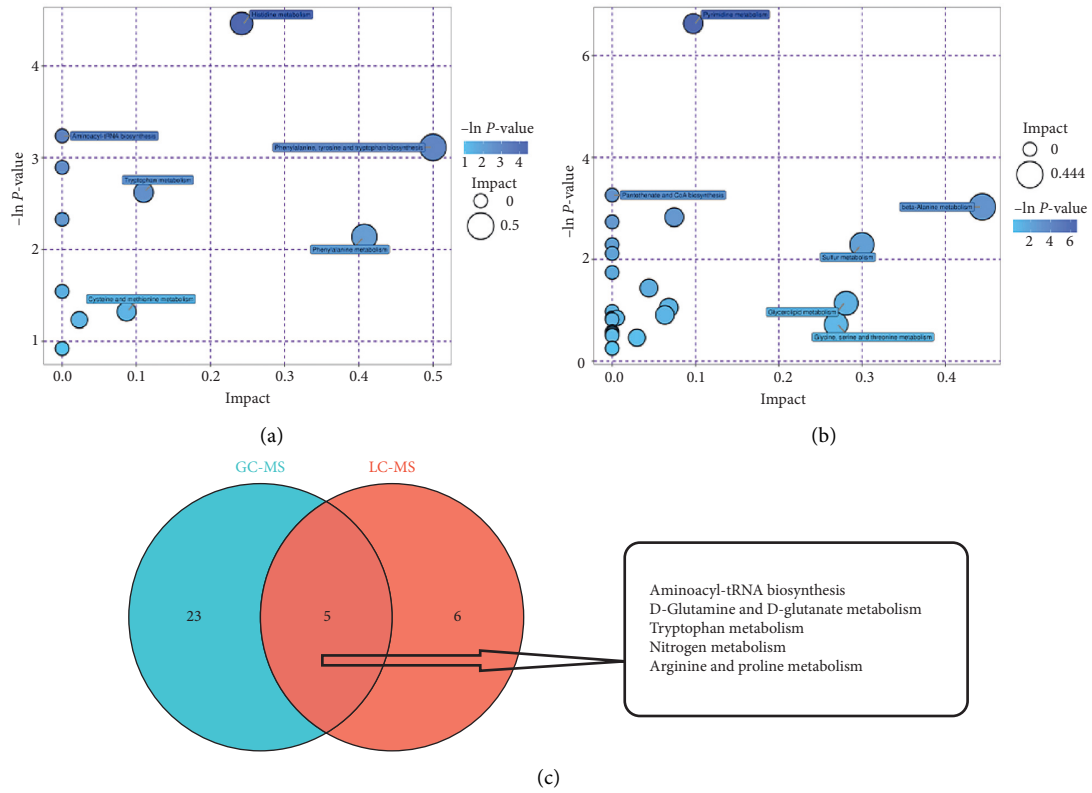


FIGURE 3: Metabolic pathway enrichment analysis of differential metabolites. (a) Pathway analysis of group M versus group T based on mass spectrometry combined with high-performance liquid chromatography. (b) Pathway analysis of group M versus group T based on mass spectrometry combined with gas chromatography. Each bubble represents a metabolic pathway; the bubble size represents the influence factor, the larger the size, the larger the influence factor; the vertical coordinate of the bubble and the color of the bubble indicate the *P* value of the enrichment analysis; the darker the color, the smaller the *P* value, the more significant the enrichment.

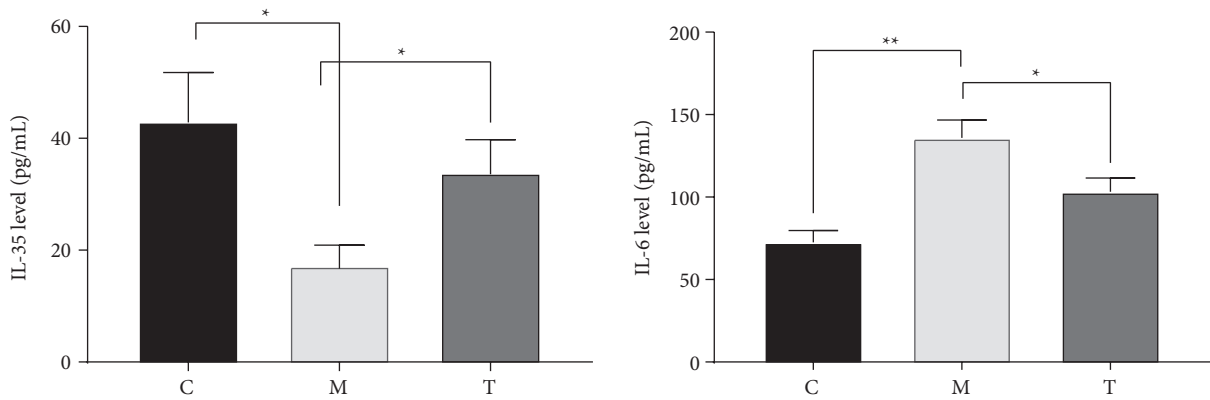


FIGURE 4: Comparison of serum levels of inflammatory factors IL-35 and IL-6 in three groups of mice.

In this experiment, a total of 38 differential metabolites were screened based on mass spectrometry coupled with the high-performance liquid phase, 120 differential metabolites were screened based on mass spectrometry coupled with gas phase, and a total of  $\alpha$ -glucose and  $\beta$ -glucose were analyzed based on NMR test results.

Measuring metabolite concentrations by metabolomics only tells half the story. Equally important is to understand pathway activity, which can be quantified as the flow of material per unit time, i.e., metabolic flux. In this experiment, we took intersections of pathways enriched by differential metabolites in the M and T groups for both mass

spectrometry coupled with high-performance liquid and gas phases, yielding a total of five common pathways, namely, amino acid tRNA biosynthesis, D-glutamine and D-glutamate metabolism, tryptophan metabolism, nitrogen metabolism, and arginine and proline metabolism.

Amino tRNA is a substrate for translation and plays a key role in determining how the genetic code is interpreted into amino acids. The function of aminyl-tRNA synthesis is to precisely match amino acids to tRNAs containing the corresponding anticodons [15]. Aminyl-tRNA synthetase is essential for the physical interpretation of the genetic code [16], and in addition to its function in protein synthesis, it is involved in various cellular processes such as immune and inflammatory responses, angiogenesis, and apoptosis [17,18]. Just one study showed that the pentose phosphate pathway, aminyl-tRNA biosynthesis, and pyrimidine metabolism are the main pathways altered in hypothyroidism [19]. Glutamate is a key excitatory neurotransmitter responsible for maintaining cognitive function and neuronal plasticity [20], while metabolites associated with glutamate metabolism, 2-ketoglutarate, L-aspartate, and fumarate are associated with the gut microbiota, and their alterations may affect human health [21]. Some studies have indicated that glycerophospholipid, glutamine, and glutamate metabolism, and related metabolites are potential key targets for common molecular mechanisms linking HIV to NCDs through inflammation and oxidative stress [22]. Tryptophan is an essential aromatic amino acid consisting of a  $\beta$ -carbon attached to the 3-position of the indole group. Although tryptophan is the least abundant amino acid in proteins and cells, it is a biosynthetic precursor for a large number of microbial and host metabolites [23,24]. Tryptophan metabolism in the intestine is the direct conversion of tryptophan by intestinal microorganisms into several molecules, such as indoles and their derivatives. And many of these indole derivatives, in turn, are ligands for aryl hydrocarbon receptors [25]. Aryl hydrocarbon receptor signaling is thought to be a key component of the immune response at the barrier site and thus can maintain intestinal homeostasis by acting on epithelial renewal, barrier integrity, and many immune cell types [26]. Arginine is a nonessential or semiessential amino acid that plays an important role in a variety of biological functions including cell proliferation, survival, and protein synthesis. It is also a precursor for the production of nitric oxide, polyamines, proline, creatinine, and glutamate. As a multifunctional amino acid, arginine plays an important role in physical health by being involved in tissue damage and chronic metabolic diseases [27]. Arginine has also been associated with endothelial function, inflammation, and airway hyperresponsiveness [28]. Just one study indicated that arginine and proline metabolic pathways are related to asthma pathogenesis [29]. The above combined with the results of the present experiment could suggest that Yanghe decoction may maintain homeostasis by altering the relevant metabolic pathways and thus improving the disease. In addition, the above pathways have shown relevance to inflammation as well as immune cells. For this reason, we also investigated the effect of Yanghe decoction.

Inflammation is a comprehensive physiological response to tissue damage, which is caused by physical injury, infection, exposure to toxins, or other types of trauma [30]. There is growing evidence that inflammation is a major factor in the progression of many diseases, including autoimmune thyroiditis [31]. The results of the present study showed that serum inflammatory factor IL-35 was significantly lower and IL-6 was significantly higher in mice in the model group compared with the normal control group, whereas serum inflammatory factor IL-35 was significantly higher and IL-6 was significantly lower in mice treated based on Yanghe decoction compared with the model group. This may be due to the effect of one or a combination of herbs in the composition of Yanghe decoction. Deer antler tablets have antifatigue, anti-inflammatory, and analgesic effects, while deer antler peptides are the main active ingredients obtained by isolation from deer antler tablets [32]. It has been shown that in osteoblasts, antler peptides block TNF- $\alpha$ -mediated inhibition of osteoblastogenesis and inhibit osteoclastogenesis through the nuclear factor- $\kappa$ B (NF- $\kappa$ B)/p65 pathway. In addition, deer antler peptides reduce levels of interleukin 1 $\beta$  and interleukin 6, as well as oxidative responses induced by increased catalase activity and reduced malondialdehyde levels [33]. Previous studies have also indicated that Yanghe decoction may improve the symptoms of Hashimoto's thyroiditis and reduce inflammation [34]. This could suggest that Yanghe decoction can effectively reduce the inflammatory response in Hashimoto's thyroiditis, but whether the specific mechanism is related to metabolic pathways remains to be explored.

## 5. Conclusion

In summary, we detected multiple metabolites that can be altered by Yanghe decoction by NMR and mass spectrometry coupled with gas or liquid chromatography, and most of them were related to aminyl-tRNA biosynthesis, D-glutamine and D-glutamine metabolism, tryptophan metabolism, nitrogen metabolism, and arginine and proline metabolic pathways. In addition, Yanghe decoction can effectively reduce serum inflammatory factor levels in mice with Hashimoto's thyroiditis.

Although we identified the metabolites that can be altered by Yanghe decoction and the pathways that are highly affected, there are still shortcomings in this study. We only observed the metabolomic profile of plasma, and further studies should evaluate serum, urine, cerebrospinal fluid, and brain samples to accurately reflect the pathological changes in Hashimoto's thyroiditis and the therapeutic mechanisms of Yanghe decoction.

## Data Availability

All data generated or analyzed during this study are included in this article.

## Conflicts of Interest

The authors declare that they have no conflicts of interest.



## References

- [1] X. Lai, Y. Xia, B. Zhang, J. Li, and Y. Jiang, "A meta-analysis of Hashimoto's thyroiditis and papillary thyroid carcinoma risk," *Oncotarget*, vol. 8, no. 37, 62424 pages, 2017.
- [2] M. Ralli, D. Angeletti, M. Fiore et al., "Hashimoto's thyroiditis: an update on pathogenic mechanisms, diagnostic protocols, therapeutic strategies, and potential malignant transformation," *Autoimmunity Reviews*, vol. 19, Article ID 102649, 2020.
- [3] Y. Min, X. Wang, H. Chen, and G. Yin, "The exploration of Hashimoto's Thyroiditis related miscarriage for better treatment modalities," *International Journal of Medical Sciences*, vol. 17, no. 16, pp. 2402–2415, 2020.
- [4] T. Akamizu and N. J. E. Amino, "Hashimoto's Thyroiditis," 2017, <https://pubmed.ncbi.nlm.nih.gov/25905412/>.
- [5] G. Graceffa, R. Patrone, S. Vieni et al., "Association between Hashimoto's thyroiditis and papillary thyroid carcinoma: a retrospective analysis of 305 patients," *BMC Endocrine Disorders*, vol. 19, pp. 1–6, 2019.
- [6] D. Mao, L. Feng, and H. J. E.-B. C. Gong, "The antitumor and immunomodulatory effect of Yanghe decoction in breast cancer is related to the modulation of the JAK/STAT signaling pathway," *Evidence-Based Complementary and Alternative Medicine*, vol. 2018, Article ID 8460526, 9 pages, 2018.
- [7] X. Xu, Y. Wan, L. Gong, Z. Ma, and T. J. M. Xu, "Chinese herbal medicine Yanghe decoction for knee osteoarthritis: a protocol for systematic review and meta-analysis," *Medicine*, vol. 99, 2020.
- [8] H. Xia, D. Cao, F. Yang et al., "Jiawei Yanghe decoction ameliorates cartilage degradation in vitro and vivo via Wnt/ $\beta$ -catenin signaling pathway," *Biomedicine & Pharmacotherapy*, vol. 122, Article ID 109708, 2020.
- [9] L. Zeng and K. Yang, "Exploring the pharmacological mechanism of Yanghe Decoction on HER2-positive breast cancer by a network pharmacology approach," *Journal of Ethnopharmacology*, vol. 199, pp. 68–85, 2017.
- [10] J. Li, X. Liu, H. Chen et al., "Multi-targeting chemoprevention of Chinese herb formula Yanghe Huayan decoction on experimentally induced mammary tumorigenesis," *BMC Complementary and Alternative Medicine*, vol. 19, pp. 48–15, 2019.
- [11] C. Jang, L. Chen, and J. D. Rabinowitz, "Metabolomics and isotope tracing," *Cell*, vol. 173, no. 4, pp. 822–837, 2018.
- [12] M. M. Rinschen, J. Ivanisevic, M. Giera, and G. Siuzdak, "Identification of bioactive metabolites using activity metabolomics," *Nature Reviews Molecular Cell Biology*, vol. 20, no. 6, pp. 353–367, 2019.
- [13] D. S. Wishart, "Metabolomics for investigating physiological and pathophysiological processes," *Physiological Reviews*, vol. 99, pp. 1819–1875, 2019.
- [14] E. Riekeberg and R. J. F. Powers, "New frontiers in metabolomics: from measurement to insight," *F1000Res*, vol. 6, 2017.
- [15] M. Ibba and D. Söll, "Aminoacyl-tRNA synthesis," *Annual Review of Biochemistry*, vol. 69, no. 1, pp. 617–650, 2000.
- [16] C. S. Francklyn and P. Mullen, "Progress and challenges in aminoacyl-tRNA synthetase-based therapeutics," *Journal of Biological Chemistry*, vol. 294, no. 14, pp. 5365–5385, 2019.
- [17] X. Gao, R. Guo, Y. Li et al., "Contribution of upregulated aminoacyl-tRNA biosynthesis to metabolic dysregulation in gastric cancer," *Journal of Gastroenterology and Hepatology*, vol. 36, no. 11, pp. 3113–3126, 2021.
- [18] C. Zhang, X. Lin, Q. Zhao et al., "YARS as an oncogenic protein that promotes gastric cancer progression through activating PI3K-Akt signaling," *Journal of Cancer Research and Clinical Oncology*, vol. 146, no. 2, pp. 329–342, 2020.
- [19] A. Muñoz-Prieto, L. G. González-Arostegui, I. Rubiç et al., "Untargeted metabolomic profiling of serum in dogs with hypothyroidism," *Research in Veterinary Science*, vol. 136, pp. 6–10, 2021.
- [20] F. J. Vázquez-Santiago, R. J. Noel, J. T. Porter, and R.-A. VJJon, "Glutamate metabolism and HIV-associated neurocognitive disorders," *Journal of NeuroVirology*, vol. 20, pp. 315–331, 2014.
- [21] M. Wang, J. Wan, H. Rong et al., "Alterations in gut glutamate metabolism associated with changes in gut microbiota composition in children with autism spectrum disorder," *mSystems*, vol. 4, pp. e00321–00318, 2019.
- [22] Y. Ding, H. Lin, X. Chen et al., "Comprehensive metabolomics profiling reveals common metabolic alterations underlying the four major non-communicable diseases in treated HIV infection," *EBioMedicine*, vol. 71, Article ID 103548, 2021.
- [23] L. M. Alkhalaf and K. S. Ryan, "Biosynthetic manipulation of tryptophan in bacteria: pathways and mechanisms," *Chemistry & Biology*, vol. 22, no. 3, pp. 317–328, 2015.
- [24] A. Agus, J. Planchais, and H. Sokol, "Gut microbiota regulation of tryptophan metabolism in health and disease," *Cell Host & Microbe*, vol. 23, no. 6, pp. 716–724, 2018.
- [25] T. D. Hubbard, I. A. Murray, and G. H. Perdew, "Indole and tryptophan metabolism: endogenous and dietary routes to Ah receptor activation," *Drug Metabolism and Disposition*, vol. 43, no. 10, pp. 1522–1535, 2015.
- [26] B. Lamas, J. M. Natividad, and H. Sokol, "Aryl hydrocarbon receptor and intestinal immunity," *Mucosal Immunology*, vol. 11, no. 4, pp. 1024–1038, 2018.
- [27] S. Zou, X. Wang, P. Liu, C. Ke, and S. Xu, "Arginine metabolism and deprivation in cancer therapy," *Biomedicine & Pharmacotherapy*, vol. 118, Article ID 109210, 2019.
- [28] D. Liang, C. N. Ladvá, R. Golan et al., "Perturbations of the arginine metabolome following exposures to traffic-related air pollution in a panel of commuters with and without asthma," *Environment International*, vol. 127, pp. 503–513, 2019.
- [29] K. D. Quinn, M. Schedel, Y. Nkrumah-Elie et al., "Dysregulation of metabolic pathways in a mouse model of allergic asthma," *Allergy*, vol. 72, no. 9, pp. 1327–1337, 2017.
- [30] P. Arulsevan, M. T. Fard, W. S. Tan, S. Gothai, S. Fakurazi, and M. E. Norhaizan, "Role of antioxidants and natural products in inflammation," *Oxidative Medicine and Cellular Longevity*, vol. 2016, Article ID 5276130, 15 pages, 2016.
- [31] D.-H. Wu, L. Xu, G.-Q. Xie, Y.-S. Fan, J. J. E.-bC. Zhou, and A. Medicine, "The pungent and hot chinese herbs cause heat syndrome in rats by affecting the regulatory T cells," *Evidence-Based Complementary and Alternative Medicine*, vol. 2019, Article ID 9824906, 9 pages, 2019.
- [32] F. Wu, H. Li, L. Jin et al., "Deer antler base as a traditional Chinese medicine: a review of its traditional uses, chemistry and pharmacology," *Journal of Ethnopharmacology*, vol. 145, no. 2, pp. 403–415, 2013.
- [33] Y. Wang and X. Xiao, "Clinical efficacy of modified Yanghe decoction in ankylosing spondylitis: a randomized controlled trial," *Medical Science Monitor*, vol. 24, pp. 2912–2918, 2018.
- [34] Be Ma, D. Chen, Y. Liu et al., "Yanghe decoction suppresses the experimental autoimmune thyroiditis in rats by improving NLRP3 inflammasome and immune dysregulation," *Frontiers in Pharmacology*, vol. 12, p. 1527, 2021.

## Research Article

# Synovitis Ointment Improved Knee Osteoarthritis by Suppressing SDF-1/CXCR4 Signaling Pathway

Jin Zhang,<sup>1</sup> Min Zhao,<sup>1</sup> Jing Liu,<sup>2</sup> Ke Wang,<sup>1</sup> Xiang Cai,<sup>3</sup> Wei Xiao,<sup>1</sup> Le Wang,<sup>2</sup> Mang Wang,<sup>2</sup> Lei Zhang ,<sup>1</sup> and Chi Zhang <sup>1</sup>

<sup>1</sup>Department of Orthopedic, Wuhan Hospital of Traditional Chinese Medicine, Wuhan 430014, China

<sup>2</sup>Department of Acupuncture, Wuhan Hospital of Traditional Chinese Medicine, Wuhan 430014, China

<sup>3</sup>Department of Surgery, Wuhan Hospital of Traditional Chinese Medicine, Wuhan 430014, China

Correspondence should be addressed to Lei Zhang; 233637948@qq.com and Chi Zhang; 4564352@qq.com

Received 17 March 2022; Revised 6 May 2022; Accepted 1 June 2022; Published 1 July 2022

Academic Editor: Ruchika Garg

Copyright © 2022 Jin Zhang et al. This is an open access article distributed under the Creative Commons Attribution License, which permits unrestricted use, distribution, and reproduction in any medium, provided the original work is properly cited.

**Objective.** Knee osteoarthritis (KOA) remains a challenge for clinicians worldwide and lacks major advancements in treatment. In this study, we investigated the mechanism of synovitis ointment interference on KOA. **Methods.** SD rats were used to establish KOA models and were randomly divided into five groups: the control group, the KOA group, the KOA + synovitis ointment group, the KOA + Western medicine group, and the KOA + Chinese medicine group. Detection of pathological injury of the joint was observed through HE staining. Enzyme-linked immunosorbent assay (ELISA) was used to measure the expression of SDF-1, CXCR4, MMP-9, and MMP-13. Effects of synovitis ointment on bone cell fibrosis were detected through Masson staining, and the relative mRNA expression of PLOD2, COL1A1, TIMP1, and TGF- $\beta$  was observed using the real-time quantitative (RT-PCR) method. **Results.** Mankin's score and the knee diameters showed that the KOA model has been successfully established; compared with the OA group, the synovitis ointment group improved the pathological injury of the knee joint. Compared with the KOA group, the synovitis ointment group, the KOA + Western medicine group, and the KOA + Chinese medicine group significantly decreased the expression of SDF-1, CXCR4, MMP-9, and MMP-13. Synovitis ointment reduced the relative content of bone cell fiber compared to that in the KOA group. While, the relative mRNA expression of PLOD2, COL1A1, TIMP1, and TGF- $\beta$  was significantly decreased in the synovitis ointment group. **Conclusion.** Synovitis ointment inhibited the inflammation and bone cell fibrosis of KOA, and the mechanism was related to the SDF-1/CXCR4 signaling pathway.

## 1. Introduction

Knee osteoarthritis (KOA) is one of the joint degenerative diseases leading to disability in the elderly [1]. Its incidence is increasing year by year and the patient have the tendency of being younger, which seriously threatens the health of humans and the quality of life [2, 3]. As the pathogenesis and etiology of KOA are still inaccurate, it is difficult to obtain satisfactory results in the clinical treatment of KOA. Previous studies have shown that cartilage damage could cause synovial inflammation, and chondrocyte-mediated inflammation played a key role in the occurrence and development of osteoarthritis [4]. Therefore, effective inhibition of

inflammation might have a great significance in delaying or even reversing the process of the KOA.

Chemokine SDF-1 (CXCL12) is a cytokinin bound to a specific G protein-coupled receptor (CXCR4; CD184) and plays an important role in physiological and pathological processes [5, 6]. Studies have shown that in patients with KOA, the SDF-1/CXCR4 pathway was involved in maintaining or promoting the inflammatory process [7]. It affected the proliferation of blood vessels through MMPs, promoted cell proliferation and migration, inhibited cell apoptosis, and promoted inflammation-driven colorectal cancer [8, 9]. Meanwhile, bone cell fibrosis was an important indicator in the development of KOA [10]. PLOD2,

COL1A1, TIMP1, and TGF- $\beta$  were generally considered fibrosis markers [11]. Thus, inhibiting inflammation and bone cell fibrosis may be a potential method for the treatment of KOA.

In recent years, traditional Chinese medicine had a significant effect on KOA, which could effectively reduce the risk of total knee replacement [12]. Studies had shown that Fang Sheng Yu decoction combined with Wu Ling powder [13] and Tian Nan Xing decoction combined with Bu Shen Huo Xue decoction could relieve the pain in knee joint and improve the function of the knee joint [14, 15]. Synovitis ointment was made with Radix Aconiti Konii, Radix Aconiti, Radix Noctis, Kaschin, Kaempferi, Hyacinth, *Asarum*, and Baijiu. It had the functions of anti-inflammatory and analgesic, expelling wind and cold, promoting blood circulation, and removing dampness. The direct external application could reduce inflammation and analgesia and repair the synovium of cartilage tissue. In the long-term clinical treatment of KOA, synovitis ointment significantly ameliorated the symptoms of KOA and improved the health and quality of life. However, the specific mechanism of synovitis ointment on KOA is still unclear. In this study, through the animal experiment, the mechanism of KOA treated with synovitis ointment was studied, which provided a scientific basis for clinical application and improved the quality of life of the elderly. This was of great significance to improve the physical quality of the people and social development.

## 2. Materials and Methods

**2.1. Experimental Animals.** Thirty specific pathogen-free (SPF) male SD rats (200  $\pm$  10 g, 6 weeks) were purchased from the China Three Gorges University (Hubei, China). Rats were fed at (22–26)°C with 12 h day/night cycle and free access to water and food for 7 d. All animal experiments confirmed to the relevant regulations of the Hubei Provincial Animal Management Committee's "Ethics Certificate for Experimental Animals." The animal study protocol was approved (approval no: SYXK (E) 2018–0104). Experiments were conducted in accordance with the ethical guidelines of the Hubei Provincial Animal Management Commission (permit no. 42010200004453).

**2.2. Establishment of the KOA Model.** All rats were anesthetized by intraperitoneal injection of pentobarbital sodium at 40 mg/kg. A longitudinal incision (2 cm) was made on one side of the knee to expose the knee joint. Then, the meniscus on one side of the knee was removed, and a cotton ball was used to stop the bleeding. The incision was sutured with 5–0 silk thread. Finally, all the rats were normally fed and conducted treatment in the 6th week of modeling.

**2.3. Animal Grouping.** Rats were randomly divided into five groups: the control group, the KOA group, the KOA + synovitis ointment group, the KOA + western medicine group, and the KOA + Chinese medicine group. The KOA model was established for all rats except for the control group rats. In the

TABLE 1: The primer sequences.

Gene	Primer sequences	Product length (bp)
PLOD2-F	GAACATTACGGCAAGTGGT	192
PLOD2-R	GGCAAATCCCTTGGTGTA	
COL1A1-F	AGATGTCCTATGGCTATGATGAG	288
COL1A1-R	CTGTTCCAGGCAATCCAC	
TIMP1-F	GGCATCCTCTTGTGCTATCATT	281
TIMP1-R	CTGCGGTTCTGGGACTTGTG	
TGF- $\beta$ -F	ACCGCAACAACGCAATCTAT	206
TGF- $\beta$ -R	ACCAAGGTAACGCCAGGAAT	
GAPDH-F	CAAGTTCAACGGCACAG	138
GAPDH-R	CCAGTAGACTCCACGACAT	

KOA + synovitis ointment group, rats were treated with 5 g synovitis ointment for 6 hours per day on the knee joint. In the KOA + Western medicine group, rats were treated with 0.4 g diclofenac cream (Sino US Tianjin Shike Pharmaceutical Co., Ltd., Tianjin, China) for each of the knee joint every day for 6 hours. In the KOA + Chinese medicine group, rats were treated with 5 g Golden Powder Cream for 6 hours per day on the knee joint. All the KOA rats were treated for 4 weeks.

**2.4. Synovitis Ointment and Golden Powder Cream.** Synovitis ointment is made from 50 g of Aconiti Kusnezoffii Radix, 50 g of Aconiti Radix, 50 g of Arisaematis Rhizoma, 50 g of Nardostachyos Radix et Rhizoma, 50 g of Rhizoma Kaempferiae, 50 g of Corydalis Rhizoma, and 20 g of Asari Radix et Rhizoma. Collect the powder and add 3 times the mass of alcohol to stir into a plaster, and 5 g plaster was placed in gauze for treatment. Golden Powder Cream: in accordance with the records of Chinese Pharmacopoeia, Radix Trichosanthis (320 g), Angelicae Dahuricae Radix (160 g), Curcumae Longae Rhizoma (160 g), Rhei Radix et Rhizoma (160 g), Phellodendri Chinensis Cortex (160 g), Atractylodis Rhizoma (64 g), Magnoliae Officinalis Cortex (64 g), *Citrus reticulata* Blanco (64 g), Radix Rhizoma Glycyrrhizae (64 g), and Arisaematis Rhizoma (64 g) were ground into a fine powder and prepared into a paste with honey. The ratio of Golden Powder Cream and honey is 3:1.5 g plaster was placed in gauze for treatment.

**2.5. Sampling and Tissue Preparation.** Blood samples were collected from the abdominal aorta. Serum samples were obtained by centrifugation at 4°C. The bone tissues were cut into tissue blocks and then fixed with decalcification solution for 2 d. Next, the tissues were permeabilized by xylene, embedded with paraffin, and cut into 3  $\mu$ m sections, which were normally conducted in a 42°C water bath and dried.

**2.6. HE Staining.** The paraffin sections were dewaxed by xylene (Sinopharm Chemical Reagent Co., Ltd., Shanghai, China) and a series of ethanol (Sinopharm Chemical Reagent Co., Ltd., Shanghai, China). Then, HE staining was performed and observed under a microscope (Leica, Wet-klar, Germany).

**2.7. Masson Staining.** The paraffin sections were dehydrated and stained with a drop of hematoxylin staining solution and

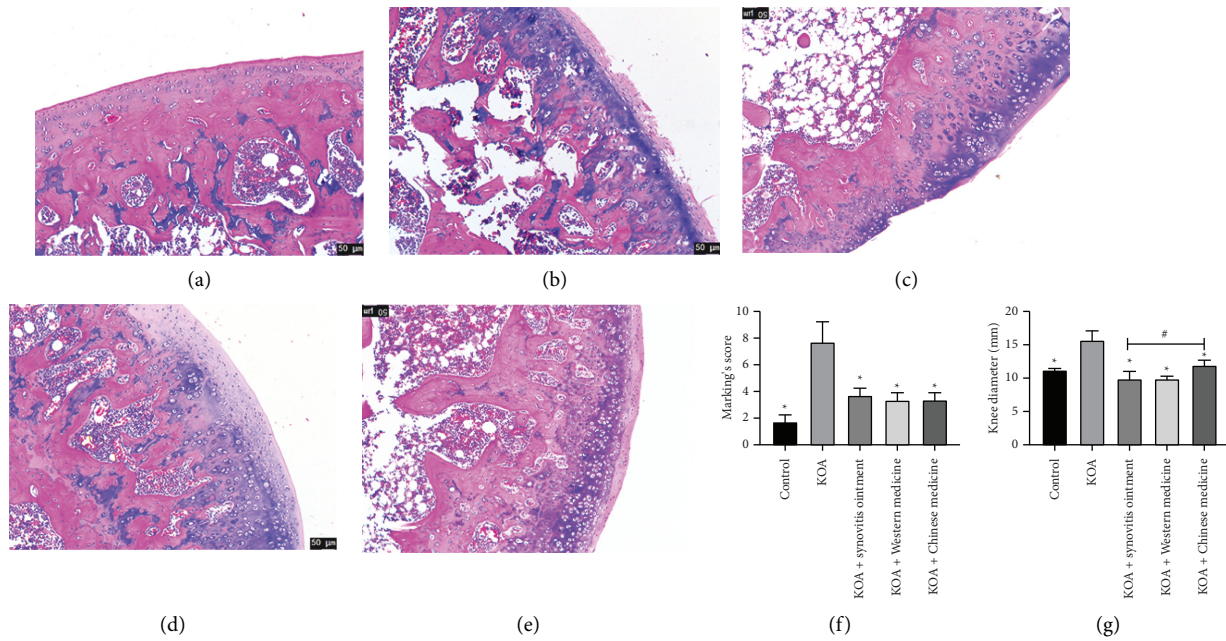


FIGURE 1: Mankin's score and knee diameter of joint tissue in the KOA model. The HE staining of joint tissue. (a) The control group. (b) The KOA group. (c) The KOA + synovitis ointment group. (d) The KOA + Western medicine group. (e) The KOA + Chinese medicine group. Mankin's score (f) and knee diameter (g) of joint tissue.

ferric chloride aqueous solution for 5 min and then differentiated with a drop of ethanol hydrochloride. The morphological changes in cartilage tissues were observed under a microscope.

**2.8. Real-Time Quantitative (RT-PCR) Methods.** 100 mg tissue samples were put into TRIzol (Ambion, Shanghai, China) for mRNA extraction. The cDNA was obtained through a reverse transcriptase kit (TAKARA, Dalian, China) with gDNA remover. The relative mRNA expression of PLOD2-F, COL1A1, TIMP1, and TGF- $\beta$  was performed in duplicate to determine an endogenous control of glyceraldehyde-3-phosphate dehydrogenase (GAPDH). The primer (Wuhan Tianyi Huayu Gene Technology Co., Ltd., Wuhan, China) sequences are given in Table 1.

**2.9. Enzyme-Linked Immunosorbent Assay (ELISA).** The serum samples were collected and concentrations of MMP-9, MMP-13, SDF-1, and CXCR4 were measured by using specific rat enzyme-linked immunosorbent assay (ELISA) kits (Wuhan Beinlai Biotechnology Co., Ltd., Wuhan, China) as per the manufacturer's instructions.

**2.10. Statistics.** All data were expressed as mean  $\pm$  SD and conducted using the SPSS 21.0 software. One-way analysis of variance (ANOVA) was used for comparisons between groups and  $P < 0.05$  was considered statistically significant. Multiple comparisons between groups were performed using Student's *t*-tests. Histological analyses were performed by two experienced investigators who were double-blinded.

### 3. Results

**3.1. Effects of Synovitis Ointment on Mankin's Score and Knee Diameter in the KOA Model.** To investigate the effect of synovitis ointment on KOA development and progression, we observed the cartilage tissue damage of the knee joint through HE staining and measured the diameter of the knee joint in rats. In the control group (Figure 1(a)), no histological changes were observed. In contrast, severe damage in HE sections from the KOA group was observed (Figure 1(b)). Full-thickness cartilage defect and microfracture in the fibrocartilage were seen in this group. The KOA + synovitis ointment group (Figure 1(c)) showed lower levels of damage than that of the KOA group. Regarding Mankin's score and knee diameter (Figures 1(f)–1(g)), Mankin's score in control, KOA + synovitis ointment, KOA + Western medicine, and KOA + Chinese medicine groups were low, but high scores were observed in the KOA group. In addition, the knee diameters in the KOA group were significantly higher than that of other groups ( $P < 0.05$ ). This demonstrated that synovitis ointment was favorable to KOA recovery.

**3.2. Effects of Synovitis Ointment on the Expression of SDF-1, CXCR4, MMP-9, and MMP-13.** To unravel the effects of synovitis ointment on SDF-1/CXCR4, we examined the expression of SDF-1, CXCR4, MMP-9, and MMP-13 in serum under different treatment conditions through the ELISA method (Figure 2). The levels of SDF-1, CXCR4, MMP-9, and MMP-13 were higher in the KOA group than those in groups with drug treatment. This finding confirmed that synovitis ointment was likely to suppress the osteoarthritis of the knee inflammation through downregulating the SDF-1/CXCR4 signaling pathway.

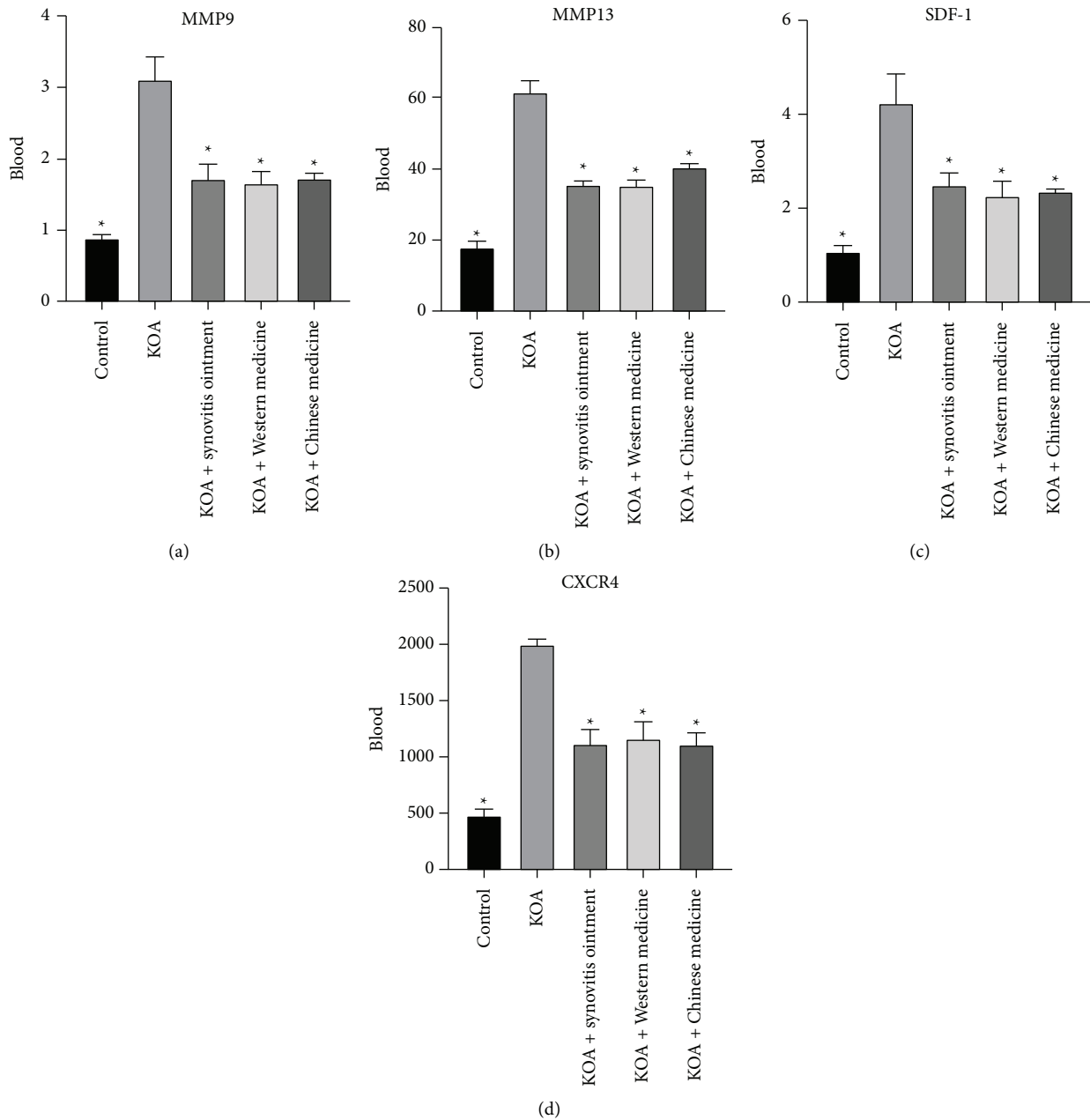


FIGURE 2: The expression of MMP-9 (a), MMP-13 (b), SDF-1 (c), and (d) CXCR4 in serum. The results are presented as the mean  $\pm$  SD,  $n = 6$ . \* $P < 0.05$  vs. control.

**3.3. Effects of Synovitis Ointment on Bone Cells Fibrosis.** To determine the effect of synovitis ointment on bone cells fibrosis, Masson staining was used for the cartilage collagen fiber staining. In the KOA group (Figure 3(b)), brighter and wider area blue was observed when compared to the control group (Figure 3(a)). The application of synovitis ointment caused significant reduction in the formation of bone cell fibrosis (Figure 3(c)). These results indicated that synovitis ointment was able to inhibit the increase of bone cell fibrosis.

**3.4. Effects of Synovitis Ointment on the Relative mRNA Expression of PLOD2, COL1A1, TIMP1, and TGF- $\beta$ .** To verify the effects of synovitis ointment on bone cells fibrosis, through RT-PCR assays, we examined the relative mRNA expression of PLOD2, COL1A1, TIMP1, and TGF- $\beta$  under different treatment conditions (Figure 4). The levels of PLOD2, COL1A1, TIMP1, and TGF- $\beta$  were significantly higher in those lacking drug treatments than those treated with synovitis ointment ( $P < 0.05$ ). This further proved that synovitis ointment treated osteoarthritis of the knee through inhibiting osteocytes fibrosis.



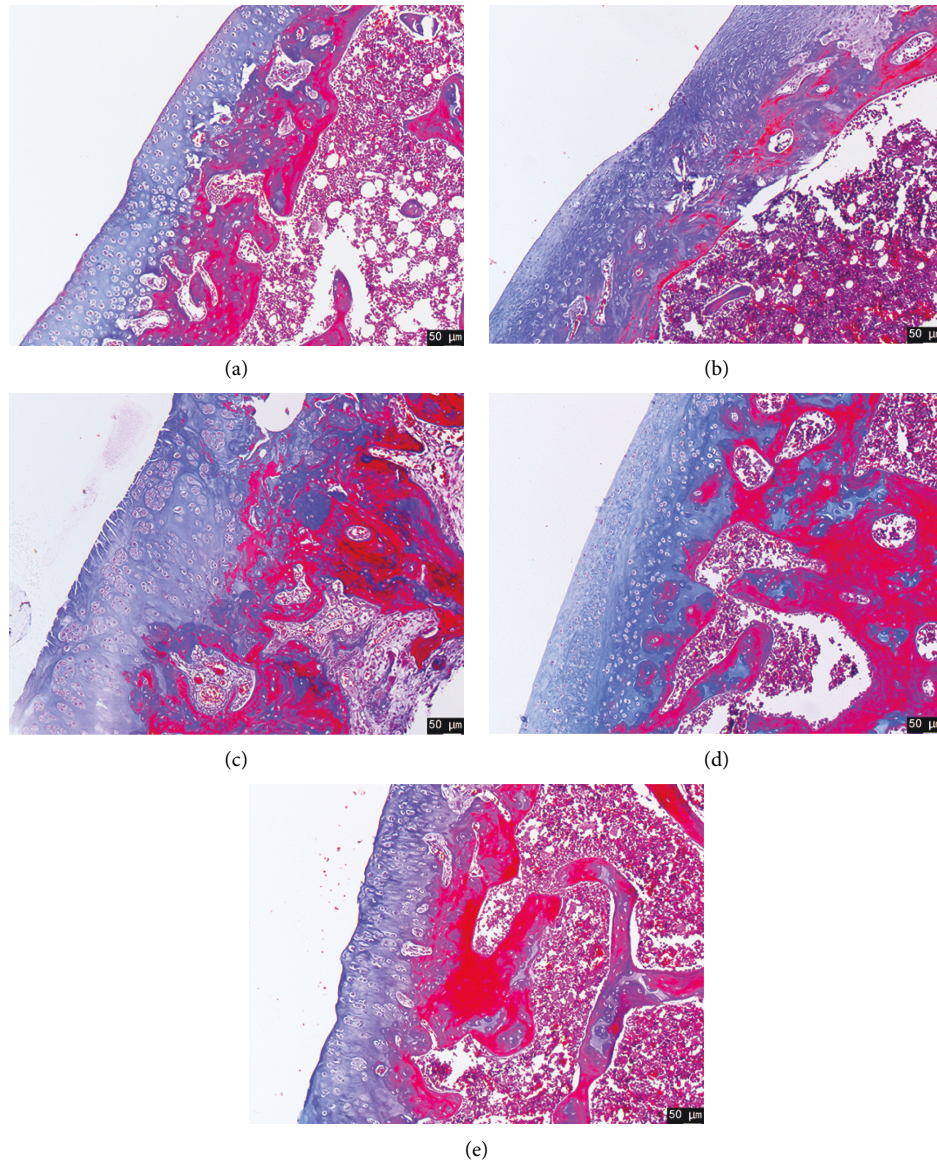


FIGURE 3: The Masson staining of joint tissue in the KOA model. (a) The control group. (b) The KOA group. (c) The KOA + synovitis ointment group. (d) The KOA + Western medicine group. (e) The KOA + Chinese medicine group.

#### 4. Discussion

KOA is known as a chronic degenerative disease and a significant public health problem, which has become one of the main reasons affecting the elderly life quality [16]. At present, there are several methods for treatment of KOA such as non-specific anti-inflammatory, electrotherapy, acupuncture, Chinese medicine, intraarticular injection of drugs, and weight loss and psychotherapy. Among them, traditional Chinese medicine synovitis ointment in the treatment of KOA has its unique curative effect. But its specific mechanism of action is rarely involved and not specific in-depth. In this study, we removed the meniscus of the knee to construct the model of KOA and confirmed it was constructed successfully through Mankin's score. Rats knee transverse diameter and HE results showed synovitis cream could effectively alleviate the symptoms of KOA.

SDF-1 is a member of CXCL12 chemokine family, which is secreted by many kinds of cells and has chemotactic and proliferative effects. It is regarded as a specific index of inflammatory response. CXCR4, as its specific receptor, is a G protein-coupled receptor, which is mainly expressed in immune cells and plays an important role in cell growth and development [17]. As a pair of important inflammatory response chemokines, the SDF-1/CXCR4 signaling pathway plays an important role in the occurrence and development of KOA [18]. MMP-9 and MMP-13 are important members of the matrix metalloproteinase (MMP) family. MMP-13, known as collagenase-13, plays a regulatory and pivotal role in the cascade of activation of MMPs. It is not only regulated by a variety of MMPs factors but also participates in the degradation process of ECM after activation. MMP-9 is a gelatinase, and activated MMP-9 can directly degrade ECM and promote the



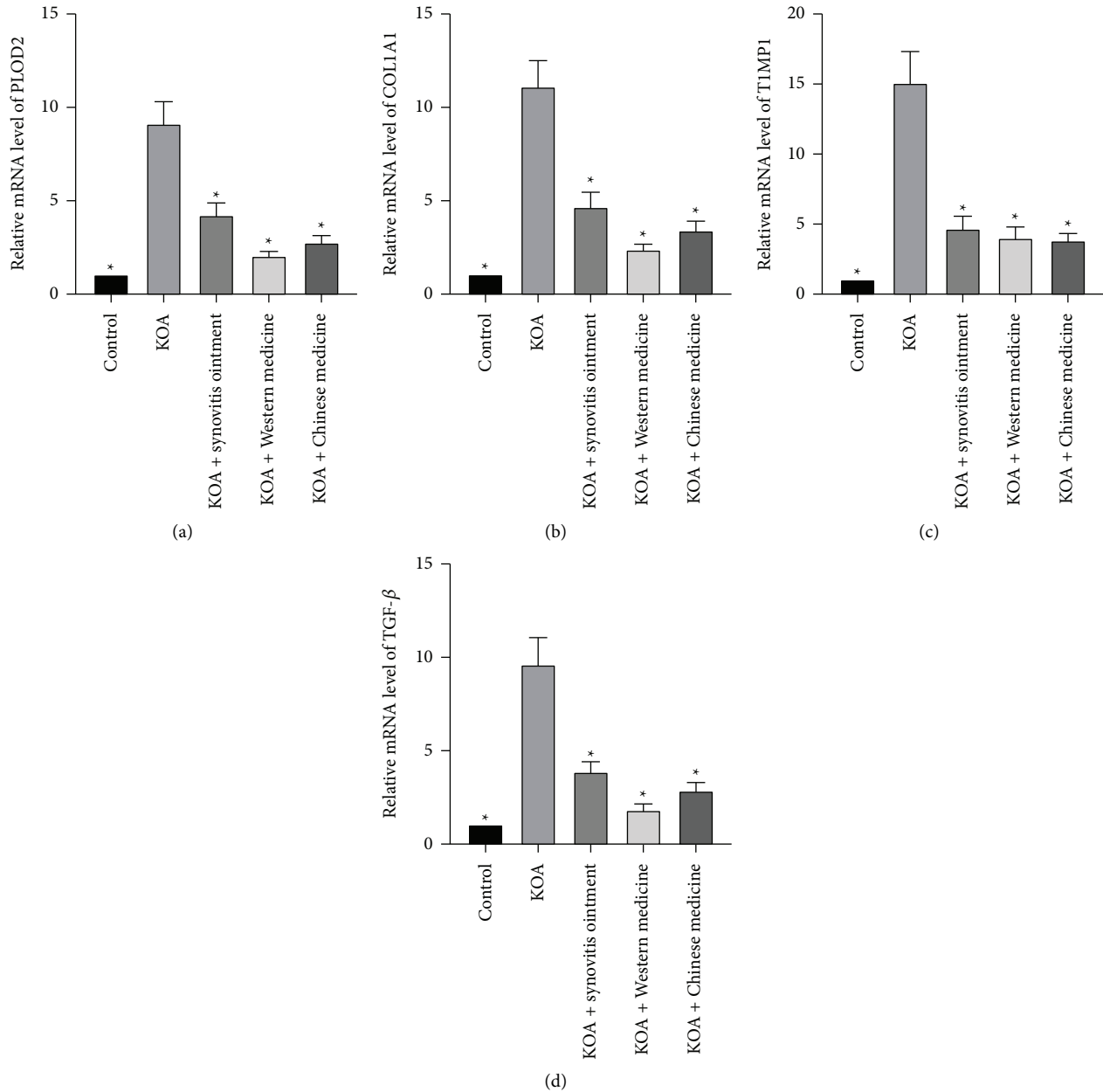


FIGURE 4: The relative mRNA expression of PLOD2 (a), COL1A1 (b), TIMP1 (c), and TGF- $\beta$  (d) of joint tissue in KOA rats. The results are presented as the mean  $\pm$  SD,  $n = 6$ . \* $P < 0.05$  vs. control.

occurrence and development of physiological and pathological osteolysis. It was widely believed that MMPs are involved in the occurrence and development of cartilage degenerative changes, and MMP-13 and MMP-9 play an important role in the degradation of cartilage extracellular matrix [19]. In this study, we found that the expression levels of SDF-1, CXCR4, MMP-9, and MMP-13 in KOA rats increased, which is consistent with reports in the literature. After applying with synovitis ointment, the expression levels of SDF-1, CXCR4, MMP-9, and MMP-13 reduced significantly in KOA rats. These results indicated that the mechanism of synovitis ointment alleviating knee arthritis is related to reducing the expression of SDF-1, CXCR4, MMP-9, and MMP-13.

KOA is most likely to invade articular cartilage during its occurrence and development. Cartilage damage and degeneration are one of the important signs of KOA. Before early morphologic changes in articular cartilage, different degrees of synovitis can be observed including synovial edema, hyperplasia, and fibrosis [20]. Synovial inflammation and articular cartilage damage interact and influence each other during KOA. Articular cartilage wear particles, and other degradation products can induce macrophage-like synovial cells to swallow and remove these debris, stimulate the inflammation of the surrounding synovial tissue, promote the secretion of joint fluid from fibroblast-like synovial cells, and cause joint

swelling [21]. Hence, we measured the levels of fibrosis markers PLOD2, COL1A1, TIMP1, and TGF- $\beta$  in bone tissue through RT-PCR. In the KOA groups, PLOD2, COL1A1, TIMP1, and TGF- $\beta$  levels were increased. As expected, synovitis ointment decreased the levels of PLOD2, COL1A1, TIMP1, and TGF- $\beta$ . Studies suggested that synovitis ointment could reduce arthritis inflammation through reducing synovial fibrosis.

## 5. Conclusion

Synovitis ointment reduces the expression of SDF-1, CXCR4, MMP-9, and MMP-13 in rats with KOA, decreases the increase of knee joint diameter, alleviates KOA injury, inhibits the expression of PLOD2, COL1A1, TIMP1, and TGF- $\beta$  mRNA to prevent osteoblast fibrosis, and finally promotes knee joint recovery. The target of synovitis cream is related to osteoclast fibrosis. In the future, we will conduct further research on the inhibition of osteoclast fibrosis by synovitis ointment and expect to discover and prove the target of synovitis ointment for the treatment of KOA.

## Data Availability

The data used to support the findings of this study are available from the corresponding author upon request.

## Conflicts of Interest

The authors declare that they have no conflicts of interest.

## Authors' Contributions

Lei Zhang and Chi Zhang participated in conceiving the hypothesis, designing experiments, analyzing data, and writing the manuscript. Jing Zhang and Min Zhao participated in executing experiments and analyzing data. Jing Liu and Ke Wang participated in executing experiments and analyzing data. Xiang Cai participated in executing experiments and analyzing data. Wei Xiao and Le Wang participated in executing experiments and analyzing data. Mang Wang participated in executing experiments and analyzing data. Jin Zhang and Min Zhao contributed equally.

## Acknowledgments

This work was supported by the key projects of Chinese Medicine Research of Hubei Provincial Health and Health Commission (ZY2019Z009) and Wuhan Health Care Commission Chinese Medicine Research (no. WZ20Z01).

## References

- [1] S. H. Kan, K. P. Chan, and Y. K. Chiu, "Non-surgical Treatment of Knee Osteoarthritis," *Hong Kong Medical Journal*, vol. 25, no. 2, pp. 127–133, 2019.
- [2] D. J. Hunter Hunter and S. J. L. Bierma-Zeinstra, "Osteoarthritis," *The Lancet*, vol. 393, pp. 1745–1759, Article ID 10182, 2019.
- [3] D. Spitaels, P. Mamouris, B. Vaes et al., "Epidemiology of knee osteoarthritis in general practice: a registry-based study," *BMJ Open*, vol. 10, no. 1, Article ID e031734, 2020.
- [4] S. J. Osteoarthritis, "Cartilage," *Osteoarthritis Year in Review*, vol. 2018, 2019.
- [5] B. A. Teicher and S. Fricker, "CXCL12 (SDF-1)/CXCR4 pathway in cancer," *Clinical Cancer Research*, vol. 16, no. 11, pp. 2927–2931, 2010.
- [6] R. Janssens, S. Struyf, P. J. C. Proost, and M. Immunology, "The Unique Structural and Functional Features of CXCL12," *Cellular & Molecular Immunology*, vol. 15, 2017.
- [7] T. Nanki, K. Takada, Y. Komano Komano et al., "Chemokine receptor expression and functional effects of chemokines on B cells: implication in the pathogenesis of rheumatoid arthritis," *Arthritis Research and Therapy*, vol. 11, no. 5, Article ID R149, 2009.
- [8] F. Wei, D. C. Moore, Y. Li et al., "Attenuation of osteoarthritis via blockade of the SDF-1/CXCR4 signaling pathway," *Arthritis Research and Therapy*, vol. 14, no. 4, Article ID R177, 2012.
- [9] Z. Zhao, X. Ma, and S. Jianxiong, "Naringin Enhances Endothelial Progenitor Cell (EPC) Proliferation and Tube Formation Capacity through the CXCL12/CXCR4/PI3K/Akt Signaling Pathway," *Chemical Biology Interactions*, vol. 286, pp. 45–51, 2018.
- [10] R. M. Fleischmann, H. Bliddal, F. J. Blanco et al., "A phase II trial of lutikizumab, an anti-interleukin-1 $\alpha/\beta$  dual variable domain immunoglobulin, in knee osteoarthritis patients with synovitis," in *Arthritis & Rheumatology*, vol. 71, no. 7, pp. 1056–1069, 2019.
- [11] K. K. Kim, D. Sheppard, and H. A. J. C. S. H. P. B. Chapman, "TGF- $\beta$ 1 signaling and tissue fibrosis," *Cold Spring Harbor Perspectives in Biology*, vol. 10, no. 4, Article ID a022293, 2017.
- [12] P. C. Lo, F. C. Lin, Y. C. Tsai, and S. K. J. M. Lin, "Traditional Chinese medicine therapy reduces the risk of total knee replacement in patients with knee osteoarthritis," *Medicine*, vol. 98, no. 23, Article ID e15964, 2019.
- [13] H. N. Zhou, H. Y. Li Li, W. H. Xu Xu, Y. Y. Wei, R. X. Yu Yu, and Y. M. Wang Chen, "Study on the action mechanism of Wuling Powder on treating osteoporosis based on network pharmacology," *Chinese Journal of Natural Medicines*, vol. 19, no. 1, pp. 28–35, 2021.
- [14] S. Y. Liu, X. F. Meng, S. W. Liu, C. L. Hao, L. F. Li Li, and N. Zhang, "Effect of Bushen Huoxue decoction on inhibiting osteogenic differentiation of vascular smooth cells by regulating OPG/RANK/RANKL system in vascular calcification," *Annals of Translational Medicine*, vol. 7, no. 6, Article ID 125, 2019.
- [15] S. H. Feng, F. Xie, H. Y. Yao, G. B. Wu, X. Y. Sun, and J. Yang, "The mechanism of Bushen Huoxue decoction in treating intervertebral disc degeneration based on network pharmacology," *Annals of Palliative Medicine*, vol. 10, no. 4, pp. 3783–3792, 2021.
- [16] L. S. Lohmander, A. Östenberg Östenberg, M. Englund, and H. J. A. Roos, "High prevalence of knee osteoarthritis, pain, and functional limitations in female soccer players twelve years after anterior cruciate ligament injury," *Arthritis & Rheumatism*, vol. 50, no. 10, pp. 3145–3152, 2004.
- [17] N. Geribaldi-Doldán, C. Fernández-Ponce, R. N. Quiroz, I. Sánchez-Gomar, and E. N. J. FiO. Quiroz, "The Role of Microglia in Glioblastoma," *Frontiers in Oncology*, vol. 10, 2021.
- [18] H. Qin, X. Zhao, Y. J. Hu, S. Wang, Y. Ma Ma, and B. HeShenWanCuiYu, "Inhibition of SDF-1/CXCR4 Axis to

alleviate abnormal bone formation and angiogenesis could improve the subchondral bone microenvironment in osteoarthritis,” *BioMed Research International*, vol. 2021, no. 9, pp. 1–13, 2021.

- [19] R. Normasari, M. Murniati, and M. Sciences, “Leptin inhibit the effect of pioglitazone in reducing MMP-9 and MMP-13 of IL-1 $\beta$ -induced chondrocytes,” *Journal of Agromedicine and Medical Sciences*, vol. 12, 1970.
- [20] Q. Wei, N. Kong, X. Liu et al., “Pirfenidone attenuates synovial fibrosis and postpones the progression of osteoarthritis by anti-fibrotic and anti-inflammatory properties in vivo and in vitro,” *Journal of Translational Medicine*, vol. 19, no. 1, Article ID 157, 2021.
- [21] M. Qadri, “Synovial Fibrosis in Osteoarthritis of the Knee: Mechanism of Development and Potential Therapeutic Targets,” *Pharmaceutical Sciences (PhD) Dissertations*, vol. 5, 2021.

## Research Article

# Loquat Leaf Extract Enhances Muscle Contraction-Induced Activation of Protein Synthesis Signaling in Rat Skeletal Muscle

Yung-Li Hung,<sup>1</sup> Riki Kosugi,<sup>2</sup> Toshiharu Natsume,<sup>3</sup> and Shuichi Machida<sup>4</sup> 

<sup>1</sup>Institute of Health and Sports and Medicine, Juntendo University, 1-1 Hirakagakuendai, Inzai, Chiba 270-1695, Japan

<sup>2</sup>Faculty of Health and Sports Science, Juntendo University, 1-1 Hirakagakuendai, Inzai, Chiba 270-1695, Japan

<sup>3</sup>COI Project Center, Juntendo University, 2-1-1 Hongo, Bunkyo, Tokyo 113-8421, Japan

<sup>4</sup>Graduate School of Health and Sports Science, Juntendo University, 1-1 Hirakagakuendai, Inzai, Chiba 270-1695, Japan

Correspondence should be addressed to Shuichi Machida; machidas@juntendo.ac.jp

Received 5 December 2021; Revised 22 April 2022; Accepted 13 June 2022; Published 24 June 2022

Academic Editor: Ruchika Garg

Copyright © 2022 Yung-Li Hung et al. This is an open access article distributed under the Creative Commons Attribution License, which permits unrestricted use, distribution, and reproduction in any medium, provided the original work is properly cited.

Loquat (*Eriobotrya japonica* (Thunb.) Lindl.) leaves are traditionally used to improve muscle weakness, but their effects on muscle protein synthesis require further research. Therefore, we aimed to investigate whether loquat leaf extract (LLE) enhances muscle contraction-induced activation of muscle protein synthesis signaling. Male Wistar rats (12 weeks old,  $n = 6$ /group) were categorized into water treatment (CON) and LLE treatment (LLE) groups. The rats were administered distilled water or LLE (1.5 g/kg/day) once a day by oral gavage for 7 days. On day 7, at 3 h post-LLE administration, the gastrocnemius muscle in the right leg of each rat was stimulated by electrical muscle stimulation (EMS) (100 Hz, 30 V) through five sets of 10 isometric contractions (7 s contraction, 3 s rest) with 3 min interset intervals. The rats were then sacrificed, and the gastrocnemius muscles of both legs were excised at 3 h post-EMS. The phosphorylation levels of mammalian target of rapamycin complex 1 (mTORC1) signaling pathway molecules (Akt, mTOR, and p70S6K) were determined by Western blotting. Regarding the muscle contraction-induced protein synthesis signaling pathway, Akt phosphorylation at Ser473 was not significantly different between the CON and LLE groups. mTOR phosphorylation at Ser2448 was increased by EMS but did not show a significant difference between the CON and LLE groups. p70S6K phosphorylation at Thr389 was significantly increased in response to EMS, whereas the LLE group showed significantly higher p70S6K phosphorylation at Thr389 than that in the CON group. This suggests that LLE enhances muscle contraction-induced activation of p70S6K phosphorylation in rat skeletal muscles.

## 1. Introduction

Skeletal muscle constitutes approximately 40% of human bodyweight; it is a key component of daily physical activity and contributes to the quality of life. Skeletal muscle mass and strength decrease because of aging and disease [1]. Severe loss of skeletal muscle mass and strength, as in sarcopenia and chronic kidney disease-related muscle wasting, leads to reduced mobility [2]. Maintaining skeletal muscle mass for normal physical activity and quality of life in patients with such diseases is rather challenging. In this context, therapeutic strategies for maintaining or increasing muscle mass are important for preserving mobility in later years.

Mammalian target of rapamycin complex 1 (mTORC1) is a key regulatory factor in the initiation of mRNA translation and is known to regulate skeletal muscle protein synthesis and subsequent muscle hypertrophy [3]. The upstream components of the mTORC1 pathway are involved in phosphoinositide 3-kinase (PI3K)/Akt signaling. The 70 kDa ribosomal protein S6 kinase (p70S6K), which plays an important role in mRNA translation initiation, is a key downstream target of mTORC1. Thus, mTORC1 signaling (Akt-mTOR-p70S6K) is thought to be involved in mTORC1 activity and subsequent muscle protein synthesis [4].

Several traditional herbal medicines, such as Go-sha-jinki-Gan, *Astragalus* polysaccharides, and *Astragali radix*,

show potential therapeutic effects in sarcopenia and disease-related muscle wasting [5–7]. However, clinical trials on the use of traditional herbal medicines in treating sarcopenia and disease-related muscle wasting remain lacking and require further investigation in future. Loquat (*Eriobotrya japonica* (Thunb.) Lindl.) leaves have been used as traditional herbal medicine in several countries to treat cough and nausea [8, 9]. Loquat leaf extract (LLE) has been shown to effectively protect against aging-induced skeletal muscle loss [10]. Furthermore, a previous study has shown that LLE supplements inhibit dexamethasone-induced reduction in muscle strength in Sprague-Dawley rats [11]. Overall, these results suggest the possibility of using LLE as a therapeutic agent to prevent skeletal muscle atrophy. Enhancing muscle protein synthesis and reducing muscle breakdown are important treatment options for muscle weakness. However, the effects of LLE on muscle protein synthesis remain unknown.

Resistance exercises improve skeletal muscle mass by muscle protein synthesis via the mTORC1 signaling pathway [12]. A previous study has demonstrated that LLE enhances mTORC1 signaling (Akt-mTOR-p70S6K) [10]. A combination of balanced nutrition and exercise is considered an effective strategy for increasing muscle mass. We thus hypothesized that LLE stimulates mTORC1 signaling and enhances mTORC1 signaling in combination with resistance exercise. To test our hypothesis, we investigated the effects of LLE alone and in combination with resistance exercise on the mTORC1 signaling pathway in rat skeletal muscles. Overall, the aim of this study was to investigate whether LLE enhances muscle contraction-induced activation of protein synthesis signaling.

## 2. Materials and Methods

**2.1. Loquat Leaf Extraction.** Dried loquat leaves (China, HB60511) were purchased from Uchidawakanyaku (Tokyo, Japan). LLE was prepared as previously described, with modifications [7, 11]. Twenty grams of LLE was crushed into a powder, soaked in 200 ml distilled water at  $23 \pm 1^\circ\text{C}$  for 30 min, and boiled at low heat for 30 min. The decoction was passed through a mesh filter and centrifuged at 4000 rpm for 12 min at  $23 \pm 1^\circ\text{C}$ . The supernatant was filtered and stored at  $-80^\circ\text{C}$  until use. The LLE concentration was approximately 0.25 g/ml. High-performance liquid chromatography (HPLC) showed that the amount of ursolic acid (UA) was 7.16 mg/100 mL of LLE and 0.4 mg/kg bodyweight/day.

**2.2. Animal Experiments.** The study protocol was approved by the Juntendo University Animal Care Committee (19-07). A previously described electrical muscle stimulation (EMS)-induced muscle contraction protocol was followed [13] with some modifications. Twelve male Wistar rats (12 weeks old) were divided into two groups and administered either LLE or distilled water following a week of acclimation. The rats were purchased from Japan SLC, Inc. (Shizuoka, Japan) and housed under controlled environmental conditions ( $23 \pm 1^\circ\text{C}$ ,  $55 \pm 5\%$  relative humidity) under a 12 h light/dark cycle with ad libitum access to water and a standard

laboratory diet. The rats were administered LLE (1.5 g/kg/day) [11] or distilled water intragastrically by oral gavage using feeding needles (Fuchigami Kikai, Kyoto, Japan) under light isoflurane anesthesia, once a day for 7 days. All groups were starved for 12 h prior to the seventh day of administration. On day 7, 3 h after administration, the rats were anesthetized in an induction chamber with 3.0% isoflurane mixed with 21%  $\text{O}_2$  and 78%  $\text{N}_2$ . The hair on the right lower hind limb was shaved and removed using a depilatory cream. Each anesthetized rat was then placed prone in a cradle specifically designed for stimulating the right gastrocnemius muscle. Throughout a typical experiment, anesthesia was maintained by gas inhalation through a facemask that continuously supplied 2.0% isoflurane mixed with 21%  $\text{O}_2$  and 78%  $\text{N}_2$ , using an open-circuit gas anesthesia machine. One electrode was placed at the knee joint, and the other was placed at the heel. The foot was fixed to the pedal at  $90^\circ$  to stretch the right gastrocnemius muscle. The electrical stimulator was used to discharge monophasic rectangular pulses. The gastrocnemius muscle of the right leg of the rats was subjected to EMS (100 Hz, 30 V) through five sets of 10 isometric contractions (7 s contraction, 3 s rest) with 3 min interset intervals. The rats were sacrificed by heart removal, and gastrocnemius muscles were collected 3 h after EMS. The gastrocnemius muscles of both legs were obtained from rats in the water treatment (CON) and LLE treatment (LLE) groups ( $n = 6/\text{group}$ ).

**2.3. Western Blot Analysis.** The gastrocnemius muscles were frozen and powdered in liquid nitrogen followed by homogenization in T-PER Tissue Protein Extraction Reagent (Thermo Scientific, Waltham, MA, USA) containing protease (Thermo Scientific) and phosphatase inhibitors (Roche, Basel, Switzerland). Protein concentration was measured using the BCA protein assay reagent according to the manufacturer's instructions (Thermo Scientific). Muscle protein extracts (20  $\mu\text{g}$ ) were separated by electrophoresis on a 10% SDS polyacrylamide gel and electroblotted onto PVDF membranes. The membranes were incubated with 5% skim milk in Tris-buffered saline/Tween 20 (TBST) for 1 h at  $23 \pm 1^\circ\text{C}$ , followed by overnight incubation with primary antibodies at  $4^\circ\text{C}$ . All antibodies were purchased from Cell Signaling Technology (Danvers, MA, USA), including phospho-Akt Ser473 (cat. no. 4060), total Akt (cat. no. 4691), phospho-mTOR Ser2448 (cat. no. 5536), total mTOR (cat. no. 2983), phospho-p70S6K Thr389 (cat. no. 9234), and total p70S6K (cat. no. 2708). Blots were washed thrice with TBST and incubated with a horseradish peroxidase-conjugated secondary antibody (1 : 5000 dilution) for 1 h at  $23 \pm 1^\circ\text{C}$ . Blots were again washed thrice with TBST and developed using an ECL chemiluminescence substrate (Amersham, Buckinghamshire, UK). Band intensities were quantified using the Image Lab v.5.2.1 software (Bio-Rad Laboratories, Hercules, CA, USA). The blots were then stained with Ponceau S to verify equal protein loading.

**2.4. Statistical Analysis.** All data are expressed as mean  $\pm$  standard deviation (SD). Statistical analysis was

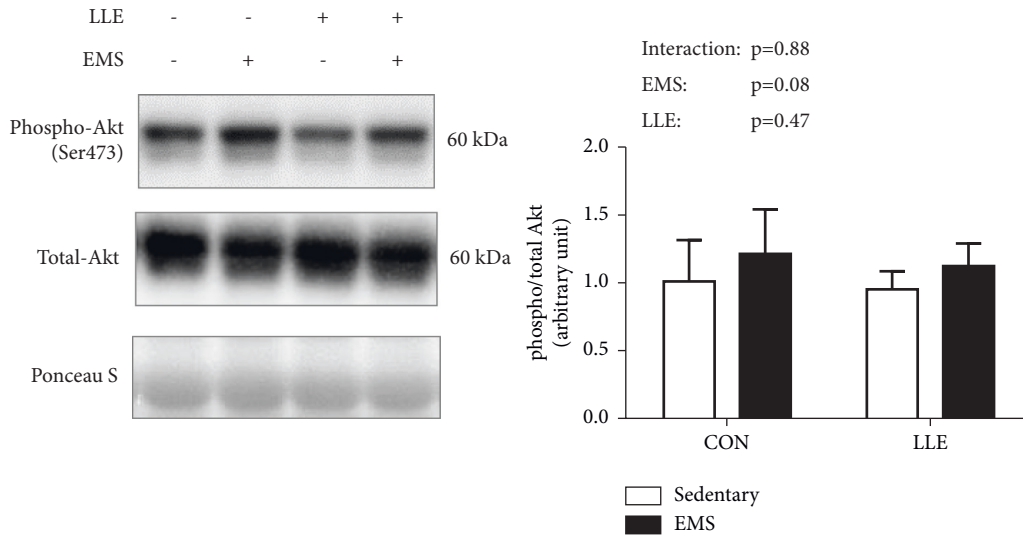


FIGURE 1: Effects of LLE administration and muscle contraction on the expression of phosphorylated Akt (Ser473). Representative blots of phosphorylated Akt (Ser473) proteins corresponding to total Akt protein, followed by Ponceau S staining to verify equal protein loading. Values are presented as mean  $\pm$  SD ( $n = 6$ ); \*  $p < 0.05$ .

performed using two-way ANOVA followed by Tukey's post hoc test using the GraphPad Prism 5 software (San Diego, CA, USA). Statistical significance was set at  $p < 0.05$ .

### 3. Results and Discussion

**3.1. Bodyweight, Water Intake, and Diet Intake.** Bodyweight, water intake, and diet intake were not significantly different between the LLE and distilled water groups after 7 days (data not shown).

**3.2. Muscle Contraction-Induced Muscle Protein Synthesis Signaling.** Regarding muscle contraction-induced mTORC1 (Akt-mTOR-p70S6K) signaling, Akt phosphorylation at Ser473 was not affected in response to EMS (Figure 1). mTOR phosphorylation at Ser2448 increased in response to EMS, but was not significantly different between the CON and LLE groups (Figure 2). p70S6K phosphorylation at Thr389 was significantly increased in response to EMS, whereas the LLE group showed significantly higher p70S6K phosphorylation at Thr389 compared with the CON group (Figure 3).

### 4. Discussion

In the present study, we investigated the effects of loquat (*Eriobotrya japonica* (Thunb.) Lindl.) leaf extract on muscle contraction-induced activation of protein synthesis signaling. Our results indicate that LLE administration alone did not affect mTORC1 signaling, but it enhanced muscle contraction-induced mTORC1 signaling via activation of p70S6K phosphorylation at Thr389 in rat skeletal muscles. These findings suggest that the effect of LLE administration on mTORC1 signaling was not additive, but synergistic with muscle contraction. On the other hand, our results

demonstrate that LLE administration dramatically increased p70S6K phosphorylation at Thr389, but did not significantly change Akt phosphorylation at Ser473 compared with that in the control group. In a previous study, Akt phosphorylation (Ser473) was affected by LLE treatment in vitro [10]. Thus, the effects of LLE may differ between in vitro and in vivo settings.

Previous studies have demonstrated a relationship between mTOR/p70S6K and muscle protein synthesis. Ogasawara and Suginoara reported that promotion of muscle protein synthesis by resistance exercise (transcutaneous electrical stimulation to induce muscle contraction) was regulated by mTOR (both rapamycin-sensitive mTORC1 and rapamycin-insensitive mTORC1 or mTORC2) [14]. However, a recent study reported that exercise-induced protein synthesis is independent of mTOR/p70S6K. You et al. reported that protein synthesis by mechanical loading is mTORC1-independent in myotectomy-induced muscle hypertrophy [15]. Different experimental methods for inducing muscle hypertrophy-like electrical stimulation or myotectomy-induced muscle hypertrophy may also result in different pathways of muscle protein synthesis. Therefore, the relationship between mTOR/p70S6K expression and muscle protein synthesis remains unclear. We did not elucidate the relationship between mTOR/p70S6K and muscle protein synthesis induced by EMS in this study either. However, the EMS-induced increase in muscle protein synthesis is regulated by mTOR/p70S6K signaling [14].

Figueiredo et al. demonstrated that mTOR Ser2448 is part of a negative feedback loop mechanism involving p70S6K phosphorylation [16]. However, mTOR Ser2448 phosphorylation has been shown to induce muscle contraction-induced activation of mTORC1 and p70S6K phosphorylation in previous studies [17, 18]. Furthermore, suppression of Akt Ser473 phosphorylation was found to reduce p70S6K Thr389



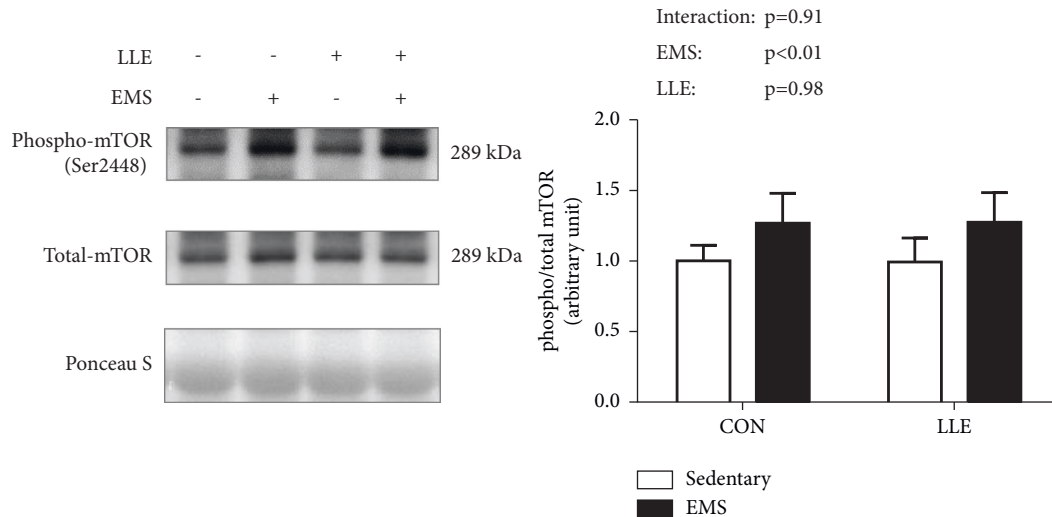


FIGURE 2: Effects of LLE administration and muscle contraction on the expression of phosphorylated mTOR (Ser2448). Representative blots of phosphorylated mTOR (Ser2448) proteins corresponding to total mTOR protein, followed by Ponceau S staining to verify equal protein loading of proteins. Values are presented as mean  $\pm$  SD ( $n=6$ ); \*  $p < 0.05$ .

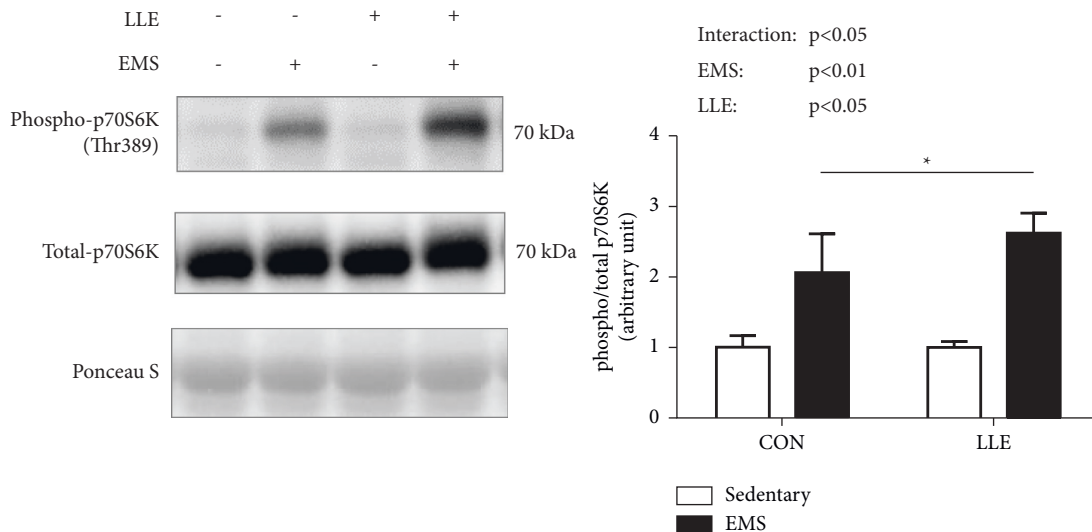


FIGURE 3: Effects of LLE administration and muscle contraction on the expression of phosphorylated p70S6K (Thr389). Representative blots of phosphorylated p70S6K (Thr389) protein corresponding to total p70S6K protein, followed by Ponceau S staining to verify equal protein loading. Values are presented as mean  $\pm$  SD ( $n=6$ ); \*  $p < 0.05$ .

phosphorylation in a previous study [19]. Taken together, the findings demonstrate that phosphorylation of Akt Ser473, mTOR Ser2448, and p70S6K Thr389 is activated by muscle contraction and plays central roles in muscle contraction-induced muscle protein synthesis.

Many active compounds, including UA, have been identified in LLE. An *in vivo* study showed that UA reduces muscle atrophy and stimulated hypertrophy [20]. Furthermore, UA enhances p70S6K phosphorylation at Thr389 but does not affect Akt phosphorylation at Ser473 in response to resistance exercise [21]. In contrast, chronic administration of UA (6 weeks) was found to affect Akt phosphorylation in a previous study [22]. However, a single administration of UA did not affect Akt phosphorylation (ser473) [21]. Thus, the

effect of LLE may differ between single and chronic administrations. These findings are consistent with those of the present study. Here, we investigated the effects of LLE on mTORC1 signaling at 3 h after muscle contraction. Ogasawara et al. indicated that UA enhanced p70S6K phosphorylation at Thr389 6 h after resistance exercise, but did not affect Akt phosphorylation at Ser473 [21]. The main effect of UA on the muscle contraction-induced mTORC1 signaling is thought to occur via p70S6K. Our results suggest that LLE augments mTORC1 signaling through activation of p70S6K at Thr389. However, further studies are needed to determine the optimal time point for contraction-induced protein synthesis after muscle contraction following LLE administration.

This study has some limitations. First, we assessed only one time point after muscle contraction. Second, the examined protein synthesis signaling pathway was only limited to the mTORC1 (Akt-mTOR-p70S6K) signaling pathway. Thus, it did not examine the upstream components of the mTORC1 pathway, which are known to be involved in Akt and extracellular signal-regulated kinase 1/2 (ERK1/2) signaling [23], and the downstream targets of mTORC1, including eukaryotic initiation factor 4E-binding protein 1 (4E-BP1) and p70S6K, both of which play important roles in mRNA translation initiation. Third, muscle protein synthesis was not assessed in this study. These limitations need to be addressed in future studies.

## 5. Conclusions

Overall, our results indicate that LLE enhances muscle contraction-induced activation of p70S6K phosphorylation at Thr389 in rat skeletal muscles.

## Data Availability

The data used to support the findings of this study are available from the corresponding author upon request.

## Disclosure

A part of this manuscript was presented at the 10th International Conference on Frailty Sarcopenia Research and Geroscience (ICFSR) on March 11–13, 2020, Toulouse, France.

## Conflicts of Interest

The authors declare that they have no conflicts of interest.

## Acknowledgments

This work was supported by grants-in-aid from JSPS KAKENHI (16K12940, 16H03205, 19K22820 to SM, and 19K19887 to Y-LH), Institute of Health and Sports and Medicine, Juntendo University, Japanese Center for Research on Women in Sports at Juntendo University, and a grant-in-aid for Scientific Research from the Society for Women's Health Science Research (ROHTO Pharmaceutical Co., Ltd.). The authors would like to thank Mr. Onur Cirak for providing support with experiments.

## References

- [1] F. Landi, M. Camprubi-Robles, D. E. Bear et al., "Muscle loss: the new malnutrition challenge in clinical practice," *Clinical Nutrition*, vol. 38, no. 5, pp. 2113–2120, 2019.
- [2] H. Watanabe, Y. Enoki, and T. Maruyama, "Sarcopenia in chronic kidney disease: factors, mechanisms, and therapeutic interventions," *Biological and Pharmaceutical Bulletin*, vol. 42, no. 9, pp. 1437–1445, 2019.
- [3] S. C. Bodine, T. N. Stitt, M. Gonzalez et al., "Akt/mTOR pathway is a crucial regulator of skeletal muscle hypertrophy and can prevent muscle atrophy in vivo," *Nature Cell Biology*, vol. 3, no. 11, pp. 1014–1019, 2001.
- [4] C. A. Goodman, "Role of mTORC1 in mechanically induced increases in translation and skeletal muscle mass," *Journal of Applied Physiology (1985)*, vol. 127, no. 2, pp. 581–590, 2019.
- [5] Y. Kishida, S. Kagawa, J. Arimitsu et al., "Go-sha-jinki-Gan (GJG), a traditional Japanese herbal medicine, protects against sarcopenia in senescence-accelerated mice," *Phytomedicine*, vol. 22, no. 1, pp. 16–22, 2015.
- [6] L. Lu, Y.-F. Huang, D.-X. Chen et al., "Astragalus polysaccharides decrease muscle wasting through Akt/mTOR, ubiquitin proteasome and autophagy signalling in 5/6 nephrectomised rats," *Journal of Ethnopharmacology*, vol. 186, pp. 125–135, 2016.
- [7] R. Nozaki, Y.-L. Hung, K. Takagi et al., "Differential protective effects of Radix astragali, herbal medicine, on immobilization-induced atrophy of slow-twitch and fast-twitch muscles," *Biomedical Research*, vol. 41, no. 3, pp. 139–148, 2020.
- [8] Y. Liu, W. Zhang, C. Xu, and X. Li, "Biological activities of extracts from loquat (*Eriobotrya japonica* Lindl.): a review," *International Journal of Molecular Sciences*, vol. 17, no. 12, p. 1983, 2016.
- [9] T. M. Kim, K. R. Paudel, and D. W. Kim, "Eriobotrya japonica leaf extract attenuates airway inflammation in ovalbumin-induced mice model of asthma," *Journal of Ethnopharmacology*, vol. 253, Article ID 112082, 2019.
- [10] B. Sung, S. Y. Hwang, M. J. Kim et al., "Loquat leaf extract enhances myogenic differentiation, improves muscle function and attenuates muscle loss in aged rats," *International Journal of Molecular Medicine*, vol. 36, no. 3, pp. 792–800, 2015.
- [11] K. K. Noh, K. W. Chung, B. Sung et al., "Loquat (*Eriobotrya japonica*) extract prevents dexamethasone-induced muscle atrophy by inhibiting the muscle degradation pathway in sprague dawley rats," *Molecular Medicine Reports*, vol. 12, no. 3, pp. 3607–3614, 2015.
- [12] R. Ogasawara, K. Kobayashi, A. Tsutaki et al., "mTOR signaling response to resistance exercise is altered by chronic resistance training and detraining in skeletal muscle," *Journal of Applied Physiology (1985)*, vol. 114, no. 7, pp. 934–940, 2013.
- [13] T. Natsume, T. Yoshihara, and H. Naito, "Electromyostimulation with blood flow restriction enhances activation of mTOR and MAPK signaling pathways in rat gastrocnemius muscles," *Applied Physiology Nutrition and Metabolism*, vol. 44, no. 6, pp. 637–644, 2019.
- [14] R. Ogasawara and T. Suginoara, "Rapamycin-insensitive mechanistic target of rapamycin regulates basal and resistance exercise-induced muscle protein synthesis," *The FASEB Journal*, vol. 32, no. 11, pp. 5824–5834, 2018.
- [15] J.-S. You, R. M. McNally, B. L. Jacobs et al., "The role of raptor in the mechanical load-induced regulation of mTOR signaling, protein synthesis, and skeletal muscle hypertrophy," *The FASEB Journal*, vol. 33, no. 3, pp. 4021–4034, 2019.
- [16] V. C. Figueiredo, J. F. Markworth, and D. Cameron-Smith, "Considerations on mTOR regulation at serine 2448: implications for muscle metabolism studies," *Cellular and Molecular Life Sciences*, vol. 74, no. 14, pp. 2537–2545, 2017.
- [17] Y. Makanae, S. Ato, K. Kido, and S. Fujita, "Dietary Aronia melanocarpa extract enhances mTORC1 signaling, but has no effect on protein synthesis and protein breakdown-related signaling, in response to resistance exercise in rat skeletal muscle," *Journal of the International Society of Sports Nutrition*, vol. 16, p. 60, 2019.
- [18] C. E. Mazo, A. C. D'Lugos, K. R. Sweeney et al., "The effects of acute aerobic and resistance exercise on mTOR signaling and autophagy markers in untrained human skeletal muscle,"

- European Journal of Applied Physiology*, vol. 121, no. 10, pp. 2913–2924, 2021.
- [19] J. N. Winter, L. S. Jefferson, and S. R. Kimball, “ERK and Akt signaling pathways function through parallel mechanisms to promote mTORC1 signaling,” *American Journal of Physiology—Cell Physiology*, vol. 300, no. 5, pp. C1172–C1180, 2011.
- [20] S. D. Kunkel, M. Suneja, S. M. Ebert et al., “mRNA expression signatures of human skeletal muscle atrophy identify a natural compound that increases muscle mass,” *Cell Metabolism*, vol. 13, no. 6, pp. 627–638, 2011.
- [21] R. Ogasawara, K. Sato, K. Higashida, K. Nakazato, and S. Fujita, “Ursolic acid stimulates mTORC1 signaling after resistance exercise in rat skeletal muscle,” *American Journal of Physiology—Endocrinology and Metabolism*, vol. 305, no. 6, pp. E760–E765, 2013.
- [22] S. D. Kunkel, C. J. Elmore, K. S. Bongers et al., “Ursolic acid increases skeletal muscle and brown fat and decreases diet-induced obesity, glucose intolerance and fatty liver disease,” *PLoS One*, vol. 7, no. 6, Article ID e39332, 2012.
- [23] M. Miyazaki, J. J. McCarthy, M. J. Fedele, and K. A. Esser, “Early activation of mTORC1 signalling in response to mechanical overload is independent of phosphoinositide 3-kinase/Akt signalling,” *The Journal of Physiology*, vol. 589, no. 7, pp. 1831–1846, 2011.

## Review Article

# Bioactive Natural Products against Systemic Arterial Hypertension: A Past 20-Year Systematic and Prospective Review

**Maisa Gomes da Silva** <sup>1</sup>, **Sara Léa Fortes Barbosa** <sup>1,2</sup>, **Diego Santos Silva** <sup>1</sup>,  
**Isadora Basílio Meneses Bezerra** <sup>1</sup>, **Érika Alves Bezerra** <sup>1,2</sup>, **Angélica Gomes Coelho** <sup>1</sup>,  
**Ilmara Cecília Pinheiro da Silva Moraes** <sup>1</sup>, **Luis Mário Rezende-Júnior** <sup>1</sup>,  
**Iolanda Souza do Carmo** <sup>2</sup>, **José de Sousa Lima-Neto** <sup>3</sup>,  
**Simón Gabriel Comerma-Steffensen** <sup>4,5</sup>, **Antônia Maria das Graças Lopes Citó** <sup>2</sup>  
and **Daniel Dias Rufino Arcanjo** <sup>1</sup>

<sup>1</sup>Department of Biophysics and Physiology, Federal University of Piauí, Teresina, Piauí, Brazil

<sup>2</sup>Department of Chemistry, Federal University of Piauí, Teresina, Piauí, Brazil

<sup>3</sup>Faculty of Pharmacy, Federal University of Piauí, Teresina, Piauí, Brazil

<sup>4</sup>Pulmonary and Cardiovascular Pharmacology, Department of Biomedicine, Aarhus University, Aarhus, Denmark

<sup>5</sup>Department of Biomedical Sciences/Animal Physiology, Veterinary Faculty, Central University of Venezuela, Maracay, Aragua, Venezuela

Correspondence should be addressed to Daniel Dias Rufino Arcanjo; [daniel.arcanjo@ufpi.edu.br](mailto:daniel.arcanjo@ufpi.edu.br)

Received 3 January 2022; Accepted 24 May 2022; Published 20 June 2022

Academic Editor: Jelena Zivkovic

Copyright © 2022 Maisa Gomes da Silva et al. This is an open access article distributed under the Creative Commons Attribution License, which permits unrestricted use, distribution, and reproduction in any medium, provided the original work is properly cited.

**Background.** Systemic arterial hypertension is one of the most common cardiovascular risks, corresponding to 45% of deaths involving CVDs. The use of natural products, such as medicinal plants, belongs to a millennial part of human therapeutics history and has been employed as an alternative anti-hypertensive treatment. **Objective.** The present review aims to prospect some natural products already experimentally assayed against arterial hypertension through scientific virtual libraries and patent documents over the past 20 years. **Search strategy.** This is a systematic review of the adoption of the PRISMA protocol and a survey of the scientific literature that synthesizes the results from published articles between 2001 and 2020 concerning the use of medicinal plants in the management of hypertension, including which parts of the plant or organism are used, as well as the mechanisms of action underlying the anti-hypertensive effect. Furthermore, a technological prospection was also carried out in patent offices from different countries in order to check technologies based on natural products claimed for the treatment or prevention of hypertension. **Inclusion criteria.** Scientific articles where a natural product had been experimentally assayed for anti-hypertensive activity (part of plants, plant extracts, and products derived from other organisms) were included. **Data extraction and analysis.** The selected abstracts of the articles and patent documents were submitted to a rigorous reading process. Those articles and patents that were not related to anti-hypertensive effects and claimed potential applications were excluded from the search. **Results.** Eighty specimens of biological species that showed anti-hypertensive activity were recovered, with 01 representative from the kingdom Fungi and 02 from the kingdom Protista, with emphasis on the families Asteraceae and Lamiaceae, with 6 representatives each. Leaves and aerial parts were the most used parts of the plants for the extraction of anti-hypertensive products, with maceration being the most used extraction method. Regarding phytochemical analyses, the most described classes of biomolecules in the reviewed works were alkaloids, terpenes, coumarins, flavonoids, and peptides, with the reduction of oxidative stress and the release of NO among the mechanisms of action most involved in this process. Regarding the number of patent filings, China was the country that stood out as the main one, with 813 registrations. **Conclusion.** The anti-hypertensive activity of natural products is still little explored in Western countries. Besides, China and India have shown more results in this area than other countries, confirming the strong influence of traditional medicine in these countries.

## 1. Introduction

Arterial hypertension (AH) is a complex, multifactorial, and polygenic disease dependent on diet, demographic, and genetic factors, resulting from the imbalance of several systems, considered a public health problem and a risk factor for cardiovascular diseases (CVD), promoting heart failure, kidney failure, and stroke. Defined by blood pressure levels, AH is characterized by persistent and sustained elevation of blood pressure (BP), that is, systolic BP (SBP) greater than or equal to 140 mm·Hg and/or diastolic BP (DBP) greater than or equal to 90 mm·Hg [1].

CVDs are the leading cause of death, hospitalizations, and outpatient care worldwide, including in developing countries such as Brazil. In 2017, complete and revised data from DATASUS showed the occurrence of 1,312,663 deaths in total, with a percentage of 27.3% for CVD, with AH associated with 45% of these cardiac deaths [2, 3]. Recently, a study led by Imperial College London in collaboration with the World Health Organization (WHO) showed that the number of adults with hypertension between 30 and 79 years of age has increased from 650 million to 1.28 billion over the past 30 years, mainly in developing countries. The study revealed that the prevalence of AH decreased in high-income countries (Canada, Peru, and Switzerland), while in low-income countries (Dominican Republic, Jamaica, Paraguay, Hungary, and Poland), there was a significant increase. The factors involved in this increase would be the aging of the population and greater exposure to other risk factors [4]. Projections show that by 2030, 41.4% of US adults will have hypertension, an increase of 8.4% from 2012 estimates [5].

Determined by the product of cardiac output (CO) and peripheral vascular resistance (PVR), blood pressure is regulated by neural, renal, humoral, endothelial, and local control mechanisms of cardiovascular and renal functions. In this way, SAH can develop from abnormalities in any homeostatic control mechanisms of PVR and/or CD [6]. Thus, the pathophysiology of AH involves changes in its different mechanisms (baroreflex dysfunction, increased sympathetic activation, alterations in the renin-angiotensin-aldosterone system, increased NAD(P)H oxidase activity, oxidative stress, and endothelial dysfunction) [7], whose common trait is endothelial dysfunction, characterized by the low availability of nitric oxide (NO) and the consequent local imbalance between factors of relaxation and constriction of arterioles [8].

Classically, the treatment of AH consists of the use of anti-hypertensive therapy, which, associated or not with other methods, such as lifestyle modifications, can effectively reduce morbidity and mortality related to this condition [7]. This information becomes of great relevance for both the academic community and the scientific community, as a way of designing new intervention strategies, so that the individual with this disease can achieve greater success in its control and treatment. Thus, pharmacological and non-pharmacological measures protect against endothelial

dysfunction by helping to preserve cardiovascular function through the reduction of oxidative stress and other mechanisms [9]. Figure 1 summarizes some physiological mechanisms towards therapeutic approaches that can be addressed.

Although more than 50% of existing medicines are synthesized from substances extracted from plants and herbs, the search for active ingredients present in plants, thus creating the first medicines with the characteristics that we know today, began only in the twentieth century—nineteenth century, according to historical records [10]. Among the drugs used in clinical practice whose origin comes from natural products, we can mention ephedrine (from *Ephedra sinica*), aspirin (from *Salix alba*), lovastatin (from *Monascus purpureus*), and reserpine (from *Rauwolfia serpentina*), for example [11].

Based on such knowledge, the objective of this study was to develop a systematic evaluation of the research carried out over the past 20 years on natural products with anti-hypertensive activity, extracting relevant information from scientific articles and patents.

## 2. Material and Methods

Through the adoption of the PRISMA protocol, a systematic review was carried out using scientific articles that addressed the anti-hypertensive activity of natural products. Following the guideline proposed by Sampaio and Mancini [12], the following question was formulated: “How many natural products have proven anti-hypertensive activity and been described in scientific articles published over the past 20 years?” Thus, a search was carried out in May 2020 in the main virtual libraries: Capes Periodical Portal, SciELO (Scientific Electronic Library Online), and portal BVS (Virtual Health Library), using the following terms: anti-hypertensive OR hypertension AND “natural product” OR “medicinal plant.” The articles should have been published between 2001 and 2020 and written in English, Portuguese, and Spanish. In the VHL Regional Portal, only articles with full text available were evaluated (Figure 2).

After cataloging, the reading of the abstract of the articles was performed by two researchers independently. Scientific articles in which a natural product had been experimentally tested for anti-hypertensive activity (parts of plants, plant extracts, and products derived from other organisms) were accepted and articles that were not intended to evaluate the anti-hypertensive function, and those related to synthetic or semisynthetic products were excluded. Subsequently, information was extracted on the species used (family, chemical constituents, and mechanisms of action) for the construction of the work.

Concomitantly, a prospective technological study was carried out in order to verify the patents deposited and published over the past 20 years, in order to obtain a current view related to the technologies used for medicinal plants in the prevention of hypertension. A search was carried out from databases associated with the INPI (National Institute

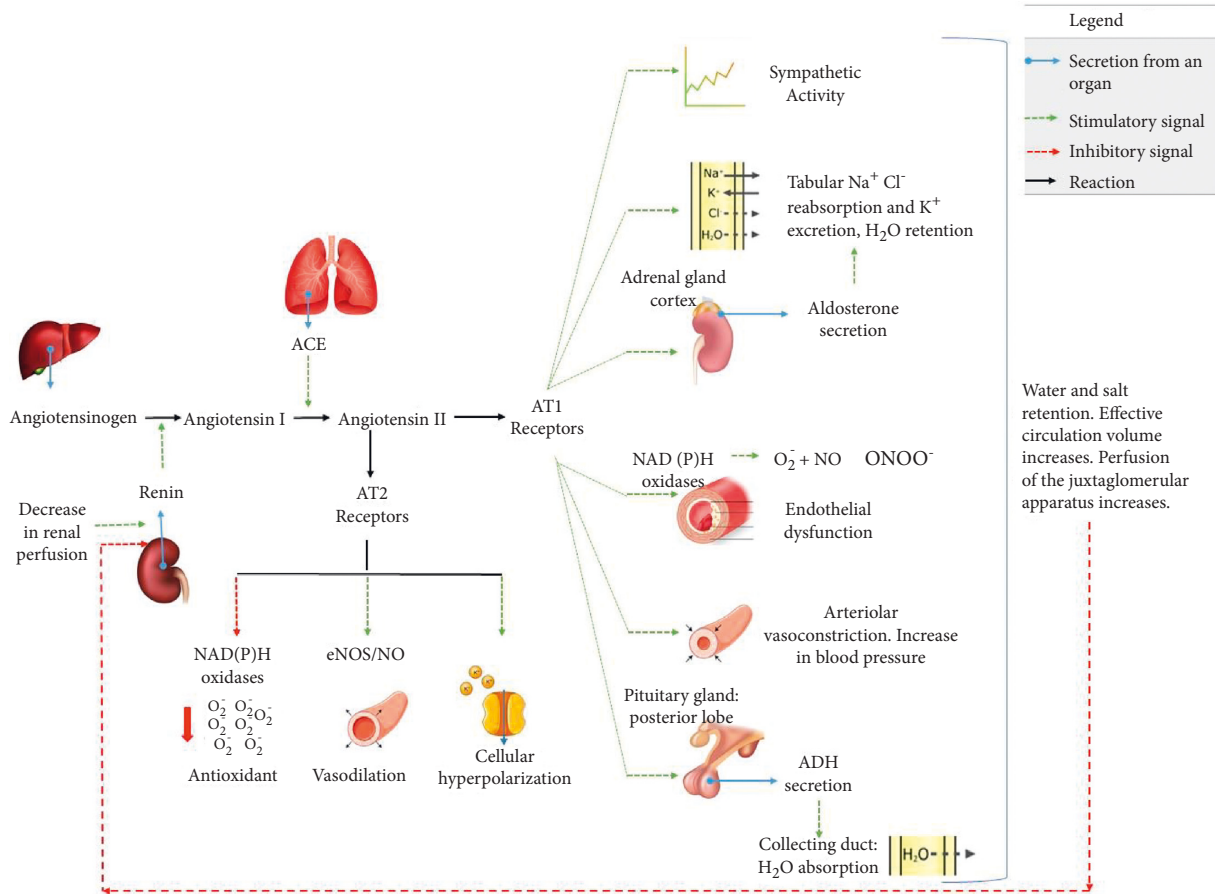


FIGURE 1: Main mechanisms and signaling pathways involved in blood pressure control.

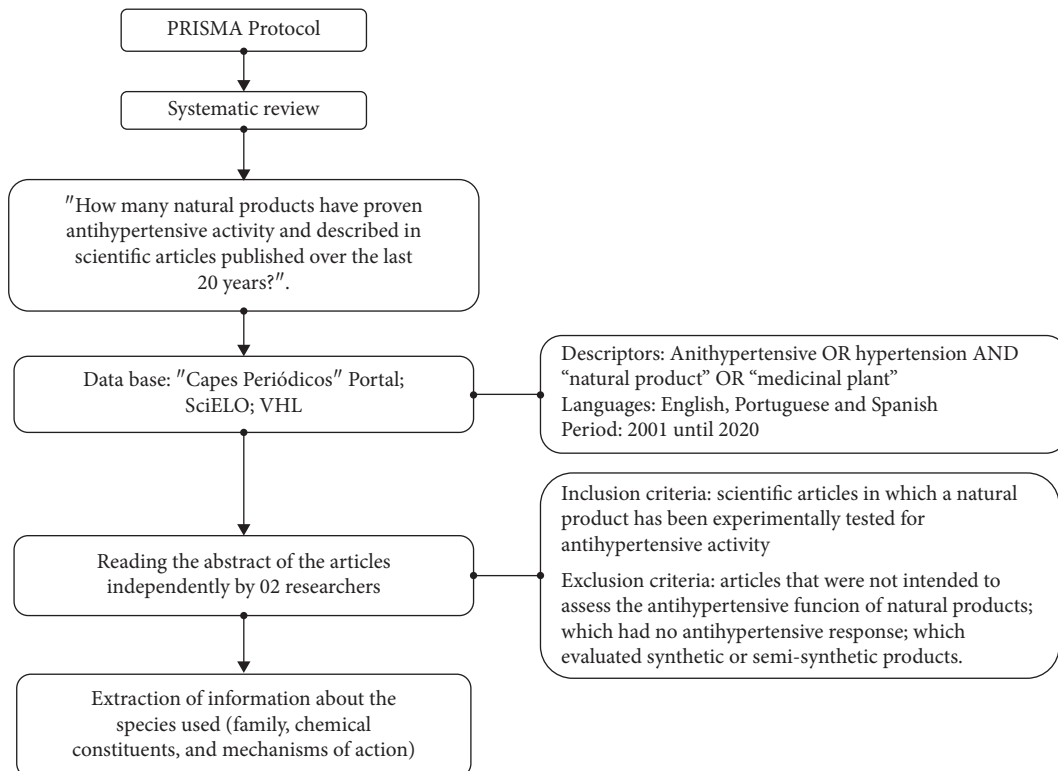


FIGURE 2: Process of the research and treatment protocol of scientific production articles about natural products that possess anti-hypertensive activity.



of Industrial Property), the USPTO (United States Patent and Trademark Office), the EPO (European Patent Office), the WIPO (World Intellectual Property Organization), and the LATIPAT, using the keywords: medicinal plant (s) and herb(s) associated with the words hypertension, anti-hypertensive, and hypotensive activity. In the case of duplication, the patent of the database other than WIPO was recorded. After an exploratory reading of the titles and abstracts, those that were in accordance with the objective of the study were selected and fully analyzed.

### 3. Results and Discussion

The search for the terms associated with hypertension, anti-hypertensive drugs, natural products, and medicinal plants in three selected virtual libraries yielded a total of 219,519 scientific articles published between the years 2001 and 2020. Of this total, 3,813 came from the search on the Capes Periodicals Portal, 3,203 from SciELO and 212, 503 from the VHL portal. Ninety-five articles were selected after applying the inclusion and exclusion criteria. Within these works, 80 specimens of biological species that showed anti-hypertensive activity were identified, with 01 representative of the Fungi kingdom and 02 of the Protista kingdom (Table 1). Species from the most different families were found, especially the Asteraceae and Lamiaceae families, with 6 representatives each (Figure 3).

The Asteraceae family is one of the largest of the angiosperms group, with about 180 genera, being considered one of the most important sources of plant species of therapeutic interest [13]. In Brazil, it covers the phytogeographic domains of the Caatinga, Amazon, Pantanal, Pampa, Atlantic Forest, and Cerrado [14]. It bears great importance for the composition of the vegetation of different places, being one of the richest families [15]. Its plants can produce a wide variety of secondary compounds; the most common compounds are phenolic acids, polyacetylenes, flavonoids, coumarins, benzofurans, and terpenoids such as monoterpenes, diterpenes, triterpenes, sesquiterpenes, and especially sesquiterpene lactones [16].

In turn, the Lamiaceae family, with 295 genera and about 7,775 species, another great representative of angiosperms [17], is a group with a cosmopolitan distribution, occurring mainly in open savannas and mountainous regions with a tropical to subtropical climate [18]. Being represented in Brazil by 34 genera and 498 species, the species of this family produce a wide variety of secondary metabolites [19] and accumulate substances with great structural diversity, such as steroids, flavonoids, iridoids, and terpenoids, including triterpenes. The latter are known to have anti-tumor, anti-HIV, anti-inflammatory, anti-oxidant, anti-bacterial, and anti-fungal activities, among others [20]. Thus, other members of these families deserve to be studied.

Popular observations on the use and effectiveness of medicinal plants significantly contribute to the dissemination of the therapeutic virtues of plants, frequently prescribed, for the medicinal effects they produce, despite not having their known chemical constituents. Indirectly, this type of medicinal culture draws the interest of researchers in

studies involving multidisciplinary areas, such as botany, pharmacology, and phytochemistry, which together enrich the knowledge about the world flora [21].

In general, the choice of a particular medicinal plant is made through the ethnopharmacological approach. Once the plant species to be studied is defined, the place of the collection is also defined, as well as the part of the plant that will be investigated (root, stem bark, stem, branches, leaves, flowers, and fruits) for carrying out the phytochemical study. Thus, in a project that links phytochemistry with pharmacology, the part of the plant that is used in folk medicine should be chosen for collection [21]. During the survey, it was observed that the leaves and aerial parts, roots, and seeds were the most used parts of the plants for the extraction of anti-hypertensive products, as shown in Figure 4(a).

The search for bioactive compounds of natural origin has increased considerably over the past two decades, mainly due to their preventive potential and in the treatment of cardiovascular, chronic, and neurodegenerative diseases [22]. In this sense, finding efficient extractive methods as well as the characterization of bioactive compounds from natural sources is a great challenge for researchers. Extractive methods for obtaining plant extracts include maceration, infusion, percolation, decoction, continuous hot extraction (Soxhlet), countercurrent extraction, microwave-assisted extraction, ultrasound, supercritical fluid, and turbolysis. In addition to the extractive methods, there are several factors that influence the extraction, such as the part of the plant material used, its origin, the degree of processing, the particle size, the solvent used, the extraction time, temperature, polarity, solvent concentration [23], and how communities do it [24]. Maceration was the most used extraction method in the research reviewed, followed by infusion/decoction and parallel Soxhlet. Other techniques such as percolation and critical superfluid extraction occurred less frequently (Figure 4(b)).

In order to quantify and qualify the chemical constituents of plant extracts, whose beneficial effects of some substances of certain species act as a key factor for the development of research bases for future applications of these bioactives [25], a preliminary phytochemical investigation is carried out to recognize the chemical constituents and/or assess their presence in the species being studied [26]. Specifically, phytochemical screening makes it possible to carry out preliminary tests to identify the presence of chemical compounds in certain plant species and thus link them to possible biological activities.

For example, alkaloids have anti-bacterial, anti-fungal, anti-plasmodic, and anti-tumor properties [27, 28] due to the ability to destabilize biological membranes. They also have the ability to inhibit the synthesis of DNA and RNA by binding to nucleic acids and intercalating into the double helix [29]. Examples of alkaloids currently used are morphine (analgesics), scopolamine (anti-cholinergics), theophylline (diuretics), vincristine (anti-tumours), and codeine (anti-tussives) [30].

Flavonoids are the most numerous compounds in angiosperms and have anti-inflammatory, anti-allergic, anti-ulcerogenic, anti-viral, anti-proliferative, anti-oxidant,

TABLE 1: Chemical constituents related to the anti-hypertensive effect of the species, mechanisms of action, study model used, and other relevant information in the publications of 2001–2020.

Species	Family	Used part (s)	Chemical constituents/ classification	Mechanisms of action	Study model	Reference
<i>Agelanthus dodoneifolius</i>	Loranthaceae	No data	Dodonein (lactone)	Blockade of the L- type calcium channels and inhibition of carbonic anhydrase in smooth muscle cells	<i>Ex vivo</i> assays for vasodilation in rat aortic rings; <i>in vitro</i> assay by the culture of vascular smooth muscle cells and determination of messenger RNA of carbonic anhydrase isozyme A in smooth muscle cells	[33]
<i>Allium cepa</i>	Amaryllidaceae	Rhizome	Diallyl thiosulphinate, methyl allyl thiosulphinate, allylmethyl thiosulphinate, protocatechuic acid, vanillic acid, p- hydroxybenzoic acid, ferulic acid, protocatechuic acid, vanillic acid, p- hydroxybenzoic acid, <i>ferulic</i> acid, and sinapinic acid	Inhibition of angiotensin- converting enzyme	<i>In vitro</i> angiotensin- converting enzyme inhibitory assay	[34]
<i>Allium sativum</i>	Amaryllidaceae	Rhizome	S-allyl cysteine	Inhibition of angiotensin- converting enzyme	<i>In vivo</i> assays with mice with fructose- induced hypertension	[35]
<i>Alpinia zerumbet</i>	Zingiberaceae	Leaves	Routine and kaempferol- 3-O- $\beta$ -D-glucuronide (flavonoids)	Stimulates NO/ cGMP pathway	<i>Ex vivo</i> tests of isolation of the superior mesenteric artery of rats	[36]
<i>Annona muricata</i>	Annonaceae	Leaves	Roseoside, isolariciresinol 9-O- $\beta$ -D- xyloside, massonanoside B, icaraside E4, and nicotiflorin	Anti-oxidant, anti- inflammatory, and anti-vascular remodeling properties and reduced AT1 receptor expression	<i>In vitro</i> assay in angiotensin II (Ang II) stimulated H9C2 cells	[37]
<i>Angelica dahurica</i>	Apiaceae	Root	Imperatorin	Reduction of oxidative stress and prevention of hypertension- related renal injury	<i>In vivo</i> assay in rats with renovascular hypertension and <i>ex vivo</i> assays that evaluate the cellular redox state	[38]
<i>Angelica decursiva</i>	Apiaceae	Root	Decursin and nodakenin	Opening of the potassium channels	Assays in rat aortic arteries	[39]
<i>Apium graveolens</i>	Apiaceae	Seed	3-n-butylphthalide	Reduction of renal fibrosis; reduction of oxidative stress; decreased levels of TNF- $\alpha$ , IL-6, and NF- $\kappa$ B	<i>In vivo</i> assays with spontaneously hypertensive rats	[40]

TABLE 1: Continued.

Species	Family	Used part (s)	Chemical constituents/ classification	Mechanisms of action	Study model	Reference
<i>Arbutus andrachne</i>	Ericaceae	Root, leaves, and fruit	Phenols, flavonoids, tannins, and anthocyanins	Reduction of oxidative stress	<i>Ex vivo</i> tests for vasodilation in rat aorta rings with intact endothelium; <i>ex vivo</i> assays that evaluate the cellular redox state	[41]
<i>Arbutus unedo</i>	Ericaceae	Root	Tannins and flavonoid (quercetin and tannic acid)	Stimulation of the endothelial nitric oxide synthase and activation of muscarinic receptors Activation of muscarinic receptors in the heart, reducing the heart rate and increasing peripheral resistance	<i>Ex vivo</i> tests for vasodilation in rat aorta rings with intact endothelium	[42]
<i>Azadirachta indica</i>	Meliaceae	Leaves	No data	Activation of the l- arginine-nitric oxide pathway	<i>In vivo</i> assay in rats with hypertension induced by DOCA- salt injection	[43]
<i>Berberis vulgaris</i>	Berberidaceae	Fruit	No data	Activation of the l- arginine-nitric oxide pathway	<i>In vivo</i> assay in rats with hypertension induced by DOCA- salt injection, <i>in vitro</i> studies in aortic rings, and <i>in vitro</i> studies in the isolated perfused mesenteric beds	[44]
<i>Bidens pilosa</i>	Asteraceae	Leaves	Alkaloids, saponins, flavonoids, polyacetylenes and triterpenes, phenylheptatriyne, linoleic acid, and linolic acid	Blocking of calcium channels	<i>Ex vivo</i> assays for vasodilation in rat aortic rings	[45]
<i>Boerhavia diffusa</i>	Nyctaginaceae	Root	Culubin (diterpenoid)	Blocking of calcium channels	<i>In vivo</i> assay in rats with hypertension caused by obesity induced by a lipid- rich diet	[46]
<i>Cassia tora</i>	Fabaceae	Seed	Chrysofanol, Aurantium Obtusine, alaternine, and chrysobthysin (anthraquinones)	Inhibition of angiotensin- converting enzyme	<i>In vitro</i> assays	[47]
<i>Cecropia pachystachya</i>	Urticaceae	Leaves	Ambaina and ambainina, long-chain carboxylic acids, and $\beta$ -sitosterol	Sympathic blockade in vessels and tachycardia by vagal inhibition in the heart	<i>In vivo</i> assay in normotensive Wistar rats through cannulation of internal carotid artery	[48]
<i>Cleistanthus collinus</i>	Phyllanthaceae	Leaves	Cleistanthin A and B (glycosides)	Inhibition of angiotensin- converting enzyme	<i>In silico</i> molecular interaction	[49]

TABLE 1: Continued.

Species	Family	Used part (s)	Chemical constituents/ classification	Mechanisms of action	Study model	Reference
<i>Crataegus tanacetifolia</i>	Rosaceae	Leaves	Hyperoside	Increase in kidney NOS activity, diuretic activity, and efflux of water and sodium, preventing hyperlipidemia and decrease in body weight	<i>In vivo</i> assay in normal male Wistar albino and L-NAME-induced hypertensive rats	[50]
<i>Codonopsis lanceolata</i>	Campanulaceae	Rhizome	Lancemaside A	Increase in NO levels by eNOS (inducible NO synthase)	<i>In vitro</i> assay in human umbilical vein endothelial cells	[51]
<i>Coffea</i>	Rubiaceae	Fruit	Chlorogenic acids	Stimulation of the endothelial nitric oxide synthase	A double-blind, randomized, placebo-controlled study in humans	[52]
<i>Coix lachryma-jobi</i>	Poaceae	Seed	Glutelin hydrolyzate	Inhibition of angiotensin-converting enzyme	<i>In vivo</i> assays in hypertensive rats	[53]
<i>Cordyceps sinensis*</i>	Clavicipitaceae	Entire organism	Mannose, glucose, and galactose (polysaccharide fraction)	Increase in NO levels and decrease of the levels of endothelin-1, epinephrine, noradrenaline, angiotensin II, and TGF- $\beta$ 1	<i>In vivo</i> assays with spontaneously hypertensive rats	[54]
<i>Coriandrum sativum</i>	Apiaceae	Fruit	Camphor, camphene, carvone, cineole, cimene, coriandrine, limonene, linoleic acid, myrcene, myristic acid, oleic acid, palmitic acid, $\alpha$ -phenyltriene, $\beta$ -phenylandrene, and $\alpha$ -terpinene, among others	Blockade of calcium channels, interaction with muscarinic receptors and diuretic effect	<i>In vivo</i> assays in normotensive mice and <i>ex vivo</i> assays in isolated tissue preparations	[55]
<i>Crocus sativus</i>	Iridaceae	Flower	Crocin, crocetin, and Safranal	Release of nitric oxide, reduction of oxidative stress, and modulation of the renin-angiotensin system	<i>In vivo</i> assay in rats through cannulation of arteries and femoral veins of rats with hypertension induced by Ang-II <i>In vivo</i> assays in mice with hypertension by chronic inhibition of nitric oxide and <i>ex vivo</i> assay in isolated tissue preparations	[56]
<i>Croton schiedeanus</i>	Euphorbiaceae	Aerial parts (stem and leaves)	Flavonoids, diterpenoids, and phenylbutanoids	Stimulation of NO/cGMP pathway	<i>In vivo</i> assays in mice with chronic inhibition of nitric oxide and <i>ex vivo</i> assay in isolated tissue preparations	[9]
<i>Cucurbita pepo</i>	Cucurbitaceae	Seed	Cucurbitacins (triterpenes); lutein, carotene, and beta carotene(carotenoids); unsaturated linoleic and oleic acids	Increase of NO levels	<i>In vivo</i> assays in mice with chronic inhibition of nitric oxide and <i>in vitro</i> assays	[57]

TABLE 1: Continued.

Species	Family	Used part (s)	Chemical constituents/ classification	Mechanisms of action	Study model	Reference
<i>Curcuma spp.</i>	Zingiberaceae	Rhizome	Curcumin, demethoxycurcumin, and bisdemethoxycurcumin	Blocking of calcium channels and the partial inhibition of $\beta$ - adrenergic receptors	<i>Ex vivo</i> vasodilation assay on intact endothelium pigs basilar arteries pre- contracted	[58]
<i>Cyclocarya paliurus</i>	Juglandaceae	Leaves and seeds	Polysaccharides	Reduction of oxidative stress	<i>In vitro</i> and <i>in vivo</i> assays using hypertensive rats	[59]
<i>Dendranthema indicum</i>	Asteraceae	Flower	Linarin	Modulation of the Renin-angiotensin system	<i>In vivo</i> assays with spontaneously hypertensive rats	[60]
<i>Dicksonia sellowiana</i>	Dicksoniaceae	Leaves	Polyphenols	Reduction of oxidative stress, activation of the pathway PI3K/ Akt/eNOS	<i>Ex vivo</i> tests on isolated tissues; <i>in vitro</i> assay on pig endothelial cell culture; <i>in vivo</i> tests with spontaneously hypertensive rats	[61]
<i>Dioscorea opposita</i>	Dioscoreaceae	Rhizome	Saponins, starch, mucopolysaccharides, protein, amino acids, mucilage, and polyphenols	Inhibition of angiotensin II converting enzyme, inhibition of endothelin-1 and reduction of oxidative stress	<i>In vivo</i> assay in rats with renovascular hypertension and <i>ex vivo</i> assays that evaluate the cellular redox state	[62]
<i>Eclipta alba</i>	Asteraceae	Aerial parts	Culubin (diterpenoid)	Diuresis due to increase in sodium excretion	<i>In vivo</i> assay in rats with hypertension caused by obesity induced by a lipid- rich diet	[46]
<i>Eucommia ulmoides</i>	Eucommiaceae	Stem bark	Wogonin (flavonoid)	Inhibition of the intracellular release of $Ca^{2+}$ and the extracellular influx of $Ca^{2+}$	<i>Ex vivo</i> testing on isolated tissue preparations	[63]
<i>Ficus deltoidea</i>	Moraceae	Leaves	$\beta$ -amyrin, lupeol, $\beta$ -amyrin cinnamate and bergapten, tanacetene, $\beta$ -elemene, stigmaterol, $\beta$ -sitosterol, lupenone, and $\alpha,\beta$ -amyrenone, as well as alkaloids, saponin, phenols, flavonoids, and tannins	Modulation of the renin-angiotensin- aldosterone system, anti- oxidant and endothelial system	<i>In vivo</i> assays with spontaneously hypertensive rats	[64]
<i>Gardenia jasminoides</i>	Rubiaceae	Fruit	Crocetin (carotenoid)	Increase in NO levels by eNOS and iNOS (inducible NO synthase)	<i>In vivo</i> assays with spontaneously hypertensive rats, <i>ex vivo</i> vasodilation assay on intact endothelium mouse aorta rings, and <i>in vitro</i> assays	[65]
<i>Glycine Max</i>	Fabaceae	Seed	Equol (flavonoid)	Diuresis by an increase in sodium excretion and increases transcription of the enzyme eNOS	A double-blind, randomized, placebo-controlled study in humans	[66]

TABLE 1: Continued.

Species	Family	Used part (s)	Chemical constituents/ classification	Mechanisms of action	Study model	Reference
<i>Gomphrena celosioides</i>	Amaranthaceae	Aerial parts	Phenolic acids and flavonoids	Increased levels of bradykinin, prostaglandins, and NO	<i>In vivo</i> assays in hypertensive animals	[67]
<i>Hibiscus sabdariffa</i>	Malvaceae	Flower	Anthocyanins	Increase in NO by activation of PI3K/Akt/eNOS pathway and activation of potassium channels	<i>Ex vivo</i> rat assays in isolated tissue preparations	[68]
<i>Inula viscosa</i>	Asteraceae	Leaves	Phenolic compounds and flavonoids	Inhibition of angiotensin-converting enzyme	<i>In vivo</i> assays in hypertensive adult rats	[69]
<i>Leersia hexandra</i>	Poaceae	Aerial parts	Not identified	Anti-oxidative and lipid-lowering effect	<i>In vivo</i> assays with hypertensive rats induced by oral administration of ethanol	[70]
<i>Lippia origanoides</i>	Verbenaceae	Aerial parts	Naringenin and pinocembrin (flavonoids), quercetin (flavonol), and luteolin (flavones)	Activation of calcium-activated potassium channels and increase in cAMP and cytosolic cGMP	<i>In vivo</i> assays in mice with hypertension by chronic inhibition of nitric oxide	[71]
<i>Lithocarpus polystachys</i>	Fagaceae	Leaves	florizine, fluoxetine, quercetin, dihydrochalcone-20-b-D-glucopyranoside, luteolin, and quercetin (Flavonoids)	Modulation of the renin-angiotensin-aldosterone system and reduction of oxidative stress	<i>In vivo</i> assays with spontaneously hypertensive rats and normotensive rats; <i>in vitro</i> assays	[72]
<i>Lonchocarpus xuul</i>	Fabaceae	Root	Dihydrospinochalcone-A and isocordoin	Activation of potassium channels and activation of NO/sCG/PKG pathway	<i>In vivo</i> assay in spontaneously hypertensive rats; <i>ex vivo</i> testing on isolated tissue preparations; molecular interaction <i>in silico</i>	[73]
<i>Lycopersicon esculentum</i>	Solanaceae	Fruit	$\alpha$ -tocopherol and the carotenoids: lycopene, $\beta$ -carotene, phytoene, and phytofluene	Attenuation of inflammatory signaling by the inhibition of the NF- $\kappa$ B transcription factor in endothelial cells	A double-blind, randomized, placebo-controlled study in humans; <i>in vitro</i> assay on human endothelial cell culture	[74]
<i>Mentha x villosa</i>	Lamiaceae	Leaves	No data	Active vascular relaxation	<i>In vivo</i> assay in rats with hypertension induced by DOCA-salt injection	[75]
<i>Mesona procumbens</i>	Lamiaceae	Leaves	Caffeic acid (polyphenol)	Reduction of oxidative stress	<i>In vivo</i> assay in spontaneously hypertensive rats and <i>ex vivo</i> assay evaluating the cellular redox state	[63]



TABLE 1: Continued.

Species	Family	Used part (s)	Chemical constituents/ classification	Mechanisms of action	Study model	Reference
<i>Mimosa caesalpiniiifolia</i>	Fabaceae	Inflorescences	Gallic acid, rutin, quercetin, and vicenine (flavonoids)	Activation of the muscarinic and ganglionic pathways and blockade of the transmembrane calcium influx	<i>In vivo</i> assay in normotensive mice; <i>ex vivo</i> testing on isolated tissue preparations	[76]
<i>Mitragyna ciliata</i>	Rubiaceae	Stem Bark	Alkaloids (mitragynine, mitraphylline, and rhynophylline) and/or flavonoid	Blocking of calcium channels	<i>Ex vivo</i> rat assays in guinea pig and rat isolated aortic rings	[77]
<i>Mixture containing Pine densiflora,</i>	Pinaceae	Leaves	Roseoside, isolariciresinol 9-O- $\beta$ -D-xyloside, massonioside B, icaricide E4, and nicotiflorin	Anti-oxidant, anti-inflammatory, and anti-vascular remodeling properties and reduced AT1 receptor expression	<i>In vitro</i> assay in Angiotensin II (Ang II)-stimulated H9C2 cells	[37]
<i>Momordica charantia</i>	Cucurbitaceae	Leaves	Roseoside, isolariciresinol 9-O- $\beta$ -D-xyloside, massonioside B, icaricide E4, and nicotiflorin	Anti-oxidant, anti-inflammatory, and anti-vascular remodeling properties and reduced AT1 receptor expression	<i>In vitro</i> assay in Angiotensin II (Ang II) stimulated H9C2 cells	[37]
<i>Morinda citrifolia</i>	Rubiaceae	Root	Alkaloids, phenolic compounds, sterols, flavonoids, tannins, coumarins, and anthraquinones	Blocking of calcium channels and release of intracellular calcium Alleviation of vascular dysfunction and oxidative stress,	<i>Ex vivo</i> rat assays in tissue preparations isolated from rats	[78]
<i>Moringa oleifera</i>	Moringaceae	Leaves	Nitrile, glucosinolates and thiocarbamate glycosides, flavonoids, phenolic acids, tannins, quercetin-3-O-glucoside, kaempferol-3-O-glucoside, Niazicin-A, Niazimin-A, and Niaziminin-B	blunted adrenergic-mediated vasoconstriction, promoted endothelium-dependent vasorelaxation; inhibition of angiotensin-converting enzyme	<i>In vivo</i> assay in L-NAME-treated rats; <i>in vitro</i> angiotensin-converting enzyme inhibitory assay; <i>in silico</i> molecular interaction	[79–81]
<i>Moringa stenopetala (Baker f.)</i>	Moringaceae	Leaves	Alkaloids, flavonoids, and saponins	Inhibition of carbonyl anhydrase Reduction of oxidative stress	<i>In vivo</i> assay on mice	[82]
<i>Musa sapientum</i>	Musaceae	Fruit peel	( $\pm$ )-7, 8-Dihydroxy-3-methyl-isochromanone-4 (polyphenol)	and increase in NO by activation of pathway PI3K/Akt/eNOS	<i>In vivo</i> assay in spontaneously hypertensive rats	[83]

TABLE 1: Continued.

Species	Family	Used part (s)	Chemical constituents/ classification	Mechanisms of action	Study model	Reference
<i>Nardostachys jatamansi</i>	Caprifoliaceae	Rhizome	Jatamansone, calarene, spirojatamol, aristolone, valencene and patchouli alcohol, $\alpha$ -pinene, and $\beta$ -maaliene	Inhibition of angiotensin-converting enzyme	<i>In vitro</i> angiotensin-converting enzyme inhibitory assay	[84]
<i>Onopordum acanthium</i>	Asteraceae	Seed	(E)-1-oxo-3, 4-dihydro-1-H-isochromen-7-yl-3-(3, 4-dihydroxyphenyl) acrylate	Inhibition of angiotensin-converting enzyme	Molecular interaction <i>in silico in vitro</i> assays	[85]
<i>Orthosiphon stamineus</i>	Lamiaceae	Leaves	No data	Modulation of $\alpha$ 1-adrenergic receptors and AT1 and increase in levels of NO	A parallel-group, randomized, placebo-controlled study in humans; rings of aorta of spontaneously hypertensive rats	[86]
<i>Panax notoginseng</i>	Araliaceae.	Root	Ginsenoside Rg1 and Rb1	NO/sGC/cGMP pathway and $\beta$ 2-adrenergic receptors	<i>Ex vivo</i> rat assays in isolated tissue preparations (aortic ring model)	[87]
<i>Peperomia pellucida</i>	Piperaceae	Leaves	2, 3, 5-trimethoxy-9-(12, 14, 15-trimethoxybenzyl)-1H-indene and pellucidin A	Inhibition of angiotensin-converting enzyme	<i>In vitro</i> angiotensin-converting enzyme inhibitory assay	[88]
<i>Phaseolus vulgaris</i>	Fabaceae	Seed	Catechins, flavonoids, and $\gamma$ -aminobutyric acid (GABA)	Inhibition of angiotensin-converting enzyme and modulation of pressure via GABA.	<i>In vitro</i> assays	[89]
<i>Phoenix dactylifera</i>	Arecaceae	Fruits	Squalene, lauric acid, palmitic acid, caprate, stearate, vitamin E, $\beta$ -sitosterol, phytol, linolenic acid, isosorbide, coumarins, and taurine	Inhibition of angiotensin-converting enzyme	<i>In vitro</i> enzyme inhibition assays	[90]
<i>Piper nigrum</i>	Piperaceae	Seed	Piperine (alkaloid)	Reduces oxidative stress	<i>In vivo</i> assay in rats with hypertension caused by obesity induced by a lipid-rich diet	[91]
<i>Prunus persica</i>	Rosaceae	Aerial parts	Amygdalin, cyanogenic glycosides, prunasin, caffeic acid, chlorogenic acid, kaempferol, p-coumaric acid, prussic acid, quercetin, quercitrin, quinic acid, tannin, and ursolic acid	NO-sGC-cGMP, vascular prostacyclin, and muscarinic receptor transduction pathway	<i>Ex vivo</i> rat assay in isolated tissue preparations (aortic ring model)	[92]
<i>Rauvolfia serpentina</i>	Apocynaceae	Roots	Reserpine, ajmalicine, serpentinine, ajmalimine, ajmaline, rescinnamidine, rescinnamine, reserpiline, serpentine, indobidine, yohimbine, and deserpidine	Protecting the liver and renal architectures	<i>In vivo</i> assay in rats with hypertension induced by high salt diet	[93]

TABLE 1: Continued.

Species	Family	Used part (s)	Chemical constituents/ classification	Mechanisms of action	Study model	Reference
<i>Rubus rosifolius</i>	Rosaceae	Leaves	Escauphic acid, flavonoids, and triterpenes	Diuretic effect	<i>In vivo</i> assay in hypertensive male rats	[94]
		Root	Lithospermic acid B	Inhibition of angiotensin- converting enzyme	<i>Ex vivo</i> assays for vasodilation in rat aortic rings	[95]
<i>Salvia miltiorrhiza</i>	Lamiaceae	Root	<i>Tanshinoato</i> of <i>magnesium B</i>	Increase in NO levels	<i>In vivo</i> assay in rats with phenylephrine- induced hypertension	[96]
<i>Salvia scutellarioides</i>	Lamiaceae	Aerial parts	Alkaloids, triterpenes, lignans, and flavonoids	Vasodilation, which activates compensatory physiological responses such as the renin- angiotensin- aldosterone system, and increase in concentrations of epinephrine and vasopressin	<i>In vivo</i> assay in L- NAME-treated rats	[97]
<i>Sargassum siliquastrum**</i>	Sargassaceae	Entire organism	<i>Sargachromenol D</i>	Induced depolarization	<i>In vivo</i> assay in rat basilar arteries	[98]
<i>Sceletium tortuosum</i>	Mesembrythemaceae	Leaves	Mesembrine (alkaloid)	Inhibition of aldosterone synthesis	<i>In vitro</i> assay on the culture of human adrenocortical carcinoma cells	[99]
<i>Solanum donianum</i>	Solanaceae	Leaves	Unreported	Inhibition of angiotensin- converting enzyme	<i>In vitro</i> angiotensin- converting enzyme inhibitory assay	[100]
<i>Spirulina maxima**</i>	Cyanophyceae	It has no true tissues	Phycocyanin	Increases transcription of the enzyme eNOS	Cohort study with humans	[101]
<i>Taraxacum officinale</i>	Asteraceae	Leaves and root	Saponins, alkaloids, phenols, flavonoids, tannins, and glycosides	Increase in NO levels by eNOS (inducible NO synthase)	<i>In vivo</i> assay in L- NAME-treated rats and with spontaneously hypertensive rats	[102]
<i>Taxus chinensis var. mairei</i>	Taxaceae Gray	Leaves	Palmitic acid, 9-octan- dienate of hexadecanil, and octan-3-ol	Reduction of the level of angiotensin II and increase in NO levels	<i>In vivo</i> assays with mice with hypertension by chronic nitric oxide inhibition and <i>in vitro</i> assays	[103]
<i>Terminalia superba</i>	Combretaceae	Stem bark	Saponins, glycosides, flavonoids, and chalcones	Reduction of oxidative stress	<i>In vivo</i> assays with mice with glucose- induced hypertension (GHR); <i>ex vivo</i> assays that evaluate the cellular redox state	[104]

TABLE 1: Continued.

Species	Family	Used part (s)	Chemical constituents/ classification	Mechanisms of action	Study model	Reference
<i>Ulmus wallichiana</i>	Ulmaceae	Stem bark	Flavonoids analogous to quercetin	Modulation of the renin-angiotensin- aldosterone system and stimulation of NO/cGMP pathway	<i>In vivo</i> assay in spontaneously hypertensive rats and assays in rats with salt and mineralocorticoid- induced hypertension, and with rats with chronic inhibition of nitric oxide	[105]
<i>Urtica dioica</i>	Urticaceae	Aerial parts	No data	An important bradycardia, which is independent of cholinergic and 1- adrenergic receptors	<i>Ex vivo</i> assays in isolated Langendorff perfused rat heart and vasodilation in rat aortic rings A double-blind, randomized, placebo-controlled study in humans	[42]
<i>Vaccinium virgatum</i>	Ericaceae	Fruit	Anthocyanins and polyphenols	Stimulation of NO/ cGMP pathway	A double-blind, randomized, placebo-controlled study in humans	[106]
<i>Vaccinium corymbosum</i>	Ericaceae	Fruit	Anthocyanins and polyphenols	Stimulation of NO/ cGMP pathway	A double-blind, randomized, placebo-controlled study in humans	[106]
<i>Vitex cienkowskii</i>	Lamiaceae	Stem bark	Tetra-acetyl jugasterone C	Stimulation of NO/ cGMP pathway and blockade of transmembrane calcium influx	<i>Ex vivo</i> tests on preparations of tissues isolated from rats	[107]
<i>Zea mays</i>	Poaceae	Seed	Corn peptide	Inhibition of angiotensin- converting enzyme	<i>In vivo</i> assay in spontaneously hypertensive rats and <i>in vitro</i> assays	[108]

\*Fungus species and \*\*species of seaweed.

hepatoprotective, anti-thrombic, and anti-carcinogenic activities [29, 30]. Tannins are phenolic compounds that have the property of complexing with metal ions and macromolecules such as proteins and polysaccharides, so they play the role of anti-oxidant and protector against herbivores and microorganisms. They are used as anti-septics, astringents, anti-diarrheals, wound healing, burns, and inflammation due to their ability to precipitate proteins [29–31]. They also have the ability to stimulate phagocytic cells [30].

Terpenes make up some essential oils and, therefore, act to attract pollinators. They also have insecticidal, anti-microbial, hepatoprotective, analgesic, anti-inflammatory, anti-microbial, and hemolytic action, among others [29, 31]. Triterpenes have anti-inflammatory, analgesic, cardiovascular, and anti-tumor effects [32].

Saponins have the ability to decrease the surface tension of water and, *in vitro*, cause erythrocyte hemolysis. They alter membrane permeability by lipophilic action and complexation with lipids and cell membrane proteins, which causes cell destruction. Therefore, they have toxic characteristics [31]. They also perform molluscicidal, anti-fungal, anti-

microbial, anti-parasitic, anti-viral, cytotoxic, and anti-tumor functions [30].

Phenolic compounds have the ability to neutralize free radicals, inhibiting the risk of cardiovascular disease, diabetes, tumors, and inflammatory processes. Coumarins are used for dermatoses, psoriasis, vitiligo, and other skin diseases; they are also anti-coagulants and laxatives, such as anthraquinones. Catechins are anti-oxidants, thermogenic, anti-inflammatory, and anti-carcinogenic. Steroids have cardiogenic functions, activators of anabolism, precursors of vitamin D, and contraceptives [30].

Regarding phytochemical analyses, the most described classes of biomolecules in the reviewed works were alkaloids, terpenes, coumarins, flavonoids, and peptides (Table 1). Thus, when relating them to anti-hypertensive activity, the focus of the prospective studies, we observed that alkaloids, such as reserpine and alstonine, reduce the availability of norepinephrine and, therefore, act as vasodilators. Flavonoids such as quercetin and rutin are primarily active in the myocardium and reduce cardiac output. Linoleic acid inhibits atherosclerosis-generating deposits of cholesterol and

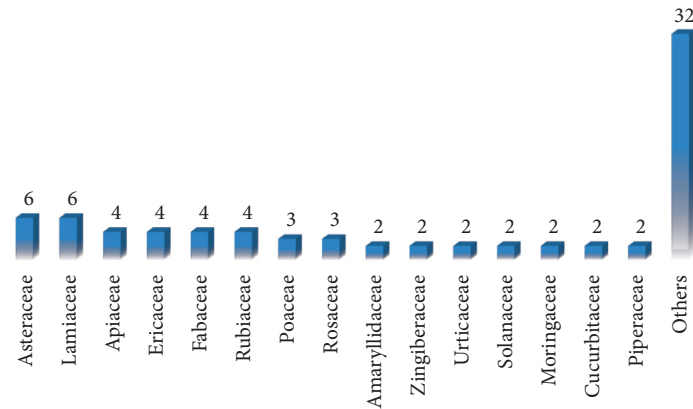


FIGURE 3: Distribution of the main families used in scientific research on natural products with anti-hypertensive activity published in the virtual libraries portal BVS, CAPES, and SciELO from 2001 to 2020.

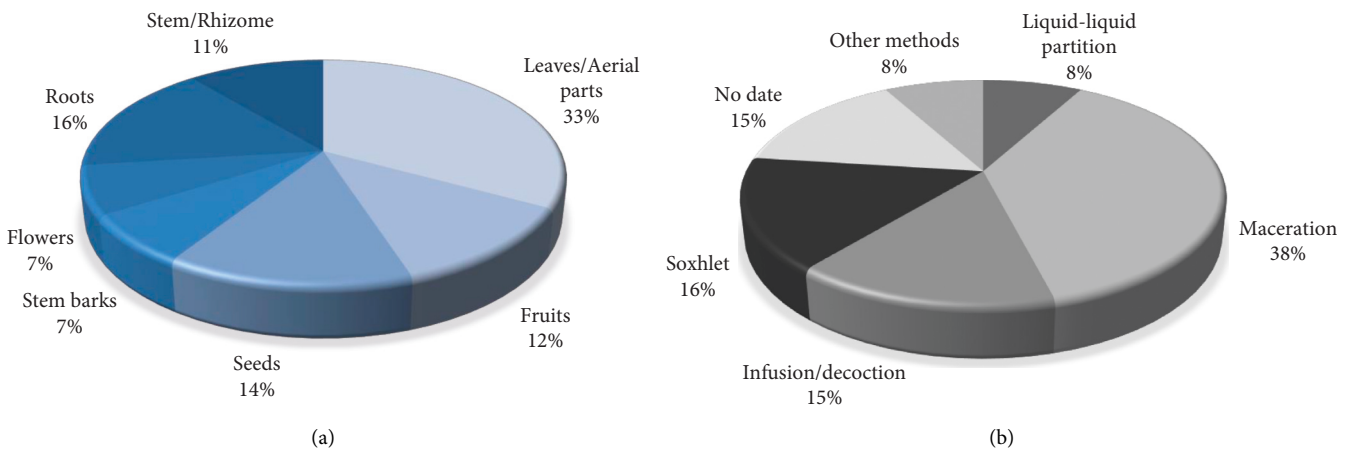


FIGURE 4: Percentages of the main chosen plant parts (a) and the main extractive methods (b) used to obtain the different natural products with anti-hypertensive activity retrieved from the virtual libraries BVS, CAPES, and SciELO over the period between 2001 and 2020.

triglycerides [109]. Phenolic compounds are anti-oxidants responsible for scavenging free radicals, capable of minimizing the harmful effects of ROS, and considered potential for the prevention of cardiovascular diseases [36].

The control of BP is made through two main mechanisms: neural and humoral. The neural mechanism is made by the autonomic nervous system composed of the sympathetic and parasympathetic systems, which act by increasing or decreasing heart rate as well as acting on peripheral vascular resistance. Humoral control is carried out by several substances that directly interfere with peripheral vascular resistance. Thus, the increase in vasodilating substances such as NO can contribute to an improvement in SAH. On the other hand, the renin-angiotensin system (RAS) plays a fundamental role due to its vasoconstrictor action, mainly through angiotensin II (Ang II) [110].

The classic view of the RAS is given by the production of angiotensinogen by the liver, being released into the circulation, where it is found in high concentrations. In the circulation, angiotensinogen undergoes the action of renin, a glycoproteolytic enzyme of renal origin [111]. After being

synthesized and released into circulation, renin promotes the conversion of angiotensinogen into Angiotensin I (Ang I) [112], and this is converted into angiotensin II (Ang II) by the catalytic action of angiotensin-converting enzyme (ACE) [113]. This conversion occurs almost exclusively in the vessels of the lungs, catalyzed by the ACE present in the endothelium of the pulmonary vessels.

The effects of Ang II are mediated by two distinct types of receptors:  $AT_1$  and  $AT_2$ , and the greatest interaction of this peptide occurs via the  $AT_1$  receptors, causing vasoconstrictor action, arrhythmogenic effect, cell proliferation, thrombosis, coagulation, inflammation, and hypertrophy of vascular smooth muscle [114, 115]. This Ang II signaling pathway with  $AT_1$  receptors is carried out by the activation of the G protein, with consequent activation of phospholipase C- $\beta$  and formation of 1,4,5-triphosphate and diacylglycerol, which in turn increases the intracellular concentration of calcium leading to vasoconstriction [116]. In addition to these effects, it is known that  $\eta$  Ang II via  $AT_1$  receptors stimulates aldosterone secretion by the zona glomerulosa of the adrenal cortex [117]. Contrary to this, the interaction of Ang II with the  $AT_2$  receptor has an

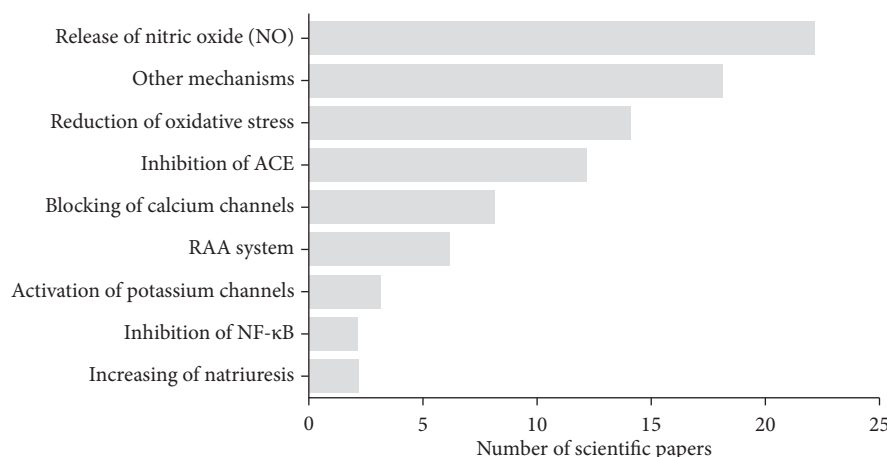


FIGURE 5: Distribution of the anti-hypertensive mechanisms elucidated in the scientific research of natural products with anti-hypertensive activity published in the virtual libraries BVS Portal, CAPES, and SciELO in the period of 2001 to 2020.

antagonistic effect on the action of the Ang II axis-AT<sub>1</sub> receptor, resulting in the formation of NO, and consequent vasodilation [118].

In addition to the physiological effects of controlling cardiovascular function, Ang II is also involved in the pathophysiology of cardiovascular diseases since this peptide induces the formation of reactive oxygen species (ROS) in the endothelium and vascular smooth muscle [119]. This process occurs via AT<sub>1</sub> receptors and consequent activation of the enzyme NAD(P)H oxidase [120], which reduces the oxygen molecule, forming O<sub>2</sub><sup>-</sup>. The latter is dismutated to H<sub>2</sub>O<sub>2</sub> by the action of the enzyme superoxide dismutase (SOD) or reacts with NO to form peroxynitrite (ONOO<sup>-</sup>) mainly under pathophysiological conditions [121].

The lower availability of NO favors greater activity of endothelin-1 (ET-1) or endothelium-derived contracting factor (EDCF) promotes endothelial cell growth and vasoconstriction and, therefore, participates in the pathogenesis of oxidative stress of SAH [122, 123]. Thus, vascular oxidative stress would result in SAH, since vasoconstrictor factors would be in preponderance in relation to vasodilator factors.

NO biosynthesis comprises one of the most important functions of L-arginine metabolism in the body. NO is formed from the terminal nitrogen of guanidine present in L-arginine, under the catalytic action of the enzyme nitric oxide synthase (eNOS), generating equimolar concentrations of L-citrulline and NO [124]. Once released, NO rapidly diffuses from the generating cell (endothelial cells) to the target cell (smooth muscle of the blood vessel), where it interacts with the heme group of soluble guanylate cyclase (GCs) stimulating its catalytic activity, leading to the formation of cGMP, which in turn decreases intracellular calcium (Ca<sup>2+</sup>) levels, reducing vascular tone. The mechanisms by which the NO/cGMP pathway induces vasodilation include inhibition of inositol-1,4,5-triphosphate (IP<sub>3</sub>) generation, increased cytosolic Ca<sup>2+</sup> sequestration, myosin light chain dephosphorylation, inhibition of Ca<sup>2+</sup> influx, activation of protein kinase, stimulation of membrane Ca<sup>2+</sup> ATPase, and opening of K<sup>+</sup> channels [125].

Regarding the mechanisms of action used in research cataloged to support the anti-hypertensive effect of the species evaluated, NO release, reduction of oxidative stress, ACE inhibition, Ca<sup>2+</sup> channel block, RAAS modulation, activation of K<sup>+</sup> channels, inhibition of nuclear kappa transcription factor (NF-κB), and increase in natriuresis can be observed (Figure 5). Among the possible study models, the research was carried out in *in vivo*, *ex vivo*, *in vitro*, and *in silico* studies, including studies in humans (Table 1).

As for the number of patents deposited in the databases according to the keywords used, it was observed that the WIPO database markedly recovered 925 documents, followed by the EPO and USPTO, with only 6 and 2 documents, respectively. In the others, INPI and LATIPAT, no patents were found. This may suggest a lack of interest on the part of research centers or industries to innovate in anti-hypertensive products, even though hypertension is one of the main causes of death in the world and 25% of currently available drugs originate from medicinal plants [126].

China was the country with the highest number of patent filings with 813 registrations. The other countries and their respective patent offices showed very low values when compared to China: the Republic of Korea with 75, the United Kingdom with 15, the World Intellectual Property Organization with 12, the European Patent Office with 7, Japan with 6, the United States with 2, and Canada, Russia, and France with 1 each (Figure 6). Although Brazil is a country rich in biodiversity and one that develops a lot of research on medicinal plants, research in the patent databases revealed a lack of interest in the development of technologies with market potential related to anti-hypertensive herbal medicines.

The superiority in the number of patents filed by China is related to the economic and technological position of this country in relation to the world scenario, as China has been increasingly establishing itself as a producer of knowledge and technological development, mainly through the work of pharmaceutical multinationals, electronics, and food, as well as the implementation of scholarship programs to encourage research. At the same time, traditional Chinese medicine is



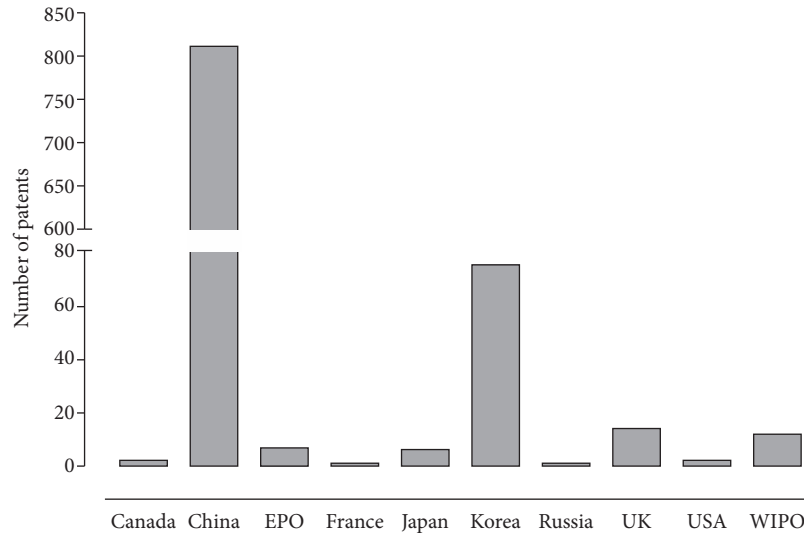


FIGURE 6: Distribution of patents deposited in accordance with the depositary office in the INPI (National Institute of Industrial Property, Brazil), the USPTO (United States Patent and Trademark Office), the EPO (European Patent Office), the WIPO (World Intellectual Property Organization), and the LATIPAT.

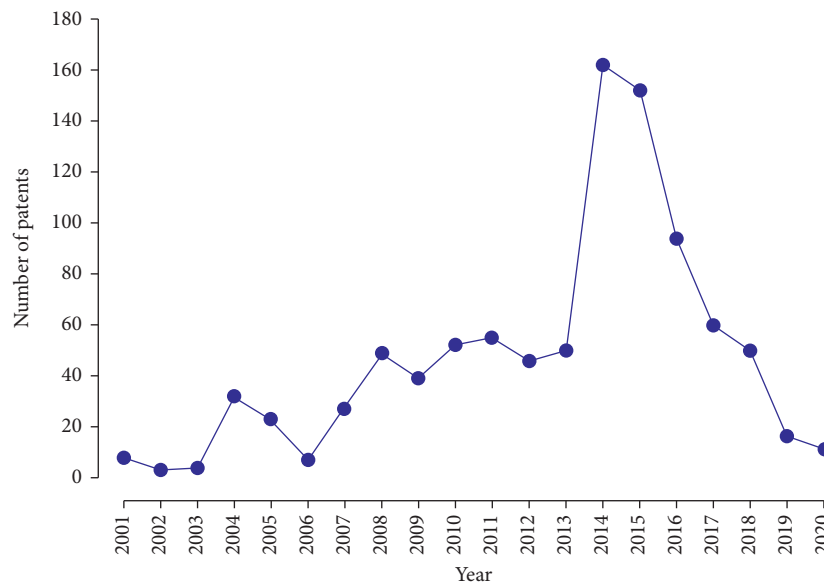


FIGURE 7: Patent deposit evolution over the past 20 years on the bases of the INPI (National Institute of Industrial Property, Brazil), the USPTO (United States Patent and Trademark Office), the EPO (European Patent Office), the WIPO (World Intellectual Property Organization), and the LATIPAT.

accompanied by a vast agricultural experience, which favors the study and development of technological alternatives that take advantage of the therapeutic potential of different plant species, especially regarding such promising applicability, for example, prevention and treatment of hypertension [127].

As for the temporal evolution of the number of patent filings (Figure 7), the sharp increase in the years 2014 and 2015 is noticeable. Regarding this increase, it is important to mention that in 2010 in the National Patent Development Strategy in China, the government defined benchmarks for future performance by 2015, setting the number of patent applications to reach two million, which would quadruple the number of applications in 2010, so that by

2015, China would be among the top two countries in a number of invention patents granted to national applicants. Such targets may have greatly influenced the significant increase in the number of patents registered in 2014 and 2015 [128].

#### 4. Conclusion

From this perspective, the anti-hypertensive activity of natural products is still little explored, especially in Western countries. In this sense, China and India have shown more results in this area than other countries, confirming the strong influence of traditional medicine in these countries.

Leaves and aerial parts were the main fractions of plants with potential exploitation. The maceration technique was the most used in obtaining the extract. The Fabaceae family was the most cited, which may indicate that more plant species belonging to this family should be studied regarding the anti-hypertensive potential. The largest number of patents related to anti-hypertensive herbs is deposited in WIPO. China is the country that invests most in research with the technological development of products from medicinal plants for the treatment and prevention of hypertension. This study was able to provide theoretical subsidies for future research with medicinal plants on the use of natural products as a coadjuvant in the treatment of systemic arterial hypertension.

### Conflicts of Interest

The authors declare that there are no conflicts of interest.

### Acknowledgments

The authors are grateful to UFPI (Universidade Federal do Piauí, Brazil), CNPQ (Conselho Nacional Para Desenvolvimento Científico e Tecnológico, Brazil), and FAPEPI (Fundação de Amparo à Pesquisa do Estado do Piauí, Brazil) for the financial support.

### References

- [1] I. K. M. Watanabe and D. E. Casarini, "Sistema renina angiotensina, novas evidências na fisiopatologia da hipertensão: importância para a prática clínica," *Journal of the Society of Cardiology of the State of São Paulo*, vol. 25, no. 1, pp. 14–18, 2015.
- [2] "Brasil Ministério da Saúde. DATASUS/MS/SVS/CGIAE—Sistema de Informações sobre Mortalidade SIM Disponível em," vol. 116, no. 3, pp. 516–658, 2020.
- [3] "Brasil Ministério da Saúde. DATASUS. Sistema de Informações Hospitalares do SUS(SIH/SUS) Disponível em," vol. 25, no. 1, 2020.
- [4] NCD Risk Factor Collaboration (NCD-RisC), "Worldwide trends in hypertension prevalence and progress in treatment and control from 1990 to 2019: a pooled analysis of 1201 population-representative studies with 104 million participants," *Lancet*, vol. 398, no. 10304, pp. 957–980, 2021.
- [5] A. S. Go, D. Mozaffarian, V. L. Roger et al., "Heart disease and stroke statistics-2013 update," *Circulation*, vol. 127, no. 1, pp. e6–e245, 2013.
- [6] A. F. Sanjuliani, "Fisiopatologia da hipertensão arterial: conceitos teóricos úteis para a prática clínica," *SOCERJ Magazine*, vol. 15, no. 4, pp. 210–218, 2002.
- [7] M. O. C. Pereira, D. A. Batista, D. R. M. Souza, I. L. N. Isabel Luiza do Nascimento Ginú, and S. K. P. Porpino, "Mechanisms involved in the pathophysiology of arterial hypertension: a literature review," *VI International Congress on Human Aging*, 2019.
- [8] W. B. Kannel and M. Larson, "Long-term epidemiologic prediction of coronary disease," *Cardiology*, vol. 82, pp. 137–152, 1993.
- [9] M. T. Páez, D. C. Rodríguez, D. F. López et al., "Croton schiedeanus schldt prevents experimental hypertension in rats induced by nitric oxide deficit," *Brazilian Journal of Pharmaceutical Sciences*, vol. 49, no. 4, pp. 865–871, 2013.
- [10] J. B. Calixto and J. M. Siqueira Júnior, "Drug development in Brazil: challenges. Bahia Medical Gazette," *Bahia*, vol. 78, 2008.
- [11] B. Baharvand-ahmadi, M. Bahmani, P. Tajeddini, M. Rafeian-kopaei, and N. Naghdi, "An ethnobotanical study of medicinal plants administered for the treatment of hypertension," *Journal of Renal Injury Prevention*, vol. 5, no. 3, pp. 123–128, 2016.
- [12] R. Sampaio and M. Mancini, "Systematic review studies: a guide to a judicious synthesis of scientific evidence," *Brazilian Journal of Physiotherapy*, vol. 11, no. 1, pp. 83–89, 2007.
- [13] W. S. Judd, C. S. Campbell, E. A. Kellogg, P. F. Stevens, and M. J. Donoghue, *Plant Systematics: A Phylogenetic Approach*, Sinauer Associates, Sunderland, MA, USA, 2009.
- [14] J. N. Nakajima, T. V. Junqueira, F. S. Freitas, and A. M. Teles, "Comparative analysis of red lists of the Brazilian flora: Asteraceae," *Rodriguesia*, vol. 63, pp. 39–54, 2012.
- [15] G. M. Barroso, A. L. Peixoto, C. L. F. Ichaso, C. G. Costa, E. F. Guimarães, and H. C. Lima, "Sistemática de Angiospermas do Brasil. Universidade federal de Viçosa," *Imprensa Universitária*, vol. 3, pp. 237–314, 1991.
- [16] L. M. Calabria, V. P. Emerenciano, M. T. Scotti, and T. J. Mabry, "Secondary chemistry of compositae," *Systematics, Evolution, and Biogeography of Compositae Cap 5*, International Association for Plant Taxonomy, Bratislava, Slovakia, 2009.
- [17] J. S. Vianna, "Anatomical, morphological and chemical characterization of chemotypes of *Ocimum gratissimum* Lineu," *Master's Degree in Agricultural Sciences—University of Brasilia*, vol. 78, 2009.
- [18] I. J. L. D. Basílio, M. F. Agra, E. A. Rocha, C. K. A. Leal, and H. F. Abrantes, "Estudo farmacobotânico comparativo das folhas de *Hyptis pectinata* (L.) Poit. e *Hyptis suaveolens* (L.) Poit. (Lamiaceae)," *Acta Farmaceutica Bonaerense*, vol. 25, no. 4, pp. 518–525, 2006.
- [19] R. M. Harley, "Dicotyledones: Lamiales (except Acanthaceae including Avicenniaceae)," *The Families and Genera of Vascular Plants*, vol. 7, 2004.
- [20] G. d. F. Lemes, P. H. Ferri, and M. N. Lopes, "Constituintes químicos de *Hyptidendron canum* (pohl ex benth)," *New Chemistry*, vol. 34, no. 1, pp. 39–42, 2011.
- [21] M. A. M. Maciel, A. C. Pinto, V. F. Veiga, N. F. Grynberg, and A. Echevarria, "Medicinal plants: the need for multidisciplinary studies," *New Chemistry*, vol. 25, no. 3, pp. 429–438, 2002.
- [22] G. Joana Gil-Chávez, J. A. Villa, J. Fernando Ayala-Zavala et al., "Technologies for extraction and production of bioactive compounds to be used as nutraceuticals and food ingredients: an overview," *Comprehensive Reviews in Food Science and Food Safety*, vol. 12, no. 1, pp. 5–23, 2013.
- [23] P. Tiwari, B. Kumar, M. Kaur, G. Kaur, and H. Kaur, "Phytochemical screening and extraction: a review," *International Pharmaceutica Science*, vol. 1, no. 1, pp. 98–106, 2011.
- [24] N. Brouwer, Q. Liu, D. Harrington et al., "An ethnopharmacological study of medicinal plants in new south wales," *Molecules*, vol. 10, pp. 1252–1262, 2005.
- [25] D. V. D. Morais, M. M. Moreira, F. d. L. Silva et al., "Dalbergia ecastaphyllum leaf extracts: in vitro inhibitory potential against enzymes related to metabolic syndrome, inflammation and neurodegenerative diseases," *Journal of*

- Social Sciences Biological Sciences*, vol. 41, no. 1, Article ID e46622, 2019.
- [26] J. C. F. D. Costa and J. Hoscheid, "Phytochemical profile and evaluation of antimicrobial activity of aqueous and ethanolic extracts of *Cecropia pachystachya* leaves," *Fitos Magazine*, vol. 12, no. 2, pp. 175–185, 2018.
- [27] D. B. d. Silva, M. d. F. C. Matos, S. T. Nakashita et al., "Isolamento e avaliação da atividade citotóxica de alguns alcalóides oxaporfínicos obtidos de *annonaceae*," *Química Nova*, vol. 30, no. 8, pp. 1809–1812, 2007.
- [28] M. C. Henrique, S. M. Nunomura, and A. M. Pohlit, "Alcaloides indólicos de cascas de *Aspidosperma vargasii* e *A. desmanthum*," *Química Nova*, vol. 33, no. 2, pp. 284–287, 2010.
- [29] C. M. O. Simões, E. P. Schenkel, G. Gosmann, J. C. P. Mello, L. A. Mentz, and P. R. Petrovick, *Porto Alegre: Editor of UFRGS; Florianópolis*, UFSC Publisher, 2007.
- [30] N. G. F. D. Bessa, J. C. M. Borges, F. P. Beserra et al., "Prospecção fitoquímica preliminar de plantas nativas do cerrado de uso popular medicinal pela comunidade rural do assentamento vale verde—Tocantins," *Revista Brasileira de Plantas Mediciniais*, vol. 15, no. 4, pp. 692–707, 2013.
- [31] H. S. Luz, A. C. G. Santos, F. C. Lima, and K. R. G. Machado, "Prospecção fitoquímica de *Himatanthus drasticus* Plumel (*Apocynaceae*), da mesorregião leste maranhense," *Revista Brasileira de Plantas Mediciniais*, vol. 16, no. 3, pp. 657–662, 2014.
- [32] Y. Ikeda, A. Murakami, and H. Ohigashi, "Ursolic acid: an anti- and pro-inflammatory triterpenoid," *Molecular Nutrition and Food Research*, vol. 52, no. 1, pp. 26–42, 2008.
- [33] G. Carre, M. Ouedraogo, C. Magaud et al., "Vasorelaxation induced by dodoneine is mediated by calcium channels blockade and carbonic anhydrase inhibition on vascular smooth muscle cells," *Journal of Ethnopharmacology*, vol. 169, pp. 8–17, 2015.
- [34] G. Oboh, A. O. Ademiluyi, O. M. Agunloye, A. O. Ademosun, and B. G. Ogunsakin, "Inhibitory effect of garlic, purple onion, and white onion on key enzymes linked with type 2 diabetes and hypertension," *Journal of Dietary Supplements*, vol. 16, no. 1, pp. 105–118, 2019.
- [35] S. M. Asdaq and M. N. Inamdar, "Potential of garlic and its active constituent, S-allyl cysteine, as antihypertensive and cardioprotective in presence of captopril," *Phytomedicine*, vol. 17, no. 13, pp. 1016–1026, 2010.
- [36] C. P. Victório, R. M. Kuster, R. S. De Moura, and C. L. S. Lage, "Vasodilator Activity of Extracts of Field *Alpinia Purpurata* (Vieill) K. Schum and *A. Zerumbet* (Pers.) Burt et Smith Cultured in Vitro," *Brazilian Journal of Pharmaceutical Sciences*, vol. 45, no. 3, pp. 507–514, 2009.
- [37] E. Y. Hong, T. Y. Kim, G. U. Hong et al., "Inhibitory effects of roseoside and icariside E4 isolated from a natural product mixture (NO-ap) on the expression of angiotensin II receptor 1 and oxidative stress in angiotensin II-stimulated H9c2 cells," *Molecules*, vol. 24, no. 3, pp. 1–13, 2019.
- [38] Y.-J. Cao, X. He, N. Wang, and L.-C. He, "Effects of imperatorin, the active component from *radix angelicae* (*baizhi*), on the blood pressure and oxidative stress in 2K,1C hypertensive rats," *Phytomedicine*, vol. 20, no. 12, pp. 1048–1054, 2013.
- [39] B. Kim, Y. Kwon, S. Lee, K. Lee, I. Ham, and H. Y. Choi, "Vasorelaxant effects of *angelica decursiva* root on isolated rat aortic rings," *BMC Complementary and Alternative Medicine*, vol. 17, no. 1, pp. 474–478, 2017.
- [40] J. Zhu, Y. Zhang, and C. Yang, "Protective effect of 3-n-Butylphthalide against hypertensive nephropathy in spontaneously hypertensive rats," *Molecular Medicine Reports*, vol. 11, no. 2, pp. 1448–1454, 2015.
- [41] E. Abidi, J. Habib, A. Yassine, N. Chahine, T. Mahjoub, and A. Elkak, "Effects of methanol extracts from roots, leaves, and fruits of the Lebanese strawberry tree (*arbutus andrachne*) on cardiac function together with their antioxidant activity," *Pharmaceutical Biology*, vol. 54, no. 6, pp. 1035–1041, 2016.
- [42] A. Legssyer, A. Ziyat, H. Mekhfi et al., "Cardiovascular effects of *urtica dioica* L. in isolated rat heart and aorta," *Phytotherapy Research*, vol. 16, no. 6, pp. 503–507, 2002.
- [43] I. Obiefuna and R. Young, "Concurrent administration of aqueous *Azadirachta indica* (neem) leaf extract with DOCA-salt prevents the development of hypertension and accompanying electrocardiogram changes in the rat," *Phytotherapy Research*, vol. 19, no. 9, pp. 792–795, 2005.
- [44] Z. Fatehi-Hassanabad, M. Jafarzadeh, A. Tarhini, and M. Fatehi, "The antihypertensive and vasodilator effects of aqueous extract from *Berberis vulgaris* fruit on hypertensive rats," *Phytotherapy Research*, vol. 19, no. 3, pp. 222–225, 2005.
- [45] T. B. Nguelefack, T. Dimo, E. P. N. Mbuyo, P. V. Tan, S. V. Rakotonirina, and A. Kamanyi, "Relaxant effects of the neutral extract of the leaves of *Bidens pilosa* Linn on isolated rat vascular smooth muscle," *Phytotherapy Research*, vol. 19, no. 3, pp. 207–210, 2005.
- [46] R. C. Verma, P. Shankar, S. Dwivedi, and R. K. Dixit, "Effects of *eclipta alba* and *boerhaavia diffusa* on normal blood pressure and hypertension in rats and their comparison with amlodipine," *International Journal of Pharma Sciences and Research*, vol. 3, pp. 1832–1838, 2012.
- [47] S. K. Hyun, H. Lee, S. S. Kang, H. Y. Chung, and J. S. Choi, "Inhibitory activities of *Cassia tora* and its anthraquinone constituents on angiotensin-converting enzyme," *Phytotherapy Research*, vol. 23, no. 2, pp. 178–184, 2009.
- [48] A. E. Consolini and G. N. Migliori, "Cardiovascular effects of the south American medicinal plant *cecropia pachystachya* (*ambay*) on rats," *Journal of Ethnopharmacology*, vol. 96, no. 3, pp. 417–422, 2005.
- [49] B. Vijayakumar, S. Parasuraman, R. Raveendran, and D. Velmurugan, "Identification of natural inhibitors against angiotensin I converting enzyme for cardiac safety using induced fit docking and MM-GBSA studies," *Pharmacognosy Magazine*, vol. 10, no. 39, pp. S639–S644, 2014.
- [50] Z. Ç. Koçyıldız, H. Birman, V. Olgaç, K. Akgün-Dar, G. Melikoğlu, and A. H. Meriçli, "*Crataegus tanacetifolia* leaf extract prevents L-NAME-induced hypertension in rats: a morphological," *Study Pharmacological Research*, vol. 20, no. 1, pp. 66–70, 2006.
- [51] Y. S. Lee, H. Kim, J. Kim, G. H. Seol, and K. W. Lee, "Lancemaside A, a major triterpene saponin of *codonopsis lanceolata* enhances regulation of nitric oxide synthesis via ENOS activation," *BMC Complementary and Alternative Medicine*, vol. 19, no. 1, pp. 110–119, 2019.
- [52] T. Watanabe, Y. Arai, Y. Mitsui et al., "The blood pressure-lowering effect and safety of chlorogenic acid from green coffee bean extract in essential hypertension," *Clinical and Experimental Hypertension*, vol. 28, no. 5, pp. 439–449, 2006.
- [53] B. Li, L. Qiao, L. Li et al., "Novel Antihypertensive Peptides Derived from *Adlay* (*Coix lachryma-jobi* L. var. *ma-yuen* Stapf) Glutelin," *Molecules*, vol. 22, no. 4, pp. 1–2, 2017.
- [54] F. Xiang, L. Lin, M. Hu, and X. Qi, "Therapeutic efficacy of a polysaccharide isolated from *cordyceps sinensis* on

- hypertensive rats," *International Journal of Biological Macromolecules*, vol. 82, pp. 308–314, 2016.
- [55] Q. Jabeen, S. Bashir, B. Lyoussi, and A. H. Gilani, "Coriander fruit exhibits gut modulatory, blood pressure lowering and diuretic activities," *Journal of Ethnopharmacology*, vol. 122, no. 1, pp. 123–130, 2009.
- [56] A. F. Plangar, A. Anaegoudari, A. Khajavirad, and M. N. Shafei, "Beneficial cardiovascular effects of hydro-alcoholic extract from crocus sativus in hypertension induced by angiotensin II," *Journal of Pharmacopuncture*, vol. 22, no. 2, pp. 95–101, 2019.
- [57] A. E. M. K. El-Mosallamy, A. A. Sleem, O. M. E. Abdel-Salam, N. Shaffie, and S. A. Kenawy, "Antihypertensive and cardioprotective effects of pumpkin seed oil," *Journal of Medicinal Food*, vol. 15, no. 2, pp. 180–189, 2012.
- [58] J. Akter, M. Z. Islam, M. A. Hossain et al., "Endothelium-independent and calcium channel-dependent relaxation of the porcine cerebral artery by different species and strains of turmeric," *Journal of Traditional and Complementary Medicine*, vol. 9, no. 4, pp. 297–303, 2019.
- [59] Q. Li, J. Hu, J. Xie, S. Nie, and M.-Y. Xie, "Isolation, structure, and bioactivities of polysaccharides from cyclocarya paliurus (batal.) iljinskaja," *Annals of the New York Academy of Sciences*, vol. 1398, no. 1, pp. 20–29, 2017.
- [60] Y. Qiaoshan, C. Suhong, S. Minxia, M. Wenjia, L. Bo, and L. Guiyuan, "Preparative purification of linarin extracts from dendranthema indicum flowers and evaluation of its anti-hypertensive effect. Evidence-based complement," *Alternative Medicine*, vol. 2014, Article ID 394276, 7 pages, 2014.
- [61] Y. D. Rattmann, E. Anselm, J.-H. Kim et al., "Natural product extract of Dicksonia sellowiana induces endothelium-dependent relaxations by a redox-sensitive src- and akt-dependent activation of eNOS in porcine coronary arteries," *Journal of Vascular Research*, vol. 49, no. 4, pp. 284–298, 2012.
- [62] N. Amat, R. Amat, S. Abdureyim et al., "Aqueous extract of Dioscorea opposita thunb. Normalizes the hypertension in 2K1C hypertensive rats," *BMC Complementary and Alternative Medicine*, vol. 14, no. 1, p. 36, 2014.
- [63] C.-T. Yeh, W.-H. Huang, and G.-C. Yen, "Antihypertensive effects of hsian-tsoa and its active compound in spontaneously hypertensive rats," *The Journal of Nutritional Biochemistry*, vol. 20, no. 11, pp. 866–875, 2009.
- [64] N. A. Azis, R. Agarwal, N. M. Ismail et al., "Blood pressure lowering effect of Ficus deltoidea var kunstleri in spontaneously hypertensive rats: possible involvement of renin-angiotensin-aldosterone system, endothelial function and anti-oxidant system," *Molecular Biology Reports*, vol. 46, no. 3, pp. 2841–2849, 2019.
- [65] S. Higashino, Y. Sasaki, J. C. Giddings et al., "Crocin, a carotenoid from Gardenia jasminoides Ellis, protects against hypertension and cerebral thrombogenesis in stroke-prone spontaneously hypertensive rats," *Phytotherapy Research*, vol. 28, no. 9, pp. 1315–1319, 2014.
- [66] Z.-m. Liu, S. C. Ho, Y.-m. Chen, Y. J. Xie, Z.-g. Huang, and W.-h. Ling, "Research protocol: effect of natural S-equal on blood pressure and vascular function- a six-month randomized controlled trial among equal non-producers of postmenopausal women with prehypertension or untreated stage 1 hypertension," *BMC Complementary and Alternative Medicine*, vol. 16, no. 1, p. 89, 2016.
- [67] P. C. de Paula Vasconcelos, D. R. Spessotto, J. V. Marinho et al., "Mechanisms underlying the diuretic effect of Gomphrena celosioides mart (Amaranthaceae)," *Journal of Ethnopharmacology*, vol. 202, pp. 85–91, 2017.
- [68] M. Sarr, S. Ngom, M. O. Kane et al., "In vitro vasorelaxation mechanisms of bioactive compounds extracted from Hibiscus sabdariffa on rat thoracic aorta," *Nutrition and Metabolism*, vol. 6, no. 1, p. 45, 2009.
- [69] Z. Hakkou, A. Maciuk, V. Leblais et al., "Antihypertensive and vasodilator effects of methanolic extract of inula viscosa: biological evaluation and POM analysis of cynarin, chlorogenic acid as potential hypertensive," *Biomedicine and Pharmacotherapy*, vol. 93, pp. 62–69, 2017.
- [70] D. C. Bilanda, Y. C. Tcheutchoua, P. D. Djomeni Dzeufiet et al., "Antihypertensive activity of leersia hexandra sw. (poaceae) aqueous extract on ethanol-induced hypertension in wistar rat," *Evidence-based complement Alternative Medicine*, vol. 2019, p. 9, Article ID 2897867, 2019.
- [71] A. G. Coelho, J. S. Lima Neto, A. K. S. Moura et al., "Optimization and standardization of extraction method from lippia origanoides H.B.K.: focus on potential anti-hypertensive applications," *Industrial Crops and Products*, vol. 78, pp. 124–130, 2015.
- [72] S.-Z. Hou, S.-J. Xu, D.-X. Jiang et al., "Effect of the flavonoid fraction of lithocarpus polystachyus rehd. On spontaneously hypertensive and normotensive rats," *Journal of Ethnopharmacology*, vol. 143, no. 2, pp. 441–447, 2012.
- [73] G. Avila-Villarreal, O. Hernández-Abreu, S. Hidalgo-Figueroa et al., "Antihypertensive and vasorelaxant effects of dihydrospinochalcone-A isolated from lonchocarpus xuul lundell by NO production: computational and ex vivo approaches," *Phytomedicine*, vol. 20, no. 14, pp. 1241–1246, 2013.
- [74] A. Armoza, Y. Haim, A. Basiri, T. Wolak, E. Paran, and E. Paran, "Tomato extract and the carotenoids lycopene and lutein improve endothelial function and attenuate inflammatory NF- $\kappa$ B signaling in endothelial cells," *Journal of Hypertension*, vol. 31, no. 3, pp. 521–529, 2013.
- [75] S. Lahlou, R. Ferreira Lima Carneiro-Leão, and J. H. Leal-Cardoso, "Cardiovascular effects of the essential oil of mentha x villosa in DOCA-salt-hypertensive rats," *Phytotherapy Research*, vol. 9, no. 8, pp. 715–720, 2002.
- [76] M. E. P. Santos, L. H. P. Moura, M. B. Mendes et al., "Hypotensive and vasorelaxant effects induced by the ethanolic extract of the mimosa caesalpinifolia benth (Mimosaceae) inflorescences in normotensive rats," *Journal of Ethnopharmacology*, vol. 164, pp. 120–128, 2015.
- [77] A. Dongmo, M. A. Kamanyi, P. V. Tan, M. Bopelet, W. Vierling, and H. Wagner, "Vasodilating properties of the stem bark extract of Mitragyna ciliata in rats and Guinea pigs," *Phytotherapy Research*, vol. 18, no. 1, pp. 36–39, 2004.
- [78] A. H. Gilani, S.-U.-R. Mandukhail, J. Iqbal et al., "Antispasmodic and vasodilator activities of Morinda citrifolia root extract are mediated through blockade of voltage dependent calcium channels," *BMC Complementary and Alternative Medicine*, vol. 10, no. 1, 2010.
- [79] D. Aekthamarat, P. Pannangpetch, and P. Tangsucharit, "Moringa oleifera leaf extract lowers high blood pressure by alleviating vascular dysfunction and decreasing oxidative stress in L-NAME hypertensive rats," *Phytomedicine*, vol. 54, pp. 9–16, 2019.
- [80] L. K. Acaram and C. L. Chichioco Hernandez, "Anti-hypertensive effect of moringa oleifera lam," *Cogent Biology*, vol. 5, no. 1, 2019.
- [81] H. Khan, V. Jaiswal, S. Kulshreshtha, and A. Khan, "Potential angiotensin converting enzyme inhibitors from moringa


- oleifera," *Recent Patents on Biotechnology*, vol. 13, no. 3, pp. 239–248, 2019.
- [82] N. Fekadu, H. Basha, A. Meresa, S. Degu, B. Girma, and B. Geleta, "Diuretic activity of the aqueous crude extract and hot tea infusion of *moringa stenopetala* (baker f.) cufod. Leaves in rats," *Journal of Experimental Pharmacology*, vol. 9, pp. 73–80, 2017.
- [83] R. Bai, J. Liu, Y. Zhu et al., "Chiral separation, configurational identification and antihypertensive evaluation of ( $\pm$ ) -7,8-Dihydroxy-3-Methyl-Isochromanone-4," *Bioorganic and Medicinal Chemistry Letters*, vol. 22, no. 20, pp. 6490–6493, 2012.
- [84] B. Bose, D. Tripathy, A. Chatterjee, P. Tandon, and S. Kumaria, "Secondary metabolite profiling, cytotoxicity, anti-inflammatory potential and in vitro inhibitory activities of *nardostachys jatamansi* on key enzymes linked to hyperglycemia, hypertension and cognitive disorders," *Phyto-medicine*, vol. 55, pp. 58–69, 2019.
- [85] N. Sharifi, E. Souri, S. A. Ziai, G. Amin, M. Amini, and M. Amanlou, "Isolation, identification and molecular docking studies of a new isolated compound, from *onopordon acanthium*: a novel angiotensin converting enzyme (ACE) inhibitor," *Journal of Ethnopharmacology*, vol. 148, no. 3, pp. 934–939, 2013.
- [86] V. Trimarco, C. S. Cimmino, M. Santoro et al., "Nutraceuticals for blood pressure control in patients with high-normal or grade 1 Hypertension180," *High Blood Press. Cardiovascular Prevention*, vol. 19, no. 3, pp. 117–122, 2012.
- [87] Y. C. Loh, C. S. Tan, Y. S. Ch'ng, C. H. Ng, Z. Q. Yeap, and M. F. Yam, "Mechanisms of action of *panax notoginseng* ethanolic extract for its vasodilatory effects and partial characterization of vasoactive compounds," *Hypertension Research*, vol. 42, no. 2, pp. 182–194, 2019.
- [88] I. Ahmad, N. Ambarwati, B. Elya et al., "A new angiotensin-converting enzyme inhibitor from *peperomia pellucida* (L.) kunth," *Asian Pacific Journal of Tropical Biomedicine*, vol. 9, 2019.
- [89] R. I. Limón, E. Peñas, M. I. Torino, C. Martínez-Villaluenga, M. Dueñas, and J. Frias, "Fermentation enhances the content of bioactive compounds in kidney bean extracts," *Food Chemistry*, vol. 172, pp. 343–352, 2015.
- [90] O. C. Obode, A. H. Adebayo, and C. Li, "Gas chromatography-mass spectrometry analysis and in vitro inhibitory effects of *phoenix dactylifera* L. On key enzymes implicated in hypertension," *Journal of Pharmacy and Pharmacognosy Research*, vol. 8, no. 5, pp. 475–490, 2020.
- [91] P. Brahmanaidu, H. Nemani, B. Meriga, S. K. Mehar, S. Potana, and S. Ramgopalrao, "Mitigating efficacy of piperine in the physiological derangements of high fat diet induced obesity in sprague dawley rats," *Chemico-Biological Interactions*, vol. 221, pp. 42–51, 2014.
- [92] B. Kim, K. Kim, S. Lee et al., "Endothelium-dependent vasorelaxant effect of *prunus persica* branch on isolated rat thoracic aorta," *Nutrients*, vol. 11, 2019.
- [93] S. M. A. Shah, S. A. R. Naqvi, N. Munir, S. Zafar, M. Akram, and J. Nisar, "Antihypertensive and antihyperlipidemic activity of aqueous methanolic extract of *Rauwolfia serpentina* in albino rats," *Dose-Response*, vol. 18, no. 3, pp. 1–7, 2020.
- [94] P. Souza, T. Boeing, L. B. Somensi et al., "Diuretic effect of extracts, fractions and two compounds 2 $\alpha$ ,3 $\beta$ ,19 $\alpha$ -trihydroxy-urs-12-en-28-oic acid and 5-hydroxy-3,6,7,8,4'-pentamethoxyflavone from *rubus rosaefolius* Sm. (Rosaceae) leaves in rats," *Naunyn-Schmiedeberg's Archives of Pharmacology*, vol. 390, no. 4, pp. 351–360, 2017.
- [95] D. G. Kang, H. Oh, H. T. Chung, and H. S. Lee, "Inhibition of angiotensin converting enzyme by lithospermic acid B isolated from *radix salviae miltiorrhiza bunge*," *Pharmacological Research*, vol. 17, no. 8, pp. 917–920, 2003.
- [96] S. Leung and K. Man, "Effects of the aqueous extract of *salvia miltiorrhiza* (danshen) and its magnesium tanshinoate B-enriched form on blood pressure," *Phytotherapy Research*, vol. 24, no. 5, pp. 769–774, 2010.
- [97] J. O. R. Amírez, C. Ms, M. A. P. Alacios, and O. S. G. Utiérrez, "Estudio del efecto antihipertensivo de *La salvia scutellaroides* en un modelo de Ratas hipertensas," *Colombia Médica*, vol. 37, no. 1, pp. 53–60, 2006.
- [98] B. G. Park, W. S. Shin, S. Oh, G. M. Park, N. I. Kim, and S. Lee, "A novel antihypertension agent, *sargachromenol D* from marine Brown algae, *sargassum siliquastrum*, exerts dual action as an L-type Ca<sup>2+</sup> channel blocker and Endothelin A/B2 receptor antagonist," *Bioorganic and Medicinal Chemistry*, vol. 25, no. 17, pp. 4649–4655, 2017.
- [99] A. C. Swart and C. Smith, "Modulation of glucocorticoid, mineralocorticoid and androgen production in H295 cells by trimesemine, a mesembrine-rich scelenium extract," *Journal of Ethnopharmacology*, vol. 177, pp. 35–45, 2016.
- [100] C. M. Rodríguez-García, J. C. Ruiz-Ruiz, L. Peraza-Echeverría et al., "Antioxidant, antihypertensive, anti-hyperglycemic, and antimicrobial activity of aqueous extracts from twelve native plants of the yucatan coast," *PLoS One*, vol. 14, no. 3, pp. 1–17, 2019.
- [101] P. V. Torres-Duran, A. Ferreira-Hermosillo, and M. A. Juárez-Oropeza, "Antihyperlipemic and antihypertensive effects of *spirulina maxima* in an open sample of Mexican population: a preliminary report," *Lipids in Health and Disease*, vol. 6, p. 33, 2007.
- [102] O. O. Aremu, C. M. Tata, C. R. Sewani-Rusike et al., "Acute and sub-chronic antihypertensive properties of *Taraxacum officinale* leaf (TOL) and root (TOR)," *Transactions of the Royal Society of South Africa*, vol. 74, no. 2, pp. 132–138, 2019.
- [103] W. X. Yang, Z. G. Zhao, L. H. Wang, S. J. Yu, and Z. S. Liang, "Control of hypertension in rats using volatile components of leaves of *taxus chinensis* var," *Mayori Journal of Ethnopharmacology*, vol. 141, no. 1, pp. 309–313, 2012.
- [104] E. N. L. Tom, C. Demougeot, O. B. Mtopi et al., "The aqueous extract of *Terminalia superba* (combretaceae) prevents glucose-induced hypertension in rats," *Journal of Ethnopharmacology*, vol. 133, no. 2, pp. 828–833, 2011.
- [105] A. A. Syed, S. Lahiri, D. Mohan et al., "Evaluation of antihypertensive activity of *ulmus wallichiana* extract and fraction in SHR, DOCA-salt- and l-NAME-induced hypertensive rats," *Journal of Ethnopharmacology*, vol. 193, pp. 555–565, 2016.
- [106] S. A. Johnson, A. Figueroa, N. Navaei et al., "Daily blueberry consumption improves blood pressure and arterial stiffness in postmenopausal women with pre- and stage 1-hypertension: a randomized, double-blind, placebo-controlled clinical trial," *Journal of the Academy of Nutrition and Dietetics*, vol. 115, no. 3, pp. 369–377, 2015.
- [107] A. B. Dongmo, P. A. Nkeng-Efouet, K. P. Devkota et al., "Tetra-acetylajugasterone a new constituent of *vitex cincinnoskii* with vasorelaxant activity," *Phytomedicine*, vol. 21, no. 6, pp. 787–792, 2014.
- [108] Y. Wang, H. Chen, X. Wang et al., "Isolation and identification of a novel peptide from zein with antioxidant and antihypertensive activities," *Food and Function*, vol. 6, no. 12, pp. 3799–3806, 2015.

- [109] K. Zeka, K. Ruparelia, R. Arroo, R. Budriesi, and M. Micucci, "Flavonoids and their metabolites: prevention in cardiovascular diseases and diabetes," *Diseases*, vol. 5, no. 3, p. 19, 2017.
- [110] J. E. Hall and M. E. Hall, *GUYTON & HALL—Treatise on Medical Physiology*, Elsevier, Amsterdam, Netherlands, 2021.
- [111] W. S. Peart, "Evolution of renin," *Hypertension*, vol. 18, 1991.
- [112] M. N. James and A. R. Sielecki, "Stereochemical analysis of peptide bond hydrolysis catalyzed by the aspartic proteinase penicillopepsin," *Biochemistry*, vol. 24, no. 14, pp. 3701–3713, 1985.
- [113] M. K. Raizada and A. J. Ferreira, "ACE2: a new target for cardiovascular disease therapeutics," *Journal of Cardiovascular Pharmacology*, vol. 50, no. 2, pp. 112–119, 2007.
- [114] A. M. Allen, J. Zhuo, and F. A. Mendelsohn, "Localization and function of angiotensin AT1 receptors," *American Journal of Hypertension*, vol. 13, pp. 31S–38S, 2000.
- [115] H. M. Siragy, M. de Gasparo, and R. M. Carey, "Angiotensin type 2 receptor mediates valsartan-induced hypotension in conscious rats," *Hypertension*, vol. 35, no. 5, pp. 1074–1077, 2000.
- [116] M. A. Araújo, B. S. Menezes, C. Lourenço, E. R. Cordeiro, R. R. Gatti, and L. R. Goulart, "O polimorfismo A1166C do receptor tipo 1 da angiotensina II no infarto agudo do miocárdio," *Arquivos Brasileiros de Cardiologia*, vol. 83, no. 5, pp. 404–408, 2004.
- [117] T. Watanabe, T. A. Barker, and B. C. Berk, "Angiotensin II and the endothelium: diverse signals and effects," *Hypertension*, vol. 45, no. 2, pp. 163–169, 2005.
- [118] J. W. Rush and C. D. Aultman, "Vascular biology of angiotensin and the impact of physical activity," *Applied Physiology Nutrition and Metabolism*, vol. 33, no. 1, pp. 162–172, 2008.
- [119] R. M. Touyz and E. L. Schiffrin, "Signal transduction mechanisms mediating the physiological and pathophysiological actions of angiotensin II in vascular smooth muscle cells," *Pharmacological Reviews*, vol. 52, no. 4, pp. 639–672, 2000.
- [120] J. M. Luther and N. J. Brown, "The renin-angiotensin-aldosterone system and glucose homeostasis," *Trends in Pharmacological Sciences*, vol. 32, no. 12, pp. 734–739, 2011.
- [121] A. M. Briones and R. M. Touyz, "Oxidative stress and hypertension: current concepts," *Current Hypertension Reports*, vol. 12, no. 2, pp. 135–142, 2010.
- [122] W. O. Sampaio and R. A. S. Santos, "Aplicações clínicas dos mecanismos fisiopatológicos da hipertensão arterial. Sistema renina-angiotensina: bases fisiopatológicas," *Revista Brasileira de História*, vol. 11, no. 1, pp. 67–70, 2004.
- [123] F. Portaluppi, B. Boari, and R. Manfredini, "Oxidative stress in essential hypertension," *Current Pharmaceutical Design*, vol. 10, no. 14, pp. 1695–1698, 2004.
- [124] S. Moncada, R. M. Palmer, and E. A. Higgs, "Nitric oxide: physiology, pathophysiology, and pharmacology," *Pharmacological Reviews*, vol. 43, no. 2, pp. 109–142, 1991.
- [125] L. J. Ignarro, G. M. Buga, K. S. Wood, R. E. Byrns, and G. Chaudhuri, "Endothelium-derived relaxing factor produced and released from artery and vein is nitric oxide," *Proceedings of the National Academy of Sciences of the United States of America*, vol. 84, no. 24, pp. 9265–9269, 1987.
- [126] C. Viegas, V. da S. Bolzani, and E. J. Barreiro, "Natural Products and Modern Medicinal Chemistry," *New Chemistry*, vol. 29, no. 2, pp. 326–337, 2006.
- [127] C. O. Fisch, J. H. Block, and P. G. Sandner, "Chinese university patents: quantity, quality, and the role of subsidy programs," *The Journal of Technology Transfer*, vol. 41, pp. 60–84, 2016.
- [128] H. Zhang, "Patent institution, innovation and economic growth in China," in *Book: Deepening Reform for China's Long-Term Growth and Development*, ANU Press, Canberra, Australia, 2014.



## Research Article

# ***Reineckia carnea* Alleviates the Production of Inflammatory Cytokines and MUC5AC in Rats with Chronic Obstructive Pulmonary Disease**

Wei Liu <sup>1</sup>, Jiang Li,<sup>2</sup> Tongyao Li,<sup>3</sup> Youliang Xie,<sup>4</sup> and Caihong Luo<sup>5</sup>

<sup>1</sup>Respiratory Medicine, The Second Affiliated Hospital of Guizhou University of Chinese Medicine, Guiyang, China

<sup>2</sup>Prescription Teaching and Research Office, Guizhou University of Chinese Medicine, Guiyang, China

<sup>3</sup>Respiratory Medicine, Qianxinan Hospital of Traditional Chinese Medicine, Guiyang, China

<sup>4</sup>Department of Internal Medicine, Xiangxiang People's Hospital, Xiangtan, China

<sup>5</sup>Geriatric Respiratory Department, Henan Electric Power Hospital, Zhengzhou, China

Correspondence should be addressed to Wei Liu; [liuwei202012262020@126.com](mailto:liuwei202012262020@126.com)

Received 15 March 2022; Revised 22 April 2022; Accepted 27 May 2022; Published 16 June 2022

Academic Editor: Ruchika Garg

Copyright © 2022 Wei Liu et al. This is an open access article distributed under the Creative Commons Attribution License, which permits unrestricted use, distribution, and reproduction in any medium, provided the original work is properly cited.

**Background.** *Reineckia carnea* (RC), a perennial evergreen herb which belongs to *Reineckia* Kunth (Liliaceae), can be used for clearing the lungs and relieving cough, reducing phlegm and anti-inflammatory effects. Moreover, chronic obstructive pulmonary disease (COPD) is characterized by airway and lung inflammation and increased secretion of airway mucus. Therefore, RC has the potential to treat COPD. **Methods.** NR8383 cells were cultured and treated with various concentrations of RC (100 mg/mL, 10 mg/mL, 1 mg/mL, 100 µg/mL, 10 µg/mL, 1 µg/mL, 100 ng/mL, and 10 ng/mL). Cell viability and levels of interleukin (IL)-1β, cyclooxygenase-2 (COX-2), and prostaglandin E2 (PGE2) in the cell culture supernatant or rat serum were analyzed using CCK-8 and enzyme-linked immunosorbent assay (ELISA), respectively. Sprague Dawley rats were assigned to mock, COPD model, RC (0.67 g/kg, 1.35 g/kg, and 2.7 g/kg), and ambroxol (5.4 mg/kg) groups. Western blot and quantitative polymerase chain reaction (qPCR) analyses were used to evaluate the protein and mRNA expression levels of mucin 5AC (MUC5AC) and Toll-like receptor 4 (TLR4). **Results.** The results showed that *Reineckia carnea* (RC) extract (RCE) inhibited the proliferation of NR8383 cells and suppressed the production of IL-1β, PGE2, and COX-2 in NR8383 cells. Moreover, RCE decreased the levels of IL-1β, PGE2, and COX-2 in the serum of rats with COPD and alleviated the expression of TLR4 and MUC5AC induced by COPD in rat lung tissue. **Conclusion.** RCE alleviated COPD by inhibiting the expression of COPD-induced inflammatory cytokines and MUC5AC in rats.

## 1. Introduction

Patients with chronic obstructive pulmonary disease (COPD) exhibit airway mucus hypersecretion with chest tightness, shortness of breath, fatigue aggravation, phlegm, and viscous mucus, resulting in airflow limitation. If not treated in a timely manner, progression to airway obstruction and asphyxia can occur [1, 2]. At present, COPD is often treated by inhaled bronchodilators and glucocorticoids, but there are many adverse reactions and the inhaled drugs are carried out by sputum due to the excessive secretion of airway mucus, which cannot exert their efficacy [3]. Therefore, the development of safe and effective

treatments is urgently needed. Many studies have found that airway mucus hypersecretion is an important pathophysiological characteristic of COPD and an independent risk factor for COPD development and prognosis, and exists at all stages of disease occurrence and development [4, 5]. Although a study has demonstrated an important role of IL-1β/COX-2 in airway mucus hypersecretion [6], the molecular mechanism of airway mucus hypersecretion in COPD still needs to be elucidated.

Airway mucus hypersecretion in COPD is caused by a variety of factors, including inflammatory factors, oxidative stress, and multiple signaling pathways. In the IL-1β/COX-2 signaling pathway, interleukin-1β, cyclooxygenase-2 (COX-2),

prostaglandin 2 (PGE<sub>2</sub>), and MUC5AC participate in the inflammatory reaction and lead to an increase in secretion from the glands, leading to airway mucus hypersecretion. Toll-like receptor (TLR) is a kind of innate immune receptor activated by the outer membrane lipopolysaccharide of Gram-negative bacteria and promotes the phosphorylation of a series of downstream factors [7]. TLR4 can regulate the inflammatory response. Studies have shown that TLR4 can activate the nuclear factor kappa-B (NF- $\kappa$ B) signaling pathway and regulate the expression of inflammation-related factors. As the earliest inflammatory factor, IL-1 $\beta$  participates in the whole inflammatory process in COPD. Therefore, there may be a connection between TLR4 and IL-1 $\beta$ , leading to the inflammatory reaction and mucus hypersecretion.

*Reineckia carnea* (RC) is a Liliaceae plant, and the whole plant mainly contains various chemical components such as steroids, flavonoids, lignans, terpenes, and organic acids, which have pharmacological activities such as antihemolysis, relieving cough, reducing phlegm, anti-inflammatory, analgesic, and hypoglycemic effects, and killing snails [8, 9]. Therefore, RC is commonly used to treat various diseases, especially respiratory diseases, such as lung dryness and cough, and is used by the Miao group to treat bronchitis, pneumonia, and other diseases [10]. Extensive research at the Guiyang College of traditional Chinese medicine has shown that RCE can effectively dilute sputum and reduce sputum secretion in patients with COPD. Furthermore, modern pharmacological studies have shown that RCE relieves cough, resolves phlegm, reduces inflammation, reduces airway secretion, and inhibits airway mucosal hypersecretion in COPD [11]. In addition, a study showed that after being injected subcutaneously with a 4500 mg/kg injection made with RC, all 12 mice died within 7 days [12].

The above studies have shown that RC can be used to treat COPD. Therefore, in this study, we explored the molecular mechanism by which RCE inhibits inflammation in COPD, with a focus on the IL-1 $\beta$ /Cox-2 signaling pathway, via animal experiments in vivo and cells assay in vitro, which provides strong evidence for its clinical use in the treatment of COPD. Moreover, ambroxol hydrochloride is an expectorant commonly used for the treatment of COPD, with anti-inflammatory and antioxidant effects. Therefore, ambroxol hydrochloride was selected as a control in the analyses of the therapeutic effect of RCE.

## 2. Materials and Methods

**2.1. Animals.** Ninety healthy male Sprague Dawley (SD) rats without specific antigens were provided by Chongqing Tengxin Biotechnology Co., Ltd. Before the experiment, the 6- to 8-week-old rats, weighing 180–220 grams, acclimatized for a week in a clear plastic cage with free of specific pathogens, a constant 12-hour light-dark cycle, and free access to water and chow.

**2.2. Establishment of COPD Rat Models.** Sixty-seven rats were randomly selected to construct COPD rat models. COPD rat models were established in 12 weeks by intranasal instillation

of lipopolysaccharide (LPS) and cigarette smoke inhalation, as previously described [8, 13, 14]. 200  $\mu$ L LPS (catalog number: ST1470, Beyotime, Shanghai, China) (30  $\mu$ g/6  $\mu$ L) was administered to SD rats via the nasal cavity on days 1, 29, and 57. The rats were exposed to cigarette (China Tobacco Guizhou Industrial, Co., Ltd) smoke in an in-house glass fumigation box (70 cm  $\times$  50 cm  $\times$  30 cm) for 30 min, 5 days per week for 12 weeks from days 2 to 84 (except on days 29 and 57). Subsequently, 12 COPD rats and 12 healthy rats were randomly selected to determine whether the COPD model was established successfully by HE staining of lung tissues and observing the lung pathological characteristics. The evaluation indices for successful model establishment were as follows: infiltration of inflammatory cells on the surface of the peripheral airway, bronchus, and bronchioles; hyperplasia and hypertrophy of the mucous glands and an increase in goblet cells; injury of the small airway, hyperplasia of collagen and scar tissue, and stenosis of the airway cavity; dilation and destruction of respiratory bronchioles, irregular expansion of alveoli, and formation of pulmonary bullae; hyperplasia of the smooth muscle of pulmonary arterioles; and infiltration of inflammatory cells in the vascular wall.

**2.3. RCE Preparation.** The RCE was prepared using the traditional method as previously described [8, 15]. In brief, 3000 g of dried RC was pulverized to a crude product and extracted with 15 times distilled water for 3 times, 2 h each time. The decoction was filtered and concentrated under pressure to obtain the extract which was dried and weighed. The extract was 645.36 g and the yield was 21.51%. Yield (%) = (weight of extract (g)  $\div$  weight of RC (g))  $\times$  100%.

**2.4. Animal Groups.** The remaining COPD rats were randomly divided into 5 groups, COPD model, low-dose RC (LD-RC), medium-dose RC (MD-RC), high-dose RC (HD-RC), and ambroxol groups. Each group consisted of 11 rats, and the remaining 11 healthy rats were used as the negative control group named the mock group.

**2.5. Treatment of Each Group of Animals.** Based on the amount of medicine used per unit body surface area, the amount of medicine used in rats is about 6.3 times that of humans [8]. The daily dosage of RC for adults is 15–30 g, so the dosage for rats is 1.35–2.7 g/kg. The low-, medium-, and high-dose RC were 0.67 g/kg, 1.35 g/kg, and 2.7 g/kg, respectively, which converted to RCE were 0.14 g/kg, 0.29 g/kg, and 0.58 g/kg, respectively. The daily dosage of ambroxol (Shanxi C&Y Pharmaceutical Group Co., Ltd) for adults is 60 mg, so the dosage for rats is 5.4 mg/kg. The drugs were separately dissolved in 3 mL of saline and gavaged to the corresponding groups of rats once a day for 17 days.

In the mock and COPD model groups, normal saline (3 mL/rat) was delivered by gavage once a day for 17 days. The experiments of this study were completed according to the requirements of the Animal Experiment Ethics Committee of the Guizhou University of Traditional Chinese Medicine.

**2.6. Cell Culture.** Rat alveolar macrophages and NR8383 cells (Xiamen Immocell Biotechnology Co., Ltd, catalog number: IM-R006) were cultured in an RPMI 1640 medium (Gibco, New York, USA) containing 10% fetal bovine serum (FBS, Gibco) at 37°C and 5% CO<sub>2</sub>. NR8383 cells were cultured in suspension, and the solution was changed in 2-3 days.

**2.7. CCK-8 Assay.** NR8383 cells were cultured overnight in 96-well plates at a density of 10000 cells per well. The cells were treated with different concentrations of RCE (1, 10, and 100 mg/mL; 1, 10, and 100 µg/mL; 10 and 100 ng/mL) or ambroxol (MedChemExpress, catalog number: HY-B1039) (10, 20, and 30 µg/mL). After 24 h, the cells were detected using CCK-8 (MedChemExpress, catalog number: HY-K0301, Shanghai, China) and a microplate reader (Bio Tek) according to the manufacturer's instructions. Results are presented as the mean ± standard deviation (SD) of six wells.

**2.8. Cell Immunohistochemistry.** The NR8383 cells were treated with 100 mg/mL RC or 30 µg/mL ambroxol. After 24 h, the cells were fixed on the slides with 0.4% paraformaldehyde, which was incubated successively with 0.5% Triton X-100 (Thermo Fisher Scientific, catalog number: R21902) for 20 min and then with 3% H<sub>2</sub>O<sub>2</sub> for 15 min. After being incubated with 5% FBS for 30 min, the cells were incubated with the TLR4 antibody (Abcam, catalog number: ab22048, dilution rate: 1:100) or MUC5AC antibody (Abcam, catalog number: ab3649, dilution rate: 1:100) for 2 h, followed by HRP-conjugated goat anti-mouse IgG (Abcam, catalog number: ab205719, dilution rate: 1:1000) for 1 h. Subsequently, the cells were stained with a DAB Immunohistochemistry Color Development Kit (Sangon Biotech, catalog number: E670033) and the nuclei were stained with hematoxylin. The cells were viewed under a microscope and photographed. The experiments were performed thrice independently.

**2.9. Enzyme-Linked Immunosorbent Assay (ELISA).** The levels of IL-1β, PGE<sub>2</sub>, and COX-2 in the cell culture supernatant or serum were determined by Rat IL-1 beta ELISA kit (Abcam, catalog number: ab255730), Rat PGE<sub>2</sub> ELISA Kit (Wuhan Fine Biotech Co., Ltd, catalog number: ER1800), ELISA kits, and Rat COX-2 ELISA Kit (CUSABIO TECHNOLOGY, catalog number: CSB-E13399r) according to the manufacturer's instructions. The experiments were performed more than three times independently.

**2.10. Isolation of RNA and Quantitative PCR (qPCR).** RNA was isolated from the lung tissues of rats using an RNA reagent (Takara, Kusatsu, Japan) and we used a PrimeScript™ RT Master Mix (Takara, catalog number: RR036Q) to reverse transcribe into cDNA. And then we employed the obtained cDNA, TB Green® Fast qPCR Mix (Takara, catalog number: RR430S), the Bio-Rad iQ5 Real-Time PCR System, and primers which are shown in Table 1, to perform qPCR. The data are expressed as the mean ± SD of three independent experiments.

**2.11. Western Blot Analysis.** Western blotting was used to examine the expression of MUC5AC and TLR4. In order to extract proteins, we added RIPA buffer (Beyotime, Shanghai, China) to the ground tissue and added protease inhibitors (Roche, Basel, Switzerland). To measure the protein concentrations, we used the BCA Protein Analysis Kit (Pierce, Rockford, IL, USA) according to the manufacturer's instructions. Thereafter, we put 50 µg of protein lysate in each SDS-PAGE well to separate proteins and transferred the proteins to a PVDF membrane which was then sealed with 5% milk at room temperature for 1 hour, followed by overnight incubation with TLR4 antibody (Abcam, catalog number: ab217274, dilution rate: 1:300), MUC5AC antibody (Abcam, catalog number: ab3649, dilution rate: 1:1000), or β-actin antibody (Abcam, catalog number: ab6276, dilution rate: 1:5000), at 4°C. After the membrane was washed with TBST, we incubated the membrane with HRP-conjugated goat anti-rabbit IgG (Abcam, catalog number: ab205718, dilution rate: 1:10000), or HRP-conjugated goat anti-mouse IgG (Abcam, catalog number: ab205719, dilution rate: 1:10000) for 1 hour at room temperature. The Pierce™ ECL Western Blotting Substrate (Thermo Scientific, catalog number: 32109) was used for luminescent detection. A gel imaging system was used to collect images, and Image Lab 3 was used to analyze gray values. Protein levels were normalized against β-actin. The experiments were performed thrice independently.

**2.12. Statistical Analysis.** We used the SPSS 20.0 software for statistical analyses. To compare the differences between two groups and between multiple groups, we performed Student's *t*-test (unpaired) and analysis of variance (ANOVA), respectively. A value of *P* < 0.05 was regarded as statistically significant.

### 3. Results

**3.1. RCE Inhibits the Production of IL-1β, PGE<sub>2</sub>, and COX-2 in NR8383 Cells.** We investigated the effects of various concentrations of RC on the proliferation of NR8383 cells. For RC concentrations of 1 mg/mL, 10 mg/mL, and 100 mg/mL, cell proliferation gradually decreased in a concentration-dependent manner (Figure 1(a), *P* < 0.05). Compared with cells not treated with RC (mock group), there was no significant difference in cell proliferation after the cells were treated with 100 ng/mL and 10 ng/mL RC (Figure 1(a), *P* < 0.05). As the ambroxol concentration increased, cell proliferation decreased in a concentration-dependent manner (Figure 1(a), *P* < 0.05). Based on these results, an RC concentration of 100 mg/mL and ambroxol concentration of 30 µg/mL were selected for further analyses, and the levels of IL-1β, PGE<sub>2</sub>, and COX-2 in the NR8383 culture medium were analyzed. RCE and ambroxol inhibited the production of IL-1β, PGE<sub>2</sub>, and COX-2 (Figure 1(b), *P* < 0.01). The expression of MUC5AC and TLR4 in NR8383 cells was evaluated by immunohistochemistry. Compared with the mock group, MUC5AC and TLR4 levels in the RC and ambroxol groups were significantly (*P* < 0.01) lower (Figure 2).

TABLE 1: Oligonucleotide primers targeting rat genes for qPCR.

Gene	Forward primer sequence (5'-3')	Reverse primer sequence (5'-3')
MUC5AC	AATGGCTACCTGAAGGTGGTGG	AAACTCGCTGGATTCTGGACTG
TLR4	AACATGAGTCACAACAACCTAC	TATTCACATATAACAAGCAACAG
$\beta$ -Actin	TCTGTGATGCCCTTAGATGTGC	AATGGGGTTCAACGGGTTAC

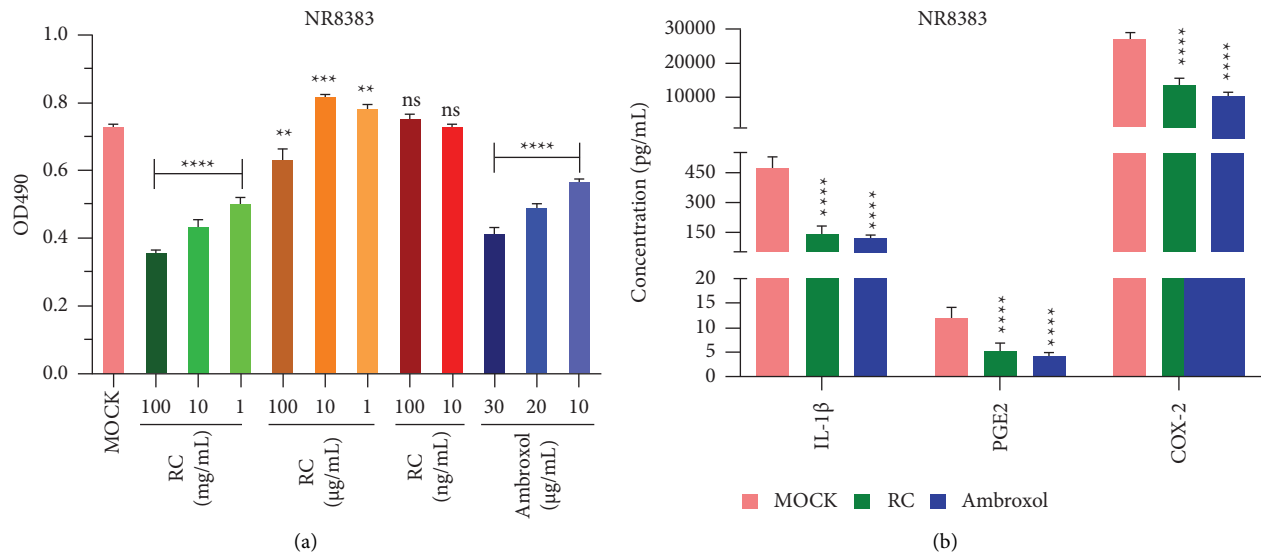


FIGURE 1: RCE inhibits the production of IL-1 $\beta$ , PGE2, and COX-2 in NR8383 cells. (a) The effects of RC and ambroxol on NR8383 cell proliferation. (b) After the NR8383 cells were treated with 100 mg/mL RC or 30  $\mu$ g/mL ambroxol for 24 h, the effects of RCE and ambroxol on the production of IL-1 $\beta$ , PGE2, and COX-2 in NR8383 cells. RC: *Reineckia carnea*, ns: not significant, \*\* $P < 0.01$ , \*\*\* $P < 0.001$ , \*\*\*\* $P < 0.0001$ .

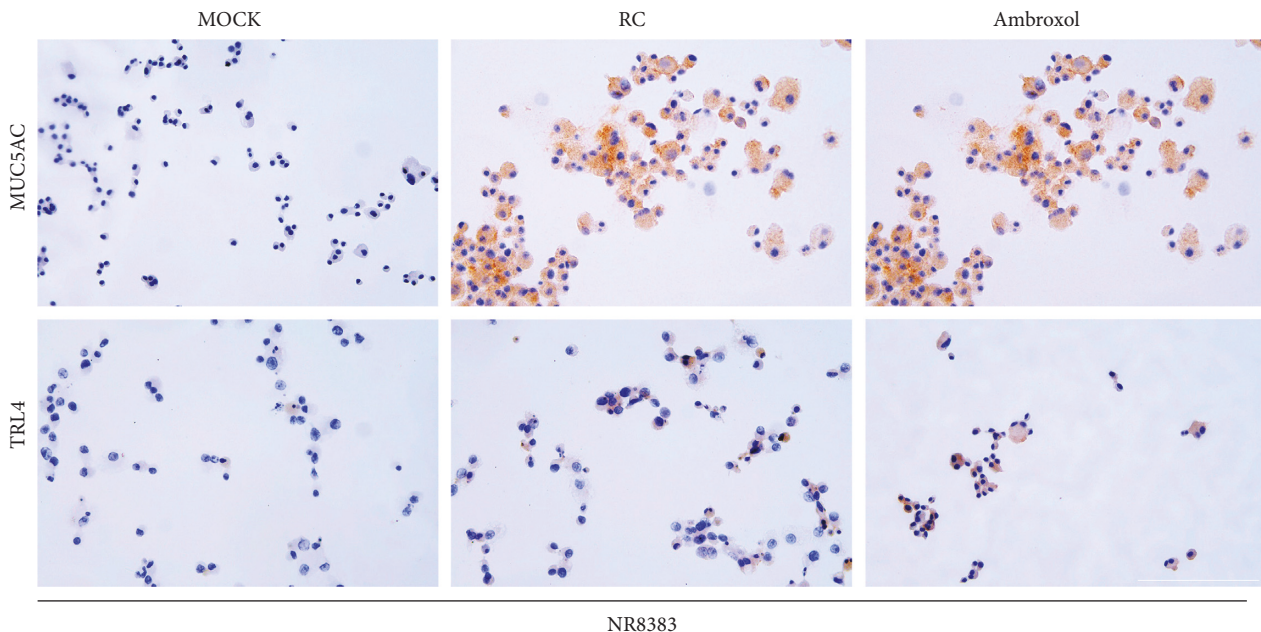


FIGURE 2: Immunohistochemical representative images show the expression of MUC5AC and TLR4 in RC- or ambroxol-treated NR8383 cells. RC: *Reineckia carnea*.

3.2. RCE Decreases the Levels of IL-1 $\beta$ , PGE2, and COX-2 in Serum of COPD Model. To investigate the molecular mechanism of RCE treatment of COPD, we constructed a COPD rat model. After the models were treated with RCE or

ambroxol, the serum was collected to detect the levels of IL-1 $\beta$ , PGE2, and COX-2. As shown in Figure 3, compared with the mock group, the levels of IL-1 $\beta$ , PGE2, and COX-2 in the model group were significantly higher (Figure 3,  $P < 0.01$ ).

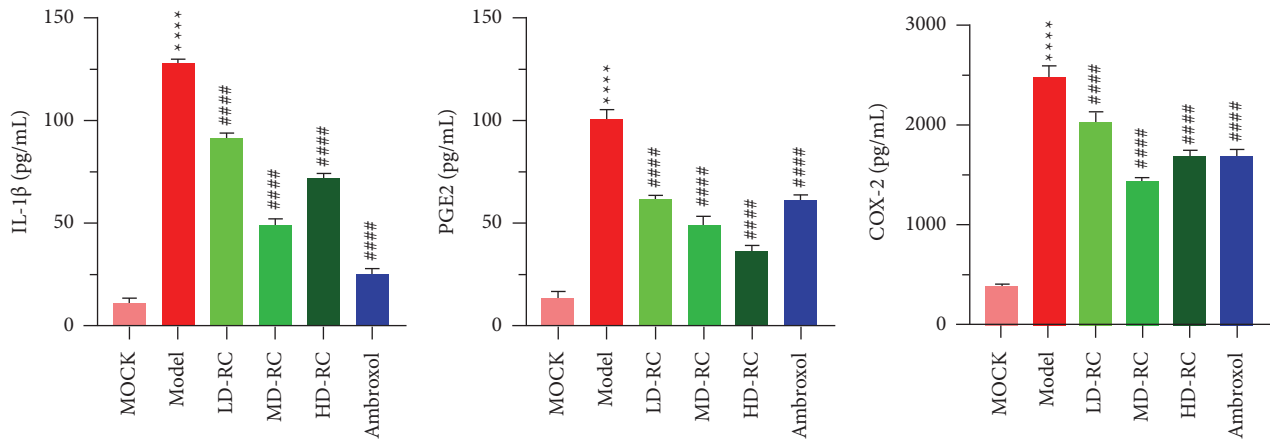


FIGURE 3: The ELISA results of the serum levels of IL-1 $\beta$ , PGE2, and COX-2. LD-RC: The rats were given a low dose of *Reineckia carnea* extract (0.14 g/kg) dissolved in 3 mL of saline. MD-RC: The rats were given a medium dose of *Reineckia carnea* extract (0.29 g/kg) dissolved in 3 mL of saline. HD-RC: The rats were given a high dose of *Reineckia carnea* extract (0.58 g/kg) dissolved in 3 mL of saline. \*\*\*\* $P < 0.0001$  vs. mock; #### $P < 0.0001$  vs. Model.

Compared with the model group, the levels of IL-1 $\beta$ , PGE2, and COX-2 were lower in the RC and ambroxol groups (Figure 3,  $P < 0.01$ ). These results indicate that RCE has similar effects as ambroxol in reducing inflammatory indices in rats with COPD.

**3.3. RCE Downregulates the COPD-Induced Expression of MUC5AC and TLR4 in Rat Lung Tissues.** Next, the expression levels of MUC5AC and TLR4 in different groups were analyzed. The mRNA levels of MUC5AC and TLR4 in the model group were significantly higher than those in the mock group (Figure 4(a),  $P < 0.01$ ). After the rats with COPD were treated with RCE or ambroxol, the mRNA levels of MUC5AC and TLR4 were significantly decreased (Figure 4(a),  $P < 0.05$ ).

Western blot analysis showed that MUC5AC and TLR4 levels in the model group were significantly higher than those in the mock group (Figures 4(b) and 4(c),  $P < 0.01$ ). The levels of TLR4 and MUC5AC proteins in the lung tissues of COPD rats treated with RCE or Ambroxol were significantly lower than those in the model group (Figures 4(b) and 4(c),  $P < 0.01$ ). Together, RCE attenuated COPD-induced TLR4 and MUC5AC expression.

## 4. Discussion

COPD, an inflammatory disease in the lung parenchyma and respiratory tract, is caused by continued inhalation of toxic substances, predominantly cigarette smoke [4, 16]. Moreover, LPS can cause inflammation [17]. Therefore, we used cigarette smoke and LPS to generate a rat COPD model. Furthermore, the IL-1 $\beta$ /COX-2 signaling pathway can cause airway mucus hypersecretion in COPD [18]. Inflammatory factors bind to corresponding receptors to activate COX-2, leading to increased secretion [19]. Airway mucus hypersecretion in COPD is related to an inflammatory reaction [20]. COX-2 is transformed into prostaglandin products *in vivo*. After the transformation, prostaglandin E2 is activated,

increasing vascular permeability and dilating blood vessels, causing mucosal edema, increasing gland secretion, and affecting airway ventilation and ventilation function [21]. In this study, we evaluated the effect of RCE on inflammatory response in rat alveolar macrophages *in vitro* and *in vivo*. RCE and ambroxol had similar effects; they reduced the levels of IL-1 $\beta$ , PGE2, and COX-2 to relieve COPD.

In addition, COX-2 is an inducible enzyme that is rapidly synthesized when cells are stimulated by various factors. It can be induced in bronchial epithelial cells and alveolar epithelial cells. Macrophages in alveoli are the main inflammatory cells expressing COX-2. When IL-1 $\beta$  binds to its receptor, the activity of COX-2 is increased. COX-2 has a catalytic role in the conversion of arachidonic acid to PGE and PGE2 under the action of PGE synthetase [22]. PGE2 can increase vascular permeability and dilate blood vessels, resulting in bronchial mucosal edema, increased gland secretion, and airway obstruction by exudates [23]. The expression of MUC5AC and TLR4 in rat alveolar macrophages was detected by immunohistochemistry. Compared with the mock group, MUC5AC and TLR4 levels in the RC and ambroxol groups were significantly lower. IL-1 $\beta$  contributes to the early inflammatory response and can be secreted by a variety of cells, including epithelial cells, macrophages, and neutrophils. Lappalainen et al. used a transgenic animal model to show that IL-1 $\beta$  can cause alveolar septum enlargement, tracheal wall thickening, and increased mucus secretion, consistent with the pathological changes in COPD. IL-1 $\beta$  can activate macrophages and other inflammatory cells to release inflammatory mediators, which can cause pulmonary inflammation, characterized by macrophage and granulocyte infiltration. IL-1 $\beta$  may be a cause of chronic lung inflammation.

RCE relieves cough, resolves phlegm, and has anti-inflammatory effects [24]. It is often used to treat cough, bronchitis, pneumonia, and other diseases by the Miao group in China. RCE-4 from RC, which suppresses the PI3K/Akt/mTOR signaling pathway and NF- $\kappa$ B activation, and has an antiproliferative effect on HeLa cells, so RC mainly reduces inflammation and oxidative stress [1].



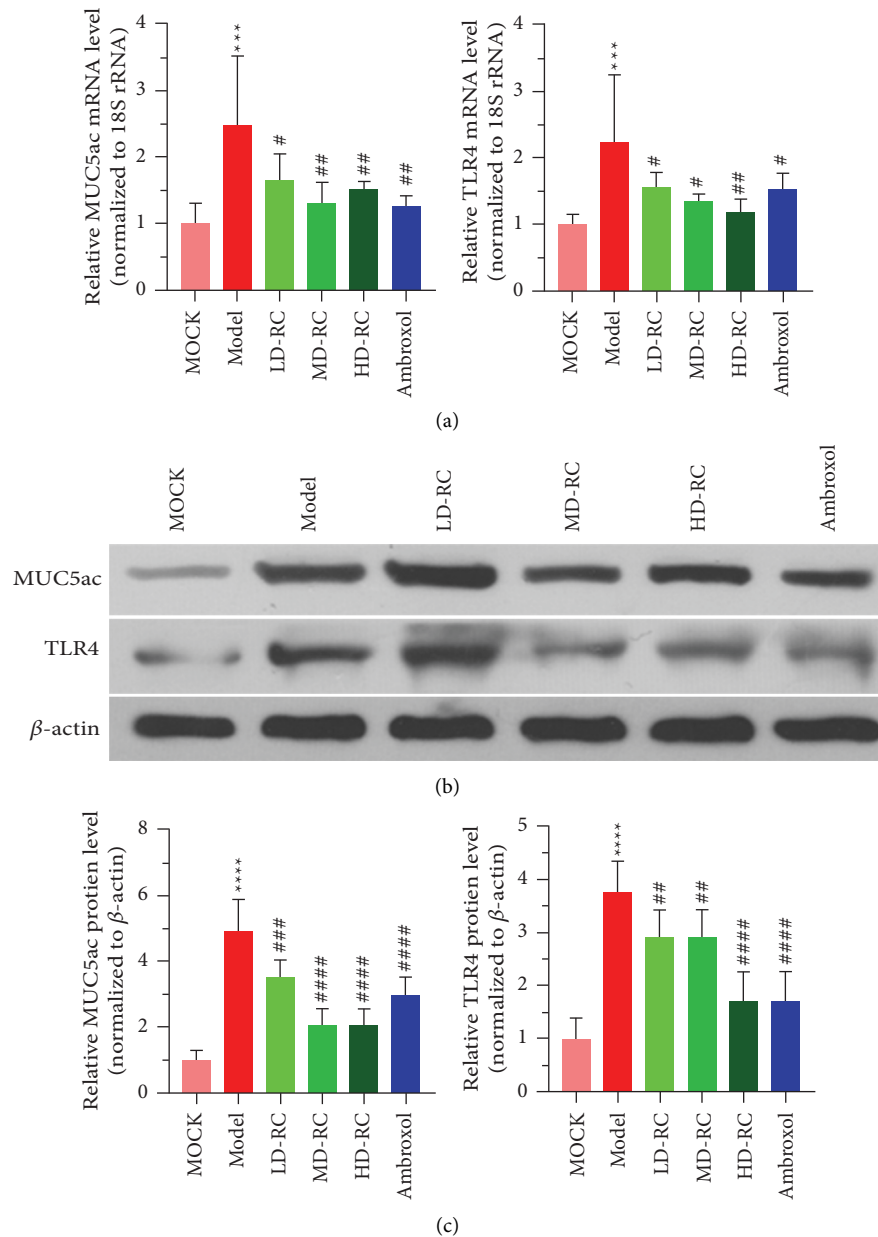


FIGURE 4: RCE downregulates the COPD-induced expression of MUC5AC and TLR4 in rat lung tissues. (a) The expression levels of MUC5AC and TLR4 in different groups. (b) The results of western blot analysis of MUC5AC and TLR4 levels. (c) Histogram of relative expression levels of TLR4 and MUC5AC proteins. LD-RC: The rats were given a low dose of *Reineckia carnea* extract (0.14 g/kg) dissolved in 3 mL of saline. MD-RC: The rats were given a medium dose of *Reineckia carnea* extract (0.29 g/kg) dissolved in 3 mL of saline. HD-RC: The rats were given a high dose of *Reineckia carnea* extract (0.58 g/kg) dissolved in 3 mL of saline. \* \* \*  $P < 0.001$ , \* \* \* \*  $P < 0.0001$  vs. mock; # $P < 0.05$ , ## $P < 0.01$ , ### $P < 0.001$ , and #### $P < 0.0001$  vs. Model.

Studies have shown that RCE can improve lung function and reduce sputum secretion in patients with COPD; however, few studies have examined the molecular mechanisms underlying its effects. ELISA was used to analyze the effects of various concentrations of RC on the serum levels of IL-1 $\beta$ , PGE2, and COX-2 in a rat model of COPD. Levels of IL-1 $\beta$ , PGE2, and COX-2 were high in the mock group. RCE and ambroxol could inhibit the secretion of airway mucus in rats with COPD. For some concentrations, the effects of RCE were more potent than those of ambroxol.

TLR is an innate immune receptor involved in the regulation of the inflammatory response. In COPD, the inflammatory response activates the IL-1 $\beta$ /COX-2 signaling pathway, leading to MUC5AC overexpression and airway mucus hypersecretion. Various factors activate the TLR4 receptor, which regulates the expression of inflammatory factors and causes inflammatory reactions via various enzymes. The overexpression of IL-1 $\beta$  can increase the activity of COX-2, increase the synthesis of PGE2, increase blood permeability and vasodilation, cause

bronchial mucosal edema, increase secretion from glands, and lead to airway restriction. Based on analyses of protein and mRNA levels, MUC5AC and TLR4 were upregulated in the mock group, indicating that mucus hypersecretion in COPD is related to the high expression of these loci. MUC5AC and TLR4 were inhibited by both RC and ambroxol ( $P < 0.01$ ).

The expression levels of MUC5AC and TLR4 were analyzed by PCR and western blotting analyses. As the RC concentration increased, the mRNA and protein expression levels of MUC5AC and TLR4 in rats with COPD decreased significantly, and a similar effect was observed in the ambroxol group. The results showed that ambroxol could inhibit airway mucus hypersecretion in COPD; however, medium and high doses of RC were more effective than those of ambroxol. Lu et al. confirmed that sequential treatment with Tongsai and Bufe Yishen granules during acute exacerbations of chronic obstructive pulmonary disease risk window (AECOPD-RW) periods reduces the inflammatory response, improves pulmonary function, and shortens the recovery course, particularly when Chinese and Western medicines are integrated [25]. In a recent study, it was shown that Bufe Yishen granules combined with electroacupuncture was effective in the treatment of COPD in rats, and the combination is superior to either strategy alone [26]. Lin et al. have shown that curcumin inhibits LPS-induced airway mucus hypersecretion and inflammation which are important pathophysiological features of chronic inflammatory airway diseases [27].

The study was based on rats and rat cells, and the results cannot be directly transferable to humans, which is a limitation of the study.

## 5. Conclusion

In conclusion, our results revealed that RCE inhibited the proliferation of NR8383 cells, and suppressed the production of IL-1 $\beta$ , PGE2, and COX-2 in NR8383 cells. Moreover, RCE alleviated the expression of IL-1 $\beta$ , PGE2, COX-2, TLR4, and MUC5AC induced by COPD. This study preliminarily revealed the molecular mechanism of RCE treatment of COPD to provide a theoretical basis for the treatment of COPD by RC and for better exploitation and quality control of RC.

## Data Availability

The datasets used and analyzed during the current study are available from the corresponding author on reasonable request.

## Ethical Approval

Ethical approval for this study was obtained from the Ethical Review Committee of Experimental Animals of the Guizhou University of Traditional Chinese Medicine. The present study followed international, national, and/or institutional guidelines for humane animal treatment and complied with relevant legislation.

## Conflicts of Interest

The authors declare that they have no conflicts of interest.

## Authors' Contributions

Wei Liu and Jiang Li designed this study. Tongyao Li and Youliang Xie were responsible for obtaining data. Wei Liu and Jiang Li were responsible for analyzing data and interpretation of data. Wei Liu and Jiang Li drafted the manuscript. Tongyao Li and Youliang Xie revised the manuscript. All the authors approved the version to be published and agree to be accountable for all aspects of the work in ensuring that questions related to the accuracy or integrity of any part of the work are appropriately investigated and resolved. Wei Liu and Jiang Li contributed equally to this work.

## Acknowledgments

This study was supported by China Regional Science Foundation Project of the National Natural Science Foundation of China (grant no. 81760774) and Science and Technology Talents Support Program of the Guizhou Education Committee (grant no. Guizhou Education Cooperation KY [2016]076).

## References

- [1] C. Bai, X. Yang, K. Zou et al., "Anti-proliferative effect of RCE-4 from *Reineckia carnea* on human cervical cancer HeLa cells by inhibiting the PI3K/Akt/mTOR signaling pathway and NF- $\kappa$ B activation," *Naunyn-Schmiedeberg's Archives of Pharmacology*, vol. 389, no. 6, pp. 573–584, 2016.
- [2] L. Tanner and A. B. Single, "Animal models reflecting chronic obstructive pulmonary disease and related respiratory disorders: translating pre-clinical data into clinical relevance," *Journal of Innate Immunity*, vol. 12, no. 3, pp. 203–225, 2020.
- [3] Chronic Obstructive Pulmonary Disease Committee RS, Chinese Medical Association, and Working Committee of Chronic Obstructive Pulmonary Disease of Respiratory Doctors Branch CMDA, "Guidelines for the diagnosis and management of chronic obstructive pulmonary disease revised version 2021," *Chinese Journal of Tuberculosis and Respiratory Diseases*, vol. 44, pp. 170–205, 2021.
- [4] K. Akata and S. F. van Eeden, "Lung macrophage functional properties in chronic obstructive pulmonary disease," *International Journal of Molecular Sciences*, vol. 21, no. 3, p. 853, 2020.
- [5] M. Samsuzzaman, M. S. Uddin, M. A. Shah, and B. Mathew, "Natural inhibitors on airway mucin: molecular insight into the therapeutic potential targeting MUC5AC expression and production," *Life Sciences*, vol. 231, Article ID 116485, 2019.
- [6] L. Zhou, Y. Liu, X. Chen et al., "Over-expression of nuclear factor- $\kappa$ B family genes and inflammatory molecules is related to chronic obstructive pulmonary disease," *International Journal of Chronic Obstructive Pulmonary Disease*, vol. 13, pp. 2131–2138, 2018.
- [7] J. Li and Z. Ye, "The potential role and regulatory mechanisms of muc5ac in chronic obstructive pulmonary disease," *Molecules (Basel, Switzerland)*, vol. 25, 2020.



- [8] J. B. Chen, L. J. Zhang, N. N. Qiu et al., "Study on fluid extract from herba euphorbiae in the treatment of chronic obstructive pulmonary disease and its mechanism," *Journal of Guizhou Medical University*, vol. 45, pp. 1412–1416, 2020.
- [9] H. Liu, J. Q. Yang, L. Xiong, and Y. Wang, "Study on chemical constituents and pharmacological activities of *Reineckia carnea*," *Chinese Traditional Patent Medicine*, vol. 34, pp. 1785–1789, 2012.
- [10] N. Han, C. Chang, Y. Wang, T. Huang, Z. Liu, and J. Yin, "The *in vivo* expectorant and antitussive activity of extract and fractions from *Reineckia carnea*," *Journal of Ethnopharmacology*, vol. 131, no. 1, pp. 220–223, 2010.
- [11] Y. Zhang, J. Du, J. Xu, G. Yao, L. Wang, and L. Zhang, "Pharmacological study of total Saponins from *Reineckia carnea* on hemolysis, relieving a cough, abolishing phlegm and anti-inflammation," *Medical Journal of the Chinese People's Armed Police Forces*, vol. 17, pp. 282–284, 2006.
- [12] D. W. Qiu and J. Du, *GUIZHOU SHIDA MIAOYAO YANJIU: Traditional Chinese Medicine*, Ancient Books Publishing House, Shanghai, China, 2008.
- [13] M. Jia, W. H. Fan, Q. H. Qin, H. Zhang, and Y. L. Chen, "Cigarette dust particles induced lung function injury of chronic obstructive pulmonary disease in mice," *Chinese Journal of Pathophysiology*, vol. 35, pp. 1915–1920, 2019.
- [14] Y. Cheng, W. L. Tao, X. M. Zhang, Z. S. Yang, and J. Chen, "Experimental study on the building animal model of chronic obstructive pulmonary disease," *World Journal of Integrated Traditional and Western Medicine*, vol. 11, pp. 445–448, 2016.
- [15] X. Xu, B. Wu, Y. Li et al., "Isolation and identification of chemical constituents from Miao medicine *reineckia carnea* in Guizhou," *Chinese Journal of Experimental Traditional Medical Formulae*, vol. 24, pp. 56–61, 2018.
- [16] C. Wang, J. Zhou, J. Wang et al., "Progress in the mechanism and targeted drug therapy for COPD," *Signal Transduction and Targeted Therapy*, vol. 5, no. 1, p. 248, 2020.
- [17] Q. Ren, S. Zhao, C. Ren, and Z. Ma, "Retracted: astragalus polysaccharide alleviates LPS-induced inflammation injury by regulating miR-127 in H9c2 cardiomyoblasts," *International Journal of Immunopathology and Pharmacology*, vol. 32, Article ID 2058738418759180, 2018.
- [18] F. Tang and C. Ling, "Curcumin ameliorates chronic obstructive pulmonary disease by modulating autophagy and endoplasmic reticulum stress through regulation of SIRT1 in a rat model," *Journal of International Medical Research*, vol. 47, no. 10, pp. 4764–4774, 2019.
- [19] B. Chen, W.-J. You, S. Xue et al., "Overexpression of farnesoid X receptor in small airways contributes to epithelial to mesenchymal transition and COX-2 expression in chronic obstructive pulmonary disease," *Journal of Thoracic Disease*, vol. 8, no. 11, pp. 3063–3074, 2016.
- [20] X. Wang, X. Yang, Y. Li et al., "Lyn kinase represses mucus hypersecretion by regulating IL-13-induced endoplasmic reticulum stress in asthma," *EBioMedicine*, vol. 15, pp. 137–149, 2017.
- [21] M. Zago, J. A. Sheridan, H. Traboulsi et al., "Low levels of the AhR in chronic obstructive pulmonary disease (COPD)-derived lung cells increases COX-2 protein by altering mRNA stability," *PLoS One*, vol. 12, no. 7, Article ID e0180881, 2017.
- [22] A. Puratchikody, A. Umamaheswari, N. Irfan et al., "A novel class of tyrosine derivatives as dual 5-LOX and COX-2/mPGES1 inhibitors with PGE2 mediated anticancer properties," *New Journal of Chemistry*, vol. 43, no. 2, pp. 834–846, 2019.
- [23] M.-Y. Ho, S.-M. Liang, S.-W. Hung, and C.-M. Liang, "Retraction: MIG-7 controls COX-2/PGE2-mediated lung cancer metastasis," *Cancer Research*, vol. 79, no. 17, p. 4553, 2019.
- [24] L. Zheng, D. Zhang, Y. Li et al., "Three new steroidal components from the roots of *Reineckia carnea*," *Natural Product Research*, vol. 35, no. 7, pp. 1159–1166, 2019.
- [25] X. Lu, Y. Li, J. Li et al., "Sequential treatments with Tongsai and Bufei yishen granules reduce inflammation and improve pulmonary function in acute exacerbation-risk window of chronic obstructive pulmonary disease in rats," *Evidence-Based Complementary and Alternative medicine*, vol. 2016, Article ID 1359105, 2016.
- [26] J. Ma, Y. Tian, J. Li et al., "Effect of Bufei Yishen granules combined with electroacupuncture in rats with chronic obstructive pulmonary disease via the regulation of TLR-4/NF- $\kappa$ B signaling," *Evidence-Based Complementary and Alternative Medicine*, vol. 2019, Article ID 6708645, 14 pages, 2019.
- [27] X.-P. Lin, C. Xue, J.-M. Zhang, W.-J. Wu, X.-Y. Chen, and Y.-M. Zeng, "Curcumin inhibits lipopolysaccharide-induced mucin 5AC hypersecretion and airway inflammation via nuclear factor erythroid 2-related factor 2," *Chinese Medical Journal*, vol. 131, no. 14, pp. 1686–1693, 2018.

## Research Article

# Network Pharmacology and Pharmacological Mechanism of CV-3 in Atrial Fibrillation

Zundong Wang <sup>1</sup>, Zhen Zeng,<sup>1</sup> Yongsheng Hu,<sup>2</sup> Hengcan Sun,<sup>1</sup> Ying Tang,<sup>3</sup> and Weiqin Liu <sup>1</sup>

<sup>1</sup>Guizhou University of Traditional Chinese Medicine, Guiyang 550025, China

<sup>2</sup>Department of Intensive Care Unit, The Second Affiliated Hospital, Guizhou University of Traditional Chinese Medicine, Guiyang 550003, China

<sup>3</sup>Department of Intensive Care Unit, The First Affiliated Hospital, Guizhou University of Traditional Chinese Medicine, Guiyang 550001, China

Correspondence should be addressed to Weiqin Liu; [liuwq0222@outlook.com](mailto:liuwq0222@outlook.com)

Received 28 February 2022; Revised 8 April 2022; Accepted 17 May 2022; Published 14 June 2022

Academic Editor: Ruchika Garg

Copyright © 2022 Zundong Wang et al. This is an open access article distributed under the Creative Commons Attribution License, which permits unrestricted use, distribution, and reproduction in any medium, provided the original work is properly cited.

The high fatality and disability rate of atrial fibrillation (AF) strongly promote the development of pathogenesis and treatment of AF that is of great value. The present research attempted to clarify potential mechanisms of Mujiangzi oil (CV-3) in treating AF by constructing an AF cardiomyocytes model and using a network pharmacology approach. The experiment was divided into 4 groups: control, an AF model, AF + CV-3-treated, and the AF + verapamil group. Flow cytometry and the MTT assay were employed to detect cell apoptosis and cell viability, respectively. The main active components of CV-3 and predicted targets were obtained firstly, and molecular docking was performed. In the AF model, the cell apoptosis was aggravated, but inhibited in the CV-3-treated group. In addition, the cell viability was recovered after CV-3 treatment compared with the model group. Five potential active compounds of CV-3 were collected, including effective ingredients N-decanoic acid, spathulenol, copaene,  $\beta$ -panasinsene, and eucalyptol. Among them, N-decanoic acid and spathulenol was demonstrated to bind to PTGS2 with binding energy of  $-4.08$  and  $-7.09$  kcal/mol, respectively, and hydrogen bonds interaction were found. The present study indicated that CV-3 could alleviate AF cardiomyocytes apoptosis and improve cardiomyocytes viability, and N-decanoic acid and spathulenol may be the key components of CV-3 in treatment of AF by regulating PTGS2. This study provided the possible target PTGS2 and the understanding of molecular mechanisms of CV-3 in treating AF.

## 1. Introduction

Atrial fibrillation (AF) is a frequently encountered arrhythmia disease with an increasing incidence based on recent studies. In China, there are more than 4.87 million patients with atrial fibrillation over 35 years old, with a total prevalence rate of 0.71%. People over 75 years of age have the prevalence rate of nearly 3% [1]. The main population of AF in China is the elderly, and AF can cause cardiac insufficiency and vascular embolism, with high fatality and disability rates, and serious harm to human health [2]. With the arrival of an aging society in China, it is expected that the number of patients and the total prevalence will increase

significantly in the future [3–5]. In addition, AF can also cause palpitations, fatigue, chest tightness, cognitive dysfunction, impaired exercise tolerance, and other common clinical symptoms, which affect the quality of life of patients [6, 7].

Western medicine's treatment of atrial fibrillation is mainly classified into drug and nondrug therapies [8]. The former includes heart rhythm control drugs (such as digitalis, beta blockers (esmolol, propranolol, and metoprolol), calcium antagonists (Verapamil and diltiazem), sinus rhythm maintenance drugs (such as propafenone), non-antiarrhythmic drugs (such as RAAS inhibitors, anti-inflammatory, and antioxidants), and anticoagulation therapy;

nondrug treatments include catheter ablation, internal atrial cardioversion defibrillator, pacemaker implantation, and surgical maze [9–13]. Clinical practice has shown that antiarrhythmic drugs have limited effect in maintaining sinus rhythm and have relatively severe toxic side effects [14]. Although surgical treatment can cure AF, patients are not highly accepted due to high treatment costs and high risks. As the research on traditional Chinese medicine (TCM) advances, increasing preparations of TCM have been applied for AF clinically. Meanwhile, the effectiveness and safety have received widespread attention [15]. TCM produces satisfactory effects in AF treatment, with few toxic and side effects. AF patients benefit much in improving clinical signs and symptoms as well as quality of life [16,17].

Mujiangzi oil (CV-3) is the volatile oil extracted from *Cinnamomum migao* H.W.Li, which is one of the top ten Miao medicines in Guizhou, China [18]. As early as the 1960s, scholars discovered that folks used CV-3 to treat chest pain, chest tightness, and asthma and has achieved good effects. It has been found in clinical research to improve arrhythmia and slow down the heart rate. In addition, studies have found that CV-3 has antiarrhythmic effects, can slow down the heart rate, dilate coronary arteries, enhance myocardial blood supply, and reduce myocardial oxygen consumption [19]. It also reduces the expression of LTCC protein in atrial muscle cells of AF rats to improve intracellular calcium ion overload and so on, so as to play a therapeutic effect on AF [20].

In the present study, the possible active and key components of CV-3 in treating AF was explored by employing network pharmacology. It is expected to offer an insight into the pharmacology mechanism of CV-3 in AF treatment and clinical application.

## 2. Materials and Methods

**2.1. Isolation and Culture of Primary Cardiomyocytes.** Animal procedures were performed in accordance with the experimental animal use and management guidelines of the Guizhou University of Traditional Chinese Medicine Experimental Animal Committee. Six 1 d neonatal SD rats were supplied by Chongqing Ensiweier Biotechnology Co., Ltd. The heart of neonatal SD rats was opened and obtained and placed in D-hank's solution precooled at 4°C. After washing, the left and right atria were taken out and cut into pieces of about 1 mm<sup>3</sup> in size. We need to transfer the chopped cardiac tissue and digestion solution into a 15 ml centrifuge tube, and we then digest in water bath at 37°C for 10 min. We need to collect the supernatant, and complete Dulbecco's Modified Eagle Medium (DMEM, BasalMedia, China) was added to terminate the digestion, and the digestion was repeated 7–8 times. We need to filter to remove residual tissue pieces, centrifuge at 1000 rpm for 8 min for the removal of the supernatant, add complete medium to resuspend the cells, and inoculate them in a 10 cm Petri dish.

Cardiomyocytes were cultured with DMEM + 10% fetal bovine serum (FBS, Hyclone, USA) + 1% penicillin/streptomycin (P/S, Beyotime, China). Culture conditions were set at 37°C, 95% air, and 5% carbon dioxide. These cells were

treated with CV-3 (93.75 μM) and verapamil (10 μM, Solarbio, China) in the positive control group for 24 h.

**2.2. Cardiomyocyte AF Model Preparation.** Copper electrodes were used at 0.3 mm thickness, 15 cm length, 10 cm width, and 10.0 cm electrode space. The electrodes were aligned in parallel and positioned using an insulator for conduction prevention between both electrodes. When the cells adhered to about 80% of the cells observed by an inverted microscope, the culture plate was placed in an electric field in 37°C, 5% CO<sub>2</sub> incubator, and stimulated with the BL-420 biological function experimental system. The stimulation frequency was 10 Hz, and the intensity was 1.5 V/cm for continuous stimulation for 24 hours.

**2.3. Cell Flow Cytometry.** Primary neonatal rat cardiomyocytes were plated in 6-well plates at 1 × 10<sup>5</sup> cells/mL of density, and the modeling process was performed, respectively. After modeling, we collect the cell culture medium and iron wall cells, centrifuge at 1 000 rpm for 5 min, remove the supernatant, harvest the cells, and resuspend the cells in PBS with care and count them. We take 0.5~1 × 10<sup>5</sup> resuspended cells, centrifuge at 1000 rpm for 5 min, and abandon the supernatant followed by supplementing 195 μL Annexin V-FITC-A (Beyotime, China) to resuspend the cells. Another 5 μL Annexin V-FITC-A was added and mixed gently. We need to incubate for 10 min at room temperature (20–25°C) away from light. We then centrifuge at 1000 rpm for 5 min, followed by the removal of the supernatant, and 190 μL Annexin V-FITC-A binding solution was added to resuspend with care. Of 10 μL, PI staining solution was supplemented and mixed gently for incubation on an ice bath avoiding light. Finally, immediately proceed to flow cytometry detection (CytoFLEX, USA).

**2.4. 3-(4,5-Dimethylthiazol-2-yl)-2,5-diphenyltetrazolium Bromide Thiazolyl Blue (MTT) Assay.** Primary neonatal rat cardiomyocytes were inoculated in 96-well plates at about 1 × 10<sup>5</sup> cells/mL. Following 48 h, the cells were processed for model construction. After modeling, we take out the 96-well plate, aspirate the old culture medium, add CV-3 and verapamil to the experimental group, and culture for 24 h. The culture medium was discarded and added with 5 mg/mL MTT solution (Solarbio, China) for incubation for 4 h. We terminate the culture, add 150 μL of dimethyl sulfoxide, and place on a shaker to shake mildly for 10 min. The absorbance of wells was measured at 490 nm in an enzyme-linked immunosorbent meter.

**2.5. Network Pharmacology.** The BATMAN-TCM (<http://bionet.ncpsb.org/batman-tcm/>) platform and the TCMSP (<http://lsp.nwu.edu.cn/tcmsp.php>) database were employed to sort out active components and putative targets of CV-3. We input “Atrial Fibrillation” as keywords in GeneCards (<https://www.genecards.org/>), and AF-related targets were collected. Overlapped targets were obtained after the predicted CV-3 and AF targets were uploaded to the SangerBox

(<http://sangerbox.com/>). Subsequently, potential mechanisms of CV-3 on AF were explored by constructing a protein-protein interaction (PPI) network diagram using STRING (<https://string-db.org/>). Cytoscape 3.6.1 was utilized to plot a CV-3 compound-target network. GO analysis and KEGG pathway enrichment were performed by import the 24 core targets using adjusted  $P$  values. And, enrichment analysis results were visualized ultimately.

**2.6. Molecular Docking.** The 3D structure of N-decanoic acid and spathulenol was initially obtained from the TCMSP website. Meanwhile, the 3D structure of the key target PTGS2 was collected from the Protein Data Bank (PDB, <http://www.rcsb.org/pdb>). The AutoDock 4.2.6 software was adopted to add hydrogen to the receptor protein and for charge treatment. Molecular docking was subsequently carried out between the receptor protein and the ligand small molecule by AutoDock Vina 1.1.2. Confirmation was obtained by docking, and binding energy was scored. The best binding energy was obtained and analyzed. The interrelationship of receptor protein and the ligand was ultimately visualized using PyMOL software.

**2.6.1. Preparation of Ligand.** The three-dimensional structures of ligands were obtained from TCMSP. The mol2 format of ligands were transformed by using OpenBabel 3.1.1 and imported in AutoDock Tools 1.5.7 to gain pdbqt format ligands.

**2.6.2. Preparation of Protein.** The 3D structure of the receptor PTGS2 was collected from PDB. PyMOL 2.5.2 was used to remove water molecules. The original ligand combined with the receptor was deleted and subsequently obtained docking box space coordinates by employing GetBox Plugin. Hydrogens were added, and charges were neutralized to the receptor and saved as pdbqt file.

**2.7. Statistical Analysis.** The described experiments were repeated three times independently, and all of the obtained measurement data were presented as mean  $\pm$  standard deviation. Statistical analysis was conducted using the GraphPad Prism 8.0.1 software. Multiple group comparison applied one-way analysis of variance (ANOVA) and Tukey's post hoc tests. The values of  $P$  less than 0.05 were considered. The difference was statistically significant.

### 3. Results

**3.1. CV-3 Inhibits Cardiomyocytes Apoptosis and Improves Cell Viability.** We firstly detected the apoptosis and cell viability of CV-3 in cardiomyocytes by flow cytometry and MTT assay. As illustrated in Figures 1(a) and 1(b), compared with control, cell apoptosis was perceivably elevated ( $P < 0.01$ ) in the model, while the cardiomyocytes apoptosis in the cardiomyocyte AF model group could be remarkably inhibited by incubating with CV-3 and verapamil ( $P < 0.01$ ). And, the comparable effect in inhibiting the cell apoptosis

was found in CV-3 and verapamil. Furthermore, we have detected the cell viability of cardiomyocytes in each group. The control group was set as one hundred percent, as analyzed, and cell viability was greatly decreased in the model group versus the control group ( $P < 0.01$ ). After CV-3 and verapamil treatment, cell viability was effectively recovered.

**3.2. Components and Potential Targets of CV-3.** Active components and targets of CV-3 were sorted out via BATMAN-TCM and TCMSP databases. There were 5 active components and 79 targets obtained. We subsequently sorted out 3 185 AF disease target genes via retrieval of the GeneCards database. The drug targets and disease genes presented 24 overlapped targets in the Venn diagram (Figure 2(a)). We then plotted a diagram of a PPI network by importing the obtained 24 overlapped targets into Cytoscape and STRING (Figures 2(b) and 2(c)). As the illustration of figures, PTGS2, ESR1, PGR, and PLG might act as key targets of CV-3 in AF treatment as they had more edge connections to nodes. We ultimately constructed a drug-compound-target-disease network using overlapped targets, active components and corresponding targets of CV-3 (Figure 2(d)). Among active compounds, N-decanoic acid and spathulenol ranked at the top of degree centrality (DC) values which were employed as potential key compounds of CV-3.

**3.3. GO Analysis and KEGG Pathway Enrichment.** To verify biological responses following AF treatment using CV-3, GO analysis of the 8 AF-related disease genes was conducted via processes of BP, CC, and MF. BP analysis revealed that related terms included oxidation-reduction process, positive regulation of transcription from RNA polymerase II promoter, and inflammatory response (Figure 3(a)). CC analysis indicated that extracellular exosome and extracellular region ranked at the top of gene ratio values (Figure 3(b)). MF analysis suggested that most related terms were positive regulation of steroid hormone receptor activity, enzyme binding, and sequence-specific DNA binding (Figure 3(c)). The top 3 entries analyzed using KEGG pathway enrichments are presented in Figure 3(d).

**3.4. Molecular Docking Analysis.** An AutoDock software was used to perform the docking studies of the potential two key components of CV-3 and PTGS2 protein. Through network pharmacology analysis and literature review [21], we select the top 2 chemical components of Chinese medicine reagents with the network topology attribute DC value of N-decanoic acid, spathulenol, and key target gene PTGS2 (PDB ID: 5F1A) for molecular docking. The results showed that the binding energy of PTGS2 and N-decanoic acid is  $-4.08$  kcal/mol, and the binding energy of PTGS2 and spathulenol is  $-7.09$  kcal/mol. The amino acid residues of PTGS2 formed three hydrogen bond interactions and one hydrogen bond interaction with N-decanoic acid and spathulenol, respectively. Molecular docking results showed that CV-3 might affect AF by regulating PTGS2 (Figures 4(a) and 4(b)).

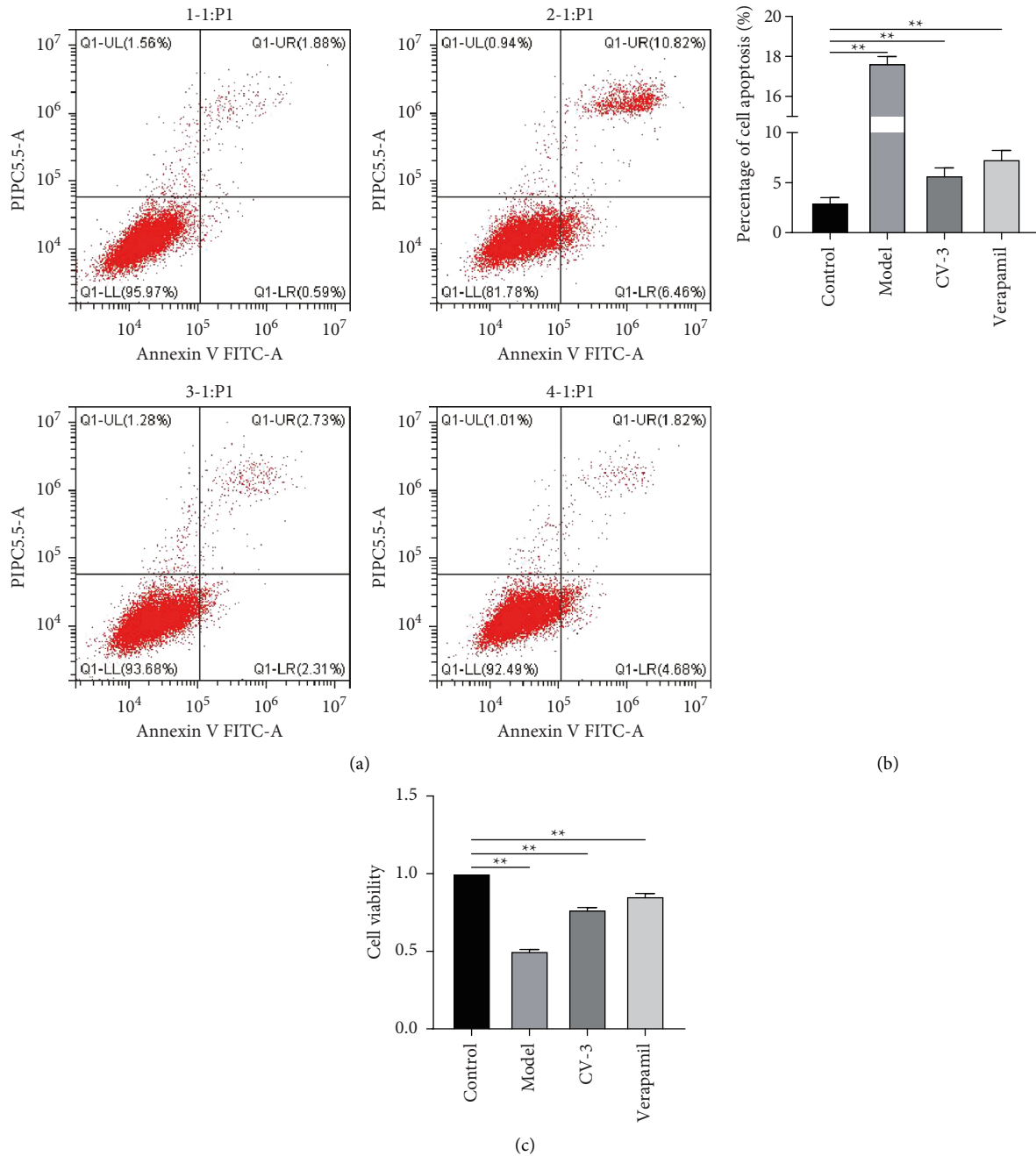


FIGURE 1: Effect of CV-3 on the apoptosis and cell viability in cardiomyocytes. (a) CV-3 reduced apoptosis of cardiomyocytes. (b) The cell apoptosis diagram with statistical analysis. (c) The cell viability diagram of cardiomyocytes. Multiple group comparison applied ANOVA and Tukey's post hoc tests.  $**P < 0.01$  compared to the control group.

#### 4. Discussion

Arrhythmia is an important type of cardiovascular disease, which can cause heart function damage and failure, increase the risk of stroke, lead to disorders of the physiological system, and even cause sudden cardiac death, which is a serious threat to human life and health. AF is recognized as a frequently encountered arrhythmia disease [22]. It has a high incidence and serious complications. Long-term illnesses are prone to complications such as heart failure and arterial embolism, which also endanger human health [23, 24]. At

present, the clinical treatment of AF is not ideal. Radio-frequency ablation is expensive, the recurrence rate is high, the effective rate of chemotherapy is low, and most drugs have obvious side effects. Therefore, research on the treatment of AF has been attracting attention. In recent years, TCM is considered to be a new way to treat AF, but there are still few studies on its mechanism of action [15, 25].

TCM has a remarkable curative effect in antiarrhythmia with few side effects. There are no reports of side effects, such as arrhythmia, caused by Chinese patent medicines commonly used in clinical practice. The severity of symptoms in

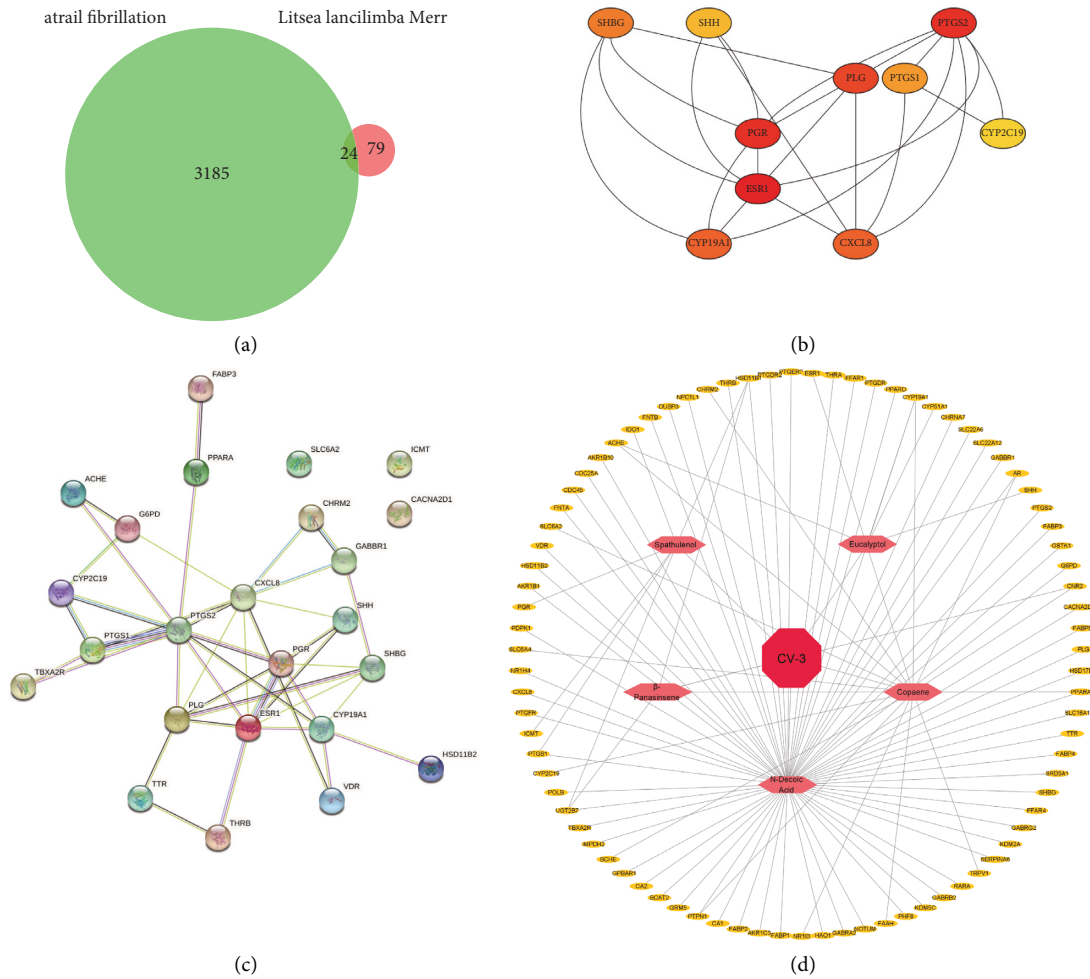


FIGURE 2: The active components and potential targets of CV-3 in AF treatment. (a) Overlapped targets of CV-3 and AF presented in the Venn diagram. (b, c) Analysis of the 24 overlapped targets in a protein-protein interaction (PPI) network using STRING and Cytoscape, respectively. (d) The drug-compound-target-disease network of CV-3 in treating AF. Pink nodes represent the 5 components of CV-3, yellow nodes represent key targets of AF, and red represents CV-3.

AF patients is often affected by the ventricular rate [26]. Controlling the ventricular rate can improve the hemodynamic status of heart failure. At the same time, it may also improve the long-term prognosis by preventing or reversing tachycardia cardiomyopathy. Studies have found that Chinese medicine can control the ventricular rate and improve symptoms [27]. In addition, studies have found that Chinese medicine can improve atrial remodeling, reverse atrial remodeling caused by AF, and improve prognosis [28, 29].

*Cinnamomum migao* H.W.Li mainly distributed in the southwest of China, whose dried and mature fruit is one of the top ten Miao medicines in Guizhou, is a plant fruit used in medicine and food. It is a traditional medicinal material of the Miao and Buyi nationalities and is often used to treat abdominal distension, abdominal pain, chest tightness, and vomiting [30]. CV-3 is the volatile oil extracted from it [18]. It has been used to treat arrhythmia in the folk. Modern medical research has confirmed that it can improve arrhythmia and slow heart rate. Studies have shown that the drug can improve the ultrastructure of left ventricular myocytes, inhibit cell apoptosis, inflammatory factors, and

slow down mitochondrial oxidative damage. However, in contrast to extensive research on the efficacy of the drug, the molecular mechanism of CV-3 is less studied, which may be related to the multipathway, multitarget, and synergistic characteristics of TCM. Though CV-3 has a lot of research on the clinical efficacy of TCM in AF treatment, its multitarget, and multichannel mode of action, the study of its pharmacological mechanism has always been a difficult problem. At present, studies have shown that oxidative stress response, regulation of ion channels in the body, regulation of calcium homeostasis, and other links are the main mechanisms of action of various AF drugs [31, 32]. TCM compounds are characterized by multicomponent and multi-target effects and can pass multiple simultaneous intervention of AF in each link and have a certain effect on stabilizing cell membrane potential, regulating intracellular calcium overload, anti-inflammatory response, and oxidative stress response [32, 33].

Therefore, this article conducts network pharmacology research on CV-3 in the treatment of AF and speculates the possible mechanism of therapeutic efficacy after Chinese

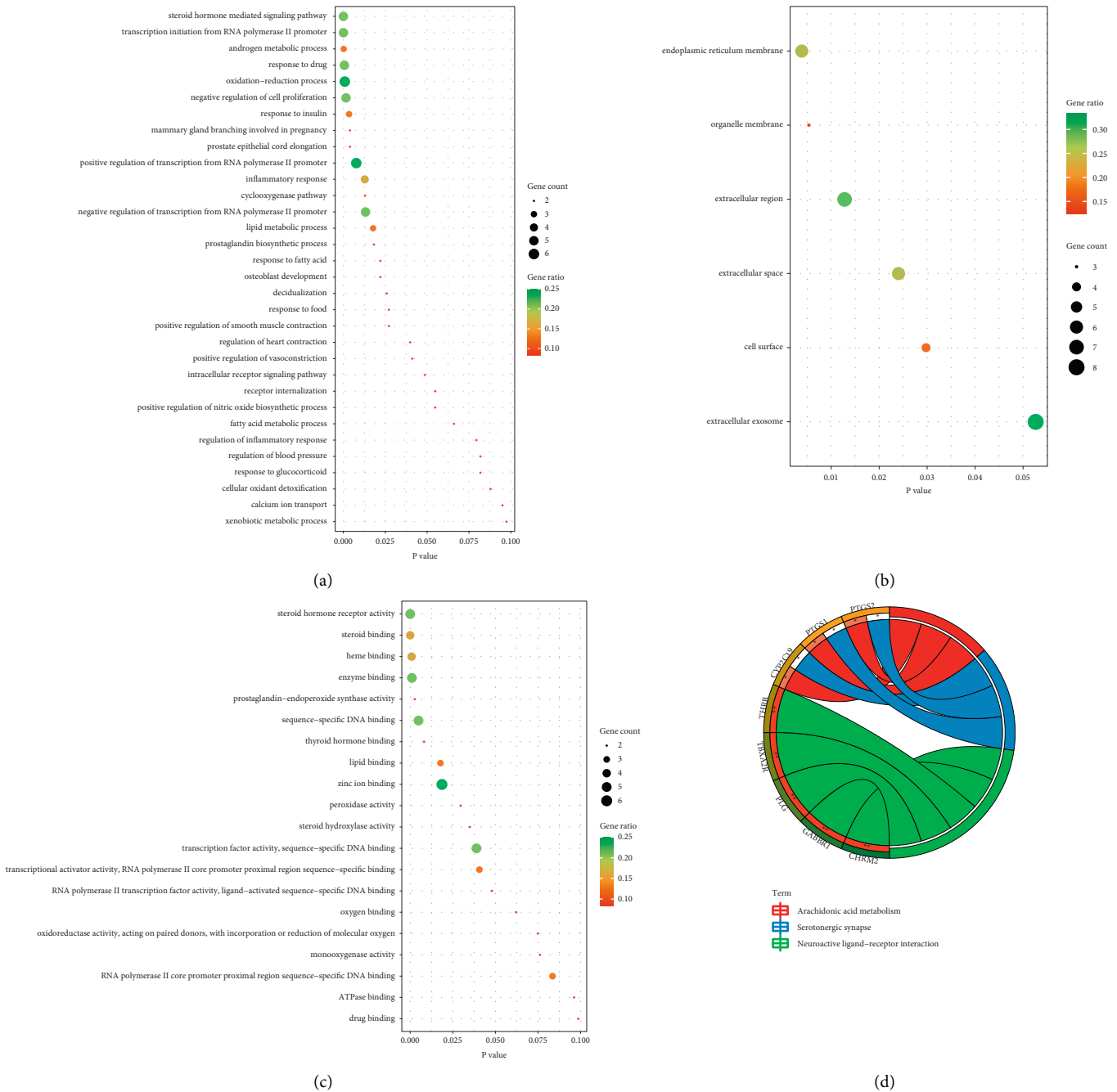


FIGURE 3: GO analysis and KEGG pathway enrichment of CV-3 candidate targets against AF. (a) Analysis of target GO terms in biological processes, (b) cellular components, and (c) molecular functions. (d) Circle of candidate targets by KEGG pathway enrichment. Percentage of gene count enriched in the GO term of the 8 key targets, gene ratio magnitude is represented in green and red. The gene count is indicated using the circle size meaning the number of genes enriched in the GO term. The outermost circle on the right represents names of signaling pathways, and genes are on the left. The left inner circle represents the significance of *p* values of genes corresponding to pathways.

medicine administration for AF treatment. This article first isolated and cultured cardiomyocytes from the heart of neonatal rats and constructed an AF model of cardiomyocytes by means to explore the effect of CV-3 on AF cardiomyocytes. The results indicated that the apoptosis of AF cardiomyocytes increased significantly. After adding CV-3, the apoptosis was significantly inhibited, and the ability to inhibit the apoptosis was equivalent to verapamil. In addition, we tested the cell

survival rate of the cell control group, the model group, and the drug group through the MTT experiment. Our experimental results showed that CV-3 can improve the survival rate of AF model cells, and its survival rate is comparable to verapamil, suggesting that CV-3 has a better effect on improving the survival rate of AF cells.

Subsequently, we use network pharmacology to query CV-3 and AF targets through the database, perform PPI



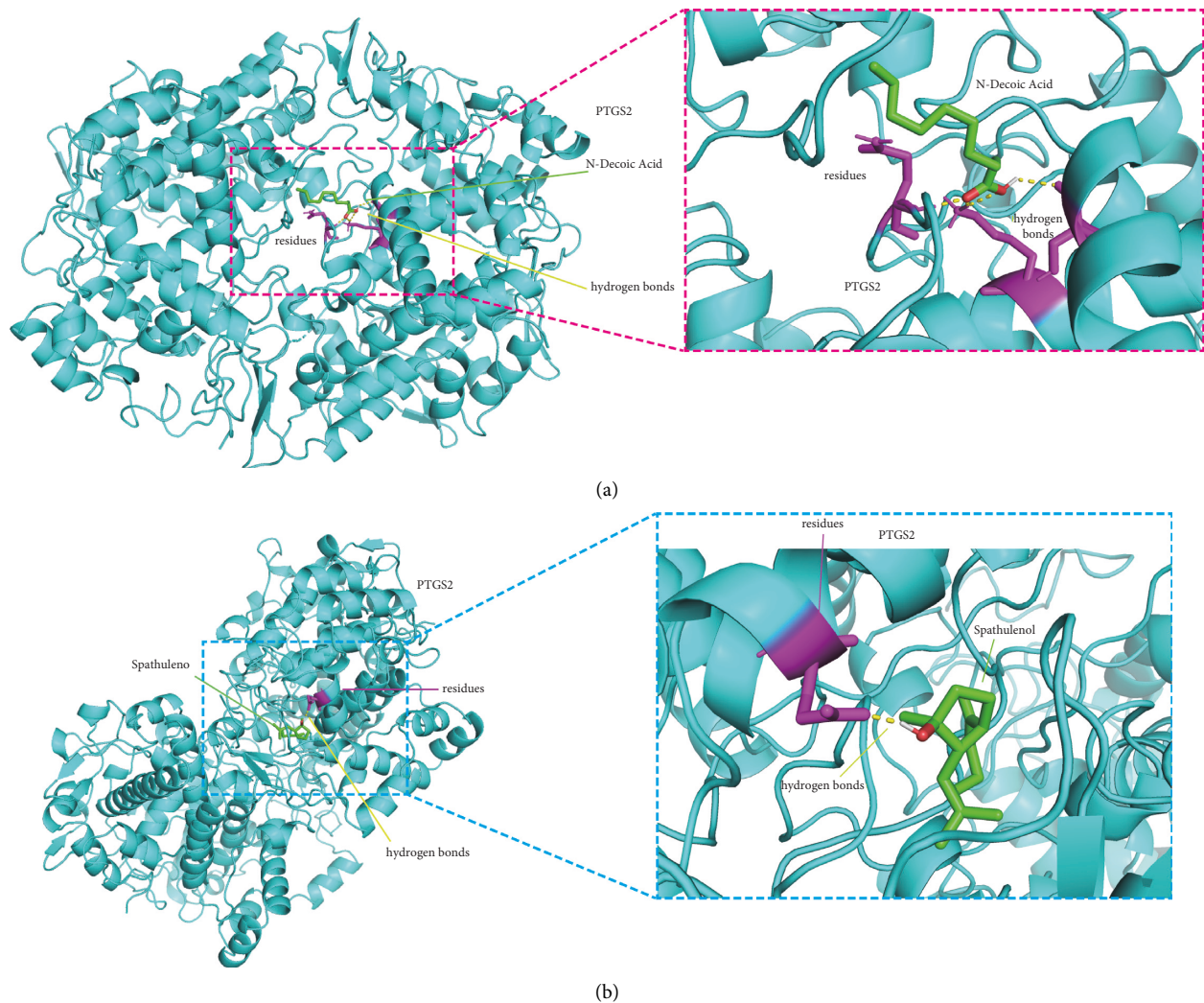


FIGURE 4: Molecular docking analysis between the two key components of CV-3 and PTGS2. (a) Docking studies of human PTGS2 with N-decanoic acid and (b) spathulenol. Protein structures are shown as cyan cartoon and molecules as green sticks. Residues involved in hydrogen bonding interaction (yellow dash lines) have been shown in stick (purple).

analysis on intersection genes, and find node genes that exert a pivotal role in the network through interaction relationships. The results showed that the possible core components of CV-3 are N-decanoic acid and spathulenol, and its potential disease targets may be PTGS2, ESR1, PGR, and PLG. PTGS2 can be induced to normally produce prostaglandins that regulate responses to physiological stress including infection and inflammation [34, 35]. ESR1 is found to be associated with lone AF [36]. Further analysis of GO and KEGG, the enrichment results show that the relevant pathways of CV-3 in the treatment of AF include the oxidation-reduction process and inflammatory response, which contribute to further elucidation of the mechanism of action of CV-3. Growing evidence have suggested that inflammatory and oxidative mechanisms involve the promotion of AF and that some inflammatory pathways may contribute to AF [33–37]. The core components, N-decanoic acid, spathulenol, and PTGS2 with the largest number of nodes, were selected for molecular docking analysis. Molecular docking results revealed that binding energy between both molecules and

protein was  $-4.08$  and  $-7.09$  kcal/mol, respectively, forming three hydrogen bonds and one hydrogen bond with the protein residues. These results indicate that N-decanoic acid and spathulenol may be the active components of CV-3. The oxidation-reduction and inflammatory response may be essential in treating AF by CV-3 and are related to the protein function of PTGS2.

## 5. Conclusion

The present work explored the efficacy of CV-3 against AF using a cardiomyocyte AF model on a network pharmacology approach. Taken together, the findings in present research revealed that CV-3 might act as a role in regulating the oxidation-reduction process, inflammatory response and cell apoptosis, and arachidonic acid metabolism has the likelihood of contributing to treating AF. PTGS2, ESR1, PGR, and PLG may be the key target gene of CV-3 in the treatment of AF. N-decanoic acid and spathulenol as active ingredients of CV-3 were of great significance in AF

treatment by targeting PTGS2. Taken together, CV-3 could be introduced as a multicomponent, multitarget, and multipathway therapy for AF, which provided a potential drug and effective targets against AF.

## Data Availability

The data provided in this study are available upon request.

## Disclosure

Zundong Wang and Zhen Zeng are co-first authors.

## Conflicts of Interest

The authors declare that they have no conflicts of interest.

## Acknowledgments

This work was supported by the National Natural Science Foundation of China (81760910), the Guizhou Provincial Science and Technology Plan Project ([2018] 2770), and Guizhou University of Traditional Chinese Medicine Intramural Project (no. [2019] 55).

## References

- [1] Z. Wang, Z. Chen, X. Wang et al., "The disease burden of atrial fibrillation in China from a national cross-sectional survey," *The American Journal of Cardiology*, vol. 122, no. 5, pp. 793–798, 2018.
- [2] I. AlAwwa, R. Al-Hindi, N. Alfraihat et al., "Prevalence and associated factors of undiagnosed atrial fibrillation among end-stage renal disease patients on maintenance haemodialysis: a cross-sectional study," *BMC Cardiovascular Disorders*, vol. 20, no. 1, Article ID 186, 2020.
- [3] I. Hwang, J. W. Park, O. S. Kwon et al., "Spatial changes in the atrial fibrillation wave-dynamics after using antiarrhythmic drugs: a computational modeling study," *Frontiers in Physiology*, vol. 12, Article ID 733543, 2021.
- [4] L.-H. Li, C.-S. Sheng, B.-C. Hu et al., "The prevalence, incidence, management and risks of atrial fibrillation in an elderly Chinese population: a prospective study," *BMC Cardiovascular Disorders*, vol. 15, no. 1, p. 31, 2015.
- [5] G. Y. H. Lip, L. Fauchier, S. B. Freedman et al., "Atrial fibrillation," *Nature Reviews Disease Primers*, vol. 2, no. 1, Article ID 16016, 2016.
- [6] F. Witassek, A. Springer, L. Adam et al., "Health-related quality of life in patients with atrial fibrillation: the role of symptoms, comorbidities, and the type of atrial fibrillation," *PLoS One*, vol. 14, no. 12, Article ID e0226730, 2019.
- [7] K. T. Gleason, S. Nazarian, and C. R. Dennison Himmelfarb, "Atrial fibrillation symptoms and sex, race, and psychological distress," *Journal of Cardiovascular Nursing*, vol. 33, no. 2, pp. 137–143, 2018.
- [8] Y. Xiao, X. Wang, J. Yang et al., "Huatian Dingji Decoction intervening in atrial fibrillation: protocol for a randomized double-blind single-simulated placebo-controlled clinical trial," *Trials*, vol. 22, no. 1, Article ID 693, 2021.
- [9] A. Amin, A. Houmsse, A. Ishola, J. Tyler, and M. Houmsse, "The current approach of atrial fibrillation management," *Avicenna Journal of Medicine*, vol. 6, no. 1, pp. 8–16, 2016.
- [10] National Institute for Health and Care Excellence, *Clinical Guidelines, in Atrial Fibrillation: Diagnosis and Management*, National Institute for Health and Care Excellence (NICE), London, England, Copyright © NICE 2021, 2021.
- [11] G. A. Dan and D. Dobrev, "Antiarrhythmic drugs for atrial fibrillation: imminent impulses are emerging," *IJC Heart & Vasculature*, vol. 21, pp. 11–15, 2018.
- [12] S. Suzuki, T. Yamashita, T. Otsuka et al., "Identifying risk patterns in older adults with atrial fibrillation by hierarchical cluster analysis: a retrospective approach based on the risk probability for clinical events," *IJC Heart & Vasculature*, vol. 37, Article ID 100883, 2021.
- [13] R. Nagarakanti, A. Slee, and S. Saksena, "Left atrial reverse remodeling and prevention of progression of atrial fibrillation with atrial resynchronization device therapy utilizing dual-site right atrial pacing in patients with atrial fibrillation refractory to antiarrhythmic drugs or catheter ablation," *Journal of Interventional Cardiac Electrophysiology*, vol. 40, no. 3, pp. 245–254, 2014.
- [14] J. Camm, "Antiarrhythmic drugs for the maintenance of sinus rhythm: risks and benefits," *International Journal of Cardiology*, vol. 155, no. 3, pp. 362–371, 2012.
- [15] Y. Dong, J. Liao, K. Yao, W. Jiang, and J. Wang, "Application of traditional Chinese medicine in treatment of atrial fibrillation," *Evidence-based Complementary and Alternative Medicine*, vol. 2017, Article ID 1381732, 2017.
- [16] X. Cai, Y. Wang, Z. Li, Y. Zhang, D. Wang, and X. Yan, "Chinese herbal medicine for patients with atrial fibrillation," *Medicine*, vol. 96, no. 50, Article ID e9228, 2017.
- [17] Z. Wang, Z. Tang, W. Zhu, L. Ge, and J. Ge, "Efficacy and safety of traditional Chinese medicine on thromboembolic events in patients with atrial fibrillation: a systematic review and meta-analysis," *Complementary Therapies in Medicine*, vol. 32, pp. 1–10, 2017.
- [18] Y. Li, X. Liu, X. Lin et al., "Chemical compound cinobufotalin potently induces FOXO1-stimulated cisplatin sensitivity by antagonizing its binding partner MYH9," *Signal Transduction and Targeted Therapy*, vol. 4, no. 12, pp. 48–50, 2019.
- [19] J. Wang, J. Liu, and A. Wen, "Research progress on the seedling medicine plant in *Cinnamomum migao* Guizhou Province," *Heilongjiang Agricultural Sciences*, no. 5, pp. 157–160, 2015.
- [20] B. Wu, F. Wang, and Y. Tang, "Therapeutic effect of cinnamomum migao oil on atrial fibrillation in rats," *Lishizhen Medicine and Materia Medica Research*, vol. 30, no. 9, pp. 2128–2130, 2019.
- [21] X. Xie, Y. T. Ma, Z. Y. Fu et al., "Association of polymorphisms of PTGS2 and CYP8A1 with myocardial infarction," *Clinical Chemistry and Laboratory Medicine*, vol. 47, no. 3, pp. 347–352, 2009.
- [22] C. R. Wyndham, "Atrial fibrillation: the most common arrhythmia," *Texas Heart Institute Journal*, vol. 27, no. 3, pp. 257–267, 2000.
- [23] N. A. Bosch, J. Cimini, and A. J. Walkey, "Atrial fibrillation in the ICU," *Chest*, vol. 154, no. 6, pp. 1424–1434, 2018.
- [24] S. Andole and P. Harbinson, "Arterial embolism of axillary artery secondary to atrial fibrillation," *BMJ Case Reports*, vol. 2011, Article ID bcr1020103449, 2011.
- [25] Y. Zhang, X. Zhang, X. Zhang et al., "Molecular targets and pathways contributing to the effects of wexin keli on atrial fibrillation based on a network pharmacology approach," *Evidence-based Complementary and Alternative Medicine*, vol. 2020, Article ID 8396484, 2020.
- [26] M. Kranert, T. Shchetynska-Marinova, T. Berghoff et al., "Arterial stiffness is associated with increased symptom

- burden in patients with atrial fibrillation,” *Canadian Journal of Cardiology*, vol. 36, no. 12, pp. 1949–1955, 2020.
- [27] S. Fu, J. Zhang, X. Gao et al., “Clinical practice of traditional Chinese medicines for chronic heart failure,” *Heart Asia*, vol. 2, no. 1, pp. 24–27, 2010.
- [28] M. Gong, M. Yuan, L. Meng et al., “Wenxin keli regulates mitochondrial oxidative stress and homeostasis and improves atrial remodeling in diabetic rats,” *Oxidative Medicine and Cellular Longevity*, vol. 2020, pp. 1–17, Article ID 2468031, 2020.
- [29] T. Mao, J. Zhang, Y. Qiao, B. Liu, and S. Zhang, “Uncovering synergistic mechanism of Chinese herbal medicine in the treatment of atrial fibrillation with obstructive sleep apnea hypopnea syndrome by network pharmacology,” *Evidence-based Complementary and Alternative Medicine*, vol. 2019, Article ID 8691608, 2019.
- [30] D. Qiu, H. Li, and S. Zhao, “Materia medica research on mi gao,” *China Journal of Traditional Chinese Medicine and Pharmacy*, vol. 8, no. 02, pp. 19-20+26-64, 1993.
- [31] M. Gao, J. Wang, Z. Wang et al., “An altered expression of genes involved in the regulation of ion channels in atrial myocytes is correlated with the risk of atrial fibrillation in patients with heart failure,” *Experimental and Therapeutic Medicine*, vol. 5, no. 4, pp. 1239–1243, 2013.
- [32] P. Korantzopoulos, K. Letsas, N. Fragakis, G. Tse, and T. Liu, “Oxidative stress and atrial fibrillation: an update,” *Free Radical Research*, vol. 52, no. 11-12, pp. 1199–1209, 2018.
- [33] P. Korantzopoulos, K. P. Letsas, G. Tse, N. Fragakis, C. A. Goudis, and T. Liu, “Inflammation and atrial fibrillation: a comprehensive review,” *Journal of Arrhythmia*, vol. 34, no. 4, pp. 394–401, 2018.
- [34] M. J. Lucido, B. J. Orlando, A. J. Vecchio, and M. G. Malkowski, “Crystal structure of aspirin-acetylated human cyclooxygenase-2: insight into the formation of products with reversed stereochemistry,” *Biochemistry*, vol. 55, no. 8, pp. 1226–1238, 2016.
- [35] B. J. Orlando and M. G. Malkowski, “Crystal structure of rofecoxib bound to human cyclooxygenase-2,” *Acta Crystallographica F structural biology communications*, vol. 72, no. 10, pp. 772–776, 2016.
- [36] K. Golubić, A. Šmalcelj, J. Sertić, and L. Juricic, “Estrogen receptor 1 gene (TA)<sub>n</sub> polymorphism is associated with lone atrial fibrillation in men,” *Croatian Medical Journal*, vol. 55, no. 1, pp. 38–44, 2014.
- [37] W. Xie, G. Santulli, S. R. Reiken et al., “Mitochondrial oxidative stress promotes atrial fibrillation,” *Scientific Reports*, vol. 5, no. 1, Article ID 11427, 2015.

## Research Article

# Phillyrin Prevents Ovariectomy-Induced Osteolysis by Inhibiting Osteoclast Differentiation

Geng Zhang,<sup>1</sup> Ying Zhang,<sup>2</sup> Cong Wang,<sup>1</sup> Chenhe Zhou,<sup>1</sup> and Shigui Yan <sup>1</sup>

<sup>1</sup>Department of Orthopedic Surgery, Second Affiliated Hospital, School of Medicine, Zhejiang University, Hangzhou, China

<sup>2</sup>Department of Orthopedic Surgery, Taizhou Hospital of Traditional Chinese Medicine, Taizhou, China

Correspondence should be addressed to Shigui Yan; [y214180268@zju.edu.cn](mailto:y214180268@zju.edu.cn)

Received 28 February 2022; Revised 23 April 2022; Accepted 25 April 2022; Published 10 June 2022

Academic Editor: Ruchika Garg

Copyright © 2022 Geng Zhang et al. This is an open access article distributed under the Creative Commons Attribution License, which permits unrestricted use, distribution, and reproduction in any medium, provided the original work is properly cited.

Postmenopausal osteoporosis is a metabolic disease caused by an imbalance between osteoclasts and osteoblasts. At present, the drug strategy for treating postmenopausal osteoporosis has some limitations and is unable to satisfy the demands of patients. *Phillyrin* (*Phil*) is an herbal extract from *Forsythiae Fructus*, with an inhibitory effect on osteolysis. In this study, we described the role of *Phil* in ovariectomy-induced osteoporosis and its effect on osteoclast differentiation *in vitro*. Eighteen female C57BL/6 mice were randomly divided into three groups: sham group (sham surgery and injection with 0.9% normal saline), ovariectomized group (ovariectomy and injection with 0.9% normal saline), and *Phil* group (ovariectomy and injecting *Phil* with 100 mg/kg for 2 days). Mice were sacrificed after 6-week *Phil* administration and femurs were harvested for microcomputed tomography (micro-CT) and histomorphology analyses. *In vitro*, we used different concentrations of *Phil* to study its effect on osteoclastogenesis. The results showed that the BV/TV, Tb.Th, and Tb.N in trabecular bone were increased in the *Phil* group compared with the OVX group, and the trabecular bone mass was remarkably decreased in the OVX group compared with the sham group. The number of osteoclasts was increased in the OVX group compared to the sham group, and the number and area of osteoclasts were decreased in the *Phil* group compared to the control group. Compared with the OVX group, the number and area of osteoclasts were reduced in the *Phil* group. In conclusion, *Phil* could inhibit the formation of osteoclasts, promote the growth of bone trabecular, and relieve osteoporosis caused by ovariectomy, with a certain clinical adoption value.

## 1. Introduction

Osteoporosis is a metabolic bone disease by the increased risk of fragility fractures [1], which is a major health problem worldwide. Presently, there are 10 million patients with osteoporosis in the United States and 27.6 million in Europe. In China, 11.7% of patients suffer from osteoporosis, most of whom are postmenopausal women and the elderly [2]. Osteoporosis can cause pain in the waist and lower back, which results in shortened body length and hunchback. It can even cause fractures, limb dysfunction, and death [3]. Osteoporosis not only leads to low quality of life [4] but also brings a heavy financial burden to patients and their families [5]. It is estimated that the annual expenditure of treating fragile osteoporotic fractures in the US by 2025 will increase by \$25 billion [6] and that in China will be as high as 132

billion Yuan by 2035. Therefore, the prevention and treatment of osteoporosis are of great significance [7].

Currently, drugs used for the treatment of osteoporosis have their disadvantages and side effects to varying degrees. For example, the long-term application of menopausal hormone therapy drugs may cause cardiocerebral vascular events, thrombosis, endometrial cancer, and breast cancer [8]. The long-term use of bisphosphonates may lead to complications, such as mandibular necrosis [9]. Salmon calcitonin can increase the risk of tumors; however, its continuous use generally does not exceed 3 months [10, 11]. Selective estrogen receptor modulators, such as raloxifene, may also cause cardiovascular and cerebrovascular accidents as well as venous thrombosis [12]. Teriparatide has limitations of high cost, long duration of treatment, and late drug requirement [13]. Strontium ranelate may cause serious



adverse cardiovascular and cerebrovascular reactions, including drug eruptions with eosinophilia and systemic symptoms [14, 15]. Therefore, a drug with fewer side effects is expected to inhibit osteoclast differentiation and improve osteogenesis. *Forsythiae Fructus*, a Chinese herbal medicine, was proposed.

*Forsythiae Fructus* is a commonly used herb in traditional Chinese medicine. It has a substantial curative effect on the treatment of fever, carbuncle, gonorrhoea, inflammation, and erysipelas [16]. *Phillyrin (Phil)* is a lignan extracted from the dried fruit of *Forsythiae Fructus*, which has several pharmacological effects. It includes anti-oxidation, antiobesity, antiviral, anti-inflammation, and antipyretic effects. Besides, *Phil*'s melting point is between 184°C and 185°C, and it is the crystalline powder [17, 18]. According to the clinical study, *Phil* has an inhibitory effect on osteolysis of lipopolysaccharide (LPS) rat skulls [19]. However, there are few clinically relevant studies.

To further explore whether *Phil* could affect osteolysis and alleviate or treat osteoporosis, *Phil* was adopted on the ovariectomized (OVX) mice to evaluate the changes of bone mineral density in the mice, thus exploring the role of *Phil* in OVX-induced osteoporosis. It was hoped to provide effective treatment methods for patients with osteoporosis clinically.

## 2. Materials and Methods

**2.1. Animal and Grouping.** Eighteen healthy female C57BL/6 mice (10 weeks old and weighing approximately 20 g) were obtained from Slac Laboratory Animal (Shanghai, China). Mice were raised under specific pathogen-free conditions (20–25°C, 60% humidity, 12/12 h light/dark) and given free access to water and food. The animal experiments were approved by the Animal Care and Use Committee of Zhejiang University following the Guide for the Care and Use of Laboratory Animals published by the United States National Institutes of Health (NIH).

Mice were randomly divided into three groups: sham group ( $n = 6$ ; sham operation with 0.9% normal saline (NS)), OVX group ( $n = 6$ ; OVX mice administered with 0.9% NS), and *Phil* group ( $n = 6$ ; OVX mice administered with *Phil* (Changsha Heking Biotechnology Co., Ltd., China) at a dose of 100 mg/kg every other day).

**2.2. Surgical Procedure.** Animals were anesthetized with an intraperitoneal injection of 5 mg/kg pentobarbital sodium (Sigma-Aldrich, Saint Louis, MO, USA) and fixed on the operating table in a prone position. An incision was made over the bilateral scapular line of the spine near the lower edge of the ribs under aseptic conditions to expose the retroperitoneal tissue. Then, the deep pink granular ovarian tissue was detected on both sides, the fallopian tubes and distal ovarian vessels were ligated, and the ovaries were removed. After cleaning the wound, the muscle, fascial layers, and skin were closed. Finally, buprenorphine was injected to reduce pain, and the mice were placed in the prone or lateral position in a breeding box to allow for recovery. For the sham controls, the incision was closed after

the aforementioned procedures without any further intervention. Simultaneously, the experimental groups received intraperitoneal *Phil* (Aladdin, Los Angeles, CA, USA) every other day from day 3 after the operation. Mice were sacrificed after 6 weeks, and femurs were fixed with 4% paraformaldehyde (BOSTER, Wuhan, China) and then stored at 4°C with 70% ethanol until use.

**2.3. Microcomputed Tomography (Micro-CT) Scanning.** The femurs of mice in the three groups were scanned by using the Scanco $\mu$ CT100 scanner (Scanco Medical AG, Bassersdorf, Switzerland). The scan parameters were as follows. The X-ray energy was set to –70 kV and 200 mA, the exposure time was –300 ms, and the region of interest was set to 10  $\mu$ m around the metaphysis of the talus. According to the two-dimension data, the cone-beam reconstruction software (SkyScan) was adopted to reconstruct CT images into three-dimensional images. From the three-dimensional images, the ratio of bone volume to tissue volume (BV/TV), the structural model index, trabecular number (Tb.N), trabecular thickness (Tb.Th), and trabecular separation (Tb.Sp) were measured and analyzed.

**2.4. Histological Analysis.** For histological processing, right femurs ( $n = 6$ /group) were subjected to decalcification in 10% ethylenediaminetetraacetic acid (EDTA) for 21 days and then embedded in paraffin. The samples were sectioned, mounted on glass slides, deparaffinized in dimethyl benzene, dealkylated in xylene, soaked in alcohol with a reduced concentration gradient, and finally immersed in distilled water for staining experiment. Sections were subjected to tartrate-resistant acid phosphatase (TRAP) (Sigma-Aldrich, Saint Louis, MO, USA) and hematoxylin and eosin (H&E) (Sigma-Aldrich, Saint Louis, MO, USA) staining following the manufacturer's protocol and then imaged under a light microscope (Olympus BX51, Tokyo, Japan). The histomorphometric parameters, including trabecular BV/TV, the number of TRAP + osteoclasts normalized to the bone area, the percentage of osteoclast surface per bone surface (Oc/BS, %), and the number of osteoclasts per unit bone perimeter (N.Oc/BS, mm), were calculated using the ImageJ software (NIH, Bethesda, MD, USA).

**2.5. In Vitro Osteoclast Differentiation.** Primary bone marrow monocytes were isolated and cultured in a complete medium (alpha-modification of Eagle's medium supplemented with 10% fetal bovine serum (Gibco-BRL, Sydney, Australia), 1% Penicillin-Streptomycin Liquid (KeyGEN, Nanjing, China)) with 25 ng/mL macrophage colony-stimulating factor (M-CSF) (R&D systems, Minneapolis, MN, USA) at 5% CO<sub>2</sub> and 37°C until macrophages formed. Macrophages were inoculated into the osteoclastogenic medium at a density of  $8 \times 10^3$  cells/well in 96-well plates to induce osteoclast differentiation (complete medium supplemented with 25 ng/mL M-CSF and 25 ng/mL receptor activator for nuclear factor- $\kappa$  B ligand (RANKL)) (R&D systems, Minneapolis, MN, USA) and were treated with

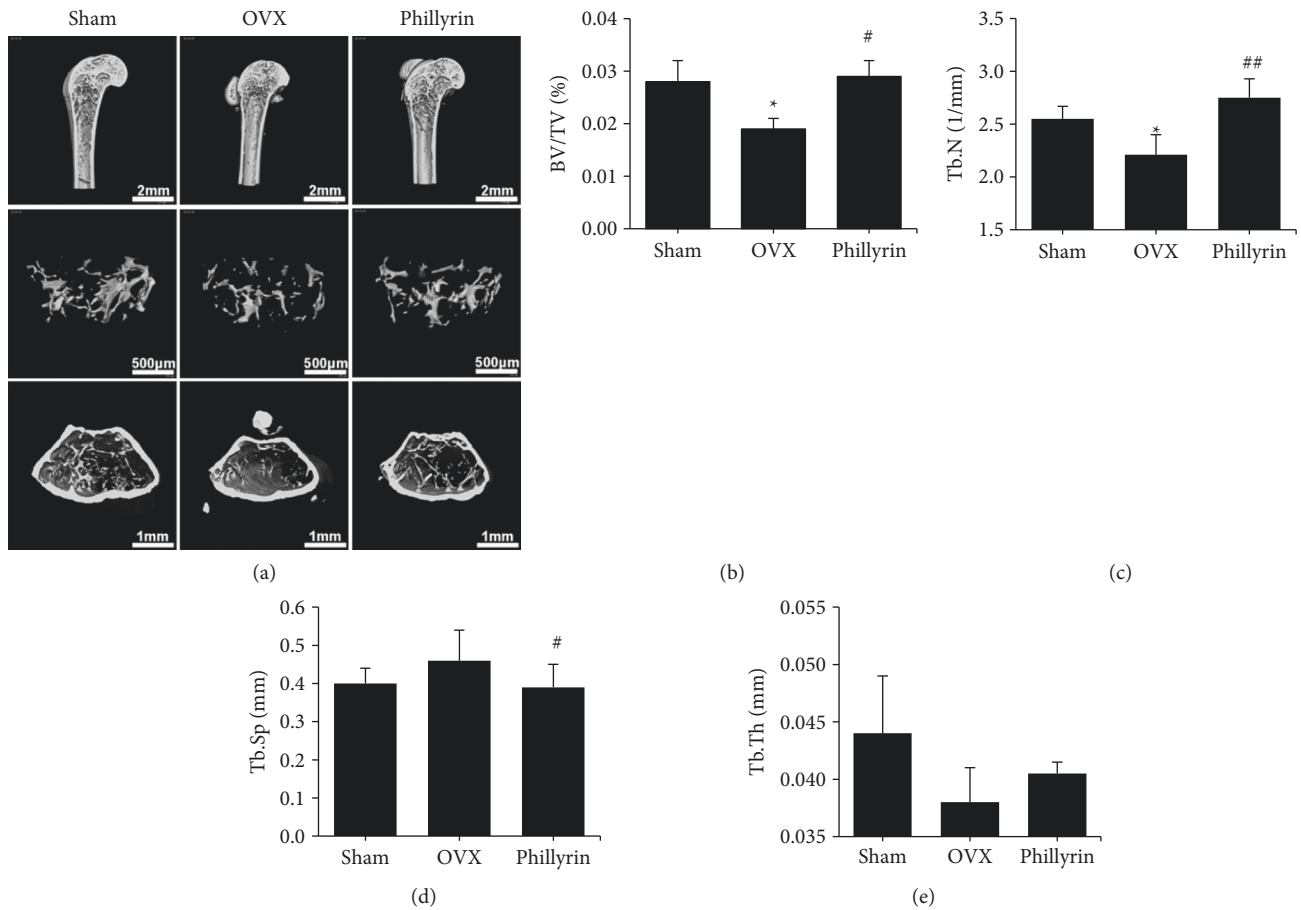


FIGURE 1: *Phillyrin* (*Phil*) prevented ovariectomized (OVX)-induced bone loss in trabecular bone. (a) Reconstruction of representative 3D microcomputed tomography (micro-CT) images of proximal femurs trabecular bone in each group. Scale bar = 2 mm, 500  $\mu$ m, and 1 mm. (b-e) The BV/TV, Tb.N, Tb.Sp, and Tb.Th values of the micro-CT data were analyzed from each sample. All values represent the mean  $\pm$  SD ( $n=6$ ). \* $P < 0.05$  and \*\* $P < 0.01$  vs. the Sham group. # $P < 0.05$  and ## $P < 0.01$  vs. the OVX group. BV/TV, bone volume to tissue volume ratio; Tb.N, number of trabeculae; Tb.Th, trabecular thickness; Tb.Sp, trabecular separation.

different doses of *Phil* (5 and 10  $\mu$ M). Media were replaced every other day. After 4 days, the cells were fixed in 2.5% glutaraldehyde for 30 min and stained with a TRAP Staining Kit following the manufacturer's guidelines. The number of TRAP-stained cells having no less than five nuclei was counted using a light microscope, and the area of the cells was measured.

**2.6. Statistical Analysis.** All the data are presented as the mean  $\pm$  SD of at least three independent tests. Statistical analysis was performed using one-way analysis of variance and followed by Tukey's post hoc analysis. Statistical significance was established at  $P < 0.05$ .

### 3. Results

**3.1. *Phil* Prevented OVX-Induced Bone Loss in Trabecular Bone.** To study the role of *Phil* in preventing bone loss, a murine model of OVX-induced osteoporosis was established and treated with *Phil*. After a 6-week treatment, the proximal femurs were scanned using micro-CT. The results are shown in Figure 1. Compared with that of the sham group, the

trabecular bone mass decreased in OVX groups. Moreover, this change was reversed in the drug-administered group. We observed an increase in the BV/TV, Tb.Th, and Tb.N in the trabecular bone of the *Phil*-treated group, compared with that of the OVX group.

To further verify the protective functions of *Phil* against trabecular bone loss, the right femurs were decalcified and assessed by histomorphology. H&E staining (Figure 2) showed that the femoral trabecular mass in the OVX group was observably reduced, compared with that in the sham operation group; whereas, the mitigative effect could be observed in the *Phil*-treated groups, which was consistent with the micro-CT scan.

**3.2. *Phil* Inhibited Osteoclastogenesis In Vivo.** Considering the important role that osteoclasts play in osteolysis, we evaluated whether *Phil* exerted an inhibitory effect on osteoclastogenesis *in vivo*. Figure 3 illustrates that compared with that in the sham group, an increased number of osteoclasts was found in the OVX group. *Phil* injection significantly reduced the OVX-induced increase in the number and size of osteoclasts.

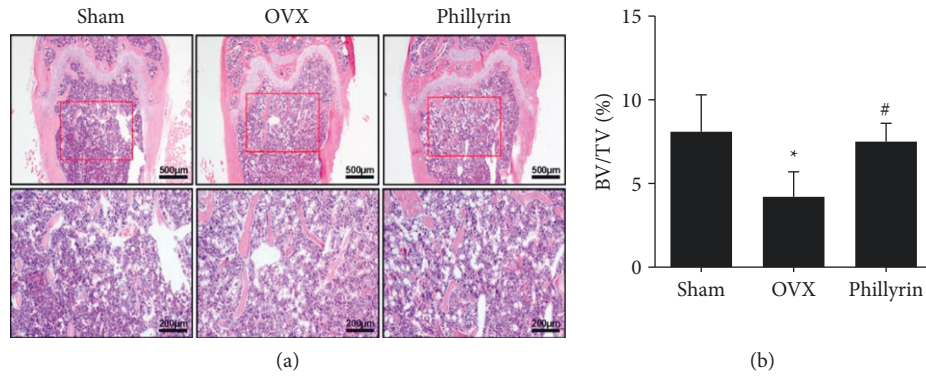


FIGURE 2: *Phillyrin* (*Phil*) prevented ovariectomized OVX-induced bone loss *in vivo*. (a) Histomorphological analysis was performed by hematoxylin and eosin (H&E) staining. Scale bar = 500 and 200 μm. (b) The bone volume to tissue volume ratio (BV/TV) of histomorphological sections was measured and quantified. All values represent the mean ± SD ( $n = 6$ ). \* $P < 0.05$  and \*\* $P < 0.01$  vs. the Sham group. # $P < 0.05$  and ## $P < 0.01$  vs. the OVX group.

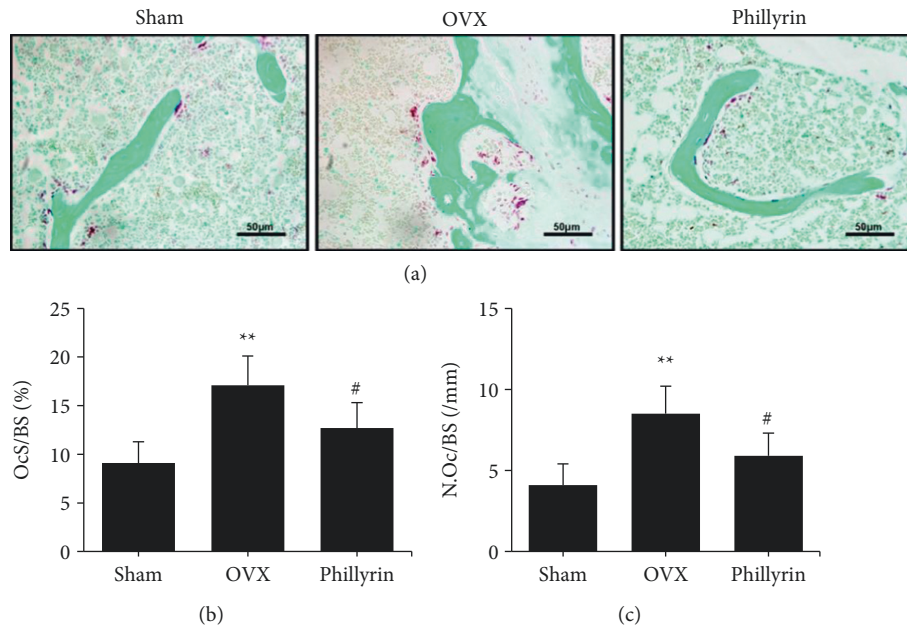


FIGURE 3: *Phillyrin* (*Phil*) inhibited osteoclastogenesis *in vivo*. (a) Tartrate-resistant acid phosphatase (TRAP) staining was performed on decalcified parts of distal femurs. Scale bar = 50 μm. (b, c) The OcS/BS and N.Oc/BS values were measured with TRAP-stained sections. All values represent the mean ± SD ( $n = 6$ ). \* $P < 0.05$  and \*\* $P < 0.01$  vs. the Sham group. # $P < 0.05$  and ## $P < 0.01$  vs. the OVX group.

OcS/BS, percentage of osteoclast surface per bone surface; N.Oc/BS, number of osteoclasts per unit bone circumference.

**3.3. *Phil* Attenuated Osteoclast Differentiation *In Vitro*.** To examine whether *Phil* has an attenuation effect on osteoclast differentiation, primary bone marrow monocytes were isolated and investigated *in vitro*. In Figure 4, the number and area of osteoclasts were reduced in the *Phil* group compared with the OVX group. Moreover, at higher doses of *Phil*, less number of osteoclasts was observed. These results demonstrated that *Phil* attenuated osteoclast differentiation in a dose-dependent manner *in vitro*.

## 4. Discussion

Osteoporosis, which affects millions of people worldwide, is an enormous and growing public health challenge. Currently, many drugs and methods for the clinical treatment of osteoporosis are available, such as estrogen replacement therapy and bisphosphonates. However, the lack of clinical evidence supporting their long-term therapeutic effect and the possibility of adverse reactions keep many patients, who may profit from these drug therapies, from taking the drugs [20]. In this study, we proved that *Phil* protects against bone loss caused by estrogen deficiency by inhibiting the differentiation of osteoclasts. Therefore, we believe that *Phil* might be a potential drug for the treatment of osteoporosis.



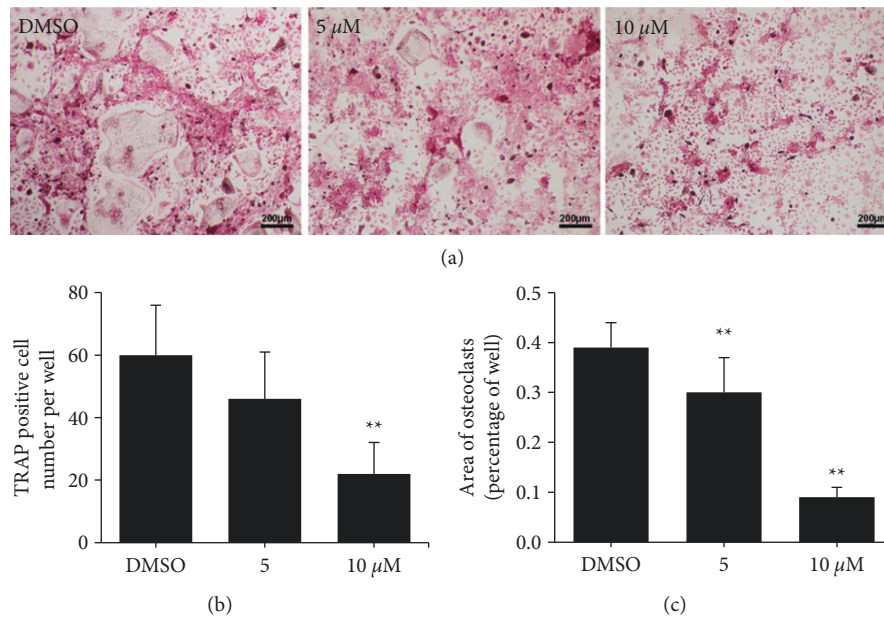


FIGURE 4: *Phillyrin* (*Phil*) attenuated osteoclast differentiation *in vitro*. (a) Representative tartrate-resistant acid phosphatase (TRAP) staining images from bone marrow macrophages (BMMs) treated with dimethyl sulfoxide (DMSO) or different doses of *Phil* in the presence of receptor activator for nuclear factor- $\kappa$  B ligand (RANKL) and macrophage colony-stimulating factor (M-CSF) for 4 days. Scale bar = 200  $\mu$ m. (b, c) The area of TRAP-positive multinuclear osteoclasts were measured and the number was quantified ( $\geq 3$  nuclei) in each well of the 96-well plate. All values represent the mean  $\pm$  SD. \* $P < 0.05$  and \*\* $P < 0.01$ .

Animal models for osteoporosis include disuse osteoporosis, glucocorticoid-induced osteoporosis, and postmenopausal osteoporosis [21]. An OVX animal is a typical experimental model of postmenopausal osteoporosis caused by estrogen deficiency in which the mice model mimics humans in terms of estrogen deficiency-induced postmenopausal osteoporosis. Therefore, the model is widely used to evaluate and develop new drugs for postmenopausal osteoporosis [22]. Previous studies have shown that osteoporosis in mice due to estrogen deficiency is always accompanied by weight gain and uterine weight loss [23]. This phenomenon was also observed in our experiment, which indicates that the OVX surgery was effective and that the model was successfully established.

*F. suspensa* (Thunb.) Vahl (Oleaceae) is a traditional herbal medicine that has been widely employed for the clinical treatment of several infectious diseases [24]. Furthermore, it is widely applied in the food and cosmetic industries as a component of our daily lives [25, 26]. Moreover, previous experimental studies have reported the therapeutic effect of *Phil* in certain diseases. For example, *Phil* can be developed as a therapeutic agent to treat influenza A virus infection [27], improve glucose and lipid metabolism abnormalities in obese patients [28], and play a protective role in LPS-induced osteolysis [19]. In our study, both micro-CT and H&E staining results showed that the bone mass was decreased, and the number of osteoclasts was increased in the TRAP-stained histological sections from the OVX groups. After the drug intervention, a dose-dependent preventive effect was found. Micro-CT and H&E staining results showed that the dose (100 mg/kg for 2 days) in the experiment significantly inhibited the bone loss in the OVX

groups. Simultaneously, TRAP staining showed that a decreased number of osteoclasts in the OVX groups. Moreover, *in vitro* experiments demonstrated that the application of this drug could suppress the differentiation of osteoclasts in a concentration-dependent manner. Therefore, our results suggested that *Phil* could attenuate OVX-induced bone loss *in vivo* and osteoclast differentiation *in vitro* in a concentration-dependent manner.

In summary, this study indicates that *Phil* inhibits OVX-induced osteolysis by inhibiting osteoclast differentiation. Our results demonstrated that *Phil* might be a novel and effective anti-osteoporosis agent.

## 5. Conclusion

*Phil* was applied for the ovariectomized (OVX) mice to evaluate changes in bone mineral density and explore the role of *Phil* in osteoporosis induced by OVX. The results showed that *Phil* was helpful to inhibit the formation of osteoclasts, promote the growth of bone trabecular, and relieve osteoporosis caused by ovariectomy, with the value of clinical adoption. However, this experiment uses animal models as the research objects, so it needs to be further explored in the clinic before the clinical adoption. Furthermore, through this experiment, *Phil* can effectively inhibit bone loss, with good development prospects.

## Data Availability

The data used to support the findings of this study are available from the corresponding author upon request.

## Conflicts of Interest






The authors declare no conflicts of interest.

## References

- [1] T. Willson, S. D. Nelson, J. Newbold, R. E. Nelson, and J. LaFleur, "The clinical epidemiology of male osteoporosis: a review of the recent literature," *Clinical Epidemiology*, vol. 7, pp. 65–76, 2015.
- [2] T. Saito, J. M. Sterbenz, S. Malay, L. Zhong, M. P. MacEachern, and K. C. Chung, "Effectiveness of anti-osteoporotic drugs to prevent secondary fragility fractures: systematic review and meta-analysis," *Osteoporosis International*, vol. 28, no. 12, pp. 3289–3300, 2017.
- [3] A. S. Nazrun, M. N. Tzar, S. A. Mokhtar, and I. N. Mohamed, "A systematic review of the outcomes of osteoporotic fracture patients after hospital discharge: morbidity, subsequent fractures, and mortality," *Therapeutics and Clinical Risk Management*, vol. 10, pp. 937–948, 2014.
- [4] M. X. Ji and Q. Yu, "Primary osteoporosis in postmenopausal women," *Chronic Diseases and Translational Medicine*, vol. 1, no. 1, pp. 9–13, 2015.
- [5] S. Khosla, D. Burr, J. Cauley et al., "Bisphosphonate-associated osteonecrosis of the jaw: report of a task force of the American society for bone and mineral research," *Journal of Bone and Mineral Research*, vol. 22, no. 10, pp. 1479–1491, 2007.
- [6] R. Burge, B. Dawson-Hughes, D. H. Solomon, J. B. Wong, A. King, and A. Tosteson, "Incidence and economic burden of osteoporosis-related fractures in the United States, 2005–2025," *Journal of Bone and Mineral Research*, vol. 22, no. 3, pp. 465–475, 2007.
- [7] L. Si, T. M. Winzenberg, Q. Jiang, M. Chen, and A. J. Palmer, "Projection of osteoporosis-related fractures and costs in China: 2010–2050," *Osteoporosis International*, vol. 26, no. 7, pp. 1929–1937, 2015.
- [8] H. D. Nelson, L. L. Humphrey, P. Nygren, S. M. Teutsch, and J. D. Allan, "Postmenopausal hormone replacement therapy," *JAMA*, vol. 288, no. 7, pp. 872–881, 2002.
- [9] A. H. van Lierop, N. M. Appelman-Dijkstra, and S. E. Papapoulos, "Sclerostin deficiency in humans," *Bone*, vol. 96, pp. 51–62, 2017.
- [10] L.-M. Sun, M.-C. Lin, C.-H. Muo, J.-A. Liang, and C.-H. Kao, "Calcitonin nasal spray and increased cancer risk: a population-based nested case-control study," *Journal of Clinical Endocrinology & Metabolism*, vol. 99, no. 11, pp. 4259–4264, 2014.
- [11] Z. A. Peña-Rodríguez, M. Haro-García, and J. R. Benito-Navarro, "Nasal osteoma and inhaled salmon calcitonin: coincidence or consequence?" *Acta Otorrinolaringológica Española*, vol. 68, pp. 366–368, 2017.
- [12] M. S. Ominsky, S. K. Boyd, A. Varela et al., "Romosozumab improves bone mass and strength while maintaining bone quality in ovariectomized cynomolgus monkeys," *Journal of Bone and Mineral Research*, vol. 32, no. 4, pp. 788–801, 2017.
- [13] N. Hassler, A. Roschger, S. Gamsjaeger et al., "Sclerostin deficiency is linked to altered bone composition," *Journal of Bone and Mineral Research*, vol. 29, no. 10, pp. 2144–2151, 2014.
- [14] I. Pernicova, E. T. Middleton, and M. Aye, "Rash, strontium ranelate and DRESS syndrome put into perspective. European medicine agency on the alert," *Osteoporosis International*, vol. 19, no. 12, pp. 1811–1812, 2008.
- [15] P. Cacoub, V. Descamps, O. Meyer, C. Speirs, P. Belissathiot, and P. Musette, "Drug rash with eosinophilia and systemic symptoms (DRESS) in patients receiving strontium ranelate," *Osteoporosis International*, vol. 24, no. 5, pp. 1751–1757, 2013.
- [16] Z. Wang, Q. Xia, X. Liu et al., "Phytochemistry, pharmacology, quality control and future research of *Forsythia suspensa* (thunb.) vahl: a review," *Journal of Ethnopharmacology*, vol. 210, pp. 318–339, 2018.
- [17] H. Qu, Y. Zhang, Y. Wang, B. Li, and W. Sun, "Antioxidant and antibacterial activity of two compounds (forsythiaside and forsythin) isolated from *Forsythia suspensa*," *Journal of Pharmacy and Pharmacology*, vol. 60, pp. 261–266, 2008.
- [18] Q. Ma, R. Li, W. Pan et al., "Phillyrin (KD-1) exerts anti-viral and anti-inflammatory activities against novel coronavirus (SARS-CoV-2) and human coronavirus 229E (HCoV-229E) by suppressing the nuclear factor kappa B (NF- $\kappa$ B) signaling pathway," *Phytomedicine: International Journal of Phytotherapy and Phytopharmacology*, vol. 78, Article ID 153296, 2020.
- [19] J. Wang, G. Chen, Q. Zhang et al., "Phillyrin attenuates osteoclast formation and function and prevents LPS-induced osteolysis in mice," *Frontiers in Pharmacology*, vol. 10, p. 1188, 2019.
- [20] S. Khosla and L. C. Hofbauer, "Osteoporosis treatment: recent developments and ongoing challenges," *Lancet Diabetes & Endocrinology*, vol. 5, no. 11, pp. 898–907, 2017.
- [21] T. Komori, "Animal models for osteoporosis," *European Journal of Pharmacology*, vol. 759, pp. 287–294, 2015.
- [22] M. Inada, C. Matsumoto, and C. Miyaura, "Animal models for bone and joint disease. Ovariectomized and orchidectomized animals," *Clinical Calcium*, vol. 21, pp. 164–170, 2011.
- [23] Z. a. Xie, H. Yu, X. Sun et al., "A novel diterpenoid suppresses osteoclastogenesis and promotes osteogenesis by inhibiting ifrd1-mediated and ixk $\alpha$ -mediated p65 nuclear translocation," *Journal of Bone and Mineral Research*, vol. 33, no. 4, pp. 667–678, 2018.
- [24] H. X. Kuang, N. Zhang, and Z. B. Lu, "Antibacterial constituents of the unripe fruit of *Forsythia suspensa* (thunb.) vahl," *Zhongyao Tongbao*, vol. 13, pp. 62–33, 1988.
- [25] J. X. Yang, J. Liu, F. R. Li, and G. X. Hou, "Study on anti-senile and anti-oxidative activities of *Forsythia suspensa* leaves tea," *Acta Nutrimenta Sinica*, vol. 26, pp. 65–67, 2004.
- [26] M. J. Kim, T. K. Jung, H.-C. Park, and K.-S. Yoon, "Effect of hoechunyangkyeok-san extract on melanogenesis," *Journal of Cosmetics, Dermatological Sciences and Applications*, vol. 6, no. 3, pp. 85–95, 2016.
- [27] X.-Y. Qu, Q.-J. Li, H.-M. Zhang et al., "Protective effects of phillyrin against influenza a virus in vivo," *Archives of Pharmacological Research*, vol. 39, no. 7, pp. 998–1005, 2016.
- [28] M. T. Do, H. G. Kim, J. H. Choi et al., "Phillyrin attenuates high glucose-induced lipid accumulation in human HepG2 hepatocytes through the activation of LKB1/AMP-activated protein kinase-dependent signalling," *Food Chemistry*, vol. 136, no. 2, pp. 415–425, 2013.

## Research Article

# Profile of Medicinal Plants Traditionally Used for the Treatment of Skin Burns

**Hanae Naceiri Mrabti** <sup>1</sup>, **Latifa Doudach**,<sup>2</sup> **Mouna Mekkaoui**,<sup>3</sup> **Zineb Khalil**,<sup>4</sup> **Khoulood Harraqui**,<sup>5</sup> **Fozia Fozia** <sup>6</sup>, **Nidal Naceiri Mrabti**,<sup>7</sup> **Mohamed El-Shazly**,<sup>8,9</sup> **Amal Alotaibi** <sup>10</sup>, **Riaz Ullah** <sup>11</sup>, **Moulay El Abbes Faouzi**,<sup>1</sup> and **Abdelhakim Bouyahya** <sup>12</sup>

<sup>1</sup>Laboratory of Pharmacology and Toxicology, Bio Pharmaceutical and Toxicological Analysis Research Team, Faculty of Medicine and Pharmacy, Mohammed V University in Rabat, BP 6203, Rabat, Morocco

<sup>2</sup>Biomedical Engineering Department, National School of Arts and Crafts Rabat (ENSAM), Mohammed V University in Rabat, BP 6203, Rabat, Morocco

<sup>3</sup>Pharmacodynamics Research Team, Laboratory of Pharmacology and Toxicology, Faculty of Medicine and Pharmacy, Mohammed V University in Rabat, Rabat, Morocco

<sup>4</sup>Laboratory of Medicinal Chemistry, Drug Sciences Research Center, Faculty of Medicine and Pharmacy, Mohammed V University in Rabat, BP 6203, Rabat, Morocco

<sup>5</sup>Biology and Health Laboratory, Faculty of Sciences, Ibn Tofail University, P.O. Box 133, Kenitra 14000, Morocco

<sup>6</sup>Biochemistry Department, Khyber Medical University Institute of Medical Sciences, Kohat, Khyber Pakhtunkhwa, Pakistan

<sup>7</sup>Computer Chemistry and Modeling Team, Laboratory of Materials, Modeling and Environmental Engineering (LIMME), Faculty of Sciences Dhar El Mehraz, Sidi Mohamed Ben Abdellah University (USMBA), BP 1796, Atlas, 30000 Fez, Morocco

<sup>8</sup>Department of Pharmacognosy, Faculty of Pharmacy, Ain Shams University, Cairo 11566, Egypt

<sup>9</sup>Department of Pharmaceutical Biology, Faculty of Pharmacy and Biotechnology, German University in Cairo (GUC), Cairo 11835, Egypt

<sup>10</sup>Department of Basic Science, College of Medicine, Princess Nourah Bint Abdulrahman University, P.O. Box 84428, Riyadh 11671, Saudi Arabia

<sup>11</sup>Department of Pharmacognosy and MAPPRC, College of Pharmacy, King Saud University, Riyadh 11451, Saudi Arabia

<sup>12</sup>Laboratory of Human Pathologies Biology, Department of Biology, Faculty of Sciences and Genomic Center of Human Pathologies, Faculty of Medicine and Pharmacy, Mohammed V University in Rabat, Rabat, Morocco

Correspondence should be addressed to Riaz Ullah; rullah@ksu.edu.sa

Received 21 February 2022; Accepted 10 May 2022; Published 6 June 2022

Academic Editor: Ruchika Garg

Copyright © 2022 Hanae Naceiri Mrabti et al. This is an open access article distributed under the Creative Commons Attribution License, which permits unrestricted use, distribution, and reproduction in any medium, provided the original work is properly cited.

Moroccan folk healers use medicinal plants to treat several diseases including skin burns. The traditional knowledge of wound healing is not common among the general population. Only one ethnobotanical survey was carried out in Rabat, Morocco, to track the traditional use of medicinal plants in wound healing. Therefore, our report aimed to study the medicinal plants used in Taza region to treat wound healing. In total, 218 individuals participated in this survey. More than 40 medicinal plants belonging to 30 botanical families were cited as anti-burn remedies. The most commonly used medicinal plants were *Agave sisalana* L., *Nerium oleander* L., *Tetralinis articulata* Benth., *Lawsonia inermis* L., *Artemisia herba-alba* Asso., and *Trigonella foenum-graecum* L. Most of the used medicinal plants belong to Asteraceae family. Comparing our results with the previous survey, we noted that twelve plants were reported for the first time as wound healing agents. The ethnomedicinal use showed that plants leaves are the most commonly used parts. Pulverization was the selected method of preparation. The direct application of powder to the burns was the most common way of treatment. Our study revealed, for the first time, the importance of medicinal plants to treat skin burns in Taza region. Our results could be considered as the stepping stone for creating a database of wound healing medicinal plants to promote scientific studies on these plants revealing their constituents and side effects.



## 1. Introduction

The skin is the largest organ in the body and provides many important functions including organ protection, percutaneous absorption, maintenance of body shape, fluid conservation, temperature control, and sensory and disease control [1]. Skin diseases are a major health problem worldwide. Skin burns are among the most common skin traumas in all age groups. Burns are defined as the partial or total destruction of the skin covering or underlying tissue by a thermal, electrical, or chemical agent or by ionizing radiation [2]. Most burn treatments start with a topical application of a soothing, protective, and anti-infective medication to prevent infection [3]. Since Antiquity, many plants were used by indigenous peoples in different regions of the world for the treatment of wounds and burns. Usually, ointments formulated from different medicinal plants have been used as curative agents due to their widespread diversity of medicinal ingredients such as terpenoids, tannins, alkaloids, flavonoids, essential oils, phenolic compounds, saponins, and fatty acids which exhibit abundant pharmacological potential like anticancer, antidiabetic, and antimicrobial effects as well as cosmetic properties [4–7]. Besides, it has been discovered currently that some bioactive constituents improve the curative progression of burns [8–10]. These phytoconstituents are not only inexpensive but also harmless. The occurrence of many life-supporting phytoconstituents in plants has prompted scientists to scientifically evaluate these plants for potential wound healing properties [11]. The development of natural resources is a goal that is becoming more and more important in many countries. Medicinal plants are used for treatment purposes of infections. These plants are subsidized as a foundation of stimulation for new beneficial phytoconstituents as well as color, flavor, and taste of food [12–17]. The WHO indorses the assessment of the efficacy and of plant-based medications to standardize their usage and integrate them into conventional healthcare systems [18]. Traditional medicinal practices differ greatly from country to country and region to region. They are influenced by many factors including culture, history, generational anecdotes, and local healers' philosophies. According to the WHO, nearly 80% of the developing countries' population use traditional medicine as the primary source of therapy [18]. In Morocco, medicinal plants inhabit a significant room in medicinal systems and play an important part in the national economy [19], and numerous investigations showed recently remarkable results for future pharmaceutical applications [20–25]. Morocco is one of the Mediterranean countries with a long tradition of cultivating and using medicinal plants. In the northeastern part of Morocco, the use of traditional medicine is widespread, and several herbal remedies used individually or in combination with other agents are recommended for the treatment of burns. Despite the widespread use of medicinal plants, the scientific categorization of the local knowledge describing how to prescribe these plants is threatened with loss. The knowledge is usually transferred from generation to generation verbally, which affects the accuracy and spread of

information in local populations. One scientific approach to tackle this problem is to conduct surveys among certain populations and collect as much data as possible. These data are then categorized, analyzed, compared, scrutinized, and presented to the scientific and local communities in a clear reliable format to be preserved in a proper way for future generations. The widespread use of medicinal plants to treat skin burns in Morocco encouraged us to conduct surveys among local populations to understand and preserve local practices. After searching the literature, we found no ethnopharmacological surveys conducted on the use of medicinal plants for the treatment of skin burns in the northeast part of Morocco [26]. The purpose of this study was to record and summarize the traditional practices of using medicinal plants in the treatment of burns in the region of Taza. The results of this survey will guide scientists in their future pharmacological and clinical work aiming to provide scientific evidence on the use of certain medicinal plants to treat skin burns.

## 2. Materials and Methods

*2.1. Description of the Study Area.* This study was carried out in the province of Taza. This city is administratively part of the Region of Fes-Meknes. Taza is a town located in the northeast of Morocco in the Taza corridor, a mountain pass where the Rif and Middle Atlas Mountains meet. The city is the capital of its province. It is located 220 km west of Oujda and 316 km east of Rabat (Figure 1). This city covers an area of 37 km<sup>2</sup> with a population of 152,678 inhabitants in 2020. This city was selected because we observed the widespread use of medicinal plants to treat wound healing. Moreover, no ethnopharmacological study was conducted in this region to collect information about the use of medicinal plants in wound healing.

*2.2. Collection of Data.* The study was carried out from January 2021 to April 2021. Ethnobotanical knowledge was obtained through semi-assembled discussions. Interviews were carried out, and plant names in local dialect were recorded when cited. A total of 218 participants were interviewed for this survey (Table 1). The interviews were planned to register data about plants used for healing purposes of skin burns and their homegrown names, methods of preparation, parts of the plant used, drug management, and demographic characteristics of the study participants (Table 1).

## 3. Results and Discussion

*3.1. Sociodemographic Characteristics of Herbalists.* Ethnobotanical surveys require questioning herbalists, traditional healers, and/or people with long experience in medicinal plants. The data obtained from questionnaires highlight the sociodemographic characteristics of herbalists and traditional healers. In this work, the number of participants was 218 individuals practicing traditional medicine in Taza. The age of these traditional practitioners ranged



FIGURE 1: Map of the study area.

TABLE 1: Sociodemographic characteristics and experience of herbalists.

Characteristics	Number of informants ( <i>n</i> )	Frequency (%)
Age (years)		
30–50	65	29.81
50–70	91	41.74
70–90	62	28.44
Total	218	100
Gender		
Male	36	16.51
Female	182	83.49
Total	218	100
Education		
None	165	75.69
Primary	37	16.97
Secondary	12	5.50
University	4	1.83
Total	218	100
Origin of knowledge		
Family heritage	202	92.66
Traditional initiation	16	7.34
Total	218	100

between 30 and 90 years with a high rate for the age group of 50 and 70 years (Table 1). It was also noted that women actively participated in this survey (83.49%) compared with men (16.51%). This is in line with previous studies carried out in Morocco, where women were more interested in traditional medicine [27, 28]. Unfortunately, most participants did not have formal education (75.69%). However, only 16.97% have primary level, 5.5% have secondary level, and 1.83% have university level education. Most participants declared that

their knowledge was inherited from older family members (92.66%), while 7.34% acquired their knowledge from traditional practices (traditional initiation). The transmission of this traditional knowledge was carried out exclusively by families, and this can lead to the disappearance of certain information (plants not yet known) because new generations became less interested in traditional knowledge.

**3.2. The Diversity of Medicinal Plants Used to Treat Burns.** The survey revealed the importance of medicinal plants in treating burns. As listed in Table 2, [47] medicinal plants were used to treat burns. These species belong to 30 different botanical families. Different species were recognized by their vernacular names, which showed the diversity of the regional language, and the information was collected by analyzing and categorizing the location of the population. In our previous work, we showed that the region of Taza is rich in medicinal plants such as *Agave sisalana* L., *Nerium oleander* L., *Tetralinis articulata* Benth., *Lawsonia inermis* L., *Artemisia herba-alba* Asso., and *Trigonella foenum-graecum* L. which are used not only for skin burns but also for other pathologies such as diabetes and diseases related to the digestive system [27]. Despite the richness of Taza with medicinal plants, a comparison of the diversity of medicinal plants between Taza and other regions was never conducted. Only Salhi et al. [3] carried out a study including six cities in the Rabat region (Rabat, Sale, Temara, Skhirat, Khemisset, and Tiflet). In the study of Salhi et al. [3], thirty-six species belonging to 35 genera and 23 botanical families were identified.

**3.3. Medicinal Plants Previously Reported for Dermatology Uses.** The only work that was reported on the anti-burn properties of Moroccan medicinal plants was that of [3] in

TABLE 2: Medicinal plants used to treat skin burns.

Family name	Plant species [voucher no.]	Vernacular name	Parts used	Method of preparation and application	FC	Recorded literature for ethnomedicinal uses in Morocco	Recorded literature for ethnomedicinal uses worldwide
Agavaceae	<i>Agave sisalana</i> L. [RAB1371]	Sabra	Mucilage	The mucilaginous extract of the fresh leaves is applied as a poultice on burns.	0.98	Skin diseases [29] and eczema [30]	ND
Amaryllidaceae	<i>Narcissus poeticus</i> [RAB1371]	Narjis	Flowers	The flower powder is mixed with olive oil and applied as a poultice on burns.	0.44	ND	ND
Anacardiaceae	<i>Pistacia atlantica</i> Desf. [RAB1372]	Drou	Barks	The bark powder is sprinkled on burns.	0.61	Diabetes [31, 32], allergy, digestive ailments, cardiovascular diseases, diabetes [33], digestive ailments, respiratory ailments, urogenital affections [34, 35], abdominal colic [36], obesity, and hair care [37]	ND
Apiaceae	<i>Ammi visnaga</i> L. [RAB12423]	Bachnikha	Fruits	The powder of the fruits is sprinkled on burns.	0.38	ND	ND
	<i>Daucus carota</i> L. [RAB109243]	Khizzu	Roots	The juice extracted from the roots is used as a compress to clean burns.	0.22	Diabetes [32, 38], stomach disorders [29], helminthiasis [39], urinary infections [40, 41], and burns [3, 30]	Burns, skin toner [42], eczema [43]
Apocynaceae	<i>Nerium oleander</i> L. [RAB18820]	Defla	Leaves	The powder of leaves is sprinkled on burns.	0.87	ND	ND
Aristolochiaceae	<i>Aristolochia paucinervis</i> [RAB18821]	Baraztam	Leaves	The leaf powder is mixed with olive oil and applied as a poultice on burns.	0.54	Urogenital affections [34], dermatological and digestive ailments, and rheumatology [44]	ND
Asteraceae	<i>Artemisia herba-alba</i> Asso., [RAB109244]	Chih	Leaves	The leaf powder is mixed with honey and applied as a poultice on burns.	0.71	ND	ND
	<i>Insula viscosa</i> (L.) Ait. [RAB109244]	Terklan	Roots	The powder of roots is sprinkled on burns.	0.11	Diabetes, digestive system, cancer, and skin diseases [29]	ND
Asteraceae	<i>Conyza canadensis</i> L. [RAB109244]	Elatassa	Leaves	The leaf powder is mixed with olive oil and applied as a poultice on burns.	0.19	Skin diseases [29]	ND
	<i>Cynara humilis</i> [RAB79161]	Timta	Roots	The powder of roots is sprinkled on burns.	0.12	Burns [36]	ND
	<i>Atractylis resinifera</i> L. [RAB79162]	Addad	Roots	The root powder is mixed with olive oil and applied as a poultice on burns.	0.27	Skin abscesses and warts [30, 39]	ND
	<i>Calendula arvensis</i> L. [RAB14312]	Zwiwl	Flowers	The flower powder is mixed with olive oil and applied as a poultice on burns.	0.18	ND	ND
	<i>Dittrichia viscosa</i> (L.) Greuter [RAB14314]	Magraman	Leaves	The powder of leaves is sprinkled directly on burns.	0.33	Diabetes [32], digestive system [40], bronchitis [45] burns, wounds, abscesses [30], urogenital affections, fever, rheumatology, and digestive system [34]	ND
Asteraceae	<i>Matricaria chamomilla</i> [RAB15115]	Babounj	Flowers	The flower powder is mixed with olive oil and applied as a poultice on burns.	0.46	Diabetes [19, 32, 38, 45], digestive system, dermocosmetology [33, 35], antineuralgic, febrifuge, antispastic of digestive organs, emmenagogue, reduced allergy [37, 46], neuralgia, anxiety, insomnia, spasmolytic, and wounds [39, 40]	ND
	Brassicaceae	<i>Lepidium sativum</i> L. [RAB14317]	Habb rchad	Seeds	The powder of the seeds is sprinkled on the burns.	0.73	Diabetes [19, 38, 45], chronic diseases [47], cardiovascular diseases [33], bronchitis, cold, cough [45], eczema, skin ulcers and warts, stomach aches, anemia [30], and asthma [36, 48]

TABLE 2: Continued.

Family name	Plant species [voucher no.]	Vernacular name	Parts used	Method of preparation and application	FC	Recorded literature for ethnomedicinal uses in Morocco	Recorded literature for ethnomedicinal uses worldwide
Boraginaceae	<i>Borago officinalis</i> L. [RAB14318]	Lsan tour	Leaves	The latex extracted from the leaves is applied as a poultice to the burns.	0.8	Diabetes [45], anti-inflammatory, nervousness, respiratory canals, skin diseases [29, 40], colds, fever, diuretic, and laxative [39]	ND
Cannabaceae	<i>Cannabis sativa</i> L. [RAB14319]	Kif	Leaves	Burning leaves are sprinkled on burns.	0.16	Narcotics, skin diseases, and hair strengthening [30, 41, 49, 50] [40]	ND
Capparaceae	<i>Capparis spinosa</i> L. [RAB97161]	Lekbar	Seeds	The powder of the seeds is sprinkled on burns.	0.28	ND	ND
Cistaceae	<i>Cistus monspeliensis</i> [RAB97162]	Chteppa	Leaves	The leaves are applied as a poultice to burns.	0.29	Wounds [49], respiratory diseases [45], and diabetes [51]	ND
Cupressaceae	<i>Tetraclinis articulata Benth.</i> [RAB18717]	Al'Araâr	Leaves	The powder of the leaves is sprinkled directly on the burns.	0.91	ND	ND
Euphorbiaceae	<i>Euphorbia</i> sp. [RAB18717]	Loubina	Latex	The latex extracted is applied as a poultice to burns.	0.2	Skin diseases and cytotoxicity [29, 30]	ND
	<i>Ricinus communis</i> [RAB18718]	Alkharwaa	Seeds	The powder of the seeds is sprinkled on burns.	0.13	Toxic [29], diabetes [52], digestive system [40], skin diseases [30, 35], headache [36], antipyretic, rheumatism, diarrhea, laxative [53], fever [54], and hair care [44, 51]	ND
Fabaceae	<i>Trigonella foenum-graecum</i> L. [RAB24117]	Lhelba	Seeds	The seed powder is mixed with rose oil and applied as a poultice on burns.	0.89	ND	ND
	<i>Lupinus albus</i> L., [RAB21118]	Termes	Seeds	The seed powder is mixed with olive oil and applied as a poultice on the burns.	0.51	ND	ND
Gentianaceae	<i>Centaurium erythraea</i> [RAB22415]	Kassat lahya	Flowers	The flower powder is sprinkled on burns.	0.22	Diabetes [38, 45, 55], skin diseases [49], allergy, increasing energy [33], digestive system, and kidney diseases [29, 44]	ND
Juncaceae	<i>Juncus acutus</i> L. [RAB47241]	Assmar	Latex	The extracted latex is applied as a poultice to burns.	0.14	Skin diseases [29].	ND
Lamiaceae	<i>Marrubium vulgare</i> L. [RAB47249]	Mriwt	Leaves	The leaf powder is mixed with olive oil and applied as a poultice on burns.	0.26	ND	ND
	<i>Mentha pulegium</i> L.	Flio	Leaves	The leaf powder is mixed with olive oil and applied as a poultice on burns.	0.39	ND	ND
	<i>Salvia verbenaca</i> [RAB109218]	Khiyyata	Leaves	The leaf powder is sprinkled on burns.	0.46	Cardiac disease, diabetes [45], respiratory and rheumatologic conditions [34], abdominal colic, cold, fever [36], and wounds [56]	Wound healing [57], wounds [58], antiseptic on wounds [42], skin inflammations, and bacterial infections of the skin [59]
Leguminosae	<i>Lavandula angustifolia</i> [RAB109229]	Lakhzama	Leaves	The leaf powder is mixed with olive oil and applied as a poultice on burns.	0.29	Diabetes [38], digestive system [40, 44], and burns [3]	Dermatitis, furuncle, abscess, wart [60], wound healing [61].
	<i>Retama raetam</i> (Forssk.) [RAB109231]	Rtem	Leaves	The leaf powder is mixed with honey and sprinkled on the burns.	0.32	Skin diseases, toxic [29], and diabetes [32]	ND
Liliaceae	<i>Urginea maritima</i> L. [RAB23142]	Bessal lansasal	Bulb	The bulbs triturated in butter are applied as a poultice to burns.	0.11	Cattle ailments, skin disorders [29], abscesses, alopecia, sedative, hemorrhoids [30], and digestive system [44]	ND
Linaceae	<i>Linum usitatissimum</i> [RAB109227]	Zariat lkatan	Seeds	The seed powder is sprinkled on burns.	0.78	Diabetes [30, 62], asthma [47], renal disease [50], laxative, diuretic, and vermifuge [39]	Skin burns [63], wound healing [43], dermatological infections [58, 64], healing skin [42]



TABLE 2: Continued.

Family name	Plant species [voucher no.]	Vernacular name	Parts used	Method of preparation and application	FC	Recorded literature for ethnomedicinal uses in Morocco	Recorded literature for ethnomedicinal uses worldwide
Lythraceae	<i>Lawsonia inermis</i> L. [RAB109226]	Lehana	Leaves	The leaf powder is sprinkled on burns.	0.112	Wounds, dermatoses [56], burns, eczema, mycosis, boils, abscesses, chapped skin, antiseptic, healing wounds [3], eczema [30], diabetes [32], and dermatocosmetology [41]	Wound healing [65], eczema [66], wrinkled skin, abscess [67]
	<i>Punica granatum</i> [RAB109230]	Raman	Pericarp	Fruit pericarp powder is mixed with olive oil and applied as a poultice on burns.	0.54	Diabetes [30, 47, 50], stomach disorders [49], diabetes, digestive system [29, 41], eczema [39], and wounds [36].	ND
Myrtaceae	<i>Eucalyptus globulus</i> Labill. [RAB9318]	Al' Kalitouss	Leaves	The leaf powder is sprinkled on burns.	0.16	ND	ND
	<i>Myrtus communis</i> L. [RAB49621]	Arraihan	Leaves	The leaf powder is mixed with rose oil and applied as a poultice on burns.	0.5	Diabetes [30, 45], cardiac disease, hypertension, [49], cardiac weakness, and digestive system [29]	ND
Oleaceae	<i>Olea europaea</i> L. var. <i>oleaster</i> [RAB51120]	Zabouj	Leaves	The essential oil is applied as a poultice on burns.	0.25	Nervousness and anthelmintic [29]	ND
Papaveraceae	<i>Papaver rhoeas</i> L. [RAB51218]	Belaaman	Flowers	The flower powder is mixed with honey and applied as a poultice on burns.	0.9	Urogenital affections, hair care [34], against fever, sleep troubles and asthma [68], cold, antimicrobial [37], asthma, cough, improving breath, sedative, skin diseases [36], fever [30], and diabetes [19]	ND
Pinaceae	<i>Pinus halepensis</i> L. [RAB93519]	Taydá	Barks	The bark powder is mixed with olive oil and applied as a poultice on burns.	0.37	Against toothache [49] and tuberculosis [39, 41]	ND
Plantaginaceae	<i>Plantago coronopus</i> L. [RAB109241]	Massassa	Stems	The fruit stems are sprinkled on the burns.	0.12	Abscess and skin diseases [29]	ND
Rosaceae	<i>Prunus armeniaca</i> L. [RAB41111]	Machmach	Seeds	The seed powder is mixed with olive oil and applied as a poultice on burns.	0.9	Diabetes [30], face care [39], and aphrodisiac [41]	ND
Rosaceae	<i>Rosa centifolia</i> L. [RAB41113]	Lward	Flowers	The essential oil is applied as a poultice on burns.	0.52	Cosmetic and skin face [29]	ND
Rosaceae	<i>Alchemilla vulgaris</i> [RAB41114]	Gdam sbaá	Leaves	The powder of leaves is sprinkled on the burns.	0.17	ND	ND
Zingiberaceae	<i>Curcuma longa</i> L. [RAB41118]	Lkharkoum	Roots	The root powder is mixed with honey and applied as a poultice on burns.	0.89	As a condiment, tonic, calefacient, and digestive [39], digestive stimulant, for blood diseases, and against amnesia [41]	ND
Zygophyllaceae	<i>Peganum harmala</i> L. [RAB41116]	Lharmel	Seeds	The powder of seeds is sprinkled on the burns.	0.25	Induce abortion [69], diabetes [32, 38, 69, 70], hair care [30, 53, 56], spasmolytic and anthelmintic [39], toxic, sedative, nervous system disorders, rheumatism, decrease lipids [37], abdominal colic, induce abortion, anti-spasmodic, cold, diarrhea, eczema, hemorrhoids, jaundice, rheumatism, women sterility, and wounds [36]	ND

ND: not determined FC explained in the manuscript : Frequency of Citation.

the region of Rabat. Other surveys done in different Moroccan regions investigated the use of medicinal plants against different pathologies but did not focus on the use of medicinal plants against only burns. The results of the previous surveys are summarized in Table 2. A certain number of medicinal plants reported in our survey were cited in previous surveys and other ethnobotanical studies outside Morocco. However, several plants were newly cited

in our survey such as *Narcissus poeticus*, *Ammi visnaga* (L.) Lam, *Nerium oleander* L., *Artemisia herba-alba* Asso., *Calendula arvensis* L., *Capparis spinosa* L., *Tetraclinis articulata* Benth., *Trigonella foenum-graecum* L., *Lupinus albus* L., *Mentha pulegium* L., *Eucalyptus globulus* Labill. (sp.), and *Alchemilla vulgaris*. These plants were not cited in any previous ethnopharmacological investigations and deserve more intensive pharmacological evaluation.

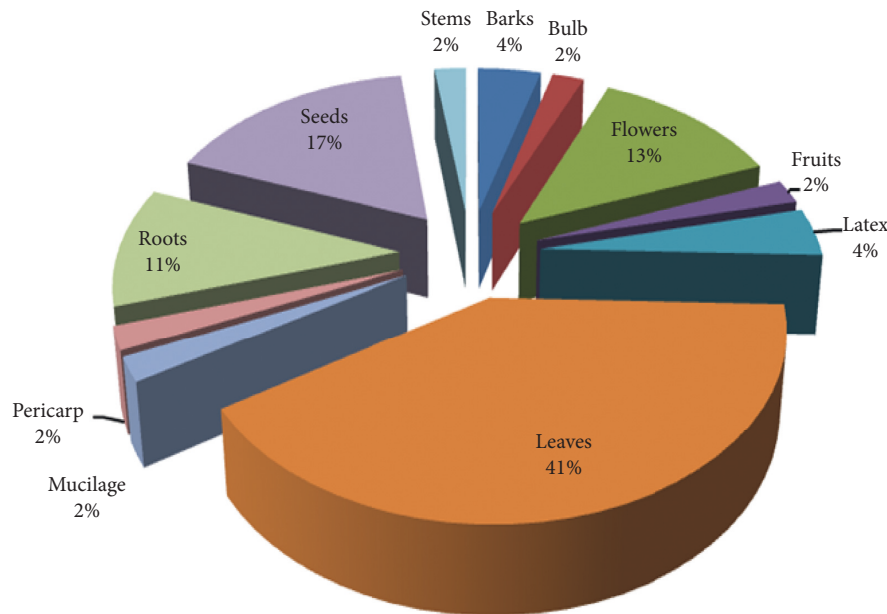


FIGURE 2: The plant parts used.

**3.4. Other Pharmacological Activities of the Reported Medicinal Plants.** Medicinal plants that showed anti-burn activity demonstrated other biological activities that need to be validated by extensive research. In our work, we carried out bibliographical research to see if the mentioned medicinal plants were subjected to experimental investigation focusing on the anti-burn activity. Certain plants were subjected to experimental investigation such as *Agave sisalana* L., *Conyza canadensis* L., and *Borago officinalis* L. (Table 2). Other species were not investigated for their wound healing activity including *Narcissus poeticus*, *Ammi visnaga* (L.) Lam, *Nerium oleander* L., *Artemisia herba-alba* Asso., *Calendula arvensis* L., *Capparis spinosa* L., *Tetraclinis articulata* Benth., *Trigonella foenum-graecum* L., *Lupinus albus* L., *Mentha pulegium* L., *Eucalyptus globulus* Labill., and *Alchemilla vulgaris*. More ethnomedicinal surveys should be carried out to preserve information on the use of medicinal plants as anti-burn agents in other regions of Morocco. Thorough medicinal surveys will allow the identification of potential plants and isolation of biologically active agents as drug leads.

**3.5. Ethnic Medicinal Characteristics: The Used Parts of Plants, Methods of Preparation, and Administration.** From the above, it is important to explore the uses of medicinal plants because they are used for the treatment of different infections. World Health Organization reports that various plant fractions and their dynamic constituents are utilized as traditional medicines of the world population [71–73].

Our data showed that the leaves were the most used parts (41%) of medicinal plants, followed by seeds (17%), flowers (13%), roots (11%), bark and latex (4% each), fruits, bulbs, stems, pericarp, and mucilage (2% each) (Figure 2). Our results were similar to the only work carried out in Morocco

by Salhi et al. [3] on plants used against skin burns. Other work carried out in Morocco on medicinal plants against different pathologies showed that the leaves were the most commonly used parts [19, 27, 28, 30, 68]. The results demonstrated that the powder was the main and simplest traditional application method used in the treatment of skin burns either alone or in combination with adjuvants such as honey, olive oil, and rose oil. Similar results were reported by Salhi et al. [3].

#### 4. Conclusion and Perspectives

We surveyed and summarized the medicinal plants used to treat skin diseases in the Taza region. The traditional knowledge demonstrated in this work showed that ethno-botanical surveys can play a decisive role in screening plants with biological properties such as wound healing activity. The results of our work can guide scientists in their selection of plants to be studied experimentally to treat burns. Other surveys should also be carried out in other regions of Morocco to highlight all the medicinal species treating skin burns in Moroccan folk medicine and thus preserve such valuable knowledge for future generations. In addition, medicinal plants that revealed healing effects in our study should be studied for their *in vivo* properties. In addition, powders of these species could be prepared as formulations for their applications against skin burns.

#### Data Availability

All the available data used to support the findings of the study are included within the article.

#### Conflicts of Interest

The authors declare no conflicts of interest.

## Acknowledgments

The authors wish to thank Princess Nourah Bint Abdulrahman University researchers, supporting project no. PNURSP2022R33), Princess Nourah Bint Abdulrahman University, Riyadh, Saudi Arabia, for financial support.

## References

- [1] K. Malik, M. Ahmad, M. Zafar et al., "An ethnobotanical study of medicinal plants used to treat skin diseases in northern Pakistan," *BMC Complementary and Alternative Medicine*, vol. 19, no. 1, pp. 210–238, 2019.
- [2] R. Bahramsoltani, M. H. Farzaei, and R. Rahimi, "Medicinal plants and their natural components as future drugs for the treatment of burn wounds: an integrative review," *Archives of Dermatological Research*, vol. 306, no. 7, pp. 601–617, 2014.
- [3] N. Salhi, A. Bouyahya, S. Fettach, A. Zellou, and Y. Cherrah, "Ethnopharmacological study of medicinal plants used in the treatment of skin burns in occidental Morocco (area of Rabat)," *South African Journal of Botany*, vol. 121, pp. 128–142, 2019.
- [4] A. Bouyahya, Y. Bakri, A. Et-Touys, I. C. C. Assemian, J. Abrini, and N. Dakka, "In vitro antiproliferative activity of selected medicinal plants from the north-west of Morocco on several cancer cell lines," *European Journal of Integrative Medicine*, vol. 18, pp. 23–29, 2018.
- [5] J. Sharifi-Rad, A. Dey, N. Koirala et al., "Cinnamomum species: bridging phytochemistry knowledge, pharmacological properties and toxicological safety for health benefits," *Frontiers in Pharmacology*, vol. 12, Article ID 600139, 2021.
- [6] A. Bouyahya, O. Belmehdi, M. El Jemli et al., "Chemical variability of *Centaureum erythraea* essential oils at three developmental stages and investigation of their in vitro antioxidant, antidiabetic, dermatoprotective and antibacterial activities," *Industrial Crops and Products*, vol. 132, pp. 111–117, 2019.
- [7] A. Bouyahya, N. El Omari, N. Elmenyiy et al., "Moroccan antidiabetic medicinal plants: ethnobotanical studies, phytochemical bioactive compounds, preclinical investigations, toxicological validations and clinical evidences; challenges, guidance and perspectives for future management of diabetes worldwide," *Trends in Food Science and Technology*, vol. 115, pp. 147–254, 2021.
- [8] M. H. Farzaei, R. Rahimi, Z. Abbasabadi, and M. Abdollahi, "An evidence-based review on medicinal plants used for the treatment of peptic ulcer in traditional Iranian medicine," *International Journal of Pharmacology*, vol. 9, no. 2, pp. 108–124, 2013.
- [9] N. Salhi, A. Bouyahya, A. Bounihi et al., "Investigation of wound healing activity *Cynara humilis* of root extracts," *Journal of Cosmetic Dermatology*, vol. 21, no. 4, pp. 1596–1609, 2021.
- [10] J. Demay, S. Halary, A. Knittel-Obrecht et al., "Anti-inflammatory, antioxidant, and wound-healing properties of cyanobacteria from thermal mud of balaruc-les-bains, France: a multi-approach study," *Biomolecules*, vol. 11, no. 1, pp. 28–21, 2020.
- [11] R. Thakur, N. Jain, R. Pathak, and S. S. Sandhu, "Practices in wound healing studies of plants," *Evidence-Based Complementary and Alternative Medicine*, vol. 2011, Article ID 438056, 17 pages, 2011.
- [12] A. Bouyahya, Y. Bakri, E. O. Khay et al., "Antibacterial, antioxidant and antitumor properties of Moroccan medicinal plants: a review," *Asian Pacific Journal of Tropical Disease*, vol. 7, no. 1, pp. 57–64, 2017.
- [13] A. Bouyahya, J. Abrini, Y. Bakri, and N. Dakka, "Phytochemical screening and evaluation of antioxidant and antibacterial activities of *Origanum compactum* extracts," *Phytotherapie*, vol. 15, 2017.
- [14] A. Bouyahya, O. Belmehdi, A. Benjouad et al., "Pharmacological properties and mechanism insights of Moroccan anticancer medicinal plants: what are the next steps?" *Industrial Crops and Products*, vol. 147, Article ID 112198, 2020.
- [15] D. Calina, A. M. Buga, M. Mitroi et al., "The treatment of cognitive, behavioural and motor impairments from brain injury and neurodegenerative diseases through cannabinoid system modulation-evidence from in vivo studies," *Journal of Clinical Medicine*, vol. 9, no. 8, p. 2395, 2020.
- [16] A. S. Alqahtani, R. Ullah, and A. A. Shahat, "Bioactive constituents and toxicological evaluation of selected antidiabetic medicinal plants of Saudi Arabia," *Evidence-Based Complementary and Alternative Medicine*, vol. 2022, Article ID 7123521, 23 pages, 2022.
- [17] U. Sarker, S. Oba, S. Ercisli, A. Assouguem, A. Alotaibi, and R. Ullah, "Bioactive phytochemicals and quenching activity of radicals in selected drought-resistant *Amaranthus tricolor* vegetable amaranth," *Antioxidants*, vol. 11, no. 3, p. 578, 2022.
- [18] L. El Fakir, M. Bourhia, A. M. Salamattullah et al., "Acute and repeated dose 60-day oral toxicity assessment of chemically characterized berberis hispanica boiss. and reut in wistar rats," *Open Chemistry*, vol. 19, no. 1, pp. 686–695, 2021.
- [19] H. N. Mrabti, N. Jaradat, M. R. Kachmar et al., "Integrative herbal treatments of diabetes in beni mellal region of Morocco," *Journal of Integrative Medicine*, vol. 17, no. 2, pp. 93–99, 2019.
- [20] B. Abdelaali, N. El Menyiy, N. El Omari et al., "Phytochemistry, toxicology, and pharmacological properties of *Origanum elongatum*," *Evidence-based Complementary and Alternative Medicine*, vol. 2021, Article ID 6658593, 12 pages, 2021.
- [21] A. Bouyahya, A. Et-Touys, J. Abrini et al., "Lavandula stoechas essential oil from Morocco as novel source of antileishmanial, antibacterial and antioxidant activities," *Biocatalysis and Agricultural Biotechnology*, vol. 12, pp. 179–184, 2017.
- [22] A. Bouyahya, F.-E. Guaouguaou, F.-E. Guaouguaou, N. Nadia Dakka, and Y. Bakri, "Pharmacological activities and medicinal properties of endemic Moroccan medicinal plant *Origanum compactum* (Benth) and their main compounds," *Asian Pacific Journal of Tropical Disease*, vol. 7, no. 10, pp. 628–640, 2017.
- [23] A. Bouyahya, Y. Bakri, O. Belmehdi, A. Et-Touys, J. Abrini, and N. Dakka, "Phenolic extracts of *Centaureum erythraea* with novel antiradical, antibacterial and antileishmanial activities," *Asian Pacific Journal of Tropical Disease*, vol. 7, no. 7, pp. 433–439, 2017.
- [24] A. Bouyahya, F. Lagrouh, N. El Omari et al., "Essential oils of mentha viridis rich phenolic compounds show important antioxidant, antidiabetic, dermatoprotective, anti-dermatophyte and antibacterial properties," *Biocatalysis and Agricultural Biotechnology*, vol. 23, Article ID 101471, 2020.
- [25] A. Bouyahya, I. C. Chadon Assemian, H. Mouzount et al., "Could volatile compounds from leaves and fruits of *Pistacia lentiscus* constitute a novel source of anticancer, antioxidant, antiparasitic and antibacterial drugs?" *Industrial Crops and Products*, vol. 128, pp. 62–69, 2019.
- [26] F. E.-Z. Amrati, M. Bourhia, M. Slighoua et al., "Traditional medicinal knowledge of plants used for cancer treatment by



- communities of mountainous areas of Fez-Meknes-Morocco,” *Saudi Pharmaceutical Journal*, vol. 29, no. 10, pp. 1185–1204, 2021.
- [27] H. Naceiri Mrabti, A. Bouyahya, N. Naceiri Mrabti, N. Jaradat, L. Doudach, and M. E. A. Faouzi, “Ethnobotanical survey of medicinal plants used by traditional healers to treat diabetes in the Taza region of Morocco,” *Evidence-Based Complementary and Alternative Medicine*, vol. 2021, Article ID 5515634, 16 pages, 2021.
- [28] M. R. Kachmar, H. Naceiri Mrabti, M. Bellahmar et al., “Traditional knowledge of medicinal plants used in the northeastern part of Morocco,” *Evidence-Based Complementary and Alternative Medicine*, vol. 2021, Article ID 6002949, 20 pages, 2021.
- [29] J. El-Hilaly, M. Hmammouchi, and B. Lyoussi, “Ethnobotanical studies and economic evaluation of medicinal plants in Taounate province (northern Morocco),” *Journal of Ethnopharmacology*, vol. 86, no. 2-3, pp. 149–158, 2003.
- [30] S. Boukhiraa, L. El Mansouria, and D. Boustaa, “Ethnobotanical studies of some medicinal and cosmetic plants used in the province of Sefrou, middle atlas of Morocco,” *The Journal of Ethnobiology and Traditional Medicine*, vol. 120, pp. 257–268, 2013.
- [31] M. Hachi, B. Ouafae, T. Hachi, E. B. Mohamed, B. Imane, and R. L. Atmane, “Contribution to the ethnobotanical study of antidiabetic medicinal plants of the central middle atlas region (Morocco),” *Lazaroa*, vol. 37, pp. 135–144, 2016.
- [32] E. Idm’Hand, F. Msanda, and K. Cherifi, “Ethnopharmacological review of medicinal plants used to manage diabetes in Morocco,” *Clinical Phytoscience*, vol. 6, no. 1, p. 18, 2020.
- [33] F. Jamila and E. Mostafa, “Ethnobotanical survey of medicinal plants used by people in oriental Morocco to manage various ailments,” *Journal of Ethnopharmacology*, vol. 154, no. 1, pp. 76–87, 2014.
- [34] A. Daoudi, M. Bammou, S. Zarkani, I. Slimani, J. Ibjibijen, and L. Nassiri, “Étude ethnobotanique de la flore médicinale dans la commune rurale d’Aguelmous province de Khénifra (Maroc),” *Phytothérapie*, vol. 14, no. 4, pp. 220–228, 2016.
- [35] A. El Alami and A. Chait, “Enquête ethnopharmacologique et ethnobotanique sur les plantes médicinales dans le haut atlas central du Maroc,” *Algerian Journal of Natural Products*, vol. 5, no. 1, pp. 427–445, 2017.
- [36] P. A. El Abbouyi, N. Filali-Ansari, P. S. Khyari, and H. Loukili, “Inventory of medicinal plants prescribed by traditional healers in El Jadida city and suburbs (Morocco),” *International Journal of Green Pharmacy*, vol. 8, no. 4, pp. 242–251, 2014.
- [37] M. El Haouari, S. El Makaoui, M. Jnah, and A. Haddaouy, “A survey of medicinal plants used by herbalists in Taza (northern Morocco) to manage various ailments,” *Journal of Materials and Environmental Sciences*, vol. 9, no. 6, pp. 1875–1888, 2018.
- [38] O. Benkhniq, B. A. Fatiha, S. Salhi, F. Mohamed, A. Douira, and L. Zidane, “Catalogue des plantes médicinales utilisées dans le traitement du diabète dans la région d’Al Haouz-Rhamna (Maroc),” *Journal of Animal and Plant Sciences*, vol. 23, no. 1, pp. 3539–3568, 2014.
- [39] A. Merzouki, F. Ed-derfoufi, and J. Molero Mesa, “Contribution to the knowledge of Rifian traditional medicine. II: folk medicine in Ksar Lakbir district (NW Morocco),” *Fitoterapia*, vol. 71, no. 3, pp. 278–307, 2000.
- [40] F. Z. Redouan, G. Benitez, B. Aboubakr et al., “The status and perception of medicinal plants by local population of Talassemtane national park (northern Morocco),” *Caspian Journal of Environmental Sciences*, vol. 18, no. 2, pp. 131–147, 2020.
- [41] J. Bellakhdar, R. Claisse, J. Fleurentin, and C. Younos, “Repertory of standard herbal drugs in the Moroccan pharmacopoea,” *Journal of Ethnopharmacology*, vol. 35, no. 2, pp. 123–143, 1991.
- [42] A. Pieroni, C. L. Quave, M. L. Villanelli et al., “Ethnopharmacognostic survey on the natural ingredients used in folk cosmetics, cosmeceuticals and remedies for healing skin diseases in the inland Marches, central-eastern Italy,” *Journal of Ethnopharmacology*, vol. 91, no. 2-3, pp. 331–344, 2004.
- [43] G. Tümen, H. Malyer, K. Başer, and S. Öz Aydın, “Plants used in anatolia for wound healing,” in *Proceedings of the 6th International Congress of Ethnobotany (ICEB 2005)*, Istanbul, Turkey, January 2006.
- [44] I. Slimani, M. Najem, L. Bachiri, E. H. Bouiamrine, and J. Ibjibijen, “Ethnobotanical survey of medicinal plants used in Zerhoun region-Morocco,” *International Journal of Innovation and Applied Studies*, vol. 15, no. 4, pp. 8466–8863, 2016.
- [45] H. Orch, A. Douira, and L. Zidane, “Étude ethnobotanique des plantes médicinales utilisées dans le traitement du diabète, et des maladies cardiaques dans la région d’Izarène (Nord du Maroc),” *Journal of Applied Biosciences*, vol. 86, no. 1, pp. 7940–7956, 2015.
- [46] H. Labiad, A. El-Tahir, M. Ghanmi et al., “Ethnopharmacological survey of aromatic and medicinal plants of the pharmacopoeia of northern Morocco,” *Ethnobotany Research and Applications*, vol. 19, pp. 1–16, 2020.
- [47] N. El Hachlafi, A. Chebat, R. Soulaymani Bencheikh, and K. Fikri-Benbrahim, “Ethnopharmacological study of medicinal plants used for chronic diseases treatment in Rabat-Sale-Kenitra region (Morocco),” *Ethnobotany Research and Applications*, vol. 20, pp. 1–23, 2020.
- [48] S. Hseini and A. Kahouadji, “Étude ethnobotanique de la flore médicinale dans la région de Rabat (Maroc Occidental),” *Complutense University of Madrid*, vol. 28, pp. 79–92, 2007.
- [49] A. Bouyahya, J. Abrini, A. Et-touys, Y. Bakri, and N. Dakka, “Indigenous knowledge of the use of medicinal plants in the north-west of Morocco and their biological activities,” *European Journal of Integrative Medicine*, vol. 13, pp. 9–25, 2017.
- [50] H. Jouad, M. Haloui, H. Rhiouani, J. El Hilaly, and M. Eddouks, “Ethnobotanical survey of medicinal plants used for the treatment of diabetes, cardiac and renal diseases in the north centre region of Morocco (Fez—boulemane),” *Journal of Ethnopharmacology*, vol. 77, no. 2-3, pp. 175–182, 2001.
- [51] M. Rhattas, A. Douira, and L. Zidane, “Étude ethnobotanique des plantes médicinales dans le Parc National de Talassemtane (Rif Occidental du Maroc),” *Journal of Applied Biosciences*, vol. 97, pp. 9187–9211, 2016.
- [52] M. Ghourri, L. Zidane, and D. Allal, “Usage des s plantes médicinales dans le traitement du diabète au Sahara marocain (Tan-Tan),” *Journal of Animal and Plant Sciences*, vol. 17, no. 1, 2013.
- [53] M. Hachi, T. Hachi, N. Belahbib, J. Dahmani, and L. Zidane, “Contribution à l’étude floristique et ethnobotanique de la flore médicinale utilisée au niveau de la ville de Khénifra (Maroc),” *International Journal of Innovation and Applied Studies*, vol. 11, no. 3, pp. 754–770, 2015.
- [54] M. E. L. Hafian, N. Benlamdini, H. Elyacoubi, and L. Zidane, “Étude floristique et ethnobotanique des plantes médicinales utilisées au niveau de la préfecture d’Agadir-Ida-Outanane (Maroc),” *Journal of Applied Biosciences*, vol. 81, 2014.



- [55] A. Tahraoui, J. El-Hilaly, Z. H. Israili, and B. Lyoussi, "Ethnopharmacological survey of plants used in the traditional treatment of hypertension and diabetes in south-eastern Morocco (Errachidia province)," *Journal of Ethnopharmacology*, vol. 110, no. 1, pp. 105–117, 2007.
- [56] S. Salhi, M. Fadli, L. Zidane, and A. Douira, "Etudes floristique et ethnobotanique des plantes médicinales de la ville de Kénitra (Maroc)," *Lazaroa*, vol. 31, no. 9, pp. 133–143, 2010.
- [57] B. Šarić-Kundalić, C. Dobeš, V. Klatte-Asselmeyer, and J. Saukel, "Ethnobotanical survey of traditionally used plants in human therapy of east, north and north-east Bosnia and Herzegovina," *Journal of Ethnopharmacology*, vol. 133, no. 3, pp. 1051–1076, 2011.
- [58] R. Y. Caverro, S. Akerreta, and M. I. Calvo, "Medicinal plants used for dermatological affections in navarra and their pharmacological validation," *Journal of Ethnopharmacology*, vol. 149, no. 2, pp. 533–542, 2013.
- [59] R. Dawid-Pač, "Medicinal plants used in treatment of inflammatory skin diseases," *Advances in Dermatology and Allergology*, vol. 3, no. 3, pp. 170–177, 2013.
- [60] C. L. Quave, A. Pieroni, and B. C. Bennett, "Dermatological remedies in the traditional pharmacopoeia of vulture-alto bradano, inland southern Italy," *Journal of Ethnobiology and Ethnomedicine*, vol. 4, no. 1, pp. 5–10, 2008.
- [61] A. Koca Kutlu, D. Çeçen, S. G. Gürgen, O. Sayin, and F. Çetin, "A comparison study of growth factor expression following treatment with transcutaneous electrical nerve stimulation, saline solution, Povidone-iodine, and lavender oil in wounds healing," *Evidence-Based Complementary and Alternative Medicine*, vol. 2013, Article ID 361832, 9 pages, 2013.
- [62] M. Eddouks, M. Maghrani, A. Lemhadri, M. L. Ouahidi, and H. Jouad, "Ethnopharmacological survey of medicinal plants used for the treatment of diabetes mellitus, hypertension and cardiac diseases in the south-east region of Morocco (Tafilalet)," *Journal of Ethnopharmacology*, vol. 82, no. 2-3, pp. 97–103, 2002.
- [63] H. M. Ahmed, "Ethnopharmacobotanical study on the medicinal plants used by herbalists in Sulaymaniyah province, Kurdistan, Iraq," *Journal of Ethnobiology and Ethnomedicine*, vol. 12, no. 1, 2016.
- [64] M. Karimi and M. Mardani, "Wound antiseptic plants: an overview of the most important medicinal plants in Iran affecting wound infections," *Journal of Global Pharma Technology*, vol. 8, no. 8, pp. 18–23, 2016.
- [65] A. Adetutu, W. A. Morgan, and O. Corcoran, "Ethnopharmacological survey and in vitro evaluation of wound-healing plants used in south-western Nigeria," *Journal of Ethnopharmacology*, vol. 137, no. 1, pp. 50–56, 2011.
- [66] M. Rahmatullah, J. M. Israt, H. A. K. M. Fahmidul et al., "An ethnobotanical survey and pharmacological evaluation of medicinal plants used by the garo tribal community living in Netrakona district, Bangladesh," *Advances in Natural and Applied Sciences*, vol. 3, no. 3, pp. 402–418, 2009.
- [67] A. P. Saikia, V. K. Ryakala, P. Sharma, P. Goswami, and U. Bora, "Ethnobotany of medicinal plants used by assamese people for various skin ailments and cosmetics," *Journal of Ethnopharmacology*, vol. 106, no. 2, pp. 149–157, 2006.
- [68] R. Rhafouri, A. Aafi, T. Zair et al., "Ethnobotanical study of medicinal plants in Ifran's national park (Morocco)," *Journal of Materials and Environmental Science*, vol. 6, no. 3, pp. 619–630, 2015.
- [69] A. Ziyat, A. Legssyer, H. Mekhfi, A. Dassouli, M. Serhrouchni, and W. Benjelloun, "Phytotherapy of hypertension and diabetes in oriental Morocco," *Journal of Ethnopharmacology*, vol. 58, no. 1, pp. 45–54, 1997.
- [70] A. Merzouki, F. Ed-Derfoufi, and J. Molero-Mesa, "Contribution to the knowledge of rifian traditional medicine III: phytotherapy of diabetes in chefchaouen province (north of Morocco)," *Ars Pharmaceutica*, vol. 44, 2003.
- [71] A. Shahat, R. Ullah, A. S. Alqahtani, M. S. Alsaid, H. A. Husseiny, and O. T. R. Meanazel, "Hepatoprotective effect of eriobotrya japonica leaf extract and its various fractions against carbon tetra chloride induced hepatotoxicity in rats," *Evidence-Based Complementary and Alternative Medicine*, vol. 2018, Article ID 3782768, 8 pages, 2018.
- [72] R. Ullah, A. S. Alqahtani, O. M. A. Noman, A. M. Alqahtani, S. Ibenmoussa, and M. Bourhia, "A review on ethno-medicinal plants used in traditional medicine in the Kingdom of Saudi Arabia," *Saudi Journal of Biological Sciences*, vol. 27, no. 10, pp. 2706–2718, 2020.
- [73] S. Mussarat, R. Amber, A. Tariq et al., "Ethnopharmacological assessment of medicinal plants used against livestock infections by the people living around Indus river," *BioMed Research International*, vol. 2014, Article ID 616858, 14 pages, 2014.

## Research Article

# Phytochemical Profiling, Antioxidant Activity, and *In Silico* Analyses of *Sterculia villosa* and *Vernonia patula*

Chadni Lyzu,<sup>1</sup> Saikat Mitra,<sup>2</sup> Kahkashan Perveen,<sup>3</sup> Zidan Khan,<sup>4</sup> Abu Montakim Tareq ,<sup>4</sup> Najat A. Bukhari,<sup>3</sup> Fohad Mabood Husain,<sup>5</sup> Evena Parvin Lipy,<sup>1</sup> Dipa Islam,<sup>1</sup> Mahmuda Hakim,<sup>1</sup> Talha Bin Emran ,<sup>6,7</sup> and Marjan Ganjali Dashti<sup>8</sup>

<sup>1</sup>Biomedical and Toxicological Research Institute, Bangladesh Council of Scientific and Industrial Research (BCSIR), Dr. Quadrat-I-Khuda Road, Dhanmondi, Dhaka 1205, Bangladesh

<sup>2</sup>Department of Pharmacy, Faculty of Pharmacy, University of Dhaka, Dhaka 1000, Bangladesh

<sup>3</sup>Department of Botany & Microbiology, College of Science, King Saud University, Riyadh-11495, Saudi Arabia

<sup>4</sup>Department of Pharmacy, International Islamic University Chittagong, Chittagong 4318, Bangladesh

<sup>5</sup>Department of Food Science and Nutrition, College of Food and Agriculture, King Saud University, Riyadh 11421, Saudi Arabia

<sup>6</sup>Department of Pharmacy, BGC Trust University Bangladesh, Chittagong 4381, Bangladesh

<sup>7</sup>Department of Pharmacy, Faculty of Allied Health Sciences, Daffodil International University, Dhaka 1207, Bangladesh

<sup>8</sup>Department of Biological Sciences, University of Texas at Dallas, 800 W Campbell Road, Richardson 75080, TX, USA

Correspondence should be addressed to Talha Bin Emran; talhabmb@gmail.com

Received 7 February 2022; Revised 9 March 2022; Accepted 6 May 2022; Published 6 June 2022

Academic Editor: Jelena Zivkovic

Copyright © 2022 Chadni Lyzu et al. This is an open access article distributed under the Creative Commons Attribution License, which permits unrestricted use, distribution, and reproduction in any medium, provided the original work is properly cited.

Our study aims to evaluate the chemical profiles and antioxidant activities of a methanolic extract of *Sterculia villosa* bark (MESV) and a methanolic extract of the *Vernonia patula* whole plant (MEVP). The chemical profiling of MESV and MEVP was performed via gas chromatography-mass spectrometry (GC-MS), which identified 52 and 33 chemical compounds, respectively. The 2,2-diphenyl-1-picrylhydrazyl (DPPH) assay indicated that both MESV and MEVP displayed concentration-dependent scavenging activities, and half-maximal inhibitory concentration (IC<sub>50</sub>) values for MEVP, MESV, and ascorbic acid were 305.30, 555.44, and 36.32  $\mu\text{g/mL}$ , respectively. The total flavonoid content (TFC) and total phenolic content (TPC) of MESV were  $81.44 \pm 2.70$  mg quercetin equivalents (QE)/g dry extract and  $62.58 \pm 1.93$  mg gallic acid equivalent (GAE)/g dry extract, whereas these values for MEVP were  $291.31 \pm 6.61$  mg QE/g dry extract and  $58.99 \pm 3.16$  mg GAE/g dry extract, respectively. Molecular docking studies were also evaluated, and absorption, distribution, metabolism, and excretion (ADME) and toxicological properties were assessed. Therefore, these two plants, *S. villosa* and *V. patula*, showed potential options for further advanced studies into oxidative stress.

## 1. Introduction

Plants containing natural bioactive compounds have been used in traditional medicinal practices worldwide since ancient times, and plants represent a source of potential medicines [1]. The scope of plants as a source of new drugs remains generally unexplored, as only a small fraction of approximately 250,000–500,000 plant species have been biologically or pharmacologically screened [2]. Phytochemicals with antioxidant properties are of particular interest because chronic disorders [3] exacerbated by oxidative stress (OS) have become the leading cause of

death [4]. Plant-derived compounds possess potent antioxidant properties that may inhibit OS by counteracting reactive oxygen species (ROS) and maintaining redox homeostasis [5, 6]. Several attempts have been undertaken to identify phytochemical compounds [4, 7] and assess their potential as antioxidants [8, 9], antimicrobials [10], antidiabetics, and anti-inflammatory compounds [11, 12]. The therapeutic potential of plants is commonly associated with their antioxidant and anticancer properties [2, 13–16].

Oxidation refers to the removal of electrons during a reaction by an atom, molecule, or ion and can occur



following the formation of elevated amounts of ROS. ROS are formed during natural cellular metabolic processes by living organisms, including byproducts of aerobic metabolism. ROS include hydrogen peroxide ( $H_2O_2$ ), superoxide anion ( $O_2^-$ ), and hydroxyl radicals ( $OH\bullet$ ), which all have inherent chemical properties and provide reactivity to various biological objectives [17]. ROS are also correlated with the concept of OS, and ROS can damage lipids, proteins, and DNA [18]. OS is a complicated process involving the generation of ROS and reactive nitrogen species (RNS) [19, 20]. ROS are produced by persistent metabolic processes and can regulate various biological and pathological processes, such as lipid peroxidation, immune response, and phagocyte activation [21]. Furthermore, excessive ROS generation can trigger oxidative damage by targeting the unsaturated fatty acids in membranes and thiol groups in proteins [22, 23]. Many chronic health problems have been associated with excessive lipid peroxidation, and free radicals have been implicated in the induction of several neuropsychiatric conditions and might mediate neuronal malfunctions associated with depression [24, 25]. OS has been identified as a significant contributor to the progression of degenerative and chronic diseases, such as malignant growths [26], diabetes, immune problems, joint inflammation, and cardiovascular and neurodegenerative diseases [27].

*Sterculia villosa* (Family: Sterculiaceae, Bengali name: Udal) is a deciduous tree with large, long-stalked, deeply lobed leaves and yellow flowers. *S. villosa* can be found in subtropical and tropical regions, including Bangladesh [7]. The plant is traditionally used as a diuretic and aphrodisiac agent [28] and is often used by Indian people to cure inflammation through traditional medicinal practices [29]. *Vernonia patula* (Family: Asteraceae, Bengali name: Kukshim) is an annual weed that is geographically disseminated throughout Bangladesh and is known as purple fleabane. This plant has significant medicinal value, used for fever reduction, headaches, malaria, common cold, and intestinal and stomach problems [30]. The bioactive compounds derived from these two plants have been reported to have antioxidant activities in prior studies [31, 32]. However, prior studies did not attempt to identify specific bioactive compounds.

Therefore, the present research attempted to identify the bioactive constituents of these two species through gas chromatography-mass spectrometry (GC-MS) analysis and explored the antioxidant efficacy of the compounds found in *S. villosa* and *V. patula*. GC-MS has been widely highlighted as an important analytical tool for secondary metabolite profiling, such as steroids, phenolics, and alkaloids, and can also identify sugars, fatty acids, amino acids, and other macromolecules found in plants and nonplant sources [33–36]. Identifying the bioactive profile may improve the identification of the key components responsible for various biological activities and contribute to the discovery of underlying principles of these effects.

To explore the possible mechanisms of action associated with the compounds identified from *S. villosa* and *V. patula*, we also performed molecular docking and absorption, distribution, metabolism, and excretion (ADME)/toxicity

(T) studies to reveal the potential target(s) of the identified antioxidant components.

## 2. Materials and Methods

**2.1. Chemicals.** Phosphate buffer, potassium ferricyanide, trichloroacetic acid, ferric chloride, ascorbic acid, 2,2-diphenyl-1-picrylhydrazyl (DPPH), and Folin-Ciocalteu Reagent were all purchased from Sigma-Aldrich, St. Louis, MO, USA.

**2.2. Collection and Preparation of *S. villosa* and *V. patula* Extracts.** Whole *S. villosa* and *V. patula* plants were collected from the Chittagong Hill-Tracts region of Bangladesh, and plants were authenticated and identified by a renowned taxonomist from the Bangladesh Council of Scientific and Industrial Research (BCSIR). The bark of *S. villosa* and the whole *V. patula* plant were washed with distilled water. The plant parts were cut into small pieces and dried. The dried materials were crushed into a fine pure powder using an electric blender. The powder was then stored in separate airtight containers. To obtain the extracts, the powders were placed in airtight containers, hexane was added at a sample to solvent ratio of 1:3, and the sample was subjected to uninterrupted stirring at 150 rpm for 90 minutes. The stirring was discontinued, and the sample was allowed to sit for 30 minutes, after which the hexane was decanted from the sample by filtration. Fresh hexane was added to the sample, and the process was repeated three times. After the final repetition, the hexane was decanted, and the sample was filtered under vacuum to completely remove all hexane, resulting in a defatted sample. The defatted crude powder was placed in an airtight container, and aqueous (95%) methanol was added at a sample to solvent ratio of 1:10. The sample was then subjected to 7 days of repeated 40/20-minute shaking/sonication cycles of uninterrupted agitation on a shaker machine at 150 rpm and ultrasonic vibrations in a sonicator machine at 55°C. The mixture was then filtered through Whatman #1 filter paper, and the filtrate was collected. This procedure was repeated thrice to extract all phytochemicals from the sample. All obtained filtrates were combined, and the methanol was evaporated in a rotary evaporator machine (Buchi, Postfach, Switzerland). The filtrates were lyophilized to complete dryness at  $-70^\circ\text{C}$  in a freeze drier (SP Scientific, Stone Ridge, NY, USA), collected into a Petri dish, covered and wrapped properly, and stored at  $4^\circ\text{C}$  until further experiments.

**2.3. GC-MS Analysis.** The methanolic extract of *S. villosa* (MESV) and the methanolic extract of *V. patula* (MEVP) were evaluated in a mass spectrometer (TQ 8040, Shimadzu Corporation, Kyoto, Japan) using the electron impact ionization (EI) technique and a gas chromatograph (GC-17A, Shimadzu Corporation) with a merged silica capillary column (Rxi-5 ms; 0.25 m film, 30 m long and internal diameter 0.32 mm) coated with DB-1 (J&W). The oven temperature was set at  $70^\circ\text{C}$  (0 min);  $10^\circ\text{C}$ ,  $150^\circ\text{C}$  (5 min);  $12^\circ\text{C}$ ,  $200^\circ\text{C}$  (15 min); and  $12^\circ\text{C}$ ,  $220^\circ\text{C}$  (5 min), with a clamp time of

TABLE 1: Tentative compounds identified from the methanolic extract of *Sterculia villosa* by gas chromatography-mass spectrometry (GC-MS) analysis.

Sl. no.	Name	Molecular formula	Nature	RT	m/z	Area
1	Heptanal	C <sub>7</sub> H <sub>14</sub> O	Aldehyde	4.146	44.00	879969
2	Benzaldehyde, 2-methyl	C <sub>8</sub> H <sub>8</sub> O	Aldehyde	4.872	120.00	359567
3	Glucitol, 6-O-nonyl	C <sub>15</sub> H <sub>32</sub> O <sub>6</sub>	Sugar alcohol	4.118	73.00	665996
4	L-Arabinitol	C <sub>5</sub> H <sub>12</sub> O <sub>5</sub>	Sugar alcohol	6.119	44.00	19425
5	$\alpha$ -Isomethyl ionone	C <sub>14</sub> H <sub>22</sub> O	Ketone	6.134	150.00	531076
6	Eucalyptol	C <sub>10</sub> H <sub>18</sub> O	Monoterpenoid	6.566	154.00	273748
7	Vanillin	C <sub>8</sub> H <sub>8</sub> O <sub>3</sub>	Phenolic aldehyde	7.246	151.00	375524
8	Prednisone	C <sub>21</sub> H <sub>26</sub> O <sub>5</sub>	Glucocorticoid	7.922	44.00	18826
9	Bioallethrin	C <sub>19</sub> H <sub>26</sub> O <sub>3</sub>	Ester	7.974	137.00	267302
10	Sorbitol	C <sub>6</sub> H <sub>14</sub> O <sub>6</sub>	Sugar alcohol	8.872	137.00	507045
11	$\beta$ -D-glucopyranose, 4-O- $\beta$ -D-galactopyranosyl	C <sub>12</sub> H <sub>22</sub> O	Carbohydrate	9.665	43.00	94028
12	Santolinatriene	C <sub>10</sub> H <sub>16</sub>	Hydrocarbon	9.314	180.00	285758
13	Vanillin, acetate	C <sub>10</sub> H <sub>10</sub> O <sub>4</sub>	Phenyl acetate	9.603	151.00	205675
14	Guanosine	C <sub>10</sub> H <sub>13</sub> N <sub>5</sub> O <sub>5</sub>	Purine nucleoside	9.603	151.00	205675
15	Trans-11-Tetradecenyl acetate	C <sub>16</sub> H <sub>30</sub> O <sub>2</sub>	Fatty acid	9.665	43.00	148058
16	D-Galactonic acid, $\gamma$ -lactone	C <sub>6</sub> H <sub>10</sub> O <sub>6</sub>	Acid	10.092	73.00	77114
17	Isopulegol	C <sub>10</sub> H <sub>18</sub> O	Terpenoid alcohol	10.359	127.00	99917
18	Benzaldehyde, 4-hydroxy-3,5-dimethoxy	C <sub>9</sub> H <sub>10</sub> O <sub>4</sub>	Aldehyde	10.463	182.00	393615
19	Naphthalene, 2-butyldecahydro-	C <sub>14</sub> H <sub>26</sub>	Hydrocarbon	10.697	137.00	256786
20	3-buten-2-one, 3-methyl-4-(3,5,6-trimethyl-3-cyclohexen-1-yl)	C <sub>14</sub> H <sub>22</sub> O	Alkane	10.852	43.00	71620
21	Cis-p-Mentha-2,8-dien-1-ol	C <sub>10</sub> H <sub>18</sub> OS	Monoterpenoid	10.949	167.00	162613
22	Trans-Sesquisabinene hydrate	C <sub>15</sub> H <sub>26</sub> O	Sesquiterpenoid	10.949	167.00	162613
23	2-methoxy-6-methylaniline	C <sub>8</sub> H <sub>11</sub> NO	Amine	11.439	137.00	4066243
24	$\beta$ -carotene	C <sub>40</sub> H <sub>56</sub>	Carotene	11.440	43.00	140490
25	Aprobarbital	C <sub>10</sub> H <sub>14</sub> N <sub>2</sub> O <sub>3</sub>	Barbiturate derivatives	11.697	167.00	179001
26	Spiro[3.4]octan-5-one	C <sub>8</sub> H <sub>12</sub> O	Ketone	12.006	124.00	283819
27	2-dodecen-1-yl(-)succinic anhydride	C <sub>16</sub> H <sub>26</sub> O <sub>3</sub>	Anhydride	12.130	196.00	61469
28	Phytol	C <sub>20</sub> H <sub>40</sub> O	Diterpene alcohol	12.520	43.00	22833
29	Digitoxin	C <sub>41</sub> H <sub>64</sub> O <sub>13</sub>	Dardenolide glycoside	12.520	43.00	22833
30	Chrysanthemic acid	C <sub>10</sub> H <sub>16</sub> O <sub>2</sub>	Fatty acid	13.455	44.00	26500
31	<i>n</i> -hexadecanoic acid	C <sub>16</sub> H <sub>32</sub> O <sub>2</sub>	Fatty acid	13.459	43.00	490715
32	$\beta$ -Asarone	C <sub>12</sub> H <sub>16</sub> O <sub>3</sub>	Phenylpropanoid	14.068	208.00	181791
33	Benzenepropanoic acid, 2,5-dimethoxy	C <sub>11</sub> H <sub>14</sub> O <sub>4</sub>	Organic acid	14.166	167.00	1864637
34	Decanoic acid, 2,3-dihydroxypropyl ester	C <sub>15</sub> H <sub>30</sub> O <sub>4</sub>	Organic acid	14.167	43.00	135871
35	9,12-octadecadienoic acid, methyl ester, (E,E)	C <sub>19</sub> H <sub>34</sub> O <sub>2</sub>	Monodecanoylglycerol	15.180	67.00	321453
36	7-hexadecenoic acid, methyl ester, (Z)	C <sub>17</sub> H <sub>32</sub> O <sub>2</sub>	Fatty acid methyl ester	15.244	55.00	182330
37	Citronellol	C <sub>10</sub> H <sub>20</sub> O	Monoterpenoid	15.348	71.00	332135
38	Undec-10-ynoic acid	C <sub>11</sub> H <sub>18</sub> O <sub>2</sub>	Fatty acid	15.490	43.00	139829
39	Undecanal	C <sub>10</sub> H <sub>21</sub> CHO	Aldehyde	16.205	73.00	40669
40	6-octadecenoic acid, methyl ester, (Z)	C <sub>19</sub> H <sub>36</sub> O <sub>2</sub>	Fatty acid	17.385	44.00	11503
41	Dodecanal	C <sub>12</sub> H <sub>24</sub> O	Aldehyde	18.284	44.00	14479
42	Nerolidol	C <sub>15</sub> H <sub>26</sub> O	Sesquiterpene	19.001	69.00	148917
44	Cyclohexane, eicosyl	C <sub>26</sub> H <sub>52</sub>	Cycloalkane	19.826	83.00	225697
45	Glycerol 1-palmitate	C <sub>19</sub> H <sub>38</sub> O <sub>4</sub>	Monoacylglycerols	20.134	43.00	311470
46	Hexadecanal	C <sub>16</sub> H <sub>32</sub> O	Aldehyde	20.515	149.00	114505
47	Meprobamate	C <sub>9</sub> H <sub>18</sub> N <sub>2</sub> O <sub>4</sub>	Carbamate	21.299	83.00	196437
48	Daucol	C <sub>15</sub> H <sub>26</sub> O <sub>2</sub>	Oxanes	21.447	151.00	211187
49	Methotrexate	C <sub>20</sub> H <sub>22</sub> N <sub>8</sub> O <sub>5</sub>	Antimetabolites	22.280	44.00	20613
50	Estradiol	C <sub>18</sub> H <sub>24</sub> O <sub>2</sub>	Steroid	22.871	272.00	407509
51	Octadecanoic acid, 2-hydroxy-1,3-propanediyl ester	C <sub>39</sub> H <sub>72</sub>	Fatty acid	23.790	43.00	126991
52	Mebutamate	C <sub>10</sub> H <sub>20</sub> N <sub>2</sub> O <sub>4</sub>	Carbamate	24.538	207.00	124804
53	Androsta-3,5-dien-3-ol, 17-acetyl-3-O-( <i>t</i> -butyldimethylsilyl)	C <sub>27</sub> H <sub>44</sub> O <sub>2</sub> Si	Steroids	25.401	207.00	39398

10 min. The inlet temperature was 260°C. The flow rate of the column was 0.6 mL/min helium gas at constant pressure (90 kPa). The GC to MS interface temperature was 280°C. The MS was used in scanning mode, with a scanning range of

40–350 amu. The ionization mode was EI, and the mass range was 50–550 m/z. One microliter of the sample was injected in the splitless injection mode. The total GC-MS course time was 50 min. The compounds in the peak areas

TABLE 2: Tentative compounds identified from the methanolic extract of *Vernonia patula* by gas chromatography-mass spectrometry (GC-MS) analysis.

Sl. no.	Name	Molecular formula	Nature	RT	m/z	Area
1	Cystine	C <sub>6</sub> H <sub>12</sub> N <sub>2</sub> O <sub>4</sub> S <sub>2</sub>	Amino acid	8.235	44.00	13166
2	D-alanine	C <sub>3</sub> H <sub>7</sub> NO <sub>2</sub>	α-amino acid	9.045	44.00	18522
3	Propanamide	C <sub>3</sub> H <sub>7</sub> NO	Amide	9.630	44.00	13580
4	(-)-norephedrine	C <sub>9</sub> H <sub>13</sub> NO	Sympathomimetic agent	9.765	44.00	16785
5	Norpseudoephedrine	C <sub>9</sub> H <sub>13</sub> NO	Alkaloid	9.765	44.00	16785
6	Dl-phenylephrine	C <sub>9</sub> H <sub>13</sub> NO	Sympathomimetic amine	9.765	44.00	16785
7	Octodrine	C <sub>8</sub> H <sub>19</sub> N	Amine	10.040	44.00	3381
8	1,2-ethanediamine, N-(2-aminoethyl)	C <sub>4</sub> H <sub>13</sub> N <sub>3</sub>	Amine	10.480	44.00	16968
9	Chlorodifluoroacetamide	C <sub>2</sub> H <sub>3</sub> ClFNO	Amide	11.250	44.00	7827
10	Cathine	C <sub>9</sub> H <sub>13</sub> NO	Alkaloid	11.916	44.00	9982
11	Phloroglucitol	C <sub>6</sub> H <sub>6</sub> O <sub>3</sub>	Polyphenol	12.666	44.00	31436
12	2-octynoic acid	C <sub>8</sub> H <sub>12</sub> O <sub>2</sub>	Fatty acid	12.945	44.00	39571
13	Glutaraldehyde	C <sub>5</sub> H <sub>8</sub> O <sub>2</sub>	Aldehyde	13.275	44.00	42367
14	Methyl stearate	C <sub>19</sub> H <sub>38</sub> O <sub>2</sub>	Fatty acid methyl ester	13.457	74.00	972212
15	Dibutyl phthalate	C <sub>16</sub> H <sub>22</sub> O <sub>4</sub>	Ester	13.454	44.00	30188
16	DL-cystine	C <sub>6</sub> H <sub>12</sub> N <sub>2</sub> O <sub>4</sub> S <sub>2</sub>	Amino acid	14.154	44.00	5343
17	Epinephrine, (β)-, 3TMS derivative	C <sub>9</sub> H <sub>13</sub> NO <sub>3</sub>	Catecholamine	14.894	73.00	367947
18	1-Dodecyne	C <sub>12</sub> H <sub>24</sub>	Alkene	14.752	44.00	5199
19	10-Undecenal	C <sub>11</sub> H <sub>20</sub> O	Aldehyde	15.489	55.00	142292
20	Phytol	C <sub>20</sub> H <sub>40</sub> O	Diterpene alcohol	15.348	71.00	227781
21	Piperazine	C <sub>4</sub> H <sub>10</sub> N <sub>2</sub>	Amine	15.341	44.00	34992
22	D-Galactonic acid, γ-lactone	C <sub>6</sub> H <sub>10</sub> O <sub>6</sub>	Sugar acid	16.727	44.00	23032
23	3,3'-Iminobispropylamine	C <sub>6</sub> H <sub>17</sub> N <sub>3</sub>	Nitrile	18.149	44.00	34648
24	Glutaraldehyde	C <sub>5</sub> H <sub>8</sub> O <sub>2</sub>	Aldehyde	18.805	44.00	27858
25	Hexanal	C <sub>6</sub> H <sub>12</sub> O	Aldehyde	19.670	44.00	17611
26	Folic acid	C <sub>19</sub> H <sub>19</sub> N <sub>7</sub> O <sub>6</sub>	Vitamin	20.190	44.00	28606
27	Undecanal	C <sub>11</sub> H <sub>22</sub> O	Aldehyde	20.132	43.00	145198
28	Epinephrine, (β)-, 3TMS derivative	C <sub>18</sub> H <sub>37</sub> NO <sub>3</sub> Si <sub>3</sub>	Hormone	21.914	73.00	295654
29	3,3-dimethylpiperidine	C <sub>7</sub> H <sub>15</sub> N	Alkaloid	21.935	44.00	6210
30	Nonanal	C <sub>9</sub> H <sub>18</sub> O	Aldehyde	23.435	44.00	12399
31	1-eicosanol	C <sub>20</sub> H <sub>42</sub> O	Fatty alcohol	24.546	59.00	7793425
32	Glucitol, 6-O-nonyl	C <sub>15</sub> H <sub>32</sub> O <sub>6</sub>	Alcohol	25.403	73.00	294332
33	Androsta-3,5-dien-3-ol, 17-acetyl-3-O-(t-butyl 4-acetyl-3,5-dimethyl-2-pyrrolicarboxylate)	C <sub>13</sub> H <sub>19</sub> NO <sub>3</sub>	Ester	31.157	207.00	67432

were classified by comparison with the national institute of standards and technology (NIST) GC-MS library version 08-S [37].

**2.4. Antioxidant Activity.** The experiments were performed in triplicate.

**2.4.1. 2,2-Diphenyl-1-Picrylhydrazyl (DPPH) Free Radical Scavenging Activity.** The extracts were evaluated for antioxidant activity using DPPH, as described in the literature [38]. In this experiment, 3 mg of each extract was added to 1 mL 50% methanol (v/v), and ascorbic acid (0.3 g) stock solution was added to 1 mL 50% methanol (v/v) as a positive control. The serial dilution technique was applied to obtain MEVP, MESV, and ascorbic acid at concentrations of 500, 250, 125, 62.5, 31.25, and 15.625 µg/mL. A 0.1 mL aliquot of each concentration of extract solution in methanol was combined with 1.0 mL freshly formulated DPPH-methanol solution (0.1 mM) and 0.45 mL 50 mM Tris (hydroxymethyl)

aminomethane (THAM) hydrochloride buffer (pH 7.40). The reaction was allowed to develop for 30 minutes, and absorbances were estimated at 517 nm. The corresponding inhibition rates were measured using the following equation:

$$\text{DPPH scavenged (\%)} = \left[ \frac{(A - B)}{A} \right] \times 100, \quad (1)$$

where  $A$  is the absorbance in the presence of extract or standard and  $B$  is the absorbance of the control.

**2.4.2. Total Phenolic Content (TPC).** The total phenolic content (TPC) of MESV and MEVP was determined using an oxidizing agent, Folin-Ciocalteu Reagent (FCR), according to the method described by Ali Reza et al. [39]. A 1 mL volume of FCR was diluted in 9 mL purified water, and then, 2.5 mL diluted FCR was combined with 2.5 mL (20%) of Na<sub>2</sub>CO<sub>3</sub> and 500 µg/mL extract. Purified water was added to obtain a final volume of 10 mL. The solution was

incubated for 20 min (250°C), and the absorbance was observed at 765 nm in triplicate. Gallic acid was used as the standard for the calculation of TPC, and the values were obtained according to the standard gallic acid curve ( $y = 0.0039x + 0.0406$ ;  $R^2 = 0.9981$ ). TPC was determined according to the following equation, in gallic acid equivalents (GAE; mg/g):

$$\text{TPC} = \text{equivalent reagent (Conc.)} \times \frac{\text{volume of total content}}{\text{conc. of sample taken}} \quad (2)$$

**2.4.3. Total Flavonoid Content (TFC).** The total flavonoid content (TFC) of MESV and MEVP was evaluated as previously described by Ali Reza et al. [39]. The TFC was calculated by mixing 0.5 mL extract with 1.5 mL methanol and adding 0.1 mL  $\text{AlCl}_3$  (10%), 0.1 mL  $\text{CH}_3\text{CO}_2\text{K}$  (1 M), and 2.8 mL distilled water. The mixture was incubated at 25°C for 30 min, and later, the absorbance was taken at 415 nm. The blank solution contained all of the reagents except for the extract. The TFC calculation was measured in quercetin equivalents (QE; mg/g), using quercetin as the standard.

**2.5. Statistical Analysis.** Values are reported as the mean  $\pm$  standard error of the mean (SEM;  $n = 3$ ).  $^aP < 0.05$ ,  $^bP < 0.01$ , and  $^cP < 0.001$  are used to identify significant differences for extract values compared with those for ascorbic acid, two-way analysis of variance (ANOVA), followed by Dunnett's test.

## 2.6. In Silico Molecular Docking

**2.6.1. Protein Preparation.** The 3D structure of urate oxidase (PDB: 1R4U) [40] and glutathione reductase (PDB: 3GRS) [41] was retrieved from the Protein Data Bank (.pdb format) [42] to evaluate the antioxidant effect. The 3D protein structure was assembled and refined using the method described by Uddin et al. [43].

**2.6.2. Ligand Preparation.** Identified compounds from *S. villosa* and *V. patula* were obtained from the PubChem databases in SDF format. Ligprep (Schrödinger v11.1) was used to prepare the ligand by maintaining OPLS3 force field [44]. The possible ionization state was generated at specific pH values ( $7.0 \pm 2.0$ ).

**2.6.3. Receptor Grid Generation.** Receptor grid generation was performed in Schrödinger v11.1, using the default parameters, with the van der Waals scaling factor and charge cutoff set to 1.00 and 0.25, respectively. A cubic box was placed on the geometrical center of the selected active site of the selected receptor, and a size setting of  $14 \text{ \AA} \times 14 \text{ \AA} \times 14 \text{ \AA}$  was used for molecular docking.

**2.6.4. Glide Standard Precision (SP) Ligand Docking and MM-GBSA Calculation.** Standard Precision (SP) flexible docking was performed using Glide (Schrödinger v11.1)

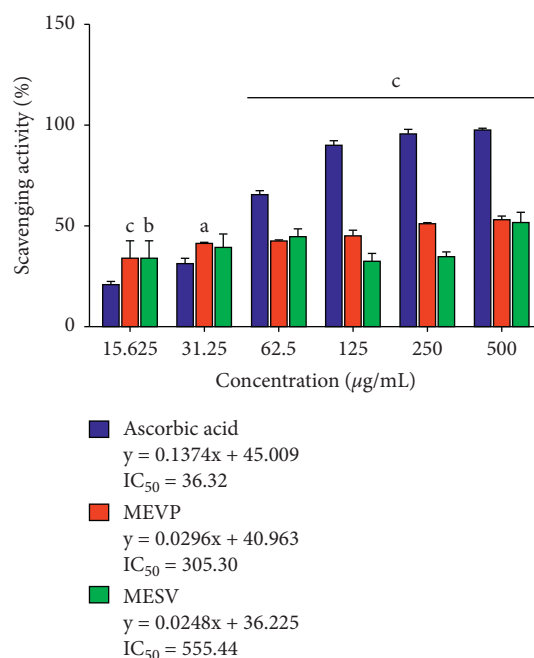


FIGURE 1: DPPH scavenging activity of methanolic extract of *Sterculia villosa* (MESV) and methanolic extract of *Vernonia patula* (MEVP) compared against the standard compound, ascorbic acid. Values are presented as the mean  $\pm$  SEM ( $n = 3$ ).  $^aP < 0.05$ ,  $^bP < 0.01$ , and  $^cP < 0.001$ ; significant compared with ascorbic acid (two-way ANOVA, followed by Dunnett's test).

[43, 45, 46]. The default parameters for the van der Waals scaling factor (0.80) and partial charge cutoff (0.15) were retained, and the docking score was recorded. The Schrödinger Prime MM-GBSA (OPLS3) was used for determining the binding energy of each ligand and the targeted receptor (kcal/mol) [47–49].

**2.6.5. In Silico Study: Determination of Pharmacokinetic Parameters by SwissADME.** The pharmacokinetic parameters used to assess the drug-likeness properties of the identified compounds were determined using SwissADME (<http://www.swissadme.ch/>). An orally active drug requires that each of the compounds adheres to the drug-like properties established by Lipinski and Veber's rule [50].

**2.6.6. In Silico Study: Toxicological Properties Prediction by ProTox Webserver.** The toxicological properties of the compounds were predicted with the assistance of the ProTox online server. The current study evaluated the toxicity profiles of selected compounds based on mutagenicity, carcinogenicity, hepatotoxicity, and toxicity class [51].

## 3. Results and Discussion

**3.1. GC-MS Analysis.** In a previous study, four triterpenoids were isolated and identified as bauerenyl acetate (I), friedelin (II), epifriedelanol (III), 20 (30)-taraxastene-3 betas, and 21  $\alpha$ -diol (IV) [30]. Several phytoconstituents from *S. villosa*



TABLE 3: Total phenolic content (TPC) and total flavonoid content (TFC) of methanolic extract of *Sterculia villosa* (MESV) and methanolic extract of *Vernonia patula* (MEVP).

Subject	TPC (mg GAE/g extract)	TFC (mg QE/g extract)
MESV	62.58 ± 1.93	81.44 ± 2.70
MEVP	58.99 ± 3.16	291.31 ± 6.61
Regression equation	$y = 0.0039x + 0.0406$ ; $R^2 = 0.9981$	$y = 0.0102x - 0.0637$ ; $R^2 = 0.9693$

TABLE 4: Molecular docking scores for identified compounds in *Sterculia villosa*.

Sl. no.	Compounds	1R4U (kcal/mol)	1R4U (MM-GBSA)	3GRS (kcal/mol)	3GRS (MM-GBSA)
1	Heptanal	—	—	-2.166	-25.325
2	Benzaldehyde, 2-methyl	-4.477	-26.2735	-5.789	-25.545
3	Glucitol, 6-O-nonyl	-3.25	-42.1814	-5.897	-62.624
4	L-Arabinitol	-3.335	-34.4304	-4.144	-28.63
5	$\alpha$ -Isomethyl ionone	-3.844	-33.9885	-5.359	-33.515
6	Eucalyptol	-4.195	-19.6369	-4.072	-12.525
7	Vanillin	-4.841	-29.0303	-5.561	-27.446
8	Prednisone	—	—	—	—
9	Bioallethrin	-2.75	-31.6861	-4.487	-35.818
10	Sorbitol	-2.968	-31.4369	-4.206	-36.397
11	$\beta$ -D-glucopyranose, 4-O- $\beta$ -D-galactopyranosyl	—	—	—	—
12	Santolinatriene	—	—	-3.349	-22.086
13	Vanillin, acetate	-4.874	-29.5427	-5.452	-35.791
14	Guanosine	-5.706	-42.3794	-7.029	-54.903
15	Trans-11-tetradecenyl acetate	+1.755	-35.467	-0.89	-54.627
16	D-galactonic acid, $\gamma$ -lactone	-5.106	-37.522	-5.364	-42.959
17	Isopulegol	-3.824	-32.1878	-6.033	-37.453
18	Benzaldehyde, 4-hydroxy-3,5-dimethoxy	-5.606	-37.7501	-5.56	-29.723
19	Naphthalene, 2-butyldecahydro	—	—	-5.423	-28.689
20	3-buten-2-one, 3-methyl-4-(3,5,6-trimethyl-3-cyclohexen-1-yl)-	-3.845	-32.3274	-4.502	-32.991
21	Cis-p-mentha-2,8-dien-1-ol	-3.743	-21.7445	-4.478	-16.731
22	Trans-sesquisabinene hydrate	-3.878	-24.5584	-4.885	-31.788
23	2-methoxy-6-methylaniline	-4.43	-26.2716	-5.738	-24.997
24	$\beta$ -carotene	-2.503	-48.5021	-6.133	-52.201
25	Aprobarbital	-6.266	-42.6018	-4.711	-23.22
26	Spiro[3.4]octan-5-one	-4.707	-24.2297	-4.684	-24.887
27	2-dodecen-1-yl(-)succinic anhydride	-1.704	-41.2219	-3.745	-53.132
28	Phytol	-1.004	-48.5855	-4.22	-36.0226
29	Digitoxin	-6.249	-61.3721	-7.396	-66.1619
30	Chrysanthemic acid	-3.833	-33.8038	-4.539	-32.3551
31	n-hexadecanoic acid	+0.47	-42.1025	-0.504	-44.2263
32	$\beta$ -asarone	-4.783	-40.5895	-5.033	-34.2406
33	Benzenepropanoic acid, 2,5-dimethoxy	-3.937	-42.1905	-5.359	-39.4505
34	Decanoic acid, 2,3-dihydroxypropyl ester	+0.681	-44.3904	-0.803	-52.772
35	9,12-octadecadienoic acid, methyl ester, (E,E)	+0.566	-45.4668	-1.483	-55.2765
36	7-hexadecenoic acid, methyl ester, (Z)	+0.652	-44.276	-1.171	-55.5193
37	Citronellol	-1.556	-26.2224	-3.03	-24.686
38	Undec-10-ynoic acid	+2.834	-38.9058	+2.186	-42.1098
39	6-octadecenoic acid, methyl ester, (Z)	-0.038	-44.8963	-0.423	-53.3609
40	Dodecanal	+2.452	-35.2648	+1.413	-40.0126
41	Nerolidol	-0.608	-34.4431	-2.001	-42.6634
42	Cyclohexane, eicosyl	-1.655	-46.9117	-2.967	-44.6644
43	Glycerol 1-palmitate	-2.579	-43.5815	-5.126	-47.6573
44	Hexadecanal	+1.286	-43.6651	-0.438	-46.5658
45	Meprobamate	-5.174	-45.9961	-5.719	-42.9626
46	Daucol	—	—	—	—
47	Methotrexate	-5.849	-61.4026	-8.457	-58.4485
48	Estradiol	-5.068	-33.4644	-5.8	-33.9768
49	Octadecanoic acid, 2-hydroxy-1,3-propanediyl	—	—	-1.109	-51.6491
50	Mebutamate	-5.359	-40.317	-6.05	-29.296
51	Androsta-3,5-dien-3-ol, 17-acetyl-3-O-(t-butyl)	—	—	—	—
52	Ascorbic acid (control)	-4.655	-37.8208	-5.965	-33.9373

TABLE 5: Molecular docking scores for identified compounds in *Vernonia patula*.

Sl. No.	Compounds	1R4U (kcal/mol)	1R4U (MM-GBSA)	3GRS (kcal/mol)	3GRS (MM-GBSA)
1	Cystine	-4.03	-41.7648	-3.399	-36.8961
2	D-alanine	-5.953	-15.5837	-5.036	-15.1612
3	Propanamide	-2.634	-18.48	-3.847	-26.3392
4	(-)-norephedrine	-5.79	-25.9004	-6.047	-29.0084
5	Norpseudoephedrine	-5.79	-25.9004	-6.047	-29.0084
6	DL-phenylephrine	-4.823	-31.1556	-5.544	-34.4102
7	Octodrine	-2.424	-26.1646	-3.653	-25.4794
8	1,2-ethanediamine, N-(2-aminoethyl)	-2.227	-19.1913	-3.182	-22.3522
9	Chlorodifluoroacetamide	-4.071	-15.6083	-5.072	-23.672
10	Cathine	-5.79	-25.9004	-6.047	-29.0084
11	Phloroglucitol	-5.858	-25.276	-5.854	-24.6614
12	2-octynoic acid	-2.58	-32.7105	-3.556	-29.6861
13	Glutaraldehyde	-3.026	-19.8291	-2.555	-25.0008
14	Methyl stearate	+1.332	-40.0523	-0.447	-51.2734
15	Dibutyl phthalate	-1.334	-37.2661	-2.763	-45.1367
16	Epinephrine, $\beta$ -, 3TMS derivative	—	—	—	—
17	1-dodecyne	+5.184	-27.4357	+3.225	-39.3134
18	10-undecenal	+2.981	-32.3244	+2.797	-34.283
19	Phytol	-1.004	-48.5855	-4.22	-36.0226
20	Piperazine	-4.933	-18.7799	-4.204	-21.361
21	D-galactonic acid, $\gamma$ -lactone	-5.106	-37.522	-5.364	-42.9587
22	3,3'-iminobispropylamine	—	—	—	—
23	Glutaraldehyde	-3.026	-19.8291	-2.555	-25.0008
24	Hexanal	-1.698	-24.1357	-2.712	-19.7671
25	Folic acid	-6.038	-49.7423	-8.243	-55.9741
26	Undecanal	+1.756	-32.3068	+1.482	-39.983
27	3,3-dimethylpiperidine	—	—	—	—
28	Nonanal	-1.868	-28.3973	-1.738	-32.1394
29	1-Eicosanol	+1.381	-54.2076	-2.03	-52.5786
30	Ascorbic acid (control)	-4.655	-37.8208	-5.965	-33.9373

and *V. patula* were identified in the current study. The MESV and MEVP may have potential therapeutic properties due to the presence of these bioactive phytoconstituents. The study was performed using GC-MS, one of the most widely used methods for phytoconstituent separation. The investigation of MESV and MEVP via GC-MS identified 52 and 33 phytochemical compounds, respectively (Tables 1 and 2). Figures S1 and S2 depict typical chromatograms for MESV and MEVP, respectively. Figures S3 and S4 depict the typical fragmentation pattern of compounds identified from MESV and MEVP, respectively. The major phytoconstituents in MESV included terpenoids, phytosterols, esters, acids, and other organic compounds. The major compounds isolated from MESV included mebutamate (RT: 24.538), octadecanoic acid, 2-hydroxy-1,3-propanediyl (RT: 23.790), estradiol (RT: 22.871), methotrexate (RT: 22.280), daucol (RT: 21.447), meprobamate (RT: 21.299), hexadecanal (RT: 20.515), glycerol 1-palmitate (RT: 20.134), and cyclohexane, eicosyl- (RT: 19.826). The major compounds isolated from MEVP included silanol, trimethyl-, phosphite (3:1) (RT: 31.157), androsta-3,5-dien-3-ol, 17-acetyl-3-O-(t-butyl 4-acetyl-3,5-dimethyl-2-pyrrolicarboxylate) (RT: 31.157), glucitol, 6-O-nonyl- (RT: 25.403), 1-eicosanol (RT: 24.546), nonanal (RT: 23.435), 3,3-dimethylpiperidine (RT: 21.935), epinephrine, ( $\beta$ -), 3TMS derivative (RT: 21.914), undecanal (RT: 20.132), folic acid (RT: 20.190), and hexanal (RT: 19.670).

**3.2. Antioxidant Activity.** Compared with the standard antioxidant, ascorbic acid, the inhibitory rate of MEVP gradually increased with increasing concentrations, ranging from 15.625 to 500  $\mu\text{g/mL}$ . A similar increase in inhibition was observed for increasing concentrations of MESV in the same concentration range. The maximum scavenging activity was observed at 500  $\mu\text{g/mL}$  for all three tested compounds, with values of 52.42%, 53.89%, and 98.33% for MESV, MEVP, and ascorbic acid, respectively (Figure 1). The  $\text{IC}_{50}$  values for MEVP, MESV, and ascorbic acid were determined to be 305.30, 555.44, and 36.32  $\mu\text{g/mL}$ , respectively.

The extracts were found to be potently active in the DPPH scavenging activity assay. The antioxidant activity of MESV and MEVP against DPPH is thought to be attributable to their hydrogen-donating capacity, suggesting that the extracts have the capacity to donate protons and can be used as primary antioxidants. The TPC and TFC were assessed using the regression equations for gallic acid ( $y = 0.0039x + 0.0406$ ;  $R^2 = 0.9981$ ) and quercetin ( $y = 0.0102x - 0.0637$ ;  $R^2 = 0.9693$ ), respectively. The TFC for MESV was higher ( $81.44 \pm 2.70$  mg QE/g dry extract) than the TPC ( $62.58 \pm 1.93$  mg GAE/g dry extract; Table 3). In MEVP, the TFC was higher ( $291.31 \pm 6.61$  mg QE/g dry extract) than the TPC ( $58.99 \pm 3.16$  mg GAE/g dry extract; Table 3).

Based on the TFC and TPC assays, the *S. villosa* and *V. patula* extracts contained significant amounts of flavonoid and phenolic contents, indicating that these plants'



TABLE 6: Interactions and bond distances between selected compounds identified in *Sterculia villosa* and the receptors following: urate oxidase (PDB: 1R4U) and glutathione reductase (PDB: 3GRS) binding sites.

Proteins	Ligands	Hydrogen bond interactions		Hydrophobic interactions	
		Amino acid residue	Distance (Å)	Amino acid residue	Distance (Å)
1R4U	Aprobarbital	ARG-176	2.27, 2.35	HIS-256	4.39
		VAL-227	1.89	LEU-170	5.20
		GLN-228	2.02, 2.02	PHE-159	4.13
	Digitoxin	—	—	SER-226	3.66
		LEU-163	2.09	ASP-165	2.69
		ASP-165	1.79	TYR-167	2.70
		TYR-167	2.17	PHE-258	5.49, 4.36, 4.21
		ILE-177	2.38	LEU-170	5.20, 5.39
	Methotrexate	—	—	GLU-259	2.38
		—	—	ARG-176	2.83, 2.34
		—	—	TYR-167	2.70
		—	—	LEU-170	5.20, 5.39
GLU-259		3.06	HIS-256	4.72	
HIS-256		1.98	ARG-176	2.71	
ILE-177		1.88	LEU-170	4.81, 4.48, 4.44	
Guanosine	LEU-170	2.72	THR-168	2.72	
	THR-169	2.54	—	—	
	THR-168	2.14	—	—	
	ASN-254	1.98, 2.01	PHE-159	2.69	
Benzaldehyde, 4-hydroxy-3,5-dimethoxy	ARG-176	1.90	GLN-228	2.42	
	GLN-228	1.96	—	—	
Ascorbic acid	LEU-287	2.50	ARG-176	2.73, 5.03	
	HIS-265	2.58	TYR-257	2.34	
	ILE-177	1.99	—	—	
	GLU-259	2.14	TYR-257	6.50	
	TYR-257	5.46	—	—	
	ILE-177	3.63, 4.43	—	—	
	HIS-256	4.03	—	—	
	GLU-259	4.18	—	—	

TABLE 6: Continued.

Proteins	Ligands	Hydrogen bond interactions		Hydrophobic interactions	
		Amino acid residue	Distance (Å)	Amino acid residue	Distance (Å)
3GRS	Methotrexate	PHE-181	5.46	VAL-61	5.99, 4.88
		ASP-104	3.81	GLY-50	5.20
		ASN-60	3.18	THR-156	4.62, 3.40
		THR-57	4.17	—	—
		GLU-50	4.76	—	—
		SER-51	3.01	—	—
		LYS-296	5.25, 4.24	MET-159	4.99
		THR-162	3.08	PRO-160	6.97
		GLY-158	3.93	HIS-158	4.87
		THR-156	4.50	VAL-61	5.19
3GRS	Digitoxin	GLU-50	3.87	GLY-56	3.78
		—	—	GLU-50	4.43
		—	—	HIS-52	4.87
		GLU-50	3.76	GLU-50	5.28, 5.38
		HOH-482	3.24	GLY-56	3.61
		ASP-331	4.05	THR-156	4.85
		GLY-158	3.87	ALA-155	4.28
		THR-57	4.22, 3.74	GLY-157	3.75
		HOH-490	3.63	GLY-330	3.78
		—	—	ALA-342	7.47
3GRS	$\beta$ -Carotene	—	—	CYS-63	4.63, 4.21
		—	—	PHE-372	6.26
		—	—	VAL-370	5.21, 4.21
		—	—	LEU-338	5.55, 4.45
		—	—	PRO-340	4.49
		—	—	TYR-197	6.03
		—	—	HIS-52	6.18
		—	—	HIS-129	5.57
		THR-156	4.74	VAL-61	4.73
		ARG-291	6.02	LYS-53	4.06
3GRS	Mebutamate	HOH-490	3.68	HIS-52	4.17
		THR-57	3.85	—	—
		ASP-178	4.21	—	—
		GLU-50	4.60, 4.15, 4.93	GLY-157	3.71
		HOH-490	3.11	GLY-27	3.38
		THR-57	3.67	—	—
		ALA-155	4.10	—	—
		—	—	—	—
		—	—	—	—
		—	—	—	—

TABLE 7: Interactions and bond distances between selected compounds identified in *Vernonia patula* and the receptors following: urate oxidase (PDB: 1R4U) and glutathione reductase (PDB: 3GRS) binding sites.

Proteins	Ligands	Hydrogen bond interactions		Hydrophobic interactions	
		Amino acid residue	Distance (Å)	Amino acid residue	Distance (Å)
1R4U	Folic acid	TYR-257	2.18, 1.94, 2.62	LEU-170	5.08
		HIS-256	2.54	ARG-176	4.60, 4.96
		LEU-287	1.70, 2.00	—	—
		GLN-288	2.24, 2.36	—	—
		ARG-176	4.11	—	—
	D-alanine	HIS-256	3.51	—	—
		ASN-254	4.86	—	—
		ILE-177	3.64	—	—
		TYR-257	4.52	—	—
	Phloroglucitol	ARG-176	6.43	—	—
		GLN-228	4.01	—	—
		TRP-160	1.79, 2.04	—	—
		ALA-225	1.97	—	—
	(-)-norephedrine	TRP-160	1.79, 2.04	—	—
		ALA-225	1.97	—	—
	Norpseudoephedrine	HIS-256	4.03	TYR-257	6.50
		GLU-259	4.18	—	—
	Ascorbic acid	TYR-257	5.46	—	—
		ILE-177	4.43, 3.63	—	—
		PHE-181	4.83	VAL-61	6.25, 5.49
		ASP-104	3.62	HIS-52	4.41
	Folic acid	LYS-53	4.79	GLU-50	4.67
		GLU-50	4.75, 3.36	—	—
		THR-57	3.59	—	—
		THR-156	5.15	—	—
	(-)-norephedrine	HOH-490	3.67	—	—
THR-156		3.73	GLY-27	3.96	
GLU-50		4.51	ALA-130	6.54	
—		—	HIS-129	6.37	
3GRS	Norpseudoephedrine	THR-156	3.73	GLY-27	3.96
		GLU-50	4.51	ALA-130	6.54
	—	—	HIS-129	6.37	
	Cathine	THR-156	3.73	GLY-27	3.96
GLU-50		4.51	ALA-130	6.54	
Phloroglucitol	—	—	HIS-129	6.37	
	TYR-197	5.77	—	—	
	THR-339	3.17	—	—	
	ASP-331	4.49	—	—	
Ascorbic acid	THR-57	3.67	GLY-157	3.71	
	ALA-155	4.10	GLY-27	3.38	
	GLU-50	4.93, 4.15	—	—	
	HOH-490	3.11	—	—	

phenolic components may predominantly consist of flavonoids in glycosidic forms; glycosidic flavonoids tend to concentrate in polar solvents, which are more effective than less polar solvents for the removal of phenolic compounds from plant materials [52, 53]. Previous research showed that the presence of phenolic compounds, such as flavonoids, correlates with high levels of antioxidant activity and health benefits [54].

**3.3. Molecular Docking Study.** The results for the molecular docking simulation study for the five compounds and control with the highest docking scores identified from *S. villosa* and *V. patula* extracts are shown in Tables 4 and 5, respectively. To

evaluate the antioxidant attributes, the selected compounds from each plant extract were subjected to docking against urate oxidase (PDB: 1R4U) and glutathione reductase (PDB: 3GRS). For the compounds identified in *S. villosa*, the five selected compounds, ordered according to docking score for urate oxidase (PDB: 1R4U), were as follows: aprobarbital > digitoxin > methotrexate > guanosine > benzaldehyde, 4-hydroxy-3,5-dimethoxy-. Then, the order for docking scores when docked with glutathione reductase (PDB: 3GRS) in case of compounds identified in *S. villosa* is as follows: methotrexate > digitoxin > guanosine >  $\beta$ -carotene > mebutamate. For *V. patula* extract, the five selected compounds according to docking scores for urate oxidase (PDB: 1R4U) were as follows: folic acid > d-alanine > phloroglucitol > (-)-norephedrine  $\geq$

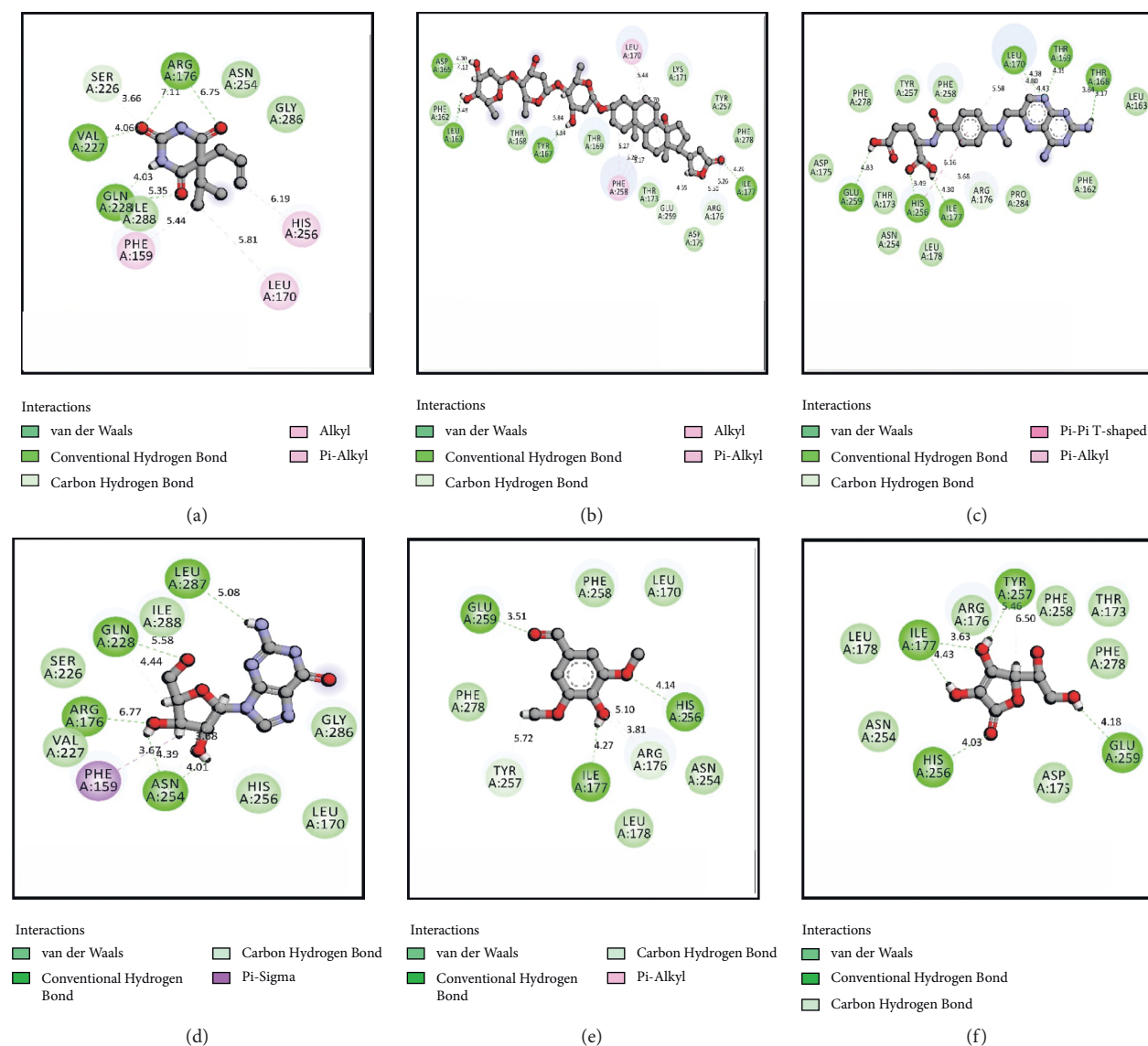


FIGURE 2: 2D representations of the best docking scores between urate oxidase (PDB: 1R4U) and (a) aprobarbital: conventional hydrogen bond (ARG-176, VAL-227, GLN-228), van der Waals bond (ILE-288), and alkyl and pi-alkyl bond (PHE-159, LEU-170, HIS-256); (b) digitoxin: conventional hydrogen bond (ASP-165, LEU-163, TYR-167, and ILE-177), carbon-hydrogen bond (ARG-176, GLU-259, TYR-167, and ASP-165), and alkyl and pi-alkyl bond (LEU-170, PHE-258); (c) methotrexate: conventional hydrogen bond (GLU-259, HIS-256, ILE-177, THR-168, THR-169, and LEU-170), pi-pi T-shaped bond (HIS-256), and pi-alkyl bond (LEU-170); (d) guanosine: conventional hydrogen bond (LEU-287, ARG-176, and ASN-254), carbon-hydrogen bond (GLN-228, ASN-254), and pi-sigma bond (PHE-159); (e) benzaldehyde, 4-hydroxy-3,5-dimethoxy-: conventional hydrogen bond (HIS-256, ILE-177, and GLU-259), carbon-hydrogen bond (ARG-176), and pi-alkyl bond (ARG-176); (f) ascorbic acid (control): conventional hydrogen bond (TYR-257, ILE-177, HIS-256, and GLU-259) and carbon-hydrogen bond (TYR-257).

norpseudoephedrine. When the docking simulation was carried out on the compounds from *V. patula* with glutathione reductase (PDB: 3GRS), the following order of docking score was found: folic acid > (-)-norephedrine  $\geq$  norpseudoephedrine  $\geq$  cathine > phloroglucitol. The molecular docking simulations between the selected compounds and the protein are further demonstrated in Tables 6 and 7. Furthermore, the 2D representations of the ligand-protein interactions are presented in Figures 2 and 3 for compounds in *S. villosa* and in Figures 4 and 5 for compounds in *V. patula*.

**3.4. ADME and Toxicological Study.** The ADME properties are markers of pharmacokinetic characteristics and were used to assess oral bioavailability based on the Lipinski and Veber rules. The data for each compound were retrieved from the SwissADME online server, as shown in Tables 8 and 9 for *S. villosa* and *V. patula*, respectively. Digitoxin was found to violate three of the parameters, and  $\beta$ -carotene violated two parameters, while one parameter of the Lipinski rule was violated by methotrexate and guanosine, among compounds identified in *S. villosa*. Only folic acid, which

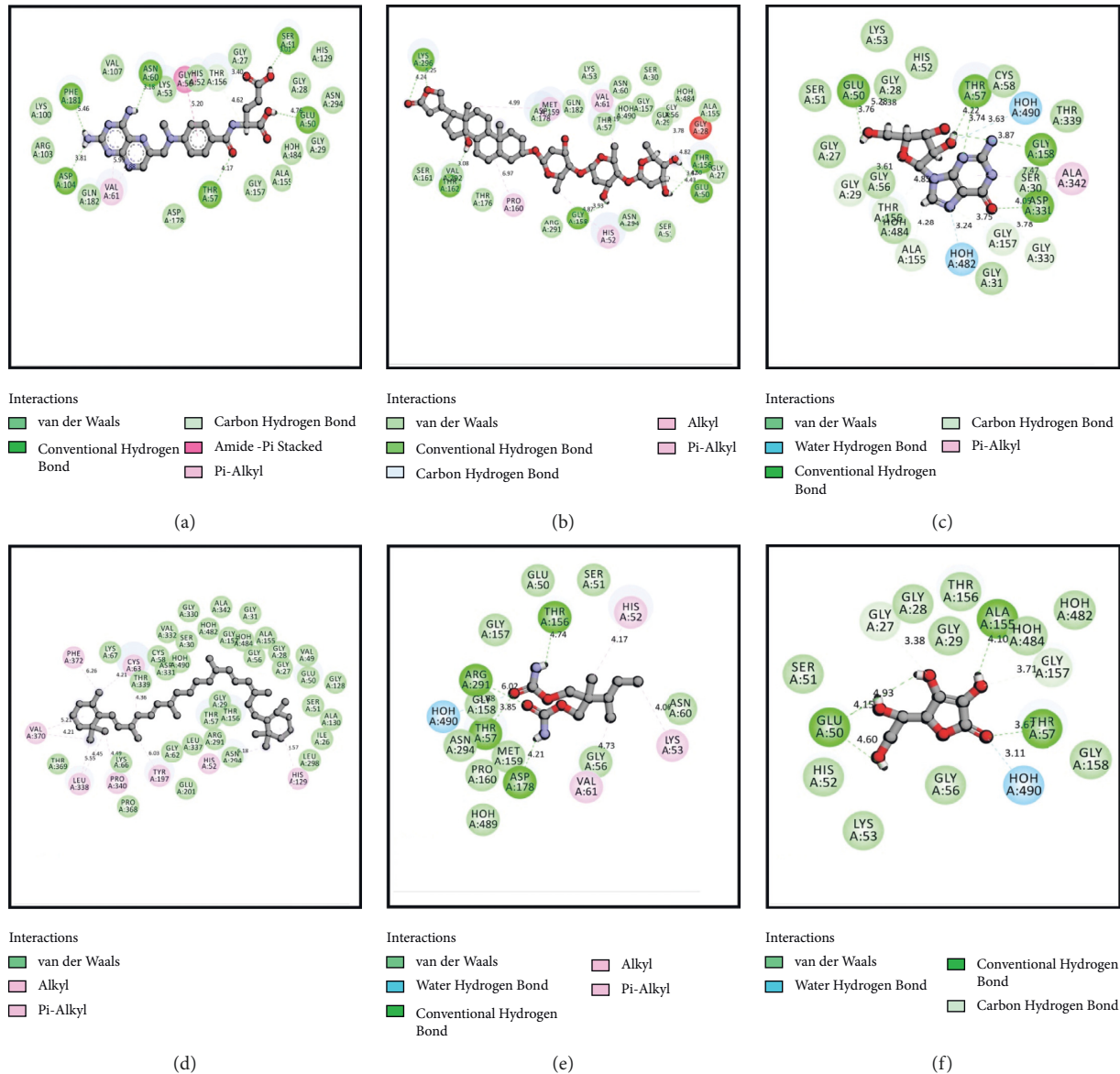


FIGURE 3: 2D representations of the best docking scores between glutathione reductase (PDB: 3GRS) and (a) methotrexate: conventional hydrogen bond (SER-51, ASN-60, PHE-181, ASP-104, THR-57, and GLU-50), carbon-hydrogen bond (THR-156), amide-pi stacked bond (GLY-50), and pi-alkyl bond (VAL-61); (b) digitoxin: conventional hydrogen bond (THR-156, GLU-50, GLY-158, THR-162, and LYS-296), alkyl and pi-alkyl bond (MET-159, PRO-160, HIS-52, and VAL-61), and carbon-hydrogen bond (GLY-56); (c) guanosine: conventional hydrogen bond (GLY-158, THR-57, ASP-331, and GLU-50), water hydrogen bond (HOH-482), carbon-hydrogen bond (GLY-157, ALA-155, THR-156, GLY-29, GLU-50, and GLY-330), and pi-alkyl bond (ALA-342); (d)  $\beta$ -carotene: alkyl and pi-alkyl bond (LEU-338, VAL-370, PRO-340, TYR-197, CYS-63, HIS-52, and HIS-129); (e) mebutamate: conventional hydrogen bond (ASP-178, THR-57, ARG-291, and THR-156), water hydrogen bond (HOH-490), and alkyl and pi-alkyl bond (VAL-61, LYS-53, and HIS-52); (f) ascorbic acid (control): conventional hydrogen bond (ALA-155, THR-57, and GLU-50), water hydrogen bond (HOH-490), and carbon-hydrogen bond (GLY-157).

violated one parameter, was found to violate these rules among the compounds identified in *V. patula*.

The toxicity profiles for each of the selected compounds in the two extracts are evaluated through the ProTox online server and are presented in Tables 10 and 11. These results showed that none of the selected compounds from *S. villosa* are associated with the hepatotoxic property.  $\beta$ -carotene was found to have mutagenicity while two of the compounds, namely, aprobarbital and mebutamate, were associated with carcinogenic properties among the compounds identified in *V. patula*.

In this study, molecular docking simulations were performed to associate and reciprocate the in vitro experimental findings. The extracts from *S. villosa* and *V. patula* were subjected to GC-MS to identify chemical compounds, and those compounds with potential pharmacological activity were subjected to a molecular docking simulation against urate oxidase (PDB: 1R4U) and glutathione reductase (PDB: 3GRS) to evaluate the antioxidant properties in silico. The five compounds from each plant extract with the highest docking scores against two distinctive receptors were

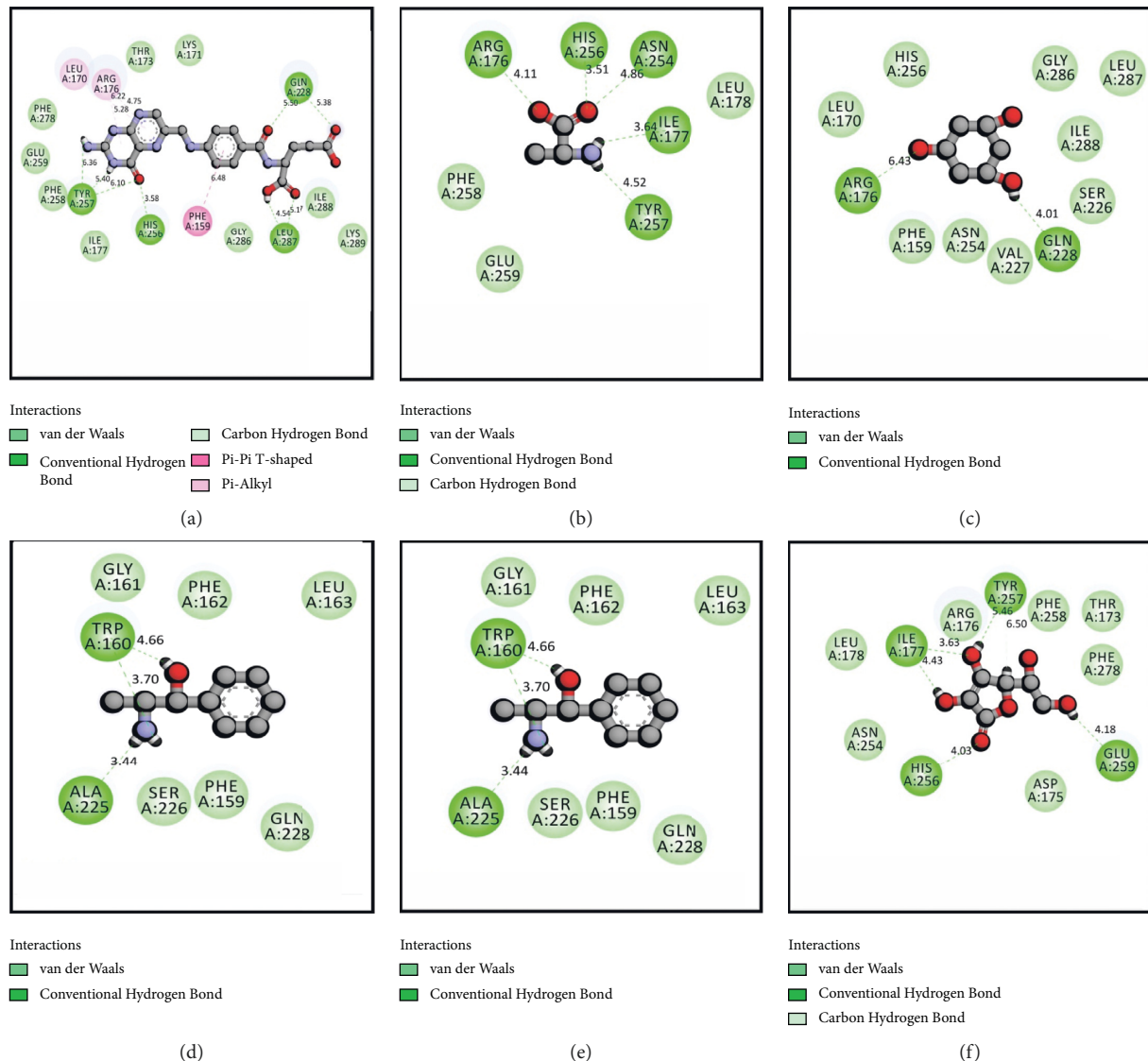


FIGURE 4: 2D representations of the best docking scores between urate oxidase (PDB: 1R4U) and (a) folic acid: conventional hydrogen bond (GLN-228, LEU-287, HIS-256, and TYR-257), pi-alkyl bond (ARG-176), and pi-pi T-shaped bond (PHE-159); (b) D-alanine: conventional hydrogen bond (ARG-176, HIS-256, ASN-254, ILE-177, and TYR-257); (c) phloroglucitol: conventional hydrogen bond (ARG-176, GLN-228); (d) (-)-norephedrine: conventional hydrogen bond (TRP-160, ALA-225); (e) norpseudoephedrine: conventional hydrogen bond (TRP-160, ALA-225); (f) ascorbic acid (control): conventional hydrogen bond (TYR-257, ILE-177, HIS-256, GLU-259).

selected for further analysis. Aprobarbital had the highest docking score ( $-6.266$ ) among the compounds identified in *S. villosa* when the docking simulation was preceded against urate oxidase (PDB: 1R4U). It exhibits a better score than the control, ascorbic acid ( $-4.655$ ). Aprobarbital formed conventional hydrogen bonds with the following amino acid residues in urate oxidase: ARG-176, VAL-227, and GLN-228. Aprobarbital also forms alkyl and pi-alkyl bonds with HIS-256, LEU-170, and PHE-159 and a carbon-hydrogen bond with SER-226 when binding with the active site of urate oxidase to exert an antioxidant effect. When the compounds were docked against glutathione reductase and compared to the control, methotrexate was found to have a significant binding affinity ( $-8.457$ ). When bonded with methotrexate, it formed a conventional hydrogen bond with

SER-51, ASN-60, PHE-181, ASP-104, THR-57, and GLU-50. One carbon-hydrogen bond with THR-156, one amide-pi stacked bond with GLY-50), and one pi-alkyl bond with VAL-61 were also reported. Folic acid possessed the best result ( $-6.038$ ) for the compounds identified in *V. patula* in case of urate oxidase (PDB: 1R4U). Folic acid formed conventional hydrogen bonds with TYR-257, HIS-256, LEU-287, and GLN-228. A pi-pi bond was formed with PHE-159, and a pi-alkyl bond was formed with LEU-170 and ARG-176. Folic acid also possessed better ligand-protein interaction ( $-8.243$ ) in case of glutathione reductase (PDB: 3GRS). It has formed a conventional hydrogen bond with PHE-181, LYS-53, THR-156, THR-57, GLU-50, and ASP-104, one water hydrogen bond with HOH-490, one pi-pi stacked bond with HIS-52, and one pi-alkyl with VAL-61. All



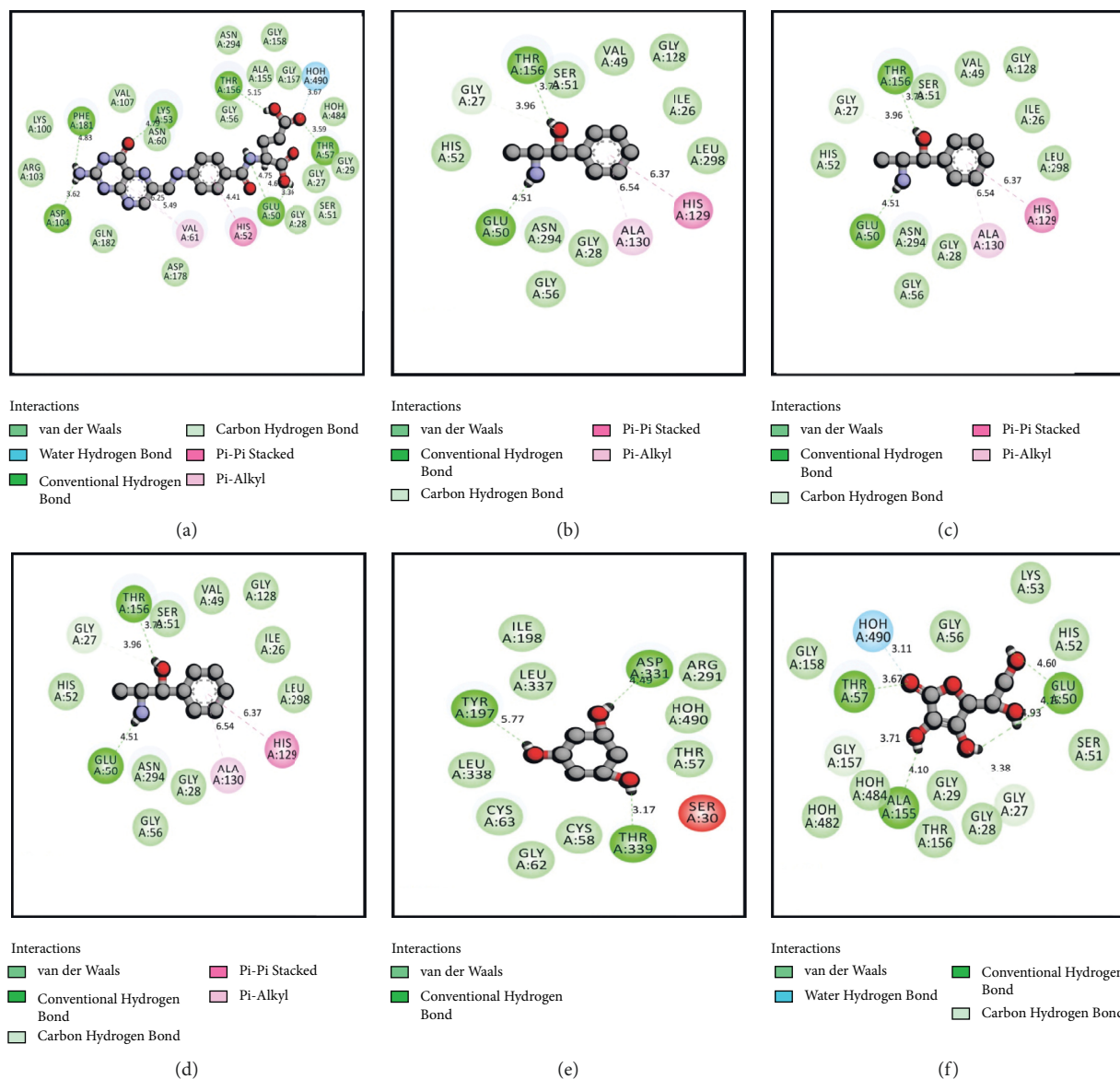


FIGURE 5: 2D representations of the best docking scores between glutathione reductase (PDB: 3GRS) and (a) folic acid: conventional hydrogen bond (PHE-181, LYS-53, THR-156, THR-57, GLU-50, and ASP-104), water hydrogen bond (HOH-490), pi-pi stacked bond (HIS-52), and pi-alkyl bond (VAL-61); (b) (-)-norephedrine: conventional hydrogen bond (THR-156, GLU-50), pi-pi stacked bond (HIS-129), pi-alkyl bond (ALA-130), and carbon-hydrogen bond (GLY-27); (c) norpseuodphedrine: conventional hydrogen bond (THR-156, GLU-50), pi-pi stacked bond (HIS-129), pi-alkyl bond (ALA-130), and carbon-hydrogen bond (GLY-27); (d) cathine: conventional hydrogen bond (THR-156, GLU-50), pi-pi stacked bond (HIS-129), pi-alkyl bond (ALA-130), and carbon-hydrogen bond (GLY-27); (e) phloroglucitol: conventional hydrogen bond (ASP-331, TYR-197, and THR-339); (f) ascorbic acid (control): conventional hydrogen bond (GLU-50, ALA-155, THR-57), water hydrogen bond (HOH-490), and carbon-hydrogen bond (GLY-157, GLY-27).

TABLE 8: Physicochemical properties associated with good oral bioavailability for the isolated compounds from *Sterculia villosa*.

Compounds	Lipinski rules				Lipinski's violations	Veber rules	
	MW <500	HBA <10	HBD <5	Log <i>P</i> ≤5		nRB ≤10	TPSA ≤140
Aprobarbital	210.23	3	2	0.82	0	3	75.27
Digitoxin	764.94	13	5	2.61	3	7	182.83
Methotrexate	454.44	9	5	-0.50	1	10	210.54
Guanosine	283.24	7	5	-2.02	1	2	159.51
Benzaldehyde, 4-hydroxy-3,5-dimethoxy	182.17	4	1	0.93	0	3	55.76
Mebutamate	232.28	4	2	1.05	0	8	104.64
β-carotene	536.87	0	0	11.11	2	10	0

Here, MW, molecular weight (g/mol); HBA, hydrogen bond acceptor; HBD, hydrogen bond donor; Log *P*, lipophilicity; nRB: number of rotatable bonds; TPSA: topological polar surface area.

TABLE 9: Physicochemical properties associated with good oral bioavailability for the isolated compound from *Vernonia patula*.

Compounds	Lipinski rules			Log <i>P</i> ≤5	Lipinski's violations ≤1	Veber rules	
	MW <500	HBA <10	HBD <5			nRB ≤10	TPSA ≤140
Folic acid	441.40	9	6	-0.36	1	10	213.28
D-alanine	89.09	3	1	-1.46	0	1	63.32
(-)-norephedrine	151.21	2	2	1.11	0	2	46.25
Norpseudoephedrine	151.21	2	2	1.11	0	2	46.25
Cathine	151.21	2	2	1.11	0	2	46.25
Phloroglucitol	132.16	3	3	-0.30	0	0	60.69

Here, MW, molecular weight (g/mol); HBA, hydrogen bond acceptor; HBD, hydrogen bond donor; Log *P*, lipophilicity; nRB: number of rotatable bonds; TPSA: topological polar surface area.

TABLE 10: Toxicological properties of the identified compounds from *Sterculia villosa*.

Compounds	Mutagenicity	Carcinogenicity	Hepatotoxicity	Toxicity class
Aprobarbital	NM	Carcinogenic	NH	II
Digitoxin	NM	NC	NH	I
Methotrexate	NM	NC	NH	I
Guanosine	NM	NC	NH	II
Benzaldehyde, 4-hydroxy-3,5-dimethoxy-	NM	NC	NH	IV
Mebutamate	NM	Carcinogenic	NH	IV
$\beta$ -carotene	Mutagenic	NC	NH	IV

NM: nonmutagenic; NC: noncarcinogenic; NH: nonhepatotoxic; Class I ( $LD_{50} \leq 5$ ); Class II ( $5 < LD_{50} \leq 50$ ); Class III ( $50 < LD_{50} \leq 300$ ); Class IV ( $300 < LD_{50} \leq 2000$ ); Class V ( $2000 < LD_{50} \leq 5000$ ); Class VI ( $LD_{50} > 5000$ ).

TABLE 11: Toxicological properties of the identified compounds from *Vernonia patula*.

Compound	Mutagenicity	Carcinogenicity	Hepatotoxicity	Toxicity class
Folic acid	NM	NC	NH	III
D-alanine	NM	NC	NH	III
(-)-norephedrine	NM	NC	NH	III
Norpseudoephedrine	NM	NC	NH	III
Cathine	NM	NC	NH	III
Phloroglucitol	NM	NC	NH	VI

NM: nonmutagenic; NC: noncarcinogenic; NH: nonhepatotoxic; Class I ( $LD_{50} \leq 5$ ); Class II ( $5 < LD_{50} \leq 50$ ); Class III ( $50 < LD_{50} \leq 300$ ); Class IV ( $300 < LD_{50} \leq 2000$ ); Class V ( $2000 < LD_{50} \leq 5000$ ); Class VI ( $LD_{50} > 5000$ ).

of the compounds having the highest docking score were significantly better than the control in terms of ligand-protein interaction. This suggested that these compounds have good potential as a promising antioxidant agent. All of the compounds were also subjected to the evaluation of ADME and toxicological properties. The Lipinski rule of five states that orally administered agents should have the following properties: molecular weight <500 amu, hydrogen bond acceptor sites <10, hydrogen bond donor sites <5, and lipophilicity value (Log *P*) ≤ 5. Veber's rules recommend a number of rotatable bonds ≤ 10 and topological polar surface area ≤ 140. According to these rules, a compound or potential medicinal agent cannot violate all of the parameters while still presenting good oral bioavailability [55, 56]. Among the two compounds with the highest docking scores identified for each plant species, aprobarbital did not violate any of the parameters, whereas folic acid and methotrexate had violated one parameter of the Lipinski rule of five, which is within the acceptable range. Thus, these compounds are considered safe for *in vivo* administration to an animal model. In the *S. villosa* extract, all other compounds, except digitoxin, methotrexate, guanosine, and  $\beta$ -carotene, also

met all of the criteria for the Lipinski rule. In the *V. patula* extract, all compounds meet all components of the rules except for folic acid. Additionally, the toxicity prediction showed that none of the identified compounds in *S. villosa* is played hepatotoxicity. When it comes to carcinogenicity, all of the compounds were free from carcinogenic properties except aprobarbital and mebutamate. In addition to that, only  $\beta$ -carotene was associated with mutagenic properties. By contrast, in the *V. patula* extract, all of the compounds were free from mutagenic, carcinogenic, and hepatotoxic properties. Therefore, the selected compounds from *S. villosa* and *V. patula* may represent promising antioxidant agents, as further supported by the molecular docking study.

#### 4. Conclusions

This study reported the potential antioxidant effects of methanolic bark extract of *S. villosa* and methanolic whole-plant extract of *V. patula*; this might be due to their chemical constituents. These chemical compounds may offer antioxidant activities, as assessed by the molecular

docking study. Further advanced studies remain necessary to identify the potential compounds responsible for antioxidant activities displayed by these two plants, *S. villosa* and *V. patula*.

## Data Availability

Available data are presented in the manuscript.

## Conflicts of Interest

The authors declare no conflicts of interest.

## Acknowledgments

The authors would like to acknowledge the support provided by Researchers Supporting Project Number (RSP-2021/358), King Saud University, Riyadh, Saudi Arabia. This article is an outcome of a R&D project of the Institute of Food Science and Technology (IFST), Bangladesh Council of Scientific and Industrial Research (BCSIR), Dhaka, Bangladesh. The authors are cordially expressing their gratitude to the authority of the BCSIR for providing necessary funds for this study. The authors are also grateful to Biomedical and Toxicological Research Institute (BTRI) for providing facilities to conduct the research. The authors would like to extend their sincere appreciation to the Research and Development (R & D) Grant (Group: Biology, Medical Science and Nutrition Science; FY 2019-2020; SL. No. 135; FY 2020-2021; SL. No. 23; Reg. No. 43), and Special Allocation Grant (Group: Biological Science; FY: 2021-2022; Gr. SL. 349 BS), Ministry of Science and Technology, People's Republic of Bangladesh for awarding research grants to Dr. Talha Bin Emran, Department of Pharmacy, BGC Trust University Bangladesh, Chittagong 4381, Bangladesh.

## Supplementary Materials

The following are available online at <http://www.mdpi.com/xxx/s1>. Figure S1: total ionic chromatogram (TIC) of methanol extract of *Sterculia villosa* (MESV). Figure S2: total ionic chromatogram (TIC) of methanol extract of *Vernonia patula* (MEVP). Figure S3: fragmentation pattern of compounds identified from the methanol extract of *Sterculia villosa* (MESV). Figure S4: fragmentation pattern of compounds identified from the methanol extract of *Vernonia patula* (MEVP). (*Supplementary Materials*)

## References

- [1] N. Stanković, T. Mihajilov-Krstev, B. Zlatković et al., "Antibacterial and antioxidant activity of traditional medicinal plants from the balkan peninsula," *NJAS: Wageningen Journal of Life Sciences*, vol. 78, no. 1, pp. 21–28, 2016.
- [2] H. C. Voon, R. Bhat, and G. Rusul, "Flower extracts and their essential oils as potential antimicrobial agents for food uses and pharmaceutical applications," *Comprehensive Reviews in Food Science and Food Safety*, vol. 11, no. 1, pp. 34–55, 2012.
- [3] S. Mitra, S. R. Prova, S. A. Sultana et al., "Therapeutic potential of indole alkaloids in respiratory diseases: a comprehensive review," *Phytomedicine*, vol. 90, Article ID 153649, 2021.
- [4] N. Alam, N. Banu, M. A. I. Aziz et al., "Chemical profiling, pharmacological insights and in silico studies of methanol seed extract of *sterculia foetida*," *Plants*, vol. 10, no. 6, p. 1135, 2021.
- [5] K. Mazumder, A. Nabila, A. Aktar, and A. Farahnaky, "Bioactive variability and in vitro and in vivo antioxidant activity of unprocessed and processed flour of nine cultivars of Australian lupin species: a comprehensive substantiation," *Antioxidants*, vol. 9, no. 4, p. 282, 2020.
- [6] S. Mitra, A. M. Tareq, R. Das et al., "Polyphenols: a first evidence in the synergism and bioactivities," *Food Reviews International*, vol. 2022, pp. 1–23, 2022.
- [7] A. Ghani, *Medicinal Plants of Bangladesh with Chemical Constituents and Uses*, p. 183, Asiatic Society of Bangladesh, Dhaka, Bangladesh, 2003.
- [8] M. A. R. B. Shovo, M. R. Tona, J. Mouah et al., "Computational and pharmacological studies on the antioxidant, thrombolytic, anti-inflammatory, and analgesic activity of *molineria capitulata*," *Current Issues in Molecular Biology*, vol. 43, no. 2, pp. 434–456, 2021.
- [9] N. A. Al-Dhabi and M. Valan Arasu, "Quantification of phytochemicals from commercial spirulina products and their antioxidant activities," *Evidence-Based Complementary and Alternative Medicine*, vol. 2016, Article ID 7631864, 13 pages, 2016.
- [10] T. Dutta, A. Paul, M. Majumder, R. A. Sultan, and T. B. Emran, "Pharmacological evidence for the use of *Cissus assamica* as a medicinal plant in the management of pain and pyrexia," *Biochemistry and Biophysics Reports*, vol. 21, p. 100715, 2020.
- [11] A. S. Ray and H. R. Chowdhury, "Pharmacognostic, phytochemical and antioxidant studies of *gardenia latifolia aiton*: an ethnomedicinal tree plant," *International Journal of Pharmacognosy and Phytochemical Research*, vol. 10, no. 5, pp. 216–228, 2018.
- [12] K. Barathkannan, B. Venkatadri, A. Khusro et al., "Chemical analysis of *Punica granatum* fruit peel and its in vitro and in vivo biological properties," *BMC Complementary Alternative Medicine*, vol. 16, no. 1, p. 264, 2016.
- [13] V. Furlan, J. Konc, and U. Bren, "Inverse molecular docking as a novel approach to study anticarcinogenic and anti-neuro-inflammatory effects of curcumin," *Molecules*, vol. 23, no. 12, p. 3351, 2018.
- [14] K. Kores, S. Lešnik, U. Bren, D. Janežič, and J. Konc, "Discovery of novel potential human targets of resveratrol by inverse molecular docking," *Journal of Chemical Information and Modeling*, vol. 59, no. 5, pp. 2467–2478, 2019.
- [15] N. Abdullah Al-Dhabi, M. Valan Arasu, and T. S. Rejiniemon, "Vitro antibacterial, antifungal, antibiofilm, antioxidant, and anticancer properties of isosteviol isolated from endangered medicinal plant *Pittosporum tetraspermum*," *Evidence-Based Complementary and Alternative Medicine*, vol. 2015, Article ID 164261, 11 pages, 2015.
- [16] A. Batool, G. A. Miana, M. Alam et al., "Bioassay-guided fractionation and isolation of Arctigenin from *Saussurea heteromalla* for in vitro and in silico cytotoxic activity against HeLa cells," *Physiological and Molecular Plant Pathology*, vol. 117, Article ID 101749, 2022.
- [17] F. I. Fahad, N. Barua, M. S. Islam et al., "Investigation of the pharmacological properties of *lepidagathis hyalina* nees through experimental approaches," *Life*, vol. 11, no. 3, pp. 180–216, 2021.
- [18] M. Z. Uddin, M. S. Rana, S. Hossain et al., "In vivo neuro-protective, antinociceptive, anti-inflammatory potential in

- Swiss albino mice and in vitro antioxidant and clot lysis activities of fractionated *Holigarna longifolia* Roxb. bark extract," *Journal of Complementary and Integrative Medicine*, vol. 17, no. 1, pp. 1–10, 2020.
- [19] M. S. H. Kabir, M. M. Hossain, M. I. Kabir et al., "Phytochemical screening, Antioxidant, Thrombolytic, alpha-amylase inhibition and cytotoxic activities of ethanol extract of *Stuednera colocasifolia* K. Koch leaves," *Journal of Young Pharmacists*, vol. 8, no. 4, p. 391, 2016.
- [20] T. A. Bristy, N. Barua, A. Montakim Tareq et al., "Deciphering the pharmacological properties of methanol extract of *Psychotria calocarpa* leaves by in vivo, in vitro and in silico approaches," *Pharmaceuticals*, vol. 13, no. 8, pp. 183–224, 2020.
- [21] G. Bartosz, "Free radicals in biology and medicine," *Cell Biology International*, vol. 24, no. 10, p. 764, 2000.
- [22] B. Halliwell and O. I. Aruoma, "DNA damage by oxygen-derived species its mechanism and measurement in mammalian systems," *FEBS Letters*, vol. 281, no. 1–2, pp. 9–19, 1991.
- [23] M. S. Cooke, M. D. Evans, M. Dizdaroglu, and J. Lunec, "Oxidative DNA damage: mechanisms, mutation, and disease," *FASEB J*, vol. 17, no. 10, pp. 1195–1214, 2003.
- [24] Z. Mahmud, T. B. Emran, N. Qais, S. C. Bachar, M. Sarker, and M. M. N. Uddin, "Evaluation of analgesic, anti-inflammatory, thrombolytic and hepatoprotective activities of roots of *Premna esculenta* (Roxb)," *Journal of Basic and Clinical Physiology and Pharmacology*, vol. 27, no. 1, pp. 63–70, 2016.
- [25] C. D. Pandya, K. R. Howell, and A. Pillai, "Antioxidants as potential therapeutics for neuropsychiatric disorders," *Progress in Neuro-Psychopharmacology and Biological Psychiatry*, vol. 46, pp. 214–223, 2013.
- [26] M. Valko, C. J. Rhodes, J. Moncol, M. Izakovic, and M. Mazur, "Free radicals, metals and antioxidants in oxidative stress-induced cancer," *Chemico-Biological Interactions*, vol. 160, no. 1, pp. 1–40, 2006.
- [27] B. Uttara, A. Singh, P. Zamboni, and R. Mahajan, "Oxidative stress and neurodegenerative diseases: a review of upstream and downstream antioxidant therapeutic options," *Current Neuropharmacology*, vol. 7, no. 1, pp. 65–74, 2009.
- [28] R. Kumar, N. Suman, and S. Dash, "Traditional uses of plants by tribals of Amarakantak region, Madhya Pradesh," *Indian Journal of Traditional Knowledge*, vol. 03, no. 4, pp. 383–390, 2004.
- [29] N. D. Namsa, H. Tag, M. Mandal, P. Kalita, and A. K. Das, "An ethnobotanical study of traditional anti-inflammatory plants used by the Lohit community of Arunachal Pradesh, India," *Journal of Ethnopharmacology*, vol. 125, no. 2, pp. 234–245, 2009.
- [30] S. Palit, R. H. Bhuiyan, J. Aklima, T. B. Emran, and R. Dash, "A study of the prevalence of thalassemia and its correlation with liver function test in different age and sex group in the Chittagong district of Bangladesh," *Journal of Basic and Clinical Pharmacy*, vol. 3, no. 4, p. 352, 2012.
- [31] P. S. Wu, J. Jeng, J. J. Yang, V. Kao, J. H. Yen, and M. J. Wu, "Vernonia patula (Dryand.) Merr. and *Leucas chinensis* (Retz.) R. Brown exert anti-inflammatory activities and relieve oxidative stress via Nrf2 activation," *Journal of Ethnopharmacology*, vol. 262, Article ID 113155, 2020.
- [32] M. Z. Uddin, T. Bin Emran, A. Kumar Nath, Md. Ismail Hossain, M. Alamgir, and S. Rana, "In vitro antioxidative, fibrinolytic and phytochemical effects of different extracts of *sterculia villosa* barks," *International Journal of Research in Pharmaceutical and Biosciences*, vol. 2, no. 1, pp. 1–9, 2015.
- [33] D. G. Robertson, "Metabonomics in toxicology: a review," *Toxicological Sciences*, vol. 85, no. 2, pp. 809–822, 2005.
- [34] A. R. Fernie, R. N. Trethewey, A. J. Krotzky, and L. Willmitzer, "Metabolite profiling: from diagnostics to systems biology," *Nature Reviews Molecular Cell Biology*, vol. 5, no. 9, pp. 763–769, 2004.
- [35] D. B. Kell, M. Brown, H. M. Davey, W. B. Dunn, I. Spasic, and S. G. Oliver, "Metabolic footprinting and systems biology: the medium is the message," *Nature Reviews Microbiology*, vol. 3, no. 7, pp. 557–565, 2005.
- [36] J. Rohloff, "Analysis of phenolic and cyclic compounds in plants using derivatization techniques in combination with GC-MS-based metabolite profiling," *Molecules*, vol. 20, no. 2, pp. 3431–3462, 2015.
- [37] A. M. Tareq, S. Farhad, A. B. M. Neshar Uddin et al., "Chemical profiles, pharmacological properties, and in silico studies provide new insights on *Cycas pectinata*," *Heliyon*, vol. 6, no. 6, Article ID e04061, 2020.
- [38] E. J. Garcia, T. L. C. Oldoni, S. M. d. Alencar, A. D. Loguercio, and R. H. M. Grande, "Antioxidant activity by DPPH assay of potential solutions to be applied on bleached teeth," *Brazilian Dental Journal*, vol. 23, no. 1, pp. 22–27, 2012.
- [39] A. S. M. Ali Reza, M. S. Hossain, S. Akhter et al., "In vitro antioxidant and cholinesterase inhibitory activities of *Elaeostema papillosum* leaves and correlation with their phytochemical profiles: a study relevant to the treatment of Alzheimer's disease," *BMC Complementary Alternative Medicine*, vol. 18, no. 1, p. 123, 2018.
- [40] P. Retailleau, N. Colloc'h, D. Vivarès et al., "Complexed and ligand-free high-resolution structures of urate oxidase (Uox) from *Aspergillus flavus*: a reassignment of the active-site binding mode," *Acta Crystallographica Section D Biological Crystallography*, vol. 60, no. 3, pp. 453–462, 2004.
- [41] P. A. Karplus and G. E. Schulz, "Refined structure of glutathione reductase at 1.54 Å resolution," *Journal of Molecular Biology*, vol. 195, no. 3, pp. 701–729, 1987.
- [42] D. S. Goodsell, "The protein Data Bank," *At. Evid*, vol. 13, 2016.
- [43] M. J. Uddin, A. S. M. Ali Reza, M. Abdullah-Al-Mamun et al., "Antinociceptive and anxiolytic and sedative effects of methanol extract of *Anisomeles indica*: an experimental assessment in mice and computer aided models," *Frontiers in Pharmacology*, vol. 9, 2018.
- [44] E. Harder, W. Damm, J. Maple et al., "OPLS3: a force field providing broad coverage of drug-like small molecules and proteins," *Journal of Chemical Theory and Computation*, vol. 12, no. 1, pp. 281–296, 2016.
- [45] R. A. Friesner, J. L. Banks, R. B. Murphy et al., "Glide: a new approach for rapid, accurate docking and scoring. 1. Method and assessment of docking accuracy," *Journal of Medicinal Chemistry*, vol. 47, no. 7, pp. 1739–1749, 2004.
- [46] R. A. Friesner, R. B. Murphy, M. P. Repasky et al., "Extra precision glide: docking and scoring incorporating a model of hydrophobic enclosure for protein-ligand complexes," *Journal of Medicinal Chemistry*, vol. 49, no. 21, pp. 6177–6196, 2006.
- [47] E. Lionta, G. Spyrou, D. Vassilatis, and Z. Cournia, "Structure-based virtual screening for drug discovery: principles, applications and recent advances," *Current Topics in Medicinal Chemistry*, vol. 14, no. 16, pp. 1923–1938, 2014.



- [48] S. A. Sakib, A. M. Tareq, A. Islam et al., "Anti-inflammatory, thrombolytic and hair-growth promoting activity of the n-hexane fraction of the methanol extract of *Leea indica* leaves," *Plants*, vol. 10, no. 6, p. 1081, 2021.
- [49] F. Chen, H. Liu, H. Sun et al., "Assessing the performance of the MM/PBSA and MM/GBSA methods. 6. Capability to predict protein-protein binding free energies and re-rank binding poses generated by protein-protein docking," *Physical Chemistry Chemical Physics*, vol. 18, no. 32, pp. 22129–22139, 2016.
- [50] C. A. Lipinski, F. Lombardo, B. W. Dominy, and P. J. Feeney, "Experimental and computational approaches to estimate solubility and permeability in drug discovery and development settings," *Advanced Drug Delivery Reviews*, vol. 64, no. SUPPL, pp. 4–17, 2012.
- [51] P. Banerjee, A. O. Eckert, A. K. Schrey, and R. Preissner, "ProTox-II: a webserver for the prediction of toxicity of chemicals," *Nucleic Acids Research*, vol. 46, no. W1, pp. W257–W263, 2018.
- [52] C. Pattanaik, C. S. Reddy, and N. K. Dhal, "Phytomedicinal study of coastal sand dune species of Orissa," *Indian Journal of Traditional Knowledge*, vol. 7, no. 2, pp. 263–268, 2008.
- [53] A. Al-Rifai, A. Aqel, T. Al-Warhi, S. M. Wabaidur, Z. A. Al-Othman, and A. Y. Badjah-Hadj-Ahmed, "Antibacterial, antioxidant activity of ethanolic plant extracts of some *Convolvulus* species and their DART-ToF-MS profiling," *Evidence-Based Complementary and Alternative Medicine*, vol. 2017, Article ID 5694305, 9 pages, 2017.
- [54] S. Sakanaka, Y. Tachibana, and Y. Okada, "Preparation and antioxidant properties of extracts of Japanese persimmon leaf tea (kakinoha-cha)," *Food Chemistry*, vol. 89, no. 4, pp. 569–575, 2005.
- [55] J. J. Li, D. D. Holsworth, and L. Y. Hu, "Molecular properties that influence the oral bioavailability of drug candidates," *Chemtracts*, vol. 16, no. 7, pp. 439–442, 2003.
- [56] F. J. Duffy, M. Devocelle, and D. C. Shields, "Computational approaches to developing short cyclic peptide modulators of protein–protein interactions," *Methods in Molecular Biology*, vol. 1268, pp. 241–271, 2015.

## Research Article

# Bioassay's Directed Isolation-Structure Elucidation and Molecular Docking of Triterpenes from *Persea duthiei* against Biologically Important Microbial Proteins

Najeeb Ullah <sup>1</sup>, Shan Zeb,<sup>2</sup> Fozia <sup>3</sup>, Shah Rukh,<sup>1</sup> Shafiullah Khan <sup>4</sup>, Ijaz Ahmad <sup>2</sup>, Shakeel Ahmad,<sup>2</sup> Nisar Ahmad,<sup>5</sup> Amal Alotaibi <sup>6</sup>, and Riaz Ullah <sup>7</sup>

<sup>1</sup>Department of Biochemistry, Bahauddin Zakariya University, Multan, Punjab, Pakistan

<sup>2</sup>Department of Chemistry, Kohat University of Science & Technology, Kohat, KPK, Pakistan

<sup>3</sup>Biochemistry Department, Khyber Medical University Institute of Medical Sciences, Kohat, KPK, Pakistan

<sup>4</sup>Department of Pharmacy, Abasyn University, Ring Road, Peshawar 25120, KPK, Pakistan

<sup>5</sup>Department of Botanical & Environmental Sciences, Kohat University of Science & Technology, Kohat 26000, KPK, Pakistan

<sup>6</sup>Department of Basic Science, College of Medicine, Princess Nourah Bint Abdulrahman University, P.O. Box 84428, Riyadh 11671, Saudi Arabia

<sup>7</sup>Department of Pharmacognosy (MAPPRC), College of Pharmacy, King Saud University, Riyadh, Saudi Arabia

Correspondence should be addressed to Riaz Ullah; rullah@ksu.edu.sa

Received 21 February 2022; Accepted 19 April 2022; Published 27 May 2022

Academic Editor: Ruchika Garg

Copyright © 2022 Najeeb Ullah et al. This is an open access article distributed under the Creative Commons Attribution License, which permits unrestricted use, distribution, and reproduction in any medium, provided the original work is properly cited.

The research work presented in this study is mainly concerned with the bioactivity-directed phytochemical and biological evaluation of *Persea duthiei*. *Persea duthiei* is a typical medicinal plant used to treat a variety of ailments such as asthma, edema, and bronchitis. Ethyl acetate, n-hexane, n-butanol, and compounds that are soluble in water were used to examine the antibacterial as well as antifungal capacities of the plant. The antibacterial activity of the soluble parts of ethyl acetate and n-hexane against *Escherichia coli*, *Staphylococcus aureus*, *Salmonella typhi*, and *Bacillus subtilis* was high, even though there was no activity against *Pseudomonas aeruginosa*. Likewise, the n-hexane and ethyl acetate fractions were found to have substantial efficacy against several fungal strains such as *Aspergillus flavus*, *Aspergillus fumigates*, *Fusarium solani*, and *Aspergillus niger*, but not against *Candida glabrata*. Among the studied fractions, the ethyl acetate soluble fraction had potent antibacterial activity against all of the tested species. This fraction was submitted to phytochemical analysis utilizing various chromatographic methods for the extraction of various pure components. As a consequence, four compounds were isolated, and their structures were elucidated using various spectroscopic methods such as IR, EIMS, HR-EIMS, <sup>1</sup>H-NMR, <sup>13</sup>C-NMR, NOESY, COSY, HMBC, and HMQC. Urs-12-en-3 $\beta$ -ol ( $\alpha$ -amyrine) (1), Urs-12-ene-2 $\alpha$ -3 $\beta$ -diol (chamaedrydiol) (2), 3 $\beta$ -hydroxyurs-12-en-28-aldehyde (ursolic aldehyde) (3), and 12-oleanex-3 $\beta$ -ol ( $\beta$ -amyrine) (4) were extracted. Compounds 1, 2, 3, and 4 were examined for antibacterial and antifungal activity and found to have zones of inhibition ranging from 0 to 11 mm against tested bacteria strains and percent inhibition ranging from 0 to 25 percent against fungus strains. Compounds 1 and 4 showed strong efficacy against the investigated fungal species, with a 25% inhibition rate. In the case of antibacterial activity, compounds 4 and 1 showed potent activity with zones of inhibition of 11 mm and 10 mm, respectively. Compounds 2 and 3 were observed to have nonsignificant antimicrobial activity. However, docking studies reflected the complex formation of compound 1 with beta-hydroxyacyl-ACP dehydratase HadAB and *S. aureus* tyrosyl-tRNA synthetase and compound 2 with topoisomerase II DNA gyrase complex, and they were reported to have antibacterial properties. Similarly, compound 4 was discovered to be well compatible with the lanosterol 14-demethylase (fungal enzyme) and is thus regarded as having antifungal capabilities. Chimera software was used to identify the binding pockets of these complexes. These results indicated that *Persea duthiei* is a valuable source of medicinal compounds for medication development.



## 1. Introduction

Humans as well as other living organisms are the victims of disease-causing microorganisms (including bacteria and viruses). Besides being disease-causing agents, these microorganisms are gaining resistance against antibiotics as diagnosed in many hospitals throughout the world [1]. With the increase in gaining multidrug resistance among microorganisms, the discovery of broad-spectrum antibiotics with modified and improved activity is gaining more interest in order to overcome diseases. Nature is a gift for us that is rich in antimicrobial ingredients; among them plants are rich in medicinal ingredients. The application of plants as a source of effective medicine is an urge throughout the world [2]. Medicinal plants are used to treat a variety of disorders mainly due to their low cost and high efficacy. However, the limited knowledge about their dosage, safety, liability, and harmful or allergic ingredients prevents doctors from prescribing them for medicinal purposes [3]. The reasons behind multiple antibiotic resistance in many microbial strains are their gene mutations, alternation in microbial structure, and excessive intake of nonspecific antibiotics for the treatment of various disorders. These modifications induce the treatment of microbial infections with the help of herbal medicines. Although a large number of medicinal plants have been examined in order to evaluate their antimicrobial properties, there is still a gap in satisfactory screening. Medicinal plants are a rich source of phytochemicals like alkaloids, flavonoids, glycosides, lactones, resins, sterols, tannins, and volatile oils, due to the natural synthesis of these bioactive compounds in plants. Phytochemicals are biologically active compounds that play a leading role in the treatment of various infections including microbial infections and inflammation [4–6]. The gain of resistance against drugs is a main issue in the identification of drugs for the therapy of microbial infections. Therefore, it is our urgent need to reduce the consumption of antibiotics by providing treatments for microbial infection with the help of novel natural drugs. This urge is fulfilled by the utilization of medicinal plants as well as their phyto-constituents as suitable antimicrobial drugs. *Persea* is a genus in the Lauraceae family that belongs to the oldest subtribe. In the Buner area of Pakistan, *Persea duthiei* is known by the local name “Gul-e-namair.” It is found mostly in Pakistan, India, and Burma and is also found across the western Himalayas [7]. Medicinal plants are used for the treatment of different infections. These plants contributed as a source of inspiration to novel therapeutic compounds as well as color, flavor, and taste of food [8, 9].

*Persea duthiei* is a medicinal plant with valuable medicine properties; the rootstocks, in particular, are bitter, acrid, hot, harsh, and vigorous. It is most commonly used to treat asthma, emphysema, bronchitis, pain, bad breath, blood problems, and vomiting [10]. The oils of *Persea duthiei*'s fruits, leaves, and flowers were studied, and forty components were discovered. One of its oils, i.e., sesquiterpenoids, is present with a percentage of 84.2% in flower, 83% in fruit, and 35.7% in leaves. Other major components (36%) of leaf oil are monoterpene hydrocarbons. Sesquiterpenoids are

represented by  $\alpha$ -pinene (10%), limonene (10.1%), p-cymene (3.5%),  $\beta$ -pinene (10%), (E)-nerolidol (13.2%),  $\beta$ -caryophyllene (5.8%), epi-cubebol (5.8%), and  $\beta$ -eudesmol (4%). Besides epi-cubebol in flower oil, the (E)-nerolidol is also present in great quantity [11]. *Persea* genus is rich in phytochemical contents like flavonoids, terpenes, alkaloids, phytosterols ( $\beta$ -sitosterol), and essential oils [12].

The antibacterial activity of crude extract and several solvent soluble fractions derived from *Persea duthiei* is reported in this research. The plant's ethyl acetate soluble fraction was discovered to have the most antibacterial potential; thus, it was subjected to column chromatography. Four chemicals (1–4) were recovered as a result of sequential column chromatography of the ethyl acetate soluble fraction. Modern spectroscopic approaches, including 1D and 2D NMR techniques, were used to determine the structures of compounds 1–4 (Figure 1). Both physical and spectral data of compounds 1–4 agreed completely with those previously published in the literature [13–15]. Despite the fact that the structures of compounds 1–4 have been disclosed previously, we are presenting their antibacterial activity and docking investigations against key microbial proteins for the first time.

## 2. Materials and Methods

**2.1. Collection of Plant.** A plant taxonomist, Professor Mehboob Ur Rehman, in the Plant Sciences Section of Postgraduate Jahanzeb College, Saidu Sharif, Swat, Pakistan, collected the plant *Persea duthiei* and identified it with a specimen voucher number HPGJC 127 lodged there.

**2.2. Extraction and Fractionation.** The entire plant *Persea duthiei* was collected, dried in shade with the presence of air, sliced, and powdered to a coarse (fine) consistency. At room temperature, the powdered plant, weighing six kg, was extracted three times with methanol (MeOH). This methanolic extract was then evaporated in rotary evaporator under low pressure, yielding dark green thick (like syrup) residue; dried; and weighed. It weighed around 711 grams. Then, this residue was partitioned into different sections with the help of a separating funnel. This methanolic extract was subsequently divided into solvents with varying polarity, such as n-hexane, n-butanol, EtOAc, and water soluble fractions. The antibacterial activity of the crude extract and subsequent soluble fractions was tested, with the ethyl acetate fraction proving to be the most effective.

**2.3. Isolation of Pure Compounds.** The extract's ethyl acetate fraction (eighty-six grams) was subjected to column chromatography. For the process of elution, different solvents having different polarities were used. Elution was performed using the solvents having a gradient of increasing polarity, with the sequence of ascending polarity being (n-hexane)  $\rightarrow$  (n-hexane-ethyl acetate)  $\rightarrow$  (pure ethyl acetate)  $\rightarrow$  (ethyl acetate-methanol) and the final elution being pure methanol.

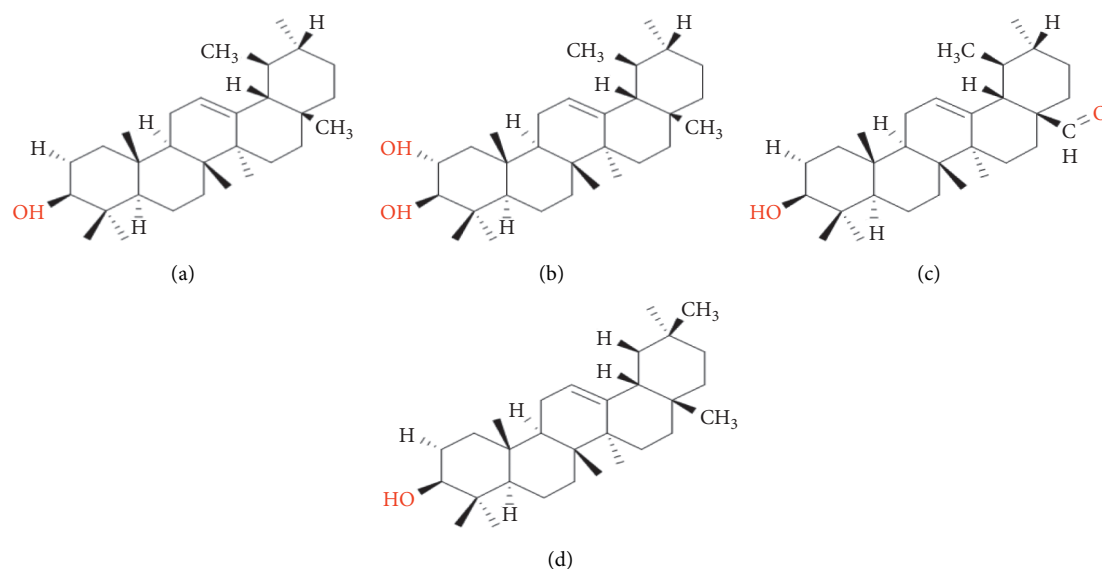


FIGURE 1: The structure of four isolated compounds: (a) compound 1; (b) compound 2; (c) compound 3; (d) compound 4.

After that, the eluted fractions with identical TLC characteristics were blended together. As a result of the compilation procedure, four (04) subfractions were obtained: F1, F2, F3, and F4. These four (04) subfractions were then submitted to repeated column chromatography for further purification. Fraction F1 was rechromatographed after being eluted with n-hexane-ethyl acetate (8:2). One pure chemical was obtained from fraction F1 [13]. Elution in the (6:4) fraction of n-hexane-ethyl acetate yielded fraction F2, which was then subjected to column chromatography. This fraction produced two compounds, 2 [11] and 3 [16], on successive chromatography eluted with two different ratios of n-hexane-ethyl acetate (9:1 and 1.5:8.5), respectively. Fraction F4 was separated and then subjected to column chromatography after being eluted with n-hexane-ethyl acetate in a ratio of 3:7. One pure chemical, 4 [13], was also obtained from this fraction, which was eluted using n-hexane-ethyl acetate (4:6).

**2.4. Bioscreening.** To assess their antimicrobial potential, soluble fractions of different solvents and their components extracted, 1 to 4, from *Persea duthiei* were tested for their antibacterial and antifungal activity.

**2.4.1. Microbial Strains.** The fractions of *Persea duthiei* in different solvents (ethyl acetate, methanol, n-butanol, and n-hexane) and the pure compounds 1–4 were tested against ten microbial species. *Bacillus subtilis*, *Escherichia coli*, *Pseudomonas aeruginosa*, *Salmonella typhi*, and *Staphylococcus aureus* are the five bacterial pathogens, while *Aspergillus flavus*, *Aspergillus fumigates*, *Aspergillus niger*, *Candida glabrata*, and *Fusarium solani* are the five fungal pathogens. The microbes were taken from Dr. Panjwani Center for Molecular Medicine and Drug Research at the University of Karachi in Pakistan (ICCBS).

**2.4.2. Antibacterial Assay.** Various strains of bacterial species were subcultured in order to create a freshly cultured bacterial species for the evaluation of antibacterial activity. As a result, each colony from a different bacterial strain was injected into the nutrient broth and cultivated for one day at room temperature (37°C). The dissolved 19 g nutritious agar medium in 1 L distilled water was then autoclaved at 121°C for half an hour. After chilling, the media were put onto 14 cm Petri plates to make 75 mL of solid media. In these solid media, 7 holes were drilled with a sterile cork borer (8 mm). To evaluate the antibacterial activity of various fractions, the agar diffusion method was used. Each bacterial strain was inoculated in its own Petri dish. To make the stock solution, 15 mg per mL of each part was combined with DMSO (dimethyl sulfoxide). In such precise holes, 100 L solution of each fraction, DMSO solution as a negative control, and doxycycline as a positive control were employed. The bacterial cultures along with solvent soluble fractions were cultivated for 24 hours at 37 degrees Celsius. According to the prior protocol [17], the zone of each hole was measured in millimeters.

**2.4.3. Antifungal Assay.** To obtain fresh cultures for each species, the old fungal strains were subcultured. For cultivating fungal strains, nutrient broth medium was utilized, and the resultant cultures were cultured at 280°C for 7 days. The disc diffusion method was employed to assess antifungal activity in different solvent soluble fractions of this plant. Through point inoculation, the fungal strains were injected on distinct agar media, namely, Potato Dextrose Agar (PDA) plates. The experiment next employed 100 microL of the store solution (12 mg from each fraction dissolved in 2 ml of DMSO); pure DMSO as a negative control; and 12 mg/mL antibiotic, i.e., miconazole, as a positive control. The activity of each strain was assessed after 7-day (280°C) incubation [17].

## 2.5. Physical and Spectral Data of Compounds 1–4

2.5.1. *Urs-12-en-3 $\beta$ -ol* (1). Amorphous solid; M.P 188°C; IR (KBr)  $\text{cm}^{-1}$  3512, 1638;  $^1\text{H-NMR}$  ( $\text{CDCl}_3$ , 400 MHz);  $\square$  5.11 (1H, t,  $J = 3.6$  Hz, H-12), 3.22 (1H, dd,  $J = 10.4, 7.2$  Hz, H-3), 2.35 (2H, m, H-11), 1.98 (1H, m, H-9), 1.95 (2H, m, H-1), 1.89 (1H, m, H-18), 1.68 (2H, m, H-15), 1.52–1.60 (9H, m, H-19, 16, 7, 6, 2), 1.40–149 (5H, m, H-20, 21, 22), 1.11 (3H, s,  $\text{CH}_3$ ), 1.05 (3H, s,  $\text{CH}_3$ ), 0.99 (3H, s,  $\text{CH}_3$ ), 0.97 (3H, s,  $\text{CH}_3$ ), 0.89 (1H, m, H-5), 0.85 (3H, s,  $\text{CH}_3$ ), 0.83 (3H, s,  $\text{CH}_3$ ), 0.81 (3H, s,  $\text{CH}_3$ ), 0.79 (3H, s,  $\text{CH}_3$ );  $^{13}\text{C-NMR}$  ( $\text{CDCl}_3$ , 125 MHz);  $\square$  139.60 (C-13), 124.40 (C-12), 77.22 (C-3), 59.07 (C-18), 55.18 (C-5), 47.72 (C-9), 42.09 (C-14), 41.54 (C-22), 40.02 (C-8), 39.68 (C-19), 39.62 (C-20), 38.72 (C-1), 38.06 (C-4), 36.96 (C-10), 33.76 (C-17), 32.66 (C-7), 31.27 (C-21), 28.14 (C-15, 23, 28), 27.25 (C-2), 26.63 (C-16), 23.39 (C-11), 23.28 (C-27), 21.40 (C-30), 18.37 (C-6), 17.48 (C-29), 16.81 (C-26), 15.63 (C-24), 15.60 (C-25); HREI-MS:  $m/z$  calc for  $\text{C}_{30}\text{H}_{50}\text{O}$   $[\text{M}]^+$  426.386 and was found as 426.382 [13].

2.5.2. *Urs-12-ene-2 $\alpha$ -3 $\beta$ -Diol* (2). Amorphous solid; M.P 219–220°C; IR (KBr)  $\text{cm}^{-1}$  3510, 1635;  $^1\text{H-NMR}$  ( $\text{CDCl}_3$ , 400 MHz);  $\square$  5.32 (1H, t,  $J = 3.8$  Hz, H-12), 3.68 (1H, m, H-2), 3.01 (1H, d,  $J = 7.6$  Hz, H-3), 2.09–2.02 (5H, m, H-11, 1, 9), 1.98 (1H, m, H-18), 1.74 (2H, m, H-15), 1.63 (2H, m, H-22), 1.60–1.51 (9H, m, H-21, 6, 16, 7, 19), 1.40 (1H, m, H-20), 1.23 (3H, s,  $\text{CH}_3$ ), 1.05 (3H, s,  $\text{CH}_3$ ), 1.02 (3H, s,  $\text{CH}_3$ ), 1.00 (3H, s,  $\text{CH}_3$ ), 0.98 (3H, s,  $\text{CH}_3$ ), 0.90 (1H, m, H-5), 0.89 (3H, s,  $\text{CH}_3$ ), 0.81 (3H, s,  $\text{CH}_3$ ), 0.77 (3H, s,  $\text{CH}_3$ );  $^{13}\text{C-NMR}$  ( $\text{CDCl}_3$ , 125 MHz);  $\square$  139.60 (C-13), 124.17 (C-12), 83.98 (C-3), 69.04 (C-2), 59.03 (C-18), 55.20 (C-5), 47.66 (C-9), 42.13 (C-14), 41.50 (C-1, 22), 40.07 (C-8), 39.64 (C-19), 39.58 (C-20), 38.34 (C-4), 37.12 (C-10), 33.37 (C-17), 32.82 (C-7), 31.23 (C-21), 28.39 (C-23, 28), 28.06 (C-16), 26.55 (C-15), 23.42 (C-11), 23.26 (C-27), 21.41 (C-30), 18.33 (C-6), 17.46 (C-29), 16.97 (C-26), 16.89 (C-25), 16.78 (C-24); HREI-MS:  $m/z$  calc for  $\text{C}_{30}\text{H}_{50}\text{O}_2$   $[\text{M}]^+$  442.381 and was found as 442.377 [14].

2.5.3. *3 $\beta$ -Hydroxyurs-12-en-28-Aldehyde* (3). Yellowish amorphous solid; M.P 219–220°C; IR (KBr)  $\text{cm}^{-1}$  3516, 3511, 1696;  $^1\text{H-NMR}$  ( $\text{CDCl}_3$ , 400 MHz);  $\square$  9.20 (1H, s, CHO), 5.30 (1H, t,  $J = 3.6$  Hz, H-12), 3.12 (1H, dd,  $J = 7.6, 4.8$  Hz, H-3), 2.61 (2H, m, H-22), 2.31–2.30 (3H, m, H-11,9), 1.97 (3H, m, H-1, 18), 1.86–1.80 (4H, m, H-21,2), 1.65 (2H, m, H-15), 1.58–1.49 (8H, m, H-6, 16, 7, 19, 20), 1.11 (3H, s,  $\text{CH}_3$ ), 1.06 (3H, s,  $\text{CH}_3$ ), 0.96 (3H, s,  $\text{CH}_3$ ), 0.94 (3H, s,  $\text{CH}_3$ ), 0.90 (3H, s,  $\text{CH}_3$ ), 0.88 (3H, s,  $\text{CH}_3$ ), 0.84 (1H, m, H-5), 0.75 (3H, s,  $\text{CH}_3$ );  $^{13}\text{C-NMR}$  ( $\text{CDCl}_3$ , 125 MHz);  $\square$  207.56 (C-28), 137.80 (C-13), 123.26 (C-12), 77.22 (C-3), 55.21 (C-5), 55.21 (C-18), 52.63 (C-17), 47.57 (C-9), 42.18 (C-14), 40.42 (C-8), 38.99 (C-19), 38.70 (C-1), 38.62 (C-20), 38.50 (C-4), 36.95 (C-10), 32.75 (C-7), 31.88 (C-21), 30.19 (C-22), 25.50 (C-23), 27.75 (C-2,15), 26.75 (C-16), 23.31 (C-11,27), 21.08 (C-30), 18.31 (C-6), 17.22 (C-24,26), 16.66 (C-29), 15.62 (C-25); HREI-MS:  $m/z$  calc for  $\text{C}_{30}\text{H}_{48}\text{O}$   $[\text{M}]^+$  440.365 and was found as 440.361 [15].

2.5.4. *12-Oleanex-3 $\beta$ -ol* (4). Solid; IR (KBr)  $\text{cm}^{-1}$  3510, 1636;  $^1\text{H-NMR}$  ( $\text{CDCl}_3$ , 400 MHz);  $\square$  5.11 (1H, t,  $J = 3.6$  Hz, H-12), 3.21 (1H, dd,  $J = 12, 4$  Hz, H-3), 2.33 (2H, m, H-11), 2.28 (1H, m, H-9), 1.98 (1H, m, H-18), 1.94 (2H, m, H-1), 1.68 (2H, m, H-15), 1.65 (2H, m, H-2), 1.57–151 (8H, m, H-6,16,7,19), 1.48–142 (4H, m, H-21,22), 1.20 (3H, s,  $\text{CH}_3$ ), 1.12 (3H, s,  $\text{CH}_3$ ), 1.11 (3H, s,  $\text{CH}_3$ ), 0.96 (3H, s,  $\text{CH}_3$ ), 0.90 (3H, s,  $\text{CH}_3$ ), 0.89 (3H, s,  $\text{CH}_3$ ), 0.85 (3H, s,  $\text{CH}_3$ ), 0.82 (1H, m, H-5), 0.76 (3H, s,  $\text{CH}_3$ );  $^{13}\text{C-NMR}$  ( $\text{CDCl}_3$ , 125 MHz);  $\square$  145.30 (C-13), 122.68 (C-12), 79.04 (C-3), 55.22 (C-5), 47.63 (C-9,18), 45.89 (C-19), 41.12 (C-14), 39.27 (C-4,8), 38.42 (C-1,22), 37.08 (C-10), 33.80 (C-21), 32.66 (C-7), 32.21 (C-17), 30.18 (C-20), 33.06 (C-30), 28.11 (C-28), 27.69 (C-16), 27.19 (C-2,15), 25.91 (C-23), 23.41 (C-11), 23.28 (C-27), 23.57 (C-29), 18.32 (C-6), 17.06 (C-26), 15.56 (C-25), 15.33 (C-24); HREI-MS:  $m/z$  calc for  $\text{C}_{30}\text{H}_{50}\text{O}$   $[\text{M}]^+$  426.386 and was found as 426.382 [13].

2.6. *Docking Study*. Molecular docking facilitates the comparison of potential binding interactions of identified chemical compounds with targeted proteins. The three-dimensional or 3D shape of targeted proteins (*S. aureus*. tyrosyl-tRNA synthetase, topoisomerase II DNA gyrase, beta-hydroxyacyl-ACP dehydratase HadAB, and lanosterol 14-demethylase enzyme with PDB codes 1JIJ, 2XCT, 4RLT, and 4WMZ) was obtained from RCSB PDB [18]. ChemDraw Professional v17 was used to sketch the ligand molecules [19]. The structures of receptors were generated with the help of the MakeReceptor Wizard module of the OpenEye Scientific Software, and the ligands' correct conformers were prepared with the help of the OMEGA module of the same software [20]. The structures of receptors and conformers of ligands were required before performing the protocol of molecular docking in the FRED ligand docking module. This software demands input conformers for each targeted compound. For that purpose, the ligands' conformers were developed with the help of OMEGA 3.0.0 [21]. For the generation of multiple conformers, the default setting of OMEGA was utilized. For the generation of grids of receptors the Pdb2Receptor grid generation module was used. The grids were tailored to each individual protein. For example, the grid against the *S. aureus* gyrase complex was developed around ciprofloxacin, but the grid against the *S. aureus* tyrosyl-tRNA synthetase complex was built around co-crystal SB-239629 ligand. Additionally, against co-crystallized *S. cerevisiae* and beta-hydroxyacyl-ACP dehydratase HadAB, the grid was formed around co-crystallized fluconazole ligand and fisetin. Boundary box for each targeted protein was spacious enough to cover the overall binding region, and it was obtained by setting it at the default value. The docking process was optimized by re-docking between the active sites of the targeted protein and the co-crystal ligand. The FRED module constructed different poses for each targeted ligand, and the pose with the lowest chemguass4 value was chosen for further analysis. The Discovery Studio client v16.1.0 was used to analyze the optimal docked binding relationship [22].

### 3. Results and Discussion

The methanolic extract prepared from *Persea duthiei* plant was partitioned into n-hexane, ethyl acetate, n-butanol, and water-soluble portions to isolate the physiologically essential parts. As a result, four terpenoids with structures similar to those indicated in Figure 1 were revealed. The antibacterial and antifungal properties were tested on the soluble fractions as well as the separated pure components.

**3.1. Antibacterial Activity of Fractions.** The antibacterial activity of *Persea duthiei* extract is shown in Table 1. *Persea duthiei* was tested for antibacterial efficacy against five different bacteria strains (*E. coli*, *B. subtilis*, *P. aeruginosa*, *S. typhi*, and *S. aureus*). With the exception of *P. aeruginosa*, all studied microorganisms showed significant efficiency in relation to the ethyl acetate and n-hexane fractions (Table 1). The ethyl acetate fraction inhibited *E. coli*, *B. subtilis*, *P. aeruginosa*, *S. typhi*, and *S. aureus* in zones of 8 mm, 3 mm, 16 mm, 9 mm, and 12 mm, respectively. However, against *E. coli*, *B. subtilis*, *P. aeruginosa*, *S. typhi*, and *S. aureus*, the percentage of n-hexane had the zones of inhibition of 11 mm, 2 mm, 7 mm, 10 mm, and 8 mm. Because the inhibition zone for the n-butanol and the aqueous fraction is so much smaller, they have less antibacterial activity.

**3.2. Antifungal Activity of Fractions.** Table 2 shows the antifungal activity of *Persea duthiei*'s various solvent soluble separated fractions. All of the fungus strains examined demonstrated strong activity against the ethyl acetate and n-hexane fractions. It is also clear from Table 2 that each fungal strain shows 100 percent growth against aqueous fractions of *Persea duthiei*. However, the butanol fractions showed antifungal activity against only two strains (*A. flavus* and *F. solani*).

**3.3. Structural Elucidation of Compounds 1–4 Isolated from *Persea duthiei*.** The ethyl acetate soluble fraction was submitted to column chromatography since it showed the maximum activity of all the fractions examined, giving four chemicals (1–4).

**3.3.1. Urs-12-en-3 $\beta$ -ol ( $\alpha$ -Amyrine) (1).** Compound 1 was synthesized in powder form with amorphous nature and melted at 188°C. The compound's chemical formula was determined as C<sub>30</sub>H<sub>50</sub>O using HR-EIMS with a molecular peak ion at m/z 426. Compound 1 in its IR spectra indicated a hydroxyl group maximum absorption at 3512 cm<sup>-1</sup> and a carbon-carbon double bond absorption peak at 1638 cm<sup>-1</sup>. Both <sup>13</sup>C- and <sup>1</sup>H-NMR spectra were found to be very similar to those reported for compound 1 [13] and are provided in the experimental section of the article.

**3.3.2. Urs-12-ene-2 $\alpha$ -3 $\beta$ -Diol (Chamaedrydiol) (2).** This compound was synthesized as an amorphous solid using an n-hexane-ethyl acetate (6:4) solvent system and a melting

point of 219–2200°C. HR-EIMS and <sup>13</sup>C-NMR (DEPT, BB) confirmed compound 2's molecular formula as C<sub>31</sub>H<sub>52</sub>O<sub>2</sub>, with a peak of molecular ion at m/z 456. In the IR spectra, OH group presented its absorption bands at 3510 cm<sup>-1</sup>, while a double bond (C=C) had absorption bands at 1635 cm<sup>-1</sup>. The physical and other spectrum data above validated the structure of compound 2 as Urs-12-ene-2-3-diol (chamaedrydiol), which agrees with those reported in the literature [13] and is also included in the experimental portion of the paper [12].

**3.3.3. 3 $\beta$ -Hydroxyurs-12-en-28-Aldehyde (Ursolic Aldehyde) (3).** Through column chromatography, an amorphous solid of yellow color material, i.e., compound 3, was recovered from F4 fraction using an n-hexane to ethyl acetate ratio of 7:3. When compound 3 was exposed to the iodine chamber, it appeared as a yellow spot. The provided compound's IR spectra reflected the absorption for the OH at 3511 cm<sup>-1</sup>, for the carbonyl group at 1696 cm<sup>-1</sup>, and for the C=C olefinic at 3516 cm<sup>-1</sup>. HR-EIMS technology revealed a peak for molecular ion at m/z 440.00, confirming the chemical formula C<sub>30</sub>H<sub>48</sub>O<sub>2</sub> (calc for C<sub>30</sub>H<sub>48</sub>O<sub>2</sub>, 440.00). The <sup>13</sup>C-NMR and <sup>1</sup>H-NMR spectrum data for compound 3 [15, 23] were found to be extremely similar to those available in literature and are included in the experimental portion of the paper.

**3.3.4. 12-Oleanex-3 $\beta$ -ol ( $\beta$ -Amyrine) (4).** After washing with methanol, the amorphous solid of compound 4, i.e.,  $\beta$ -amyrine, was isolated in the ethyl acetate soluble fraction of *Persea duthiei*'s MeOH extract and crystallized to a colorless needle-like crystal. HR-EIMS was used to detect a molecular ion peak at m/z 426.38, which corresponded to the C<sub>30</sub>H<sub>50</sub>O as its chemical formula. Infrared spectra represent absorption peaks for the OH group at 3510 cm<sup>-1</sup> and a trisubstituted double bond at 1636 cm<sup>-1</sup>. Compound 4's <sup>1</sup>H-NMR spectra and <sup>13</sup>C-NMR assignment were indistinguishable from those described in the literature for  $\beta$ -amyrine [13], which is also supplied in the article's experimental section.

**3.4. Bio-screening of Compounds.** Antibacterial and antifungal properties were tested on the four identified compounds, 1–4, at a concentration of 28 g/ml. Compound 4 was shown to be more active than compounds 2 and 3, whereas compound 1 had the second highest level of antibacterial activity for all the targeted bacterial strains with the exception of *B. subtilis* as mentioned in Table 3. Compounds 4 and 1 showed antibacterial activity for the investigated bacterial strains. However, in terms of antifungal activity, compound 1 demonstrated the most activity against all fungal strains, followed by compound 4. Table 4 shows that compounds 2 and 3 have no substantial action.

**3.5. Structure-Activity Relationship of Isolated Compounds.** The antimicrobial activities of all the four isolated compounds were examined by evaluating the structure-activity relationship of these compounds.

TABLE 1: Zones of inhibition in millimeters showing antibacterial activities of isolated fractions of *Persea duthiei* against different bacterial strains (15 mg/ml).

S. No.	Fractions	<i>E. coli</i>	<i>P. aeruginosa</i>	<i>S. typhi</i>	<i>B. subtilis</i>	<i>S. aureus</i>
1	n-Hexane	11	2	7	10	8
2	Ethyl acetate	8	3	16	9	12
3	n-Butanol	1	4	3	2	5
4	Aqueous	3	1	5	2	3
5	Doxycycline	16	19	24	22	20

TABLE 2: Antifungal activity (% inhibition) of different fractions (15 mg/ml) [17] isolated from *Persea duthiei* against five fungi strains.

S. No.	Fractions	<i>A. flavus</i>	<i>A. fumigates</i>	<i>A. niger</i>	<i>F. solani</i>	<i>C. glabrata</i>
1	n-Hexane	+, +	+	+, +	+	+
2	Ethyl acetate	+, +	+	+, +	+, +	+
3	n-Butanol	+	-	-	+	-
4	Aqueous	-	-	-	-	-
5	Miconazole	+, +, +, +	+, +, +, +	+, +, +, +	+, +, +, +	+, +, +, +

Note. (-) 100% growth; (+) 75% growth; (+, +) 50% growth; (+, +, +) 25% growth; (+, +, +, +) no growth.

TABLE 3: Zones of inhibition in millimeters showing antibacterial activities of isolated compounds 1–4 (28  $\mu$ g/ml) of *Persea duthiei* against different bacterial strains.

S. No.	Compounds	<i>E. coli</i>	<i>P. aeruginosa</i>	<i>S. typhi</i>	<i>B. subtilis</i>	<i>S. aureus</i>
1	Compound 1	7	8	10	1	2
2	Compound 2	8	5	0	0	3
3	Compound 3	0	5	2	0	7
4	Compound 4	9	11	9	1	5
5	Levofloxacin	16	19	24	22	20

TABLE 4: Antifungal activity (% inhibition) of compounds 1–4 (28  $\mu$ g/ml) isolated from *Persea duthiei* against five fungi strains.

S. No.	Compounds	<i>A. flavus</i>	<i>A. fumigates</i>	<i>A. niger</i>	<i>F. solani</i>	<i>C. glabrata</i>
1	Compound 1	+	+	+	+	+
2	Compound 2	+	-	-	-	-
3	Compound 3	-	+	-	-	-
4	Compound 4	+	+	-	+	-
5	Clotrimazole	+, +, +, +	+, +, +, +	+, +, +, +	+, +, +, +	+, +, +, +

Note. (-) 100% growth; (+) 75% growth; (+, +) 50% growth; (+, +, +) 25% growth; (+, +, +, +) no growth.

Compound 1 (i.e.,  $\alpha$ -amyryne), a pentacyclic triterpene, is a pharmacological important compound that exhibits antimicrobial and anti-inflammatory as well as anticancer properties [16, 24]. Compound 1 ( $\alpha$ -amyryne) shows more antimicrobial activity against each targeted microbial strain. The reason behind the pharmacological importance of  $\alpha$ -amyryne is represented by evaluating the structure-activity relationship of compound 1. The presence of OH group at R2 is involved in the formation of H-bonding with the membrane proteins of bacteria, ultimately leading to lysis or rupture of microbial cell [25] that is represented in their zone of inhibition for bacterial strains (Table 3) and percent inhibition for fungal strains (Table 4). Compound 2 (i.e., chamaedrydiol) has minimum antimicrobial activities compared to the other 3 compounds. The reason behind this least activity is exhibited in its structure. It has two adjacent OH groups at R1 and R2 positions; these adjacent OH groups generally reduce the strength of H-bonding, thereby resulting in the least activity against bacteria and fungi [26].

Compound 3 (i.e., ursolic aldehyde) has the least antibacterial activity against three strains of bacteria (*S. typhi*, *P. aeruginosa*, and *S. aureus*) and has near to zero antibacterial activity against *E. coli* and *B. subtilis*. This low or no activity of (ursolic aldehyde) is based on the presence of carbonyl group (C=O) at the R3 position. This carbonyl group hinders the antimicrobial activity of compounds [23, 27]. However, the presence of the OH group at R2 is involved in the formation of H-bond with microbial membrane protein, so this compound has weak antimicrobial activity [27]. Compound 4, (i.e.,  $\beta$ -amyryne) is also a pentacyclic triterpene; its pharmacological as well as antibacterial activities are similar to those of compound 1. The antibacterial activities of both compounds are also relatable to each other [24, 25].

3.6. *Molecular Docking Studies.* The predicted binding relationship of ligands with physiologically significant targeted

TABLE 5: FRED chemguass4 score of compounds 1–4 and co-crystallized reported ligand against docking with bacterial enzyme beta-hydroxyacyl-ACP dehydratase HadAB (PDB ID: 4rlt).

Compound code	FRED chemguass4 score
Compd_1	-11.85
Compd_2	-10.34
Compd_3	-11.07
Compd_4	-10.55
4RLT_cc	-14.85

proteins is evaluated using molecular docking. Each isolated chemical was subjected to docking studies to identify its directing of binding inside the pockets at the active site of the target proteins. HadAB, *S. aureus* tyrosyl-tRNA synthetase, and topoisomerase II DNA gyrase, along with one fungus protein, lanosterol 14-demethylase (CYP51), were examined to determine whether they may be exploited as therapeutic targets for antibacterial and antifungal drug development. Tables 5–8 show the binding affinity of all compounds under investigation against 3 bacterial and one fungal proteins using the FRD docking program's chemguass4 score. FRED uses multi-conformer docking techniques, which entail generating a number of conformers with low energy one at a time and firmly docking each one.

Bacterial beta-hydroxyacyl-ACP dehydratase HadAB is an enzyme that is involved in catalyzing the dehydration step of bacterial fatty acid elongation [28]. The formation of complex having this enzyme with the targeted compounds can inhibit the significant role of this dehydratase enzyme ultimately leading to antibacterial therapy. By putative binding of four isolated compounds with this enzyme in docking studies, the FRED score of all compounds is obtained and represented in Table 5. The values of the FRED score indicate that compound 1 has a more putative binding with this enzyme, having -11.85 FRED score. Structure-activity relationship also represents the comparatively more antibacterial activity of compound 1 against bacterial strains. The docking results suggest that the hydroxyl group as well as the hydrophobic portion of these compounds is interfering with the microbial proteins through various intermolecular interactions. Further, crystallographic studies can confirm the part of the compound interacting with the proteins.

Figure 2 depicts the synthesis of compound 1 in association with beta-hydroxyacyl-ACP dehydratase HadAB.

In docking study, three parameters were assessed: the binding affinity expressed in kcal/mol, the bonding interactions between the amino acid residues of the target protein and the atoms of the ligand, and the bond distance of these interactions, as shown in Table 9.

*S. aureus* tyrosyl-tRNA synthetase is a bacterial enzyme, catalyzing the activation of tyrosine and its transfer to tRNA during translation of various important bacterial proteins [29]. The putative binding of four isolated compounds with this enzyme is evaluated in FRD docking software. FRED scores of all compounds are obtained and represented in Table 7. The values of FRED score indicate that compound 1 has a more putative binding affinity with this enzyme, with a

TABLE 6: FRED chemguass4 score of compounds 1–4 and co-crystallized ligand against docking in bacterial enzyme *S. aureus* tyrosyl-tRNA synthetase (PDB ID: 1jjj).

Compound code	FRED chemguass4 score
Compd_1	-8.23
Compd_2	-6.90
Compd_3	-7.89
Compd_4	-7.02
Co-crystallized ligand	-14.64

TABLE 7: FRED chemguass4 score of compounds 1–4 and co-crystallized ligand against docking in bacterial enzyme topoisomerase II DNA gyrase (PDB ID: 2xct).

Compound code	FRED chemguass4 score
Compd_1	-1.33
Compd_2	-1.48
Compd_3	-0.72
Compd_4	-0.99
Co-crystallized ligand	-3.25

TABLE 8: FRED chemguass4 score of compounds 1–4 and co-crystallized ligand against docking with fungal enzyme, i.e., Lanosterol 14 $\alpha$ -demethylase enzyme (PDB ID: 4wmz).

Compound code	FRED chemguass4 score
Compd_1	-12.62
Compd_2	-12.72
Compd_3	-12.44
Compd_4	-12.89
Co-crystallized ligand	-11.25

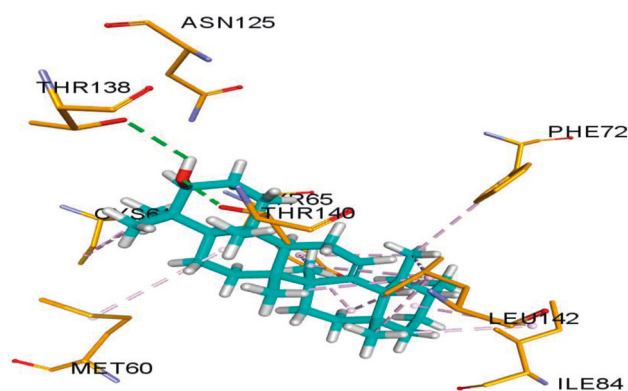


FIGURE 2: Putative binding interaction of compound 1 with the bacterial enzyme HadAB. Residues of compound 1 are interacting with the enzyme active site amino acid residues like THR138 and THR140 (shown in yellow sticks) at the active site of bacterial beta-hydroxyacyl-ACP dehydratase HadAB [25] through hydrogen bond (dotted lines in green).

FRED score of -8.23. Compound 1 has a higher antibacterial activity than compound 2 against the bacterial strains, as shown by the structure-activity relationship.

The formation of compound 1-*S. aureus* tyrosyl-tRNA synthetase complex is represented in Figure 3. Three parameters were evaluated using docking analysis: first is the



TABLE 9: Molecular docking analysis of compound 1 against bacterial enzyme beta-hydroxyacyl-ACP dehydratase HadAB (PDB ID: 4rlt) on the basis of the type of bonds, the bond distances, and the interacting amino acids.

Bond type	Bond distance (Å)	Interacting amino acid of target
Hydrogen bond	2.71	A:THR140:OG1
Hydrogen bond	2.94	A:THR138:OG1
Hydrogen bond	2.71	A:THR140:OG1
Hydrogen bond	2.94	A:THR138:OG1
Hydrogen bond	2.71	A:THR140:OG1
Hydrogen bond	2.94	A:THR138:OG1
Hydrophobic	4.64	A:ILE84
Hydrophobic	4.82	A:LEU142
Hydrophobic	5.49	A:LEU142
Hydrophobic	5.24	B:MET60
Hydrophobic	5.45	A:LEU142
Hydrophobic	5.26	A:ILE84
Hydrophobic	4.58	A:LEU142
Hydrophobic	5.18	A:LEU142
Hydrophobic	3.71	A:CYS61
Hydrophobic	4.79	A:CYS61
Hydrophobic	5.03	A:TYR65
Hydrophobic	5.13	A:TYR65
Hydrophobic	5.06	A:TYR65
Hydrophobic	5.41	A:PHE72

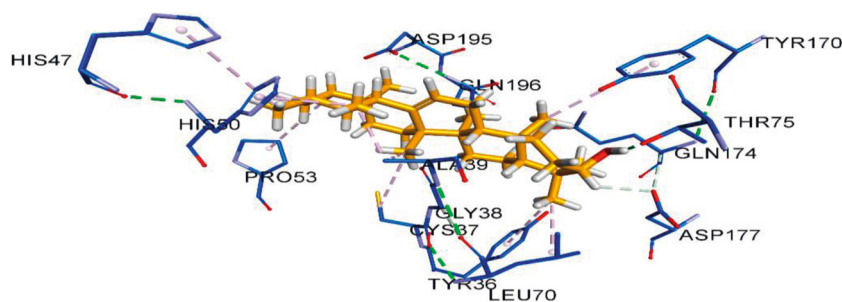


FIGURE 3: Putative binding interaction of compound 1 against bacterial *S. aureus* tyrosyl-tRNA synthetase. The THR75 (interacting with OH group of compound 1) and ASP177 (interacting with hydrogen atom of compound 1) residues of *S. aureus* tyrosyl-tRNA synthetase are hydrogen-bonded with OH group of compound 1, similar to its hydrogen bond formation with SB-284485 as previously reported. Similarly, HIS50 residue is also present in the active site of *S. aureus* tyrosyl-tRNA synthetase that interacts through hydrophobic bonding with the hydrophobic part of compound 1 in a similar fashion to that between SB-239629 and *S. aureus* tyrosyl-tRNA synthetase [30].

TABLE 10: Molecular docking analysis of compound 1 against bacterial enzyme *S. aureus* tyrosyl-tRNA synthetase (PDB ID: 1jjj) based on the type of bonds, bond distances, and interacting amino acids.

Bond type	Bone distance (Å)	Interacting amino acid of target
Hydrogen bond	1.84	A:THR75:OG1
Hydrogen bond	3.04	A:ASP177:OD1
Hydrogen bond	1.84	A:THR75:OG1
Hydrogen bond	3.04	A:ASP177:OD1
Hydrophobic	3.55	A:ALA39
Hydrophobic	4.17	A:ALA39
Hydrophobic	4.83	A:PRO53
Hydrophobic	4.28	A:CYS37
Hydrophobic	3.55	A:LEU70
Hydrophobic	4.84	A:TYR36
Hydrophobic	5.19	A:HIS47
Hydrophobic	4.44	A:HIS50
Hydrophobic	3.48	A:HIS50
Hydrophobic	5.14	A:TYR170

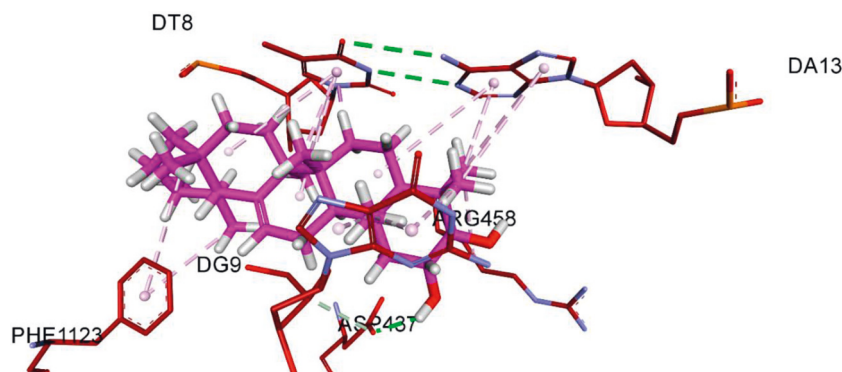


FIGURE 4: Putative binding interactions of compound 2 against bacterial topoisomerase II DNA gyrase. The ASP437 residue (shown in red) located at the active site of topoisomerase II DNA gyrase forms H-bond (dotted line in green) with OH group of compound 2, in a similar way to hydrogen bond formation between the GSK299423 inhibitor and the enzyme [32].

TABLE 11: Molecular docking analysis of compound 2 against bacterial enzyme topoisomerase II DNA gyrase (PDB ID: 2xct) on the basis of the type of bonds, bond distances, and interacting amino acids.

Bond type	Bond distance (Å)	Interacting amino acid of target
Hydrogen bond	2.21	B:ASP437:OD2
Hydrophobic	1.60	E:DT8
Hydrophobic	4.26	B:ARG458
Hydrophobic	4.78	D:PHE1123
Hydrophobic	5.11	D:PHE1123
Hydrophobic	4.17	D:PHE1123
Hydrophobic	4.77	E:DT8
Hydrophobic	4.93	E:DT8
Hydrophobic	4.58	E:DT8
Hydrophobic	3.71	E:DT8
Hydrophobic	3.31	G:DG9
Hydrophobic	3.52	G:DG9
Hydrophobic	4.35	G:DG9
Hydrophobic	5.02	H:DA13
Hydrophobic	4.93	H:DA13
Hydrophobic	5.36	H:DA13
Hydrophobic	3.50	H:DA13
Hydrophobic	4.08	H:DA13
Hydrogen bond	2.21	B:ASP437:OD2
Hydrogen bond	2.21	B:ASP437:OD2

binding affinity expressed in kcal/mol, second is the interactions between the amino acid residues of the target protein and the atoms of ligand, and third is the bond distance of these interactions as represented in Table 10.

Topoisomerase II DNA gyrase is a bacterial enzyme that is involved in introducing turns in DNA (i.e., negative superhelical turns), so it is involved in the replication of bacterial strains [31]. However, the formation of a complex having bioactive compounds with this enzyme can retard the normal replication of microbes. The putative binding of four isolated compounds with this enzyme was evaluated with FRD docking software. FRED scores of all compounds are

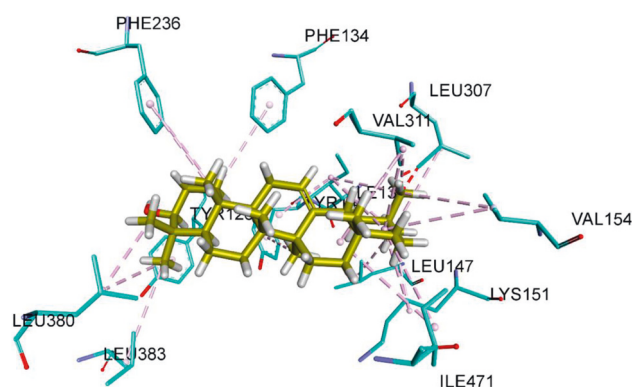


FIGURE 5: Putative binding interaction of compound 4 against fungal lanosterol 14 $\alpha$ -demethylase enzyme. The amino acids LEU380, LEU383, and VAL311 in the hydrophobic core of the enzyme located in the active site are involved in the hydrophobic Van der Waals bonding with the hydrophobic residues of compound 4 [35].

obtained and represented in Table 7. The values of FRED score show that compound 2 has more putative binding with this enzyme, with a FRED score of  $-1.48$ .

The formation of compound 2–topoisomerase II DNA gyrase complex is represented in Figure 4. Three parameters were evaluated using docking analysis: first is the binding affinity expressed in kcal/mol, second is the bonding interactions between the amino acid residues of the target protein and the atoms of ligand, and third is the bond distance of these interactions as shown in Table 11.

Lanosterol 14 $\alpha$ -demethylase is a fungal enzyme, involved in the synthesis of a necessary component (ergosterol) of the cell membrane in fungi [33]. Inhibition of this enzyme leads to reduction of ergosterol in fungal cell membrane and formation of toxic metabolites [34]. Both these effects are fungistatic for many pathogenic fungi. For the synthesis of novel antifungal medications, this enzyme has gained much importance. Docking studies revealed that compound 4 showed more stable complex with this enzyme, with chemguass4 score of  $-12.89$ , than the other three compounds (Table 8).

The formation of compound 4–lanosterol 14 $\alpha$ -demethylase complex is represented in Figure 5. Three

TABLE 12: Molecular docking analysis of compound 4 against the fungal enzyme lanosterol 14 $\alpha$ -demethylase enzyme (PDB ID: 4wmz) on the basis of the type of bonds, bond distances, and interacting amino acids.

Bond type	Bond distance (Å)	Interacting amino acid of protein
Hydrophobic	5.43	A:ILE139
Hydrophobic	5.31	A:ILE139
Hydrophobic	4.67	A:LYS151
Hydrophobic	5.05	A:VAL154
Hydrophobic	4.99	A:VAL311
Hydrophobic	4.47	A:VAL311
Hydrophobic	5.46	A:ILE471
Hydrophobic	5.35	A:ILE471
Hydrophobic	3.57	A:VAL311
Hydrophobic	4.58	A:ILE139
Hydrophobic	4.62	A:LEU147
Hydrophobic	4.15	A:LYS151
Hydrophobic	4.93	A:LEU307
Hydrophobic	4.69	A:ILE139
Hydrophobic	4.68	A:VAL154
Hydrophobic	3.90	A:VAL311
Hydrophobic	3.97	A:LEU380
Hydrophobic	4.20	A:LEU380
Hydrophobic	5.21	A:LEU383
Hydrophobic	4.79	A:TYR126
Hydrophobic	5.32	A:PHE134
Hydrophobic	5.34	A:TYR140
Hydrophobic	5.20	A:PHE236
Hydrophobic	4.76	A:PHE236

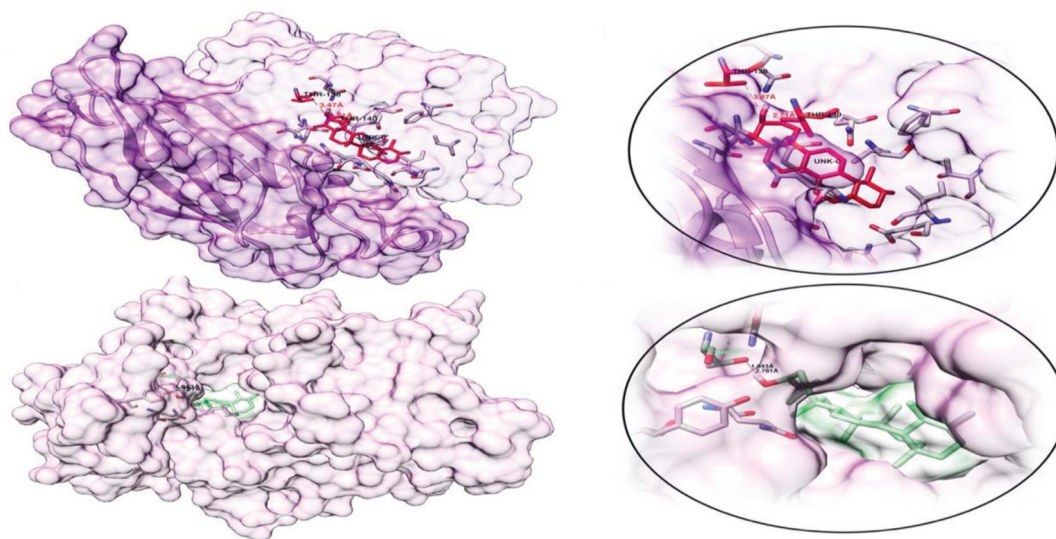


FIGURE 6: The visualization of binding pockets of enzyme  $\beta$ -hydroxyacyl-ACP dehydratase (PDB ID: 4rlt) (a, b) and tyrosyl-tRNA synthetase (PDB ID: 1jjj) (c, d) with  $\alpha$ -amyrine. Compound 1 (depicted as a stick) is embedded in the binding pockets of enzymes. (a, b) Binding of compound 1 in the active site of enzyme  $\beta$ -hydroxyacyl-ACP dehydratase through active site residues GLN86 and GLN89 of  $\beta$ 2 strand and THR138, THR140, and LEU142 of  $\beta$ 5 strand forming hydrogen bond with the hydroxyl groups of the ligand. (c, d) Compound 1 bound to the tyrosyl-tRNA synthetase' active site residue THR75 that is involved in the formation of hydrogen bond with the OH group of compound 1.

parameters were evaluated using docking analysis: first is the binding affinity expressed in kcal/mol, second is the interactions between the amino acid residues of the target protein and the atoms of ligand, and third is the bond distance of these interactions as listed in Table 12.

The docking results between the enzymes  $\beta$ -hydroxyacyl-ACP dehydratase (PDB ID: 4rlt) and tyrosyl-tRNA synthetase (PDB ID: 1jjj) with compound 1 are visualized in 3 dimensions and shown in Figure 6. Similarly, the binding pocket visualization and active site residue interaction of

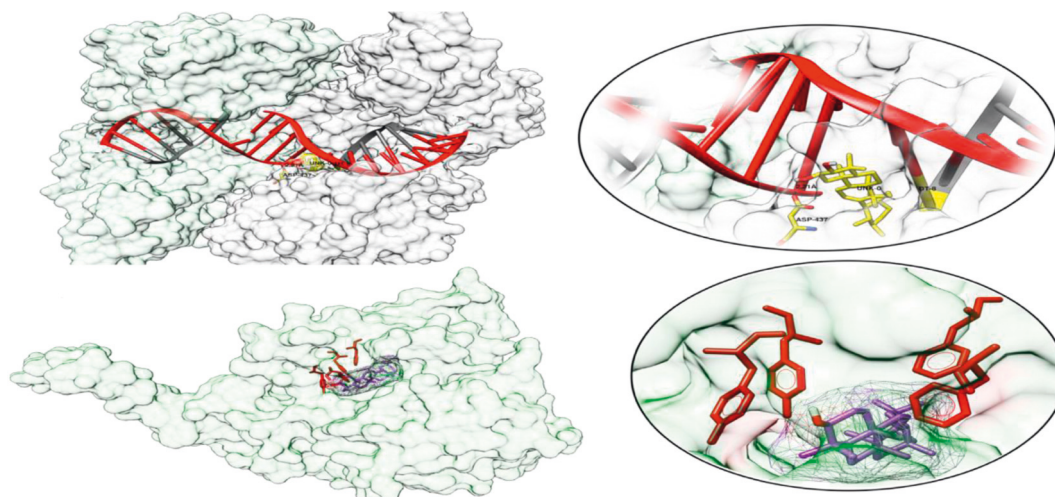


FIGURE 7: Visualization of binding pockets. (a, b) The interaction between compound 2 and topoisomerase II DNA gyrase (PDB ID: 2xct) enzyme is depicted. Compound 2 (shown in yellow sticks) is involved in the formation of hydrogen bond with the DNA (red and gray) and also interacts with the ASP437 residue of this enzyme. (c, d) Docked complex of lanosterol 14 $\alpha$ -demethylase enzyme (PDB ID: 4wmz) with compound 4 is depicted. This enzyme has a hydrophobic pocket (lined with VAL, LEU, PHE, and TYR), and interestingly the PHE and TYR form a hydrophobic tunnel (residues shown in red sticks) that may facilitate the stabilization and subsequent co-crystallization through the hydrophobic core of compound 4.

topoisomerase II DNA gyrase (PDB ID: 2xct) with chamaedrydiol and lanosterol 14 $\alpha$ -demethylase enzyme (PDB ID: 4wmz) with compound 4 are shown in Figure 7. The 3D visualizations were performed by Chimera software [35].

#### 4. Conclusion

The findings of this article concluded that *Persea duthiei* showed potent antibacterial and antifungal properties due to having bioactive ingredients (phytochemicals). Among different solvent soluble fractions, ethyl acetate and n-hexane fractions exhibited decent antimicrobial potency. Ethyl acetate soluble fraction yielded four compounds that served as antimicrobial target inhibitors/prodrugs. Compound 1 ( $\alpha$ -amyrine) and compound 4 ( $\beta$ -amyrine) showed more significant antimicrobial properties due to their potential interaction with the microbial membrane proteins. Molecular docking studies also reflected the antimicrobial activities (antibacterial as well as antifungal activities) of these compounds by indicating the putative binding interaction with the bacterial enzyme (beta-hydroxyacyl dehydratase, tyrosyl-tRNA synthetase, and topoisomerase II DNA gyrase) and fungal enzyme (lanosterol 14 $\alpha$ -demethylase) active sites, respectively. These findings may be helpful in modifying these reported compounds, targeting the biologically significant proteins, and may help in the development of new and advanced broad-spectrum antibiotics. Further, the authors will crystallize and subsequently co-crystallize these important microbial proteins along with these four terpenoids to see their interactions in real natural environment, leading to *in vivo* inhibition studies.

#### Data Availability

All the available data are incorporated in the manuscript and can be obtained from the research supervisor Dr. Ijaz Ahmad.

#### Conflicts of Interest

The authors declare no conflicts of interest.

#### Acknowledgments

The authors wish to thank Princess Nourah Bint Abdulrahman University Researchers Supporting Project number (PNURSP2022R33), Princess Nourah Bint Abdulrahman University, Riyadh, Saudi Arabia, for financial support.

#### References

- [1] P. D. Abeysinghe, "Antibacterial activity of aqueous and ethanol extracts of mangrove species collected from Southern Sri Lanka," *Asian Journal of Pharmaceutical and Biological Research*, vol. 2, pp. 79–83, 2012.
- [2] B. Malesh and S. Satish, "Antimicrobial activity of some important medicinal plant against plant and human pathogen," *World Journal of Agricultural Sciences*, vol. 4, pp. 839–843, 2008.
- [3] C. Walter, Z. K. Shinwari, I. Afzal, and R. N. Malik, "Antibacterial activity in herbal products used in Pakistan," *Pakistan Journal of Botany*, vol. 43, pp. 155–162, 2011.
- [4] I. Bushra, A. Waheed, A. Rehman et al., "Antimicrobial activity OF malva neglecta and nasturtium microphyllum," *International Journal of Research in Ayurveda and Pharmacy*, vol. 3, no. 6, pp. 808–810, 2012.
- [5] Y.-C. Lin, C.-C. Lin, Y.-C. Chu, C.-W. Fu, and J.-H. Sheu, "Bioactive diterpenes, norditerpenes, and sesquiterpenes from a formosan soft coral cespitularia sp," *Pharmaceuticals*, vol. 14, no. 12, p. 1252, 2021.
- [6] N. Uddin, N. Ali, Z. Uddin et al., "Evaluation of cholinesterase inhibitory potential of different genotypes of ziziphus nummularia, their HPLC-UV, and molecular docking analysis," *Molecules*, vol. 25, no. 21, p. 5011, 2020.
- [7] S. Ahmad, J. A. Khader, R. Ullah et al., "Phytochemical analysis and antimicrobial activity of *Persea duthiei*," *African*



- Journal of Pharmacy and Pharmacology*, vol. 6, no. 48, pp. 3302–3304, 2012.
- [8] A. S. Alqahtani, R. Ullah, and A. A. Shahat, “Bioactive constituents and toxicological evaluation of selected anti-diabetic medicinal plants of Saudi Arabia,” *Evidence-Based Complementary and Alternative Medicine*, vol. 2022, Article ID 712, 23 pages, 2022.
  - [9] U. Sarker, S. Oba, S. Ercisli, A. Assouguem, A. Alotaibi, and R. Ullah, “Bioactive phytochemicals and quenching activity of radicals in selected drought-resistant *Amaranthus tricolor* vegetable *Amaranth*,” *Antioxidants*, vol. 11, no. 3, p. 578, 2022.
  - [10] R. Gupta, *Flora of Nainitalensis*, Navyug Traders, New Delhi, India, 1968.
  - [11] R. C. Padalia, S. C. Joshi, D. S. Bisht, and C. S. Mathela, “Essential oil composition of *Persea duthiei*,” *Chemistry of Natural Compounds*, vol. 45, no. 5, pp. 745–747, 2009.
  - [12] J. M. Álvarez, L. E. Cuca, A. Carrasco-Pancorbo, A. B. Ruiz-Muelle, I. Fernández, and A. Fernández-Gutiérrez, “Phenolic constituents of leaves from *Persea caerulea* ruiz & pav; mez (Lauraceae),” *Biochemical Systematics and Ecology*, vol. 67, pp. 53–57, 2016.
  - [13] M. A. Saeed and A. Sabir, “Irritant potential of some constituents from the seeds of *Caesalpinia bonducella* (L.) Fleming,” *Journal of Asian Natural Products Research*, vol. 5, no. 1, pp. 35–41, 2003.
  - [14] F. de Sousa Menezes, Â. S. Borsatto, N. A. Pereira, F. J. de Abreu Matos, and M. A. C. C. Kaplan, “Chamaedrydiol, an ursane triterpene from *Marsypianthes chamaedrys*,” *Phytochemistry*, vol. 48, no. 2, pp. 323–325, 1998.
  - [15] L. Fu, S. Zhang, N. Li et al., “Three new triterpenes from *nerium oleander* and biological activity of the isolated compounds,” *Journal of Natural Products*, vol. 68, no. 2, pp. 198–206, 2005.
  - [16] L. H. Vázquez, P. Javier, and N. Arturo, “The pentacyclic triterpenes amyryns: a review of sources and biological activities,” *Phytochemicals-A Global Perspective of Their Role in Nutrition and Health*, 2013.
  - [17] J. P. Fan and C. H. He, “Single step preparative separation of barbinervic acid and its epimer (rotungenic acid), along with two other pentacyclic triterpene acids from the leaves of *Diospyros kaki* using HSCCC,” *Journal of Liquid Chromatography & Related Technologies*, vol. 29, no. 6, pp. 815–826, 2006.
  - [18] S. A. Khan, S. U. Khan, N. Ullah et al., “Isolation, structure elucidation and in silico prediction of potential drug-like flavonoids from *onosma chitralicum* targeted towards functionally important proteins of drug-resistant bad bugs,” *Molecules*, vol. 26, no. 7, p. 2048, 2021.
  - [19] X. Z. Feng, G. G. T. B. H. Weissig, and S. P. E. Bourne, “Conformational transition in DNA on a cold surface,” *Nucleic Acids Research*, vol. 28, no. 2, pp. 593–596, 2000.
  - [20] P. Elmer, *Chem Bio Draw Profesional Version (15.0. 0.106)*, Cambridge Soft, Waltham, MA, USA, 2017.
  - [21] O. Toolkit, *OpenEye Scientific Software*, OEChem Toolkit, Santa Fe, NM, USA, 2019.
  - [22] N. Santa Fe, *FRED. In Version 3.0.0*, OpenEye Scientific Software, Santa Fe, NM, USA, 2013.
  - [23] F. J. Luna-Vázquez, C. Ibarra-Alvarado, A. Rojas-Molina et al., “Role of nitric oxide and hydrogen sulfide in the vasodilator effect of ursolic acid and uvaol from black cherry *Prunus serotina* fruits,” *Molecules*, vol. 21, no. 1, p. 78, 2016.
  - [24] B. Biovia, *Discovery Studio Client*, Dassault Systemes, San Diego, CA, USA, 2015.
  - [25] D. Nocedo-Mena, S. Arrasate, E. Garza-González et al., “Molecular docking, SAR analysis and biophysical approaches in the study of the antibacterial activity of ceramides isolated from *Cissus incisa*,” *Bioorganic Chemistry*, vol. 109, 2021.
  - [26] L. F. Scatena, M. G. Brown, and G. L. Richmond, “Water at hydrophobic surfaces: weak hydrogen bonding and strong orientation effects,” *Science*, vol. 292, no. 5518, pp. 908–912, 2001.
  - [27] N. N. Q. Vo, E. O. Fukushima, and T. Muranaka, “Structure and hemolytic activity relationships of triterpenoid saponins and sapogenins,” *Journal of Natural Medicines*, vol. 71, no. 1, pp. 50–58, 2017.
  - [28] Y. Dong, X. Qiu, N. Shaw et al., “Molecular basis for the inhibition of  $\beta$ -hydroxyacyl-ACP dehydratase HadAB complex from *Mycobacterium tuberculosis* by flavonoid inhibitors,” *Protein & Cell*, vol. 6, no. 7, pp. 504–517, 2015.
  - [29] N. Zhu, Y. Lin, D. Li et al., “Identification of an anti-TB compound targeting the tyrosyl-tRNA synthetase,” *Journal of Antimicrobial Chemotherapy*, vol. 70, no. 8, pp. 2287–2294, 2015.
  - [30] X. Qiu, C. A. Janson, W. W. Smith et al., “Crystal structure of *Staphylococcus aureus* tyrosyl tRNA synthetase in complex with a class of potent and specific inhibitors,” *Protein Science*, vol. 10, pp. 2008–2016, 2001.
  - [31] T. Khan, K. Sankhe, V. Suvarna, A. Sherje, K. Patel, and B. Dravyakar, “DNA gyrase inhibitors: progress and synthesis of potent compounds as antibacterial agents,” *Biomedicine & Pharmacotherapy*, vol. 103, pp. 923–938, 2018.
  - [32] B. D. Bax, P. F. Chan, D. S. Eggleston et al., “Type IIA topoisomerase inhibition by a new class of antibacterial agents,” *Nature*, vol. 466, no. 7309, pp. 935–940, 2010.
  - [33] A. A. Sagatova, M. V. Keniya, R. K. Wilson, B. C. Monk, and J. D. A. Tyndall, “Structural insights into binding of the antifungal drug fluconazole to *Saccharomyces cerevisiae* lanosterol 14 $\alpha$ -demethylase,” *Antimicrobial Agents and Chemotherapy*, vol. 59, no. 8, pp. 4982–4989, 2015.
  - [34] P. Watson, M. Rose, S. Ellis, H. England, and S. Kelly, “Defective sterol C5-6 desaturation and azole resistance: a new hypothesis for the mode of action of azole antifungals,” *Biochemical and Biophysical Research Communications*, vol. 164, no. 3, pp. 1170–1175, 1989.
  - [35] Z. Yang, K. Lasker, D. Schneidman-Duhovny et al., “UCSF Chimera, MODELLER, and IMP: an integrated modeling system,” *Journal of Structural Biology*, vol. 179, no. 3, pp. 269–278, 2012.

## Research Article

# Protective Effect of Salvianolic Acid A against N-Methyl-N-Nitrosourea-Induced Retinal Degeneration

Yumei Zhou,<sup>1,2</sup> Weiwei Xu,<sup>1</sup> Anqi Liu,<sup>1</sup> Ye Tao,<sup>1</sup> Qun Wang,<sup>1</sup> Yanfeng Yang,<sup>1</sup> Liqiang Wang <sup>1</sup> and Yifei Huang <sup>1</sup>

<sup>1</sup>Department of Ophthalmology, Chinese PLA General Hospital, Beijing, China

<sup>2</sup>Department of Ophthalmology, China Emergency General Hospital, Beijing, China

Correspondence should be addressed to Liqiang Wang; liqiangw301@163.com and Yifei Huang; 301yk@sina.com

Received 16 March 2022; Revised 22 April 2022; Accepted 25 April 2022; Published 26 May 2022

Academic Editor: Ruchika Garg

Copyright © 2022 Yumei Zhou et al. This is an open access article distributed under the Creative Commons Attribution License, which permits unrestricted use, distribution, and reproduction in any medium, provided the original work is properly cited.

**Objective.** Retinal degeneration (RD) is a serious, irreversible, and blinding eye disease, which seriously affects the visual function and quality of life of patients. At present, there is no effective method to treat RD. The final outcome of its development is photoreceptor cell oxidation and apoptosis. Therefore, looking for safe, convenient, and effective antioxidant therapy is still the key research field of Rd. In this study, the mice model of RD was induced by N-methyl-N-nitrosourea (MNU) *in vivo* to explore the therapeutic effect and mechanism of salvianolic acids (Sal A) on RD. *In vitro*, the protective effect of Sal A on MNU injured 661 W cell line of mouse retina photoreceptor cone cells was investigated preliminarily. **Methods.** Male C57BL/6 mice (7–8 weeks old) received a single intraperitoneal injection (ip) of 60 mg/kg MNU or vehicle control. Treatment groups then received Sal-A 0.5 mg/kg and 1.0 mg/kg via daily intravenous injections. On day 7, functional and morphological examinations were performed, including photopic and scotopic electroretinography (ERG) and hematological analyses to observe functional changes and damage to the outer nuclear layer (ONL). On the 3rd and 7th days, the levels of superoxide dismutase (SOD) activity and malondialdehyde (MDA) content were determined. The expression of retinal Bax, Bcl-2, and caspase-3 was quantified by Western blot and RT-PCR assays. 661 W strain of mice retinal photoreceptor cone cells were cultured *in vitro* and treated with 1  $\mu$ m MNU. The cells in the treatment group were given 50  $\mu$ M Sal A as an intervention. The growth of 661 W cells was observed and recorded under an inverted light microscope, and the activity of cells was detected by the MTT method. **Results.** Sal A treatment was effective against MNU-induced RD in mice at both 0.5 mg/kg/d and 1.0 mg/kg/d doses, and the protective effect was dose-dependent. Sal A can alleviate MNU-mediated alterations to retinal ERG activity and can support maintenance of the thickness of the ONL layer. Sal A treatment increases the expression of retinal SOD and reduces the lipid peroxidation product MDA, suggesting that its protective effect is related to the oxidation resistance. It can offset changes to the expression of apoptotic factors in the retina caused by MNU treatment. Sal A mitigates MNU-mediated damage to cultured mice photoreceptor cone cells 661 W *in vitro*. **Conclusion.** Sal A alleviates the damage caused by MNU to retinal photoreceptor cells *in vivo* and *in vitro*, and its protective effect is related to its antioxidant and antiapoptotic activities.

## 1. Introduction

Retinal degeneration (RD) is a common ophthalmic condition that impairs the visual function significantly. It is characterized by progressive apoptosis, which finally results in the death of photoreceptor cells and blindness [1, 2]. Reactive oxygen species (ROS) has been considered as the key factor of photoreceptor cell apoptosis in RD [3]. ROS can activate the poly-ADP ribose polymerase (PARP) in

photoreceptor nucleus, so as to regulate the expression level of apoptosis inducing factor (AIF), and finally touch the apoptosis of photoreceptor cells [4].

There is currently no effective treatment for RD yet. In recent years, a variety of *in vivo*, *in vitro*, and clinical experimental treatment methods have been studied for RD, such as traditional neurotrophic therapy, calcium antagonistic therapy, antiapoptosis/antioxidant therapy, growth factor therapy, as well as new gene therapy, stem cell therapy,



retinal transplantation, artificial retina etc., which have made progress to a certain extent. However, the toxic and side effects of treatment or complex administration methods are the difficulties that limit the research of RD treatment [5–11]. So, the search for safe, convenient, and effective antioxidant therapies is an important research strategy with regard to RD. One effective means to study RD is to use chemical agents, such as N-methyl-N-nitrosourea (MNU), to make animal models. MNU is a nitrophthalamine alkylate with strong mutagenic ability that has been shown to be particularly effective in a variety of tissues [12–14]. In the field of ophthalmology, MNU has been successfully used to induce cataracts, corneal diseases, and animal models of RD [15, 16]. With regard to RD in particular, MNU has been shown to selectively induce photoreceptor cell degradation through the induction of oxidative stress *in vitro* and *in vivo* [4, 17].

In this study, we investigate the potential of salvianolic acid A (Sal A) to inhibit MNU-induced retinal photoreceptor cell apoptosis. Sal A (Figure 1) has a convenient preparation, and it is known to exert few adverse reactions *in vivo*. Because Sal A has a strong antioxidant capacity [18, 19], we predicted that it would protect the retina from damage and thus delay the occurrence and development of RD.

## 2. Materials and Methods

**2.1. Animals.** Male 7-week-old C57BL/6 mice were bought from Viton Lever Company in Beijing, China. They were kept in an air-conditioned facility with a room temperature of 18°C–23°C, humidity of 40%–65%, and a 12-hour light/dark cycle. They were fed normal chow and water ad libitum. The animal study protocol no. is 20161111.

**Animal ethics statement:** Our animal study was performed the ARVO's Statement on the Use of Animals in Ophthalmology and Vision Research.

**2.2. Drugs and Reagents.** MNU (Sigma; St. Louis, MO, USA) was kept at –20°C in the dark, diluted in normal saline containing 0.05 percent acetic acid, and given to mice intraperitoneally (ip) in a single dosage of 60 mg/kg. Sal A-lyophilized powder (purity >98%) was dissolved in normal saline (NS) and injected intravenously into the tails of mice.

### 2.3. Experimental Methods

**2.3.1. Animal Treatments.** Mice were randomly divided into 5 groups (10 mice in each group). Two groups were considered control groups, and they received a single dose of vehicle (NS containing 0.05% acetic acid) ip. Mice in one of the negative control groups (NC) received a tail vein injection of NS on days 1 through 7. Mice in the other negative control group (NC + Sal-A) were injected with Sal A at a dose of 1.0 mg/kg body weight (bw) via the tail vein on each of days 1 through 7.

Mice in three of the groups received a single dose of 60 mg MNU/kg bw ip and then were treated as follows. One group of mice (the MNU group) received a tail vein injection of NS (5 mL/kg/d) on days 1 through 7. A second group of

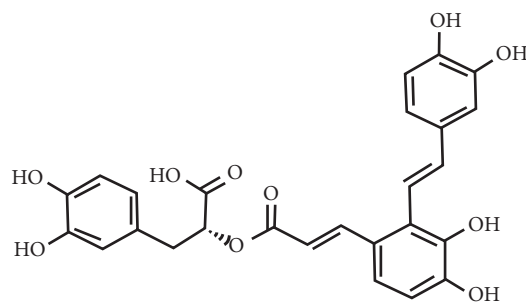


FIGURE 1: Chemical structure of Sal (A). Molecular formula:  $C_{26}H_{22}O_{10}$ ; M.W.:494.45.

mice (the MNU + Sal A (0.5) group) received an initial injection of Sal A at a dose of 0.5 mg/kg bw into the tail vein within 1 h of MNU treatment. Then, from days 1 through 7, the mice were injected with Sal A (0.5 mg/kg bw) everyday through the tail vein. The third group of mice (the MNU + Sal A (1.0) group) were treated similarly to the MNU + Sal A (0.5) group, except that the dose of Sal A was 1.0 mg/kg bw every day.

**2.3.2. Electroretinogram (ERG) Analysis.** After 7 days of MNU administration, the mice were examined by ERG. After 24 hr of dark adaptation, mice were anesthetized by ip injection of chlorpromazine (15 mg/kg) and ketamine 60 mg/kg (Pfizer, USA). Compound tropicamide eye drops (Santen Pharmaceuticals, Japan) were administered to dilate the pupils, and the corneas were anesthetized with cocaine hydrochloride eye drops (Santen Pharmaceutical Co., Japan). On the recording stage under dim red light, the recording electrode was placed on the limbus, and the reference electrode and the ground electrode were placed on the cheek and tail, respectively. The b-wave amplitude and latency were recorded with a single flash stimulation.

**2.3.3. Collection of Mice Eyeballs.** After the mice were deeply anesthetized, right eyeballs were taken and fixed in 4% paraformaldehyde for 12 hours, marked at the top with toluidine blue, and then embedded in paraffin. The left eyeball was removed and preserved in liquid nitrogen.

**2.3.4. Histopathological Assessment of Retinal Morphology.** Routine paraffin-embedded specimens were sagittally sectioned through the optic nerve, and 5  $\mu$ m thick sections were made. After staining with hematoxylin and eosin (HE), light microscopy (OLMPUS BX51) was used to observe the tissues, and images were analyzed with ImageView software. The thickness of the outer nuclear layer (ONL) of the retina was measured at an interval of 200  $\mu$ m up and down the vertical axis. Each measurement was performed 5 times.

**2.3.5. Determination of the Superoxide Dismutase Activity (SOD) and Malonaldehyde (MDA) Content.** The retinal tissue was homogenized and centrifuged at 500 g for 5 minutes at 4°C in PBS containing 0.5 percent Triton X-100

(pH 7.4). The activity of superoxide dismutase (SOD) in the supernatant was determined using a SOD Assay Kit (Biyuntian Biotechnology Co., Ltd., China). The SOD activity was determined using a spectrophotometer to measure the absorbance at 560 nm, and the findings were reported in units per mg protein.

The malondialdehyde (MDA) level was determined using a colorimetric thiobarbituric acid test kit (Biyuntian Biotechnology Co., Ltd., China). The MDA intensity was determined at 532 nm using a spectrophotometer, and the lipid peroxide levels in the presence of MDA were expressed as nmol/mg protein.

**2.3.6. Determination of the Expression Levels of Apoptosis-Related Genes by Western Blotting and Reverse Transcription Polymerase Chain Reaction (RT-PCR) Assays.** *Western Blotting.* Slices of retinal tissues were added to cell lysis solution to remove cellular proteins, which were then separated using SDS-PAGE. The transfer of the proteins to nitrocellulose membranes was prevented using 5% nonfat milk powder. Anti-Bax, anti-BCL-2, anti-caspase-3, and anti-actin primary monoclonal mouse antibodies were bought from Abcam and utilized at dilutions of 1:1000. The secondary antibody, goat anti-mouse IgG, was obtained and utilized at a dilution of 1:1000 from Biyuntian Biotechnology Co., Ltd. Photographs were taken using the gel imaging equipment, and the gray value was analyzed using the program Image J. The expression level was estimated as the ratio of the target protein's optical density to that of actin.

*RT-PCR.* The Trizol reagent was used to extract RNA from retinal tissues. Spectroscopic analysis was conducted to quantify the RNA, which was subsequently reverse-transcribed into a single-stranded cDNA. The relative expression levels of actin, Bax, Bcl-2, and caspase-3 genes were adjusted and measured using gene-specific primers and 25 cycles of cDNA amplification. The primers of Bax, Bcl-2, and caspase-3 were referenced [20].

**2.3.7. Cell Experiments. Cell Grouping.** 661 W cells (from ATCC) are a mice retinal photoreceptor cone cell line. Treatments were initiated when cells reached 70% to 80% confluence. The medium was removed and replaced with fresh media-containing treatments according to 4 treatment groups, as follows. A culture medium containing 1  $\mu$ M MNU was added to cells of the MNU group. A culture medium containing 1  $\mu$ M MNU and 50  $\mu$ M Sal A was added to cells of the MNU + Sal-A group. A culture medium lacking additives was added to the NC (the normal control). A culture medium containing 50  $\mu$ M Sal A was added to cells of the NC + Sal-A group.

*Cell Growth.* Cell growth was monitored and recorded consistently with an inverted optical microscope.

*Cell Viability Assay.* The MTT method was used to find out how healthy the cells that had been treated were, and the absorbance (A) value was found by setting a spectrophotometer to 490 nm. To figure out how many cells were alive, we used this formula: cell viability (percentage) = A for treatment groups/A

for control groups  $\times 100$ . The average of five tests that were done again is used to figure out the result.

**2.3.8. Statistical Analysis.** Data are expressed as mean  $\pm$  standard deviation and were subjected to analysis of variance (ANOVA). Differences for which  $P < 0.05$  were considered statistically significant.

### 3. Results

**3.1. Changes to the Retinal ERG Activity.** On day 7, the MNU-treated group's b-wave amplitudes of retinal ERGs were substantially lower than those of the equivalent NC group in both photopic and scotopic circumstances ( $P < 0.01$ , Figure 2). The b-waves of mice in the MNU group were low and flat, suggesting that MNU caused significant damage to the retinas. In the treatment groups, Sal A was found to significantly inhibit the MNU-invoked decrease of the b-wave amplitude ( $P < 0.01$ ) in a dose-dependent manner ( $P < 0.01$ ). The b-wave amplitude of the NC + Sal-A group was not significantly different from that of the normal control NC group, indicating that the administration of Sal A alone did not affect the electrical activity of the normal mouse retina.

**3.2. Detection of ONL Thickness in Each Group on Day 7.** The retinal ONL of the MNU-treated mice became thinner over time ( $P < 0.01$ , Figure 3), and the ONL layer in this group was basically eliminated by day 7. The thickness of the two Sal A treatment groups was significantly greater than that of the MNU group ( $P < 0.01$ ), and the average ONL thickness of the MNU + Sal A (1.0) group was significantly greater than that of the MNU + Sal A (0.5) group ( $P < 0.01$ ). There was no significant difference in the ONL layer thickness between the NC + Sal-A group and the NC group.

**3.3. Effects of Sal A on the SOD Activity and MDA Content in Retinal Tissues.** As seen in Figure 4, in the MNU-treated group, the SOD activity was considerably lowered ( $P < 0.01$ ) and MDA content was significantly elevated ( $P < 0.01$ ) compared to those in the NC group on day 3. The SOD activity in the retinas of both Sal A treatment groups was probably greater than that in the MNU group ( $P < 0.01$ ), and the high-dose group had considerably increased SOD activity than the low-dose group ( $P < 0.01$ ). MDA concentrations in the retinas of Sal A-treated mice were considerably lower than those in the MNU group ( $P < 0.01$ ), and the high-dose group had significantly lower MDA concentrations than the low-dose group ( $P < 0.01$ ).

On day 7 of the treatment program, the mean retinal SOD activity of the MNU group continued to decrease with time ( $P < 0.01$ ), and the MDA level continued to increase ( $P < 0.01$ ). While the retinal SOD activity of the two Sal A treatment groups continued to decrease ( $P < 0.01$ ), the SOD activity in the retinas of mice treated with Sal A remained significantly higher than that of the MNU group ( $P < 0.01$ ). MDA levels in the retinas from both treatment groups continued to increase ( $P < 0.01$ ) but remained significantly

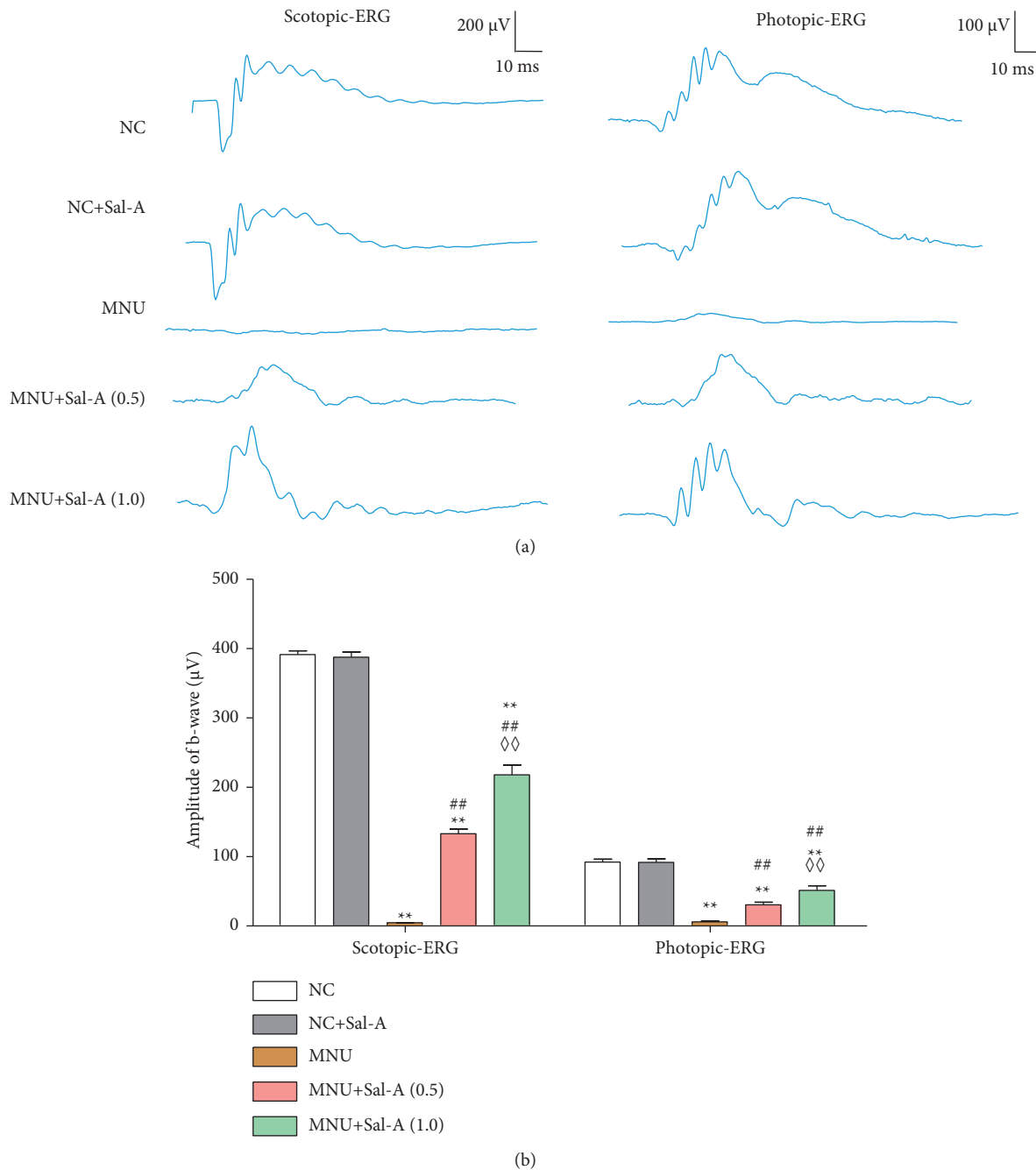


FIGURE 2: Results of ERGs performed under scotopic and photopic conditions. (a): Representative waveforms of scotopic and photopic ERGs from mice at day 7 post-MNU treatment. (b): Quantitative analysis of scotopic and photopic ERG b-wave amplitudes ( $n = 10$ ). \* $P < 0.05$ , \*\* $P < 0.01$  vs. NC group; # $P < 0.05$ , ## $P < 0.01$  vs. MNU group;  $\diamond P < 0.05$ ,  $\diamond\diamond P < 0.01$  MNU + Sal A (1.0) vs. MNU + Sal A (0.5).

lower than those in the MNU group ( $P < 0.01$ ). No significant differences were found between levels of SOD or MDA in the NC groups treated with Sal A and with vehicle control ( $P > 0.05$ ).

**3.4. Effect of Sal A on the Expression Levels of Apoptosis-Related Genes.** As illustrated in Figures 5 and 6, both Western blotting and quantitative real-time PCR experiments revealed that on day 3 of the treatment regimen, the levels of

expression of the retinal proapoptotic genes Bax and caspase 3 were significantly higher in the MNU-treated group than in the NC group ( $P < 0.01$ ). They were all considerably lower than the MNU group ( $P < 0.01$ ), while being significantly higher than the NC group ( $P < 0.01$ ). The expression of these genes was significantly greater in the MNU + Sal A (0.5) group than in the MNU + Sal A (1.0) group ( $P < 0.01$ ), showing that proapoptotic genes were expressed more in the low-dose group than in the high-dose group. The anti-apoptotic gene Bcl-2 expression was substantially decreased

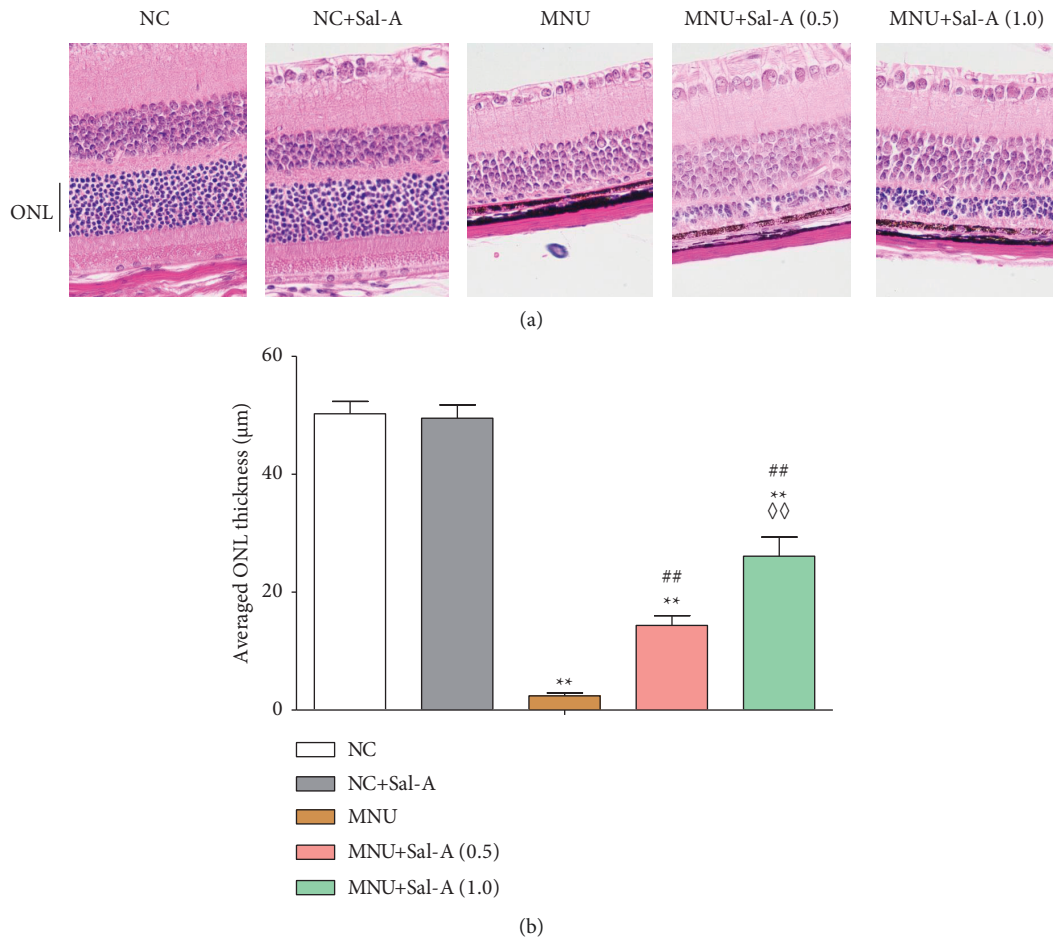


FIGURE 3: Changes in retinal morphology of mice in each group on day 7 after MNU treatment. (a): Representative photograph of the central retina sectioned along the vertical axis ( $\times 400$ ). (b): Histogram analysis of ONL thickness in each group ( $n = 10$ ). \* $P < 0.05$ , \*\* $P < 0.01$  vs. NC group; # $P < 0.05$ , ## $P < 0.01$  vs. MNU group; ◇ $P < 0.05$ , ◇◇ $P < 0.01$  MNU + Sal A (1.0) vs. MNU + Sal A (0.5).

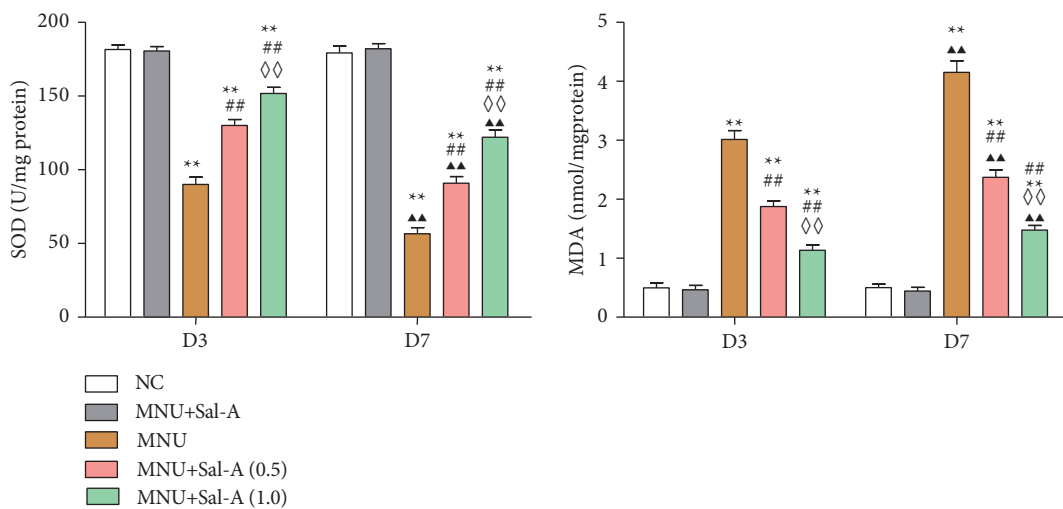


FIGURE 4: Histogram analysis of SOD activity and MDA content in retina of mice in each group on day 3 (D3) and day 7 (D7) ( $n = 10$ ). \* $P < 0.05$ , \*\* $P < 0.01$  vs. NC group; # $P < 0.05$ , ## $P < 0.01$  vs. MNU group; ◇ $P < 0.05$ , ◇◇ $P < 0.01$  MNU + Sal A (1.0) vs. MNU + Sal A (0.5). ▲ $P < 0.05$ , ▲▲ $P < 0.01$  vs. the value at day 3 in the same group.

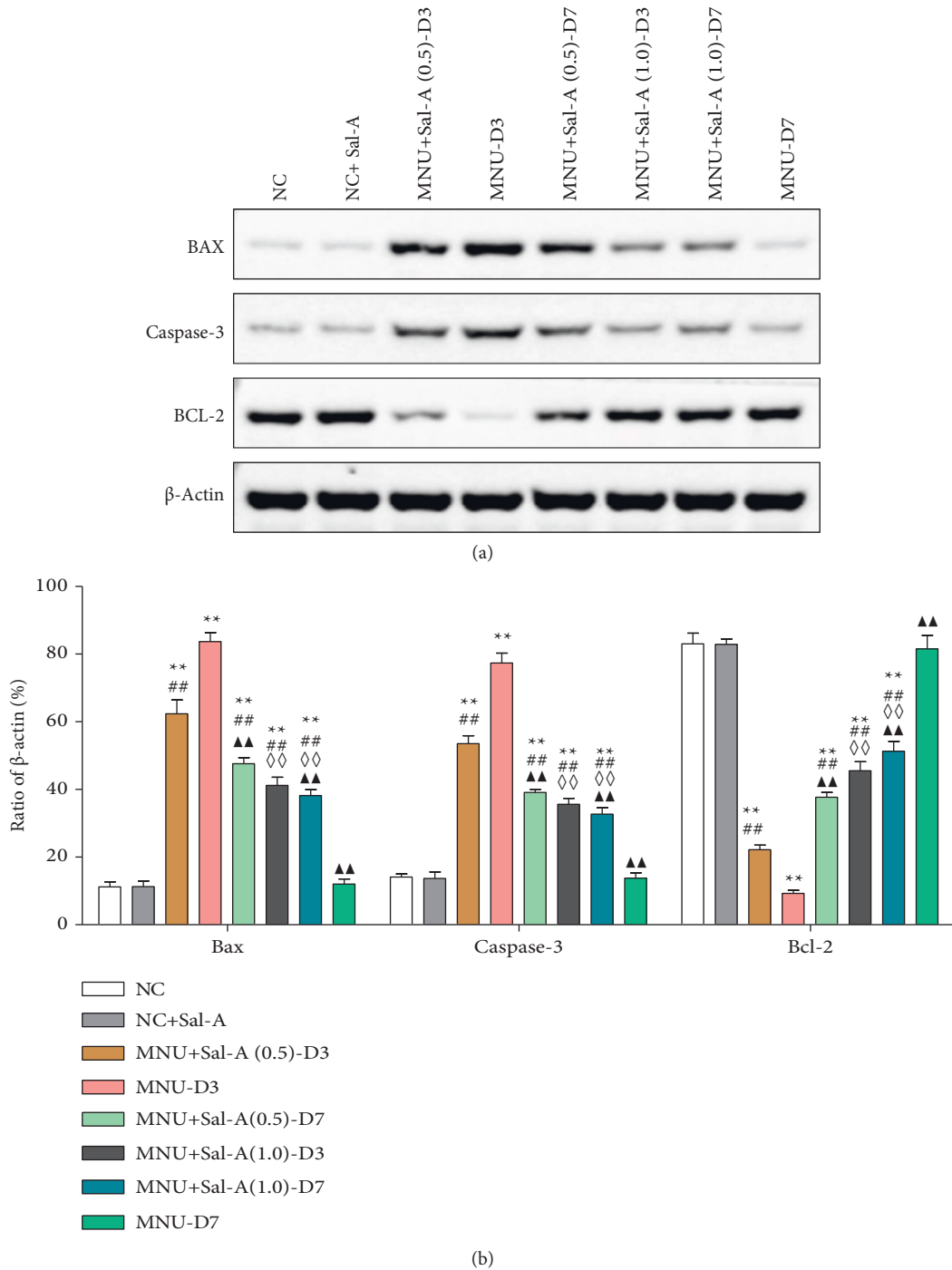


FIGURE 5: (a): Western blotting was utilized to compare Bax, caspase 3, and Bcl-2 protein expression in the retinas of mice in each group. (b): Levels of Bax, Bcl-2, and caspase 3 protein expression in each group’s retinal tissues were measured ( $n = 10$ ). \* $P < 0.05$ , \*\* $P < 0.01$  vs. NC group; # $P < 0.05$ , ## $P < 0.01$  vs. MNU group;  $\diamond P < 0.05$ ,  $\diamond\diamond P < 0.01$  MNU + Sal A (1.0) vs. MNU + Sal A (0.5).  $\blacktriangle P < 0.05$ ,  $\blacktriangle\blacktriangle P < 0.01$  vs. the value at day 3 in the same group.

in mice treated with MNU ( $P < 0.01$ ) compared to animals treated with NC. The Bcl-2 gene expression was considerably greater in the treatment group that received Sal A alone than in the MNU group ( $P < 0.01$ ). The expression of this antiapoptotic gene was significantly lower in the MNU + Sal A (0.5) group than in the MNU + Sal A (1.0) group ( $P < 0.01$ ), indicating that it was expressed less in the low-dose group

than in the high-dose group. Between the NC + Sal A and NC groups, there were no significant changes in the expression of the three apoptosis-related genes ( $P > 0.05$ ).

At day 7, the expression levels of Bax, caspase-3, and Bcl-2 were restored to normal in the MNU group, and there was no significant difference between the MNU group and the normal NC group ( $P > 0.05$ ). On the seventh day, the ONL of



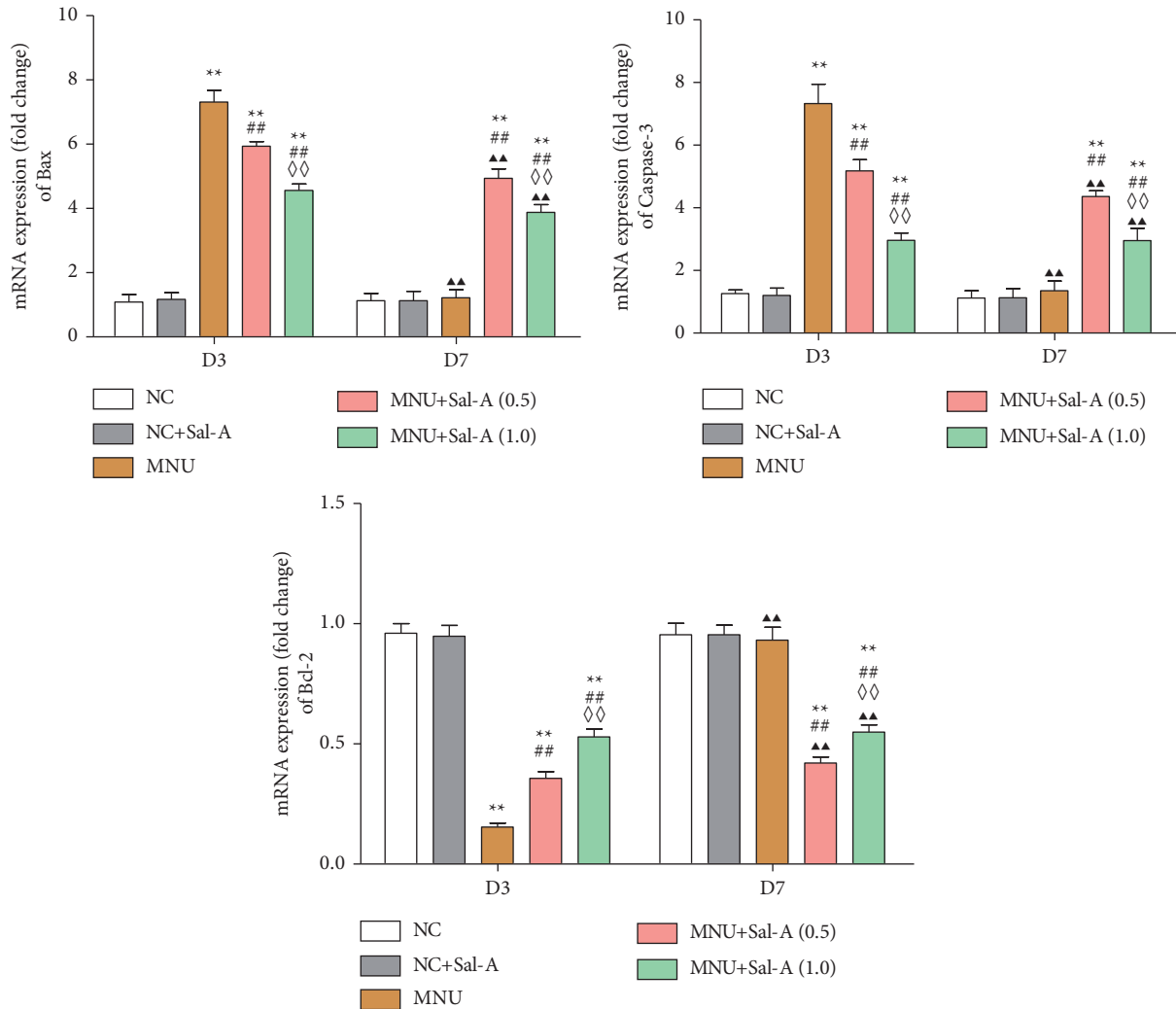


FIGURE 6: Changes of mRNA in the levels of expression of Bax, caspase 3, and Bcl-2 in the retinas of mice in each group. The levels of expression of the mRNA of the three indicators on day 3 (D3) and day 7 (D7) of the treatment regimen as determined by RT-PCR. Data were normalized to the expression of the mRNA coding for  $\beta$  actin ( $n=10$ ). \* $P < 0.05$ , \*\* $P < 0.01$  vs. NC group; # $P < 0.05$ , ## $P < 0.01$  vs. MNU group; ◇ $P < 0.05$ , ◇◇ $P < 0.01$  MNU + Sal A (1.0) vs. MNU + Sal A (0.5). ▲ $P < 0.05$ , ▲▲ $P < 0.01$  vs. the value at day 3 in the same group.

the retina was essentially atrophic, and photoreceptor cells had undergone apoptosis. As a result, the observed amount of apoptotic gene expression was the same as the expression of other normal retinal structures, which was normal. While Bax and caspase 3 expression levels were considerably higher in the Sal A treatment group than in the normal control NC group ( $P < 0.01$ ), and The two genes were expressed at a greater level in the MNU + Sal A (0.5) group than in the high-dose MNU + Sal A (1.0) group ( $P < 0.01$ ). Both treatment groups had a lower Bcl-2 expression than the NC group ( $P < 0.01$ ), and the MNU + Sal A (0.5) group had a lower Bcl-2 expression than the MNU + Sal A (1.0) group ( $P < 0.01$ ). Between the NC+Sal A and NC groups, there was no significant change in the expression of the three apoptotic genes ( $P > 0.05$ ).

**3.5. Morphological Changes of 661 W Cells.** Cells were treated in the noted ways and then were incubated for 12 hr and

24 hr after treatment, and the morphologies were then observed under light microscopy (Figure 7(a)). The adherent growth of cells in the NC group and the NC + Sal-A group was consistent with each other, and the cells were completely confluent at 24 h. On the other hand, the cells treated with MNU shrank and began to fall off at 12 h, and most cells detached from the substrate by 24 h post-treatment. In the MNU + Sal-A group, however, while a small number of cells detached from the substrate at 12 h, some cells remained adhered to the plate and grew well at 24 h.

**3.6. Effects of Treatments on Cell Viability.** The viability of cells in the MNU group, as measured by MTT assays, was significantly lower than that in the NC group at 12 h ( $P < 0.01$ , Figure 7(b)), and continued to decrease at 24 h ( $P < 0.01$ ). Although the viability of cells in the MNU + Sal-A group was continued to decrease with time ( $P < 0.01$ ), but significantly higher than cells treated only with MNU



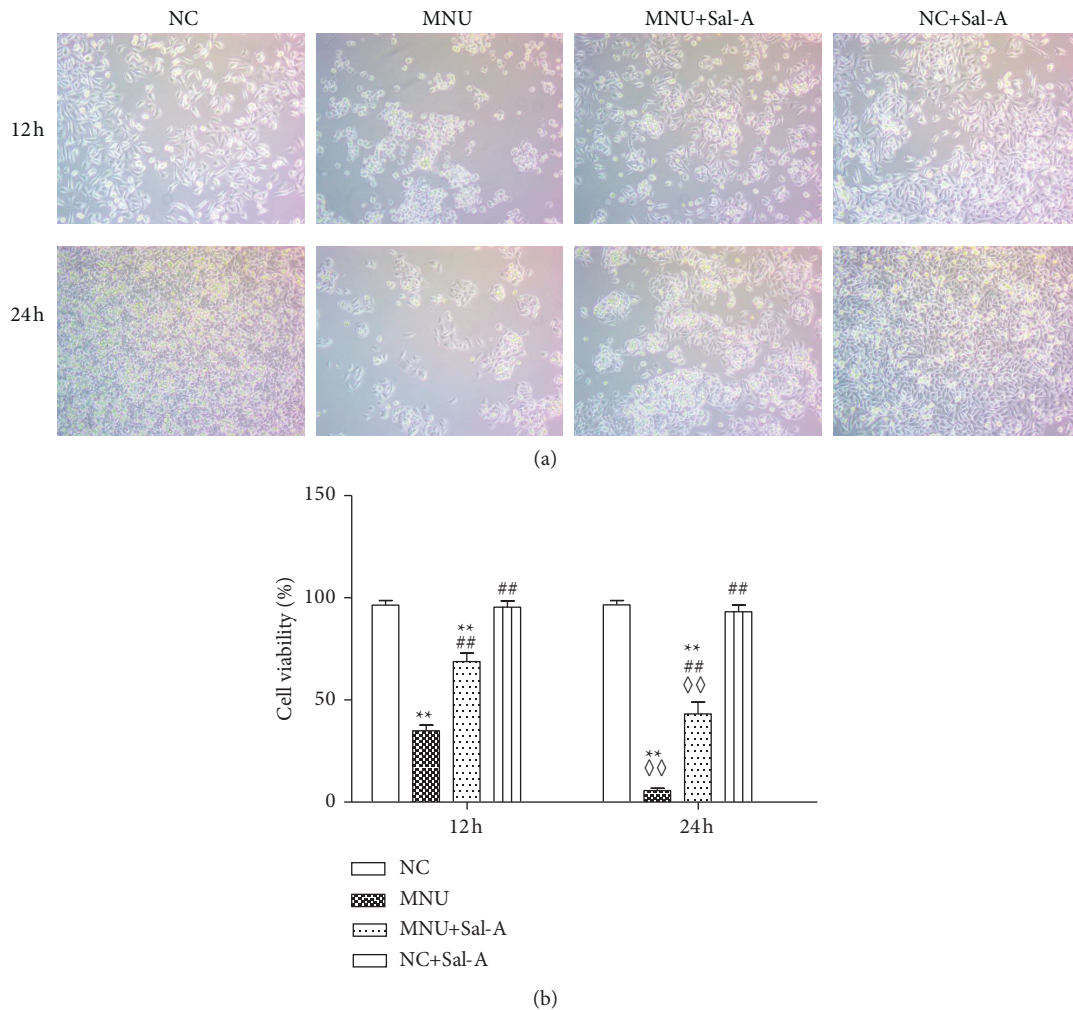


FIGURE 7: (a):Morphologies of 661 W cells at 12 and 24 h after treatment. 661 W cells in each group were observed with an inverted light microscope ( $\times 100$ ). (b) Cell viability of 661 W cell line upon the noted treatment ( $n = 10$ ). \* $P < 0.05$ , \*\* $P < 0.01$  vs. NC group; # $P < 0.05$ , ## $P < 0.01$  vs. MNU group; ◇ $P < 0.05$ , ◇◇ $P < 0.01$  vs.12 h value in the same group.

( $P < 0.01$ ). The viability of cells treated only with Sal A group was not significantly different from that of the NC group ( $P > 0.05$ ), indicating that Sal A itself did not affect cell activity.

#### 4. Discussion

Sal A, a water-soluble phenolic acid extracted from *Salvia miltiorrhiza*, has been demonstrated to exhibit a broad spectrum of pharmacological effects, including antioxidant and anti-inflammatory properties, myocardial ischemia protective, antithrombotic, neuroprotective, and antifibrotic effects [21–26]. In fact, Sal A has one of the strongest antioxidative effects that has been identified among natural products to date, and it has been shown to remove superoxide anions and hydroxyl radicals from the environment and to prevent lipid peroxidation [27, 28]. A study of effects of Sal A application to the eye found that it was able to delay the formation of cataracts, reduce peroxidation products, and improve cellular antioxidant capacity in an animal model induced by 50% galactose [29]. Because of the strong

activity of Sal A, an arginine-glycine-aspartic acid-conjugated polyethyleneimine particle loaded with Sal A has been created for choroidal neovascularization-targeted anti-angiogenesis therapy [18].

In the present study, we explored the therapeutic effect of Sal A on MNU-induced degeneration of photoreceptor cells. The RD model induced by MNU has good reproducibility and high specificity and is widely used in studies of the pathological mechanisms of RD and in drug screening [30, 31]. A single ip of 40 to 70 mg/kg MNU in adult rodents can produce morphological and functional changes, such as a significant reduction in photoreceptor cells and a low level or disappearance of ERG waveforms on days 3 through 7, and a stable RD model can be formed [32–34]. In this experiment, 7 days after a single administration of 60 mg/kg MNU to adult mice, retinal ERG analyses indicated a clear damage to the tissue, and the retinal ONL thickness was significantly reduced. It has been found that the apoptosis of photoreceptor cells induced by MNU is closely related to oxidative stress, and reactive oxygen species (ROS) have been considered to be a key factor in the apoptosis of

photoreceptor cells [4, 35]. ROS activate members of the Bax/Bak family of proteins, and this activation ultimately leads to a caspase-mediated apoptosis cascade [3, 36]. In this study, the retinal SOD activity of mice treated with MNU decreased with time, while the level of MDA increased over time. As SOD is a key enzyme involved in scavenging-free radicals, and MDA levels are a proxy for ROS-mediated damage to lipids; these results support the idea that MNU-induced damage to retinal tissue is associated with oxidative stress.

In the present study, it was shown that Sal A did not affect the waveform of retinal ERG or retinal ONL thickness in normal mice, but it counteracted the decline of the b-wave in the ERG of mice treated with MNU, thereby improving the electrophysiology of retinas of MNU-treated mice. Sal A was also found to maintain ONL thickness in this mice model of RD. Daily administration of Sal A at 0.5 mg/kg and at 1.0 mg/kg had significant dose-dependent protective effects. These results are consistent with the conclusion that Sal A treatment can at least partially alleviate MNU-induced retinal morphological and functional damage.

Studies on the mechanism of the protective effect mediated by Sal A show that it can increase the activity of SOD in mice retinas and can reduce the levels of the lipid peroxidation product MDA, suggesting that its protective effect may be related to the enriching of endogenous antioxidants. This enrichment would relieve MNU-induced oxidative stress in retinal tissues. Through Western blotting and RT-PCR experiments, effects of MNU and Sal A on the expression of the proapoptotic genes Bax and caspase 3 and the antiapoptotic gene Bcl-2 were detected. It was found that Sal A can increase the levels of Bcl-2 mRNA and decrease the levels of Bax and caspase 3 mRNA within the retina, indicating that its protective effect is closely related to an antiapoptotic mechanism.

In addition, we studied the effects of MNU and Sal A *in vitro*. We found that the treatment of cultured 661 W cells with 1  $\mu$ M MNU can induce damage and reduce cell viability, which is consistent with literature reports [15]. Other *in vitro* studies have shown that Sal A can inhibit H<sub>2</sub>O<sub>2</sub>-induced reductions of retinal pigment epithelial cell viability by inhibiting apoptosis and reducing ROS production [19]. It has also been found to protect oxidized LDL-induced retinal pigment epithelial cells from inflammation and oxidative damage [37, 38]. In the present study, we showed that treatment of normally cultured 661 W cells with Sal A is not associated with observable toxic effects. Importantly, though, treatment with Sal A can protect these cells against the damage caused by MNU and can delay MNU-induced decreases of cell viability.

## 5. Conclusions

In conclusion, our study shows that Sal A can ameliorate MNU-induced photoreceptor degeneration *in vitro* and *in vivo*. Moreover, its mechanism is closely related to anti-oxidation and antiapoptosis. Sal A should thus be examined further as a potential safe and effective new therapy for the clinical treatment of RD.

## Data Availability

No data were used to support this study.

## Conflicts of Interest

The authors declare that they have no conflicts of interest.

## Acknowledgments

This study was supported by the National Natural Science Foundation of China (No.81770887), National Key R&D Program of China (Project No. 2017YFA0103200), and Medical Development Research Fund of China Emergency General Hospital (No:K201714).

## References

- [1] R. K. Koenekeop, "Why do cone photoreceptors die in rod-specific forms of retinal degenerations?" *Ophthalmic Genetics*, vol. 30, no. 3, pp. 152–154, 2009.
- [2] S. Strong, G. Liew, and M. Michaelides, "Retinitis pigmentosa-associated cystoid macular oedema: pathogenesis and avenues of intervention," *British Journal of Ophthalmology*, vol. 101, no. 1, pp. 31–37, 2017.
- [3] S. Hisano, Y. Koriyama, K. Ogai, K. Sugitani, and S. Kato, "Nitric oxide synthase activation as a trigger of n-methyl-n-nitrosourea-induced photoreceptor cell death," *Retinal Degenerative Diseases*, vol. 854, pp. 379–384, 2016.
- [4] K. Tsuruma, M. Yamauchi, Y. Inokuchi, S. Sugitani, M. Shimazawa, and H. Hara, "Role of oxidative stress in retinal photoreceptor cell death in N-methyl-N-nitrosourea-treated mice," *Journal of Pharmacological Sciences*, vol. 118, no. 3, pp. 351–362, 2012.
- [5] M. Kuro, K. Yoshizawa, N. Uehara, H. Miki, K. Takahashi, and A. Tsubura, "Calpain inhibition restores basal autophagy and suppresses MNU-induced photoreceptor cell death in mice," *in vivo*, vol. 25, no. 4, pp. 617–623, 2011.
- [6] D. Athanasiou, M. Aguila, J. Bellingham et al., "The molecular and cellular basis of rhodopsin retinitis pigmentosa reveals potential strategies for therapy," *Progress in Retinal and Eye Research*, vol. 62, no. 1, pp. 1–23, 2018.
- [7] J. Zhang, D. Xu, H. Ouyang et al., "Neuroprotective effects of methyl 3,4 dihydroxybenzoate in a mouse model of retinitis pigmentosa," *Experimental Eye Research*, vol. 162, pp. 86–96, 2017.
- [8] Wu J, Cho E, Willett WC, Sastry SM, and Schaumberg DA, "Intakes of lutein, zeaxanthin, and other carotenoids and age-related macular degeneration during 2 decades of prospective follow-up," *JAMA Ophthalmology*, vol. 133, no. 12, pp. 1415–1424, 2015.
- [9] D. Tsikas, "Assessment of lipid peroxidation by measuring malondialdehyde (MDA) and relatives in biological samples: analytical and biological challenges," *Analytical Biochemistry*, vol. 524, pp. 13–30, 2017 May 1.
- [10] K. Srinivasan, "Antioxidant potential of spices and their active constituents," *Critical Reviews in Food Science and Nutrition*, vol. 54, no. 3, pp. 352–372, 2014.
- [11] C. F. Wang, J. R. Yuan, D. Qin et al., "Protection of tauroursodeoxycholic acid on high glucose-induced human retinal microvascular endothelial cells dysfunction and streptozotocin-induced diabetic retinopathy rats," *Journal of Ethnopharmacology*, vol. 185, pp. 162–70, 2016.

- [12] H. H. El-Diasty, H. El-Sayyad, S. Refaat, and H. A. El-Gha-weet, "Efficacy of quercetin-sensitized cisplatin against n-nitroso-nmethylurea induced testicular carcinogenesis in wistar rats," *The Asian Pacific Journal of Cancer Prevention*, vol. 22, no. 1, pp. 75–84, 2021.
- [13] A. I. Faustino-Rocha, R. Ferreira, P. A. Oliveira, A. Gama, and M. Ginja, "N-Methyl-N-nitrosourea as a mammary carcinogenic agent," *Tumor Biology*, vol. 36, pp. 9095–9117, 2015.
- [14] J. Y. Lee, N. Kim, Y. J. Choi et al., "Effect of N-methyl-N-nitrosourea on helicobacter-induced gastric carcinogenesis in C57BL/6 mice," *Journal of Cancer Prevention*, vol. 21, no. 3, pp. 182–186, 2016.
- [15] Y. Qu, R. Li, X. Li et al., "Development of animal models for lens and corneal diseases using N-methyl-N-nitrosourea," *Investigative Ophthalmology & Visual Science*, vol. 61, no. 8, p. 38, 2020.
- [16] A. Tsubura, K. Yoshizawa, M. Kuwata, and N. Uehara, "Animal models for retinitis pigmentosa induced by MNU; disease progression, mechanisms and therapeutic trials," *Histology & Histopathology*, vol. 25, pp. 933–944, 2010.
- [17] J. Wang, X. Chen, F. Wang et al., "OFD1, as a ciliary protein, exhibits neuroprotective function in photoreceptor degeneration models," *PLoS One*, vol. 11, no. 5, Article ID e0155860, 2016.
- [18] G. H. Du, Y. Qiu, Y. E. Tian, and J. T. Zhang, "Prevention of galactose-induced cataractogenesis in rats by salvianolic acid A," *Yao Xue Bao*, vol. 30, no. 8, pp. 561–566, 1995.
- [19] J. Zhang, J. Zhu, L. Zhao et al., "RGD-modified multifunctional nanoparticles encapsulating salvianolic acid A for targeted treatment of choroidal neovascularization," *Journal of Nanobiotechnology*, vol. 19, no. 1, p. 196, 2021.
- [20] Z. Changizi, A. Moslehi, A. H. Rohani, and A. Eidi, "Chlorogenic acid induces 4T1 breast cancer tumor's apoptosis via p53, Bax, Bcl-2, and caspase-3 signaling pathways in BALB/c mice," *Journal of Biochemical and Molecular Toxicology*, vol. 35, no. 2, Article ID e22642, 2021.
- [21] T. J. Lin, K. J. Zhang, and G. T. Liu, "Effects of salvianolic acid A on oxygen radicals released by rat neutrophils and on neutrophil function," *Biochemical Pharmacology*, vol. 51, no. 9, pp. 1237–1241, 1996.
- [22] K. S. Oh, B. K. Oh, J. Mun, H. W. Seo, and B. H. Lee, "Salvianolic acid A suppress lipopolysaccharide-induced NF-kappaB signaling pathway by targeting IKKbeta," *International Immunopharmacology*, vol. 11, pp. 1901–1906, 2011.
- [23] X. L. Li, J. P. Fan, J. X. Liu, and L. N. Liang, "Salvianolic acid A protects neonatal cardiomyocytes against hypoxia/reoxygenation-induced injury by preserving mitochondrial function and activating Akt/GSK-3β signals," *Chinese Journal of Integrative Medicine*, vol. 25, no. 1, pp. 23–30, 2019.
- [24] R. Wang, F. Song, S. Li, B. Wu, Y. Gu, and Y. Yuan, "Salvianolic acid A attenuates CCl4-induced liver fibrosis by regulating the PI3K/AKT/mTOR, Bcl-2/Bax and caspase-3/cleaved caspase-3 signaling pathways," *Drug Design, Development and Therapy*, vol. 13, pp. 1889–1900, 2019.
- [25] F. H. P. Tan, A. C. J. Ting, B. G. Leow, N. Najimudin, N. Watanabe, and G. Azzam, "Alleviatory effects of Danshen, Salvianolic acid A and Salvianolic acid B on PC12 neuronal cells and *Drosophila melanogaster* model of Alzheimer's disease," *Journal of Ethnopharmacology*, vol. 279, Article ID 114389, 2021.
- [26] M. Y. Chien, C. H. Chuang, C. M. Chern et al., "Salvianolic acid A alleviates ischemic brain injury through the inhibition of inflammation and apoptosis and the promotion of neurogenesis in mice," *Free Radical Biology and Medicine*, vol. 99, pp. 508–519, 2016.
- [27] C. H. Liu, Y. Y. Hu, X. L. Wang, P. Liu, and L. M. Xu, "Effects of salvianolic acid-A on NIH/3T3 fibroblast proliferation, collagen synthesis and gene expression," *World Journal of Gastroenterology*, vol. 6, no. 3, pp. 361–364, 2000 Jun.
- [28] Y. S. Huang and J. T. Zhang, "Antioxidative effect of three water-soluble components isolated from *Salvia miltiorrhiza* in vitro," *Yao Xue Bao*, vol. 27, no. 2, pp. 96–100, 1992.
- [29] Y. Liu and J. Zhang, "THydroxyl radical scavenging effect of Salvianolic acids," *Chinese Journal of Pharmaceutical*, vol. 3, pp. 43–50, 1994.
- [30] Y. Gao, X. G. Deng, Q. N. Sun, and Z. Q. Zhong, "Ganoderma spore lipid inhibits N-methyl -N -nitrosourea-induced retinal photoreceptor apoptosis in vivo," *Experimental Eye Research*, vol. 90, pp. 397–404, 2010.
- [31] Y. Koriyama, K. Ogai, K. Sugitani, S. Hisano, and S. Kato, "Geranylgeranylacetone suppresses N-methyl-N-nitrosourea-Induced photoreceptor cell loss in mice," *Advances in Experimental Medicine & Biology*, vol. 854, pp. 237–243, 2016.
- [32] K. Yoshizawa and A. Tsubura, "Characteristics of N-methyl-N-nitrosourea-induced retinal degeneration in animals and application for the therapy of human retinitis pigmentosa," *Nippon Ganka Gakkai Zasshi*, vol. 109, no. 6, pp. 327–337, 2005.
- [33] Y. Emoto, K. Yoshizawa, Y. Kinoshita, M. Yuki, T. Yuri, and A. Tsubura, "Susceptibility to N-methyl-N-nitrosourea-induced retinal degeneration in different rat strains," *Journal of Toxicologic Pathology*, vol. 29, no. 1, pp. 67–71, 2016.
- [34] Y. Y. Chen, S. L. Liu, D. P. Hu, Y. Q. Xing, and Y. Shen, "N -methyl- N -nitrosourea-induced retinal degeneration in mice," *Experimental Eye Research*, vol. 121, pp. 102–113, 2014.
- [35] Y. Emoto, K. Yoshizawa, Y. Kinoshita, M. Yuki, T. Yuri, and A. Tsubura, "Green tea extract attenuates MNU-induced photoreceptor cell apoptosis via suppression of heme oxygenase-1," *Journal of Toxicologic Pathology*, vol. 29, no. 1, pp. 61–65, 2016.
- [36] Y. Wooff, N. Fernando, J. H. C. Wong et al., "Caspase-1-dependent inflammasomes mediate photoreceptor cell death in photo-oxidative damage-induced retinal degeneration," *Scientific Reports*, vol. 10, no. 1, p. 2263, 2020.
- [37] H. Zhang, Y. Y. Liu, Q. Jiang et al., "Salvianolic acid A protects RPE cells against oxidative stress through activation of Nrf2/HO-1 signaling," *Free Radical Biology and Medicine*, vol. 69, pp. 219–228, 2014.
- [38] K. Mao, W. Shu, Q. Qiu, Q. Gu, and X. Wu, "Salvianolic acid A protects retinal pigment epithelium from OX-LDL-induced inflammation in an age-related macular degeneration model," *Discovery Medicine*, vol. 23, no. 125, pp. 129–147, 2017.



## Research Article

# Ameliorative Potential of Resveratrol in Dry Eye Disease by Restoring Mitochondrial Function

Jingyao Chen, Weijia Zhang, Yixin Zheng, and Yanze Xu 

Department of Ophthalmology, Yan An Hospital Affiliated to Kunming Medical University, Kunming, China

Correspondence should be addressed to Yanze Xu; xuyanze6@kmmu.edu.cn

Received 28 January 2022; Revised 29 March 2022; Accepted 18 April 2022; Published 26 May 2022

Academic Editor: Ruchika Garg

Copyright © 2022 Jingyao Chen et al. This is an open access article distributed under the Creative Commons Attribution License, which permits unrestricted use, distribution, and reproduction in any medium, provided the original work is properly cited.

**Background and Significance.** Dry eye disease (DED) is a prevalent optic surface illness with a high incidence worldwide that is caused by a variety of factors, including mitochondrial dysfunction. Resveratrol has been confirmed to protect the eye surface in DED, and as an antioxidant, resveratrol can maintain mitochondrial function. Therefore, we investigated whether resveratrol can improve DED by restoring mitochondrial function. **Methods.** The mitochondrial dysfunction of HCE-2 human corneal epithelial cells was induced by high osmotic pressure exposure and treated with resveratrol (50  $\mu$ M). Western blotting was used to detect the expression of the antioxidant proteins SOD2, GPx, and SIRT1, and flow cytometry was used to detect cell apoptosis and ROS production. The DED mouse model was induced by 0.2% benzalkonium chloride (BAC) and treated with resveratrol. The tear yield was measured by the phenol cotton thread test, the density of cup cells in the conjunctiva was measured by periodic acid-Schiff (PAS) staining, and the expression levels of SIRT1, GPx, and SOD2 in lacrimal glands were detected by Western blotting. **Results.** In hypertonic conditions, the apoptosis of HCE-2 cells increased, the expression of the antioxidant proteins SOD2 and GPx decreased, ROS production increased, and the expression of SIRT1 protein, an essential regulator of mitochondrial function, was downregulated. Treatment with resveratrol reversed the mitochondrial dysfunction mediated by high osmotic pressure. In the DED mouse model, resveratrol treatment promoted tear production and goblet cell number in DED mice, decreased corneal fluorescein staining, upregulated SIRT1 expression, and induced SOD2 and GPx expression in DED mice. **Conclusion.** Resveratrol alleviates mitochondrial dysfunction by promoting SIRT1 expression, thus reducing ocular surface injury in mice with dry eye. This study suggests a new path against DED.

## 1. Introduction

DED is a prevalent ocular surface disorder caused by inadequate production of tears and excessive tear evaporation. Of note, the prevalence of DED in the world population ranges from 6 to 34%, and the prevalence of DED is higher in the aging population [1]. Thus, effective therapeutic strategies are urgently needed for remitting DED.

Emerging evidence indicates that mitochondrial dysfunction is responsible for pathological processes, including but not limited to neurodegenerative disease [2], cancer [3], and DED [4]. Studies have shown that mitochondrial function is a crucial component in the progression of DED. For example, DDIT4 knockdown restores mitochondrial function under hyperosmolarity and preserves the viability of human corneal epithelial cells [5]. Moreover, the

modulation of mitochondrial homeostasis is related to the outcome of DED [6]. Recent studies suggest that antioxidant administration may restore mitochondria. Resveratrol (3,5,4'-trihydroxy-trans-stilbene), a natural plant product, has been reported to have antioxidant effects and maintain mitochondrial function [7, 8]. The protective role of resveratrol in mitochondrial dysfunction-related diseases, such as cardiac diseases [9], hypoxic ischemic injury [10], and neurodegenerative disorders [11], has been well established. It is worth noting that the function of resveratrol in protecting the ocular surface in experimental DED has been reported [12]. However, the underlying mechanism by which resveratrol ameliorates DED remains obscure.

Mammalian sirtuin 1 (SIRT1) is an exceedingly conserved NAD(+)-dependent deacetylase that has been reported to be engaged in the regulation of mitochondrial

biogenesis [13]. Aberrant expression of SIRT1 leads to mitochondrial dysfunction, thereby enhancing pathological processes [14]. Earlier research revealed that the expression of SIRT1 is decreased in the condition of diabetic dry eye [15], indicating that SIRT1 may function in DED. It is well known that resveratrol is a potent activator of SIRT1 [16]. Currently, the antioxidative effect of resveratrol is achieved by upregulating SIRT1 expression [17]. For instance, resveratrol improves mitochondria and protects against metabolic disease by activating SIRT1 [18]. Resveratrol activates SIRT1 to alleviate cardiac dysfunction through mitochondrial regulation [19]. However, the correlation between resveratrol and SIRT1 in DED is unknown.

Thus, we demonstrate that resveratrol treatment attenuates hyperosmolarity-induced mitochondrial dysfunction in human corneal epithelial cells (HCEpiCs). SIRT1 is reduced in hyperosmolarity-treated HCEpiCs, while resveratrol upregulates SIRT1 expression. Moreover, we found that resveratrol restores mitochondrial function by inducing SIRT1 expression. Consistently, resveratrol ameliorated dry eye symptoms in the DED mouse model. Thus, our results establish a novel mechanism by which resveratrol attenuates DED by facilitating SIRT1 expression.

## 2. Materials and Methods

**2.1. Cell Culture and Treatment.** Human corneal epithelial cells HCE-2[50.B1] (CRL-11135) were acquired from ATCC (Manassas, VA, USA). Cells were cultured at 37°C in 5% CO<sub>2</sub> humidity in 10% fetal bovine serum (FBS, Gibco) and 1% v/v penicillin/streptomycin (Gibco) in Dulbecco's modified Eagle's medium (DMEM, Gibco). For the DED cell model, HCEpiCs were treated with 0 or 94 mM NaCl in the medium and treated at isotonic and high osmolarity (312 and 500 mOsM) for 24 h. For resveratrol treatment, HCEpiCs were administered at 50 μM, and the vehicle (alcohol) had a final concentration of 0.5% (nontoxic for cells) [20].

**2.2. Cell Apoptosis Assay.** The apoptosis of the indicated cells was analyzed by an Annexin V-FITC apoptosis detection kit (C1062S, Beyotime). Briefly, cells were collected and resuspended in PBS. After centrifugation, the suspension was discarded, and the cells were resuspended in buffer. Subsequently, 5 μl of Annexin V-FITC and 10 μl of propidium iodide staining solution were added. After incubating at room temperature in the dark for 10–20 minutes, the cells were placed on ice and analyzed by flow cytometry.

**2.3. Measurement of ROS Levels.** The ROS level in the indicated cells was measured by an ROS assay kit (ab113851, Abcam). Briefly, HCEpiCs were stained with DCFDA for 30 minutes at 37°C.

**2.4. Western Blot.** Proteins isolated from HCEpiCs and lacrimal glands were measured by a BCA assay kit (P0012S, Beyotime). Approximately 40 μg of protein was separated by sodium dodecyl sulfate-polyacrylamide gel electrophoresis

(SDS-PAGE) and transferred to PVDF membranes (1620177, BioRad). PVDF membranes were blocked in 5% nonfat milk and incubated with the primary antibodies at 4°C overnight. After washing with TBST three times, the membranes were incubated with secondary antibodies. Finally, the bands were measured with an ECL reagent kit (A38555, Thermo Scientific™).

**2.5. Animal Model and Treatment.** Seventy female C57BL/6 mice (Certificate number: SCXK(Dian)K2020-0004) aged 6–8 weeks were purchased from the Animal Center of Kunming Medical University. The mice were instilled with 5 μL of 0.2% BAC (Sigma-Aldrich) solution in both the eyes, twice a day, for 2 consecutive weeks, to induce the mouse DED model [21]. After the successful establishment of the DED model, the mice were randomly divided into 3 groups (15 mice in each group): DED group, DED mice with alcohol administration, and DED mice with resveratrol administration, and the mice without BAC induction were used as the normal control group. Resveratrol (5 μL/eye) was administered 3 times/day in both the eyes for two weeks. Eventually, the mice were euthanized by CO<sub>2</sub> asphyxiation, and the entire eye tissue, including the conjunctiva and eyeball, was removed for further analysis.

**2.6. Corneal Fluorescein Staining.** 1 μL of 1% sodium fluorescein was dropped into the inferior conjunctival sac using a micropipette; then, punctate staining on the corneal surface was evaluated in a blind fashion. Cobalt blue light was used for inspection and photographic recording under a slit-lamp microscope with 0 points for no staining of corneal fluorescein, 1 point for one-quarter staining, 2 points for less than half staining, 3 points for more than half staining, and 4 points for more than half staining [22].

**2.7. Tear Production.** The tear output was analyzed using phenol red cotton threads (Tianjin Jingming) [23]. The phenol red thread was positioned in the lateral canthus of the eye for 60 seconds, and then, thread wetting measurements were recorded.

**2.8. Periodic Acid-Schiff (PAS) Staining.** The eyeball was embedded and sliced into 5 μm thick divisions. Each division was stained with periodic acid-Schiff (PAS) [24]. The goblet cell density was quantified.

**2.9. Statistical Analysis.** All data are expressed as the mean ± SEM. GraphPad software was used to analyze and draw figures. The statistical significance of differences was evaluated by the two-tailed Student's *t*-test or two-way ANOVA. All *p* values were considered statistically significant when values were <0.05.

## 3. Results

**3.1. Environmental Hyperosmolarity Promotes Mitochondrial Dysfunction in HCEpiCs.** To investigate the part of

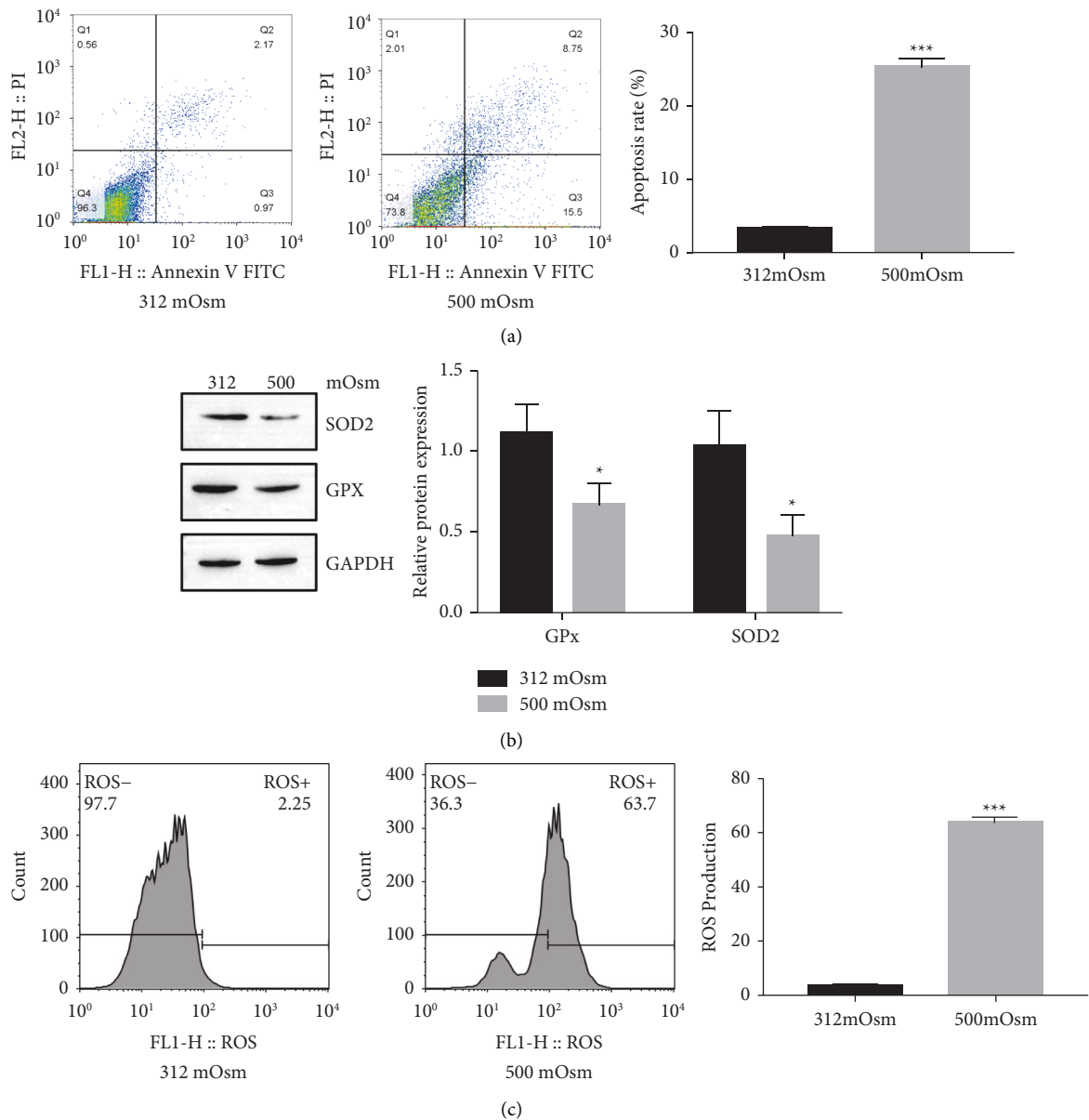


FIGURE 1: Environmental hyperosmolarity promotes mitochondrial dysfunction in HCEpiCs. (a) Apoptosis of HCEpiCs under iso and hyperosmolarities (312 and 500 mOsm) determined by flow cytometry. (b) The expression levels of the antioxidant proteins SOD2 and GPx measured by Western blotting. (c) ROS production under iso- and hyper-osmolarities determined by flow cytometry.  $n = 3$ . \* $P < 0.05$  and \*\*\* $P < 0.001$ .

mitochondria in DED, a hyperosmolarity HCEpiCs model was created using 500 mOsm medium, and HCEpiCs exposed to 312 mOsm medium were regarded as controls. As shown in Figure 1(a), after exposure to 500 mOsm medium, the apoptosis of HCEpiCs was increased. The expression levels of the antioxidant proteins SOD2 and GPx were reduced in HCEpiCs under hyperosmolarity (Figure 1(b)). Consistently, hyperosmolarity increased ROS production in HCEpiCs (Figure 1(c)).

**3.2. Resveratrol Treatment Suppresses Mitochondrial Dysfunction in HCEpiCs.** Resveratrol is reported to modulate mitochondrial function in vitro and in vivo. To understand

the function of resveratrol in mitochondrial function in HCEpiCs, hyperosmolarity-treated HCEpiCs were administered 50  $\mu\text{M}$  of resveratrol. The apoptosis of HCEpiCs was reduced by resveratrol treatment (Figure 2(a)). Resveratrol administration promoted SOD2 and GPx expression (Figure 2(b)); in contrast, ROS production was reduced (Figure 2(c)).

**3.3. Resveratrol Upregulates SIRT1 Expression in HCEpiCs.** Previous studies suggested that SIRT1 contributed to mitochondrial function maintenance [25]. SIRT1 is involved in resveratrol-mediated mitochondrial regulation [19, 26]. Here,



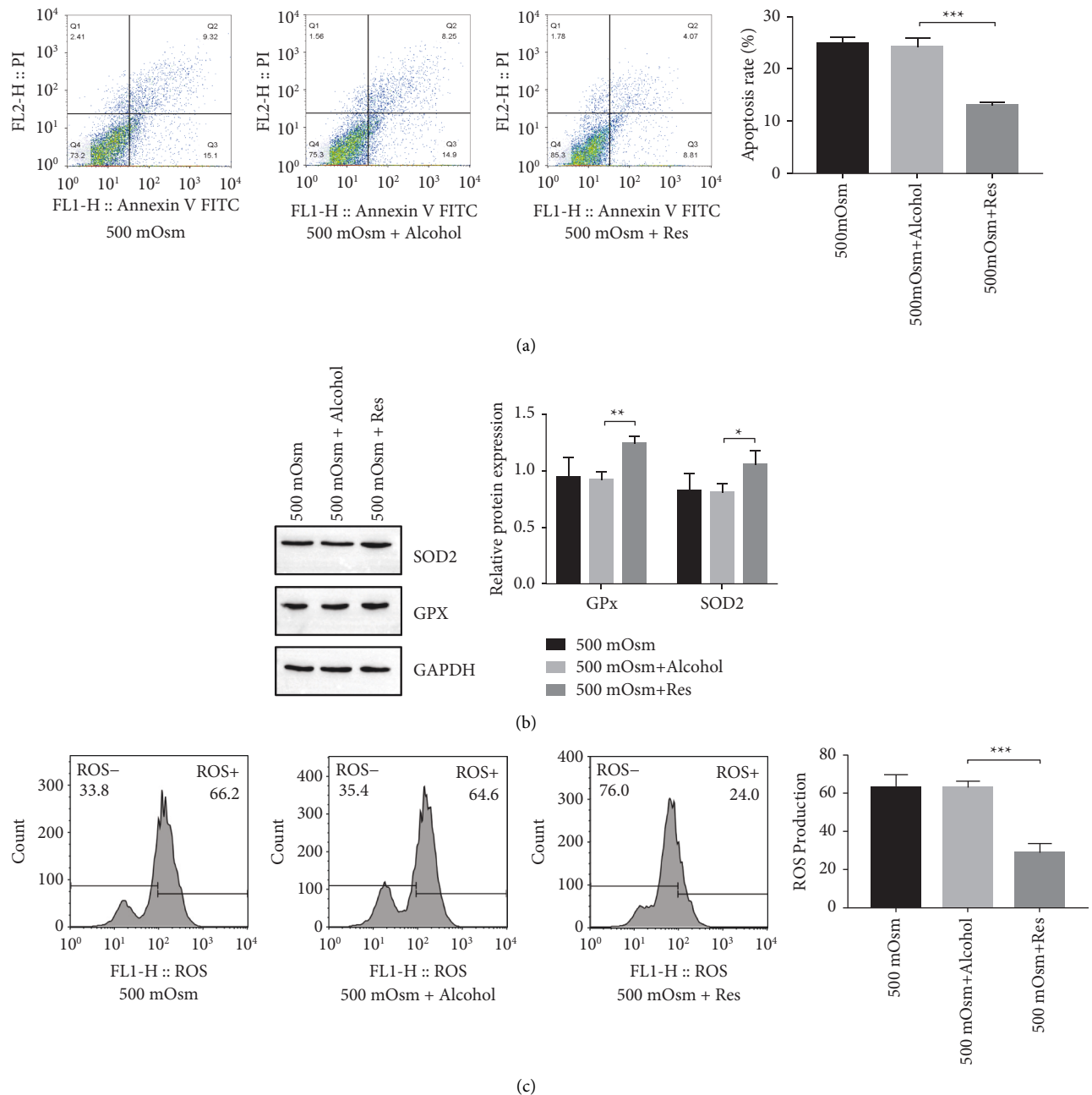


FIGURE 2: Resveratrol treatment suppresses mitochondrial dysfunction in HCEpiCs. (a) Apoptosis of HCEpiCs under hyperosmolarity (500 mOsm) with resveratrol treatment determined by flow cytometry. (b) The expression levels of the antioxidant proteins SOD2 and GPx measured by Western blotting. (c) ROS production in HCEpiCs under hyperosmolar conditions with resveratrol treatment determined by flow cytometry.  $n = 3$ . \* $P < 0.05$ , \*\* $P < 0.01$ , \*\*\* $P < 0.001$ .

we showed that SIRT1 was suppressed in HCEpiCs under hyperosmolarity (Figure 3(a)). We examined the effects of resveratrol on SIRT1 and found that the expression of SIRT1 was recovered with resveratrol treatment (Figure 3(b)).

We next asked whether SIRT1 was responsible for resveratrol-mediated mitochondrial regulation in HCEpiCs. To test this hypothesis, we introduced the SIRT1 inhibitor EX527. Treatment with EX527 counteracted the inhibitory effect of resveratrol on HCEpiCs apoptosis (Figure 3(c)) and SOD2 and GPx expression (Figure 3(d)). We also observed

that EX527 eliminated part of the inhibitory effect of resveratrol on ROS production (Figure 3(e)).

#### 3.4. Resveratrol Ameliorates DED Syndrome in Vivo via SIRT1.

Next, a DED mouse model induced by BAC ammonium chloride was used to determine the role of resveratrol in DED progression. Tear output was measured by the phenol red cotton thread test, which indicated that resveratrol-treated DED mice experienced more tear production than alcohol-

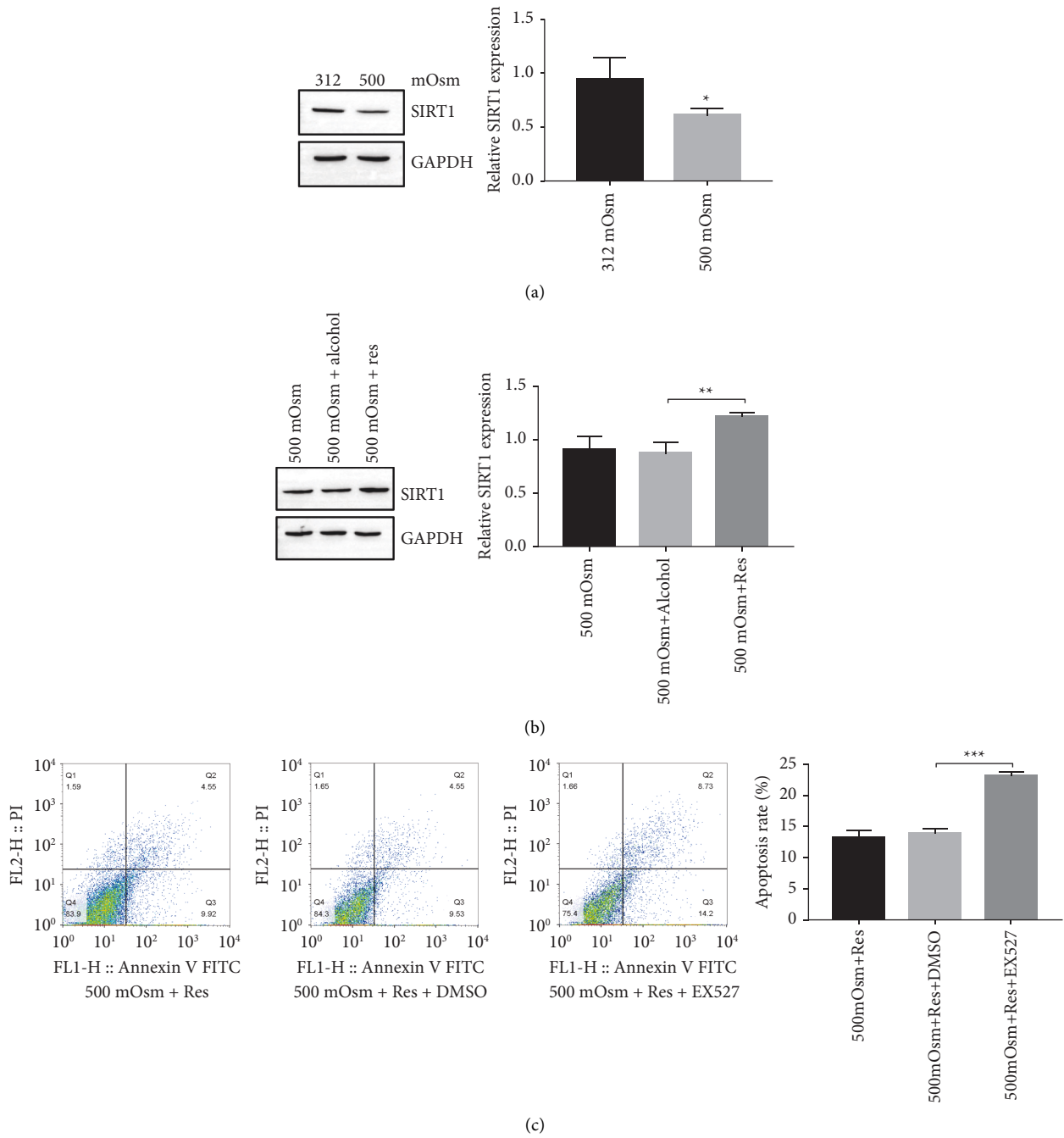


FIGURE 3: Continued.

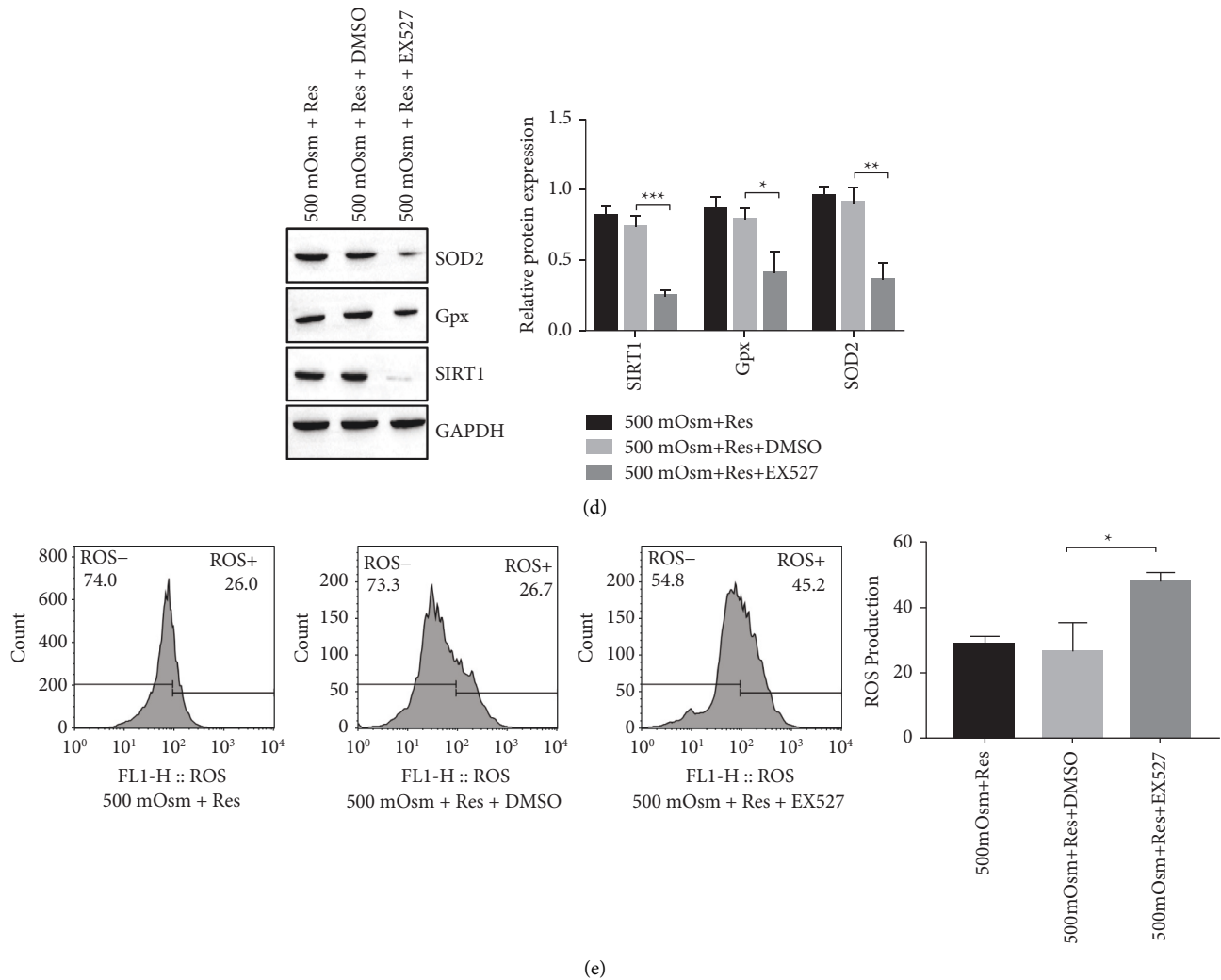


FIGURE 3: Resveratrol upregulates SIRT1 expression in HCEpiCs. (a) Expression of SIRT1 in HCEpiCs under iso- and hyper-osmolarities (312 and 500 mOsm) detected by Western blotting. (b) Expression of SIRT1 in HCEpiCs under hyperosmolarity (500 mOsm) with resveratrol treatment determined by Western blotting. (c) Apoptosis of HCEpiCs under hyperosmolar conditions treated with resveratrol and/or the SIRT1 inhibitor EX527 determined by flow cytometry. (d) Expression of SIRT1, Gpx, and SOD2 in HCEpiCs under hyperosmolarity with resveratrol and/or SIRT1 inhibitor EX527 treatment measured by Western blotting. (e) ROS production in HCEpiCs under hyperosmolar conditions treated with resveratrol and/or the SIRT1 inhibitor EX527 measured by flow cytometry.  $n = 3$ . \* $P < 0.05$ , \*\* $P < 0.01$ , \*\*\* $P < 0.001$ .

treated DED mice and DED mice (Figure 4(a)). Corneal fluorescein staining was decreased in resveratrol-treated mice (Figure 4(b)). Moreover, the number of goblet cells was increased with resveratrol administration (Figure 4(c)). These data indicated that resveratrol attenuates DED progression.

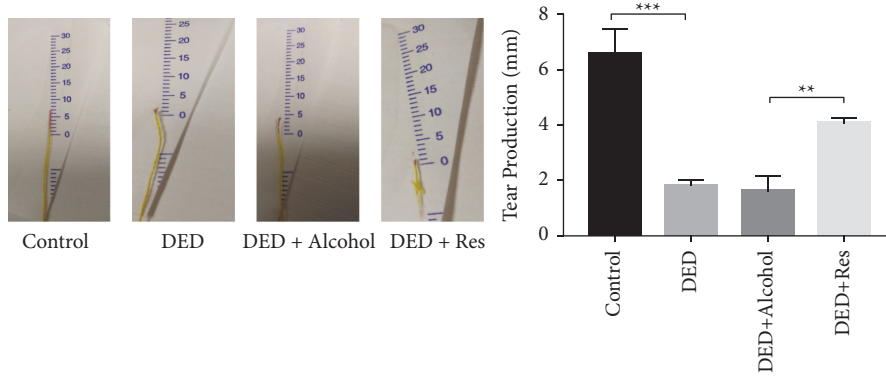
We then detected SIRT1 expression in lacrimal glands and found that SIRT1 was inhibited in DED mice and alcohol-treated DED mice, while resveratrol upregulated SIRT1 expression (Figure 4(d)). Moreover, resveratrol administration induced SOD2 and Gpx expression in the DED mouse model (Figure 4(e)).

#### 4. Discussion

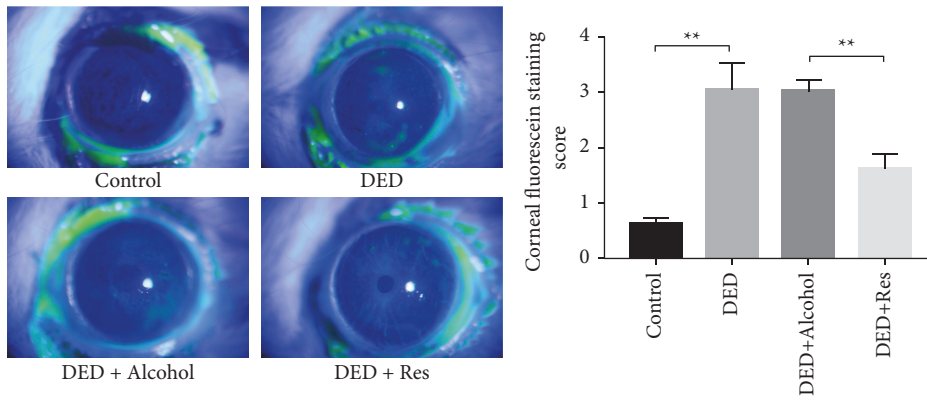
In the current research, we demonstrated that hyperosmolarity induces apoptosis and mitochondrial

dysfunction in HCEpiCs, while resveratrol restores the mitochondrial function of HCEpiCs under hyperosmolarity. Decreased expression of SIRT1 could be observed in HCEpiCs with hyperosmolarity culturing. Importantly, our results further demonstrated that SIRT1 is responsible for resveratrol-mediated mitochondrial restoration. Consistently, by establishing a DED mouse model, we found that resveratrol prevents DED syndrome. Thus, our data extended the role of resveratrol and illustrated the underlying mechanism of resveratrol in ameliorating DED.

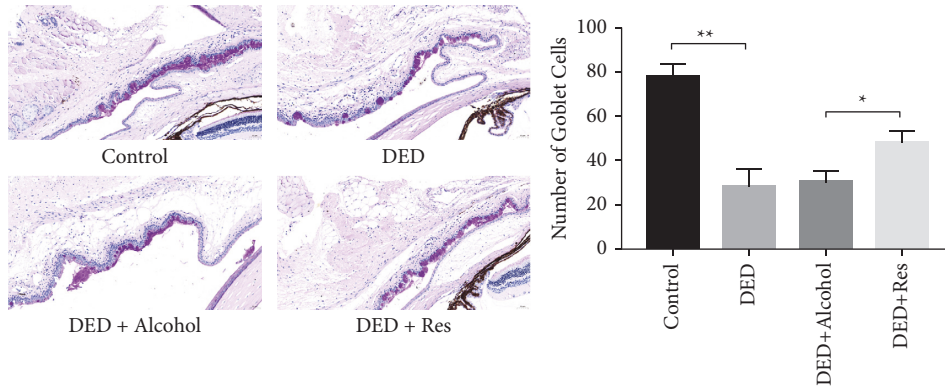
DED is a multifactorial disease and is closely related to mitochondrial function. In diabetic mice, Qu et al. [27] demonstrated that hyperglycemia-induced mitochondrial bioenergetic inadequacy of the lacrimal gland ameliorates early onset of dry eye. Bogdan et al. [28] proposed that insulin-like growth factor binding



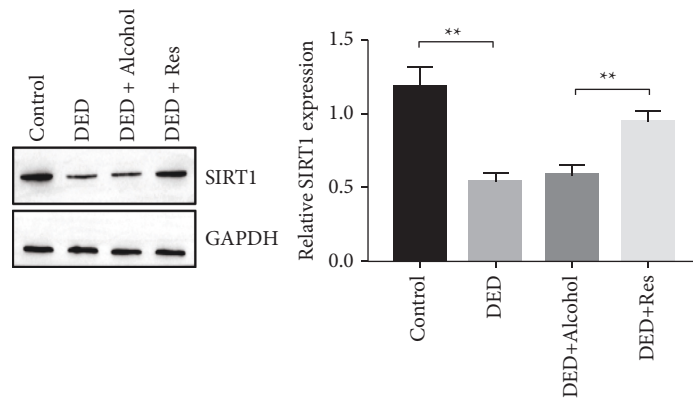
(a)



(b)



(c)



(d)

FIGURE 4: Continued.

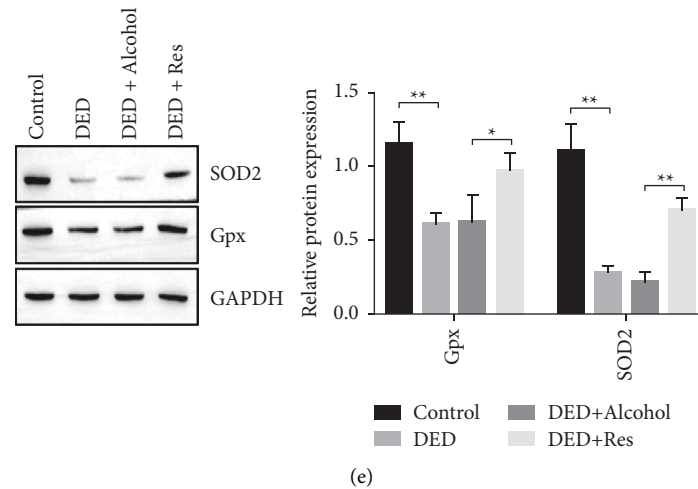


FIGURE 4: Resveratrol ameliorates DED syndrome in vivo via SIRT1. (a) The tear production in control mice, DED mice, DED mice treated with alcohol, or DED mice treated with resveratrol measured by the phenol red cotton thread test. (b) Corneal fluorescein staining in control mice, DED mice, DED mice with alcohol treatment, and DED mice treated with resveratrol. (c) Goblet cell density in the conjunctival epithelial layer measured by periodic acid-Schiff (PAS) staining. (d) Expression of SIRT1 in lacrimal glands determined by Western blotting. (e) Expression of GPx and SOD2 in lacrimal glands determined by Western blotting.  $n = 3$ . \* $P < 0.05$ , \*\* $P < 0.01$ , \*\*\* $P < 0.001$ .

protein-3 (IGFBP-3) is involved in hyperosmolar stress responses in the corneal epithelium by modulating mitochondrial function. Hyperosmolarity can increase ROS and apoptosis of HCEpiCs (Figure 1), and our results confirm this. Since antioxidants are one of the most common factors for restoring mitochondrial function and could prevent mitochondrial-associated pathology [29], we focused on resveratrol and set out to determine the role of resveratrol in DED development. Resveratrol, a common antioxidant, contributes to mitochondrial function maintenance. Kang et al. [30] showed that resveratrol protects neural cells from injury via regulation of mitochondrial biogenesis and mitophagy. In C6 astrocytes, Bobermin et al. [31] demonstrated that resveratrol prevents an increase in ROS production, a reduction in mitochondrial membrane potential ( $\Delta\Psi$ ), and bioenergetic insufficiency caused by ammonia. Importantly, several studies have indicated that resveratrol prevents DED syndrome [12, 32]. However, whether resveratrol attenuates DED development by regulating mitochondria remains unknown. Here, we found that hyperosmolarity culturing reduces the expression of the antioxidant proteins SOD2 and GPx and induces ROS levels. Resveratrol administration inhibits HCEpiCs apoptosis, increases SOD2 and GPx expression, and decreases ROS levels. Moreover, resveratrol attenuates DED syndrome and increases SOD2 and GPx expression in a DED mouse model. These results suggest that resveratrol may reduce oxidative stress and HCEpiCs apoptosis by maintaining mitochondrial function.

SIRT1 contributes to the function and biogenesis of mitochondria [33]. Of note, Samadi et al. [34] described that SIRT1 expression is suppressed in a diabetic dry eye model. Here, we also observed decreased expression of SIRT1 in HCEpiCs from a hyperosmolarity culture and DED mouse model, which was accompanied by increased levels of

oxidative stress, apoptosis, or dry eye syndrome. In addition, resveratrol was previously shown to be critical in SIRT1 activation [35]. In the next experiment, we demonstrated that resveratrol treatment reversed SIRT1 expression in HCEpiCs under hyperosmolarity and DED in mice, while the SIRT1 inhibitor EX527 rescued the inhibitory effect of resveratrol on mitochondrial dysfunction in HCEpiCs. This finding suggests that resveratrol ameliorates mitochondrial dysfunction via SIRT1.

It was proposed in early studies that the antioxidant resveratrol is critical in preventing DED syndrome, but the mechanism remains unclear. Our results demonstrate that resveratrol can restore mitochondrial function in HCEpiCs and inhibit HCEpiCs apoptosis. Furthermore, our findings indicate that SIRT1 is the major effector in resveratrol-regulated DED development. Therefore, our results show that resveratrol/SIRT1 plays a significant role in DED development, which is beneficial to DED therapy.

## 5. Conclusion

In summary, we found that resveratrol reversed hyperosmolarity-mediated mitochondrial dysfunction in HCEpiCs, and we demonstrated that resveratrol alleviated mitochondrial dysfunction by promoting SIRT1 expression. At the same time, it has been proven in animal experiments that resveratrol can reduce ocular surface damage in a mouse model of DED. Finally, resveratrol improved the effect of DED by restoring mitochondrial function, and this study provides new ideas for the treatment of DED.

## Data Availability

The datasets generated during and/or analyzed during the current study are available from the corresponding author upon request.

## Conflicts of Interest

The authors declare that they have no conflicts of interest.

## Acknowledgments

This work was supported by grants from the National Natural Science Foundation of China (82000869), the Training Plan of Medical Reserve Talents of Yunnan Health Committee (H-2019058), Basic Research Plan of Yunnan Province (2019FE001(-157)), and Kunming Health Science and Technology Personnel Training Project (2019-sw-04).

## References

- [1] J. Wu, X. Wu, H. Zhang et al., "Dry eye disease among Mongolian and han older adults in grasslands of northern China: prevalence, associated factors, and vision-related quality of life," *Frontiers of Medicine*, vol. 8, Article ID 788545, 2021.
- [2] N. M. C. Connolly, P. Theurey, V. Adam-Vizi et al., "Guidelines on experimental methods to assess mitochondrial dysfunction in cellular models of neurodegenerative diseases," *Cell Death & Differentiation*, vol. 25, no. 3, pp. 542–572, 2018.
- [3] L. Liu, F. Wang, Y. Tong, L. F. Li, Y. Liu, and W. Q. Gao, "Pentamidine inhibits prostate cancer progression via selectively inducing mitochondrial DNA depletion and dysfunction," *Cell Proliferation*, vol. 53, no. 1, Article ID e12718, 2020.
- [4] S. Seen and L. Tong, "Dry eye disease and oxidative stress," *Acta Ophthalmologica*, vol. 96, no. 4, pp. e412–e420, 2018.
- [5] B. Wang, L. Peng, H. Ouyang et al., "Induction of DDIT4 impairs autophagy through oxidative stress in dry eye," *Investigative Ophthalmology & Visual Science*, vol. 60, no. 8, pp. 2836–2847, 2019.
- [6] L. Li, R. Jin, Y. Li et al., "Effects of Eurya japonica extracts on human corneal epithelial cells and experimental dry eye," *Experimental and Therapeutic Medicine*, vol. 20, no. 2, pp. 1607–1615, 2020.
- [7] A. Di Credico, G. Gaggi, P. Izzicupo, I. Bucci, and A. Di Baldassarre, "Resveratrol enhances the cytotoxic activity of lymphocytes from menopausal women," *Antioxidants*, vol. 10, no. 12, 2021.
- [8] M. S. Kumaran, G. Dabas, A. B. Kapadia, and D. Parsad, "Resveratrol-induced thrombocytopenia: inadvertent side-effect of a commonly used antioxidant," *Dermatologic Therapy*, vol. 31, no. 1, 2018.
- [9] A. Arinno, N. Apaijai, S. C. Chattipakorn, and N. Chattipakorn, "The roles of resveratrol on cardiac mitochondrial function in cardiac diseases," *European Journal of Nutrition*, vol. 60, no. 1, pp. 29–44, 2021.
- [10] P. B. Ham 3rd and R. Raju, "Mitochondrial function in hypoxic ischemic injury and influence of aging," *Progress in Neurobiology*, vol. 157, pp. 92–116, 2017.
- [11] C. Wang, J. Yuan, and J. Du, "Resveratrol alleviates acute lung injury through regulating PLSCR-3-mediated mitochondrial dysfunction and mitophagy in a cecal ligation and puncture model," *European Journal of Pharmacology*, vol. 913, Article ID 174643, 2021.
- [12] A. Abengózar-Vela, C. S. Schaumburg, M. E. Stern, M. Calonge, A. Enríquez-de-Salamanca, and M. J. González-García, "Topical quercetin and resveratrol protect the ocular surface in experimental dry eye disease," *Ocular Immunology and Inflammation*, vol. 27, no. 6, pp. 1023–1032, 2019.
- [13] Y. Huang, J. Lu, L. Zhan et al., "Resveratrol-induced Sirt1 phosphorylation by LKB1 mediates mitochondrial metabolism," *Journal of Biological Chemistry*, vol. 297, no. 2, Article ID 100929, 2021.
- [14] M. Ding, N. Feng, D. Tang et al., "Melatonin prevents Drp1-mediated mitochondrial fission in diabetic hearts through SIRT1-PGC1 $\alpha$  pathway," *Journal of Pineal Research*, vol. 65, no. 2, Article ID e12491, 2018.
- [15] W. Chen, B. Lin, S. Xie et al., "Naringenin protects RPE cells from NaIO<sub>3</sub>-induced oxidative damage in vivo and in vitro through up-regulation of SIRT1," *Phytomedicine*, vol. 80, Article ID 153375, 2021.
- [16] C. Sawda, C. Moussa, and R. S. Turner, "Resveratrol for Alzheimer's disease," *Annals of the New York Academy of Sciences*, vol. 1403, no. 1, pp. 142–149, 2017.
- [17] Y. W. Kao, S. K. Hsu, J. Y. Chen et al., "Curcumin metabolite tetrahydrocurcumin in the treatment of eye diseases," *International Journal of Molecular Sciences*, vol. 22, no. 1, 2020.
- [18] G. Björklund, M. Dadar, N. Martins et al., "Brief challenges on medicinal plants: an eye-opening look at ageing-related disorders," *Basic and Clinical Pharmacology and Toxicology*, vol. 122, no. 6, pp. 539–558, 2018.
- [19] S. Ma, J. Feng, R. Zhang et al., "SIRT1 activation by resveratrol alleviates cardiac dysfunction via mitochondrial regulation in diabetic cardiomyopathy mice," *Oxidative Medicine and Cellular Longevity*, vol. 2017, Article ID 4602715, 15 pages, 2017.
- [20] X. Zhang, X. Liu, F. Wan et al., "Protective effect of resveratrol against hydrogen peroxide-induced oxidative stress in bovine skeletal muscle cells," *Meat Science*, vol. 185, Article ID 108724, 2021.
- [21] S. P. Bang, C. Y. Yeon, N. Adhikari et al., "Cyclosporine A eyedrops with self-nanoemulsifying drug delivery systems have improved physicochemical properties and efficacy against dry eye disease in a murine dry eye model," *PLoS One*, vol. 14, no. 11, Article ID e0224805, 2019.
- [22] M. L. Ratay, S. C. Balmert, E. J. Bassin, and S. R. Little, "Controlled release of an HDAC inhibitor for reduction of inflammation in dry eye disease," *Acta Biomaterialia*, vol. 71, pp. 261–270, 2018.
- [23] B. Ma, Y. Zhou, R. Liu et al., "Pigment Epithelium-Derived Factor (PEDF) Plays Anti-inflammatory Roles in the Pathogenesis of Dry Eye Disease," *The Ocular Surface*, vol. 20, 2021.
- [24] M. Qu, X. Qi, Q. Wang et al., "Therapeutic Effects of STAT3 Inhibition on Experimental Murine Dry Eye," *Investigative Ophthalmology & Visual Science*, vol. 60, no. 12, pp. 3776–3785, 2019.
- [25] T. G. Biel, S. Lee, J. A. Flores-Toro et al., "Sirtuin 1 suppresses mitochondrial dysfunction of ischemic mouse livers in a mitofusin 2-dependent manner," *Cell Death & Differentiation*, vol. 23, no. 2, pp. 279–290, 2016.
- [26] Q. Zhao, Z. Tian, G. Zhou et al., "SIRT1-dependent mitochondrial biogenesis supports therapeutic effects of resveratrol against neurodevelopment damage by fluoride," *Theranostics*, vol. 10, no. 11, pp. 4822–4838, 2020.
- [27] M. Qu, L. Wan, M. Dong, Y. Wang, L. Xie, and Q. Zhou, "Hyperglycemia-induced severe mitochondrial bioenergetic deficit of lacrimal gland contributes to the early onset of dry eye in diabetic mice," *Free Radical Biology and Medicine*, vol. 166, pp. 313–323, 2021.
- [28] E. D. Bogdan, W. L. Stuard, R. Titone, and D. M. Robertson, "IGFBP-3 mediates metabolic homeostasis during



- hyperosmolar stress in the corneal epithelium,” *Investigative Ophthalmology & Visual Science*, vol. 62, no. 7, p. 11, 2021.
- [29] S. S. Santos, J. B. Moreira, M. Costa et al., “The mitochondrial antioxidant Sirtuin3 cooperates with lipid metabolism to safeguard neurogenesis in aging and depression,” *Cells*, vol. 11, no. 1, 2021.
- [30] R. R. Kang, Q. Sun, K. G. Chen et al., “Resveratrol prevents benzo(a)pyrene-induced disruption of mitochondrial homeostasis via the AMPK signaling pathway in primary cultured neurons,” *Environmental pollution (Barking, Essex: 1987)*, vol. 261, Article ID 114207, 2020.
- [31] L. D. Bobermin, D. O. Souza, C.-A. Gonçalves, and A. Quincozes-Santos, “Resveratrol prevents ammonia-induced mitochondrial dysfunction and cellular redox imbalance in C6 astroglial cells,” *Nutritional Neuroscience*, vol. 21, no. 4, pp. 276–285, 2018.
- [32] R. Shetty, M. Subramani, P. Murugeswari et al., “Resveratrol rescues human corneal epithelial cells cultured in hyperosmolar conditions: potential for dry eye disease treatment,” *Cornea*, vol. 39, no. 12, pp. 1520–1532, 2020.
- [33] A. Isaacs-Ten, M. Moreno-Gonzalez, C. Bone et al., “Metabolic Regulation of Macrophages by SIRT1 Determines Activation during Cholestatic Liver Disease in Mice,” *Cellular and Molecular Gastroenterology and Hepatology*, vol. 13, 2021.
- [34] M. Samadi, S. G.-G. Aziz, and R. Naderi, “The effect of tropisetron on oxidative stress, SIRT1, FOXO3a, and claudin-1 in the renal tissue of STZ-induced diabetic rats,” *Cell Stress & Chaperones*, vol. 26, no. 1, pp. 217–227, 2021.
- [35] F. Akhondzadeh, A. Astani, R. Najjari et al., “Resveratrol suppresses interleukin-6 expression through activation of sirtuin 1 in hypertrophied H9c2 cardiomyoblasts,” *Journal of Cellular Physiology*, vol. 235, no. 10, pp. 6969–6977, 2020.

## Research Article

# Inhibitory Effects of Mongolian Medicine Yihe-Tang on Continuous Darkness Induced Liver Steatosis in Zebrafish

Rigaiqiqige Sa, Chi Feng, Hongxia Bai, Xiaoyu Yin, Lei Song, Xiaodong Hu, Rui Xu, Xinshan Li, Wu Dong , and Jingfeng Yang 

Inner Mongolia Key Laboratory of Toxicant Monitoring and Toxicology, College of Animal Science and Technology, Inner Mongolia Minzu University, Tongliao, Inner Mongolia 028000, China

Correspondence should be addressed to Jingfeng Yang; yangjf@imun.edu.cn

Received 14 January 2022; Revised 30 April 2022; Accepted 6 May 2022; Published 20 May 2022

Academic Editor: Jelena Zivkovic

Copyright © 2022 Rigaiqiqige Sa et al. This is an open access article distributed under the Creative Commons Attribution License, which permits unrestricted use, distribution, and reproduction in any medium, provided the original work is properly cited.

The constant dark induction (DD) causes lipid degeneration and nonalcoholic fatty liver disease (NAFLD) in zebrafish, which might be closely related to the imbalance of gut microbiota and require in-depth study. In this study, a total of 144 zebrafish were divided into four groups, including the control group, Yihe-Tang group, constant dark group, and constant dark + Yihe-Tang group, and were treated with constant darkness (except control and Yihe-Tang groups) for 21 days. The bodyweights of zebrafish were recorded after 8 d, 15 d, and 22 d. The sequencing analysis of gut microbiota, detection of liver histopathological changes, and comparison of lipid metabolism-related gene expression levels were performed on the 22<sup>nd</sup> day of the experiment. The results showed that the Yihe-Tang could inhibit the constant dark-induced increase in zebrafish weight and liver steatosis. As compared to the control group, the dark treatment could alter the composition of gut microbiota in zebrafish, increase the relative abundance of harmful bacteria, and decrease the *Cetobacterium* and *Bacteroides* to *Firmicutes* ratio in the intestines. The abundance of Proteobacteria in the constant dark + Yihe-Tang group was close to that in the control group and that of Fusobacteria and *Cetobacterium* increased, especially the *Cetobacterium*, which increased significantly. The constant dark treatment caused an abnormal expression of liver lipid-related genes, inhibited lipid metabolism, and promoted fat accumulation. However, the Yihe-Tang could restore these changes to the level of the control group. This study indicated that Yihe-Tang could restore the constant dark-induced liver lipid degeneration. We hypothesized that *Cetobacterium* could significantly inhibit steatosis.

## 1. Introduction

In recent years, the incidence of nonalcoholic fatty liver disease (NAFLD) has been increased, causing severe health problems. NAFLD includes simple steatosis, nonalcoholic steatohepatitis (NASH), liver fibrosis, and cirrhosis [1]. It is a liver disease caused by the disorders of glucolipid metabolism and characterized by the deposition of lipids in hepatocytes. Its causative factors generally include a high-fat diet, drugs, and other factors in addition to exogenous intake of alcohol. NAFLD has now become a significant cause of chronic liver disease worldwide with a prevalence as high as 24% [2]. The effective prevention and treatment of NAFLD and NASH are needed to avoid their progression to end-stage liver diseases. Many factors, such as genetics, obesity, poor lifestyle habits, and imbalance of gut microbiota, have

been reported to be highly related to the prevalence of NAFLD [3]. There is a strong correlation between gut microbiota and NAFLD [4]. In 1998, Marshall formally proposed the “gut-liver axis” concept [5]. The core function of this axis is the two-way communication between the intestine and liver, influencing each other. This means that liver can affect the intestines, especially causing changes in the composition of gut microbiota, which in turn affects the liver. Therefore, using the “gut-liver axis” as a target, the mechanism of action of the environment or drugs on NAFLD is investigated using the compositional analysis of gut microbiota. At the same time, this treatment method could also result in the significant upregulation of lipid synthesis-related genes, such as *ppar-p* and *fasn*, in zebrafish liver and also resulted in the significant downregulation of lipolysis-related genes, such as *cpt1* and *acadm*. These results

indicated that the changes in gut microbiota might lead to the deposition of fats in the zebrafish liver [6].

Yihe-Tang was produced according to the “Drug Standards of the Chinese Ministry of Health (Mongolian Drugs)” and approved by the Affiliated Hospital of Inner Mongolia Minzu University (approval number: Z15021057), which is responsible for the standardization of drugs to ensure their contents. Yihe-Tang is composed of *Carthamus tinctorius* L., *Terminalia chebula* Retz., *Melia toosendan*, *Inula helenium* L., *Gardenia jasminoides* J. Ellis., *Corydalis bungeana* Turcz., *Dolomiaea souliei* (Franch.) C. Shih., *Neopicrorhiza scrophulariiflora* (Pennell) D. Y. Hong., *Gentiana macrophylla* Pall., *Ophiopogon japonicus* (L. f.) Ker Gawl., *Punica granatum* L., *Pyrus ussuriensis* Maxim., *Cyrtomium fortunei* J. Sm., *Gentiana dahurica* Fisch., *Chrysanthemum indicum* L., *Asarum heterotropoides* F. Schmidt., *Coriandrum sativum* L., *Momordica cochinchinensis* (Lour.) Spreng., *Sus scrofa domestica* Brisson, *Tussilago farfara* L., *Scabiosa comosa* Fisch., *Dianthus superbus* L., *Dracocephalum moldavica* L., *Trogopterus xanthipes*, and *Amomum kravanh* Pierre ex Gagnep. In rat models, Yihe-Tang could inhibit the alcohol-induced fatty liver by reducing the increase in glucose-deficient transferrin [7]. A study by Haosoqiqige et al. also suggested that Yihe-Tang had a therapeutic effect on the AFLD [8]. Yihe-Tang has a protective effect on the liver and has been widely used in Mongolian areas for treating liver inflammation and other liver-related diseases. However, the studies on Yihe-Tang are limited and the mechanism of action of its mixed preparation is still unclear. Several studies have reported the mechanism of action of a single decoction component in Yihe-Tang. For example, gardenoside components inhibit the NAFLD-induced oxidative stress and inflammation by upregulating the Nrf2 and modulating the protein expression and AMPK/PI3K/mTOR signaling pathway [9] or improve NAFLD by upregulating PPAR- $\alpha$  [10]. *Terminalia chebula* Retz (chebulinic acid) upregulates the Heme oxygenase-1 (HO-1) and NAD(P)H quinone oxidoreductase-1 (NQO1) expression levels in L-02 cells in order to resist the tert-butyl hydrogen peroxide (t-BHP-) induced oxidative stress [11]. The safflower yellow (SY) component inhibits inflammatory response, promotes collagen degradation, and regulates gut microbiota [12]. Based on the previous studies' results, Yihe-Tang might have an antioxidative stress effect or play a protective role by regulating the gut microbiota. In this study, an NAFLD animal model of zebrafish was established and the regulatory effects of Yihe-Tang on the gut microbiota of zebrafish were studied.

Zebrafish (*Danio rerio*) is a widely used experimental animal model. It has the advantages of being small and easy to raise, fast growth and development, high breeding function, and drug sensitivity. In particular, the circadian rhythm and characteristic sleep state of zebrafish are similar to those of mammals and its genetic background is highly similar to humans [13]. In this study, zebrafish were used as experimental animal models. Liver steatosis was induced through the dark environment treatment and their body weight, histological changes in liver, changes in the composition of gut microbiota, and expression of lipid

metabolism-related genes were determined. The effects of Yihe-Tang on the recovery of the changes in zebrafish's gut microbiota and liver metabolism caused by the dark environment were further investigated.

## 2. Material and Methods

**2.1. Medicines and Materials.** Yihe-Tang was purchased from the Affiliated Hospital of Inner Mongolia Minzu University (approval number: Z15021057). The total RNA extraction kit, reverse transcription kit, and other drugs were purchased from Sigma-Aldrich (St. Louis, MO).

**2.2. Feeding and Light/Dark Cycle of Zebrafish.** Zebrafish (AB line) were used as experimental animals. The breeding zebrafish were maintained at  $28 \pm 1^\circ\text{C}$  in the circulating zebrafish aquacultures (Aisho, Beijing, China) with a light/dark cycle of 14/10 h. The 4-month-old zebrafish ( $n = 144$ ) were taken from the 12 aquariums, respectively (12 zebrafish were placed in each tank according to the male to female ratio of 1:1). These fish tanks were randomly assigned to each experimental group ( $n = 3$  per group) and labeled as control, constant dark, Yihe-Tang, and constant dark + Yihe-Tang groups. Yihe-Tang was administered by feeding. First, the diet was supplemented with 3.5 mg Yihe-Tang/g of basal diet (the drug content was about 0.35% of the feed weight). The daily diet intake of zebrafish was calculated to be 4% of their total body weight and their average body weight was  $0.28 \pm 0.003$  g. The daily feeding diet was  $0.0112 \pm 0.00012$  g and the average daily dose of Yihe-Tang per fish was  $39.2 \pm 0.42$   $\mu\text{g}$ . The feed was given daily at 8:00 am and 4 pm for 26 days. The first five days were considered preparatory experiment time and the next 21 days as formal experiment periods. For creating a dark environment, all the fish tanks were placed in a dark box. The feed was given gradually during the pretest period in order to ensure that the zebrafish consumed all the feed. Also, the feed residuals were checked during changing the water in the main experiment. The daily feeding rate was calculated as follows: daily feeding rate (%/d) =  $100 \times \text{total feed consumed} / \text{days} \times (\text{initial body weight} + \text{final body weight}) / 2$  [14].

**2.3. Hematoxylin-Eosin Staining (H&E) and Oil Red O (ORO) Staining of the Liver Tissues.** The zebrafish in each group were treated for 8 d, 15 d, 22 d, and their livers were collected and fixed with 4% paraformaldehyde (PFA) for 16 h. Then, the livers were rinsed with phosphate-buffered saline (PBS) and dehydrated with 60, 70, 80, 90, 95, and 100% ethanol. The ethanol was then replaced by 100% for paraffin embedding. The prepared tissue sections were then stained with H&E for microscopic observation and analysis. Similarly, for the ORO staining, the liver tissues were fixed with 4% PFA for 16 h and the iced tissue sections were prepared by optimal cutting temperature (OCT) embedding. After preparation, the tissues were rinsed with 60% propylene glycol, stained with ORO stain, counterstained with safranwood, sealed with glycerin gelatin, and observed under a microscope.

#### 2.4. Sample Collection and Sequencing of Gut Microbiota.

The livers and intestines were obtained using sterile surgical instruments on a clean bench. The livers were immediately put into a cryotube for RNA extraction. A sterile cotton swab was dipped into the intestinal contents of the intestines and immediately put into a cryotube, which was then stored in liquid nitrogen in a refrigerator at  $-80^{\circ}\text{C}$  and used for 16S *rRNA* gene sequencing ( $n=6$ ). The 16S *rRNA* gene sequencing was performed by Nuovo Zhiyuan (Beijing, China). The genomic DNA (gDNA) from each sample was extracted using the sodium dodecyl sulfate (SDS) method and the polymerase chain reaction (PCR) amplification was performed using specific primers (barcode label), template DNA ( $1\text{ ng}/\mu\text{l}$ ), and Phusion® high-fidelity PCR Master Mix (New England Biolabs, USA). For the identification of gut microbiota, the following gene regions were amplified: V3-V4 hypervariable region of 16S *rRNA* gene for the identification of gut bacterial diversity, V4 hypervariable region of 18S *rRNA* gene for the identification of gut eukaryotic microbial diversity, and *ITS1* region for the identification of gut fungal diversity, 16S V3-V4/16S V4-V5/16SV5-V7, Archaea 16S V4-V5/Archaea 16S V8, 18S V9, and *ITS2* gene regions. The amplified PCR products were detected on 2% agarose gel and the target bands were recovered using a gel recovery kit (QIAGEN, Germany). The sequencing library was constructed with a TruSeq® DNA PCR-Free Sample Preparation Kit (Illumina, USA). Qubit and q-PCR were used for the quantification of library and the qualified libraries were sequenced using a NovaSeq 6000 sequencing platform (Illumina, USA).

**2.5. RNA Extraction and qRT-PCR Analysis.** According to research [6], TRIzol reagent (Ambion, USA) was used to extract the total RNA from zebrafish liver tissues. A total of 250 ng of the extracted RNA samples with OD 230/260 and OD 260/280 of greater than 1.8 were reverse transcribed to obtain cDNA. The TB Green Premix Ex Tax II kit was used for qRT-PCR analysis. The primer sequences used in the study are listed in Table 1 and 18S was used as an internal reference gene, and the changes in the relative expression of genes were calculated using the  $2^{-\Delta\Delta\text{Ct}}$  method.

**2.6. Statistical Analyses.** One-way analysis of variance (ANOVA) and *t*-test were used for the data analysis and the significance threshold level was set to  $P < 0.05$ . All the data were expressed as mean  $\pm$  standard error of the mean (SEM).

### 3. Results

**3.1. Effects of Yihe-Tang on the Weight Gain of Zebrafish Induced by the Dark.** In order to analyze the effects of Yihe-Tang on the weight gain of zebrafish induced by the constant darkness, their body weights were measured on 8 d, 15 d, and 22 d of the treatments. The results showed that the average daily weight showed an increasing trend in the constant dark group which tended to increase in each period. As compared to the control group, the average daily

TABLE 1: The primers for RT-qPCR.

Gene	Primer sequences (5'-3')	Forward/Reverse
18s	TCGCTAGTTGGCATCGTTTATG	Forward
ID: 100037361	TCGCTAGTTGGCATCGTTTATG	Reverse
fasn	GCACCGGTACTAAGGTTGGA	Forward
ID: 559001	ACACAACCGACCATCTGTCA	Reverse
acadm	AGGTTTTGAGGGCAGGTGTT	Forward
ID:406283	TCTGCTGCTCGGTTAGTTCA	Reverse
cpt1	ATGAGGAGCACCAAGAATG	Forward
ID: 122874692	TGGGAAAAGCGTAAAGAAAAG	Reverse
mgst	GATATGTGGCGCTAACCGGA	Forward
ID: 449784	ATGCTGAATCCCACCCACAG	Reverse

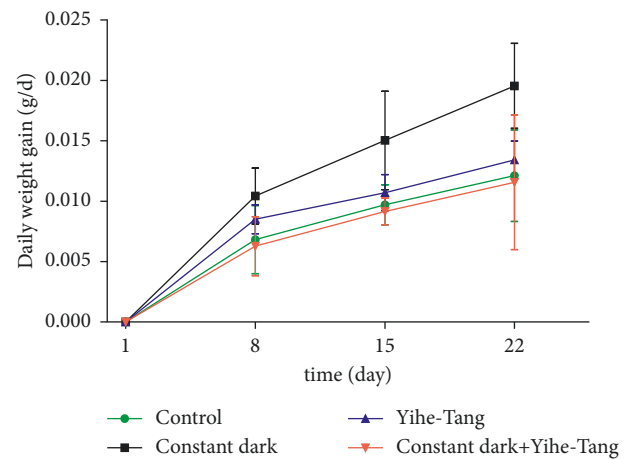


FIGURE 1: Effects of Yihe-Tang on the constant dark-induced weight gain of zebrafish. Experimental setup included four groups; control, Yihe-Tang, constant dark, and constant dark + Yihe-Tang group. The bodyweights of zebrafish were measured on 8 d, 15 d, and 22 d of the treatment ( $n=25$  d).

weights of zebrafish in the constant dark group increased by 53%, 54%, and 62%, respectively, while those in the constant dark + Yihe-Tang group returned to the control level (Figure 1).

#### 3.2. Effects of Yihe-Tang on the Pathological Changes of Liver Tissue Induced by the Constant Darkness in Zebrafish.

After the 8 d, 14 d, and 22 d of constant dark induction, the zebrafish livers were collected for H&E staining. The results showed that the zebrafish liver had no significant changes in each period. The liver cells were regularly arranged with dense chromosomes and visible nuclei in the control and Yihe-Tang treatment groups. However, in the constant dark group, the zebrafish liver showed a small amount of steatosis after 8 d and severe steatosis after 14 and 22 d of constant dark treatment (Figures 2(g) and 2(k)). As compared to the control group, the vacuolation of fish liver tissue increased by 13.93 times ( $P < 0.05$ ) in the constant dark group (Figure 2(m)). After the Yihe-Tang treatment (constant dark + Yihe-Tang group), the zebrafish liver tissues did not show a significant increase in the degeneration of fats and

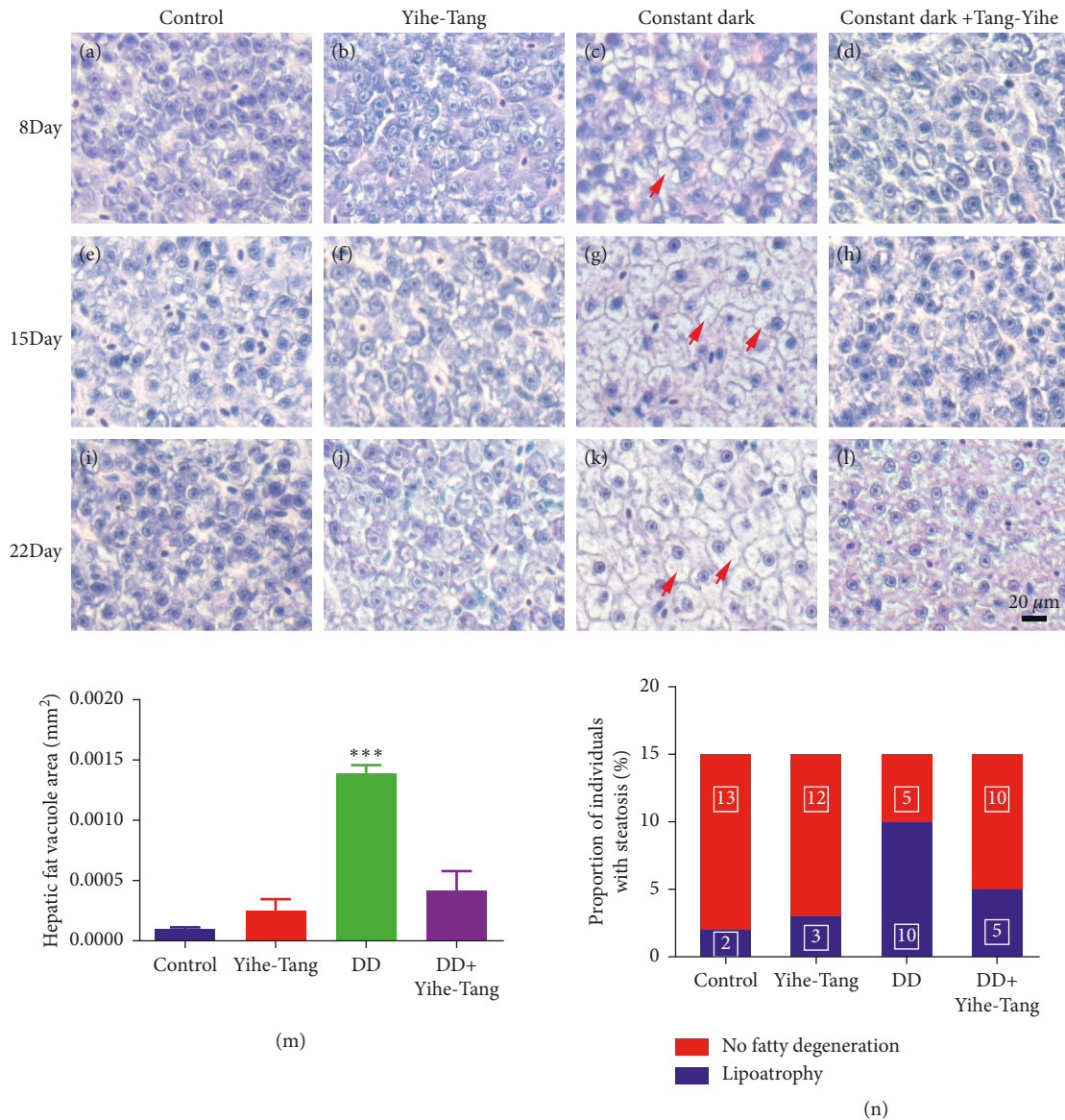


FIGURE 2: Effects of Yihe-Tang on the degeneration of fats in the zebrafish liver tissues induced by the constant darkness. ImageJ software was used to quantify the liver vacuole area. Control group: (a), (e), and (i); Yihe-Tang group: (b), (f), and (j); constant dark group: (c), (g), and (k); constant dark + Yihe-Tang group: (d), (h), and (l); (m): quantification of void area, (n): fatty degeneration scale,  $n = 15$ , scale bar = 20  $\mu\text{m}$ .

vacuoles after the 8 d and 15 d of constant dark treatment. However, the degeneration of fats and vacuoles in the liver at 22 d was significantly lower in the constant dark + Yihe-Tang group than that in the constant dark group ( $P < 0.05$ ); the fats were 30% of those in the dark treatment group (Figure 2(d)). The statistical results showed that the constant dark + Yihe-Tang group significantly reduced the constant dark-induced steatosis (Figures 2(m) and 2(n)).

**3.3. Improving Effects of Yihe-Tang on the Hepatic Fat Accumulation Induced by the Constant Darkness in Zebrafish.** The ORO staining results showed that there was no lipid accumulation in the control group. As compared to the control group, a large number of red lipid droplets were

accumulated in the constant dark-induced group. However, the accumulation of lipid droplets in the constant dark + Yihe-Tang group improved significantly as compared to the constant dark group, as shown in Figure 3. The results showed that the Yihe-Tang could improve the fat accumulation induced by the constant dark treatment.

**3.4. Effects of Yihe-Tang on the Dark-Induced Changes in Gut Microbiota.** A comparative analysis of the gut microbiota of the four different treatment groups was performed based on 16S rRNA gene sequencing technology. A total of 80563 raw sequence reads were obtained from the 24 gut samples, among which 76355 high-quality sequence reads were obtained after the screening and filtering for subsequent



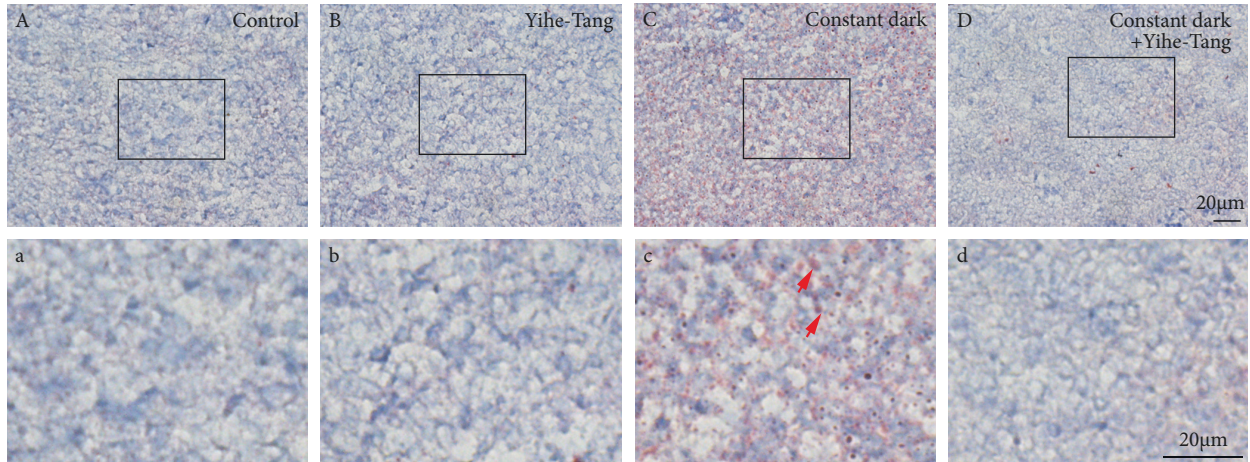


FIGURE 3: Improving effect of Yihe-Tang on the constant dark-induced liver fat accumulation in zebrafish. The zebrafish were divided into control, constant dark, Yihe-Tang, and constant dark + Yihe-Tang groups, after 21 d of treatment ( $n = 3$ ). Their liver tissues were collected and stained with Oil Red O to detect the histological changes in the liver of zebrafish.  $N = 3$ , scale bar =  $20 \mu\text{m}$ .

analysis. A threshold of 0.97 was selected for the clustering analysis and comparison, resulting in a total of 9,321 operational taxonomic units (OTUs). About 99.2% of these microbes were clustered into common phyla against the four treatment groups (Figure 4(a)). The alpha diversity indices (Shannon and Simpson indices) of the zebrafish gut microbiota increased significantly ( $P < 0.05$ ) in the constant dark + Yihe-Tang group as compared to the control group, while the species and chao1 indices were also significantly higher ( $P < 0.05$ ) (Figure 4(b)). Principal coordinate analysis (PCoA) plots showed that the clustering of microbial communities in each group was different (Figure 4(c)).

Based on the results of OTU species annotation, the top ten species with the highest abundance were selected and classified in the phyla, orders, families, and genera and were analyzed comparatively using the cumulative plots of the species relative abundance. The analysis at the phylum level revealed that there was no significant difference in the gut microbiota of Yihe-Tang group as compared to the control group; the relative abundance of phylum Proteobacteria increased significantly in the dark group, while that of *Clostridium* (Fusobacteria) decreased significantly. The relative abundance of Proteobacteria in the constant dark + Yihe-Tang group was similar to that in the control group, while the relative abundance of *Fusobacteria* was significantly reduced in the constant dark + Yihe-Tang group but tended to increase as compared to the constant dark group (Figure 5(a)). At the genus level, the highest relative abundance of *Cetobacterium* was found in the Yihe-Tang group, which was a dominant species in this treatment group, while its abundance was significantly reduced in the constant dark group. Interestingly, the relative abundance of *Cetobacterium* significantly increased in the constant dark + Yihe-Tang groups (Figure 5(b)).

The prediction of microbial functions based on the dominant gut microbiota in each treatment group showed that the functions of microbiota, including metabolic function, cellular transformation, human disease, and environmental information feedback, were higher in the constant dark group as compared to the control group. Two

functions, including the organic system and genetic information feedback, were lower in the constant dark group than those in the control group. The Yihe-Tang treatment could restore all these functional microbiotas (Figure 6).

**3.5. Effect of Yihe-Tang on the Expression of Lipid Metabolism-Related Genes.** When the zebrafish were treated with and without Yihe-Tang in a constant dark for 22 days, the expression levels of the genes associated with fat metabolism were analyzed using RT-PCR. The results showed that constant dark induction significantly reduced the mRNA expression levels of *cpt1*, *acadm*, and *mgst*, which decreased by 15%, 55%, and 48% (Figure 7(a)–7(c)), respectively as compared to the control group ( $P < 0.05$ ). On the contrary, the constant dark induction increased the mRNA expression level of *fasn* by 7.6 times as compared to the control group ( $P < 0.05$ ) (Figure 7(d)). However, the gene expression levels in the constant dark + Yihe-Tang group were recovered to the control level ( $P < 0.05$ ).

## 4. Discussion

The constant dark environment for a long time causes liver steatosis in zebrafish, which can be relieved after treatment with Yihe-Tang. In this study, the analysis of gut microbiota in zebrafish showed that the constant dark induction increased the abundance of harmful gut microbiota and significantly decreased the relative abundance of genus *Cetobacterium*. In contrast, the treatment with Yihe-Tang could significantly restore the abundance of genus *Cetobacterium*. We hypothesized that *Cetobacterium* could significantly inhibit steatosis. At the genetic level, the constant dark treatment caused significant changes in the expression levels of lipid metabolism-related genes. However, Yihe-Tang also significantly restored this change. The experimental results indicated that the changes in steatosis and gene regulation caused by the constant dark treatment might be related to the changes in the gut microbiota of zebrafish.



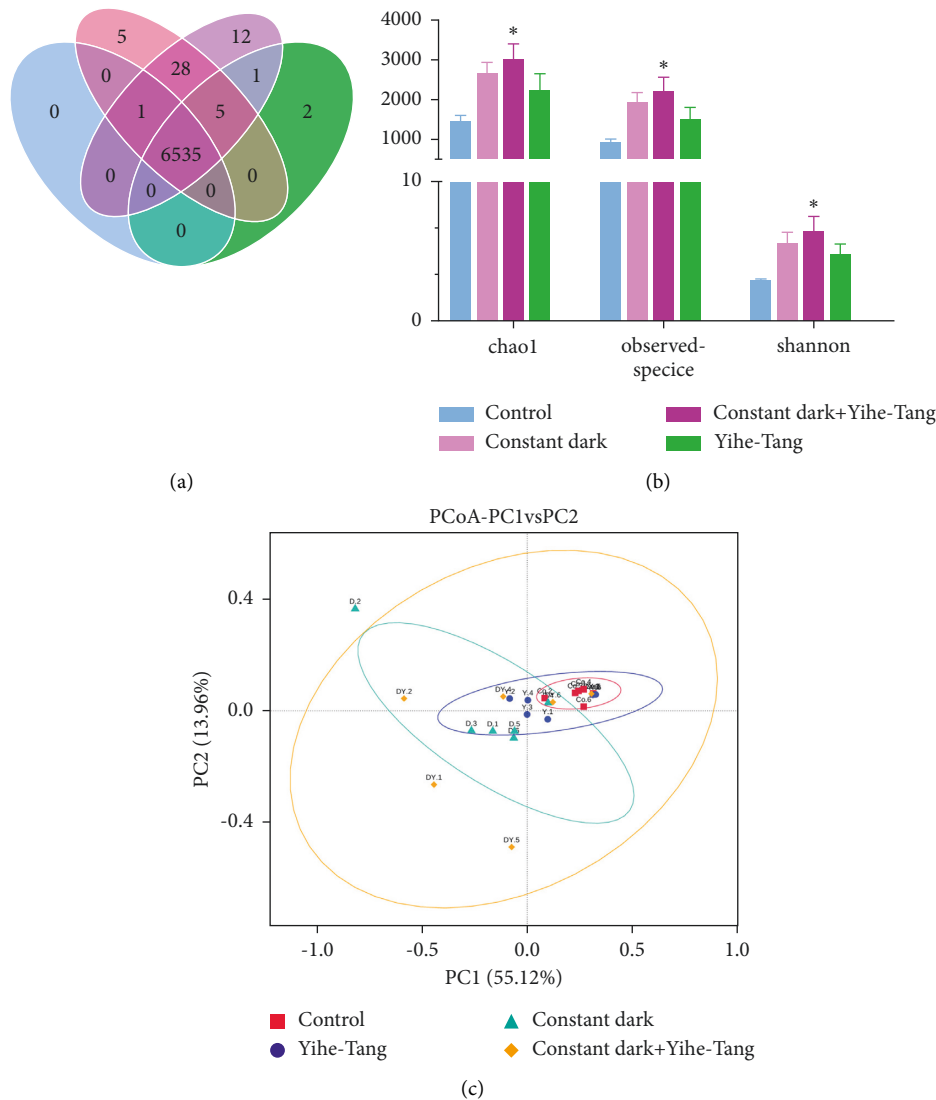


FIGURE 4: Effects of Yihe-Tang on the changes of zebrafish gut microbiota caused by the constant dark treatment. (a) Venn diagram summarizes the number of standards and different OTUs. (b) Microbial diversity index. (c) PCoA analysis. The horizontal and vertical axes in (c) represent the different principal components, and the percentage represents the contribution value of the main element to the sample difference. The data are expressed as mean, standard error (SE) of the mean ( $n = 6$ ). “\*” indicates a significant difference ( $P < 0.05$ ).

Chen et al. used Chinese herbal medicine (919 syrup) in the NAFLD rat models and showed a reduction in the weight of rats and improvement in the liver histopathological changes caused by NAFLD [15], which was consistent with the present study. Hung et al. found that Pingtang No. 5 Capsule (PT5, a traditional Chinese medicine compound of Alisma Decoction) could inhibit the accumulation of liver lipids and liver cell damage and reduce the bodyweight in NAFLD mice [16].

In order to study the inhibitory effect of Yihe-Tang on fat accumulation, Uzhitunashun et al. showed that Yihe-Tang inhibited the alcohol-induced abnormal apoptosis of rat liver cells, thereby improving the liver function [17]. In fatty acid synthesis, *fasn* is a downstream gene in the *srebp1* pathway and a key fat synthesis enzyme, which is closely related to the production and accumulation of fat. The *cpt1* gene plays a key role in lipolysis  $\beta$ -oxidation. The *acadm*

gene is a key lipolytic gene [18]. The constant dark induction caused a significant decrease in the mRNA expression levels of *cpt1* and *acadm* genes, indicating that the dark had a low effect on fat degradation. The Yihe-Tang treatment could significantly upregulate the expression levels of *cpt1* and *acadm*, indicating that the treatment with Yihe-Tang could promote the fat degradation function of the liver in zebrafish. The *fasn* is an important gene, regulating the fatty acid synthesis, which is involved in the entire process of fatty acid synthesis. The constant dark treatment significantly increased the mRNA expression level of *fasn*, which was restored by Yihe-Tang treatment. In addition, the *mgst* is a decomposing enzyme related to oxidative stress metabolites [19]. It is highly expressed in various organs. Its antioxidant effects can protect liver cells [20–22]. The present study showed that the constant dark induction could reduce the expression level of *mgst* gene. At the same time,

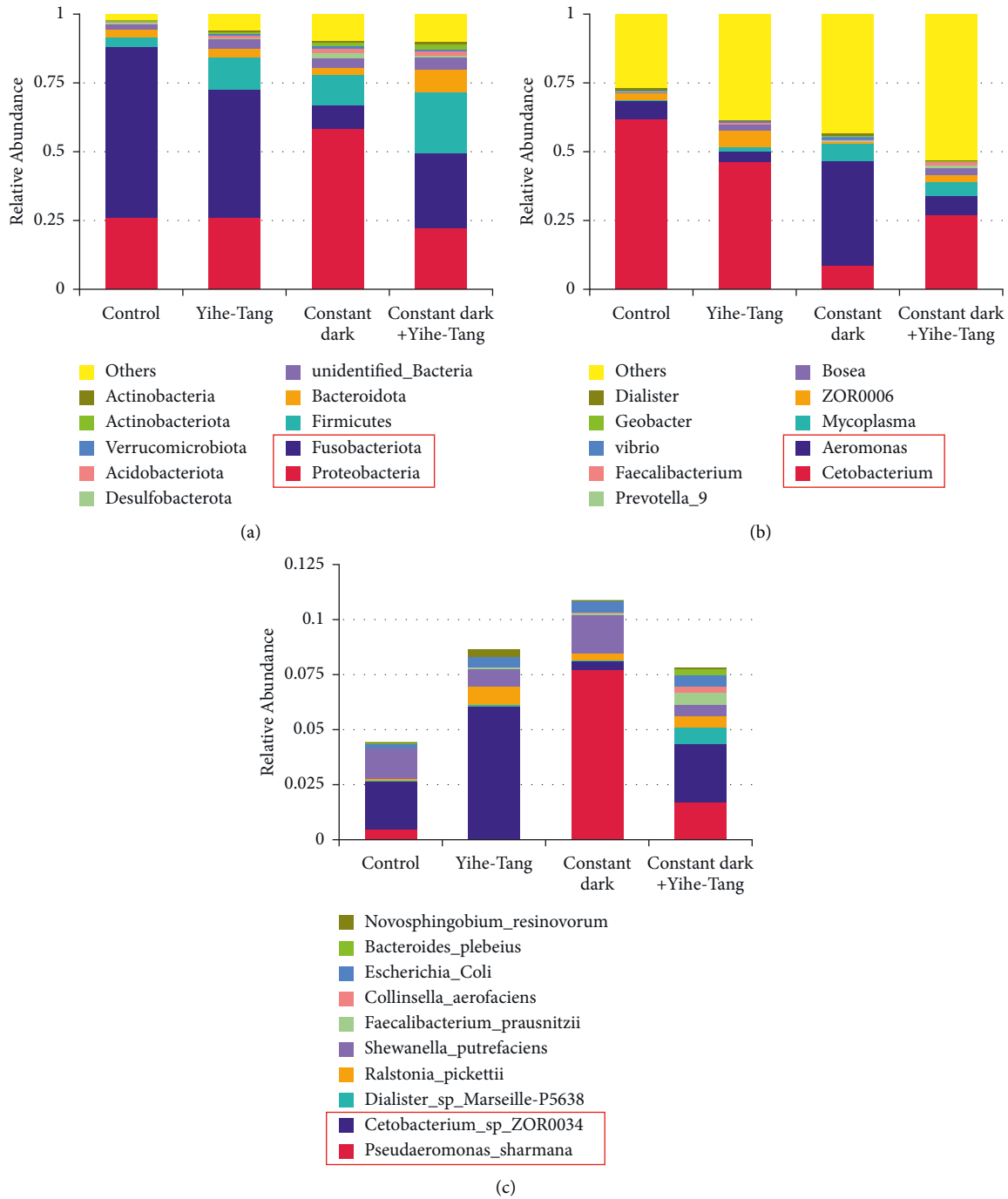


FIGURE 5: Effect of Yihe-Tang on the relative abundance of gut microbiota in zebrafish. (a) Relative abundance at the phylum level, (b) relative abundance at the genus level, and (c) relative abundance at the species level. The data of the top ten microbial communities with the highest relative abundances were selected from the above four groups.

the Yihe-Tang could significantly increase the expression level of *mgst* gene, indicating that Yihe-Tang could enhance the liver's ability to break down lipids.

Feng et al. showed that the constant dark induction could significantly affect the gut microbiota and liver metabolism in zebrafish and indicated that the changes in gut microbiota could affect the liver metabolism in zebrafish [6]. Since the liver is connected to the gut microbiota through the "gut-liver axis," the pathogenesis of NAFLD is

closely related to the gut microbiota, which has been a hot research topic in recent years. In this study, *16S rRNA* gene sequencing technology was used to detect the effects of Yihe-Tang on the gut microbiota of zebrafish. The effects of Yihe-Tang on the gut microbiota of zebrafish under dark treatment were observed. As compared to the control group, the constant dark induction could reduce the ratio of Firmicutes to Bacteroides (F/B) in the gut microbiota of zebrafish, while the Yihe-Tang treatment could significantly increase the

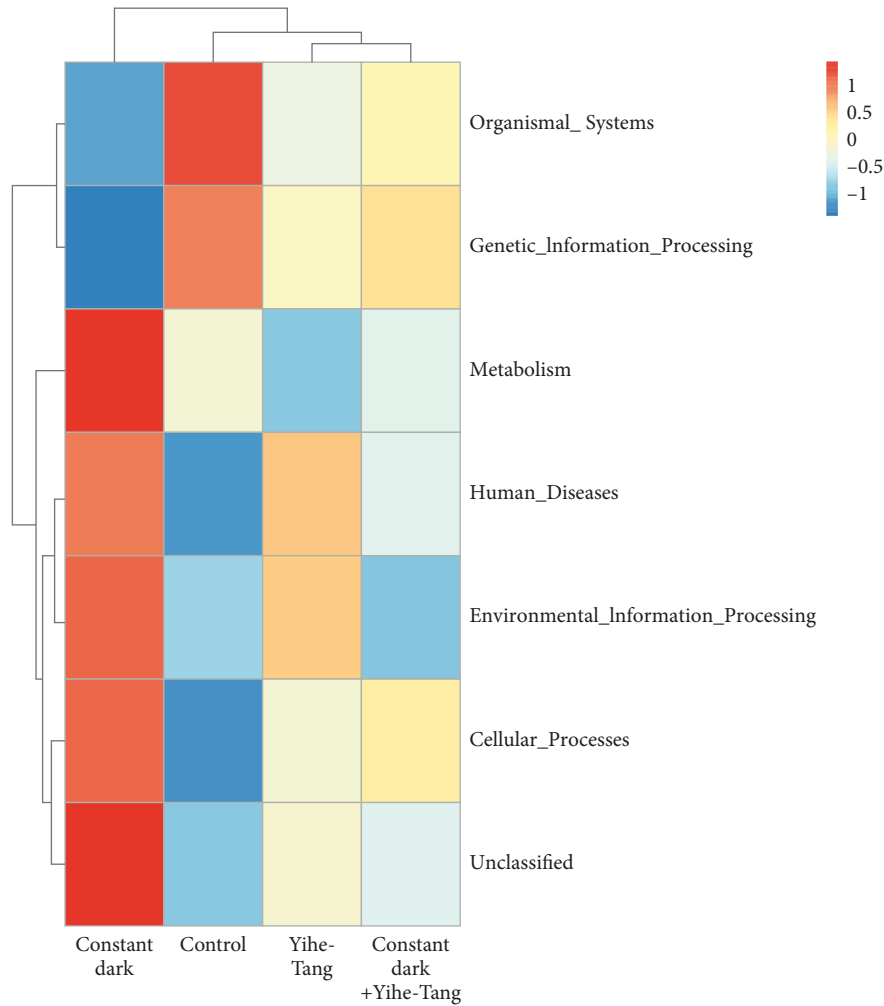


FIGURE 6: Clustering heat map for predicting the function of gut microbiota. The red color indicates that the abundance of gut microbiota was large or the corresponding annotation function was enhanced and vice versa for the blue color. Four groups were analyzed and compared and the microbial colonies with the highest abundances were selected for drawing.

richness of gut microbial community. The F/B ratio also increased. A study showed that the constant dark environment could cause a significant decrease in the proportion of Bacteroides and Firmicutes in the zebrafish intestines, thereby leading to metabolic disorders, fat accumulation, and weight gain in zebrafish [5]. These gut bacteria are related to obesity and diabetes, as well as energy absorption [23]. The F/B ratio can be used as an indicator of obesity [24]. In this study, the relative abundances of Fusobacteria were 7.38 times and 2.38 times lower in the constant dark and Yihe-Tang groups, respectively, as compared to the control group.

The short-chain fatty acids (SCFAs) are metabolites of *Cetobacterium* and regulate lipid metabolism as a substrate for lipid synthesis [25]. The correlation between SCFAs and NAFLD has been focused on in recent years. Studies have shown that the regulation of SCFAs by *Cetobacterium* plays an important role in maintaining the health of zebrafish intestines [26]. In this study, as compared to the control group, the constant dark induction could reduce the abundance of *Cetobacterium* in

the zebrafish intestines and cause lipid degeneration in the liver. However, the intervention of Yihe-Tang increased the abundance of *Cetobacterium* and inhibited steatosis. The result indicated that Yihe-Tang might exert an anti-inflammatory effect by regulating the production of SCFAs by *Cetobacterium*. *Cetobacterium*, accounting for 70% of the fish gut microbiota, is a rod-shaped Gram-negative anaerobic bacterial genus, which ferments SCFAs, including acetate, propionate, and butyrate [14, 27], among which acetate is the main fermentation product [28]. Canfora et al. reported that both the acetate and propionate increased the plasma acetate concentrations (fasting condition), promoted fat oxidation, and decreased the circulating free glycerol concentrations after the rectal administration of acetate or propionate during fasting and postprandial conditions (oral glucose load) [29]. In addition, acetate could also affect appetite by secreting the gut hormones, such as glucagon-like peptide 1 and peptide YY, in order to enhance host energy and substrate metabolism, increase fat oxidation and energy expenditure, and reduce systemic fat synthesis [30].

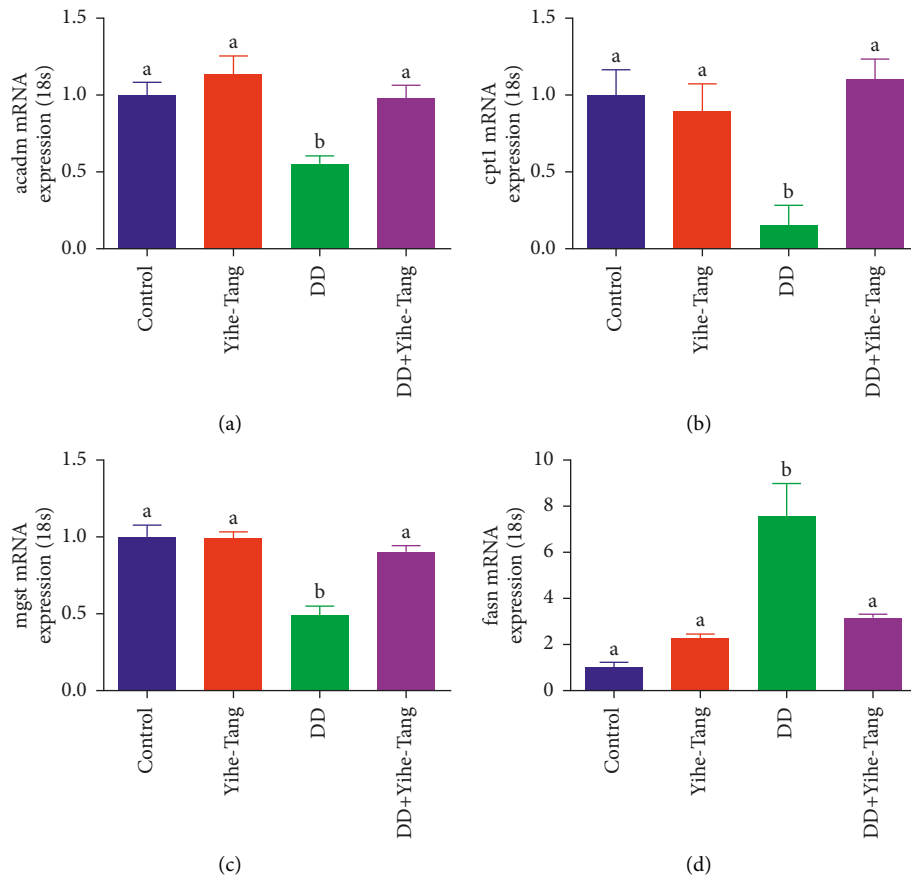


FIGURE 7: Yihe-Tang restored the constant dark-induced changes in the expression levels of lipid metabolism-related genes. Zebrafish were treated with dark in the control, Yihe-Tang, constant dark, and constant dark + Yihe-Tang groups for 22 days and the liver tissues were collected for RT-PCR analysis. (a): *acadm*, (b): *cpt1*, (c): *mgst*, and (d): *fasn*. Data are expressed as mean  $\pm$  standard error (SEM) ( $n = 9$ ), and different letters indicate significant differences ( $P < 0.05$ ).

Therefore, restoring the abundance of *Cetobacterium* can effectively supplement acetate, thereby effectively inhibiting fat accumulation and steatosis.

Circadian clocks regulate metabolism and energy homeostasis in the liver and other peripheral tissues [31]. Human and rodent studies have clearly shown that hepatic fat accumulation and steatosis are closely associated with insulin resistance [32]. In the insulin-resistant states, insulin loses its ability to inhibit the production of glucose, while still promoting hepatic lipid synthesis even in a hyperactive state [33]. Perry et al. reported that acetate could activate the parasympathetic nervous system, which in turn promoted the secretion of glucose-stimulated insulin [34]. Consistent with mammalian findings, the addition of acetate to the diet promoted insulin secretion and glucose utilization in zebrafish, thereby suggesting a conservative role of acetate in regulating glucose homeostasis [14]. In adult zebrafish, the abundance of *Cetobacterium* and intestinal acetic acid levels were highly correlated, suggesting that the positive effects of *Cetobacterium* on glucose homeostasis in zebrafish were mediated by the production of acetic acid [31]. This suggested that the acetate-brain-insulin secretion axis is conserved between fish and mammals, revealing a specific

intestinal “*Cetobacterium*-brain” pathway, which regulates glucose homeostasis in zebrafish [14].

## 5. Conclusions

Yihe-Tang could inhibit the increase in zebrafish weight caused by the constant dark induction and inhibit lipid degeneration in the zebrafish liver cells. This inhibition was closely related to the recovery of zebrafish gut microbiota. We hypothesized that *Cetobacterium* could significantly inhibit steatosis. For example, Yihe-Tang reduced the abundances of the phylum Proteobacteria, increased those of the phylum Fusobacterium and genus *Cetobacterium*, and increased the F/B ratio. At the same time, the constant dark induction caused an abnormal expression of liver lipid metabolism-related genes, which was reversed by Yihe-Tang. This study showed that the recovery effects of Yihe-Tang on the dark-induced liver metabolism disorder in zebrafish were closely related to the recovery of *Cetobacterium*.

## Data Availability

The study data are available from the corresponding author upon request.

## Conflicts of Interest

The authors declare no conflicts of interest.

## Acknowledgments

This study was funded by the National Natural Science Foundation of China (82060672) supported by the Program for Innovative Research Team in Universities of Inner Mongolia Autonomous Region (NMGIRT2216), Natural Science Foundation of Inner Mongolia Autonomous Region of China (2020MS08103), Open Project Program of Inner Mongolia Key Laboratory of Toxicant Monitoring and Toxicology, China (MDK2017013, MDK2018029, and MDK2019076), and Open Project Program of Inner Mongolia Research Institute of Traditional Mongolian Medicine Engineering Technology China (MDK2020002).

## References

- [1] C. Estes, Q. M. Anstee, M. T. Arias-Loste et al., "Modeling NAFLD disease burden in China, France, Germany, Italy, Japan, Spain, United Kingdom, and USA for the period 2016-2030," *Journal of Hepatology*, vol. 69, no. 4, pp. 896-904, 2018.
- [2] Z. Younossi, M. Stepanova, A. J. Sanyal et al., "The conundrum of cryptogenic cirrhosis: adverse outcomes without treatment options," *Journal of Hepatology*, vol. 69, no. 6, pp. 1365-1370, 2018.
- [3] Z.-C. Chi, "Gut microecological imbalance and nonalcoholic fatty liver disease," *Journal of General Surgery for Clinicians*, vol. 5, no. 2, pp. 1-6, 2017.
- [4] J. P. Liu, W. L. Zou, S. J. Chen et al., "Effects of different diets on intestinal microbiota and nonalcoholic fatty liver disease development," *World Journal of Gastroenterology*, vol. 22, no. 32, pp. 7353-7364, 2016.
- [5] K. Miura and H. Ohnishi, "Role of gut microbiota and Toll-like receptors in nonalcoholic fatty liver disease," *World Journal of Gastroenterology*, vol. 20, no. 23, pp. 7381-7391, 2014.
- [6] C. Feng, Sarigaiqiqige, W. Liu, H. Chen, W. Dong, and J. Yang, "Effect of dark environment on intestinal flora and expression of genes related to liver metabolism in zebrafish (*Danio rerio*)," *Comparative Biochemistry and Physiology. Toxicology & Pharmacology*, vol. 249, Article ID 109100, 2021.
- [7] R.-T.-N.-S. Wu, "Effect of Yihe-Tang on glucose deficient transferrin in alcoholic fatty liver model rats," *Journal of Medicine & Pharmacy of Chinese Minorities*, vol. 22, no. 10, pp. 61-63, 2016.
- [8] S.-Q.-Q.-G. Hao, "To explore the therapeutic effect of Mongolian medicine Yihe-Tang on alcoholic fatty liver," *World Latest Medicine Information*, vol. 18, no. 33, p. 149, 2018.
- [9] B. Shen, H. Feng, J. Cheng et al., "Geniposide alleviates non-alcohol fatty liver disease via regulating Nrf2/AMPK/mTOR signalling pathways," *Journal of Cellular and Molecular Medicine*, vol. 24, no. 9, pp. 5097-5108, 2020.
- [10] Y. Zhang, Y. Ding, X. Zhong et al., "Geniposide acutely stimulates insulin secretion in pancreatic  $\beta$ -cells by regulating GLP-1 receptor/cAMP signaling and ion channels," *Molecular and Cellular Endocrinology*, vol. 430, no. 9, pp. 89-96, 2016.
- [11] X.-H. Feng, H.-Y. Xu, J.-Y. Wang, S. Duan, Y.-C. Wang, and C.-M. Ma, "In vivo hepatoprotective activity and the underlying mechanism of chebulinic acid from Terminalia chebula fruit," *Journal of Phytomedicine*, vol. 83, Article ID 153479, 2021.
- [12] H. Fu, X. Liu, L. Jin et al., "Safflower yellow reduces DEN-induced hepatocellular carcinoma by enhancing liver immune infiltration through promotion of collagen degradation and modulation of gut microbiota," *Food & Function*, vol. 12, no. 21, pp. 10632-10643, 2021.
- [13] G. Vatine, D. Vallone, Y. Gothilf, and N. S. Foulkes, "It's time to swim! Zebrafish and the circadian clock," *FEBS Letters*, vol. 585, no. 10, pp. 1485-1494, 2011.
- [14] A. Wang, Z. Zhang, Q. Ding et al., "Intestinal Cetobacterium and acetate modify glucose homeostasis via parasymphathetic activation in zebrafish," *Gut Microbes*, vol. 13, no. 1, pp. 1-15, 2021.
- [15] M. Chen, J. Xing, D. Pan, X. Peng, and P. Gao, "Chinese herbal medicine mixture 919 syrup alleviates nonalcoholic fatty liver disease in rats by inhibiting the NF-kappaB pathway," *Biomedicine & Pharmacotherapy*, vol. 128, Article ID 110286, 2020.
- [16] T.-C. Hung, N. Zhao, C. Huang et al., "Exploring the mechanism of PingTang No.5 capsule on nonalcoholic fatty liver disease through network pharmacology and experimental validation," *Biomedicine & Pharmacotherapy*, vol. 138, Article ID 111408, 2021.
- [17] N.-R.-S. Bao, *Study on the Mechanism of Mongolian Medicine "Yihe-Tang" on NAFLD*, Inner Mongolia Medical University, Inner Mongolia, China, 2014.
- [18] Y.-S. Shieh, Y.-S. Chang, J.-R. Hong et al., "Increase of hepatic fat accumulation by liver specific expression of Hepatitis B virus X protein in zebrafish," *Biochimica et Biophysica Acta (BBA)-Molecular and Cell Biology of Lipids*, vol. 1801, no. 7, pp. 721-730, 2010.
- [19] P. J. Jakobsson, R. Morgenstern, J. Mancini, A. Ford-Hutchinson, and B. Persson, "Membrane-associated proteins in eicosanoid and glutathione metabolism (MAPEG). A widespread protein superfamily," *American Journal of Respiratory and Critical Care Medicine*, vol. 161, no. 2, pp. S20-S24, 2000.
- [20] J. Chen, S. Xiao, Y. Deng, X. Du, and Z. Yu, "Cloning of a novel glutathione S-transferase 3 (GST3) gene and expression analysis in pearl oyster, *Pinctada martensii*," *Fish & Shellfish Immunology*, vol. 31, no. 6, pp. 823-830, 2011.
- [21] J.-H. Kim, S. Raisuddin, J.-S. Rhee, Y.-M. Lee, K.-N. Han, and J.-S. Lee, "Molecular cloning, phylogenetic analysis and expression of a MAPEG superfamily gene from the pufferfish *Takifugu obscurus*," *Comparative Biochemistry and Physiology-Part C: Toxicology & Pharmacology*, vol. 149, no. 3, pp. 358-362, 2009.
- [22] J. Fu and P. Xie, "The acute effects of microcystin LR on the transcription of nine glutathione S-transferase genes in common carp *Cyprinus carpio* L.," *Aquatic Toxicology*, vol. 80, no. 3, pp. 261-266, 2006.
- [23] A. L. Komaroff, "The microbiome and risk for obesity and diabetes," *JAMA*, vol. 317, no. 4, pp. 355-356, 2017.
- [24] P. Roca-Saavedra, V. Mendez-Vilabrille, J. M. Miranda et al., "Food additives, contaminants and other minor components: effects on human gut microbiota-a review," *Journal of Physiology & Biochemistry*, vol. 74, no. 1, pp. 69-83, 2018.
- [25] J. He, P. Zhang, L. Shen et al., "Short-chain fatty acids and their association with signalling pathways in inflammation, glucose and lipid metabolism," *International Journal of Molecular Sciences*, vol. 21, no. 17, p. 6356, 2020.
- [26] M. Xie, Y. Xie, Y. Li et al., "Stabilized fermentation product of *Cetobacterium somerae* improves gut and liver health and

- antiviral immunity of zebrafish,” *Fish & Shellfish Immunology*, vol. 13, no. 120, pp. 56–66, 2021.
- [27] M.-X. Xie, W. Zhou, Y.-D. Xie et al., “Effects of *Cetobacterium somerae* fermentation product on gut and liver health of common carp (*Cyprinus carpio*) fed diet supplemented with ultra-micro ground mixed plant proteins,” *Aquaculture*, vol. 543, Article ID 736943, 2021.
- [28] W. Huang, Y. Man, C. Gao et al., “Short-chain fatty acids ameliorate diabetic nephropathy via GPR43-mediated inhibition of oxidative stress and NF- $\kappa$ B signaling,” *Oxidative Medicine and Cellular Longevity*, vol. 2020, Article ID 4074832, 21 pages, 2020.
- [29] E. E. Canfora, C. M. van der Beek, J. W. E. Jocken et al., “Colonic infusions of short-chain fatty acid mixtures promote energy metabolism in overweight/obese men: a randomized crossover trial,” *Scientific Reports*, vol. 7, no. 1, p. 2360, 2017.
- [30] M. A. G. Hernández, E. E. Canfora, J. W. E. Jocken, and E. E. Blaak, “The short-chain fatty acid acetate in body weight control and insulin sensitivity,” *Nutrients*, vol. 11, no. 8, p. 1943, 2019.
- [31] O. Froy and M. Garaulet, “The circadian clock in white and Brown adipose tissue: mechanistic, endocrine, and clinical aspects,” *Endocrine Reviews*, vol. 39, no. 3, pp. 261–273, 2018.
- [32] P. M. Titchenell, M. A. Lazar, and M. J. Birnbaum, “Unraveling the regulation of hepatic metabolism by insulin,” *Trends in Endocrinology and Metabolism*, vol. 28, no. 7, pp. 497–505, 2017.
- [33] F. W. B. Sanders and J. L. Griffin, “De novolipogenesis in the liver in health and disease: more than just a shunting yard for glucose,” *Biological Reviews*, vol. 91, no. 2, pp. 452–468, 2016.
- [34] R. J. Perry, L. Peng, N. A. Barry et al., “Acetate mediates a microbiome-brain- $\beta$ -cell axis to promote metabolic syndrome,” *Nature*, vol. 534, no. 7606, pp. 213–217, 2016.



## Research Article

# Phytochemical Analysis, Antioxidant, Antimicrobial, and Anti-Swarming Properties of *Hibiscus sabdariffa* L. Calyx Extracts: *In Vitro* and *In Silico* Modelling Approaches

Bechr Hamrita <sup>1</sup>, Noumi Emira <sup>2,3</sup>, Adele Papetti <sup>4</sup>, Riadh Badraoui <sup>2,5</sup>,  
Lamjed Bouslama <sup>6</sup>, Mohamed-Iheb Ben Tekfa,<sup>1</sup> Assia Hamdi <sup>7</sup>, Mitesh Patel <sup>8</sup>,  
Abdelbaset Mohamed Elsbali <sup>9</sup>, Mohd Adnan <sup>2</sup>, Syed Amir Ashraf <sup>10</sup>,  
and Mejdi Snoussi <sup>2,11</sup>

<sup>1</sup>Research Unit URI7ES30 “Virology & Antiviral Strategies”, Institute of Biotechnology, University of Monastir, Monastir, Tunisia

<sup>2</sup>Department of Biology, College of Science, University of Hail, Hail, P.O. Box 2440, Saudi Arabia

<sup>3</sup>Laboratory of Bioresources: Integrative Biology & Recovery, High Institute of Biotechnology, University of Monastir, Monastir, Tunisia

<sup>4</sup>Laboratory of Nutraceutical & Food Chemical-Toxicological Analysis, Department of Drug Sciences, University of Pavia, Pavia, Italy

<sup>5</sup>Section of Histology-Cytology, Medicine Faculty of Tunis, University of Tunis El Manar, Road Djebel Lakhdar, 1007 La Rabta, Tunis, Tunisia

<sup>6</sup>Laboratory of Bioactive Substances, Center of Biotechnology of Borj Cedria, University of Tunis El Manar, Tunisia

<sup>7</sup>Laboratory of Chemical, Pharmaceutical and Pharmacological Development of Drugs, Faculty of Pharmacy of Monastir, University of Monastir, Monastir, Tunisia

<sup>8</sup>Department of Biotechnology, Parul Institute of Applied Sciences and Centre of Research for Development, Parul University, Vadodara 391760, Gujarat, India

<sup>9</sup>Department of Clinical Laboratory Science, College of Applied Sciences-Qurayyat, Jouf University, Sakakah, Saudi Arabia

<sup>10</sup>Department of Clinical Nutrition, College of Applied Medical Sciences, University of Hail, Hail, P.O. Box 2440, Saudi Arabia

<sup>11</sup>Laboratory of Genetics, Biodiversity and Valorisation of Bioresources, High Institute of Biotechnology, University of Monastir, Monastir, Tunisia

Correspondence should be addressed to Abdelbaset Mohamed Elsbali; [aeelasbali@ju.edu.sa](mailto:aeelasbali@ju.edu.sa) and Mohd Adnan; [drmohdadnan@gmail.com](mailto:drmohdadnan@gmail.com)

Received 4 March 2022; Revised 25 April 2022; Accepted 27 April 2022; Published 20 May 2022

Academic Editor: Sekar Vijayakumar

Copyright © 2022 Bechr Hamrita et al. This is an open access article distributed under the Creative Commons Attribution License, which permits unrestricted use, distribution, and reproduction in any medium, provided the original work is properly cited.

The aim of this study was to investigate the phytochemical composition of dried Roselle calyx (*Hibiscus sabdariffa* L.) using both ethanolic and aqueous extracts. We report the antimicrobial activities against a wide range of bacteria, yeast, and fungi. The antioxidant activities were tested using 2,2-diphenyl-1-picrylhydrazyl (DPPH), hydroxyl, and 2-2'-azinobis-(3-ethylbenzthiazoline-6-sulfonic acid) radical scavenging assays. We report also for the first time the effect of the swarming motility in *Pseudomonas aeruginosa* PAO1. Our results showed that the tested two extracts were a rich source of phenols, flavonoids, and tannins with different degrees. Additionally, eleven phytoconstituents were identified by LC/MS technique (*Hibiscus* acid: 3-caffeoylquinic acid, 5-caffeoylquinic acid, 5-feruloylquinic acid, cyanidin 3-o-glucoside, myricetin, quercetin 7-o-rutinoside, quercetin 3-o-glucoside, delphinidin 3-o-sambubioside, and kaempferol 3-o-p-coumaroyl-glucoside). Also, it was shown that the calyx extract can scavenge 86% of the DPPH radical, while the rate of 53% and 23% of inhibition of the DPPH was obtained only at the concentration of 125 and 50 µg/mL, and a small inhibition was made at a concentration of 5 µg/mL. Roselle extracts inhibited the growth of the selected microorganisms at low concentrations, while higher concentrations are needed to completely kill them. However, no activity against CVB-3 was recorded for both extracts. In addition, the obtained extracts reduced the swarming motility of *P. aeruginosa* at 2.5 mg/ml. The docking simulation showed acceptable binding affinities (up to -9.6 kcal/mol) and interaction with key residues of 1JJI, 2QZW, and 2UVO. The obtained results highlighted the potential use of Roselle extract as a source of phytoconstituents with promising antimicrobial, antioxidant, and anti-quorum sensing activities.

## 1. Introduction

The plants still show a beneficial role in the treatment of various human pathologies. Isolation and extraction of plant compounds are imperative to understand their impact on the prevention and treatment of serious illness [1]. Several reports have been executed on natural antioxidants for decades to decipher protection against diseases linked to powerful oxidative stress and to the various damages induced by the presence of free radicals. Generally, oxidative stress is associated with several diseases, including cancer, neurodegenerative diseases, diabetes and inflammatory diseases, and aging process [2].

Actually, it has been proven that plants have shown a various range of compounds with antioxidant activities such as polyphenols as secondary metabolites. This component has been shown as strongly natural antioxidants of the vegetable world [3]. Currently, they are used against heart conditions, headaches, colds, wounds, and various skin infections, as well as insecticides and herbicides [4]. Natural phytocompounds can offer us a possible alternative to antibacterial agents [5].

In other way, previous studies have shown also that plants and their derived extracts are effective and may be of potential to inhibit bacterial QS system and biofilm [6]. In fact, QS and biofilm installation among resistant bacteria prove a major problem in human existence [7]. Several works have shown that resistance among bacteria or in QS and biofilm formation has motivated the treatment with plants and their derived extracts. Plants and their different extracts have been used to treat bacterial aggression and used as anti-QS compounds [6]. QS plays a crucial role in biofilm installation and virulence factor production [8].

*Hibiscus sabdariffa* L. (HS) is a plant from the Malvaceae family, which normally grows in subtropical and tropical regions around the world. “Zobo” is a local drink known in Nigeria from a medicinal herb HS, used in folk medicine to treat hypertension [4]. Various works have been carried out targeting the physiological effects of its calyces, focused on various aqueous and organic extracts rich in bioactive compounds such as tocopherols, polyphenols, flavonoids, and organic acids such as malic acids, oxalic acids, and also shikimic acid [9].

Extracts from the HS calyces have shown several essential biological activities and may include antibacterial properties. *In vitro* studies have proven the effectiveness of HS in inhibiting pathogenic strains such as *E. coli*. The aqueous, ethanolic, and methanolic extracts from HS have shown good efficacy against enterohemorrhagic *E. coli* (EHEC) O157:H7 [10]. In addition, other researchers have noted that the methanolic extract from HS has potent bactericidal activity against clinical isolates of uropathogenic *E. coli* (UPEC) [11].

Another study revealed that the aqueous extract of HS shows an inhibitory effect against *Ascaris galliivium* in

poultry. In addition, the coloring part from the calyces would also be fatal for *Mycobacterium tuberculosis* [12]. Roselle has also shown significant effects in India, such as aphrodisiac, astringent, cholagogue, demulcent, digestive, diuretic, emollient, purgative, refrigerant resolvent, sedative, stomachic, and tonic. Roselle is noted also as being a popular treatment for abscesses, bilious conditions, coughs, dysuria, scurvy, and cancer [11, 13–15]. According to the literature, several studies have proven its uses in the treatment of different diseases such as cancer, abscesses, bilious conditions, and cough, pathologies directly linked to microbial infections [16]. *In vivo* studies have shown that the anthocyanins of Hibiscus, a part of natural phenolic pigments present in the dried flower of Roselle and *H. rosa-sinensis*, have proven cardioprotective, hypocholesterolemic, and hepatoprotective effects [5].

In addition, other phenolic compounds, which have been isolated from dried HS flowers such as anthocyanin pigments and other phenolic compounds (*Hibiscus* protocatechuic acid), have shown that a protective role against tert-butyl hydroperoxide (t-BHP) induces oxidative stress, so hepatotoxicity has been noted *in vitro* and *in vivo* [17]. In addition, other work has shown that polyphenols, which are extracted from HS, have the ability to inhibit the accumulation and storage of triglycerides, to minimize the harmful effect of oxidative damage and the secretion of inflammatory adipokines, which directly target the infiltration of macrophages into adipose tissue [18, 19]. *In vitro*, the polyphenolic extract from HS has shown remarkable efficiency. These studies have shown that these compounds prevent fatty liver in hyperlipidemic mice by regulating gene expression applied in the regulation of glucose and lipid homeostasis and by lowering blood pressure and regulating endothelial function [18, 20].

To find new therapeutic resources with a powerful antioxidant effect, the objective of this work was to assess the antioxidant potentials, the antimicrobial activities, and the anti-swarming properties of the aqueous methanolic compounds of *H. sabdariffa* in relationship with its phytochemical composition. Furthermore, the intermolecular interactions of *H. sabdariffa* identified compounds and some targeted receptors (1JII, 2QZW, and 2UVO) were assessed using *in silico* molecular docking approach.

## 2. Materials and Methods

**2.1. Preparation of the Extracts.** The fresh parts of the Roselle were collected in March 2017 in Biskra (Algeria). In the laboratory, the collected parts of Roselle calyces were washed with sterile distilled water. Ten grams of the powdered dried plant material was soaked in 100 ml of pure methanol or pure distilled water for 48 h. The homogenate was filtered using Whatman’s filter paper. The final solution was concentrated, and the methanol was removed using a rotary evaporator. The small volume was later freeze-dried and kept in the freezer at 4°C for further studies.

**2.2. Biological Material.** In this work, the antifungal activity of the different extracts was tested against several fungi belonging to the genera *Aspergillus*, *Fusarium*, and *Penicillium* including the species *Aspergillus niger* DSM 63263, *Fusarium oxysporum*, *Penicillium expansum* DSM 994, *P. citrinum* DSM 1997, *P. simplicissimum* DSM 1097, *A. versicolor* DSM 1993, and *A. niger*. Four yeast strains were also tested namely *Candida albicans* ATCC 2019, *C. parapsilosis* ATCC 22019, *C. kefir* ATCC 6258, and *C. tropicalis* ATCC 06-085. The antibacterial activity was tested against nine bacterial strains frequently isolated from human infections and food poisoning: *Staphylococcus aureus* ATCC 25923, *S. epidermidis* CIP 106510, *Escherichia coli* ATCC 35218, *Listeria monocytogenes* ATCC 19115, *Pseudomonas aeruginosa* ATCC 27853, *Enterococcus faecalis* ATCC 29212, *Salmonella typhimurium* ATCC 1408, *Bacillus cereus* ATCC 11778, and *Vibrio parahaemolyticus* ATCC 17802. For cytotoxicity and antiviral activities, Vero cells, herpes virus type 2, and Coxsackievirus type 3 were used.

### 2.3. Phytochemical Screening of *H. sabdariffa* Extracts

**2.3.1. Polyphenol's Evaluation.** The Folin-Ciocalteu protocol [21] was used for the evaluation of total phenolic compounds in selected parts of plants. For the experiment, 1000  $\mu$ L of extracts was added to 5 ml of Folin-Ciocalteu reagent (mixed with distilled water 1:10 v/v) and 4 ml (75 g/L) of sodium carbonate. The samples were vortexed for 15 s and left to stand for 30 min at 40°C for staining. The absorbance was determined at a wavelength of 765 nm using the Thermo Scientific Spectrascan UV 2700 dual-beam spectrophotometer. The concentration of each plant extract was 0.1 g/ml. Phenol levels were calculated in mg/g of n-propyl gallate equivalent.

**2.4. Flavonoid Estimation.** The level of total flavonoids was determined using the procedure already described by Haddaji et al. [21]. In summary, 2 mL of distilled water and a  $\text{NaNO}_2$  (0.15 ml; 5%) solution were added to 0.5 ml of plant extract. After 6 min of incubation at room temperature, a solution of  $\text{AlCl}_3$  (0.15 ml, 1.1%) was added and allowed to stand for six minutes. Subsequently, a solution of NaOH (2 ml, 4%) was added to the mixture. Immediately, the distilled water was added (5 ml). Then, the mixture is allowed to stand for 15 minutes, and the color intensity was measured at 510 nm. The results were reported in mg of catechin equivalent (EC) per gram of the extract.

**2.5. Determination of Total Tannins.** The quantification of total tannins in both extracts was estimated using the same protocol described by Haddaji et al. [21]. For the experiment, 50  $\mu$ L of each extract was appropriately diluted and mixed with a volume of 1.5 ml of 4% vanillin and then added to 750  $\mu$ L of concentrated HCl. After vigorous stirring, the mixture was incubated for 20 min at room temperature. Then, the absorbance was measured at 500 nm [22]. The

contents of condensed tannins are expressed in mg of equivalent catechin per gram of extract.

**2.6. RP-HPLC-DAD-ESI-MS<sup>n</sup> Analysis.** To obtain a profile of polyphenolic composition of methanolic and aqueous extracts, an HPLC-DAD-ESI/MS<sup>n</sup> analysis was carried out. Ten milligrams of dried samples was solubilized in 10 ml of the mobile phase, and 5  $\mu$ L was injected in the Thermo Finnigan Surveyor Plus HPLC System (Thermo Fisher Scientific, Waltham, MA), equipped with a Surveyor UV-Vis photodiode array detector (PAD), connected to an LCQ Advantage MAX ion trap mass spectrometer through an ESI source (Thermo Fisher Scientific, Waltham, MA). The analysis was performed on a Gemini C18 analytical column (150 mm  $\times$  2.0 mm i.d., 5  $\mu$ m) with a Hypersil GOLD C18 guard column (10 mm  $\times$  2.1 mm i.d., 5  $\mu$ m; both from Phenomenex, Torrance, CA). A binary mobile phase was used, and it consisted of eluents A and B, which were 0.1% formic acid aqueous solution and acetonitrile, respectively. Analytes were eluted in a linear gradient from 5% to 95% B in 70 min at a flow rate of 0.3 ml/min, 30°C. Each run was followed by column reconditioning. The chromatogram was recorded at 315 nm (hydroxycinnamic acids), 370 nm (flavonols), and 520 nm (anthocyanins). Spectral data were acquired in the range of 190–600 nm for all peaks. The ion trap was operated in data-dependent, full-scan (100–1800  $m/z$ ), and MS/MS mode to obtain fragment ions ( $m/z$ ) with a collision energy of 30% and an isolation width of 3  $m/z$ . ESI source parameters were optimized to an ionization voltage of 4 kV, a capillary temperature of 320°C, a sheath gas flow rate of 15 arbitrary units, and an auxiliary gas flow rate of 10 arbitrary units. Thermo Fisher Scientific Excalibur 2.0 software was used for data acquisition and processing.

**2.7. Antioxidant Activities of *H. sabdariffa* Extracts.** The antioxidant activity of the extracts was studied by three methods: the trapping power of the free radical DPPH, that of the radical ABTS, and the power of reduction of ferric ions (FRAP).

**2.8. Scavenging Activity of DPPH Radical.** The DPPH radical scavenging activity was evaluated using the protocol of Moraes-de-Souza et al. [23] after rectifications. The reaction was composed of 30  $\mu$ L of extract, 3 ml of methanol, and 0.270 ml of a solution of 0.5 mM 2,2-diphenyl-1-picrylhydrazyl (DPPH) radical solution in methanol. The absorbance was measured in an ELx800 microplate reader (BioTek Instrument, Inc., Winooski, VT, USA) at 517 nm, after 45 min of incubation. The antioxidant activity was calculated using the following equation:

$$\% \text{inhibition} = \left[ \frac{(A \text{ control} - A \text{ sample})}{A \text{ control}} \right] \times 100, \quad (1)$$

where  $A_{\text{control}}$  = absorbance of negative control at the moment of solution preparation and  $A_{\text{sample}}$  = absorbance of sample after 45 min.

The antioxidant activity was expressed as  $IC_{50}$  (mg/mL), which represented the extract concentrations scavenging 50% of DPPH radicals [21].

**2.9. Scavenging Activity of ABTS Radical.** The ABTS radical scavenging activity was evaluated using the protocol referred to Re et al. [24] after rectifications. 7 mM of 2,2'-azinobis (3-ethylbenzothiazoline-6-sulfonic acid) (ABTS) was added to the distilled water. The radical cation ABTS ( $ABTS \cdot +$ ) was generated in the presence of ABTS and 2.45 mM potassium persulfate (final concentration), and then, the mixture will be placed in the dark at room temperature for 12 to 16 h before use.

The dilution of the  $ABTS^+$  solution was performed with water to an absorbance of 0.70 ( $\pm 0.02$ ) at 734 nm. The reaction mixture is composed of 0.07 ml of the HS extract and 3 ml of the ABTS radical. Then, this mixture is incubated for 7 min, and the absorbance reading was taken using a spectrophotometer at 734 nm. The antioxidant activity was calculated using the following equation:

$$\% \text{inhibition} = \left[ \frac{(A_{\text{control}} - A_{\text{sample}})}{A_{\text{control}}} \right] \times 100, \quad (2)$$

where  $A_{\text{control}}$  = absorbance of negative control at the moment of solution preparation and  $A_{\text{sample}}$  = absorbance of sample after 6 min.

The  $EC_{50}$  values were evaluated from the curves, which show the concentration of the extract required to scavenge 50% of the free radical ABTS. The  $EC_{50}$  is generally defined to determine the amount or concentration of extracts required to scavenge 50% of free radicals.

**2.10. Ferric Reducing Antioxidant Power (FRAP) Methods.** This technique is based on the microplate reader. Indeed, volumes of the order of 0.5 ml of the different concentrations of the extracts tested were mixed with a sodium phosphate buffer (200 mmol/l, pH 6.6, 0.5 ml) and ferricyanide of potassium (1% w/v, 0.5 ml). The mixture was incubated at 50°C for 20 minutes, and then, trichloroacetic acid (10% w/v, 0.5 ml) was added. Afterwards, 0.8 ml of the mixture was poured into the 48-well microplates, and then, the deionized water (0.8 ml) and the ferric chloride (0.1% w/v, 0.16 ml) were added. Absorbance was measured at 690 nm. The concentration of the extract, which gives 0.5 absorbance ( $EC_{50}$ ), was estimated from the graph, which reports the evaluation of the absorbance at 690 nm as a function of the concentrations of the extract.

### 2.11. Screening for Antimicrobial Activities

**2.11.1. Disc Diffusion Method.** Antibacterial activity was carried out by the disc diffusion method [25] against nine Gram-positive and Gram-negative type bacterial strains. The

same technique was used to study the antifungal activity of HS extracts against four *Candida* species on Sabouraud chloramphenicol agar plate at 30°C for 17–26 h.

The optical density of all bacteria was adjusted to 0.5 McFarland turbidity standards and 2 McFarland for yeast strains with a DENSIMAT (bioMérieux). The suspension was used to inoculate Mueller Hinton/Sabouraud chloramphenicol Petri dishes using a sterile cotton swab. The plant extract was prepared at a final concentration of about 100 mg/ml. Sterile filter paper discs (6 mm in diameter) were impregnated with 10  $\mu$ l of plant extract that was placed on the cultured plates. After 1.5–3 h at 4°C, the treated Petri dishes were incubated at 27 or 36°C for 17–24 h. For fungi, a spore solution ( $10^6$  spore/mL) was used to inoculate the potato dextrose agar Petri dishes that were incubated for 48 h at 37°C.

The treated Petri dishes were placed at 4°C for 1.5–3 h and then incubated at 37°C for 17–24 h. The inhibition of microorganism growth was evaluated by measuring the diameter of the transparent inhibition zone around each disc. The average of three measurements was recorded. The susceptibility of the standard (ampicillin and amphotericin B) was determined at a final concentration of about 10 mg/disc.

**2.12. Microdilution Assay.** The determination of MICs and MBCs was performed by dilution technique in a liquid medium used for bacteria [25], yeast [26], and fungi [27]. For the experiment, 95  $\mu$ l of Sabouraud broth (yeast and fungi) or Mueller Hinton broth (bacteria), 5  $\mu$ l of bacterial or fungal suspension, and 100  $\mu$ l of dilution of the extract were tested. The negative control well contains 195  $\mu$ l of enrichment broth without extract and 5  $\mu$ l of suspension of the microorganism to be tested. The final volume in each well is 200  $\mu$ l. After incubation at 37°C for 24 h for bacteria and yeast and 48 h for fungi, the lowest concentration, at which there was no turbidity, was also regarded as MIC value of the extract. MBC/MFC is defined as the concentration of extract that totally inhibits the growth of microorganisms tested confirmed on MH/SC/PDA agar. According to Zahin et al. [28], plant extract exerted two types of activities: a bacteriostatic/fungistatic (MBC/MIC  $\geq 4$ ) and bactericidal/fungicidal activity (MBC/MIC  $< 4$ ).

**2.13. Study of Antiviral Activity.** Vero cells (ATCC No. CCL-81) were cultivated in RPMI 1640 supplemented with 10% fetal bovine serum (FBS) mixed with 1% penicillin (100 U/ml), 1% streptomycin (100 mg/ml), and 1% fungizone (2.5 mg/ml). Vero cells were grown in a solution composed of RPMI containing 5% FBS, placed in sterile 96-well, 24-well flat-bottomed plates at  $1 \text{ g}/10^4$  cells/well, at 37°C, and incubated under 5%  $\text{CO}_2$  humidified atmosphere at 37°C.

The stock solutions were diluted serially with RPMI media without FBS to obtain many extract concentrations. In general, the final concentration of DMSO in the working concentration was below 0.5%. The determination of the cytotoxic concentration of the two extracts was performed on 96-well flat-bottomed plates. One hundred  $\mu$ l of  $\frac{1}{2}$  diluted

extracts starting from 2.5 mg/mL concentration was deposited on cells in confluence. Vero cells treated with 0.5% DMSO in PBS were used as negative control. All experiments were performed in triplicates. Then, the plate was incubated under 5% CO<sub>2</sub>, humidified atmosphere at 37°C. After 72 h, the extract dilutions were substituted with 100 µL of the MTT solution (5 mg/mL) and incubated for 4 h at 37°C. Then, the formazan crystals were dissolved with DMSO and the plate was read on an ELISA reader at a 570 nm wavelength to measure the optical density. 50% cytotoxic concentration (CC<sub>50</sub>) of crude plant extracts, which is the concentration that causes 50% cell cytotoxicity of Vero cells, was determined by linear regression.

**2.14. Viruses and Antiviral Activity.** Antiviral activity was performed on the same 96-well flat-bottom plates. Confluent Vero cells were infected with 50 TCID<sub>50</sub> (50% tissue culture infective dose) of CVB-4 in the presence of 100 µL of ½ diluted extracts starting from CC<sub>50</sub>. Following 1 h of incubation, the medium was removed, and the cells were washed with PBS. Vero cells infected without extract were used as a virus control. All experiments were performed in triplicates. Then, the plate was incubated under 5% CO<sub>2</sub> humidified atmosphere at 37°C. After 48 h, the medium was substituted with 100 µL of the MTT solution (5 mg/mL) and incubated for 4 h at 37°C. Then, the formazan crystals were dissolved with DMSO and the plate was read on an ELISA reader at a 570 nm wavelength to measure the optical density. 50% inhibitory concentration (IC<sub>50</sub>) of crude plant extract, which is the concentration that reduces the optical density by 50% in comparison with the cell control, was determined by linear regression.

**2.15. Anti-Swarming Motility Test.** In swarming assays, overnight cultures of the test bacteria (*P. aeruginosa* ATCC 27853) were point inoculated (5 µL) at the center of swarming plates consisting of 1% peptone, 0.5% NaCl, 0.5% agar, and 0.5% of filter-sterilized D-glucose with various concentrations of Hibiscus aqueous methanolic extracts (0.5, 1, 2.5, and 10 mg/ml). The plate without the extract was maintained as control. The plates were incubated at an appropriate temperature in the upright position at 37°C for 18 h. The swarming migration was recorded by following swarm fronts of the bacterial cells.

**2.16. In Silico Molecular Docking and Intermolecular Interactions.** The biological activity of the compounds identified by RP-HPLC-DAD-ESI-MS<sup>n</sup> analysis was confirmed by *in silico* molecular docking and interaction assay. The active sites of some selected receptors (TyrRS from *S. aureus*; PDB ID: 1JIJ, aspartic proteinase from *Candida albicans*, PDB ID: 2QZW, and wheat germ agglutinin, PDB ID: 2UVO) have been targeted to assess the antibacterial/antimicrobial and antiviral effects, respectively. The tridimensional structures of the targeted proteins were obtained from RCSB. ChemDraw was used to draw the chemical structures of the previously identified 17 compounds

[29, 30]. The docking approach was based on the CHARMM force field after processing ligands and receptors: polar hydrogen and Kollman charges. The binding affinity and the hydrogen bond calculations were assessed as previously reported [29, 31–33]. These receptors have been selected because they are highly involved in the bacterial, viral, and quorum sensing processes and are commonly targeted in pharmaceutical studies as they are parts of the treatment pathways [34, 35].

**2.17. Statistical Analysis.** All the analyses were run in triplicate and averaged. All values are expressed as mean ± standard deviation. The CC<sub>50</sub>, EC<sub>50</sub>, and IC<sub>50</sub> values were estimated by extrapolating the graph plotted with software Microsoft Excel 2007. Mean values were compared using multiple comparison of Duncan's test with the SPSS statistical software program (SPSS v.16). The difference was statistically significant when  $p < 0.05$ .

### 3. Results

**3.1. Phytochemical Composition of the Obtained Extracts.** The phytochemical composition of both methanolic and aqueous extracts of Hibiscus calyces is summarized in Table 1. Phenolic compounds are secondary metabolites whose presence is highly influenced by environmental and genetic factors. Their contents vary according to the plant and/or studied organ. Indeed, the methanolic extract of Hibiscus has a polyphenol content in the order of 19.58 ± 0.08 mg EAG/g of dry extract, which has been found to be lower than the aqueous extract of the same plant of 22.71 ± 0.08 mg EAG/g of dry extract.

According to the results obtained, it is noted that the flavonoids are the most abundant phenolic compounds in the flower of Hibiscus with an amount of 22.49 ± 1.04 mg EC/g of the aqueous extract. The extracts showed also low content of tannin molecules. These values are in the order of 8.4 ± 0.7 mg EC/g of the dry extract for the aqueous extract and about 1.16 ± 0.16 mg EC/g of dry extract for the methanolic extract of the Hibiscus calyces.

A list of compounds identified in methanolic and aqueous extracts by LC-MS is reported in Table 2. The methanolic extract contained two anthocyanins, which were detected in positive ionization mode, i.e., delphinidin 3-*O*-sambubioside (compound 10) and cyanidin 3-*O*-glucoside (compound 6). Both of them fragmented giving the aglycone ions at  $m/z$  of 303 and 287, which corresponded to the loss of sambubiose and glucose moieties, respectively. Four flavonols were also detected. Myricetin (compound 7) ionized to give an ion at  $m/z$  of 319, and it was confirmed by comparing its behavior with that of the standard, as well as the identity of quercetin 3-*O*-glucoside ( $m/z$  465) (compound 9). Another quercetin derivative (compound 8) was present; it fragmented giving a base peak an ion at  $m/z$  of 303 and a very intense parent ion at  $m/z$  of 302, thus indicating the linkage position of the sugar moiety on the aglycone and leading to the correct identification of the disaccharide [39]. Kaempferol 3-*O*-*p*-coumaroyl-gucoside (compound 11) was

TABLE 1: Phytochemical study of the methanolic and aqueous extracts from *H. sabdariffa* calyces. mg EGA/g extract: mg equivalent gallic acid/g extract; mg EC/g extract: mg equivalent catechin/g extract.

Compound	Aqueous extract (HE)	Methanolic extract (HM)
Total polyphenols (mg EGA/g extract)	22.71 ± 0.08	19.58 ± 0.08
Flavonoids (mg EC/g extract)	22.49 ± 1.04	16.3 ± 1.85
Tannins (mg EC/g extract)	8.4 ± 0.7	1.16 ± 0.10

TABLE 2: MS and MS/MS data of compounds detected in methanolic and aqueous extracts.

N	RT (min)	Precursor ion (m/z)	HPLC-ESI-MS <sup>n</sup> m/z (% of base peak)	Compound identity	References
1	12.90	189	MS <sup>2</sup> [189]: 171 (20), 127 (100)	Hibiscus acid	Amaya-Cruz <i>et al.</i> , [36]; Rodriguez-Medina <i>et al.</i> , [37]
2	34.21	341	MS <sup>2</sup> [341]: 179 (100), 135 (20)	Caffeic acid derivative	Amaya-Cruz <i>et al.</i> [36]
3	37.62	353	MS <sup>2</sup> [353]: 191 (100), 179 (60), 135 (10)	3-Caffeoylquinic acid	Carazzone <i>et al.</i> , [38]
4	38.22	353	MS <sup>2</sup> [353]: 191 (100), 179 (10)	5-Caffeoylquinic acid	Carazzone <i>et al.</i> , [38]
5	39.92	367	MS <sup>2</sup> [367]: 191 (100), 173 (25)	5-Feruloylquinic acid	Carazzone <i>et al.</i> , [38]
6 <sup>a</sup>	45.41	449 <sup>+</sup>	MS <sup>2</sup> [449]: 287 (100)	Cyanidin 3-O-glucoside	Amaya-Cruz <i>et al.</i> , [36]
7 <sup>a</sup>	54.50	319	—	Myricetin	Borrás-Linares <i>et al.</i> , [10]
8	62.47	611 <sup>+</sup>	MS <sup>2</sup> [611]: 303 (100), 302 (70), (100)	Quercetin 7-O-rutinoside	Shi <i>et al.</i> , [39]
9 <sup>a</sup>	65.02	465 <sup>+</sup>	MS <sup>2</sup> [465]: 303 (85), 303 (100)	Quercetin 3-O-glucoside	Rodriguez-Medina <i>et al.</i> , [37]
10	67.31	597 <sup>+</sup>	MS <sup>2</sup> [597]: 303 (100)	Delphinidin 3-O-sambubioside	Borrás-Linares <i>et al.</i> , [10]
11	72.56	595 <sup>+</sup>	MS <sup>2</sup> [595]: 449 (55), 287 (80), 286 (100)	Kaempferol 3-O-p-coumaroyl-glucoside	Fernández-Arroyo <i>et al.</i> , [40]

RT: retention time; <sup>a</sup>compared with standard compound; <sup>+</sup>positive ionization mode.

identified thanks to its fragmentation pattern, which was consistent with the loss of the glucose and of the acyl-glucose moieties, respectively.

### 3.2. Biological Activities of the Different Extracts Obtained

**3.2.1. Antimicrobial Activity.** The antimicrobial activities were evaluated using the disc diffusion test to determine the diameters of the bacterial growth inhibition zones. The liquid microdilution assay was carried out to evaluate the minimum inhibitory concentrations (MICs) and the minimum bactericidal concentrations (MBCs). The inhibition of microbial growth (bacteria and yeasts) resulted in the appearance of a halo around each disc impregnated with the extract to be tested.

The results of the agar diffusion assay reveal that the antibacterial activity of the extracts is dependent from the target bacterium. Indeed, the Hibiscus aqueous extract showed moderate antimicrobial activity with a diameter zone inhibition of 18.33 mm. It is noted that the highest antimicrobial activity was obtained with the same extract against *L. monocytogenes* strain ATCC 19115 with a mean zone of growth inhibition value of 21 mm. In fact, the Hibiscus methanolic extracts showed a zone inhibition of 17.12 mm. According to studies confirmed by Kalemba and Cunicka [41], the sensitivity of a microorganism certainly depends on the composition variability of the extract and also of the microorganism itself. The antifungal activity has shown variation in growth inhibition. In fact, the inhibition diameter of yeast with methanolic extract was about 14 mm; however, it

was ranging from 14 to 17 mm, when the aqueous extract was used. All these results are summarized in Table 3.

The determination of MICs and MBCs/MFCs showed that the Hibiscus extracts in liquid medium are very active on all tested bacteria and yeasts but with different degrees. In addition, these extracts appear to be more effective on bacteria than yeasts with lower MICs and MBCs compared with those recorded for yeasts. In the liquid medium, the lowest MIC values are recorded with the Hibiscus aqueous extract (MICs: 9.375 mg/ml) and the lowest CMFs by the same plant methanolic extract (MFCs: 18.75 to 37.5 mg/ml). It is the same for the bacteria tested by the Hibiscus aqueous extract with similar MICs in all bacteria (2,342 mg/ml) and CMBs ranging from 4.68 to 9.375 mg/ml. All these results are expressed in Table 3. The antifungal activity results of the different methanolic and aqueous extracts tested on two strains of fungi according to the microdilution method recorded that the minimum inhibitory concentrations vary from 75 to 150 mg/ml (Table 4).

**3.3. Cytotoxicity and Antiviral Activities.** Hibiscus extracts showed low cytotoxicity on Vero cell lines with CC<sub>50</sub> of 946 and 1250 µg/ml, respectively, for methanolic and aqueous extracts. However, no activity against CVB-3 was recorded for both extracts.

**3.4. Study of the Antioxidant Activity of the Extracts Obtained.** The antioxidant activity of the extracts was evaluated by the DPPH method. This method makes to evaluate the ability of



TABLE 3: Determination of MICs, MBCs, and MBC/MIC ratio of *H. sabdariffa* methanolic and aqueous extracts compared with amphotericin and ampicillin.

	<i>H. sabdariffa</i> aqueous extract				<i>H. sabdariffa</i> methanolic extract				Ampicillin		
	IZ*	MIC*	MBC**	MBC/ MIC ratio	IZ	MIC	MBC	MBC/ MIC ratio	IZ	MIC	MBC
<i>S. aureus</i> ATCC 25923	18 ± 0 <sup>a</sup>	2.342	9.375	4	17 ± 1 <sup>a</sup>	2.342	4.68	2	26.66 ± 1.15 <sub>b</sub>	0.25	0.40
<i>S. epidermidis</i> CIP 106510	19 ± 2 <sup>b</sup>	2.342	9.375	4	15.33 ± 0.57 <sup>a</sup>	2.342	4.68	2	22.67 ± 0.57 <sup>c</sup>	0.25	0.40
<i>E. coli</i> ATCC 35218	17 ± 1 <sup>b</sup>	2.342	9.375	4	15 ± 1 <sup>b</sup>	2.342	9.375	4	11.67 ± 1.52 <sup>a</sup>	0.023	3
<i>L. monocytogenes</i> ATCC 19115	21 ± 1 <sup>c</sup>	9.375	18.75	2	16.66 ± 0.57 <sup>b</sup>	2.342	9.375	4	12.33 ± 0.57 <sup>a</sup>	0.023	0.093
<i>E. faecalis</i> ATCC 29212	19.33 ± 0.57 <sup>c</sup>	9.375	37.5	4	18 ± 0 <sup>b</sup>	2.342	9.375	4	13.66 ± 0.57 <sup>a</sup>	0.023	0.093
<i>S. typhimurium</i> ATCC 1408	18 ± 0 <sup>a</sup>	9.375	>75	>4	17 ± 2 <sup>a</sup>	2.342	9.375	4	17.33 ± 1.15 <sup>a</sup>	0.023	0.093
<i>B. cereus</i> ATCC 11778	20 ± 2 <sup>a</sup>	9.375	18.75	2	19.33 ± 0.57 <sup>a</sup>	2.342	9.375	4	26.33 ± 1.52 <sup>b</sup>	0.25	0.40
<i>V. parahaemolyticus</i> ATCC 17802	17.33 ± 0.57 <sup>b</sup>	9.375	37.5	4	17.33 ± 0.57 <sup>b</sup>	2.342	9.375	4	13.33 ± 0.57 <sup>a</sup>	0.011	3
<i>P. aeruginosa</i> ATCC 27853	16 ± 2 <sup>a</sup>	9.375	18.75	2	18.33 ± 1.52 <sup>a</sup>	2.342	9.375	4	22.66 ± 0.57 <sup>b</sup>	0.011	1.5
Yeasts	IZ*	MIC	MFC * *	MFC/ MIC ratio	IZ	MIC	MFC	MFC/ MIC ratio	Amphotericin B		
<i>Candida albicans</i> ATCC 2019	15 ± 1 <sup>a</sup>	9.375	37.5	4	14.33 ± 0.57 <sup>a</sup>	9.375	37.5	4	14.66 ± 0.57 <sup>a</sup>	0.024	0.781
<i>Candida parapsilosis</i> ATCC 22019	14 ± 1 <sup>b</sup>	9.375	37.5	4	15 ± 1 <sup>b</sup>	9.375	37.5	4	10.33 ± 0.57 <sup>a</sup>	0.195	0.39
<i>Candida krusei</i> ATCC 6258	17.66 ± 1.52 <sup>b</sup>	9.375	37.5	4	10 ± 1 <sup>a</sup>	9.375	18.75	2	12 ± 0 <sup>a</sup>	0.097	0.195
<i>Candida tropicalis</i> ATCC 06-085	17 ± 1 <sup>c</sup>	9.375	37.5	4	15 ± 1 <sup>b</sup>	9.375	37.5	4	6 ± 0 <sup>a</sup>	0.39	0.25

The diameter of the disc is 6 mm. The letters (a–c) indicate a significant difference between the different inhibition zones according to the Duncan test ( $p < 0.05$ ). MIC: minimal inhibitory concentration expressed as mg/ml; MBC: minimal bactericidal concentration expressed as mg/ml; MFC: minimal fungicidal concentration expressed as mg/ml.

TABLE 4: Determination of the MIC and MFC values of the different extracts tested on seven fungal strains (expressed in mg/mL).

Strains tested	<i>H. sabdariffa</i> methanolic extract		<i>H. sabdariffa</i> aqueous extract	
	MIC*	MFC**	MIC	MFC
<i>Aspergillus niger</i> DSM 63263	75	150	5	150
<i>Fusarium oxysporum</i>	150	>150	5	>150
<i>Penicillium expansum</i> DSM 1994	150	>150	5	>150
<i>Penicillium citrinum</i> DSM 1997	150	>150	5	>150
<i>Penicillium simplicissimum</i> DSM 1097	75	>150	5	>150
<i>Aspergillus versicolor</i> DSM 1993	150	>150	5	>150
<i>Aspergillus niger</i>	150	150	5	150

MIC: minimal inhibitory concentration (mg/ml); MFC: minimal fungicidal concentration (mg/ml).

phenolic compounds to inhibit the DPPH radical. The results showed that both Roselle extracts were able to scavenge the DPPH free radical with different degrees (IC<sub>50</sub> value about 2.793 ± 0.044 mg/ml for methanolic extract and 2.471 ± 0.024 mg/ml for the aqueous one). For the radical ABTS<sup>\*\*</sup>, the results obtained showed that the Hibiscus methanolic extract has the highest antioxidant activity with an EC<sub>50</sub> value of 1.918 ± 0.06 mg/ml as compared to its aqueous extract of 2.082 ± 0.0035 mg/ml. The presence of reducing agents in plant extracts causes the Fe<sup>3+</sup>/ferricyanide complex to be reduced to the ferrous form. The results

obtained show that the Hibiscus aqueous and methanolic extracts have low EC<sub>50</sub> values of about 0.578 ± 0.016 and 0.676 ± 0.026 mg/ml, respectively. All these data are summarized in Table 5.

### 3.5. Anti-Quorum Sensing Activity

**3.5.1. Anti-Swarming Activity.** Swarming migrations play an important role in quorum sensing biofilm formation, and we tried to examine the anti-QS potential of Hibiscus aqueous

TABLE 5: Comparative analysis of the results for the antioxidant activities obtained by DPPH, FRAP, and ABTS tests as compared to ascorbic acid.

<i>H. sabdariffa</i>	DPPH IC <sub>50</sub> (mg/mL)	ABTS EC <sub>50</sub> (mg/mL)	FRAP EC <sub>50</sub> (mg/mL)
Methanolic extract	2.793 ± 0.044	2.082 ± 0.035	0.676 ± 0.026
Aqueous extract	2.471 ± 0.024	1.918 ± 0.060	0.578 ± 0.016
Ascorbic acid	0.022 ± 0.00058	0.0209 ± 0.0016	0.09 ± 0.007

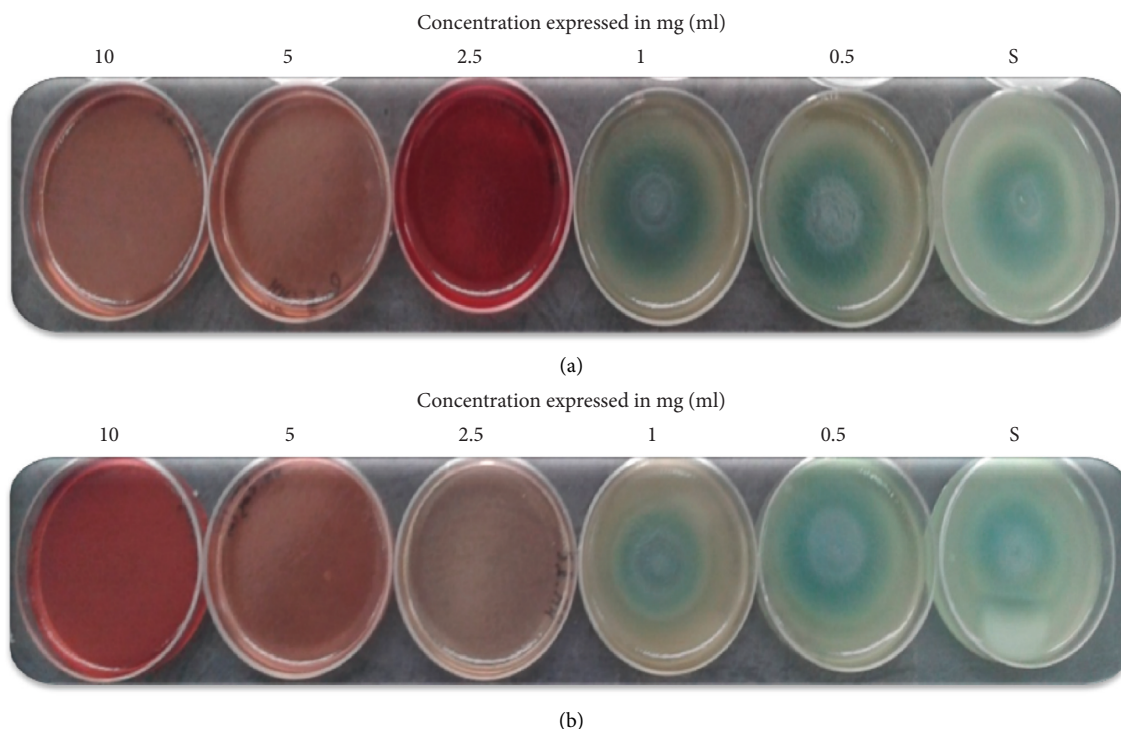


FIGURE 1: Anti-swarming activity of the methanolic and aqueous extracts from *H. sabdariffa* calyces tested against *P. aeruginosa* PAO1 strain. (a): methanolic extract and (b): aqueous extract; S: standard.

and methanolic extracts against motility in PAO1 strain. Our results indicated that HS extracts inhibited the swarming of PAO1 at the three tested concentrations (2.5, 5, and 10 mg/ml) (Figure 1). However, a high inhibition in the migration of PAO1 was obtained at 2.5 mg/ml. At high concentration of both tested extracts, a reduction in the intensity of the green coloration of the pigment “pyocyanin” was noted. All these data are summarized in Table 6.

**3.6. In Silico Results.** The molecular interactions of the plant-identified compounds and some targeted macromolecules involved in the biological activities are reported in Table 7. The in silico data reported in this study correspond to the better positions with both best binding affinity and RMSD equal to zero, as commonly reported in molecular interactions’ studies [42–44]. The compounds were predicted to establish different binding affinities reaching  $-9.6$  for 1JII,  $-7.5$  for 2QZW, and  $-6.9$  for 2UVO. This might be related to the structure-activity relationship [30, 32, 33, 43]. Figures 2–4 exhibit 3D and 2D illustrations of the top 3 complexes with the highest binding scores.

TABLE 6: Evaluation of the anti-swarming activity of aqueous and methanolic extracts from *H. sabdariffa* against *P. aeruginosa* PAO1.

Mean diameter ± SD (mm)	Concentration of extracts in (mg/ml)					Standard
	0.5	1	2.5	5	10	
Aqueous extract	2.7 ± 0.25	1.2 ± 0.25	0	0	0	10.6 ± 0.57
Methanolic extract	9.6 ± 1.52	8.3 ± 0.57	0	0	0	9.5 ± 0.25

## 4. Discussion

Hydroxycinnamic acid derivatives were the compounds mostly present in the aqueous extract in addition to a less concentration of compounds 7, 8, 9, and 11. In fact, two different isomers of caffeoylquinic acids (CQAs) were detected and they were identified as 3-CQA (compound 3) and 5-CQA (compound 4) according to the different intensities of a fragment ion at  $m/z$  of 179 and the presence of an ion at  $m/z$  of 135 only in MS/MS fragmentation of 3-CQA [45]. A similar fragmentation pattern was registered for compound 5, identified as 5-feruloylquinic acid.

TABLE 7: Binding energy, conventional hydrogen bonds, and the closest interacting residues of 1JII, 2QZW, and 2UVO for TyrRS from *S. aureus*, the aspartic proteinase from *Candida albicans*, and the wheat germ agglutinin in complex with N-acetyl-D-glucosamine, respectively.

No.	Affinity (Kcal/mol)	Conventional H-bonds	Closest interacting residues	Distance to closest interacting residue (Å)
<i>TyrRS from S. aureus</i> (PDB ID: 1JII)				
1	-7.1	11	Lys <sup>84</sup> , Arg <sup>88</sup> , Arg <sup>88</sup> , Tyr <sup>170</sup> , Gln <sup>174</sup> , Gln <sup>196</sup> , Asp <sup>80</sup> , Gly <sup>38</sup> , Gln <sup>196</sup> , Asp <sup>80</sup> , Gln <sup>196</sup>	Asp <sup>80</sup> (2.25)
2	-9.1	7	Lys <sup>84</sup> , Lys <sup>84</sup> , Asn <sup>124</sup> , Asp <sup>195</sup> , Asp <sup>177</sup> , Gln <sup>174</sup> , Gln <sup>190</sup>	Gln <sup>174</sup> (1.92)
3	-9.1	6	Cys <sup>37</sup> , Asp <sup>40</sup> , Thr <sup>75</sup> , Tyr <sup>170</sup> , Thr <sup>75</sup> , Asp <sup>195</sup> , Ala <sup>39</sup> , Gly <sup>192</sup> , Leu <sup>70</sup>	Thr <sup>75</sup> (2.20)
4	-8.6	5	Asp <sup>40</sup> , Gly <sup>193</sup> , Asp <sup>177</sup> , Gly <sup>38</sup> , Asp <sup>195</sup> , Ala <sup>39</sup> , Gly <sup>192</sup> , Leu <sup>70</sup>	Asp <sup>195</sup> (2.09)
5	-8.9	8	Gly <sup>38</sup> , Asp <sup>80</sup> , Arg <sup>88</sup> , Arg <sup>88</sup> , Gly <sup>193</sup> , Val <sup>191</sup> , Gln <sup>174</sup> , Asp <sup>40</sup> , Ala <sup>39</sup> , Lys <sup>84</sup> , Asp <sup>195</sup> , Asp <sup>195</sup> , His <sup>50</sup> , His <sup>50</sup> , Pro <sup>53</sup>	Arg <sup>88</sup> (1.82)
6	-9.6	6	Tyr <sup>36</sup> , Gln <sup>190</sup> , Asp <sup>177</sup> , Asp <sup>40</sup> , Thr <sup>75</sup> , Asp <sup>40</sup> , Ala <sup>39</sup> , Asp <sup>195</sup> , Ala <sup>39</sup> , Ala <sup>39</sup>	Thr <sup>75</sup> (1.87)
7	-8.2	7	Lys <sup>84</sup> , Arg <sup>88</sup> , Tyr <sup>170</sup> , Gln <sup>174</sup> , Gly <sup>193</sup> , Gln <sup>196</sup> , Asp <sup>40</sup> , Cys <sup>37</sup> , His <sup>50</sup> , His <sup>50</sup> , Asp <sup>195</sup> , Asp <sup>195</sup> , Asp <sup>80</sup> , Pro <sup>53</sup> , His <sup>50</sup> , Phe <sup>54</sup> , Cys <sup>37</sup>	Tyr <sup>170</sup> (1.57)
8	-8.8	11	Asp <sup>40</sup> , Asn <sup>124</sup> , Gln <sup>174</sup> , Gln <sup>174</sup> , Gly <sup>193</sup> , Gln <sup>196</sup> , Asp <sup>177</sup> , Asp <sup>177</sup> , Asp <sup>195</sup> , Gly <sup>49</sup> , Gln <sup>190</sup> , His <sup>50</sup> , Gly <sup>38</sup> , Asp <sup>40</sup> , His <sup>50</sup> , Ala <sup>39</sup> , Ala <sup>39</sup>	Asp <sup>40</sup> (1.60)
9	-8.3	9	Cys <sup>37</sup> , Lys <sup>84</sup> , Lys <sup>84</sup> , Arg <sup>88</sup> , Arg <sup>88</sup> , Gln <sup>174</sup> , Asp <sup>40</sup> , Thr <sup>75</sup> , Asp <sup>40</sup> , Asp <sup>40</sup> , Asp <sup>195</sup> , Asp <sup>195</sup> , Cys <sup>37</sup> , His <sup>50</sup> , Tyr <sup>36</sup> , Ala <sup>39</sup> , Pro <sup>53</sup>	Lys <sup>84</sup> (2.24)
10	-9.4	4	Lys <sup>84</sup> , Lys <sup>84</sup> , Arg <sup>88</sup> , Asp <sup>177</sup> , Asp <sup>80</sup> , Asp <sup>80</sup> , Leu <sup>70</sup>	Lys <sup>84</sup> (2.50)
<i>Aspartic proteinase from Candida albicans</i> (PDB ID: 2QZW)				
1	-5.2	5	Asp <sup>218</sup> , Thr <sup>221</sup> , Asp <sup>218</sup> , Asp <sup>218</sup> , Asp <sup>86</sup>	Asp <sup>86</sup> (2.13)
2	-6.2	6	Gly <sup>85</sup> , Asn <sup>131</sup> , Arg <sup>192</sup> , Arg <sup>195</sup> , Thr <sup>221</sup> , Glu <sup>193</sup>	Asn <sup>131</sup> (2.01)
3	-5.7	5	Asn <sup>131</sup> , Arg <sup>195</sup> , Thr <sup>221</sup> , Asp <sup>32</sup> , Gly <sup>34</sup>	Asp <sup>32</sup> (2.14)
4	-4.1	2	Gly <sup>220</sup> , Glu <sup>193</sup> , Asp <sup>86</sup> , Asp <sup>218</sup> , Ile <sup>30</sup> , Ile <sup>123</sup>	Glu <sup>193</sup> (2.42)
5	-0.3	3	Ser <sup>35</sup> , Gly <sup>220</sup> , Gly <sup>220</sup> , Asp <sup>86</sup> , Asp <sup>218</sup> , Asp <sup>218</sup> , Gly <sup>85</sup> , Tyr <sup>84</sup> , Leu <sup>216</sup> , Ala <sup>335</sup>	Gly <sup>220</sup> (1.87)
6	-7.8	2	Arg <sup>195</sup> , Asp <sup>86</sup> , Asp <sup>86</sup> , Asp <sup>218</sup> , Asp <sup>218</sup> , Gly <sup>85</sup> , Leu <sup>216</sup> , Ala <sup>335</sup>	Asp <sup>86</sup> (2.60)
7	26.3	4	Asp <sup>86</sup> , Asp <sup>218</sup> , Leu <sup>217</sup> , Thr <sup>33</sup> , Ser <sup>35</sup> , Thr <sup>221</sup> , Arg <sup>192</sup> , Glu <sup>193</sup> , Leu <sup>216</sup> , Leu <sup>216</sup>	Thr <sup>221</sup> (1.47)
8	32.6	6	Gly <sup>34</sup> , Gly <sup>34</sup> , Gly <sup>220</sup> , Gly <sup>220</sup> , Glu <sup>193</sup> , Ala <sup>303</sup> , Gly <sup>220</sup> , Asp <sup>218</sup> , Asp <sup>218</sup> , Thr <sup>221</sup> , Ile <sup>305</sup> , Leu <sup>216</sup> , Ala <sup>303</sup> , Ile <sup>305</sup> , Ala <sup>335</sup>	Gly <sup>220</sup> (2.47)
9	31.2	2	Glu <sup>193</sup> , Asp <sup>218</sup> , Glu <sup>193</sup> , Asp <sup>218</sup> , Ser <sup>35</sup> , Gly <sup>85</sup> , Ser <sup>35</sup> , Thr <sup>221</sup> , Ser <sup>336</sup> , Asp <sup>32</sup> , Asp <sup>32</sup> , Ile <sup>123</sup> , Tyr <sup>84</sup> , Tyr <sup>84</sup> , Ile <sup>123</sup> , Ile <sup>30</sup>	Ser <sup>35</sup> (1.66)
10	-7.5	4	Gly <sup>220</sup> , Gly <sup>34</sup> , Glu <sup>193</sup> , Ala <sup>303</sup> , Asp <sup>218</sup> , Asp <sup>218</sup> , Leu <sup>216</sup> , Ala <sup>303</sup> , Ala <sup>335</sup>	Glu <sup>193</sup> (2.10)
<i>Wheat germ agglutinin</i> (PDB ID: 2UVO)				
1	-5.1	8	Arg <sup>45</sup> , Arg <sup>45</sup> , Gln <sup>49</sup> , Tyr <sup>66</sup> , NAG <sup>1174</sup> , Tyr <sup>64</sup> , NDG <sup>1173</sup> , NA <sup>1174</sup>	Tyr <sup>64</sup> (2.32)
2	3.2	6	Cys <sup>55</sup> , Asn <sup>58</sup> , Asn <sup>58</sup> , Gln <sup>59</sup> , Gln <sup>59</sup> , Gln <sup>59</sup> , Pro <sup>82</sup> , Ile <sup>87</sup> , Phe <sup>69</sup> , Pro <sup>82</sup> , Leu <sup>102</sup>	Gln <sup>59</sup> (1.72)
3	-1.1	5	Ser <sup>43</sup> , Arg <sup>45</sup> , NDG <sup>1173</sup> , NAG <sup>1174</sup> , Ser <sup>43</sup> , Thr <sup>42</sup> , Ser <sup>43</sup> , Tyr <sup>66</sup>	Ser <sup>43</sup> (1.92)
4	-4.8	1	Tyr <sup>66</sup> , NAG <sup>1174</sup> , Tyr <sup>64</sup>	Tyr <sup>66</sup> (2.15)
5	4.8	3	Cys <sup>55</sup> , Gln <sup>59</sup> , Cys <sup>55</sup> , Leu <sup>102</sup> , Gly <sup>81</sup> , Phe <sup>69</sup> , Pro <sup>99</sup> /Asn <sup>100</sup> , Pro <sup>82</sup> , Pro <sup>99</sup> , Leu <sup>102</sup> , Pro <sup>82</sup> , Ile <sup>87</sup> , Pro <sup>99</sup>	Cys <sup>55</sup> (2.00)
6	-6.9	2	Arg <sup>45</sup> , Tyr <sup>64</sup> , Tyr <sup>64</sup> , Tyr <sup>64</sup> , Tyr <sup>66</sup>	Tyr <sup>64</sup> (1.74)
7	15.4	6	Gly <sup>70</sup> , Gly <sup>52</sup> , Gln <sup>59</sup> , Cys <sup>83</sup> , Ala <sup>85</sup> , Cys <sup>83</sup> , Gly <sup>81</sup> , Cys <sup>110</sup> , Cys <sup>83</sup> , Cys <sup>55</sup> , Cys <sup>61</sup> , Asn <sup>100</sup> , Gln <sup>79</sup> /Gly <sup>80</sup> , Pro <sup>82</sup> , Cys <sup>60</sup> , Cys <sup>74</sup> , Pro <sup>99</sup> , Pro <sup>99</sup>	Cys <sup>83</sup> (1.75)
8	19.8	6	Ser <sup>43</sup> , Ser <sup>43</sup> , Lys <sup>44</sup> , Lys <sup>44</sup> , Gly <sup>38</sup> , Gln <sup>59</sup> , Thr <sup>42</sup> , Lys <sup>44</sup> , Gly <sup>38</sup> , Cys <sup>103</sup> , Cys <sup>117</sup> , Gly <sup>113</sup> /Ser <sup>114</sup> , Gly <sup>113</sup> /Ser <sup>114</sup> , Lys <sup>44</sup> , Cys <sup>55</sup> , Cys <sup>67</sup> , Cys <sup>117</sup> , Leu <sup>112</sup> , Ala <sup>125</sup> , Ala <sup>39</sup>	Lys <sup>44</sup> (2.15)
9	16	6	Gly <sup>81</sup> , Ile <sup>87</sup> , Asn <sup>100</sup> , Asn <sup>58</sup> , Cys <sup>110</sup> , Gly <sup>52</sup> , Gly <sup>47</sup> , Gly <sup>80</sup> , Gly <sup>81</sup> , Asn <sup>100</sup> , Ala <sup>53</sup> , Gln <sup>79</sup> , Phe <sup>69</sup> , Phe <sup>69</sup> , Phe <sup>69</sup> , Pro <sup>82</sup> , Ile <sup>87</sup> , Pro <sup>82</sup> , Ile <sup>87</sup> , Pro <sup>82</sup> , Leu <sup>102</sup>	Asn <sup>58</sup> (1.67)
10	6.3	3	Arg <sup>45</sup> , Tyr <sup>66</sup> , NAG <sup>1174</sup> , Tyr <sup>64</sup>	Tyr <sup>66</sup> (1.92)

Another caffeic acid derivative was present and its fragmentation gave as the base peak an ion at  $m/z$  of 179, indicating a hexose linked to the acidic moiety (compound 2). Hibiscus acid (compound 1) was also present; it is the lactone derivative of hydroxycitric acid and fragment losing a water molecule and the  $\text{CO}_2$ . The presence of these molecules in *Hibiscus* extracts was already reported in the literature with the exception of cyanidin 3-*O*-glucoside; in

fact, the sambubioside derivative was generally detected [36, 46, 47].

The obtained results are in agreement with those previously described in the international bibliography concerning these two studied plants. In this way, it has been demonstrated that the crude extract of *Hibiscus* plant has an antibacterial activity directed against strains of *Streptococcus mutans* isolated from the oral cavity with a minimal

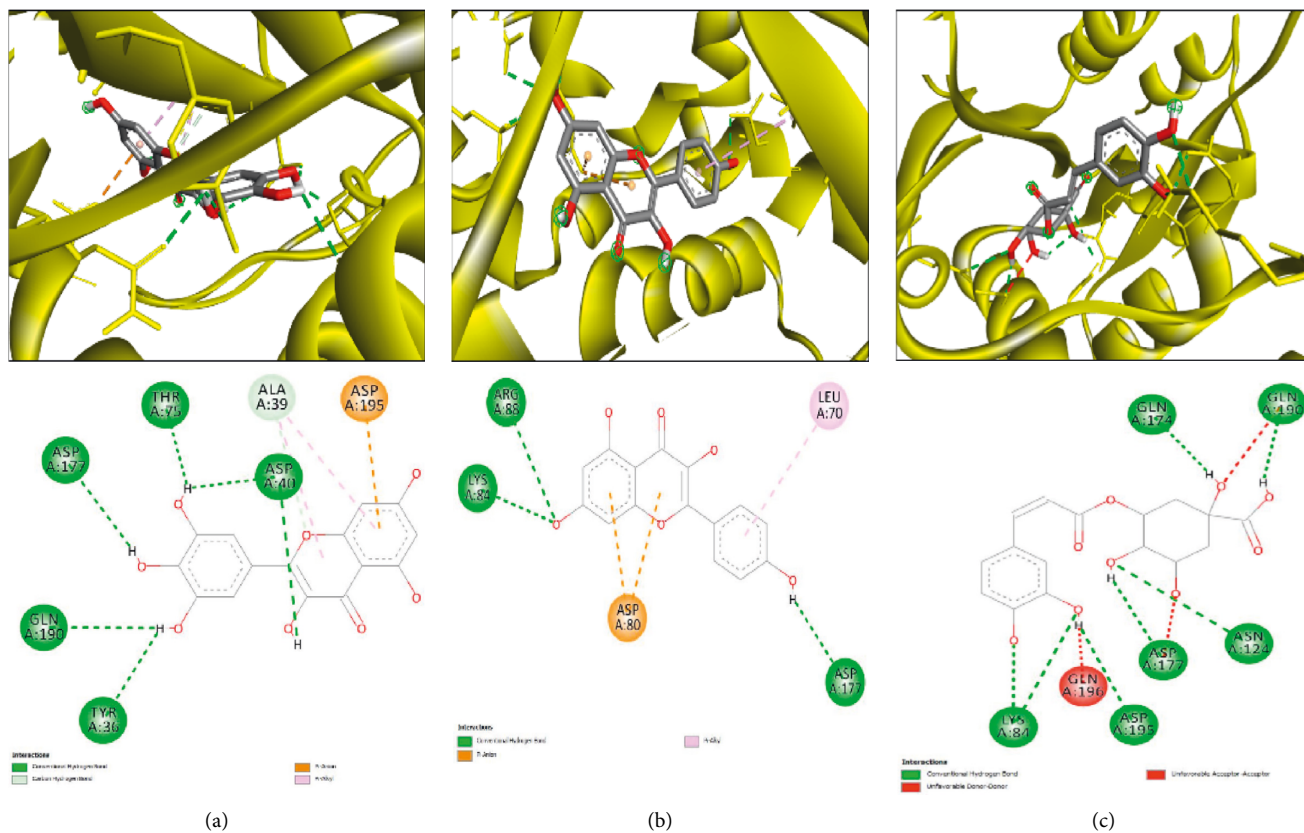


FIGURE 2: 3D illustration (a-c) and the corresponding 2D diagram of interactions (a'-c') for the compounds with the best docking scores of 13, 17, and 9 ( $-9.6$ ,  $-9.4$ , and  $-9.1$  kcal/mol) with the active site of 1JJ.

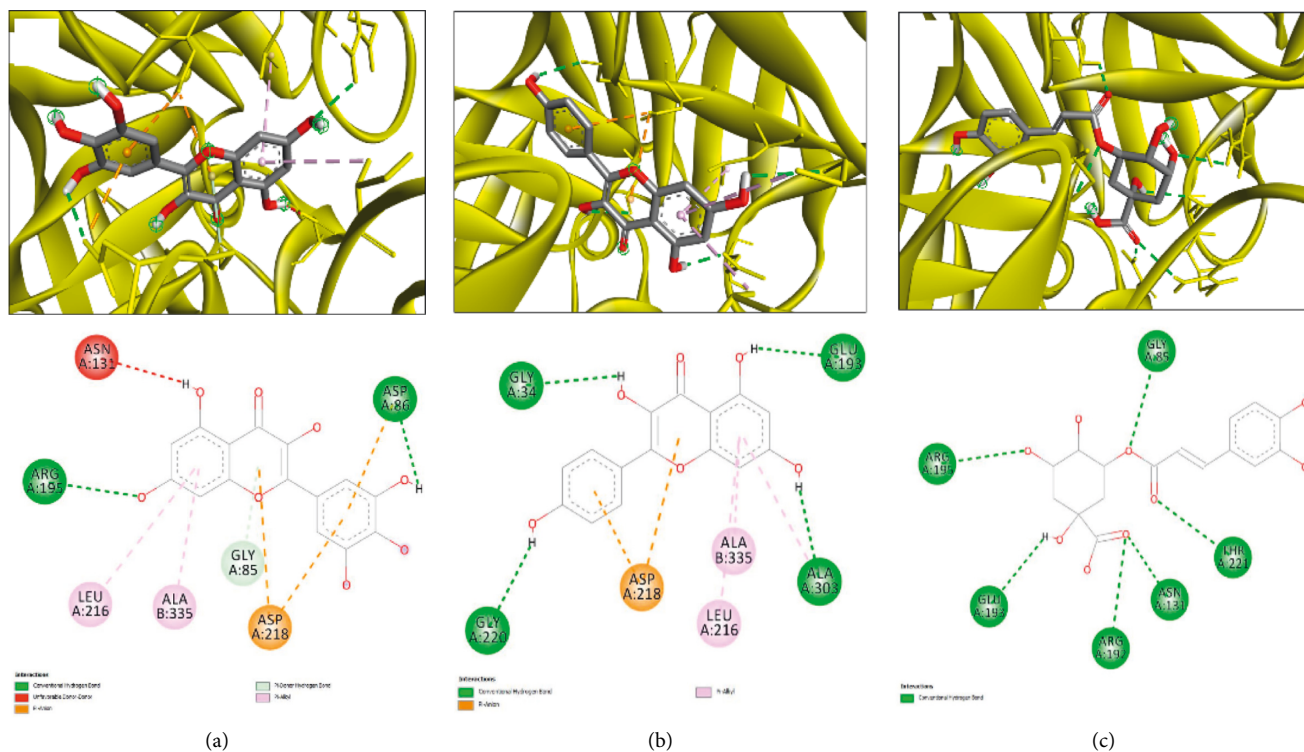


FIGURE 3: 3D illustration (a-c) and the corresponding 2D diagram of interactions (a'-c') for the compounds with the best docking scores of 13, 17, and 9 ( $-7.8$ ,  $-7.5$ , and  $-6.2$  kcal/mol) with the active site of 2QZW.



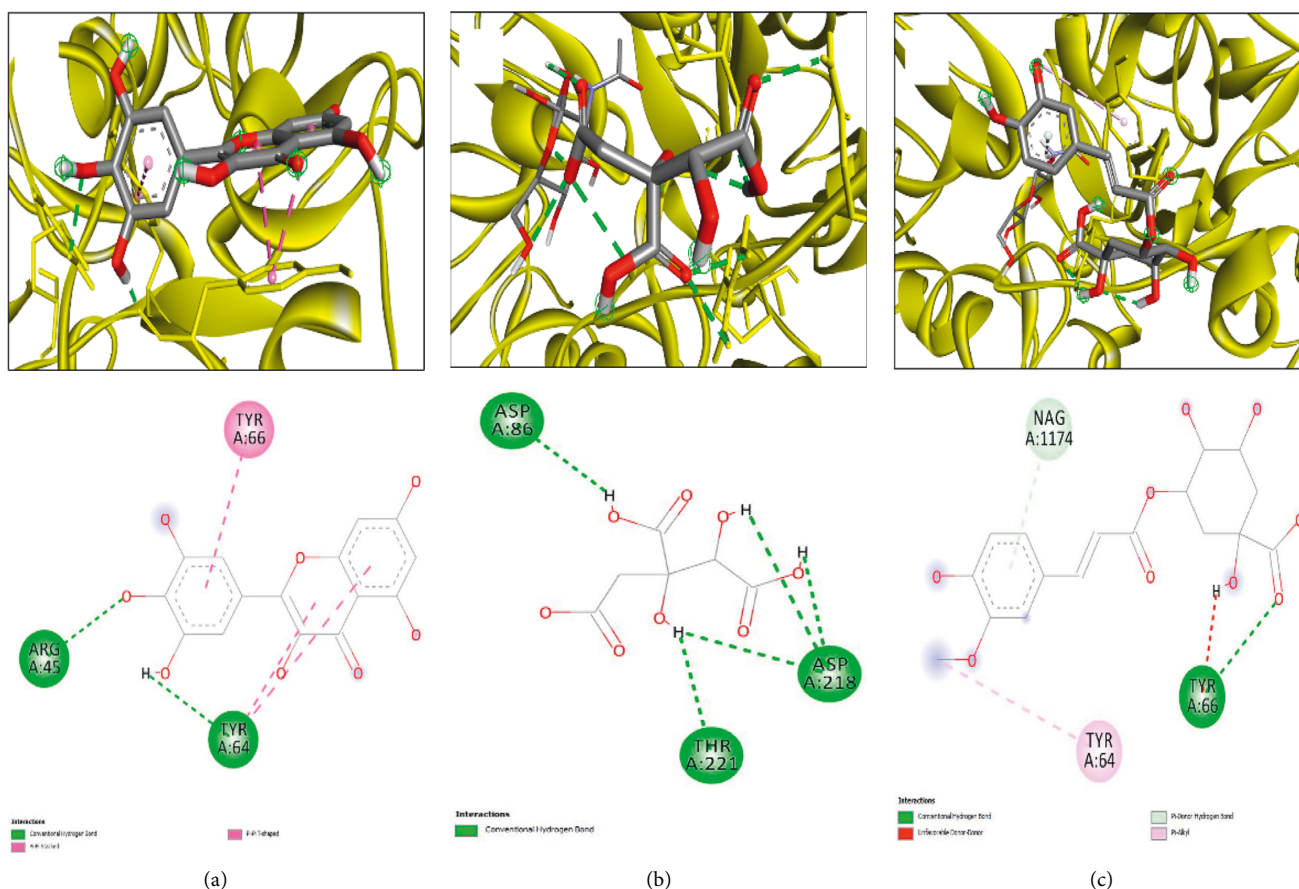


FIGURE 4: 3D illustration (a–c) and the corresponding 2D diagram of interactions (a'–c') for the compounds with the best docking scores of 13, 8, and 11 (–6.9, –5.1, and –4.8 kcal/mol) with the active site of 2UVO.

inhibitory concentration in the order of 2.5 mg/ml [48] and the species of *Campylobacter* sp. (*Campylobacter jejuni*, *Campylobacter coli*, and *Campylobacter fetus*) that contaminate beef, pork, and poultry meat with inhibitory concentrations ranging from 96 to 152  $\mu\text{g/ml}$  [49]. In addition, Olaley and Rocha [50] have shown that the methanol Hibiscus water extract has antibacterial activity against several Gram-positive and Gram-negative bacteria including the following species: *S. aureus*, *Bacillus stearothermophilus*, *Micrococcus luteus*, *Serratia marcescens*, *Clostridium sporogenes*, *Escherichia coli*, *K. pneumoniae*, *Bacillus cereus*, and *P. fluorescence*. This author has also shown that this same extract is not active against yeast *Candida albicans* [50].

In 2017, Quing et al. showed that the raw Hibiscus seed extract is active against three Gram-negative strains such as *Salmonella*, *Shigella*, and *Enterobacter*. In 2015, Borrás-Linares and his collaborators showed that the ethanolic extract of 25 varieties of Hibiscus was active against *E. coli*, *S. enteritidis*, *M. luteus*, and *S. aureus* strains with inhibition zones ranging from 16 to 22 mm for *S. aureus* and from 10 to 18 mm for the *M. luteus* strain. Gram-negative strains were the most resistant with an inhibition diameter ranging from 10 to 16 mm for both *E. coli* and *S. enteritidis* strains [10]. Recently, Abdallah [5] has shown that the Hibiscus

methanolic extract of calyx grown in Sudan is active against antibiotic-resistant strains of *Acinetobacter baumannii* with inhibition zone diameters of  $11.3 \pm 0.3$  and  $13.6 \pm 0.3$  mm and MIC and MBC values ranging from 25 to 50 mg/ml and 50 to 100 mg/ml, respectively. *Hibiscus* extract has also been shown to have activity against strains of *C. albicans* isolated from urinary tract infections and to inhibit biofilm formation by this yeast [11].

Both extracts show a proportional increase in the inhibition percent of the DPPH radical depending on the used concentration. These inhibition percentages exceed 50% at very low concentrations of tested extracts. The inhibition percentages reveal a proportional decrease in the DPPH radical until its total disappearance at a concentration of 10 mg/ml for all the tested extracts. From the curves of the various extracts, the concentration of antioxidant necessary to remove 50% of a quantity of DPPH (at equilibrium), it is the effective concentration ( $EC_{50}$ ). The low  $EC_{50}$  values indicate the effectiveness of the extract and thus are a better and powerful antioxidant. The  $EC_{50}$  values calculated for the DPPH activity are 2.793 and 2.471 mg/ml for aqueous and methanolic HS extracts, respectively. The antioxidant activity is associated with the phenolic composition, which is in agreement with our results, since the extracts, which have higher phenolic compound contents, are the extracts having

the more pronounced antioxidant activity [51]. The results recorded for the estimation of the anti-swarming activity proved that the tested extracts significantly decreased the mobility of PAO1.

The molecular docking approach showed that for H-bond interactions, which are considerably associated with pharmaceutical effects and drug design [29, 31, 32, 44], the highest number of H-bonds was found with Hibiscus acid (Lys<sup>84</sup>, Arg<sup>88</sup>, Arg<sup>88</sup>, Tyr<sup>170</sup>, Gln<sup>174</sup>, Gln<sup>196</sup>, Asp<sup>80</sup>, Gly<sup>38</sup>, Gln<sup>196</sup>, Asp<sup>80</sup>, and Gln<sup>196</sup>) and quercetin 3-O-glucoside (Asp<sup>40</sup>, Asn<sup>124</sup>, Gln<sup>174</sup>, Gln<sup>174</sup>, Gly<sup>193</sup>, Gln<sup>196</sup>, Asp<sup>177</sup>, Asp<sup>177</sup>, Asp<sup>195</sup>, Gly<sup>49</sup>, and Gln<sup>190</sup>). The latter complex was reinforced with a supplementary network of interactions involving His<sup>50</sup> and Ala<sup>39</sup> (twice for each) and Gly<sup>38</sup> and Asp<sup>40</sup> (once for each). These compounds established 11 conventional H-bonds with 1JJ, particularly with some key residues such as Asp<sup>40</sup>, Asp<sup>80</sup>, and Gln<sup>196</sup>. Furthermore, all the compounds were deeply embedded within the pocket region and showed close vicinity to the targeted proteins. For instance, the close vicinity was predicted for 1JJ-quercetin 7-O-rutinoside (1.57 Å), 2QZW-quercetin 7-O-rutinoside (1.47 Å), and 2UVO-3-caffeoylquinic acid (1.72 Å). In this context, it has been reported that closely related ligand-amino acid/receptor complexes may enhance the biological activity [31–33, 44]. Besides, for each targeted receptor, most of the identified compounds were predicted to occupy almost the same region, which may support the possible synergistic effects. In fact, it was reported that the use of the whole plant extract was suggested to be much better [32, 34, 43]. Overall, the *in silico* showed that the biological effect of *H. sabdariffa* compounds are thermodynamically possible. The computationally proved effects include (i) antibacterial via tyrosyl-tRNA synthetase from *S. aureus*, which is largely responsible for hospital-acquired infections [52]; (ii) antifungal as assessed against the secreted aspartic protease (SAP-1) of *C. albicans*; and (iii) anti-quorum sensing through the wheat germ agglutinin. Such effects, explored using *in vitro* and/or *in vivo* approaches, would be of crucial importance and support our findings. The *in silico* findings, particularly the molecular interactions between ligands and receptors, would be confirmed and validated by molecular dynamic simulations.

This study demonstrated also that both Hibiscus extracts inhibit the swarming motility of *P. aeruginosa* PAO1. Swarming motility is strongly involved in pathogenesis by aiding in the attachment of *P. aeruginosa* to the host tissue and colonizing the surfaces of the medical devices such as catheters [53]. Swimming is another major form of *P. aeruginosa* PAO1 motility, in which bacteria swim in aqueous environments via the flagellum [54]. *P. aeruginosa* exhibits swarming motility, which helps in initial attachment and later in relocation of biofilm from one site to another [55]. Moreover, swarming motility is important in early stages of biofilm formation by *P. aeruginosa* cells and confers to bacteria an extra advantage in tolerating the antibiotics [56]. In this study, it has been found that the exposure of PAO1 with Hibiscus extracts significantly impaired swarming motility of this bacterium. This finding is consistent with other studies that proved the repression of

swarming of *P. aeruginosa* PAO1 by clove extracts and ginseng [57].

## 5. Conclusions

The results obtained indicate that *H. sabdariffa* L. is rich in natural antioxidant compounds, antimicrobial agent, and anti-swarming factor. Taken together, these biological properties may allow the tested extracts from *H. sabdariffa* to be considered as having the potential to be candidate in the design of new therapeutic strategies for microbial infections, and may lead to the development of novel bioactive molecules for industrial needs. Further studies, such as the use of other isolation and purification techniques of the active compounds and *in vivo* studies, would help to elucidate the mode of action of the observed beneficial effects of the aqueous and methanolic extracts.

## Data Availability

All data generated or analyzed during this study are included in this article.

## Conflicts of Interest

The authors declare no conflicts of interest.

## Acknowledgments

AME extends his appreciation to the Deanship of Scientific Research at Jouf University for funding his work through research grant number: DSR-2021-01-0366.

## References

- [1] B. H. Ali, N. A. Wabel, and G. Blunden, "Phytochemical, pharmacological and toxicological aspects of Hibiscus sabdariffa L.: a review," *Phytotherapy Research*, vol. 19, no. 5, pp. 369–375, 2005.
- [2] M. Battino, F. Giampieri, D. Cianciosi et al., "The roles of strawberry and honey phytochemicals on human health: a possible clue on the molecular mechanisms involved in the prevention of oxidative stress and inflammation," *Phytomedicine*, vol. 86, Article ID 153170, 2021.
- [3] E. O. Farombi and A. Fakoya, "Free radical scavenging and antigenotoxic activities of natural phenolic compounds in dried flowers of Hibiscus sabdariffa L.," *Molecular Nutrition & Food Research*, vol. 49, pp. 1120–1128, 2005.
- [4] T. Panda, N. Mishra, and B. K. Pradhan, "Folk Knowledge on Medicinal Plants Used for the Treatment of Skin Diseases in Bhadrak District of Odisha, India," *Medicinal & Aromatic Plants*, vol. 5, 2016.
- [5] E. M. Abdallah, "Antibacterial activity of Hibiscus sabdariffa L. calyces against hospital isolates of multidrug resistant *Acinetobacter baumannii*," *Journal of Acute Disease*, vol. 5, no. 6, pp. 512–516, 2016.
- [6] A. S. Gibot, "Fighting the enemy properly," *Critical Care Medicine*, vol. 32, pp. 1223–1224, 2004.
- [7] S. A. Rogers, R. W. Huigens III, J. Cavanagh, and C. Melander, "Synergistic effects between conventional antibiotics and 2-aminoimidazole-derived antibiofilm agents," *Antimicrobial Agents and Chemotherapy*, vol. 10, pp. 2112–2118, 2010.



- [8] T. R. De Kievit, R. Gillis, S. Marx, C. Brown, and B. H. Iglewski, "Quorum-sensing genes in *Pseudomonas aeruginosa* biofilms: their role and expression patterns," *Applied and Environmental Microbiology*, vol. 67, pp. 1865–1873, 2001.
- [9] S. O. Babalola, A. O. Babalola, and O. C. Aworh, "Compositional attributes of the calyces of roselle (*Hibiscus sabdariffa* L.," *Journal of Food Technology in Africa*, vol. 6, no. 4, pp. 133–134, 2001.
- [10] I. I. Borrás-Linares, S. D. Fernández-Arroyo, P. A. Arráez-Roman et al., "Characterization of phenolic compounds, anthocyanidin, antioxidant and antimicrobial activity of 25 varieties of Mexican Roselle (*Hibiscus sabdariffa*)," *Industrial Crops and Products*, vol. 69, pp. 385–394, 2015.
- [11] I. Alshami and A. E. Alharbi, "Antimicrobial activity of *Hibiscus sabdariffa* extract against uropathogenic strains isolated from recurrent urinary tract infections," *Asian Pacific Journal of Tropical Disease*, vol. 4, no. 4, pp. 317–322, 2014.
- [12] P. N. Fauziyah, E. Y. Sukandar, and D. K. Ayuningtyas, "Combination effect of antituberculosis drugs and ethanolic extract of selected medicinal plants against multi-drug resistant *Mycobacterium tuberculosis* isolates," *Scientia Pharmaceutica*, vol. 85, no. 1, pp. 10–14, 2017.
- [13] B. J. Adegunloye, J. O. Omoniyi, O. A. Owolabi, O. P. Ajagbonna, O. A. Sofola, and H. A. Coker, "Mechanisms of the blood pressure lowering effect of the calyx extract of *Hibiscus sabdariffa* in rats," *African Journal of Medicine & Medical Sciences*, vol. 25, pp. 235–238, 1996.
- [14] M. B. Ali, W. M. Salih, A. H. Mohamed, and A. M. Homeida, "Investigation of the antispasmodic potential of *Hibiscus sabdariffa* calyces," *Journal of Ethnopharmacology*, vol. 31, no. 2, pp. 249–257, 1991.
- [15] S. Zhou, R. Sauve, T. Fish, and T. W. Thannhauser, "Salt-induced and salt-suppressed proteins in tomato leaves," *Journal of the American Society for Horticultural Science*, vol. 134, no. 2, pp. 289–294, 2009.
- [16] A. Malacrida, D. Maggioni, A. Casseti, G. Nicolini, G. Cavaletti, and M. Miloso, "Antitumoral effect of *Hibiscus sabdariffa* on human squamous cell carcinoma and multiple myeloma cells," *Nutrition and Cancer*, vol. 68, no. 7, pp. 1161–1170, 2016.
- [17] C. J. Wang, J. M. Wang, W. L. Lin, C. Y. Chu, F. P. Chou, and T. H. Tseng, "Protective effect of *Hibiscus* anthocyanins against tert-butyl hydroperoxide-induced hepatic toxicity in rats," *Food and Chemical Toxicology*, vol. 38, pp. 411–416, 2000.
- [18] M. Herranz-López, M. Olivares-Vicente, M. Boix-Castejón, N. Caturla, E. Roche, and V. Micol, "Differential effects of a combination of *Hibiscus sabdariffa* and *Lippia citriodora* polyphenols in overweight/obese subjects: a randomized controlled trial," *Scientific Reports*, vol. 9, no. 1, pp. 1–12, 2019.
- [19] J. Joven Jorge, E. Espinel, A. Rull et al., "Plant-derived polyphenols regulate expression of miRNA paralogs miR-103/107 and miR-122 and prevent diet-induced fatty liver disease in hyperlipidemic mice," *Biochimica et Biophysica Acta (BBA) - General Subjects*, vol. 1820, no. 7, pp. 894–899, 2012.
- [20] J. Joven, I. March, E. Espinel et al., "*Hibiscus sabdariffa* extract lowers blood pressure and improves endothelial function," *Molecular Nutrition & Food Research*, vol. 58, no. 6, pp. 1374–1378, 2014.
- [21] F. Haddaji, A. Papetti, E. Noumi et al., "Bioactivities and in silico study of *Pergularia tomentosa* L. phytochemicals as potent antimicrobial agents targeting type IIA topoisomerase, TyrRS, and Sap1 virulence proteins," *Environmental Science and Pollution Research*, vol. 28, no. 20, pp. 25349–25367, 2021.
- [22] R. Julkunen-Tiitto, "Phenolic constituents in the leaves of northern willows: methods for the analysis of certain phenolics," *Journal of Agricultural and Food Chemistry*, vol. 33, no. 2, pp. 213–217, 1985.
- [23] R. A. Moraes-de-Souza, T. L. C. Oldoni, M. A. B. Regitano-d'Arce, and S. M. Alencar, "Antioxidant activity and phenolic composition of herbal infusions consumed in Brazil activid and antioxidante y compuestos fenólicos en infusiones herbarias consumid as en Brasil," *CyTA - Journal of Food*, vol. 6, no. 1, pp. 41–47, 2008.
- [24] R. Re, N. Pellegrini, A. Proteggente, A. Pannala, M. Yang, and D. C. Rice-Evans, "Antioxidant activity applying an improved ABTS radical cation decolorization assay," *Free Radical Biology and Medicine*, vol. 26, pp. 1231–1237, 1999.
- [25] M. Snoussi, N. Trabelsi, A. Dehmeni et al., "Phytochemical analysis, antimicrobial and antioxidant activities of *Allium roseum* var. *odoratissimum* (Desf.) Coss extracts," *Industrial Crops and Products*, vol. 89, pp. 533–542, 2016.
- [26] E. Noumi, M. Snoussi, H. Hajlaoui, E. Valentin, and A. Bakhrouf, "Antifungal properties of *Salvadora persica* and *Juglans regia* L. extracts against oral *Candida* strains," *European Journal of Clinical Microbiology & Infectious Diseases*, vol. 29, no. 1, pp. 81–88, 2010.
- [27] B. Djihane, N. Wafa, S. Elkhamssa, A. E. Maria, and Z. M. Mihoub, "Chemical constituents of *Helichrysum italicum* (Roth) G. Don essential oil and their antimicrobial activity against Gram-positive and Gram-negative bacteria, filamentous fungi and *Candida albicans*," *Saudi Pharmaceutical Journal*, vol. 25, no. 5, pp. 780–787, 2017.
- [28] M. Zahin, S. Hasan, F. Aqil, M. S. A. Khan, F. M. Husain, and I. Ahmad, "Screening of certain medicinal plants from India for their anti-quorum sensing activity," *Indian Journal of Experimental Biology*, vol. 48, no. 12, pp. 1219–1224, 2010.
- [29] K. Hchicha, M. Korb, R. Badraoui, and H. Naili, "A novel sulfate-bridged binuclear copper (II) complex: structure, optical, ADMET and in vivo approach in a murine model of bone metastasis," *New Journal of Chemistry*, vol. 45, no. 31, pp. 13775–13784, 2021.
- [30] I. M. M. Othman, M. A. M. Gad-Elkareem, H. A. Radwan et al., "Synthesis, structure-activity relationship and in silico studies of novel pyrazolothiazole and thiazolopyridine derivatives as prospective antimicrobial and anticancer agents," *ChemistrySelect*, vol. 6, no. 31, pp. 7860–7872, 2021.
- [31] A. Akacha, R. Badraoui, T. Rebai, and L. Zourgui, "Effect of *Opuntia ficus indica* extract on methotrexate-induced testicular injury: a biochemical, docking and histological study," *Journal of Biomolecular Structure and Dynamics*, pp. 1–11, 2020.
- [32] R. Badraoui, M. Adnan, F. Bardakci, and M. M. Alreshidi, "Chloroquine and hydroxychloroquine interact differently with ACE2 domains reported to bind with the coronavirus spike protein: mediation by ACE2 polymorphism," *Molecules*, vol. 26, no. 3, p. 673, 2021.
- [33] N. Zammal, M. Saeed, N. Bouali et al., "Antioxidant and anti-inflammatory effects of zingiber officinale roscoe and allium subhirsutum: in silico, biochemical and histological study," *Foods*, vol. 10, no. 6, p. 1383, 2021.
- [34] M. Alreshidi, E. Noumi, L. Bouslama et al., "Phytochemical screening, antibacterial, antifungal, antiviral, cytotoxic, and anti-quorum-sensing properties of *teucrium polium* L. Aerial parts methanolic extract," *Plants*, vol. 9, no. 11, 2020.

- [35] D. Schwefel, C. Maierhofer, J. G. Beck et al., "Structural basis of multivalent binding to wheat germ agglutinin," *Journal of the American Chemical Society*, vol. 132, no. 25, pp. 8704–8719, 2010.
- [36] D. Amaya-Cruz, I. F. Pérez-Ramírez, J. Pérez-Jiménez, G. M. Nava, and R. Reynoso-Camacho, "Comparison of the bioactive potential of Roselle (*Hibiscus sabdariffa* L.) calyx and its by-product: phenolic characterization by UPLC-QTOF MSE and their anti-obesity effect in vivo," *Food Research International*, vol. 126, Article ID 108589, 2019.
- [37] C. Rodríguez-Medina, B. D. Raúl, M. M. Vicente et al., "Direct characterization of aqueous extract of *Hibiscus sabdariffa* using HPLC with diode array detection coupled to ESI and ion trap MS," *Journal of Separation Science*, vol. 32, no. 20, 2009.
- [38] C. Carazzone, D. Mascherpa, G. Gazzani, and A. Papetti, "Identification of phenolic constituents in red chicory salads (*Cichorium intybus*) by high-performance liquid chromatography with diode array detection and electrospray ionisation tandem mass spectrometry," *Food Chemistry*, vol. 138, pp. 1062–1071, 2013.
- [39] P. Shi, Q. He, Y. Song, H. Qu, and Y. Cheng, "Characterization and identification of isomeric flavonoid O-diglycosides from genus *Citrus* in negative electrospray ionization by ion trap mass spectrometry and time-of-flight mass spectrometry," *Analytica Chimica Acta*, vol. 598, no. 1, 2007.
- [40] S. Fernández-Arroyo, I. C. Rodríguez-Medina, R. Beltrán-Debón et al., "Quantification of the polyphenolic fraction and in vitro antioxidant and in vivo anti-hyperlipemic activities of *Hibiscus sabdariffa* aqueous extract," *Food Research International*, vol. 44, pp. 1490–1495, 2011.
- [41] D. Kalembe and A. Kunicka, "Antibacterial and antifungal properties of essential oils," *Current Medicinal Chemistry*, vol. 10, no. 10, pp. 813–829, 2003.
- [42] M. Allouche, S. Ishak, M. Ben Ali et al., "Molecular interactions of polyvinyl chloride microplastics and beta-blockers (diltiazem and bisoprolol) and their effects on marine meiofauna: combined in vivo and modeling study," *Journal of Hazardous Materials*, vol. 431, Article ID 128609, 2022.
- [43] R. Badraoui, M. Saoudi, W. S. Hamadou et al., "Antiviral effects of Artemisinin and its derivatives against SARS-CoV-2 main proteases: computational evidences and interactions with ACE2 allelic variants," *Pharmaceuticals*, vol. 15, no. 2, p. 129, 2022.
- [44] N. Mhadhbi, N. Issaoui, W. S. Hamadou et al., "Physicochemical properties, pharmacokinetics, molecular docking and in-vitro pharmacological study of a cobalt (II) complex based on 2-aminopyridine," *ChemistrySelect*, vol. 7, no. 3, Article ID e202103592, 2022.
- [45] M. N. Clifford, W. Zheng, and N. Kuhnert, "Profiling the chlorogenic acids of aster by HPLC-MSn, Phytochemical Analysis," *An International Journal of Plant Chemical and Biochemical Techniques*, vol. 17, no. 6, pp. 384–393, 2006.
- [46] M. Herranz-López, M. Olivares-Vicente, J. A. Encinar et al., "Multi-targeted molecular effects of *Hibiscus sabdariffa* polyphenols: an opportunity for a global approach to obesity," *Nutrients*, vol. 9, no. 8, 2017.
- [47] D. M. Rasheed, A. Porzel, A. Frolov, H. R. El Seedi, L. A. Wessjohann, and M. A. Farag, "Comparative analysis of *Hibiscus sabdariffa* (roselle) hot and cold extracts in respect to their potential for  $\alpha$ -glucosidase inhibition," *Food Chemistry*, vol. 250, pp. 236–244, 2018.
- [48] O. C. Afolabi, F. T. Ogunsoola, and A. O. Coker, "Susceptibility of Cariogenic *Streptococcus mutans* to extracts of *Garcinia kola*, *Hibiscus sabdariffa*, and *Solanum americanum*," *West African Journal of Medicine*, vol. 27, no. 4, pp. 230–3, 2008.
- [49] M. Yin and C. Chao, "Anti-Campylobacter, anti-aerobic, and anti-oxidative effects of roselle calyx extract and protocatechuic acid in ground beef," *International Journal Of Food Microbiology*, vol. 127, 2008.
- [50] M. T. Olalye and J. B. T. Rocha, "Commonly used tropical medicinal plants exhibit distinct in vitro antioxidant activities against hepatotoxins in rat liver," *Experimental and Toxicologic Pathology*, vol. 58, no. 6, pp. 433–438, 2007.
- [51] L. M. Cheung, P. C. K. Cheung, and V. E. C. Ooi, "Antioxidant activity and total phenolics of edible mushroom extracts," *Food Chemistry*, vol. 81, no. 2, pp. 249–255, 2003.
- [52] A. Borelli, E. Ruge, J. H. Lee et al., "X-ray structures of Sap1 and Sap5: Structural comparison of the secreted aspartic proteinases from *Candida albicans*," *Proteins: Structure, Function, and Bioinformatics*, vol. 72, no. 4, pp. 1308–1319, 2008.
- [53] J. D. ShROUT, D. L. Chopp, C. L. Just, M. Hentzer, M. Givskov, and M. R. Parsek, "The impact of quorum sensing and swarming motility on *Pseudomonas aeruginosa* biofilm formation is nutritionally conditional," *Molecular Microbiology*, vol. 62, no. 5, pp. 1264–1277, 2006.
- [54] M. H. Rashid and A. Kornberg, "Inorganic polyphosphate is needed for swimming, swarming, and twitching motilities of *Pseudomonas aeruginosa*," *Proceedings of the National Academy of Sciences of the United States of America*, vol. 97, no. 9, pp. 4885–4890, 2000.
- [55] J. C. Taganna, J. P. Quanico, R. M. G. Perono, E. C. Amor, and W. L. Rivera, "Tannin-rich fraction from *Terminalia catappa* inhibits quorum sensing (QS) in *Chromobacterium violaceum* and the QS-controlled biofilm maturation and LasA staphylolytic activity in *Pseudomonas aeruginosa*," *Journal Of Ethnopharmacology*, vol. 134, no. 3, 2011.
- [56] M. T. Butler, Q. Wang, and R. M. Harshey, "Cell density and mobility protect swarming bacteria against antibiotics," *Proceedings of the National Academy of Sciences USA*, vol. 107, pp. 3776–3781, 2010.
- [57] T. Krishnan, W. F. Yin, and K. G. Chan, "Inhibition of quorum sensing-controlled virulence factor production in *Pseudomonas aeruginosa* PAO1 by Ayurveda spice clove (*Syzygium aromaticum*) bud extract," *Sensors*, vol. 12, pp. 4016–4030, 2012.

## Research Article

# Study on the Mechanism of Shenjing Guben Prescription Regulating PI3K and NRF2 Signaling Pathway in the Treatment of Immune Infertility

Handu Liu <sup>1</sup>, Jianguo Xue,<sup>2</sup> and Hui Mo<sup>1</sup>

<sup>1</sup>Faculty of Chinese Medicine, Macau University of Science and Technology, Wai Long Avenue, S.A.R. 999078, Taipa, Macau

<sup>2</sup>Andrology, Affiliated Hospital of Nanjing University of Chinese Medicine, Nanjing, China

Correspondence should be addressed to Handu Liu; handuliu2021@163.com

Received 8 January 2022; Revised 9 February 2022; Accepted 14 February 2022; Published 13 May 2022

Academic Editor: Ruchika Garg

Copyright © 2022 Handu Liu et al. This is an open access article distributed under the Creative Commons Attribution License, which permits unrestricted use, distribution, and reproduction in any medium, provided the original work is properly cited.

**Objective.** To explore the mechanism of Shenjing Guben prescription (SP) in the treatment of immune infertility by regulating PI3K-NRF2/p38 signal pathway. **Methods.** 60 adult male SD rats were randomly divided into control group (NC group), ACN group, low concentration AP intervention group (low group), middle concentration SP intervention group (middle group), and high concentration SP intervention group (high group). 12 rats in each group were administered by gavage once a day, 6 days/w, and the rats were killed after 28 days. Bilateral testis and epididymis were removed and weighed and organ coefficients were calculated, and testicular histopathological sections were prepared to evaluate the changes of testicular tissue structure. The relative expression levels of PI3K, MKK7, JNK, p38 mRNA, and protein in testis were measured by QRT-PCR and western blot. **Results.** (1) Compared with the control group, the proportion of grade A and B sperms in ACN group increased significantly, and the proportion of grade D sperm decreased significantly ( $P < 0.05$ ). After SP intervention, compared with ACN group, there was no significant difference in the proportion of sperm at all levels in low, medium, and high SP intervention groups ( $P > 0.05$ ). (2) Compared with the control group, the sperm VCL, VSL, VAP, and mad in ACN group increased significantly, and the BCF decreased significantly ( $P < 0.05$ ). After SP intervention, compared with ACN group, there was no significant difference in sperm motility parameters among low, medium, and high SP intervention groups ( $P > 0.05$ ). (3) Compared with the control group, the activities of AKP and SDH in testicular tissue of rats in ACN group decreased significantly ( $P < 0.05$ ). After SP intervention, compared with ACN group, AKP activity increased significantly and LDH activity decreased significantly in low, medium, and high SP intervention groups ( $P < 0.05$ ). (4) Compared with the control group, the expression levels of PI3K, p-PI3K, MKK7, p-MKK7, JNK, p-JNK, p38, and p-p38 proteins and the ratios of p-JNK/JNK and p-p38/p38 increased in the testis of ACN group ( $P < 0.05$ ). After SP intervention, compared with ACN group, the protein expression levels of PI3K, p-PI3K, MKK7, p-MKK7, JNK, p-JNK, p38, and p-p38 in testicular tissue of SP intervention group decreased, and the ratio of p-JNK/JNK and p-p38/p38 decreased ( $P < 0.05$ ). **Conclusion.** SP can reduce the oxidative stress of testis induced by ACN and inhibit the activation of PI3K-NRF2/p38 signal pathway.

## 1. Introduction

Acrylonitrile (ACN), also known as ethylene cyanogen, is a colorless, flammable, volatile liquid with bitter almond flavor. ACN is an important organic chemical synthetic monomer. It is an important raw material for manufacturing synthetic resin, synthetic rubber, synthetic plastics, synthetic fiber, and acrylamide [1]. ACN can also be detected in

cigarette smoke and automobile exhaust. Therefore, low-dose environmental exposure cannot be ignored. ACN and CEO can also combine with biological macromolecules such as protein or DNA to consume GSH in tissues. The depletion of GSH will reduce the antioxidant capacity of the body, and cytochrome P450 metabolizing ACN can produce more free radicals in the metabolic process, further increasing the load of oxidative stress. ACN is a highly toxic compound. It is a

mutagen and suspected carcinogen in humans. Its exposure will increase the risk of lung cancer and astrocytoma [2].

Traditional Chinese medicine recognizes that kidney deficiency and blood stasis are the fundamental pathogenesis throughout the whole process. The basic guiding principle of clinical treatment is the method of kidney activating blood circulation. Based on many years of clinical practice experience and the principle of kidney tonifying method, traditional Chinese medicine is committed to the clinical and basic research of kidney tonifying and blood activating traditional Chinese medicine in the treatment of sperm deficiency infertility. Shenjing Guben prescription consists of pilose antler, cinnamon, red ginseng, *Astragalus membranaceus*, *Rehmannia glutinosa*, polygonatum, *Polygonum multiflorum*, *Cornus officinalis*, raspberry, etc. SP can upregulate the expression of Caspase-7 in spermatozoa and inhibit the function of spermatozoa. Ginseng pill can protect spermatozoa by upregulating the expression of Caspase-7 in spermatozoa. However, the overactivation of primitive spermatheca is an important pathological mechanism leading to dor. PI3K-jnk/p38 signal pathway is to maintain the primitive spermatozoa in the static state of bubbles, and the initiation of supplementary growth is an important regulatory factor. In the dormant state of primitive spermatozoa, the activity is inhibited. Once the signal is activated, the primitive spermatozoa will be activated, growth into the vesicle pool of sperm. Granulosa cell apoptosis is the central link in the induction of sperm atresia. PI3K-jnk/p38 signaling pathway plays a key regulatory role in the apoptotic pathway. Oxidative stress is an important factor to start the apoptotic process. The essence of apoptosis is the result of the destruction of the dynamic balance between intracellular oxidation system and antioxidant system. PI3K-jnk/p38 signal pathway is the most important endogenous antioxidant stress signal pathway found so far, which is of great significance to maintain the normal growth and development of sperm [3]. Gutierrez et al. found that SP can protect mouse cardiomyocytes from injury induced by lipoteichoic acid by inhibiting the activation of JNK and p38 [4]. Zhang et al. found that SP can improve the decrease of SOD and GSH PX activity and the increase of MDA content, downregulate the expression of Caspase-3 and Bax, upregulate the expression of Bcl-2, show antioxidant and anti-apoptotic characteristics, and promote the recovery of neural function in rats after spinal cord injury [5]. Dang et al. found that SP can downregulate the expression of Caspase-3, suggesting that SP can inhibit germ cell apoptosis and reduce the inflammatory response caused by ACN by downregulating NF signal [6]. Li et al. [7]. found that SP can reduce inflammatory factors in mouse lung tissue, prevent the phosphorylation of p38 and JNK, upregulate the expression of Bcl-2, and downregulate the expression of Bax and Caspase-3, suggesting that SP can play a protective role in LPS induced acute lung injury by reducing inflammatory response, inhibiting p38 MAPK and JNK signaling pathway and apoptosis [8]. Lin et al. found that SP inhibited dopamine-induced melanocyte apoptosis by reducing the production of ROS and inhibiting the activation of JNK and p38 MAPK signaling pathways [9].

## 2. Method

**2.1. Experimental Animals.** There were 60 adult male SD rats, weighing 180~220 g. The experiment was approved by the ethics committee of our hospital. Sixty male SD rats were randomly divided into five groups with 12 rats in each group according to their body weight: control group (NC group), ACN group, low concentration SP intervention group (low group), medium concentration SP intervention group (middle group), and high concentration AP intervention group (high group). ACN and AP were prepared into the required dose with corn oil and were administered by gavage according to the gavage amount of 5 ml/kg. The gavage amount was adjusted by weighing every two days. Low, medium, and high SP intervention groups were given ACN 30 minutes after SP gavage. Once a day for 28 consecutive days, the dose selection of ACN was determined according to the previous study. SP showed antioxidant effect in rat testicular tissue in the range of 234~468 mg/kg. Therefore, this study established the model of reproductive injury induced by ACN by 46 mg/kg ACN for 28 days and intervened with 117, 234, and 351 mg/kg SP at the same time. The feeding temperature is 21~24°C, and the relative humidity is 40%~60%. The laboratory is illuminated day and night for 12 hours. It is fed with ordinary feed and can eat and drink freely.

**2.2. Sperm Density.** Select the left epididymis of 6 rats in each group, cut 3 openings laterally in the epididymis, put it into an ampoule containing 0.9% normal saline, bathe in water at 37°C for 50 minutes, and suck sperm suspension for 10 minutes. It was added to the sperm counting plate and determined by computer-aided sperm analysis (CASA). The following parameters were measured: (1) sperm density: the number of sperm per ml of semen ( $\times 10^6/\text{ml}$ ). (2) Sperm motility and mobility: sperm can be divided into four grades according to different movement modes: grade A sperm is fast linear forward moving sperm, and straight fine velocity (VSL)  $\geq 25 \mu\text{m/s}$ ; grade B spermatozoa are slow or nonlinear forward motile spermatozoa with VSL ranging from 5 to 25  $\mu\text{m/s}$ ; grade C sperms are nonforward motile sperm with VSL  $< 5 \mu\text{m/s}$ ; grade D sperms are immobile sperm. (3) Sperm viability refers to the percentage of "a + B + C" sperm in semen. (4) Sperm motility refers to the percentage of "a + B" sperm in semen.

**2.3. Determination of Testicular Tissue Marker Enzymes.** Take the right testis of 8 rats in each group, cut 100~200 mg and put it into the glass homogenizer. Add precooled 0.9% normal saline according to the ratio of tissue (g): homogenization medium (ML) = 1:9, grind it fully in ice water bath, centrifuge at 2500 rpm for 10 min, absorb the supernatant, and prepare 10% testicular tissue homogenate. Detect the activities of alkaline phosphatase (AKP), acid phosphatase (ACP), succinate dehydrogenase (SDH), and lactate dehydrogenase (LDH) according to the steps on the instructions of the kit.

**2.4. Determination of Oxidative Stress-Related Indexes.** Take 10% testicular tissue homogenate and determine the contents of GSH and MDA and the activities of SOD, GSH PX, and catalase (CAT) according to the operation steps on the manual. Take the right testicular tissue of rats with the same number, add precooled 0.9% normal saline according to the ratio of testicular tissue (g): homogenate medium (ML) = 1 : 4, grind in ice water bath to obtain 20% testicular tissue homogenate, centrifuge at 12000 rpm for 5 min, and absorb the supernatant to detect the total antioxidant capacity (T-AOC).

**2.5. RT-PCR.** RT-PCR was used to detect the mRNA expression of PI3K, MKK7, p38, JNK, Bax, and Bcl-2 in testicular tissue. Total testicular RNA was extracted with Trizol reagent. According to the supplier's instructions, use the primerscript first strand cDNA synthesis kit from 2  $\mu$ l total RNA synthesis cDNA. Use SYBR premix ex Taq  $\mu$  II kit and 10  $\mu$ l SYBR premix ex Taq for <sup>™</sup> II kit for real-time quantification <sup>™</sup>. The expression level of the gene was normalized to  $\beta$ -actin. The expression level of actin mRNA. Real-time polymerase chain reaction was performed using an applied biological system type 7500. The reaction conditions are 95°C 5 min, 95°C 30 s, 63°C 50 s, 72°C 60 s, 30 cycles, and 72°C 5 min. The relative expression of the target gene is calculated by  $2^{-\Delta\Delta CT}$ .

**2.6. Protein Expression Was Detected by Western Blot.** Total tissue protein was extracted and quantified by BCA protein analysis kit. Total protein was isolated by 10% SDS-PAGE (20  $\mu$ g) and it was transferred to polyvinylidene fluoride (PVDF) membrane. 5% skimmed milk powder was dissolved in Tris buffer solution containing 0.1% Tween 20 for blocking and then incubated with MKK7, p-MKK7, p38, p-p38, JNK, p-JNK, and Caspase-9 antibodies at 4°C overnight. On the 2nd day, the membrane was washed with PBS for 3 times, and the Goat antirabbit IgG antibody coupled with horseradish peroxidase (HRP) was incubated at room temperature for 1 h. Add an appropriate amount of ECL light solution in the darkroom for development and fixation. After scanning the strip, analyze the gray value with ImageJ software to calculate the relative expression of protein.

**2.7. Apoptosis of Rat Testicular Cells Was Detected by TUNEL Method.** Take rat testicular tissue sections for dewaxing and hydration; hydrogen peroxide is treated at room temperature for 10 min and washed with water; after incubation with protease K diluted with 0.01 mol/L TBS 1 : 200 at 37°C for 10 min, rinse with 0.01 mol/L TBS for 3 times for 5 min each time; take 1 TDT and 1 dig-d-utp respectively  $\mu$  50. Add 18  $\mu$ l labeling buffer, mix well, add it to the slices, incubate at 37°C for 2 hours, and rinse with 0.01 mol/L TBS for 3 times for 5 minutes each time; plus 50  $\mu$  L blocking solution, incubate at 37°C for 30 min and throw off the blocking solution; add biotinylated antidigoxin antibody diluted 100 times with antibody diluent and react at 37°C for 30 min. Rinse 3 times with 0.01 mol/L TBS for 5 min each time; SABC diluted 100

times with antibody diluent was added. After reacting at 37°C for 30 min, 0.01 mol/L TBS was rinsed for 4 times for 5 min each time; take one drop of A, B, and C in DAB kit, add 1 ml deionized water, mix well, add it to the slice for color development, and wash with water; hematoxylin is lightly counterstained, washed, dried, and sealed.

**2.8. Statistical Analysis.** SPSS 20.0 and GraphPad Prism 5.0 software were used for data processing. The measurement data were expressed by mean  $\pm$  standard deviation, one-way ANOVA was compared among multiple groups, and LSD test was used for pairwise comparison.  $P < 0.05$ , the difference was considered to be statistically significant.

### 3. Results

**3.1. General Conditions and Organ Coefficient Changes of Rats.** During the experiment, the rats in ACN group showed salivation, and irritability in the second week, and no abnormal behavior was observed in other groups. There was no significant difference in body weight between groups before the experiment ( $P > 0.05$ ). After the experiment, there was no significant difference in testicular wet weight and testicular organ coefficient between groups ( $P > 0.05$ ). Compared with the control group, the wet weight and organ coefficient of epididymis in ACN group were significantly lower ( $P < 0.05$ ); after SP intervention, compared with ACN group, the wet weight and organ coefficient of epididymis in low SP intervention group were significantly higher ( $P < 0.05$ ); the organ coefficient of epididymis in SP intervention group increased significantly ( $P < 0.05$ ) (Tables 1 and 2).

**3.2. Changes of Sperm Density in Rats.** There was no significant difference in sperm density between groups ( $P > 0.05$ ). Compared with the control group, the proportion of grade A and B sperm in ACN group increased significantly, and the proportion of grade D sperm decreased significantly ( $P < 0.05$ ); after SP intervention, compared with ACN group, there was no significant difference in the proportion of sperm at all levels in low, medium, and high SP intervention groups ( $P > 0.05$ ).

**3.3. Changes of Sperm Motility Parameters in Rats.** Compared with the control group, the sperm VCL, VSL, VAP, and mad in ACN group increased significantly, and the BCF decreased significantly ( $P < 0.05$ ); after AP intervention, compared with ACN group, there was no significant difference in sperm motility parameters among low, medium, and high SP intervention groups ( $P > 0.05$ ). See Figure 1.

**3.4. Morphological Changes of Rat Testis.** The pathological sections of testicular tissue of rats in each group were observed under light microscope. The seminiferous tubules in testicular tissue of rats in the control group were complete and closely arranged; spermatogenic cells at different



TABLE 1: General condition and organ coefficient changes in rats.

Group	Weight (g)	Orchis		Epididymis	
		Wet weight (g)	Organ coefficient	Wet weight (g)	Organ coefficient
NC	349.64 ± 24.20	3.15 ± 0.23	0.92 ± 0.07	1.11 ± 0.07	0.33 ± 0.04
ACN	333.64 ± 20.14	2.99 ± 0.15	0.91 ± 0.05	0.99 ± 0.07	0.31 ± 0.02
Low	329.41 ± 18.47	3.04 ± 0.28	0.93 ± 0.09	1.05 ± 0.05	0.33 ± 0.03
Middle	315.63 ± 13.87	3.08 ± 0.21	0.99 ± 0.10	0.99 ± 0.06	0.34 ± 0.04
High	312.54 ± 14.02	2.90 ± 0.56	0.93 ± 0.03	0.95 ± 0.15	0.31 ± 0.05

TABLE 2: Changes in sperm density in rats.

Group	Sperm density	Sperm movement mode			
		A level	B level	C level	D level
NC	5.73 ± 1.19	6.02 ± 2.14	11.46 ± 2.98	40.31 ± 2.58	42.31 ± 4.78
ACN	6.68 ± 2.48	12.34 ± 3.52	15.64 ± 4.20	42.12 ± 4.69	29.321 ± 8.15
Low	6.39 ± 2.87	10.57 ± 4.79	14.24 ± 4.58	42.64 ± 5.80	32.64 ± 10.42
Middle	5.97 ± 2.45	10.54 ± 4.25	14.79 ± 1.35	42.43 ± 6.25	32.65 ± 8.12
High	5.96 ± 1.42	10.53 ± 3.25	14.98 ± 2.31	43.12 ± 4.02	31.58 ± 5.61

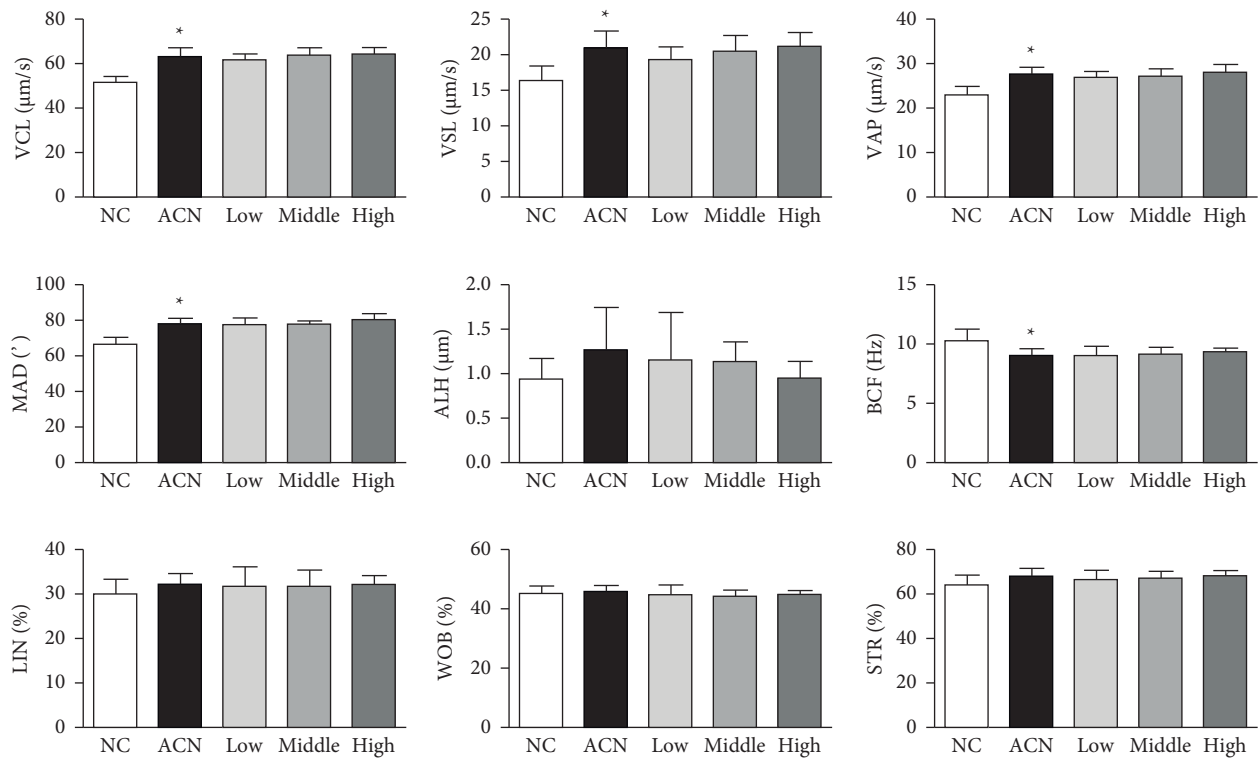


FIGURE 1: Changes in sperm motility parameters in rats.

developmental stages can be seen in the seminiferous tubules. Spermatogonia, primary spermatocytes, secondary spermatocytes, and spermatocytes can be seen from the basement membrane to the lumen. The cell layers are clear and orderly; mature sperm can be seen in the lumen; interstitial cells can be seen in groups between seminiferous tubules. In ACN group, the seminiferous tubules were atrophic and deformed, and the diameter of seminiferous tubules became smaller; the number of spermatogenic cell

layers decreased significantly, the number of primary spermatocytes and secondary spermatocytes decreased, and the number of mature sperms in the lumen was very small; the number of stromal cells decreased. In the low SP intervention group, only some seminiferous tubules were damaged, the number of spermatogenic cell layers and the number of mature sperms decreased; in the SP intervention group, the wall of spermatogenic tubules was relatively complete and arranged regularly, only a few layers of



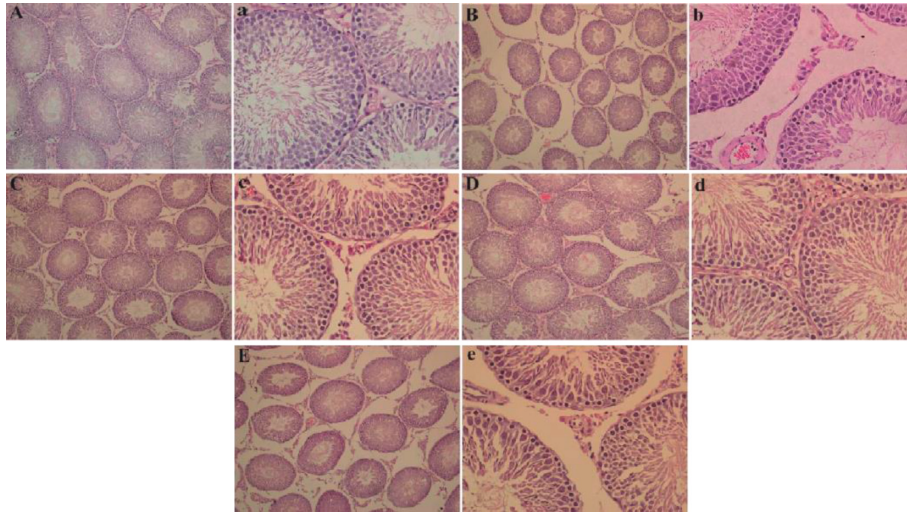


FIGURE 2: Changes in the tissue morphology of the testis in rats.

spermatogenic cells were reduced, and spermatogenic cells and mature sperm at all levels were seen in the lumen; in the high SP intervention group, the seminiferous tubules shrank and the diameter became smaller; the number and layers of spermatogenic cells decreased, the number of mature sperms decreased, and the number of stromal cells decreased.

**3.5. Changes of Marker Enzymes in Rat Testis.** Compared with the control group, the activities of AKP and SDH in testicular tissue of rats in ACN group decreased significantly ( $P < 0.05$ ); after SP intervention, compared with ACN group, AKP activity increased significantly and LDH activity decreased significantly in low, medium, and high SP intervention groups ( $P < 0.05$ ).

**3.6. Expression Level of PI3K-NRF2/p38 Pathway-Related Genes.** The results of RT-PCR showed that compared with the control group, the relative expression levels of PI3K, MKK7, JNK, and p38 mRNA in testis of rats in ACN group increased ( $P < 0.05$ ); after SP intervention, compared with ACN group, the relative expression levels of MKK7, JNK, and p38 mRNA in testicular tissue of rats in low SP intervention group decreased ( $P < 0.05$ ); the relative expression level of JNK mRNA in testicular tissue of rats in SP intervention group decreased ( $P < 0.05$ ).

**3.7. Expression Level of PI3K-NRF2/p38 Pathway-Related Proteins.** Compared with the control group, the expression levels of PI3K, p-PI3K, MKK7, p-MKK7, JNK, p-JNK, p38, and p-p38 proteins and the ratios of p-JNK/JNK and p-p38/p38 increased in the testis of ACN group ( $P < 0.05$ ); after SP intervention, compared with ACN group, the expression levels of PI3K, p-PI3K, MKK7, p-MKK7, JNK, p-JNK, p38, and p-p38 protein in testicular tissue of rats in low SP intervention group decreased, and the ratio of p-JNK/JNK and p-p38/p38 decreased ( $P < 0.05$ ); the expression levels of PI3K, p-PI3K, MKK7, p-MKK7, JNK, p-JNK, p38, and

p-p38 proteins and the ratio of p-PI3K/PI3K and p-JNK/JNK in testicular tissue of rats in middle SP intervention group decreased ( $P < 0.05$ ); the ratios of p-PI3K/PI3K and p-JNK/JNK in testicular tissue of rats in high SP intervention group decreased ( $P < 0.05$ ).

#### 4. Discussion

Sperm density, motility, and morphology are important indicators reflecting sperm quality. They can reflect the damage degree of exogenous chemicals to male reproductive system and evaluate male reproductive toxicity [10]. In this study, Casa system was used to analyze the quality of rat sperm. Casa system organically combines computer technology and advanced image processing technology. Through the observation of sperm movement, Casa system provides accurate data of various indexes of sperm quality and improves the detection speed and objectivity of results. This study found that the proportion of grade A and B sperms in ACN group increased significantly, the proportion of grade D sperm decreased significantly, and the sperm mobility and motility were significantly higher than those in the control group, suggesting that the increase of sperm motility may be caused by transient stress caused by short-term exposure to ACN [11]. There were no significant changes in sperm density, viability, and motility after SP intervention compared with ACN group, suggesting that SP had little effect on sperm density in this study, which may be related to the shorter action time [12].

Histopathological examination can reflect the damage of chemicals to target organs. It is one of the important items to evaluate the toxicity of exogenous chemicals. In this experiment, we observed that the seminiferous tubules in ACN group shrank and deformed, the number of stromal cells decreased, the layers of spermatogenic cells decreased and arranged disorderly, and the number of mature sperms in the lumen decreased [11]. The above situation of each dose of SP intervention group has been improved to a certain extent. The effect of low and medium SP intervention group is more

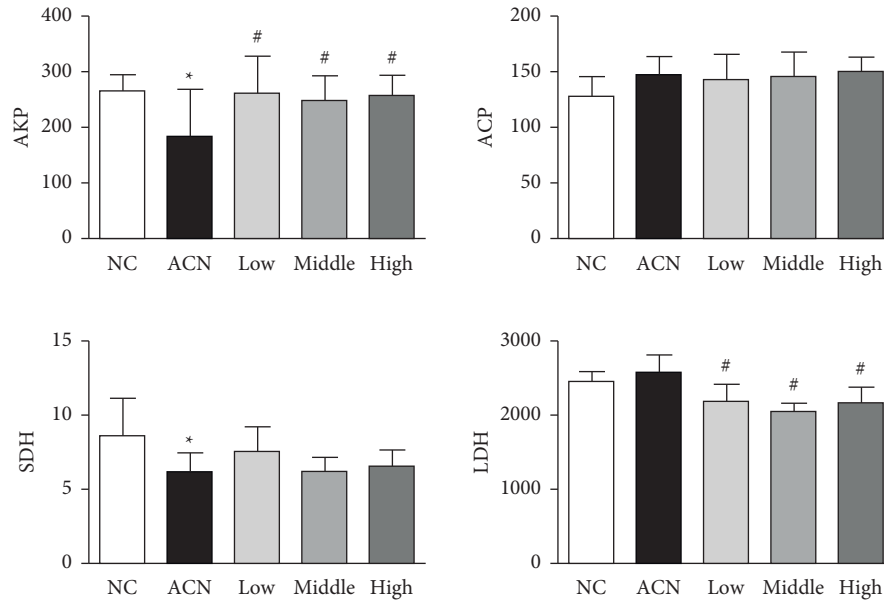


FIGURE 3: Changes in the rat testis marker enzymes.

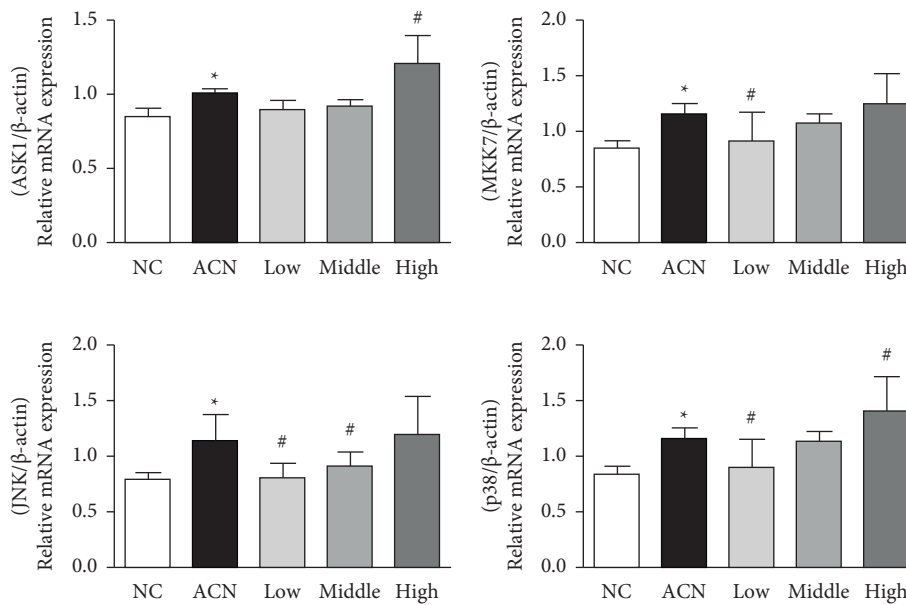


FIGURE 4: Expression levels of genes associated in the PI3K 1-NRF2/p38 pathway.

obvious, which is similar to the result of organ coefficient, suggesting that SP has a certain protective effect on testicular injury induced by ACN. KP, ACP, LDH, and SDH are testicular marker enzymes, which play an important role in spermatogenesis and maturation, and are closely related to testicular function. AKP is mainly involved in the transport of nutrients in spermatogenic cells and is closely related to the proliferation and division of spermatogenic cells [13]. ACP is related to the degeneration of spermatogenic epithelium and the phagocytosis of testicular Sertoli cells. It mostly exists in the lysosome of Sertoli cells. It has the ability to remove damaged and aging cells. It plays an important role in maintaining the normal metabolism and

physiological function of spermatogenic cells [14]. Its activity can be used as an indicator to measure whether spermatogenic disorder occurs. SDH mainly exists in the mitochondria of seminiferous tubules and spermatogenic cells. It provides energy for spermatogenic cells by catalyzing fructose into sorbitol. It plays an important role in sperm energy metabolism. Its activity can be used as an index to evaluate the function of sperm mitochondria. At the same time, it is also a marker enzyme for testicular pill maturity, sperm functional maturity, and perfect morphology. LDH belongs to glycolytic enzyme system, which is mainly distributed in seminiferous tubules and spermatogenic cells [15]. It participates in sperm energy metabolism and is also

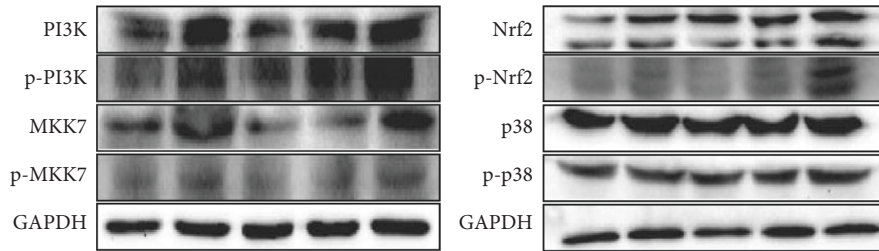


FIGURE 5: The protein expression levels associated with the PI3K-NRF2 pathway.

related to the maturation of spermatogenic epithelium. It is a marker enzyme of spermatogenic cell maturation. Xin et al. exposed male rats to ACN subchronic. The results showed that 10 mg/kg ACN could significantly increase the activity of LDH in testicular tissue and slightly increase the activities of AKP, ACP, and SDH. Then, with the increase of dose, the activities of LDH, ACP, and SDH in testicular tissue decreased [16]. The results showed that the activities of AKP and SDH decreased significantly in ACN group, indicating that ACN can affect the transport of testicular nutrients, interfere with testicular energy metabolism and the maturation of testicular spermatogenic epithelium, and cause a certain degree of damage to testis. After SP intervention, compared with ACN group, AKP activity increased significantly and LDH activity decreased significantly in low, medium, and high SP intervention groups, suggesting that SP can improve the above changes of testicular marker enzymes caused by ACN, that is, it can improve testicular energy metabolism and maturation of spermatogenic epithelium [17].

Under normal circumstances, oxidation and anti-oxidation in the body are in dynamic balance. When the free radicals produced by exogenous chemicals on the body exceed its scavenging capacity, it will lead to the excess of free radicals, the balance state will be broken, and the oxidative damage of cells and tissues will be caused [18]. ACN and its metabolite CEO can covalently combine with GSH to form adducts. At the same time, the released CN can induce the production of ROS, trigger free radical reaction, lipid peroxidation, and produce MDA and other active products. MDA is the product of lipid peroxidation. It has a strong toxic effect on the body. It can destroy the structure of biological macromolecules such as nucleic acid and protein [19]. It is an important physiological index of oxidative stress and lipid peroxidation. Sod can specifically scavenge  $O_2^-$ , inhibit oxygen free radical reaction and lipid peroxidation, and resist the damage caused by oxygen free radicals to cells. GSH is a kind of nonenzymatic small molecule antioxidant, which has the physiological functions of antioxidation, antiaging, and scavenging free radicals [20]. It can combine with the toxic compounds entering the body and urge them to be excreted from the body to neutralize the toxicity. GSH PX is an important peroxidase in the body. It can catalyze the reduction of toxic peroxides to nontoxic hydroxyl compounds and protect the structure and function of cell membrane from damage. Cat is a free radical scavenger and a marker enzyme of peroxisome. It can promote the decomposition of  $H_2O_2$  into molecular oxygen and water, so as to protect tissues and

cells from  $H_2O_2$  damage [21]. T-AOC represents the comprehensive effect of enzymatic and nonenzymatic antioxidant capacity of the body, mainly reflects the dynamic balance of ROS in the internal environment, and is often used to evaluate the antioxidant capacity of the body. Zhao et al. found that after exposure to 50 mg/kg ACN for 13 weeks, the content of MDA in rat testis increased significantly and the activity of GSH PX decreased significantly. Under the experimental conditions, compared with the control group, the activity of GSH PX and the level of T-AOC in testicular tissue of ACN group decreased significantly, the content of MDA increased to a certain extent, and the content of GSH, the activity of SOD, and the level of cat decreased to a certain extent, suggesting that ACN leads to oxidative stress injury in testicular tissue of rats [22]. Some researchers found that SP can increase the activity of SOD in serum and GSH PX in the liver and reduce the content of MDA. Kilani et al. found that SP can significantly reduce MDA content and improve SOD activity and T-AOC level in hyperuricemia rats. Chen Junyi and others found that SP has a protective effect on lipid peroxidation and DNA damage of rat sperm caused by ACN [23]. 468 mg/kg SP can reduce ROS production, MDA content, SOD activity, and sperm DNA damage. The results showed that after SP intervention, compared with ACN group, the content of GSH and the level of T-AOC in testicular tissue in low SP intervention group were significantly increased, the content of MDA was reduced, and the activities of SOD, GSH PX, and cat were increased; in the SP intervention group, the content of MDA in testicular tissue decreased to a certain extent, and the content of GSH, the activity of SOD and cat, and the level of T-AOC increased to a certain extent, suggesting that SP can improve the oxidative stress of rat testicular tissue induced by ACN [24].

Oxidative stress can mediate the activation of many intracellular pathways, such as the study by MAPK et al. There are cross and feedback between these channels, which affect each other. MAPK is a kind of serine/threonine protein kinase, which can transmit exogenous signals down through multilevel protein kinase cascade reaction [25] and then regulate gene and cell physiological response to environmental changes. It exists widely in vivo. At present, four MAPK family members have been identified, namely, p38 MAPK, JNK, extracellular signal regulated kinase 1/2 (ERK1/2), and extracellular signal regulated kinase-5 (ERK5). They can play an important role in regulating cell growth, differentiation, and apoptosis. The MAPK signaling pathway is composed of three protein kinases, including MAP2K and MAP3K, which are associated with a variety of diseases, such



as tumors, autoimmune diseases and diabetes, and developmental abnormalities [26]. When stimulated by growth factors, cytokines, or other factors, MAP3K-MAP2K-mapk phosphorylation is activated step by step. Serine/threonine residue phosphorylation of channel protein is the main way of MAPK pathway activation. Different exogenous stimuli activate different MAPK signaling pathways and then phosphorylate different downstream substrates, including various transcription factors and protein kinases, which eventually lead to a series of biochemical reactions such as cell proliferation, differentiation, and apoptosis [27]. PI3K is a member of MAP3K family. It is ROS sensitive and is the key in oxidative stress-mediated apoptosis. After oxidative stress, the Thr 845 site of PI3K is phosphorylated and then activated. Activated PI3K can phosphorylate downstream MKK4 and MKK7. Activated MKK4 and MKK7 activate JNK by phosphorylating Thr 183 and Tyr 185. They can also phosphorylate downstream MKK3 and MKK6. Activated MKK3 and MKK6 activate p38 by phosphorylating Thr 180 and Tyr 182. The results of this study showed that compared with the control group, the relative expression levels of PI3K, MKK7, JNK, and p38 mRNA, the expression levels of PI3K, p-PI3K, MKK7, p-MKK7, JNK, p-JNK, p38, and p-p38 protein, and the ratio of p-JNK/JNK and p-p38/p38 increased in ACN group; after SP intervention, compared with ACN group, the relative expression levels of MKK7, JNK, and p38 mRNA, the expression levels of PI3K, p-PI3K, MKK7, p-MKK7, JNK, p-JNK, p38, and p-p38 protein and the ratio of p-JNK/JNK and p-p38/p38 decreased in low SP intervention group [28]; The relative expression level of JNK mRNA, the expression level of PI3K, p-PI3K, MKK7, p-MKK7, JNK, p-JNK, p38, and p-p38 protein and the ratio of p-PI3K/PI3K and p-JNK/JNK decreased in the middle SP intervention group. The ratio of p-JNK/JNK and p-p38/p38 in testicular tissue of rats in high SP intervention group decreased, suggesting that SP can inhibit the activation of PI3K-NRF2/p38 signal pathway induced by ACN.

In conclusion, SP can reduce ACN induced testicular oxidative stress, inhibit the activation of PI3K-NRF2/p38 signaling pathway, and then inhibit mitochondrial mediated apoptosis. This study detected the related indicators of testicular oxidative stress and speculated that SP may play a protective role by reducing oxidative stress, but ROS was not detected and there was no direct evidence. Therefore, ROS level should be detected in future research. In this study, SP intervention can improve the sperm quality and testicular injury induced by ACN, but the changes of various indexes after different doses of SP intervention do not show consistent results. In future research, we can refine the grouping and explore the best dose of SP for the protection of ACN reproductive injury.

### Data Availability

No data were used in this study.

### Conflicts of Interest

The authors declare that they have no conflicts of interest.

### References

- [1] J. E. Miller, S. H. Ahn, S. P. Monsanto, K. Khalaj, M. Koti, and C. Tayade, "Implications of immune dysfunction on endometriosis associated infertility," *Oncotarget*, vol. 8, no. 4, pp. 7138–7147, 2017.
- [2] K. Kolanska, J. Alijotas-Reig, J. Cohen et al., "Endometriosis with infertility: a comprehensive review on the role of immune deregulation and immunomodulation therapy," *American Journal of Reproductive Immunology*, vol. 85, no. 3, Article ID e13384, 2021.
- [3] J. Fu, R. Yao, and Y. Luo, "Immune infertility should be positively diagnosed using an accurate method by monitoring the level of anti-ACTL7a antibody," *Scientific Reports*, vol. 6, no. 1, pp. 1–8, 2016.
- [4] J. Fu, R. Yao, Y. Luo et al., "Anti-GAPDH antibodies: a biomarker of immune infertility," *Cell and Tissue Research*, vol. 364, no. 1, pp. 199–207, 2016.
- [5] T. T. Lao, J. S. M. Mak, and T. C. Li, "Hepatitis B virus infection status and infertility causes in couples seeking fertility treatment—indicator of impaired immune response?" *American Journal of Reproductive Immunology*, vol. 77, no. 4, Article ID e12636, 2017.
- [6] S. Dutta, P. Sengupta, and M. F. Hassan, "Role of toll-like receptors in the reproductive tract inflammation and male infertility," *Chemical Biology Letters*, vol. 7, no. 2, pp. 113–123, 2020.
- [7] A. Sood, D. Cole, and F. Abdollah, "Endocrine, sexual function, and infertility side effects of immune checkpoint inhibitor therapy for genitourinary cancers," *Current Urology Reports*, vol. 19, no. 9, pp. 1–9, 2018.
- [8] T. Rantsi, H. Öhman, M. Puolakkainen et al., "Predicting tubal factor infertility by using markers of humoral and cell-mediated immune response against *Chlamydia trachomatis*," *American Journal of Reproductive Immunology*, vol. 80, no. 5, Article ID e13051, 2018.
- [9] K. Yamaguchi, "Tacrolimus treatment for infertility related to maternal-fetal immune interactions," *American Journal of Reproductive Immunology*, vol. 81, no. 4, Article ID e13097, 2019.
- [10] E. Nagy and B. E. Nagy, "Coping with infertility: comparison of coping mechanisms and psychological immune competence in fertile and infertile couples," *Journal of Health Psychology*, vol. 21, no. 8, pp. 1799–1808, 2016.
- [11] C. Walker, S. Ghazisaeidi, B. Collet, A. Boisvert, and M. Culty, "In utero exposure to low doses of genistein and di-(2-ethylhexyl) phthalate (DEHP) alters innate immune cells in neonatal and adult rat testes," *Andrology*, vol. 8, no. 4, pp. 943–964, 2020.
- [12] X.-L. Zhang and X.-Y. Zhao, "Regulatory effect of Zishen Yutai pill on the biological behavior of Oocytes in immune infertility model rats," *Chinese Journal of Integrated Traditional and Western Medicine*, vol. 37, no. 3, pp. 351–355, 2017.
- [13] G. Massei, D. Cowan, D. Eckery et al., "Effect of vaccination with a novel GnRH-based immun contraceptive on immune responses and fertility in rats," *Heliyon*, vol. 6, no. 4, Article ID e03781, 2020.
- [14] A. M. Padma, A. B. Alshaiikh, M. J. Song et al., "Decellularization protocol-dependent damage-associated molecular patterns in rat uterus scaffolds differentially affect the immune response after transplantation," *Journal of Tissue Engineering and Regenerative Medicine*, vol. 15, no. 7, pp. 674–685, 2021.
- [15] T.-J. Ye and H.-X. Cheng, "Therapeutic efficacy of moxibustion plus medicine in the treatment of infertility due to

- polycystic ovary syndrome and its effect on serum immune inflammatory factors,” *Journal of Acupuncture and Tuina Science*, vol. 18, no. 4, pp. 269–275, 2020.
- [16] B. Santoso, A. Sa’adi, S. R. Dwiningsih et al., “Soluble immune checkpoints CTLA-4, HLA-G, PD-1, and PD-L1 are associated with endometriosis-related infertility,” *American Journal of Reproductive Immunology*, vol. 84, no. 4, Article ID e13296, 2020.
- [17] S. H. Zhou, Y. F. Deng, Z. W. Weng, H. W. Weng, and Z. D. Liu, “Traditional Chinese medicine as a remedy for male infertility: a review,” *The World Journal of Men’s Health*, vol. 37, no. 2, pp. 175–185, 2019.
- [18] S. Dutta, P. Sengupta, and B. S. Chhikara, “Reproductive inflammatory mediators and male infertility,” *Chemical Biology Letters*, vol. 7, no. 2, pp. 73–74, 2020.
- [19] T. Rantsi, P. Joki-Korpela, H. Öhman et al., “*Chlamydia trachomatis*-induced cell-mediated and humoral immune response in women with unexplained infertility,” *American Journal of Reproductive Immunology*, vol. 80, no. 1, Article ID e12865, 2018.
- [20] T. Homma, Y. Takeda, S. Sakahara et al., “Heterozygous SOD1 deficiency in mice with an NZW background causes male infertility and an aberrant immune phenotype,” *Free Radical Research*, vol. 53, no. 11–12, pp. 1060–1072, 2019.
- [21] Y. Liu, K. Zhao, Z. Xiong et al., “Transcriptional activation and regulation of urokinase plasminogen activator induced by LPS through MyD88 independent pathway in rat Sertoli cells,” *Folia Histochemica et Cytobiologica*, vol. 59, no. 4, pp. 236–244, 2021.
- [22] N. I. Rizk, M. S. Rizk, and A. S. Mohamed, “Attenuation of sleep deprivation dependent deterioration in male fertility parameters by vitamin C,” *Reproductive Biology and Endocrinology*, vol. 18, no. 1, pp. 1–13, 2020.
- [23] A. M. El-Shehawi, S. El-Shazly, M. Ahmed et al., “Transcriptome analysis of testis from HFD-induced obese rats (*Rattus norvegicus*) indicated predisposition for male infertility,” *International Journal of Molecular Sciences*, vol. 21, no. 18, p. 6493, 2020.
- [24] S. Dutta, P. Sengupta, and S. Chakravarthi, “Adiponectin: ‘a metabolic ballcock’modulating immune responses and male reproduction,” *Chemical Biology Letters*, vol. 8, no. 4, pp. 171–182, 2021.
- [25] N. Lorzadeh and N. Kazemirad, “The role of natural killer cells and mast cells in female infertility and associated treatment Outcomes,” *Current Women’s Health Reviews*, vol. 16, no. 2, pp. 102–106, 2020.
- [26] J.-F. Xia, Y. Inagaki, J.-F. Zhang, L. Wang, and P. p. Song, “Chinese medicine as complementary therapy for female infertility,” *Chinese Journal of Integrative Medicine*, vol. 23, no. 4, pp. 245–252, 2017.
- [27] C. E. Okechukwu, “Does the use of mobile phone affect male fertility? A mini-review,” *Journal of Human Reproductive Sciences*, vol. 13, no. 3, p. 174, 2020.
- [28] S. Wang, J. Jiang, and X. Lu, “Progress on therapy of infertility by integrated traditional Chinese and western medicine,” *Advances in Reproductive Sciences*, vol. 8, no. 4, pp. 175–185, 2020.

## Research Article

# Gambogic Acid and Piperine Synergistically Induce Apoptosis in Human Cholangiocarcinoma Cell via Caspase and Mitochondria-Mediated Pathway

Rittibet Yapasert <sup>1</sup> and Ratana Banjerdpongchai <sup>1,2</sup>

<sup>1</sup>Department of Biochemistry, Faculty of Medicine, Chiang Mai University, Chiang Mai 50200, Thailand

<sup>2</sup>Center for Research and Development of Natural Products for Health, Chiang Mai University, Chiang Mai 50200, Thailand

Correspondence should be addressed to Ratana Banjerdpongchai; [ratana.b@cmu.ac.th](mailto:ratana.b@cmu.ac.th)

Received 17 March 2022; Accepted 25 April 2022; Published 12 May 2022

Academic Editor: Jelena Zivkovic

Copyright © 2022 Rittibet Yapasert and Ratana Banjerdpongchai. This is an open access article distributed under the Creative Commons Attribution License, which permits unrestricted use, distribution, and reproduction in any medium, provided the original work is properly cited.

Most cholangiocarcinoma (CCA) patients undergo chemotherapy as a therapeutic approach due to the disease's frequently late diagnosis. However, because CCA is resistant to currently available treatments, the prognosis for this cancer is still quite poor. Combination therapy has emerged as a novel and promising strategy in cancer treatment, as monotherapy frequently results in tumor recurrence and drug resistance. Gambogic acid has been shown to have a synergism with other compounds in combating certain cancer cells. Moreover, piperine has been shown to improve the efficacy of numerous chemotherapy drugs and other anticancer natural substances. However, no research has been done on the combination of these two compounds in the treatment of bile duct cancer. In this study, the cytotoxic activity was determined by using the MTT assay, and then, the combined effect was assessed by using the combination index (CI). We found that the combination of gambogic acid and piperine inhibited cell viability more effectively than either treatment alone, and it also demonstrated a synergistically cytotoxic effect against CCA cells. Interestingly, the findings allowed the use of lower concentrations of gambogic acid in cancer treatment when combined with piperine, which could reduce its adverse effect on normal cholangiocytes. Furthermore, the combination of the two compounds increased CCA cell death by inducing apoptosis via both the extrinsic and intrinsic or mitochondria-mediated pathways, as determined by caspase-3, -8, and -9 activity and the reduction of mitochondrial transmembrane potential ( $\Delta\Psi_m$ ). It is possible that the use of these two natural compounds together could be a promising strategy for the treatment of bile duct cancer.

## 1. Introduction

Primary hepatic cancer, often known as liver cancer, is classified into two histopathological types: hepatocellular carcinoma (HCC) and cholangiocarcinoma (CCA). HCC is the most frequent type of liver cancer around the world [1]. CCA is highly prevalent in Thailand and is the most common pathogenic form, accounting for more than 80% of all detected primary liver cancer [2, 3]. CCA is still associated with high mortality rates, particularly in the northeast of Thailand, due to its aggressiveness and the poor prognosis generally in patients suffering from this disease [1, 4, 5]. At present, only about a quarter of CCA patients are candidates for surgical excision of the tumor, with the majority of the

patients undergoing chemotherapy as a type of treatment [6]. Unfortunately, CCA cannot resist standard treatment by using several tolerance pathways [7, 8]. As a result, it is critical to find a novel drug with great efficacy for CCA treatment [9, 10].

Gambogic acid (see Figure 1(a)) is the major xanthonoid derived from the brownish resin of the *Garcinia hanburyi* tree in Southeast Asia [11, 12]. Previous studies have revealed its anticancer efficacy both *in vitro* and *in vivo*. In preclinical research, the cytotoxicity and the effect on apoptosis induction of gambogic acid were demonstrated. Gambogic acid can inhibit HCC and CCA cell proliferation, induce cell cycle arrest at the G0/G1 phase, and then induce apoptosis through both the mitochondria-dependent and



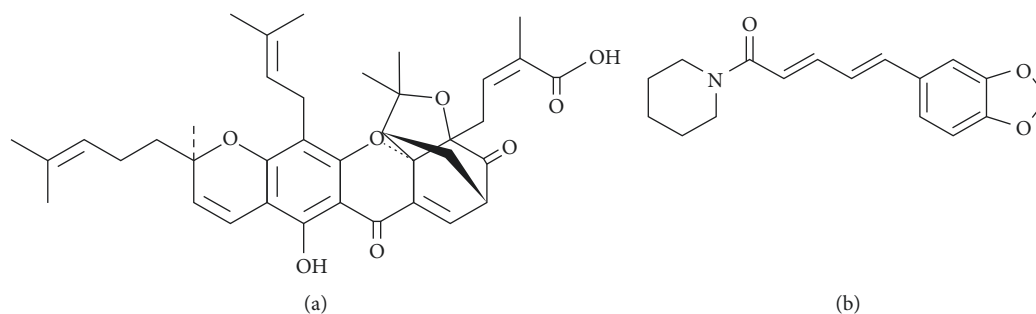


FIGURE 1: Chemical structure of (a) gambogic acid and (b) piperine.

extrinsic death receptor pathways [13–16]. However, in animal studies, this compound has been shown to cause a variety of adverse effects as well as severe systemic toxicity [17–20].

Piperine (see Figure 1(b)) is a major alkaloid isolated from *Piper nigrum* (black pepper) and *Piper longum* L. (long pepper) [21], both of which are used in culinary and traditional medicine around the world. Piperine has several pharmacological effects, including anticonvulsant [22], antioxidant [23], antiinflammatory [24], antiangiogenic [25], antibacterial [26], and anticancer activities. It has been shown in recent research to be cytotoxic to a variety of human cancer cells [27–29]. Furthermore, piperine can induce mitochondria-mediated apoptosis in HCC cells [30]. These findings imply that it may have a therapeutic potential against CCA. Intriguingly, it is a known bioavailability enhancer for various chemotherapeutic agents and other anticancer natural compounds because of its inhibitory effect on p-glycoprotein or multidrug resistance protein 1 (MDR1) activity [31, 32].

Monotherapy frequently results in tumor recurrence and drug resistance [33], whereas combination therapy has emerged as a novel and promising strategy in cancer treatment [34, 35]. Given their similar killing mechanisms, we intended to test whether these two natural chemicals when combined have greater anticancer potential while having fewer negative effects on normal cells (cholangiocytes). In the present study, we examined the effects of gambogic acid and piperine alone or in combination on CCA cell proliferation and apoptosis. Our studies demonstrated that cotreatment of gambogic acid with piperine enhanced the cytotoxic effect and apoptosis in CCA cells, while decreasing toxicity in normal cholangiocytes when compared to a single compound treatment, suggesting that the combination of these two compounds may deliver a novel and advantageous option for treatment of CCA patients.

## 2. Materials and Methods

**2.1. Chemical Compounds.** Gambogic acid (purity  $\geq 95\%$ ) was purchased from Cayman Chemical (2752-65-0) (Ann Arbor, MI, USA). Piperine (P49007) (purity  $\geq 97\%$ ) and gemcitabine (G6423) (purity  $\geq 98\%$ ) were purchased from Sigma-Aldrich (St. Louis, MO, USA). Ham's F-12 (21700-

075), fetal bovine serum (FBS), phosphate-buffered saline (PBS), and trypsin-EDTA solution were purchased from Gibco (Grand Island, NY, USA). 3-(4,5-Dimethylthiazol-2-yl)-2,5-diphenyltetrazolium bromide (MTT), 3,3'-dihexyloxycarbocyanine iodide (DiOC<sub>6</sub>), and dimethyl sulfoxide (DMSO) were purchased from Sigma Chemical, Inc. (St. Louis, MO, USA). Annexin-V-FLUOS staining kit and protease inhibitor cocktail tablets were obtained from Roche Diagnostics (Rotkreuz, Switzerland). The substrates of caspase-9 (LEHD-para-nitroaniline; LEHD-p-NA), caspase-8 (IETD-para-nitroaniline; IETD-p-NA), and caspase-3 (DEVD-para-nitroaniline; DEVD-p-NA) were obtained from Invitrogen (Thermo Fisher Scientific Inc., Waltham, MA, USA).

**2.2. Cell Culture.** Human cholangiocarcinoma cell lines (KKU-100, HUCCA-1, and KKU-213) and an immortalized human cholangiocyte cell line (MMNK-1) were obtained from the Japanese Collection of Research Bioresources (JCRB) Cell Bank, Japan. All cell lines were cultured in a Ham's F-12 medium with NaHCO<sub>3</sub>, 100 U/mL penicillin, and streptomycin. The medium was adjusted to a pH of 7.2 and supplemented with 10% heat-inactivated fetal bovine serum. Cells were cultured at 37°C in an incubator supplied with 5% of CO<sub>2</sub>.

**2.3. Cell Viability Assay.** The 3-(4,5 dimethylthiazol-2-yl)-2,5 diphenyltetrazolium bromide (MTT) assay [36] was performed by seeding cells in a 96-well culture plate. The stock solutions of gambogic acid (100 mM), piperine (2 M), and gemcitabine (2 M) in DMSO were used to prepare test solutions in different concentrations in Ham's F-12 medium using a 2-fold serial dilution method. The final concentration of DMSO for treatment was less than 0.1%. Cells were treated with gambogic acid, piperine, or gemcitabine (positive control) in various concentrations for a 24-hour incubation period. The cell viability in each concentration of compounds was compared to that of the untreated condition [37].

**2.4. Determination of the Combination Index.** Synergism, additivity, or antagonism between compounds was quantitated based on the Chou–Talalay method [38, 39]. The

combination index (CI) value between two compounds A and B was calculated using CompuSyn Software (available by free downloading from <http://www.combosyn.com>) [40] employing the following equation:

$$CI = \left( \frac{C_{A,X}}{IC_{X,A}} \right) + \left( \frac{C_{B,X}}{IC_{X,B}} \right). \quad (1)$$

$IC_{X,A}$  and  $IC_{X,B}$  are concentrations of each component alone that have an  $X$  percent effect, whereas  $C_{A,X}$  and  $C_{B,X}$  are concentrations of compounds in combination that have the same effect. Interpretation of the value was referenced by following criteria: CI values more than 1 indicate antagonism, CI values equal to 1 indicate additivity, and CI values less than 1 indicate synergism [41, 42].

**2.5. Apoptosis Assay.** Apoptotic cell quantification was performed as previously described [43]. In brief, after compound treatment with gambogic acid and/or piperine for 24 hours, floating and adhering cells were collected and then washed with phosphate-buffered saline (PBS). After that, cells were stained with Annexin V-fluorescein isothiocyanate (FITC) and propidium iodide (PI) fluorescence dye for 15 minutes and analyzed by using a flow cytometer (CyAn ADP, Beckman Coulter, USA).

**2.6. Determination of Mitochondrial Transmembrane Potential ( $\Delta\Psi_m$ ).** This procedure was performed in accordance with the previously described method [43]. After treatment with gambogic acid and/or piperine for 24 hours, suspending and adhering cells were collected and then washed with PBS before being stained for 15 minutes at 37°C with 40 nM 3,3'-dihexyloxycarbocyanine iodide (DiOC<sub>6</sub>). Flow cytometry was then performed to examine the stained cells (CyAn ADP, Beckman Coulter, USA).

**2.7. Determination of Caspases-3, -8, and -9 Activities.** Caspases activity was performed according to the manufacturer's protocols by using specific substrates and colorimetric analysis. After treatment with gambogic acid and/or piperine for 24 hours, floating and adhering cells were collected and then washed with PBS. After that, the cells were lysed by using a lysis buffer and proteins were extracted. Protein extracts were incubated with caspase-3 (DEVD-p-NA), caspase-8 (IETD-p-NA), and caspase-9 (LEHD-p-NA) chromogenic substrates at 37°C for an hour. The optical density was measured by using a microplate reader (BioTek, Winooski, VT, USA) at the wavelength of 405 nm [43].

**2.8. Statistical Analysis.** All data were analyzed by using statistic SPSS Software version 20 and were presented as the mean  $\pm$  standard deviation (SD) from repeated three independent experiments. Statistical analysis was performed using one-way analysis of variance (ANOVA) followed by a comparison between groups by Tukey's test when more than three groups were analyzed and using Student's  $t$ -test when

two groups were compared. Statistical significance was considered with values of  $p < 0.05$ .

### 3. Results and Discussion

**3.1. Effects of Gambogic Acid and Piperine on CCA Cell Viability.** We examined the cytotoxic effect of gambogic acid and piperine on the cell viability of human CCA cell lines, including KKU-100, HuCCA-1, and KKU-213 compared to that on normal cholangiocyte MMNK-1 cells. Cells were treated with various concentrations of gambogic acid or piperine for 24 hours. We found that gambogic acid and piperine significantly inhibited viability of all CCA cells in a concentration-dependent manner (see Figure 2). Gemcitabine, a first-line drug for cholangiocarcinoma [42], was used as a positive control. Gambogic acid presented the lowest IC<sub>50</sub> value in all the cancer cell lines (Table 1). However, piperine was found to be more selectively toxic, particularly against KKU-100 and HuCCA-1 cells than other compounds.

**3.2. Piperine Enhanced the Cytotoxic Effect of Gambogic Acid against CCA Cells.** To determine whether piperine could enhance the cytotoxicity of gambogic acid, CCA cells were treated with gambogic acid, piperine or in combination. The concentration of piperine was fixed at the IC<sub>50</sub> value of each cell line, whereas gambogic acid concentrations ranged from 0 to 100  $\mu$ M. As shown in Figure 3(a), combining gambogic acid with piperine provided a synergistic anticancer effect by presenting CI values at different levels of cytotoxic effect (fraction affected, Fa) that were less than 1. However, piperine could not synergistically enhance the toxicity of gemcitabine on CCA cells (see Figure 3(b)). Interestingly, Table 2 exhibits that combination treatment of gambogic acid with piperine could reduce gambogic acid concentration when compared to a single treatment, resulting in a lower toxicity to normal cells.

**3.3. Enhancement Effect of Piperine on Gambogic Acid-Induced Apoptotic Cell Death.** Previous research has shown that gambogic acid and piperine can induce apoptosis in various cancer cells [13–15, 30]. Together with the current study, it suggested that cotreatment of gambogic acid and piperine could result in a synergistic cytotoxic effect. Hence, to elucidate the potential enhancement effect of piperine on gambogic acid-induced cell death via apoptosis, we investigated the effects of gambogic acid, piperine, and combined treatment on apoptosis in CCA cell lines. As shown in Figure 4, apoptotic cells were quantitated by Annexin V-fluorescein isothiocyanate (FITC) and propidium iodide (PI) double staining, and the result showed that the percentage of early and late apoptotic cells of combined condition was increased significantly as compared with a single treatment.

**3.3.1. The Combination Treatment Increased Apoptosis via Caspase Activation.** To further confirm the combined effect

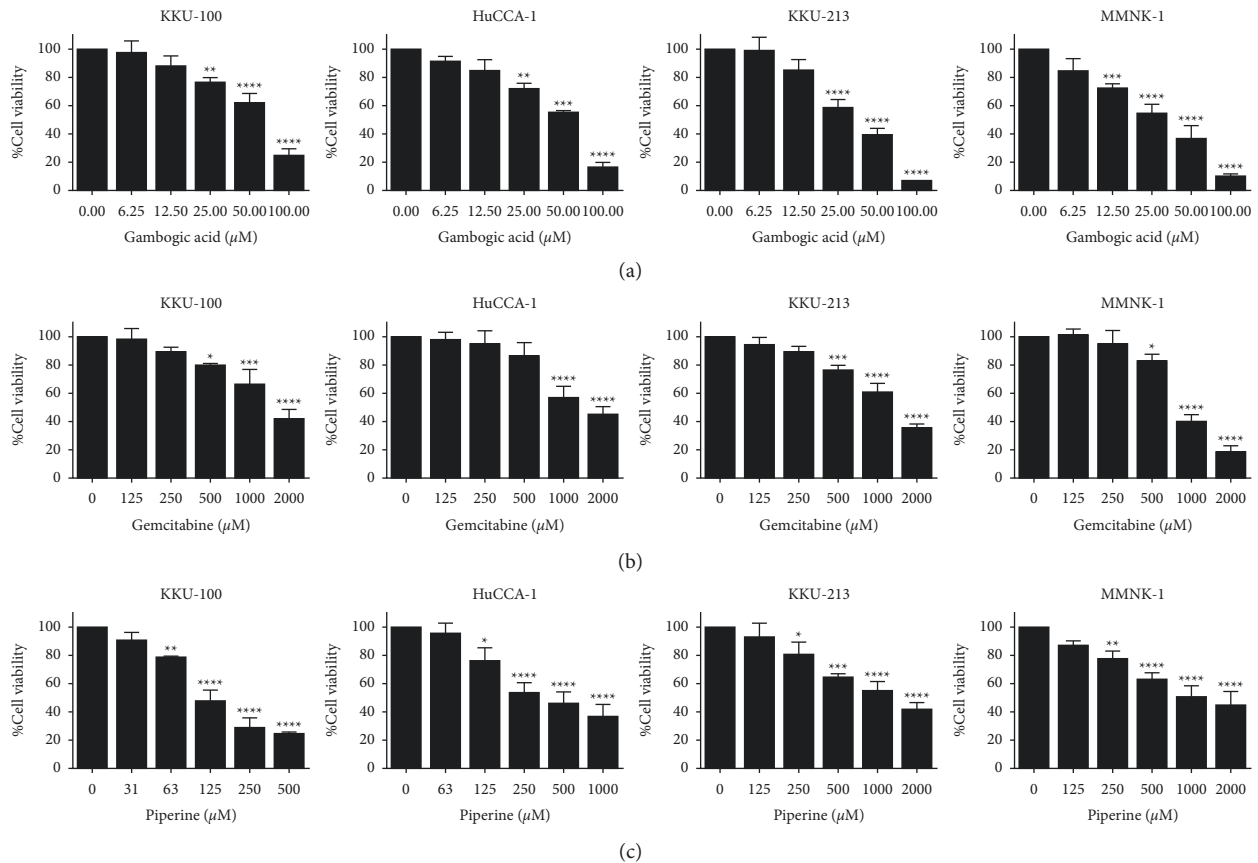


FIGURE 2: Cytotoxic effect of gambogic acid, gemcitabine, and piperine against CCA cell lines and normal cholangiocytes. KKKU-100, HuCCA-1, KKKU-213, and MMNK-1 cells were treated with indicated concentrations of gambogic acid (a), gemcitabine (b), and piperine (c) for 24 h. After that, cell viability was measured using the MTT assay. Results are shown as mean  $\pm$  SD values from three repeated independent experiments. In addition, \*  $p < 0.05$ , \*\*  $p < 0.01$ , \*\*\*  $p < 0.001$ , and \*\*\*\*  $p < 0.0001$  when compared with the control (without treatment).

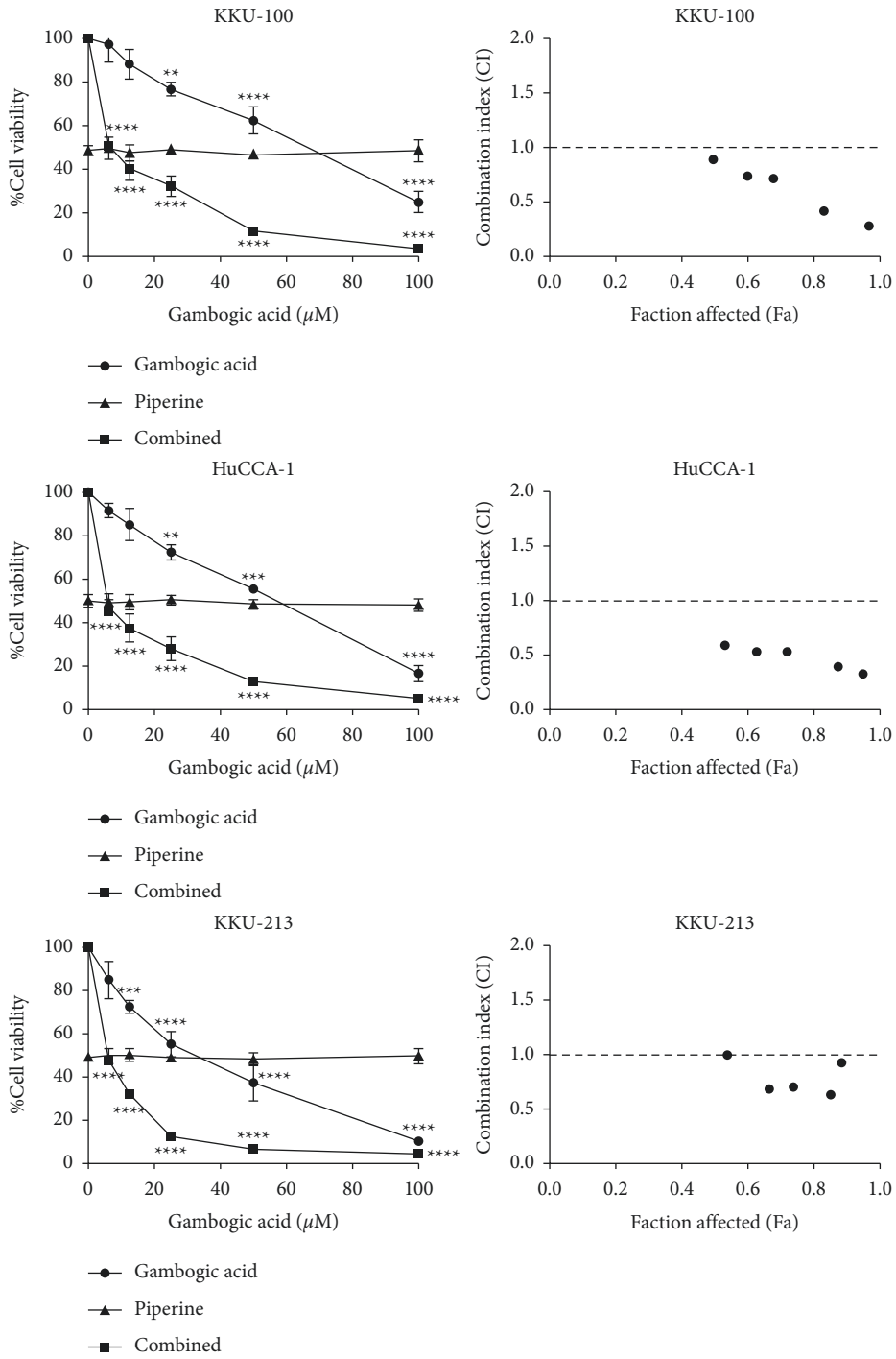
TABLE 1: Inhibitory concentration at 50% cell viability ( $IC_{50}$ ) of gambogic acid, gemcitabine, and piperine on CCA cell lines compared to normal cholangiocyte (MMNK-1) and the selectivity index (SI) of each compound.

Cell type	Cell lines	Values	Gambogic acid	Piperine	Gemcitabine
CCA	KKU-100	$IC_{50}$ ( $\mu M$ )	$63.2 \pm 2.5^{****}$	$119.1 \pm 3.6^{****,####}$	$1,674.7 \pm 7.9$
		SI	0.5	9.4	0.5
	HUCCA-1	$IC_{50}$ ( $\mu M$ )	$53.4 \pm 5.8^{****}$	$299.5 \pm 2.4^{****,####}$	$1,590.1 \pm 6.1$
		SI	0.6	3.7	0.5
	KKU-213	$IC_{50}$ ( $\mu M$ )	$35.7 \pm 1.2^{****}$	$1,148.3 \pm 7.3^{****}$	$1,423.5 \pm 4.5$
		SI	0.9	1.0	0.5
Normal	MMNK-1	$IC_{50}$ ( $\mu M$ )	$31.7 \pm 4.8$	$1,115.0 \pm 6.7$	$768.5 \pm 2.3$

Note. The selectivity index (SI) is the  $IC_{50}$  ratio value between MMNK-1 and CCA cells. SI value less than 2 indicates general toxicity of the compound [44]. Results are shown as mean  $\pm$  SD,  $n = 3$ . \*\*\*\*  $p < 0.0001$ , significantly lower than the  $IC_{50}$  value of gemcitabine of an individual cell; ####  $p < 0.0001$ , significantly lower than the  $IC_{50}$  value of MMNK-1.

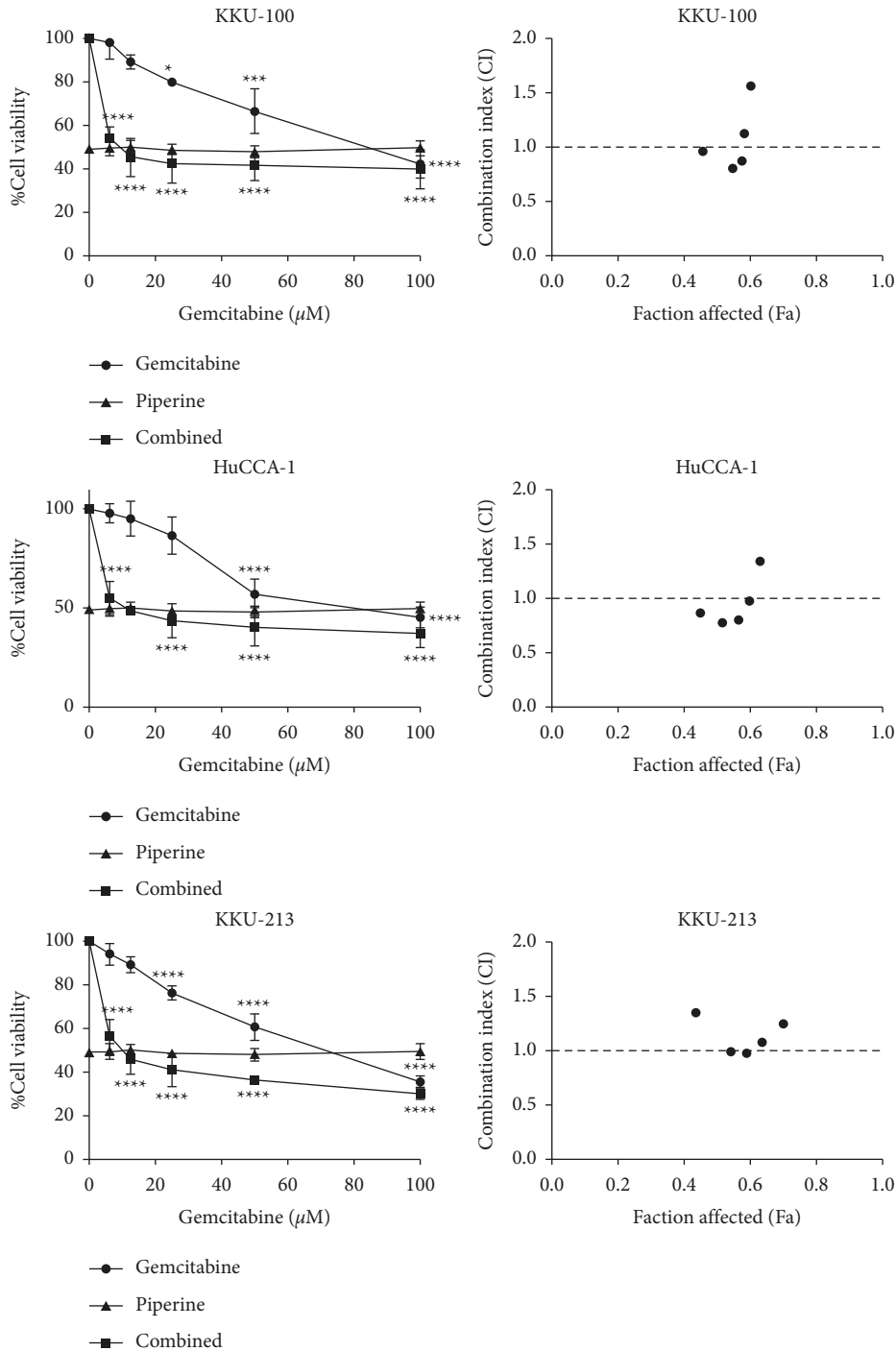
on apoptosis induction via caspase activation, we measured caspase-3, -8, and -9 activities after treatment with gambogic acid, piperine, or a combination of two compounds for 24 hours. As shown in Figure 5, when compared to a single treatment, the activities of caspases-3, -8, and -9 increased significantly after treatment with a combination of two compounds. These results indicated that the combined treatment enhanced apoptotic cell death through both extrinsic (caspase-8) and intrinsic (caspase-9) pathways.

3.3.2. *The Combination of Gambogic Acid and Piperine Induced the Mitochondria-Mediated Apoptosis Pathway.* Depolarization of the mitochondrial transmembrane potential ( $\Delta\Psi_m$ ) as a result of mitochondrial outer membrane permeabilization (MOMP) has been shown to contribute to apoptosis induction [45, 46]. Hence, the effect of the combination treatment on the modulation of mitochondrial transmembrane potential was investigated. The mitochondrial transmembrane potential was determined by using a



(a)

FIGURE 3: Continued.



(b)

FIGURE 3: Combination effects of gambogic acid or gemcitabine with piperine on CCA cells. Dose-response curves (left) and CI values at different levels of fraction affected (Fa) (right) of (a) gambogic acid plus piperine and (b) gemcitabine plus piperine. Results are shown as mean  $\pm$  SD values from three repeated independent experiments. In addition, \* $p < 0.05$ , \*\* $p < 0.01$ , \*\*\* $p < 0.001$ , and \*\*\*\* $p < 0.0001$  when compared with the control.

DiOC<sub>6</sub> fluorescence probe. The results revealed that the percentage of cells with a loss of mitochondrial transmembrane potential increased significantly after treatment with a combination of two compounds when compared to a single treatment (see Figure 6).

#### 4. Discussion

Because of the disease's frequent late diagnosis, chemotherapy is recommended for more than seventy percent of cholangiocarcinoma (CCA) patients [9]. However, many

TABLE 2: Cell viability of MNNK-1 at combined concentrations which could inhibit CCA cell viability at 50% (IC<sub>50</sub>).

CCA cell lines	Gambogic acid ( $\mu\text{M}$ )	Gemcitabine ( $\mu\text{M}$ )	Piperine ( $\mu\text{M}$ )	% cell viability of MNNK-1
KKU-100	54.9	—	157.1	77.2 $\pm$ 4.8
	—	1,482.6	157.1	53.4 $\pm$ 6.6
HUCCA-1	42.7	—	455.4	70.0 $\pm$ 2.5
	—	1,549.6	455.4	54.7 $\pm$ 3.1
KKU-213	25.7	—	1,220.1	66.6 $\pm$ 5.6
	—	1,197.2	1,206.5	47.1 $\pm$ 8.9

Note. The combined concentrations which could inhibit CCA cell viability at 50% were calculated using CompuSyn software.

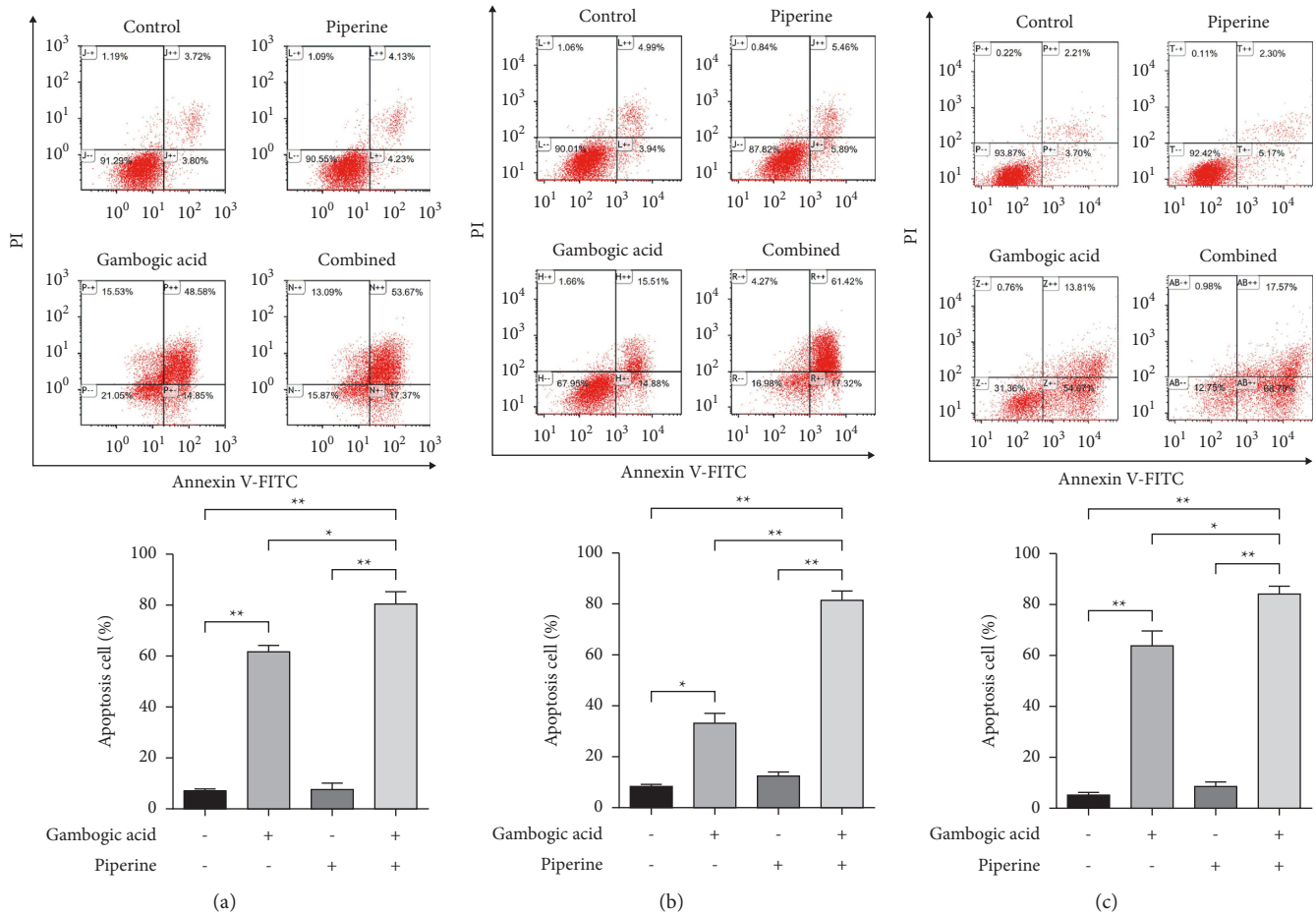


FIGURE 4: The combination of gambogic acid and piperine significantly induced apoptosis in CCA cells. KKU-100 (a), HuCCA-1 (b), and KKU-213 (c) were treated with gambogic acid at IC<sub>50</sub>, piperine at IC<sub>10</sub> (33.2  $\mu\text{M}$ , 80.7  $\mu\text{M}$  and 155.3  $\mu\text{M}$  for KKU-100, HuCCA-1, and KKU-213 cells, respectively), or combination of both for 24 hours. Then, the cells were stained with Annexin V-FITC/PI and analyzed by flow cytometry to examine apoptotic cells. Bar graphs represented the percentage of apoptotic cells. Results are shown as mean  $\pm$  SD values from three repeated independent experiments. \*  $p < 0.05$  and \*\*  $p < 0.01$  compared with control (without treatment).

studies have demonstrated that there were many mechanisms of CCA cells in chemoresistance, such as reduced drug absorption and metabolism, as well as impairment of the apoptotic mechanism [47], which has resulted in a relatively poor response to existing chemotherapeutic drugs [48, 49]. Furthermore, many chemotherapeutic drugs have considerable side effects that cause patient intolerance and treatment failure. As a result, substantial efforts have been

focused on finding novel and effective anticancer drugs with little or no side effects. However, the combination treatment appears to have significant potential benefits due to the reduction of side effects, the synergistic/combined antitumor effects, and the ability to overcome drug resistance [35].

Gambogic acid is the major active compound derived from *Garcinia hanburyi* [11, 12]. Previous studies have shown that it has a high efficacy anticancer effect via



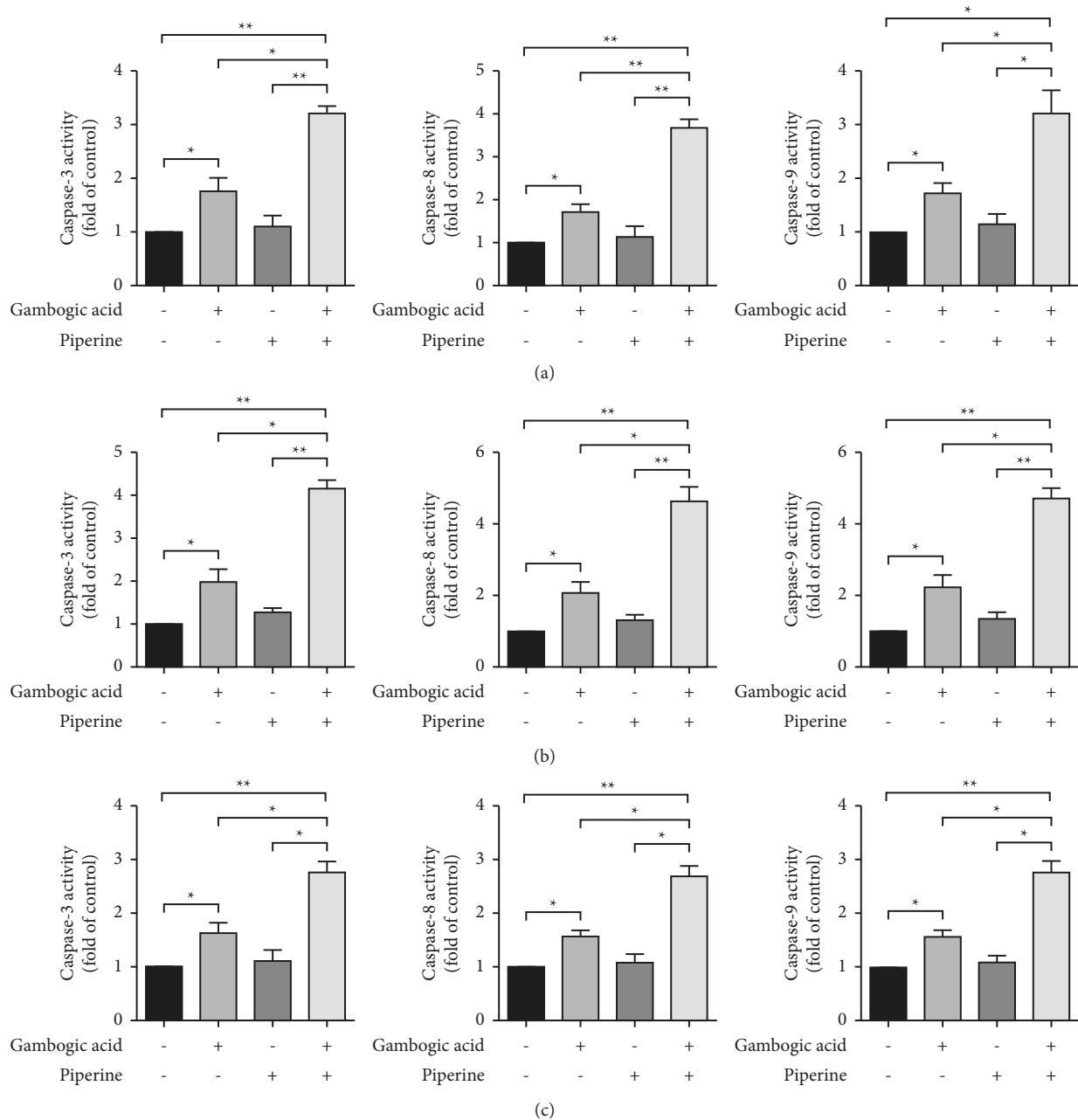


FIGURE 5: The combination of gambogic acid and piperine induced apoptosis via caspase activation. Caspase-3, -8, and -9 activities are shown after KKU-100 (a), HuCCA-1 (b), and KKU-231 (c) were treated with gambogic acid or piperine compared with the combined effect of the two compounds. Results are shown as mean  $\pm$  SD from three repeated independent experiments. \*  $p < 0.05$  and \*\*  $p < 0.01$  compared with the control.

apoptosis induction. However, in animal studies, this compound causes many adverse effects [17–20]. One of the best options to reduce adverse reactions is cotreatment with other compounds or drugs that can enhance its activity but can reduce the toxic side effects [50]. There have been several studies that suggest a synergistic antitumor effect when gambogic acid is combined with other drugs or natural compounds [51]. Piperine, isolated from black pepper (*Piper nigrum*) and long pepper (*Piper longum*) [21], is well known as an antioxidant, antiproliferative, antiinflammatory, and

anticancer agent [31, 52–55]. Moreover, it is a bioavailability enhancer for chemotherapeutic drugs and other anticancer compounds [30–32, 55]. Nevertheless, there has not been any research on its enhancement activity when combined with gambogic acid.

In the current study, the cytotoxic effects of gambogic acid and piperine were determined compared to positive control and gemcitabine. The result showed that gambogic acid, piperine, and gemcitabine inhibited the viability of cholangiocarcinoma (CCA) cells including KKU-100,

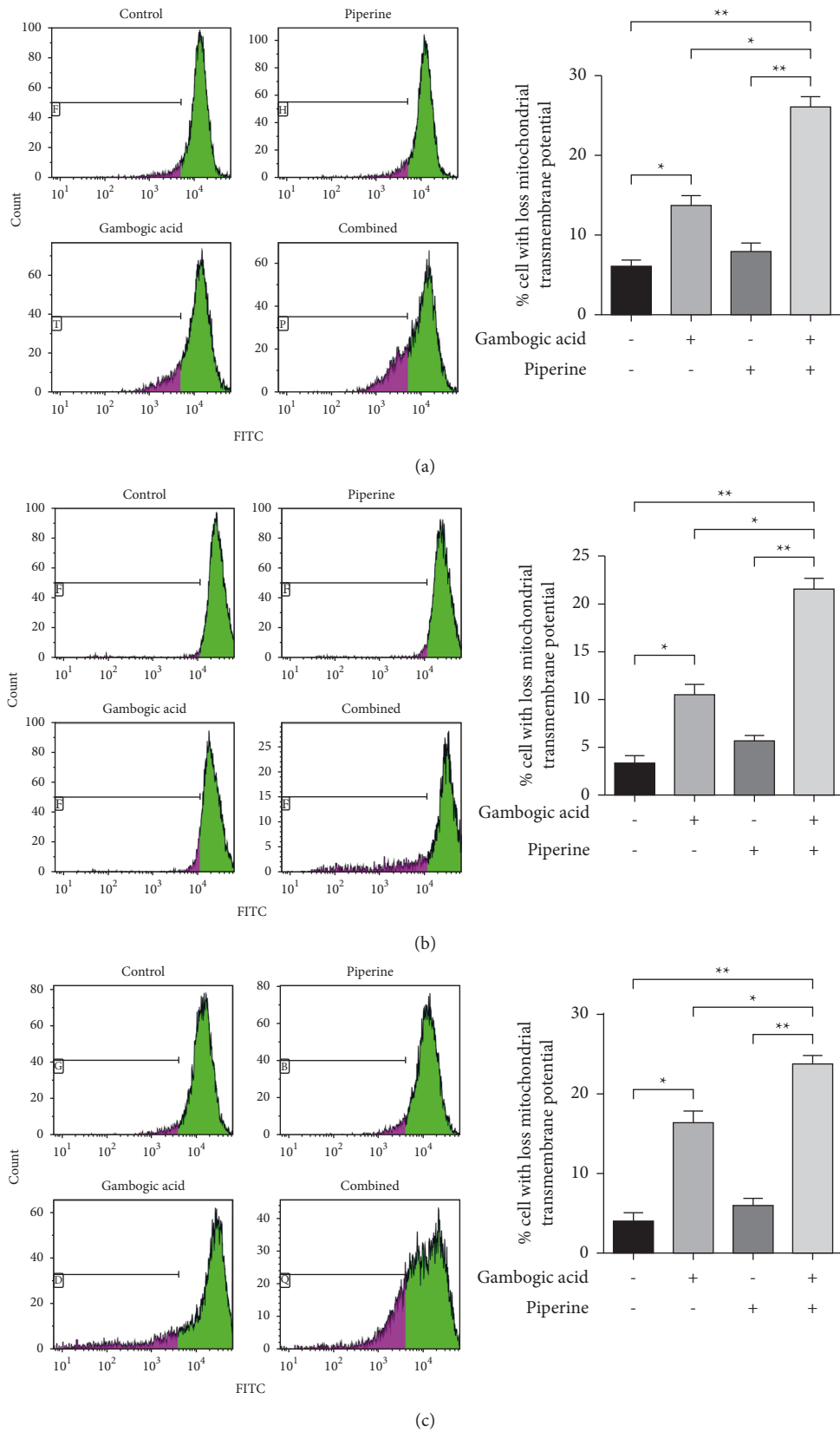


FIGURE 6: The combination of gambogic acid and piperine induced apoptosis via a mitochondrial pathway. After treatment, Kku-100 (a), HuCCA-1 (b), and Kku-231 (c) cells were stained with DiOC<sub>6</sub> and analyzed by flow cytometry to examine the disruption of mitochondrial transmembrane potential. Bar graphs are presented as the percentage of the cells with a loss of mitochondrial transmembrane potential. Results are shown as mean  $\pm$  SD,  $n = 3$ . \*  $p < 0.05$  and \*\*  $p < 0.01$  compared with the control.

HuCCA-1, and KKKU213 in a concentration-dependent manner. Intriguingly, gambogic acid has the lowest IC<sub>50</sub> value in all CCA cell lines. In addition, piperine was found to be more selectively toxic than the other phytochemicals (gambogic acid), especially against KKKU-100 and HuCCA-1 cells. However, gemcitabine had the highest IC<sub>50</sub> value and was nonselectively toxic to cancer cells.

The Chou–Talalay method was used to calculate the fractional inhibition (Fa) and combination index (CI) from the percentage of cell viability. The Fa-CI plots or the Chou–Talalay plots for drug combination in Figure 3 provide the quantitative determination of drug interactions, where CI values less than 1, equal to 1, and more than 1 indicate synergism, additive effect, and antagonism, respectively [56]. Combining gambogic acid with piperine provided a synergistic anticancer effect by presenting combination index (CI) values at different levels of the cytotoxic effect (fraction affected, Fa) that were less than 1. On the other hand, piperine could not synergistically enhance the toxicity of gemcitabine towards CCA cells. Furthermore, the combined concentrations which could inhibit CCA cell viability at 50% (IC<sub>50</sub>) were calculated and then were used for investigating the cell viability of normal cholangiocyte (MNNK-1). According to the synergism of piperine and gambogic acid, when compared to a single treatment, this combination decreased the concentration of gambogic acid, resulting in less toxicity to normal cells because gambogic acid exhibited nonselective toxicity, whereas piperine was found to be selectively toxic to cancer cells.

Flow cytometric analysis of apoptotic cells demonstrated that gambogic acid, piperine, and a combined treatment significantly increased the percentage of apoptotic cells compared to a single treatment. This was consistent with a significant increase in the percentage of cells with the loss of the mitochondrial transmembrane potential ( $\Delta\Psi_m$ ) and the enhanced activities of caspase-3, caspase-8 (extrinsic pathway mediator), and caspase-9 (intrinsic pathway mediator) after cotreatment with gambogic acid and piperine when compared to a single treatment. These results indicated that the combination treatment synergistically inhibited CCA cell viability and was associated with apoptotic regulated cell death induction via both extrinsic and intrinsic or mitochondria-mediated pathways.

## 5. Conclusions

The purpose of this study was to demonstrate that the combination of gambogic acid and piperine synergistically suppressed cholangiocarcinoma cell (KKU-100, HuCCA-1, and KKKU213) viability more efficiently than either therapy alone. Interestingly, when combined with piperine, the findings allowed the use of lower concentrations of gambogic acid in cancer treatment, perhaps reducing its adverse effect on normal cholangiocytes. In addition, the combination of the two agents enhanced apoptotic death of CCA cells through caspase and mitochondria-mediated pathways, as measured by caspase activity and the alteration of

mitochondrial transmembrane potential. Taken together, the current study found that cotreatment of gambogic acid and piperine exhibited a synergistic anticancer effect on CCA cells through apoptosis induction, providing a new strategy for bile duct cancer complementary therapy. However, the mechanisms of piperine in enhancing the effects of gambogic acid should be investigated further.

## Data Availability

The results presented to demonstrate the findings of the current study are accessible from the corresponding author upon request.

## Conflicts of Interest

The authors declare that they have no conflicts of interest.

## Authors' Contributions

RY and RB designed the research. RY performed the experiments and analyzed the results. RY and RB wrote the manuscript draft. All authors read and agreed to the published version of the manuscript.

## Acknowledgments

The authors are grateful to the Faculty of Medicine, Chiang Mai University (grant number 113/2565), Pre Square Wellness Co., Ltd., and Chiang Mai Genetics Laboratory Co., Ltd., for supporting the present study. This research was partially supported by Chiang Mai University and the Center for Research and Development of Natural Products for Health.

## References

- [1] B. Blechacz, "Cholangiocarcinoma: current knowledge and new developments," *Gut and liver*, vol. 11, no. 1, pp. 13–26, 2017.
- [2] B. Sripa and C. Pairojkul, "Cholangiocarcinoma: lessons from Thailand," *Current Opinion in Gastroenterology*, vol. 24, no. 3, pp. 349–356, 2008.
- [3] S. Kamsa-ard, S. Kamsa-ard, V. Luvira, K. Suwanrungruang, P. Vatanasapt, and S. Wiangnon, "Risk factors for cholangiocarcinoma in Thailand: a systematic review and meta-analysis," *Asian Pacific Journal of Cancer Prevention: Asian Pacific Journal of Cancer Prevention*, vol. 19, no. 3, pp. 605–614, 2018.
- [4] C. Varamo, C. Peraldo-Neia, P. Ostano et al., "Establishment and characterization of a new intrahepatic cholangiocarcinoma cell line resistant to gemcitabine," *Cancers*, vol. 11, no. 4, p. 519, 2019.
- [5] S. Woradet, N. Songserm, S. Promthet, and D. M. Parkin, "Health-related quality of life and survival of cholangiocarcinoma patients in northeastern region of Thailand," *PLoS One*, vol. 11, no. 9, Article ID e0163448, 2016.
- [6] W. Wattanawongdon, C. Hahnvajjanawong, N. Namwat et al., "Establishment and characterization of gemcitabine-resistant human cholangiocarcinoma cell lines with multidrug resistance and enhanced invasiveness," *International Journal of Oncology*, vol. 47, no. 1, pp. 398–410, 2015.

- [7] G. Fava, "Molecular mechanisms of cholangiocarcinoma," *World Journal of Gastrointestinal Pathophysiology*, vol. 1, no. 1, p. 12, 2010.
- [8] H.-J. Wu and P.-Y. Chu, "Role of cancer stem cells in cholangiocarcinoma and therapeutic implications," *International Journal of Molecular Sciences*, vol. 20, no. 17, p. 4154, 2019.
- [9] J. J. G. Marin, E. Lozano, E. Herrera et al., "Chemoresistance and chemosensitization in cholangiocarcinoma," *Biochimica et Biophysica Acta - Molecular Basis of Disease*, vol. 1864, no. 4, pp. 1444–1453, 2018.
- [10] J. J. G. Marin, E. Herrera, E. Lozano, R. I. R. Macias, and O. Briz, "Models for understanding resistance to chemotherapy in liver cancer," *Cancers*, vol. 11, no. 11, p. 1677, 2019.
- [11] H. Auterhoff, H. Frauendorf, W. Liesenklas, and C. Schwandt, "The chief constituents of gamboge resins. 1. Chemistry of gamboge," *Archiv der Pharmazie und Berichte der Deutschen Pharmazeutischen Gesellschaft*, vol. 295/67, pp. 833–846, 1962.
- [12] W. Liesenklas and H. Auterhoff, "The constitution of gambogic acid and its isomerization. 4. Chemistry of gum-resin," *Archiv der Pharmazie und Berichte der Deutschen Pharmazeutischen Gesellschaft*, vol. 299, no. 9, pp. 797–798, 1966.
- [13] J. Li, X. Wang, Y. Shao, X. Lu, and B. Chen, "A novel exploration of a combination of gambogic acid with TiO<sub>2</sub> nanofibers: the photodynamic effect for HepG2 cell proliferation," *Materials*, vol. 7, no. 9, pp. 6865–6878, 2014.
- [14] H. Gu, X. Wang, S. Rao et al., "Gambogic acid mediates apoptosis as a p53 inducer through down-regulation of mdm2 in wild-type p53-expressing cancer cells," *Molecular Cancer Therapeutics*, vol. 7, no. 10, pp. 3298–3305, 2008.
- [15] P. N. H. Lee and W. S. Ho, "Antiproliferative activity of gambogic acid isolated from *Garcinia hanburyi* in Hep3B and Huh7 cancer cells," *Oncology Reports*, vol. 29, no. 5, pp. 1744–1750, 2013.
- [16] K. Suksen, K. Janpipatkul, S. Reabroi et al., "Gambogic acid inhibits wnt/ $\beta$ -catenin signaling and induces ER stress-mediated apoptosis in human cholangiocarcinoma," *Asian Pacific Journal of Cancer Prevention*, vol. 22, no. 6, pp. 1913–1920, 2021.
- [17] Y.-t. Liu, K. Hao, X.-q. Liu, and G.-j. Wang, "Metabolism and metabolic inhibition of gambogic acid in rat liver microsomes," *Acta Pharmacologica Sinica*, vol. 27, no. 9, pp. 1253–1258, 2006.
- [18] K. Hao, X.-Q. Liu, G.-J. Wang, and X.-P. Zhao, "Pharmacokinetics, tissue distribution and excretion of gambogic acid in rats," *European Journal of Drug Metabolism & Pharmacokinetics*, vol. 32, no. 2, pp. 63–68, 2007.
- [19] J. Dai, *The Preparation of a Kind of Gambogic Acid Injection*.
- [20] L. Cai, N. Qiu, M. Xiang et al., "Improving aqueous solubility and antitumor effects by nanosized gambogic acid-mPEG2000 micelles," *International Journal of Nanomedicine*, vol. 9, pp. 243–255, 2014.
- [21] K. Izawa, Y. Amino, M. Kohmura, Y. Ueda, and M. Kuroda, "4.16-Human-Environment interactions-taste," *Comprehensive Natural Products II*, Elsevier, pp. 631–671, Amsterdam, Netherlands.
- [22] R. D'Hooge, Y. Q. Pei, A. Raes, P. Lebrun, P. P. van Bogaert, and P. P. de Deyn, "Anticonvulsant activity of piperine on seizures induced by excitatory amino acid receptor agonists," *Arzneimittel Forschung*, vol. 46, no. 6, pp. 557–560, 1996.
- [23] K. Selvendiran, S. M. Banu, and D. Sakthisekaran, "Protective effect of piperine on benzo (a) pyrene-induced lung carcinogenesis in Swiss albino mice," *Clinica Chimica Acta*, vol. 350, no. 1-2, pp. 73–78, 2004.
- [24] X. Ying, X. Chen, S. Cheng, Y. Shen, L. Peng, and H. z. Xu, "Piperine inhibits IL- $\beta$  induced expression of inflammatory mediators in human osteoarthritis chondrocyte," *International Immunopharmacology*, vol. 17, no. 2, pp. 293–299, 2013.
- [25] C. D. Doucette, A. L. Hilchie, R. Liwski, and D. W. Hoskin, "Piperine, a dietary phytochemical, inhibits angiogenesis," *The Journal of Nutritional Biochemistry*, vol. 24, no. 1, pp. 231–239, 2013.
- [26] D. M. Hikal, "Antibacterial activity of piperine and black pepper oil," *Biosciences biotechnology research Asia*, vol. 15, no. 4, pp. 877–880, 2018.
- [27] L.-h. Lai, Q.-h. Fu, Y. Liu et al., "Piperine suppresses tumor growth and metastasis *in vitro* and *in vivo* in a 4T1 murine breast cancer model," *Acta Pharmacologica Sinica*, vol. 33, no. 4, pp. 523–530, 2012.
- [28] A. Samykutty, A. V. Shetty, G. Dakshinamoorthy et al., "Piperine, a bioactive component of pepper spice exerts therapeutic effects on androgen dependent and androgen independent prostate cancer cells," *PLoS One*, vol. 8, no. 6, Article ID e65889, 2013.
- [29] L. Si, R. Yang, R. Lin, and S. Yang, "Piperine functions as a tumor suppressor for human ovarian tumor growth via activation of JNK/p38 MAPK-mediated intrinsic apoptotic pathway," *Bioscience Reports*, vol. 38, no. 3, 2018.
- [30] V. Gunasekaran, K. Elangovan, and S. Niranjali Devaraj, "Targeting hepatocellular carcinoma with piperine by radical-mediated mitochondrial pathway of apoptosis: an *in vitro* and *in vivo* study," *Food and Chemical Toxicology*, vol. 105, pp. 106–118, 2017.
- [31] R. A. Rather and M. Bhagat, "Cancer chemoprevention and piperine: molecular mechanisms and therapeutic opportunities," *Frontiers in Cell and Developmental Biology*, vol. 6, p. 10, 2018.
- [32] S. J. Hewlings and D. S. Kalman, "Curcumin: a review of its effects on human health," *Foods*, vol. 6, no. 10, p. 92, 2017.
- [33] M. M. Gottesman, T. Fojo, and S. E. Bates, "Multidrug resistance in cancer: role of ATP-dependent transporters," *Nature Reviews Cancer*, vol. 2, no. 1, pp. 48–58, 2002.
- [34] T. A. Yap, A. Omlin, and J. S. De Bono, "Development of therapeutic combinations targeting major cancer signaling pathways," *Journal of Clinical Oncology*, vol. 31, no. 12, pp. 1592–1605, 2013.
- [35] R. B. Mokhtari, T. S. Homayouni, N. Baluch et al., "Combination therapy in combating cancer," *Oncotarget*, vol. 8, no. 23, pp. 38022–38043, 2017.
- [36] J. C. Stockert, A. Blázquez-Castro, M. Cañete, R. W. Horobin, and Á. Villanueva, "MTT assay for cell viability: intracellular localization of the formazan product is in lipid droplets," *Acta Histochemica*, vol. 114, no. 8, pp. 785–796, 2012.
- [37] R. Yapasert, N. Lertprasertsuk, S. Subhawa, J. Poofery, B. Sripanidkulchai, and R. Banjerdpongchai, "Antitumor efficacy of the herbal recipe benja amarit against highly invasive cholangiocarcinoma by inducing apoptosis both *in vitro* and *in vivo*," *International Journal of Molecular Sciences*, vol. 21, no. 16, p. 5669, 2020.
- [38] T.-C. Chou and P. Talalay, "Quantitative analysis of dose-effect relationships: the combined effects of multiple drugs or enzyme inhibitors," *Advances in Enzyme Regulation*, vol. 22, pp. 27–55, 1984.
- [39] L. Zhao, M. G. Wientjes, and J. L. S. Au, "Evaluation of combination chemotherapy: integration of nonlinear regression, curve shift, isobologram, and combination index

- analyses," *Clinical Cancer Research*, vol. 10, no. 23, pp. 7994–8004, 2004.
- [40] T. Chou and N. Martin, *CompuSyn for Drug Combinations: PC Software and User's Guide: A Computer Program for Quantitation of Synergism and Antagonism in Drug Combinations, and the Determination of IC50 and ED50 and LD50 Values*, ComboSyn Inc, Paramus, NJ, USA, 2005.
- [41] J. L. Hernandez, L. Padilla, S. Dakhel et al., "Therapeutic targeting of tumor growth and angiogenesis with a novel anti-S100A4 monoclonal antibody," *PLoS One*, vol. 8, no. 9, Article ID e72480, 2013.
- [42] Z. Zou, L. Xie, J. Wei et al., "Synergistic anti-proliferative effects of gambogic acid with docetaxel in gastrointestinal cancer cell lines," *BMC Complementary and Alternative Medicine*, vol. 12, no. 1, pp. 58-59, 2012.
- [43] R. Yapasert, B. Sripanidkulchai, M. Teerachaisakul, K. Banchuen, and R. Banjerdpongchai, "Anticancer effects of a traditional Thai herbal recipe Benja Amarit extracts against human hepatocellular carcinoma and colon cancer cell by targeting apoptosis pathways," *Journal of Ethnopharmacology*, vol. 254, 2020.
- [44] R. B. Badisa, S. F. Darling-Reed, P. Joseph, J. S. Cooperwood, L. M. Latinwo, and C. B. Goodman, "Selective cytotoxic activities of two novel synthetic drugs on human breast carcinoma MCF-7 cells," *Anticancer Research*, vol. 29, no. 8, pp. 2993–2996, 2009.
- [45] J. D. Ly, D. R. Grubb, and A. Lawen, "The mitochondrial membrane potential ( $\delta\psi_m$ ) in apoptosis; an update," *Apoptosis*, vol. 8, no. 2, pp. 115–128, 2003.
- [46] E. Gottlieb, S. Armour, M. Harris, and C. Thompson, "Mitochondrial membrane potential regulates matrix configuration and cytochrome c release during apoptosis," *Cell Death & Differentiation*, vol. 10, no. 6, p. 709, 2003.
- [47] L. Fouassier, M. Marzioni, M. B. Afonso et al., "Signalling networks in cholangiocarcinoma: molecular pathogenesis, targeted therapies and drug resistance," *Liver International*, vol. 39, pp. 43–62, 2019.
- [48] J. Jg Marin, E. Lozano, O. Briz, R. Al-Abdulla, M. A Serrano, and R. Ir Macias, "Molecular bases of chemoresistance in cholangiocarcinoma," *Current Drug Targets*, vol. 18, no. 8, pp. 889–900, 2017.
- [49] R. I. Macias, "Cholangiocarcinoma: biology, clinical management, and pharmacological perspectives," *ISRN hepatology*, vol. 2014, 2014.
- [50] R. J. Tallarida, "Quantitative methods for assessing drug synergism," *Genes & cancer*, vol. 2, no. 11, pp. 1003–1008, 2011.
- [51] Y. Liu, Y. Chen, L. Lin, and H. Li, "Gambogic acid as a candidate for cancer therapy: a review," *International Journal of Nanomedicine*, vol. 15, Article ID 10385, 2020.
- [52] J.-J. Lu, J.-L. Bao, X.-P. Chen, M. Huang, and Y.-T. Wang, "Alkaloids isolated from natural herbs as the anticancer agents," *Evidence-Based Complementary and Alternative Medicine*, vol. 2012, Article ID 485042, 12 pages, 2012.
- [53] L. Freire-de-Lima, T. S. Ribeiro, G. M. Rocha et al., "The toxic effects of piperine against *Trypanosoma cruzi*: ultrastructural alterations and reversible blockage of cytokinesis in epimastigote forms," *Parasitology Research*, vol. 102, no. 5, pp. 1059–1067, 2008.
- [54] R. A. Rafiq, B. A. Ganai, and S. A. Tasduq, "Piperine promotes ultraviolet (UV)-B-induced cell death in B16F10 mouse melanoma cells through modulation of major regulators of cell survival," *RSC Advances*, vol. 5, no. 16, pp. 11884–11894, 2015.
- [55] A. Tawani, A. Amanullah, A. Mishra, and A. Kumar, "Evidences for Piperine inhibiting cancer by targeting human G-quadruplex DNA sequences," *Scientific Reports*, vol. 6, no. 1, pp. 39239–39312, 2016.
- [56] T.-C. Chou, "Preclinical versus clinical drug combination studies," *Leukemia and Lymphoma*, vol. 49, no. 11, pp. 2059–2080, 2008.



## Research Article

# Orientin Enhances Colistin-Mediated Bacterial Lethality through Oxidative Stress Involvement

Madonsela Khumbulani,<sup>1</sup> Kazeem Adekunle Alayande ,<sup>2</sup> and Saheed Sabiu <sup>1</sup>

<sup>1</sup>Department of Biotechnology and Food Science, Faculty of Applied Sciences, Durban University of Technology, Durban, South Africa

<sup>2</sup>Unit for Environmental Sciences and Management, North-West University, Potchefstroom, South Africa

Correspondence should be addressed to Saheed Sabiu; [sabius@dut.ac.za](mailto:sabius@dut.ac.za)

Received 3 March 2022; Revised 19 April 2022; Accepted 22 April 2022; Published 9 May 2022

Academic Editor: Sekar Vijayakumar

Copyright © 2022 Madonsela Khumbulani et al. This is an open access article distributed under the Creative Commons Attribution License, which permits unrestricted use, distribution, and reproduction in any medium, provided the original work is properly cited.

Bacterial resistance to colistin has prompted the search for alternative strategies to enhance antibacterial potential. Combination therapy remains one of the viable strategies in antibacterial therapy and has been proven to be effective in reducing the risk of resistance. In this study, the potential of orientin for enhancing the antibacterial activity of colistin was assessed against *Klebsiella pneumoniae* and *Pseudomonas aeruginosa* *in vitro*. The involvement of oxidative stress in such enhancement was also assessed. The minimum inhibitory concentrations (MICs) of colistin and orientin were 16 µg/mL and 64 µg/mL against *K. pneumoniae* and 64 µg/mL and 256 µg/mL against *P. aeruginosa* respectively. For the combination therapy, orientin potentiates the antibacterial effect of colistin with a friction inhibitory concentration index (FICI) of 0.37 and 0.31 against *K. pneumoniae* and *P. aeruginosa*, respectively. This observation suggests a synergistic interaction, with the MIC of colistin being reduced by 3- and 4-fold in the presence of orientin against *K. pneumoniae* and *P. aeruginosa*, respectively. Additionally, treatment with the combination of colistin and orientin induced oxidative stress against both organisms through increased cellular levels of superoxide anion radicals with concomitant increase in NAD<sup>+</sup>/NADH and ADP/ATP ratios. These findings suggest that orientin enhanced colistin in the killing of the test bacteria and the cotreatment of colistin and orientin induced oxidative stress, through reactive oxygen species generation, which consequently facilitated bacterial lethality without causing drug-drug interactions. Although, the data presented in this study has supported the capability of orientin for strengthening antibacterial activity of colistin toward the fight against drug-resistant Gram-negative bacteria, studies focusing on the exact target and mechanism of action of orientin are underway.

## 1. Introduction

Antibiotic resistance remains a persistent health challenge, claiming more than 750000 deaths each year and this has been largely attributed to the overuse and misuse of antibiotics coupled with bacterial evolution [1]. Some bacteria resist antibiotics by altering their genetic material and thus forming antibiotic-resistant genes [2]. While antibiotics such as glycopeptides, aminoglycosides, macrolides, and derivatives through chemical modification of existing antibiotics have been used as improved alternatives in overcoming bacterial resistance to antibiotics, available evidence suggests that adverse effect, continuous resistance evolution,

and cost have undermined their application, hence presenting them as less effective [1]. Even colistin, which has been used as a last resort whenever the use of aminoglycosides, quinolones, and β-lactams is not effective [3], has now been reported to be less potent due to resistance from several bacterial strains [4].

Over the years, plant secondary metabolites have gained research interest due their diverse pharmacological properties including antibacterial, antiviral, antifungal, antioxidant, and anti-inflammatory activities [5]. Specifically, both Gram-negative and Gram-positive bacterial strains have shown susceptibility to several isolated compounds from plants including phenolics [6]. Studies have also implicated



phenolics in antibacterial combination therapy with conventional antibiotics, and such combination therapy has been reported to enhance the antibacterial potential of antibiotics [7, 8].

Antimicrobial combination therapy is one of the viable strategies in clinical practice and has been used to enhance therapeutic action of antibiotics against multidrug-resistant bacterial strains of several infectious diseases [9], to mitigate toxicity [10], and to prevent the emergence of drug resistance [11, 12]. Antibiotics can be used in combination with other antibiotics or with other antibacterial agents. For instance, colistin has been reported to exhibit synergistic action against *Acinetobacter baumannii* when combined with phenolic acids. Besides enhancing the bacterial lethality of conventional antibiotics, phenolic acids such as gallic acid, caffeic acid, and protocatechuic acid with a catechol functional group have been found to act as redox cycluser in a manner that generates reactive oxygen species (ROS) and semiquinone [13]. The ROS generated in the process have been documented to contribute toward bacterial killing *in vitro* [13].

Among the C-glycosylated flavonoids, orientin, iso-orientin, vitexin, and isovitexin are the most frequently implicated therapeutics due to their high stability [14], with orientin finding significant antibacterial applications against *Staphylococcus aureus*, *Escherichia coli*, and *Bacillus subtilis* [14, 15]. Additionally, orientin has a catechol functional group (Figure 1) and may generate ROS as a by-product during catechol oxidation. It is therefore hypothesized that the use of orientin in combination therapy with colistin could enhance the effectiveness of colistin against the ever-increasing infectious diseases caused by pathogenic bacteria that are becoming more difficult to treat. Hence, in this study, the ability of orientin to potentiate colistin against multidrug-resistant Gram-negative bacteria (*Klebsiella pneumoniae* and *Pseudomonas aeruginosa*) was evaluated *in vitro*. The involvement of ROS in such enhancement through monitoring of some important oxidative stress biomarkers was also investigated, while the tendency of the combination of colistin and orientin to cause drug-drug interaction was established *in silico*.

## 2. Materials and Methods

**2.1. Bacterial Cultures, Antibiotics, and Test Compounds.** The *Klebsiella pneumoniae* and *Pseudomonas aeruginosa* strains used in this study were obtained from Anatech Analytical Technology, Olivedale, Gauteng, South Africa. Colistin and orientin were procured from Merck, South Africa, and their stock solutions were prepared by weighing and subsequent dissolution in sterile distilled water. The resulting stock solutions were then preserved at 4°C until further use.

**2.2. In Vitro Antibacterial Evaluation.** Before the determination of minimum inhibitory concentration (MIC), agar well diffusion assay was employed [16], to test whether *K. pneumoniae* and *P. aeruginosa* were susceptible to colistin

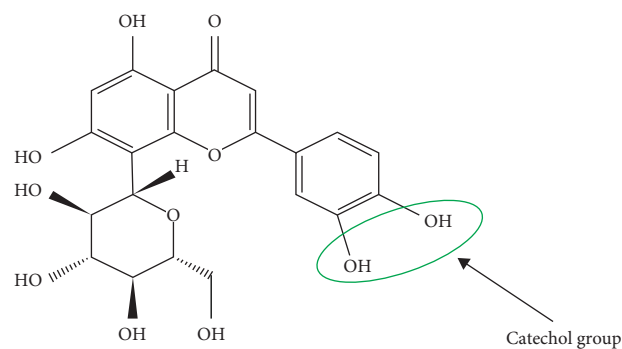


FIGURE 1: Structure of orientin (<https://pubmed.ncbi.nlm.nih.gov/>).

and orientin. Briefly, the surface of the agar plates was inoculated with 100  $\mu$ L of the exponential phase microbial inoculum (*K. pneumoniae* and *P. aeruginosa*). Following inoculation, a hole was bored on the surface of the plate with the tip of a sterile cork borer. Thereafter, 50  $\mu$ L of varying concentrations of colistin and orientin solution was then introduced into the well. The plates were then incubated at 37°C for 24 h. Thereafter, the broth microdilution assay for MIC determination was performed as earlier reported [16], following the clinical and laboratory standard institute guidelines [17] for both orientin and colistin. This was then followed by the evaluation of the minimum bactericidal concentrations (MBCs) against *K. pneumoniae* and *P. aeruginosa*. In brief, two-fold serial dilutions of orientin and colistin were prepared for the determination of the MIC. The bacterial suspensions were prepared by transferring colonies aseptically into sterile saline (0.85%). The turbidity was adjusted to 0.5 McFarland standards using spectrophotometer at 600 nm. The prepared orientin (1024  $\mu$ g/mL) and colistin (512  $\mu$ g/mL) solutions were mixed with the bacterial suspension in a 96-well microtiter plate. After adequate mixing, the microtiter plate was then incubated at 37°C for 24 h. The experiment was done in triplicate, and the MICs in the two organisms were determined from the well with the lowest concentration showing no turbidity bacterial growth. For the MBC determination, on the other hand, nutrient agar plates were used for plating the dilutions representing at least two concentrations of colistin and orientin above the MIC, followed by incubation for 48 h at 37°C, and the colonies were counted to determine the viable CFU/mL.

**2.3. Checkerboard Assay.** For the determination of the combined antibacterial effect of orientin with colistin against *K. pneumoniae* and *P. aeruginosa*, checkerboard assay was employed as previously described [18]. Using the prepared stock solution of orientin and colistin, two-fold serial dilutions were performed in Mueller–Hinton broth (MHB) in sterile 96-well microtiter plates in decreasing concentrations. The standardized (0.5 McFarland) suspensions of *K. pneumoniae* and *P. aeruginosa* were inoculated into the wells of the microtiter plates. The wells containing the broth but no bacteria served as negative controls, and the ones with

both broth and suspension of either *K. pneumoniae* or *P. aeruginosa* suspensions represented positive controls. The friction inhibitory concentration index (FICI) was then calculated to evaluate the combined effect of colistin and orientin using the following formula:

$$\text{FICI} = \frac{\text{MIC of orientin in combination with colistin}}{\text{MIC of orientin alone}} + \frac{\text{MIC of colistin in combination with orientin}}{\text{MIC of colistin alone}} \quad (1)$$

The probable combined effect of colistin and orientin was established in accordance with an earlier method [19], where an FICI of 0.5 or below signifies synergism, values above 0.5 and less than 4 indicate indifferent interaction, and values above 4.0 indicate antagonistic effect.

**2.4. Time-Kill Susceptibility Test.** The rate at which treatment with either colistin or orientin and their combination kills bacteria (*K. pneumoniae* and *P. aeruginosa*) over time was evaluated [13, 20]. Using a 96-well microtiter plate, 50  $\mu\text{L}$  of MHB was added in each well followed by the addition of colistin, orientin, and combination of colistin with orientin. Following the addition of antimicrobial agents, 50  $\mu\text{L}$  of the standard inoculum of *K. pneumoniae* and *P. aeruginosa* was inoculated into the wells of the microtiter plates. The growth control wells were comprised of only MHB and bacterial inoculum. Thereafter, the microtiter plates were incubated at 37°C to measure the optical density at 0, 2, 4, 6, 8, and 24 h after the addition of bacterial inoculum. The time-kill curves were plotted as the decrease in the optical density within the experimentation period.

## 2.5. Oxidative Stress Biomarker Assays

**2.5.1. NAD<sup>+</sup>/NADH Assay.** The ratio of NAD<sup>+</sup>/NADH in *K. pneumoniae* and *P. aeruginosa* cells treated with colistin, orientin, and their combination was estimated based on the procedure outlined in NAD<sup>+</sup>/NADH quantification kit (Sigma-Aldrich, MAK 037). The bacterial cells at exponential phase were incubated with colistin (with or without orientin) and with orientin alone at a resulting concentration of 4  $\times$  MIC for each treatment for 30 minutes at 37°C. After incubation, cold phosphate buffer saline (pH 7.5) was utilized to wash bacterial cells, followed by centrifugation (2000  $\times$ g, 5 minutes). Treated cells were frozen/thawed for two cycles on dry ice for 20 minutes followed by 10 minutes at room temperature using NAD<sup>+</sup>/NADH extraction buffer. Thereafter, samples were centrifuged (13000  $\times$ g, 10 minutes) to separate the cell-free extract. Subsequently, NAD<sup>+</sup>/NADH extraction buffer (50  $\mu\text{L}$ ) was used to treat 50  $\mu\text{L}$  of the cells and then followed by the addition of 100  $\mu\text{L}$  of master mix (NAD cycling buffer and NAD cycling enzyme). After complete mixing, the reaction was incubated for 5 minutes at room temperature. Thereafter, the absorbance was read at 450 nm following the addition of NADH de-veloper (10  $\mu\text{L}$ ) and incubation for 2 h at room temperature.

The ratio of NAD<sup>+</sup>/NADH in the samples was then determined using the following equation:

$$\frac{\text{NAD}^+}{\text{NADH ratio}} = \frac{\text{NADtotal} - \text{NADH}}{\text{NADH}} \quad (2)$$

where NAD<sup>+</sup><sub>total</sub> is the amount of total NAD<sup>+</sup> (NAD<sup>+</sup> + NADH) in the unknown sample (treated bacterial cells) (pmole) from the standard curve and NADH is the amount of NADH in treated bacterial cells (pmole) from the standard curve.

**2.5.2. ADP/ATP Assay.** For the determination of ADP/ATP ratio, the procedure outlined in ADP/ATP ratio quantification kit (Sigma-Aldrich, MAK 135) was employed. The *K. pneumoniae* and *P. aeruginosa* cells at exponential phase were treated with colistin (with or without orientin) and with orientin alone (with a resulting concentration of 4  $\times$  MIC for each treatment) and incubated for 30 minutes at 37°C. An equal volume of ATP reagent (90  $\mu\text{L}$ ) was mixed with the cells and incubated for 1 minute at room temperature. Luminescence (relative light units) was read for ATP assay (RLU<sub>A</sub>). The luminescence for ATP (RLU<sub>B</sub>) was read to provide the background before ADP measurement after the mixture was incubated for 10 minutes. After reading (RLU<sub>B</sub>), ADP reagent (5  $\mu\text{L}$ ) was added and mixed immediately, and the luminescence (RLU<sub>C</sub>) was read after 1 minute. Then ADP/ATP ratio was estimated using the following equation:

$$\frac{\text{ADP}}{\text{ATP ratio}} = \frac{\text{RLU}_C - \text{RLU}_B}{\text{RLU}_A} \quad (3)$$

**2.5.3. Superoxide Anion Radical Assay.** The *K. pneumoniae* and *P. aeruginosa* cells were grown into exponential phase. Following incubation, the cells were further incubated with 0.5 mL of 4  $\times$  MIC of colistin, orientin, and their combination (with a resulting concentration of 4  $\times$  MIC) for 30 minutes at 37°C. Thereafter, 0.25 mL of nitroblue tetrazolium (1 mg/ml) was added and incubated for another 30 minutes at 37°C. Following incubation, 0.05 mL of 0.1 mM HCl was added, followed by centrifugation at 1500  $\times$ g for 20 minutes. The nitroblue tetrazolium that was reduced in the pellets was extracted and further diluted with 0.8 mL of phosphate-buffered saline (pH 7.5). A microtiter plate reader absorbance was then used to read the absorbance at 575 nm. Thereafter, the amount of superoxide anion radical generated was calculated using a molar extinction coefficient of 3-(4,5-dimethylthiazol-2 $\gamma$ -1)-2,5-diphenyltetrazolium bromide formazan (17000 M<sup>-1</sup>·cm<sup>-1</sup> at pH 7.4–8) as described by [13] and then converted to percentage.

**2.6. Evaluation of Probable Drug-Drug Interaction between Colistin and Orientin.** For molecular docking, the crystal structure of cytochrome 3A4 (CYP3A4) was obtained from RCSB protein data bank (<https://www.rcsb.org/>) and used as rigid molecule receptor for colistin, orientin, ketocozazole, and rifampicin. The 3D structures of colistin and

TABLE 1: Antibacterial activities of colistin and orientin and their friction inhibitory concentration index.

Test isolates	Zone of inhibition (mm)		MIC ( $\mu\text{g}/\text{mL}$ )		MBC ( $\mu\text{g}/\text{mL}$ )		FICI	Interactions
	Colistin	Orientin	Colistin	Orientin	Colistin	Orientin		
<i>K. pneumoniae</i>	23	25	16	64	128	512	0.37	Synergistic
<i>P. aeruginosa</i>	18	11	64	256	256	1024	0.31	Synergistic

MIC: minimum inhibitory concentration, MBC: minimum bactericidal concentration, and FICI: friction inhibitory concentration index.

rifampicin were obtained from ChemSpider (<http://www.chemspider.com/>) while those of orientin and ketoconazole were obtained from PubChem in sdf format (<https://pubchem.ncbi.nlm.nih.gov/>). The nonstandard residues, complexes such as nonessential water molecules, and heteroatoms that were bound to the active site of CYP3A4 were removed using UCSF Chimera 1.15 software to prepare CYP3A4 for docking. Gasteiger charges were added to the molecule, and nonpolar hydrogens atoms were merged into carbon atoms prior to docking. The grid box, with a spacing of 1 Å and size of  $31.13 \times 30.54 \times 26.54$  pointing toward  $x$ ,  $y$ , and  $z$  directions, was firstly defined to dock the compounds to the binding site of CYP3A4. The binding energies of colistin and orientin were then compared with those of conventional inhibitor (ketoconazole) and inducer (rifampicin) of CYP3A4. Furthermore, SwissADME (<http://www.swissadme.ch/>) was utilized to predict the ADMET properties of colistin and orientin against CYP3A4.

**2.7. Statistical Analysis.** GraphPad Prism version 5.0 using one-way ANOVA was utilized to analyze the *in vitro* results, followed by nonparametric tests to detect any significant difference ( $p < 0.05$ ) between the treatment means. The results are presented as mean  $\pm$  standard error of the mean (SEM).

### 3. Results

**3.1. Antibacterial Activity.** The results obtained from the agar well diffusion assay revealed that the test organisms were susceptible to colistin and orientin, with larger zones of inhibition observed against *K. pneumoniae* compared to *P. aeruginosa* (Figure S1). The zones of inhibition obtained with colistin (256  $\mu\text{g}/\text{mL}$ ) were 23 mm and 18 mm against *K. pneumoniae* and *P. aeruginosa*, respectively, while they were 11 mm and 25 mm for *P. aeruginosa* and *K. pneumoniae*, respectively, following treatment with orientin (512  $\mu\text{g}/\text{mL}$ ) (Table 1). Furthermore, the data obtained with respect to MICs of the test compounds revealed that colistin and orientin had values less than  $\leq 64 \mu\text{g}/\text{mL}$  with MBC ranging between 128 and 512  $\mu\text{g}/\text{mL}$  against *K. pneumoniae*, while they had MICs  $\leq 256 \mu\text{g}/\text{mL}$  with MBC ranging between 256 and 1024  $\mu\text{g}/\text{mL}$  against *P. aeruginosa* (Table 1). From the checkerboard assay, it was observed that the combination of colistin and orientin resulted in a synergistic interaction as the FICI was 0.37 and 0.31 against *K. pneumoniae* and *P. aeruginosa*, respectively (Table 1).

**3.2. Time-Kill Analysis.** Treatment with colistin and orientin alone as well as their combination resulted in decreased number of viable bacterial cells measured as the optical density of *K. pneumoniae* which decreased after 2 h of treatment and remained constant throughout the 24 h exposure time (Figure 2(a)). For *P. aeruginosa*, only the combination of colistin and orientin showed an observable reduction in optical density after 2 h of treatment and was maintained over the 24 h exposure period (Figure 2(b)). A noticeable increase in viable cells was however observed in treatments with colistin and orientin alone after 24 h of exposure (Figure 2(b)).

**3.3. Oxidative Stress Markers.** The results of involvement of ROS/oxidative stress in the bacterial lethality of the test compounds are presented in Figures 3–5. The cellular levels of  $\text{NAD}^+/\text{NADH}$  and  $\text{ADP}/\text{ATP}$  ratios increased significantly ( $p < 0.05$ ) in both *K. pneumoniae* and *P. aeruginosa* cells following treatment with test compounds relative to cells treated with sterile distilled water (control) (Figures 2–4). The *K. pneumoniae* and *P. aeruginosa* cells treated with colistin and orientin as well as their combination were significantly different ( $p < 0.05$ ) regarding generation of superoxide anion radical compared to cells treated with sterile distilled water, with the combined treatment having the most profound effect in each case (Figures 5(a) and 5(b)).

**3.4. Drug-Drug Interactions.** From the molecular docking results, colistin and orientin had binding energy values of  $-8.0 \text{ kcal/mol}$  and  $-9.0 \text{ kcal/mol}$  with 10 and 5 hydrogen bonds, respectively (Table 2, Figures S2 and S3). These values are more or less the same as those of ketoconazole ( $-9.5 \text{ kcal/mol}$ ) and rifampicin ( $-7.7 \text{ kcal/mol}$ ), but with 2 and 3 hydrogen bonds, respectively (Table 2, Figures S4 and S5). A further probe into their probable drug-drug interaction tendency with SwissADME predicts both colistin and orientin to be neither inducers nor inhibitors of CYP3A4 (Table 2).

### 4. Discussion

Due to the devastating effect of multidrug-resistant strains of Gram-negative bacteria, the reuse of colistin has been advocated and becoming increasingly embraced [4]. However, despite their efficacy, some Gram-negative bacteria belonging to the Enterobacteriaceae family such as *K. pneumoniae* and *P. aeruginosa*, which are implicated in diseases such as bacteremia, septicemia, hospital acquired

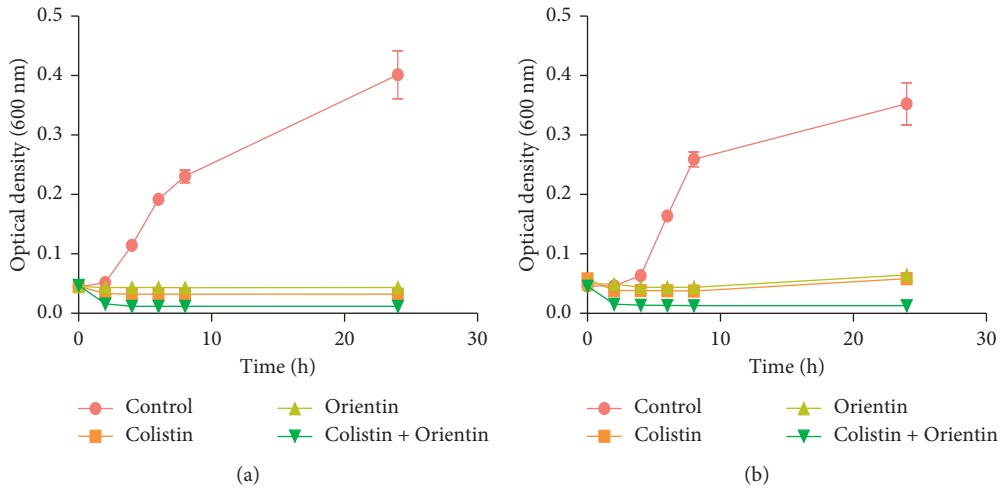


FIGURE 2: Time-kill growth curves of (a) *K. pneumoniae* and (b) *P. aeruginosa* treated with 4×MIC of colistin, orientin, and their combination. No significant difference ( $p < 0.05$ ) was observed with colistin and orientin alone.

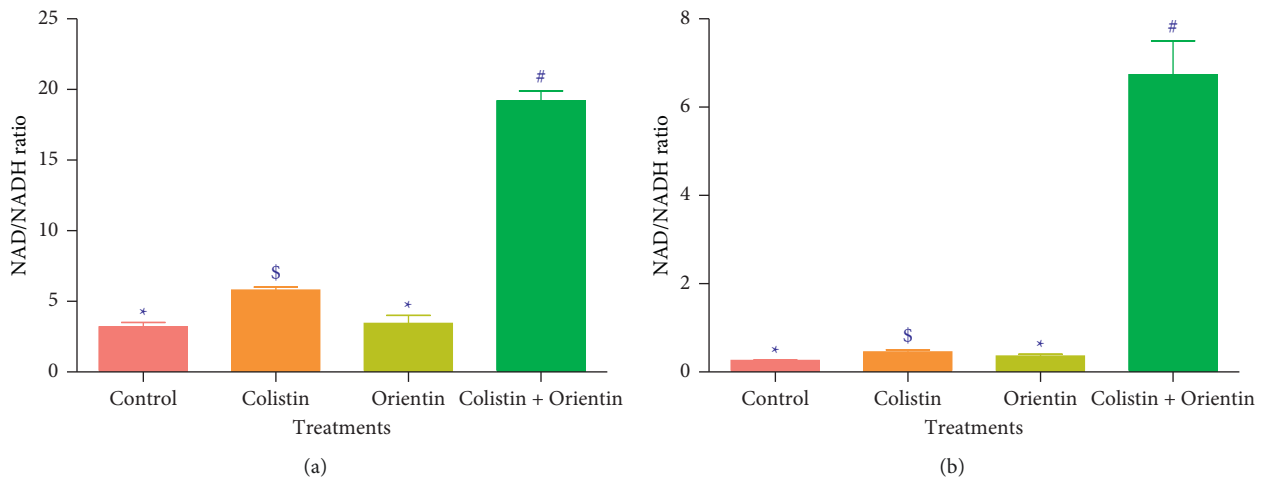


FIGURE 3: NAD<sup>+</sup>/NADH ratio in (a) *K. pneumoniae* and (b) *P. aeruginosa* treated with dH<sub>2</sub>O, colistin, orientin, and colistin with orientin (4×MIC). Bars with different symbols are significantly different ( $p < 0.05$ ) from each other.

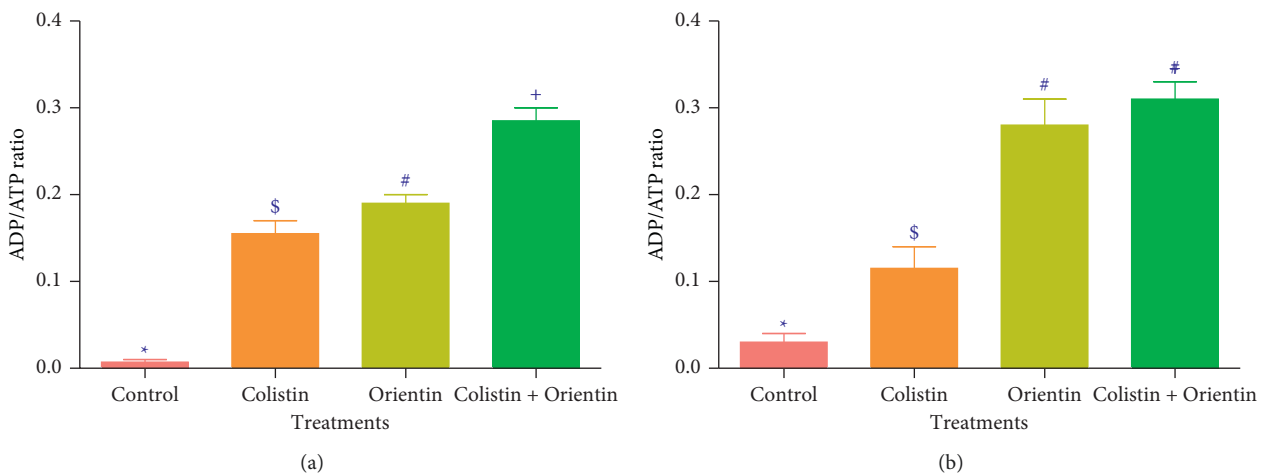


FIGURE 4: ADP/ATP ratio in (a) *K. pneumoniae* and (b) *P. aeruginosa* cells treated with dH<sub>2</sub>O, colistin, orientin, and colistin with orientin (4×MIC). Bars with different symbols are significantly different ( $p < 0.05$ ) from each other.

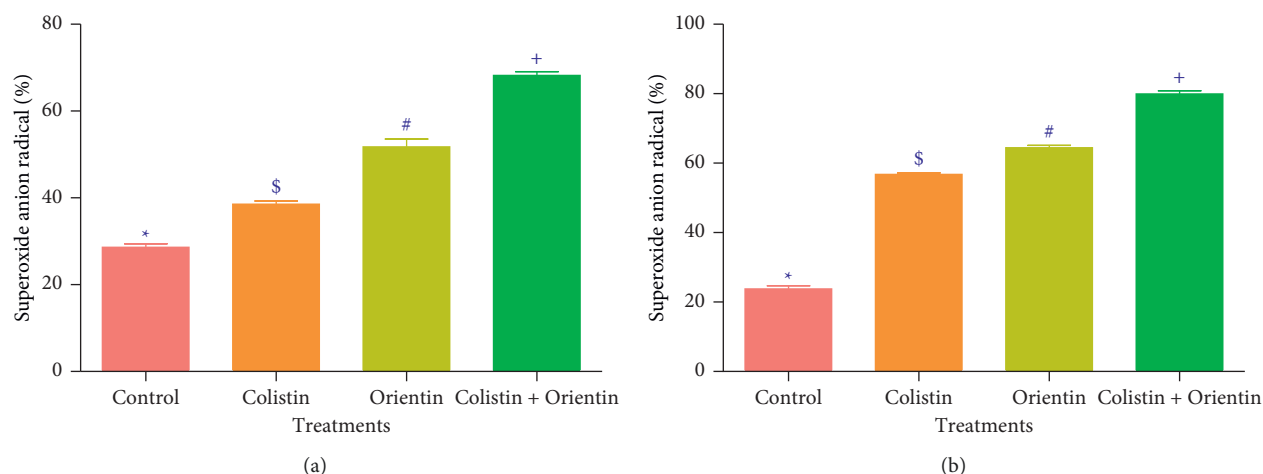


FIGURE 5: Superoxide anion radical generated following the treatment with colistin, orientin, and combination of colistin with orientin at  $4 \times \text{MIC}$  against (a) *K. pneumoniae* and (b) *P. aeruginosa*. Bars with different symbols are significantly different ( $p < 0.05$ ).

TABLE 2: Interactions and binding energies of the compounds and standards against CYP3A4 protein.

Protein	Compounds	Binding energy score (kcal/mol)	No. of hydrogen bonds	Hydrogen bonds interactions	SwissADME remarks	
					Inhibitor	Inducer
CYP3A4	Colistin	-8.0	10	Cys 442, Ala 305, Pro 434, Thr 433, Arg 372, Ala 370, Gly 481, Phe 213, Ser 119	No	No
	Orientin	-9.0	5	Ala 370, Arg 106, Glu 374, Arg 105	No	No
	Ketoconazole	-9.5	2	Ile 443, Gly 444	Yes	No
	Rifampicin	-7.7	3	Arg 105, Arg 212	No	Yes

pneumonia and lung infections, and ventilator-associated pneumonia, have remained consistently resistant to colistin [3]. Since colistin is regarded as the last hope for treating infections caused by Gram-negative bacteria, strategies to overcome this menace are highly needed. Among the available strategies, combination therapy has been recognized as one of the viable options in enhancing the antibacterial potency of antibiotics [9]. Previously, it has also been reported that phenolics with catechol functional group such as protocatechuic acid, ferulic acid, and gallic acid possess antibacterial activity against both Gram-negative and Gram-positive bacteria, and ROS involvement has been demonstrated as an important contributor to the process [13, 21–23]. In this study, the combination of colistin with orientin, a catechol functional group bearing flavonoid, was evaluated against *K. pneumoniae* and *P. aeruginosa*. The observed high MIC values of orientin relative to colistin in the current study are not surprising because colistin is a conventional antibiotic that has been modified while orientin is a mere plant secondary metabolite that could be further modified to enhance its antibacterial effect. Nevertheless, judging by a previous submission [24] that MIC values  $> 1000 \mu\text{g/mL}$  should be avoided for crude extract and isolated compounds and that MIC range of phyto-compounds should be between 100 and  $1000 \mu\text{g/mL}$  to be classified as antimicrobials [25], the results from this study regarding the MIC values can be regarded as remarkable for

orientin with significant activity against the test organisms as its MIC values were less than  $1000 \mu\text{g/mL}$ .

Combination therapy allows the use of lower concentrations and therefore minimizes the advent of probable toxicity [26, 27]. The type of interaction that results from the combination of colistin and orientin against both *K. pneumoniae* and *P. aeruginosa* was synergistic as the FICI was 0.37 and 0.31, respectively. Based on the FICI values obtained in this study, orientin reduced the MIC value of colistin by three- and fourfold against *K. pneumoniae* and *P. aeruginosa*, respectively. This not only suggests that orientin enhanced the antibacterial activity of colistin, but also is indicative of its propensity to act on a different target other than the cell membrane like colistin [28]. In a previous study [8], morin and quercetin (flavonoids) enhanced the activity of ciprofloxacin and tetracycline against *Staphylococcus aureus* CECT 796, ciprofloxacin against *S. aureus* 1199B, and tetracycline against methicillin-resistant strains. This was said to be associated with the existence, amount, and degree of substitution of hydroxyl or methyl groups on the benzene ring. Hence, these properties could also have had a crucial role in the antibacterial activity of orientin in addition to its catechol group. In addition to checkerboard assay, time-kill kinetics further supported the synergistic interaction of colistin and orientin as both *K. pneumoniae* and *P. aeruginosa* cells were completely killed following treatment with their combination. These results suggest that



the combination of colistin with orientin at the investigated concentrations was bactericidal against both isolates. However, the observed regrowth of *P. aeruginosa* cells after 24 h of treatment with either colistin or orientin alone could mean that colistin and orientin alone were bacteriostatic against *P. aeruginosa* at the investigated concentrations. This observation is in line with the report of Abreu et al. [8], where the regrowth of *S. aureus* SA1199B was observed after 8 h, following treatment with rutin, demonstrating the bacteriostatic effect of rutin at the investigated concentration.

The generation of ROS is regarded as one of the important aspects of antibiotics that induce oxidative stress in bacteria with subsequent contribution to its lethality [29]. Of the ROS generating pathways involved in bacterial lethality, the tricarboxylic acid (TCA) cycle plays a significant role [30]. According to Adam-Vizi and Chinopoulos [31], ROS, particularly superoxide anion radicals, are mainly produced in the mitochondria, and their production is associated with high NAD<sup>+</sup>/NADH levels. In this study, the high levels of NAD<sup>+</sup>/NADH ratio produced in the cotreatment relative to the single treatments particularly against *K. pneumoniae* could signify the involvement of oxidative stress in the killing of *K. pneumoniae* and *P. aeruginosa*. In addition to the increased NAD<sup>+</sup>/NADH ratio, the increased ADP/ATP ratio in *K. pneumoniae* and *P. aeruginosa* cells treated with colistin, orientin, and their combination may be indicative of ATP accumulation which could have resulted from the inhibition of energy-consuming processes such as phase I of glycolysis [30]. This inhibition could further inhibit the primary electron flow pathway (oxidation of NADH to NAD<sup>+</sup> in the TCA cycle) together with the electron transport chain, and this could be transferred to oxygen molecules by side reactions to produce ROS as earlier reported [32]. Previous studies have implicated and documented the elevation of ROS, particularly superoxide anion radical, as one of the common mechanisms for bactericidal antimicrobials [32, 33]. The elevation of superoxide anion radical in the cells treated with either colistin, orientin, or their combination may be attributable to ROS generation. However, the elevation of superoxide anion radical was more observed in the cotreatment regimen. This could be due to the inhibition of electron transport chain activities, and this observation is consistent with the study of Ajiboye et al. [34], where only the cotreatment of colistin with phenolic acids increased the generation of superoxide anion radicals against both the wild type and mutant strains of *A. baumannii*.

A major issue associated with combination therapy is drug-drug interaction (DDI) which could result in serious harm to patients and even lead to death [35]. The CYP3A4 is one of the most vital isoenzymes belonging to the P450 family and is responsible for metabolism of several (> 60%) drugs, hence potentiating a crucial biological and medicinal application [36, 37]. Studies have revealed a higher risk of adverse effects and negative impact on the efficacy of coadministered drugs under influence of CYP3A4 [38, 39]. Thus, assessing the probable interactions between therapeutic agents and CYP3A4 is imperative to their application. According to Tallei [40], the formation of hydrogen bonds is

one of the indices that could be used to establish the pattern of interactions between a ligand and a suitable receptor, which will, in turn, dictate the biological properties of the resulting complex. In this study, molecular docking against CYP3A4 revealed that the combination of colistin and orientin will not result in DDI when coadministered. This was evident from the observation that the number of hydrogen bonds formed in ketoconazole and rifampicin complexes was less than 5 contrary to those of colistin and orientin. Additionally, the observed hydrogen bonds with Ile 443, Gly 444, Arg 105, and Arg 212 at the binding pockets of CYP3A4 with either ketoconazole or rifampicin, which were absent in complexes with orientin and colistin, could be another good reason why neither colistin nor orientin is an inducer or an inhibitor of CYP3A4. This was further corroborated by the SwissADME prediction, thus allaying the fear of DDI in the event of coadministration of colistin and orientin.

## 5. Conclusion

The emergence of antibiotic-resistant Gram-negative bacteria has continued to prompt the need for alternative strategies to overcome this menace. Combination therapy is one of the strategies that are gaining much interest as it addresses issues relating to resistance, while providing broad-spectrum antibacterial activity with reduced toxicological concerns. In this study, it was demonstrated that orientin potentiates colistin in the killing of *K. pneumoniae* and *P. aeruginosa* through the reduced MIC of colistin from 16 to 2 µg/mL against *K. pneumoniae* and from 64 to 4 µg/mL against *P. aeruginosa*. Furthermore, the increased level of NAD<sup>+</sup>/NADH and ADP/ATP ratios coupled with the generation of superoxide anion radicals revealed that the cotreatment of colistin and orientin induced oxidative stress, in a manner that enhanced bacterial lethality. Even though orientin acted synergistically with colistin, the exact mechanism through which orientin does this is still not clearly known. Hence, studies on information about the exact target and mechanism of antibacterial action of orientin are imperative and highly recommended.

## Data Availability

The data used to support the findings of this study are included within the article.

## Conflicts of Interest

The authors declare no potential conflicts of interest.

## Authors' Contributions

SS designed, supervised, and acquired funding for the study. KM performed the laboratory work. KM, KAA, and SS contributed to the interpretation of the results. KM wrote the original draft of the manuscript. All authors read and approved the final version for publication.



## Supplementary Materials

Additional data for the results of the antibacterial activities of colistin and orientin as well as those of the molecular docking are presented in the supplementary file (Figures S1–S5). (*Supplementary Materials*)

## References

- [1] W. C. Reygaert, “An overview of the antimicrobial resistance mechanisms of bacteria,” *AIMS Microbiology*, vol. 4, no. 3, pp. 482–501, 2018.
- [2] E. Goldman, “Antibiotic abuse in animal agriculture: exacerbating drug resistance in human pathogens,” *Human and Ecological Risk Assessment: An International Journal*, vol. 10, no. 1, pp. 121–134, 2004.
- [3] S. Biswas, J.-M. Brunel, J.-C. Dubus, M. Reynaud-Gaubert, and J.-M. Rolain, “Colistin: an update on the antibiotic of the 21st century,” *Expert Review of Anti-infective Therapy*, vol. 10, no. 8, pp. 917–934, 2012.
- [4] Z. Aghapour, P. Gholizadeh, K. Ganbarov et al., “Molecular mechanisms related to colistin resistance in enterobacteriaceae,” *Infection and Drug Resistance*, vol. 12, pp. 965–975, 2019.
- [5] C. L. Gorlenko, H. Y. Kiselev, E. V. Budanova, A. A. Zamyatnin, and L. N. Ikryannikova, “Plant secondary metabolites in the battle of drugs and drug-resistant bacteria: new heroes or worse clones of antibiotics?” *Antibiotics*, vol. 9, no. 4, p. 170, 2020.
- [6] A. Adamczak, M. Ożarowski, and T. M. Karpiński, “Antibacterial activity of some flavonoids and organic acids widely distributed in plants,” *Journal of Clinical Medicine*, vol. 9, no. 1, p. 109, 2019.
- [7] R. Musumeci, A. Speciale, R. Costanzo et al., “*Berberis aetnensis* C. Presl. extracts: antimicrobial properties and interaction with ciprofloxacin,” *International Journal of Antimicrobial Agents*, vol. 22, no. 1, pp. 48–53, 2003.
- [8] A. C. Abreu, S. C. Serra, A. Borges et al., “Combinatorial activity of flavonoids with antibiotics against drug-resistant *Staphylococcus aureus*,” *Microbial Drug Resistance*, vol. 21, no. 6, pp. 600–609, 2015.
- [9] P. J. Petersen, P. Labthavikul, C. H. Jones, and P. A. Bradford, “*In vitro* antibacterial activities of tigecycline in combination with other antimicrobial agents determined by checkerboard and time-kill kinetic analysis,” *Journal of Antimicrobial Chemotherapy*, vol. 57, no. 3, pp. 573–576, 2006.
- [10] E. Gradelski, L. Valera, D. Bonner, and J. Fung-Tomc, “Synergistic activities of gatifloxacin in combination with other antimicrobial agents against *Pseudomonas aeruginosa* and related species,” *Antimicrobial Agents and Chemotherapy*, vol. 45, no. 11, pp. 3220–3222, 2001.
- [11] G. P. Allen, R. Cha, and M. J. Rybak, “*In vitro* activities of quinupristin-dalfopristin and cefepime, alone and in combination with various antimicrobials, against multidrug-resistant *Staphylococci* and *Enterococci* in an *in vitro* pharmacodynamic model,” *Antimicrobial Agents and Chemotherapy*, vol. 46, no. 8, pp. 2606–2612, 2002.
- [12] G. R. Zimmermann, J. Lehár, and C. T. Keith, “Multi-target therapeutics: when the whole is greater than the sum of the parts,” *Drug Discovery Today*, vol. 12, no. 1–2, pp. 34–42, 2007.
- [13] T. O. Ajiboye, E. Skiebe, and G. Wilharm, “Phenolic acids potentiate colistin-mediated killing of *Acinetobacter baumannii* by inducing redox imbalance,” *Biomedicine & Pharmacotherapy*, vol. 101, pp. 737–744, 2018.
- [14] J. Xiao, E. Capanoglu, A. R. Jassbi, and A. Miron, “Advance on the flavonoid C-glycosides and health benefits,” *Critical Reviews in Food Science and Nutrition*, vol. 56, no. 1, pp. S29–S45, 2016.
- [15] D. Barreca, E. Bellocco, U. Leuzzi, and G. Gattuso, “First evidence of C- and O-glycosyl flavone in blood orange (*Citrus sinensis* (L.) Osbeck) juice and their influence on antioxidant properties,” *Food Chemistry*, vol. 149, pp. 244–252, 2014.
- [16] M. Balouiri, M. Sadiki, and S. K. Ibnsouda, “Methods for *in vitro* evaluating antimicrobial activity: a review,” *Journal of Pharmaceutical Analysis*, vol. 6, no. 2, pp. 71–79, 2016.
- [17] CLSI, *Performance Standards for Antimicrobial Susceptibility Testing. CLSI Supplement M100*, Clinical and Laboratory Standards Institute, Wayne, PA, USA, 28th edition, 2018.
- [18] S. Bajaksouzian, M. A. Visalli, M. R. Jacobs, and P. C. Appelbaum, “Activities of levofloxacin, ofloxacin, and ciprofloxacin, alone and in combination with amikacin, against *Acinetobacters* as determined by checkerboard and time-kill studies,” *Antimicrobial Agents and Chemotherapy*, vol. 41, no. 5, pp. 1073–1076, 1997.
- [19] D. J. Winston, W. G. Ho, D. A. Bruckner, and R. E. Champlin, “Beta-lactam antibiotic therapy in febrile granulocytopenic patients: a randomized trial comparing cefoperazone plus piperacillin, ceftazidime plus piperacillin, and imipenem alone,” *Annals of Internal Medicine*, vol. 115, no. 11, pp. 849–859, 1991.
- [20] D. F. Basri, L. W. Xian, N. I. Abdul Shukur, and J. Latip, “Bacteriostatic antimicrobial combination: antagonistic interaction between epsilon- $\epsilon$ -viniferin and vancomycin against methicillin-resistant *Staphylococcus aureus*,” *BioMed Research International*, vol. 2014, Article ID 461756, 8 pages, 2014.
- [21] H. Sakagami and K. Satoh, “Prooxidant action of two antioxidants: ascorbic acid and gallic acid,” *Anticancer Research*, vol. 17, no. 1A, pp. 221–224, 1997.
- [22] M. Y. Moridani, H. Scobie, A. Jamshidzadeh, P. Salehi, and P. J. O’Brien, “Caffeic acid, chlorogenic acid, and dihydrocaffeic acid metabolism: glutathione conjugate formation,” *Drug metabolism and disposition: The Biological Fate of Chemicals*, vol. 29, no. 11, pp. 1432–1439, 2001.
- [23] M. L. Zeraik, M. S. Petrônio, D. Coelho et al., “Improvement of pro-oxidant capacity of protocatechuic acid by esterification,” *PLoS One*, vol. 9, no. 10, Article ID e110277, 2014.
- [24] J. L. Rios and M. C. Recio, “Medicinal plants and antimicrobial activity,” *Journal of Ethnopharmacology*, vol. 100, no. 1–2, pp. 80–84, 2005.
- [25] M. Simões, R. N. Bennett, and E. A. S. Rosa, “Understanding antimicrobial activities of phytochemicals against multidrug resistant bacteria and biofilms,” *Natural Product Reports*, vol. 26, no. 6, pp. 746–757, 2009.
- [26] R. C. Tellis, S. Vidyasagar, M. Moosabba, and R. C. Tellis, “Activity of antibiotic combinations against multidrug resistant *Pseudomonas aeruginosa*: a study from South India,” *International Journal of Current Microbiology and Applied Sciences*, vol. 2, no. 4, pp. 27–34, 2016.
- [27] N. Ul Islam, E. Khan, M. Naveed Umar et al., “Enhancing dissolution rate and antibacterial efficiency of azithromycin through drug-drug cocrystals with paracetamol,” *Antibiotics*, vol. 10, no. 8, p. 939, 2021.
- [28] I. H. N. Bassolé and H. R. Juliani, “Essential oils in combination and their antimicrobial properties,” *Molecules*, vol. 17, no. 4, pp. 3989–4006, 2012.
- [29] M. N. Al-Hasan, J. W. Wilson, B. D. Lahr et al., “ $\beta$ -lactam and fluoroquinolone combination antibiotic therapy for

- bacteremia caused by gram-negative bacilli,” *Antimicrobial Agents and Chemotherapy*, vol. 53, no. 4, pp. 1386–1394, 2009.
- [30] A. V. Akhova and A. G. Tkachenko, “ATP/ADP alteration as a sign of the oxidative stress development in *Escherichia coli* cells under antibiotic treatment,” *FEMS Microbiology Letters*, vol. 353, no. 1, pp. 69–76, 2014.
- [31] V. Adam-Vizi and C. Chinopoulos, “Bioenergetics and the formation of mitochondrial reactive oxygen species,” *Trends in Pharmacological Sciences*, vol. 27, no. 12, pp. 639–645, 2006.
- [32] J. O. Aribisala, S. Nkosi, I. Idowu et al., “Astaxanthin-mediated bacterial lethality: evidence from oxidative stress contribution and molecular dynamics simulation,” *Oxidative Medicine and Cellular Longevity*, vol. 2021, no. 24, Article ID 7159652, 2021.
- [33] M. A. Kohanski, D. J. Dwyer, and J. J. Collins, “How antibiotics kill bacteria: from targets to networks,” *Nature Reviews Microbiology*, vol. 8, no. 6, pp. 423–435, 2010.
- [34] T. O. Ajiboye, M. Aliyu, I. Isiaka et al., “Contribution of reactive oxygen species to (+)-catechin-mediated bacterial lethality,” *Chemico-Biological Interactions*, vol. 258, pp. 276–287, 2016.
- [35] R. L. Slaughter and D. J. Edwards, “Recent advances: the cytochrome P450 enzymes,” *The Annals of Pharmacotherapy*, vol. 29, no. 6, pp. 619–624, 1995.
- [36] G. R. Wilkinson, “Drug metabolism and variability among patients in drug response,” *New England Journal of Medicine*, vol. 352, no. 21, pp. 2211–2221, 2005.
- [37] L. Basheer and Z. Kerem, “Interactions between CYP3A4 and dietary polyphenols,” *Oxidative Medicine and Cellular Longevity*, vol. 2015, Article ID 854015, 15 pages, 2015.
- [38] D. G. Bailey, J. M. O. Arnold, J. D. Spence, and J. D. Spence, “Grapefruit juice-drug interactions,” *British Journal of Clinical Pharmacology*, vol. 58, no. 7, pp. S831–S840, 2004.
- [39] S. Sabiu and K. Idowu, “An insight on the nature of biochemical interactions between glycyrrhizin, myricetin and CYP3A4 isoform,” *Journal of Food Biochemistry*, vol. 46, no. 3, Article ID e13831, 2021.
- [40] T. E. Tallei, A. Y. Fatimawali, A. Yelnetty et al., “An analysis based on molecular docking and molecular dynamics simulation study of bromelain as anti-SARS-CoV-2 variants,” *Frontiers in Pharmacology*, vol. 12, Article ID 717757, 2021.

## Research Article

# Zhuye Shigao Decoction Combined with Qingqi Huatan Pills in Alleviating the Acute Exacerbation of Chronic Obstructive Pulmonary Disease (Phlegm-Heat Stagnating in the Lungs) via the IL-6-Mediated JAK1/STAT3 Signaling Pathway

Yunkun Chen and Wenbin Zhang 

Department of Respiratory and Critical Care Medicine, Chongqing Traditional Chinese Medicine Hospital, No. 40, Daomenkou, Yuzhong District, Chongqing 400011, China

Correspondence should be addressed to Wenbin Zhang; 56871072@qq.com

Received 18 January 2022; Revised 7 March 2022; Accepted 31 March 2022; Published 6 May 2022

Academic Editor: Ruchika Garg

Copyright © 2022 Yunkun Chen and Wenbin Zhang. This is an open access article distributed under the Creative Commons Attribution License, which permits unrestricted use, distribution, and reproduction in any medium, provided the original work is properly cited.

Chronic obstructive pulmonary disease (COPD) is a chronic disease with a long course which is often induced by an acute exacerbation of the disease by a respiratory tract infection. We aimed to explore the effect of Zhuye Shigao Decoction combined with Qingqi Huatan Pills on the regulation of the interleukin (IL)-6-mediated JAK1/STAT3 signaling pathway in rats with an acute exacerbation of COPD (phlegm-heat stagnating in the lungs). A model of COPD rats with lung phlegm-heat stagnation was established by smoking and intratracheal injection of lipopolysaccharide (LPS). The rats were randomly divided into eight groups: normal control, model control, three doses of herbs group, and three doses of herbs + itacitinib groups. The lung function indexes were measured by using a lung function tester, and changes in pathological features of all groups were observed by hematoxylin-eosin (HE) staining. The mRNA expression and protein expression levels in lung tissues were determined by real-time quantitative polymerase chain reaction (RT-qPCR), western blot, and immunohistochemical assay, respectively. Following treatment, IL-6 expression in lung tissues was significantly reduced compared with the model group. The results demonstrated that the medication was effective in alleviating the persistent airflow limitation and pathological features in COPD rats. Expression of JAK1/STAT3 in lung tissues was remarkably decreased. The JAK1/STAT3 pathway was inhibited, while SOCS3 expression was upregulated in the drug-treated groups compared with model control. However, after the addition of itacitinib (JAK1 inhibitor), the efficacy in each group was evidently impaired compared with herbs alone. Taken together, Zhuye Shigao Decoction combined with Qingqi Huatan Pills could improve the persistent airflow limitation and reduce lung inflammation and pathological changes of COPD possibly by regulating the expression of the IL-6-mediated JAK1/STAT3 pathway.

## 1. Introduction

Respiratory diseases cause a huge health burden worldwide. November 17, 2021, is World COPD Day. The Global Initiative for Chronic Obstructive Lung Disease (GOLD) has announced that COPD has affected 300 million people around the globe and has ended the lives of over 3 million people each year, making it the third leading cause of death worldwide [1].

COPD is a chronic inflammatory disease that progressively affects obstructive airflow limitation in the lungs. The manifestations include dyspnoea, coughing, coughing up mucus (sputum), and wheezing [2, 3]. This progressive airflow limitation eventually leads to airway remodeling and lung parenchymal destruction, and the progression of the disease is irreversible. In addition, the lung functions of COPD patients undergo a progressively abnormal decline and then chronic respiratory failure [4]. As one of the top

three leading causes of death in China, the diagnostic rate varied from 23.61% to 30.00%. The medical cost ranged from 72 to 3,565 USD per year, accounting for 33.33% to 118.09% of the local average annual income [5]. Patients with COPD have been significantly impacted by health problems with poor quality of life (QOL).

Nevertheless, the pathogenesis of COPD has not yet been fully clarified. It is speculated that this disease is related to smoking, occupational dust, chemicals, air pollution, chronic inflammation of airway epithelial cells, enhanced oxidative stress response, imbalance of protease and anti-protease systems, and that the whole process is related to a multitude of cytokines and signal channels [6–8].

In temporary, the chronic inflammation mechanism of airway epithelial cells is universally accepted, involving a variety of inflammatory cells, cytokines, and inflammatory mediators. The Janus tyrosine kinase/signal transducer and activator of transcription (JAK1/STAT3) pathway plays an important role in the process of acute exacerbation of chronic obstructive pulmonary disease (AECOPD). It can mediate cell proliferation, differentiation, migration, apoptosis, and other biological reactions [9–11]. External stimuli either smoking or infection first activate airway epithelial cells to release massive inflammatory mediators, neutrophils, and macrophages. Meanwhile, additional inflammation-related cells in the body are accumulated in the airway in an active state allowing to accelerate the production of inflammatory mediators. Subsequently, more inflammatory cells are generated, recruited, and then combined with JAK receptors to activate the JAK1/STAT3 signaling pathway, triggering the acute COPD attack. In epithelial and immune cells, STAT3 serves as a key component of the JAK/STAT pathway. It can be activated by IL-6 intracellular, and then the expression of numerous proinflammatory genes in the lung is induced [12, 13]. The suppressors of cytokine signaling (SOCS3) can counteract interferon (IFN)- $\gamma$ /STAT1 and IL-12/STAT4, IL-4/STAT6, growth hormone (GH)/STAT5, and IL-6/STAT3 [14]. In addition, SOCS3 has been identified as a negative feedback regulator of the JAK/STAT pathway [15] and has been demonstrated to be a target for inhibiting the activation of the JAK/STAT pathway in various inflammatory diseases [16].

Massive experimental studies have been conducted on the efficacy of traditional Chinese medicine (TCM) in the treatment of COPD-related signal transduction pathways, and findings have revealed that TCM treatment produces satisfactory effects on alleviating clinical symptoms and enhancing patients' physical fitness. It can also benefit patients with less number of attacks and a better quality of life, which is of important significance to the clinical study [4].

Some scholars have established a rat model of COPD and found that the percentage of pulmonary artery fiber, serum IL-6 content, and the expression of p-JAK2 and p-STAT3 are decreased after the intervention of Baofei Dingchuan Decoction, indicating that it can significantly reduce the weight of pulmonary blood vessels and improve lung functions of COPD rats [17].

Zhao Mei et al. have demonstrated the outstanding efficacy of Qingjin Huatan granules in the treatment of

AECOPD with phlegm-heat stagnation. They have reported that AECOPD inflammation can be inhibited by down-regulating p-STAT1, p-STAT3, p-JAK2, and JAK2 proteins and gene expression, and upregulating SOCS3 protein and gene expression [18]. Although there are various studies on JAK/STAT in TCM, there has been no research on the inflammatory response caused by the JAK1/STAT3 pathway mediated by IL-6.

This study intended to administer several doses of Zhuye Shigao Decoction combined with Qingqi Huatan Pills and different doses of herbs + itacitinib to intervene in the COPD rat model. The changes in lung function and lung tissue pathology were observed, and the expression of IL-6, JAK1, STAT3, and SOCS3 mRNA and proteins related to the JAK1/STAT3 pathway involved in chronic airway inflammation were determined. It is hypothesized that IL-6 initiated the expression of the STAT3 gene to mediate the inflammatory response caused by the JAK1/STAT3 pathway and promote the occurrence of AECOPD.

## 2. Materials and Methods

**2.1. Animals.** A total of 48 male specific-pathogen-free grade SD rats (6 for each group) weighing  $200 \pm 50$  g and aged 10 to 12 weeks were purchased. All animals had adaptive feeding for 7 days in a clean and ventilated environment. The room temperature was set at  $23 \pm 2^\circ\text{C}$  and atmosphere humidity at  $60 \pm 5\%$ . Food and water were supplied ad libitum. The color of the fur, food intake, and behaviors were recorded.

**2.2. Model Establishment and Grouping.** The composition of Zhuye Shigao Decoction combined with Qingqi Huatan Pills included 15 g of light bamboo leaves, 30 g of raw gypsum, 15 g of French *Pinellia*, 20 g of *Ophiopogon japonicus*, 10 g of ginseng, 6 g of licorice, 10 g of scutellaria, 30 g of melon seeds, 12 g of dannan star, 15 g of tangerine peel, 10 g of bitter almonds, 15 g of *Citrus aurantium*, 30 g of *Houttuynia cordata*, 10 g of *Bulbus Fritillariae Thunbergii*, and 15 g of Zhuru. All of the herbs were purchased from the Department of Pharmacy at the Chongqing Hospital of Traditional Chinese Medicine and produced by Sichuan Kangmei Pharmaceutical to ensure experimental results were reliable. According to the dosage of medication, the animals were divided into low ( $5 \text{ g}\cdot\text{kg}^{-1}/\text{d}$ ), medium ( $10 \text{ g}\cdot\text{kg}^{-1}/\text{d}$ ), and high-dose ( $15 \text{ g}\cdot\text{kg}^{-1}/\text{d}$ ) intervention groups. The dosage was determined based on our previous study and the published literature of modern medical laboratory zoology [19, 20]. Each drug was prepared according to the specific dosage, dissolved in distilled water, and finally adjusted to a crude drug amount of 2 g/mL.

The COPD model of rats was induced by cigarette smoke combined with lipopolysaccharide after 1 week of adaptive feeding [21]. There were eight groups with six rats in each one: normal control, model control, three doses of herbs group, and three doses of herbs + itacitinib group according to the weight based on the random number table method. The different doses of herbs with or without itacitinib ( $30 \text{ mg/kg}$ ) were administered by gavage and subcutaneous

injection, respectively. Apart from the normal control group (NC), on the 1<sup>st</sup> and 14<sup>th</sup> days, all rats were anesthetized with 4% pentobarbital sodium and the tracheas were exposed to 200  $\mu$ L of lipopolysaccharide (LPS, 1 g/mL). Rats were placed into a 50 cm  $\times$  40 cm  $\times$  40 cm glass smoked poisoning box and exposed to the smoke from the ignition of an appropriate amount of sawdust and 20 cigarettes mixture from day 2 to 30. The rats were exposed to smoke twice per day (30 min each time) and rested two days a week to establish the experimental model. After the COPD model was successfully established, the herbal treatment with or without itacitinib was given to the rats for 14 consecutive days, while the NC and model control were given equal saline.

**2.3. Histopathology.** The right lung tissue of rats was fixed with 4% formaldehyde, routinely embedded in paraffin and cut into 5  $\mu$ m serial sections. The sections were then progressively dewaxed with xylene, dehydrated with ethanol, stained with eosin and hematoxylin, and sealed with neutral gum. The morphological changes of the bronchus and lung tissues were observed under a light microscope and analyzed (Jetta Company, Shanghai, China).

**2.4. Immunohistochemistry.** Immunohistochemistry (IHC) analysis was carried out by using MaxVision<sup>TM</sup> techniques (Maixin Bio, China) based on the manufacturer's instructions. Firstly, the lung tissue was fixed by 4% paraformaldehyde (Solarbio, Shanghai, China), dehydrated, and paraffin embedded. The 5  $\mu$ m thick slides were obtained. The deparaffinization and hydration were performed, the slides were then incubated with 3% H<sub>2</sub>O<sub>2</sub> (Sinopharm, China) for 10 min and 0.1% trypsin (Beyotime, China) for 20 min. The primary antibodies were incubated at 4°C overnight and then incubated with HRP-polymer-conjugated secondary antibodies at 37°C for 1 h. The slides were then stained by using the chromogenic reagent diaminobenzidine (DAB, Zhongshan, Beijing, China) for 3 min and counterstained with hematoxylin (Jiancheng, Nanjing, China). An inverted microscope (Olympus, Japan) was employed for image acquisition. The primary antibodies anti-IL-6, anti-JAK1, anti-STAT3, and anti-SOCS3 were purchased from Cell Signaling Technology (CST).

**2.5. ELISA Assay.** The rats were anesthetized by intraperitoneal injection of 4% sodium pentobarbital. The serum of each group was collected. The sample was taken at -80°C and prepared in advance. The detection was performed strictly according to the instructions of the ELISA kit manufacturer (R&D Systems, Emeryville, CA, USA). Firstly, the diluted primary antibody was added to the appropriate wells and incubated for 2 h at room temperature. A blocking solution of 300  $\mu$ L was added to each well and incubated for 1 h at room temperature after three cycles of washing with 0.05% Tween-20. Then, the plate was washed twice with a wash solution. The diluted biotinylated detection antibody was added and incubated for 1 h at 37°C, and the plate was washed three times. Subsequently, 100  $\mu$ L of diluted AKP

conjugated streptavidin was added and incubated for 1 h at room temperature. The plate was emptied and washed three times for a total of 15 min and washed five more times. The substrate was collected for color development for 30 min at room temperature. Finally, 0.05 mL of 2 M of H<sub>2</sub>SO<sub>4</sub> was added to each well and immediately read with a plate reader at 405–410 nm.

**2.6. Quantification of mRNA.** The expression quantification of IL-6, JAK1, STAT3, and SOCS3 mRNA in rat lung tissue was detected by reverse transcription quantitative real-time polymerase chain reaction (RT-PCR) technology. The lung tissue was collected, and total RNA was extracted from the tissue by the TRIzol method. The subsequent reverse transcription into cDNA was performed using Superscript II RT (Invitrogen, China). cDNA was amplified by adding equivalent amounts of initial RNA quantity to the reaction mix including 12.5  $\mu$ L of SYBR Green (Invitrogen), forward and reverse primers (10 pmol/ml), with 0.5  $\mu$ L for each primer, and nuclease-free water to final volumes of 25  $\mu$ L per well. Relative fold changes were quantified using the 2<sup>- $\Delta\Delta$ Ct</sup> formula. Primers used were as follows: IL-6-F, 5'- CTCC CAACAGACCTGTCTATAC-3'; IL-6-R, 5'- CCATTGCA CAACTCTTTTCTCA-3'; JAK1-F, 5'-TCTGTTTGCTCAG GGACAGT-3'; JAK1-R, 5'- AGCCATCCCTAGACACT CGT-5'; STAT3-F, 5'- ATCACGCCTTCTACAGACTGC-3'; STAT3-R, 5'- CATCCTGGAGATTCTCTACCACT-3'; SOCS3-F, 5'- CCTGCGCCTCAAGACCTTC-3'; SOCS3-R, 5'- GTCAGTGGCTCCAGTAGAA-3'; GAPDH-F, 5'-AG GTCGGTGTGAACGGATTG-3'; and GAPDH-R, 5'-TG TAGACCATGTAGTTGAGGTCA-3'.

**2.7. Western Blot.** The western blot (WB) assay was used to detect the expression changes of STAT1 and STAT3 in rat lung tissues. Stored rat lung tissues were lysed using RIPA reagent (Beyotime, China), prepared and detected using protein gel electrophoresis. Proteins were transferred to a PVDF membrane, blocked, and incubated with diluted primary antibody, and then secondary antibody. The primary and secondary antibodies were incubated for 1 h and 1–2 h, respectively. Protein visualization was conducted using an enhanced chemiluminescence detection kit (Solarbio, China). The Image J 1.8.0 software was used to determine the optical density values of protein bands and the internal control  $\beta$ -actin, and the relative density of the protein in each group was calculated from the ratio of the two. Immunoblotting was performed and blots were probed with antibodies against IL-6, JAK1, STAT3, SOCS3, and  $\beta$ -actin (CST, USA).

**2.8. Statistical Analysis.** Statistical analysis was performed using GraphPad Prism software, version 8.0.1. The data were reported as the mean  $\pm$  standard error (SD). Differences between groups were analyzed using one-way ANOVA with Tukey analysis of variance for comparison of more than two groups. *P* values of <0.05 were considered statistically significant.

### 3. Results

**3.1. The IL-6 Expression in Lung Tissue Is Inhibited.** Various methodologies were used to detect the expression of IL-6 in lung tissues. The results of immunohistochemical experiments are shown in Figure 1(a). Compared with NC, the number of brown-positive cells in MC was significantly increased. Compared with MC, the positive cells in the herbs intervene group were significantly reduced, and the decline was most significant in the high-dose herbs group. Itacitinib was utilized to block the JAK-STAT3 pathway transduction. In medium- and high-dose herbs + itacitinib groups, the positive cells were decreased compared with the MC but increased evidently compared with the corresponding herbs treated group. However, no apparent decrease in the number of positive cells was observed in the low-dose herbs + itacitinib group. In addition, WB was used to detect the expression of IL-6 protein, and semiquantitative analysis was performed based on the gray value, as shown in Figure 1(c). It is revealed that the expression of IL-6 was upregulated in the model group, and the expression of IL-6 could be significantly downregulated in the herbs intervention group. While IL-6 expression was increased in herbs + itacitinib groups compared with herb groups; however, it was still lower than the model control. Moreover, the gene expression was detected using RT-qPCR, and the expression trend was consistent with immunohistochemistry and WB results (Figure 1(b)).

**3.2. The Lung Function Is Improved and Pathological Changes in Lung Tissues Are Reduced.** The peak inspiratory flow (PIF), peak expiratory flow (PEF), and minute ventilation volume (MV) were measured for detecting lung functions of rats, as shown in Figure 2, compared with NC, PIF, PEF, and MV were decreased significantly in MC, indicating airflow limitation, pulmonary ventilation dysfunction, and successful COPD modeling. The values of PIF, PEF, and MV in the herbs treated group were increased remarkably in contrast to MC. The value of PIF in the herbs + itacitinib groups was also increased markedly (Figure 2(a)), whereas those of PEF and MV were increased only in the medium- and high-dose herbs + itacitinib groups (Figures 2(b) and 2(c)). Compared with the herbs + itacitinib groups, the PIF and MV values of the herbs group were significantly higher than the corresponding dose intervention groups ( $P < 0.05$ ), and the PEF value was also increased, but there were no statistics in the low-dose herbs group. These findings demonstrated that all doses of herbs could improve lung airflow limitation and ventilatory dysfunction, and the improvement effect on lung function was significantly reduced after inhibiting JAK-STAT3 signal transduction.

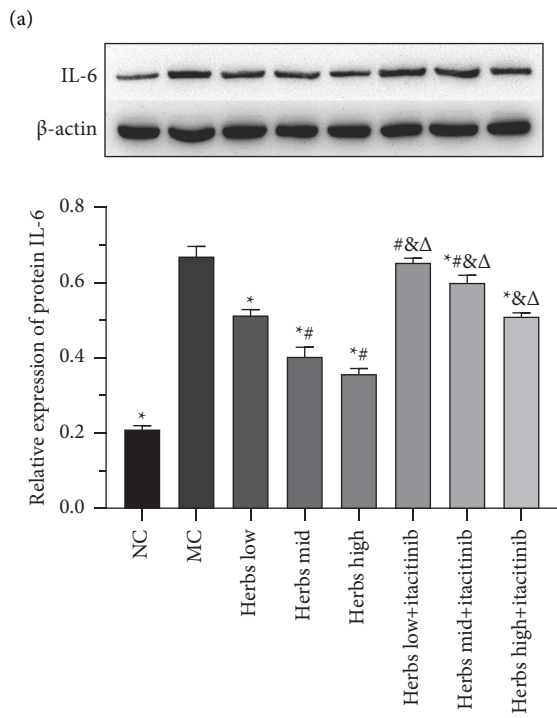
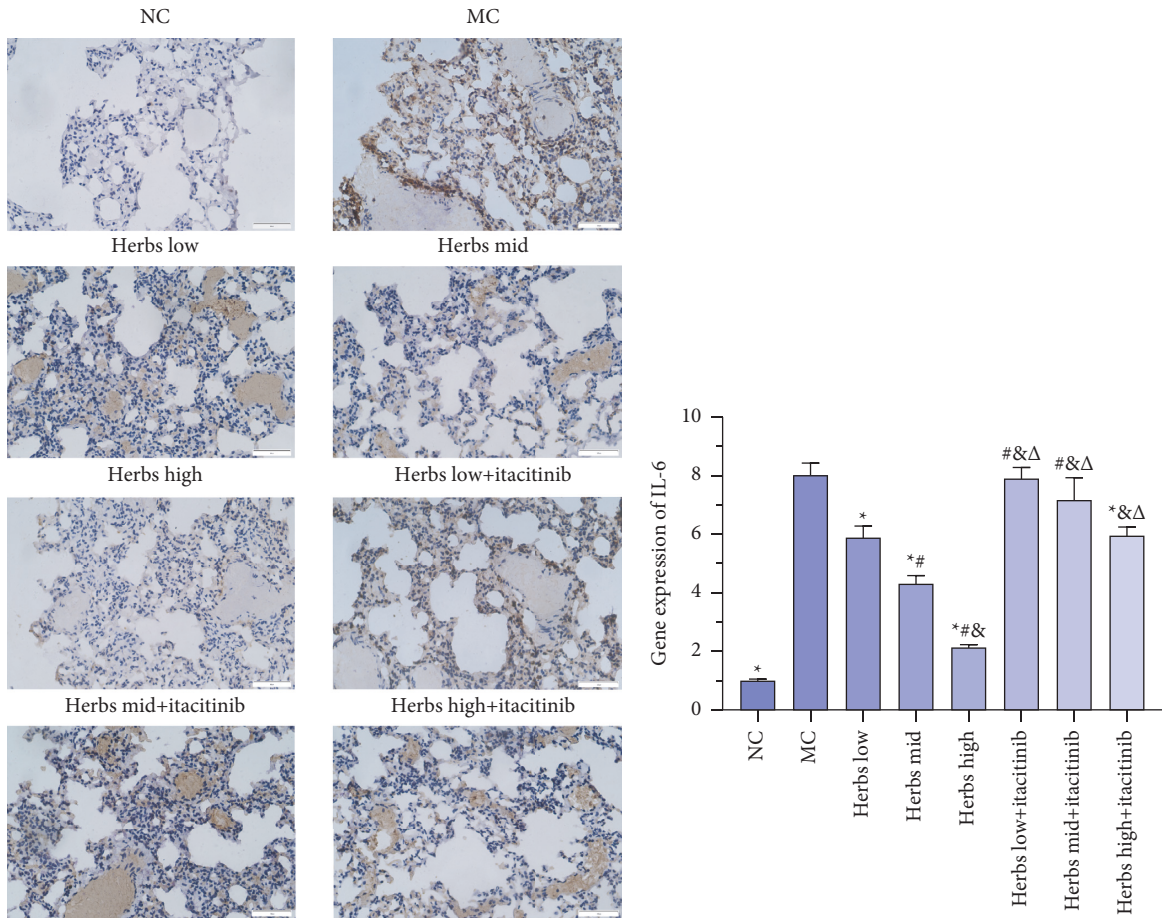
The changes in lung tissue histopathology were observed using HE staining. The lung tissue of the rats in NC was clearly visible, and the bronchial wall structure was relatively regular, without obvious damage. Only a small infiltration of inflammatory cells was seen, mucus plugs and mucus were not observed, and the congestion and edema of the mucous membrane were not observed (Figure 2(d)). The lung tissue

of MC showed glandular hyperplasia in multiple locations, a large number of inflammatory cells were infiltrated, and the tube wall thickened. The structure of the alveolar wall was severely damaged, thinned, and broken, allowing the formation of pulmonary bullae, and the number of alveoli was reduced. Compared with MC, the lung tissue pathology in the herbs mid and high groups was significantly attenuated. The bronchial wall thinning, partial shedding, inflammatory cell infiltration, congestion, and edema were alleviated, and pulmonary bullae were reduced. And the destruction of the alveolar cavity, expansion, and fusion were eased. In the herbs low + itacitinib group, the lung tissue pathology was not significantly improved compared with the herbs intervention groups. While the alveolar expansion and fusion, inflammatory cell infiltration, and mucosal congestion were improved in the herbs mid + itacitinib group. Moreover, the pathological improvement of the herbs high + itacitinib group was better than that of the herbs mid + itacitinib group.

**3.3. Changes in Serum Cytokine Levels.** The rat serum was collected for ELISA and the results are shown in Figure 3. The serum levels of IFN- $\gamma$ , IL-4, IL-4R, IL-12, and IL-12R in MC were significantly increased compared with NC. Compared with the MC, the levels of IFN- $\gamma$ , IL-4, IL-4R, IL-12, and IL-12R in the serum of rats in each dose group of herbs decreased remarkably, and the herbs high group had the strongest effect. The cytokine content in the herbs + itacitinib group increased compared with different doses of herbs groups. It was found that all dose groups of herbs were effective in reducing serum inflammatory factors in COPD model rats, and the high-dose group produced the best effect, while the ability of herbs to decrease serum inflammatory factors in the herbs + itacitinib group was reduced.

**3.4. Expression of the JAK1/STAT3 Signaling Pathway in Lung Tissues.** The results of the immunohistochemistry experiment are shown in Figure 4(a). The number of JAK1 brown-positive cells in the lung tissue sections of the MC was increased significantly compared with NC. Compared with MC, the number of positive cells in the herbs treatment was significantly reduced, most notably in the high-dose group. After the addition of itacitinib to inhibit the JAK-STAT3 pathway, positive cells in the herbs mid and high + itacitinib groups were lower than those in the MC, while in the herbs low + itacitinib group, no significant decline in the number of positive cells was observed. WB was subsequently employed to detect the expression of JAK1 and STAT3 proteins and semiquantitatively analyzed based on the gray value, as shown in Figures 4(b), 4(d), and 4(f), and the expression of JAK1 and STAT3 was increased in the MC, and the difference was significant. The herbs could significantly downregulate JAK1 and STAT3 expression. After the JAK-STAT3 was blocked by itacitinib, the expression of JAK1 and STAT3 was increased in each dose group of herbs compared with the corresponding herbs dose of the itacitinib-free group, and the difference was significant. In





(c)

FIGURE 1: IL-6 expression is inhibited in lung tissues. (a) The photomicrographs of immunohistochemical staining for IL-6 among lung tissue samples are displayed. The nucleus is colored in blue and the positive cells are colored in brown (scale bar is 50 μm, ×400). (b) The relative IL-6 gene expression. (c) Western blot analysis of IL-6 in lung tissues. Each group in the strip chart is consistent with the below semiquantitative analysis on the basis of the intensity of the strip chart. Error bars represent SD,  $n = 3$ . \*, #, &, and Δ represent  $P$  values <0.05 which are considered statistically significant. \* versus MC (model control), # versus herbs low, & versus herbs mid, and Δ versus herbs high.

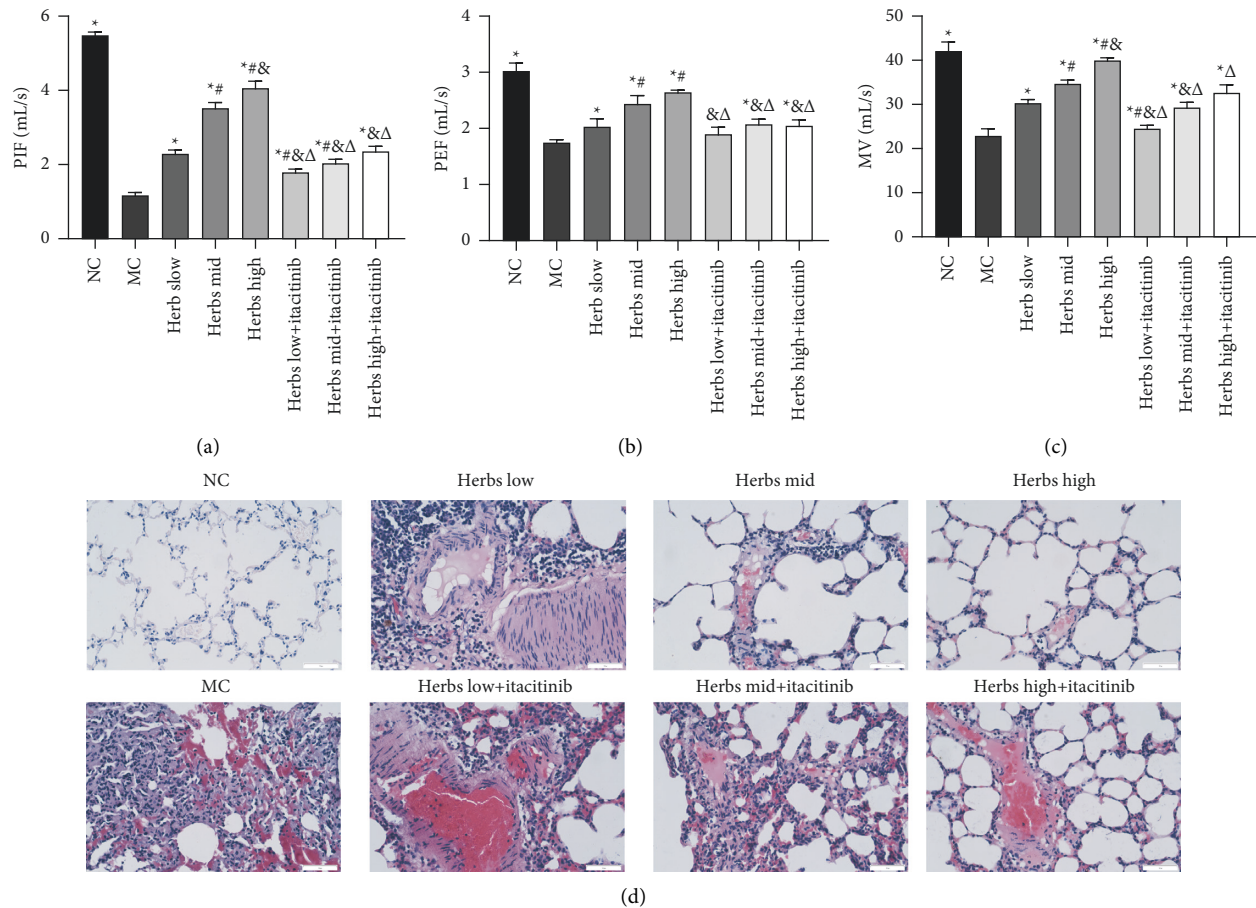


FIGURE 2: Zhuye Shigao Decoction combined with Qingqi Huatan Pills is able to improve lung function and alleviate pathological changes in lung tissue. (a) PIF, (b) PEF, and (c) MV detection as shown in the diagram. (d) HE staining for the lung tissue of SD rats (scale bar is 50  $\mu\text{m}$ ,  $\times 400$ ). Error bars represent SD,  $n = 3$ . \*, #, &, and  $\Delta$  represent  $P$  values  $< 0.05$  which are considered statistically significant. \* versus MC (model control), # versus herbs low, & versus herbs mid, and  $\Delta$  versus herbs high.

addition, the immunohistochemical staining results of STAT3 are shown in Figure 4(e). RT-qPCR showed that compared with the NC, the expression of JAK1 and STAT3 mRNA in the lung tissue of rats was significantly increased in the model control. Herbs treatment could significantly reduce the expression of JAK1 and STAT3 mRNA levels. After the interference of JAK1 inhibitor itacitinib, the JAK1 and STAT3 mRNA expression of the herbs treated group was increased remarkably (Figures 4(c) and 4(g)).

**3.5. SOCS3 Expression Is Upregulated in Lung Tissue.** SOCS3 protein expression in rat lung tissue was detected by WB and IHC (Figure 5(a)–5(c)). The SOCS3 brown positive cells in the lung tissue sections of the MC were significantly reduced (Figure 5(b)). Compared with the MC, the number of positive cells in the herb mid and high groups was significantly increased. In the herbs + itacitinib group, there was no significant change in the number of positive cells compared with the MC, except for the herbs high + itacitinib group. The expression of SOCS3 mRNA in lung tissue was detected by RT-qPCR which was significantly reduced in MC (Figure 5(d)). The herbs treatment could significantly

increase the expression of SOCS3 mRNA. In the presence of itacitinib, SOCS3 mRNA in each herbs dose group decreased, and there was no significant difference in herbs low and mid group compared with MC (Figure 5(d)).

#### 4. Discussion

COPD is one of the common respiratory diseases in the clinic which is mostly characterized by continuous airflow limitation, and seriously affects the quality of life and safety of patients [22]. The inducing factors are mainly related to the chronic inflammatory reaction of the airway and lung tissue caused by harmful gases or particles in the environment, and they are the continuous airway inflammatory reaction. COPD airway inflammation involves all airways and lung tissues, involving macrophages, neutrophils, IL-8, TNF- $\alpha$ , cytokines, and inflammatory mediators [23, 24]. Inflammatory factors play a dominant role in the occurrence and development of COPD, and IL-6 is an important proinflammatory factor in the complex inflammatory cell-cytokine network in the airway inflammation of COPD. Studies have shown that IL-6 is elevated to various degrees in sputum, lung parenchyma, and blood in COPD patients

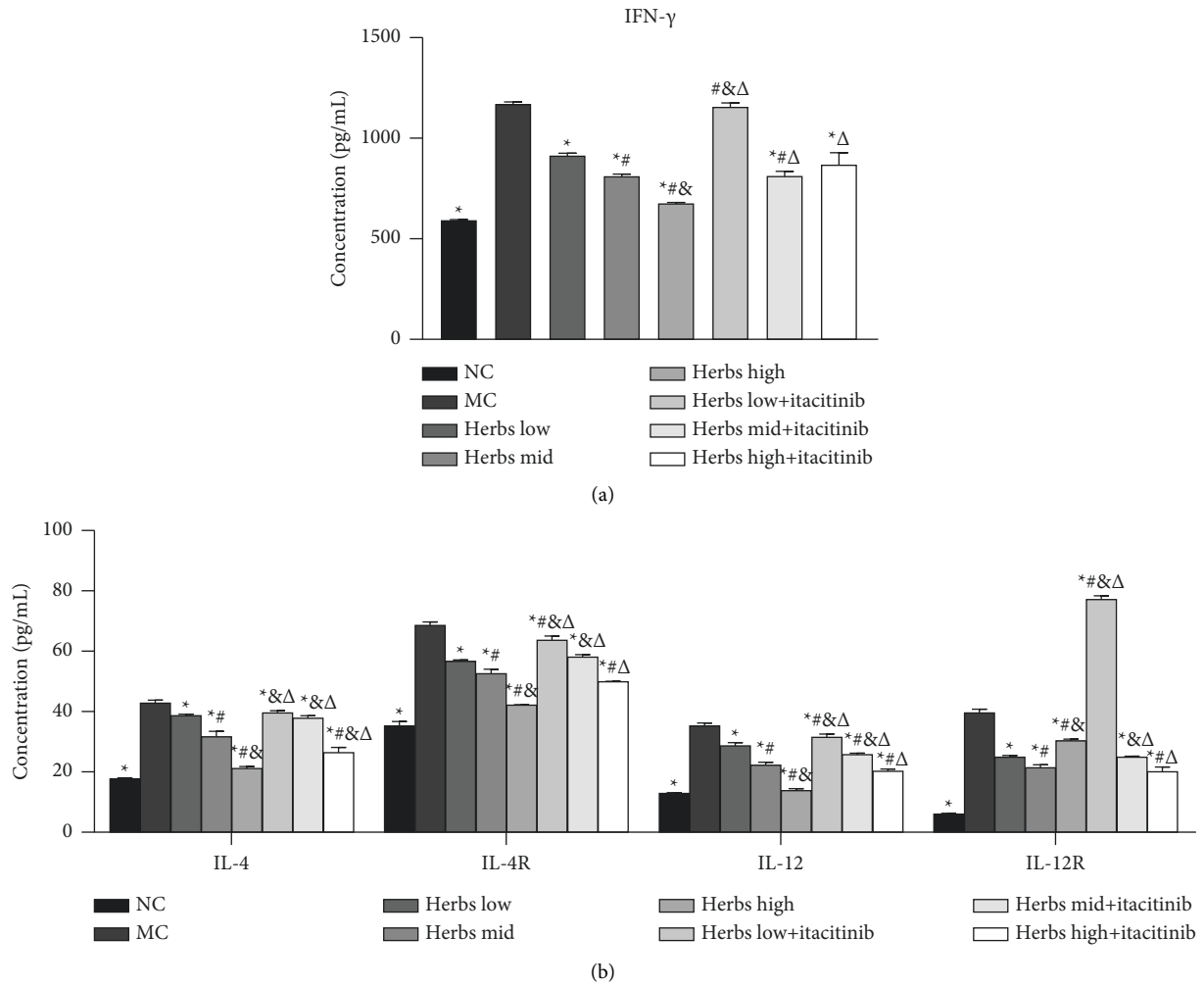
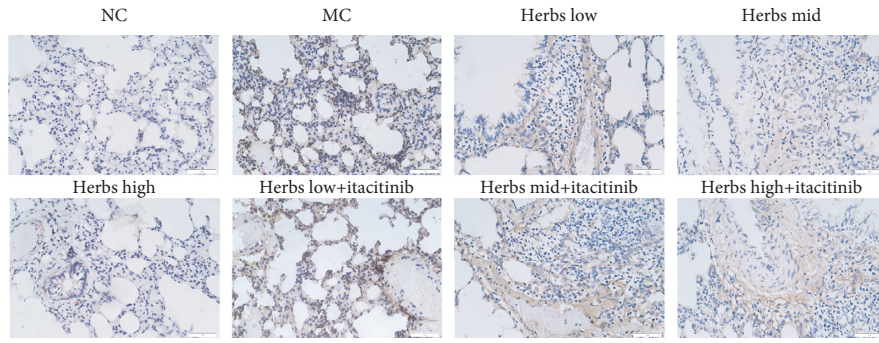


FIGURE 3: Cytokines level in serum is detected by ELISA. (a) IFN- $\gamma$  concentration in serum. (b) IL-4, IL-4R, IL-12, and IL-12R were measured by ELISA. Error bars represent SD,  $n = 3$ . \*, #, &, and  $\Delta$  represent  $P$  values  $< 0.05$  which are considered statistically significant. \* versus MC (model control), # versus herbs low, & versus herbs mid, and  $\Delta$  versus herbs high.

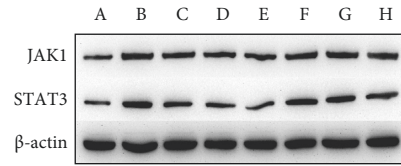
[25, 26]. Continuous activation and overexpression of STAT1 and STAT3 in airway epithelial cells are closely related to airway inflammation [27], which is widely involved in mediating the expression and regulation of inflammatory cytokines. The study has reported that several inflammatory cells can release inflammatory factors and inflammatory chemokines under the COPD mechanism and participate in cell proliferation, differentiation, apoptosis, inflammatory response, and other pathophysiological mechanisms through the JAK/STAT signaling pathway [28].

In this experiment, the COPD model rats were prepared by combining smoking and LPS, using different doses of TCM Zhuye Shigao Decoction combined with Qingqi Huatan Pills to gavage rats. It was found that each dose group of herbs could improve the lung function of rats' PIF, PEF, and MV, and relieve lung airflow limitation and ventilatory dysfunction, thereby alleviating lung tissue disease and bronchial wall inflammation. It was also confirmed that IL-6, JAK1, and STAT3 mRNA and protein were significantly highly expressed in COPD rats, indicating that the occurrence and development of COPD were closely related

to the continuous activation and overexpression of JAK1/STAT3 and abnormal signal transduction pathways in lung tissues, and the activation level of STAT3 was closely and positively correlated to IL-6. It is reported that cytokines play a role in regulating gene transcription by acting on cell surface receptors by activating signal transducers, that is, sending out a series of signal molecules and transmitting the stimulating signal to the target gene in the nucleus. The expression of the proinflammatory factor IL-6 was significantly increased under the combined induction of smoking and LPS. IL-6R on the cell surface was combined, further inducing phosphorylation of JAK1. JAK1 activation quickly combines with STAT3 to phosphorylate STAT3 and activate it. STAT3 could regulate the transcription and expression of related genes. The TCM Zhuye Shigao Decoction combined with Qingqi Huatan Pills could reduce the expression of IL-6, JAK1, and STAT3 mRNA and protein in lung tissues and inhibit the serum cytokines IFN- $\gamma$ , IL-4, IL-4R, IL-12, and IL-12R. T cells secreting IFN- $\gamma$  in the airways of COPD patients increase, and IFN- $\gamma$  levels in patients with COPD were increased. IFN- $\gamma$  coordinates the infiltration of T cells

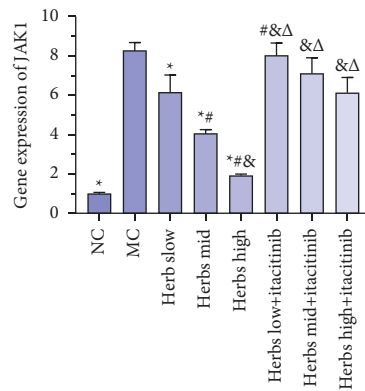


(a)

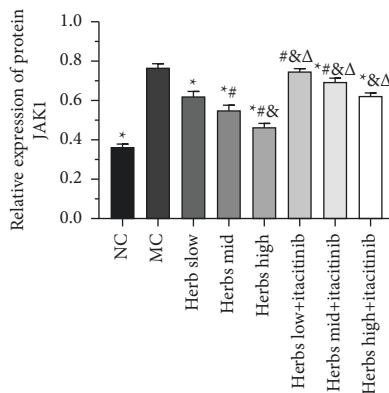


A: NC (normal control); B: MC (model control);  
 C: Herbs low D: Herbs mid; E: Herbs high;  
 F: Herbs low+itacitinib; G: Herbs mid+itacitinib;  
 H: Herbs high+itacitinib

(b)



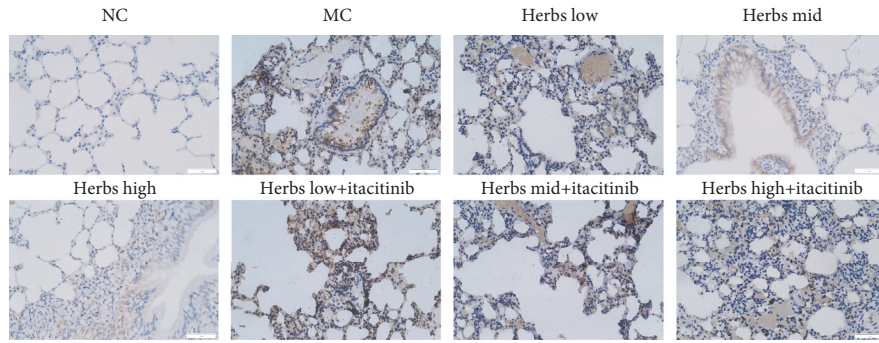
(c)



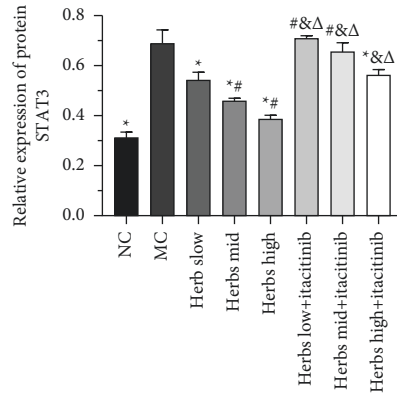
(d)

FIGURE 4: Continued.

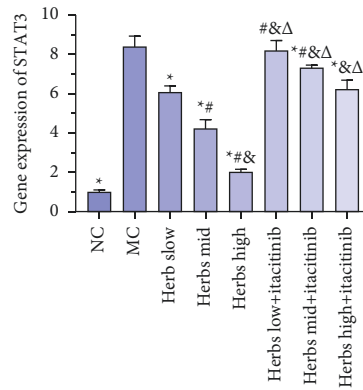




(e)



(f)



(g)

FIGURE 4: Expression of the JAK1/STAT3 signaling pathway of lung tissue in each group. (a) JAK1 protein expression of lung tissue detected by immunohistochemistry is presented by photomicrographs. The nucleus is colored in blue and the positive cells are colored in brown (scale bar is 50  $\mu\text{m}$ ,  $\times 400$ ). (b) The strip chart of JAK1 and STAT3,  $\beta$ -actin was used as the internal reference. (c) The relative JAK1 gene expression. (d) Semiquantitative analysis based on the intensity of strip chart for JAK1 in lung tissue. (e) STAT3 protein expression of lung tissue detected by immunohistochemistry was presented by photomicrographs. The nucleus is colored in blue and the positive cells are colored in brown (scale bar is 50  $\mu\text{m}$ ,  $\times 400$ ). (f) Semiquantitative analysis of STAT3 expression. (g) Gene expression of STAT3. Error bars represent SD,  $n = 3$ . \*, #, &, and  $\Delta$  represent  $P$  values  $< 0.05$  which are considered statistically significant. \* versus MC (model control), # versus herbs low, & versus herbs mid, and  $\Delta$  versus herbs high.

in COPD lungs by upregulating CXC-chemokine receptor (CXCR) 3 on these cells and the release of chemokines that activate CXCR3 [29]. Previous studies have found that IL-4 and IL-12 are significantly elevated in AECOPD patients [30]. By using itacitinib for JAK-STAT3 pathway intervention, compared with their corresponding doses of itacitinib free groups, the expressions of IL-6, JAK1, and STAT3 mRNA and protein in the lung tissue of each dose

group of herbs were significantly increased, and serum IFN- $\gamma$ , IL-4, IL-4R, IL-12, and IL-12R also increased significantly.

Cytokines are important factors in the JAK/STAT signaling pathway, which are transmitted from the cell membrane to the nucleus, and the inhibitor of cytokine transduction (SOCS) is transduced by the JAK/STAT signal and has a negative regulatory effect by specifically negatively

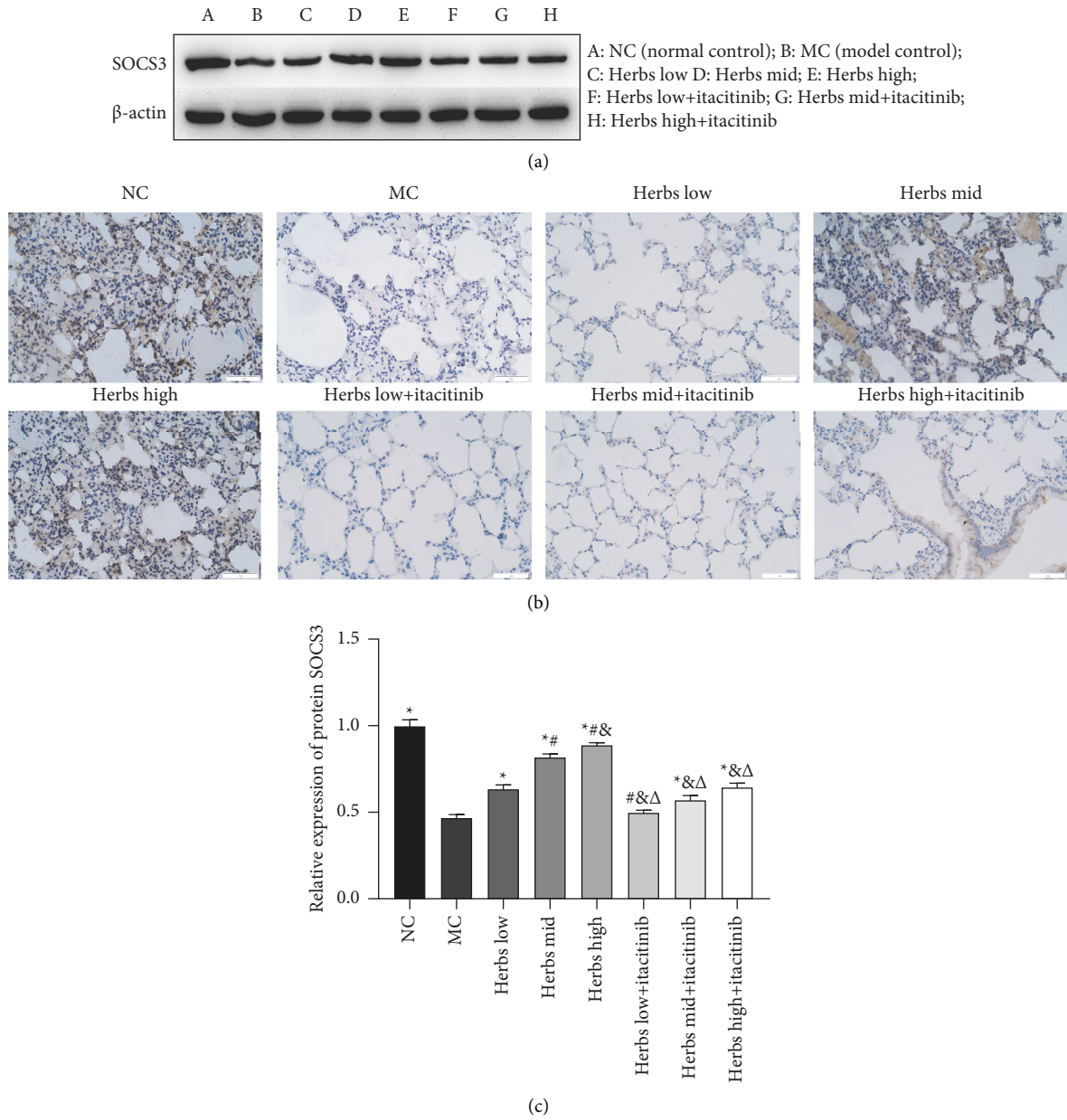


FIGURE 5: Continued.



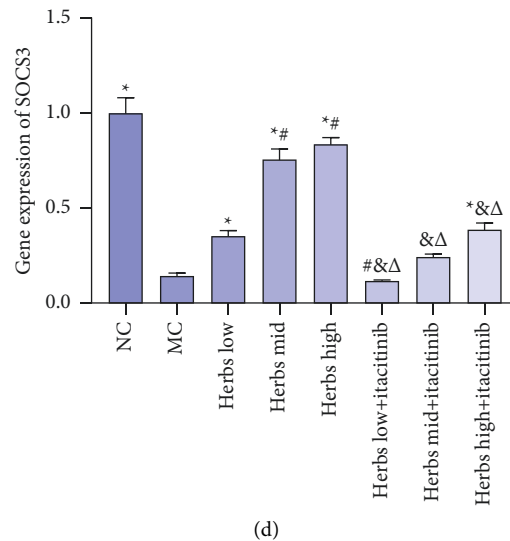


FIGURE 5: SOCS3 expression is upregulated in lung tissue. (a) Western blot analysis of SOCS3 in lung tissue,  $\beta$ -actin was used as the internal reference. (b) The photomicrographs of immunohistochemical staining for SOCS3 among lung tissue samples are displayed. The nucleus is colored in blue and the positive cells are colored in brown (scale bar is 50  $\mu$ m,  $\times$ 400). (c) Semiquantitative analysis on the basis of the intensity of protein bands in eight groups. (d) The relative SOCS3 gene expression. Error bars represent SD,  $n = 3$ . \*, #, &,  $\Delta$  represent  $P$  values  $< 0.05$  which are considered statistically significant. \* versus MC (model control), # versus herbs low, & versus herbs mid, and  $\Delta$  versus herbs high.

regulating the induction and activation of the JAK/STAT pathway [31]. SOCS3 is activated to negatively regulate the JAK/STAT pathway, and it is generally believed that SOCS3 is the target gene of STATs and can directly inhibit the activation of STATs at present [32]. WB, IHC, and RT-qPCR assays were used to detect the expression of SOCS3 in lung tissues. The results showed that Zhuye Shigao Decoction combined with Qingqi Huatan Pills could significantly increase the SOCS3 expression of mRNA and protein in lung tissues. In contrast to the corresponding itacitinib free Herbs intervention group, the expression of SOCS3 mRNA and protein in the lung tissue of the herbs group in the presence of itacitinib was significantly reduced.

## 5. Conclusions

The described results revealed that Zhuye Shigao Decoction combined with Qingqi Huatan Pills could alleviate the continuous airflow limitation of COPD and reduce lung inflammation and pathological changes. It has been demonstrated that the herbs can downregulate the overexpression and continuous activation of JAK1 and STAT3 in the JAK/STAT signaling pathway based on IL-6 and upregulate SOCS3 to negatively regulate JAK/STAT signals, thereby inhibiting the AECOPD attack. In addition, JAK/STAT3 can be used as the main target for the treatment of COPD patients that are overactivated by JAK/STAT3. Further research after the intervention of TCM will provide basic support for the treatment of AECOPD with TCM and prevent its occurrence and development. However, the study was short of methodology on molecular mechanism exploration and was limited to the COPD rat investigation. Moreover, the herbs' adverse effects were not investigated.

Subsequent research is needed to mainly focus on the limitations mentioned above.

## Data Availability

The data used to support the findings of this study are included within the article.

## Conflicts of Interest

The authors declare no conflicts of interest.

## Acknowledgments

This study was sponsored by the Natural Science Foundation of Chongqing, China (No. cstc2020jcyj-msxmX1084).

## References

- [1] Global Strategy for Prevention, "Diagnosis and management of COPD," 2020, <https://goldcopd.org/gold-reports/>.
- [2] S. P. Kukrety, J. D. Parekh, and K. L. Bailey, "Chronic obstructive pulmonary disease and the hallmarks of aging," *Lung India: Official Organ of Indian Chest Society*, vol. 35, no. 4, pp. 321–327, 2018.
- [3] M. Joshi and B. Varkey, "Editorial," *Current Opinion in Pulmonary Medicine*, vol. 25, no. 2, pp. 129–131, 2019.
- [4] P. Lange, B. Celli, A. Agustí et al., "Lung-function trajectories leading to chronic obstructive pulmonary disease," *New England Journal of Medicine*, vol. 373, no. 2, pp. 111–122, 2015.
- [5] B. Zhu, Y. Wang, J. Ming, W. Chen, and L. Zhang, "Disease burden of COPD in China: a systematic review," *International Journal of Chronic Obstructive Pulmonary Disease*, vol. 13, pp. 1353–1364, 2018.

- [6] X.-X. Lv, S.-S. Liu, K. Li, B. Cui, C. Liu, and Z.-W. Hu, "Cigarette smoke promotes COPD by activating platelet-activating factor receptor and inducing neutrophil autophagic death in mice," *Oncotarget*, vol. 8, no. 43, pp. 74720–74735, 2017.
- [7] J. Chen, L. Dai, T. Wang, J. He, Y. Wang, and F. Wen, "The elevated CXCL5 levels in circulation are associated with lung function decline in COPD patients and cigarette smoking-induced mouse model of COPD," *Annals of Medicine*, vol. 51, pp. 314–329, 2019.
- [8] M. Yang, M. Kohler, T. Heyder et al., "Proteomic profiling of lung immune cells reveals dysregulation of phagocytotic pathways in female-dominated molecular COPD phenotype," *Respiratory Research*, vol. 19, no. 1, p. 39, 2018.
- [9] L. Yew-Booth, M. A. Birrell, M. S. Lau et al., "JAK-STAT pathway activation in COPD," *European Respiratory Journal*, vol. 46, no. 3, pp. 843–845, 2015.
- [10] H. Kuusanmäki, O. Dufva, E. Parri et al., "Drug sensitivity profiling identifies potential therapies for lymphoproliferative disorders with overactive JAK/STAT3 signaling," *Oncotarget*, vol. 8, no. 57, pp. 97516–97527, 2017.
- [11] C. Wang, Z. Li, X. Liu et al., "Effect of liuweibuqi capsule, a Chinese patent medicine, on the JAK1/STAT3 pathway and MMP9/TIMP1 in a chronic obstructive pulmonary disease rat model," *Journal of Traditional Chinese Medicine*, vol. 35, no. 1, pp. 54–62, 2015.
- [12] W. Huan, Z. Tianzhu, L. Yu, and W. Shumin, "Effects of ergosterol on COPD in mice via JAK3/STAT3/NF- $\kappa$ B pathway," *Inflammation*, vol. 40, no. 3, pp. 884–893, 2017.
- [13] W. E. Naugler and M. Karin, "The wolf in sheep's clothing: the role of interleukin-6 in immunity, inflammation and cancer," *Trends in Molecular Medicine*, vol. 14, no. 3, pp. 109–119, 2008.
- [14] A. Dalpke and K. Heeg, "Suppressors of cytokine signaling proteins in innate and adaptive immune responses," *Archivum Immunologiae et Therapiae Experimentalis*, vol. 51, no. 2, pp. 91–103, 2003.
- [15] J. A. Chaves de Souza, A. V. Nogueira, P. P. Chaves de Souza et al., "SOCS3 expression correlates with severity of inflammation, expression of proinflammatory cytokines, and activation of STAT3 and p38 MAPK in LPS-induced inflammation in vivo," *Mediators of Inflammation*, vol. 2013, Article ID 650812, 10 pages, 2013.
- [16] A. Suzuki, T. Hanada, K. Mitsuyama et al., "Cis3/Socs3/Ssi3 plays a negative regulatory role in Stat3 activation and intestinal inflammation," *Journal of Experimental Medicine*, vol. 193, no. 4, pp. 471–482, 2001.
- [17] F. He, Y. Shen, and J. Xu, "Effect of Baofei dingchuan decoction on JAK/STAT signal transduction pathway of pulmonary artery in rats with chronic obstructive pulmonary disease," *Journal of Traditional Chinese Medicine*, vol. 58, no. 21, pp. 1856–1859, 2017.
- [18] M. Zhao, G. Xu, and J. Li, "Effect of qingjin huatan granule on JAK/STAT signal pathway in lung tissue of rats with chronic obstructive pulmonary disease in acute exacerbation stage," *Journal of Traditional Chinese Medicine*, vol. 60, no. 8, pp. 696–700, 2019.
- [19] Z. Wen-bin, L. Wen-hui, and F. Ying-kai, "Add and subtract therapy of Zhuye Shigao decoction combined with Qingqi huatan Pills on chronic obstructive pulmonary disease at acute and aggravating period," *Chinese Journal of Experimental Traditional Medicine Formula*, vol. 23, no. 11, pp. 200–205, 2017.
- [20] X. Shi, *Xiandai Yixue Shiyuan Dongwuxue [M]*, People's Military Medical Press, Beijing, China, 2000.
- [21] D. Lin, S. Li, C. Hou, X. Xu, S. Guo, and Q. Wang, "Exploring the biological mechanism of qi deficiency syndrome with chronic obstructive pulmonary disease (COPD) based on integrated pharmacology," *Journal of Traditional Chinese Medical Sciences*, vol. 8, no. 1, pp. 72–81, 2021.
- [22] M. K. Tulic, T. Piche, and V. Verhasselt, "Lung-gut cross-talk: evidence, mechanisms and implications for the mucosal inflammatory diseases," *Clinical and Experimental Allergy*, vol. 46, no. 4, pp. 519–528, 2016.
- [23] T. Victoni, E. Barreto, V. Lagente, and V. F. Carvalho, "Oxidative imbalance as a crucial factor in inflammatory lung diseases: could antioxidant treatment constitute a new therapeutic strategy?" *Oxidative Medicine and Cellular Longevity*, vol. 2021, Article ID 6646923, 11 pages, 2021.
- [24] V. Beasley, P. V. Joshi, A. Singanayagam, P. L. Molyneaux, S. L. Johnston, and P. Mallia, "Lung microbiology and exacerbations in COPD," *International Journal of Chronic Obstructive Pulmonary Disease*, vol. 7, pp. 555–569, 2012.
- [25] H. Xu, X. Shi, X. Li et al., "Neurotransmitter and neuropeptide regulation of mast cell function: a systematic review," *Journal of Neuroinflammation*, vol. 17, no. 1, p. 356, 2020.
- [26] M. S. Caetano, H. Zhang, A. M. Cumpian et al., "IL6 blockade reprograms the lung tumor microenvironment to limit the development and progression of K-ras-mutant lung cancer," *Cancer Research*, vol. 76, no. 11, pp. 3189–3199, 2016.
- [27] J. H. Gong, D. Shin, S. Y. Han et al., "Blockade of airway inflammation by kaempferol via disturbing tyk-STAT signaling in airway epithelial cells and in asthmatic mice," *Evid Based Complement Alternat Med*, vol. 2013, Article ID 250725, 10 pages, 2013.
- [28] B. J. Jenkins, "Transcriptional regulation of pattern recognition receptors by JAK/STAT signaling, and the implications for disease pathogenesis," *Journal of Interferon and Cytokine Research*, vol. 34, no. 10, pp. 750–758, 2014.
- [29] A. Mitra, S. Vishweswaraiah, T. A. Thimraj et al., "Association of elevated serum GM-CSF, IFN- $\gamma$ , IL-4, and TNF- $\alpha$  concentration with tobacco smoke induced chronic obstructive pulmonary disease in a south Indian population," *International Journal of Inflammation*, vol. 2018, Article ID 2027856, 10 pages, 2018.
- [30] B. Wei and C. Sheng Li, "Changes in Th1/Th2-producing cytokines during acute exacerbation chronic obstructive pulmonary disease," *Journal of International Medical Research*, vol. 46, no. 9, pp. 3890–3902, 2018.
- [31] R. T. Uren and A. M. Turnley, "Regulation of neurotrophin receptor (Trk) signaling: suppressor of cytokine signaling 2 (SOCS2) is a new player," *Frontiers in Molecular Neuroscience*, vol. 7, p. 39, 2014.
- [32] X. D. Li, X. M. Li, J. W. Gu, and X. C. Sun, "MiR-155 regulates lymphoma cell proliferation and apoptosis through targeting SOCS3/JAK-STAT3 signaling pathway [J]," *European Review for Medical and Pharmacological Sciences*, vol. 24, no. 14, pp. 7577, 2020.

## Research Article

# Efficiency of *Coriandrum sativum* (Linn.) and *Petroselinum crispum* (Mill.) in Enhancing Iron Absorption: An *In Silico* and *In Vitro* Approach

T. Sangeetha <sup>1</sup>, K. Syed Ibrahim <sup>2</sup>, S. Deepa <sup>2</sup>, B. Balamuralikrishnan <sup>3</sup>, M. Arun,<sup>4</sup>  
S. Velayuthaprabhu <sup>5</sup>, K. M. Saradhadevi <sup>6</sup> and A. Vijaya Anand <sup>1</sup>

<sup>1</sup>Department of Human Genetics and Molecular Biology, Bharathiar University, Coimbatore, Tamil Nadu, India

<sup>2</sup>PG & Research Department of Botany, PSG College of Arts and Science, Coimbatore, Tamil Nadu, India

<sup>3</sup>Department of Food Science and Biotechnology, Sejong University, Seoul, Republic of Korea

<sup>4</sup>Department of Obstetrics and Gynaecology, Centre for Perinatal and Reproductive Medicine, University of Perugia, Perugia, Italy

<sup>5</sup>Department of Biotechnology, Bharathiar University, Tamil Nadu, Coimbatore, India

<sup>6</sup>Department of Biochemistry, Bharathiar University, Tamil Nadu, Coimbatore, India

Correspondence should be addressed to A. Vijaya Anand; avahgmb@buc.edu.in

Received 8 March 2022; Revised 11 April 2022; Accepted 12 April 2022; Published 30 April 2022

Academic Editor: Ruchika Garg

Copyright © 2022 T. Sangeetha et al. This is an open access article distributed under the Creative Commons Attribution License, which permits unrestricted use, distribution, and reproduction in any medium, provided the original work is properly cited.

*Coriandrum sativum* (Linn.) and *Petroselinum crispum* (Mill.) are the common herbs used for culinary purposes in daily life. The chlorophyll pigment in plants is being identified with various medicinal values, whereas iron is an essential micronutrient for the proper metabolism of the human body. The current research has been aimed at predicting the role of *C. sativum* and *P. crispum* in enhancing iron absorption via an *in vitro* approach. *C. sativum* and *P. crispum* have been analyzed for their capability of being a source of chlorophyll and iron concentration. The extracts prepared from solvents like carbinol, petroleum ether, and water were subjected to the identification of phytoconstituents through gas chromatography-mass spectrometry analysis, and the identified compounds were subjected to *in silico* studies against the iron-binding receptor, transferrin, to depict the binding affinity of the identified compounds. The carbinol extract was then put through *in vitro* analytical studies in Caco2 cell lines with a concentration of 500 µg/ml. Current research has shown that the leaves of *C. sativum* and *P. crispum* are an excellent source of chlorophyll and iron and has also suggested that these herbs efficiently enhance the absorption of iron in human intestinal cells.

## 1. Introduction

*Coriandrum sativum* (Linn.), commonly called coriander, and *Petroselinum crispum* (Mill.), commonly called Chinese coriander or parsley, belong to the Apiaceae family. Table 1 shows the family characterization of *C. sativum* and *P. crispum*. These two plants are most efficiently used in the medicinal field as well as in the culinary areas [1]. The phytochemical compounds present in these plants are being identified to have various medicinal purposes, including anti-inflammatory, neuroprotectivity, antidiabetic, anti-cancer, antibacterial, and antifungal activities [2–5]. One of

the most important micronutrients needed by the human body is iron [6]. Approximately about 8.7 mg and 14.8 mg of iron are needed per day by men and women, respectively [7]. The improper iron supplementation affects the transportation of oxygen directly since iron is an essential component in the formation of erythrocytes, which are composed of a protein called hemoglobin that is majorly involved in oxygen transport [8]. Deficiency in the iron content may be due to various reasons like improper iron absorption by the intestine, excess loss of iron, or improper intake of iron. The duodenum and jejunum are the parts of the small intestine involved in iron absorption [9]. Anemia is

TABLE 1: Scientific classification of coriander and parsley.

Classification	Coriander	Parsley
Super kingdom	Eukaryota	Eukaryota
Kingdom	Viridiplantae	Viridiplantae
Phylum	Streptophyta	Streptophyta
Subphylum	Streptophytina	Streptophytina
Class	Magnoliopsida	Magnoliopsida
Order	Apiales	Apiales
Suborder	Apiineae	Apiineae
Family	Apiaceae	Apiaceae
Subfamily	Apiioideae	Apiioideae
Tribe	Coriandreae	Apiiae
Genus	<i>Coriandrum</i>	<i>Petroselinum</i>
Species	<i>Sativum</i>	<i>Crispum</i>

the predominant clinical condition caused as a result of iron deficiency, whereas iron deficiency may also be life-threatening in the event of occurring as a comorbidity along with heart and kidney failure [10]. The concentrations of iron in the herbs *C. sativum* and *P. crispum* are found to be present in significant concentrations, yet the clinical significance and pathophysiology of iron absorption in the intestines from these herbs are still unclear. Hence, the human colon adenocarcinoma (Caco2) cell lines, which are mainly derived from colon carcinoma, are mainly used in studies related to the intestinal epithelial barrier. The current study has been aimed at analyzing the effectiveness of the leaf extracts of *C. sativum* and *P. crispum* in the absorption of iron by human intestinal cells *via in vitro* studies using Caco2 cell lines. The iron absorption enhancement by using the plant extracts may provide an effective and easy way of treating the acquired iron deficiency in human individuals.

## 2. Materials and Methods

**2.1. Plant Collection.** The seeds of plants *C. sativum* and *P. crispum* have been sown and grown in partial sunlight, and the plant identification has been done after the plant has reached its complete growth (Plant Identification Number: 2998, 2999; Department of Botany, St. Joseph's College, Tiruchirapalli, Tamil Nadu, India). The leaves of the plants had been collected just before the flowering stage, and the fresh leaves were subjected to chlorophyll estimation, while the remaining leaves were dried in the shade for further analysis.

**2.2. Chlorophyll Estimation.** The fresh leaves of *C. sativum* and *P. crispum* were crushed into a fluid by using 80% acetone in a mortar and pestle. The fluid was then centrifuged and the supernatant was collected in a 100 ml standard flask. The centrifugation with 80% acetone has been repeated until a clear supernatant is obtained. The obtained supernatant was then made up to 100 ml with 80% acetone and the solution was taken for colorimetric analysis at 645 nm and 663 nm. The concentration of chlorophyll has been calculated using the Arnon formula [11], chlorophyll content =  $[20.2 (A_{645}) + 8.02 (A_{663})/1000 \times \text{weight}] \times \text{volume}$ , with the obtained values.

TABLE 2: Chlorophyll estimation of *C. sativum* and *P. crispum* leaves.

Sample	Absorbance at 645 nm		Absorbance at 663 nm	
	<i>C. sativum</i>	0.38	$\bar{x} = \mathbf{0.38}$	0.82
	0.37		0.81	
	0.39		0.83	
<i>P. crispum</i>	0.43	$\bar{x} = \mathbf{0.43}$	0.85	$\bar{x} = \mathbf{0.85}$
	0.44		0.84	
	0.42		0.86	

Footnotes:  $\bar{x}$  - average

The bold numbers has been defined in the footnotes as "average."

TABLE 3: Iron estimation in *C. sativum* and *P. crispum* leaves.

Sample	Optical density values at 540 nm	Iron
Estimated (mg/ml)		
Blank	0.00	0
Standard 01 (10 $\mu\text{g/ml}$ standard)	0.08	0.01
Standard 02 (20 $\mu\text{g/ml}$ standard)	0.16	0.02
Standard 03 (30 $\mu\text{g/ml}$ standard)	0.25	0.03
Standard 04 (40 $\mu\text{g/ml}$ standard)	0.31	0.04
Standard 05 (50 $\mu\text{g/ml}$ standard)	0.35	0.05
<i>C. sativum</i> —fresh (solvent: phosphate buffer saline)	0.21	0.86
	0.23	0.93
	0.22	0.90
	0.12	0.50
<i>C. sativum</i> —dried (solvent: phosphate buffer saline)	0.15	0.63
	0.13	0.53
	0.10	0.43
<i>P. crispum</i> —fresh (solvent: phosphate buffer saline)	0.11	0.46
	0.10	0.43
	0.2	0.01
<i>P. crispum</i> —dried (solvent: phosphate buffer saline)	0.2	0.01
	0.3	0.02
	0.26	1.06
<i>C. sativum</i> —fresh (solvent: 30% sulfuric acid)	0.26	1.06
	0.25	1.00
	0.15	0.63
<i>C. sativum</i> —dried (solvent: 30% sulfuric acid)	0.18	0.76
	0.14	0.60
	0.12	0.50
<i>P. crispum</i> —fresh (solvent: 30% sulfuric acid)	0.11	0.46
	0.10	0.43
	0.04	0.02
<i>P. crispum</i> —dried (solvent: 30% sulfuric acid)	0.04	0.02
	0.05	0.02

The bold numbers has been defined in the footnotes as "average."

**2.3. Iron Estimation.** The shade-dried leaves of *C. sativum* and *P. crispum* were used for the estimation of iron by using the thiocyanate method [12]. 1 in 10 dilutions of the stock standard, which was prepared by using ferrous ammonium sulphate and 30% sulfuric acid in demineralized water, was used as the working standard solution, followed by the addition of 30% sulfuric acid, potassium persulphate, and potassium thiocyanate as reagents during the analysis. The optical density values were recorded at 540 nm in the colorimeter.

TABLE 4: Compounds scrutinized for molecular docking.

S. no.	Name of the compound
1	Cyclopenta[C]Furo[3',2':4,5] furo[2,3-h][1]benzopyran-11(1h)-one, 2,3,6a,9a-tetrahydro-1,3-dihydroxy-4-methoxy-
2	Butanedioic acid, 2,3-Bis (benzoyloxy)-, (2r,3r)
3	Benzyl beta-D-glucoside
4	1-Beta-D-Ribofuranosylimidazo[1,2 B] pyrazole-7-carbonitrile
5	(4e)-6,7-Dihydro-2,1,3-benzoxadiazol-4(5h)-one oxime
6	1,2-O-(1-Methylethylidene) hexofuranose
7	5,7-Dimethylpyrazolo[1,5-A] pyrimidin-2(1h)-one
8	4-Hydroxy-3-pentyl-cyclohexanone
9	2,4-Dihydroxy-2,5-dimethyl-3(2h)-Furan-3-one
10	2-Undecenoic acid
11	Ethyl 1-thio-Alpha-L-arabinofuranoside
12	3,5-Dodecadiyne, 2-methyl-
13	1h-Pyrazole-5-carboxamide, N-(2-hydroxyethyl)-
14	Methyl 1-methyl-3-oxocyclopentanecarboxylate
15	Butane, 2-(2,2-dichloro-1,3-dimethylcyclopropyl)-
16	Ethanimidothioic acid, 2-(dimethyl)
17	Gamma-guanidinobutyric_acid
18	Isocitronellol
19	Piracetam
20	2,3,4,5-Tetrahydroxypentanal
21	2-Amino-3-hydroxypyridine
22	Ribitol
23	2,3-Dimethylfumaric acid
24	1-Deoxy-D-arabitol
25	5-Hydroxymethylfurfural
26	Diazene, Bis(1,1-dimethylethyl)-
27	Pentanedioic acid, dimethyl ester
28	2(5h)-Furanone, 5-methyl-
29	Pyrrolidin-1-acetic acid
30	Butanedioic acid, monomethyl ester
31	2,5-Furandione
32	Dimethylamine, N-(diisopropylphosphino)methyl-
33	2-Aminoethanethiol hydrogen sulfate (ester)
34	2-Methyl-1,3,4-oxadiazole
35	N-Methoxy-N-methylacetamide
36	Ethane, 1,1-diethoxy-
37	2-Methylpyrrolidine
38	2-Propen-1-ol
39	Butane, 2-isothiocyanato-
40	2,2'-Bioxirane
41	Pyrrolidine

**2.4. Molecular Docking.** The dried leaves of *C. sativum* and *P. crispum* were subjected to Soxhlet extraction by using three different solvents, carbinol, petroleum ether, and water. The extracts obtained were then subjected to gas chromatography-mass spectrometry (GC-MS) analysis. The phytochemical compounds were then subjected to virtual screening using the SwissADME software to scrutinize the compounds based on pharmacokinetic properties and drug-likeness, which includes the Lipinski rule. The scrutinized compounds are then analyzed for their binding capacity with the iron-binding receptor, transferrin (IKAS), via molecular docking by using AutoDock Vina (version 1.1.2).

**2.5. In Vitro Studies.** The culturing of Caco2 cells was performed using Dulbecco's modified Eagle's medium with high glucose containing 10% fetal bovine serum. The

cultured cells were then treated with 0.25% trypsin and centrifuged at 300g. Then 200  $\mu$ l of the suspension obtained was loaded in a 96-well microtiter plate and incubation at 37°C in 5% carbon dioxide for 24 hours was carried out. The five different test concentrations (62.5  $\mu$ l, 125  $\mu$ l, 250  $\mu$ l, 500  $\mu$ l, and 1000  $\mu$ l) of the carbinol extracts of *C. sativum* and *P. crispum* leaves were added to the medium and the incubation was repeated, followed by the addition of 10% 3-(4,5-dimethylthiazolyl-2)-2,5-diphenyltetrazolium bromide (MTT) reagent and the incubation was extended for 3 hours. The cells were then absorbed at 570 nm and 630 nm to depict the IC<sub>50</sub> value. Following the MTT assay (cytotoxicity test), the cells were tested for the iron content present in them, and then the iron uptake by the cells was analyzed after treating the cells with the carbinol extracts of *C. sativum* and *P. crispum* by using the inductively coupled plasma mass spectrometry (ICPMS).



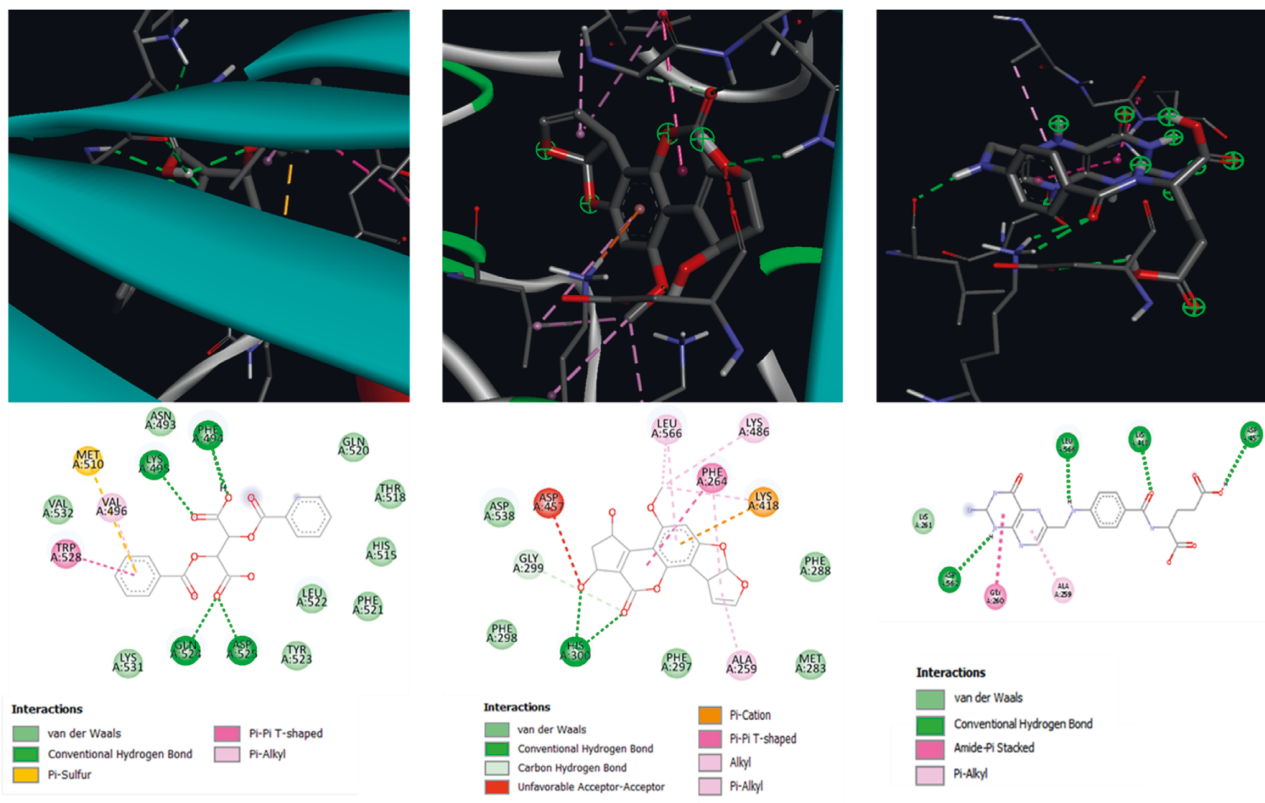


FIGURE 1: Docking of compound (a) butanedioic acid, 2,3-Bis(Benzoyloxy)-, (2r,3r) (b) Cyclopenta (c) Furo[3',2':4,5]Furo[2,3-H][1] Benzopyran-11(1h)-One,2,3,6a,9a-Tetrahydro-,3-Dihydroxy-4-Methoxy, and (d): Control drug: diclofenac with transferrin receptor.

### 3. Results

**3.1. Chlorophyll Estimation.** The chlorophyll estimation of *C. sativum* and *P. crispum* leaves yielded the tabulated results when absorbed at 645 nm and 663 nm (Table 2). The amount of chlorophyll present in *C. sativum* and *P. crispum* was observed to be 1.07 mg/g and 1.82 mg/g, respectively.

**3.2. Iron Estimation.** The estimation of iron in both fresh and dried leaves of *C. sativum* and *P. crispum* gave the tabulated results (Table 3) when absorbed at 540 nm, and the calculation used for iron estimation is  $(\text{observed value} \div n) \times (\text{volume} \div 1000)$  mg/ml, whereas “n” represents the volume of sample added for the analysis; in the current experiment,  $n = 3$  ml. The iron content was found to be higher in both the plant leaves when processed with 30% sulfuric acid with phosphate buffer saline solution. The iron content observed in the fresh leaves was 34% higher than the iron content seen in dried *C. sativum* leaves in phosphate buffer saline, whereas fresh leaves of *P. crispum* showed a 43% higher yield. In the case of 30% sulfuric acid as a solvent, the yield of fresh leaves of *C. sativum* was 38% higher and the yield of *P. crispum* was 44% higher than the dried leaves of the respective plants. On comparing *C. sativum* and *P. crispum*, the yield of *C. sativum* was 55% higher than the iron content of *P. crispum*.

**3.3. Molecular Docking.** Based on the GC-MS analysis that was performed preliminarily, the phytochemicals obtained from *C. sativum* and *P. crispum* by using three different

solvents (carbinol, petroleum ether, and water) yielded about 1761 (901 + 860) identified compounds and 37 (20 + 17) unknown compounds, respectively. Among the three solvents, carbinol was found to yield more compounds than petroleum ether and water. Carbinol extracted about 309 (304 identified + 5 unknown) compounds from *C. sativum* and 327 (325 identified + 2 unknown) compounds from *P. crispum* leaves, whereas 300 and 246 compounds were extracted using petroleum ether from *C. sativum* and *P. crispum*, respectively using water as the solvent (results obtained from preliminary work, the data has not shown). Hence, our further analysis used compounds from carbinol extracts of both *C. sativum* and *P. crispum* leaves.

Following the compound identification, based on the virtual screening, only 42 compounds were selected for molecular docking based on their pharmacokinetic and pharmacodynamic properties (Table 4). Transferrin, an iron receptor, was selected as the target, and the binding affinity was observed. The cyclopenta[c]furo[3',2':4,5] furo[2,3-h][1] benzopyran-11(1h)-one, 2, 3, 6a, 9a-tetrahydro-1,3-dihydroxy-4-methoxy and 2,3-dibenzoyltartaric acid-(2R,3R)- are the top two compounds with higher binding affinity when compared with the control drug. 2,3-Dibenzoyltartaric acid- (2R,3R)- showed hydrogen bonds with four different amino acids: lysine, phenylalanine, glutamine, aspartic acid, and cyclopenta[c]furo[3',2':4,5] furo[2,3-h][1] benzopyran-11(1h)-one,2,3,6a,9a-tetrahydro-1,3-dihydroxy-4-methoxy showed two hydrogen bonds with histidine alone,



TABLE 5: Cytotoxicity test of *C. sativum* and *P. crispum* on Caco2 cell line.

% Viability	Test concentrations ( $\mu\text{g/ml}$ )						
	Blank	Untreated	62.5	125	250	500	1000
<i>C. sativum</i>	-	100	110.08	111.13	110.43	114.75	108.49
<i>P. crispum</i>	-	100	108.00	116.34	117.44	125.53	105.46

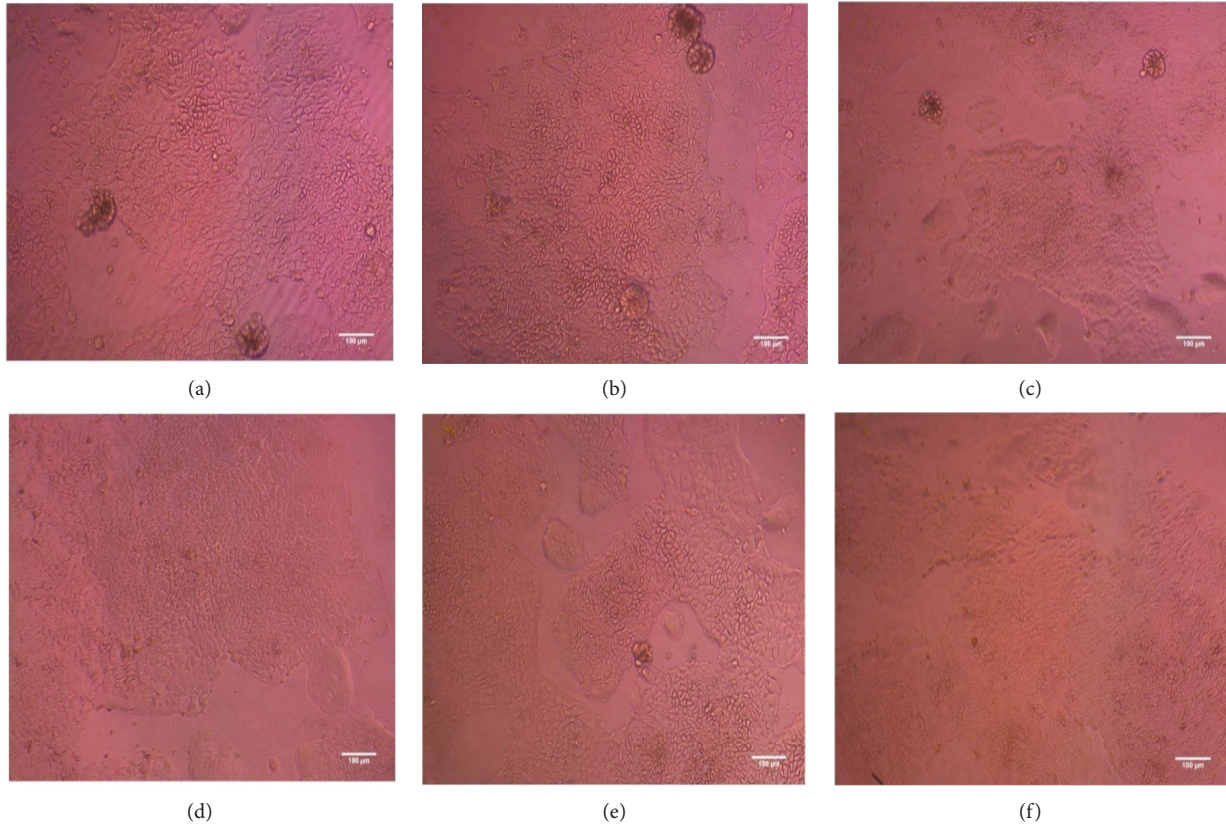


FIGURE 2: Cytotoxicity analysis on Caco2 Cells with *C. sativum* extracts with different concentrations (a) Untreated (b) 62.5  $\mu\text{g/ml}$  (c) 125  $\mu\text{g/ml}$  (d) 250  $\mu\text{g/ml}$  (e) 500  $\mu\text{g/ml}$  (f) 1000  $\mu\text{g/ml}$ ] (Both the figures 2(a) and 3(a) are the same images of the untreated cells).

whereas the control drug, folic acid, showed four hydrogen bonds with three different amino acids, two bonds with aspartic acid, and one each with lysine and leucine (Figures 1(a) and 1(c)) of the transferrin receptor.

**3.4. In Vitro Analysis.** The carbinol extracts of *C. sativum* and *P. crispum* leaves were nontoxic to the Caco2 cells. Table 5 shows the test concentration and viability rate of Caco2 cells. The cells did not show any decline in viability and subsequent cell growth has also been observed, indicating that *C. sativum* and *P. crispum* extracts enhance cell proliferation and viability. Figures 2 and 3 show the cytotoxicity tests of extracts on Caco2 cells. Followed by a cytotoxicity test, the *C. sativum* and *P. crispum* extracts showed 0.67 mg/L and 0.91 mg/L of iron concentration in their carbinol extracts, respectively, when analyzed using ICPMS. After the quantification, the

iron uptake of the cells was recorded and tabulated (Table 6).

The Caco2 cells treated with iron alone failed to absorb the iron, whereas the cells treated with the extracts showed excellent iron absorption. 48.51% of the total iron added was absorbed by the cells treated with *C. sativum* extracts, and 8.24% of the iron was absorbed by the *P. crispum* extracts. The apparent permeability of the cells treated with *C. sativum* extracts was moderate ( $1.18 \times 10^6 \text{ cm/s}$ ) and *P. crispum* extracts showed a lower permeability rate ( $2.01 \times 10^7 \text{ cm/s}$ ), whereas the untreated cells did not show any permeability across the membrane (0 cm/s).

#### 4. Discussion

Chlorophyll is the pigment present in plant parts that has been proved to have medicinal properties. The chlorophyll derivatives influence the metabolism of lipids in a positive

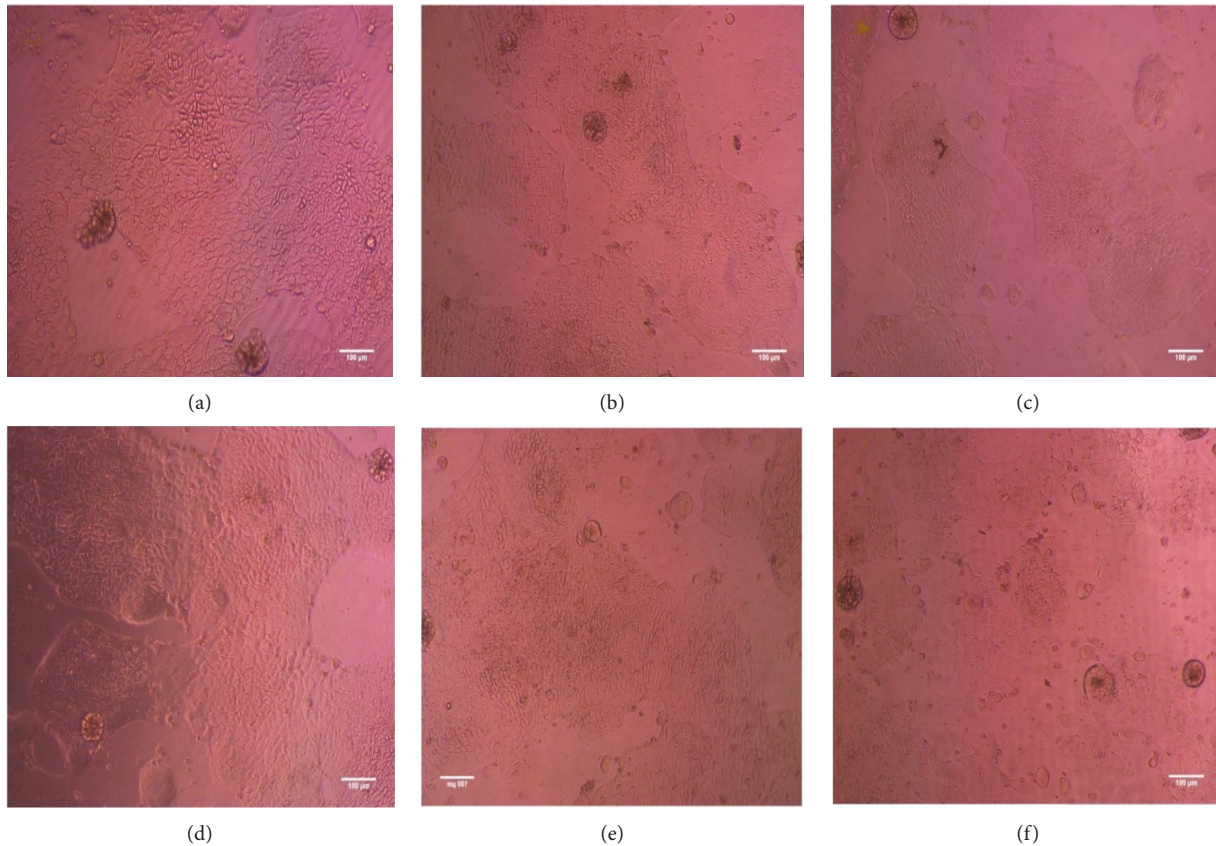


FIGURE 3: Cytotoxicity analysis on Caco2 Cells with *P. crispum* with different concentrations. (a) Untreated; (b) 62.5 µg/ml; (c) 125 µg/ml; (d) 250 µg/ml; (e) 500 µg/ml; (f) 1000 µg/ml. Both Figures 2(a) and 3(a) are the same images of the untreated cells.

TABLE 6: Iron absorption analysis.

Sample	Quantity of iron added to cells (µg)	Quantified iron (mg/L)	Quantity of iron taken up by cells (µg)	Iron uptake by Caco2 cells (µg)
Untreated	0	0.51	<b>0.51</b>	<b>0</b>
<i>C. sativum</i> treated	1.34	1.16	<b>1.16</b>	<b>0.65</b>
<i>P. crispum</i> treated	1.82	0.66	<b>0.66</b>	<b>0.15</b>

Concentration of the extracts used: 500 µg/mL

manner, which can be further used in the management of obesity [13]. *C. sativum* leaves have been shown to have the highest concentrations of about 14 µg/mL and the lowest of about 9.5 µg/mL of chlorophyll [14]. About 0.42 mg/g of iron has been estimated in the leaves of *C. sativum*, whereas their seeds were composed of 0.16 mg/g of iron [15]. The *C. sativum* leaves were also found to be rich in antioxidants [16]. A chlorophyll concentration of around  $16.57 \pm 3.2$  mg/g to  $10.97 \pm 2.6$  mg/g has been estimated in the commercially bought *C. sativum* leaves [17]. About 2.2 mg/g of chlorophyll has been quantified from the leaves of coriander [18]. The current research on the estimation of chlorophyll in the leaves of *C. sativum* has yielded 1.07 mg/g, which is considered significant. The *C. sativum* leaves exhibited 0.835 mg/g of chlorophyll, whereas *P. crispum* leaves showed an estimate of 1.282 mg/g in their fresh leaves [19]. The

leaves of chlorophyll content were found to be  $0.0263 \pm 0.0019$  mg/g in the leaves of *P. crispum* [20]. A study by Arnold et al. [21] has revealed that the chlorophyll concentration in the leaves of *P. crispum* is 0.632 mg/g, whereas about 0.185 mg/g to 1.8 mg/mL of chlorophyll was found in the study performed by Kuzma et al. [22] and Paulert et al. [23] in the leaves of *P. crispum*. Parsley leaves were examined for chlorophyll content in their baby greens variety and showed significantly higher values, i.e., 18.36 mg/g [24]. The parsley leaves showed a similar quantity of chlorophyll in the current research as well.

Iron is the micronutrient that has a major role in the chlorophyll synthesis of plants [25,26]. In human beings, the role of iron is significant. From the transportation of oxygen to tissues to storage and energy employment, iron plays an irreplaceable role in the physiological functions of the



human body [27]. Iron is the major component of the hemoglobin molecule, a pigment in red blood cells that is involved in the transportation of oxygen throughout the body [28]. On examining the presence of iron, the *C. sativum* showed 0.42 mg/g in the leaves and 0.16 mg/g in the seeds [28]. Around 1.06 mg/g of iron has been estimated in the leaves of *C. sativum* in the study performed by Vanisha and Monika [29]. The leaves of *P. crispum* have been suggested to contain 6.2 mg/100g iron [30]. The iron content was also notably higher in fresh as well as dried leaves, and also in the extracts prepared by using the soxhlet extraction method, indicating the leaves of *C. sativum* and *P. crispum* are significant iron sources. On the other hand, the extracts of coriander leaves showed an effective chelating nature with iron [31], indicating the iron metabolism can be influenced by coriander leaves, whereas parsley leaves are proved to have components involved in the treatment of anxiety and depression [32]. The nanoparticles produced from the parsley leaves may be used effectively against iron deficiency, anemia condition, in rats [33]. A study by Lakshmana Prabhu et al. [34] has reported that phytochemicals such as 3,4',5,7-tetrahydroxyflavone and quercetin have a good binding affinity when analyzed for the antiasthma properties [34]. The extracts of seeds of *C. sativum* have been examined for their anti-cancer properties *via* docking of phytochemicals, and the rutin molecule has been found to have the highest binding affinity [35]. In the present study, cyclopenta[c]furo[3',2':4,5] furo[2,3-h] [1]benzopyran-11(1h)-one,2,3,6a,9a-tetrahydro-1,3-dihydroxy-4-methoxy and (2R,3R)-2,3-dibenzoyltartaric acid have shown an excellent binding affinity with the transferrin receptor, suggesting the positive influence in the enhancement of iron absorption.

Caco2 cell lines have been observed to be a better way to estimate iron absorption in human cells. The bioavailability, as well as the uptake of iron by Caco2 cells, has shown a considerable outcome [36]. In addition, iron uptake by the human epithelial cells can be correlated more efficiently by using *in vitro* studies, which involve the Caco2 cell lines [36,37]. The iron uptake by Caco2 cells in the current research has also shown noteworthy results that strongly suggest the utilization of *C. sativum* and *P. crispum* leaves for the enhancement of iron absorption in human beings.

## 5. Conclusion

The chlorophyll content of *C. sativum* and *P. crispum* leaves were sufficiently significant in their concentration, suggesting the rich chlorophyll nature of these two plants. The iron concentration of these two plants was considered suggestive and higher. The number of phytoconstituents in the leaf extracts of *C. sativum* and *P. crispum* has been observed to be considerably higher in all the three solvents analyzed. Among the identified compounds, the two compounds, cyclopenta[c]furo[3',2':4,5] furo[2,3-h] [1]benzopyran-11(1h)-one,2,3,6a,9a-tetrahydro-1,3-dihydroxy-4-methoxy and (2R,3R)-2,3-dibenzoyltartaric acid have shown a better binding affinity with the iron-binding receptor when compared with the control drug. The *in vitro* studies yielded very suggestive results on enhancing the iron

absorption efficiently in the human intestinal cells by these two plants. The iron deficiency can be effectively treated by using these two plants as the *in vitro* studies have suggested an excellent iron absorption in cells treated with plant extracts.

## Data Availability

The datasets generated during and/or analyzed during the current study are available from the corresponding author on reasonable request.

## Conflicts of Interest

The authors declare no conflicts of interest.

## Acknowledgments

The authors acknowledge the authorities of the Institution and the fellow researchers for rendering moral support in completing the manuscript.

## References

- [1] S. Koppula, R. Alluri, and S. R. Kopalli, "Coriandrum sativum attenuates microglia mediated neuroinflammation and MPTP-induced behavioral and oxidative changes in Parkinson's disease mouse model," *EXCLI J*, vol. 20, no. 20, pp. 835–850, 2021.
- [2] S. D. Kothalawala, D. Edward, J. C. Harasgama et al., "Immunomodulatory activity of a traditional Sri Lankan concoction of *Coriandrum sativum* L and *Coscinium fenestratum* G," *Evidence-based Complementary and Alternative Medicine*, vol. 2020, pp. 1–10, 2020.
- [3] L. Elmas, M. Secme, R. Mammadov, U. Fahrioglu, and Y. Dodurga, "The determination of the potential anticancer effects of *Coriandrum sativum* in PC-3 and LNCaP prostate cancer cell lines," *Journal of Cellular Biochemistry*, vol. 120, no. 3, pp. 3506–3513, 2019.
- [4] A. S. Jesuthasan and D. I. Uluwaduge, "Ethnobotanics used in folk medicine of Tamil culture in Sri Lanka: a scientific review," *Journal of Integrative Medicine*, vol. 15, no. 1, pp. 19–26, 2017.
- [5] R. H. Vekaria, M. N. Patel, P. N. Bhalodiya, V. Patel, T. R. Desai, and P. R. Tigar, "Evaluation of neuroprotective effect of *Coriandrum sativum* Linn. against ischemic-reperfusion insult in brain," *International Journal of Phyto-pharmacology*, vol. 2, pp. 186–193, 2012.
- [6] J. Chen, N. N. Zhang, Q. Pan et al., "Hydrogen sulphide alleviates iron deficiency by promoting iron availability and plant hormone levels in glycine max seedlings," *BMC Plant Biology*, vol. 20, no. 1, p. 383, 2020.
- [7] H. Finnamore, J. Le Couteur, M. Hickson, M. Busbridge, K. Whelan, and C. L. Shovlin, "Hemorrhage-adjusted iron requirements, hematinics and hepcidin define hereditary hemorrhagic telangiectasia as a model of hemorrhagic iron deficiency," *PLoS One*, vol. 8, no. 10, 2013.
- [8] G. Verna, A. Sila, M. Liso et al., "Iron-enriched nutritional supplements for the 2030 pharmacy shelves," *Nutrients*, vol. 13, no. 2, p. 378, 2021.
- [9] T. Ems, K. St Lucia, and M. R. Huecker, *Biochemistry, Iron Absorption. [Updated 2021 Apr 26]. in: StatPearls [Internet]. StatPearls Publishing, Treasure Island, FL, USA, Available*

- from: <https://www.ncbi.nlm.nih.gov/books/NBK448204/>, 2021.
- [10] J. Rossler, F. Schoenrath, B. Seifert et al., "Iron deficiency is associated with higher mortality in patients undergoing cardiac surgery: a prospective study," *British Journal of Anaesthesia*, vol. 124, no. 1, pp. 25–34, 2020.
  - [11] D. I. Arnon, "Copper enzymes in isolated chloroplasts. Polyphenoloxidase in beta vulgaris," *Plant Physiology*, vol. 24, no. 1, pp. 1–15, 1949.
  - [12] J. Woods and M. Mellon, "Thiocyanate method for iron: a spectrophotometric study," *Industrial & Engineering Chemistry Analytical Edition*, vol. 13, no. 8, pp. 551–554, 1941.
  - [13] H. G. Lee, Y. A. Lu, J. G. Je et al., "Effects of ethanol extracts from Grateloupia elliptica, a red seaweed, and its chlorophyll derivative on 3t3-l1 adipocytes: suppression of lipid accumulation through downregulation of adipogenic protein expression," *Marine Drugs*, vol. 19, no. 2, p. 91, 2021.
  - [14] Z. Rabiei, S. J. Hosseini, H. Pirdashti, and S. Hazrati, "Physiological and biochemical traits in coriander affected by plant growth-promoting rhizobacteria under salt stress," *Heliyon*, vol. 6, no. 10, Article ID e05321, 2020.
  - [15] U. Rajeshwari and B. Andallu, "Medicinal benefits of coriander (*Coriandrum sativum* L.)," *Spatula DD*, vol. 1, p. 51, 2011.
  - [16] S. Bhat, P. Kaushal, M. Kaur, and H. K. Sharna, "Coriander (*Coriandrum sativum* L.): processing, nutritional and functional aspects," *African Journal of Plant Science*, vol. 8, no. 1, pp. 25–33, 2014.
  - [17] S. Priyadarshi, H. Khanum, R. Ravi, B. B. Borse, and M. M. Naidu, "Flavour characterisation and free radical scavenging activity of coriander (*Coriandrum sativum* L.) foliage," *Journal of Food Science & Technology*, vol. 53, no. 3, pp. 1670–1678, 2016.
  - [18] G. Kofidis, A. Giannakoula, and I. F. Ilias, "Growth, anatomy and chlorophyll fluorescence of coriander plants (*Coriandrum sativum* L.) treated with prohexadione-calcium and daminozide," *Acta Biologica Cracoviensia - Series Botanica*, vol. 50, p. 55, 2008.
  - [19] K. Kathirvel, Y. Garipey, O. R. S. A. T. Valerie, and V. Raghavan, "Microwave drying - a promising alternative for the herb processing industry," *CSBE 2006 Annual Conference Proceedings*, vol. 06, no. 212, pp. 02–16, 2006.
  - [20] S. Najla, R. Sanoubar, and R. Murshed, "Morphological and biochemical changes in two parsley varieties upon water stress," *Physiology and Molecular Biology of Plants*, vol. 18, no. 2, pp. 133–139, 2012.
  - [21] C. Arnold, U. Schwarzenbolz, and V. Bohm, "Carotenoids and chlorophylls in processed xanthophyll-rich food," *Lebensmittel-Wissenschaft und -Technologie- Food Science and Technology*, vol. 57, no. 1, pp. 442–445, 2014.
  - [22] P. Kuzma, B. Druzynska, and M. Obiedzinski, "Optimization of extraction conditions of some polyphenolic compounds from parsley leaves (*Petroselinum crispum*)," *Acta Scientiarum Polonorum Technologia Alimentaria*, vol. 13, no. 2, pp. 145–154, 2014.
  - [23] R. Paulert, R. Ascrizzi, S. Malatesta et al., "*Ulva intestinalis* extract acts as biostimulant and modulates metabolites and hormone balance in basil (*Ocimum basilicum* L.) and parsley (*Petroselinum crispum* L.)," *Plants*, vol. 10, no. 7, p. 1391, 2021.
  - [24] C. El-Nakhel, A. Pannico, G. Graziani et al., "Mineral and antioxidant attributes of *Petroselinum crispum* at different stages of ontogeny: microgreens v s baby greens," *Agronomy*, vol. 11, no. 5, p. 857, 2021.
  - [25] S. S. Jangra, V. K. Madan, I. Singh, and Dusyant, "Comparative analysis of phytochemical profile and antioxidant activity of coriander (*Coriandrum sativum* L.)," *Asian Journal of Chemistry*, vol. 30, no. 3, pp. 508–512, 2018.
  - [26] H. A. H. Said-Al Ahl and E. A. Omer, "Effect of spraying with zinc and/or iron on growth and chemical composition of coriander (*Coriandrum sativum* L.) harvested at three stages of development," *Journal of Medicinal Food Plants*, vol. 1, pp. 30–46, 2009.
  - [27] G. J. Kontoghiorghes, A. Kolnagou, T. Demetriou, M. Neocleous, and C. N. Kontoghiorghes, "New era in the treatment of iron deficiency anaemia using trimaltol iron and other lipophilic iron chelator complexes: historical perspectives of discovery and future applications," *International Journal of Molecular Sciences*, vol. 22, no. 11, p. 5546, 2021.
  - [28] T. Ravingerova, L. Kindernay, M. Bartekova et al., "The molecular mechanisms of iron metabolism and its role in cardiac dysfunction and cardioprotection," *International Journal of Molecular Sciences*, vol. 21, no. 21, p. 7889, 2020.
  - [29] S. N. Vanisha and S. Monika, "Carotene content of coriander leaves (*Coriandrum sativum*), amaranth, red (*Amaranthus* sp), green garlic (*Allium sativum*) and mogri (*Raphanus caudatus*) and its products," *Journal of Applied Pharmaceutical Science*, vol. 4, no. 08, pp. 069–074, 2014.
  - [30] M. Rezazad and F. Farokhi, "Protective effect of Petroselinum crispum extract in abortion using prostadin-induced renal dysfunction in female rats," *Avicenna Journal of Phytomedicine*, vol. 4, no. 5, pp. 312–319, 2014.
  - [31] R. Talaei, A. Kheirollah, H. Babaahmadi Rezaei, E. Mansouri, and G. Mohammadzadeh, "The protective effects of hydroalcoholic extract of *Coriandrum sativum* in rats with experimental iron-overload condition," *Jundishapur Journal of Natural Pharmaceutical Products*, vol. 13, no. 2, Article ID e65028, 2017.
  - [32] I. Es-Safi, H. Mechchate, A. Amaghnoije et al., "The potential of parsley polyphenols and their antioxidant capacity to help in the treatment of depression and anxiety: an in vivo subacute study," *Molecules*, vol. 26, no. 7, p. 2009, 2021.
  - [33] S. M. El-Bahr, A. M. Elbakery, N. El-Gazzar et al., "Biosynthesized iron oxide nanoparticles from *Petroselinum crispum* leaf extract mitigate lead-acetate-induced anemia in male albino rats: hematological, biochemical and histopathological features," *Toxics*, vol. 9, no. 6, p. 123, 2021.
  - [34] S. Lakshmana Prabu, A. Umamaheswari, V. Tamilselvan, and V. Brithvi, "In silico analysis of *Coriandrum Sativum* against sPLA2 as a therapeutic target protein for Antiasthmatic activity," *International Journal of Research in Pharmacology & Pharmacotherapeutics*, pp. 55–64, 2016.
  - [35] H. Mechchate, R. Costa de Oliveira, I. Es-Safi et al., "Anti-leukemic activity and molecular docking study of a polyphenolic extract from coriander seeds," *Pharmaceuticals*, vol. 14, no. 8, p. 770, 2021.
  - [36] A. P. Au and M. B. Reddy, "Caco-2 cells can be used to assess human iron bioavailability from a semipurified meal," *Journal of Nutrition*, vol. 130, no. 5, pp. 1329–1334, 2000.
  - [37] S. Kalgaoonkar and B. Lonnerdal, "Effects of dietary factors on iron uptake from ferritin by Caco-2 cells," *The Journal of Nutritional Biochemistry*, vol. 19, no. 1, pp. 33–39, 2008.

## Review Article

# The Multiple Pharmacologic Functions and Mechanisms of Action of Guizhi Fuling Formulation

Jie Gao <sup>1,2</sup>, Jianmei Yang <sup>3</sup>, Zhiyuan Lu <sup>1</sup>, Xianwen Dong <sup>4</sup>, and Ying Xu <sup>1</sup>

<sup>1</sup>Department of Physiology, School of Basic Medicine, Shanghai University of Traditional Chinese Medicine, 1200 Cailun Road, Shanghai 201203, China

<sup>2</sup>Department of Rehabilitation Medicine, Affiliated Hospital of Nantong University, 20 Xisi Road, Nantong 226001, Jiangsu, China

<sup>3</sup>Department of Traditional Chinese Medicine, Shanghai Xuhui District Central Hospital, Shanghai 200031, China

<sup>4</sup>Department of Children Rehabilitation Medicine, The Fifth Affiliated Hospital of Zhengzhou University, Zhengzhou 450052, China

Correspondence should be addressed to Xianwen Dong; [xianwen.2004@163.com](mailto:xianwen.2004@163.com) and Ying Xu; [yingxu612@shutcm.edu.cn](mailto:yingxu612@shutcm.edu.cn)

Received 10 December 2021; Accepted 9 April 2022; Published 29 April 2022

Academic Editor: Jelena Zivkovic

Copyright © 2022 Jie Gao et al. This is an open access article distributed under the Creative Commons Attribution License, which permits unrestricted use, distribution, and reproduction in any medium, provided the original work is properly cited.

**Objectives.** Guizhi Fuling Formulation (GZFL), a traditional Chinese medical formulation, consists of Cinnamomi Ramulus, Paeoniae Radix Alba (or Paeoniae Radix Rubra), Moutan Cortex, Persicae Semen, and Poria, with multiple therapeutic functions such as sedation, antitumor activity, anti-inflammation, and neuroprotection. However, its clinical applications remain relatively fragmented, and the underlying mechanisms of GZFL in different diseases are still not very certain. Further research and summary in both application and mechanisms remain to be needed for human health and the best use of GZFL. Therefore, we summarized the multiple pharmacologic effects and possible mechanisms of action of GZFL according to recent 17 years of research. **Methods.** We retrieved four English and two Chinese databases using these keywords (the formulation name or its synonyms) and searched articles written in English from January 2006 up to February 2022. **Key Findings.** GZFL exhibits multiple pharmacologic advantages in gynecologic diseases and other expanding diseases such as cancer, blood, and vascular disease, renal failure, inflammation, and brain injury. Possibly due to its diverse bioactive components and pharmacologic activities, GZFL could target the multiple signaling pathways involved in regulating blood circulation, inflammatory and immune factors, proliferation, apoptosis, and so on. **Conclusion.** This review suggests that GZFL displays promising therapeutic effects for many kinds of diseases, which have been beyond the scope of the original prescription for gynecologic diseases. In this way, we wish to provide a reference and recommendation for further preclinic and clinic studies.

## 1. Introduction

Guizhi Fuling Formulation (GZFL) is an ancient Chinese herbal formulation. GZFL was recorded first in *Synopsis of Prescriptions of the Golden Chamber* (<https://apps.who.int/iris/handle/10665/206952>). This classic tome of traditional Chinese medicine was written by Zhang Zhongjing (AD 150–219), a renowned physician of the Eastern Han Dynasty (AD 25–220).

GZFL is composed of five herbal ingredients according to Chinese Pharmacopeia: Cinnamomi Ramulus (*Cinnamomum cassia* Presl), Paeoniae Radix Alba/Paeoniae Radix Rubra (*Paeonia lactiflora* Pall and *Paeonia veitchii* Lynch),

Moutan Cortex (*Paeonia suffruticosa* Andrews), Persicae Semen (*Prunus persica* (L.) Batsch and *Prunus davidiana* (Carr.) Franch), and Poria (*Poria cocos* (Schw.) Wolf) [1]. The five herbal ingredients from GZFL are mixed at the same ratio in preparations including honey pills, capsules, decoctions, and tablets for the therapeutic method of different diseases. In addition, GZFL is termed differently in different countries: “Guizhi Fuling Wan”, “Guizhi Fuling decoction”, “Guizhi Fuling capsule”, and “Guizhi Fuling tablets” in China; Keishibukuryogan (KBG), K-06, and TJ-25 in Japan; Gyejibokryeong-hwan (GBH) in Korean; and TU-025 in the USA [2–4]. GZFL has been used in different countries.

However, the scientific botanical species of these five herbal ingredients are different according to Pharmacopeia in different countries. For example, KBG consists of the Cinnamomi cortex, Radix Paeoniae, Cortex Moutan, Poria, and Semen Persicae. GBH is composed of Cinnamomi Ramulus, Poria, Moutan Cortex, Semen Persicae, and Paeoniae radix. TU-025 comprises Cinnamon bark, Peony root, Peach kernel, Poria sclerotium, and Moutan bark.

GZFL was utilized widely to invigorate blood circulation and remove blood stasis. It has achieved obvious effects on various gynecologic diseases in China for more than 1000 years, such as dysmenorrhea, ovarian cysts, and uterine fibroids [5]. Moreover, an increasing number of clinical and experimental data have demonstrated that GZFL possesses potent sedative, analgesic, antitumor, anti-inflammatory, and neuroprotective properties without eliciting adverse effects [6]. Thus, GZFL has also been used to treat microvascular inflammation in the skin [7], bladder cancer [8], uterine fibroids [9], and brain injury [10]. Due to these multiple and attractive therapeutic functions, the bioactivity of GZFL has gained enormous attention, thereby leading to the increasing interest in exploring its pharmacological functions and mechanisms of action.

The active ingredients from GZFL are complex. Pharmacologic studies have shown that GZFL consists of cinnamic acid, cinnamaldehyde, paeoniflorin, albiflorin, gallic acid, ethyl gallate, benzoylpaeoniflorin, and benzoic acid [11–13]. Cinnamic acid and cinnamaldehyde are derived from the crude drugs of Cinnamomi Ramulus, which has antimicrobial, anti-inflammatory, and neuroprotective effects [14–16] and has also been reported to be an immune suppressor [17]. Paeoniflorin and albiflorin are derived from Paeoniae Radix Alba. Paeoniflorin can alleviate some inflammatory and autoimmune diseases, such as endoplasmic reticulum stress-associated vascular inflammation [18] and rheumatoid arthritis [19], and also has improving effects on glutamate-induced damage in PC12 cells and bupivacaine-induced cytotoxicity in SH-SY5Y cells [20, 21]. Albiflorin has antidepressant-like effects by increasing hippocampal expression of 5-hydroxytryptamine (5-HT)/norepinephrine (NE) and brain-derived neurotrophic factor (BDNF) [22] and also ameliorates obesity by modulating the expression of thermogenic genes [23]. Gallic acid and ethyl gallate are derived from Moutan Cortex. Gallic acid can improve ulcerative colitis by suppressing inflammation [24] and also exert neuroprotective effects on memory and long-term potentiation (LTP) impairment by decreasing lipid peroxidation and expression of proinflammatory cytokines in the cortex of rats with traumatic brain injury [25]. Ethyl gallate exhibits antioxidant and anticancer capacities in mice with oral cancer [26]. Benzoylpaeoniflorin and benzoic acids are the main active ingredients of Paeoniae Radix and Moutan Cortex, which can prevent hydrogen peroxide (H<sub>2</sub>O<sub>2</sub>)-induced cytotoxicity in primary neurons from the rat cortex and improve dysmenorrhea by suppressing uterus contraction [27]. However, the synergistic interactions of active ingredients remain unclear and the underlying mechanisms of GZFL in different diseases, such as gynecologic diseases, cancers, blood, and vascular disease, are still not very certain.

Therefore, in this review, we summarize the clinical therapeutic efficacy and pharmacologic mechanisms of GZFL documented in clinical and experimental studies in recent years, trying to explain the underlying mechanisms in different diseases which may instruct clinical treatment in the future.

## 2. Methods

We retrieved four English and two Chinese databases (PubMed, Web of Science, Science Direct, Wiley Online Library, CNKI, Wanfang Data), combining searching these keywords (the formulation name or its synonyms) in the Medical Subject Headings (MeSH) field and in the title/abstract. All types of clinical and experimental investigations were considered for inclusion. We only searched articles written in English and published in peer-reviewed journals from January 2006 up to February 2022. Studies using GZFL in any preparations (pills, capsules, decoctions, and tablets) were included. The studies which involved the following ineligible interventions were excluded: (1) combined other herbs, modified GZFL, or active ingredients from GZFL; (2) qualitative assessments and studies without statistical significance; (3) GZFL utilized external or topical administration methods. The name of each herbal ingredient was included according to the *Chinese Pharmacopeia*.

## 3. Gynecologic Diseases

**3.1. Dysmenorrhea.** Dysmenorrhea is the most common gynecologic disorder. It presents as cramps in the abdomen/back during/before menstruation. The main contributor to dysmenorrhea is obviously reduced blood flow caused by enhanced activities and abnormal contractions of the uterus, which induces sensitization of peripheral nerves [28].

A clinical research indicated that GZFL displayed obviously therapeutic effects on patients with primary and secondary dysmenorrhea with the indications such as sweating, heat intolerance, cold sensation in the lower back, and a tense abdomen [29, 30]. GZFL is used widely to treat secondary dysmenorrhea with uterine fibroids. A randomized clinical trial reported that GZFL significantly alleviated dysmenorrhea in patients with uterine fibroids by improving blood stasis and inducing smooth blood flow [3, 4]. In addition, one randomized controlled trial provided support for the positive effects of GZFL on dysmenorrhea and the accompanying acne vulgaris related to menstruation in adults women [12].

Various experimental studies have been carried out to analyze the pharmacologic mechanisms of GZFL in dysmenorrhea. It was reported that GZFL effectively reduced lamina propria edema and displayed a directly inhibitory effect against cyclooxygenase-2 (COX-2) expression, but there is no effect on COX-2 expression in the uterine tissues of oxytocin-induced ICR mice [31]. However, a study in human umbilical vein endothelial cells showed that GZFLs act on downregulating the mRNA levels of COX-1 and COX-2 [32]. Moreover, another *in vivo* study has demonstrated that GZFL significantly improved primary dysmenorrhea with uterine contraction by decreasing the releases of nitric oxide



(NO), prostaglandin (PG)  $F_{2a}$ ,  $Ca^{2+}$  concentration, expression of COX-2, and oxytocin receptor in the uterine tissue of oxytocin-induced mice. At the same time, GZFL and its components could suppress spontaneous and oxytocin-induced contractions in uterine strips and reduce intracellular  $Ca^{2+}$  levels in oxytocin-induced myometrial cells, suggesting that GZFL might exert relaxant effects upon uterine contraction to relieve pain [33]. In addition, an integrative urinary metabolomic study indicated that GZFL treatment reduced the enhanced writhing times and  $PGF_{2a}/PGE_2$  ratio in plasma of rats with primary dysmenorrhea induced by oxytocin injection. Notably, urinary metabolic deviations of those rats were decreased after GZFL treatment, suggesting that GZFL showed therapeutic effects on primary dysmenorrhea by regulating several metabolic pathways [34].

To further understand for mechanisms and effects of GZFL on primary dysmenorrhea, a pharmacokinetic-pharmacodynamic (PK-PD) model was applied to study the PK processes of several bioactive ingredients from GZFL in plasma: gallic acid, amygdalin, albiflorin, prunasin, and cinnamic acid. Results showed that GZFL significantly decreased the number of spiral arteries and inflammatory cells in uterine tissues of rats with primary dysmenorrhea induced by estradiol benzoate and oxytocin. Moreover, their bioactive ingredients were likely to have key roles in blocking platelet aggregation and thrombosis by increasing the  $PGE_2/PGF_{2\alpha}$  ratio and 6-Keto-Prostaglandin  $F_{1\alpha}$  (6-Keto- $PGF_{1\alpha}$ )/thromboxane  $B_2$  (TXB<sub>2</sub>) ratio in plasma of rats with primary dysmenorrhea after GZFL treatment [35].

Therefore, in light of these clinical and experimental studies, we conclude that GZFL possesses the potential for improving primary and secondary dysmenorrhea by regulating the levels of inflammatory factors, intracellular  $Ca^{2+}$ , and several metabolic pathways.

**3.2. Uterine Fibroids.** Uterine fibroids (also termed “uterine leiomyomas” or “uterine myomas”) are the most common benign tumor in fertile women. About 50% of uterine fibroids are symptomatic and elicit abdominal pain or extension during menstruation, pressure symptoms, and fertility problems [36]. Surgery is invasive, and hormonal drugs have obvious side effects, so GZFL and several other herbal medicines have been used widely as an alternative treatment for uterine fibroids in China [37, 38]. GZFL was reported to relieve pelvic pain, alleviate the uterine fibroid symptoms and reduce uterine size and fibroids volume in women with symptomatic uterine fibroids [39]. And meta-analyses of clinical trials have indicated that the combined treatment of GZFL and mifepristone might be more advantageous than the use of mifepristone alone for shrinking the volume of fibroids and reducing uterine size. Meanwhile, GZFL plus mifepristone showed less adverse events in comparison to mifepristone alone [3]. Previous research reported that GZFL drug serum was collected from Sprague Dawley (SD) rats and used to treat uterine leiomyoma cells in patients. Results showed that GZFL drug serum possessed the potential to inhibit the proliferation and promote the apoptosis of leiomyoma cells by enhancing the expression of

tuberous sclerosis 2 (TSC2) and forkhead box O (FOXO), which are associated with the 14-3-3 $\gamma$  signal pathway [40]. However, one study on SD rats model of uterine fibroids and human uterine leiomyoma cells demonstrated that GZFL inhibited uterine fibroids growth by modulating Mediator complex subunit 12 (Med12)-mediated wingless-type (Wnt)/ $\beta$ -Catenin signaling pathway [41]. Another research on estradiol-induced endometrial hyperplasia mice showed GZFL ameliorated endometrial hyperplasia through promoting p62-Keap1-NRF2-mediated ferroptosis [42]. The therapeutic mechanism seems multiple. A network pharmacology method was used to identify the pharmacologic mechanism of GZFL against uterine fibroids at the systematic level. This investigation indicated that GZFL exhibited significant therapeutic effects on uterine fibroids through inhibiting proliferation and promoting apoptosis by multiple signaling pathways: Wnt/ $\beta$ -catenin, retinoic acid (RA), epidermal growth factor (EGF), and insulin-like growth factor-1 (IGF-1) [9].

**3.3. Endometriosis.** About 10% of reproductive-age women suffer from endometriosis, a common estrogen-dependent benign disease, which is characterized by pelvic pain, dysmenorrhea, and infertility [43]. In Asia, several herbal formulations (including GZFL) are widely accepted as a kind of alternative medicine to treat endometriosis [44].

Meta-analyses of 10 randomized controlled trials involving 1052 women with endometriosis demonstrated that the combined treatment of GZFL and mifepristone (progesterone antagonist) had obvious benefits in terms of improving the prevalence of pregnancy and decreasing the prevalence of recurrence of endometriosis compared with the use of mifepristone alone. Similarly, GZFL also exhibited adjuvant effects on reducing the level of estradiol and progesterone in the serum of women with endometriosis without serious adverse effects. Thus, GZFL is considered to be an additional therapeutic approach for endometriosis patients [45].

Furthermore, studies on pharmacologic mechanisms have reported that GZFL can induce serious apoptosis and deter the proliferation and metastasis of endometrial cells in a rat with endometriosis by reversing suppression of survivin and the B-cell lymphoma (Bcl)-2/BCL2-associated X protein (Bax) ratio, which is related to the mitochondrial apoptotic pathway. Thus, GZFL is considered to be a potent apoptosis inducer and a therapeutic drug for endometriosis [46].

In addition, GZFL has been shown to significantly lower the volume of endometrial explants in endometriosis rats by immunologic regulation, including decreasing expressions of monocyte chemoattractant protein (MCP)-1 and intercellular adhesion molecules (ICAM)-1 and increasing the number of cluster of differentiation (CD)4<sup>+</sup> lymphocytes and the activity of natural killer (NK) cells [47].

In general, the pharmacologic mechanisms of GZFL in improving endometriosis could involve regulating apoptosis and the inflammatory responses as well as other targets.

**3.4. Climacteric Syndrome.** Climacteric syndrome is caused by a decrease in hormonal activity during menopause. This leads to vasomotor symptoms, mood disorders, night sweats,

hot flashes, insomnia, and osteoporosis [48–50]. These symptoms usually affect a woman's quality of life severely.

Accumulating studies have shown that the use of herbal medicine is an alternative method for improving climacteric syndrome in women who cannot receive hormone replacement therapy [51, 52]. One clinical study found that GZFL treatment for 12 weeks elicited significant beneficial effects for patients with climacteric symptoms, such as vasomotor symptoms and melancholia. Moreover, the therapeutic effects of GZFL on these patients could be evaluated by identifying a polymorphism of the estrogen receptor  $\beta$  (ER $\beta$ ) gene, which is involved in climacteric disorders [51]. In perimenopausal and postmenopausal women in Japan, GZFL treatment was shown to be more efficacious than other Kampo formulations in terms of improving sleep disturbance, perspiration, and reducing blood pressure and heart rate [52]. In addition, various studies have shown that GZFL displays beneficial effects on hot flashes in menopausal women [53]. A retrospective case series reported that young women with hot flashes showed improvement after GZFL treatment, possibly by regulating a calcitonin gene-related peptide- (CGRP-) induced temperature rise on the skin without estrogenic activity [54]. Furthermore, a randomized controlled trial in the USA demonstrated that GZFL could obviously decrease the frequency and severity of hot flashes when compared before and after a 3-month intervention in postmenopausal women. However, unlike the clinical experience in Asia, GZFL did not significantly ameliorate hot flashes or sleep quality compared with that obtained using a placebo. This study suggested that future investigations on traditional Asian medicines should consider several potentially important methodological factors [2].

These clinical studies detailed above demonstrated the therapeutic potential of GZFL for the climacteric syndrome.

**3.5. Polycystic Ovary Syndrome.** Polycystic ovary syndrome (PCOS) is a common reproductive endocrine disease in women and the etiology is complex. Besides reproductive dysfunction, the pathological manifestations of PCOS commonly involve insulin resistance and hyperandrogenism [55, 56] and display an inflammatory state [57].

Studies *in vivo* have reported that GZFL efficiently reduced fasting blood glucose, fasting insulin level, and insulin resistance index in plasma of PCOS rats with insulin resistance [58, 59]. The amelioration of insulin resistance was claimed under the mechanism of regulating intestinal flora to reduce tumor necrosis factor- $\alpha$  (TNF- $\alpha$ ), interleukin-6 (IL-6), and hypersensitive C-reactive protein (HS-CRP) in plasma [58]. In addition, the GZFL-treated rats had lower productions of testosterone, luteinizing hormone (LH), and follicle-stimulating hormone (FSH) compared with PCOS rats and lower LH/FSH ratios. These beneficial trends for normal ovulation were due to the GZFL's effects on inhibiting granulosa cell autophagy and promoting follicular development via restoring the phosphatidylinositol-3-kinase (PI3K)/AKT/mammalian target of rapamycin (mTOR) pathway [59].

## 4. Cancers

**4.1. Bladder Cancer.** Studies have indicated the suppressive effects of GZFL on bladder cancer *in vitro* and *in vivo*. For instance, *in vitro* data indicated that GZFL interfered with cell-cycle progression *via* activation of phosphorylated cell cycle checkpoint kinase2 (CHK2) and cell cycle regulatory protein P21, and induction of apoptosis, in human bladder cancer cell lines. However, GZFL exhibited only weak toxicity to normal human urothelial cells [60]. Another molecular mechanism demonstrates that GZFL could arrest cell cycles efficiently, suppress proliferation, and induce apoptosis in mouse bladder cancer cells (MB49) through increasing levels of reactive oxygen species (ROS) and activating ataxia telangiectasia-mutated (ATM)/CHK2 and ATM/P53 pathways. Furthermore, intravesical GZFL therapy has shown greater inhibitory effects on tumor growth than that of mitomycin C and *Bacillus Calmette-Guérin* vaccine in mice with orthotopic bladder tumors [8].

Taken together, these studies mentioned above support the notion that GZFL is a potential drug for bladder cancer by using intravesical therapy.

**4.2. Ovarian Cancer.** Ovarian cancer is a common malignant tumor for women aged >40 years. Radical surgery and chemotherapy are standard treatments for ovarian cancer [61]. However, resistance to chemotherapy agents has greatly restricted their use. Obviously, chemoresistant metastasis hinders survival and is a major cause of death [62].

GZFL has been used to treat ovarian cancer for more than 20 years in the clinic, which could increase chemotherapy efficacy, minimize side effects, and reduce chemoresistance. Explicitly, the microarray analyses have shown that GZFL treatment could deter the cell cycle, invasion, and migration-related genes in ovarian cancer cell lines SKOV3 by inhibiting protein kinase B (AKT)/glycogen synthase kinase 3  $\beta$  (GSK3 $\beta$ ) signaling pathway. Meanwhile, GZFL also reduced tumor growth/metastasis to the lung in xenograft mice [63]. In addition, one study reported that GZFL had a therapeutic potential against cisplatin-resistant ovarian cancers *in vitro* and *in vivo* by suppressing the expression level and function of permeability glycoprotein (P-gp) through blockage of the PI3K/AKT/mTOR pathway. Furthermore, the inhibitory effect of GZFL on tumor growth has been found in cisplatin resistance in human ovarian cancer cell line SKOV3/DDP xenograft nude mice [64]. What's more, serum derived from rats administered with GZFL extract in cisplatin-resistant human ovarian cancer SKOV3/DDP cells was a promising way to overcome cisplatin-resistant by inhibiting the expression of metadherin (MTDH), inducing the expression of phosphatase and tensin homolog (PTEN), and improving the interaction between MTDH and PTEN [65].

**4.3. Cervical Cancer.** Cervical cancer is the primary cause of death among all gynecologic cancers. The imbalance of expression of matrix metalloproteinases (MMPs) and tissue inhibitors of metalloproteinases (TIMPs) can result in

degradation of the extracellular matrix (ECM), which is a pivotal stage in tumor invasion [66]. One study reported that GZFL might restore the balance of MMPs/TIMPs and inhibit ECM degradation by decreasing MMPs activities and increasing TIMPs activities in HeLa cells which, eventually, interfered with the growth and invasion of cervical cancer cells *in vitro* and *in vivo* [67].

**4.4. Breast Cancer.** Breast cancer is one of the women's most common cancer, and there is an upward trend in the incidence. An experimental study found that the active pharmaceutical ingredient and its fraction from the GZFL capsule had a strong potential to deter the proliferation of human breast cancer MCF-7 cells and MDA-MB-231 cells in different doses and suppress the rate of cell growth in human umbilical vein endothelial cells (HUVECs) proliferation without toxicity [68]. In addition, the other study found that GZFL culture suppressed the proliferation of MCF-7 cells in the S phase by reducing the expression of CyclinA2, Cdk2, and EGFR [69]. In addition, GZFL exhibited the anti-proliferation, proapoptosis, and antiangiogenesis activities in MDA-MB-231 cells mainly through inhibiting the PI3K and the mitogen-activated protein kinase (MAPK) signaling pathways [70].

**4.5. Malignant Melanoma.** Melanoma is an aggressive cutaneous cancer with a poor prognosis and high mortality. Meanwhile, cutaneous melanoma is the most prevalent type. Accumulating evidence reported that long noncoding RNAs (lncRNAs) highly expressed in malignant melanoma cells could promote cellular proliferation, migration, and invasion [71, 72].

One of those abnormal lncRNAs, TPT1-AS1, can target and bind to miR-671-5p and negatively regulate its level. However, miR-671-5p played a key role in suppressing osteosarcoma cell proliferation by blocking the cell cycle [73]. One study reported that GZFL might suppress the proliferation, migration, and invasion of human cutaneous malignant melanoma cells through the regulation of the TPT1-AS1/miR-671-5p molecular pathway [74].

## 5. Blood and Vascular Disease

Consolidated evidence indicates that GZFL has various effects on blood stasis by reducing blood viscosity and platelet aggregation, increasing blood flow rate and erythrocyte deformability, as well as dilation of arteries [75]. Patients suffering varicose veins in the legs often complain of subjective symptoms (malaise, numbness, coldness, pain, and pruritus) that lower their quality of life. One clinical study reported that GZFL relieved "oketsu" (impaired microcirculation, blood congestion) and skin perfusion pressure in patients with varicose veins in the legs [75].

The symptoms of sensory sequelae after a stroke are usually cold sensations and numbness, which result from an unregulated vasomotor system and low peripheral blood flow [76]. A clinical investigation using a visual analog scale (VAS) found that GZFL alleviated cold sensations and numbness in

22 stroke patients by improving the skin perfusion temperature through an increase in peripheral blood flow [77].

In addition, GZFL had improving effects on articular symptoms and endothelial dysfunction in rheumatoid arthritis (RA) patients by reducing plasma levels of soluble vascular cell adhesion molecule-1 (sVCAM)-1 and lipid peroxide (LPO) [78]. A clinical trial demonstrated that GZFL significantly increased the mean value of the natural logarithmic-scaled reactive hyperemia index (LRHI) and decreased levels of nonesterified fatty acid (NEFA), malondialdehyde, and sVCAM-1 in serum, which contribute to GZFL's beneficial effects on endothelial function in metabolic syndrome patients [79].

A study using live imaging techniques showed that GZFL possessed an antioketsu effect on microcirculation in murine subcutaneous vessels, including amelioration of arterioles vasodilation and erythrocyte congestion, increasing blood velocity in the subcutaneous capillary. Furthermore, the authors found that the effect of GZFL on improving oketsu was related to an increase in NO levels in the mesenteric arterial endothelium of rats [80]. In addition, impaired microcirculation can be caused by other factors, such as platelets/leukocytes aggregation on endothelial cells. A study using screen filtration pressure showed that GZFL and its main constituent (Moutan Cortex and Cinnamomi Ramulus) were associated with the inhibitory effects on collagen-induced platelet aggregation and impaired microcirculation in whole blood samples from guinea pigs [81].

High cholesterol concentrations in serum have key roles in the progression of hypercholesterolemia and nonalcoholic fatty liver disease (NAFLD), which are critical risk factors for many cardiovascular diseases, including atherosclerosis, hypertension, and myocardial infarction [82]. One study reported that GZFL improved atherosclerosis by down-regulating the levels of triglyceride (TG), alkaline phosphatase (ALP), alanine aminotransferase (ALT), and ICAM-1 (a marker of activation of the endothelial cell) in the serum, as well ICAM-1 expression in the aorta, of rats fed a high-cholesterol diet [83]. Analysis of network pharmacology and molecular docking confirmed that AKT1, caspase-3 (CASP3), MAPK1, MAPK3, NOS2, and prostaglandin-endoperoxide synthase 2 (PTGS2) were GZFL's potential target genes against atherosclerosis [84]. Besides, GZFL alleviated Coronary Heart Disease (CHD) syndromes (such as elevated ST segment, increased levels of serum creatine kinase-MB (CK-MB) and lactic dehydrogenase (LDH), abnormal histopathological features) and downregulated TNF- $\alpha$  and IL-6 levels in acute myocardial ischemia (AMI) rats induced with isoproterenol [85].

Therefore, GZFL shows the potential for inhibiting the development of blood stagnation, vascular endothelial dysfunction, and atheromatous plaque by exerting anti-oxidative, anti-inflammatory, and immunoregulatory effects against many blood and vascular diseases.

## 6. Renal Failure

Chronic renal failure is the most common complication of diabetes mellitus. Furthermore, in recent years, increasing

numbers of patients suffering from diabetic nephropathy have required dialysis therapy, which lead to a rise in the cost of cure [86].

Notably, traditional herbal medicines are considered to be an effective alternative medicine for diabetic nephropathy. One study in spontaneously diabetic WBN/Kob rats reported that GZFL obviously reduced urinary excretion of proteins and serum levels of creatinine, inhibited oxidative stress by decreasing 8-Hydroxy-deoxyguanosine (8-OHdG) release in urine and kidneys and hepatic lipid peroxidation, and showed protective effects on renal function by suppressing transforming growth factor  $\beta_1$  (TGF- $\beta_1$ )-induced fibronectin release in the renal cortex [87]. Similarly, GZFL has been exhibited to significantly reduce the levels of blood urea nitrogen and urinary excretion of proteins and mRNA expressions of osteopontin, TGF- $\beta_1$ , and fibronectin in the remnant kidney of nephrectomized rats. Thus, these studies suggest that GZFL can help to retard the aggravation of chronic renal failure [88].

Recently, several studies have indicated that solute carrier organic anion transporters (OATs), as membrane proteins, regulate the reabsorption and excretion of renal metabolic substrates and toxins, which are considered to be novel drug targets for nephrotoxicity [89]. Furthermore, the pharmacologic effects of GZFL on the functions of renal transporters have been investigated. GZFL can suppress the substrate-uptake activities of urate transporter 1 (URAT1), OAT1, and OAT3 in *Xenopus oocytes* and HEK293 human kidney embryonic cells [90]. Therefore, GZFL has been seriously considered to be a nephroprotective agent.

## 7. Inflammation

Accumulating studies have presented experimental evidence of GZFL for the treatment of inflammation. An abnormal immune reaction can trigger chronic inflammation in skin diseases such as psoriasis, chronic pigmented purpura, and atopic dermatitis. Thus, regulation of immune homeostasis and inflammation in the skin may be an efficacious therapeutic approach against skin disease [91].

A study reported that GZFL treatment alleviated the disease severity using clinical assessments (SCORAD index and VAS score) in patients with atopic dermatitis, particularly those presenting with chronic lichenification. Conversely, the level of serum lactate dehydrogenase (LDH) was also decreased significantly in atopic dermatitis patients after GZFL treatment according to laboratory assessments [92]. Studies have shown that GZFL treatment significantly suppressed levels of migration inhibitory factor (MIF, an initiator of proinflammatory cytokines) [93] and subsequent production of IL-6, IL-8, TNF- $\alpha$ , COX-2, and inducible nitric oxide synthase (iNOS) in lipopolysaccharide- (LPS-) stimulated cultured human dermal microvascular endothelial cells (HDMECs). These results imply that GZFL exhibited a potential for improving microvascular inflammation-mediated skin disease, such as chronic pigmented purpura [7]. In addition, GZFL extract significantly reduced levels of chemokine (macrophages are derived from chemokines (MDC), regulated upon activation of normal T cell

expressed sequence (RANTES)), and production of IL-8 and IL-8 mRNA in TNF- $\alpha$ /interferon-gamma- (IFN- $\gamma$ -) stimulated HaCaT human keratinocytes by blocking the signal transducer and activator of transcription 1 (STAT1) pathway, which contributed to the anti-inflammatory effect of GZFL on skin disorders [94]. Taken together, those data suggest that GZFL is a potent therapeutic drug for inflammation-associated skin diseases.

In addition, GZFL and its active complex can inhibit the inflammatory response by decreasing the secretion of IL-1 $\beta$ , TNF- $\alpha$ , and PGE2 in LPS-induced RAW264.7 cells [95]. Furthermore, proinflammatory chemokines factors contribute to the development of atherosclerosis and NAFLD. GZFL can downregulate the expression of MCP-1 and its receptor CC chemokine receptor 2 (CCR2) in the liver and adipose tissue to improve atherosclerosis in rats fed a high-cholesterol diet [83]. Furthermore, another study on neuroinflammation reported that GZFL also decreased levels of proinflammatory factors, such as NO, IL-1 $\beta$ , TNF- $\alpha$ , iNOS, COX-2, macrophage inhibitory protein- (MIP-) 1 $\alpha$ , MCP-1, and IFN- $\gamma$  inducible protein- (IP-) 10, RANTES, in LPS-stimulated BV2 microglia by blocking nuclear factor-kappa B (NF- $\kappa$ B), extracellular signal-regulated kinase (Erk), c-Jun N-terminal kinase (JNK), and PI3K/AKT pathways. On the contrary, GZFL could increase the expression of anti-inflammatory factors, including IL-10 and Heme oxygenase 1 (HO-1), in LPS-stimulated BV2 microglia through activation of nuclear factor-E2-related factor-2 (NRF2) and cyclic adenosine monophosphate-response element-binding protein (CREB) pathways, suggesting that GZFL exhibited an anti-inflammatory effect on microglia-related neuroinflammatory disorders [96].

## 8. Brain Injury

Disability and death are common outcomes of ischemic stroke and are characterized by the interruption of cerebral blood flow. The postischemic inflammatory response exacerbates neuronal damage and loss, leading to neurological dysfunction in patients suffering from ischemic stroke. However, efficacious treatment approaches against stroke are lacking.

In Asia, extensive experiences and clinical research have indicated that traditional herbal medicine has beneficial effects on postischemic rehabilitation in stroke patients [97]. Studies demonstrated that GZFL administration elicits significant protective effects against cerebral ischemia/reperfusion injury through decreasing infarct areas and water contents of brain tissue in stroke rats, which is attributed to the anti-inflammatory properties of GZFL. As expected, GZFL treatment not only obviously reduced the levels of TNF- $\alpha$  and IL-1 $\beta$  but also elevated IL-10 levels in serum and brain tissue of rats with cerebral ischemia/reperfusion injury [10].

Recently, diabetes mellitus has been reported to induce neuronal loss and cognitive deficits [98]. One study showed that GZFL treatment ameliorated memory impairment in streptozotocin- (STZ-) induced hyperglycemic mice. Moreover, GZFL significantly reduced the number of

TABLE 1: Summary of pharmacologic effects and targets of Guizhi Fuling Formulation (GZFL).

Diseases	Pharmacological effects and targets	Patient/Model	Refs.
Primary and secondary dysmenorrhea	Improvement (to some degree) in >80% of patients	Patients	[29]
	Induces smooth blood flow	Patients	[4]
	Improves acne vulgaris	Patients	[12]
	Reduces lamina propria edema and COX-2 expression	Oxytocin-induced ICR mice	[31]
	Downregulates the mRNA expressions of COX-1 and COX-2	Human umbilical vein endothelial cells	[32]
	Decreases NO, $\text{PGF}_{2\alpha}$ , $\text{Ca}^{2+}$ , COX-2, OTR in uterine tissue	Oxytocin-induced ICR mice	[33]
	suppresses uterus contractions, restrains intracellular $\text{Ca}^{2+}$	Oxytocin-induced uterine strips and myometrial cells	[33]
	Reduces writhing times, $\text{PGF}_{2\alpha}/\text{PGE}_2$ ratio in plasma, urinary metabolic deviations	Oxytocin-induced rats	[34]
	Reduces writhing times, and the number of spiral arteries and inflammatory cells in uterine tissues;	Estradiol benzoate- and oxytocin-induced rats	[35]
	Increases $\text{PGE}_2/\text{PGF}_{2\alpha}$ , 6-Keto- $\text{PGF}_{1\alpha}/\text{TXB}_2$ ratio in plasma	Patients	[3]
Reduces uterine size and fibroids volume	Patients	[39]	
Relieves pelvic pain and the uterine fibroid symptoms and reduces the uterine size and fibroids volume			
Suppresses proliferation and promotes apoptosis and increases TSC2, FOXO by regulating the 14-3-3 $\gamma$ signal pathway	Human uterine leiomyoma cells	[40]	
Inhibits uterine fibroids growth by modulating Med12-mediated wnt/ $\beta$ -catenin signaling pathway	Estradiol benzoate- and progesterone-induced SD rats	[41]	
Ameliorates endometrial hyperplasia through promoting p62-Keap1-NRF2-mediated ferroptosis	Human uterine leiomyoma cells	[42]	
Inhibits proliferation and induces apoptosis by multiple pathways	hyperplasia mice	[9]	
Improves pregnancy rate, and decreases the recurrence rate	Network pharmacology	[45]	
Reduces estradiol and progesterone in serum	Patients	[45]	
Decreases the ratio of Bcl-2/Bax, survivin			
Increases caspase-3 and caspase-9	Endometrial cells of rats	[44, 46]	
Increases the percentage of $\text{CD4}^+$ T cells, activity of NK cell			
Decreases MCP-1 and ICAM-1	Endometriosis model in rats	[47]	
Improves vasomotor symptoms, melancholia	Patients	[51]	
Improves sleep disturbance, perspiration, and reduces blood pressure, heart rate	Patients	[52]	
Ameliorates hot flashes by regulating CGRP	Patients	[54]	
Decreases the frequency and severity of hot flashes	Patients	[2]	
Improves insulin resistance via regulating intestinal flora to control inflammation			
Improves insulin resistance	PCOS rats with insulin resistance	[58]	
Inhibits granulosa cell autophagy and promotes follicular development to attenuate ovulation disorder by restoring PI3K/AKT/mTOR pathway			
			[59]

TABLE 1: Continued.

Diseases	Pharmacological effects and targets	Patient/Model	Refs.
Bladder cancer	Interferes with cell cycle progression by activating CHK2 and P21 Activates ATM/CHK2 and ATM/P53 pathways	Human bladder cancer cells	[60]
	Suppresses cell cycle, invasion, and migration-related genes by inhibiting the AKT/GSK3 $\beta$ pathway	Mouse bladder cancer cells Orthotopic bladder cancer mice HEY and SKOV3 cells	[8] [63]
Ovarian cancer	Reduces tumor growth and metastasis Decreases P-gp by blocking the PI3K/AKT/mTOR pathway	Xenograft mice SKOV3 and SKOV3/DDP cells	[64]
	Inhibits tumor growth Inhibits MTDH expression, induces PTEN expression, and improves the interaction between MTDH and PTEN	SKOV3/DDP xenograft nude mice SKOV3 cells and its cisplatin-resistant SKOV3/DDP cells	[65]
Cervical cancer	Restores the MMP-TIMP balance Suppresses degradation of the extracellular matrix	Human cervical cancer (HeLa) cells	[67]
	Interferes with tumor growth and invasion Inhibits the proliferation Suppresses cell growth rate	HeLa human cervical cancer xenograft mice MCF-7 and MDA-mb-231 cells HUVCEs	[68]
Breast cancer	Inhibits the proliferation by reducing the expression of CyclinA2, Cdk2, and EGFR	MCF-7 cell	[69]
	Inhibits proliferation, angiogenesis and promotes apoptosis by regulating the PI3K and the MAPK pathways	MDA-MB-231 cells	[70]
Malignant melanoma	Inhibits the proliferation, migration, and invasion by regulating the molecular axis of lncRNA TPT1-AS1/mir-671-5p	Human cutaneous malignant melanoma cells A375	[74]
	Improves subjective symptoms, "oketsu", and skin perfusion pressure	Patients	[75]
Varicose veins legs Cold sensation and numbness after stroke	Increases peripheral blood flow	Stroke patients	[77]
	Reduces sVCAM-1 and LPO Increases LRHI	Patients	[78]
Rheumatoid arthritis	Decreases NEFAs, sVCAM-1, and malondialdehyde	Patients	[79]
	Induces vasodilation, increases blood velocity Decreases endothelial NO production	Mice subcutaneous vessels and rat mesenteric arterioles	[80]
Metabolic syndrome	Improves impaired microcirculation Downregulates TG, ALP, ALT and ICAM-1	Whole blood of guinea pigs High-cholesterol-diet rats	[81] [83]
	Alleviates CHD syndromes and regulates inflammatory responses	Isoproterenol-induced AMI rats	[85]
Oketsu (ischemia)	Reduces urinary protein excretion and serum creatinine, 8-OHdG, lipid peroxidation, fibronectin, and TGF- $\beta$ 1	Spontaneously diabetic WBN/Kob rats	[87]
	Reduces blood urea nitrogen and urinary protein excretion, as well as mRNA expressions of osteopontin, TGF- $\beta$ 1, and fibronectin	Nephrectomized rats	[88]
Platelet aggregation Atherosclerosis Coronary heart disease Diabetic renal disease	Suppresses substrate-uptake activities of URAT1, OAT1, and OAT3	<i>Xenopus</i> oocytes and HEK293 cells	[90]
Blood and vascular disease			
Renal failure			
Chronic renal failure			
Nephrotoxicity			



TABLE 1: Continued.

Diseases	Pharmacological effects and targets	Patient/Model	Refs.
Inflammation-related diseases	<p>Atopic dermatitis Alleviates disease severity and reduces serum LDH</p> <p>Chronic pigmented purpura Suppresses MIF, IL-6, IL-8, TNF-<math>\alpha</math>, COX-2, and iNOS</p> <p>Inflammatory skin disorders Reduces chemokine production and p-STAT1</p> <p>Inflammatory response Decreases IL-1<math>\beta</math>, TNF-<math>\alpha</math> and PGE2</p> <p>Atherosclerosis Downregulates MCP-1 and its receptor CCR2</p> <p>Neuroinflammatory disorders Decreases NO, IL-1<math>\beta</math>, TNF-<math>\alpha</math>, iNOS, COX-2, MIP-1<math>\alpha</math>, MCP-1, IP-10, RANTES, NF-<math>\kappa</math>B, erk, JNK, and PI3K/AKT</p> <p>Cerebral ischemia/reperfusion injury Increases IL-10, HO-1, NRF2, and CREB</p> <p>Decreases infarct area and water content of brain tissue</p> <p>Reduces TNF-<math>\alpha</math>, IL-1<math>\beta</math> increases IL-10 in serum and brain tissue</p>	<p>Patients</p> <p>LPS-stimulated HDMECs</p> <p>TNF-<math>\alpha</math> and IPN-<math>\gamma</math>-induced HaCaT cells</p> <p>LPS-induced RAW264.7 cells</p> <p>High-cholesterol-diet rats</p> <p>LPS-induced BV2 microglia</p> <p>Rats</p>	<p>[92]</p> <p>[7]</p> <p>[94]</p> <p>[95]</p> <p>[83]</p> <p>[96]</p> <p>[10]</p>
Brain injury	<p>Hyperglycemia and diabetes mellitus Improves memory deficits</p> <p>Reduces TUNEL<sup>+</sup> cells and caspase-3<sup>+</sup> cells</p> <p>Reduces caspase-3</p> <p>Increases Bcl-2</p> <p>Increases body weight and food intake</p> <p>Improves depressive-like behavior</p> <p>Reduces corticosterone in plasma</p> <p>Decreases IL-1<math>\beta</math>, IL-6, and TNF-<math>\alpha</math></p>	<p>STZ-induced hyperglycemic mice and rats</p> <p>Reserpine-induced mice</p>	<p>[99]</p> <p>[100]</p>
Other diseases	<p>Depression Increases BDNF and p-CREB in the hippocampus</p> <p>Obesity Decreases leptin, TG, and cholesterol</p> <p>Immune-related disease Enhances CD80 and CD86 and CD25/CD69 ratio</p>	<p>SHR rats and the DIO mice</p> <p>Spleen T lymphocytes</p>	<p>[101]</p> <p>[102]</p>

TUNEL<sup>+</sup> cells and caspase-3<sup>+</sup> cells in the cortex and hippocampus of STZ-induced hyperglycemic rats. Similarly, the increased protein levels of caspase-3 and reduced Bcl-2 were reversed in the cortex and hippocampus by GZFL treatment in STZ-induced hyperglycemic rats [99]. A depression-related study found that GZFL could reverse the decreased body weight and food intake in reserpine-induced depression mice. Furthermore, GZFL improved depressive-like behaviors by regulating immune/endocrine dysfunction in depression mice, as evidenced by a decrease in corticosterone levels in plasma and mRNA expressions of proinflammatory factors in the hippocampus after GZFL treatment through activation of the BDNF-CREB pathway [100].

In general, these results mentioned above suggest that GZFL treatment may be beneficial for patients with ischemia or diabetes mellitus-induced brain injury and depression.

## 9. Other Therapeutic Effects

Other therapeutic effects of GZFL have been reported in clinical and experimental studies. After GZFL treatment, dietary-induced obese mice showed an obvious decrease in serum levels of leptin, liver levels of TG, and cholesterol. In addition, GZFL also reduced the adipocyte accumulation and steatosis in the liver of dietary-induced obese mice by suppressing expressive of lipid metabolism-associated genes such as peroxisome proliferator-activated receptor- $\gamma$  (PPA $\gamma$ ) and sterol-regulated element-binding protein 1 (SERBP1) [101]. GZFL and its active components exhibited immunomodulatory effects by enhancing the expression of CD80 and CD86 in splenic lymphocytes and the CD25/CD69 ratio in splenic T lymphocytes, suggesting that the pharmacologic mechanism of GZFL is also involved in the regulation of lymphocyte activation [102].

## 10. Safety and Toxicity

Security and toxicity evaluations of traditional Chinese medicine have drawn concerns. Negative side effects or toxicity of GZFL have been observed in patients with the gynecologic disease [103]. GZFL was not found to cause detectable carcinogenic or genotoxic effects in other studies [104, 105]. GZFL has been assessed for efficacy and safety in the treatment of dysmenorrhea by the USA Food and Drug Administration [106, 107]. Gratifyingly, GZFL has been exhibited to be very safe and efficacious with little adverse reaction in other studies [6, 108].

## 11. Conclusion

In summary, this review suggests that GZFL displays promising therapeutic effects for many kinds of diseases, which have been beyond the scope of the original prescription for gynecologic diseases. Moreover, a large number of clinical and experimental researches demonstrated that GZFL also was used to treat cancer, blood and vascular disease, renal failure, inflammation, and brain injury. Possibly due to its diverse bioactive components and pharmacologic activities, GZFL could target multiple signaling

pathways involved in various diseases, such as blood circulation, inflammatory and immune factors, proliferation, and apoptosis. The multiple pharmacologic effects and possible mechanisms of action of GZFL are summarized in Table 1. Notably, anti-inflammatory and immunomodulatory effects of GZFL play a central role in treating various diseases, indicating that GZFL possesses a potential for strengthening the body resistance to eliminate pathogenic factors and optimize the body function, which conform to the strategy of the overall treatment in traditional medicine. However, much of the actual data from *in vivo* and *in vitro* experiments have sufficiently demonstrated obvious potential for GZFL to improve certain diseases, including cancer, renal failure, and brain injury, which are difficult to extrapolate these data to the clinical experiments. Thus, in order to prove the potential of GZFL in patients, a large number of rigorous designed and well-controlled clinical researches are required, which relate to the cellular and animal data to supply a strong cause-and-effect for their therapeutic potentials against the above diseases. At present, its deeply molecular mechanisms underlying different pharmacodynamic effects are not fully understood. Accordingly, in the future, we should fully combine GZFL's physical and chemical properties and conduct a new innovative research mode "from bedside to bench to bedside" to examine the pharmacodynamic effects and underlying mechanisms of GZFL and thereby enlighten the development of Chinese classic herbal formulation.

## Data Availability

The data are included in the article as table.

## Ethical Approval

This review was approved by the Ethics Committee of Shanghai University of Traditional Chinese Medicine (PZSHUTCM200904011) on September 4, 2020.

## Disclosure

Jie Gao, Jianmei Yang, and Zhiyuan Lu are the co-first authors.

## Conflicts of Interest

The authors declare no competing financial interests.

## Authors' Contributions

Jie Gao, Jianmei Yang, and Zhiyuan Lu contributed equally to this work. Ying Xu and Xianwen Dong provided ideas for this review. Jie Gao, Jianmei Yang, and Zhiyuan Lu conducted data analysis and interpretation. Ying Xu mainly wrote the manuscript. Jianmei Yang helped revise the manuscript. All authors read and approved the final manuscript. Correspondence should be addressed to Ying Xu and Xianwen Dong. Jie Gao, Jianmei Yang and Zhiyuan Lu contributed equally to this work.

## Acknowledgments

The authors appreciated Xingyu Wang for collecting data. This research was financially supported by grants from the General Program of the National Natural Science Foundation of China (Grant 82174003 and 81773927 to Y. X.), Henan Province key scientific research projects in Colleges and Universities (21A320058), and Key projects jointly constructed by Henan Provincial Health Commission and Ministry of Health (SBGJ202002123).

## References

- [1] C. P. Commission, *Chinese Pharmacopoeia*, China Medical Science Press, Beijing, China, 2015.
- [2] G. A. Plotnikoff, K. Watanabe, C. Torkelson, J. La Valleur, and D. M. Radosevich, "The TU-025 keishibukuryogan clinical trial for hot flash management in postmenopausal women: results and lessons for future research," *Menopause*, vol. 18, no. 8, pp. 886–892, 2017.
- [3] N. N. Chen, M. Han, and H. Yang, "Chinese herbal medicine Guizhi Fuling Formula for treatment of uterine fibroids: a systematic review of randomised clinical trials," *BMC Complementary and Alternative Medicine*, vol. 14, p. 2, 2014.
- [4] J. Jung, J. A. Lee, and M. M. Ko, "Gyejibongnyong-hwan, a herbal medicine for the treatment of dysmenorrhoea with uterine fibroids: a protocol for a randomised controlled trial," *BMJ Open*, vol. 6, no. 11, Article ID e013440, 2021.
- [5] Z. Su, N. Li, and L. Cao, "[Main progress on studies of pharmacological activities and clinical applications of Guizhi Fuling capsule]," *Zhongguo Zhongyao Zazhi*, vol. 40, no. 6, pp. 989–992, 2015.
- [6] W. Y. Jeon, S. E. Jin, and C. S. Seo, "Safety assessment of Gyejibokryeong-hwan water extract: study of acute and subacute toxicity, and influence on drug metabolizing enzymes," *Journal of Ethnopharmacology*, vol. 240, Article ID 111913, 2020.
- [7] Y. Yoshihisa, M. Furuichi, M. Ur Rehman, C. Ueda, T. Makino, and T. Shimizu, "The traditional Japanese formula keishibukuryogan inhibits the production of inflammatory cytokines by dermal endothelial cells," *Mediators of Inflammation*, vol. 2010, Article ID 804298, 2010.
- [8] C. C. Lu, C. H. Shen, and C. B. Chang, "Guizhi Fuling Wan as a novel agent for intravesical treatment for bladder cancer in mouse model," *Molecular Medicine*, vol. 28, 2014.
- [9] L. Zeng, K. Yang, H. Liu, and G. Zhang, "A network pharmacology approach to investigate the pharmacological effects of Guizhi Fuling Wan on uterine fibroids," *Experimental and Therapeutic Medicine*, vol. 14, no. 5, pp. 4697–4710, 2017.
- [10] T. J. Li, Y. Qiu, J. Q. Mao, P. Y. Yang, Y. C. Rui, and W. S. Chen, "Protective effects of Guizhi-Fuling-Capsules on rat brain ischemia/reperfusion injury," *Journal of Pharmacological Sciences*, vol. 105, no. 1, pp. 34–40, 2015.
- [11] H. Satomi, Y. Mori, and B. Makino, "Clustering analysis of keishibukuryogan formulas by use of self-organizing maps," *Chemical and Pharmaceutical Bulletin*, vol. 58, no. 11, pp. 1497–1501, 2021.
- [12] K. I. Kim, H. J. Nam, M. Kim, J. Lee, and K. Kim, "Effects of herbal medicine for dysmenorrhea treatment on accompanied acne vulgaris: a study protocol for a randomized controlled trial," *BMC Complementary and Alternative Medicine*, vol. 17, no. 1, p. 318, 2017.
- [13] J. H. Kim, C. S. Seo, and H. K. Shin, "Development of validated determination of the eleven marker compounds in Gyejibokryeong-hwan for the quality assessment using HPLC analysis," *Archives of Pharmacal Research*, vol. 38, no. 1, pp. 52–62, 2014.
- [14] S. Yilmaz, M. Sova, and S. Ergun, "Antimicrobial activity of trans-cinnamic acid and commonly used antibiotics against important fish pathogens and nonpathogenic isolates," *Journal of Applied Microbiology*, vol. 43, 2014.
- [15] L. Zhang, Z. Zhang, and Y. Fu, "Trans-cinnamaldehyde improves memory impairment by blocking microglial activation through the destabilization of iNOS mRNA in mice challenged with lipopolysaccharide," *Neuropharmacology*, vol. 110, pp. 503–518, 2014.
- [16] Y. Zhao, H. Deng, and K. Li, "Trans-cinnamaldehyde improves neuroinflammation-mediated NMDA receptor dysfunction and memory deficits through blocking NF-kappaB pathway in presenilin1/2 conditional double knockout mice," *Brain, Behavior, and Immunity*, vol. 82, pp. 45–62, 2017.
- [17] F. Roth-Walter, A. Moskovskich, and C. Gomez-Casado, "Immune suppressive effect of cinnamaldehyde due to inhibition of proliferation and induction of apoptosis in immune cells: implications in cancer," *PLoS One*, vol. 9, no. 10, Article ID e108402, 2018.
- [18] J. Chen, M. Zhang, and M. Zhu, "Paeoniflorin prevents endoplasmic reticulum stress-associated inflammation in lipopolysaccharide-stimulated human umbilical vein endothelial cells via the IRE1alpha/NF-kappaB signaling pathway," *Food & Function*, vol. 9, no. 4, pp. 2386–2397, 2019.
- [19] J. L. Shu, X. Z. Zhang, and L. Han, "Paeoniflorin-6'-O-benzene sulfonate alleviates collagen-induced arthritis in mice by downregulating BAFF-TRAF2-NF-kappaB signaling: comparison with biological agents," *Acta Pharmacologica Sinica*, vol. 13, 2012.
- [20] D. Wang, Q. R. Tan, and Z. J. Zhang, "Neuroprotective effects of paeoniflorin, but not the isomer albiflorin, are associated with the suppression of intracellular calcium and calcium/calmodulin protein kinase II in PC12 cells," *Journal of Molecular Neuroscience*, vol. 51, no. 2, pp. 581–590, 2013.
- [21] L. Chen, Q. Li, H. Wang, Q. Chen, Y. Wu, and Y. Shang, "Paeoniflorin attenuated bupivacaine-induced neurotoxicity in SH-SY5Y cells via suppression of the p38 MAPK pathway," *Journal of Cellular Biochemistry*, vol. 14, 2019.
- [22] Y. L. Wang, J. X. Wang, and X. X. Hu, "Antidepressant-like effects of albiflorin extracted from *Radix paeoniae Alba*," *Journal of Ethnopharmacology*, vol. 179, pp. 9–15, 2020.
- [23] M. Y. Jeong, J. Park, and D. H. Youn, "Albiflorin ameliorates obesity by inducing thermogenic genes via AMPK and PI3K/AKT in vivo and in vitro," *Metabolism*, vol. 73, pp. 85–99, 2015.
- [24] L. Zhu, P. Gu, and H. Shen, "Gallic acid improved inflammation via NF-kappaB pathway in TNBS-induced ulcerative colitis," *International Immunopharmacology*, vol. 67, pp. 129–137, 2016.
- [25] M. A. Mirshekar, A. Sarkaki, and Y. Farbood, "Neuroprotective effects of gallic acid in a rat model of traumatic brain injury: behavioral, electrophysiological, and molecular studies," *Iran J Basic Med Sci*, vol. 21, no. 10, pp. 1056–1063, 2016.
- [26] S. Mohan, K. Thiagarajan, and R. Chandrasekaran, "Evaluation of ethyl gallate for its antioxidant and anticancer properties against chemical-induced tongue carcinogenesis

- in mice," *Biochemical Journal*, vol. 474, no. 17, pp. 3011–3025, 2019.
- [27] S. H. Kim, M. K. Lee, K. Y. Lee, S. H. Sung, J. Kim, and Y. C. Kim, "Chemical constituents isolated from *Paeonia lactiflora* roots and their neuroprotective activity against oxidative stress in vitro," *Journal of Enzyme Inhibition and Medicinal Chemistry*, vol. 24, no. 5, pp. 1138–1140, 2018.
- [28] M. Y. Dawood, "Primary dysmenorrhea: advances in pathogenesis and management," *Obstetrics & Gynecology*, vol. 108, no. 2, pp. 428–441, 2020.
- [29] T. Yoshino, K. Katayama, and Y. Horiba, "The difference between the two representative kampo formulas for treating dysmenorrhea: an observational study," *Evid Based Complement Alternat Med*, vol. 2016, Article ID 3159617, 2016.
- [30] X. Xiong, C. T. Che, F. Borrelli, K. D. Moudgil, and G. Caminiti, "Evidence-Based TAM classic herbal formula: from myth to science," *Evid Based Complement Alternat Med*, vol. 2017, Article ID 9493076, 2017.
- [31] W. Zheng, M. Li, and Y. Wang, "Guizhi fuling capsule exhibits antidysemorrhoea activity by inhibition of cyclooxygenase activity," *Evid Based Complement Alternat Med*, vol. 2020, Article ID 8607931, 2020.
- [32] Y. Zheng, G. Xin, G. Gong, T. T. Dong, P. Li, and K. W. K. Tsim, "Evaluation of anti-inflammatory components of Guizhi fuling capsule, an ancient Chinese herbal formula, in human umbilical vein endothelial cells," *Evid Based Complement Alternat Med*, vol. 2020, Article ID 2029134, 2020.
- [33] L. Sun, L. N. Liu, and S. B. Zong, "Traditional Chinese medicine Guizhi Fuling capsule used for therapy of dysmenorrhea via attenuating uterus contraction," *Journal of Ethnopharmacology*, vol. 191, pp. 273–279, 2015.
- [34] Z. Xiong, L. Lang, X. Gao, W. Xiao, Z. Wang, and L. Zhao, "An integrative urinary metabolomic study of the therapeutic effect of Guizhi Fuling capsule on primary dysmenorrheal rats based (1)H NMR and UPLC-MS," *Journal of Pharmacy Biomedicine Analytical*, vol. 164, pp. 750–758, 2013.
- [35] Y. Cheng, Y. Chu, and X. Su, "Pharmacokinetic-pharmacodynamic modeling to study the anti-dysmenorrhea effect of Guizhi Fuling capsule on primary dysmenorrhea rats," *Phytomedicine*, vol. 48, pp. 141–151, 2012.
- [36] B. S. Levy, "Modern management of uterine fibroids," *Acta Obstetrica et Gynecologica Scandinavica*, vol. 87, no. 8, pp. 812–823, 2011.
- [37] J. P. Liu, H. Yang, Y. Xia, and F. Cardini, "Herbal preparations for uterine fibroids," *Cochrane Database of Systematic Reviews*, vol. 4, Article ID CD005292, 2015.
- [38] M. Li, A. Hung, and A. W. H. Yang, "Guizhi Fuling Wan for uterine fibroids: a systematic review of in vivo studies," *Journal of Ethnopharmacology*, vol. 245, p. 112177, 2009.
- [39] W. Meng, W. L. Lin, and W. F. Yeung, "Randomized double-blind trial comparing low dose and conventional dose of a modified traditional herbal formula Guizhi Fuling Wan in women with symptomatic uterine fibroids," *Journal of Ethnopharmacology*, vol. 283, Article ID 114676, pp. 1872–7573, 2011, (Electronic).
- [40] Q. Shen, W. Ye, X. Hu, C. Zhao, L. Zhou, and X. Zhu, "The effects of Guizhi fuling capsule drug serum on uterine leiomyoma cells and its mechanism," *Evid Based Complement Alternat Med*, vol. 2016, Article ID 2393640, 2016.
- [41] L. Chen, H. Chen, and Q. Yang, "Guizhi Fuling Capsule inhibits uterine fibroids growth by modulating Med12-mediated Wnt/beta-Catenin signaling pathway," *Journal of Ethnopharmacology*, vol. 290, Article ID 115115, 2015.
- [42] M. Zhang, T. Zhang, and C. Song, "Guizhi Fuling Capsule ameliorates endometrial hyperplasia through promoting p62-Keap1-NRF2-mediated ferroptosis," *Journal of Ethnopharmacology*, vol. 274, Article ID 114064, 2014.
- [43] M. Ulukus, H. Cakmak, and A. Arici, "The role of endometrium in endometriosis," *Journal of the Society for Gynecologic Investigation*, vol. 13, no. 7, pp. 467–476, 2015.
- [44] S. Kong, Y. H. Zhang, and C. F. Liu, "The complementary and alternative medicine for endometriosis: a review of utilization and mechanism," *Evid Based Complement Alternat Med*, vol. 2014, Article ID 146383, 2014.
- [45] W. Meng, N. Ta, and F. Wang, "Add-on effect of Guizhi Fuling formula to mifepristone for endometriosis: a meta-analysis of randomized controlled trials," *Medicine (Baltimore)*, vol. 98, no. 33, Article ID e16878, 2015.
- [46] C. Hu, Z. Wang, and Z. Pang, "Guizhi fuling capsule, an ancient Chinese formula, attenuates endometriosis in rats via induction of apoptosis," *Climacteric*, vol. 17, no. 4, pp. 410–416, 2015.
- [47] X. Ji, J. Gao, and X. Cai, "Immunological regulation of Chinese herb Guizhi Fuling Capsule on rat endometriosis model," *Journal of Ethnopharmacology*, vol. 134, no. 3, pp. 624–629, 2016.
- [48] E. K. Kwak, H. S. Park, and N. M. Kang, "Menopause knowledge, attitude, symptom and management among midlife employed women," *J Menopausal Med*, vol. 20, no. 3, pp. 118–125, 2012.
- [49] A. Bien, E. Rzonca, G. Iwanowicz-Palus, and M. Panczyk-Szeptuch, "The influence of climacteric symptoms on women's lives and activities," *International Journal of Environmental Research and Public Health*, vol. 12, no. 4, pp. 3835–3846, 2019.
- [50] L. A. Morrison, D. E. Brown, and L. L. Sievert, "Voices from the hilo women's health study: talking story about menopause," *Health Care for Women International*, vol. 35, no. 5, pp. 529–548, 2018.
- [51] T. Namiki, H. Sato, and Y. Matsumoto, "Identification of a predictive biomarker for the beneficial effect of keishibukuryogan, a kampo (Japanese traditional) medicine, on patients with climacteric syndrome," *Evid Based Complement Alternat Med*, vol. 2014, Article ID 962109, 2014.
- [52] M. Terauchi, S. Hiramitsu, and M. Akiyoshi, "Effects of three Kampo formulae: tokishakuyakusan (TJ-23), Kamishoyosan (TJ-24), and Keishibukuryogan (TJ-25) on Japanese peri- and postmenopausal women with sleep disturbances," *Archives of Gynecology and Obstetrics*, vol. 284, no. 4, pp. 913–921, 2013.
- [53] M. Li, A. Hung, H. Li, and A. W. H. Yang, "A classic herbal formula Guizhi fuling wan for menopausal hot flashes: from experimental findings to clinical applications," *Biomedicine*, vol. 7, p. 3, 2012.
- [54] K. Cho, Y. Kim, W. Jung, and T. Kim, "Effect of Gui-zhi-fuling-wan on hot flashes in young patients: a retrospective case series," *J Acupunct Meridian Stud*, vol. 4, no. 2, pp. 129–133, 2011.
- [55] O. Osibogun, O. Ogunmoroti, and E. D. Michos, "Polycystic ovary syndrome and cardiometabolic risk: opportunities for cardiovascular disease prevention," *Trends in Cardiovascular Medicine*, vol. 30, no. 7, pp. 399–404, 2011.
- [56] M. Liu, S. Murthi, and L. Poretsky, "Polycystic ovary syndrome and gender identity," *Yale Journal Biology Medicine*, vol. 93, no. 4, pp. 529–537, 2016.

- [57] S. G. Shamasbi, S. Ghanbari-Homayi, and M. Mirghafourvand, "The effect of probiotics, prebiotics, and synbiotics on hormonal and inflammatory indices in women with polycystic ovary syndrome: a systematic review and meta-analysis," *European Journal of Nutrition*, vol. 59, no. 2, pp. 433–450, 2016.
- [58] Z. Ying, L. Yin, L. Min, H. XiaoDan, and Z. Hongqiu, "Guizhi fuling wan, Chinese herbal medicine, ameliorates insulin sensitivity in PCOS model rats with insulin resistance via remodeling intestinal homeostasis," *Frontiers in Endocrinology*, vol. 24, 2018.
- [59] M. Liu, H. Zhu, Y. Zhu, and X. Hu, "Guizhi Fuling Wan reduces autophagy of granulosa cell in rats with polycystic ovary syndrome via restoring the PI3K/AKT/mTOR signaling pathway," *Journal of Ethnopharmacology*, vol. 270, Article ID 113821, pp. 1872–7573, 2016, (Electronic).
- [60] C. C. Lu, M. Y. Lin, and S. Y. Chen, "The investigation of a traditional Chinese medicine, Guizhi Fuling Wan (GFW) as an intravesical therapeutic agent for urothelial carcinoma of the bladder," *BMC Complementary and Alternative Medicine*, vol. 13, p. 44, 2017.
- [61] S. Vaughan, J. I. Coward, and R. C. Bast, "Rethinking ovarian cancer: recommendations for improving outcomes," *Nature Reviews Cancer*, vol. 11, no. 10, pp. 719–725, 2016.
- [62] R. C. Bast, "Molecular approaches to personalizing management of ovarian cancer," *Annals of Oncology*, vol. 22, no. Suppl 8, 2019.
- [63] F. Tao, S. Ruan, W. Liu, L. Wang, Y. Xiong, and M. Shen, "Fuling granule, a traditional Chinese medicine compound, suppresses cell proliferation and TGFbeta-induced EMT in ovarian cancer," *PLoS One*, vol. 11, no. 12, Article ID e0168892, 2012.
- [64] L. Han, X. Guo, and H. Bian, "Guizhi fuling wan, a traditional Chinese herbal formula, sensitizes cisplatin-resistant human ovarian cancer cells through inactivation of the PI3K/AKT/mTOR pathway," *Evid Based Complement Alternat Med*, vol. 2016, 2016.
- [65] L. Han, X. Y. Cao, and Z. Chen, "Overcoming cisplatin resistance by targeting the MTDH-PTEN interaction in ovarian cancer with sera derived from rats exposed to Guizhi Fuling wan extract," *BMC Complementary Medicine and Therapies*, vol. 20, p. 1, 2019.
- [66] C. V. Hojilla, F. F. Mohammed, and R. Khokha, "Matrix metalloproteinases and their tissue inhibitors direct cell fate during cancer development," *British Journal of Cancer*, vol. 89, no. 10, pp. 1817–1821, 2016.
- [67] Z. Yao and Z. Shulan, "Inhibition effect of Guizhi-Fuling-decoction on the invasion of human cervical cancer," *Journal of Ethnopharmacology*, vol. 120, no. 1, pp. 25–35, 2015.
- [68] L. L. Yu Zi-ru, J.-hua Wang, Z.-Z. Wang, W. Xiao, and D. U. Guan-hua, "Effect of Guizhi fuling capsule and its ingredients on human breast cancer cells proliferation," *Chinese Journal of Integrated Traditional and Western Medicine*, vol. 2, pp. 202–207, 2018.
- [69] L. L. Jiang Shi-hong, Y.- Wu, and L.-D. Xia, "Zhang pei-xu mechanism of Guizhi fuling wan in inhibiting proliferation of human breast cancer MCF-7 cells," *China Journal of Experimental Traditional Medical Formulae*, vol. 15, pp. 132–136, 2014.
- [70] D. Yifei, Q. Weijie, and Y. Xiankuo, "Guizhi Fuling Decoction inhibiting the PI3K and MAPK pathways in breast cancer cells revealed by HTS2 technology and systems pharmacology," *Computational and Structural Biotechnology Journal*, vol. 18, 2017.
- [71] X. Chen, J. Gao, Y. Yu, Z. Zhao, and Y. Pan, "LncRNA FOXD3-AS1 promotes proliferation, invasion and migration of cutaneous malignant melanoma via regulating miR-325/MAP3K2," *Biomedicine & Pharmacotherapy*, vol. 120, 2017.
- [72] H. Jiang, G. Huang, and N. Zhao, "Long non-coding RNA TPT1-AS1 promotes cell growth and metastasis in cervical cancer via acting AS a sponge for miR-324-5p," *Journal of Experimental & Clinical Cancer Research*, vol. 37, no. 1, p. 169, 2012.
- [73] C. Xin, S. Lu, and Y. Li, "miR-671-5p inhibits tumor proliferation by blocking cell cycle in osteosarcoma," *DNA and Cell Biology*, vol. 38, no. 9, pp. 996–1004, 2015.
- [74] B. Zhang, "Guizhi Fuling pills inhibit the proliferation, migration and invasion of human cutaneous malignant melanoma cells by regulating the molecular axis of LncRNA TPT1-AS1/miR-671-5p," *Cellular and Molecular Biology*, vol. 66, no. 5, pp. 148–154, 2016.
- [75] S. Hayashi, S. Shibutani, and H. Okubo, "Examination of clinical efficacy of keishibukuryogan on non-specific complaints associated with varicose veins of the lower extremity," *Ann Vasc Dis*, vol. 7, no. 3, pp. 266–273, 2017.
- [76] H. Naver, C. Blomstrand, S. Ekholm, C. Jensen, T. Karlsson, and G. Wallin, "Autonomic and thermal sensory symptoms and dysfunction after stroke," *Stroke*, vol. 26, no. 8, pp. 1379–1385, 2013.
- [77] K. Fujita, T. Yamamoto, T. Kamezaki, and A. Matsumura, "Efficacy of keishibukuryogan, a traditional Japanese herbal medicine, in treating cold sensation and numbness after stroke: clinical improvement and skin temperature normalization in 22 stroke patients," *Neurologia Medico-Chirurgica*, vol. 50, no. 1, pp. 1–5, 2012, discussion 5–6.
- [78] K. Nozaki, H. Hikiami, H. Goto, T. Nakagawa, N. Shibahara, and Y. Shimada, "Keishibukuryogan (gui-zhi-fu-ling-wan), a Kampo formula, decreases disease activity and soluble vascular adhesion molecule-1 in patients with rheumatoid arthritis," *Evid Based Complement Alternat Med*, vol. 3, no. 3, pp. 359–364, 2012.
- [79] Y. Nagata, H. Goto, and H. Hikiami, "Effect of keishibukuryogan on endothelial function in patients with at least one component of the diagnostic criteria for metabolic syndrome: a controlled clinical trial with crossover design," *Evidence-Based Complementary and Alternative Medicine*, vol. 2012, Article ID 359282, 2020.
- [80] T. Tomita, A. Hirayama, H. Matsui, and K. Aoyagi, "Effect of keishibukuryogan, a Japanese traditional kampo prescription, on improvement of microcirculation and oketsu and induction of endothelial nitric oxide: a live imaging study," *Evid Based Complement Alternat Med*, vol. 2017, Article ID 3620130, 2017.
- [81] K. Terawaki, M. Noguchi, M. Yuzurihara, Y. Omiya, Y. Ikarashi, and Y. Kase, "Keishibukuryogan, a traditional Japanese medicine, inhibits platelet aggregation in Guinea pig whole blood," *Evid Based Complement Alternat Med*, vol. 2015, Article ID 295706, 2015.
- [82] A. R. Mohamed, W. F. El-Hadidy, and H. F. Manna, "Assessment of the prophylactic role of aspirin and/or clopidogrel on experimentally induced acute myocardial infarction in hypercholesterolemic rats," *Drugs in R & D*, vol. 14, no. 4, pp. 233–239, 2017.
- [83] W. Qian, J. Hasegawa, S. Tsuno, Y. Endo, A. Matsuda, and N. Miura, "Effects of kampo formulas on the progression of hypercholesterolemia and Fatty liver induced by high-cholesterol diet in rats," *Yonago Acta Medica*, vol. 57, no. 4, pp. 147–158, 2019.

- [84] A. Y. Lee, J. Y. Lee, and J. M. Chun, "Exploring the mechanism of gyejibokryeong-hwan against atherosclerosis using network pharmacology and molecular docking," *Plants*, vol. 9, p. 12, 2016.
- [85] B. L. Duan, L. T. Han, and S. P. Ming, "Fuling-guizhi herb pair in coronary heart disease: integrating network pharmacology and in vivo pharmacological evaluation," *Evidence-Based Complementary and Alternative Medicine*, vol. 2020, 2020.
- [86] E. Ritz and S. R. Orth, "Nephropathy in patients with type 2 diabetes mellitus," *New England Journal of Medicine*, vol. 341, no. 15, pp. 1127–1133, 2017.
- [87] T. Nakagawa, H. Goto, H. Hikiyami, T. Yokozawa, N. Shibahara, and Y. Shimada, "Protective effects of keishibukuryogan on the kidney of spontaneously diabetic WBN/Kob rats," *Journal of Ethnopharmacology*, vol. 110, no. 2, pp. 311–317, 2018.
- [88] T. Nakagawa, I. Tashiro, and M. Fujimoto, "Keishibukuryogan reduces renal injury in the early stage of renal failure in the remnant kidney model," *Evid Based Complement Alternat Med*, vol. 2011, Article ID 914249, 2011.
- [89] N. Anzai, Y. Kanai, and H. Endou, "Organic anion transporter family: current knowledge," *Journal of Pharmacological Sciences*, vol. 100, no. 5, pp. 411–426, 2016.
- [90] H. S. Lee, H. J. Shin, M. Cho, S. H. Lee, and D. S. Oh, "Inhibitory effects of Kampo medicines, Keishibukuryogan and Shakuyakukanzoto, on the substrate uptake activities of solute carrier organic anion transporters," *Journal of Pharmacological Sciences*, vol. 138, no. 4, pp. 279–283, 2013.
- [91] M. Pasparakis, I. Haase, and F. O. Nestle, "Mechanisms regulating skin immunity and inflammation," *Nature Reviews Immunology*, vol. 14, no. 5, pp. 289–301, 2017.
- [92] M. Mizawa, T. Makino, H. Hikiyami, Y. Shimada, and T. Shimizu, "Effectiveness of keishibukuryogan on chronic-stage lichenification associated with atopic dermatitis," *ISRN Dermatol*, vol. 2012, Article ID 158598, 2012.
- [93] T. Shimizu, H. Niizeki, and O. Takeuchi, "Induction of macrophage migration inhibitory factor precedes the onset of acute tonsillitis," *Mediators of Inflammation*, vol. 13, no. 4, pp. 293–295, 2016.
- [94] S. Jeong, H. Lim, and C. Seo, "Anti-inflammatory actions of herbal formula Gyejibokryeong-hwan regulated by inhibiting chemokine production and STAT1 activation in HaCaT cells," *Biological and Pharmaceutical Bulletin*, vol. 38, no. 3, pp. 425–434, 2012.
- [95] Z. Z. Zhang, X. Z. Zhang, and N. Li, "Study on anti-inflammation effect and involved mechanism of Guizhi Fuling capsule and its active complex," *Zhongguo Zhongyao Zazhi*, vol. 40, no. 6, pp. 993–998, 2017.
- [96] B. K. Park, Y. H. Kim, and Y. R. Kim, "Antineuroinflammatory and neuroprotective effects of gyejibokryeong-hwan in lipopolysaccharide-stimulated BV2 microglia," *Evid Based Complement Alternat Med*, vol. 2019, Article ID 7585896, 2019.
- [97] H. Kim, "Neuroprotective herbs for stroke therapy in traditional eastern medicine," *Neurological Research*, vol. 27, no. 3, pp. 287–301, 2017.
- [98] Z. G. Li, W. Zhang, G. Grunberger, and A. A. Sima, "Hippocampal neuronal apoptosis in type 1 diabetes," *Brain Research*, vol. 946, no. 2, pp. 221–231, 2019.
- [99] K. J. Wu, Y. F. Chen, H. Y. Tsai, C. R. Wu, and W. G. Wood, "Guizhi-Fuling-Wan, a traditional Chinese herbal medicine, ameliorates memory deficits and neuronal apoptosis in the streptozotocin-induced hyperglycemic rodents via the decrease of Bax/Bcl2 ratio and caspase-3 expression," *Evid Based Complement Alternat Med*, vol. 2012, Article ID 656150, 2012.
- [100] B. K. Park, Y. R. Kim, and Y. H. Kim, "Antidepressant-like effects of gyejibokryeong-hwan in a mouse model of reserpine-induced depression," *BioMed Research International*, vol. 2018, Article ID 5845491, 2018.
- [101] F. Gao, S. Yokoyama, and M. Fujimoto, "Effect of keishibukuryogan on genetic and dietary obesity models," *Evid Based Complement Alternat Med*, vol. 2015, Article ID 801291, 2015.
- [102] Y. P. Jiang, X. Wu, and N. Li, "Research on immune-modulation effects and its mechanisms of Guizhi Fuling capsule and its active ingredient combination," *Zhongguo Zhongyao Zazhi*, vol. 40, no. 15, pp. 3068–3071, 2016.
- [103] G. Q. Wang, Y. Gao, F. M. Liu, R. L. Wei, and Y. M. Xie, "Post-marketing surveillance on Guizhi Fuling Jiaonang based on literature review," *Zhongguo Zhongyao Zazhi*, vol. 43, no. 4, pp. 820–832, 2018.
- [104] M. Kanitani, N. Nishimura, H. Edamoto, and Y. Kase, "Keishibukuryogan is not carcinogenic in Sprague-Dawley rats," *Journal of Toxicologic Pathology*, vol. 29, no. 2, pp. 103–110, 2017.
- [105] M. Lee, C. Seo, H. Ha, E. Park, J. Kim, and H. Shin, "The genotoxicity of an aqueous extract of Gyejibokryeong-hwan," *BMC Complementary and Alternative Medicine*, vol. 18, no. 1, p. 21, 2015.
- [106] Y. X. Zhong, X. L. Jin, and S. Y. Gu, "Integrated identification, qualification and quantification strategy for pharmacokinetic profile study of Guizhi Fuling capsule in healthy volunteers," *Scientific Reports*, vol. 6, Article ID 31364, 2015.
- [107] X. Lei, J. Chen, C. X. Liu, J. Lin, J. Lou, and H. C. Shang, "Status and thoughts of Chinese patent medicines seeking approval in the US market," *Chinese Journal of Integrative Medicine*, vol. 20, no. 6, pp. 403–408, 2016.
- [108] S. E. Jin, C. S. Seo, M. Y. Lee, H. K. Shin, M. J. Yang, and H. Ha, "Sub-chronic toxicity of gyejibokryeong-hwan in sprague-dawley rats," *Journal of Ethnopharmacology*, vol. 224, pp. 441–450, 2012.



## Research Article

# Naringin Alleviates H<sub>2</sub>O<sub>2</sub>-Inhibited Osteogenic Differentiation of Human Adipose-Derived Stromal Cells via Wnt/ $\beta$ -Catenin Signaling

Xufang Yang <sup>1</sup>, Jianjiang Dong <sup>2</sup>, Yankun Hao <sup>3</sup>, Yucheng Qi <sup>4</sup>, Jun Liang <sup>5</sup>,  
Lei Yan <sup>2</sup> and Wenting Wang <sup>6</sup>

<sup>1</sup>Department of Pathophysiology, Mudanjiang Medical University, Mudanjiang 157011, China

<sup>2</sup>Department of Histology and Embryology, Mudanjiang Medical University, Mudanjiang 157011, China

<sup>3</sup>Department of Medical Function, Mudanjiang Medical University, Mudanjiang 157011, China

<sup>4</sup>Basic Medical College, Mudanjiang Medical University, Mudanjiang 157011, China

<sup>5</sup>Stem Cell Institute, Mudanjiang Medical University, Mudanjiang 157011, China

<sup>6</sup>Department of Physiology, Mudanjiang Medical University, Mudanjiang 157011, China

Correspondence should be addressed to Wenting Wang; wangwenting@mdjmu.edu.cn

Received 18 February 2022; Revised 30 March 2022; Accepted 15 April 2022; Published 29 April 2022

Academic Editor: Ruchika Garg

Copyright © 2022 Xufang Yang et al. This is an open access article distributed under the Creative Commons Attribution License, which permits unrestricted use, distribution, and reproduction in any medium, provided the original work is properly cited.

Osteoporosis is an age-related systemic bone disease that places a heavy burden on patients and society. In this study, we aimed to investigate the effects of naringin (NAR) on the osteogenic differentiation of human adipose-derived stromal cells (ADSCs). The results demonstrated that NAR pretreatment effectively abated H<sub>2</sub>O<sub>2</sub>-induced cell death and ROS accumulation in ADSCs undergoing osteogenic differentiation (ADSCs-OD). In addition, we also observed that the impaired extracellular matrix mineralization and ALP activity in H<sub>2</sub>O<sub>2</sub>-stimulated ADSCs-OD were notably rescued by NAR pretreatment. Moreover, the effects of H<sub>2</sub>O<sub>2</sub> exposure on Wnt/ $\beta$ -catenin signaling in ADSCs-OD were largely reversed by NAR pretreatment. Collectively, our findings indicated that NAR could protect ADSCs-OD against H<sub>2</sub>O<sub>2</sub>-inhibited osteogenic differentiation.

## 1. Introduction

Osteoporosis is a common disease characterised by a systemic impairment of bone mass, strength, and microarchitecture which increases the propensity of fragility fractures [1]. Osteoporosis seriously affects patients' life quality and places a heavy burden on society. At the cellular level, this disease is caused by an imbalance between osteoclast-mediated bone resorption and osteoblast-mediated bone formation [2]. In 2001, adipose-derived stromal cells (ADSCs) were extracted for the first time by digestion of human adipose tissues [3]. ADSCs are abundant and can be easily acquired [4]. The in vitro and in vivo osteogenetic capability makes ADSCs a promising source of seed cells in bone tissue engineering [5].

Traditional Chinese medicines (TCMs) have long been used to prevent and treat osteoporosis. They have fewer adverse reactions and are more suitable for long-term use compared with chemically synthesized medicines [6]. Naringin (NAR), a bioflavonoid abundant in grapefruit and other related citrus fruit species, has numerous biological and pharmacological properties [7]. It has been shown to prevent ovariectomy-induced osteoporosis and promote osteoclasts apoptosis via mitochondria-mediated apoptosis pathway [8]. In this study, we aimed to investigate the effects of NAR on the osteogenic differentiation of human ADSCs.

## 2. Materials and Methods

**2.1. Human Samples.** The samples of human abdominal fat were obtained from 10 donors (the average age was

33.6 ± 4.8; 5 males, 5 females) who underwent liposuction at hospital. Patients with healthy physical examination results were included. Patients with malignant tumors, autoimmune diseases, congenital diseases, and genetic diseases were excluded. None of the participants had systemic diseases or infections. This study was approved by the ethics committee of the hospital, and written informed consent was obtained from all participants.

**2.2. Isolation and Culture of ADSCs.** The samples of human abdominal fat were washed twice with 10 ml phosphate-buffered saline (PBS) to remove blood and grease, digested with collagenase type I solution (Sigma-Aldrich, St. Louis, MO, USA) for 1 h at 37°C, and filtered through 250 µm filters. Following centrifugation (500 × g, 5 min, 3×), the cells were collected and cultured in Dulbecco's modified Eagle's medium (DMEM; Invitrogen, Carlsbad, CA, USA) containing 10% fetal bovine serum (FBS; HyClone, Logan, UT, USA) and 1% penicillin/streptomycin at 37°C in a humidified incubator with 5% CO<sub>2</sub>. Cells at passage 3 were used in the following experiments.

**2.3. Osteogenic Induction and NAR Treatment.** To induce osteogenic differentiation, ADSCs seeded in 24-well plates (1 × 10<sup>4</sup> cells/well) were treated with osteogenic medium (OM), which consisted of standard culture medium supplemented with 0.1 mM dexamethasone, 7 mM sodium β-glycerophosphate, and 200 µM ascorbic acid. The medium was renewed every 2 d. After 14 d, cells were stained with Alizarin red S to confirm the existence of mineralized nodules.

The experiments were divided into four groups:

- (i) ADSCs in Group 1 were cultured in OM for 14 d.
- (ii) After incubation in OM for 48 h, ADSCs in Group 2 were treated with 0.2 mM H<sub>2</sub>O<sub>2</sub> for 4 h. The supernatant was then discarded, and ADSCs were further cultured in OM for 12 d.
- (iii) ADSCs in Group 3 were cultured in OM for 24 d. Then, 0.1 mM NAR was added to each well, and ADSCs were further cultured for 13 d.
- (iv) After incubation in OM for 24 h, ADSCs in Group 4 were treated with 0.1 mM NAR for 24 h. Then 0.2 mM H<sub>2</sub>O<sub>2</sub> was added to each well. After additional 4 h, the supernatant was discarded, and ADSCs were further cultured in OM + 0.1 mM NAR for 12 d.

**2.4. Alizarin Red S (ARS) Staining Assay.** The cells were fixed in 4% paraformaldehyde, and stained with 0.1% ARS staining solution (pH 4.2; Sigma-Aldrich). After 1 h, the stained cells were observed by a light microscope (Olympus, Tokyo, Japan).

**2.5. Alkaline Phosphatase (ALP) Staining Assay.** The cells were fixed in 4% paraformaldehyde, and stained with BCIP/

NBT working solution (Beyotime, Shanghai, China). After 0.5 h, the stained cells were observed by a light microscope.

**2.6. Cell Viability Analysis.** Cell viability was determined by the MTT assay. The cells were seeded into 96-well plates. After the aforementioned treatments, 20 µl MTT solution (5 mg/l; Sigma-Aldrich) was added to each well. After additional 4 h, the supernatant was discarded, and 150 µl DMSO was added to dissolve the violet formazan crystals. The absorbance was measured at 570 nm using a microplate reader (Molecular Devices, Sunnyvale, CA, USA).

**2.7. Measurement of Intracellular ROS Accumulation.** Intracellular ROS production was detected with DCFH-DA fluorescent probe (Sigma-Aldrich). The cells were incubated with 20 µl DCFH-DA solution at 37°C for 30 min. The fluorescence intensity was measured by using a FACScan flow cytometer (BD Biosciences, Franklin lakes, NJ, USA).

**2.8. RT-qPCR Analysis.** Total RNA was extracted from cells using TRIzol reagent (Invitrogen), and then reverse-transcribed into cDNA by the PrimeScript RT reagent Kit (TaKaRa, Dalian, China). PCR amplifications were then carried out using a SYBR Green PCR Kit (TaKaRa) on a 7500 Fast Real-Time Sequence detection system (Applied Biosystems, Foster City, CA, USA). The data were analyzed using 2-ΔΔCt method [9], and β-actin was employed as an internal control.

**2.9. Western Blot Analysis.** Cell lysates were prepared with RIPA buffer (Beyotime). Identical quantity of protein samples were separated by SDS-polyacrylamide gels, and transferred to PVDF membranes (Millipore, Billerica, MA, USA). Following blocking in 5% nonfat milk for 1 h, the membranes were incubated with specific primary antibodies and HRP-conjugated secondary antibody. The protein bands were visualized by the Immobilon ECL substrate kit (Millipore), and β-actin was employed as an internal control.

**2.10. Statistical Analysis.** All statistical analyses were performed using the GraphPad Prism 6.0 software (GraphPad Software, Inc., La Jolla, CA, USA). Data were expressed as mean ± standard deviation (SD) of three repeated experiments. The significance of differences between groups was assessed by one-way analysis of variance followed by Tukey's test. Values of *p* < 0.05 were considered to indicate a statistically significant result.

### 3. Results

We first confirmed that treatment with 0.1 mM NAR for 13 d did not have any significant effect on the survival of ADSCs undergoing osteogenic differentiation (ADSCs-OD), as determined by the MTT assay, but 4 h of exposure with 0.2 mM H<sub>2</sub>O<sub>2</sub> notably reduced cell viability, and this toxic effect was markedly rescued by NAR pretreatment (Figure 1(a)). In addition, NAR pretreatment also

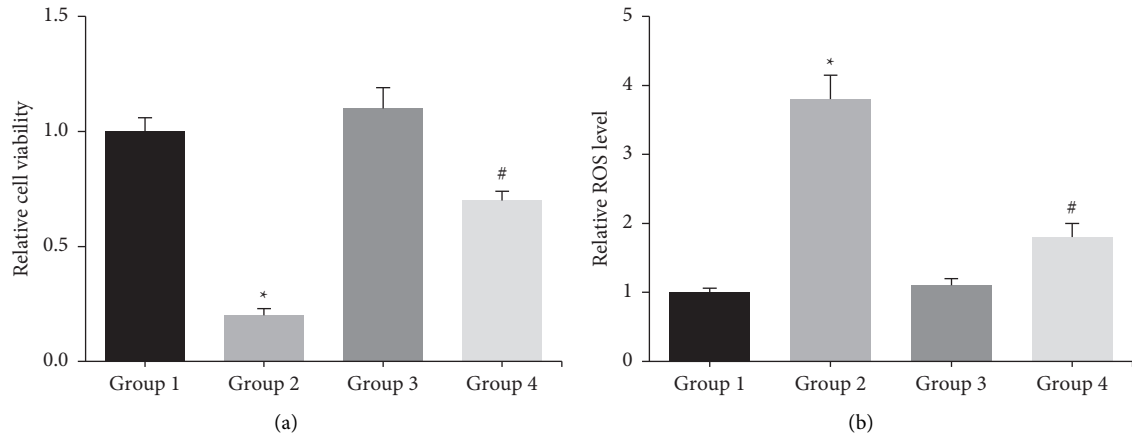


FIGURE 1: (a) The viability of ADSCs-OD was detected by MTT assay. (b) The intracellular ROS accumulation in ADSCs-OD was detected by DCFH-DA staining. \* $p < 0.05$  vs. Group 1; # $p < 0.05$  vs. Group 2.

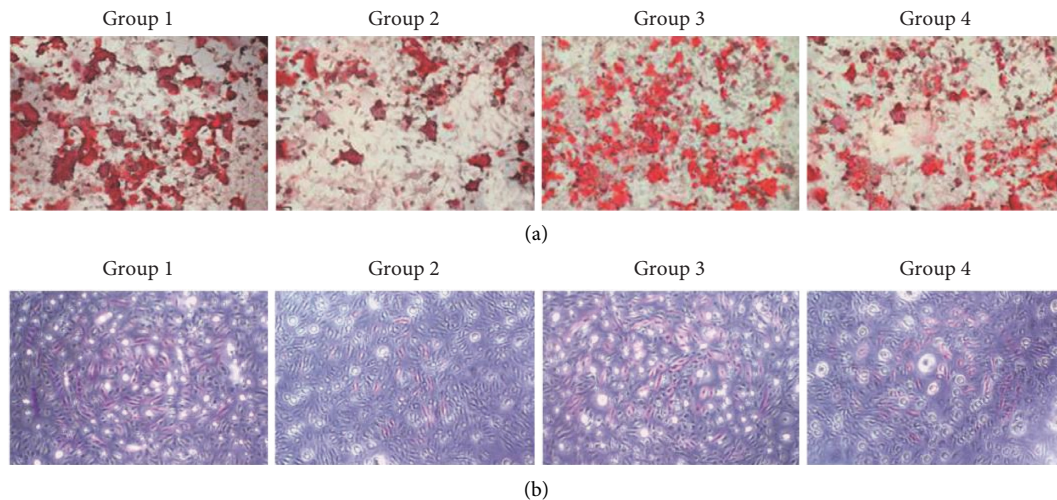


FIGURE 2: (a) The extracellular matrix mineralization in ADSCs-OD was detected by ARS staining. (b) The ALP activity in ADSCs-OD was detected by ALP staining.

dramatically reduced the  $H_2O_2$ -induced ROS accumulation in ADSCs-OD (Figure 1(b)).

Moreover, as shown in Figure 2, the impaired extracellular matrix mineralization and ALP activity in  $H_2O_2$ -stimulated ADSCs-OD were significantly blocked by NAR pretreatment.

Through RT-qPCR analysis, we noted that after  $H_2O_2$  exposure, the mRNA levels of osteogenesis-related genes, such as OCN and RUNX2, were significantly reduced in ADSCs-OD, but these effects were obviously restored by NAR pretreatment (Figure 3).

Furthermore, through western blot analysis, we observed that the effects of  $H_2O_2$  exposure on the expression levels of Wnt/ $\beta$ -catenin signaling-related proteins, such as  $\beta$ -catenin and FOXO3a, in ADSCs-OD were largely reversed by NAR pretreatment (Figure 4).

#### 4. Discussion

Osteoblasts play a major role in bone formation. ADSCs can be differentiated into osteoblasts under specific induction, and improving the osteogenic differentiation ability of ADSCs is of critical importance for bone regeneration. Oxidative stress, resulting from excessive generation of reactive oxygen species (ROS), inhibits osteoblastic differentiation of bone cells [10]. This research used  $H_2O_2$ -induced oxidative stress model, and we confirmed that NAR pretreatment could reduce the oxidative damage caused by  $H_2O_2$  in ADSCs-OD. The inhibition of osteoblastic differentiation caused by  $H_2O_2$  was featured by the reduction of ALP activity, a critical regulator of bone matrix mineralization [11]. Patients with osteoporosis often have lower OCN and RUNX2 compared to healthy people [12]. This

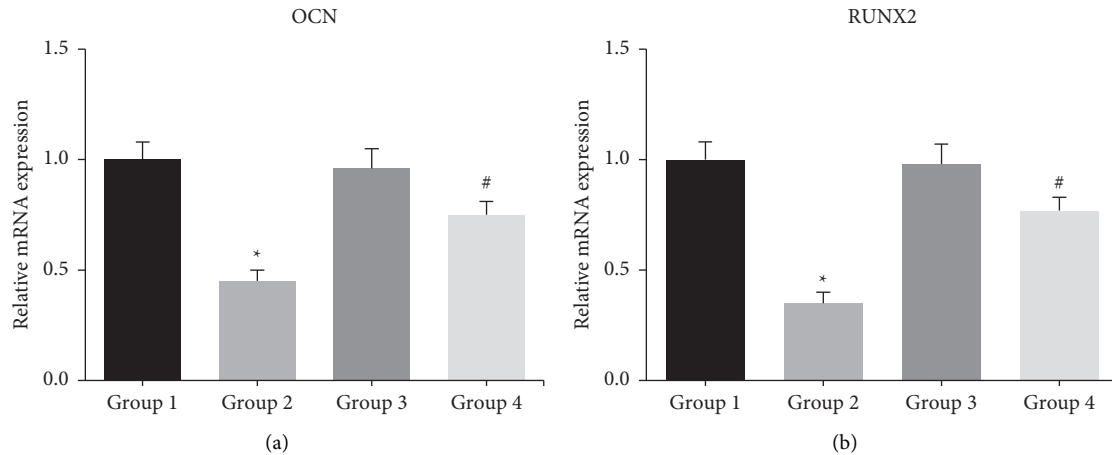


FIGURE 3: The mRNA levels of osteogenesis-related genes in ADSCs-OD were detected by RT-qPCR analysis. \* $p < 0.05$  vs. Group 1; # $p < 0.05$  vs. Group 2.

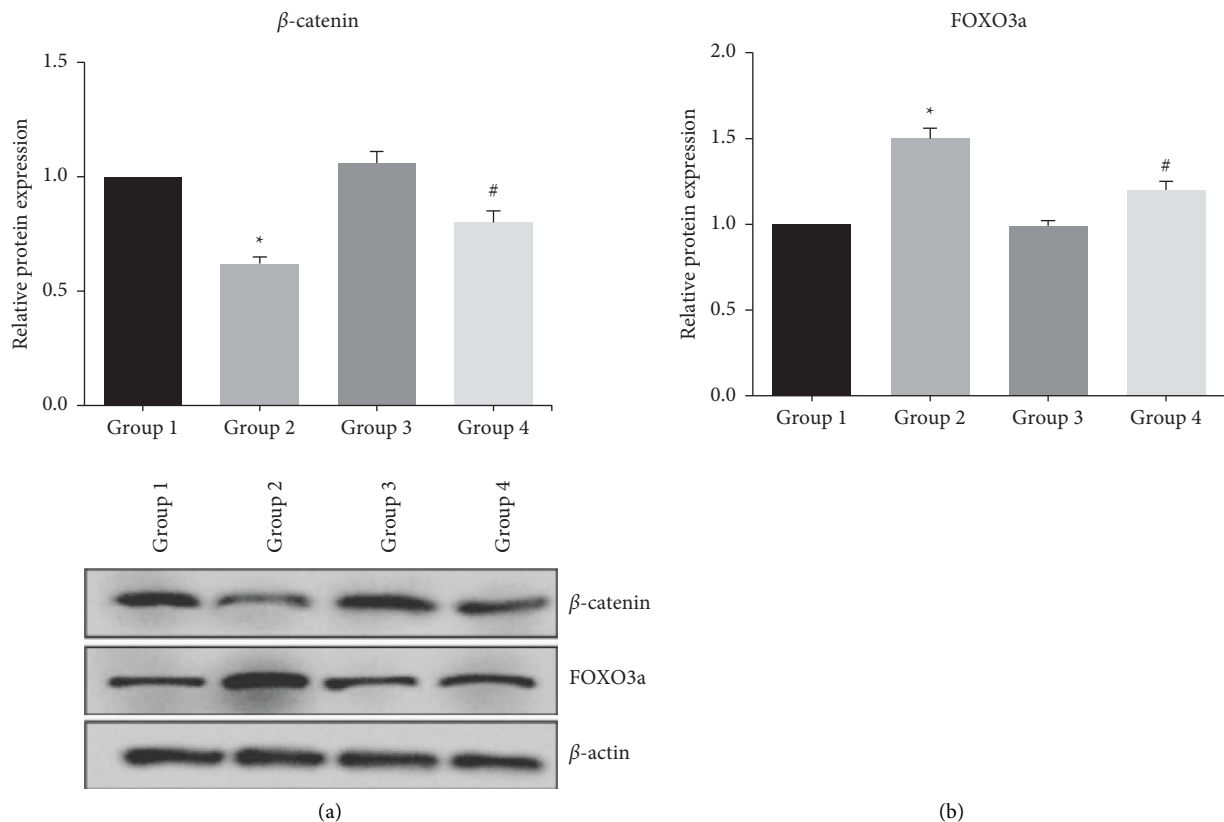


FIGURE 4: The expression levels of Wnt/ $\beta$ -catenin signaling-related proteins in ADSCs-OD were detected by western blot analysis. \* $p < 0.05$  vs. Group 1; # $p < 0.05$  vs. Group 2.

study further showed that  $H_2O_2$ -inhibited osteogenic differentiation was notably rescued by NAR pretreatment.

Wnt/ $\beta$ -catenin signaling is involved in the regulation of diverse pathophysiological processes, and it also plays a key role in osteogenesis by determining the differentiation of stem cells into mature osteoblasts rather than into chondrocytes and adipocytes [13]. Attenuation of Wnt/ $\beta$ -catenin signaling may be responsible for decreased bone formation

and increased bone marrow adiposity [14]. Oxidative stress antagonizes Wnt/ $\beta$ -catenin signaling in osteoblast precursors by activating FOXO3a transcription factor [15]. The present study also verified that the effects of  $H_2O_2$  exposure on Wnt/ $\beta$ -catenin signaling in ADSCs-OD were obviously reversed by NAR pretreatment.

In conclusion, our study provides promising evidence that NAR could protect ADSCs-OD against  $H_2O_2$ -inhibited

osteogenic differentiation. Therefore, NAR may be a potential therapeutic approach for treating patients with osteoporosis.

### Data Availability

The data used to support the findings of this study are available from the corresponding author upon request.

### Conflicts of Interest

The authors declare no conflicts of interest.

### Acknowledgments

This work was supported by the scientific research projects of basic scientific research in colleges and universities operating expenses of Heilongjiang Province in 2019, China (grant no. 2019-KYYWF-0994).

### References

- [1] T. D. Rachner, S. Khosla, and L. C. Hofbauer, "Osteoporosis: now and the future," *The Lancet*, vol. 377, no. 9773, pp. 1276–1287, 2011.
- [2] M. T. Drake, B. L. Clarke, and E. M. Lewiecki, "The pathophysiology and treatment of osteoporosis," *Clinical Therapeutics*, vol. 37, no. 8, pp. 1837–1850, 2015.
- [3] P. A. Zuk, M. Zhu, P. Ashjian et al., "Human adipose tissue is a source of multipotent stem cells," *Molecular Biology of the Cell*, vol. 13, no. 12, pp. 4279–4295, 2002.
- [4] R. A. Sabol, A. C. Bowles, A. Cote, R. Wise, N. Pashos, and B. A. Bunnell, "Therapeutic potential of adipose stem cells," *Advances in Experimental Medicine & Biology*, vol. 1341, 2018.
- [5] B. Levi and M. T. Longaker, "Concise review: adipose-derived stromal cells for skeletal regenerative medicine," *Stem cells*, vol. 29, no. 4, pp. 576–582, 2011.
- [6] J. An, H. Yang, Q. Zhang et al., "Natural products for treatment of osteoporosis: the effects and mechanisms on promoting osteoblast-mediated bone formation," *Life Sciences*, vol. 147, pp. 46–58, 2016.
- [7] R. Chen, Q.-L. Qi, M.-T. Wang, and Q.-Y. Li, "Therapeutic potential of naringin: an overview," *Pharmaceutical Biology*, vol. 54, no. 12, pp. 3203–3210, 2016.
- [8] F. Li, X. Sun, J. Ma et al., "Naringin prevents ovariectomy-induced osteoporosis and promotes osteoclasts apoptosis through the mitochondria-mediated apoptosis pathway," *Biochemical and Biophysical Research Communications*, vol. 452, no. 3, pp. 629–635, 2014.
- [9] K. J. Livak and T. D. Schmittgen, "Analysis of relative gene expression data using real-time quantitative PCR and the 2- $\Delta\Delta$ CT method," *Methods*, vol. 25, no. 4, pp. 402–408, 2001.
- [10] X.-c. Bai, D. Lu, J. Bai et al., "Oxidative stress inhibits osteoblastic differentiation of bone cells by ERK and NF- $\kappa$ B," *Biochemical and Biophysical Research Communications*, vol. 314, no. 1, pp. 197–207, 2004.
- [11] L. Hessele, K. A. Johnson, H. C. Anderson et al., "Tissue-nonspecific alkaline phosphatase and plasma cell membrane glycoprotein-1 are central antagonistic regulators of bone mineralization," *Proceedings of the National Academy of Sciences*, vol. 99, no. 14, pp. 9445–9449, 2002.
- [12] A. E. Handschin, M. Egermann, O. Trentz et al., "Cbfa-1 (Runx-2) and osteocalcin expression by human osteoblasts in heparin osteoporosis in vitro," *Clinical and Applied Thrombosis*, vol. 12, no. 4, pp. 465–472, 2006.
- [13] M. Rossini, D. Gatti, and S. Adami, "Involvement of WNT/ $\beta$ -catenin signaling in the treatment of osteoporosis," *Calcified Tissue International*, vol. 93, no. 2, pp. 121–132, 2013.
- [14] S. Iyer, E. Ambrogini, S. M. Bartell et al., "FOXOs attenuate bone formation by suppressing Wnt signaling," *Journal of Clinical Investigation*, vol. 123, no. 8, pp. 3409–3419, 2013.
- [15] M. Almeida, L. Han, M. Martin-Millan, C. A. O'Brien, and S. C. Manolagas, "Oxidative stress antagonizes Wnt signaling in osteoblast precursors by diverting  $\beta$ -catenin from T cell factor- to forkhead box O-mediated transcription," *Journal of Biological Chemistry*, vol. 282, no. 37, pp. 27298–27305, 2007.

## Research Article

# Efficacy and Mechanism of *Mallotus furetianus* Müll. Arg. Extract on Nonalcoholic Fatty Liver Disease

Daobin Lin,<sup>1</sup> Yi Ding,<sup>2</sup> Yabo Cheng,<sup>3</sup> Yubin Chen,<sup>4</sup> Yunting Tang,<sup>4</sup> Xiaowen Wu,<sup>4</sup> and Yawei Cheng<sup>2</sup> 

<sup>1</sup>Department of Cardiology, Hainan Provincial Hospital of Traditional Chinese Medicine, Haikou 570293, China

<sup>2</sup>Department of Disease Prevention, Hainan Provincial Hospital of Traditional Chinese Medicine, Haikou 570293, China

<sup>3</sup>Department of Wrist, Sichuan Orthopedic Hospital, Chengdu 610041, China

<sup>4</sup>Department of Disease Prevention, Hainan Hospital of Traditional Chinese Medicine Affiliated to Guangzhou University of Chinese Medicine, Haikou 570100, China

Correspondence should be addressed to Yawei Cheng; [chengyawei1990@outlook.com](mailto:chengyawei1990@outlook.com)

Received 21 December 2021; Revised 11 March 2022; Accepted 5 April 2022; Published 28 April 2022

Academic Editor: Ruchika Garg

Copyright © 2022 Daobin Lin et al. This is an open access article distributed under the Creative Commons Attribution License, which permits unrestricted use, distribution, and reproduction in any medium, provided the original work is properly cited.

Nonalcoholic fatty liver disease (NAFLD) is currently the major cause of chronic liver disease globally. To observe the sedative effect of *Mallotus furetianus* extract (MFE) on NAFLD and the potential molecular mechanism, a high-fat diet (HFD) was used to induce NAFLD in rats for 8 weeks. Rats were orally given MFE (1.7 g/kg, 2.5 g/kg, and 3.3 g/kg) every day. Serum and liver biochemical indexes were detected. 16S rDNA sequencing was performed to test the changes in the gut microbiota. Mass spectrometry was used to analyze the changes in blood and liver metabolites and to perform a joint analysis of differential flora and differential metabolites. The results showed that MFE alleviated liver injury and decreased hepatic lipids content. ELISA analysis certificated that MFE reduced inflammation levels in rats fed with HFD. Compared to HFD rats with a normal diet, MFE significantly changed the overall structure of the intestinal flora and the composition of the intestinal microbes destroyed by HFD. In addition, MFE changes the metabolic levels of lipids and proteins in HFD rats. In conclusion, MFE effectively treated NAFLD and significantly improved the overall structure and intestinal microbial composition of the intestinal microbiota. The abundance of *Bacteroides fragilis* and *Escherichia coli* increased significantly in the partridge tea treatment group.

## 1. Introduction

NAFLD has now become an important cause of chronic liver disease in developed countries. The prevalence of NAFLD in adult people is 10% to 30%, of which 10% to 20% are nonalcoholic steatohepatitis (NASH). The incidence of liver cirrhosis is as high as 25% within 10 years [1, 2]. NAFLD covers many disease states, such as fatty liver, nonalcoholic steatohepatitis, fibrosis, cirrhosis, and hepatocellular carcinoma. Various levels of metabolic factors such as insulin resistance, dyslipidemia, and inflammation are increasingly regarded as the main pathogenic factors leading to liver steatosis, but the specific pathogenesis of NAFLD is complex and unclear [3, 4]. In addition, there is currently no

approved treatment for NAFLD, so new treatments to treat this complex liver disease are urgently needed [3, 4].

*Mallotus furetianus* is an economic plant from Hainan Island in China. Its leaves are used as an aromatic beverage and as a folk remedy for the treatment of cholecystitis [5]. The extract also has antioxidant and antiatherosclerotic activities. The water extract can reduce intracellular lipid accumulation in oleic acid-induced fat degeneration of liver cancer cells [5]. These results indicate that MF is effective in treating liver steatosis.

The intestinal flora has an important regulatory effect on NAFLD. The intestinal flora could affect the intestinal permeability, the luminal metabolism of cholecystic acid, lipoprotein lipase, endogenous alcohol, and toxic



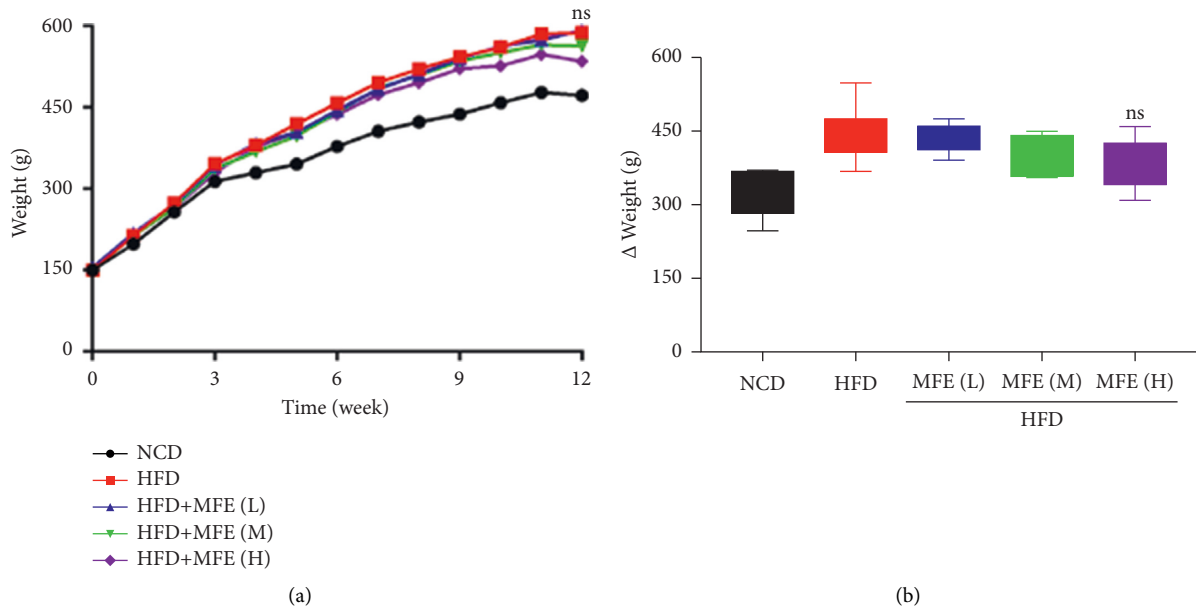


FIGURE 1: MFE does not affect weight in rats fed with HFD. (a) The body weight curve from 0 to 12 weeks after treatment ( $n = 7-9$ ). (b) The change in overall body weight within 12 weeks. Data were expressed as mean  $\pm$  SEM. ns, no significance.

compounds [6, 7]. Increased intestinal permeability and lipoprotein lipase production in intestinal diseases contribute to the pathogenesis of NAFLD. The gut microbiota, which affects bile cholic acid biosynthesis in the course of NAFLD by regulating the liver-like protein X receptor (FXR) and HF-induced liver steatosis, inhibits the gut by changing the gut microbiota [8, 9]. The fermentation of short-chain fatty acids and carbohydrates produced by intestinal microorganisms helps to inhibit fat synthesis and accelerate the oxidation of fat in the liver. Some enzymes produced by gut microbes convert choline in food into toxic compounds, which are then absorbed by the liver, leading to liver damage and inflammation. In addition, the intestinal flora is the primary source of endogenous alcohol, and in patients with NASH. Large numbers of bacteria have been reported to produce alcohol [10–12]. Treatment with probiotics or prebiotics to relieve NAFLD is effective, further confirming the influence of intestinal flora on NAFLD. Therefore, regulating the intestinal flora is a potential treatment for NAFLD. In this study, HFD was used to induce NAFLD in rats, and 16S rDNA sequencing and metabolomics were used to analyze the regulatory effect and molecular mechanism of MFE on NAFLD.

## 2. Materials and Methods

**2.1. Experimental Animals.** Fifty male Wistar rats (200–250 g, 4–6 weeks old) were obtained from the Shanghai Laboratory Animal Center of Chinese Academy of Sciences (Shanghai, China). The animals were fed with standard laboratory feed and allowed to drink tap water at will. All animals were appropriately treated in accordance with the institutional animal care guidelines approved by the Experimental Animal Ethical Committee of Hainan Provincial

Hospital of Traditional Chinese Medicine (IACUC-20200112-02).

**2.2. Treatment of Rats.** Fifty rats were divided into 5 groups randomly: normal-chow diet (NCD) ( $n = 10$ ); HFD ( $n = 10$ ); HFD + MFE (1.7 g/kg) ( $n = 10$ ); HFD + MFE (2.5 g/kg) ( $n = 10$ ); and HFD + MFE (3.3 g/kg) ( $n = 10$ ). MFE is dissolved in physiological saline solution. The rats were fed HFD, and MFE was administered daily for 8 weeks.

**2.3. Analysis of Serum ALT/AST Activities.** The blood sample was stored at 4°C for 2 hours and then centrifuged at 860  $\times$ g for 15 minutes before serum collection. The kit was used to measure serum ALT and AST according to the manufacturer's instructions [10–12].

**2.4. Assessment of IL-1 $\beta$ , IL-6, TNF $\alpha$ , and ADS/LEP.** For each rat, commercial ELISA kits were utilized to quantify the level of serum tumor inflammatory factors (IL-1 $\beta$ , IL-6, and TNF $\alpha$ ) and serum ADS/LEP, in accordance with the manufacturer's instructions [13].

**2.5. Liver Histological Evaluation.** Liver sections were fixed in 10% formalin solution for 24 hours and then embedded in paraffin. The specimen sections (5  $\mu$ m) were stained with hematoxylin-eosin (H&E) to observe the histology of liver damage. Oil red O staining was performed to observe the accumulation of lipids in the liver [14].

**2.6. DNA Extraction, PCR Amplification, and MiSeq Sequencing.** Samples were stored at  $-80^{\circ}\text{C}$  until the DNA is extracted. QIAamp DNA Stool Mini Ki was used to extract

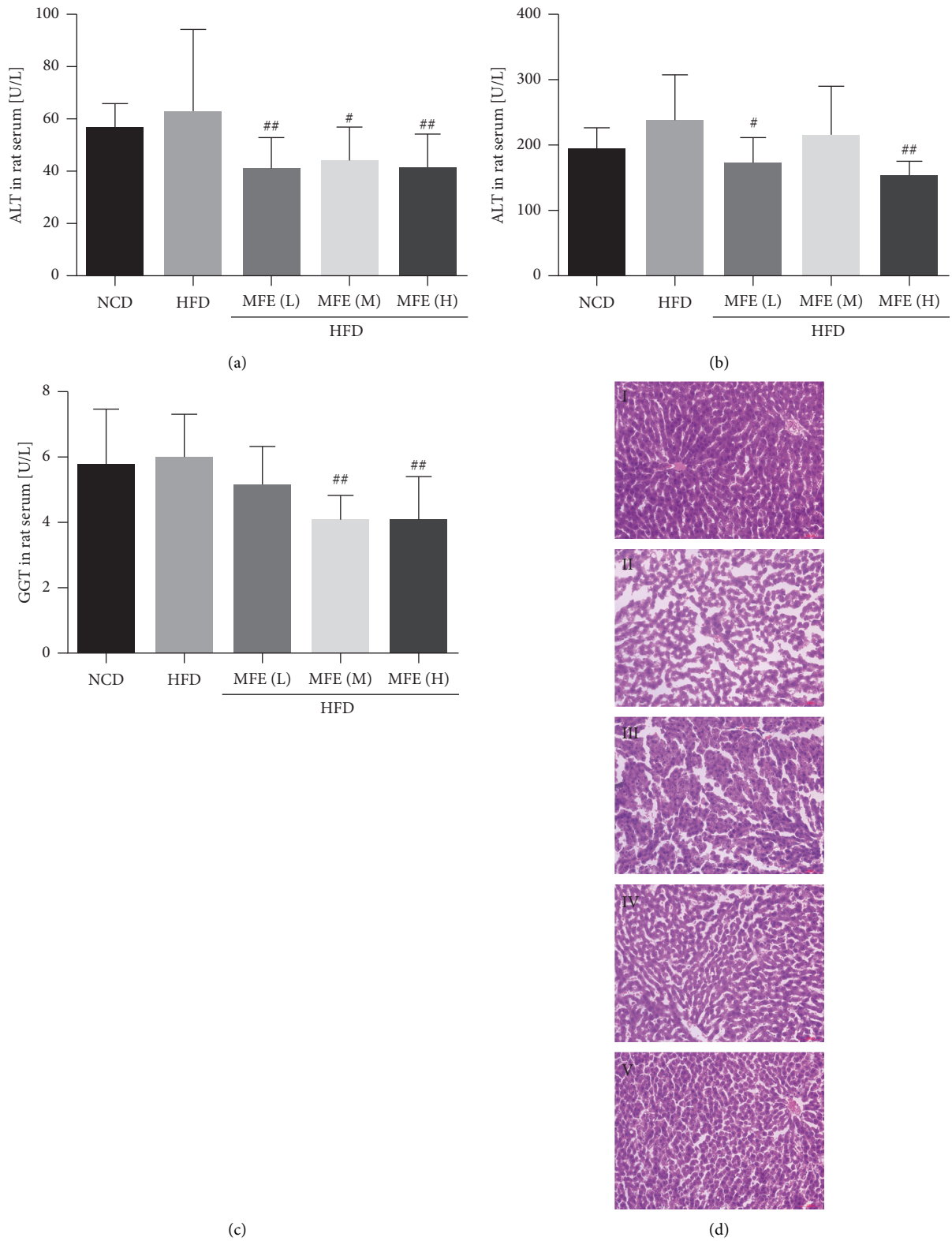


FIGURE 2: MFE reduced liver injury in rats fed with HFD, with 10 rats in each group. (a) Detection of serum ALT activity. (b) Detection of serum AST activity. (c) Detection of serum GGT activity ( $n = 10$ ). (d) Liver H&E staining. Magnification, 200 times. (I) NCD, (II) HFD, (III) HFD + MFE (1.7 g/kg), (IV) HFD + MFE (2.5 g/kg), and (V) HFD + MFE (3.3 g/kg). Data were expressed as mean  $\pm$  SEM. <sup>#</sup> $P < 0.05$ , <sup>##</sup> $P < 0.01$ .

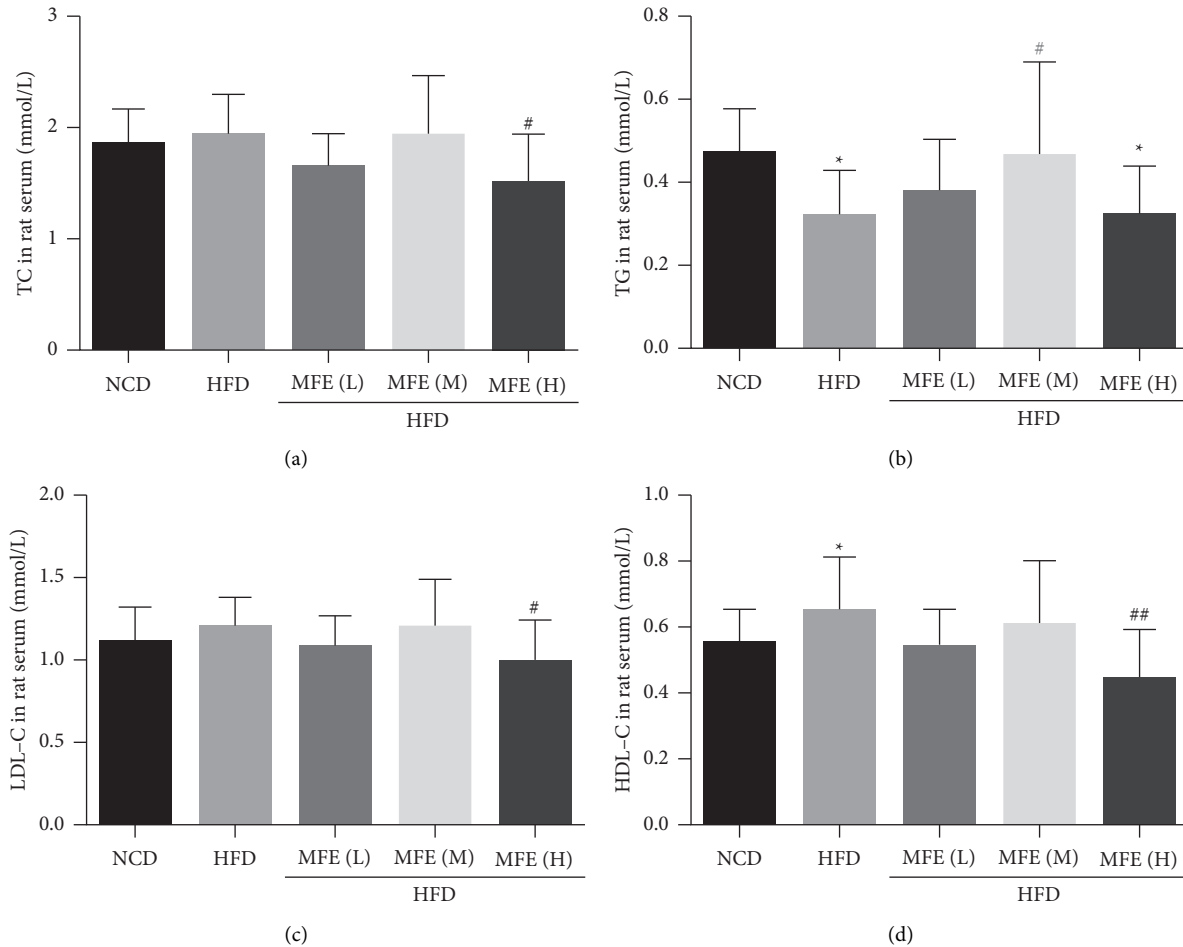


FIGURE 3: MFE reduced hepatic lipids accumulation in rats fed with HFD. (a) The content of serum TC ( $n = 10$ ). (b) The content of serum TG ( $n = 10$ ). (c) The content of serum LDL-C ( $n = 10$ ). (d) Serum HDL-C ( $n = 10$ ). Data were expressed as mean  $\pm$  SEM. <sup>#</sup> $P < 0.05$ , <sup>##</sup> $P < 0.01$ .

all genomic DNA from each sample. As mentioned earlier, PCR amplification and MiSeq sequencing were performed. In summary, Phusion High-Fidelity PCR Master Mix and HF buffer (New England Biolabs, UK) were used to amplify the V4-V5 region of the bacterial 16S rDNA. Barcode index PCR primers 515F and 926R were used. The amplicon library with the AXYGEN AxyPrep DNA Gel Extraction Kit (AXYGEN Scientific, Union City, CA, USA) was purified, normalized with FTC-3000™ Real-Time PCR, using the MiSeq instrument (Illumina), using  $2 \times 300$  cycles of V3 reagents. The cassette is sequenced.

**2.7. Bioinformatics Analysis.** The original sequencing reads were optimized, and bioinformatics analysis was performed. Simply put, the original data are demultiplexed according to the barcode. Trimmomatic (version 0.35) was used to eliminate poor-quality base pairs. FLASH (version 1.2.11) and mothur (version 1.33.3) were used to merge and filter the truncated reads. The multivariate statistical analysis was carried out with mothur, UPARSE (USEARCH version v8.1.1756), and R (version 3.2.3). The clean labels are aggregated in OTU and then assigned to the corresponding

taxon according to the Silva 119 database. The multifactor analysis was performed to assess the total structural changes in the intestinal flora, and the sparse curve and alpha diversity were tested to assess the richness and diversity of each group of intestinal flora. The main coordinate analysis (PCoA) was performed based on the UniFrac distance and the UniFrac tree. mothur and R were used to analysis of  $\alpha$ -diversity and  $\beta$ -diversity [15].

**2.8. Metabolomic Analysis.** A liquid chromatography (LC) quadrupole mass spectrometry (MS) amino acid analysis system with two independent liquid phase time-of-flight (LC-time) mass spectrometry platforms was used to measure the level of metabolites in the serum. For liver samples, the above 3 LC-MS platforms were analyzed by methanol/water extraction.

**2.9. Statistical Analysis.** Data are expressed as mean  $\pm$  standard error of mean (SEM). Significant differences were determined by one-way analysis of variance (one-way ANOVA) and LSD post test.  $P < 0.05$  was considered statistically significant.

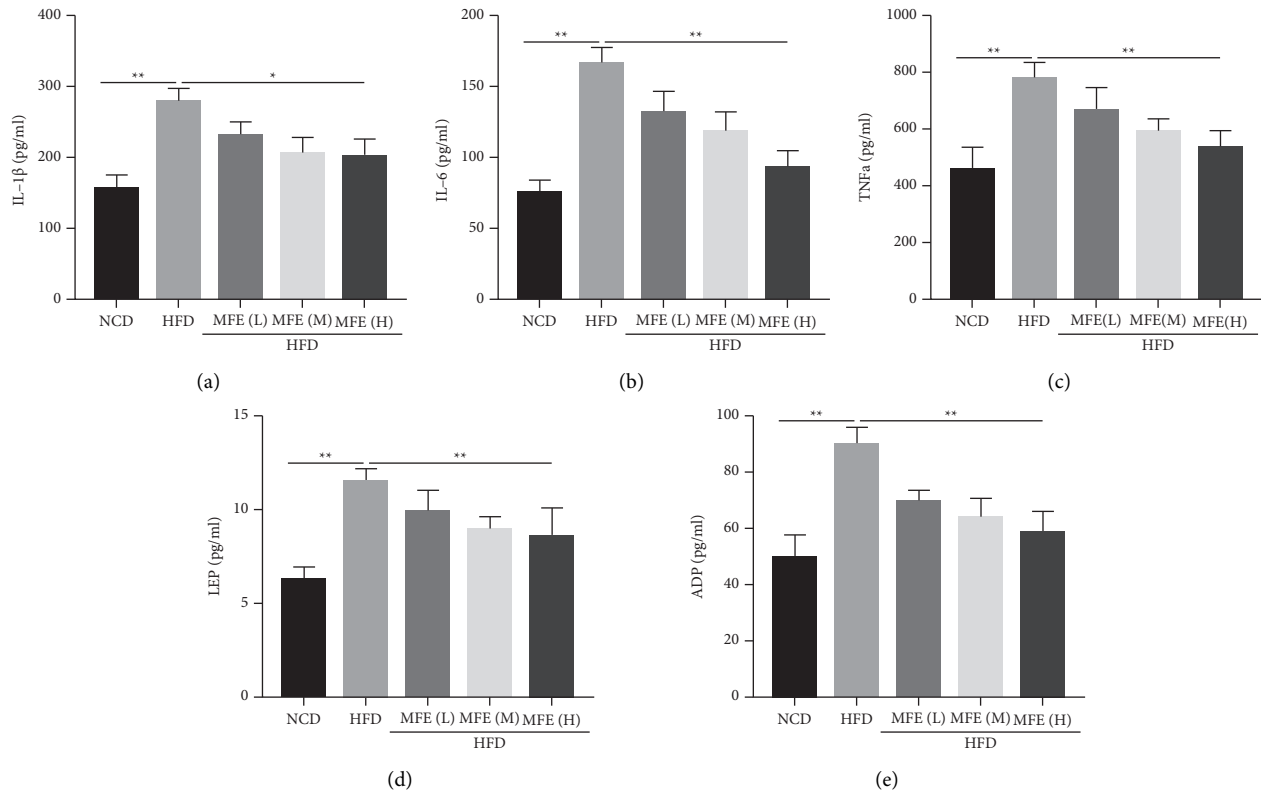


FIGURE 4: MFE reduced inflammation levels in rats fed with HFD. (a) The content of serum IL-1 $\beta$  ( $n = 10$ ). (b) The content of serum IL-6 ( $n = 10$ ). (c) The content of serum TNFa ( $n = 10$ ). (d) The content of serum LEP ( $n = 10$ ). (e) The content of serum ADP ( $n = 10$ ). Data were expressed as mean  $\pm$  SEM. \* $P < 0.05$ , \*\* $P < 0.01$ .

### 3. Results

**3.1. MFE Does Not Affect Weight in Rats Fed with HFD.** After pathological examination confirmed that the model was successfully established, rats were given 1.7 g/(kg·d), 2.5 g/(kg·d), and 3.3 g/(kg·d) partridge tea solution by intragastric administration, and the normal group and the model group were given 10 ml/(kg·d) body weight distilled water orally. The administration period was 4 weeks, during which all rats were fed with basic feed and free drinking water, and weighed once a week. Figure 1(a) shows the body weight curve from 0 to 12 weeks after treatment. No significant differences were found between the groups. Figure 1(b) is the change in overall body weight within 12 weeks. It can be said that MFE has no effect on weight gain from a high-fat diet.

**3.2. MFE Reduced Liver Injury in Rats Fed with HFD.** As shown in Figures 2(a)–2(c), MFE (1.7, 2.5, and 3.3 g/kg) reduced the increased serum ALT, AST, and GGT activities induced by HFD in rats. Moreover, the effect of MFE (3.3 g/kg) was better than the other two doses. The liver H&E staining results indicated that MFE could reduce HFD-induced liver steatosis in rats (Figure 2(d)).

**3.3. MFE Reduced Hepatic Lipids Accumulation in Rats Fed with HFD.** The results showed that MFE (1.7, 2.5, and 3.3 g/

kg) reduced the increased contents of serum TC, TG, LDL-C, and HDL-C induced by HFD in rats. In addition, the effect of 3.3 g/kg MFE was better than the other dose (Figure 3).

**3.4. MFE Reduced Inflammation Levels in Rats Fed with HFD.** Next, the expression of inflammation factors was detected in rats. The results showed that MFE (1.7, 2.5, and 3.3 g/kg) reduced the increased contents of serum IL-1 $\beta$ , IL-6, TNFa, LEP, and ADP induced by HFD in rats (Figure 4). Moreover, the effect of 3.3 g/kg MFE was better than the other dose.

**3.5. MFE Changed the Composition of the Gut Microbiota.** 16S rDNA sequencing generated 593,121 high-quality sequences and 1,625 OTUs from 30 stool samples. Wien image analysis showed that the overall microbial diversity between the three groups was significantly different (Figure 5(a)). The dilution curve shows that the depth of the current sequence is sufficient and OTU is common (Figure 5(b)). According to the weighted and unweighted table of PCoA results, compared with the control group, the structure of the intestinal flora of the HFD group with the second major component (PC2) changed, and these changes were reversed after high-dose MFE administration (Figures 5(c) and 5(d)). Weighted and unweighted UniFrac trees show three different microbial communities in each group (Figures 5(e) and 5(f)).

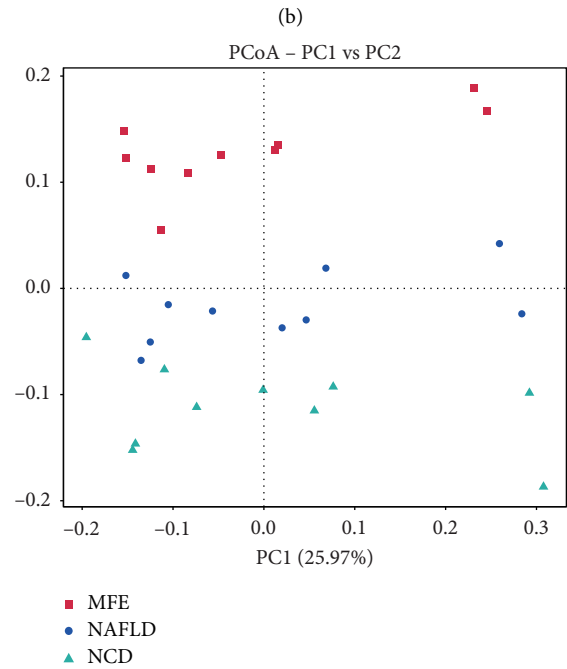
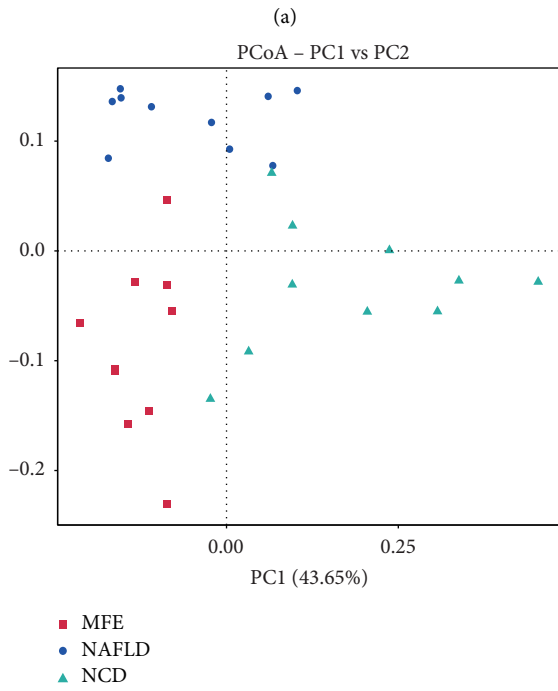
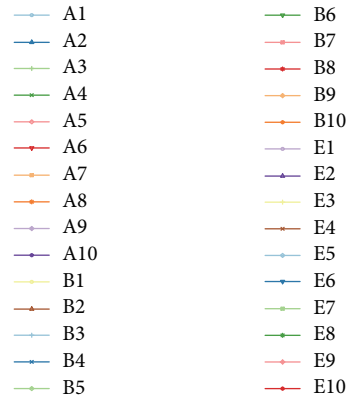
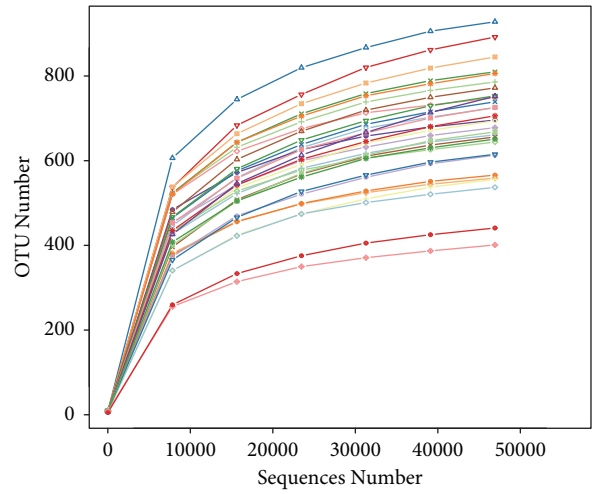
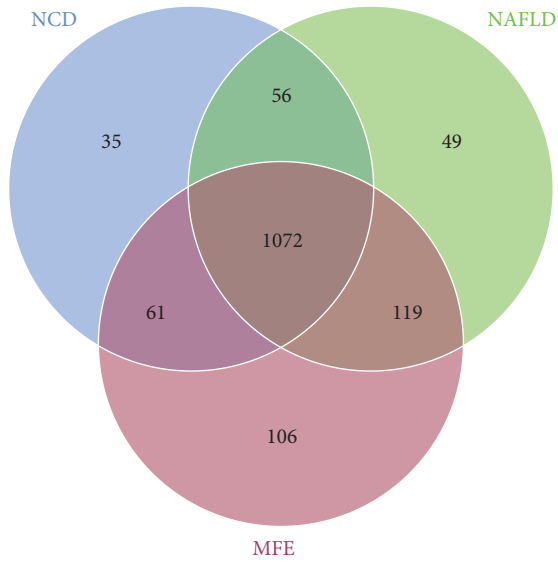


FIGURE 5: Continued.

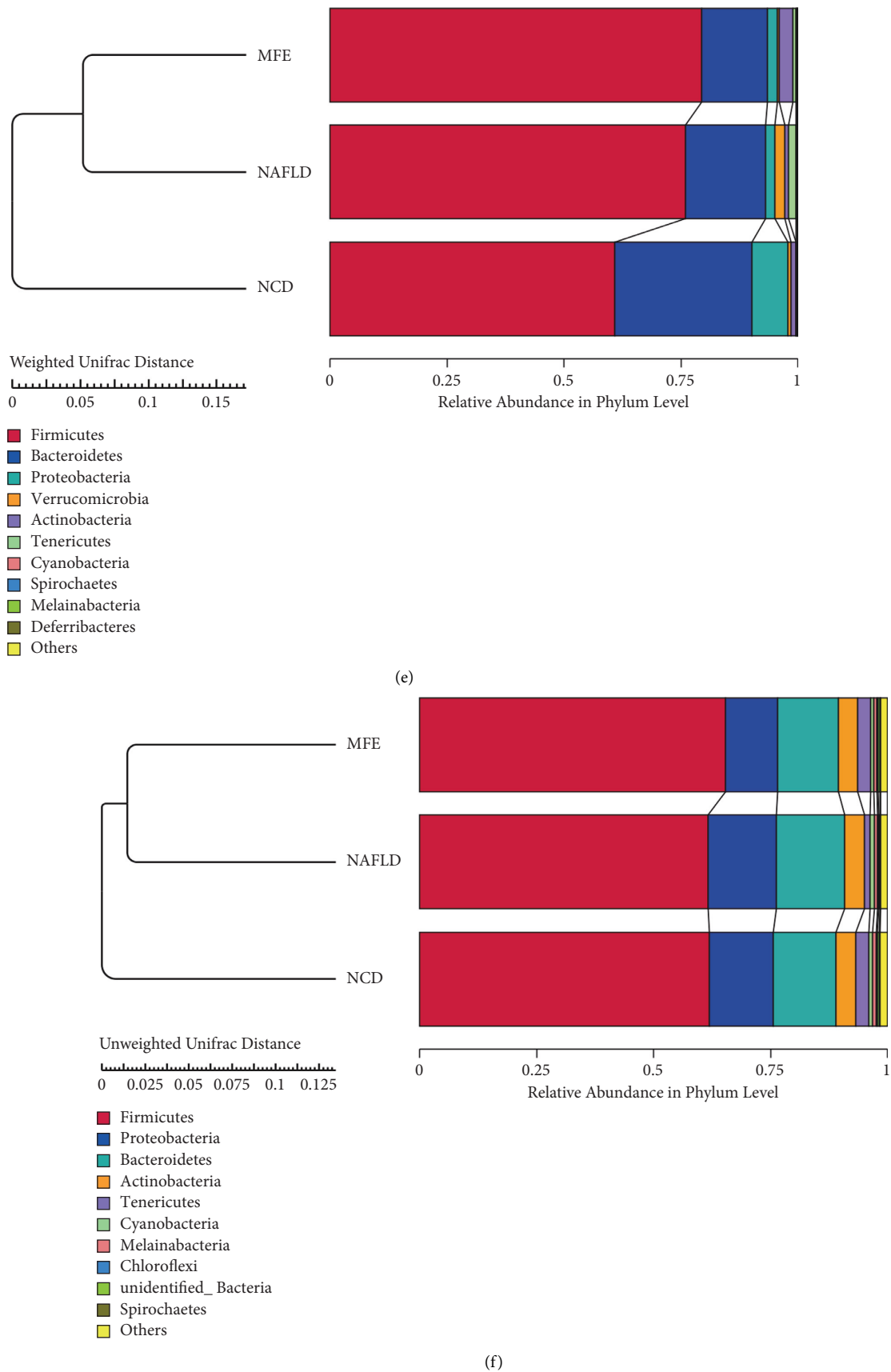


FIGURE 5:  $\alpha$ -Diversity analysis and structural changes of the gut microbiota. (a) Venn picture of multiple samples. (b) Rarefaction curves. (c) Weighted table of PCoA results. (d) Unweighted table of PCoA results. (e) Weighted UniFrac trees. (f) Unweighted UniFrac trees.



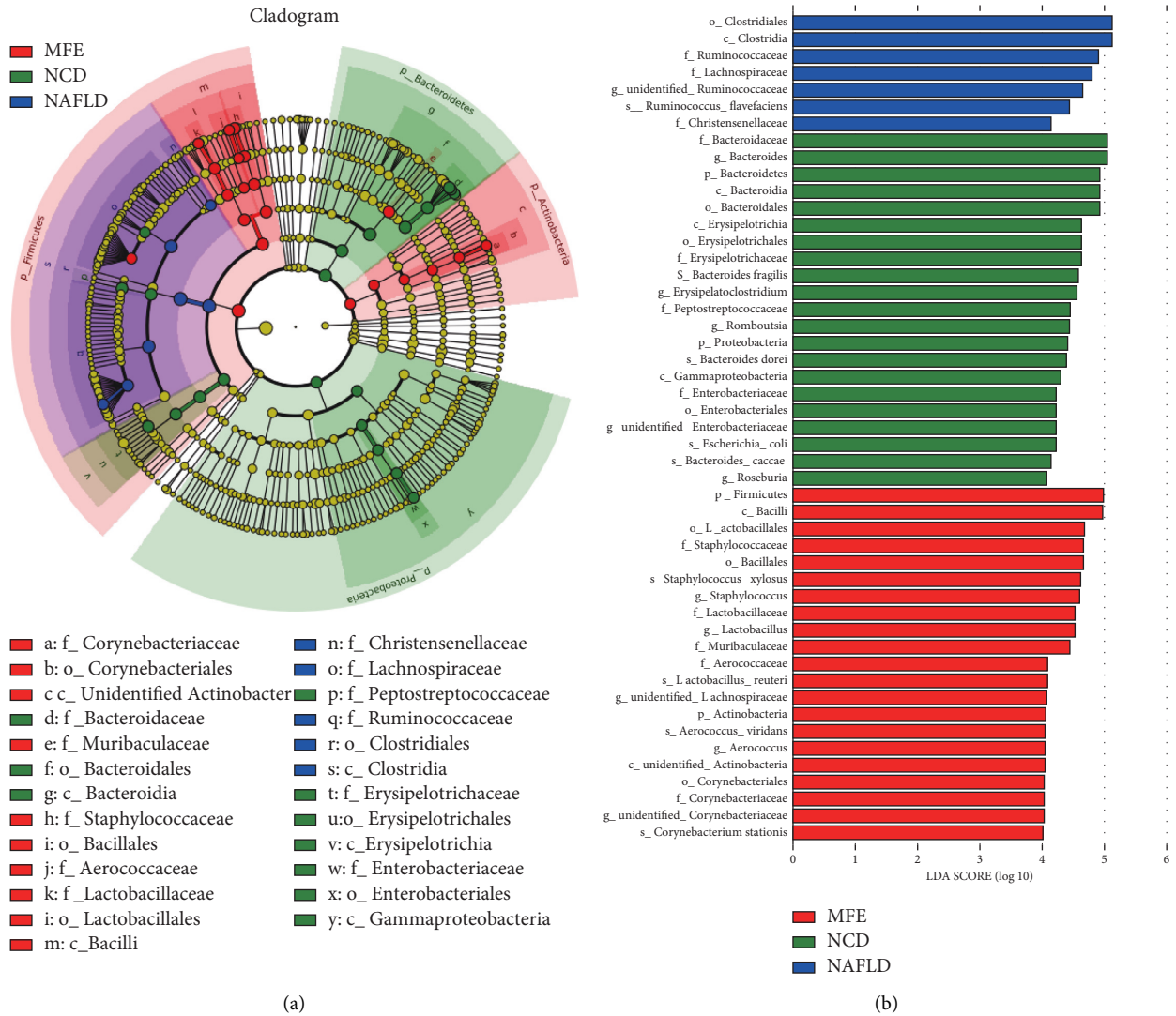
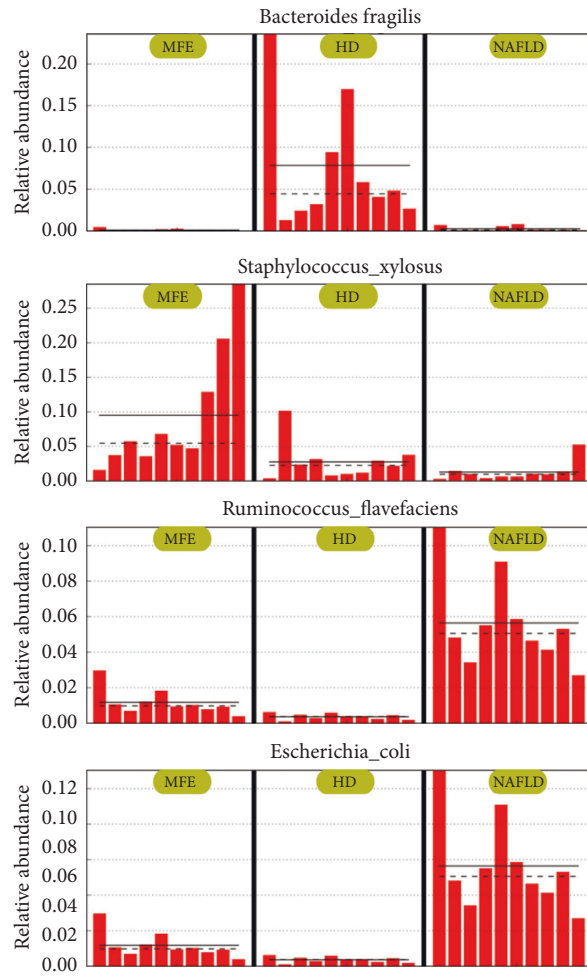


FIGURE 6: Continued.



(c)

FIGURE 6: Continued.

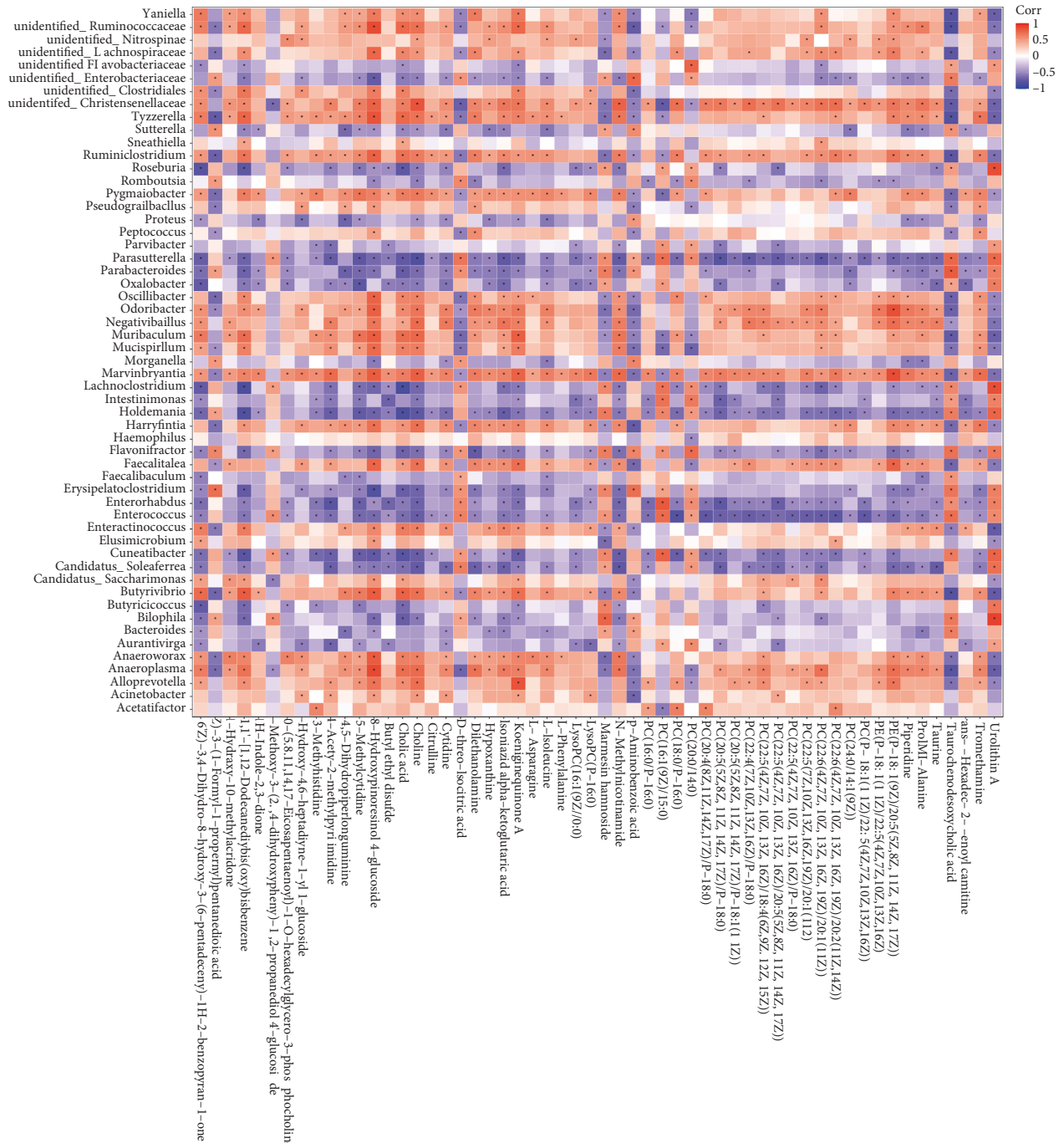


FIGURE 6: LefSe analysis of the flora with statistical differences between the three groups. (a) Clade diagram. (b) Histogram. (c) The relative abundance of biomarker samples in each group. (d) Combined analysis of 16S flora analysis data and metabolome.

In addition, LefS was performed to analyze the statistical differences between the three groups. In the clade diagram, the circles radiating from the inside to the outside indicate the order level from the strain to the genus (or species). Each small circle of different degrees represented a level of the level, and the diameter of the small circle was proportional to the relative frequency. Species without a significant difference were colored yellow and biomarkers of different species

were colored according to the group. The red knot represented the microbiome that plays an important role in the MFE group, and the green knot represented the microbiome that plays an important role in the MFE high-dose group. The blue knot represented the microbial taxa that play an important role in the NAFLD group (Figure 6(a)).

The LDA value distribution histogram showed species with an LDA score greater than 4, showing species with

significant differences in abundance in different groups, and the length of the histogram represented the impact of different species (Figure 6(b)). Further analysis of the relative abundance of the biomarker in each group of samples found that *Bacteroides fragilis* and *Escherichia coli* in the NCD group were significantly higher than those in the other two groups, *Staphylococcus xylosus* in the MFE group was significantly higher than that in the other two groups, and *Ruminococcus flavefaciens* in the NAFLD group was significantly higher than the other two groups (Figure 6(c)). In addition, we combined the 16S flora analysis data with the metabolome. We found that the abundance of *Bacteroides* was negatively correlated with the contents of 3R, 6'Z)-3,4-dihydro-8-hydroxy-3-(6-pentadecenyl)-1H-2-benzopyran-1-one, 4,5-dihydropiperlonguminine, 8-hydroxypinoresinol 4-glucoside, cytidine, hypoxanthine, isoniazid alpha-ketoglutaric acid, L-isoleucine, and prolyl-alanine, and positively correlated with the contents of taurochenodesoxycholic acid, p-aminobenzoic acid, and marmesin rhamnoside (Figure 6(d)).

#### 4. Discussion

In recent years, NAFLD has become more and more common in the world, which has attracted widespread attention from researchers and doctors [16]. Studies have shown that a variety of Chinese herbal medicines and natural active ingredients extract have good therapeutic prospects for NAFLD [17–19]. These studies provide new ideas for the treatment of NAFLD to find effective drugs from traditional Chinese medicine. MFE has a lipid-lowering effect and is widely used in the treatment of NAFLD [20]. MFE has a lipid-lowering effect on the blood and liver of rats with HFD fed [5]. HFD is widely used to induce experimental NAFLD in mice, and its pathology is very similar to human NAFLD [21]. In this study, liver TG, CT levels, and liver histopathology and staining showed that MFE reduced liver lipid accumulation in high-fat diet rats. These results further confirmed the protective effect of MFE on NAFLD and proved the great potential of MFE in the clinical treatment of NAFLD.

Elevated serum ALT and AST activities are usually signs of liver cell damage. Liver cell damage was related to the occurrence of NAFLD [22]. The results indicated that MFE also reduced the increased ALT/AST activity in the serum of HFD-fed rats, suggesting that it has a protective effect on liver cell damage during the progression of NAFLD. To determine the causes of weight loss and anti-inflammatory effects, we analyzed the gut microbiota of rats. The  $\alpha$ -diversity analysis showed that the microbial accumulation of liraglutide in NAFLD rats was significantly reduced and not reversed. The  $\beta$ -diversity analysis shows that liraglutide has a significant influence on the composition of the intestinal flora. Hence, we speculate that liraglutide may have received a healthier composition of the intestinal flora, that is beneficial for lipid metabolism and inhibits inflammation.

Previous studies have shown that *Phascolarctobacterium*, *Blautia*, *Ruminococcus*, *Clostridium*, etc., in

the samples of the NAFLD group are significantly increased, and they all have the ability to ferment to produce short-chain fatty acids (SCFAs) in the human intestine. Studies have shown that NAFLD affects the intestinal SCFA content. The level of SCFAs detected in the feces of NAFLD patients is increased, and the concentration of SCFAs produced by bacterial fermentation is relatively higher, suggesting a more adequate energy intake. The content of *Lachnospiraceae* in the NAFLD group was significantly reduced. *Lachnospiraceae* is a butyrate-producing bacteria. Its reduced content can significantly reduce the content of butyrate in SCFAs. Butyrate can be used as an important energy source for colon cells and also participates in inhibiting inflammation and enhanced screen long function. These indicate that the concentration of SCFAs in the intestinal tract of NAFLD is increased, which may only be due to the increase in the content of some of them, such as acetic acid [23]. We combined the 16S flora analysis data with the metabolome and found that the contents of (3R, 6'Z)-3,4-dihydro-8-hydroxy-3-(6-pentadecenyl)-1H-2-benzopyran-1-one, 4,5-dihydropiperlonguminine, 8-hydroxypinoresinol 4-glucoside, cytidine, hypoxanthine, isoniazid alpha-ketoglutaric acid, L-isoleucine, prolyl-alanine, taurochenodesoxycholic acid, p-aminobenzoic acid, and marmesin rhamnoside were correlated with the flora in the NAFLD group. This study is consistent with previous studies, showing that the intestinal flora can regulate metabolic pathways and participate in regulating the life activities of the body.

#### 5. Conclusion

MFE reduced liver damage and lipid accumulation in NAFLD rats. MFE significantly improved the overall structure and intestinal microbial composition of the intestinal microbiota. The abundance of *Bacteroides fragilis* and *Escherichia coli* increased significantly in the MFE treatment group. In future research, we will further clarify the molecular regulation mechanism and target of MFE based on molecular docking, affinity chromatography, and coprecipitation experiments and lay a better research foundation for the clinical application of MFE.

#### Data Availability

The data used to support this research are included within this manuscript.

#### Conflicts of Interest

The authors declare that they have no conflicts of interest.

#### Acknowledgments

This research was supported by the Hainan Provincial Basic and Applied Basic Research Program (Natural Science Field) High-Level Talent Project (2019RC383).

## References

- [1] M. S. Mundi, S. Velapati, J. Patel, T. A. Kellogg, B. K. Abu Dayyeh, and R. T. Hurt, "Evolution of NAFLD and its management," *Nutrition in Clinical Practice*, vol. 35, no. 1, pp. 72–84, 2020.
- [2] A. A. Kolodziejczyk, D. Zheng, O. Shibolet, and E. Elinav, "The role of the microbiome in NAFLD and NASH," *EMBO Molecular Medicine*, vol. 11, no. 2, 2019.
- [3] M. Meroni, M. Longo, A. Rustichelli, and P. Dongiovanni, "Nutrition and genetics in NAFLD: the perfect binomium," *International Journal of Molecular Sciences*, vol. 21, no. 8, p. 2986, 2020.
- [4] M. Gjorgjieva, C. Sobolewski, D. Dolicka, M. Correia de Sousa, and M. Foti, "miRNAs and NAFLD: from pathophysiology to therapy," *Gut*, vol. 68, no. 11, pp. 2065–2079, 2019.
- [5] E. Yoshikawa, I. Matsui-Yuasa, X. Huang, Y. Kobayashi, and A. Kojima-Yuasa, "Mallotus furetianus extract protects against ethanol-induced liver injury via the activation of the cAMP-PKA pathway," *Food Sciences and Nutrition*, vol. 8, no. 7, pp. 3936–3946, 2020.
- [6] J. Chen and L. Vitetta, "Gut microbiota metabolites in NAFLD pathogenesis and therapeutic implications," *International Journal of Molecular Sciences*, vol. 21, no. 15, p. 5214, 2020.
- [7] J. Aron-Wisnewsky, C. Vigliotti, J. Witjes et al., "Gut microbiota and human NAFLD: disentangling microbial signatures from metabolic disorders," *Nature Reviews Gastroenterology & Hepatology*, vol. 17, no. 5, pp. 279–297, 2020.
- [8] A. Pérez-Montes de Oca, M. T. Julian, A. Ramos, M. Puig-Domingo, and N. Alonso, "Microbiota, fiber, and NAFLD: is there any connection?" *Nutrients*, vol. 12, no. 10, p. 3100, 2020.
- [9] E. E. Canfora, R. C. R. Meex, K. Venema, and E. E. Blaak, "Gut microbial metabolites in obesity, NAFLD and T2DM," *Nature Reviews Endocrinology*, vol. 15, no. 5, pp. 261–273, 2019.
- [10] Y. Ji, Y. Yin, L. Sun, and W. Zhang, "The molecular and mechanistic insights based on gut-liver Axis: nutritional target for non-alcoholic fatty liver disease (NAFLD) improvement," *International Journal of Molecular Sciences*, vol. 21, no. 9, p. 3066, 2020.
- [11] G. Svegliati-Baroni, B. Patricio, G. Lioci, M. P. Macedo, and A. Gastaldelli, "Gut-pancreas-liver Axis as a target for treatment of NAFLD/NASH," *International Journal of Molecular Sciences*, vol. 21, no. 16, p. 5820, 2020.
- [12] J. Henao-Mejia, E. Elinav, C. Jin et al., "Inflammasome-mediated dysbiosis regulates progression of NAFLD and obesity," *Nature*, vol. 482, no. 7384, pp. 179–185, 2012.
- [13] F. Zhang, L. Wang, J. J. Wang, P. f. Luo, X. t. Wang, and Z. f. Xia, "The caspase-1 inhibitor AC-YVAD-CMK attenuates acute gastric injury in mice: involvement of silencing NLRP3 inflammasome activities," *Scientific Reports*, vol. 6, no. 1, p. 24166, 2016.
- [14] X. Gao, S. Guo, S. Zhang, A. Liu, L. Shi, and Y. Zhang, "Correction to: matrine attenuates endoplasmic reticulum stress and mitochondrion dysfunction in nonalcoholic fatty liver disease by regulating SERCA pathway," *Journal of Translational Medicine*, vol. 17, no. 1, p. 277, 2019.
- [15] N. Zhang, J. Tao, L. Gao et al., "Liraglutide attenuates non-alcoholic fatty liver disease by modulating gut microbiota in rats administered a high-fat diet," *BioMed Research International*, vol. 2020, Article ID 2947549, 10 pages, 2020.
- [16] P. Rada, A. Gonzalez-Rodriguez, C. Garcia-Monzon, and A. M. Valverde, "Understanding lipotoxicity in NAFLD pathogenesis: is CD36 a key driver?" *Cell Death & Disease*, vol. 11, no. 9, p. 802, 2020.
- [17] K. I. Zheng, J. G. Fan, J. P. Shi et al., "From NAFLD to MAFLD: a "redefining" moment for fatty liver disease," *Chinese Medical Journal*, vol. 133, no. 19, pp. 2271–2273, 2020.
- [18] K. Garg, S. Brackett, I. B. Hirsch, and S. K. Garg, "NAFLD/NASH and diabetes," *Diabetes Technology & Therapeutics*, vol. 22, no. S1, pp. S-174–S-186, 2020.
- [19] Q. Chen, T. Wang, J. Li et al., "Effects of natural products on fructose-induced nonalcoholic fatty liver disease (NAFLD)," *Nutrients*, vol. 9, no. 2, p. 96, 2017.
- [20] X. Huang, M. Xu, T. Shirahata et al., "Anti-steatosis compounds from leaves of *Mallotus furetianus*," *Natural Product Research*, vol. 32, no. 12, pp. 1459–1462, 2018.
- [21] J. Willebrords, I. V. A. Pereira, M. Maes et al., "Strategies, models and biomarkers in experimental non-alcoholic fatty liver disease research," *Progress in Lipid Research*, vol. 59, pp. 106–125, 2015.
- [22] D. W. Kim, J. Ock, K. W. Moon, and C. H. Park, "Association between Pb, Cd, and Hg exposure and liver injury among Korean adults," *International Journal of Environmental Research and Public Health*, vol. 18, no. 13, p. 6783, 2021.
- [23] Y. N. Ming, J. Y. Zhang, X. L. Wang et al., "Liquid chromatography mass spectrometry-based profiling of phosphatidylcholine and phosphatidylethanolamine in the plasma and liver of acetaminophen-induced liver injured mice," *Lipids in Health and Disease*, vol. 16, no. 1, p. 153, 2017.

## Research Article

# Deciphering the Molecular Mechanism of Red Raspberry in Apoptosis of Liver Cancer Cells

Linlin Song,<sup>1</sup> Qi Li,<sup>2</sup> Hui Shi,<sup>3</sup> and Hui Yue<sup>4</sup> 

<sup>1</sup>College of Pharmacy, Jiamusi University, Jiamusi 154007, Heilongjiang, China

<sup>2</sup>Department of Biochemistry, Mudanjiang Medical University, Mudanjiang 157011, Heilongjiang, China

<sup>3</sup>Pharmacy Department, First Affiliated Hospital of Jiamusi University, Jiamusi 154007, Heilongjiang, China

<sup>4</sup>Department of Pathology, Mudanjiang Medical University, Mudanjiang 157011, Heilongjiang, China

Correspondence should be addressed to Hui Yue; 3321091931@stu.cpu.edu.cn

Received 22 February 2022; Accepted 15 April 2022; Published 27 April 2022

Academic Editor: Ruchika Garg

Copyright © 2022 Linlin Song et al. This is an open access article distributed under the Creative Commons Attribution License, which permits unrestricted use, distribution, and reproduction in any medium, provided the original work is properly cited.

Red raspberry contains a variety of bioactive ingredients and has high edible and medicinal value. Red raspberry extractions (RREs) have strong antioxidant capacity and anticancer ability *in vivo* and *in vitro*. This study was to explore the specific mechanism of RREs inhibiting the proliferation of liver cancer HepG2 cells and provide a theoretical basis for the prevention and treatment of liver cancer by RREs. HepG2 cells were cultured *in vitro*, and MTT assay was adopted to detect the effect of RREs on HepG2 cell activity. Colony formation assay was applied to detect the growth and proliferation of cells, cell apoptosis was detected by flow cytometry, and dichloro-dihydro-fluorescein diacetate (DCFH-DA) assay was adopted to detect the effect of RREs on the production of reactive oxygen species (ROS) in cells. The effect of RREs on cell mitochondrial membrane potential was evaluated by mitochondrial membrane potential assay kit with JC-1 (JC-1 assay), and western blot was used to detect the expression of apoptosis-related proteins (B-cell lymphoma-2 (Bcl-2), Bcl-2-associated  $\alpha$  (Bax), and Caspase-3), thus investigating the effect of RREs on the molecular mechanism of HepG2 cell apoptosis. The results showed that RREs could inhibit the proliferation activity of HepG2 cells and promote their apoptosis in a concentration-dependent manner. The level of ROS in HepG2 cells interfered by RREs increased markedly, while the cell mitochondrial membrane potential decreased sharply. As the concentration of HepG2 increased, the mitochondrial membrane potential reduced steeply. Western blot results showed that the expression of apoptosis-related protein Bcl-2 in the RREs treatment group dropped, but the expression of Bax and Caspase-3 rose. In summary, RREs could inhibit the proliferation of liver cancer HepG2 cells and promote their apoptosis. This inhibition might be executed by inducing HepG2 cells to produce ROS, a decrease in Bcl-2/Bax protein ratio, and an obvious reduction in mitochondrial membrane potential.

## 1. Introduction

Cancer is a serious threat to human life and health. However, radiotherapy and chemotherapy, the main methods of cancer treatment, have certain side effects and limitations [1]. Therefore, it is imperative to develop new drugs and treatment methods. Studies suggested that there are two different manifestations between tumor cells and normal cells. On the one hand, tumor cells are under oxygen pressure due to relatively high ROS content [2, 3]. On the other hand, tumor cells contain lower enzymes and non-enzymatic antioxidants. Thus, the two different

manifestations make tumor cells more sensitive to ROS [4, 5]. Besides, the existence of these two differences provides a biochemical basis for selectively killing tumor cells by increasing ROS [6]. The free radicals are used for selective antitumor to achieve therapeutic effects [7, 8], which have attracted more and more attention from researchers.

Red raspberry contains a lot of active substances, such as phenolic acids, flavonoids, proanthocyanidins, and ellagic acid [9, 10]. Proanthocyanidins and ellagic acid have certain preventive and therapeutic effects on tumors [11]. At present, most of the domestic research on red raspberries focus on the identification of active ingredients and the



separation of biologically active substances [12, 13], and there are relatively few studies on the specific anticancer mechanisms. It is expected that RREs can prevent and treat oxidative stress-related diseases by protecting the body through antioxidant effect. In addition, ROS can be used to selectively kill cancer cells to treat cancer for antioxidants can promote oxidation under certain conditions. To gain a deeper understanding of antioxidant and oxidative stress, and to better understand the relationship between free radicals and tumors, the specific mechanism of RREs inhibiting the proliferation of liver cancer cells was explored in this work, hoping to provide new ideas for the prevention and treatment of liver cancer.

## 2. Materials and Methods

**2.1. Cell Culture.** Human liver cancer cell line HepG2 was purchased from Shanghai Honsun Biological Technology Co., Ltd., China. HepG2 cells were cultured in a 37°C and 5% CO<sub>2</sub> incubator with the Roswell Park Memorial Institute (RPMI) 1640 complete medium (containing 10% fetal bovine serum, 100 µg/mL penicillin, and 100 µg/mL streptomycin). Besides, the medium was changed every two days. When the confluence of the cells reached 70%–80%, trypsin was used for digestion and passage or experiments.

**2.2. Extraction Method of Red Raspberry.** The frozen red raspberry fruit was taken out, thawed at room temperature (25°C), and pulped. There was reflux and extraction for three times (material-to-liquid ratio was m(g): V(mL) = 1:8, temperature was 60°C, and extraction solvents were distilled water, 50% ethanol solution, and 100% ethanol solution in turn). Then, it was centrifuged at 3,000 r/min for 10 minutes, combined with the supernatant, and distilled under reduced pressure. Besides, the concentrates were combined, and the mixture was frozen and dried. Finally, the collected RREs were stored at –80°C.

**2.3. MTT Assay.** The effect of RREs on the cell activity of human liver cancer cell line HepG2 was analyzed. Cells were inoculated in a 96-well plate at  $2 \times 10^4$  cells/well, and 200 µL RPMI 1640 culture medium was added to each well. After the cells adhered to the wall, the RREs were added at the concentration of 0, 5, 10, 20, 60, 80, 120, and 160 mg/mL. Six auxiliary wells were set up in each group. 48 hours after the addition of the drug, 20 µL of MTT was added to each well under dark conditions. After four hours of incubation, the medium and MTT were discarded. Then, 150 µL dimethyl sulfoxide (DMSO) was added to each well, which was shaken for 5 minutes, and the optical density (OD) of each well was measured at the absorbance of 490 nm. The inhibition rate of different concentrations of drugs on cell activity was calculated, and the half inhibitory concentration of RREs on the activity of HepG2 cells was also calculated. Besides, the growth inhibition of the cells was measured 48 hours after the drug was added, and the cell inhibition rate of different concentrations of RREs was calculated. Cell inhibition

$$\text{rate} = \frac{\text{experimental group}}{\text{blank control group}} \times 100\%. \quad (1)$$

**2.4. Clone Formation Experiment.** Cloning experiments were performed using the method in reference [14]. The effect of RREs on the growth and proliferation status of cells were observed. The cells were inoculated in a 6-well plate at 1,000 cells/well, and 3 mL culture medium was added to each well. After the cells adhered to the wall, a blank group, a 30 mg/mL RREs group, and a 60 mg/mL RREs group were set up. Next, the RREs groups were added with different concentrations of drugs, and the blank group was added with an equal volume of normal saline. The culture solution was discarded after 14 days of culture, and phosphate buffer saline (PBS) was utilized to rinse the cells carefully for twice. Each well was added with 5 mL of 4% paraformaldehyde to fix the cells for 15 minutes. Then, the fixative was discarded, and the above was rinsed with distilled water twice and added with an appropriate amount of crystal violet staining solution to soak for 15 minutes. The staining solution was slowly washed off with running water, and then it was dried in the air. After picture taking, the software was adopted to count the number of colonies formed by the clones. Clone formation

$$\text{rate} = \frac{\text{number of clones forming cell colony}}{\text{number of inoculated cells}} \times 100\%. \quad (2)$$

**2.5. Cell Apoptosis Detected by Flow Cytometry.** The method in reference [15] was used to detect apoptosis of HepG2 cells in each group. HepG2 cells grown in the logarithmic phase were inoculated in a 6-well plate at a concentration of  $3 \times 10^5$  cells/mL and cultured in an incubator with 2 mL per well at 37°C and 5% CO<sub>2</sub> saturated humidity for 24 hours. Then, the control group, 30 mg/mL RREs group, and 60 mg/mL RREs group were set up. After a culture of 48 hours, the cells were collected, washed with precooled PBS 3 times, and added with 195 µL Annexin V-FITC binding solution. The cells were gently resuspended, and 5 µL Annexin V-FITC and 10 µL of propidium iodide staining solution were added, which was mixed gently. Finally, cells were incubated at room temperature under dark conditions for 10–20 minutes and then detected by flow cytometry.

**2.6. Cell ROS Detection.** ROS levels in HepG2 cells in each group were detected using the method in reference [16]. The HepG2 cells growing in the logarithmic phase were collected for resuspension and inoculated in a 6-well plate at a density of  $3 \times 10^5$  cells/mL. An untreated group, a 30 mg/mL RREs group, and a 60 mg/mL RREs group were set in this study. After a culture of 48 hours, the medium was incubated with 10 mmol/L DCFH-DA at 37°C for 30 min and then washed with PBS for 3 times. After the treatment, pictures were taken under a fluorescence microscope immediately, and light should be avoided carefully during the operation.

### 2.7. Detection of Cell Mitochondrial Membrane Potential.

The mitochondrial membrane potential of HepG2 cells in each group was detected by the method in reference [17]. After the cells were passaged, the cells were inoculated in a 96-well plate. When the cells were 60% full, they were processed. The drug treatment group was added with 30 mg/mL and 60 mg/mL RREs, and a serum-free medium was used for the control group. Six wells were repeated at each concentration and incubated for 48 hours in an incubator. The medium was discarded, and the wells were washed with sterile PBS for three times and added with 100  $\mu$ L JC-1 staining solution to stain for 30 minutes. After staining, sterile PBS was used to wash for 3 times, and 100  $\mu$ L of PBS was added and placed in a multifunction microplate detector to measure the fluorescence intensity. The decrease in the fluorescence intensity ratio indicated that the mitochondrial membrane potential decreased.

**2.8. Western Blot.** HepG2 cells were cultured routinely and inoculated in 6-well plates at  $2 \times 10^5$ /well. After the liver cancer HepG2 cells were treated by RREs at different concentrations (30 and 60 mg/mL) for 48 hours, the cells in each group were collected and added with the cell lysis buffer to lyse the cells for protein extraction. The loading amount was 30  $\mu$ g. The protein was separated by 10% polyacrylamide gel electrophoresis and then transferred to the polyvinylidene fluoride (PVDF) membrane. The 5% skimmed milk solution was used to seal the plate at room temperature for 1 hour, and Bcl-2 (1 : 3000), Bax (1 : 3000) or Caspase-3 (1 : 3000), and  $\beta$ -actin primary antibody were added for incubation overnight at 4°C. After three times of washing with tris buffered saline tween (TBST) the next day, 1 : 2,000 diluted horseradish peroxidase-labeled rabbit secondary antibody was added and then incubated for 1 hour at room temperature. After the membrane was washed with TBST, the target band was detected by chemiluminescence method, and the band gray-scale analysis was performed. The experiment was repeated 3 times.

**2.9. Statistical Analysis.** SPSS 22.0 was employed for data processing, the data were expressed as mean  $\pm$  standard deviation ( $\bar{x} \pm s$ ), and the one-way analysis of variance was applied in this study.  $P < 0.05$  indicated that the difference was statistically considerable.

## 3. Results

**3.1. HepG2 Cell Activity.** After HepG2 cells were treated with different concentrations of RREs for 48 hours, RREs showed inhibitory effect on the activity of liver cancer HepG2 cells, which was concentration-dependent. The 50% inhibitory concentration of RREs against HepG2 cell activity was 48.37 mg/mL, while the lower concentration of RREs had no obvious inhibitory effect on cell proliferation (Figure 1).

**3.2. HepG2 Cell Proliferation.** The results of the colony formation experiment revealed that the cells in the control group grew vigorously and the colonies were evenly

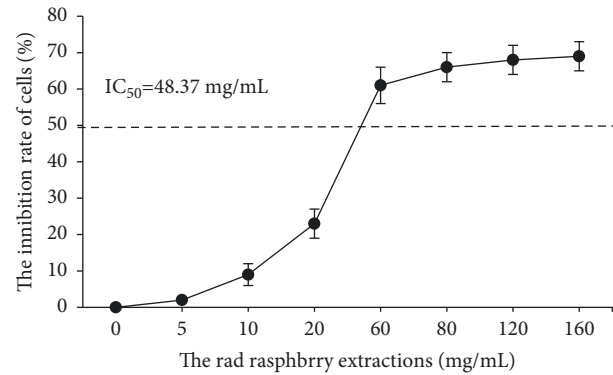


FIGURE 1: The inhibitory rate of different concentrations of RREs on the proliferation of liver cancer HepG2 cells.

dispersed. After being treated with RREs, the formation of the number of colonies was reduced steeply by RREs at a concentration of 30 mg/mL and 60 mg/mL ( $P < 0.05$ ), and the effect of 60 mg/mL was more significant (Figure 2).

**3.3. HepG2 Cell Apoptosis.** Compared with the control group, both early and late apoptosis elevated obviously ( $P < 0.05$ ) after the treatment of 30 mg/mL and 60 mg/mL RREs for 48 hours, which was concentration-dependent, suggesting that RREs treatment could induce HepG2 cell apoptosis (Figure 3).

**3.4. ROS Measurement Results.** The change of intracellular ROS content is shown in Figure 4 after 30 mg/mL and 60 mg/mL RREs were used for treatment for 48 hours. Thus, RREs treatment could substantially increase the intracellular ROS level.

**3.5. Measurement Results of Cell Mitochondrial Membrane Potential.** Figure 5 indicates that the RREs treatment for 48 hours decreased the mitochondrial membrane potential of HepG2 cells in a concentration-dependent manner after HepG2 cells were incubated with different concentrations of RREs.

**3.6. Western Blot Test Results.** To explore the specific mechanism of RREs promoting the apoptosis of liver cancer HepG2 cells, western blot was applied to detect the expression of Bcl-2, Bax, and Caspase-3. Compared with the control group, RREs could sharply inhibit the expression of Bcl-2 ( $P < 0.05$ ) but enhance the expression of Bax and Caspase-3 ( $P < 0.05$ ), thereby reducing the ratio of Bcl-2/Bax (Figure 6).

## 4. Discussion

Red raspberries are extensively applied in medical research and have certain effects on tumors, diabetes, and cardiovascular and cerebrovascular diseases [18]. Moreover, red raspberry juice or extractions have been proven to inhibit tumor growth in vivo and in vitro [19]. The experimental

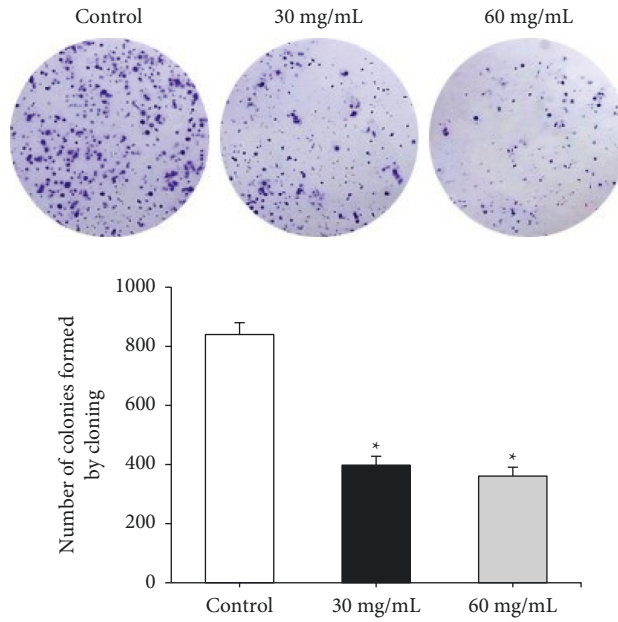


FIGURE 2: Effect of RREs on the proliferation of liver cancer cells determined by plate clone formation assay. \* Compared to the control group,  $P < 0.05$ .

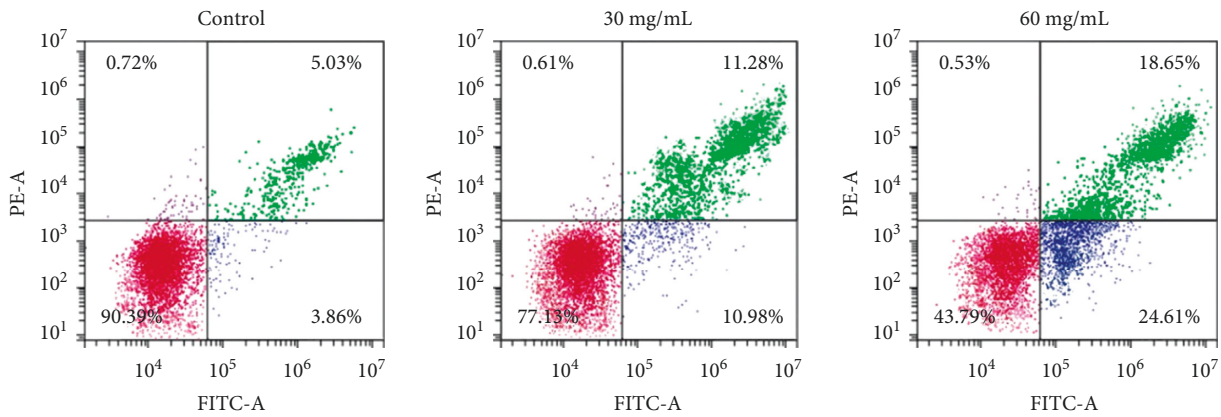


FIGURE 3: The effect of RREs on HepG2 cell apoptosis detected by flow cytometry.

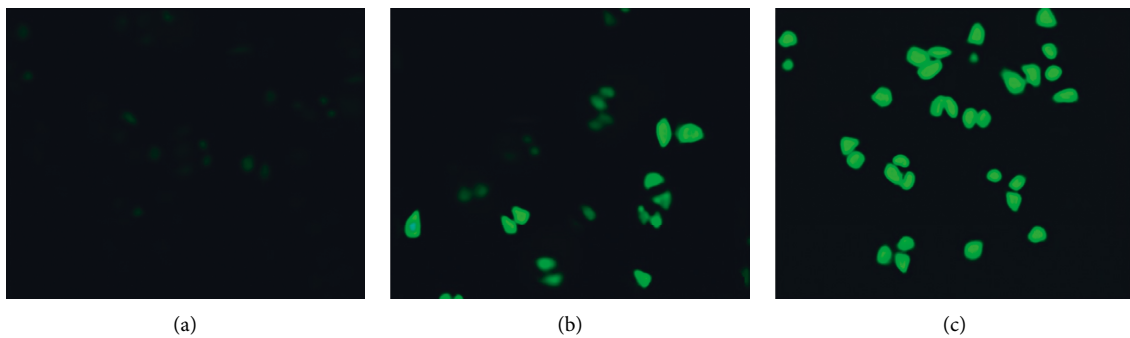


FIGURE 4: Effects of RREs on ROS production in HepG2 cells.

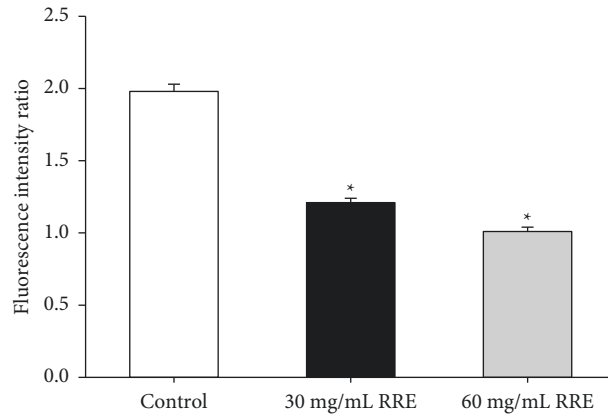


FIGURE 5: Effects of RREs on mitochondrial membrane potential reduction in HepG2 cells. \*Compared to the control group,  $P < 0.05$ .

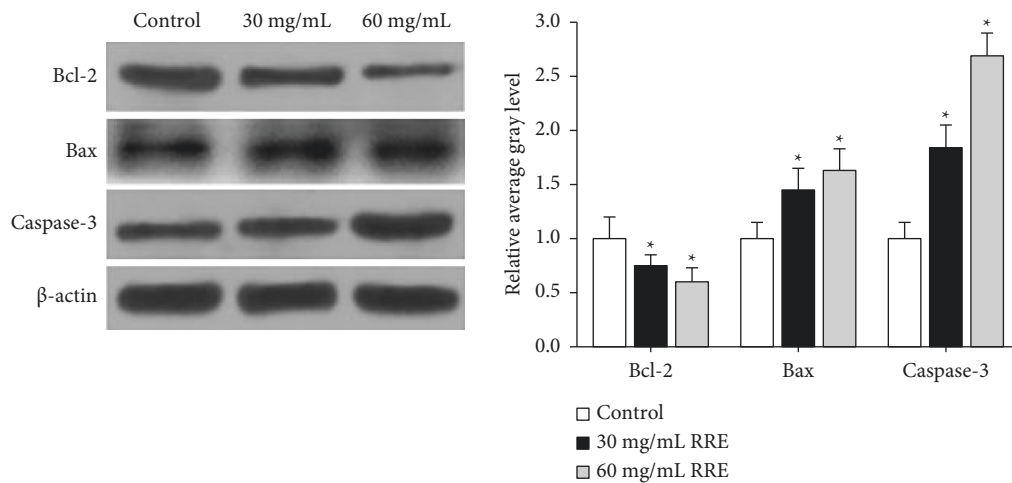


FIGURE 6: The effect of RREs on Bcl-2, Bax, and Caspase-3 protein expression detected by western blot. \*Compared to the control group,  $P < 0.05$ .

results of this study showed that RREs had a marked inhibitory effect on the proliferation of liver cancer cells in vitro. Besides, the inhibitory effect becomes more obvious, with the concentration growth of the RREs.

In recent years, research on red raspberry anticancer is more inclined to the specific molecular mechanisms of chemical composition anticancer, including research on signaling pathways, oxidative stress, cell cycle block, apoptosis, and angiogenesis [20, 21]. Lee et al. (2016) [22] pointed out that red raspberry component sanguin H-6 (SH-6) could suppress the proliferation of ovarian cancer cells A2780. The experimental results suggested that SH-6 could pass P38, mitogen-activated protein kinase (MARK), and Caspase-8-dependent BID decomposition pathways to induce apoptosis of ovarian cancer cell A2780.

The proapoptotic and antiapoptotic proteins in the Bcl-2 family in normal cells are at a relatively stable level [23]. When cells are stimulated by apoptotic factors, the upstream apoptotic signaling pathway is activated, and proapoptotic proteins are activated and translocated to mitochondria [24]. The Bax gene induces mitochondrial fragmentation and the release of cytochrome C, which activates the Caspase

cascade, leading to apoptosis [25]. What's more, Bcl-2 can inhibit the opening of mitochondrial permeability transition pore (MPTP), avoid the activation of the Caspase system, and prevent cell apoptosis [26]. The experimental results of this study indicated that RREs could reduce the expression of Bcl-2 protein in HepG2 cells, increase the expression of Bax protein to elevate the ratio of Bax/Bcl-2, promote the activation of Caspase-3, and cause cell apoptosis.

The key of cancer treatment is to inhibit the cancer cell proliferation and to induce cancer cell death, and ROS-mediated mitochondrial pathway apoptosis plays a critical role in the treatment of cancer [27]. Therefore, the ROS-mediated mitochondrial apoptosis pathway was used as a clue in this study to investigate the effect of RREs on mitochondrial membrane ROS production of liver cancer cells, and the effect of RREs induced ROS production on mitochondrial membrane potential of apoptotic cells, so as to reveal the effect and mechanism of RREs on liver cancer cells. From the research results, it could be inferred that RREs induced HepG2 cell apoptosis by generating ROS to disrupt the normal redox balance in the cell, which made the mitochondrial structure change, so as to disrupt the

mitochondrial membrane potential and destroy the normal function of mitochondria, thereby leading to apoptosis of HepG2 cells. Studies have speculated that RREs may induce HepG2 cell apoptosis through ROS-mediated mitochondrial pathway.

## 5. Conclusions

To explore the therapeutic effect of RREs on hepatocellular carcinoma, HepG2 cells were treated with RREs, and the mechanism of its effect on cell proliferation and apoptosis was detected. The results suggested that RREs may inhibit the proliferation and apoptosis of HCC cells by inducing ROS production, decreasing Bcl-2/Bax ratio, and significantly decreasing mitochondrial membrane potential of HepG2 cells, thus inhibiting the progression of HCC. However, the *in vitro* assay was adopted to analyze the inhibitory effect of RREs treatment on HepG2 cells, without combining signal pathway or transcriptome data for specific analysis. In future studies, animal models of liver cancer will be further constructed and the specific effects of RREs on liver cancer will be verified in *in vivo* experiments. In conclusion, this study provides reference for finding new therapeutic methods for hepatocellular carcinoma.

## Data Availability

The data used to support the findings of this study are available from the corresponding author upon request.

## Conflicts of Interest

The authors declare no conflicts of interest.

## Acknowledgments

This work was supported by the Young Creative Talent Projects of Jiamusi University (JMSUQP2021024).

## References



- [1] K. Ikegame and M. Terashima, "Perioperative chemotherapy for gastric cancer," *Gan To Kagaku Ryoho*, vol. 47, no. 4, pp. 569–573, 2020.
- [2] Z. Zhao, J. Gao, C. Li, X. Xu, Y. Hu, and S. Huang, "Reactive oxygen species induce endothelial differentiation of liver cancer stem-like sphere cells through the activation of akt/IKK signaling pathway," *Oxidative Medicine and Cellular Longevity*, vol. 2020, no. 5, Article ID 1621687, 11 pages, 2020.
- [3] H. Chen, Y. Li, Y. Zhu et al., "Advanced glycation end products promote ChREBP expression and cell proliferation in liver cancer cells by increasing reactive oxygen species," *Medicine*, vol. 96, no. 33, Article ID e7456, 2017.
- [4] R. Yuan, H. Xu, X. Liu et al., "Zinc-doped copper oxide nanocomposites inhibit the growth of human cancer cells through reactive oxygen species-mediated NF- $\kappa$ B activations," *ACS Applied Materials & Interfaces*, vol. 8, no. 46, pp. 31806–31812, 2016.
- [5] S. H. Wu, C. C. Chyau, J. H. Chen, S. F. Tu, H. H. Lin, and F. P. Chou, "Anti-cancerous effects of *Wasabia japonica* extract in Hep3B liver cancer cells via ROS accumulation, DNA damage and p73-mediated apoptosis," *Journal of Functional Foods*, vol. 14, pp. 445–455, 2015.
- [6] C. Stefania, T. Cristian, P. Claudia et al., "Hypoxia up-regulates SERPINB3 through HIF-2 $\alpha$  in human liver cancer cells," *Oncotarget*, vol. 6, no. 4, pp. 2206–2221, 2015.
- [7] T. Sakurai, N. Yada, T. Watanabe et al., "Cold-inducible RNA-binding protein promotes the development of liver cancer," *Cancer Science*, vol. 106, no. 4, pp. 352–358, 2015.
- [8] N. Wang, H. Liu, G. Liu et al., "Yeast  $\beta$ -D-glucan exerts antitumour activity in liver cancer through impairing autophagy and lysosomal function, promoting reactive oxygen species production and apoptosis," *Redox Biology*, vol. 32, Article ID 101495, 2020.
- [9] G. D. Noratto, B. P. Chew, and L. M. Atienza, "Red raspberry (*Rubus idaeus* L.) intake decreases oxidative stress in obese diabetic (db/db) mice," *Food Chemistry*, vol. 227, pp. 305–314, 2017.
- [10] O. Ozarda, A. Barla Demirköz, M. Özdemir, and Murat, "Sensory characteristics and antioxidant capacity of red raspberry extract as a preservative in fruit flavoured beverages," *Journal of Food Science & Technology*, vol. 52, no. 10, pp. 6687–6694, 2015.
- [11] S. I. Xu, C. Qin-qin, B. I. Jin-feng, W. U. Xin-ye, and L. I. Zhao-lu, "Research progress in main functional compounds in raspberry," *Science and Technology of Food Industry*, vol. 36, no. 4, pp. 376–381, 2015.
- [12] S. C. Debnath, "A scaled-up system for *in vitro* multiplication of thiazuron-induced red raspberry shoots using a bioreactor," *Journal of Horticultural Science and Biotechnology*, vol. 85, no. 2, pp. 94–100, 2015.
- [13] M. Hang, J. Shelby, L. Weixi et al., "Evaluation of polyphenol anthocyanin-enriched extracts of blackberry, black raspberry, blueberry, cranberry, red raspberry, and strawberry for free radical scavenging, reactive carbonyl species trapping, anti-glycation, anti- $\beta$ -amyloid aggregation, and microglial neuroprotective effects," *International Journal of Molecular Sciences*, vol. 19, no. 2, p. 461, 2018.
- [14] C. Schulz, F. Jung, and J. H. Küpper, "Inhibition of phase-1 biotransformation and cytostatic effects of diphenyleneiodonium on hepatoblastoma cell line HepG2 and a CYP3A4-overexpressing HepG2 cell clone," *Clinical Hemorheology and Microcirculation*, vol. 79, no. 1, pp. 231–243, 2021.
- [15] Y. D. Gao, A. Zhu, L. D. Li et al., "Cytotoxicity and underlying mechanism of evodiamine in HepG2 cells," *Beijing da xue xue bao. Yi xue ban = Journal of Peking University. Health sciences*, vol. 53, no. 6, pp. 1107–1114, 2021.
- [16] G. Zhou, M. Qin, X. Zhang, J. Yang, and H. Yu, "Topotecan induces hepatocellular injury via ASCT2 mediated oxidative stress," *Gastroenterología Y Hepatología*, vol. 44, no. 1, pp. 1–12, 2021.
- [17] Y. Y. Zhu, H. Y. Huang, and Y. L. Wu, "[Retracted] Anti-cancer and apoptotic activities of oleanolic acid are mediated through cell cycle arrest and disruption of mitochondrial membrane potential in HepG2 human hepatocellular carcinoma cells," *Molecular Medicine Reports*, vol. 23, no. 6, p. 440, 2021.
- [18] M. Sousa, V. Machado, R. Costa et al., "Red raspberry phenols inhibit angiogenesis: a morphological and subcellular analysis upon human endothelial cells," *Journal of Cellular Biochemistry*, vol. 117, no. 7, pp. 1604–1612, 2016.
- [19] K. Durgo, A. Belščak-Cvitanović, A. Stančić, J. Franekić, and D. Komes, "The bioactive potential of red raspberry (*Rubus idaeus* L.) leaves in exhibiting cytotoxic and cytoprotective activity on human laryngeal carcinoma and colon

- adenocarcinoma,” *Journal of Medicinal Food*, vol. 15, no. 3, pp. 258–268, 2012.
- [20] B. M. Burton-Freeman, A. K. Sandhu, and I. Edirisinghe, “Red raspberries and their bioactive polyphenols: cardiometabolic and neuronal health links,” *Advances in Nutrition*, vol. 7, no. 1, pp. 44–65, 2016.
- [21] G. Noratto, B. P. Chew, and I. Ivanov, “Red raspberry decreases heart biomarkers of cardiac remodeling associated with oxidative and inflammatory stress in obese diabetic db/db mice,” *Food & Function*, vol. 7, no. 12, pp. 4944–4955, 2016.
- [22] D. Lee, H. Ko, Y. J. Kim et al., “Inhibition of A2780 human ovarian carcinoma cell proliferation by a *Rubus* component, sanguin H-6,” *Journal of Agricultural and Food Chemistry*, vol. 64, no. 4, pp. 801–805, 2016.
- [23] X. Zhao, K. Jiang, B. Liang, and X. Huang, “Anticancer effect of xanthohumol induces growth inhibition and apoptosis of human liver cancer through NF- $\kappa$ B/p53-apoptosis signaling pathway,” *Oncology Reports*, vol. 35, no. 2, pp. 669–675, 2016.
- [24] T. Mitupatum, K. Aree, S. Kittisenachai et al., “mRNA expression of Bax, bcl-2, p53, cathepsin B, caspase-3 and caspase-9 in the HepG2 cell line following induction by a novel monoclonal ab Hep88 mAb: cross-talk for paraptosis and apoptosis,” *Asian Pacific Journal of Cancer Prevention*, vol. 17, no. 2, pp. 703–712, 2016.
- [25] N. Jiang, Y. Li, and D. Y. Ruan, “Sa1688 aberrantly regulated dysadherin and bcl-2/bax2 enhances tumorigenesis and DNA targeting drug resistance of liver cancer stem cells,” *Gastroenterology*, vol. 148, no. 4, 2015.
- [26] N. Jiang, Y. Li, and D. Y. Ruan, “Effect of aberrantly regulated dysadherin and Bcl-2/Bax2 on tumorigenesis and DNA targeting drug resistance of liver cancer stem cells,” *Journal of Clinical Oncology*, vol. 33, no. 15, Article ID e15167, 2015.
- [27] J. Liese, T. M. Hinrichs, M. Lange, and S. Fulda, “Cotreatment with sorafenib and oleanolic acid induces reactive oxygen species-dependent and mitochondrial-mediated apoptotic cell death in hepatocellular carcinoma cells,” *Anti-Cancer Drugs*, vol. 30, no. 3, p. 1, 2019.



## Research Article

# Photoprotective Potential, Cytotoxicity, and UPLC-QTOF/MS Analysis on Bioactive Solvent Fractions of *Moringa concanensis* Nimmo Bark

Rameshkumar Santhanam <sup>1,2</sup>, Thiruventhan Karunakaran <sup>3,4</sup>,  
Kandhasamy Sowndhararajan,<sup>5</sup> Muhammad Faiz Zulkifli,<sup>1</sup>  
Mouriya Govindan Kothandaraman,<sup>1</sup> Veerasamy Aravindhnan,<sup>5</sup>  
and Wan Iryani Wan Ismail<sup>1,2</sup>

<sup>1</sup>Faculty of Science and Marine Environment, Universiti Malaysia Terengganu, Kuala Nerus 21030, Terengganu, Malaysia

<sup>2</sup>Biological Security and Sustainability Research Group (BIOSES), Faculty of Science and Marine Environment, Universiti Malaysia Terengganu, Kuala Nerus 21030, Terengganu, Malaysia

<sup>3</sup>Centre for Drug Research, Universiti Sains Malaysia, Gelugor, Pulau Pinang 11800, Malaysia

<sup>4</sup>School of Chemical Sciences, Universiti Sains Malaysia, Gelugor, Pulau Pinang 11800, Malaysia

<sup>5</sup>Department of Botany, Kongunadu Arts and Science College (Autonomous), Coimbatore 641029, Tamil Nadu, India

Correspondence should be addressed to Rameshkumar Santhanam; [ramesh@umt.edu.my](mailto:ramesh@umt.edu.my) and Thiruventhan Karunakaran; [thiruventhan@usm.my](mailto:thiruventhan@usm.my)

Received 31 January 2022; Revised 3 April 2022; Accepted 5 April 2022; Published 23 April 2022

Academic Editor: Jelena Zivkovic

Copyright © 2022 Rameshkumar Santhanam et al. This is an open access article distributed under the Creative Commons Attribution License, which permits unrestricted use, distribution, and reproduction in any medium, provided the original work is properly cited.

*Moringa concanensis* Nimmo (Moringaceae) belongs to the same family of *M. oleifera* (miracle tree) and is a medicinal plant traditionally used by Indians to treat various ailments related to diabetes, tumours, inflammation, and blood pressure. Despite its versatility, the photoprotective properties of the plant remain unclear. This study revealed the UV-protective properties of its methanol bark extract and respective subfractions, chloroform, hexane, and ethyl acetate through total phenolic and flavonoid content (TPC & TFC), antioxidant (DPPH), sun protecting factor (SPF) value, and UV absorption spectra analysis. This study also investigated on the inhibitory effect of the tested samples on collagenases and elastase, which are well-known for their role in the skin. The cytotoxic and H<sub>2</sub>O<sub>2</sub> scavenging properties of *M. concanensis* in 3T3-L1 cells were explored. Finally, the phytochemical profiling of the active fraction was conducted through UPLC-QTOF/MS analysis. Among the tested fractions, the chloroform fraction of *M. concanensis* showed the highest TPC (30.92 ± 0.71 mg GAE/DW), TFC (29.05 ± 0.09 mg QE/DW), and antioxidant properties (IC<sub>50</sub>-6.616 ± 1.90 μgml<sup>-1</sup>). Additionally, chloroform fraction demonstrated the highest SPF value, 10.46 at 200 μgml<sup>-1</sup>, compared to the other tested fractions. All the fractions showed a broad absorption spectrum covering both UVA and UVB ranges. The chloroform fraction of *M. concanensis* also showed collagenase (50%) and elastase (IC<sub>50</sub>-2.95 ± 1.23 μgml<sup>-1</sup>) inhibition properties similar to the positive control. Cytotoxic results revealed that the chloroform fraction of *M. concanensis* prevented the H<sub>2</sub>O<sub>2</sub>-induced oxidative damage in 3T3-L1 cells even at lower concentrations (1.56 μgml<sup>-1</sup>). UPLC-QTOF/MS analysis tentatively identified the presence of bioactive flavonoids and phenolics such as astragalin, quercetin, isoquercetin, and caffeic acid in the active fraction of *M. concanensis* bark. Overall, it is suggested that the chloroform fraction of *M. concanensis* bark has the potency to be used as an active ingredient in sunscreen products.

## 1. Introduction

In recent times, the intensity of ultraviolet (UV) radiation reaching the earth's surface has increased due to ozone depletion by releasing human-made chemicals into the

atmosphere. [1]. Three types of UV (200–400 nm) radiations are available: UVA (320–400 nm), UVB (290–320 nm), and UVC (200–290 nm). UV radiation-stimulated skin damage is highly influenced by its wavelength, intensity, and exposure time [2]. UV radiation directly interacts with the

skin, which leads to the activation of several signaling cascades in the skin layers. Excessive doses of UVA and UVB rays are widely considered the leading causative agent for sunburns, early aging, DNA damage, wrinkle formation, oxidative stress, and skin cancer. [3]. In particular, UVA radiation produces immediate skin pigmentation and skin alterations related to premature aging *via* penetrating the deeper layers of the skin, whereas UVB is responsible for skin damage, including erythema and sunburn, by inducing late pigmentation. UVB is also associated with changes in cellular DNA and can provoke skin cancer [4]. Both rays are capable of promoting lipid peroxidation, which is strongly associated with the generation of reactive oxygen species (ROS) [5]. The excessive production of ROS leads to direct DNA damage; stimulation of proinflammatory cytokines such as IL-1 (interleukin-1), IL-6 (interleukin-6), and TNF- $\alpha$  (tumor necrosis factor); activation of signaling pathways; and the release of matrix metalloproteinases. Over-expression of these biomarkers could damage the matrix proteins such as elastin and collagen, which finally results in phototoxic reactions such as photoallergy, photosensitivity, photoaging, and photocarcinogenesis [6, 7].

Nowadays, sunscreen-based photoprotection is one of the essential strategies utilized to prevent UV-induced damage and other skin-related disorders. Sunscreens can protect the skin from sunburn, sun allergy rash, immune suppression, and other harmful effects induced by UV radiation. These sunscreens are made up of different organic and inorganic filters to protect the skin [3, 4]. Synthetic-based sunscreens are now becoming a serious threat to consumers and a threat to marine lives and the environment. A wide range of novel hypoallergenic cosmetics has been developed using natural products due to the adverse effect of synthetic sunscreen ingredients. Specifically, plant-based products are in high demand due to their myriad benefits such as antioxidant, anti-inflammatory, and immune enhancers [3–9]. Compared to synthetic filters, compounds, fractions, and extracts from plant sources offer a broad range of UV absorption. Several natural products are incorporated into sunscreen products. Previous research reported the usage of numerous traditional plants such as *Moringa oleifera* Lam, *Zanthoxylum rhetsa* (Roxb.) DC., *Parentuccella latifolia* Caruel, and *Nephelium lappaceum* L., *Camellia sinensis* L. Kuntze, and other plant extracts or fractions that are rich in polyphenols were described to possess appreciable sunscreen properties *via* targeting free radicals, inflammatory pathways (NF- $\kappa$ B, MAPK) and cytokines, and matrix metalloproteinases (MMP1, MMP3, MMP9, etc.) [2, 3, 6, 8, 10, 11]. Though there are studies that revealed the photoprotective potency of some traditional medicinal plants, it remains limited.

*Moringa concanensis* Nimmo is an important traditional medicinal plant in the family of Moringaceae mainly spotted in the Western Ghats of India and also widely distributed in Asian and Arab countries [12]. This species looks almost similar to the well-known medicinal, nutritional value species *M. oleifera*. However, it has some distinct features such as bipinnate leaves, a strong central trunk with an extremely distinctive layer of very furrowed bark, and the petals and

sepals of the flower have green patches at the tip. Moreover, the leaves and flowers of *M. concanensis* are larger compared to *M. oleifera* [13]. In Indian traditional systems of medicine, *M. concanensis* is mainly used to treat fertility problems. The leaves and bark of this species were used to treat skin tumours, tiredness, high blood pressure, jaundice, eye problems, diabetes, and swellings [14] with a wide range of therapeutic properties. Studies revealed that the ethanol extract of *M. concanensis* extract exhibited hyperglycaemic activity and showed protective activity against oxidative tissue damage in the pancreas, liver, and kidney [15]. In this study, the photoprotective properties of various solvent fractions of the *M. concanensis* bark were revealed for the first time using biochemical assays such as total phenolic (TPC) and flavonoid content (TFC), DPPH free radical scavenging activity, SPF value determination, and UVA/UVB absorption spectra analysis. Moreover, the inhibitory effect of the plant extract towards collagenase and elastase was also shown using gelatin digestion and antielastase assay. The cytotoxic and H<sub>2</sub>O<sub>2</sub> damage preventive potential of the extracts and fractions were assessed through the cell culture technique using MTT assay. The potential metabolites present in the active fraction responsible for the biological properties of *M. concanensis* bark were identified through UPLC-QTOF/MS analysis.

## 2. Materials and Methods

**2.1. Chemical and Reagents.** Solvents such as hexane (CAS No. 110-54-3), chloroform (CAS No. 67-66-3), methanol (CAS No. 67-56-1), and ethyl acetate (CAS No. 141-78-6) used for extraction are of analytical grade obtained from Merck Millipore (Darmstadt, Germany). Collagenase from *Clostridium histolyticum* (CAS No. 9001-12-1), N-succinyl-ala-ala-ala-*p*-nitroanilide (AAPVN, CAS No. 52299-14-6), 2,2-diphenyl-1-picrylhydrazyl (DPPH, CAS, No. 1898-66-4), gelatin (CAS No. 9000-70-8), porcine elastase (CAS No. 39445-21-1), Coomassie blue R-250 (CAS No. 6104-59-2), ascorbic acid (AA) (CAS No. 50-81-7), epigallocatechin gallate (EGCG, CAS No. 989-51-5), Tris-HCl (CAS No. 1185-53-1), agarose (CAS No. 9012-36-6), acetic acid (CAS No. 64-19-7), dimethyl sulfoxide (DMSO, CAS No. 67-68-5), and 3-(4,5-dimethylthiazol-2-yl)-2,5-diphenyltetrazolium bromide (MTT, CAS No. 57360-69-7) were purchased from Sigma-Aldrich Chemicals (St. Louis, MO, USA). Dulbecco's modified Eagle's medium (DMEM, CAT No. 11-995-073), TrypLE Express (CAT No. 12604-013), fetal bovine serum (FBS, CAT No. 26-140-079), and penicillin/streptomycin (CAT No. 15140-122) were purchased from Gibco (Life Technologies, California, USA).

**2.2. Samples Collection and Extraction.** The stem bark of *M. concanensis* was collected from Madukkarai, Coimbatore, Tamil Nadu, India. The plant specimen was authenticated, and plant identification certificate was given by Dr. G.V.S. Moorthy, Head of Office, Southern Regional Centre (Letter No. BSI/SRC/5/23/2018/Tech-437), Botanical Survey of India, Coimbatore, Tamil Nadu, India. The Voucher specimen

(BUH-VA-3203/2018) was submitted to the Herbarium of Department of Botany, Bharathiar University, Coimbatore, Tamil Nadu, India. The crude methanolic extract (28 g) from dried and powdered bark (600 g) of *M. concanensis* was obtained using ultrasound-assisted extraction technique according to the literature [6].

**2.3. Liquid-Liquid Partitioning.** Various solvent fractions of the crude methanol extract of *M. concanensis* were subjected to liquid-liquid partitioning technique using different solvents based on their polarity. Initially, 15 g of the methanol crude extract was mixed with equal volume of hexane and water (1 : 1) and loaded into the separating funnel. After few agitations, the hexane fraction was removed and the chloroform was added to the separating funnel. Then, the same process was repeated with ethyl acetate. Finally using rotavapor, the resultant fractions such as hexane (3.1 g), chloroform (6.2 g), and ethyl acetate (1.8 g) were obtained and dried under vacuum and lyophilized [11].

**2.4. Total Phenolic Content.** The total phenolic content for all the solvent fractions of *M. concanensis* bark was determined using the Folin–Ciocalteu method [16]. Briefly, 50  $\mu\text{L}$  of the sample (1  $\text{mgmL}^{-1}$ ) in methanol was mixed with 50  $\mu\text{L}$  distilled water, 50  $\mu\text{L}$  of 10% Folin–Ciocalteu's phenol reagent, and 50  $\mu\text{L}$  of 1 M sodium carbonate solution in a 96-well microwell plate and incubated for 60 min at room temperature without exposing it to light. Methanol was used as a blank. The absorbance of the reaction mixture was measured using a microplate reader at 750 nm. The total phenolic content was determined through calibration curve using gallic acid (7.81, 15.62, 31.25, 62.5, 125, 250, and 500  $\mu\text{g mL}^{-1}$ ) as standard. Results are expressed as milligram gallic acid equivalents (GAE) per gram of dry plant extract. All tests were done in triplicates.

**2.5. Total Flavonoid Content.** The total flavonoid content for all the fractions of *M. concanensis* bark was determined using spectrophotometric method [16]. 100  $\mu\text{L}$  of the plant extract (1  $\text{mgmL}^{-1}$ ) and standard solutions of quercetin (7.81, 15.62, 31.25, 62.5, 125, 250, and 500  $\mu\text{g mL}^{-1}$ ) in methanol solution were mixed with 100  $\mu\text{L}$  of 2%  $\text{AlCl}_3$  solution. Reaction mixtures were incubated for an hour at room temperature. The absorbance was measured using Tecan Infinite F200 Pro plate reader at  $\lambda_{\text{max}}$  415 nm. Total flavonoid contents were expressed as mg quercetin equivalent (QE) per gram of dry plant extract. Experiments were done in triplicates.

**2.6. DPPH Scavenging Activity Assay.** The crude extract and the fractions of *M. concanensis* bark were tested for their free radical scavenging properties using DPPH free radical scavenging assay [16, 17]. Briefly, 0.12 mM DPPH in methanol was prepared and mixed with various concentrations of test samples at 1 : 1 ratio (100  $\mu\text{L}$ ). Ascorbic acid was used as the positive control. Test samples and DPPH solution were incubated at room temperature for 30 min in the dark. After the incubation, the absorbance value of the

mixture was recorded on a microwell plate reader at 570 nm. The experiment was done in triplicates. The DPPH radical scavenging activity was calculated using the formula:

$$\begin{aligned} &\text{DPPH radical scavenging activity (\%)} \\ &= \frac{[(\text{Abs}_{\text{control}} - \text{Abs}_{\text{sample}})]}{[(\text{Abs}_{\text{control}})]} \times 100, \end{aligned} \quad (1)$$

where  $\text{Abs}_{\text{control}}$  is the absorbance of DPPH radical + methanol and  $\text{Abs}_{\text{sample}}$  is the absorbance of DPPH radical + samples/positive control.

**2.7. SPF Value Determination.** The *in vitro* SPF value of the crude extract and solvent fractions of *M. concanensis* were obtained by the method described in the literature [16]. Briefly, the absorbance value of the test sample (200  $\mu\text{g mL}^{-1}$ ) was determined on a UV-Visible spectrophotometer at 5 nm intervals within the range of 290–320 nm. The SPF value was then calculated by using the formula:

$$\text{SPF spectrophotometric} = \frac{\text{CF}}{290} \times \sum_{290}^{320} \text{EE}(\lambda) \times I(\lambda) \times \text{Abs}(\lambda), \quad (2)$$

where CF is the correction factor (= 10),  $\text{EE}(\lambda)$  is the erythemal effect spectrum,  $I(\lambda)$  is the solar intensity spectrum,  $\text{Abs}(\lambda)$  is the absorbance of test sample, where  $\text{EE}(\lambda) \times I(\lambda)$  are constants. Methanol was used as a blank, and measurements were made in triplicate.

**2.8. UVA/UVB Absorption Spectra.** The UV absorption spectrum of the crude extract and solvent fractions of *M. concanensis* (100  $\mu\text{g mL}^{-1}$  in methanol) were measured over a wavelength range of 200–400 nm on a UV-Visible spectrophotometer using a quartz cell (1 cm). The UV absorption spectrum of the samples tested was compared with the positive control, epigallocatechin gallate (EGCG) prepared with the same concentration.

**2.9. Gelatin Digestion Assay.** The gelatin digestion assay was done according to the method described by Santhanam et al. [6] with slight modifications. Agarose (2%) was prepared in a collagenase buffer (50 mM Tris-HCl, 10 mM  $\text{CaCl}_2$ , 0.15 M NaCl, pH 7.8) and porcine gelatin (0.15%). The mixture was transferred into a petri dish and left at room temperature for 1 h for solidification. Later, the wells were made using a sterile 200  $\mu\text{L}$  microtip. Then, 25  $\mu\text{L}$  of the samples was incubated with 25  $\mu\text{L}$  of bacterial collagenase-1 (0.1  $\text{mgmL}^{-1}$ ) for 1 h. Finally, the reaction mixture (50  $\mu\text{L}$ ) was loaded into the well and further incubated overnight. EGCG was used as a positive control. The next day, the petri dish was visualized by the Coomassie brilliant blue staining method. The degree of gelatin digestion was determined by measuring the area of the light translucent zone formed after destaining over a blue background.

**2.10. Antielastase Assay.** The antielastase activity of the various solvent fractions of *M. concanensis* was determined according to the methods of Santhanam et al. [6], with minor modifications. The assay was performed in Tris-HCl buffer (0.2 mM, pH 8.0). The stock solution of porcine pancreatic elastase (PE-E.C. 3.4.21.36) was dissolved in sterile water. N-succinyl-ala-ala-ala-p-nitroanilide (AAPVN) was dissolved in 1 mL Tris-HCl (0.2 mM) buffer (pH 8.0), and the samples were dissolved in buffer. Then, the test samples and elastase were incubated for 15 minutes before adding the substrate to start the reaction. The final reaction mixture contains a buffer, 0.8 mM AAPVN, 50  $\mu\text{g mL}^{-1}$  PE, and the test samples at various test concentrations in a total volume of 250  $\mu\text{L}$ . EGCG served as the positive control while water served as the negative control. The absorbance value was measured using a Tecan Infinite F200 Pro plate reader (Tecan Group Ltd., Männedorf, Switzerland) at 410 nm.

Enzyme inhibition activity (%)

$$= \frac{[(\text{Abs}_{\text{control}} - \text{Abs}_{\text{sample}})]}{[\text{Abs}_{\text{control}}]} \times 100. \quad (3)$$

**2.11. Cell Culture.** 3T3-L1 cells were maintained in complete Dulbecco's modified Eagle's medium (DMEM) high-glucose media according to the method of Raseetha et al. [18] with slight modification. The media were supplemented with 10% fetal bovine serum (FBS) and 5% of penicillin-streptomycin in a humidified 5% CO<sub>2</sub> incubator at 37°C. Once the cell reaches 70–80% confluence, it was utilized for seeding and treatment.

**2.11.1. Cytotoxicity.** Cells cytotoxicity was performed using MTT assay based on the method described by Raseetha et al. [18]. The cells were seeded at a density of  $1 \times 10^5$  cells/well in 96-well plates. Once the cell reaches 80% confluence, the 100  $\mu\text{L}$  of various concentrations of methanol extract and solvent fractions of *M. concanensis* and positive control EGCG were treated in each well. After 24 h, 20  $\mu\text{L}$  of MTT was added to the cells and it was incubated at 37°C for 4 h. The medium was replaced with 100  $\mu\text{L}$  DMSO, and the absorbance for each well was measured at 570 nm on Tecan Infinite F200 Pro plate reader. Cytotoxicity assay was conducted to determine the range of concentrations of the active fraction. Experiments were performed in triplicates.

**2.11.2. Protective Effect of Samples against H<sub>2</sub>O<sub>2</sub>-Induced Oxidative Damage in 3T3-L1 Cells.** The protective effect of *M. concanensis* fractions against H<sub>2</sub>O<sub>2</sub> was performed according to Chen et al. [19] with slight modification. The 3T3-L1 cells were seeded on 96-well plates at a density of  $1 \times 10^5$  (in 100  $\mu\text{L}$  medium) per well and incubated at 37°C for 24 h. Once the cell reaches the confluence, the medium was replaced with 100  $\mu\text{L}$  of samples with various concentrations (0–100  $\mu\text{g mL}^{-1}$ ) and positive control (ascorbic acid) for 18 h. Then, the cells were treated with H<sub>2</sub>O<sub>2</sub> (125  $\mu\text{M}$ ) to induce oxidative damage, and the dose concentration was fixed based

on the current study. After 6 h, the medium was removed, and the cells were washed thrice with PBS. Next, the MTT solution was added and the cells were further incubated for 4 h. Finally, the formazan crystals were dissolved in DMSO (100  $\mu\text{L}$  per well), and the absorbance value was measured at 540 nm using Tecan Infinite F200 Pro plate reader [20].

**2.12. Ultrapformance Liquid Chromatography Quadrupole Time-of-Flight Mass Spectrometry (UPLC-QTOF/MS) Analysis.** Phytochemical profiling in chloroform fractions of *M. concanensis* was conducted via ultrapformance liquid chromatography (UPLC-MS) analysis. The analysis was carried out using Waters ACQUITY ultrapformance LC system (Waters, Milford, MA, USA). Chromatographic separation of the respective extract was conducted using a selected column (ACQUITY UPLC HSS T3, 100 mm  $\times$  2.1 mm  $\times$  1.8 m, Waters, Manchester, UK) maintained at 40°C. The UPLC systems were connected to Vion IMS QTOF detector (Waters, Milford, MA, USA). The mobile phases used in the analysis were 0.1% formic acid (A) and acetonitrile (B). The composition of mobile phases was consisted of the following multistep linear gradient: 0 min, 1% B and 99% A; 0.5 min, 1% B and 99% A; 16.00 min, 35% B and 65% A; 18.00 min, 100% B and 0% A; and 20.00 min, 1% B and 99% A, respectively. The injection volume used for the sample was 1  $\mu\text{L}$  while the flow rate was set at 0.6 mL/min. The data were obtained from the UHPLC system coupled with Vion IMS QTOF hybrid mass spectrometer from waters, equipped with a LockSpray ion source. The ion source was operated in negative electrospray ionization (ESI) mode by applying specific conditions such as the capillary voltage at 1.50 kV, reference capillary voltage at 3.00 kV, source temperature at 120°C, desolvation gas temperature at 550°C, desolvation gas flow at 800 L/h, and cone gas flow at 50 L/h, respectively. Nitrogen (>99.5%) was used as desolvation and cone gas. Data were acquired in high-definition MSE (HDMSE) mode ranging between  $m/z$  50 and 1500 at 0.1 s/scan. Hence, two independent scans with different collision energies (CE) were alternatively obtained during the run: a low-energy (LE) scan at a fixed CE of 4 eV and a high-energy (HE) scan where the CE was ramped from 10 to 40 eV. Argon (99.999%) was used as collision-induced-dissociation (CID) gas. Data interpretation was carried out using Waters UNIFI Scientific Information System database. Resolved peaks were further identified with the assistance of reported values from previous literature and are shown in Table 1.

**2.13. Statistical Analysis.** All the data were represented as mean  $\pm$  SD. Statistical analyses were performed using GraphPad Prism version 5 with one-way ANOVA followed by Dunnett's test.  $p$  values < 0.05 were considered to be statistically significant.

### 3. Results and Discussion

**3.1. Total Phenolic and Flavonoid Contents.** It is well established that phenolic compounds from various plants are strongly associated with their biological properties.

TABLE 1: Compounds tentatively identified in the chloroform fraction from the methanol extract of *M. concanensis* bark using UPLC-QTOF/MS analysis.

Peak no.	Tentative identification	Elemental composition	Calculated m/z [M-H] <sup>-</sup>	Observed m/z [M-H] <sup>-</sup>	Retention time	References
1	Kaempferol-3- <i>O</i> -rutinoside	C <sub>27</sub> H <sub>30</sub> O <sub>15</sub>	593.1507	593.1512	6.65	[21]
2	Astragalin	C <sub>21</sub> H <sub>20</sub> O <sub>11</sub>	447.0927	447.0937	7.50	[21]
3	Quercetin-3- <i>O</i> -glucuronide	C <sub>21</sub> H <sub>18</sub> O <sub>13</sub>	477.0670	477.0685	7.83	—
4	Tetra- <i>O</i> -galloyl-glucoside	C <sub>34</sub> H <sub>28</sub> O <sub>22</sub>	787.0994	787.1005	8.11	—
5	Kaempferol-3- <i>O</i> -glucuronosyl methyl ester	C <sub>22</sub> H <sub>20</sub> O <sub>12</sub>	475.0876	475.0867	8.61	[21]
6	Isoquercetin	C <sub>21</sub> H <sub>20</sub> O <sub>12</sub>	463.0877	463.0884	8.63	[21]
7	Caffeic acid	C <sub>9</sub> H <sub>8</sub> O <sub>4</sub>	179.0344	179.0352	9.01	[21]
8	Hydroxy-methoxy-cinnamic acid	C <sub>10</sub> H <sub>10</sub> O <sub>4</sub>	193.0501	193.0511	9.38	—
9	Sinapic acid	C <sub>11</sub> H <sub>12</sub> O <sub>5</sub>	223.0607	223.0613	10.04	—
10	Kaempferol 3- <i>O</i> -arabinoside	C <sub>20</sub> H <sub>18</sub> O <sub>10</sub>	417.0822	417.0844	10.40	—
11	Secoisolariciresinol	C <sub>20</sub> H <sub>26</sub> O <sub>6</sub>	361.1651	361.1656	10.43	—
12	Kaempferol-3- <i>O</i> -rhamnoside	C <sub>21</sub> H <sub>20</sub> O <sub>10</sub>	431.0978	431.0995	10.91	[21]
13	Quercetin-3- <i>O</i> -glucuronide-methyl-ester	C <sub>22</sub> H <sub>20</sub> O <sub>13</sub>	491.0826	491.0842	10.99	—
14	Quercetin	C <sub>15</sub> H <sub>10</sub> O <sub>7</sub>	301.0348	301.0351	11.93	[21]
15	Eugenol	C <sub>10</sub> H <sub>12</sub> O <sub>2</sub>	163.0759	163.0765	12.47	[21]
16	Naringenin	C <sub>15</sub> H <sub>12</sub> O <sub>5</sub>	271.0607	271.0615	13.07	—
17	Trimethoxyflavone	C <sub>18</sub> H <sub>16</sub> O <sub>5</sub>	311.0920	311.0929	13.32	—
18	Demethoxycurcumin	C <sub>20</sub> H <sub>18</sub> O <sub>5</sub>	337.1076	337.1085	15.53	—
19	Sanleng acid	C <sub>18</sub> H <sub>34</sub> O <sub>5</sub>	329.2328	329.2339	15.62	[21]
20	Licoricone	C <sub>22</sub> H <sub>22</sub> O <sub>6</sub>	381.1338	381.1335	15.65	—

Hence, it would be worthwhile to determine the total phenolic and flavonoid contents in the plant extracts [10]. The total phenolic and flavonoid contents of methanol extract and its fractions of *M. concanensis* bark are presented in Table 2. The total phenolic ( $30.920 \pm 0.71$  mg GAE/g DW) and flavonoid ( $29.054 \pm 0.09$  mg QE/g DW) contents were found to be higher in the chloroform fraction followed by hexane fraction. Phenolic components are regarded as powerful antioxidants and act in redox-sensitive signaling cascades to prevent DNA damage [11].

Data expressed as mean  $\pm$  SD,  $n = 3$ . Data with different alphabet superscript letters show significant difference at  $p < 0.05$ , among different solvents, with multiple comparisons (one-way ANOVA, followed by Dunnett's test).

### 3.2. Antioxidant Activity of *M. concanensis* Bark Fractions

**3.2.1. Free Radical Scavenging Assay.** The free radical scavenging capacity of the crude methanol extract and other fractions of *M. concanensis* bark were determined using the DPPH assay, and the results are shown in Figure 1. All the samples exhibited varying degrees of concentration-dependent DPPH radical scavenging activity. In that, the chloroform fraction showed the strongest DPPH radical scavenging activity with the IC<sub>50</sub> value of  $6.616 \pm 1.90$   $\mu\text{g mL}^{-1}$  followed by ethyl acetate fraction (IC<sub>50</sub> =  $13.4 \pm 2.22$   $\mu\text{g mL}^{-1}$ ) which is comparable to the positive control, ascorbic acid (AA). Gori et al. [22] revealed the photoprotective effect of 11 medicinal plants *Atalantia ceylanica* (Arn.) Oliv, *Argyrea populifolia* Choisy, *Hibiscus furcatus* Roxb. ex DC, *Ipomoea mauritiana* Jacq, *Lasia spinosa* (L.) Thw, *Leucas zeylanica* (L.) W.T.Aiton, *Olex zeylanica* Wall., *Ophiorrhiza mungo* Linn., *Plectranthus*

TABLE 2: Total phenolic and flavonoid contents of the methanol extract and its fractions from the bark of *M. concanensis*.

Fractions	Total phenolics mg GAE/g DW	Total flavonoids mg QE/g DW
Methanol	$9.858 \pm 0.036^d$	$3.655 \pm 0.061^d$
Hexane	$14.306 \pm 0.073^b$	$9.089 \pm 0.193^b$
Chloroform	$30.920 \pm 0.717^a$	$29.054 \pm 0.099^a$
Ethyl acetate	$12.154 \pm 0.158^c$	$4.055 \pm 0.056^c$

*amboinicus* (Lour.), and *Mollugo cerviana* (L.) Ser. where the plant that showed high SPF values is closely related to its antioxidant properties. Numerous studies also suggested that the plant fraction which shows high free scavenging properties offers significant protection towards UV-induced damage [16, 22].

### 3.3. Protective Effect of the *M. concanensis* Fractions against UV

**3.3.1. Sunscreen Protection Factor (SPF) Value.** SPF value refers to the efficacy of test samples that protects the development of UV radiation-induced erythema [23]. It is a measure of UVB protection offered by sunscreen products. As the value increases, the percentage of UVB protection increases. As shown in Table 3, at the concentration of  $200$   $\mu\text{g mL}^{-1}$ , the chloroform fraction of *M. concanensis* bark exhibited the highest SPF value ( $10.50 \pm 0.23$  with  $>87\%$  of UVB protection) compared to the other fractions such as ethyl acetate and hexane. The SPF value of the most active ingredient epigallocatechin gallate (EGCG) from *Camellia sinensis* (Green

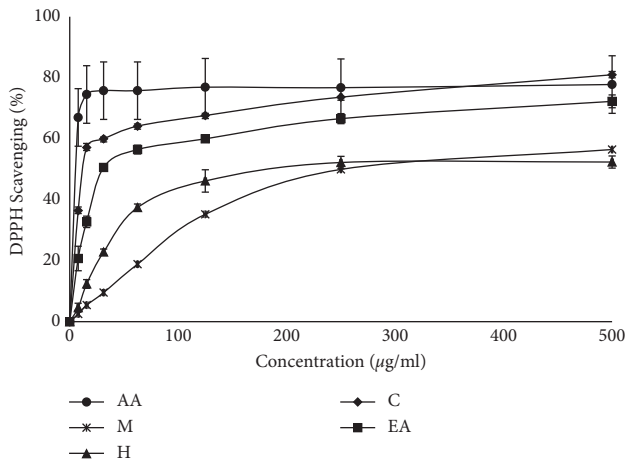


FIGURE 1: DPPH radical scavenging activity of the methanol extract and its fractions from the bark of *M. concanensis*. AA, ascorbic acid; M, methanol extract; H, hexane extract; C, chloroform extract; EA, ethyl acetate extract. ( $n = 3$ ).

TABLE 3: The sun protection factor (SPF) value and UVB protection effect of the methanol extract and its fractions from the bark of *M. concanensis*.

Samples ( $200 \mu\text{gml}^{-1}$ )	SPF value	UVB protection (%)
Methanol	$4.37 \pm 0.17^{***}$	>75
Hexane	$5.49 \pm 0.01^{***}$	>75
Chloroform	$10.50 \pm 0.23^{ns}$	>87
Ethyl acetate	$5.18 \pm 0.01^{***}$	>75
Epigallocatechin gallate	$10.34 \pm 0.21$	>87

Data are expressed as mean  $\pm$  SD,  $n = 3$ . Data represent a significant difference at (\*\*\*)  $p$  value < 0.05, among different solvent fractions compared with the positive control (EGCG), using one-way ANOVA, followed by Dunnett's test.

Tea) is  $10.34 \pm 0.21$ , which is almost like the SPF value of the chloroform fraction of *M. concanensis* bark. The literature revealed that the seed oil from *M. concanensis* could be a good candidate for sunscreen formulation [24]. The bark extract of medicinal plants such as *Curatella americana* L and *Amburana cearensis* (Allemão) A.C. Sm. showed SPF values 14.74 and 12.21 at  $0.2 \text{ mgmL}^{-1}$  which is suggested to be the promising source of future skin care products [25]. Similarly, the bark extract of *M. concanensis* could also be utilized as one of the encouraging ingredients in natural product sunscreen formulation.

**3.3.2. UV Absorption Spectra.** UV absorption spectra of various solvent fractions of *M. concanensis* and the positive control EGCG are shown in Figure 2. The results showed that all the fractions of *M. concanensis* have a wide range of UV absorption; however, among the other fractions, the chloroform fraction of *M. concanensis* showed a broad spectrum of UV absorption which covers UVA (320–400 nm), UVB (280–320 nm), and also UVC (200–280 nm). The positive control EGCG showed the absorption under the UVB range only. Similar patterns of results were observed in the active fraction of *Zanthoxylum rhetsa* (Roxb.) DC. bark extract which is suggested to be utilized in broad-spectrum sunscreen

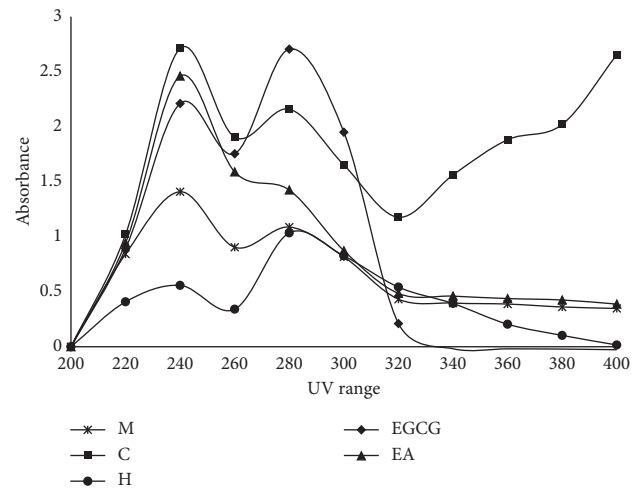


FIGURE 2: UV absorption spectra of the methanol extract and its fractions from the bark of *M. concanensis*. M, methanol extract; C, chloroform extract; H, hexane extract; EGCG, epigallocatechin gallate; EA, ethyl acetate extract ( $n = 3$ ).

formulations [6]. Compared to the active fraction of *Z. rhetsa*, the UV absorption spectra of *M. concanensis* bark are high. At present, several studies and regulatory bodies recommend using broad-spectrum natural sunscreen to prevent the damages such as wrinkling and sunburns induced by both UVA and UVB, respectively [26]. The results revealed that the chloroform fraction of *M. concanensis* bark could be an optional ingredient to be used in a natural broad-spectrum sunscreen formulation.

**3.4. Gelatin Digestion Assay.** Collagenases are one of the important matrix metalloproteinases responsible for the breakdown of collagen present in the skin layers. Studies revealed that continuous exposure of UV radiation could increase the level of collagenases that might damage the matrix proteins and cause wrinkle formation as well as lead to premature aging [27]. The collagenase inhibitory activity of extract and various solvent fractions of *M. concanensis* are presented in Table 4. Compared to the extract and other fractions, the chloroform fraction showed appreciable collagenase inhibitory activity of 50% at the concentration of  $200 \mu\text{gml}^{-1}$  which is comparable to that of EGCG. However, the hexane and ethyl acetate fractions exhibited a weaker collagenase inhibition activity. Studies revealed that various parts of medicinal plants such as leaves extracts (methanol) of *Aegle marmelos* (L.) Correa, *Acalypha indica* Linn, *Calotropis gigantea* (L.) W.T. Aiton, *Nerium oleander* L., and *Nyctanthes arbor-tristis* Linn and a rhizome extract of *Acorus calamus*. Linn at the concentration of  $1 \text{ mgmL}^{-1}$  showed 50% collagenase inhibitory activity [28], whereas the ethyl acetate fraction of the bark extract of *Z. rhetsa* showed 50% collagenase inhibition at the concentration of  $500 \mu\text{gml}^{-1}$  [6].

**3.5. Antielastase.** Elastase is a serine protease, responsible for the breakdown of elastin, an important protein responsible for skin elasticity [29]. The inhibitory activity of



TABLE 4: Gelatin digestion activity of the methanol extract and its fractions from the bark of *M. concanensis*.

Samples (200 $\mu\text{g mL}^{-1}$ )	Zone inhibition (mm)	Enzyme inhibition (%)
Control	20 $\pm$ 0.81	0
EGCG	10 $\pm$ 0.47***	50
Chloroform	10 $\pm$ 1.24***	50
Hexane	16 $\pm$ 0.47***	20
Ethyl acetate	16 $\pm$ 0.47***	20
Methanol	18 $\pm$ 0.81	10

Data are expressed as mean  $\pm$  SD,  $n = 3$ . Data represent significant differences at (\*\*\*)  $p$  value  $< 0.05$ , among different solvent fractions compared with negative control (water), using one-way ANOVA, followed by Dunnett's test.

methanol extract and its fractions of *M. concanensis* on elastase enzyme were examined. Figure 3 and Table 5 show the effect of methanol extract and its fractions of *M. concanensis* bark against elastase enzyme activity. Among different fractions tested, the chloroform fraction exhibited remarkable elastase inhibition activity with the  $\text{IC}_{50}$  value of  $2.957 \pm 1.23 \mu\text{g mL}^{-1}$  than the standard EGCG ( $\text{IC}_{50}$ - $39.32 \pm 1.41 \mu\text{g mL}^{-1}$ ). These findings demonstrated that chloroform fraction of *M. concanensis* may have antiaging potentials by inhibiting elastase enzyme production and delaying the degradation of elastin fibers. Researchers suggested that the plant fraction that is rich in phenolics and flavonoids is reported to possess significant antielastase activity. The ethyl acetate fraction of *Garcinia daedalanthera* Pierre. stem bark extract possesses 43.96  $\pm$  12.53% elastase inhibitory effect at the concentration of 100 ppm [30]. In this study, the chloroform fraction of *M. concanensis* bark exhibited  $>50\%$  of elastase inhibitory effect at the concentration of  $31.25 \mu\text{g mL}^{-1}$ .

### 3.6. Cytotoxicity of *M. concanensis* Fractions in Cell Culture (3T3-L1 Cell Lines)

**3.6.1. MTT Assay.** Cytotoxic effect of various solvent fractions of *M. concanensis* was tested in 3T3-L1 cells with a wide range of concentration (0–500  $\mu\text{g mL}^{-1}$ ). Results revealed that all the fractions of *M. concanensis* bark except the chloroform fraction were nontoxic to the cells up to 250  $\mu\text{g mL}^{-1}$ . However, the chloroform fraction of *M. concanensis* was toxic to the cells at the concentration  $>25 \mu\text{g mL}^{-1}$ , where it showed the strongest cytotoxic activity against 3T3-L1 cells by reducing the cell viability to 16.5% at the concentration of 62.5  $\mu\text{g mL}^{-1}$ , Figure 4. This is the first study to reveal the cytotoxic effect of various solvent fractions of *M. concanensis* bark against the preadipocyte cells. Previously, the ethanol extract of the leaves of *M. concanensis* was also reported to be nontoxic to 3T3-L1 adipocytes up to 100  $\mu\text{g mL}^{-1}$  until 24 h of treatment [15]. Balamurugan et al. [31] tested the crude ethanol extract of *M. concanensis* leaves and bark against HepG2 cell lines and revealed that both parts of *M. concanensis* strongly inhibit the growth of cancerous cells in a dose-dependent manner. In another study, the methanolic root bark extract of *M. concanensis* was found to be toxic against HepG2 cells,

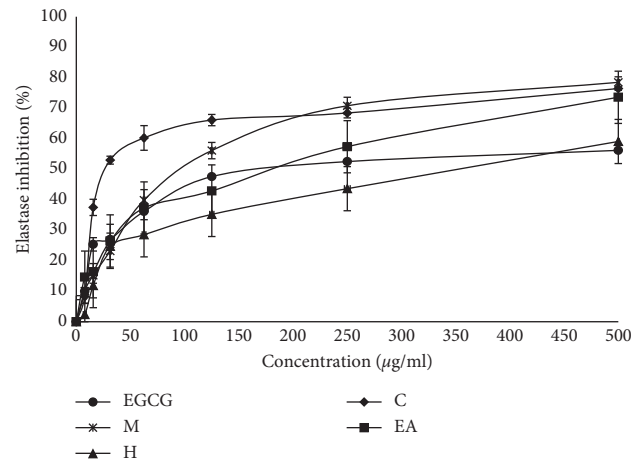


FIGURE 3: Antielastase activity of the methanol extract and its fractions from the bark of *M. concanensis*. Data are expressed as mean  $\pm$  SD,  $n = 3$ .

TABLE 5:  $\text{IC}_{50}$  values of elastase inhibition activity of the methanol extract and its fractions from the bark of *M. concanensis*.

Samples	$\text{IC}_{50}$ ( $\mu\text{g mL}^{-1}$ )
EGCG	39.32 $\pm$ 1.41
Methanol	88.53 $\pm$ 1.95**
Hexane	78.11 $\pm$ 1.72*
Chloroform	2.957 $\pm$ 1.23**
Ethyl acetate	176.7 $\pm$ 2.20***

Data expressed as mean  $\pm$  SD,  $n = 3$ . Data represent significant differences at  $p$  value  $< 0.05$ , among different solvent fractions compared with the positive control (EGCG), using one-way ANOVA, followed by Dunnett's test.

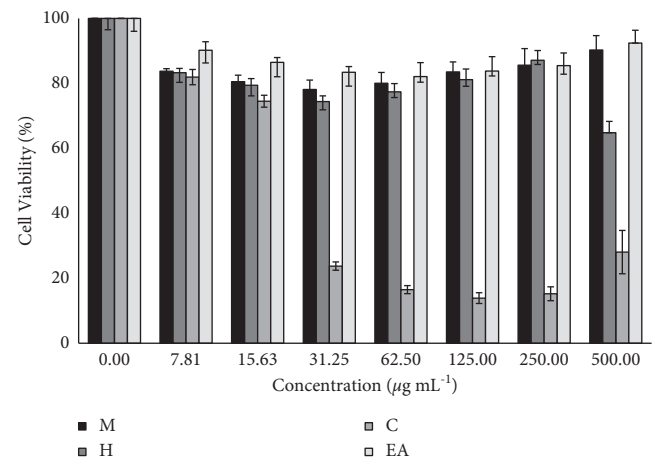


FIGURE 4: Cytotoxic effect of the methanol extract and various solvent fractions of *M. concanensis* bark treated with 3T3 mouse fibroblasts for 24 h data expressed as mean  $\pm$  SD,  $n = 3$ .

whereas it does not induce toxic effect against A549 and HT-29 cell line which demonstrates its selective cytotoxicity [21]. In this study, the crude methanol extract of *M. concanensis* bark does not induce any toxicity against 3T3-L1 cells up to 500  $\mu\text{g mL}^{-1}$ . Since the other solvent fractions of *M. concanensis* bark have toxic effect  $>250 \mu\text{g mL}^{-1}$  and the chloroform fraction has toxic effect  $>25 \mu\text{g mL}^{-1}$ , on an average, we reduced

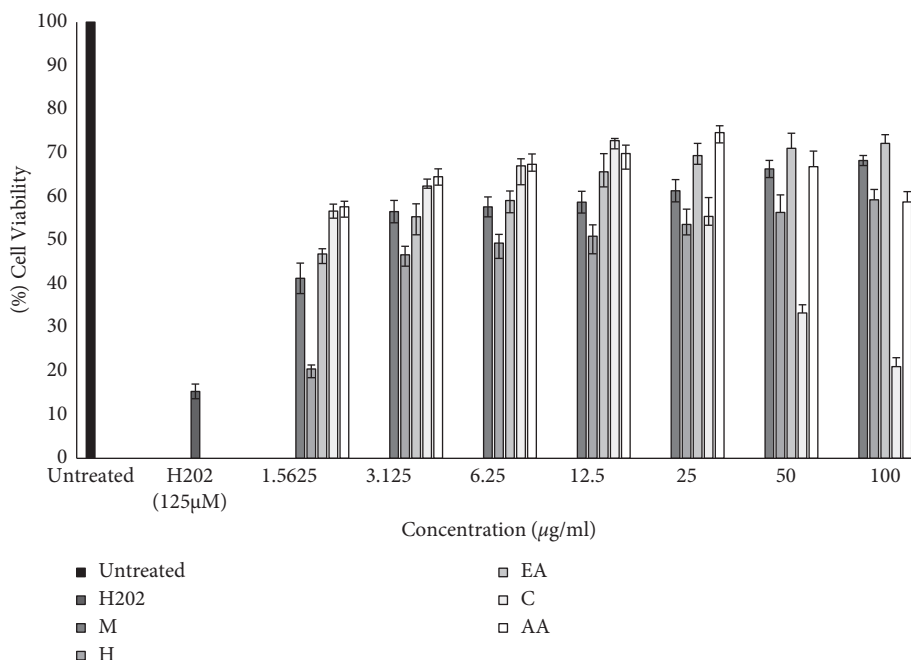


FIGURE 5: Protective effect of various solvent fractions of *M. concanensis* bark against  $H_2O_2$ -induced oxidative damage in 3T3-L1 cells treated for 24 h. Data are expressed as mean  $\pm$  SD,  $n = 3$ . Data represent significant difference at  $p$  value  $< 0.05$ , among different solvent fractions of *M. concanensis* bark (various concentrations) compared with the  $H_2O_2$  ( $125 \mu M$ ), using one-way ANOVA, followed by Dunnett's test.

the concentration range of all the extracts/fractions to  $0\text{--}100 \mu g mL^{-1}$  for further assay.

**3.6.2.  $H_2O_2$ -Induced Damage.** The protective effect of various solvent fractions of *M. concanensis* bark against  $H_2O_2$ -induced oxidative damage in 3T3-L1 was determined and shown in Figure 5. From the results, it has been clear that the  $H_2O_2$  ( $125 \mu M$ ) reduced the viability of cells to 15.35% after 6 h of treatment, whereas the cells pretreated with various solvent fractions of *M. concanensis* bark prevented the cells from oxidative damage. However, the level of protection by each fraction varies and it depends on the concentration and constituents present in each sample. The chloroform fraction of *M. concanensis* bark offers significant protection against  $H_2O_2$ -induced damage even at low concentration, where the viability of cells treated with  $1.56 \mu g mL^{-1}$  protects 56% of cells which was comparable to that of positive control, AA (cell viability—57%). As the concentration increases, up to  $12.5 \mu g mL^{-1}$ , the chloroform fraction prevented the cells up to 72% where AA prevented up to 69%. However, at the concentration of  $25 \mu g mL^{-1}$  and above, the viability of cells treated with chloroform fraction got drastically reduced. This might be due to the overdose of chemical constituents present in it. Similar patterns of results were obtained in the cytotoxicity assay, and at low concentration ( $<15 \mu g mL^{-1}$ ), the chloroform fraction was nontoxic to 3T3-L1 cells. As the concentration increases, the chloroform fraction is toxic. As reported, the extracts and fractions of various parts of *M. concanensis* are cytotoxic to different cancer cell lines like HepG2 [31, 32], and the chloroform fraction of *M. concanensis* bark could offer a significant cytotoxic effect

in other cancerous cell lines. Further research is needed to evaluate the selective cytotoxic effect of chloroform fraction of *M. concanensis* bark.

From this study, it has been evident that compared to other fractions, the chloroform fraction of *M. concanensis* bark has a high sunscreen protection factor value, broad-spectrum UV absorption, appreciable DPPH scavenging, anticollagenase, antielastase, high phenolic, and high flavonoid content. Additionally, it also prevents the  $H_2O_2$ -induced oxidative damage in 3T3-L1 cells which was comparable to that of positive control, AA.

**3.7. UPLC-QTOF/MS Analysis.** From this study, it has been identified that the chloroform fraction is the bioactive fraction of *M. concanensis* bark. UPLC-QTOF/MS analysis was found to be a convenient method to determine the presence of possible phytoconstituents in the studied fraction through the exact mass detection. Polyphenolic compounds such as phenolic acids and flavonoids are naturally abundant and commonly found in the genus *Moringa*. Bioactive flavonoids such as quercetin, hyperoside, astragalin, isoquercetin, kaempferol-3-*O*-rutinoside, and rutin were reported previously in this genus especially in the species, *Moringa oleifera* [20]. In this study, 20 different phytoconstituents were identified in the chloroform fraction obtained from the methanol extract of *M. concanensis* bark using UPLC-QTOF/MS analysis, Table 1. The result indicated that the chloroform fraction contains a complex mixture of bioactive tentative annotated phenolics such as kaempferol-3-*O*-rutinoside, astragalin, quercetin-3-*O*-glucuronide, kaempferol 3-*O*-glucuronopyranosyl methyl ester, isoquercetin, kaempferol-

3-*O*-arabinoside, kaempferol-3-*O*-rhamnoside, quercetin-3-*O*-glucuronide-methyl ester, eugenol, quercetin, and caffeic acid. The assignments were carried out on a prediction basis and detailed phytochemistry studies required to be carried out on this species for the affirmation of the presence of the predicted metabolites in the studied fraction/extract in the future. This comprehensive phytochemical profiling analysis has revealed the structural diversity of phenolics and their similar structural patterns as well as the biological potency of the studied fractions.

Moreover, the findings are in agreement with the results obtained from the total phenolic and total flavonoids evaluation conducted on the respective fractions. The existence of flavonoids, especially flavonols, could possibly be the main contributors to photoprotective properties especially in collagenase and elastase inhibitory activities through a synergistic effect [33]. Furthermore, the presence of carbonyl and hydroxyl moieties in the main scaffold of the flavonols might be played the role in giving the inhibitory effects which allow them to bind to metalloenzymes like collagenase and elastase that could alter or inhibit metabolic pathways [34]. However, further studies are required in relation to the detailed identification and isolation of bioactive metabolites from the bark of *M. concanensis* as well as molecular mechanisms of their photoprotective potentials.

#### 4. Conclusion

In summary, the result obtained from the phytochemical analysis showed that chloroform fractions of *M. concanensis* have the highest DPPH, TPC, and TFC values. The photoprotective study also demonstrated a high SPF value for chloroform fractions and gave the same UVB protection as its positive control, EGCG. Besides that, the chloroform fractions have a much broader spectrum of UV absorption that covers both UVA and UVB when compared to others. The inhibitory effect of *M. concanensis* chloroform fractions towards elastase and collagenase proved that the plant extract has potential biological properties that can reduce the breakdown of collagen and elastin within the skin. *In vitro* study showed that some of the fractions possessed low cytotoxicity towards the 3T3-L1 cell line even at higher concentrations (methanol, hexane, and ethyl acetate). However, chloroform fractions obtained from the plant extract exhibit high cytotoxic activity even at lower concentrations (ranging from 31.25 to 500  $\mu\text{g mL}^{-1}$ ). All the fractions displayed protective effect against  $\text{H}_2\text{O}_2$ -induced oxidative damage in 3T3-L1 cells, with methanol, hexane, and ethyl acetate having a higher cell viability percentage even at higher concentrations (50 and 100  $\mu\text{g mL}^{-1}$ ). Various metabolites especially bioactive flavonols that were tentatively identified using UPLC-QTOF/MS analysis might be the source for the high photoprotective activity. Based on these results, *M. concanensis* has the potential to be a new applicant as an active component in pharmaceutical and cosmetics formulation. However, detailed preclinical research is needed to demonstrate the individual or synergistic effect of the bioactive components involved in the photoprotective mechanism of *M. concanensis*.

#### Data Availability

Data used to support the findings of this study are obtained from the corresponding author.

#### Conflicts of Interest

The authors declare that there are no conflicts of interest.

#### Authors' Contributions

R.S., K.S., and T.K. conceptualized the study; R.S. was responsible for methodology; W.I.W.I., R.S., and T.K. validated the data; M.F.Z., R.S., and T.K. performed formal analysis and investigation; A.V. was responsible for resources; R.S., M.F.Z., and G.K.M. performed experiments; R.S., K.S., T.K., M.F.Z., and V.S. prepared the original draft and reviewed and edited the manuscript; R.S. and W.I.W.I. supervised the study and were responsible for funding acquisition; all authors have read and agreed to the published version of the manuscript.

#### Acknowledgments

The authors would like to thank Universiti Malaysia Terengganu and Universiti Sains Malaysia for the facilities provided. This research was funded by Universiti Malaysia Terengganu, Malaysia, under the Talent and Publication Enhancement Research Grant (TAPE-RG) scheme. Vote Number: 55256.

#### References

- [1] A. Verma, H. N. Kushwaha, A. K. Srivastava et al., "Piperine attenuates UV-R induced cell damage in human keratinocytes via NF- $\kappa$ B, Bax/Bcl-2 pathway: an application for photoprotection," *Journal of Photochemistry and Photobiology B: Biology*, vol. 172, pp. 139–148, 2017.
- [2] Y.-S. Wang, S.-S. Zhou, C.-Y. Shen, and J.-G. Jiang, "Isolation and identification of four antioxidants from *Rhodiola crenulata* and evaluation of their UV photoprotection capacity *in vitro*," *Journal of Functional Foods*, vol. 66, Article ID 103825, 2020.
- [3] M. Radice, S. Manfredini, P. Ziosi et al., "Herbal extracts, lichens and biomolecules as natural photo-protection alternatives to synthetic UV filters. A systematic review," *Fito-terapia*, vol. 114, pp. 144–162, 2016.
- [4] G. Schneider, F. L. Figueroa, J. Vega et al., "Photoprotection properties of marine photosynthetic organisms grown in high ultraviolet exposure areas: cosmeceutical applications," *Algal Research*, vol. 49, Article ID 101956, 2020.
- [5] H. Sies, "Nutritional protection against skin damage from sunlight," *Oncology Research Featuring Preclinical and Clinical Cancer Therapeutics*, vol. 15, pp. 462–463, 2006.
- [6] R. K. Santhanam, S. Fakurazi, S. Ahmad et al., "Inhibition of UVB-induced pro-inflammatory cytokines and MMP expression by *Zanthoxylum rhetsa* bark extract and its active constituent hesperidin," *Phytotherapy Research*, vol. 32, no. 8, pp. 1608–1616, 2018.
- [7] A. Kammeyer and R. M. Luiten, "Oxidation events and skin aging," *Ageing Research Reviews*, vol. 21, pp. 16–29, 2015.

- [8] M. D. Mota, A. N. da Boa Morte, L. C. R. C. e. Silva, and F. A. Chinalia, "Sunscreen protection factor enhancement through supplementation with Rambutan (*Nephelium lappaceum* L) ethanolic extract," *Journal of Photochemistry and Photobiology B: Biology*, vol. 205, Article ID 111837, 2020.
- [9] N. Saewan and A. Jimtaisong, "Natural products as photoprotection," *Journal of Cosmetic Dermatology*, vol. 14, no. 1, pp. 47–63, 2015.
- [10] D. Lin, M. Xiao, J. Zhao et al., "An overview of plant phenolic compounds and their importance in human nutrition and management of type 2 diabetes," *Molecules*, vol. 21, no. 10, Article ID 1374, 2016.
- [11] Y. C. Boo, "Can plant phenolic compounds protect the skin from airborne particulate matter?" *Antioxidants*, vol. 8, no. 9, p. 379, 2019.
- [12] V. Ravichandran, G. Arunachalam, N. Subramanian, and B. Suresh, "Pharmacognostical and phytochemical investigations of *Moringa concanensis* (Moringaceae) an ethnomedicine of Nilgiris," *Journal of Pharmacognosy and Phytotherapy*, vol. 1, pp. 76–81, 2009.
- [13] M. Manzoor, F. Anwar, T. Iqbal, and M. I. Bhangar, "Physico-chemical characterization of *Moringa concanensis* seeds and seed oil," *Journal of the American Oil Chemists' Society*, vol. 84, no. 5, pp. 413–419, 2007.
- [14] S. Anbazhakan, R. Dhandapani, P. Anandhakumar, and S. Balu, "Traditional medicinal knowledge on *Moringa concanensis* Nimmo of perambalur district, tamilnadu," *Ancient Science of Life*, vol. 26, pp. 42–45, 2007.
- [15] B. B. Balakrishnan, K. Krishnasamy, and K. C. Choi, "*Moringa concanensis* Nimmo ameliorates hyperglycemia in 3T3-L1 adipocytes by upregulating PPAR-gamma, C/EBP alpha via Akt signaling pathway and STZ- induced diabetic rats," *Biomedicine & Pharmacotherapy*, vol. 103, pp. 719–728, 2018.
- [16] R. Santhanam, S. Ahmad, F. Abas, I. S. Ismail, Y. Rukayadi, and K. Shaari, "Photoprotective properties of *Zanthoxylum rhetsa*: an in vitro analysis," *Journal of Chemical and Pharmaceutical Research*, vol. 5, pp. 1512–1520, 2013.
- [17] C. Wang, X. Gao, R. K. Santhanam et al., "Effects of polysaccharides from *Inonotus obliquus* and its chromium (III) complex on advanced glycation end-products formation,  $\alpha$ -amylase,  $\alpha$ -glucosidase activity and H<sub>2</sub>O<sub>2</sub>-induced oxidative damage in hepatic L02 cells," *Food and Chemical Toxicology*, vol. 116, pp. 335–345, 2018.
- [18] S. Raseetha, M. F. Zulkifli, M. Nurul-Nabilah, W. I. W. Ismail, and L. Jayasinghe, "Inhibition of lipid accumulation in 3T3-L1 adipocytes by chlorogenic acid derived from green coffee (*Robusta* sp.) beans and pulps," *Malaysian Applied Biology*, vol. 46, pp. 163–170, 2017.
- [19] W. Chen, Y. Liu, G. Xue, L. Zhang, and S. Shao, "Diazoxide protects L6 skeletal myoblasts from H<sub>2</sub>O<sub>2</sub>-induced apoptosis via the phosphatidylinositol-3 kinase/Akt pathway," *Inflammation Research*, vol. 65, pp. 53–60, 2016.
- [20] H. Lin, H. Zhu, J. Tan et al., "Comparative analysis of chemical constituents of *Moringa oleifera* leaves from China and India by ultra-performance liquid chromatography coupled with quadrupole-time-of-flight mass spectrometry," *Molecules*, vol. 24, no. 5, p. 942, 2019.
- [21] M. Vijayarajan and R.-M. Pandian, "Cytotoxicity of methanol and acetone root bark extracts of *Moringa concanensis* against A549, hep-G2 and HT-29 cell lines," *J. Acad. ind. Res.*, vol. 5, pp. 45–49, 2016.
- [22] A. Gori, C. Brunetti, L. B. dos Santos Nascimento et al., "Photoprotective role of photosynthetic and non-photosynthetic pigments in *Phillyrea latifolia*: is their "Antioxidant" function prominent in leaves exposed to severe summer drought?" *International Journal of Molecular Sciences*, vol. 22, no. 15, p. 8303, 2021.
- [23] K. Geoffrey, A. N. Mwangi, and S. M. Maru, "Sunscreen products: rationale for use, formulation development and regulatory considerations," *Saudi Pharmaceutical Journal*, vol. 27, no. 7, pp. 1009–1018, 2019.
- [24] S. Kale, G. Gajbhiye, and N. Chaudhari, "Determination and comparison of in vitro SPF of topical formulation containing lutein ester from Formulation and in- vitro Evaluation of *Moringa concanensis*, Nimmo. Seed Oils Sunscreen Cream," *Int. J. Pharmtech Res*, vol. 2, pp. 2060–2062, 2010.
- [25] A. R. Nunes, A. L. M. Rodrigues, D. B. de Queiróz et al., "Photoprotective potential of medicinal plants from Cerrado biome (Brazil) in relation to phenolic content and antioxidant activity," *Journal of Photochemistry and Photobiology B: Biology*, vol. 189, pp. 119–123, 2018.
- [26] N. Lionetti and L. Rigano, "The new sunscreens among formulation strategy, stability issues, changing norms, safety and efficacy evaluations," *Cosmetics*, vol. 4, no. 2, p. 15, 2017.
- [27] K. Maeda, "Analysis of ultraviolet radiation wavelengths causing hardening and reduced elasticity of collagen gels in vitro," *Cosmetics*, vol. 5, no. 1, p. 14, 2018.
- [28] S. Iswarya, N. Radhakrishnan, V. Kavitha, A. B. Mandal, and A. Gnanamani, "Collagenase inhibition activity of Indian medicinal plants: an approach to moderate collagen turnover," *International Journal of Bioassays*, vol. 3, pp. 2075–2078, 2014.
- [29] T. S. Thring, P. Hili, and D. P. Naughton, "Anti-collagenase, anti-elastase and anti-oxidant activities of extracts from 21 plants," *BMC Complementary and Alternative Medicine*, vol. 9, no. 1, p. 27, 2009.
- [30] N. S. S. Ambarwati, B. Elya, Y. Desmiaty, and H. Omar, "Anti-elastase of leaves and stem bark extract of *Garcinia daedalanthera* Pierre," *International Journal of Pharma Sciences and Research*, vol. 12, pp. 592–596, 2020.
- [31] V. Balamurugan, V. Balakrishnan, P. J. Robinson, and M. Ramakrishnan, "Anti-cancer and apoptosis-inducing effects of *Moringa concanensis* using hepG2 cell lines," *Bangladesh Journal of Pharmacology*, vol. 9, pp. 604–609, 2014.
- [32] D. Sivakumar, R. Manikandan, and P. Velu, "Antimicrobial activity of *Moringa concanensis* flower against human pathogens and its cytotoxic effects on HepG2 cell Line," *Research Journal of Microbiology*, vol. 15, pp. 51–60, 2020.
- [33] B. Y. Sin and H. P. Kim, "Inhibition of collagenase by naturally-occurring flavonoids," *Archives of Pharmacal Research*, vol. 28, no. 10, pp. 1152–1155, 2005.
- [34] N. Ł. Zofia, Z. D. Martyna, Z. Aleksandra, and B. Tomasz, "Comparison of the antiaging and protective properties of plants from the Apiaceae family," *Oxidative Medicine and Cellular Longevity*, vol. 2020, Article ID 5307614, 2020.

## Research Article

# Systematic Elaboration of the Pharmacological Targets and Potential Mechanisms of ZhiKe GanCao Decoction for Preventing and Delaying Intervertebral Disc Degeneration

Wanqing Sun <sup>1</sup>, Yuan Chen <sup>2</sup>, and Miao Li <sup>3,4</sup>

<sup>1</sup>Third Intenal Department, Hunan Rehabilitation Hospital, Hunan, China

<sup>2</sup>The Maternal and Child Health of Liu Yang, Hunan Province, China

<sup>3</sup>Department of Pediatric Orthopedics, Hunan Children's Hospital, Changsha 410007, China

<sup>4</sup>The School of Pediatrics, Hengyang Medical School, University of South China, Changsha 410007, China

Correspondence should be addressed to Miao Li; miaoli2022@163.com

Received 12 December 2021; Accepted 15 March 2022; Published 22 April 2022

Academic Editor: Jelena Zivkovic

Copyright © 2022 Wanqing Sun et al. This is an open access article distributed under the Creative Commons Attribution License, which permits unrestricted use, distribution, and reproduction in any medium, provided the original work is properly cited.

**Background.** ZhiKe GanCao Decoction (ZKGCD) is a commonly used traditional Chinese medicine in the clinical treatment of intervertebral disc degeneration (IDD). However, its active ingredients and mechanism of action remain unclear. This study aims to propose the systematic mechanism of ZKGCD action on IDD based on network pharmacology, molecular docking, and enrichment analysis. **Methods.** Firstly, the common target genes between ZKGCD and IDD were identified through relevant databases. Secondly, the protein-protein interaction (PPI) network of common genes was constructed and further analyzed to determine the core active ingredients and key genes. Thirdly, gene ontology (GO) and Kyoto Encyclopedia of Genes and Genomes (KEGG) enrichment analysis of common genes were performed. Finally, the stability of the binding between core active ingredients and key genes was verified by molecular docking analysis. **Results.** “Intersecting genes-active components” network consists of 154 active ingredients and 133 common genes. The ten key genes are AKT1, TNF, IL6, TP53, IL1B, JUN, CASP3, STAT3, MMP9, and MAPK3. Meanwhile, quercetin (Mol000098), luteolin (Mol000006), and kaempferol (Mol000422) are the most important core active ingredients. The main signal pathways selected by KEGG enrichment analysis includes AGE-RAGE signaling pathway in diabetic complications (hsa04933), TNF signaling pathway (hsa04668), IL-17 signaling pathway (hsa04657), cellular senescence (hsa04218), apoptosis (hsa04210), and PI3K-Akt signaling pathway (hsa04151), which are mainly involved in inflammation, apoptosis, senescence, and autophagy. **Conclusion.** This study provides a basis for further elucidating the mechanism of action of ZKGCD in the treatment of IDD and offers a new perspective on the conversion of the active ingredient in ZKGCD into new drugs for treating IDD.

## 1. Introduction

Low back pain (LBP) is one of the most common global health problems, and it has been younger in recent years [1]. According to the Global Burden of Diseases Survey, LBP ranks among the top causes of disability [2, 3]. Intervertebral disc degeneration (IDD) is the most significant factor in LBP patients (40%) [4]. The vast majority of studies have suggested that LBP caused by IDD may be closely related to local inflammatory, but the specific mechanism is not yet fully understood [5, 6]. Therefore, the current pretreatment of

IDD is still based on a single symptomatic treatment, and the main clinical drugs used are nonsteroidal anti-inflammatory drugs (NSAIDs) [7, 8]. There is a lack of effective noninvasive methods to control, slow down, and reverse the progression of IDD.

Traditional Chinese medicine (TCM) has been used for thousands of years in Eastern countries and is widely used to treat various diseases [9, 10]. In recent years, an increasing number of scholars have advocated a novel treatment method combining TCM and Western medicine. ZhiKe GanCao Decoction (ZKGCD) is a classic empirical formula

for the treatment of IDD, which was developed by Professor Gong Zhengfeng with his years of clinical experience [11]. Professor Gong Zhengfeng is one of China’s leading traditional Chinese medicine practitioners and has received many national honors. ZKGCD is mainly composed of *Aurantii Fructus* (Pinyin: ZhiKe (ZK)), *Licorice* (Pinyin: GanCao (GC)), *Angelicae Sinensis Radix* (Pinyin: DangGui (DG)), *Radix Salvia* (DanShen (DS)), *Sparganii rhizome* (Pinyin: SanLeng (SL)), *Curcumae rhizome* (Ezhu (EZ)), *Semen Pharbitidis* (Pinyin: QianNiuZi (QNZ)) (Table 1). The main effect of this formula is to invigorate blood circulation and remove blood stasis, which can alleviate the patient’s pain by improving the local microenvironment of the herniation and the nerve root [11]. Currently, ZKGCD is mainly used by TCM practitioners to treat cervical and lumbar spine disorders and skeletal muscle disorders associated with inflammation [12–15]. However, the specific mechanism of action has not been elucidated and verified. Then, TCM is characterized by multiple components, multiple targets, and multiple mechanisms, which limited the elucidation of specific therapeutic mechanisms.

The emergence of network pharmacology presents a new opportunity. Recent studies have confirmed that network pharmacology has good predictive performance in the study of different drug-disease interactions [16–19]. Network pharmacology is mainly used to explain the relationship among herbs, compounds, targets, signaling pathways, and diseases with a specific approach. Currently, network pharmacology has been successfully applied to study the relationship between herbal medicines and skeletal muscle diseases and to demonstrate the complex mechanisms of TCM diseases based on multiple compounds, multiple targets, and multiple pathways. In addition, gene ontology (GO) and Kyoto Encyclopedia of Genes and Genomes (KEGG) analysis combined with network pharmacology may provide more valuable and complementary information, thus further improving the predictive performance of potentially effective mechanisms.

This study aimed to explore the main active ingredients, potential targets, and signaling pathways of ZKGCD for the treatment of IDD based on the network pharmacology approach and to provide theoretical support for clinical practice. In addition, the reliability of the results was further confirmed by molecular docking. Figure 1 illustrates the detailed workflow of this study.

## 2. Methods

**2.1. Selection of Intersecting Genes for ZKGCD and IDD Target Genes.** The formula of this study is ZKGCD, which contains seven herbs: *Aurantii Fructus* (Pinyin: ZhiKe (ZK)), *Licorice* (Pinyin: GanCao (GC)), *Angelicae Sinensis Radix* (Pinyin: DangGui (DG)), *Radix salvia* (DanShen (DS)), *sparganii rhizome* (Pinyin: SanLeng (SL)), *curcumae rhizome* (Ezhu(EZ)), *semen pharbitidis* (Pinyin: QianNiuZi (QNZ)). We used the Traditional Chinese Medicine Systems Pharmacology (TCMSP) database (<https://tcm-sp-e.com/>) [20] to select the active ingredients of each herb in ZKGCD and set oral bioavailability (OB)  $\geq 30\%$  and drug-likeness (DL)  $\geq$

TABLE 1: Scientific names for all herbs in ZhiKe GanCao Decoction.

Pin Yin	Latin name
ZhiKe (ZK)	<i>Aurantii Fructus</i>
GanCao (GC)	<i>Licorice</i>
DangGui (DG)	<i>Angelicae Sinensis Radix</i>
DanShen (DS)	<i>Radix Salvia</i>
SanLeng (SL)	<i>Sparganii Rhizome</i>
Ezhu(EZ)	<i>Curcumae Rhizome</i>
QianNiuZi (QNZ)	<i>Semen Pharbitidis</i>

0.18. Meanwhile, the target genes corresponding to each active ingredient were obtained from the DrugBank database (<https://go.drugbank.com/>) [21] and UniProt database (<https://www.UniProt.org>) [22].

We integrated a total of 5 databases of target genes for IDD, namely Online Mendelian Inheritance in Man (OMIM) (<https://omim.org/>) [23], GeneCards database (<https://www.genecards.org/>) [24], Comparative Toxicogenomics Database (CTD) (<http://ctdbase.org/>) [25], DrugBank database (<https://go.drugbank.com/>) [21], and DisGeNet database (<https://www.disgenet.org/>) [26]. Finally, the obtained genes were uniformly named through the UniProt database.

The intersection gene set was obtained based on the above two gene sets by constructing Venn diagrams, which are potential target genes for ZKGCD treatment of IDD.

### 2.2. Network Construction and Core Gene Identification.

In this study, we used Cytoscape software [27] to construct the “intersecting genes-active components” network and the “IDD-key genes-active ingredients-herbs” network to show the relationships among ZKGCD, seven herbs, intersection genes and IDD. In the network, the degree represents the number of edges shared by each node. Based on the degree of each active ingredient in the two networks, we used the top three active ingredients as the main active ingredients. Then, protein-protein interaction (PPI) network was obtained by importing all the intersecting genes into the STRING database (<https://www.string-db.org/>) [28] with *Homo sapiens* and 0.4 moderate confidence for filter conditions. At the same time, the TSV file was obtained. Finally, the obtained TSV file was imported into Cytoscape software to visualize the PPI network of intersected genes, and the PPI network was analyzed by MCODE and CytoHubba plugin in Cytoscape to acquire clusters and key genes with 12 kinds of topological measures.

**2.3. Enrichment Analysis of Intersecting Genes.** To further clarify the potential specific mechanism of the ZKGCD treatment IDD, we used the clusterProfiler package of R software to perform enrichment analysis for the intersection gene set, mainly including gene ontology (GO) and Kyoto Encyclopedia of Genes and Genomes (KEGG) enrichment analysis [29]. On the one hand, GO analysis was used to explore the potential relationship of intersecting genes with IDD treatment at three levels: cellular components (CCs), molecular functions (MFs), and biological processes (BPs).



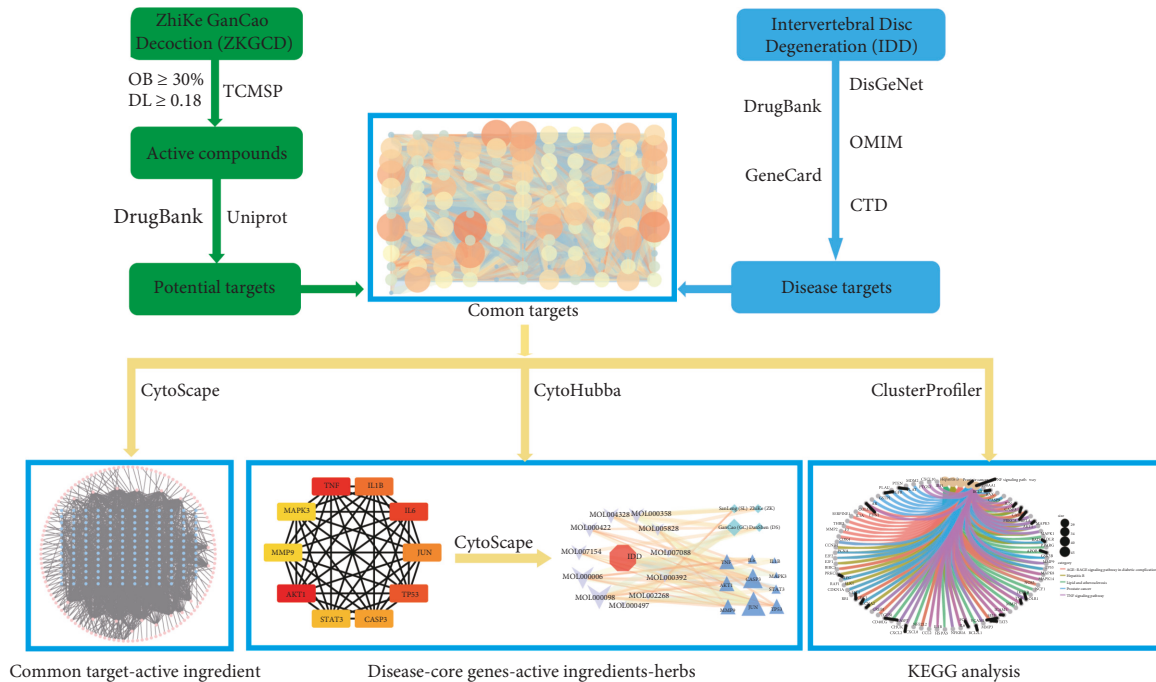


FIGURE 1: Flow chart of the study. OB: oral bioavailability. DL: drug-likeness.

On the other hand, KEGG analysis reveals the main pathways of action of the target genes.

**2.4. Verification of Stability for Core Genes and Active Ingredients.** In this study, we mainly used molecular docking analysis to clarify whether there is a good stability between our selected key genes and the corresponding active ingredients. The stereo structures of key genes and active ingredients (small molecule ligands) were downloaded from the RCSB PDB database (<https://www.rcsb.org/>) and PubChem database (<https://pubchem.ncbi.nlm.nih.gov/>), respectively. And then, they were preprocessed by PyMol 2.4.0 and ChenBio3D software. Finally, we used AutoDock Vina to calculate the binding energy based on the hydrogenation reaction of proteins and small-molecule ligands.

### 3. Results

**3.1. Bioactive Components and Drug Targets for ZKGCD.** A total of 194 active ingredients from seven herbs in ZKGCD were obtained from the TCMSP database based on two selection conditions ( $OB \geq 30\%$  and  $DL \geq 0.18$ ). Among them, 5 active ingredients were derived from ZK, 92 from GC, 2 from DG, 65 from DS, 5 from SL, 3 from EZ, and 22 from QNZ (Supplementary Table 1). Then, 186 active ingredients were obtained after removing the repeats. Finally, 267 targets of ZKGCD were obtained by sorting the corresponding targets of 186 active compounds through DrugBank and UniProt databases (Supplementary Table 2).

**3.2. Potential Target Genes of ZKGCD for the Treatment of IDD.** We obtained a total of 2166 nonduplicated IDD-related genes from five databases OMIM, GeneCards, CTD,

DrugBank, and DisGeNet database based on the keyword of Intervertebral disc degeneration. Then, we analyzed the intersection gene set of ZKGCD targets and IDD-related genes through online analysis (<http://bioinformatics.ps.ugent.be/webtools/Venn/>) and obtained the intersection gene set containing 133 drug-disease targets, which are potential target genes of ZKGCD treatment for IDD (Figure 2 and Supplementary Table 3).

**3.3. Construction of “Intersecting Genes-Active Components” Network.** According to the relationship between drug targets and bioactive ingredients, we established the “intersection gene-active ingredient” network through Cytoscape software, which contains 1278 edges, 133 intersection genes, and 154 active ingredients (Figure 3). Then, we performed statistical analysis for this network structure and found that quercetin (Mol000098), luteolin (Mol000006), and kaempferol (Mol000422) were the top three degrees, which indicated that these three components correspond to the largest number of intersecting genes. Therefore, they may be the key components of ZKHCD for the treatment of IDD. The top 10 active ingredients were screened according to the degree value, as shown in Table 2.

**3.4. Construction of Protein-Protein Interaction (PPI) Network and Key Genes Network.** All 133 intersecting genes were imported into the STRING database to construct the PPI network and visualized it by Cytoscape (Figure 4). Then, based on the results of 12 topological algorithms, we selected the top 10 key genes based on degree values, namely AKT1, TNF, IL6, TP53, IL1B, JUN, CASP3, STAT3, MMP9, and MAPK3 (Figure 4). Additionally, a total of three clusters were identified in the PPI network by the cluster analysis

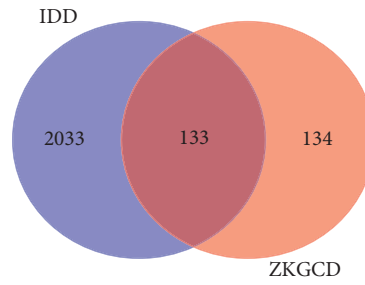
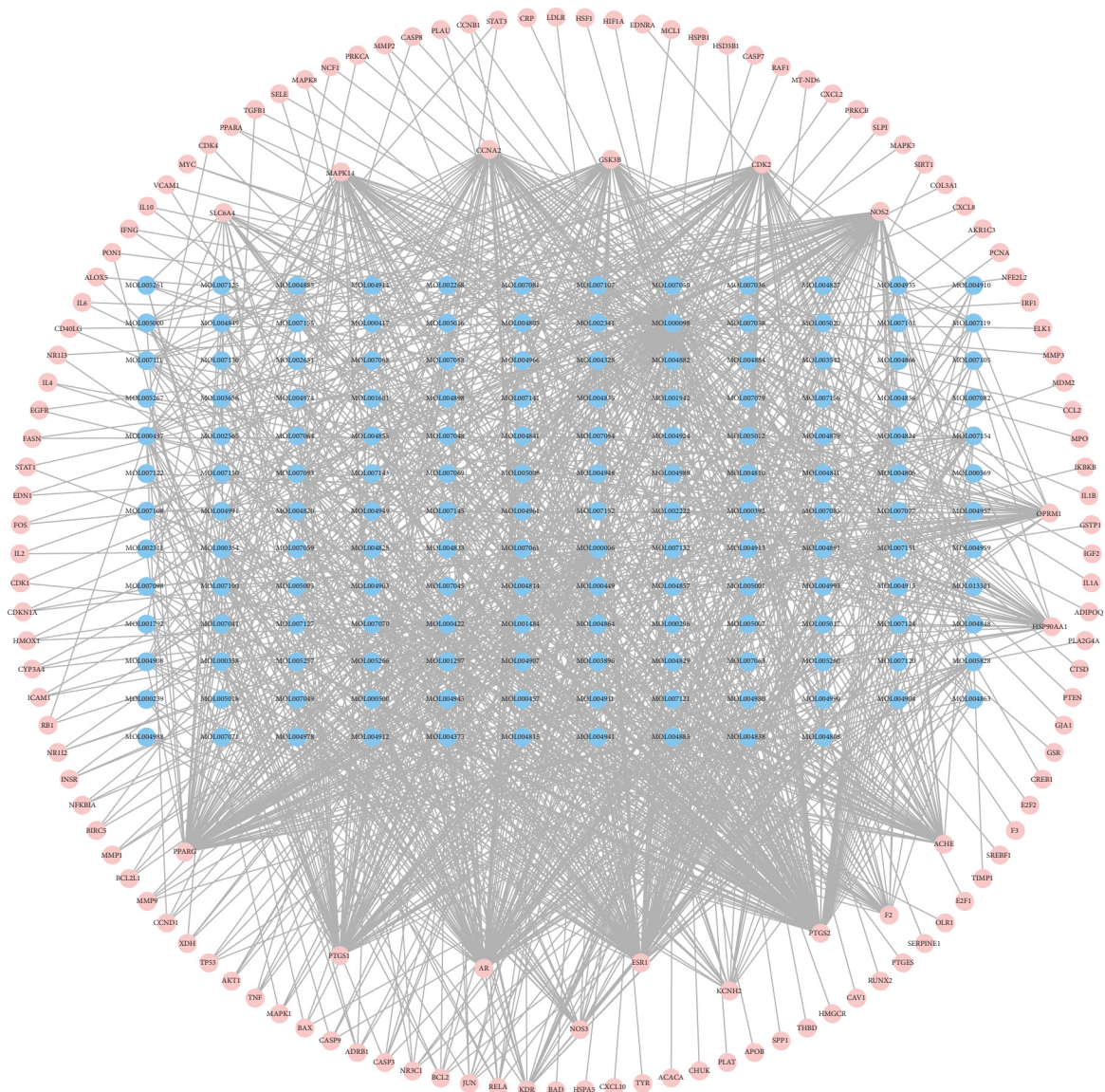


FIGURE 2: Venn diagrams of intersecting genes between IDD and active ingredients in ZKGCD. IDD: intervertebral disc degeneration. ZKGCD: ZhiKe GanCao Decoction.



function with the MCODE plugin (Figure 5, Table 3). We found that the first cluster contained 10 key genes, further confirming the credibility of key gene selection.

3.5. Construction of “Diseases-Key Genes-Active Ingredients-Herbs” Network. To further elaborate the relationship between ZKGCD and IDD, we identified 11 bioactive

TABLE 2: Basic information of 11 active components in ZKGCD.

Molecule ID	Molecule name	PubChem CID	OB (%)	DL	Source (herb name)	Targeted key genes
MOL000098	Quercetin	5280343	46.43	0.28	GanCao	AKT1, MMP9, TNF, JUN, IL6, CASP3, TP53, IL1B
MOL000006	Luteolin	5280445	36.16	0.25	DanShen	AKT1, MMP9, TNF, JUN, IL6, CASP3, TP53
MOL000422	Kaempferol	5280863	41.88	0.24	GanCao	AKT1, TNF, JUN, CASP3
MOL004328	Naringenin	932	59.29	0.21	ZhiKe, GanCao	AKT1, MAPK3, CASP3
MOL000392	Formononetin	5280378	69.67	0.21	GanCao, SanLeng	JUN
MOL005828	Nobiletin	72344	61.67	0.52	ZhiKe	MMP9, JUN, TP53
MOL007154	Tanshinone IIA	164676	49.89	0.40	DanShen	MMP9, JUN, CASP3, TP53
MOL000497	Licochalcone A	5318998	40.79	0.29	GanCao	STAT3
MOL000354	Isorhamnetin	5281654	49.60	0.31	GanCao	/
MOL004373	Anhydrocaritin	44259058	45.41	0.44	QianNiuZi	/

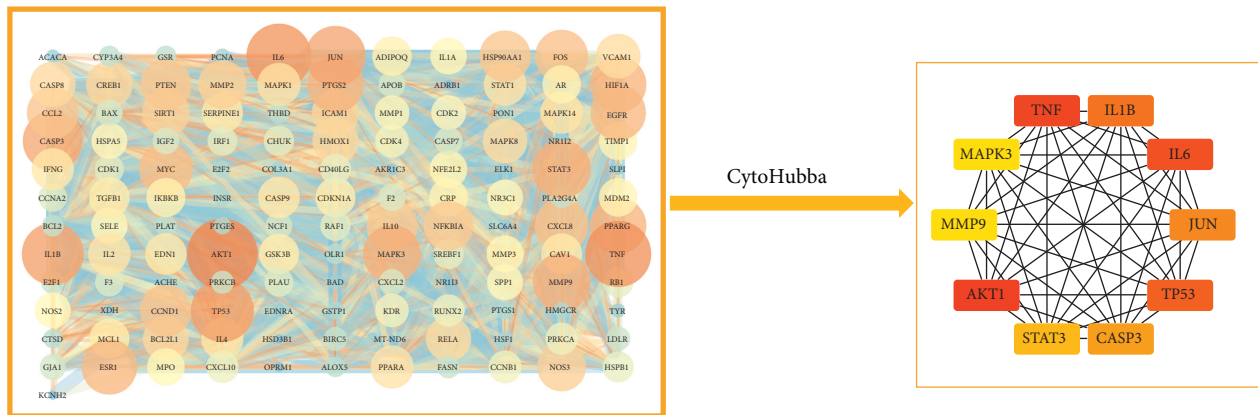


FIGURE 4: Protein-protein interaction (PPI) network and key gene network.

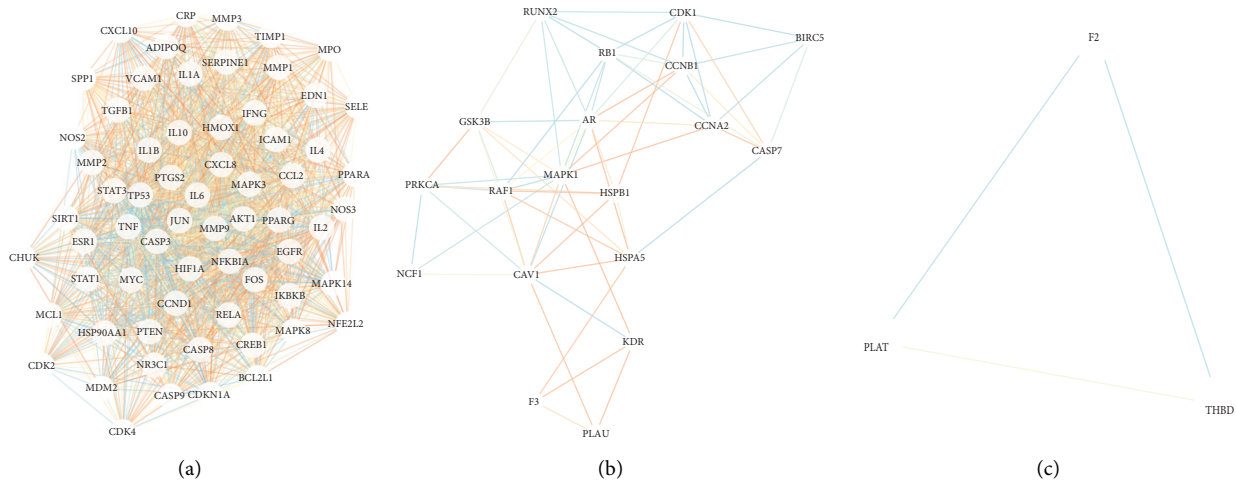


FIGURE 5: Three clusters of common genes by MCODE plugin in Cytoscape.

ingredients and 4 herbs corresponding to 10 key genes, and the relationship among them is shown in Figure 6 (Supplementary Table 4). The 11 bioactive ingredients are quercetin (Mol000098), luteolin (Mol000006), kaempferol (Mol000422), beta-sitosterol (Mol000358), naringenin (Mol004328), nobiletin (Mol005828), formononetin (Mol000392), licochalcone A (Mol000497),

cryptotanshinone (Mol007088), tanshinone IIA (Mol007154), and rhein (Mol002268). The 4 herbs are ZhiKe (ZK), GanCao (GC), DanShen (DS), and SanLeng (SL). Analyzing the “diseases-key genes-active ingredients-herbs” network revealed the highest degree of quercetin, the second degree of luteolin, and the third degree of kaempferol, which were consistent with the results of the “intersecting genes-



TABLE 3: Cluster information of the protein-protein interaction (PPI) network for common genes.

Cluster	Score	Nodes	Edges	Gene names
1	50.156	65	1605	MMP2, TGFB1, SERPINE1, MPO, CCL2, CDK4, MYC, IL2, MDM2, IFNG, IL4, NR3C1, CRP, CDK2, MAPK3*, IL1A, STAT3*, ICAM1, TP53*, VCAM1, NOS3, MMP3, BCL2L1, CXCL8, SELE, CXCL10, JUN*, MMP9*, MMP1, EDN1, SPP1, NOS2, MAPK8, CASP9, HSP90AA1, SIRT1, IKBKB, HIF1A, PPARG, ESR1, IL10, CASP8, STAT1, PTEN, EGFR, PPARA, ADIPOQ, MCL1, AKT1*, CHUK, IL1B*, FOS, NFKBIA, PTGS2, NFE2L2, CREB1, TNF*, CCND1, CASP3*, RELA, IL6*, MAPK14, CDKN1A, HMOX1, TIMP1
2	7	19	63	NCF1, HSPB1, RAF1, AR, F3, PLAU, CCNB1, BIRC5, MAPK1, GSK3B, CAV1, CDK1, KDR, PRKCA, RB1, RUNX2, CCNA2, CASP7, HSPA5
3	3	3	3	F2, THBD, PLAT

\* Core genes are highlighted in red.

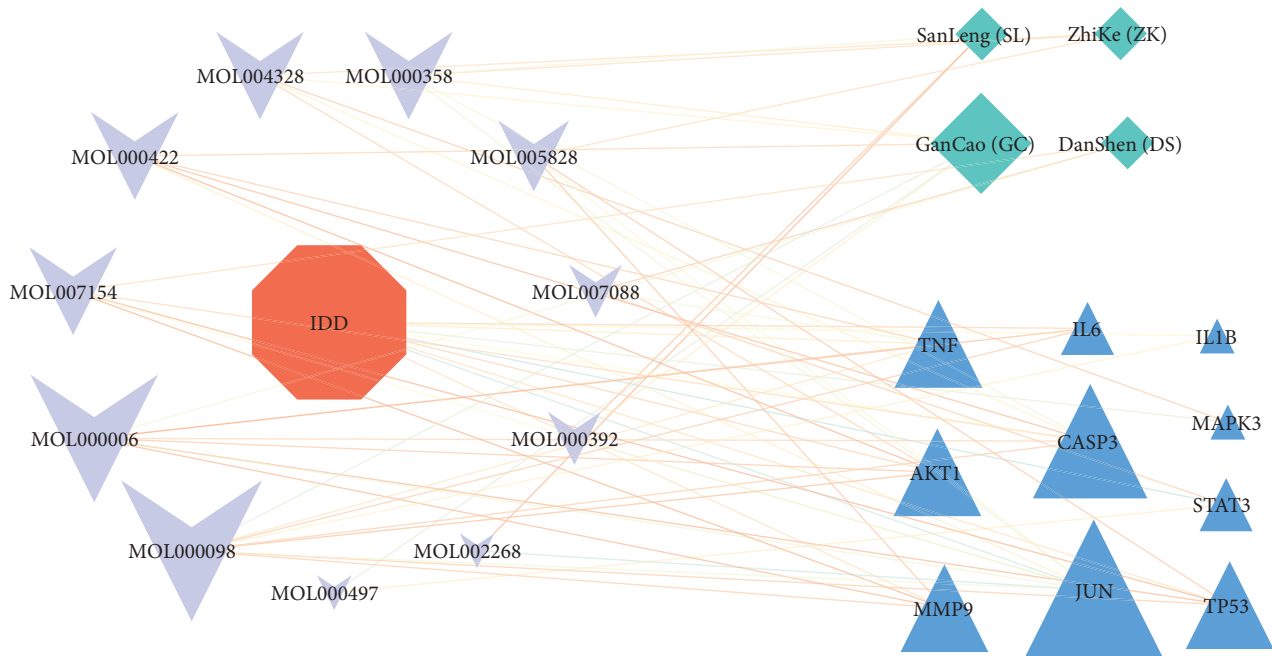


FIGURE 6: “IDD-key genes-active ingredients-herbs” network. Red pentagons represent diseases, dark blue triangles represent key genes, purple inverted triangles represent active ingredients associated with core genes, and light blue rectangles represent herbs. The size of each node represents the number of degrees.

active components” network analysis. Eight of the 11 bio-active ingredients are among the top 10 active ingredients in the “intersecting genes-active components” network.

**3.6. Enrichment Analysis for GO Function and KEGG Pathway.** Based on R platform, we conducted GO function and KEGG pathway enrichment analysis for 133 intersected genes. A total of 2610 results were obtained by GO functional enrichment analysis, including 2423 BPs, 50 CCs, and 137 MFs. Among them, biological processes are mainly related to response to oxidative stress, response to reactive oxygen species, cellular response to reactive oxygen species, reactive oxygen species metabolic process, and regulation of apoptotic signaling pathway. As for CCs, the results showed that it was mainly related to membrane raft, cyclin-dependent protein kinase holoenzyme complex, RNA

polymerase II transcription regulator complex, nuclear chromatin, and vesicle lumen. The MFs are mainly related to cytokine activity, DNA-binding transcription activator activity, cytokine receptor binding, and receptor ligand activity. Figure 7 exhibits the top 10 for each category, and details of the GO analysis results are listed in Supplementary Table 5.

We used KEGG pathway enrichment analysis to further and comprehensively elaborate the potential mechanism of ZK/GCD in delaying the IDD process. Finally, a total of 172 potential related pathways are enriched, mainly involving inflammation, apoptosis, senescence, and autophagy, which are specifically manifested as AGE-RAGE signaling pathway in diabetic complications (hsa04933), TNF signaling pathway (hsa04668), IL-17 signaling pathway (hsa04657), cellular senescence (hsa04218), apoptosis (hsa04210), and PI3K-Akt signaling pathway (hsa04151) (Table 4).

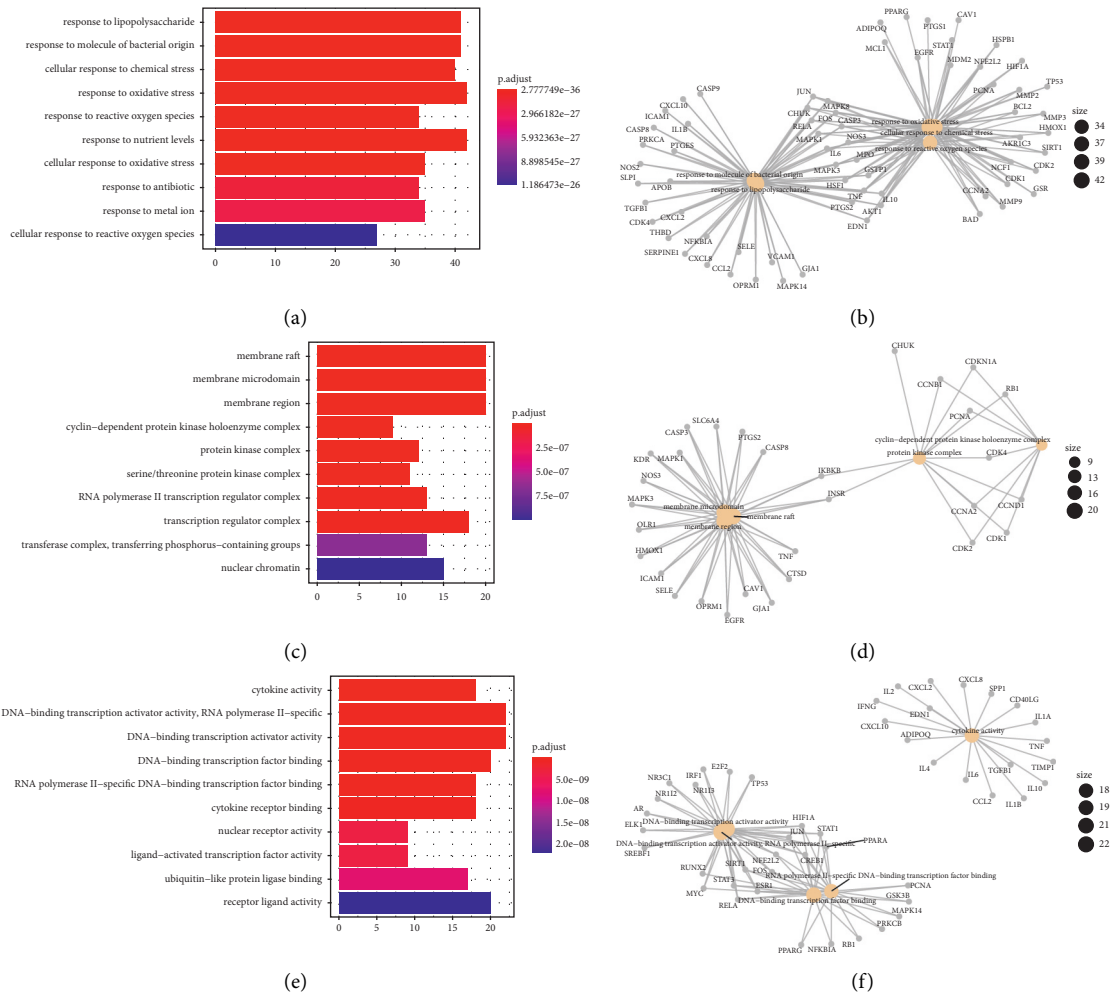


FIGURE 7: GO enrichment analysis of common genes. (a) Top 10 significantly enriched terms in biological processes (BPs). (b) Subnetwork showing the top five BP terms and related genes. (c) Top 10 significantly enriched terms in cellular components (CCs). (d) Subnetwork shows the top five CC terms and related genes. (e) Top 10 significantly enriched terms in molecular functions (MFs). (f) Subnetwork shows the top five MF terms and related genes.

TABLE 4: The main related pathways for IDD are in the top 30.

ID	Description	p. adjust	Count
hsa04933	AGE-RAGE signaling pathway in diabetic complications	3.36E-34	30
hsa04668	TNF signaling pathway	1.53E-26	29
hsa04657	IL-17 signaling pathway	4.17E-26	27
hsa04218	Cellular senescence	5.35E-19	26
Hsa04210	Apoptosis	3.71E-18	24
Hsa04151	PI3K-Akt signaling pathway	2.00E-16	33

Particularly, we visualized the first 30 pathways of enrichment results according to adjusted  $P$  values (Figure 8). Detailed information of the GO analysis results is listed in Supplementary Table 5.

**3.7. Molecular Docking between Key Genes and Active Ingredients.** Binding energy is considered to be one of the key indicators to verify the stability of the conformation of the bound protein and active ingredient. At the same time,

the stability of the conception increases as the binding energy decreases. For this reason, we performed molecular docking analysis on 10 key genes and the top 3 bioactive components, and the results are shown in Figure 9. The results of molecular docking showed that all binding energies were lower than  $-5.0$  kcal/mol, which on the other hand reflected that ZKGCD acted through multiple targets in the treatment of IDD. In addition, we found that quercetin, the most important bioactive component of ZKGCD, obtained the highest binding energy of 10.5 kcal/mol for

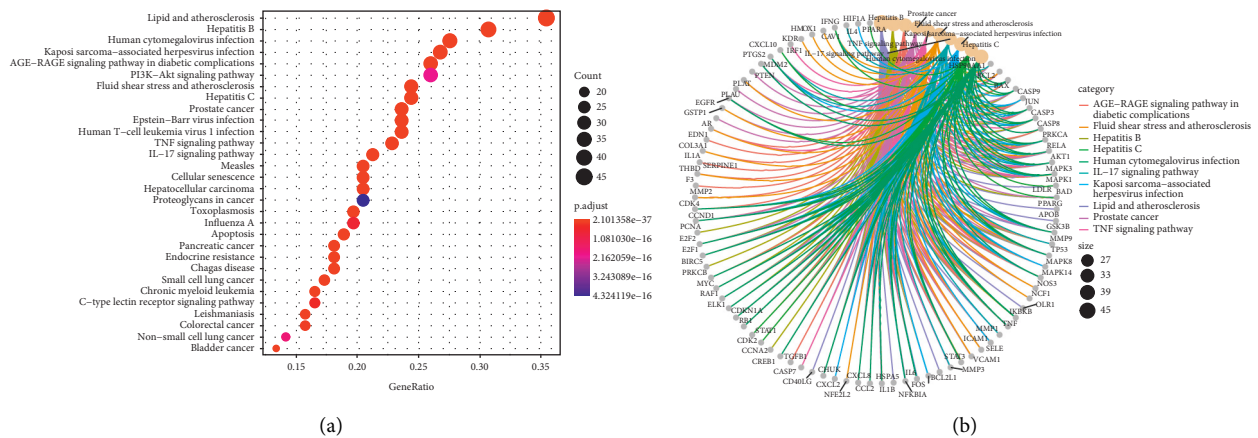


FIGURE 8: KEGG pathway enrichment analysis of common genes. (a) The 30 pathways with the lowest adjusted  $p$  values. The darker the color, the smaller the adjusted  $p$  value. The larger the circle, the greater the number of target genes in the term. (b) Subnetwork shows the top five KEGG pathways and related genes.

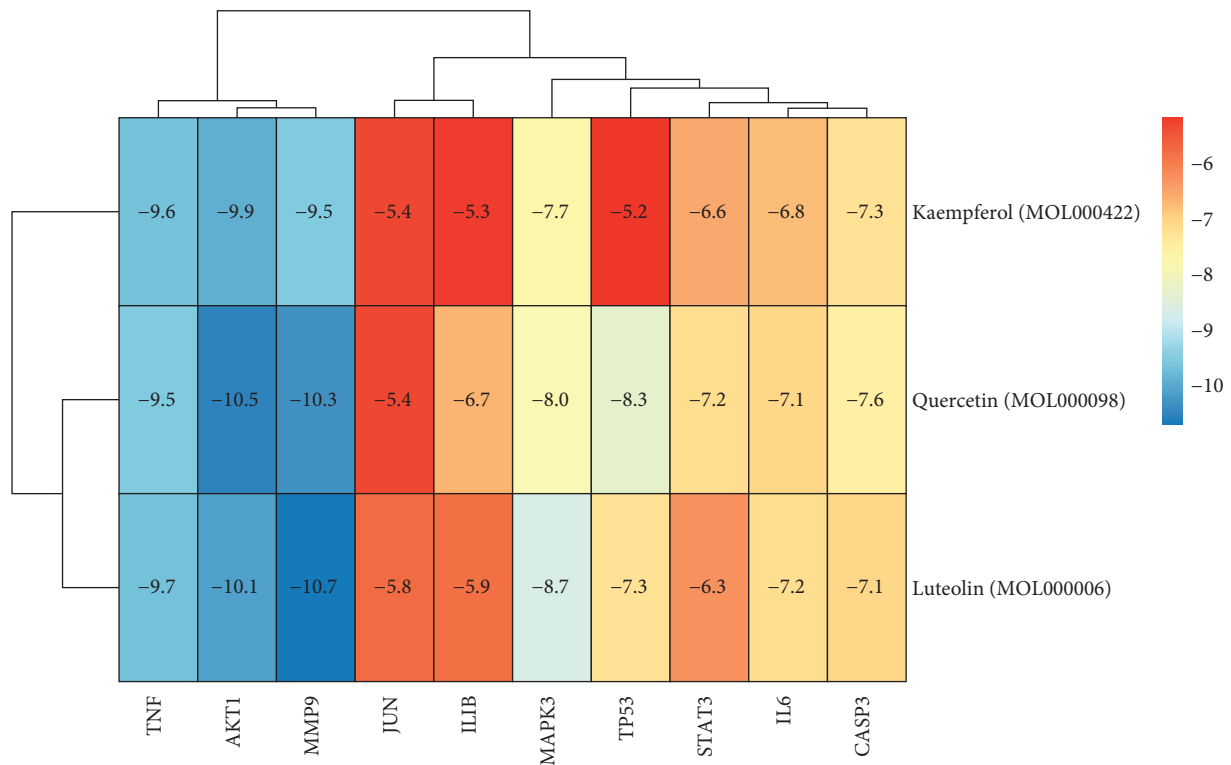


FIGURE 9: Heat map of binding energy between 10 core genes and top three active ingredients by molecular docking.

binding to the protein AKT1. Similarly, the highest binding energy of 9.9 kcal/mol was obtained for kaempferol binding to AKT1. However, for luteolin, the binding to MMP9 was required to obtain the highest binding energy of 10.7 kcal/mol. Moreover, we showed the structure of the interaction between each bioactive ingredient and the key protein with the strongest binding activity, whereas, for quercetin, we selected two key proteins (Figure 10).

#### 4. Discussion

With the increasing intensity of modern work, the incidence of IDD is increasing. Currently, the generally recognized mechanisms of IDD may be related to the enrichment of inflammatory factors, senescence, and apoptosis of nucleus pulposus cells (NPC) and degradation of extracellular matrix (ECM). However, there is a lack of effective noninvasive



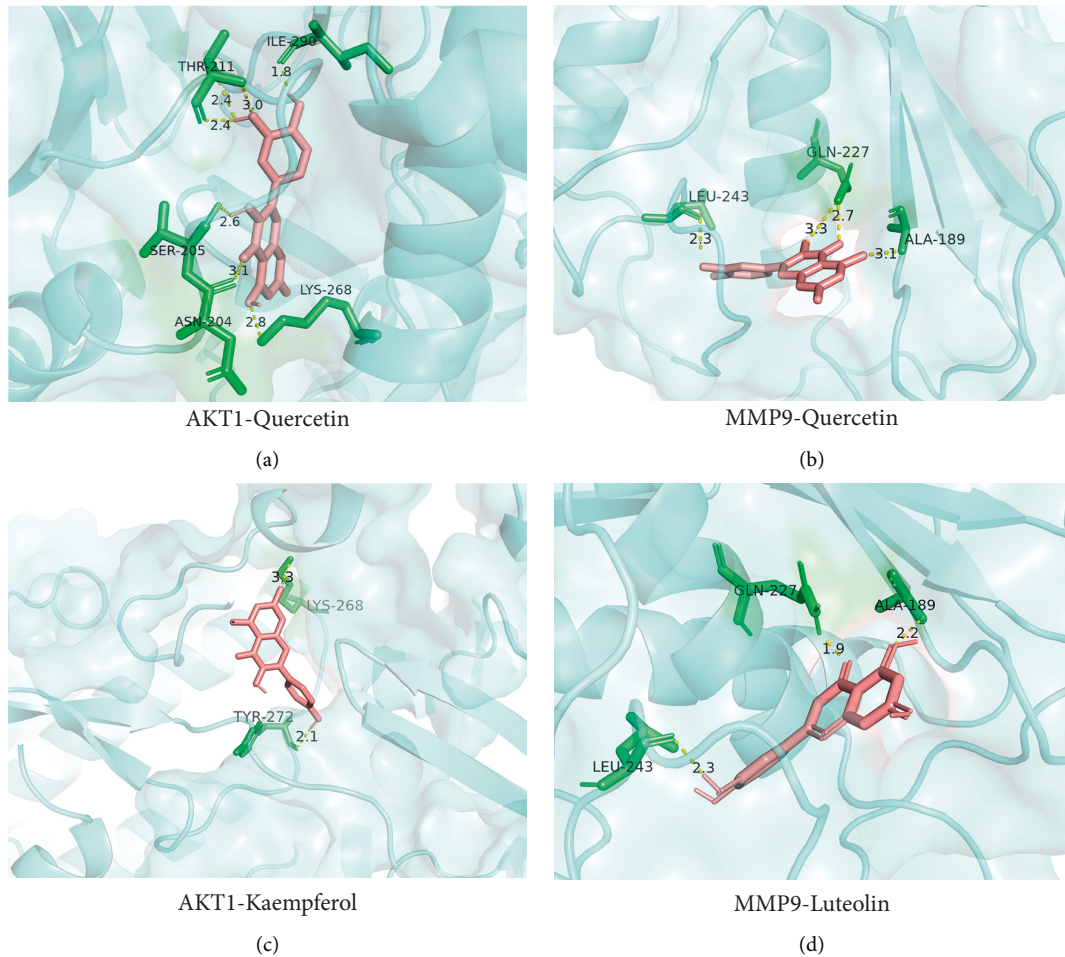


FIGURE 10: Four examples of conformations for some core compounds and key genes.

treatment for IDD before it progresses to surgery. Single NSAIDs are mainly used to relieve painful symptoms, but it is accompanied by a series of side effects. Since herbs taken from nature have no or very few side effects, it has been used as a supplement to western medicine. ZKGCD, a traditional Chinese medicine compound, has been used to treat musculoskeletal diseases. However, the specific therapeutic mechanism of ZKGCD is not clear, which limited the application of ZKGCD in clinical practice. This study used network pharmacology theories, molecular docking techniques, high-throughput data analysis, and a series of related tools to visualize the specific relationships among drug active ingredients, key targets, important signaling pathways, and disease.

In this study, a total of 154 active ingredients were selected, among which quercetin (Mol000098), luteolin (Mol000006), and kaempferol (Mol000422) were identified as the core active ingredients. Quercetin is one of the main active components of licorice, which is a natural flavonoid with antioxidant and anti-inflammatory effects and widely exists in various plants. Several studies have shown that quercetin can delay IDD progression through multiple signaling pathways, mainly including (1) quercetin can prevent IDD by regulating p38 MAPK-mediated autophagy

[30]; (2) quercetin can promote SIRT1-dependent autophagy to prevent IDD [31]; (3) QUE inhibits the expression of SASP and senescence phenotype in NPC and improves the progression of IDD through Nrf2/NF- $\kappa$ B axis [32]. Luteolin, also a natural flavonoid, has anti-inflammatory and anticatabolic effects as its most important effects, which are opposed to the underlying mechanisms of IDD development. Therefore, it is reasonable that luteolin has a therapeutic effect on IDD. The most significant effect of kaempferol is anti-inflammatory, which has been shown to have beneficial effects on chronic inflammatory diseases, including IDD [33]. In addition, experimental studies have shown that kaempferol reduces inflammation mainly by increasing the levels of IL-10 and IL-6, which are anti-inflammatory and proinflammatory factors, respectively [34]. The major pathological features of IVDD are the elevated expression of inflammatory mediators, increased senescence and apoptosis of nucleus pulposus cells (NPCs), and degradation of the extracellular matrix [5, 6]. Therefore, regulating inflammation and oxidative stress is a crucial step in the treatment of IDD. Quercetin, luteolin, and kaempferol all have anti-inflammatory effects. We speculate that, on the one hand, the combination of multiple components may have produced a synergistic effect. On the other hand, other

bioactive components may have promoted the antioxidant effect of luteolin. In addition, several studies have shown that the majority of herbal formulas with quercetin, kaempferol, and luteolin as the core bioactive components have regulated effects on inflammation, oxidative stress, and apoptosis, which is consistent with the potential mechanism of ZKGCD for IDD [35–38].

According to the ten key targets selected by the PPI network and topology algorithm, and the results of GO function enrichment and KEGG pathway enrichment analysis, the final results all mainly focused on the regulation of inflammatory response, oxidative stress response, reactive oxygen metabolism, and apoptotic signaling pathway. AKT1 is a serine/threonine protein kinase involved in a variety of biological processes. AKT activation depends on the PI3K pathway. Furthermore, studies have confirmed that the pathogenesis of disc lesions may be related to end-plate sclerosis, increased oxidative stress, and AGE/RAGE-mediated interactions. TNF and IL6, as typical inflammatory factors, are associated with our selected core active components and potential mechanisms (TNF signaling pathway and IL-17 signaling pathway) that are complementary to each other. The enrichment results also suggested that two pathways, including cellular senescence and apoptosis, may play a very important role in the treatment of IDD. On the one hand, senescence of NPC is a key factor in IDD, and delaying NPC senescence may be beneficial for alleviating IDD [39, 40]. On the other hand, endoplasmic reticulum (ER) stress and ECM degradation are important factors in the development of IDD. Autophagy can effectively repair ER stress and maintain ECM homeostasis [41]. Moreover, TP53 and CASP3, among the key targets, are mainly associated with induction of apoptosis and senescence, which further confirmed the potential of ZKGCD in treating IDD. However, we must acknowledge that the results of this study were confirmed by experiments in other studies, lacking our own in vivo experimental validation.

## 5. Conclusion

In conclusion, this study systematically elucidated the potential mechanisms of ZKGCD for the treatment of IDD based on a network pharmacology approach, molecular docking technique, and GO and KEGG enrichment analysis. The results indicated that quercetin (Mol000098), luteolin (Mol000006), and kaempferol (Mol000422) were the main bioactive components, which may alleviate the occurrence and development of IDD through the AGE-RAGE signaling pathway in diabetic complications, TNF signaling pathway, IL-17 signaling pathway, cellular senescence, apoptosis, and PI3K-Akt signaling pathway. This study demonstrated the characteristics of multicomponent, multitarget, and multipathway of ZKGCD and provided potential targets and a basis for the development of new drugs and experimental studies for the subsequent treatment of IDD.

## Data Availability

The data used to support the findings of this study are included within the article.

## Conflicts of Interest

The authors declare that they have no conflicts of interest.

## Acknowledgments

This study is supported by “1233 Young Talents Program” of Hunan Children’s Hospital.

## Supplementary Materials

Supplementary Table 1: ingredients of each herb contained in ZKGCD (OB  $\geq$  30%, DL  $\geq$  0.18). Supplementary Table 2: potential targets related to active ingredients in ZKGCD. Supplementary Table 3: intersection genes and corresponding active ingredients. Supplementary Table 4: relationship among key genes, active ingredients, and herbs. Supplementary Table 5: detailed information of GO and KEGG enrichment analysis for common targets. (*Supplementary Materials*)

## References

- [1] C. Maher, M. Underwood, and R. Buchbinder, “Non-specific low back pain,” *The Lancet*, vol. 389, no. 10070, pp. 736–747, 2017.
- [2] S. Safiri, A.-A. Kolahi, M. Noori et al., “Burden of anemia and its underlying causes in 204 countries and territories, 1990–2019: results from the Global Burden of Disease Study 2019,” *Journal of Hematology & Oncology*, vol. 14, no. 1, p. 185, 2021.
- [3] T. Driscoll, G. Jacklyn, J. Orchard et al., “The global burden of occupationally related low back pain: estimates from the Global Burden of Disease 2010 study,” *Annals of the Rheumatic Diseases*, vol. 73, no. 6, pp. 975–981, 2014.
- [4] B. I. Martin, R. A. Deyo, and S. K. Mirza, “Expenditures and health status among adults with back and neck problems,” *JAMA*, vol. 299, no. 6, pp. 656–664, 2008.
- [5] J. Dowdell, M. Erwin, T. Choma, A. Vaccaro, J. Iatridis, and S. K. Cho, “Intervertebral disk degeneration and repair,” *Neurosurgery*, vol. 80, no. 3S, pp. S46–s54, 2017.
- [6] M. A. Adams and P. J. Roughley, “What is intervertebral disc degeneration, and what causes it?” *Spine*, vol. 31, no. 18, pp. 2151–2161, 2006.
- [7] P. D. D. M. Roelofs, R. A. Deyo, B. W. Koes, R. J. P. M. Scholten, and M. W. van Tulder, “Nonsteroidal anti-inflammatory drugs for low back pain,” *Spine*, vol. 33, no. 16, pp. 1766–1774, 2008.
- [8] N. Henschke, C. G. Maher, K. M. Refshauge et al., “Prognosis in patients with recent onset low back pain in Australian primary care: inception cohort study,” *BMJ*, vol. 337, p. a171, 2008.
- [9] Y. Wu, F. Zhang, K. Yang et al., “SymMap: an integrative database of traditional Chinese medicine enhanced by symptom mapping,” *Nucleic Acids Research*, vol. 47, no. D1, pp. D1110–d1117, 2019.
- [10] X. Zhang, Y. Yang, F. Zhang et al., “Traditional Chinese medicines differentially modulate the gut microbiota based on their nature (Yao-Xing),” *Phytomedicine*, vol. 85, Article ID 153496, 2021.
- [11] H. W. Li, Z. G. Zhang, and K. L. Xu, “30 cases of lumbar disc herniation treated with modified ZhiKe GanCao Decoction,” *Hennan Traditional Chinese Medicine*, vol. 31, pp. 170–171, 2011.

- [12] K. L. Xu and H. Jianag, "64 cases of acute lumbar disc herniation treated with ZhiKe GanCao Decoction," *The Journal of Traditional Chinese Orthopedics and Traumatology*, vol. 22, p. 67, 2010.
- [13] F. Shen, "Clinical observation on treatment of cervical spondylosis with ZhiKe GanCao Decoction," *Zhejiang Journal of Integrated Traditional Chinese and Western Medicine*, vol. 29, p. 9, 2019.
- [14] J. T. Sun, Y. W. Li, and X. F. Shen, "The experimental study of Zhike Gancao Decoction on inflammation and degeneration of lumbar disc protrusion model in rats," *Journal of Emergency in Traditional Chinese Medicine*, vol. 25, pp. 1488–1492, 2016.
- [15] G. L. Dai, Single-segmental Fusion and Adjacent Level Decompression Combined with Clinical Observation of ZhiKe GanCao Decoction in Treating Lumbar Degenerative Diseases, 2020.
- [16] J. Yang, M. Zhang, Q. Song et al., "Integrating network pharmacological and experimental models to investigate the therapeutic effects of baicalin in glaucoma," *Chinese Medicine*, vol. 16, no. 1, p. 124, 2021.
- [17] Y. Kuang, Y. Chai, H. Su, J.-Y. Lo, X. Qiao, and M. Ye, "A network pharmacology-based strategy to explore the pharmacological mechanisms of Antrodia camphorata and antcin K for treating type II diabetes mellitus," *Phytomedicine*, vol. 96, Article ID 153851, 2022.
- [18] Y. D. Yu, W. J. Hou, J. Zhang, Y. T. Xue, and Y. Li, "Network pharmacology and molecular docking-based analysis on bioactive anticoronary heart disease compounds in *Trichosanthes kirilowii maxim* and *bulbus allii macrostemi*," *Evid Based Complement Alternat Med*, vol. 2021, Article ID 6704798, 2021.
- [19] B. Shi, C. Lu, X. Liu, L. Zhou, K. Wang, and X. Tao, "Pharmacological mechanisms underlying the androgen-reducing effects of Shaoyao Gancao Decoction determined by network pharmacology and molecular docking," *Minerva Medica*, 2021.
- [20] J. Ru, P. Li, J. Wang et al., "TCMSP: a database of systems pharmacology for drug discovery from herbal medicines," *Journal of Cheminformatics*, vol. 6, no. 1, p. 13, 2014.
- [21] D. S. Wishart, Y. D. Feunang, A. C. Guo et al., "DrugBank 5.0: a major update to the DrugBank database for 2018," *Nucleic Acids Research*, vol. 46, no. D1, pp. D1074–d1082, 2018.
- [22] "UniProt: a hub for protein information," *Nucleic Acids Research*, vol. 43, pp. D204–D212, 2015.
- [23] J. S. Amberger, C. A. Bocchini, F. Schiettecatte, A. F. Scott, and A. Hamosh, "OMIM.org: online Mendelian Inheritance in Man (OMIM), an online catalog of human genes and genetic disorders," *Nucleic Acids Research*, vol. 43, no. D1, pp. D789–D798, 2015.
- [24] M. Rebhan, V. Chalifa-Caspi, J. Prilusky, and D. Lancet, "GeneCards: integrating information about genes, proteins and diseases," *Trends in Genetics*, vol. 13, no. 4, p. 163, 1997.
- [25] A. P. Davis, C. J. Grondin, R. J. Johnson et al., "The comparative Toxicogenomics database: update 2019," *Nucleic Acids Research*, vol. 47, no. D1, pp. D948–d954, 2019.
- [26] J. Pinero, A. Bravo, N. Queralt-Rosinach et al., "DisGeNET: a comprehensive platform integrating information on human disease-associated genes and variants," *Nucleic Acids Research*, vol. 45, pp. D833–d839, 2017.
- [27] P. Shannon, A. Markiel, O. Ozier et al., "Cytoscape: a software environment for integrated models of biomolecular interaction networks," *Genome Research*, vol. 13, no. 11, pp. 2498–2504, 2003.
- [28] D. Szklarczyk, A. L. Gable, D. Lyon et al., "STRING v11: protein-protein association networks with increased coverage, supporting functional discovery in genome-wide experimental datasets," *Nucleic Acids Research*, vol. 47, no. D1, pp. D607–d613, 2019.
- [29] G. Yu, L.-G. Wang, Y. Han, and Q.-Y. He, "clusterProfiler: an R package for comparing biological themes among gene clusters," *OMICS: A Journal of Integrative Biology*, vol. 16, no. 5, pp. 284–287, 2012.
- [30] S. Zhang, W. Liang, Y. Abulizi et al., "Quercetin alleviates intervertebral disc degeneration by modulating p38 MAPK-mediated autophagy," *BioMed Research International*, vol. 2021, Article ID 6631562, 2021.
- [31] D. Wang, X. He, D. Wang et al., "Quercetin suppresses apoptosis and attenuates intervertebral disc degeneration via the SIRT1-autophagy pathway," *Frontiers in Cell and Developmental Biology*, vol. 8, Article ID 613006, 2020.
- [32] Z. Shao, B. Wang, Y. Shi et al., "Senolytic agent Quercetin ameliorates intervertebral disc degeneration via the Nrf2/NF- $\kappa$ B axis," *Osteoarthritis and Cartilage*, vol. 29, no. 3, pp. 413–422, 2021.
- [33] J. Ren, Y. Lu, Y. Qian, B. Chen, T. Wu, and G. Ji, "Recent progress regarding kaempferol for the treatment of various diseases," *Experimental and Therapeutic Medicine*, vol. 18, pp. 2759–2776, 2019.
- [34] J. Zhu, H. Tang, Z. Zhang et al., "Kaempferol slows intervertebral disc degeneration by modifying LPS-induced osteogenesis/adipogenesis imbalance and inflammation response in BMSCs," *International Immunopharmacology*, vol. 43, pp. 236–242, 2017.
- [35] Y. Cui, H. Wang, D. Wang et al., "Network pharmacology analysis on the mechanism of huangqi sijunzi decoction in treating cancer-related fatigue," *Journal of healthcare engineering*, vol. 2021, Article ID 9780677, 2021.
- [36] S.-H. Feng, F. Xie, H.-Y. Yao, G.-B. Wu, X.-Y. Sun, and J. Yang, "The mechanism of Bushen Huoxue decoction in treating intervertebral disc degeneration based on network pharmacology," *Annals of Palliative Medicine*, vol. 10, no. 4, pp. 3783–3792, 2021.
- [37] N. Suga, A. Murakami, H. Arimitsu, T. Nakamura, Y. Nakamura, and Y. Kato, "Luteolin suppresses 5-hydroxytryptamine elevation in stimulated RBL-2H3 cells and experimental colitis mice," *Journal of Clinical Biochemistry & Nutrition*, vol. 69, no. 1, pp. 20–27, 2021.
- [38] Q. Zhang, X. Li, J. Li et al., "Mechanism of anti-inflammatory and antibacterial effects of QingXiaoWuWei decoction based on network pharmacology, molecular docking and in vitro experiments," *Frontiers in Pharmacology*, vol. 12, Article ID 678685, 2021.
- [39] J. Lin, J. Du, X. Wu et al., "SIRT3 mitigates intervertebral disc degeneration by delaying oxidative stress-induced senescence of nucleus pulposus cells," *Journal of Cellular Physiology*, vol. 236, no. 9, pp. 6441–6456, 2021.
- [40] Y. Sun, X. Li, X. Yang, B. Chen, and W. Zhang, "Small extracellular vesicles derived from adipocytes attenuate intervertebral disc degeneration in rats by rejuvenating senescent nucleus pulposus cells and endplate cells by delivering exogenous NAMPT," *Oxidative Medicine and Cellular Longevity*, vol. 2021, Article ID 9955448, 2021.
- [41] Z. Lin, L. Ni, C. Teng et al., "Eicosapentaenoic acid-induced autophagy attenuates intervertebral disc degeneration by suppressing endoplasmic reticulum stress, extracellular matrix degradation, and apoptosis," *Frontiers in Cell and Developmental Biology*, vol. 9, Article ID 745621, 2021.

## Research Article

# Effect of Licochalcone-A Combined with *Rab23* Gene on Proliferation of Glioma U251 Cells

Yindong Mu <sup>1</sup>, Jianjiang Dong <sup>1</sup>, Hong Cui <sup>2</sup>, Jiangping Hu <sup>1</sup>, Jun Liang <sup>3</sup>,  
and Lei Yan <sup>1</sup>

<sup>1</sup>Department of Histology and Embryology, Mudanjiang Medical University, Mudanjiang 157011, China

<sup>2</sup>Department of Pharmacy, Hongqi Hospital Affiliated to Mudanjiang Medical University, Mudanjiang 157011, China

<sup>3</sup>Stem Cell Institute, Mudanjiang Medical University, Mudanjiang 157011, China

Correspondence should be addressed to Lei Yan; [yanlei@mdjmu.edu.cn](mailto:yanlei@mdjmu.edu.cn)

Received 18 February 2022; Accepted 4 April 2022; Published 22 April 2022

Academic Editor: Ruchika Garg

Copyright © 2022 Yindong Mu et al. This is an open access article distributed under the Creative Commons Attribution License, which permits unrestricted use, distribution, and reproduction in any medium, provided the original work is properly cited.

This research aimed to explore the effect of Licochalcone-A (LCA) combined with *Rab23* gene on the proliferation, migration, and invasion of glioma U251 cells through the Wnt/ $\beta$ -catenin signaling pathway. The glioma U251 cell line was taken as the research object, and the *Rab23* overexpression plasmid was constructed. According to the treatment method, U251 cells were rolled into blank control group (BC), *Rab23* overexpression plasmid transfection group (*Rab23*),  $25 \mu\text{mol}\cdot\text{L}^{-1}$  LCA treatment group (LCA), and *Rab23* overexpression plasmid transfection combined with  $25 \mu\text{mol}\cdot\text{L}^{-1}$  LCA treatment group (*Rab23* + LCA). Subsequently, the ability of cell proliferation, migration, and invasion of each group was detected by methyl thiazolyl tetrazolium (MTT) assay, scratch healing test, and Transwell cell invasion test, respectively. Western blot was implemented to detect the expression differences of cell proliferation antigen Ki-67, apoptosis-related proteins Bcl-2 and Bax, and Wnt/ $\beta$ -catenin pathway-related proteins  $\beta$ -catenin, glycogen synthase kinase-3 (GSK3 $\beta$ ), Axin2, and c-myc. The results showed the successful construction of *Rab23* overexpression and stable transfection U251 cell line. After grouping and treatments, the cell proliferation, migration, and invasion ability of the *Rab23* group, LCA group, and *Rab23* + LCA group was substantially reduced relative to BC group ( $P < 0.05$ ). In addition, the cell proliferation, migration, and invasion ability of *Rab23* + LCA group decreased relatively more significantly. The expression levels of Ki-67, Bcl-2,  $\beta$ -catenin, and c-myc in the *Rab23*, LCA, and *Rab23* + LCA groups were greatly lower versus those of BC group. Moreover, the protein expression levels of Bax, GSK3 $\beta$ , and Axin2 were considerably increased ( $P < 0.05$ ), while the expression of protein in *Rab23* + LCA group increased notably. These findings indicate that LCA combined with *Rab23* gene can inhibit the proliferation, migration, and invasion of glioma U251 cells through the Wnt/ $\beta$ -catenin signaling and can promote cell apoptosis.

## 1. Introduction

At present, the mortality rate of malignant tumors accounts for about 24% of all causes of death, and the incidence and mortality rate of nervous system tumors account for the top ten of all malignant tumors. The pathogenesis of primary central nervous system tumors is not clear and has the characteristics of strong invasion, high recurrence rate, and high mortality, among which glioma accounts for more than 50% [1]. The current standard clinical treatment of glioma is surgery combined with chemotherapy or radiotherapy. Glioma is highly

invasive, and the prognosis of patients is very poor, with the recurrence rate reaching 100%, while the 5-year survival rate is less than 5% [2]. Multidisciplinary treatment, including surgery, radiotherapy, and chemotherapy, is the standard treatment for glioma, but the survival time of most patients after treatment does not exceed two years [3]. Therefore, the development of new drugs for killing glioma cells is of great significance for reducing the recurrence rate and mortality after treatment and improving the quality of life of patients and the prognosis.

Chinese herbal medicine is one of the preferred methods of modern medicine to treat diseases, and the antitumor activity

and the advantages of low side effects of Chinese herbal medicine have also received extensive attention from people. Licochalcone-A (LCA) extracted from licorice is a kind of natural active brass, and it has antitumor activity [4]. At present, many studies confirmed that LCA had excellent anticancer effects, such as in liver cancer [5], gastric cancer [6], breast cancer [7], and bladder cancer [8]. The process of tumor cell invasion and metastasis is regulated by multiple genes and steps. *Rab23* gene is a member of the Ras oncogene family. Studies confirmed that the *Rab23* gene played an imperative role in the occurrence and progression of tumors [9]. In addition, the overexpression of *Rab23* gene can inhibit the proliferation activity of glioma cells [10]. In recent years, studies verified that the disorder and excessive activation of the Wnt signaling pathway can participate in the biological processes of glioma cell proliferation, migration, and invasion [11].

However, the mechanism of *Rab23* gene combined with LCA in the invasion and metastasis of glioma remains to be explored. In this research, glioma U251 cells were deemed as the research object, and the effects on cell proliferation, migration, and invasion were explored through overexpression of *Rab23* and LCA treatment. Then, the mechanism of Wnt/ $\beta$ -catenin pathway in the proliferation, migration, and invasion of glioma U251 cells was preliminarily explored.

## 2. Materials and Methods

**2.1. Experimental Materials.** The glioma cell line U251 was purchased from ATCC, USA. Fetal bovine serum, high glucose DMEM, penicillin mixture, and trypsin were all purchased from Gibco, USA. LCA powder (molecular formula:  $C_{21}H_{22}O_4$ ; molecular weight: 338.40; purity  $\geq 96.0\%$ ), dimethyl sulfoxide preparation, and methyl thiazolyl tetrazolium (MTT) kit were purchased from Sigma, USA. A 4% paraformaldehyde was purchased from Invitrogen, USA. Radio immunoprecipitation assay (RIPA) cell lysate was purchased from Beyotime Institute of Biotechnology, China. Bicinchoninic acid (BCA) kit and horseradish peroxidase-labeled goat anti-mouse IgG antibody were purchased from Thermo Company, USA. The ultrasensitive ECL chemiluminescence kit was purchased from Advansta, USA. Mouse anti-human Ki-67,  $\beta$ -catenin, GSK3 $\beta$ , Axin2, c-myc, Bcl-2, Bax, and GAPDH were all purchased from Cell Signaling, USA. Puromycin was purchased from Merck, USA. Lentiviral Vector Particle was purchased from China Jikai Gene. The cell culture dishes were purchased from Corning Costar, USA.

### 2.2. Experimental Methods

**2.2.1. Cultivation of Glioma U251 Cells.** Glioma U251 cells were cultured in Dulbecco's modified eagle medium (DMEM) containing 10% fetal bovine serum (FBS) and  $100\text{ UL}^{-1}$  penicillin streptomycin, and placed in a  $37^\circ\text{C}$  thermostatic cell culture incubator (Thermo Company, USA) containing 5%  $\text{CO}_2$ . When the degree of cell fusion reached 80%, the cells were digested with trypsin and passed at a rate of 1 : 4. In this study, 2–13 generations of cells with the best culture activity were used for subsequent experiments.

**2.2.2. Grouping and Transfection of Glioma U251 Cells.** The glioma U251 cells were rolled into blank control group (BC), *Rab23* transfection group (*Rab23*), LCA group (LCA), and *Rab23* + LCA group (*Rab23* + LCA). The cells in *Rab23* group were transfected with *Rab23* overexpression plasmid; cells in LCA group were treated with  $25\ \mu\text{mol}\cdot\text{L}^{-1}$  LCA; and the cells in the *Rab23* + LCA group were transfected with *Rab23* overexpression plasmid and  $25\ \mu\text{mol}\cdot\text{L}^{-1}$  LCA.

The cells were transfected according to the instructions of Lentiviral Vector Particle. Glioma U251 cells were inoculated into 96-well plates, and  $1 \times 10^5\ \text{TU}\cdot\text{mL}^{-1}$  transfection solution ( $2\ \mu\text{L}$  virus mixed with  $98\ \mu\text{L}$  DMEM containing 10% FBS) was added into each well when the fusion degree reached about 70%. After 12 h of culture, the original medium was discarded, and conventional cell medium was added to culture for 3 days for fluorescence observation. After 7 days of culture, the cells were inoculated into 24-well plates when the fluorescence expression of the cells exceeded 70%. Routine cell culture medium containing  $1\ \text{mg}\cdot\text{L}^{-1}$  puromycin was added for culture for 7 days, to obtain stable overexpression of *Rab23* cell lines. Western blot was performed to detect the expression of *Rab23* in glioma U251 cell lines transfected with lentivirus.

**2.2.3. MTT Assay.** The cells were seeded into 96-well cell culture plates at a density of  $1 \times 10^7\ \text{cells}\cdot\text{mL}^{-1}$ , the inoculation volume was  $100\ \mu\text{L}$  per well, and five replicates were set in each group. When the degree of cell fusion reached about 80%, the cells were passed and grouped. After 48 h of culture, the original medium of cells in each well was removed, and  $20\ \mu\text{L}$  MTT working solution was added to each well successively. The cell culture plates were replaced in a  $37^\circ\text{C}$  constant temperature cell incubator containing 5%  $\text{CO}_2$  and incubated in dark place for 4 h. Then, the original MTT working fluid of cells in each well was removed, and  $150\ \mu\text{L}$  dimethyl sulfoxide reagent was added to each well successively. The MTT working fluid in each well was shaken at low speed for 10 min avoiding light. Finally, the absorbance (OD) of cells in each well was measured at 490 nm using a microplate analyzer (BioTek, USA). The relative viability of cells was calculated according to the equation: (average absorbance in the test group/average absorbance in the blank group)  $\times 100\%$ .

**2.2.4. Scratch Healing Test.** Cells were seeded in a 6-well cell culture plate with the density of  $4 \times 10^5\ \text{cells}\cdot\text{mL}^{-1}$ , and cultured for 24 h. When the degree of cell fusion reached about 80%, the sterilized  $100\ \mu\text{L}$  pipettor head was used to scratch the monolayer cells perpendicular to the bottom of the orifice plate. The cells were gently washed with phosphoric acid buffer (PBS) 3 times. After transfection and administration, new cell medium was added to each well for further culture for 24 h. A microscope (Nikon, Japan) was employed to take pictures of monolayer cells with different field of view and the width of the scratches is measured. The cell scratch healing rate was calculated according to the equation: (scratch width of 0 h – scratch width of 24 h)/scratch width of 0 h  $\times 100\%$ .

**2.2.5. Transwell Chamber Cell Invasion Test.** Cell concentration was adjusted to  $2 \times 10^5$  cells·mL<sup>-1</sup>, and transfected and administered, respectively. After 24 h of normal culture, serum-free starvation lasted for 12 h. After trypsin digestion, the cell density was adjusted to  $1 \times 10^5$  cells·mL<sup>-1</sup> using serum-free medium. Then, 50 mg·L<sup>-1</sup> Matrigel 1 : 8 diluent was used to coat the upper compartment surface of the membrane at the bottom of the Transwell chamber, and the solution was fixed in an incubator for 30 min. After this, the residual liquid in the chamber was removed, and 50  $\mu$ L serum-free culture medium was added to each well, hydrated for 30 min. Then, 200  $\mu$ L cell suspension was taken and placed in Transwell chamber of 24-well plate. The experiment was repeated for three times in each group. A quantity of 500  $\mu$ L high glucose DMEM containing 20% FBS was added into the lower chamber, and put into 37°C constant temperature cell incubator containing 5% CO<sub>2</sub> for 24 h. Three days later, the Transwell chamber was removed, the matrix glue and cells in the chamber were gently wiped with a sterile cotton swab, and 4% paraformaldehyde solution was added to fix the cells for 5 min. Then, the residual liquid was discarded, and 4 g·L<sup>-1</sup> crystal violet solution was added for staining for 20 min. Then, the cells were washed for 3 times with PBS. Ten fields were randomly selected from each sample. The cells transferred to the subcellular membrane were counted using an inverted microscope (Nikon, Japan) and averaged.

**2.2.6. Western Blot.** The treated cells of each group were taken, RIPA cell lysate was added, and the supernatant was taken after centrifugation at 12,000 rpm for 20 min. According to the instructions of the BCA kit, the total protein concentration was measured at 570 nm using an enzyme plate analyzer. Then, Western blot analysis was performed on 40  $\mu$ g protein. After 10% sodium dodecyl sulfate-polyacrylamide gel electrophoresis (SDS-PAGE) gel electrophoresis, transfer blot was performed, and the membrane was sealed overnight with 5% skimmed milk at 4°C. Mouse anti-human Ki-67 (1 : 1000), Bcl-2 (1 : 1000), Bax (1 : 1000),  $\beta$ -catenin (1 : 1000), GSK3 $\beta$  (1 : 1000), Axin2 (1 : 1000), c-myc (1 : 1000), and GAPDH (1 : 1000) primary antibodies were added, and sealed overnight at 4°C. Then, horseradish peroxidase (HRP) labeled goat anti-rat IgG (1 : 2000) secondary antibody was added and incubated at room temperature for 2 h. According to the instructions of the ECL chemiluminescence kit, the color of protein bands was developed. After exposure, ECL chemiluminescence instrument (Bio-Rad, USA) was utilized for development and fixing. Quantity One was then employed to analyze the gray value of the target protein bands. The relative expression of target protein was calculated according to the equation: gray value of target protein band/gray value of GAPDH band.

**2.3. Statistical Methods.** SPSS 19.0 was employed for statistical analysis. The test data were all expressed as mean plus or minus standard deviation ( $\bar{x} \pm s$ ), and differences were compared by one-way ANOVA analysis.  $P < 0.05$  was considered statistically significant.

### 3. Results

**3.1. Evaluation of Stable Transformation of U251 Cells Overexpressing Rab23.** The fluorescence expression in U251 cells after transfection was observed with an inverted fluorescence microscope. Figure 1(a) shows that after transfection with the empty vector and the Rab23 overexpression vector, the U251 cells all had green fluorescence expression, and they were evenly distributed in the cytoplasm. Western blot detection results of Rab23 protein expression in cells in Figure 1(b) showed that there was no significant difference in Rab23 protein expression between the blank control group and the transfected empty vector group ( $P > 0.05$ ). In contrast to blank control group and the transfected empty vector group, the Rab23 protein expression level in the cells of the Rab23 overexpression plasmid transfection group was remarkably increased ( $P < 0.05$ ).

**3.2. Detection of U251 Cell Proliferation Inhibition by MTT Assay.** MTT assay was adopted to detect the differences in cell proliferation levels of U251 cells in different treatment groups after 48 hours of grouping treatment. Figure 2 presents that the cell proliferation activity of the Rab23 group, the LCA group, and the Rab23 + LCA group was greatly reduced compared to that of the BC group ( $P < 0.05$ ). The cell proliferation activity of the Rab23 + LCA group was considerably reduced relative to that of Rab23 group and the LCA group ( $P < 0.05$ ), while there was no obvious difference in the cell proliferation activity between the Rab23 group and the LCA group ( $P > 0.05$ ).

**3.3. Scratch Healing Test to Detect the Migration Ability of U251 Cells.** The scratch healing test was performed to evaluate the migration ability of U251 cells in different treatment groups, and the results are shown in Figure 3. From Figure 3(a), there was no substantial difference in the scratch healing degree among the four groups of cells at 0 h of the scratch. After 24 h of scratching, the scratches in the BC group healed significantly, the scratches in the Rab23 group and the LCA group were obvious, and the scratches in the Rab23 + LCA group were more obvious. Figure 3(b) shows that compared to the BC group, the healing of the scratches of the cells in the Rab23 group, the LCA group, and the Rab23 + LCA group was notably reduced ( $P < 0.05$ ). In contrast to the Rab23 group and the LCA group, the scratch healing of the cells in the Rab23 + LCA group was remarkably reduced ( $P < 0.05$ ), while there was no great difference in the scratch healing of the cells between the Rab23 group and the LCA group ( $P > 0.05$ ).

**3.4. Transwell Chamber Test to Evaluate Invasion Ability of U251 Cells.** The Transwell chamber test was implemented to evaluate the invasion ability of U251 cells in different treatment groups, and the results are shown in Figure 4. Figure 4(a) shows that the cell invasion staining of the Rab23 group, the LCA group, and the Rab23 + LCA group was obviously less than that of the BC group, and the cell invasion staining of the Rab23 + LCA group was the least. The number of positive



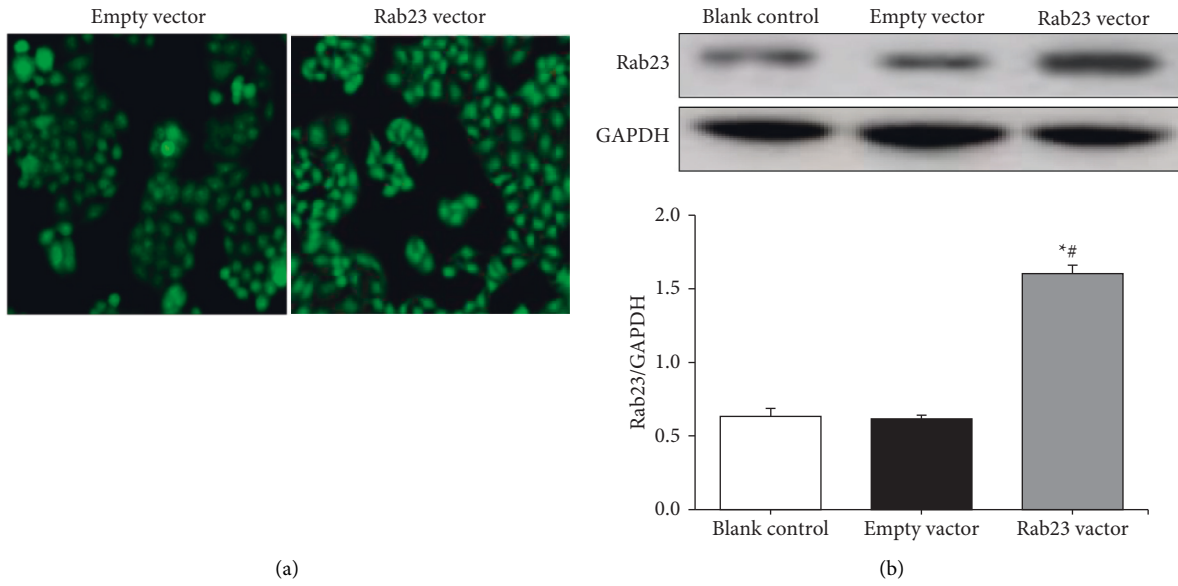


FIGURE 1: Identification of U251 cells with stable empty vector and overexpressing Rab23. (a) Micrograph of U251 cells ( $\times 200$ ); (b) Rab23 protein expression. In contrast to blank control group,  $*P < 0.05$ ; in contrast to empty vector transfection group,  $\#P < 0.05$ .

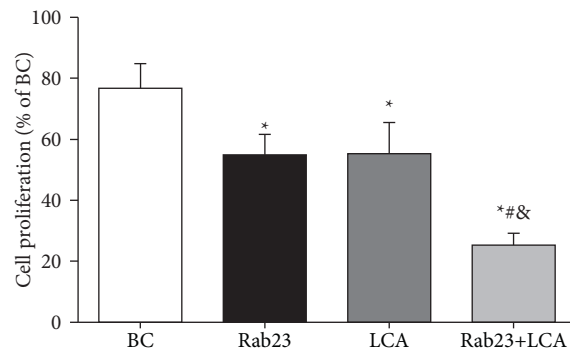


FIGURE 2: A comparison of U251 cell proliferation activity in each group.  $*P < 0.05$  versus BC group;  $\#P < 0.05$  versus Rab23 group;  $\&P < 0.05$  versus LCA group.

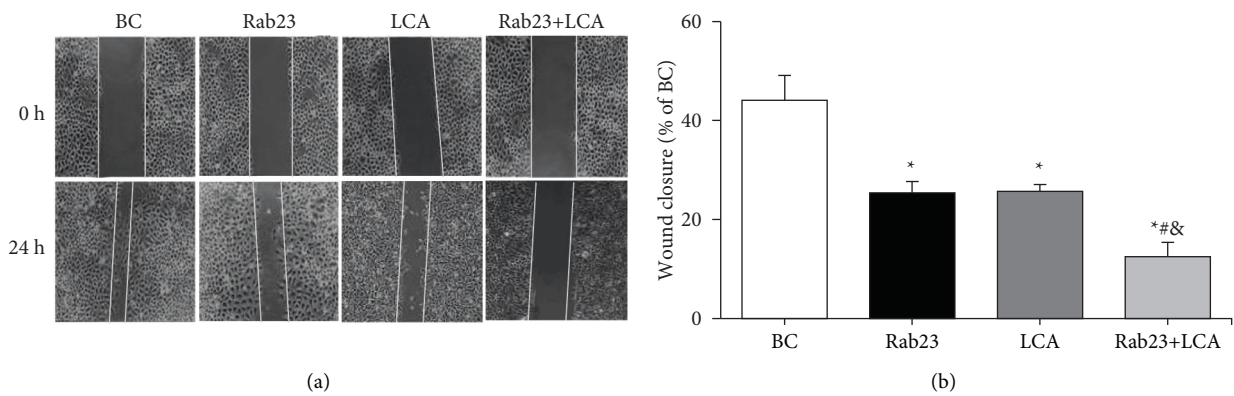


FIGURE 3: A comparison of scratch healing degree of U251 cells in each group. (a) Microscopic image of cell scratch ( $\times 100$ ); (b) statistical graph of cell scratch healing.  $*P < 0.05$  versus BC group;  $\#P < 0.05$  versus Rab23 group;  $\&P < 0.05$  versus LCA group.

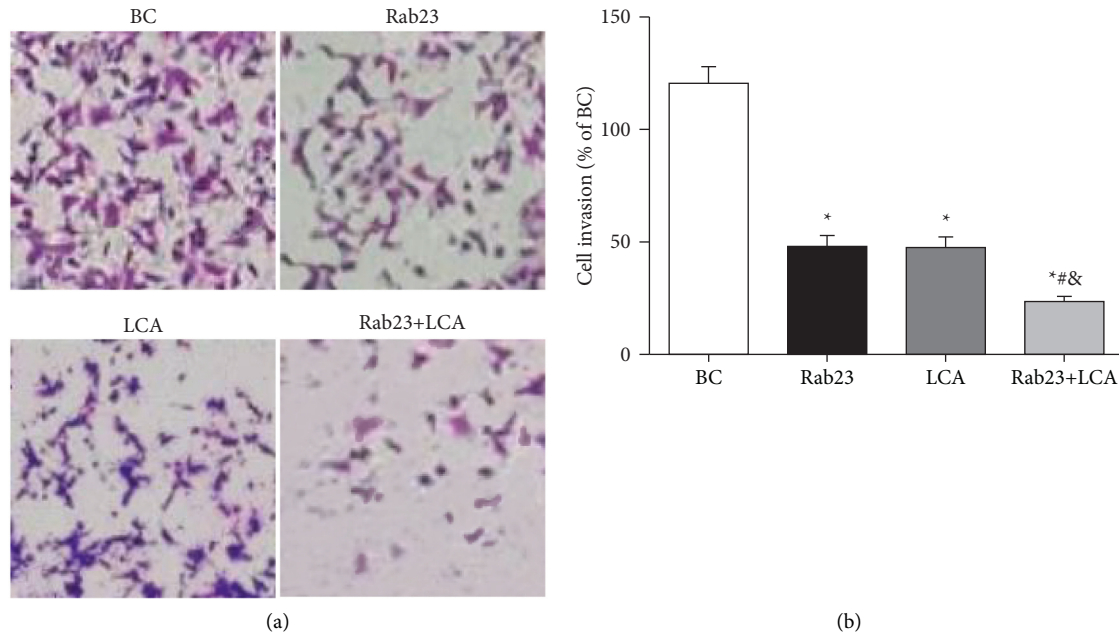


FIGURE 4: A comparison of U251 cell invasion levels in each group. (a) Cell invasion staining map ( $\times 100$ ); (b) cell invasion level statistics. \* $P < 0.05$  versus BC group; # $P < 0.05$  versus Rab23 group; & $P < 0.05$  versus LCA group.

U251 cells stained was counted. Figure 4(b) shows that compared with the BC group, the cell invasion level of the Rab23 group, the LCA group, and the Rab23 + LCA group was substantially reduced ( $P < 0.05$ ). The cell invasion level of the Rab23 + LCA group was evidently inferior to that of Rab23 group and the LCA group ( $P < 0.05$ ), while the Rab23 group and the LCA group had no remarkable difference in the cell invasion level ( $P > 0.05$ ).

**3.5. Western Blot Detection of Ki-67 and Apoptosis-Related Protein Expression in U251 Cells.** Western blot was adopted to detect the differences in the expression of Ki-67 antigen and apoptosis-related proteins Bcl-2 and Bax in U251 cells in different treatment groups. The results are shown in Figure 5. Figure 5(a) shows that the expression of Ki-67 and Bcl-2 protein in the Rab23 group, the LCA group, and the Rab23 + LCA group were significantly reduced relative to those of BC group, while the Bax protein expression was significantly increased. The gray value difference of target protein in each group was counted. From Figures 5(b), 5(c), and 5(d), the expression of Ki-67 and Bcl-2 protein in the Rab23 group, the LCA group, and the Rab23 + LCA group were notably reduced in contrast to BC group, while the Bax protein expression was greatly increased ( $P < 0.05$ ). Compared with the Rab23 group and the LCA group, the expression of Ki-67 and Bcl-2 protein in the Rab23 + LCA group was reduced, and the Bax protein expression was increased greatly ( $P < 0.05$ ). However, there were no significant differences in the expression of Ki-67, Bcl-2, and Bax proteins between Rab23 group and LCA group ( $P > 0.05$ ).

**3.6. Western Blot Detection of Wnt/ $\beta$ -Catenin Related Protein Expression in U251 Cells.** Western blot was performed to detect differences in the expression of Wnt/ $\beta$ -catenin

signaling-related proteins  $\beta$ -catenin, GSK3 $\beta$ , Axin2, and c-myc in U251 cells in different treatment groups. The results are shown in Figure 6. Figure 6(a) shows that, compared with the BC group, the expression of  $\beta$ -catenin and c-myc protein in the Rab23 group, the LCA group, and the Rab23 + LCA group was considerably reduced, while the expression of GSK3 $\beta$  and Axin2 protein was substantially increased.

The differences in the gray value of the target protein of each group of cells were statistically analyzed. Figures 6(b)–6(d) show that the expression of  $\beta$ -catenin and c-myc protein in the Rab23 group, LCA group, and Rab23 + LCA group was greatly lower than that of the BC group ( $P < 0.05$ ). The expression of  $\beta$ -catenin and c-myc protein in the Rab23 + LCA group was notably lower than that in the Rab23 group and the LCA group ( $P < 0.05$ ). From Figures 6(c)–6(e), the expression of GSK3 $\beta$  and Axin2 protein in the Rab23 group, LCA group, and Rab23 + LCA group was remarkably inferior to that in the BC group ( $P < 0.05$ ). The expression of GSK3 $\beta$  and Axin2 protein in the Rab23 + LCA group was evidently lower than that in the Rab23 group and the LCA group ( $P < 0.05$ ). However, there was no significant difference in the expression of  $\beta$ -catenin, GSK3 $\beta$ , Axin2, and c-myc in the cells of Rab23 group and LCA group ( $P > 0.05$ ).

## 4. Discussion

Glioma is a primary intracranial tumor with high incidence and high degree of malignancy, and the average survival time of patients is relatively short [12]. *Rab23* gene is closely related to the progression of cancer. Studies found that overexpression of Rab23 can inhibit the proliferation activity of cancer cells and promoted cell apoptosis [13]. At present,

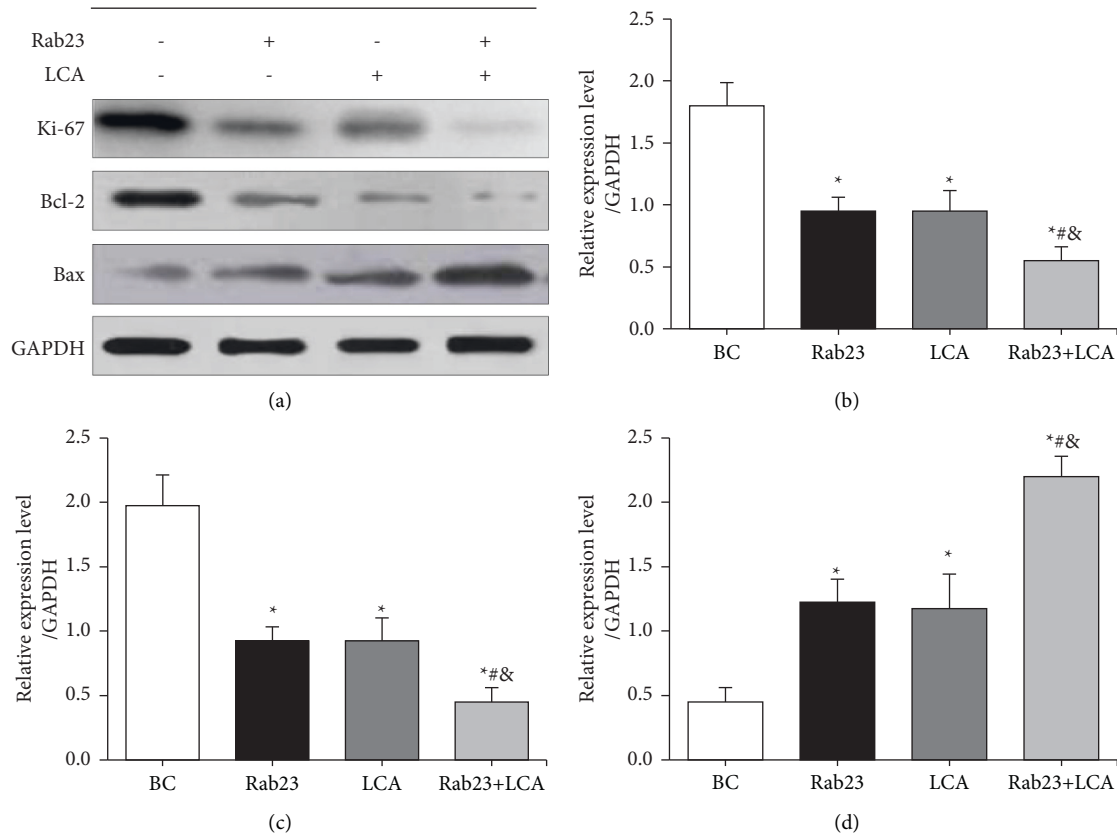


FIGURE 5: The differences in the expression of proliferation antigens and apoptosis proteins of U251 cells in each group. (a) Western blot; (b) relative expression of Ki-67 protein; (c) relative expression statistics chart of Bcl-2 protein; (d) relative expression statistics chart of Bax protein. \* $P < 0.05$  versus BC group; # $P < 0.05$  versus Rab23 group; & $P < 0.05$  versus LCA group.

the standard treatment for glioma is surgery combined with chemotherapy and radiotherapy, but the treatment efficiency is still unsatisfactory. LCA is a Chinese herbal extract with anti-inflammatory, antiviral, and antitumor properties, and studies showed that LCA can inhibit the proliferation activity of various tumor cells [14, 15]. Therefore, the potential molecular mechanisms of the effects of overexpression of Rab23 and LCA on proliferation, migration, and invasion of glioma U251 cells were explored. The results showed that overexpression of Rab23 and LCA treatment could inhibit the proliferation, migration, and invasion ability of human glioma U251 cells. Moreover, the inhibition effect of overexpression of Rab23 combined with LCA on proliferation, migration, and invasion of human glioma U251 cells was significantly superior to that of single treatment group. These results indicated that overexpression of Rab23 and LCA could inhibit the proliferation, migration, and invasion of glioma U251 cells, and the combined treatment had a better effect.

Studies revealed that LCA can activate mitochondrial-dependent endogenous apoptosis, and can downregulate the level of antiapoptotic protein Bcl-2 and upregulate the level of proapoptotic protein Bax [16, 17]. The balance of Bcl-2 and Bax protein expression levels determines the state of cell survival or apoptosis [18]. Therefore, this work further examined the changes in the expression of Bcl-2 and Bax proteins in cells.

Western blot results showed that overexpression of Rab23, LCA simple treatment, and combined treatment can reduce the expression level of Bcl-2 protein and can promote the expression level of Bax protein. Among these proteins, the Bcl-2 protein level decreased and the Bax protein level increased obviously in the combined treatment group, indicating that overexpression of Rab23 and LCA can also promote the apoptosis of glioma U251 cells by regulating the expression levels of Bcl-2 and Bax protein, thus playing an antitumor effect.

Wnt/ $\beta$ -catenin signaling pathway participates in the regulation of tumor cell growth and differentiation, and activation of Wnt/ $\beta$ -catenin signaling pathway can participate in the process and metastasis of glioma cells [19, 20]. Studies revealed that inhibiting the Wnt/ $\beta$ -catenin signaling pathway can inhibit the proliferation and migration of glioma cells [21].  $\beta$ -Catenin is a positive regulator of this pathway, and GSK3 $\beta$  and Axin can form a "destruction complex" and bind to  $\beta$ -catenin [22]. In tumor cells, the Wnt signaling pathway was activated to transfer  $\beta$ -catenin, which in turn lead to the activation of downstream target genes c-myc, thus promoting tumor development [23]. Studies suggested that Axin expression was downregulated in glioma cells, and the activation of GSK3 $\beta$  can promote the proliferation and differentiation of glioma cells [24, 25]. Western blot results showed that overexpression of Rab23, LCA alone, and combined treatment can downregulate  $\beta$ -catenin

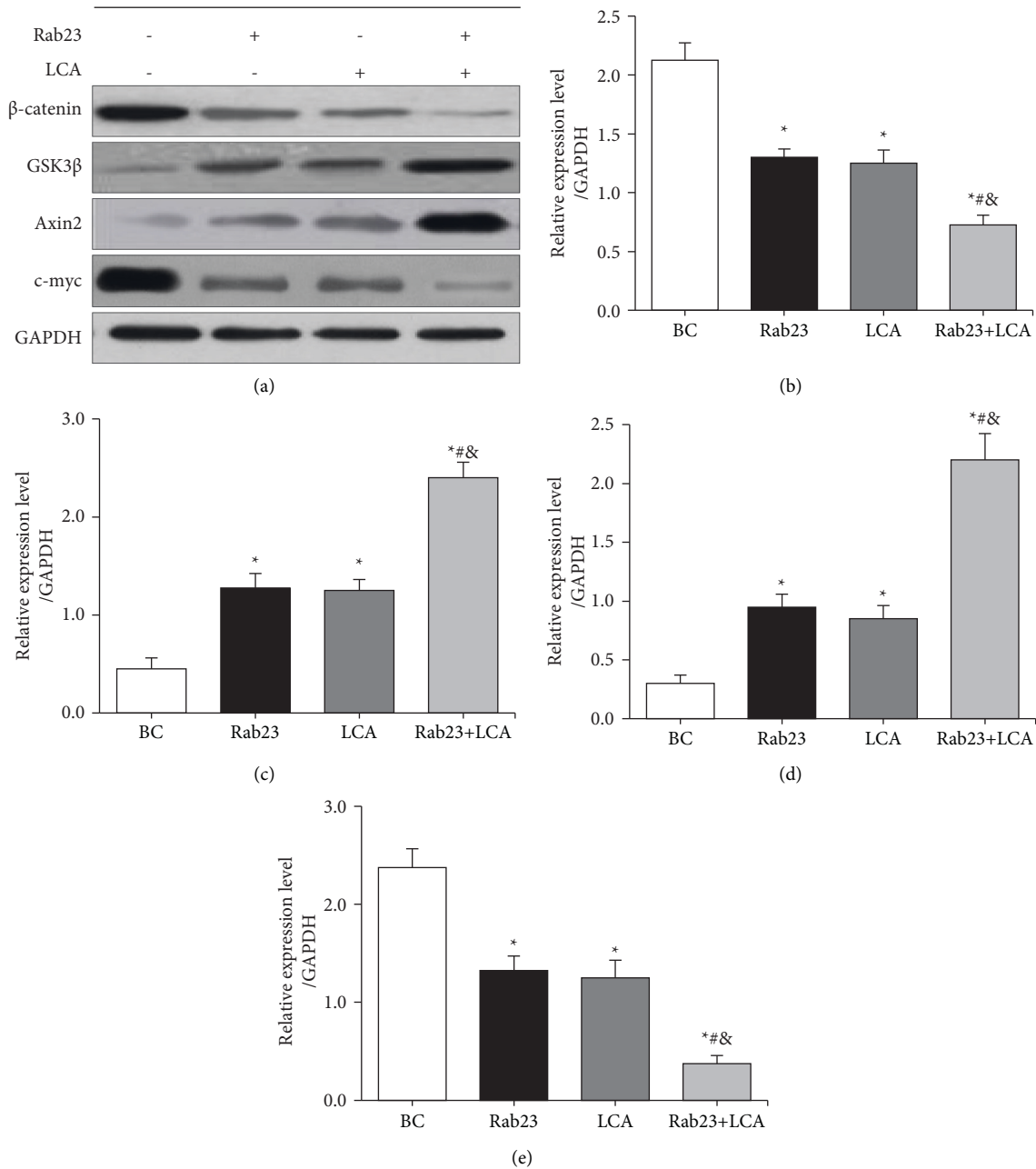


FIGURE 6: Differences in Wnt/ $\beta$ -catenin pathway-related protein expression in U251 cells in each group. (a) Western blot; (b) relative expression of  $\beta$ -catenin protein; (c) relative expression of GSK3 $\beta$  protein; (d) relative expression of Axin2 protein; (e) statistical graph of relative expression of c-myc protein. \* $P < 0.05$  versus BC group; # $P < 0.05$  versus Rab23 group; & $P < 0.05$  versus LCA group.

and c-myc protein levels in glioma U251 cells, which can upregulate GSK3 $\beta$  and Axin2 protein levels.

## 5. Conclusion

In summary, the results of this study preliminarily showed that overexpression of Rab23 and LCA can effectively inhibit the proliferation, migration, and invasion of glioma cells through the Wnt/ $\beta$ -catenin signaling, and promoted cell apoptosis. In this study, only glioma cells were used as experimental subjects, and the inhibitory effects of LCA on the proliferation, invasion, and migration of glioma cells

were verified in vitro. However, whether LCA can prolong survival and other specific mechanisms remain to be explored. Therefore, in future studies, animal glioma models will be further prepared to explore the effects of LCA treatment on the blood-brain barrier, tumor immune inflammatory microenvironment, and survival rate in animal models, thereby comprehensively exploring the effect of LCA treatment on glioma. Meanwhile, the interaction between LCA and Rab23 gene will be further explored. The effect of overexpression of Rab23 combined with LCA was even obvious. This study can provide a new research direction for the clinical treatment of glioma.

## Data Availability

The data used to support the findings of this study are available from the corresponding author upon request.

## Conflicts of Interest

The authors declare no conflicts of interest.

## Acknowledgments

This work was supported by the <https://doi.org/10.13039/501100005046> Natural Science Foundation of Heilongjiang Province, China (No. LH2020H077).

## References

- [1] E. Aliotta, S. W. Dutta, X. Feng et al., "Automated apparent diffusion coefficient analysis for genotype prediction in lower grade glioma: association with the T2-FLAIR mismatch sign," *Journal of Neuro-Oncology*, vol. 149, no. 2, pp. 325–335, 2020.
- [2] M. Li, S. Han, and X. Shi, "In situ dendritic cell vaccination for the treatment of glioma and literature review," *Tumor Biology*, vol. 37, no. 2, pp. 1797–1801, 2016.
- [3] S. Wulfovich, S. Tucker, M. Levy, and J. R. Crawford, "Incidental cerebellar dermoid cyst mimicking low grade glioma in a teenager," *BMJ Case Reports*, vol. 14, no. 2, Article ID e241227, 2021.
- [4] B. A. M. Cantelli, T. A. Bitencourt, T. T. Komoto, R. O. Belebani, M. Marins, and A. L. Fachin, "Caffeic acid and licochalcone a interfere with the glyoxylate cycle of *trichophyton rubrum*," *Biomedicine & Pharmacotherapy*, vol. 96, pp. 1389–1394, 2017.
- [5] C. Qiu, T. Zhang, W. Zhang et al., "Licochalcone a inhibits the proliferation of human lung cancer cell lines a549 and h460 by inducing g2/m cell cycle arrest and er stress," *International Journal of Molecular Sciences*, vol. 18, no. 8, p. 1761, 2017.
- [6] W. Hao, X. Yuan, L. Yu et al., "Licochalcone a-induced human gastric cancer bgc-823 cells apoptosis by regulating ros-mediated maps and pi3k/akt signaling pathways," *Scientific Reports*, vol. 5, no. 1, p. 10336, 2015.
- [7] L. F. B. Bortolotto, F. R. Barbosa, G. Silva et al., "Cytotoxicity of trans-chalcone and licochalcone a against breast cancer cells is due to apoptosis induction and cell cycle arrest," *Biomedicine & Pharmacotherapy*, vol. 85, pp. 425–433, 2016.
- [8] Y.-Y. Zhang, C.-T. Huang, S.-M. Liu et al., "Licochalcone a exerts antitumor activity in bladder cancer cell lines and mice models," *Tropical Journal of Pharmaceutical Research*, vol. 15, no. 6, pp. 1151–1157, 2016.
- [9] Y. Wu, X. Wei, H. Feng, S. Wang, J. Liu, and T. Wang, "Lncrna nnt-as1 inhibits the progression of prostate cancer by modulating mir-320a/rab23 axis," *European Urology Open Science*, vol. 19, no. Supplement 2, p. e665, 2020.
- [10] Q. Liu, H. Tang, X. Liu et al., "Mir-200b as a prognostic factor targets multiple members of rab family in glioma," *Medical Oncology*, vol. 31, no. 3, p. 859, 2014.
- [11] W. Han, J. Shi, J. Cao, B. Dong, and W. Guan, "Current advances of long non-coding rnas mediated by wnt signaling in glioma," *Pathology, Research & Practice*, vol. 216, no. 8, Article ID 153008, 2020.
- [12] H. K. Rooprai, P. Lawrence, S. Keshavarz et al., "Draq7 as an alternative to mtt assay for measuring viability of glioma cells treated with polyphenols," *Anticancer Research*, vol. 40, no. 10, pp. 5427–5436, 2020.
- [13] C. Kaid, P. B. G. Silva, B. A. Cortez, C. O. Rodini, P. Semedo-Kuriki, and O. K. Okamoto, "miR-367 promotes proliferation and stem-like traits in medulloblastoma cells," *Cancer Science*, vol. 106, no. 9, pp. 1188–1195, 2015.
- [14] M. K. Park, J. Ji, K. Haam et al., "Licochalcone a inhibits hypoxia-inducible factor-1 $\alpha$  accumulation by suppressing mitochondrial respiration in hypoxic cancer cells," *Biomedicine & Pharmacotherapy*, vol. 133, no. 2, Article ID 111082, 2021.
- [15] T. H. Kang, J. H. Seo, H. Oh, G. Yoon, J. I. Chae, and J. H. Shim, "Licochalcone a suppresses specificity protein 1 as a novel target in human breast cancer cells," *Journal of Cellular Biochemistry*, vol. 118, no. 12, pp. 4652–4663, 2017.
- [16] Y.-T. Yo, G.-S. Shieh, K.-F. Hsu, C.-L. Wu, and A.-L. Shiau, "Licorice and licochalcone-a induce autophagy in Incap prostate cancer cells by suppression of bcl-2 expression and the mtor pathway," *Journal of Agricultural and Food Chemistry*, vol. 57, no. 18, pp. 8266–8273, 2009.
- [17] M. M. Rafi, R. T. Rosen, A. Vassil et al., "Modulation of bcl-2 and cytotoxicity by licochalcone-a, a novel estrogenic flavonoid," *Anticancer Research*, vol. 20, no. 4, pp. 2653–2658, 2000.
- [18] M. Nazeri, A. Mirzaie-Asl, M. Saidijam, and M. Moradi, "Methanolic extract of *artemisia absinthium* prompts apoptosis, enhancing expression of bax/bcl-2 ratio, cell cycle arrest, caspase-3 activation and mitochondrial membrane potential destruction in human colorectal cancer hct-116 cells," *Molecular Biology Reports*, vol. 47, no. 11, pp. 8831–8840, 2020.
- [19] W. Yang, Y. Li, R. Gao, Z. Xiu, and T. Sun, "MHC class I dysfunction of glioma stem cells escapes from CTL-mediated immune response via activation of wnt/ $\beta$ -catenin signaling pathway," *Oncogene*, vol. 39, no. 5, pp. 1098–1111, 2019.
- [20] H. Ni, D. Ji, J. Li, Z. Zhao, and J. Zuo, "The nuclear transporter importin-11 regulates the wnt/ $\beta$ -catenin pathway and acts as a tumor promoter in glioma," *International Journal of Biological Macromolecules*, vol. 176, pp. 145–156, 2021.
- [21] X. Yue, F. Lan, and T. Xia, "Hypoxic glioma cell-secreted exosomal miR-301a activates wnt/ $\beta$ -catenin signaling and promotes radiation resistance by targeting TCEAL7," *Molecular Therapy*, vol. 27, no. 11, pp. 1939–1949, 2019.
- [22] S. Ikeda, S. Kishida, H. Yamamoto, H. Murai, and A. A. Kikuchi, "A negative regulator of the wnt signaling pathway, forms a complex with gsk-3 $\beta$  and  $\beta$ -catenin and promotes gsk-3 $\beta$ -dependent phosphorylation of  $\beta$ -catenin," *The EMBO Journal*, vol. 17, no. 5, pp. 1371–1384, 2014.
- [23] F. Liu, L. Wan, H. Zou, Z. Pan, W. Zhou, and X. Lu, "PRMT7 promotes the growth of renal cell carcinoma through modulating the  $\beta$ -catenin/C-MYC axis," *The International Journal of Biochemistry & Cell Biology*, vol. 120, Article ID 105686, 2020.
- [24] J. Lu, F. Zhang, D. Zhao et al., "ATRA-inhibited proliferation in glioma cells is associated with subcellular redistribution of  $\beta$ -catenin via up-regulation of Axin," *Journal of Neuro-Oncology*, vol. 87, no. 3, pp. 271–277, 2008.
- [25] B. K. Verma and P. Kondaiah, "Regulation of  $\beta$ -catenin by IGFBP2 and its cytoplasmic actions in glioma," *Journal of Neuro-Oncology*, vol. 149, no. 11, pp. 209–217, 2020.



## Research Article

# Fucoxanthin, a Marine Carotenoid, Suppresses *Mycoplasma pneumoniae*-Triggered Inflammatory Cytokine Production and Promotes Bacterial Clearance in a Murine Model

Hongbo Wu <sup>1</sup>, Shu Li <sup>2</sup>, Linlin Wang <sup>3</sup>, Jun Liang <sup>4</sup>, Lei Yan <sup>5</sup>,  
and Jianjiang Dong <sup>5</sup>

<sup>1</sup>Department of Pediatrics, Beijing Luhe Hospital, Capital Medical University, Beijing 100000, China

<sup>2</sup>Department of Medical Function, Mudanjiang Medical University, Mudanjiang 157011, China

<sup>3</sup>Department of Library, Mudanjiang Medical University, Mudanjiang 157011, China

<sup>4</sup>Stem Cell Institute, Mudanjiang Medical University, Mudanjiang 157011, China

<sup>5</sup>Department of Histology and Embryology, Mudanjiang Medical University, Mudanjiang 157011, China

Correspondence should be addressed to Jianjiang Dong; [dongjianjiang@mdjmu.edu.cn](mailto:dongjianjiang@mdjmu.edu.cn)

Received 18 February 2022; Accepted 5 April 2022; Published 21 April 2022

Academic Editor: Ruchika Garg

Copyright © 2022 Hongbo Wu et al. This is an open access article distributed under the Creative Commons Attribution License, which permits unrestricted use, distribution, and reproduction in any medium, provided the original work is properly cited.

*Mycoplasma pneumoniae* (MP), an atypical bacterium, is a common pathogenetic organism of respiratory infection in children. In the present study, we analyzed the beneficial role of fucoxanthin (Fx), a marine carotenoid, in a murine model of MP. C57BL/6 mice were inoculated once intranasally with  $10^7$  CFU of *M. pneumoniae*, and we found that Fx treatment markedly decreased BAL (quantitative bronchoalveolar lavage) *M. pneumoniae* concentrations and alleviated airway obstruction in the infected mice. Moreover, the concentrations of proinflammatory cytokines, including IL-6, TNF- $\alpha$  and IL-1 $\beta$ , were significantly decreased by Fx treatment in the BAL samples of infected mice. In vitro study further indicated that Fx treatment markedly suppressed the production of proinflammatory cytokines in mouse peritoneal macrophages after *M. pneumoniae* infection. In conclusion, this may be the first study to report the protective role of Fx against *M. pneumoniae* infection, providing a potential therapeutic agent for MP.

## 1. Introduction

Mycoplasmas are the smallest (50–300 nm in diameter) free-living organisms. *Mycoplasma pneumoniae* (MP) is recognized as a worldwide cause of community-acquired pneumonia in children and young adolescents [1]. MP in children is an acute lung inflammation caused by atypical *Mycoplasma* infection, accounting for about 10%–40% of community-acquired pneumonia in children. In clinical manifestations, severe complications such as bronchiectasis, necrotizing pneumonia, even fatal pneumonia, and damage of multisystem function may occur in children with MP infection. In this situation, the therapeutic effect is poor and the hospitalization time is prolonged [2]. The strong inflammatory responses induced by *M. pneumoniae* are closely related to the pathogenic factors to induce pneumonia [3]. Thus, there is an urgent need to identify more appropriate methods to alleviate inflammatory responses in MP.

In recent years, natural products draw great attention from scientists around the world. Fucoxanthin (Fx; Figure 1(a)), a natural product of carotenoids, is widely recognized as a potential drug source obtained from marine algae [4]. This compound has a wide range of pharmacological properties, including antioxidant, anti-inflammatory, and antimicrobial activities [5, 6]. Fx also attenuates LPS-induced acute lung injury and ameliorates the inflammatory responses [7]. The objective of the present study was to determine the beneficial role of Fx in a murine model of MP, as well as the related underlying mechanisms.

## 2. Materials and Methods

**2.1. *M. pneumoniae* Preparation.** *M. pneumoniae* wild-type (WT) strain M129, obtained from American Type Cell Collection (Manassas, VA, USA), was cultured in SP4 broth in culture flasks at 37°C. After 72 h, *M. pneumoniae* were



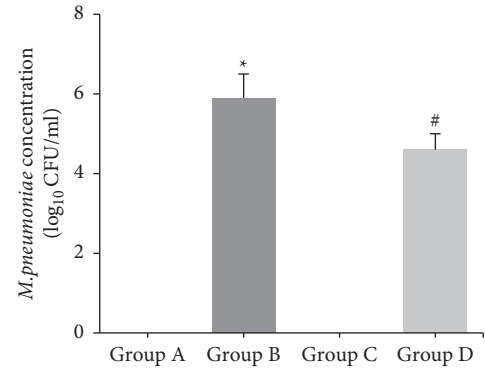
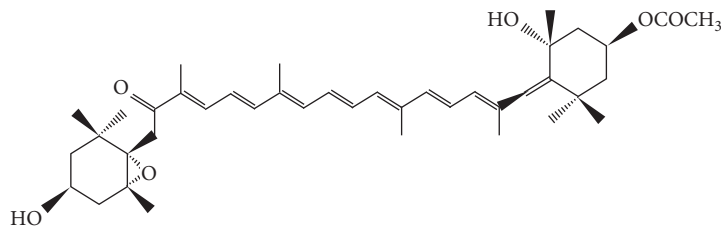


FIGURE 1: (a) The chemical structure of fucoxanthin (Fx). (b) The concentrations of *M. pneumoniae* in the BAL samples of mice. \* $P < 0.05$  vs. group A; # $P < 0.05$  vs. group B.

harvested by centrifugation and resuspended in PBS solution to achieve a concentration in the range of  $10^8$ – $10^9$  CFU/ml. Aliquots were stored at  $-80^\circ\text{C}$ .

**2.2. Animals and Treatments.** Forty male C57BL/6 mice, purchased from Shanghai Laboratory Animal Center (Shanghai, China), were housed under a 12-hour light/dark cycle in a temperature-controlled room ( $22$ – $24^\circ\text{C}$ ). The animals were supplied with water and standard chow ad libitum. All animal care and experimental protocols were approved by the ethics committee of hospital. All efforts were made to minimize animal suffering.

Fx (purity  $\geq 95\%$  by HPLC) was purchased from Sigma-Aldrich (St. Louis, MO, USA) and dissolved in DMSO before use.

The mice were allowed to acclimate to new environment for 1 week and then randomized into four groups ( $n = 10$ /group). On day 0, the mice in group A were treated with  $100\ \mu\text{l}$  vehicle solution (PBS solution containing  $25\ \text{mM}$  HCl) by nasal drops, while the mice in group C and group D were successively given Fx orally at a dose of  $50\ \text{mg/kg}$  for five days. Then, the mice in group B and group D were inoculated intranasally infected with *M. pneumoniae* M129 ( $10^7$  CFU in  $50\ \mu\text{l}$  of SP4 broth) on day 1. On day 5, the mouse lungs were lavaged with  $1\ \text{ml}$  of sterile saline. Cell-free bronchoalveolar lavage (BAL) fluid samples were stored at  $-80^\circ\text{C}$ . Whole-lung specimens (including the trachea and both lungs) were collected, fixed in buffered formalin, dehydrated in  $70\%$  ethanol, cut in  $4\ \mu\text{m}$  thick sections, and stained with hematoxylin and eosin. Morphometric analysis was performed under an optical microscope.

**2.3. Measurement of Cytokine Production.** The concentrations of IL-6, TNF- $\alpha$ , and IL-1 $\beta$  in culture supernatants were measured using specific ELISA kits (Affymetrix-eBioscience, Santa Clara, CA, USA), according to the manufacturer's instructions.

**2.4. Cell Culture and Treatments.** Peritoneal macrophages were isolated from male C57BL/6 mice, as previously described [8]. The isolated macrophages were seeded into 6-

TABLE 1: Abbreviations and full names.

Abbreviation	Full name
MP	<i>Mycoplasma pneumoniae</i>
Fx	Fucoxanthin
CFU	Colony forming unit
BAL	Bronchoalveolar lavage
IL-6	Interleukin-6
TNF- $\alpha$	Tumor necrosis factor- $\alpha$
IL-1 $\beta$	Interleukin-1 $\beta$
WT	Wild-type
PBS	Phosphate buffer solution
DMSO	Dimethyl sulfoxide
ELISA	Enzyme-linked immunosorbent assay
FBS	Fetal bovine serum
RPMI	Roswell Park Memorial Institute
SD	Standard deviation

well plates and cultured in the RPMI-1640 medium (HyClone, Logan, UT, USA), containing  $10\%$  fetal bovine serum (FBS; HyClone) at  $37^\circ\text{C}$  in a humidified incubator with  $5\%$   $\text{CO}_2$ .

Cells in group A were treated with vehicle (DMSO). Cells in group C and group D were treated with  $20\ \mu\text{M}$  Fx. After 2 h, cells in group D were infected with *M. pneumoniae* ( $20\ \text{CFU/ml}$ ) for another 24 h. Cells in group B were infected with *M. pneumoniae* ( $20\ \text{CFU/ml}$ ) for 24 h without Fx treatment.

**2.5. Statistical Analysis.** All statistical analyses were carried out using GraphPad Prism 6.0 software (GraphPad Software, Inc., La Jolla, CA, USA). The data were expressed as the mean  $\pm$  standard deviation (SD). Differences among two or more independent groups were analyzed using Student's *t*-test or one-way analysis of variance followed by Tukey's test. *P* values of less than  $0.05$  were considered as statistically significance.

### 3. Results

All abbreviations and their full names are given in Table 1.

As shown in Figure 1(b), the concentration of MP was observed in the BAL samples of mice in groups A and

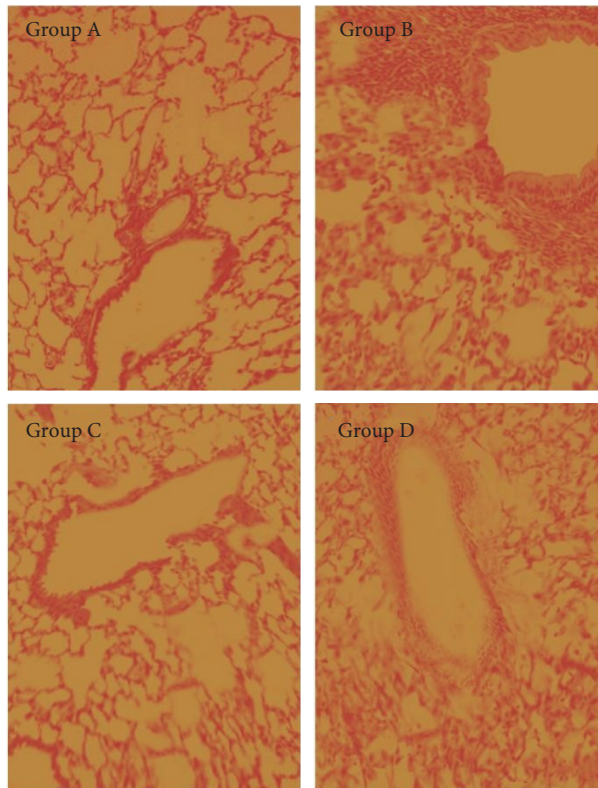


FIGURE 2: The pathological changes in lung tissues of mice.

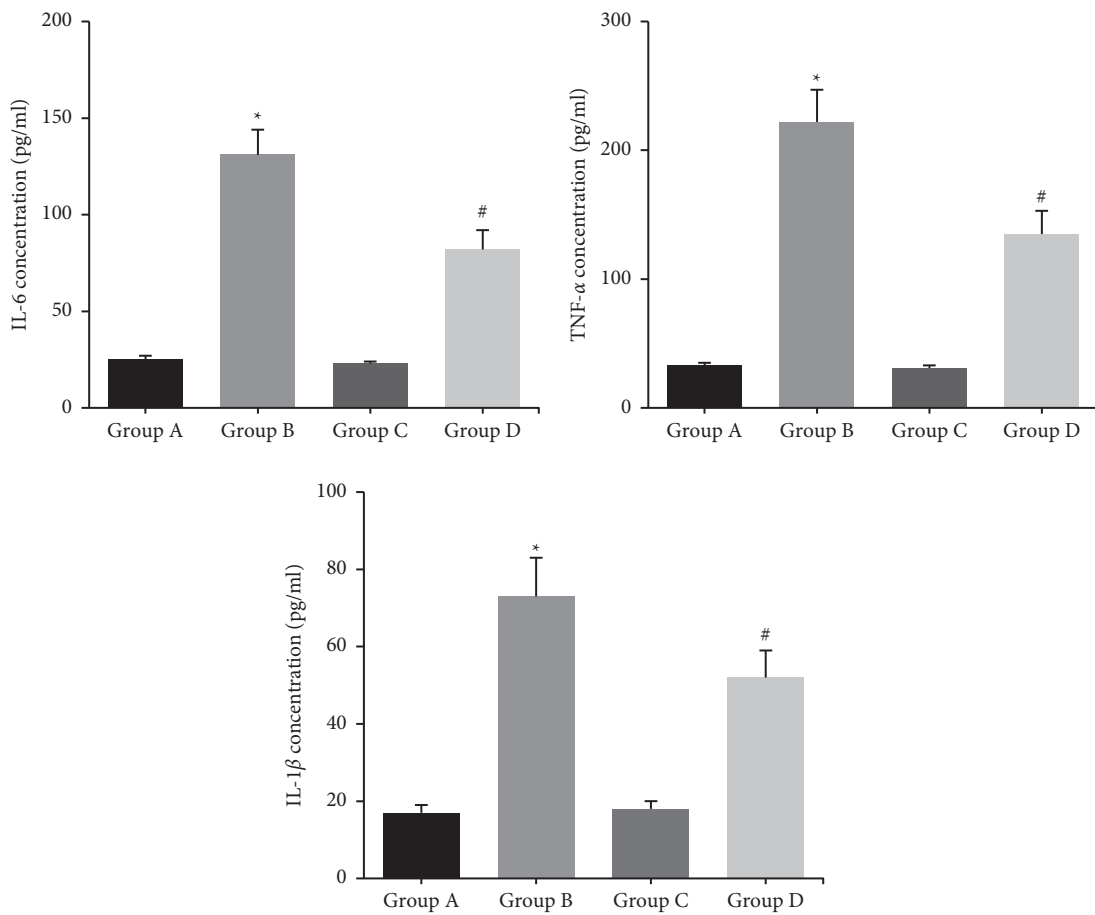


FIGURE 3: The concentrations of proinflammatory cytokines in the BAL samples of mice. \* $P < 0.05$  vs. group A; # $P < 0.05$  vs. group B.

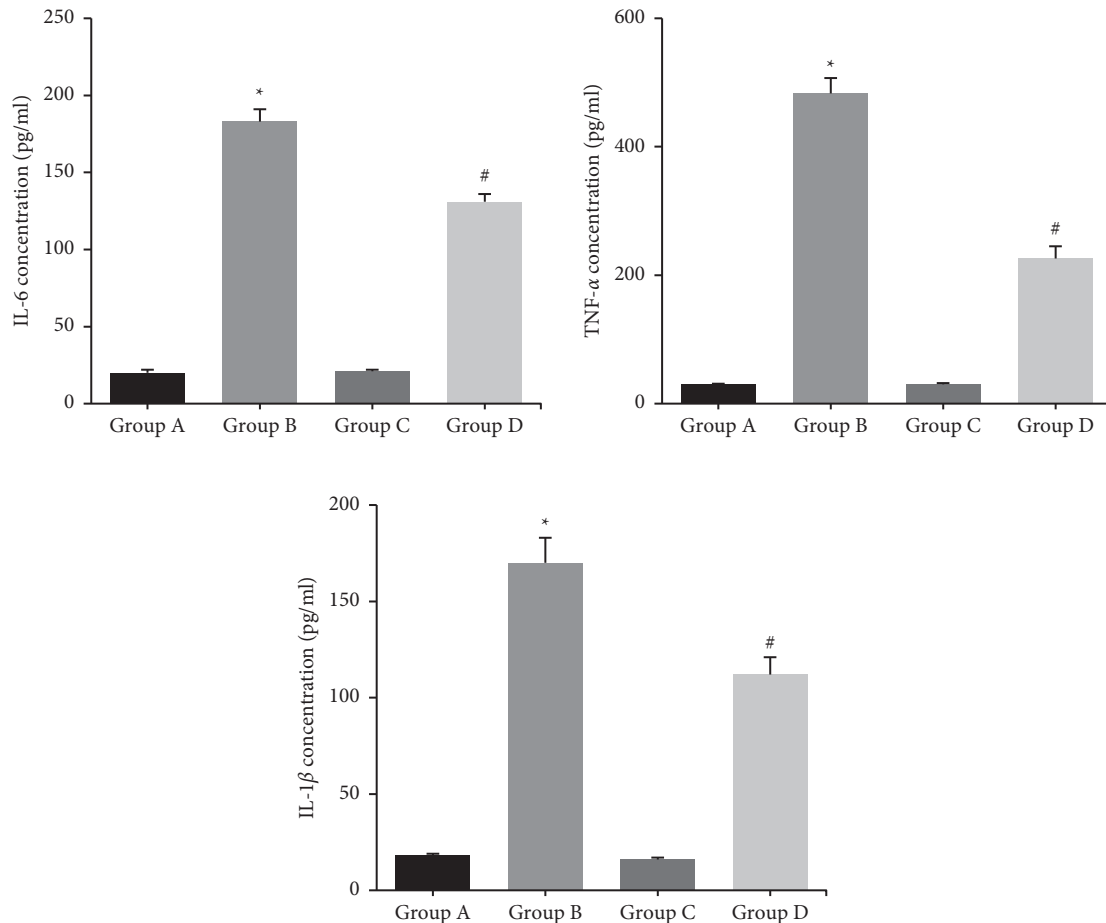


FIGURE 4: The concentrations of proinflammatory cytokines in the mouse peritoneal macrophages. \* $P < 0.05$  vs. group A; # $P < 0.05$  vs. group B.

C. After comparison, it was found that the concentration of MP in the BAL samples of mice in group B was significantly higher than that in group A ( $P < 0.05$ ); the concentration of MP in the BAL samples of mice in group D was significantly lower than that in group B ( $P < 0.05$ ).

As shown in Figure 2, the lung histomorphology of mice in groups A and C was normal, the lung tissues of mice in group B showed significant pathological changes of alveolar wall thickening and bronchial stenosis, while the inflammatory infiltration status in the lung tissues of mice in group D was significantly alleviated.

Figure 3 shows that the concentrations of IL-6, TNF- $\alpha$ , and IL-1 $\beta$  in BAL samples of group B were significantly higher than those of group A ( $P < 0.05$ ); the concentrations of IL-6, TNF- $\alpha$ , and IL-1 $\beta$  in BAL samples of group D mice were significantly lower than those of group B ( $P < 0.05$ ); there was no statistically significant difference in the concentrations of IL-6, TNF- $\alpha$ , and IL-1 $\beta$  in BAL samples of groups A and C ( $P > 0.05$ ).

Figure 4 shows that the concentrations of IL-6, TNF- $\alpha$ , and IL-1 $\beta$  in peritoneal macrophages of group B were significantly higher than those of group A ( $P < 0.05$ ); the concentrations of IL-6, TNF- $\alpha$ , and IL-1 $\beta$  in peritoneal macrophages of group D were significantly lower than those of group B ( $P < 0.05$ ); there was no statistically

significant difference in the concentrations of IL-6, TNF- $\alpha$ , and IL-1 $\beta$  in peritoneal macrophages of groups A and C ( $P > 0.05$ ).

#### 4. Discussion

MP is a community-acquired infection occurring mainly in children. Drug development for MP is still a tough challenge. Previous studies have shown that inoculation with *M. pneumoniae* induces significant airway obstruction in mice [9]. Consistent with this, in the present research, we successfully established the murine model of MP, and we observed that Fx treatment could promote the clearing of *M. pneumoniae* infection and protect the mouse lung from *M. pneumoniae*-induced injury, as evidenced by the alleviation of airway obstruction.

The pathogenesis of MP infection is attributed to an excessive immune response, and cytokine content is closely related to the severity of MP [10]. Zhao et al. [11] concluded that IL-6 level in bronchoalveolar lavage fluid in children with severe MP was significantly higher than that in children with mild MP, indicating that IL-6 is closely related to the severity of MP. The changes in the contents of proinflammatory cytokines IL-6, TNF- $\alpha$ , and IL-1 $\beta$  in BAL samples from MP-infected mice were examined using

ELISA, and it was found that the levels of proinflammatory factors in BAL samples from MP mice were significantly higher than those from normal mice, while Fx treatment significantly decreased the concentrations of proinflammatory cytokines. Macrophages are one of the major immune cells that internalize MP during infection [12]. Collins et al. [13] demonstrated that TNF- $\alpha$  levels significantly increased in MP-infected mice and their macrophages. Vitro analysis also confirmed that Fx treatment significantly inhibited the production of proinflammatory cytokines IL-6, TNF- $\alpha$ , and IL-1 $\beta$  in peritoneal macrophages of mice after MP infection. In conclusion, to our knowledge, this may be the first study to report the protective role of Fx against *M. pneumoniae* infection, providing a potential therapeutic reagent for MP.

## 5. Conclusions

In order to investigate the inflammatory response and the therapeutic effect of Fx after MP infection, the MP mice model was obtained by MP pathogen infection, and Fx was used for the treatment of mice. The results showed that the lung tissues of MP mice had obvious pathological changes, and the contents of proinflammatory cytokines IL-6, TNF- $\alpha$ , and IL-1 $\beta$  in bronchoalveolar lavage fluid and macrophages were significantly increased. However, after treatment with Fx, the histopathological changes and proinflammatory factor levels in the lungs of MP mice were significantly improved. The above results confirmed that Fx can play a protective role after MP infection by reducing the inflammatory response of the body. The results can provide a reference for the research and development and selection of new drugs for the clinical treatment of MP.

## Data Availability

The data used to support the findings of this study are available from the corresponding author upon request.

## Conflicts of Interest

The authors declare that they have no conflicts of interest.

## Acknowledgments

This work was supported by the Natural Science Foundation of Heilongjiang Province, China (LH2020H077).

## References

- [1] T. P. Atkinson, M. F. Balish, and K. B. Waites, "Epidemiology, clinical manifestations, pathogenesis and laboratory detection of mycoplasma pneumoniae infections," *FEMS Microbiology Reviews*, vol. 32, no. 6, pp. 956–973, 2008.
- [2] P. R. Wood, J. C. Kampschmidt, P. H. Dube et al., "Mycoplasma pneumoniae and health outcomes in children with asthma," *Annals of Allergy, Asthma & Immunology*, vol. 119, no. 2, pp. 146–152, 2017.
- [3] T. Shimizu, "Inflammation-inducing factors of mycoplasma pneumoniae," *Frontiers in Microbiology*, vol. 7, p. 414, 2016.
- [4] N. D'Orazio, E. Gemello, M. Gammone, M. de Girolamo, C. Ficoneri, and G. Riccioni, "Fucoxantin: a treasure from the sea," *Marine Drugs*, vol. 10, no. 12, pp. 604–616, 2012.
- [5] M. Liu, W. Li, Y. Chen, X. Wan, and J. Wang, "Fucoxanthin: a promising compound for human inflammation-related diseases," *Life Sciences*, vol. 255, Article ID 117850, 2020.
- [6] T. M. Karpiński and A. Adamczak, "Fucoxanthin—an anti-bacterial carotenoid," *Antioxidants*, vol. 8, no. 8, p. 239, 2019.
- [7] X. Li, R. Huang, K. Liu et al., "Fucoxanthin attenuates LPS-induced acute lung injury via inhibition of the TLR4/MyD88 signaling axis," *Aging*, vol. 13, no. 2, pp. 2655–2667, 2020.
- [8] X. Zhang, R. Goncalves, and D. M. Mosser, "The isolation and characterization of murine macrophages," *Current Protocols in Immunology*, vol. 83, no. 1, 2008.
- [9] M. Fonseca-Aten, A. M. Rios, A. Mejías et al., "Mycoplasma pneumoniae induces host-dependent pulmonary inflammation and airway obstruction in mice," *American Journal of Respiratory Cell and Molecular Biology*, vol. 32, no. 3, pp. 201–210, 2005.
- [10] X.-F. Xu, X.-J. Li, J.-L. Liu, L. Wu, and Z.-M. Chen, "Serum cytokine profile contributes to discriminating *M. pneumoniae* pneumonia in children," *Cytokine*, vol. 86, pp. 73–78, 2016.
- [11] J. Zhao, Y. Li, and W. Zhang, "The clinical significance of IL-6s and IL-27s in Bronchoalveolar lavage fluids from children with mycoplasma pneumoniae pneumonia," *BMC Infectious Diseases*, vol. 20, no. 1, p. 331, 2020.
- [12] A. Athamna, M. R. Kramer, and I. Kahane, "Adherence of *Mycoplasma pneumoniae* to human alveolar macrophages," *FEMS Immunology and Medical Microbiology*, vol. 15, no. 2-3, pp. 135–141, 1996.
- [13] K. L. Collins, U. S. Younis, S. Tanyaratsrisakul et al., "Angiotensin-(1-7) peptide hormone reduces inflammation and pathogen burden during mycoplasma pneumoniae infection in mice," *Pharmaceutics*, vol. 13, no. 10, p. 1614, 2021.

## Research Article

# Effect of Zhujingqiaoyun Receptivity of Infertility with Kidney Deficiency Based on Ultrasonic Evaluation

Xiaoli Mao,<sup>1</sup> WeiMao,<sup>2</sup> Ling Zhong,<sup>1</sup> Zhun Qu,<sup>1</sup> Huimin Chen,<sup>1</sup> Qiaomin Wang,<sup>1</sup> and Jingjing He<sup>1</sup> 

<sup>1</sup>Wuhan Hospital of Traditional Chinese Medicine, Wuhan, China

<sup>2</sup>Department of Huawei Outpatients, Peking University Shenzhen Hospital, Shenzhen, China

Correspondence should be addressed to Jingjing He; [hjj2021hjj2021@163.com](mailto:hjj2021hjj2021@163.com)

Received 16 February 2022; Revised 7 March 2022; Accepted 4 April 2022; Published 21 April 2022

Academic Editor: Ruchika Garg

Copyright © 2022 Xiaoli Mao et al. This is an open access article distributed under the Creative Commons Attribution License, which permits unrestricted use, distribution, and reproduction in any medium, provided the original work is properly cited.

**Objective.** This study aims to explore the effect of the prescription for Zhujingqiaoyun receptivity in patients with infertility. **Methods.** This project is a prospective randomized controlled clinical study, including infertility diagnostic criteria and dialectical kidney deficiency patients. 60 cases were randomly divided into 2 groups: the control group, where medication complex packing estradiol tablets were given, and the treatment group, on the basis of the control group, which was given Zhujingqiaoyun receptivity plus or minus. Transvaginal ultrasound was used to observe the endometrial thickness, endometrial volume, endometrial blood supply, and other aspects of patients in the two groups to evaluate the endometrial receptivity before and after treatment, and to record the pregnancy rate and safety of patients in the two groups after three menstrual cycles. **Results.** There was no significant difference in age, course of disease, and endometrial thickness between the two groups ( $P > 0.05$ ). Before and after treatment, the endometrial thickness of the two groups increased significantly, and the uterine artery blood flow pulsatility index (PI) and resistance index (RI) decreased significantly ( $P < 0.05$ ). The endometrial volume in the control group was significantly lower than that in the treatment group, and the difference was statistically significant ( $P < 0.05$ ). The endometrial FI and VFI in the control group were significantly lower than those in the treatment group, and the difference was statistically significant ( $P < 0.05$ ). In the treatment group, 30 cases were treated for 3 months, and 11 of those were pregnant (36.7%). There were 30 cases in the control group, and 5 cases were pregnant (16.67%). Both groups had good safety. SPSS 22.0 statistical software was used for the chi-square test. **Conclusion.** Zhujingqiaoyun receptivity on endometrial receptivity can treat infertility patients with good efficacy, increasing endometrial thickness and reducing uterine artery blood flow index. It is worthy of clinical promotion to improve pregnancy rates.

## 1. Introduction

Couples who live together for one year without contraception and have a normal sex life and fail to conceive are called infertile. Infertility is one of the three major diseases affecting human life and health. At the same time, infertility is also a difficult disease that causes common concern all over the world. According to the relevant survey data, the incidence rate of infertility in China is 10% to 15%. One of the main reasons for female infertility is ovulation disorders. Ovulation-related infertility accounts for 25% to 30% of the causes of infertility [1]. The latter mainly depends on

endometrial receptivity. Improving endometrial receptivity and increasing the implantation rate is the key to improve the pregnancy rate.

Endometrial receptivity means that the endometrium is in a state where the blastocyst can be positioned, adhered, and invaded, and the endometrial stroma changes at the same time, which leads to embryo implantation [2]. The embryo can be implanted smoothly, and excellent endometrial receptivity is essential. There are many clinical indicators to evaluate endometrial receptivity. Pinocytosis is a morphological indicator. Its acquisition is an invasive operation, and its clinical application is limited. Nowadays,



three-dimensional color ultrasound is often used to monitor endometrial anatomy and physiological parameters to indirectly reflect endometrial receptivity [3]. Traditional Chinese medicine believes that the kidney is the main reproductive organ. For the treatment of infertile patients, Cang Fu Dao Tan decoction is added to strengthen the spleen and reduce phlegm. Phlegm wet removal can promote the development of follicles and improve the pregnancy rate [4, 5]. To improve the endometrial capacity, traditional Chinese medicine believes that tonifying the kidneys and promoting blood circulation is important [6]. Studies have found that the use of kidney-tonifying traditional Chinese medicine can thicken endometrial thickness and improve uterine arterial blood supply, thereby improving endometrial tolerance and increasing clinical pregnancy rate [7]. It is found that in traditional Chinese medicine, kidney deficiency and blood stasis are the main pathogenesis of low endometrial receptivity. Traditional Chinese medicine can improve endometrial receptivity and pregnancy rate by reducing blood flow resistance, increasing endometrial thickness, and improving endometrial type and endocrine hormone environment [6]. The theory of traditional Chinese medicine believes that the kidney is the main reproductive. The kidney is the origin of the congenital, and the spleen is the origin of the acquired, so the treatment is based on tonifying the kidney and strengthening the spleen, regulating Chong Ren, and has achieved good clinical effect. This study showed that the basic pathogenesis of the disease was based on deficiency, kidney deficiency, phlegm and blood stasis, so attention should be paid to the combination of promoting blood circulation and tonifying the kidney and spleen in treatment [8]. The formula in this test consists of tonifying the kidney and spleen, regulating qi, reducing phlegm and promoting blood circulation, taking dryness and dampness as the basic laws, as well as tonifying the kidney and promoting blood circulation. The whole party played kidney-tonifying spleen, resolving phlegm and promoting blood circulation [9].

In recent years, Chinese medicine has made some progress in the etiology, pathogenesis, treatment, curative effect observation, and mechanism of infertility. Dr. Shengyang Xu, a national-famous and old traditional Chinese medicine practitioner, summarized the previous experience and combined it with his own clinical experience for many years, putting forward that the disease is based on kidney deficiency, mixed with phlegm dampness or blood stasis. In the treatment, the method of tonifying the kidney, activating blood circulation, and resolving phlegm is adopted, which has significant curative effects in inducing ovulation, improving endometrial receptivity, and improving the pregnancy rate. Therefore, this study intends to explore the effect of the prescription for Zhujingqiaoyun receptivity in patients with infertility.

## 2. Methods

**2.1. Participants.** This study was verified by the Research and the Ethics Committee of Wuhan Hospital of Traditional Chinese Medicine, where the patients recognized the study

procedure by signing the consent form and approval letter. This unit was facilitated with the staff having a specialized multidisciplinary team, comprising physiotherapy, dietetics, occupational therapy, medical and nursing.

By the principle of randomized control, 60 infertile women were divided into two groups: the treatment group and the control group, with 30 cases in each group.

The inclusion criteria were as follows: (1) meet the diagnostic and syndrome differentiation criteria of traditional Chinese medicine and Western medicine; (2) the reproductive ability of the spouse is normal; (3) the size and shape of uterus and ovary are normal after imaging and laparoscopy, and at least one fallopian tube is unobstructed after salpingography or hydrotherapy; (4) ovulation occurred in 3 natural ovulation cycles monitored by B-ultrasound; (5) no history of estrogen/progesterone uses within 3 months before admission; (6) there was no history of pelvic and uterine surgery within 6 months before admission; (7) sign informed consent; and (8) approved by the ethics committee.

The exclusion criteria were as follows: (1) a history of endocrine diseases; (2) endometritis and *tuberculosis*; (3) there are uterine malformations, endometriosis, and other diseases that cause abnormal uterine cavity morphology and lead to infertility; (3) received sex hormone treatment in recent 3 months; and (4) those who are allergic to drugs or allergic constitution.

**2.2. Study Protocol.** Control group: oral complex packing estradiol tablets were given from the 5th day of menstrual or withdrawal bleeding. 1 tablet, quaque die (qd), 21-day continuous treatment is a course of treatment. The drug is stopped for 1 week, regardless of menstrual cramps. The abovementioned steps were repeated for treatment for 3 consecutive courses.

Treatment group: on the basis of the control group, oral prescription for Zhujingqiaoyun receptivity (12 g *Rehmannia glutinosa*, 15 g *Cuscuta chinensis* Lam., 15 g *Morinda officinalis*, 15 g *Cistanche salsa*, 12 g *Cornus officinalis*, 15 g *Lyciumbarbarum* L., 15 g *Carapax Testudinis*, 10 g *Angelica sinensis*, 5 g *Rhizoma Chuanxiong*, 12 g *Paeoniae Radix Alba*, 15 g *Salvia miltiorrhiza* Bunge, 10 g *Rhizomacyperis*, and 12 g *Rhizoma Atractylodis macrocephalae*) was added. Decoction of traditional Chinese medicine in accordance with the requirements of "Management Regulations of Traditional Chinese Medicine Decoction Room in Medical Institutions" issued by the National Chinese Medicine (2009) No. 3, using drinking water that meets national health standards for decoction. Each dose of Chinese medicine was concentrated and filtered into 2 bags of liquid medicine, 200 ml/bag, divided into morning and evening. Starting from the fifth day of menstruation, one payment was made every day, and 21 days were taken as a course of treatment. The medication is stopped for 1 week. After menstrual cramps, the abovementioned steps were repeated for 3 consecutive courses of treatment. The medication was stopped in the case of pregnancy. Cold, greasy, and irritating foods were avoided during the medication.



TABLE 1: General information comparison.

Group	N	Age	Course of disease	Endometrial thickness (mm)
Control group	30	28.62 ± 3.72	4.65 ± 1.06	7.35 ± 0.98
Treatment group	30	28.43 ± 3.27	4.72 ± 1.24	7.31 ± 0.84

TABLE 2: Comparison of three-dimensional ultrasonic parameters between two groups after treatment.

Group	N	Endometrial volume	VI%	FI	VFI
Control group	30	3.76 ± 0.78	4.65 ± 1.06	23.07 ± 2.58	1.12 ± 0.38
Treatment group	30	5.23 ± 0.84*	4.72 ± 1.24	24.36 ± 2.18	1.26 ± 0.29

Note.  $P < 0.05^*$ .

**2.3. Observation Index and Curative Effect Standard.** After pregnancy determination treatment, blood/urine human chorionic gonadotropin (HCG) was detected. If it is (+), it indicates pregnancy. Then, the clinical pregnancy was diagnosed by transvaginal ultrasonography (35 days after ovulation) as an intrauterine gestational sac, fetal bud, or fetal heart. Pregnancy rate = number of clinical pregnancies/total number of cases × 100%.

Transvaginal three-dimensional color Doppler detection: (1) when the whole segment of the endometrium is displayed on the sagittal section of the uterus by transvaginal two-dimensional color Doppler, the thickness of the double-layer endometrium is measured at the place 10 mm away from the uterine fundus. After three consecutive measurements, the average value is calculated to observe the endometrial type and endometrial peristalsis. At the same time, after adding color on the sagittal section of the uterus, at the junction of myometrium and endometrium, the Doppler spectrum was taken out from the brightest part of the color blood flow of the low return vocal cord. The PI and RI were measured, and the average value was calculated after three consecutive measurements. (2) The 3D function key was enabled, the multiplane mode was applied, the volume angle to 120° was set, the sampling frame was adjusted to fully wrap the inner membrane, and the 3D volume data were obtained and stored after starting the volume scanning. The virtual organ computer-aided analysis (vol) software was used to draw the contour manually. The angle between each face of the extracted volume data was set to 30°. The intimal contour was drawn, 6 different sections were traced, and the three-dimensional volume of the intima was automatically obtained.

**2.4. Statistical Analysis.** SPSS 22.0 statistical software was used for data analysis. When the measurement data conform to the normality and homogeneity of variance, the mean ± standard deviation ( $\bar{x} \pm s$ ) is used for statistical description.  $P < 0.05$  was statistically significant,  $P < 0.01$  was statistically significant.

### 3. Results

**3.1. General Information Comparison.** There was no significant difference in age, course of disease, and endometrial thickness between the two groups ( $P > 0.05$ ) (Table 1).

**3.2. Comparison of Efficacy Indexes between the Two Groups before and after Treatment.** Before and after treatment, the endometrial thickness of the two groups increased significantly (Table 2 and Figure 1), and the uterine artery blood flow PI and RI decreased significantly ( $P < 0.05$ ). The endometrial volume in the control group was significantly lower than that in the treatment group, and the difference was statistically significant ( $P < 0.05$ ). The endometrial FI and VFI in the control group were significantly lower than those in the treatment group, and the difference was statistically significant ( $P < 0.05$ ) (Table 3).

**3.3. Comparison of Pregnancy Rate between Two Groups after Treatment.** In the treatment group, 30 cases were treated for 3 months, and 11 of those were pregnant (36.7%). There were 30 cases in the control group, and 5 cases were pregnant (16.67%). It could be seen that the pregnancy rate of the experimental group was significantly higher than that of the control group, but the difference was not statistically significant by the chi-square ( $X^2$ ) test ( $P = 0.82$ ) ( $P > 0.05$ ).

**3.4. Safety Observation.** There was 1 patient in the treatment group who had mild diarrhea during medication, which did not affect normal work and life and was not treated with special treatment, but spontaneously relieved after two days. In the control group, 2 patients showed nausea symptoms, which did not affect their normal work and life, did not stop treatment, and then were relieved by themselves. No adverse reactions occurred in other patients. There were no abnormalities in blood and urine routine, electrocardiogram, liver and kidney function before and after treatment.

### 4. Discussion

Traditional Chinese medicine believes that the kidney stores the essence and governs reproduction and is connected to the uterus through the veins, which is the innate foundation and the root of gestation [10]. The essence of the kidney is filled, the qi and blood flow through the channels, and the endometrium is nourished, which is the material basis for the implantation of the fertilized egg and the continued pregnancy [11, 12]. Insufficient kidney essence, lack of source of essence and blood, inability to promote the circulation of qi and blood, endometrial and embryonic uterus cannot be nurtured, the uterus is unable to consolidate the fetal element,

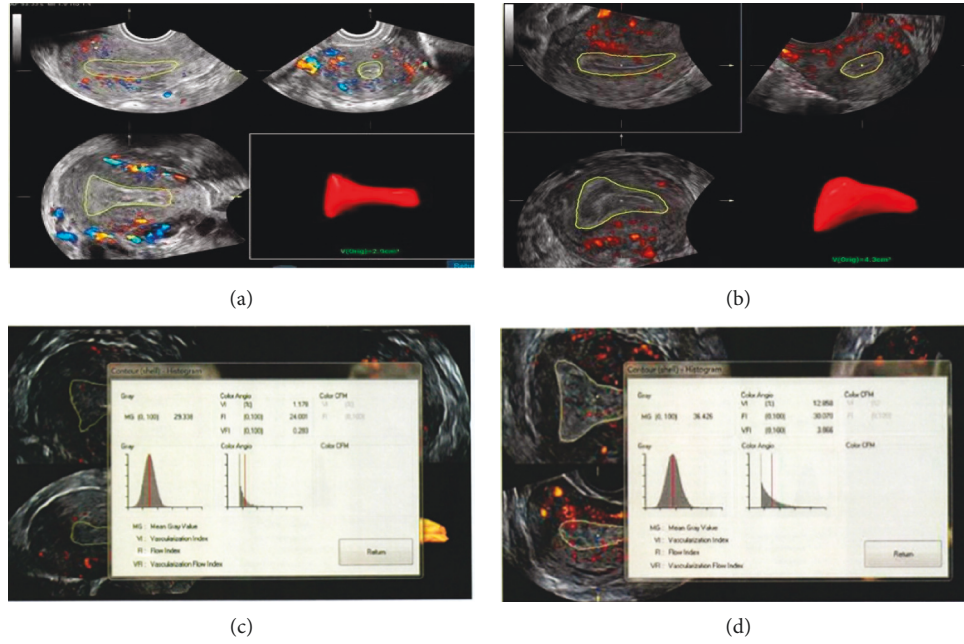


FIGURE 1: (a, b) After three-dimensional power Doppler imaging, the endometrial volume of the two groups was measured by voice software. (c) (d) After three-dimensional power Doppler imaging, the blood flow histogram function was used to obtain the endometrial VL, FI, and VFI of the two groups.

TABLE 3: Comparison of efficacy indexes between the two groups before and after treatment.

Group	N	Time	Endometrial thickness (mm)	PI	RI
Control group	30	Before treatment	$7.35 \pm 0.98$	$2.53 \pm 0.72$	$0.92 \pm 0.12$
		After treatment	$7.87 \pm 0.86$	$2.49 \pm 0.68$	$0.86 \pm 0.08$
Treatment group	30	Before treatment	$7.31 \pm 0.84$	$2.56 \pm 0.80$	$0.90 \pm 0.10$
		After treatment	$8.34 \pm 0.91^*$	$2.31 \pm 0.55$	$0.81 \pm 0.07$

Note.  $P < 0.05^*$ .

the material basis for gestation and growth is lacking, and the fetus loses its implantation soil, leading to infertility. Western medicine believes that after the fertilized egg is implanted into the endometrium, the growth of the endometrium must be synchronized with the fertilized egg to ensure the stability of embryo implantation [13]. This stability is called endometrial receptivity. Western medicine mainly improves the endometrial capacity by supplementing progesterone, estrogen, and using anticoagulant drugs, and strives to synchronize with follicular development, but the coordination is not good. Clomiphene citrate tablets have the effect of promoting ovulation and are currently commonly used drugs for the treatment of infertility, but they can inhibit the synthesis of estrogen, causing retardation of endometrial growth, a high ovulation rate, but a low pregnancy rate [14].

At present, the application of endometrial thickness to evaluate endometrial receptivity is still controversial. Some scholars believe that pregnancy rates decrease significantly when endometrial thickness is less than 7 mm. Dickey et al. [15] found that endometrial thickness in the pregnant group was significantly higher than that in the nonpregnant group, and they believed that endometrial thickness was an important factor in predicting pregnancy. However, Zollner

et al. [16] believed that endometrial thickness had no statistical difference between pregnant and nonpregnant women and could not predict pregnancy. The endometrial thickness of the two groups after treatment was significantly different from that before treatment ( $P < 0.05$ ). The therapeutic effect was better in the treatment group. It indicates that in the treatment of infertility patients, adding the treatment of Zhujingqiaoyun receptivity can increase the endometrial thickness.

Three-dimensional energy Doppler ultrasound can evaluate all blood vessels in the overall volume of an organ or tissue, which can accurately, intuitively, and truly reflect the blood perfusion in the area of interest. The parameters include VI, vascular index, which represents the ratio of color voxel value in the region of interest to the total voxel and represents the vascular density within the observed intimal volume, expressed as a percentage. The FI, or blood flow index, is interested in all color voxel intensity averages (i.e., the sum of the weighted color voxel divided by the total number of all the colors of the body element), which is all the average color value of blood flow or blood cell density. This prompts interest in the endovascular blood cell energy reflected by endovascular blood, the more the FI, the higher.

VFI refers to the average color intensity of the total voxels in the area of interest; that is, the sum of all the color voxels divided by all the voxels. VFI reflects not only the vascular density of the tissue but also the blood cell density of the tissue [17]. The results of this study show that the endometrial volume in the control group was significantly lower than that in the treatment group, and the difference was statistically significant ( $P < 0.05$ ). The endometrial FI and VFI in the control group were significantly lower than those in the treatment group, and the difference was statistically significant ( $P < 0.05$ ).

In the treatment group, there were 30 patients, 11 of whom were pregnant after treatment, with a pregnancy rate of 36.67%. In the control group, there were 30 patients, 5 of whom were pregnant after treatment, and the pregnancy rate was 16.67%. The pregnancy rate in the treatment group was significantly higher than that in the control group, but the difference was not statistically significant ( $P > 0.05$ ), which may be related to the small sample size and short treatment time.

## 5. Conclusion

According to the results of the trial, Zhujingqiaoyun receptivity on endometrial receptivity can increase the endometrial thickness and improve the endometrial type of infertility patients on ovulation day, reduce the uterine artery blood flow resistance, and other endometrial receptivity indicators. Therefore, Zhujingqiaoyun receptivity can treat infertility patients with good efficacy, increasing endometrial thickness, and reducing uterine artery blood flow index. It is worthy of clinical promotion to improve pregnancy rates.

## Data Availability

The data used to support this study are available from the corresponding author upon request.

## Conflicts of Interest

The authors declare that they have no conflicts of interest.

## Authors' Contributions

Xiaoli Mao and Mao Wei contributed equally to this study.

## Acknowledgments

This study was supported by the Wuhan Medical Research Project (WZ20C12) and the Hubei Medical Research Project (No. ZY2021Q016).






## References

- [1] H. J. Choi, T. W. Chung, M. J. Park et al., "Water-extracted tubers of *Cyperus rotundus* L. enhance endometrial receptivity through leukemia inhibitory factor-mediated expression of integrin  $\alpha V\beta 3$  and  $\alpha V\beta 5$ ," *Journal of Ethnopharmacology*, vol. 208, no. 17, pp. 16–23, 2017.
- [2] J. Miravet-Valenciano, M. Ruiz-Alonso, E. Gómez, and J. A. Garcia-Velasco, "Endometrial receptivity in eutopic endometrium in patients with endometriosis: it is not affected and let me show you why," *Fertility and Sterility*, vol. 108, no. 1, pp. 28–31, 2017.
- [3] J. L. Cai, L. L. Liu, Y. Q. Hu et al., "Polychlorinated biphenyls impair endometrial receptivity in vitro via regulating mir-30d expression and epithelial mesenchymal transition," *Toxicology*, vol. 365, pp. 25–34, 2016.
- [4] B. Imani, M. J. Eijkemans, E. R. te Velde, J. F. Habbema, and B. C. Fauser, "A nomogram to predict the probability of live birth after clomiphene citrate induction of ovulation in normogonadotropic oligoamenorrheic infertility," *Fertility and Sterility*, vol. 77, no. 1, pp. 91–97, 2002.
- [5] S. Franks, J. Stark, and K. Hardy, "Follicle dynamics and anovulation in polycystic ovaries syndrome," *Human Reproduction Update*, vol. 14, no. 5, p. 539, 2008.
- [6] The Rotterdam Eshre/Asrm-Sponsored Pcos Workshop Group, "Revised 2003 consensus diagnostic criteria and long-term health risks related to polycystic ovaries syndrome [J]," *Fertility and Sterility*, vol. 81, no. 1, pp. 19–25, 2004.
- [7] L. J. Webber, S. Stubbs, J. Stark et al., "Formation and early development of follicles in the polycystic ovary," *The Lancet*, vol. 362, no. 9389, pp. 1017–1021, 2003.
- [8] A. Requena, J. Herrero, J. Landeras et al., "Use of letrozole in assisted reproduction: a systematic review and meta-analysis," *Human Reproduction Update*, vol. 14, no. 6, pp. 571–582, 2008.
- [9] S. Rath and R. Sharma, "Surgical approach for polycystic ovarian syndrome in management of infertility," *Medical Journal Armed Forces India*, vol. 62, no. 2, pp. 119–122, 2006.
- [10] M. Singh, P. Chaudhry, and E. Asselin, "Bridging endometrial receptivity and implantation: network of hormones, cytokines, and growth factors," *Journal of Endocrinology*, vol. 210, no. 1, pp. 5–14, 2011.
- [11] A. Zhioua, H. Elloumi, S. Fourati et al., "Morphometric analysis of the human endometrium during the implantation window: light and transmission electron microscopy study," *Journal de Gynecologie Obstetrique et Biologie de la Reproduction*, vol. 41, no. 3, pp. 235–242, 2012.
- [12] D. M. Zhang, J. X. Wei, J. Wang, S. Liu, and Q. Yan, "Difucosylated oligosaccharide LewisY is contained within integrin  $\alpha v \beta 3$  on RL95-2 cells and required for endometrial receptivity," *Fertility and Sterility*, vol. 95, no. 4, pp. 1446–1451.e1, 2011.
- [13] N. Mariee, T. C. Li, and S. M. Laird, "Expression of leukaemia inhibitory factor and interleukin 15 in endometrium of women with recurrent implantation failure after IVF; correlation with the number of endometrial natural killer cells," *Human Reproduction*, vol. 27, no. 7, pp. 1946–1954, 2012.

- [14] H. Dechaud, E. Bessueille, P. J. Bousquet, L. Reyftmann, S. Hamamah, and B. Hedone, "Optimal timing of ultrasonographic and Doppler evaluation of uterine receptivity to implantation," *Reproductive BioMedicine Online*, vol. 16, no. 3, pp. 368–375, 2008.
- [15] Y. Gonen and R. F. Casper, "Prediction of implantation by the sonographic appearance of the endometrium during controlled ovarian stimulation for in vitro fertilization (IVF)," *Journal of In Vitro Fertilization and Embryo Transfer*, vol. 7, no. 3, pp. 146–152, 1990.
- [16] I. Y. Jarvela, P. Sladkevicius, S. Kelly, K. Ojha, S. Campbell, and G. Nargund, "Evaluation of endometrial receptivity during in vitro fertilization using three-dimensional power Doppler ultrasound," *Ultrasound in Obstetrics and Gynecology*, vol. 26, no. 7, pp. 765–769, 2005.
- [17] S. Kupesic, I. Bekavac, D. Bjelos, and A. Kurjak, "Assessment of endometrial receptivity by transvaginal color Doppler and three-dimensional power Doppler ultrasonography in patients undergoing in vitro fertilization procedures," *Journal of Ultrasound in Medicine*, vol. 20, no. 2, pp. 125–134, 2001.

## Research Article

# Topical Application of *Premna integrifolia* Linn on Skin Wound Injury in Rats Accelerates the Wound Healing Process: Evidence from *In Vitro* and *In Vivo* Experimental Models

Saeed Ali Alsareii <sup>1</sup>, Nasser A. N. Alzerwi <sup>2</sup>, Mansour Yousef AlAsmari,<sup>1</sup>  
Abdulrahman Manaa Alamri <sup>1</sup>, Mater H. Mahnashi <sup>3</sup> and Ibrahim Ahmed Shaikh <sup>4</sup>

<sup>1</sup>Department of Surgery, College of Medicine, Najran University, Najran, Saudi Arabia

<sup>2</sup>Department of Surgery, College of Medicine, Majmaah University, Ministry of Education, Al-Majmaah City, Saudi Arabia

<sup>3</sup>Department of Pharmaceutical Chemistry, College of Pharmacy, Najran University, Najran, Saudi Arabia

<sup>4</sup>Department of Pharmacology, College of Pharmacy, Najran University, Najran, Saudi Arabia

Correspondence should be addressed to Mater H. Mahnashi; matermaha@gmail.com

Received 19 January 2022; Accepted 1 April 2022; Published 13 April 2022

Academic Editor: Sekar Vijayakumar

Copyright © 2022 Saeed Ali Alsareii et al. This is an open access article distributed under the Creative Commons Attribution License, which permits unrestricted use, distribution, and reproduction in any medium, provided the original work is properly cited.

**Background.** When the skin and tissues within the body are injured, the healing process begins. Medicinal herbs have been used to cure wounds since time immemorial. The antimicrobial and antioxidant activity possessed by *P. integrifolia* may accelerate wound healing. **Objectives.** To assess the wound healing activity of *Premna integrifolia* extract (PIE) by employing in-vivo experimental animal models and an in-vitro migration scratch assay. Furthermore, to assess its cytotoxicity using the MTT assay. **Methods.** Wistar albino rats were used for the *in vivo* wound healing models. The animals were divided into four groups at random: Group I was untreated. Group II was vehicle control (ointment base). Group III was PIE ointment (5% W/W). Group IV was standard (povidone-iodine ointment) (5% W/W). The ointments were applied directly to the wounds as described above until they healed completely. The wound contraction percentage and tensile strength were calculated. The MTT test was used to determine the viability of the test extract against the fibroblast cells. The scratch assay was used *in vitro* to determine the wound healing potential of the test drug.  $P \leq 0.05$  values were considered statistically significant. **Results.** *Premna integrifolia* extract did not possess any noticeable cytotoxicity to the cell line and showed an  $IC_{50}$  of 185.98  $\mu\text{g/ml}$ . The wound contraction potential of PIE ointment-treated animals was considerably greater ( $P \leq 0.001$ ) on days 4, 8, 12, 16, and 20 when compared to the control group. The percentage of wound contraction on day 20 was 99.92% in PIE-treated animals compared to 83.23% in untreated animals. Compared to the untreated group, the duration of full epithelization was significantly ( $P \leq 0.01$ ) shorter in the test group. When compared to the incision control group, the animals treated with PIE ointment had significantly higher ( $P \leq 0.001$ ) tensile strength. In addition, animals given the test drug had a significant ( $P \leq 0.001$ ) increase in total protein and hydroxyproline. In the *in vitro* scratch assay, test drug-treated cells demonstrated greater cell migration. Histology images confirmed that the test drug-treated group had epithelial tissue proliferation and keratinization. **Conclusion.** The current study found that *Premna integrifolia* improved wound healing activity both *in vitro* and *in vivo*. These findings indicate that *Premna integrifolia* extract has wound-healing potential and could be a viable source of nutraceuticals with wound-healing properties.

## 1. Introduction

A wound is a rupture in the continuity of a living tissue's cellular, functional, and anatomical properties caused by chemical, physical, thermal, immunological, or microbial

assaults [1]. To restore the structural integrity of the damaged tissue, a sequence of activities must occur, including cell migration, proliferation, interaction, differentiation, bimolecular interactions, matrix component creation, and a complicated signaling network [2].



The regulation of the acute wound healing process is determined by interacting processes at the cellular, molecular, and extracellular matrix levels and concludes with wound closure in extended periods of time [3]. Physiological healing can be divided into three stages: inflammation, proliferation, and remodeling [4]. However, an asymmetry between metalloproteinases (MMPs) and the associated tissue inhibitors of metalloproteinase (TIMPs) may impede the healing process throughout the inflammatory phase, particularly during the tissue formation phase. Chronic wounds are used to characterize this type of injury [4, 5]. Although the mechanism underlying this chronic wound is complex, it is frequently linked to other comorbid disorders, such as diabetes, obesity, vascular insufficiency, or high blood pressure. Local hypoxia, bacterial colonization, and repeated ischemia-reperfusion damage, as well as cellular and systemic alterations, are the most common symptoms associated with chronic wounds [6].

Skin injury has been considered to be a complicated process. The current wound management strategies for resolving minor to severe injuries include irrigation, debridement, proteolytic enzymes, antibiotics, and tissue grafts, however, they have been linked to severe downsides, such as invasiveness and cost [7]. The emergence of antibacterial resistance combined with the high cost and slow rate of new antibiotic development increases wound-related mortality and morbidity. The rise of resistant bacterium strains, particularly those that cause wounds, such as *Pseudomonas* and *Acinetobacter* species that are multidrug-resistant, vancomycin-resistant *Staphylococcus aureus* (VRSA), and methicillin-resistant *Staphylococcus aureus* (MRSA), remains a global public health concern. As a result, wound infection continues to be the most common cause of nonhealing wounds and continues to be a considerable burden for both patients and caregivers [8, 9]. Apart from being expensive, the drugs utilized in the management of wounds pose issues, such as hypersensitivity reactions and resistance [10]. Herbal medicines can solve the adverse effects, costs, and antimicrobial resistance issues. The antimicrobial activity possessed by the phytoconstituents in herbal extracts may aid in wound healing [11]. The effectiveness of antimicrobials in wound healing is well-established and reinforces their role in accelerating wound healing with either systemic or topical use [10–12].

Since the dawn of time, medicinal herbs have been utilized to treat wounds. Natural products, particularly plant secondary metabolites, such as isoprenoids, phenolics, and alkaloids, have been shown to be the most effective sources of novel wound healing agents [13]. *Premna integrifolia* Linn. (Lamiaceae) is a common shrub with 40 species found in tropical and subtropical locations around the world, including the United States, India, Australia, Bangladesh, and China. Although this genus has several species, only two of them, *P. latifolia* and *P. integrifolia*, are known to have medicinal properties [14].

Several diseases, including bronchitis, diabetes, edema, chyluria, dyspepsia, inflammation, liver problem, constipation, piles, and fever can be treated with the roots of *P. integrifolia* [15]. Anticoagulant, antiarthritic,

antihyperglycemic, and antimicrobial characteristics have also been reported for the plant [15]. It protects against cardiovascular diseases since it contains alkaloids and iridoid glycosides [16].

*P. integrifolia* ethanolic extract exhibits potent antidiabetic, analgesic, antibacterial, antiulcer, and antioxidant properties [15]. *P. integrifolia* leaf extracts were found to have hepatoprotective properties against carbon tetrachloride and paracetamol-induced liver damage [15]. However, no research has been done on the plant's effectiveness in wound healing. The current study was carried out to evaluate the wound-healing property of *P. integrifolia*, utilizing the incision wound model and excision wound model, in perspective of its anti-inflammatory and antibacterial characteristics.

## 2. Materials and Methods

**2.1. *Premna integrifolia* Extract.** The standardized extract of *Premna integrifolia* was procured from Vital Herbs Z-26/27 Commercial Enclave, Uttam Nagar, New Delhi, India.

**2.2. Ointment Formulation.** A simple ointment (British Pharmacopoeia) was prepared using white soft paraffin, cetostearyl alcohol, hard paraffin, and wool fat [17].

Procedure: hard paraffin (5 g) was melted in a beaker over a water bath to make the 100 g simple ointment base. The remaining ingredients were added in the descending order of melting point: cetostearyl alcohol (5 g), white soft paraffin (85 g), and wool fat (5 g). All of the ingredients were melted in a water bath while being constantly stirred until they were completely homogeneous. The mixture was taken off the heat and stirred until it was completely cool. Five grams of *P. integrifolia* extract were mixed with a portion of the simple ointment base to make a 5% (w/w) ointment. The rest of the simple ointment base was gradually added and thoroughly mixed in. The prepared ointment was stored in a clean and dry container, away from heat. The ointment was used for topical application on the wounds for 20 consecutive days during the experiment.

**2.3. Animals.** Male and female Wistar albino rats ( $\approx 200$  g) were maintained under typical ambient conditions of humidity and temperature ( $25 \pm 0.5$  C) and a 12 h light/dark cycle. The rats were given a conventional pellet diet and free access to water. The animal research was carried out at the institute with the Najran University Scientific Research Ethical Committee's approval, vide number 443-41-49631-DS.

**2.4. Acute Dermal Toxicity.** The goal of the study was to figure out what the therapeutic dose of the standardized extract should be. The extract's acute cutaneous toxicity was tested by applying an ointment containing extract at the highest concentrations of 5% (w/w) to the rats' shaved backs. The study was conducted in accordance with OECD Guidelines No. 434 [18].



**2.5. Wound Healing Activity.** With six animals in each group, the animals were divided into four major groups: control, base, test, and standard. The control group was not given any treatment. The base (vehicle) control group received only the ointment base. The test group was given ointment with a high concentration of extract (5% w/w) mixed into a simple ointment base. Cipladine (5% w/w povidone-iodine ointment) was used on the control group.

**2.6. Excision Wound Model.** The animals were divided into four groups at random: Group I: untreated excision; Group II: vehicle control (ointment base); Group III: PIE ointment (5% W/W); Group IV: standard (povidone-iodine ointment 5% W/W). Ketamine (0.5 ml/kg b. w. i.p.) was used to anesthetize the rats. On the shaved backs of the rats, a full-

thickness excision wound of circular area (about 250 mm<sup>2</sup>) and 2 mm depth was made 30 minutes after the injection of ketamine. Day 0 was designated as the day of the wounding (Figure 1). The topical application of the ointments as indicated above was used to treat the wounds until they were totally healed. On days 0, 4, 8, 12, 16, and 20, the wounds were observed, and the area of the wound and the mean percent wound contraction were assessed. The number of days required for the dead tissue to fall without any remaining raw wound was used to calculate the epithelization duration [19].

**2.7. Wound Healing Rate [20].** Wound healing rate is given by

$$\% \text{ of wound closure} = \frac{\text{wound area on day 0} - \text{wound area on day } n}{\text{wound area on day 0}} \times 100. \quad (1)$$

### 3. Estimation of Biochemical Markers

**3.1. Hydroxyproline Estimation.** The hydroxyproline content of resected wound tissues was determined on day 20 of the experiment. The tissue samples were dried in a hot air oven at 60°C, and thereafter, they were hydrolyzed for four hours at 130°C in 6 N HCl. The hydrolysates were neutralized to pH 7.0 and oxidized with Chloramine-T for 20 minutes. The reaction was stopped after 5 minutes by adding 0.4 M perchloric acid and developing color with Ehrlich's reagent at 60°C. The materials were examined in an ultraviolet spectrophotometer at 557 nm after complete stirring. The hydroxyproline concentration of the tissue samples was determined using a pure L-hydroxyproline standard curve [21].

**3.2. Protein Estimation.** Protein estimation was determined on day 20 of the experiment. Tissue specimens were homogenized overnight in 0.1 N NaOH. The homogenate (2 mL) was placed in a vial and centrifuged for 15 minutes at 5000 rpm. 1 mL of supernatant was added to 1 mL of reagent (50 mL of 2% Na<sub>2</sub>CO<sub>3</sub> in 0.1 N NaOH + 2 mL of 0.5 percent CuSO<sub>4</sub> in 1% sodium potassium tartrate) in a separate vial. At room temperature, the samples were incubated for 15 minutes. Each sample received 100 mL of Folin-Ciocalteu reagent, which was left at room temperature for 30 minutes. A UV-vis spectrophotometer was used to measure absorbance at 670 nm within 30 minutes [22].

**3.3. Incision Wound Model.** Ketamine (0.5 ml/kg b. w. i.p.) was used to anesthetize the rats. Thirty minutes after the rats were given ketamine, sterilized scalpels were used to make 6 cm long and 2 mm deep incision wounds on their shaved backs (figure 1(b)). The skin was held together by stitching it at 0.5 cm intervals with black silk. Stitching was done with surgical thread (number. 000) and a curved needle (no. 9).

The continuous thread on both wound edges was tightened to ensure that the wounds were properly closed. The wounds of the animals in each group were treated for 10 days with the topical treatment of the ointments as indicated above. The day of the wounding was counted as day 0. On the eighth postwounding day, the sutures were removed, and the tensile strength of the skin, defined as the weight in grams necessary to tear open the skin/wound, was determined using a tensiometer on day 10 [23].

**3.4. MTT Assay.** The MTT test was used to determine whether the test extract was viable against L929 Mouse transformed fibroblast cell line. Different concentrations of the test extract (50–250 µg/ml) were added to the fibroblast cell lines. The fibroblast cell lines were cultured for 24 hours in DMEM. After that, 10 µl MTT (3-(4, 5-dimethyl-thiazol-2-yl)-2, 5-diphenyl tetrazolium bromide) was added to each well and allowed to sit for 2 hours. After dissolving the formazan crystals with dimethyl sulfoxide (DMSO), absorbance was measured at 570 nm in a microtitre plate [24]. Cisplatin is the known standard cytotoxic drug, and it was used as a control to compare the results of the test drug.

**3.5. In Vitro Wound Healing Activity.** The trypsinized cells were aspirated into a 5 ml centrifuge tube. Centrifugation at 300 x g yielded a cell pellet. The cell count was adjusted in each well of the 12-well plate using DMEM. Then, 1 ml DMEM containing 100 µl of the cell suspension was added, and the plate was incubated at 37°C and 5% CO<sub>2</sub> for 24 hours to achieve 100% confluence as a monolayer. A new 200 µl pipette tip was used to scratch the monolayer gently and slowly over the center of the well. To remove the detached cells, gently wash the well twice with medium after scratching. Refill the well with fresh media after washing the cells twice with 1x Phosphate Buffered Saline (PBS). The PBS was sucked out. With 1 ml of new medium, 25 µl of varied

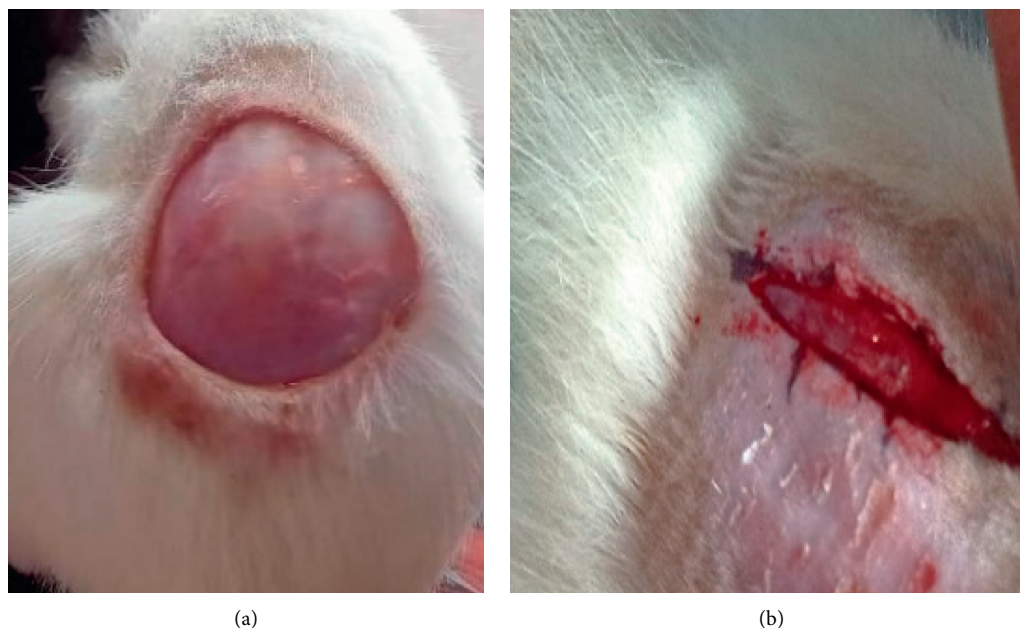


FIGURE 1: (a) Circular excision wound on day 0. (b) Linear incision wound on day 0.

test concentrations from the stock of test medications were introduced to the appropriate wells. The images of the scratched monolayers were obtained at different time intervals of 0 hours, 12 hours, and 24 hours, followed by a 24-hour incubation of the plate at 37°C and 5% CO<sub>2</sub>. By measuring the gap distance at 4X resolution using Mag-Vision Software, the gap distance was quantified [25].

The rate of migration was calculated using the below formula:

$$Rm = \frac{(W_i - W_t)}{T}, \quad (2)$$

where  $Rm$ : rate of cell migration ( $\mu\text{m}/\text{h}$ );  $W_i$ : initial wound width ( $\mu\text{m}$ );  $W_t$ : final wound width ( $\mu\text{m}$ );  $T$ : duration of migration (hours)

#### 4. Antibacterial and Antifungal Activity

**4.1. Agar-Well Diffusion Method.** Petri plates containing 25 ml of optimized media were seeded using a glass rod with 24 hr-old cultures of *Candida albicans* strains for assessing antifungal activity and *Escherichia coli* (Gram +ve) and *Bacillus cereus* (Gram -ve) strains for assessing antibacterial activity. The spread plate method was followed, and the wells were made using a well-borer. A stock concentration of 100 mg in 1 ml and a standard drug (Itracanzole and ciprofloxacin) of 30  $\mu\text{l}$  were used. The plates were then incubated at 37°C for 24 hours. The antimicrobial activity was confirmed by measuring the diameter of the inhibition zone formed around the well.

**4.2. Histological Examination.** At the conclusion of the experiment, skin biopsies were taken from the rats and preserved in a buffered formaldehyde solution (10% v/v).

Tissue samples were treated and fixed in paraffin wax on a regular basis. Hematoxylin and eosin were used to stain the longitudinal sections (5 mm) of healed lesions. On coded slides, the microscopic examination was done blindly using a light microscope.

**4.3. Statistical Analysis.** The data was statistically analyzed using GraphPad Prism® version 5.01 (GraphPad Software, USA) using one-way analysis of variance, followed by Tukey's post hoc test.  $P < 0.05$  was used as a cut-off point for statistical significance.

### 5. Results

**5.1. Acute Dermal Toxicity Test.** There were no signs of inflammation or edema after applying a 5% w/w ointment dose during the first 24 hours. In addition, 14 days after topical application of the PIE ointment, no mortality or signs of toxicity were observed.

**5.2. MTT Assay.** Phytochemicals have long been researched for their therapeutic characteristics, however, their cytotoxic effects on the cell type of interest are often overlooked. However, there has been an increasing trend to examine this crucial component in recent years. The MTT assay was used to check the cytotoxicity of the test extract against a fibroblast cell line. The test extract was less cytotoxic to the normal cell line than the control drug cisplatin. The cell line treatment with various doses of test extract had no discernible cytotoxicity and showed an IC<sub>50</sub> of 185.98  $\mu\text{g}/\text{ml}$ . However, at a concentration of 250  $\mu\text{g}/\text{ml}$  of test extract, a little reduction in cell viability was observed (Figure 2). These results showed that *P. integrifolia* extract was not cytotoxic and that its medicinal potential may be

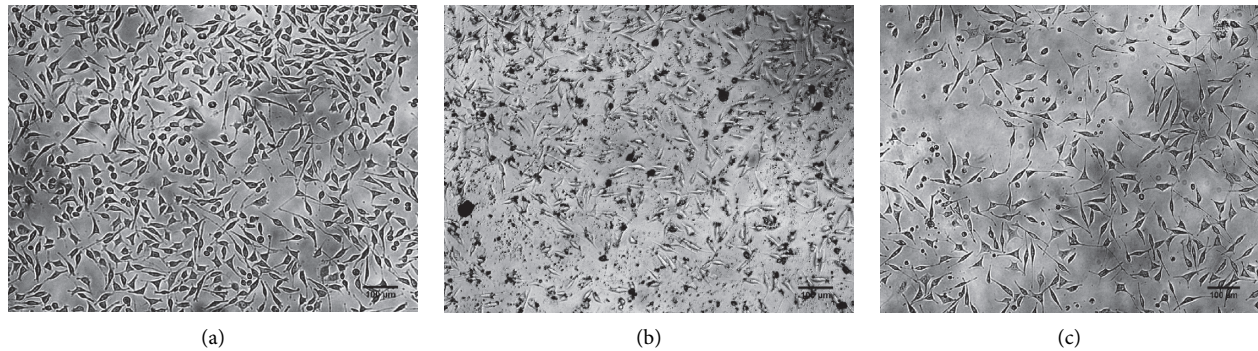


FIGURE 2: Pictographs. (a) Untreated. (b) *Premna integrifolia* extract (250 µg/ml). (c) Cisplatin.

investigated further. In contrast, cells treated with cisplatin showed maximum toxicity. Cisplatin inhibits cell proliferation by a cytotoxic mechanism, characterized by DNA damage and the modulation of oxidative stress. Exposure to oxidative stress can upset regular biological functions. Cisplatin also induces reactive oxygen species that trigger DNA damage, leading to cell death. Cell death occurs upon the immediate activation of numerous signaling pathways.

**5.3. Effect of the Standardized Extract of *Premna integrifolia* on Percentage Wound Contraction and Epithelialization Period.** Table 1 and Figure 3 show the results of wound-healing activity using the excision wound model. The percentage wound-healing values shown in the table are for excision control, base, test extract, and the standard group at 0, 4, 8, 12, 16, and 20 days. The wound-contracting ability of animals treated with the ointment containing 5% (w/w) test extract was shown to be considerably higher ( $P < 0.001$ ) on days 4, 8, 12, 16, and 20 when compared to the excision control group (Figure 4). On day four after wounding, the control group animals had firm thrombus edema and exudates on the wound area (group I), while a comparatively soft thrombus with a decrease in inflammation and no noticeable discharge was observed in the PIE ointment (group III) and standard treated group (group IV). The generation of reddish connective tissue was detected in the animals of groups III and IV on day eight. In group IV, however, it was noticed earlier (on the eighth day after wounding) than in group III. In comparison to group I, the animals treated with standard and PIE ointment significantly ( $P < 0.001$ ) improved wound-healing effects in the rat models and aided in wound contraction from day 4 to day 20.

The complete epithelization period for group I animals was 17 days, while epithelization times for group III and group IV animals were 11 and 8.6 days, respectively. In comparison to the untreated group, the full epithelization duration was significantly ( $P < 0.01$ ) shorter in groups III and IV. The wound-healing effect of PIE ointment was found to be comparable to that of the commercially available 5% w/w povidone-iodine ointment (standard).

**5.4. Hydroxyproline Content.** The animals treated with the test extract exhibited significantly ( $71.72 \pm 0.79$  µg/100 mg of

tissue) higher hydroxyproline content than the excision control. The standard control group showed  $90.41 \pm 0.9241$  µg/100 mg of tissue [figure 5(a)].

**5.5. Protein Estimation.** The levels of total protein in the tissue were found to be  $131 \pm 3.26$ ,  $107.2 \pm 2.45$ ,  $78.17 \pm 2.3$ ,  $67.50 \pm 2.26$  µg/100 mg of tissue in the standard, test extract, base, and excision control groups, respectively. The animals treated with the test and standard drug have shown a significant ( $P < 0.001$ ) increase in total protein level compared with the excision control animals [figure 5(b)].

**5.6. Incision Wound Study.** The tensile strength of the incision wound was used to assess the influence of the wound-healing activities in this model. The results are provided as the mean weight in Gram  $\pm$  SEM, necessary to burst open the sutured incision (Table 2 and Figures 6 and 7). When compared to the incision control group, the animals treated with PIE ointment had considerably higher ( $P = 0.001$ ) tensile strength. ( $P < 0.001$ ) tensile strength.

**5.7. In Vitro Wound-Healing Cell Migration Assay.** Scratch assay is a frequently used *in vitro* technique for determining a compound's wound-healing potential. In the current study, the mouse fibroblast cell line was treated with *Premna integrifolia* for 24 hours. Cell migration was captured at different time intervals of 0 hrs, 6 hrs, 12 hrs, and 24 hrs. The results showed that the PI extract (18 µg/mL) filled the scratch gap by 87.89 percent in 24 hours. Table 3 shows the percentage of wound closure at various time periods in untreated, extract-treated, and standard drug-treated cells. When compared to the control, the test extract caused the fibroblast cells to migrate, resulting in a higher percentage of wound closure. At 24 hours, 96.53% of the gap in the cells treated with the standard drug had been closed, which was almost similar compared to the test drug. In the standard and the extract-treated cells, the images demonstrate greater cell migration (Figure 8).

**5.8. In Vitro Antimicrobial Activity.** The data obtained from the standard antimicrobial assay of *Premna integrifolia* were compared with that of the standard drugs. The antimicrobial

TABLE 1: Effect of PIE on wound diameter, wound area, and percentage of wound contraction in an excision wound model.

Groups	Wound diameter (mm)				Area (mm sq)				Percentage wound contraction (%)									
	D0	D4	D8	D12	D0	D4	D8	D12	D0	D4	D8	D12	D16	D20				
Excision (control)	24.5 ± 0.58	23.7 ± 0.5	22.5 ± 0.5	15.5 ± 0.58	12.5 ± 0.58	10 ± 0.82	471.4 ± 22.2	442.9 ± 18.4	397.6 ± 20.4	188.8 ± 14.5	122.9 ± 11.3	78.9 ± 8.83	0	5.8 ± 0.87	15.51 ± 2.89	59.88 ± 3.54	73.89 ± 2.71	83.23 ± 2.97
Base	24.7 ± 0.5	23.5 ± 0.58	22.2 ± 0.43	13 ± 0.82	12.5 ± 1.29	8 ± 0.82	481 ± 19.2	433.7 ± 21.3	388.8 ± 17.7	133.1 ± 16.67	123.6 ± 12.4	50.6 ± 6.63	0	9.64 ± 1.34	19.11 ± 2.12	72.30 ± 3.57	74.13 ± 5.28	89.46 ± 2.13
Extract (PIE)	25 ± 0.5	21.5 ± 0.58	17.5 ± 1.12	10.5 ± 1.29	4 ± 1.41	0.5 ± 0.58	481 ± 19.2	363.1 ± 19.5	241.4 ± 25.5	87.5 ± 11.3	13.7 ± 2.8	0.4 ± 0.11	0	24.43 ± 3.32*	49.70 ± 6.32**	81.75 ± 4.6**	97.15 ± 1.58**	99.92 ± 0.09**
STD (povidone-iodine)	24.5 ± 0.58	20 ± 1.41	15 ± 0.71	8.75 ± 0.96	2.7 ± 0.96	0	471.4 ± 22.2	315.2 ± 20.4	177 ± 19.2	60.6 ± 9.47	6.5 ± 0.9	0.0	0	32.75 ± 5.85**	62.28 ± 5.49**	87.20 ± 2.31**	98.64 ± 0.90**	100 ± 0**

Values are expressed as mean ± SEM for 6 animals per group. \* $P < 0.01$ . \*\* $P < 0.001$  compared with controls (ANOVA followed by post hoc tests for multiple comparisons).



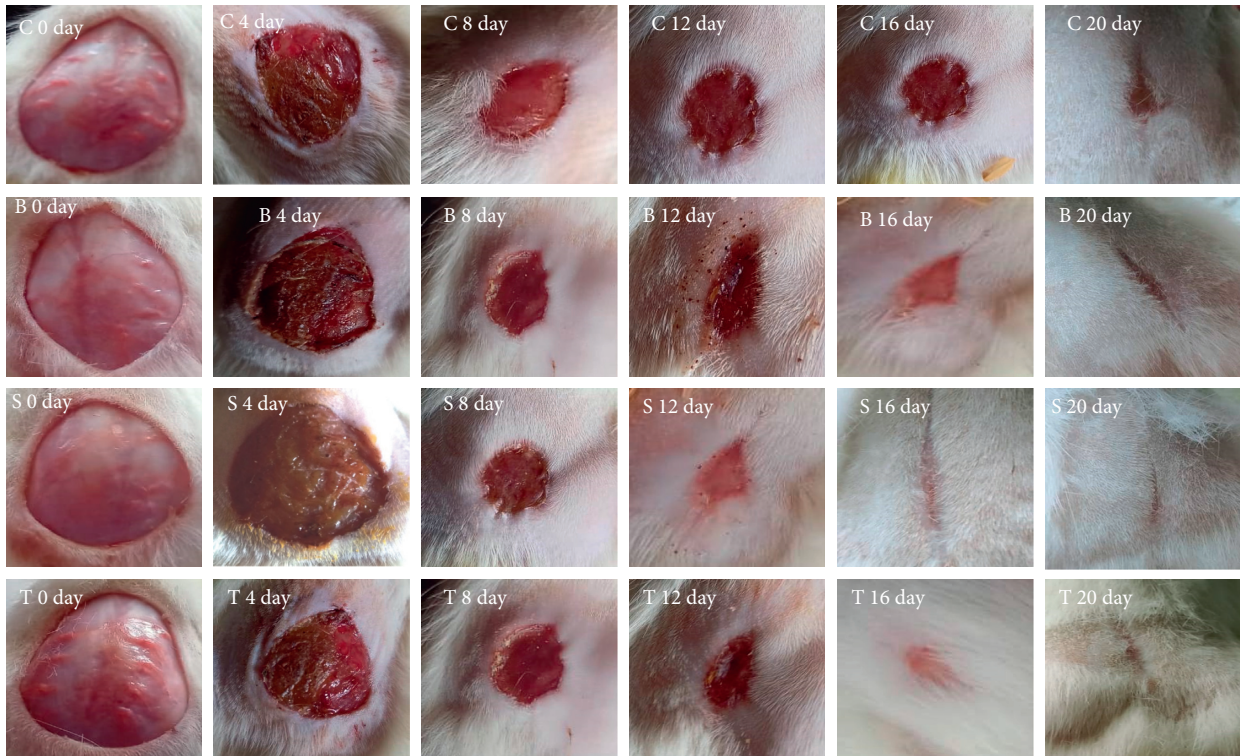


FIGURE 3: Photos depicting the effect of PIE ointment on excision wound model across different stages of the study.

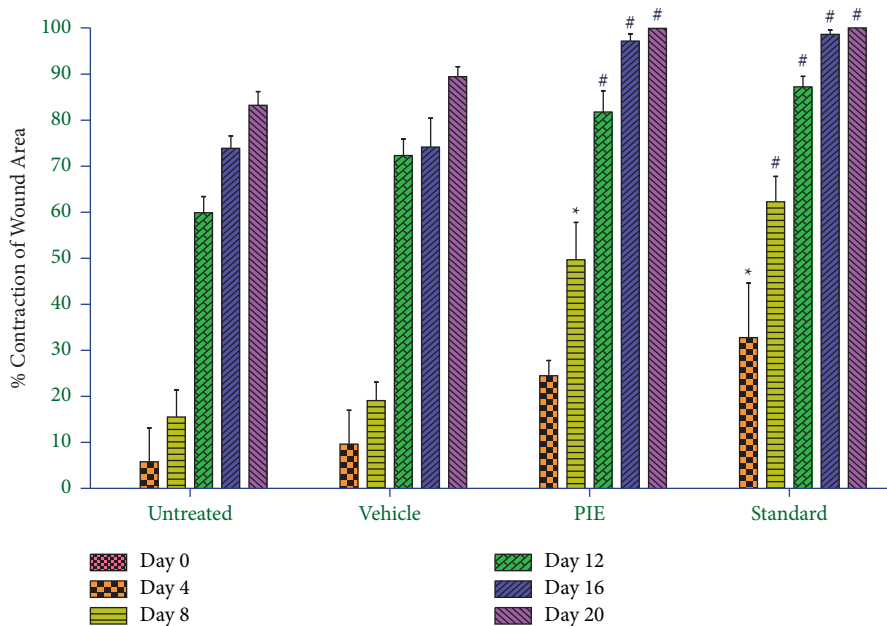


FIGURE 4: The percentage contraction of the wound area was employed as an evaluation criterion for *in vivo* wound-healing activity using an incision wound model. Values are expressed as mean  $\pm$  SEM for 6 animals per group. \* $P < 0.01$ . # $P < 0.001$  compared with controls (ANOVA followed by post hoc tests for multiple comparisons).

assay test results showed a promising outcome when compared to that of standard antimicrobial agents. The results showed that *E. coli* (Gram -ve), *B. cereus* (Gram +ve), and *C. albicans* strains were susceptible to the tested drug with the inhibition zone diameter of 20 mm, 07 mm, and 9 mm, respectively (Table 4 and Figure 9).

5.9. *Histopathological Study.* On the twentieth day, the histological investigations of the skin in the excision wounds were done, and the histopathological features of the tissue from all groups of animals are depicted in Figure 10. Animals in group I (A) (excision control) had inflammatory cells, decreased collagen fibers, fibroblast cells, and blood

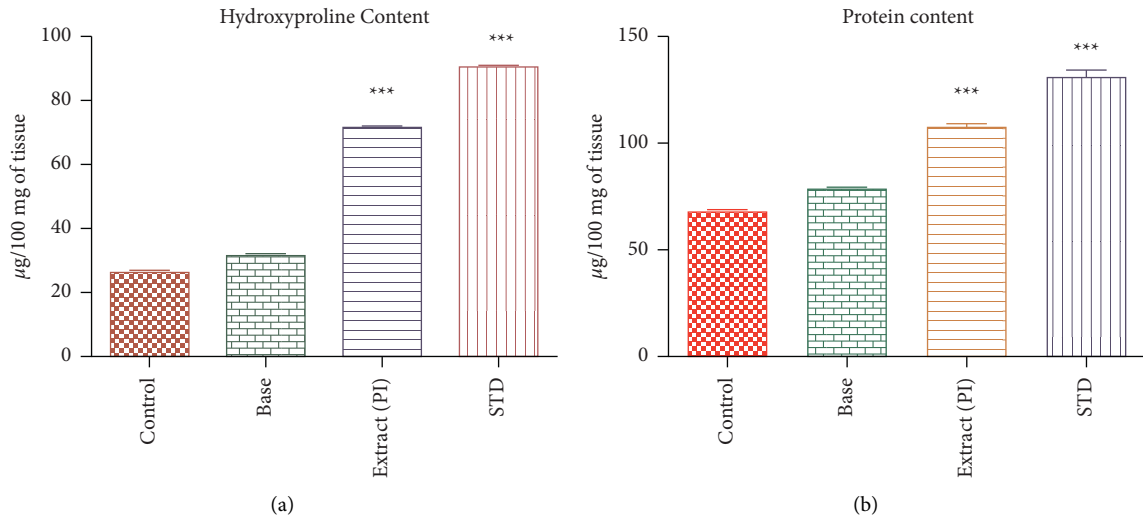


FIGURE 5: (a) The hydroxyproline content of various animal groups’ granulation tissues. (b) Protein content in the granulation tissues of different animal groups.

TABLE 2: Effect of PIE on tensile strength in the incision wound-healing model.

S. no.	Groups	Tensile strength (gm)
1	Incision control	768.0 ± 4.041
2	Base	862.5 ± 3.030
3	Extract (PIE)	1090 ± 16.09***
4	STD (povidone-iodine)	1204 ± 12.39***

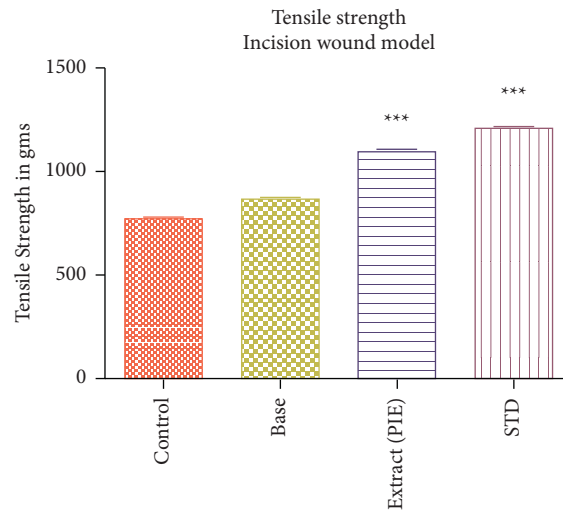


FIGURE 6: The effect of PIE ointment on tensile strength in incision wound model in Wister rats.

vessels, as well as apparent scar tissue. Group II (B) (base treatment) exhibited necrotic cells and fewer collagen fibers and blood vessels. However, as compared to the control, group III (C) (PIE ointment) revealed significantly more fibroblast cells, blood vessels, and well-organized collagen fibers. Group IV (D) (standard) demonstrated complete tissue regeneration as evidenced by increased fibroblast cells, collagen fibers, and blood vessels, as well as decreased inflammatory cells. Both the extract ointment-treated and

standard groups demonstrated epithelial tissue proliferation and keratinization.

## 6. Discussion

Wound-healing is a sophisticated process that takes place when the skin and other soft tissues of the body are damaged. Wound-healing is a dynamic process that involves numerous chemical pathways with the goal of returning the



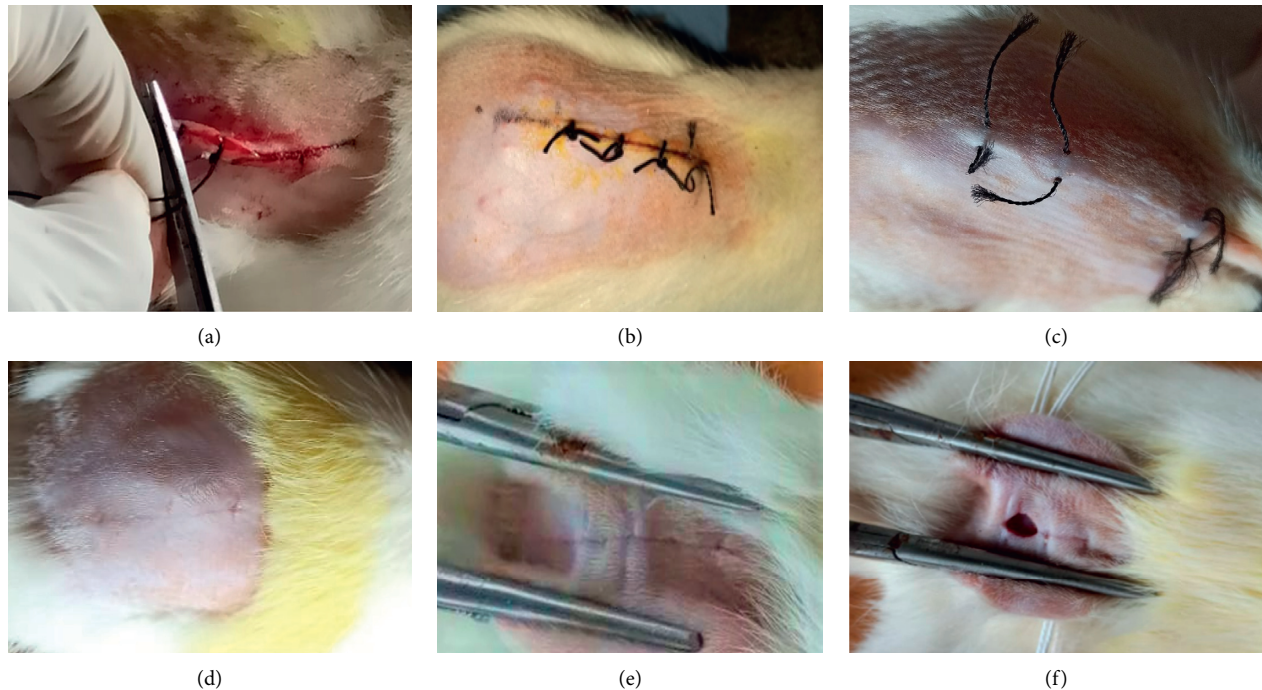


FIGURE 7: Photos depicting the effect of PIE ointment on the incision wound model across different stages of the study. (a) Wound suturing on day 0. (b) Wound-healing on day 8. (c) Wound-healing on day 12. (d) Wound-healing on day 16. (e) Tensile strength of test drug-treated animal wound on day 20 (wound did not open after applying 1090 g of weight). (f) Tensile strength of control animal wound on day 20 (sutured wound opened after applying 768 g of weight).

TABLE 3: The percentage of cell migration (wound closure) of STD and test samples at different time intervals.

S. no	Test sample	Duration	Cell migration in $\mu\text{m}$	Percentage wound closure (24 h)
1	Untreated	12 hours	5.08	16.90%
		24 hours	4.589	
2	Standard drug	12 hours	15.12	96.53%
		24 hours	21.65	
3	<i>Premna integrifolia</i>	12 hours	21.44	87.89%
		24 hours	22.07	

wounded cellular structure to its original form [26]. The conventional wound-healing cascade consists of three sequential and overlapping steps: inflammation, proliferation, and remodeling [27].

To further understand the extended usage of crude plant extracts or purified secondary metabolites in wound healing, a variety of *in vitro* investigations have been conducted. Several medicinal plants have been identified as medicinally relevant and important in both traditional and modern scientific studies [28]. *P. integrifolia* is an edible plant and has culinary uses. Its leaves are eaten by the inhabitants of the Coromandel coast, India. In Vietnam, the aromatic leaves are used to cook in some braise or stir fry dishes [29]. Thus, the consumption of this plant may also help heal gastric ulcers. Although *P. integrifolia*'s medical benefits have been known for decades, they are yet to be scientifically verified.

In the current study, we used *in vitro* assays and *in vivo* animal models to examine the wound-healing characteristics of *Premna integrifolia*.

In the current investigation, the topical administration of PIE (5% w/w) ointment promoted wound healing in both excision and incision wound types in rats. Recent research has suggested that triterpenoids, flavonoids, and tannins play an important role in wound healing through various mechanisms, including wound contraction, increased rate of epithelialization, and prevention of secondary bacterial infection [30, 31]. Previous studies on *Premna integrifolia* found the presence of sterols, flavonoids, tannins, and saponins, all of which aid in wound healing.

In our investigation, the test extract-treated groups exhibited a larger area of wound contraction than the excision control and ointment base groups. Furthermore, the tensile strength of PIE ointment was higher than the incision control animals. It could be related to increased fibroblast activity, increased collagen synthesis, antioxidant, anti-inflammatory [32], and antibacterial properties of the plant. In the current study, the antimicrobial activity of PIE was assessed, and it showed good antibacterial and antifungal potential.

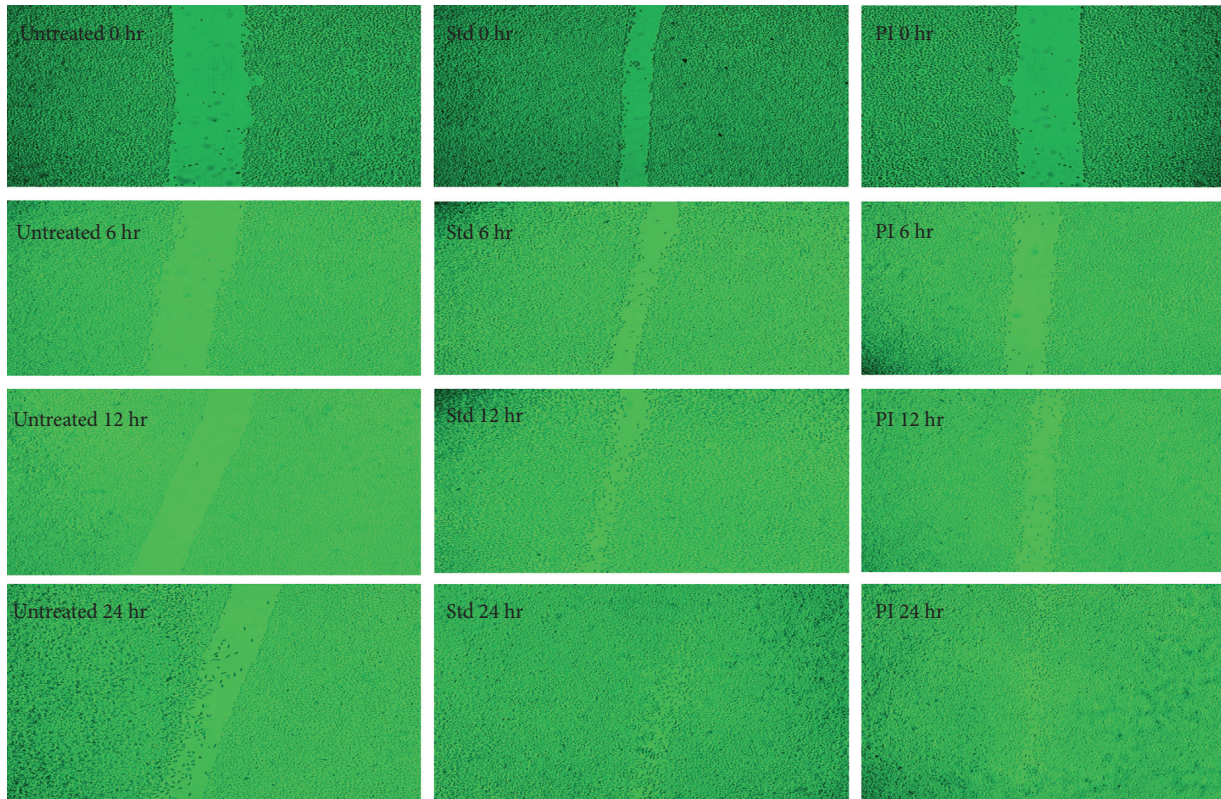


FIGURE 8: Microscopical photos illustrating *Premna integrifolia*'s ability to heal wounds *in vitro*. Images were taken at 0, 6, 12, and 24 hours after the mice fibroblast cells were cultured in the presence or absence of the test and standard drugs.

TABLE 4: Antimicrobial activity of test drug as depicted by the zones of inhibition (mm).

Test drug	<i>Escherichia coli</i> (Gram -ve)			<i>Bacillus cereus</i> (Gram +ve)			<i>Candida albicans</i> (fungi)					
	Control (ciprofloxacin): 29 mm	Conc. 1	Conc. 2	Conc. 3	Control (ciprofloxacin): 22 mm	Conc. 1	Conc. 2	Conc. 3	Control (Itraconazole): 13 mm	Conc. 1	Conc. 2	Conc. 3
<i>Premna integrifolia</i>	0 mm	0 mm	20 mm	0 mm	0 mm	7 mm	0 mm	7 mm	9 mm			

Wound contraction shortens healing time by lowering wound size and the volume of extracellular matrix needed to repair the injury. The wound-healing property of the PIE was parallel to that of povidone-iodine ointment, which is used as a standard treatment for wound-healing. Povidone-iodine is a well-known antibacterial medication that is used to prevent persistent wound infections.

Collagen is an extracellular protein found in the granulation tissue of a regenerating wound, assisting wound resilience and tissue matrix integrity [33, 34]. Controlled synthesis and the deposition of new collagen and its maturation are essential for wound healing [35]. In the current study, wound contraction was substantially higher in PIE-treated animals compared to the control group, which could be attributable to increased collagen synthesis. It could be related to the presence of phenolic compounds [25, 28], however, flavonoids may also help prevent secondary wound infections because they have antiviral and antibacterial properties [36]. This study focuses on hydroxyproline levels as a biochemical measure of collagen turnover. Significantly higher ( $P \leq 0.001$ ) hydroxyproline content in the granulation tissue of PIE ointment-treated rats shows an elevated

level of collagen content, which leads to rapid wound-healing, and this significant finding could be attributed to the presence of flavonoids [37]. Subsequently, the tensile strength of the treated wounds increased, which could be attributed to higher collagen levels and collagen fiber stabilization [38].

There was no indication of pus build-up, polymorphonuclear cell infiltration, fibrin deposition, or edema in animal lesions in the drug-treated group. Wound infection is the most common cause of delayed healing of skin wounds. Some of the most common bacteria that cause wound infection are *P. aeruginosa*, *E. coli*, *S. pyogenes*, *S. aureus*, and *Corynebacterium sp.* [39]. PIE previously demonstrated antibacterial action against *B. subtilis*, *S. lutea*, *E. coli*, *Pseudomonas sp.*, *X. campestris*, and *K. pneumoniae* [40]. In the present study, PIE exhibited good antibacterial and antifungal activity, which might be one of the mechanisms responsible for its wound-healing potential. It has been previously reported that plants rich in polyphenols exhibit significant antibacterial activity [41, 42].

The *in vitro* MTT assay is well-known for testing the cytotoxicity of test drugs against fibroblast cell lines. In this



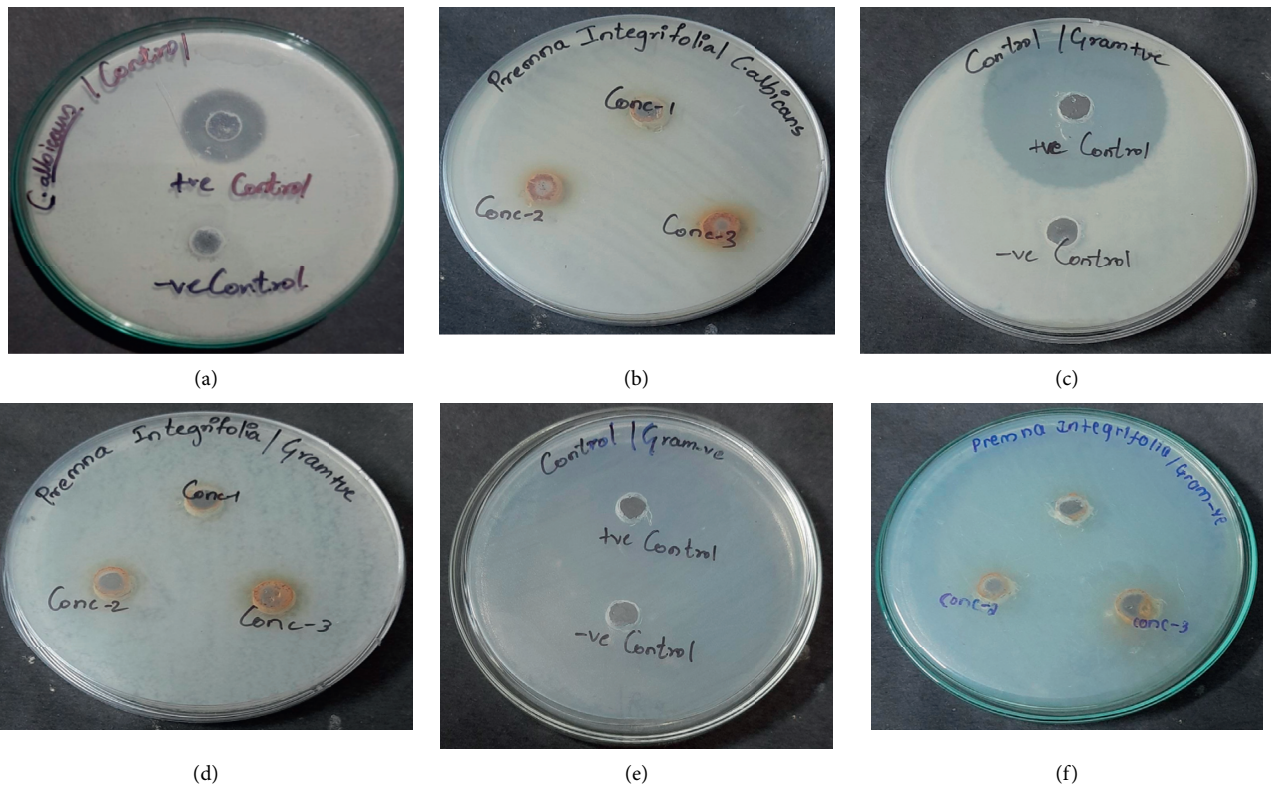


FIGURE 9: Antimicrobial activity of *P. integrifolia* against *C. albicans*: control itraconazole (a) and drug-treated (b). *B. cereus*: control ciprofloxacin (c) and drug-treated (d). *E. coli*: control ciprofloxacin (e) and drug-treated (f).

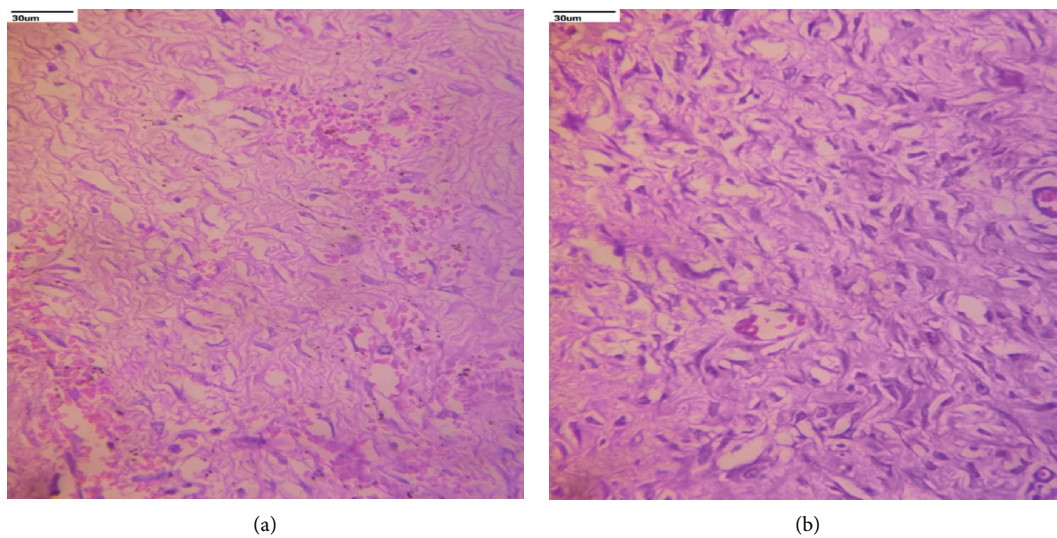


FIGURE 10: Continued.

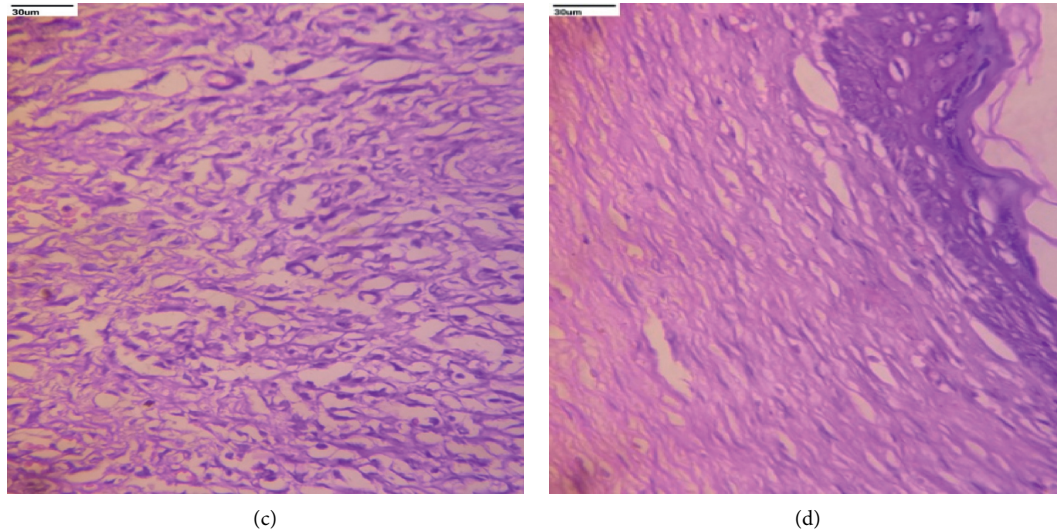


FIGURE 10: Histopathology analysis of newly healed tissue on day 20 post-treatment with PIE ointment. (a) Group I (excision control). (b) Group II (base treatment). (c) Group III (PIE ointment). (d) Group IV (Standard-Povidone-Iodine).

experiment, fibroblast cells were treated with PIE at various concentrations (50–250  $\mu\text{g/ml}$ ) and showed minimal or very minor toxicity to the fibroblast cells [43].

In the scratch-healing assay, scratching forms a “wound gap” in a cell monolayer, and the “healing” of this breach by cell proliferation and migration toward the center of the gap is recorded and frequently analyzed [44]. Factors affecting cell migration and/or proliferation can cause the gap to “heal” at a quicker or slower rate. This assay is easy to use and affordable, and the experimental settings can be simply changed to suit varied needs.

In the present study, when fibroblast cells were treated with *P. integrifolia* extract, we found that they migrated better toward the artificially created wound. It indicates that the extract hastens wound healing by causing fibroblast migration. A similar study on *A. saccata* leaves extract found that its methanolic extract stimulated the migration of fibroblasts while also increasing the expression of wound-healing genes [28].

One of the primary benefits of the scratch method is that it approximates cell mobility *in vivo* to some extent. Endothelial cells (ECs) migrate into the wound region to mend the wound. Furthermore, migration patterns mimic the behavior of these cells during *in vivo* migration, whether as a loosely connected population (e.g., fibroblasts) or as sheets of cells (e.g., epithelium and ECs). Another advantage of this experiment is its ability to investigate extracellular matrix and cell-cell interactions as regulators of cell migration [44].

## 7. Conclusion

The present research demonstrated that *Premna integrifolia* enhanced wound-healing activity *in vitro* and *in vivo*. The obtained results showed that the application of PIE on wounds induced considerable wound contraction and accelerated healing. Furthermore, the extract was

determined to have good antibacterial activity and had no cytotoxic effects. These findings show that *Premna integrifolia* extract possesses wound-healing potential and could be a viable source for isolating natural wound-healing phytochemicals. However, further clinical trials are warranted to extrapolate the results of this study in human beings.

### 7.1. Limitations, Economic Aspects, and Applied Suggestions.

In the field of regenerative medicine for wound repair, most wounds are currently treated with supportive measures, such as appropriate wound dressing, maintaining hygiene, and prophylactic antibiotic use rather than drugs that innately boost the healing process. Drugs for wound healing should ideally be designed so that they are effective and provide quick results, reduce patient morbidity and suffering, and, most importantly, are cost-effective. *Premna integrifolia* ointment shows excellent promise for the future of wound healing while also being cost-effective. The animal models for wound healing are not devoid of their limitations. There are differences in the anatomy and physiology of rodents and human skin. The architecture of human skin is not reflected by the loose skin and dense hair on the rodent skin. There is no single animal model that can capture the heterogeneity and complexity of human wounds. The ultimate challenge remains to be the reproducibility and translation of preclinical data into clinical reality. Rat wounds heal primarily through contraction, reducing the importance of re-epithelialization and granulation unless a splinting technique is used, and they are less tractable genetically than mice.

## Data Availability

The data related to this research are included in the Results section.

## Conflicts of Interest

The authors declare no conflicts of interest.

## Authors' Contributions

Conceptualization was done by Saeed Ali Alsareii, Mater Mahnashi, and Ibrahim Shaikh. Data curation was done by Nasser A. N Alzerwi and Mansour Yousef AlAsmari. Funding acquisition was done by Saeed Ali Alsareii. The investigation was done by Mansour Yousef AlAsmari, Abdulrahman Manaa Alamri, and Mater Mahnashi. Methodology was given by Saeed Ali Alsareii, Nasser A. N Alzerwi, Mater Mahnashi, and Ibrahim Shaikh. Project administration was done by Mansour Yousef AlAsmari, Abdulrahman Manaa Alamri, and Ibrahim Shaikh. Resources were provided by Abdulrahman Manaa Alamri. Supervision was done by Nasser A. N Alzerwi. Writing contributions are as follows: the original draft was prepared by Mater Mahnashi and Ibrahim Shaikh. Review and editing were done by Saeed Ali Alsareii, Mansour Yousef AlAsmari, Abdulrahman Manaa Alamri, and Ibrahim Shaikh.

## Acknowledgments

The authors are thankful to the Deanship of Scientific Research at Najran University for funding this work under the Research Groups Funding program grant code (NU/RG/MRC/11/4).

## References

- [1] S. Mulkalwar, L. Behera, P. Golande, R. Manjare, and H. Patil, "Evaluation of wound healing activity of topical phenytoin in an excision wound model in rats," *International Journal of Basic & Clinical Pharmacology*, vol. 4, no. 1, p. 139, 2015.
- [2] M. Shrimanker, N. Patel, H. Modi, and R. Dave, "A review: screening models for wound healing activity in animals," *American Journal of PharmTech Research*, vol. 3, pp. 2249–3387, 2013.
- [3] P. Stephens, M. Caley, and M. Peake, "Alternatives for animal wound model systems," *Methods in Molecular Biology*, vol. 1037, pp. 177–201, 2013.
- [4] V. Iorio, L. D. Troughton, and K. J. Hamill, "Laminins: roles and utility in wound repair," *Advances in Wound Care*, vol. 4, no. 4, pp. 250–263, 2015.
- [5] C. Tyavambiza, P. Dube, M. Goboza, S. Meyer, A. M. Madiehe, and M. Meyer, "Wound healing activities and potential of selected african medicinal plants and their synthesized biogenic nanoparticles," *Plants*, vol. 10, no. 12, p. 2635, 2021.
- [6] S. Schreml, R. M. Szeimies, L. Prantl, S. Karrer, M. Landthaler, and P. Babilas, "Oxygen in acute and chronic wound healing," *British Journal of Dermatology*, vol. 163, no. 2, pp. 257–268, 2010.
- [7] M. B. Dreifke, A. A. Jayasuriya, and A. C. Jayasuriya, "Current wound healing procedures and potential care," *Materials Science and Engineering: C*, vol. 48, pp. 651–662, 2015.
- [8] W.-P. Sandar, S. Saw, A. M. V. Kumar, B. S. Camara, and M.-M. Sein, "Wounds, antimicrobial resistance and challenges of implementing a surveillance system in Myanmar: a mixed-methods study," *Tropical Medicine and Infectious Disease*, vol. 6, no. 2, p. 80, 2021.
- [9] F. R. DeLeo and H. F. Chambers, "Reemergence of antibiotic-resistant *Staphylococcus aureus* in the genomics era," *Journal of Clinical Investigation*, vol. 119, no. 9, pp. 2464–2474, 2009.
- [10] B. A. Lipsky, M. Dryden, F. Gottrup, D. Nathwani, R. A. Seaton, and J. Stryja, "Antimicrobial stewardship in wound care: a position paper from the British society for antimicrobial chemotherapy and European wound management association," *Journal of Antimicrobial Chemotherapy*, vol. 71, no. 11, pp. 3026–3035, 2016.
- [11] K. Ravishankar, G. V. N. Kiranmayi, Y. R. Prasad, and L. Devi, "Wound healing activity in rabbits and antimicrobial activity of *Hibiscus hirtus* ethanolic extract," *Brazilian Journal of Pharmaceutical Sciences*, vol. 54, no. 4, 2018.
- [12] R. Madaan, S. Kumar, G. Bansal, and A. Sharma, "Estimation of total phenols and flavonoids in extracts of *Actaea spicata* roots and antioxidant activity studies," *Indian Journal of Pharmaceutical Sciences*, vol. 73, no. 6, pp. 666–669, 2011.
- [13] M. Pérez, P. Robres, B. Moreno et al., "Comparison of antibacterial activity and wound healing in a superficial abrasion mouse model of *Staphylococcus aureus* skin infection using photodynamic therapy based on methylene blue or mupirocin or both," *Frontiers of Medicine*, vol. 8, Article ID 673408, 2021.
- [14] P. Mali, "Premna integrifolia L.: a review of its biodiversity, traditional uses and phytochemistry," *Ancient Science of Life*, vol. 35, no. 1, pp. 4–11, 2015.
- [15] P. Mali, "Pharmacological potentials of Premna integrifolia L.," *Ancient Science of Life*, vol. 35, no. 3, pp. 132–142, 2016.
- [16] S. M. Al-Reza, M. Rokonzaman, M. Afroz, M. I. Hussain, M. A. Rashid, and A. Rahman, "Chemical composition and antioxidant activity of essential oil and organic extracts of Premna integrifolia Linn.," *Brazilian Archives of Biology and Technology*, vol. 59, 2016.
- [17] British Pharmacopoeia (BP), *Department of Health and Social Security Scottish Home and Health department*, Office of the British Pharmacopoeia Commission, vol. 2, p. 713, UK, 1988.
- [18] OECD, *Guideline for Testing of Chemicals: Draft Updated Test Guideline 434 on Acute Dermal Toxicity*, pp. 1–12, OECD, Paris, France, 2015.
- [19] B. S. Nayak, M. Anderson, and L. M. Pinto Pereira, "Evaluation of wound-healing potential of Catharanthus roseus leaf extract in rats," *Fitoterapia*, vol. 78, no. 7-8, pp. 540–544, 2007.
- [20] M. S. Kumar, S. Kirubanandan, R. Sripriya, and P. K. Sehgal, "Triphala promotes healing of infected full-thickness dermal wound," *Journal of Surgical Research*, vol. 144, no. 1, pp. 94–101, 2008.
- [21] J. F. Woessner Jr, "The determination of hydroxyproline in tissue and protein samples containing small proportions of this imino acid," *Archives of Biochemistry and Biophysics*, vol. 93, no. 2, pp. 440–447, 1961.
- [22] O. Lowry, N. Rosebrough, A. L. Farr, and R. Randall, "Protein measurement with the Folin phenol reagent," *Journal of Biological Chemistry*, vol. 193, no. 1, pp. 265–275, 1951.
- [23] M. Singh, R. Govindarajan, V. Nath, A. K. S. Rawat, and S. Mehrotra, "Antimicrobial, wound healing and antioxidant activity of *Plagiochasma appendiculatum* Lehm. et Lind.," *Journal of Ethnopharmacology*, vol. 107, no. 1, pp. 67–72, 2006.
- [24] D. Gerlier and N. Thomasset, "Use of MTT colorimetric assay to measure cell activation," *Journal of Immunological Methods*, vol. 94, no. 1-2, pp. 57–63, 1986.
- [25] Y. Chen, "Scratch wound healing assay," *Bio-protocol*, vol. 2, no. 5, 2012.



- [26] R. A. F. Clark, "Cutaneous tissue repair: basic biologic considerations. I," *Journal of the American Academy of Dermatology*, vol. 13, no. 5, pp. 701–725, 1985.
- [27] T. Kondo and Y. Ishida, "Molecular pathology of wound healing," *Forensic Science International*, vol. 203, no. 1–3, pp. 93–98, 2010.
- [28] S. R. Bolla, A. Mohammed Al-Subaie, R. Yousuf Al-Jindan et al., "In vitro wound healing potency of methanolic leaf extract of *Aristolochia saccata* is possibly mediated by its stimulatory effect on collagen-1 expression," *Heliyon*, vol. 5, no. 5, Article ID e01648, 2019.
- [29] A. H. Sturtevant, *Edible Plants of the World*, Dover Publications, Mineola, NY, 1972.
- [30] S. Lodhi and A. K. Singhai, "Wound healing effect of flavonoid rich fraction and luteolin isolated from *Martynia annua* Linn. on streptozotocin induced diabetic rats," *Asian Pacific Journal of Tropical Medicine*, vol. 6, no. 4, pp. 253–259, 2013.
- [31] K. Li, Y. Diao, H. Zhang et al., "Tannin extracts from immature fruits of *Terminalia chebula* Fructus Retz. promote cutaneous wound healing in rats," *BMC Complementary and Alternative Medicine*, vol. 11, no. 1, p. 86, 2011.
- [32] R. H. Gokani, S. K. Lahiri, D. D. Santani, and M. B. Shah, "Evaluation of anti-inflammatory and antioxidant activity of *Premna integrifolia* root," *Journal of Complementary and Integrative Medicine*, vol. 8, no. 1, 2011.
- [33] S. W. Hassan, M. G. Abubakar, R. A. Umar, A. S. Yakubu, H. M. Maishanu, and G. Ayeni, "Pharmacological and toxicological properties of leaf extracts of *kingelia africana* (Bignoniaceae)," *Journal of Pharmacology and Toxicology*, vol. 6, no. 2, pp. 124–132, 2011.
- [34] T. Ponrasu and L. Suguna, "Efficacy of *annona squamosa* L in the synthesis of glycosaminoglycans and collagen during wound repair in streptozotocin induced diabetic rats," *BioMed Research International*, vol. 2014, Article ID 124352, 10 pages, 2014.
- [35] A. Puratchikody, C. Devi, and G. Nagalakshmi, "Wound healing activity of *cyperus rotundus* linn," *Indian Journal of Pharmaceutical Sciences*, vol. 68, no. 1, p. 97, 2006.
- [36] J. Yang, J. Guo, and J. Yuan, "In vitro antioxidant properties of rutin," *Lebensmittel-Wissenschaft und -Technologie- Food Science and Technology*, vol. 41, no. 6, pp. 1060–1066, 2008.
- [37] S. Lodhi, A. P. Jain, V. K. Sharma, and A. K. Singhai, "Wound-healing effect of flavonoid-rich fraction from *Tephrosia purpurea* Linn. On streptozotocin-induced diabetic rats," *Journal of Herbs, Spices, & Medicinal Plants*, vol. 19, no. 2, pp. 191–205, 2013.
- [38] A. L. Udupa, D. R. Kulkarni, and S. L. Udupa, "Effect of *Tridax procumbens* extracts on wound healing," *International Journal of Pharmacognosy*, vol. 33, no. 1, pp. 37–40, 1995.
- [39] M. Senthil Kumar, R. Sripriya, H. Vijaya Raghavan, and P. K. Sehgal, "Wound healing potential of *Cassia fistula* on infected albino rat model," *Journal of Surgical Research*, vol. 131, no. 2, pp. 283–289, 2006.
- [40] A. Rahman, Z. Sultana Shanta, M. A. Rashid et al., "In vitro antibacterial properties of essential oil and organic extracts of *Premna integrifolia* Linn," *Arabian Journal of Chemistry*, vol. 9, pp. S475–S479, 2016.
- [41] M. H. Mahnashi, B. A. Alyami, Y. S. Alqahtani et al., "Phytochemical profiling of bioactive compounds, anti-inflammatory and analgesic potentials of *Habenaria digitata* Lindl.: molecular docking based synergistic effect of the identified compounds," *Journal of Ethnopharmacology*, vol. 273, Article ID 113976, 2021.
- [42] M. Sheriff Maqbul, A. M. Alshabi, A. Abdullatif Khan et al., "Comparative study of *moringa oleifera* with *moringa peregrina* seed oil using GC-MS and its antimicrobial activity against *Helicobacter pylori*," *Oriental Journal of Chemistry*, vol. 36, no. 03, pp. 481–492, 2020.
- [43] R. Abu-Dahab, "Antiproliferative activity of selected medicinal plants of Jordan against a breast adenocarcinoma cell line (MCF7)," *Scientia Pharmaceutica*, vol. 75, no. 3, pp. 121–136, 2007.
- [44] C.-C. Liang, A. Y. Park, and J.-L. Guan, "In vitro scratch assay: a convenient and inexpensive method for analysis of cell migration in vitro," *Nature Protocols*, vol. 2, no. 2, pp. 329–333, 2007.



## Research Article

# Efficacy and Safety of Zuojin Pill for the Treatment of Chronic Nonatrophic Gastritis: A Randomized Active-Controlled Clinical Trial

Ruilin Wang,<sup>1</sup> Yanling Wang,<sup>2</sup> Zheng Lu,<sup>2</sup> Jing Jing,<sup>1</sup> Zhongxia Wang,<sup>1</sup> Tingting He,<sup>1</sup> Miao Tian,<sup>1</sup> Zongyang Yuan,<sup>1</sup> Yanfei Cui,<sup>1</sup> Wenya Rong,<sup>3</sup> Xiao Ma ,<sup>4</sup> and Yanling Zhao <sup>5</sup>

<sup>1</sup>Division of Integrative Medicine, The Fifth Medical Center, General Hospital of PLA, Beijing 100039, China

<sup>2</sup>Senior Department of Hepatology, The Fifth Medical Center, General Hospital of PLA, Beijing 100039, China

<sup>3</sup>School of Chinese Medicine, Southern Medical University, Guangzhou 510515, China

<sup>4</sup>School of Pharmacy, Chengdu University of Traditional Chinese Medicine, Chengdu 611137, China

<sup>5</sup>Department of Pharmacy, General Hospital of PLA, Beijing 100039, China

Correspondence should be addressed to Xiao Ma; [tobymaxiao@163.com](mailto:tobymaxiao@163.com) and Yanling Zhao; [zhaoyl2855@126.com](mailto:zhaoyl2855@126.com)

Received 3 January 2022; Accepted 25 March 2022; Published 7 April 2022

Academic Editor: Jelena Zivkovic

Copyright © 2022 Ruilin Wang et al. This is an open access article distributed under the Creative Commons Attribution License, which permits unrestricted use, distribution, and reproduction in any medium, provided the original work is properly cited.

**Objective.** Zuojin pill (ZJP) is used as the classical prescription for a wide variety of digestive diseases. However, there is a lack of direct evidence for its use in the treatment of chronic nonatrophic gastritis (CNG). In particular, there is a lack of rigorous trials of randomized controlled designs. In this study, a randomized active-controlled clinical trial was performed to verify the efficacy and safety of ZJP in detail. **Methods.** Patients with CNG were divided into the ZJP group and the Marzulene-S granule group. Patients were enrolled from September 2019 to February 2021 (ChiCTR2000040549). Endoscopy and histology scores were evaluated as the primary outcome measure. The *Helicobacter pylori* positive rate and the disappearance rate of symptoms were also measured to reflect the outcomes. Finally, adverse events were also calculated as the index of safety. **Results.** A total of 68 eligible patients were enrolled in this trial and randomly divided into two groups with baseline comparability. ZJP was able to improve the red plaques as well as bile reflux scores compared with Marzulene-S granule ( $P = 0.043$  and  $P = 0.019$ , respectively). Moreover, it also remarkably alleviated the active chronic inflammation score ( $P = 0.043$ ). However, there was no difference between the *Helicobacter pylori* positivity rate ( $P = 0.752$ ). The symptom scores of abdominal distension ( $P = 0.004$ ), belching ( $P = 0.010$ ), and loss of appetite ( $P = 0.019$ ) were alleviated by ZJP, but nausea and vomiting were not ( $P = 0.616$ ). ZJP can also be considered safe with no obvious adverse effects. **Conclusion.** ZJP might decrease mucosal injury and alleviate symptoms in CNG. In addition, more large-scale clinical trials should be carried out to further confirm its clinical efficacy and safety.

## 1. Introduction

Chronic gastritis refers to the chronic infiltration of inflammation in the gastric mucosa and is the most common disease worldwide. It can be divided into three types: nonatrophic gastritis (CNG), atrophic gastritis (CG), and other special types. Recent data from the *Digestive Endoscopy Branch of the Chinese Medical Association* indicated that approximately 49.3% of patients with upper gastrointestinal symptoms were diagnosed with CNG. Further evidence

suggested that CNG can develop into CG without proper treatment. Patients who had CG with premalignant gastric lesions were shown to carry a remarkable risk of gastric cancer within 10 years of follow-up. Even in the short term, symptomatic patients might have a decreased quality of life due to nonspecific dyspeptic symptoms, such as epigastric discomfort, belching, distention, nausea, and even loss of appetite. However, there is still a lack of a specific medicine for CNG treatment due to the complex pathogenesis. *Helicobacter pylori* (*Hp*) infection is believed to be the primary

cause of CNG, and therapy involving the eradication of *Hp* is applied worldwide. Clarithromycin-containing regimens are recommended as first-line drugs. However, the increasing rate of antibiotic resistance has already influenced the treatment of CNG [1]. Moreover, proton pump inhibitors (PPIs), such as omeprazole, esomeprazole, and lansoprazole, are also important medicines that could reduce the damage to the mucosa that is induced by gastric acid. Studies have indicated that PPIs are associated with a series of adverse effects, including osteoporosis, hypomagnesemia, *Clostridium difficile* colitis, and cardiovascular morbidity [2, 3]. In addition, bismuth quadruple therapy is also widely employed as a first-line treatment. However, current studies have suggested that it might cause short-term dysbiosis of the gut microbiota and lead to adverse effects [4]. Specific medicine with ideal efficacy that can improve the quality of life is urgently needed for CNG patients.

It has long been recognized that traditional medicine still demonstrates unique therapeutic characteristics in the modern clinical system [5, 6]. Artemisinin, derived from *Artemisia annua* L. (Qinghao), is one of the most commonly used medicines to efficiently fight against malaria. The original plant was first recorded by Ge Hong in *A Handbook of Prescriptions for Emergencies* and was applied to relieve malaria symptoms. It is widely thought to be a gift from traditional Chinese medicine to the world [7]. Apart from artemisinin, Maxingshigan decoction and Yinqiao powder have also been recently used to fight against complex diseases. These two prescriptions are thought to be antiplague formulae in traditional Chinese medicine. In 2011, the combination of these two formulae was demonstrated to reduce the fever resolution period of patients with H1N1 influenza virus infection compared with oseltamivir in a prospective randomized controlled trial [8]. Lianhua-qingwen capsule, one type of traditional Chinese patent medicine that is made from the combination of Maxingshigan decoction and Yinqiao powder, was further confirmed to be effective in alleviating coronavirus disease 2019 (COVID-19) pneumonia in the clinic [9]. Therefore, it could serve as a crucial source for drug development from traditional Chinese medicine.

Zuojin pill (ZJP) was initially created by Danxi Zhu in his *Danxi's Experiential Therapy*, which is a well-known formula that has been used since the 15th century. Two kinds of herbal medicine containing the root of *Coptischinensis* Franch. and the fruit of *Euodia ruticarpa* (A. Juss.) Benth. are involved in this prescription at a ratio of 6:1 (w/w). It is used for the pattern of liver fire invading the stomach, which represents specific symptoms, including heartburn, dyspepsia, vomiting, and abdominal distension, in traditional Chinese medicine. This pattern occurs in a wide variety of digestive diseases in modern clinics [10]. Hence, it is recognized as the principle medicine for the treatment of patients suffering from gastritis, gastroesophageal reflux disease, gastric ulcer, and even gastric carcinoma [11]. Several preclinical pharmacologic experiments also suggested that the Zuojin pill could significantly reduce gastric mucosal injury by inhibiting the regulation of the NF- $\kappa$ B signaling pathway and reducing the inflammatory response

[12, 13]. All these studies provide indirect data that confirm the therapeutic efficacy of the Zuojin pill on CNG. However, there is a lack of direct evidence, especially with rigorous trials of randomized controlled designs. In this study, an open-label, randomized controlled trial was performed to verify the efficacy and safety of the Zuojin pill in detail. The results will definitely guide clinical applications.

## 2. Methods and Design

**2.1. Participant Diagnosis.** Patients with CNG were recruited from September 2019 to February 2021 at the Fifth Medical Center of PLA General Hospital, Beijing, China. The protocol was approved by the Ethics Committee at Fifth Medical Center of PLA General Hospital (approval number: 2019087D). All procedures and the purpose of the trial were clearly explained to all participants. Consent was obtained prior to participation. Participants with CNG were diagnosed according to the current standards of the Chinese Consensus on Chronic Gastritis (Shanghai, 2017).

**2.1.1. Clinical Manifestations.** Nonspecific dyspepsia, such as epigastric pain, distention, belching, acid regurgitation, nausea, vomiting, and loss of appetite, was the clinical manifestations of symptomatic patients. The physical sign was slight epigastric pain or mild discomfort in the upper abdomen.

**2.1.2. Endoscopic and Histopathological Diagnosis.** Endoscopic and histopathological examinations were the main references for CNG diagnosis. The essential characteristics of CNG are red plaques with punctuates, patches, and striae. Coarse and uneven mucosa, hemorrhagic spots or plaques, oedematous mucosa, and exudates without atrophic changes were also seen under endoscopy. Furthermore, no atrophic changes or intestinal metaplasia were found in the histopathological examination of the gastric mucosa.

## 2.2. Inclusion, Exclusion, Rejection, and Withdrawal Criteria

**2.2.1. Inclusion Criteria.** The inclusion criteria were as follows: participants were diagnosed with CNG according to the Chinese Consensus on Chronic Gastritis; participants were diagnosed with liver fire invading stomach syndrome, according to TCM syndrome differentiation; participants were between 20 and 70 years of age; participants voluntarily provided written informed consent.

**2.2.2. Exclusion Criteria.** The exclusion criteria were as follows: patients who underwent gastric-related surgery; patients with atrophic changes, intestinal metaplasia, or suspected malignant changes in the gastric mucosa; patients who also had other systemic diseases in the heart, liver, lung, kidney, or blood system; female patients who are planning to have a baby, are currently pregnant, or are lactating; patients with life-threatening illnesses, such as tumors and AIDS; patients who received other kinds of medicine in the 2 weeks

before recruitment; and patients who were judged as inappropriate to be enrolled in the trial by investigators.

**2.2.3. Rejection Criteria.** The rejection criteria were as follows: patients who were misdiagnosed; patients who did not take the proper drug dosage; and patients who could not complete the follow-up.

**2.2.4. Withdrawal Criteria.** The withdrawal criteria were as follows: patients who quit the clinical trial voluntarily and patients who were intolerant to the Zuojin pill or conventional therapy. Adverse events occurred during the trial. These adverse events included severe hepatic injury, malignant tumors, or hemorrhage of the digestive tract, and thus, a patient with these events was unlikely to complete the procedure.

**2.3. Intervention.** Participants assigned to the control group received Marzulene-S granule (2.01 g/day, three times a day, for 12 weeks). One granule of Marzulene-S weighed 0.67 g and contained 663.3 mg L-glutamine and 2.0 mg sodium guaienate. Participants in the treatment group received the Zuojin pill (6.0 g/day, twice a day, for 12 weeks). Zuojin pill was available from the Department of Pharmacy in the Fifth Medical Center of PLA General Hospital. A chemical analysis was performed to ensure the homogeneity of the prescription. During the treatment, a healthy lifestyle with a light diet, regular work and rest, and proper exercise were required, and smoking, alcohol consumption, and the consumption of spicy foods were prohibited. Patients with *Helicobacter pylori* also received clarithromycin-containing regimens for eradication. A follow-up was scheduled every 4 weeks following the treatment. Patients received conventional treatment if they did not obtain full recovery of CNG after the trial.

#### 2.4. Outcome Measures

**2.4.1. Primary Outcome.** The score of endoscopy evaluation, involving red plaques, erosion, hemorrhage, and bile reflux, was compared between the control group and the treatment group (Supplementary Table 1). The grade of histopathological changes, including chronic inflammation and active chronic inflammation, was also evaluated (Supplementary Table 2). The standard was set according to the Chinese Consensus on Chronic Gastritis.

#### 2.4.2. Secondary Outcomes

(1) *Helicobacter pylori* positive rate. The *Helicobacter pylori* positive rate in patients was also evaluated for the treatment.

(2) *Symptom scores.* Changes in each symptom score, including abdominal distension, belching, nausea, vomiting, and loss of appetite, were compared to reflect the quality of life (Supplementary Table 3).

**2.4.3. Subgroup Analysis.** Subgroup analysis based on *Hp* infection was also conducted with all the outcome measures.

**2.5. Safety Outcome.** Patients were interviewed every 4 weeks to record adherence and identify adverse events. Routine tests, including blood, urine, and stool tests, electrocardiogram, and liver and renal function tests, were performed at baseline. If the adverse events were relevant to the medication, patients were followed until their adverse events were resolved or there was no clinical significance.

**2.6. Preparation and HPLC-MS/MS Analysis of Zuojin Pill.** The preparation and HPLC-MS/MS analysis of the Zuojin pill were conducted according to a previous method.

**2.6.1. Preparation of Zuojin Pill Extracts and Standard Samples.** The root of *Coptis chinensis* Franch. and the fruit of *Euodia ruticarpa* (A. Juss.) Benth. were weighed and added at 6:1 ratio. They were soaked for 30 min in pure water (1/10, w/v). After that, it was extracted twice by heating (1 h at a time). The filtrate was rotationally evaporated, condensed, and dried into a dry powder for preservation. The weight ratio of the Zuojin pill was 23.48%. Berberine hydrochloride, *Coptis chinensis* alkaloid, palmatine, magnolia alkaloid, evodiamine, rutaecarpine, and dehydroevodiamine were purchased from Chengdu Chroma-Biotechnology Co., Ltd. (China). Carbamazepine (internal standard) was purchased from the National Institutes for Food and Drug Control. Berberine hydrochloride, *Coptis chinensis* alkaloid, palmatine, magnolia alkaloid, evodiamine, rutaecarpine, and dehydroevodiamine were prepared to standard concentrations of 1.1, 5.15, 1.6, 2.55, 12, 17, and 0.5  $\mu\text{g}/\text{mL}$  in methanol/water (1:1, v:v). Aliquots of all standards and internal standards were stored at  $-20^{\circ}\text{C}$ . Linearity was measured using a freshly prepared calibration pool of the mixed standards that was diluted to 1/2, 1/4, 1/10, 1/20, 1/40, 1/100, 1/500, and 1/1000 to obtain 9 final standard concentrations. The final concentration of the internal standard was 10  $\mu\text{g}/\text{mL}$ . Each concentration was prepared in three replicates. The calibration curve was prepared by determining the best fit of the peak area ratio (peak area of analyte/internal standard) versus concentration. The calibration curves were constructed using linear regression with  $1/x$  or  $1/x^2$  weighting factors. The results were used to calculate the overall linearity.

**2.6.2. HPLC-MS/MS Analysis.** The chromatographic separation was carried out on a Shim-pack GIS C18 column (10 mm  $\times$  2.1 mm, 3  $\mu\text{m}$ ) fitted on a Jasper HPLC system. The mobile phases were 0.1% formic acid (A) and acetonitrile (B). The flow rate was set to 0.3 mL/min. The column temperature was maintained at  $40^{\circ}\text{C}$ . The following gradient program was used: the initial mixture of 90% A and 10% B was held for 0.5 min; the linear gradient was increased to 70% B in 5 min and held for 2 min; then the linear gradient was increased to 90% B in 0.1 min and held for 1 min; then return to the initial conditions in 0.1 min, followed by

3.3 min of equilibration. The total run time was 12 min, and the injection volume was 2  $\mu$ L. Mass spectra were obtained using an API 3200 equipped with a TurboIon electrospray (ESI) interface set in the positive mode (needle voltage +5500 V). The mass spectrometry conditions were as follows: CUR, 20 psi; Gas 1 and Gas 2, 55 psi; IS: 5500 V; gas temperature: 550°C. The acquisition dwell time for each transition monitored was 50 ms.

**2.7. Statistical Analyses.** A series of statistical analyses were conducted by SPSS 26.0. Continuous variables are expressed as 'mean  $\pm$  standard', and categorical variables are expressed as frequencies (percentages). Student's *t*-test, Mann-Whitney test, or Chi-square test was used to compare baselines in different circumstances. For the comparison of variations from baseline to endpoint, Student's *t*-test and Wilcoxon signed-ranks test were performed according to normal or nonnormal variables, respectively. Moreover, the Wilcoxon test was applied to analyze the differences in the endoscopic scores and symptom scores between groups. The Chi-square test or Fisher's exact test was used for the symptom disappearance rate. All statistical tests were two-sided. The levels of  $P < 0.05$  and  $P < 0.01$  were assumed to be statistically significant and markedly significant, respectively.

### 3. Results

**3.1. Participant Distribution.** Seventy patients with endoscopy evaluation were determined to be eligible. However, one patient had liver cirrhosis, and one patient refused to sign the informed consent forms. Thus, a total of 68 patients were eligible for inclusion in this trial according to the CONSORT statement (Figure 1). All 68 patients were randomly assigned to the control group and treatment group. Thirty-four patients were assigned to the treatment group. This group included 22 men and 12 women, and the average age was  $56.20 \pm 9.33$  years. Thirty-four patients were included in the control group. This group included 17 men and 17 women, and the average age was  $53.91 \pm 10.92$  years. Two patients were excluded due to loss of follow-up, 1 patient deviated from the protocol, and 1 patient had poor compliance.

**3.2. Baseline Characteristics.** There was no significant difference in age, sex, endoscopic scores, histopathological changes, or symptom scores between the two groups. Moreover, the number of patients with *H. pylori* (positive) in the treatment group (44.12%, 15/34) and that in the control group (52.94%, 18/34) were also comparable ( $P = 0.355$ ) (Table 1).

**3.3. Endoscopy and Histology Evaluation Scores.** Zuojin pill was able to improve the red plaques and the bile reflux scores compared with Marzulene-S granule ( $P = 0.043$  and  $P = 0.019$ , respectively). However, there was no significant difference in the erosion score between patients who

received the Zuojin pill and the Marzulene-S granule ( $P = 0.769$ ). Although the Zuojin pill had a trend of decreasing hemorrhage compared with Marzulene-S granule, it did not reach statistical significance ( $P = 0.405$ ) (Table 2). In addition, the grade of histopathological changes in chronic inflammation was not significantly different between the two therapies ( $P = 0.055$ ). However, the Zuojin pill markedly alleviated the active chronic inflammation score compared with the Marzulene-S granule ( $P = 0.043$ ) (Table 2).

**3.4. Helicobacter pylori Positive Rate.** There was no difference in the *Helicobacter pylori* positive rate between the patients in the Zuojin pill group (14.70%, 5/34) and those in the Marzulene-S granule group (20.59%, 7/34) (Figure 2(a)).

**3.5. Symptom Scores.** The disappearance rates of symptoms in patients treated with the Zuojin pill were  $0.76 \pm 0.78$  for abdominal distension,  $0.18 \pm 0.58$  for belching,  $0.35 \pm 0.77$  for nausea and vomiting, and  $0.29 \pm 0.52$  for loss of appetite. These rates in the Marzulene-S granule group were  $1.29 \pm 0.68$ ,  $0.68 \pm 0.94$ ,  $0.26 \pm 0.66$ , and  $0.68 \pm 0.77$ , respectively. Zuojin pill significantly alleviated the symptoms of abdominal distension, belching, and loss of appetite compared with Marzulene-S granule ( $P = 0.004$ ,  $P = 0.010$ ,  $P = 0.019$ ). However, there was no difference in the symptoms of nausea and vomiting between the two groups ( $P = 0.616$ ) (Figure 2(b)).

**3.6. Subgroup Analysis.** Because *Hp* infection is thought to be the main cause of CNG, a subgroup analysis based on *Hp* infection was also conducted. The results indicated that the Zuojin pill could significantly decrease active chronic inflammation compared with Marzulene-S granule treatment in patients with *Hp* infection ( $P = 0.033$ ). Moreover, the Zuojin pill was able to alleviate red plaques ( $P = 0.016$ ), chronic inflammation ( $P = 0.005$ ), and abdominal distension ( $P = 0.012$ ) compared with Marzulene-S granule treatment in patients without *Hp* infection (Table 3).

**3.7. Adverse Events.** Adverse events included constipation (1 case in the Zuojin pill group) and dizziness (1 case in the Zuojin pill group and 2 cases in the Marzulene-S granule group). None of the cases were determined to be related to the medication.

**3.8. HPLC-MS Analysis of Zuojin Pill.** Seven major compounds were identified, including berberine hydrochloride, *Coptis chinensis* alkaloid, palmatine, magnolia alkaloid, evodi-amine, rutaecarpine, dehydroevodi-amine, and carbamazepine, which was the internal standard (Supplementary Figure 1).

## 4. Discussion

**4.1. The Insight into CNG from Mechanism to Treatment.** CNG is a common digestive disease but has a wide variety of complex mechanisms that require further investigation. The



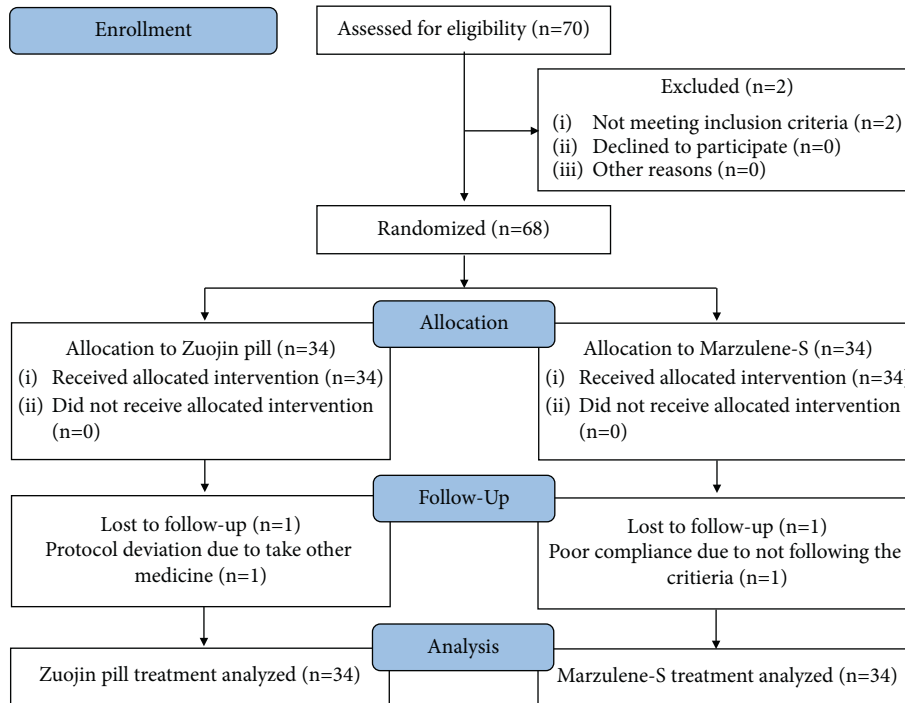


FIGURE 1: Standard CONSORT flowchart of the clinical trial.

TABLE 1: Comparison of baseline characteristics (mean ± SD).

Variables	Zuojin pill (n = 34)	Marzulene-S granule (n = 34)	P value
Gender (male/female)	22/12	17/17	0.327
Age	56.20 ± 9.33	53.91 ± 10.92	0.355
Red plaques	2.09 ± 0.83	2.15 ± 0.92	0.770
Erosion	2.09 ± 0.83	2.15 ± 0.66	0.747
Hemorrhage	1.62 ± 1.10	1.38 ± 0.95	0.350
Bile reflux	1.65 ± 0.69	1.76 ± 0.85	0.535
Chronic inflammation	2.35 ± 0.64	2.26 ± 0.66	0.581
Active chronic inflammation	2.20 ± 0.81	2.06 ± 0.78	0.447
Positive <i>Hp</i> rate	15 (44.1%)	18 (52.9%)	0.628
Abdominal distension	2.82 ± 0.39	2.68 ± 0.59	0.228
Belching	2.15 ± 0.36	2.29 ± 0.46	0.148
Nausea and vomiting	2.47 ± 0.67	2.38 ± 0.74	0.594
Loss of appetite	2.79 ± 0.50	2.76 ± 0.50	0.804

Notes: *Hp*, *Helicobacter pylori*.

TABLE 2: Comparison of endoscopy and histology evaluation after treatment (mean ± SD).

Variables	Zuojin pill (n = 34)	Marzulene-S granule (n = 34)	P value
Red plaques	1.15 ± 0.92	1.62 ± 0.95	0.043
Erosion	1.82 ± 0.83	1.88 ± 0.81	0.769
Hemorrhage	0.38 ± 0.74	0.53 ± 0.71	0.405
Bile reflux	0.26 ± 0.57	0.74 ± 0.99	0.019
Chronic inflammation	1.47 ± 0.96	1.91 ± 0.90	0.055
Active chronic inflammation	1.29 ± 1.12	1.82 ± 1.00	0.043

traditional concept of ‘one target, one disease’ seems inadequate for the determination of this crucial pathogenesis and is a limited approach for treatment [14, 15]. Therefore, the recent recognition of the pathogenesis of this disease

could be beneficial to improving the therapeutic options. It is widely believed that the progression of CNG, CAG, gastric intestinal metaplasia (GIM), and gastric cancer (GC) occurs through a thoroughly programmed deterioration with

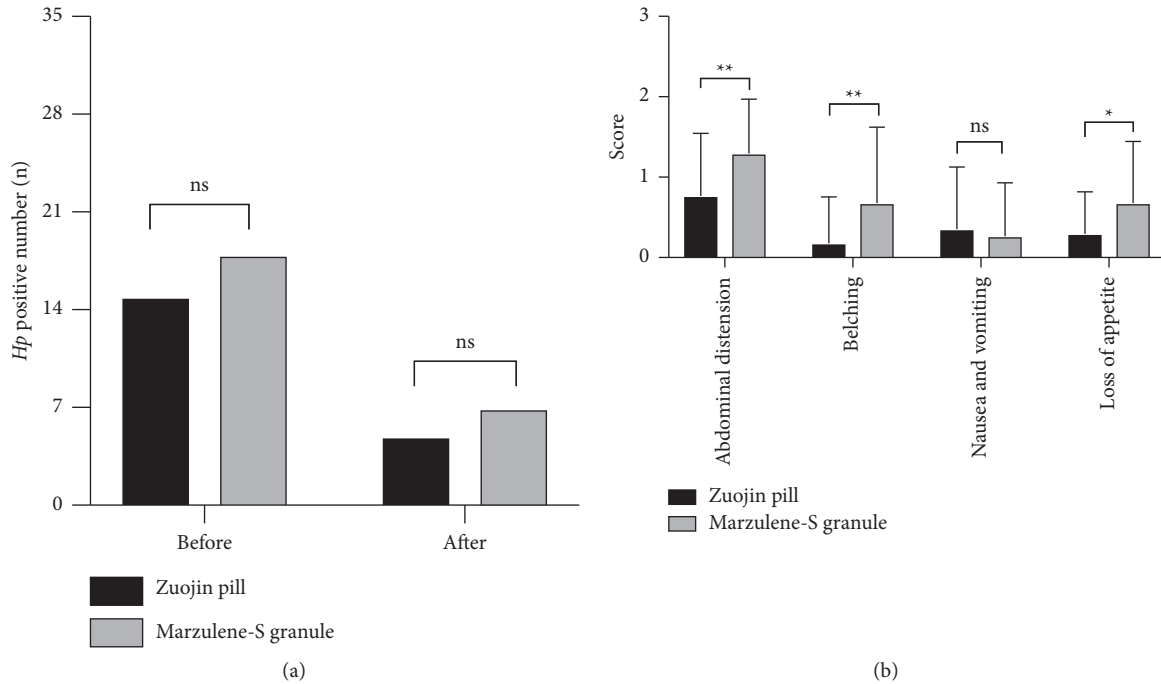


FIGURE 2: Comparison of secondary outcome measures. (a) *Helicobacter pylori* positive patients before and after treatment. (b) Symptom scores after treatment. \*  $P < 0.05$  compared with the Marzulene-S granule group; \*\*  $P < 0.01$  compared with the Marzulene-S granule group; ns: No significance).

TABLE 3: Subgroup comparison based on *Helicobacter pylori* infection after treatment (mean  $\pm$  SD).

Variables	Zuojin pill	Marzulene-S granule	P value
<i>Helicobacter pylori</i> infection positive	N = 15	N = 18	
Red plaques	1.40 $\pm$ 1.12	1.56 $\pm$ 0.92	0.665
Erosion	2.07 $\pm$ 0.80	2.11 $\pm$ 0.83	0.877
Hemorrhage	0.53 $\pm$ 0.83	0.67 $\pm$ 0.77	0.636
Bile reflux	0.47 $\pm$ 0.74	0.83 $\pm$ 1.04	0.263
Chronic inflammation	1.87 $\pm$ 0.99	1.78 $\pm$ 0.88	0.786
Active chronic inflammation	1.27 $\pm$ 1.10	2.06 $\pm$ 0.94	0.033
Abdominal distension	1.00 $\pm$ 0.84	1.39 $\pm$ 0.70	0.157
Belching	0.27 $\pm$ 0.70	0.78 $\pm$ 1.00	0.107
Nausea and vomiting	0.54 $\pm$ 0.92	0.39 $\pm$ 0.78	0.627
Loss of appetite	0.40 $\pm$ 0.63	0.83 $\pm$ 0.78	0.095
<i>Helicobacter pylori</i> infection negative	N = 19	N = 16	
Red plaques	0.95 $\pm$ 0.70	1.69 $\pm$ 1.01	0.016
Erosion	1.63 $\pm$ 1.01	1.62 $\pm$ 0.72	0.980
Hemorrhage	0.26 $\pm$ 0.65	0.38 $\pm$ 0.62	0.609
Bile reflux	0.16 $\pm$ 0.50	0.38 $\pm$ 0.88	0.369
Chronic inflammation	1.16 $\pm$ 0.83	2.06 $\pm$ 0.93	0.005
Active chronic inflammation	1.32 $\pm$ 1.16	1.56 $\pm$ 1.03	0.514
Abdominal distension	0.58 $\pm$ 0.69	1.19 $\pm$ 0.66	0.012
Belching	0.10 $\pm$ 0.46	0.56 $\pm$ 0.89	0.077
Nausea and vomiting	0.21 $\pm$ 0.63	0.12 $\pm$ 0.50	0.664
Loss of appetite	0.21 $\pm$ 0.42	0.50 $\pm$ 0.73	0.152

organized steps. CNG is accompanied by various biological factors, such as *Helicobacter pylori* infection, excessive inflammation, oxidative stress, and DNA damage and repair.

*Helicobacter pylori* is a Gram-negative pathogenic bacterium that has been found to colonize in the gastric mucosa

of a large population worldwide. The progress of *Helicobacter pylori* infection is believed to be the initiating cause of gastritis, and this has been established for almost a century [16]. However, the investigation into its role in inducing inflammatory responses in gastritis has never ended.



Traditional concepts recognize that *Helicobacter pylori* activates inflammation through various pathways that are associated with modifying TLR ligands [17]. Moreover, the most recent research indicates that *Helicobacter pylori* could exacerbate gastric inflammation by triggering C-type lectin receptors to modify host cholesterol [18]. *Helicobacter pylori* infection is widely associated with inflammation and the dysregulation of metabolites, which affects the progression of gastritis to a great extent. Oxidative stress, which plays a double-edged role, has also received increasing attention for its role in the progression of gastritis. First, redox homeostasis and antioxidant defense are highly needed to maintain homeostasis of the gastric epithelium due to excessive exposure to harsh conditions involving digestive enzymes, an aggressive pH environment, and bacteria [19]. For instance, the products of lipid peroxidation, including HNE and its protein/histidine adducts, are thought to be closely related to the pathogenesis of numerous gastric diseases [20]. Interestingly, a beneficial role has emerged for HNE in eradicating *Helicobacter pylori* infection. A study from Grasberger indicated that the dual oxidases (DUOX) enzyme complex was able to prevent gastric colonization by alleviating *Helicobacter pylori* and the inflammatory response [21]. In addition, DNA damage and repair are another important cause of chronic gastritis. The *p42.3* gene is a typical tumorigenesis promoter in various cancers [22]. It has been proven that both *Helicobacter pylori* and inflammatory factors can significantly enhance *p42.3* expression at the protein level. This gene was also positively associated with the severity of injury to the gastric mucosa. Thus, the damage caused by *p42.3* might be a significant regulator that affects CNG [23].

It is critically important to reverse the complex signaling network associated with CNG progression. The concept of a combination medication for CNG, such as triple therapy, is to maintain the surrounding stability. This concept has lasted at least 2000 years since the development of traditional Chinese medicine. Zuojin pill is used to treat various gastric diseases that are associated with network regulation. Its gastroprotective effect has been revealed at the molecular level during the past decade. Rhizoma Coptidis, one of the constituents in the Zuojin pill, was able to alleviate chronic gastritis with *Helicobacter pylori* infection. Our previous pharmacological research revealed that this effect was due to palmatine. It might ameliorate *Helicobacter pylori*-induced chronic gastritis by inhibiting MMP-10 through the ADAM17/EGFR signaling pathway [24]. Moreover, this action was also related to a metabolite network involving taurine and hypotaurine metabolism, glycerophospholipid metabolism, and pentose and glucuronate interconversions [25]. Another compound, berberine, which is derived from Rhizoma Coptidis, also demonstrates a beneficial effect on chronic gastritis. Research has indicated that berberine is able to suppress the IRF8-IFN- $\gamma$  signaling axis to inhibit progression [26]. Apart from Rhizoma Coptidis, the research on the effects of Fructus Evodiae on gastritis has also vastly improved. Rutaecarpine, one of the main quinazolino carboline alkaloids, exerts a remarkable gastroprotective effect against mucosal injury induced by ethanol. This effect

is highly associated with the suppression of the nuclear translocation of NF- $\kappa$ B p65 and its downstream signaling factors. The antioxidant role of this compound also involves the activation of the PI3K/AKT signaling pathway [27]. Thus, the components of the Zuojin pill are integral to the mechanisms of its effects.

#### 4.2. The Guidance of TCM from Bedside to Bench to Bedside.

Establishing an approach that connects basic research and clinical practice has long been an aim in medical science. In the past two decades, translational medicine has been considered a suitable concept for bridging this gap. It acts as a robust bi-directional link between research and application to enhance the rapid clinical translation and provide further feedback for basic research results [28]. During this progress, basic research knowledge can be translated to clinical application. It thus provides more advanced concepts, techniques, tools, and methods to address the diagnosis and treatment of diseases. Moreover, clinical researchers also ruminate the basic advances to further amend deficiencies in basic research. These relationships are commonly called ‘from bench to bedside’, ‘from bedside to bench’, or ‘B2B’ [29]. Thereafter, chemicals were developed for various diseases via this approach [30].

As the cornerstone of traditional medicine, herbal medicine has been recognized as an important source for drug development [31, 32]. Moreover, modern basic research offers deep insight into this clinical application and promotes further indication of its use. Thus, many medicines experience the process of ‘from bedside to bench to bedside’ to find the optimal guidance in TCM. The anti-influenza virus efficacy of Yinqiao powder (Yinqiaosan) is an outstanding example. This formula is found in ‘*Wen Bing TiaoBian*’, which is the basis of the theoretical research on the warm-heat disease in TCM. It consists of nine herbal components, such as *Flos Lonicerae*, *Fructus forsythiae*, *Fructus arctii*, and *Herba Schizonepetae*. Yinqiao powder and its modified formulae have a long history in the treatment of the common cold, fever, coughing, and other respiratory infectious diseases. Furthermore, researchers found that Yinqiao powder is able to inhibit the influenza-A virus based on an infected embryonated hen egg model [33]. In 2011, a modified formula of Yinqiao powder demonstrated remarkable efficacy in reducing the time to fever resolution in patients combating H1N1 influenza virus infection in the clinic [8]. This model sheds light on the translational medicine approach for TCM and bridges the gap between clinical experience and medicinal therapy. In addition, our previous research also confirmed the gastroprotective effect of the Zuojin pill and its components against mucosal injury. Thus, a clinical trial will provide clinical evidence for the value of the Zuojin pill for further application in CNG.

#### 4.3. The Indication of Current Research from Results to Application.

This research mainly focused on the efficacy of the Zuojin pill on CNG in the clinic. The results suggested that the Zuojin pill was able to alleviate several indices of mucosal injury under endoscopy and histology. It could downregulate red plaques and bile reflux but not erosion and hemorrhage,

indicating the selectivity of Zuojin pill action. In addition, it could remarkably alleviate active chronic inflammation. This action is critically important in anti-inflammation. Therefore, this efficacy coincides with our previous experimental results [27]. Furthermore, the efficacy of the Zuojin pill in alleviating symptoms of abdominal distension, belching, and loss of appetite was remarkable, indicating an integral improvement in quality of life. However, this result should be interpreted with caution. The concept of ‘pattern’ is the core factor for differentiating disease and further treatment in traditional Chinese medicine. That is, the Zuojin pill might be more suitable for CNG patients with a pattern of liver fire invading the stomach in TCM. Patients with this kind of pattern might achieve higher efficacy. Thus, subgroup trials with different patterns are needed for further exploration. Regarding the *Helicobacter pylori* positivity rate, the Zuojin pill did not demonstrate a significant difference compared to the Marzulene-S granule. This is because the main targets of the Zuojin pill focus more on downstream signaling pathways involved in inflammatory regulation. Furthermore, safety was also observed during the whole trial. However, all the cases with adverse events were ultimately determined to have no relation to the medication. Therefore, Zuojin pill treatment could be considered safe.

**4.4. The Limitations of the Current Research.** Overall, this trial strictly abided by the clinical standard from design to the determination to calculation. However, there still exists improvement in three aspects. First, a multicenter randomized clinical trial with large sample size is needed for further exploration. Only by performing this kind of trial can the evidence reported here be applied to guide gastritis treatment. Second, this research mainly uses the modern clinical index of CNG. Zuojin pill alleviates various symptoms. Therefore, the index of TCM symptoms should also be evaluated to obtain further clinical data. Finally, a comprehensive investigation of the specific mechanisms is still needed. Due to the current progress of multiomics techniques, the exploration of combined metabolomics and proteomics is urgently needed to predict possible molecular mechanisms and indicate the cure index.

## 5. Conclusion

Zuojin pill is able to decrease the mucosal injury of CNG and alleviate the related symptoms to elevate the life of quality. It is also safe for patients to use. In addition, more large-scale clinical trials with longer intervention durations should be carried out to further prove its clinical efficacy and safety.

## Data Availability

Data are available in ChiCTR2000040549.

## Conflicts of Interest

The authors declare that this research was conducted in the absence of any commercial or financial relationships that could be construed as a potential conflict of interest.

## Authors' Contributions

RW, YW, and JJ analyzed the data and wrote the manuscript. ZW, TH, and MT collected and analyzed the samples. ZY, YC, and WR amended the paper. XM and YZ (corresponding authors) conceived and coordinated the study and critically amended the paper.

## Acknowledgments

This work was supported by the Major Program of National Natural Science Foundation of China (no. 82192915), the National Key R&D Program of China (nos. 2018YFC1704500 and 2018YFC1704504), and Fund of China Medicine Education Association (2020KTY001).

## Supplementary Materials

Supplementary Table 1: score of endoscopy evaluation. Supplementary Table 2: grade of histopathological changes. Supplementary Table 3: symptom scores evaluation. Supplementary Figure 1: the HPLC-MS analysis of the Zuojin pill. (*Supplementary Materials*)

## References

- [1] J. P. Schubert, J. Gehlert, C. K. Rayner et al., “Antibiotic resistance of *Helicobacter pylori* in Australia and New Zealand: a systematic review and meta-analysis,” *Journal of Gastroenterology and Hepatology*, vol. 36, no. 6, pp. 1450–1456, 2021.
- [2] Y. Liu, X. Zhu, R. Li, J. Zhang, and F. Zhang, “Proton pump inhibitor ugeniang and potentially inappropriate prescribing analysis: insights from a single-centred retrospective study,” *BMJ Open*, vol. 10, no. 11, Article ID e040473, 2020.
- [3] O. Sattayalertyanyong, P. Thitilertdecha, and C. Auesomwang, “The inappropriate use of proton pump inhibitors during admission and after discharge: a prospective cross-sectional study,” *International Journal of Clinical Pharmacy*, vol. 42, no. 1, pp. 174–183, 2020.
- [4] P.-I. Hsu, C.-Y. Pan, J. Y. Kao et al., “*Helicobacter pylori* eradication with bismuth quadruple therapy leads to dysbiosis of gut microbiota with an increased relative abundance of Proteobacteria and decreased relative abundances of Bacteroidetes and Actinobacteria,” *Helicobacter*, vol. 23, no. 4, Article ID e12498, 2018.
- [5] S. Law, A. W. Leung, and C. Xu, “Is traditional Chinese medicine, “radix *Ilicis Pubescentis*” possible for treating cardiovascular disease?” *Traditional and Integrative Medicine*, vol. 5, no. 4, pp. 177–179, 2020.
- [6] N. Nayeibi, A. Esteghamati, A. Meysamie et al., “The effects of the *Melissa officinalis* L. based product on metabolic parameters in patients with type 2 diabetes mellitus: a randomized double-blinded controlled clinical trial,” *Journal of Complementary & Integrative Medicine*, vol. 16, no. 3, Article ID 20180088, 2019.
- [7] Y. Tu, “Artemisinin-A gift from traditional Chinese medicine to the world (nobel lecture),” *Angewandte Chemie International Edition*, vol. 55, no. 35, pp. 10210–10226, 2016.
- [8] C. Wang, B. Cao, Q.-Q. Liu et al., “Oseltamivir compared with the Chinese traditional therapy maxingshigan-yinqiaosan in the treatment of H1N1 influenza,” *Annals of Internal Medicine*, vol. 155, no. 4, pp. 217–225, 2011.

- [9] X. Chen, Y. Wu, C. Chen et al., "Identifying potential anti-COVID-19 pharmacological components of traditional Chinese medicine Lianhuaqingwen capsule based on human exposure and ACE2 biochromatography screening," *Acta Pharmaceutica Sinica B*, vol. 11, no. 1, pp. 222–236, 2021.
- [10] W. Guo, J. Huang, N. Wang et al., "Integrating network pharmacology and pharmacological evaluation for deciphering the action mechanism of herbal formula Zuojin pill in suppressing hepatocellular carcinoma," *Frontiers in Pharmacology*, vol. 10, p. 1185, 2019.
- [11] S. Li, M. Huang, G. Wu et al., "Efficacy of Chinese herbal formula sini Zuojin decoction in treating gastroesophageal reflux disease: clinical evidence and potential mechanisms," *Frontiers in Pharmacology*, vol. 11, p. 76, 2020.
- [12] Q. S. Wang, X. N. Zhu, H. L. Jiang, G. F. Wang, and Y. L. Cui, "Protective effects of alginate-chitosan microspheres loaded with alkaloids from *Coptis chinensis* Franch. and *Evodia rutaecarpa* (Juss.) Benth. (Zuojin Pill) against ethanol-induced acute gastric mucosal injury in rats," *Drug Design, Development and Therapy*, vol. 9, pp. 6151–6165, 2015.
- [13] J. Wang, T. Zhang, L. Zhu, C. Ma, and S. Wang, "Anti-ulcerogenic effect of Zuojin Pill against ethanol-induced acute gastric lesion in animal models," *Journal of Ethnopharmacology*, vol. 173, pp. 459–467, 2015.
- [14] E. E. Schadt, S. H. Friend, and D. A. Shaywitz, "A network view of disease and compound screening," *Nature Reviews Drug Discovery*, vol. 8, no. 4, pp. 286–295, 2009.
- [15] X. Ma, Y. Jiang, W. Zhang et al., "Natural products for the prevention and treatment of cholestasis: a review," *Phytotherapy Research*, vol. 34, no. 6, pp. 1291–1309, 2020.
- [16] K. M. Fock, D. Y. Graham, and P. Malfertheiner, "*Helicobacter pylori* research: historical insights and future directions," *Nature Reviews Gastroenterology & Hepatology*, vol. 10, no. 8, pp. 495–500, 2013.
- [17] S. Nagai, H. Mimuro, T. Yamada et al., "Role of Peyer's patches in the induction of *Helicobacter pylori*-induced gastritis," *Proceedings of the National Academy of Sciences*, vol. 104, no. 21, pp. 8971–8976, 2007.
- [18] M. Nagata, K. Toyonaga, E. Ishikawa et al., "*Helicobacter pylori* metabolites exacerbate gastritis through C-type lectin receptors," *Journal of Experimental Medicine*, vol. 218, no. 1, Article ID e20200815, 2021.
- [19] J. Kanner and T. Lapidot, "The stomach as a bioreactor: dietary lipid peroxidation in the gastric fluid and the effects of plant-derived antioxidants," *Free Radical Biology and Medicine*, vol. 31, no. 11, pp. 1388–1395, 2001.
- [20] A. Cherkas and N. Zarkovic, "4-Hydroxynonenal in redox homeostasis of gastrointestinal mucosa: implications for the stomach in health and diseases," *Antioxidants*, vol. 7, no. 9, p. 118, 2018.
- [21] H. Grasberger, M. El-Zaatari, D. T. Dang, and J. L. Merchant, "Dual oxidases control release of hydrogen peroxide by the gastric epithelium to prevent *Helicobacter felis* infection and inflammation in mice," *Gastroenterology*, vol. 145, no. 5, pp. 1045–1054, 2013.
- [22] L. Mao, W. Sun, W. Li et al., "Cell cycle-dependent expression of p42.3 promotes mitotic progression in malignant transformed cells," *Molecular Carcinogenesis*, vol. 53, no. 5, pp. 337–348, 2014.
- [23] P. Chen, Y. Cui, Q. Y. Fu, Y. Y. Lu, J. Y. Fang, and X. Y. Chen, "Positive relationship between p42.3 gene and inflammation in chronic non-atrophic gastritis," *Journal of Digestive Diseases*, vol. 16, no. 10, pp. 568–574, 2015.
- [24] X. Chen, R. Wang, C. Bao et al., "Palmatine ameliorates *Helicobacter pylori*-induced chronic atrophic gastritis by inhibiting MMP-10 through ADAM17/EGFR," *European Journal of Pharmacology*, vol. 882, Article ID 173267, 2020.
- [25] X. Chen, J. Zhang, R. Wang et al., "UPLC-Q-TOF/MS-Based serum and urine metabolomics study on the ameliorative effects of palmatine on *Helicobacter pylori*-induced chronic atrophic gastritis," *Frontiers in Pharmacology*, vol. 11, p. 586954, 2020.
- [26] T. Yang, R. Wang, J. Zhang et al., "Mechanism of berberine in treating *Helicobacter pylori* induced chronic atrophic gastritis through IRF8-IFN- $\gamma$  ugeniang axis suppressing," *Life Sciences*, vol. 248, Article ID 117456, 2020.
- [27] S. Ren, Y. Wei, R. Wang et al., "Rutaecarpine ameliorates ethanol-induced gastric mucosal injury in mice by modulating genes related to inflammation, oxidative stress and apoptosis," *Frontiers in Pharmacology*, vol. 11, Article ID 600295, 2020.
- [28] F.-M. Chen, Y.-M. Zhao, Y. Jin, and S. Shi, "Prospects for translational regenerative medicine," *Biotechnology Advances*, vol. 30, no. 3, pp. 658–672, 2012.
- [29] D. R. Moore, "Reverse translation: clearing a path from bedside to bench," *Nature*, vol. 454, no. 7202, p. 274, 2008.
- [30] A. Gabizon, H. Shmeeda, E. Tahover et al., "Development of promitil, a ugenia prodrug of mitomycin c in PEGylated liposomes: from bench to bedside," *Advanced Drug Delivery Reviews*, vol. 154–155, pp. 13–26, 2020.
- [31] S. H. Mosavat, M. Heydari, M. H. Hashempur, and S. M. Dehghani, "Use of complementary and alternative medicine among paediatric patients with hepatogastrointestinal diseases," *Eastern Mediterranean Health Journal*, vol. 24, no. 10, pp. 1018–1025, 2018.
- [32] S. Parveen, A. A. Khan, and Q. A. Khan, "Antihyperlipidemic effect of seeds of jamun (*Ugenia jambolana*) in subjects of intermediate hyperglycemia: a pilot study," *Traditional and Integrative Medicine*, vol. 5, no. 4, pp. 191–197, 2021.
- [33] X. Wang, O. Hao, W. Wang, X. Ying, and H. Wang, "Evaluation of the use of different solvents to extract the four main components of Yinqiaosan and their in vitro inhibitory effects on influenza-A virus," *The Kaohsiung Journal of Medical Sciences*, vol. 26, no. 4, pp. 182–191, 2010.



## Research Article

# Artemisinin Alleviates Cerebral Ischemia/Reperfusion Injury via Regulation of the Forkhead Transcription Factor O1 Signaling Pathway

Xiaogang Yang<sup>1</sup> and Ke Wu<sup>2</sup> 

<sup>1</sup>Department of Neurosurgery, Affiliated Hospital of Yan'an University, Yan'an 716000, Shanxi Province, China

<sup>2</sup>Department of Neurosurgery, Xichang People's Hospital, Xichang 615000, Sichuan Province, China

Correspondence should be addressed to Ke Wu; [ruidou50834399@163.com](mailto:ruidou50834399@163.com)

Received 24 January 2022; Revised 9 March 2022; Accepted 19 March 2022; Published 5 April 2022

Academic Editor: Ruchika Garg

Copyright © 2022 Xiaogang Yang and Ke Wu. This is an open access article distributed under the Creative Commons Attribution License, which permits unrestricted use, distribution, and reproduction in any medium, provided the original work is properly cited.

The effect and mechanism of artemisinin therapy on cerebral ischemia-reperfusion injury (CIRI) was analyzed in this work. 100 healthy male C57BL/6 mice were selected and randomly divided into the sham group (no treatment), CIRI model group (IR), IR + artemisinin posttreatment group (IR + Arte), EX527 + IR group (EX527 + IR), and EX527 + IR + artemisinin posttreatment group (EX527 + IR + Arte), with 20 mice in each group. The cerebral infarct volumes of mice in different groups were measured by the 2,3,5-triphenyltetrazolium chloride (TTC) staining method. The neurological function scores and oxidative stress levels of mice in different groups were measured and compared. In addition, the expressions of silent information regulator 1 (SIRT1), forkhead transcription factor O1 (FOXO1), and p53 protein in brain tissue were detected. The results showed that the contents of reactive oxygen species (ROS) and malondialdehyde (MDA) in the EX527 + IR group and EX527 + IR + Arte group were significantly higher than those in the IR + Arte group ( $P < 0.05$ ). The expressions of SIRT1 protein in the brain tissue of the IR group and EX527 + IR group were much lower than that of the sham group ( $P < 0.01$ ); compared with the IR + Arte group, the expression of the X527 + IR group in the brain tissue was greatly reduced ( $P < 0.05$ ). The expression levels of FOXO1 protein and p53 protein in the brain tissue of mice in the IR group and EX527 + IR group were higher than those in the sham group ( $P < 0.01$ ). It was concluded that artemisinin treatment can reduce oxidative stress damage and alleviate CIRI through the SIRT1/FOXO1 signaling pathway, thereby achieving neuroprotective effects.

## 1. Introduction

Ischemic stroke is a sudden and acute disorder of cerebral blood circulation, which has a high morbidity, fatality, and disability rate [1]. Among the current treatment methods for ischemic stroke, thrombolysis with recombinant tissue-type plasminogen activator and mechanical recanalization to establish cerebral blood flow reperfusion are the best treatment options, but it is easy to cause cerebral ischemia-reperfusion injury (CIRI) [2]. CIRI is an irreversible process, which is related to factors such as mitochondrial dysfunction, oxidative stress, apoptosis, inflammation, and ion imbalance in the body [3]. Artemisinin is an extract from the Compositae plant *Artemisia annua*. Current research results

show that artemisinin has immunomodulatory, anti-inflammatory, antiapoptotic, and antifibrosis effects [4, 5]. Artemisinin can effectively reduce the myocardial CIRI through antioxidant and scavenging oxygen free radicals [6]. However, there are currently few studies on artemisinin posttreatment on brain protection, and its mechanism is not yet known [7].

Silent information regulator 1 (SIRT1) is a histone deacetylase that relies on nicotinamide adenine dinucleotide ( $\text{NAD}^+$ ), and it participates in cell proliferation, senescence, apoptosis, oxidative stress, and inflammatory reactions by cooperating with various factors such as forkhead transcription factor O1 (FOXO1) and nuclear transcription factor- $\kappa\text{B}$  (NF- $\kappa\text{B}$ ) [8, 9]. It has been reported that the SIRT1/

FOXO1 signaling pathway has a cerebral protective effect in a variety of brain diseases such as CIRI and subarachnoid hemorrhage [10]. Curcumin can reduce myocardial CIRI and large CIRI by activating the SIRT1/FOXO1 signaling pathway [11]. Chinese researchers Zhang et al. [12] pointed out that artemisinin has a certain effect on rat myocardial CIRI, but there is no report on the effect of artemisinin posttreatment on large CIRI and the specific mechanism.

## 2. Materials and Methods

**2.1. Experimental Reagents.** The experimental reagents included the malondialdehyde (MDA) kit (Nanjing Jiancheng Bioengineering Institute), superoxide dismutase (SOD) kit (Nanjing Jiancheng Bioengineering Institute), glutathione peroxidase (GSH-Px) kit (Nanjing Jiancheng Bioengineering Institute), MitoCheck Complex I Activity Assay Kit (Cayman Islands, USA), 2,3,5-triphenyltetrazolium chloride (TTC, Beijing Soleibo Biotechnology Co., Ltd.), paraformaldehyde (Hebei Tianda Chemical Co., Ltd.), and dihydroethidium (DHE).

**2.2. Experimental Animals and Their Grouping.** 100 healthy male C57BL/6 mice aged 7–8 weeks and weighing 20–25 g were selected in this study; 5 mice per cage were housed in specified pathogen free (SPF) laboratory, with the room temperature of 25°C, relative humidity of about 55%, under 12-hour light conditions, and free drinking and eating. After 2 weeks of adaptive rearing, all mice were randomly divided into 5 groups: sham group (sham, no treatment), ischemia-reperfusion (IR) group (CIRI model), IR + artemisinin posttreatment group (IR + Arte), EX527 + IR group (EX527 + IR), and EX527 + IR + artemisinin posttreatment group (EX527 + IR + Arte), with 20 animals in each group. The details of time and route of administration are given in Table 1. All animal procedures in this experiment were approved by the Experimental Animal Management Committee, and the experimental methods were carried out in accordance with the approved guidelines.

**2.3. Establishment of the Mice CIRI Model and Treatment Methods of Mice in Different Groups.** A mouse middle cerebral artery occlusion model (MACO) [13] was used to establish a CIRI model, which was modified on this basis. During the operation, the mice were anesthetized with a mixture of oxygen and isoflurane, the neck and chest hair were removed, and the mice were fixed on the operating table in a supine position. A heating pad was adopted to maintain the rectal body temperature of mice at  $37 \pm 1^\circ\text{C}$ . After routine disinfection of the head and neck, the anterior median incision of the neck was bluntly separated under a microscope to fully expose the right common carotid artery and external carotid artery of the mice. A 6-0 monofilament nylon thread with a length of 11 mm and poly-L-lysine-coated was inserted into the internal carotid artery through the common carotid artery to block the blood flow of the middle cerebral artery, induce ischemia for 30 minutes, and remove the thread plug for reperfusion. After the operation,

the mice were resuscitated on a constant temperature plate at  $37^\circ\text{C}$  and then returned to room temperature for 24 hours.

Artemisinin was first completely dissolved in absolute ethanol and then diluted to normal saline at a volume ratio of 1:9. The mice except the sham group were injected intraperitoneally with artemisinin 10 minutes before brain tissue reperfusion. The dosage was 25 mg/kg. Before model construction, mice in the EX527 + IR and EX527 + IR + Arte groups were intraperitoneally injected with EX527 at a dose of 5 mg/kg, once every two days, for a total of 3 times.

**2.4. Measurement of Neurological Function Score and Cerebral Infarct Volume.** After 24 hours of reperfusion, mice in different groups were scored by three experimenters with unclear information about grouping, surgery, and dosage of mice individually with reference to Liang et al. [14] method mechanical energy neurological function score, and the average value was calculated and recorded. The normal state was rated as 0; the left front paw of the mouse could not be fully extended was rated as 1; the mouse turned to the left when awake was rated as 2 points; the mouse still had left side dumping in the resting state was rated as 3 points; and the mice were unable to walk or roll was rated as 4 points.

24 hours after reperfusion, pentobarbital sodium was used for anesthesia, the skin was cut along the middle of the mouse neck, the left mouse carotid artery was separated, the brain tissue was completely separated, weighed and sliced, and the thickness was about 2 mm. 2% 2,3,5-triphenyltetrazolium chloride (TTC) dye solution (Sigma-Aldrich, USA) was added for 30 min at  $37^\circ\text{C}$  under dark conditions, and 4% paraformaldehyde (Hebei Tianda Chemical Co., Ltd.) was added overnight. Then, the photos were taken. Red indicated normal brain tissue, and unstained indicated brain tissue in the infarct area. The infarct volume of mice in different groups was calculated.

**2.5. Detection on Oxidative Stress Level, Mitochondrial Complex I (MCI), and ROS Activity.** The malondialdehyde (MDA) kit (Nanjing Jiancheng Institute of Bioengineering), superoxide dismutase (SOD) kit (Nanjing Jiancheng Institute of Bioengineering), and glutathione peroxidase (GSH-Px) kit (Nanjing Jiancheng Institute of Bioengineering) were used to detect MDA, SOD, and GSH-Px contents in mouse brain tissues of different groups. The MitoCheck Complex I Activity Assay Kit (Cayman, USA) was used to detect the activity of MCI in the main member of the reactive oxygen species family in the brain tissue of different groups of mice.

The brain tissue was embedded with optimum cutting temperature compound (OCT) glue and frozen at  $-80^\circ\text{C}$  for 1 min. After taking it out, the tissue was wrapped in tin foil and stored in the refrigerator at  $-80^\circ\text{C}$  for later use. The tissue was cut into slices of about  $10 \mu\text{m}$  using a cryostat (Meikang, Germany), added with 10 mol/L dihydroethidium (DHE), and then treated at  $37^\circ\text{C}$  for 30 minutes. Next, it was photographed with a confocal microscope (Olympus, Japan) to analyze the fluorescence intensity with the Image Pro Plus software.

TABLE 1: Time and route of administration.

Group	Administration time	Route of administration	Dose
Sham	10 minutes before brain tissue reperfusion	Intraperitoneal injection	25 mg/kg
IR	Before model construction	Intraperitoneal injection	5 mg/kg
IR + Arte	Before model construction	Intraperitoneal injection	5 mg/kg
EX527 + IR	Before model construction	Intraperitoneal injection	5 mg/kg
EX527 + IR + Arte	Before model construction	Intraperitoneal injection	5 mg/kg

**2.6. Western Blot (WB) to Detect Brain Tissue Protein Content.** The tissue was rinsed with precooled phosphate buffer saline (PBS) and put into a homogenizer, added with 500  $\mu$ L of protein lysis solution for grinding, and fully lysed to extract total protein. The protein content was determined by the bicinchoninic acid (BCA) method. The sodium dodecyl sulfate polyacrylamide gel electrophoresis (SDS-PAGE) was adopted to separate the cellular proteins; the protein was transferred to polyvinylidene fluoride (PVDF) membrane by the wet transfer method and then sealed with 5% skimmed milk. After adding with primary antibodies diluted 1:1000, the tissue was incubated overnight at 4°C, thoroughly washed 3 times with Tris-buffered saline Tween (TBST), added with horseradish peroxidase-conjugated secondary antibody, and then incubated at room temperature for 2 hours. After it was thoroughly washed 3 times with TBST, the tissue was added with color-developing solution and automatically exposed on the developing instrument to take pictures for grayscale scanning. Finally, the protein expression level was analyzed according to the gray value.

**2.7. Statistical Analysis.** SPSS 19.0 was used for data statistics and analysis. Measurement data were expressed in the form of mean  $\pm$  standard deviation ( $\bar{x} \pm s$ ), and counting data were displayed in the form of percentage (%). Measurement data that obeyed the normal distribution were expressed by the *t*-test, or otherwise, they were expressed by Wilcoxon. In the test, one-way analysis of variance was used for comparison between groups, and  $P < 0.05$  indicated that the difference was statistically significant.

### 3. Results

**3.1. Comparison on Neurological Function Score Results in Different Groups of Mice.** The neurological function scores of mice in different groups were compared, as shown in Figure 1. The neurological function scores of mice in the IR group, EX527 + IR + Arte group, and EX527 + IR group were much higher than those in the sham group ( $P < 0.01$ ), and compared with the sham group, there was a statistical difference in the IR + Arte group ( $P < 0.05$ ). The neurological function scores of the mice in the IR + Arte group and EX527 + IR + Arte group were statistically different from those in the IR group ( $P < 0.05$ ), and those in the EX527 + IR group and EX527 + IR + Arte group were visibly greater than the score in the IR + Arte group ( $P < 0.05$ ).

**3.2. Comparison on Cerebral Infarct Volume in Different Groups of Mice.** The results of TTC staining in the brain

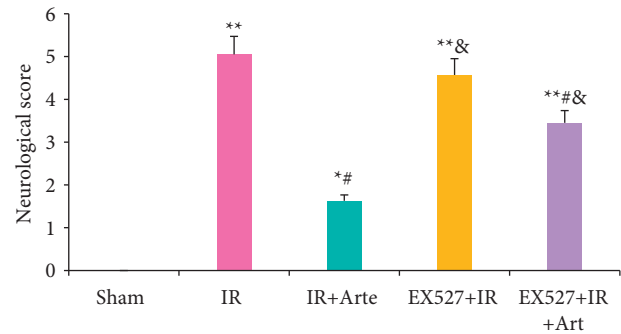


FIGURE 1: Comparison on neurological function score results in different groups of mice. \*, #, & Difference was statistically great compared with the sham group, IR group, and IR + Arte group, respectively ( $P < 0.05$ ). \*\*Statistically extremely great difference in contrast to the sham group ( $P < 0.01$ ).

tissue of mice in different groups are shown in Figure 2(a). As it was shown, most of the area of TTC in the brain tissue of the IR group was unstained, and the TTC staining in the sham group was basically red. The cerebral infarct volume of mice in the IR group, EX527 + IR + Arte group, and EX527 + IR group was extremely obviously larger than that of the sham group ( $P < 0.01$ ), and there was a statistical difference between the IR + Arte group and the sham group ( $P < 0.05$ ). The cerebral infarct volume of mice in the IR + Arte group and EX527 + IR + Arte group was greatly different from that of the IR group ( $P < 0.05$ ) and that in the EX527 + IR group and EX527 + IR + Arte group was dramatically larger than the IR + Arte group ( $P < 0.05$ ) (Figure 2(b)).

**3.3. Analysis of ROS Level and Oxidative Stress Level in Brain Tissue of Mice with Acute CIRI.** The ROS levels in the brain tissues of mice in different groups were detected and analyzed, and the results are shown in Figure 3. The ROS levels in the brain tissues of mice in the IR group, EX527 + IR + Arte group, and EX527 + IR group were much higher than those in the sham group ( $P < 0.01$ ). Compared with the IR group, the ROS levels of the mice in the IR + Arte group and EX527 + IR + Arte group were statistically different ( $P < 0.05$ ) and that in the mice in the EX527 + IR group and EX527 + IR + Arte group were remarkably higher in contrast to the IR + Arte group ( $P < 0.05$ ).

The MDA contents in the brain tissues of mice in different groups were detected and analyzed, and the results are shown in Figure 4. The MDA content in the brain tissues of mice in the IR group, EX527 + IR + Arte group, and



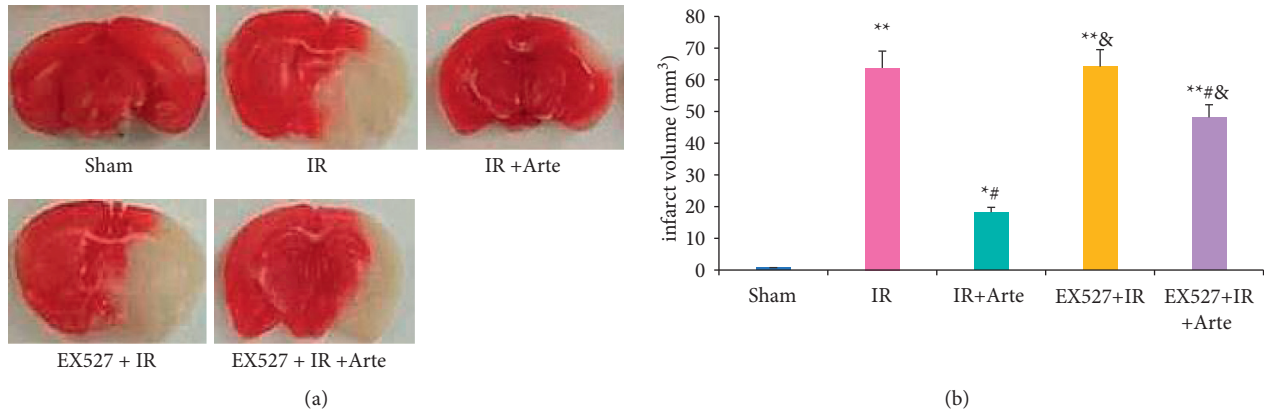


FIGURE 2: Comparison on cerebral infarct volume in different groups of mice. (a) TTC staining results. (b) The comparison of cerebral infarct volume. \*, #, & Difference was statistically great compared with the sham group, IR group, and IR + Arte group, respectively ( $P < 0.05$ ). \*\*Statistically extremely great difference in contrast to the sham group ( $P < 0.01$ ).

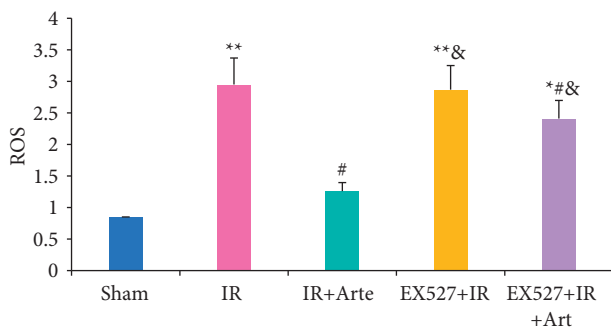


FIGURE 3: Comparison on ROS levels in brain tissue of mice with acute CIRI. \*, #, & Difference was statistically great compared with the sham group, IR group, and IR + Arte group, respectively ( $P < 0.05$ ). \*\*Statistically extremely great difference in contrast to the sham group ( $P < 0.01$ ).

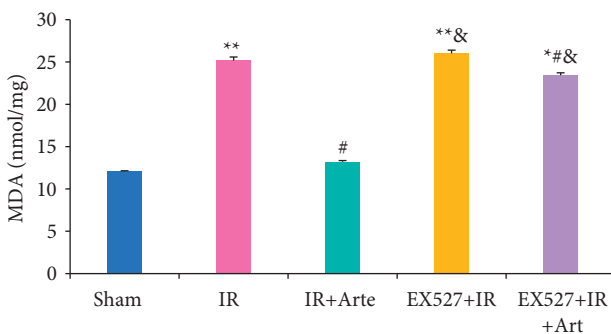


FIGURE 4: Comparison on MDA contents in brain tissue of mice with acute CIRI. \*, #, & Difference was statistically great compared with the sham group, IR group, and IR + Arte group, respectively ( $P < 0.05$ ). \*\*Statistically extremely great difference in contrast to the sham group ( $P < 0.01$ ).

EX527 + IR group was much higher than those in the sham group, showing extremely statistical differences ( $P < 0.01$ ). Compared with the IR group, the MDA contents of the mice in the IR + Arte group and EX527 + IR + Arte group were statistically different ( $P < 0.05$ ) and those in the mice in the

EX527 + IR group and EX527 + IR + Arte group were remarkably higher in contrast to the IR + Arte group ( $P < 0.05$ ).

The SOD contents in the brain tissues of mice in different groups were detected and analyzed, and the results are shown in Figure 5. The SOD contents in the brain tissues of mice in the IR group, EX527 + IR + Arte group, and EX527 + IR group were much lower than those in the sham group, showing extremely statistical differences ( $P < 0.01$ ). Compared with the IR group, the SOD contents of the mice in the IR + Arte group and EX527 + IR + Arte group were statistically different ( $P < 0.05$ ) and those in the mice in the EX527 + IR group and EX527 + IR + Arte group were remarkably lower in contrast to the IR + Arte group ( $P < 0.05$ ).

The GSH-Px contents in the brain tissues of mice in different groups were detected and analyzed, and the results are shown in Figure 6. The GSH-Px contents in the brain tissues of mice in the IR group, EX527 + IR + Arte group, and EX527 + IR group were much lower than those in the sham group, showing extremely statistical differences ( $P < 0.01$ ). Compared with the IR group, the GSH-Px contents of the mice in the IR + Arte group and EX527 + IR + Arte group were statistically different ( $P < 0.05$ ) and those in the mice in the EX527 + IR group and EX527 + IR + Arte group were remarkably lower in contrast to the IR + Arte group ( $P < 0.05$ ).

**3.4. Analysis on Protein Expression Related to the SIRT1/FOXO1 Signaling Pathway in Different Groups of Mice.** The SIRT1, FOXO1, and p53 protein expressions in the SIRT1/FOXO1 signaling pathway in the brain tissue of different groups of mice were analyzed, as shown in Figure 7. The expression of SIRT1 protein in the brain tissue of the IR group and EX527 + IR group was greatly lower than that of the sham group ( $P < 0.01$ ), that in the IR + Arte and EX527 + IR + Arte groups was statistically significant in contrast to that in the sham group ( $P < 0.05$ ), that in the IR + Arte group/EX527 + IR + Arte group and the EX527 + IR + Arte group was greatly different from that of the IR group ( $P < 0.05$ ), that in the EX527 + IR group was

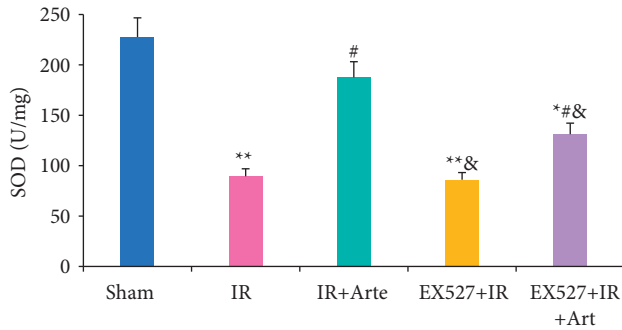


FIGURE 5: Comparison on SOD contents in brain tissue of mice with acute CIRI. \*, #, & Difference was statistically great compared with the sham group, IR group, and IR + Arte group, respectively ( $P < 0.05$ ). \*\* Statistically extremely great difference in contrast to the sham group ( $P < 0.01$ ).

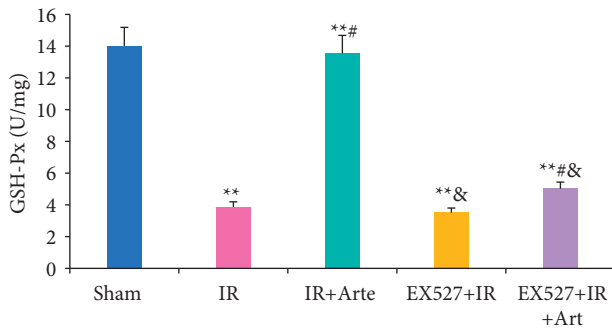


FIGURE 6: Comparison on GSH-Px contents in brain tissue of mice with acute CIRI. \*, #, & Difference was statistically great compared with the sham group, IR group, and IR + Arte group, respectively ( $P < 0.05$ ). \*\* Statistically extremely great difference in contrast to the sham group ( $P < 0.01$ ).

lower visibly compared with that in the IR + Arte group ( $P < 0.05$ ), and that in the brain tissue of the EX527 + IR + Arte group was lower greatly than that of the IR + Arte group ( $P < 0.05$ ). The expressions of FOXO1 protein and p53 protein in the brain tissue of mice in the IR group and EX527 + IR group were observably higher than the expression in the sham group ( $P < 0.01$ ), those in the brain tissue of the mice in the IR + Arte and EX527 + IR + Arte groups were statistically different from the sham group ( $P < 0.05$ ), those in the IR + Arte group, EX527 + IR + Arte group, and EX527 + IR + Arte group were extremely different from those of the IR group ( $P < 0.05$ ), those in the EX527 + IR group was higher than that in IR + Arte group ( $P < 0.05$ ), and those in the brain tissue of the EX52 + IR + Arte group was significantly higher than that of the IR + Arte group ( $P < 0.05$ ).

**3.5. Activity Analysis on MCI in Rat Brain Tissue.** The activity of MCI in the brain tissue of mice in different groups was analyzed, as shown in Figure 8. The activity of MCI in the brain tissue of mice in the IR group and EX527 + IR group was extremely lower than that in the sham group ( $P < 0.01$ ) and that in EX527 + IR + Arte group was

significantly different from that in the sham group ( $P < 0.05$ ); it in the IR + Arte group, EX527 + IR + Arte group, and EX527 + IR + Arte group was greatly different from that of the IR group ( $P < 0.05$ ), and the activity of MCI in the EX527 + IR and EX527 + IR + Arte groups was lower in contrast to the IR + Arte group ( $P < 0.05$ ).

## 4. Discussion

Oxidative stress can promote the occurrence and development of CIRI by inducing cell apoptosis and promoting inflammation [15, 16], and it plays an important role in CIRI. Studies have pointed out that inhibiting oxidative stress can effectively improve the blood-brain barrier caused by CIRI [17]. Ischemia-reperfusion will induce a large amount of ROS in the body, which will further initiate the process of inflammation and apoptosis, leading to neuronal cell death and aggravation of penumbra area damage [18]. Artemisinin has anti-inflammatory, antiapoptotic, and antioxidant effects [19] and is an antimalarial drug recognized by the World Health Organization. Current research results show that artemisinin can reduce myocardial fibrosis by downregulating the expression of transforming growth factor  $\beta$ 1 protein, inhibit ventricular remodeling after myocardial infarction, and ultimately achieve a protective effect on the heart [20]. Franke et al. [21] pointed out that artemisinin can improve myocardial ischemia-reperfusion injury through an antioxidant mechanism. The results of this study showed that the levels of ROS and MDA in the brain tissue of mice in the IR group, EX527 + IR + Arte group, and EX527 + IR group were extremely higher than those in the sham group ( $P < 0.01$ ), and those in the EX527 + IR group and EX527 + IR + Arte group were higher than those in the IR + Arte group ( $P < 0.05$ ). The contents of SOD and GSH-Px in the brain tissue of mice in the IR group, EX527 + IR + Arte group, and EX527 + IR group were much lower than those in the sham group ( $P < 0.01$ ), those in the IR + Arte group and EX527 + IR + Arte group were different from those in the IR group ( $P < 0.05$ ), and those in the EX527 + IR group and EX527 + IR + Arte group were lower compared with the IR + Arte group ( $P < 0.05$ ). In addition, the contents of ROS and MDA in the brain tissue of the IR group of mice increased greatly after ischemia-reperfusion, while the contents of SOD and GSH-Px decreased obviously. It shows that obvious oxidative stress damage has occurred after ischemia and reperfusion. After treatment with artemisinin, the content of ROS and MDA decreased, while the content of SOD and GSH-Px increased observably. It shows that artemisinin may improve oxidative stress damage after ischemia-reperfusion through antioxidant. Furthermore, the SIRT1 molecular-specific blocker EX527 was used to block the SIRT1/FOX1 signaling pathway. The results showed that the levels of ROS and MDA in the brain tissue of the mice in the EX527 + IR + Arte group were higher than those in the artemisinin-treated group, indicating that the SIRT1 signal is blocked, and the protective effect of artemisinin on the brain is weakened. MCI is an important member of the reactive oxygen species family, and it also plays an important role in the production of reactive oxygen species after cerebral

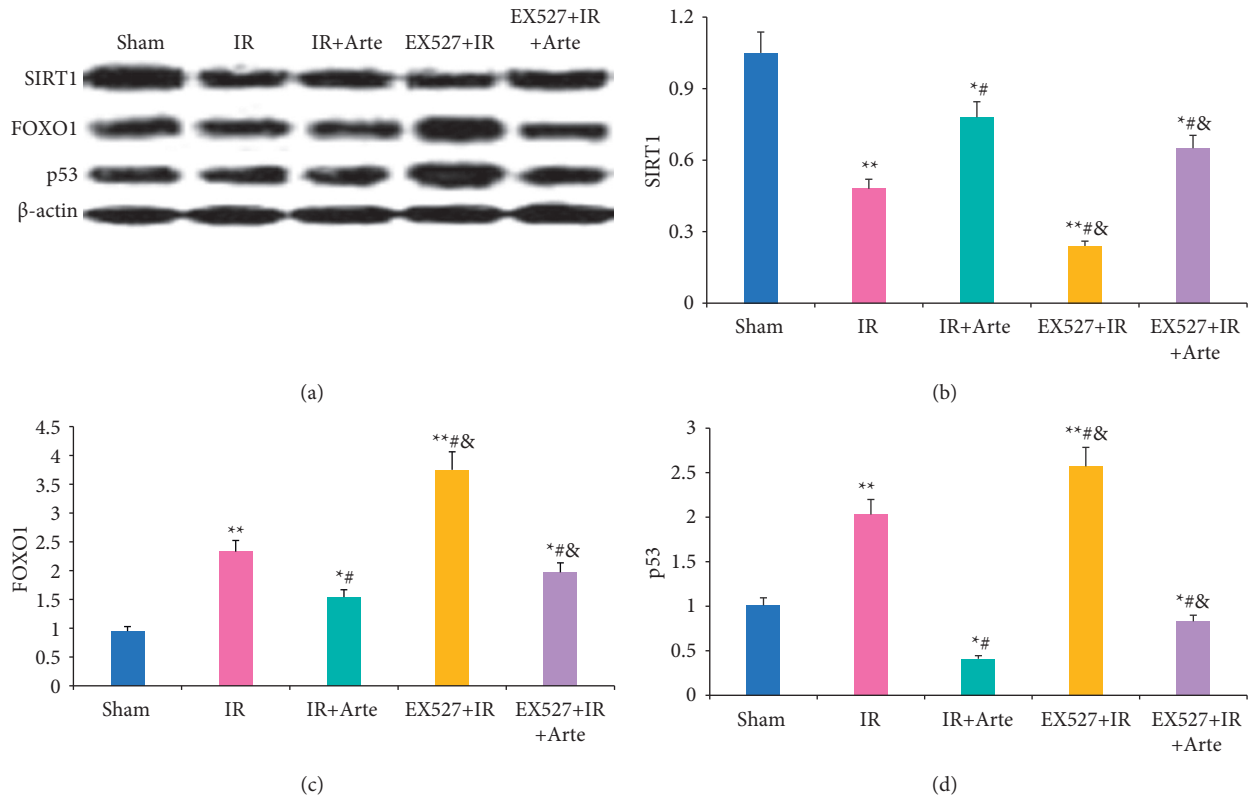


FIGURE 7: Analysis on protein expression related to the SIRT1/FOXO1 signaling pathway in different groups of mice. (a) The WB band. (b)–(d) The comparisons of SIRT1, FOXO1, and p53 expression levels. \*, #, & Difference was statistically great compared with the sham group, IR group, and IR + Arte group, respectively ( $P < 0.05$ ). \*\* Statistically extremely great difference in contrast to the sham group ( $P < 0.01$ ).

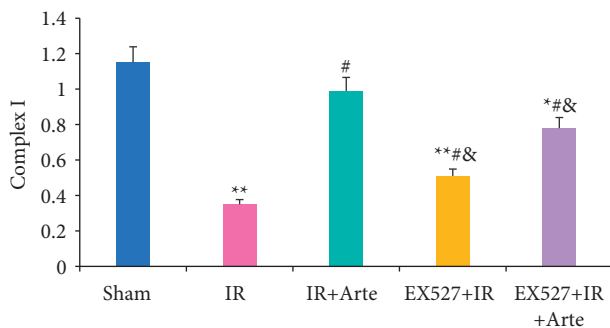


FIGURE 8: Comparison of activity on MCI in rat brain tissue. \*, #, & Difference was statistically great compared with the sham group, IR group, and IR + Arte group, respectively ( $P < 0.05$ ). \*\* Statistically extremely great difference in contrast to the sham group ( $P < 0.01$ ).

ischemia and reperfusion [22]. The results in this study found that the activity of CMI in the brain tissue of mice in the IR group and EX527 + IR group was much lower than that in the sham group ( $P < 0.01$ ), that in the EX527 + IR + Arte group was lower compared with the sham group with a statistical difference ( $P < 0.05$ ), and that in EX527 + IR and EX527 + IR + Arte groups was lower in contrast to the IR + Arte group ( $P < 0.05$ ). It suggests that the activity of MCI is significantly inhibited after CIRI, and it is increased greatly after artemisinin treatment, indicating that

artemisinin can alleviate oxidative stress damage by activating MCI activity. After CIRI, a large number of free radicals will be produced in the body, and the activity of MCI will decrease, leading to damage to the nerves [23]. Artemisinin activates the activity of MCI to alleviate the damage of CIRI.

## 5. Conclusion

It explored the role of artemisinin in CIRI and its specific regulatory mechanism in the SIRT1/FOXO1 signaling pathway. It was found that artemisinin can improve cerebral infarction volume and oxidative stress damage by regulating the SIRT1/FOXO1 signaling pathway, relieving CIRI, and then achieving the neuroprotective effect. The results could provide a reference for the clinical treatment of CIRI. The disadvantage of this work was that only the oxidative stress factors in the SIRT1/FOXO1 signaling pathway were detected, while the apoptosis-related factors in this pathway were not analyzed. In future works, it would further analyze whether oxidative stress factors in the SIRT1/FOXO1 signaling pathway were involved in the protective effect of artemisinin on acute CIRI.

## Data Availability

The data used to support the findings of this study are included within the article.

## Conflicts of Interest

The authors declare that they have no conflicts of interest.

## Acknowledgments

This study was supported by the Shaanxi Scientific Research Project “Clinical study on pharmacokinetic changes of three cephalosporins in cerebrospinal fluid based on HPLC” (2017SF-257, to Xiaogang Yang) and Yan’an Scientific Research Project “Study on bFGF expression after craniocerebral injury and its effect on fracture healing” (2017KS-05, to Xiaogang Yang).

## References

- [1] F. Herpich and F. Rincon, “Management of acute ischemic stroke,” *Critical Care Medicine*, vol. 48, no. 11, pp. 1654–1663, 2020.
- [2] A. A. Rabinstein, “Update on treatment of acute ischemic stroke,” *Continuum: Lifelong Learning in Neurology*, vol. 26, no. 2, pp. 268–286, 2020.
- [3] G. S. Silva and R. G. Nogueira, “Endovascular treatment of acute ischemic stroke,” *Continuum: Lifelong Learning in Neurology*, vol. 26, no. 2, pp. 310–331, 2020.
- [4] A. M. Talman, J. Clain, R. Duval, R. Ménard, and F. Arieu, “Artemisinin bioactivity and resistance in malaria parasites,” *Trends in Parasitology*, vol. 35, no. 12, pp. 953–963, 2019.
- [5] Y. Tu, “Artemisinin-A gift from traditional Chinese medicine to the world (nobel lecture),” *Angewandte Chemie International Edition*, vol. 55, no. 35, pp. 10210–10226, 2016.
- [6] Y. K. Wong, C. Xu, K. A. Kalesh et al., “Artemisinin as an anticancer drug: recent advances in target profiling and mechanisms of action,” *Medicinal Research Reviews*, vol. 37, no. 6, pp. 1492–1517, 2017.
- [7] S.-P. Lin, J.-X. Wei, J.-S. Hu et al., “Artemisinin improves neurocognitive deficits associated with sepsis by activating the AMPK axis in microglia,” *Acta Pharmacologica Sinica*, vol. 42, no. 7, pp. 1069–1079, 2021.
- [8] V. Singh and S. Ubaid, “Role of silent information regulator 1 (SIRT1) in regulating oxidative stress and inflammation,” *Inflammation*, vol. 43, no. 5, pp. 1589–1598, 2020.
- [9] Y. Wu, X. Meng, C. Huang, and J. Li, “Emerging role of silent information regulator 1 (SIRT1) in hepatocellular carcinoma: a potential therapeutic target,” *Tumor Biology*, vol. 36, no. 6, pp. 4063–4074, 2015.
- [10] H. Kudo, O. Takeichi, K. Makino, K. Hatori, and B. Ogiso, “Expression of silent information regulator 2 homolog 1 (SIRT1) in periapical granulomas,” *Journal of Oral Science*, vol. 60, no. 3, pp. 411–417, 2018.
- [11] S. Broussy, H. Laaroussi, and M. Vidal, “Biochemical mechanism and biological effects of the inhibition of silent information regulator 1 (SIRT1) by EX-527 (SEN0014196 or selisistat),” *Journal of Enzyme Inhibition and Medicinal Chemistry*, vol. 35, no. 1, pp. 1124–1136, 2020.
- [12] X. Zhang, Y. Li, Y. Wang et al., “Dexmedetomidine post-conditioning suppresses myocardial ischemia/reperfusion injury by activating the SIRT1/mTOR axis,” *Bioscience Reports*, vol. 40, no. 5, Article ID BSR20194030, 2020.
- [13] L. Liu, H. Chen, J. Jin et al., “Melatonin ameliorates cerebral ischemia/reperfusion injury through SIRT3 activation,” *Life Sciences*, vol. 239, Article ID 117036, 2019.
- [14] J. Liang, Q. Wang, J.-Q. Li, T. Guo, and D. Yu, “Long non-coding RNA MEG3 promotes cerebral ischemia-reperfusion injury through increasing pyroptosis by targeting miR-485/AIM2 axis,” *Experimental Neurology*, vol. 325, Article ID 113139, 2020.
- [15] X. J. Wu, X. H. Sun, S. W. Wang, J. L. Chen, Y. H. Bi, and D. X. Jiang, “Mifepristone alleviates cerebral ischemia-reperfusion injury in rats by stimulating PPAR  $\gamma$ ,” *European Review for Medical and Pharmacological Sciences*, vol. 22, no. 17, pp. 5688–5696, 2018.
- [16] G. Zuo, D. Zhang, R. Mu et al., “Resolvin D2 protects against cerebral ischemia/reperfusion injury in rats,” *Molecular Brain*, vol. 11, no. 1, p. 9, 2018.
- [17] S. Liao, N. Apajjai, N. Chattipakorn, and S. C. Chattipakorn, “The possible roles of necroptosis during cerebral ischemia and ischemia/reperfusion injury,” *Archives of Biochemistry and Biophysics*, vol. 695, Article ID 108629, 2020.
- [18] W. Liang, C. Lin, L. Yuan et al., “Preactivation of Notch1 in remote ischemic preconditioning reduces cerebral ischemia-reperfusion injury through crosstalk with the NF- $\kappa$ B pathway,” *Journal of Neuroinflammation*, vol. 16, no. 1, p. 181, 2019.
- [19] Y. Liao, J. Cheng, X. Kong et al., “HDAC3 inhibition ameliorates ischemia/reperfusion-induced brain injury by regulating the microglial cGAS-STING pathway,” *Theranostics*, vol. 10, no. 21, pp. 9644–9662, 2020.
- [20] X. Guan, Z. Li, S. Zhu et al., “Galangin attenuated cerebral ischemia-reperfusion injury by inhibition of ferroptosis through activating the SLC7A11/GPX4 axis in gerbils,” *Life Sciences*, vol. 264, Article ID 118660, 2021.
- [21] M. Franke, M. Bieber, P. Kraft, A. N. R. Weber, G. Stoll, and M. K. Schuhmann, “The NLRP3 inflammasome drives inflammation in ischemia/reperfusion injury after transient middle cerebral artery occlusion in mice,” *Brain, Behavior, and Immunity*, vol. 92, pp. 221–231, 2021.
- [22] Q. Pan, H. Su, D. Hui, and C. X. Hu, “Mir-149-5p can reduce myocardial apoptosis induced by myocardial ischaemia reperfusion by inhibiting the expression of il-6,” *Acta Medica Mediterranea*, vol. 36, no. 1, pp. 641–646, 2020.
- [23] M. A. Perrone, F. Iellamo, B. Donatucci, G. Caminiti, and M. Lombardo, “Oxidative stress, redox state and antioxidant supplementation in physical exercise and professional sports: a brief review,” *Acta Medica Mediterranea*, vol. 36, no. 2, pp. 1245–1251, 2020.



## Review Article

# Antiosteoporosis Studies of 20 Medicine Food Homology Plants Containing Quercetin, Rutin, and Kaempferol: TCM Characteristics, *In Vivo* and *In Vitro* Activities, Potential Mechanisms, and Food Functions

Dayue Shen <sup>1</sup>, Yating Feng <sup>1</sup>, Xilan Zhang <sup>1</sup>, Le Gong <sup>1</sup>, Jing Liu <sup>1</sup>, Yuanping Li <sup>2</sup>,  
and Hui Liao <sup>2</sup>

<sup>1</sup>School of Pharmacy, Shanxi Medical University, Taiyuan 030001, China

<sup>2</sup>Department of Pharmacy, Fifth Hospital of Shanxi Medical University (Shanxi Provincial People's Hospital), Taiyuan 030012, China

Correspondence should be addressed to Hui Liao; huiliao@263.net

Received 30 January 2022; Revised 28 February 2022; Accepted 5 March 2022; Published 31 March 2022

Academic Editor: Sekar Vijayakumar

Copyright © 2022 Dayue Shen et al. This is an open access article distributed under the Creative Commons Attribution License, which permits unrestricted use, distribution, and reproduction in any medium, provided the original work is properly cited.

Dietary nutraceutical compounds have been evidenced as backbone for bone health in recent years. It is reported that medicine food homology (MFH) plants have multiple nutraceutical compounds. Based on our literature research, 20 MFH plants caught our attention because they contain three popular antiosteoporosis compounds simultaneously: quercetin, rutin, and kaempferol. According to traditional Chinese medicine (TCM), their characteristics including natures, flavors, attributive to meridian tropism, and efficacies were listed. The relationships between TCM efficacies, such as “heat clearing,” “tonic,” and “the interior warming,” and antiosteoporosis pharmacological actions such as antioxidant and immune regulation were discussed. The *in vivo* antiosteoporosis effects of the 20 MFH plants were summarized. The *in vitro* antiosteoporosis activities and related mechanisms of the 20 plants and quercetin, rutin, kaempferol were detailed. The TGF- $\beta$ -Smad signaling, fibroblast growth factor, and Wnt/ $\beta$ -catenin signaling on bone formation and the RANKL signaling, NF- $\kappa$ B signaling, and macrophage-colony-stimulating factor on bone resorption were identified. From food point, these 20 MFH plants could be classified as condiment, vegetable, fruit, tea and related products, beverage, etc. Based on the above discussion, these 20 MFH plants could be used as daily food supplements for the prevention and treatment against osteoporosis.

## 1. Introduction

Osteoporosis is a systemic metabolic bone disease characterized by bone mass decrease and microstructural degradation, which may increase the risk of bone fracture and lead to high mortality [1]. China National Health Commission conducted an osteoporosis epidemiological survey in 2018. The results showed that osteoporosis has become an important health problem for middle-aged and elderly people in China: the incidence of osteoporosis was 19% in people over 50 years old and even reached 32% in over 65 years old [2]. It is confirmed that factors such as age, sex, weight, and diabetes are significant predictors of osteoporosis in the

Chinese people [3]. Estrogen deficiency and aging are the main causes for disturbances in bone remodeling activity and bone loss [4]. The current drugs for the treatment of osteoporosis include bisphosphonates, estrogen, receptor activator of nuclear factor kappa B ligand (RANKL) inhibitors, etc. These drugs play important roles clinically, but their serious side effects limit their clinical use [5, 6].

Scientific reports suggest that natural Chinese medicine therapies appear to have both the anabolic and anticatabolic effects for the treatment of osteoporosis by promoting bone formation and attenuating imbalanced bone resorption, leading to improved bone mineral density and reducing bone microstructural degradation. A wide range of natural

compounds were identified to bear this potential. The identified natural compounds are summarized such as kaempferol, icariin, and berberine [7]. The classic and bone-specific drugs in natural Chinese medicines for the treatment of osteoporosis were reviewed comprehensively on the treatment of osteoporosis that had been deeply and definitely studied [8]. These studies provide a critical overview of alternative medicine for the treatment and prevention of osteoporosis.

Dietary nutraceuticals as backbone for bone health in Chinese medicine therapies have been evidenced in recent years. The nutraceutical compounds such as ginsenosides and quercetin identified from medicinal plants can reverse/slow down osteoporosis. Most of these compounds are inexpensive and have no side effect [9]. Some nutraceutical compounds are from medicine food homology (MFH) plants, such as ginsenosides from ginseng [10].

“The list of MFH species” was updated by the National Health Commission in 2014, and a total of 94 MFH plants were included in this list [11]. Compared with modern dietary nutrition, MFH plants have unique beneficial concepts, such as the holism, and diet suggestions based on different syndromes. On the other hand, the MFH research has some limitations such as lack of evidence-based data and difficult to evaluate the active ingredients [12]. From the point of pharmacological research, some nutraceutical compounds, mainly including quercetin, resveratrol, curcumin, rutin, and kaempferol [9], showed more and more antiosteoporosis evidences recently.

Based on PubMed, Scopus, Wanfang, and CNKI database, the literature of the five popular nutraceutical compounds [9] on antiosteoporosis effects was searched, and the results showed that most of the relevant studies are on resveratrol, quercetin, and curcumin (Figure 1). Further literature studies showed an interesting result: quercetin, rutin, and kaempferol were present in more MFH plants than curcumin and resveratrol (Figure 2, the 38 references did not show). Based on above information, the 20 MFH plants that contain quercetin, rutin, and kaempferol simultaneously were discussed in this manuscript. Their characteristics according to the theory of traditional Chinese medicine (TCM) are summarized in Table 1, the *in vitro* antiosteoporosis research is detailed in Table 2, and the *in vivo* antiosteoporosis research is detailed in Table 3 and Figure 3. Their antiosteoporosis mechanisms related to quercetin, rutin, and kaempferol are identified in Figure 4. This review finally explored the possibilities of the 20 MFH plants as antiosteoporosis food supplementation, as shown in Figure 5.

## 2. TCM Characteristics

**2.1. Four Natures and Five Flavors.** The properties and actions of Chinese herbs are mainly summarized as the four natures and five flavors, meridian tropism, and toxicity. Four natures and five flavors are also known as the properties and tastes of Chinese herbs. Cold-cool and hot-warm are two completely different categories of natures [55]. As shown in Table 1, there are ten herbs in the cold-cool category and six

in the hot-warm category. In addition, there are also some herbs known as neutral ones whose cold or hot nature is not so remarkable and whose action is relatively mild. Among the 20 MFH plants, there are four herbs with neutral properties.

The five flavors of Chinese herbs refer to the five different tastes: pungent, sweet, sour, bitter, and salty [56]. Actually, the five flavors are not only the true reflection of the taste of drugs but also the high generalization of the effects of herb medicines. Since the theory of five tastes was applied to summarize therapeutic effects, the “taste” of five tastes has gone beyond the scope of the real taste of herb medicines. From Table 1, we could see that there are 9 MFH plants with sweet taste (alone or dominated), 5 MFH plants with pungent taste, 2 MFH plants with sour, and 4 MFH plants with bitter taste.

**2.2. Attributive to Meridian Tropism.** Meridian tropism refers to that herbs often produce their therapeutic effects on some portion of a human body in preference. If certain herb can work on several meridians, which means the herb can be used widely to treat the disorders of these meridians. From Table 1, we could see that only 2 MFH plants point a single meridian, and the other 18 MFH plants have more than two meridians. The meridian tropisms include spleen and liver (10 MFH plants, separately), lung (9 MFH plants), stomach (7 MFH plants), and kidney (6 MFH plants).

In TCM, kidney deficiency is the main pathogenesis of osteoporosis based on the theory of “kidney governing bones” [57]. On the other hand, modern clinical and pre-clinical research showed that liver-spleen-kidney insufficiency may result in the development of diabetic osteoporosis [58]. In this case, it is necessary to develop an objective and comprehensive method to evaluate and understand the antiosteoporosis effects of the 17 MFH plants attributed to the liver, spleen, and kidney.

**2.3. Traditional Efficacies and Modern Antiosteoporosis Actions.** According to some research, there was a certain relationship between TCM efficacies and modern pharmacological actions [59]. In order to find the relationships between traditional efficacies of the 20 MFH plants such as “heat clearing” and “diaphoretics with cool property” and modern antiosteoporosis pharmacological action, we will provide some information and references as follows.

“Clearing away heat” in TCM displays a variety of biological activities and mainly antioxidant and anti-inflammatory actions [59, 60]. Attenuating effect of *P. oleracea* extract on chronic constriction injury-induced neuropathic pain in rats was related to its antioxidative and anti-inflammatory effects [61]. *H. cordata* crude extract administration inhibited fever in rats, reduced the number of leukocytes, and restored serum complement levels [62]. A recent study demonstrated a broad range of biological activities of *P. vulgaris*, including immune modulatory, antiviral, anti-inflammatory, antioxidant, and antidiabetic [63]. Chemical compositions and antioxidant activities of *C. album* were identified, and dietary intakes of



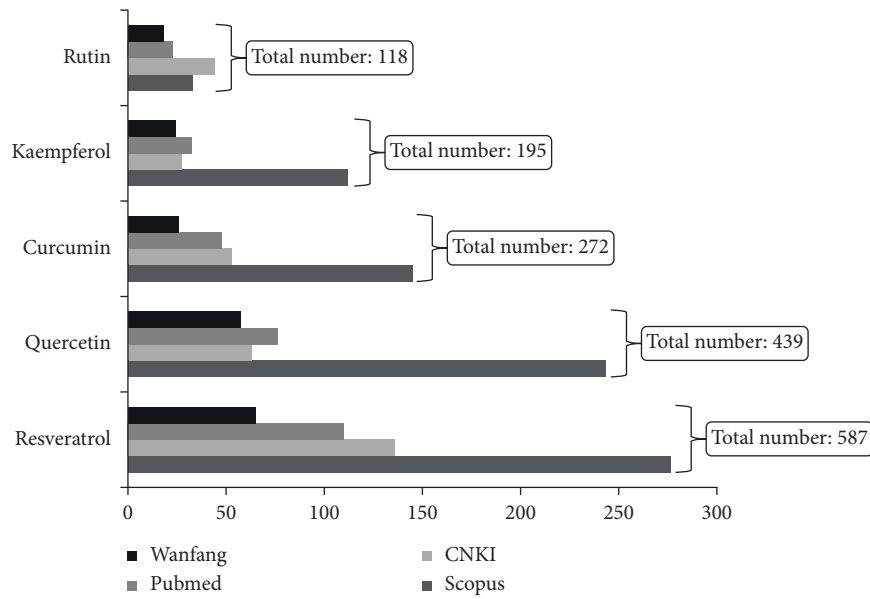


FIGURE 1: Antiosteoporosis literature research of five popular nutraceutical compounds [9]. Abbreviations: CNKI, China National Knowledge Infrastructure; Wanfang, Wanfang Database.

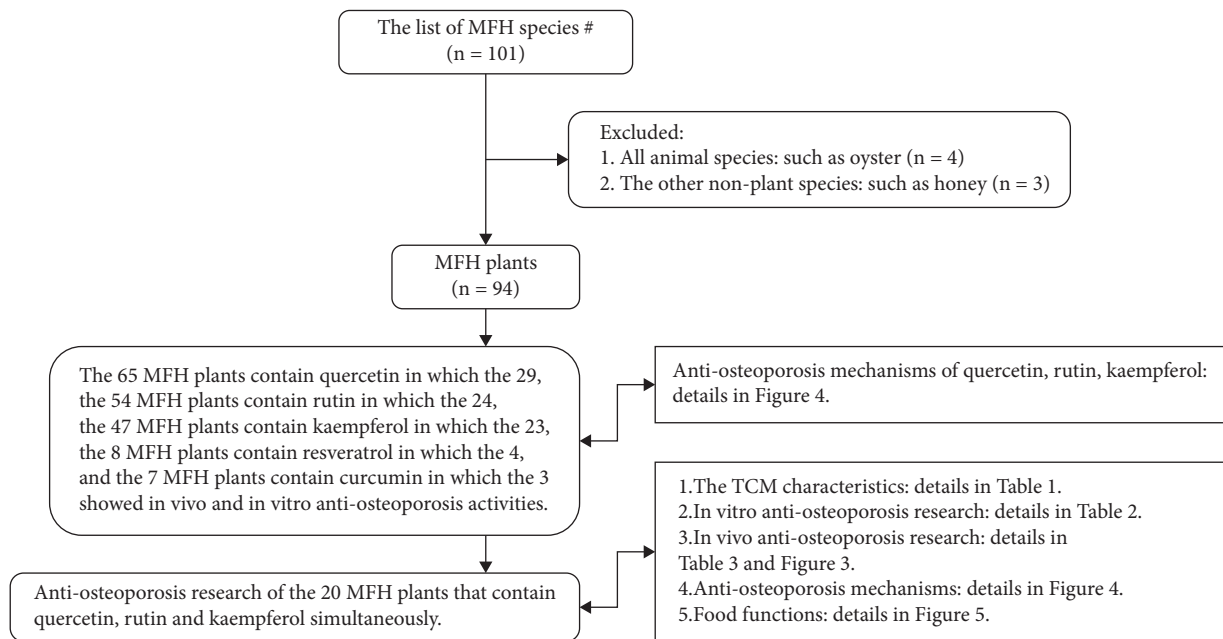


FIGURE 2: Antiosteoporosis research of the 20 MFH plants that contain quercetin, rutin, and kaempferol. Notes. <sup>#</sup>The list of MFH species is according to “The management about medicine food homology catalog” issued by the National Health Commission of the People’s Republic of China in 2014 [11]. Abbreviations: MFH, medicine food homology; TCM, traditional Chinese medicine.

health-promoting components were also estimated [64]. The antioxidant activities, antiglycation effects, and inhibition activities on  $\alpha$ -glucosidase and  $\alpha$ -amylase of seven extracts from *H. acerba* were confirmed *in vitro* [65]. The health-promoting activities attributed to *C. intybus* include anti-inflammatory, antimutagenic, antifungal, and antioxidative qualities [66].

Chinese herbs “with cool property” also show important pharmacological effects on antioxidant activities [67]. Mulberry leaves extract ameliorated alcohol-induced liver

damages through reduction of acetaldehyde toxicity and inhibition of apoptosis induced by oxidative stress signals [68]. Antioxidant effects of *C. morifolium* could be potent phytochemical agents to reduce low-density lipoprotein (LDL) oxidation and prevent the progression of atherosclerosis [69].

Traditional “tonic” efficiency is normally related with immune regulation effects [70]. Ginseng has been used worldwide for its miracle “tonic” effects, especially for its immunomodulatory activities [71]. The fruits of *M. alba* have

TABLE 1: The list of 20 medicine food homology plants and their TCM characteristics.

Classification in TCM <sup>&amp;</sup>	Botanical name*	English name <sup>†</sup> (Chinese name*)	Nature*	Flavor*	Attributive to meridian tropism*	Efficiency in TCM*
Heat-clearing CMHs	<i>Portulaca oleracea</i>	Purslane (Machixian)	Cold	Sour	Intestine, liver, and spleen	Clears away heat and relieves toxins, cools the blood, and stops bleeding.
	<i>Houttuynia cordata</i>	Heartleaf Houttuynia herb (Yuxingcao)	Slight cold	Pungent	Lung	Clears away heat and relieves toxins, treats carbuncle and promotes pus drainage, and promotes diuresis to treat stranguria.
	<i>Prunella vulgaris</i>	Common selfheal spike (Xiakucao)	Cold	Bitter and pungent	Liver and gallbladder	Clears away liver-fire and disperses stagnation.
	<i>Canarium album</i>	Immature Tomentosa Terminalia (Qingguo)	Cool	Sweet and sour	Stomach and lung	Clears away heat and relieves toxins, eases the throat, and resolves phlegm.
	<i>Hovenia acerba</i>	Raisin tree seed (Zhijuzi)	Neutral	Sweet and bitter	Stomach	Clears away heat and promotes diuresis, and relieves alcohol toxins.
	<i>Cichorium intybus</i>	Chicory (Juju)	Cool	Bitter and salty	Spleen, liver, and bladder	Clears away liver-fire, relieves constipation, and promotes diuresis.
Tonics	<i>Panax ginseng</i>	Ginseng (Renshen)	Neutral	Sweet and slightly bitter	Spleen, lung, and heart	Invigorates renal <i>qi</i> , strengthens <i>qi</i> of the spleen and lung, promotes production of the body fluids to quench thirst, and calms the mind to promote intelligence.
	<i>Morus alba</i>	Mulberry fruit (Sangshen)	Cold	Sweet	Heart, liver and kidney	Nourishes <i>yin</i> and enriches the blood, nourishes the liver, and invigorates the kidney.
	<i>Polygonatum sibiricum</i>	Siberian Solomon's seal rhizome (Huangjing)	Neutral	Sweet	Spleen, lung, and kidney	Moistens the lung and nourishes the kidney, invigorates the kidney, and benefits <i>qi</i> .
	<i>Lycium barbarum</i>	Wolfberry fruit (Gouqizi)	Neutral	Sweet	Liver and kidney	Tonifies the kidney and benefits essence, and nourishes the liver and improves eyesight.
The interior warming CMHs	<i>Rubus chingii</i>	Palmleaf raspberry fruit (Fupenzi)	Warm	Sweet and sour	Liver and kidney	Benefits the kidney to preserve the essence and reduces the frequency of urination, and nourishes the liver to treat eye diseases.
	<i>Eugenia caryophyllata</i>	Clove (Dingxiang)	Warm	Pungent	Spleen, stomach, and kidney	Warms the middle energizer to low the adverse rising <i>qi</i> , and promotes circulation of <i>qi</i> and alleviates pain.
	<i>Zanthoxylum schinifolium</i> / <i>Zanthoxylum bungeanum</i>	Bunge pricklyath pericarp (Huajiao)	Hot	Pungent	Spleen, stomach, and kidney	Warms the middle energizer to alleviate pain.
Diaphoretics with pungent-cool property	<i>Alpinia officinarum</i>	Lesser galangal rhizome (Gaoliangjiang)	Hot	Pungent	Spleen and stomach	Expels cold and relieves pain, and warms the spleen and stomach to stop vomiting.
	<i>Morus alba</i>	Mulberry leaf (Sangye)	Cold	Bitter and sweet	Lung and liver	Expels wind and heat, clears away lung heat and moisturizes dryness, and clears away liver-fire to treat eye diseases.
	<i>Chrysanthemum morifolium</i>	Chrysanthemum flower (Juhua)	Cold	Bitter and pungent	Lung and liver	Expels wind and clears away heat, clears liver-fire to treat eye diseases, and eliminates toxic substances.

TABLE 1: Continued.

Classification in TCM <sup>§</sup>	Botanical name*	English name <sup>#</sup> (Chinese name*)	Nature*	Flavor*	Attributive to meridian tropism*	Efficiency in TCM*
Phlegm resolving, antitussive and antiasthmatic CMHs	<i>Siraitia acerba</i>	Siraitia fruit (Luohanguo)	Cool	Sweet	Lung and spleen	Resolves phlegm and arrests cough, clears away lung heat and eases throat, and moistens the intestine to relieve constipation.
	<i>Hippophae rhamnoides</i>	Sea buckthorn fruit (Shaji)	Warm	Sour and astringent	Lung, spleen, stomach, and liver	Resolves phlegm and arrests cough, and nourishes the spleen and stomach.
CMHs for invigorating the blood and removing blood stasis	<i>Crocus sativus</i>	Saffron crocus style and stigma (Xihonghua)	Warm	Pungent	Heart and liver	Promotes blood circulation to remove blood stasis, promotes menstruation, and alleviates pain.
Dampness-removing CMHs	<i>Coix lacryma-jobi</i>	Adlay (Yiyiren)	Cold	Sweet	Spleen, stomach, and lung	Promotes diuresis to resolve dampness and invigorates the spleen, treats <i>Bi</i> -syndrome, and clears away heat to drain the pus.

Notes. \*Botanical name, Chinese name, natures, flavors, attributive to meridian tropism, and efficiency in TCM are according to Chinese Pharmacopoeia (Chinese Pharmacopoeia Commission, China Medical Science Press, Beijing, China, 2020). <sup>#</sup>English name is according to the Chinese Herbal Medicine Name Dictionary (Z. W. Xie, Beijing Science and Technology Press, Beijing, China, 2004). <sup>§</sup>Classification in TCM is according to the Science of Chinese Materia Medica (D. C. Tang and J. Y. Xun, Publishing House of Shanghai University of TCM, Shanghai, China, 2003). Abbreviations: TCM, traditional Chinese medicine; CMHs, Chinese medicine herbs.

TABLE 2: *In vitro* research of the 20 medicine food homology plants on osteoblastogenesis and osteoclastogenesis process.

Botanical name*	On osteoblastogenesis process	On osteoclastogenesis process	References
<i>Portulaca oleracea</i>	Purslane on human osteoblasts.	(1) The extract on RANKL-induced primary mice BMMS. (2) The extract on primary mice osteoclast cells.	[13–15]
<i>Prunella vulgaris</i>	The extract on glucocorticoids-induced BMMSCs by activating the Smad pathway.		[16]
<i>Canarium album</i>		The extract on RANKL-induced RAW264.7 cells.	[17]
<i>Hovenia acerba</i>	The extract on calvarial osteoblasts from the calvaria of ICR mice at postnatal day, via Wnt/ $\beta$ -catenin pathway.		[18]
<i>Panax ginseng</i>	(1) Ginsenoside Rb1 on aluminum chloride-induced rat osteoblasts. (2) Ginsenoside Rb2 on hydrogen peroxide-induced osteoblastic MC3T3-E1 cells, via reduction of oxidative damage. (3) Ginsenoside Rg3 on osteoblastic MC3T3-E1 cells.	(1) Ginsenoside Rb1 on RANKL-induced RAW264.7 cells, via NF- $\kappa$ B and MAPKs pathways (2) Ginsenoside Rb2 on RANKL-induced RAW264.7 cells, via NF- $\kappa$ B and STAT3 (3) Ginsenoside Rg3 on RANKL-induced RAW264.7 cells, via RANKL, JNK, and p38 MAPK pathways.	[19–24]
<i>Polygonatum sibiricum</i>	The polysaccharide on primary mice BMMSCs, via ERK/GSK-3 $\beta$ / $\beta$ -catenin and Wnt/ $\beta$ -catenin pathways.	The polysaccharide on RANKL-induced primary mice BMMS.	[25–27]
<i>Lycium barbarum</i>	The polysaccharides on the osteoblast MC3T3-E1 cell line.		[28]
<i>Rubus chingii</i>	Seven compounds on primary rat osteoblasts.	Seven compounds on primary rat osteoclasts.	[29]
<i>Zanthoxylum schinifolium</i> / <i>Zanthoxylum bungeanum</i>		The extract on RANKL-induced RAW264.7 cells.	[17]
<i>Alpinia officinarum</i>	The extract on primary rat osteoblasts isolated from newborn rat calvariae.	The extract on RANKL-induced primary mice BMMS.	[30, 31]
<i>Chrysanthemum morifolium</i>	Linarin on the osteoblast MC3T3-E1 cell line, via BMP-2/Runx2 pathway.		[32]

TABLE 2: Continued.

Botanical name*	On osteoblastogenesis process	On osteoclastogenesis process	References
<i>Siraitia acerba</i>	Mogroside V on primary rat osteoblasts isolated from newborn rat calvariae.		[33]
<i>Crocus sativus</i>	(1) Crocin on the osteoblast MC3T3-E1 cell line. (2) Crocin and crocetin on primary rat BMMSCs.	Crocin on RANKL-induced primary mice BMMs, via JNK and NF-κB pathways.	[34–36]
<i>Coix lacryma-jobi</i>	(1) The extract on the primary rat osteoblasts isolated from the calvaria of fetal rats (18 days old) via the ERK-regulated pathway. (2) The water extract of adlay seeds in cultured neonatal rat calvariae.		[37, 38]

Notes. \* Botanical name are according to Chinese Pharmacopoeia (Chinese Pharmacopoeia Commission, China Medical Science Press, Beijing, China, 2020). Abbreviations: RANKL, receptor activator for nuclear factor κB ligand. BMMs, bone marrow-derived macrophages; BMMSCs, bone marrow mesenchymal stem cells; ICR, Institute of Cancer Research; NF-κB, nuclear factor kappa B; MAPK, mitogen-activated protein kinases; p38 MAPK, p38 mitogen-activated protein kinase; STAT3, signal transducer and activator of transcription protein 3; JNK, c-Jun N-terminal kinase; ERK, extracellular signal regulated kinase; GSK-3β, glycogen synthase kinase-3β; Wnt, wingless; BMP-2, bone morphogenetic protein 2; Runx2, runt-related transcription factor 2.

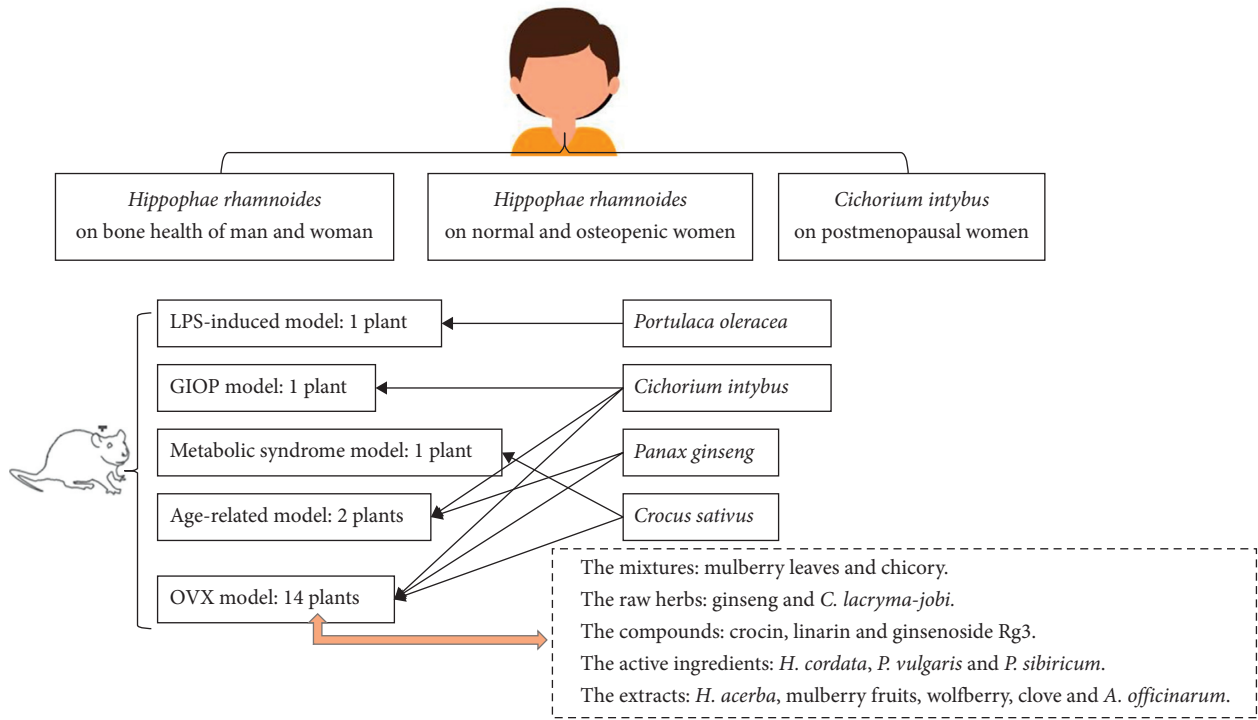


FIGURE 3: *In vivo* clinical and animal research of medicine food homology plants. Abbreviations: LPS, lipopolysaccharide; GIOP, glucocorticoid-induced osteoporosis; OVX, ovariectomy.

TABLE 3: *In vivo* animal research of the 15 medicine food homology plants.

Botanical name*	Model	Dose	Route	Intervention time	Main improved results	Reference
<i>Portulaca oleracea</i>	The extract in LPS-induced osteolysis male mice.	250 mg/kg	Administered orally	Every 2 days for 8 days	Bone loss, bone erosion, and the number of TRAP-positive osteoclasts↓ BV/TV, Tb.Sp, and Tb.N↑	[13]
<i>Houttuynia cordata</i>	The essential oil in OVX mice.	10 and 20 mg/kg	I.g.	12 weeks	ALP, TRAP, TNF-α, IL-1β, and MDA↓ SOD, parameters of bone morphometry, and biomechanical properties↑	[39]

TABLE 3: Continued.

Botanical name*	Model	Dose	Route	Intervention time	Main improved results	Reference
<i>Prunella vulgaris</i>	The flavonoids in OVX rats.	10%	I.g.	12 weeks	ALP, the number of osteoclasts, and bone resorption perimeter percentage↓ OPG, BMD, and the relative volume and thickness of trabecular bone↑	[40]
<i>Hovenia acerba</i>	(1) The extract in normal 8-week-old male mice.	200 mg/kg	I.p.	5 sequential days each week for 4 weeks	Trabecular bone, BV/TV and Tb.N, femoral bone mass, and thickness and area of femoral cortical bone↑ Trabecular or cortical femoral bone loss↓	[18]
	(2) Methyl vanillate in OVX mice.		Administrated orally	5 sequential days each week for 4 weeks	BV/TV, Tb.N, trabecular bone volume↑	
<i>Cichorium intybus</i>	(1) Chicory inulins and a mixture of inulins-isoflavones in OVX rats.	385 mg/day	In water	2 months	BMD↑	[41]
	(2) Chicory inulin in growing male rats.	5 and 10 g/100 g diet	In diet	22 weeks	WBBMC and WBBMD↑	[42]
	(3) A purified native inulin, a reformulated inulin, and a dehydrated chicory in young male rats.	7.5% inulin in the diet	In diet	3 months	Mg absorption, BMD, and breaking load↑	[43]
	(4) The chicory extracts in GIOP rats.	100 mg/kg	Administrated orally	3 times per week for 8 weeks	Ca, P, BMD, BMC↑ PTH, ALP↓	[44]
<i>Panax ginseng</i>	(1) Ginseng on osteoporosis in OVX rats in which inflammation was induced.	100 and 200 mg/kg	Administrated orally	20 days	BMD↑ OC, TNF- $\alpha$ , IL-1 $\beta$ , IL-6↓	[45]
	(2) Ginsenoside Rg3 in OVX rats	20 mg/kg	I.p.	Every 2 days for 5 weeks	Thickness, number, and density of trabeculae, osteogenesis↑	[19]
	(3) Ginseng extracts in 112-week-old male rats.	300 mg/kg/day	Administrated orally	8 weeks	Total BMD in the tibia, osteoblast↑	[46]
<i>Morus alba</i>	The extract in OVX rats.	0.5% or 1%	Tube feeding	8 weeks	ALP, fragile structure was reduced↓ Trabecular thickness↑	[47]
<i>Polygonatum sibiricum</i>	(1) The polysaccharide in OVX rats.	100, 200, and 400 mg/kg	I.g.	Every 2 days for 35 days	BMD, BGP↑ ALP, TRAP, and TNF- $\alpha$ ↓	[48]
	(2) The polysaccharide on osteoporotic fracture, which is established by OVX rats.	100, 500, and 1000 mg/kg	I.g.	8 weeks	TRAP and PINP↓ ALP, OPG, the maximum tibial load, elastic load, BMD, BGP, GPR48, and BMP-2 protein↑	[49]
<i>Lycium barbarum</i>	The extract in OVX mice.	1 and 100 mg/kg	Administrated orally	6 weeks.	BMC, BMD, CON, calcium↑ Hypertrophy of the epiphyseal plate ↓	[50]
<i>Eugenia caryophyllata</i>	The extract in OVX rats.		Administrated orally	4 weeks	AP, TRAP, urinary phosphate, and creatinine↓ Ca, bone density, bone mineral content, bone tensile strength↑	[51]



TABLE 3: Continued.

Botanical name*	Model	Dose	Route	Intervention time	Main improved results	Reference
<i>Alpinia officinarum</i>	The extract in OVX rats.	300 mg/kg	I.g.	12 weeks	OP↓ Bone strength↑	[30]
<i>Crocus sativus</i>	(1) Crocin in OVX rats.	5, 10, and 20 mg/kg	Administrated orally	16 weeks	BMD of L4 vertebrae and femurs, skeletal remodeling, bone-turnover markers↑ Oxidative stress status in bone tissue↓	[52]
	(2) Crocin in metabolic syndrome-induced osteoporosis rats.	5 and 10 mg/kg	I.g.	5 sequential days each week for 12 weeks	OCN, longitudinal, and perpendicular forces of femurs↑ TRAP, CTX1, IL-6, TNF-α, oxidative stress in femur distal epiphysis tissues↓	[53]
<i>Morus alba</i>	The combined extract of mulberry leaf and <i>Polygonum odoratum</i> in OVX rats.	5, 150, and 300 mg/kg	Administrated orally	3 months	Oxidative stress and osteoclast density↓ Osteoblast density and cortical thickness, serum Ca, ALP, and OCN↑	[54]
<i>Chrysanthemum morifolium</i>	Linarin in OVX mice	50 and 150 mg/kg	I.g.	8 weeks	BMD, BV/TV, BS/TV, and Tb.N↑ ALP and OCN↓	[32]
<i>Coix lacryma-jobi</i>	(1) The adlay diet and adlay extract in OVX mice.	10% and 30% in diet	In diet	4 weeks	ALP, Ca, and BMD↑	[37]
	(2) The extract in OVX rats.	300 μg/mL	Administrated orally	4 weeks	ALP, Ca↑ TRAP↓	[38]

Notes. \* Botanical name are according to Chinese Pharmacopoeia (Chinese Pharmacopoeia Commission, China Medical Science Press, Beijing, China, 2020). Abbreviations: ALP, alkaline phosphatase; BMD, bone mineral density; BGP, bone Gla protein; BMP-2, bone morphogenetic protein-2; BV/TV, bone volume/total volume; CTXI, collagen cross-linking carboxy-terminal telopeptide, type I; GIOP, glucocorticoid-induced osteoporosis; GPR48, G protein-coupled receptor 48; IL-1β, interleukin-1β; LPS, lipopolysaccharide; MDA, malondialdehyde; OCN, osteocalcin; OP, osteopontin; OPG, osteoprotegerin; OVX, ovariectomy; PINP, procollagen type I N-terminal propeptide; PTH, parathyroid hormone; SOD, superoxide dismutase; Tb.N, trabecular number; Tb.Sp, trabecular separation; TNF-α, tumor necrosis factor-α; TRAP, tartrate-resistant acid phosphatase; WBBMC, whole-body bone mineral content; WBBMD, whole-body bone mineral density.

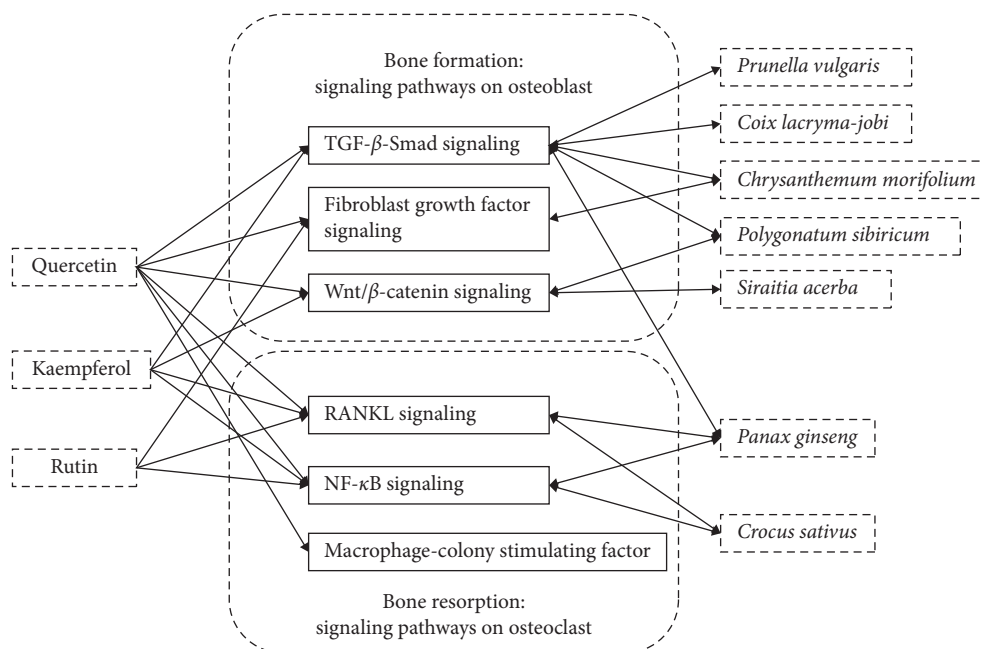


FIGURE 4: Mechanism research of quercetin, kaempferol, rutin, and medicine food homology plants on bone formation and bone resorption. Abbreviations: TGF-β, transforming growth factor-β; Smad, suppressor of mothers against decapentaplegic; Wnt, wingless; RANKL, receptor activator for nuclear factor kappa B ligand; NF-κB, nuclear factor kappa B.

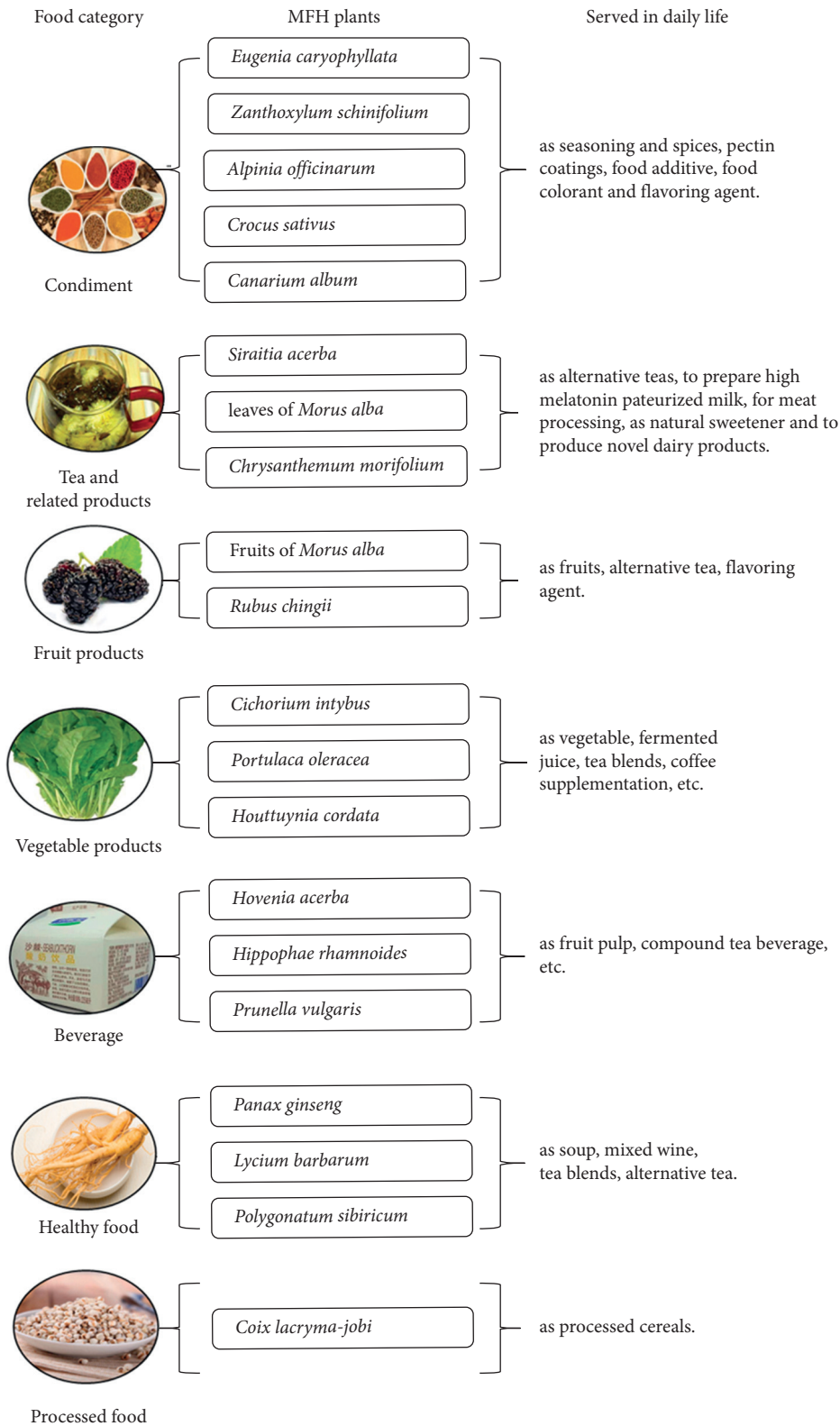


FIGURE 5: Food functions of the 20 MFH plants. Abbreviation: MFH, medicine food homology.

been traditionally used as a “tonic” to enhance immune responses [72]. *P. sibiricum* participated in the protection against immunosuppression in cyclophosphamide-treated mice, highlighting its potential as an

immunostimulant [73]. Several clinical studies in healthy subjects showed that consumption of wolfberry juice improves general wellbeing and immune functions [74]. It is reported that antiosteoporotic activity is related to

the regulation of immune functions and antioxidant activity [75]. In this case, traditional “tonic”, “clearing away heat” efficiency, and “with cool property” could explain the antiosteoporotic activity from the point of antioxidant and immune-regulatory activities.

It is interesting that “the interior warming” efficiency could be understood from the point of penetration enhancement activity of essential oils from *E. caryophyllata*, *Z. schinifolium*, and *A. officinarum* [76]. Flurbiprofen is one of the most potent nonsteroidal anti-inflammatory drugs with very low bioavailability of approximately 12% after transdermal administration, compared with that after oral administration. The essential oils from *A. officinarum* could be used as an oil phase and a penetration enhancer that help transdermal delivery of flurbiprofen [77]. Further study in ovariectomy (OVX) rats showed that osteogenic efficacy can be enhanced by kaempferol through an engineered layer-by-layer matrix [78]. That might explain the anti-osteoporosis effect of “the interior warming” efficiency based on penetration enhancement activity of essential oil and kaempferol.

From a modern perspective of the cardiovascular system, it seems easy to understand the ancient efficiency of “activating blood circulation and removing blood stasis.” In TCM, the antiosteoporotic effect of some traditional herbs is ascribed to their action on liver and blood stasis as main therapeutic targets defining osteoporosis [79], but the research of MFH plants with “removing blood stasis” efficiency on antiosteoporosis effect should be conducted further.

For more than 300 years, *S. grosvenorii* has been used as a natural sweetener and as a traditional medicine for the treatment of pharyngitis and pharyngeal pain, as well as an antitussive remedy in China [80]. Its ancient antitussive efficiency is similar to modern terms but difficult to understand from the antiosteoporosis point. The mechanisms of adlay were confirmed in regulating the water transport on the spleen deficiency and wet dampness rat model [81]. It is also hard to understand its antiosteoporosis effects from the point of “dampness removing.”

Based on the above discussion, some traditional efficacies of MFH plants might be related with modern antioxidant and immune-regulatory activities, and latter are associated with antiosteoporosis effects.

### 3. In Vivo Clinical Studies

Postmenopausal women tend to be susceptible to primary osteoporosis due to its association with estrogen deficiency. Aside from physical activity, nutrition and diet in adequate proportions are suggested to be an important tool for ameliorating osteoporosis and bone health issues in postmenopausal women [82]. There were three clinical studies that correlated with postmenopausal women [83–85].

The first clinical study was a test of a mixture of chicory oligofructose and long-chain inulin on 15 postmenopausal women ( $72.2 \pm 6.4$  years). The women were treated with the mixture for 6 weeks using a double-blind, placebo-controlled, crossover design [83].

The second one was a study about sea buckthorn oil fatty acid, which was tested on normal and osteopenic women. A total of 1865 female subjects (20–79 years old) were enrolled in this study. The results showed that the intake of the oil fatty acids seemed to be positively associated with bone mineral density (BMD), which is obtained by dividing the bone width by the bone mineral content (BMC) at both the hips and the lumbar spine in normal and osteopenic women [84].

The last one was about omega-3 polyunsaturated fatty acids from sea buckthorn, which was studied on bone health of 20 males and 3 females for 6 weeks in a randomized, 3-period crossover design. The results indicated that sea buckthorn may have a protective effect on bone metabolism via a decrease in bone resorption in the presence of consistent levels of bone formation [85].

In summary, clinical antiosteoporosis studies of the 20 MFH plants are still limited. The popular compounds such as quercetin and kaempferol have not reported clinical research till now [9]. Well-designed clinical studies will help discover the antiosteoporosis evidences of these MFH plants and also compounds.

### 4. In Vivo Animal Studies

**4.1. OVX Models.** Animal models of osteoporosis are appropriate tools for establishing new prevention strategies and more effective treatment modalities, of which the OVX rat model is the most commonly used [86]. From Figure 3, we could see that the 14 MFH plants were tested on OVX animal models and they all had positive effects on bone health. These 14 MFH plants were tested on mixtures [41, 54], single herbs [18, 30, 37, 45, 47, 50, 51], and active ingredients [19, 32, 39, 40, 48, 52] separately.

The combined extract of mulberry leaves and *Polygonum odoratum* were also tested [54]. Chicory inulins and a mixture of inulins-isoflavones were compared in OVX rats. The results showed that there were no apparent histological changes in rats treated with inulins and the mixture [41].

The tested two raw herbs were ginseng [45] and adlay [37]. The tested extracts were from *H. acerba* [18], mulberry fruits [47], wolfberry [50], clove [51], and *A. officinarum* [30].

The tested active ingredients included the essential oil of *H. cordata* [39], the flavonoids from *P. vulgaris* [40], and the polysaccharide from *P. sibiricum* [48]. The tested nutritional compounds included crocin from saffron [52], linarin from chrysanthemum [32], ginsenoside Rg3 from ginseng [19], etc.

Based on OVX models, the effects of *P. sibiricum* were reported on an OVX-induced fracture model that was established by broken femoral shaft in OVX rats. The related research showed that *P. sibiricum* improved the biomechanical properties and BMD of fracture rats by regulating bone repair and bone metabolic factors [49]. Most studies have reported that polysaccharides, flavonoids, and saponins are the main bioactive compounds in *P. sibiricum*, which play important roles on antioxidation [87]. That suggested that the antifracture effect of

*P. sibiricum* might be related with its antioxidation activities.

*In vitro* cultured rat femoral metaphyseal tissues isolated from an OVX model were used for the research of adlay extract. The results showed that adlay seeds could reverse the decreased calcium levels induced by parathyroid hormone in cultured metaphyseal tissues [38].

**4.2. Age-Related Models.** Bone health is important throughout the whole human life: infancy, adolescence, adulthood, and old age. Age-related model studies in this review included a nutraceutical compound from chicory on growing rats [42] and young rats [43] and extracts and compounds from ginseng on aged animals [19, 46, 88].

Inulin, a nutraceutical compound from chicory, showed its effects on whole-body BMC, whole-body bone area, and whole-body BMD in growing male rats (4-5 weeks old). The results also showed that chicory inulin not only increases calcium absorption but also increases mineral parameters in whole-body bones [42].

Furthermore, a purified native inulin, a reformulated inulin based on a combination of short- and long-chain fructans, and a dehydrated chicory were tested in 3-month-old young male rats, and the experiment was continued for 3 months. The results showed that bone parameters had a significant positive improvement by the chicory diet, whereas the purified inulin diets were less effective. The particular effects of the chicory crude fraction on digestive fermentation and bone parameters suggest possible synergisms between inulin-type fructans and other nutrients [43].

It is well known that aging leads to impaired bone regulation, resulting in an imbalance between bone homeostasis and pathological bone mass [89]. Using natural 112-week-old male rats, some research indicated that the extracts from ginseng might be a potential alternative medicine for the prevention and treatment of natural aging-induced osteoporosis in humans [46]. Ginsenosides are pharmacologically active compounds that are often extracted from *P. ginseng* for their medicinal properties. Many ginsenosides can promote bone formation and inhibit bone resorption, such as Rb1, Rb2 [88], and Rg3 [19]. We are interested that these ginsenosides have effects on aging-induced osteoporosis in the following research.

As we discussed before, estrogen deficiency and aging are the main causes for disturbances in bone remodeling activity and bone loss [4]. The current drugs for the osteoporosis include estrogen treatment [5, 6]. Estrogen is involved in the regulation activity of osteoblasts and osteoclasts, directly through estrogen receptor (ER)- $\alpha$  and ER- $\beta$ . In the last decades, *in vitro* and *in vivo* results have revealed that *P. ginseng* and its active compounds are equipped with hormone analogous effects. There is evidence that ginsenosides Rg1 exert estrogen-like effect via the activation of ER- $\alpha$  [90].

**4.3. Glucocorticoid-Induced Models.** Glucocorticoid-induced osteoporosis (GIOP) that is mainly featured as low bone density and increased risk of fracture is prone to occur with

the administration of excessive glucocorticoids [91]. Chicory showed bone protection against GIOP in rats, and the protective effects were related to its flavonoids and inulin [44]. Estrogen is involved in the regulation activity of bone, indirectly through parathyroid hormone (PTH). The chicory extracts can decrease PTH in GIOP rats [44].

**4.4. Metabolic Syndrome Models.** Metabolic syndrome is a serious health problem. Complications of metabolic syndrome include osteoporosis. Antiosteoporotic activities of crocin from saffron were evaluated in a rat model of metabolic syndrome-induced osteoporosis. Crocin enhanced both the longitudinal and perpendicular bone strength (bone strength means the ratio of the maximum load value to the BMC per millimeter of specimen length) of femurs. That enhanced effects of crocin mitigated oxidative stress in femur distal epiphysis tissues [53].

**4.5. LPS-Induced Bone Loss Model.** Injection of lipopolysaccharide (LPS) rapidly induced trabecular bone loss through stimulation of osteoclast differentiation. The protective effect of purslane on LPS-induced bone loss was confirmed. Purslane exhibited its antiosteoclastogenic activity based on its anti-inflammatory and antioxidative properties [13].

## 5. In Vitro Studies

The homeostasis of bones is jointly maintained by osteoblasts, osteoclasts, bone marrow mesenchymal stem cells (BMMSCs), and other cells [92]. Osteoporosis is produced by an imbalance between osteoblastogenesis and osteoclastogenesis processes during bone metabolism. Inflammation and high reactive oxygen enhance osteoclastogenesis while reducing osteoblastogenesis by inducing osteoblast apoptosis and suppressing osteoblastic proliferation and BMMSC differentiation [93].

**5.1. On Osteoblastogenesis Processes.** A total of 12 MFH plants were reported to have a positive regulatory effect on osteoblast differentiation. The extracts from *H. acerba* [18], *A. officinarum* [30], and mogroside V from *S. grosvenorii* [33]. The above three samples were tested on calvarial osteoblasts from the rat/mice calvaria at postnatal day. The polysaccharides from *L. barbarum* [28], and three compounds including crocin [34], linarin via bone morphogenetic proteins 2(BMP-2)/runt-related transcription factor 2 (Runx2) pathway [42], and ginsenoside Rb2 via a reduction of oxidative damage [20] were all tested on the osteoblast MC3T3-E1 cell line. The results showed that osteoblast differentiation could be induced by the above extracts and compounds [18, 20, 28, 30, 33, 34, 42].

Comparison of seven compounds from *R. chingii* was carried out on primary rat osteoblasts [29]. Purslane was tested on primary human osteoblasts [14], and the adlay extract was tested on primary rat osteoblasts isolated from the calvaria of fetal rats (18 days old) via an extracellular

signal regulated kinase (ERK) pathway [37]. The promoting effects on osteoblast differentiation could be seen in the related results [14, 29, 37].

The effects of two MFH plants and their active ingredients on BMMSCs were reported. *P. vulgaris* protected glucocorticoids-induced osteogenesis inhibition in BMMSCs through activating the suppressor of mothers against decapentaplegic (Smad) pathway [16]. The polysaccharide from *P. sibiricum* was tested on primary mice BMMSCs [25, 26]. Crocin and crocetin, two major compounds from saffron, were compared and their effects on osteogenic differentiation of BMMSCs isolated from rats were tested [35]. Ginsenoside Rb1 from ginseng was reported to alleviate aluminum chloride-induced rat osteoblast dysfunction [21].

**5.2. On Osteoclastogenesis Processes.** Osteoclasts are functional cells and play a major role in pathological bone resorption. They are derived from hematopoietic precursors and undergo a series of differentiation and fusion steps in response to various humoral factors. RANKL-induced osteoclast formation is considered as an important canonical pathway [94].

According to current studies, two MFH plants were only tested on RANKL-induced osteoclastogenesis processes *in vitro*: both *C. album* and *Z. schinifolium* were tested on the RANKL-induced RAW 264.7 cell line [17]. The two MFH plant extracts from purslane [15] and *A. officinarum* [31] and the polysaccharide from *P. sibiricum* [25, 27] were also tested on RANKL-induced osteoclastogenesis processes on primary bone marrow-derived macrophages (BMMs).

The active compounds research included the following: crocin by regulating c-Jun N-terminal kinase (JNK) and nuclear factor kappa B (NF- $\kappa$ B) signaling pathways [36]; ginsenoside Rg3 via RANKL, JNK, and p38 mitogen-activated protein kinase (MAPK) pathways [22]; ginsenoside Rb1 via NF- $\kappa$ B and MAPKs pathways [23]; and ginsenoside Rb2 via NF- $\kappa$ B and STAT3 [24] were all tested and their effects on RANKL-induced RAW264.7 cells were defined.

## 6. Mechanism Studies

Signaling pathways are key players in the commitment and differentiation of osteoblasts and osteoclasts. A number of studies have identified key signals in the process of osteogenesis. From Figure 4, it seems that three compounds have more signaling research than MFH plants. Among the three compounds, quercetin is the most used one in pathway studies: transforming growth factor- $\beta$  (TGF- $\beta$ )-Smad signaling, fibroblast growth factor (FGF) signaling, wingless (Wnt)/ $\beta$ -catenin signaling in bone formation and RANKL signaling, NF- $\kappa$ B signaling, and macrophage colony-stimulating factor (M-CSF) in bone resorption.

**6.1. TGF- $\beta$ -Smad Signaling.** The TGF- $\beta$  superfamily members bind and signal through dual type I and II transmembrane receptors, containing serine/threonine kinase domains. Smad proteins play key roles in transmitting

signals from receptor to nucleus. One of the members of TGF- $\beta$  superfamily, BMPs is critical in osteogenesis. The activation of MAPKs including ERK, JNK, and p38 is regulated by BMP-2 in osteoblastic cells [9].

The interaction of BMP-2 and TGF- $\beta$  with their respective receptors results in the upregulation of osteogenic genes and osteoclastogenic genes via activation of Smad proteins and/or inhibition of MAPKs. Quercetin may have positive or negative effects on the levels of BMP-2, TGF- $\beta$ , and Smad protein in bone cells [95]. The research found that kaempferol increased cell growth, secretion of osteoblast growth factor, and the level of BMP receptor II in opossum kidney cells. Findings from this study implied that kaempferol stimulated kidney repair, which indirectly stimulates bone formation [5].

The 5 MFH plants showed their effects on TGF- $\beta$ -Smad signaling: the polysaccharide from Siberian Solomon's seal rhizome on primary mice BMMSCs via ERK [25], the extracts from common selfheal spike on glucocorticoids-induced BMMSCs by activating the Smad pathway [16], the adlay extract on the primary rat osteoblasts via the ERK pathway [37], compound linarin from chrysanthemum flowers on the osteoblast MC3T3-E1 cell line via BMP-2 [32], and the compound ginsenoside Rb1 from ginseng alleviated aluminum chloride-induced rat osteoblast dysfunction via the increased TGF- $\beta$  and BMP-2 expression [21].

**6.2. FGF Signaling.** The FGFs are the family members of secreted polypeptides. FGFs bind to FGF tyrosine kinase receptors (FGFRs) and then take part in a number of biological events critical in endochondral and intramembranous ossification. It has been demonstrated that FGF activates runt-related transcription factor 2 (Runx2) by MAPKs pathways and thus helps bone formation [9].

The treatment of MC3T3-E1 cells with rutin can significantly increase the expression of Runx2 gene, and significant differences were found among groups in which different concentrations were used [96]. The majority of studies have reported osteoblastogenesis-activating effects of quercetin via increased Runx2 levels, with a few exceptions. These discrepancies may be related to the cell types and doses of quercetin used [95]. Studies have shown that chrysanthemum flowers activate the transcription factor Runx2 through MAPKs pathways, therefore promoting bone formation [32].

**6.3. Wnt/ $\beta$ -Catenin Signaling.** The canonical Wnt/ $\beta$ -catenin signaling pathway has a central regulatory role in bone metabolism. The activation of Wnt signaling leads to the expression of the Wnt-targeted gene Runx2, which is essential for osteoblast differentiation [95]. In unstimulated conditions,  $\beta$ -catenin is sequestered into a destruction complex consisting of axis inhibition protein 2 (Axin-2), casein kinase 1 alpha (CK1 $\alpha$ ), adenomatous polyposis coli (APC), and glycogen synthase kinase-3 beta (GSK3 $\beta$ ). Higher levels of  $\beta$ -catenin signaling upregulate the



expression of genes implicated in the differentiation of osteoblasts [9].

Quercetin rescued LPS-induced impairment of osteogenesis in murine osteoblastic MC3T3-E1 cells by enhancing the protein levels of Wnt3 and  $\beta$ -catenin and decreasing the protein level of GSK3 $\beta$  [95]. The stimulation of SaOS-2 cells by kaempferol resulted in an increased activity of Wnt signaling responsive reporter construct, Axin-2, and, subsequently, stabilization of Wnt signaling-mediated transcription factor  $\beta$ -catenin, probably leading to the activation of Wnt-targeted genes for osteogenesis [97].

The polysaccharide from Siberian Solomon's seal rhizome was tested on primary mice BMMSCs. The results showed that the polysaccharide promoted the osteogenic differentiation of BMMSCs. This effect was due to the increased nuclear accumulation of  $\beta$ -catenin, resulting in a higher expression of osteoblast-related genes [25]. One of the ingredients in raisin tree seeds was reported to activate the Wnt/ $\beta$ -catenin pathway to induce osteogenic differentiation of calvarial osteoblasts [18].

**6.4. RANKL Signaling.** RANKL, an important member of tumor necrosis factor (TNF) superfamily, is also known as osteoclast differentiation factor (ODF). The binding of extracellular signaling factor RANKL to RANK activates signaling cascades by recruiting adapter protein tumor necrosis factor receptor-associated factor 6 (TRAF6), which leads to multiple downstream events such as activation of MAPKs (ERK, p38, and JNK) and NF- $\kappa$ B [9].

Numerous studies have found that quercetin inhibits the formation of osteoclast-like cells, bone resorption pit, and F-actin ring formation in murine macrophage RAW264.7 cells, human peripheral-blood mononuclear cells (PBMCs), or bone marrow macrophages treated with M-CSF and/or RANKL [95].

In RAW264.7 cells treated with RANKL, kaempferol was shown to abrogate RANKL-induced cells, the indicator for osteoclast differentiation. The downregulation of osteoclastogenic factors including RANKL, nuclear factor of activated T-cells cytoplasmic 1, and TRAF6 was also observed in kaempferol-treated cells [5].

The effects of rutin on the development and activity of osteoclasts *in vitro* were compared with the effects of 17 $\beta$ -estradiol. The anti-resorbing properties of rutin were mainly mediated by ER proteins through the inhibition of RANK protein or the activation of caspases [98]. On the other hand, the research *in silico* interaction of rutin with the RANK/RANKL system in diabetoporosis showed that the initial interaction of RANK with rutin will facilitate the bond of RANK to RANKL. This is in contrast to previous findings that rutin decreases the activity of RANKL [99].

Ginsenoside Rg3 is one of the most promising compounds of ginseng with numerous biological activities. Inhibition of osteoclast differentiation by ginsenoside Rg3 in RAW264.7 cells via RANKL, JNK, and p38 MAPK pathways was observed [22].

Crocin, an important compound from saffron crocus style and stigma, inhibited RANKL-induced phosphorylation of JNK in BMMs. The results suggested that the inhibitory effect of crocin on the differentiation of osteoclast precursors into mature osteoclasts may be mediated by the regulation of JNK phosphorylation [36].

**6.5. NF- $\kappa$ B Signaling.** NF- $\kappa$ B is a set of nuclear factors that bind to consensus DNA sequences called  $\kappa$ B sites and is essential for osteoclast formation and survival. Abnormal activation of NF- $\kappa$ B signaling in osteoclasts is associated with excessive osteoclastic activity and observed in osteolytic conditions frequently. Modulators of NF- $\kappa$ B signaling pathways have a great therapeutic potential in bone disease. NF- $\kappa$ B signaling pathways are strictly regulated by cytokines such as RANKL, TNF- $\alpha$ , and IL-1, which differentially regulate classical and/or alternative NF- $\kappa$ B pathways to maintain bone homeostasis in osteoclastic cells [100]. Curcumin, an important dietary nutraceutical compound derived from the Indian spice turmeric, has been shown to inhibit both NF- $\kappa$ B activation and osteoclastogenesis induced by RANKL [100].

Several studies using genetically engineered mouse models suggested that the NF- $\kappa$ B pathway plays a key role in RANKL-induced osteoclast development and function [9].

Both quercetin and kaempferol potentially protect the bone through their anti-inflammatory property on osteoblastic cells via inhibition of NF- $\kappa$ B nuclear translocation [5, 9]. Similarly, rutin inhibits osteoclast formation by decreasing reactive oxygen species and TNF- $\alpha$  by inhibiting activation of NF- $\kappa$ B [101].

Three compounds crocin [36], ginsenoside Rb1 [23], and ginsenoside Rb2 [24] showed their inhibition on RANKL-induced osteoclastogenesis by regulating NF- $\kappa$ B signaling pathways.

**6.6. Macrophage-Colony-Stimulating Factor.** Osteoclasts are specialized bone-resorbing cells regulated by RANKL and M-CSF. When monocytes were stimulated with M-CSF, mature osteoclasts were formed, and quercetin decreased this osteoclastogenesis [102].

## 7. Food Functions

TCM nutrition is an ancient but burgeoning discipline, and its main goal is to use food as a means to achieve balance and harmony within the body [12]. From the point of food supplementation, the viewpoints of MFH plants conform to today's food requirements of returning to a natural and green healthy life and seem easy to accept [103]. Take some examples, the edible flowers such as chrysanthemum [104], the vegetable such as chicory [105], and wild edible plants such as purslane [106] are all distributed all over the world and have been consumed as food since ancient times.

According to the "Measures for the Administration of Food Production Licensing," the State Administration for Market Supervision and Administration updated the "Catalogue of Food Production Licensing" in 2020 [107].

Food functions of the 20 MFH plants were discussed as the following catalogues: condiment (5 MFH plants), tea and related products (3 MFH plants), vegetable products (3 MFH plants), beverages (3 MFH plants), healthy food (3 MFH plants), fruit products (2 MFH plants), and processed food (1 MFH plant).

**7.1. Condiments.** Both clove and *A. officinarum* are normally served as seasoning in daily life. The effectiveness of pectin coatings enriched with clove essential oil was investigated to preserve bream fillets during refrigeration. The results showed that pectin coating along with clove oil was effective in inhibiting bacterial growth especially in Gram-negative bacteria [108].

*Z. schinifolium* is distributed in more than 20 provinces in China including Sichuan. Sichuan-*Z. schinifolium* are also a popular food additive and widely used in cooking with the history of more than 1000 years for both medicinal and economic values [109].

Saffron, stigmas of *C. sativus*, is one of the most precious spices used as a food colorant and flavoring agent and is widely consumed in culinary for its famous and unique color. Crocin is the typical carotenoid pigment of saffron that gives food a rich golden-yellow tinge [110], and crocin also plays an important role as a nutraceutical compound and exhibits antiosteoporosis effects according to our review.

*C. album*, normally called Chinese olive, is a tropical and semitropical fruit of the family Burseraceae, widely cultivated in Taiwan, Southeast China, and other regions of Asia. Some findings suggest that Chinese olive may ameliorate metabolic dysfunction in diabetic rats under high-fat diet challenge [111].

**7.2. Tea and Related Products.** Both the fruits and leaves of *M. alba* have nutritional and medicinal values and could be served as tea. Mulberry fruits with high concentrations of anthocyanins are favored by consumers as fruits because of their good taste, bright color, and high nutritional value [112]. Findings indicated that mulberry leaves and soybean are both good sources of melatonin and free tryptophan and can be applied to prepare high-melatonin pasteurized milk [113].

Mulberry leaves and mulberry fruits have different clinical efficiencies according to TCM, but they both showed antiosteoporosis effects on OVX models [47, 54]. The phenolic profile of mulberry leaves was characterized by the presence of a high number of flavonol derivatives, mainly glycosylated forms of quercetin and kaempferol [114]. LC-MS analysis also revealed that the contents of four flavonoid glycosides including kaempferol rhamnosylhexoside increased after digestion of mulberry fruits [115]. Another popular tea in China is made from chrysanthemum flower [116]. As a novel natural antioxidant, chrysanthemum could be used for the meat processing industry [117].

*Siraitia* fruits have been used as a natural sweetener for more than 300 years [80]. The research of *Siraitia* fruit extract supplementation on the chemical, microbial, and

sensory properties of probiotic yogurt showed that it offers a promising option as a dietary supplement to produce novel dairy products that have high nutritional and bioactivity values [118].

**7.3. Vegetable Productions.** Purslane is a popular wild edible plant. Wild edible plants are gaining importance as they are potential sources of food due to their nutritional value, besides showing positive health effects and offering innovative applications in haute cuisine [106].

*H. cordata* is a popular vegetable in Asian countries [119] and is an important traditional Chinese medicine used in heat clearing and detoxifying, swelling and discharging pus, promoting diuresis, and relieving stranguria [120]. It was reported that fermented juice of *H. cordata* can improve diabetic symptoms by enhancing insulin sensitivity, reducing oxidative stress, and suppressing inflammation [121].

Chicory is a perennial herb and is cultivated worldwide. So far, chicory has been used mainly in animal feed but also in several cases in the food industry: as salad, for teas and tea blends, for coffee supplementation, and as a source for the inulin production. Nowadays, there is an increasing interest in chicory utilization for food production and supplementation. Some compounds present in chicory, such as kaempferol, inulin, and oligofructose may be considered as potential carriers of food functionality [105].

**7.4. Beverage.** Herbal teas or herbal drinks are traditional beverages that are prevalent in many cultures around the world. *P. vulgaris* L. is as a major plant in the Chinese traditional functional beverage Guangdong herbal tea for the treatment of fevers, diarrhea, and sore mouth [122].

*H. acerba* has long been used as traditional folk remedies for alcohol intoxication. The antihangover effect of *H. acerba* extract was examined in a randomized controlled crossover trial. The results suggest that a favorable effect of *H. acerba* beverage on alcohol hangovers might be associated with enhancing homeostatic regulation of inflammatory response [123].

Eighteen novel smoothie products containing sea buckthorn (25–50%) with other fruits and vegetables were analyzed. The results showed that sea buckthorn enriched the flavonols in smoothies and provided the most sensory attractive [124].

**7.5. Healthy Food.** The related research showed that wolfberry ameliorates osteoporosis in OVX mice by improving several important parameters including BMC, BMD, and bone-turnover markers such as osteocalcin and calcium levels in serum [37]. Wolfberry has been used as a tonic medicine and a long-term healthy food, which can be served as nutritional soup [125]. Several clinical studies in healthy subjects show that consumption of wolfberry juice improves general wellbeing and immune functions [74].

As another nutrition is this study, the safety and effectiveness of ginseng in different regions including American ginseng, Korean ginseng, and Asian ginseng were

supported by some research [126] and already accepted in the East and West. Ginseng can be served as mixed wine, tea blends, alternative tea, soup, etc [107].

*P. sibiricum* is widely distributed in most regions in the south of the Yangtze River in China. It has served as a Taoist health potion such as soup and food ingredient since ancient times and functions to nourish the liver and kidney and prolong life [127].

## 8. Conclusive Remarks

Based on the literature research, 20 MFH plants are discussed in this review. Their common features are they all contain quercetin, rutin, and kaempferol and they all showed antiosteoporosis activities, *in vivo* and *in vitro*. The TCM characteristics including natures, flavors, attributive to meridian tropism, and efficiencies of the 20 MFH plants are compared. We have tried to explain their traditional efficiencies with pharmacological actions. Based on antiosteoporosis pathway research of quercetin, rutin, and kaempferol, more mechanisms of the 20 MFH plants should be evidenced for further application. At the same time, how to evaluate the actions of these compounds in the MFH plants is another problem that should be solved. Anyway, as food and food supplementation, these MFH plants with multiple nutraceutical compounds can be served as multiple food forms in our daily life. This is the focus of our concern.

## Abbreviations

APC:	Adenomatosis polyposis coli
AXIN:	Axis inhibition protein 2
BMC	Bone mineral content
(g/cm):	
BMD	Bone mineral density
(g/cm <sup>2</sup> ):	
BMMs:	Bone marrow-derived macrophages
BMMSCs:	Bone marrow mesenchymal stem cells
BMPs:	Bone morphogenetic proteins
CK1:	Casein kinase 1 alpha
ER:	Estrogen receptor
ERK:	Extracellular signal regulated kinase
FGF:	Fibroblast growth factor
FGFRs:	FGF tyrosine kinase receptors
GIOP:	Glucocorticoid-induced osteoporosis
GSK3 $\beta$ :	Glycogen synthase kinase-3 beta
JNK:	C-Jun n-terminal kinase
LDL:	Low-density lipoprotein
LPS:	Lipopolysaccharide
MAPKs:	Mitogen-activated protein kinases
M-CSF:	Macrophage-colony-stimulating factor
MFH:	Medicine food homology
NF- $\kappa$ B:	Nuclear factor kappa B
ODF:	Osteoclast differentiation factor
OVX:	Ovariectomy
PBMCs:	Human peripheral-blood mononuclear cells
PTH:	Parathyroid hormone
RANKL:	Receptor activator for nuclear factor $\kappa$ B ligand
RUNX2:	Runt-related transcription factor 2

SMAD:	Suppressor of mothers against decapentaplegic
STAT3:	Signal transducer and activator of transcription protein 3
TCM:	Traditional Chinese medicine
TGF- $\beta$ :	Transforming growth factor- $\beta$
WNT:	Wingless
TNF:	Tumor necrosis factor
TRAF6:	Tumor necrosis factor receptor-associated factor 6.

## Data Availability

All the authors declare that the readers can access the conclusions from the five figures and three tables. All the figures and tables are summarized based on the references.

## Additional Points

Chemical compounds mentioned in this article: Crocetin (PubChem CID: 5281232); Crocin (PubChem CID: 5281233); Curcumin (PubChem CID: 969516); Ginsenoside Rb1 (PubChem CID: 9898279); Ginsenoside Rb2 (PubChem CID: 6917976); Ginsenoside Rg3 (PubChem CID: 9918693); Inulin (PubChem CID: 24763); Kaempferol (PubChem CID: 5280863); Linarin (PubChem CID: 5317025); Quercetin (PubChem CID: 5280343); Rutin (PubChem CID: 5280805); Resveratrol (PubChem CID: 445154); Genistein (PubChem CID: 5280961).

## Conflicts of Interest

The authors declare there are no conflicts of interest.

## Acknowledgments

This study was supported by Wu Jieping Medical Foundation (No. 320.6750.2021-08-10) and Wu Jieping Medical Foundation (No. 320.6750.2021-08-11), the Key R&D Project of Shanxi Province (International Scientific and Technological Cooperation, Independent Topics, No. 201903D421061), and the Basic Research Program of Shanxi Province (No. 202103021224370).

## References

- [1] W. Zhang, K. Xue, Y. Gao et al., "Systems pharmacology dissection of action mechanisms of dipsaci Radix for osteoporosis," *Life Science*, vol. 235, Article ID 116820, 2019.
- [2] Osteoporosis and Bone Mineral Disease Branch of Chinese Medical Association, "Epidemiological survey of osteoporosis in China and the results of the "healthy bones" special action released," *Chinese Journal of Osteoporosis and Bone Mineral Research*, vol. 12, no. 4, pp. 317-318, 2019.
- [3] R. Cui, L. Zhou, Z. Li, Q. Li, Z. Qi, and J. Zhang, "Assessment risk of osteoporosis in Chinese people: relationship among body mass index, serum lipid profiles, blood glucose, and bone mineral density," *Clinical Interventions in Aging*, vol. 11, pp. 887-895, 2016.
- [4] C. Yang, P. Yang, P. Liu, H. Wang, E. Ke, and K. Li, "Targeting filamin a alleviates ovariectomy-induced bone

- loss in mice via the WNT/ $\beta$ -catenin signaling pathway," *Cellular Signalling*, vol. 90, Article ID 110191, 2022.
- [5] S. K. Wong, K. Y. Chin, and S. Ima-Nirwana, "The osteoprotective effects of kaempferol: the evidence from in vivo and in vitro studies," *Drug Design, Development and Therapy*, vol. 13, pp. 3497–3514, 2019.
  - [6] I. Khorsand, R. Kashef, M. Ghazanfarpour, E. Mansouri, S. Dashti, and T. Khadivzadeh, "The beneficial and adverse effects of raloxifene in menopausal women: a mini review," *Journal of Menopausal Medicine*, vol. 24, no. 3, pp. 183–187, 2018.
  - [7] T. Wang, Q. Liu, W. Tjhioc et al., "Therapeutic potential and outlook of alternative medicine for osteoporosis," *Current Drug Targets*, vol. 18, no. 9, pp. 1051–1068, 2017.
  - [8] J. He, X. Li, Z. Wang et al., "Therapeutic anabolic and anticatabolic benefits of natural Chinese medicines for the treatment of osteoporosis," *Frontiers in Pharmacology*, vol. 10, p. 1344, 2019.
  - [9] M. K. Pandey, S. C. Gupta, D. Karelia, P. J. Gilhooley, M. Shakibaei, and B. B. Aggarwal, "Dietary nutraceuticals as backbone for bone health," *Biotechnology Advances*, vol. 36, no. 6, pp. 1633–1648, 2018.
  - [10] J. Wang, H. Wang, X. Mou et al., "The advances on the protective effects of Ginsenosides on myocardial ischemia and ischemia-reperfusion injury," *Mini Reviews in Medicinal Chemistry*, vol. 20, no. 16, pp. 1610–1618, 2020.
  - [11] L. Xue, L. Gao, X. Qin, G. Du, and Y. Zhou, "A review of recent literature on anti-aging activity of medicinal and edible traditional Chinese herbs," *Food Science*, vol. 38, no. 15, pp. 302–309, 2017.
  - [12] X. Zhao, X. Tan, H. Shi, and D. Xia, "Nutrition and traditional Chinese medicine (TCM): a system's theoretical perspective," *European Journal of Clinical Nutrition*, vol. 75, no. 2, pp. 267–273, 2021.
  - [13] J. Y. Kim, H. M. Oh, S. C. Kwak et al., "Purslane suppresses osteoclast differentiation and bone resorbing activity via inhibition of Akt/GSK3 $\beta$ -c-Fos-NFATc1 signaling in vitro and prevents lipopolysaccharide-induced bone loss in vivo," *Biological and Pharmaceutical Bulletin*, vol. 38, no. 1, pp. 66–74, 2015.
  - [14] M. D'Imperio, G. Brunetti, I. Gigante et al., "Integrated in vitro approaches to assess the bioaccessibility and bioavailability of silicon-biofortified leafy vegetables and preliminary effects on bone," *In Vitro Cellular & Developmental Biology—Animal*, vol. 53, no. 3, pp. 217–224, 2017.
  - [15] M. Erkhembaatar, E. J. Choi, H. Y. Lee, C. H. Lee, Y. R. Lee, and M. S. Kim, "Attenuated RANKL-induced cytotoxicity by *Portulaca oleracea* ethanol extract enhances RANKL-mediated osteoclastogenesis," *BMC Complementary and Alternative Medicine*, vol. 15, no. 226, pp. 1–7, 2015.
  - [16] L. Xi, Y. F. Zhang, Z. J. Zhao, D. S. Pan, and W. Liang, "*Prunella vulgaris* L protects glucocorticoids-induced osteogenesis inhibition in bone marrow mesenchymal stem cells through activating the Smad pathway," *European Review for Medical and Pharmacological Sciences*, vol. 24, no. 10, pp. 5691–5696, 2020.
  - [17] F.-F. Xu, Y. Ding, and H.-D. Zhang, "Antioxidant and anti-osteoporosis activities of extracts from 15 kinds of Chinese herbal medicines," *Journal of Chinese Institute of Food Science and Technology*, vol. 17, no. 6, pp. 240–248, 2017.
  - [18] P. H. Cha, W. Shin, M. Zahoor, H. Y. Kim, S. Min do, and K. Y. Choi, "Hovenia dulcis thunb extract and its ingredient methyl vanillate activate Wnt/ $\beta$ -catenin pathway and increase bone mass in growing or ovariectomized mice," *PLoS One*, vol. 9, no. 1, Article ID e85546, 2014.
  - [19] X. Zhang, F. Huang, X. Chen, X. Wu, and J. Zhu, "Ginsenoside Rg3 attenuates ovariectomy-induced osteoporosis via AMPK/mTOR signaling pathway," *Drug Development Research*, vol. 81, no. 7, pp. 875–884, 2020.
  - [20] Q. Huang, B. Gao, Q. Jie et al., "Ginsenoside-Rb2 displays anti-osteoporosis effects through reducing oxidative damage and bone-resorbing cytokines during osteogenesis," *Bone*, vol. 66, pp. 306–314, 2014.
  - [21] Y. Zhu, C. Hu, P. Zheng et al., "Ginsenoside Rb1 alleviates aluminum chloride-induced rat osteoblasts dysfunction," *Toxicology*, vol. 368–369, pp. 183–188, 2016.
  - [22] M. H. Siddiqi, M. Z. Siddiqi, S. Kang et al., "Inhibition of osteoclast differentiation by ginsenoside Rg3 in RAW264.7 cells via RANKL, JNK and p38 MAPK pathways through a modulation of cathepsin K: an in silico and in vitro study," *Phytotherapy Research*, vol. 29, no. 9, pp. 1286–1294, 2015.
  - [23] B. Cheng, J. Li, J. Du, X. Lv, L. Weng, and C. Ling, "Ginsenoside Rb1 inhibits osteoclastogenesis by modulating NF- $\kappa$ B and MAPKs pathways," *Food and Chemical Toxicology*, vol. 50, no. 5, pp. 1610–1615, 2012.
  - [24] F. Cong, J. Liu, C. Wang et al., "Ginsenoside Rb2 inhibits osteoclast differentiation through nuclear factor-kappaB and signal transducer and activator of transcription protein 3 signaling pathway," *Biomedicine & Pharmacotherapy*, vol. 92, pp. 927–934, 2017.
  - [25] L. Du, M. N. Nong, J. M. Zhao, X. M. Peng, S. H. Zong, and G. F. Zeng, "Polygonatum sibiricum polysaccharide inhibits osteoporosis by promoting osteoblast formation and blocking osteoclastogenesis through Wnt/ $\beta$ -catenin signaling pathway," *Science Report*, vol. 6, Article ID 32261, 2016.
  - [26] X. Peng, J. He, J. Zhao et al., "Polygonatum sibiricum polysaccharide promotes osteoblastic differentiation through the ERK/GSK-3 $\beta$ / $\beta$ -catenin signaling pathway in vitro," *Rejuvenation Research*, vol. 21, no. 1, pp. 44–52, 2018.
  - [27] B. Li, P. Wu, W. Fu et al., "The role and mechanism of miRNA-1224 in the polygonatum sibiricum polysaccharide regulation of bone marrow-derived macrophages to osteoclast differentiation," *Rejuvenation Research*, vol. 22, no. 5, pp. 420–430, 2019.
  - [28] H. Zhang, L. Zheng, and Z. Yuan, "Lycium barbarum polysaccharides promoted proliferation and differentiation in osteoblasts," *Journal of Cellular Biochemistry*, vol. 120, no. 4, pp. 5018–5023, 2019.
  - [29] W.-Q. Liang, G.-J. Xu, D. Weng, B. Gao, X.-F. Zheng, and Y. Qian, "Anti-osteoporotic components of *Rubus chingii*," *Chemistry of Natural Compounds*, vol. 51, no. 1, pp. 47–49, 2015.
  - [30] Y. Su, Y. Chen, Y. Liu et al., "Antiosteoporotic effects of alpinia officinarum hance through stimulation of osteoblasts associated with antioxidant effects," *Journal of Orthopaedic Translation*, vol. 4, pp. 75–91, 2016.
  - [31] K. S. Shim, C. J. Lee, N. H. Yim, M. J. Gu, and J. Y. Ma, "Alpinia officinarum stimulates osteoblast mineralization and inhibits osteoclast differentiation," *American Journal of Chinese Medicine*, vol. 44, no. 6, pp. 1255–1271, 2016.
  - [32] J. Li, L. Hao, J. Wu, J. Zhang, and J. Su, "Linarin promotes osteogenic differentiation by activating the BMP-2/RUNX2 pathway via protein kinase a signaling," *International Journal of Molecular Medicine*, vol. 37, no. 4, pp. 901–910, 2016.
  - [33] S. Yao, L. Liao, J. Qin, and H. Wei, "Mogrosin V promotes bone formation by stimulating osteoblast proliferation and

- differentiation," *Chinese Journal of Tissue Engineering Research*, vol. 23, no. 29, pp. 4701–4706, 2019.
- [34] Z. Nie, S. Deng, L. Zhang, S. Chen, Q. Lu, and H. Peng, "Crocin protects against dexamethasone-induced osteoblast apoptosis by inhibiting the ROS/Ca<sup>2+</sup>-mediated mitochondrial pathway," *Molecular Medicine Reports*, vol. 20, no. 1, pp. 401–408, 2019.
- [35] F. Kalalinia, H. Ghasim, S. Amel Farzad, E. Pishavar, M. Ramezani, and M. Hashemi, "Comparison of the effect of crocin and crocetin, two major compounds extracted from saffron, on osteogenic differentiation of mesenchymal stem cells," *Life Sciences*, vol. 208, pp. 262–267, 2018.
- [36] L. Shi, S. Zhao, Q. Chen, Y. Wu, J. Zhang, and N. Li, "Crocin inhibits RANKL-induced osteoclastogenesis by regulating JNK and NF- $\kappa$ B signaling pathways," *Molecular Medicine Reports*, vol. 17, no. 6, pp. 7947–7951, 2018.
- [37] R. S. Yang, Y. H. Lu, W. Chiang, and S. H. Liu, "Osteoporosis prevention by adlay (yī yī: the seeds of coix lachryma-jobi L. Var. ma-yuen stapf) in a mouse model," *Journal of Traditional and Complementary Medicine*, vol. 3, no. 2, pp. 134–138, 2013.
- [38] R. S. Yang, W. Chiang, Y. H. Lu, and S. H. Liu, "Evaluation of osteoporosis prevention by adlay using a tissue culture model," *Asia Pacific Journal of Clinical Nutrition*, vol. 17, no. 1, pp. 143–146, 2008.
- [39] D. Huang, X. Deng, Y. Wu, Z. Lin, and L. Zeng, "Preventive effect of essential oil of *Houttuynia cordata* on osteoporosis in ovariectomized mice and its mechanism," *Central South Pharmacy*, vol. 17, no. 1, pp. 25–29, 2019.
- [40] H. Liu, Y. Zhong, and D. Wu, "Inhibitory effect of *Prunella vulgaris* L. flavonoids on osteoporosis in ovariectomized rats," *Modern Food Science and Technology*, vol. 30, no. 8, pp. 6–11, 2014.
- [41] M. Rivera-Huerta, V. L. Lizárraga-Grimes, I. G. Castro-Torres et al., "Functional effects of prebiotic fructans in colon cancer and calcium metabolism in animal models," *BioMed Research International*, vol. 2017, Article ID 9758982, 10 pages, 2017.
- [42] M. B. Roberfroid, J. Cumps, and J. P. Devogelaer, "Dietary chicory inulin increases whole-body bone mineral density in growing male rats," *Journal of Nutrition*, vol. 132, no. 12, pp. 3599–3602, 2002.
- [43] C. Demigné, H. Jacobs, C. Moundras et al., "Comparison of native or reformulated chicory fructans, or non-purified chicory, on rat cecal fermentation and mineral metabolism," *European Journal of Nutrition*, vol. 47, no. 7, pp. 366–374, 2008.
- [44] W. G. Hozayen, M. A. El-Desouky, H. A. Soliman, R. R. Ahmed, and A. K. Khaliefa, "Antiosteoporotic effect of petroselinum crispum, ocimum basilicum and *Cichorium intybus* L. in glucocorticoid-induced osteoporosis in rats," *BMC Complementary and Alternative Medicine*, vol. 16, no. 165, pp. 1–11, 2016.
- [45] U. Avsar, E. Karakus, Z. Halici et al., "Prevention of bone loss by panax ginseng in a rat model of inflammation-induced bone loss," *Cellular and Molecular Biology*, vol. 59, no. Suppl, pp. OL1835–OL1841, 2013.
- [46] H. J. Kim, K. H. Park, D. H. Kim, H. J. Chae, G. H. Sung, and Y. O. Kim, "In vitro assessments of bone microcomputed tomography in an aged male rat model supplemented with *Panax ginseng*," *Saudi Journal of Biological Sciences*, vol. 25, no. 6, pp. 1135–1139, 2018.
- [47] H. Y. Jao, J. D. Hsu, Y. R. Lee, C. S. Lo, and H. J. Lee, "Mulberry water extract regulates the osteoblast/osteoclast balance in an ovariectomic rat model," *Food & Function*, vol. 7, no. 12, pp. 4753–4763, 2016.
- [48] G. F. Zeng, Z. Y. Zhang, L. Lu et al., "Protective effects of polygonatum sibiricum polysaccharide on ovariectomy-induced bone loss in rats," *Journal of Ethnopharmacology*, vol. 136, no. 1, pp. 224–229, 2011.
- [49] S. Ye and Y. Li, "Effect of polysaccharide on bone repair and bone metabolic factor in rats with osteoporotic fracture," *Chinese Journal of Clinical Pharmacology*, vol. 35, no. 18, pp. 2128–2131, 2019.
- [50] M. H. Kim, J. E. Lee, J. S. Lee, and W. M. Yang, "Improvement of osteoporosis by lycium chinense administration in ovariectomized mice," *Journal of the Chinese Medical Association*, vol. 80, no. 4, pp. 222–226, 2017.
- [51] S. Karmakar, M. Choudhury, A. S. Das, A. Maiti, S. Majumdar, and C. Mitra, "Clove (*Syzygium aromaticum* Linn) extract rich in eugenol and eugenol derivatives shows bone-preserving efficacy," *Natural Product Research*, vol. 26, no. 6, pp. 500–509, 2012.
- [52] P. C. Cao, W. X. Xiao, Y. B. Yan et al., "Preventive effect of crocin on osteoporosis in an ovariectomized rat model," *Evidence-Based Complementary and Alternative Medicine*, vol. 2014, Article ID 825181, 11 pages, 2014.
- [53] M. M. Algandaby, "Crocin attenuates metabolic syndrome-induced osteoporosis in rats," *Journal of Food Biochemistry*, vol. 43, no. 7, Article ID e12895, 2019.
- [54] S. Sungkamanee, J. Wattanathorn, S. Muchimapura, and W. Thukham-Mee, "Antiosteoporotic effect of combined extract of morus alba and polygonum odoratum," *Oxidative Medicine and Cellular Longevity*, vol. 2014, Article ID 579305, 9 pages, 2014.
- [55] H. Liao, L. K. Banbury, and D. N. Leach, "Antioxidant activity of 45 Chinese herbs and the relationship with their TCM characteristics," *Evidence-Based Complementary and Alternative Medicine*, vol. 5, no. 4, pp. 429–434, 2008.
- [56] D. C. Tang, *Science of Chinese Materia Medica*, House of Shanghai University of Traditional Chinese Medicine, Shanghai, China, 2003.
- [57] Z. Ma, X. Li, Y. Chen et al., "Comprehensive evaluation of the combined extracts of epimedii folium and ligustri lucidi fructus for PMOP in ovariectomized rats based on MLP-ANN methods," *Journal of Ethnopharmacology*, vol. 268, Article ID 113563, 2021.
- [58] R. Ma, R. Zhu, L. Wang et al., "Diabetic osteoporosis: a review of its traditional Chinese medicinal use and clinical and preclinical research," *Evidence-Based Complementary and Alternative Medicine*, vol. 2016, Article ID 3218313, 13 pages, 2016.
- [59] J. G. Ren, D. Z. Wang, L. Lei, L. Kang, and J. X. Liu, "Preliminary analysis on relationship between traditional efficacy of Chinese medicine and modern pharmacological action," *Zhongguo Zhongyao Zazhi*, vol. 42, no. 10, pp. 1979–1983, 2017.
- [60] Q. Q. Wang, S. Han, X. X. Li et al., "Nuezhenide exerts anti-inflammatory activity through the NF- $\kappa$ B pathway," *Current Molecular Pharmacology*, vol. 14, no. 1, pp. 101–111, 2021.
- [61] F. Forouzanfar, H. Hosseinzadeh, M. B. Khorrami, S. Asgharzade, and H. Rakhshandeh, "Attenuating effect of Portulaca oleracea extract on chronic constriction injury induced neuropathic pain in rats: an evidence of anti-oxidative and anti-inflammatory effects," *CNS & Neurological Disorders - Drug Targets*, vol. 18, no. 4, pp. 342–349, 2019.

- [62] Y. Lu, Y. Jiang, L. Ling, Y. Zhang, H. Li, and D. Chen, "Beneficial effects of *Houttuynia cordata* polysaccharides on "two-hit" acute lung injury and endotoxic fever in rats associated with anti-complementary activities," *Acta Pharmaceutica Sinica B*, vol. 8, no. 2, pp. 218–227, 2018.
- [63] K. B. Roh, D. Park, and E. Jung, "Inhibitory effects of *prunella vulgaris* L. extract on 11 $\beta$ -HSD1 in human skin cells," *Evidence-Based Complementary and Alternative Medicine*, vol. 2018, Article ID 1762478, 8 pages, 2018.
- [64] D. Perez-Balladares, M. Castaneda-Teran, M. G. Granda-Albuja et al., "Chemical composition and antioxidant activity of the main fruits, tubers and legumes traditionally consumed in the Andean regions of Ecuador as a source of health-promoting compounds," *Plant Foods for Human Nutrition*, vol. 74, no. 3, pp. 350–357, 2019.
- [65] D. T. Wu, W. Liu, M. L. Xian et al., "Polyphenolic-protein-polysaccharide complexes from *hovenia dulcis*: insights into extraction methods on their physicochemical properties and in vitro bioactivities," *Foods*, vol. 9, no. 4, p. 456, 2020.
- [66] I. C. Nwafor, K. Shale, and M. C. Achilonu, "Chemical composition and nutritive benefits of chicory (*Cichorium intybus*) as an ideal complementary and/or alternative livestock feed supplement," *Scientific World Journal*, vol. 2017, Article ID 7343928, 11 pages, 2017.
- [67] Y. Q. Liu, M. C. Cheng, L. X. Wang, N. Zhao, H. B. Xiao, and Z. T. Wang, "Functional analysis of cultured neural cells for evaluating cold/cool- and hot/warm-natured Chinese herbs," *The American Journal of Chinese Medicine*, vol. 36, no. 4, pp. 771–781, 2008.
- [68] H. W. Liang, T. Y. Yang, C. S. Teng et al., "Mulberry leaves extract ameliorates alcohol-induced liver damages through reduction of acetaldehyde toxicity and inhibition of apoptosis caused by oxidative stress signals," *International Journal of Medical Sciences*, vol. 18, no. 1, pp. 53–64, 2021.
- [69] H. H. Lin, A. L. Charles, C. W. Hsieh, Y. C. Lee, and J. Y. Ciou, "Antioxidant effects of 14 Chinese traditional medicinal herbs against human low-density lipoprotein oxidation," *Journal of Traditional and Complementary Medicine*, vol. 5, no. 1, pp. 51–55, 2015.
- [70] Q. Wu and Y. Hu, "Integrated network pharmacology and molecular docking strategy to explore the mechanism of medicinal and edible *astragalus radix*-*atractylodes macrocephalae rhizoma* acting on pneumonia via immunomodulation," *Journal of Food Biochemistry*, vol. 44, no. 12, Article ID e13510, 2020.
- [71] B. Ma, W. L. Kan, H. Zhu, S. L. Li, and G. Lin, "Sulfur fumigation reducing systemic exposure of ginsenosides and weakening immunomodulatory activity of ginseng," *Journal of Ethnopharmacology*, vol. 195, pp. 222–230, 2017.
- [72] S. B. Kim, B. Y. Chang, Y. H. Jo et al., "Macrophage activating activity of pyrrole alkaloids from *morus alba* fruits," *Journal of Ethnopharmacology*, vol. 145, no. 1, pp. 393–396, 2013.
- [73] Z. Chen, J. Liu, X. Kong, and H. Li, "Characterization and immunological activities of polysaccharides from *polygonatum sibiricum*," *Biological and Pharmaceutical Bulletin*, vol. 43, no. 6, pp. 959–967, 2020.
- [74] J. Cheng, Z. W. Zhou, H. P. Sheng et al., "An evidence-based update on the pharmacological activities and possible molecular targets of *lycium barbarum* polysaccharides," *Drug Design, Development and Therapy*, vol. 9, pp. 33–78, 2015.
- [75] Y. Xi, T. Jiang, J. Yu et al., "Preliminary studies on the anti-osteoporosis activity of baohuoside I," *Biomedicine & Pharmacotherapy*, vol. 115, Article ID 108850, 2019.
- [76] J. Yao, Q. Jiang, X. Zhu et al., "Cytotoxicity and penetration enhancement activity of essential oils from warming the interior medicinals with hot or warm property in terms of Traditional Chinese Medicine," *Journal of Traditional Chinese Medicine*, vol. 38, no. 2, pp. 257–265, 2018.
- [77] J. Dong, X. M. Zhu, F. Y. Wu et al., "Development of galangal essential oil-based microemulsion gel for transdermal delivery of flurbiprofen: simultaneous permeability evaluation of flurbiprofen and 1,8-cineole," *Drug Development and Industrial Pharmacy*, vol. 46, no. 1, pp. 91–100, 2020.
- [78] G. K. Gupta, A. Kumar, V. Khedgikar et al., "Osteogenic efficacy enhancement of kaempferol through an engineered layer-by-layer matrix: a study in ovariectomized rats," *Nanomedicine*, vol. 8, no. 5, pp. 757–771, 2013.
- [79] Y. Guo, Y. Li, L. Xue et al., "*Salvia miltiorrhiza*: an ancient Chinese herbal medicine as a source for anti-osteoporotic drugs," *Journal of Ethnopharmacology*, vol. 155, no. 3, pp. 1401–1416, 2014.
- [80] X. Gong, N. Chen, K. Ren et al., "The fruits of *siraitia grosvenorii*: a review of a Chinese food-medicine," *Frontiers in Pharmacology*, vol. 10, p. 1400, 2019.
- [81] X. Han, X. Ji, H. Zhao et al., "Mechanisms of coix seed compositions in the treatment of spleen deficiency and wet dampness zheng," *African Journal of Traditional, Complementary and Alternative Medicines*, vol. 14, no. 4, pp. 239–246, 2017.
- [82] B. L. Ilesanmi-Oyelere and M. C. Kruger, "Nutrient and dietary patterns in relation to the pathogenesis of postmenopausal osteoporosis—a literature review," *Life*, vol. 10, no. 10, p. 220, 2020.
- [83] L. Holloway, S. Moynihan, S. A. Abrams, K. Kent, A. R. Hsu, and A. L. Friedlander, "Effects of oligofructose-enriched inulin on intestinal absorption of calcium and magnesium and bone turnover markers in postmenopausal women," *The British Journal of Nutrition*, vol. 97, no. 2, pp. 365–372, 2007.
- [84] J. Lavado-García, R. Roncero-Martin, J. M. Moran et al., "Long-chain omega-3 polyunsaturated fatty acid dietary intake is positively associated with bone mineral density in normal and osteopenic Spanish women," *PLoS One*, vol. 13, no. 1, Article ID e0190539, 2018.
- [85] A. E. Griel, P. M. Kris-Etherton, K. F. Hilpert, G. Zhao, S. G. West, and R. L. Corwin, "An increase in dietary n-3 fatty acids decreases a marker of bone resorption in humans," *Nutrition Journal*, vol. 6, no. 2, pp. 1–8, 2007.
- [86] N. Yousefzadeh, K. Kashfi, S. Jeddi, and A. Ghasemi, "Ovariectomized rat model of osteoporosis: a practical guide," *EXCLI Journal*, vol. 19, pp. 89–107, 2020.
- [87] G. Wang, Y. Fu, J. Li et al., "Aqueous extract of *Polygonatum sibiricum* ameliorates ethanol-induced mice liver injury via regulation of the Nrf2/ARE pathway," *Journal of Food Biochemistry*, vol. 45, no. 1, Article ID e13537, 2021.
- [88] N. Yang, D. Liu, X. Zhang et al., "Effects of ginsenosides on bone remodelling for novel drug applications: a review," *Chinese Medicine*, vol. 15, no. 42, pp. 1–15, 2020.
- [89] N. Imerb, C. Thonusin, N. Chattipakorn, and S. C. Chattipakorn, "Aging, obese-insulin resistance, and bone remodeling," *Mechanism of Ageing and Development*, vol. 191, Article ID 111335, 2020.
- [90] M. Tian, L. N. Li, R. R. Zheng, L. Yang, and Z. T. Wang, "Advances on hormone-like activity of *Panax ginseng* and ginsenosides," *Chinese Journal of Natural Medicines*, vol. 18, no. 7, pp. 526–535, 2020.



- [91] J. Wu, Z. Zeng, Y. Li et al., "Cycloastragenol protects against glucocorticoid-induced osteogenic differentiation inhibition by activating telomerase," *Phytotherapy Research*, vol. 35, no. 4, pp. 2034–2044, 2021.
- [92] Y. Jiang, P. Zhang, X. Zhang, L. Lv, and Y. Zhou, "Advances in mesenchymal stem cell transplantation for the treatment of osteoporosis," *Cell Proliferation*, vol. 54, no. 1, Article ID e12956, 2021.
- [93] H. T. Huang, T. L. Cheng, S. Y. Lin et al., "Osteoprotective roles of green tea catechins," *Antioxidants*, vol. 9, no. 11, p. 1136, 2020.
- [94] W. Feng, J. Guo, and M. Li, "RANKL-independent modulation of osteoclastogenesis," *Journal of Oral Biosciences*, vol. 61, no. 1, pp. 16–21, 2019.
- [95] S. K. Wong, K. Y. Chin, and S. Ima-Nirwana, "Quercetin as an agent for protecting the bone: a review of the current evidence," *International Journal of Molecular Sciences*, vol. 21, no. 7, p. 6648, 2020.
- [96] X. W. Liu, B. Ma, Y. Zi, L. B. Xiang, and T. Y. Han, "Effects of rutin on osteoblast MC3T3-E1 differentiation, ALP activity and Runx2 protein expression," *European Journal of Histochemistry*, vol. 65, no. 1, p. 3159, 2021.
- [97] A. R. Sharma and J. S. Nam, "Kaempferol stimulates WNT/ $\beta$ -catenin signaling pathway to induce differentiation of osteoblasts," *Journal of Nutritional Biochemistry*, vol. 74, Article ID 108228, 2019.
- [98] C. M. Rassi, M. Lieberherr, G. Chaumaz, A. Pointillart, and G. Cournot, "Modulation of osteoclastogenesis in porcine bone marrow cultures by quercetin and rutin," *Cell and Tissue Research*, vol. 319, no. 3, pp. 383–393, 2005.
- [99] I. Z. Akbar, F. R. P. Dewi, and B. Setiawan, "In silico interaction of the active compounds of *scurrula atropurpurea* with the RANK/RANKL/OPG system in diabetoporosis," *Acta Informatica Medica*, vol. 27, no. 1, pp. 8–11, 2019.
- [100] J. Xu, H. F. Wu, E. S. M. Ang et al., "NF-kappaB modulators in osteolytic bone diseases," *Cytokine & Growth Factor Reviews*, vol. 20, no. 1, pp. 7–17, 2009.
- [101] T. W. Kyung, J. E. Lee, H. H. Shin, and H. S. Choi, "Rutin inhibits osteoclast formation by decreasing reactive oxygen species and TNF-alpha by inhibiting activation of NF-kappaB," *Experimental & Molecular Medicine*, vol. 40, no. 1, pp. 52–58, 2008.
- [102] H. R. Kim, B. M. Kim, J. Y. Won et al., "Quercetin, a plant polyphenol, has potential for the prevention of bone destruction in rheumatoid arthritis," *Journal of Medicinal Food*, vol. 22, no. 2, pp. 152–161, 2019.
- [103] Y. Hou and J. G. Jiang, "Origin and concept of medicine food homology and its application in modern functional foods," *Food & Function*, vol. 4, no. 12, pp. 1727–1741, 2013.
- [104] J. Zheng, B. Lu, and B. Xu, "An update on the health benefits promoted by edible flowers and involved mechanisms," *Food Chemistry*, vol. 340, Article ID 127940, 2021.
- [105] J. Perović, V. Tumbas Šaponjac, J. Kojić et al., "Chicory (*Cichorium intybus* L.) as a food ingredient—nutritional composition, bioactivity, safety, and health claims: a review," *Food Chemistry*, vol. 336, Article ID 127676, 2021.
- [106] A. G. Pereira, M. Fraga-Corral, P. García-Oliveira et al., "Culinary and nutritional value of edible wild plants from northern Spain rich in phenolic compounds with potential health benefits," *Food & Function*, vol. 11, no. 10, pp. 8493–8515, 2020.
- [107] "Announcement of the state administration for market regulation on revising and publishing the classification catalogue of food production license," 2021, [http://www.gov.cn:8080/zhengce/zhengceku/2020-03/27/content\\_5496236.htm](http://www.gov.cn:8080/zhengce/zhengceku/2020-03/27/content_5496236.htm).
- [108] T. Nisar, X. Yang, A. Alim, M. Iqbal, Z. C. Wang, and Y. Guo, "Physicochemical responses and microbiological changes of bream (*Megalobrama ambycephala*) to pectin based coatings enriched with clove essential oil during refrigeration," *International Journal of Biological Macromolecules*, vol. 124, pp. 1156–1166, 2019.
- [109] C. Tan, C. Wu, Y. Huang, C. Wu, and H. Chen, "Identification of different species of zanthoxyl pericarpium based on convolution neural network," *PLoS One*, vol. 15, no. 4, Article ID e0230287, 2020.
- [110] M. A. Farag, N. Hegazi, E. Dokhalahy, and A. R. Khattab, "Chemometrics based GC-MS aroma profiling for revealing freshness, origin and roasting indices in saffron spice and its adulteration," *Food Chemistry*, vol. 331, Article ID 127358, 2020.
- [111] S. Upadhyay, P. K. Tripathi, M. Singh, S. Raghavendhar, M. Bhardwaj, and A. K. Patel, "Evaluation of medicinal herbs as a potential therapeutic option against SARS-CoV-2 targeting its main protease," *Phytotherapy Research*, vol. 34, no. 12, pp. 3411–3419, 2020.
- [112] H. Li, Z. Yang, Q. Zeng et al., "Abnormal expression of bHLH3 disrupts a flavonoid homeostasis network, causing differences in pigment composition among mulberry fruits," *Horticulture Research*, vol. 7, no. 83, pp. 1–19, 2020.
- [113] J. Sangsopha, N. P. Johns, J. Johns, and A. Moongngarm, "Dietary sources of melatonin and benefits from production of high melatonin pasteurized milk," *Journal of Food Science & Technology*, vol. 57, no. 6, pp. 2026–2037, 2020.
- [114] E. M. Sánchez-Salcedo, M. Tassotti, D. Del Rio, F. Hernández, J. J. Martínez, and P. Mena, "(Poly)phenolic fingerprint and chemometric analysis of white (*Morus alba* L.) and black (*Morus nigra* L.) mulberry leaves by using a non-targeted UHPLC-MS approach," *Food Chemistry*, vol. 212, pp. 250–255, 2016.
- [115] D. Hu, Y. Xu, J. Xie, C. Sun, X. Zheng, and W. Chen, "Systematic evaluation of phenolic compounds and protective capacity of a new mulberry cultivar J33 against palmitic acid-induced lipotoxicity using a simulated digestion method," *Food Chemistry*, vol. 258, pp. 43–50, 2018.
- [116] H. Du, S. S. Li, Q. Wu et al., "Analysis of active compounds and antioxidant activity assessment of six popular Chinese juhua teas," *Natural Product Communications*, vol. 10, no. 3, pp. 495–498, 2015.
- [117] I. A. Khan, W. Xu, D. Wang et al., "Antioxidant potential of chrysanthemum morifolium flower extract on lipid and protein oxidation in goat meat patties during refrigerated storage," *Journal of Food Science*, vol. 85, no. 3, pp. 618–627, 2020.
- [118] M. Abdel-Hamid, E. Romeih, Z. Huang, T. Enomoto, L. Huang, and L. Li, "Bioactive properties of probiotic set-yogurt supplemented with *Siraitia grosvenorii* fruit extract," *Food Chemistry*, vol. 303, Article ID 125400, 2020.
- [119] C. K. Chan, G. Pan, and W. Chan, "Analysis of aristolochic acids in *houuttynia cordata* by liquid chromatography-tandem mass spectrometry," *Journal of Mass Spectrometry*, vol. 56, no. 4, p. e4652, 2020.
- [120] Q. Ma, R. Wei, Z. Wang et al., "Bioactive alkaloids from the aerial parts of *houuttynia cordata*," *Journal of Ethnopharmacology*, vol. 195, pp. 166–172, 2017.

- [121] W. Sakuludomkan, R. Yeewa, S. Subhawa, C. Khanaree, A. I. Bonness, and T. Chewonarin, "Effects of fermented *Houttuynia cordata* thunb. on diabetic rats induced by a high-fat diet with streptozotocin and on insulin resistance in 3T3-L1 adipocytes," *Journal of Nutrition and Metabolism*, vol. 2021, Article ID 6936025, 15 pages, 2021.
- [122] Z. Qu, J. Zhang, H. Yang et al., "*Prunella vulgaris* L., an edible and medicinal plant, attenuates scopolamine-induced memory impairment in rats," *Journal of Agricultural and Food Chemistry*, vol. 65, no. 2, pp. 291–300, 2017.
- [123] H. Kim, Y. J. Kim, H. Y. Jeong et al., "A standardized extract of the fruit of *hovenia dulcis* alleviated alcohol-induced hangover in healthy subjects with heterozygous ALDH2: a randomized, controlled, crossover trial," *Journal of Ethnopharmacology*, vol. 209, pp. 167–174, 2017.
- [124] K. Tkacz, A. Wojdyło, I. P. Turkiewicz, and P. Nowicka, "Anti-diabetic, anti-cholinesterase, and antioxidant potential, chemical composition and sensory evaluation of novel sea buckthorn-based smoothies," *Food Chemistry*, vol. 338, Article ID 128105, 2021.
- [125] C. Lin, S. M. Cao, E. T. Chang et al., "Chinese nonmedicinal herbal diet and risk of nasopharyngeal carcinoma: a population-based case-control study," *Cancer*, vol. 125, no. 24, pp. 4462–4470, 2019.
- [126] M. Sadeghian, S. Rahmani, M. Zendejdel, S. A. Hosseini, and A. Zare Javid, "Ginseng and cancer-related fatigue: a systematic review of clinical trials," *Nutrition and Cancer*, vol. 73, no. 8, pp. 1270–1281, 2021.
- [127] S. Huang, H. Yuan, W. Li et al., "*Polygonatum sibiricum* polysaccharides protect against MPP-Induced neurotoxicity via the Akt/mTOR and Nrf2 pathways," *Oxidative Medicine and Cellular Longevity*, vol. 2021, Article ID 8843899, 13 pages, 2021.

## Research Article

# Inhibitory Potential of Shen-Shuai-Ling Formulation on Renal Interstitial Fibrosis via Upregulation of PLZF

Na Song,<sup>1</sup> Haitao Tu,<sup>2</sup> Ying Li ,<sup>3</sup> Weijian Xiong,<sup>3</sup> Ling Zhang,<sup>3</sup> Hong Liu,<sup>3</sup> Weisen Ding,<sup>3</sup> Mei Long,<sup>3</sup> Dewei Ren,<sup>3</sup> and Jin Zhong<sup>3</sup>

<sup>1</sup>Department of Oncology, Chongqing Hospital of Traditional Chinese Medicine, Chongqing 400021, China

<sup>2</sup>Department of Nephrology, The First Affiliated Hospital of Guangzhou University of Chinese Medicine, Guangzhou 510405, China

<sup>3</sup>Department of Nephrology, Chongqing Hospital of Traditional Chinese Medicine, Chongqing 400021, China

Correspondence should be addressed to Ying Li; ylv219752@163.com

Received 2 November 2021; Accepted 27 January 2022; Published 31 March 2022

Academic Editor: Ruchika Garg

Copyright © 2022 Na Song et al. This is an open access article distributed under the Creative Commons Attribution License, which permits unrestricted use, distribution, and reproduction in any medium, provided the original work is properly cited.

**Background.** Renal interstitial fibrosis (RIF) is an important cause of kidney disease, which seriously affects people's health. As a traditional Chinese medicine, Shen-Shuai-Ling Formulation (SSLF) has obvious kidney function. However, the therapeutic effect of SSLF on RIF and its molecular mechanism are still unclear. **Methods.** First, the potential targets and pathways of SSLF for RIF were predicted by network pharmacology, and then, the binding of luteolin and target protein to SSLF was verified by molecular docking and Co-IP experiments. Finally, the effects of SSLF and luteolin on PLZF and (Pro) renin receptor (PRR) were verified by western blot and qPCR experiments. Angiotensin (Ang)-1, Ang-2, and transforming growth factor- $\beta$  (TGF- $\beta$ ) were the indexes of renal interstitial fibrosis. **Results.** Through the drug-active component-target network diagram, we found that luteolin has the most connections, and promyelocytic leukemia zinc finger (PLZF) is the target protein. GO analysis and KEGG pathway analysis of targets were performed using Cytoscape ClueGO. Molecular docking experiments and Co-IP are used to prove that luteolin and PLZF can be combined. Western blot and qPCR results showed that both SSLF and luteolin significantly upregulated the expression of PLZF and decreased the levels of PRR, Ang-1, Ang-2, and TGF- $\beta$ . The overexpression of PLZF decreased the expression of PRR, the knockdown of PLZF increased the expression of PRR, and the overexpression of PRR decreased the expression of Ang-1, Ang-2, and TGF- $\beta$ . **Conclusions.** SSLF inhibits PRR and renal interstitial fibers by the upregulation of PLZF levels.

## 1. Introduction

Chronic kidney disease (CKD) is a disease in which renal structural or functional abnormalities last longer than 3 months. RIF is a common pathological feature of CKD. RIF is the replacement of normal tissue by fibrous tissue and renal failure following chronic and persistent renal injury. Inhibition of RIF is significant in the treatment of CKD.

Excessive accumulation of extracellular matrix (ECM) in the kidneys is an important cause of RIF [1, 2]. TGF- $\beta$  plays a key role in regulating the upstream factors produced by ECM. Ang-2 is of great significance in regulating TGF- $\beta$  upstream factors. PRR plays an important role in regulating

the production of Ang-2 [3]. In 2002, a new member of the PRR upstream of the renin-angiotensin system (RAS) was found to be located primarily on the cell surface and at cell intervals, particularly perinuclear spaces [4, 5]. PRR is involved in the production of Ang-2 mainly through two pathways: proteolytic pathway and nonproteolytic pathway [6, 7].

PLZF is also known as zinc finger and BTB (Broad-complex, Tramtrack, and Bric-a-brac) domain containing 16 (ZBTB16) or zinc finger protein 145 (Zfp145). In humans, the PLZF gene is located at position 23 (11q23) of the long arm of chromosome 11, and the gene expression product is a transcription factor composed of 673 amino acids [8, 9]. It is

highly conserved in humans, mice, and rats. PLZF is a transcription factor that can act as both a transcriptional inhibitor and a transcriptional activator, and the mechanism of its activation is not known at present. Meanwhile, it has not been elucidated whether PLZF acts as an activator or as a determinant of repression. It is found that renin-treated HEK293 cells can cause PLZF nuclear translocation, and then, PLZF is recruited into the promoter of the PRR gene, which inhibits PRR transcription.

SSLF is a prescription developed by Xin Zheng, a master of traditional Chinese medicine with more than 60 years of clinical experience [10]. SSLF has apparent effects on improving renal function and delaying the progression of CKD and can significantly relieve clinical symptoms such as constipation and abdominal distension.

To study SSLF's functional mechanism and understand its potential inhibitory role in renal fibrosis, we first predicted the possible targets and pathways of SSLF for renal fibrosis using network pharmacology molecular docking, and then, we used molecular docking and Co-IP experiments to verify the binding of SSLF and its luteolin to target proteins. Finally, western blot and qPCR experiments were used to find the mechanism of SSLF and luteolin in inhibiting renal fibrosis.

## 2. Materials and Methods

**2.1. Experimental Herbal Formulation.** SSLF is composed of Herba Rhubarb (DH), Herba Codonopsis pilosula (DS), Herba Astragalus membranaceus (HQ), Herba Stony dragon (ML), Herba Safflower (HH), Herba Ganoderma lucidum (JLZ), Herba Angelica sinensis (DG), Herba Salvia miltiorrhiza (RS), Herba Epimedium (YYH), and Herba Dandelion (PGY). SSLF used in our research was processed by the Chongqing Institute of Traditional Chinese Medicine (Chongqing, China).

**2.2. Cell Cultures and Experimental Treatments.** Human kidney 2 (HK-2) cells were purchased from the American Type Culture Collection (ATCC) (Manassas, USA). HK-2 cells were cultured in DMEM/F12 medium (Gibco). In addition, ten 6-week-old male SD rats were given 20 mg/kg SSLF intragastrically for 7 days. The animal experiment was approved by the Animal Ethics Committee of the Chongqing Hospital of Traditional Chinese Medicine. Rats were euthanized, and serum was collected on day 8. HK-2 cells were seeded and exposed to drug-containing serum or blank serum for 24 hours. HK-2 cells were treated with 10 ng/ml TGF- $\beta$  and 100 nM renin for 24 hours.

**2.3. Network Pharmacology-Based Analysis.** The active components of SSLF were retrieved from the website <http://www.swisstargetprediction.ch/>. The genes related to human RIF were selected from the GeneCards (<https://www.genecards.org/>) disease database. The PPI network was constructed by STRING database (<https://string-db.org/>), and the drug-component-target network was constructed by Cytoscape 3.6.0. The GO analysis and KEGG pathway analysis were performed on 86

target sites with Cytoscape ClueGO, and the enrichment analysis results were visualized.

**2.4. Molecular Docking.** The 3D structure of luteolin was obtained from the TCMSP (<https://tcmsp.com/tcmsp.php>), the 3D structure of the key target protein was retrieved from the Protein Data Bank (<http://www.rcsb.org/pdb>), the receptor protein was hydrogenated by AutoDock 4.2.6 software, the charge was calculated, and the receptor protein and ligand molecules were molecularly docked by AutoDock Vina 1.1.2. The confirmation was obtained by docking, the binding energy was scored, and the best binding energy was obtained for graph analysis. PyMOL was used as a three-dimensional graph to show the interaction between the receptor protein and a small molecule of ligand.

**2.5. Western Blot Analysis.** Cells were collected and added to RIPA lysate including PMSF and proteinase inhibitor cocktail. The supernatant was transferred into a precooled 1.5 mL centrifuge tube and centrifuged at 13000 rpm for 20 min for concentration determination. 30  $\mu$ g/well of total protein was boiled at 100°C for 10 min, separated by 10% polyacrylamide gel electrophoresis (SPS-PAGE), then transferred to a PDVF membrane, closed with 5% skim milk for 1 h at room temperature, and washed 3 times with TBST, 5 min each time. 3% BSA primary antidilution solution was diluted with 1:1000~2000, incubated at 4°C overnight, and incubated with secondary antidilution solution (1:1000) for 1 h on the next day.

**2.6. Coimmunoprecipitation.** Luteolin was labeled with biotin by EZ-Link™ Biotin-LC-Hydrazide (Thermo Scientific). After 24 h incubation, the cells were collected by centrifugation and precooled RIPA buffer was added. The suspension was centrifuged for 15 min. The protein A agarose beads were added and centrifuged for 15 minutes to remove the protein A agarose beads. Add rabbit anti at 4°C overnight. Protein A agarose beads were added to capture the antigen-antibody complex at 4°C overnight. Agarose beads-antigen antibody complexes were collected by centrifugation. The samples were boiled for 5 min. After boiling, the samples were detected by SDS-PAGE electrophoresis.

**2.7. qPCR.** Total RNA was extracted from the sample using TRIzol reagent (Takara, Japan). cDNA was reverse-transcribed using the PrimeScript™ RT kit (Takara, Japan). The response system and procedures for qRT-PCR are described in the instructions of the TB Green Premix Ex Taq II (Takara, Japan), using the CFX96 Real-Time System (Bio-Rad, USA). The relative expression level of genes was calculated by the  $2^{-\Delta\Delta CT}$  algorithm. Primer sequence of each gene is as follows: PLZF-F(GCTACTGTGCAAGGCCAAC CA), PLZF-R(GCGGTGGAAGAGGATCTCAAACA), PRR-F (GGTAGGGAAGGCAAACCTCAGTG), PRR-R(ATTGA GGGGGAGTGAACCTGAGAAC), Ang-1-F(AAGATTGCT TCAGCCAGCGTC), Ang-1-R(AGGTGACTTTGGCTAC

AAGCATTGT), Ang-2-F(TTCAACCTCGCTGTGGCTGA), Ang-2-R(AACTTTGCACATCACAGGTCCAA), TGF- $\beta$ 1-F(AATACAGCAACAATTCCTGGCGA), TGF- $\beta$ 1-R(CG CAACTCCGGTGACATCAA), GAPDH-F(CTGGGC TACTGAGCACC), and GAPDH-R(AAGTGGTCGTTG AGGGCAATG).

**2.8. Statistical Analysis.** SPSS 23.0 was used to analyze the data. The mean of two groups of independent samples was compared by *t*-test, and the mean of multiple groups of samples was analyzed by one-way ANOVA ( $p < 0.05$ ). All the experiments were repeated three times independently, and the results are expressed as the mean value  $\pm$  standard deviation.

### 3. Results

**3.1. Common Targets and Network Visualization of SSLF and RIF.** In order to study the role of SSLF in RIF, we first predicted 747 targets of SSLF active components in the SwissTargetPrediction database, screened 414 targets of RIF-related genes in the GeneCards database, and obtained 86 intersection genes by intersection analysis (Figure 1(a)). Then we use UpSet plot to visualize the intersection gene between the components of SSLF (Figure 1(b)). We use the STRING database to obtain the protein-interaction network and put the network into the Cytoscape 3.6 to obtain the visual protein interaction network diagram (Figure 1(c)). The network diagram shows that STAT3, VEGFA, and AKT1 are in the central position. Finally, we use Cytoscape 3.6 to analyze SSLF and its components and targets and draw a drug-active component-target network diagram. We find that luteolin has the most connections, and PLZF is the target protein (Figure 1(d)).

**3.2. GO and KEGG Pathway Enrichment Analyses.** In order to explore the function of SSLF and the role of potential targets in signaling pathways, we used Cytoscape ClueGO to analyze 86 targets by GO and KEGG pathway and visualized the enrichment analysis results. The GO enrichment analysis shows that, in biological process (BP), it is related to acute inflammatory response, hormone metabolic process, positive regulation of protein localization to the membrane, and negative regulation of gene silencing by RNA (Figure 2(a)). In molecular function (MF), it is associated with the regulation of protein binding, protein phosphatase binding, and growth factor receptor binding (Figure 2(b)). In cellular component (CC), it may be associated with membrane microdomain, clathrin-coated vesicle membrane, and basal plasma membrane (Figure 2(c)). Analysis of the KEGG pathway revealed that 86 potential targets of SSLF for renal fibrosis were primarily associated with the PI3K-Akt signaling pathway, the Rap1 signaling pathway, and the HIF-1 signaling pathway (Figure 2(d)).

**3.3. Interaction between Luteolin and Target Protein.** In order to investigate the effect of luteolin in SSLF on PLZF and core target protein, we first select the key component luteolin and

core target genes AKT1 (PDB ID : 1UNQ), VEGFA (PDB ID : 3V2A), STAT3 (PDB ID : 4ZIA), and PLZF (PDB ID : 1BUO) for molecular docking. The binding energies of luteolin and core target proteins were 5.58 kcal/mol (AKT1), 5.25 kcal/mol (VEGFA), 4.08 kcal/mol (STAT3), and 6.48 kcal/mol (PLZF). The amino acid residues (LEU29, ARG28, ALA47, and LEU84) of luteolin and PLZF form hydrogen bonds. The amino acid residues of luteolin and PLZF (ALA-30, GLY-31, GYS-34, GLU-85, GEN-81, HIS-46, and PHE-45) form hydrophobic interactions (Figures 3(a)–3(d)). To verify the relationship between luteolin and PLZF and its target proteins, we labeled luteolin with biotin and observed whether luteolin could bind to PLZF and other target proteins. The Co-IP results show that luteolin can be combined with PLZF (Figure 3(e)). Therefore, we wondered whether SSLF and luteolin could inhibit renal fibrosis by regulating PLZF.

**3.4. SSLF and Luteolin Upregulate PLZF Levels in HK-2 Cells.** In order to verify whether SSLF can regulate PLZF, we first added renin to induce fibrosis of HK-2 cells. The experiment was divided into two groups: the control group and the model group. The model group was divided into three groups. The first group was low-dose SSLF (20% of rat serum concentration) and the second group was medium-dose SSLF (40% of rat serum concentration). The third group was high-dose SSLF (60% of rat serum concentration). The effect of SSLF sum on PLZF was detected by western blot experiment and qPCR experiment. The western blot results showed that SSLF significantly upregulated the expression of PLZF and decreased the levels of PRR, Ang-1, Ang-2, and TGF- $\beta$ . The qPCR results were consistent with the western blot results (Figures 4(a) and 4(b)). Similarly, the results showed that luteolin could upregulate the expression of PLZF and decrease the levels of PRR, Ang-1, Ang-2, and TGF- $\beta$  (Figures 4(c) and 4(d)). Recently, it has been found that renin in HEK293 cells can cause nuclear translocation of PLZF, and then PLZF is recruited to the promoter of the PRR gene, which inhibits PRR transcription. We have confirmed that luteolin can bind to PLZF, and we suspect that luteolin can regulate downstream fibrosis by upregulating PLZF to inhibit PRR expression.

**3.5. PLZF Reduced the Levels of Ang-1, Ang-2, and TGF- $\beta$  by Inhibiting PRR in HK-2 Cells.** In order to study the effect of PLZF on the PRR of a downstream target gene, we first constructed an overexpression cell model and a knockdown model of PLZF. We used western blot and qPCR experiments to verify the effect of PLZF on PRR. The results showed that overexpression of PLZF could decrease the expression level of PRR, knockdown of PLZF could increase the expression level of PRR, and the expression levels of Ang-1, Ang-2, and TGF- $\beta$  were consistent with those of PRR (Figures 5(a) and 5(b)). It was found that renin-treated HEK293 cells resulted in PLZF nuclear translocation, and then PLZF was recruited to the promoter of the PRR gene, which inhibited PRR transcription.

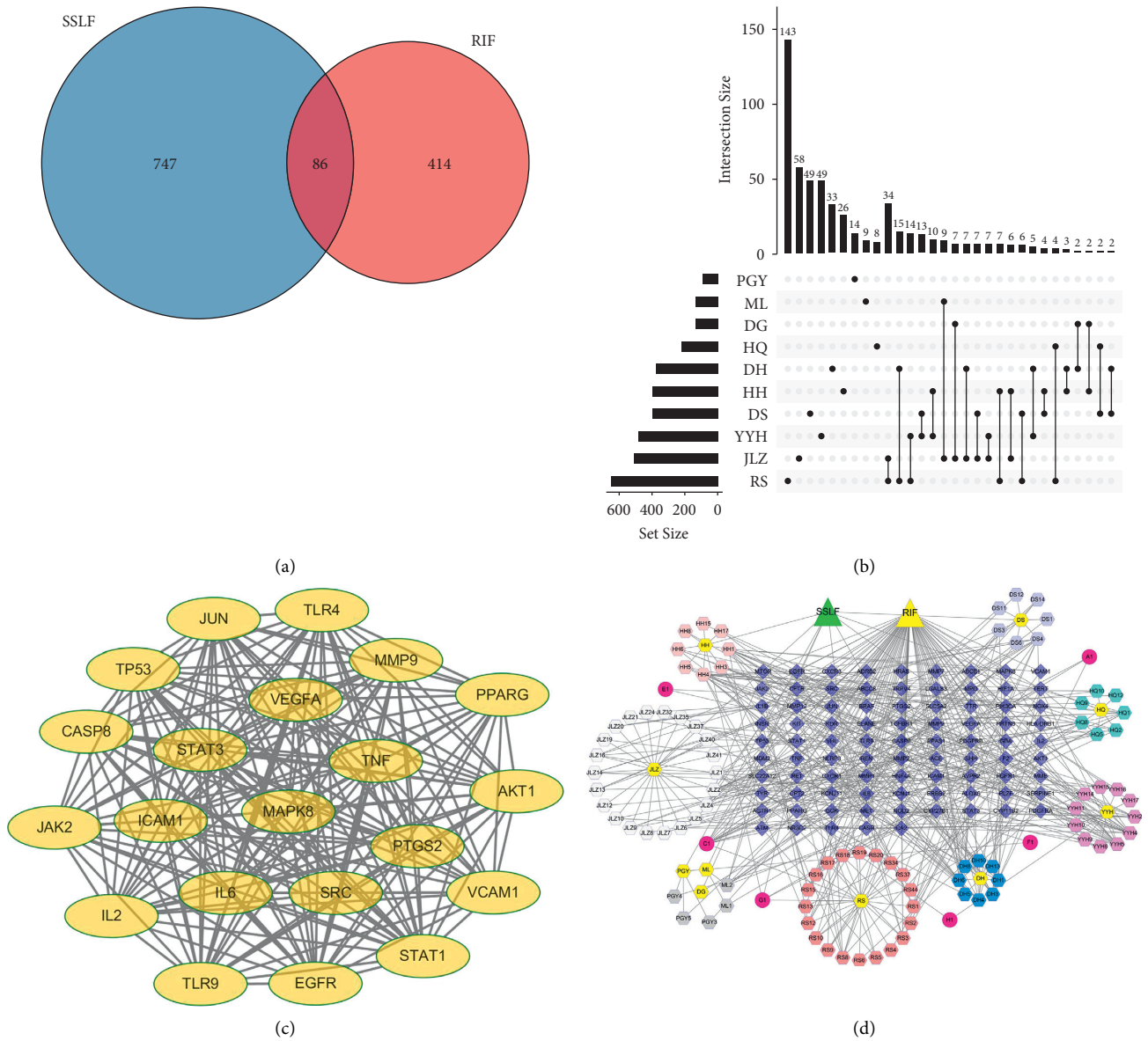


FIGURE 1: Analysis of key components and core targets of SSLF therapy for RIF based on network pharmacology. (a) Venn diagram of the intersection gene between SSLF and RIF target. (b) Venn diagram of the target intersection gene. (c) Protein-protein interaction network. Edges represent protein-protein interactions. (d) SSLF-compound-target-RIF network. In this network, the blue diamonds represent candidate targets of SSLF against RIF, and the yellow hexagon represents active compounds in SSLF.

To verify whether PLZF inhibits PRR expression, we induced fibrosis in HK-2 cells with renin and found that the addition of the positive drug TGF- $\beta$  reduced PLZF levels and increased the index of PRR and other indices of renal interstitial fibrosis. In cells overexpressing PLZF, PRR significantly increased the levels of other indices of renal interstitial fibrosis, suggesting that PLZF did inhibit the index levels of renal interstitial fibrosis by inhibiting PRR expression, and qPCR also validated the same conclusion (Figures 5(c) and 5(d)).

#### 4. Discussion

CKD is a disease in which renal structural or functional abnormalities last longer than 3 months. At present, CKD is a worldwide public health problem. The prevalence rate increases year by year. With the prolongation of the disease course and the development of the disease, some patients will enter end-stage renal disease (ESRD) [11, 12]. End-stage renal disease patients are in the final stage of chronic renal failure caused by various primary or secondary renal



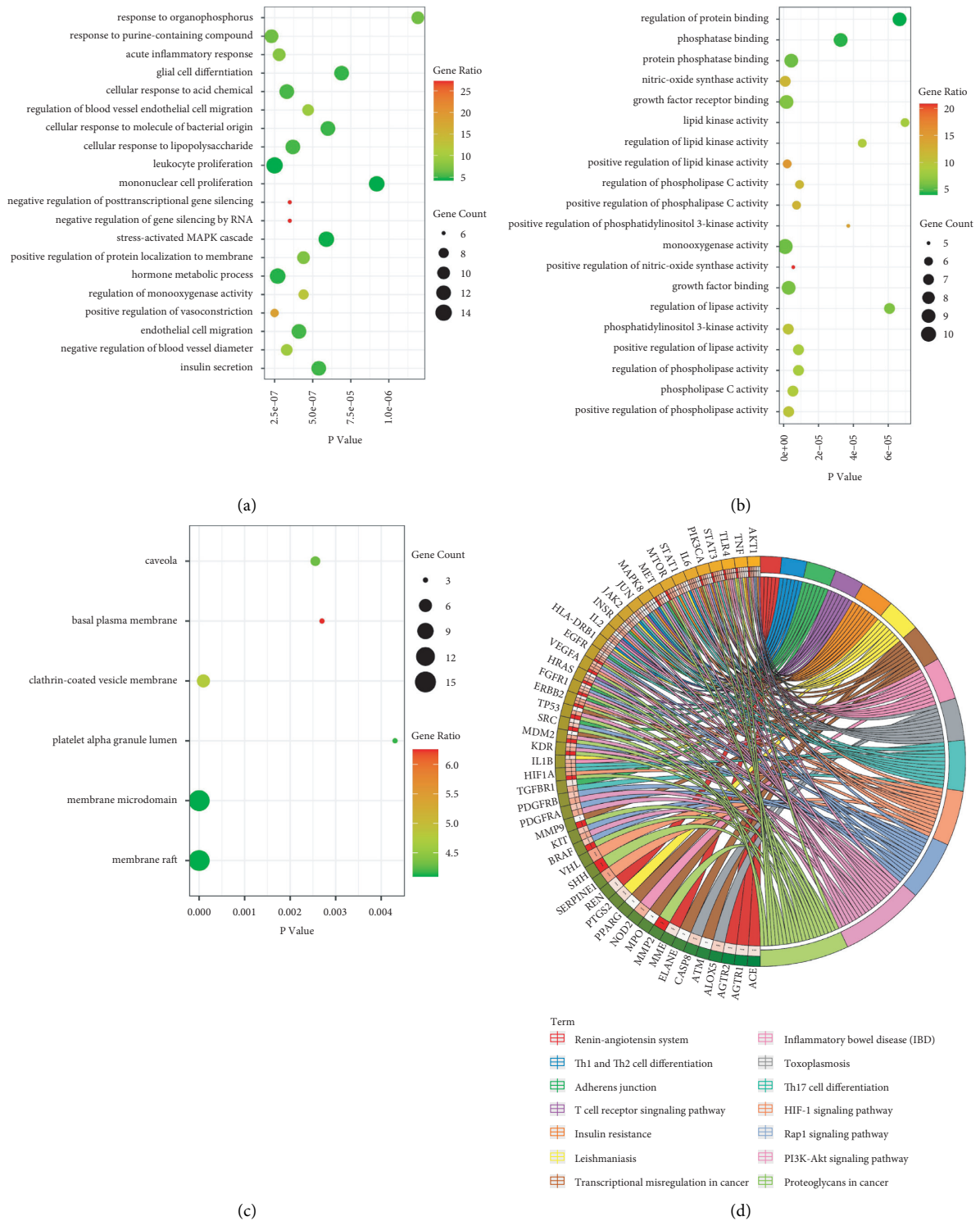


FIGURE 2: GO and KEGG pathway enrichment analyses of SSLF for RIF. (a-c) The bubble graph shows biological process, cellular component, molecular function, and the intersection gene GO analysis. The left Y-axis is the name of the GO path, and the abscissa is *p* value. The larger the circle is, the greater the number of genes compared to this path. The darker the color is, the higher the proportion of genes compared to this path. (d) KEGG pathway enrichment analysis circle diagram. In the outermost layer of the circle, signaling pathway names are displayed in the right side and gene names are displayed in the left side. The inner ring on the left indicates the significant *p* value of gene corresponding pathway.

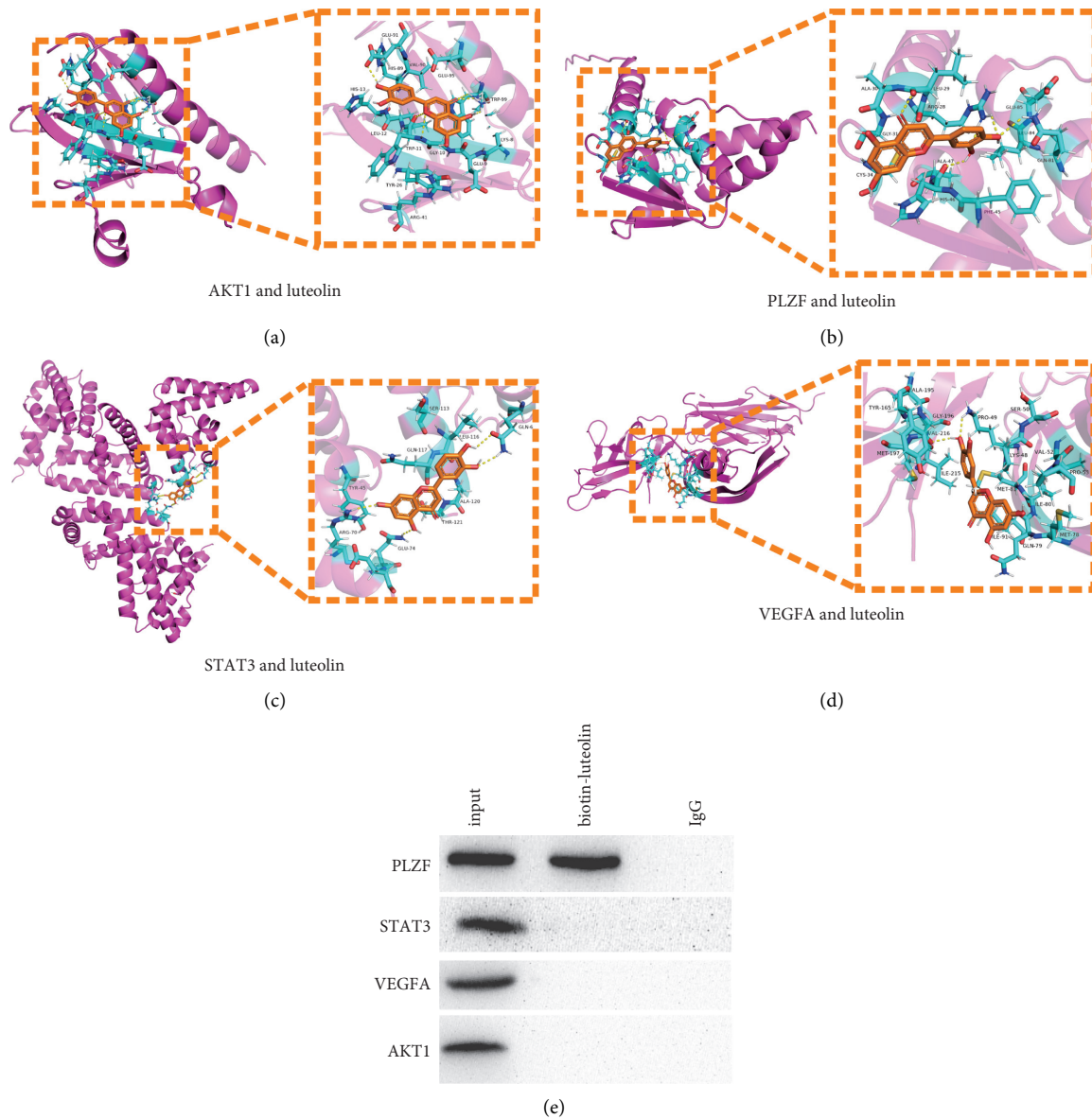


FIGURE 3: Luteolin and core targets for molecular docking. (a–d) The molecular docking of AKT1, PLZF, STAT3, VEGFA, and luteolin. The yellow line represents the hydrogen bonds; the blue sticks represent amino acid residues. (e) Coimmunoprecipitation assay shows PLZF-luteolin interactions in HK-2 cells.

diseases, which are the key diseases endangering human health worldwide. RIF is an important cause of ESRD, in which excessive accumulation and precipitation of ECM in the kidneys lead to the pathogenesis of renal fibrosis. The associated molecular signaling pathways that affect ECM accumulation are complex and include a variety of cytokines as well as hormonal, metabolic, and kinetic factors [13–15]. SSLF contains Herba Rhubarb (DH), Herba Codonopsis pilosula (DS), Herba Astragalus membranaceus (HQ), Herba Stony dragon (ML), Herba Safflower (HH), Herba Ganoderma lucidum (JLZ), Herba Angelica sinensis (DG), Herba Salvia miltiorrhiza (RS), Herba Epimedium (YYH), and Herba Dandelion (PGY). SSLF has apparent effects on improving renal function and delaying the progression of CKD.

To study SSLF's functional mechanism and understand its potential inhibitory role in renal fibrosis, first, we found that STAT3, VEGFA, and AKT1 of the intersection genes of SSLF and RIF are the core proteins in the intersection genes. Using the SSLF-compound-target-RIF network, we found that luteolin, the monomeric drug, has the most connections, and PLZF is the target protein. In order to study the effect of SSLF on PLZF, we used molecular docking and IP experiments to find that the key component of SSLF, luteolin, can bind to PLZF. At present, the mechanism of transcriptional inhibition of PLZF is that PLZF binds to the promoter of the target gene through nine zinc finger structures at the C-terminal, and then its N-terminal BTB/POZ domain recruits nuclear coinhibitory complexes. The physiological functions of PLZF mainly include regulating

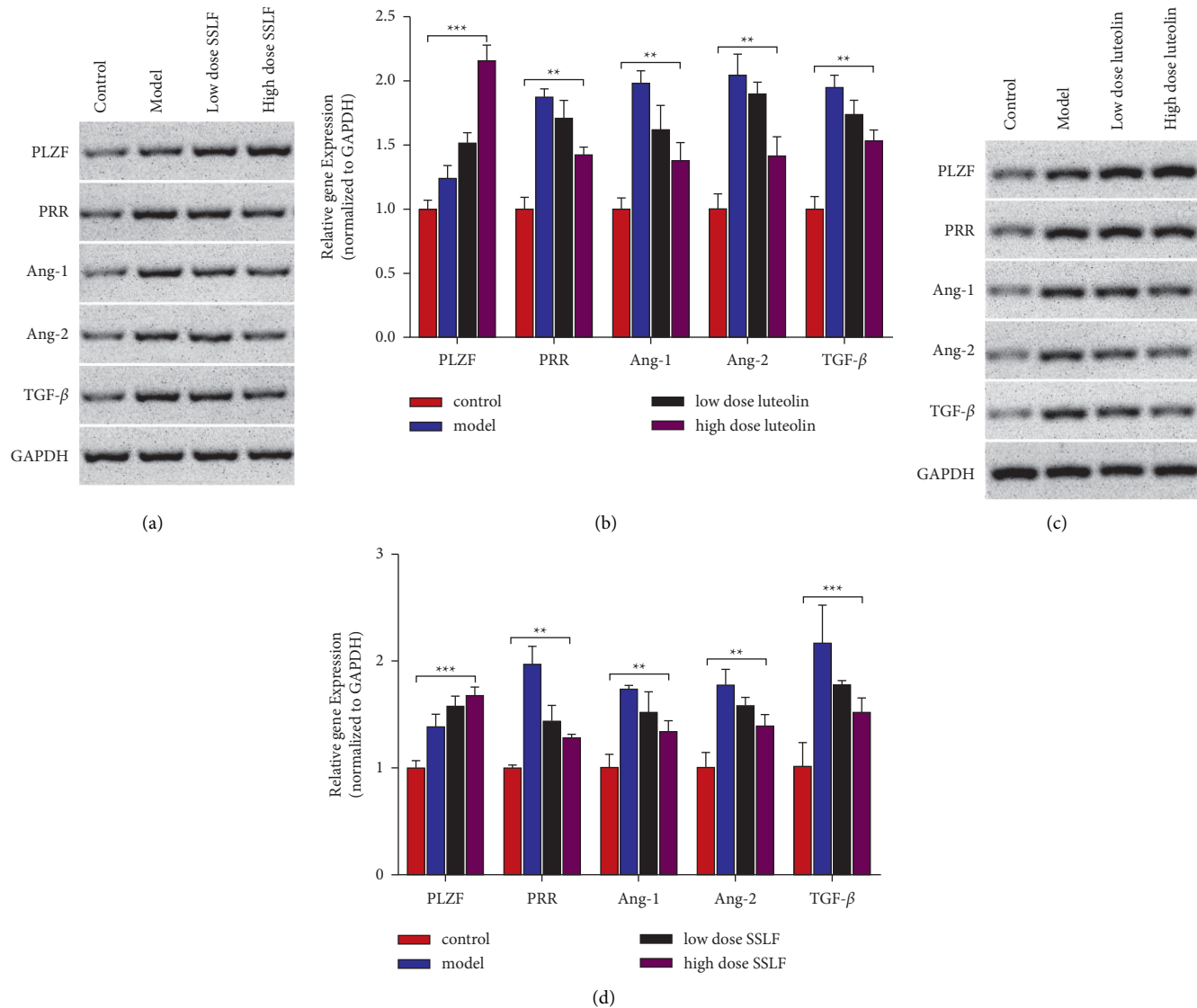


FIGURE 4: SSLF and luteolin upregulation of PLZF levels. (a, b) Protein and gene expression of PLZF, PRR, Ang-1, Ang-2, and TGF- $\beta$ . Western blot and qPCR analyses were performed after treatment with different concentrations of medicated rat serum containing SSLF. (c, d) Protein and gene expression of PLZF, PRR, Ang-1, Ang-2, and TGF- $\beta$ . Western blot and qPCR analyses were performed after treatment with different concentrations of luteolin (5  $\mu$ M, 10  $\mu$ M, and 20  $\mu$ M). Data are represented as mean  $\pm$  SD ( $n \geq 3$  experiments). \* $p < 0.05$ , \*\* $p < 0.01$ , \*\*\* $p < 0.001$ , and \*\*\*\* $p < 0.0001$  as determined using Student's *t*-test (two groups) or one-way ANOVA, followed by Tukey's test (more than two groups).

the differentiation of hematopoietic cells, maintaining the stability of the hematopoietic progenitor cell pool, maintaining the normal development of bone and the renewal of male germ cells, participating in the development of nerve cells, regulating the cell cycle, and participating in cell growth, proliferation, differentiation, and apoptosis. Recent studies have shown that PLZF also participates in immune response and has environmental-dependent anticancer and antitumor effects [16–21].

TGF- $\beta$  is the most effective factor affecting ECM accumulation, which can stimulate ECM production and inhibit ECM degradation. Ang-2 is a member of RAS, and RAS is one of the important pathways closely related to TGF- $\beta$ . The classical RAS is mainly the conversion of renin to Ang-2.

Renin is an important hormone secreted by RAS, which can catalyze the conversion of angiotensinogen to Ang-1, and Ang-1 is subsequently cleaved by ACE to Ang-2. It is found that injection of Ang-2 in rats can increase the expression of glomerular TGF- $\beta$ , and blocking the activity of Ang-2 can significantly reduce the expression of TGF- $\beta$ , reduce the formation of ECM, and effectively slow down the progression of disease [22, 23]. It has been reported that PRR plays an important role in regulating the production of Ang-2 [24]. PRR is mainly located on the cell surface and at cell intervals, especially perinuclear spaces. PRR is involved in the production of Ang-2 mainly through two pathways: the proteolytic pathway and the nonproteolytic pathway [25, 26].

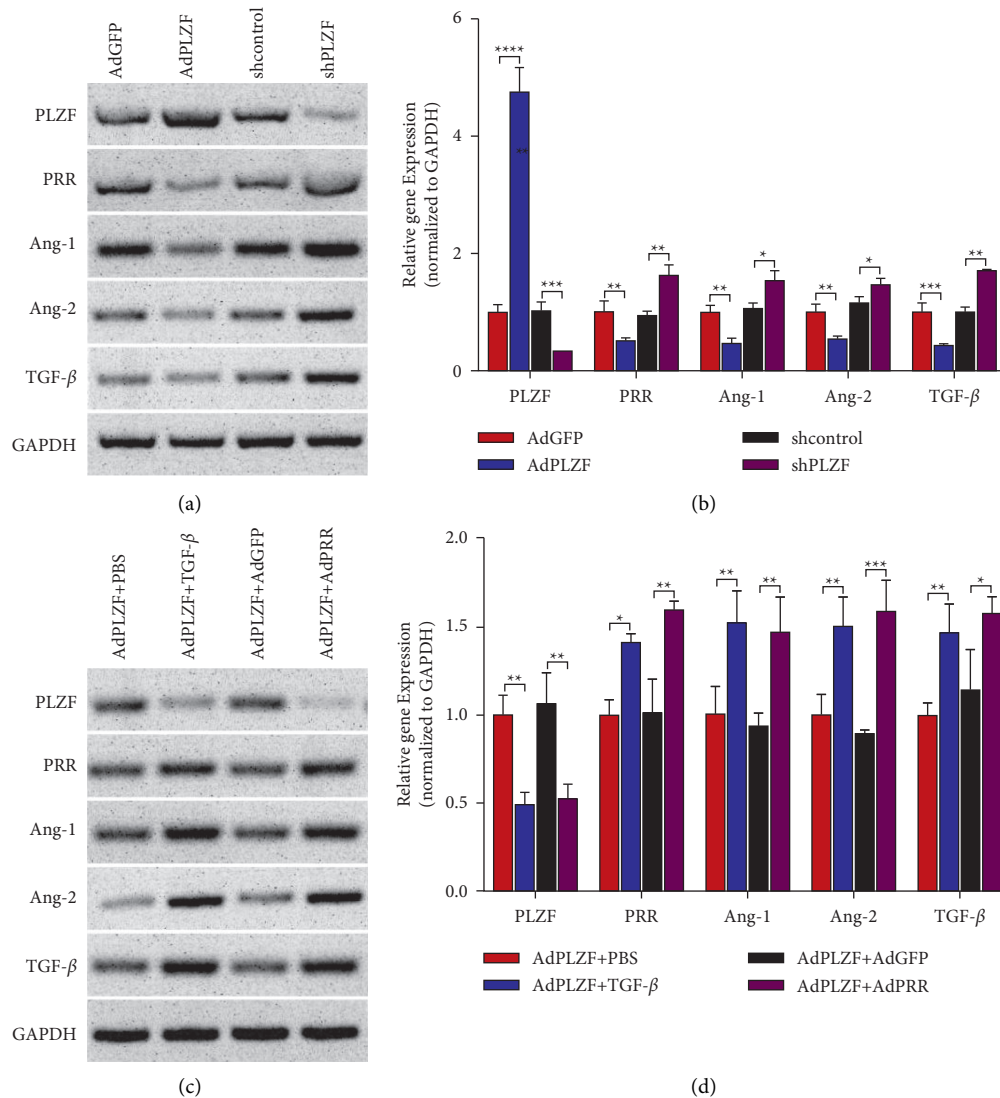


FIGURE 5: PLZF inhibits PRR expression in HK-2 cells. (a, b) Protein and gene expression of PLZF, PRR, Ang-1, Ang-2, and TGF- $\beta$ . Western blot and qPCR results of overexpression of PLZF and PLZF upon knockdown. (c, d) Protein and gene expression of PLZF, PRR, Ang-1, Ang-2, and TGF- $\beta$ . Western blot and qPCR results of overexpression of PRR. Data are represented as mean  $\pm$  SD ( $n \geq 3$  experiments). \*  $p < 0.05$ , \*\*  $p < 0.01$ , \*\*\*  $p < 0.001$ , and \*\*\*\*  $p < 0.0001$  as determined using Student's  $t$ -test (two groups) or one-way ANOVA, followed by Tukey's test (more than two groups).

To investigate whether SSLF regulates PLZF, we first used renin to induce fibrosis in HK-2 cells. Then, western blot and qPCR experiments showed that SSLF could significantly upregulate the expression of PLZF and decrease the expression of PRR and other indices of renal interstitial fibrosis. Then we also found that luteolin, a key component of SSLF, could upregulate the expression of PLZF and reduce the expression of PRR and other renal interstitial fibrosis markers. The present study found that renin-treated HEK293 cells resulted in nuclear translocation of PLZF, and then PLZF was recruited to the promoter of the PRR gene. We then found that overexpression of PLZF inhibited PRR levels and other indices of renal interstitial fibrosis using western blot and qPCR in a renin-induced model of renal interstitial fibrosis. The knockdown of PLZF resulted in a significant increase in the PRR levels in cells and a significant increase in other indices of renal interstitial

fibrosis, and qPCR also validated the same conclusion. This suggests that PLZF can indeed regulate PRR expression. In addition, we found that TGF- $\beta$  reduced the PLZF levels and inhibited PRR and other indices of renal interstitial fibrosis. To verify that PLZF affects renal interstitial fibrosis by regulating PRR, we overexpressed PRR, and western blot and qPCR results showed that, in HK-2 cells, PRR significantly increased the levels of other indices of renal interstitial fibrosis, suggesting that PLZF does inhibit renal interstitial fibrosis by inhibiting PRR expression.

## 5. Conclusions

We first predicted the possible targets and pathways of SSLF for RIF using network pharmacology, and then we used molecular docking and IP experiments to verify the binding

of SSLF and its key component, luteolin, to target proteins. Finally, using western blot and qPCR experiments, we found that SSLF and luteolin could upregulate the expression of PLZF and inhibit the level of PRR. In future studies, we will further verify the effect of SSLF and luteolin in regulating renal interstitial fibrosis through PLZF in animal models and collect clinical data to analyze the relationship between the consumption of SSLF and the expression level of PLZF in the body to provide a basis for better clinical applications.

## Data Availability

The data supporting the research are included in this study.

## Disclosure

Na Song and Haitao Tu are co-first authors.

## Conflicts of Interest

The authors declare no conflicts of interest.

## Acknowledgments

This research was supported by the National Natural Science Foundation of China (no. 81904012) and Chongqing Province Natural Scientific Foundation (nos. cstc2018jcyj-AX0783, cstc2018jcyjAX0808, cstc2020jcyj-msxmX0036, and cstc2019jxjl130007).


## References

- [1] V. Thallas-Bonke, C. Lindschau, B. Rizkalla et al., "Attenuation of extracellular matrix accumulation in diabetic nephropathy by the advanced glycation end product cross-link breaker ALT-711 via a protein kinase C- $\alpha$ -dependent pathway," *Diabetes*, vol. 53, no. 11, pp. 2921–2930, 2004.
- [2] T. Inoguchi, T. Sonta, H. Tsubouchi et al., "Protein kinase C-dependent increase in reactive oxygen species (ROS) production in vascular tissues of diabetes: role of vascular NAD(P)H oxidase," *Journal of the American Society of Nephrology: Journal of the American Society of Nephrology*, vol. 14, pp. S227–32, 2003.
- [3] J. C. K. Leung, L. Y. Y. Chan, M. A. Saleem, P. W. Mathieson, S. C. W. Tang, and K. N. Lai, "Combined blockade of angiotensin II and prorenin receptors ameliorates podocytic apoptosis induced by IgA-activated mesangial cells," *Apoptosis*, vol. 20, pp. 907–920, 2015.
- [4] G. Nguyen, F. Delarue, C. Burcklé, L. Bouzahir, T. Giller, and J.-D. Sraer, "Pivotal role of the renin/prorenin receptor in angiotensin II production and cellular responses to renin," *Journal of Clinical Investigation*, vol. 109, no. 11, pp. 1417–1427, 2002.
- [5] Z. Shan, A. E. Cuadra, and M. K. Raizada, "Characterization of a functional (pro)renin receptor (PRR) in brain neuron," *The FASEB Journal*, vol. 22, 2008.
- [6] G. Nguyen and D. N. Muller, "The biology of the (Pro)Renin receptor," *Journal of the American Society of Nephrology*, vol. 21, no. 1, pp. 18–23, 2009.
- [7] A. H. M. N. Nabi and F. Suzuki, "Biochemical properties of renin and prorenin binding to the (pro)renin receptor," *Hypertension Research*, vol. 33, no. 2, pp. 91–97, 2010.
- [8] Y. Jin, H. Z. Nenseth, and F. Saaticioglu, "Role of PLZF as a tumor suppressor in prostate cancer," *Oncotarget*, vol. 8, no. 41, pp. 71317–71324, 2017.
- [9] D. Rohle, J. Popovici-Muller, N. Palaskas et al., "An inhibitor of mutant IDH1 delays growth and promotes differentiation of glioma cells," *Science*, vol. 340, no. 6132, pp. 626–630, 2013.
- [10] H. Liu, W. Xiong, and X. Zheng, "Academic thought and clinical experience of TCM master ZHENG Xin in treating diabetic nephropathy," *China Journal of Traditional Chinese Medicine and Pharmacy*, vol. 31, pp. 4547–4549, 2016.
- [11] V. A. Luyckx, D. Z. I. Cherney, and A. K. Bello, "Preventing CKD in developed countries," *Kidney international reports*, vol. 5, no. 3, pp. 263–277, 2020.
- [12] Y. Zha and Q. Qian, "Protein nutrition and malnutrition in CKD and ESRD," *Nutrients*, vol. 9, 2017.
- [13] A. B. Farris and R. B. Colvin, "Renal interstitial fibrosis," *Current Opinion in Nephrology and Hypertension*, vol. 21, no. 3, pp. 289–300, 2012.
- [14] A. Shrestha, R.-C. Che, and A.-H. Zhang, "Role of aldosterone in renal fibrosis," *Advances in Experimental Medicine and Biology*, vol. 1165, pp. 325–346, 2019.
- [15] Y. B. Y. Sun, X. Qu, G. Caruana, and J. Li, "The origin of renal fibroblasts/myofibroblasts and the signals that trigger fibrosis," *Differentiation*, vol. 92, no. 3, pp. 102–107, 2016.
- [16] M. Barna, N. Hawe, L. Niswander, and P. P. Pandolfi, "Plzf regulates limb and axial skeletal patterning," *Nature Genetics*, vol. 25, no. 2, pp. 166–172, 2000.
- [17] J. E. Dick and S. Doulatov, "The role of PLZF in human myeloid development," *Annals of the New York Academy of Sciences*, vol. 1176, no. 1, pp. 150–153, 2009.
- [18] Y.-H. Ching, L. A. Wilson, and J. C. Schimenti, "An allele separating skeletal patterning and spermatogonial renewal functions of PLZF," *BMC Developmental Biology*, vol. 10, no. 1, p. 33, 2010.
- [19] M. V. Bernardo, E. Yelo, L. Gimeno, J. A. Campillo, and A. Parrado, "Identification of apoptosis-related PLZF target genes," *Biochemical and Biophysical Research Communications*, vol. 359, no. 2, pp. 317–322, 2007.
- [20] A. K. Savage, M. G. Constantinides, J. Han et al., "The transcription factor PLZF directs the effector program of the NKT cell lineage," *Immunity*, vol. 29, no. 3, pp. 391–403, 2008.
- [21] R. M. Hobbs and P. P. Pandolfi, "Shape-shifting and tumor suppression by PLZF," *Oncotarget*, vol. 1, no. 1, pp. 3–5, 2010.
- [22] G. Vega, S. Alarcón, and R. San Martín, "The cellular and signalling alterations conducted by TGF- $\beta$  contributing to renal fibrosis," *Cytokine*, vol. 88, pp. 115–125, 2016.
- [23] B. Sutariya, D. Jhonsa, and M. N. Saraf, "TGF- $\beta$ : the connecting link between nephropathy and fibrosis," *Immunopharmacology and Immunotoxicology*, vol. 38, no. 1, pp. 39–49, 2016.
- [24] Q. Xu, D. D. Jensen, H. Peng, and Y. Feng, "The critical role of the central nervous system (pro)renin receptor in regulating systemic blood pressure," *Pharmacology & Therapeutics*, vol. 164, pp. 126–134, 2016.
- [25] Q. Li and M. K. Raizada, "Is (pro)renin receptor a multifunctional receptor?" *Hypertension (Dallas, Tex.: 1979)*, vol. 55, pp. 1308–1309, 2010.
- [26] T. Yang, "Crosstalk between (Pro)renin receptor and COX-2 in the renal medulla during angiotensin II-induced hypertension," *Current Opinion in Pharmacology*, vol. 21, pp. 89–94, 2015.



## Research Article

# GC-MS Analysis and Various In Vitro and In Vivo Pharmacological Potential of *Habenaria plantaginea* Lindl.

Mater H. Mahnashi,<sup>1</sup> Yahya S. Alqahtani,<sup>1</sup> Bandar A. Alyami,<sup>1</sup> Ali O. Alqarni,<sup>1</sup> Mohammad Ahmed Alshrahili,<sup>2</sup> Mahrous A. Abou-Salim,<sup>3</sup> Mohammed N. Alqahtani,<sup>4</sup> Sadaf Mushtaq,<sup>5</sup> Abdul Sadiq,<sup>6</sup> and Muhammad Saeed Jan <sup>7</sup>

<sup>1</sup>Department of Pharmaceutical Chemistry, College of Pharmacy, Najran University, Najran, Saudi Arabia

<sup>2</sup>Armed Forces Hospital Jazan, Jazan, Saudi Arabia

<sup>3</sup>Al-Azhar University, Faculty of Pharmacy, Pharmaceutical Organic Chemistry, Assiut 71524, Egypt

<sup>4</sup>Ahad Rufaidah General Hospital, Abha-Ahad Rufaidah, Jazan, Saudi Arabia

<sup>5</sup>ELMS College, Springfield Street, Chicopee, MA, USA

<sup>6</sup>Department of Pharmacy, Faculty of Biological Sciences, University of Malakand, Chakdara 18000, Dir (L), KP, Pakistan

<sup>7</sup>Department of Pharmacy, University of Swabi, Anbar 23561, Swabi, KPK, Pakistan

Correspondence should be addressed to Muhammad Saeed Jan; saeedjanpharmacist@gmail.com

Received 30 December 2021; Accepted 14 March 2022; Published 31 March 2022

Academic Editor: Ruchika Garg

Copyright © 2022 Mater H. Mahnashi et al. This is an open access article distributed under the Creative Commons Attribution License, which permits unrestricted use, distribution, and reproduction in any medium, provided the original work is properly cited.

**Background.** The current study aims to give a scientific origin for employing *Habenaria plantaginea* Lindl. as a potential candidate against nociception, inflammation, and pyrexia. The pharmacological studies were performed on crude extract and subfractions. In the gas chromatography-mass spectroscopy analysis, a total of 21 compounds were identified. The plant samples were displayed for in vitro anti-inflammatory potentials. The observed IC<sub>50</sub> for chloroform against cyclooxygenase-2 and 5-lipoxygenase enzymes was 33.81 and 26.74 µg/mL, respectively. The in vivo activities were prerequisites with the acute toxicity studies. In carrageenan-induced inflammation, the chloroform fraction exhibited 46.15% inhibition similar to that of standard drug diclofenac sodium 47.15%. Likewise, in the acetic acid-induced writhing test, the ethyl acetate fraction displayed 71.42% activity, which was dose-dependent as that of standard drug. In Brewer's yeast-induced antipyretic activity, a significant decrease in rectal volume was observed after 30, 60, and 90 minutes. Moreover, the results of this study indicated that the chloroform and ethyl acetate fractions inhibited nociception, inflammation, and pyrexia dose dependently. Likewise, mechanistic insights indicated that naloxone antagonized the antinociceptive effect of chloroform and ethyl acetate fractions, thereby signifying the involvement of opioidergic mechanisms respectively. These results suggest that these molecules present in this plant have synergistically beneficial potential for the cure and management of analgesia, inflammation, and pyrexia.

## 1. Introduction

New drug from a natural source with a desirable profile is tremendously an inspiring task in the field of clinical research [1]. Nociceptive pain induces activation of sensory nerve fibers when the stimulus overshoots the noxious intensity [2]. Chemical, thermal, and mechanical stimuli are the various common types of nociceptive pain which might further be alienated into deep, visceral, superficial somatic,

and somatic pain [3]. The visceral part of the organ is extremely sensitive to inflammation, ischemia, and stretch but is not sensitive to the other stimuli that induce pain in other parts of the body [4]. Deep somatic pain initiates in blood vessels, muscles, tendons, bones, and ligaments after the stimulations of nociceptors in these organs. This type of pain is dull and poorly localized. Muscle sprain and breaking bones are the most common examples of deep somatic pain [5]. When the nociceptors in superficial and skin tissues



activate, they induce superficial pain, which is very sharp. Minor burns and minor wounds are the most common examples of superficial pain [6]. Pain is a sign to propel a person from deleterious conditions to protect a damaged part of the body after healing. After removing the toxic stimuli, most of the pain sensation disappears but in some cases, pain perception remains for a long time after removing the damaging stimuli. Inflammation is a complicated protective response involving immune cells, blood vessels, and molecular mediators of the body to harmful stimuli, damaged cells, or invading microbes [6, 7]. The main role of inflammation is to eliminate of necrotic cells, damaged tissues, and injured cells and to start the tissue repairing process of the body [8]. The immune response of the body is not specific of a body to irritation, infection, and injury, which may be acute or chronic [9].

The clinical hallmarks of inflammations in Latin are rubor (redness), calor (warmth), tumor (swelling), and dolor (pain). The characteristics of inflammation were first described by the Roman physician Aulus Cornelius Celsus (Aurelius) [10]. The body response against the invading microbes or any other foreign substances is the innate immune system that is specific for specific microorganisms that enter into the body [11]. Inflammation is divided into two types: acute and chronic inflammation.

Presently, mild-to-moderate pain, inflammation, and pyrexia are managed with NSAIDs, but there are serious limitations of these therapies [12]. For example, there is well-documented evidence that continuous use of NSAIDs displays toxicity such as GIT ulceration, bleeding, perforation, cardiovascular disorders, and analgesic nephropathy. Hence, across the globe, extensive search is in progress in the area of medical management of pain and inflammation to find out new remedies [13]. This new drug discovery acts as alternative drugs to traditional analgesics including NSAIDs and narcotics.

*Hebanaria* genus is associated with the Orchidaceae family, which may consist of about 850 genera and 35000 species [14, 15]. Orchids were employed as the basis of conventional remedy for a very long time to cure various disorders such as arthritis, syphilis, stomach problem, acidity, tumor, jaundice, boils, inflammations, piles, hepatitis, malaria, blood dysentery, pyrexia, sexually transmitted ailments, tuberculosis, cholera, wounds, eczema, vermifuge, and diarrhea [16–18]. *Bulbophyllum neilgherrense*, a traditional therapeutic plant, has lately been assessed as a mediator of inflammation and analgesia [19]. The anti-inflammatory properties of orchids from South Africa have also been studied [20]. No scientific evaluation has been reported for the investigation of pharmacological features of *H. plantaginea*. In our previous study, we have also explored *H. digitata*, which belongs to the same family for its anti-inflammatory and analgesic potential [21].

We have deliberated this research work to explore the pyrexia, analgesia, and anti-inflammatory properties of *H. plantaginea* based on ethnomedicinal exploitation and previous literature assessment. Furthermore, we have indomitable phytochemicals via GC-MS methods. Evaluation of these unexplored plants can potentially lead to the

generation of new molecules for drug development and better medicine.

## 2. Materials and Methods

**2.1. Chemicals and Drugs.** For anti-inflammatory in vitro assay, the enzyme COX-2 (Catalog no. C0858) and 5-LOX (Catalog no. 437996) were acquired from the Sigma-Aldrich GmbH, USA. The substrate arachidonic acid (CAT no. 150384), linoleic acid (CAS no. 60-33-3), and their cofactor solution materials TMPD (CAS no. 637-01-4), hematin (CAS no. 15489-90-4), and glutathione (CAS no. 70-18-8) were purchased from Sigma-Aldrich, Germany. Carrageenan (CAS no. 9064-67-7), naloxone, and AA (CAS No: 506-32-1) were also acquired from Sigma-Aldrich, Germany. Buffer solution containing  $\text{KH}_2\text{PO}_4$  and  $\text{K}_2\text{HPO}_4$  and solvents employed were of pure class. Celecoxib and Montelukast was purchased from Pfizer pharmaceutical and Libra (Pvt.) Limited. Tramadol and Diclofenac were purchased from Alliance Pharmaceuticals, Pakistan.

**2.2. Plant Material, Collection, and Extraction.** The *H. plantaginea* plant was collected from the Dir (L) KPK, Pakistan, in mid of April and then was identified via Prof. Muhammad Ilyas, Department of Botany, University of Swabi, Swabi KPK, Pakistan. The sample of the said plant was kept and recorded at herbarium having voucher number H.UOS.20-2. The aerial pieces of the plant (15 kg) were soaked with uncontaminated water and were sheltered desiccated for 21 days. The sheltered desiccated pieces of plants were firstly incised into minor pieces and then via grinder changed into coarse fine particles (7.5 kg). The pulverized substance was then macerated in the 26 L methanol (80%) for 21 days. Afterward, the entire substance was filtered using the muslin cloth and consequently by the Whatman filter paper. Then, the filtrate was transferred to a rotary evaporator (40°C) for further extraction [2, 22]. The last gloomy green color hard methanolic extort of *H. plantaginea* was attained weighing 650 g.

**2.3. Fractionation.** Methanol extort was decanted quietly in the separating funnel having a closed stopper. The Hp. Cr was mixed with the same amount of 500 ml hexane and water. The separating funnel was shaken vigorously for proper mixing of all the ingredients and then reserved at the correct position via a stand to prepare two separate layers: the *n*-hexane and water layer. The layer of *n*-hexane was alienated. A similar process was repeated two times through 500 ml of hexane. The organic layers which were separated three times were then mixed and concentrated in decreased pressure via rotary evaporator having a temperature of 40°C. The obtained concentrated weight of Hex. was 27.6 g. Similarly, the identical protocol was applied with the further solvents via raising the polarization of solvents. Following solvent fractions acquired was basically of ethyl acetate, chloroform, and Bt., having weights of 30, 42, and 94 g correspondingly. In last, the aqueous stratum was concentrated with a weight of 140 g [23].

**2.4. GC-MS Analysis (Phytochemistry).** The tandem gas chromatography/mass spectrometry procedure of crude extract was executed by Agilent USB:393752 gas chromatograph (Agilent Technologies, Palo Alto, CA, USA) having an HHP-5MS 5% phenyl methyl siloxane tubular-column (30.0 m × 0.25 mm × 0.25 μm film thickness: Restek, Bellefonte, PA, USA) prepared through the Agilent HP; 5973 mass selective detector having the effective mode of electron (Ionization energy; 70 eV) performance in the parallel investigational ambiance as exemplification, intended for gas chromatography [10, 24].

### 2.5. In Vitro Pharmacological Activities

**2.5.1. COX-2 Activity.** The in vitro COX-2 scavenging activity was conceded through the previous explained normal protocol [25]. The COX-2 solution of the enzyme was equipped to have 300 U ml<sup>-1</sup> concentrations. For enzyme activation, the enzyme solution (10 μl) was placed on ice for 5 minutes. Likewise, total of 50 μl cofactor mixture with 0.9 mM glutathione, 1 mM hematin, and 0.24 mM TMPD within 0.1 M Tris HCl buffer (pH 8.0) was added to a mixture of the solution of enzyme. Consequently, plant samples (20 μl) including different concentrations (1000–31.25 μg ml<sup>-1</sup>) along with 60 μl of the solution of the enzyme were placed at room temperature for five minutes. Similarly, 30 mM AA (20 μl) was added for starting the reaction. After that, the solution mixture was incubated for 5 min. After the incubation, the absorbance of the solution mixture was recorded at 570 nm using UV-visible spectrophotometer. The COX-2 enzyme inhibition was indomitable from per unit time of absorbance value. The IC<sub>50</sub> values were resolute by plotting the reticence of enzyme beside different test fraction concentrations. Celecoxib was employed as a positive control (standard drug).

**2.5.2. 5-LOX Assay.** The inhibitory potential of 5-LOX on the *H. plantaginea* various fractions was carried out as per the previously reported procedure. Firstly, various dilutions were made ranging from 31.25 to 1000 μg/mL. Afterward, the 5-LOX enzyme having 10,000 U ml<sup>-1</sup> solutions was prepared. Linoleic acid (80 mM) was used as a substrate in this assay. Likewise, phosphate buffer (50 mM) was ready with 6.3 pH. The various fractions of the plant samples were mixed in phosphate buffer solution and lipoxygenase enzyme (250 μl each) was mixed with it and incubated for 5 minutes at normal room temperature. Then, 0.6 mM of substrate solution (1000 μl) was added with that of the solution containing enzyme and shaken; after that, absorbance was deliberated at 234 nm. The experimental procedures were carried out thrice. In our activity, the standard drug employed was zileuton [26]. The % inhibition was calculated by the following equation:

$$\text{Percentage Inhibition} = \frac{\text{Control Abs.} - \text{Sample Abs.}}{\text{Control Abs.}} \times 100. \quad (1)$$

### 2.6. In Vivo Pharmacological Activities

**2.6.1. Animals.** Albino mice of either sex were used in all experimental work and all experiments were conducted in the time range from 8.00 am to 5.00 pm. Food and water were available to all animals. The light-and-dark cycle was conserved with a temperature of 22 ± 2°C and which has an exhaust fan facility. At the end of all experimental processes, animals were sacrificed by scheduled 1 method and appropriately disposed of according to ethical guidelines of the institution. The experimental albino mice were employed as per authorization of the ethical board having letter number: UOS. Ph. 40121 Department of Pharmacy, University of Swabi, Pakistan.

**2.6.2. Acute Toxicity.** The acute toxicity was carried out on investigational albino mice. All animals were alienated into different sets having test and control groups. Every group has 5 tested animals. The *H. plantaginea* tested samples were administered per oral at various doses (25 to 2000 mg kg<sup>-1</sup>) according to body weight. For the dose preparation, Tween-80 was employed. After administration of various doses, the experimental mice were pragmatic for up to 3 days for any minor allergic reactions and abnormal behavior [27].

**2.6.3. Antinociceptive Activity.** We used two standard models for the evaluation of antinociceptive activity in mice: acetic acid-induced writhes and hot plate models [28, 29].

**(1) Acetic Acid-Induced Writhes.** Animals were deprived of food and water for 2 hours before starting the experimental procedure. Animals were divided into various groups. The acetic acid at a dose of 10 ml/kg (1%) was administered intraperitoneally into the animal, which leads to constrictions of the abdomen. This constriction was counted for 20 minutes [23]. Diclofenac sodium at a dose of 50 mg/kg was taken as a reference standard. Crude extract and their subsequent fractions were given at doses of 100 mg/kg, while 0.9% sodium chloride was taken as a control group. The standard drug, test drug, and normal saline were administered intraperitoneally to different groups of animals 30 minutes before the administration of acetic acid.

**(2) Hot Plate Test.** All the animals were habituated to the laboratory environment at least 2 hours before experimental procedures. Analgesimeter was used for the evaluation of analgesic activity on hot plate [30]. The hot plate temperatures were kept at 54.0 ± 0.1°C. Animals were subjected to pretest and all those animals that show latency time less than 30 seconds were selected. The selected animals were then arranged into various groups like normal saline group, standard group, and other potent fractions of the tested samples. The normal saline, standard drug, and various fractions of the test sample were administered intraperitoneally. The latency time of animals on the hot plates at intervals of 30, 60, and 90 minutes was calculated.

(3) *Effect of Naloxone on Antinociceptive Activity of Various Fractions on Hot Plate Model Experimental Protocol.* For the evaluation of the mechanism of the *H. plantaginea*, naloxone and tramadol were given to the animals. The animals were divided into ten groups, each group containing six animals ( $n=6$ ). All the animals were acclimatized to the laboratory environment 1 hour before the start of experimental work. In this study, albino mice of either sex were used through experiments and are exposed to the hot plate having a temperature of  $54.0 \pm 0.1^\circ\text{C}$ . All the animals were subjected to pretest. All those animals were selected which shows latency time less than 30 seconds and the other animals were rejected to circumvent tissue damage [29]. After completion of the pretest, tramadol at a dose of 5 mg/kg was injected intraperitoneally and the latency time was recorded at 30, 60, and 90 minutes. In the antagonistic activity, naloxone at a dose of 1 mg/kg was administered subcutaneously 10 minutes before tramadol administrations [31].

#### 2.6.4. Anti-Inflammatory Activity

(1) *Carrageenan-Induced Inflammation.* Carrageenan-induced paw edema was used for evaluation of anti-inflammatory activity [32]. All the animals of either sex were arranged into five groups each having six animals. All the animals were fasted overnight but have free excess to water. Diclofenac sodium (50 mg/kg) as a standard drug, normal saline as a control group, and various fractions at a dose of 100 mg/kg were administered 30 minutes before administration of 0.05 ml of 1% carrageenan into the subplantar area of the paw. A high-sensitivity instrument digital plethysmometer was used for measuring a small volume change in hind paw developed in the form of edema after injection of carrageenan. Reading was taken on a plethysmometer before and after carrageenan administrations up to 5 hours at an interval of 1 hour.

#### 2.6.5. Antipyretic Activity

(1) *Brewer's Yeast-Induced Pyrexia.* For the evaluation of antipyretic study, Brewer's yeast model was used in which 20% Brewer's yeast was injected subcutaneously leading to hyperpyrexia [33]. All the animals were fasted overnight having free excess to water only and are arranged into various groups, each group containing 6 animals. With the help of a digital thermometer, rectal temperatures were recorded after 24-hour administration of Brewer's yeast. All those animals were selected which shows the rise in temperature up to  $0.3\text{--}0.5^\circ\text{C}$ . Group 1 received normal saline at a dose of 10 ml/kg, group 2 received standard drug at a dose of 150 mg/kg, and groups 3, 4, and 5 received test drug at a dose of 100 mg/kg body weight intraperitoneally. Rectal temperature was recorded after administration of all groups at an interval of 30 minutes, 60 minutes, and 90 minutes. Lubricants such as olive oil were used for insertion into the animal rectum and were maintained for 30 seconds for temperature record (Figure 1).

2.6.6. *Analysis of Data.* The results of all the experimental works were demonstrated as mean  $\pm$  SEM of all the groups having six animals. The  $\text{IC}_{50}$  values were calculated through SPSS software. One-way ANOVA statistical tools were used for the assessment and differences of various means, which follow two-way ANOVA followed by Bonferroni's posttest by using GraphPad Prism version 5. During statistical analysis, the value of  $P$  that is less than 0.05 was considered to be statistically significant.

### 3. Results

3.1. *GC-MS Analysis.* The GC-MS analysis of Hp. Cr was executed and recognized twenty-two (22) molecules in it. The structure of all the known molecules is exhibited in Figure 2. GC-MS identification depends on the corresponding of spectral peak, the fragmentation pattern of its peak and mass through the identified library is established inside the apparatus. For that reason, occasionally it is probably because of the fact that basic two molecules will have the same fragmentation pattern and mass spectra, but it is not an ordinary case. Furthermore, all the details about the new molecule present inside of plant were not installed in GC-MS library, so there is the probability of not identifying those new molecules. Full details of GC-MS analysis are summarized in Table 1. The compounds 2, 4, 5 were previously reported for their anti-inflammatory potential while compound 6 was reported as antihemorrhagic, analgesic, diuretic, antipyretic, and insecticide activities.

#### 3.2. In Vitro Pharmacological Activates

3.2.1. *Cox-2 Assay.* In this assay, various fractions like Hp. Chf and Hp. EtAc exhibited excellent COX-2 inhibition as shown in Table 2. Hp. Chf showed that the highest COX-2 inhibitory potential observed was  $77.40 \pm 0.25$ ,  $72.41 \pm 0.30$ ,  $65.79 \pm 1.28$ ,  $61.32 \pm 0.68$ , and  $56.49 \pm 0.73\%$ ; activity was monitored for the fraction Hp. Chf at concentration of 1000, 500, 250, 125, and  $62.5 \mu\text{g mL}^{-1}$ , respectively, with  $\text{IC}_{50}$  value of  $33.81 \mu\text{g mL}^{-1}$ . Likewise, Hp. EtAc exhibited second highest inhibitory potential observed:  $76.38 \pm 0.76$ ,  $69.37 \pm 0.52$ ,  $62.90 \pm 1.16$ ,  $54.48 \pm 0.54$ , and  $45.56 \pm 0.69$  with  $\text{IC}_{50}$  value  $87.56 \mu\text{g mL}^{-1}$ , respectively. Celecoxib demonstrated  $84.51 \pm 0.30$ ,  $77.84 \pm 0.27$ ,  $73.50 \pm 2.26$ ,  $65.74 \pm 0.16$ , and  $61.56 \pm 0.28$  with  $\text{IC}_{50}$  value  $23.30 \mu\text{g mL}^{-1}$  respectively. All the other fractions displayed good-to-moderate activity in this assay.

3.2.2. *5-LOX Assay.* In this assay, Hp. Chf exhibited highest activity against with  $81.73 \pm 0.37$ ,  $75.27 \pm 1.37$ ,  $69.62 \pm 0.11$ ,  $63.81 \pm 0.51$ , and  $59.08 \pm 0.12$  percent inhibition at concentration of 1000, 500, 250, 125, and  $62.5 \mu\text{g mL}^{-1}$ , respectively. The  $\text{IC}_{50}$  value measured from the dose-response curve was  $26.74 \mu\text{g mL}^{-1}$ . Similarly, Hp. EtAc exhibited  $80.47 \pm 0.70$ ,  $73.57 \pm 0.43$ ,  $65.12 \pm 0.94$ ,  $57.76 \pm 1.09$ , and  $49.38 \pm 0.50$  with  $\text{IC}_{50}$  value  $67.51 \mu\text{g mL}^{-1}$ , respectively. The standard drug linoleic acid displayed  $87.66 \pm 0.45$ ,  $81.64 \pm 0.42$ ,  $76.01 \pm 1.61$ ,  $70.46 \pm 0.32$ , and  $64.50 \pm 0.02$  inhibition at concentration

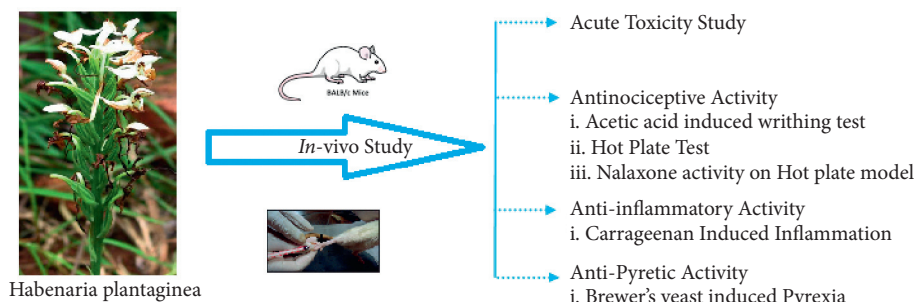


FIGURE 1: Schematic diagram of the in vivo experimental animal design.

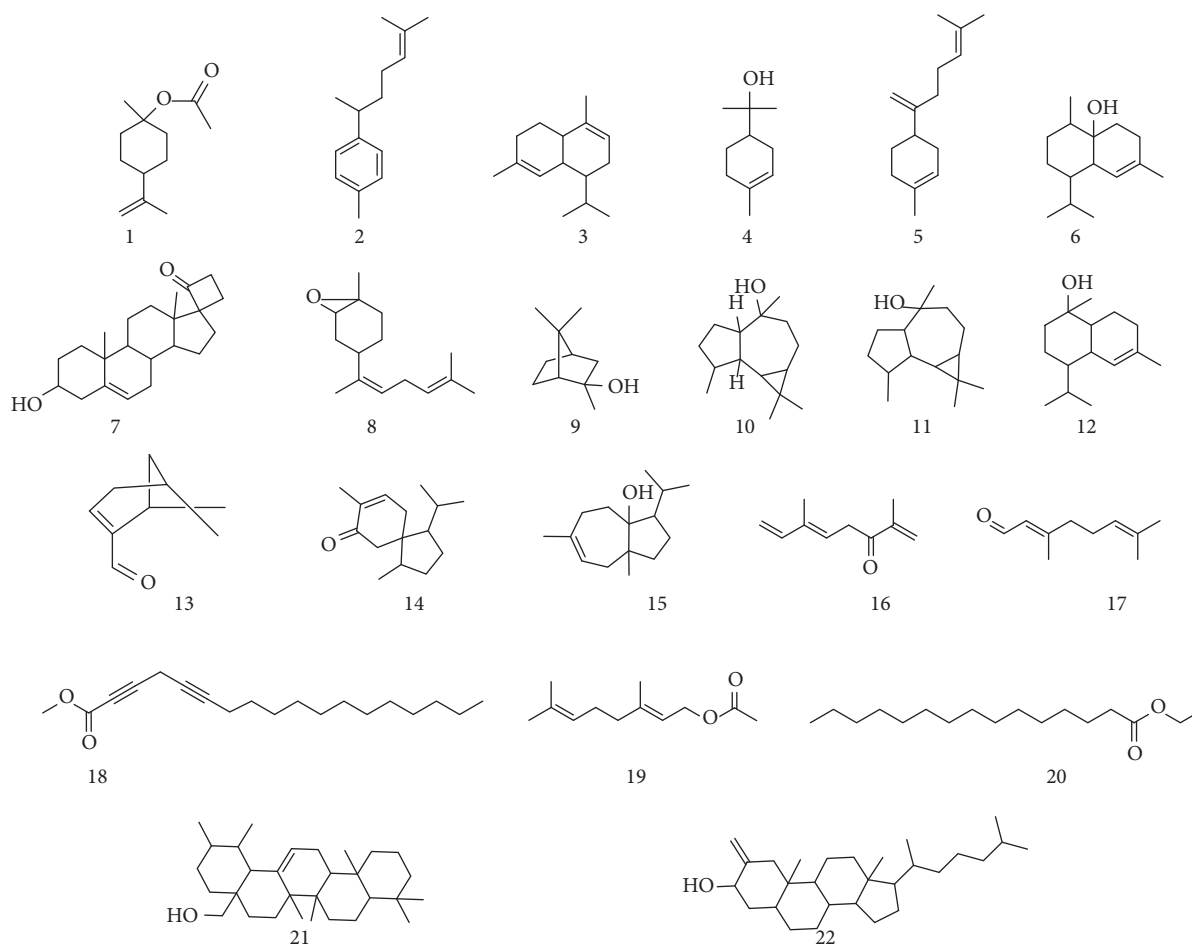


FIGURE 2: Identified compounds' structures in *Habenaria plantaginea*.

ranging from 1000 to  $62.5 \mu\text{g mL}^{-1}$ , respectively, attaining the  $\text{IC}_{50}$  value of  $17.47 \mu\text{g mL}^{-1}$  as shown in Table 2.

### 3.3. In Vivo Pharmacological Activities

**3.3.1. Acute Toxicity Result.** In the acute toxicity studies, no mortality and no changes in behavior were noticed in the investigational mice. Based on the observation in the acute toxicity result, a dose of 2000 mg/kg was measured as the safest dose. The information of the doses specified to mice is presented in Table 3.

### 3.3.2. Evaluation of Antinociceptive Activity

**(1) Acetic Acid-Induced Writhing Activity.** A significant decrease in the number of writhing was observed in animals treated with standard drug (50 mg/kg I/P) as compared to the normal saline control group. The number of writhes exhibited by the standard group is 10.33 with 74.70% of inhibition, while the Hp. Chf and Hp. EtAc have also reversed the effect of acetic acid and displayed number of writhes  $16.17 \pm 0.10$  and  $11.67 \pm 0.60$  ( $P < 0.001$ ) with  $60.39 \pm 0.42$ , and  $71.42 \pm 0.55\%$  of inhibition, respectively, at a dose of 100 mg/kg I/P (Figure 3).

TABLE 1: GC-MS details of identified compounds.

S. no.	Chemical name	Common name/synonym	Formula
1	1-Methyl-4-(prop-1-en-2yl)cyclohexyl acetate	Beta-terpinyl acetate	C <sub>12</sub> H <sub>20</sub> O <sub>2</sub>
2	1-Methyl-4-(6-methyl hept-5-en-2-yl)benzene	Alpha-curcumene	C <sub>15</sub> H <sub>22</sub>
3	1-Isopropyl-4,7-dimethyl-1,2,4a,5,6,8a-hexahydronaphthalene	Not identified	C <sub>15</sub> H <sub>24</sub>
4	2-(4-Methylcyclohex-3-enyl)propan-2-ol	Alpha-terpineol	C <sub>10</sub> H <sub>18</sub> O
5	1-Methyl-4-(6-methylhepta-1,5-dien-2-yl)cyclohex-1-ene	β-Bisabolene	C <sub>15</sub> H <sub>24</sub>
6	1-Isopropyl-4,7-dimethyl-1,2,3,4,4a,5,6,8a-octahydronaphthalen-4a-ol	Cadina-1(6),4-diene	C <sub>15</sub> H <sub>26</sub> O
7	Spiro[androst-5-ene-17,1'-cyclobutan]-2'-one,3-hydroxy-	Not identified	C <sub>22</sub> H <sub>32</sub> O <sub>2</sub>
8	(Z)-1-Methyl-4-(6-methylhepta-2,5-dien-2-yl)-7-oxa-bicyclo[4.1.0]heptane	Not identified	C <sub>15</sub> H <sub>24</sub> O
9	2,7,7-Trimethylbicyclo[2.2.1]heptan-2-ol	Isoborneol	C <sub>10</sub> H <sub>18</sub> O
10	1,1,4,7-Tetramethyl-decahydro-1H-cyclopropa[e]azulen-4-ol	Viridiflorol	C <sub>15</sub> H <sub>26</sub> O
11	1,1,4,7-Tetramethyl-decahydro-1H-cyclopropa[e]azulen-4-ol	Globulol	C <sub>15</sub> H <sub>26</sub> O
12	4-Isopropyl-1,6-dimethyl-1,2,3,4,4a,7,8,8a-octahydronaphthalen-1-ol	δ-Cadinol	C <sub>15</sub> H <sub>26</sub> O
13	4,6-Dimethylcyclohex-1-enecarbaldehyde	Not identified	C <sub>9</sub> H <sub>14</sub> O
14	Spiro [4.5]dec-6-en-8-one, 1,7-dimethyl-4-(1-methylethyl)-	Acorenone 1	C <sub>15</sub> H <sub>24</sub> O
15	(Z)-3-isopropyl-6,8 a-dimethyl-1,2,3,3a,4,5,8,8a-octahydroazulen-3a-ol	Bullnesol	C <sub>15</sub> H <sub>26</sub> O
16	(E)-3,7-dim ethylocta-1,5,7-trien-3-one	Hotrienol	C <sub>10</sub> H <sub>14</sub> O
17	(E)-3,7-dimethylocta-2,6-dienal	Not identified	C <sub>10</sub> H <sub>16</sub> O
18	Methyl octadeca-2,5-dienoate	Methyl 2,5-octadecadienoate	C <sub>19</sub> H <sub>30</sub> O <sub>2</sub>
19	(E)-3,7-dim ethylocta-2,6-dienyl acetate	1-Octanol	C <sub>12</sub> H <sub>20</sub> O <sub>2</sub>
20	Ethyl pentadecanoate	n-Pentadecanoic acid ethyl ester	C <sub>17</sub> H <sub>34</sub> O <sub>2</sub>
21	(1,2,6a,6b,9,9,12a-heptamethyl-1,2,3,4,4a,5,6,6a,6b,7,8,8a,9,10,11,12,12a,12b,13,14b-icosahydricen-4a yl)methanol	Not identified	C <sub>30</sub> H <sub>50</sub> O
22	10,13-Dimethyl-2-methylene-17-(6-methylheptan-2-yl)-hexadecahydro-1H-cyclopenta[a]phenanthren-3-ol	Not identified	C <sub>28</sub> H <sub>48</sub> O

(2) *Evaluation of Antinociceptive Activity on Hot Plate Model after 30 Minutes.* A significant increase in the latency time was observed in animals treated with standard drug (tramadol 5 mg/kg I/P) as compared to the vehicle control group. The latency time after 30 minutes observed in the positive control group was 17.23 with 47.59 ± 0.71% analgesic activity at 100 mg/kg body weight. The Hp. Chf fraction of the plant has reversed the latency time 14.33 ± 0.44 ( $P < 0.01$ ) with 36.99 ± 0.94% inhibition of thermal stimuli significantly at the dose of 100 mg/kg I/P. The Hp. EtAc also reversed the effect significantly causing 29.62 ± 0.84 ( $P < 0.05$ ) % inhibitions at the dose of 100 mg/kg (Table 4).

(3) *Evaluation of Antinociceptive Activity on Hot Plate Model Result after 60 Minutes.* A significant increase in the latency time was observed in animals treated with standard drug (tramadol 5 mg/kg I/P) as compared to the vehicle control group after 60 minutes ( $P < 0.001$ ). The fraction Hp. Chf has reversed the analgesic potential causing 44.16 ± 0.70% inhibition ( $P < 0.01$ ) significantly at the dose of 100 mg/kg I/P. The tested fraction Hp. EtAc having latency time in 14 seconds, which has also reversed the good effect of thermal stimuli with 35.50 ± 0.50% inhibition ( $P < 0.05$ ) significantly at the dose of 100 mg/kg (Table 4).

(4) *Evaluation of Antinociceptive Activity on Hot Plate Model Result after 90 Minutes.* A significant increase in the latency time was observed in animals treated with standard drug (tramadol 5 mg/kg I/P) as compared to the vehicle control group with latency time 13.27 ( $P < 0.001$ ) causing 34.69 ± 0.56 of % inhibition. The Hp. Chf fractions reversed

the pain effect significantly with latency time 11.25 ( $P < 0.01$ ) causing percent analgesic inhibitions 22.93 ± 0.60 at the dose of 100 mg/kg I/P. The Hp. EtAc fraction displayed a latency time of 8.8 causing a very low effect as contrasted to the negative control at the same dose. Results were shown in Table 4.

(5) *Mechanistic Antinociceptive Activity of Various Fractions on Hot Plate Model.* It depicts the tramadol antinociceptive activity, which shows that standard drug morphine (5 mg/kg) possesses a significant result, 34.10 ± 0.20 ( $P < 0.001$ ) % inhibition; the tested fraction Hp. Chf at a dose of 100 mg/kg causes 58.23 ± 0.44 ( $P < 0.001$ ) % inhibition while Hp. EtAc exhibited significant result 43.39 ± 0.52 ( $P < 0.001$ ). Table 5 represents the effects of naloxone after 30, 60, and 90 minutes in hot plate test. The data were expressed as means ± SEM ( $n = 6$ ).

3.3.3. *Evaluation of Anti-Inflammatory Activity Test Results.* A significant decrease in paw volume was observed in animals treated with standard drug (diclofenac sodium 10 mg/kg I/P) as compared to the vehicle control group. The percent increase in paw volume in the positive control group is decreased from the first 1<sup>st</sup> to 5<sup>th</sup> h with 30.01 ± 0.10 to 23.20 ± 0.40 ( $P < 0.001$ ) causing 34.76 ± 0.56 to 55.38 ± 0.80% edema volume inhibition from the 1<sup>st</sup> to 5<sup>th</sup> hours, respectively. The Hp. Chf displayed 32.61 ± 0.88 percent inhibition at the 1<sup>st</sup> h and till significant 46.15 ± 0.10 at the 5<sup>th</sup> h. The next most potent activity was shown by Hp.

TABLE 2: Results of in vitro cyclooxygenase and lipoxygenase inhibitory activity.

Name	Concentration	COX-2% inhibition (mean $\pm$ SEM)	COX-2 IC <sub>50</sub> ( $\mu$ g/ ml)	5-LOX % inhibition (mean $\pm$ SEM)	5-LOX IC <sub>50</sub> ( $\mu$ g/ ml)
Hp. Chf	1000	77.40 $\pm$ 0.25***	33.81	81.73 $\pm$ 0.37***	26.74
	500	72.41 $\pm$ 0.30**		75.27 $\pm$ 1.37***	
	250	65.79 $\pm$ 1.28***		69.62 $\pm$ 0.11***	
	125	61.32 $\pm$ 0.68*		63.81 $\pm$ 0.51***	
	62.5	56.49 $\pm$ 0.73**		59.08 $\pm$ 0.12***	
Hp. EtAc	1000	76.38 $\pm$ 0.76***	87.56	80.47 $\pm$ 0.70***	67.51
	500	69.37 $\pm$ 0.52***		73.57 $\pm$ 0.43***	
	250	62.90 $\pm$ 1.16***		65.12 $\pm$ 0.94***	
	125	54.48 $\pm$ 0.54***		57.76 $\pm$ 1.09***	
	62.5	45.56 $\pm$ 0.69***		49.38 $\pm$ 0.50***	
Hp. Cr	1000	65.94 $\pm$ 0.71***	200	71.50 $\pm$ 0.56***	106.99
	500	58.28 $\pm$ 0.54***		65.40 $\pm$ 0.55***	
	250	52.65 $\pm$ 0.91***		59.36 $\pm$ 0.57***	
	125	45.30 $\pm$ 0.55***		51.30 $\pm$ 0.52***	
	62.5	37.63 $\pm$ 0.98***		44.37 $\pm$ 0.58***	
Hp. Hex	1000	64.55 $\pm$ 0.51***	217.93	66.42 $\pm$ 0.46***	171.05
	500	57.55 $\pm$ 0.67***		60.53 $\pm$ 0.41***	
	250	51.40 $\pm$ 0.44***		52.68 $\pm$ 0.64***	
	125	45.67 $\pm$ 0.55***		47.46 $\pm$ 0.47***	
	62.5	37.33 $\pm$ 0.62**		40.51 $\pm$ 0.62***	
Hp. Bt	1000	60.35 $\pm$ 0.51***	438.39	63.45 $\pm$ 0.59***	328.34
	500	51.27 $\pm$ 0.58***		55.49 $\pm$ 0.60***	
	250	43.41 $\pm$ 0.55***		46.23 $\pm$ 0.44***	
	125	34.40 $\pm$ 0.76*		37.50 $\pm$ 0.61**	
	62.5	27.24 $\pm$ 0.80*		31.47 $\pm$ 0.46*	
Hp. Aq	1000	68.83 $\pm$ 1.07***	141.2	72.37 $\pm$ 0.54***	132.27
	500	61.39 $\pm$ 0.60***		64.00 $\pm$ 0.20***	
	250	56.58 $\pm$ 0.56***		57.15 $\pm$ 0.91***	
	125	49.29 $\pm$ 0.43***		51.15 $\pm$ 0.61***	
	62.5	41.37 $\pm$ 0.58***		40.40 $\pm$ 0.68***	
Celecoxib	1000	84.51 $\pm$ 0.30	23.20	87.66 $\pm$ 0.45	—
	500	77.84 $\pm$ 0.27		81.64 $\pm$ 0.42	
	250	73.50 $\pm$ 2.26		—	
	125	65.74 $\pm$ 0.16		—	
	62.5	61.56 $\pm$ 0.28		—	
Montelukast	1000	—	—	87.66 $\pm$ 0.45	17.47
	500	—		81.64 $\pm$ 0.42	
	250	—		76.01 $\pm$ 1.61	
	125	—		70.46 $\pm$ 0.32	
	62.5	—		64.50 $\pm$ 0.02	

The values are presented as mean  $\pm$  SEM ( $n=5$ ). The asterisk shows that the significance levels in comparison with that of the negative control. Data were analyzed via two-way ANOVA followed by Bonferroni's posttest. \* $P < 0.05$ , \*\* $P < 0.01$ , and \*\*\* $P < 0.001$ .

TABLE 3: Group of animals and drug quantities are given for acute toxicity studies with various fractions of *H. plantaginea*.

Groups	Animals	Conc. ( $\mu$ g/mL)
1	5	25
2	5	50
3	5	100
4	5	200
5	5	300
6	5	400
7	5	500
8	5	1000
9	5	2000



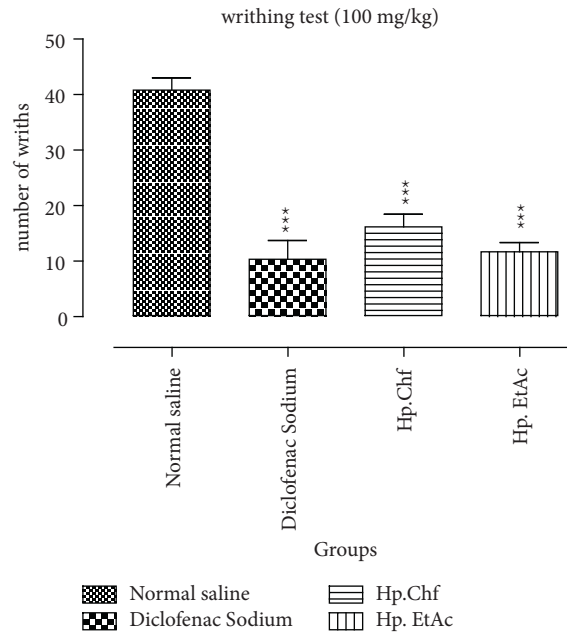


FIGURE 3: Analgesic activities through acetic acid-induced writhing potential in mice. The data were expressed as means  $\pm$  SEM ( $n = 6$ ). Data were analyzed via two-way ANOVA followed by Bonferroni's posttest. \*\*\* $P < 0.001$ . ### Comparison of standard drug to the normal saline group.

TABLE 4: Antinociceptive activity of *H. plantaginea* assessed using the hot plate test.

Treatment	Dose (mg/kg)	Latency time in seconds (mean $\pm$ SEM)		
		After 30 min	After 60 min	After 90 min
Normal saline	10 ml/kg	9.03 $\pm$ 0.40	10.05 $\pm$ 0.30	8.67 $\pm$ 0.65
Standard	5 mg/kg	17.23 $\pm$ 0.33***	19.56 $\pm$ 0.52***	13.27 $\pm$ 0.25***
Hp. Chf	100 mg/kg	14.33 $\pm$ 0.44**	16.17 $\pm$ 0.42**	11.25 $\pm$ 0.52**
Hp. EtAc	100 mg/kg	12.83 $\pm$ 0.52*	14.00 $\pm$ 0.10***	8.83 $\pm$ 0.80*

The data represent analgesic activities through hot plate test in mice. The data were expressed as means  $\pm$  SEM ( $n = 6$ ) analyzed via two-way ANOVA followed by Bonferroni's posttest. \* $P < 0.05$ ; \*\* $P < 0.01$ ; \*\*\* $P < 0.001$ ; and ns: not significant.

TABLE 5: Results of analgesic activity following hot plate model and opioid receptors evaluation study.

Samples	Dose (mg/kg)	Reaction time on hot plate		
		30 min	60 min	90 min
Normal saline	10 ml/kg	10.12 $\pm$ 0.42	10.12 $\pm$ 0.57	10.12 $\pm$ 0.33
Normal saline + NLX	10 ml/kg + 1	10.14 $\pm$ 0.71	10.14 $\pm$ 0.47	10.14 $\pm$ 0.60
Morphine	5	21.64 $\pm$ 0.59	23.64 $\pm$ 0.70	19.64 $\pm$ 0.60
Morphine + NLX	5 + 1	14.26 $\pm$ 0.94	16.60 $\pm$ 0.66	12.40 $\pm$ 0.88
Hp. EtAc	100	19.96 $\pm$ 0.05	22.26 $\pm$ 0.04	24.80 $\pm$ 0.07
Hp. EtAc + NLX	100 + 1	11.30 $\pm$ 0.03	13.70 $\pm$ 0.09	16.60 $\pm$ 0.48
Hp. Chf	100	20.42 $\pm$ 0.08	25.60 $\pm$ 0.05	28.10 $\pm$ 0.55
Hp. Chf + NLX	100 + 1	8.53 $\pm$ 0.30	9.98 $\pm$ 0.59	14.40 $\pm$ 0.71

While after 60 minutes, the standard drug tramadol possesses a significant result ( $P < 0.01$ ). Hp. Chf and Hp. EtAc fractions displayed dose-dependent result causing  $61.01 \pm 0.45$  ( $P < 0.001$ ) and  $38.45 \pm 0.50$  ( $P < 0.01$ ) analgesic effect at the dose of 100 mg/kg. Similarly, after 90 minutes, tramadol again exhibited a significant result ( $P < 0.01$ ), while tested fraction Hp. EtAc has  $33.06 \pm 0.33$  ( $P < 0.01$ )% potential. Likewise, tested fraction Hp. Chf at 100 mg/kg body weight exhibited dose-dependent results as that of the standard drug causing  $48.75 \pm 0.56$  ( $P < 0.001$ )% inhibitions.

EtAc at the 4th h ( $43.40 \pm 0.42$ ) after carrageenan induction (Figure 4).

**3.3.4. Evaluation of Brewer's Yeast-Induced Antipyretic Activity Result.** The subcutaneous injection of yeast suspension

noticeably elevated the rectal temperature after administration. A significant decrease in rectal volume was observed after 30, 60, and 90 minutes with  $34.20 \pm 0.42$ ,  $33.02 \pm 0.10$ , and  $35.50 \pm 0.52^\circ\text{C}$  ( $P < 0.001$ ) in animals treated with standard drug (50 mg/kg I/P) as compared to the vehicle control group. The tested fraction Hp. Chf also reduced the

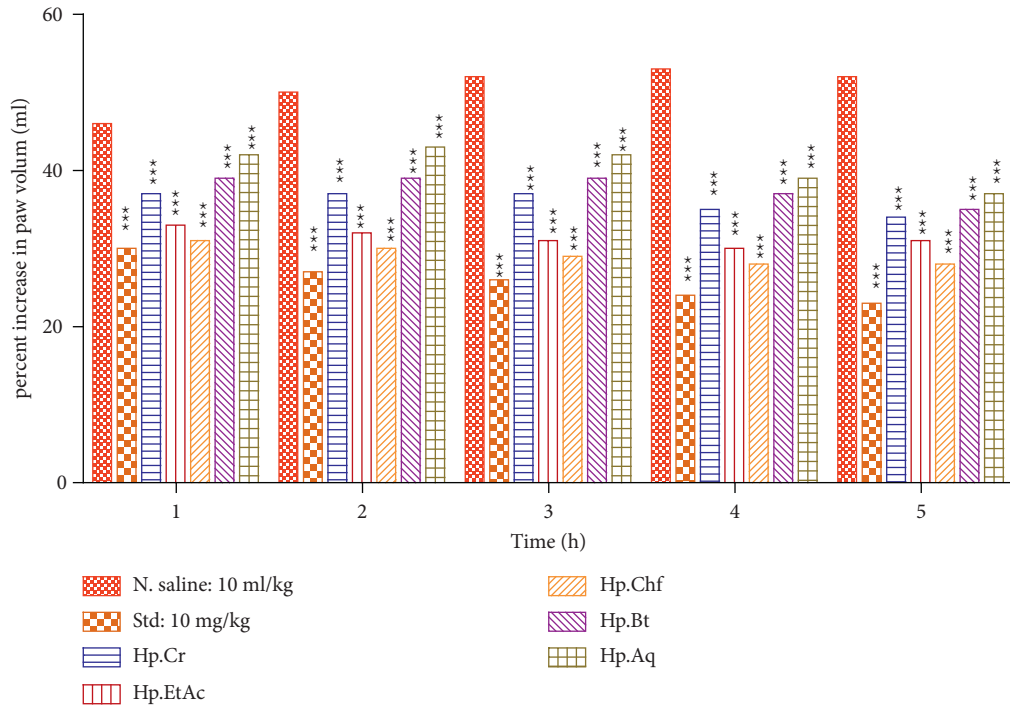


FIGURE 4: Carrageenan-induced anti-inflammatory potential in mice. The data were expressed as means  $\pm$  SEM ( $n = 6$ ). Data were analyzed via two-way ANOVA followed by Bonferroni's posttest. \*\*\* $P < 0.001$ .

rectal temperature significantly at 30, 60, and 90 minutes causing  $34.10 \pm 0.56$ ,  $32.88 \pm 0.66$ , and  $34.10 \pm 0.20^\circ\text{C}$  ( $P < 0.001$ ) at 100 mg/kg i/p. The other fraction like Hp. EtAc also revealed good reduction in rectal volume after 60 minutes,  $36.20 \pm 0.40^\circ\text{C}$  ( $P < 0.01$ ) (Figure 5).

#### 4. Discussion

Currently, several investigational drugs have been developed by scientists to control pain and inflammation but still the therapy is not completely satisfactory [34, 35]. Due to a considerable increase in the field of medicine, disease and disorder treatment with new inventions increase tremendously. The evolutions of synthetic compounds and alternate medicine are searching out in which the possibilities of adverse effects should be minimized as compared to existing drugs. For the treatment and management of pain, inflammation, and pyrexia, the use of NSAIDs leads to severe abnormalities and complications which causes cardiac and kidney abnormality, gastric and intestinal bleeding, and so on (Wolfe et al., 1999) [27]. The human COX enzyme is a dimer of COX-1 and COX-2 subunits and catalyzes the oxidation of AA to generate  $\text{PGG}_2$  followed by reduction into  $\text{PGH}_2$  [36]. The prostaglandins  $\text{PGG}_2$  and  $\text{PGH}_2$  are the precursors of signaling molecules in various diseases including inflammation, cardiovascular problems, and cancer [37]. The catalytic domain of each subunit of the dimer comprises cyclooxygenase and peroxidase active sites on either side of the heme prosthetic group [38]. The nonselective NSAIDs target the COX-1 and COX-2 enzymes to block the formation of inflammatory signaling precursors leading to acute inflammation, cancer, and cardiovascular

diseases [39]. For example, aspirin acetylates Ser-530 on the cyclooxygenase active site and inactivates the enzyme by interfering with the binding of AA to Ser-530 in each of the two subunits [40].

For the evaluation of antinociceptive activity acetic acid-induced writhing model, pain in the peripheral origin is induced through the injection of irritant chemicals, such as acetic acid [41]. In the activity of abdominal constrictions, which are induced by acetic acid, the synthesis of prostaglandins plays a key role [42] through the action of the essential enzymes such as cyclooxygenase-II, which cause an increase in pain perception at sensory nerve endings. Perception of pain through COX pathway and activation of the sensory pathways in the peritoneum of mice encourage abdominal constrictions and a viscerosomatic reflex was observed in response to acetic acid (algesiogenics) [43]. At the terminal of the abdominal peritoneum sensory afferents, neurons possess adrenergic receptors like  $\alpha$ -adrenoceptors,  $\beta$ -adrenoceptors, and some opioid receptors. The generations of pain impulses become depressed with the activation of these receptors by the appropriate agonists but in the mice peritoneum, an interaction was found between opioid receptors and  $\alpha$ -adrenoceptors [44, 45]. The central and peripheral processes are involved in abdominal constrictions [46].

The inflammatory process along with neurons of the dorsal horn is activated in the later phase of nociception [47]. It was suggested that in hot plate test determination of central pain mechanisms the nociceptive responses are integrated supraspinally [48].

In Figure 1, the study of antinociceptive activity on mice was evaluated through acetic acid induced writhing model,

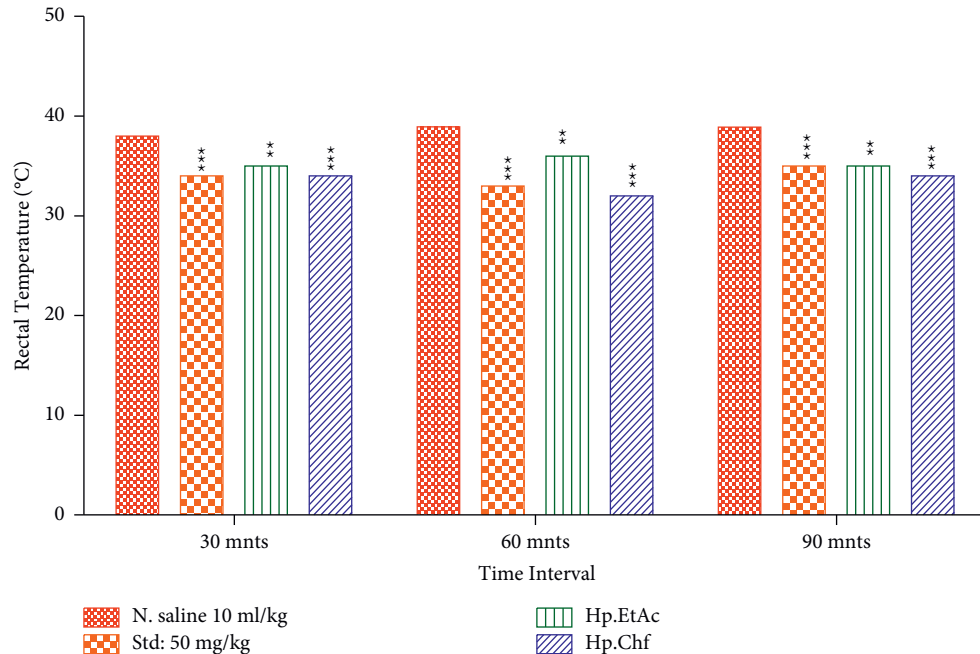


FIGURE 5: Anti-inflammatory activities through Brewer's yeast-induced pyrexia in mice. The data were expressed as means  $\pm$  SEM ( $n = 6$ ). Data were analyzed via two-way ANOVA followed by Bonferroni's posttest. \*\*\* $P < 0.001$ .

which shows a significant decrease in the number of writhes in animals treated with standard drug being 10.33 with 74.70% of inhibition at a dose of 50 mg/kg I/P. The potent fractions of *H. plantaginea* like Hp. Chf and Hp. EtAc at the dose of 100 mg/kg body weight I/p show a significant effect with the number of writhes:  $16.17 \pm 0.10$  and  $11.67 \pm 0.60$  causing  $60.39 \pm 0.42$  and  $71.42 \pm 0.55\%$  of inhibition, respectively ( $P < 0.001$ ), in acetic acid-induced analgesia. Hot plat test has been performed to distinguish whether the various fractions have a central or peripheral antinociceptive effect. Standard drug shows a significant  $47.59 \pm 0.71\%$  inhibition ( $P < 0.001$ ) resulting in prolonging the latency time at various intervals while in tested fractions Hp. Chf exhibited a significant result causing  $36.99 \pm 0.94$  and  $44.16 \pm 0.70$  ( $P < 0.01$ ) after 30 and 60 minutes at a dose of 100 mg/kg I/P in hot plate evaluation test. The tramadol antagonistic nociceptive activity was evaluated by utilizing the hot plate test [49]. The antinociceptive effect of tramadol (5 mg/kg) was reversed significantly by opioid antagonist naloxone (1 mg/kg) causing  $34.10 \pm 0.20$  ( $P < 0.01$ ), and the Hp. EtAc and Hp. Chf fractions have shown a significant result:  $43.39 \pm 0.52$  ( $P < 0.01$ ) and  $29.76 \pm 0.66$  ( $P < 0.01$ ) percent inhibition after 30 minutes at a dose of 100 mg/kg, respectively.

For the evaluation of antipyretic activity, fungal pyrogens present in Brewer's yeast induce pyrexia in rodents. Recommended guidelines for the evaluation of antipyretic activities show that Brewer's yeast should be administered subcutaneously [50]. Upon administration of Brewer's yeast, several inflammatory mediators such as transcription factors, cytokines like IL-6 and TNF-, and enzymes involved in the synthesis of PGE<sub>2</sub> are released [51]. The retardations of these mediators are accountable for the antipyretic effects

(Rawlins, 1973). The cause of pyrexia induced with the administration of Brewer's yeast may be due to the production of prostaglandins [52]. Upon administration of various reactions of the *H. plantaginea* at high doses such as 100 mg/kg on the base of body weight I/P and standard drug paracetamol the rectal temperature of mice were significantly at 30, 60, and 90 minutes with  $34.20 \pm 0.42$ ,  $33.02 \pm 0.10$ , and  $35.50 \pm 0.52^\circ\text{C}$  ( $P < 0.001$ ) reduced, which shows that the tested fraction possesses antipyretic activity. The possible mechanism of the Hp. Chf ( $34.10 \pm 0.56$  at 30 minutes) fraction and standard drug paracetamol may be the inhibition of PGs, which shows its antipyretic activities.

The most common model used for the study of inflammation is carrageenan-induced paw edema [53]. The most important parameter of inflammation is the formation of edema, which is considered for the evaluation of anti-inflammatory activity of selected compounds [54]. PGE<sub>2</sub> and Bradykinin release at the site of inflammation induced carrageenan [55, 56]. A biphasic response was investigated with the injection of carrageenan in the paw of the mice in which multiple mediators are released which leads inflammation (Cuzzocrea et al., 1999). This study shows that Hp. Chf fraction of *H. plantaginea* significantly displayed  $32.61 \pm 0.88$  percent inhibition at the 1st h and till significant  $46.15 \pm 0.10$  at the 5th h. The next potent activity was shown by Hp. EtAc at the 4th h ( $43.40 \pm 0.42$ ) after carrageenan induction. The results demonstrate that the both fractions affect the early and late phases of inflammation.

During the pain and inflammatory progression, the release of free radicals like ROS that cause the proinflammatory cytokines (IL1 $\beta$ , TNF- $\alpha$ , and IL-6), production of cell lyses, and COX and LOX expression are responsible for various diseases [57, 58]. The inhibitory result of the

various fractions of *H. plantaginea* against COX-2 and 5-LOX enzyme was assessed that were extensively employed to conclude the anti-inflammatory capacity of the fractions [59] and is generally employed for the evaluation of analgesic and anti-inflammatory potential of various fractions. Based on the result attained from the current study, the COX-2 and 5-LOX scavenging potential of Hp. Chf (IC<sub>50</sub> 33.81 and 26.74 µg/mL) exhibited comparable and dose-dependent results to that of standard drug celecoxib and montelukast (IC<sub>50</sub> 23.20 and 17.47 µg/mL) [60]. The in vitro analgesic and anti-inflammatory capacity of various fractions contribute to strengthening the anti-inflammatory, antipyretic, and analgesic potentials.

This study possesses significant importance in the development of new natural product research, which permits us to predict that the said plant has new drugs that contain antinociceptive, antipyretic, and anti-inflammatory properties. The natural products are free from common side effects possessed by traditional NSAIDs, which minimize economic burden and increase patient compliance. The current study possesses a base for the development of new drugs, which require detailed pharmacological study on different animal models.

## 5. Conclusions

Based on current results, it might be clear that *H. plantaginea* plant has anti-inflammatory potential and also possesses analgesic and antipyretic compounds. Further, *H. plantaginea* may be a good candidate for complementary and alternative therapy. This might be free from common side effects passed by traditional NSAIDs. This study also gives investigational and scientific justification for the ethnomedicinal use of *H. plantaginea* plant as analgesic, anti-inflammatory, and antipyretic.

## Abbreviations

AA:	Arachidonic acid
Aq:	Aqueous
Bt:	Butanol
Cr:	Crude extract
Chf:	Chloroform
COX:	Cyclooxygenase
EtAc:	Ethyl acetate
GC-MS:	Gas chromatography-mass spectroscopy
GIT:	Gastrointestinal tract
Hp:	<i>Habenaria plantaginea</i>
IL-6:	Interleukine-6
KH <sub>2</sub> PO <sub>4</sub> :	Potassium dihydrogen phosphate
K <sub>2</sub> HPO <sub>4</sub> :	Dipotassium hydrogen phosphate
LOX:	Lipoxygenase
NSAIDs:	Nonsteroidal anti-inflammatory drugs
PGH <sub>2</sub> :	Prostaglandin H <sub>2</sub>
ROS:	Reactive oxygen species
SEM:	Standard error means
TMPD:	N,N,N-Tetramethyl-p-phenylenediamine dihydrochloride
TNF-α:	Tumor necrosis factor-alpha.

## Data Availability

Data will be available from the corresponding author upon request.

## Conflicts of Interest

There are no conflicts of interest declared by all the authors regarding the publication of this paper.

## Acknowledgments

The authors would like to express their gratitude and thanks to the Deanship of Scientific Research at Najran University for funding this paper under the code NU/-/MRC/10/375.

## References

- [1] B. Kalra, S. Kalra, and S. Bajaj, "Vulvodinia: an unrecognized diabetic neuropathic syndrome," *Indian journal of endocrinology and metabolism*, vol. 17, p. 787, 2013.
- [2] S. M. M. Shah, F. Ullah, S. M. H. Shah, M. Zahoor, and A. Sadiq, "Analysis of chemical constituents and antinociceptive potential of essential oil of *Teucrium Stocksianum* bioss collected from the North West of Pakistan," *BMC Complementary and Alternative Medicine*, vol. 12, p. 244, 2012.
- [3] A. Zeb, S. Ahmad, F. Ullah, M. Ayaz, and A. Sadiq, "Antinociceptive activity of ethnomedicinally important analgesic plant *Isodon rugosus* Wall. ex Benth: mechanistic study and identifications of bioactive compounds," *Frontiers in Pharmacology*, vol. 7, p. 200, 2016.
- [4] M. Ayaz, M. Junaid, F. Ullah et al., "Molecularly characterized solvent extracts and saponins from *Polygonum hydropiper* L. show high anti-angiogenic, anti-tumor, brine shrimp, and fibroblast NIH/3T3 cell line cytotoxicity," *Frontiers in Pharmacology*, vol. 7, p. 74, 2016.
- [5] A. Zeb, F. Ullah, M. Ayaz, S. Ahmad, and A. Sadiq, "Demonstration of biological activities of extracts from *Isodon rugosus* wall. ex benth: separation and identification of bioactive phytoconstituents by GC-MS analysis in the ethyl acetate extract," *BMC Complementary and Alternative Medicine*, vol. 17, pp. 1–16, 2017.
- [6] S. Akbar, F. Subhan, M. Shahid et al., "6-Methoxyflavanone abates cisplatin-induced neuropathic pain apropos anti-inflammatory mechanisms: a behavioral and molecular simulation study," *European Journal of Pharmacology*, vol. 872, Article ID 172972, 2020.
- [7] M. Abdollahi, H. Karimpour, and H. R. Monsef-Esfehani, "Antinociceptive effects of *Teucrium polium* L total extract and essential oil in mouse writhing test," *Pharmacological Research*, vol. 48, no. 1, pp. 31–35, 2003.
- [8] M. S. Jan, M. Shahid, S. Ahmad et al., "Synthesis of pyrrolidine-2, 5-dione based anti-inflammatory drug: in vitro COX-2, 5-LOX inhibition and in vivo anti-inflammatory studies," *Latin American Journal of Pharmacy*, vol. 38, pp. 2287–2294, 2019.
- [9] A. Munir, A. Khushal, K. Saeed et al., "Synthesis, in-vitro, in-vivo anti-inflammatory activities and molecular docking studies of acyl and salicylic acid hydrazide derivatives," *Bioorganic Chemistry*, vol. 104, Article ID 104168, 2020.
- [10] M. Ayaz, M. Junaid, F. Ullah et al., "GC-MS analysis and gastroprotective evaluations of crude extracts, isolated

- saponins, and essential oil from *Polygonum hydropiper* L,” *Frontiers in Chemistry*, vol. 5, p. 58, 2017.
- [11] X. Tong, X. Li, M. Ayaz et al., “Neuroprotective studies on *Polygonum hydropiper* L. essential oils using transgenic animal models,” *Frontiers in Pharmacology*, p. 2290, 2021.
  - [12] M. S. Jan, S. Ahmad, F. Hussain et al., “Design, synthesis, in-vitro, in-vivo and in-silico studies of pyrrolidine-2, 5-dione derivatives as multitarget anti-inflammatory agents,” *European Journal of Medicinal Chemistry*, vol. 186, Article ID 111863, 2020.
  - [13] A. T. Khalil, M. Ovais, J. Iqbal et al., “Microbes-mediated synthesis strategies of metal nanoparticles and their potential role in cancer therapeutics,” in *Seminars in Cancer Biology*, Elsevier, Amsterdam, Netherlands, 2021.
  - [14] S. Ahmad, M. H. Mahnashi, B. A. Alyami et al., “Synthesis of michael adducts as key building blocks for potential analgesic drugs: in vitro, in vivo and in silico explorations,” *Drug Design, Development and Therapy*, vol. 15, p. 1299, 2021.
  - [15] M. W. Chase, K. M. Cameron, J. V. Freudenstein et al., “An updated classification of *Orchidaceae*,” *Botanical Journal of the Linnean Society*, vol. 177, pp. 151–174, 2015.
  - [16] M. M. Hossain, “Therapeutic orchids: traditional uses and recent advances—an overview,” *Fitoterapia*, vol. 82, pp. 102–140, 2011.
  - [17] J.-M. Kong, N.-K. Goh, L.-S. Chia, and T.-F. Chia, “Recent advances in traditional plant drugs and orchids,” *Acta Pharmacologica Sinica*, vol. 24, pp. 7–21, 2003.
  - [18] P. Ramos, G. A. Colareda, M. A. Rosella, S. L. Debenedetti, E. D. Spegazzini, and A. E. Consolini, “Phytochemical profile and anti-inflammatory effect of the orchid *Catasetum macroglossum*,” *Latin American Journal of Pharmacy*, vol. 31, pp. 62–67, 2012.
  - [19] V. G. Nair, P. K. Prajapati, K. Nishteswar, V. Unnikrishnan, and M. B. Nariya, “Analgesic and anti-inflammatory activities of *Bulbophyllum neilgherrense* wight. pseudobulb: a folklore plant,” *Ayu*, vol. 39, p. 76, 2018.
  - [20] M. Chinsamy, J. Finnie, and J. Van Staden, “Anti-inflammatory, antioxidant, anti-cholinesterase activity and mutagenicity of South African medicinal orchids,” *South African Journal of Botany*, vol. 91, pp. 88–98, 2014.
  - [21] M. H. Mahnashi, B. A. Alyami, Y. S. Alqahtani et al., “Phytochemical profiling of bioactive compounds, anti-inflammatory and analgesic potentials of *Habenaria digitata* Lindl.: molecular docking based synergistic effect of the identified compounds,” *Journal of Ethnopharmacology*, vol. 273, Article ID 113976, 2021.
  - [22] A. Zeb, A. Sadiq, F. Ullah, S. Ahmad, and M. Ayaz, “Phytochemical and toxicological investigations of crude methanolic extracts, subsequent fractions and crude saponins of *Isodon rugosus*,” *Biological Research*, vol. 47, p. 57, 2014.
  - [23] A. Sadiq, A. Zeb, F. Ullah et al., “Chemical characterization, analgesic, antioxidant, and anticholinesterase potentials of essential oils from *Isodon rugosus* wall. ex. Benth,” *Frontiers in Pharmacology*, vol. 9, p. 623, 2018.
  - [24] R. Zafar, H. Ullah, M. Zahoor, and A. Sadiq, “Isolation of bioactive compounds from *Bergenia ciliata* (haw.) sternb rhizome and their antioxidant and anticholinesterase activities,” *BMC Complementary and Alternative Medicine*, vol. 19, pp. 1–13, 2019.
  - [25] S. M. M. Shah, A. Sadiq, S. M. H. Shah, and F. Ullah, “Antioxidant, total phenolic contents and antinociceptive potential of *Teucrium stocksianum* methanolic extract in different animal models,” *BMC Complementary and Alternative Medicine*, vol. 14, pp. 1–7, 2014.
  - [26] F. Alam, K. M. Din, R. Rasheed et al., “Phytochemical investigation, anti-inflammatory, antipyretic and antinociceptive activities of *Zanthoxylum armatum* DC extracts-in vivo and in vitro experiments,” *Heliyon*, vol. 6, Article ID e05571, 2020.
  - [27] A. Sadiq, U. Rashid, S. Ahmad et al., “Treating hyperglycemia from *Eryngium caeruleum* M. Bieb: in-vitro  $\alpha$ -glucosidase, antioxidant, in-vivo antidiabetic and molecular docking-based approaches,” *Frontiers in Chemistry*, vol. 8, p. 1064, 2020.
  - [28] N. F. M. Rocha, E. R. V. Rios, A. M. R. Carvalho et al., “Antinociceptive and anti-inflammatory activities of (–)- $\alpha$ -bisabolol in rodents,” *Naunyn-Schmiedeberg’s archives of pharmacology*, vol. 384, pp. 525–533, 2011.
  - [29] F. Subhan, M. Abbas, K. Rauf, M. Arfan, R. Sewell, and G. Ali, “The role of opioidergic mechanism in the activity of *Bacopa monnieri* extract against tonic and acute phasic pain modalities,” *Pharmacologyonline*, vol. 3, pp. 903–914, 2010.
  - [30] A. M. Mahmoud, M. M. EL-Wekil, M. H. Mahnashi, M. F. Ali, and S. A. Alkahtani, “Modification of N, S co-doped graphene quantum dots with p-aminothiophenol-functionalized gold nanoparticles for molecular imprint-based voltammetric determination of the antiviral drug sofosbuvir,” *Microchimica Acta*, vol. 186, pp. 1–8, 2019.
  - [31] N. Ahmad, F. Subhan, N. U. Islam, M. Shahid, F. U. Rahman, and K. Fawad, “A novel pregabalin functionalized salicylaldehyde derivative afforded prospective pain, inflammation, and pyrexia alleviating propensities,” *Archiv der Pharmazie*, vol. 350, Article ID e201600365, 2017.
  - [32] C. A. Winter, E. A. Risley, and G. W. Nuss, “Anti-inflammatory and antipyretic activities of indo-methacin, 1-(p-chlorobenzoyl)-5-methoxy-2-methyl-indole-3-acetic acid,” *Journal of Pharmacology and Experimental Therapeutics*, vol. 141, pp. 369–376, 1963.
  - [33] M. M. Al-Harbi, S. Qureshi, M. M. Ahmed, M. Raza, G. A. Miana, and A. H. Shah, “Studies on the anti-inflammatory, antipyretic and analgesic activities of santonin,” *The Japanese Journal of Pharmacology*, vol. 64, pp. 135–139, 1994.
  - [34] R. K. Portenoy and K. M. Foley, “Chronic use of opioid analgesics in non-malignant pain: report of 38 cases,” *Pain*, vol. 25, pp. 171–186, 1986.
  - [35] D. Rozen and G. W. Grass, “Perioperative and intraoperative pain and anesthetic care of the chronic pain and cancer pain patient receiving chronic opioid therapy,” *Pain Practice*, vol. 5, pp. 18–32, 2005.
  - [36] W. L. Smith, Y. Urade, and P. J. Jakobsson, “Enzymes of the cyclooxygenase pathways of prostanoïd biosynthesis,” *Chemical Reviews*, vol. 111, pp. 5821–5865, 2011.
  - [37] E. M. Smyth, T. Grosser, M. Wang, Y. Yu, and G. A. Fitzgerald, “Prostanoids in health and disease,” *The Journal of Lipid Research*, vol. 50, pp. S423–S428, 2009.
  - [38] M. G. Malkowski, S. L. Ginell, W. L. Smith, and R. M. Garavito, “The productive conformation of arachidonic acid bound to prostaglandin synthase,” *Science*, vol. 289, pp. 1933–1937, 2000.
  - [39] A. J. Vecchio, D. M. Simmons, and M. G. Malkowski, “Structural basis of fatty acid substrate binding to cyclooxygenase-2,” *Journal of Biological Chemistry*, vol. 285, pp. 22152–22163, 2010.
  - [40] M. J. Lucido, B. J. Orlando, A. J. Vecchio, and M. G. Malkowski, “Crystal structure of aspirin-acetylated human cyclooxygenase-2: insight into the formation of

- products with reversed stereochemistry,” *Biochemistry*, vol. 55, pp. 1226–1238, 2016.
- [41] S. Gawade, “Acetic acid induced painful endogenous infliction in writhing test on mice,” *Journal of Pharmacology and Pharmacotherapeutics*, vol. 3, p. 348, 2012.
- [42] H. Matsumoto, H. Naraba, A. Ueno et al., “Induction of cyclooxygenase-2 causes an enhancement of writhing response in mice,” *European Journal of Pharmacology*, vol. 352, pp. 47–52, 1998.
- [43] L. R. Ballou, R. M. Botting, S. Goorha, J. Zhang, and J. R. Vane, “Nociception in cyclooxygenase isozyme-deficient mice,” *Proceedings of the National Academy of Sciences*, vol. 97, pp. 10272–10276, 2000.
- [44] A. Gray, P. Spencer, and R. Sewell, “The involvement of the opioidergic system in the antinociceptive mechanism of action of antidepressant compounds,” *British Journal of Pharmacology*, vol. 124, pp. 669–674, 1998.
- [45] A. M. Gray, M. J. Nevinson, and R. D. Sewell, “The involvement of opioidergic and noradrenergic mechanisms in nefopam antinociception,” *European Journal of Pharmacology*, vol. 365, pp. 149–157, 1999.
- [46] Z. A. Zakaria, L. Y. Wen, N. I. A. Rahman, A. H. A. Ayub, M. R. Sulaiman, and H. K. Gopalan, “Antinociceptive, anti-inflammatory and antipyretic properties of the aqueous extract of *Bauhinia purpurea* leaves in experimental animals,” *Medical Principles and Practice*, vol. 16, pp. 443–449, 2007.
- [47] A. Tjølsen, A. Lund, and K. Hole, “Antinociceptive effect of paracetamol in rats is partly dependent on spinal serotonergic systems,” *European Journal of Pharmacology*, vol. 193, pp. 193–201, 1991.
- [48] H. Hosseinzadeh and H. M. Younesi, “Antinociceptive and anti-inflammatory effects of *Crocus sativus* L. stigma and petal extracts in mice,” *BMC Pharmacology*, vol. 2, p. 7, 2002.
- [49] F. Noble, C. Smadja, O. Valverde et al., “Pain-suppressive effects on various nociceptive stimuli (thermal, chemical, electrical and inflammatory) of the first orally active enkephalin-metabolizing enzyme inhibitor RB 120,” *Pain*, vol. 73, pp. 383–391, 1997.
- [50] P. Thangaraj, “Antipyretic activity,” *Pharmacological Assays Of Plant-Based Natural Products*, Springer, Berlin Germany, 2016.
- [51] R. Dangarembizi, K. Erlwanger, C. Rummel, J. Roth, M. Madziva, and L. Harden, “Brewer’s yeast is a potent inducer of fever, sickness behavior and inflammation within the brain,” *Brain, Behavior, and Immunity*, vol. 68, pp. 211–223, 2018.
- [52] Q. J. Pittman, X. Chen, A. Mouihate, M. Hirasawa, and S. Martin, “Arginine vasopressin, fever and temperature regulation,” *Progress Brain Research*, vol. 119, pp. 383–392, 1998.
- [53] F. Nantel, D. Denis, R. Gordon et al., “Distribution and regulation of cyclooxygenase-2 in carrageenan-induced inflammation,” *British Journal of Pharmacology*, vol. 128, pp. 853–859, 1999.
- [54] C. J. Morris, “Carrageenan-induced Paw Edema in the rat and mouse,” *Inflammation Protocols*, Springer, Berlin, Germany, 2003.
- [55] J. B. Calixto, M. M. Campos, M. F. Otuki, and A. R. Santos, “Anti-inflammatory compounds of plant origin. Part II. Modulation of pro-inflammatory cytokines, chemokines and adhesion molecules,” *Planta Medica*, vol. 70, pp. 93–103, 2004.
- [56] J. I. Gallin, I. M. Goldstein, and R. Snyderman, *Inflammation: Basic Principles and Clinical Correlates*, Lippincott Williams & Wilkins, Philadelphia, PA, USA, 1999.
- [57] A. Ahmad, F. Ullah, A. Sadiq et al., “Comparative cholinesterase,  $\alpha$ -glucosidase inhibitory, antioxidant, molecular docking, and kinetic studies on potent succinimide derivatives,” *Drug Design, Development and Therapy*, vol. 14, p. 2165, 2020.
- [58] B. Alam, F. Akter, N. Parvin et al., “Antioxidant, analgesic and anti-inflammatory activities of the methanolic extract of piper betle leaves,” *Avicenna Journal of Phytomedicine*, vol. 3, p. 112, 2013.
- [59] B. Aouey, A. Samet, H. Fetoui, M. Simmonds, and M. Bouaziz, “Anti-oxidant, anti-inflammatory, analgesic and antipyretic activities of grapevine leaf extract (*vitis vinifera*) in mice and identification of its active constituents by LC-MS/MS analyses,” *Biomedicine & Pharmacotherapy*, vol. 84, pp. 1088–1098, 2016.
- [60] E.-M. Choi and J.-K. Hwang, “Antiinflammatory, analgesic and antioxidant activities of the fruit of *Foeniculum vulgare*,” *Fitoterapia*, vol. 75, pp. 557–565, 2004.



## Research Article

# Wenyang Huazhuo Tuihuang Formula Inhibits the Th17/Treg Cell Imbalance and Protects against Acute-on-Chronic Liver Failure

Xiufeng Wang,<sup>1</sup> Yunqing Zhong,<sup>2</sup> Rongzhen Zhang ,<sup>1</sup> Yueqiao Chen,<sup>1</sup> Minggang Wang ,<sup>1</sup> Chao Lv,<sup>1</sup> and Dewen Mao <sup>1</sup>

<sup>1</sup>Department of Liver Disease Area 1, The First Affiliated Hospital of Guangxi University of Chinese Medicine, Nanning 530201, China

<sup>2</sup>Department of Pulmonary Disease, Guangxi International Zhuang Medicine Hospital, Nanning, China

Correspondence should be addressed to Dewen Mao; mdwboshi2005@163.com

Received 31 December 2021; Revised 22 February 2022; Accepted 7 March 2022; Published 30 March 2022

Academic Editor: Ruchika Garg

Copyright © 2022 Xiufeng Wang et al. This is an open access article distributed under the Creative Commons Attribution License, which permits unrestricted use, distribution, and reproduction in any medium, provided the original work is properly cited.

**Objective.** Acute-on-chronic liver failure (ACLF) is a group of chronic liver diseases and caused by acute internal and external liver injury. Wenyang Huazhuo Tuihuang (WYHZTH) formula had a good clinical effect on promoting the resolution of jaundice. The aim of this study is to further investigate the mechanism of the WYHZTH formula in the ACLF rat model. **Methods.** The ACLF rat model was constructed by combining human serum albumin with LPS and D-gal. WYHZTH was used to intervene and treat. The cytokines IL-17, IL-23, IL-10, and TGF- $\beta$  were detected by ELISA and fluorescence-quantitative PCR. Flow cytometry was used to detect the percentage of Th17 and Treg cells in the peripheral blood and liver tissues of each group of rats. The pathological changes in the liver tissue were detected by hematoxylin-eosin staining, immunohistochemistry, and electron microscopy. **Results.** Compared with the ACLF group, the WYHZTH formula and Thy significantly decreased the levels of ALT, AST, and CHE in the ACLF group. After drug intervention, apoptosis was significantly reduced. The PCNA expression decreased in the ACLF model group but increased in the WYHZTH or Thy group. Under transmission electron microscope, hepatocytes in the ACLF group showed obvious necrosis. After drug intervention, hepatocyte necrosis was reduced with most of the structure returning to normal. **Conclusion.** This present study demonstrated that WYHZTH formula may protect against acute-on-chronic liver failure, which may be related to the inhibition of Th17/Treg cell imbalance.

## 1. Introduction

Liver failure is a serious clinical syndrome, which is characterized by massive necrosis of hepatocytes caused by various acute or chronic injuries caused by drinking, hepatotoxic drugs, or virus infection, such as hepatitis B virus (HBV) and hepatitis C virus (HCV) [1–3]. Acute-on-chronic liver failure (ACLF) is a concept that was first widely used in liver disease intensive care units to distinguish patients who were treated with artificial livers as a way to liver transplantation [4]. In 2009, the Asia Pacific Association for the Study of the Liver (APASL) first defined the concept of ACLF. ACLF is an acute injury of liver function that occurs on the basis of chronic liver disease, and it is related to multiple organ failure and high mortality [5–7]. Therefore,

new strategies to prevent the disease progression of liver failure are urgently required.

In recent years, Th17/Treg balance in liver failure has become a research hotspot [8, 9]. CD4+ T lymphocytes, as helper T cells, play an important regulatory role in the body's immune response and inflammatory response, and Treg/Th17 is derived from the initial CD4+ T cells (Th0), which antagonize each other in differentiation and function, and is closely related to the inflammatory response, which is involved in the occurrence of viral hepatitis, cirrhosis, and acute or chronic liver failure [10–13].

Currently, the treatment of liver failure mostly adopts comprehensive measures such as removing the cause and regulating immune function, but there is still no breakthrough progress, and there are many complications and

high mortality. So far, there was no western medicine that could inhibit the progress of ACLF, while in a previous study, Wenyang Huazhuo Tuihuang (WYHZTH) formula is composed of Baifu tablets, dried ginger, Yin Chen, raw rhubarb, Chishao, *Polygonum cuspidatum*, ginseng, atractylodes, and licorice, which have a good clinical effect on promoting the resolution of jaundice and removing the dampness of the liver, gallbladder, spleen, and stomach, thereby clearing away heat and removing fire. At the same time, studies have pointed out that it also has a diuretic effect [14, 15], which shows a delightful prospect for liver function [16].

Our study was to deeply explore the mechanism of WYHZTH formula in the ACLF rat model. We intended to use Wenyang Huazhuo Tuihuang Recipe (WYHZTHR) to treat the ACLF model, evaluate the expression changes of CD4+ T cell subsets, clarify the protective effect of WYHZTHR on liver tissue damage, explore the targets of action of Chinese medicine in the treatment of ACLF, and provide a new theoretical basis for the prevention and treatment of ACLF by Chinese medicine.

## 2. Materials and Methods

**2.1. Materials.** The herbal WYHZTH formula was decocted by the Traditional Chinese Medicine Laboratory Center of the First Affiliated Hospital of Guangxi University after the identification of crude drugs was confirmed. Thymopentin injection (M107827, Aladdin), 20% human serum albumin (HSA), D-galactosamine (D-Gal), and lipopolysaccharide (LPS) were purchased from Sigma. The other reagents used were as follows: hematoxylin-eosin (Cat. No. E8090, G1140, G8590, Solarbio); protein marker, BCA protein concentration determination kit (Cat. No. XY-MY-0112, XY-MY-0096, Shanghai Xuanya), PVDF membrane, ECL luminescence reagent (Cat. No. XF-P3360, ZDSJ140, Xinfan Company), Tween-20 (Cat. No. PW0028, LEAGEN Company); RIPA tissue cell rapid lysate (Cat. No. BL504A, Biosharp); Nephryn, Podocin, LC3-I/II, Beclin1, P62, AMPK, and GAPDH protein primary antibody (Cat. Nos. PAB40854, PAB44275, PAB34124, PAB44768, PAB35470, PAB30970, and PAB36269, Bioswamp); p-AMPK and p-ULK1 (Cat. Nos. 50081S and 14202S, CST); goat anti-rabbit IgG (Cat. No. SAB43714, Bioswamp); and MaxVision™ secondary antibody and HRP-polymer (Cat. No. Kit-5020, Maixin).

**2.2. Animal Model.** Sprague Dawley (SD) rats, equal number of rats of either sex, 8 weeks old, weighing about 250 g, with a total of 90 were used. The animals come from Three Gorges University. Laboratory animal license number: SYXK (E) 2018-0104, certificate No. 42010200003097. They were raised under SPF conditions. The temperature was 22–26°C, relative humidity 50–60%, artificial light and dark for 12 hours, and adaptive feeding for 1 week.

According to the random number table method, 15 rats were selected as the normal control group and the other 75 rats were model groups. 20% human serum albumin was

used to construct a rat model of liver cirrhosis [17]. The rats were injected with 20% human serum albumin at 15 mg/kg through the tail vein twice a week, and the model was formed after 6 weeks. Based on liver cirrhosis, the ACLF rat model was constructed by intraperitoneal injection of lipopolysaccharide (LPS 100 µg/kg) and D-galactosamine (D-Gal 400 mg/kg) [17].

**2.3. Drug Intervention and Animal Groups.** After the model was successfully constructed, the rats were divided into 6 groups for drug intervention, each with 15 rats: ① Normal control group (NC): no treatment, fed with ordinary feed; ② Acute-on-chronic liver failure model group (ACLF): equal volume of drinking water gavage. ③ Thymopentin group (ACLF + Thy): thymopentin 0.11 mg/(kg·d) injected and administered for 6 weeks; ④ WYHZTH low-dose group (ACLF + WYHZTH-L): 0.23 g/(kg·d) was given by intragastric administration for 6 weeks; ⑤ WYHZTH middle-dose group (ACLF + WYHZTH-M): 0.46 g/(kg·d) suspension was gavaged for 6 weeks; and ⑥ WYHZTH high-dose group (ACLF + WYHZTH-H): 0.92 g/(kg·d) suspension was gavaged for 6 weeks. The WYHZTH group and the thymopentin group were planned to be administered by gavage 5 days before the model was started, continued until 48 h after the success of the model, twice a day with an interval of 12 h, and the amount of gavage liquid was 2 mL/100 g per day.

**2.4. General Behavior Observation.** During the experiment, the body weight (BW) of the rats was recorded every week, and the weight changes of the rats in each group compared with the NC group were statistically analyzed.

**2.5. Biochemical Index Detection.** After aseptic blood collection from the abdominal aorta, the whole blood was centrifuged at 3000 rpm for 15 min, and the serum was collected. The alanine aminotransferase (ALT), aspartate aminotransferase (AST), and cholinesterase (CHE) in the serum were detected by an automatic biochemical analyzer.

**2.6. HE Staining.** After the drug intervention completed, all rats were sacrificed. The liver tissue was dissected and then fixed with 4% paraformaldehyde solution for more than 24 hours, dehydrated with absolute ethanol, respectively, at 70%, 80%, 90%, and 95% gradient elution for 30 min, dehydrated with absolute ethanol twice and transparent with xylene, embedded in paraffin, and cut into tissue slices with a thickness of 5 µm. After staining, the pathological changes in the liver tissue were observed, especially hepatocyte damage, and photos were taken under a light microscope.

**2.7. TUNEL Method.** According to the literature [18], after fixation, the liver tissue is paraffin-embedded and sectioned. The sections had undergone routine dewaxing and hydration. According to TUNEL test kit instructions, DAB was added into the sections for color rendering and restained

with hematoxylin. 5 high-power lens fields were randomly selected; each lens count 100 hepatocyte nuclei in each field, and the percentage of apoptotic cells was calculated.

**2.8. Immunohistochemical Assay.** After antigen retrieval, paraffin sections were placed in 3% H<sub>2</sub>O<sub>2</sub> and blocked for 10 minutes to eliminate endogenous peroxidase activity. And then, it was blocked and incubated with 10% goat serum for 30 min. Primary antibody (proliferating cell nuclear antigen, PCNA, 1 : 200 dilution) was added and incubated at 4°C in a humidified box overnight. Then, the secondary antibody (1 : 200) was added dropwise and incubated at 37°C for 30 min. The substrate DAB was added to develop color. When the color change of the section was observed, the staining solution was washed off with tap water immediately. Hematoxylin was counterstained for 3 min, differentiated with 1% hydrochloric acid and alcohol, and rinsed with tap water for 10 min. Gradient alcohol dehydration was performed. Xylene is transparent, and the film is mounted with a neutral gum. The regeneration of liver cells is observed, and pictures were captured under a microscope.

**2.9. Transmission Electron Microscope.** The liver specimens were fixed with 2.5% glutaraldehyde and 1% hungry acid, embedded in epoxy resin and sectioned after being dehydrated by ethanol and acetone, and then double stained with saturated uranyl acetate and lead citrate. Finally, we observed the change in the ultrastructure of the liver tissue under a transmission electron microscope.

**2.10. Enzyme-Linked Immunosorbent Assay.** The serum of rats was collected in each group, 50 μL of different concentrations of standards and samples to be tested on the ELISA plate and 50 μL PBS were added to the blank wells. 50 μL of enzyme-labeled IL-17, IL-23, IL-10, or TGF-β antibody was added to each well, except for blank wells. After sealing the plate with a sealing film, incubate at 37°C for 30 min, carefully remove the sealing film, discard the liquid, and spin dry. 50 μL of A developer and 50 μL of B developer were added and develop the color at 37°C for 10 min in the dark. Finally, 50 μL of stop solution was added to stop the reaction and the absorbance (OD value) of each well was measured at 450 nm wavelength. A standard curve was drawn with the concentrations of the standards as the abscissa and the OD values as the ordinate, and the concentration of IL-17, IL-23, IL-10, and TGF-β was calculated in the sample according to the OD value.

**2.11. Real-Time Fluorescence Quantitative PCR.** The total RNA of liver tissue was extracted by the Trizol method; reverse transcription was performed according to the TAKARA rapid cDNA first-strand generation kit; the generated cDNA was used as a template for fluorescence quantitative PCR amplification. Designing and synthesizing of each qRT-PCR primer: IL-17-F CCCTCA-GACTACCTCAACCG, IL-17-R GCTCTCAGGC TCCCTCTTC; IL-23-F TGCTGCTCACGGTCACTT, IL-

23-RGCTTTGTGGCATCCTGG; IL-10-FGGTTGTCGTCT CATTCTGAAAGA, IL-10-R GGTAGAGGACCCAAG TTCGTTAAGA; TGF-β-F ACCAACTATTGCTTCAG CTC, TGF-β-RCTTGCAGGAGCGCACGATCA; FOXP3-FCTGGGAAGATGGCATTGAC, FOXP3-RCACTCTC-CACTCGCACAAA; GAPDH-FCCTTCCGTGTTCCCTAC, GAPDH-RGACAACCTGTTCCCTCA. All primers were synthesized by Wuhan Tianyi Huiyuan Company. PCR reaction conditions were as follows: predenaturation at 95°C for 3 min; 95°C for 5 s, 56°C for 10 s, 72°C for 25 s, total 40 cycles, and 72°C for 10 min. The Bio-Rad fluorescent quantitative PCR instrument was used to determine the Ct value. The Ct value is standardized with the Ct value of GAPDH, and the relative fold is calculated by  $2^{-\Delta\Delta Ct}$ , and the data are recorded and carried out by ABIprism7300SDS software.

**2.12. Flow Cytometry.** 1 ml of anticoagulated whole blood sample was taken from each group of rats. After separating the cells, IL-17 and CD4 labeling were used and the frequency of Th cells was detected. Meanwhile, CD4, CD25, and Foxp3 labeling was used, and the frequency of Treg cells was detected on a flow cytometer.

**2.13. Statistical Analysis.** SPSS 21.0 was used for data analysis. The *t*-test for the comparison of the two sample means was statistically processed. The data were expressed as the  $\bar{x} \pm s$ , and the comparison of percentages was performed by the  $\chi^2$  test; the comparison between multiple groups was performed by one-way ANOVA analysis, and  $P < 0.05$  indicates the difference was significant.

### 3. Results

**3.1. Effect of WYHZTH on the Body Weight of ACLF Rats.** After the success of the acute-on-chronic liver failure model, the weight of rats in the ACLF group gradually decreased over time. After 4 weeks, the weight in the ACLF group was significantly lower than that in the NC group ( $P < 0.01$ ). Compared with the ACLF group, the weights in the ACLF + WYHZTH-L/M/H group were all increased ( $P < 0.05$ ), and the weight in the ACLF + WYHZTH-H group and the ACLF + Thy group was significantly improved, which was gradually increased with the increase of the WYHZTH dose ( $P < 0.05$ , Table 1).

**3.2. The Level of Serum Liver Function Indexes in ACLF Rats after WYHZTH Treatment.** In order to explore the effect of WYHZTH on the liver function of ACLF models, after the drug intervention was completed, we measured ALT, AST, and CHE in the serum. It was found that the levels of ALT and AST in the ACLF group were higher than those in the NC group ( $P < 0.001$ ). Instead, the level of CHE was lower in the ACLF group. After treatment, the levels of ALT and AST in different doses of WYHZTH groups were significantly lower than those in the ACLF group ( $P < 0.05$ ), but CHE was increased. Meanwhile, the content of ALT, AST, and CHE

TABLE 1: The effect of WYHZTH on body weight of rats with acute-on-chronic liver failure ( $\bar{x} \pm s$ ,  $n = 6$ ).

Group	BW (g)		
	0 week	4 weeks	8 weeks
NC	266.37 ± 6.28	407.53 ± 4.21	478.53 ± 5.38
ACLF	259.60 ± 4.53	373.62 ± 6.42**	419.30 ± 5.46***
ACLF + Thy	260.28 ± 2.72	398.53 ± 6.23##	462.83 ± 6.34###
ACLF + WYHZTH-L	267.12 ± 2.64	368.53 ± 5.65	416.35 ± 2.35
ACLF + WYHZTH-M	265.42 ± 5.77	383.29 ± 1.59#	440.86 ± 6.71##
ACLF + WYHZTH-H	269.53 ± 3.26	401.78 ± 3.65##	466.54 ± 3.87###

vs. NC group, \* $P < 0.05$ , \*\* $P < 0.01$ , \*\*\* $P < 0.001$ ; vs. ACLF group; # $P < 0.05$ , ## $P < 0.01$ , ### $P < 0.001$ .

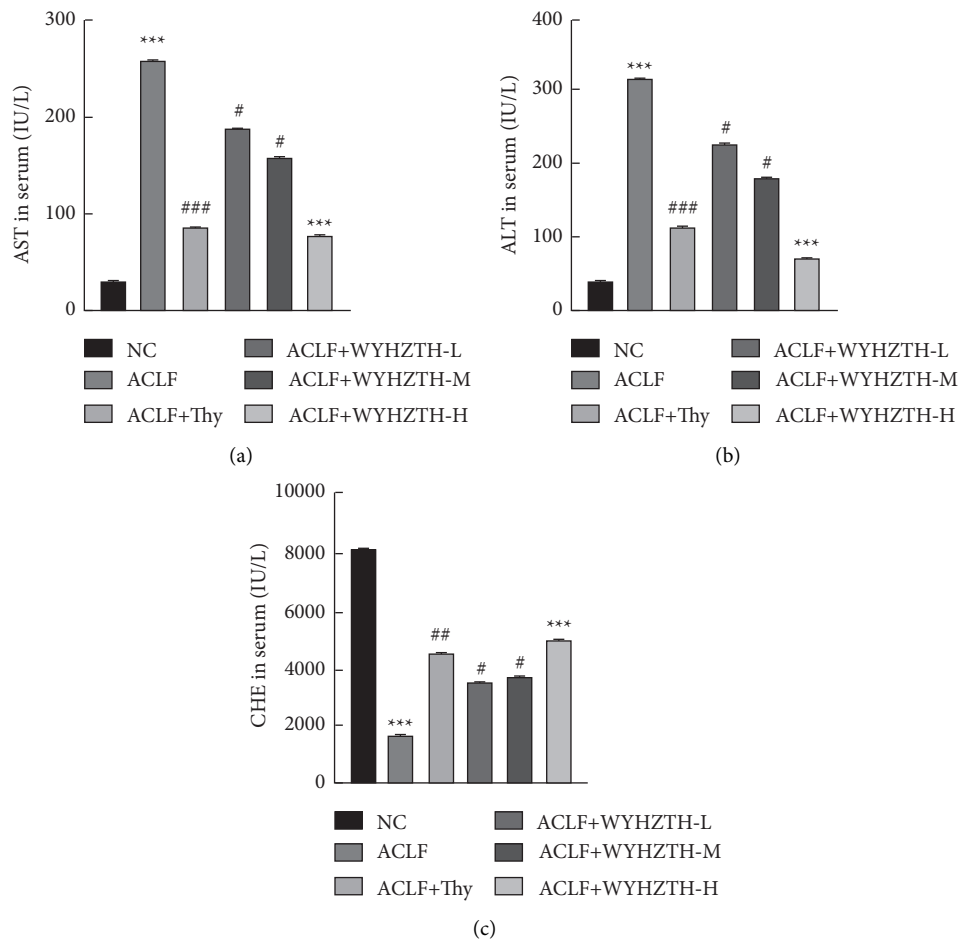


FIGURE 1: Effect of WYHZTH on the level of serum liver function indexes in ACLF rats. (a) The quantification of AST in serum of rats from different groups; (b) the concentration of ALT in serum of rats from different groups; (c) the concentration of CHE in serum of rats from different groups. vs. NC group, \* $P < 0.05$ , \*\* $P < 0.01$ , \*\*\* $P < 0.001$ ; vs. DN group, # $P < 0.05$ , ## $P < 0.01$ , ### $P < 0.001$ .

gradually changed with the WYHZTH dose increasing (Figure 1).

**3.3. Effect of WYHZTH on the Morphology of Liver Tissue in ACLF Rats.** In order to further demonstrate the role of WYHZTH in the process of acute-on-chronic liver failure, the changes in the liver tissue structure of rats in each group were observed by HE staining (Figure 2(a)) and TUNEL staining for apoptosis change in the liver tissue (Figure 2(b)).

Compared with the NC group, it was easy to find that the ACLF group showed ballooning and vacuolar degeneration of hepatocytes and the liver sinusoids dilated and congested in a small area, with a small amount of inflammatory cell infiltration outside the blood vessels and bile ducts. The degree of hyperemia and inflammatory cell infiltration in the ACLF + Thy group and the ACLF + WYHZTH group at different doses were significantly reduced (Figure 2(a)). It showed that the ACLF group significantly induced apoptosis in liver tissue in TUNEL staining. However, after drug

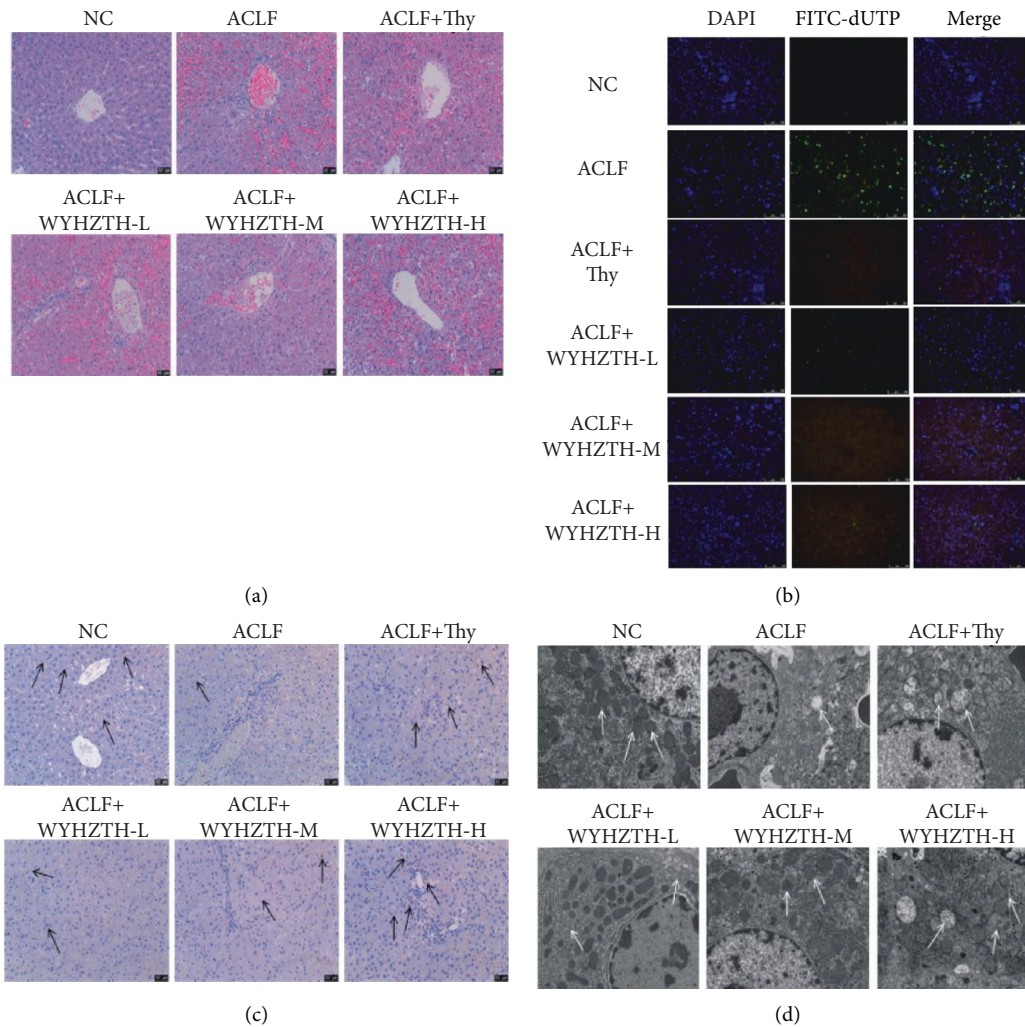


FIGURE 2: Effect of WYHZTH on the morphology of liver tissue in ACLF rats. (a) The liver tissue injury of rats in each group was observed by HE staining (200x); (b) the apoptosis change of liver tissue was tested by TUNEL staining (200x); (c) immunohistochemistry detected the expression of hepatocytes protein PCNA (200x); (d) ultrastructural changes of liver tissue in rats under electron microscope (6000x).

intervention, there were some little green fluorescent spots; that is, apoptosis was significantly reduced (Figure 2(b)). The PCNA expression in the NC group was uniformly diffused, but expression decreased in the ACLF model group. In ACLF + Thy group and the different dose WYHZTH groups, PCNA increased in varying degrees. The arrows represented the local expression of PCNA (Figure 2(c)). Under transmission electron microscope, hepatocytes in the ACLF group showed obvious necrosis, mitochondria swelled, and cristae fractured or even disappeared, lipid droplets were seen in the cytoplasm, and lysosomes were significantly increased. After drug intervention, hepatocytes necrosis was reduced, and the degree of lesions was significantly reduced with most of the structure returning to normal. The arrows represented the distribution of mitochondrial cristae (Figure 2(d)).

#### 3.4. Expression of Inflammatory Factors IL-17, IL-23, IL-10, and TGF- $\beta$ in Serum and Liver Tissue of Rats. In order to

clarify whether WYHZTH plays a role in improving the inflammatory injury of liver in ACLF, we first detected the expression of inflammatory factors IL-17, IL-23, IL-10, and TGF- $\beta$  in the serum in each group of rats by ELISA. The results showed that the expressions of IL-17, IL-23, and IL-10 in the ACLF group were higher obviously than those in the NC group ( $P < 0.001$ ); meantime, TGF- $\beta$  was also increased in the ACLF group ( $P < 0.001$ , Figures 3(a)–3(d)). The levels of inflammatory factors in the ACLF + Thy and ACLF + WYHZTH-M/H groups were significantly lower than those in the ACLF group ( $P < 0.05$ , Figures 3(a)–3(d)). Moreover, as the dose of WYHZTH increasing, the expression of inflammatory factors and TGF- $\beta$  gradually decreased. In the high-dose group, inflammatory factors and TGF- $\beta$  were significantly reduced ( $P < 0.001$ , Figures 3(a)–3(d)), which was basically close to the normal level.

In contrast to the cytokine level in the serum of rats, we further detected the mRNA levels of IL-17, IL-23, IL-10, TGF- $\beta$ , and FOXP3 in liver tissues by fluorescence quantitative PCR. The results showed that compared to the NC

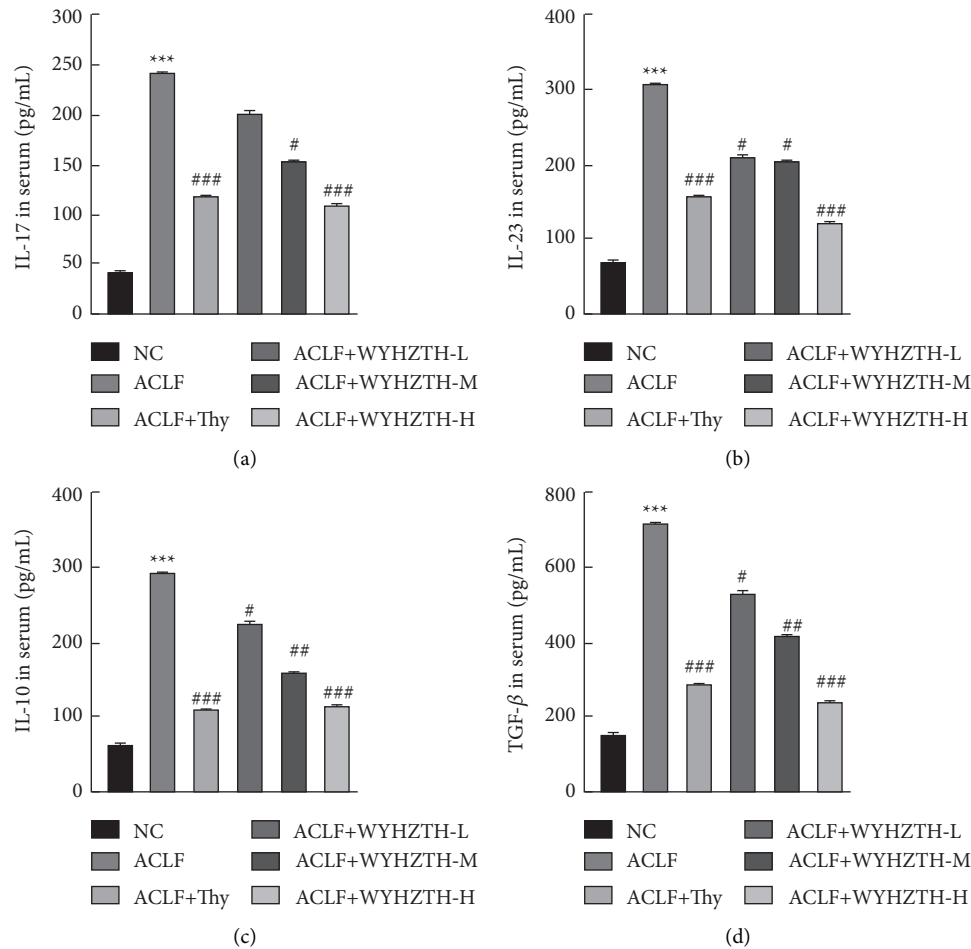


FIGURE 3: Expression of inflammatory factors IL-17, IL-23, IL-10, and TGF- $\beta$  in serum of rats from different groups: (a) the concentration of IL-17 in serum of rats in each group; (b) the expression of IL-23 in serum from different groups; (c, d) the concentration of IL-10 and TGF- $\beta$  in serum of rats from different groups. vs. NC group, \* $P < 0.05$ , \*\* $P < 0.01$ , \*\*\* $P < 0.001$ ; vs. ACLF group, # $P < 0.05$ , ## $P < 0.01$ , ### $P < 0.001$ .

group, the ACLF group IL-17, IL-23, TGF- $\beta$ , and FOXP3 mRNA levels were significantly upregulated (all  $P < 0.05$ , Figure 4), but IL-10 mRNA was downregulated. After drug treatment, the expression of IL-17, IL-23, TGF- $\beta$ , and FOXP3 was significantly reduced in ACLF + Thy and different doses of WYHZTH groups ( $P < 0.05$ , Figures 3(a)–3(d)). Meantime, the expression of inflammatory factors, TGF- $\beta$  and FOXP3, all gradually changed with the dose of WYHZTH increasing.

**3.5. The Frequency of Th17 and Treg Cells in the Peripheral Blood of Rats with ACLF and/or WYHZTH Intervention.** Studies have shown that the number of Th17 cells and Treg cells is closely related to the occurrence and progression of ACLF, so we further tested the frequency of Th17 and Treg cells in the peripheral blood of rats with ACLF and/or WYHZTH intervention to clarify the mechanism, by which WYHZTH can alleviate the occurrence and development of ACLF. Our results showed that the ratio of CD4+IL-17+ Th cells in the ACLF group was significantly higher than that in the NC group (Figure 5(a)), but after WYHZTH

intervention, the ratio of CD4+IL-17+ Th cells decreased (Figure 5(a)), which gradually decreased with increasing dose. However, the opposite was true for CD4+CD25+Foxp3+ Treg cells. The ratio of Treg cells in the ACLF group was significantly lower than that in the NC group (Figure 5(b)), but after WYHZTH intervention, Treg cells gradually increased (Figure 5(b)), which was also dose-dependent with WYHZTH.

## 4. Discussion

Acute-on-chronic liver injury manifested as jaundice and coagulopathy [19, 20]. In APASL revised in 2014, the concept has been improved and high 28-day mortality rate has been added [21]. It is usually related to sudden trigger events, and the 90-day mortality rate increased due to multisystem organ failure [22, 23]. Acute-on-Chronic Liver Failure in Cirrhosis (CANONIC) is a large-scale prospective study of patients with decompensated acute liver cirrhosis. A multicenter study [24] aims to distinguish patients with high short-term mortality risk among people with decompensated cirrhosis and develops the definition of ACLF.



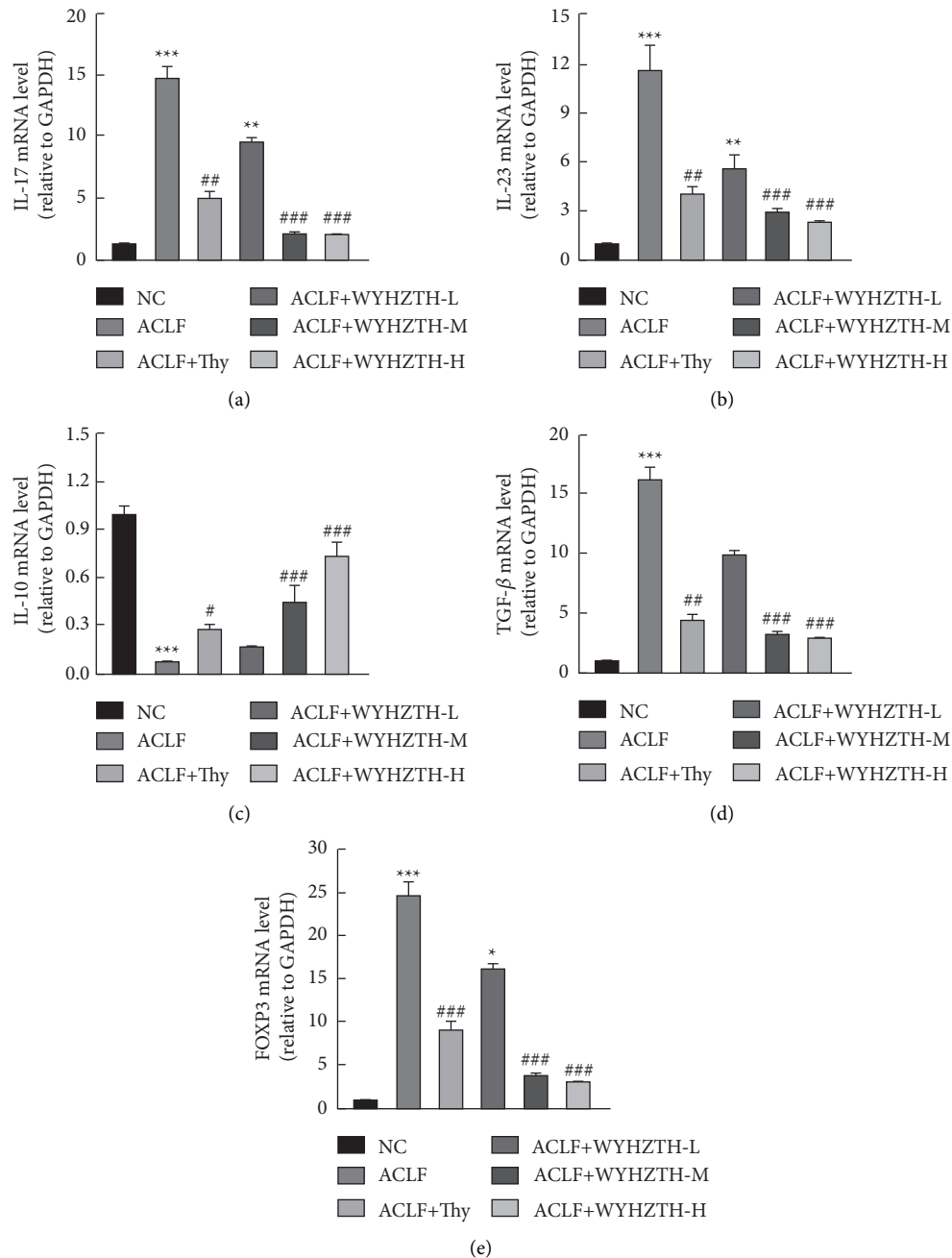


FIGURE 4: The mRNA level of IL-17, IL-23, IL-10, TGF- $\beta$ , and FOXP3 in liver tissue of rats from different groups. (a) The mRNA level of IL-17 in liver tissue of rat in each group; (b) the mRNA level of IL-23 in liver tissue from different groups; (c-e) the mRNA level of IL-10, TGF- $\beta$ , and FOXP3 in liver tissue of rats from different groups. vs. NC group, \* $P < 0.05$ , \*\* $P < 0.01$ , \*\*\* $P < 0.001$ ; vs. ACLF group, # $P < 0.05$ , ## $P < 0.01$ , ### $P < 0.001$ .

Among the earlier published studies included alcohol or bacteria-induced liver cirrhosis, decompensated liver cirrhosis, and ACLF [25]. This study found that systemic inflammation already exists when liver cirrhosis is decompensated, manifested by increased plasma inflammatory factors, renin and copeptin. These indicators are higher in ACLF patients. IL-6, IL-8, TNF- $\alpha$ , IL-10, and IL-1 are different in bacteria-induced ACLF and alcohol-induced ACLF. The severity of systemic inflammation is closely related to the frequency and severity of ACLF. The

latter study included ACLF patients related to chronic hepatitis B in China [26]. The difference from the previous study is that it is not limited to the analysis of various factors in plasma but extends the scope of the study to immune cells. This study found that ACLF patients had higher peripheral blood white blood cell counts than those without ACLF. The neutrophil-to-lymphocyte ratio (NLR) is related to the death of severe hepatitis B patients. NLR can independently predict the occurrence and short-term mortality of ACLF.

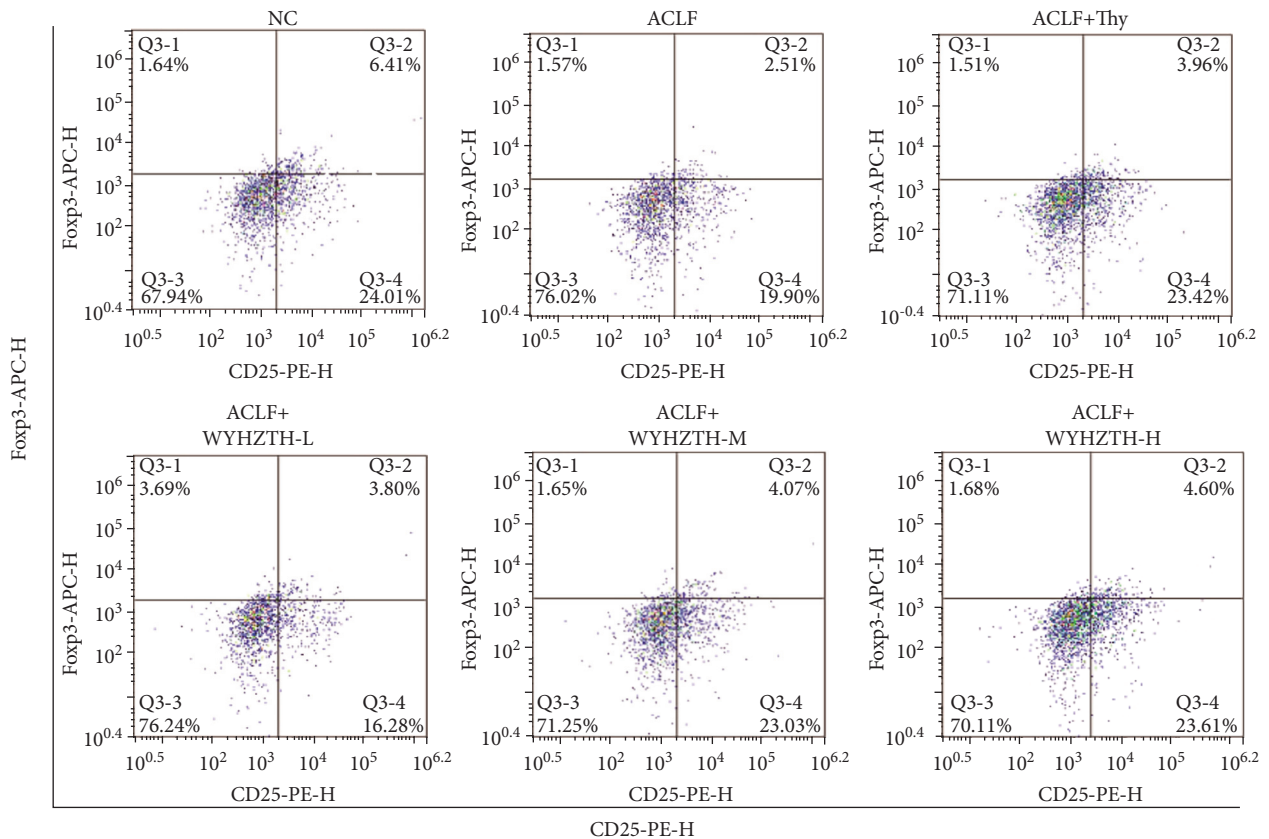
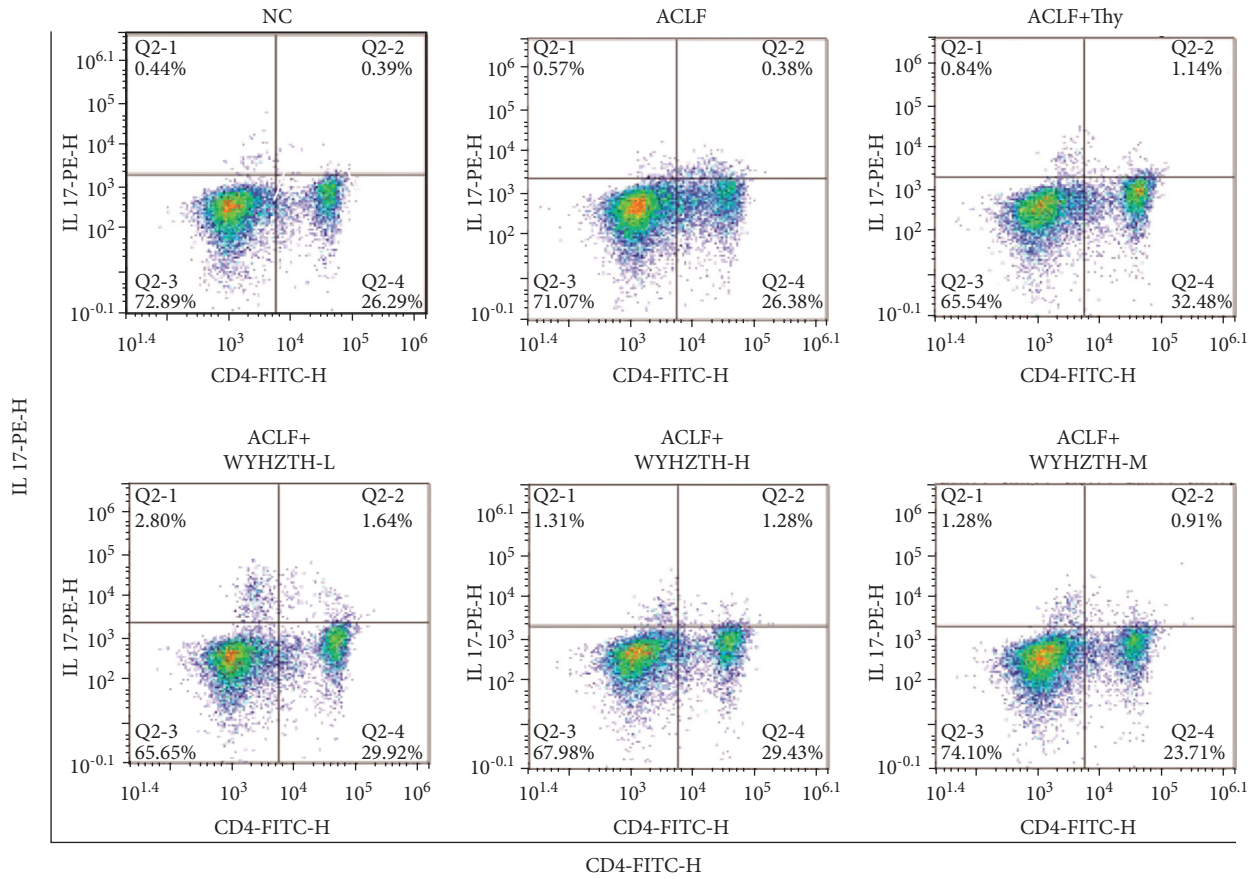


FIGURE 5: The frequency of Th17 and treg cells in the peripheral blood of rats with ACLF and/or WYHZTH intervention. (a) Flow cytometry detected IL-17 and CD4 labeled Th17 cells; (b) flow cytometry detected the frequency of CD25+Foxp3+ treg cells.

So far, the Th17/Treg balance in liver failure has become a research hotspot. CD4+ T lymphocytes, as helper T cells, play an important regulatory role in the body's immune system and inflammatory response, and Treg/Th17 is derived from the initial CD4+ T cells (Th0), which antagonize each other in differentiation and function, and is closely related. Treg cells mostly secrete IL-10, TGF- $\beta$ , and other cytokines to exert their inhibitory function, and Th17 cells mostly secrete IL-17, IL-23, TNF- $\alpha$ , etc. to exert their proinflammatory effects. Under normal physiological conditions, the body is in a balanced state. Once its steady state changes, it will affect the outcome of immune and inflammatory responses, which is closely related to the occurrence and progression of some immune diseases and inflammatory diseases. Th17 and Treg cells are derived from the same naive T cells [27, 28]. Under normal circumstances, the two maintain a balance, which is beneficial to the maintenance of the body's immune system in a stable state. Th17/Treg imbalance leads to excessive inflammatory response, which is involved in the occurrence of hepatitis, cirrhosis, and liver failure [26]. Liu et al. [29] compared the Th17/Treg ratio in patients with chronic hepatitis B with different disease progression levels in healthy people and a series of correlation analyses and confirmed that Th17/Treg is common in chronic HBV infection. The Th17/Treg ratio can more accurately reflect the progress of HBV infection-related liver disease. Shi Wenjuan [30] used ELISA to detect cytokines in the serum of 33 patients with ACHBLF and found that cytokines are related to the pathogenesis of ACHBLF with high levels of IL-17 and IL-35. The expression may be related to the occurrence of chronic hepatitis plus acute liver failure. Kan et al. [31] believed that ACHBLF patients have varying degrees of immune dysfunction. Th17/Treg imbalance is involved in the occurrence of hepatocyte inflammatory necrosis and can reflect the degree of liver inflammatory response. The above studies show that Treg cells, Th17 cells, and Treg/Th17 ratio are closely related to the progression of ACLF, and their role in the pathogenesis of ACLF is not very clear. Therefore, further in-depth research will provide more in-depth research on the pathogenesis and treatment of liver failure. Scientific theoretical basis.

Recently, the role of Th17/Treg balance in liver failure has become a hotspot. Treg cells mainly secrete IL-10, TGF- $\beta$ , and other cytokines to exert their inhibitory function, but Th17 cells mostly secrete IL-17, IL-23, TNF- $\alpha$ , and other cytokines to exert their proinflammatory effects [32–34]. So we further tested the frequency of Th17 and Treg cells in the rats with ACLF and/or WYHZTH intervention, by which WYHZTH can improve the balance of Th17/Treg cells so as to maintain the stable secretion of inflammatory factors and alleviate the happening of ACLF.

Many clinical studies have reported on the advantages of traditional Chinese medicine in the treatment of liver failure, believing that it will enhance immune function and antiviral efficacy, thereby improving life quality. Traditional Chinese medicine does not have the name of "liver failure." According to the symptom, it can be treated from

"jaundice," "paste yellow," "abrupt yellow," "heavenly yellow," and other diseases. Although ACLF is caused by an epidemic virus when you feel it, it is due to the lack of righteousness in the body, and the epidemic virus can also cause damp heat, stagnation of blood, and loss of righteousness. With the in-depth study of liver failure, it is not difficult to find that spleen-yang deficiency and kidney-yang deficiency are more obvious in liver failure. Therefore, the method of invigorating the yang has become one of the common methods for the treatment of ACLF. The Center of Liver Diseases in the Guangxi University believes that the pathogenesis of ACLF can be summarized as poisonous turbidity and injury based on the theory of the Fuyang school of "yang governs yin from view" and liver failure "toxin-poisonous disease." In the liver, qi deficiency and weakness, blood flow is not smooth; long-term qi deficiency will damage Yang. Combined with the research results of the research group's previous retrospective investigations, it is suggested that ACLF has certain characteristics of TCM syndrome distribution and evolution. Prolonged illness can easily lead to a loss of yang in the body. Yang deficiency and blood stasis yellow syndrome is the main type of ACLF [35]. According to this, the corresponding treatment methods should be to nourish yang, cultivate soil, detoxify, remove blood stasis, and retreat yellow, and condense the prescription of warming yang, dissolving turbidity, and retreating yellow. This prescription is an effective compound based on the treatment of acute liver failure with Jiedu Huayu Granules. Long-term clinical practice has shown that this prescription has good clinical effects in promoting the resolution of jaundice and reducing the mortality of liver failure. The whole prescription consists of Baifu tablets, dried ginger, *Atractylodes macrocephala*, *Yinchen*, raw rhubarb, red peony root, knotweed, ginseng, and licorice. The combination of all the medicines has the effect of warming the sun to transform the turbidity, promoting blood circulation and relieving jaundice. The addition of Wenyang Huazhuo Tuihuang Decoction can reduce the proinflammatory factor IL-32 level and increase the inflammation inhibitory factor IL-10 level in patients with HBV-related ACLF, which has a certain regulatory effect on immune disorders [36]. But the specific mechanism of action is currently unclear.

## 5. Conclusion

In summary, our study established a rat ACLF model and found that WYHZTH can protect against liver failure by improving Th17/Treg balance, reducing liver damage, and playing a beneficial role in the ACLF rats. The mechanism of ACLF liver injury was elucidated from the perspective of congenital immunity, and the targets of action of Chinese medicine were explored in the treatment of ACLF, which will provide an effective target for the treatment and prognosis of ACLF. On the other hand, that also laid the foundation for our next research into the specific mechanism of WYHZTH and its relationship with innate immunity.

## Data Availability

The data used to support the findings of this study are available from the corresponding author upon request.

## Conflicts of Interest

All authors declare that there are no conflicts of interest.

## Acknowledgments

The present study was supported by the Nature Science Foundation of Guangxi Province (grant nos. 2018GXNSFBA281031 and 2018GXNSFGA281002).

## References

- [1] J. Bernuau, B. Rueff, and J.-P. Benhamou, "Fulminant and subfulminant liver failure: definitions and causes," *Seminars in Liver Disease*, vol. 6, no. 2, pp. 97–106, 1986.
- [2] P. Farci, H. J. Alter, A. Shimoda et al., "Hepatitis C virus-associated fulminant hepatic failure," *New England Journal of Medicine*, vol. 335, no. 9, pp. 631–634, 1996.
- [3] V. J. Navarro and J. R. Senior, "Drug-related hepatotoxicity," *New England Journal of Medicine*, vol. 354, no. 7, pp. 731–739, 2006.
- [4] L. L. Kjaergard, J. Liu, B. Als-Nielsen, and C. Gluud, "Artificial and bioartificial support systems for acute and acute-on-chronic liver failure," *JAMA*, vol. 289, no. 2, pp. 217–222, 2003.
- [5] G. Zaccherini, E. Weiss, and R. Moreau, "Acute-on-chronic liver failure: definitions, pathophysiology and principles of treatment," *JHEP Reports*, vol. 3, Article ID 100176, 2020.
- [6] Q. Li, J. Wang, M. Lu, Y. Qiu, and H. Lu, "Acute-on-chronic liver failure from chronic-hepatitis-B, who is the behind scenes," *Frontiers in Microbiology*, vol. 11, 2020.
- [7] Z. Yu, Y. Zhang, Y. Cao et al., "A dynamic prediction model for prognosis of acute-on-chronic liver failure based on the trend of clinical indicators," *Scientific Reports*, vol. 11, no. 1, pp. 1810–1817, 2021.
- [8] S. J. Yu, R. Jiang, Y. Z. Mazzu et al., "Epigallocatechin-3-gallate prevents triptolide-induced hepatic injury by restoring the Th17/treg balance in mice," *The American Journal of Chinese Medicine*, vol. 44, no. 6, pp. 1221–1236, 2016.
- [9] X. S. Liang, C. Z. Li, Z. Ying, and M.-B. Wan, "Changes of Treg and Th17 cells balance in the development of acute and chronic hepatitis B virus infection," *BMC Gastroenterology*, vol. 12, no. 1, pp. 43–48, 2012.
- [10] A. A. Aleem, E. Rahman, and A. Elgonimy, "Evaluation of CD4+CD25+ regulatory T cells in patients with hepatocellular carcinoma and liver cirrhosis," *Egyptian Journal of Hospital Medicine*, vol. 43, no. 1, pp. 182–191, 2011.
- [11] J.-Q. Lian, X.-Q. Wang, Y. Zhang, C.-X. Huang, and X.-F. Bai, "Correlation of circulating TLR2/4 expression with CD3+/4+/8+ T cells and treg cells in HBV-related liver cirrhosis," *Viral Immunology*, vol. 22, no. 5, pp. 301–308, 2009.
- [12] S. Nasser and K. Paul, "CD4+ T cell responses in hepatitis C virus infection," *World Journal of Gastroenterology*, vol. 13, no. 36, pp. 4831–4838, 2007.
- [13] R. Tang, Z. Lei, X. Wang et al., "Hepatitis B envelope antigen increases Tregs by converting CD4+CD25 T cells into CD4+CD25+Foxp3+tregs," *Experimental and Therapeutic Medicine*, vol. 20, no. 4, pp. 116–120, 2020.
- [14] X. Y. Li, C. Z. Meng, B. Y. Ye et al., "Qiao Chengli's experiences in the treatment of nephritic syndrome with wenyang huazhuo therapy," *World Journal of Integrated Traditional and Western Medicine*, vol. 2, no. 7, pp. 56–61, 2019.
- [15] L. F. Zhang, Q. Wang, L. Yang, N. Liu, Y. Shan, and H. Bian, "Effect of Wenyang Huazhuo Tongluo decoction on VEGF, CTGF and ET-1 levels in systemic sclerosis mice," *Science Technology and Engineering*, vol. 25, no. 3, pp. 50–57, 2018.
- [16] P. An, S. Dong, X. F. Li et al., "Wenyang Huazhuo Fang exerts transient receptor potential cation channel subfamily C member-dependent nephroprotection in a rat model of doxorubicin-induced nephropathy," *Journal of Traditional Chinese Medicine: English Edition*, vol. 40, no. 4, p. 8, 2020.
- [17] X. H. Liu, Y. Chen, and J. Zhang, "The construction of acute-on-chronic liver failure rat model and its pathological mechanism explore," *Guide Paper of Technology*, vol. 25, no. 18, pp. 32–37, 2007, in Chinese.
- [18] A. E. Feldstein, A. Canbay, P. Angulo et al., "Hepatocyte apoptosis and fas expression are prominent features of human nonalcoholic steatohepatitis," *Gastroenterology*, vol. 125, no. 2, pp. 437–443, 2003.
- [19] S. Rao, I. Ashraf, F. Mir, S. Samiullah, J. Ibdah, and V. Tahan, "Dual infection with hepatitis B and epstein-barr virus presenting with severe jaundice, coagulopathy and hepatitis B virus chronicity outcome: 1996," *Official Journal of the American College of Gastroenterology ACG*, vol. 180, pp. 170–172, 2016.
- [20] S. K. Sarin, A. Choudhury, M. K. Sharma et al., "Acute-on-chronic liver failure: consensus recommendations of the Asian Pacific association for the study of the liver (APASL): an update," *Hepatology International*, vol. 13, no. 4, pp. 353–390, 2019.
- [21] S. Sarin, C. Kedarisetty, Z. Abbas et al., "Acute-on-chronic liver failure: consensus recommendations of the Asian Pacific association for the study of the liver (APASL)," *Hepatology International*, vol. 11, no. 5, pp. 41–43, 2014.
- [22] R. Jalan, P. Gines, J. C. Olson et al., "Acute-on chronic liver failure," *Journal of Hepatology*, vol. 57, no. 6, pp. 1336–1348, 2012.
- [23] J. C. Olson and P. S. Kamath, "Acute-on-chronic liver failure: concept, natural history, and prognosis," *Current Opinion in Critical Care*, vol. 17, pp. 165–169, 2011.
- [24] R. Moreau, R. Jalan, G. Pere et al., "Acute-on-chronic liver failure is a distinct syndrome that develops in patients with acute decompensation of cirrhosis," *Gastroenterology*, vol. 144, no. 7, pp. 1426–1437, 2013.
- [25] J. Clària, R. E. Stauber, M. J. Coenraad et al., "Systemic inflammation in decompensated cirrhosis: characterization and role in acute-on-chronic liver failure," *Hepatology*, vol. 64, no. 4, pp. 1249–1264, 2016.
- [26] W. Wu, H. Yan, H. Zhao et al., "Characteristics of systemic inflammation in hepatitis B-precipitated ACLF: differentiate it from no-ACLF," *Liver International*, vol. 38, pp. 248–257, 2017.
- [27] E. S. J. Edwards, J. J. Bosco, P. M. Aui et al., "Predominantly antibody-deficient patients with non-infectious complications have reduced naive B, treg, Th17, and Tfh17 cells," *Frontiers in Immunology*, vol. 10, pp. 2593–2597, 2019.
- [28] X. Zhong, W. Gao, N. Degauque et al., "Reciprocal generation of Th1/Th17 and treg cells by B1 and B2 B cells," *European Journal of Immunology*, vol. 37, no. 9, pp. 2400–2404, 2010.
- [29] H. Liu, J. You, H. Chen et al., "The role of helper T lymphocyte 17 regulatory T lymphocyte balance in the progression of

- hepatitis B virus infection-related liver disease,” *Chinese General Practice*, vol. 19, no. 18, pp. 2121–2125, 2016.
- [30] W. Shi, J. Jia, C. Li, and H. Wang, “The expression and significance of Th17/treg cytokines in patients with chronic hepatitis B acute liver failure,” *Liver*, vol. 21, no. 2, pp. 92–94, 2016.
- [31] Y. Kan, J. Gan, W. Sun, and T. Feng, “Changes of Th17 and treg in patients with HBV-related chronic acute liver failure and their clinical relevance,” *Liver*, vol. 21, no. 2, pp. 90–91, 2016.
- [32] C. Li, H. Yang, X. Rao, X. Qiu, and J. Dou, “The research progress of Th17 cells and treg cells in regulating tumor immunity,” *Pharmaceutical Biotechnology*, vol. 69, 2017.
- [33] P. Bhattacharya, S. Ghosh, S. A. Ejazi et al., “Induction of IL-10 and TGF $\beta$  from CD4+CD25+FoxP3+ T cells correlates with parasite load in Indian Kala-Azar patients infected with leishmania donovani,” *PLoS Neglected Tropical Diseases*, vol. 10, no. 2, Article ID e0004422, 2016.
- [34] K. H. G. Mills, A. Allen, S. Edwards et al., “S-16,” *Cytokine*, vol. 70, no. 1, p. 24, 2014.
- [35] D. Mao, N. Wang, N. Tang, F. Long, and X. Chen, “Investigation on the constitution of traditional Chinese medicine in 232 patients with liver failure in Guangxi,” *Journal of Integrated Traditional Chinese and Western Medicine Liver Disease*, vol. 25, no. 4, pp. 201–202, 2015.
- [36] X. Wang, L. Zhao, Y. Zhong, R. Zhang, and D. Mao, “Effect of Wenyang Huazhuo Tuihuang decoction on serum IL-32, IL-10 and T cell subsets in patients with HBV-related ACLF,” *Guangxi Traditional Chinese Medicine*, vol. 42, no. 246, pp. 1–3, 2019.

## Research Article

# Acetyl-11-Keto- $\beta$ -Boswellic Acid (AKBA) Prevents Lipopolysaccharide-Induced Inflammation and Cytotoxicity on H9C2 Cells

Danial Taherzadeh,<sup>1,2</sup> Vafa Baradaran Rahimi,<sup>3</sup> Hamed Amiri,<sup>1</sup> Sajjad Ehtiati,<sup>1,2</sup> Roghayeh Yahyazadeh,<sup>4,5</sup> Seyed Isaac Hashemy <sup>1,2</sup> and Vahid Reza Askari <sup>4,5,6</sup>

<sup>1</sup>Department of Clinical Biochemistry, Faculty of Medicine, Mashhad University of Medical Sciences, Mashhad, Iran

<sup>2</sup>Surgical Oncology Research Center, Mashhad University of Medical Sciences, Mashhad, Iran

<sup>3</sup>Department of Cardiovascular Diseases, Faculty of Medicine, Mashhad University of Medical Sciences, Mashhad, Iran

<sup>4</sup>Applied Biomedical Research Center, Mashhad University of Medical Sciences, Mashhad, Iran

<sup>5</sup>Department of Pharmaceutical Sciences in Persian Medicine, School of Persian and Complementary Medicine, Mashhad University of Medical Sciences, Mashhad, Iran

<sup>6</sup>Department of Persian Medicine, School of Persian and Complementary Medicine, Mashhad University of Medical Sciences, Mashhad, Iran

Correspondence should be addressed to Vahid Reza Askari; askariv@mums.ac.ir

Received 24 December 2021; Accepted 15 March 2022; Published 30 March 2022

Academic Editor: Jelena Zivkovic

Copyright © 2022 Danial Taherzadeh et al. This is an open access article distributed under the Creative Commons Attribution License, which permits unrestricted use, distribution, and reproduction in any medium, provided the original work is properly cited.

Acetyl-11-keto-beta-boswellic acid (AKBA), the major component of *Boswellia serrata*, exhibits anti-inflammatory activities. This in vitro study investigated the protective effects of AKBA against lipopolysaccharide (LPS)-induced cardiac dysfunction. In this study, the H9C2 cardiomyocytes were pretreated with AKBA (2.5, 5, and 10  $\mu$ M for 24 h), and then cotreated with LPS for another 24 h. The MTT assay, ELISA test kits, and quantitative real-time PCR analysis assessed the cell viability, levels of proinflammatory factors (IL- $\beta$ , IL-6, TNF- $\alpha$ , and PGE2), and the gene expression of IL- $\beta$ , IL-6, TNF- $\alpha$ , iNOS, and COX-2, respectively. The nitric oxide (NO) and thiol levels were also measured using a biochemical assay. The results indicated that LPS exposure markedly reduced cell viability and total thiol content, but increased the inflammatory cytokines, NO metabolites, and gene expression of proinflammatory mediators in H9C2 cells. AKBA pretreatment significantly altered the mentioned factors induced by LPS. Our results demonstrated that AKBA might be a promising therapeutic agent for treating sepsis-related cardiac dysfunction in the future.

## 1. Introduction

Sepsis is a lethal condition caused by an overreaction of the immune system to infection that can lead to tissue damage, multiple organ failure, and even death [1–4]. Myocardial dysfunction is one of the prominent sepsis features that has proved to be associated with a high mortality risk for septic patients [5, 6]. Many studies have reported the crucial role of proinflammatory cytokines in myocardial oxidative damage that commonly occurs in the course of sepsis [7]. Throughout these severe inflammatory conditions, the

elevating production of multiple proinflammatory mediators, such as interleukin-1beta (IL-1 $\beta$ ), IL-6, tumour necrosis factor- $\alpha$  (TNF- $\alpha$ ), and nitric oxide (NO), eventually lead to cardiac depression, oedema, and necrosis in the myocardial cells [2–4, 8]. According to previous studies, the systemic inflammatory response is stimulated by damage-associated molecular patterns (DAMPs) such as lipopolysaccharide (LPS) as a bacterial endotoxin, which can induce inflammatory signalling pathways through toll-like receptor-4 (TLR-4) in cardiomyocytes [3, 9, 10]. The LPS/TLR-4 complex formation can activate further inflammatory



signalling cascades associated with several transcription factors, particularly the nuclear factor-kappa B (NF- $\kappa$ B) pathway, which stands as the primary signalling cascade in initiating the process of intracellular inflammation [3, 10, 11]. Considering the activation of inflammation by NF- $\kappa$ B, the intensified proinflammatory cytokines can accumulate intracellular oxygen free radicals (ROS) and automatically impair the structure and function of cardiomyocytes [7, 10, 12–14]. The available pharmacological approaches, such as using nonsteroidal anti-inflammatory drugs (NSAIDs), are minimal due to their controversial and various adverse effects [7, 10, 13–15]. It is consequently necessary to consider efficient therapeutic interventions to prevent sepsis-induced cardiomyopathy. There is growing evidence on natural compounds, especially plants' secondary metabolites, are capable of representing optimal therapeutic effects in alleviating LPS-induced cardiotoxicity [6, 16].

Acetyl-11-keto- $\beta$ -boswellic acid (AKBA), as a plant-derived-bioactive pentacyclic triterpene, has been isolated from *Boswellia serrata* (BS) [4, 10, 17]. The remarkable biological features of AKBA have been repeatedly indicated, including antioxidant [18], antitumour [19], antimicrobial activity [20], anti-inflammatory [4, 10, 13, 14], neuroprotective [2, 14], and other beneficial qualities [13, 14, 21]. Recently, the cardioprotective activities of pentacyclic triterpenoid compounds have been paid the attention of many researchers. In one study, two natural compounds with a similar chemical structure (boswellic acid and oleanolic acid) have been investigated on high glucose-induced toxicity in the H9C2 cardiomyocyte cell line. This study showed that these compounds attenuate apoptosis by reducing the activity of NF- $\kappa$ B, lowering ROS production, and enhancing the glutathione redox cycle [22]. Further studies also reported the protective impacts of AKBA against the consequences of myocardial ischemia-reperfusion (I/R) injury in a rat model by modulating the oxidative-inflammatory cascades [23]. Based on the abovementioned data, this work aimed to investigate the effects of AKBA on lipopolysaccharide (LPS)-induced cell injury in H9C2 cells.

## 2. Methods and Materials

**2.1. Chemicals and Reagents.** AKBA (Calbiochem), DMEM culture media, fetal bovine serum (FBS), penicillin plus streptomycin (pen/strep), dimethyl sulfoxide (DMSO), LPS (*Escherichia coli* O55:B5 purified by phenol extraction, L2880 SIGMA), and other chemicals used were of cell culture and analytical grade from Sigma-Aldrich (St. Louis, MO, USA). A proliferation assay kit (MTT) was provided from Roche Diagnostic (Mannheim, Germany). ELISA kits (PGE2, IL-6, IL-1 $\beta$ , and TNF- $\alpha$ ) were supplied from IBL International (USA).

**2.2. Cell Viability Assay.** In this study, we first evaluated the viability of H9C2 cells in the presence of AKBA (2.5, 5, and 10  $\mu$ M) to better understand the working solution selected based on nontoxic concentration. In brief, the cells were

treated with different concentrations of AKBA (2.5, 5, and 10  $\mu$ M) for 48 h, and then the cell viability was evaluated employing the MTT assay. Once the nontoxicity of the applied concentrations towards cells was ascertained, the protective effects of AKBA were assessed. In the next step, we evaluated the effects of the concentrations of AKBA (2.5, 5, and 10  $\mu$ M) on LPS-induced (10  $\mu$ g/ml) by culturing  $7 \times 10^3$  H9C2 cells in a 96-well plate. In review, the cells were pretreated with different concentrations of AKBA (2.5, 5, and 10  $\mu$ M) for 24 h, and then were cocultured with LPS (10  $\mu$ g/ml) for another 24 h. In the end, the cell viability was measured by applying an MTT assay. For the MTT assay, briefly, 10  $\mu$ L of MTT solution with a final concentration of 5 mg/ml was appended to each well to be incubated for 3 h. After discarding the medium culture (RPMI-1640), 100  $\mu$ L of DMSO was used to dissolve the formed formazan crystals. The absorption of the 96-well plate was recorded by an ELISA reader (Awareness Inc., USA) at 570 nm and 620 nm [7].

**2.3. Experimental Procedure and Grouping.** The protective effects of AKBA against LPS-induced cardiomyocyte toxicity were evaluated as a model of septic shock. Initially, the cells were pretreated with AKBA (2.5, 5, and 10  $\mu$ M) for 24 h, and then were coexposed with LPS (10  $\mu$ g/ml) for another 24 h. After that, we assessed the changes in both gene expression (in the cell lysate, using real-time PCR) and protein (in the supernatant, using ELISA) levels of proinflammatory biomarkers, including TNF- $\alpha$ , IL-1 $\beta$ , IL-6, PGE2, iNOS, COX-2, and nitric oxide metabolites (NO). Total thiol content was also assessed as an antioxidant marker in the lysate. Experimental groups were as follows:

Group 1: control group, H9C2 cells received a complete media culture and the solvent of AKBA with neither AKBA nor LPS for 48 h

Group 2: LPS group, H9C2 cells received a complete media culture and the solvent of AKBA and LPS (10  $\mu$ g/ml) for 48 h

Groups 3, 4, and 5: AKBA treated groups, H9C2 cells received a complete media culture and AKBA (2.5, 5, and 10  $\mu$ M) for 24 h, and then coincubated with LPS (10  $\mu$ g/ml) for another 24 h

AKBA was dissolved in DMSO, which was serially diluted with a complete medium that contained the final DMSO concentration at a lower percentage than 0.1% v/v throughout all of the experiments. We selected the concentrations of AKBA according to the preliminary results of the cell viability by the MTT assay, and a similar study evaluated the antioxidative effects of AKBA (2.5–10  $\mu$ M) [16].

**2.4. Measuring Total Protein Levels.** The Bradford protein assay was carried out to quantify the total protein concentration in a sample using the Coomassie Brilliant Blue G-250 dye [24–27]. First, the dye (10 mg) was dissolved in 50 ml of ethanol (96%), and then phosphoric acid (85%) (10 ml) was added, and the volume of the solution reached

100 ml. Thereafter, bovine serum albumin (BSA, 4 mg/ml) solution was prepared as a standard curve. Then, after sample pouring (20  $\mu$ l), a Bradford reagent (200  $\mu$ l) was added to the 96-well microplate. Finally, after 5 minutes, the absorption was read out at 595 nm with a microplate reader [24–27].

**2.5. Evaluation of the Protein Levels of Inflammatory Biomarkers.** The ELISA assay evaluated the IL-1 $\beta$ , IL-6, TNF- $\alpha$ , and PGE2 levels as inflammatory mediators, which were carried out in accordance with the manufacturers' protocol, IBL company [6, 7, 24, 26, 28], USA. In summary,  $1.5 \times 10^6$  cells were cultured in a 6-well plate overnight, and they were treated according to the experimental grouping section. The supernatant of cells was then used for the required measurements, and the lysates were collected for gene expression studies.

**2.6. Gene Expression Assessment.** A real-time PCR technique was performed through the SYBR Green procedure's employment to assess the possible impacts of different AKBA concentrations on the levels of TNF- $\alpha$ , IL-1 $\beta$ , IL-6, and COX-2 as well as iNOS related mRNA. Rotor-Gene 6000 was involved as a real-time reaction detection system, and GAPDH was considered a reference gene [7, 24, 26]. We procured the required real-time PCR primers in a similar design to those mentioned in previous studies [29]; the primer specificity was blasted and confirmed by applying NCBI Primer-BLAST. The primer sequences are detailed in Table 1. The real-time PCR reaction contained 5  $\mu$ L of amplicon master mix, 0.4  $\mu$ L of each primer (1  $\mu$ M), 0.2  $\mu$ L of DEPC water, and 50 ng of cDNA. Meanwhile, the prepared conditions for PCR were set at 95°C for 3 min and then followed by 45 cycles of 95°C for 20 sec, annealing temperature (55–65°C) for 5 sec, and 72°C for 10 sec. As the last step, we examined the values of gene expression levels by using the  $\Delta\Delta C_t$  method and reported the fold-change values as  $2^{-(\Delta\Delta C_t)}$  to the control group.

**2.7. Evaluation NO Metabolites and Thiol Content Level.** The nitrite oxide metabolite levels were measured based on the measurement of nitrite (NO<sup>-2</sup>) as the stable and the final NO product by the Griess method described elsewhere [30]. The NO levels were assessed in the supernatant at 540 nm by using the standard curve of different nitrite concentrations [6, 7, 24, 26–28].

The total thiol content was evaluated through a colorimetric method, which was set according to the reaction of total thiol content with Ellman reagent (5,5'-dithiobis (2-nitrobenzoic acid) (Sigma-Aldrich) [31]. This particular reaction results in the formation of yellow-coloured TNB (5-thio-2-nitrobenzoic acid) that can be quantified at 412 nm [6, 7, 24, 26–28].

**2.8. Statistical Analysis.** We displayed the obtained results as mean  $\pm$  SEM. The gathered data were analysed by GraphPad Prism 6 (GraphPad Software, San Diego, CA, USA) software. Besides, the one-way analysis of variance (ANOVA) test was

carried out with Tukey-Kramer's post hoc multiple comparisons test according to the variance's homogeneity. By statistics, probability (*P*) values of less than 0.001, 0.01, and 0.05 were considered significant differences in all of the performed calculations.

### 3. Results

**3.1. AKBA Alleviates LPS-Induced Cytotoxicity in H9C2 Cells.** As shown in Figure 1(a), in comparison to the control group, there were no significant changes in the level of cell viability of H9C2 cells incubated with various concentrations of AKBA (2.5, 5, and 10  $\mu$ M) for 48 h. Incubation of the cells with LPS (10  $\mu$ g/mL) for 48 h led to a significant reduction in the level of cell viability compared to the control group ( $P < 0.001$ ; Figure 1(b)). However, treatment with AKBA (5 and 10  $\mu$ M) notably increased the level of cell viability in the presence of LPS stimulation ( $P < 0.05$  and 0.001, respectively; Figure 1(b)).

**3.2. AKBA Inhibits LPS-Induced Inflammatory Cytokines Production in H9C2 Cells.** To demonstrate the anti-inflammatory effects of AKBA, we assessed the production levels of proinflammatory cytokines, including TNF- $\alpha$ , IL-6, IL-1 $\beta$ , and PGE2, which contributed to LPS-induced cardiomyopathy. As illustrated in Figures 2(a)–2(d), the production levels of TNF- $\alpha$ , IL-6, IL-1 $\beta$ , and PGE2 were significantly elevated in H9C2 cells following the LPS (10  $\mu$ g/mL) stimulation in comparison to the control group ( $P < 0.001$  for all cases). However, pretreatment of the cells with AKBA (2.5, 5, and 10  $\mu$ M) dramatically decreased the production of TNF- $\alpha$  ( $P < 0.001$  for all cases; Figure 2(a)), IL-1 $\beta$  ( $P < 0.001$  for all cases; Figure 2(b)), and IL-6 ( $P < 0.001$  for all cases; Figure 2(c)) in a concentration-dependent manner, compared to the LPS group. Although AKBA exerted reducing effects on the level of PGE2, this effect was statistically significant only at two higher concentrations of AKBA (5 and 10  $\mu$ M) in comparison to the LPS group ( $P < 0.001$  for both cases; Figure 2(d)).

**3.3. AKBA Attenuates the Gene Expression Levels of Inflammatory Cytokines in H9C2 Cells.** Our study evaluated the capability of AKBA in suppressing the transcription of proinflammatory mediators in our study using the real-time PCR (qPCR) technique. According to Figures 3(a)–3(e), treatment of H9C2 cells with LPS (10  $\mu$ g/mL) caused a significant enhancement in proinflammatory genes' expression levels (IL-1 $\beta$ , TNF- $\alpha$ , IL-6, iNOS, and COX-2). We revealed that three nontoxic concentrations of AKBA (2.5, 5, and 10  $\mu$ M) exhibited notable suppressive impacts on the expression levels of proinflammatory mediators (IL-1 $\beta$ , TNF- $\alpha$ , IL-6, iNOS, and COX-2), in a concentration-dependent manner, compared to the LPS group ( $P < 0.001$ –0.01 for all cases; Figures 3(a)–3(e)).

**3.4. AKBA Decreased Nitric Oxide Level and Increased Thiol Level.** We investigated the antioxidant effect of AKBA in

TABLE 1: List of primers sequence (from 5' to 3') [7, 29].

Gene name	5'-3' primer	Sequence Accession Number
<i>tnf-<math>\alpha</math></i>	FW CACCTCTCAAGCAGAGCACAG	M98820
	RW GGGTTCCATGGTGAAGTCAAC	
<i>cox-2</i>	FW AAATGGGCTCCCTCTCATCAGTTC	X66539
	RW TCTGCTTGGTGGTTTGCTACGAC	
<i>il-1<math>\beta</math></i>	FW TGATGCTACCATCTGGCTTCGG	S67722
	RW GTTTGGAAACAGTCGCTCGTCATC	
<i>il-6</i>	FW CATTGGAAGTGAAGCGTTTCG	L12562
	RW CAGCTGGGCTGTACAAACCTT	
<i>inos</i>	FW TCCTACCCCAACTTCCAATGCTC	E02522
	RW TTGGATGGTCTTGGTCCTTAGCC	
<i>gapdh</i>	FW GTATTGGGCGCCTGGTCACC	AB017801
	RW CGCTCCTGGAAGATGGTGATGG	

FW, forward primer; RW, reverse primer; GAPDH, glyceraldehyde-3-phosphate dehydrogenase.

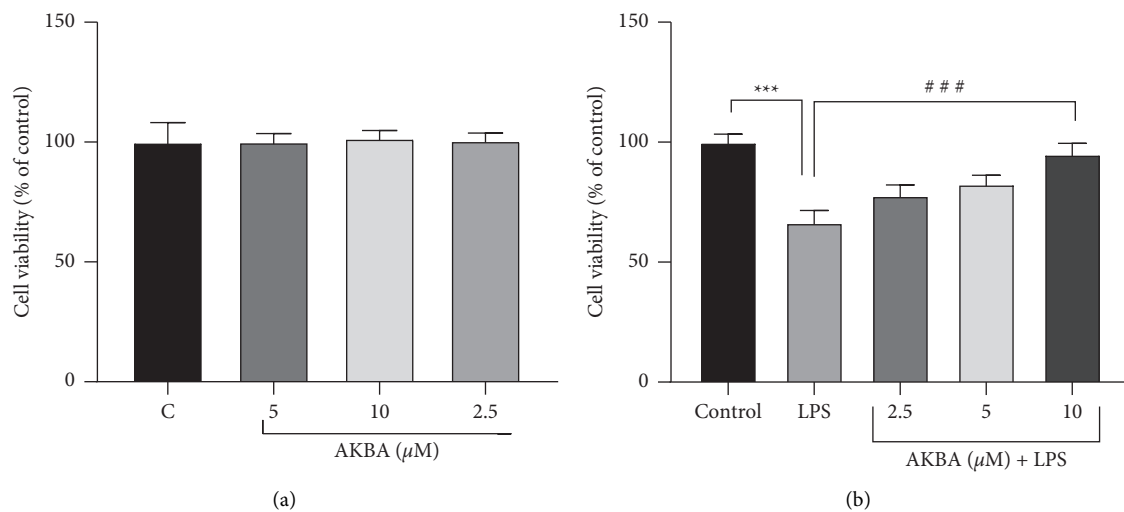


FIGURE 1: H9C2 cell viability in the presence of AKBA alone and with LPS. Effect of AKBA (2.5–10  $\mu$ M) on cell viability (a). The survival of the H9C2 cell line was evaluated when treated with LPS (10  $\mu$ g/ml) and 24 h of pretreatment with AKBA then exposure with LPS (b).  $n = 6$  per group. Error bars indicate standard error mean (SEM) \*\*\* $P < 0.001$  vs. control and ### $P < 0.001$  vs. LPS.

LPS-stimulated H9C2 cells by detecting the levels of nitric oxide (NO) and thiol [32] in the culture medium. According to the obtained results, LPS at a concentration of 10  $\mu$ g/mL led to a significant enhancement in the level of NO ( $P < 0.001$ ; Figure 4(a)) and a significant reduction in the level of total thiol content ( $P < 0.001$ ; Figure 4(b)), compared to the control group.

In contrast, pretreatment with AKBA (2.5, 5, and 10  $\mu$ M) caused a significant inhibition of NO production compared to the LPS-treated group ( $P < 0.001$ –0.01 for all cases; Figure 4(a)). Moreover, preincubation of the cells with AKBA (2.5, 5, and 10  $\mu$ M) resulted in a marked increase in the levels of total thiol content in a concentration-dependent manner compared to the LPS group ( $P < 0.001$ –0.01 for all cases; Figure 4(b)).

#### 4. Discussion

To the best of our knowledge, the present work is the first study to investigate the potential protective effects of AKBA against LPS-induced cardiomyopathy. Here, we used an in

vitro H9C2 model of myocardial injury to explore the protective mechanism of AKBA on LPS-induced cardiac dysfunction [33]. Our study results showed that LPS increased the levels of proinflammatory mediators (IL-1 $\beta$ , TNF- $\alpha$ , IL-6, and PGE2) and nitric oxide (NO), whereas it reduced the cell viability of H9C2 cells as well as the level of total thiol content. However, pretreatment with various concentrations of AKBA (2.5, 5, and 10  $\mu$ M) could dramatically enhance the cell viability and the content of total thiol content. Furthermore, AKBA significantly suppressed the expression of proinflammatory factors and NO production, indicating that AKBA might be effective against LPS-induced inflammatory responses. We also found that the gene expression of COX-2 and iNOS was down-regulated by AKBA pretreatment.

It is well established that LPS, as an exogenous ligand of TLR4, induces inflammatory processes involved in severe cardiac injury [34]. LPS-mediated activation of initiates NF- $\kappa$ B dependent signalling pathways, resulting in the overproduction of various proinflammatory mediators, such as COX-2, iNOS, IL-1 $\beta$ , IL-6, and TNF- $\alpha$  [6, 24, 26–28, 35, 36].

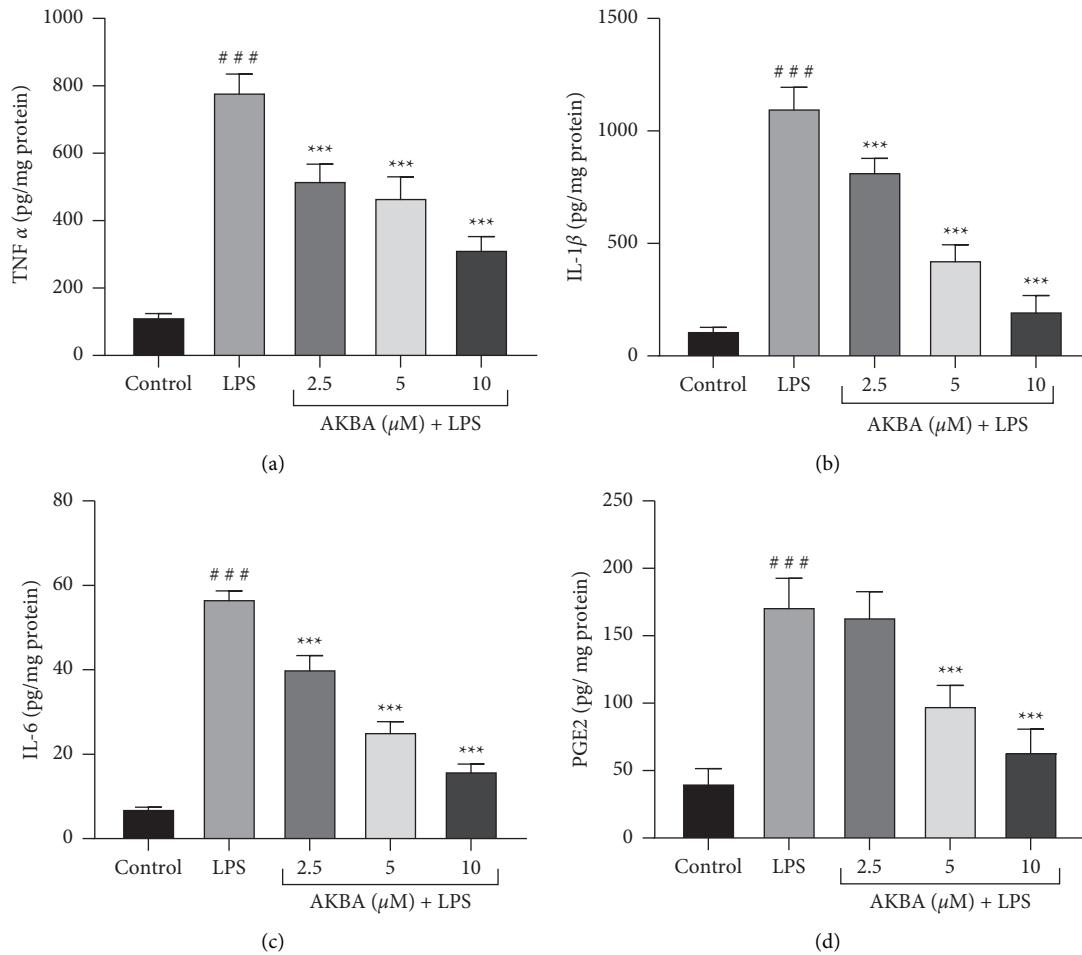


FIGURE 2: Effect of AKBA and LPS on the level of TNF- $\alpha$  (a), IL-1 $\beta$  (b), IL-6 (c), and PGE2 (d). The cells were pretreated with AKBA for 24 h, then incubated with LPS for another 24 h, and levels of TNF- $\alpha$ , IL-1 $\beta$ , IL-6, and PGE2 were evaluated by an ELISA assay. The data are the mean  $\pm$  SEM ( $n = 6$  per group). ### $P < 0.001$  vs. control and \*\*\* $P < 0.001$  vs. LPS.

Excessive production of proinflammatory cytokines plays a vital role in developing many inflammatory disorders, including sepsis-induced myocardial dysfunction [37]. Meanwhile, several studies have investigated the role of TNF- $\alpha$  in the pathogenesis of LPS-induced acute cardiac injury and have shown that high concentrations of TNF- $\alpha$  promoted the expression of specific cytokines and mediators involved in LPS-induced septic cardiomyopathy [6, 24, 26–28, 38, 39]. IL-6 is another important proinflammatory factor that can directly cause myocardial damage by stimulating nitric oxide synthase activity and NO production [40]. Besides, several published studies have reported that cytokines such as IL-1 $\beta$  may act as cardiodepressant inflammatory mediators during sepsis [6, 24, 26–28, 41]. Hence, inhibiting the production of inflammatory cytokines can be a critical molecular target for novel anti-inflammatory therapeutic approaches. In the present study, LPS notably stimulated the release of proinflammatory cytokines from H9C2 cardiomyocytes, consistent with previous reports [42]. The anti-inflammatory activity of AKBA has been investigated using several models of inflammation. Previous studies have reported that AKBA

inhibits the generation of proinflammatory cytokines through down-regulation of the NF- $\kappa$ B pathway [43]. For example, Chao Wei et al. evaluated the neuroprotective function of AKBA in a mouse model of Alzheimer's disease. Their findings indicated that AKBA had a strong anti-inflammatory effect on APP<sup>sw</sup>/PS1<sup>dE9</sup> mice by reducing inflammatory molecules' production through the inhibition of the NF- $\kappa$ B signalling pathway [44]. It has also been reported that the potential cardiac-protective of AKBA is likely associated with the activation of Nrf-2 related signalling cascades [23]. In another study, AKBA was shown to effectively alleviate oxygen-glucose deprivation (OGD)-induced neuroinflammation via the increased expression of Nrf2 [45].

Meanwhile, we explored the possible cardiac-protective effect of AKBA against LPS-induced inflammatory cytokine production in H9C2 cells. The results showed that AKBA pretreatment dramatically suppressed the protein and gene expression of IL-1 $\beta$ , IL-6, and TNF- $\alpha$  in LPS-exposed H9C2 cells in a concentration-dependent manner. Our results revealed that the protective effects of AKBA against LPS-induced cardiac injury were associated with inflammatory

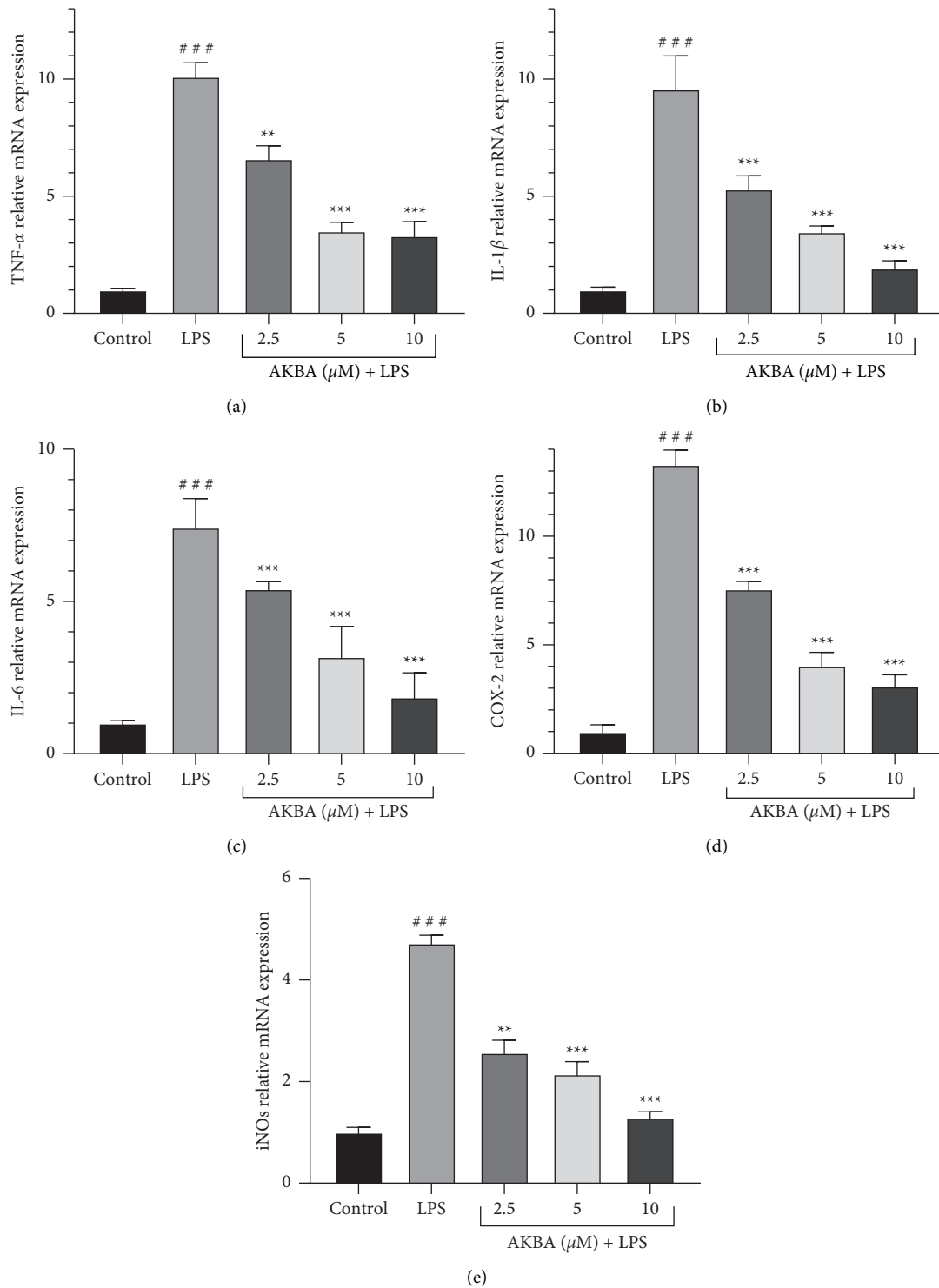


FIGURE 3: Effect of AKBA and LPS on the mRNA Level of TNF- $\alpha$  (a), IL-1 $\beta$  (b), IL-6 (c), Cox2 (d), and iNos (e). The cells were pretreated with AKBA for 24 h then incubated with LPS for another 24 h and gene expression of TNF- $\alpha$ , IL-1 $\beta$ , IL-6, Cox2, and iNos was evaluated by real time-PCR. The data are mean  $\pm$  SEM ( $n = 6$  per group). ### $P < 0.001$  vs. control, \*\* $P < 0.01$  and \*\*\* $P < 0.001$  vs. LPS.

cytokine production inhibition. The obtained results were in accordance with a previous study in which AKBA markedly reduced TNF- $\alpha$  production in the target tissue against the LPS-induced neuroinflammatory model [13]. These findings suggest that the potent anti-inflammatory properties of

AKBA may be related to its inhibitory activity on the expression of inflammatory factors.

COX-2 is an inducible isoform from cyclooxygenase that catalyses the formation of prostaglandin E<sub>2</sub> (PEG<sub>2</sub>), which is involved in many processes leading to the inflammatory

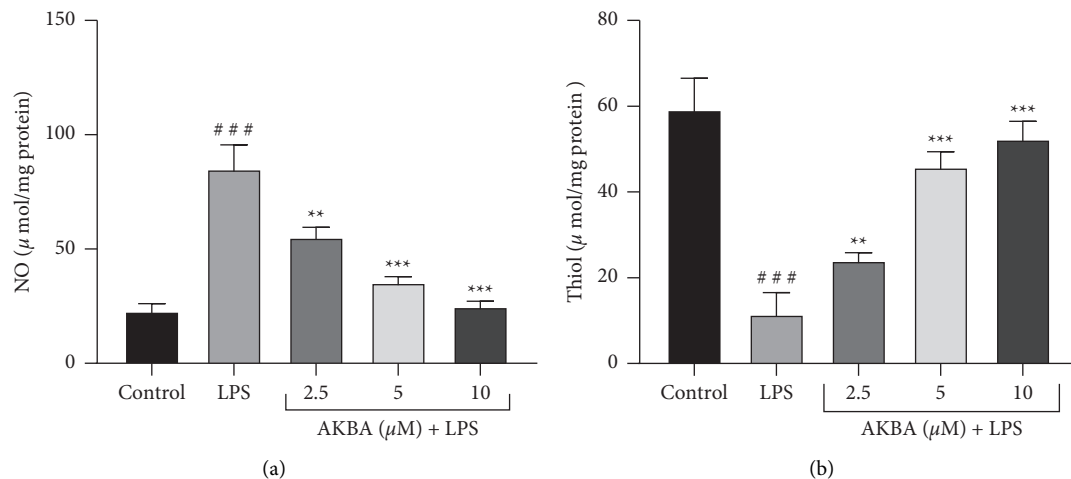


FIGURE 4: Cellular redox status including thiol state and NO state after treatment with AKBA and LPS. The cells were treated (24 hours) with various concentrations AKBA (2.5–10  $\mu\text{M}$ ) and then incubated with LPS (10  $\mu\text{g/ml}$ ) for 24 hours. The data are mean  $\pm$  SEM ( $n = 6$ ). ### $P < 0.001$  vs. control, \*\* $P < 0.001$  and \*\*\* $P < 0.001$  vs. LPS.

response [6, 24, 26–28, 46]. Many studies have shown that COX-2 enzymatic activity is significantly induced by proinflammatory stimuli such as TNF- $\alpha$  and LPS and high NO concentrations during various inflammatory conditions [47–49]. Thus, the level of COX-2 expression seems to play a pivotal role in multiple pathophysiological mechanisms, especially inflammation-related diseases [49, 50]. Likewise, several studies have proved that many natural products derived from medicinal plants with significant anti-inflammatory effects act as selective inhibitors of COX-2 activity [6, 24, 26–28, 49, 51]. In this research, we found that AKBA could efficiently suppress the mRNA expression of COX-2 in H9C2 cardiomyocytes activated with LPS. This outcome supports the hypothesis that the cardiac-protective effect of AKBA may also be attributed to the direct suppression of COX-2 gene expression. To further investigate the anti-inflammatory potential of AKBA, we measured the expression level of PEG2 in AKBA + LPS-treated H9C2 cells. Results indicated that pretreatment with AKBA meaningfully decreased the PGE2 level in LPS-activated H9C2 cells. As a result, inhibiting these inflammatory mediators' production can be an essential indicator for our anti-inflammatory agents.

Inducible nitric oxide synthase (iNOS) is commonly expressed in response to proinflammatory stimuli such as LPS and specific chemokines/cytokines in a wide range of cells. It has been found that the overproduction of NO by iNOS activity plays a crucial role in the pathophysiology of septic cardiomyopathy [52]. High NO levels lead to the induction of cellular oxidative damage via increasing the production of reactive nitrogen species (RNS) such as peroxynitrite [53]. Many previous studies have revealed that natural phytochemicals can show therapeutic effects against LPS-evoked inflammatory injury via reducing the iNOS expression and NO content [54]. In the current study, we also found a significant suppressive effect of AKBA on the expression of iNOS and the production of NO.

Similarly, antioxidant effects of AKBA have been previously reported. Manoj Kumar et al. have demonstrated that AKBA inhibits benzo (a) pyrene-induced liver toxicity by reducing NO generation [55]. Besides, Yu et al. investigated the nitric oxide inhibitory activity of bioactive compounds isolated from the resin of *Boswellia carteri*. Interestingly, their experiments showed that AKBA was one of the most potent antioxidant compounds in *Boswellia carteri* that could inhibit NO production in LPS-stimulated RAW264.7 cells [56]. These findings provide novel evidence that AKBA may attenuate inflammatory responses by suppressing iNOS-mediated NO production.

Additionally, the amount of glutathione is another parameter used in our study to evaluate the antioxidant activity of AKBA. As a nonenzymatic antioxidant compound, total thiol content has a crucial role in protecting cells from oxidative stress and maintaining cellular redox homeostasis [57]. It has been proven that a decreased level of reduced total thiol content leads to activation of the NF- $\kappa\text{B}$  pathway and enhances the expression of proinflammatory cytokines during inflammation-related disorders [58]. Consequently, the increased level of total thiol content can be part of the antioxidant defence mechanism to inhibit sepsis-induced cardiomyopathy [59]. On the other hand, natural metabolites have been shown to protect against oxidative damage in many inflammatory conditions by enhancing intracellular total thiol content [6, 24, 26–28, 49, 60]. The results of a previous study revealed that AKBA possessed antioxidant effects through elevating the reduced total thiol content levels in an experimental model of colitis [61]. Consistent with these findings, we also observed a remarkable increase of reduced total thiol content in LPS-exposed H9C2 cardiomyocytes after pretreating with AKBA. Based on this result, it can be inferred that the beneficial effects of AKBA on LPS-induced inflammation in H9C2 cells may be due to its potent antioxidant potential.

Overall, our findings demonstrate the potent anti-inflammatory and antioxidant properties of AKBA, suggesting



that it can be used as an effective therapeutic agent to lessen the inflammatory injuries caused by LPS in cardiomyocytes. However, additional *in vivo* experiments are required to further support the therapeutic potential of AKBA in sepsis-related myocardial dysfunction.

### Data Availability

The data used to support the findings of this study are available from the corresponding author upon reasonable request.

### Ethical Approval

This study does not require ethical approval.

### Consent

This study does not require the need for informed consent.

### Disclosure

Danial Taherzadeh, Vafa Baradaran Rahimi, Hamed Amiri, and Sajjad Ehtiati shared the first co-authorship.

### Conflicts of Interest

The authors declare that they have no conflicts of interest.

### Authors' Contributions

All authors equally contributed to performing the project and preparing the manuscript.

### Acknowledgments

This study was financially supported by a nonspecific grant of the research council of Mashhad University of Medical Sciences (GN 991660, 991593, and 990961).

### References

- [1] X. Wei, X. Meng, Y. Yuan, F. Shen, C. Li, and J. Yang, "Quercetin exerts cardiovascular protective effects in LPS-induced dysfunction *in vivo* by regulating inflammatory cytokine expression, NF- $\kappa$ B phosphorylation, and caspase activity," *Molecular and Cellular Biochemistry*, vol. 446, no. 1-2, pp. 43–52, 2018.
- [2] N. Marefati, F. Beheshti, P. Etemadzadeh, M. Hosseini, and A. Anaigoudari, "Gum resin extract of *Boswellia serrata* attenuates lipopolysaccharide-induced inflammation and oxidative damage in hepatic and renal tissues of rats," *Asian Pacific Journal of Tropical Biomedicine*, vol. 12, no. 1, pp. 20–25, 2022.
- [3] N. Marefati, F. Beheshti, S. Memarpour, M. Rezaei, and M. Hosseini, "The effects of pre-treatment with olibanum and its constituent, boswellic acid on synaptic plasticity impairments induced by lipopolysaccharide in rats," *Avicenna journal of phytomedicine*, vol. 11, no. 1, pp. 68–78, 2021.
- [4] N. Marefati, F. Beheshti, F. Vafae, M. Barabadi, and M. Hosseini, "The effects of incense acetate on neuro-inflammation, brain-derived neurotrophic factor and memory impairment induced by lipopolysaccharide in rats," *Neurochemical Research*, vol. 46, no. 9, pp. 2473–2484, 2021.
- [5] C.-Y. Fu, J. Chen, X.-Y. Lu et al., "Dimethyl fumarate attenuates lipopolysaccharide-induced mitochondrial injury by activating Nrf2 pathway in cardiomyocytes," *Life Sciences*, vol. 235, Article ID 116863, 2019.
- [6] R. Yahyazadeh, V. Baradaran Rahimi, A. Yahyazadeh, S. A. Mohajeri, and V. R. Askari, "Promising effects of gingerol against toxins: a review article," *Biofactors*, vol. 47, 2021.
- [7] V. Baradaran Rahim, M. T. Khammar, H. Rakhshandeh, A. Samzadeh-Kermani, A. Hosseini, and V. R. Askari, "Crocins protect cardiomyocytes against LPS-Induced inflammation," *Pharmacological Reports*, vol. 71, no. 6, pp. 1228–1234, 2019.
- [8] T. Q. C. Nguyen, T. Duy Binh, T. L. A. Pham et al., "Anti-inflammatory effects of lasia spinosa leaf extract in lipopolysaccharide-induced RAW 264.7 macrophages," *International Journal of Molecular Sciences*, vol. 21, no. 10, p. 3439, 2020.
- [9] R. Wang, D. Li, J. Ouyang et al., "Leonurine alleviates LPS-induced myocarditis through suppressing the NF- $\kappa$ B signaling pathway," *Toxicology*, vol. 422, pp. 1–13, 2019.
- [10] N. Marefati, F. Beheshti, A. Mokhtari-Zaer et al., "The effects of olibanum on oxidative stress indicators, cytokines, brain derived neurotrophic factor and memory in lipopolysaccharide challenged rats," *Toxin Reviews*, pp. 1–14, 2020.
- [11] N. Ahmed, D. S. El-Agamy, G. A. Mohammed, H. Abo-Haded, M. Elkablawy, and S. R. M. Ibrahim, "Suppression of LPS-induced hepato-and cardiotoxic effects by pulicaria petiolaris via NF- $\kappa$ B dependent mechanism," *Cardiovascular Toxicology*, vol. 20, pp. 1–9, 2019.
- [12] M. H. Al-Dossari, L. M. Fadda, H. A. Attia, I. H. Hasan, and A. M. Mahmoud, "Curcumin and selenium prevent lipopolysaccharide/diclofenac-induced liver injury by suppressing inflammation and oxidative stress," *Biological Trace Element Research*, vol. 196, no. 1, pp. 173–183, 2020.
- [13] N. Marefati, F. Beheshti, S. Memarpour et al., "The effects of acetyl-11-keto- $\beta$ -boswellic acid on brain cytokines and memory impairment induced by lipopolysaccharide in rats," *Cytokine*, vol. 131, Article ID 155107, 2020.
- [14] N. Marefati, S. Khamse, S. Khamse, S. Mansouri, M. Hosseini, and A. Anaigoudari, "Effects of boswellia serrata resin on central nervous system: a mini review," *Physiology and Pharmacology*, vol. 25, no. 4, pp. 288–295, 2021.
- [15] M. Molteni, A. Bosi, and C. Rossetti, "Natural products with toll-like receptor 4 antagonist activity," *International Journal of Inflammation*, vol. 2018, Article ID 2859135, 9 pages, 2018.
- [16] A. Rajabian, H. R. Sadeghnia, A. Hosseini, S. H. Mousavi, and M. T. Boroushaki, "3-Acetyl-11-keto- $\beta$ -boswellic acid attenuated oxidative glutamate toxicity in neuron-like cell lines by apoptosis inhibition," *Journal of Cellular Biochemistry*, vol. 121, no. 2, pp. 1778–1789, 2020.
- [17] X. Pang, Z. Yi, X. Zhang et al., "Acetyl-11-Keto- $\beta$ -Boswellic acid inhibits prostate tumor growth by suppressing vascular endothelial growth factor receptor 2-mediated angiogenesis," *Cancer Research*, vol. 69, no. 14, pp. 5893–5900, 2009.
- [18] M. Chen, M. Wang, Q. Yang et al., "Antioxidant effects of hydroxysafflor yellow a and acetyl-11-keto- $\beta$ -boswellic acid in combination on isoproterenol-induced myocardial injury in rats," *International Journal of Molecular Medicine*, vol. 37, no. 6, pp. 1501–1510, 2016.
- [19] W. Li, J. Liu, W. Fu et al., "3-O-acetyl-11-keto- $\beta$ -boswellic acid exerts anti-tumor effects in glioblastoma by arresting cell cycle at G2/M phase," *Journal of Experimental & Clinical Cancer Research*, vol. 37, no. 1, p. 132, 2018.

- [20] F. Iram, S. A. Khan, and A. Husain, "Phytochemistry and potential therapeutic actions of boswellic acids: a mini-review," *Asian Pacific Journal of Tropical Biomedicine*, vol. 7, no. 6, pp. 513–523, 2017.
- [21] B. E. Al-Dhubiab, S. S. Patel, M. A. Morsy et al., "The beneficial effect of boswellic acid on bone metabolism and possible mechanisms of action in experimental osteoporosis," *Nutrients*, vol. 12, no. 10, p. 3186, 2020.
- [22] C. Y. Chan, M. C. Mong, W. H. Liu, C. Y. Huang, and M. C. Yin, "Three pentacyclic triterpenes protect H9c2 cardiomyoblast cells against high-glucose-induced injury," *Free Radical Research*, vol. 48, no. 4, pp. 402–411, 2014.
- [23] S. M. Elshazly, D. M. Abd El Motteleb, and N. N. Nassar, "The selective 5-LOX inhibitor 11-keto- $\beta$ -boswellic acid protects against myocardial ischemia reperfusion injury in rats: involvement of redox and inflammatory cascades," *Naunyn-Schmiedeberg's archives of pharmacology*, vol. 386, no. 9, pp. 823–833, 2013.
- [24] V. Baradaran Rahimi, A. Rajabian, H. Rajabi et al., "The effects of hydro-ethanolic extract of capparid spinosa (*C. spinosa*) on lipopolysaccharide (LPS)-induced inflammation and cognitive impairment: evidence from in vivo and in vitro studies," *Journal of Ethnopharmacology*, vol. 256, Article ID 112706, 2020.
- [25] M. M. Bradford, "A rapid and sensitive method for the quantitation of microgram quantities of protein utilizing the principle of protein-dye binding," *Analytical Biochemistry*, vol. 72, no. 1-2, pp. 248–254, 1976.
- [26] P. Rahmanian-Devin, H. Rakhshandeh, V. Baradaran Rahimi et al., "Intraperitoneal lavage with *Crocus sativus* prevents postoperative-induced peritoneal adhesion in a rat model: evidence from animal and cellular studies," *Oxidative Medicine and Cellular Longevity*, vol. 2021, Article ID 5945101, 2021.
- [27] A. Jaafari, V. Baradaran Rahimi, N. Vahdati-Mashhadian et al., "Evaluation of the therapeutic effects of the hydro-ethanolic extract of portulaca oleracea on surgical-induced peritoneal adhesion," *Mediators Inflamm*, vol. 2021, Article ID 8437753, 18 pages, 2021.
- [28] M. Ghadiri, V. Baradaran Rahimi, E. Moradi et al., "Standardised pomegranate peel extract lavage prevents postoperative peritoneal adhesion by regulating TGF- $\beta$  and VEGF levels," *Inflammopharmacology*, vol. 29, no. 3, pp. 855–868, 2021.
- [29] A. Peinnequin, C. Mouret, O. Birot et al., "Rat pro-inflammatory cytokine and cytokine related mRNA quantification by real-time polymerase chain reaction using SYBR green," *BMC Immunology*, vol. 5, no. 1, p. 3, 2004.
- [30] J. Sun, X. Zhang, M. Broderick, and H. Fein, "Measurement of nitric oxide production in biological systems by using griess reaction assay," *Sensors*, vol. 3, no. 8, pp. 276–284, 2003.
- [31] I. Rahman, A. Kode, and S. K. Biswas, "Assay for quantitative determination of glutathione and glutathione disulfide levels using enzymatic recycling method," *Nature Protocols*, vol. 1, no. 6, pp. 3159–3165, 2006.
- [32] H. Lin, W. Wang, M. Lee, Q. Meng, and H. Ren, "Current status of septic cardiomyopathy: basic science and clinical progress," *Frontiers in Pharmacology*, vol. 11, p. 210, 2020.
- [33] L. Chen, P. Liu, X. Feng, and C. Ma, "Salidroside suppressing LPS-induced myocardial injury by inhibiting ROS-mediated PI3K/Akt/mTOR pathway in vitro and in vivo," *Journal of Cellular and Molecular Medicine*, vol. 21, no. 12, pp. 3178–3189, 2017.
- [34] S. Tan, Z. Long, X. Hou et al., "H2 protects against lipopolysaccharide-induced cardiac dysfunction via blocking TLR4-Mediated cytokines expression," *Frontiers in Pharmacology*, vol. 10, p. 865, 2019.
- [35] W. Tong, X. Chen, X. Song et al., "Resveratrol inhibits LPS-induced inflammation through suppressing the signaling cascades of TLR4-NF- $\kappa$ B/MAPKs/IRF3," *Experimental and Therapeutic Medicine*, vol. 19, no. 3, pp. 1824–1834, 2020.
- [36] Y.-Y. Meng, Y. Liu, Z.-F. Hu et al., "Sanguinarine attenuates lipopolysaccharide-induced inflammation and apoptosis by inhibiting the TLR4/NF- $\kappa$ B pathway in H9c2 cardiomyocytes," *Current Medical Science*, vol. 38, no. 2, pp. 204–211, 2018.
- [37] L.-j. Sun, W. Qiao, Y.-j. Xiao, L. Cui, X. Wang, and W.-d. Ren, "Naringin mitigates myocardial strain and the inflammatory response in sepsis-induced myocardial dysfunction through regulation of PI3K/AKT/NF- $\kappa$ B pathway," *International Immunopharmacology*, vol. 75, Article ID 105782, 2019.
- [38] J. An, J. Du, N. Wei, T. Guan, A. K. S. Camara, and Y. Shi, "Differential sensitivity to LPS-induced myocardial dysfunction in the isolated brown norway and DAHL S rat hearts," *Shock*, vol. 37, no. 3, pp. 325–332, 2012.
- [39] P. Zhao, Y. Wang, S. Zeng, J. Lu, T.-M. Jiang, and Y.-M. Li, "Protective effect of astragaloside IV on lipopolysaccharide-induced cardiac dysfunction via downregulation of inflammatory signaling in mice," *Immunopharmacology and Immunotoxicology*, vol. 37, no. 5, pp. 428–433, 2015.
- [40] V. P. Viswanadha, V. Dhivya, N. M. Beeraka et al., "The protective effect of piperine against isoproterenol-induced inflammation in experimental models of myocardial toxicity," *European Journal of Pharmacology*, vol. 885, Article ID 173524, 2020.
- [41] N. G. Yousif, N. R. Hadi, F. Al-Amran, and Q. A. Zigam, "Cardioprotective effects of irbesartan in polymicrobial sepsis," *Herz*, vol. 43, no. 2, pp. 140–145, 2018.
- [42] M. Zeng, M. Li, Y. Chen et al., "A new bisepoxyignan dendranlignan A isolated from chrysanthemum flower inhibits the production of inflammatory mediators via the TLR4 pathway in LPS-induced H9c2 cardiomyocytes," *Archives of Biochemistry and Biophysics*, vol. 690, Article ID 108506, 2020.
- [43] A. S. Sayed and N. S. E. D. El Sayed, "Co-administration of 3-acetyl-11-keto-beta-boswellic acid potentiates the protective effect of celecoxib in lipopolysaccharide-induced cognitive impairment in mice: possible implication of anti-inflammatory and antigitamatergic pathways," *Journal of Molecular Neuroscience*, vol. 59, no. 1, pp. 58–67, 2016.
- [44] C. Wei, J. Fan, X. Sun et al., "Acetyl-11-keto- $\beta$ -boswellic acid ameliorates cognitive deficits and reduces amyloid- $\beta$  levels in APPswe/PS1dE9 mice through antioxidant and anti-inflammatory pathways," *Free Radical Biology and Medicine*, vol. 150, 2020.
- [45] S. Ahmad, S. A. Khan, A. Kindelin et al., "Acetyl-11-keto- $\beta$ -boswellic acid (AKBA) attenuates oxidative stress, inflammation, complement activation and cell death in brain endothelial cells following OGD/reperfusion," *Neuro-Molecular Medicine*, vol. 21, no. 4, pp. 505–516, 2019.
- [46] L. Y. Lu, F. Loi, K. Nathan et al., "Pro-inflammatory M1 macrophages promote Osteogenesis by mesenchymal stem cells via the COX-2-prostaglandin E2 pathway," *Journal of Orthopaedic Research*, vol. 35, no. 11, pp. 2378–2385, 2017.
- [47] S.-B. Lee, W. S. Lee, J.-S. Shin, D. S. Jang, and K. T. Lee, "Xanthotoxin suppresses LPS-induced expression of iNOS, COX-2, TNF- $\alpha$ , and IL-6 via AP-1, NF- $\kappa$ B, and JAK-STAT

- inactivation in RAW 264.7 macrophages," *International Immunopharmacology*, vol. 49, pp. 21–29, 2017.
- [48] M. M. Gamal El-Din, M. I. El-Gamal, M. S. Abdel-Maksoud et al., "Inhibitory effects of triarylpyrazole derivatives on LPS-induced nitric oxide and PGE2 productions in murine RAW 264.7 macrophages," *Bioorganic & Medicinal Chemistry Letters*, vol. 30, no. 4, Article ID 126884, 2020.
- [49] P. Rahmanian-Devin, V. Baradaran Rahimi, M. R. Jaafari, S. Golmohammadzadeh, Z. Sanei-far, and V. R. Askari, "Noscapine, an emerging medication for different diseases: a mechanistic review," *Evidence-based Complementary and Alternative Medicine*, vol. 2021, Article ID 8402517, 16 pages, 2021.
- [50] D. Mukherjee, S. E. Nissen, and E. J. Topol, "Risk of cardiovascular events associated with selective COX-2 inhibitors," *JAMA*, vol. 286, no. 8, pp. 954–959, 2001.
- [51] H. Cao, R. Yu, Y. Choi et al., "Discovery of cyclooxygenase inhibitors from medicinal plants used to treat inflammation," *Pharmacological Research*, vol. 61, no. 6, pp. 519–524, 2010.
- [52] S. Franceschelli, M. Pesce, A. Ferrone et al., "Biological effect of Licochalcone C on the regulation of PI3K/Akt/eNOS and NF- $\kappa$ B/iNOS/NO signaling pathways in H9c2 cells in response to LPS stimulation," *International Journal of Molecular Sciences*, vol. 18, no. 4, p. 690, 2017.
- [53] A. Durand, T. Duburcq, T. Dekeyser et al., "Involvement of mitochondrial disorders in septic cardiomyopathy," *Oxidative medicine and cellular longevity*, vol. 2017, Article ID 4076348, 13 pages, 2017.
- [54] H. M.-D. Wang, L. Fu, C. C. Cheng et al., "Inhibition of LPS-induced oxidative damages and potential anti-inflammatory effects of *Phyllanthus emblica* extract via down-regulating NF- $\kappa$ B, COX-2, and iNOS in RAW 264.7 cells," *Antioxidants*, vol. 8, no. 8, p. 270, 2019.
- [55] P. Bhardwaj, M. Kumar, S. K. Dhatwalia, M. L. Garg, and D. K. Dhawan, "Acetyl-11-keto- $\beta$ -boswellic acid modulates membrane dynamics in benzo pyrene-induced lung carcinogenesis," *Molecular and Cellular Biochemistry*, vol. 460, pp. 17–27, 2019.
- [56] P.-Y. Zhang, B. Yu, W.-J. Men et al., "Acetyl- $\alpha$ -boswellic acid and Acetyl- $\beta$ -boswellic acid protects against caerulein-induced pancreatitis via down-regulating MAPKs in mice," *International Immunopharmacology*, vol. 86, Article ID 106682, 2020.
- [57] V. P. Bajic, C. Van Neste, M. Obradovic et al., "Glutathione "redox homeostasis" and its relation to cardiovascular disease," *Oxidative medicine and cellular longevity*, vol. 2019, Article ID 5028181, 14 pages, 2019.
- [58] J. T. Jones, X. Qian, J. L. J. van der Velden et al., "Glutathione S-transferase pi modulates NF- $\kappa$ B activation and pro-inflammatory responses in lung epithelial cells," *Redox Biology*, vol. 8, pp. 375–382, 2016.
- [59] V. Tsolaki, D. Makris, K. Mantzaris, and E. Zakyntinos, "Sepsis-induced cardiomyopathy: oxidative implications in the initiation and resolution of the damage," *Oxidative medicine and cellular longevity*, vol. 2017, Article ID 7393525, 11 pages, 2017.
- [60] H.-J. Fan, Z.-B. Tan, Y.-T. Wu et al., "The role of ginsenoside Rb1, a potential natural glutathione reductase agonist, in preventing oxidative stress-induced apoptosis of H9C2 cells," *Journal of Ginseng Research*, vol. 44, no. 2, pp. 258–266, 2020.
- [61] R. M. Hartmann, M. I. Morgan Martins, J. Tieppo, H. S. Fillmann, and N. P. Marroni, "Effect of *Boswellia serrata* on antioxidant status in an experimental model of colitis rats induced by acetic acid," *Digestive Diseases and Sciences*, vol. 57, no. 8, pp. 2038–2044, 2012.

## Research Article

# Folecitin Isolated from *Hypericum oblongifolium* Exerts Neuroprotection against Lipopolysaccharide-Induced Neuronal Synapse and Memory Dysfunction via p-AKT/Nrf-2/HO-1 Signalling Pathway

Umar Farooq,<sup>1</sup> Muhammad Umar Khayam Sahibzada,<sup>2</sup> Taous Khan ,<sup>1</sup> Rahim Ullah,<sup>3</sup> Muhammad Shahid,<sup>4</sup> Ameer Khusro ,<sup>5</sup> Veronique Seidel,<sup>6</sup> Magda H. Abdellattif ,<sup>7</sup> and Talha Bin Emran <sup>8</sup>

<sup>1</sup>Department of Pharmacy, COMSATS University Islamabad Abbottabad Campus, Abbottabad, Pakistan

<sup>2</sup>Department of Pharmacy, Sarhad University of Science & Information Technology, Peshawar 25100, Khyber Pakhtunkhwa, Pakistan

<sup>3</sup>Department of Pharmacy, University of Peshawar, Peshawar, Pakistan

<sup>4</sup>Department of Pharmacy, Institute of Integrative Biosciences, CECOS University of IT and Emerging Sciences, Peshawar, Khyber Pakhtunkhwa, Pakistan

<sup>5</sup>Research Department of Plant Biology and Biotechnology, Loyola College, Chennai, Tamil Nadu, India

<sup>6</sup>Natural Products Research Laboratory, Strathclyde Institute of Pharmacy and Biomedical Sciences, University of Strathclyde, Glasgow G4 0RE, UK

<sup>7</sup>Department of Chemistry, College of Science, Taif University, PO. Box 11099, Taif 21944, Saudi Arabia

<sup>8</sup>Department of Pharmacy, BGC Trust University Bangladesh, Chittagong 4381, Bangladesh

Correspondence should be addressed to Taous Khan; [taouskhan@ciit.net.pk](mailto:taouskhan@ciit.net.pk), Ameer Khusro; [armankhan0301@gmail.com](mailto:armankhan0301@gmail.com), and Talha Bin Emran; [talhabmb@gmail.com](mailto:talhabmb@gmail.com)

Received 15 January 2022; Accepted 7 March 2022; Published 28 March 2022

Academic Editor: Ruchika Garg

Copyright © 2022 Umar Farooq et al. This is an open access article distributed under the Creative Commons Attribution License, which permits unrestricted use, distribution, and reproduction in any medium, provided the original work is properly cited.

Neurodegenerative diseases, especially Alzheimer's disease (AD), are characterised with neuronal synapse and memory dysfunction, and thus, there is an urgent need to find novel therapeutic medicines that can target different pathways to restore the deficits. In this investigation, we assessed the medicinal potency of folecitin (a flavonoid isolated from *Hypericum oblongifolium* Wall.) against lipopolysaccharide (LPS)-induced amyloidogenic amyloid beta ( $A\beta$ ) production pathway-mediated memory impairment in mice. The LPS was administered intraperitoneally (i.p.) 250  $\mu\text{g}/\text{kg}/\text{day}$  for 3 consecutive weeks, followed by the coadministration of folecitin (30  $\text{mg}/\text{kg}/\text{day}$ ) with LPS for the last two weeks (2<sup>nd</sup> and 3<sup>rd</sup> week). The expression of various proteins involved in synapse, neuronal death, and  $A\beta$  generation was evaluated using the Western blot approach. Results indicated that folecitin significantly decreased LPS-induced apoptotic proteins; expressed BAX, PARP-1, and caspase-3 proteins; and inhibited BACE1 that cleaves transmembrane amyloid precursor protein and the amyloidogenic  $A\beta$  production pathway. Folecitin restored both preneuronal and postneuronal synapse, accompanied by the improvement in memory impairment. Moreover, folecitin significantly activated endogenous antioxidant proteins Nrf-2 and HO-1 by stimulating the phosphorylation of Akt proteins. These findings indicate that folecitin might be a promising target for developing novel medication to treat neurodegenerative disorders caused by neurotoxins.

## 1. Introduction

Neurological disorders (NDs), for example, Parkinson's disease (PD), Alzheimer's disease (AD), and amyotrophic lateral sclerosis (ALS), are the key progressive neurodegenerative problems worldwide. According to reports, 46.8 million individuals suffered from NDs in 2015, incurring an estimated treatment cost of US\$ 818 billion. By 2040, NDs are expected to be the 2<sup>nd</sup> most common cause of death [1]. The NDs are characterised by the depletion (or inadequate synthesis) of neurotransmitters, inflammation, aggregation of misfolded proteins, and oxidative stresses in central nervous system (CNS), for instance,  $\beta$ -amyloid and Tau proteins in AD [2, 3]. The treatment of AD uses various therapeutic agents of natural and synthetic origin [4], some of which such as the acetylcholinesterase inhibitors present adverse side effects [5]. Other treatments such as anti-Tau protein and  $\beta$ -amyloid antibodies, and  $\beta$ -secretase 1 (BACE1) inhibitors are very expensive [6, 7].

Plants have a long history of contributing to the discovery of new drugs. There are approximately 300,000 different species of higher plants worldwide, of which more than 85% have not been explored for the presence of bioactive principles [8, 9]. Plants produce a diverse range of chemicals (e.g., alkaloids, polyphenols, flavonoids, glycosides, terpenoids, and saponins) that exhibit various biological properties [10, 11]. In Asian countries, more than 120 traditional plants-based medicines are used for the management of CNS disorders [12–14]. This includes extracts and phytoconstituents from various plants such as *Panax ginseng* (ginsenosides) [15], *Curcuma longa* (curcumin) [16], *Hypericum perforatum* (hyperoside) [17], *Centella asiatica* (catechin) [18], *Bacopa monnieri* (bacosides) [19], *Withania somnifera* (withanolides) [20], and *Ginkgo biloba* (ginkgolides) [21] that exhibited promising psychotropic and neuroprotective properties.

The genus *Hypericum* (Hypericaceae) consists of herbs and shrubs found commonly in temperate regions and used as a source of natural medicines, pigments, dyes, gums, resins, and timbers [22]. Various species within the *Hypericum* genus, especially *Hypericum caprifoliatum* [23], *Hypericum perforatum* [24, 25], *Hypericum grandifolium* [26], *Hypericum oblongifolium* [27], *Hypericum polyanthemum* [28], and *Hypericum triquetrifolium* [29] have been studied for their antidepressant, antioxidant, anxiolytic, antimicrobial, antiviral, anticancer, anti-inflammatory, and antiulcerogenic properties.

*H. oblongifolium* Wall. (also known as basant, sheen chayi, and Pendant St. John's Wort) grows at altitudes of 800–1200 m within the Western Himalayas [27]. It is widely distributed in Northern Pakistan. Its flowers are yellow with persistent-withering petals, and they bloom from June to September [30]. The species is used traditionally for external wounds, hepatitis, gastric ulcers, and other gastrointestinal disorders [31]. It has potent *in vitro* antiglycation and antioxidant properties [32]. It has also demonstrated anti-proliferative activity on HT-29 human colon adenocarcinoma cells [33]. The species mainly contains flavonoids, triterpenes, and xanthenes [34].

Flavonoids are a vast category of natural polyphenolic plant pigments found in a wide variety of foods, including fruits, cereals, herbs, and drinks. Flavonoids have anticancer, cardiovascular, antioxidant, neuroprotective, and anti-inflammatory effects [35, 36]. Flavonoids are considered as potential neuroprotective compounds that can modulate cellular mechanisms implicated with neurodegeneration [35, 37–39]. Flavonoids show the characteristics of both antioxidant and signal pathway modulator. It can modulate cellular signal cascades by interacting with enzymes or receptors that are involved in activation and deactivation of signalling pathways [40, 41]. Reports suggest that a habitual intake of dietary flavonoids can reduce the risk of dementia and stroke [39]. For instance, flavonoids in fruits, vegetables, grains, etc. seem to prevent or reverse cognitive related deficits [37]. Considering the pivotal role of flavonoids, in this study, we focused on the isolation of folecitin (a flavonoid), from *H. oblongifolium*, and the evaluation of its protective activity against neuroinflammation using a lipopolysaccharide (LPS)-induced neurotoxicity assay in mice.

## 2. Materials and Methods

**2.1. Plant Materials.** Fresh leaves of *H. oblongifolium* were collected from Thandiyani, Abbottabad, KPK, Pakistan. The plant was authenticated by Dr. Banaras Khan, Department of Botany, Post Graduate College Attock city, and a voucher specimen (Atk/102/2018) was deposited in the herbarium of College.

**2.2. Extraction.** The pulverised leaves (15 kg) were macerated for 14 days in methanol:water solution (7:3) with frequent stirring using a steel rod. The resulting suspension was filtered by means of Whatman filter paper. The obtained solution was then concentrated under vacuum to afford a first crude extract. The remaining plant material was re-extracted with a fresh mixture of methanol:water (7:3) for another 7 days. After filtration, as aforementioned, the sample was concentrated under vacuum to afford a second extract. The combined crude extracts were resuspended in distilled water (1 L), and liquid-liquid partition was carried out using analytical grade solvents of increasing polarity starting with *n*-hexane, chloroform, ethyl acetate, and *n*-butanol to obtain *n*-hexane (640 g), chloroform (40 g), ethyl acetate (400 g), *n*-butanol (180 g), and aqueous (390 g) fractions.

**2.3. Isolation of Folecitin from *H. oblongifolium*.** Ethyl acetate fraction (400 g) was subjected to column chromatography over silica gel mesh size 230 (Merck), eluting with *n*-hexane:ethyl acetate having a ratio of 2:8. A total of 16 major fractions were obtained and pooled on the basis of their similar chemical profiles on thin layer chromatography (TLC) using silica gel 60 PF<sub>254</sub> plates (Merck). Fraction 14 (1.2 g) was further subjected to flash silica gel column chromatography, eluting with ethyl acetate:chloroform (1:1). Twelve major fractions were pooled based on

TLC analysis. Fractions 5–9 led to the separation of folecitin (70 mg) as yellow crystals. Folecitin was observed on TLC plates using cerium sulfate ( $\text{CeSO}_4$ ) and solid iodine, followed by heating. The structure of folecitin was determined following analysis of its  $^1\text{H}$  and  $^{13}\text{C}$  NMR, COSY, HSQC, and HMBC spectra recorded on Bruker spectrometers (Avance Av 500, 600/150 MHz) and comparison with the literature data [27]. All chemical shifts ( $\delta$ ) and coupling constants (J) were estimated in ppm and Hz.

#### 2.4. Neuroprotective Activity

**2.4.1. Ethical Approval.** All experimental animals were taken care of according to the approvals of the ethical committee of the Neuroprotective Medicine and Molecular Research Center, Ring Road Peshawar, Pakistan (Ethical committee number: NMMRC/2019/Rodents/015). Animals were handled as per the scientific procedures of the UK Animals guidelines Act 1986.

**2.4.2. Chemicals and Reagents.** Lipopolysaccharide (LPS), phosphate buffered saline tablets, polyvinylidene fluoride (PVDF) membrane, reagent for tissue protein extraction (T-PER), RNAsait solution, reagent for protein assay dye, acrylamide, bis-acrylamide, sample buffer (2X Laemmli), ammonium per sulfate (APS), trizma base, TEMED, sodium dodecyl sulfate (SDS), glycine, methanol, KCl, skim milk, NaCl, and Tween 20 were purchased from Sigma Aldrich (USA) and stored at the required temperature for further experimental purposes.

**2.4.3. Maintenance of Animals Used.** BALB/c adult male mice of 7–8 weeks old (weighing 30–32 g) were acquired from the Veterinary Research Institute, Peshawar, KPK, Pakistan. They were maintained separately in cages (Biobase, China), kept in a special room with a constant 12 h dark and 12 h light cycle at  $27 \pm 3^\circ\text{C}$ , with easy access to food and water.

**2.4.4. Experimental Groups.** Animals were arbitrarily divided into 4 experimental groups ( $n=6$ ). The total span of the experiment was 3 weeks (day 1 to day 21). The control group (C) received intraperitoneally (i.p.) normal saline for 3 consecutive weeks. Group 2 (LPS group) received LPS (i.p.) ( $250 \mu\text{g}/\text{kg}$ ) for 21 consecutive days. Group 3 (LPS + folecitin) received LPS ( $250 \mu\text{g}/\text{kg}/\text{day}$ ) for first 7 days and then continue till to the last day, while LPS was complemented by folecitin ( $30 \text{ mg}/\text{kg}$ ) from day 8 to day 21 of the experiment. The fourth and final group received folecitin ( $30 \text{ mg}/\text{kg}$ ) alone for the last two weeks of the experiment.

**2.4.5. Behavioural Tests.** Two well-known behavioural tests, the Y-maze and the Morris water maze (MWM), were conducted in order to find out the neuroprotective effect of folecitin on learning and remembrance behaviours in adult mice ( $n=6$ ).

**(1) Y-Maze Test.** The Y-Maze test consisted of 3 arms of 60 cm length, 12 cm diameter (width), and 22 cm height at an angle of  $120^\circ$  from each other [42, 43]. Briefly, all the experimental mice were allowed to receive trainings for the first 3 days (3 training trials per day). In each trial, the animals were trained for 10 min so that they could adapt to their new surroundings. After resting for 2 days, all the mice were permitted to search and walk around the Y-Maze for 8 min by keeping them in the center of the arms. A build-in camera with software was used to record the movements of mice, total arm entrances, and consecutive number of triplets. The percentage (%) of repetitions was estimated as per the equation below,

$$\text{Repetition (\%)} = (\text{consecutive sets of triplets} / \text{total number of arm entries} - 2) \times 100.$$

The changes and repetition (%) were associated positively with spatial functioning memory.

**(2) MWM Test.** The MWM test was implemented to determine the four-dimensional learning (spatial learning) and commemoration in adult mice [42]. The MWM device was made of a circular water tank of about 1.8 m in diameter and 0.6 m in height filled with normal tap water ( $25\text{--}28^\circ\text{C}$ ). Skimmed milk powder (1 kg) was added to make the water appearance opaque. A grey escape plastic platform (35.5 cm in height) was located 1 cm underneath the water surface nearby middle of any one of the four corners of the maze apparatus. This unique stage can be lowered to the bottom of the tank or raised to its typical position on the maze apparatus during behavioural learning and testing. A second stand (36.5 cm in height), black in colour, was raised 2 cm over the water layer during the first 3 days of training. The MWM was encircled by white curtains with fixed patterns in order to provide a configuration of three-dimensional signals. Observations were made using a video tracing system (HVS Image Analyzing VP-112) with the in-built software.

Briefly, all the experimental mice were allowed to receive 3 training trials (60 s per trial) per day for 3 successive days [43]. On each training test, an animal was released freely in the MWM from one of four equally spread-out starting positions round the border of the water tank. If any animal did not locate the escape stage within 80 s on any training session, it was guided and placed for 30 s on the platform. After resting for 2 days, all the animals were exposed to the latency to escape from the water maze (finding the submerged escape platform) was determined for each test day (four successive days). Again, after three-day rest, final escape latency and probe tests were carried out to estimate memory association. The time consumed in the particular quadrant by every animal was recorded.

**2.5. Western Blot.** Western blotting was carried out according to the method reported by Badshah et al. [44] with minor alterations. The mice brains were collected as quickly as possible and then homogenized in a T-PER solution. The levels of proteins in all 4 groups were



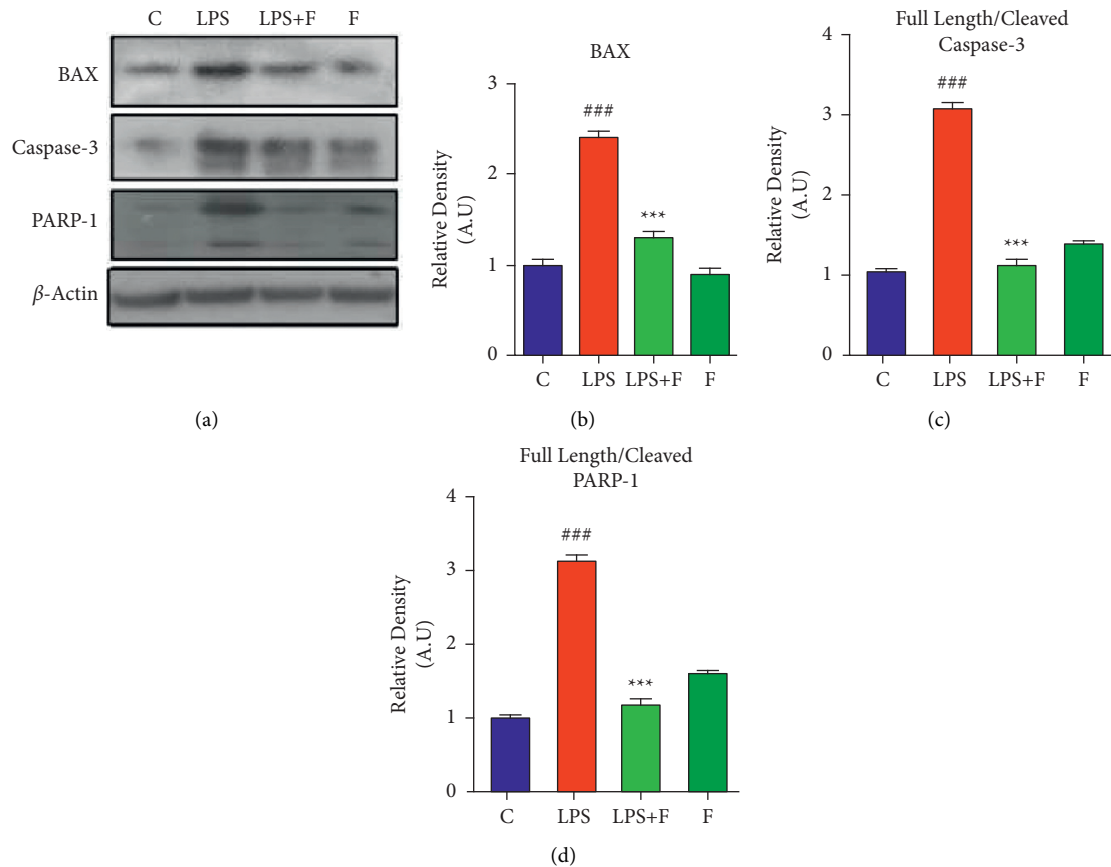


FIGURE 1: Folicitin decreased the expression of apoptotic protein markers in the mice brain. (a) Immunoblots of BAX, PARP-1, and caspase-3 in the brain homogenates of the adult mice for the experimental groups including (c) LPS, LPS + F, and F alone. Histogram of (b) BAX, (c) full-length/cleaved caspase-3, and (d) full-length/cleaved PARP-1.  $\beta$ -Actin was used as a loading control (reference control). The bands were analysed using the Image J software, and the density histograms (expressed in AU) compared to the control were organized using GraphPad Prism. Values are presented as the mean  $\pm$  SEM for the indicated proteins ( $n = 6$  mice per group). C: control, LPS: lipopolysaccharide, F: folicitin, AU: arbitrary units,  $###P < 0.001$  as compared to the C group, and  $**P < 0.01$  and  $***P < 0.001$  as compared to the LPS group.

measured using a BioRad protein assay. For each of the 4 groups, 30  $\mu$ g of the protein content was run on a 15–20% SDS-PAGE. After completing the electrophoresis process, all the proteins were shifted to a PVDF membrane (Santa Cruz Biotech, USA) over transblot (Bio-Rad). Different primary monoclonal antibodies (Santa Cruz, CA, USA) such as caspase-3, Bcl-2-associated X protein (BAX), beta-secretase-1 (BACE-1), poly (ADP-ribose) polymerase-1 (PARP-1), amyloid beta ( $A\beta$ ), synaptophysin (SYP), postsynaptic density protein 95 (PSD-95), and beta actin as well as HRP-conjugated secondary antibodies (Santa Cruz, CA, USA) were smeared. All results were visualised in a dark room on X-ray films.

**2.6. Statistical Analysis.** Results obtained were calculated as group mean  $\pm$  SEM (standard error mean) and analysed using one-way or two-way analysis of variance (ANOVA) followed by suitable *post hoc* tests. All the statistical investigations were conducted using the GraphPad Prism-5 software.  $P$  values less than 0.05 were defined as significant.

### 3. Results

**3.1. Effect of Folicitin on LPS-Induced Neuroapoptotic Protein Markers.** Different apoptotic indicators such as BAX, caspase-3, and PARP-1 protein expressions were analysed with the Western blotting technique. Results revealed that a 3-week administration of LPS-induced widespread upregulation in the adult mice brain. The LPS induced the proapoptotic BAX protein expression ( $P < 0.01$ ) and also triggered caspase-3 protein expression ( $P < 0.001$ ). Finally, LPS-induced neuronal DNA fragmentation increases PARP-1 protein expression ( $P < 0.001$ ). Interestingly, the administration of folicitin during the last 2 weeks of the experiment significantly inhibited proapoptotic-BAX ( $P < 0.001$ ), followed by low levels of caspase-3 ( $P < 0.01$ ) and PARP-1 ( $P < 0.001$ ) proteins (Figure 1).

**3.2. Effect of Folicitin on LPS-Induced  $A\beta$  Productions.** The 3-week administration of LPS significantly increased beta-secretase activity with significant ( $P < 0.001$ ) upregulation of the BACE-1 protein expression (which produces

fragments of  $A\beta$  precursor protein to cut into toxic  $A\beta$  fragments). Similarly, the expression of  $A\beta$  protein (both oligomers and monomers) was significantly ( $P < 0.001$ ) increased after LPS administration. In contrast, treatment with folicitin not only significantly ( $P < 0.05$ ) inhibited BACE-1 expression but also significantly ( $P < 0.001$ ) decreased both oligomers and monomers in the brain homogenates mixture of adult mice (Figure 2).

**3.3. Effect of Folicitin on Neuronal Synapse.** Western blot analysis revealed that systemic LPS injection reduced both SYP proteins ( $P < 0.001$ ) and PSD-95 ( $P < 0.05$ ) in the brain homogenates of mice with respect to the control group. Folicitin administration reduced the impact of LPS induction on synaptic markers and enhanced PSD-95 expression ( $P < 0.01$ ), as compared to the LPS-treated group, and SYP ( $P < 0.001$ ) (Figure 3).

**3.4. Effect of Folicitin on Stimulation of Phosphorylated-Akt (p-Akt) to Activate Nrf-2/HO-1.** The LPS administration significantly suppressed the protein expressions of p-AKT ( $P < 0.001$ ), nuclear factor erythroid 2-related factor 2 (Nrf-2) ( $P < 0.01$ ), and HO-1 ( $P < 0.001$ ), in comparison to the control group. In contrast, the administration of folicitin for two weeks significantly ( $P < 0.001$ ) stimulated phospho-Akt protein. It was accompanied by the stimulation of Nrf-2 ( $P < 0.001$ ) and HO-1 ( $P < 0.01$ ) protein expression in the brain homogenates of mice (Figure 4).

**3.5. Effect of Folicitin on Behaviour and LPS-Induced Memory Deficits.** The MWM and Y-maze tests were employed to check the memory-improving ability of folicitin. In the MWM test, LPS-treated mice showed significantly ( $P < 0.001$ ) higher mean escape latencies from day 1 to day 5. There was a gradual decrease in the mean escape latency from the start to the end of the experiment, suggesting that these mice had impaired memory. There was a little decrease in the mean latency on a daily basis from day 1 to day 5. On the other hand, the mice treated with LPS + folicitin showed better memory from day 1 to day 5. The performance of these mice was better with reduced mean escape latencies from day 1 to day 5 compared to LPS-treated mice ( $P < 0.05$ ,  $P < 0.001$ ). The experimental mice treated with folicitin alone showed escape latencies similar to the control group from the beginning to the end of the test, suggesting that they have no memory deficiency (Figure 5(a)). In the probe test, the control animal spent more time as compared to the LPS-treated animals. Among the other 2 groups, the mice treated with LPS + folicitin had spent more time ( $P < 0.001$ ) in the target quadrant, while the only folicitin-treated mice shown good memory by spending more time in the target quadrant (Figure 5(b)). The short-term memory was investigated by performing the Y-maze test. The control animals showed higher percentage of spontaneous alteration, while the LPS-treated animals displayed less percentage of spontaneous alteration ( $P < 0.001$ ). Similarly, animals treated with LPS + folicitin showed a significantly ( $P < 0.01$ )

higher percentage of spontaneous alteration, similar to the LPS-treated mice (Figure 5(c)).

## 4. Discussion

The current study reported that folicitin abrogated LPS-induced neuroapoptosis-mediated neuronal synapse dysfunction and memory impairment in the adult albino mice brain. Moreover, folicitin stimulated the p-Akt signalling pathway to activate Nrf-2 and its downstream molecule HO-1 in the brain of adult mice.

Alzheimer's disease is a neurodegenerative disorder with leading reason of death and disability [45]. In aging individuals, AD leads to a gradual impairment in cognition and neuronal dysregulation of communication. There are many evidences of involvement of neuroinflammation, apoptosis, and oxidative stress in the pathogenesis of AD and its associated neurodegenerative diseases [46]. In particular, it has been stated that the microglial activation plays a key role in triggering extreme oxidative stress when high levels of reactive oxygen species (ROS) are present [47]. Intracellular ROS in microglial cells causes inflammation and ultimately leads to neuronal cell death [48]. The level of endogenous ROS can be controlled by antioxidant molecules and anti-oxidative enzymes *via* the Nrf-2/antioxidant response element signal pathways [49].

Many reports conferred that the inclusion of LPS in rodents caused impairment of cognitive function and enhanced the level of AD-like markers, namely,  $A\beta$  and BACE-1 [44]. Several studies had reported that LPS impaired learning and memory [50, 51]. In the line with those studies, in the current report, the administration of LPS also impaired spatial learning and memory in the MWM test [44]. The MWM test results indicated that the mice receiving LPS had more mean escape time latencies and travelled longer distance to identify the escape platform. Our probe trial findings too demonstrated that LPS receiving animals' group failed in finding the exact location of the submerged platform and which is why they spent less time in the target quadrant. Animals receiving folicitin displayed a good recognition pattern and recognized the platform place and, hence, spent more time in the target quadrant.

The present study also demonstrated that folicitin significantly reduced apoptotic markers (BAX, caspase-3, and PARP-1 proteins) against LPS in the mice brain. Moreover, we hypothesized that folicitin had activated Nrf-2/HO-1 against LPS-induced oxidative stress in the brain of adult mice. Our results indicated that folicitin increased the nuclear translocation of Nrf-2/HO-1 and its production to inhibit LPS-induced oxidative stress. Of different genes involved in the antioxidative characteristics, HO-1 has been rated high, as it can exert protection via various mechanisms.

Akt acts as a signalling pathway with various functions, such as apoptosis, cell proliferation, and cellular defence, and is known to modulate Nrf-2 [52]. Cross-talk between the PI3K/Akt and Nrf-2 signalling pathways is capable of protecting cells against inflammatory and oxidative damage [53]. Subsequently, we investigated whether the Akt pathway-mediated folicitin-induced Nrf-2 activation and HO-1

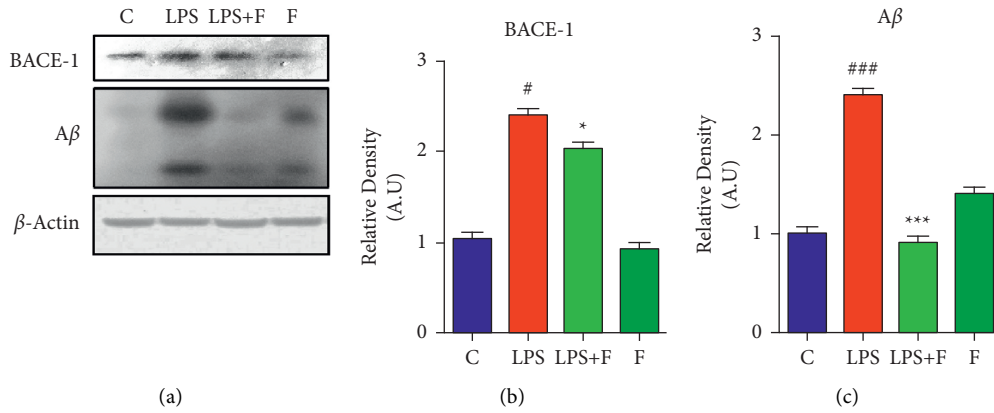


FIGURE 2: Folicitin reduced Aβ via inhibiting BACE-1 expression. (a) Immunoblots of BACE1 and Aβ in the brain homogenates of the adult mice for the experimental groups including (c) LPS, LPS + F, and F alone. Histogram of (b) BACE1 and (c) Aβ. β-Actin was used as a house-keeping loading control (reference control). The bands were analysed using the Image J software, and the density histograms (expressed in AU) compared to the control were organized using GraphPad Prism. Values are presented as the mean ± SEM for the indicated proteins (n = 6 mice per group). C: control, LPS: lipopolysaccharide, F: folicitin, AU: arbitrary units, #P < 0.05 and ###P < 0.001 as compared to the C group, and \*P < 0.05 and \*\*\*P < 0.001 as compared to the LPS group.

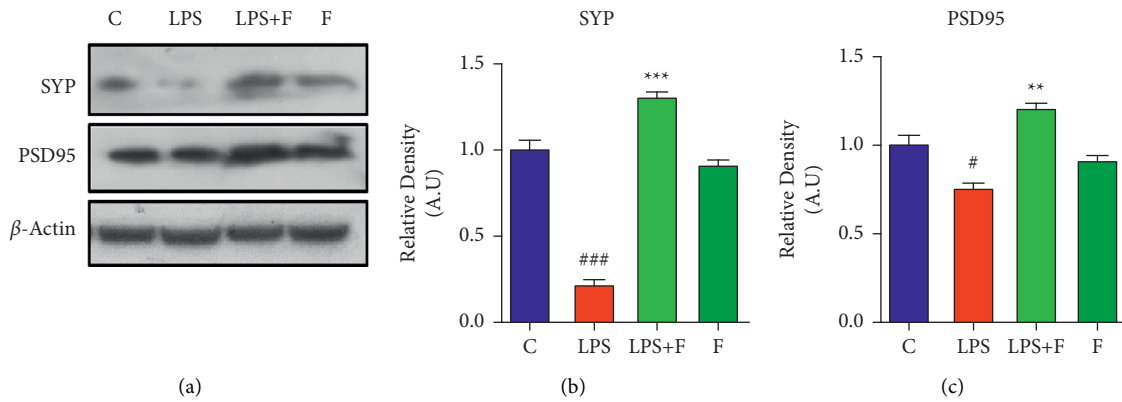


FIGURE 3: Folicitin reversed synaptic deficits induced by LPS. (a) Immunoblots of SYP and PSD95 proteins in the brain homogenates of male adult albino mice for the experimental groups including (c) LPS, LPS + F, and F alone. Histograms of (b) SYP and (c) PSD-95. β-Actin was used as a loading control (reference control). The bands were analysed using the Image J software, and the density histograms (expressed in AU) compared to the control were organized using GraphPad Prism. Values are presented as the mean ± SEM for the indicated proteins (n = 6 mice per group). C: control, LPS: lipopolysaccharide, F: folicitin, AU: arbitrary units, #P < 0.05 and ###P < 0.001 as compared to the C group, and \*\*P < 0.01 and \*\*\*P < 0.001 as compared to the LPS group.

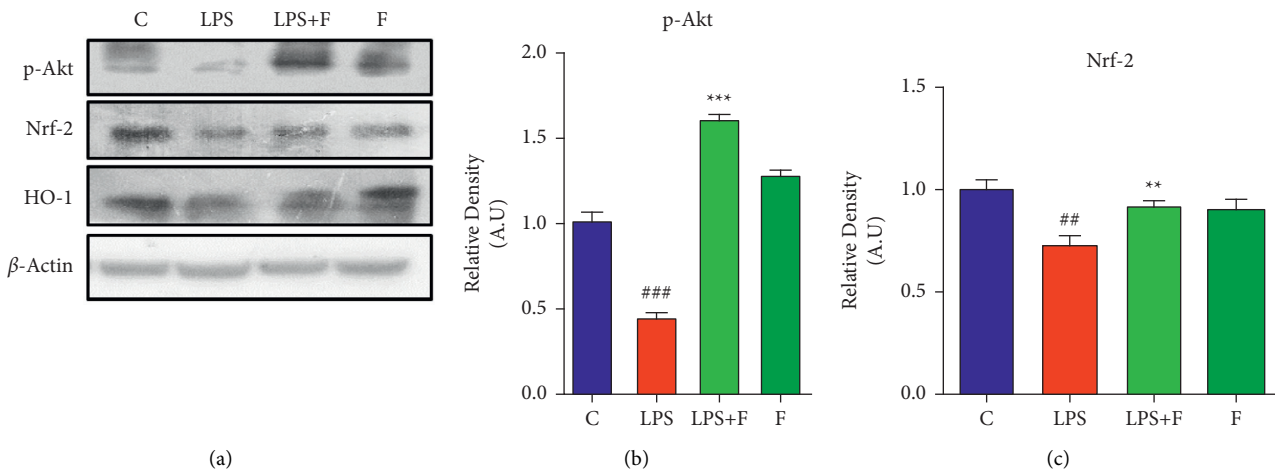


FIGURE 4: Continued.

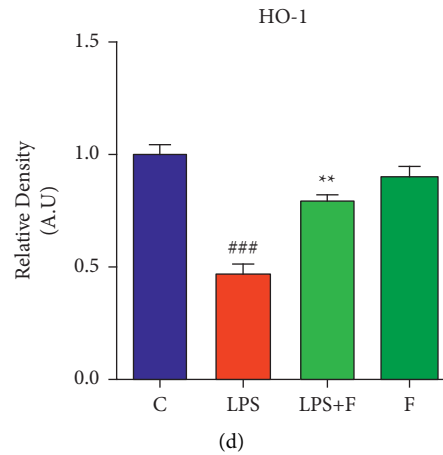


FIGURE 4: Folicitin stimulated the phosphorylated-Akt (p-Akt) to activate Nrf-2/HO-1. (a) Immunoblots of p-Akt, HO-1, and Nrf-2 proteins for the experimental groups including (c) LPS, LPS + F, and F alone. Histogram of (b) p-Akt, (c) Nrf-2, and (d) HO-1 proteins.  $\beta$ -Actin was used as a loading control (reference control). The bands were analysed using the Image J software, and the density histograms (expressed in AU) compared to the control were organized using GraphPad Prism. Values are presented as the mean  $\pm$  SEM for the indicated proteins ( $n = 6$  mice per group). C: control, LPS: lipopolysaccharide, F: folicitin, AU: arbitrary units,  $^{###}P < 0.001$  as compared to the C group, and  $^{**}P < 0.01$  and  $^{***}P < 0.001$  as compared to the LPS group.

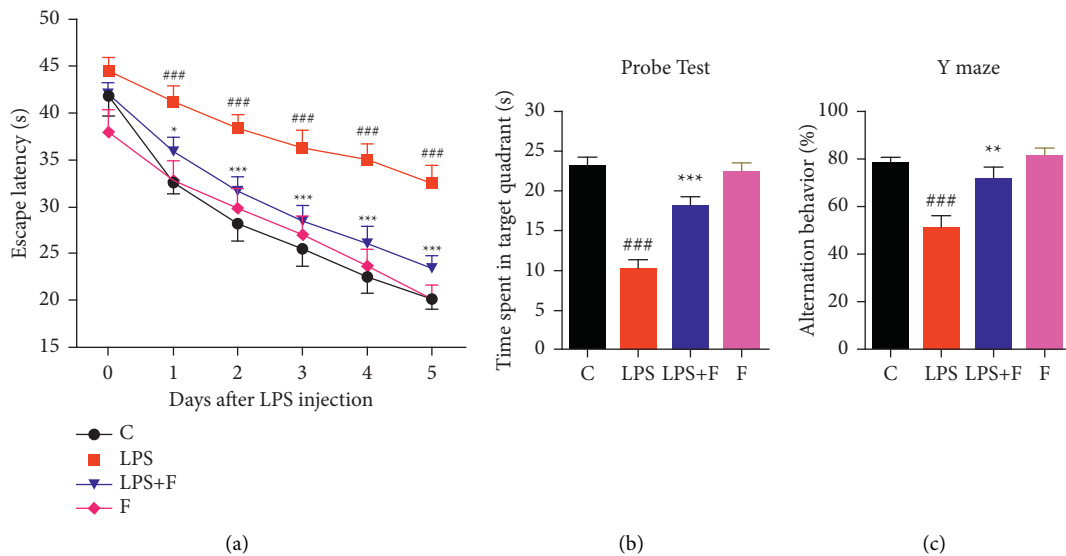


FIGURE 5: Improvement of LPS-induced memory impairment by folicitin. (a) Effect of folicitin on escape latency in the MWM test. (b) Effect of folicitin in the probe test (time consumed in the target quadrant on final day of the experiment) showed during the MWM test when the immersed platform was removed. (c) Effect of folicitin on alternation behaviour in the Y-maze test. Values are presented as the mean  $\pm$  SEM ( $n = 6$  mice per group). C: control, LPS: lipopolysaccharide, F: folicitin,  $^{###}P < 0.001$  as compared to the control group, and  $^{*}P < 0.05$ ,  $^{**}P < 0.01$ , and  $^{***}P < 0.001$  as compared to the LPS group.

expression or not. The results showed that folicitin induced a significant augmentation of the Akt phosphorylation pathway, which is directly associated with Nrf-2-mediated antioxidant response.

In this context, we used folicitin in the animal model of LPS to know its capability to reverse memory impairment. Our results revealed that folicitin significantly enhanced the LPS-inhibited endogenous antioxidant system, i.e., Nrf-2 and HO-1 accompanied by subsequent reduced expression of apoptotic markers in adult albino mice. It is followed by

the positive effect on neuronal synapse and improvement in the memory impairment in the adult animal model. Most importantly, folicitin restored the p-Akt/Nrf-2/HO-1 signalling pathway to overcome the LPS-induced amyloidogenic pathway of  $A\beta$  production in male adult mice. Considering the antioxidative potential and vital ability in enhancing memory deficits, folicitin could be the potential drug candidates against neurodegenerative disorders, especially AD. An overview of the proposed mechanisms of action of folicitin is illustrated in Figure 6.

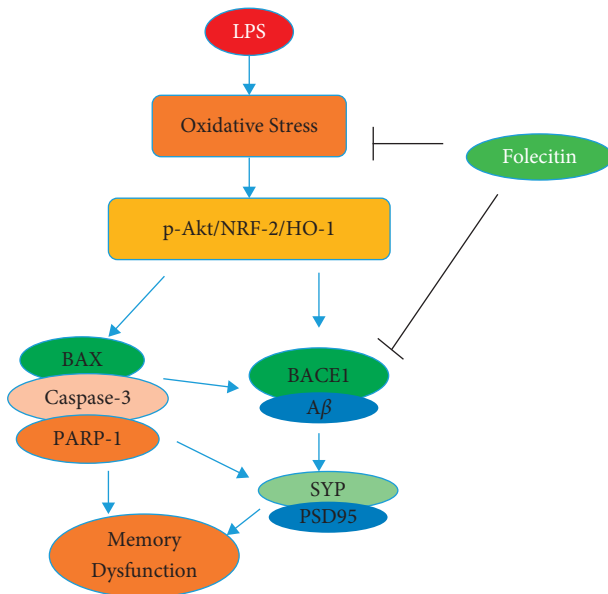


FIGURE 6: Proposed mechanism of folecitin neuroprotection action against LPS-induced oxidative stress mediated memory impairment. Folecitin activated the p-Akt/HO-1/Nrf-2 signalling pathway, leading to a reduction in oxidative stress, neurodegeneration, and associated neuronal synapse and memory impairment.

## 5. Conclusions

The administration of LPS to the brain of adult mice caused neuronal synapse and memory dysfunction. On the other hand, folecitin significantly abrogated the LPS-induced amyloidogenic  $A\beta$  production and improved the associated neuronal synapse and memory impairment. Moreover, folecitin restored the p-Akt signalling pathway to activate Nrf-2/HO-1 signalling. Owing to its neuroprotective potential and ability to improve memory deficits, folecitin might be a promising lead in designing new drugs for neurotoxin-triggered neurodegenerative problems [54].

## Data Availability

All the data are included within this manuscript.

## Conflicts of Interest

The authors declare no conflicts of interest.

## Acknowledgments

This research was funded by University Researchers Supporting Project (No. TURSP2020/91), Taif University, Taif, Saudi Arabia.

## References

- [1] N. Raz, P. Ghisletta, K. M. Rodrigue, K. M. Kennedy, and U. Lindenberger, "Trajectories of brain aging in middle-aged and older adults: regional and individual differences," *NeuroImage*, vol. 51, pp. 501–511, 2010.
- [2] Z. Asefy, A. Khusro, S. Mammadova et al., "Melatonin hormone as a therapeutic weapon against neurodegenerative diseases," *Cellular and Molecular Biology*, vol. 67, pp. 99–106, 2021.
- [3] A. H. Bhat, K. B. Dar, S. Anees et al., "Oxidative stress, mitochondrial dysfunction and neurodegenerative diseases; a mechanistic insight," *Biomedicine and Pharmacotherapy*, vol. 74, pp. 101–110, 2015.
- [4] S. Shaikh, A. Verma, S. Siddiqui et al., "Current acetylcholinesterase-inhibitors: a neuroinformatics perspective," *CNS and Neurological Disorders-Drug Targets*, vol. 13, pp. 391–401, 2014.
- [5] M. B. Colović, D. Z. Krstić, T. D. Lazarević-Pašti, A. M. Bondžić, and V. M. Vasić, "Acetylcholinesterase inhibitors: pharmacology and toxicology," *Current Neuropharmacology*, vol. 11, pp. 315–335, 2013.
- [6] E. A. Adewusi, N. Moodley, and V. Steenkamp, "Antioxidant and acetylcholinesterase inhibitory activity of selected southern African medicinal plants," *South African Journal of Botany*, vol. 77, pp. 638–644, 2011.
- [7] C. C. Felder, F. P. Bymaster, J. Ward, and N. DeLapp, "Therapeutic opportunities for muscarinic receptors in the central nervous system," *Journal of Medicinal Chemistry*, vol. 43, pp. 4333–4353, 2000.
- [8] A. M. Barata, F. Rocha, V. Lopes, and A. M. Carvalho, "Conservation and sustainable uses of medicinal and aromatic plants genetic resources for the worldwide for human welfare," *Industrial Crops and Products*, vol. 88, pp. 8–11, 2016.
- [9] M. Prasathkumar, K. Raja, K. Vasanth et al., "Phytochemical screening and *in vitro* antibacterial, antioxidant, anti-inflammatory, anti-diabetic, and wound healing attributes of *Senna auriculata* (L.) Roxb. leaves," *Arabian Journal of Chemistry*, vol. 14, Article ID 103345, 2021.
- [10] A. Batool, G. A. Miana, M. Alam et al., "Bioassay-guided fractionation and isolation of Arctigenin from *Saussurea heteromalla* for *in vitro* and *in silico* cytotoxic activity against HeLa cells," *Physiological and Molecular Plant Pathology*, vol. 117, Article ID 101749, 2022.
- [11] E. Y. Enioutina, E. R. Salis, K. M. Job, M. I. Gubarev, L. V. Krepkova, and C. M. Sherwin, "Herbal Medicines: challenges in the modern world. Part 5. status and current directions of complementary and alternative herbal medicine worldwide," *Expert Review of Clinical Pharmacology*, vol. 10, pp. 327–338, 2017.
- [12] W. Ahmad, M. Ahmad, M. U. K. Sahibzada et al., "Lipid peroxidation reduction and hippocampal and cortical neurons protection against ischemic damage in animal model using *Stellaria media*," *Saudi Journal of Biological Sciences*, vol. 29, 2021.
- [13] M. Faheem, S. Ameer, A. W. Khan et al., "A comprehensive review on antiepileptic properties of medicinal plants," *Arabian Journal of Chemistry*, vol. 15, Article ID 103478, 2022.
- [14] R. Rodrigo, A. Miranda, and L. Vergara, "Modulation of endogenous antioxidant system by wine polyphenols in human disease," *Clinica Chimica Acta*, vol. 412, pp. 410–424, 2011.
- [15] H. Y. Bao, J. Zhang, S. J. Yeo et al., "Memory enhancing and neuroprotective effects of selected ginsenosides," *Archives of Pharmacological Research*, vol. 28, pp. 335–342, 2005.
- [16] G. M. Cole, B. Teter, and S. A. Frautschy, "Neuroprotective effects of curcumin," *Advances in Experimental Medicine & Biology*, vol. 595, pp. 197–212, 2007.
- [17] A. I. Oliveira, C. Pinho, B. Sarmiento, and A. C. P. Dias, "Neuroprotective activity of *Hypericum perforatum* and its

- major components,” *Frontiers of Plant Science*, vol. 7, p. 1004, 2016.
- [18] Y. Lokanathan, N. Omar, N. N. Ahmad Puzi, A. Saim, and R. Hj Idrus, “Recent updates in neuroprotective and neuroregenerative potential of *Centella asiatica*,” *Malaysian Journal of Medical Sciences*, vol. 23, pp. 4–14, 2016.
- [19] A. S. Abdul Manap, S. Vijayabalan, P. Madhavan et al., “*Bacopa monnieri*, a neuroprotective lead in Alzheimer disease: a review on its properties, mechanisms of action, and preclinical and clinical studies,” *Drug Target Insights*, vol. 13, Article ID 1177392819866412, 2019.
- [20] H. Birla, C. Keswani, S. N. Rai et al., “Neuroprotective effects of *Withania somnifera* in BPA induced-cognitive dysfunction and oxidative stress in mice,” *Behavioral and Brain Functions*, vol. 15, p. 9, 2019.
- [21] S. K. Singh, S. Srivastav, R. J. Castellani, G. Plascencia-Villa, and G. Perry, “Neuroprotective and antioxidant effect of Ginkgo biloba extract against AD and other neurological disorders,” *Neurotherapeutics: The Journal of The American Society for Experimental NeuroTherapeutics*, vol. 16, pp. 666–674, 2019.
- [22] S. L. Crockett and N. K. B. Robson, “Taxonomy and chemotaxonomy of the genus *Hypericum*,” *Medicinal and Aromatic Plant Science and Biotechnology*, vol. 5, pp. 1–13, 2011.
- [23] A. Viana, J. C. do Rego, G. von Poser et al., “The antidepressant-like effect of *Hypericum caprifoliatum* Cham & Schlecht (Guttiferae) on forced swimming test results from an inhibition of neuronal monoamine uptake,” *Neuropharmacology*, vol. 49, pp. 1042–1052, 2005.
- [24] M. C. Dinamarca, W. Cerpa, J. Garrido, J. L. Hancke, and N. C. Inestrosa, “Hyperforin prevents  $\beta$ -amyloid neurotoxicity and spatial memory impairments by disaggregation of Alzheimer’s amyloid- $\beta$ -deposits,” *Molecular Psychiatry*, vol. 11, pp. 1032–1048, 2006.
- [25] S. S. Valvassori, C. Borges, D. V. Bavaresco et al., “*Hypericum perforatum* chronic treatment affects cognitive parameters and brain neurotrophic factor levels,” *Brazilian Journal of Psychiatry*, vol. 40, pp. 367–375, 2018.
- [26] C. Sánchez-Mateo, C. Bonkanka, and R. Rabanal, “*Hypericum grandifolium* choisy: a species native to macaronesian region with antidepressant effect,” *Journal of Ethnopharmacology*, vol. 121, no. 2, pp. 297–303, 2009.
- [27] N. Raziq, M. Saeed, M. S. Ali, S. Zafar, and M. I. Ali, “In vitro anti-oxidant potential of new metabolites from *Hypericum oblongifolium* (Guttiferae),” *Natural Product Research*, vol. 29, pp. 2265–2270, 2015.
- [28] M. Borsoi, C. Batassini, C. Lazzaretti et al., “*Hypericum polyanthemum* cyclohexane extract potentiates behavioral effects and neurodegeneration induced by nigral infusions of 6-hydroxydopamine in rats,” *Neuroscience Letters*, vol. 687, pp. 177–182, 2018.
- [29] K. H. Alzoubi, L. Abdel-Hafiz, O. F. Khabour, T. El-Elimat, M. A. Alzubi, and F. Q. Alali, “Evaluation of the effect of *Hypericum triquetrifolium* turra on memory impairment induced by chronic psychosocial stress in rats: role of BDNF,” *Drug Design Development and Therapy*, vol. 14, p. 5299, 2020.
- [30] M. Arfan, M. Ali, H. Ahmad et al., “Urease inhibitors from *Hypericum oblongifolium* WALL,” *Journal of Enzyme Inhibition and Medicinal Chemistry*, vol. 25, pp. 296–299, 2010.
- [31] J. S. Butola, S. Pant, and S. Samant, “Diversity, distribution and indigenous uses of the *Hypericum* species in Indian Himalayan region,” *Ethnobotanical Leaflets*, vol. 4, 2007.
- [32] G. Abbas, M. J. Hassan, Z. Saddiqe et al., “Non-toxic fractions of *Hypericum perforatum* and *Hypericum oblongifolium* inhibit protein glycation, free radicals production and lipid peroxidation in vitro,” *International Journal of Phytomedicine*, vol. 5, pp. 191–196, 2013.
- [33] A. Sajid, E. Ahmed, A. Sharif et al., “Bioassay directed isolation studies on *Hypericum oblongifolium*,” *Journal of the Chemical Society of Pakistan*, vol. 40, 2018.
- [34] M. Ali, A. Latif, K. Zaman et al., “Anti-ulcer xanthenes from the roots of *Hypericum oblongifolium* wall,” *Fitoterapia*, vol. 95, pp. 258–265, 2014.
- [35] K. Gopinath, D. Prakash, and G. Sudhandiran, “Neuroprotective effect of naringin, a dietary flavonoid against 3-nitropropionic acid-induced neuronal apoptosis,” *Neurochemistry International*, vol. 59, no. 7, pp. 1066–1073, 2011.
- [36] K. Saraswathi, R. Bharkavi, A. Khusro et al., “Assessment on in vitro medicinal properties and chemical composition analysis of *Solanum virginianum* dried fruits,” *Arabian Journal of Chemistry*, vol. 14, Article ID 103442, 2021.
- [37] F. Dajas, F. Rivera-Megret, F. Blasina et al., “Neuroprotection by flavonoids,” *Brazilian Journal of Medical and Biological Research*, vol. 36, no. 12, pp. 1613–1620, 2003.
- [38] D. Prakash and G. Sudhandiran, “Dietary flavonoid fisetin regulates aluminium chloride-induced neuronal apoptosis in cortex and hippocampus of mice brain,” *The Journal of Nutritional Biochemistry*, vol. 26, no. 12, pp. 1527–1539, 2015.
- [39] G. Scapagnini, V. Sonya, A. G. Nader, C. Calogero, D. Zella, and G. Fabio, “Modulation of Nrf2/ARE pathway by food polyphenols: a nutritional neuroprotective strategy for cognitive and neurodegenerative disorders,” *Molecular Neurobiology*, vol. 44, no. 2, pp. 192–201, 2011.
- [40] S. I. Ahmed, M. Q. Hayat, M. Tahir et al., “Pharmacologically active flavonoids from the anticancer, antioxidant and antimicrobial extracts of *Cassia angustifolia* Vahl,” *BMC Complementary and Alternative Medicine*, vol. 16, no. 1, pp. 1–9, 2016.
- [41] T. Ali, T. Kim, S. U. Rehman et al., “Natural dietary supplementation of anthocyanins via PI3K/Akt/Nrf2/HO-1 pathways mitigate oxidative stress, neurodegeneration, and memory impairment in a mouse model of Alzheimer’s disease,” *Molecular Neurobiology*, vol. 55, no. 7, pp. 6076–6093, 2018.
- [42] S. U. Rehman, S. A. Shah, T. Ali, J. I. Chung, and M. O. Kim, “Anthocyanins reversed D-galactose-induced oxidative stress and neuroinflammation mediated cognitive impairment in adult rats,” *Molecular Neurobiology*, vol. 54, pp. 255–271, 2017.
- [43] S. A. Shah, F. U. Amin, M. Khan et al., “Anthocyanins abrogate glutamate-induced AMPK activation, oxidative stress, neuroinflammation, and neurodegeneration in postnatal rat brain,” *Journal of Neuroinflammation*, vol. 13, pp. 1–16, 2016.
- [44] H. Badshah, T. Ali, and M. O. Kim, “Osotin attenuates LPS-induced neuroinflammation and memory impairments via the TLR4/NF $\kappa$ B signaling pathway,” *Scientific Reports*, vol. 6, pp. 1–13, 2016.
- [45] J. Weuve, L. E. Hebert, P. A. Scherr, and D. A. Evans, “Deaths in the United States among persons with Alzheimer’s disease (2010–2050),” *Alzheimer’s and Dementia*, vol. 10, pp. e40–e46, 2014.
- [46] L. Gan and J. A. Johnson, “Oxidative damage and the Nrf2-ARE pathway in neurodegenerative diseases,” *Biochimica et Biophysica Acta-Molecular Basis of Disease*, vol. 1842, pp. 1208–1218, 2014.



- [47] C. A. Cobb and M. P. Cole, "Oxidative and nitrative stress in neurodegeneration," *Neurobiology of Disease*, vol. 84, pp. 4–21, 2015.
- [48] K. Bedard and K.-H. Krause, "The NOX family of ROS-generating NADPH oxidases: physiology and pathophysiology," *Physiological Reviews*, vol. 87, pp. 245–313, 2007.
- [49] M. Pajares, A. Cuadrado, and A. I. Rojo, "Modulation of proteostasis by transcription factor NRF2 and impact in neurodegenerative diseases," *Redox Biology*, vol. 11, pp. 543–553, 2017.
- [50] K. M. Sell, S. F. Crowe, and S. Kent, "Lipopolysaccharide induces memory-processing deficits in day-old chicks," *Pharmacology Biochemistry and Behavior*, vol. 68, pp. 497–502, 2001.
- [51] A. H. Swiergiel and A. J. Dunn, "Effects of interleukin-1 $\beta$  and lipopolysaccharide on behavior of mice in the elevated plus-maze and open field tests," *Pharmacology Biochemistry and Behavior*, vol. 86, pp. 651–659, 2007.
- [52] X. Zhang, N. Tang, T. J. Hadden, and A. K. Rishi, "Akt, FoxO and regulation of apoptosis," *Biochimica et Biophysica Acta (BBA)-Molecular Cell Research*, vol. 1813, no. 11, pp. 1978–1986, 2011.
- [53] K. Y. Lim, A. O. Sasmita, A. P. K. Ling et al., "Neuroprotective mechanisms of orientin against hydrogen peroxide-induced oxidative damage in SH-SY5Y cells," *Journal of Biochemistry, Microbiology and Biotechnology*, vol. 6, no. 1, pp. 10–18, 2018.
- [54] A. Ahmad, T. Ali, H. Y. Park, H. Badshah, S. U. Rehman, and M. O. Kim, "Neuroprotective effect of fisetin against amyloid-beta-induced cognitive/synaptic dysfunction, neuroinflammation, and neurodegeneration in adult mice," *Molecular Neurobiology*, vol. 54, no. 3, pp. 2269–2285, 2017.

## Research Article

# Identification of Key Drug Targets and Molecular Mechanisms of Curcumae Rhizoma Acting on HBV-Related HCC: Weighted Correlation Network and Network Pharmacological Analyses

Mengyuan Zhao,<sup>1</sup> Yun Fu,<sup>1</sup> Lili Liu,<sup>2</sup> Yong Hou,<sup>2</sup> Mei Shi,<sup>2</sup> Hao Zhou,<sup>2</sup> and Guoliang Zhang<sup>ID</sup><sup>2</sup>

<sup>1</sup>Anhui University of Chinese Medicine, Hefei, China

<sup>2</sup>Department of Infectious Disease, The First Affiliated Hospital of Anhui University of Chinese Medicine, Hefei, China

Correspondence should be addressed to Guoliang Zhang; [guoliangzhang2022@163.com](mailto:guoliangzhang2022@163.com)

Received 8 February 2022; Revised 6 March 2022; Accepted 10 March 2022; Published 27 March 2022

Academic Editor: Ruchika Garg

Copyright © 2022 Mengyuan Zhao et al. This is an open access article distributed under the Creative Commons Attribution License, which permits unrestricted use, distribution, and reproduction in any medium, provided the original work is properly cited.

**Background.** Hepatitis B virus (HBV)-related hepatocellular carcinoma (HCC) has poor prognosis and high mortality rate. Curcumae Rhizoma, a classic Chinese medicinal herb, is often used to treat tumors. **Methods.** Active ingredients of Curcumae Rhizoma were extracted from the Traditional Chinese Medicine Database and Analysis Platform (TCMSP) database, and potential targets were predicted by the TCMSP database and Swiss Target Prediction database. The key drug targets were filtered by intersecting predicted targets, DEGs, and genes in important modules from WGCNA. Besides, the key drug targets were used to construct a network of “herb-active ingredient-target-disease” interactions and subjected to enrichment analysis and protein-protein interaction (PPI) analysis. The hub targets based on PPI analysis was evaluated by the KMplotter database. **Results.** Three active ingredients of Curcumae Rhizoma were collected with  $OB \geq 30\%$  and  $DL \geq 0.18$ , including hederagenin, wenjine, and bisdemethoxycurcumin. The key drug targets were mainly enriched in cell cycle checkpoint, DNA integrity checkpoint, and peptidyl-serine modification. Besides, Curcumae Rhizoma treatment of HBV-related HCC mainly involved the p53 signaling pathway and arachidonic acid metabolism. Finally, ESR1 and PTGS2 were identified as hub targets from PPI analysis. ESR1 was found to be correlated with survival in liver cancer patients with hepatitis. **Conclusion.** Based on WGCNA and network pharmacological analysis, our results illustrated that Curcumae Rhizoma might work through regulating multitargets and multipathways in HBV-related HCC.

## 1. Introduction

Hepatocellular carcinoma (HCC) is currently recognized as one of the most hard-to-treat malignancies, with the incidence increasing significantly over the last century [1–3]. According to the 2018 global tumor statistics, HCC is the 4th leading cause of cancer death at 8.2% [4]. It was reported by the National Cancer Center in 2019 that there were 370000 new cases of HCC in 2015, making it the 4th most common malignant tumor and the 2nd leading cause of tumor death in China, seriously threatening human life and health [5, 6]. About 80% of HCC in China are caused by hepatitis B virus (HBV) infection, making HBV-related HCC one of the major public health problems in China [6]. However, its pathogenesis has not yet been fully understood.

In the traditional treatment of HBV-related HCC, chronic HBV infection and liver malignancy are seen as two causally related but relatively independent aspects, and therefore, their treatment is divided into long-term aggressive antiviral therapy for HBV and interventional, targeted, and surgical treatments for HCC [7, 8]. Existing Western medicine treatment programs are generally combinatorial rather than comprehensive. Traditional Chinese medicine (TCM) treatment, due to its holistic view of the disease, can play a comprehensive role in controlling disease progression in the context of chronic HBV infection, including blocking precancerous changes, compensating for the limitations of Western medicine alone, prolonging survival, and improving quality of life [9, 10]. However, due to the high complexity of TCM mechanisms, the exploration

of drug targets and the screening of active ingredients is an important challenge at present.

Curcumae Rhizoma, bitter and acrid, could invigorate blood circulation, dispel blood stasis, regulate Qi, alleviate pain, dissolve accumulations, and alleviate pain [11, 12]. Curcumae Rhizoma has been reported to have anticancer activity against a variety of cancers, including breast cancer [13], gastric cancer [14], and colorectal cancer [15]. Curcumae Rhizoma or some of its active ingredients have been reported to have a better inhibitory effect on liver fibrosis and HCC [16, 17].

In this study, we obtained the GSE121248 dataset by searching datasets containing HCC tissues and paracancerous tissues with HBV infection in the GEO database. By bioinformatics techniques, we identified the significant modules and differentially expressed genes (DEGs) of the GSE121248 dataset. Using various databases and bioinformatics algorithms, we screened out active components of Curcumae Rhizoma, targets of HBV-related HCC, and key drug targets of Curcumae Rhizoma for the treatment of HBV-related HCC. The characteristics of these key targets were preliminary revealed. In summary, this study provides new targets and ideas for the treatment of HBV-related HCC with Curcumae Rhizoma.

## 2. Methods

**2.1. Curcumae Rhizoma Active Ingredient Screening and Target Prediction.** TCMSP is a traditional Chinese medicine database and analysis platform that could analyze the relationship among drugs, targets, and diseases, revealing the nature and potential mechanisms of TCM [18]. Curcumae Rhizoma was searched in the TCMSP database, and the chemical components were screened with oral bioavailability (OB)  $\geq 30\%$  and drug likeness (DL)  $\geq 0.18\%$ . The potential drug targets were also searched in the TCMSP database and Swiss Target Prediction database [19]. Then, the potential drug targets from the TCMSP database were imported into the UniProtKB database [20] for target gene name correction and elimination of nonhuman targets. The potential drug targets from the Swiss Target Prediction database were screened with probability  $> 0$ .

**2.2. GSE121248 Dataset Collection.** Gene Expression Omnibus (GEO) database [21] was utilized to search the public dataset associated with HBV-related HCC, and the GSE121248 dataset (<https://www.ncbi.nlm.nih.gov/geo/query/acc.cgi?acc=GSE121248>) provided by Wang et al. [22] was downloaded via R (version 3.6.3) package of GEOquery 2.54.1 [23]. Tissues from chronic hepatitis B induced HCC and their adjacent normal tissues were isolated, and total RNA was extracted for Affymetrix gene microarray analysis.

**2.3. WGCNA.** WGCNA is a systems biology approach to describe gene association patterns among different samples, to figure out highly synergistic gene sets, and to identify candidate biomarkers or therapeutic targets based on the

endogeneity of the gene set and the association between the gene set and the phenotype [24]. The analysis methods were previously described [25]. WGCNA was performed using top 5000 genes with maximum mean absolute deviation, a power  $\beta$  of 6, a minimal module size of 30, a deep split of 3, and an unsigned type of topological overlap matrix (TOM). Finally, 13 modules were obtained, and Spearman correlations between modules and clinical features were analyzed.

**2.4. Differential Expression Analysis.** The expression matrix of the GSE121248 dataset was filtered by transforming repeated probe signals as the median value. The limma 3.42.2 package was then used for the differential expression analysis between tumor sample from hepatocellular carcinoma patient and adjacent normal sample from hepatocellular carcinoma patient. Besides, DEGs were screened with  $|\log_{2}FC| \geq 1$  and  $P < 0.05$  and visualized as a volcano plot. Top 50 DEGs were visualized as heatmaps with the clustering method of Euclidean distances using the ComplexHeatmap 2.2.0 package [26].

**2.5. Construction of the “Herb-Active Ingredient-Target-Disease” Interaction Network.** Key drug targets were screened by intersecting predicted targets, DEGs, and genes in important modules from WGCNA. Then, the interactions among herb, active ingredients, and targets were imported into the Cytoscape software (version 3.8.3) [27] for network construction.

**2.6. Enrichment and PPI Analysis of Key Drug Targets.** Key drug targets were subjected to Gene Ontology (GO) and Kyoto Encyclopedia of Genes and Genomes (KEGG) enrichment analysis using the clusterProfiler 3.14.3 package [28], and the top 10 entries with highest generation and  $P < 0.05$  were visualized as bubble plots and chord diagrams.

Key drug targets were uploaded to the STRING database (version 11.0) [29], and interactions with a score above 0.4 were considered significant. Then, the interactions were downloaded and visualized using Cytoscape software (version 3.8.3) [27]. The common genes in top 5 genes with highest degree and bottleneck score were detected as hub targets by cytoHubba plugin [30].

**2.7. Prognostic Analysis of Hub Targets.** The hub targets were entered into the KMplotter database [31] and analyzed for prognostic value based on the hepatitis virus yes subgroup and all groups. The web was established to perform univariate and multivariate survival analyses using any custom-generated data.

**2.8. Active Ingredient Screening and Target Prediction.** The active ingredients of Curcumae Rhizoma, including hederagenin, wenjine, and bisdemethoxycurcumin, were obtained by searching the TCMSP database and screening with OB and DL parameters (Figure 1(a), Table 1). Their molecule structure was downloaded (Figures 1(b)–1(d)).

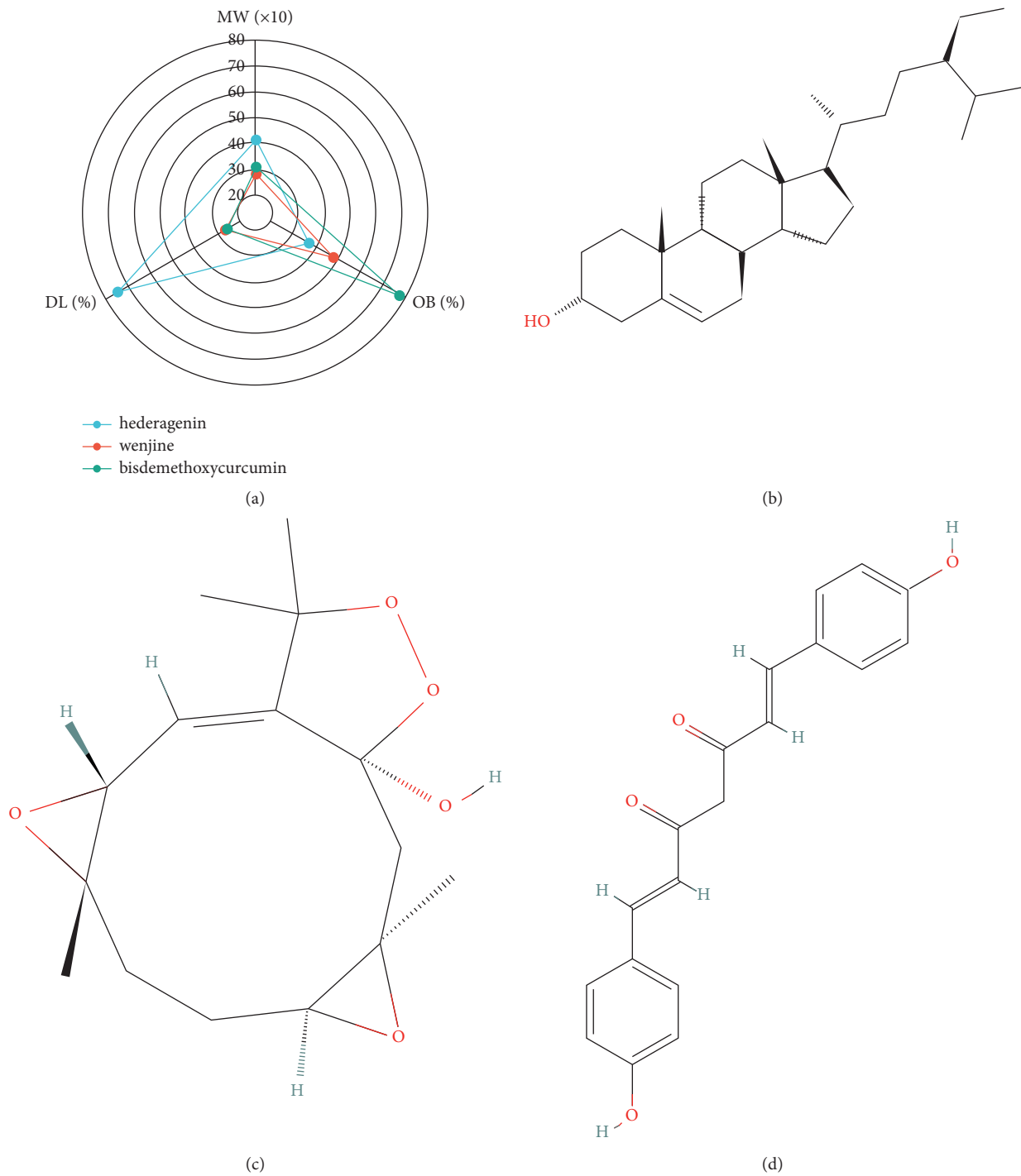
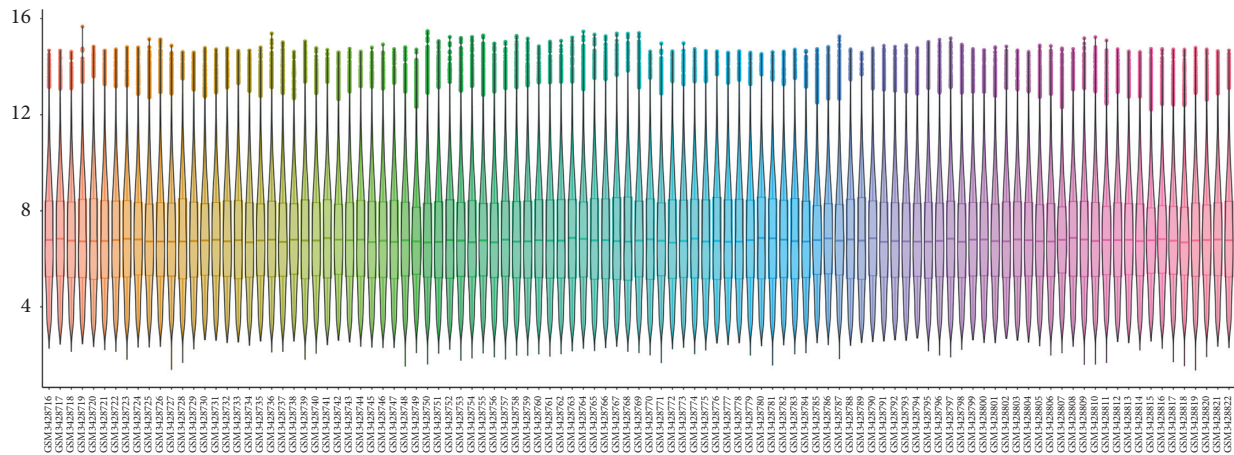


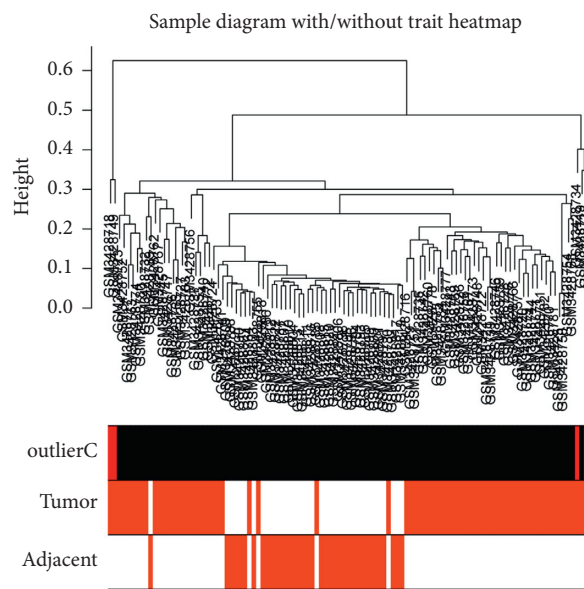
FIGURE 1: Curcumae Rhizoma active ingredients. (a) The characteristics of Curcumae Rhizoma active ingredients. (b) Hederagenin molecule structure. (c) Wenjine molecule structure. (d) Bisdemethoxycurcumin molecule structure.

TABLE 1: Potential active compounds of Curcumae Rhizoma.

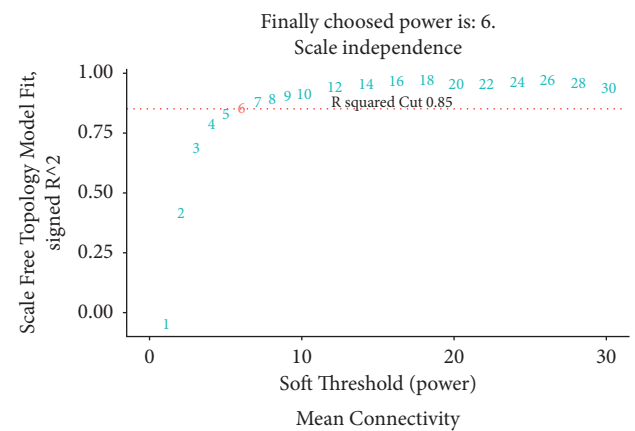
Mol. ID	Molecule name	MW	OB (%)	DL
MOL000296	Hederagenin	414.79	36.91	0.75
MOL000906	Wenjine	282.37	47.93	0.27
MOL000940	Bisdemethoxycurcumin	308.35	77.38	0.26



(a)



(b)



(c)

FIGURE 2: Expression profile preprocess and soft power determination. (a) The expression profile distribution of all liver samples. (b) Hierarchical clustering excluded outlier samples. (c) The soft-threshold power determined based on a scale-free  $R^2$  of 0.85.

Then, 22 potential targets of hederagenin were extracted from the TCMSP database. 11 potential targets of wenjine and 68 potential targets of bisdemethoxycurcumin were predicted from the Swiss Target Prediction database.

### 3. Results

**3.1. HBV-Related HCC Target Screening.** To identify HBV-related HCC targets, we downloaded the GSE121248 dataset from the GEO database. By WGCNA analysis, a power  $\beta$  of 6 was detected and 13 modules were obtained (Figures 2, 3(a)–3(c)). Among these modules, blue, brown, magenta, red, and

turquoise modules were screened as important modules since they were most significantly correlated with tumor (Figure 3(d)).

Then, expression profile of the GSE121248 dataset was subjected to differential expression analysis (Figure 4(a)). The top 50 upregulated (Figure 4(b)) and downregulated (Figure 4(c)) genes were visualized.

**3.2. Key Drug Targets and Their Features.** To identify key drug targets of Curcumae Rhizoma in treating HBV-related HCC, we collected the overlapped genes in DEGs, genes in

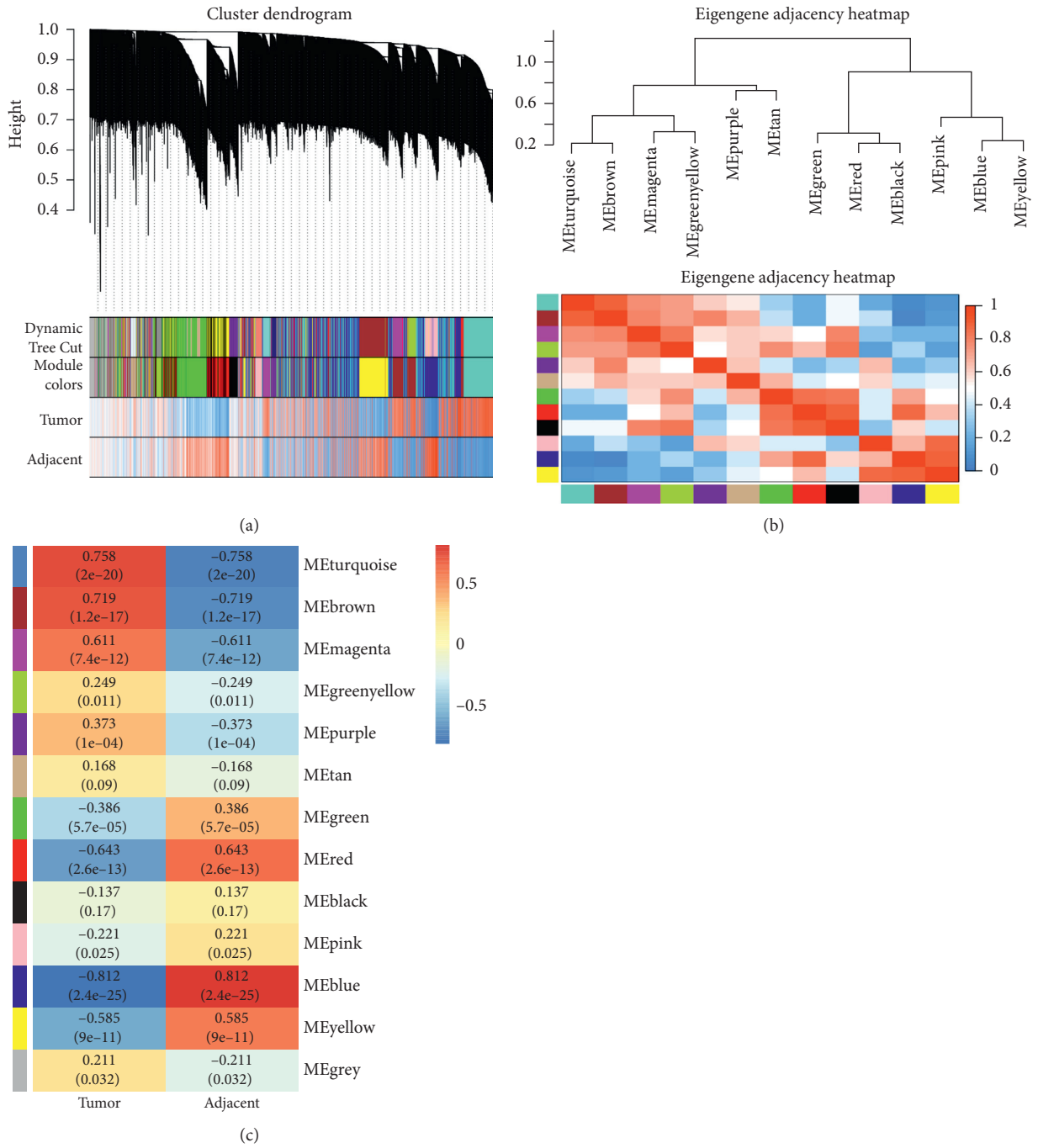


FIGURE 3: Continued.



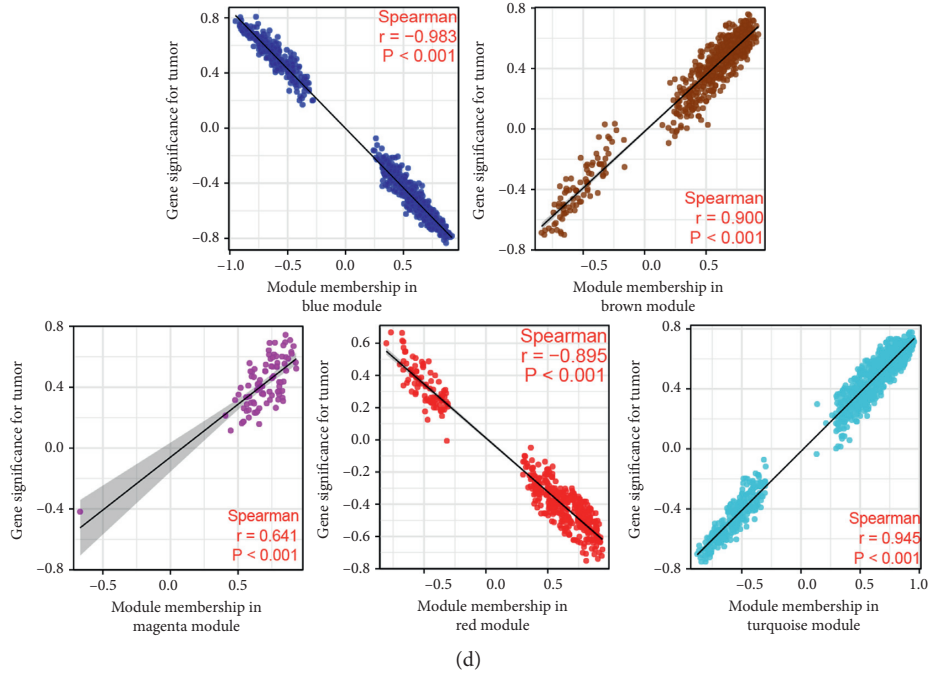


FIGURE 3: Coexpression module identification. (a) Dynamic tree cut. (b) Module correlation. (c) WGCNA module trait correlation plot with negative correlation plotted as blue color and positive correlation plotted as red color. (d) Correlation of module membership and gene significance in blue, brown, magenta, red, and turquoise modules.

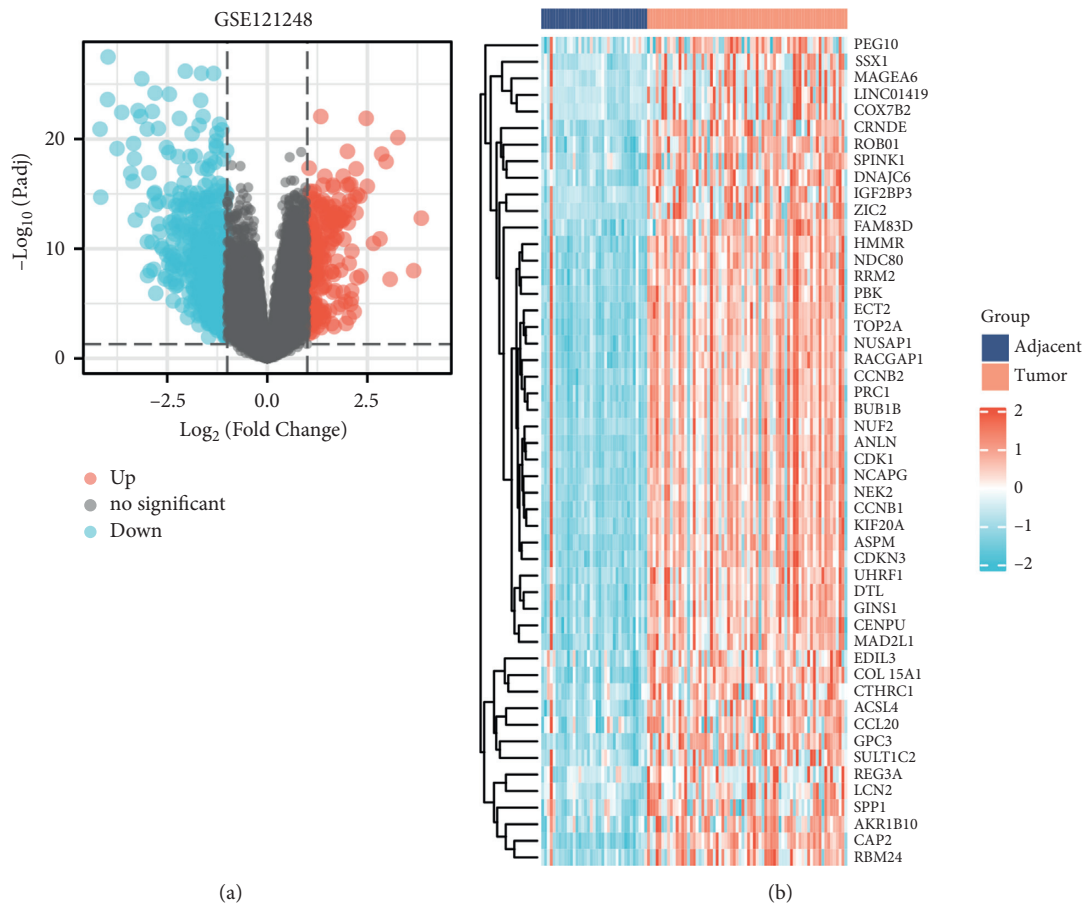


FIGURE 4: Continued.

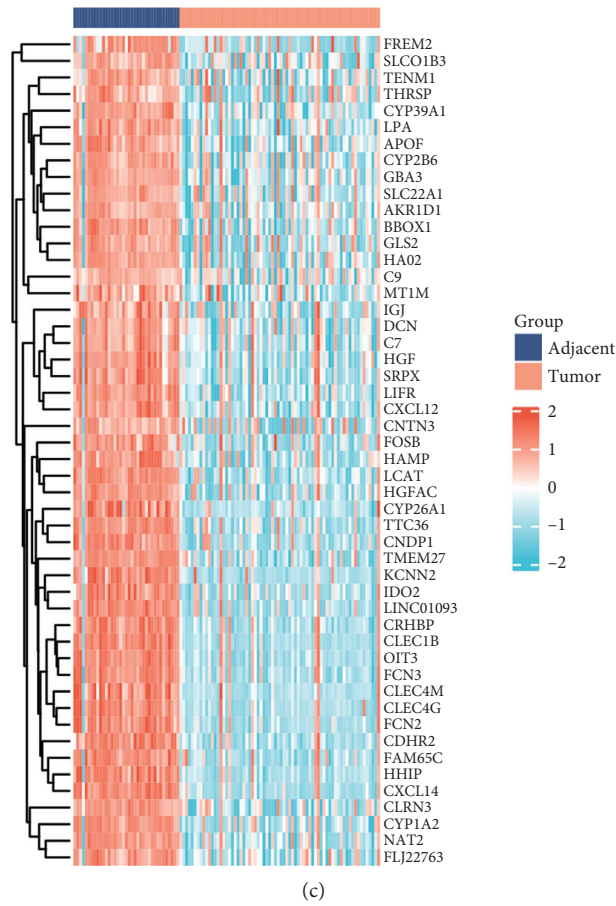


FIGURE 4: DEGs screening on the GSE121248 dataset. (a) Volcano plot with threshold of  $|\log_{2}FC| \geq 1$  and  $P_{\text{adjust}} < 0.05$ . (b) Top 50 upregulated genes. (c) Top 50 downregulated genes.

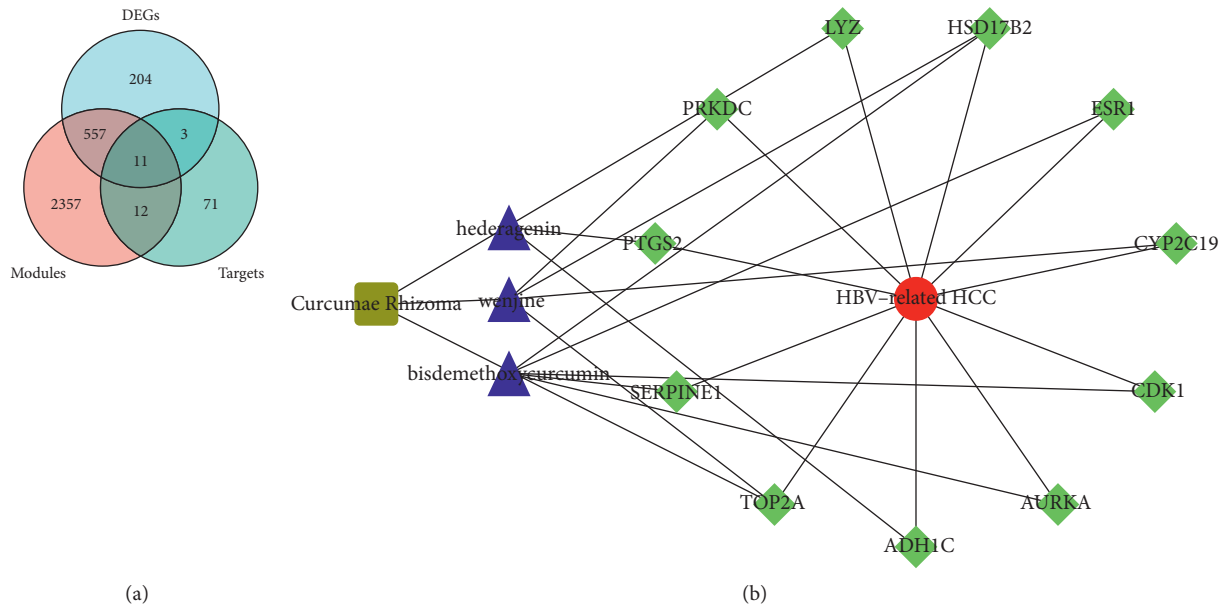


FIGURE 5: Continued.

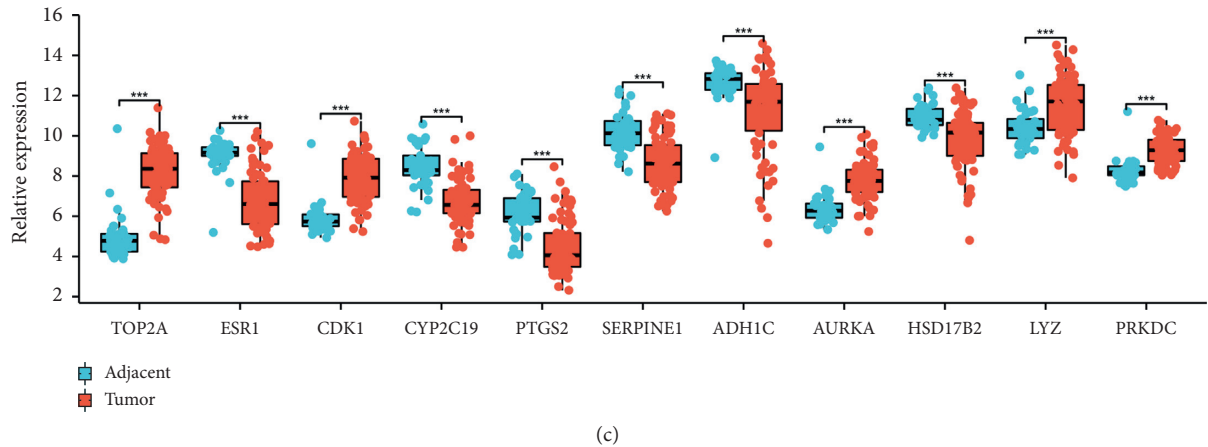


FIGURE 5: Key drug targets screening and network construction. (a) Key drug targets screening. (b) Key drug target expression in the GSE121248 dataset. (c) A network of “herb-active ingredient-target-disease” interactions.

TABLE 2: Potential targets of active compounds of Curcuma Rhizoma in HBV-related HCC.

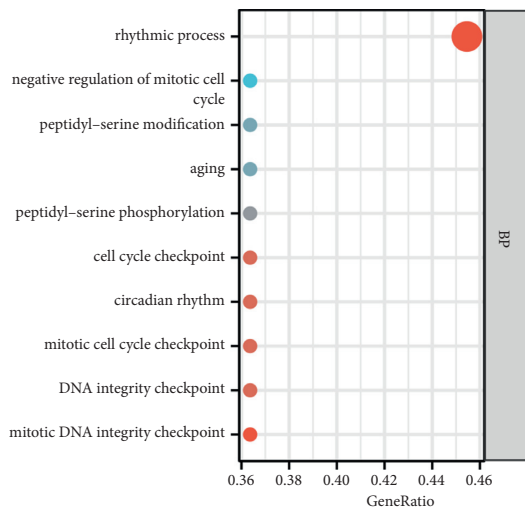
Gene symbol	Protein name	logFC	Degree	Bottleneck
TOP2A	DNA topoisomerase 2-alpha	3.261963	4	1
ESR1	Estrogen receptor	-2.27525	7	9
CDK1	Cyclin-dependent kinase 1	2.029494	4	1
CYP2C19	Cytochrome P450 2C19	-1.72843	1	1
PTGS2	Prostaglandin G/H synthase 2	-1.62628	3	2
SERPINE1	Plasminogen activator inhibitor 1	-1.55996	2	1
ADH1C	Alcohol dehydrogenase 1C	-1.4645	0	0
AURKA	Aurora kinase A	1.381586	3	1
HSD17B2	17-Beta-hydroxysteroid dehydrogenase type 2	-1.15057	1	1
LYZ	Lysozyme C	1.128273	0	0
PRKDC	DNA-dependent protein kinase catalytic subunit	1.029811	3	1

TABLE 3: Enriched GO-BP and KEGG terms of potential targets.

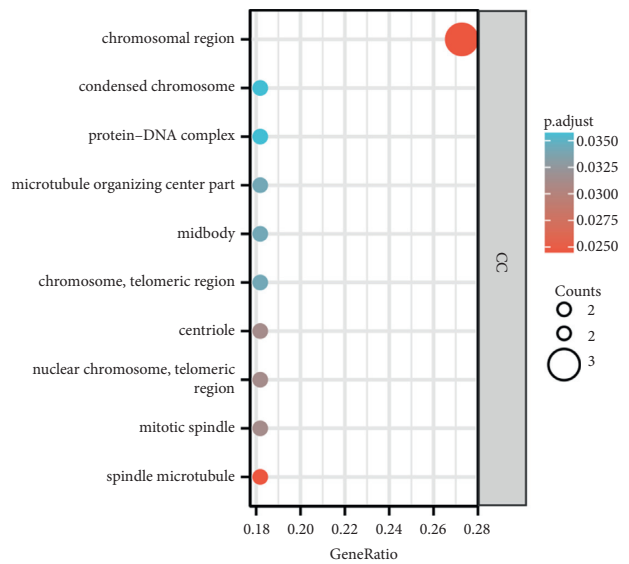
Ontology	ID	Description	GeneRatio	BgRatio	P value	P adjust	Q value	GeneID	Count	Zscore
BP	GO:0044774	Mitotic DNA integrity checkpoint	4/11	106/18670	$3.14e-07$	$1.88e-04$	$9.49e-05$	TOP2A/ CDK1/ AURKA/ PRKDC	4	2
BP	GO:0048511	Rhythmic process	5/11	295/18670	$4.07e-07$	$1.88e-04$	$9.49e-05$	TOP2A/ESR1/ CDK1/ SERPINE1/ PRKDC	5	0.447213595
BP	GO:0031570	DNA integrity checkpoint	4/11	157/18670	$1.52e-06$	$4.10e-04$	$2.07e-04$	TOP2A/ CDK1/ AURKA/ PRKDC	4	2
BP	GO:0007093	Mitotic cell cycle checkpoint	4/11	165/18670	$1.85e-06$	$4.10e-04$	$2.07e-04$	TOP2A/ CDK1/ AURKA/ PRKDC	4	2
BP	GO:0007623	Circadian rhythm	4/11	208/18670	$4.65e-06$	$4.10e-04$	$2.07e-04$	TOP2A/ CDK1/ SERPINE1/ PRKDC	4	1

TABLE 3: Continued.

Ontology	ID	Description	GeneRatio	BgRatio	P value	P adjust	Q value	GeneID	Count	Zscore
BP	GO:0000075	Cell cycle checkpoint	4/11	216/18670	$5.40e-06$	$4.10e-04$	$2.07e-04$	TOP2A/ CDK1/ AURKA/ PRKDC	4	2
BP	GO:0018105	Peptidyl-serine phosphorylation	4/11	299/18670	$1.95e-05$	$1.00e-03$	$5.04e-04$	CDK1/ PTGS2/ AURKA/ PRKDC	4	1
BP	GO:0007568	Aging	4/11	321/18670	$2.57e-05$	0.001	$5.78e-04$	CDK1/ PTGS2/ SERPINE1/ PRKDC	4	0
BP	GO:0018209	Peptidyl-serine modification	4/11	322/18670	$2.60e-05$	0.001	$5.78e-04$	CDK1/ PTGS2/ AURKA/ PRKDC	4	1
BP	GO:0045930	Negative regulation of mitotic cell cycle	4/11	338/18670	$3.15e-05$	0.001	$6.68e-04$	TOP2A/ CDK1/ AURKA/ PRKDC	4	2
KEGG	hsa05204	Chemical carcinogenesis	3/11	82/8076	$1.57e-04$	0.008	0.006	CYP2C19/ PTGS2/ ADH1C	3	-1.73205081
KEGG	hsa04913	Ovarian steroidogenesis	2/11	51/8076	0.002	0.044	0.035	PTGS2/ HSD17B2	2	-1.41421356
KEGG	hsa00590	Arachidonic acid metabolism	2/11	63/8076	0.003	0.044	0.035	CYP2C19/ PTGS2	2	-1.41421356
KEGG	hsa00982	Drug metabolism-cytochrome P450	2/11	71/8076	0.004	0.044	0.035	CYP2C19/ ADH1C	2	-1.41421356
KEGG	hsa04115	p53 signaling pathway	2/11	73/8076	0.004	0.044	0.035	CDK1/ SERPINE1	2	0



(a)



(b)

FIGURE 6: Continued.

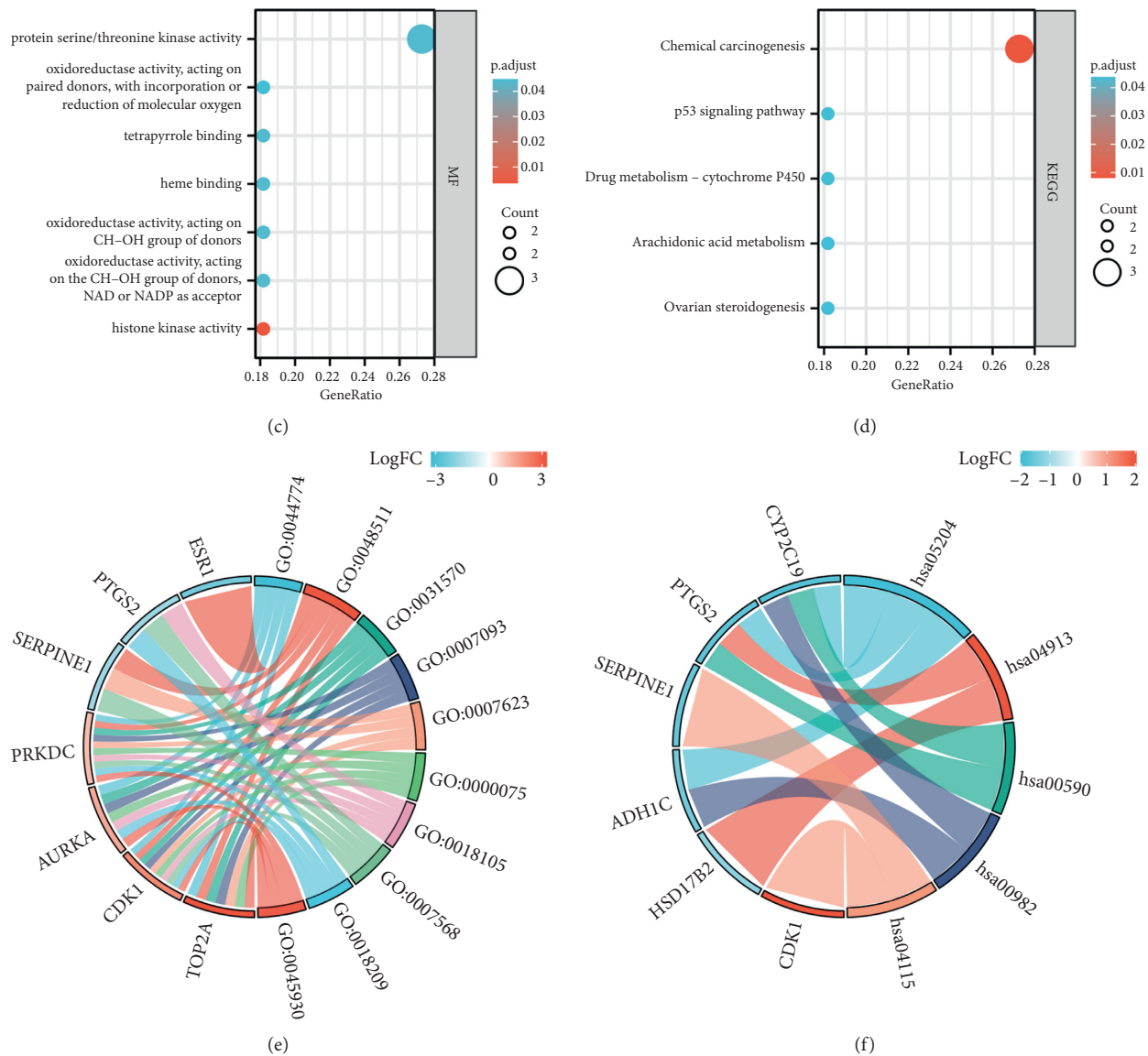


FIGURE 6: Enrichment analysis of key drug targets. (a) A bubble plot showing GO-BP analysis. (b) A bubble plot showing GO-CC analysis. (c) A bubble plot showing GO-MF analysis. (d) A bubble plot showing KEGG analysis. (e) A chord diagram showing GO-BP analysis. (f) A chord diagram showing KEGG analysis.

important modules, and predicted targets (Figure 5(a)). These genes were screened as key drug targets, including TOP2A, ESRI, CDK1, CYP2C19, PTGS2, SERPINE1, ADH1C, AURKA, HSD17B2, LYZ, and PRKDC (Table 2). Moreover, the expression levels of key drug targets were analyzed (Figure 5(b)). Then, a network of “herb-active ingredient-target-disease” interactions was constructed (Figure 5(c)).

To characterize the key drug targets, we performed GO and KEGG enrichment analyses (Table 3). The results depicted that the key drug targets mainly involved in the rhythmic process, mitotic DNA integrity checkpoint, DNA integrity checkpoint, mitotic cell cycle checkpoint, circadian rhythm, cell cycle checkpoint, peptidyl-serine phosphorylation, aging, peptidyl-serine modification, and negative regulation of mitotic cell cycle (Figure 6(a)). Besides, some

cellular component (CC) terms were also enriched, such as chromosomal region, spindle microtubule, mitotic spindle, nuclear chromosome, telomeric region, centriole, chromosome, telomeric region, midbody, microtubule organizing center part, protein-DNA complex, and condensed chromosome (Figure 6(b)). In terms of molecular function (MF), key drug targets participated in protein serine/threonine kinase activity, histone kinase activity, oxidoreductase activity, acting on the CH-OH group of donors, NAD or NADP as acceptor, oxidoreductase activity, acting on CH-OH group of donors, heme binding, tetrapyrrole binding, and oxidoreductase activity, acting on paired donors, with incorporation or reduction of molecular oxygen (Figure 6(c)). Moreover, the involved pathways included chemical carcinogenesis, ovarian steroidogenesis, arachidonic acid metabolism, drug metabolism-cytochrome P450,

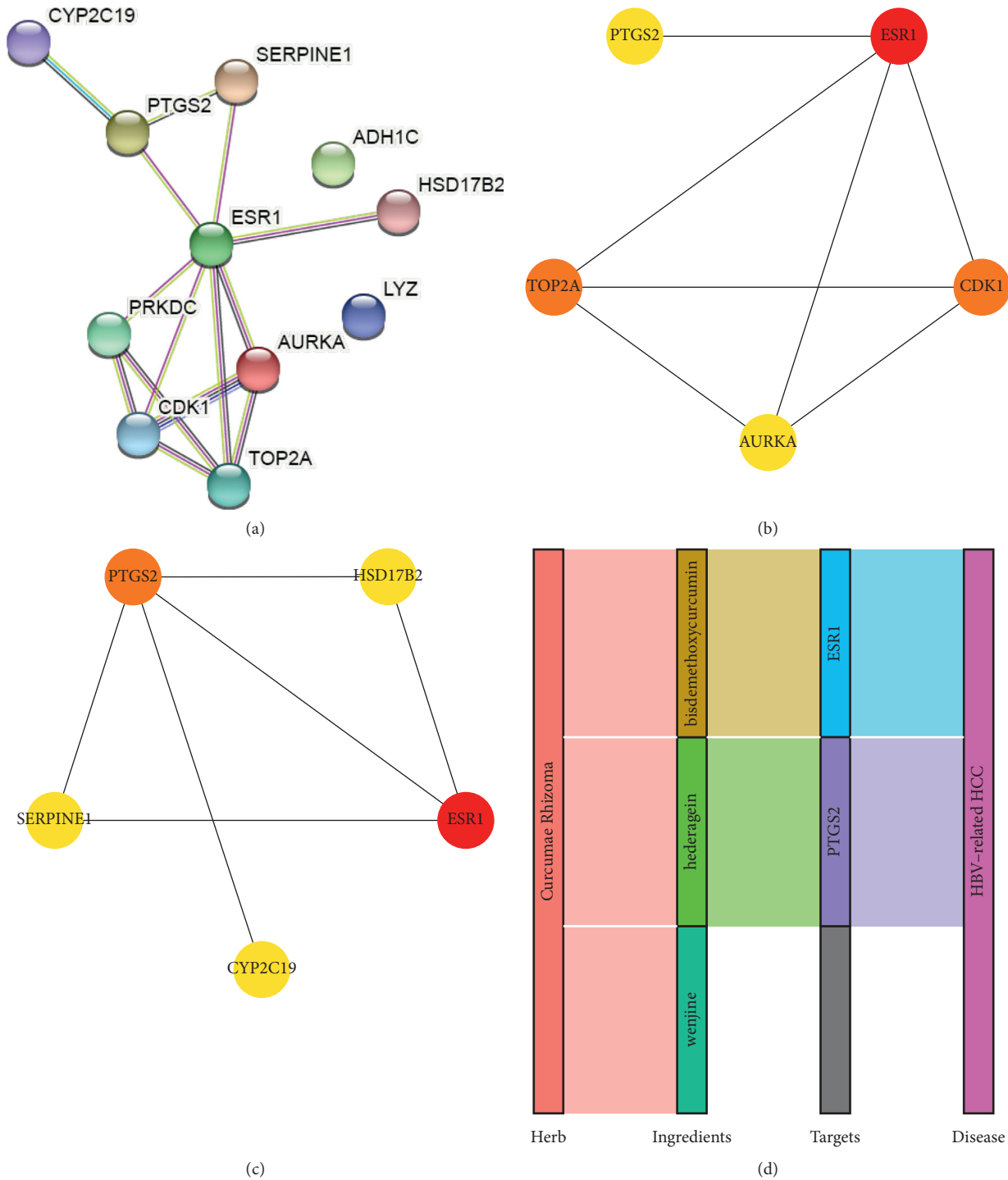


FIGURE 7: PPI analysis of key drug targets. (a) PPI network of key drug targets. (b) Top 5 key drug targets under the degree algorithm. (c) Top 5 key drug targets under the bottleneck algorithm. (d) A network of “herb-active ingredient-target-disease” interactions based on hub targets.

and p53 signaling pathway (Figure 6(d)). Combining logFC, the GO-biological process (BP) and KEGG enrichment results are shown in Figures 6(e) and 6(f).

Meanwhile, the key drug targets were subjected to PPI analysis (Figure 7(a)). In Cytoscape software, degree and bottleneck algorithm identify top 5 genes, respectively (Figures 7(b) and 7(c)). The common genes were ESR1 and

PTGS2 under two algorithms. Based on the two hub targets, a network of “herb-active ingredient-target-disease” interactions was simplified (Figure 7(d)).

**3.3. Hub Target Verification.** The hub targets, ESR1 and PTGS2, were uploaded to the KMplotter database, and the



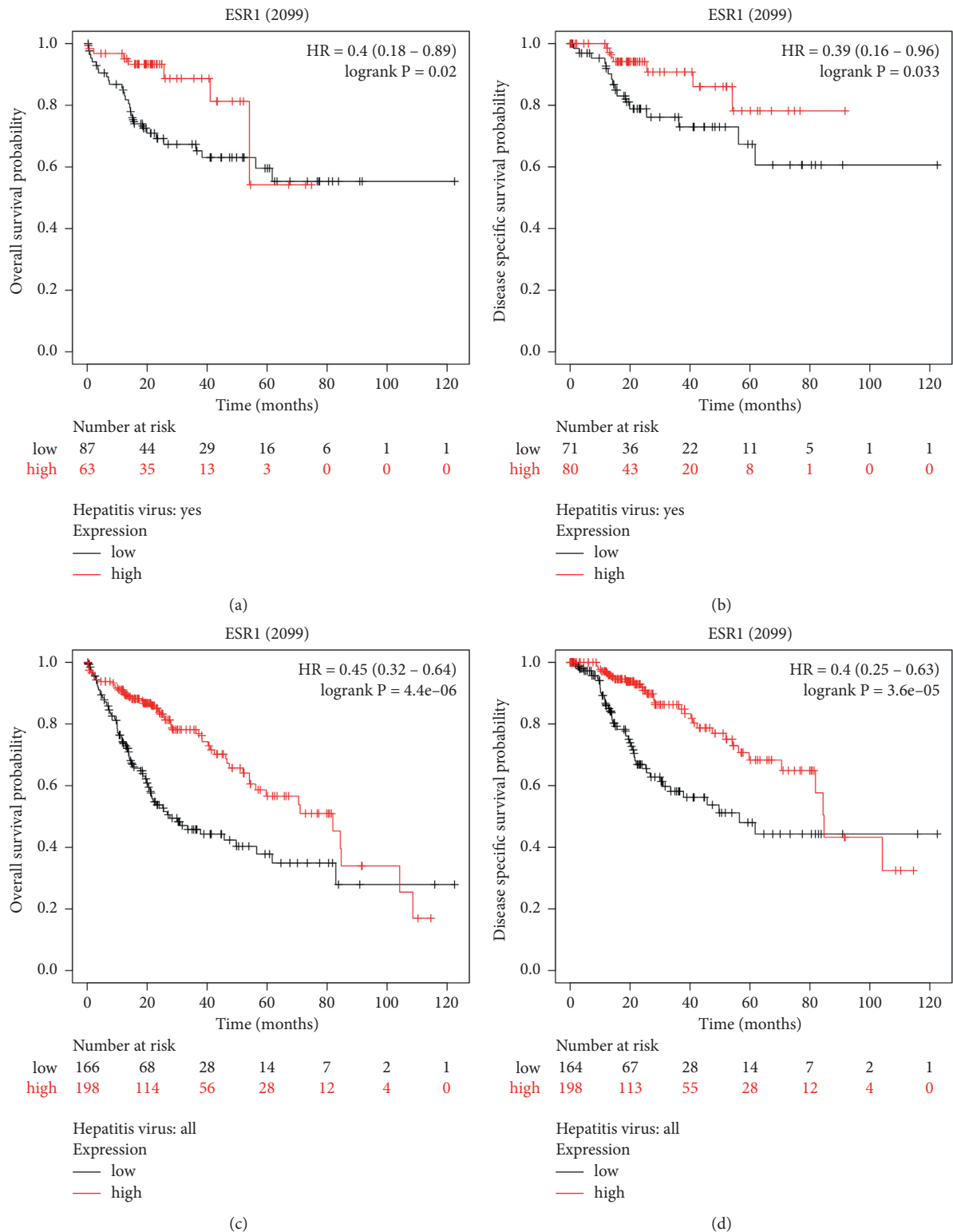


FIGURE 8: Prognostic analysis of hub targets. ESR1 expression was associated with overall survival probability (a) and disease-specific survival probability (b) in liver cancer patients with hepatitis virus. ESR1 expression was associated with overall survival probability (c) and disease-specific survival probability (d) in liver cancer patients.

prognostic analysis showed that ESR1 might be a tumor suppressor gene in HBV-related HCC (Figure 8).

#### 4. Discussion

Globally, there are nearly 887000 deaths per year from HBV infection-related diseases, of which HBV-related HCC accounts for about 38% [32]. In China, the proportion of HCC caused by HBV is as high as 84% [32]. Research on the molecular mechanisms of HBV-related HCC development is still emerging, but there is still a lack of effective biomarkers for targeted therapy. In this study, 11 key drug targets of *Curcumae Rhizoma* for the treatment of HBV-related HCC were identified through a combination of data mining and network pharmacology analysis, and these key targets were characterized. This study provided new targets and ideas for the treatment of HBV-related HCC with *Curcumae Rhizoma*.

Through the TCMSP database and Swiss Target Prediction database, we obtained three potential active ingredients of *Curcumae Rhizoma*, including hederagenin, wenyujin, and bisdemethoxycurcumin. Hederagenin reportedly mediated cytotoxicity to cancers via multipathways, for example, hederagenin inhibits proliferation and promotes apoptosis of cervical cancer CaSki cells by blocking the STAT3 pathway [33]. Hederagenin saponin extraction offers great potential as an antineoplastic drug via the mitochondrial pathway [34]. By impairing autophagy, hederagenin induced ROS accumulation, potentiating the cytotoxicity of cisplatin and paclitaxel to lung cancer cells [35]. According to Liu et al., hederagenin displayed potent antineoplastic activities against human HCC HepG2 cell line [36]. Bisdemethoxycurcumin has antitumor effects exerted through a multimechanistic mode of action [37]. For example, bisdemethoxycurcumin sensitizes nonsmall cell lung cancer cells to icotinib [38]. It enhances  $\alpha$ -PD-L1 antibody-mediated immune responses against bladder cancer [39]. It induces glioblastoma cell apoptosis [40]. Besides, it could cause a decrease in HCC cell viability and an increase in apoptosis [41, 42].

In terms of pathogenesis, GO-BP enrichment analysis suggested that the 11 key drug targets screened were involved in cell cycle checkpoint, DNA integrity checkpoint, and peptidyl-serine modification, all of which were associated with the development, progression, and metastasis of HCC [43–45]. The KEGG pathway enrichment results indicated that the p53 signaling pathway and arachidonic acid metabolism are enriched, which was supported by recent findings. HBV reportedly induce the abnormal lipid metabolism and activate Tregs through arachidonic acid signaling [46]. Hepatocytes with p53 inhibition escape death and senescence, becoming HCC progenitors [47]. *Curcumae Rhizoma* might play roles in treatment of HBV-related HCC via these biological processes and pathways.

In PPI analysis, we screened out ESR1 as a hub target. A recent study showed that ESR1 could inhibit HCC worsening [48]. ESR1 was lowly expression in liver tissues from chronic hepatitis B induced HCC in the GSE121248 dataset. Low ESR1 expression correlated with poor overall survival

and disease specific survival in liver patients, no matter whether they had hepatitis virus infection. Besides, the study by Shuying Dai et al. implied that bisdemethoxycurcumin has a good affinity with ESR1 [49]. *Curcumae Rhizoma*, modulating ESR1, could be a potential therapeutic agent against HBV-related HCC.

Although there are some limitations in this study, such as fewer *Curcumae Rhizoma* active ingredients and fewer HBV-related HCC dataset, making the findings somewhat one-sided, we used bioinformatics to screen out the key drug targets of HBV-related HCC, which will lay an important foundation for subsequent research on the therapeutic targets of HBV-related HCC with *Curcumae Rhizoma*.

#### 5. Conclusion

Based on WGCNA and network pharmacological analysis, our results illustrated that *Curcumae Rhizoma* might work through regulating multitargets and multipathways in HBV-related HCC. Therefore, it is suggested that we can refer to these relevant mechanisms in the future research of *Curcumae Rhizoma* on clinically treating HBV-related HCC. In addition, ESR1 and PTGS2 modulators are also deserved to be validated by further clinical and animal models of HBV-related HCC.

#### Data Availability

The data used to support this study are available from the corresponding author upon request.

#### Conflicts of Interest

The authors declare that they have no conflicts of interest.

#### Authors' Contributions

Mengyuan Zhao and Yun Fu contributed equally to this study.

#### Acknowledgments

This study was funded by the “Molecular Mechanism of Ruanganyin on Immune Regulation of Chronic Hepatitis B Based on PD-1/PD-L1 and CD28/CD80 Signaling Pathway” (81874451).

#### References

- [1] T. Akinyemiju, S. Abera, M. Ahmed et al., “The burden of primary liver cancer and underlying etiologies from 1990 to 2015 at the global, regional, and national level: results from the global burden of disease study 2015,” *JAMA Oncol*, vol. 3, no. 12, pp. 1683–1691, 2017.
- [2] D. Q. Huang and D. J. H. Tan, “Editorial: suboptimal ultrasound visualisation in patients undergoing surveillance for hepatocellular carcinoma,” *Alimentary Pharmacology & Therapeutics*, vol. 55, no. 6, pp. 752–753, 2022.
- [3] H. Abbas, Y. A. El-Feky, M. M. Al-Sawahli, N. M. EL-Deeb, H. B. El-Nassan, and M. Zewail, “Development and optimization of curcumin analog nano-biosomes using 21.31 full

- factorial design for anti-tumor profiles improvement in human hepatocellular carcinoma: in-vitro evaluation, in-vivo safety assay,” *Drug Delivery*, vol. 29, no. 1, pp. 714–727, 2022.
- [4] F. Bray, J. Ferlay, I. Soerjomataram, R. L. Siegel, L. A. Torre, and A. Jemal, “Global cancer statistics 2018: GLOBOCAN estimates of incidence and mortality worldwide for 36 cancers in 185 countries,” *CA: A Cancer Journal for Clinicians*, vol. 68, no. 6, pp. 394–424, 2018.
  - [5] L. Lan, Z. Fei, C. Yue, W. Ruixian, and M. Qun, “Analysis of epidemiological characteristics of malignant tumor mortality among Chinese residents in 2015,” *Chinese Journal of Epidemiology*, vol. 39, no. 1, pp. 32–34, 2018.
  - [6] M. Zhou, H. Wang, X. Zeng et al., “Mortality, morbidity, and risk factors in China and its provinces, 1990-2017: a systematic analysis for the Global Burden of Disease Study 2017,” *The Lancet*, vol. 394, no. 10204, pp. 1145–1158, 2019.
  - [7] Z. Chen, H. Xie, M. Hu et al., “Recent progress in treatment of hepatocellular carcinoma,” *American journal of cancer research*, vol. 10, no. 9, pp. 2993–3036, 2020.
  - [8] F. Kanwal and A. G. Singal, “Surveillance for hepatocellular carcinoma: current best practice and future direction,” *Gastroenterology*, vol. 157, no. 1, pp. 54–64, 2019.
  - [9] X. Wang, Z.-Y. Wang, J.-H. Zheng, and S. Li, “TCM network pharmacology: a new trend towards combining computational, experimental and clinical approaches,” *Chinese Journal of Natural Medicines*, vol. 19, no. 1, pp. 1–11, 2021.
  - [10] Z. Wu, C. Wei, L. Wang, and L. He, “Determining the traditional Chinese medicine (TCM) syndrome with the best prognosis of HBV-related HCC and exploring the related mechanism using network pharmacology,” *Evid Based Complement Alternat Med*, vol. 2021, Article ID 9991533, 13 pages, 2021.
  - [11] Y. Zhou, M. Xie, Y. Song et al., “Two traditional Chinese medicines curcumae radix and curcumae rhizoma: an ethnopharmacology, phytochemistry, and pharmacology review,” *Evidence-based Complementary and Alternative Medicine: eCAM*, vol. 2016, Article ID 4973128, 30 pages, 2016.
  - [12] Z. Lan, Y. Zhang, Y. Zhang et al., “Rapid evaluation on pharmacodynamics of Curcumae Rhizoma based on Micro-NIR and benchtop-NIR,” *Journal of Pharmaceutical and Biomedical Analysis*, vol. 200, Article ID 114074, 2021.
  - [13] Z. Zhong, H. Yu, S. Wang, Y. Wang, and L. Cui, “Anti-cancer effects of Rhizoma Curcumae against doxorubicin-resistant breast cancer cells,” *Chinese Medicine*, vol. 13, no. 1, p. 44, 2018.
  - [14] L. Wu, L. Wang, X. Tian, J. Zhang, and H. Feng, “Germacone exerts anti-cancer effects on gastric cancer through induction of cell cycle arrest and promotion of apoptosis,” *BMC Complementary Medicine and Therapies*, vol. 20, no. 1, p. 21, 2020.
  - [15] Y. Bian, G. Wang, J. Zhou et al., “Astragalus membranaceus (Huangqi) and Rhizoma curcumae (Ezhu) decoction suppresses colorectal cancer via downregulation of Wnt5/ $\beta$ -Catenin signal,” *Chinese Medicine*, vol. 17, no. 1, p. 11, 2022.
  - [16] Y. Chen, W. Liao, Z. Zhu et al., “Essential oil from the raw and vinegar-processed Rhizoma Curcumae ameliorate CCl4-induced liver fibrosis: integrating network pharmacology and molecular mechanism evaluation,” *Food & Function*, vol. 12, no. 9, pp. 4199–4220, 2021.
  - [17] H.-H. Zhang, Y. Zhang, Y.-N. Cheng et al., “Metformin in combination with curcumin inhibits the growth, metastasis, and angiogenesis of hepatocellular carcinoma in vitro and in vivo,” *Molecular Carcinogenesis*, vol. 57, no. 1, pp. 44–56, 2018.
  - [18] J. Ru, P. Li, J. Wang et al., “TCMSP: a database of systems pharmacology for drug discovery from herbal medicines,” *Journal of Cheminformatics*, vol. 6, no. 1, p. 13, 2014.
  - [19] D. Gfeller, A. Grosdidier, M. Wirth, A. Daina, O. Michielin, and V. Zoete, “SwissTargetPrediction: a web server for target prediction of bioactive small molecules,” *Nucleic Acids Research*, vol. 42, no. W1, pp. W32–W38, 2014.
  - [20] E. Boutet, D. Lieberherr, M. Tognolli, M. Schneider, and A. Bairoch, “UniProtKB/Swiss-Prot,” *Plant Bioinformatics*, vol. 406, pp. 89–112, 2007.
  - [21] T. Barrett, S. E. Wilhite, P. Ledoux et al., “NCBI GEO: archive for functional genomics data sets—update,” *Nucleic Acids Research*, vol. 41, pp. D991–D995, 2013.
  - [22] S. M. Wang, L. L. P. J. Ooi, and K. M. Hui, “Identification and validation of a novel gene signature associated with the recurrence of human hepatocellular carcinoma,” *Clinical Cancer Research*, vol. 13, no. 21, pp. 6275–6283, 2007.
  - [23] S. Davis and P. S. Meltzer, “GEOquery: a bridge between the gene expression Omnibus (GEO) and BioConductor,” *Bioinformatics*, vol. 23, no. 14, pp. 1846–1847, 2007.
  - [24] P. Langfelder and S. Horvath, “WGCNA: an R package for weighted correlation network analysis,” *BMC Bioinformatics*, vol. 9, no. 1, p. 559, 2008.
  - [25] W. Li, H. Wang, Z. Ma et al., “Multi-omics analysis of microenvironment characteristics and immune escape mechanisms of hepatocellular carcinoma,” *Frontiers in Oncology*, vol. 9, Article ID 1019, 2019.
  - [26] Z. Gu, R. Eils, and M. Schlesner, “Complex heatmaps reveal patterns and correlations in multidimensional genomic data,” *Bioinformatics*, vol. 32, no. 18, pp. 2847–2849, 2016.
  - [27] G. Su, J. H. Morris, B. Demchak, and G. D. Bader, “Biological network exploration with Cytoscape 3,” *Current protocols in bioinformatics*, vol. 47, pp. 8–24, 2014.
  - [28] G. Yu, L.-G. Wang, Y. Han, and Q.-Y. He, “clusterProfiler: an R package for comparing biological themes among gene clusters,” *OMICS: A Journal of Integrative Biology*, vol. 16, no. 5, pp. 284–287, 2012.
  - [29] D. Szklarczyk, A. L. Gable, K. C. Nastou et al., “The STRING database in 2021: customizable protein-protein networks, and functional characterization of user-uploaded gene/measurement sets,” *Nucleic Acids Research*, vol. 49, no. D1, pp. D605–D612, 2021.
  - [30] C. H. Chin, S.-H. Chen, H.-H. Wu, C.-W. Ho, M.-T. Ko, and C.-Y. Lin, “cytoHubba: identifying hub objects and sub-networks from complex interactome,” *BMC Systems Biology*, vol. 8, no. Suppl 4, p. S11, 2014.
  - [31] A. Lanczyk and B. Gyorffy, “Web-based survival analysis tool tailored for medical research (KMplot): development and implementation,” *Journal of Medical Internet Research*, vol. 23, no. 7, Article ID e27633, 2021.
  - [32] G. Wang and Z. Duan, “Guidelines for prevention and treatment of chronic hepatitis B,” *Journal of clinical and translational hepatology*, vol. 9, no. 5, pp. 769–791, 2021.
  - [33] L. Fang, M. Liu, and L. Cai, “Hederagenin inhibits proliferation and promotes apoptosis of cervical cancer CaSki cells by blocking STAT3 pathway,” *Xi Bao Yu Fen Zi Mian Yi Xue Za Zhi*, vol. 35, no. 2, pp. 140–145, 2019.
  - [34] L. Cheng, L. Shi, J. Wu et al., “A hederagenin saponin isolated from Clematis ganpiniana induces apoptosis in breast cancer cells via the mitochondrial pathway,” *Oncology Letters*, vol. 15, no. 2, pp. 1737–1743, 2018.

- [35] K. Wang, X. Liu, Q. Liu et al., “Hederagenin potentiated cisplatin- and paclitaxel-mediated cytotoxicity by impairing autophagy in lung cancer cells,” *Cell Death & Disease*, vol. 11, no. 8, p. 611, 2020.
- [36] X. Liu, L. Sun, Q.-H. Liu, B.-Q. Chen, and Y.-M. Liu, “Synthesis, characterization and anti-hepatoma activity of new hederagenin derivatives,” *Mini Reviews in Medicinal Chemistry*, vol. 20, no. 3, pp. 252–257, 2020.
- [37] M. Ramezani, M. Hatamipour, and A. Sahebkar, “Promising anti-tumor properties of bisdemethoxycurcumin: a naturally occurring curcumin analogue,” *Journal of Cellular Physiology*, vol. 233, no. 2, pp. 880–887, 2018.
- [38] M. Xiang, H.-G. Jiang, Y. Shu et al., “Bisdemethoxycurcumin enhances the sensitivity of non-small cell lung cancer cells to icotinib via dual induction of autophagy and apoptosis,” *International Journal of Biological Sciences*, vol. 16, no. 9, pp. 1536–1550, 2020.
- [39] Y. Shao, W. Zhu, J. Da et al., “Bisdemethoxycurcumin in combination with  $\alpha$ -PD-L1 antibody boosts immune response against bladder cancer,” *OncoTargets and Therapy*, vol. 10, pp. 2675–2683, 2017.
- [40] T. C. Hsia, S.-F. Peng, F.-S. Chueh et al., “Bisdemethoxycurcumin induces cell apoptosis and inhibits human brain glioblastoma GBM 8401/luc2 cell xenograft tumor in subcutaneous nude mice in vivo,” *International Journal of Molecular Sciences*, vol. 23, no. 1, 2022.
- [41] T. Y. Huang, S. F. Peng, Y. P. Huang et al., “Combinational treatment of all-trans retinoic acid (ATRA) and bisdemethoxycurcumin (BDMC)-induced apoptosis in liver cancer Hep3B cells,” *Journal of Food Biochemistry*, vol. 44, no. 2, Article ID e13122, 2020.
- [42] C. Qiu, K. Liu, S. Zhang et al., “Bisdemethoxycurcumin inhibits hepatocellular carcinoma proliferation through akt inactivation via CYLD-mediated deubiquitination,” *Drug Design, Development and Therapy*, vol. 14, pp. 993–1001, 2020.
- [43] P. Kronschnabl, A. Grünweller, R. K. Hartmann, A. Aigner, and U. Weirauch, “Inhibition of PIM2 in liver cancer decreases tumor cell proliferation in vitro and in vivo primarily through the modulation of cell cycle progression,” *International Journal of Oncology*, vol. 56, no. 2, pp. 448–459, 2020.
- [44] M. Liu, Z. Zhao, Y. Cai et al., “YTH domain family: potential prognostic targets and immune-associated biomarkers in hepatocellular carcinoma,” *Aging*, vol. 13, no. 21, pp. 24205–24218, 2021.
- [45] M. Lulli, L. Del Coco, T. Mello et al., “DNA damage response protein CHK2 regulates metabolism in liver cancer,” *Cancer Research*, vol. 81, no. 11, pp. 2861–2873, 2021.
- [46] Z. Liu, J. Wang, L. Liu et al., “Chronic ethanol consumption and HBV induce abnormal lipid metabolism through HBx/SWELL1/arachidonic acid signaling and activate Tregs in HBV-Tg mice,” *Theranostics*, vol. 10, no. 20, pp. 9249–9267, 2020.
- [47] D. Dhar, L. Antonucci, H. Nakagawa et al., “Liver cancer initiation requires p53 inhibition by CD44-enhanced growth factor signaling,” *Cancer Cell*, vol. 33, no. 6, pp. 1061–1077, 2018.
- [48] J. Yun, Y. S. Kim, M. J. Heo, M. J. Kim, A. Moon, and S. J. Kim, “ER $\alpha$  inhibits mesenchymal and amoeboidal movement of liver cancer cell via G $\alpha$ 12,” *International Journal of Cancer*, vol. 150, no. 10, pp. 1690–1705, 2022.
- [49] S. Dai, G. Zhang, F. Zhao, and Q. Shu, “Study on the molecular mechanism of the herbal couple sparganii rhizoma-curcumae rhizoma in the treatment of lung cancer based on network pharmacology,” *Evidence Based Complementary Alternative Medicine*, vol. 2021, Article ID 6664489, 17 pages, 2021.

## Research Article

# GC-MS Analysis, Heavy Metals, Biological, and Toxicological Evaluation of *Reseda muricata* and *Marrubium vulgare* Methanol Extracts

Riaz Ullah  and Ali S. Alqahtani

Department of Pharmacognosy, College of Pharmacy, King Saud University, Riyadh, Saudi Arabia

Correspondence should be addressed to Riaz Ullah; rullah@ksu.edu.sa

Received 8 February 2022; Accepted 8 March 2022; Published 21 March 2022

Academic Editor: Ruchika Garg

Copyright © 2022 Riaz Ullah and Ali S. Alqahtani. This is an open access article distributed under the Creative Commons Attribution License, which permits unrestricted use, distribution, and reproduction in any medium, provided the original work is properly cited.

The usage of herbal remedy is growing vividly all around the world. Though, ecological contamination particularly with heavy metals carries a thoughtful problem on quality of medicinal plants and their foodstuffs. In the world, 80% of the population depend on traditional medicine, while information on the levels of heavy metal such as Zn, Mn, Cu, Cr, Pb, As, Cd, and Cr in plants utilized for making of herbal remedies is unavailable. Therefore, the purpose of this study was to assess phytochemicals, biological activities, and heavy metal analysis of *Reseda muricata* and *Marrubium vulgare* grown in different parts of Saudi Arabia. Qualitative phytochemical analysis of *R. muricata* and *M. vulgare* confirmed the presence of alkaloids, flavonoids, tannins, phenol, and saponins. Methanol extracts of both *Reseda muricata* and *Marrubium vulgare* were characterized with the help of GC-MS. Antioxidants, antimicrobial, and brine shrimp lethal toxicity of the both species were also evaluated.

## 1. Introduction

The medicinal potential of plants species is because of the occurrence of secondary phytoconstituents which have numerous functions such as antioxidant, antimicrobial, cytotoxic, anticancer, and antiviral. Plants have been the main root of traditional medicines since ancient times [1–3]. The plants are used as primary healthcare all over the world, but South American countries in particular [4]. About 300–315 thousand species of plants are present on this planet, and few of these provide food to humans, aquatic, and terrestrial animals [5]. Plants are used as antimicrobial agents that are used to kill microorganisms such as bacteria and fungi or inhibit their growth [6, 7]. They also have antioxidant, anticancer, antiviral, and cytotoxic and much more effects. Antioxidants inhibit the oxidation of substrate such as free radicals [8, 9]. Cytotoxicity is the quality of being toxic to cells. Cytotoxic potential of crude extract is ascertained against various cells using methods such as MTT and brine shrimp lethality assays [10, 11]. *Reseda muricata* is an

herb belonging to family and spread in southeast Egypt. Family Resedaceae consists of 6 genera and 75 species. While, very small data about *R. muricata* appeared till date. Previously, chemical screening of *R. muricata* has reported a flavonoid trioxide, and its coumaryl ester together with some flavonoids and phenolic acids were identified from the leaves of *Reseda muricata*. Pharmacological studies of extracts of various *Reseda* species presented antifungal, antibacterial, and anti-inflammatory activities. *R. muricata* is traditionally used for the treatment of hemorrhoids, stomach aches, and diarrhea [12].

*Marrubium vulgare* is a plant of family Lamiaceae, whose genus comprises of 97 species. It is spread far and wide along the Mediterranean Sea and growing in the temperate areas of the Eurasian region. The plant has been utilized as a substitute for hops in beer breweries and is presently used to make herbal teas. In the past times, it was augmented to boiled vegetables, sauces, and salads. It is also utilized as traditional medicine. *M. vulgare* is habitually a significant foundation for the pharmaceutical and food industries. For



instance, just in India, there are 33 registered herbal formulations comprising of white horehound. *M. vulgare* showed diaphoretic, expectorant, stimulant, tonic, diuretic, and aromatic potential. Its phytochemical constituents are diterpenic lactones, phenolic compounds, and phenylpropanoids [13]. Folk usage of *Reseda muricata* fruit is reported as menstruation tonic [14]. Similarly, in Morocco, the leaf infusion utilization of *M. vulgare* is used for the treatment of metabolic disorder [15]. Furthermore, in Serbian language, *M. vulgare* is called očajnica, which means desperate woman; because its tea is considered good remedy for women who were unable to conceive and regulate menstrual cycle, it is also traditionally utilized for the treatment of respiratory and gastrointestinal disorders [16]. Medicinal uses of the plants are due to the presence of phytochemicals. The most generally responsible phytoconstituents as antidiabetic are benzoic acid derivatives, phenol and its derivatives, flavonoid, amino acid and its derivatives, vitamins, saponin, alkaloid, and carbohydrate [17]. Phytochemicals such as flavonoids, polyphenols, steroids, terpenoids, and alkaloids have balanced usages and are existed in different amounts in different plants species. The presence of these classes of phytochemicals in plants species and dietary food plays a substantial part to defend against ailment [18]. Keeping in mind the importance of these plants species, we have designed the current study to evaluate its biological potential.

## 2. Experimental

**2.1. Plant Collection.** The plants *R. muricata* and *M. vulgare* were collected from the Hawdaf Sudayer Dam on 18-3-2017 and identified by Dr. Rifayatullah, a plant taxonomist at our college. "The specimen vouchers were deposited in the Herbarium of the Medicinal Aromatic and Poisonous Plants Research Center, College of Pharmacy, King Saud University, Riyadh, Saudi Arabia, with voucher numbers SAID 326 and MV-2019, respectively."

**2.2. Extraction Procedure.** The plants *R. muricata* and *M. vulgare* parts were ground to fine powder by a mechanical grinder. The powder plant material (100 g, each) was soaked in 3 liters of methanol. The greenish methanol was filtered and evaporated with the help of a rotary evaporator. The greenish residue of methanol was further assessed for phytochemicals screening, antimicrobial, antioxidant, and cytotoxic potential using reported protocols.

**2.3. Phytochemicals Screening.** Phytochemicals such as alkaloids, flavonoids, tannins, phenols, and saponins were determined using different reagents such as Mayer's reagent and ferric chloride reagent [19–24].

**2.4. GC-MS Analysis.** Agilent GC 7890A combined with a triple axis detector 5975 C single quadrupole mass spectrometer were used for GC-MS analysis. The chromatographic column was an Agilent HP 5MS column

(30 m × 0.25 mm × 0.25 μm film thickness), with high-purity helium as the gas carrier, at a flow rate of 1 mL/min. The injector temperature was 250°C, and it was equipped with a splitless injector at 20:1. The source temperature of MS was set at 230°C, and the quad temperature was set at 150°C. The oven temperature was initially at 40°C (held for 1 min), then was increased to 150°C at 10°C min<sup>-1</sup> (held for 1 min), and then increased further to 300°C at 10°C min<sup>-1</sup> for 1 min. The injection volume was 1 μL, and the scan range was set at 50–800 mass ranges at 70 eV electron energy and the solvent delay of 3 minutes. Finally, unknown compounds were identified by comparing the spectra with that of the NIST 2008 (National Institute of Standard and Technology library). The total time required for analyzing a single sample was 29 minutes.

### 2.5. Antimicrobial Activity

**2.5.1. Agar Well Diffusion Assay (Antibacterial Activity).** Methanol extracts of the plants *R. muricata* and *M. vulgare* were evaluated for antibacterial potential using the well diffusion assay. Nutrient agar media plates were inoculated and were placed in the incubator at 37°C for 18–24 h. Wells were designed in Petri dish having 6 mm diameter with the help of sterile cork borers. Using a sterile swab, the inocula of the respective bacterial strains were spread on nutrient agar plates and then dried at 37°C for 15 min. Stock solutions of n-hexane, chloroform, ethyl acetate, and butanol extracts were prepared using DMSO as solvent. Concentration of each extract solution was kept as 2 mg/mL and 3 mg/mL. Then, 100 μL of each extract was administered in each well containing *E. coli*, *K. pneumonia*, *Xanthomonas*, and *S. aureus*. The Petri plates were placed for incubation at temperature 37°C for 24 h. The zone of inhibition in (mm) for antibacterial activity was determined after incubation. The positive control used showed antibacterial activity [25, 26].

**2.5.2. Agar Well Diffusion Assay (Antifungal Activity).** Agar well diffusion assay was used to find out the antifungal activity of *R. muricata* and *M. vulgare*. The fungal strains were first grown on Petri plates. Wells of 6 mm in diameter were made in Petri plates containing nutrient agar medium using sterile cork borers. Using a sterile swab, the inocula of the respective bacterial strains were spread on nutrient agar plates and then dried at 37°C for 15 min. Stock solutions of n-hexane, chloroform, ethyl acetate, and butanol extracts were prepared using DMSO as solvent. Concentration of each extract solution was kept as 2 mg/mL and 3 mg/mL. Then, 100 μL of each extract was administered in each well containing *Aspergillus niger*, clinical *Candida*, *Acremonium*, *Rhizopus*, and *Trichoderma*. The Petri plates were placed for incubation at temperature 37°C for 24 h. The zones of inhibition in mm for antibacterial activity were determined after incubation. The positive control used showed antibacterial activity [27, 28].



**2.6. Antioxidant Activity.** The antioxidant activity of *R. muricata* and *M. vulgare* was measured by using 2,2-diphenyl picrylhydrazyl radical (DPPH). The molecule responsible for antioxidant activity reacts with DPPH and converts it into diphenyl-picryl hydrazine having yellow color. This change in color is measured with the help of a spectrophotometer. Using the following equation, the DPPH radical inhibiting activity or antioxidant activity of the plant extract with different solvents was calculated.

$$\text{DPPH scavenged (\%)} = \frac{\text{Abs (control)} - \text{Abs (test)}}{\text{Abs (control)}} \times 100, \quad (1)$$

where Abs (control) and Abs (test) are the absorbance of the control and absorbance of the tested sample, respectively [29].

**2.7. Brine Shrimp Lethality Protocol.** The cytotoxic activity of the plant was assessed using the brine shrimp lethality bioassay method where totally 6 graded doses (3 graded doses for each plant) (1000  $\mu\text{g/mL}$ , 100  $\mu\text{g/mL}$ , and 10  $\mu\text{g/mL}$ ) were used. Brine shrimps (*Artemia salina* Leach) nauplii (Ocean 90, USA) were used as test organisms. For hatching, eggs were kept in brine with a constant oxygen supply for 48 h. The mature nauplii were then used in the experiment. DMSO was used as a solvent and also as a negative control. Vincristine sulfate was used as a reference standard in this case. To gage the percentage mortality (% M), the number of dead shrimps is divided by the total number of shrimps and is then multiplied by 100%. The death of the shrimps confirmed the presence of bioactive compounds in the plant extracts [21, 28, 30].

**2.8. Determination of Heavy Metals.** The protocol described by W. Khan et al. [31] was used. Analytical grade concentrated per chloric acid ( $\text{HClO}_4$ ) and nitric acid ( $\text{HNO}_3$ ) were used for the digestion. Samples (0.2 g) of dry grounded whole plant (each) were weighed into 100 mL beakers. Predigestion of the samples was performed with  $\text{HNO}_3$  (5 mL), followed by cooling and digestion again to  $\text{HClO}_4$  fumes. Heavy metals analyses for zinc (Zn), copper (Cu), manganese (Mn), chromium (Cr), lead (Pb), arsenic (As), cadmium (Cd), and chromium (Cr) were performed in triplicates for both medicinal plants using the atomic absorption spectrophotometer (Analyst 700, Perkin Elmer).

### 3. Results and Discussion

**3.1. GC-MS Analysis of *Reseda muricata* (RMM) and *Marrubium vulgare* (MVM) Methanol Extracts.** GC-MS analysis of *Reseda muricata* and *Marrubium vulgare* methanol extracts is shown in Figure 1, Table 1 and Figure 2, Table 2, respectively. GC-MS analysis of RMM showed 17 constituents in methanol extracts. The highest abundance of 2-propenenitrile, 3-phenyl-, (E)- followed by 1H-indole-3-acetic acid-methyl ester has been observed as shown in Figure 1. Similarly, 42 phytoconstituents were noted in the

methanol extract of MVM. 5-Methoxy-2-nitrobenzoic acid was the highest in abundance followed by hexadecanoic acid and methyl ester in MVM. Phytochemicals as collective in the extracts are responsible for biological activities of plant extracts. Therefore, detail of phytochemicals is important.

**3.2. Qualitative Phytochemicals Analysis of *R. muricata* and *M. vulgare*.** Qualitative investigation of methanol extract of *R. muricata* and *M. vulgare* confirmed the presence of different kinds of phytochemicals such flavonoids, phenols, saponins, alkaloids, and tannins, as given in Table 3.

**3.3. Antibacterial Activity.** The bacterial strains used are *E. coli*, *Klebsiella pneumonia*, *Xanthomonas*, and *Staphylococcus aureus*. The methanol extract of *R. muricata* and *M. vulgare* showed antibacterial activity (Table 4). Both the extracts showed a significant zone of inhibition against the test bacterial strain, which confirmed that the methanol extract of *R. muricata* and *M. vulgare* can be used for further investigation.

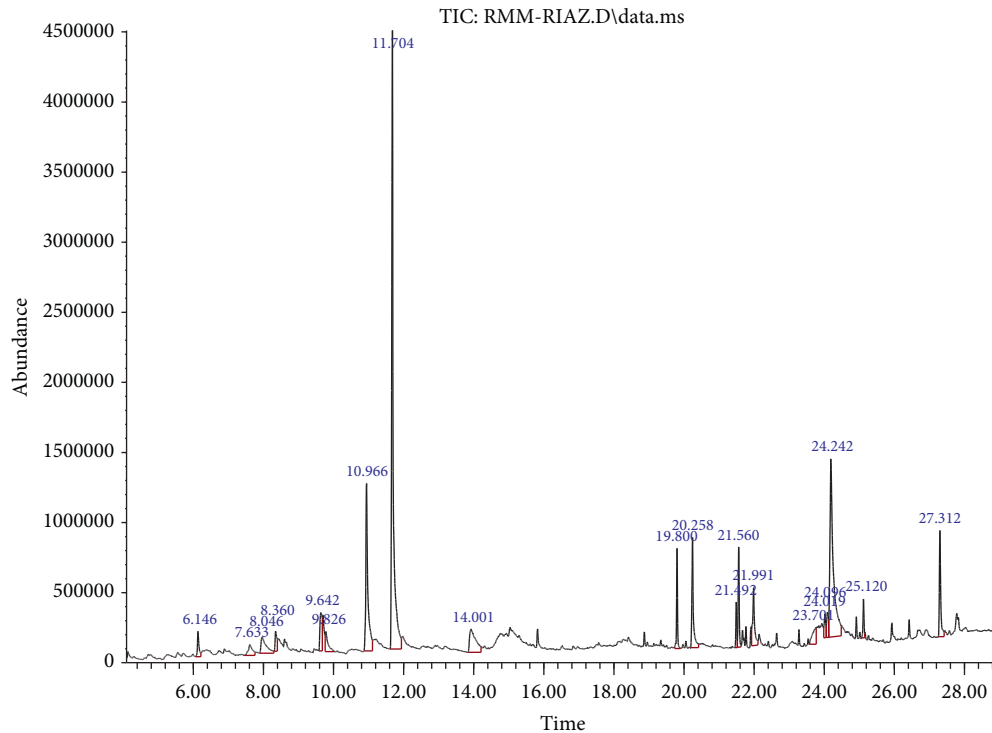
**3.4. Antifungal Activity.** *A. niger*, *Candida*, *Rhizopus*, *Acremonium*, and *Trichoderma* fungal stains were used. The results obtained are given in Table 5. The methanol extract of *R. muricata* and *M. vulgare* showed significant antifungal activities.

**3.5. Antioxidant Activity.** The DPPH free radical scavenging assay was used to evaluate the antioxidant potential of the methanol extract of *R. muricata* and *M. vulgare* which showed that both extracts are active (Table 6). The results were compared with ascorbic acid which was used as a standard antioxidant having  $\text{LC}_{50}$  31.59  $\mu\text{g/mL}$ . The  $\text{LC}_{50}$  of both extracts was above 100  $\mu\text{g/mL}$  (Table 6).

**3.6. Cytotoxicity.** Brine shrimp lethality assay (BSLA) was applied to evaluate the cytotoxicity of the extracts of *Reseda muricata*. It can be seen that with increased in concentration, the mortality rate was increased. The extracts were found to have high mortality above 1000  $\mu\text{g/mL}$  mortality rate and  $\text{LD}_{50}$ , as given in Table 7.

**3.7. Determination of Heavy Metals.** The results given in Table 8 provide the levels of heavy metal in the whole part of *R. muricata* and *M. vulgare*. These results show that the concentration of bioessential elements is within the permissible limit as well as the toxic heavy metal not detected in it.

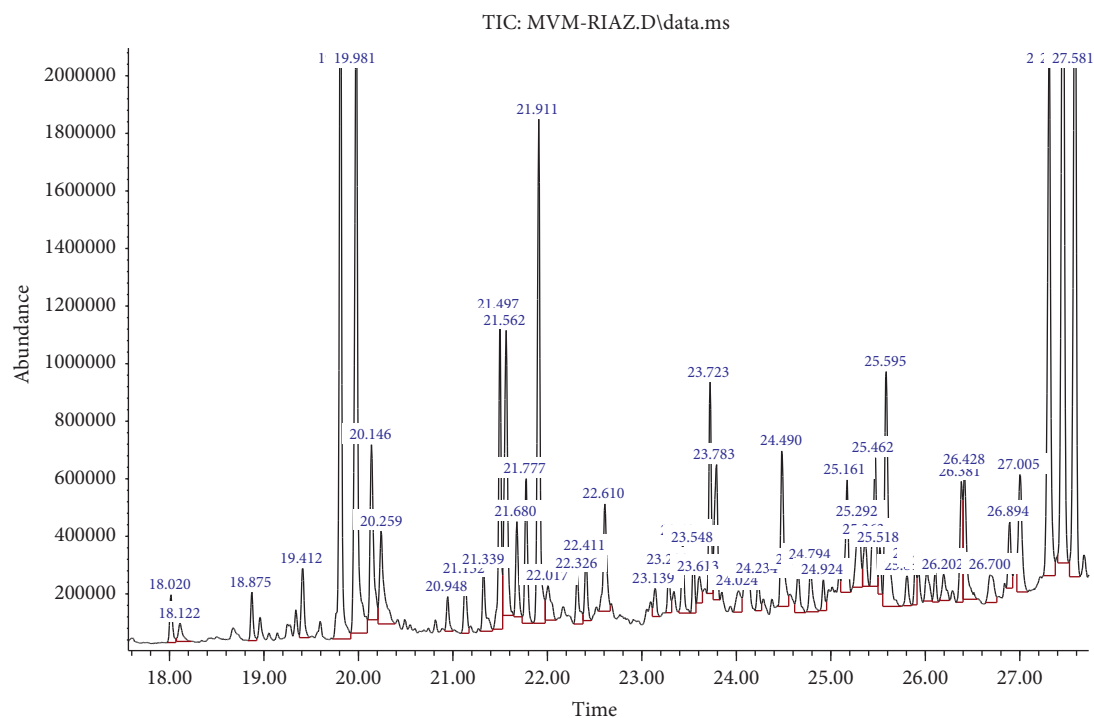
According to the FAO/WHO [31], the acceptable limit for Zn, Cu, Cr, and Mn is 27.4, 3.00, 0.02, and 2 ppm, respectively. From the given findings, it is concluded that the levels of these elements are within the standard parameters. Our study completely agreed with the results which confirmed that concentration of heavy metals in both species *R. muricata* and *M. vulgare* were within the toxic limits. Though, its concentration varies based on different

FIGURE 1: GC-MS analysis of *Reseda muricata* (RMM).TABLE 1: GC-MS analysis of *Reseda muricata* (RMM).

S. no.	Rt (min)	Area (Ab*s)	Absolute height (ab)	Name of compounds	Mol. weight (amu)
1	6.145	557970	224607	5-Isothiazolemethanol	115.009
2	7.634	643368	129714	Cyclopentanecarboxylic acid, 1-amino-	129.079
3	8.047	1190894	184042	2-Butanone, 4-hydroxy-3-methyl-	102.068
4	8.359	493253	226255	Piperazine, 1,2,4-trimethyl-	128.131
5	9.642	1203054	357987	4H-Pyran-4-one, 2,3-dihydro-3,5-dihydroxy-6-methyl-	144.042
6	9.823	719452	222876	2,5-Difluoroanisole	144.039
7	11.706	13822257	4511047	2-Propenenitrile, 3-phenyl-, (E)-	129.058
8	14.002	2029488	241307	Benzeneacetic acid, alpha-hydroxy-, methyl ester, (S)-	166.063
9	19.8	1288777	817118	Pentadecanoic acid, 14-methyl-, methyl ester	270.256
10	20.257	2262071	893465	n-Hexadecanoic acid	256.24
11	21.489	561457	434086	9,12-Octadecadienoic acid (Z,Z)-, methyl ester	294.256
12	21.558	1440001	827838	9,12,15-Octadecatrienoic acid, methyl ester, (Z,Z,Z)-	292.24
13	21.99	1513742	536962	9,12,15-Octadecatrienoic acid, (Z,Z,Z)-	278.225
14	23.704	891444	252326	2,5-Dimethylbenzonitrile	131.073
15	24.016	482012	348804	Octadecanoic acid, 3-oxo-, methyl ester	312.266
16	24.098	614148	361747	Heptadecanoic acid, 3-oxo-, methyl ester	298.251
17	24.242	8477297	1450949	1H-indole-3-acetic acid-methyl ester	204.09

environmental conditions [32]. These metals are very necessary for the development of plants, and its excess or shortage can cause serious problems in plants and humans. Zn is an essential trace nutrient for plant growth due to its role in several cell functions. It is also vital for brain growth, normal growth, bone formation, wound-healing, and behavioral response with a dietary limit in humans of 100 ppm [33]. Its deficiency causes diabetes and loss of smell and touch. Cu is important for normal plant growth, but its extreme levels (>100 ppm) can cause phytotoxicity. The concentration of Cu in seed and flower parts exceeded the

prescribed WHO limits, but its concentration was lower in leaf, stem, and root. Meanwhile, with respect to bodyweight, the acceptable lower limit of Cu is 20  $\mu\text{g}/\text{mg}$  bodyweight per day [31, 34]. In both *R. muricata* and *M. vulgare* samples, Pb, As, Cd, and Cr were not detected. Industries, sewage, air, water pollution, and the fly ash are the main sources of heavy metal contamination. These plants were collected from the Hawdaf Sudayeer Dam of Saudi Arabia, the dam constructed only to store rain water. It is away from cities and industries or industries sewage. This may be the reason why these plants are safe. A similar study reports that three other

FIGURE 2: GC-MS analysis of *Marrubium vulgare* (MVM).TABLE 2: GC-MS analysis of *Marrubium vulgare* (MVM).

S. no.	Rt (min)	Area (Ab*s)	Absolute height (ab)	Name of compounds	Mol. weight (amu)
1	15.609	917256	441083	Bicyclo[2.2.2]octane, 2-methyl-	124.125
2	18.124	192669	98391	2,10-Dodecadien-1-ol, 3,7,11-trimethyl-, (E)-(+/-)-	224.214
3	18.875	305308	206206	Bicyclo[3.1.1]heptane, 2,6,6-trimethyl-, (1.alpha.,2.beta.,5.alpha.)-	138.141
4	19.412	526019	288389	4-(1,3,3-Trimethyl-bicyclo[4.1.0]hept-2-yl)-but-3-en-2-one	206.167
5	19.813	4914762	2914174	Hexadecanoic acid, methyl ester	270.256
6	20.144	1490568	718319	Phenol, o-amino-	109.053
7	20.257	1050891	418235	n-Hexadecanoic acid	256.24
8	20.945	228251	190697	Benzenesulfinothioic acid, 4-methoxy-, S-phenyl ester	264.028
9	21.495	2040641	1171386	9,12-Octadecadienoic acid, methyl ester	294.256
10	21.564	2275132	1115652	9,12,15-Octadecatrienoic acid, methyl ester, (Z,Z,Z)-	292.24
11	21.683	650401	450996	Phytol	296.308
12	21.777	1018339	600656	Octadecanoic acid, methyl ester	298.287
13	21.908	3522375	1849605	1H-Indene, 2-butyl-5-hexyloctahydro-	264.282
14	22.015	424602	228408	1H-Indene, 5-butyl-6-hexyloctahydro-	264.282
15	22.327	421674	271332	Carane, 4,5-epoxy-, trans	152.12
16	22.409	447050	331946	1,2-Dioctylcyclopropene	264.282
17	22.609	965818	512697	7-(1,3-Dimethylbuta-1,3-dienyl)-1,6,6-trimethyl-3,8-dioxatricyclo[5.1.0.0(2,4)]octane	234.162
18	23.141	211430	218876	[1,1'-Biphenyl]-3-amine	169.089
19	23.291	283469	285892	Tricosane	324.376
20	23.435	495501	383643	Methyl 2-octylcyclopropene-1-octanoate	308.272
21	23.547	383518	362077	Methyl 18-methylnonadecanoate	326.318
22	23.61	231395	260954	2(1H)-Naphthalenone, octahydro-4a-methyl-7-(1-methylethyl)-, (4.alpha.,7.beta.,8a.beta.)-	208.183
23	23.722	1294950	935884	cis,cis-2,9-Dimethylspiro[5.5]undecane	180.188
24	23.785	1072281	649412	2-Methyl-3-(3-methyl-but-2-enyl)-2-(4-methyl-pent-3-enyl)-oxetane	222.198
25	24.023	278775	211072	3-Cyclohexene-1-carboxaldehyde, 1,3,4-trimethyl-	152.12
26	24.235	235821	253211	Butyramide, 4,N-bis(4-methoxyphenyl)-2,4-dioxo-	327.111
27	24.492	1286972	696867	3-Buten-2-one, 4-(5,5-dimethyl-1-oxaspiro[2.5]oct-4-yl)	208.146

TABLE 2: Continued.

S. no.	Rt (min)	Area (Ab*s)	Absolute height (ab)	Name of compounds	Mol. weight (amu)
28	24.654	361709	283653	1,1'-Bicyclohexyl, 2-propyl-, trans-	208.219
29	24.792	393996	301014	Cyclopropane carboxamide, 2-cyclopropyl-2-methyl-N-(1-cyclopropylethyl)-	207.162
30	25.161	935181	595906	Docosanoic acid, methyl ester	354.35
31	25.292	794788	450542	(7,7-Dimethyl-2-oxobicyclo[2.2.1]hept-1-yl)methanesulfonic acid, methyl ester	246.093
32	25.461	1111821	672632	2-Heptanone, 6-(3-acetyl-1-cyclopropen-1-yl)-3-hydroxy-6-methyl-, (R*,R*)-	224.141
33	25.593	2166410	972489	Longipinane, (E)-	206.203
34	25.805	232096	262661	Phenol, 4-methyl-2-nitro-	153.043
35	25.893	263570	304601	3,5-Dihydroxybenzamide	153.043
36	26.106	195485	282498	Ursodeoxycholic acid	392.293
37	26.425	1019036	631125	Trifluoroacetyl-.alpha.-fenchol	250.118
38	26.7	412469	265361	2,4,5,5,8a-Pentamethyl-4a,5,6,7,8,8a-hexahydro-2h-chromene	208.183
39	27.006	1106824	614740	1,4-Methanoazulene-9-methanol, decahydro-4,8,8-trimethyl-, [1S-(1.alpha.,3a.beta.,4.alpha.,8a.beta.,9R*)]-	222.198
40	27.313	4354006	2167785	Bicyclo[2.2.1]heptan-2-one, 1,7,7-trimethyl-, (+/-)-	152.12
41	27.457	6087633	2947769	5-Methoxy-2-nitrobenzoic acid	197.032
42	28.282	703407	401338	Cyclohexane-1-methanol, 3,3-dimethyl-2-(3-methyl-1,3-butadienyl)-	208.183

TABLE 3: Qualitative phytochemical analysis of *R. muricata* and *M. vulgare*.

S. no.	Plant species	Alkaloids	Flavonoids	Tannins	Phenol	Saponins
1	<i>R. muricata</i> (methanol extract)	+	+	+	+	+
2	<i>M. vulgare</i> (methanol extract)	+	+	+	+	+

TABLE 4: Antibacterial activity of methanol extract of *R. muricata* and *M. vulgare*.

Samples	Gram negative			Gram positive	
	Zone of inhibition (mm)				
	<i>E. coli</i>	<i>Klebsiella pneumoniae</i>	<i>Xanthomonas</i>	<i>Staphylococcus aureus</i>	
Negative control (DMSO)	—	—	—	—	
<i>R. muricata</i> (methanol extract)	8.03 ± 0.35	7.13 ± 0.12	5.13 ± 0.12	4.13 ± 0.22	
<i>M. vulgare</i> (methanol extract)	5.17 ± 0.35	6.12 ± 0.39	8.11 ± 0.31	6.11 ± 0.31	
Streptomycin	17.00 ± 1.02	16.20 ± 0.14	15.91 ± 0.81	18.10 ± 0.07	

TABLE 5: Antifungal activity of methanol extract of *R. muricata* and *M. vulgare*.

Samples	Zone of inhibition (mm)				
	<i>A. niger</i>	<i>Candida</i>	<i>Rhizopus</i>	<i>Acremonium</i>	<i>Trichoderma</i>
Negative control (DMSO)	—	—	—	—	—
<i>R. muricata</i> (methanol extract)	3.09 ± 0.31	4.12 ± 0.10	1.19 ± 0.91	5.11 ± 0.21	1.08 ± 0.11
<i>M. vulgare</i> (methanol extract)	2.91 ± 0.16	4.01 ± 0.29	2.10 ± 0.01	7.12 ± 0.31	0.11 ± 0.12
Flumetazole	9.89 ± 2.08	10.25 ± 1.01	4.29 ± 0.01	13.21 ± 1.22	2.22 ± 1.29

TABLE 6: LC<sub>50</sub> values of the methanol extract of *R. muricata* and *M. vulgare*.

Samples	LC <sub>50</sub> (µg/mL)
<i>R. muricata</i> (methanol extract)	154.80 ± 12.10 <sup>a</sup>
<i>M. vulgare</i> (methanol extract)	127.20 ± 10.10 <sup>b</sup>
Ascorbic acid	31.59 ± 6.01 <sup>c</sup>

Values are presented as means ± SD (n = 3). Means with different superscript (a-c) letters in the rows are significantly (p < 0.01) different from one another.

TABLE 7: Cytotoxic activity of *R. muricata* and *M. vulgare* (methanol extract).

Samples	% mortality at different concentrations			LD <sub>50</sub> (μg/mL)
	1000 μg/mL	100 μg/mL	10 μg/mL	
<i>R. muricata</i> (methanol extract)	45 ± 1.92	22 ± 2.21	10 ± 0.11	>1000
<i>M. vulgare</i> (methanol extract)	60 ± 1.87	35 ± 1.39	12 ± 1.18	>1000

TABLE 8: Heavy metal concentrations (mg/kg) of *R. muricata* and *M. vulgare* (methanol extract).

Samples	Zn	Cu	Cr	Mn	Pb	As	Cd	Cr
<i>R. muricata</i>	8.91 ± 0.02	1.98 ± 0.90	1.02 ± 0.02	0.91 ± 0.01	ND	ND	ND	ND
<i>M. vulgare</i>	5.42 ± 0.03	2.37 ± 0.12	1.91 ± 0.03	0.52 ± 0.03	ND	ND	ND	ND

species, namely, *Juniperus communis*, *Ocimum basilicum*, and *Commiphora opobalsamum* were collected from Saudi Arabia where Pb and Cd were not detected [35], which is an agreement with our findings. Concentration of Cr between 5 and 30 mg kg<sup>-1</sup> is measured serious for the plants and can affect the plant by curbing its yield. It is vital to show that lead is very hazardous both for plants and animals, especially humans. The maximum acceptable limit for food stuff is 1 mg kg<sup>-1</sup> [36]. The poisonous effects of these heavy metal are because of their hindrance with the regular body biochemistry in normal metabolic processes. Usually, Cr and arsenic are the heavy metals most often concerned in morbidity and death [37]. Likewise, the plant metabolites are fundamental phytoconstituents that display a few observable impacts in the human body. Flavonoids and alkaloids possess strong antioxidant, anticancer, and antimalarial activities. Steroids are very vital class of alcohols with variable implication. The structures are so appropriate to be efficiently transformed by the microbial activities to commercially valued constituents; otherwise, it is hard to synthesize [38]. The presence of alkaloid and tannin contents in *R. muricata* was also quantitatively and qualitatively confirmed by another study [39]. Though, till date, very fewer biological investigations have been made with *R. muricata*, *Reseda* species have been described to hold numerous biological potential such as antimicrobial, antioxidant, and anti-inflammatory, which agree with our findings. The presence of steroids in all extracts modeled a limitless anticipation. The saponins are also identified as the soap forming constituents and are commercially significant [40]. The extracts displayed a good variety of dose-reliant antimicrobial actions against the tested pathogenic fungi and bacteria. So, this plant may be useful for the preparation of broad-spectrum antibacterial drugs. To summarize, this study is a decent help for diverse folklore usages of plants, but still needed a broad study and care because different geographical conditioned may affect the heavy metal contents as well as phytochemical parameters.

#### 4. Conclusion

Traditionally, both plant species have many biological potentials. Numerous phytoconstituents, counting tannins, steroids, alkaloids, phenol, saponin, and flavonoid, are

present in methanol extract of *R. muricata* and *M. vulgare*. The presence of heavy metals such as Zn, Cu, Cr, and Mn are in permissible limits. The paper disc diffusion test displayed some significant antimicrobial effectiveness compared to the standard antibiotics. Antioxidant effectiveness possessed by a plant is certain to keep the free radicals in the body and scavenge them if they are high and a very excellent protector to DNA. Hence, this study recommended further investigation to isolate new bioactive compounds from *R. muricata* and *M. vulgare*.

#### Data Availability

The data used to support this study are included within the article.

#### Conflicts of Interest

The authors declare that they have no conflicts of interest.

#### Acknowledgments

The authors wish to thank researcher supporting project number (RSP-2021/110) at King Saud University, Riyadh, Saudi Arabia, for financial support.

#### References

- [1] R. Islam, A. S. M. A. Reza, A. A. K. Chawdhury, J. Uddin, and K. Farhana, "Evaluation of in vitro antioxidant activity and cytotoxicity of mButanolic extract of *Sidacordata* leaves," *International Journal of Biological & Pharmaceutical Research*, vol. 5, no. 2, pp. 196–200, 2014.
- [2] Y. Hara-Kudo, A. Kobayashi, Y. Sugita-Konishi, and K. Kondo, "Antibacterial activity of plants used in cooking for aroma and taste," *Journal of Food Protection*, vol. 12, no. 5, pp. 2820–2824, 2004.
- [3] D. Liu, Z. Hu, Z. Liu, B. Yang, W. Tu, and L. Li, "Chemical composition and antimicrobial activity of essential oil isolated from the cultured mycelia of *Ganoderma japonicum*," *Journal of Nanjing Medical University*, vol. 23, no. 3, pp. 168–172, 2009.
- [4] M. A. M. Maciel, A. C. Pinto, V. F. Veiga, N. F. Grynberg, and A. Echevarria, "Plantas medicinais: a necessidade de estudos multidisciplinares," *Química Nova*, vol. 25, no. 3, pp. 429–438, 2002.









- [5] M. M. Cowan, "Plant products as antimicrobial agents," *Clinical Microbiology Reviews*, vol. 12, no. 4, pp. 564–582, 1999.
- [6] R. Dabur, A. Gupta, T. K. Mandal et al., "Antimicrobial activity of some Indian medicinal plants," *African Journal of Traditional, Complementary and Alternative Medicines*, vol. 4, no. 3, pp. 313–318, 2007.
- [7] A. Zulqarnain, A. Rahim, K. Ahmad, F. Ullah, H. Ullah, and U. Nishan, "In vitro Antibacterial activity of selected medicinal plants from lower Himalayas," *Pakistan Journal of Pharmaceutical Sciences*, vol. 28, no. 2, pp. 581–587, 2015.
- [8] E. A. Brisibe, U. E. Umoren, F. Brisibe et al., "Nutritional characterisation and antioxidant capacity of different tissues of *Artemisia annua* L.," *Food Chemistry*, vol. 115, no. 4, pp. 1240–1246, 2009.
- [9] A. Karadeniz, I. Cinbilgel, S. Gun, and A. Cetin, "Antioxidant activity of some Turkish medicinal plants," *Natural Product Research*, vol. 29, pp. 1–5, 2015.
- [10] S. Pisutthanan, P. Plianbangchang, N. Pisutthanan, S. Ruanruay, and O. Muanrit, "Brine shrimp lethality activity of Thai medicinal plants in the family Meliaceae," *Naresuan University Journal*, vol. 12, no. 2, pp. 13–18, 2004.
- [11] H. Bhattacharya, Q. Xiao, and L. Lun, "Toxicity studies of nonylphenol on rosy barb (*Puntius conchonioides*): a biochemical and histopathological evaluation," *Tissue and Cell*, vol. 40, no. 4, pp. 243–249, 2008.
- [12] N. H. El-Sayed, N. M. Omara, A. K. Yousef, A. M. Farag, and T. J. Mabry, "Kaempferol triosides from *Reseda muricata*," *Phytochemistry*, vol. 57, no. 4, pp. 575–578, 2001.
- [13] M. Rezgui, M. Basma, N. Neng, J. M. Nogueira, L. Bettaieb Ben-Kaab, and M. E. Machado Araújo, "Evaluation of *marrubium vulgare* growing wild in Tunisia for its potential as a dietary supplement," *Foods*, vol. 10, no. 11, Article ID 2864, 2021.
- [14] R. Ullah, A. S. Alqahtani, O. M. A. Noman, A. M. Alqahtani, S. Ibenmoussa, and M. Bourhia, "A review on ethno-medicinal plants used in traditional medicine in the Kingdom of Saudi Arabia," *Saudi Journal of Biological Sciences*, vol. 27, no. 10, pp. 2706–2718, 2020.
- [15] N. Chaachouay, O. Benkhniq, M. Fadli, H. El Ibaoui, and L. Zidane, "Ethnobotanical and ethnopharmacological studies of medicinal and aromatic plants used in the treatment of metabolic diseases in the Moroccan Rif," *Heliyon*, vol. 5, no. 10, Article ID e02191, 2019.
- [16] M. Aćimović, K. Jeremić, N. Salaj et al., "*Marrubium vulgare* L.: a phytochemical and pharmacological overview," *Molecules*, vol. 25, no. 12, Article ID 2898, 2020.
- [17] A. S. Alqahtani, R. Ullah, and A. A. Shahat, "Bioactive constituents and toxicological evaluation of selected antidiabetic medicinal plants of Saudi Arabia," *Evidence-based Complementary and Alternative Medicine*, vol. 2022, Article ID 7123521, 23 pages, 2022.
- [18] A. Shad, S. Ahmad, R. Ullah et al., "Phytochemical and biological activities of four wild medicinal plants," *The Scientific World Journal*, vol. 2014, Article ID 857363, 7 pages, 2014.
- [19] B. S. Abhijit and R. M. Yogini, "Phytochemical analysis and antibacterial properties of some Indian medicinal plants," *International Journal of current Microbiology and Applied sciences*, vol. 4, no. 3, pp. 228–235, 2015.
- [20] H. Iqbal, K. MoneeburRahman, U. Riaz et al., "Phytochemical screening and antimicrobial activities of selected medicinal plants of Khayberpaktunkhwa Pakistan," *African Journal of Pharmacy and Pharmacology*, vol. 5, no. 6, pp. 746–750, 2011.
- [21] R. Umbreen, K. R. Muhammad, J. Shumila, B. Jasia, and S. A. Naseer, "Assessment of phytochemicals, antimicrobial and cytotoxic activities of extract and fractions from *Fagoniaolivieri* (Zygophyllaceae)," *BioMed Central complementary and alternative medicine*, vol. 13, p. 167, 2013.
- [22] M. S. El-Abyad, N. M. Morsi, D. A. Zaki, and M. T. Shaaban, "Preliminary screening of some Egyptian weeds for antimicrobial activity," *Microbios*, vol. 62, pp. 47–57, 1990.
- [23] A. J. Aldesanmi, A. Sofowora, and J. D. Leary, "Preliminary biological and phytochemical investigation of two Nigerian medicinal plants," *International Journal of crude drugs Res*, vol. 24, pp. 147–153, 1986.
- [24] G. F. S. Al-Saleh, A. Y. Gamal El-Din, J. A. Abbas, and N. A. Saeed, "Phytochemical and biological studies of medicinal plants in Bahrain: the family chenopodiaceae-Part 2," *International Journal of Pharmacognosy*, vol. 35, no. 1, pp. 38–42, 1997.
- [25] B. Mahesh and S. Satish, "Antimicrobial activity of some important medicinal plant against plant and human pathogens," *World Journal of Agricultural Sciences*, vol. 4, pp. 839–843, 2008.
- [26] C. F. Bagamboula, M. Uyttendaele, and J. Debevere, "Antimicrobial effect of spices and herbs on *Shigella sonnei* and *Shigella flexneri*," *Journal of Food Protection*, vol. 66, no. 4, pp. 668–673, 2003.
- [27] R. Dall'Agnol, A. Ferraz, and A. P. Bernardi, "Antimicrobial activity of some *Hypericum* species," *Phytomedicine*, vol. 10, pp. 511–516, 2003.
- [28] M. Al-Fatima, M. Wurster, G. Schroder, and U. Lindequist, "Antioxidant, antimicrobial and cytotoxic activities of selected medicinal plants from Yemen," *Journal of Ethnopharmacology*, vol. 11, pp. 657–666, 2007.
- [29] R. Ullah, M. S. Alsaid, A. A. Shahat et al., "Antioxidant and hepatoprotective effects of methanolic extracts of zilla spinosa and hammada elegans against carbon tetrachlorideinduced hepatotoxicity in rats," *Open Chemistry*, vol. 16, no. 1, pp. 133–140, 2018.
- [30] M. O. Ullah, M. Haque, K. F. Urmi et al., "Anti-bacterial activity and brine shrimp lethality bioassay of methanolic extracts of fourteen different edible vegetables from Bangladesh," *Asian Pacific journal of tropical biomedicine*, vol. 3, no. 1, pp. 1–7, 2013.
- [31] W. Khan, S. Subhan, D. Farhan Shams et al., "Antioxidant potential, phytochemicals composition, and metal contents of *datura alba*," *BioMed Research International*, vol. 2019, Article ID 2403718, 8 pages, 2019.
- [32] A. Chehregani, F. Mohsenzade, and F. Vaezi, "Introducing a new metal accumulator plant and the evaluation of its ability in removing heavy metals," *Toxicological and Environmental Chemistry*, vol. 91, no. 6, pp. 1105–1114, 2009.
- [33] J. P. Dzoyem and J. N. Eloff, "Anti-inflammatory, anticholinesterase and antioxidant activity of leaf extracts of twelve plants used traditionally to alleviate pain and inflammation in South Africa," *Journal of Ethnopharmacology*, vol. 160, no. 3, pp. 194–201, 2015.
- [34] J. Mohmand, S. A. M. A. S. Eqani, M. Fasola et al., "Human exposure to toxic metals via contaminated dust: bio-accumulation trends and their potential risk estimation," *Chemosphere*, vol. 132, pp. 142–151, 2015.
- [35] I. A. Maghrabi, "Determination of some mineral and heavy metals in Saudi Arabia popular herbal drugs using modern techniques," *African journal of Pharmacy and Pharmacology*, vol. 8, no. 36, pp. 893–898, 2014.



- [36] N. M. Abd Ei-Salam, I. Hussain, R. Ullah, S. Ahmad, and S. Khan, "Essential oil and heavy metals analysis of *Boerhaavia procumbens*," *Life Science Journal*, vol. 10, pp. 955–958, 2013.
- [37] H. N. Bhatti and R. A. Khera, "Biological transformations of steroidal compounds: a review," *Steroids*, vol. 77, no. 12, pp. 1267–1290, 2012.
- [38] R. A. Street, "Heavy metals in medicinal plant products - an African perspective," *South African Journal of Botany*, vol. 82, pp. 67–74, 2012.
- [39] S. S. Emam, "Comparative study of the alkaloidal and tannin contents of some *Reseda* species," *Journal of Applied Sciences Research*, vol. 6, pp. 888–896, 2010.
- [40] A. Phuyal, P. K. Ojha, B. Guragain, and N. K. Chaudhary, "Phytochemical screening, metal concentration determination, antioxidant activity, and antibacterial evaluation of *Drymaria diandra* plant," *Beni-Suef University Journal of Basic and Applied Sciences*, vol. 8, no. 1, p. 16, 2019.

## Research Article

# Cytoprotective Antioxidant, Anti-Inflammatory, and Antifibrotic Impact of Celery Seed Oil and Manuka Honey Against Cyclophosphamide-Induced Cystitis in Rabbits

**Ayman M. Mousa** <sup>1,2</sup> **Khaled S. Allemailem** <sup>1,3</sup> **Fahad A. Alhumaydhi** <sup>3</sup>  
**Faris Alrumaihi**<sup>3</sup> **Ahmad Almatroudi** <sup>3</sup> **Mohammad Aljasir** <sup>3</sup> **Ameen S. S. Alwashmi**<sup>3</sup>  
**Osamah Al Rugaie**<sup>4</sup> **Khaled E. A. Soliman**<sup>4,5</sup> **Abdullah S. M. Aljohani** <sup>6</sup>  
**Waleed Al Abdulmonem**<sup>7</sup> **Ahmed A. Ahmed**<sup>8</sup> **Arif Khan**<sup>1</sup> **Masood A. Khan**<sup>1</sup>  
**Naif AlSuhaymi**<sup>9</sup> **Mahdi H. Alsugoor**<sup>9</sup> **Wafa Abdullah Al-Megrin**<sup>10</sup> and  
**Abulmaaty M. Elsayed**<sup>11,12</sup>

<sup>1</sup>Department of Basic Health Sciences, College of Applied Medical Sciences, Qassim University, Buraydah 51452, Saudi Arabia

<sup>2</sup>Department of Histology and Cell Biology, Faculty of Medicine, Benha University, Benha 13518, Egypt

<sup>3</sup>Department of Medical Laboratories, College of Applied Medical Sciences, Qassim University, Buraydah 51452, Saudi Arabia

<sup>4</sup>Department of Basic Medical Sciences, College of Medicine and Medical Sciences, Qassim University, Unaizah 51452, Saudi Arabia

<sup>5</sup>Department of Forensic Medicine and Clinical Toxicology, Faculty of Medicine, Sohag University, Sohag 82524, Egypt

<sup>6</sup>Department of Veterinary Medicine, College of Agricultural and Veterinary Medicine, Qassim University, Buraydah 51452, Saudi Arabia

<sup>7</sup>Department of Pathology, College of Medicine, Qassim University, Buraydah 51452, Saudi Arabia

<sup>8</sup>Research Center, College of Medicine, Qassim University, Buraydah 51452, Saudi Arabia

<sup>9</sup>Department of Emergency Medical Services, Faculty of Health Sciences, AlQunfudah, Umm Al-Qura University, Makkah 21912, Saudi Arabia

<sup>10</sup>Department of Biology, Faculty of Science, Princess Nourah Bint Abdulrahman University, Riyadh 11671, Saudi Arabia

<sup>11</sup>Department of Anatomy and Histology, Faculty of Medicine, Mutah University, Mutah, Jordan

<sup>12</sup>Department of Anatomy and Embryology, Faculty of Medicine, Benha University, Benha 13518, Egypt

Correspondence should be addressed to Ayman M. Mousa; [a.mousa@qu.edu.sa](mailto:a.mousa@qu.edu.sa)

Received 19 January 2022; Accepted 1 March 2022; Published 17 March 2022

Academic Editor: Sekar Vijayakumar

Copyright © 2022 Ayman M. Mousa et al. This is an open access article distributed under the Creative Commons Attribution License, which permits unrestricted use, distribution, and reproduction in any medium, provided the original work is properly cited.

Patients treated with cyclophosphamide (CP) usually suffer from severe hemorrhagic cystitis (HC). Our previous study exhibited that mesna + celery cotherapy partially ameliorated HC. Therefore, there is a substantial need to seek alternative regimens to get complete protection against CP-induced HC. The current study investigated the effects of mesna + celery seed oil (MCSO) or mesna + manuka honey (MMH) cotherapy against CP-induced HC in adult male rabbits. The forty rabbits were divided into four equal groups and treated for three weeks. The control group (G1) received distilled water and the second group (G2) received CP (50 mg/kg/week). The third group (G3) received CP + MCSO (CPMCSO regimen), and the fourth group (G4) received CP + MMH (CPMMH regimen). The urinary bladder (UB) specimens were processed to evaluate UB changes through histopathological, immunohistochemical, ultrastructural, and biochemical investigations. In G2, CP provoked HC features (urothelial necrosis, ulceration, and sloughing), UB fibrosis, and TNF- $\alpha$  immunoexpression. Besides, CP reduced the activity of antioxidant enzymes (GPx1, SOD3, and CAT) and elevated the serum levels of NF- $\kappa$ B, TNF- $\alpha$ , IL-1B, and IL-6 cytokines in G2 rabbits. In contrast, the CPMMH regimen caused significant increments of UB protection against HC in G4 rabbits compared to the partial protection by the CPMCSO regimen in G3. Therefore, our study indicated for the first time that the novel CPMMH regimen resulted in complete UB protection against CP-induced HC via combined antioxidant, anti-inflammatory, and antifibrotic properties.

## 1. Introduction

Cyclophosphamide (CP) is an effective antineoplastic drug, which unfortunately causes multiple side effects such as hemorrhagic cystitis (HC), delayed wound healing, and nephropathy in CP-treated patients [1]. The incidence of HC in those patients may reach up to 75%, with several symptoms including frequency, dysuria, suprapubic pain, and hematuria. CP is metabolized into acrolein (urotoxic hepatic metabolite) by hepatic microsomal hydroxylation to be excreted by both kidneys into the urinary bladder (UB) [2]. Direct urothelial contact with acrolein plays a significant role in HC pathogenesis, which induces a prominent UB inflammation. Acrolein usually induces urothelial apoptosis, necrosis, and damage with subsequent ulceration of the UB [3]. Increased oxidative stress results from increased reactive oxygen species (ROS) and reactive nitrogen species (RNS) production or decreased antioxidant defense mechanisms [4]. Acrolein induces the production of numerous ROS such as hydrogen peroxide ( $H_2O_2$ ), malondialdehyde (MDA), superoxide ( $O_2^-$ ), and reduced glutathione (GSH). Besides, it enhances the formation of RNS such as peroxynitrite ( $ONOO^-$ ) from the combination of nitric oxide (NO) with  $O_2^-$  in the urothelial cells [5]. Therefore, the administration of CP usually evokes HC via overproduction of the ROS and RNS molecules, which cause UB inflammation. Cellular injury and necrosis of the UB involve several mechanisms, including lipid peroxidation of cellular membranes and DNA damage in the inflammatory areas [6]. Besides, the oxidative stress conditions induce the formation of nuclear factor kappa B (NF- $\kappa$ B), which enhances the transcription of tumor necrosis factor- $\alpha$  (TNF- $\alpha$ ), interleukin-1 $\beta$  (IL-1 $\beta$ ), and IL-6. These proinflammatory cytokines have been involved in HC pathogenesis by oxidizing the polyunsaturated fatty acids and inducing inflammation [7].

Mesna administration directly binds acrolein in the UB lumen and neutralizes it into an inert metabolite (thioether), passing safely in urine without damaging the urothelium [8]. Although it is effective for treating induced HC; however, it cannot wholly eradicate the challenging symptoms of HC in 25% of CP-treated cases [9]. Therefore, it is essential to involve other protective antioxidant agents such as celery seed oil (CSO) or manuka honey (MH) beside mesna to reduce the hazards of induced HC [10, 11]. Numerous studies focused on celery (*Apium graveolens*) and honey as effective antioxidants, which substantially reduced the cellular oxidative damage [12, 13]. Besides, their phytochemicals such as terpenoids, flavonoids, and phenolic acids could suppress the activity of proinflammatory cytokines [14].

Celery emerges as one of the most prestigious edible plants, which elicits the attention of researchers as a safe, cheap, and valid phytochemical vegetable growing mainly around the Mediterranean Sea and in Europe [15]. It belongs to the parsley family and usually acts as an effective remedy against numerous inflammatory diseases such as bronchitis, bronchial asthma, arthritis, and hepatitis [16–18]. At the same time, celery has a substantial role in inhibiting appetite,

reducing body weight, and preventing hypertension through its diuretic, antioxidant, and anti-inflammatory properties [12, 19].

In contrast, honey possesses powerful wound healing properties and prevents infections for long periods as it offers antimicrobial activity, immunomodulatory properties, and protection against wound infections [20, 21]. The monofloral MH is derived from the manuka tree and has numerous biological properties, including antioxidant, antimicrobial, and anti-inflammatory activities [22]. Regarding the dominant constituents in MH, there are high levels of flavonoids and phenolic acids (glyoxal, benzoic acid, leptosin, quercetin, and chrysin) [23]. A recent study attributed the beneficial nutritional and antioxidant effects of MH to these bioactive polyphenolics and flavonoids [24]. Besides, MH has a high potent antibacterial activity against *Staphylococcus epidermidis*, *Staphylococcus aureus*, and *Streptococcus pyogenes* due to its potential contents of peptides (abaecin), proteins (royalisin), and lysozymes [25]. Henceforth, MH has been employed as a powerful wound-healing remedy for combating various types of infections, including burns, traumatic wounds, and ulcers [26]. Our aim in the current study was to investigate the effectiveness of two novel regimens (CP + mesna + CSO (CPMCSO regimen) and CP + mesna + MH (CPMMH regimen)) against CP-induced HC in an experimental model of rabbits and to evaluate which one of the proposed regimens is more effective against HC.

## 2. Materials and Methods

**2.1. Drugs and Chemicals.** CP (Cytosan vials 500 mg) and mesna ampoules (uromitexan 400 mg) were obtained from Baxter Healthcare Company (Illinois, USA). The CSO bottles (30 mL) were purchased from Sameera Fragrance (New Delhi, India). The manufacturer extracted the oil by the steam distillation process. The main isolated natural products from the CSO included limonene, sedanolide, and 3-n-butyl phthalide, which give the characteristic odor of celery [27]. The MH bottles (250 gm) were purchased from Airborne Company (Canterbury, New Zealand). The ELISA kits of GPx1 (ABIN774992), SOD3 (ABIN6959756), CAT (ABIN628258), NF- $\kappa$ B (ABIN775386), TNF- $\alpha$  (ABIN6574142), IL-1B (ABIN6999391), and IL-6 (ABIN6957175) were purchased from antibodies-online GmbH (Aachen, Germany).

**2.2. Animals and Study Design.** Forty adult male, New Zealand rabbits were acclimatized for one week before the commencement of the current experimental study to induce a model of HC. The rabbits' age was 12 weeks, their weight was 1.4–2 kg, and they were fed a standard balanced diet *ad libitum* in metal cages at 24°C. The rabbits were divided into four groups ( $n = 10$ ) and treated for three weeks. The study protocol and procedures were approved by the Institutional Research Ethics Committee of Qassim University (Cams1-2019-2-2-I-5467), conducted following the National

Institutes of Health guide for the care and use of laboratory animals (NIH publications no. 8023, revised 1978), and complied with the ARRIVE guidelines [12]. As depicted in Figure 1, the control group (G1) received an orogastric distilled water (2 mL/kg/day), and the second group (G2) received an intraperitoneal injection (IPI) of CP (50 mg/kg/week) to induce HC [11, 28]. The CPMCSO regimen group (G3) received an IPI of CP (50 mg/kg/week) and 21 mg of mesna/kg/week plus 50  $\mu$ L of CSO/kg/day orally [29–31]. The CPMMH regimen group (G4) received an IPI of CP (50 mg/kg/week) and 21 mg of mesna/kg/week plus 1 gm of MH/kg/day orally [25].

The rabbits were anesthetized with an intramuscular injection of xylazine (6 mg/kg) and ketamine (70 mg/kg) by a professional veterinary doctor to minimize pain, anxiety, and distress effects to the animals. Once the animals became unconscious, a percutaneous intracardiac 19-gauge needle attached to a 20 mL syringe was inserted between the ribs (at the most robust heartbeat) to get blood samples for the various biochemical investigations. Then, the rabbits were euthanized by cervical decapitation to obtain UB specimens for investigating the effectiveness of CPMCSO or CPMMH regimen against CP-induced HC [32]. After ensuring death, the euthanized rabbits were disposed of appropriately following the National Research Council (USA) Guide for the Care and Use of Laboratory Animals [33]. The histopathological (HP), immunohistochemical (IHC), scanning electron microscope (SEM), and biochemical investigations were performed, as described in our previous study [34].

**2.3. Grading of Macroscopic Hematuria by the Urine Visual Color Test.** The visual color scale of the Hemostick test was used to grade the extent of hematuria from 0 to 5 in the urine samples of all groups, as described by Lee et al. [35].

**2.4. Examining the HP Structure of UB.** Small UB specimens from each rabbit were processed to get thin (4  $\mu$ m) paraffin sections suitable for staining with H&E and Masson trichrome stains, as described by Hussien et al. [36]. The UB general structure was evaluated, and the degree of UB damage (ulceration and sloughing) was rated from 0 to 3 (no, mild, moderate, and severe) by a pathologist who did not know the sequence of groups [12].

**2.5. Measurement of TNF- $\alpha$  Immunoexpression (IE) in the UB.** The UB sections were stained by the streptavidin-biotin peroxidase technique to detect the TNF- $\alpha$  IE in the UB tissues according to the manufacturer's protocol, as described by Mousa et al. [37].

**2.6. Examining the UB Ultrastructure.** The UB mucosal surface was examined by the SEM to evaluate the degree of UB ulceration and sloughing. Small specimens from each UB

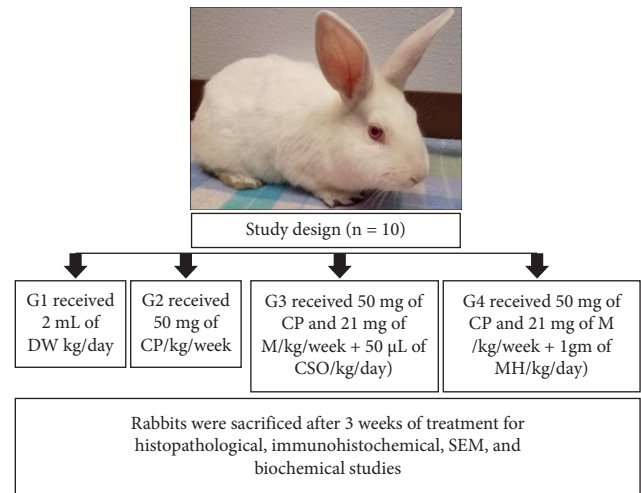


FIGURE 1: Schematic illustration of the experimental design. The control group (G1) received distilled water (DW), and the second group (G2) received cyclophosphamide (CP). The third group (G3) received CP + mesna (M) + celery seed oil (CSO) = CPMCSO regimen group. The fourth group (G4) received CP + M + manuka honey (MH) = CPMMH regimen group.

were processed to obtain thin sections of UB suitable for SEM examination as described by Poveda et al. [38].

**2.7. Morphometric Study.** “The digital CMOS, TC5PRO camera on a light microscope (Jinan, China) was used to photograph ten fields from the UB sections of each rabbit at magnification 200X to evaluate the UB structure in all groups. Besides, all sections underwent image analysis by ImageJ V1.50i (NHI/USA) to measure the UB ulcer's size and the area percentage of collagen fibers (CFs) deposition and TNF- $\alpha$  IE in the UB/10 fields” [12].

**2.8. Biochemical Measurement of the Antioxidant Enzymes and Proinflammatory Cytokines.** The serum levels of antioxidant enzymes (GPx1, SOD3, and CAT) and proinflammatory cytokines (NF- $\kappa$ B, TNF- $\alpha$ , IL-1B, and IL-6) were investigated to elucidate the effectiveness of CPMCSO and CPMMH regimens against HC. Blood sample centrifugation was conducted at 3000 rpm for 15 minutes to get serum samples stored at  $-20^{\circ}$ C for the colorimetric assay according to the manufacturer's protocol, as described by Mousa and Aldebasi [39].

**2.9. Statistical Analysis of Data.** The mean (M)  $\pm$  standard deviation (SD) of the data was analyzed statistically by the SPSS software program (IBM, USA), and the one-way ANOVA test followed by LSD was performed to evaluate the intergroup comparisons. At first, the normality tests (skewness and Kurtosis) were performed and revealed the normal data distribution.  $P \leq 0.05$  indicated statistically significant results. The GraphPad Prism software version 6.0



(GraphPad Software Inc., San Diego, CA) was used to create graphs of the analyzed data [12, 40].

### 3. Results

**3.1. CPMCSO and CPMMH Effects on the Macroscopic Hematuria Scale of UB.** Figure 2 exhibited a significant ( $P \leq 0.05$ ) elevation of the hematuria scale in G2 compared with G1 and G4 rabbits. In contrast, G4 revealed a significant ( $P \leq 0.05$ ) reduction of the hematuria scale compared with G3 rabbits.

**3.2. CPMCSO and CPMMH Effects on the UB Structure.** Figure 3 revealed a typical structure of the UB in G1 and G4 rabbits, elucidating a wholly protective role of the CPMMH regimen against HC in G4. In contrast, G2 exhibited an obvious abnormality of UB structure (urothelial vacuolar degeneration, ulceration, and sloughing) compared with G1, elucidating the harmful effects of CP on the UB of G2 rabbits. Besides, G3 revealed mild erosion and ulceration of the urothelium compared with G2, elucidating the partial protective role of the CPMCSO regimen against HC in G3 rabbits. Statistical analysis of the urothelial ulcer's size confirmed the appearance of HC in G2 compared with G1 and G4 rabbits.

**3.3. CPMCSO and CPMMH Effects on CF Deposition in the UB.** Figure 4 exhibited average deposition of CF in G1 and G4 rabbits, indicating the protective role of the CPMMH regimen against HC and UB fibrosis in G4. In contrast, G2 and G3 rabbits revealed urothelial ulceration and moderate CF deposition in the UB, indicating substantial UB fibrosis in both groups.

**3.4. CPMCSO and CPMMH Effects on TNF- $\alpha$  IE in the UB.** Figure 5 exhibited mild TNF- $\alpha$  IE in the UB of G1 and G4 rabbits, elucidating complete anti-inflammatory protection against HC by the CPMMH regimen in G4. In contrast, G2 and G3 revealed marked urothelial TNF- $\alpha$  IE, indicating a weak anti-inflammatory protective effect of the CPMCSO regimen on the UB of G3 rabbits.

**3.5. CPMCSO and CPMMH Effects on the Urothelial Ultrastructure.** SEM examination revealed the typical urothelial structure of G1 and G4 in Figure 6, indicating wholly urothelial protection by the CPMMH regimen in G4. In contrast, the urothelial ulcers were significantly increased in G2 (confirming urothelial ulceration) compared with G4 and significantly reduced in G4 compared with G3 (elucidating a partial protective role of the CPMCSO regimen on the urothelium of G3).

**3.6. CPMCSO and CPMMH Effects on the Activity of Antioxidant Enzymes.** Figure 7 revealed significant reductions in the activity of antioxidant enzymes (GPx1, SOD3, and CAT), indicating a marked induction of oxidative stress by CP administration in G2 compared with G1 and G4. In contrast,

the antioxidant activity significantly increases by the CPMMH regimen in G4 compared with G3, indicating the potent antioxidant activity of the CPMMH regimen against HC in G4 compared with the moderate antioxidant activity of the CPMMH regimen in G3.

**3.7. CPMCSO and CPMMH Effects on the Proinflammatory Cytokines.** Figure 8 reveals significantly elevated serum levels of proinflammatory cytokines (NF- $\kappa$ B, TNF- $\alpha$ , IL-1B, and IL-6) in G2 compared with G1 and G4, indicating the extensive induction of proinflammatory cytokines' production by CP administration in G2. In contrast, the CPMMH regimen caused marked reductions of the proinflammatory cytokines' levels, indicating its substantial anti-inflammatory effects on G4 compared with G3 rabbits.

### 4. Discussion

It is evident that CP-induced HC is mainly sparked by renal excretion of acrolein, which induces inflammatory reactions in the UB by enhancing the oxidative stress process and releasing the proinflammatory cytokines [28]. Therefore, finding a novel, safe, and selective therapeutic modality rich in antioxidants and anti-inflammatory agents is expected to be an enduring progression for avoiding HC. The CPMCSO and CPMMH regimens involve the coadministration of CP plus mesna and CSO or mesna and MH. Both regimens are rich in antioxidants and anti-inflammatory agents (bioactive flavonoids and polyphenols) [41].

Rabbits of the current study were treated with the CPMCSO or CPMMH regimen to determine which one of them is more protective against CP-induced HC. The main HP, IHC, and SEM features of HC appeared as urothelial degeneration, ulceration, and sloughing in G2, which were significantly attenuated with remarkable curative effects on HC by the CPMMH regimen in G4 compared with the CPMCSO regimen in G3 rabbits. Additionally, it was not surprising that CP induced a significant reduction of the antioxidant enzymes (GPx1, SOD3, and CAT) activity and significantly elevated the levels of proinflammatory cytokines (NF- $\kappa$ B, TNF- $\alpha$ , IL-1, and IL-6) in G2 compared with G1 and G4 rabbits. In contrast, the CPMMH regimen significantly elevated the antioxidants activity and significantly reduced the levels of proinflammatory cytokines in G4 compared with the CPMCSO regimen in G3 rabbits.

The pathogenesis of CP-induced HC could be explained by several studies, which reported that toxic acrolein metabolites directly contact the urothelium, induce the transcription of NF- $\kappa$ B factor, and activate the overproduction of intracellular ROS and RNS, leading to the marked formation of ONOO<sup>-</sup> [42, 43]. Besides, these substances influence the progression of HC by inducing lipid peroxidation, depleting numerous cellular proteins, and evoking the cascade of cellular proinflammatory mediators, with subsequent UB injury [44, 45]. Moreover, NO and ONOO<sup>-</sup> activation disrupts the UB integrity, exaggerates the oxidative stress process, and activates the inflammatory cells (especially

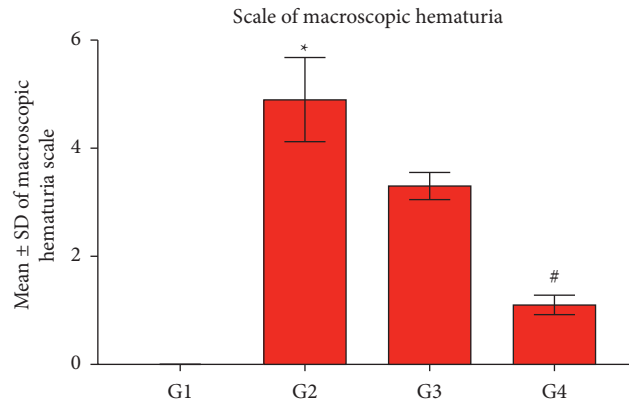


FIGURE 2: Statistical analysis of the macroscopic hematuria scale. The CP group (G2) exhibits a significant elevation of the hematuria scale compared with the control group (G1) and the CPMMH regimen group (G4). In contrast, G4 reveals a significant reduction of the hematuria scale compared with the CPMCSO regimen group (G3). \* $P \leq 0.05$  vs. G1 and G4 and # $P \leq 0.05$  vs. G3.

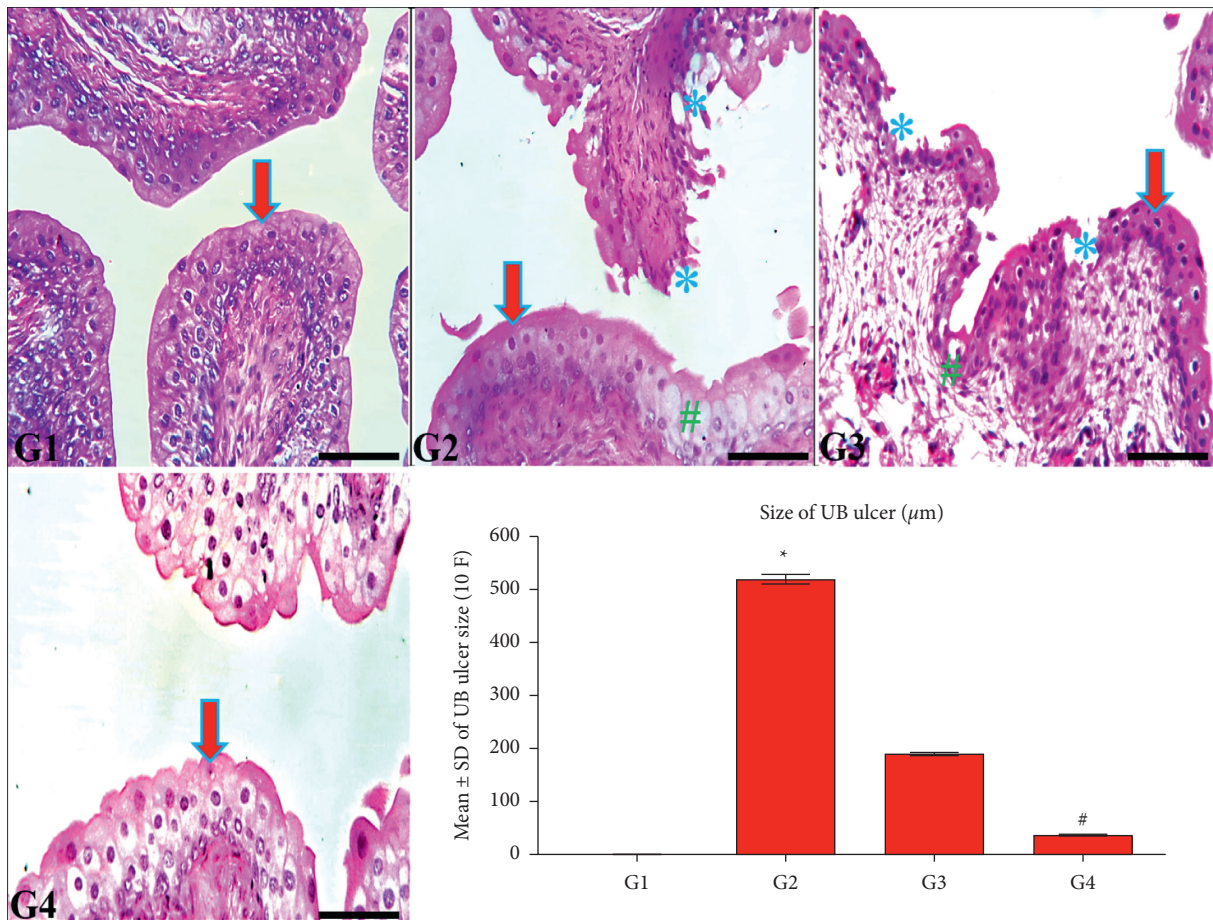


FIGURE 3: Histological structure of the urinary bladder (UB) in all groups. The UB of G1 and G4 rabbits show typical urothelial structure (arrow) compared with the marked urothelial vacuolar degeneration (#) and ulceration (\*) in G2 and G3. In contrast, G4 reveals a significant improvement of urothelial ulceration compared with G3. H&E; 200x, bar = 100 µm. Statistical analysis of the UB ulcer's size/10 fields (F). \* $P \leq 0.05$  vs. G1 and G4 and # $P \leq 0.05$  vs. G3.

macrophages), leading to potentiation of NF-κB expression and overproduction of the proinflammatory cytokines TNF-α, IL-1B, and IL-6 [46, 47].

On the other hand, mesna is transformed into dimesna, which is rapidly excreted in urine to create a nontoxic, inert

dimer (thioether) on the mucosal surface of UB by direct coupling of dimesna with acrolein [48]. Lack of mesna antioxidant and anti-inflammatory activity limits its effectiveness, leading to ineffective prevention of HC in 25% of cases treated with CP.



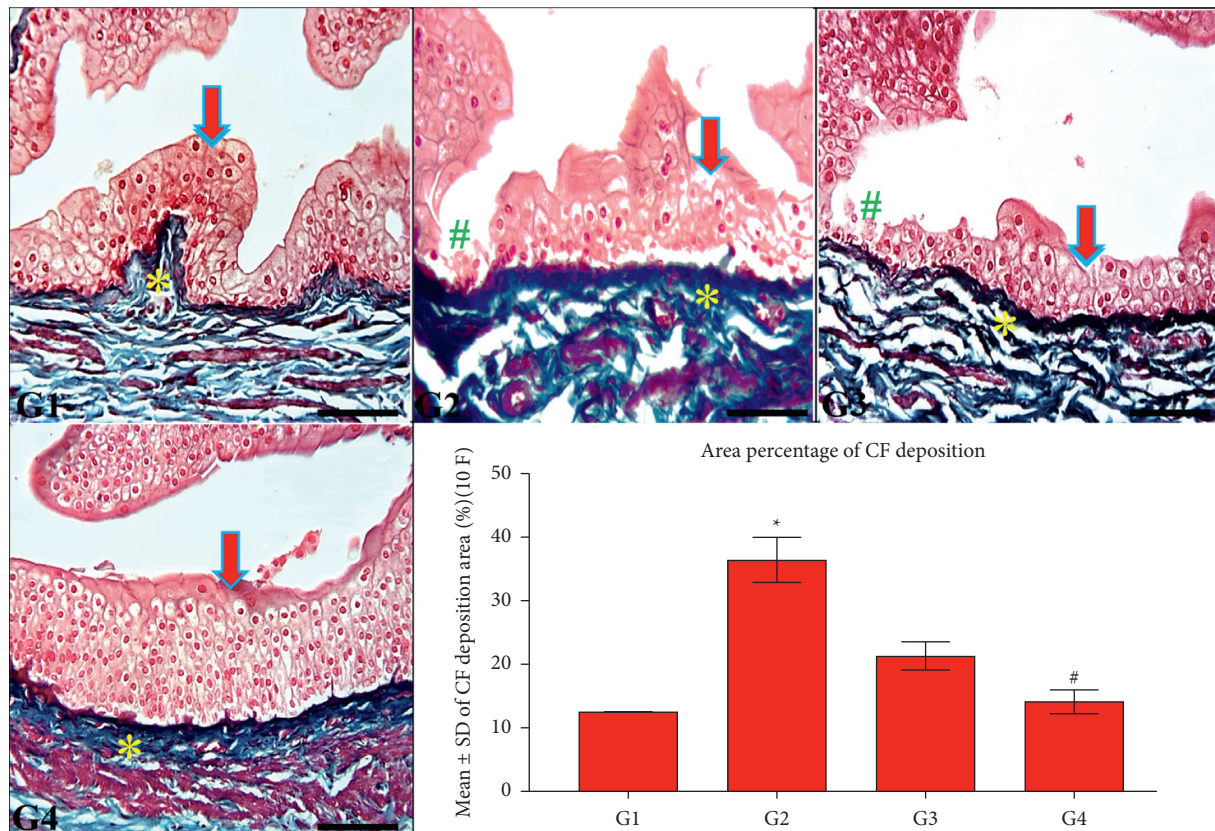


FIGURE 4: Collagen fibers (CF) deposition in the UB of all groups. G1 and G4 rabbits exhibit normal urothelial structure (arrow) and mild CF deposition (\*) in the UB. In contrast, the UB wall shows urothelial ulceration (#) and moderate CF deposition (\*) in G2 and G3 compared with G4 rabbits. Masson's trichrome; 200x, bar = 100  $\mu$ m. UB statistical analysis of CF deposition/10 (F) \* $P \leq 0.05$  vs. G1 and G4 and # $P \leq 0.05$  vs. G3.

Nowadays, numerous studies have proved that dietary modifications could become an essential adjuvant therapeutic line in minimizing UB damage by enhancing the antioxidative defense system, augmenting the anti-inflammatory effects, and abolishing the severity of UB damage [49]. Hence, numerous natural products such as celery and honey could be safe, effective, and cheap agents against HC due to their antioxidant and anti-inflammatory effects [50]. Therefore, a real need to coadministrate extra natural antioxidants and anti-inflammatory agents with mesna exists to enhance its protective role against HC. In the current work, we expected that coadministration of mesna with these agents could be a novel effective chemotherapeutic regimen for protection against CP-induced HC [51].

Indeed, the CSO has several active constituents with potent antioxidant and anti-inflammatory properties, including d-limonene, sedanolide, terpenoids, polyphenols, apiin, and apiuman [52, 53]. Therefore, the potential effects of these compounds improved the healing power of urothelium, enhanced the activity of antioxidant

enzymes (GPx1, SOD3, and CAT), and subsequently improved the CPMCSO regimen's efficacy against HC in G3 rabbits [14]. Besides, CSO has been ameliorated the damaged UB tissues via enhancing the scavenging power of free radicals and reducing the lipids peroxidation process [54, 55]. Additionally, the anti-inflammatory properties of CSO could be attributed to the inhibitory effects of apiin and apiuman against the expression of proinflammatory cytokines (NF- $\kappa$ B, TNF- $\alpha$ , IL-1B, and IL-6) [16].

On the other hand, several studies explained the healing power of MH via its various antioxidant, antimicrobial, and anti-inflammatory effects on the inflammatory response [56, 57]. The potent antioxidant capacity of MH in G4 rabbits could be attributed to its high contents of phenolic compounds, which modulate the free radical production and protect the cell components from the harmful effects of ROS [58]. At the same time, the diverse phenolic compounds and defensin-1 in MH may account for its potential antimicrobial effects [59]. Furthermore, the potent protective anti-inflammatory mechanisms of MH could be explained via the

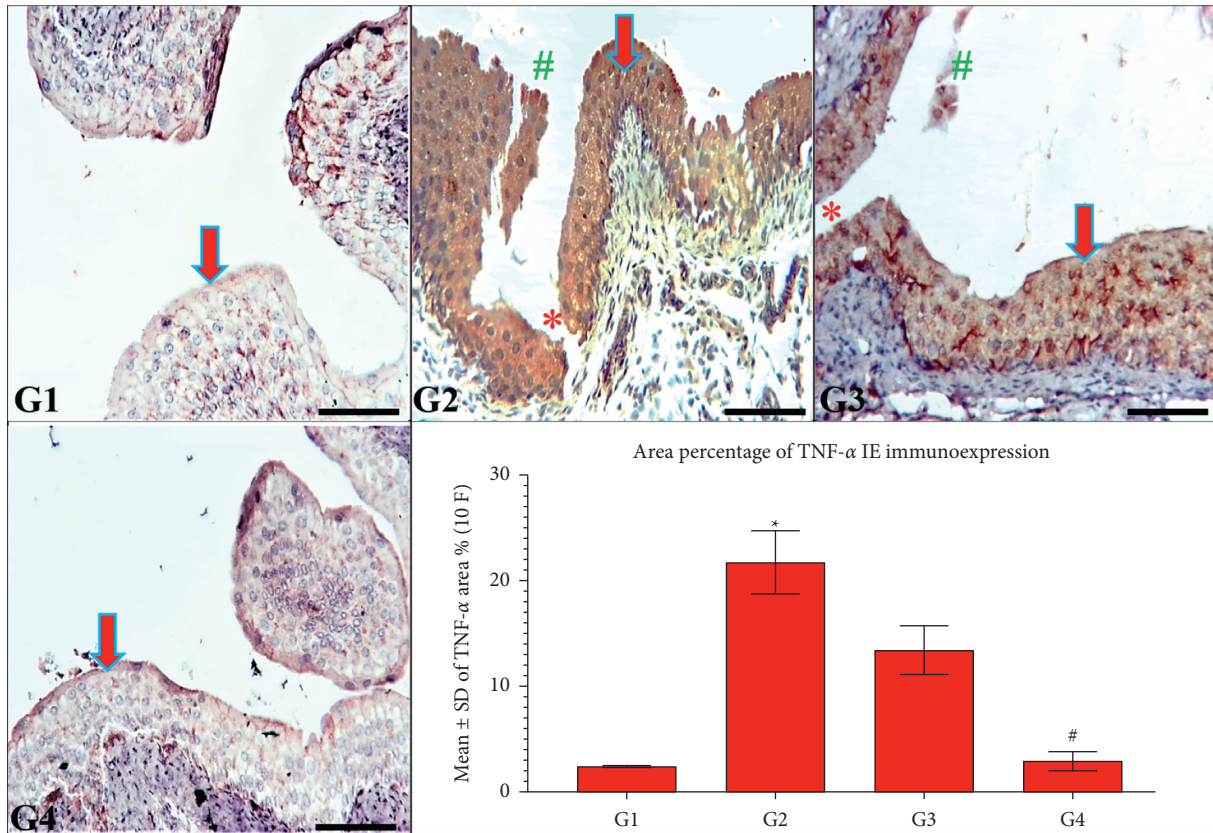


FIGURE 5: TNF- $\alpha$  immunoreactivity in the UB of all groups. G1 and G4 rabbits show typical UB structure and mild TNF- $\alpha$  IE (arrow). In contrast, G2 and G3 rabbits show urothelial ulceration (\*) and sloughing (#) with marked TNF- $\alpha$  IE (arrow) compared with G4 rabbits. TNF- $\alpha$  immunostain; 200x, bar = 100  $\mu$ m. Statistical analysis of TNF- $\alpha$  IE/10 (F) \*  $P \leq 0.05$  vs. G1 and G4 and #  $P \leq 0.05$  vs. G3.

suppression of inflammatory cells migration at the wound site, the reduction of proinflammatory cytokines (TNF- $\alpha$ , IL-1 $\beta$ , and IL-6) production, and the enhancement of fibroblasts proliferation, which improves the wound healing process [60].

To sum up, the CPMMH regimen significantly improves the antioxidants activity, reduces the NF- $\kappa$ B, TNF- $\alpha$ , IL-1 $\beta$ , and IL-6 activation, and ensures better protection of the UB in G4 rabbits compared with the partial protection against UB toxicity by the CPMCSO regimen in G3 rabbits.



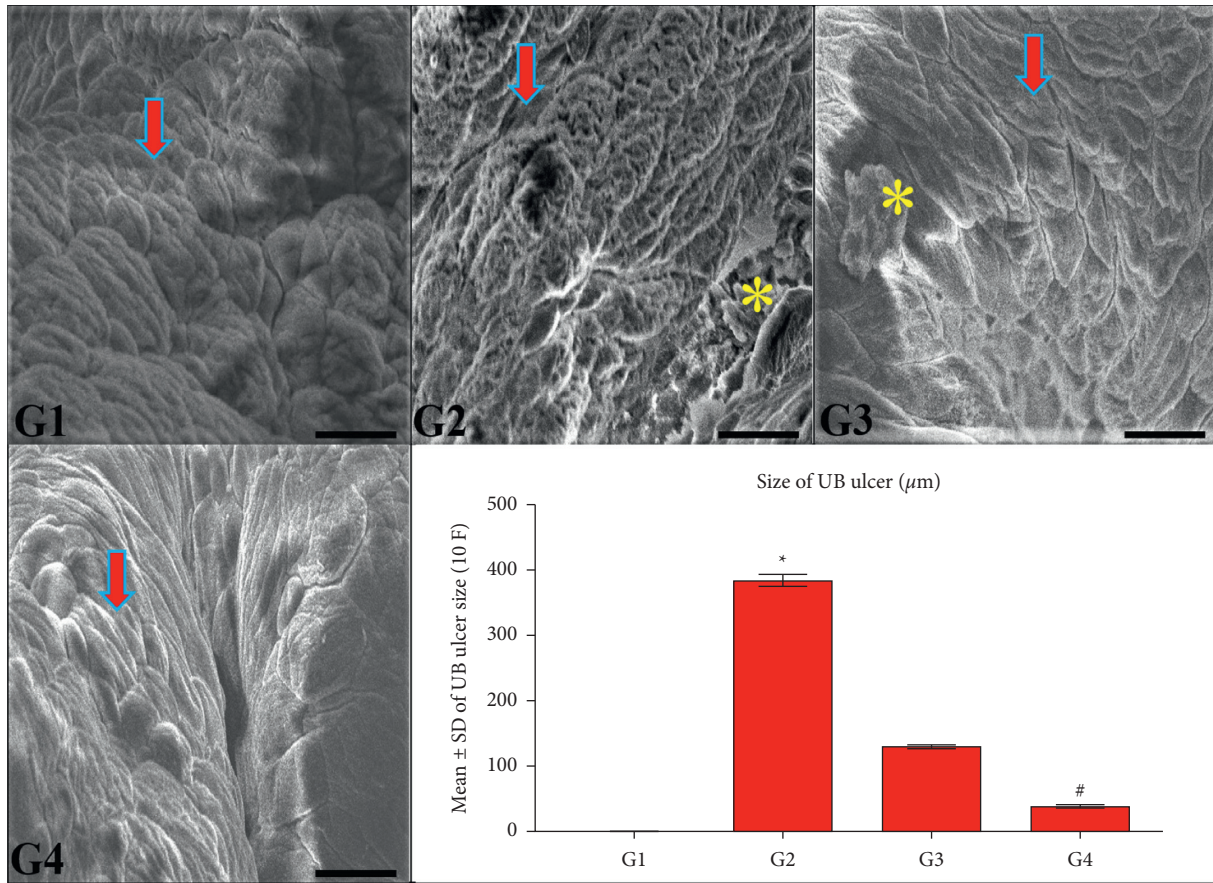


FIGURE 6: Ultrastructure of the urinary bladder’s (UB) urothelial surface in all groups. G1 and G4 show a standard urothelial surface structure (arrow). In contrast, the area percentage of urothelial ulcer (\*) significantly increases in G2 compared with G1 and G4. Besides, the urothelial ulcer significantly decreases in G4 compared with G3 (\*). SEM; 15 kv, 1000x, bar = 20 μm. Statistical analysis of the area percentage of urothelial ulcers. \* $P \leq 0.05$  vs. G1 and G4 and # $P \leq 0.05$  vs. G3.

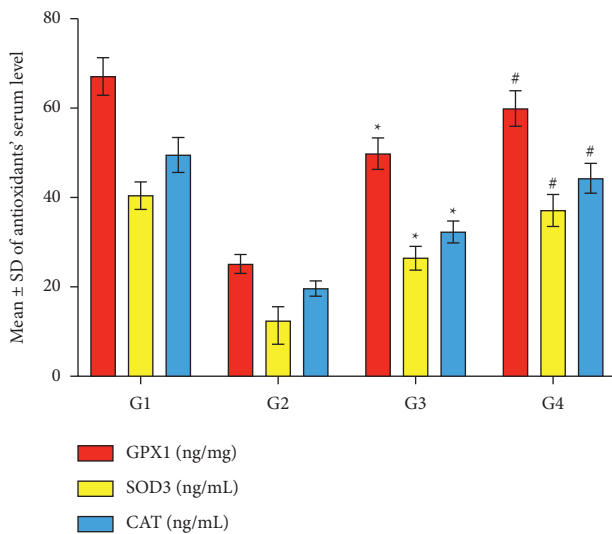


FIGURE 7: Statistical analysis of the antioxidant enzymes (GPx1, SOD3, and CAT) activity. G2 shows significant reductions in the antioxidant activity compared with G1 and G4. In contrast, the antioxidant activity shows significant elevation in G4 compared with G3. \* $P \leq 0.05$  vs. G1 and G4 and # $P \leq 0.05$  vs. G3.

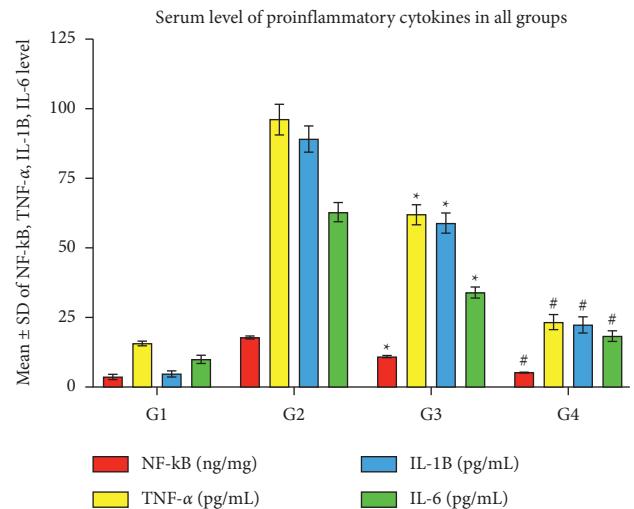


FIGURE 8: Statistical analysis of the proinflammatory cytokines (NF-κB, TNF-α, IL-1B, and IL-6). G2 shows significant elevations of the proinflammatory cytokines’ serum levels compared with G1 and G4. In contrast, G4 reveals significant reductions of the proinflammatory cytokines’ levels compared with G3. \* $P \leq 0.05$  vs. G1 and G4 and # $P \leq 0.05$  vs. G3.

## 5. Conclusion

The current study concludes that CP therapy induced apparent hazardous urothelial oxidative stress and impaired the healing process of UB, which developed HC and remarkably impeded the usage of CP against several neoplastic diseases. In contrast, the CPMMH regimen revealed marked improvement of the UB structure and caused lesser inflammation and ulceration of the urothelium. Additionally, it significantly improves the antioxidant activity of GPx1, SOD3, and CAT enzymes, reduces the NF- $\kappa$ B, TNF- $\alpha$ , IL-1B, and IL-6 cytokines activation, and ensures better protection of the UB in G4 rabbits compared with the partial protection against UB injury by the CPMCSO regimen in G3. Therefore, the CPMMH regimen seems to be more effective than the CPMCSO regimen for combating HC and could be a novel future cotherapy against CP-induced HC.

## Data Availability

All relevant data have been provided in the manuscript and supplementary material.

## Conflicts of Interest

The authors declare no conflicts of interest in this study. The funder had no role in the design, data collection, analyses, or interpretation of the study, writing the manuscript, or publishing the results.

## Authors' Contributions

A.M.M. conducted the conceptualization, funding acquisition, methodology, investigation, writing, review editing, supervision, and project administration. K.A., F.H., F.A., A.A., M.A., A.S.A., O.A., K.S., A.A., W.A., A.A., A.K., M.K., N.A., M.A., W.A., and A.M. conducted the investigation, resources, data curation, formal analysis, software validation, visualization, and writing of original draft. All authors have revised and agreed to the published version of the manuscript.

## Acknowledgments

The authors gratefully acknowledge Qassim University, represented by the Deanship of Scientific Research, on the financial support for this research under the number (Cams1-2019-2-2-I-5467) during the academic year 1440 AH/2019 AD.

## Supplementary Materials

The supplementary file includes highlights and a graphical abstract of the study. (*Supplementary Materials*)

## References

- [1] K. M. Sakthivel and C. Guruvayoorappan, "Acacia ferruginea inhibits cyclophosphamide-induced immunosuppression and urotoxicity by modulating cytokines in mice," *Journal of Immunotoxicology*, vol. 12, no. 2, pp. 154–163, 2015.
- [2] F. Patti and S. Lo Fermo, "Lights and shadows of cyclophosphamide in the treatment of multiple sclerosis," *Auto-immune Diseases*, vol. 2011, Article ID 961702, 14 pages, 2011.
- [3] I. Yildirim, A. Korkmaz, S. Oter, A. Ozcan, and E. Oztas, "Contribution of antioxidants to preventive effect of mesna in cyclophosphamide-induced hemorrhagic cystitis in rats," *Cancer Chemotherapy and Pharmacology*, vol. 54, no. 5, pp. 469–473, 2004.
- [4] E. N. Barut, S. Engin, B. Barut et al., "Uroprotective effect of ambroxol in cyclophosphamide-induced cystitis in mice," *International Urology and Nephrology*, vol. 51, pp. 803–810, 2019.
- [5] M. O. Islam, T. Bacchetti, and G. Ferretti, "Alterations of antioxidant enzymes and biomarkers of Nitro-oxidative stress in tissues of bladder cancer," *Oxidative Medicine and Cellular Longevity*, vol. 2019, Article ID 2730896, 10 pages, 2019.
- [6] O. Bayrak, I. Seckiner, M. Solakhan, M. Karakok, S. M. Erturhan, and F. Yagci, "Effects of intravesical dexamethasone on lipid peroxidation and bladder histology in a chemical cystitis animal model," *Urology*, vol. 79, no. 5, pp. 1023–1026, 2012.
- [7] E. Molaei, A. Molaei, F. Abedi, A. W. Hayes, and G. Karimi, "Nephroprotective activity of natural products against chemical toxicants: the role of Nrf2/ARE signaling pathway," *Food Sciences and Nutrition*, vol. 9, no. 6, pp. 3362–3384, 2021.
- [8] S. A. Abd El-Baset, M. R. Abd El-Haleem, R. S. Abdulkmaksoud, and A. A. A. Kattaia, "Mesna ameliorates acute lung injury induced by intestinal ischemia-reperfusion in rats," *Scientific Reports*, vol. 11, no. 1, Article ID 13356, 2021.
- [9] C. K. Batista, G. A. Brito, M. L. Souza, B. T. Leitão, F. Q. Cunha, and R. A. Ribeiro, "A model of hemorrhagic cystitis induced with acrolein in mice," *Brazilian Journal of Medical and Biological Research*, vol. 39, no. 11, pp. 1475–1481, 2006.
- [10] W. Kooti, M. Moradi, K. Peyro et al., "The effect of celery (*Apium graveolens* L.) on fertility: a systematic review," *Journal of Complementary and Integrative Medicine*, vol. 15, 2018.
- [11] A. Ozcan, A. Korkmaz, S. Oter, and O. Coskun, "Contribution of flavonoid antioxidants to the preventive effect of mesna in cyclophosphamide-induced cystitis in rats," *Archives of Toxicology*, vol. 79, no. 8, pp. 461–465, 2005.
- [12] A. M. Mousa, K. S. Allemailem, F. A. Alhumaydhi et al., "Could mesna and celery seed cotherapy modulate oxidative stress and inflammation of the urinary bladder induced by ifosfamide in rabbits?" *Journal of Inflammation Research*, vol. 14, pp. 5837–5847, 2021.
- [13] M. A. Abd El-Ghany, A. M. Ramadan, and S. F. Ghozy, "Nutraceutical effects of curcuma, ginger, celery, yeast and honey on side effects of gentamicin induced nephrotoxicity in rats," *World Applied Sciences Journal*, vol. 16, pp. 646–655, 2012.
- [14] M. S. Al Aboody, "Cytotoxic, antioxidant, and antimicrobial activities of Celery (*Apium graveolens* L.)," *Bioinformation*, vol. 17, no. 1, pp. 147–156, 2021.
- [15] B. B. Consentino, G. Virga, G. G. la Placa et al., "Celery (*Apium graveolens* L.) performances as subjected to different sources of protein hydrolysates," *Plants*, vol. 9, p. 1633, 2020.
- [16] W. Kooti and N. Daraei, "A review of the antioxidant activity of celery (*Apium graveolens* L.)," *Journal of Evidence-Based Complementary & Alternative Medicine*, vol. 22, no. 4, pp. 1029–1034, 2017.
- [17] B. Ahmed, T. Alam, M. Varshney, and S. A. Khan, "Hepatoprotective activity of two plants belonging to the Apiaceae and the Euphorbiaceae family," *Journal of Ethnopharmacology*, vol. 79, no. 3, pp. 313–316, 2002.

- [18] S. Sultana, S. Ahmed, T. Jahangir, and S. Sharma, "Inhibitory effect of celery seeds extract on chemically induced hepatocarcinogenesis: modulation of cell proliferation, metabolism and altered hepatic foci development," *Cancer Letters*, vol. 221, no. 1, pp. 11–20, 2005.
- [19] A. Safira, S. L. Savitri, A. R. B. Putri et al., "Review on the pharmacological and health aspects of *Hylocereus* or *Pitaya*: an update," *Journal of Drug Delivery and Therapeutics*, vol. 11, no. 6, pp. 297–303, 2021.
- [20] A. T. Khalil, I. Khan, K. Ahmad, Y. A. Khan, J. Khan, and Z. K. Shinwari, "Antibacterial activity of honey in north-west Pakistan against select human pathogens," *Journal of Traditional Chinese Medicine*, vol. 34, no. 1, pp. 86–89, 2014.
- [21] N. Al-Waili, K. Salom, and A. A. Al-Ghamdi, "Honey for wound healing, ulcers, and burns; data supporting its use in clinical practice," *The Scientific World Journal*, vol. 11, pp. 766–787, 2011.
- [22] J. Alvarez-Suarez, M. Gasparrini, T. Forbes-Hernández, L. Mazzoni, and F. Giampieri, "The composition and biological activity of honey: a focus on manuka honey," *Foods*, vol. 3, no. 3, pp. 420–432, 2014.
- [23] J. M. Stephens, R. C. Schlothauer, B. D. Morris et al., "Phenolic compounds and methylglyoxal in some New Zealand manuka and kanuka honeys," *Food Chemistry*, vol. 120, no. 1, pp. 78–86, 2010.
- [24] R. Mărgăoan, E. Topal, R. Balkanska et al., "Monofloral honeys as a potential source of natural antioxidants, minerals and medicine," *Antioxidants*, vol. 10, pp. 1–48, 2021.
- [25] A. Prakash, B. Medhi, P. K. Avti, U. N. Saikia, P. Pandhi, and K. L. Khanduja, "Effect of different doses of Manuka honey in experimentally induced inflammatory bowel disease in rats," *Phytotherapy Research*, vol. 22, no. 11, pp. 1511–1519, 2008.
- [26] S. Patel and S. Cichello, "Manuka honey: an emerging natural food with medicinal use," *Natural Products and Bioprospecting*, vol. 3, no. 4, pp. 121–128, 2013.
- [27] M. Ramezani, S. Nasri, and N. Yassa, "Antinociceptive and anti-inflammatory effects of isolated fractions from *Apium graveolens* seeds in mice," *Pharmaceutical Biology*, vol. 47, no. 8, pp. 740–743, 2009.
- [28] K. A. Mills, R. Chess-Williams, and C. McDermott, "Novel insights into the mechanism of cyclophosphamide-induced bladder toxicity: chloroacetaldehyde's contribution to urothelial dysfunction in vitro," *Archives of Toxicology*, vol. 93, no. 11, pp. 3291–3303, 2019.
- [29] M. A. M. Helal, "Celery oil modulates DEHP-induced reproductive toxicity in male rats," *Reproductive Biology*, vol. 14, no. 3, pp. 182–189, 2014.
- [30] N. A. El-Shinnawy, "The therapeutic applications of celery oil seed extract on the plasticizer di (2-ethylhexyl) phthalate toxicity," *Toxicology and Industrial Health*, vol. 31, no. 4, pp. 355–366, 2015.
- [31] M. P. Goren, J. M. Houle, D. A. Bush, J. T. Li, C. E. Newman, and W. P. Brade, "Similar bioavailability of single-dose oral and intravenous mesna in the blood and urine of healthy human subjects," *Clinical Cancer Research: An Official Journal of the American Association for Cancer Research*, vol. 4, pp. 2313–2320, 1998.
- [32] N. H. Shomer, K. H. Allen-Worthington, D. L. Hickman et al., "Review of rodent euthanasia methods," *Journal of the American Association for Laboratory Animal Science*, vol. 59, no. 3, pp. 242–253, 2020.
- [33] National Research Council (US) Institute for Laboratory Animal Research, *Guide for the Care and Use of Laboratory Animals*, National Academies Press, Washington, DC, USA, 2011.
- [34] N. I. Hussien and A. M. Mousa, "Could nitric oxide be a mediator of action of oxytocin on myocardial injury in rats? (Biochemical, histological and immunohistochemical study)," *General Physiology and Biophysics*, vol. 35, pp. 353–362, 2016.
- [35] J. Y. Lee, J. S. Chang, K. C. Koo, S. W. Lee, Y. D. Choi, and K. S. Cho, "Hematuria grading scale: a new tool for gross hematuria," *Urology*, vol. 82, no. 2, pp. 284–289, 2013.
- [36] N. I. Hussien, A. M. Mousa, and A. A. Shoman, "Decreased level of plasma nesfatin-1 in rats exposed to cell phone radiation is correlated with thyroid dysfunction, oxidative stress, and apoptosis," *Archives of Physiology and Biochemistry*, vol. 6, pp. 1–7, 2020.
- [37] A. M. Mousa, A. Almatroudi, A. S. Alwashmi et al., "Thyme oil alleviates Ova-induced bronchial asthma through modulating Th2 cytokines, IgE, TSLP and ROS," *Biomedicine and Pharmacotherapy*, vol. 140, Article ID 111726, 2021.
- [38] E. J. Poveda-Pagán, S. Hernández-Sánchez, L. Rhys-Jones-López, A. Palazón-Bru, and C. Lozano-Quijada, "Scanning electron microscopy examination of needle tips after different procedures of deep dry needling in humans," *Scientific Reports*, vol. 8, pp. 1–10, 2018.
- [39] A. M. Mousa and Y. H. Aldebasi, "L-carnosine mitigates interleukin-1 $\alpha$ -induced dry eye disease in rabbits via its antioxidant, anti-inflammatory, antiapoptotic, and antifibrotic effects," *Cutaneous and Ocular Toxicology*, vol. 40, no. 3, pp. 241–251, 2021.
- [40] F. A. Alhumaydhi, A. M. H. Mackawy, E. N. Morgan et al., "Potential role of folic acid in preventing male infertility associated with MTHFR gene C677T (rs1801133) polymorphism," *All Life*, vol. 14, no. 1, pp. 730–743, 2021.
- [41] S. Haldar, C. Dru, and N. A. Bhowmick, "Mechanisms of hemorrhagic cystitis," *American Journal of Clinical and Experimental Urology*, vol. 2, pp. 199–208, 2014.
- [42] A. Korkmaz, T. Topal, and S. Oter, "Pathophysiological aspects of cyclophosphamide and ifosfamide induced hemorrhagic cystitis; Implication of reactive oxygen and nitrogen species as well as PARP activation," *Cell Biology and Toxicology*, vol. 23, no. 5, pp. 303–312, 2007.
- [43] D. B. Clayton, H. A. Stephany, C. B. Ching et al., "F2-Isoprostanes as a biomarker of oxidative stress in the mouse bladder," *The Journal of Urology*, vol. 191, no. 5S, pp. 1597–1601, 2014.
- [44] J. H. Lee, J. H. Park, and M. H. Yang, "The effect of cyclophosphamide on fas-mediated apoptosis," *Journal of Korean Medical Science*, vol. 12, no. 3, pp. 185–189, 1997.
- [45] M. R. Zirak, G. Karimi, R. Rahimian, A. H. Jafarian, A. W. Hayes, and S. Mehri, "Tropisetron ameliorates cyclophosphamide-induced hemorrhagic cystitis in rats," *European Journal of Pharmacology*, vol. 883, Article ID 173310, 2020.
- [46] C.-J. Tsai, S.-S. Wang, and Y.-C. Ou, "Cyclophosphamide-induced intractable hemorrhagic cystitis treated with hyperbaric oxygenation and intravesical sodium hyaluronate," *Urological Science*, vol. 25, no. 4, pp. 155–157, 2014.
- [47] J. Hayslip, E. V. Dressler, H. Weiss et al., "Plasma TNF- $\alpha$  and soluble TNF receptor levels after doxorubicin with or without Co-administration of mesna-A randomized, cross-over clinical study," *PLoS One*, vol. 10, Article ID e0124988, 14 pages, 2015.
- [48] D. Salman, J. Swinden, J.-M. R. Peron, S. Barton, and S. Nabhani-Gebara, "New investigations into the stability of Mesna using LC-MS/MS and NMR," *Expert Review of Anticancer Therapy*, vol. 16, no. 1, pp. 123–130, 2016.
- [49] J. T. R. Keeney, X. Ren, G. Warriar et al., "Doxorubicin-induced elevated oxidative stress and neurochemical alterations



- in brain and cognitive decline: protection by MESNA and insights into mechanisms of chemotherapy-induced cognitive impairment (“chemobrain”),” *Oncotarget*, vol. 9, no. 54, pp. 30324–30339, 2018.
- [50] K. Dolati, H. Rakhshandeh, M. Golestani, F. Forouzanfar, R. Sadeghnia, and H. R. Sadeghnia, “Inhibitory effects of apium graveolens on xanthine oxidase activity and serum Uric acid levels in hyperuricemic mice,” *Preventive Nutrition and Food Science*, vol. 23, no. 2, pp. 127–133, 2018.
- [51] G. Ş. Beyhan Sağlam, E. Cikler, and Z. Ali, “Şule çetinel, feriha ercan, protective effects of 2-mercaptoethane sulfonate (mesna) on Protamine sulfate induced bladder damage 2-mercaptoetan sülfonat (mesna)’ in, Protamİ N sülfatin Tetİ Kleİği,” *Original Research*, vol. 18, pp. 6–12, 2005.
- [52] G. Q. Zheng, P. M. Kenney, J. Zhang, and L. K. T. Lam, “Chemoprevention of benzo [a] pyrene-induced forestomach cancer in mice by natural phthalides from celery seed oil,” *Nutrition and Cancer*, vol. 19, no. 1, pp. 77–86, 1993.
- [53] L. Chunliang, X. Xu, G. Liu, L. Zhuang, and D. Song, “Isolation, purification, and identification of the main phenolic compounds from leaves of celery (*Apium graveolens* L. var. dulce Mill./Pers.),” *Journal of Separation Science*, vol. 40, pp. 472–479, 2017.
- [54] H. Rouhi-Boroujeni, H. Rouhi-Boroujeni, E. Heidarian, F. Mohammadizadeh, and M. Rafieian-Kopaei, “Herbs with anti-lipid effects and their interactions with statins as a chemical antihyperlipidemia group drugs: a systematic review,” *ARYA Atherosclerosis*, vol. 11, pp. 244–251, 2015.
- [55] D.-K. Liu, C.-C. Xu, L. Zhang et al., “Evaluation of bioactive components and antioxidant capacity of four celery (*Apium graveolens* L.) leaves and petioles,” *International Journal of Food Properties*, vol. 23, no. 1, pp. 1097–1109, 2020.
- [56] F. F. Abd El-Malek, A. S. Yousef, and S. A. El-Assar, “Hydrogel film loaded with new formula from manuka honey for treatment of chronic wound infections,” *Journal of Global Antimicrobial Resistance*, vol. 11, pp. 171–176, 2017.
- [57] J. Kwiecińska-Piróg, J. Przekwas, M. Majkut, K. Skowron, and E. Gospodarek-Komkowska, “Biofilm formation reducing properties of manuka honey and propolis in proteus mirabilis rods isolated from chronic wounds,” *Microorganisms*, vol. 8, pp. 1–15, 2020.
- [58] M. Moniruzzaman, S. A. Sulaiman, M. I. Khalil, and S. H. Gan, “Evaluation of physicochemical and antioxidant properties of sourwood and other Malaysian honeys: a comparison with manuka honey,” *Chemistry Central Journal*, vol. 7, pp. 138–212, 2013.
- [59] J. Majtan, J. Bohova, M. Horniackova, J. Klaudivy, and V. Majtan, “Anti-biofilm effects of honey against wound pathogens proteus mirabilis and enterobacter cloacae,” *Phytotherapy Research*, vol. 28, no. 1, pp. 69–75, 2014.
- [60] V. Tomblin, L. R. Ferguson, D. Y. Murray, R. Schlothauer, and D. Y. Han, “Potential pathway of anti-inflammatory effect by New Zealand honeys,” *International Journal of General Medicine*, vol. 7, pp. 149–158, 2014.



## Research Article

# Mechanism of Zhen Wu Decoction in the Treatment of Heart Failure Based on Network Pharmacology and Molecular Docking

Chen-Yu Ma,<sup>1</sup> Yu-Qian Ma,<sup>2</sup> and Min Deng<sup>3</sup> 

<sup>1</sup>Cixi Third People's Hospital, Zhejiang, China

<sup>2</sup>Wenzhou Medical University, Wenzhou, China

<sup>3</sup>Emergency Medicine Department, Zhejiang Hospital of Integrated Traditional Chinese and Western Medicine, Hangzhou, China

Correspondence should be addressed to Min Deng; dengmin0607@126.com

Received 11 December 2021; Revised 10 February 2022; Accepted 14 February 2022; Published 15 March 2022

Academic Editor: Ruchika Garg

Copyright © 2022 Chen-Yu Ma et al. This is an open access article distributed under the Creative Commons Attribution License, which permits unrestricted use, distribution, and reproduction in any medium, provided the original work is properly cited.

Heart failure (HF) is a serious manifestation or advanced stage of various cardiovascular diseases, and its mortality and rehospitalization rate are still on the rise in China. Based on the network pharmacology method, 59 components of Zhen Wu decoction (ZWD) and 83 target genes related to HF were obtained. Through the PPI network, four potential therapeutic targets were identified: AKT1, IL6, JUN, and MAPK8. The beneficial components of ZWD might intervene HF through the AGE-RAGE signalling pathway in the diabetes component, fluid shear stress and atherosclerosis, the TNF signalling pathway, TB, and Kaposi sarcoma related herpesvirus infection, according to a KEGG enrichment study. The protein interaction network of candidate targets was constructed by the STRING database, and the protein interaction network was clustered by MEODE software. GO and KEGG enrichment analyses were performed on the core modules obtained by clustering. Finally, AutoDock Vina software was used for molecular docking verification of key targets and active ingredients. The result was that 75 active ingredients and 109 genes were screened as potential active ingredients and potential targets of Shengjie Tongyu decoction for CHF treatment. The main active components were quercetin, luteolin, kaempferol, dehydrated icariin, isorhamnetin, formononetin, and other flavonoids. IL-6, MAPK1, MAPK8, AKT1, VEGFA, and JUN were selected as the core targets. Molecular docking showed that the key components were well connected with the target. GO enrichment analysis showed that Shengjie Tongyu decoction could play a role through multiple biological pathways including angiogenesis, regulation of endothelial cell proliferation, binding of cytokine receptors, negative regulation of apoptotic signalling pathways, regulation of nitric oxide synthase activity, and reactive oxygen metabolism. Key pathways mainly focus on the toll-like receptor signalling pathway, nod-like receptor signalling pathway, MAPK signalling pathway, mTOR signalling pathway, JAK-STAT signalling pathway, VEGF signalling pathway, and other pathways. Through molecular docking technology, it was found that a variety of effective components in ZWD, such as kaempferol. Molecular docking technology has preliminarily verified the network pharmacology and laid a foundation for the follow-up pharmacological research.

## 1. Background

Heart failure (HF) refers to a variety of heart function or organic diseases caused by cardiac insufficiency or dysfunction, resulting in cardiac output which cannot meet the metabolic needs of the disease [1]. After the illness, organ deficiency, dyspnea, fluid retention, and so on seriously threaten the life safety of patients [2]. Heart failure (HF) is a prevalent kind of critical clinical disease. According to

cardiac systolic/diastolic dysfunction, it can be divided into systolic HF and diastolic HF. Rendering to different clinical manifestations, it can be divided into left HF, right HF, and total HF [3]. In developed countries, the mortality rate is 1.5%–2.0%, and the pervasiveness proportion of individuals more than 70 years of age is more than or equal to 10%, while in China, the mortality rate of hospitalized patients is about 4.1% [4]. Primary myocardial damage and abnormality are the main causes of HF, and in addition to cardiovascular

disease, noncardiovascular disease can also lead to it. At present, it is a chronic, spontaneous progressive disease [5]. According to the HF diagnosis and treatment quality evaluation and control index expert consensus 2021 in China, cardiac activation is the key factor that causes the development of HF. It is recommended to use the early use of sarkoba valsartan drugs to reduce the incidence rate and mortality [6]. Chinese medicine [7] is a comprehensive medical system that has been passed down for over two millennia.

Zhen Wu decoction (ZWD) comes from the treatise on febrile and miscellaneous diseases by Zhang Zhongjing. Modern research shows that it has a therapeutic effect on HF and other diseases [8]. Traditional Chinese medicine and its compounds have the characteristics of multicomponent, low selectivity, and multitarget interaction. This complexity makes it difficult to control the treatment; it lacks a reasonable and effective safety evaluation system and is relatively difficult to analyze its action and compatibility mechanism [9]. In recent years, network pharmacology has been rising in the world. It has the characteristics of multidirectional cross-fusion. It can realize the comprehensive network analysis of traditional Chinese medicine and its compound prescriptions and understand the pathogenesis of diseases from the system level. It has significant advantages and the potential to clarify the mechanism of action and explain the law of prescription composition [10, 11], because the integrity and systematicness of its research strategy correspond to the overall concept of traditional Chinese medicine and syndrome differentiation and treatment. As a result, one such study employs network pharmacology to investigate the pharmacodynamic material basis and molecular basis of Zhen Wu decoction in the therapies of HF, creates the “pharmacodynamic element goal continuum” relationship network, investigates the multicomponent, multitarget, and multichannel mechanism of Zhen Wu decoction, and preliminarily validates the results using docking study technology to provide the foundation for basic experimental research and clinical trials.

## 2. Data and Methods

**2.1. Acquisition of Effective Components and Targets of Core Drugs.** Input each medica of ZWD into TCMSP [12] data step by step (<https://tcms-pw.com/tcmsp.php>). Oral bioavailability is determined by the same principle [13]  $\geq 30\%$ , drug-like (DL)  $\geq 0.18$ , was selected to obtain the effective components and target of core drugs. At the same time, the structure of the effective components was retrieved and saved in mol2 format. Import the abovementioned targets to the UniProt [14] website (<https://www.UniProt.org/>). Gene mapping is performed towards obtaining gene symbols to the corresponding target.

**2.2. Acquisition of Disease-Drug Common Target Genes.** In the human gene database, GeneCards (<https://gene-cards.Weizmann.ac.il/v3/>) and MalaCards (<https://www.malecards.org/>) were used. To obtain the target genes of

coronary heart disease, we searched with the keyword “hyperlipidemia” in the abovementioned drug target genes, and disease target genes were introduced into the Venn diagram web (<http://bioinformatics.PSB.ugent.be/webtools/Venn/>). The common illness and therapeutic target genes were discovered.

**2.3. Construction of Protein-Protein Interaction (PPI) Network for Key Targets.** The suitable target genes of the disorders and medications mentioned above have been entered into the STRING website [15]. The species chosen as “*Homo sapiens*,” and the associated connections between protein targets were determined. Following the PPI file export, the graphs were improved with Cytoscape software, and the 10 leading essential genes (hub genes) in the PPI network were determined based on the degree values.

**2.4. GO Enrichment Analysis and KEGG Enrichment Analysis.** The illness medication commonality genes were added to the David database, and the species “*Homo sapiens*” was chosen for gene ontology (GO) and Kyoto Encyclopedia of Genes and Genomes (KEGG) signal pathway enrichment analyses [16, 17]. And the alleyway map of the signal pathways closely related to hypertension is obtained. The abovementioned results are imported into R software for visual operation of relevant results and data.

**2.5. Composition-Target-Signal Pathway Network Diagram.** Potential targets are imported into the David6.8 (HTTP://David, abcc.Ncicrf.Gov/) gene function analysis tool. The identifier is selected. The list type were set to official gene symbol, gene list, and species is limited to *Homo sapiens*. Submit List is clicked for the GO function and KEGG enrichment analysis. At the same time, the ENSG encoding corresponding to potential genes is obtained by gene ID conversion. The whole human genome is taken as the background gene. The ENSG codes obtained were imported into the OmicShare (WWW.omicshare.com/tools) website for KEGG pathway annotation number analysis. To create the network design of active ingredient, target, and signal pathways, the active ingredient, target, and signal routes were loaded into the Cytoscape 3.6.0 programme.

### 2.6. Molecular Docking Verification

- (1) The PDB structure of hub protein was acquired by researching hub genes on the RCSB PDB database (<https://www.rcsb.org/search>). The abovementioned compounds were entered into the DS programme and prepared using the “prepare ligands” feature. To locate the probable active surface area in the protein cavities, remove water, ligand classes, and irrelevant side chains from the receptors and click on receptor-ligand interactions > define and edit the binding > from receptor cavities. (3) CDOCKER INTERACTION ENERGY (molecular docking binding energy) was utilised to identify and rank the

optimum molecular conformations of every docking molecule. The findings reveal that the smaller the binding energy of the docking study conformation, the more stable the binding notion is and the more likely the reactive receptor molecule and ligand will bind.

### 3. Results

**3.1. Active Ingredients and Targets of Core Drugs.** From the TCMSP website, there are 13 active ingredients in *Paeoniae Radix Alba*, 7 active ingredients in *Atractylodes macrocephala* Koidz, 15 active ingredients in *Poria Cocos* (Schw.) Wolf, 21 active ingredients in *Aconiti Lateralis Radix Praeparata*, and 5 active ingredients in *Zingiber officinale* Roscoe, with 59 constituents (Table 1). The abovementioned effective components were input into the TCMSP website and searched for 85 effective component targets. Then, these target proteins were introduced into the UniProt website and transformed into a corresponding gene symbol.

**3.2. Common Target Genes of ZWD and HF.** 13194 genes targets of hyperlipidemia were obtained since the GeneCards website, and disease and drug boards were imported to draw Venn diagram website for Wayne map analysis, and 83 common target genes of illness and drugs were obtained, as shown in Figure 1.

**3.3. Key Target PPI Network.** As shown in Figure 2, the PPI network map was created after the 83 frequent genes were added to the string database. Targets appear as nodes and are connected by edges in a PPI network. The more dense the edges of key targets are, the larger the nodes are, which means the more important role they play in the PPI network. The hub plug-in in the Cytoscape programme is used to retrieve the top 4 hub genes (core genes) according to the degree value after the PPI network is stored in TSV format, as shown in Figure 3.

**3.4. KEGG Pathway Enrichment Analysis with GO Enrichment Analysis.** As shown in Figure 4, the 53 shared target genes of ZWD and HF were entered into the David database for ontologies (GO) enrichment research, which included three components: biological process (BP), cellular component (CC), and molecular function (MF). GO is mainly related to response to drugs, response to lipopolysaccharides, response to molecules of bacterial origin, and other BPs; membrane raft, micromembrane domain, plasma membrane raft, caveola, and other Mfs; nuclear receptor activity, live activated transcription factor activity, peptide binding, G protein-coupled amine receptor activity, and other MFs. KEGG enrichment analysis mainly involves the AGE-RAGE signalling pathway in diabetic composition, fluid shear stress and atherosclerosis, the TNF signalling pathway, tuberculosis, Kaposi sarcoma-associated herpesvirus infection, etc., as shown in Figure 5.

**3.5. Component-Target-Pathway Network Analysis of ZWD.** To more clearly show the relationship between components, targets, and pathways of ZWD in the treatment of HF, the network of pathways, active ingredients, and core targets was constructed using Cytoscape software (Figure 6). A network graph contains nodes and edges. The green node represents drugs, the blue node represents active ingredients, the yellow node represents target genes, the red node represents signalling pathways, and the black node represents disease. The network diagram can directly show that ZWD own features of multicomponent, multitarget, and multichannel interaction in hyperlipidemia.

**3.6. Molecular Docking Results.** According to the method in 1.6 for molecular verification, the docking results of each group are shown by the heat map in Figure 7. The protein group is on the horizontal axis while the ligand is on the vertical axis. The redder the color, the stronger the binding force is. Each group's first two docking results with the highest energy score are shown as three-dimensional and two-dimensional graphs. The three-dimensional graph shows the spatial relationship between the ligand and the protein. The two-dimensional graph shows the chemical bond type formed by the ligand and the amino acid group or residue of the protein. The docking scores of the AKT1 group were MOL002433, MOL002394, 56.1364 and 53.2491, respectively, as shown in Figures 8(a) and 8(b). In the IL6 group, MOL 000422 and MOL 000492, the docking scores were 74.0031 and 48.4424, respectively, as shown in Figures 8(c) and 8(d). In Jun group, MOL 000422 and MOL006129 were used, with docking scores of 75.7236 and 69.2787, as shown in Figures 8(e) and 8(f). In mapk8 group, MOL 000422 and MOL 002419, with docking scores of 48.9098 and 47.1798, as shown in Figures 8(g) and 8(h).

### 4. Discussion

HF is a range of complicated clinical syndromes, a significant manifestation or end phase of several heart illnesses [18]. It is produced by aberrant cardiac structure and/or function induced by various factors, obstructing ventricular systolic and/or diastolic function. An epidemiological survey shows that the disease is prone to people over 65 years old, with a high mortality and hospitalization rate, which causes a substantial economic burden. In recent years, modern medicine has made remarkable progress in the prevention and treatment of HF. However, there is still a lack of ideal treatment countermeasures in diuretics resistance, repeated hospitalization of HF, and the decline of quality of life. In the face of these problems, traditional Chinese medicine has a significant advantage and a broad prospect in treating HF due to its multidirectional, multitarget, multimechanism, and small side effects. The occurrence of HF is closely related to ion defects, inflammation and remodelling, myocardial hypertrophy, etc., and the discovery of new biomarkers is beneficial to its early diagnosis [19, 20].

The compensations and characteristics of old Chinese medicine diagnosis and management of HF are obvious, and

TABLE 1: Operative ingredients of ZWD.

Drug	Mol ID	Mol Name	OB	DL
<i>Paeoniae Radix Alba</i>	MOL001910	11alpha,12alpha-epoxy-3beta-23-dihydroxy-30-norolean-20-en-28,12beta-olide	64.77	0.38
<i>Paeoniae Radix Alba</i>	MOL001918	Paeoniflorgenone	87.59	0.37
<i>Paeoniae Radix Alba</i>	MOL001919	(3S,5R,8R,9R,10S,14S)-3,17-Dihydroxy-4,4,8,10,14-pentamethyl-2,3,5,6,7,9-hexahydro-1H-cyclopenta[a]phenanthrene-15,16-dione	43.56	0.53
<i>Paeoniae Radix Alba</i>	MOL001921	Lactiflorin	49.12	0.8
<i>Paeoniae Radix Alba</i>	MOL001924	Paeoniflorin	53.87	0.79
<i>Paeoniae Radix Alba</i>	MOL001925	Paeoniflorin_qt	68.18	0.4
<i>Paeoniae Radix Alba</i>	MOL001928	Albiflorin_qt	66.64	0.33
<i>Paeoniae Radix Alba</i>	MOL001930	Benzoyl paeoniflorin	31.27	0.75
<i>Paeoniae Radix Alba</i>	MOL000211	Mairin	55.38	0.78
<i>Paeoniae Radix Alba</i>	MOL000358	Beta-sitosterol	36.91	0.75
<i>Paeoniae Radix Alba</i>	MOL000359	Sitosterol	36.91	0.75
<i>Paeoniae Radix Alba</i>	MOL000422	Kaempferol	41.88	0.24
<i>Paeoniae Radix Alba</i>	MOL000492	(+)-Catechin	54.83	0.24
<i>Atractylodes macrocephala</i> Koidz	MOL000020	12-Senecioid-2E,8E,10E-atractylentriol	62.4	0.22
<i>Atractylodes macrocephala</i> Koidz	MOL000021	14-Acetyl-12-senecioid-2E,8E,10E-atractylentriol	60.31	0.31
<i>Atractylodes macrocephala</i> Koidz	MOL000022	14-Acetyl-12-senecioid-2E,8Z,10E-atractylentriol	63.37	0.3
<i>Atractylodes macrocephala</i> Koidz	MOL000028	$\alpha$ -Amyrin	39.51	0.76
<i>Atractylodes macrocephala</i> Koidz	MOL000033	(3S,8S,9S,10R,13R,14S,17R)-10,13-Dimethyl-17-[(2R,5S)-5-propan-2-yloctan-2-yl]-2,3,4,7,8,9,11,12,14,15,16,17-dodecahydro-1H-cyclopenta[a]phenanthren-3-ol	36.23	0.78

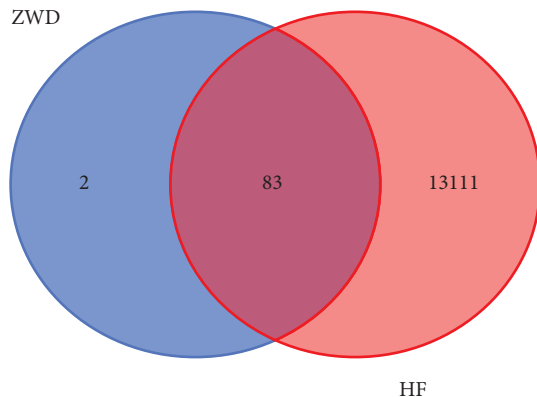


FIGURE 1: Common target genes of ZWD and HF.

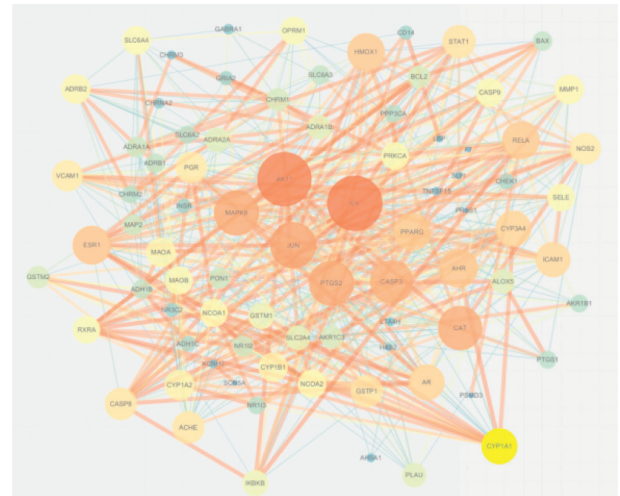


FIGURE 2: PPI network of common target genes of ZWD and HF.

rich clinical experience has been accumulated. The combination of Chinese and Western medicine allows patients to get comprehensive treatment in all directions [21]. ZWD is a classic Chinese medicine prescription for HF, and it is urgent to study its pharmacological mechanism.

In the current research, 59 dynamic apparatuses of ZWD was found, including kaempferol, paeoniflorin, (+)-catechin, 6-methylgingediacetate 2, and (R)-norcochlorine. Kaempferol blocks Akt/glycogen kinase (GSK)-3 $\beta$ . The apoptosis of the signal transduction pathway of p38 mitogen-activated protein kinase/extracellular signal-regulated kinase can inhibit apoptosis, thus improving the cardiac protection of KF. Kaempferol is a kind of flavonoid compound, which prevents the cardiac remodelling induced by angiotensin II by reducing the inflammation and oxidative stress induced by angiotensin II [22, 23]. Kaempferol significantly inhibited the expression of high glucose-induced inflammatory cytokines and ROS

production, thus reducing the fibrosis response and apoptosis in vitro. Kaempferol suppresses nuclear factors- $\kappa$ B (NF- $\kappa$ B) and nuclear translocation, and the protective action of DCM is mediated by nuclear factors-like erythrocytes 2 P45 related factor 2 (Nrf-2). Kaempferol reduced diabetes-induced cardiac fibrosis and apoptosis in type 1 diabetic mice generated by streptozotocin. These alterations were similarly associated with decreased inflammation and oxidative stress in diabetic mice's hearts [24]. Sinapine decreased the activity of the ASK1/JNK1/2/p38 signal pathway and the amplification of H9c2 cardiomyocytes in vitro. Furthermore, in mice, kaempferol was found to protect the heart and H9c2 cells from the effects of oxidative stress [25]. Catechins significantly reduced the expression level of inflammatory cytokines and

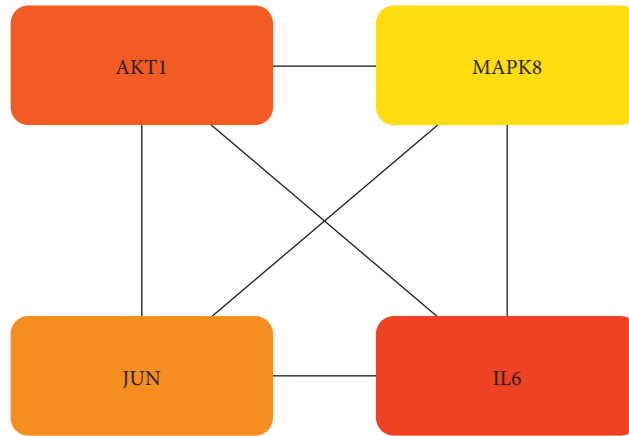


FIGURE 3: TOP4 genes of PPI network by degree value.

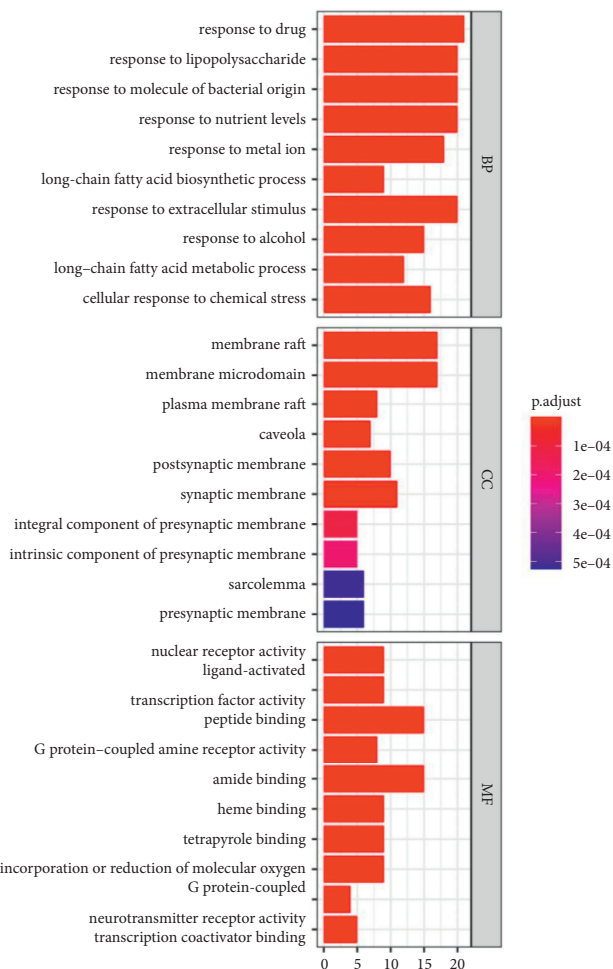


FIGURE 4: GO analysis of common target genes of ZWD and HF.

provided cardiac protection for adriamycin-induced cardiac toxicity through antioxidation and anti-inflammatory properties [26]. Catechins regulate CREB/lncRNA Miat/Akt/Gsk-3 $\beta$ . The pathway abridged the programmed cell death of myocardial cells induced by H/R [27]. Paoniflorin also inhibited collagen deposition in the heart under pressure overload, TGF $\beta$ , CTGF, I $\alpha$ , and III $\alpha$ . The expression of

collagen and phosphorylation of Smad2 and Smad3. Eonoside can inhibit the apoptosis of myocardial cells, and the introduction of AB by the cleavage of Bax and caspase 3 reduces cardiac hypertrophy, fibrosis, apoptosis, and inflammation in stress overload mice and improves left ventricular function [28]. Paoniflorin's goal is to improve remodelling induced by distress in spontaneously hypertensive rats by modulating the MAPK signalling system [29]. Paoniflorin can reduce heart remodelling and improve cardiac function, as well as reduce CVF level, collagen volume around blood vessels, and TGF in rats with HF- $\beta$ . The expression of Smad3 and 1 suggests that the potential mechanism of cardiac protection may be related to TGF- $\beta$  1/the down-down height correlation of the Smad signal path [30].

We also got 83 common target genes of disease drugs. Through PPI network analysis, we got the hub genes with the highest degree: AKT1, IL6, Jun, and MAPK8. AKT1 is a critical gene in the PI3k/Akt signalling pathway. AKT1 is involved in cell functions such as apoptosis, glucose metabolism, and cell proliferation and growth [31]. Akt activity was raised when interacting with actin and HSP90, while it was lowered when interacting with other proteins (such as CTMP and TRB3). The function of Akt in cardiovascular processes such as cell survival, growth, proliferation, angiogenesis, vasodilation, and cell metabolism is determined by its activity in downstream targets. Akt enhances cell survival by activating caspase-9, Yap, Bcl-2, and Bax. Akt mediated eNOS activation, vasodilation, and angiogenesis, as well as increased VEGF release. Through its downstream targets, GSK3 and GLUT4, Akt can boost cell metabolism.

Many cardiovascular diseases, such as atherosclerosis, cardiac hypertrophy, and vascular remodeling, are linked to changes in Akt signal transduction [32]. In the large heterogeneous HF cohort, more than 50 per cent of patients found that IL-6 levels were elevated and were associated with iron deficiency, reduced LVEF, atrial fibrillation, and poor clinical outcomes. These findings require further study of IL-6 as a potential therapeutic target in specific HF subgroups [35]. In HF, there was an inequity between proinflammatory and anti-inflammatory cytokines. The concentration of several interleukins in HF increased, including IL-1 $\beta$ , IL-6, IL-8, IL-9, IL-10, IL-13, IL-17, and IL-18 were downregulated, while IL-



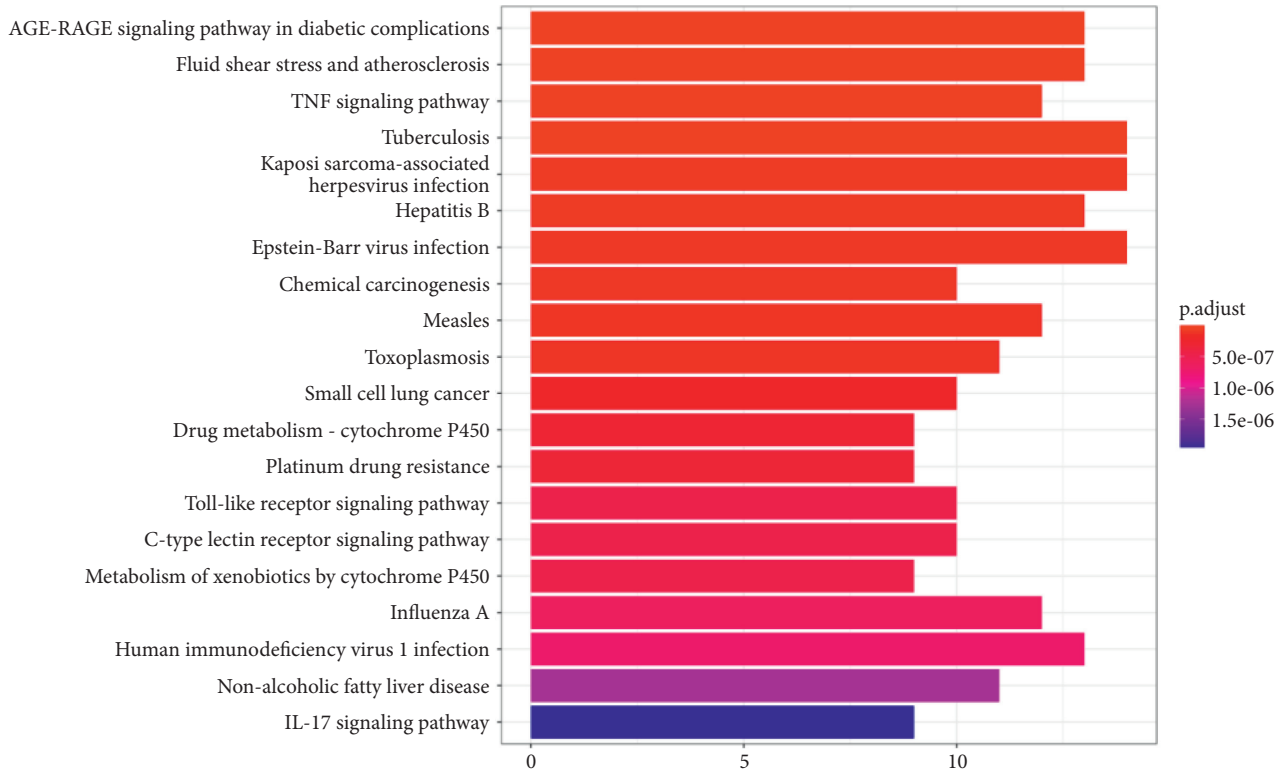


FIGURE 5: KEGG analysis of common target genes of ZWD and HF.

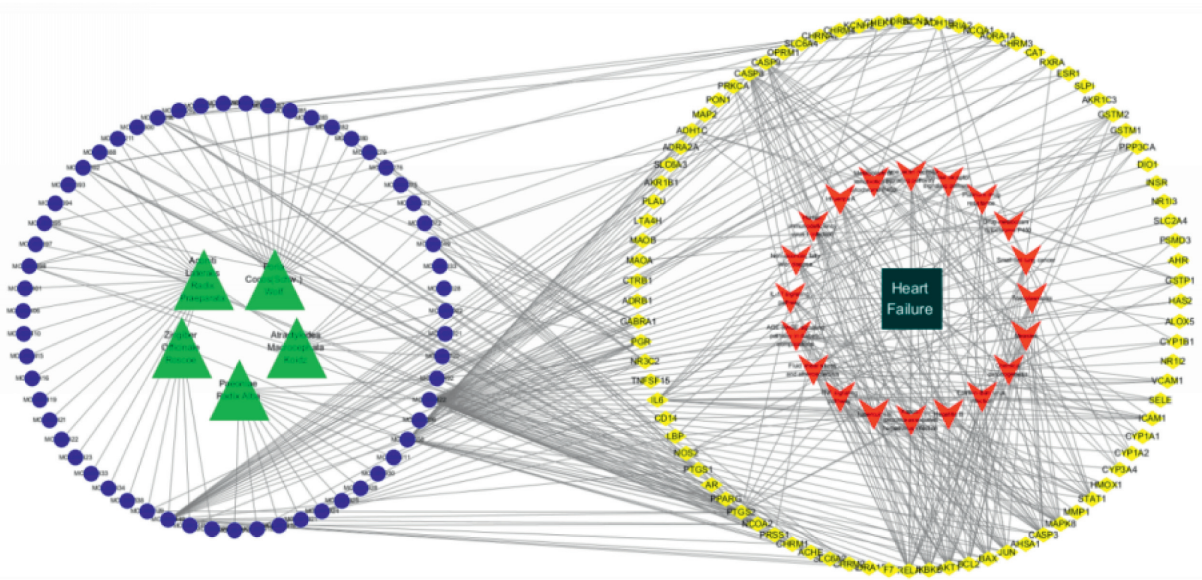


FIGURE 6: Network of component-targets pathways of ZWD treating HF.

5, IL-7, or IL-33 were downregulated [34]. The concentration of inflammatory medium is related to cardiac function, which can be an HF marker and a predictor of adverse outcome or mortality. IL-6 may cause myocardial damage and dysfunction in chronic HF syndrome caused by different reasons. As the cause of cardiomyopathy, myocarditis, rejection of allogeneic transplantation, and CHF in the condition of left ventricular assist device (LVAD), the IL-6 level in circulation

is related to the severity of left ventricular dysfunction and is also a powerful predictor of subsequent clinical results. In viral myocarditis, continuous and excessive production of IL-6 will destroy the cytokine network and virus clearance, thus promoting myocardial damage. Although IL-6 may be essential in the process of virus antigen presentation, early activation of the immune response and weakening of virus replication seem to be significant in animal models of viral



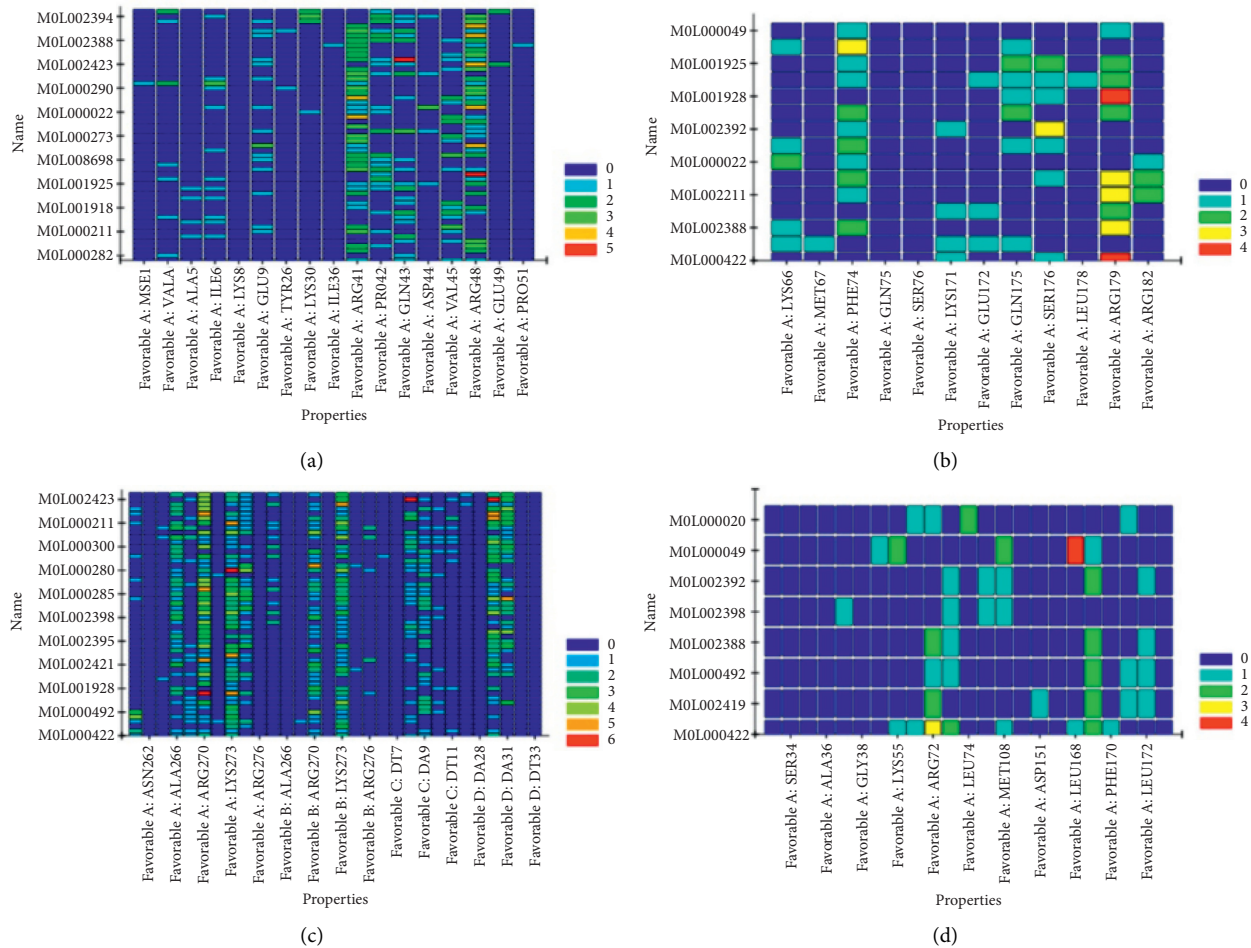


FIGURE 7: Docking heatmap of ligands and hub proteins.

myocarditis. IL-6 can induce cardiac hypertrophy by IL-6 signalling receptor glycoprotein 130 [35].

Response to the drug, lipopolysaccharide, bacterial molecule response, and other BPs; membrane raft, membrane microdomain, plasma membrane raft, caveola, and other MFs; nuclear receptor activity, live activated transcription factor activity, peptide binding, G protein-coupled amine receptor activity, and other MFs. The AGE-RAGE signalling pathway in diabetes composition, fluid shear stress and atherosclerosis, TNF signalling pathway, TB, and Kaposi sarcoma linked herpesvirus infection are all included in the KEGG enrichment study. It is known that the formation and accumulation of advanced glycation end products (ages) are accelerated in diabetes. In addition, even with improved glycemic control, ages hardly degraded and remained in diabetic vessels for a long time. Therefore, aging can explain why previously accumulated diabetic exposure may lead to the current progression of diabetic vascular complications [36]. Kaempferol can alleviate myocardial ischemia-reperfusion injury in diabetic rats by reducing the oxidative stress and inflammatory response induced by AGE-RAGE/MAPK [37]. Endothelial cells convert friction (fluid shear stress) from blood flow into biochemical signals, which influence gene expression and cell activity via specific

processes and pathways. These routes improve tissue flow by shaping the circulatory system during development, post-partum, and maturity. Atherosclerosis and vascular abnormalities are also caused by the same way [38]. TNF receptor activation in myocardial ischemia/reperfusion damage and protection has a conflicting function. Excess TNF expression and subsequent activation of TNF receptor type 1 in cardiomyocytes can result in systolic dysfunction, hypertrophy, fibrosis, and cell death.

In contrast, lower levels of TNF can result in systolic dysfunction, hypertrophy, fibrosis, and cell death. In type 2 cardiomyocytes, the presence of TNF and subsequent activation of the TNF receptor produced protective benefits. In addition to its concentration and receptor subtypes, TNF $\alpha$  the myocardial effect of CPB also depends on the duration of exposure and its location [39].

Discovery Studio (DS, v2016) is a younger breed of molecular modeling software that uses the method of the CDOCKER module to randomise search the conformational changes of molecules and then optimises each shape in the receptor active site region using the stochastic optimization method [40, 41]. We can simulate the docking of active components and target targets in the component target signalling pathway network diagram using molecular docking

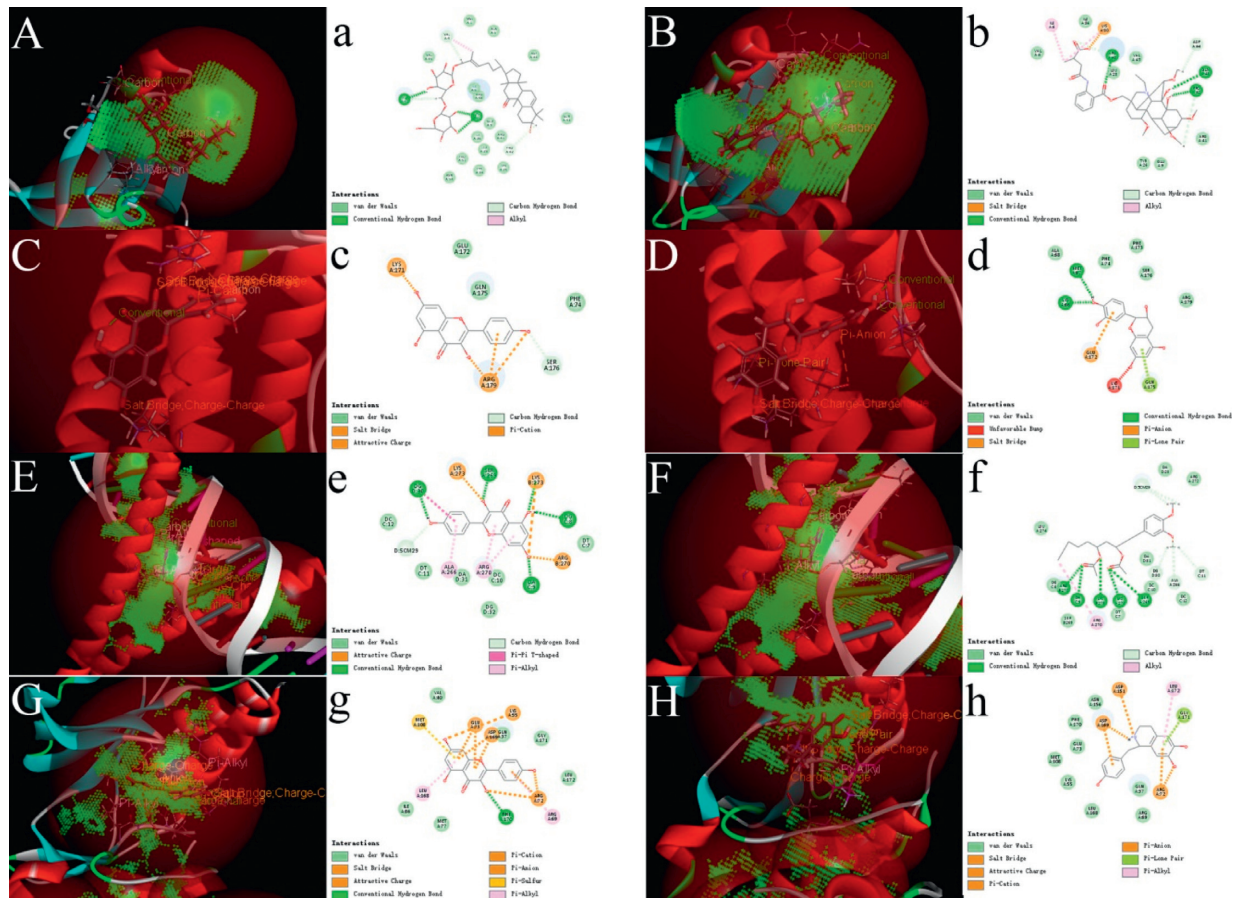


FIGURE 8: 3(d) and 2D graph of docking conformations of ligands and hub proteins.

technology, and it can help with the discovery of effective ingredients with clinical potential, drug design, and precursor optimization by analysing relevant binding parameters and binding conformation [42]. Several components, including kaempferol, P (+) - catechin, 6-methylgediacetate 2, and (R) - norcochlorine, have favourable docking conformations. The forces include the Van der Waals force, the Yanqiao force, and the PI alkyl force. Molecular docking proved that ZWD could regulate the PPI network by binding with a hub protein and intervening in HF through different signalling pathways [43].

## 5. Conclusion

Based on the network pharmacology method, 59 components of ZWD and 83 target genes related to HF were obtained. Through the PPI network, four potential therapeutic targets were identified: AKT1, IL6, Jun, and mapk8. The beneficial components of ZWD might intervene HF through the AGE-RAGE signalling pathway in diabetic composition, fluid shear stress and atherosclerosis, the TNF signalling pathway, TB, and Kaposi sarcoma related herpesvirus infection, according to a KEGG enrichment study. Through molecular docking technology, it was found that a variety of effective components in ZWD, such as kaempferol, could combine with hub protein, which preliminarily verified network pharmacology and laid a foundation for subsequent pharmacological research.

## Data Availability

The data used to support this work are available from the corresponding author on reasonable request.

## Conflicts of Interest

The authors have no conflicts of interest.

## Acknowledgments

The National Natural Science Foundation of China provided funding for this research (ID. 81973350).

## Supplementary Materials

Appendix: Supplementary materials. Table 2. Operative ingredients of ZWD (Continued). (*Supplementary Materials*)

## References



















- [1] E. Tanai and S. Frantz, "Pathophysiology of heart failure," *Comprehensive Physiology*, vol. 6, no. 1, pp. 187–214, 2015.
- [2] M. Gedela, M. Khan, and O. Jonsson, "Heart failure," *South Dakota Medicine*, vol. 68, no. 9, pp. 407–409, 2015.

- [3] D. Tomasoni, M. Adamo, C. M. Lombardi, and M. Metra, "Highlights in heart failure," *ESC Heart Failure*, vol. 6, no. 6, pp. 1105–1127, 2019.
- [4] P. D. Lopez, E. H. Cativo-Calderon, D. Otero, M. Rashid, S. Atlas, and C. Rosendorff, "The impact of environmental factors on the mortality of patients with chronic heart failure," *The American Journal of Cardiology*, vol. 146, no. 10, pp. 48–55, 2021.
- [5] M. H. F. Chaudhry, "Current hypertension reviews," *Bentham Science*, vol. 18, no. 1, p. 7, 2022.
- [6] H. Wang, J. F. Yang, Y. Huo, Heart Failure Study Group, Cardiovascular Medicine Physician Branch, and Chinese Heart Failure Center Alliance Committee of Experts, "Expert consensus on quality evaluation and control indicators of diagnosis and treatment of HF in China," *Chinese Journal of Forensic Medicine*, vol. 13, no. 3, pp. 52–62, 2021.
- [7] L. Li, H. Yao, J. Wang, Y. Li, and Q. Wang, "The role of Chinese medicine in health maintenance and disease prevention: application of constitution theory," *American Journal of Chinese Medicine*, vol. 47, no. 3, pp. 495–506, 2019.
- [8] Q. Tang, Y. Wang, and K. Li, "Zhenwu decoction for chronic heart failure," *Medicine (Baltimore)*, vol. 97, no. 29, Article ID e11559, 2018.
- [9] L. C. Matos, J. P. Machado, F. J. Monteiro, and H. J. Greten, "Understanding traditional Chinese medicine therapeutics: an overview of the basics and clinical applications," *Healthcare*, vol. 9, no. 3, p. 257, 2021.
- [10] M. Kibble, N. Saarinen, J. Tang, K. Wennerberg, S. Mäkelä, and T. Aittokallio, "Network pharmacology applications to map the unexplored target space and therapeutic potential of natural products," *Natural Product Reports*, vol. 32, no. 8, pp. 1249–1266, 2015.
- [11] A. Oulas, G. Minadakis, M. Zachariou, K. Sokratous, M. M. Bourdakou, and G. M. Spyrou, "Systems Bioinformatics: increasing precision of computational diagnostics and therapeutics through network-based approaches," *Briefings in Bioinformatics*, vol. 20, no. 3, pp. 806–824, 2019.
- [12] J. Ru, P. Li, J. Wang et al., "TCMSP: a database of systems pharmacology for drug discovery from herbal medicines," *Journal of Cheminformatics*, vol. 6, no. 1, p. 13, 2014.
- [13] J. van den Anker, M. D. Reed, K. Allegaert, and G. L. Kearns, "Developmental changes in pharmacokinetics and pharmacodynamics," *The Journal of Clinical Pharmacology*, vol. 58, no. Suppl 10, pp. S10–S25, 2018.
- [14] Consortium, "UniProt: a worldwide hub of protein knowledge," *Nucleic Acids Research*, vol. 47, no. D1, pp. D506–D515, 2019.
- [15] D. Szklarczyk, J. H. Morris, H. Cook et al., "The STRING database in 2017: quality-controlled protein-protein association networks, made broadly accessible," *Nucleic Acids Research*, vol. 45, no. D1, pp. D362–D368, 2017.
- [16] The Gene Ontology Consortium, "The gene ontology resource: 20 years and still GOing strong," *Nucleic Acids Research*, vol. 47, no. D1, pp. D330–D338, 2019.
- [17] M. Kanehisa, M. Furumichi, M. Tanabe, Y. Sato, and K. Morishima, "KEGG: new perspectives on genomes, pathways, diseases and drugs," *Nucleic Acids Research*, vol. 45, no. D1, pp. D353–D361, 2017.
- [18] M. G. Crespo-Leiro, M. Metra, L. H. Lund et al., "Advanced heart failure: a position statement of the heart failure association of the European society of cardiology," *European Journal of Heart Failure*, vol. 20, no. 11, pp. 1505–1535, 2018.
- [19] L. Adamo, C. Rocha-Resende, S. D. Prabhu, and D. L. Mann, "Reappraising the role of inflammation in heart failure," *Nature Reviews Cardiology*, vol. 17, no. 5, pp. 269–285, 2020.
- [20] P. van der Meer, H. K. Gaggin, and G. W. Dec, "ACC/AHA versus ESC guidelines on heart failure," *Journal of the American College of Cardiology*, vol. 73, no. 21, pp. 2756–2768, 2019.
- [21] S. Fu, J. Zhang, X. Gao et al., "Clinical practice of traditional Chinese medicines for chronic heart failure," *Heart Asia*, vol. 2, no. 1, pp. 24–27, 2010.
- [22] Y. Du, J. Han, H. Zhang, J. Xu, L. Jiang, and W. Ge, "Kaempferol prevents against ang II-induced cardiac remodeling through attenuating ang II-induced inflammation and oxidative stress," *Journal of Cardiovascular Pharmacology*, vol. 74, no. 4, pp. 326–335, 2019.
- [23] L. Zhang, Z. Guo, Y. Wang, J. Geng, and S. Han, "The protective effect of kaempferol on heart via the regulation of Nrf2, NF- $\kappa$ B, and PI3K/Akt/GSK-3 $\beta$  signaling pathways in isoproterenol-induced heart failure in diabetic rats," *Drug Development Research*, vol. 80, no. 3, pp. 294–309, 2019.
- [24] X. Chen, J. Qian, L. Wang et al., "Kaempferol attenuates hyperglycemia-induced cardiac injuries by inhibiting inflammatory responses and oxidative stress," *Endocrine*, vol. 60, no. 1, pp. 83–94, 2018.
- [25] H. Feng, J. Cao, G. Zhang, and Y. Wang, "Kaempferol attenuates cardiac hypertrophy via regulation of ASK1/MAPK signaling pathway and oxidative stress," *Planta Medica*, vol. 83, no. 10, pp. 837–845, 2017.
- [26] Q. Tang, Y. Wang, and K. Li, "Zhenwu decoction for chronic heart failure: protocol for a systematic review and meta-analysis," *Medicine*, vol. 97, no. 29, 2018.
- [27] L. Cong, Y. Su, D. Wei et al., "Catechin relieves hypoxia/reoxygenation-induced myocardial cell apoptosis via down-regulating lncRNA MIAT," *Journal of Cellular and Molecular Medicine*, vol. 24, no. 3, pp. 2356–2368, 2020.
- [28] H. Zhou, H.-X. Yang, Y. Yuan et al., "Paeoniflorin attenuates pressure overload-induced cardiac remodeling via inhibition of TGF $\beta$ /Smads and NF- $\kappa$ B pathways," *Journal of Molecular Histology*, vol. 44, no. 3, pp. 357–367, 2013.
- [29] X. Liu, K. Chen, Y. Zhuang et al., "Paeoniflorin improves pressure overload-induced cardiac remodeling by modulating the MAPK signaling pathway in spontaneously hypertensive rats," *Biomedicine & Pharmacotherapy*, vol. 111, pp. 695–704, 2019.
- [30] M. Liu, J. Ai, J. Feng et al., "Effect of paeoniflorin on cardiac remodeling in chronic heart failure rats through the transforming growth factor  $\beta$ 1/Smad signaling pathway," *Cardiovascular Diagnosis and Therapy*, vol. 9, no. 3, pp. 272–280, 2019.
- [31] R. Basnet and B. B. Basnet, "Overview of protein kinase B enzyme: a potential target for breast and prostate cancer," *Current Molecular Pharmacology*, vol. 14, no. 4, pp. 527–536, 2021.
- [32] P. Abeyrathna and Y. Su, "The critical role of Akt in cardiovascular function," *Vascular Pharmacology*, vol. 74, pp. 38–48, 2015.
- [33] G. Markousis-Mavrogenis, J. Tromp, W. Ouwkerk et al., "The clinical significance of interleukin-6 in HF: results from the BIOSTAT-CHF study," *European Journal of Heart Failure*, vol. 21, no. 8, pp. 965–973, 2019.
- [34] O. A. Segiet, A. Piecuch, L. Mielanczyk, and E. Nowalany-Kozielska, "Role of interleukins in HF with reduced ejection fraction," *The Anatolian Journal of Cardiology*, vol. 22, no. 6, pp. 287–299, 2019.

- [35] S. N. Goonewardena, A. B. Stein, R. E. Tsuchida, R. Rattan, D. Shah, and S. L. Hummel, "Monocyte subsets and inflammatory cytokines in acute decompensated heart failure," *Journal of Cardiac Failure*, vol. 22, no. 5, pp. 358–365, 2016.
- [36] Z. Wang, J. Zhang, L. Chen, J. Li, H. Zhang, and X. Guo, "Glycine suppresses AGE/RAGE signaling pathway and subsequent oxidative stress by restoring Glo1 function in the aorta of diabetic rats and in HUVECs," *Oxidative Medicine and Cellular Longevity*, vol. 2019, Article ID 4628962, 2019.
- [37] K. Suchal, S. Malik, S. Khan et al., "Molecular pathways involved in the amelioration of myocardial injury in diabetic rats by kaempferol," *International Journal of Molecular Sciences*, vol. 18, no. 5, Article ID 1001, 2017.
- [38] N. Baeyens, C. Bandyopadhyay, B. G. Coon, S. Yun, and M. A. Schwartz, "Endothelial fluid shear stress sensing in vascular health and disease," *Journal of Clinical Investigation*, vol. 126, no. 3, pp. 821–828, 2016.
- [39] P. Kleinbongard, R. Schulz, and G. Heusch, "TNF $\alpha$  in myocardial ischemia/reperfusion, remodeling and heart failure," *Heart Failure Reviews*, vol. 16, no. 1, pp. 49–69, 2011.
- [40] K. A. Porter, I. Desta, D. Kozakov, and S. Vajda, "What method to use for protein-protein docking?" *Current Opinion in Structural Biology*, vol. 55, pp. 1–7, 2019.
- [41] R. Dias and W. de Azevedo Jr., "Molecular docking algorithms," *Current Drug Targets*, vol. 9, no. 12, pp. 1040–1047, 2008.
- [42] J. Li, C. Lu, M. Jiang et al., "Traditional chinese medicine-based network pharmacology could lead to new multi-compound drug discovery," *Evidence-Based Complementary and Alternative Medicine*, vol. 2012, Article ID 149762, 11 pages, 2012.
- [43] Y. Han, L. Huang, G. Zhong et al., "Evaluation of the safety and efficacy of Zhenwu decoction as adjuvant therapy for the treatment of heart failure with reduced ejection fraction: A protocol for systematic review and meta-analysis," *Medicine*, vol. 101, no. 4, 2022.

## Review Article

# Traditional Uses, Phytochemistry, and Bioactivities of *Mesosphaerum suaveolens* (L.) Kuntze

José Weverton Almeida-Bezerra <sup>1</sup>, Felicidade Caroline Rodrigues <sup>1</sup>,  
José Jailson Lima Bezerra <sup>1</sup>, Anderson Angel Vieira Pinheiro <sup>2</sup>,  
Saulo Almeida de Menezes <sup>1</sup>, Aline Belém Tavares <sup>1</sup>, Adrielle Rodrigues Costa <sup>1</sup>,  
Priscilla Augusta de Sousa Fernandes <sup>3</sup>, Viviane Bezerra da Silva <sup>1</sup>,  
José Galberto Martins da Costa <sup>3</sup>, Rafael Pereira da Cruz <sup>3</sup>,  
Maria Flaviana Bezerra Moraes-Braga <sup>3</sup>, Henrique Douglas Melo Coutinho <sup>3</sup>,  
Edward Teixeira de Albergaria <sup>1</sup>, Marcos Vinicius Meiado <sup>4</sup>,  
Abolghasem Siyadatpanah <sup>5</sup>, Bonglee Kim <sup>6</sup>,  
and Antônio Fernando Moraes de Oliveira <sup>1</sup>

<sup>1</sup>Federal University of Pernambuco–UFPE, Recife 50670-901, PE, Brazil

<sup>2</sup>Federal University of Paraíba–UFPB, João Pessoa 58051-970, PB, Brazil

<sup>3</sup>Regional University of Cariri–URCA, Crato 63105-000, CE, Brazil

<sup>4</sup>Federal University of Sergipe–UFS, Itabaiana 49500-000, SE, Brazil

<sup>5</sup>Ferdows School of Paramedical and Health, Birjand University of Medical Sciences, Birjand, Iran

<sup>6</sup>Department of Pathology, College of Korean Medicine, Kyung Hee University, Seoul 02447, Republic of Korea

Correspondence should be addressed to Bonglee Kim; bongleekim@khu.ac.kr

Received 1 December 2021; Revised 28 January 2022; Accepted 16 February 2022; Published 10 March 2022

Academic Editor: Sekar Vijayakumar

Copyright © 2022 José Weverton Almeida-Bezerra et al. This is an open access article distributed under the Creative Commons Attribution License, which permits unrestricted use, distribution, and reproduction in any medium, provided the original work is properly cited.

*Mesosphaerum suaveolens* (L.) Kuntze is a species widely used traditionally in the treatment of ailments, such as stomach pain, hemorrhoids, cough, verminosis, ulcer, liver disease, fever, influenza, nasal congestion, and inflammation. This review aims to provide a survey of available information on seven international electronic databases (Google Scholar, Medline, ResearchGate, Web of Science, Scopus, Science Direct, and PubMed) about botanical aspects, traditional uses, phytochemistry, and biological activities of *M. suaveolens*. *Mesosphaerum suaveolens* is a tropical America native species, but it can be found in several parts of the world as a ruderal plant. The species is the most studied species of the genus Lamiaceae due its phytochemical aspect, especially regarding the chemical composition of its essential oil. Besides the essential oils, *M. suaveolens* is a source of numerous secondary compounds such as triterpenes, diterpenes, and phenolic compounds, which are related to its biological activities, such as allelopathic, antibacterial, antifungal, insecticidal, and larvicidal activities as described in the literature.

## 1. Introduction

Plant species, with medicinal properties that have always been part of human life, are being used both for the treatment of diseases as for food. For the treatment of diseases, they are accessible and culturally accepted, so their

use is popular since ancient civilizations [1, 2]. The Lamiaceae family is one of the most diverse and widespread in terms of the ethnomedicinal value and variety of plants with biological and medical applications [3–8]. Regarding the genus *Mesosphaerum*, previous studies demonstrate the ethnomedicinal and pharmacological importance of some



species that belong to it, such as *Mesosphaerum sidifolium* (L'Hérit.) Harley & J.F.B. Pastore, used to treat stomach disorders and headaches, as well as being used as an expectorant, carminative, and tonic. This species possesses in vivo antitumor activity against Ehrlich ascites carcinoma cells causing growth inhibition by inducing cell cycle arrest, besides not showing cytotoxicity [9]. Another species with several bioactivities is *Mesosphaerum verticillatum* (syn. *Hyptis verticillata* Jacq.) with anti-inflammatory, antimicrobial, and anticancer potentials, among other reports. Ethnomedicinal uses of this plant include cough, colds, asthma, fever, tonsillitis, uterine fibroids, bronchitis, and gastrointestinal problems [5].

In Northeast Brazil, the use of plant species as therapeutic resources is widespread, and one species present in this region is *Mesosphaerum suaveolens* (L.) Kuntze, known as “bamburral,” “erva-canudo,” or “alfazema-brava” [10]. Its leaves are mainly used to treat respiratory diseases (asthma, bronchitis, colds, and flu) and diseases related to the gastrointestinal tract [1]. Such medicinal uses are related to the chemical heterogeneity arising from the secondary metabolism of the species, a recurrent characteristic in species of the Lamiaceae family [6].

Several works in the literature indicate that *M. suaveolens* presents a high biotechnological potential, mainly regarding its essential oil [10]. In addition, a large number of studies have emphasized the biological activities of the essential oil and extracts of this species against pathogenic microorganisms to humans [6]. Taking into account that *M. suaveolens* is a medicinal species widely studied by the scientific community, the main objective of this work was to make a general review of the botanical aspects, traditional uses, phytochemistry, toxicity and biological, and pharmacological activities.

## 2. Materials and Methods

Methodologically, it was used the keywords “*Mesosphaerum suaveolens*” and its synonym “*Hyptis suaveolens*” associated to the terms “biological activity,” “bioactive,” “ethnomedicinal use,” “traditional use,” “ethnobotany,” “ethnopharmacology,” “toxicity,” “natural products,” “phytochemistry,” and “allelopathy” to collect information available on Google Scholar, Medline, ResearchGate, Web of Science, Scopus, ScienceDirect, and PubMed databases. The consideration insertion criteria of the articles were as follows: full article only, articles written in English and/or Portuguese languages, and all available and opened access articles, with no time limit determined.

It was obtained 190 articles dated between 1971 and 2021 which were grouped into some categories. (1) Botanical aspects, with information on description, classification, and geographical distribution; (2) phytochemistry; (3) ethnobotany; (4) biological activities; and (5) pharmacological activities. The trial process (collecting of the articles, reading of the abstracts, and checking the insertion criteria) took three months, and all the selected articles had been read completely and summarized in a table with the isolated chemical constituents and their respective biological activities.

## 3. Review

**3.1. Botanical Aspects: Description, Classification, and Distribution.** *Mesosphaerum suaveolens* (L.) Kuntze is an herbaceous plant belonging to the Lamiaceae family. The word “*mesosphaeron*” comes from the Greek and Latin “*mesosphaerum*,” meaning “a type of tuberose with medium-sized leaves,” while its specific epithet *suaveolens*, means “with a sweet fragrance” due to the aroma of essential oils exhaled by the trichomes present on its leaves [11, 12].

Its vernacular name varies widely according to the region of occurrence. In the northeastern region of Brazil, the species is known as “bamburral” and “alfazema-brava” and in the southern region of the country, the herbaceous plant is called “erva-canudo” and “betônica-brava” [10]. In other parts of the world, such as in India, it is known as “pignut,” “beejabandha,” “sima tulasi,” “sakavong,” “pichi tulas,” and “bushmint” [13], while in Nigeria, it is known as “false buttonweed” and in Bangladesh as “tukma” [14]. In French-speaking countries, the species is called “horehound,” “pignut,” “wild spikenard,” “gros baume,” and “*Hyptis à odeur*.” In other languages, the plant is called “chao,” “hierba de las muelas,” “menta de campo” (Spanish), “wilaiti tulsi” (Hindi), “bhustrena,” “darp tulas,” “jungli tulas” (Marathi), “sirna tulasi” (Telugu), “bilati tulas” (Bengali), “ganga tulasi” (Ora), and “bhustrena” (Sanskrit) [13].

Taxonomically, *M. suaveolens* presents as botanical synonyms *Ballota suaveolens* L., *Hyptis suaveolens* (L.) Poit., *Bystropogon suaveolens* (L.) L'Hér., *Bystropogon graveolens* Blume, *Hyptis congesta* Leonard, *Hyptis ebracteata* R.Br., *Hyptis plumierii* Poit., and *Marrubium indicum* Blanco, with *H. suaveolens* as the most widespread synonym in scientific circles. However, the current circumscription of the genus *Mesosphaerum* P. Browne was recognized in 2012 after phylogenetic studies [15].

Morphologically, *M. suaveolens* is an erect herb or subshrub that measures up to 2 m in height. Its photosynthetic quadrangular stem is hairy with closely spaced branches and nodes. It has oval leaves, serrate or cordate margin, pilose limb, acute apex, and obtuse base with opposite crossed phyllotaxis. The petioles are short, canalliculate, as are its stems. Its inflorescences consist of up to 20 flowers located around the nodes and near the leaf axils. The flowers are pedunculate, with a persistent, tubular calyx, and 5 pointed sepals. The corolla is also tubular with five lilac petals, and the lobes are evident. Its fruits are dry, indehiscent, and uniseminated, originating from a bicarpellate gynoecium. Such fruits originate dimorphic seeds, two per fruit. Morphologically, such diaspores are elongated with dorsoventral flattening, longitudinal median ridge, starting near the hilum and extending to the apex of the seed with retusa boundary with black coloration (Figure 1) [16–18].

As for the geographical distribution, *M. suaveolens* is native to tropical America; however, as it is ruderal, it ended up invading natural ecosystems in tropical and subtropical regions of the globe, so that, due to this widespread occurrence, the species is considered a pantropical ruderal species [19–22]. In Brazil, *M. suaveolens* is present in almost the entire territory [23].



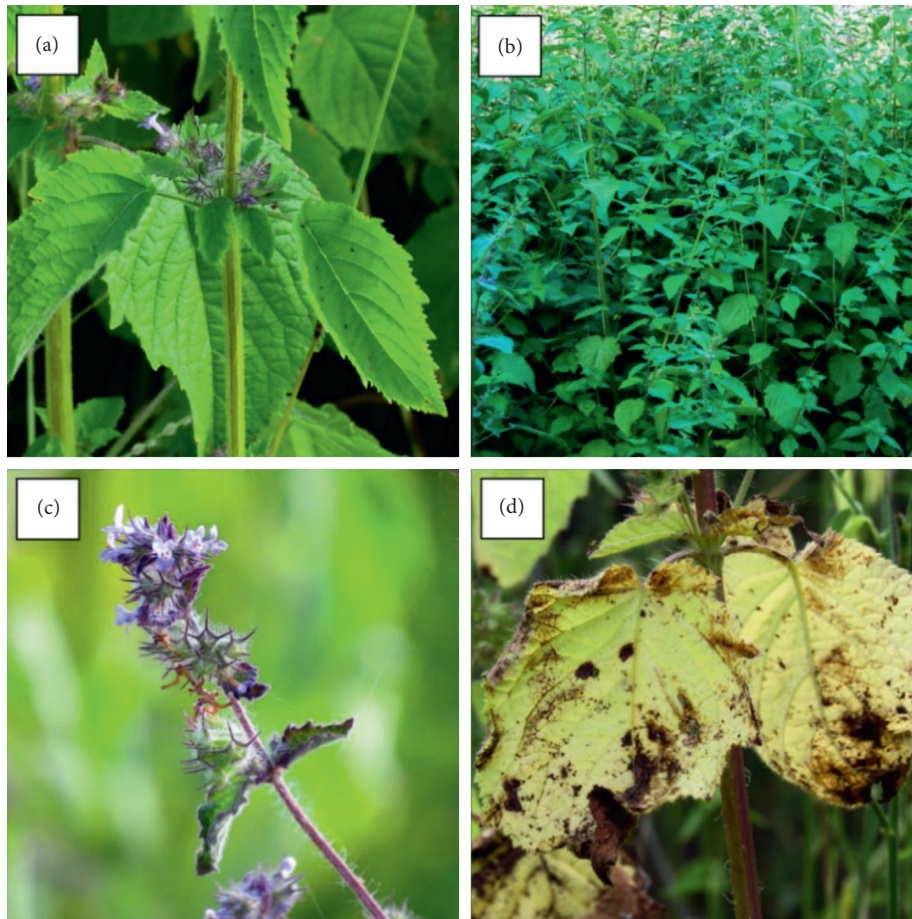


FIGURE 1: *Mesosphaerum suaveolens* (L.) Kuntze (Lamiaceae). (a) Leaves and stem. (b) Population of *M. suaveolens* in an area of Caatinga, a seasonally dry tropical forest, in Quixelô-CE, Brazil. (c) Prominence of flowers. (d) Leaves in senescence. Source: author (2018).

**3.2. Phytochemistry.** *Mesosphaerum suaveolens* is an important source of essential oils, alkaloids, flavonoids, phenols, saponins, triterpenes, and sterols [13, 24]. The essential oil of this species, obtained exclusively from its leaves, has already been chemically characterized in several studies. However, since this species exhibits a high level of genetic polymorphism and allows adaptation to changes in environmental characteristics, high variability in the composition and content of the major constituents (>20%) has been found [25]. In *M. suaveolens* extracts, terpenoids had a great predominance (mono, di, tri, and sesquiterpenes) (Table 1) (Table 1). Among the diterpenes, suaveolic acid stood out with recognized antimicrobial and allelopathic action [26]. Furthermore, phenolic acids, phenylpropanoids, flavonoids [10, 27], and fatty acids [28, 29] were also identified in different parts of *M. suaveolens* (Table 1).

**3.3. Ethnobotany.** Traditionally, *M. suaveolens* is taken to treat ailments in Brazil, Benin, India, Nigeria, Thailand, and Togo. In Brazil, the leaves in the form of infusions, decoctions, teas, and syrups are used to treat ulcers, inflammation, respiratory diseases (asthma, bronchitis, colds, flu, and sinusitis), diseases related to the gastrointestinal tract, pain, dizziness, nausea, nervousness, and constipation

[1, 56–64]. The leaves are also used to treat headaches [65], malaria [14, 66], fever [67, 68], and used to reduce labor time and labor pain [69]. The flowers of *M. suaveolens* are employed as therapeutic resources against dysmenorrhea, respiratory diseases, and as a febrifuge [70, 71].

In the Asian continent, more specifically in India, the leaves, stems, inflorescence, and roots are used to treat urinary calculi [72], stomach pain [73], healing, itching [74], boil, eczema, diabetes [75], pneumonia [76], and fever [77]. Besides that, the seeds of *M. suaveolens* are used to treat gynecological disorders such as menorrhagia, leucorrhoea, and rheumatism [78, 79]. The fresh poultice of the leaves is applied to snake bites, wounds, and mycoses [80], while the paste of the fresh leaves is also indicated for skin diseases [81].

In South Asia, in Bangladesh, traditional communities use the seeds in juice preparations to treat constipation and weakness [82, 83]; in addition, the seeds are consumed along with roots of *Bombax ceiba* to treat gonorrhoea [84, 85], and the paste of the leaves is used to treat skin infections [86]. In Togo, the leaves of the species are spent in decoction form for the treatment of gynecological disorders [87], while in Thailand, the decoction of the roots is indicated in cases of food poisoning [88]. On the African continent, more specifically in Benin and Nigeria, the whole plant of

TABLE 1: Identified constituents in *Mesosphaerum suaveolens* (L.) Kuntze (Lamiaceae).

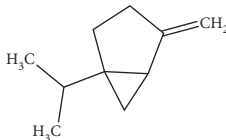
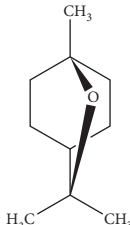
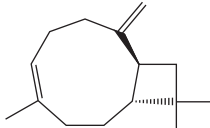
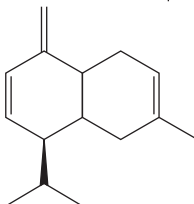
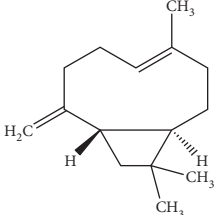
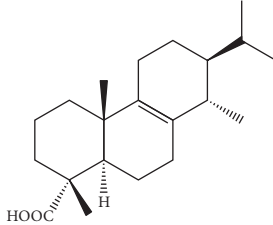
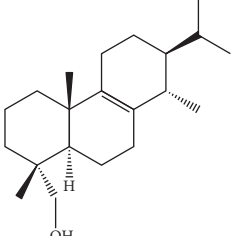
Composite	Structure	Identification method	Part of the plant	Citation
<b>Monoterpene</b>				
Sabinene		GC-MS	Leaves (essential oil)	[30–35]
Eucalyptol		GC-MS	Leaves (essential oil)	[35–37]
<b>Sesquiterpene</b>				
<i>E</i> -Caryophyllene		GC-MS	Leaves (essential oil)	[38]
Germacrene D		GC-MS	Leaves (essential oil)	[38]
$\beta$ -Caryophyllene		GC-MS	Leaves (essential oil)	[32, 33, 39, 40]
<b>Diterpenes</b>				
Mellowolic acid		$^1\text{H-NMR}$ and $^{13}\text{C-NMR}$	Leaves and stem	[26, 41]
Suaveolol		$^1\text{H-NMR}$ and $^{13}\text{C-NMR}$	Leaves	[41–43]

TABLE 1: Continued.

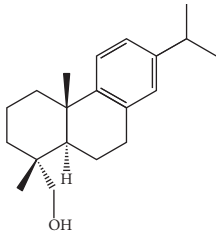
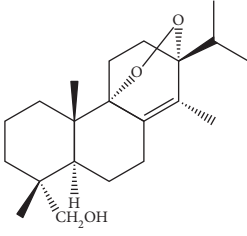
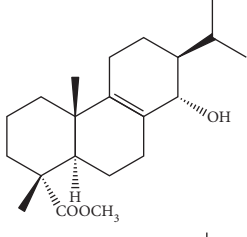
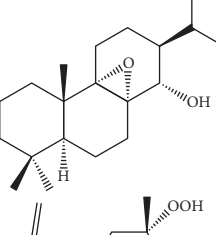
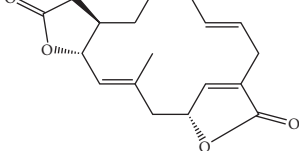
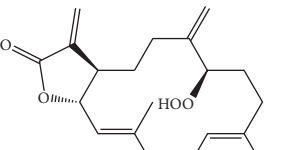
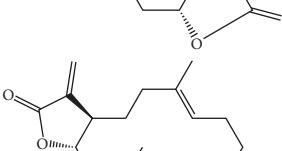
Composite	Structure	Identification method	Part of the plant	Citation
Dehydroabietinol		GC-MS, $^1\text{H-NMR}$ , and $^{13}\text{C-NMR}$	Leaves, stem, and flowers	[29, 44, 45]
$9\alpha,13\alpha$ -Epi-dioxiabiet-8(14)-en-18-ol		$^1\text{H-NMR}$ and $^{13}\text{C-NMR}$	Leaves	[46]
Methyl suaveolate		$^1\text{H-NMR}$ and $^{13}\text{C-NMR}$	Leaves	[42]
Ácido $8\alpha,9\alpha$ -epoxysuaveolic		$^1\text{H-NMR}$ and $^{13}\text{C-NMR}$	Leaves and stem	[43]
$4\alpha$ -Hydroperoxy-5-enovatodiolide		$^1\text{H-NMR}$ and $^{13}\text{C-NMR}$	Flowers	[47]
4-Methylene- $5\beta$ -hydroperoxy ovatodiolide		$^1\text{H-NMR}$ and $^{13}\text{C-NMR}$	Flowers	[47]
Ovatodiolide		$^1\text{H-NMR}$ and $^{13}\text{C-NMR}$	Flowers	[47]

TABLE 1: Continued.

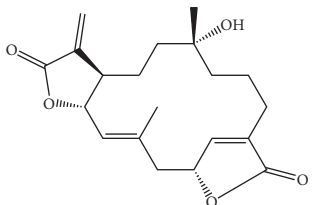
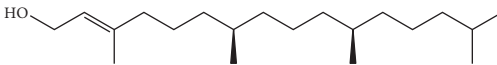
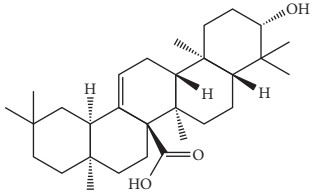
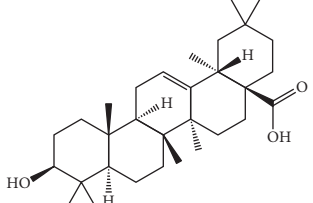
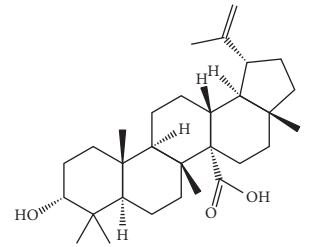
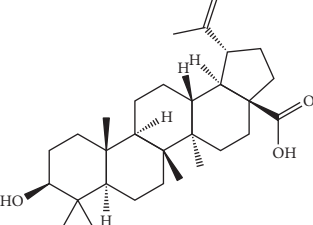
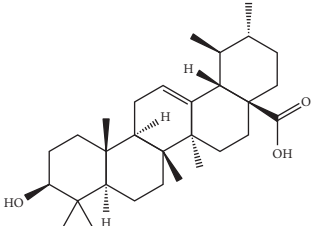
Composite	Structure	Identification method	Part of the plant	Citation
4 $\alpha$ -Hydroxy-5-enovatodiolide		$^1\text{H-NMR}$ and $^{13}\text{C-NMR}$	Flowers	[47]
Phytol		GC-MS	Flowers	[29]
Triterpenes and steroids				
$\alpha$ -Peltoboikinolic acid		$^1\text{H-NMR}$ and $^{13}\text{C-NMR}$	Root	[48]
Oleanolic acid		$^1\text{H-NMR}$ and $^{13}\text{C-NMR}$	Root	[48]
Bacosine		$^1\text{H-NMR}$ and $^{13}\text{C-NMR}$	Root	[49]
Betulinic acid		$^1\text{H-NMR}$ and $^{13}\text{C-NMR}$	Root	[49]
Ursolic acid		$^1\text{H-NMR}$ and $^{13}\text{C-NMR}$	Root, leaves, and stem	[49, 50]

TABLE 1: Continued.

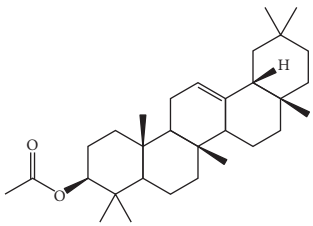
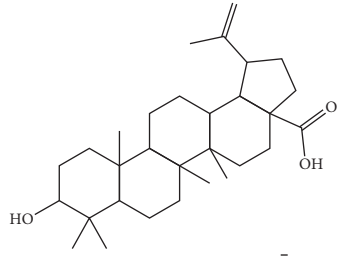
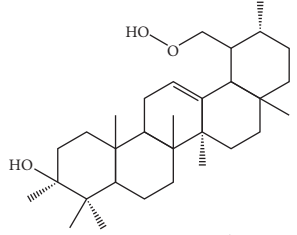
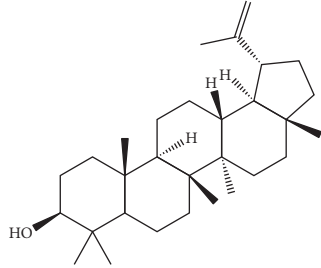
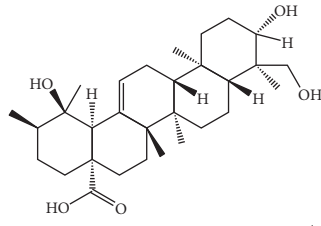
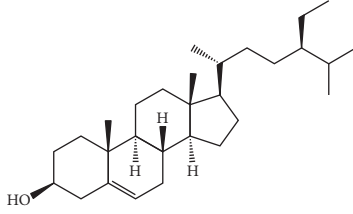
Composite	Structure	Identification method	Part of the plant	Citation
$\alpha$ -Amyrin		$^1\text{H-NMR}$ and $^{13}\text{C-NMR}$	Root	[51]
$3\beta$ -Hydroxylup-20(29)-en-28-oic acid		$^1\text{H-NMR}$ and $^{13}\text{C-NMR}$	Root	[51]
Urs-12-en-3 $\beta$ -ol-29-oic acid		$^1\text{H-NMR}$ and $^{13}\text{C-NMR}$	Leaves and stem	[53]
Lupeol		$^1\text{H-NMR}$ and $^{13}\text{C-NMR}$	Leaves	[50]
Rotundic acid		$^1\text{H-NMR}$ and $^{13}\text{C-NMR}$	Leaves and stem	[50]
$\beta$ -Sitosterol		$^1\text{H-NMR}$ and $^{13}\text{C-NMR}$	Leaves and stem	[50]

TABLE 1: Continued.

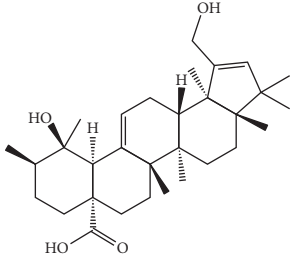
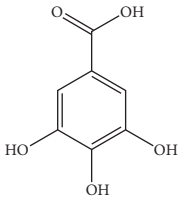
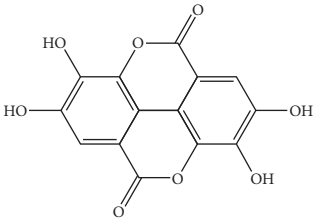
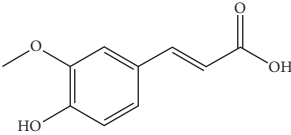
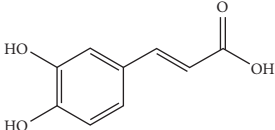
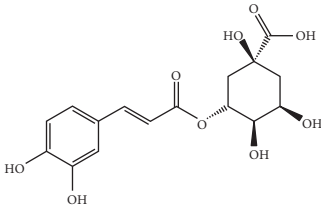
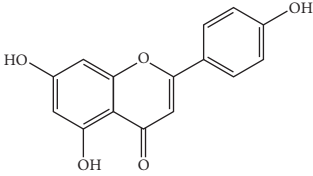
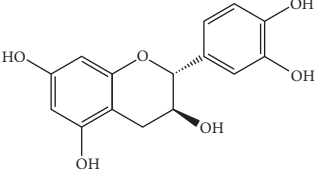
Composite	Structure	Identification method	Part of the plant	Citation
Hyptadienoic acid		$^1\text{H-NMR}$ and $^{13}\text{C-NMR}$	Leaves and stem	[53]
Phenolics				
Gallic acid		HPLC-DAD and HPTLC	Leaves and stem	[10, 27]
Ellagic acid		HPLC-DAD	Leaves and aerial parts	[6]
Ferulic acid		HPTLC	Leaves and stem	[27]
Caffeic acid		HPLC-DAD and UPLC-MS	Leaves	[6, 10, 54]
Chlorogenic acid		HPLC-DAD and HPTLC	Leaves and stem	[6, 10, 27]
Apigenin		HPLC-DAD	Leaves	[6, 10]
Catechin		HPLC-DAD	Leaves	[6, 10]



TABLE 1: Continued.

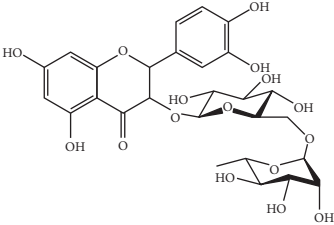
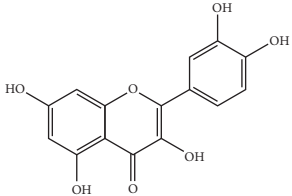
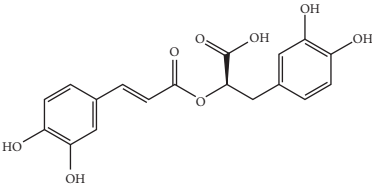
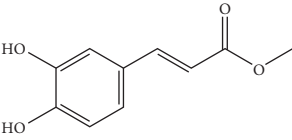
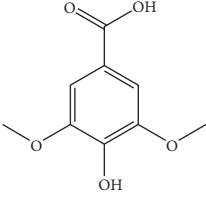
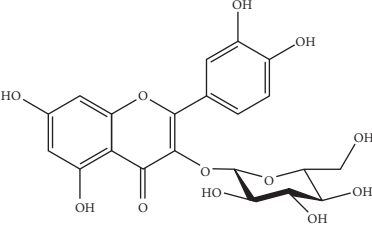
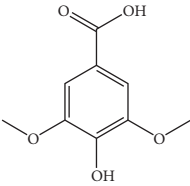
Composite	Structure	Identification method	Part of the plant	Citation
Rutin		HPLC-DAD and UPLC-MS	Leaves	[6, 10, 54]
Quercetin		HPLC-DAD and UPLC-MS	Leaves and stem	[6, 10, 27, 54]
Rosmarinic acid		UPLC-MS	Leaves	[54]
Ethyl caffeate		UPLC-MS	Leaves	[54]
Sagerinic acid		UPLC-MS	Leaves	[54]
Isoquercetin		UPLC-MS	Leaves	[54]
Syringic acid		UPLC-MS	Leaves	[54]

TABLE 1: Continued.

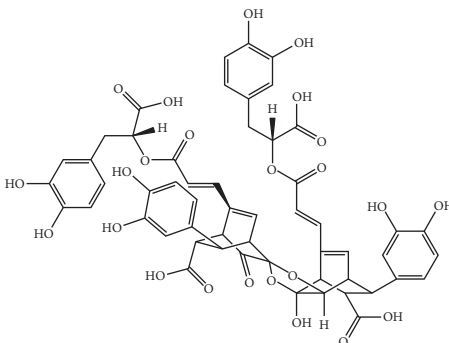
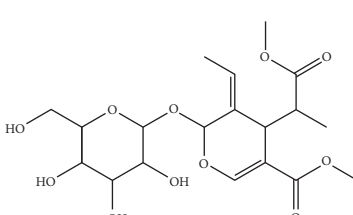
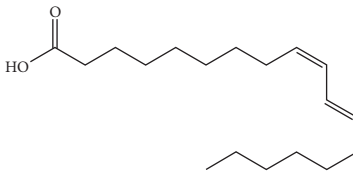
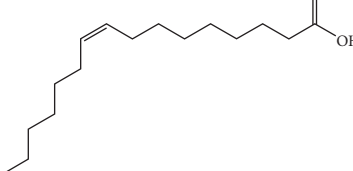
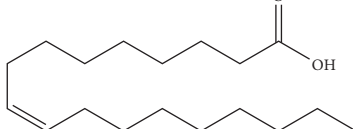
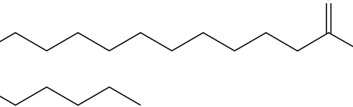
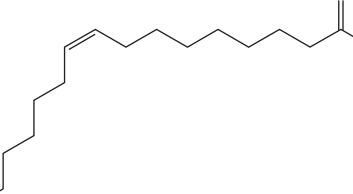
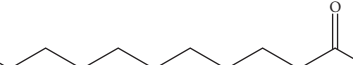
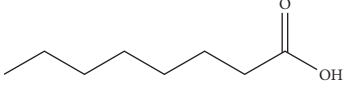
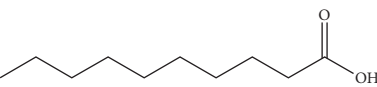
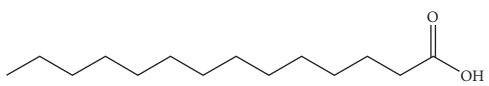
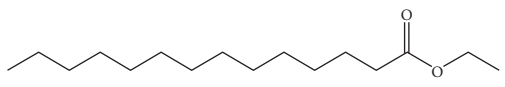
Composite	Structure	Identification method	Part of the plant	Citation
Yunnaneic acid		UPLC-MS	Leaves	[54]
Secoiridoid				
Oleoside dimethyl ester		UPLC-MS	Leaves	[54]
Fatty acids				
Linoleic acid		GC-MS	Seeds	[28]
Palmitic acid		GC-MS	Seeds and leaves	[28, 29]
Oleic acid		GC-MS	Seeds	[28]
Stearic acid		GC-MS	Seeds	[28]
Palmitoleic acid		GC-MS	Seeds	[28]
Undecanoic acid		GC-MS	Leaves	[29]

TABLE 1: Continued.

Composite	Structure	Identification method	Part of the plant	Citation
Octanoic acid		GC-MS	Leaves	[29]
<i>n</i> -Decanoic acid		GC-MS	Leaves	[29]
Tetradecanoic acid		GC-MS	Leaves	[29]
Myristic acid ethyl ester		GC-MS	Aerial parts	[55]

*M. suaveolens* is used for the treatment of candidiasis and as a blood tonic [89, 90].

From a veterinary point of view, *M. suaveolens* has also been used for the treatment of diseases in animals. Such use is reported in India for the treatment of inflammation in cattle, with the juice of the leaves being applied to the animal's eyes [91]. In Brazil, the species is employed against diarrhea [92]. In the African continent, more specifically in Kenya, the aerial parts of the plant are utilized as a repellent for the mosquito *Anopheles gambiae* Giles, 1926 (Diptera: Culicidae) [93, 94].

### 3.4. Biological Activities

**3.4.1. Allelopathic Activity.** According to Sharma et al. [95], after the establishment of *M. suaveolens* in an area, it becomes evident that the species imposes a profound impact on the local vegetation, as the number of species, richness, diversity, and uniformity is severely reduced. Although *M. suaveolens* is native to the Brazilian territory, it is distributed in different ecosystems, such as Caatinga, a seasonally dry tropical forest [20].

*Mesosphaerum suaveolens* produces numerous seeds of rapid germination and subsequent growth and thus manages to occupy and dominate environments because of its allelopathic action [96]. Islam et al. [26], for example, isolated suaveolic acid from *M. suaveolens* and demonstrated in bioassays that this diterpene exhibits allelopathic action, interfering with the growth of the caulicle and radicle of *Lepidium sativum* L. (Brassicaceae), *Lactuca sativa* L. (Asteraceae), *Lolium multiflorum* Lam. (Poaceae), and *Echinochloa crus-galli* (L.) P. Beauv. (Poaceae). Their extracts present allelopathic action against *Echinochloa crus-galli* (L.) P. Beauv. [97], *Sorghum vulgare* Pers., *Raphanus sativus* L., and *Lactuca sativa* L. [98].

Allelochemicals present in the species have been reported to act by causing oxidative stress, reduction in chlorophyll content, and inducing the formation of chromosomal aberrations [99, 100]. Such damage may occur in response to the synergistic action of the constituents.

In addition to heterotoxicity, *M. suaveolens* has been found to exhibit autotoxicity; however, its constituents affect

other species more than itself [101]. Thus, the low amounts of allelochemicals released by *M. suaveolens* affect the ecological succession of other species, but do not affect the species itself as much.

Despite reports of the allelopathic action of *M. suaveolens*, it is worth noting that most of these studies were conducted under laboratory conditions and with extracts of the plant, so these actions do not match the allelopathic actions found in the environment. Thus, it is necessary to conduct studies that simulate as much as possible the natural conditions, to affirm whether one species can affect another. Only Kapoor [99] evaluated the allelopathic action of *M. suaveolens* in conditions similar to those found in the environment, demonstrating in fact that the species has allelopathic action on *Parthenium hysterophorus* L. (Asteraceae).

*M. suaveolens* has allelochemicals from its secondary metabolism, which compromise the structure and plant diversity [102].

**3.4.2. Antimicrobial Activity.** Teas of *M. suaveolens* are used to treat diseases related to the gastrointestinal and respiratory tracts [1], so numerous researchers have hypothesized that the species exhibits biological activity against strains of pathogenic microorganisms.

Cyrille et al. [103] evaluated the antibacterial action of the hydroethanolic extract (70%) of the leaves and found that the species presented low antibacterial activity since an MIC of 3.12 mg/ml was observed against *Staphylococcus aureus* (Rosenbach, 1884) (Staphylococaceae) ATCC 25923 and *Pseudomonas aeruginosa* (Schroeter, 1872) (Pseudomonadaceae) ATCC 27853 strains. It is worth noting that MIC values obtained above 1 mg/ml (1000 µg/ml) do not reflect clinically notable activity (Van Vuuren, 2008) (Table 2).

The works evaluating the antimicrobial action of the species highlight the use of the volatile terpenes (essential oils) of the leaves (Table 2). Xu et al. [104] demonstrated that the oil of *M. suaveolens* showed antimicrobial action through the microdilution technique with MIC values of great clinical relevance, notably against *Bacillus subtilis* (Cohn, 1872) (Bacillaceae) CMCC 63501, *Escherichia coli*

TABLE 2: Antimicrobial activities of *Mesosphaerum suaveolens* (L.) Kuntze (Lamiaceae).

Extract/parts of the plant	Assay	Antimicrobial activity	Citation
Methanolic extract of the aerial parts	Disk diffusion test	<i>Candida albicans</i> (7 mm)	[105]
Essential oil from the leaves	Disk diffusion test	<i>Staphylococcus aureus</i> ATCC 29213 (27 mm) <i>Escherichia coli</i> ATCC 25922 (22 mm) <i>Trichophyton mentagrophytes</i> (15 mm) <i>Trichophyton rubrum</i> (24 mm)	[106]
Essential oil from the leaves	Dilution method	<i>Staphylococcus aureus</i> ATCC 29213 (MIC 8.82 mg/ml) <i>Streptococcus pyogenes</i> P183 (MIC 4.41 mg/ml) <i>Streptococcus pyogenes</i> P31 P183 (MIC 4.41 mg/ml) <i>Bacillus subtilis</i> (MIC 16.67 µl/ml) <i>Staphylococcus aureus</i> (MIC 1.56 µl/ml)	[106]
Essential oil from the leaves	Disk diffusion test	<i>Escherichia coli</i> (MIC 6.25 µl/ml) <i>Proteus vulgaris</i> (MIC 50 µl/ml) <i>Pseudomonas aeruginosa</i> (MIC 25 µl/ml)	[107]
Essential oil from the leaves	Disk diffusion test and dilution method	<i>Erwinia herbicola</i> MTCC 3609 (MIC 2 µl/ml) <i>Pseudomonas putida</i> MTCC 1190 (MIC 8 µl/ml) <i>Staphylococcus aureus</i> CMCC 26001 (MIC 50 µg/ml) <i>Bacillus subtilis</i> CMCC 63501 (MIC 25 µg/ml) <i>Pseudomonas aeruginosa</i> CMCC 10104 (MIC 50 µg/ml)	[108]
Essential oil from the aerial parts	Microdilution method	<i>Escherichia coli</i> CMCC 44102 (MIC 25 µg/ml) <i>Fusarium graminearum</i> (MIC 50 µg/ml) <i>Botrytis cinerea</i> (MIC 25 µg/ml) <i>Exerohilum turcicum</i> (MIC 50 µg/ml) <i>Lecanosticta acicola</i> (MIC 50 µg/ml) <i>Aeromonas caviae</i> (0.1 mm) <i>Aeromonas hydrophila</i> (0.1 mm)	[104]
Ethanol extract of the aerial parts	Disk diffusion test	<i>Ralstonia</i> spp. (0.17 mm) <i>Shigella</i> spp. (0.23 mm) <i>Trichophyton mentagrophyte</i> (15.7 mm)	[109]
Aerial parts essential oil	Disk diffusion test	<i>Trichophyton rubrum</i> (14.7 mm) <i>Microsporium gypseum</i> (13.3 mm) <i>Candida albicans</i> (13.7 mm) <i>Escherichia coli</i> ATCC 25922 (MIC 350 µl/ml)	[110]
Blossoms essential oil	Disk diffusion test	<i>Klebsiella pneumoniae</i> ATCC 23357 (MIC 400 µl/ml) <i>Salmonella typhi</i> CDC57 (MIC 450 µl/ml) <i>Escherichia coli</i> ATCC 25922 (MIC 350 µl/ml)	[111]
Flower essential oil	Disk diffusion test	<i>Klebsiella pneumoniae</i> ATCC 23357 (MIC 400 µl/ml) <i>Salmonella typhi</i> CDC57 (MIC 450 µl/ml) <i>Staphylococcus aureus</i> Meti-R (MIC 3.12 mg/ml)	[111]
Leaf hydroethanolic extract (70%)	Agar diffusion method	<i>Pseudomonas aeruginosa</i> Cefta/Imp-R (MIC 12.5 mg/ml) <i>Staphylococcus aureus</i> ATCC 25923 (MIC 3.12 mg/ml) <i>Pseudomonas aeruginosa</i> ATCC 27853 (MIC 3.12 mg/ml) <i>Staphylococcus aureus</i> Meti-R (MIC 5.37 mg/ml)	[103]
Leaves essential oil	Agar diffusion method	<i>Pseudomonas aeruginosa</i> Cefta/Imp-R (MIC 10.75 mg/ml) <i>Staphylococcus aureus</i> ATCC 25923 (MIC 5.37 mg/ml) <i>Pseudomonas aeruginosa</i> ATCC 27853 (MIC 10.75 mg/ml) <i>Escherichia coli</i> MTCC 443 (MIC 0.5 mg/ml) <i>Salmonella typhi</i> MTCC 531 (MIC 0.125 mg/ml) <i>Shigella flexneri</i> MTCC 1457 (MIC 0.5 mg/ml) <i>Vibrio vulnificus</i> MTCC 1145 (MIC 0.5 mg/ml)	[103]
Seed fixed oil	Dilution method	<i>Pseudomonas aeruginosa</i> MTCC 424 (MIC 0.125 mg/ml) <i>Lactobacillus plantarum</i> MTCC 2621 (MIC 0.125 mg/ml) <i>Lactobacillus leishmanii</i> MTCC 911 (MIC 0.25 mg/ml) <i>Staphylococcus aureus</i> MTCC 737 (MIC 0.25 mg/ml) <i>Candida tropicalis</i> MTCC 227 (MIC 0.125 mg/ml) <i>Candida albicans</i> MTCC 227 (MIC 0.25 mg/ml) <i>Escherichia coli</i> ATCC 25922 (MIC 350 µl/ml)	[112]
Essential oil from leaves	Disc diffusion method	<i>Klebsiella pneumoniae</i> ATCC 23357 (MIC 300 µl/ml) <i>Salmonella typhi</i> CDC57 (MIC 400 µl/ml)	[111]

TABLE 2: Continued.

Extract/parts of the plant	Assay	Antimicrobial activity	Citation
Hexanic extract from the seeds	Microdilution method	<i>Staphylococcus aureus</i> Meti-R (MIC 0.375 mg/ml)	[113]
		<i>Enterococcus faecalis</i> ATCC 29212 (MIC 0.1875 mg/ml)	
		<i>Escherichia coli</i> ATCC 25922 (MIC 0.1875 mg/ml)	
		<i>Pseudomonas aeruginosa</i> ATCC 15442 (MIC 0.375 mg/ml)	
		<i>Klebsiella pneumoniae</i> (MIC 0.375 mg/ml)	
Aqueous extract from the leaves	Microdilution method	<i>Acinetobacter baumannii</i> (MIC 0.375 mg/ml)	[6]
		<i>Candida albicans</i> 77 (IC <sub>50</sub> 266.4 µg/ml)	
		<i>Candida albicans</i> 40006 (IC <sub>50</sub> 300.4 µg/ml)	
		<i>Candida tropicalis</i> 23 (IC <sub>50</sub> 359.9 µg/ml)	
		<i>Candida tropicalis</i> 40042 (IC <sub>50</sub> 640.3 µg/ml)	
Aqueous extract from aerial parts	Microdilution method	<i>Candida albicans</i> 77 (IC <sub>50</sub> 18.5 µg/ml)	[6]
		<i>Candida albicans</i> 40006 (IC <sub>50</sub> 526.4 µg/ml)	
		<i>Candida tropicalis</i> 23 (IC <sub>50</sub> 25 µg/ml)	
		<i>Candida tropicalis</i> 40042 (IC <sub>50</sub> 58.62 µg/ml)	
		<i>Staphylococcus aureus</i> UCH 511 (14 mm)	
Essential oil from the leaves	Disk diffusion test	<i>Bacillus cereus</i> (10 mm)	[114]
		<i>Escherichia coli</i> NCTC 7001 (12 mm)	
		<i>Pseudomonas aeruginosa</i> UCH 655 (14 mm)	
Leaf ethanolic extract	Disk diffusion test	<i>Candida albicans</i> (16 mm)	[115]
		<i>Sclerotium rolfsii</i> (MIC 2000 mg/ml)	
Leaf hydroethanolic extract (70%)	Disk diffusion test	<i>Staphylococcus aureus</i> Meti-R (24 mm)	[116]
		<i>Staphylococcus aureus</i> ATCC 25923 (24 mm)	
		<i>Pseudomonas aeruginosa</i> Ceft/Imp-R (16 mm)	
		<i>Pseudomonas aeruginosa</i> ATCC 27853 (20 mm)	
Leaf essential oil	Disk diffusion test	<i>Staphylococcus aureus</i> Meti-R (13 mm)	[116]
		<i>Staphylococcus aureus</i> ATCC 25923 (16 mm)	
		<i>Pseudomonas aeruginosa</i> Ceft/Imp-R (0 mm)	
		<i>Pseudomonas aeruginosa</i> ATCC 27853 (0 mm)	
		<i>Staphylococcus aureus</i> (MIC 30 µg/ml)	
Leaf essential oil	Disk diffusion test	<i>Bacillus subtilis</i> (MIC 26 µg/ml)	[117]
		<i>Proteus vulgaris</i> (MIC 15 µg/ml)	
		<i>Candida albicans</i> (MIC 10 µg/ml)	
		<i>Aspergillus niger</i> (MIC 40 µg/ml)	
		<i>Pseudomonas aeruginosa</i> (MIC 28 µg/ml)	
		<i>Trichophyton mentagrophytes</i> (MIC > 100 µg/ml)	
		<i>Escherichia coli</i> (MIC 26 µg/ml)	
		<i>Klebsiella pneumoniae</i> (MIC 37 µg/ml)	
<i>Yersinia enterocolitica</i> (MIC > 100 µg/ml)			
Essential oil from the leaves	Disk diffusion test	<i>Aspergillus flavus</i> (MIC 93.8 µl/ml)	[118]
		<i>Escherichia coli</i> (7 mm)	
		<i>Bacillus subtilis</i> (8 mm)	
		<i>Vibrio cholerae</i> (9 mm)	
		<i>Shigella dysenteriae</i> (9 mm)	
Essential oil from the leaves	Disk diffusion test	<i>Corynebacterium diphtheriae</i> (10 mm)	[119]
		<i>Salmonella typhi</i> (9 mm)	
		<i>Streptococcus faecalis</i> (9 mm)	
		<i>Bacillus pumilus</i> (9 mm)	
		<i>Streptococcus pyogenes</i> (8 mm)	
		<i>Micrococcus</i> (8 mm)	
Crushed leaves	Disk diffusion test	<i>Pseudomonas solanacearum</i> (10 mm)	[120]
		<i>Aspergillus flavus</i> (56% inhibition at 5% concentration)	
Methanolic extract from the leaves	Disk diffusion test	<i>Bacillus cereus</i> (9 mm)	[121]
		<i>Bacillus subtilis</i> (3 mm)	
		<i>Bacillus megaterium</i> (1 mm)	
		<i>Staphylococcus aureus</i> (6 mm)	
		<i>Enterococcus faecalis</i> (7 mm)	
Methanolic extract from the leaves	Disk diffusion test	<i>Escherichia coli</i> (12 mm)	[121]
		<i>Salmonella typhi</i> (6 mm)	
		<i>Salmonella paratyphi</i> (5 mm)	
		<i>Pseudomonas aeruginosa</i> (3 mm)	
Methanolic extract from the leaves	Disk diffusion test	<i>Klebsiella pneumoniae</i> (4 mm)	[121]
		<i>Staphylococcus aureus</i> (6 mm)	

TABLE 2: Continued.

Extract/parts of the plant	Assay	Antimicrobial activity	Citation
Essential oil from the leaves	Microdilution method	<i>Saccharomyces cerevisiae</i> (IC <sub>50</sub> 1000 µg/ml) <i>Fusarium moniliforme</i> 7075 (IC <sub>50</sub> > 1500 µg/ml) <i>Mucor</i> sp. (IC <sub>50</sub> 750 µg/ml) <i>Candida albicans</i> (0 mm) <i>Colletotrichum capsici</i> (10 mm)	[122]
Whole plant aqueous extract	Disk diffusion test	<i>Fusarium oxysporum</i> F.sp. <i>lycopersici</i> (5 mm) <i>Klebsiella pneumoniae</i> (14 mm) <i>Escherichia coli</i> (12 mm) <i>Staphylococcus aureus</i> (0 mm) <i>Pseudomonas aeruginosa</i> (0 mm) <i>Candida albicans</i> (19 mm) <i>Colletotrichum capsici</i> (20 mm)	[123]
Whole plant ethanolic extract	Disk diffusion test	<i>Fusarium oxysporum</i> F.sp. <i>lycopersici</i> (18 mm) <i>Klebsiella pneumoniae</i> (22 mm) <i>Escherichia coli</i> (18 mm) <i>Staphylococcus aureus</i> (29 mm) <i>Pseudomonas aeruginosa</i> (12 mm) <i>Aspergillus niger</i> : 1: 6 mm 2: 11 mm 3: 0.5 mm 4: 7 mm 5: 12 mm	[123]
Ethanolic (1), chloroform (2), methanolic (3), petroleum ether (4), and aqueous (5) extracts of the whole plant	Disk diffusion test	<i>Candida albicans</i> : 1: 10 mm 2: 10.5 mm 3: 3.5 mm 4: 8.5 mm 5: 8 mm <i>Fusarium</i> sp.: 1: 12 mm 2: 11 mm 3: 3 mm 4: 12 mm 5: 19 mm	[124]
Essential oil from the leaves	Microdilution method	<i>Aspergillus fumigatus</i> ATCC 40640 (MIC 40 µl/ml) <i>Aspergillus parasiticus</i> ATCC 15517 (MIC 40 µl/ml) <i>Trichophyton mentagrophytes</i> (MIC 640 µl/ml) <i>Staphylococcus aureus</i> (MIC 160 µl/ml) <i>Streptococcus suis</i> (MIC 160 µl/ml)	[36]
Essential oil from the leaves	Microdilution method	<i>Erysipelothrix rhusiopathiae</i> (MIC 80 µl/ml) <i>Actinomyces pyogenes</i> (MIC 80 µl/ml) <i>Pasteurella multocida</i> (MIC 80 µl/ml) <i>Pseudomonas aeruginosa</i> (MIC 20 µl/ml) <i>Escherichia coli</i> (MIC 20 µl/ml) <i>Rhizoctonia solani</i> (MIC 4000 µl/l)	[125]
Essential oil from the leaves	Disk diffusion test	<i>Pythium debaryanum</i> (MIC 300 µl/l) <i>Pythium aphanidermatum</i> (MIC 300 µl/l)	[126]



TABLE 2: Continued.

Extract/parts of the plant	Assay	Antimicrobial activity	Citation
Aqueous extract of the leaves	Microdilution method	<i>Trichoderma viride</i> (IC <sub>50</sub> > 500 µl/l)	[127]
		<i>Alternaria porri</i> (IC <sub>50</sub> > 500 µl/l)	
		<i>Aspergillus parasiticus</i> (IC <sub>50</sub> > 500 µl/l)	
		<i>Aspergillus fumigatus</i> (IC <sub>50</sub> > 500 µl/l)	
		<i>Fusarium lini</i> (IC <sub>50</sub> > 500 µl/l)	
		<i>Alternaria brassicae</i> (IC <sub>50</sub> > 500 µl/l)	
		<i>Colletotrichum</i> sp. (IC <sub>50</sub> > 500 µl/l)	
		<i>Fusarium sesami</i> (IC <sub>50</sub> > 500 µl/l)	
		<i>Fusarium nivale</i> (IC <sub>50</sub> > 500 µl/l)	
		<i>Alternaria solani</i> (IC <sub>50</sub> > 500 µl/l)	
		<i>Fusarium oxysporum</i> f. sp. <i>ciceri</i> (IC <sub>50</sub> > 393.4 µl/l)	
		<i>Aspergillus niger</i> (IC <sub>50</sub> > 244.7 µl/l)	
		<i>Aspergillus sulphureus</i> (IC <sub>50</sub> > 475.4 µl/l)	
		<i>Helminthosporium oryzae</i> (IC <sub>50</sub> > 197.7 µl/l)	
		<i>Alternaria alternata</i> (IC <sub>50</sub> > 475.5 µl/l)	
<i>Alternaria tenuissima</i> (IC <sub>50</sub> > 321.1 µl/l)			
<i>Fusarium semitectum</i> (IC <sub>50</sub> > 243.5 µl/l)			
<i>Cladosporium cladosporioides</i> (IC <sub>50</sub> > 228.6 µl/l)			
<i>Drechslera aunti</i> (IC <sub>50</sub> > 411 µl/l)			
<i>Penicillium citrinum</i> (IC <sub>50</sub> > 446.7 µl/l)			
Methanolic extract of the leaves	Disk diffusion test	<i>Staphylococcus aureus</i> (6 mm)	[128]
		<i>Bacillus subtilis</i> (9 mm)	
Hexanic extract of the leaves	Microdilution method	<i>Escherichia coli</i> ATCC 10536 (IC <sub>50</sub> ≅ 200 µg/ml)	[29]
		<i>Proteus mirabilis</i> ATCC 7002 (IC <sub>50</sub> ≅ 200 µg/ml)	
		<i>Klebsiella pneumoniae</i> ATCC 10031 (IC <sub>50</sub> ≅ 400 µg/ml)	
		<i>Proteus vulgaris</i> ATCC 49132 (IC <sub>50</sub> ≅ 100 µg/ml)	
		<i>Serratia marcescens</i> FJ584421 (IC <sub>50</sub> ≅ 50 µg/ml)	
		<i>Staphylococcus aureus</i> ATCC 29213:	
		1: 13 mm	
		2: 8 mm	
		3: 8 mm	
		4: 12 mm	
<i>Listeria monocytogenes</i> ATCC 19115:			
1: 0 mm			
2: 7 mm			
3: 5 mm			
4: 0 mm			
Petroleum ether (1), chloroform (2), methanolic (3), and aqueous (4) extracts of the leaves	Disk diffusion test	<i>Escherichia coli</i> ATCC 25922:	[129]
		1: 7 mm	
		2: 10 mm	
		3: 0 mm	
		4: 0 mm	
		<i>Serratia marcescens</i> ATCC 21074:	
		1: 18 mm	
		2: 0 mm	
		3: 8 mm	
		4: 0 mm	
		<i>Aspergillus flavus</i> ATCC 32612:	
		1: 18 mm	
		2: 0 mm	
3: 0 mm			
4: 14 mm			
Leaf essential oil	Disk diffusion test	<i>Fusarium oxysporum</i> f. sp. <i>gladioli</i> MPPLU 01 (MIC 0.6 µl/ml)	[130]
Leaf essential oil	Disk diffusion test	<i>Rhizoctonia solani</i> (MIC 5.000 µg/ml)	[131]
		<i>Sclerotinia sclerotiorum</i> (MIC 5.000 µg/ml)	
		<i>Sclerotium rolfsii</i> (MIC 5.000 µg/ml)	
Leaf methanolic extract	Disk diffusion test	<i>Klebsiella pneumoniae</i> MTCC 109 (7.5 mm)	[132]
		<i>Bacillus subtilis</i> MTCC 121 (8 mm)	
Leaf essential oil	Disk diffusion test	<i>Salmonella typhi</i> MTCC 733 (7 mm)	[133]
		<i>Fusarium oxysporum</i> f.sp. <i>gladioli</i> MPPLU 01 (MIC 0.998 µg/ml)	

TABLE 2: Continued.

Extract/parts of the plant	Assay	Antimicrobial activity	Citation
Aerial parts methanolic extract	Disk diffusion test	<i>Candida albicans</i> (7 mm)	[105]
Leaf essential oil	Disk diffusion test	<i>Microsporium gypseum</i> (MIC 625 µg/ml)	[134]
		<i>Aureobasidium pullulans</i> (MIC 5.000 µg/ml)	
Essential oil from the leaves	Microdilution method	<i>Candida albicans</i> (MIC 10.000 µg/ml)	[135]
		<i>Aspergillus flavus</i> (MIC 10.000 µg/ml)	
Leaf hydroethanolic extract	Disk diffusion test	<i>Trichophyton rubrum</i> (MIC 156 µg/ml)	[136]
		<i>Cryptococcus neoformans</i> (MIC 5.000 µg/ml)	
Leaf essential oil	Microdilution method	<i>Staphylococcus aureus</i> (MIC 64 and 256 µg/ml)	[137]
		<i>Candida albicans</i> (IC <sub>50</sub> 18.15 µg/ml)	
Leaf essential oil	Microdilution method	<i>Candida tropicalis</i> (IC <sub>50</sub> 40.4 µg/ml)	[137]
		<i>Staphylococcus aureus</i> (0.7 cm)	
Leaf essential oil	Microdilution method	<i>Salmonella typhi</i> (0.52 cm)	[136]
		<i>Escherichia coli</i> (0.25 cm)	
Leaf essential oil	Microdilution method	<i>Enterococcus faecalis</i> (IC <sub>50</sub> 5.78 µg/ml)	[137]
		<i>Staphylococcus aureus</i> (IC <sub>50</sub> 68.98 µg/ml)	
Leaf essential oil	Microdilution method	<i>Bacillus cereus</i> (IC <sub>50</sub> 9.35 µg/ml)	[137]
		<i>Candida albicans</i> (IC <sub>50</sub> 6.78 µg/ml)	

(T. Escherich, 1885) (Enterobacteriaceae) CMCC 44102, and *Botrytis cinerea* (De Bary) Whetzel, 1945 (Sclerotiniaceae). The oil was also very active against *S. aureus* CMCC 26001, *P. aeruginosa* CMCC 10104, *Fusarium graminearum* Schwabe, 1839 (Nectriaceae), *Exerohilum turcicum* (Pass.) K.J. Leonard & Suggs, 1974 (Pleosporaceae), and *Lecanosticta acicola* (Thüm.) Syd., 1924 (Mycosphaerellaceae).

Besides the essential oil, the fixed oil from *M. suaveolens* seeds showed activities of clinical relevance against *E. coli* MTCC 443 (MIC 0.5 mg/ml), *Salmonella typhi* Typhi (Enterobacteriaceae) MTCC 531 (MIC 0.125 mg/ml), *Shigella flexneri* Castellani & Chalmers, 1919 (Enterobacteriaceae) MTCC 1457 (MIC 0.5 mg/ml), *Vibrio vulnificus* (Reichelt et al.) Farmer, 1980 (Vibrionaceae) MTCC 1145 (MIC 0.5 mg/ml), *P. aeruginosa* MTCC 424 (MIC 0.125 mg/ml), *Lactobacillus plantarum* (Orla-Jensen) Bergey et al., 1923 (Lactobacillaceae) MTCC 2621 (MIC 0.125 mg/ml), *Lactobacillus leishmanii* (Henneberg) Bergey et al. 1923 (Lactobacillaceae) MTCC 911 (MIC 0.25 mg/mL), *S. aureus* MTCC 737 (MIC 0.25 mg/ml), *Candida tropicalis* Berkhout, 1923 (Saccharomycetaceae) MTCC 227 (MIC 0.125 mg/ml), and *Candida albicans* Berkhout, 1923 (Saccharomycetaceae) MTCC 227 (MIC 0.25 mg/ml) (Table 2).

**3.4.3. Insecticidal Activity.** Popularly, in Kenya, the aerial parts of *M. suaveolens* are burned to repel mosquitoes of the species *Anopheles gambiae* [84, 94]. Subsequently, other researchers have highlighted that the oil has biological action against various insects, such as *A. gambiae* itself (Table 3).

Works evaluating the insecticidal action showed that the essential oil of *M. suaveolens* by fumigation showed the effect against *Callosobruchus maculatus* (Fabricius 1775; Coleoptera: Chrysomelidae) (CL<sub>50</sub> 4.7 µg/ml), *Rhyzopertha dominica* (Fabricius 1972; Coleoptera: Bostrichidae) (CL<sub>50</sub> 12 µg/ml), *Sitophilus oryzae* (Linnaeus 1763; Coleoptera: Curculionidae) (CL<sub>50</sub> 10.6 µg/ml), *Tribolium castaneum*

(Herbst 1932; Coleoptera: Tenebrionidae) (CL<sub>50</sub> 23.2 µg/ml) (Tripathi; Upadhyay 2009), and *Sitophilus granarius* (Linnaeus, 1758) (CL<sub>50</sub> 0.251 µl/insect) [138].

*Mesosphaerum suaveolens* oil showed toxicity through contact and ingestion against Mediterranean flies (*Ceratitis capitata* (Wiedemann, 1824) (Diptera: Tephritidae)) with CL<sub>50</sub> 13.041 µl/l through ingestion and CL<sub>50</sub> 0.066 µl/l through contact [30]. Canale et al. [139], when evaluating the toxicity of the oil against *Bactrocera oleae* (Rossi, 1790) (Diptera: Tephritidae), demonstrated that, by ingestion, the product showed a CL<sub>50</sub> of 4.9 mg/ml. Bezerra et al. [10] evaluated by fumigation the action of the oil and highlighted that it presents great insecticidal action with CL<sub>50</sub> of 15.5 µg/ml against adults of *Drosophila melanogaster* (Meigen, 1830) (Diptera: Drosophilidae). Also, via the fumigation test, Wangrawa et al. [35] found a CL<sub>50</sub> of 1.86 µg/ml (oil/air) against *A. gambiae*. Recently, Adjou et al. (2019) found the insecticidal action of *M. suaveolens* oil against *Tenebroides mauritanicus* (Linnaeus, 1758) (Coleoptera: Trogossitidae) with a CL<sub>50</sub> 0.35 µl/g.

**3.4.4. Repellent Activity.** Besides causing mortality in insects, the products of *M. suaveolens*, especially the essential oil of the leaves, can repel insects and arachnids of public health and economic interests (Table 4). As for Diptera, the essential oil by fumigation and the fresh leaves by contact were able to repel mosquitoes of the species *Anopheles gambiae*, malaria vector, with the former showing an effective rate of 98% repellency at a low concentration (6%) [152], while the leaves when rubbed on the body had a rate of 66.5% [153]. Besides this Diptera, *Aedes aegypti* vector of arboviruses, such as dengue, yellow fever, chikungunya, and zika, was also repelled when in contact with the ethyl acetate extract of the leaves.

As for insects of economic interest, the leaves of *M. suaveolens* showed that the phytochemicals released by the leaves can repel two species of coleoptera, being

TABLE 3: Insecticidal activities of *Mesosphaerum suaveolens* (L.) Kuntze (Lamiaceae).

Extract/parts of the plant	Assay	Insecticidal activity	Citation
		<i>Ceratitis capitata</i>	
Leaf essential oil	Fumigation	Fumigation: CL <sub>50</sub> 18.37 µl/l	[30]
	Ingestion	Ingestion: CL <sub>50</sub> 13.041 µl/l	
	Contact toxicity	Contact toxicity: CL <sub>50</sub> 0.066 µl/l	
Leaf essential oil	Fumigation	<i>Callosobruchus maculatus</i> (CL <sub>50</sub> 4.7 µg/ml)	[34]
		<i>Rhyzopertha dominica</i> (CL <sub>50</sub> 12 µg/ml)	
		<i>Sitophilus oryzae</i> (CL <sub>50</sub> 10.6 µg/ml)	
		<i>Tribolium castaneum</i> (CL <sub>50</sub> 23.2 µg/ml)	
		<i>Callosobruchus maculatus</i> (CL <sub>50</sub> 57 µg/mg)	
		<i>Rhyzopertha dominica</i> (CL <sub>50</sub> 126 µg/mg)	
Leaf essential oil	Contact toxicity	<i>Sitophilus granarius</i> (CL <sub>50</sub> 0.251 µl/insect)	[138]
Leaf essential oil	Ingestion	<i>Bactrocera oleae</i> (CL <sub>50</sub> 4.9 mg/ml)	[139]
Leaf methanolic extract	Contact	<i>Sitophilus oryzae</i> (CL <sub>50</sub> 475.9 µl/ml)	[140]
		<i>Sitophilus zeamais</i> CL <sub>50</sub> 707.4 µl/ml)	
Leaf essential oil	Fumigation	<i>Callosobruchus maculatus</i> (CL <sub>50</sub> 451.2 µl/ml)	[141]
Leaf essential oil	Fumigation	<i>Tribolium castaneum</i> (CL <sub>50</sub> 229.33 µg/ml)	[142]
Leaf infusion	Ingestion	<i>Drosophila melanogaster</i> (CL <sub>50</sub> 15.5 µg/ml)	[10]
Leaf essential oil	Fumigation	<i>Drosophila melanogaster</i> (CL <sub>50</sub> > 30.3 µg/ml)	[10]
Leaf essential oil	Contact toxicity	<i>Anopheles gambiae</i> (CL <sub>50</sub> 1.86 µg/ml)	[35]
Leaf essential oil	Toxicity by ingestion	<i>Tenebroides mauritanicus</i> (CL <sub>50</sub> 0.35 µl/g)	[142]
Leaf ethanolic extract	Fumigation	<i>Apis mellifera</i> (CL <sub>50</sub> 43.03%)	[143]
Crushed leaves	Ingestion toxicity	<i>Callosobruchus maculatus</i> (100% mortality (at 10% concentration)	[144]
Crushed leaves and flowers	Ingestion toxicity	<i>Callosobruchus maculatus</i> (CL <sub>50</sub> 73 mg/g)	[145]
Crushed leaves	Ingestion toxicity	<i>Callosobruchus maculatus</i> (20.1% of mortality)	[146]
		<i>Callosobruchus maculatus</i> (96.6% of mortality in the concentration 43.75 mg/g)	[147]
Leaf essential oil	Fumigation	<i>Sitophilus zeamais</i> (30% of mortality in the concentration 43.75 mg/g)	[148]
Leaf essential oil	Fumigation	<i>Callosobruchus maculatus</i> (CL <sub>50</sub> : 1.3 µl/l)	[149]
Leaf essential oil	Fumigation	<i>Callosobruchus maculatus</i> (CL <sub>50</sub> : >20 µl/l)	[150]
Leaf essential oil	Fumigation	<i>Callosobruchus maculatus</i> (CL <sub>50</sub> : >2.6 µl/ml)	[151]
Leaf essential oil	Fumigation	<i>Nauphoeta cinerea</i> (did not show insecticidal action)	[151]

TABLE 4: Repellent activities of *Mesosphaerum suaveolens* (L.) Kuntze (Lamiaceae).

Extract/parts of the plant	Assay	Insecticidal activity	Citation
Aerial parts essential oil	Contact	<i>Amblyomma cajennense</i> (EC <sub>50</sub> 0.55 mg/cm <sup>2</sup> )	[23]
Crushed leaves	Fumigation	<i>Callosobruchus maculatus</i> (repellency from 5 minutes of exposure)	[146]
Leaf essential oil	Fumigation	<i>Anopheles gambiae</i> (98% repellency rate at 6% concentration)	[152]
Fresh leaves	Contact	<i>Anopheles gambiae</i> (repellency rate 66.5%)	[153]
Leaf essential oil	Fumigation	<i>Sitophilus granarius</i> (repellency rate 40% at 100% concentration)	[154]
Leaf ethyl acetate extract	Contact	<i>Aedes aegypti</i> (repellency rate of 78.8% for 500 µl)	[155]
Crushed leaves (1) and twigs (2)	Contact	<i>Callosobruchus maculatus</i> :	[156]
		1: repellency index: 0.11 2: repellency index: 0.2	
Leaf essential oil	Fumigation	<i>Anopheles</i> sp. (67% repellency rate at 6.3 µg/ml concentration)	[157]
Leaf essential oil	Fumigation	<i>Ixodes ricinus</i> (repellency rate 93% at 10% concentration)	[158]

*Sitophilus granarius* and *Callosobruchus maculatus*. As for arachnid repellency, the essential oil was able to repel *Amblyomma cajennense* and *Ixodes ricinus*.

**3.4.5. Larvicidal Activity.** Besides microbiological and insecticidal activities, apolar and polar extracts of *M. suaveolens* showed larvicidal action in some studies (Table 5). Its oil, for example, showed activity against *Aedes albopictus* (Skuse, 1894) (Diptera: Culicidae) (CL<sub>50</sub>

240.3 µg/ml) [159], *Aedes aegypti* (Linnaeus, 1762) (Diptera: Culicidae) (CL<sub>50</sub> 0.4 µL/ml) [160], *Artemia salina* (Linnaeus, 1758) (Anostraca: Artemiidae) (CL<sub>50</sub> 49.72 µg/ml) [10], and *Chrysodeixis chalcites* (Esper, 1789) (Lepidoptera: Noctuidae) (CL<sub>50</sub> 2.42 µg/ml) [32].

**3.4.6. Cytotoxic Activity.** Besides microbiological and insecticidal activities, it was evidenced that *M. suaveolens* products present biologically active compounds against

TABLE 5: Larvicidal activities of *Mesosphaerum suaveolens* (L.) Kuntze (Lamiaceae).

Extract/parts of the plant	Assay	Larvicidal activity	Citation
Leaf essential oil	Acute toxicity	<i>Artemia salina</i> (CL <sub>50</sub> 49.72 µg/ml)	[10]
Leaf infusion	Acute toxicity	<i>Artemia salina</i> (CL <sub>50</sub> > 1000 µg/ml)	[10]
Leaf essential oil	Acute toxicity	<i>Chrysodeixis chalcites</i> (CL <sub>50</sub> 2.42 µg/ml)	[32]
Essential oil from leaves	Acute toxicity	<i>Aedes albopictus</i> (CL <sub>50</sub> 240.3 µg/ml)	[159]
Leaf essential oil	Acute toxicity	<i>Aedes aegypti</i> (CL <sub>50</sub> 0.4 µL/ml)	[160]
Hexanic extract (1), diethyl ether (2), dichloromethane (3), and ethyl acetate (4) from leaves	Acute toxicity	<i>Aedes aegypti</i> 1: CL <sub>50</sub> 543.66 µg/ml 2: CL <sub>50</sub> 1443.53 µg/ml 3: CL <sub>50</sub> 1292.36 µg/ml 4: CL <sub>50</sub> 853.04 µg/ml	[161]
Hexanic extract (1), diethyl ether (2), dichloromethane (3), and ethyl acetate (4) from aerial parts	Acute toxicity	<i>Anopheles stephensi</i> 1: CL <sub>50</sub> 1.52 mg/ml 2: CL <sub>50</sub> 1.49 mg/ml 3: CL <sub>50</sub> 1.39 mg/ml 4: CL <sub>50</sub> 0.94 mg/ml	[162]
Hexanic (1), isopropanolic (2), methanolic (3), acetone (4), and dimethyl sulfoxide (5) extract from the leaves	Acute toxicity	<i>Aedes albopictus</i> 1: CL <sub>50</sub> 1.52 mg/ml 2: CL <sub>50</sub> 1.52 mg/ml 3: CL <sub>50</sub> 1.52 mg/ml 4: CL <sub>50</sub> 1.52 mg/ml 5: CL <sub>50</sub> 1.52 mg/ml	[163]
Isopropanolic (1), methanolic (2), acetonic (3), dimethyl sulfoxide (4), and aqueous extract from the leaves (5)	Acute toxicity	<i>Aedes albopictus</i> 1: CL <sub>50</sub> 900 µg/ml 2: CL <sub>50</sub> 940 µg/ml 3: CL <sub>50</sub> 820 µg/ml 4: CL <sub>50</sub> 1590 µg/ml 5: CL <sub>50</sub> 1560 µg/ml	[163]
Aqueous leaf extract	Acute toxicity	<i>Anopheles stephensi</i> (CL <sub>50</sub> 26.08 mg/ml) <i>Aedes aegypti</i> (CL <sub>50</sub> 17.6 mg/ml) <i>Culex quinquefasciatus</i> (CL <sub>50</sub> 33.68 mg/ml)	[164]
Methanolic (1), chloroform (2), and petroleum ether (3) extracts of the leaves	Acute toxicity	<i>Culex quinquefasciatus</i> : 1: CL <sub>50</sub> > 300 µg/ml 2: CL <sub>50</sub> 41.93 µg/ml 3: CL <sub>50</sub> 38.39 µg/ml	[165]
Dichloromethane extract from the aerial parts	Acute toxicity	<i>Aedes aegypti</i> : 1: CL <sub>50</sub> > 300 µg/ml 2: CL <sub>50</sub> > 300 µg/ml 3: CL <sub>50</sub> 64.49 µg/ml	[165]
Aqueous extract from aerial parts	Spraying	<i>Anopheles gambiae</i> (CL <sub>50</sub> 63.5 mg/ml)	[166]
Aqueous extract from leaves and fruits	Contact toxicity	<i>Sesamia calamistis</i> (37.85% motility (300 mg/ml))	[167]
Hexanic (1), chloroform (2), ethyl acetate (3), and methanolic (4) extract from the aerial parts	Acute toxicity	<i>Mussidia nigrivenella</i> (49% motility (200 mg/g)) <i>Sesamia calamistis</i> (37% motility (200 mg/g)) <i>Eldana saccharina</i> (41% motility (200 mg/g))	[168]
Crushed aerial parts	Contact toxicity	<i>Culex quinquefasciatus</i> : 1: CL <sub>50</sub> 213.09 µg/ml 2: CL <sub>50</sub> 217.64 µg/ml 3: CL <sub>50</sub> 167.59 µg/ml 4: CL <sub>50</sub> 86.93 µg/ml	[169]
Essential oil from leaves	Ingestion toxicity	<i>Helicoverpa armigera</i> (66.7% mortality at 20% concentration)	[170]
		<i>Spodoptera frugiperda</i> (CL <sub>50</sub> 600 µg/ml)	[171]

TABLE 5: Continued.

Extract/parts of the plant	Assay	Larvicidal activity	Citation
Hexanic extract (1), chloroform (2), and ethyl acetate (3) from leaves	Ingestion toxicity	<i>Helicoverpa armigera</i> :	[172]
		1: mortality of 31.68% (concentration: 1%)	
		2: mortality of 65.28% (concentration: 1%)	
		3: mortality of 72.87% (concentration: 1%)	
		<i>Spodoptera litura</i> :	
		1: mortality of 34.09% (concentration: 1%)	
		2: mortality of 63.62% (concentration: 1%)	
		3: mortality of 74.56% (concentration: 1%)	
		<i>Earias vittella</i> :	
		1: mortality of 44.37% (concentration: 1%)	
		2: mortality of 69.28% (concentration: 1%)	
		3: mortality of 73.40% (concentration: 1%)	
Essential oil from leaves (1) and crushed leaves (2)	Contact toxicity	<i>Leucinodes orbonalis</i> :	[173]
		1: mortality of 37.57% (concentration: 1%)	
		2: mortality of 67.62% (concentration: 1%)	
Leaf essential oil	Acute toxicity	<i>Dinarmus basalis</i> :	[174]
		1: CL <sub>50</sub> 7.76 $\mu$ l 2: CL <sub>50</sub> 14.06 g <i>Aedes aegypti</i> (CL <sub>50</sub> 139.07 $\mu$ g/ml)	

TABLE 6: Cytotoxic activities of *Mesosphaerum suaveolens* (L.) Kuntze (Lamiaceae).

Extract/parts of the plant	Assay	Cytotoxic activity	Citation
Chloroform (1) and butanolic (2) extract from the leaves	MTT assay	MCF-7 cell lines	[175]
		1: IC <sub>50</sub> 12 $\mu$ g/ml 2: IC <sub>50</sub> 2.8 $\mu$ g/ml	
Ethanollic (1) and aqueous (2) extracts of the leaves	MTT assay	Human T-lymphocyte leukemia:	[176]
		1: IC <sub>50</sub> 553.52 $\mu$ g/ml 2: IC <sub>50</sub> 1356.17 $\mu$ g/ml	
Ethanollic extract of the aerial parts	MTT assay	EAC cells (IC <sub>50</sub> 10.63 $\mu$ g/ml)	[177]
		Human breast epithelial adenocarcinoma (MDA-MB-231)	
Leaf callus	MTT assay	IC <sub>50</sub> 74.66 $\mu$ g/ml	[178]
		Prostate cancer (PC-3)	
		IC <sub>50</sub> 173.21 $\mu$ g/ml	
Silver nanoparticles from the leaves	MTT assay	Human breast epithelial adenocarcinoma (MDA-MB-231)	[179]
		IC <sub>50</sub> 63.16 $\mu$ g/ml	
		Prostate cancer (PC-3)	
		IC <sub>50</sub> 52.49 $\mu$ g/ml	

cancer cells (Table 6). The activities evaluated using the MTT (3-(4,5-dimethylthiazol-2-yl)-2,5-diphenyltetrazolium bromide) assay demonstrated that the leaves are the source of the anticancer compounds against some cell types. Among these, Lautié et al. [175] evaluated the bioactivities of chlorophore and butanolic extracts against MCF-7 cell lines and showed that such products have low IC<sub>50</sub> (12 and 2.8  $\mu$ g/ml, respectively). Besides these cell lines, activities were demonstrated against EAC (Ehrlich ascites carcinoma), human breast epithelial adenocarcinoma (MDA-MB-231), and T-lymphocyte leukemia cells.

Among the studies against cancer cell lines, only the aqueous extract of the leaves showed low cytotoxicity (IC<sub>50</sub> 1,356.17  $\mu$ g/ml) when evaluated against T-lymphocyte leukemia-causing cells [176]. Concomitantly in the same study, the ethanollic extract of the same organs had moderate cytotoxicity (IC<sub>50</sub> 553.52  $\mu$ g/ml); such fact is explained by the

variation of solvent used for the extraction of the compounds.

**3.4.7. Other Biological Activities (Antiarachnidic, Antiparasitic, and Molluscicides).** In addition to the aforementioned activities, the herbaceous species present bioactive compounds against other biological organisms. Among these were highlighted parasitic organisms of humans, as reported by Shittu et al. [180], in which evaluating the trypanocidal action (*Trypanosoma brucei brucei*) in vivo of gold nanoparticles from *M. suaveolens* demonstrated that the species can cause a complete clearance of the parasite after seven days of infection. As well as in insecticidal action against malaria vectors (*Anopheles* spp.), *M. suaveolens* exhibits antiplasmodial activity (*Plasmodium falciparum* 3D7) [45, 46, 181]. Noronha et al. [181] evaluated the antiparasitic



action of the methanolic extract of *M. suaveolens* leaves and observed that the natural product has an  $IC_{50}$  of 3.906  $\mu\text{g/ml}$  against chloroquine-sensitive *Plasmodium falciparum* strains. In the study by Ziegler et al. [45], the researchers isolated a diterpene (dehydroabietinol) from the leaves and observed that the compound was able to inhibit 50% of parasite growth at a low concentration of 7.3  $\mu\text{g/ml}$ . Similarly, Chukwujekwu et al. [46] demonstrated that another diterpene (13 $\alpha$ -epi-dioxiabiet-8(14)-en-18-ol) isolated from the same organ showed an  $IC_{50}$  of 0.11  $\mu\text{g/ml}$ , against *P. falciparum* D10, being of great clinical interest.

Research involving the extracts and essential oil of *M. suaveolens* focus on insecticidal activities, so only one work aimed to evaluate the bioactive potential against Arachnida species [182]. In this study, the authors demonstrated that the essential oil of the leaves at the concentration of 31.3 mg/ml can cause 50% mortality of *Rhipicephalus (Boophilus) microplus* for engorged females, while for juvenile forms of the tick,  $CL_{50}$  is 51.6 mg/mL, demonstrating that females are more susceptible to the oil.

Salawu and Odaibo [182] evaluated the molluscicide action of the ethanolic extract of *M. suaveolens* against *Bulinus globosus*, found that the product presents both lethality in adult individuals ( $LC_{50}$  77  $\mu\text{g/ml}$ ), and also presents an ovicidal potential ( $LC_{50}$  614  $\mu\text{g/ml}$ ).

### 3.5. Pharmacological Activities

**3.5.1. Antioxidant Activity.** Narayanaswamy and Balakrishnan [84] evaluated the extracts of thirteen plants of ethnomedicinal importance and identified that *M. suaveolens* species among all had the highest activity in both aqueous and ethanolic extracts evaluated. Thus, it demonstrates that the species is a source of compounds of pharmacological interest for the development of natural antioxidant products.

Agarwal [183] showed that the methanolic extract of *M. suaveolens* leaves has potent antioxidant activity evaluated by the 2,2-diphenyl-1-picrylhydrazyl (DPPH) method with  $IC_{50}$  value = 40.91  $\mu\text{g/ml}$ , and there is about 69% free radical inhibition capacity at the highest concentration (100  $\mu\text{g/ml}$ ). It was also found that the percentage of inhibition is concentration dependent, the higher the concentration the greater the inhibition of free radicals, and that the main phytochemicals involved in this activity may be phenols and flavonoids. The methanolic extract also demonstrated antioxidant activity with assays other than DPPH, such as ferric reducing antioxidant power (FRAP) and 2,2'-azino-bis (3-ethylbenzothiazoline-6-sulfonic acid) (ABTS) [184].

Other studies have also evaluated the free radical scavenging potential by the DPPH method. Gavani and Paarakh [185] evaluated the methanolic extract of *M. suaveolens* leaves and obtained an  $IC_{50}$  of 14.04  $\mu\text{g/ml}$ . The aqueous and ethanolic extracts of the fresh leaves of *M. suaveolens* demonstrated high antioxidant activity. The former product had an  $IC_{50}$  = 20.32  $\mu\text{g/ml}$ , while the ethanolic extract had a statistically equal result to the positive control, ascorbic acid, with  $IC_{50}$  of  $7.06 \pm 0.82$  and

$6.69 \pm 0.85$   $\mu\text{g/ml}$ , respectively [186]. Such results are attributed to the phenolic compounds present in such extracts.

Iqbal et al. [187] reported that the methanolic extract of the seeds of *M. suaveolens* showed better antioxidant activity by the DPPH method ( $IC_{50}$  =  $72 \pm 0.45$   $\mu\text{g/ml}$ ) when compared to the methanolic extracts of the stem ( $IC_{50}$  =  $250 \pm 5.46$   $\mu\text{g/ml}$ ) and root ( $IC_{50}$  =  $143 \pm 2.15$   $\mu\text{g/ml}$ ).

In the work of Priyadarshini and Sujatha [188], four types of leaf extracts were evaluated; in the DPPH assay, three of the extracts had significant results, the best of them being the ethyl acetate extract with a percentage of inhibition ( $IC_{50}$  = 137  $\mu\text{g}$ ) very close to that of the standard used, ascorbic acid ( $IC_{50}$  = 127  $\mu\text{g}$ ). In this same study, the acetate extract also stood out with other tests; in the superoxide anion radical scavenging assay, the  $IC_{50}$  value = 22.94  $\mu\text{g}$ , and the standard had a value of 21.47  $\mu\text{g}$ .

In addition to leaves, antioxidant potentials of other organs such as flowers were investigated in the study by Banerjee and De [189]. However, the results were not promising, as the extract of the reproductive parts exhibited an  $IC_{50}$  of 1690.21  $\mu\text{g/ml}$  against DPPH. Antioxidant studies involving *M. suaveolens* are not restricted to extracts only. Nantitanon et al. [126] evaluated the effect of the essential oil from the leaves; however, it showed low potential to reduce free radicals ( $IC_{50}$  of 3.7200 mg/ml). Hsu et al. [190] demonstrated that the seeds also exhibit antioxidant action, as they showed moderate inhibitory activity against xanthine oxidase. In a study conducted by Lima et al. [191], it was observed that the essential oil from *M. suaveolens* leaves showed moderate  $Fe^{2+}$  chelating activity at the concentration of 480  $\mu\text{g/ml}$ .

**3.5.2. Healing Potential.** The healing potential of *M. suaveolens* leaves was evaluated by three types of extracts (petroleum ether, ethanolic, and aqueous) in different wound models (excision, incision, and healing) using albino Wistar rats [192]. In this study, it was revealed that the extract using petroleum ether had the greatest significant effect on wound healing in murine wounds. Shirwaikar et al. [193] evaluated the ethanolic extract on these same three types of wounds, also obtaining significant results which were justified by the free radical scavenging action of this species.

**3.5.3. Neuroprotective Activity.** Ghaffari et al. [184] determined the neuroprotective potential of the methanolic extract of the aerial parts of *M. suaveolens* on mouse N2A neuroblastoma cells, in which they observed that the natural product inhibits hydrogen peroxide ( $H_2O_2$ )-induced neuronal death. The authors justified this effect by the fact that the extract can regulate the activation of antioxidant and protective genes of the nerve cells. These results are promising, and the methanolic extract can be employed to treat stress-induced neurodegeneration.

**3.5.4. Anti-Inflammatory Activity.** Shenoy and Shirwaikar [194] evaluated the anti-inflammatory potential of ethanolic extract of the leaves against inflammation induced by carrageenan in albino rats; the extract showed significant results



when compared to standard ibuprofen; this result is justified by the good antioxidant activity of this extract. In the study by Grassi et al. [42], two diterpenes ( $C_{20}$ ) isolated from *M. suaveolens*, suaveolol and methyl suaveolate, showed anti-inflammatory potential when evaluated regarding the reduction of ear edema in rats. In such research, it was observed that the compounds reduced inflammation with  $ID_{50} = 0.71 \mu\text{mol}/\text{cm}^2$  (dose giving 50% edema inhibition) for suaveolol and  $ID_{50} = 0.60 \mu\text{mol}/\text{cm}^2$ ; however, despite the pharmacological effect, the results were only two to three times less active than the standard drug used in the study indomethacin ( $ID_{50} = 0.26 \mu\text{mol}/\text{cm}^2$ ).

**3.5.5. Antiulcer Activity.** *Mesosphaerum suaveolens* leaves are popularly used for the treatment of gastric ulcers; however, no active ingredient had been identified. The first study evaluating such an effect was by Vera-Arvaze et al. [43], in which such authors isolated the diterpene suaveolol from the leaves and evaluated it against an induced experimental model; the results presented indicated that this compound had a gastroprotective effect of more than 70%.

One year after the publication of the mentioned study, Jesus et al. [195] using the ethnopharmacological approach of *M. suaveolens* evaluated its antiulcer potential through the ethanolic extract and its fractions. The results for all products had high significance,  $p > 0.001$ , with the hexanic fraction of the extract being the most effective with 74% inhibition of induced gastric ulcer at a dose of 500 mg/kg.

**3.5.6. Antidiarrheal Activity.** Although *M. suaveolens* is popularly used to treat gastrointestinal disorders such as diarrhea, only the work of Shaikat et al. [196] evaluated its antidiarrheal potential. The researchers prepared ethanolic extracts of the leaves and based on the popular use, evaluated against an experimental model of diarrhea induced in mice; the results obtained show that this species presents compounds with the antidiarrheal effect ( $p > 0.001$ ) that may be acting in an isolated or synergistic way.

**3.5.7. Antihyperglycemic Activity.** The ethanolic extract of *M. suaveolens* leaves was evaluated in the in vivo experimental model of streptozotocin-induced diabetes. The extract at doses of 250 and 500 mg/kg bodyweight was administered orally over 21 days; at the end of the treatment, a decrease in the levels of triglycerides, total cholesterol, and low-density lipoprotein can be seen; these results indicate that this species has significant antidiabetic activity [197].

**3.5.8. Hepatoprotective Effect.** Ghaffari et al. [198] induced damage to livers of Wistar rats using carbon tetrachloride ( $\text{CCl}_4$ ) and subsequently administered doses of 50 and 100 ml/kg of methanolic extract of the aerial parts of *M. suaveolens*. The results were promising, demonstrating that the extract has a hepatoprotective effect, which can be explained by the antioxidant potential of the product, also demonstrated in the study.

**3.5.9. Toxicity.** A topical cream based on *M. suaveolens* essential oil was prepared based on its popular use in Thailand, where they pointed out further investigations related to its toxicity in humans. This study was conducted on Wistar rats for 28 days under 3, 10, and 30% concentration of essential oil. The results showed us that concentrations of 3 and 10% did not cause a statistically significant dermal toxicity unlike the 30% concentration in which some female rats presented signs of erythema on its shaved dorsal skin between 11 and 14 days after the cream application [199].

## 4. Conclusions

It is evident that *M. suaveolens* is the most studied species of the genus, traditionally used in the new and old world to combat several diseases. Chemically, the species is much investigated, mainly about the composition of its essential oils that can vary according to the locality of occurrence. *Mesosphaerum suaveolens* also behaves as ruderal, and its success may be due to the release of allelochemicals. The species also presents a biotechnological potential corroborated by the remarkable activity against pathogenic microorganisms, insects, and other arthropods that transmit diseases. Finally, the pharmacological applications of the species are highlighted, especially the antioxidant action found in several organs of the species.

## Data Availability

The data used to support the findings of this study are available from the corresponding author upon request.

## Conflicts of Interest

The authors declare that they have no conflicts of interest.

## Authors' Contributions

J.W.A.B. conceptualized the study. J.J.L.B. and F.C.R. developed methodology. A.A.V.P. developed software. M.F.B.M.B. and J.G.M.d.C. validated the study. F.C.R., P.A.d.S.F., and V.B.d.S. performed formal analysis. S.A.d.M. investigated the study. A.R.C. curated data. A.S. and J.W.A.B. wrote original draft. B.K. and A.B.T. reviewed and edited the article. A.F.M.d.O. and M.V.M. supervised the study. H.D.M.C administered the project. All authors have read and agreed to the published version of the manuscript.

## Acknowledgments

This research was supported by Basic Science Research Program through the National Research Foundation of Korea (NRF) funded by the Ministry of Education (NRF-2020R1I1A2066868), the National Research Foundation of Korea (NRF) grant funded by the Korea Government (MSIT) (2020R1A5A2019413), a grant of the Korea Health Technology R&D Project through the Korea Health Industry Development Institute (KHIDI), funded by the Ministry of Health and Welfare, Republic of Korea (HF20C0116), and a

grant of the Korea Health Technology R&D Project through the Korea Health Industry Development Institute (KHIDI), funded by the Ministry of Health and Welfare, Republic of Korea (HF20C0038).

## References

- [1] U. P. de Albuquerque, J. M. Monteiro, M. A. Ramos, and E. L. C. de Amorim, "Medicinal and magic plants from a public market in northeastern Brazil," *Journal of Ethnopharmacology*, vol. 110, no. 1, pp. 76–91, 2007.
- [2] J. W. Almeida Bezerra, A. Rodrigues Costa, M. A. de Freitas et al., "Chemical composition, antimicrobial, modulator and antioxidant activity of essential oil of *Dysphania ambrosioides* (L.) Mosyakin & Clemants," *Comparative Immunology, Microbiology and Infectious Diseases*, vol. 65, pp. 58–64, 2019.
- [3] S. Sharafzadeh and M. Zare, "Effect of drought stress on qualitative and quantitative characteristics of some medicinal plants from Lamiaceae family: a review," *Advances in Environmental Biology*, vol. 5, pp. 2058–2062, 2011.
- [4] C. M. Uritu, C. T. Mihai, G.-D. Stanciu et al., "Medicinal plants of the family Lamiaceae in pain therapy: a review," *Pain Research and Management*, vol. 2018, pp. 1–44, 2018.
- [5] D. Picking, R. Delgoda, I. Boulogne, and S. Mitchell, "*Hyptis verticillata* Jacq: a review of its traditional uses, phytochemistry, pharmacology and toxicology," *Journal of Ethnopharmacology*, vol. 147, no. 1, pp. 16–41, 2013.
- [6] A. R. Costa, J. W. A. Bezerra, R. P. Cruz, M. A. Freitas, V. B. Silva, and J. C. Neto, "In vitro antibiotic and modulatory activity of *Mesosphaerum suaveolens* (L.) Kuntze against *Candida* strains," *Antibiotics*, vol. 9, pp. 1–13, 2020.
- [7] R. M. Harley, J. F. B. Pastore, A. S. Soares, E. M. P. Fernando, and M. Mota, "*Mesosphaerum caatingense* (Lamiaceae), a new species from the semi-arid Caatinga region of Northeast Brazil," *Kew Bulletin*, vol. 74, pp. 1–7, 2019.
- [8] M. D. Sedano-Partida, K. P. Santos, W. R. Sala-Carvalho, C. L. Silva-Luz, and C. M. Furlan, "A review of the phytochemical profiling and biological activities of *Hyptis* Jacq.: a Brazilian native genus of Lamiaceae," *Revista Brasileira de Botanica*, vol. 43, pp. 1–16, 2020.
- [9] T. L. Rolim, D. R. P. Meireles, T. M. Batista et al., "Toxicity and antitumor potential of *Mesosphaerum sidifolium* (Lamiaceae) oil and fenchone, its major component," *BMC Complementary and Alternative Medicine*, vol. 17, pp. 347–412, 2017.
- [10] J. W. A. Bezerra, A. R. Costa, M. A. P. da Silva et al., "Chemical composition and toxicological evaluation of *Hyptis suaveolens* (L.) Poiteau (LAMIACEAE) in *Drosophila melanogaster* and *Artemia salina*," *South African Journal of Botany*, vol. 113, pp. 437–442, 2017.
- [11] D. Chakraborty and S. M. Mandal, "Glandular and nonglandular trichomes on vegetative and reproductive parts of *Hyptis suaveolens* (L.) Poit," *Phytomorphology*, vol. 56, pp. 151–159, 2006.
- [12] U. Quattrocchi, *CRC World Dictionary of Plant Names: Common Names, Scientific Names, Eponyms, Synonyms, and Etymology*, Routledge, England, UK, 1st edition, 2017.
- [13] P. P. Sharma, R. K. Roy, D. G. Anurag, and K. S. Vipin, "*Hyptis suaveolens* (L.) poit: a phyto-pharmacological review," *International Journal of Chemical and Pharmaceutical Sciences*, vol. 4, pp. 1–11, 2013.
- [14] O. S. Olorunnisola, A. Adetutu, E. A. Balogun, and A. J. Afolayan, "Ethnobotanical survey of medicinal plants used in the treatment of malarial in Ogbomoso, Southwest Nigeria," *Journal of Ethnopharmacology*, vol. 150, no. 1, pp. 71–78, 2013.
- [15] R. M. Harley and J. F. B. Pastore, "A generic revision and new combinations in the Hyptidinae (Lamiaceae), based on molecular and morphological evidence," *Phytotaxa*, vol. 58, no. 1, pp. 1–55, 2012.
- [16] M. Chatri, A. Baktiar, M. Mansyurdin, and P. Periadnadi, "Leaf trichomes morphology of *Hyptis suaveolens* (L.) poit. (Lamiaceae)," *IOP Conference Series: Materials Science and Engineering*, vol. 335, pp. 1–6, 2018.
- [17] H. J. C. Moreira and H. B. N. Bragança, *Manual de Identificação de Plantas Infestantes*, FMC Campinas, Campinas, Brazil, 2010.
- [18] J. S. R. Aluri, M. I. Vergara-Santana, and S. L. Juarez, "Floral ecology, carinal-lobe release, pollination and reproductive success in the wild and domesticated forms of *Hyptis suaveolens* (L.) Poit. (Lamiaceae) in Mexico," *Plant Species Biology*, vol. 12, no. 2-3, pp. 61–68, 1997.
- [19] P. Sharma and N. Sharma, "Mating strategies in a ruderal weed: case history of *Hyptis suaveolens* (L.) Poit," *Vegetos*, vol. 32, no. 4, pp. 564–570, 2019.
- [20] H. Padalia, V. Srivastava, and S. P. S. Kushwaha, "Modeling potential invasion range of alien invasive species, *Hyptis suaveolens* (L.) Poit. in India: comparison of MaxEnt and GARP," *Ecological Informatics*, vol. 22, pp. 36–43, 2014.
- [21] R. J. Fensham and I. D. Cowie, "Alien plant invasions on the Tiwi Islands. Extent, implications and priorities for control," *Biological Conservation*, vol. 83, no. 1, pp. 55–68, 1998.
- [22] I. D. Cowie and P. A. Werner, "Alien plant species invasive in Kakadu National Park, tropical northern Australia," *Biological Conservation*, vol. 63, no. 2, pp. 127–135, 1993.
- [23] S. F. Soares, L. M. F. Borges, R. de Sousa Braga et al., "Repellent activity of plant-derived compounds against *Amblyomma cajennense* (Acari: ixodidae) nymphs," *Veterinary Parasitology*, vol. 167, no. 1, pp. 67–73, 2010.
- [24] H. O. Edeoga, G. Omosun, and L. C. Uche, "Chemical composition of *Hyptis suaveolens* and *Ocimum gratissimum* hybrids from Nigeria," *African Journal of Biotechnology*, vol. 5, pp. 892–895, 2006.
- [25] L. C. A. Barbosa, F. T. Martins, R. R. Teixeira, M. Polo, and R. M. Montanari, "Chemical variability and biological activities of volatile oils from *Hyptis suaveolens* (L.) Poit," *Agriculturae Conspectus Scientificus*, vol. 78, pp. 1–10, 2013.
- [26] A. K. M. M. Islam, O. Ohno, K. Suenaga, and H. Kato-Noguchi, "Suaveolic acid: a potent phytotoxic substance of *Hyptis suaveolens*," *The Scientific World Journal*, vol. 2014, pp. 1–6, 2014.
- [27] D. Asha, L. Mathew, and K. S. Rishad, "Evaluation of HPTLC fingerprints of flavonoids and antioxidant activity of selected medicinal plants of Lamiaceae family," *International Journal of Pharmacognosy and Phytochemical Research*, vol. 7, pp. 240–245, 2015.
- [28] B. G. V. N. Rao and S. S. Nigam, "Chemical examination of the fixed oil from the seeds of *Hyptis suaveolens*," *Indian Oil & Soap Journal*, vol. 37, pp. 295–300, 1972.
- [29] R. Salini, M. Sindhulakshmi, T. Poongothai, and S. K. Pandian, "Inhibition of quorum sensing mediated biofilm development and virulence in uropathogens by *Hyptis suaveolens*," *Antonie Van Leeuwenhoek*, vol. 107, no. 4, pp. 1095–1106, 2015.
- [30] G. Benelli, G. Flamini, A. Canale, P. L. Cioni, and B. Conti, "Toxicity of some essential oil formulations against the Mediterranean fruit fly *Ceratitis capitata* (Wiedemann)

- (Diptera Tephritidae),” *Crop Protection*, vol. 42, pp. 223–229, 2012.
- [31] H. Lohani, H. C. Andola, and N. Chauhan, “Variations in essential oil composition and biological activity of *Hyptis suaveolens* Poit: a high value aromatic plant of the Himalaya,” *Medicinal Plants-International Journal of Phytomedicines and Related Industries*, vol. 3, no. 4, pp. 311–314, 2011.
- [32] S. Ngom, R. C. Perez, M. A. Mbow et al., “Larvicidal activity of Neem oil and three plant essential oils from Senegal against *Chrysodeixis chalcites* (Esper, 1789),” *Asian Pacific Journal of Tropical Biomedicine*, vol. 8, pp. 67–72, 2018.
- [33] Z. F. Tonzibo, A. B. Florence, G. Bédi, and J. C. Chalchat, “Chemical composition of essential oil of *Hyptis suaveolens* (L.) Poit. from Côte d’Ivoire,” *European Journal of Scientific Research*, vol. 38, pp. 565–571, 2009.
- [34] A. K. Tripathi and S. Upadhyay, “Repellent and insecticidal activities of *Hyptis suaveolens* (Lamiaceae) leaf essential oil against four stored-grain coleopteran pests,” *International Journal of Tropical Insect Science*, vol. 29, no. 04, pp. 219–228, 2009.
- [35] D. W. Wangrawa, A. Badolo, Z. Ilboudo et al., “Insecticidal activity of local plants essential oils against laboratory and field strains of anopheles gambiae s. l. (Diptera: Culicidae) from Burkina Faso,” *Journal of Economic Entomology*, vol. 111, pp. 2844–2853, 2018.
- [36] A. C. P. Moreira, E. D. O. Lima, P. A. Wanderley, E. S. Carmo, and E. L. D. Souza, “Chemical composition and antifungal activity of *Hyptis suaveolens* (L.) poit leaves essential oil against *Aspergillus* species,” *Brazilian Journal of Microbiology*, vol. 41, no. 1, pp. 28–33, 2010.
- [37] T. R. S. A. Luz, J. A. C. Leite, L. S. S. Mesquita, S. A. Bezerra, D. P. B. Silveira, and J. W. C. Mesquita, “Seasonal variation in the chemical composition and biological activity of the essential oil of *Mesosphaerum suaveolens* (L.) Kuntze,” *Industrial Crops and Products*, vol. 153, pp. 1–8, 2020.
- [38] H. B. Andrade, A. F. Braga, S. K. V. Bertolucci, B. S. Hsie, S. T. Silva, and J. E. B. P. Pinto, “Effect of plant growth regulators, light intensity and LED on growth and volatile compound of *Hyptis suaveolens* (L.) Poit *in vitro* plantlets,” *Acta Horticulturae*, vol. 1155, pp. 277–284, 2015.
- [39] M. T. Gueye, A. Diallo, S. Gueye et al., “Analysis of the composition of plant essential oil used in cereals and legumes storage in Senegal,” *Journal of Essential Oil Bearing Plants*, vol. 19, no. 2, pp. 403–409, 2016.
- [40] C. Kossouh, M. Moudachirou, V. Adjakidje, J.-C. Chalchat, and G. Figuéredo, “A comparative study of the chemical composition of the leaves and fruits deriving the essential oil of *Hyptis suaveolens* (L.) Poit. from Benin,” *Journal of Essential Oil Research*, vol. 22, no. 6, pp. 507–509, 2010.
- [41] P. S. Manchand, J. D. White, J. Fayos, and J. Clardy, “Chemical constituents of tropical plants. V. structures of suaveolic acid and suaveolol,” *Journal of Organic Chemistry*, vol. 39, no. 15, pp. 2306–2308, 1974.
- [42] P. Grassi, T. S. U. Reyes, S. Sosa, A. Tubaro, O. Hofer, and K. Zitterl-Eglseer, “Anti-inflammatory activity of two diterpenes of *Hyptis suaveolens* from El Salvador,” *Zeitschrift für Naturforschung C*, vol. 61, no. 3-4, pp. 165–170, 2006.
- [43] C. Vera-Arzave, L. C. Antonio, J. Arrieta et al., “Gastroprotection of suaveolol, isolated from *Hyptis suaveolens*, against ethanol-induced gastric lesions in Wistar rats: role of prostaglandins, nitric oxide and sulfhydryls,” *Molecules*, vol. 17, no. 8, pp. 8917–8927, 2012.
- [44] M. B. Ngassoum, L. Jirovetz, and G. Buchbauer, “Essential oil and headspace from *Hyptis suaveolens*(L.) poit. Leaves and flowers from Cameroon,” *Journal of Essential Oil Research*, vol. 11, no. 3, pp. 283–288, 1999.
- [45] H. L. Ziegler, T. H. Jensen, J. Christensen et al., “Possible artefacts in the *in vitro* determination of antimarial activity of natural products that incorporate into lipid bilayer: apparent antiplasmodial activity of dehydroabietinol, a constituent of *Hyptis suaveolens*,” *Planta Medica*, vol. 68, no. 6, pp. 547–549, 2002.
- [46] J. C. Chukwujekwu, P. Smith, P. H. Coombes, D. A. Mulholland, and J. Van Staden, “Antiplasmodial diterpenoid from the leaves of *Hyptis suaveolens*,” *Journal of Ethnopharmacology*, vol. 102, no. 2, pp. 295–297, 2005.
- [47] M. A. Arai, K. Uchida, S. K. Sadhu et al., “Hedgehog inhibitors from *Artocarpus communis* and *Hyptis suaveolens*,” *Bioorganic & Medicinal Chemistry*, vol. 23, no. 15, pp. 4150–4154, 2015.
- [48] T. N. Misra, R. S. Singh, T. N. Oiha, and J. Upadhyay, “Chemical constituents of *Hyptis suaveolens*. part I. spectral and biological studies on a triterpene acid,” *Journal of Natural Products*, vol. 44, no. 6, pp. 735–738, 1981.
- [49] T. N. Misra, R. S. Singh, and J. Upadhyay, “A natural triterpene acid from *Hyptis suaveolens*,” *Phytochemistry*, vol. 22, no. 11, pp. 2557–2558, 1983.
- [50] K. V. Rao, *Chemical Constituents of Hyptis suaveolens Poit and Solanum pubescens Willd*, Doctoral Thesis, Acharya Nagarjuna University, Guntur, AP, India, 1989.
- [51] T. N. Misra, R. S. Singh, and J. Upadhyay, “Triterpenoids from *Hyptis suaveolens* roots,” *Phytochemistry*, vol. 22, no. 2, pp. 603–605, 1983.
- [52] K. S. Mukherjee, R. K. Mukherjee, and P. K. Ghosh, “Chemistry of *Hyptis suaveolens*: a pentacyclic triterpene,” *Journal of Natural Products*, vol. 47, no. 2, pp. 377–378, 1984.
- [53] K. V. Raja Rao, L. J. M. Rao, and N. S. Prakasa Rao, “An A-ring contracted triterpenoid from *Hyptis suaveolens*,” *Phytochemistry*, vol. 29, no. 4, pp. 1326–1329, 1990.
- [54] N. Ekow Thomford, K. Dzobo, F. Adu, S. Chirikure, A. Wonkam, and C. Dandara, “Bush mint (*Hyptis suaveolens*) and spreading hogweed (*Boerhavia diffusa*) medicinal plant extracts differentially affect activities of CYP1A2, CYP2D6 and CYP3A4 enzymes,” *Journal of Ethnopharmacology*, vol. 211, pp. 58–69, 2018.
- [55] F. D. F. Machado, R. O. Formiga, G. R. M. Lima et al., “*Hyptis suaveolens* (L.) Poit protects colon from TNBS-induced inflammation via immunomodulatory, antioxidant and anti-proliferative mechanisms,” *Journal of Ethnopharmacology*, vol. 265, pp. 113153–113213, 2021.
- [56] T. A. S. Araújo, N. L. Alencar, E. L. C. Amorim, and U. P. Albuquerque, “A new approach to study medicinal plants with tannins and flavonoids contents from the local knowledge,” *Journal of Ethnopharmacology*, vol. 120, pp. 72–80, 2008.
- [57] N. Z. T. D. Jesus, J. C. D. S. Lima, R. M. D. Silva, M. M. Espinosa, and D. T. D. O. Martins, “Levantamento etnobotânico de plantas popularmente utilizadas como antiúlcera e antiinflamatórias pela comunidade de Pirizal, Nossa Senhora do Livramento-MT, Brasil,” *Revista Brasileira de Farmacognosia*, vol. 19, no. 1a, pp. 130–139, 2009.
- [58] R. V. Ribeiro, I. G. C. Bieski, S. O. Balogun, and D. T. d. O. Martins, “Ethnobotanical study of medicinal plants used by ribeirinhos in the north araguaia microregion, mato grosso, Brazil,” *Journal of Ethnopharmacology*, vol. 205, pp. 69–102, 2017.
- [59] N. J. Jacobo-Herrera, F. E. Jacobo-Herrera, A. Zentella-Dehesa, A. Andrade-Cetto, M. Heinrich, and C. Pérez-



- Plasencia, "Medicinal plants used in Mexican traditional medicine for the treatment of colorectal cancer," *Journal of Ethnopharmacology*, vol. 179, pp. 391–402, 2016.
- [60] U. B. Breitbach, M. Niehues, N. P. Lopes, J. E. Q. Faria, and M. G. L. Brandão, "Amazonian Brazilian medicinal plants described by C.F.P. von Martius in the 19th century," *Journal of Ethnopharmacology*, vol. 147, no. 1, pp. 180–189, 2013.
- [61] K. G. Gonçalves and M. C. Pasa, "A etnobotânica e as plantas medicinais na Comunidade Sucuri, Cuiabá, MT, Brasil," *Interações*, vol. 16, pp. 245–256, 2015.
- [62] A. L. D. S. Ferreira, M. C. Pasa, and C. V. Nunez, "A etnobotânica e o uso de plantas medicinais na Comunidade Barreirinho, Santo Antônio de Leverger, Mato Grosso, Brasil," *Interações*, vol. 21, pp. 817–830, 2020.
- [63] F. C. S. Oliveira, F. J. Vieira, A. N. Amorim, and R. F. M. Barros, "The use and diversity of medicinal flora sold at the open market in the city of Oeiras, semiarid region of Piauí, Brazil," *Ethnobotany Research and Applications*, vol. 22, pp. 1–19, 2021.
- [64] P. K. A. Magalhães, E. N. Araujo, A. M. Santos et al., "Ethnobotanical and ethnopharmacological study of medicinal plants used by a traditional community in Brazil's Northeastern," *Brazilian Journal of Biology*, vol. 82, pp. 1–11, 2021.
- [65] J. O. Igoli, I. C. Igwue, and N. P. Igoli, "Traditional medicinal practices among the Igede people of Nigeria," *Journal of Herbs, Spices, & Medicinal Plants*, vol. 10, no. 4, pp. 1–10, 2004.
- [66] M. A. Sonibare, P. N. Okorie, T. O. Aremu, and A. Adegoke, "Ethno-medicines for mosquito transmitted diseases from south-western Nigeria," *Journal of Natural Remedies*, vol. 15, no. 1, pp. 33–42, 2015.
- [67] M. P. Chander, C. Kartick, and P. Vijayachari, "Medicinal plants used by the nicobarese inhabiting little Nicobar island of the andaman and Nicobar archipelago, India," *Journal of Alternative & Complementary Medicine*, vol. 21, no. 7, pp. 373–379, 2015.
- [68] R. D. C. Paulino, G. P. d. S. A. Henriques, O. N. S. Moura, M. D. F. B. Coelho, and R. A. B. Azevedo, "Medicinal plants at the sítio do gois, apodi, rio grande do norte state, Brazil," *Revista Brasileira de Farmacognosia*, vol. 22, no. 1, pp. 29–39, 2012.
- [69] A. F. Attah, M. O'brien, J. Koehbach et al., "Uterine contractility of plants used to facilitate childbirth in Nigerian ethnomedicine," *Journal of Ethnopharmacology*, vol. 143, no. 1, pp. 377–382, 2012.
- [70] M. F. Agra, G. S. Baracho, K. Nurit, I. J. L. D. Basílio, and V. P. M. Coelho, "Medicinal and poisonous diversity of the flora of "Cariri Paraibano", Brazil," *Journal of Ethnopharmacology*, vol. 111, no. 2, pp. 383–395, 2007.
- [71] E. A. Rocha and M. F. Agra, "The ethnomedicinal evaluation of the Lamiaceae family of the cariris Velhos, Paraíba, Brazil," *Revista Brasileira de Ciências Farmacêuticas*, vol. 77, pp. 19–24, 1996.
- [72] K. Agarwal and R. Varma, "Ethnobotanical study of antilithic plants of Bhopal district," *Journal of Ethnopharmacology*, vol. 174, pp. 17–24, 2015.
- [73] R. Silambarasan and M. Ayyanar, "An ethnobotanical study of medicinal plants in Palamalai region of Eastern Ghats, India," *Journal of Ethnopharmacology*, vol. 172, pp. 162–178, 2015.
- [74] J. Sharma, S. Gairola, Y. P. Sharma, and R. D. Gaur, "Ethnomedicinal plants used to treat skin diseases by Tharu community of district Udham Singh Nagar, Uttarakhand, India," *Journal of Ethnopharmacology*, vol. 158, pp. 140–206, 2014.
- [75] R. Kumar and P. Saikia, "Wild edible plants of Jharkhand and their utilitarian perspectives," *Indian Journal of Traditional Knowledge*, vol. 19, pp. 237–250, 2020.
- [76] S. Talukdar and A. Gupta, "Ethnomedicinal knowledge of the Garo community of two villages in western Assam, India," *Journal of Herbal Medicine*, vol. 20, Article ID 100229, 2020.
- [77] A. K. Pandey, "An ethnobotanical study of medicinal plants in Atal Nagar (New Raipur) of Chhattisgarh, India," *International Research Journal of Plant Science*, vol. 12, pp. 01–18, 2021.
- [78] R. R. Manjula, J. K. Rao, and T. S. Reddi, "Ethnomedicine for rheumatism by the tribals of Khammam district, Andhra Pradesh," *Journal of Natural Remedies*, vol. 13, pp. 138–141, 2013.
- [79] G. M. Vidyasagar and P. Prashantkumar, "Traditional herbal remedies for gynecological disorders in women of Bidar district, Karnataka, India," *Fitoterapia*, vol. 78, no. 1, pp. 48–51, 2007.
- [80] R. Singh, S. K. Upadhyay, A. Rani et al., "Ethnobotanical study of weed flora at district Ambala, Haryana, India: comprehensive medicinal and pharmacological aspects of plant resources," *International Journal of Pharmaceutical Sciences and Research*, vol. 12, pp. 1941–1956, 2020.
- [81] R. L. Ghalme, "Ethno-medicinal plants for skin diseases and wounds from Dapoli Tehsil of Ratnagiri district, Maharashtra (India)," *Flora Fauna*, vol. 26, pp. 58–64, 2020.
- [82] M. F. Kadir, M. S. Bin Sayeed, N. I. Setu, A. Mostafa, and M. M. K. Mia, "Ethnopharmacological survey of medicinal plants used by traditional health practitioners in Thanchi, Bandarban Hill Tracts, Bangladesh," *Journal of Ethnopharmacology*, vol. 155, no. 1, pp. 495–508, 2014.
- [83] M. Rahmatullah, Z. Khatun, S. Saha et al., "Medicinal plants and formulations of Tribal healers of the Chekla clan of the Patro tribe of Bangladesh," *Journal of Alternative & Complementary Medicine*, vol. 20, no. 1, pp. 3–11, 2014.
- [84] M. Rahmatullah, A. Hasan, W. Parvin et al., "Medicinal plants and formulations used by the Soren clan of the Santal tribe in Rajshahi district, Bangladesh for treatment of various ailments," *African Journal of Traditional, Complementary, and Alternative Medicines*, vol. 9, pp. 350–359, 2012.
- [85] M. M. U. K. Mia, M. F. Kadir, M. S. Hossan, and M. Rahmatullah, "Medicinal plants of the Garo tribe inhabiting the Madhupur forest region of Bangladesh," *American-Eurasian Journal of Sustainable Agriculture*, vol. 3, pp. 165–171, 2009.
- [86] S. R. Brishty, N. I. Setu, M. Anwar et al., "Ethnobotanical study on medicinal plants for dermatological disorders at Chittagong Hill Tracts, Bangladesh," *Pharmaceutical and Biomedical Research*, vol. 6, pp. 61–90, 2020.
- [87] M. S. Kpodar, S. D. Karou, G. Katawa et al., "An ethnobotanical study of plants used to treat liver diseases in the Maritime region of Togo," *Journal of Ethnopharmacology*, vol. 181, pp. 263–273, 2016.
- [88] N. Saisor, P. Prathepha, and S. Saensouk, "Ethnobotanical study and utilization of plants in Khok Nhong Phok forest, Kosum Phisai district, northeastern Thailand," *Biodiversitas*, vol. 22, pp. 4336–4348, 2021.
- [89] B. A. Fanou, J. R. Klotoe, L. Fah et al., "Ethnobotanical survey on plants used in the treatment of candidiasis in traditional markets of southern Benin," *BMC Complementary Medicine and Therapies*, vol. 20, pp. 288–318, 2020.
- [90] D. D. Nyam, P. D. Mamwan, M. D. Sila, S. N. Dawang, C. J. Abok, and E. H. Kwon-Ndung, "Ethnobotanical survey

- of plants in Bokkos district of Bokkos local government area of plateau state,” *International Journal of Engineering Science*, vol. 10, pp. 13–21, 2021.
- [91] R. L. S. Sikarwar and V. Kumar, “Ethnoveterinary knowledge and practices prevalent among the tribals of central India,” *Journal of Natural Remedies*, vol. 5, pp. 147–152, 2005.
- [92] M. L. Marinho, M. S. Alves, M. L. C. Rodrigues et al., “A utilização de plantas medicinais em medicina veterinária: um resgate do saber popular,” *Revista Brasileira de Plantas Mediciniais*, vol. 9, pp. 64–69, 2007.
- [93] M. Rahmatullah, M. N. K. Azam, I. Malek et al., “An ethnomedicinal survey among the Marakh sect of the Garo tribe of Mymensingh district, Bangladesh,” *International Journal of PharmTech Research*, vol. 4, pp. 141–149, 2021.
- [94] A. Seyoum, K. Pålsson, S. Kung’a et al., “Traditional use of mosquito-repellent plants in western Kenya and their evaluation in semi-field experimental huts against *Anopheles gambiae*: ethnobotanical studies and application by thermal expulsion and direct burning,” *Transactions of the Royal Society of Tropical Medicine and Hygiene*, vol. 96, no. 3, pp. 225–231, 2002.
- [95] A. Sharma, D. R. Batish, H. P. Singh, V. Jaryan, and R. K. Kohli, “The impact of invasive *Hyptis suaveolens* on the floristic composition of the periurban ecosystems of Chandigarh, northwestern India,” *Flora*, vol. 233, pp. 156–162, 2017.
- [96] R. Wulff and E. Medina, “Germination of seeds in *Hyptis suaveolens* poit,” *Plant and Cell Physiology*, vol. 12, pp. 567–579, 1971.
- [97] A. K. M. Islam and H. Kato-Noguchi, “Allelopathic potential of five Labiatae plant species on barnyard grass (*Echinochloa crus-galli*),” *Australian Journal of Crop Science*, vol. 7, p. 1369, 2013.
- [98] A. C. Rodrigues, F. A. Artioli, M. Polo, L. C. A. Barbosa, and L. A. Beijo, “Efeito alelopático de folhas de bamburral [*Hyptis suaveolens* (L.) Poit.] sobre a germinação de sementes de sorgo (*Sorghum vulgare* Pers.), rabanete (*Raphanus sativus* L.) e alface (*Lactuca sativa* L.),” *Revista Brasileira de Plantas Mediciniais*, vol. 14, no. 3, pp. 487–493, 2012.
- [99] R. T. Kapoor, “Bioherbicidal potential of leaf-residue of *Hyptis suaveolens* on the growth and Physiological Parameters of *Parthenium hysterophorus* L,” *Current Research Journal of Biological Sciences*, vol. 3, pp. 341–350, 2011.
- [100] K. V. Sumitha and J. E. Thoppil, “Genotoxicity assessment of two common curing weeds: *Hyptis suaveolens* (L.) Poir. and *Leucas indica* (L.) R. Br,” *Cytotechnology*, vol. 68, no. 4, pp. 1513–1527, 2016.
- [101] J. A. Kumari and P. R. C. Prasad, “Assessing the allelopathy and autotoxicity effects of *Parthenium hysterophorus* L., *Senna uniflora* (mill.) H.S. Irwin and Barneby and *Hyptis suaveolens* (L.) poit,” *Russian Journal of Biological Invasions*, vol. 9, no. 3, pp. 290–298, 2018.
- [102] A. Islam and H. KatoNoguchi, “Plant growth inhibitory activity of medicinal plant *Hyptis suaveolens*: could allelopathy be a cause?” *Emirates Journal of Food and Agriculture*, vol. 25, no. 9, pp. 692–701, 2013.
- [103] G. K. R. Cyrille, S. O. R. O. Yaya, D. A. D. I. E. Adjehi, K. A. B. Benjamin, and D. J. E. Marcellin, “Antibacterial activity of essential oils and extracts from the leaves of *Hyptis suaveolens* and *Lippia multiflora* on multi-resistant bacteria,” *Journal of Chemistry*, vol. 8, pp. 396–403, 2015.
- [104] D.-H. Xu, Y.-S. Huang, D.-Q. Jiang, and K. Yuan, “The essential oils chemical compositions and antimicrobial, antioxidant activities and toxicity of three *Hyptis* species,” *Pharmaceutical Biology*, vol. 51, no. 9, pp. 1125–1130, 2013.
- [105] C. Wiart, S. Mogana, S. Khalifah et al., “Antimicrobial screening of plants used for traditional medicine in the state of Perak, Peninsular Malaysia,” *Fitoterapia*, vol. 75, no. 1, pp. 68–73, 2004.
- [106] S. Okonogi, S. Chansakaow, S. Vejabhikul et al., “Antimicrobial activity and pharmaceutical development of essential oil from *Hyptis suaveolens*,” *Acta Horticulturae*, vol. 678, no. 678, pp. 163–169, 2005.
- [107] B. Joy, M. Omanakutty, and M. Mathew, “Antibacterial effects and chemical composition of the essential oil of *Hyptis suaveolens* Poit leaves,” *Journal of Essential Oil Bearing Plants*, vol. 11, no. 4, pp. 384–390, 2008.
- [108] A. Pandey, P. Singh, U. Palni, and N. N. Tripathi, “In-vitro antibacterial activities of the essential oils of aromatic plants against *Erwinia herbicola* (Lohnis) and *Pseudomonas putida* (Kris Hamilton),” *Journal of the Serbian Chemical Society*, vol. 77, no. 3, pp. 313–323, 2012.
- [109] N. Rattanata, S. Daduang, S. Phaetchanla et al., “Antioxidant and antibacterial properties of selected Thai weed extracts,” *Asian Pacific Journal of Tropical Biomedicine*, vol. 4, no. 11, pp. 890–895, 2014.
- [110] R. Khonkarn, S. Okonogi, O. S. Kittipongpatana, and V. Boasoung, “Antifungal effect of *Hyptis suaveolens* oil microemulsion based carboxymethyl mungbean gel for topical delivery,” *International Journal of Pharmacy and Pharmaceutical Sciences*, vol. 7, pp. 556–561, 2015.
- [111] N. R. Tesch, R. Márquez Yáñez, X. Mendoza-Rojas et al., “Composición química y actividad antibacteriana del aceite esencial de *Hyptis suaveolens* (L.) Poit. (Lamiaceae) de los Llanos venezolanos,” *Revista Peruana de Biología*, vol. 22, pp. 103–107, 2015.
- [112] R. K. Bachheti, I. Rai, A. Joshi, and R. S. Satyan, “Chemical composition and antimicrobial activity of *Hyptis suaveolens* Poit. seed oil from Uttarakhand State, India,” *Oriental Pharmacy and Experimental Medicine*, vol. 15, no. 2, pp. 141–146, 2015.
- [113] M. S. Hossan, H. Jindal, S. Maisha et al., “Antibacterial effects of 18 medicinal plants used by the Khyang tribe in Bangladesh,” *Pharmaceutical Biology*, vol. 56, no. 1, pp. 201–208, 2018.
- [114] O. T. Asekun, O. Ekundayo, and B. A. Adeniyi, “Antimicrobial activity of the essential oil of *Hyptis suaveolens* leaves,” *Fitoterapia*, vol. 70, no. 4, pp. 440–442, 1999.
- [115] M. Chatri, D. Handayani, and S. A. Primayani, “The effect of *Hyptis suaveolens* (L.) poit extract on the growth of *Sclerotium rolfsii* with in-vitro,” *Journal of Physics: Conference Series*, vol. 1317, no. 1, Article ID 012081, 2019.
- [116] K. R. C. Goly, Y. Soro, A. Dadie, A. B. B. Kassi, and M. Djé, “Antibacterial activity of essential oils and extracts from the leaves of *Hyptis suaveolens* and *Lippia multiflora* on multi-resistant bacteria,” *Rasayan Journal of Chemistry*, vol. 8, pp. 396–403, 2015.
- [117] M. Iwu, C. Ezeugwu, C. Okunji, D. R. Sanson, and M. S. Tempesta, “Antimicrobial activity and terpenoids of the essential oil of *Hyptis suaveolens*,” *International Journal of Crude Drug Research*, vol. 28, no. 1, pp. 73–76, 1990.
- [118] B. Prakash and N. K. Dubey, “Evaluation of chemically characterised essential oils of *Coleus aromaticus*, *Hyptis suaveolens* and *Ageratum conyzoides* against storage fungi and aflatoxin contamination of food commodities,” *International Journal of Food Science and Technology*, vol. 46, pp. 754–760, 2011.

- [119] A. Kar and S. R. Jain, "Antibacterial evaluation of some indigenous medicinal volatile oils," *Qualitas Plantarum et Materiae Vegetabiles*, vol. 20, no. 3, pp. 231–237, 1971.
- [120] Y. L. Krishnamurthy, J. Shashikala, and B. Shankar Naik, "Antifungal potential of some natural products against *Aspergillus flavus* in soybean seeds during storage," *Journal of Stored Products Research*, vol. 44, no. 4, pp. 305–309, 2008.
- [121] Y. Mahida and J. S. S. Mohan, "Screening of Indian plant extracts for antibacterial activity," *Pharmaceutical Biology*, vol. 44, no. 8, pp. 627–631, 2006.
- [122] R. S. Malele, C. K. Mutayabarwa, J. W. Mwangi et al., "Essential oil of *Hyptis suaveolens* (L.) Poit. from Tanzania: composition and antifungal activity," *Journal of Essential Oil Research*, vol. 15, no. 6, pp. 438–440, 2003.
- [123] G. L. Pachkore, D. A. Dhale, and A. N. Dharasurkar, "Antimicrobial and phytochemical screening of *Hyptis suaveolens* (L. Poit) Lamiaceae," *International Multidisciplinary Research Journal*, vol. 1, pp. 01–03, 2011.
- [124] V. C. Mbatchou, S. Abdullatif, and R. Glover, "Phytochemical screening of solvent extracts from *Hyptis suaveolens* LAM for fungal growth inhibition," *Pakistan Journal of Nutrition*, vol. 9, no. 4, pp. 358–361, 2010.
- [125] W. Nantitanon, S. Chowwanapoonpohn, and S. Okonogi, "Antioxidant and antimicrobial activities of *Hyptis suaveolens* essential oil," *Scientia Pharmaceutica*, vol. 75, no. 1, pp. 35–46, 2007.
- [126] V. N. Pandey and N. K. Dubey, "Effect of essential oils from some higher plants against fungi causing damping-off disease," *Biologia Plantarum*, vol. 34, no. 1–2, pp. 143–147, 1992.
- [127] V. N. Pandey and N. K. Dubey, "Antifungal potential of leaves and essential oils from higher plants against soil phytopathogens," *Soil Biology and Biochemistry*, vol. 26, no. 10, pp. 1417–1421, 1994.
- [128] A. Rojas, L. Hernandez, R. Pereda-Miranda, and R. Mata, "Screening for antimicrobial activity of crude drug extracts and pure natural products from Mexican medicinal plants," *Journal of Ethnopharmacology*, vol. 35, no. 3, pp. 275–283, 1992.
- [129] V. Satish, V. D. Ravichandrian, U. Gavani, and P. M. Paarakh, "Antimicrobial studies on the extracts of *Cocculus hirsutus* Linn. And *Hyptis suaveolens* poit," *Indian Journal of Natural Products and Resources*, vol. 1, pp. 49–52, 2010.
- [130] N. Sharma and A. Tripathi, "Integrated management of postharvest *Fusarium* rot of gladiolus corms using hot water, UV-C and *Hyptis suaveolens* (L.) Poit. essential oil," *Postharvest Biology and Technology*, vol. 47, no. 2, pp. 246–254, 2008.
- [131] H. B. Singh and A. K. Handique, "Antifungal activity of the essential oil of *Hyptis suaveolens* and its efficacy in biocontrol measures," *Journal of Essential Oil Research*, vol. 9, no. 6, pp. 683–687, 1997.
- [132] N. U. Prakash, S. Sowmya, C. Priyadarshini et al., "Studies on bio efficacy of weeds in Tanjore district, Tamilnadu, India," *International Journal of Pharmacy and Pharmaceutical Sciences*, vol. 4, pp. 132–134, 2012.
- [133] A. Tripathi, N. Sharma, and V. Sharma, "In vitro efficacy of *Hyptis suaveolens* L. (Poit.) essential oil on growth and morphogenesis of *Fusarium oxysporum* f.sp. *gladioli* (Massey) Snyder & Hansen," *World Journal of Microbiology and Biotechnology*, vol. 25, no. 3, pp. 503–512, 2009.
- [134] P. H. A. Zollo, L. Biyiti, F. Tchoumboungang, C. Menut, G. Lamaty, and P. Bouchet, "Aromatic plants of tropical Central Africa. part XXXII. chemical composition and antifungal activity of thirteen essential oils from aromatic plants of Cameroon," *Flavour and Fragrance Journal*, vol. 13, no. 2, pp. 107–114, 1998.
- [135] J. W. A. Bezerra, F. C. Rodrigues, A. R. Costa, K. S. Pereira, N. R. Vieira, and G. Oliveira Lôbo, "*Mesosphaerum suaveolens* (Lamiaceae): source of antimicrobial and antioxidant compounds," *Research, Society and Development*, vol. 9, Article ID e575986161, 2020.
- [136] S.-A. Oscar, C.-N. Antonio, G.-V. Marina, R.-S. Elsa, and V.-A. Gabriel, "Phytochemical screening, antioxidant activity and *in vitro* biological evaluation of leave extracts of *Hyptis suaveolens* (L.) from south of Mexico," *South African Journal of Botany*, vol. 128, pp. 62–66, 2020.
- [137] N. T. Chung, L. T. Huong, D. N. Dai, and I. A. Ogunwande, "Chemical compositions of essential oils and antimicrobial activity of *Hyptis suaveolens* (L.) Poit. (Lamiaceae) from Vietnam," *European Journal of Medicinal Plants*, vol. 31, pp. 114–123, 2020.
- [138] B. Conti, A. Canale, P. L. Cioni, G. Flamini, and A. Rifici, "*Hyptis suaveolens* and *Hyptis spicigera* (Lamiaceae) essential oils: qualitative analysis, contact toxicity and repellent activity against *Sitophilus granarius* (L.) (Coleoptera: Dryophthoridae)," *Journal of Pest Science*, vol. 84, no. 2, pp. 219–228, 2011.
- [139] A. Canale, G. Benelli, B. Conti et al., "Ingestion toxicity of three Lamiaceae essential oils incorporated in protein baits against the olive fruit fly, *Bactrocera oleae* (Rossi) (Diptera Tephritidae)," *Natural Product Research*, vol. 27, no. 22, pp. 2091–2099, 2013.
- [140] O. F. Olotuah, "Laboratory evaluation of pesticidal activities of *Hyptis suaveolens* in pest management," *International Journal of Agricultural Research*, vol. 8, no. 2, pp. 101–106, 2013.
- [141] P. S. Jaya, P. Singh, B. Prakash, and N. K. Dubey, "Insecticidal activity of *Ageratum conyzoides* L., *Coleus aromaticus* Benth. and *Hyptis suaveolens* (L.) Poit essential oils as fumigant against storage grain insect *Tribolium castaneum* Herbst," *Journal of Food Science & Technology*, vol. 51, no. 9, pp. 2210–2215, 2014.
- [142] E. S. Adjou, D. Chougourou, and M. M. Soumanou, "Insecticidal and repellent effects of essential oils from leaves of *Hyptis suaveolens* and *Ocimum canum* against *Tenebroides mauritanicus* (L.) isolated from peanut in post-harvest," *Journal of Consumer Protection and Food Safety*, vol. 14, no. 1, pp. 25–30, 2019.
- [143] C. I. Abramson, P. A. Wanderley, M. J. A. Wanderley, J. C. R. Silva, and L. M. Michaluk, "The effect of essential oils of sweet fennel and pignut on mortality and learning in africanized honeybees (*Apis mellifera* L.) (Hymenoptera: apidae)," *Neotropical Entomology*, vol. 36, no. 6, pp. 828–835, 2007.
- [144] C. O. Adedire and L. Lajide, "Toxicity and oviposition deterrence of some plant extracts on cowpea storage bruchid, *Callosobruchus maculatus* Fabricius," *Journal of Plant Diseases and Protection*, vol. 106, pp. 647–653, 1999.
- [145] O. M. Azeez and O. O. R. Pitan, "Influence of cowpea variety on the potency and deterrent indices of six plant powders against the seed bruchid, *Callosobruchus maculatus* (Fabricius) (Coleoptera: Bruchidae)," *Archives of Phytopathology and Plant Protection*, vol. 48, no. 5, pp. 441–451, 2015.
- [146] S. J. Boeke, I. R. Baumgart, J. J. A. Van Loon, A. Van Huis, M. Dicke, and D. K. Kossou, "Toxicity and repellence of African plants traditionally used for the protection of stored



- cowpea against *Callosobruchus maculatus*,” *Journal of Stored Products Research*, vol. 40, no. 4, pp. 423–438, 2004.
- [147] B. N. Iloba and T. Ekrakene, “Comparative assessment of insecticidal effect of *Azadirachta indica*, *Hyptis suaveolens* and *Ocimum gratissimum* on *Sitophilus zeamais* and *Callosobruchus maculatus*,” *Journal of Biological Sciences*, vol. 6, pp. 626–630, 2006.
- [148] Z. Ilboudo, L. C. B. Dabiré, R. C. H. Nébié et al., “Biological activity and persistence of four essential oils towards the main pest of stored cowpeas, *Callosobruchus maculatus* (F.) (Coleoptera: Bruchidae),” *Journal of Stored Products Research*, vol. 46, no. 2, pp. 124–128, 2010.
- [149] Z. Ilboudo, C. L. Dabiré-Binso, F. Sankara, R. C. H. Nébié, and A. Sanon, “Optimizing the use of essential oils to protect stored cowpeas from *Callosobruchus maculatus* (Coleoptera: Bruchinae) damage,” *African Entomology*, vol. 23, no. 1, pp. 94–100, 2015.
- [150] S. M. Kéita, C. Vincent, J. P. Schmit, S. Ramaswamy, and A. Bélanger, “Effect of various essential oils on *Callosobruchus maculatus* (F.) (Coleoptera: Bruchidae),” *Journal of Stored Products Research*, vol. 36, pp. 355–364, 2000.
- [151] J. W. A. Bezerra, F. A. Grangeiro Neto, J. T. Pereira Filho et al., “Chemical composition and insecticide activity of essential oil of *Mesosphaerum suaveolens* against *Nauphoeta cinerea*,” *Journal of Agricultural Studies*, vol. 8, no. 2, pp. 352–361, 2020.
- [152] A. Z. Abagli, T. B. C. Alavo, F. Avlessi, and M. Moudachirou, “Potential of the bush mint, *Hyptis suaveolens* essential oil for personal protection against mosquito biting,” *Journal of the American Mosquito Control Association*, vol. 28, no. 1, pp. 15–19, 2012.
- [153] K. Pålsson and T. G. Jaenson, “Plant products used as mosquito repellents in Guinea Bissau, West Africa,” *Acta Tropica*, vol. 72, pp. 39–52, 1999.
- [154] G. Benelli, G. Flamini, A. Canale, I. Molfetta, P. L. Cioni, and B. Conti, “Repellence of *Hyptis suaveolens* whole essential oil and major constituents against adults of the granary weevil *Sitophilus granarius*,” *Bulletin of Insectology*, vol. 65, pp. 177–183, 2012.
- [155] T. G. T. Jaenson, K. Pålsson, and A.-K. Borg-Karlson, “Evaluation of extracts and oils of mosquito (Diptera: Culicidae) repellent plants from Sweden and Guinea-Bissau,” *Journal of Medical Entomology*, vol. 43, no. 1, pp. 113–119, 2006.
- [156] B. A. d. Melo, A. J. Molina-Rugama, K. Haddi, D. T. Leite, and E. E. d. Oliveira, “Repellency and bioactivity of Caatinga Biome plant powders against *Callosobruchus maculatus* (Coleoptera: Chrysomelidae: Bruchinae),” *Florida Entomologist*, vol. 98, no. 2, pp. 417–423, 2015.
- [157] C. Vongsombath, K. Pålsson, L. Björk, A. K. Borg-Karlson, and T. G. Jaenson, “Mosquito (Diptera: Culicidae) repellency field tests of essential oils from plants traditionally used in Laos,” *Journal of Medical Entomology*, vol. 49, pp. 1398–1404, 2014.
- [158] T. Ashitani, S. S. Garboui, F. Schubert et al., “Activity studies of sesquiterpene oxides and sulfides from the plant *Hyptis suaveolens* (Lamiaceae) and its repellency on *Ixodes ricinus* (Acari: ixodidae),” *Experimental & Applied Acarology*, vol. 67, no. 4, pp. 595–606, 2015.
- [159] B. Conti, G. Benelli, G. Flamini et al., “Larvicidal and repellent activity of *Hyptis suaveolens* (Lamiaceae) essential oil against the mosquito *Aedes albopictus* Skuse (Diptera: Culicidae),” *Parasitology Research*, vol. 110, no. 5, pp. 2013–2021, 2012.
- [160] A. A. Amusan, A. B. Idowu, and F. S. Arowolo, “Comparative toxicity effect of bush tea leaves (*Hyptis suaveolens*) and orange peel (*Citrus sinensis*) oil extract on larvae of the yellow fever mosquito *Aedes aegypti*,” *Tanzania Journal of Health Research*, vol. 7, pp. 174–178, 2005.
- [161] S. Tennyson, K. J. Ravindran, and S. Arivoli, “Bioefficacy of botanical insecticides against the dengue and chikungunya vector *Aedes aegypti* (L.) (Diptera: Culicidae),” *Asian Pacific Journal of Tropical Biomedicine*, vol. 2, pp. 1842–1844, 2012.
- [162] S. Arivoli, K. J. Ravindran, and T. Samuel, “Larvicidal efficacy of plant extracts against the malarial vector *Anopheles stephensi* Liston (Diptera: Culicidae),” *World Journal of Medical Sciences*, vol. 7, pp. 77–80, 2012.
- [163] R. Yadav, V. Tyagi, S. N. Tikar et al., “Differential larval toxicity and oviposition altering activity of some indigenous plant extracts against dengue and chikungunya vector *Aedes albopictus*,” *Journal of Arthropod-Borne Diseases*, vol. 8, no. 2, pp. 174–185, 2014.
- [164] D. Elumalai, M. Hemavathi, C. V. Deepaa, and P. K. Kaleena, “Evaluation of phytosynthesised silver nanoparticles from leaf extracts of *Leucas aspera* and *Hyptis suaveolens* and their larvicidal activity against malaria, dengue and filariasis vectors,” *Parasite Epidemiology and Control*, vol. 2, no. 4, pp. 15–26, 2017.
- [165] I. Hari and N. Mathew, “Larvicidal activity of selected plant extracts and their combination against the mosquito vectors *Culex quinquefasciatus* and *Aedes aegypti*,” *Environmental Science and Pollution Research*, vol. 25, no. 9, pp. 9176–9185, 2018.
- [166] J. Abok, A. Ombugadu, A. Ombugadu, and G. Angbalaga, “*Hyptis suaveolens* extract exhibits larvicidal activity against *Anopheles gambiae* Larvae,” *Tropical Journal of Natural Product Research*, vol. 2, no. 5, pp. 245–249, 2018.
- [167] C. Adda, P. Atachi, K. Hell, and M. Tamò, “Potential use of the bushmint, *Hyptis suaveolens*, for the control of infestation by the pink stalk borer, *Sesamia calamistis* on maize in southern Benin, West Africa,” *Journal of Insect Science*, vol. 11, p. 33, 2011.
- [168] K. Agboka, A. K. Mawufe, M. Tamò, and S. Vidal, “Effects of plant extracts and oil emulsions on the maize cob borer *Mussidia nigrivenella* (Lepidoptera: Pyralidae) in laboratory and field experiments,” *International Journal of Tropical Insect Science*, vol. 29, no. 04, pp. 185–194, 2009.
- [169] K. Kovendan, K. Murugan, C. Panneerselvam et al., “Laboratory and field evaluation of medicinal plant extracts against filarial vector, *Culex quinquefasciatus* Say (Diptera: Culicidae),” *Parasitology Research*, vol. 110, no. 6, pp. 2105–2115, 2012.
- [170] K. P. Kumar, P. N. Rao, and A. Tanweer, “*Helicoverpa armigera* larval control with certain plant products in the cotton agro-ecosystem,” *Pestology*, vol. 24, pp. 9–13, 2000.
- [171] C. W. G. de Menezes, G. A. Carvalho, D. S. Alves et al., “Biocontrol potential of methyl chavicol for managing *Spodoptera frugiperda* (Lepidoptera: Noctuidae), an important corn pest,” *Environmental Science and Pollution Research*, vol. 27, no. 5, pp. 5030–5041, 2020.
- [172] M. Pavunraj, K. Baskar, M. G. Paulraj, S. Ignacimuthu, and S. Janarthanan, “Phagodeterrence and insecticidal activity of *Hyptis suaveolens* (Poit.) against four important lepidopteran pests,” *Archives of Phytopathology and Plant Protection*, vol. 47, no. 1, pp. 113–121, 2014.
- [173] A. Sanon, M. N. Ba, L. C. B. Dabiré, R. C. H. Nébié, and J. P. Monge, “Side effects of grain protectants on biological control agents: how *Hyptis* plant extracts affect parasitism

- and larval development of *Dinarmus basalis*,” *Phytoparasitica*, vol. 39, no. 3, pp. 215–222, 2011.
- [174] T. I. Silva, A. C. Leite Alves, F. R. Azevedo, C. Araújo Marco, H. R. Santos, and R. Azevedo, “Actividad larvicida de aceites esenciales en *Aedes aegypti* L. (Diptera: Culicidae),” *Idesia*, vol. 35, pp. 63–70, 2017.
- [175] E. Lautié, R. Quintero, M. A. Fliniaux, and M. L. Villarreal, “Selection methodology with scoring system: application to Mexican plants producing podophyllotoxin related lignans,” *Journal of Ethnopharmacology*, vol. 120, pp. 402–412, 2008.
- [176] S. Musika and K. Indrapichate, “Cytotoxicity and apoptosis induction of Mintweed (*Hyptis suaveolens* L. Poit) leaf extracts on human T-leukemia cell line, Jurkat cells,” *World Journal of Pharmacy and Pharmaceutical Sciences*, vol. 3, pp. 304–317, 2014.
- [177] S. Gurunagarajan and B. Pemaiah, “Comparative studies on cytotoxic effect of *Hyptis suaveolens* Poit. and *Leonotis nepeatefolia* R. Br. against EAC cell lines,” *Journal of Pharmacy Research*, vol. 4, pp. 1222–1224, 2011.
- [178] S. Botcha and S. D. Prattipati, “Callus extract mediated green synthesis of silver nanoparticles, their characterization and cytotoxicity evaluation against MDA-MB-231 and PC-3 cells,” *BioNanoScience*, vol. 10, pp. 1–12, 2019.
- [179] S. Botcha and S. D. Prattipati, “Green synthesis of silver nanoparticles using *Hyptis suaveolens* (L.) Poit leaf extracts, their characterization and cytotoxicity evaluation against PC-3 and MDA-MB 231 cells,” *Biologia*, vol. 74, no. 7, pp. 783–793, 2019.
- [180] O. K. Shittu, B. Lawal, A. A. Ojo, and A. S. Yisa, “Polyethylene glycol-modified nanocarrier encapsulation of diminazene aceturate improved haematobiochemical recovery in *Trypanosoma brucei* infected rats,” *Polish Journal of Natural Sciences*, vol. 34, pp. 317–332, 2019.
- [181] M. Noronha, S. Guleria, D. Jani, L. B. George, H. Highland, and R. B. Subramanian, “Ethnobotanical database based screening and identification of potential plant species with antiplasmodial activity against chloroquine-sensitive (3D7) strain of *Plasmodium falciparum*,” *Asian Pacific Journal of Tropical Biomedicine*, vol. 8, p. 92, 2018.
- [182] O. T. Salawu, T. O. fnm Odaibo, and B. A., “The molluscicidal effects of *Hyptis suaveolens* on different stages of *Bulinus globosus* in the laboratory,” *African Journal of Biotechnology*, vol. 10, no. 50, pp. 10241–10247, 2011.
- [183] K. Agarwal, “Antioxidant activity and phytochemical analysis of *Hyptis suaveolens* (L.) Poit,” *Journal of Advanced Pharmacy Education & Research*, vol. 3, pp. 541–549, 2013.
- [184] H. Ghaffari, B. J. Ghassam, S. Chandra Nayaka, K. Ramachandra Kini, and H. S. Prakash, “Antioxidant and neuroprotective activities of *Hyptis suaveolens* (L.) Poit. against oxidative stress-induced neurotoxicity,” *Cellular and Molecular Neurobiology*, vol. 34, no. 3, pp. 323–331, 2014.
- [185] U. Gavani and P. M. Paarakh, “Antioxidant activity of *Hyptis suaveolens* poit,” *International Journal of Pharmacology*, vol. 4, no. 3, pp. 227–229, 2008.
- [186] J. W. A. Bezerra, F. C. Rodrigues, A. R. Costa et al., “*Mesospaerum suaveolens* (L.) Kuntze (pignut) a medicinal plant with antioxidant potential and abundant polyphenols,” *Revista Cubana de Plantas Medicinales*, vol. 24, 2019.
- [187] D. Iqbal, A. B. Dukhyil, and M. S. Khan, “Geno-protective, free radical scavenging and antimicrobial potential of *Hyptis suaveolens* Methanolic fraction: an *in-vitro* study,” *Journal of Pharmaceutical Research International*, vol. 2021, pp. 46–57, 2021.
- [188] S. D. Priyadarshini and V. Sujatha, “Antioxidant and cytotoxic studies on two known compounds isolated from *Hyptis suaveolens* leaves,” *International Journal of Pharmacy and Pharmaceutical Sciences*, vol. 5, pp. 283–290, 2013.
- [189] A. Banerjee and B. De, “Antioxidant activity of ethnomedicinally used flowers of West Bengal, India,” *International Journal of Pharmacognosy and Phytochemical Research*, vol. 6, pp. 622–635, 2014.
- [190] F.-C. Hsu, S.-F. Tsai, and S.-S. Lee, “Chemical investigation of *Hyptis suaveolens* seed, a potential antihyperuricemic nutraceutical, with assistance of HPLC-SPE-NMR,” *Journal of Food and Drug Analysis*, vol. 27, no. 4, pp. 897–905, 2019.
- [191] E. E. Lima, A. R. Costa, J. W. Almeida-Bezerra et al., “Phytochemistry, chelating and reducing potential of *Mesospaerum suaveolens* (L.) Kuntze (Lamiaceae) essential oil,” *Research, Society and Development*, vol. 9, no. 11, Article ID e1099119333, 2020.
- [192] C. Shenoy, M. B. Patil, and R. Kumar, “Wound healing activity of *Hyptis suaveolens* (L.) poit (Lamiaceae),” *International Journal of PharmTech Research*, vol. 1, pp. 737–744, 2009.
- [193] A. Shirwaikar, R. Shenoy, A. L. Udupa, S. L. Udupa, and S. Shetty, “Wound healing property of ethanolic extract of leaves of *Hyptis suaveolens* with supportive role of antioxidant enzymes,” *Indian Journal of Experimental Biology*, vol. 41, pp. 238–241, 2003.
- [194] R. Shenoy and A. Shirwaikar, “Anti inflammatory and free radical scavenging studies of *Hyptis suaveolens* (Labiatae),” *Indian Drugs*, vol. 39, pp. 574–577, 2002.
- [195] N. Z. T. Jesus, H. S. Falcão, G. R. M. Lima et al., “*Hyptis suaveolens* (L.) Poit (Lamiaceae), a medicinal plant protects the stomach against several gastric ulcer models,” *Journal of Ethnopharmacology*, vol. 150, no. 3, pp. 982–988, 2013.
- [196] M. Z. H. Shaikat, M. T. Hossain, and G. Azam, “Phytochemical screening and anti-diarrhoeal activity of *Hyptis suaveolens*,” *International Journal of Applied Research in Natural Products*, vol. 5, pp. 1–4, 2012.
- [197] S. B. Mishra, A. Verma, A. Mukerjee, and M. Vijayakumar, “Anti-hyperglycemic activity of leaves extract of *Hyptis suaveolens* L. Poit in streptozotocin induced diabetic rats,” *Asian Pacific Journal of Tropical Medicine*, vol. 4, no. 9, pp. 689–693, 2011.
- [198] H. Ghaffari, B. J. Ghassam, and H. Prakash, “Hepatoprotective and cytoprotective properties of *Hyptis suaveolens* against oxidative stress-induced damage by  $CCl_4$  and  $H_2O_2$ ,” *Asian Pacific Journal of Tropical Medicine*, vol. 5, no. 11, pp. 868–874, 2012.
- [199] W. Niwatananun, K. Niwatananun, A. Titwan, and S. Okonogi, “Safety of topical formulations containing *Hyptis suaveolens* bioactive compound,” *International Workshop on Bioencapsulation*, vol. 6, pp. 1–5, 2007.

## Review Article

# Harnessing the Natural Toxic Metabolites in COVID-19

**Ali Bahrami** <sup>1,2</sup>, **Mohammad Taheri** <sup>3</sup>, **Mohammad Reza Arabestani** <sup>3</sup>,  
**Meysam Soleimani** <sup>2</sup>, **Mojdeh Mohammadi** <sup>4</sup>, **Fatemeh Golabchi**,<sup>1,2</sup>  
**Maryam Banitorfi**,<sup>1,2</sup> **Seyed Mostafa Hosseini** <sup>3</sup>, **Sodabe Khodabandehlou**,<sup>4</sup>  
**and Fatemeh Nouri** <sup>2</sup>

<sup>1</sup>Student Research Committee, Hamadan University of Medical Sciences, Hamadan, Iran

<sup>2</sup>Department of Pharmaceutical Biotechnology, School of Pharmacy, Hamadan University of Medical Sciences, Hamadan, Iran

<sup>3</sup>Department of Microbiology, Faculty of Medicine, Hamadan University of Medical Sciences, Hamadan, Iran

<sup>4</sup>Department of Pharmacology and Toxicology, School of Pharmacy, Hamadan University of Medical Sciences, Hamadan, Iran

Correspondence should be addressed to Mohammad Taheri; motaheri360@gmail.com and Fatemeh Nouri; fatemenouri1@gmail.com

Received 6 November 2021; Revised 16 January 2022; Accepted 9 February 2022; Published 7 March 2022

Academic Editor: Jelena Zivkovic

Copyright © 2022 Ali Bahrami et al. This is an open access article distributed under the Creative Commons Attribution License, which permits unrestricted use, distribution, and reproduction in any medium, provided the original work is properly cited.

SARS-CoV-2 is a novel coronavirus and the cause of the recent pandemic; it is an enveloped  $\beta$ -coronavirus. SARS-CoV-2 appear in the Wuhan City of China for the first time and outspread worldwide quickly. Due to its person-to-person fast transmission, COVID-19 is becoming a global problem. SARS-CoV-2 enter into cells by using ACE2 receptors that are numerous in the lungs and finally can cause acute respiratory distress syndrome (ARDS). Dry cough, sore throat, fever, body pain, headache, GIT discomfort, diarrhoea, and fatigue are some of the COVID-19 symptoms. There is no definite and certain treatment for disease caused by SARS-CoV-2 till now. Some pharmacological effects of toxins, toxoids, and venoms have been proven, and their effects on some diseases have been evaluated. This study aimed to investigate the role of toxins, toxoids, and venom in the pathophysiology of COVID-19 disease.

## 1. Background

Acute respiratory syndrome coronavirus 2 (SARS-CoV-2) is characterized by severe cytokine syndrome following inflammation. The pathogenesis of SARS-CoV-2 is such that in the first stage, viral binding to epithelial cells occurs with a minimal innate immune response. In the second stage, we see increased viral replication along with an active immune response and the spread of the virus to the lower respiratory tract, which may also affect the digestive and cardiovascular systems. In the third stage, events such as hypoxia, the penetration of the virus into the entire respiratory tract, and finally acute respiratory distress syndrome (ARDS) occur, which the fatal rate is potentially high [1].

SARS-CoV-2 affects the lungs the most, but it can also attack the brain and cause unpredictable nervous defects by crossing the blood-brain barrier [2]. SARS-CoV-2 is transmitted person-to-person through viral airborne

droplets. This infection has several clinical symptoms such as dry cough, sore throat, fever, body pain, headache, abdominal discomfort, diarrhoea, and fatigue. In the acute phase, it can cause pneumonia, acute respiratory failure, encephalopathy, multiorgan dysfunction, and death. Because angiotensin-converting enzyme 2 (ACE2) is one of the major receptors identified for SARS-CoV-2 and is predominantly expressed in the lungs, the lungs are involved in coronavirus infection. This receptor can also be found in the gastrointestinal tract, the cardiovascular system, the brain, and other organs [3–5].

Various data and treatments for SARS-CoV-2 infection are being reviewed. We previously examined the impact of serum electrolytes, trace elements, and heavy metals in COVID-19 [6, 7]. Toxins are small molecules, peptides, or proteins secreted by prokaryotic and eukaryotic cells and provide defence ability for them [8]. Phospholipases, proteases, and ion channel modulators are their primary targets.

Many toxins are multifunctional and have several biological targets which may have no relation with their toxic role [9]. Some toxin-derived peptides are now being used to treat type 2 diabetes, hypertension, neuropathic pain, and other medical disorders [10–13]. Some data confirm the effect of bee venom (BV) on preventing COVID-19 and improving it [1]. Some other data ignore the BV effect on preventing COVID-19 and hypothesize that less SARS-CoV-2 infection in beekeepers is due to their less exposure to other people [3]. A low dose of botulinum neurotoxin (BoNT) can reduce the symptoms of COVID-19, and so, it could be used in treatment lines [14]. It has demonstrated that the rate of DTP vaccination has an inverse correlation with COVID-19 prevalence [15]. Cobrotoxin has an anti-inflammatory effect and also can restore the CD4/CD8 ratio and perform immunoprotective activity against SARS-CoV-2 [16]. Tetrodotoxin is an inhibitor of  $M^{Pro}$  of SARS-CoV-2 and so can affect the virus [17]. This study aimed to investigate the role of toxins, toxoids, and venom in the pathophysiology of COVID-19 disease.

## 2. Method

The bibliographic search was performed on PubMed, Scopus, and Web of Science databases in Sep 2021. Search keywords including “toxin” OR “aflatoxin” OR “botulinum toxin A” OR “dioxin” OR “diphtheria toxin” OR “exotoxin” OR “pertussis toxin” OR “tetanus toxin” OR “tetradotoxin” OR “trichothecenes” OR “Shiga toxin” OR “cholera toxin B” OR “bufotoxin” OR “ochratoxin A” OR “Anthrax toxin” AND “coronavirus 2019” OR “COVID-19” OR “SARS-CoV-2” in all fields. Any languages or date restrictions were not applied. Identified studies were screened by title, abstract, and full text. The reference list of identified studies was also evaluated to increment the sensitivity and choice of most literature which we could not identify in the database. Greatest sensitivity search was initiated, 167 articles on external databases were found and collected by a researcher using the Endnote software. Then, unifying the articles from all the cited databases and bringing out duplicate articles, the two researchers separately investigated all the articles and excluded the articles that includes irrelevance of title to toxins and COVID-19, absence of keywords in the title or abstract of studies, and the inclusion index criteria. Afterwards, several articles after reviewing titles and abstracts were excluded. The existing publications were carefully assessed, the relevant study was chosen, and the data for the studies were appraised based on the title, examined technique, sample size, and so on. Finally, 38 articles were analyzed after acquiring relevant papers and determining the limitations of the search strategy. During the examination of publications in 2021, we discovered 30 new articles that were included in the study (search strategy was shown in Figure 1).

## 3. Results

**3.1. Bee Venom.** Apitherapy means the use of bee stings to treat certain diseases. However, the results regarding the effectiveness of this method are controversial [3]. Bee venom

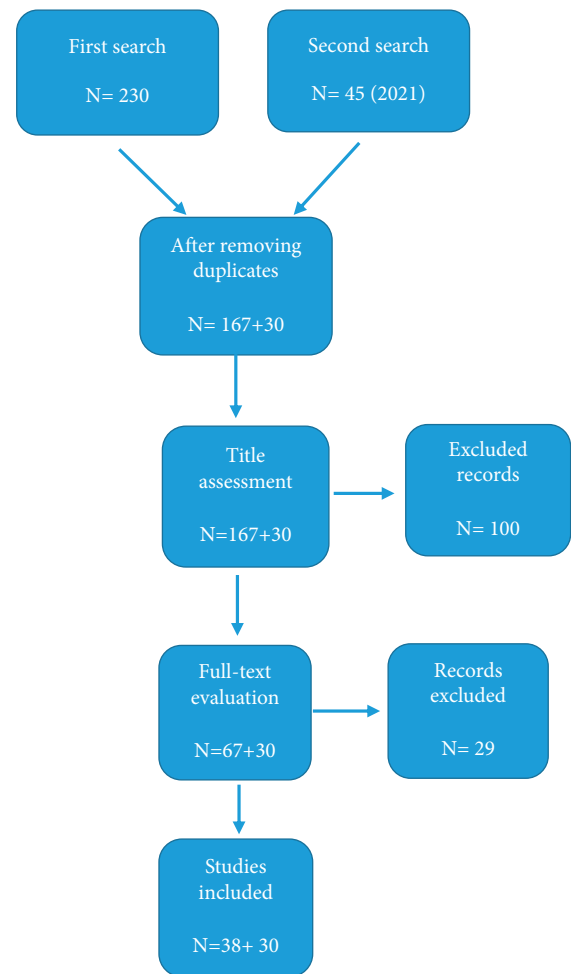


FIGURE 1: Flow chart of the search strategy.

(BV) has antiviral properties because of the presence of melittin and phospholipase A2 (PLA2). Both agents work against enveloped and nonenveloped viruses, and they work against H1N1 and HIV by using antagonist activity against IL-6, IL-8, interferon, and TNF- $\alpha$ . BV vaccination is also a way to protect against cytomegalovirus. In modern medicine, bee venom is used to treat Parkinson’s disease, multiple sclerosis, and arthritis [1, 18–20].

According to a study in Hubei Province in China, none of the 5115 local beekeepers had covid-19 symptoms. 5 apitherapists and 121 patients who received apitherapy were also interviewed. Two of the apitherapists, although exposed to suspected or confirmed covid-19 victims without protection, showed no signs of COVID-19. Also, none of the 121 patients was infected with COVID-19, even though 3 of them were exposed to relatives infected with SARS-CoV-2. They suggested that BV therapy, due to the presence of melittin and phospholipase A2, which have a strong anti-inflammatory function, could help support recovery because even if the patient recovers from the initial SARS-CoV-2 infection, and it may have long-term effects which are known as long-covid because PLA2 binds to the membrane *in vivo*, causes antibodies to bind with the cell membrane, and stimulates CD8 T cells [1]. Bee venom increases the



differentiation of FOXP3-expressing cells in CD4 T cells and mature CD4 thymocytes [21, 22]. Yang et al. believe that the effect of BV on the immune system and increasing the differentiation of human regulatory T cells plays an important role in controlling COVID-19 [18]. Also, Block et al. believe that the anti-inflammatory and antimicrobial properties of BV derivatives may help prevent long-term fibrotic destruction of the lungs. It has demonstrated that IL-10 increase in beekeepers due to their persistent exposure to BV. IL-10 is an anti-inflammatory cytokine that reduces inflammatory cytokines IL-1 and TNF-alpha and so, BV can decrease the cytokine storm [3, 23].

A study conducted in Germany did not confirm the results of apitherapy in SARS-CoV-2. The study found that beekeepers were not immune to SARS-CoV-2 infections. The hypothesis that beekeepers will not be infected with SARS because of immunity due to bee stings is not supported by the data of this study. Some factors like how long they had been a beekeeper, the total number of bee stings received, the number of bee stings received in the year 2020, and potential allergic reactions to bee stings do not have any effect on the severity of COVID-19. However, beekeepers' reactions to bee stings are one of the elements that influence two COVID-19 symptoms, including tiredness and sore throat soreness. These symptoms are more pronounced in beekeepers who are more sensitive to bee stings. The fact that beekeepers are less affected by SARS-CoV-2 infection may be due to their personality traits, which tend to spend more time alone and therefore less exposed to contact with other humans and COVID-19. BV and the melittin it contains can regulate Th1 and other immune cells and are used to lower viral load and reduce the severity of interstitial pneumonia in PRRSV-infected pigs. These effects may also be crucial in the case of SARS-CoV-2 pneumonia, but these effects were only achieved when BV was administered through the nasal or rectal route. The various effects of BV on the immune system and its resistance to SARS-CoV-2 should be considered as an indicator of the level of the immune response, rather than as a definite therapy strategy [3].

**3.2. Botulinum Neurotoxin (BoNT).** The use of therapeutic botulinum neurotoxin (BoNT) against SARS-CoV-2 is also being considered. Botulinum toxins are powerful neurotoxins that can cause muscle paralysis and acute respiratory arrest in humans, but a mild dose of the pure form of Botox therapy is known to reduce the common clinical symptoms of COVID-19 including chronic cough, dyspnoea, pneumonia, acute respiratory failure, abnormal circulation, cardiac defects, and various neurological deficits. A low dose of purified BoNT is also used in many diseases such as strabismus, blepharospasm, chronic migraine, and overactive bladder. Therapeutic BoNT can be used as a method of preventing SARS-CoV-2 infection in high-risk populations. To reduce its side effects, antioxidants can also be used along with treatment. It reported that the side effects of therapeutic BoNT are temporary and reversible, and the action of this toxin in very mild doses is relatively safe [24]. There are some reports that therapeutic BoNT in very mild doses can

suppress many human diseases by 10 to 20 units [25–28]. It also can migrate from the site of intramuscular injection to the brain and other organs. The beneficial effects of a single therapeutic dose are probably long-lasting. Designing a multifaceted drug to fight SARS-CoV-2 infection can be effective, and therapeutic BoNT can be a good option [14]. In a study in France, 193 patients who used BoNT/A in different doses for different purposes such as migraines and facial palsy were evaluated, and a critical contrast between the number of infected people within the common populace and the number of patients injected with BoNT/A who appeared signs of COVID-19 has seen [29].

**3.3. Tetanus and Diphtheria.** There is evidence suggesting that a tetanus toxoid vaccine could reduce the severity of COVID-19 symptoms. A connection between tetanus toxin and the COVID-19 spike glycoprotein as well as a similar connection between the tetanus toxin protein sequence and other coronaviruses was observed [30]. Also, neurological symptoms and temporomandibular joint (TMJ) pain, which are common symptoms of tetanus disease, have been reported in several COVID-19 patients. Also, in comparison between the United States and other countries where tetanus vaccination rates were lower, an inverse correlation was observed between tetanus vaccination rates and mortality rates [31, 32]. We know the DTP vaccine contains toxoids of tetanus, diphtheria, and pertussis, and it is noteworthy that there is a correlation between the rate of DTP vaccination in children worldwide and the rate of asymptomatic COVID-19. A similar association is observed in pregnant women, who are advised to receive two flu and Tdap vaccines in the third month of pregnancy [30]. As a result, it may be inferred that tetanus and diphtheria vaccines may have a protective effect against COVID-19 in both children as well as adults who are up-to-date on their tetanus vaccination. Two other studies also noted a reduction in the severity of COVID-19 in children and its possible association with DTP vaccination and suggested that the DTP vaccine could stimulate the immune system. In one case, it was concluded that the DTP vaccine is the only vaccine with a high potential for cross-reactivity with COVID-19 spike protein [15, 33]. CRM197, a modified diphtheria toxin found in the Hib vaccine, and rubella vaccine are highly similar to SARS-CoV-2 proteins, suggesting that they may have some anti-SARS-CoV-2 activity [34].

**3.4. Cobrotoxin.** Cobrotoxin, a short-chain  $\alpha$ -neurotoxin from *Naja naja atra* venom (NNAV), may be effective in treating COVID-19 patients and inhibiting SARS-CoV-2 infection. The inflammatory cytokine storm causes aggravation of lung disease in COVID-19 patients, in addition to other deadly consequences. As a result, in addition to attempting to restrict virus replication, anti-inflammatory medication is an important method of combating COVID-19 disease. Cobrotoxin and alpha-neurotoxins have anti-inflammatory activity and prevent the binding of the nuclear factor- $\kappa$ B to DNA, which is a transcription factor that regulates the expression of genes involved in the

TABLE 1: Data summary.

Bee venom	IL-1 and TNF- $\alpha$ decrease because of an increase in cytokine IL-10 due to bee venom, so, cytokines storm could be weakened. Also, bee venom contains melittin and phospholipase A2 that have an antagonist effect on IL-6, IL-8, interferon, and TNF- $\alpha$ . [1, 3, 18–20, 23]. Less infection in bee keepers is due to their less exposure to other people not because of bee venom [3].
Botulinum neurotoxin (BoNT)	A mild dose of the pure BoNT can reduce the common clinical symptoms of COVID-19 including chronic cough, dyspnoea, pneumonia, acute respiratory failure, abnormal circulation, cardiac defects, and various neurological deficits [14].
Tetanus and diphtheria	Tetanus toxin and diphtheria toxin both are similar to SARS-CoV-2 proteins, and so, the administration of the DTP vaccine may have a protective effect against SARS-CoV-2 [30, 34].
Cobrotoxin	Cobrotoxin prevents the expression of inflammatory genes and also balances the ratio of CD4/CD8 cells and performs immunoprotective activity [16].
Tetrodotoxin	Tetrodotoxin is a potential M <sup>Pro</sup> inhibitor of SARS-CoV-2. So, it may affect SARS-CoV-2 [17].

inflammatory response, thereby reducing the transcription of inflammatory genes. Cobrotoxin inhibits CD8 T cell proliferation more than that of CD4 T cells, and since COVID-19 cellular immune responses are induced by overexpression and hyperactivation of cytotoxic T lymphocytes [35], cobrotoxin can restore the CD4/CD8 ratio and perform an immunoprotective activity [16].

**3.5. Tetrodotoxin.** Tetrodotoxin is a sodium channel blocker and acts on the nervous system message delivery [36]. The toxicity of tetrodotoxin is 1200 times more than cyanide. One of the important drug targets in coronaviruses is the main protease (M<sup>Pro</sup>) due to its important role in controlling replicate complex activity and its vital role in viral replication and transcription [37, 38]. Tetrodotoxin is a potential M<sup>Pro</sup> inhibitor of SARS-CoV-2 which may be a potential compound against SARS-CoV-2 according to the results of the ligand-based approaches [17].

**3.6. Snake Venoms.** Nature is known to offer numerous biotherapeutics from animal venoms, green growth, and plant that have been generally utilized in conventional medication. Among these bioresources, snake poison shows numerous bioactivities such as antiviral, antiplatelet, antithrombotic, anti-inflammatory, antimicrobial, and antitumoral. Snake venom contains a mixture of amino acids, proteins, peptides, nucleotides, lipids, carbohydrates, and metal elements along with proteins [39, 40]. Several studies have reported that snake venom ingredients have antiviral activity against measles, Sendai, dengue, yellow fever, and human immunodeficiency virus [41–43]. Snake venoms are a complex combination of proteins and peptides. Venom serine proteases (SVSPs), snake venom metalloproteinases (SVMPs), secreted phospholipases A2 (SV-PLA2s), C-type lectins, and disintegrins are the major groups of snake venom components, while the minor group includes nucleotidases (Ntases), phosphodiesterases (PDEs), cysteine-rich secretory proteins, L-amino acid oxidases, Kunitz peptides, three-finger peptides (3FTX), and natriuretic peptides [44–48]. Bradykinin-potentiating peptide 10C (BPP-10C) isolated from *Bothrops jararaca* can decrease angiotensin II by inhibiting the ACE and increase bradykinin 2-receptor [49–51] that both have a role in the pathogenesis of SARS-CoV-2 [52–55], and it can be

considered as an anti-SARS-CoV-2 agent [56]. Kunitz-type peptides ((also called bovine pancreatic trypsin inhibitors) (BPTIs)) are 50 to 60 amino acid components found in the snake venoms that inhibit the catalytic site of serine proteases [57]; so, they are potential antiviral agents because transmembrane protease serine-2 (TMPRSS2) activity is required for SARS-CoV-2 entry [58, 59]. Clinical information has appeared that numerous patients with serious COVID-19 display coagulation anomalies such as microvascular thrombosis and venous or blood vessel thrombosis [60–63]. Snake venoms are wealthy sources of bioactive particles interfering with the blood coagulation cascade and platelet aggregation [64, 65]. Phospholipase A2s (PLA2s) are one of the main components of snake venoms [66]. HDP-1 and HDP-2 are PLA2s that are isolated from *V. nikolskii* and could inhibit SARS-CoV-2 binding to ACE2 [67]. So, they can be effective in improving COVID-19 [68].

## 4. Discussion

Coronavirus pandemic induced by SARS-CoV-2 has been the cause of high burden worldwide. On 4 February 2022, the WHO announced 383,510,000 confirmed coronavirus illness 2019 cases and 5,700,000 deaths due to COVID-19. Although wide research has been carried out on the finding of effective therapeutics, so far there are no approved treatments against COVID-19. In the present study, harnessing natural toxic metabolites have been prioritized to make a review focusing on the efficacy of these metabolites as therapeutic agents [69]. Chloroquine/hydroxyl chloroquine combined with azithromycin had been used to improve COVID-19, but the results were controversial [70]. Remdesivir was the only approved antiviral drug for COVID-19 that was administrated for severe patients [71]. Some evidence indicates that toxins, toxoids, and venoms might be effective against SARS-CoV-2 through their anti-inflammatory, M<sup>Pro</sup> inhibitory, or antiviral effect. Due to the presence of melittin and phospholipase A2 (PLA2) in BV, it has antiviral effects on some enveloped and nonenveloped viruses. We know that after curing COVID-19, also some long-term effects may remain. BV has also a positive effect on recovery from long-COVID-19 [1]. Another idea is that fewer infected beekeepers are due to their less contact with other people and not for the effect of BV [3]. A low dose of pure botulinum toxin can reduce some symptoms of



COVID-19-like acute respiratory failure and dyspnoea [14]. Tetanus toxin is similar to SARS-CoV-2 spike proteins and has been demonstrated that there is a correlation between DTP vaccination and the severity of COVID-19. Also, the rate of COVID-19 infection in pregnant women who received the TDaP vaccine decreases [30]. CRM197 that is a modified diphtheria toxin is similar to SARS-CoV-2 proteins and is present in some vaccines such as Hib and rubella. So, these vaccines may also have a protective effect on COVID-19 [34]. Cobrotoxin regulates the expression of genes involved in the inflammatory response and can prevent cytokines storm that causes more lung damage. Also, CD4/CD8 ratio that is imbalanced in COVID-19 can restore by cobrotoxin [16, 35]. Tetrodotoxin inhibits main protease ( $M^{Pro}$ ) and affects the replication of the virus [17]. Toxins, toxoids, and venoms may have effects on SARS-CoV-2 disease and prevent disease or reduce its symptoms. In addition, to achieve definitive results and efficacy of natural toxic metabolites comprehensive studies are needed (the data summary is presented in Table 1).

## 5. Conclusion

In this study, we investigated the role of toxins, toxoids, and venom on the pathophysiology of COVID-19 as an inflammatory disease. We discussed BV, botulinum toxin, tetanus toxin or toxoid, diphtheria toxin or modified toxin, cobrotoxin, and tetrodotoxin, which can be impressive in the pathophysiology of COVID-19. More surveys and clinical assessments are needed for better knowledge about the effect of toxins on COVID-19.

## Data Availability

The data that appeared in this study are already publicly available in the literature.

## Ethical Approval

This study was approved by the Ethics Committee of Hamadan University of Medical Sciences (IR.UMSHA.REC.1400.441).

## Conflicts of Interest

The authors declared no potential conflicts of interest.

## Authors' Contributions

Mohammad Taheri and Fatemeh Nouri contributed equally to this work.

## Acknowledgments

The authors are thankful to the Hamadan University of Medical Sciences for the financial support. This work was supported financially by Hamadan University of Medical Sciences, Hamadan, Iran (grant no. 140008046326).

## References

- [1] K. I. Kasozi, G. Niedbala, M. Alqarni et al., "Bee venom—a potential complementary medicine candidate for SARS-CoV-2 infections," *Frontiers in Public Health*, vol. 8, p. 755, 2020.
- [2] M. A. Erickson, E. M. Rhea, R. C. Knopp, and W. A. Banks, "Interactions of SARS-CoV-2 with the blood-brain barrier," *International Journal of Molecular Sciences*, vol. 22, no. 5, 2021.
- [3] H. Männle, J. Hübner, and K. Münstedt, "Beekeepers who tolerate bee stings are not protected against SARS-CoV-2 infections," *Toxicon: Official Journal of the International Society on Toxinology*, vol. 187, pp. 279–284, 2020.
- [4] C. Huang, Y. Wang, X. Li et al., "Clinical features of patients infected with 2019 novel coronavirus in Wuhan, China," *Lancet*, vol. 395, no. 10223, pp. 497–506, 2020.
- [5] V. Izda, M. A. Jeffries, and A. H. Sawalha, "COVID-19: a review of therapeutic strategies and vaccine candidates," *Clinical Immunology*, vol. 222, Article ID 108634, 2021.
- [6] M. Taheri, A. Bahrami, P. Habibi, and F. Nouri, *A Review on the Serum Electrolytes and Trace Elements Role in the Pathophysiology of COVID-19. Biological Trace Element Research*, Humana Press Inc., Totowa, NJ, USA, 2020.
- [7] A. Bahrami, M. R. Arabestani, M. Taheri et al., "Exploring the role of heavy metals and their derivatives on the pathophysiology of COVID-19," *Biological Trace Element Research*, pp. 1–12, 2021.
- [8] A. Shapira and I. Benhar, "Toxin-based therapeutic approaches," *Toxins*, vol. 2, no. 11, pp. 2519–2583, 2010.
- [9] I. Kerkis, A. R. de Brandão Prieto da Silva, C. Pompeia, J. Tytgat, and P. L. de Sá Junior, "Toxin bioprotides: exploring toxin biological activity and multifunctionality," *Cellular and Molecular Life Sciences*, vol. 74, no. 4, pp. 647–661, 2017.
- [10] G. F. King, "Venoms as a platform for human drugs: translating toxins into therapeutics," *Expert Opinion on Biological Therapy*, vol. 11, no. 11, pp. 1469–1484, 2011.
- [11] A. Schmidtke, J. Lötsch, R. Freynhagen, and G. Geisslinger, "Ziconotide for treatment of severe chronic pain," *Lancet*, vol. 375, no. 9725, pp. 1569–1577, 2010.
- [12] V. O. Zambelli, K. F. M. Pasqualoto, G. Picolo, A. M. Chudzinski-Tavassi, and Y. Cury, "Harnessing the knowledge of animal toxins to generate drugs," *Pharmacological Research*, vol. 112, pp. 30–36, 2016.
- [13] R. S. Norton, "Enhancing the therapeutic potential of peptide toxins," *Expert Opinion on Drug Discovery*, vol. 12, no. 6, pp. 611–623, 2017.
- [14] M. Kandasamy, "Perspectives for the use of therapeutic Botulinum toxin as a multifaceted candidate drug to attenuate COVID-19," *Medicine in Drug Discovery*, vol. 6, Article ID 100042, 2020.
- [15] G. Ietto, "Sars - CoV-2: reasons of epidemiology of severe ill disease cases and therapeutic approach using trivalent vaccine (tetanus, diphtheria and Bordetella pertussis)," *Medical Hypotheses*, vol. 141, Article ID 109779, 2020.
- [16] F. Lin, P. F. Reid, and Z.-h. Qin, "Cobrotoxin could be an effective therapeutic for COVID-19," *Acta Pharmacologica Sinica*, vol. 41, no. 9, pp. 1258–1260, 2020.
- [17] W. Y. Law, M. R. Asaruddin, S. A. Bhawani, and S. Mohamad, "Pharmacophore modelling of vanillin derivatives, favipiravir, chloroquine, hydroxychloroquine, monolaurin and tetrodotoxin as MPro inhibitors of severe acute respiratory syndrome coronavirus-2 (SARS-CoV-2)," *BMC Research Notes*, vol. 13, no. 1, p. 527, 2020.

- [18] W. Yang, F.-I. Hu, and X.-f. Xu, "Bee venom and SARS-CoV-2," *Toxicon*, vol. 181, pp. 69-70, 2020.
- [19] S. Bogdanov, *Biological and Therapeutic Properties of Bee Venom*, The Bee Venom Book, Muehlethurnen, Switzerland, 2016.
- [20] Y. Al Naggar, J. P. Giesy, M. M. Abdel-Daim, M. J. Ansari, S. N. Al-Kahtani, and G. Yahya, "Fighting against the second wave of COVID-19: can honeybee products help protect against the pandemic?" *Saudi Journal of Biological Sciences*, vol. 28, 2020.
- [21] I. Caramalho, A. Melo, E. Pedro et al., "Bee venom enhances the differentiation of human regulatory T cells," *Allergy*, vol. 70, no. 10, pp. 1340-1345, 2015.
- [22] W. G. Lima, J. C. M. Brito, and W. S. Cruz Nizer, "Bee products as a source of promising therapeutic and chemoprophylaxis strategies against COVID -19 (SARS-CoV -2)," *Phytotherapy Research*, vol. 35, no. 2, pp. 743-750, 2021.
- [23] J. Block, *High Risk COVID-19: Potential Intervention at Multiple Points in the COVID-19 Disease Process via Prophylactic Treatment with Azithromycin or Bee Derived Products*, Preprints.org, Basel, Switzerland, 2020.
- [24] U. Muthane and D. Panikar, "Botulinum toxins: pharmacology and its current therapeutic evidence for use," *Neurology India*, vol. 51, no. 4, pp. 455-460, 2003.
- [25] P. Nigam and A. Nigam, "Botulinum toxin," *Indian Journal of Dermatology*, vol. 55, no. 1, pp. 8-14, 2010.
- [26] S. S. Arnon, R. Schechter, T. V. Inglesby et al., "Botulinum toxin as a biological weapon," *JAMA*, vol. 285, no. 8, pp. 1059-1070, 2001.
- [27] Z. F. Dembek, L. A. Smith, and J. M. Rusnak, "Botulism: cause, effects, diagnosis, clinical and laboratory identification, and treatment modalities," *Disaster Medicine and Public Health Preparedness*, vol. 1, no. 2, pp. 122-134, 2007.
- [28] Z. Feng, Q. Sun, L. He et al., "Optimal dosage of botulinum toxin type A for treatment of glabellar frown lines," *Dermatologic Surgery*, vol. 41, no. 1, pp. S56-S63, 2015.
- [29] D. Batifol, P. J. Finiels, S. Galmiche, P. Jammet, and M. de Boutray, "Could treatment with botulinum toxin protect against subsequent infection with COVID-19?" *Journal of Stomatol Oral Maxillofac Surgery*, 2021.
- [30] C. D. Rickett, K. J. Maschhoff, and S. R. Sukumar, "Does tetanus vaccination contribute to reduced severity of the COVID-19 infection?" *Medical Hypotheses*, vol. 146, Article ID 110395, 2021.
- [31] H. Sadeghi, Z. Robati, and M. J. Saharkhiz, "Variability in Zataria multiflora Bioss. essential oil of twelve populations from Fars province, Iran," *Industrial Crops and Products*, vol. 67, pp. 221-226, 2015.
- [32] M. F. Nagoor Meeran, H. Javed, H. Al Taei, S. Azimullah, and S. K. Ojha, "Pharmacological properties and molecular mechanisms of thymol: prospects for its therapeutic potential and pharmaceutical development," *Frontiers in Pharmacology*, vol. 8, p. 380, 2017.
- [33] P. A. Reche, "Potential cross-reactive immunity to SARS-CoV-2 from common human pathogens and vaccines," *Frontiers in Immunology*, vol. 11, Article ID 586984, 2020.
- [34] C. Pawlowski, A. Puranik, H. Bandi et al., "Exploratory analysis of immunization records highlights decreased SARS-CoV-2 rates in individuals with recent non-COVID-19 vaccinations," *Scientific Reports*, vol. 11, no. 1, Article ID 4741, 2021.
- [35] A. Ganji, I. Farahani, B. Khansarinejad, A. Ghazavi, and G. Mosayebi, "Increased expression of CD8 marker on T-cells in COVID-19 patients," *Blood Cells, Molecules, and Diseases*, vol. 83, Article ID 102437, 2020.
- [36] V. Bane, M. Lehane, M. Dikshit, A. O'Riordan, and A. Furey, "Tetrodotoxin: chemistry, toxicity, source, distribution and detection," *Toxins*, vol. 6, no. 2, pp. 693-755, 2014.
- [37] V. C. C. Cheng, S. K. P. Lau, P. C. Y. Woo, and K. Y. Yuen, "Severe acute respiratory syndrome coronavirus as an agent of emerging and reemerging infection," *Clinical Microbiology Reviews*, vol. 20, no. 4, pp. 660-694, 2007.
- [38] X. Xue, H. Yu, H. Yang et al., "Severe acute respiratory syndrome coronavirus as an agent of emerging and reemerging infection," *Journal of Virology*, vol. 82, no. 5, pp. 2515-2527, 2008.
- [39] D. Georgieva, R. K. Arni, and C. Betzel, "Proteome analysis of snake venom toxins: pharmacological insights," *Expert Review of Proteomics*, vol. 5, no. 6, pp. 787-797, 2008.
- [40] J. J. Calvete, P. Juárez, and L. Sanz, "Snake venomomics. Strategy and applications," *Journal of Mass Spectrometry*, vol. 42, no. 11, pp. 1405-1414, 2007.
- [41] V. D. M. Muller, R. R. Russo, A. C. Oliveira Cintra et al., "Crotoxin and phospholipases A2 from *Crotalus durissus terrificus* showed antiviral activity against dengue and yellow fever viruses," *Toxicon*, vol. 59, no. 4, pp. 507-515, 2012.
- [42] G. Borkow and M. Ovadia, "Selective lysis of virus-infected cells by cobra snake cytotoxins: a sendai virus, human erythrocytes, and cytotoxin model," *Biochemical and Biophysical Research Communications*, vol. 264, no. 1, pp. 63-68, 1999.
- [43] R. Meenakshisundaram, S. Sweni, and P. Thirumalaikolundusubramanian, "Hypothesis of snake and insect venoms against Human Immunodeficiency Virus: a review," *AIDS Research and Therapy*, vol. 6, p. 25, 2009.
- [44] T. Tasoulis and G. K. Isbister, "A review and database of snake venom proteomes," *Toxins*, vol. 9, no. 9, 2017.
- [45] J. Slagboom, J. Kool, R. A. Harrison, and N. R. Casewell, "Haemotoxic snake venoms: their functional activity, impact on snakebite victims and pharmaceutical promise," *British Journal of Haematology*, vol. 177, no. 6, pp. 947-959, 2017.
- [46] M. Ameziani, F. Chérifi, H. Kiheli et al., "Isolation and functional identification of an antiplatelet RGD-containing disintegrin from cerastes cerastes venom," *The Protein Journal*, vol. 39, no. 5, pp. 574-590, 2020.
- [47] S. Saoud, F. Chérifi, T. Benhassine, and F. Laraba-Djebbari, "Purification and characterization of a platelet aggregation inhibitor and anticoagulant Cc 5<sub>NTase</sub>, CD 73-like, from *Cerastes cerastes* venom," *Journal of Biochemical and Molecular Toxicology*, vol. 31, no. 5, 2017.
- [48] A. Munawar, S. Ali, A. Akrem, and C. Betzel, "Snake venom peptides: tools of biodiscovery," *Toxins*, vol. 10, no. 11, p. 474, 2018.
- [49] A. C. M. Camargo, D. Ianzer, J. R. Guerreiro, and S. M. T. Serrano, "Bradykinin-potentiating peptides: beyond captopril," *Toxicon*, vol. 59, no. 4, pp. 516-523, 2012.
- [50] D. M. Lopes, N. E. G. Junior, P. P. C. Costa et al., "A new structurally atypical bradykinin-potentiating peptide isolated from *Crotalus durissus cascavella* venom (South American rattlesnake)," *Toxicon*, vol. 90, pp. 36-44, 2014.
- [51] C. W. Chi, S. Z. Wang, L. G. Xu, M. Y. Wang, S. S. Lo, and W. D. Huang, "Structure-function studies on the bradykinin potentiating peptide from Chinese snake venom (*Agkistrodon halys* Pallas)," *Peptides*, vol. 6, no. 3, pp. 339-342, 1985.
- [52] D. Gurwitz, "Angiotensin receptor blockers as tentative SARS-CoV-2 therapeutics," *Drug Development Research*, vol. 81, no. 5, pp. 537-540, 2020.

- [53] M. Hoffmann, H. Kleine-Weber, S. Schroeder et al., "SARS-CoV-2 cell entry depends on ACE2 and TMPRSS2 and is blocked by a clinically proven protease inhibitor," *Cell*, vol. 181, no. 2, pp. 271–280, 2020.
- [54] R. Lu, X. Zhao, J. Li et al., "Genomic characterisation and epidemiology of 2019 novel coronavirus: implications for virus origins and receptor binding," *The Lancet*, vol. 395, no. 10224, pp. 565–574, 2020.
- [55] F. L. van de Veerdonk, M. G. Netea, M. van Deuren et al., "Kallikrein-kinin blockade in patients with COVID-19 to prevent acute respiratory distress syndrome," *Elife*, vol. 9, 2020.
- [56] A. S. Gouda and B. Mégarbane, "Snake venom-derived bradykinin-potentiating peptides: a promising therapy for COVID -19?" *Drug Development Research*, vol. 82, no. 1, pp. 38–48, 2021.
- [57] L.-s. Chang, C. Chung, H.-B. Huang, and S.-r. Lin, "Purification and characterization of a chymotrypsin inhibitor from the venom of *Ophiophagus hannah* (King Cobra)," *Biochemical and Biophysical Research Communications*, vol. 283, no. 4, pp. 862–867, 2001.
- [58] S. Seyedpour, B. Khodaei, A. H. Loghman et al., "Targeted therapy strategies against SARS-CoV-2 cell entry mechanisms: a systematic review of in vitro and in vivo studies," *Journal of Cellular Physiology*, vol. 236, no. 4, pp. 2364–2392, 2021.
- [59] F. Chérifi and F. Laraba-Djebari, "Bioactive molecules derived from snake venoms with therapeutic potential for the treatment of thrombo-cardiovascular disorders associated with COVID-19," *The Protein Journal*, vol. 40, no. 6, pp. 799–841, 2021.
- [60] N. Tang, D. Li, X. Wang, and Z. Sun, "Abnormal coagulation parameters are associated with poor prognosis in patients with novel coronavirus pneumonia," *Journal of Thrombosis and Haemostasis*, vol. 18, no. 4, pp. 844–847, 2020.
- [61] M. Levi, J. Thachil, T. Iba, and J. H. Levy, "Coagulation abnormalities and thrombosis in patients with COVID-19," *The Lancet Haematology*, vol. 7, no. 6, pp. e438–e440, 2020.
- [62] J. D. McFadyen, H. Stevens, and K. Peter, "The emerging threat of (Micro) Thrombosis in COVID-19 and its therapeutic implications," *Circulation Research*, vol. 127, no. 4, pp. 571–587, 2020.
- [63] J. E. Gómez-Mesa, S. Galindo-Coral, M. C. Montes, and A. J. Muñoz Martín, "Thrombosis and coagulopathy in COVID-19," *Current Problems in Cardiology*, vol. 46, no. 3, Article ID 100742, 2021.
- [64] T. Matsui, Y. Fujimura, and K. Titani, "Snake venom proteases affecting hemostasis and thrombosis," *Biochimica et Biophysica Acta*, vol. 1477, no. 1-2, pp. 146–156, 2000.
- [65] Y. Yamazaki and T. Morita, "Snake venom components affecting blood coagulation and the vascular system: structural similarities and marked diversity," *Current Pharmaceutical Design*, vol. 13, no. 28, pp. 2872–2886, 2007.
- [66] J. M. Gutiérrez and B. Lomonte, "Phospholipases A2: unveiling the secrets of a functionally versatile group of snake venom toxins," *Toxicon: Official Journal of the International Society on Toxinology*, vol. 62, pp. 27–39, 2013.
- [67] A. E. Siniavin, M. A. Streltsova, M. A. Nikiforova et al., "Snake venom phospholipase A2s exhibit strong virucidal activity against SARS-CoV-2 and inhibit the viral spike glycoprotein interaction with ACE2," *Cellular and Molecular Life Sciences*, vol. 78, no. 23, pp. 7777–7794, 2021.
- [68] B. Kalita, A. J. Saviola, S. P. Samuel, and A. K. Mukherjee, "State-of-the-art review - a review on snake venom-derived antithrombotics: potential therapeutics for COVID-19-associated thrombosis?" *International Journal of Biological Macromolecules*, vol. 192, pp. 1040–1057, 2021.
- [69] D. Shokri and M. Rabbani khorasgani, "Evaluation of carbapenems resistance and frequency of *Klebsiella pneumoniae* carbapenemase (KPC) enzyme in *Klebsiella pneumoniae* strains isolated from clinical samples and determination of their acquired resistant profiles," *Journal of Ilam University of Medical Sciences*, vol. 24, no. 3, pp. 18–30, 2016.
- [70] K. E. da Silva, T. R. Varella, G. M. d. S. Bet et al., "High mortality rate associated with KPC-producing *Enterobacter cloacae* in a Brazilian hospital," *American Journal of Infection Control*, vol. 46, no. 1, pp. 108–110, 2018.
- [71] P. Tarighi, S. Eftekhari, M. Chizari, M. Sabernavaei, D. Jafari, and P. Mirzabeigi, "A review of potential suggested drugs for coronavirus disease (COVID-19) treatment," *European Journal of Pharmacology*, vol. 895, Article ID 173890, 2021.

## Research Article

# Mechanism of Huoluo Xiaoling Dan in the Treatment of Psoriasis Based on Network Pharmacology and Molecular Docking

Ke Gong <sup>1,2</sup>, Wen Guo,<sup>1,2</sup> Kaiqing Du,<sup>1,2</sup> Fang Wang,<sup>3</sup> Mengli Li,<sup>2</sup> and Jianhui Guo <sup>1,2</sup>

<sup>1</sup>Hebei Province Cangzhou Hospital of Integrated Traditional and Western Medicine, Cangzhou, China

<sup>2</sup>Department of Traditional Chinese Medicine Surgery, Hebei University of Chinese Medicine, Shijiazhuang, China

<sup>3</sup>Traditional Chinese Medicine Hospital of Jiaozuo City, Henan Province, Jiaozuo, China

Correspondence should be addressed to Jianhui Guo; guojianhui618@163.com

Received 5 November 2021; Revised 19 December 2021; Accepted 20 December 2021; Published 27 February 2022

Academic Editor: Ruchika Garg

Copyright © 2022 Ke Gong et al. This is an open access article distributed under the Creative Commons Attribution License, which permits unrestricted use, distribution, and reproduction in any medium, provided the original work is properly cited.

**Objective.** To explore the mechanism of the action of Huoluo Xiaoling Dan (HLXLD) in the treatment of psoriasis based on network pharmacology and molecular docking. **Methods.** The main active components and targets of HLXLD were collected from CMSP, and the targets related to psoriasis were collected from GeneCards, OMIM, TTD, DisGeNET, and DrugBank. Drug disease target genes were obtained by Venny tools, drug-component-target networks were constructed and analyzed, and pathway enrichment analysis was performed. AutoDockTools is used to connect the core components and the target, and PyMOL software is used to visualize the results. **Results.** 126 active components (such as quercetin, luteolin, tanshinone IIA, dihydrotanshinlactone, and beta-sitosterol) and 238 targets of HLXLD were screened out. 1,293 targets of psoriasis were obtained, and 123 drug-disease targets were identified. Key targets included AKT1, TNF, IL6, TP53, VEGFA, JUN, CASP3, IL1B, STAT3, PTGS2, HIF1A, EGF, MYC, EGFR, MMP9, and PPARG. Enrichment analysis showed that 735 GO analysis and 85 KEGG pathways were mainly involved in biological processes such as response to the drug, inflammatory response, gene expression, and cell proliferation and apoptosis, as well as signal pathways such as cancer, TNF, HIF-1, and T cell receptor. Molecular docking showed that there was strong binding activity between the active ingredient and the target protein. **Conclusions.** HLXLD could treat psoriasis through multicomponents, multitargets, and multipathways, which provides a new theoretical basis for further basic research and clinical application.

## 1. Introduction

Psoriasis was a common inflammatory reactive skin disease with erythema and scaly lesions as the main manifestations, accompanied by varying degrees of pruritus, with a chronic course and easy recurrence [1]. The pathogenesis of the disease was not completely clear, and the etiology was complex, which was related to genetic, environmental, immune, and other factors [2]. Syndrome differentiation and treatment was a unique advantage of traditional Chinese medicine (TCM).

TCM treatment of psoriasis is mostly based on blood, and blood stasis syndrome is one of the most common syndromes [3]. In recent years, many doctors had treated psoriasis from the perspective of collateral disease theory. Based on the Huoluo Xiaoling Dan (HLXLD) composed of Radix Salviae (Danshen (DS)), Angelica Sinensis (Danggui (DG)), Frankincense (Ru Xiang(RS)), and Myrrha (Moyao

(MY)), they have added and subtracted according to the syndrome and achieved good results [4, 5], but the molecular mechanism of the treatment has not been clear.

Therefore, this study through network pharmacology to predict the potential targets and signal pathways of HLXLD in the treatment of psoriasis and combines it with molecular docking technology to assist verification, to provide a certain theoretical basis for the in-depth study of HLXLD in the treatment of psoriasis.

## 2. Materials and Methods

**2.1. Screening of Active Components and Targets of HLXLD.** On the Traditional Chinese Medicine Database and Analysis Platform [6] (TCMSP, <https://www.tcmospw.com/>), the names of four Chinese herbal medicines were input in succession to obtain the corresponding chemical

compounds and related information. According to the principle of pharmacokinetics (ADME), the oral bioavailability (OB)  $\geq 30\%$  and drug-likeness (DL)  $\geq 0.18$  were set as the screening conditions to obtain the effective components and corresponding targets of each drug of HLXLD. The Uniprot database [7] (<http://www.uniprot.org/>) was used to screen the target genes from human attributes and was verified, and the target names were standardized into official symbols.

### 2.2. Collection of Target Proteins Associated with Psoriasis.

To ensure the comprehensiveness and accuracy of the data, the potential targets of psoriasis in GeneCards [8] (<https://www.genecards.org/>), OMIM [9] (<https://omim.org/>), TTD [10] (<http://db.idrblab.net/ttd/>), DisGeNET [11] (<https://www.disgenet.org/>), and Drugbank [12] (<https://go.drugbank.com/>) were searched with “psoriasis” as keywords. In the GeneCards database, the score indicates the closeness between the target and the disease, so the target with a score greater than the median was set as the potential target of psoriasis. The targets obtained from the above disease database were combined, and the repetition was removed to get the psoriasis-related targets, and the Uniprot database is used to standardize the target names through the above methods.

### 2.3. Identification of Potential Therapeutic Targets of HLXLD in the Treatment of Psoriasis.

The two target sets were input, respectively, to the Venny 2.1.0 to acquire the common targets, and the Venn diagram was drawn to obtain the potential targets of HLXLD in the treatment of psoriasis.

### 2.4. Construction of the Drug-Compound-Target Network.

The obtained active components of HLXLD and the potential targets for psoriasis treatment were imported into Cytoscape 3.8.2 [13] software to draw the drug-compound-target network diagram for visual analysis, in which “node” was used to represent drugs, components, or targets, and “edge” was used to represent the relationship between nodes. The network parameters of each node were analyzed based on the network analyzer and cytoNCA plugins.

### 2.5. Construction of Protein-Protein Interaction (PPI) Network Map and Core Targets' Screening.

The potential targets screened above were imported into the STRING [14] (<https://www.string-db.org/>), “Homo sapiens” was selected, the minimum required interaction score was set to  $\geq 0.4$ , the free nodes were hidden, the PPI network was built, and the corresponding files were exported. The downloaded results were uploaded to Cytoscape3.8.2 software for analysis. The network analyzer and cytoNCA plugins were used for topology analysis. The core targets were screened by taking the median of 2 times of degree, and the median of Betweenness Centrality (BC) and Closeness Centrality (CC) as card values.

### 2.6. Gene Ontology (GO) Functional Enrichment and Kyoto Encyclopedia of Genes and Genomes (KEGG) Pathway Analysis.

The previously obtained potential targets were imported into the DAVID database [15] (<https://david.ncicrf.gov/>), and the species was defined as “Homo sapiens.” The GO function and KEGG pathway enrichment of common target genes of HLXLD and psoriasis were analyzed. The results were visualized by using Bioinformatics online mapping tool (<http://www.bioinformatics.com.cn/>), and the network diagram of “disease-pathway-target-component drug” was constructed by using Cytoscape 3.8.2.

### 2.7. Molecular Docking.

Molecular docking was applied for the key components with the top 5 degree values in the drug-compound-target network and the core targets with the top 5 degree values in the PPI network. The protein structure of the core target was downloaded from the PDB [16] database (<https://www.rcsb.org/>). The selection criteria [17] are as follows: (1) X-ray structures with a resolution of 2.5 Å or better were included, if available; (2) if two or more structures were available, that with the best solution was selected; (3) a structure with a ligand bound to its nucleotide-binding site was selected; (4) non-modified and non-phosphorylated residues found in the binding site were selected with priority; (5) the organism was human. The small molecular structure of key components was downloaded from the TCMSP database. The PyMOL 2.4.0 [18] software was used to dehydrate, hydrogenate, and separate the original ligand of the core target protein. The molecular docking was completed in the AutoDockVina [19] software. When the binding energy was negative, it indicated that the receptor and ligand can bind spontaneously; when the binding energy was less than  $-5 \text{ kcal mol}^{-1}$ , it indicated that there was good binding activity between the receptor and the ligand [17]. The results with higher activity were visualized by PyMOL 2.4.0.

## 3. Results

### 3.1. Screening of Active Components and Targets of HLXLD.

Through TCMSP database retrieval, DS, DG, RX, and MY had 66, 8, 9, and 45 active ingredients, respectively. A total of 126 active components of HLXLD were obtained after merging and removing duplicates, and the corresponding target proteins were further obtained. After being transformed into standard gene names in the UniProt database and removing duplicates, a total of 238 predicted targets were obtained.

### 3.2. Collection of Target Proteins Associated with Psoriasis.

After merging and removing the duplication of acne disease target genes collected by GeneCards, OMIM, TTD, DisGeNET, and DrugBank databases, a total of 1,923 related target proteins were obtained. After matching the target genes of the active components of HLXLD with the target genes related to psoriasis, the intersection was taken, and 123 common genes were obtained through the Venn diagram (Figure 1).

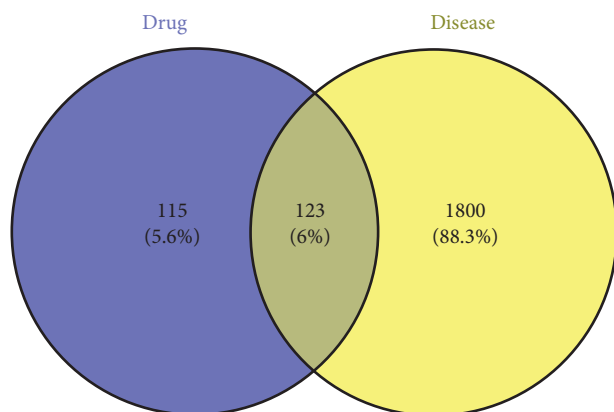


FIGURE 1: Venn diagram of intersecting targets of HLXLD and psoriasis.

### 3.3. Construction of the Drug-Compound-Target Network.

The active components and the corresponding targets of HLXLD in the treatment of psoriasis were introduced into the Cytoscape 3.8.2 software to construct the network diagram of the drug-compound-target network which included 225 points and 759 edges (Figure 2). Among them, the red hexagon node represents the drug, the light blue diamond node represents the effective components of DS, the orange diamond node represents the effective components of DG, the dark blue diamond node represents the effective components of RX, the purple diamond node represents the effective components of MY, the pink diamond node represents the common components of DG and MY, and the green square node represents the action target. After network topology analysis, the median of degree, BC, and CC was set as the card values. Among the effective active ingredients screened out, quercetin (MOL000098) had the highest degree value, acting on 93 drug targets. In the descending order, luteolin (MOL000006) acted on 37 drug targets, tanshinone IIA (MOL007154) acted on 22 drug targets, and dihydrotanshinlactone (MOL007100) acted on 18 drug targets,  $\beta$ -sitosterol (MOL000358) acted on 17 drug targets. Table 1 shows that the 27 key drug components were analyzed by topology. Figure 2 and Table 1 show the characteristics of HLXLD in the treatment of psoriasis with multicomponent and multitarget.

### 3.4. PPI Network Construction and Topology Analysis.

123 intersection targets brought in the STRING database to set up the PPI network (Figure 3). The network consists of 123 points and 2,413 edges, with an average degree of 39.2. Imported into Cytoscape 3.8.2 software, network analyzer and cytoNCA plugins were used to further analyze the PPI network, and 16 targets with degree  $\geq 74$ , BC  $\geq 0.0021906$ , and CC  $\geq 0.57819905$  were selected. These targets played a key role in the PPI network and are the core targets of HLXLD in the treatment of psoriasis. The core protein interaction was further visualized (Figure 4). There were 16 nodes and 240 edges in the network. The size and color of nodes reflect the size of the degree. The larger the node, the more red color indicates the higher degree. The thickness of

edges reflects the size of the connection score between nodes. The thicker the color indicates the larger the connection score between nodes. The basic information is shown in Table 2.

**3.5. GO Enrichment Analysis.** 123 common targets were enriched and analyzed by the David database, and a total of 735 were obtained, including 588 biological process (BP), 49 cellular component (CC), and 98 molecular function (MF). The top 20 results were selected according to the *P* value to draw the bubble chart (Figures 5–7). The smaller the *P* value, the more the color of the point tends to red, the more the number of enriched genes, and the larger the area of the point.

### 3.6. KEGG Pathway Enrichment Analysis.

A total of 85 pathways were obtained by KEGG pathway enrichment analysis. The top 20 results were selected according to the *P* value to draw the bubble diagram (Figure 8). The disease-pathway-target-compound-drug network is further constructed through Cytoscape 3.8.2 (Figure 9). The network consists of 179 points (including 1 disease, 20 pathways, 78 targets, 76 components, and 4 drugs) and 844 edges.

### 3.7. Molecular Docking of Main Active Components with Core Targets.

Quercetin, luteolin, tanshinone IIA,  $\beta$ -sitosterol, and dihydrotanshinlactone ranked among the top 5 key components in the drug-compound-target network. The top 5 targets with degree value in the core target PPI network were AKT1, TNF, IL6, TP53, and VEGFA. The above components and targets were docked by the AutoDockVina software. The results are shown in Table 3. The average binding energy was  $-6.65 \text{ kcal mol}^{-1}$ , among which tanshinone IIA-TNF,  $\beta$ -sitosterol-TNF,  $\beta$ -sitosterol-TP53, and tanshinone IIA-TP53 had the highest affinity. The molecular docking results showed that all binding energies were negative, and most of them were less than  $-5.0 \text{ kcal mol}^{-1}$ . The binding pattern diagram was drawn by PyMOL 2.4.0 for the docking results with binding energy  $\leq -9 \text{ kcal mol}^{-1}$  (Figure 10).

## 4. Discussion

The course of psoriasis was prolonged and easy to relapse. The skin lesions of psoriasis were thick and dark, and there were obvious abnormalities in the microcirculation of patients with psoriasis [20, 21]. These clinical characteristics were closely related to the “blood stasis” factor of TCM, which was very consistent with the thought of “long illness entering the collaterals” in the theory of collateral diseases. As a classic prescription for the treatment of collateral diseases, HLXLD was from Integrating Chinese and Western Medicine and was composed of DS, DG, RX, and MY. Danshensu could effectively improve the skin lesions of the psoriasis mouse model induced by imiquimod (IMQ). The higher the concentration, the more obvious the improvement of skin lesions. At the same time, it could also reduce



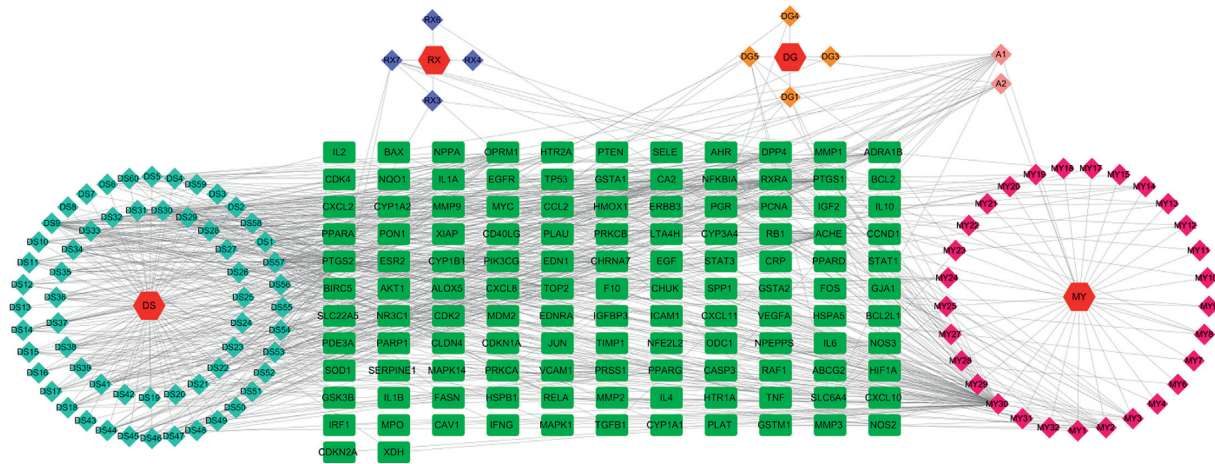


FIGURE 2: The drug-compound-target network of HLXLD.

TABLE 1: The drug components of HLXLD in the treatment of psoriasis.

MOL ID	Molecule name	OB	DL	Degree	Source
MOL000098	Quercetin	46.43	0.28	96	MY
MOL000006	Luteolin	36.16	0.25	38	DS
MOL007154	Tanshinone IIA	49.89	0.40	23	DS
MOL000358	Beta-sitosterol	36.91	0.75	19	DG, MY
MOL007100	Dihydrotanshinlactone	38.68	0.32	18	DS
MOL007088	Cryptotanshinone	52.34	0.40	16	DS
MOL007093	Danshexinkum D	38.88	0.55	16	DS
MOL007119	Milrinone I	49.68	0.32	14	DS
MOL007108	Isocryptotanshinone	54.98	0.39	14	DS
MOL007124	Neocryptotanshinone II	39.46	0.23	13	DS
MOL007041	2-Isopropyl-8-methylphenanthrene-3,4-dione	40.86	0.23	13	DS
MOL007049	4-Methylenemiltirone	34.35	0.23	13	DS
MOL007098	Deoxyneocryptotanshinone	49.40	0.29	12	DS
MOL007105	Epidanshenspiroketallactone	68.27	0.31	12	DS
MOL001601	1,2,5,6-Tetrahydrotanshinone	38.75	0.36	12	DS
MOL000449	Stigmasterol	43.83	0.76	11	DG, MY
MOL007111	Isotanshinone II	49.92	0.40	11	DS
MOL007094	Danshenspiroketallactone	50.43	0.31	11	DS
MOL007061	Methylenetanshinquinone	37.07	0.36	11	DS
MOL007145	Salviolone	31.72	0.24	11	DS
MOL001004	Pelargonidin	37.99	0.21	10	MY
MOL007122	Miltirone	38.76	0.25	10	DS
MOL007127	1-Methyl-8,9-dihydro-7H-naphtho[5,6-g]benzofuran-6,10,11-trione	34.72	0.37	10	DS
MOL007036	5,6-Dihydroxy-7-isopropyl-1,1-dimethyl-2,3-dihydrophenanthren-4-one	33.77	0.29	9	DS
MOL007125	Neocryptotanshinone	52.49	0.32	10	DS
MOL007059	3- $\beta$ -Hydroxymethylenetanshinquinone	32.16	0.41	10	DS
MOL007069	Przewaquinone C	55.74	0.40	10	DS

the expression of Yes-related protein (YAP) in skin lesions [22]. YAP was highly expressed in psoriasis and could participate in the pathogenesis by regulating the proliferation and apoptosis of keratinocytes [23]. Salvanolic acid B could improve the skin lesions of IMQ-induced psoriasis mouse models by inhibiting the PI3K/AKT pathway and downregulating the expression of keratin markers [24]. Angelica polysaccharides could downregulate the protein expression of NF- $\kappa$ B in peripheral blood mononuclear cells and reduce the secretion of IFN- $\gamma$  in patients with psoriasis [25]. Mastic acid was also widely used in the clinic because of

its strong anti-inflammatory ability [26]. A clinical trial in Italy used boswellic acid to treat psoriasis with an effective rate of up to 70% [27]. Myrrhosterone could significantly inhibit the proliferation of HaCaT cells, induce apoptosis, downregulate the expression of psoriasis-related genes mRNA, and reduce the severity of skin lesions in mice with psoriasis [28]. However, the target and signal pathways of psoriasis treatment from the perspective of “collateral disease theory” have still been unclear. TCM had the characteristics of multicomponent, multitarget, and multichannel in the treatment of diseases. Therefore, combined with the

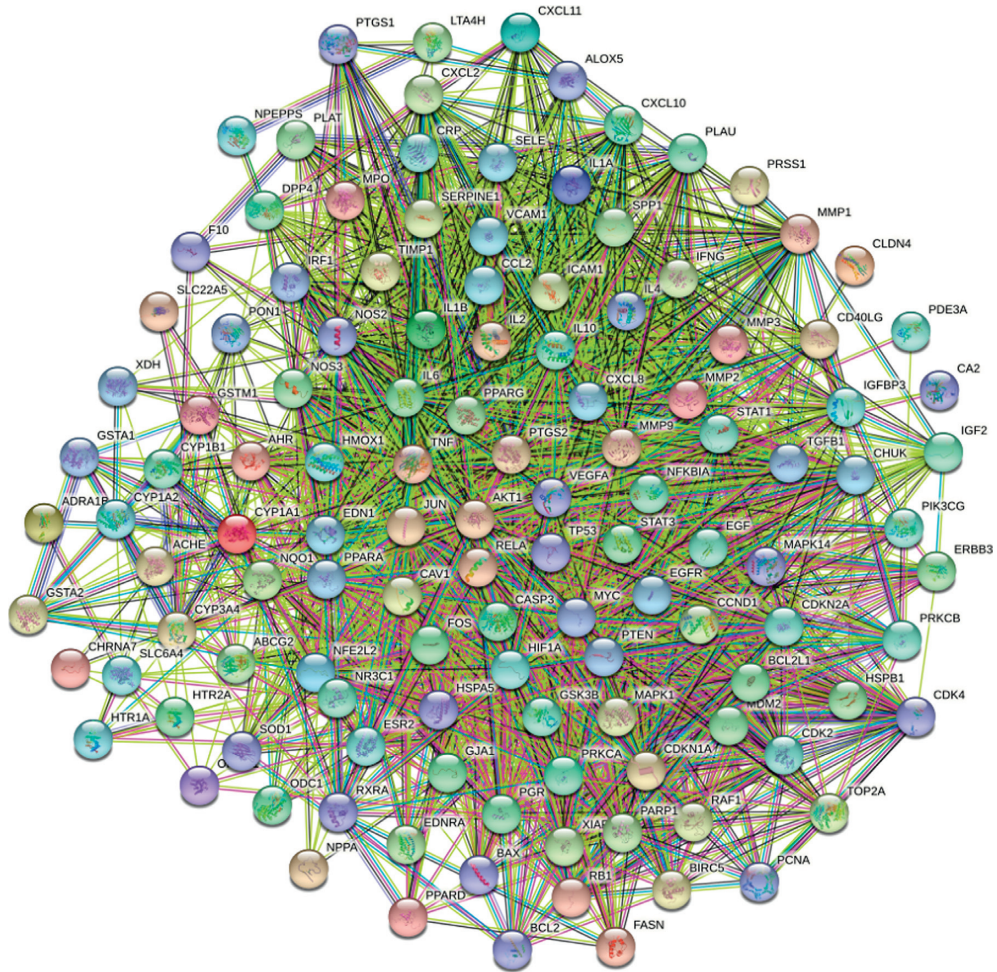


FIGURE 3: The PPI network of HLXLD in the treatment of psoriasis.

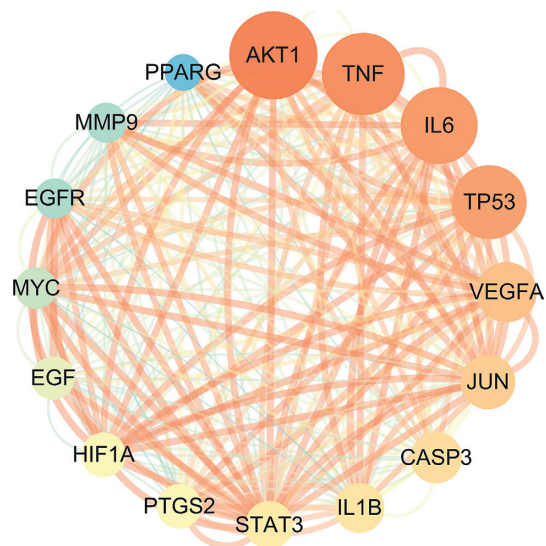


FIGURE 4: Core target PPI network.

TABLE 2: The core target topological parameters of HLXLD in the treatment of psoriasis.

Gene	Gene name	BC	DC	Degree
AKT1	RAC-alpha serine/threonine-protein kinase	0.06452241	0.82993197	97
TNF	Tumor necrosis factor	0.05075691	0.81879195	95
IL6	Interleukin-6	0.03833700	0.80794702	93
TP53	Cellular tumor antigen p53	0.03368498	0.80263158	92
VEGFA	Vascular endothelial growth factor A	0.01953143	0.77707006	87
JUN	Transcription factor AP-1	0.03194387	0.76250000	85
CASP3	Caspase-3	0.01684584	0.75776398	83
IL1B	Interleukin-1 beta	0.01865965	0.75308642	82
STAT3	Signal transducer and activator of transcription 3	0.01224804	0.74390244	81
PTGS2	Prostaglandin G/H synthase 2	0.01437445	0.73493976	79
HIF1A	Hypoxia-inducible factor 1-alpha	0.01139618	0.73493976	79
EGF	Proepidermal growth factor	0.01558726	0.73053892	78
MYC	Myc proto-oncogene protein	0.01512287	0.72189349	77
EGFR	Epidermal growth factor receptor	0.02954812	0.72189349	76
MMP9	Matrix metalloproteinase-9	0.02061406	0.72619048	76
PPARG	Peroxisome proliferator-activated receptor gamma	0.01436399	0.71764706	74

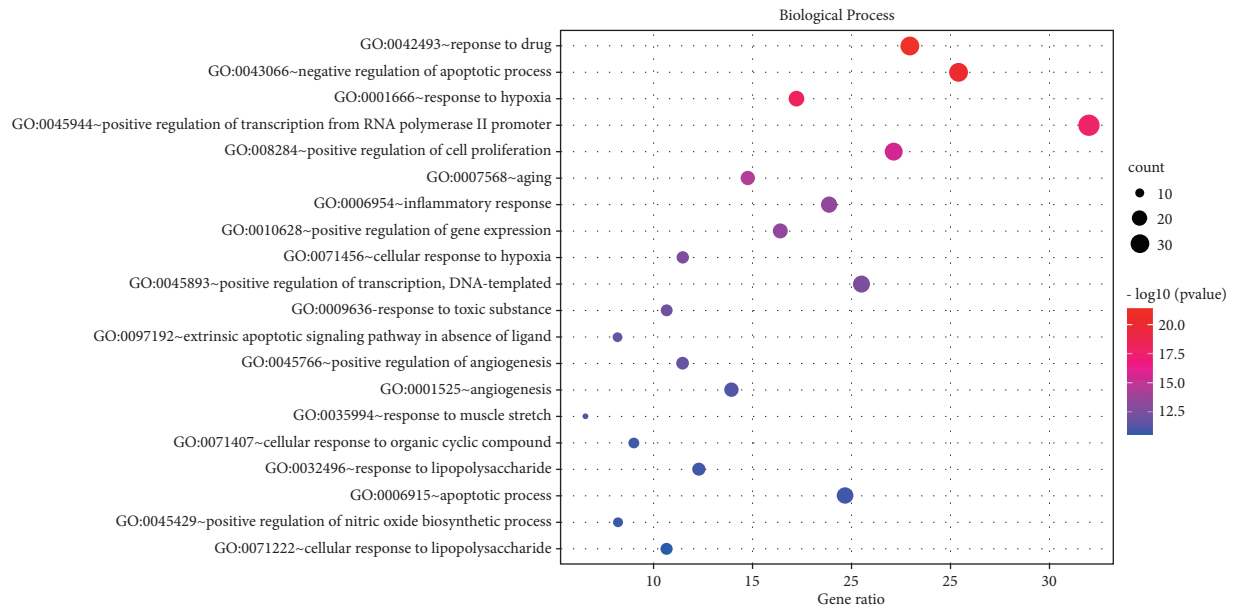


FIGURE 5: BP enrichment analysis of 123 nodes.

big-data analysis method of network pharmacology, this study aimed to explore the mechanism of HLXLD in the treatment of psoriasis and provide theoretical support for follow-up research.

The results showed that there are 123 potential targets of HLXLD in the treatment of psoriasis, involving 98 active components of HLXLD. According to topological analysis, the main components were quercetin, luteolin, tanshinone IIA,  $\beta$ -sitosterol, etc., as shown in Table 1. Previous studies have shown that quercetin and luteolin could inhibit the activation of the NF- $\kappa$ B pathway, reduce the levels of serum inflammatory factors such as TNF- $\alpha$ , IL-6, and IL-17, and significantly reduce the PASI score of IMQ-induced psoriasis mouse models [29–31]. In addition, quercetin could significantly reduce the expression level of tyrosine kinase in HaCaT cells [32]. Luteolin could promote the expression of HSP90 in HaCaT cells, reduce the ratio of Th1/Th2 and

Th17/Treg in the immune cells of psoriasis mice, and inhibit the increase of Th1 and Th17 in peripheral blood [33]. Tanshinone IIA could inhibit the proliferation of keratinocytes and induce apoptosis in mouse models of psoriasis, thereby reducing the appearance of skin lesions [34, 35]. Another study found that cryptotanshinone could reduce epidermal hyperplasia by inhibiting the activation of STAT3 [36].

The potential target PPI network of HLXLD in the treatment of psoriasis (Figure 3) had selected the core targets by topological analysis (Figure 4), indicating that HLXLD may treat psoriasis by acting on core targets such as AKT1, TNF, IL6, TP53, VEGFA, JUN, CASP3, IL1 $\beta$ , STAT3, PTGS2, HIF1A, EGF, MYC, EGFR, MMP9, and PPARG. Many studies have shown that the excessive proliferation of psoriasis keratinocytes was closely related to the increase of AKT1 levels in skin lesions [37, 38]. The dysregulation of the



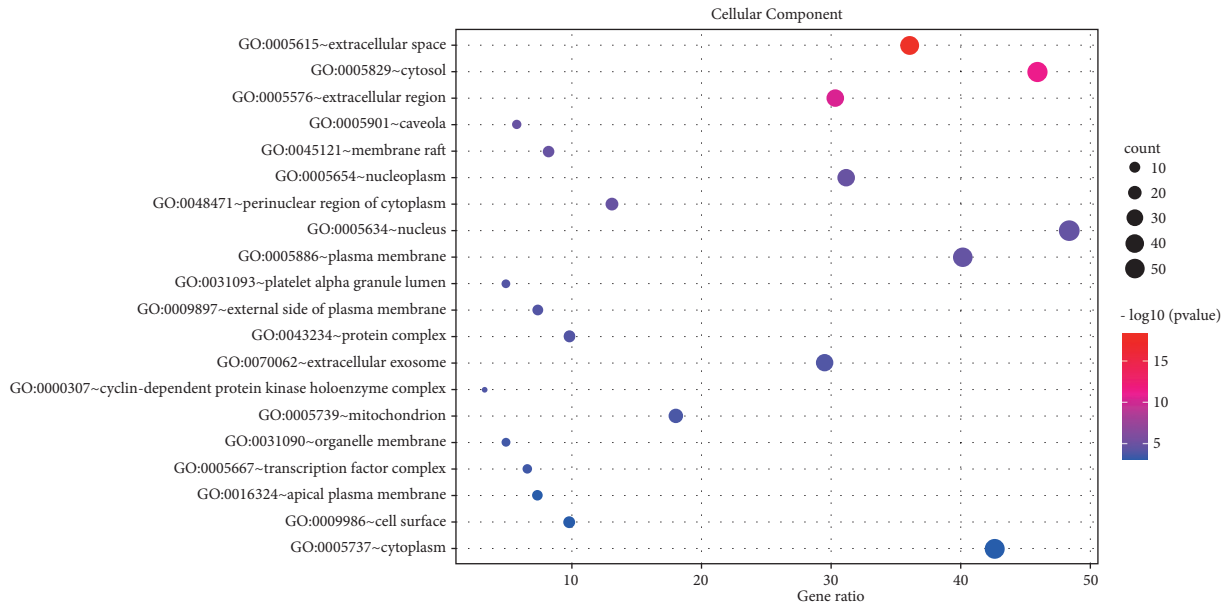


FIGURE 6: CC enrichment analysis of 123 nodes.

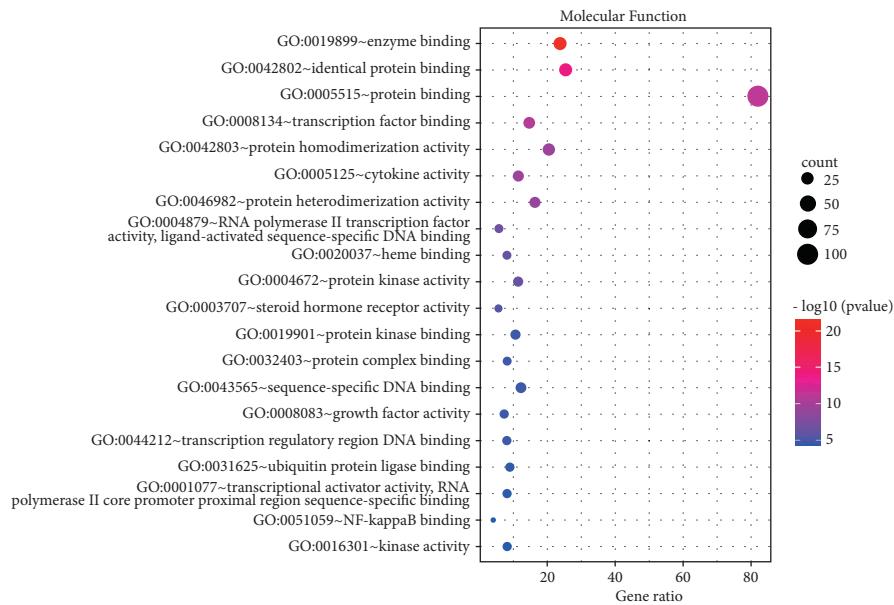


FIGURE 7: MF enrichment analysis of 123 nodes.

Akt-FOXO1 pathway led to T cell dysfunction, which was also widespread in patients with psoriasis [39]. Inflammation-related factors such as TNF, IL6, and IL1 $\beta$  were abnormal throughout the pathogenesis of psoriasis [40]. Growth factors and their receptors such as VEGFA, EGF, and EGFR were also inextricably linked with psoriasis [41–44]. The above point of view had long become a consensus in dermatology. The protein P53 encoded by TP53 was called the “Genome Guardian.” During the cell cycle, p53 could not only repair cell cycle arrest in the G1 phase through the expression of p21 but also mediate cell death through the Bcl-2/Bax pathway [45]. Moorchung’s study found that p53 was an important protein that

regulated the apoptosis process of psoriasis epidermal cells [46]. A clinical study used UV to treat psoriasis. After the course of treatment, it was found that p53 and Foxp3 decreased significantly, and it was speculated that p53 was an essential protein for UV-induced Foxp3 transcription [47]. c-JUN was a pathway closely related to a variety of autoimmune diseases. c-JUN activation could stimulate the production of inflammatory factor IL-6, thereby further aggravating the inflammatory response in psoriasis skin lesions [48]. Bears found that the expression of CASP3 was positively correlated with the condition of psoriasis, especially with the early psoriasis lesions located at the extremities [49]. STAT3 could regulate T cell differentiation.

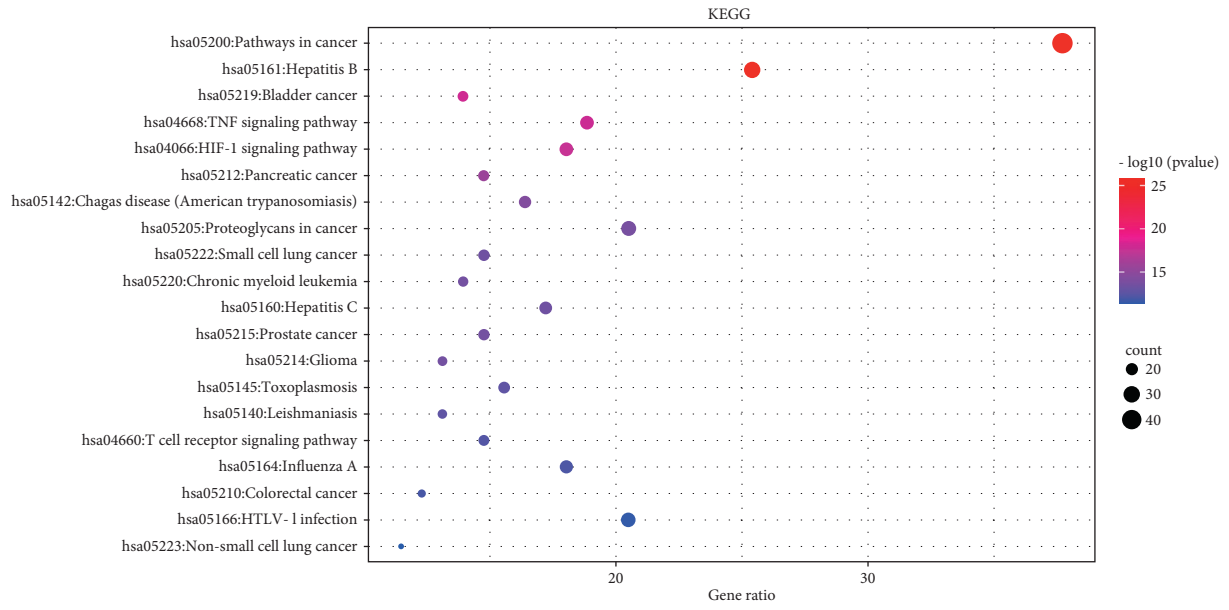


FIGURE 8: The top 20 pathways of KEGG enrichment.

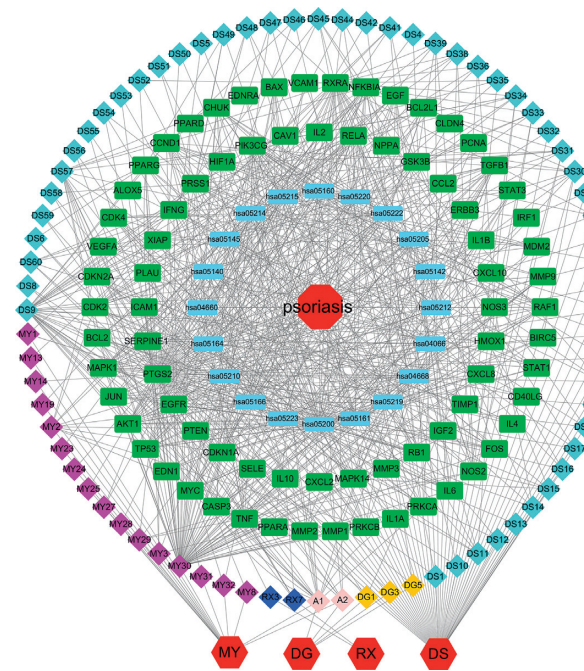


FIGURE 9: The disease-pathway-target-compound-drug network.

TABLE 3: Molecular docking results.

Active ingredient	Binding energy (kcal·mol <sup>-1</sup> )				
	AKT1	TNF	IL6	TP53	VEGFA
Quercetin	-4.49	-5.13	-4.9	-5.52	-4.23
Luteolin	-6.21	-7.4	-4.48	-6.07	-5.41
Tanshinone IIA	-7.97	-9.42	-6.84	-9.07	-7.73
$\beta$ -Sitosterol	-7.99	-9.30	-6.8	-9.27	-6.50
Dihydrotanshinlactone	-6.07	-6.82	-5.48	-7.2	-6.13

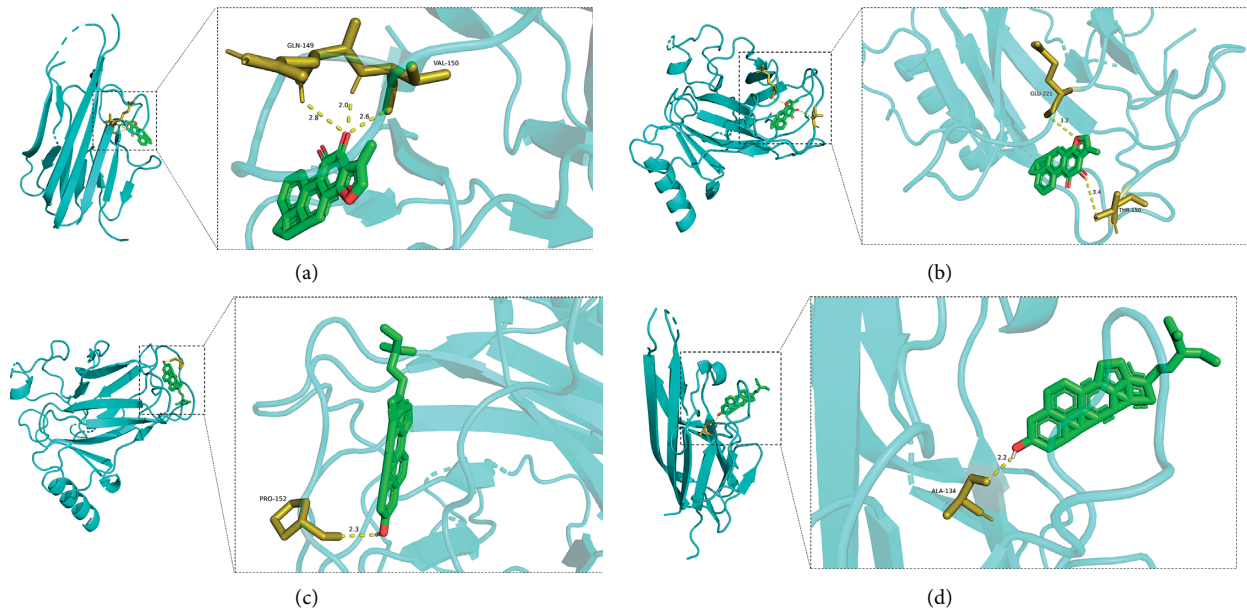


FIGURE 10: Molecular docking mode. (a) Tanshinone IIA-TNF, (b) beta-sitosterol-TNF, (c) beta-sitosterol-TP53, and (d) tanshinone IIA-TP53.

Studies have found that mice with high expression of the STAT3 pathway can spontaneously develop psoriasis-like skin lesions [50]. In the pathogenesis of psoriasis, the STAT3 pathway was involved in regulating the secretion of Th17 cytokines. When the STAT3 pathway was overactive, it could promote the excessive proliferation of keratinocytes and the production of IL6 and IL17. These cytokines, in turn, trigger Th17 and STAT3 signaling pathways, resulting in a sustained inflammatory response [51]. In addition, STAT3 also activated the transcription of related genes by targeting its promoter region, thereby forming a regulatory feedback loop that affected the proliferation and apoptosis of HaCaT cells [52]. Studies have found that HIF1A levels in patients with psoriasis were significantly higher than those in normal patients and were positively correlated with microvessel density in skin lesions [53]. Many other studies have reported that the protein expression levels of PPARG [54], MMP9 [55], and MYC [56] were also strongly correlated with the incidence of psoriasis.

The results of GO functional enrichment analysis and KEGG pathway enrichment showed that the mechanism of HLXLD treatment of psoriasis mainly focuses on drug response, negative regulation of apoptosis process, hypoxia response, positive regulation of RNA polymerase II promoter transcription, and positive regulation of cells. Proliferation, aging, inflammation, positive regulation of gene expression, positive regulation of transcription, DNA templating, etc., and the pathways related to the treatment of psoriasis by HLXLD mainly involved pathways in cancer (including multisystem and multiorgan cancers), TNF signaling pathway, HIF-1 signaling pathway, T cell receptor signaling pathway, etc. At present, more and more pieces of evidence supported the correlation between cancer and psoriasis. Several meta-analyses and retrospective studies [57–60] have found that the risk of cancer in patients with

psoriasis was higher than that of normal people, especially skin cancer, lymphatic cancer [58], colorectal cancer [59] and lung cancer [60], etc. TNF had strong biological activity and played an important role in the pathogenesis of psoriasis. The TNF/IL23/IL17A axis was also widely involved in the body's immune response, promoting the occurrence of psoriasis inflammatory response and the proliferation of epidermal cells [61]. The increase of HIF-1 in keratinocytes helped promote angiogenesis and skin inflammation [62]. Another study found that HIF1A might promote the glycolysis process of psoriasis Vulgaris by increasing the expression of CD147 and GLUT1 [63]. From an immune perspective, psoriasis was a chronic skin disease associated with T cell-mediated inflammation. The activation of T cells promoted the proliferation and migration of keratinocytes, thereby causing or accelerating the progression of the disease. At present, most monoclonal antibody preparations were aimed at this mechanism and block downstream inflammatory mediators such as TNF and IL17A to treat psoriasis [64].

## 5. Conclusion

To sum up, based on the network pharmacology method, this study systematically expounded the relationship between HLXLD in the treatment of psoriasis through multicomponent, multitarget, and multichannel, and verifies the strong binding activity between key components and core targets by molecular docking technology. The results showed that HLXLD might act on AKT1, IL6, TNF, TP53, VEGFA, EGF, EGFR, CXCL8, MMP9, MAPK8, and other targets through active components such as quercetin, luteolin, tanshinone IIA,  $\beta$ -Sitosterol, and dihydrodanshenlide, involving multiple signal pathways such as cancer signaling pathway, TNF signaling pathway, HIF-1 signaling pathway,



and T cell receptor signaling pathway, participating in the drug reaction, inflammatory reaction, gene expression, cell proliferation, and apoptosis, to play a role in the treatment of psoriasis, which provided a theoretical basis for the further application of HLXLD in the clinic. However, because this study mainly relied on the network database, there were still some limitations. The specific drug action mechanism needs further experimental verification in vivo and in vitro.

## Data Availability

The data used to support this study are available from the corresponding author upon request.

## Conflicts of Interest

The authors declare that they have no conflicts of interest.

## Acknowledgments

This study was funded by a Scientific Research Project of Hebei Administration of Traditional Chinese Medicine (nos. 2020461 and 2022230).

## References

- [1] H. Li, L. Hu, and Y. Zheng, "Analysis of the epidemiological burden of psoriasis in China based on the big data of global burden of disease study (GBD)," *The Chinese Journal of Dermatovenereology*, vol. 35, no. 4, pp. 386–392, 2021.
- [2] J. Z. Hu, S. D. Billings, D. Yan, and A. P. Fernandez, "Histologic comparison of tumor necrosis factor- $\alpha$  inhibitor-induced psoriasis and psoriasis vulgaris," *Journal of the American Academy of Dermatology*, vol. 83, no. 1, pp. 71–77, 2020.
- [3] Y. Cao, K. Zhu, and F. Pan, "Modern literature study on syndrome distribution and Chinese medicine medication regularity in treatment of psoriasis vulgaris," *Journal of Guangzhou University of Traditional Chinese Medicine*, vol. 37, no. 6, pp. 1198–1201, 2020.
- [4] Y. Ji, W. Li, Y. Lin, Z. Shuchan, and L. Xuan, "Discussion on the treatment of plaque psoriasis with fire acupuncture combined with cotton moxibustion based on collateral disease theory," *Journal of Liaoning University of Traditional Chinese Medicine*, vol. 24, no. 1, pp. 143–146, 2022.
- [5] J. Guo, W. Guo, and H. Li, "Clinical observation on Treating 30 cases of psoriasis vulgaris from collateral disease," *Guiding Journal of Traditional Chinese Medicine and Pharmacy*, vol. 18, no. 11, pp. 40–41, 2012.
- [6] J. Ru, P. Li, J. Wang et al., "TCMSP: a database of systems pharmacology for drug discovery from herbal medicines," *Journal of Cheminformatics*, vol. 6, no. 1, 2014.
- [7] A. Bateman, M. Martin, and S. Orchard, "UniProt: the universal protein knowledgebase in 2021," *Nucleic Acids Research*, vol. 49, no. D1, pp. D480–D489, 2021.
- [8] G. Stelzer, N. Rosen, I. Plaschkes et al., "The GeneCards suite: from gene data mining to disease genome sequence analyses," *Current Protocols in Bioinformatics*, vol. 54, no. 1, pp. 1–30, 2016.
- [9] A. Hamosh, J. S. Amberger, C. Bocchini, A. F. Scott, and S. A. Rasmussen, "Online mendelian inheritance in man (OMIM): victor McKusick's magnum opus," *American Journal of Medical Genetics, Part A*, vol. 185, no. 11, pp. 3259–3265, 2021.
- [10] Y. Wang, S. Zhang, F. Li et al., "Therapeutic target database 2020: enriched resource for facilitating research and early development of targeted therapeutics," *Nucleic Acids Research*, vol. 48, no. D1, pp. D1031–D1041, 2019.
- [11] J. Piñero, J. M. Ramírez-Anguita, J. Saúch-Pitarch et al., "The DisGeNET knowledge platform for disease genomics: 2019 update," *Nucleic Acids Research*, vol. 48, no. D1, pp. D845–D855, 2019.
- [12] D. S. Wishart, Y. D. Feunang, A. C. Guo et al., "DrugBank 5.0: a major update to the DrugBank database for 2018," *Nucleic Acids Research*, vol. 46, no. D1, pp. D1074–D1082, 2018.
- [13] E. Ragueneau, A. Shrivastava, J. H. Morris, N. del-Toro, H. Hermjakob, and P. Porras, "IntAct App: a Cytoscape application for molecular interaction network visualization and analysis," *Bioinformatics*, vol. 37, no. 20, pp. 3684–3685, 2021.
- [14] D. Szklarczyk, A. L. Gable, K. C. Nastou et al., "The STRING database in 2021: customizable protein-protein networks, and functional characterization of user-uploaded gene/measurement sets," *Nucleic Acids Research*, vol. 49, no. D1, pp. D605–D612, 2021.
- [15] D. W. Huang, B. T. Sherman, and R. A. Lempicki, "Systematic and integrative analysis of large gene lists using DAVID bioinformatics resources," *Nature Protocols*, vol. 4, no. 1, pp. 44–57, 2009.
- [16] H. M. Berman, J. Westbrook, Z. Feng et al., "The protein data bank," *Nucleic Acids Research*, vol. 28, no. 1, pp. 235–242, 2000.
- [17] K.-Y. Hsin, S. Ghosh, and H. Kitano, "Combining machine learning systems and multiple docking simulation packages to improve docking prediction reliability for network pharmacology," *PLoS One*, vol. 8, no. 12, Article ID e83922, 2013.
- [18] B. H. Mz, "Shortcuts for faster image creation in PyMOL," *Protein Science: A Publication of the Protein Society*, vol. 29, no. 1, pp. 268–276, 2020.
- [19] O. Trott and A. J. Olson, "AutoDock Vina: improving the speed and accuracy of docking with a new scoring function, efficient optimization, and multithreading," *Journal of Computational Chemistry*, vol. 31, no. 2, pp. 455–461, 2010.
- [20] X. Dong, S. Luo, and Y. Bai, "Study on current situation of TCM treatment for psoriasis," *Beijing Journal of Traditional Chinese Medicine*, vol. 40, no. 8, pp. 806–810, 2021.
- [21] W. Fei, H. Tang, S. Yang, and C. J. D. Venerool, "Changes of cutaneous microcirculatory in psoriasis," *The Chinese Journal of Dermatovenereology*, vol. 32, no. 6, pp. 714–717, 2018.
- [22] J. Jia, X. Mo, J. Liu et al., "Mechanism of danshensu-induced inhibition of abnormal epidermal proliferation in psoriasis," *European Journal of Pharmacology*, vol. 868, Article ID 172881, 2020.
- [23] J. Jia, C. Li, J. Yang et al., "Yes-associated protein promotes the abnormal proliferation of psoriatic keratinocytes via an amphiregulin dependent pathway," *Scientific Reports*, vol. 8, no. 1, Article ID 14513, 2018.
- [24] S. Wang, L. Zhu, Y. Xu, Z. Qin, and A. Xu, "Salvianolic acid B ameliorates psoriatic changes in imiquimod-induced psoriasis on BALB/c mice by inhibiting inflammatory and keratin markers via altering phosphatidylinositol-3-kinase/protein kinase B signaling pathway," *Korean Journal of Physiology and Pharmacology*, vol. 24, no. 3, pp. 213–221, 2020.
- [25] H. Jing, H. Zhou, and D. Duan, "The influence of angelica polysaccharide on the expression of NF- $\kappa$ B and IFN- $\gamma$  in co-culture of peripheral blood mononuclear cells and

- keratinocytes from psoriatic patients,” *China Journal of Leprosy and Skin Diseases*, vol. 29, no. 12, pp. 769–772, 2013.
- [26] T. Efferth and F. Oesch, “Anti-inflammatory and Anti-cancer Activities of Frankincense: Targets, Treatments and toxicities,” *Seminars in Cancer Biology*, vol. 20, 2020.
- [27] G. Maramaldi, S. Togni, F. Di Pierro, and M. Biondi, “A cosmeceutical formulation based on boswellic acids for the treatment of erythematous eczema and psoriasis,” *Clinical, Cosmetic and Investigational Dermatology*, vol. 7, p. 321, 2014.
- [28] Y. Shen, *The Role and Mechanisms of Guggulsterone in Keratinocytes[D]*, Shandong University, Jinan, China, 2020.
- [29] H. Chen, C. Lu, H. Liu et al., “Quercetin ameliorates imiquimod-induced psoriasis-like skin inflammation in mice via the NF- $\kappa$ B pathway,” *International Immunopharmacology*, vol. 48, pp. 110–117, 2017.
- [30] W. Zhou, M. Hu, X. Zang et al., “Luteolin attenuates imiquimod-induced psoriasis-like skin lesions in BALB/c mice via suppression of inflammation response,” *Biomedicine & Pharmacotherapy*, vol. 131, Article ID 110696, 2020.
- [31] Z. Weng, A. B. Patel, M. Vasiadi, A. Therianou, and T. C. Theoharides, “Luteolin inhibits human keratinocyte activation and decreases NF- $\kappa$ B induction that is increased in psoriatic skin,” *PLoS One*, vol. 9, no. 2, Article ID e90739, 2014.
- [32] S. Sundarajan, M. P. Nandakumar, D. Prabhu, J. Jeyaraman, and M. Arumugam, “Conformational insights into the inhibitory mechanism of phyto-compounds against Src kinase family members implicated in psoriasis,” *Journal of Biomolecular Structure and Dynamics*, vol. 38, no. 5, pp. 1398–1414, 2020.
- [33] J. Lv, D. Zhou, Y. Wang et al., “Effects of luteolin on treatment of psoriasis by repressing HSP90,” *International Immunopharmacology*, vol. 79, Article ID 106070, 2020.
- [34] F. Li, R. Xu, Q. Zeng et al., “Tanshinone IIA inhibits growth of keratinocytes through cell cycle arrest and apoptosis: underlying treatment mechanism of psoriasis,” *Evidence-based complementary and alternative medicine*, vol. 2012, Article ID 927658, 2012.
- [35] L. Kuai, Y. Luo, K. Qu et al., “Transcriptomic analysis of the mechanisms for alleviating psoriatic dermatitis using taodan granules in an imiquimod-induced psoriasis-like mouse model,” *Frontiers in Pharmacology*, vol. 12, Article ID 632414, 2021.
- [36] L. Tang, S. He, X. Wang et al., “Cryptotanshinone reduces psoriatic epidermal hyperplasia via inhibiting the activation of STAT3,” *Experimental Dermatology*, vol. 27, no. 3, pp. 268–275, 2018.
- [37] X. Yang, X. Wang, and X. Zhang, “Role of Akt in epidermal proliferation in psoriasis vulgaris,” *Chinese Journal of Dermatovenereology of Integrated Traditional and Western Medicine*, vol. 20, no. 3, pp. 241–245, 2021.
- [38] Q. Duan, G. Wang, M. Wang et al., “LncRNA RP6-65G23.1 accelerates proliferation and inhibits apoptosis via p-ERK1/2/p-AKT signaling pathway on keratinocytes,” *Journal of Cellular Biochemistry*, vol. 121, no. 11, pp. 4580–4589, 2020.
- [39] B. Li, J. Lei, L. Yang et al., “Dysregulation of akt-FOXO1 pathway leads to dysfunction of regulatory T cells in patients with psoriasis,” *Journal of Investigative Dermatology*, vol. 139, no. 10, pp. 2098–2107, 2019.
- [40] A. W. Armstrong and C. Read, “Pathophysiology, clinical presentation, and treatment of psoriasis,” *JAMA*, vol. 323, no. 19, pp. 1945–1960, 2020.
- [41] A. Luengas-Martinez, J. Hardman-Smart, R. Paus, and H. S. Young, “Vascular endothelial growth factor-A as a promising therapeutic target for the management of psoriasis,” *Experimental Dermatology*, vol. 29, no. 8, pp. 687–698, 2020.
- [42] F. Benhadou, E. Glitzner, A. Brisebarre et al., “Epidermal autonomous VEGFA/Flt1/Nrp1 functions mediate psoriasis-like disease,” *Science Advances*, vol. 6, no. 2, Article ID eaax5849, 2020.
- [43] B. Ehst, Z. Wang, J. Leitenberger et al., “Synergistic induction of IL-23 by TNF $\alpha$ , IL-17A, and EGF in keratinocytes,” *Cytokine*, vol. 138, Article ID 155357, 2021.
- [44] W. Wang, Y. He, and H. Xu, “Update of epidermal growth factor receptor signaling pathway in the pathogenesis of related skin diseases,” *China Journal of Leprosy and Skin Diseases*, vol. 36, no. 11, pp. 697–700, 2020.
- [45] G. Sa and T. Das, “Anti cancer effects of curcumin: cycle of life and death,” *Cell Division*, vol. 3, no. 1, p. 14, 2008.
- [46] N. Moorchung, B. Vasudevan, S. Dinesh Kumar, and A. Muralidhar, “Expression of apoptosis regulating proteins p53 and bcl-2 in psoriasis,” *Indian Journal of Pathology & Microbiology*, vol. 58, no. 4, pp. 423–426, 2015.
- [47] D. Zhang, Y. Chen, L. Chen et al., “Ultraviolet irradiation promotes FOXP3 transcription via p53 in psoriasis,” *Experimental Dermatology*, vol. 25, no. 7, pp. 513–518, 2016.
- [48] Z. Wei, T. Li, Y. Sun et al., “Daturaturin A, a withanolide in Datura metel L., induces HaCaT autophagy through the PI3K-Akt-mTOR signaling pathway,” *Phytotherapy Research*, vol. 35, no. 3, pp. 1546–1558, 2021.
- [49] S. M. M. Bebars, D. R. Al-Sharaky, M. A. Gaber, and D. R. Afify, “Immunohistochemical expression of caspase-3 in psoriasis,” *Journal of Clinical and Diagnostic Research: Journal of Clinical and Diagnostic Research*, vol. 11, no. 7, pp. C1–C5, 2017.
- [50] M. Morelli, C. Scarponi, L. Mercurio et al., “Selective immunomodulation of inflammatory pathways in keratinocytes by the janus kinase (JAK) inhibitor tofacitinib: implications for the employment of JAK-targeting drugs in psoriasis,” *Journal of immunology research*, vol. 2018, Article ID 7897263, 2018.
- [51] F. Xu, J. Xu, X. Xiong, and Y. Deng, “Salidroside inhibits MAPK, NF- $\kappa$ B, and STAT3 pathways in psoriasis-associated oxidative stress via SIRT1 activation,” *Redox Report*, vol. 24, no. 1, pp. 70–74, 2019.
- [52] Z. Yang, Z. Chen, C. Wang, P. Huang, M. Luo, and R. Zhou, “STAT3/SH3PXD2A-AS1/miR-125b/STAT3 positive feedback loop affects psoriasis pathogenesis via regulating human keratinocyte proliferation,” *Cytokine*, vol. 144, Article ID 155535, 2021.
- [53] A. G. Abdou, A. G. A. Farag, M. Hammam, D. M. Taie, and R. A. Abdelaziz, “Immunohistochemical expression HIF1 $\alpha$  in chronic plaque psoriasis, an association with angiogenesis and proliferation,” *Journal of Immunoassay and Immunochemistry*, vol. 39, no. 3, pp. 249–262, 2018.
- [54] S. Blunder, T. Krimbacher, V. Moosbrugger-Martinz, R. Gruber, M. Schmuth, and S. Dubrac, “Keratinocyte-derived IL-1 $\beta$  induces PPARG downregulation and PPARD upregulation in human reconstructed epidermis following barrier impairment,” *Experimental Dermatology*, vol. 30, no. 9, pp. 1298–1308, 2021.
- [55] L. M. Amezcua-Guerra, R. Bojalil, J. Espinoza-Hernandez et al., “Serum of patients with psoriasis modulates the production of MMP-9 and TIMP-1 in cells of monocytic lineage,” *Immunological Investigations*, vol. 47, no. 7, pp. 725–734, 2018.

- [56] D. Cibrian, H. de la Fuente, and F. Sánchez-Madrid, "Metabolic pathways that control skin homeostasis and inflammation," *Trends in Molecular Medicine*, vol. 26, no. 11, pp. 975–986, 2020.
- [57] A. M. Trafford, R. Parisi, E. Kontopantelis, C. E. M. Griffiths, and D. M. Ashcroft, "Association of psoriasis with the risk of developing or dying of cancer," *JAMA Dermatology*, vol. 155, no. 12, pp. 1390–1403, 2019.
- [58] S. Vaengebjerger, L. Skov, A. Egeberg, and N. D. Loft, "Prevalence, incidence, and risk of cancer in patients with psoriasis and psoriatic arthritis," *JAMA Dermatology*, vol. 156, no. 4, pp. 421–429, 2020.
- [59] A. E. Prizment, A. Alonso, A. R. Folsom et al., "Association between psoriasis and incident cancer: the Iowa's Women's Health Study," *Cancer Causes & Control*, vol. 22, no. 7, pp. 1003–1010, 2011.
- [60] Z. C. Chiesa Fuxench, D. B. Shin, A. Ogdie Beatty, and J. M. Gelfand, "The risk of cancer in patients with psoriasis," *JAMA Dermatology*, vol. 152, no. 3, pp. 282–290, 2016.
- [61] K. Furue, T. Ito, G. Tsuji, T. Kadono, and M. Furue, "Psoriasis and the TNF/IL23/IL17 axis," *Societa italiana di dermatologia e sifilografia*, vol. 154, no. 4, pp. 418–424, 2019.
- [62] W.-J. Zhu, P. Li, L. Wang, and Y.-C. Xu, "Hypoxia-inducible factor-1: a potential pharmacological target to manage psoriasis," *International Immunopharmacology*, vol. 86, Article ID 106689, 2020.
- [63] W. Tang, T. Long, F. Li et al., "HIF-1 $\alpha$  may promote glycolysis in psoriasis vulgaris via upregulation of CD147 and GLUT1," *Journal of Central South University*, vol. 46, no. 4, pp. 333–344, 2021.
- [64] F. Zhou, Z. Zhu, J. Gao et al., "NFkB1 mediates Th1/Th17 activation in the pathogenesis of psoriasis," *Cellular Immunology*, vol. 331, pp. 16–21, 2018.

## Research Article

# Molecular Mechanism Investigation on Monomer Kaempferol of the Traditional Medicine Dingqing Tablet in Promoting Apoptosis of Acute Myeloid Leukemia HL-60 Cells

Dandan Zheng,<sup>1</sup> Yongming Zhou,<sup>2</sup> Yong Liu,<sup>1</sup> Lihai Ma,<sup>1</sup> and Lingzhan Meng<sup>1</sup> 

<sup>1</sup>Department of Oncology, Chongqing Hospital of Traditional Chinese Medicine, Chongqing, China

<sup>2</sup>Department of Hematology, Yueyang Hospital of Integrated Traditional Chinese and Western Medicine, Shanghai University of Traditional Chinese Medicine, Shanghai, China

Correspondence should be addressed to Lingzhan Meng; [lingzhanmeng@outlook.com](mailto:lingzhanmeng@outlook.com)

Received 2 December 2021; Accepted 17 January 2022; Published 24 February 2022

Academic Editor: Ruchika Garg

Copyright © 2022 Dandan Zheng et al. This is an open access article distributed under the Creative Commons Attribution License, which permits unrestricted use, distribution, and reproduction in any medium, provided the original work is properly cited.

The traditional medicine Dingqing Tablet produces effective efficacy in treating acute myeloid leukemia, but its specific mechanism remains to be investigated. Dingqing Tablet consists of Codonopsis, Indigo Naturalis, Cortex Moutan, Radix Notoginseng, Citrus Reticulata, and Eolite. The active components of Dingqing Tablets were screened by the TCMSP database. Meanwhile, the SwissTargetPrediction database was utilized to predict the corresponding targets. Relevant disease targets of acute myeloid leukemia were obtained from GeneCards. The obtained targets of Dingqing Tablets and genes of acute myeloid leukemia were used, and the overlapped genes were presented in the Venn diagram. A drug-component-target network was constructed via Cytoscape 3.6.0 software. Molecular docking methodology was also used with AutoDock Vina 1.1.2. Furthermore, the effects of kaempferol on the proliferation and apoptosis of HL-60 cells were identified using 3-(4,5)-dimethylthiazolo(-z-y1)-3,5-diphenyltetrazoliumromide (MTT), 5-Ethynyl-2'-deoxyuridine (EDU), flow cytometry, and TdT-mediated dUTP nick-end labeling (TUNEL) assays. The combination of kaempferol and AKT1 was verified using an immunoprecipitation (IP) experiment and the effects of Kaempferol on HL-60 cell apoptosis by western blot (WB) and qPCR. The key component kaempferol and the core target gene AKT1 were sorted out using a drug-component target network diagram. Molecular docking results revealed that the binding energy between kaempferol and AKT1 was lower than -5 kcal/mol. MTT and EDU assays indicated that kaempferol markedly inhibited the proliferation of HL-60 cells. Flow cytometry and TUNEL assays suggested that kaempferol substantially promoted HL-60 cell apoptosis. IP assay results testified that kaempferol could bind to AKT1, thereby reducing the level of P-AKT and promoting HL-60 cell apoptosis. The monomer kaempferol of Dingqing Tablet could promote apoptosis of HL-60 cells, and the mechanism might correlate with the combination of kaempferol and AKT1, reducing the level of P-AKT and promoting the expression of the apoptotic signaling pathway.

## 1. Introduction

Acute myeloid leukemia (AML) is recognized as a highly heterogeneous disorder and the most common acute leukemia developed in adults [1]. The American Cancer Society's 2021 estimate of leukemia in the United States is that there will be 20,240 new cases of AML, mostly adults, and about 11,400 deaths from acute myeloid leukemia, almost all of which occur in adults. AML is one of the most common types of leukemia in adults. AML is fairly rare overall, accounting for only about 1% of all cancers [2]. It is

characterized by an abnormal proliferation of leukemia cells in the bone marrow. The clinical manifestations are anemia, hemorrhage, infection and pyrexia, organ infiltration, and metabolic abnormalities [3]. Currently, chemotherapy and stem cell transplantation are widely applied in the treatment of AML [4]. However, the prevalence of chemotherapy resistance and relapse remains a challenge for AML patients. Meanwhile, the five-year survival rate is still very low [5]. Further and deeper investigations have found that AML pathogenesis is complicated with multiple genes, multiple factors, and even multiple molecules involved [6, 7]. As AML

patients develop general conditions of chemotherapy resistance, recurrence, and low survival rates, there is an urgent need to explore new biomarkers applied in diagnosing the occurrence, development, and prognosis of AML, as well as to discover novel therapeutic targets.

Dingqing Tablet serves as effective preparation for the treatment of leukemia. It has been developed by the team led by Professor Huang Zhenqiao from Yueyang Hospital of Integrated Traditional Chinese and Western Medicine, Shanghai University of Traditional Chinese Medicine, under the principles of Chinese medicine. This prescription consists of Codonopsis, Indigo Naturalis, Cortex Moutan, Radix Notoginseng, Citrus Reticulata, and Eolite [8]. Kaempferol is a main component of Cortex Moutan [9]. Kaempferol is also known as kaempferide with the chemical name of 3,5, 7-trihydroxy-2-(4-hydroxyphenyl)-4h-1-benzopyran 4-ketone, which belongs to the flavonol compounds [10]. This flavonoid compound is extensively present in edible plants and traditional natural medicines. Numerous preclinical studies have revealed that kaempferol and kaempferitrin exhibit extensive biological activities, including anticancer, anti-inflammation, antimicrobe, antioxidant, protection of both cardiovascular, and neuron as well as antidiabetes [11–13].

As a major intracellular signal transduction pathway [14], the PI3K-Akt signaling pathway is essential in promoting cell proliferation and inhibiting apoptosis in the body by influencing the activation of multiple downstream effector molecules [15]. Akt serves as a serine/threonine protein kinase (molecular weight 57 kD) [16]. The Bcl-2 family includes homodimers and heterodimers of which the formation and balance are of great significance to cell survival or apoptosis [17]. p-Akt promotes the phosphorylate of the Ser136/Ser112 residues of Bad, while Bcl-2 or Bcl-xl inhibited the phosphorylate of Bad [18]. The PI3K-Akt pathway activation enables phosphorylate the Ser184 residue of Bax, allowing Bax to stay in the cytoplasm, thereby promoting the formation of heterodimers and inhibiting cell apoptosis [18].

This research predicted the active ingredients and relevant targets of Dingqing Tablet employing a network pharmacology technique. The overlapped targets with disease target genes were subsequently obtained. Followed by core targets identification, we also conducted GO and KEGG pathway analysis and screened out the component kaempferol in Cortex Moutan. Molecular docking was subsequently conducted with the core target AKT1. Moreover, flow cytometry and TUNEL assays testified that kaempferol promoted apoptosis of HL-60 cells and determined that kaempferol and AKT could bind to each other and reduce the phosphorylation of AKT.

## 2. Materials and Methods

**2.1. Cell Culture and Drug Treatment.** Human leukemia cell line HL60 was purchased from American Type Culture Collection (ATCC). Culture medium utilized RPMI 1640 containing 10% inactivated fetal bovine serum, streptomycin, penicillin (each 100 U/mL), NaHCO<sub>3</sub> (2 g/L), and

HEPES (2.4 g/L) at PH 7.2–7.4, and incubation was performed at 37°C constant temperature and 5% CO<sub>2</sub>. Cells at the logarithmic growth phase were collected for further experiments, which were treated using kaempferol (25, 50, and 100 μM), and the positive control was treated using all-trans retinoic acid (ATRA) (10 μM).

**2.2. Network Pharmacological Analysis.** Through the network pharmacology approach, principal components and action targets of Dingqing Tablets were predicted. Firstly, the active ingredients of Dingqing Tablets (Codonopsis, Indigo Naturalis, Cortex Moutan, Radix Notoginseng, Citrus Reticulata, and Eolite) were retrieved from the TCMSP database [19] (<https://tcmspw.com/tcmsp.php>), and their corresponding targets were predicted using the SwissTargetPrediction website [20]. Human AML-related genes were sorted out from the gene disease database [21], and then a PPI protein interaction network diagram was constructed using String [22], and a drug-component-target network diagram was plotted using Cytoscape 3.6.0. A Cytoscape plugin ClueGO was used for GO and KEGG pathway analysis on the 92 targets, and visualization of the enrichment analysis results was processed [23].

**2.3. Molecular Docking.** The 3D structure of kaempferol was exported from TCMSP (<https://tcmspw.com/tcmsp.php>), and AKT 3D structure was retrieved from the Protein Data Bank [24] (<http://www.rcsb.org/pdb>). The receptor protein was added with hydrogen and calculated charge using AutoDock 4.2.6 software [25], docked with a ligand using AutoDock Vina 1.1.2 software. The docking results and the scores of binding energy were obtained. Those parts with the best binding energy were utilized for plotting. The 3D images plotted using PyMOL [26] presented the interaction between the receptor protein and the ligand.

**2.4. MTT Assay.** HL-60 cells were inoculated into a 96-well plate and followed by 6 d incubation. After being supplemented with 20 μL MTT solution [27] in the wells, cell incubation was conducted, lasting for 4 h until being terminated. To each well, 150 μL DMSO was added and shaken for 10 min [28]. The light absorption of each hole was measured on an enzyme-linked immunosorbent monitor at the wavelength of 490 nm for colorimetry. Cell growth curves were recorded and plotted [29].

**2.5. EDU Assay.** The HL-60 cells were planted to a 24-well plate. In light of the instructions of the EdU kit, a 2x EdU reaction solution was prepared and added to the 24-well plate. The cells were incubated in the dark for 2 h after the supplement of the reaction solution, fixed with 4% paraformaldehyde at room temperature for 20 min, supplemented with 500 μL 0.3% Triton X-100, and reacted at room temperature for 10 min. Then, PBS was employed to rinse the cells 3 times. AZIDE 555-Click reaction solution was freshly prepared, supplied 200 μL to each well, and incubated 30 min at room temperature avoiding light. After the



reaction was completed, the solution was removed and followed by PBS washing 3 times, the nuclei were subsequently counterstained using Hoechst for further immunofluorescence. Observe and take pictures under an inverted microscope. Observation and photograph were performed under an inverted microscope [30].

**2.6. Flow Cytometry.** The cells were evenly inoculated into a 6-well plate, digested using trypsin after 48 h transfection, and collected after centrifugation. Following two cycles of washing with precooled PBS, the cells were added with 400  $\mu$ L of  $1 \times$  Annexin V binding solution and suspended at a concentration of about  $1 \times 10^6$  cells/mL. The solution was transferred to a flow cytometry tube, supplied with 5  $\mu$ L Annexin V-FITC staining solution and mixed well gently. Incubation was followed under 4°C for 15 min avoiding light, supplemented with 10  $\mu$ L PI staining solution again and gently mixed, incubated for 5 min at 4°C in the dark followed by immediate detection by flow cytometry [31].

**2.7. TUNEL Assay.** The cell slides processed in experiments were treated with paraformaldehyde for 15–30 min at room temperature, washed 3 times with PBS, added with blocking solution, and incubated at room temperature for 10 min. Rinsed again with PBS, the slides were added with membrane solution and incubated 30 min at room temperature. The mixture of TUNEL reaction was prepared and mixed with 50  $\mu$ L TdT + 450  $\mu$ L fluorescein-labeled dUTP solution. Following reaction at room temperature for about 30 min, a 50  $\mu$ L mixture was supplied for reaction in a wet chamber avoiding light at 37°C for 60 min. Following 3 cycles of washing with PBS, one PBS was dripped, and the apoptotic cells were observed using a fluorescence microscope (the excitation and detection wavelength were 450–500 nm and 515–565 nm, respectively) [32].

**2.8. Coimmunoprecipitation Assay.** Biotin-labeled kaempferol, the kit used EZ-Link™ Biotin-LC-Hydrazide (Thermo Scientific), and the procedures were followed following the operating instructions. Biotin-labeled kaempferol was inoculated into HL-60 cell suspension, cultured for 24 h, and centrifuged to collect the cells. Precooled RIPA Buffer was added, and the cells were collected for centrifugation at 14 000 g 15 min. Protein A agarose was prepared following two cycles of bead washing with PBS. To each 1 mL of total protein, 100  $\mu$ L Protein A agarose beads (50%) were added and centrifuged at 14 000 g for 15 min. Rabbit antibody was subsequently added, and the antigen-antibody mixture was slowly shaken at 4°C overnight, added with 100  $\mu$ L protein A agarose beads, and shaken slowly overnight at 4°C. Instantaneous centrifugation was performed at 14 000 rpm for 5 s before the collection of agarose bead-antigen-antibody complex and followed by electrophoresis [33].

**2.9. WB Assay.** The cells were harvested for lysis using IP lysis buffer. Following centrifugation at 4°C 13 000 rpm 20 min, the supernatant was obtained, and the protein was

harvested. 10% SPS-PAGE was employed to separate the total protein, which was then transferred to PDVF, blocked with milk at room temperature for 1 h with subsequent TBST washing 3 times. Primary antibody was supplied and incubated overnight at 4°C, and second antibody was supplied the next day and incubated for 1 h for ECL coloration [34].

**2.10. qPCR Assay.** Extraction of total RNA was conducted employing Trizol reagent (Takara, Japan). The first reversely transcribed cDNA strand used the PrimeScript™ RT kit (Takara, Japan). When determining relative gene expression, the reaction system and procedures of qPCR referred to instructions of TBGreenPremixExTaqII (Takara, Japan), and the instrument was CFX96Real-TimeSystem (Bio-Rad, USA). The  $2^{-\Delta\Delta CT}$  algorithm was used to calculate the relative gene expression levels [34].

**2.11. Data Analysis.** The experimental data obtained were exhibited as mean  $\pm$  standard deviation (SD). Student's *t*-test was performed for pairwise comparison and one-way analysis of variance (ANOVA) for multiple group comparison to assess the significance of statistical data using GraphPad Prism 7.0 software (LaJolla, CA, USA). *p* values less than 0.05 were regarded as the difference was statistically significant.

### 3. Results

**3.1. Overlapped Targets and Network Visualization of Drugs and Diseases.** To explore the actions of Dingqing Tablet on leukemia HL-60 cells, we initially determined the active ingredients and relevant targets of Dingqing Tablets. There were 707 targets sorted from Dingqing Tablet and 585 targets from human AML (Figure 1(a)). The overlapped genes of Radix Notoginseng, Citrus Reticulata, Codonopsis, Cortex Moutan, Indigo Naturalis, and Eolite and human AML were 37, 6, 97, 15, 102, and 58, respectively (Figure 1(b)). A PPI protein interaction network diagram was constructed through String (Figure 1(c)). The drugs, ingredients, and targets were visualized via Cytoscape 3.6, we found that MDP2 (kaempferol), DS6 (luteolin), XH (eolite), and E1 (quercetin) were the key ingredients in Dingqing Tablet, and AKT and STAT3 were the core target genes with top degrees (Figure 1(d)).

**3.2. Molecular Docking.** We selected the key ingredient kaempferol and the core target genes AKT1 (PDB ID: 1UNQ) and XDH (PDB ID: 5DN2) to conduct molecular docking with its corresponding chemical components. As shown in Figure 2, the binding energies of AKT1 and the main chemical components kaempferol (Figure 2(a)), isoindigo (Figure 2(b)), luteolin (Figure 2(c)), and quercetin (Figure 2(d)) were  $-5.16$ ,  $-5.91$ ,  $-5.37$ , and  $-5.45$  kcal/mol, respectively. The binding between kaempferol and AKT1 exhibited that the amino acid residues Arg48 and Tyr38 generated hydrogen bond

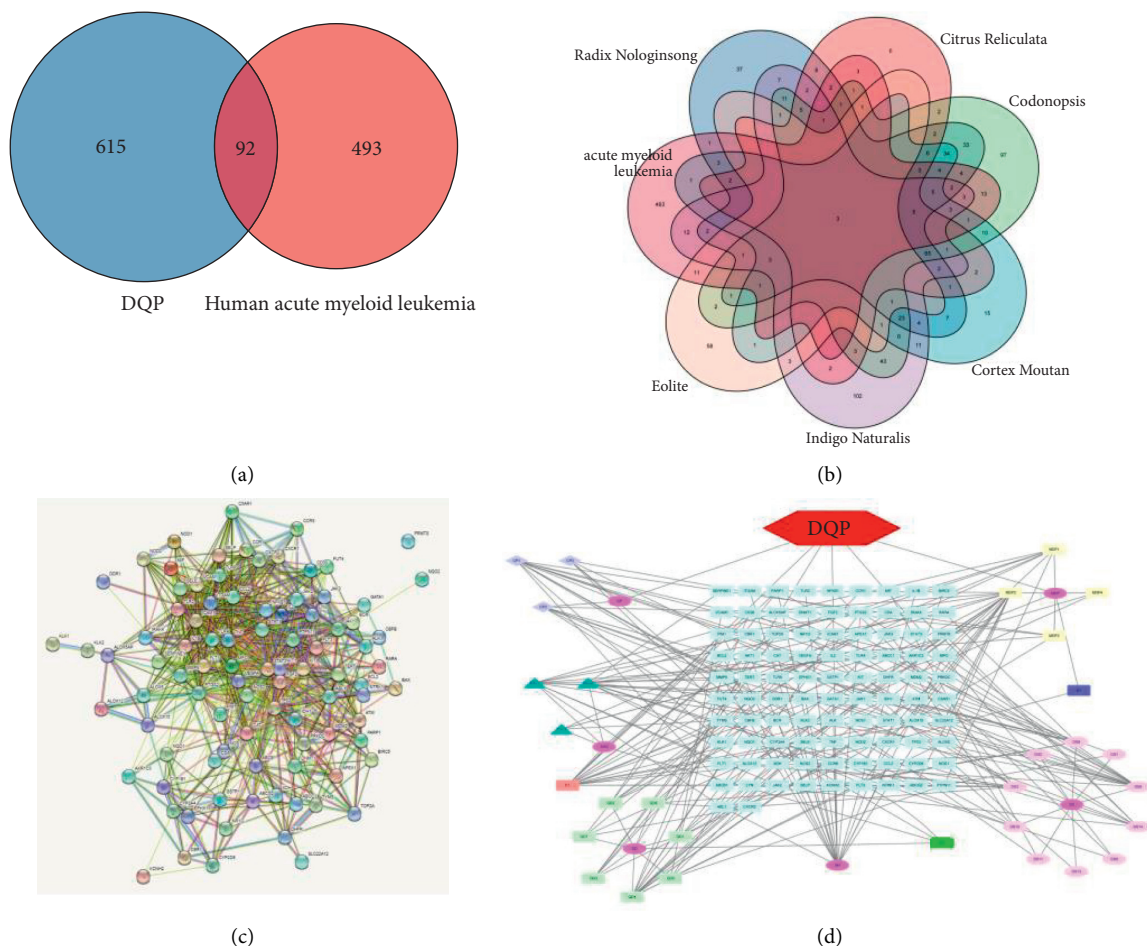


FIGURE 1: Analysis of the regulatory network of Dingqing tablets-key components-targets-acute myeloid leukemia based on network pharmacology. (a) Venn diagram of overlapped genes between Dingqing Tablet and human AML targets. (b) Venn diagrams of overlapped genes between Radix Notoginseng, Citrus Reticulata, Codonopsis, Cortex Moutan, Indigo Naturalis, and Eolite and human AML targets. (c) Protein-protein interaction analysis of 92 proteins. (d) Drug-active ingredient-target gene network diagram. DQP represented the compound drug Dingqing Tablet, and SSQ, CP, DS, MDP, QD, and XH, respectively, represented the six herbs containing in Dingqing Tablet: Radix Notoginseng, Citrus Reticulata, Codonopsis, Cortex Moutan, Indigo Naturalis, and Eolite.

interactions, while the amino acid residues Pro51, Glu49, Ile36, Leu28, Lys30, Ile6, Val4, and kaempferol formed hydrophobic interactions.

**3.3. GO and KEGG Pathway Enrichment Analysis.** We had a further illustration of the target function of Dingqing Tablet and the role of potential targets in the signaling pathway and analyzed the 92 targets through GO and KEGG pathway analysis employing a Cytoscape plugin ClueGO. Meanwhile, visualization of the enrichment analysis results was processed. As shown in Figure 3, GO analysis indicated that the most prominent biological processes included negative regulation of small molecule metabolic process and translation repressor activity; and those included in cell components and molecular functions were ligand-activated transcription factor activity, mRNA regulatory element binding, myeloid cell differentiation, and nuclear receptor activity (Figure 3(a)). KEGG pathway analysis results

revealed that the 92 potential targets of Dingqing Tablet in AML treatment were mainly correlated with the MAPK signaling pathway and PI3K-Akt signaling pathway (Figure 3(b)).

**3.4. Monomer of Dingqing Tablet Inhibits the Proliferation of HL-60.** To explore influences of Dingqing Tablet monomer kaempferol on the proliferation of HL-60, we divided HL-60 into a Control group, a Cisplatin group, a 25  $\mu\text{M}$  kaempferol group, a 50  $\mu\text{M}$  kaempferol group, and a 100  $\mu\text{M}$  kaempferol group. We detected the cell proliferation using MTT assays, and the results revealed that ATRA and 100  $\mu\text{M}$  kaempferol could markedly suppress the proliferation of HL-60 cells on day 4 ( $p = 0.0213$  and  $p = 0.0306$ ) (Figure 4(a)). Furthermore, the action of kaempferol on the proliferation ability of HL-60 cells was detected using EDU experiment, and the results revealed that 100  $\mu\text{M}$  kaempferol could markedly suppress the proliferation ability of HL-60 cells (Figures 4(b)–4(c)).

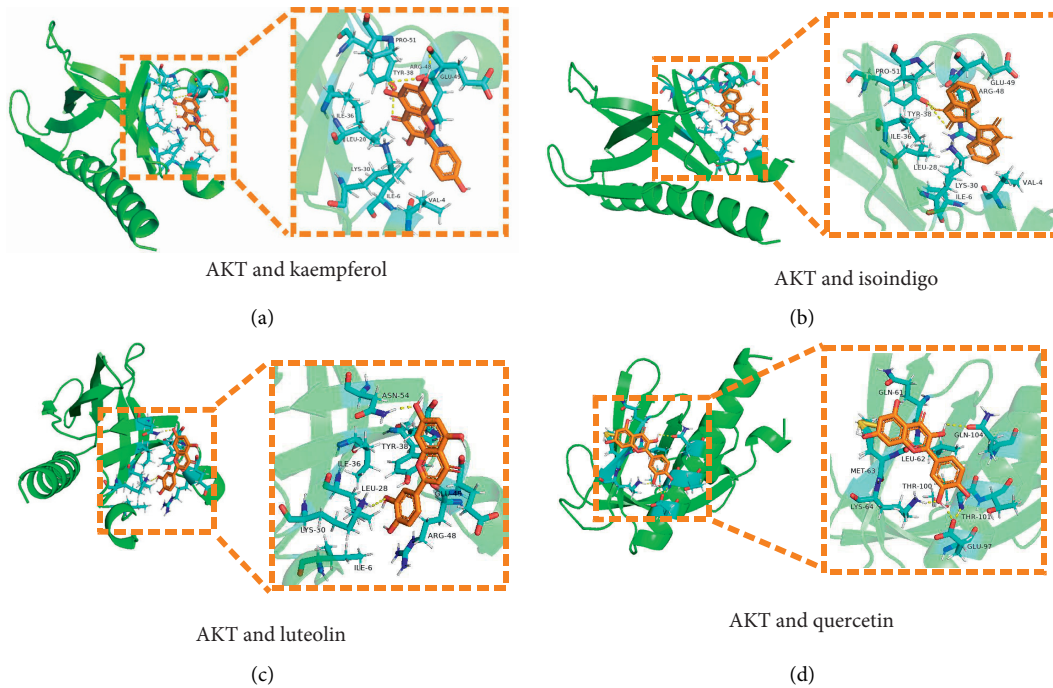


FIGURE 2: Molecular docking of the key components in Dingqing Tablet and the core target AKT1. (a) Molecular docking of AKT and kaempferol. (b) Molecular docking of AKT1 and isoindigo. (c) Molecular docking between AKT1 and luteolin. (d) Molecular docking between AKT1 and quercetin.

### 3.5. Monomer of Dingqing Tablet Promotes HL-60 Apoptosis.

To clarify the effect of kaempferol on HL-60 apoptosis, we performed flow cytometry and TUNEL assays to determine whether kaempferol acted on HL-60 cell apoptosis. Flow cytometry results revealed that the 100  $\mu$ M kaempferol group substantially promoted apoptosis of HL-60 cells compared with the control group (Figures 5(a) and 5(c)). And TUNEL assays indicated that 100  $\mu$ M kaempferol remarkably elevated the percentage of TUNEL+ cells (%) compared with the control group (Figures 5(b) and 5(d)).

### 3.6. Kaempferol Dingqing Tablet Combined with AKT to Promote the AKT-Bcl2 Signaling Pathway Activation.

To explore whether kaempferol was correlated with the downstream apoptosis signaling pathway of AKT1, WB results indicated that kaempferol could increase the expression of apoptotic proteins by inhibiting P-AKT levels (Figures 6(a) and 6(b)). Meanwhile, kaempferol could markedly promote apoptosis of HL-60 detected by qPCR (Figure 6(c)). As verification of the relationship between kaempferol and AKT1 was required, we labeled kaempferol with biotin to observe whether it could bind to AKT1 or not. IP results revealed that kaempferol could combine with AKT1 (Figure 6(d)).

## 4. Discussion

AML is a malignant clonal disease originating from the hematopoietic system. The leukemia cells lose control in proliferation and develop differentiation dysfunction and apoptosis obstruction during cell cycles [35]. They can

aggregate in the bone marrow and certain hematopoietic tissues in a great number, thereby inhibiting the normal hematopoietic function of bone marrow and infiltrating multiple organs [36]. As techniques in chemotherapy, specifically targeted therapy, and bone marrow transplantation advance constantly in recent years, the treatment effect has been continuously improved [36]. The overall disease remission rate of AML patients can reach 50% to 80%. However, approximately 65% of patients remain to undergo relapse within 3 to 5 years [37]. The overall survival rate of adults is only 24% to 28% [38].

Traditional Chinese medicine presents unique benefits in antitumor and immune function regulation of the body. In recent years, Chinese medicine has been commenced gradually in clinically treating malignant hematological diseases [39]. Despite the fact that Dingqing Tablet developed by the team led by Professor Huang Zhenqiao can effectively treat leukemia, its specific mechanism has not yet been elucidated. We screened the traditional Chinese medicine monomer kaempferol and AKT interaction using network pharmacology and molecular docking and verified its downstream apoptosis signaling pathway.

First, the 38 active ingredients of Dingqing Tablet and their corresponding 615 targets were identified. A total of 92 overlapped targets of Dingqing Tablet and AML targets were obtained subsequently. Second, the constructed PPI network diagram via the String platform revealed that proteins VEGFA, STAT3, AKT1, and TNF were located in the center of the network and interacted more frequently with other factors. The results suggested that AKT1 might be a key target for the AML treatment. The drugs, ingredients, and

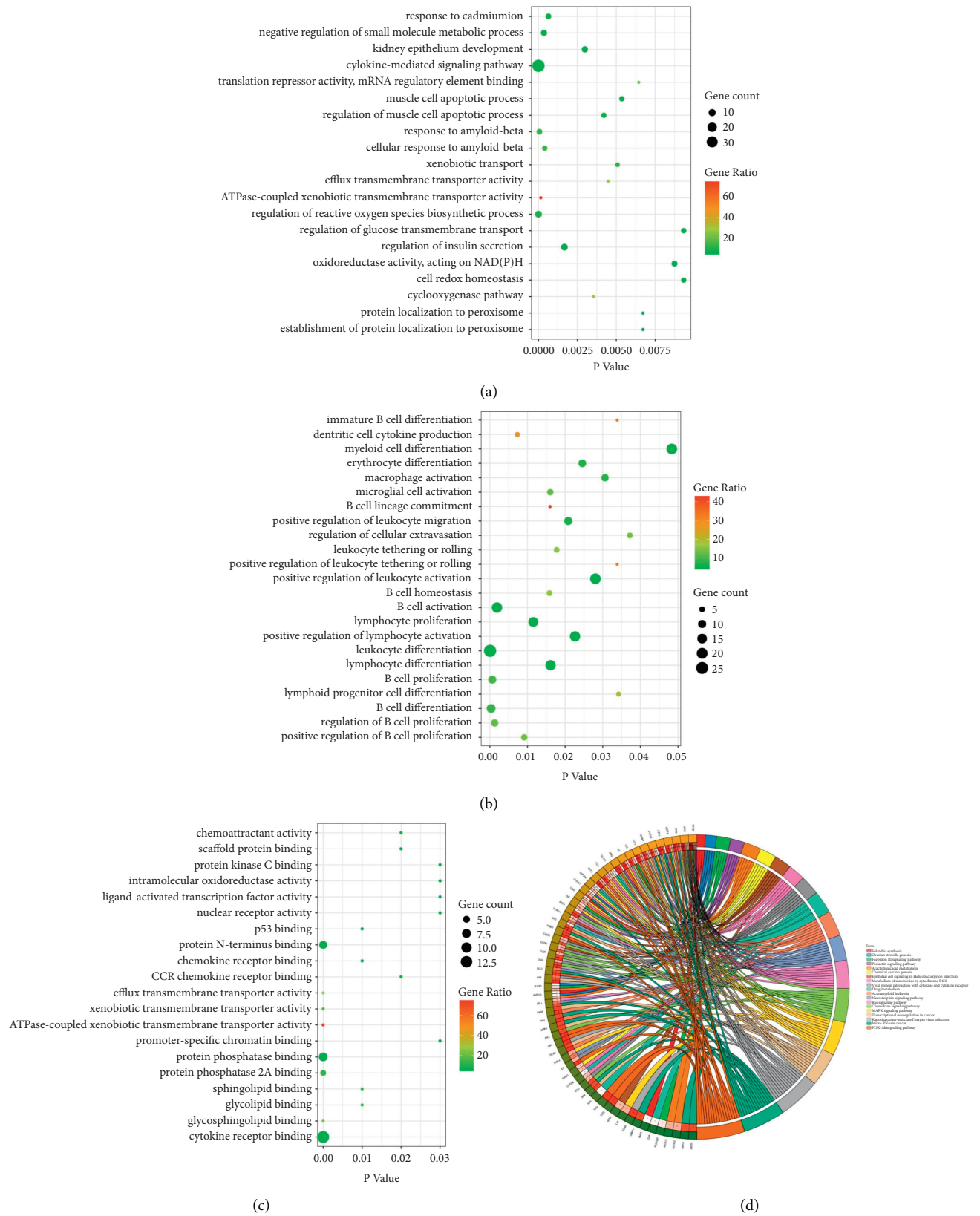


FIGURE 3: GO and KEGG pathway enrichment analysis of Dingqing Tablet in AML treatment (a, b, c) Bubble charts of biological process, immune response, the molecular function of overlapped genes using GO analysis. The Y-axis on the left represented entry names of GO analysis, and the X-axis represented  $p$  values. Big circles represented that more genes were aligned with the pathway, and darker colors represented a higher proportion of the aligned genes in the pathway. (d) Analysis results of KEGG pathway enrichment. The outermost circle on the right indicated entry names of the signaling pathways, and the left indicated genes. The inner circle on the left indicated the significance of  $p$  values of the pathways corresponding to the gene.



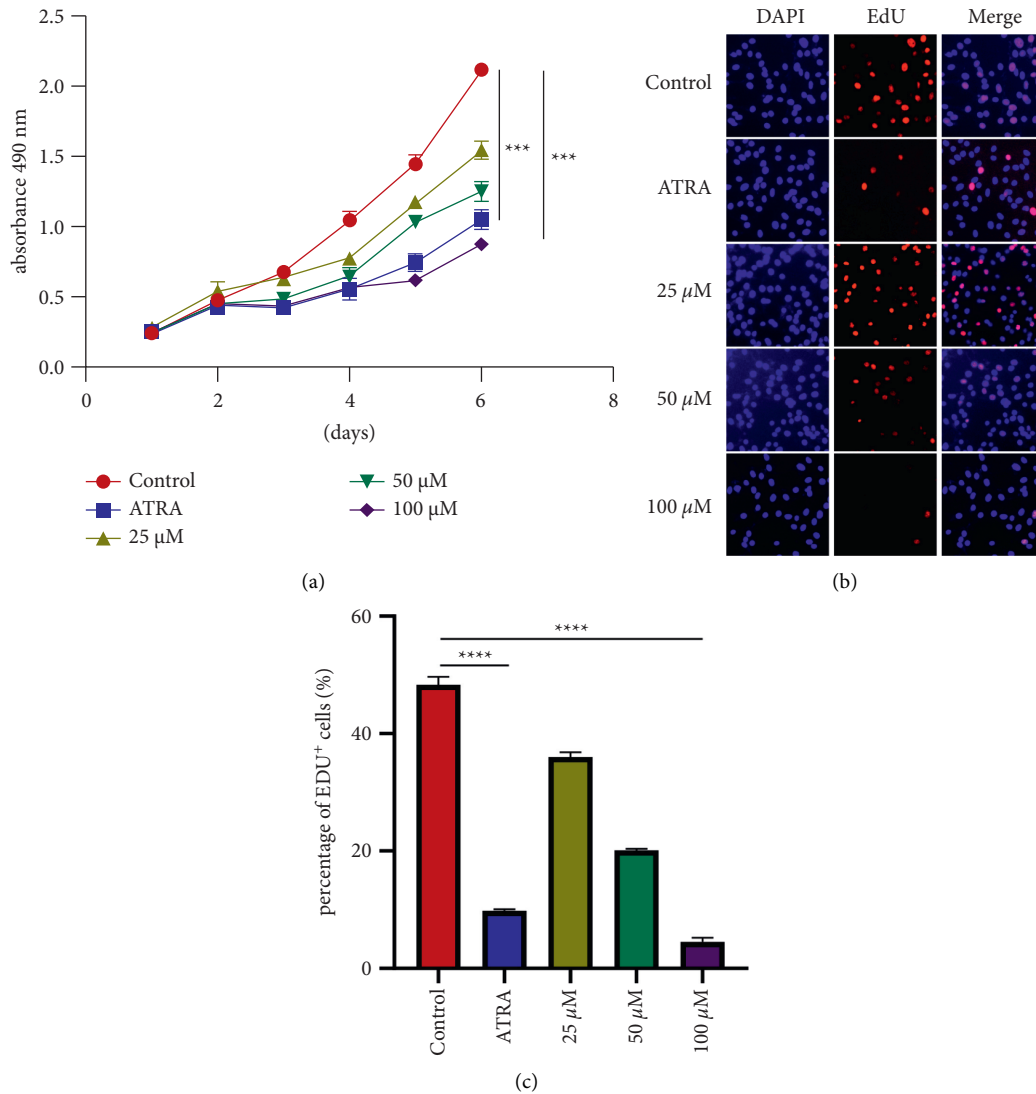


FIGURE 4: Kaempferol inhibits HL-60 cell proliferation. (a) HL-60 cell growth curves. HL-60 cells were treated with kaempferol (25  $\mu$ M, 50  $\mu$ M, and 100  $\mu$ M) and ATRA (10  $\mu$ M) for 72 h (b, c) Representative images (b) and quantification (c) were obtained via EdU incorporation assays. HL-60 cells were treated with kaempferol (25  $\mu$ M, 50  $\mu$ M, and 100  $\mu$ M) and ATRA (10  $\mu$ M) for 48 h. Data were represented as mean  $\pm$  SD ( $n \geq 3$ ). \*  $p = 0.05$ , \*\*  $p = 0.01$ , \*\*\*  $p = 0.001$ , \*\*\*\*  $p = 0.0001$  as determined using Student's  $t$ -test for pairwise comparison or one-way ANOVA, followed by Tukey's test for multiple group comparison.

targets were visualized using the Cytoscape software. We found that kaempferol, luteolin, Eolite, and quercetin had the most connections, and they might be the key ingredients of Dingqing tablet. Next, we carried out molecular docking, and the binding energies between AKT1 and the main chemical components kaempferol, isoindigo, luteolin, and quercetin were  $-5.91$ ,  $-5.16$ ,  $-5.37$ , and  $-5.45$  kcal/mol, respectively, of which kaempferol and AKT1 had the lowest binding energy. It was obvious that kaempferol was very likely to treat AML by acting on AKT1. Recently, a great number of studies have reported that kaempferol can promote tumor cell apoptosis by regulating the PI3K-AKT pathway [39–41].

Subsequently, the function of the targets of Dingqing Tablet was testified and whether the potential targets played a role in the signaling pathway was also assessed. The 92 targets

were analyzed using GO and KEGG pathway analysis with the Cytoscape ClueGO software. GO analysis results demonstrated that the collected targets might affect the negative regulation of the small molecule metabolic process and translation repressor activity in the biological process. Through analyses of cell components and molecular functions, the previously described targets might influence mRNA regulatory element binding, myeloid cell differentiation, ligand-activated transcription factor activity, and nuclear receptor activity. KEGG pathway analysis results exhibited that the 92 potential targets of Dingqing Tablet in AML treatment were mainly correlated with both PI3K-Akt and MAPK signaling pathways, of which AKT served as a core protein of the PI3K-Akt signaling pathway. We hypothesized that kaempferol in Dingqing Tablet directly acted on AKT to treat AML by regulating the PI3K-Akt signaling pathway.



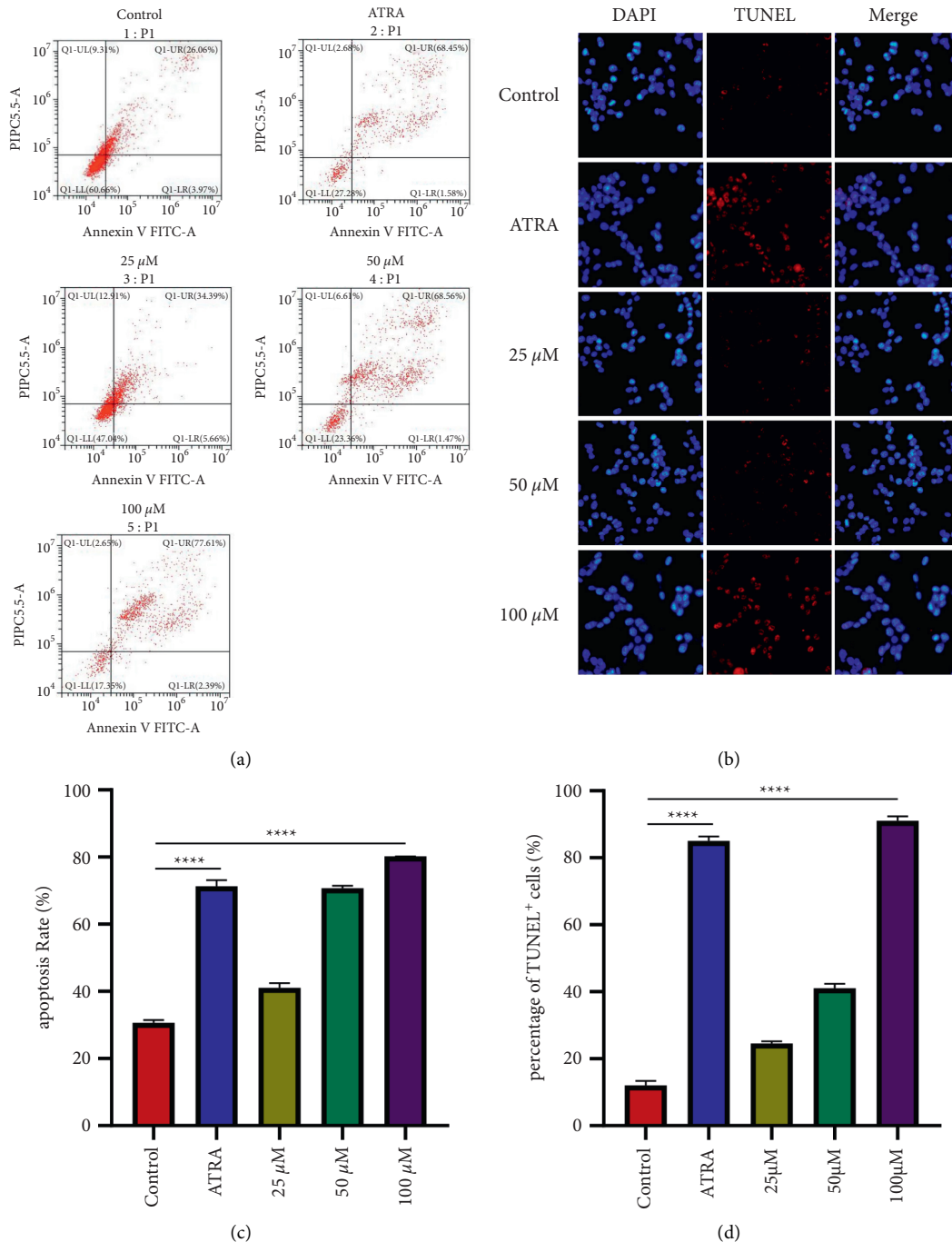


FIGURE 5: Kaempferol promotes apoptosis of HL-60 cells. (a) Flow cytometry analysis of apoptosis was performed following kaempferol treatment (25 μM, 50 μM, and 100 μM) and ATRA (10 μM). (b) TUNEL analysis of apoptosis following kaempferol treatment (25 μM, 50 μM, and 100 μM) and ATRA (10 μM). (c) Quantification of cell death detected in Figure 4(c). (d) Quantification of TUNEL+ cell in Figure 4(b). Data obtained were expressed as mean ± SD ( $n \geq 3$ ). \* $p = 0.05$ , \*\* $p = 0.01$ , \*\*\* $p = 0.001$ , \*\*\*\* $p = 0.0001$  based on Student's  $t$ -test (two groups) or one-way ANOVA and Tukey's test for more than two groups.

To clarify how the monomer of Dingqing Tablet kaempferol acted on the proliferation of HL-60, we conducted MTT experiments, which suggested that kaempferol could inhibit the proliferation of HL-60 cells. Furthermore, an EDU experiment was conducted to determine the effect of kaempferol on the proliferation ability of HL-60 cells, and consistent results were obtained. To explore the effect of

kaempferol on HL-60 apoptosis, we performed flow cytometry and TUNEL experiments, which proved that kaempferol promoted HL-60 cell apoptosis.

To verify the intrarelationship between kaempferol and core targets AKT1 and VEGFA, we employed a biotin-labeled IP technique to observe the binding of kaempferol target proteins. IP results suggested that kaempferol could

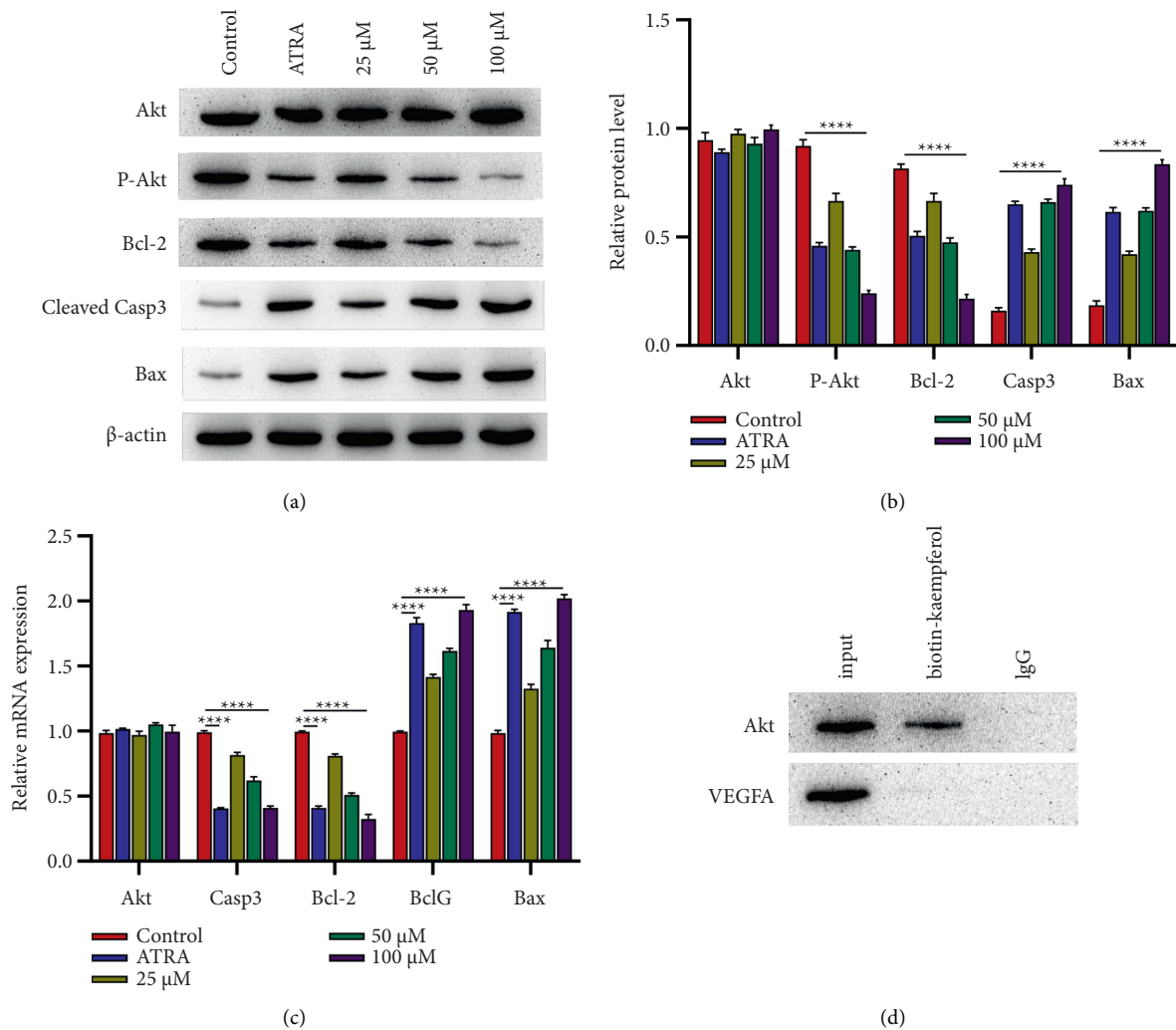


FIGURE 6: Kaempferol promotes the expression of apoptotic pathway. (a) Protein expressions of Akt, P-Akt, Bcl2, Cleaved Casp3, and Bax. HL-60 cell treatment presented as in Figure 4(a) and the protein isolation and analysis by western blotting. GAPDH expression served as an internal control. (b) TUNEL findings after kaempferol treatment (25  $\mu$ M, 50  $\mu$ M, and 100  $\mu$ M) and ATRA (10  $\mu$ M). (c) mRNA expression levels of the indicated genes were measured by qRT-PCR. (d) Coimmunoprecipitation assay shows AKT1-kaempferol interactions in HL-60 cells. Data were expressed as mean  $\pm$  SD ( $n \geq 3$ ). \*  $p = 0.05$ , \*\*  $p = 0.01$ , \*\*\*  $p = 0.001$ , \*\*\*\*  $p = 0.0001$  based on Student's  $t$ -test (two groups) or one-way ANOVA and Tukey's tests for more than two groups.

combine with AKT1. To explore whether kaempferol was linked to the AKT1 downstream apoptosis signaling pathway, WB and qPCR results demonstrated that kaempferol could elevate the expression of apoptotic proteins and reduce the expression of anti-apoptotic proteins by suppressing P-AKT levels. qPCR assays also proved that kaempferol could promote apoptosis of HL-60 cells. The previously described experiments demonstrated that kaempferol could bind to AKT1, thereby reducing the levels of P-AKT and promoting apoptosis of HL-60 cells.

Taken together, the main components and targets of Dingqing Tablet were predicted in a network pharmacological approach. Meanwhile, molecular docking was employed to determine the key components kaempferol and the core overlapped protein AKT1. The IP experiment demonstrated that kaempferol and AKT1 could interact with

each other, and further findings indicated that kaempferol reduced the levels of P-AKT and promoted apoptosis of HL-60 by binding to AKT1.

## 5. Conclusion

The monomer kaempferol of Dingqing Tablet could promote apoptosis of HL-60 cells. The mechanism of Dingqing Tablet might correlate with the combination of kaempferol and AKT1, reducing the level of P-AKT and promoting the expression of the apoptotic signaling pathway.

## Data Availability

The data used to support the research were included within this manuscript.

## Conflicts of Interest

The authors declare that they have no conflicts of interest.

## Authors' Contributions

Zheng Dandan and Zhou Yongming contributed equally to this paper.

## Acknowledgments

The research was funded by Special Project for Performance Incentive and Guidance of Scientific Research Institutions in Chongqing, grant number: jxyn2019-2-2.

## References

- [1] M. Ibáñez, E. Such, E. Onecha et al., "Analysis of SNP array abnormalities in patients with DE NOVO acute myeloid leukemia with normal karyotype," *Scientific Reports*, vol. 10, p. 5904, 2020.
- [2] K. Ahmadmehrabi, A. R. Haque, A. Aleem, E. A. Griffiths, and G. W. Roloff, "Targeted therapies for the evolving molecular landscape of acute myeloid leukemia," *Cancers*, vol. 13, no. 18, p. 4646, 2021.
- [3] Y. Yuan, Q. Wu, J. Zhao et al., "Investigation of pathogenesis and therapeutic targets of acute myeloid leukemia based on untargeted plasma metabolomics and network pharmacology approach," *Journal of Pharmaceutical and Biomedical Analysis*, vol. 195, Article ID 113824, 2021.
- [4] J. Guan, P. Liu, A. Wang, and B. Wang, "Long non-coding RNA ZEB2-AS1 affects cell proliferation and apoptosis via the miR-122-5p/PLK1 axis in acute myeloid leukemia," *International Journal of Molecular Medicine*, vol. 46, pp. 1490–1500, 2020.
- [5] X. Yang, Y. Wang, S. Pang et al., "LINC00665 promotes the progression of acute myeloid leukemia by regulating the miR-4458/DOCK1 pathway," *Scientific Reports*, vol. 11, no. 1, p. 5009, 2021.
- [6] Y. Zhang, H.-X. Chen, S.-Y. Zhou et al., "Sp1 and c-Myc modulate drug resistance of leukemia stem cells by regulating survivin expression through the ERK-MSK MAPK signaling pathway," *Molecular Cancer*, vol. 14, no. 1, p. 56, 2015.
- [7] Y. Li, X. Lv, X. Ge et al., "Mutational spectrum and associations with clinical features in patients with acute myeloid leukaemia based on next-generation sequencing," *Molecular Medicine Reports*, vol. 19, pp. 4147–4158, 2019.
- [8] D. Zheng, W. Sun, and Y. Zhou, "Impacts of dingqing tablets on the proliferation and apoptosis of HL-60 cells in human leukemia," *World Journal of Integrated Traditional and Western Medicine*, vol. 12, pp. 1037–1040, 2017.
- [9] H. Chunnian, P. Yong, F. Yuxiong, P. Bing, W. Zhe, and X. Peigen, "Quick comparison of Radix Paeonia Alba, Radix Paeonia Rubra, and Cortex Moutan by high performance liquid chromatography coupled with monolithic columns and their chemical pattern recognition," *Pharmacognosy Magazine*, vol. 8, pp. 237–243, 2012.
- [10] J. Ren, Y. Lu, Y. Qian, B. Chen, T. Wu, and G. Ji, "Recent progress regarding kaempferol for the treatment of various diseases," *Experimental and Therapeutic Medicine*, vol. 18, pp. 2759–2776, 2019.
- [11] R. I. Castro, O. Forero-Doria, L. Soto-Cerda, A. Peña-Neira, and L. Guzmán, "Protective effect of pitao ((R. & P.) molina) polyphenols against the red blood cells lipoperoxidation and the LDL oxidation," *Evidence-based Complementary and Alternative Medicine: eCAM*, vol. 2018, Article ID 1049234, 9 pages, 2018.
- [12] E. Oskoueian, N. Abdullah, and A. Oskoueian, "Effects of flavonoids on rumen fermentation activity, methane production, and microbial population," *BioMed Research International*, vol. 2013, Article ID 349129, 8 pages, 2013.
- [13] L. Li, Y. Shao, H. Zheng, and H. Niu, "Kaempferol regulates miR-15b/bcl-2/TLR4 to alleviate OGD-induced injury in H9c2 cells," *International Heart Journal*, vol. 61, no. 3, pp. 585–594, 2020.
- [14] Q. Wang, J. Luo, R. Sun, and J. Liu, "MicroRNA-1297 suppressed the Akt/GSK3 signaling pathway and stimulated neural apoptosis in an sevoflurane exposure model," *Journal of International Medical Research*, vol. 49, Article ID 300060520982104, 2021.
- [15] T. Lu, M. Zong, S. Fan, Y. Lu, S. Yu, and L. Fan, "Thioredoxin 1 is associated with the proliferation and apoptosis of rheumatoid arthritis fibroblast-like synoviocytes," *Clinical Rheumatology*, vol. 37, no. 1, pp. 117–125, 2018.
- [16] Q. Yan, H. Luo, B. Wang et al., "Correlation between PKB/Akt, GSK-3 $\beta$  expression and tubular epithelial-mesenchymal transition in renal allografts with chronic active antibody-mediated rejection," *Experimental and Therapeutic Medicine*, vol. 13, no. 5, pp. 2217–2224, 2017.
- [17] Y.-J. Kim, T. Tsang, G. R. Anderson, J. M. Posimo, and D. C. Brady, "Inhibition of BCL2 family members increases the efficacy of copper chelation in brafv600e-driven melanoma," *Cancer Research*, vol. 80, no. 7, pp. 1387–1400, 2020.
- [18] Q. Ma, X. Wang, H. Wang, W. Song, Q. Wang, and J. Wang, "HMGN5 silencing suppresses cell biological progression via AKT/MAPK pathway in human glioblastoma cells," *BioMed Research International*, vol. 2020, Article ID 8610271, 13 pages, 2020.
- [19] J. Ru, P. Li, J. Wang et al., "TCMSP: a database of systems pharmacology for drug discovery from herbal medicines," *Journal of Cheminformatics*, vol. 6, no. 1, p. 13, 2014.
- [20] A. Daina, O. Michielin, and V. Zoete, "SwissTargetPrediction: updated data and new features for efficient prediction of protein targets of small molecules," *Nucleic Acids Research*, vol. 47, no. W1, pp. W357–W364, 2019.
- [21] G. Stelzer, N. Rosen, I. Plaschkes et al., "The GeneCards suite: from gene data mining to disease genome sequence analyses," *Current Protocols in Bioinformatics*, vol. 54, p. 1, 2016.
- [22] D. Szklarczyk, A. L. Gable, D. Lyon et al., "STRING v11: protein-protein association networks with increased coverage, supporting functional discovery in genome-wide experimental datasets," *Nucleic Acids Research*, vol. 47, no. D1, pp. D607–D613, 2019.
- [23] J. Reimand, R. Isserlin, V. Voisin et al., "Pathway enrichment analysis and visualization of omics data using g:Profiler, GSEA, Cytoscape and EnrichmentMap," *Nature Protocols*, vol. 14, no. 2, pp. 482–517, 2019.
- [24] S. K. Burley, H. M. Berman, G. J. Kleywegt, J. L. Markley, H. Nakamura, and S. Velankar, "Protein data bank (PDB): the single global macromolecular structure archive," *Methods in Molecular Biology*, vol. 1607, pp. 627–641, 2017.
- [25] S. M. Rizvi, S. Shakil, and M. Haneef, "A simple click by click protocol to perform docking: AutoDock 4.2 made easy for non-bioinformaticians," *EXCLI Journal*, vol. 12, pp. 831–857, 2013.
- [26] B. H. M. Mooers and M. E. Brown, "Templates for writing PyMOL scripts," *Protein Science*, vol. 30, no. 1, pp. 262–269, 2021.

- [27] P. Kumar, A. Nagarajan, and P. D. Uchil, "Analysis of cell viability by the MTT assay," *Cold Spring Harbour Protocols*, vol. 2018, 2018.
- [28] M. H. Jokar, S. Sedighi, and M. Moradzadeh, "A comparative study of anti-leukemic effects of kaempferol and epigallocatechin-3-gallate (EGCG) on human leukemia HL-60 cells," *Avicenna Journal of Phytomedicine*, vol. 11, pp. 314–323, 2021.
- [29] X. L. Zhang, B. F. An, and G. C. Zhang, "MiR-27 alleviates myocardial cell damage induced by hypoxia/reoxygenation via targeting TGFBR1 and inhibiting NF- $\kappa$ B pathway," *The Kaohsiung Journal of Medical Sciences*, vol. 35, no. 10, pp. 607–614, 2019.
- [30] T. Ma, T. Qiao, Z. Yuan et al., "Long noncoding RNA JAKMIP2-AS1 promotes the growth of colorectal cancer and indicates poor prognosis," *OncoTargets and Therapy*, vol. 14, pp. 763–772, 2021.
- [31] J.-J. Zeng, H.-D. Wang, Z.-W. Shen, X.-D. Yao, C.-J. Wu, and T. Pan, "Curcumin inhibits proliferation of synovial cells by downregulating expression of matrix metalloproteinase-3 in osteoarthritis," *Orthopaedic Surgery*, vol. 11, no. 1, pp. 117–125, 2019.
- [32] H. Herrmann, M. Kneidinger, S. Cerny-Reiterer et al., "The Hsp32 inhibitors SMA-ZnPP and PEG-ZnPP exert major growth-inhibitory effects on D34+/CD38+ and CD34+/CD38- AML progenitor cells," *Current Cancer Drug Targets*, vol. 12, no. 1, pp. 51–63, 2012.
- [33] Y. Pang, Y. Zhao, Y. Wang et al., "TNFAIP8 promotes AML chemoresistance by activating ERK signaling pathway through interaction with Rac1," *Journal of Experimental & Clinical Cancer Research*, vol. 39, no. 1, p. 158, 2020.
- [34] W. Dorsey, P. Tchounwou, and B. Ford, "Neuregulin 1- $\beta$ eta cytoprotective role in AML 12 mouse hepatocytes exposed to pentachlorophenol," *International Journal of Environmental Research and Public Health*, vol. 3, no. 1, pp. 11–22, 2006.
- [35] J. Gao, F. Wang, P. Wu, Y. Chen, and Y. Jia, "Aberrant LncRNA expression in leukemia," *Journal of Cancer*, vol. 11, no. 14, pp. 4284–4296, 2020.
- [36] W.-T. Zhang, G.-X. Zhang, and S.-S. Gao, "The potential diagnostic accuracy of circulating MicroRNAs for leukemia: a meta-analysis," *Technology in Cancer Research & Treatment*, vol. 20, Article ID 15330338211011958, 2021.
- [37] Y. Li, M. Zhang, M. Sheng et al., "Therapeutic potential of GSK-J4, a histone demethylase KDM6B/JMJD3 inhibitor, for acute myeloid leukemia," *Journal of Cancer Research and Clinical Oncology*, vol. 144, no. 6, pp. 1065–1077, 2018.
- [38] M.-K. Song, B.-B. Park, and J.-E. Uhm, "Targeted therapeutic approach based on understanding of aberrant molecular pathways leading to leukemic proliferation in patients with acute myeloid leukemia," *International Journal of Molecular Sciences*, vol. 22, no. 11, p. 5789, 2021.
- [39] Y. Sun, G. B. Lenon, and A. W. H. Yang, "Phellodendri cortex: a phytochemical, pharmacological, and pharmacokinetic review," *Evidence-Based Complementary and Alternative Medicine: eCAM*, vol. 2019, Article ID 7621929, 45 pages, 2019.
- [40] Z. Chen, T. Lin, X. Liao et al., "Network pharmacology based research into the effect and mechanism of Yinchenhao Decoction against Cholangiocarcinoma," *Chinese Medicine*, vol. 16, no. 1, p. 13, 2021.
- [41] M. Jiang, W. Wang, J. Zhang et al., "Protective effects and possible mechanisms of actions of bushen cuyun recipe on diminished ovarian reserve induced by cyclophosphamide in rats," *Frontiers in Pharmacology*, vol. 11, p. 546, 2020.

## Research Article

# Ethnopharmacological-Based Validation of *Polyalthia suberosa* Leaf Extract in Neurological, Hyperalgesic, and Hyperactive Gut Disorders Using Animal Models

Ruhul Amin <sup>1</sup>, Cristina Quispe,<sup>2</sup> Jesús Herrera-Bravo <sup>3,4</sup>, Md. Mizanur Rahman,<sup>5</sup> Radmila Novakovic,<sup>6</sup> Sevgi Durna Daştan,<sup>7,8</sup> Atul Kabra,<sup>9</sup> and Javad Sharifi-Rad <sup>10</sup>

<sup>1</sup>Faculty of Pharmaceutical Science, Assam Down Town University, Panikhaiti, Guwahati, Assam, India

<sup>2</sup>Facultad de Ciencias de La Salud, Universidad Arturo Prat, Avda. Arturo Prat 2120, Iquique 1110939, Chile

<sup>3</sup>Departamento de Ciencias Básicas, Facultad de Ciencias, Universidad Santo Tomas, Chile

<sup>4</sup>Center of Molecular Biology and Pharmacogenetics, Scientific and Technological Bioresource Nucleus, Universidad de La Frontera, Temuco 4811230, Chile

<sup>5</sup>Pharmacy Department, Daffodil International University, Dhaka, Bangladesh

<sup>6</sup>Institute of Pharmacology, Clinical Pharmacology and Toxicology, Medical Faculty, University of Belgrade, Belgrade, Serbia

<sup>7</sup>Department of Biology, Faculty of Science, Sivas Cumhuriyet University, Sivas 58140, Turkey

<sup>8</sup>Beekeeping Development Application and Research Center, Sivas Cumhuriyet University, Sivas 58140, Turkey

<sup>9</sup>University School of Pharmaceutical Sciences, Chandigarh University, Gharuan, Mohali-140413, Punjab, India

<sup>10</sup>Facultad de Medicina, Universidad del Azuay, Cuenca, Ecuador

Correspondence should be addressed to Javad Sharifi-Rad; [javad.sharifrad@gmail.com](mailto:javad.sharifrad@gmail.com)

Received 8 November 2021; Revised 24 November 2021; Accepted 29 January 2022; Published 17 February 2022

Academic Editor: Smail Aazza

Copyright © 2022 Ruhul Amin et al. This is an open access article distributed under the Creative Commons Attribution License, which permits unrestricted use, distribution, and reproduction in any medium, provided the original work is properly cited.

*Polyalthia suberosa* (Roxb.) is a plant used to cure coughs, dysentery, fevers, joint aches, rheumatic pain, inflammation, and a variety of skin diseases. The aim of the study was to evaluate the ethyl acetate extract of *Polyalthia suberosa* (*P. suberosa*) leaves and their effects on mice for neuropharmacological, analgesic, and antidiarrheal activities. For neurological studies, the hole cross, hole board, open field, and thiopental sodium-induced sleep duration measurement methodologies were used. The castor oil-induced diarrhea inhibition test was used to assess antidiarrheal action, and the acetic acid-induced writhing inhibition test was used to determine analgesic effectiveness. The extract was given in doses of 250 and 500 mg kg<sup>-1</sup> body weight. As a standard drug, diazepam at a dosage of 3 mg kg<sup>-1</sup> was used. The extract was also given to groups, and sleep time was measured and recorded. The onset of the anxiolytic effect of the extract at both doses was found to be significant ( $p < 0.001$ ), and sleep time increased to 273 minutes. For assessing analgesic activity, the extract along with standard diclofenac was administered and found to be 55.02 percent and 64.33 percent, respectively, for the extracts, and diclofenac was found to be 67.44 percent ( $p < 0.001$ ). For antidiarrheal activity, it was compared with the standard drug, loperamide. The decrease for plant extracts was 50.07 percent and 70.06 percent at 250 mg kg<sup>-1</sup> and 500 mg kg<sup>-1</sup>, respectively, whereas it was 85.01 percent for loperamide (3 mg kg<sup>-1</sup>) ( $p < 0.00$ ). In this study, it was found that ethyl acetate extract of *Polyalthia suberosa* leaves had strong CNS depressant, analgesic, and antidiarrheal activities, which indicates that it may be used in contemporary medicine.

## 1. Introduction

Traditional medicine, like modern medicine, has exploded in popularity in Bangladesh in recent years. Traditional medicines (TM) in different forms have been utilized in our

nation as a crucial way of treating illnesses and managing various health issues since the dawn of time [1]. In the previous several years, traditional remedies have seen exponential development in recent years, and these treatments are gaining appeal on both sides of the Atlantic. Because of



their natural nature and fewer adverse effects, they are used in both developing and developed nations. There are several traditional medications available. Medicinal herbs, minerals, and organic substances are all used. The World Health Organization (WHO) has compiled a list of 21,000 plants utilized for medical reasons all around the globe [2, 3].

Sedatives and hypnotics are medicines that may relieve anxiety and provide a relaxing effect while allowing you to sleep. Currently, these medicines are widely used to treat a variety of mental problems, including anxiety and sleeplessness. Long-term use of these presently available sedative-hypnotic therapies, on the other hand, seems to have adverse effects ranging from respiratory, digestive, and immune system damage to decreased cognitive performance, physical dependence, and tolerance [4]. Numerous herbal medications have been shown to be active in the central nervous system (CNS) and may have the ability to treat chronic diseases including anxiety, depression, migraines, and epilepsy that do not respond well to conventional treatments. For many years, people in different parts of the globe have used herbal remedies to treat emotional disorders, and as a consequence, the search for new pharmacotherapy from medicinal plants has exploded in the past decade [5]. Medicinal plants are valuable treasures with a diverse range of compounds that are frequently used in conventional medicine to prevent, relieve, or cure a variety of human diseases in various parts of the world [6, 7], and about 80% of people in developing countries rely on herbal medicine to treat their illnesses [8]. There are a few medicinal plants that have neuropharmacological action and have fewer adverse effects than conventional medications. The presence of alkaloids, glycosides, and flavonoids in high concentrations in plant extracts has sedative, anxiolytic, and antiepileptic effects [9]. Analgesic effects are attributed to phenols and particular flavonoids such as normal, quercetin, and luteolin [10, 11]. Plants containing phytoconstituents such as tannins, alkaloids, saponins, flavonoids, steroids, and or terpenoids have antidiarrheal action [12]. *Polyalthia suberosa* (synonym: *Uvaria suberosa* Roxb.; family: Annonaceae) is a short, tiny tree that is extensively spread in Bangladesh, the West Indies, the Philippines, India, Sri Lanka, Malaysia, and Myanmar. Fruits are often used to prevent diarrhea. Lung issues are treated using fruits and herbs. Coughs, colds, and diarrhea are treated with the leaves. It is also utilized as an anti-HIV drug and for flatulence [13]. The bark is used as a febrifuge to prevent diarrhea and dysentery. This is an analgesic and laxative that is readily astringent. Seeds have a diuretic, sedative, and soporific action. Latex is utilized as an inexpensive filler for dental cavities in the tropics [14, 15]. The goal of this research was to see whether the ethyl acetate extract of *Polyalthia suberosa* leaves had any neuropharmacological, analgesic, or antidiarrheal properties.

## 2. Materials and Methods

**2.1. Plant Collection and Extraction.** During the month of December 2018, the leaves of *Polyalthia suberosa* were completely collected by us from Sundarban, Bangladesh. The sample was identified by Sr. Scientist Mahabuba Sultana at Bangladesh's National Herbarium in Mirpur, Dhaka. A voucher

specimen (DACB: 46476) was submitted for future reference. The plant's leaves were gathered and cleaned in freshwater before being chopped into tiny pieces and shred-dried for up to ten days. Capacitor start motor, China dish, crushed the dried leaves into a fine powder. Cold extraction of 560 g of powder in 900 ml of 90% methanol in a clean and sealed glass jar for fourteen days at room temperature with periodic shaking and stirring yielded the crude extract. The whole combination was then coarsely filtered using a piece of clean, white cotton material, followed by filter paper. The extract was concentrated first in a rotary evaporator at low pressure and then in the open air. It was discovered that the yield was 5.5 percent w/w. In all the studies, freshly produced extracts were utilized.

**2.2. Phytochemical Screening.** Using conventional chemical assays, several phytochemical groups such as alkaloids, glycosides, flavonoids, tannins, gums, saponins, and steroids have been recognized by distinctive color change. The presence of carbohydrates was determined using the Mulish and Fehling tests [16, 17]. Proteins were detected using the Biuret test. The presence of phytochemical analysis in plant extracts and ethanolic aqueous solutions was determined using the following conventional procedures [18–21].

**2.2.1. Test for Tannins.** The 0.5 g extract was mixed with 10 ml of bromine water. The presence of tannins was shown by the decolorization of bromine water.

**2.2.2. Test for Saponins.** In a test tube, 5.0 mL of distilled water was combined with an aqueous crude plant extract and aggressively stirred. The foam was combined with a few drops of olive oil and violently agitated, revealing the presence of saponins in the foam.

**2.2.3. Tests for Flavonoids**

(1) *Shinoda Test.* Magnesium ribbons and concentrated HCl were combined with aqueous crude plant extract, and the pink hue indicated flavonoid content.

(2) *Alkaline Reagent Test.* We combined 2 ml of 2.0 percent NaOH with aqueous plant crude extract and obtained an intense yellow tint, which became colorless when we added 2 drops of diluted acid to the mixture. Flavonoids were found in this sample.

**2.2.4. Tests for Glycosides**

(1) *Liebermann's Test.* We mixed aqueous plant crude extract with 2.0 mL of acetic acid and 2 mL of chloroform. After cooling the liquid, we added concentrated H<sub>2</sub>SO<sub>4</sub>. The entity of an aglycone, the steroidal portion of glycosides, was shown in green.

(2) *Keller–Kiliani Test.* A 4.0 mL solution of glacial acetic acid was combined with 10 mL of aqueous plant extract and 1 mL of concentrated H<sub>2</sub>SO<sub>4</sub> to make a Keller–Kiliani

combination. Between the layers, a brown ring developed, indicating the presence of cardiac steroidal glycosides.

(3) *Salkowski's Test*. To the aqueous plant crude extract, we added 2 mL of concentrated  $\text{H}_2\text{SO}_4$ . The presence of the steroidal aglycone portion of the glycoside resulted in a reddish-brown tint.

2.2.5. *Test for Terpenoids*. The 5 ml of aqueous plant extract was mixed with 2.0 ml of chloroform and evaporated on the water route before being heated with 3 ml of concentrated  $\text{H}_2\text{SO}_4$ . The entity of terpenoids appeared as a grayish color.

2.2.6. *Test for Steroids*. To the 5 ml of aqueous plant crude extract, 2 ml of chloroform and concentrated  $\text{H}_2\text{SO}_4$  were added. A red hue occurred in the bottom chloroform layer, indicating the presence of steroids.

2.3. *Experimental Animals*. This study utilized Swiss albino mice that were 4-5 weeks old and weighed 25–28 g on average. The mice were procured from the Pharmacology Lab, Pharmacy Department of Jahangirnagar University. The mice were maintained in a regular setting for 10 days and were given a standard pellet diet and free access to water. The study protocol was authorized by Daffodil International University's Institutional Animal Ethics Committee in

Dhaka, Bangladesh (Ref. FAHSREC/DIU/2019/1005, dated December 6, 2019).

#### 2.4. Evaluation of Neuropharmacological Activity

2.4.1. *Thiopental Sodium-Induced Sleeping Time*. The test was carried out according to the instructions [22]. Negative control groups, positive control groups, and test groups were used to split the mice into four groups (I and II). In four cages, each group of six mice was maintained separately. The mice in the negative control group were given 10 ml  $\text{kg}^{-1}$  body weight of 1 percent (v/v) Tween-80 orally in distilled water. The mice in the positive control group were given 3 mg  $\text{kg}^{-1}$  body weight of the conventional medication diazepam. Mice in research groups I and II were given crude extract at dosages of 250 and 500 mg  $\text{kg}^{-1}$  body weight, respectively. With the use of a needle, all dosages were given orally. After 30 minutes, all sleep-inducing groups received thiopental sodium (40 mg  $\text{kg}^{-1}$ ) intraperitoneally. All the animals began to sleep at the same time. The mice were placed in the inverted posture after being put to sleep, and after the sedation was finished, the mice returned to normal, and the time was recorded. The hypnotic effect index was calculated as the time between the loss and recovery of the righting reflex. Latency was defined as the period between the thiopental sodium injection and the onset of sleep. The following formula was used to determine the percentage of effect:

$$\text{effect (\%)} = \frac{\text{average duration of loss of righting reflex in the test group}}{\text{average duration of loss of righting reflex in the control group}} \times 100. \quad (1)$$

2.4.2. *Open Field Test*. In this study, 24 mice were chosen at random and split into four groups: negative control, positive control, and test groups (I and II). The negative control group received just 1% (v/v) Tween-80 at a dosage of 10 ml  $\text{kg}^{-1}$  body weight, whereas the positive group received the standard medication, diazepam, as an oral solution at a dose of 3 mg  $\text{kg}^{-1}$  body weight. The research groups (I and II) were given oral doses of 250 mg  $\text{kg}^{-1}$  and 500 mg  $\text{kg}^{-1}$  body weight of plant extract solution. Orally, both dosages were given with the help of sterile feeding. The animals were placed separately in one of the corners of square grids (100 cm  $\times$  100 cm  $\times$  40 cm) after being diagnosed. The number of squares traversed by the mice was tracked for 3 minutes at 0, 30, 60, 90, and 120 minutes throughout the observation period. The experiment was conducted in a completely quiet setting [23].

2.4.3. *Hole Board Test*. The mice were split into four groups, each with six mice weighing 25–28 g. Group I received 1 percent Tween-80, Group II received diazepam at a dosage of 3 mg  $\text{kg}^{-1}$  body weight, and Groups III and IV received 250 mg  $\text{kg}^{-1}$  and 500 mg  $\text{kg}^{-1}$  body weight, respectively, of ethyl acetate extract of *Polyalthia suberosa* (leaves). Mice

were placed near the screen's edge at the start of the experiment. For the whole observation period, the number of head dips in the holes for a period of 3 minutes was tallied at 0, 30, 60, 90, and 120 minutes. The experiment was carried out in a sound-proofed room [24].

2.4.4. *Hole Cross Test*. Following their respective care of the community, the mice were separately placed in the cage's darker chamber, divided by a wall with a hole in the dark and white chambers. At 0, 30, 60, 90, and 120 minutes, the total number of crossings from one chamber to the other by the mice of each group was tallied. The experiment was carried out in a sound-proofed room [25, 26].

#### 2.5. Evaluation of Analgesic Activity

2.5.1. *Acetic Acid-Induced Writhing Test*. For the analgesic test, the mice were split into four groups. Each group consists of six mice. The first group is for distilled water and is a controlled group. Group 2 was the control group, which received diclofenac sodium BP (10 mg  $\text{kg}^{-1}$ ). Alcoholic extract (250 mg  $\text{kg}^{-1}$  and 500 mg  $\text{kg}^{-1}$ ) was given to groups 3 and 4. After 45 minutes, each mouse was given a 10 ml  $\text{kg}^{-1}$

body weight injection of 0.7 percent acetic acid. After 15 minutes of IP administration of acetic acid, the number of writhing responses for each animal was recorded for 3

minutes, and the mean abdominal writhes for each group were calculated [27]. The percentage inhibition was calculated using the following formula:

$$\text{inhibition (\%)} = \frac{\text{mean number of writhes (control)} - \text{mean number of writhes (drugs)}}{\text{mean number of writhes (control)}} \quad (2)$$

## 2.6. Evaluation of Antidiarrheal Activity

**2.6.1. Castor Oil-Induced Diarrheal Test.** All animals were checked for diarrhea before the experiment by giving them 0.5 ml of castor oil orally, and the animals that started having diarrhea were chosen for the test. Following the screening, twenty-six mice were chosen and split into four groups, each with six mice. Prior to the trial, mice were fasted for 18 hours with free access to water. Group 1 received distilled water (10 ml kg<sup>-1</sup> body weight) as a control, whereas Group 2 received a standard treatment (loperamide 3 mg kg<sup>-1</sup> body weight). The extract was administered in different dosages to groups 3 and 4 (250 mg kg<sup>-1</sup> and 500 mg kg<sup>-1</sup>, respectively). Both mice were given 0.5 mL of castor oil orally 30 minutes after the treatment to initiate diarrhea and were placed in cages on blotting paper. The paper may be changed at any time. For each group of animals, the quantity of diarrheal feces was recorded and the percentage of defecation inhibition was computed throughout the 4 h observation period [28, 29].

**2.7. Data Analysis.** The results are presented as an average SEM. One-way variance analysis (ANOVA) was used in the statistical analysis, which was followed by Dunnett's post hoc test, a sleep time test, and a hole board test. Two-way ANOVA was used for the hole cross test and open field test, followed by Bonferroni's post hoc testing. The statistical analysis was carried out with the help of Microsoft Excel 2007 software.

## 3. Results

**3.1. Phytochemical Screening.** The presence of reducing tannin, alkaloid, glycoside, steroid, flavonoid, phenol, carbohydrate, and terpenoid, as well as the lack of saponins, was found in the crude ethyl acetate extract of *Polyalthia suberosa* (leaves) in a chemical community (Table 1).

### 3.2. Evaluation of Neuropharmacological Activity

**3.2.1. Thiopental Sodium-Induced Sleeping Time.** When we gave *Polyalthia suberosa* leaf extract at 250 mg kg<sup>-1</sup> and 500 mg kg<sup>-1</sup> dosages to thiopental sodium patients, their sleeping duration was altered. In comparison with the control group, the behavior of extracts shows that it lowers latent duration and boosts or prolongs the sleeping time (Table 2).

**3.2.2. Open Field Test.** Although the impact of diazepam was greater compared to the results of crude extracts, the crude extracts exhibited a statistically significant decrease in mouse movements when compared to placebo. At each measured dosage of 250, 500, and 1000 mg kg<sup>-1</sup>, decreased activity was seen at the second observation and lasted until the fourth observation (Table 3).

**3.2.3. Hole Cross Test.** Although the impact of diazepam was strong compared to the crude extract testing, the crude extracts demonstrated a statistically significant decrease in locomotor activity in mice at any dosage tested (250 and 500 mg kg<sup>-1</sup>). The 2nd persistent observation to the 4th observation revealed a decrease in locomotor operation (Table 4 and Figure 1).

**3.2.4. Hole Board Test.** Although the impact of diazepam was strong compared to the findings of the crude extracts, the crude extracts at each dosage exhibited a significant decrease in the frequency of head dips relative to the placebo in the hole board check. The effect started on the experiment's second observation and continued until the fourth observation (Table 5 and Figure 2).

### 3.3. Evaluation of Analgesic Activity

**3.3.1. Acetic Acid-Induced Writhing Test.** At oral dosages of 250 and 500 mg kg<sup>-1</sup> body weights of mice, the crude extract inhibited writhing by 55.02 percent and 64.33 percent, respectively. The conventional medication diclofenac sodium, on the other hand, showed a 67.44 percent inhibition at a dose of 10 mg kg<sup>-1</sup> body weight (Table 6).

### 3.4. Evaluation of Antidiarrheal Activity

**3.4.1. Castor Oil-Induced Test.** The extract had a significant antidiarrheal effect in mice in a castor oil-induced diarrhea test. When compared to the untreated control group, the extract significantly reduced the incidence of defecation ( $p < 0.001$ ) and dose lowered the total quantity of diarrheal feces. At 250 and 500 mg kg<sup>-1</sup> dosages of the extract, the percentage inhibition of diarrhea was 50.07 percent and 70.06 percent, respectively. The percentage suppression of diarrhea by loperamide HCl (3 mg kg<sup>-1</sup>) was 85.01 percent ( $p < 0.001$ , vs control) (Table 7 and Figure 3).

TABLE 1: Phytochemical test results of extract of *Pterocarpus indicus*.

Tested groups	Ethyl acetate extract of <i>P. suberosa</i> (leaves)
Tannins	+
Alkaloids	+
Glycosides	+
Saponins	-
Steroids	+
Flavonoids	+
Phenol	+
Carbohydrate	+
Terpenoid	+

TABLE 2: Effect of *Polyalthia suberosa* on thiopental sodium-induced sleeping time in mice (mean  $\pm$  SEM,  $n = 6$ ).

Group	Dose	Latent period	Sleeping time	% effect
Control (1% v/v Tween-80: water)	10 ml kg <sup>-1</sup>	87.33 $\pm$ 1.45	136.67 $\pm$ 9.53	0.0
Standard (diazepam)	3 mg kg <sup>-1</sup>	2.6 $\pm$ 0.88	337.8 $\pm$ 14.19***	96.94
PS-250	250 mg kg <sup>-1</sup>	40 $\pm$ 7.21***	251.67 $\pm$ 6.57***	51.53
PS-500	500 mg kg <sup>-1</sup>	50.66 $\pm$ 3.84***	273 $\pm$ 8.76***	41.01

\*indicates  $p < 0.05$ , \*\*indicates  $p < 0.01$ , and \*\*\*indicates  $p < 0.001$  when compared with control.

TABLE 3: Effect of *Polyalthia suberosa* on the open field test in mice (mean  $\pm$  SEM,  $n = 6$ ).

Group	Dose	Number of movements (% of movement inhibition)				
		0 min	30 min	60 min	90 min	120 min
Control	10 ml kg <sup>-1</sup>	26.5 $\pm$ 0.64	27.75 $\pm$ 0.47	28.0 $\pm$ 0.63	27.5 $\pm$ 0.65	27.5 $\pm$ 0.64
Standard	3 mg kg <sup>-1</sup>	20.5 $\pm$ 0.28***	13.0 $\pm$ 0.41***	10.5 $\pm$ 0.65***	9.25 $\pm$ 0.48***	8.25 $\pm$ 0.48***
PS-250	250 mg kg <sup>-1</sup>	24.0 $\pm$ 0.40**	18.25 $\pm$ 0.47***	16.5 $\pm$ 0.64***	15.55 $\pm$ 0.64***	15.73 $\pm$ 0.85***
PS-500	500 mg kg <sup>-1</sup>	23.25 $\pm$ 0.48**	16.0 $\pm$ 0.41***	13.5 $\pm$ 0.65***	13.25 $\pm$ 0.48***	13.5 $\pm$ 0.64***

\*indicates  $p < 0.05$ , \*\*indicates  $p < 0.01$ , and \*\*\*indicates  $p < 0.001$  when compared with control.

TABLE 4: Effect of *Polyalthia suberosa* on the hole cross test in mice (mean  $\pm$  SEM,  $n = 6$ ).

Group	Dose	Number of head dips				
		0 min	30 min	60 min	90 min	120 min
Control	10 ml kg <sup>-1</sup>	5 $\pm$ 0.70	6.2 $\pm$ 0.37	6.2 $\pm$ 0.48	6.6 $\pm$ 0.40	8.6 $\pm$ 0.24
Standard	3 mg kg <sup>-1</sup>	1.6 $\pm$ 0.51	1.2 $\pm$ 0.37*	1.6 $\pm$ 0.40**	1.2 $\pm$ 0.58**	0.2 $\pm$ 0.20**
PS-250	250 mg kg <sup>-1</sup>	0.0 $\pm$ 0.0	3.25 $\pm$ 1.65	3.75 $\pm$ 1.44*	2.5 $\pm$ 1.32	2.0 $\pm$ 1.23**
PS-500	500 mg kg <sup>-1</sup>	0.0 $\pm$ 0.0	0.25 $\pm$ 0.25*	0.75 $\pm$ 0.48**	2.25 $\pm$ 1.31	2.25 $\pm$ 1.31**

\*indicates  $p < 0.05$ , \*\* indicates  $p < 0.01$ , and \*\*\* indicates  $p < 0.001$  when compared with control.

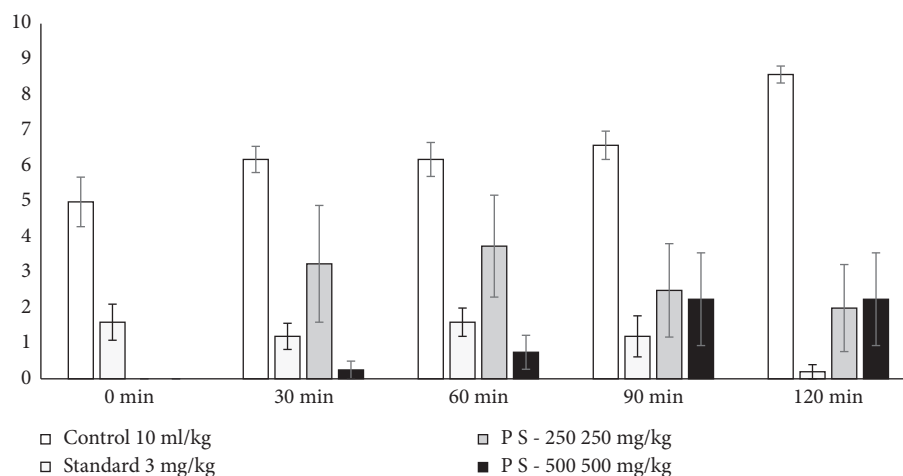
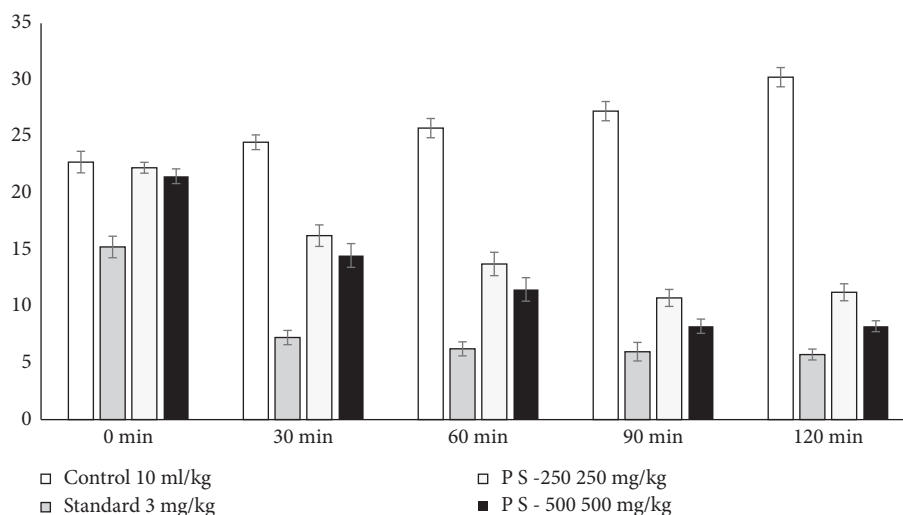
FIGURE 1: *Polyalthia suberosa* on the hole cross test in mice.

TABLE 5: Effect of *Polyalthia suberosa* on the hole board test in mice (mean  $\pm$  SEM,  $n = 6$ ).

Group	Dose	Number of movements (% of movement inhibition)				
		0 min	30 min	60 min	90 min	120 min
Control	10 ml kg <sup>-1</sup>	22.75 $\pm$ 0.95	24.5 $\pm$ 0.65	25.75 $\pm$ 0.85	27.25 $\pm$ 0.85	30.25 $\pm$ 0.85
Standard	3 mg kg <sup>-1</sup>	15.25 $\pm$ 0.95***	7.25 $\pm$ 0.63***	6.25 $\pm$ 0.62***	6 $\pm$ 0.82***	5.75 $\pm$ 0.48***
PS-250	250 mg kg <sup>-1</sup>	22.25 $\pm$ 0.48	16.25 $\pm$ 0.95***	13.75 $\pm$ 1.03***	10.75 $\pm$ 0.75***	11.25 $\pm$ 0.75***
PS-500	500 mg kg <sup>-1</sup>	21.5 $\pm$ 0.65	14.5 $\pm$ 1.05***	11.5 $\pm$ 1.04***	8.25 $\pm$ 0.63***	8.25 $\pm$ 0.48***

\*indicates  $p < 0.05$ , \*\*indicates  $p < 0.01$ , and \*\*\*indicates  $p < 0.001$  when compared with control.

FIGURE 2: *Polyalthia suberosa* on the hole board test in mice.TABLE 6: Analgesic activity of *Polyalthia suberosa* on acetic acid-induced writhing in mice (mean  $\pm$  SEM,  $n = 6$ ).

Treatment	Dose	Number of writhing (mean $\pm$ SEM)	% inhibition
Control (distilled water)	10 ml kg <sup>-1</sup>	21.50 $\pm$ 2.92	00
Standard (diclofenac sodium)	10 mg kg <sup>-1</sup>	7.0 $\pm$ 0.52***	67.44%
PS-250	250 mg kg <sup>-1</sup>	9.67 $\pm$ 1.38***	55.02%
PS-500	500 mg kg <sup>-1</sup>	7.67 $\pm$ 0.72***	64.33%

\*indicates  $p < 0.05$ , \*\*indicates  $p < 0.01$ , and \*\*\*indicates  $p < 0.001$  when compared with control.

TABLE 7: Effect of *Polyalthia suberosa* in the castor oil-induced diarrheal test.

Group	Dose	Total number of feces (mean $\pm$ SEM)	% inhibition of defecation	Total number of diarrhoeal feces (mean $\pm$ SEM)	% inhibition of diarrhea
Control	10 ml kg <sup>-1</sup>	9.67 $\pm$ 0.88	00	6.67 $\pm$ 0.67	00
Standard (loperamide)	3 mg kg <sup>-1</sup>	2.33 $\pm$ 0.33	76	1 $\pm$ 0.0***	85.01
PS-250 mg	250 mg kg <sup>-1</sup>	5.33 $\pm$ 0.88	44.89	3.33 $\pm$ 0.89***	50.07
PS-500 mg	500 mg kg <sup>-1</sup>	4 $\pm$ 0.58	58.64	2 $\pm$ 0.58***	70.06

\*indicates  $p < 0.05$ , \*\*indicates  $p < 0.01$ , and \*\*\*indicates  $p < 0.001$  when compared with control.

#### 4. Discussion

Phytochemical analysis revealed the presence of alkaloids, tannins, terpenoids, flavonoids, phenols, and steroids in *Polyalthia suberosa* extracts in the current study. The existence of these phytochemical substances has been linked to *Polyalthia suberosa*'s biological activity. The effects of secondary bioactive metabolites of *Polyalthia suberosa* on neuropharmacology, analgesia, and antidiarrhea were investigated in this study. Vivo hypnosis, open field, hole

board, and hole cross methods all provide neuropharmacological impact. Beyond basic movement, the open field test assesses a variety of aspects of behavior [30, 31].

The open board test (HBT) is a scientific research method for measuring anxiety, tension, and emotion in animals [32]. It is possible to measure a wide range of processes because of its measurement capabilities. It is a common test in pharmacology, but the results are not always obvious. External symptoms were estimated through hole cross checks to complete the approval of anxiousness. Some



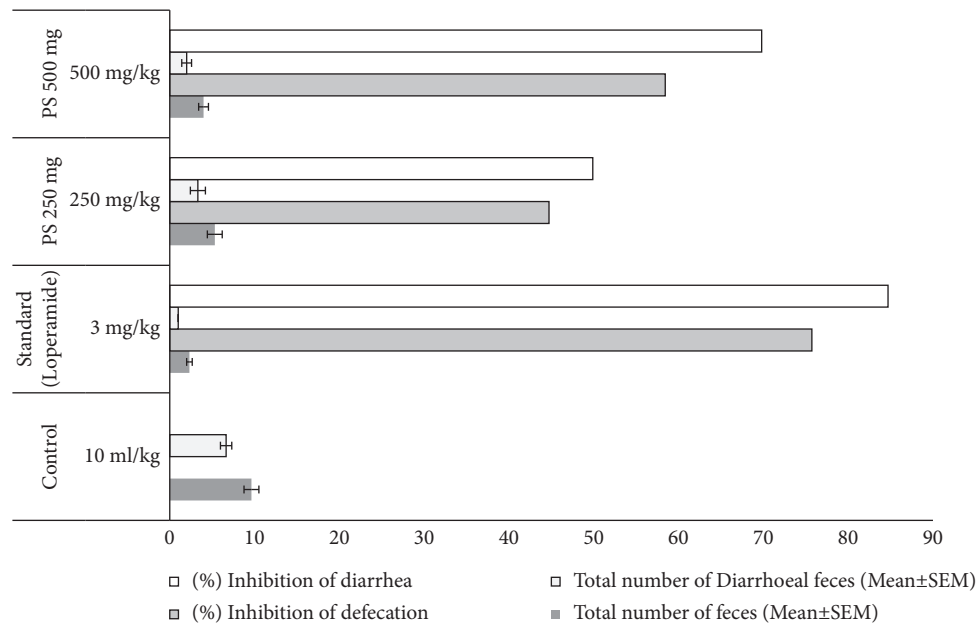


FIGURE 3: Neuropharmacological, analgesic, and antidiarrheal activity of *Polyalthia suberosa* leaf extract in Swiss albino mice.

studies have found that plant extracts rich in alkaloids, glycosides, and flavonoids have sedative, anxiolytic, and antiepileptic properties that interfere with their properties at the benzodiazepine site of the GABAergic complex structure or are immediate or aberrant modulators that are responsible for increases in GABA activity in the brain that cause drowsiness and facies [33, 34]. It seems that the phytochemicals included in the extract of *Polyalthia suberosa* leaves contribute to the relaxing and sleep-inducing actions on the CNS, at least to a limited degree. We started our investigation to see how the effect of *Polyalthia suberosa*'s CNS wretchedness differs from the uncontrolled locomotory behavior of mice in hole cross and open field experiments. The oral organization of the test removal at dosages of 250 and 500 mg kg<sup>-1</sup> resulted in a substantial decrease in the number of holes traversed and sleepiness to a new condition, which was reversed when the CNS stimulating agent was used. Each of the parts that were tested got a motion critique. Another big impact was created, and this one was much worse than the hole board test. By examining the exploratory behaviors of rats, this test is established as a method of evaluating the potential anxiolytic and narcotic effects of any operator. The behavior of animals plummeting their heads is definitely linked to their mental tension [35]. According to this view, the declaration of anxiolytic condition in animals may be represented by an increase in head-plunging behavior [36], while a decrease in head-plunging was regarded as related to the depressive effect [37, 38].

The acetic acid-induced writhing procedure was used to evaluate the extract's analgesic effectiveness. Acetic acid raised the levels of local endogenous chemicals such as PGE<sub>2</sub>, PGF<sub>2</sub>, lipoxygenase products, acetylcholine, and histamine, which are responsible for pain sensation in the peritoneal fluids [39–41]. As the concentration of the extract was raised, the inhibition of writhing in mice grew, and the former acquired a remarkable inhibition of writhing similar

to normal diclofenac sodium (Table 6). Analgesic action is known to be mediated by a variety of flavonoids, alkaloids, and steroids [42]. The phytochemical community of leaf extract research has revealed several important phytochemicals, such as alkaloids, tannins, and flavonoids. These polyphenolic chemicals are thought to be responsible for the leaf extract's analgesic action.

Diarrhea is described as irregular defecation with a poor consistency of feces, which may be caused by a disturbance in water and electrolyte transport in the intestines. The active metabolite of castor oil, ricinoleic acid, stimulates the release of endogenous prostaglandins and peristaltic activity in the small intestine, resulting in alterations in the intestinal mucosa's electrolyte permeability [43, 44]. The crude ethyl acetate extract of *Polyalthia suberosa* (leaves) showed a statistically significant decrease in the incidence and frequency of diarrhea in experimental animals, according to our findings. In the castor oil-induced diarrhea research in mice, the *Polyalthia suberosa* extract exhibited a significant antidiarrheal effect at both dosages.

## 5. Conclusion

The results of this research show that *Polyalthia suberosa* leaf extract possesses outstanding antidepressant, analgesic, and antidiarrheal properties. In mice, the extract depresses the CNS and possesses numerous sedative and anticonvulsant properties. Finally, the results of this study provide evidence for the plant's potential application in ethnomedicine while also providing early data on the plant's core behavior. Consequently, these findings offer fresh information on plant development, which may lead to the identification of medicines derived from natural sources. To isolate the bioactive chemicals and explain the precise processes responsible for the pharmacological actions found in this plant, further chemical and pharmacological research is needed.

## Data Availability

The data used to support the findings of this study are available from the corresponding author upon request.

## Conflicts of Interest

The authors declare that they have no conflicts of interest.

## References

- [1] Z. Labu, K. Jahan, and F. J. B. J. O.D. D. Rahman, "Therapeutics. Current official status of traditional medicine and their used as in chronic diseases," *Evidence-Based Complementary and Alternative Medicine*, vol. 1, pp. 93–104, 2013.
- [2] X. Zhang and W. H. Organization, "Traditional medicine strategy 2002 2005," 2002.
- [3] World Health Organization, *WHO Global Report on Traditional and Complementary Medicine 2019*, World Health Organization, Geneva, Switzerland, 2019.
- [4] M. Moniruzzaman, A. Rahman, A. J. E.-B. C. Ferdous, and A. Medicine, "Evaluation of sedative and hypnotic activity of ethanolic extract of *Scoparia dulcis* Linn," *Evidence-Based Complementary and Alternative Medicine*, vol. 2015, Article ID 873954, 6 pages, 2015.
- [5] S. A. Mirshafa, M. Azadbakht, and N. Ahangar, "Study of antidepressant and sedative-hypnotic activity of hydro-alcoholic extract of *Asperugo procumbens* L. aerial parts in mice," *Iranian Journal of Pharmaceutical Research: Iranian Journal of Pharmaceutical Research*, vol. 12, pp. 529–35, 2013.
- [6] P. Sheng-Ji, "Ethnobotanical approaches of traditional medicine studies: some experiences from Asia," *Pharmaceutical Biology*, vol. 39, no. 1, pp. 74–79, 2001.
- [7] E. A. Palombo and T. E. O. N. P. Derivatives, "Phytochemicals from traditional medicinal plants used in the treatment of diarrhoea: modes of action and effects on intestinal function," *Phytotherapy Research*, vol. 20, no. 9, pp. 717–724, 2006.
- [8] K. Pathak and R. J. J. I. J. O. H. M. Das, "Herbal medicine-a rational approach in health care system," *Pharmaceutical Biology*, vol. 1, pp. 86–89, 2013.
- [9] R. Awad, F. Ahmed, N. Bourbonnais-Spear et al., "Ethnopharmacology of Q'eqchi' Maya antiepileptic and anxiolytic plants: effects on the GABAergic system," *Journal of Ethnopharmacology*, vol. 125, no. 2, pp. 257–264, 2009.
- [10] R. Arslan, N. Bektas, and Y. Ozturk, "Antinociceptive activity of methanol extract of fruits of *Capparis ovata* in mice," *Journal of Ethnopharmacology*, vol. 131, no. 1, pp. 28–32, 2010.
- [11] D. Deliorman Orhan, A. Hartevioğlu, E. Küpeli, and E. Yesilada, "In vivo anti-inflammatory and antinociceptive activity of the crude extract and fractions from *Rosa canina* L. fruits," *Journal of Ethnopharmacology*, vol. 112, no. 2, pp. 394–400, 2007.
- [12] S. Umer, A. Tekewe, N. Kebede, and a. medicine, "Anti-diarrhoeal and antimicrobial activity of *Calpurnia aurea* leaf extract," *BMC Complementary and Alternative Medicine*, vol. 13, pp. 21–25, 2013.
- [13] Z. J. J. O.B. Labu and P. Research, "Phytochemical screening and in vitro study of antioxidant, anti-diarrhoeal and analgesic activities of Hydromethanol extracts," *Evidence-Based Complementary and Alternative Medicine*, vol. 2, pp. 52–63, 2013.
- [14] P. Tuchinda, M. Pohmakotr, B. Munyoo, V. Reutrakul, and T. Santisuk, "An azaanthracene alkaloid from *Polyalthia suberosa*," *Phytochemistry*, vol. 53, no. 8, pp. 1079–1082, 2000.
- [15] N. Yasmen, M. Aziz, A. Tajmim et al., "Analgesic and anti-inflammatory activities of diethyl ether and n-hexane extract of *polyalthia suberosa* leaves," *Evidence-Based Complementary and Alternative Medicine*, vol. 2018, Article ID 5617234, 8 pages, 2018.
- [16] J. H. Foulger, "The use of the molisch ( $\alpha$ -NAPHTHOL) reactions in the study of sugars in biological fluids," *Journal of Biological Chemistry*, vol. 92, no. 2, pp. 345–353, 1931.
- [17] H. Fehling, "Die quantitative Bestimmung von Zucker und Stärkmehl mittelst Kupfervitriol," *Annalen der Chemie und Pharmacie*, vol. 72, no. 1, pp. 106–113, 1849.
- [18] A. Ghani, "Medicinal Plants of Bangladesh: Chemical Constituents and Uses," Asiatic society of Bangladesh, Dhaka, Bangladesh, 1998.
- [19] T. Subedi, "A study on the medicinal chemistry of curcuma longa," *Himalayan Biodiversity*, vol. 23, pp. 39–46, 2019.
- [20] H. Kiliani, "Ueber den Nachweis der digitalis-glycoside und ihrer spaltungsprodukte durch eisenhaltige schwefelsäure," *Archiv der Pharmazie*, vol. 234, no. 3-4, pp. 273–277, 1896.
- [21] O. Debiyi and F. J. I. Sofowora, "Pytochemical screening of medicinal plants," *International Journal of Phytotherapy and Phytopharmacology*, vol. 3, pp. 234–246, 1978.
- [22] R. A. Turner and P. J. A. P. Hebban, "Analgesics: screening methods in pharmacology," *International Journal of Phytotherapy and Phytopharmacology*, vol. 100, 1965.
- [23] B. D. Gupta, P. C. Dandiya, and M. L. Gupta, "A psychopharmacological analysis of behaviour in rats," *Japanese Journal of Pharmacology*, vol. 21, no. 3, pp. 293–298, 1971.
- [24] Y. Oztürk, S. Aydin, R. Beis, K. H. Başer, and H. Berberoğlu, "Effects of *Hypericum perforatum* L. and *Hypericum calycinum* L. extracts on the central nervous system in mice," *Phytomedicine: International Journal of Phytotherapy and Phytopharmacology*, vol. 3, pp. 139–146, 1996.
- [25] S. J. Uddin, J. A. Shilpi, M. T. Rahman, M. Ferdous, R. Rouf, and S. D. Sarker, "Assessment of neuropharmacological activities of *Pandanus foetidus* (Pandanaceae) in mice," *Die Pharmazie*, vol. 61, pp. 362–364, 2006.
- [26] K. Takagi, M. Watanabe, and H. Saito, "Studies of the spontaneous movement of animals by the hole cross test; effect of 2-dimethylaminoethanol and its acyl esters on the central nervous system," *Japanese Journal of Pharmacology*, vol. 21, no. 6, pp. 797–810, 1971.
- [27] R. Koster, "Acetic acid for analgesic screening," *Proceedings of Federation Proceedings (Fed Proc)*, vol. 13, p. 412, 2013.
- [28] F. G. Shoba and M. Thomas, "Study of anti-diarrhoeal activity of four medicinal plants in castor-oil induced diarrhoea," *Journal of Ethnopharmacology*, vol. 76, no. 1, pp. 73–76, 2001.
- [29] F. Awouters, C. J. Niemegeers, F. M. Lenaerts, and P. A. Janssen, "Delay of castor oil diarrhoea in rats: a new way to evaluate inhibitors of prostaglandin biosynthesis," *Journal of Pharmacy and Pharmacology*, vol. 30, pp. 41–45, 1978.
- [30] J. T. Arnason and M. A. Bernards, "Impact of constitutive plant natural products on herbivores and pathogens The present review is one in the special series of reviews on animal-plant interactions," *Canadian Journal of Zoology*, vol. 88, no. 7, pp. 615–627, 2010.
- [31] S. Y. Gbedema, "Anti-plasmodial evaluation of extracts of selected Ghanaian medicinal plants and other bioactivities of isolates of *polyalthia longifolia* Var. *Pendula* (Annonaceae)," 2014.
- [32] M. R. Rahman, M. Ali, M. Sharif, and A. J. M. C. S. R. Tajmim, "A review study on the traditional plants has potential antidepressant property," *Evidence-Based Complementary and Alternative Medicine*, vol. 4, Article ID 00100, 2017.

- [33] I. Ishola, S. Olayemi, O. Yemitan, and E. J. D. R. Umeh, "Antidepressant and anxiolytic effects of the methanol root extract of *Capparis thoningii*: involvement of monoaminergic," *Cholinergic and GABAergic Systems*, vol. 65, pp. 205–213, 2015.
- [34] Z. Liu, J. Silva, A. S. Shao et al., "Flavonoid compounds isolated from Tibetan herbs, binding to GABAA receptor with anxiolytic property," *Journal of Ethnopharmacology*, vol. 267, Article ID 113630, 2021.
- [35] R. Estrada-Reyes, C. López-Rubalcava, L. Rocha, G. Heinze, A. R. González Esquinca, and M. Martínez-Vázquez, "Anxiolytic-like and sedative actions of *Rollinia mucosa*: possible involvement of the GABA/benzodiazepine receptor complex," *Pharmaceutical Biology*, vol. 48, no. 1, pp. 70–75, 2010.
- [36] H. Takeda, M. Tsuji, and T. Matsumiya, "Changes in head-dipping behavior in the hole-board test reflect the anxiogenic and/or anxiolytic state in mice," *European Journal of Pharmacology*, vol. 350, no. 1, pp. 21–29, 1998.
- [37] S. E. File and S. Pellow, "Intrinsic actions of the benzodiazepine receptor antagonist Ro 15-1788," *Psychopharmacology*, vol. 88, no. 1, pp. 1–11, 1986.
- [38] H. Viola, C. Wasowski, M. Levi de Stein et al., "Apigenin, a component of *Matricaria recutita* Flowers, is a central benzodiazepine receptors-ligand with anxiolytic effects," *Planta Medica*, vol. 61, no. 3, pp. 213–216, 1995.
- [39] T. B. Huq, M. S. Rahman, M. A. Nure et al., "Evaluation of pharmacological activities of methanol extract of *Ixora cuneifolia* leaves," *Evidence-Based Complementary and Alternative Medicine*, vol. 2, pp. 1–9, 2017.
- [40] N. Muhammad, M. Saeed, H. Khan, and A. medicine, "Antipyretic, analgesic and anti-inflammatory activity of *Viola betonicifolia* whole plant," *BMC Complementary and Alternative Medicine*, vol. 12, pp. 59–68, 2012.
- [41] H. Khan, M. Saeed, and N. Muhammad, "Antipyretic, analgesic and anti-inflammatory activity of *viola betonicifolia* whole plant," 2012.
- [42] S. Rahman and E. Medicine, "Antioxidant, analgesic, cytotoxic and antidiarrheal activities of ethanolic *Zizyphus mauritiana* bark extract," *Oriental Pharmacy and Experimental Medicine*, vol. 12, no. 1, pp. 67–73, 2012.
- [43] H. V. Ammon, P. J. Thomas, and S. F. Phillips, "Effects of oleic and ricinoleic acids on net jejunal water and electrolyte movement. Perfusion studies in man," *Journal of Clinical Investigation*, vol. 53, no. 2, pp. 374–379, 1974.
- [44] J. Galvez, A. Zarzuelo, M. Crespo, M. Lorente, M. Ocete, and J. Jiménez, "Antidiarrhoeic activity of *euphorbia hirta* extract and isolation of an active flavonoid constituent," *Planta Medica*, vol. 59, no. 4, pp. 333–336, 1993.

## Research Article

# Ethnobotanical Study of Medicinal Plants Used as Therapeutic Agents to Manage Diseases of Humans

**Sanae Achour,<sup>1,2</sup> Mohamed Chebaibi ,<sup>2</sup> Hanane Essabouni,<sup>3</sup> Mohammed Bourhia ,<sup>4</sup> Lahcen Ouahmane,<sup>4</sup> Ahmad Mohammad Salamatullah ,<sup>5</sup> Mourad A M Aboul-Soud,<sup>6</sup> and John P. Giesy<sup>7,8,9,10</sup>**

<sup>1</sup>Laboratory of Pharmacology and Toxicology, University Hospital Hassan II, Fez, Morocco

<sup>2</sup>Biomedical and Translational Research Laboratory, Faculty of Medicine and Pharmacy of the Fez, University of Sidi Mohamed Ben Abdellah, BP 1893, Km 22, Road of Sidi Harazem, Fez, Morocco

<sup>3</sup>Department of Biology, Faculty of Sciences Dhar El Meharz, University of Sidi Mohamed Ben Abdellah, Fez, Morocco

<sup>4</sup>Laboratory of Microbial Biotechnology, Agro-Sciences and Environment (BioMAGe), Cadi Ayyad University, Marrakesh, Morocco

<sup>5</sup>Department of Food Science & Nutrition, College of Food and Agricultural Sciences, King Saud University, P. O. Box 2460, Riyadh 11451, Saudi Arabia

<sup>6</sup>Department of Clinical Laboratory Sciences, College of Applied Medical Sciences, King Saud University, P.O. Box 10219, Riyadh 11433, Saudi Arabia

<sup>7</sup>Toxicology Centre, University of Saskatchewan, 44 Campus Drive, Saskatoon, SK, Canada S7N 5B3

<sup>8</sup>Department of Veterinary Biomedical Sciences, University of Saskatchewan, Saskatoon, SK, Canada S7N 5B4

<sup>9</sup>Department of Integrative Biology, Center for Integrative Toxicology, Michigan State University, East Lansing, MI 48824, USA

<sup>10</sup>Department of Environmental Science, Baylor University, One Bear Place #97266, Waco, TX 76798-7266, USA

Correspondence should be addressed to Mohamed Chebaibi; mohamed.chebaibi@usmba.ac.ma and Mohammed Bourhia; bourhiamohammed@gmail.com

Received 4 November 2021; Revised 5 January 2022; Accepted 11 January 2022; Published 17 February 2022

Academic Editor: Sekar Vijayakumar

Copyright © 2022 Sanae Achour et al. This is an open access article distributed under the Creative Commons Attribution License, which permits unrestricted use, distribution, and reproduction in any medium, provided the original work is properly cited.

**Objective.** This work aimed to survey medicinal plants used in phytotherapy in the Fez-Boulemane region, Morocco. **Methods.** A comprehensive ethnobotanical survey was conducted using a questionnaire to collect data from thirty herbalists on medicinal plants used for therapeutic purposes in the Fez-Boulemane region, Morocco. **Results.** The mean age of herbalists interviewed was 52.13 years. Forty percent of the herbalists were illiterate, and 73% referred to the experiences of their parents as knowledge of the properties and uses of medicinal plants. One hundred and eight medicinal plants belonging to 51 botanical families were recommended by herbalists in the region of Fez-Boulemane, Morocco, for treatment. According to the respondents, *Lawsonia inermis* L., *Rosmarinus officinalis* L., and *Lavandula coronopifolia* L. were the most used plants with the percentage of 13%, 12%, and 11%, respectively. Most plants had been involved in the treatment of digestive disorders (25%) and osteoarticular diseases (24%). Some (7.4%) of the plants mentioned in our survey were potentially toxic. **Conclusion.** It was learned that irrational use of toxic plants and unknown compositions of recipes are recommended to consumers. As a result, particular attention should be paid to risks related to plants used in traditional treatment without scientific validation. It is envisaged that increasing awareness, by conducting educational campaigns and transferring evidence-based scientific knowledge, on traditional treatments among the local population is expected to have beneficial impacts on health and disease management.

## 1. Introduction

Traditional medicine is very ancient, and it is the sum of all knowledge, skills, and practices based on the theories, beliefs, and experiences specific to various cultures, whether explicable or not, and for which is used in the preservation of health, as well as in the prevention, diagnosis, improvement, or treatment of physical and mental illnesses [1]. The therapeutic effects of medicinal plants and their uses in several medicines encourage people to use herbal medicine to cure physical and mental illnesses. Morocco, by its geographical position and climate conditions, has a rich and varied flora, made up of more than 4,200 species, including 500 to 600 species that are used in traditional medicine [2, 3].

Medicinal plants are widely used by the Moroccan population to cure diseases [4–6]. Illiteracy, the limited income of the Moroccan population, and sociocultural factors, in general, have resulted in a relatively large demand for treatment using plants. This frequent use is due to the belief of people that plants are natural products and have no adverse or toxic effects [7, 8]. Products used are often a “variegation” of plants; the knowledge and requirements of preparation and consumption are generally not mastered [9]. Previous studies conducted by the Anti-Poison and Pharmacovigilance Center in Morocco (CAPM) have shown that plants are involved in 3 to 5% of all poisoning across the country [9, 10]. There is no official, traditional, and well-coded pharmacopeia for Morocco. Due to the absence of legislation and control, limitations such as little regulation of collection, sale, or use of plants exist. The lack of any formal studies of the medicinal plants used in Morocco has also limited the valuation of these species and development of their use by modern medicine [9]. There was no systematic listing of plants used in medicine in Morocco, and much of the information available was of an oral nature with little committed to writing. For the above reasons, it was deemed necessary to conduct an ethnobotanical survey among herbalists of the Fez-Boulemane region of Morocco in order to collect as much information as possible concerning the therapeutic uses of medicinal plants used by the indigenous population of the Fez-Boulemane-Morocco region.

## 2. Materials and Methods

**2.1. Study Area.** The region of Fez-Boulemane is a part of the Middle Atlas, Morocco (Figure 1), which is located in the center-north of the Kingdom. It is considered as a crossroad between the east and northeast of the Kingdom. The Fez-Boulemane region is subject to three climates: a continental climate in the north, a cold and humid climate in mountainous areas, and a semiarid climate in the high hills of Boulemane. The region also includes one of the largest forests in Morocco and extends over most of the northern slope of the elevated and mountainous plateau, extending from Imilchil to Midelt, known as the Eastern High Atlas. Thus, due to its geographical position and its climatic conditions, this region has a rich and varied flora that includes several species used in traditional medicine.

**2.2. Data Collection.** Between April and September 2016, an ethnobotanical survey was conducted for four provinces in the Fez-Boulemane region, including Moulay Yacoub, Fez, Sefrou, and Boulemane. The questionnaire was divided into two parts; the first concerned sociodemographic and professional parameters of herbalists, including age, sex, locality, level of education, years of experience, and source of acquisition of knowledge; the second part was reserved for ethnobotanical indices, including plants used, methods of preparation, and pathologies treated.

**2.3. Identification of Plants.** Identification of botanical names has been verified following the “Flore Pratique du Maroc” (Practical Flora of Morocco). Each plant has been registered under a specific number and deposited at the Herbarium of Biomedical and Translational Research Laboratory (BTRL), Sidi Mohammed Ben Abdellah University, Fez, Morocco.

**2.4. Statistical Analyses.** The sociodemographic data were analyzed by a simple descriptive statistical analysis using percentages and frequencies. Ethnobotanical data were analyzed using percentages and relative frequency of citation. Data entry and statistical analysis were performed by SPSS v.21 software.

## 3. Results

### 3.1. Sociodemographic and Professional Parameters

**3.1.1. Sociodemographic Data.** Among the thirty herbalists interviewed, the age varied between 20 years and 70 years, with an average age of  $52.13 \pm 13.17$  years. Eighty-seven percent of herbalists questioned were in urban areas, with the other 13% in rural areas. Forty percent of herbalists were illiterate, and 20% had a primary school and 10% had a secondary school education (Table 1).

**3.2. Professional Data.** Fifteen herbalists (50%) had professional experience between 13 and 20 years, and 7 of them had been practicing this profession for more than 20 years. Twenty-eight of the herbalists had received no training in herbal medicine. Concerning the source of information, 73% of herbalists refer to the experiences of their parents to use medicinal plants as remedies for specific diseases, 18% use radio broadcasts, and 7% use books. This study showed that 23 of the herbalists (77%) are not members of any association of herbalists, while 7 (23%) are registered in associations (National Authority of Herbalists in Morocco) (Table 2).

### 3.3. Ethnobotanical Data

**3.3.1. Collection and Conservation of Plants.** Twenty-six of the herbalists (87%) bought plants from distributors, and 13% of them reported that they picked some plants from forests according to a calendar open all year. Most herbalists (22%) kept plants in a dry place, 19% in glass bottles, 13% in



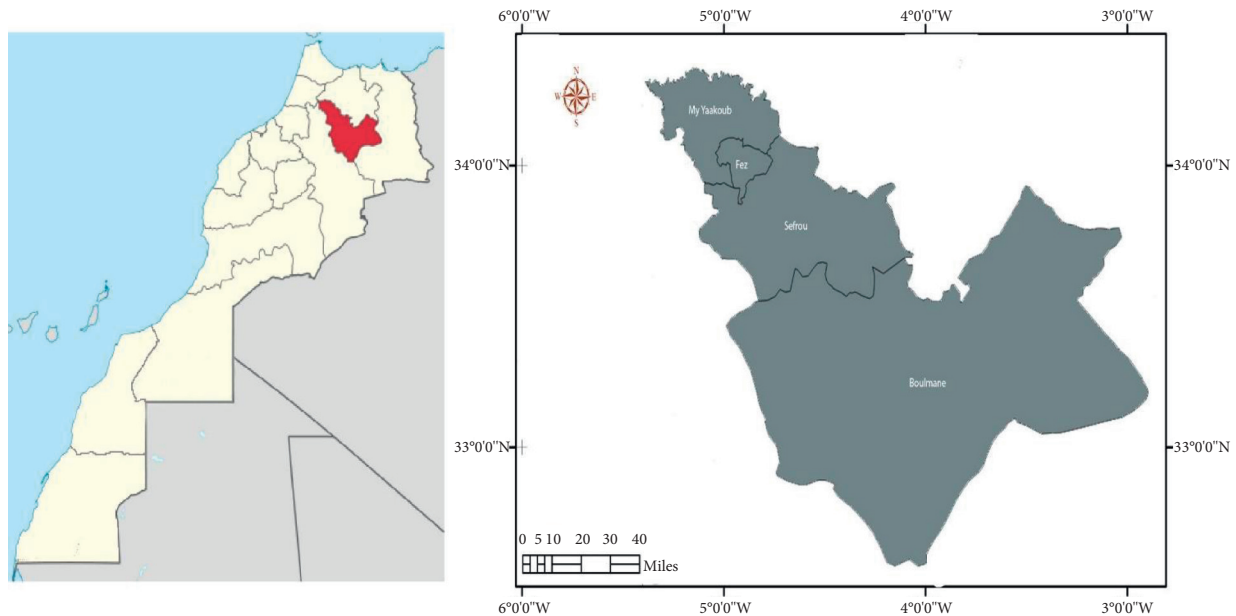


FIGURE 1: Map of the study area, prepared by QGIS software.

cloth bags, and 5% in plastic bags, and only 8% is kept away from light. Concerning the duration of the conservation of plants, it never exceeds 1 year.

**3.3.2. Mode of Utilization of Medicinal Plants.** Method of preparation, parts used, and route of administration: in total, nine parts of plants are used in traditional medicine including the seed, roots, whole plant, leaves, flower, aerial part, gum, and fruit. The percentage of use of these different parts showed that the leaves and the aerial part are the most cited with 20% and 27%, respectively. The whole plant, fruit, and root take the second place with a respective percentage of 12% and 11% (Figure 2). Decoction and infusion are the two most used preparation methods with 42% and 24%, respectively (Figure 3). The oral route was the most used (60%), followed by the cutaneous route (31%). Most customers (67%) request prepared mixtures, and 33% prefer the use of separate medicinal plants.

Among the most demanded plants by customers, we note *Lawsonia inermis* L. (13%) and *Rosmarinus officinalis* L. (12%), followed by *Carum carvi* L. and *Lavandula coronopifolia* L. (11%) (Table 3).

**Pathologies treated with plants:** most people use medicinal plants for the treatment of digestive disorders (25%), osteo-articular diseases (24%), and urogenital diseases (12%) (Table 4). Several groups of medicinal plants are used in the treatment of diseases in the region of Fez-Boulemane (Table 5).

**3.3.3. Toxic Plants and Mixtures.** Toxic plants recommended by herbalists: some plants used by the local population for treatments can cause toxic effects. These included *Atractylis gummifera* L. (15%) followed by *Peganum harmala* L. (14%) and *Papaver somniferum* L. (12%) (Table 6).

Mixtures proposed by herbalists: it was difficult to obtain information on the mixtures because the herbalists' answers remained vague and evasive; herbalists prefer to sell ground and prepared mixtures. For fairly well-known mixtures, herbalists sell recipes without description, and the components are always sold in a powder format (Table 7).

## 4. Discussion

According to floristic and ethnobotanical studies of the medicinal flora of the Eastern High Atlas conducted between 2012 and 2013, only 20% of the population preferred modern medicine [11]. In southeastern Morocco, 70.7% of individuals practice phytotherapy [12]. The results of the two studies confirm ours since 75.1% of the population studied use phytotherapy. A total of 108 species belonging to 51 families, of which Lamiaceae, Apiaceae, and Asteraceae are the most represented medicinal plants used by the population of the region. These results were consistent with those of a survey conducted in eastern Morocco [13], which showed that the most represented botanical families in eastern Morocco are 53 species of Asteraceae, 34 species of Lamiaceae, 29 species of Fabaceae, 28 species of Apiaceae, 17 species of Liliaceae, and 17 species of Poaceae. Among the 108 species used in phytotherapy, the most often identified are the same species used by the population of the Rabat region of Morocco [14].

While various parts of plants are used, aerial parts were the most used part, with 27.5%, followed by the leaves with 20.0%. According to several floristic and ethnobotanical studies of medicinal plants, aerial parts are the parts most used in phytotherapy [11, 15]. The use of aerial parts, including stems and leaves or leaves only, can be explained by ease of harvesting and also availability of these parts

TABLE 1: Distribution of herbalists according to sociodemographic characteristics.

Variables	Number of respondents Proportion (%)	
Sex		
Male	28	93
Female	2	7
Locality		
City	26	87
Village	4	13
Age (years)		
<25	1	3
25–45	5	17
>45	24	80
Mean age	52.13	
Level of education		
Illiterate	12	40
Primary level	15	50
Secondary level	3	10
University	0	0

TABLE 2: Distribution of herbalists according to professional characteristics.

Variables	Number of respondents Proportion (%)	
Years of experience		
<6 years	2	6
7–12 years	6	20
13–20 years	15	50
>20 years	7	23
Source of acquisition of knowledge		
Ancestral experience	22	73
Radio	5	17
Books	2	7
TV	1	3

throughout the year. Another reason is that the aerial part is the seat of photosynthesis [16–18].

Various therapeutic practices are used by local populations, namely, decoction, infusion, powdered preparation, fumigation, poultice, maceration, raw, and cooking. Most plants are involved in the treatment of digestive disorders (18.3%), pathologies linked to metabolism and secretion (14.7%), pathologies of the respiratory system (11.4%), and also bone and joint diseases (10%). Our results are in agreement with the works of Tahri et al. [15]. The methods for preparation mostly are decoction, infusion, and powder, with a rate of 39.93%, 26.46%, and 16.63%, respectively. It has been reported that preparations of plants are administered internally, via oral ingestion or rectally by enemas, in 65.71% of cases, or externally, by local application, in 31.42% [19]. This agrees with our study where the oral route remains the main mode of use of plants (66.4%) of the time. More than 50% of the Moroccan population uses combinations of two or more plants, which are, in most cases, sold by herbalists.

Medicinal plants are complex mixtures of various molecules. Their composition is often unknown and made

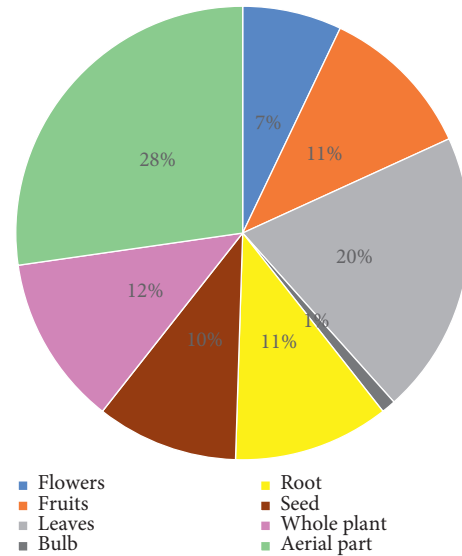


FIGURE 2: Parts of plants used by herbalists in Fez-Boulemane region, Morocco.

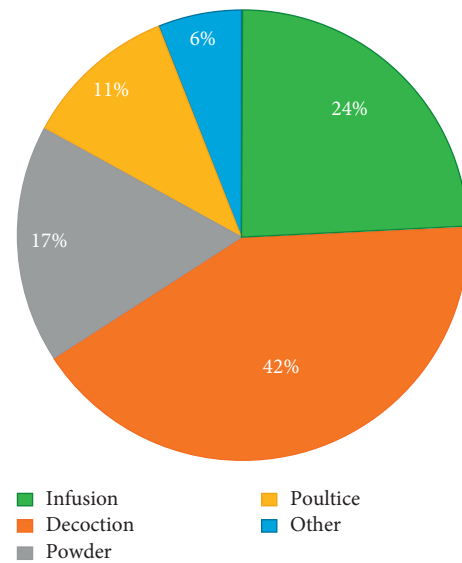


FIGURE 3: Methods of preparation cited by herbalists in the region of Fez-Boulemane.

up of molecules with known biological activity, including heterosides, alkaloids, anthocyanins, tannins, and steroids. These constituents can, at sufficient concentrations, cause toxicity via multiple mechanisms of action [20]. Combining plants can be used as a mechanism for masking the toxicity of herbal preparations in several African countries [21]. Contents of these constituents can “naturally” vary from one preparation to another; among the plants used, 14.8% are toxic. The study was conducted on uses of medicinal plants in the circle of Mechra Bel Ksiri region of western Morocco, which showed that only 27% of the population, especially the oldest subjects, understand that plants can be toxic [13]. Alternatively, in the study presented here, 96.7% of people using medicinal

TABLE 3: Species of plants most requested by customers in the Fez-Boulemane region of Morocco.

Plant number	Botanical name	Families	Common name	Moroccan vernacular name	Frequency of citation
BTRL16E1	<i>Ammodaucus leucotrichus</i> Coss. and Dur.	Apiaceae	Ammodaucus	Kemmoun souffi	12
BTRL16E2	<i>Carum carvi</i> L.	Apiaceae	Caraway	Kerouiya	23
BTRL16E3	<i>Euphorbia resinifera</i> L.	Euphorbiaceae	Euphorbia	Daghmous	9
BTRL16E4	<i>Herniaria fontanesii</i> L.	Caryophyllaceae	Smooth rupturewort	Herrast lehjar	20
BTRL16E5	<i>Lavandula coronopifolia</i> L.	Lamiaceae	Lavandula	Lekhzama	22
BTRL16E6	<i>Lawsonia inermis</i> L.	Lythraceae	Henna	L-henna	28
BTRL16E7	<i>Matricaria chamomilla</i> L.	Asteraceae	Camomile	Babounj	8
BTRL16E8	<i>Nigella sativa</i> L.	Ranunculaceae	Nigella	H'bat Ibaraka, sanouj	16
BTRL16E9	<i>Origanum compactum</i> Benth L.	Lamiaceae	Oregano	Za'atar, zoukni	21
BTRL16E10	<i>Pennisetum typhoides</i> L.	Poaceae	Pearl millet	Illan	13
BTRL16E11	<i>Rosmarinus officinalis</i> L.	Lamiaceae	Rosemary	Azel	26
BTRL16E12	<i>Ziziphus lotus</i> L.	Rhamnaceae	Ziziphus lotus	Sedra	10

TABLE 4: Distribution of pathologies treated with phytotherapy in Fez-Boulemane region, Morocco.

Pathology	Frequency of citation	Proportion (%)
Digestive disorders	42	25
Osteoarticular diseases	39	24
Urogenital diseases	21	12
Metabolic disorders	16	10
Skin disorders	10	6
Cardiovascular diseases	10	6
Parasitic diseases	8	5
Respiratory diseases	7	4
Food poisoning	6	4
Carcinogenic diseases	5	3
Liver disease	2	1

TABLE 5: Distribution of pathologies treated with phytotherapy in the Fez-Boulemane region of Morocco.

Ailment	Plants
Pathologies of digestive disorders	<i>Pennisetum typhoides</i> L., <i>Artemisia absinthium</i> L., <i>Ceratonia siliqua</i> L., <i>Cinnamomum zeylanicum</i> L., <i>Citrullus colocynthis</i> L., <i>Citrus limonia</i> L., <i>Coriandrum, Sativum</i> L., <i>Crocus sativus</i> L., <i>Fragaria vesca</i> L., <i>Mentha piperita</i> L., <i>Myristica fragrans</i> Houtt., <i>Nigella sativa</i> L., <i>Ocimum basilicum</i> L., <i>Ormenis mixta</i> L., <i>Papaver somniferum</i> L., <i>Peganum harmala</i> L., <i>Phoenix dactylifera</i> L., <i>Pimpinella anisum</i> L., <i>Prunus amygdalus</i> L., <i>Punica granatum</i> L., <i>Raphanus sativus</i> L., <i>Rosa centifolia</i> L., <i>Rosmarinus officinalis</i> L., <i>Ruta graveolens</i> L., <i>Salvadora persica</i> L., <i>Sesamum indicum</i> L., <i>Thymus vulgaris</i> L., <i>Trigonella foenum-graecum</i> L., <i>Vitis vinifera</i> L., <i>Zea mays</i> L., <i>Zingiber officinale</i> L.
Metabolic disorders	<i>Artemisia absinthium</i> L., <i>Euphorbia resinifera</i> L., <i>Nerium oleander</i> L., <i>Artemisia herba-alba</i> Asso, <i>Brassica rapa</i> L., <i>Trigonella foenum-graecum</i> , <i>Glycyrrhiza glabra</i> L., <i>Armoracia rusticana</i> L., <i>Origanum majorana</i> L., <i>Aristolochia baetica</i> L., <i>Salvia officinalis</i> L., <i>Cinnamomum verum</i> L., <i>Trigonella foenum-graecum</i> , <i>Linum usitatissimum</i> L., <i>Punica granatum</i> L., <i>Ficus carica</i> L., <i>Eugenia caryophyllata</i> Thunb., <i>Olea europaea</i> L., <i>Nigella sativa</i> L., <i>Rhamnus alaternus</i> L., <i>Prunus dulcis</i> L., <i>Ruta montana</i> L., <i>Zingiber officinale</i> L., <i>Atropa belladonna</i> L., <i>Brassica rapa</i> L., <i>Rosmarinus officinalis</i> L., <i>Viola odorata</i> L., <i>Cinnamomum zeylanicum</i> L., <i>Eugenia caryophyllata</i> Thunb., <i>Mentha piperita</i> L., <i>Marrubium vulgare</i> L., <i>Myristica fragrans</i> Houtt., <i>Ocimum basilicum</i> L., <i>Ormenis mixta</i> L., <i>Papaver rhoeas</i> L., <i>Papaver somniferum</i> L., <i>Petroselinum sativum</i> Hoffm., <i>Phoenix dactylifera</i> L., <i>Pimpinella anisum</i> L., <i>Prunus amygdalus</i> L., <i>Thymus vulgaris</i> L., <i>Zingiber officinale</i> L.

TABLE 5: Continued.

Ailment	Plants
Urogenital diseases	<i>Citrullus colocynthis</i> L., <i>Ocimum basilicum</i> L., <i>Ormenis mixta</i> L., <i>Papaver somniferum</i> L., <i>Peganum harmala</i> L., <i>Petroselinum sativum</i> Hoffm., <i>Pimpinella anisum</i> L., <i>Rosa centifolia</i> L., <i>Ruta graveolens</i> L., <i>Zingiber officinale</i> L., <i>Myristica fragrans</i> Houtt., <i>Atropa belladonna</i> L., <i>Olea europaea</i> L., <i>Petroselinum sativum</i> Hoffm., <i>Punica granatum</i> L., <i>Raphanus sativus</i> L., <i>Herniaria hirsuta</i> L., <i>Lavandula vera</i> L., <i>Peganum harmala</i> L.
Skin diseases	<i>Argania spinosa</i> L., <i>Citrus limonia</i> L., <i>Corylus avellana</i> L., <i>Lawsonia inermis</i> L., <i>Peganum harmala</i> L., <i>Prunus amygdalus</i> Mill., <i>Raphanus sativus</i> L., <i>Rosa centifolia</i> L., <i>Ruta graveolens</i> L., <i>Sesamum indicum</i> L., <i>Attractylis gummifera</i> L., <i>Peganum harmala</i> L., <i>Lavandula vera</i> L., <i>Delphinium staphisagria</i> L., <i>Ziziphus lotus</i> L., <i>Thymelaea microphylla</i> L.
Cardiovascular diseases	<i>Allium sativum</i> L., <i>Argania spinosa</i> L., <i>Atropa belladonna</i> L., <i>Brassica rapa</i> L., <i>Cinnamomum zeylanicum</i> L., <i>Corylus avellana</i> L., <i>Nigella sativa</i> L., <i>Olea europaea</i> L., <i>Papaver rhoeas</i> L., <i>Punica granatum</i> L., <i>Rosmarinus officinalis</i> L., <i>Sesamum indicum</i> L., <i>Thymus vulgaris</i> L., <i>Trigonella foenum-graecum</i> L., <i>Viola odorata</i> L., <i>Vitis vinifera</i> L., <i>Prunus amygdalus</i> L.
Osteoarticular diseases	<i>Cinnamomum camphora</i> L., <i>Citrus limonia</i> L., <i>Myristica fragrans</i> Houtt., <i>Papaver somniferum</i> L., <i>Rosmarinus officinalis</i> L., <i>Ruta graveolens</i> L., <i>Thymus vulgaris</i> L., <i>Vitis vinifera</i> L., <i>Zea mays</i> L., <i>Zingiber officinale</i> L., <i>Pennisetum typhoides</i> L., <i>Citrullus colocynthis</i> L., <i>Alpinia officinarum</i> Hance.

TABLE 6: Distribution of recommended toxic plants by herbalists in the region of Fez-Boulemane, Morocco.

Botanical name	Common name	Moroccan vernacular name	Frequency of citation	Proportion (%)
<i>Aristolochia longa</i> L.	Long aristolochi	Bereztem	14	11
<i>Attractylis gummifera</i> L.	Distaff thistle	Daad, chouk el aalk	20	15
<i>Atropa belladonna</i> L.	Belladonna	Belaydour	13	10
<i>Citrullus colocynthis</i> L.	Bitter apple	Hadja, tafzazte	11	8
<i>Delphinium staphisagria</i> L.	Stavesacre	Habat ras	9	7
<i>Myristica fragrans</i> Houtt.	Nutmeg	L'goza	4	3
<i>Nerium oleander</i> L.	Nerium	Deffla, Alili	15	11
<i>Nigella sativa</i> L.	Nigella	h'bat lbaraka, sanouj	7	5
<i>Papaver somniferum</i> L.	Opium poppy	Kharchakha	16	12
<i>Peganum harmala</i> L.	Wild rue	L'harmal	18	14
<i>Urginea maritima</i> L.	Squill	Åanssla	6	4

TABLE 7: Mixtures offered by herbalists in the region of Fez-Boulemane, Morocco.

Mixture	Common name	Botanical name	Mode of use
Mixture against cancer	Aristolochia baetica	<i>Aristolochia baetica</i> L.	All mixed with pure honey; it is advisable to take a small scoop every morning until healing
	Fenugreek	<i>Trigonella foenum-graecum</i> L.	
	Euphorbia White wormwood	<i>Euphorbia resinifera</i> L. <i>Artemisia herba-alba</i> L.	
	Ajuga iva White horehound	<i>Ajuga iva</i> L. <i>Marrubium vulgare</i> L.	
Mixture against digestive disorders	Black caraway	<i>Nigella sativa</i> L.	The plants are powdered and mixed with honey, a teaspoon on an empty stomach
	Anise	<i>Pimpinella anisum</i> L.	
	Fennel	<i>Foeniculum vulgare</i> L.	
Mixture against rheumatism	Nutmeg	<i>Myristica fragrans</i> Houtt.	All mixed with honey; it is advisable to take a spoonful of coffee 3 times a day before meals
	Ammodaucus	<i>Ammodaucus leucotrichus</i> Coss. and Dur.	
	Ginger	<i>Zingiber officinale</i> L.	
	Alpinia	<i>Alpinia officinarum</i> L.	

TABLE 7: Continued.

Mixture	Common name	Botanical name	Mode of use
Mixture against hair loss	Wild rue	<i>Peganum harmala</i> L.	The two plants are mixed with olive oil and used as an antihair loss treatment. This mixture is preceded by onion juice application on the hair.
	Lavandula	<i>Lavandula coronopifolia</i> L.	
Mixture for the treatment of diabetes	Black caraway	<i>Nigella sativa</i> L.	Powdered <i>Nigella</i> mixes with dried white horehound and olive leaves and powdered madder roots
	White horehound	<i>Marrubium vulgare</i> L.	
	Olea europaea	<i>Olea europaea</i> L.	
	Rose madder	<i>Rubia tinctorum madder</i> L.	
Mixture in case of fever	Eucalyptus	<i>Eucalyptus globulus</i> L.	Fumigation
	White horehound	<i>Marrubium vulgare</i> L.	
	Ammi visnaga	<i>Ammi visnaga</i> L.	
	Dried cloves	<i>Syzygium aromaticum</i> L.	
	Turnip	<i>Brassica rapa</i> L.	
	Sage	<i>Salvia officinalis</i> L.	
Mixture for ovarian stimulation	Oregano	<i>Origanum vulgare</i> L.	Leaf decoction
	Chamomile	<i>Matricaria chamomilla</i> L.	
	Fenugreek	<i>Trigonella foenum-graecum</i> L.	
	Liquorice	<i>Glycyrrhiza glabra</i> L.	
	Alpinia	<i>Alpiniaofficinarum</i> L.	

plants in the Fez-Boulemane region, Morocco, understood the concept of toxicity and that some plants could be toxic. The best-known toxic plant is thistle, which is no longer used for therapeutic purposes. Three hundred and twenty-eight or 54.6% of users of medicinal plants have observed undesirable effects, including toxicity or aggravation of the disease. This can be explained by the lack of awareness among tutors about risks of toxic effects associated with the use of plants or by uninformed use of plants, without respecting the dose, the parts used, nor the method of preparation. Toxicities of several plants used by the population of the region of Fez-Boulemane of Morocco including *Atractylis gummifera* L. have been demonstrated in controlled clinical studies. Toxicity of this plant is due to two diterpene glucosides, atractyloside and carboxyatractyloside, which inhibit mitochondrial oxidative phosphorylation [22]. *Herniaria hirsuta* is another nephrotoxic plant that is the cause of several cases of renal lithiasis received by the Hassan II hospital center in Fez (CHU Fez) [23]. Use of *Aristolochia longa* L. as an anticancer plant in Morocco can, due to aristolochic acid, cause interstitial nephritis and DNA adducts to the kidney [23]. Interstitial nephritis is also referred to as tubulointerstitial nephritis and is inflammation of the area of the kidney known as the renal interstitium, which consists of a collection of cells, extracellular matrix, and fluid surrounding the renal tubules. Most of the harmful effects of medicinal plants are not due to inherent toxicities of medicinal plants, but rather are due to errors in identification, involuntary contamination, and noncompliance with the adequate dose or interactions with drugs [19]. In this survey, 61.7% of the population uses plants in combination with synthetic pharmaceuticals, which can increase risks of side effects and can result in frank toxicities. Pharmacokinetic interactions of herbal

products can affect absorption, distribution, and elimination of certain prescribed drugs. In other cases, interactions can promote increases in concentrations and cause undesirable side effects.

## 5. Conclusions

Morocco has a rich and variable flora, which, in part, explains the frequent use of plants for therapeutic, cosmetic, and gastronomic purposes. However, the irrational, anarchic, and uncontrolled consumption of plants can be responsible for poisoning, which can be life-threatening. Thus, our study allowed us to describe the relative importance given to the use of phytotherapy by the population of the region of Fez-Boulemane and to confirm the persistent use of plants for therapeutic purposes, despite the revolution of medical technology and availabilities of modern synthetic pharmaceuticals. It was learned that toxic plants and unknown compositions of recipes are also sold to consumers. Hence, the interest in raising awareness among population about the dangers is associated with the use of non-scientifically validated plants for treatment.

## Data Availability

The data used to support the findings of this study are included within the article.

## Conflicts of Interest

The authors declare no conflicts of interest.

## Authors' Contributions

Sanae Achour conceptualized and supervised the study and provided methodology. Mohamed Chebaibi conceptualized



the study, performed statistical analysis, and wrote the original draft. Hanane Essabouni and Mohammed Bourhia conceptualized and investigated the study. Ahmad Mohammad Salamatullah, Mourad A. M. Aboul-Soud, and John P. Giesy wrote the original draft and edited and reviewed the article.

## Acknowledgments




The authors extend their appreciation to Researchers Supporting Project number (RSP-2022R437), King Saud University, Riyadh, Saudi Arabia.

## References

- [1] WHO, *General Guidelines for Methodologies on Research and Evaluation of Traditional Medicine*, WHO, Geneva, 2000.
- [2] M. Fennane, *Proposals for Important Areas for Plants in Morocco (ZIP Morocco)*, Institut Scientifique, Rabat, Morocco, 2004.
- [3] M. Rejdali, *The Flora of Morocco: Current State and Prospects for Conservation. Biological Diversity and Valorization of Medicinal Plants*, pp. 17–22, Actes Edition, 1996.
- [4] M. Abouri, A. El Mousadik, and F. Msanda, “An ethnobotanical survey of medicinal plants used in the Tata Province, Morocco,” *International Journal of Medicinal Plants Research*, vol. 1, no. 7, pp. 99–123, 2012.
- [5] J. Bellakhdar, R. Claisse, J. Fleurentin, and C. Younos, “Repertory of standard herbal drugs in the Moroccan pharmacopoea,” *Journal of Ethnopharmacology*, vol. 35, no. 2, pp. 123–143, 1991.
- [6] J. El Amri, K. El Badaoui, and T. Zair, “Ethnobotanical study of medicinal plants in the region El Hajeb (central Morocco),” *Journal of Research in Biology*, vol. 4, no. 8, pp. 1568–1580, 2015.
- [7] M. Zekkour, *The risks of phytotherapy, monographs of the most common toxic plants in Morocco*, Ph.D. thesis, Faculty of Medicine and Pharmacy, Rabat, Morocco, 2008.
- [8] M. Chebaibi, D. Bousta, I. Iken et al., “Ethnopharmacological survey of medicinal plants used in traditional treatment of kidney diseases in fez-meknes region, Morocco,” *Phytothérapie*, vol. 18, no. 2, pp. 99–114, 2020.
- [9] A. Khattabi, N. Rhalem, and A. Chabat, “Plants and public health,” *Toxicologie Maroc*, vol. 2, 2010.
- [10] L. Ouammi, N. Rhalem, and R. Aghandous, “Epidemiological profile of poisoning in Morocco from 1980 to 2007,” *Toxicologie Maroc*, vol. 1, pp. 8–13, 2009.
- [11] N. Benlamdini, M. Elhafian, A. Rochdi, and L. Zidane, “Étude floristique et ethnobotanique de la flore médicinale du Haut Atlas oriental (Haute Moulouya),” *Journal of applied biosciences*, vol. 78, no. 1, pp. 6771–6787, 2014.
- [12] L. El Rhaffari and A. Zaid, “Practice of phytotherapy in the south-east of Morocco (Tafilalet): an empirical knowledge for a renovated pharmacopoeia,” *Knowledge Sources to Future Medicines*, pp. 293–318, 2002.
- [13] M. Kahouadji, “Contribution to an ethnobotanical study of medicinal plants in eastern Morocco,” Graduate Diploma of 3rd Cycle. Mohamed I University, 1995.
- [14] S. Hseini and A. Kahouadji, “Ethnobotanical study of medicinal flora in the region of Rabat (western Morocco),” *Lazaroa*, vol. 28, pp. 9–92, 2007.
- [15] N. Tahri, A. El Basti, and L. Zidane, “Ethnobotanical study of medicinal plants in the province of Settat (Morocco),” *Kastamonu University Journal of Forestry Faculty*, vol. 12, no. 2, pp. 192–208, 2012.
- [16] M. Barkaoui, A. Katiri, H. Boubaker, and F. Msanda, “Ethnobotanical survey of medicinal plants used in the traditional treatment of diabetes in Chtouka Ait Baha and Tiznit (Western Anti-Atlas), Morocco,” *Journal of Ethnopharmacology*, vol. 198, pp. 338–350, 2017.
- [17] M. Eddouks, M. Ajebli, and M. Hebi, “Ethnopharmacological survey of medicinal plants used in Daraa-Tafilalet region (Province of Errachidia), Morocco,” *Journal of Ethnopharmacology*, vol. 198, pp. 516–530, 2017.
- [18] A. Ziyat, A. Legssyer, H. Mekhfi, A. Dassouli, M. Serhrouchni, and W. Benjelloun, “Phytotherapy of hypertension and diabetes in oriental Morocco,” *Journal of Ethnopharmacology*, vol. 58, no. 1, pp. 45–54, 1997.
- [19] A. Zeggwagh, Y. Lahlou, and Y. Bousliman, “Investigation of the toxicological aspects of herbal medicine used by an herbalist in Fez, Morocco,” *The Pan African Medical Journal*, vol. 14, 2013.
- [20] M. Chebaibi, D. Bousta, L. Chbani, I. Iken, and S. Achour, “Evaluation of acute toxicity of plants’ mixture used in traditional treatment of kidney diseases in Morocco,” *Pharmacognosy Research*, vol. 11, no. 2, pp. 155–161, 2019.
- [21] T. Omara, “Antimalarial plants used across Kenyan communities,” *Evidence-based Complementary and Alternative Medicine*, vol. 2020, 2020.
- [22] C. Daniele, S. Dahamna, O. Firuzi, N. Sekfali, L. Saso, and G. Mazzanti, “Atractylis gummifera L. poisoning: an ethnopharmacological review,” *Journal of Ethnopharmacology*, vol. 97, no. 2, pp. 175–181, 2005.
- [23] N. Touiti, S. Achour, I. Iken, M. Chebaibi, and T. Sqalli Houssaini, “Nephrotoxicity associated with herbal medicine use, experience from Morocco,” *Toxicologie Analytique et Clinique*, vol. 31, no. 3, pp. 145–152, 2019.

## Research Article

# Evaluation of Antioxidant, Cytotoxic, Anti-Inflammatory, Antiarthritic, Thrombolytic, and Anthelmintic Activity of Methanol Extract of *Lepidagathis hyalina* Nees Root

Shafiqul Islam,<sup>1</sup> Fowzul Islam Fahad,<sup>1</sup> Arifa Sultana,<sup>2</sup> Syed Al Jawad Sayem,<sup>1</sup> Shawon Baran Roy,<sup>1</sup> Mohammad Nazmul Islam ,<sup>1</sup> Arpita Roy ,<sup>3</sup> and Mohammed Abu Sayeed <sup>1</sup>

<sup>1</sup>Department of Pharmacy, International Islamic University Chittagong, Chittagong-4318, Bangladesh

<sup>2</sup>Department of Pharmacy, Faculty of Pharmacy, University of Dhaka, Dhaka-1000, Bangladesh

<sup>3</sup>Department of Biotechnology, School of Engineering & Technology, Sharda University, Greater Noida, India

Correspondence should be addressed to Mohammad Nazmul Islam; nazmul@iuc.ac.bd, Arpita Roy; arbt2014@gmail.com, and Mohammed Abu Sayeed; pmasayeed@yahoo.com

Received 31 December 2021; Revised 17 January 2022; Accepted 20 January 2022; Published 15 February 2022

Academic Editor: Ruchika Garg

Copyright © 2022 Shafiqul Islam et al. This is an open access article distributed under the Creative Commons Attribution License, which permits unrestricted use, distribution, and reproduction in any medium, provided the original work is properly cited.

*Lepidagathis hyalina* Nees is an ethnomedicinally potential Asian herb, locally used to treat cardiovascular diseases and coughs. The study was intended to evaluate qualitative and quantitative investigation to ensure numerous pharmacological properties of methanol extracts of *L. hyalina* Nees root (MELHR). MELHR manifested strong radical scavenging activity in the reducing power and DPPH (1, 1-diphenyl-2-picrylhydrazyl) assays, and phenol and flavonoid in the quantitative assays. In the study of the thrombolytic assay, MELHR showed moderate explicit percentage of clot lysis ( $29.39 \pm 1.40\%$ ) with moderate ( $135.35 \mu\text{g/mL}$ ) toxic properties. The *in vitro* anti-inflammatory activity was evaluated by the inhibition of hypotonicity-induced RBC hemolysis, whereas the plant extract exhibited a significant ( $p < 0.005$ ) dose-dependent inhibition and the highest inhibition was found  $55.01 \pm 3.22\%$  at  $1000 \mu\text{g/mL}$  concentration. Moreover, the MELHR also showed significant ( $p < 0.005$ ) dose-dependent potentiality on protein denaturation which is considered as antiarthritic activity, and the peak inhibition was found significant ( $71.97 \pm 2.71\%$ ) at  $1000 \mu\text{g/mL}$  concentration. MELHR also exhibited the dose-dependent and statistically significant anthelmintic potential on aquarium worm (*Tubifex tubifex*). So, the present investigation suggests that *L. hyalina* could be the best choice for the management of cardiovascular, inflammation, arthritis, and anthelmintic diseases. Further investigation should be necessary to determine behind the mechanism of bioactivity and therapeutic potential of this plant.

## 1. Introduction

Free radicals are major concern for biological evolution and also have certain beneficial effects on some species [1]. An imbalance between the accumulation and production of ROS in tissues causes oxidative stress [2, 3]. Oxidative stress triggers inflammation, which in chronic conditions results in atherosclerosis formation, thrombosis, plaque rupture, myocardial injury, and failure like serious cardiac diseases [4, 5]. Different epidemiological studies express that some inflammatory mediators not only facilitate the proliferation of

malignant cells in the microenvironment of the tumor, but also induce metastasis and angiogenesis and redefine the responses of hormones, chemotherapeutic agents, and overall adaptive immunity [6]. Some bioactive compounds such as capsaicin, catechins, lycopenes, cucurbitacin B, isoflavones, phenethyl isothiocyanate, benzyl isothiocyanate, and piperlongumine have been proved to exert effective pharmacological activities to treat cancer [7]. Certain phytochemicals like thymol, berberine, curcumin, lycopene, epigallocatechin, resveratrol, vanillin, and sulforaphane may also reduce the possibility of the onset of several types of cancer [8–11].

Arthritis becomes a common cause of disability in developed countries nowadays, which is attributed to pain, restricted joint movement, and synovial membrane inflammation [12, 13]. Fibroblast-like synoviocytes (FLSs) facilitate both the propagation of joint damage and inflammation by producing proinflammatory mediators like matrix metalloproteins (MMPs), interleukins (IL6, IL8), and prostaglandins (PGE2) [14]. For this reason, anti-inflammatory agents can also be used as a long-term treatment of rheumatoid arthritis [15]. Thrombolytic agents activate plasminogen to plasmin, which clears the fibrin mesh. As a result, the clot becomes soluble and blood flow gets normalized [16]. As the consequences of inflammation spread over a wide range of actions like asthma and atherosclerosis, multitargeted therapeutic approaches can be appeared prevailing over combination therapy or just single-target drugs [17, 18]. Besides, the antioxidant properties containing agents may prevent inflammation and thrombotic as well as help to prevent cardiovascular diseases [19].

Helminthiasis (worm infestation) is a macroparasitic ailment in which parasitic worms such as nematodes, trematodes, cestodes, and other parasitic worms infest the human and animal body and cause a variety of disorders like pneumonia, malnutrition, eosinophilia, anemia, etc. It exacerbates global economic and social difficulties, particularly in tropical areas [20]. According to the World Health Organization, helminthiasis affects 1.5 billion people or 24% of the world's population [21]. However, in developing countries, it has become a major public health issue owing to anthelmintic misuse, which has resulted in the development of anthelmintic resistance in parasitic worms [22].

However, antioxidants (e.g., arginine, glutathione, taurine, selenium, tea polyphenols, superoxide dismutase, and vitamin C, E, and A) overcome the oxidative stress by scavenging free radicals [2,3]. Unfortunately, plenty of synthetic agents used for the treatment of these diseases have potential side effects and also cannot afford adequate therapeutic significance [23, 24]. Therefore, the drugs, which can generate effect against parasitic worms, scavenge RONS, inhibit inflammation, exhibit thrombolytic activities, and give minimal side effect, would be a jackpot in the drug development process [25]. Plants have diversified phytochemicals obtained from secondary metabolism [26] that give diversified biological activities including some good pharmacological actions [27]. For instance, lichens, *Allium sativum* (garlic), and *Hydrastis canadensis* are good options of antimicrobial activities with lesser side effects than their synthetic counterparts like streptomycin and Aureomycin [28]. So, the popularity of traditional medicine is increasing in both developed and developing countries for its low cost and less side effects [29]. Additionally, incorporating plant-derived bioactive compounds in the conventional system is also increasing day by day.

*Lepidagathis hyalina*, also known as Curved Lepidagathis, is a wild herb from the *Acanthaceae* family that has various therapeutic potentials including antimicrobial and antidiabetic activities [30, 31]. This plant has been

reported in various subtropical locations across the world, particularly in the Indian subcontinent. In Bangladesh, it is mostly found in hill tract regions which have a long history of use in the treatment of coughs and cardiovascular disorders [30, 32]. According to a prior study, a biological substance called triterpenoid saponin ((3- $\beta$ -O-[ $\alpha$ -L-rhamnopyranosyl (1 $\rightarrow$ 4)O- $\beta$ -D-glucopyranosyl] 16- $\alpha$ -hydroxy-olean-12-en (13)-28-oic acid)) identified in the leaves of this plant has antibacterial and antifungal properties, and also the stem part of this plant manifested several pharmacological properties which are reported as antioxidant, thrombolytic, antidepressant, and anxiolytic activity [30, 32]. To verify its ethnomedicinal uses, we aim to investigate several *in vitro* tests on *Lepidagathis hyalina* Ness.

## 2. Methods and Materials

**2.1. Chemicals.** Sodium carbonate, ferric chloride, folin-ciocalteu reagent (FCR), trichloroacetic acid, methanol, potassium ferrocyanide, potassium acetate, aluminum chloride, hydrochloric acid, and sulfuric acid were purchased from Merck (Darmstadt, Germany). Diclofenac sodium and levamisole were brought from ACME Laboratories Ltd. (Dhaka, Bangladesh). Sodium acetate, quercetin, and 1, 1-diphenyl-2-picrylhydrazyl (DPPH) were collected from Sigma Chemical Co. (St. Louis, USA). Lyophilized streptokinase vial (1500000 IU) and vincristine sulfate (1 mg/vial) were gained from Beacon Pharmaceutical Ltd. (Dhaka, Bangladesh). Ultraviolet-Vis spectrophotometer (Shimadzu, Japan) was applied to take absorbance for this experiment. Specified reference-tagged chemicals were used in this research project which was an analytical grade reagent.

**2.2. Collection.** The roots of *Lepidagathis hyalina* Ness were collected as fresh condition from the Golden Temple Hill area, Bandarban, Chittagong, Bangladesh. After collection, the plant taxonomy was authenticated by Prof. Dr. Sheikh Bokhtear Uddin (Department of Botany, University Chittagong, Chittagong-4331, Bangladesh), and also identified and confirmed by Prof. Dr. Abu Sayeed (Department of Pharmacy, International Islamic University Chittagong, Chittagong-4318, Bangladesh).

The roots of *L. hyalina* were washed and stored in shade at low temperature for two weeks and after that ground into coarse powder through a blender machine. The blended powder of root was put in an impermeable container with a sufficient volume of methanol at room temperature for 10–14 days, and the mixed solution shook vigorously. A rotary evaporator was applied to filter the mixed solution at 40–50°C. By this process, a deep green sticky semisolid was formed and kept in a refrigerator until further study. All of the research design and protocols have been approved and authenticated by the P&D committee (Pharm-P&D17/08'-19), Department of Pharmacy, International Islamic University Chittagong, Chittagong, Bangladesh.

**2.3. Phytochemical Screening.** MELHS was experimented for preliminary qualitative phytochemical analysis through the standard determination method of phytochemicals (e.g., quinones, carbohydrates, alkaloids, reducing sugar, polyphenols, phenols, flavonoids, resins, glycoside, phlobatannins, xanthoproteins, triterpenoids, coumarins, cardial glycoside, cholesterol, etc.) [33].

#### 2.4. Antioxidant Activity Test

**2.4.1. DPPH Radical Scavenging Assay.** Free radical scavenging assay of methanol extract of *L. hyalina* Ness roots (MELHR) was examined through the method described by Tayab et al. [34]. The DPPH reagent used all concentrations of MELHR and kept 30 mins in the darkened room. After incubation, the absorbance was recorded at 517 nm using a UV spectrophotometer against a blank solution. Ascorbic acid was subjected as a reference standard. The free radical scavenging assay was calculated by the equation as follows:

$$\% \text{ scavenging activity} = \frac{A_c - A_s}{A_c} \times 100. \quad (1)$$

Here,  $A_c$  = absorbance of the control and  $A_s$  = absorbance of the sample.

**2.4.2. Reducing Power Assay.** The method of Sarkar et al. was conducted to evaluate the reducing power assay of MELHR [35]. 1 milliliter of several serial diluted concentrations (62.5 to 1000  $\mu\text{g}/\text{mL}$ ) was made and then mixed with 2.5 ml of 0.2 M phosphate buffer (pH 6.6) and 1% potassium ferricyanide. At 50°C temperature, the mixed solution was incubated for reaction completion. About 2.5 ml of 10% trichloroacetic acid was added and centrifuged the mixer for 10 mins at 3000 rpm. The formed supernatant solution was dispelled after centrifuging period. Then, a half milliliter of 0.1% ferric chloride and 2.5 milliliter distilled water were summed up and then investigated the absorbance at 700 nm on a UV spectrophotometer. The blank and reference standard that applied in this experiment was phosphate buffer and ascorbic acid, respectively.

**2.4.3. Total Phenolic Content Test.** The total phenolic content of MELHR was measured by the following method, where gallic acid is used as standard [36]. 1 ml of extract solution and 1 ml of the standard solution containing different concentrations were taken to the different test tubes. 5 ml diluted FCR and 5 ml solution containing different concentrations of 7.5% sodium carbonate were added to each test tube one after another. The test tubes were incubated at 25°C for 20 minutes to facilitate the reaction. The test tubes and a blank sample were placed in the UV machine, and absorbance was taken to 760 nm. A standard curve was generated based on the gallic acid, and total phenolic content (TPC) was calculated.

**2.4.4. Total Flavonoid Content Test.** The content of total flavonoid content of MELHR was measured by aluminum chloride colorimetric method using quercetin as standard

[32]. 1 mL of extract solution and 1 ml of standard solution containing different concentrations were taken to the different test tubes. 3 ml methanol, 200  $\mu\text{l}$  aluminum chloride (10%), 200  $\mu\text{l}$  of 1 M potassium acetate, and 5.6 milliliters of distilled water were added to each test tube one after another. The final mixture was placed in incubation for 30 minutes to facilitate the reaction. Then, the sample, standard, and a blank were placed into UV machine, and absorbance was measured at 420 nm. Total flavonoid content was shown as mg of quercetin equivalent/gm of dried extract.

**2.5. Brine Shrimp Lethality Bioassay.** The cytotoxic properties of MELHR were investigated by the method of Alam et al. with slight modification [37]. *Artemia salina* leaches (brine shrimp eggs) were subjected as test organisms to evaluate the toxic potential. To develop artificial seawater, the seawater (38 g/L) and 1N NaOH were mixed well and adjust the pH 8.5. After that, shrimp eggs were hatched in this mixer and placed at room temperature under a constant oxygen supply. Around 2 days were allowed for maturing the shrimp eggs into larvae which were named nauplii. The crude extract was dissolved in DMSO (5 mg/mL) with artificial seawater and considered as a test sample which was led to serial dilution and obtained several concentrations (31.25 to 1000  $\mu\text{g}/\text{mL}$ ). Vincristine sulfate was used in this experiment as a positive control as the preceding method in serial concentrations between 0.125  $\mu\text{g}/\text{mL}$  to 10  $\mu\text{g}/\text{mL}$ . In each experimental vial, ten alive nauplii were added and incubated at room temperature under the light. After incubation, an amplifying glass was applied to calculate the living nauplii in each vial and record the number. The mortality percentage of nauplii was figured out according to the equation:

$$\text{percentage (\% of mortality)} = \frac{N_0 - N_1}{N_0} \times 100, \quad (2)$$

where  $N_0$  = number of nauplii taken and  $N_1$  = number of nauplii alive.

#### 2.6. Anti-Inflammatory Assessment

**2.6.1. Erythrocyte Suspension Preparation.** Alsever solution (0.5% citric acid, 0.8% sodium citrate, 2% dextrose, and 0.42% sodium chloride) was taken and equally mixed with fresh whole blood that was taken from some healthy volunteers. Then, the blood solution was centrifuged at 3000 g for 10 mins. After that, isosaline was subjected to wash the packed cells, then made 10% v/v solution, and kept at 4°C before use in this experiment.

**2.6.2. Hypotonic-Induced Human Red Blood Cell Hemolysis.** The anti-inflammatory effects of MELHR were inspected on hemolysis of human red blood cells (HRBCs) induced by a hypotonic solution and were evaluated using the described method with slight modification [18]. Different concentrations (31.25 to 1000  $\mu\text{g}/\text{mL}$ ) of crude extract and diclofenac sodium were taken, and then, add 0.5 mL of stock

erythrocyte (RBC) suspension, 1 mL of 10 mM sodium phosphate buffer (pH 7.4), and 2 mL of hypotonic solution (50 mM sodium chloride), respectively. 0.5 mL of stock erythrocyte (RBC) suspension and the hypotonic-buffered solution were mixed and considered as a control sample solution. The different mixer that was made in this experiment was incubated for half an hour at 37°C temperature and then centrifuged for 20 mins at 3000 g. After centrifugation, the supernatant solution was subjected to calculate the absorbance at 560 nm on a UV spectrophotometer. The percentage of inhibition was counted through the equation as follows:

$$\text{percentage (\% of inhibition)} = \frac{OD_1 - OD_2}{OD_1} \times 100, \quad (3)$$

where  $OD_1$  = optical density of the hypotonic-buffered saline solution and  $OD_2$  = optical density of test sample in a hypotonic solution.

**2.7. Antiarthritic Assay.** The antiarthritic activity of MELHR was investigated by the method of the protein denaturation technique [18]. The reaction mixture of test solution (0.5 mL) consisted of 5% w/v aqueous solution of bovine albumin (0.45 mL) and test sample (0.05 mL), and the control solution (0.5 mL) comprised a mixture of 0.45 mL bovine serum albumin (5% of w/v aqueous solution) and 0.05 mL of distilled water. Different concentrations (31.25 to 1000  $\mu\text{g}/\text{mL}$ ) of MELHR and diclofenac sodium were taken. 1N HCl was applied to adjust the pH 6.3 of the solutions and then incubated first for 20 mins at 37°C temperature. After that, all solutions were kept in an incubator for half an hour again at 57°C. After the incubation process, all the solutions were cooled, and then add 2.5 milliliters of phosphate buffer. The UV-visible spectrophotometer was subjected to measure the absorbance of the solutions at 416 nm. The control manifests 100% protein denaturation. The following equation was used to measure the percentage inhibition of protein denaturation:

$$\text{percentage (\% of inhibition)} = \frac{A_C - A_S}{A_C} \times 100, \quad (4)$$

where  $A_C$  = absorbance of the control and  $A_S$  = absorbance of the sample.

**2.8. Thrombolytic Activity.** The *in vitro* thrombolytic assay was performed using streptokinase vial in the same method described by Hasnat et al. [38]. 0.5 ml of venous blood withdrawn from healthy volunteers was placed in ten sterile microcentrifuge tubes which were previously weighed. Each tube was placed in incubation for 45 min at 37°C or clot formation. When the clot formation is completed, serum was gently removed from each test tube without disrupting the clot. 100  $\mu\text{l}$  of (10 mg/ml) methanol extract was added to the preweighed clot. 100  $\mu\text{l}$  streptokinase was added to the positive control group and 100  $\mu\text{l}$  of distilled water in the negative control group. All the tubes were further incubated for 90 min at 37°C for clot lysis. After removing the fluid, the

weight of the clot was further measured and the difference in weight was calculated. The percentage clot lysis was computed using the formula:

$$\% \text{ clot lysis} = \left( \frac{\text{weight of clot after removing the fluid}}{\text{weight of clot}} \right) \times 100. \quad (5)$$

**2.9. Anthelmintic Activity.** The anthelmintic activity of crude extracts was measured by the method described by Ajaiyeoba et al. with some minor modifications [39]. In this experiment, the aquarium worm *Tubifex tubifex* was subjected to find out anthelmintic potential because it has anatomical similarity and belongs to the same group of intestinal worms. The sludge worm used in this experiment was collected from the aquarium shop of Chittagong. The experiment was divided into several groups; whereas the negative control group consists of only distilled water, the positive control group consisted of the standard drug levamisole (1 mg/mL), and the test group consisted of different concentrations (5, 8 and 10 mg/mL) of crude extracts, respectively. In this investigation, 10 to 12 worms were placed in each Petri dish in five different groups. Then, 3 mL of the different concentrations of all groups was added to the Petri dish. The initial time, paralysis time, and the death time of the worms were observed and recorded carefully, in which paralysis time and death time of worms were considered as the evaluation of the anthelmintic activity of this experiment. When the worm's movement could not be observed after shaking vigorously, the paralysis time and the death time considered by the confirmation of worm's movement could not be observed either after shaking or when dipped in slightly warm water.

**2.10. Statistical Analysis.** GraphPad Prism version 7.00 (GraphPad Software Inc., San Diego, CA) was used to analyze the experimental results. The data were presented as mean  $\pm$  SEM (standard error mean), in which \* $p < 0.05$ , \*\* $p < 0.01$ , and \*\*\* $p < 0.001$  were considered as statistically significant. The one-way ANOVA was measured by following Dunnett's test compared to the negative control. All the assays were conducted as triplicate and repeated three times each for the consistency of the result and statistical function.

### 3. Results

**3.1. Phytochemical Screening.** The qualitative phytochemical experiment of methanolic extracts of *L. hyalina* Nees root (MELHR) manifested the presence of carbohydrates, quinones, alkaloids, reducing sugar, phenols, polyphenols, flavonoids, triterpenoids, coumarins, and cardiac glycosides. The yield of this experiment is summarized in Table 1.

#### 3.2. Antioxidant Effect

**3.2.1. DPPH Radical Scavenging Assay.** The antioxidant activity of MELHR was investigated by DPPH free radical



TABLE 1: Result of phytochemical screening of methanolic extract of *L. hyalina* Nees roots (MELHR).

Phytochemicals	Test types	Appearance	Results
Carbohydrates	Molisch's test	Reddish color ring form	++
Quinones	HCl test	Yellow color present	+
Alkaloids	Wagner test	A reddish-brown color	++
	Mayer's test	Yellow color	+
Reducing sugar	Benedict's test	Reddish color precipitate form	++
	Fehling's test:	Red precipitate form	++
Phenols	FeCl <sub>3</sub> test	Violet color form	++
Polyphenols	Ferric cyanide test	Blue-green color form	+
Flavonoids	Lead acetate test	Fluorescence yellow color form	++
Resins	FeCl <sub>3</sub> test	No precipitation	-
Glycosides	Shinoda test	No deep red color	-
Phlobatannins	HCl test	No reddish precipitate form	-
Xanthoproteins	Xanthoprotein test	No reddish-brown precipitate form	-
Triterpenoids	Salkowski's test	Reddish-brown color form	+
Coumarins	Ammonia test	Green color form	++
Cardial glycosides	Legal test	Brown color	+
Cholesterols	General test	No red rose color	-

++: Highly present; +: moderately present; -: absent.

scavenging. The crude extract manifests potential antioxidant properties which were presented in Figure 1. The maximum antioxidant potency (76.18%) of MELHR has shown at 500  $\mu\text{g}/\text{ml}$  concentration, while standard ascorbic acid demonstrates a 97.49% effect at the same concentration. Here, the potentiality of scavenging properties was increased compared with the increased concentration. The  $\text{IC}_{50}$  values of MELHR and ascorbic acid were 189.01% and 20.59%, respectively, which was estimated via linear regression formula.

**3.2.2. Reducing Power Activity.** Reducing power is related to antioxidant properties in which the components containing reducing power can decrease the oxidized intermediated lipid peroxidation process. The reducing power properties of MELHR and ascorbic acid are summarized in Figure 2. We can see that both extract and standard displayed increased absorbance with the increased concentrations. The peak absorbance of MELHR was found 0.451 at 1000  $\mu\text{g}/\text{ml}$  concentration, whereas the standard has shown 1.88 absorbance at the same concentrations.

**3.2.3. Total Flavonoid and Phenol Contents.** The total flavonoid and phenol content of the crude extract was estimated quantitatively. The result is displayed in Table 2. The flavonoid and phenolic potentials of MELHR were found at  $41.40 \pm 0.204$  mg QE/gm and  $98.61 \pm 0.064$  mg GAE/gm, respectively. Here, MELHR was carried out through linear regression equation (for flavonoid activity, equation stands as  $y = 0.0102x - 0.0637$ ; for phenol assay, it was  $y = 0.0039x + 0.033$ ).

**3.3. Cytotoxic Activity.** The potential of cytotoxicity of crude extract was evaluated via brine shrimp cytotoxic assay. The fatality result of plant extract was assessed in Figure 3. Here, the  $\text{LC}_{50}$  value of MELHR was 135.35  $\mu\text{g}/\text{mL}$  which was demonstrated via linear regression equation

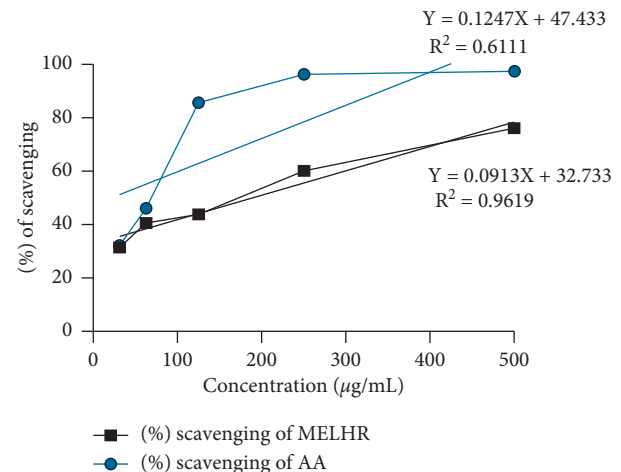


FIGURE 1: Percentage of radical scavenging activity by the DPPH (1, 1-diphenyl-2-picrylhydrazyl) assay of the MELHR (methanolic extract of *L. hyalina* Nees root) and standard drug ascorbic acid (AA) at differ concentrations.

( $y = 0.0691x + 40.647$ ) and the average percentage of mortality was 63.33%.

**3.4. Anti-Inflammatory Effect.** The *in vitro* anti-inflammatory potential of MELHR is assessed in Figure 4, in which crude extracts manifest dose-dependently and significantly ( $p < 0.05$ ) increased the anti-inflammatory properties. The peak percentage of inhibition of hemolysis by hypotonic solution and heat-induced hemolysis of crude extract was found  $55.01 \pm 3.22$  at 1000  $\mu\text{g}/\text{mL}$  concentration, whereas diclofenac Na manifested  $82.46 \pm 1.92$  at the same concentration.

**3.5. Antiarthritic Effect.** The antiarthritic activity of MELHR on protein denaturation is presented in Figure 5. The plant extract showed dose-dependent inhibitory potency when

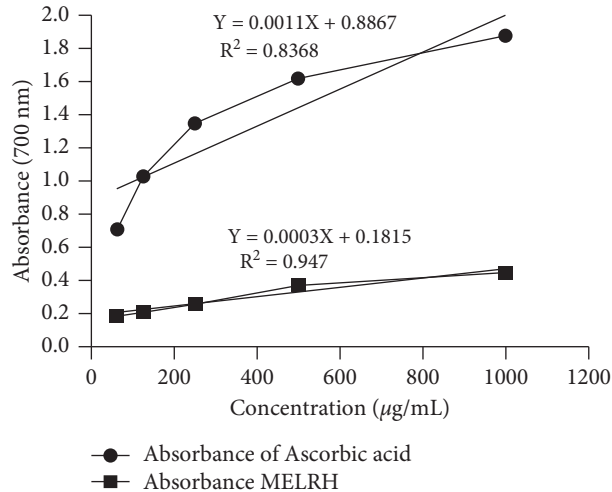


FIGURE 2: Reducing power of MELHR and standard drug ascorbic acid (AA) at different concentrations.

TABLE 2: Total phenol and flavonoid contents of methanol extract of *Lepidagathis hyalina* Ness root (MELHR).

Tested extract	Total phenol content (mg GAE/g dried extract)	Total flavonoid content (mg QE/g dried extract)
MELHR	98.61 ± 0.064	41.40 ± 0.204

MELHR: methanolic extract of *L. hyalina* Ness root.

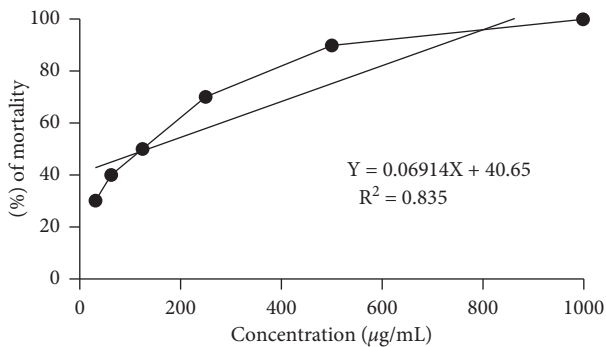


FIGURE 3: Percentage of mortality of brine shrimp at different concentrations of methanolic extract of *L. hyalina* Nees (MELHR).

compared to diclofenac sodium. The percentage of inhibition was 21.71 ± 3.53, 28.15 ± 1.88, 44.58 ± 2.03, 55.41 ± 3.25, 60.64 ± 1.22, and 71.97 ± 2.71 for MELHR; and 65.3 ± 1.09, 74.87 ± 0.89, 79.73 ± 0.82, 82.59 ± 1.4, 86.44 ± 0.73, and 93.59 ± 0.22 for diclofenac sodium at the concentration of 31.25, 62.5, 125, 250, 500, and 1000 µg/mL, respectively.

**3.6. Thrombolytic Effect.** The thrombolytic property of MELHR is shown in Figure 6. The experimental record uncovers that MELHR has significantly ( $p < 0.005$ ) moderate (29.39 ± 1.40%) clot lysis properties compared with both positive and negative controls.

**3.7. Anthelmintic Effect.** The anthelmintic activity of MELHR was investigated on *Tubifex tubifex* worms which finding summarized in Table 3. In this investigation, at the 5, 8, 10 µg/mL concentrations the extract manifested significant paralysis time 13.2 ± 0.842, 7.37 ± 0.684, and

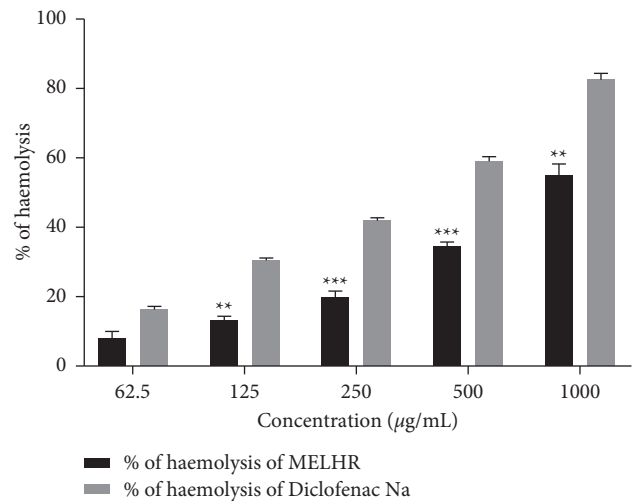


FIGURE 4: In vitro anti-inflammatory activity (membrane stabilizing assay) of methanolic extract of *L. hyalina* Ness root (MELHR). Values are expressed as mean ± SEM ( $n = 3$ ); \*  $p < 0.05$  is statistically significant comparison with diclofenac Na followed by Dunnett's test.

4.5 ± 0.65 min; and death time 36.16 ± 3.096, 27.3 ± 2.197, and 15.53 ± 1.88 min, respectively, whereas the standard drug levamisole showed paralysis and death time 3.17 ± 0.189 and 6.5 ± 0.384 min, respectively, at 1 µg/mL. The result indicated that the effect of anthelmintic was directly proportional to the concentrations of crude extract.

## 4. Discussion

Despite the availability of modern medicines, medicinal plants in developing countries are becoming increasingly

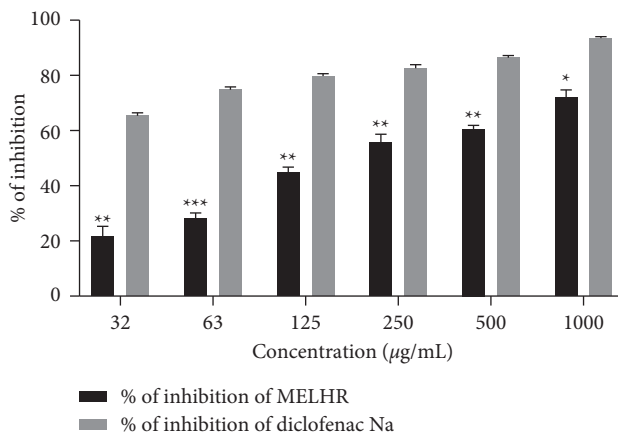


FIGURE 5: *In vitro* antiarthritic activity (inhibition of protein denaturation assay) of methanolic extract of *L. hyalina* Ness root (MELHR). Values are presented as mean ± SEM; one-way analysis of variance (ANOVA) followed by Dunnett’s test. \*\*  $p < 0.01$  and \*\*\*  $p < 0.001$  are considered as significant compared with the diclofenac Na.

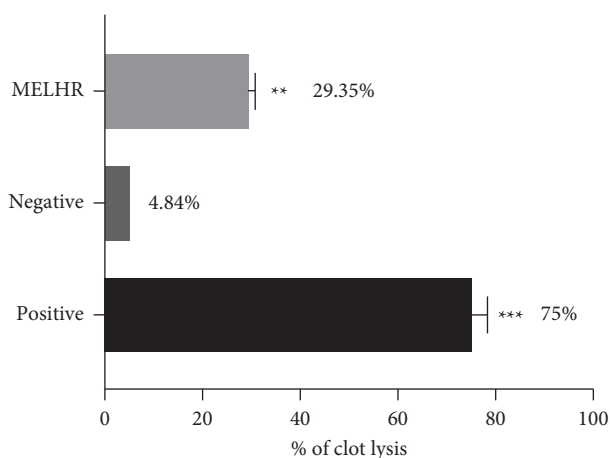


FIGURE 6: *In vitro* thrombolytic activity of MELHR. Values are presented as mean ± SEM; one-way analysis of variance (ANOVA) followed by Dunnett’s test. \*  $p < 0.05$ , \*\*  $p < 0.01$ , and \*\*\*  $p < 0.001$  are considered as significant compared with control.

TABLE 3: Anthelmintic activity of methanolic extract of *Lepidagathis hyalina* Ness root (MELHR).

Treatment and concentration	Time taken for paralysis in min	Time taken for death in min
Levamisole (1 µg/mL)	3.17 ± 0.189	6.5 ± 0.384
MELHR (5 µg/mL)	13.2 ± 0.842***	36.16 ± 3.096***
MELHR (8 µg/mL)	7.37 ± 0.684**	27.3 ± 2.197***
MELHR (10 µg/mL)	4.5 ± 0.65	15.53 ± 1.88*

MELHR: methanolic extract of *L. hyalina* Ness root.

popular as primary healthcare products because of their low cost and low side effects and toxicity [40, 41]. In this study, we conducted various tests to assess different health benefits like antioxidant, anti-inflammatory, antiarthritic, thrombolytic, cytotoxic, and antianthelmintic of the methanolic extract of *Lepidagathis hyalina* roots. Phytochemical screening of the methanolic extract of *L. hyalina* roots confirmed the presence of a wide range of chemical entities such as carbohydrates, quinones, alkaloids, reducing sugar, phenols, polyphenols, flavonoids, triterpenoids, coumarins, and cardiac glycoside that can be associated with several pharmacological activities given by the plant extract.

The numerous artificial antioxidants have been replaced with plant-based polyphenols and flavonoids in recent years. Nature source antioxidants are obviously safer to consume than artificial antioxidants, which are suspected of harmful effects on health [8, 42]. The extracts of the plant were compared with conventional antioxidant ascorbic acid, which exhibited a dose-dependent antioxidant activity in DPPH testing. The IC<sub>50</sub> values of crude extract were found 189.01%, which by comparison with ascorbic acid stand as 20.59%. Then, the connection of methanol extracts between TPC, TFC, reducing power, and DPPH was analyzed, indicating that MELHR has strong antioxidant potentiality

[19]. However, the brine shrimp lethality test is a common technique to test cytotoxic action along with ion channel interference, enzyme inhibition, and antibacterial activity [43].  $LC_{50}$  at low concentration with a quick response indicates that the plant extract is quite potent to give cytotoxic activity [16].

Since the membrane of erythrocytes is regarded to be analogous to the lysosomal membrane, the erythrocyte membrane stabilization test is considered to be an efficient tool for the anti-inflammatory drug screening process. The extracellular release of lysosomal contents by activated neutrophils is an important phenomenon in the pathophysiology of inflammation that is why membrane stabilization tests play a crucial role to assess inflammation [44, 45]. Both MELHR and diclofenac Na treatment groups significantly increased the percentage of hemolysis in a dose-dependent manner. Thus, the plant extract exhibited an anti-inflammatory effect in medium to high doses. One of the most well-known origins of arthritic diseases is the denaturation of tissue proteins. Denaturation of proteins can result in the production of autoantigens in some arthritic disorders [46, 47]. It might be caused by changes in electrostatic, hydrophobic, disulphide, and hydrogen bonds in proteins [47]. Here, the *in vitro* antiarthritic activity of MELHR was summarized in terms of inhibition of the protein denaturation method. The study demonstrated that both the standard drug and the plant extract increase inhibition level gradually with the increase in doses, but diclofenac Na was observed to give better results than plant extract indicating a better antiarthritic effect.

Thrombosis occurs as a result of hypercoagulation of the blood, damage to blood vessels, and blockage of blood flow within blood vessels. It is a life-threatening vascular complication of arthritis, myocardial infarction, pulmonary embolism, cerebrovascular ischemia, stroke, and venous embolism. Furthermore, venous thrombosis has been identified as the second greatest cause of cancer-related mortality [48]. The plant extract significantly ( $p < 0.05$ ) reduced the percentage of clot lysis (29.35%) as moderate scale compared with standard. A significant difference between the percentage values of clot lysis of positive and treatment groups indicates the efficiency of plant extract to exert effective thrombolytic activity. In a previous study, carbon tetrachloride extract and dichloromethane soluble extract have shown an almost similar level of activity ( $24.89 \pm 0.23$  and  $23.59 \pm 1.29\%$ , respectively) against streptokinase standard [49].

As part of a study to assess anthelmintic action, it was discovered that the crude extract causes dose-dependent paralysis, ranging from loss of mobility to death. The plant extract's paralysis and death time were compared to that of the standard medication levamisole. The anthelmintic activity of the test extract steadily increased, although at a higher concentration than levamisole. The fact that the plant extract includes a combination of components, but levamisole is a single component utilized as a medicine, might be the explanation. It was obtained from the previous studies that alkaloid, phenol, tannin, and terpenoids play an important role to give anthelmintic activity [50–52].

## 5. Conclusions

The complied pharmacological results indicated that this plant has a strong potentiality for the treatment of several diseases like arthritis, inflammation, cancer, etc. In our investigation, MELHR has been proved to have promising radical scavenging properties. Additionally, MELHR possesses significant arthritis, anti-inflammatory, thrombolytic, and anthelmintic activity with moderate toxic effects. This potentiality of MELHR could be due to the several bioactive compounds that are found in phytochemical analysis. Overall, *L. hyalina* Nees could be considered as a potential source for discovering the secondary metabolites which could be used for numerous pharmacological applications, and further studies are required to reveal the mechanism behind its potentiality.

## Abbreviations

MELHR:	Methanol extract of <i>Lepidagathis hyalina</i> Nees root
BSA:	Bovine serum albumin
DPPH:	1, 1-Diphenyl-2-picrylhydrazyl
FCR:	Folin-ciocalteu reagent
SEM:	Standard error mean
TPC:	Total phenol content
TFC:	Total flavonoid content
UV:	Ultraviolet.

## Data Availability

The data used to support the findings of this study are included within the article.

## Conflicts of Interest

The authors declare that they have no conflicts of interest.

## Authors' Contributions

M.S.I. and F.I.F. combined, investigated, planned, and designed the research. M.A.S. and M.N.I. arranged the whole facilities for the experimental research. M.S.I., F.I.F., A.S., and S.B.R. prepared the extract and carried out experimental work, data collection, evaluation, and literature search. M.S.I., F.I.F., A.R., and S.A.J.S. imparted in study design and interpreted the results putting efforts on statistical analysis with M.A.S. and M.N.I. M.S.I., F.I.F., A.S., and M.N.I. participated in the manuscript draft and have thoroughly checked and revised the manuscript for necessary format changes. M.N.I. and M.A.S. supervised the entire research work and reviewed and edited the manuscript. All authors read and agreed on the final version of the manuscript.

## Acknowledgments

The authors are thankful to the Department of Pharmacy, International Islamic University Chittagong (IIUC), Bangladesh, for research facilities and other logistic supports.

This work was conducted with the individual funding of all authors.

## References

- [1] J. Rahman, A. M. Tareq, M. M. Hossain et al., "Biological evaluation, DFT calculations and molecular docking studies on the antidepressant and cytotoxicity activities of *Cycas pectinata* buch.-ham. compounds," *Pharmaceuticals*, vol. 13, no. 9, p. 232, 2020.
- [2] A. Roy, "A review on the alkaloids an important therapeutic compound from plants," *IJPB*, vol. 3, no. 2, pp. 1–9, 2017.
- [3] M. N. Islam, A. Rauf, F. I. Fahad et al., "Superoxide dismutase: an updated review on its health benefits and industrial applications," *Critical Reviews in Food Science and Nutrition*, vol. 61, pp. 1–19, 2021.
- [4] F. J. Pashkow, "Oxidative stress and inflammation in heart disease: do antioxidants have a role in treatment and/or prevention?" *International Journal of Inflammation*, vol. 2011, Article ID 514623, 2011.
- [5] P. R. Moreno and V. Fuster, "New aspects in the pathogenesis of diabetic atherothrombosis," *Journal of the American College of Cardiology*, vol. 44, no. 12, pp. 2293–2300, 2004.
- [6] A. Mantovani, P. Allavena, A. Sica, and F. Balkwill, "Cancer-related inflammation," *Nature*, vol. 454, no. 7203, pp. 436–444, 2008.
- [7] A. Roy, S. Datta, K. S. Bhatia, P. Jha, and R. Prasad, "Role of plant derived bioactive compounds against cancer," *South African Journal of Botany*, vol. 147, 2021.
- [8] A. Roy, A. Anand, S. Garg et al., "Structure-based in silico investigation of agonists for proteins involved in breast cancer," *Evidence-Based Complementary and Alternative Medicine*, vol. 2022, Article ID 7278731, 2022.
- [9] C. R. Sahoo, S. K. Paidasetty, and R. N. Padhy, "The recent development of thymol derivative as a promising pharmacological scaffold," *Drug Development Research*, vol. 82, no. 8, pp. 1079–1095, 2021.
- [10] V. Sachdeva, A. Roy, and N. Bharadvaja, "Current prospects of nutraceuticals: a review," *Current Pharmaceutical Biotechnology*, vol. 21, no. 10, pp. 884–896, 2020.
- [11] A. Roy, S. Ahuja, and N. Bharadvaja, "A review on medicinal plants against cancer," *Journal of Plant Sciences and Agricultural Research*, vol. 2, no. 1, pp. 8–12, 2017.
- [12] J. Sellam and F. Berenbaum, "The role of synovitis in pathophysiology and clinical symptoms of osteoarthritis," *Nature Reviews Rheumatology*, vol. 6, no. 11, p. 625, 2010.
- [13] Y. Li, R. Kakkar, and J. Wang, "In vivo and in vitro approach to anti-arthritis and anti-inflammatory effect of crocetin by alteration of nuclear factor- $\kappa$ B-related factor 2/hem oxygenase (HO)-1 and NF- $\kappa$ B expression," *Frontiers in Pharmacology*, vol. 9, p. 1341, 2018.
- [14] A. Mor, S. B. Abramson, and M. H. Pillinger, "The fibroblast-like synovial cell in rheumatoid arthritis: a key player in inflammation and joint destruction," *Clinical Immunology*, vol. 115, no. 2, pp. 118–128, 2005.
- [15] J. S. Bang, H. M. Choi, B.-J. Sur et al., "Anti-inflammatory and antiarthritic effects of piperine in human interleukin 1 $\beta$ -stimulated fibroblast-like synoviocytes and in rat arthritis models," *Arthritis Research & Therapy*, vol. 11, no. 2, pp. 1–9, 2009.
- [16] T. A. Chowdhury, A. M. Kamal, K. A. A. Chowdhury, A. Chy, and K. Ashfaq, "Cytotoxic & thrombolytic activity of methanolic extract of *Macaranga denticulata* Bark," *The Pharma Innovation*, vol. 4, no. 5, p. 36, 2021.
- [17] S. Hajra, A. Mehta, P. Pandey, J. John, and P. Mehta, "Antibacterial property of crude ethanolic extract of *Mikania micrantha*," *Asian Journal of Experimental Biological Sciences*, vol. 2010, pp. 158–160, 2010.
- [18] P. Ansari, M. J. Uddin, M. M. Rahman et al., "Anti-inflammatory, anti-diarrheal, thrombolytic and cytotoxic activities of an ornamental medicinal plant: *Persicaria orientalis*," *Journal of Basic and Clinical Physiology and Pharmacology*, vol. 28, no. 1, pp. 51–58, 2017.
- [19] N. Alluri, R. Bv, H. Kumari, and M. Majumdar, "Evaluation of in vitro antioxidant, anti-inflammatory and thrombolytic activities of *Scilla hyacinthina*, an endangered medicinal plant," *International Journal of Pharmacy and Pharmaceutical Sciences*, vol. 7, no. 13, pp. 84–88, 2015.
- [20] A. R. Williams, C. Fryganas, A. Ramsay, I. Mueller-Harvey, and S. M. Thamsborg, "Direct anthelmintic effects of condensed tannins from diverse plant sources against *Ascaris suum*," *PLoS One*, vol. 9, no. 5, p. e97053, 2014.
- [21] P. M. Jourdan, P. H. Lamberton, A. Fenwick, and D. G. Addiss, "Soil-transmitted helminth infections," *The Lancet*, vol. 391, no. 10117, pp. 252–265, 2018.
- [22] M. Stenson, J. Van der Merwe, R. Vorster, P. Viljoen, and J. A. Van Wyk, "Anthelmintic resistance in South Africa: surveys indicate an extremely serious situation in sheep and goat farming," *Onderstepoort Journal of Veterinary Research*, vol. 66, no. 4, 1999.
- [23] W. Hassan, C. Eduardo Barroso Silva, I. U. Mohammadzai, J. Batista Teixeira da Rocha, and J. Landeira-Fernandez, "Association of oxidative stress to the genesis of anxiety: implications for possible therapeutic interventions," *Current Neuropharmacology*, vol. 12, no. 2, pp. 120–139, 2014.
- [24] O. Berton and E. J. Nestler, "New approaches to antidepressant drug discovery: beyond monoamines," *Nature Reviews Neuroscience*, vol. 7, no. 2, pp. 137–151, 2006.
- [25] J.-M. Kong, N.-K. Goh, L.-S. Chia, and T.-F. Chia, "Recent advances in traditional plant drugs and orchids," *Acta Pharmacologica Sinica*, vol. 24, no. 1, pp. 7–21, 2003.
- [26] D. Krishnaiah, R. Sarbatly, and A. Bono, "Phytochemical antioxidants for health and medicine a move towards nature," *Biotechnology and Molecular Biology Reviews*, vol. 2, no. 4, pp. 97–104, 2007.
- [27] K. S. Bhatia, S. Garg, A. Anand, and A. Roy, "Evaluation of different phytochemicals against BRCA2 receptor," *Bio-interface Research in Applied Chemistry*, vol. 12, no. 2, pp. 1670–1681, 2021.
- [28] M. G. Jinukuti and A. Giri, "Antimicrobial activity of phytopharmaceuticals for prevention and cure of diseases," *Annals of Phytomedicine*, vol. 2, no. 2, pp. 28–46, 2013.
- [29] M. Ekor, "The growing use of herbal medicines: issues relating to adverse reactions and challenges in monitoring safety," *Frontiers in Pharmacology*, vol. 4, p. 177, 2014.
- [30] R. Yadava, "A new biologically active triterpenoid saponin from the leaves of *Lepidagathis hyalina* Nees," *Natural Product Letters*, vol. 15, no. 5, pp. 315–322, 2001.
- [31] M. A. H. Mollik, B. C. Panday, and M. Badruddaza, *Abstract B73: Complementary and Alternative Medicine and the Development of Self in Chronic Diseases: A Prospective, Multi-center Observational Survey in the Munshiganj District of Bangladesh*, AACR, Philadelphia, PA, USA, 2010.
- [32] F. I. Fahad, N. Barua, M. Islam et al., "Investigation of the pharmacological properties of *Lepidagathis hyalina* nees through experimental approaches," *Life*, vol. 11, no. 3, p. 180, 2021.

- [33] B. Guha, M. Arman, M. N. Islam et al., "Unveiling pharmacological studies provide new insights on *Mangifera longipes* and *Quercus gomeziana*," *Saudi Journal of Biological Sciences*, vol. 28, no. 1, pp. 183–190, 2021.
- [34] M. A. Tayab, K. A. A. Chowdhury, and M. Javed, "Antioxidant-rich *Woodfordia fruticosa* leaf extract alleviates depressive-like behaviors and impede hyperglycemia," *Plants*, vol. 10, no. 2, p. 287, 2021.
- [35] T. Sarkar, K. K. Bharadwaj, M. Salauddin, S. Pati, and R. Chakraborty, "Phytochemical characterization, antioxidant, anti-inflammatory, anti-diabetic properties, molecular docking, pharmacokinetic profiling, and network pharmacology analysis of the major phytoconstituents of raw and differently dried *Mangifera indica* (himsagar cultivar): an in vitro and in silico investigations," *Applied Biochemistry and Biotechnology*, vol. 194, pp. 1–38, 2021.
- [36] N. Banu, N. Alam, M. Nazmul Islam et al., "Insightful valorization of the biological activities of *Panicum heloch* leaves through experimental and computer-aided mechanisms," *Molecules*, vol. 25, no. 21, p. 5153, 2020.
- [37] S. Alam, N. U. Emon, S. Shahriar et al., "Pharmacological and computer-aided studies provide new insights into *Milletia peguensis* Ali (Fabaceae)," *Saudi Pharmaceutical Journal*, vol. 28, no. 12, pp. 1777–1790, 2020.
- [38] A. Hasanat, M. S. H. Kabir, M. A. Ansari et al., "*Ficus cunia* Buch.-Ham. ex Roxb. (leaves): an experimental evaluation of the cytotoxicity, thrombolytic, analgesic and neuropharmacological activities of its methanol extract," *Journal of Basic and Clinical Physiology and Pharmacology*, vol. 304 pages, 2019.
- [39] E. Ajaiyeoba, P. Onocha, and O. Olarenwaju, "In vitro anthelmintic properties of *Buchholzia coriacea* and *Gynandropsis gynandra* extracts," *Pharmaceutical Biology*, vol. 39, no. 3, pp. 217–220, 2001.
- [40] A. Roy and N. Bharadwaja, "Effect of various culture conditions on shoot multiplication and GC-MS analysis of *Plumbago zeylanica* accessions for plumbagin production," *Acta Physiologiae Plantarum*, vol. 40, no. 11, pp. 1–11, 2018.
- [41] A. Roy and N. Bharadwaja, "Qualitative analysis of phyto-compounds and synthesis of silver nanoparticles from *Centella asiatica*," *Innovative Techniques in Agriculture*, vol. 1, no. 2, pp. 88–95, 2017.
- [42] A. Roy and N. Bharadwaja, "Establishment of root suspension culture of *Plumbago zeylanica* and enhanced production of plumbagin," *Industrial Crops and Products*, vol. 137, pp. 419–427, 2019.
- [43] J. H. Cardellina, R. W. Fuller, W. R. Gamble et al., "Evolving strategies for the selection, dereplication and prioritization of antitumor and HIV-inhibitory natural products extracts," in *Bioassay Methods in Natural Product Research and Drug Development*, pp. 25–35, Springer, Berlin, Germany, 1999.
- [44] M. Škerget, P. Kotnik, M. Hadolin, A. R. Hraš, M. Simonič, and Ž. Knez, "Phenols, proanthocyanidins, flavones and flavonols in some plant materials and their antioxidant activities," *Food Chemistry*, vol. 89, no. 2, pp. 191–198, 2005.
- [45] T. M. Saleem, A. Azeem, C. Dilip, C. Sankar, N. Prasanth, and R. Duraisami, "Anti-inflammatory activity of the leaf extracts of *Gendarussa vulgaris* nees," *Asian Pacific Journal of Tropical Biomedicine*, vol. 1, no. 2, pp. 147–149, 2011.
- [46] E. Umapathy, E. Ndebia, A. Meeme et al., "An experimental evaluation of *Albuca setosa* aqueous extract on membrane stabilization, protein denaturation and white blood cell migration during acute inflammation," *Journal of Medicinal Plants Research*, vol. 4, no. 9, pp. 789–795, 2010.
- [47] S. S. Volluri, S. R. Bammidi, S. C. Chippada, and M. Vangalapati, "In-vitro anti-arthritic activity of methanolic extract of *Bacopa monniera*," *International Journal of Chemical Environmental and Pharmaceutical Research*, vol. 2, pp. 156–159, 2011.
- [48] A. Roy, N. Jauhari, and N. Bharadwaja, "Medicinal plants as a potential source of chemopreventive agents," in *Anticancer Plants: Natural Products and Biotechnological Implements*, pp. 109–139, Springer, Singapore, 2018.
- [49] M. M. Miah, P. Das, Y. Ibrahim, M. S. Shajib, and M. A. Rashid, "In vitro antioxidant, antimicrobial, membrane stabilization and thrombolytic activities of *Dioscorea hispida* Dennst," *European Journal of Integrative Medicine*, vol. 19, pp. 121–127, 2018.
- [50] A. Paul, M. Adnan, M. Majumder, and N. Kar, "Anthelmintic activity of *Piper sylvaticum* Roxb. (family: piperaceae): in vitro and in silico studies," *Clinical Phytoscience*, vol. 4, no. 1, pp. 1–7, 2018.
- [51] M. Salhan, B. Kumar, P. Tiwari, P. Sharma, H. K. Sandhar, and M. Gautam, "Comparative anthelmintic activity of aqueous and ethanolic leaf extracts of *Clitoria ternatea*," *International Journal of Drug Development & Research*, vol. 3, no. 1, pp. 62–69, 2011.
- [52] S. Banik, G. A. Hury, and M. S. Hussain, "Elucidation of phytochemical and pharmacological nature of methanolic extract of *Ixora cuneifolia*," *Asian Journal of Medicine and Health*, vol. 1, no. 5, pp. 1–7, 2016.



## Research Article

# Shen-Shuai-Ling Formulation Attenuates Renal Interstitial Fibrosis in Chronic Kidney Disease by Regulating SHH-Gli1 Signaling Pathway

Ying Li,<sup>1</sup> Haitao Tu,<sup>2</sup> Yan Luo <sup>1</sup>, Weijian Xiong <sup>2</sup>, Hong Liu,<sup>1</sup> Yanying Xiong,<sup>1</sup> Qin Zhang,<sup>1</sup> Huihui Li,<sup>1</sup> and Xuan Gao<sup>1</sup>

<sup>1</sup>Department of Nephrology, Chongqing Hospital of Traditional Chinese Medicine, Chongqing 400021, China

<sup>2</sup>Department of Nephrology, The First Clinical Hospital of Guangzhou Medical University, Guangzhou 510405, China

Correspondence should be addressed to Yan Luo; yanluoyl2021@outlook.com and Weijian Xiong; xw558369@163.com

Received 2 November 2021; Accepted 5 January 2022; Published 12 February 2022

Academic Editor: Ruchika Garg

Copyright © 2022 Ying Li et al. This is an open access article distributed under the Creative Commons Attribution License, which permits unrestricted use, distribution, and reproduction in any medium, provided the original work is properly cited.

**Background.** Shen-Shuai-Ling Formulation (SSLF) has apparent effects on improving renal function, delaying the progression of chronic kidney disease (CKD). **Methods.** Fifty male SD rats were randomly divided into 5 groups: Sham group, Model group, SSLF group, CPN group, and C + S group. The morphological changes and the collagen fibers of the rat kidneys were observed by HE staining. The expression of  $\alpha$ -SMA, Col I, SHH, Gli1, and snail1 was detected by Western blot and qPCR. Then, the cells were divided into the control group, SHH group, and SHH + SSLF serum group. **Results.** Compared with the Model group, the fibrosis in SSLF, CPN, and C + S groups was significantly alleviated. And, compared with those in the Model group, the expression of  $\alpha$ -SMA, Col I, SHH, Gli1, Snail in SSLF, CPN, and C + S groups decreased remarkably. **Conclusions.** SSLF remarkably improves renal function and alleviates renal interstitial fibrosis in UUO rats.

## 1. Introduction

CKD has become a prominent public health issue in the world. The global prevalence of CKD in 2017 was 9.1% (697.5 million cases). Nearly one-third of CKD cases occurred in China (132.3 million) or India (115.11 million), with more than 10 million cases in 10 countries and more than 1 million cases in 79 countries. In 2017, CKD caused 1.2 million deaths and was the 12th leading cause of death in the world [1, 2]. The prevention and treatment of CKD and its related diseases pose an immense challenge to the global health system. The main pathological changes of renal interstitial fibrosis (RIF) include myofibroblasts activation, abnormal deposition of the extracellular matrix, and progressive increase of fibrous scars [3, 4]. RIF is a common route and pathological feature in the development of all kinds of CKD leading to end-stage kidney disease. It has been confirmed that the severity of RIF is closely linked to the degree of renal function declination. It is an effective

indicator of the disease prognosis. Therefore, it is of great significance to study the mechanism of RIF in order to delay the pathological process of CKD and preserve renal function.

In recent years, a large number of studies have proved that SHH (Sonic hedgehog) signaling pathway is involved in the progress of liver, lung, and bile duct fibrosis [5–8]. Thus, the SHH signaling pathway has become a focus in tissue fibrosis research. Studies have shown that SHH is highly expressed in damaged renal tubular epithelial cells and mainly functions on proliferation and activation of interstitial fibroblasts [9–12]. Many domestic and international experiments have confirmed that the inhibition of the SHH signaling pathway could significantly reduce renal fibrosis and protect renal function [13]. Inhibition of Gli1, a marker protein in the SHH-Gli1 signaling pathway, is the emphasis of research. The expression of Gli1 is a reliable indicator of the activation of the SHH signaling pathway. Scholars abroad have also found that activation of SHH can be precisely controlled by regulating the expression of Snail. Therefore, it is particularly

important to seek a treatment scheme to block the activation of the SHH signaling pathway.

SSLF is a prescription developed by Xin Zheng, a master of Traditional Chinese Medicine with more than 60 years of clinical experience [14]. SSLF contains rhubarb, keel, oyster, Dangshen, astragalus, fungus *Ganoderma lucidum*, *Epidemium*, safflower, angelica, *salvia miltiorrhiza*, and dandelion [15]. SSLF has apparent effects on improving renal function, delaying the progression of CKD, and can significantly relieve clinical symptoms such as constipation and abdominal distension. To study SSLF's functional mechanism and understand its potential inhibitory role in renal fibrosis, this study utilizes the UUO model to mimic renal interstitial fibrosis in rats and administers SSLF and/or other medication to them. The pathological changes and cell proliferation in renal fibrosis and the effects of SSLF on the expression of SHH, Gli1, and snail1 protein have been analyzed. The relationship between SSLF and the SHH signaling pathway and the underlying mechanism of SSLF's inhibitory function against RIF is discussed in our study.

## 2. Materials and Methods

**2.1. Animals and Cells.** Fifty clean-grade male SD rats (7 weeks old,  $200 \pm 20$ g) were purchased from the Laboratory Animal Center of Chongqing Institute of Traditional Chinese Medicine (Animal license No. SCXK:20120001). Normal rat kidney interstitial fibroblasts (NRK-49F) were purchased from the American Type Culture Collection (ATCC, Manassas, VA). The animal study was performed according to the National Standards for Laboratory Animals. The animal experiment was approved by the Animal Ethics Committee of Chongqing Hospital of Traditional Chinese Medicine.

**2.2. Experimental Herbal Formulation.** SSLF is composed of rhubarb, *Codonopsis pilosula*, *Astragalus membranaceus*, *Osmunda cinnamomea*, *Ostreagastnunb*, *Carthamus tinctorius*, *Ganoderma lucidum*, *Angelica sinensis*, *Salvia miltiorrhiza*, *Epidemium brevicornu* Maxim, and dandelion, etc. SSLF used in our research was processed by the Chongqing Institute of Traditional Chinese Medicine.

**2.3. Reagents and Instruments.** Antibodies used in our experiments included anti-SHH, anti-Gli1, anti-snail1, and anti-GAPDH antibodies (Affinity Biosciences, China). PVDF membrane, BCA Protein Assay Kit, and BeyoECL Moon kit were acquired from Beyotime Biotechnology, China. Cyclopamine was purchased from Selleck Chemicals, USA. Experimental instruments included AU400 automatic biochemical analyzer (OLYMPUS, Japan), BX51T-PHD-J11 microscope (OLYMPUS Company, Japan), image acquisition system CMOS (OLYMPUS Company, Japan), and Image-Pro Plus (Media Cybernetics Company, USA), etc.

### 2.4. Animal Model and Experimental Design

**2.4.1. Experimental Animals.** The animal experiment was approved by the Animal Ethics Committee of Chongqing

Hospital of Traditional Chinese Medicine. Fifty clean-grade male SD rats were randomly divided into five groups with 10 rats in each group: Sham operation (Sham) group, Model group, SSLF group, CPN group, and S + C group. The Sham group were first sedated with 5% sodium pentobarbital. Then, their abdominal cavities were cut open to expose left ureters. Blunt dissection was performed on the left ureters before the closure of abdominal cavities by stratified suture. Besides the Sham group, all the other groups underwent the same surgical procedures to establish UUO model rats: after anesthesia with 5% sodium pentobarbital, the rats' left ureters were exposed and bluntly dissected. Double ligation with 4-0 surgical suture on the upper 1/3 of the ureters was applied to cut off the ureters before closing abdominal cavities. The SSLF group were given 20 mg/kg SSLF intragastrically for 14 days. The dosage was calculated according to Experimental Pharmacology [9]. The rats in the Sham group and Model group were intragastrically given 20 mg/kg of distilled water for 14 days. The CPN group were continuously injected with 10 mg/kg/d of Cyclopamine for 14 days. The S + C group were intragastrically injected with 20 mg/kg/d of SSLF and intraperitoneally injected with 10 mg/kg/d of Cyclopamine for 14 days. After 14 days, tissues and blood were harvested from the rats fasted for 12 hours. SSLF has no obvious side effects [16].

**2.4.2. Detection of Blood Biochemical Indexes.** The blood samples of rats were taken through the tail vein. The samples were settled at room temperature for one hour and centrifuged at 3500 rpm for 5 minutes. The clear supernatant was used for serum SCr and BUN analysis by an automatic biochemical analyzer.

**2.4.3. Histopathological Analysis of the Renal Tissue.** The rats' renal tissue was fixed in 4% paraformaldehyde for 24 hours, embedded in paraffin, and sectioned. The 3  $\mu$ m thick sections were dewaxed, treated with gradient ethanol, stained with Hematoxylin and Eosin (HE), and sealed with neutral resin. The renal tissue was observed by a microscope. The nuclei appeared to be pink or red under the microscope.

**2.4.4. Analysis of Renal Tissue Fibrosis.** The renal tissue was collected and immersed in a 4% paraformaldehyde tissue fixative. After dehydration, permeation, waxing, and embedding, 2  $\mu$ m tissue sections were produced with a pathological slicer. PAS (Periodic Acid-Schiff) and Masson staining were performed on the sections. Pathological semiquantitative analysis of glomeruli and tubules was performed using a light microscope. The degree of glomerular sclerosis was determined by selecting 50 glomeruli under 400 times magnification from each slide, and the sclerotic index of the glomeruli was calculated according to the average points.

The severity of sclerotic disease was scored from 1 to 4 points. The mesangial sclerotic area less than 25% was scored as 1 point; the sclerotic area between 25% and 50% was scored as 2 points; the sclerotic area between 50% and 75%

was scored as 3 points; the sclerotic area larger than 75% was scored as 4 points. The interstitial score of the renal tubules was analyzed under 200 times magnification; 10 tubules per visual field were observed. According to the range of renal tubular atrophy, tubular type, stromal cell infiltration, and fibrosis, scores of 0 to 3 were assigned: 0 for none, 1 for less than 25%, 2 for 25%–50%, and 3 for 50–75%.

**2.4.5. The Expression of Fibrosis-Related Proteins Detected by Western Blot.** Renal tissue protein was extracted, quantified, and visualized by Western blot after electrophoresis, membrane transfer, and antibody incubation. Primary antibodies (1:1000 dilution) for  $\alpha$ -SMA, Collagen I, SHH, Gli1, and Snail were added for overnight incubation at 4°C on a shaking bed, respectively. Then, the secondary antibody at 1:2000 dilution was added, and the membranes were incubated at 37°C for 120 min. After applying ECL color reagent and dark chamber exposure imaging, the gray value of the images was analyzed by Quantity One software. The ratio of the target protein to the GAPDH band absorbance value was calculated to reflect the expression level of the target proteins.

### 2.5. In Vitro Experiments

**2.5.1. NRK-49F Cells Stimulated by SHH.** NRK-49F cells purchased from ATCC (Manassas, VA) were utilized in the in vitro experiments. The cells were treated with 10% fetal bovine serum, 100000 units/L penicillin, and 100 mg/L streptomycin in the DMEM medium. The activation of NRK-49F cells was induced for 24-, 48-, or 72-hour by 100 ng/L human SHH protein (StemRD Inc., Burlingame, CA). The expression of snail1 and Gli1 in vitro was evaluated by Western blot analysis.

**2.5.2. Preparation of SSLF-Containing Serum.** Fifty clean-grade male SD rats were given 20 mg/kg of SSLF per day intragastrically. After 7 days, blood was harvested from the rats fasted for 12 hours. The blood samples of rats were settled at room temperature for one hour and centrifuged at 3500 rpm for 5 minutes to obtain SSLF serum stock.

**2.5.3. Administration of SSLF In Vitro.** A humidified incubator with 5% CO<sub>2</sub> at 37°C was used to culture the NRK-49F cells. The cells were divided into the following groups: the untreated control group (control); SHH group (SHH) in which cells were induced for 48 hours by 100 ng/L human SHH protein; and SHH + SSLF group (SHH + SSLF) in which cells were treated with 10% SSLF serum, 100000 units/L penicillin, and 100 mg/L streptomycin in the DMEM medium and induced for 48 hours by 100 ng/L human SHH protein. An equal amount of nuclear and cytoplasmic extracts was tested for the expression of Gli1, snail1, Collagen I,  $\alpha$ -SMA, and PCNA by Western blot.

**2.5.4. Network Pharmacology.** The main targets of the Shenhueling formula were predicted by network

pharmacology. The effective active ingredients of SSLF and related targets were searched in TCMSP. Rheumatoid arthritis-related genes were selected according to the GeneCards disease database, and the PPI protein interaction network was constructed to carry out GO enrichment analysis and KEGG pathway enrichment analysis of key targets.

**2.6. Statistical Analysis.** Data analysis was carried out using SPSS 17.0 software. The quantitative data were expressed as mean  $\pm$  SEM ( $\bar{x} \pm s$ ). Independent-samples *t*-test or ANOVA was applied for the statistical analysis. Pairwise comparisons were performed using *t*-tests. *p* value less than 0.05 was considered statistically significant.

## 3. Results

**3.1. Network Pharmacological Analysis.** We used TCMSP to find 10 major components of SSLF and Swiss TargetPrediction to predict 774 drug target genes. The intersection of drug target genes and 414 targets of renal interstitial fibrosis resulted in a total of 86 targets, which were involved in biological processes and functions such as acute inflammatory response, protein binding, and growth factor receptor binding. The compounds targeting SHH were identified as quercetin, CLR, and epoxyganoderiol A, respectively, which were regarded as the major bioactive compounds (Figure 1).

### 3.2. Animal Experiments

**3.2.1. SCr and BUN Levels in Each Group.** Compared with the Sham group, the SCr and BUN levels in all the other groups were significantly higher ( $p < 0.05$ ). In comparison with the Model group, SCr and BUN levels in SSLF, CPN, and S + C groups were significantly lower ( $p < 0.05$ ). In comparison with the S + C group, SCr and BUN in SSLF and CPN groups were significantly higher ( $p < 0.05$ ). There was no significant difference between the SSLF and CPN groups (Figure 2).

**3.2.2. Observation of Kidney Samples in Each Group.** The kidneys from the Sham group were of normal size, dark red color, and soft to the touch. In the Model group, the left kidneys were obviously swollen and had a dark brown color. The renal capsules were tense; turbid fluid could be seen in the incision. The calyces of the renal pelvis were dilated and deformed, and the renal cortex appeared to be significantly thinner compared with that of the Sham group. The kidneys in SSLF, CPN, and S + C groups were found to be swollen and dark brown; however, their renal cortex appeared to be slightly thicker than that of the Model group.

**3.2.3. Histopathological Changes in Renal Tissues.** The HE staining of the Sham group showed normal renal tissue structure. The tubules in renal tissues were arranged neatly, and the basement membrane was continuous. No

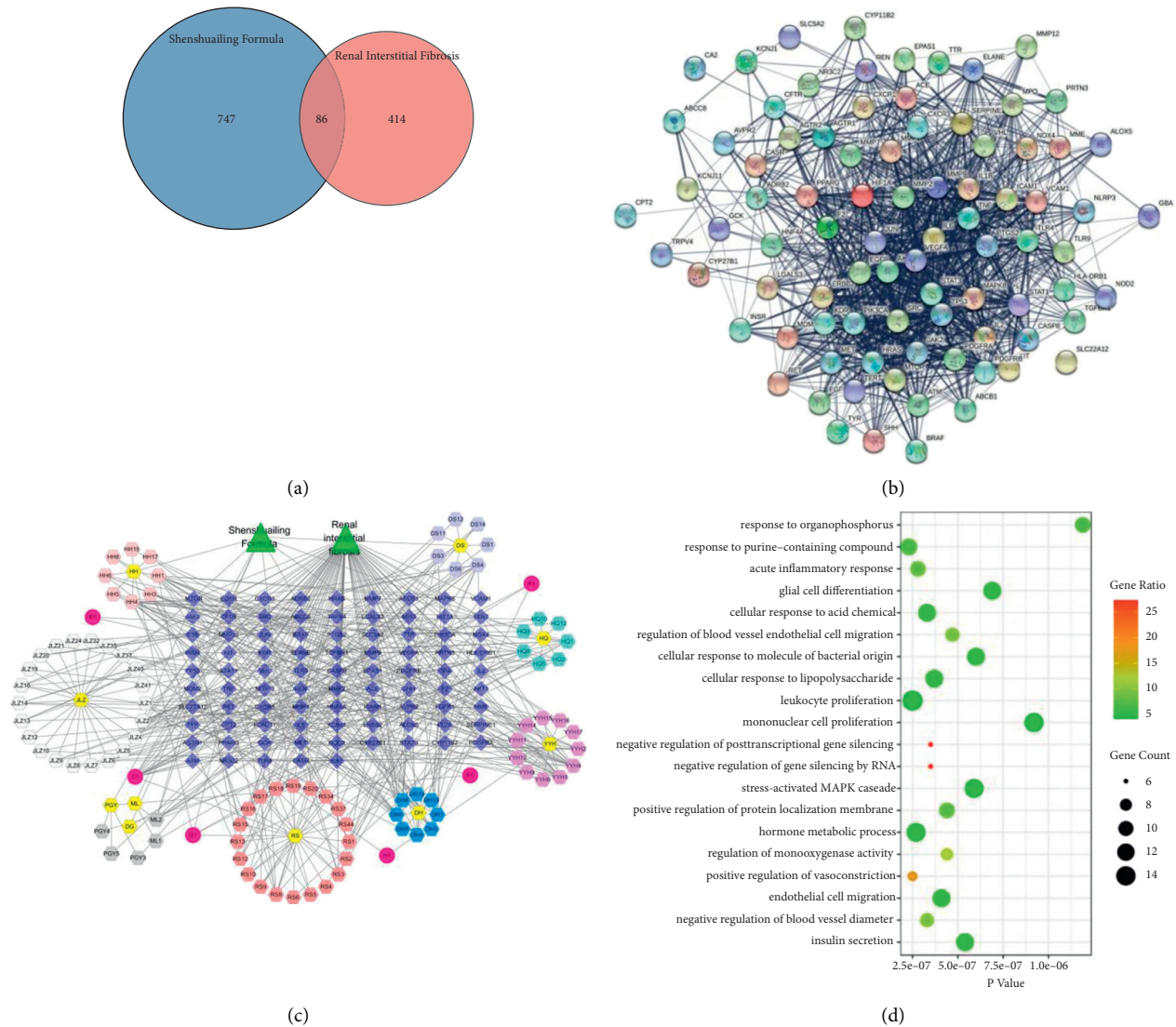


FIGURE 1: SSLF on renal interstitial fibrosis by network pharmacology analysis. (a) Venn diagrams of intersections of drug and disease targets. (b) String analysis protein interaction network diagram. (c) Drug-active ingredient-target network diagram. (d) Bubble map was analyzed by GO of intersection gene.

inflammatory infiltration in the stroma area was found. Compared with the Sham group, the renal tubules in the Model group were obviously dilated and atrophied. Fibrous tissue proliferated in the cortical medulla. The renal interstitial area expanded, and the infiltration of inflammatory cells was apparent. Compared with the Model group, there was less infiltration of renal interstitial inflammatory cells in the SSLF, CPN, and S + C groups. The dilatation and atrophy of renal tubules and fiber proliferation were also alleviated. No significant histopathological differences were seen in the SSLF, CPN, and S + C groups. However, the S + C group appeared to have less pathological changes (Figure 3).

**3.2.4. Effects of SSLF on Collagen Fiber Deposition Rate.** According to the method described in paragraph 1.4.4, the kidney samples from each group were counted and scored. There were no obvious changes in the glomerulus and renal

tubule in the Sham group. In the Model group, there were marked changes in the glomerulus, the renal tubule, and the interstitial tissue. The mesangial matrix had increased with hyperplastic mesangial cells, and the wall of the glomerulus was thickened. The capillary was expanded or occluded, and some of the pellets had segmental or spherical sclerosis. The renal tubule was atrophic and exhibited an expanded small tube. A large amount of the protein tube appears, accompanied by widened renal interstitial and infiltration of inflammatory cells. Renal stroma also showed microvascular lesions, with focal distribution, disordered structure, deformation, and reduction of the capillary cavity. The morphological changes in the C+S and CPN groups were slightly improved; the injury scores of glomeruli and tubules were significantly reduced. PAS staining showed that compared with the Model group, the glomerular score in the SSLF group had decreased by 10% ( $p < 0.05$ ), the CPN group had decreased by 12% ( $p < 0.05$ ), and the C + S group had

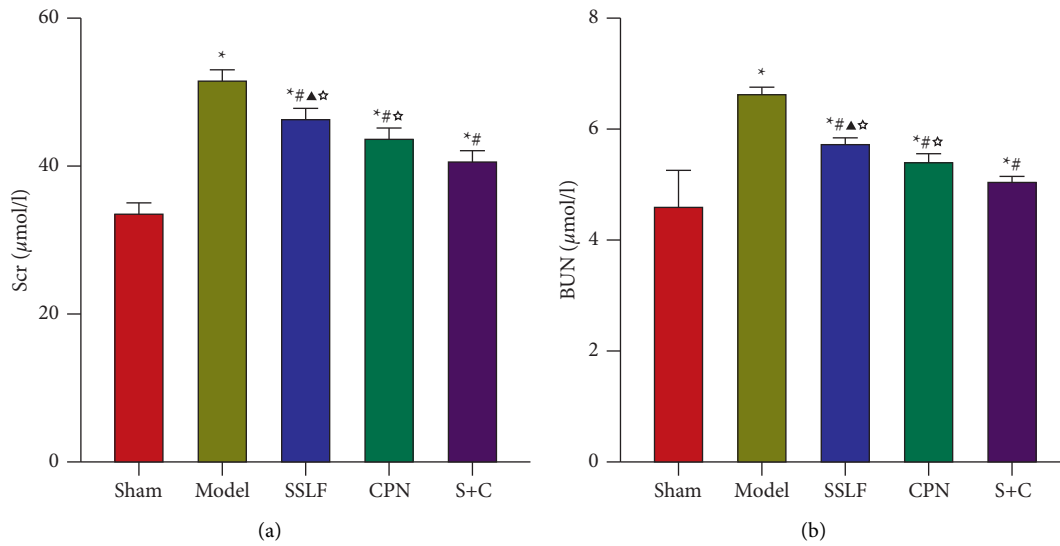


FIGURE 2: Levels of SCr and BUN in renal tissues in each group. (a) Levels of SCr in renal tissues in each group. (b) Levels of SCr in renal tissues in each group. \*  $p < 0.05$  compared with the Sham group; #  $p < 0.05$  compared with the Model group; ^  $p < 0.05$  compared with the S + C group; ▲  $p > 0.05$  compared with the CPN group.

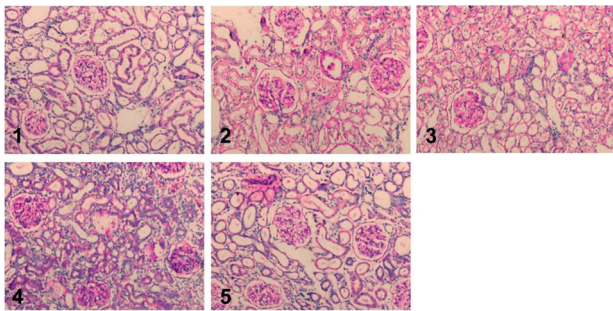


FIGURE 3: Histopathological changes in each group. 1: Sham group; 2: Model group; 3: SSLF group; 4: CPN group; 5: C + S group (HE staining,  $\times 200$ ).

decreased by 26% ( $p < 0.05$ ). There were no significant differences between the SSLF and CPN groups. The renal tubule stroma scores revealed by Masson staining showed that, in comparison with that in the Model group, the score of the SSLF group had decreased by 9% ( $p < 0.05$ ), and that of the C + S group had decreased by 14% ( $p < 0.05$ ). And the glomerular score of C + S group had decreased by nearly 21% ( $p < 0.05$ ). (Figures 4 and 5).

**3.2.5. Western Blot and qPCR Analysis.** The results of Western blot and qPCR showed the protein expression of  $\alpha$ -SMA, Collagen I, SHH, Gli1, and snail1 in the renal tissue of the Model group were significantly higher than those of the Sham group ( $p < 0.05$ ). And the protein expressions of  $\alpha$ -SMA, Collagen I, SHH, Gli1, and snail1 in the renal tissue of SSLF, CPN, and C + S groups were significantly lower than those of the Model group ( $p < 0.05$ ). There was no significant difference in the expression of fibrotic protein markers between CPN and S + C groups ( $p > 0.05$ ). (Figure 6).

### 3.3. In Vitro Experimental Results

**3.3.1. NRK-49F Cells Stimulated by SHH.** In comparison with the untreated control, the expressions of snail1 and Gli1 in NRK-49F cells stimulated by SHH (100 ng/ml) were significantly increased. Western blot and qPCR showed that the expression of snail1 and Gli1 in NRK-49F cells had increased in a time-dependent manner upon SHH stimulation. The expression of snail1 and Gli1 peaked at 48 h; thus, we set 48 h as the time point for follow-up experiments (Figure 7).

**3.3.2. Effects of SSLF In Vitro.** The expressions of Gli1, snail1, Collagen I,  $\alpha$ -SMA, and PCNA in control and SHH and SHH + SSLF groups were detected by Western blot and qPCR at 48h. The expressions of Gli1, snail1, Collagen I,  $\alpha$ -SMA, and PCNA in the SHH + SSLF group were significantly lower than those in the SHH group ( $p < 0.05$ ). The SHH and SHH + SSLF groups had higher levels of Gli1, snail1, Collagen I,  $\alpha$ -SMA, and PCNA expression, compared with control ( $p < 0.05$ ). (Figure 8).

## 4. Discussion

Shen-Shuai-Ling Formulation (SSLF) is a prescription from Traditional Chinese Medicine master Zheng Xin who has more than 60 years of experience. Master Zheng is proficient in the four classics of Traditional Chinese Medicine. Integrating classical and modern knowledge, he specializes in using Chinese herbal medicine to treat renal diseases. SSLF protects renal function by purging turbid toxin, tonifying healthy Qi, improving self-immunity, improving renal blood homeostasis, etc. It reflects the Traditional Chinese Medicine theory of strengthening body resistance and eliminating pathogens.



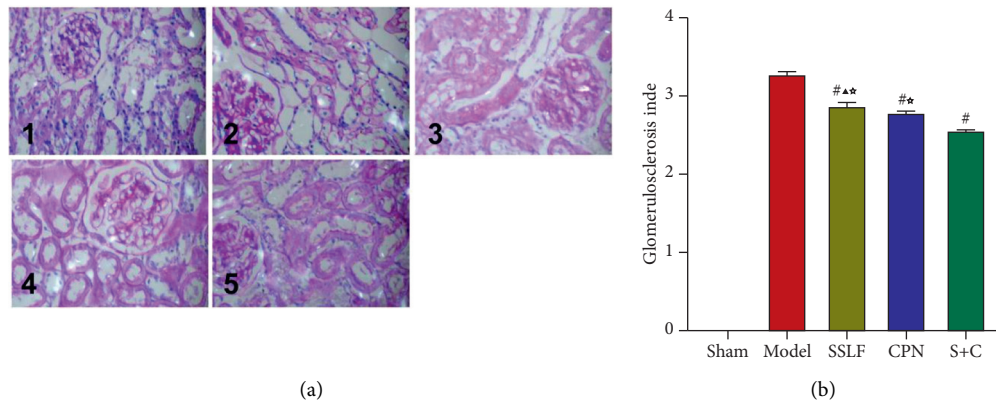


FIGURE 4: PAS staining to observe renal tissue fibrosis in each group. (a) 1: Sham group. 2: Model group. 3: SSLF group. 4: CPN group. 5: C + S group (PAS staining,  $\times 400$ ). (b) The scores of glomerulosclerosis index in PAS staining. <sup>#</sup> $p < 0.01$  versus Model group, <sup>\*</sup> $p < 0.05$  versus S + C group, <sup>▲</sup> $p > 0.05$  versus CPN group.

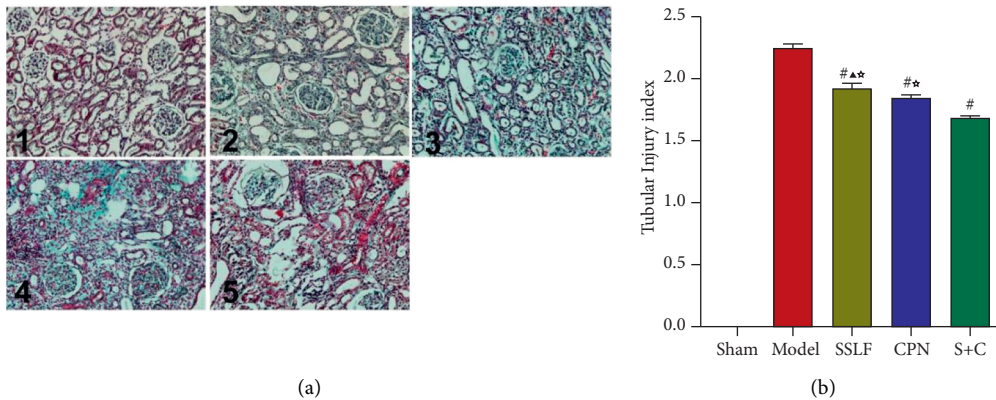


FIGURE 5: Masson staining to observe renal tissue fibrosis in each group. (a) 1: Sham group; 2: Model group; 3: SSLF group; 4: CPN group; 5: C + S group (Masson staining,  $\times 200$ ). (b) The scores of tubular injury index in Masson staining. <sup>#</sup> $p < 0.01$  compared with the Model group, <sup>\*</sup> $p < 0.05$  compared with the S + C group, and <sup>▲</sup> $p > 0.05$  compared with the CPN group.

To study the molecular mechanism of SSLF in the treatment of renal interstitial fibrosis, we screened out major bioactive compounds from SSLF and offered a new understanding of the protection mechanism of SSLF against renal interstitial fibrosis by network pharmacology method. We found that SHH is a common target of SSLF and renal interstitial fibrosis and the SHH signaling pathway has become a focus in tissue fibrosis research, so we chose SHH as the target gene and its downstream signaling pathway to study.

In the clinical study, the serum levels of SCr and BUN of the patients treated with SSLF for one course of treatment have significantly decreased. The results of the present study show that serum levels of SCr and BUN in the UUO rat model are significantly higher than those in the Sham group, suggesting that the UUO model has been successfully established. The serum levels of SCr and BUN in the SSLF treated group are significantly reduced, suggesting that SSLF has protective effects on the renal function of the UUO model rats. There is no significant difference in renal function between the CPN and SSLF groups. And the serum levels of SCr and BUN in the S + C group are the lowest, suggesting that SSLF and CPN have a synergistic effect.

Clinically, the cortex of renal tissue is thinned by a Color Doppler ultrasound of chronic kidney disease. In the Model group, the left kidneys look swollen and dark brown. Manifestations such as tight capsule, turbid effusion, dilatation and deformation of renal pelvis and calyces, and the thinner-than-normal renal cortex indicate the success of UUO model establishment. In the SSLF group, the kidneys are also swollen and dark brown. But the renal cortex is slightly thicker than that in the Model group, suggesting that SSLF has alleviated renal tissue damage and slowed down the progression of renal disease. HE staining reveals that the renal tubules in the Model group are obviously dilated, atrophic, and fibroblastic, accompanied by an increased area of renal interstitium and infiltration of inflammatory cells. According to PAS and Masson staining, the Model group have obvious collagen fiber deposition in renal interstitium, their renal tubules are atrophic or dilated, and there are apparent pathological changes such as glomerular sclerosis and microvascular disease. However, these indicators have been significantly alleviated in SSLF, CPN, and C + S groups according to the scoring system. Col I protein in the ECM can be produced in large quantities after myofibroblast



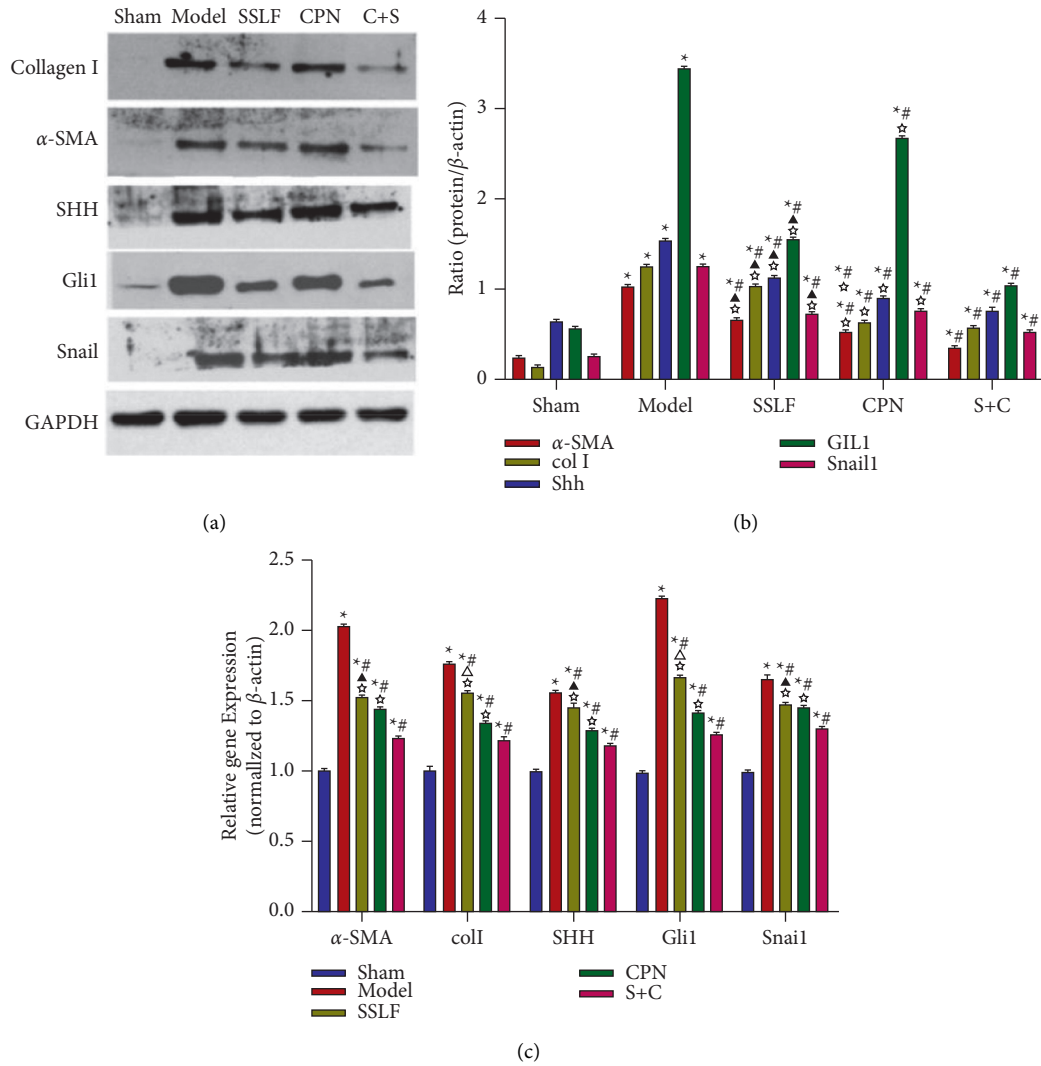


FIGURE 6: Levels of  $\alpha$ -SMA, Col I SHH, Gli1, and snail1 in renal tissues in each group. (a) Levels of  $\alpha$ -SMA, Col I SHH, Gli1, and snail1 were measured by Western blot. (b) Quantitative analysis. (c) Levels of  $\alpha$ -SMA, Col I SHH, Gli1, and snail1 were measured by qPCR. Data were expressed as mean  $\pm$  SEM. \*  $p < 0.05$  compared with the Sham group, #  $p < 0.05$  compared with the Model group,  $\Delta$   $p < 0.05$  compared with the CPN group,  $\star$   $p < 0.05$  compared with the S + C group,  $\blacktriangle$   $p > 0.05$  compared with the CPN group, and  $\star$   $p > 0.05$  compared with the C + S group.

activation. Normally, Col I plays a role in repairing damaged tissues, but the persistent inflammatory reaction can cause myfibroblasts to continuously secrete extracellular matrix protein. The expression of  $\alpha$ -SMA, a marker of myfibroblast activation, increases as the organ fibrosis exacerbates. Excessive extracellular matrix protein deposition eventually evolves into renal fibrosis. In the Model group, the expressions of  $\alpha$ -SMA and Col I have significantly increased, indicating severe renal inflammation. Upon SSLF and/or CPN intervention, the expression of  $\alpha$ -SMA and Col I decreases significantly in myfibroblasts, indicating that SSLF and/or CPN can inhibit the excessive secretion of  $\alpha$ -SMA and Col I. Thus, SSLF and CPN are able to suppress renal pathological changes and tissue fibrosis alone or synergistically.

Renal interstitial fibrosis (RIF) is a common pathway and pathological feature in various chronic kidney diseases

leading to end-stage renal disease. In this process, effective nephrons are gradually lost and renal function declines progressively. The study has confirmed that the severity of RIF is closely related to the degree of renal function declination, and it is a reliable index to determine the prognosis. It has been found that the expression of SHH in renal tubular epithelial cells is significantly upregulated in patients with chronic kidney disease (CKD) with different causes. And other studies have confirmed it in various rat renal fibrosis models as well, suggesting that SHH signaling pathway activation is a common pathological outcome in many kidney diseases [17]. In classical activation of the SHH signaling pathway, SHH binds to the membrane receptor transmembrane protein patched (PTCH) after automatic catalytic cleavage, which relieves the inhibition of smoothed (SMO). SMO activates Gli1 phosphorylation, and then Gli1 enters the nucleus in full-length to initiate the transcription

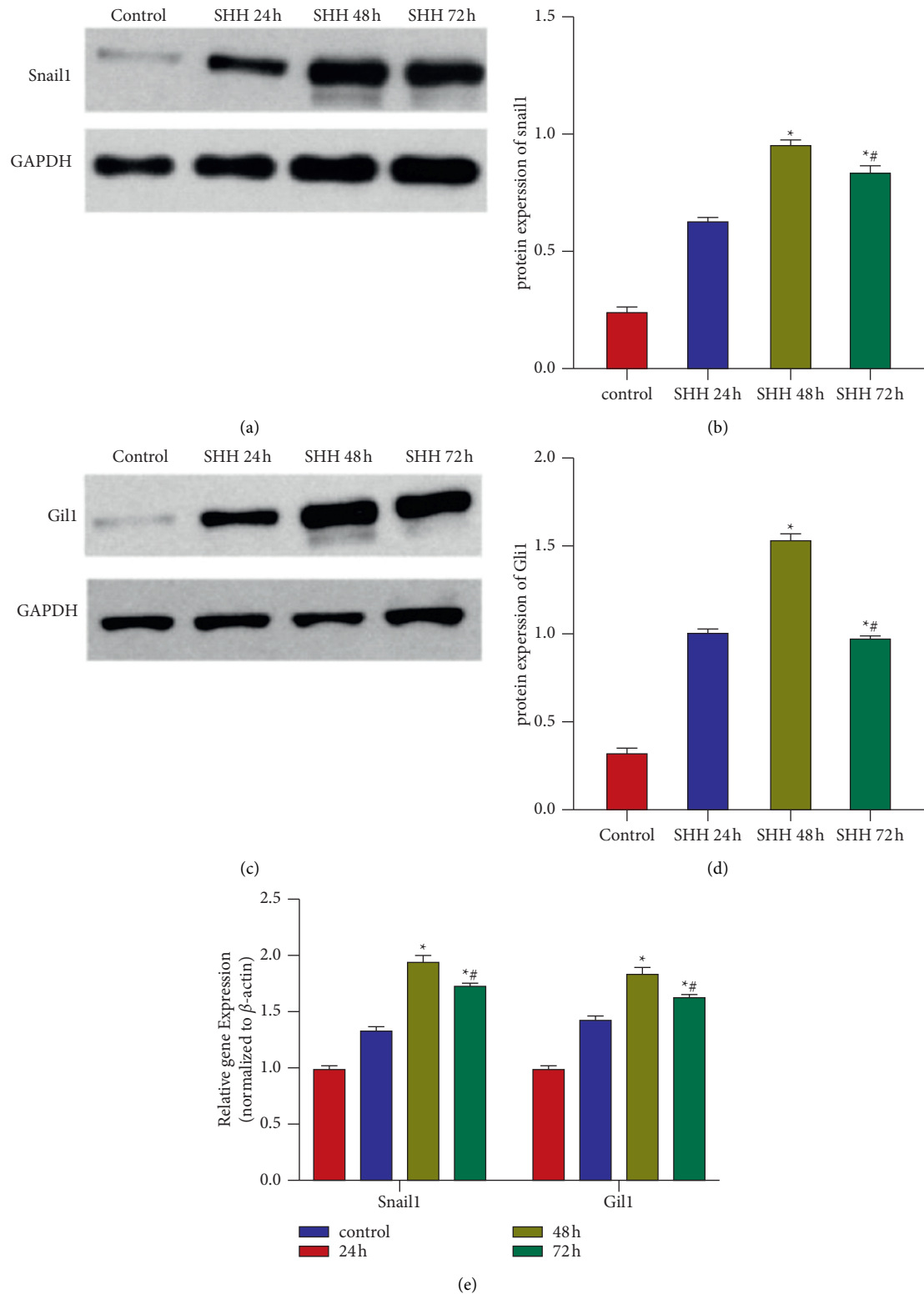


FIGURE 7: Levels of snail1 and Gli1 in renal tissues in each group. (a, b) Levels of snail1 were measured by Western blot. (c, d) Levels of snail1 and Gli1 were measured by Western blot. (e) Levels of snail1 and Gli1 in renal tissues were measured by qPCR. Data were expressed as mean  $\pm$  SEM. \*  $p < 0.05$  compared with the Control group; #  $p < 0.05$  compared with the SHH 48 h group.

of the target gene [18, 19]. Gli1 is an important multifunctional transcription factor in the SHH signaling pathway, and its activation is a reliable indicator of SHH signaling

activity. The SHH-Gli1 pathway is involved in the development of RIF by promoting cell proliferation [20, 21]. Through the study of Gli1-lacZ knockout rats, it has been

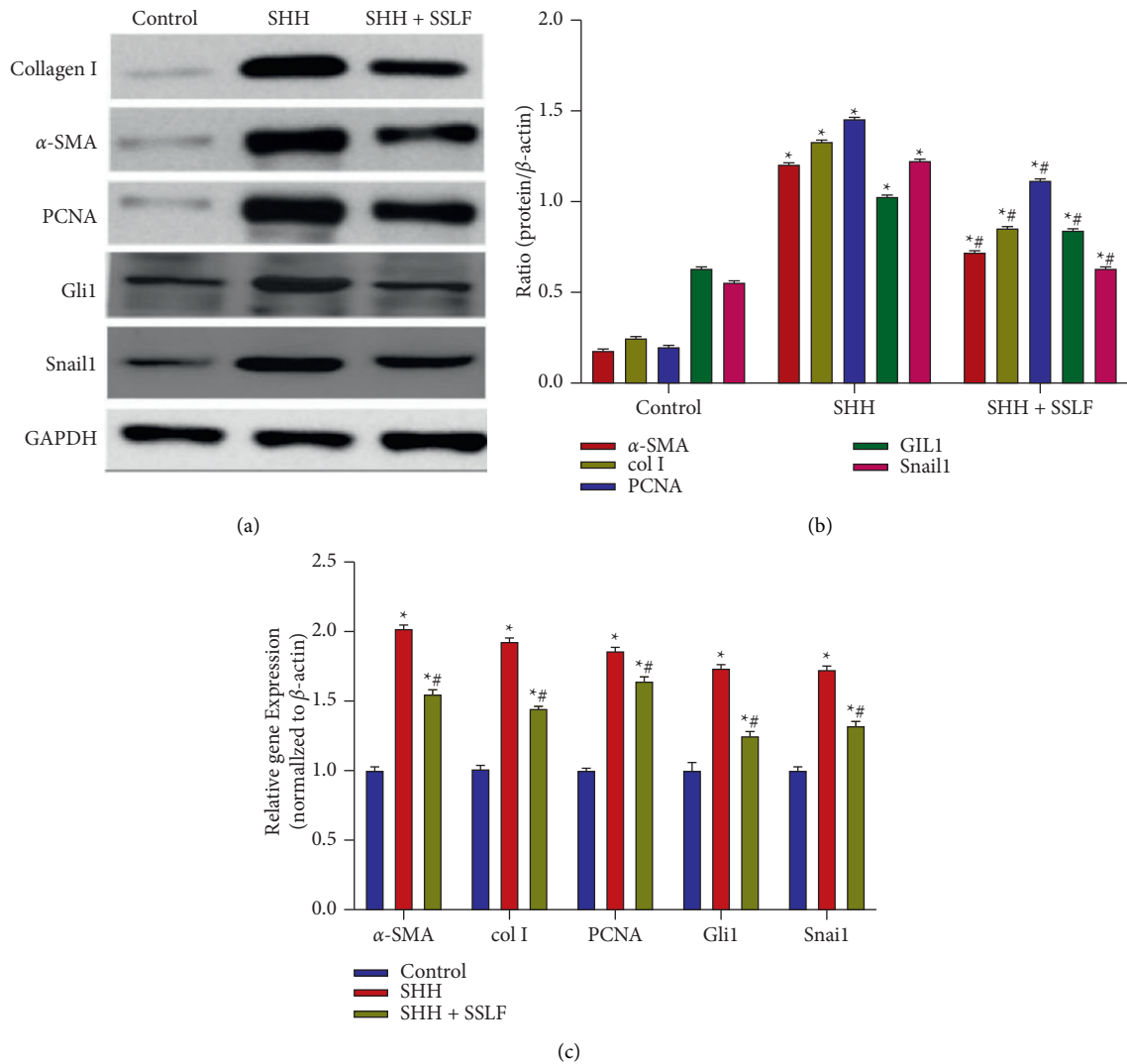


FIGURE 8: Levels of Snail1 and Gli1 in renal tissues in each group. (a) Levels of collagen,  $\alpha$ -SMA, PCNA, Gli1, and snail1 were measured by Western blot. (b) Quantitative analysis. (c) Levels of collagenI,  $\alpha$ -SMA, PCNA, Gli1, and snail1 were measured by qPCR. Data were expressed as mean  $\pm$  SEM. \* $p < 0.05$  compared with the control group; # $p < 0.05$  compared with the SHH 48 h group.

revealed that the SHH-Gli1 pathway is essential in renal fibrosis [22]. A recent study has found that the SHH-Gli1 pathway can induce the expression of transcription factor snail1 [23]. Further study has found that activation of SHH-Gli1 can sophistically upregulate the expression of  $\alpha$ -SMA and Collagen III via snail1 in RIF [24,25]. Therefore, it is suggested that the SHH-Gli1-snail1 signaling pathway plays an important role in RIF. In the present study, SSLF and/or CPN inhibit the elevated expression of SHH, Gli1, and snail1 in UUO model rats. We can preliminarily speculate that SSLF and CPN downregulate the SHH-Gli1-snail1 signaling pathway.

Based on the results of in vivo experiments, NRK-49F cells are stimulated with SHH (100 ng/ml). The Gli1 and snail1 expressions in the cells have increased and peaked at 48h, indicating the activation of the SHH-Gli1-snail1 signaling pathway upon SHH stimulation. When SSLF is applied to the cells, the expressions of Gli1 and snail1 are significantly inhibited at 48h. Moreover, the expressions of

$\alpha$ -SMA, Col I, and PCNA exhibit apparent reduction. Thus, SSLF can significantly inhibit the expression of fibrotic proteins. These results suggest that SSLF inhibits the activation of the SHH-Gli1-snail1 signaling pathway and the proliferation of fibrotic cells, which may be the mechanism of its protective effect against renal fibrosis.

## 5. Conclusion

SSLF can remarkably improve renal function and alleviate renal interstitial fibrosis both in vivo and in vitro. And the underlying mechanism may be related to the inhibition of the SHH-Gli1-Snail signaling pathway.

## Data Availability

The data used to support the findings of this study are available from the corresponding author upon request.

## Conflicts of Interest

The authors declare no conflicts of interest.

## Acknowledgments

This research was supported by the National Natural Science Foundation of China (No. 81904012), Chongqing Province Natural Scientific Foundation (cstc2017jcyjAX0465, cstc2019jxjl130022, and cstc2018jxjl130048), and Foundation for Distinguished Young Talents (Natural Science) in Higher Education of Guangdong, China (No. 2018KQNCX043).

## References

- [1] E. F. Carney, "The impact of chronic kidney disease on global health," *Nature Reviews Nephrology*, vol. 16, no. 5, p. 251, 2020.
- [2] Lancet, "Global, regional, and national burden of chronic kidney disease, 1990-2017: a systematic analysis for the Global Burden of Disease Study," *Lancet (London, England)*, vol. 2020, no. 395, pp. 709-733, 2017.
- [3] A. A. Eddy, "Molecular basis of renal fibrosis," *Pediatric Nephrology*, vol. 15, no. 3-4, pp. 290-301, 2000.
- [4] B. D. Humphreys, "Mechanisms of renal fibrosis," *Annual Review of Physiology*, vol. 80, no. 1, pp. 309-326, 2018.
- [5] D. Zhou, R. J. Tan, and Y. Liu, "Sonic hedgehog signaling in kidney fibrosis: a master communicator," *Science China Life Sciences*, vol. 59, no. 9, pp. 920-929, 2016.
- [6] A. Pan, L. Chang, A. Nguyen, and A. W. James, "A review of hedgehog signaling in cranial bone development," *Frontiers in Physiology*, vol. 4, p. 61, 2013.
- [7] S. I. Chung, H. Moon, H.-L. Ju et al., "Hepatic expression of Sonic Hedgehog induces liver fibrosis and promotes hepatocarcinogenesis in a transgenic mouse model," *Journal of Hepatology*, vol. 64, no. 3, pp. 618-627, 2016.
- [8] N. Cigna, E. Farrokhi Moshai, S. Brayer et al., "The hedgehog system machinery controls transforming growth factor- $\beta$ -dependent myofibroblastic differentiation in humans," *American Journal of Pathology*, vol. 181, no. 6, pp. 2126-2137, 2012.
- [9] Y. Zhang, *Experimental Pharmacology*, People's Health Publishing House, Beijing, China, 2nd edition, 1996.
- [10] E. Ó hAinmhire, H. Wu, Y. Muto et al., "A conditionally immortalized Gli1-positive kidney mesenchymal cell line models myofibroblast transition," *American Journal of Physiology - Renal Physiology*, vol. 316, no. 1, pp. F63-F75, 2019.
- [11] M. C. Kugler, T.-A. Yie, Y. Cai, J. Z. Berger, C. A. Loomis, and J. S. Munger, "The Hedgehog target Gli1 is not required for bleomycin-induced lung fibrosis," *Experimental Lung Research*, vol. 45, no. 1-2, pp. 22-29, 2019.
- [12] Y. Li, W. Xiong, J. Yang et al., "Attenuation of inflammation by emodin in lipopolysaccharide-induced acute kidney injury via inhibition of toll-like receptor 2 signal pathway," *Iranian journal of kidney diseases*, vol. 9, pp. 202-208, 2015.
- [13] Y. Bai, H. Lu, C. Lin et al., "Sonic hedgehog-mediated epithelial-mesenchymal transition in renal tubulointerstitial fibrosis," *International Journal of Molecular Medicine*, vol. 37, no. 5, pp. 1317-1327, 2016.
- [14] H. Liu, W. Xiong, and X. Zheng, "Academic thought and clinical experience of TCM master ZHENG Xin in treating diabetic nephropathy," *China Journal of Traditional Chinese Medicine And Pharmacy*, vol. 31, pp. 4547-4549, 2016.
- [15] Y. Chen, G. Zhang, J. Huang, and X. Zheng, "Influence of bushen capsule and shenshuailing on emotional kidney function," *Chongqing medical Journal*, vol. 33, pp. 1257-1258, 2004.
- [16] Y. Chen, G. Li, G. Zhang, J. Huang, D. Zhi, and X. Zheng, "Experimental study on the protective effect of kidney medicine on renal function of animals with renal failure caused by adenine," *Chinese Journal of Traditional Medical Science and Technology*, vol. 10, pp. 279-281, 2003.
- [17] W. Chen, Z.-Q. Zhou, Y.-Q. Ren et al., "Effects of long non-coding RNA LINC00667 on renal tubular epithelial cell proliferation, apoptosis and renal fibrosis via the miR-19b-3p/LINC00667/CTGF signaling pathway in chronic renal failure," *Cellular Signalling*, vol. 54, pp. 102-114, 2019.
- [18] A. V. D. S. Faria, A. I. Akyala, K. Parikh et al., "Smoothed-dependent and -independent pathways in mammalian non-canonical Hedgehog signaling," *Journal of Biological Chemistry*, vol. 294, no. 25, pp. 9787-9798, 2019.
- [19] A. N. Singh and N. Sharma, "Epigenetic modulators as potential multi-targeted drugs against hedgehog pathway for treatment of cancer," *The Protein Journal*, vol. 38, no. 5, pp. 537-550, 2019.
- [20] D. Tampe and M. Zeisberg, "Potential approaches to reverse or repair renal fibrosis," *Nature Reviews Nephrology*, vol. 10, no. 4, pp. 226-237, 2014.
- [21] Y. Liu, "New insights into epithelial-mesenchymal transition in kidney fibrosis," *Journal of the American Society of Nephrology*, vol. 21, no. 2, pp. 212-222, 2010.
- [22] A. A. Rauhauser, C. Ren, D. Lu et al., "Hedgehog signaling indirectly affects tubular cell survival after obstructive kidney injury," *American Journal of Physiology - Renal Physiology*, vol. 309, no. 9, pp. F770-F778, 2015.
- [23] V. Bhuria, J. Xing, T. Scholta et al., "Hypoxia induced Sonic Hedgehog signaling regulates cancer stemness, epithelial-to-mesenchymal transition and invasion in cholangiocarcinoma," *Experimental Cell Research*, vol. 385, no. 2, Article ID 111671, 2019.
- [24] W. He and C. Dai, "Key fibrogenic signaling," *Current pathobiology reports*, vol. 3, no. 2, pp. 183-192, 2015.
- [25] Y. Zhang, S. Wang, S. Liu, C. Li, and J. Wang, "Role of Smad signaling in kidney disease," *International Urology and Nephrology*, vol. 47, no. 12, pp. 1965-1975, 2015.

## Research Article

# ***Camelina sativa* Oil Treatment Alleviates Castor Oil-Induced Diarrhea in ICR Mice by Regulating Intestinal Flora Composition**

**Jie Zhu** <sup>1,2</sup>, **Liqin Yu**<sup>1,2</sup>, **Yi Fan** <sup>1,2</sup>, **Huanan Zhang**<sup>1,2</sup>, **Feifei Li**<sup>1,2</sup>, **Xiao Li**<sup>1,2</sup>, **Yue Wei**<sup>1,2</sup>, and **Zhiyao Wang**<sup>1,2</sup>

<sup>1</sup>Henan Napu Biotechnology Co., Ltd., Zhengzhou, Henan 450000, China

<sup>2</sup>Henan Academy of Sciences, Zhengzhou, Henan 450000, China

Correspondence should be addressed to Yi Fan; orchid\_21@163.com

Received 25 November 2021; Accepted 15 January 2022; Published 8 February 2022

Academic Editor: Ruchika Garg

Copyright © 2022 Jie Zhu et al. This is an open access article distributed under the Creative Commons Attribution License, which permits unrestricted use, distribution, and reproduction in any medium, provided the original work is properly cited.

Diarrhea, occurring due to intestinal flora disturbance, is potentially lethal, and its current treatments have adverse effects such as constipation and vomiting. *Camelina sativa* oil (CSO) is a cooking ingredient and natural remedy used in several countries; however, its pharmacological effects on intestinal health remain unknown. Here, we explored the CSO treatment effects on intestinal flora in male ICR mice with castor oil-induced diarrhea. The rate and degree of loose stools, the diarrhea index, serum inflammatory indices, fecal short-chain fatty acids (SCFAs), and the diversity and abundance of intestinal flora were measured. Castor oil-administered mice experienced diarrhea, reduced intestinal flora diversity and fecal SCFAs concentrations, altered intestinal flora composition, and increased serum proinflammatory indices. In contrast, CSO treatment relieved diarrhea, improved intestinal flora composition, and increased the relative abundance of *Lactobacillus* and *Lachnospiraceae*. Additionally, CSO significantly increased the concentrations of fecal propionic acid, valeric acid, isovaleric acid, and serum sIgA, while it reduced those of serum interleukin-17. These findings suggest that CSO could be a promising preventive agent against diarrhea.

## 1. Introduction

Diarrhea results from altered electrolyte absorption/secretion or nonabsorbable/osmotically active substances ingested from foods that accumulate in the intestinal lumen. It is a potentially lethal disease worldwide, particularly in infants, young children, and immune-compromised patients [1, 2], causing more than 0.5 million deaths of children annually [3, 4]. Long-term diarrhea in children can lead to malnutrition, growth retardation, and affect the immune system [5, 6]. In addition, diarrhea is also a common problem that affects up to 5% of adults [7]; this may lead to dehydration and have negative effects on the quality of life and work productivity [8].

A few clinical options to treat diarrhea include oral rehydration, antisecretory agents, probiotics, intestinal adsorbents, antibacterial and antiviral drugs, and the opioid receptor agonist loperamide [9]. Vomiting and constipation are the common adverse events of racecadotril and

loperamide during the treatment of diarrhea; these cannot be effectively alleviated [10]. Antibiotics and antiviral treatments are intended to target specific pathogenic microorganisms; however, they pose considerable health challenges, which are extensive and unpredictable [11]. Therefore, to date, diarrhea treatment remains challenging, and there has been a continuous effort to identify avenues to stop diarrhea in a safe, simple, and inexpensive manner.

The intestinal flora is the “second genome” of the human body; it plays a vital role in the development of immune organs, human health, aging, and the occurrence of diseases. It ferments food to produce large quantities of short-chain fatty acids (SCFAs) that are pivotal signaling factors between the intestinal flora and the host [12–14]. Disturbances in the intestinal flora can lead to metabolic disorders, intestinal inflammatory diseases, metabolic syndrome, immune dysfunction, and other diseases [15, 16]. Intestinal flora and diarrhea-related diseases are closely related, including inflammatory bowel disease, malnourishment, and irritable

bowel syndrome [17–19].  $\omega$ -3 polyunsaturated fatty acids ( $\omega$ -3 PUFAs), such as eicosapentaenoic acid (EPA) and docosahexaenoic acid (DHA), are essential nutrients for human beings. These are synthesized only minimally in mammals; therefore, they must be obtained through dietary sources.  $\omega$ -3 PUFAs exert potent anti-inflammatory effects via modulating membrane structure, attenuation of nuclear factor-kappa B (NF- $\kappa$ B) activation, and stimulation of peroxisome proliferator-activated receptors, resulting in the reduced production of inflammation-related factors [20].  $\omega$ -3 PUFAs could modulate the diversity and composition of the intestinal flora. A clinical study on  $\omega$ -3 PUFAs discovered that the abundance of *Lactobacillus* in intestinal flora increases at least two-fold following intervention with 4000 mg of EPA and DHA daily for 8 weeks; however, these large doses cause considerable treatment-emergent adverse events, including heartburn and acid regurgitation, and particularly in relation to dyspeptic symptoms [21]. Notably, several clinical studies have attempted to treat diarrhea-related diseases using fish oil, which is rich in EPA and DHA; however, the findings are discrepant, and the efficacy of the treatment remains to be fully elucidated [22].

*Camelina sativa* is an oilseed plant common in Europe and Asia and belongs to the *Cruciferae* family. *C. sativa* oil (CSO) contains >35% of  $\alpha$ -linolenic acid (ALA), a dietary precursor of EPA and DHA. *C. sativa* has good agronomic properties and is suitable for growth in cold and arid areas, making CSO economical and a readily available replacement for fish oil. Additionally, CSO is a novel cooking ingredient in the United States, Canada, and many other countries [23]. Moreover, concerns regarding the nutraceutical effects of CSO are few and only focused on its hyperlipidemic effect [24]; however, the effect of CSO on intestinal health remains obscure.

Castor oil is often used in experiments to induce diarrhea because of its reproducibility and stability [25, 26]. Castor oil stimulates intestinal mucosal cells and reduces the active absorption of Na<sup>+</sup> and K<sup>+</sup>, thereby inducing intestinal inflammation and diarrhea [27, 28]. The present study was designed to investigate the effect of preventive CSO administration on the intestinal flora of mice with castor oil-induced diarrhea. Our findings may facilitate the development of CSO administration as an alternative measure to treat and prevent diarrhea.

## 2. Materials and Methods

**2.1. Animals.** Adult male (6-week-old) ICR mice (18–22 g) were purchased from Hunan Slake Jingda Experimental Animal Co., Ltd. (Changsha, China) and acclimatized to laboratory conditions for at least 1 week prior to the beginning of the experiments. Mice were kept in a room with a controlled temperature of 22–24°C, a stable humidity of 45–55%, and a 12-h light-dark cycle throughout the trial, and were allowed free access to water and food (standard mouse-breeding feed consisting of corn, soybean protein, flour, fish powder, brewer's yeast powder, vegetable oil, amino acids, calcium hydrogen phosphate, stone powder, salt, and compound vitamins; Beijing Huanyu Zhongke

Biotechnology Co., Ltd., Beijing, China). The animal experiments were performed in accordance with the Regulations on the Administration of Experimental Animals issued by the Ministry of Science and Technology of China and approved by the animal welfare and ethic committee of Henan Napu Biotechnology Co., Ltd. (experiment approval number: HNP. No20210325002). An overview of the experimental procedures is shown in Figure 1.

**2.2. Preventive Administration of CSO.** CSO, which mainly contained 37.2% ALA, 16.6% linoleic acid, 15.8% eicosenoic acid, and 10.9% oleic acid, was produced in our laboratory from cold-pressed *Camelina* seed harvested in Henan province, China (CSO yield: 28.0%). Fifty mice (10 mice/group) were fed separately and randomly assigned to five groups: the control (Ctrl) and model (Md) groups were treated with 10 mL/kg body weight (BW) of normal saline; the CSO low-dose (Md\_CSOL) and high-dose (Md\_CSOH) groups were treated with 1.0 mL/kg BW and 2.0 mL/kg BW of CSO (equivalent to the recommended daily intake amounts for humans generally regarded as safe), respectively; and the positive control group (Md\_MP) was treated with 3.0 g/kg BW of montmorillonite power (0.3 g/mL). All test substances were administered intragastrically at 9:00 am once daily for ten consecutive days.

**2.3. Castor Oil-Mediated Induction of Diarrhea.** Castor oil was administered to mice from day 7 of the experiment at 20 mL/kg BW for four consecutive days intragastrically at 2:00 pm to induce diarrhea. Normal saline, instead of castor oil, was administered to the Ctrl group. On day 10, after castor oil or normal saline treatment, the bedding in the cage was removed and replaced with filter paper of an appropriate size to observe feces, and the diarrhea status of mice was recorded for 5 h. The numbers of fecal and loose stool evacuations, as well as the rate of loose stool, degree of loose stool, and diarrhea index, were calculated according to a previously described method [29]. The rate of loose stool was defined as the percentage of the number of loose stools among the total fecal evacuations. The degree of loose stool indicated the level of loose stools and was graded according to the diameter of the stain formed by the loose stools on the filter paper. The degree of loose stool was rated as follows: (1) diameter of the stain <1 cm; (2) diameter of the stain  $\geq$ 1 cm and <1.9 cm; (3) diameter of the stain  $\geq$ 2 cm and  $\leq$ 3 cm; and (4) diameter of the stain >3 cm. The longest and shortest diameters were measured for stains with irregular shapes, and the average was calculated. The diarrhea index was calculated as follows: the rate of loose stool  $\times$  degree of loose stool.

**2.4. Sample Collection and Processing.** Fresh fecal samples were collected in sterile centrifuge tubes on day 10 and immediately stored at –80°C until further determination. Plasma was collected from the eyeball, separated from whole blood by centrifugation (1,200  $\times$  g) at 4°C for 10 min, and



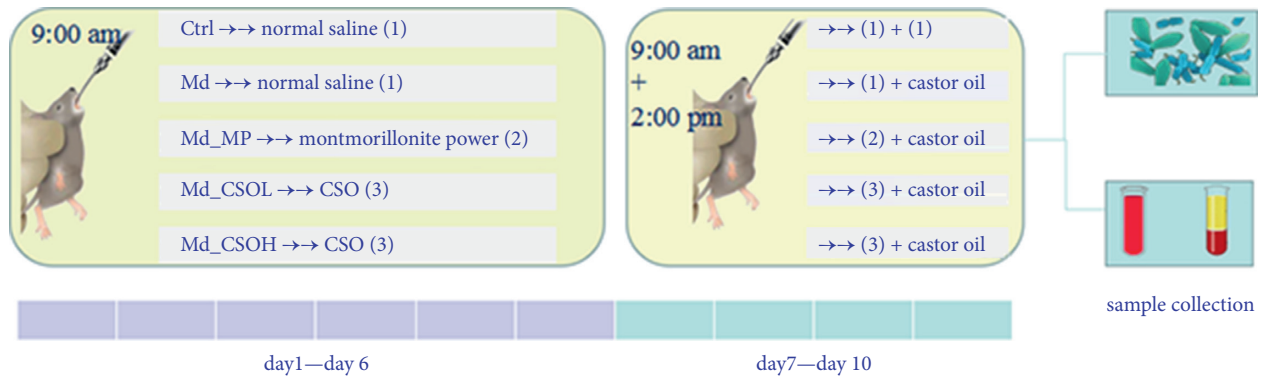


FIGURE 1: Experimental procedures.

immediately stored at  $-80^{\circ}\text{C}$  until subsequent determination.

**2.5. High-Throughput Sequencing of Microbial 16S rDNA.** Total microbial genomic DNA was extracted from the fecal samples (5 mice/Md\_MP group and 6 mice/other groups) using the E. Z. N. ATM Mag-Bind soil DNA kit (Omega, Norcross, GA, USA). DNA quantity and concentration were measured using gel electrophoresis. The bacterial 16S rDNA V3–V4 variable region was amplified using forward primer 341F (5'-CCTACGGGNGGCWGCAG-3') and reverse primer 805R (5'-GACTACHVGGGTATCTAATCC-3'). The DNA library was quantified using 2% agarose gel electrophoresis and a Qubit 3.0 fluorimeter (Thermo Fisher Scientific, Waltham, MA, USA) and sequenced on the Illumina MiSeq™ platform (Illumina, San Diego, CA, USA). The original data were filtered by removing primer connector sequences and low-quality bases; the effective data for each sample were obtained and used for further operational taxonomic unit (OTU) analysis.

**2.6. SCFAs Analysis.** Concentrations of five SCFAs (acetic, propionic, butyric, isobutyric, valeric, and isovaleric acids) in the feces were measured using gas chromatography. Fecal samples were accurately weighed and placed in 2-mL centrifuge tubes; methanol was added at a ratio of 1:5 (mg:  $\mu\text{L}$ ) and stirred with a homogenizer (IKA, Staufen im Breisgau, Germany) for 30 s until uniformly dispersed. Concentrated sulfuric acid was added to adjust the pH of the suspension to 2.0 to 3.0. After vortexing the mixture for 30 s and incubating for 10 min at ambient temperature, the samples were centrifuged ( $4,800 \times g$ ) at  $4^{\circ}\text{C}$  for 10 min. The supernatants were collected and injected into a gas chromatograph (aGC-2010 Plus; CD-WAX 30 m  $\times$  0.32 mm  $\times$  0.25  $\mu\text{m}$ ; Shimadzu, Tokyo, Japan) with a flame ionization detector temperature. The oven temperature was set to  $100^{\circ}\text{C}$ , held for 2 min, and then raised to  $200^{\circ}\text{C}$  at  $15^{\circ}\text{C}/\text{min}$  (held for 10 min). The detector temperature was controlled at  $260^{\circ}\text{C}$ . The flow rates of make-up gas ( $\text{N}_2$ ),  $\text{H}_2$ , and air were 3.0, 40, and 400 mL/min, respectively. A sample volume of 1.0  $\mu\text{L}$  was injected at  $260^{\circ}\text{C}$  using a split ratio of  $\sim 5:1$ . The runtime for each sample was 15 min.

**2.7. Inflammatory Index Determination.** Proinflammatory indices, including those of interleukin (IL)-6, IL-1 $\beta$ , IL-17, interferon (IFN)- $\gamma$ , and tumor necrosis factor-alpha (TNF- $\alpha$ ), and the anti-inflammatory index of secretory immunoglobulin A (sIgA) were measured using commercial ELISA kits (Elabscience, Wuhan, China).

**2.8. Correlation Analysis among Indices.** We explored the relationships among indices, including SCFAs/inflammatory index, SCFAs/genus-level intestinal flora, SCFAs/SCFAs, and inflammatory index/inflammatory index, to investigate their respective interactions.

**2.9. Statistical Analysis.** Statistical analysis and result visualization were performed using SPSS (v.25.0) and R software (v3.6.0). Descriptive statistics were used for single-group data, and an independent sample *t*-test was used for two-group comparisons. Data were analyzed using either one-way analysis of variance and a post hoc LSD test for three-group comparisons when the data conformed to a normal distribution and the variance was homogeneous or Tamhane's T2 test when the data were nonnormally distributed. Differences were considered significant at  $p < 0.05$ . Spearman's correlation coefficients with 95% confidence intervals were performed to analyze the relationship between the parameters.

### 3. Results

**3.1. Effects of CSO Treatment on Body Weights in Mice with Castor Oil-Induced Diarrhea.** We observed significant changes in mouse defecation, specifically loose stool, after treatment with castor oil, indicating the successful establishment of a murine diarrhea model. The feces excreted by mice in the Ctrl group were dry, granular, and soft throughout the experimental period. Mice in the Md group excreted soft, loose, or watery stool after the administration of castor oil for four days. Additionally, they showed gloomy spirits, with loose hair and little movement. The body weights of mice in the Md group on day 10 were slightly lower, and the rate of loose stool (0.23 vs. 0.00,  $p < 0.01$ ), degree of loose stool (1.68 vs. 0.00,  $p < 0.01$ ), and diarrhea index (0.38 vs. 0.00,  $p < 0.01$ ) of mice in the Md group were

markedly higher in comparison with those in the Ctrl group. The state of mood in mice from the Md\_MP, Md\_CSOL, and Md\_CSOH groups improved, and the body weights of mice in these groups were slightly higher; the rate of loose stool (0.05 vs. 0.23,  $p < 0.01$ ; 0.07 vs. 0.23,  $p < 0.01$ ), degree of loose stool (0.62 vs. 1.68,  $p < 0.05$ ; 0.62 vs. 1.68  $p < 0.01$ ), and diarrhea index (0.07 vs. 0.38,  $p < 0.01$ ; 0.09 vs. 0.38,  $p < 0.01$ ) of mice in the Md\_MP and Md\_CSOH groups were significantly lower than those in the Md group, indicating that CSO and MP treatments could effectively inhibit castor oil-induced diarrhea (Figures 2(a) and 2(b)).

**3.2. Effects of CSO Treatment on Intestinal Flora Disturbance Induced by Castor Oil.** The Venn diagram shows the number of common and unique OTUs and displays the diversity and overlap of OTU numbers in samples. There were 712 OTUs detected in samples, and OTU numbers in the Ctrl, Md, Md\_MP, Md\_CSOL, and Md\_CSOH groups were 655, 619, 630, 622, and 625, respectively (Figure 3). There were 578 common OTUs in the Ctrl and Md groups, accounting for 88.24% of OTUs in the Ctrl group, implying that the administration of castor oil induced intestinal flora disturbance. There were 597, 583, and 584 common OTUs in the Ctrl and Md\_MP, Md\_CSOL, and Md\_CSOH groups, accounting for 91.14%, 89.01%, and 89.16% of OTUs in the Ctrl group, respectively. This indicated that the preventive administration of MP and CSO alleviates the intestinal flora disorder induced by castor oil.

$\alpha$ -Diversity is a critical parameter for investigating the diversity of intestinal flora, along with OTUs, Shannon, Chao, and Ace indices, the values of which are positively correlated with the diversity of intestinal flora in samples. The coverage index refers to the coverage of each sample library. The test result is approaching the actual sample if the coverage index is closer to 1. The average coverage index of each group was 1.0, indicating that the probability of undetected sequences in samples was low and that results were reliable (Figure 4(a)). The values of OTUs (395.33 vs. 476.67,  $p < 0.01$ ), Shannon (3.18 vs. 3.88,  $p < 0.01$ ), Chao (508.90 vs. 584.20,  $p < 0.01$ ), and Ace (511.78 vs. 571.28,  $p < 0.01$ ) indices in the Md group were significantly lower in comparison with those in the Ctrl group (Figures 4(b)–4(e)). This implied that castor oil administration markedly reduced the diversity of intestinal flora. The abovementioned indices were slightly higher with the preventive administration of CSO and MP, relative to those in the MP group; however, there was no significant difference.

**3.3. Effects of CSO Treatment on the Phylum-Level Composition of Intestinal Flora.** Noticeable changes in the phylum-level composition of intestinal flora were observed after castor oil treatment (Figure 5). The Md group mice displayed a decreased relative abundance of the phylum Firmicutes (8.84% vs. 33.45%,  $p < 0.05$ ) and Firmicutes: Bacteroidetes (F/B) ratio (0.13 vs. 0.61) and an increased relative abundance of the phylum Proteobacteria (8.19% vs. 2.76%) and Verrucomicrobia (13.51% vs. 0.48%) in comparison with

those in the Ctrl group. Conversely, the relative abundance of Firmicutes and the F/B ratio in the Md\_MP (16.11% vs. 8.84% and 0.29 vs. 0.13, respectively), Md\_CSOL (9.91% vs. 8.84% and 0.14 vs. 0.13, respectively), and Md\_CSOH (15.19% vs. 8.84% and 0.25 vs. 0.13, respectively) groups were slightly higher in comparison with those in the Md group; in contrast, the relative abundance of Proteobacteria was lower (6.25% vs. 8.19%, 4.18% vs. 8.19%, and 7.41 vs. 8.19%, respectively).

**3.4. Effects of CSO Treatment on the Genus-Level Composition of Intestinal Flora.** The dominant genera in the intestinal flora were *Porphyromonadaceae*, *Lactobacillus*, *Bacteroides*, *Lachnospiraceae*, *Alistipes*, *Prevotella*, *Barnesiella*, and *Clostridiales* (*Clostridium\_XVIII*, *Clostridium\_XIVa*, and *Clostridiales*) in the Ctrl group, whereas those in the Md group included *Porphyromonadaceae*, *Bacteroides*, *Akkermansia*, *Prevotella*, *Lactobacillus*, and *Enterobacteriaceae*, accounting for >87% of the total genera (Figure 6). The relative abundance of *Lactobacillus* (4.21% vs. 24.01%,  $p < 0.01$ ), *Lachnospiraceae* (2.00% vs. 7.44%,  $p < 0.01$ ), and *Clostridiales* (0.78% vs. 2.13%,  $p < 0.01$ ) was significantly decreased, and that of *Akkermansia* (13.45% vs. 0.47%) was increased in the Md group in comparison with those in the Ctrl group. The relative abundance of *Lactobacillus* and *Lachnospiraceae* in Md\_MP (7.85% vs. 4.21% and 3.99% vs. 2.00%, respectively), Md\_CSOL (5.21% vs. 4.21% and 2.95% vs. 2.00%, respectively), and Md\_CSOH (7.38% vs. 4.21% and 4.48% vs. 2.00%, respectively) groups increased slightly but with no statistical difference in comparison with those in the Md group. Notably, *Alistipes*, *Ruminococcaceae*, *Oscilibacter*, and *Odoribacter* were detected in the Ctrl group but not in the Md group, whereas *Escherichia*, *Shigella* and *Erysipelotrichaceae* were detected only in the Md group.

**3.5. Effects of CSO Treatment on SCFA Concentrations in Feces.** Acetic acid was the most abundant SCFA in feces, followed by propionic, isobutyric, valeric, isovaleric, and butyric acids. The concentrations of acetic acid (1217.86 vs. 4105.70 mg/g,  $p < 0.01$ ), propionic acid (278.84 vs. 547.86 mg/g,  $p < 0.01$ ), and isobutyric acid (140.29 vs. 401.82 mg/g,  $p < 0.01$ ) were significantly decreased in the fecal samples from castor oil-treated mice in the Md group in comparison with those in the Ctrl group (Figures 7(a), 7(b), and 7(d)). The concentrations of propionic acid (454.13 vs. 278.84 mg/g,  $p < 0.01$ ), valeric acid (208.84 vs. 103.19 mg/g,  $p < 0.01$ ), and isovaleric acid (124.08 vs. 92.68 mg/g,  $p < 0.05$ ) were significantly increased (Figures 7(b), 7(e), and 7(f)), whereas those of other SCFAs, including acetic acid, butyric acid, and isobutyric acid, were slightly increased in the fecal samples of the Md\_CSOL group in comparison with those in the Md group. The concentration of isovaleric acid (150.99 vs. 92.68 mg/g,  $p < 0.01$ ) in fecal samples of Md\_CSOH mice was markedly higher than that in the Md group (Figure 7(f)), indicating that CSO regulates the concentrations of intestinal SCFAs. Interestingly, MP treatment had no positive effect on SCFA concentrations; the amounts of acetic acid (446.96 vs. 1217.86 mg/g,  $p < 0.01$ ), propionic acid (25.75 vs. 278.84 mg/g,  $p < 0.01$ ), butyric acid

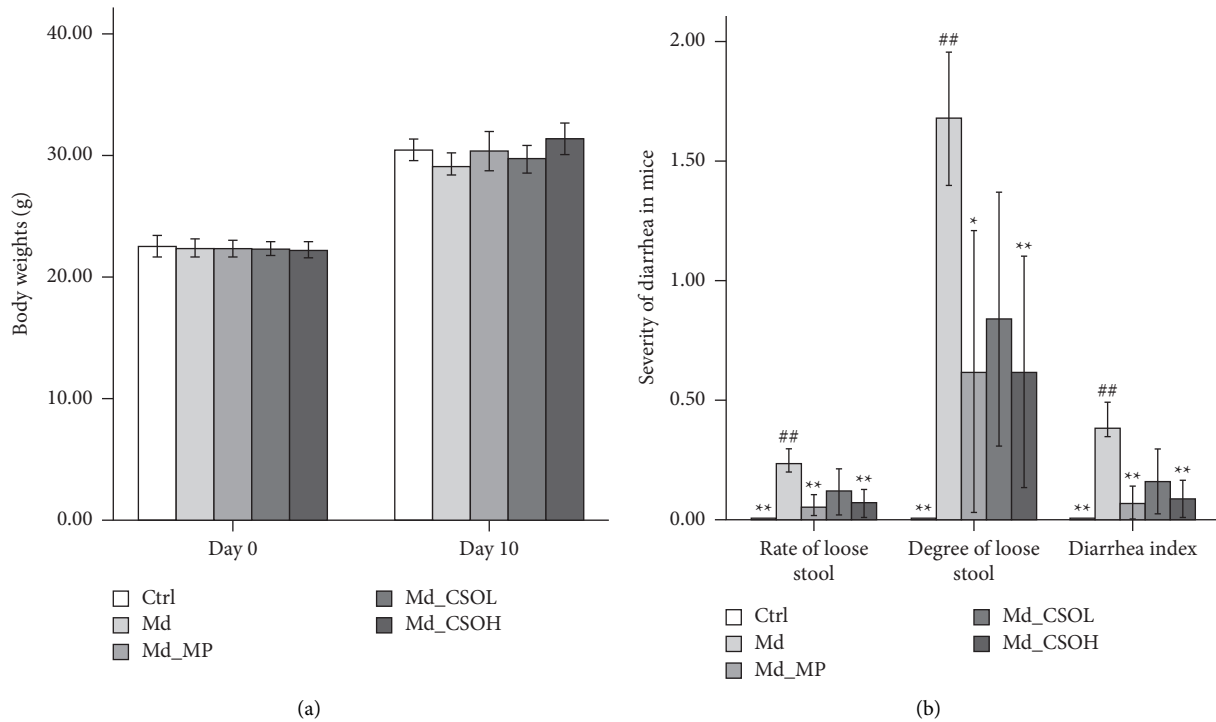


FIGURE 2: Influence of *Camelina sativa* oil (CSO) on the body weights of mice with diarrhea induced by using castor oil. (a) Body weights of mice in different groups; (b) severity of diarrhea in mice of different groups (vs model (Md) group, \* $p < 0.05$ , \*\* $p < 0.01$ ; vs control (Ctrl) group, #  $p < 0.05$ , ##  $p < 0.01$ ).

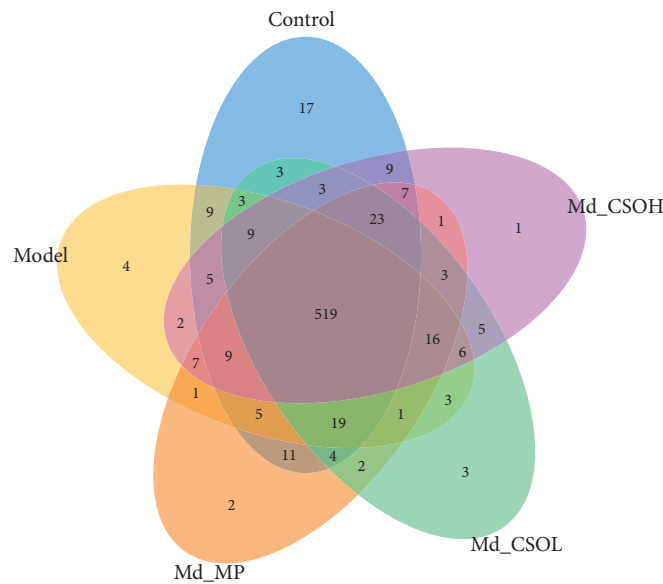


FIGURE 3: Venn chart of intestinal flora. Unique and common OTUs among different groups (control group (blue), model group (yellow), Md\_MP group (orange), Md\_CSOL group (green), and Md\_CSOH group (pink)) as well as the common OTUs among them (gray).

(11.95 vs. 68.58 mg/g,  $p < 0.01$ ), and isobutyric acid (35.27 vs. 140.29 mg/g,  $p < 0.01$ ) were markedly lower than those in the Md group (Figures 7(a)–7(d)).

**3.6. Effects of CSO Treatment on the Inflammatory Index.** Compared with those in the Ctrl group, IL-1 $\beta$  (41.21 vs. 23.09 pg/mL,  $p < 0.01$ ), IL-6 (168.90 vs. 121.44 pg/mL,

$p < 0.05$ ), and IL-17 concentrations (468.56 vs. 354.70 pg/mL,  $p < 0.01$ ) in the sera from mice in the Md group were markedly elevated (Figures 8(a)–8(c)), whereas IFN- $\gamma$ , TNF- $\alpha$ , and sIgA levels were not affected by the administration of castor oil (Figures 8(d)–8(f)). IL-17 levels in the sera of mice in the Md\_CSOL (380.79 vs. 468.56 pg/mL,  $p < 0.01$ ) and Md\_CSOH groups (322.08 vs. 468.56 pg/mL,  $p < 0.01$ ) were significantly decreased

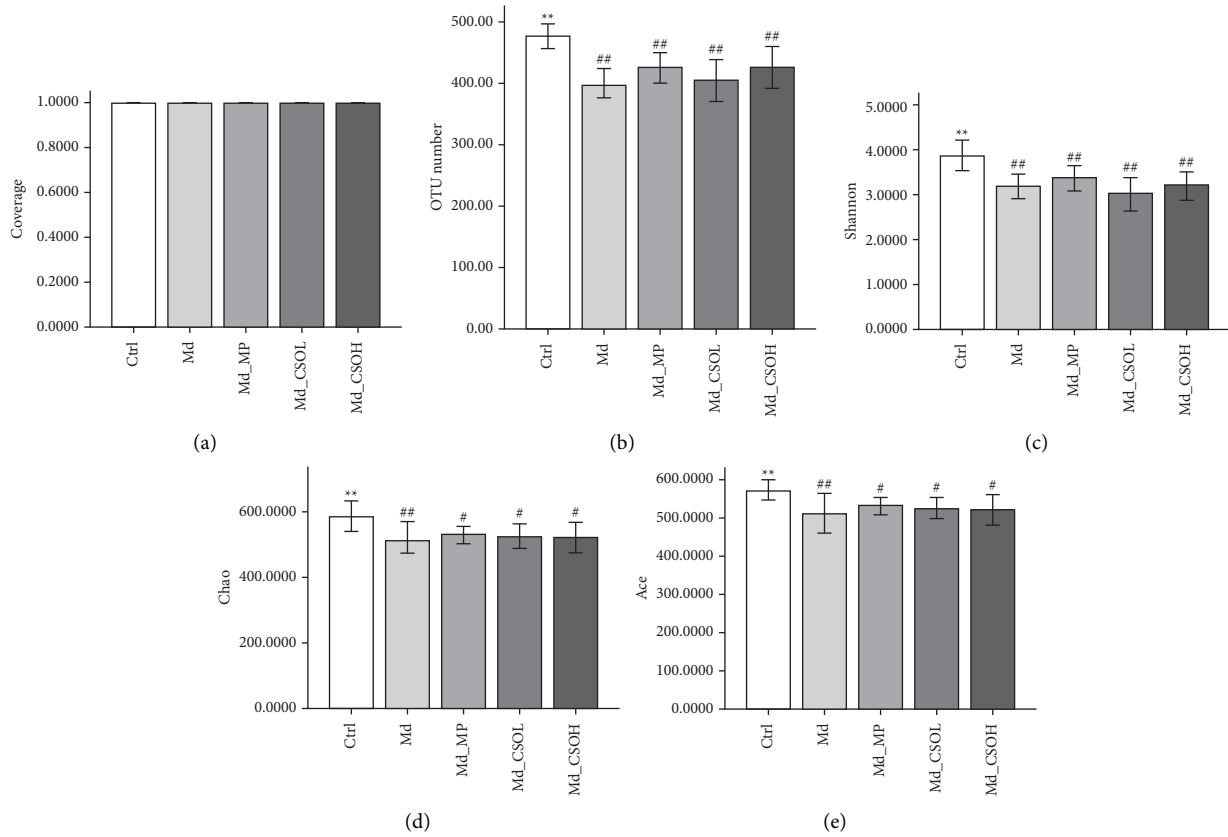


FIGURE 4:  $\alpha$ -Diversity of mouse intestinal microbiota in different treatment groups. (a) Coverage; (b) OTU numbers; (c) Shannon; (d) Chao; and (e) Ace indices (vs model (Md) group, \* $p < 0.05$ , \*\* $p < 0.01$ ; vs control (Ctrl) group, # $p < 0.05$ , ## $p < 0.01$ ).

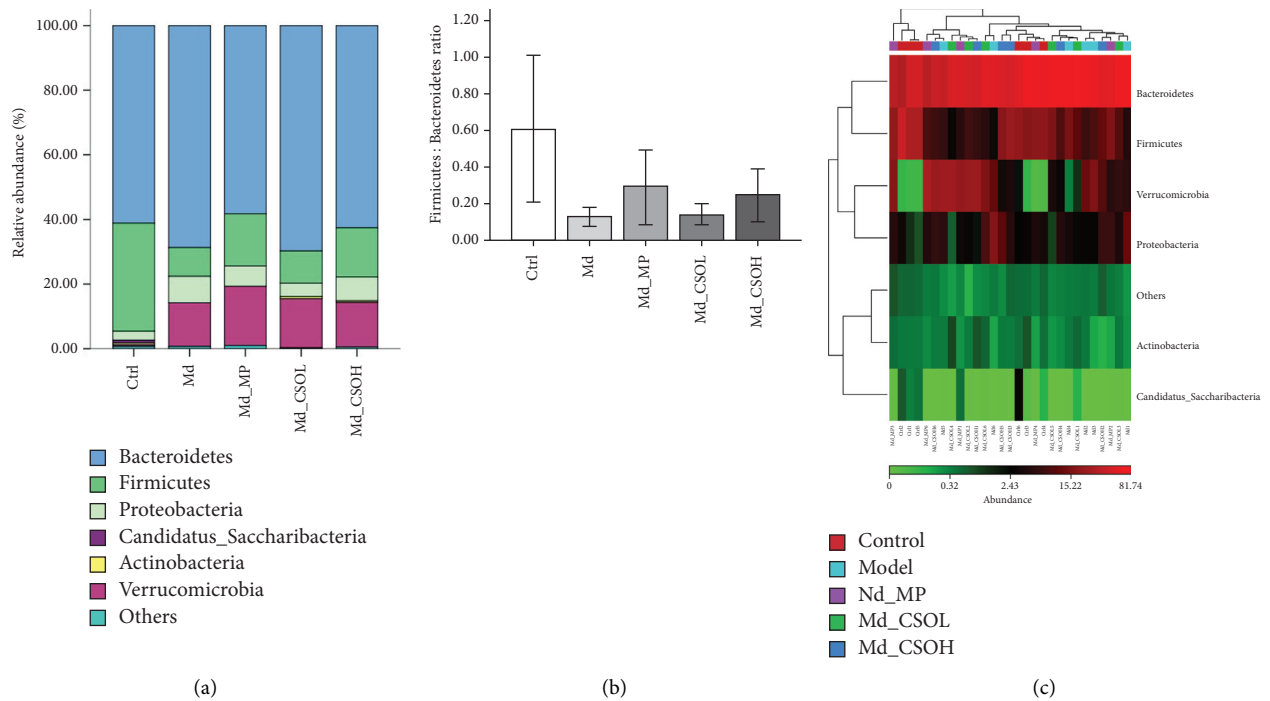


FIGURE 5: CSO altered the phylum-level composition of the intestinal flora. (a) Relative abundance of phyla in mouse intestinal flora; (b) Firmicutes-to-Bacteroidetes (F/B) ratios in different groups; (c) the phylum-level heatmap of samples.

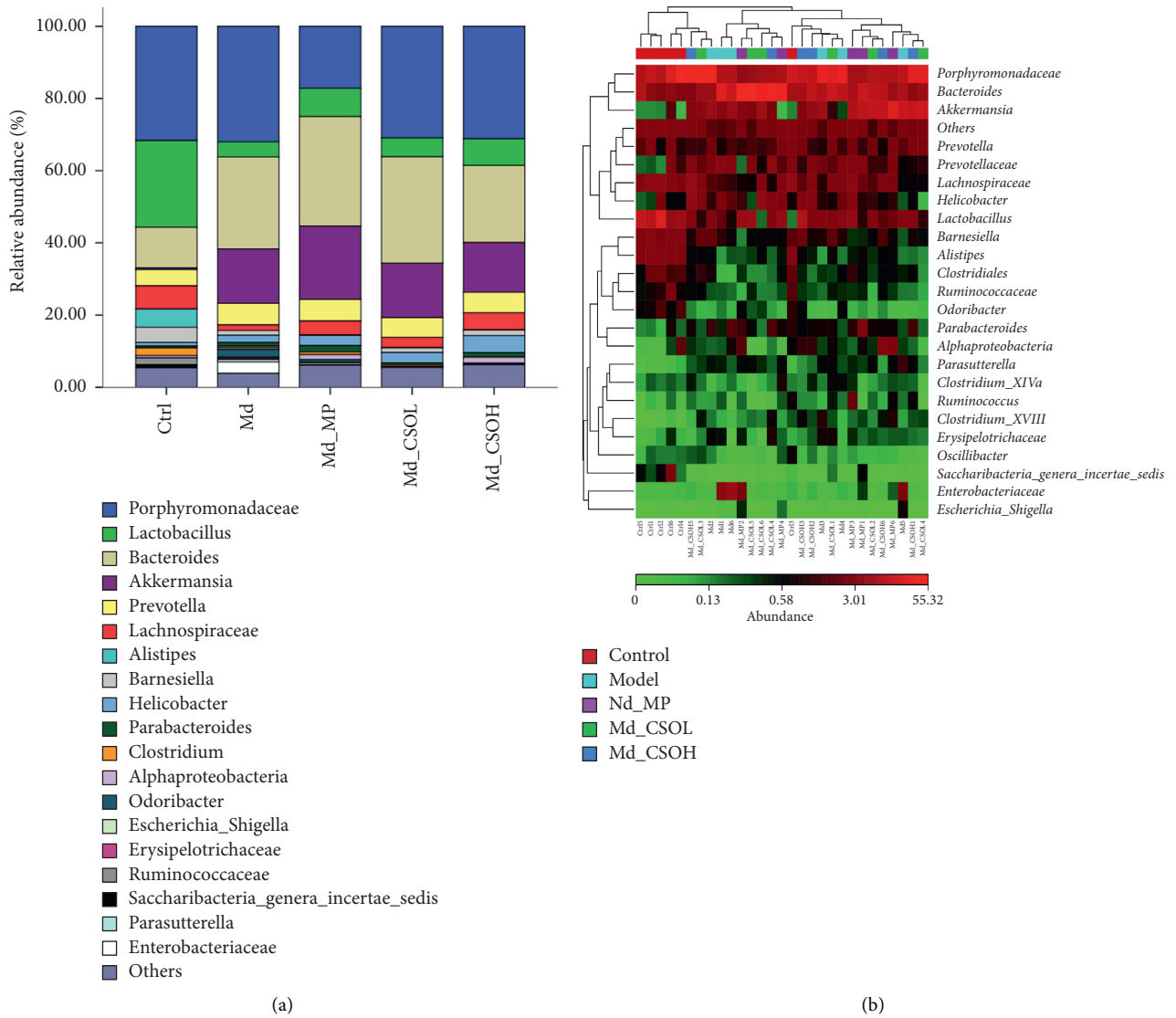


FIGURE 6: CSO altered the genus-level composition of the intestinal flora. (a) The relative abundance of the genus in mouse intestinal flora; (b) genus-level heatmap of samples.

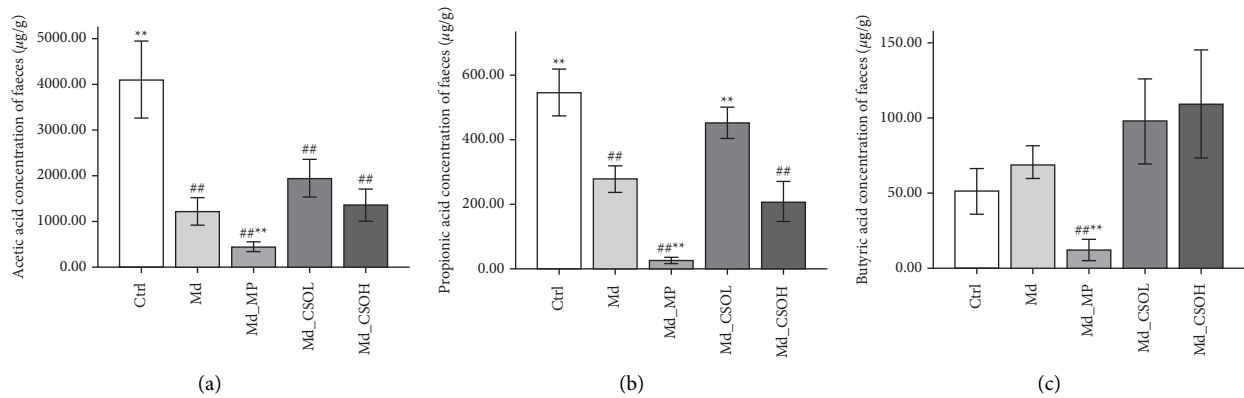


FIGURE 7: Continued.

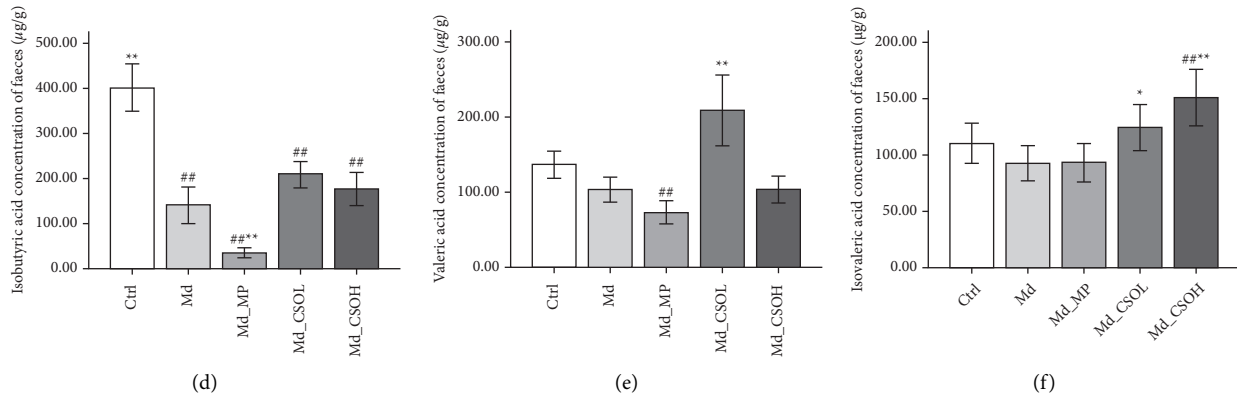


FIGURE 7: Fecal short-chain fatty acids (SCFAs) concentrations in different treatment groups. (a) Acetic acid; (b) propionic acid; (c) butyric acid; (d) isobutyric acid; (e) valeric acid; (f) isovaleric acid (vs model (Md) group, \*  $p < 0.05$ , \*\*  $p < 0.01$ ; vs control (Ctrl) group, #  $p < 0.05$ , ##  $p < 0.01$ ).

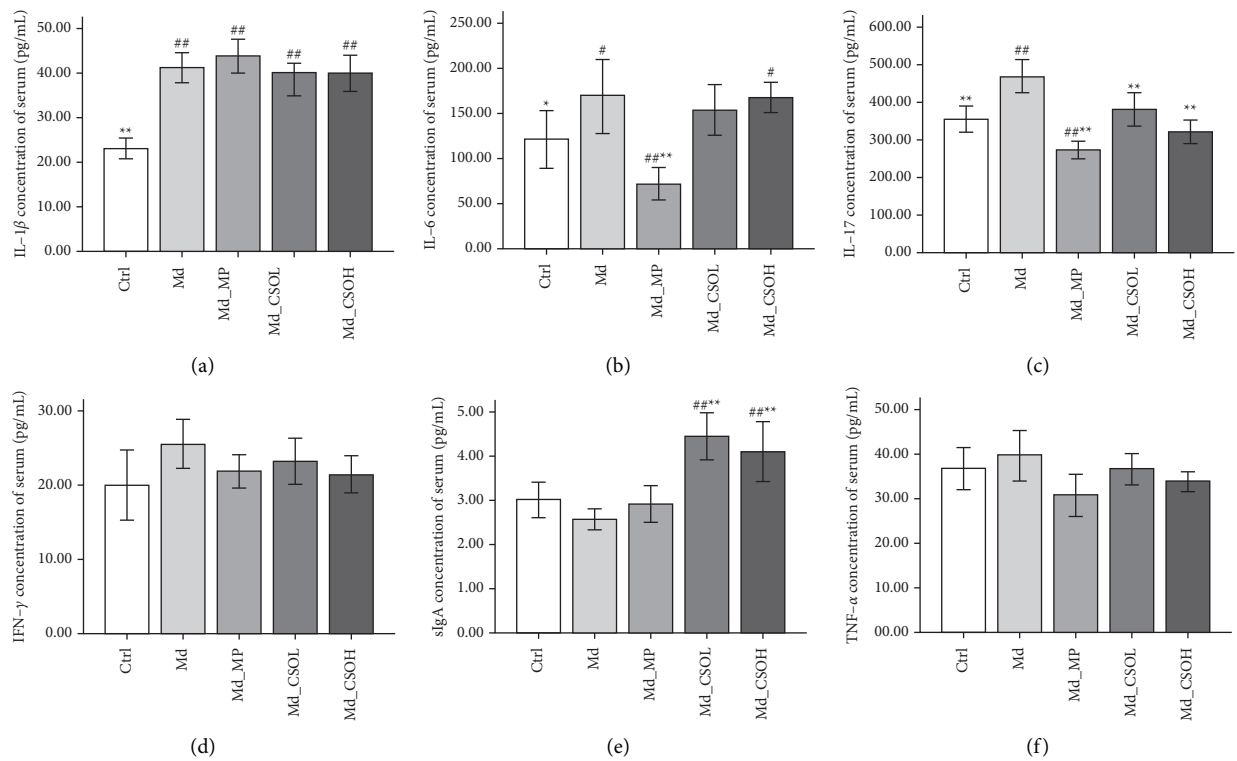


FIGURE 8: Inflammatory index in sera of mice in different treatment groups. (a) Interleukin 1 $\beta$  (IL-1 $\beta$ ); (b) interleukin 6 (IL-6); (c) interleukin 17 (IL-17); (d) interferon  $\gamma$  (IFN- $\gamma$ ); (e) secretory immunoglobulin A (sIgA); (f) tumor necrosis factor alpha (TNF- $\alpha$ ) (vs model (Md) group, \*  $p < 0.05$ , \*\*  $p < 0.01$ ; vs control (Ctrl) group, #  $p < 0.05$ , ##  $p < 0.01$ ).

(Figure 8(c)), whereas sIgA levels were markedly increased in the Md\_CSOL (4.44 vs. 2.56 pg/mL,  $p < 0.01$ ) and Md\_CSOH (4.10 vs. 2.56 pg/mL,  $p < 0.01$ ) groups (Figure 8(e)), compared with those in the Md group. IL-6 (72.04 vs. 168.90 pg/mL,  $p < 0.01$ ) and IL-17 (273.93 vs. 468.56 pg/mL,  $p < 0.01$ ) levels in sera from mice in the Md\_MP group decreased significantly, compared with those from mice in the Md group (Figures 8(b) and 8(c)).

**3.7. Correlation Analysis.** Heatmap visualization illustrated the correlation coefficients among SCFAs, relative abundance of genus-level intestinal flora, and inflammation indices (Figure 9). There were negative correlations between *Parabacteroides* ( $p < 0.05$ ), *Bacteroides* ( $p < 0.05$ ), *Helicobacter* ( $p < 0.01$ ), *Akkermansia* ( $p < 0.05$ ), and serum IL-1 $\beta$  ( $p < 0.01$ ) and intestinal acetic acid levels. Additionally, we observed negative correlations between *Parabacteroides* ( $p < 0.01$ ), *Helicobacter* ( $p < 0.01$ ), *Akkermansia*



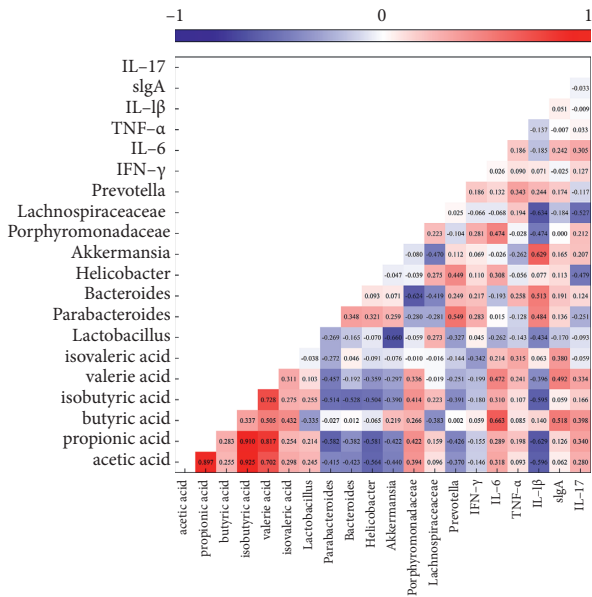


FIGURE 9: Heatmap of Spearman's correlation between short-chain fatty acids, genus level of intestinal flora, and the inflammation index ( $n = 29$ ).

( $p < 0.05$ ), *Prevotella* ( $p < 0.05$ ), and serum IL-1 $\beta$  ( $p < 0.01$ ) and intestinal propionic acid levels. Moreover, intestinal butyric acid levels were negatively correlated with *Lachnospiraceae* ( $p < 0.05$ ); intestinal isobutyric acid levels were negatively correlated with the abundance of *Parabacteroides* ( $p < 0.01$ ), *Bacteroides* ( $p < 0.01$ ), *Helicobacter* ( $p < 0.01$ ), *Prevotella* ( $p < 0.05$ ), and serum IL-1 $\beta$  levels ( $p < 0.01$ ), respectively. *Porphyrionadaceae* was significantly positively correlated with acetic acid ( $p < 0.05$ ), propionic acid ( $p < 0.05$ ), and isobutyric acid levels ( $p < 0.05$ ). Furthermore, butyric acid and valeric acid were positively correlated with IL-6 ( $p < 0.01$  and  $p < 0.05$ , respectively) and sIgA ( $p < 0.05$  and  $p < 0.05$ , respectively). Notably, we observed a statistically significant correlation among SCFAs.

#### 4. Discussion

In this study, we discussed the feasibility of the economic and convenient use of CSO to prevent diarrhea. We demonstrated that preventive CSO treatment markedly ameliorated castor oil-induced diarrhea in mice. The findings regarding CSO-specific mechanisms included the following: (i) improvement of the overall intestinal flora diversity; (ii) modulation of intestinal flora composition, especially elevating the relative abundance of *Lactobacillus* and *Lachnospiraceae*; (iii) enhancement of intestinal SCFA concentrations, including propionic acid and isovaleric acid; and (iv) decreased expression of proinflammatory factors along with increased sIgA expression.

The majority of previous  $\omega$ -3 PUFA studies focused on their contributions to human health, including decreasing the risk of cardiovascular disease, breast and colorectal cancers, and promoting joint health. The tested substances were primarily seafood, especially fatty fish. The main components of them are EPA and DHA, which are often

used as dietary supplements and ingredients of pharmaceutical preparations [30, 31]. Few studies have attempted to characterize ALA, a fat found in plant food, and its effect on intestinal diseases; small amounts of ALA can be metabolized to EPA and DHA after absorption. The main users and providers of  $\omega$ -3 PUFAs are fatty fish; however, they are a finite and limited resource. Therefore, it is important to alleviate the global shortfall in these key nutrients through the agriculture industry [32]. Reviews on  $\omega$ -3 PUFAs for the self-regulation of the inflammatory response and cardiovascular disease suggest that ALA differs from EPA and DHA in terms of the expression and activation of cyclooxygenase-2 and the outcomes of clinical studies [33, 34]. The fatty acid composition in plant oil is complex and includes  $\omega$ -3 and  $\omega$ -6 PUFAs, such as arachidonic acid, which is associated with promoting inflammation. Intake of  $\omega$ -3 PUFAs through plant oil can lead to an increase in the amount of  $\omega$ -6 PUFAs. Therefore, it is reasonable to speculate that investigating the impact of CSO on diarrhea not only expands the understanding of ALA and CSO but also promotes human health.

Our findings indicated that castor oil significantly decreased the diversity and composition of intestinal flora by decreasing the relative abundance of the phylum Firmicutes and increasing the relative abundance of Proteobacteria and Verrucomicrobia without affecting that of Bacteroidetes. Firmicutes and Bacteroidetes are the main intestinal phyla that regulate host inflammation and adaptive immunity. The F/B ratio is considered an indicator of health status, especially in the intestine [35]. An elevated F/B ratio indicates that the body is in a state of inflammation and immunological imbalance. Excessive growth of Firmicutes can produce metabolic endotoxins, such as lipopolysaccharides, that trigger systemic inflammation [25, 36]. However, in this study, we obtained a contradictory result; the F/B ratio decreased with diarrhea and intestinal inflammation. This was consistent with the results reported by Jacobs et al. [37]. The intestinal flora in both Crohn's disease and ulcerative colitis exhibits a general decrease in taxonomic diversity relative to that in the healthy intestinal flora. In addition, there is a phylum-level decrease in Firmicutes and an increase in Proteobacteria. The difference could be due to the different environmental influences, such as diets, and distinct species, including humans and mice. Firmicutes comprise several genera of outstanding relevance in healthcare, such as *Staphylococcus* and *Listeria*, which are pathogenic, and lactic acid bacteria, which are used as probiotics and in the preparation of food products [38]. Members of the genus *Lactobacillus* are associated with good intestinal health. *Lactobacillus* can inhibit pathogen colonization via the production of several acidic metabolites, mainly acetic acid and lactic acid [39]. The relative abundances of the dominant genera *Lactobacillus* and *Lachnospiraceae* were significantly decreased after the castor oil treatment, leading to a lower F/B ratio with diarrhea.

Furthermore, we found that the relative abundances of *Akkermansia*, *Bacteroides*, *Parabacteroides*, and *Helicobacter* were negatively correlated with SCFAs and positively correlated with proinflammation indicators. The abundance of

*Akkermansia* and *Bacteroides* positively correlates with proinflammation pathways, including the IFN signaling pathway and T cell and monocyte expression of NF- $\kappa$ B [40], which was consistent with the results in this study. SCFAs participate in host immune regulation and enhance the intestinal barrier [41]. We observed positive correlations between SCFAs and sIgA, which represents the first line of mucosal immunity and is essential for the intestinal barrier. sIgA coating and steric hindrance can prevent microbial adhesions from contacting and interacting with the epithelium. sIgA can also specifically inhibit pathogens by directly recognizing receptor-binding domains, such as that of reovirus type 1 [42].

The connections between ALA and intestinal flora are not fully elucidated. Dietary  $\omega$ -3 PUFAs (DHA and EPA) can improve the health of patients with inflammatory bowel disease. This is achieved by reverting the disordered intestinal flora to a healthy state by decreasing the F/B ratio, inhibiting the production of proinflammatory factors, such as TNF- $\alpha$  and IL-17, promoting the production of anti-inflammatory factors, such as IL-10, and increasing the content of SCFAs [43–46]. In this study, the preventive administration of CSO decreased the levels of the proinflammatory factor IL-17 and increased the levels of the anti-inflammatory factors, sIgA, and SCFAs. The discrepancy in the F/B ratio trend can be attributed to the different effects of ALA and DHA/EPA and the presence of several fatty acids (not only ALA) in CSO. Noriega et al. reported that supplementation with  $\omega$ -3 PUFAs at a daily dose of 600 mg through a fish protein diet for 2 weeks leads to an increase in Firmicutes and a decrease in those of Bacteroidetes and Actinobacteria; this is consistent with the findings of this study [47].

## 5. Conclusions

CSO treatment could regulate intestinal flora and the expression of inflammatory factors. In addition, it improved the levels of SCFAs in the feces of mice, preventing or alleviating diarrhea. Therefore, CSO administration can be a promising strategy for preventing diarrhea. However, this study has several limitations. This study evaluated the CSO pretreatment of mice by treating them with CSO and then inducing diarrhea; therefore, the result is focused on the preventive effect of CSO. The efficacy of CSO for treating diarrhea remains uncertain. SCFAs exert anti-inflammatory effects, and the intestinal flora directly influences the availability of ALA; therefore, further studies are needed to determine whether the interaction between ALA and intestinal flora can enhance the anti-inflammatory effect of CSO.

## Data Availability

The data used to support the research are included within this manuscript.

## Conflicts of Interest

The authors declare that there are no conflicts of interest.

## Authors' Contributions

Yi Fan was responsible for conceptualization of the study; Jie Zhu and Yi Fan developed the methodology; Liqin Yu was responsible for software; Jie Zhu and Feifei Li validated the study; Jie Zhu and Huanan Zhang contributed to formal analysis; Jie Zhu, Liqin Yu, Huanan Zhang, and Feifei Li were responsible for investigation; Xiao Li was responsible for resources; Jie Zhu and Yue Wei contributed to data curation; Jie Zhu prepared the original draft; Jie Zhu and Xiao Li reviewed and edited the manuscript; Yue Wei and Zhiyao Wang were responsible for visualization; Yi Fan was responsible for supervision of the study; Jie Zhu, Huanan Zhang, and Liqin Yu were responsible for project administration; Zhiyao Wang was involved in funding acquisition. All authors have read and agreed to the published version of the manuscript.

## Acknowledgments

This research was funded by the Henan Academy of Sciences (Projects of Special Foundation for Major Scientific Research supported by Henan Academy of Sciences (no. 190113004) and Projects of Basic Scientific Research supported by Henan Academy of Sciences (no. 200613114)).

## References







- [1] K. H. Keddy, "Old and new challenges related to global burden of diarrhoea," *The Lancet Infectious Diseases*, vol. 18, no. 11, pp. 1163–1164, 2018.
- [2] R. E. Black, S. Cousens, H. L. Johnson et al., "Global, regional, and national causes of child mortality in 2008: a systematic analysis," *The Lancet*, vol. 375, no. 9730, pp. 1969–1987, 2010.
- [3] R. Black, O. Fontaine, L. Lamberti et al., "Drivers of the reduction in childhood diarrhoea mortality 1980–2015 and interventions to eliminate preventable diarrhoea deaths by 2030," *Journal of Global Health*, vol. 9, no. 2, Article ID 020801, 2019.
- [4] M. A. da Cruz Gouveia, M. T. C. Lins, and G. A. P. da Silva, "Acute diarrhea with blood: diagnosis and drug treatment," *Jornal de Pediatria*, vol. 96, no. S1, pp. 20–28, 2020.
- [5] S. Bhatnagar, R. Kumar, R. Dua, S. Basu, and P. Kumar, "Outcome of children with severe acute malnutrition and diarrhea: a cohort study," *Pediatric Gastroenterology, Hepatology & Nutrition*, vol. 22, no. 3, pp. 242–248, 2019.
- [6] R. H. J. Bandsma, K. Sadiq, and Z. A. Bhutta, "Persistent diarrhoea: current knowledge and novel concepts," *Paediatrics and International Child Health*, vol. 39, no. 1, pp. 41–47, 2019.
- [7] O. Gómez-Escudero and J. M. Remes-Troche, "Approach to the adult patient with chronic diarrhea: a literature review," *Revista de Gastroenterología de México*, vol. 86, pp. 387–402, 2021.
- [8] M. Pimentel, "Evidence-based management of irritable bowel syndrome with diarrhea," *American Journal of Managed Care*, vol. 24, no. 3S, pp. S35–S46, 2018.
- [9] Y. X. Li, S. T. Xia, X. H. Jiang et al., "Gut microbiota and diarrhea: an updated review," *Frontiers in Cellular and Infection Microbiology*, vol. 11, Article ID 625210, 2021.
- [10] M. Eberlin, M. Chen, T. Mueck, and J. Däbritz, "Racecadotril in the treatment of acute diarrhea in children: a systematic, comprehensive review and meta-analysis of randomized

- controlled trials,” *BMC Pediatrics*, vol. 18, no. 124, p. 124, 2018.
- [11] M. A. Silverman, L. Konnikova, and J. S. Gerber, “Impact of antibiotics on necrotizing enterocolitis and antibiotic-associated diarrhea,” *Gastroenterology Clinics of North America*, vol. 46, no. 1, pp. 61–76, 2017.
  - [12] B. L. Zhou, Y. T. Yuan, S. S. Zhang et al., “Intestinal flora and disease mutually shape the regional immune system in the intestinal tract,” *Frontiers in Immunology*, vol. 11, Article ID 575, 2020.
  - [13] V. Ronan, R. Yeasin, and E. C. Claud, “Childhood development and the microbiome: the intestinal microbiota in maintenance of health and development of disease during childhood development,” *Gastroenterology*, vol. 160, no. 2, pp. 495–506, 2021.
  - [14] C. Martin-Gallausiaux, L. Marinelli, H. M. Blottière, P. Larraufie, and N. Lapaque, “SCFA: mechanisms and functional importance in the gut,” *Proceedings of the Nutrition Society*, vol. 80, no. 1, pp. 37–49, 2021.
  - [15] C. Z. Shi, H. Li, X. Qu et al., “High fat diet exacerbates intestinal barrier dysfunction and changes gut microbiota in intestinal-specific ACF7 knockout mice,” *Biomedicine & Pharmacotherapy*, vol. 110, pp. 537–545, 2019.
  - [16] R. V. Luthold, G. R. Fernandes, A. C. Franco-de-Moraes, L. G. D. Folchetti, and S. R. G. Ferreira, “Gut microbiota interactions with the immunomodulatory role of vitamin D in normal individuals,” *Metabolism*, vol. 69, pp. 76–86, 2017.
  - [17] H. Furuhashi, K. Isshi, and R. Inoue, “Effect of salacia species extract on gut microbiota composition in patients with diarrhea-predominant irritable bowel syndrome: a multicenter, double-blind, randomized, placebo-controlled study,” *Gastroenterology*, vol. 158, p. S-95, 2020.
  - [18] R. M. Kambale, F. I. Nancy, G. A. Ngaboyeka, J. B. Kasengi, L. B. Bindels, and D. Van der Linden, “Effects of probiotics and synbiotics on diarrhea in undernourished children: systematic review with meta-analysis,” *Clinical Nutrition*, vol. 40, no. 5, pp. 3158–3169, 2021.
  - [19] Y. Peng, Y. M. Yan, P. Wan et al., “Prebiotic effects in vitro of anthocyanins from the fruits of lycium ruthenicum murray on gut microbiota compositions of feces from healthy human and patients with inflammatory bowel disease,” *LWT-Food Science and Technology*, vol. 149, Article ID 111829, 2021.
  - [20] A. M. Darwesh, D. K. Sosnowski, T. Y. Lee, H. Keshavarz-Bahaghighat, and J. M. Seubert, “Insights into the cardioprotective properties of *n*–3 PUFAs against ischemic heart disease via modulation of the innate immune system,” *Chemico-Biological Interactions*, vol. 308, pp. 20–44, 2019.
  - [21] H. Watson, S. Mitra, F. C. Croden et al., “A randomised trial of the effect of omega-3 polyunsaturated fatty acid supplements on the human intestinal microbiota,” *Gut*, vol. 67, no. 11, pp. 1974–1983, 2018.
  - [22] A. Belluzzi, “N-3 fatty acids for the treatment of inflammatory bowel diseases,” *Proceedings of the Nutrition Society*, vol. 61, no. 3, pp. 391–395, 2002.
  - [23] H. D. Belayneh, R. L. Wehling, E. Cahoon, and O. N. Ciftci, “Extraction of omega-3-rich oil from camelina sativa seed using supercritical carbon dioxide,” *The Journal of Supercritical Fluids*, vol. 104, pp. 153–159, 2015.
  - [24] T. Meuronen, M. A. Lankinen, A. Fauland et al., “Intake of camelina sativa oil and fatty fish alter the plasma lipid mediator profile in subjects with impaired glucose metabolism—a randomized controlled trial,” *Prostaglandins Leukotrienes and Essential Fatty Acids*, vol. 159, pp. 102–143, 2020.
  - [25] W. L. Chen, X. Y. Peng, J. X. Yu et al., “FengLiao affects gut microbiota and the expression levels of Na<sup>+</sup>/H<sup>+</sup> exchangers, aquaporins and acute phase proteins in mice with castor oil-induced diarrhea,” *PLoS One*, vol. 15, no. 7, Article ID e0236511, 2020.
  - [26] M. A. F. Tagne, H. Akaou, P. A. Noubissi et al., “Effect of hydroethanolic extract of *bixa orellana* linn (bixaceae) leaves on castor oil-induced diarrhea in swiss albino mice,” *Gastroenterology Research and Practice*, vol. 2019, Article ID 6963548, 8 pages, 2019.
  - [27] M. C. Roberts, L. L. Clarke, and C. M. Johnson, “Castor-oil induced diarrhoea in ponies: a model for acute colitis,” *Equine Veterinary Journal*, vol. 21, no. S7, pp. 60–67, 1989.
  - [28] Y. Maniyar, P. Bhixavatimath, and N. Agashikar, “Antidiarrheal activity of flowers of *ixora coccinea* linn in rats,” *Journal of Ayurveda & Integrative Medicine*, vol. 1, no. 4, pp. 287–291, 2010.
  - [29] G. Zhou, Z. Hu, and Y. Wang, “An inquiry into preparing diarrhea model of mice and application of diarrhea index,” *Chinese Traditional Herbal Drugs*, vol. 25, no. 4, pp. 195–199, 1994.
  - [30] D. Li, M. L. Wahlqvist, and A. J. Sinclair, “Advances in *n*–3 polyunsaturated fatty acid nutrition,” *Asia Pacific Journal of Clinical Nutrition*, vol. 28, no. 1, pp. 1–5, 2019.
  - [31] M. B. Flak, R. A. Colas, E. Muñoz-Atienza, M. A. Curtis, J. Dalli, and C. Pitzalis, “Inflammatory arthritis disrupts gut resolution mechanisms, promoting barrier breakdown by prophyromonas gingivalis,” *JCI Insight*, vol. 4, no. 13, Article ID e125191, 2019.
  - [32] D. R. Tocher, M. B. Betancor, M. Sprague, R. Olsen, and J. Napier, “Omega-3 long chain polyunsaturated fatty acids, EPA and DHA: bridging the gap between supply and demand,” *Nutrients*, vol. 11, no. 1, pp. 89–108, 2019.
  - [33] A. S. Abdelhamid, T. J. Brown, J. S. Brainard et al., “Omega-3 fatty acids for the primary and secondary prevention of cardiovascular disease,” *Cochrane Database of Systematic Reviews*, vol. 11, no. 11, Article ID CD003177, 2018.
  - [34] J. Korbecki, R. Bobiński, and M. Dutka, “Self-regulation of the inflammatory response by peroxisome proliferator-activated receptors,” *Inflammation Research*, vol. 68, no. 6, pp. 443–458, 2019.
  - [35] C. J. Chang, C. S. Lin, C. C. Lu et al., “Ganoderma lucidum reduces obesity in mice by modulating the composition of the gut microbiota,” *Nature Communications*, vol. 6, no. 1, p. 7489, 2015.
  - [36] D. I. Poppleton, M. Duchateau, V. Hourdel et al., “Outer membrane proteome of *veillonella parvula*: a diderm firmicute of the human microbiome,” *Frontiers in Microbiology*, vol. 8, Article ID 1215, 2017.
  - [37] J. P. Jacobs, M. Goudarzi, N. Singh et al., “A disease-associated microbial and metabomics state in relatives of pediatric inflammatory bowel disease patients,” *Cellular and Molecular Gastroenterology Hepatology*, vol. 2, no. 6, pp. 750–766, 2016.
  - [38] V. F. Lanza, A. P. Tedim, J. L. Martínez, F. Baquero, and T. M. Coque, “The plasmidome of firmicutes: impact on the emergence and the spread of resistance to antimicrobials,” *Microbiology Spectrum*, vol. 3, no. 2, 2015.
  - [39] E. J. C. Goldstein, K. L. Tyrrell, and D. M. Citron, “Lactobacillus species: taxonomic complexity and controversial susceptibilities,” *Clinical Infectious Disease*, vol. 60, no. S2, pp. S98–S107, 2015.
  - [40] M. Derrien, P. Van Baarlen, G. Hooiveld, E. Norin, M. Müller, and W. M. de Vos, “Modulation of mucosal immune response, tolerance, and proliferation in mice colonized by the

- mucin-degrader akkermansia muciniphila,” *Frontiers in Microbiology*, vol. 2, Article ID 166, 2011.
- [41] H. Zeng, S. Umar, B. Rust, D. Lazarova, and M. Bordonaro, “Secondary bile acids and short chain fatty acids in the colon: a focus on colonic microbiome, cell proliferation, inflammation, and cancer,” *International Journal of Molecular Sciences*, vol. 20, no. 5, p. 1214, 2019.
- [42] Y. Li, L. Ji, and T. X. Chen, “The effect of secretory IgA in the mucosal immune system,” *Biomedicine Research International*, vol. 2020, Article ID 2032057, 6 pages, 2020.
- [43] A. Belluzzi, “Polyunsaturated fatty acids ( $n-3$  PUFAs) and inflammatory bowel disease (IBD): pathogenesis and treatment,” *European Review Medical and Pharmacological Sciences*, vol. 8, pp. 225–229, 2004.
- [44] T. Babcock, A. Kurland, W. Helton, A. Rahman, K. Anwar, and N. Espat, “Inhibition of activator protein-1 transcription factor activation by omega-3 fatty acid modulation of mitogen-activated protein kinase signaling kinases,” *Journal of Parenteral and Enteral Nutrition*, vol. 27, no. 3, pp. 176–180, 2003.
- [45] A. Awoyemi, M. Trøseid, H. Arnesen, S. Solheim, and I. Seljeflot, “Effects of dietary intervention and  $n-3$  PUFA supplementation on markers of gut-related inflammation and their association with cardiovascular events in a high-risk population,” *Atherosclerosis*, vol. 286, pp. 53–59, 2019.
- [46] M. L. Santoru, C. Piras, A. Murgia et al., “Cross sectional evaluation of the gut-microbiome metabolome axis in an Italian cohort of IBD patients,” *Scientific Reports*, vol. 7, no. 1, p. 9523, 2017.
- [47] B. S. Noriega, M. A. Sanchez-Gonzalez, D. Salyakina, and J. Coffman, “Understanding the impact of omega-3 rich diet on the gut microbiota,” *Case Reportin Medicine*, vol. 2016, Article ID 3089303, 6 pages, 2016.

## Research Article

# Network Pharmacology- and Molecular Docking-Based Identification of Potential Phytocompounds from *Argyrea capitiformis* in the Treatment of Inflammation

Ahmad J. Obaidullah <sup>1</sup>, Mohammed M. Alanazi <sup>1</sup>, Nawaf A. Alsaif,<sup>1</sup> Ashwag S. Alanazi,<sup>2</sup> Hussam Albassam <sup>3</sup>, Alanazi AZ <sup>3</sup>, Osama I. Alwassil <sup>4</sup>, Ali M. Alqahtani <sup>5</sup> and Abu Montakim Tareq<sup>6</sup>

<sup>1</sup>Department of Pharmaceutical Chemistry, College of Pharmacy, King Saud University, P.O. Box 2457, Riyadh 11451, Saudi Arabia

<sup>2</sup>Department of Pharmaceutical Sciences, College of Pharmacy, Princess Nourah Bint Abdulrahman University, Riyadh 84428, Saudi Arabia

<sup>3</sup>Department of Pharmacology and Toxicology, College of Pharmacy, King Saud University, P.O. Box 2457, Riyadh 11451, Saudi Arabia

<sup>4</sup>Department of Pharmaceutical Sciences, College of Pharmacy, King Saud bin Abdulaziz University for Health Sciences, Riyadh 11481, Saudi Arabia

<sup>5</sup>Department of Pharmacology, College of Pharmacy, King Khalid University, Abha 62529, Saudi Arabia

<sup>6</sup>Department of Pharmacy, International Islamic University Chittagong, Chittagong 4318, Bangladesh

Correspondence should be addressed to Ahmad J. Obaidullah; aobaidullah@ksu.edu.sa

Received 18 December 2021; Revised 3 January 2022; Accepted 15 January 2022; Published 31 January 2022

Academic Editor: Ruchika Garg

Copyright © 2022 Ahmad J. Obaidullah et al. This is an open access article distributed under the Creative Commons Attribution License, which permits unrestricted use, distribution, and reproduction in any medium, provided the original work is properly cited.

The methanolic extract of *Argyrea capitiformis* stem was examined for anti-inflammatory activities following network pharmacology analysis and molecular docking study. Based on gas chromatography-mass spectrometry (GC-MS) analysis, 49 compounds were identified from the methanolic extract of *A. capitiformis* stem. A network pharmacology analysis was conducted against the identified compounds, and Kyoto Encyclopedia of Genes and Genomes (KEGG) pathway analysis and Gene Ontology analysis of biological processes and molecular functions were performed. Six proteins (IL1R1, IRAK4, MYD88, TIRAP, TLR4, and TRAF6) were identified from the KEGG pathway analysis and subjected to molecular docking study. Additionally, six best ligand efficiency compounds and positive control (aspirin) from each protein were evaluated for their stability using the molecular dynamics simulation study. Our study suggested that IL1R1, IRAK4, MYD88, TIRAP, TLR4, and TRAF6 proteins may be targeted by compounds in the methanolic extract of *A. capitiformis* stem to provide anti-inflammatory effects.

## 1. Introduction

Inflammation describes a biological process that occurs in tissues to protect the host against harmful stimuli, such as microorganisms and abnormal or damaged cells. Inflammation stimulates the immune system and regulates protective responses via immune cells, blood vessels, and molecular biological agents [1, 2]. Many chronic diseases, including cardiovascular and gastrointestinal illnesses,

diabetes, rheumatism, and cancer, are associated with upregulated inflammation [3]. Chronic diseases represent a major human health concern according to the World Health Organization (WHO). The incidence of chronic inflammation-related disorders is expected to steadily increase in the United States (US) over the next 30 years. Approximately 125 million people in the US were diagnosed with chronic diseases in 2000, with 61 million (21%) having multiple conditions [4–6]. Typically, cellular and molecular

mechanisms and interactions among various factors can efficiently limit the potential damage and prevent further infection during an acute inflammatory response, resulting in the eventual repair of cellular homeostasis following the resolution of acute inflammation. However, uncontrolled acute inflammation can develop into chronic inflammation, causing a range of chronic inflammatory diseases [7]. Three out of five people worldwide die from chronic inflammatory conditions, such as stroke, respiratory infections, cardiovascular diseases, cancers, diabetes, and obesity [4–6]. A growing interest in the use of medicinal plants has developed for the treatment and management of diseases in an effort to identify safer and more efficient anti-inflammatory agents for the prevention of inflammatory conditions rather than using synthetic anti-inflammatory drugs [8].

*Argyrea capitiformis* (Poir.) Ooststr. is a member of the Convolvulaceae family of the *Argyrea* genus, which is not toxic and has medicinal and ornamental uses [9, 10]. Traditionally, a paste made from the leaves of *A. capitiformis* has been used as an effective treatment of bruising on the legs. *A. capitiformis* has also been used in traditional medicine as a purgative and to treat sexual debility and ear pain [10–12]. Several studies have been reported for the *Argyrea* species, including antioxidant, anti-inflammatory, immunomodulatory, and CNS activities with several bioactive compounds [13–15]. However, no such study has been evaluated for *A. capitiformis* except the recent study on the methanolic extract of *A. capitiformis* leaves that suppressed the nuclear factor- $\kappa$ B (NF- $\kappa$ B) pathway and inhibited the lipopolysaccharide-induced production of nitric oxide and inducible nitric oxide synthase in RAW 264.7 cells, demonstrating anti-inflammatory activities [9]. However, the chemical compounds found in *A. capitiformis* that are responsible for these anti-inflammatory effects and the underlying mechanisms remain unknown. Further research is necessary to identify the potential lead compounds responsible for these biological anti-inflammatory outcomes.

Network pharmacology has become a widely accessible analysis method following the increased availability of biomedical data sets during the postgenomic period, supporting the growth of the fields of systems biology and polypharmacology [16]. Complex compound-gene and compound-protein interactions can be evaluated systematically to develop a prototype for efficient therapy. New therapeutic mechanisms may be discovered by network pharmacology analysis, which is oriented toward a “multi-goals, multi-disease” paradigm rather than “one target, one drug” [17–19]. Network pharmacology represents an effective method for selecting and elucidating the synergistic effects among bioactive chemicals through the mechanistic exploration of effects on multiple disease pathways [19, 20]. Additionally, spectrometric and chromatographic technologies used in the initial evaluation of medicinal plants provide valuable information on bioactive activities that aid in the selection of biologically active species. Alkaloids, phenolic compounds, organic acids, esters, and amino acids are among the chemicals that GC-MS can detect quickly and accurately. Thus, in this investigation, GC-MS was used to

detect and identify phytochemical constituents in *A. capitiformis* [21–24].

The network pharmacology approach connects targeted genes with the effects of bioactive compounds; thus, the present study was designed to elucidate the anti-inflammatory effects of the methanolic extract of *A. capitiformis* stem using a network pharmacology approach. Bioactive compounds in the methanolic extract of *A. capitiformis* stem were identified for this study using gas chromatography-mass spectrometry (GC-MS) analysis, followed by a molecular docking assay to investigate potential ligand-receptor interactions, including the assessment of binding affinity and stability.

## 2. Materials and Methods

**2.1. Plant Extraction.** The stems of *A. capitiformis* were collected from the Sitakunda Eco-park, Chittagong, Bangladesh, in March 2020 and later identified by a taxonomist. The stems were subjected to air-drying and ground to a coarse powder. The powder (200 g) was soaked in methanol (1 L) for 7 days [25, 26]. Subsequently, the extract was filtered through Whatman filter paper and evaporated at 45°C. After the evaporation, 2.67 g of the black methanol extract yield (1.34%) was collected in an amber glass vial and refrigerated at 4°C until further use.

**2.2. GC-MS Analysis.** An Agilent GC 7890A (Agilent Technologies Inc., Wilmington, DE, USA), combined with a triple-axis detector 5975 C single-quadrupole mass spectrometer, was used for GC-MS analysis. The chromatographic column was an Agilent HP 5MS column (30 m  $\times$  0.25 mm  $\times$  0.25  $\mu$ m film thickness), using high-purity helium as the gas carrier at a flow rate of 1 mL per min. The injector temperature was 230°C, and the sample was injected using a splitless injector at 20:1. The temperature was set primarily to 40°C (held for 1 min), raised to 150°C at a rate of 5°C per min (held for 2 min), before being increased to 300°C at a rate of 5°C per min (held for 10 min). The temperature of the MS ion source was set to 150°C, and the temperature of the inlet line was set to 280°C. The scan range was set between 50 and 550 mass, with 70 eV electron energy and a 4-min solvent delay. Finally, by comparing the spectra against the NIST 2008 database (National Institute of Standard and Technology library), tentative compounds were identified. The total analysis time required for the sample was 65 min [27].

**2.3. Network Pharmacology.** The network pharmacology analysis was performed using the STITCH platform (<http://stitch.embl.de/>) to identify putative associations between the identified compounds and target genes. Multiple compound targets were identified using the *Homo sapiens* genome [27–29]. Multiple functional nodes and edges were identified in the network. Kyoto Encyclopedia of Genes and Genomes (KEGG) analysis was performed on the components identified in the network to obtain a biological interpretation of



the vast list of potential targets and to identify potential anti-inflammatory pathways that are targeted.

The STRING (search tool for retrieval of interacting genes) database (<https://string-db.org>), which includes predicted protein-protein interactions (PPIs), was used to predict functional protein interactions [30].

#### 2.4. Molecular Docking Study

**2.4.1. Protein Selection and Preparation.** Six targeted proteins were selected from the KEGG analysis: interleukin 1 (IL-1) receptor type 1 (IL1R1; PDB: 1ITB) [31], IL-1 receptor-associated kinase 4 (IRAK4; PDB: 6EGA) [32], myeloid differentiation factor 88 (MYD88; PDB: 4EO7) [33], TIR domain-containing adaptor protein (TIRAP; PDB: 4FZ5) [34], Toll-like receptor 4 (TLR4; PDB: 3FXI) [35], and tumor necrosis factor (TNF) receptor-associated factor 6 (TRAF6; PDB: 3HCT) [36]. Protein structures were retrieved in .pdb format from the Protein Data Bank (<http://www.rcsb.org/pdb>). The proteins were prepared using Schrödinger (Maestro v11.1), utilizing the force field OPLS3 [27].

**2.4.2. Ligand Preparation.** We selected 47 compounds identified from *A. capitiformis*, according to the qualitative GC-MS analysis, which we submitted to the molecular docking study. The selected compounds were retrieved in .sdf format from the PubChem database. In addition, aspirin (CID: 2244) was utilized in this study as a positive anti-inflammatory control. The three-dimensional (3D) structures of the selected compounds were constructed in Schrödinger using LigPrep (Maestro v11.1), utilizing the force field OPLS3.

**2.4.3. Grid Generation and Molecular Docking.** To create receptor grids and execute a molecular docking analysis, Glide (Schrödinger, Maestro v11.1) was used. The grids were generated in Glide with the default settings and the OPLS3 force field. A cubic box with a boundary box (14 Å × 14 Å × 14 Å) was specified for the receptors. All docking studies were conducted using Glide's standard precision (SP) and flexible docking modes, and the lowest docking score for each ligand was recorded.

**2.4.4. MM-GBSA and Ligand Efficiency Analysis.** The free energies of binding ( $\Delta G$ ; kcal/mol) for each ligand and the target receptors were calculated using the Schrödinger software package Prime/MM-GBSA module (OPLS3) [37, 38]. The ligand efficiency (LE) was assessed for each ligand by obtaining the ratio of  $\Delta G$  to the number of heavy atoms (NHA):  $LE = -(\Delta G)/NHA$  [39].

**2.5. Molecular Dynamics Simulation.** The molecular dynamics simulation study was conducted in YASARA dynamics by the aid of AMBER14 force field [40, 41]. The docked complexes were optimized and cleaned, and hydrogen bond network system was oriented. The cubic simulation cell was created where the TIP3P solvation model

was used with periodic boundary conditions [42]. The simulation system was neutralized at 310 K temperature, pH 7.4, and 0.9% NaCl. The initial energy minimization was conducted by steepest grained algorithms by simulating annealing methods. The long-range electrostatic interactions were calculated by the particle mesh Ewald (PME) methods with a cutoff radius of 8.0 Å [43, 44]. The simulation time step was set as 2.0 fs. The simulation trajectories were saved after 100 ps and finally run for 20 ns by following the constant pressure and Berendsen thermostat [45]. The simulation trajectories were used to calculate the root-mean-square deviation, solvent accessible surface area, radius of gyration, and hydrogen bond [46–54].

### 3. Results

**3.1. GC-MS Analysis.** In this work, methanol was utilized as the solvent for extraction, resulting in a 1.34% yield. The GC-MS analysis of the *A. capitiformis* stem methanolic extract revealed 49 compounds with different retention times and peak areas (Table 1 and Figure S1). The methanolic extract contained the following identified compounds: stigmast-4-en-3-one (20.78%, RT: 58.161); hexadeca-2,6,10,14-tetraen-1-ol, 3,7,11,16-tetramethyl-, (E,E,E)- (18.36%, RT: 51.477); urs-9(11),12-dien-3-one (10.35%, RT: 58.55); urs-9(11),12-dien-3-ol (6.89%, RT: 55.077); 2-(2-hydroxy-2-phenylethyl)-3,5,6-trimethylpyrazine (5.21%, RT: 22.438); longipinane, (E)- (3.86%, RT: 61.245); urs-12-ene (2.95%, RT: 57.274); 2-hydrazino-8-hydroxy-4-phenylquinoline (2.29%, RT: 50.688); and friedelin (2.01%, RT: 59.511).

**3.2. Network Construction and Biological Process Analysis.** A KEGG pathway analysis of potential target genes (IL1R1, IRAK4, MYD88, TIRAP, TLR4, and TRAF6) revealed signaling pathways related with anti-inflammatory effects (see Table 2). Figure S2 shows the PPI network with 12 proteins (IL1R1, IRAK2, MYD88, IRAK4, IRAK2, MYD88, TIRAP, TRAF6, TLR3, TLR4, TLR5, and TLR6), all of which have anti-inflammatory effects. Tables S1 and S2 represent the biological processes and molecular functions of the genes interacting with the compounds, respectively. Protein-protein interaction (PPI) status of 10 proteins with co-expression is demonstrated in Table S3.

**3.3. Molecular Docking and Simulation.** A total of 47 compounds docking results are presented in Tables 3–8, which show the findings. Aspirin has been used as a positive control for this study. This study's findings reveal that binding energies of most of the ligands to receptors are negative, as later validated by MM-GBSA analysis. The proteins and ligands' molecular interaction is presented in Supplementary Materials (Tables S4–S9). To better understand the docking score, we have studied the ligand efficiency, which demonstrated excellent support for molecular docking scores. The molecular dynamics simulation of the targeted receptors (IL1R1, IRAK4, MYD88, TIRAP, TLR4, and TRAF6) against the best stable compounds is presented in Figures 1–6.

TABLE 1: GC-MS analysis of the methanolic extract of *Argyrea capitiformis* stem.

Sl. no.	RT (min)	Area	PA (%)	Compounds	MW (amu)
1	7.081	579298	0.105693	Methylcyclohexane	98.11
2	9.965	3399237	0.620188	Phenol	94.042
3	10.079	1001603	0.182742	Sulcatone	126.104
4	10.148	780660	0.142431	Butanoic acid, 2,3-dimethyl-, ethyl ester	144.115
5	10.348	865180	0.157852	1,2-Cyclohexanedione	112.052
6	11.601	1689097	0.308175	4-Methyl-1,5-heptadiene	110.11
7	16.104	925883	0.168927	Catechol	110.037
8	16.373	5726885	1.044866	Coumaran	120.058
9	18.359	4206254	0.767428	Hydroquinone	110.037
10	18.879	2153554	0.392914	p-Vinylguaicol	150.068
11	19.412	630941	0.115115	Gamma-pyrone	136.125
12	20.916	2138840	0.39023	4-Ethylresorcinol	138.068
13	22.438	28577337	5.213916	2-(2-Hydroxy-2-phenylethyl)-3,5,6-trimethylpyrazine	242.142
14	25.225	2487140	0.453777	Ethanone, 1-(3,4-dimethoxyphenyl)-	180.079
15	25.563	4005631	0.730825	Spathulenol	220.183
16	25.694	2465579	0.449843	Caryophyllene oxide	220.183
17	26.295	639699	0.116713	Cyclopentanecarboxaldehyde, 2-methyl-3-methylene-	124.089
18	27.314	1610820	0.293893	Epiglobulol	222.198
19	27.668	1426632	0.260288	4(1H)-Pyrimidinone, 6-hydroxy-	112.027
20	28.126	1109370	0.202404	Cyclododecanone, 2-methylene-	194.167
21	28.481	1911669	0.348783	2,3-Dehydro-4-oxo-7,8-dihydro-beta-ionone	206.131
22	28.767	1292504	0.235816	Diepicedrene-1-oxide	220.183
23	29.213	10432471	1.903397	Coniferol	180.079
24	33.848	7982629	1.456425	n-Hexadecanoic acid	256.24
25	36.206	6006919	1.095958	Methyl 6,9,12-hexadecatrienoate	264.209
26	36.44	14533536	2.651634	Phytol	296.308
27	45.59	1109241	0.20238	1,3,6,10-Cyclotetradecatetraene, 3,7,11-trimethyl-14-(1-methylethyl)-, [S-(E,Z,E,E)]-	272.25
28	46.574	5222376	0.952819	(Z,E)-Farnesol	222.198
29	47.054	5942094	1.084131	Geranyl acetate	332.272
30	47.215	4894168	0.892938	Farnesol acetate	264.209
31	47.426	5740162	1.047289	3-Furaldehyde	96.021
32	47.781	1179960	0.215283	trans-13-Docosamide	337.334
33	48.542	6365219	1.16133	Squalene	410.391
34	48.782	5112411	0.932756	2'H-Androsta-2,4,6-trieno [3,2-c]pyrazol-17.beta.-ol, 17-methyl-, acetate (ester)	366.231
35	49.686	6003161	1.095273	Spiro[2H-indole-2,8'(7'H)-[3, 7]methano[2H]furo[4,3,2-hi]indolizine]-2'a(3'H)-carboxylic acid, 4'-ethylidene-1,3,4',5',8',8'b-hexahydro-3-oxo-, methyl ester	366.158
36	49.83	2892843	0.527797	Chola-5,22-dien-3-ol, (3.beta.,22Z)-	342.292
37	50.236 and 52.536	2523311 and 4290679	0.460376 and 0.782831	Curan-17-oic acid, 2,16-didehydro-20-hydroxy-19-oxo-, methyl ester	354.158
38	50.47	7587558	1.384345	Geranylgeraniol	290.261
39	50.688	12575157	2.294329	2-Hydrazino-8-hydroxy-4-phenylquinoline	251.106
40	51.477	100609821	18.35619	Hexadeca-2,6,10,14-tetraen-1-ol, 3,7,11,16-tetramethyl-, (E,E,E)-	290.261
41	52.811	4449457	0.8118	Cycloartenol	426.386
42	55.077	37780051	6.892945	Ursa-9(11),12-dien-3-ol	424.371
43	57.274	16193192	2.954437	Urs-12-ene	410.391
44	58.161	113880865	20.77749	Stigmast-4-en-3-one	412.371
45	58.55	56736847	10.3516	Ursa-9(11),12-dien-3-one	422.355
46	58.962	3509209	0.640253	C(14a)-homo-27-nor-14-beta-gammaceran-3-alpha-ol	428.402
47	59.511	11017163	2.010074	Friedelin	426.386
48	60.575	21170007	3.862453	Longipinane, (E)-	206.203
49	61.245	2733077	0.498648	Lanosterol	426.386

Note. MW: molecular weight; RT: retention time.

TABLE 2: KEGG analysis of the genes targeted by compounds.

Pathway ID	Pathway description	Observed gene count	False discovery rate	Matching proteins in network (labels)
05204	Chemical carcinogenesis	12	$3.6E-15$	<i>SULT1A1, SULT1A2, SULT1A3, UGT1A1, UGT1A10, UGT1A3, UGT1A4, UGT1A6, UGT1A7, UGT1A8, UGT1A9, UGT2B15</i>
00053	Ascorbate and aldarate metabolism	9	$1.21E-14$	<i>UGT1A1, UGT1A10, UGT1A3, UGT1A4, UGT1A6, UGT1A7, UGT1A8, UGT1A9, UGT2B15</i>
00040	Pentose and glucuronate interconversions	9	$1.49E-13$	<i>UGT1A1, UGT1A10, UGT1A3, UGT1A4, UGT1A6, UGT1A7, UGT1A8, UGT1A9, UGT2B15</i>
00860	Porphyrin and chlorophyll metabolism	9	$9.94E-13$	<i>UGT1A1, UGT1A10, UGT1A3, UGT1A4, UGT1A6, UGT1A7, UGT1A8, UGT1A9, UGT2B15</i>
00983	Drug metabolism—other enzymes	9	$1.27E-12$	<i>UGT1A1, UGT1A10, UGT1A3, UGT1A4, UGT1A6, UGT1A7, UGT1A8, UGT1A9, UGT2B15</i>
00500	Starch and sucrose metabolism	9	$4.62E-12$	<i>UGT1A1, UGT1A10, UGT1A3, UGT1A4, UGT1A6, UGT1A7, UGT1A8, UGT1A9, UGT2B15</i>
00140	Steroid hormone biosynthesis	9	$6.95E-12$	<i>UGT1A1, UGT1A10, UGT1A3, UGT1A4, UGT1A6, UGT1A7, UGT1A8, UGT1A9, UGT2B15</i>
00830	Retinol metabolism	9	$1.44E-11$	<i>UGT1A1, UGT1A10, UGT1A3, UGT1A4, UGT1A6, UGT1A7, UGT1A8, UGT1A9, UGT2B15</i>
00982	Drug metabolism—cytochrome P450	9	$2.81E-11$	<i>UGT1A1, UGT1A10, UGT1A3, UGT1A4, UGT1A6, UGT1A7, UGT1A8, UGT1A9, UGT2B15</i>
00980	Metabolism of xenobiotics by cytochrome P450	9	$4.52E-11$	<i>UGT1A1, UGT1A10, UGT1A3, UGT1A4, UGT1A6, UGT1A7, UGT1A8, UGT1A9, UGT2B15</i>
04620	Toll-like receptor signaling pathway	9	$1.83E-09$	<i>CD289, IRAK4, MYD88, TIRAP, TLR3, TLR4, TLR5, TLR6, TRAF6</i>
05152	Tuberculosis	8	$3.14E-06$	<i>CD289, IRAK2, IRAK4, MYD88, TIRAP, TLR4, TLR6, TRAF6</i>
<b>04064</b>	<b>NF-kappa B signaling pathway</b>	<b>6</b>	<b><math>1.35E-05</math></b>	<b><i>IL1R1, IRAK4, MYD88, TIRAP, TLR4, TRAF6</i></b>
05142	Chagas disease (American trypanosomiasis)	6	$2.09E-05$	<i>CD289, IRAK4, MYD88, TLR4, TLR6, TRAF6</i>
05133	Pertussis	5	$7.9E-05$	<i>IRAK4, MYD88, TIRAP, TLR4, TRAF6</i>
05162	Measles	5	0.00154	<i>CD289, IRAK4, MYD88, TLR4, TRAF6</i>
05140	Leishmaniasis	4	0.00164	<i>IRAK4, MYD88, TLR4, TRAF6</i>
04210	Apoptosis	4	0.00332	<i>IL1R1, IRAK2, IRAK4, MYD88</i>
05144	Malaria	3	0.00825	<i>CD289, MYD88, TLR4</i>
05145	Toxoplasmosis	4	0.00895	<i>IRAK4, MYD88, TLR4, TRAF6</i>
05134	Legionellosis	3	0.0113	<i>MYD88, TLR4, TLR5</i>
05161	Hepatitis B	4	0.0182	<i>MYD88, TIRAP, TLR3, TLR4</i>
05164	Influenza A	4	0.0332	<i>IRAK4, MYD88, TLR3, TLR4</i>
05132	Salmonella infection	3	0.0337	<i>MYD88, TLR4, TLR5</i>
05168	Herpes simplex infection	4	0.0362	<i>CD289, MYD88, TLR3, TRAF6</i>

Bold indicates the main pathway and proteins responsible for this study.

#### 4. Discussion

Plants have been used throughout the history of traditional medicine to induce a variety of biological effects, and extensive pharmaceutical resources have recently been devoted to the identification and investigation of new remedies, including those derived from plants. A critical issue encountered by researchers who perform phytoscience is that a single plant can harbor a wide range of bioactive chemicals [55, 56]. The pharmaceutical industry relies on phytochemicals to develop new drugs and therapeutic agents. Finding natural bioactive components is the first step in developing novel drugs. Screening plant extracts for therapeutically active chemicals is a novel strategy. It is important to know that plants have a lot of different types of phytochemicals, which have a lot of different biological properties. These include antioxidant, anti-inflammatory,

antidiarrhea, antiulcer, and anticancer activities [57–59]. Determining which compounds are responsible for the biological activities associated with plant materials can help understand toxicities, determine suitable doses, and identify ideal methods for compound extraction. The successful acquisition of components from plant materials depends primarily on the solvent used during the extraction process [60, 61]. The stem methanolic extract was analyzed by GC-MS analysis, and the results indicated 49 different chemicals with varying retention times and peak areas.

The network pharmacology analysis was performed to evaluate potential interactions between the identified chemical compounds and proteins, followed by multiple comparisons to determine the number of genes responsible for the anti-inflammatory effects, which was represented by the STITCH platform (Figure 7). Table 2 shows the results of KEGG pathway analysis performed on potential target

TABLE 3: Docking scores and ligand efficiencies of compounds from the methanolic extract of *Argyrea capitiformis* stems binding with IL1R1 (PDB: 1ITB).

Compounds	IL1R1 (1ITB)			
	DS*	MM-GBSA*	NHA	LE*
Methylcyclohexane	-3.416	-8.53477	7	1.22
Phenol	-4.567	-20.6083	7	2.94
Sulcatone	-3.319	-22.5701	9	2.51
Butanoic acid, 2,3-dimethyl-, ethyl ester	-3.695	-22.6538	10	2.27
1,2-Cyclohexanedione	-3.772	-15.6443	8	1.96
4-Methyl-1,5-heptadiene	-0.264	-15.0204	8	1.88
Catechol	-4.755	-24.1451	8	3.02
Coumaran	-4.368	-18.8456	9	2.09
Hydroquinone	-4.703	-21.6152	8	2.70
p-Vinylguaiaicol	-3.965	-17.0656	11	1.55
Gamma-pyrone	—	—	—	—
4-Ethylresorcinol	-4.791	-19.4157	10	1.94
2-(2-Hydroxy-2-phenylethyl)-3,5,6-trimethylpyrazine	-3.768	-18.6465	18	1.04
Ethanone, 1-(3,4-dimethoxyphenyl)-	-5.147	-24.0973	13	1.85
Spathulenol	—	—	—	—
Caryophyllene oxide	—	—	—	—
Cyclopentanecarboxaldehyde, 2-methyl-3-methylene-	-3.819	-14.8427	9	1.65
Epiglobulol	—	—	—	—
4(1H)-Pyrimidinone, 6-hydroxy-	-5.289	-22.2826	8	2.79
Cyclododecanone, 2-methylene-	-3.031	-15.4537	14	1.10
2,3-Dehydro-4-oxo-7,8-dihydro-beta-ionone	—	—	—	—
Diepicedrene-1-oxide	-3.253	-20.532	16	1.28
Coniferol	-4.551	-25.8365	13	1.99
Methyl 6,9,12-hexadecatrienoate	-0.024	-27.9609	19	1.47
Phytol	-0.765	-31.806	21	1.51
1,3,6,10-Cyclotetradecatetraene, 3,7,11-trimethyl-14-(1-methylethyl)-, [S-(E,Z,E,E)]-	—	—	—	—
(Z,E)-Farnesol	-1.134	-28.241	16	1.77
Geranyl acetate	-3.607	-33.7371	24	1.41
Farnesol, acetate	-1.636	-37.7206	24	1.57
3-Furaldehyde	-4.663	-17.5816	7	2.51
trans-13-Docosamide	-3.73	-41.2676	24	1.72
Squalene	-3.241	-26.5894	30	0.89
Chola-5,22-dien-3-ol, (3.beta.,22Z)-	-3.62	-23.7437	25	0.95
Curan-17-oic acid, 2,16-didehydro-20-hydroxy-19-oxo-, methyl ester	—	—	—	—
Geranylgeraniol	-1.699	-26.6476	21	1.27
2-Hydrazino-8-hydroxy-4-phenylquinoline	-5.348	-26.1207	19	1.37
Cycloartenol	-2.877	-17.9477	31	0.58
Ursa-9(11),12-dien-3-ol	—	—	—	—
Urs-12-ene	-2.712	-25.2104	30	0.84
Stigmast-4-en-3-one	-2.78	-23.2611	30	0.78
Ursa-9(11),12-dien-3-one	—	—	—	—
C(14a)-Homo-27-nor-14-beta-gammaceran-3-alpha-ol	—	—	—	—
Friedelin	—	—	—	—
Longipinane, (E)-	—	—	—	—
Lanosterol	-3.249	-26.5783	31	0.86
Aspirin	-4.26	-21.1433	13	1.63

Note. DS: docking score; NHA: number of heavy atoms; LE: ligand efficiency. \*Results presented in kcal/mol.

genes, which identified signaling pathways associated with anti-inflammatory actions. Analyses of biological processes and molecular functions, which identified proteins and pathways with significant values, were also performed (Table S1). A comparison of the compound-gene interaction network and the protein-protein interaction network was performed to reveal biological and molecular functions (Table S2). From a molecular and functional perspective, these findings can assist in understanding the computational rules of compounds that have the potential

to treat diseases. For example, protein kinase C (PKC) binding is known to treat inflammatory diseases [62], and the present results showed that binding with TIRAP, UGT1A10, and UGT1A7 was significant ( $p=0.0447$ ) and similar to that for PKC. Also, retinoic acid binding has a great impact on the immune system and the inflammatory response. Our findings identified the genes *UGT1A1*, *UGT1A3*, *UGT1A7*, *UGT1A8*, and *UGT1A9* as being the most significant interactions for the compounds in our extract ( $p=2.69E-06$ ).

TABLE 4: Docking scores and ligand efficiencies of compounds from the methanolic extract of *Argyrea capitiformis* stems binding with IRAK4 (PDB: 6EGA).

Compounds	IRAK4 (6EGA)			
	DS*	MM-GBSA*	NHA	LE*
Methylcyclohexane	-5.343	-28.5422	7	4.08
Phenol	-6.799	-30.4637	7	4.35
Sulcatone	-4.611	-34.0534	9	3.78
Butanoic acid, 2,3-dimethyl-, ethyl ester	-5.338	-27.5643	10	2.76
1,2-Cyclohexanedione	-5.827	-26.2939	8	3.29
4-Methyl-1,5-heptadiene	-2.392	-31.5398	8	3.94
Catechol	-6.363	-35.5712	8	4.45
Coumaran	-7.179	-34.9848	9	3.89
Hydroquinone	-6.568	-30.1474	8	3.77
p-Vinylguaiaicol	-6.906	-45.639	11	4.15
Gamma-pyrone	-5.242	-25.8647	10	2.59
4-Ethylresorcinol	-6.961	-33.0487	10	3.30
2-(2-Hydroxy-2-phenylethyl)-3,5,6-trimethylpyrazine	-7.589	-47.6142	18	2.65
Ethanone, 1-(3,4-dimethoxyphenyl)-	-7.704	-38.3452	13	2.95
Spathulenol	—	—	—	—
Caryophyllene oxide	—	—	—	—
Cyclopentanecarboxaldehyde, 2-methyl-3-methylene-	-6.889	-34.1045	9	3.79
Epiglobulol	—	—	—	—
4(1H)-Pyrimidinone, 6-hydroxy-	-6.247	-19.6834	8	2.46
Cyclododecanone, 2-methylene-	—	—	—	—
2,3-Dehydro-4-oxo-7,8-dihydro-beta-ionone	-6.224	-26.8822	15	1.79
Diepicedrene-1-oxide	—	—	—	—
Coniferol	-7.225	-49.0664	13	3.77
Methyl 6,9,12-hexadecatrienoate	-3.841	-51.8616	19	2.73
Phytol	-4.092	-37.6416	21	1.79
1,3,6,10-Cyclotetradecatetraene, 3,7,11-trimethyl-14-(1-methylethyl)-, [S-(E,Z,E,E)]-	—	—	—	—
(Z,E)-Farnesol	-4.144	-53.635	16	3.35
Geranyl acetate	-7.613	-46.7163	24	1.95
Farnesol acetate	-4.638	-48.5373	24	2.02
3-Furaldehyde	-6.301	-28.4227	7	4.06
trans-13-Docosenamide	-6.62	-55.939	24	2.33
Squalene	-7.603	-73.1988	30	2.44
Chola-5,22-dien-3-ol, (3.beta.,22Z)-	-7.25	-36.8492	25	1.47
Curan-17-oic acid, 2,16-didehydro-20-hydroxy-19-oxo-, methyl ester	—	—	—	—
Geranylgeraniol	-4.383	-54.1471	21	2.58
2-Hydrazino-8-hydroxy-4-phenylquinoline	-6.639	-35.0611	19	1.85
Cycloartenol	-3.914	-28.0451	31	0.90
Ursa-9(11),12-dien-3-ol	—	—	—	—
Urs-12-ene	-5.048	-24.8357	30	0.83
Stigmast-4-en-3-one	-7.199	-25.6365	30	0.85
Ursa-9(11),12-dien-3-one	—	—	—	—
C(14a)-homo-27-nor-14-beta-gammaceran-3-alpha-ol	—	—	—	—
Friedelin	—	—	—	—
Longipinane, (E)-	—	—	—	—
Lanosterol	-6.524	-29.9751	31	0.97
Aspirin	-6.798	-31.0373	13	2.39

Note. DS: docking score; NHA: number of heavy atoms; LE: ligand efficiency. \*Results presented in kcal/mol.

As shown in Table 2, KEGG pathway analysis for inflammatory responses identified *IL1R1*, *IRAK4*, *MYD88*, *TIRAP*, *TLR4*, and *TRAF6* in the NF- $\kappa$ B signaling pathway, which has a  $p$ -value of  $1.35E-05$ . Similar results were demonstrated for the inflammatory response in the biological process analysis, which identified the MYD88-dependent TLR signaling pathway ( $p = 2.19E-07$ ; *IRAK2*, *IRAK4*, *MYD88*, *TIRAP*, *TLR4*, *TLR5*, *TLR6*, and *TRAF6*), the TLR4 signaling pathway ( $p = 9.14E-07$ ; *IRAK2*, *IRAK4*, *MYD88*, *TIRAP*, *TLR3*, *TLR4*, *TLR6*, and *TRAF6*), the TLR1:

TLR2 signaling pathway ( $p = 2.31E-06$ ; *IRAK2*, *IRAK4*, *MYD88*, *TIRAP*, *TLR4*, *TLR6*, and *TRAF6*), the TLR 2 pathway ( $p = 2.54E-06$ ; *IRAK2*, *IRAK4*, *MYD88*, *TIRAP*, *TLR4*, *TLR6*, and *TRAF6*), the TLR signaling pathway ( $p = 3.15E-06$ ; *IRAK2*, *IRAK4*, *MYD88*, *TIRAP*, *TLR3*, *TLR4*, *TLR5*, and *TRAF6*), positive regulation of interleukin-6 production ( $p = 2.06E-05$ ; *MYD88*, *TIRAP*, *TLR3*, *TLR4*, *TLR6*, and *TRAF6*), NF- $\kappa$ B signaling ( $p = 0.000393$ ; *IRAK2*, *TIRAP*, *TLR3*, *TLR4*, and *TRAF6*), NF- $\kappa$ B signaling ( $p = 0.000601$ ; *IRAK4*, *MYD88*, *TIRAP*, *TLR3*, *TLR4*, *TLR6*,

TABLE 5: Docking scores and ligand efficiencies of compounds from the methanolic extract of *Argyrea capitiformis* stems binding with MYD88 (PDB: 4EO7).

Compounds	MYD88 (4EO7)			
	DS*	MM-GBSA*	NHA	LE*
Methylcyclohexane	-2.691	-2.45925	7	0.35
Phenol	-3.654	-5.09725	7	0.73
Sulcatone	-1.726	-8.41174	9	0.93
Butanoic acid, 2,3-dimethyl-, ethyl ester	-1.597	-2.95307	10	0.29
1,2-Cyclohexanedione	-3.341	-6.76768	8	0.85
4-Methyl-1,5-heptadiene	0.155	-14.7508	8	1.84
Catechol	-3.771	-8.25542	8	1.03
Coumaran	—	—	—	—
Hydroquinone	-3.855	-12.4109	8	1.55
p-Vinylguaiacol	-3.207	-14.8801	11	1.35
Gamma-pyrone	—	—	—	—
4-Ethylresorcinol	-4.822	-13.2875	10	1.33
2-(2-Hydroxy-2-phenylethyl)-3,5,6-trimethylpyrazine	-3.247	-32.6507	18	1.81
Ethanone, 1-(3,4-dimethoxyphenyl)-	-3.317	-10.222	13	0.79
Spathulenol	—	—	—	—
Caryophyllene oxide	-2.647	-17.446	16	1.09
Cyclopentanecarboxaldehyde, 2-methyl-3-methylene-	—	—	—	—
Epiglobulol	—	—	—	—
4(1H)-pyrimidinone, 6-hydroxy-	-4.189	-6.98163	8	0.87
Cyclododecanone, 2-methylene-	—	—	—	—
2,3-Dehydro-4-oxo-7,8-dihydro-beta-ionone	—	—	—	—
Diepicedrene-1-oxide	—	—	—	—
Coniferol	-3.03	-22.5252	13	1.73
Methyl 6,9,12-hexadecatrienoate	—	—	—	—
Phytol	0.454	-26.4647	21	1.26
1,3,6,10-Cyclotetradecatetraene, 3,7,11-trimethyl-14-(1-methylethyl)-, [S-(E,Z,E,E)]-	—	—	—	—
(Z,E)-Farnesol	0.368	-26.3771	16	1.65
Geranyl acetate	-2.457	-29.1004	24	1.21
Farnesol, acetate	0.023	-20.0217	24	0.83
3-Furaldehyde	—	—	—	—
trans-13-Docosenamide	-2.916	-42.0383	24	1.75
Squalene	-2.59	-40.4505	30	1.35
Chola-5,22-dien-3-ol, (3.beta.,22Z)-	-2.236	-7.69418	25	0.31
Curan-17-oic acid, 2,16-didehydro-20-hydroxy-19-oxo-, methyl ester	—	—	—	—
Geranylgeraniol	0.094	-25.417	21	1.21
2-Hydrazino-8-hydroxy-4-phenylquinoline	-3.068	-7.45669	19	0.39
Cycloartenol	-1.726	-21.1763	31	0.68
Ursa-9(11),12-dien-3-ol	—	—	—	—
Urs-12-ene	-1.704	-11.5462	30	0.38
Stigmast-4-en-3-one	-1.772	-19.7209	30	0.66
Ursa-9(11),12-dien-3-one	—	—	—	—
C(14a)-homo-27-nor-14-beta-gammaceran-3-alpha-ol	—	—	—	—
Friedelin	—	—	—	—
Longipinane, (E)-	-2.592	-11.7102	15	0.78
Lanosterol	-1.84	-21.6645	31	0.69
Aspirin	-1.659	-5.81427	13	0.45

Note. DS: docking score; NHA: number of heavy atoms; LE: ligand efficiency. \*Results presented in (kcal/mol).

and *TRAF6*), TLR5 signaling pathway ( $p = 0.000712$ ; *IRAK2*, *IRAK4*, *MYD88*, *TLR5*, and *TRAF6*), and TLR10 signaling pathway ( $p = 0.000712$ ; *IRAK2*, *IRAK4*, *MYD88*, *TLR5*, *TRAF6*). Six genes were identified as being associated with the NF- $\kappa$ B signaling pathway, suggesting anti-inflammatory effects, in support of a previous study that identified the inhibition of NF- $\kappa$ B functional pathways in RAW 264.7 cells following treatment with a methanolic extract of *A. capitiformis* leaves [9].

Although a remarkable amount of functional and structural data has been compiled for each identified protein, our knowledge regarding protein-protein relationships remain scattered. The purpose of the STRING database is the collection, scoring, integration, and complementation with computational predictions for all public sources of PPIs [63–66]. In the present study, 10 proteins (*IL1R1*, *IRAK4*, *IRAK2*, *MYD88*, *TIRAP*, *TRAF6*, *TLR3*, *TLR4*, *TLR5*, and *TLR6*) were used to analyze a PPI network (Figure S2), which



TABLE 6: Docking scores and ligand efficiencies of compounds from the methanolic extract of *Argyrea capitiformis* stems binding with TIRAP (PDB: 4FZ5).

Compounds	TIRAP (4FZ5)			
	DS*	MM-GBSA*	NHA	LE*
Methylcyclohexane	-3.814	-19.0091	7	2.72
Phenol	-4.448	-21.4312	7	3.06
Sulcatone	-2.879	-15.5041	9	1.72
Butanoic acid, 2,3-dimethyl-, ethyl ester	-3.225	-19.8212	10	1.98
1,2-Cyclohexanedione	-4.658	-18.7199	8	2.34
4-Methyl-1,5-heptadiene	-0.875	-18.4864	8	2.31
Catechol	-4.501	-22.731	8	2.84
Coumaran	-4.133	-19.5103	9	2.17
Hydroquinone	-5.072	-21.6796	8	2.71
p-Vinylguaiaicol	-3.458	-17.6974	11	1.61
Gamma-pyronene	-3.944	-18.1058	10	1.81
4-Ethylresorcinol	-5.971	-29.5938	10	2.96
2-(2-Hydroxy-2-phenylethyl)-3,5,6-trimethylpyrazine	-4.304	-25.9223	18	1.44
Ethanone, 1-(3,4-dimethoxyphenyl)-	-5.243	-24.616	13	1.89
Spathulenol	—	—	—	—
Caryophyllene oxide	—	—	—	—
Cyclopentanecarboxaldehyde, 2-methyl-3-methylene-	-4.868	-20.8151	9	2.31
Epiglobulol	—	—	—	—
4(1H)-pyrimidinone, 6-hydroxy-	-4.845	-15.1979	8	1.89
Cyclododecanone, 2-methylene-	-2.974	-20.1319	14	1.44
2,3-Dehydro-4-oxo-7,8-dihydro-beta-ionone	-4.032	-21.7031	15	1.45
Diepicedrene-1-oxide	—	—	—	—
Coniferol	-4.855	-32.2717	13	2.48
Methyl 6,9,12-hexadecatrienoate	0.105	-31.8802	19	1.68
Phytol	0.856	-29.859	21	1.42
1,3,6,10-Cyclotetradecatetraene, 3,7,11-trimethyl-14-(1-methylethyl)-, [S-(E,Z,E,E)]-	—	—	—	—
(Z,E)-Farnesol	0.289	-15.1735	16	0.95
Geranyl acetate	-1.574	-25.783	24	1.07
Farnesol, acetate	0.333	-14.545	24	0.61
3-Furaldehyde	-4.332	-17.5272	7	2.50
trans-13-Docosenamamide	-1.763	-31.4792	24	1.31
Squalene	-1.678	-23.5817	30	0.79
Chola-5,22-dien-3-ol, (3.beta.,22Z)-	-2.807	-23.4983	25	0.94
Curan-17-oic acid, 2,16-didehydro-20-hydroxy-19-oxo-, methyl ester	—	—	—	—
Geranylgeraniol	0.085	-9.16848	21	0.44
2-Hydrazino-8-hydroxy-4-phenylquinoline	-4.084	-24.5226	19	1.29
Cycloartenol	-1.963	-29.9984	31	0.97
Ursa-9(11),12-dien-3-ol	—	—	—	—
Urs-12-ene	-2.561	-20.6408	30	0.69
Stigmast-4-en-3-one	—	—	—	—
Ursa-9(11),12-dien-3-one	-3.348	-39.9359	31	1.29
C(14a)-homo-27-nor-14-beta-gammaceran-3-alpha-ol	—	—	—	—
Friedelin	—	—	—	—
Longipinane, (E)-	—	—	—	—
Lanosterol	-1.716	-27.5587	31	0.89
Aspirin	-4.343	-23.6086	13	1.82

Note. DS: docking score; NHA: number of heavy atoms; LE: ligand efficiency. \*Results presented in kcal/mol.

were all significantly ( $p < 1.0e - 16$ ) related to anti-inflammatory functions. Signals from the various TLRs are diverse, but all TLRs are activated by the binding of TIR-containing adaptor proteins (e.g., TIRAP activates MYD88, and TRAM activates TRIF). IRAK4, IRAK1, IRAK2, and TRAF6 are all activated by MYD88. MYD88 binding results in the phosphorylation and release of IRAK1 from the cell membrane into the cytoplasm, where it interacts with and activates the transforming growth factor- $\beta$ -activated kinase 1 (TAK1)

downstream. TAK1 activates the IKK $\beta$ -to-I $\kappa$ B- $\alpha$ -to-NF- $\kappa$ B pathway, inducing the transcription of proinflammatory genes. TAK1 also influences gene expression by activating mitogen-activated protein kinase (MAPK) cascades. TRAF6,  $\beta$ RIP1, and TAK1 are activated by the binding of TLR with TRIF, resulting in the activation of MAPK, interferon regulatory factor 3 (IRF3), NF- $\kappa$ B, and interferon- transcription activation. The TRIF pathway also promotes the release of proinflammatory cytokines, although to a lesser

TABLE 7: Docking scores and ligand efficiencies of compounds from the methanolic extract of *Argyrea capitiformis* stems binding with TLR4 (PDB: 3FXI).

Compounds	TLR4 (3FXI)			
	DS*	MM-GBSA*	NHA	LE*
Methylcyclohexane	-5.225	-25.2088	7	3.60
Phenol	-6.387	-32.1845	7	4.59
Sulcatone	-5.227	-37.5653	9	4.17
Butanoic acid, 2,3-dimethyl-, ethyl ester	-4.588	-32.241	10	3.22
1,2-Cyclohexanedione	-6.231	-26.8612	8	3.36
4-Methyl-1,5-heptadiene	-2.573	-35.6785	8	4.45
Catechol	-6.224	-35.1395	8	4.39
Coumaran	-6.217	-31.1228	9	3.46
Hydroquinone	-5.879	-32.0765	8	4.01
p-Vinylguaiaicol	-6.497	-41.7567	11	3.79
Gamma-pyronene	-5.859	-28.5764	10	2.86
4-Ethylresorcinol	-7.636	-30.7191	10	3.07
2-(2-Hydroxy-2-phenylethyl)-3,5,6-trimethylpyrazine	-7.775	-47.2615	18	2.63
Ethanone, 1-(3,4-dimethoxyphenyl)-	-7.127	-35.528	13	2.73
Spathulenol	—	—	—	—
Caryophyllene oxide	—	—	—	—
Cyclopentanecarboxaldehyde, 2-methyl-3-methylene-	-6.018	-29.885	9	3.32
Epiglobulol	—	—	—	—
4(1H)-pyrimidinone, 6-hydroxy-	-5.805	-25.5615	8	3.19
Cyclododecanone, 2-methylene-	—	—	—	—
2,3-Dehydro-4-oxo-7,8-dihydro-.beta.-ionone	-6.232	-10.5536	15	0.70
Diepicedrene-1-oxide	—	—	—	—
Coniferol	-7.058	-52.0494	13	4.003
Methyl 6,9,12-hexadecatrienoate	-2.949	-48.4222	19	2.55
Phytol	-3.527	-48.9579	21	2.33
1,3,6,10-Cyclotetradecatetraene, 3,7,11-trimethyl-14-(1-methylethyl)-, [S-(E,Z,E,E)]-	—	—	—	—
(Z,E)-Farnesol	-3.612	-49.9903	16	3.12
Geranyl acetate	-6.867	-47.3758	24	1.97
Farnesol, acetate	-4.062	-56.2792	24	2.34
3-Furaldehyde	-5.191	-27.4652	7	3.92
trans-13-Docosenamide	-5.443	-52.2716	24	2.18
Squalene	-6.729	-40.8575	30	1.36
Chola-5,22-dien-3-ol, (3.beta.,22Z)-	—	—	—	—
Curan-17-oic acid, 2,16-didehydro-20-hydroxy-19-oxo-, methyl ester	—	—	—	—
Geranylgeraniol	-3.692	-42.9074	21	2.04
2-Hydrazino-8-hydroxy-4-phenylquinoline	-5.647	0.186151	19	-0.009
Cycloartenol	—	—	—	—
Ursa-9(11),12-dien-3-ol	—	—	—	—
Urs-12-ene	—	—	—	—
Stigmast-4-en-3-one	—	—	—	—
Ursa-9(11),12-dien-3-one	—	—	—	—
C(14a)-homo-27-nor-14-beta-gammaceran-3-alpha-ol	—	—	—	—
Friedelin	—	—	—	—
Longipinane, (E)-	—	—	—	—
Lanosterol	—	—	—	—
Aspirin	-6.329	-35.694	13	2.75

Note. DS: docking score; NHA: number of heavy atoms; LE: ligand efficiency. \*Results presented in kcal/mol.

degree than the MYD88 pathway. TLRs are a class of specific receptors that are key players in mounting an effective innate immune response to infection [67–69].

Subsequently, gene co-occurrence can be used to identify gene families whose patterns exhibit similarity across genomes. Three types of analyses have been used to examine genomes (neighborhood, fusion, gene co-occurrence) based on the systemic comparison of all-against-all genomes to evaluate the impacts of historical genome restructurings,

genetic gains and losses, and gene fusion [70, 71]. In the present study, 100% sequence conservation was observed for the ten proteins (IL1R1, IRAK4, IRAK2, MYD88, TIRAP, TRAF6, TLR3, TLR4, TLR5, and TLR6) selected for the PPI network analysis, as shown in Figure S3. Additionally, gene coexpression was also studied in the present study, as summarized in Table S3 and Figure S4. The coexpression pathway is predicated by performing gene-by-gene correlation testing across many gene expression databases.

TABLE 8: Docking scores and ligand efficiencies of compounds from the methanolic extract of *Argyrea capitiformis* stems binding with TRAF6 (PDB: 3HCT).

Compounds	TRAF6 (3HCT)			
	DS*	MM-GBSA*	NHA	LE*
Methylcyclohexane	-4.23	-15.5462	7	2.22
Phenol	-4.75	-17.0982	7	2.44
Sulcatone	-3.224	-22.1931	9	2.47
Butanoic acid, 2,3-dimethyl-, ethyl ester	-3.328	-17.6969	10	1.77
1,2-Cyclohexanedione	-5.406	-17.7531	8	2.22
4-Methyl-1,5-heptadiene	-1.225	-18.4899	8	2.31
Catechol	-4.53	-18.205	8	2.28
Coumaran	-3.768	-20.8505	9	2.32
Hydroquinone	-4.795	-18.3408	8	2.29
p-Vinylguaiaicol	-4.303	-17.778	11	1.62
Gamma-pyronene	-4.133	-21.4044	10	2.14
4-Ethylresorcinol	-5.48	-19.6712	10	1.97
2-(2-Hydroxy-2-phenylethyl)-3,5,6-trimethylpyrazine	-5.119	-41.8887	18	2.33
Ethanone, 1-(3,4-dimethoxyphenyl)-	-5.708	-29.3694	13	2.26
Spathulenol	—	—	—	—
Caryophyllene oxide	—	—	—	—
Cyclopentanecarboxaldehyde, 2-methyl-3-methylene-	-5.198	-20.7855	9	2.31
Epiglobulol	—	—	—	—
4(1H)-pyrimidinone, 6-hydroxy-	-5.483	-15.5853	8	1.95
Cyclododecanone, 2-methylene-	-4.619	-3.58279	14	0.26
2,3-Dehydro-4-oxo-7,8-dihydro-beta-ionone	-4.327	-25.9777	15	1.73
Diepicedrene-1-oxide	—	—	—	—
Coniferol	-3.698	-31.781	13	2.44
Methyl 6,9,12-hexadecatrienoate	0.144	-27.9098	19	1.47
Phytol	1.098	-20.446	21	0.97
1,3,6,10-Cyclotetradecatetraene, 3,7,11-trimethyl-14-(1-methylethyl)-, [S-(E,Z,E,E)]-	—	—	—	—
(Z,E)-Farnesol	-0.033	-18.0454	16	1.13
Geranyl acetate	-2.742	-22.1469	24	0.92
Farnesol, acetate	-0.582	-27.6353	24	1.15
3-Furaldehyde	-4.911	-16.8696	7	2.41
trans-13-Docosenamide	-2.779	-43.4455	24	1.81
Squalene	-2.1	-40.8237	30	1.36
Chola-5,22-dien-3-ol, (3.beta.,22Z)-	-2.904	-21.7666	25	0.87
Curan-17-oic acid, 2,16-didehydro-20-hydroxy-19-oxo-, methyl ester	—	—	—	—
Geranylgeraniol	-0.313	-26.3103	21	1.253
2-Hydrazino-8-hydroxy-4-phenylquinoline	-4.282	-21.7512	19	1.14
Cycloartenol	-2.32	-17.571	31	0.57
Ursa-9(11),12-dien-3-ol	—	—	—	—
Urs-12-ene	-2.153	-13.0659	30	0.44
Stigmast-4-en-3-one	-2.229	-18.7231	30	0.62
Ursa-9(11),12-dien-3-one	—	—	—	—
C(14a)-homo-27-nor-14-beta-gammaceran-3.alpha.-ol	—	—	—	—
Friedelin	—	—	—	—
Longipinane, (E)-	—	—	—	—
Lanosterol	-2.204	-16.5677	31	0.53
Aspirin	-4.81	-26.889	13	2.07

Note. DS: docking score; NHA: number of heavy atoms; LE: ligand efficiency. \*Results presented in kcal/mol.

STRING reconstructs and maps this enormous series of experiments, which is stored on the NCBI database along with transcript data [63, 72]. The present findings suggested co-expression among the ten selected proteins (IL1R1, IRAK4, IRAK2, MYD88, TIRAP, TRAF6, TLR3, TLR4, TLR5, and TLR6) in *Homo sapiens*. In addition, co-expression (transferred) of three more genes was observed in *Gallus gallus*, *Mus musculus*, and *Rattus norvegicus*.

Structure-based drug discovery is gradually becoming a key technique for facilitating the rapid and cost-effective

discovery and optimization of lead compounds. The use of a rational, structure-based drug design strategy is more efficient than conventional drug development techniques because this approach seeks to understand the molecular basis of diseases and incorporates information regarding the biological target's 3D structure during the drug design process [37]. A molecular docking study was incorporated into the present study to predict the complex structure formed by ligand-protein binding and analyze the ligand's conformational space within the protein-binding site. A score function

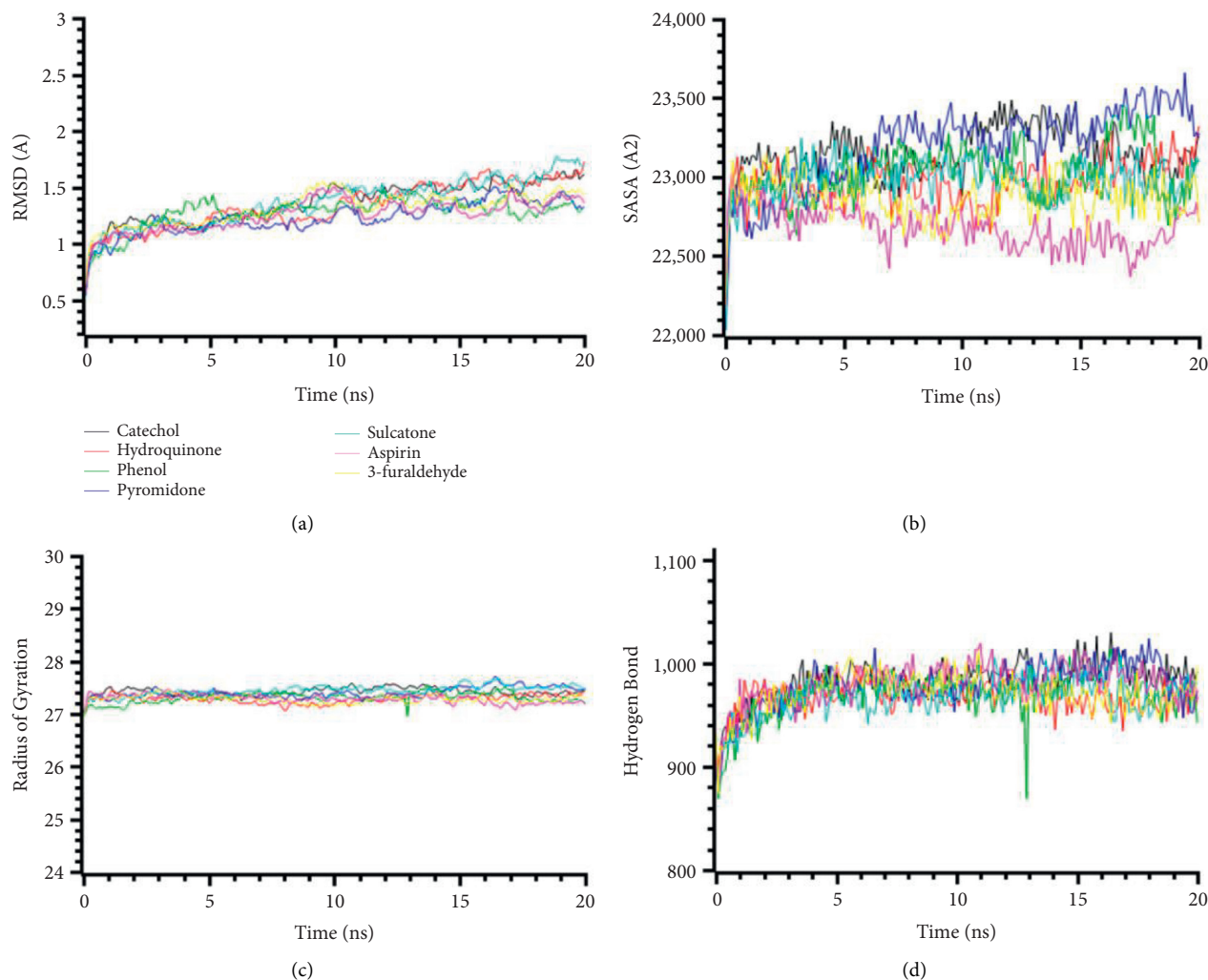


FIGURE 1: Molecular dynamics simulation of the best ligand efficiencies for compounds against IL1R1 (PDB: 1ITB). (a) Root-mean-square deviation of the complexes (RMSD). (b) Solvent accessible surface area (SASA). (c) Radius of gyration (Rg). (d) Hydrogen bond analysis from the simulation system.

is then used for each docking analysis to assess the free energy of the interaction between the protein and ligand [37, 73, 74]. Additionally, the LE is calculated, which can enrich docking functions and allow for the coordination between docking outcomes and experimental results. Critical information regarding a molecule's properties, such as the NHA, can then be combined into a single table [39].

IL-1 controls a range of innate immune pathways, making it a key regulator of inflammation [75]. Two IL-1 cell surface receptors and a decoy receptor have been identified, including IL1R1 and IL1R2. First, IL-1 binds with IL1R1, inducing the formation of a heterodimer between IL1R1 and either IL-1RAcP or IL1R3, followed by IL-1 receptor-associated kinase (IRAK) and MyD88. The inflammatory response induced by IL1R1 occurs when IL1R1 binds with either the IL-1 $\alpha$  or IL-1 $\beta$  ligands, whereas the T-lymphocytes, fibroblastic cells, epithelial cells, and endothelial cells have been indicated [76–78]. In the present study, selected six target proteins based on the network pharmacology analysis for the molecular docking study: IL1R1 (PDB:

1ITB), IRAK4 (PDB: 6EGA), and MYD88 (PDB: 4EO7) was used for the docking study. For IL1R1 (PDB: 1ITB), the majority of the 47 tested compounds demonstrated good docking scores, except for 12 compounds (Table 3). Among the 33 compounds with good docking scores, catechol (3.02), phenol (2.94), 4(1H)-pyrimidinone, 6-hydroxy- (2.79), hydroquinone (2.70), 3-furaldehyde (2.51), and sulcatone (2.51) showed the best ligand efficiencies, compared with the LE value of 1.63 for the positive control aspirin (Table S4 and Figure S5). The compounds with the best ligand efficiencies were found to interact with LYS-93 by H-bond (distances  $>4$  Å), and catechol interacted via two H-bonds. Similar findings were also observed for the positive control aspirin. According to an earlier study, the noncontiguous binding epitope containing LYS-93 was identified for IL-1 $\beta$  [79].

IRAK4 (PDB: 6EGA) also exhibited similar findings in the docking experiment, with only 12 compounds that did not display any interactions. Catechol (4.45), phenol (4.35), p-vinylguaicol (4.15), methylcyclohexane (4.08), 3-furaldehyde (4.06), and 4-methyl-1,5-heptadiene (3.94) showed

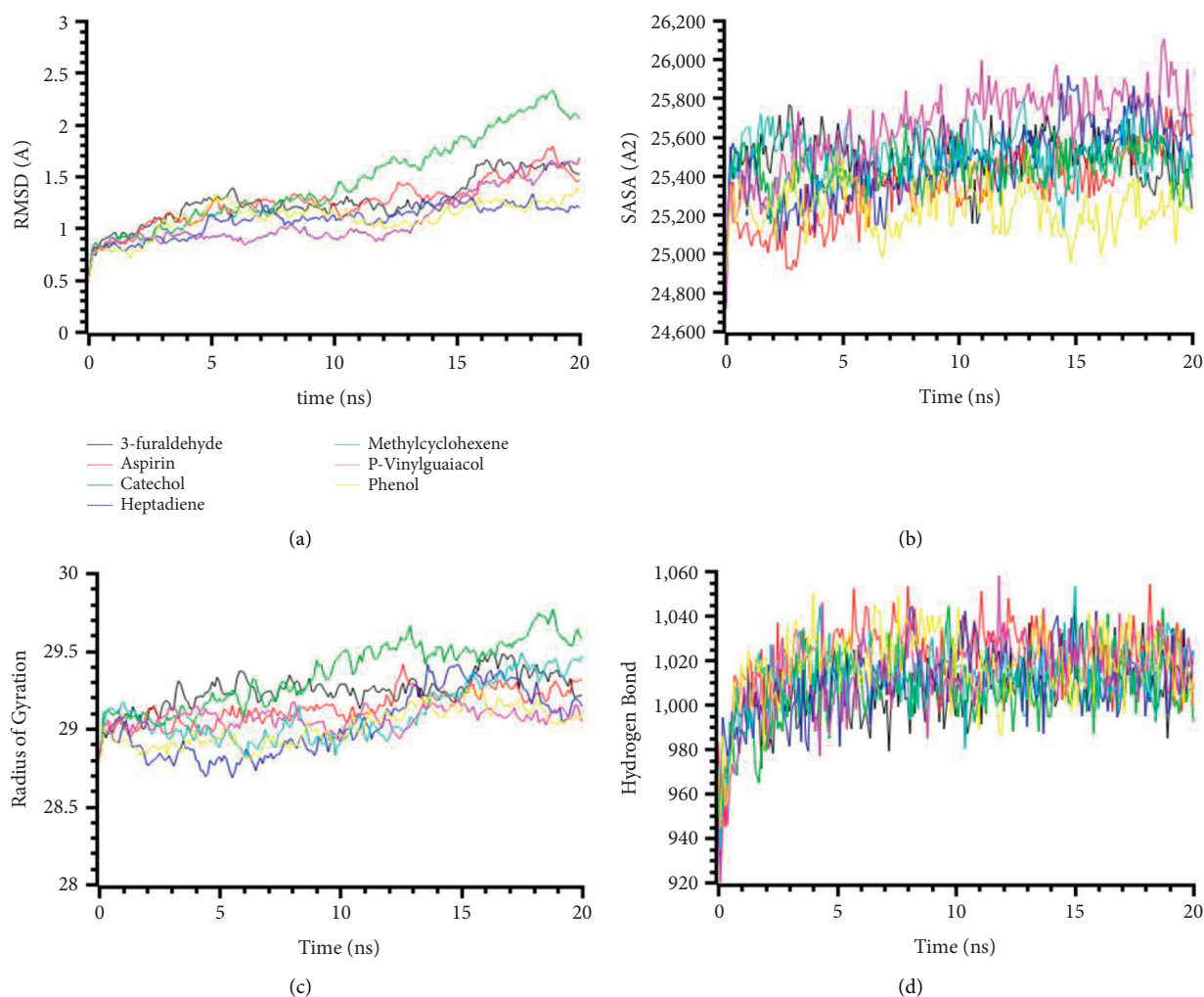


FIGURE 2: Two-dimensional representations of the best ligand efficiencies for compounds against IRAK4 (PDB: 6EGA). (a) Root-mean-square deviation of the complexes (RMSD). (b) Solvent accessible surface area (SASA). (c) Radius of gyration (Rg). (d) Hydrogen bond analysis from the simulation system.

the best LE values, as shown in Table 4. The LE value of aspirin was 2.39. The molecular interactions between the compounds with the best LE values and IRAK4 (PDB: 6EGA) are presented in Table S5 and Figure S6. ASP-329 formed H-bonds with catechol (4.02, 3.48 Å), p-vinylguaiacol (4.05, 4.06 Å), phenol (3.49 Å), and aspirin (4.24 Å), whereas no H-bond interactions were observed for 4-methyl-1,5-heptadiene or methylcyclohexane. Additionally, 3-furaldehyde interacted with MET-265 (4.0 Å) via one H-bond. Remarkably, ASP-329, MET-265, and LYS-213 were all reported to interact with IRAK4 in a previous study [32].

Additionally, MYD88 (PDB: 4EO7) was also studied as a potential target of the anti-inflammatory effects of the methanolic extract of *A. capitiformis* stems. In the molecular docking experiment, 29 compounds were found to interact with MYD88 (Table 5). The best LE values for MYD88 (PDB: 4EO7) were identified for 4-methyl-1,5-heptadiene (1.84), 2-(2-hydroxy-2-phenylethyl)-3,5,6-trimethylpyrazine (1.81), trans-13-docosenamide (1.75), coniferol (1.73), (Z, E)-farnesol (1.65), and hydroquinone (1.55). The

positive control aspirin had an LE value of 0.45, which was lower than the LE values for 24 of the identified compounds. The molecular interactions between the compounds with the best LE values and MYD88 (PDB: 4EO7) are presented in Table S6 and Figure S7. ASP-156 was reported to form H-bonds with coniferol, 2-(2-hydroxy-2-phenylethyl)-3,5,6-trimethylpyrazine, and (Z,E)-farnesol, whereas hydroquinone interacted with ASP-156 through the formation of hydrophobic bonds (3.51 Å). No H-bond interactions were reported for 4-methyl-1,5-heptadiene. The other compound, trans-13-docosenamide, interacted with ARG-160 (5.21 Å) and GLU-159 (4.36 Å) via H-bonds.

TIRAP, also known as MYD88 adapter-like (Mal), is an important link between MYD88 and the receptor complex formed by TLR2 and TLR4 activation following bacterial infection [32]. MYD88 activates IRAK1 and IRAK4 and eventually activates TRAF6, causing the prototypic inflammatory transcription factor NF- $\kappa$ B to translocate to the nucleus [80, 81]. TIRAP is the second adaptor that has been identified to mediate NF- $\kappa$ B activation through the activation

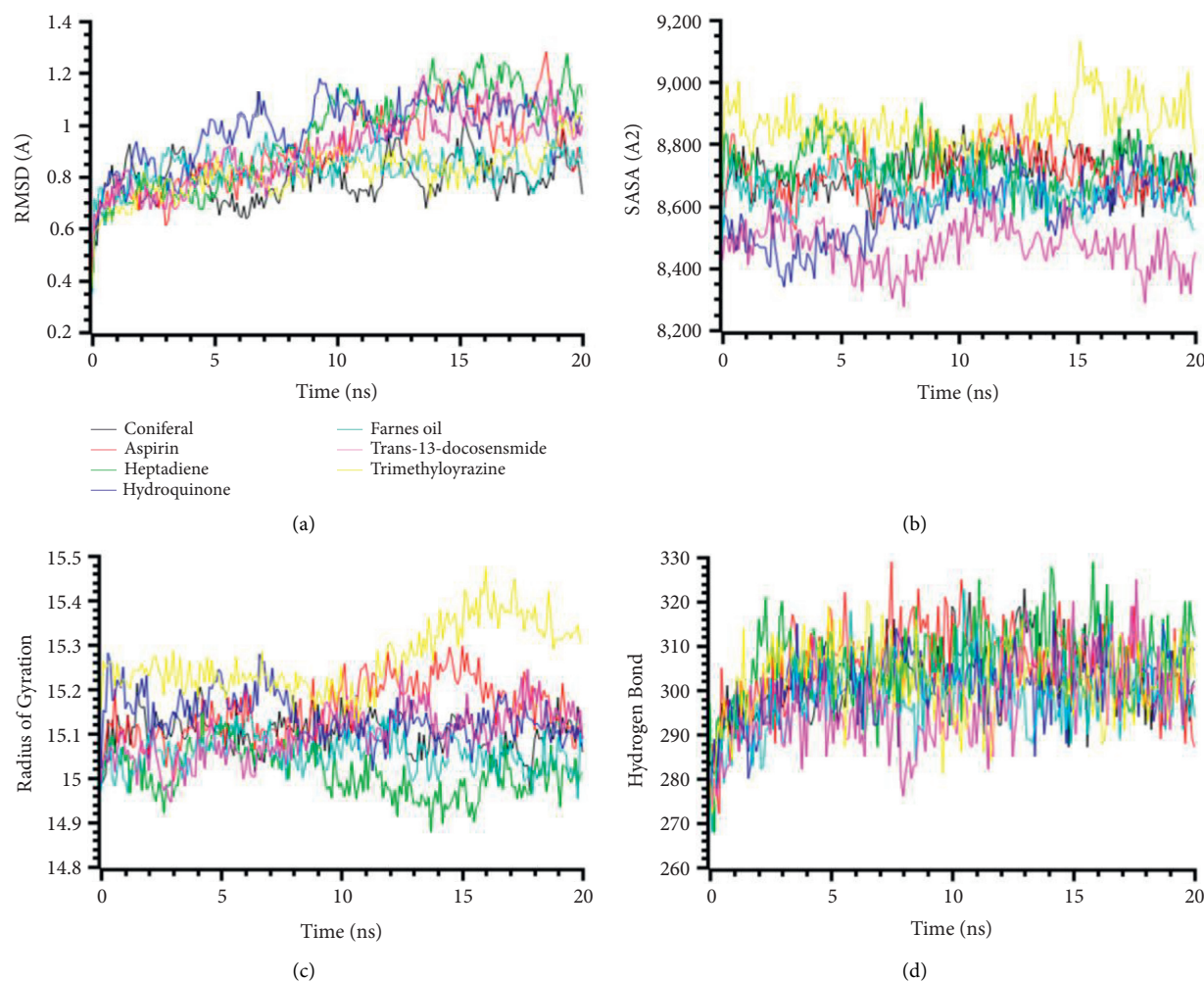


FIGURE 3: Two-dimensional representations of the best ligand efficiencies for compounds against MYD88 (4EO7). (a) Root-mean-square deviation of the complexes (RMSD). (b) Solvent accessible surface area (SASA). (c) Radius of gyration (Rg). (d) Hydrogen bond analysis from the simulation system.

of TLR4 and TLR2 signaling pathways [82–85]. The molecular docking of TIRAP (PDB: 4FZ5) was examined against the 45 compounds identified in the methanolic extract of *A. capitiformis* stems, of which 35 demonstrated interactions and 10 did not (Table 6). The best interacting compounds were phenol (3.06), 4-ethylresorcinol (2.96), catechol (2.84), methylcyclohexane (2.72), hydroquinone (2.71), and 3-furaldehyde (2.50), compared with the positive control aspirin, which exhibited an LE of 1.82 (Figure S8). The molecular interactions between the compounds with the best LE values and TIRAP (PDB: 4FZ5) are presented in Table S7. LEU-107 formed H-bond with 3-furaldehyde, catechol, phenol, and aspirin, and a hydrophobic interaction was also observed for catechol, methylcyclohexane, and phenol. Another protein residue, LYS-210, interacted with 3-furaldehyde, 4-ethylresorcinol, hydroquinone, and phenol via hydrophobic interactions. In a previous study, LYS-210 was reported to form a hydrophobic interaction with NF- $\kappa$ B [86].

In addition, TLR4 (PDB: 3FXI) was compared against 45 compounds found in the methanolic extract of *A. capitiformis* stems, although 17 compounds did not

interact with TLR4 (Table 7). Phenol (4.59), 4-methyl-1,5-heptadiene (4.45), catechol (4.39), sulcatone (4.17), hydroquinone (4.01), and coniferol (4.003) displayed the highest LE values, whereas aspirin showed an LE value of 2.75. The molecular interactions between the compounds with the best LE values and TLR4 (PDB: 3FXI) are presented in Table S8 and Figure S9. SER-441 was found to form H-bond interactions with phenol and sulcatone, whereas hydrophobic interactions were exhibited for phenol, hydroquinone, catechol, and coniferol. VAL-82 interacted via hydrophobic interactions with coniferol, 4-methyl-1,5-heptadiene, catechol, phenol, and hydroquinone. In a previous study, SER-441 was reported to interact strongly with apigenin-7-O-glucoside [87]. Similar interactions were also observed for ILE-80 and VAL-82 [88].

Finally, TRAF6 (PDB: 3HCT) was assessed against the 45 chemicals found in the methanolic extract of *A. capitiformis* stems, of which 34 were identified as interacting (Table 8). Sulcatone (2.47), phenol (2.44), coniferol (2.44), 3-furaldehyde (2.41), 2-(2-hydroxy-2-phenylethyl)-3,5,6-trimethylpyrazine (2.33), and coumaran (2.32) displayed the



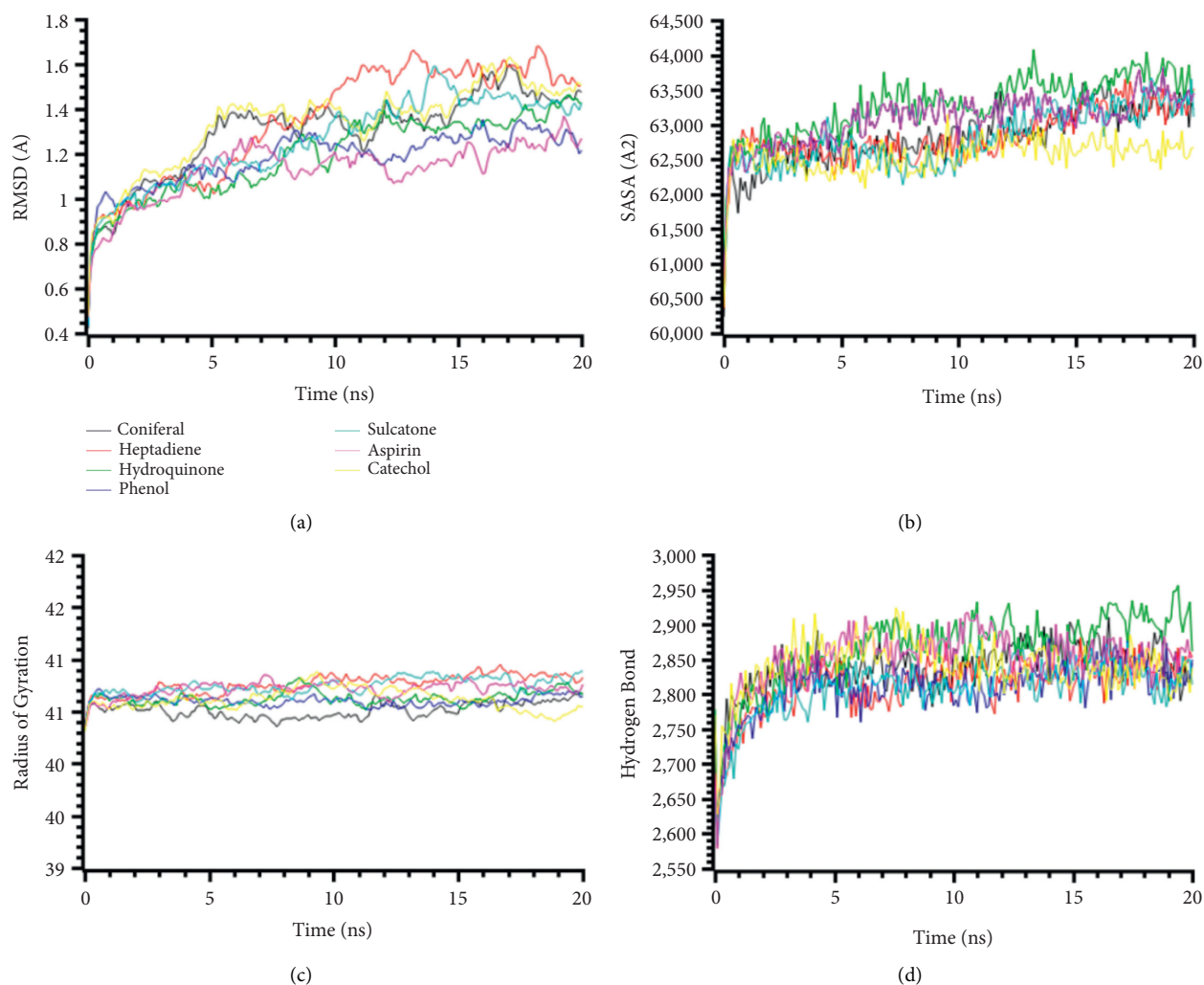


FIGURE 4: Two-dimensional representations of the best ligand efficiencies for compounds against TIRAP (PDB: 4FZ5). (a) Root-mean-square deviation of the complexes (RMSD). (b) Solvent accessible surface area (SASA). (c) Radius of gyration (Rg). (d) Hydrogen bond analysis from the simulation system.

highest LE values compared with aspirin (2.07). The molecular interactions between the compounds with the best LE values and TRAF6 (PDB: 3HCT) are presented in Table S9 and Figure S10. ARG-6 formed H-bond interactions with coniferyl, 2-(2-hydroxy-2-phenylethyl)-3,5,6-trimethylpyrazine, and aspirin, whereas hydrophobic interactions were identified for 2-(2-hydroxy-2-phenylethyl)-3,5,6-trimethylpyrazine and sulcatone. GLN-54 also formed H-bond interactions with multiple compounds, including 2-(2-hydroxy-2-phenylethyl)-3,5,6-trimethylpyrazine and 3-furaldehyde.

The root-mean-square deviations from the C-alpha atoms from the docked complexes IL1R1 (PDB: 1ITB) proteins are illustrated in Figure 1. The complexes' RMSD values were calculated to find out the deviations among the simulation complexes and structural stability. Figure 1(a) demonstrates that the complexes had similar RMSD profiles and did not fluctuate much in the simulation trajectories. The RMSD profile of the complexes reached the steady state after 5 ns and maintained the structural stability till the last

periods of the simulations, which defines the stability of the complexes. The SASA of the complexes was analyzed to find out the change in the surface area. The higher SASA represents the expansion of the surface area of the protein, whereas the lower SASA indicates the truncated nature of the complexes. Figure 1(b) shows that the complexes were in a stable state in SASA. The radius of gyration defines the lability and mobility of the complexes, where Figure 1(c) indicates the lower deviations. The hydrogen bond patterning follows a similar stable profile (Figure 1(d)).

The molecular dynamics simulation of IRAK4 (PDB: 6EGA) is presented in Figure 2. The RMSD of the complexes had a stable trend in the RMSD profile for all the complexes except catechol. The higher RMSD of these complexes defines the higher flexibility of these compounds in the simulating environments (Figure 2(a)). The SASA profile of the complexes was stable, did not fluctuate much, and had a steady trend in SASA (Figure 2(b)). This SASA profile correlates with the stable and rigid profile of the complexes (Figure 2(c)). The radius of gyration and hydrogen bond

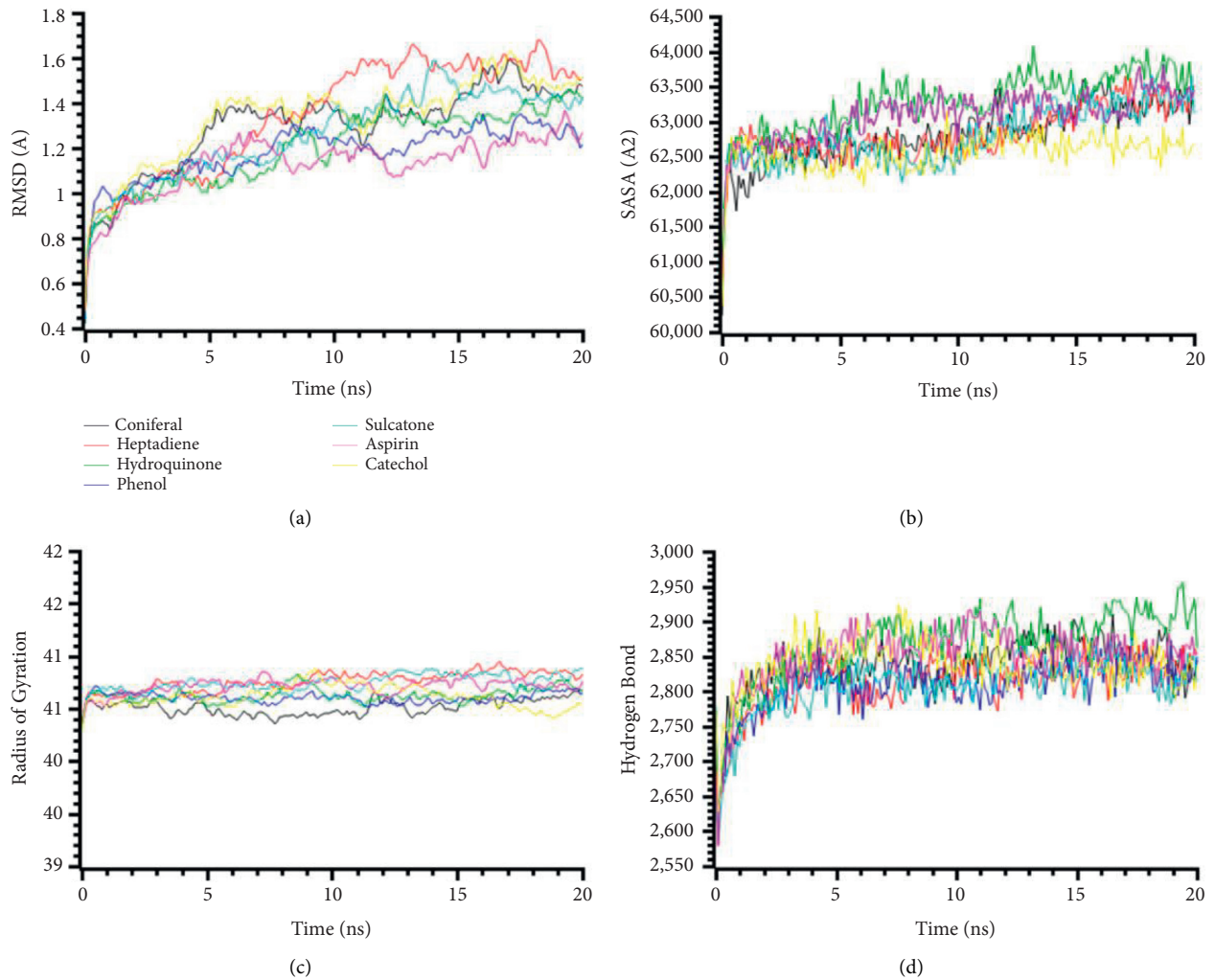


FIGURE 5: Two-dimensional representations of the best ligand efficiencies for compounds against TLR4 (PDB: 3FXI). (a) Root-mean-square deviation of the complexes (RMSD). (b) Solvent accessible surface area (SASA). (c) Radius of gyration (Rg). (d) Hydrogen bond analysis from the simulation system.

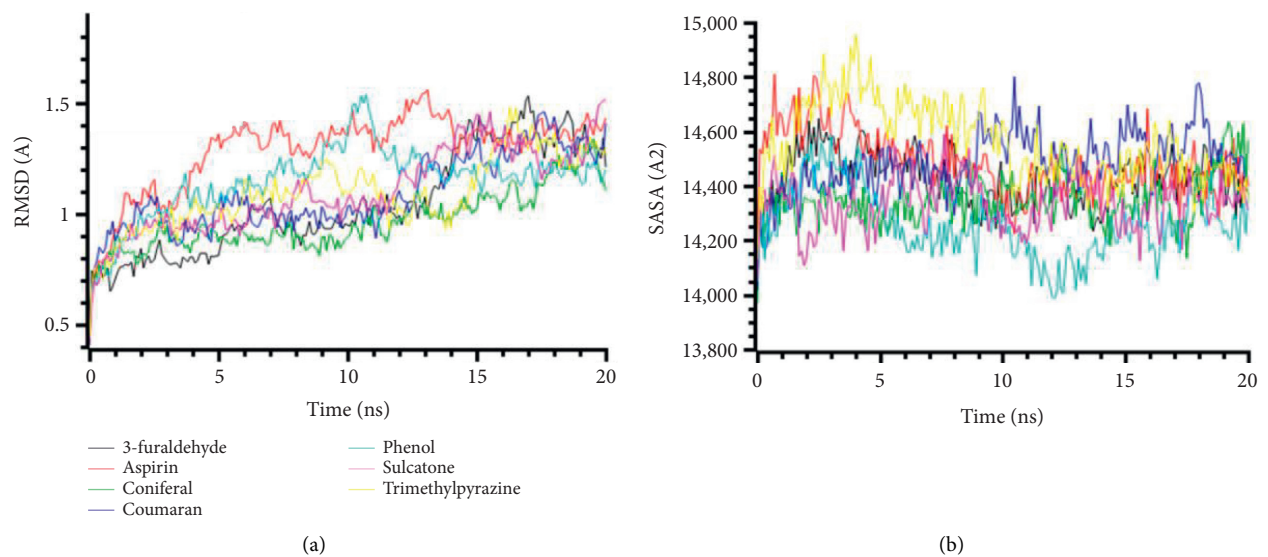


FIGURE 6: Continued.

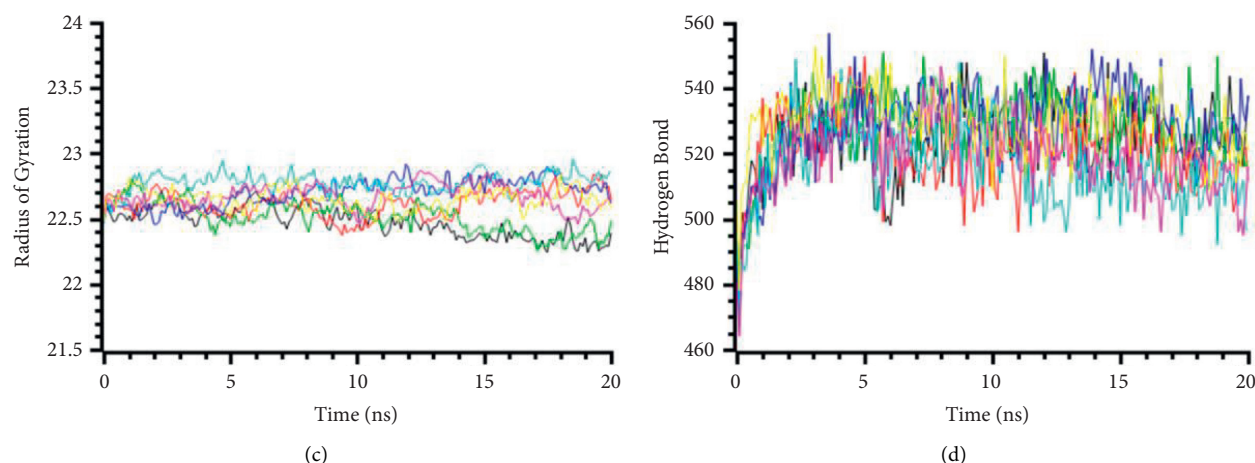


FIGURE 6: Two-dimensional representations of the best ligand efficiencies for compounds against TRAF6 (PDB: 3HCT). (a) Root-mean-square deviation of the complexes (RMSD). (b) Solvent accessible surface area (SASA). (c) Radius of gyration (Rg). (d) Hydrogen bond analysis from the simulation system.

pattern systems were similar and did not change too much in the simulations (Figure 2(d)).

The RMSD of the MYD88 (4EO7) protein complexes had a lower level of fluctuations, and lower deviations were observed across the compounds. All compounds had a lower RMSD than 2.5 Å in whole simulation periods (Figure 3(a)). The SASA of the MYD88 (4EO7) complexes were stable, but the complex of trans-13-docosenamide had a lower SASA than the other complexes. This SASA profile of trans-13-docosenamide defines the MYD88 (4EO7) experienced the condensed conformation upon binding with the corresponding ligands (Figure 3(b)). The 2-(2-Hydroxy-2-phenylethyl)-3,5,6-trimethylpyrazine complexes had a higher Rg than other complexes, which defines the complexes' flexible nature than other complexes (Figure 3(c)). These complexes also had a higher SASA in Figure 3(b), which depicts the changes in the confirmations than other complexes in simulated environments. The hydrogen-bonding pattern of the complexes for MYD88 (4EO7) protein was found stable and did not change too much in simulations (Figure 3(d)).

The RMSD profile of TIRAP (PDB: 4FZ5) complexes is illustrated in Figure 4. All complexes from TIRAP (PDB: 4FZ5) protein had an initial rise of RMSD due to a higher degree of flexibility but stabilized subsequently after 5 ns times. The complex 4-ethylresorcinol had a higher RMSD than the other complexes, which might be responsible for the more remarkable conformational changes and the flexibility of the compounds (Figure 4(a)). The SASA of the complexes had a stable and similar trend for all the compounds. But the complex phenol had a lower SASA profile at the last phase of SASA, which defines the complexes' truncated nature in simulations (Figure 4(b)). The radius of gyration profile of the complexes had a lower trend, which correlates with the less flexibility of the complexes (Figure 4(c)). The hydrogen bond patterning of the complexes had a stable profile in Figure 4(d).

The molecular dynamics simulation study of the TLR4 (PDB: 3FXI) and complexes was done to analyze the structural deviation in the docked structure. The root-mean-square deviations of all complexes are illustrated in Figure 5(a). The RMSD value of the complexes initially followed the upper trend from the beginning. This might be happening due to the higher flexibility level. But all the complexes from TLR4 (PDB: 3FXI) had a stable profile after 10 ns times and followed a similar trend until the last periods, demonstrating structural stability. The SASA of the TLR4 (PDB: 3FXI) complexes had lowered the degree of the deviations from the beginning and followed lower fluctuations, which define no changes in the surface area of the complexes (Figure 5(b)). The Rg and hydrogen bond patterns of the simulation systems were stable and did not change too much, which correlates with the structural stability (Figures 5(c) and 5(d)).

The docked complexes from the TRAF6 (PDB: 3HCT) protein and their simulation descriptors are illustrated in Figure 6. The RMSD profile of the TRAF6 (PDB: 3HCT) complexes defines that the phenol and aspirin had a higher level of RMSD than other complexes, which correlates with the comparative higher degree of the deviations of the complexes. All complexes had reached a stable state after 5 ns of the simulation times. Moreover, the complexes exhibit RMSD lower than 2.5 Å, which defines the complexes with a higher rigidity degree (Figure 6(a)). The SASA profile of the complexes had a lower deviation, as illustrated in Figure 6(b). The phenol had a lower SASA value than all the compounds, indicating the truncated nature of the protein complexes compared with the others. Moreover, the radius of gyration from Figure 6(c) demonstrates that the complexes had a lower degree of deviations, and no significant higher fluctuations were observed. This Rg profile indicates the complexes had lower mobility and flexibility during the simulation times. The hydrogen bond pattern of the complexes was stable during the simulations (Figure 6(d)).

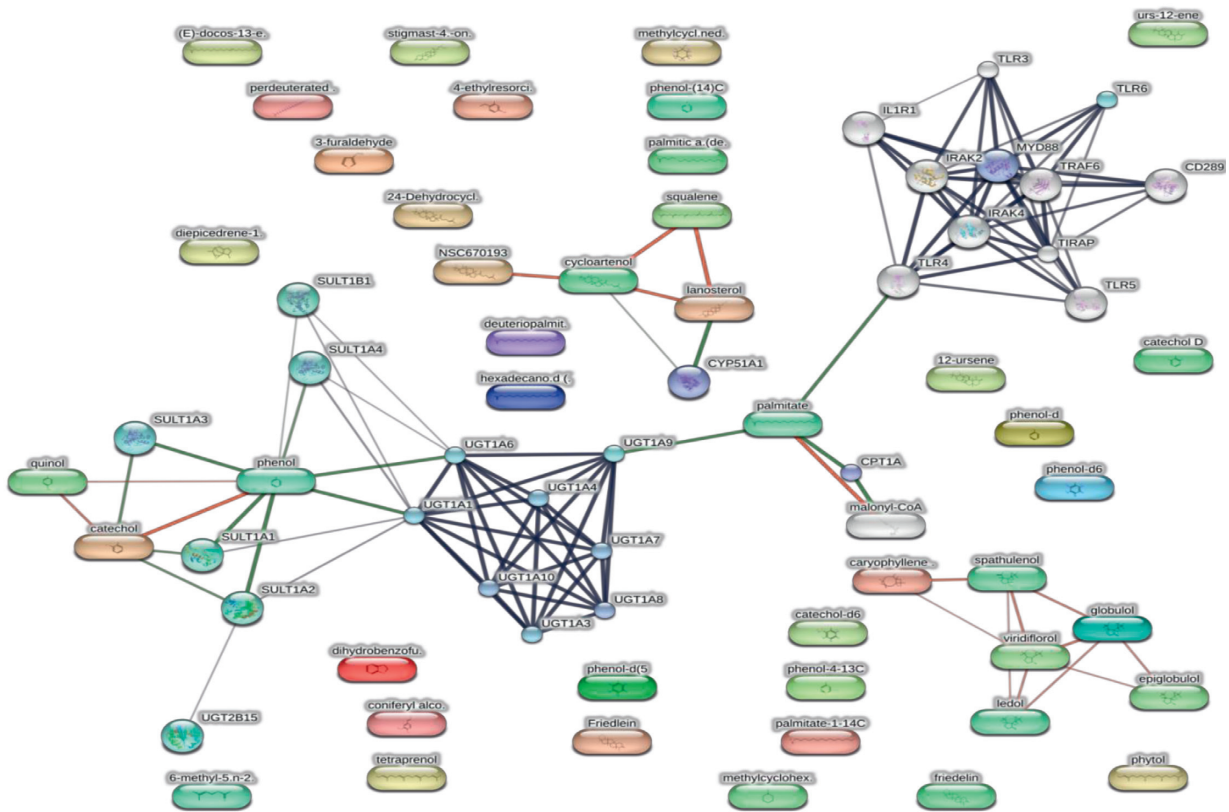


FIGURE 7: Network pharmacology presentation of phytoconstituents, targets, and pathways.

## 5. Conclusions

The network pharmacology analysis revealed key pathways involved in the anti-inflammatory activities induced by the chemical compounds found in the methanolic extract of *A. capitiformis* stem. Six inflammation pathways were obtained from the KEGG pathway analysis (*IL1R1*, *IRAK4*, *MYD88*, *TIRAP*, *TLR4*, and *TRAF6*), and molecular docking studies of these pathways revealed that the identified chemical compounds had strong binding affinities with these pathway components. The current study discovered that 3-furaldehyde, phenol, catechol, and hydroquinone were effective anti-inflammatory compounds found within the methanolic extract of *A. capitiformis* and played an important part in the inflammation pathway by targeting these six proteins. Additional *in vitro* and *in vivo* experiments will be helpful to validate and optimize the findings of this study.

## Abbreviations

GC-MS: Gas chromatography-mass spectrometry  
 KEGG: Kyoto Encyclopedia of Genes and Genomes  
 WHO: World Health Organization  
 NF- $\kappa$ B: Nuclear factor-kappa B  
 STRING: Search Tool for Retrieval of Interacting Genes  
 PPIs: Protein-protein interactions  
 IL: Interleukins

PKC: Protein kinase C  
 MAPK: Mitogen-activated protein kinase  
 IRF: Interferon regulatory factor  
 IRAK: Receptor-associated kinase  
 TLR: Toll-like receptor  
 3D: Three-dimensional  
 PDB: Protein Data Bank  
 RMSD: Root-mean-square deviation of the complexes  
 SASA: Solvent accessible surface area  
 Rg: Radius of gyration.

## Data Availability

The data are available within the manuscript and also accessible from the corresponding author upon request.

## Conflicts of Interest

The authors declare no conflicts of interest.

## Authors' Contributions

Ahmad J. Obaidullah, Mohammed M. Alanazi, Nawaf A. Alsaif, Ashwag S. Alanazi, Hussam Albassam, Osama I. Alwassil, and Alanazi AZ conducted the study and performed the corresponding data analysis, prepared figures, and drafted the manuscript. Abu Montakim Tareq, Mohammed M. Alanazi, and Ahmad J. Obaidullah



supervised the study, performed the data analysis, prepared the figure, and contributed to writing with Shafi Mahmud and Ali M. Alqahtani. Ahmad J. Obaidullah, Mohammed M. Alanazi, and Abu Montakim Tareq were responsible for writing, review, and editing of the manuscript. All the authors approved the final version of the manuscript.

## Acknowledgments

The authors extend their appreciation to the Deanship of Scientific Research at King Saud University for funding this work through research no. RG-1441-398.

## Supplementary Materials

Table S1: biological processes of the genes targeted by the compounds; Table S2: molecular functions of the genes interacting with the compounds; Table S3: protein-protein interaction (PPI) status of 10 proteins with coexpression; Table S4: molecular interactions with the best ligand efficiencies for compounds binding with IL1R1 (PDB: 1ITB); Table S5: molecular interactions with the best ligand efficiencies for compounds binding with IRAK4 (PDB: 6EGA); Table S6: molecular interactions with the best ligand efficiencies for compounds binding with MYD88 (4EO7); Table S7: molecular interactions with the best ligand efficiencies for compounds binding with TIRAP (PDB: 4FZ5); Table S8: molecular interactions with the best ligand efficiencies for compounds binding with TLR4 (PDB: 3FXI); and Table S9: molecular interactions with the best ligand efficiencies for compounds binding with TRAF6 (PDB: 3HCT). Figure S1: GC-MS chromatograph of the methanolic extract of *Argyrea capitiformis* stem; Figure S2: protein-protein interaction (PPI) network of 10 proteins; Figure S3: gene co-occurrence of 10 proteins for *Homo sapiens*; Figure S4: gene coexpression of 10 proteins in PPI network; and Figure S5: two-dimensional representations of the best ligand efficiencies for compounds binding with IL1R1 (PDB: 1ITB). 3-Furaldehyde (A), 4(1H)-pyrimidinone, 6-hydroxy- (B), catechol (C), hydroquinone (D), phenol (E), sulcatone (F), and aspirin (G) are shown. Figure S6: two-dimensional representations of the best ligand efficiencies for compounds binding to IRAK4 (PDB: 6EGA). 3-Furaldehyde (A), 4-methyl-1,5-heptadiene (B), catechol (C), methylcyclohexane (D), p-vinylguaiacol (E), phenol (F), and aspirin (G) are shown. Figure S7: two-dimensional representations of the best ligand efficiencies for compounds binding to MYD88 (4EO7). (Z,E)-farnesol (A), 2-(2-hydroxy-2-phenylethyl)-3,5,6-trimethylpyrazine (B), 4-methyl-1,5-heptadiene (C), coniferol (D), hydroquinone (E), trans-13-docosenamide (F), and aspirin (G) are shown. Figure S8: two-dimensional representations of the best ligand efficiencies for compounds binding to TIRAP (PDB: 4FZ5). 3-Furaldehyde (A), 4-ethylresorcinol (B), catechol (C), hydroquinone (D), methylcyclohexane (E), phenol (F), and aspirin (G) are shown. Figure S9: two-dimensional representations of the best ligand efficiencies for compounds against TLR4 (PDB: 3FXI). 4-Methyl-1,5-heptadiene (A), catechol (B), coniferol

(C), hydroquinone (D), phenol (E), sulcatone (F), and aspirin (G) are shown. Figure S10: two-dimensional representations of the best ligand efficiencies for compounds against TRAF6 (PDB: 3HCT). 2-(2-Hydroxy-2-phenylethyl)-3,5,6-trimethylpyrazine (A), 3-furaldehyde (B), coniferol (C), coumaran (D), phenol (E), sulcatone (F), and aspirin (G) are shown. (*Supplementary Materials*)

## References

- [1] F. O. Martinez, L. Helming, and S. Gordon, "Alternative activation of macrophages: an immunologic functional perspective," *Annual Review of Immunology*, vol. 27, no. 1, pp. 451–483, 2009.
- [2] A. Kauppinen, T. Suuronen, J. Ojala, K. Kaarniranta, and A. Salminen, "Antagonistic crosstalk between NF- $\kappa$ B and SIRT1 in the regulation of inflammation and metabolic disorders," *Cellular Signalling*, vol. 25, no. 10, pp. 1939–1948, 2013.
- [3] P. Libby, "Inflammatory mechanisms: the molecular basis of inflammation and disease," *Nutrition Reviews*, vol. 65, no. 12, pp. S140–S146, 2007.
- [4] I. P. Barcelos, R. M. Troxell, and J. S. Graves, "Mitochondrial dysfunction and multiple sclerosis," *Biology*, vol. 8, no. 2, 2019.
- [5] D.-H. Tsai, M. Riediker, A. Berchet et al., "Effects of short- and long-term exposures to particulate matter on inflammatory marker levels in the general population," *Environmental Science and Pollution Research*, vol. 26, no. 19, pp. 19697–19704, 2019.
- [6] P. Deepak, J. E. Axelrad, and A. N. Ananthakrishnan, "The role of the radiologist in determining disease severity in inflammatory bowel diseases," *Gastrointestinal endoscopy clinics of North America*, vol. 29, no. 3, pp. 447–470, 2019.
- [7] Y. Zhou, Y. Hong, and H. Huang, "Triptolide attenuates inflammatory response in membranous glomerulo-nephritis rat via downregulation of NF- $\kappa$ B signaling pathway," *Kidney & Blood Pressure Research*, vol. 41, no. 6, pp. 901–910, 2016.
- [8] O. Oguntibeju, "Medicinal plants with anti-inflammatory activities from selected countries and regions of Africa," *Journal of Inflammation Research*, vol. 11, pp. 307–317, 2018.
- [9] G. H. Yeum, B. R. So, S. M. Eum, and S. K. Jung, "Evaluation of anti-inflammatory effect by regulating NF- $\kappa$ B pathway of *Argyrea capitata* (Vahl) Choisy extract in LPS-induced RAW 264.7 macrophages," *Korean Journal of Food Science and Technology*, vol. 52, no. 3, pp. 249–254, 2020.
- [10] H. Singh, P. A. Dhole, R. Saravanan, and P. K. Baske, "Ethnomedicinal plants used in sexual disorder in Balangir and Deogarh districts, Odisha, India," *International Journal of Current Science*, vol. 20, no. 3, pp. 57–62, 2017.
- [11] G.-T. Chen, Y. Lu, M. Yang, J.-L. Li, and B.-Y. Fan, "Medicinal uses, pharmacology, and phytochemistry of Convolvulaceae plants with central nervous system efficacies: a systematic review," *Phytotherapy Research*, vol. 32, no. 5, pp. 823–864, 2018.
- [12] A. H. Atta, N. H. Mohamed, S. M. Nasr, and S. M. Mounier, "Phytochemical and pharmacological studies on *Convolvulus fatmensis* Ktze," *Journal of Natural Remedies*, vol. 7, no. 1, p. 109, 2007.
- [13] V. Galani, B. Patel, and N. Patel, "*Argyrea speciosa* (Linn. f.) sweet: a comprehensive review," *Pharmacognosy Reviews*, vol. 4, no. 8, pp. 172–178, 2010.
- [14] A. Meher, A. Kumar, and P. Ranjan, "A literature review on *Argyrea nervosa* (burm. F.) bojer," *International Journal of*

- Research in Ayurveda and Pharmacy*, vol. 2, pp. 1501–1504, 2011.
- [15] A. B. Gokhale, A. S. Damre, and M. N. Saraf, “Investigations into the immunomodulatory activity of *Argyrea speciosa*,” *Journal of Ethnopharmacology*, vol. 84, no. 1, pp. 109–114, 2003.
  - [16] S. Wang, Y. Tong, T. B. Ng et al., “Network pharmacological identification of active compounds and potential actions of Erxian decoction in alleviating menopause-related symptoms,” *Chinese Medicine*, vol. 10, no. 1, pp. 19–12, 2015.
  - [17] S. Li and B. Zhang, “Traditional Chinese medicine network pharmacology: theory, methodology and application,” *Chinese Journal of Natural Medicines*, vol. 11, no. 2, pp. 110–120, 2013.
  - [18] Y.-q. Zhang, X. Mao, Q.-y. Guo, N. Lin, and S. Li, “Network pharmacology-based approaches capture essence of Chinese herbal medicines,” *Chinese Herbal Medicines*, vol. 8, no. 2, pp. 107–116, 2016.
  - [19] J.-w. Liang, M.-y. Wang, K. M. Olounfeh, N. Zhao, S. Wang, and F.-h. Meng, “Network pharmacology-based identification of potential targets of the flower of *Trollius chinensis* Bunge acting on anti-inflammatory effects,” *Scientific Reports*, vol. 9, no. 1, p. 8109, 2019.
  - [20] Y. Guo, Q. Nie, A. L. MacLean, Y. Li, J. Lei, and S. Li, “Multiscale modeling of inflammation-induced tumorigenesis reveals competing oncogenic and oncoprotective roles for inflammation,” *Cancer Research*, vol. 77, no. 22, pp. 6429–6441, 2017.
  - [21] T. Yi, S.-M. Li, J.-Y. Fan et al., “Comparative analysis of EPA and DHA in fish oil nutritional capsules by GC-MS,” *Lipids in Health and Disease*, vol. 13, no. 1, p. 190, 2014.
  - [22] A. M. Juszczak, M. Zovko-Končić, and M. Tomczyk, “Recent trends in the application of chromatographic techniques in the analysis of luteolin and its derivatives,” *Biomolecules*, vol. 9, no. 11, p. 731, 2019.
  - [23] S. Razack, K. Kumar, I. Nallamuthu, M. Naika, and F. Khanum, “Antioxidant, biomolecule oxidation protective activities of *Nardostachys jatamansi* DC and its phytochemical analysis by RP-HPLC and GC-MS,” *Antioxidants*, vol. 4, no. 1, pp. 185–203, 2015.
  - [24] N. Konappa, A. C. Udayashankar, S. Krishnamurthy, C. K. Pradeep, S. Chowdappa, and S. Jogaiah, “GC-MS analysis of phytoconstituents from *Amomum nilgircum* and molecular docking interactions of bioactive serverogenin acetate with target proteins,” *Scientific Reports*, vol. 10, no. 1, p. 16438, 2020.
  - [25] A. M. Tareq, S. Farhad, A. B. M. Neshar Uddin et al., “Chemical profiles, pharmacological properties, and in silico studies provide new insights on *Cycas pectinata*,” *Heliyon*, vol. 6, no. 6, Article ID e04061, 2020.
  - [26] M. A. Rahman, R. Sultana, T. Bin Emran et al., “Effects of organic extracts of six Bangladeshi plants on in vitro thrombolysis and cytotoxicity,” *BMC Complementary and Alternative Medicine*, vol. 13, no. 1, p. 25, 2013.
  - [27] A. J. Obaidullah, M. M. Alanazi, N. A. Alsaif et al., “Deeper insights on *Cnesmone javanica* blume leaves extract: chemical profiles, biological attributes, network pharmacology and molecular docking,” *Plants*, vol. 10, no. 4, 2021.
  - [28] P. Khanal, B. M. Patil, B. K. Mandar, Y. N. Dey, and T. Duyu, “Network pharmacology-based assessment to elucidate the molecular mechanism of anti-diabetic action of *Tinospora cordifolia*,” *Clinical Phytoscience*, vol. 5, no. 1, pp. 1–9, 2019.
  - [29] M. F. Mahomoodally, S. Jugreet, K. I. Sinan et al., “Pharmacological potential and chemical characterization of *bridelia ferruginea* benth—a native tropical african medicinal plant,” *Antibiotics*, vol. 10, no. 2, p. 223, 2021.
  - [30] D. Szklarczyk, A. Franceschini, S. Wyder et al., “STRING v10: protein-protein interaction networks, integrated over the tree of life,” *Nucleic Acids Research*, vol. 43, pp. D447–D452, 2015.
  - [31] G. P. A. Vigers, L. J. Anderson, P. Caffes, and B. J. Brandhuber, “Crystal structure of the type-I interleukin-1 receptor complexed with interleukin-1 $\beta$ ,” *Nature*, vol. 386, no. 6621, pp. 190–194, 1997.
  - [32] L. Wang, R. Ferrao, Q. Li et al., “Conformational flexibility and inhibitor binding to unphosphorylated interleukin-1 receptor-associated kinase 4 (IRAK4),” *Journal of Biological Chemistry*, vol. 294, no. 12, pp. 4511–4519, 2019.
  - [33] G. A. Snyder, C. Cirl, J. Jiang et al., “Molecular mechanisms for the subversion of MyD88 signaling by TcpC from virulent uropathogenic *Escherichia coli*,” *Proceedings of the National Academy of Sciences*, vol. 110, no. 17, pp. 6985–6990, 2013.
  - [34] J.-R. Woo, S.-M. Kim, S. E. Shoelson, and S.-Y. Park, “X-ray crystallographic structure of TIR-domain from the human TIR-domain containing adaptor protein/MyD88-adaptor-like protein (TIRAP/MAL),” *Bulletin of the Korean Chemical Society*, vol. 33, no. 9, pp. 3091–3094, 2012.
  - [35] B. S. Park, D. H. Song, H. M. Kim, B.-S. Choi, H. Lee, and J.-O. Lee, “The structural basis of lipopolysaccharide recognition by the TLR4-MD-2 complex,” *Nature*, vol. 458, no. 7242, pp. 1191–1195, 2009.
  - [36] Q. Yin, S.-C. Lin, B. Lamothe et al., “E2 interaction and dimerization in the crystal structure of TRAF6,” *Nature Structural & Molecular Biology*, vol. 16, no. 6, pp. 658–666, 2009.
  - [37] E. Lionta, G. Spyrou, D. Vassilatis, and Z. Cournia, “Structure-based virtual screening for drug discovery: principles, applications and recent advances,” *Current Topics in Medicinal Chemistry*, vol. 14, no. 16, pp. 1923–1938, 2014.
  - [38] F. Chen, H. Liu, H. Sun et al., “Assessing the performance of the MM/PBSA and MM/GBSA methods. 6. Capability to predict protein-protein binding free energies and re-rank binding poses generated by protein-protein docking,” *Physical Chemistry Chemical Physics*, vol. 18, no. 32, pp. 22129–22139, 2016.
  - [39] A. T. Garcia-Sosa, C. Hetényi, and U. Maran, “Drug efficiency indices for improvement of molecular docking scoring functions,” *Journal of Computational Chemistry*, vol. 31, no. 1, pp. 174–184, 2010.
  - [40] J. Wang, R. M. Wolf, J. W. Caldwell, P. A. Kollman, and D. A. Case, “Development and testing of a general amber force field,” *Journal of Computational Chemistry*, vol. 25, no. 9, pp. 1157–1174, 2004.
  - [41] H. Land and M. S. Humble, “YASARA: a tool to obtain structural guidance in biocatalytic investigations,” *Methods in Molecular Biology*, vol. 1685, pp. 43–67, 2018.
  - [42] M. F. Harrach and B. Drossel, “Structure and dynamics of TIP3P, TIP4P, and TIP5P water near smooth and atomistic walls of different hydroaffinity,” *The Journal of Chemical Physics*, vol. 140, no. 17, Article ID 174501, 2014.
  - [43] M. J. Harvey and G. De Fabritiis, “An implementation of the smooth particle mesh ewald method on GPU hardware,” *Journal of Chemical Theory and Computation*, vol. 5, no. 9, pp. 2371–2377, 2009.
  - [44] U. Essmann, L. Perera, M. L. Berkowitz, T. Darden, H. Lee, and L. G. Pedersen, “A smooth particle mesh Ewald method,” *The Journal of Chemical Physics*, vol. 103, no. 19, pp. 8577–8593, 1995.



- [45] E. Krieger and G. Vriend, "New ways to boost molecular dynamics simulations," *Journal of Computational Chemistry*, vol. 36, no. 13, pp. 996–1007, 2015.
- [46] S. Mahmud, M. A. R. Uddin, G. K. Paul et al., "Virtual screening and molecular dynamics simulation study of plant-derived compounds to identify potential inhibitors of main protease from SARS-CoV-2," *Briefings in Bioinformatics*, vol. 22, no. 2, pp. 1402–1414, 2021.
- [47] S. S. Bappy, S. Sultana, J. Adhikari et al., "Extensive immunoinformatics study for the prediction of novel peptide-based epitope vaccine with docking confirmation against envelope protein of Chikungunya virus: a computational biology approach," *Journal of Biomolecular Structure and Dynamics*, vol. 39, no. 4, pp. 1139–1154, 2021.
- [48] M. A. Khan, S. Mahmud, A. S. M. R. U. Alam, M. E. Rahman, F. Ahmed, and M. Rahmatullah, "Comparative molecular investigation of the potential inhibitors against SARS-CoV-2 main protease: a molecular docking study," *Journal of biomolecular structure & dynamics*, vol. 39, no. 16, pp. 6317–6323, 2021.
- [49] S. K. Pramanik, S. Mahmud, G. K. Paul et al., "Fermentation optimization of cellulase production from sugarcane bagasse by *Bacillus pseudomycoloides* and molecular modeling study of cellulase," *Current Research in Microbial Sciences*, vol. 2, Article ID 100013, 2021.
- [50] K. H. Chowdhury, M. R. Chowdhury, S. Mahmud et al., "Drug repurposing approach against novel coronavirus disease (COVID-19) through virtual screening targeting SARS-CoV-2 main protease," *Biology*, vol. 10, no. 1, 2020.
- [51] M. Munia, S. Mahmud, M. Mohasin, and K. M. K. Kibria, "In silico design of an epitope-based vaccine against choline binding protein A of *Streptococcus pneumoniae*," *Informatics in Medicine Unlocked*, vol. 23, Article ID 100546, 2021.
- [52] A. Rakib, Z. Nain, S. A. Sami et al., "A molecular modelling approach for identifying antiviral selenium-containing heterocyclic compounds that inhibit the main protease of SARS-CoV-2: an in silico investigation," *Briefings in Bioinformatics*, vol. 22, no. 2, pp. 1476–1498, 2021.
- [53] S. Mahmud, M. A. R. Uddin, M. Zaman et al., "Molecular docking and dynamics study of natural compound for potential inhibition of main protease of SARS-CoV-2," *Journal of Biomolecular Structure & Dynamics*, vol. 39, no. 16, pp. 6281–6289, 2020.
- [54] M. Z. Uddin, A. Paul, A. Rakib et al., "Chemical profiles and pharmacological properties with in silico studies on *elastostema papillosum* wedd," *Molecules*, vol. 26, no. 4, p. 809, 2021.
- [55] B. Petrovska, "Historical review of medicinal plants' usage," *Pharmacognosy Reviews*, vol. 6, no. 11, pp. 1–5, 2012.
- [56] I. Ahmad, F. Aqil, and M. Owais, *Modern Phytomedicine: Turning Medical Plants into Drugs*, Wiley VCH, Weinheim, Germany, 2006.
- [57] K. Nisha, M. Darshana, G. Madhu, and M. K. Bhupendra, "GC-MS analysis and anti-microbial activity of *Psidium guajava* (leaves) grown in Malva region of India," *International Journal of Drug Development & Research*, vol. 3, no. 4, pp. 237–245, 2011.
- [58] K. Gopalakrishnan and R. Udayakumar, "GC-MS analysis of phytocompounds of leaf and stem of *Marsilea quadrifolia* (L.)," *International Journal of Biochemistry Research & Review*, vol. 4, no. 6, pp. 517–526, 2014.
- [59] T. Starlin, P. S. Prabha, P. Saravana Prabha, B. K. A. Thayakumar, and V. K. Gopalakrishnan, "Screening and GC-MS profiling of ethanolic extract of *Tylophora pauciflora*," *Bioinformation*, vol. 15, no. 6, pp. 425–429, 2019.
- [60] T. Efferth, P. C. H. Li, V. S. B. Konkimalla, and B. Kaina, "From traditional Chinese medicine to rational cancer therapy," *Trends in Molecular Medicine*, vol. 13, no. 8, pp. 353–361, 2007.
- [61] K. Ghazi-Moghadam, H. M. Inançlı, N. Bazazy, P. K. Plinkert, T. Efferth, and S. Sertel, "Phytomedicine in otorhinolaryngology and pulmonology: clinical trials with herbal remedies," *Pharmaceuticals*, vol. 5, no. 8, pp. 853–874, 2012.
- [62] D. J. Loegering and M. R. Lennartz, "Protein kinase C and toll-like receptor signaling," *Enzyme Research*, vol. 2011, Article ID 537821, 7 pages, 2011.
- [63] D. Szklarczyk, A. L. Gable, D. Lyon et al., "STRING v11: protein-protein association networks with increased coverage, supporting functional discovery in genome-wide experimental datasets," *Nucleic Acids Research*, vol. 47, no. D1, pp. D607–D613, 2019.
- [64] L. Xie and P. E. Bourne, "Functional coverage of the human genome by existing structures, structural genomics targets, and homology models," *PLoS Computational Biology*, vol. 1, no. 3, p. e31, 2005.
- [65] M. Uhlen, P. Oksvold, L. Fagerberg et al., "Towards a knowledge-based human protein atlas," *Nature Biotechnology*, vol. 28, no. 12, pp. 1248–1250, 2010.
- [66] "UniProt: The universal protein knowledgebase," *Nucleic Acids Research*, vol. 45, no. D1, pp. D158–D169, 2017.
- [67] N. J. Gay and M. Gangloff, "Structure and function of Toll receptors and their ligands," *Annual Review of Biochemistry*, vol. 76, no. 1, pp. 141–165, 2007.
- [68] T. Kawai and S. Akira, "Signaling to NF- $\kappa$ B by toll-like receptors," *Trends in Molecular Medicine*, vol. 13, no. 11, pp. 460–469, 2007.
- [69] T. Kawai and S. Akira, "The role of pattern-recognition receptors in innate immunity: update on Toll-like receptors," *Nature Immunology*, vol. 11, no. 5, pp. 373–384, 2010.
- [70] M. Huynen, B. Snel, W. Lathe III, and P. Bork, "Predicting protein function by genomic context: quantitative evaluation and qualitative inferences," *Genome Research*, vol. 10, no. 8, pp. 1204–1210, 2000.
- [71] L. Skrabanek, H. K. Saini, G. D. Bader, and A. J. Enright, "Computational prediction of protein-protein interactions," *Molecular Biotechnology*, vol. 38, no. 1, pp. 1–17, 2008.
- [72] T. Barrett, S. E. Wilhite, P. Ledoux et al., "NCBI GEO: archive for functional genomics data sets—update," *Nucleic Acids Research*, vol. 41, pp. D991–D995, 2013.
- [73] A. Lavecchia and C. Giovanni, "Virtual screening strategies in drug discovery: a critical review," *Current Medicinal Chemistry*, vol. 20, no. 23, pp. 2839–2860, 2013.
- [74] T. Cheng, Q. Li, Z. Zhou, Y. Wang, and S. H. Bryant, "Structure-based virtual screening for drug discovery: a problem-centric review," *The AAPS Journal*, vol. 14, no. 1, pp. 133–141, 2012.
- [75] C. A. Dinarello, "Immunological and inflammatory functions of the interleukin-1 family," *Annual Review of Immunology*, vol. 27, no. 1, pp. 519–550, 2009.
- [76] P. Martin, G. Palmer, S. Vigne et al., "Mouse neutrophils express the decoy type 2 interleukin-1 receptor (IL-1R2) constitutively and in acute inflammatory conditions," *Journal of Leukocyte Biology*, vol. 94, no. 4, pp. 791–802, 2013.
- [77] K. Shimizu, A. Nakajima, K. Sudo et al., "IL-1 receptor type 2 suppresses collagen-induced arthritis by inhibiting IL-1 signal on macrophages," *The Journal of Immunology*, vol. 194, no. 7, pp. 3156–3168, 2015.
- [78] C. Brikos, R. Wait, S. Begum, L. A. J. O'Neill, and J. Saklatvala, "Mass spectrometric analysis of the endogenous type I

- interleukin-1 (IL-1) receptor signaling complex formed after IL-1 binding identifies IL-1RAcP, MyD88, and IRAK-4 as the stable components,” *Molecular & Cellular Proteomics*, vol. 6, no. 9, pp. 1551–1559, 2007.
- [79] R. Sarabu, J. P. Cooper, C. M. Cook, P. Gillespie, A. V. Perrotta, and G. L. Olson, “Design and synthesis of small molecule interleukin-1 receptor antagonists based on a benzene template,” *Drug Design and Discovery*, vol. 15, no. 3, pp. 191–198, 1998.
- [80] L. A. J. O’Neill, “The interleukin-1 receptor/Toll-like receptor superfamily: 10 years of progress,” *Immunological Reviews*, vol. 226, no. 1, pp. 10–18, 2008.
- [81] S. Akira, S. Uematsu, and O. Takeuchi, “Pathogen recognition and innate immunity,” *Cell*, vol. 124, no. 4, pp. 783–801, 2006.
- [82] K. A. Fitzgerald, E. M. Palsson-McDermott, A. G. Bowie et al., “Mal (MyD88-adaptor-like) is required for toll-like receptor-4 signal transduction,” *Nature*, vol. 413, no. 6851, pp. 78–83, 2001.
- [83] T. Horng, G. M. Barton, and R. Medzhitov, “TIRAP: an adaptor molecule in the Toll signaling pathway,” *Nature Immunology*, vol. 2, no. 9, pp. 835–841, 2001.
- [84] T. Horng, G. M. Barton, R. A. Flavell, and R. Medzhitov, “The adaptor molecule TIRAP provides signalling specificity for toll-like receptors,” *Nature*, vol. 420, no. 6913, pp. 329–333, 2002.
- [85] M. Yamamoto, S. Sato, H. Hemmi et al., “Essential role for TIRAP in activation of the signalling cascade shared by TLR2 and TLR4,” *Nature*, vol. 420, no. 6913, pp. 324–329, 2002.
- [86] O. Kadioglu, J. Nass, M. E. Saeed, B. Schuler, and T. Efferth, “Kaempferol is an anti-inflammatory compound with activity towards NF- $\kappa$ B pathway proteins,” *Anticancer Research*, vol. 35, no. 5, pp. 2645–2650, 2015.
- [87] W. A. H. M. Karunarathne, I. M. N. Molagoda, K. T. Lee et al., “Anthocyanins from *Hibiscus syriacus* L. attenuate LPS-induced inflammation by inhibiting the TLR4-mediated NF- $\kappa$ B signaling pathway,” in *Proceedings of the Plant Resources Society of Korea Conference*, p. 92, Seoul, Korea, November 2019.
- [88] Q. U. Ain, M. Batool, and S. Choi, “TLR4-Targeting therapeutics: structural basis and computer-aided drug discovery approaches,” *Molecules*, vol. 25, no. 3, p. 627, 2020.

## Research Article

# Insecticidal, Antimalarial, and Antileishmanial Effects of Royal Jelly and Its Three Main Fatty Acids, *trans*-10-Hydroxy-2-decenoic Acid, 10-Hydroxydecanoic Acid, and Sebacic Acid

Abeer Mousa Alkhaibari <sup>1</sup> and Abdullah D. Alanazi <sup>2</sup>

<sup>1</sup>Department of Biology, Faculty of Science, University of Tabuk, Tabuk 71491, Saudi Arabia

<sup>2</sup>Department of Biological Science, Faculty of Science and Humanities, Shaqra University, Ad-Dawadimi 11911, Saudi Arabia

Correspondence should be addressed to Abeer Mousa Alkhaibari; [aalkhaibari@ut.edu.sa](mailto:aalkhaibari@ut.edu.sa)

Received 23 November 2021; Revised 31 December 2021; Accepted 4 January 2022; Published 20 January 2022

Academic Editor: Sekar Vijayakumar

Copyright © 2022 Abeer Mousa Alkhaibari and Abdullah D. Alanazi. This is an open access article distributed under the Creative Commons Attribution License, which permits unrestricted use, distribution, and reproduction in any medium, provided the original work is properly cited.

Natural products and their derivatives as an inexpensive, accessible, and useful alternative medicine are broadly applied for the treatment of a wide range of diseases and infectious ones. The present study was designed to evaluate the insecticidal, antimalarial, antileishmanial, and cytotoxic effects of royal jelly and its three main fatty acids (*trans*-10-hydroxy-2-decenoic acid (10-H2DA), 10-hydroxydecanoic acid (10-HDAA), sebacic acid (1,10-decanedioic acid)). Insecticidal activity of RJ and 10-H2DA, 10-HDAA, and sebacic acid was performed against healthy 4th instar larvae at  $25 \pm 2^\circ\text{C}$ . Antiplasmodial and antileishmanial effects of RJ and 10-H2DA, 10-HDAA, and sebacic acid were also performed against chloroquine-resistant *Plasmodium falciparum* K1-strain and *Leishmania major* amastigotes according to the Malstat method and macrophage model, respectively. In addition, the level of nitric oxide (NO) production in J774-A1 macrophages cells, plasma membrane permeability, and caspase-3-like activity and cytotoxicity effects of RJ and 10-H2DA, 10-HDAA, and sebacic acid against human embryonic kidney 293 (HEK239T cells) were evaluated. Considering the insecticidal activity, the results showed that the lethal concentration 50% value for RJ, 10-H2DA, 10-HDAA, and sebacic acid was 24.6, 31.4, 37.8, and 44.7  $\mu\text{g}/\text{mL}$ , respectively. RJ, 10-H2DA, 10-HDAA, and sebacic acid showed potent ( $P < 0.0001$ ) antileishmanial effects with  $\text{IC}_{50}$  values ranging from 2.4 to 8.4  $\mu\text{g}/\text{mL}$ . Various concentrations of RJ, 10-H2DA, 10-HDAA, and sebacic acid significantly ( $P < 0.05$ ) increased the production of NO, plasma membrane permeability, and caspase-3-like activity level as a dose-dependent response. Considering the cytotoxicity, SIs  $> 10$  of these compounds exhibited their specificity to parasites and safety against human HEK239T normal cells. The results of the present investigation revealed the promising insecticidal, antimalarial, and antileishmanial effects of RJ and its three main fatty acids (10-H2DA, 10-HDAA, and sebacic acid). However, more studies are required to confirm the mechanisms of action mode of these compounds as well as their efficacy in animal models and clinical settings.

## 1. Introduction

According to the World Health Organization (WHO) reports, vector-borne diseases account for nearly 17% of all infectious diseases, with a mortality rate of 700,000 deaths each year [1]. *Aedes aegypti* is considered as the principal vector recognized to transmit a number of important vector-borne infections such as malaria, dengue, chikungunya, and Zika [2, 3]. Today, one of the most important approaches for controlling insects is the use of

insecticides (e.g., diflubenzuron, alpha-cypermethrin, malathion, and deltamethrin) [4, 5]. The current studies demonstrated that the too much and persistent use of chemical and synthetic insecticides has reduced their efficacy and raised various ecological concerns such as emerging of drug resistance to insecticides, ecological imbalance, and outcomes to animals [6, 7]. Accordingly, these problems and limitations have led researchers to pay more attention to finding novel insecticides with high efficacy and eco-friendly properties around the world.

Malaria is a serious vector-borne infection, which causes about 430,000 deaths yearly, generally in African children [8]. Among the *Plasmodium* species in human, *Plasmodium vivax* and *P. falciparum* are well known as the most common and deadly *Plasmodium* species, respectively [9, 10]. In recent decades, there have been numerous reports on side effects as well as drug resistance of *Plasmodium* spp. (mainly *P. falciparum* malaria) to current antimalarial drugs [11]. So finding and introducing a new antimalarial drug especially from natural resources with the lower toxicity and the highest performance is necessary for malaria treatment.

Leishmaniasis as a neglected tropical infection is caused by the parasitic species *Leishmania*, which infects about 12 million people each year in 98 countries worldwide [12]. The disease is observed in humans in different forms, including cutaneous leishmaniasis, cutaneous-mucosal leishmaniasis, and visceral leishmaniasis [13]. In chemotherapy as the most important method of treating leishmaniasis, various drugs such as meglumine antimoniate and Pentostam are used; however, the previous studies have reported that the majority of the synthetic antileishmanial drugs have been associated with some disadvantages and limitations such as emerging drug resistance and adverse side effects [14, 15].

From a long time ago, natural products have been well known as a valuable and effective resource for treating a broad spectrum of diseases, including cardiovascular, cancers, and neurological [16]. Among the natural products, beehive derivatives and products including royal jelly, honey, and propolis are considered as one of the best health-promoting products [17]. Royal jelly (RJ) is a gelatinous material secreted from the apical glands of young nurse honey bees with various pharmacological and biological benefits such as anticancer, antioxidant, anti-inflammatory, and antimicrobial [18–20]. Considering the compounds in RJ, previous studies have demonstrated that the main composition of RJ is water (50–60%), proteins (18%), carbohydrates (7–18%), and lipids (3–8%), respectively [21]. The lipid composition of RJ consists of 80–85% fatty acids, composed of proteins that are attributed to its biological properties [22]. Reviews showed that the major fatty acids present in RJ are (i) *trans*-10-hydroxy-2-decenoic acid (10-H2DA), an unsaturated hydroxyl fatty acid which consists of >50% of the free FAs; (ii) 10-hydroxydecanoic acid (10-HDAA), as a saturated hydroxyl fatty acid, 10-HDAA; (iii) sebatic acid (SEA, 1,10-decanedioic acid), a dicarboxylic fatty acid, comprising 3.3% of the total acids in RJ [23, 24].

Based on what has been said about the biological and pharmacological activities of RJ and also the limitations, problems, and side effects of the current insecticidal, antileishmanial, and antimalarial agents, in this study, we decided to assess the insecticidal, antiplasmodial, antileishmanial, and cytotoxic effects of RJ and its three main fatty acids (10-H2DA, 10-HDAA, and sebatic acid).

## 2. Materials and Methods

**2.1. Royal Jelly.** Royal jelly materials were obtained from Langstroth hives containing colonies of the *A. mellifera* grown in Tabuk, Saudi Arabia, from June 2021. Samples were

dissolved with normal saline and filtered under a vacuum by means of filter paper (Whatman membrane, England). Samples (50 mg) were diluted in distilled water and then ultrasonicated for 1 h. In the next step, the sample solution was centrifuged at 6000 rpm for 10 minutes, whereas the upper phase was applied as the sample solution and was stored at  $-20^{\circ}\text{C}$  until testing.

### 2.2. Secondary Metabolites Contents

**2.2.1. Total Phenol Content.** The total phenol content in the RJ sample was assessed based on the technique explained by Singleton et al. [25]. To do this, 50  $\mu\text{L}$  of RJ solution (50 mg/mL) was added to 250  $\mu\text{L}$  of Folin-Ciocalteu's reagent (0.2 N) for 6 min, and then 0.2 mL of sodium carbonate (7.5%) was put into the tested tubes. After 120 min incubation at room temperature, the absorbance of suspension was determined at 760 nm. Distilled water was used as the blank solution. Total phenol content was reported as mg gallic acid equivalents (GAE)/g.

**2.2.2. Total Flavonoid Content.** The determination of flavonoid content was performed according to the method explained by El-Guendouz et al. In this way, 200  $\mu\text{L}$  of RJ solution was poured into the tubes with 200  $\mu\text{L}$  aluminum chloride (20%). The tubes were then incubated at room temperature for 60 min, and their absorbance was determined at 420 nm [26]. The total flavonoid content was reported as milligram of quercetin equivalents per gram of RJ (mg QE/g RJ).

**2.2.3. Total Protein Content.** Bradford technique was used to determine the protein content. Briefly, the RJ sample (200 mg) was added to a tube containing 10 mL methanol/water (50/50; v/v); the suspension was sonicated for 1 h. In the next step, the pH of the suspension was adjusted to 2.5 with phosphoric acid and was then diluted 10 times. Next, 5 mL of Bio-Rad reagent was mixed with 250  $\mu\text{L}$  of RJ solutions, and the absorbance of the mixture was determined at 595 nm. The total protein content was reported as a percentage by means of the bovine serum albumin standard curve [27].

**2.3. Chemicals.** *trans*-10-hydroxy-2-decenoic acid, 10-hydroxydecanoic acid, sebatic acid (1,10-decanedioic acid), and MTT (3-(4,5-dimethylthiazol-2-yl)-2,5-diphenyltetrazolium bromide) powder in high purity were purchased from Sigma-Aldrich (Germany).

**2.4. Insecticidal Activity.** *Ae. aegypti* eggs were provided from the Department of Biology, Faculty of Science, University of Tabuk, Saudi Arabia. The insecticidal effects of RJ, 10-H2DA, 10-HDAA, and sebatic acid were carried out based on the method described by Huong et al. [28]. To do this, various concentrations of RJ, 10-H2DA, 10-HDAA, and sebatic acid (12.5, 25, 50, and 100  $\mu\text{g}/\text{mL}$ ) were put in a 500 mL beaker, and 150 mL water was added with 20 healthy 4th instar larvae at  $25 \pm 2^{\circ}\text{C}$ . Larva mortality was determined after 24 h of

incubation; lethal concentration 50% (LC<sub>50</sub>) was calculated via the Probit test in SPSS software for RJ, 10-H2DA, 10-HDAA, and sebacic acid. All tests were carried out in triplicate, and during experiments, no nutritional complement was added, whereas DMSO was considered as the control group.

**2.5. Antiplasmodial Activity.** The Malstat method was used to determine the antiplasmodial effects of different concentrations of RJ, 10-H2DA, 10-HDAA, and sebacic acid (12.5, 25, 50, and 100 µg/mL) against *P. falciparum* K1-strain [29]. Parasites were firstly incubated with the human erythrocytes (red blood cells, RBC) in RPMI-1640 medium improved with 10% human serum at 37°C with low oxygen atmosphere (3% O<sub>2</sub>, 4% CO<sub>2</sub>, and 93% N<sub>2</sub>). The infected human RBC (0.2 mL, 1% parasitaemia, and 2% hematocrit) were treated with various concentrations of RJ, 10-H2DA, 10-HDAA, and sebacic acid in each well and were incubated for 3 days. Then, tested plates were frozen at -20°C. In the next step, in a new plate, 0.1 mL of Malstat reagent was mixed with 0.02 mL of suspension of hemolysed parasite and incubated for 15 min at 21°C. After this time, 0.02 mL of NBT/PES solution was added to the plates and was incubated again for 120 min in the dark. Finally, the absorbance of each well was recorded at 655 nm with the ELISA reader. The 50% inhibitory concentrations (IC<sub>50</sub>) were also calculated via the Probit test in SPSS software.

**2.6. Antileishmanial Effects.** *L. major* promastigotes (MRHO/IR/75/ER) and murine macrophage cells (J774-A1) were cultured at RPMI 1640 complemented with 15% heat-inactivated fetal calf serum (FCS), streptomycin (100 µg/mL), and penicillin (200 IU/mL) and at Dulbecco's modified eagle's medium (DMEM) improved with 10% FCS at 37°C in 5% CO<sub>2</sub>. Firstly, J774-A1 cells (5 × 10<sup>5</sup> cells/mL) were transferred in sterile 6-cell plates (with 1 cm<sup>2</sup> coverslip implanted on their floor) and incubator at 37°C for 24 hours with 5% CO<sub>2</sub> to adhere to macrophages. After 24 hours, the plates were removed from the incubator and washed with sterile warm saline phosphate buffer. Then, 1 mL of *L. major* promastigotes (5 × 10<sup>6</sup>) in the stationary phase was added to plates and kept warm at 37°C for 4 hours; then, the wells were washed with RPMI1640 medium to remove free promastigotes. In the next step, 1 mL of RPMI1640 medium containing different concentrations of RJ, 10-H2DA, 10-HDAA, and sebacic acid (1, 2, 4, and 8 µg/mL) and MA was added to the wells and was incubated for 48 hours. The slides were then fixed with methanol and stained with Gamisa dye diluted with water in a ratio of 1:10. The results were estimated by calculating the mean number of amastigotes inside 100 macrophages. The IC<sub>50</sub> values were also calculated via the Probit test in SPSS software. Examinations were carried out in triplicate [30].

**2.7. Plasma Membrane Permeability.** In order to determine the plasma membrane permeability, *L. major* (1 × 10<sup>6</sup> cells/mL) were incubated with different concentrations of

RJ, 10-H2DA, 10-HDAA, and sebacic acid (12.5, 25, 50, and 100 µg/mL) and then Sytox Green stain was applied based on the kit instructions. Nontreated parasites and those treated with 2.5% of Triton X-100 (Sigma-Aldrich) were determined as the negative and positive control, respectively. The plasma membrane permeability was calculated by means of a microplate reader (BMG Labtech, Germany) for 4 h [30].

**2.8. Effect on Nitric Oxide (NO) Production.** The effect of RJ, 10-H2DA, 10-HDAA, and sebacic acid on the NO release of macrophage cells was performed via Griess reaction for nitrites. In summary, macrophage cells (1 × 10<sup>6</sup> cells/mL) were exposed with various concentrations of RJ, 10-H2DA, 10-HDAA, and sebacic acid (1, 2, and 4 µg/mL) for 72 h. Then, 0.1 mL of collected supernatants was transferred into a 96-well microplate, and 60 µL of Griess reagents A and B was put within each well. Lastly, the production of NO was determined by reading the plates at 540 nm in an ELISA reader (BioTek-ELX800) [30].

**2.9. Evaluating the Caspase-3-Like Activity of Extract-Treated Promastigotes.** Caspase-3-like activity of *L. major* promastigotes treated with RJ, 10-H2DA, 10-HDAA, and sebacic acid was assessed through the colorimetric protease (Sigma, Germany) technique according to the manufacturer guidelines. In this way, the caspase-3-like activity level was measured based on the rate of color spectrophotometric produced through the release of a molecule (pNA attached to the substrate) under the enzyme caspase-3 activity. Briefly, the promastigotes (10<sup>6</sup>) were incubated with RJ, 10-H2DA, 10-HDAA, and sebacic acid for 48 h and were centrifuged at 700 rpm for 5 minutes at 4°C. In the next step, the cell residue was lysed, and the cell lysate was centrifuged again at 20,000 rpm for 10 minutes. Lastly, supernatant of reaction (5 µL) was added to the 85 µL of buffer, and 10 µL of caspase 3 (pNA-DEVD-Ac) solution and the mixture was incubated for 120 min at 37°C. The caspase-3-like activity was determined through the light absorption at 405 nm with the ELISA reader [29].

**2.10. Cytotoxicity Effects.** The cytotoxic effect of RJ, 10-H2DA, 10-HDAA, and sebacic acid against human embryonic kidney 293 (HEK239T cells) was evaluated using the colorimetric MTT (3-(4,5-dimethylthiazol-2-yl)-2,5-diphenyltetrazolium bromide) assay according to the method described elsewhere [30]. HEK239T cells were cultured in DMEM, supplemented with 10% fetal bovine serum and streptomycin (100 µg/mL) and penicillin (200 IU/mL). Next, HEK239T cells (5 × 10<sup>4</sup>/mL) were treated with RJ, 10-H2DA, 10-HDAA, and sebacic acid (12.5, 25, 50, 100, and 200 µg/mL) for 48 h in microplates at 37°C with 5% CO<sub>2</sub>. The 50% cytotoxic concentrations (CC<sub>50</sub> values) were calculated by means of the Probit test in SPSS software. Selectivity indices (CC<sub>50</sub>/IC<sub>50</sub>) were also recorded for each tested drug [27].



**2.11. Statistical Analysis.** The statistical analysis was performed by the SPSS statistical package, version 22.0 (SPSS, Inc.). To compare the results among tested groups, we applied the unpaired samples *t*-test, one-way analysis of variance (ANOVA), and Dunnett's test.  $P < 0.05$  was measured statistically significant.

### 3. Results

**3.1. Secondary Metabolites Contents of RJ.** The findings of the secondary metabolites analysis of RJ displayed that total phenolic and flavonoid content were  $83.6 \pm 0.31$  (mg GEA/g DW) and  $1.78 \pm 0.023$  (mg QE/g DW), respectively; the results also showed that the total protein content of the RJ sample was 11.3% (Table 1).

**3.2. Insecticidal Effects.** Table 2 revealed that the larvicidal effects of RJ, 10-H2DA, 10-HDAA, and sebacic acid were remarkable ( $P < 0.001$ ) against *Ae. aegypti* larva. The results showed that among the tested compounds sebacic acid and RJ displayed the lowest and highest larvicidal effects against *Ae. aegypti* larva with the  $LC_{50}$  of 44.7 and 24.6  $\mu\text{g/mL}$ , respectively.

**3.3. Antimalarial Activity.** The obtained findings demonstrated that RJ, 10-H2DA, 10-HDAA, and sebacic acid had considerable ( $P < 0.001$ ) antiplasmodial effects against *P. falciparum*. The  $IC_{50}$  value for RJ was 7.62  $\mu\text{g/mL}$ , while the  $IC_{50}$  value for 10-H2DA, 10-HDAA, and sebacic acid was 2.41, 2.65, and 3.1  $\mu\text{g/mL}$ , respectively (Table 3), indicating that the lowest and highest antimalarial activities were observed in RJ and 10-H2DA, respectively.

**3.4. Antileishmanial Effects.** Our findings also exhibited that RJ, 10-H2DA, 10-HDAA, and sebacic acid had considerable ( $P < 0.001$ ) antileishmanial effects against intracellular amastigotes of *L. major*. The  $IC_{50}$  value for RJ was 8.14  $\mu\text{g/mL}$ , while the  $IC_{50}$  value for 10-H2DA, 10-HDAA, and sebacic acid was 3.8, 3.77, and 4.13  $\mu\text{g/mL}$ , respectively (Table 4). These findings indicated that although all tested compounds showed higher antileishmanial effects against intracellular amastigotes of *L. major*, the lowest and highest antileishmanial activities were observed in RJ and 10-H2DA, respectively.

**3.5. Cytotoxicity Effects.** Considering the cytotoxicity effects of RJ, 10-H2DA, 10-HDAA, and sebacic acid, the obtained results of the MTT assay demonstrated that  $CC_{50}$  value for RJ, 10-H2DA, 10-HDAA, and sebacic acid was 117.3, 74.4, 81.3, and 92.6  $\mu\text{g/mL}$ ; subsequently, their  $SI > 10$  of these compound exhibited their specificity to parasites and safety against human HEK239T normal cells (Table 5), indicating that among the tested compounds the lowest and highest cytotoxic effects were observed in RJ and sebacic acid, with the  $SI$  value of 13.9 and 22.4, respectively.

**3.6. The Effect on the Plasma Membrane Permeability.** Here, we evaluated the plasma membrane permeability of the *L. major* promastigotes treated with RJ, 10-H2DA, 10-

HDAA, and sebacic acid. The results of relative fluorescence units revealed that the promastigotes treated with RJ, 10-H2DA, 10-HDAA, and sebacic acid as a dose-dependent response changed the permeability of plasma membrane by Sytox Green (Figure 1).

**3.7. Evaluating NO Production.** As shown in Figure 2, various concentrations of RJ, 10-H2DA, 10-HDAA, and sebacic acid (1, 2, and 4  $\mu\text{g/mL}$ ) significantly ( $P < 0.05$ ) increased the production of NO as a dose-dependent pattern in comparison to the nontreated macrophage cells as a dose-dependent response. The results also showed that, among the tested compounds, RJ and 10-H2DA displayed the highest stimulation of NO production.

**3.8. Effect on the Caspase-3-Like Activity.** The caspase-3-like activity of parasites treated with RJ, 10-H2DA, 10-HDAA, and sebacic acid was assessed through the colorimetric protease. The results exhibited that RJ, 10-H2DA, 10-HDAA, and sebacic acid significantly induced caspase-3 activation as a dose-dependent response ranging from 9.4 to 27.2% in comparison with the control (Figure 3). Based on the obtained results, among the tested compounds, 10-H2DA and 10-HDAA displayed the maximum induction of caspase-3 activity.

### 4. Discussion

From the last centuries, natural products have been well known as valuable resources of bioactive and useful ingredients for medical, industrial, and agricultural purposes [31]. In recent years, natural products have been evaluated for several procedures in the pest control insecticidal, ovicidal, and evaluation as a repellent [32–34]. The present study aimed to assess the insecticidal, antiplasmodial, antileishmanial, and cytotoxic effects of RJ and its three fatty acids (10-H2DA, 10-HDAA, and sebacic acid). We found that sebacic acid and RJ displayed the lowest and highest larvicidal effects against *Ae. aegypti* larva, respectively. At present, there is no specific criterion in the recommendations of the WHO for estimating the larvicidal activity of natural products, but several studies have reported some criteria to demonstrate the efficacy of insecticides derived from natural products [35, 36]. For example, Komalamisra et al. [37] have revealed that natural products with the  $LC_{50}$  value of less than 50 mg/L are promising and active, while the products with the  $LC_{50}$  values between 50 to 100 mg/L were moderately active. In addition, natural products with the  $LC_{50}$  value between 100 and 750 mg/L and  $>750$  mg/L were effective and inactive, respectively. Another investigation conducted by Kiran et al. [38] reported that natural products with the  $LC_{50}$  less than 100 mg/L are considered as a potent larvicidal effect. However, these criteria are depended on some factors such as exposure time and the source of larvae, which can affect the  $LC_{50}$  values of tested natural products [39]. Hence, our results exhibited the relevant and promising insecticidal effects of RJ, 10-H2DA,



TABLE 1: The results of measurement of the secondary metabolites contents of royal jelly.

Total content	Test	Amount
Phenolic	Folin–Ciocalteu’s reagent colorimetric	83.6 ± 0.31 mg GEA/g DW
Flavonoids	Aluminum chloride (AlCl <sub>3</sub> 2%) colorimetric	1.78 ± 0.023 mg QE/g DW
Protein	Bradford method	11.3%

TABLE 2: Larvicidal activity of royal jelly and its three main fatty acids (*trans*-10-hydroxy-2-decenoic acid (10-H2DA), 10-hydroxydecanoic acid (10-HDAA), and sebacic acid (1,10-decanedioic acid)) against *Ae. aegypti* larva.

Drug	Insecticidal activity LC <sub>50</sub> (µg/mL)
Royal jelly	24.6
10-H2DA	31.4
10-HDAA	37.8
Sebacic acid	44.7

TABLE 3: Antimalarial activity of royal jelly and its three main fatty acids (*trans*-10-hydroxy-2-decenoic acid (10-H2DA), 10-hydroxydecanoic acid (10-HDAA), and sebacic acid (1,10-decanedioic acid)) against *P. falciparum* K1-strain.

Drug	Antimalarial activity IC <sub>50</sub> (µg/mL)
Royal jelly	7.62 ± 0.65
10-H2DA	2.41 ± 0.155
10-HDAA	2.65 ± 0.182
Sebacic acid	3.1 ± 0.213
Chloroquine sulphate	0.53 ± 0.213

Data are presented as the mean ± SD.

TABLE 4: Antileishmanial activity of royal jelly and its three main fatty acids (*trans*-10-hydroxy-2-decenoic acid (10-H2DA), 10-hydroxydecanoic acid (10-HDAA), and sebacic acid (1,10-decanedioic acid)) against intracellular amastigotes of *Leishmania major*.

Drug	Antileishmanial effect IC <sub>50</sub> (µg/mL)
Royal jelly	8.4 ± 0.74
10-H2DA	3.8 ± 0.22
10-HDAA	3.77 ± 0.46
Sebacic acid	4.13 ± 0.51
Meglumine antimoniate	13.6 ± 1.15

Data are presented as the mean ± SD.

TABLE 5: Cytotoxic effects of royal jelly and its three main fatty acids (*trans*-10-hydroxy-2-decenoic acid (10-H2DA), 10-hydroxydecanoic acid (10-HDAA), and sebacic acid (1,10-decanedioic acid)) and their selectivity index (SI) against human HEK293T normal cells.

Drug	Cytotoxicity effect CC <sub>50</sub> (µg/mL)	SI
Royal jelly	117.3	13.9
10-H2DA	74.4	19.5
10-HDAA	81.3	21.5
Sebacic acid	92.6	22.4

Data are presented as the mean ± SD.

10-HDAA, and sebacic acid, according to the criterion reported by Komalamisra et al. [37] and Kiran et al. [38].

Our findings demonstrated that RJ, 10-H2DA, 10-HDAA, and sebacic acid had considerable ( $P < 0.001$ ) antiplasmodial effects against *P. falciparum* with the IC<sub>50</sub> values 7.62, 2.41, 2.65, and 3.1 µg/mL, respectively. In addition, we found that RJ, 10-H2DA, 10-HDAA, and sebacic acid had considerable ( $P < 0.001$ ) antileishmanial effects against the intracellular amastigotes of *L. major* with the IC<sub>50</sub> value 8.14, 3.8, 3.77, and 4.13 µg/mL, respectively. Today, there has been rising attention in evaluating the pharmacological and chemical properties of bee-related products as

a substitute antiparasitic treatment [40]. Previously, it has been proven that bee-related products such as honey, propolis, bee pollen, and bee venom are widely used as herbal therapies for treating various infectious diseases in various parts of the world [41]. Several investigations have shown the promising *in vitro* and/or *in vivo* antiparasitic effects of bee-related products against a wide range of protozoa and helminths such as *Schistosoma* spp., *Trypanosoma* spp., *Leishmania* spp., and *Plasmodium* spp. [42]. Considering the antimicrobial mechanisms of bee products, previous studies displayed that these compounds have several antimicrobial mechanisms such as (i) disruption of

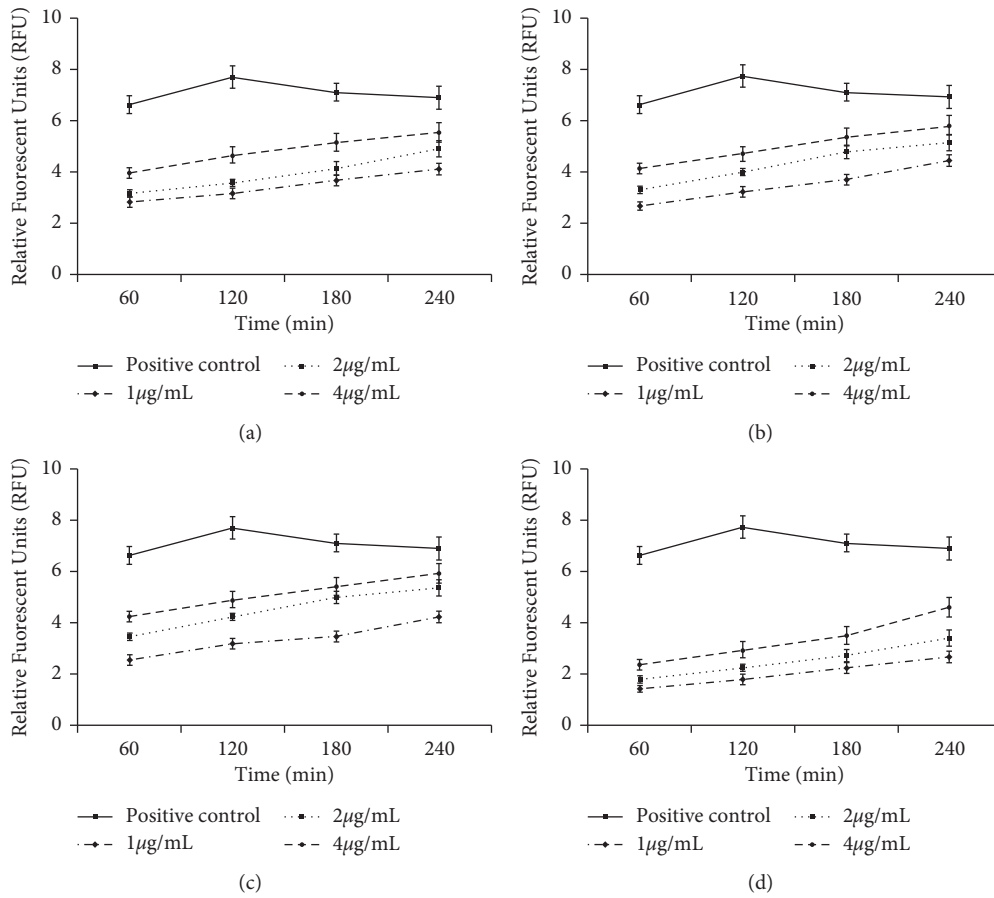


FIGURE 1: The plasma membrane permeability of the *Leishmania major* promastigotes treated with RJ (a), 10-H2DA (b), 10-HDAA (c), and sebacic acid (d). The results exhibited of relative fluorescence units revealed that the promastigotes treated with RJ, 10-H2DA, 10-HDAA, and sebacic acid as a dose-dependent response changed the permeability of plasma membrane by Sytox Green. Data are presented as the mean  $\pm$  SD ( $n = 3$ ).

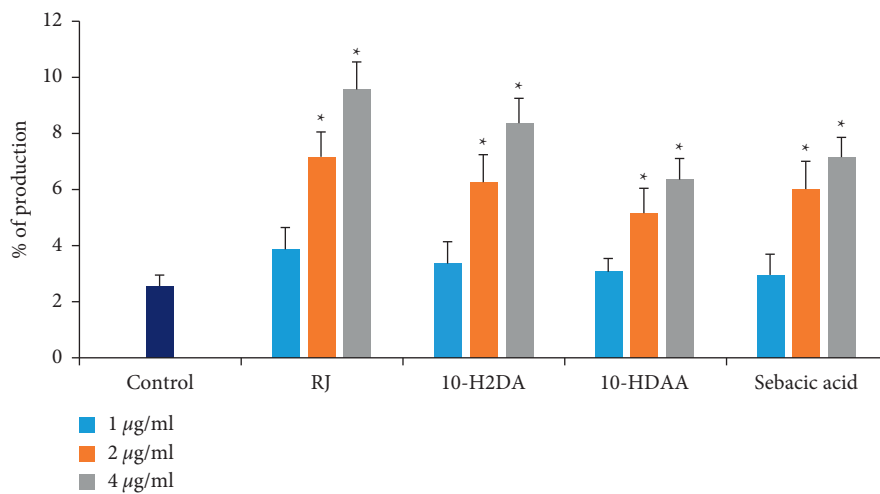


FIGURE 2: Comparison of NO production in J774-A1 macrophage cells after treatment with various concentrations of royal jelly and its three main fatty acids (*trans*-10-hydroxy-2-decenoic acid (10-H2DA), 10-hydroxydecanoic acid (10-HDAA), and sebacic acid). Data are presented as the mean  $\pm$  SD ( $n = 3$ ). \* $P < 0.05$  shows that the difference was statistically significant in comparison with control.

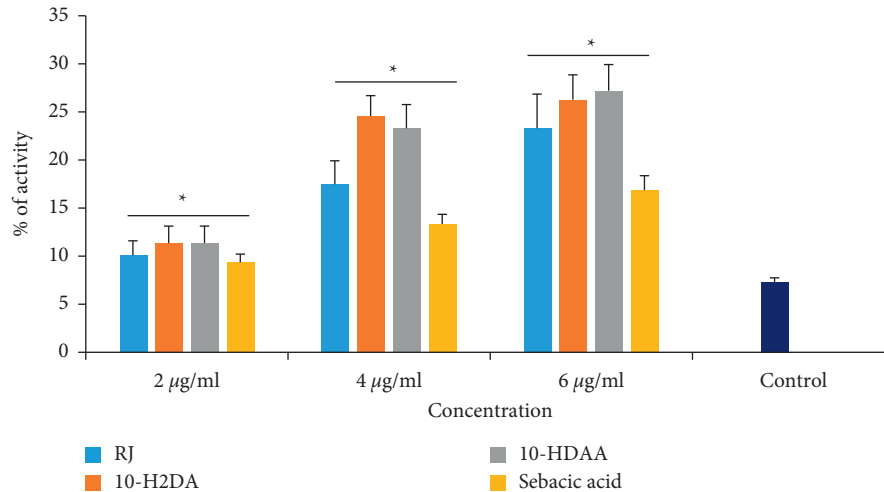


FIGURE 3: The caspase-3-like activity of promastigotes treated with RJ, 10-H2DA, 10-HDAA, and sebacic acid using the colorimetric protease methods. The results exhibited that RJ, 10-H2DA, 10-HDAA, and sebacic acid significantly induced caspase-3 activation as a dose-dependent response. Data are presented as the mean  $\pm$  SD ( $n = 3$ ). \* $P < 0.05$  shows that the difference was statistically significant in comparison with control.

cell wall, (ii) stimulation of macrophages via the production of reactive oxygen species (ROS) and nitrogen metabolites, (iii) promoting the activation of host immune responses by stimulating the production of some cytokines, and (iv) the induction of apoptosis-like mechanisms [43–50].

We found that the 10-H2DA, 10-HDAA, and sebacic acid as the major fatty acids present in RJ had potent insecticidal, antileishmanial, and antiplasmodial effects. Reviews have previously demonstrated that fatty acids demonstrated their antimicrobial mechanisms through suppressing the cellular energy production, inhibition of the DNA/RNA replication, inhibition of enzyme activity, nutrient uptake disorders, generation of peroxidation, and autooxidation degradation products, as well as cytoplasmic membrane disruption [51, 52]. Therefore, it can be suggested that the insecticidal, antiplasmodial, and antileishmanial effects of RJ are due to the existence of these constituents in RJ.

Nowadays, it has been demonstrated that NO, which is produced by a number of immune cells, plays a critical role in the immune-mediated response for eliminating intracellular pathogens [53]. We reported that RJ, 10-H2DA, 10-HDAA, and sebacic acid (1, 2, and 4  $\mu\text{g}/\text{mL}$ ) significantly ( $P < 0.05$ ) increased the production of NO as a dose-dependent pattern in comparison to the nontreated macrophage cells. These results suggest that although RJ, 10-H2DA, 10-HDAA, and sebacic acid triggered the NO production as an important intracellular antimicrobial mechanism, supplementary surveys and analyses are required to evaluate the importance of NO and eliminate other factors.

Previous studies have exhibited that the rupture plasma membrane is one of the key action modes to inhibit the growth of intracellular pathogens [31, 40]. We found that the promastigotes treated with RJ, 10-H2DA, 10-HDAA, and

sebacic acid changed the permeability of the plasma membrane by Sytox Green as a dose-dependent response.

Apoptosis is one of the important processes that basically links pathogen survival to its ability to induce controlled death [43]. Among the caspases, as the main mediators of apoptosis, caspase-3 is considered one of the key caspases that predominantly triggered death protease and successively prompt cell death [45]. Here, we found that RJ, 10-H2DA, 10-HDAA, and sebacic acid significantly induced caspase-3 activation as a dose-dependent response ranging from 9.4 to 27.2% in comparison with the control. Considering the cytotoxicity effects of RJ, 10-H2DA, 10-HDAA, and sebacic acid, the obtained results of the MTT assay demonstrated that the  $CC_{50}$  value for RJ, 10-H2DA, 10-HDAA, and sebacic acid was 117.3, 74.4, 81.3, and 92.6, respectively; subsequently, their  $SI > 10$  of these compound exhibited their specificity to parasites and safety against human HEK239T normal cells.

## 5. Conclusion

The results of the present investigation revealed the promising insecticidal, antiplasmodial, and antileishmanial effects of RJ and its three main fatty acids (10-H2DA, 10-HDAA, and sebacic acid) against healthy 4th instar larvae of *Ae. aegypti*, chloroquine-resistant *P. falciparum* K1-strain, and *L. major* amastigotes, respectively. Although the main mechanisms of action in these natural products are clearly understood, our study revealed that RJ, 10-H2DA, 10-HDAA, and sebacic acid displayed their antimicrobial mechanism through the plasma membrane permeability, triggering the NO production, and the induction of apoptosis. More studies are required to confirm the efficacy of these compounds, especially in animal models and clinical settings.

## Data Availability

All data generated or analyzed during this study are included in this published paper.

## Consent

Not applicable.

## Conflicts of Interest

All authors declare that they have no conflicts of interest.

## Acknowledgments

The authors thank the staff members of the Biological Science Department, Faculty of Science and Humanities, Shaqra University, and the staff members of the Department of Biology, Faculty of Science, University of Tabuk, Saudi Arabia, for their technical support.

## References












- [1] WHO, "Vector-borne diseases. Fact sheets 2017," 2019, <https://www.who.int/news-room/factsheets/detail/vector-borne-diseases>.
- [2] J. A. Souza-Neto, J. R. Powell, and M. Bonizzoni, "Aedes aegypti vector competence studies: a review," *Infection, Genetics and Evolution*, vol. 67, pp. 191–209, 2019.
- [3] J. R. Powell and W. J. Tabachnick, "History of domestication and spread of Aedes aegypti—a review," *Memórias do Instituto Oswaldo Cruz*, vol. 108, no. suppl 1, pp. 11–17, 2013.
- [4] N. Sutthanont, S. Attrapadung, and S. Nuchprayoon, "Larvicidal activity of synthesized silver nanoparticles from Curcuma zedoaria essential oil against Culex quinquefasciatus," *Insects*, vol. 10, no. 1, p. 27, 2019.
- [5] T. Chareonviriyaphap, M. J. Bangs, W. Suwonkerd, M. Kongmee, V. Corbel, and R. Ngoen-Klan, "Review of insecticide resistance and behavioral avoidance of vectors of human diseases in Thailand," *Parasites & Vectors*, vol. 6, no. 1, p. 280, 2013.
- [6] R. Pavela, "Larvicidal effects of various Euro-Asiatic plants against Culex quinquefasciatus Say larvae (Diptera: Culicidae) Parasitol," *Parasitology Research*, vol. 102, no. 3, pp. 555–559, 2008.
- [7] A. Abdul Rahuman, G. Gopalakrishnan, P. Venkatesan, and K. Geetha, "Isolation and identification of mosquito larvicidal compound from Abutilon indicum (Linn.)," *Parasitology Research*, vol. 102, no. 5, pp. 981–988, 2008.
- [8] M. Bannister-Tyrrell, K. Verdonck, S. Hausmann-Muela, C. Gryseels, J. M. Ribera, and K. P. Grietens, "Defining micro-epidemiology for malaria elimination: systematic review and meta-analysis," *Malaria Journal*, vol. 16, no. 1, pp. 1–20, 2017.
- [9] K. Sabina, "Prevalence and epidemiology of malaria in Nigeria: a review," *International Journal of Research in Pharmacy and Biosciences*, vol. 4, no. 8, pp. 10–12, 2017.
- [10] R. E. Cibulskis, P. Alonso, J. Aponte et al., "Malaria: global progress 2000–2015 and future challenges," *Infectious diseases of poverty*, vol. 5, no. 1, pp. 1–8, 2016.
- [11] G. Newby, J. Hwang, K. Koita et al., "Review of mass drug administration for malaria and its operational challenges," *The American Journal of Tropical Medicine and Hygiene*, vol. 93, no. 1, pp. 125–134, 2015.
- [12] I. Kevric, M. A. Cappel, and J. H. Keeling, "New world and old world Leishmania infections: a practical review," *Dermatologic Clinics*, vol. 33, no. 3, pp. 579–593, 2015.
- [13] I. Sharifi, M. R. Aflatoonian, M. H. Daei Parizi et al., "Visceral leishmaniasis in Southeastern Iran: a narrative review," *Iranian Journal of Parasitology*, vol. 12, no. 1, pp. 1–11, 2017.
- [14] L. Monzote, "Current treatment of leishmaniasis: a review," *The Open Antimicrobial Agents Journal*, vol. 1, no. 1, 2009.
- [15] L. F. Oliveira, A. O. Schubach, M. M. Martins et al., "Systematic review of the adverse effects of cutaneous leishmaniasis treatment in the New World," *Acta Tropica*, vol. 118, no. 2, pp. 87–96, 2011.
- [16] G. M. Cragg and D. J. Newman, "Natural products: a continuing source of novel drug leads," *Biochimica et Biophysica Acta (BBA)-General Subjects*, vol. 1830, no. 6, pp. 3670–3695, 2013.
- [17] V. R. Pasupuleti, L. Sammugam, N. Ramesh, and S. H. Gan, "Honey, propolis, and royal jelly: a comprehensive review of their biological actions and health benefits," *Oxidative Medicine and Cellular Longevity*, vol. 2017, Article ID 1259510, 2017.
- [18] C. I. Pavel, L. A. Mărghitaş, O. Bobiş et al., "Biological activities of royal jelly—review," *Scientific Papers Animal Science and Biotechnologies*, vol. 44, no. 2, pp. 108–118, 2011.
- [19] M. F. Ramadan and A. Al-Ghamdi, "Bioactive compounds and health-promoting properties of royal jelly: a review," *Journal of Functional Foods*, vol. 4, no. 1, pp. 39–52, 2012.
- [20] J. Kocot, M. Kielczykowska, D. Luchowska-Kocot, J. Kurzepa, and I. Musik, "Antioxidant potential of propolis, bee pollen, and royal jelly: possible medical application," *Oxidative Medicine and Cellular Longevity*, vol. 2018, Article ID 7074209, 2018.
- [21] S. Ahmad, M. G. Campos, F. Fratini, S. Z. Altaye, and J. Li, "New insights into the biological and pharmaceutical properties of royal jelly," *International Journal of Molecular Sciences*, vol. 21, no. 2, p. 382, 2020.
- [22] S. Kolayli, H. Sahin, Z. Can, O. Yildiz, M. Malkoc, and A. Asadov, "A member of complementary medicinal food: anatolian royal jellies, their chemical compositions, and antioxidant properties. J. Evid. Based complement," *Alternative Medicine*, vol. 21, pp. NP43–NP48, 2016.
- [23] V. A. Isidorov, S. Bakier, and I. Grzech, "Gas chromatographic-mass spectrometric investigation of volatile and extractable compounds of crude royal jelly," *Journal of Chromatography B*, vol. 885–886, pp. 109–116, 2012.
- [24] E. Melliou and I. Chinou, "Chemistry and bioactivity of royal jelly from Greece," *Journal of Agricultural and Food Chemistry*, vol. 53, no. 23, pp. 8987–8992, 2005.
- [25] V. L. Singleton, R. Orthofer, and R. M. Lamuela-Raventós, "Analysis of total phenols and other oxidation substrates and antioxidants by means of Folin-Ciocalteu reagent," *Oxidants and Antioxidants Part A*, vol. 299, pp. 152–178, 1999.
- [26] S. El-Guendouz, S. Aazza, B. Lyoussi, M. D. Antunes, M. L. Faleiro, and M. G. Miguel, "Anti-acetylcholinesterase, antidiabetic, anti-inflammatory, antityrosinase and anti-xanthine oxidase activities of Moroccan propolis," *International Journal of Food Science and Technology*, vol. 51, no. 8, pp. 1762–1773, 2016.
- [27] K. Hartfelder, M. M. G. Bitondi, C. S. Brent et al., "Standard methods for physiology and biochemistry research in Apis mellifera," *Journal of Apicultural Research*, vol. 52, no. 1, pp. 1–48, 2013.
- [28] L. T. Huong, N. H. Hung, D. N. Dai et al., "Chemical compositions and mosquito larvicidal activities of essential

- oils from Piper species growing wild in Central Vietnam,” *Molecules*, vol. 24, no. 21, p. 3871, 2019.
- [29] M. T. Makler, R. C. Piper, J. A. Williams et al., “Parasite lactate dehydrogenase as an assay for Plasmodium falciparum drug sensitivity,” *The American Journal of Tropical Medicine and Hygiene*, vol. 48, no. 6, pp. 739–741, 1993.
- [30] A. E. Albalawi, S. Abdel-Shafy, A. Khudair Khalaf et al., “Therapeutic potential of green synthesized copper nanoparticles alone or combined with meglumineantimoniate (glucantime®) in cutaneous leishmaniasis,” *Nanomaterials*, vol. 11, no. 4, p. 891, 2021.
- [31] H. Yuan, Q. Ma, L. Ye, and G. Piao, “The traditional medicine and modern medicine from natural products,” *Molecules*, vol. 21, no. 5, p. 559, 2016.
- [32] A. Asadollahi, M. Khoobdel, A. Zahraei-Ramazani, S. Azarmi, and S. H. Mosawi, “Effectiveness of plant-based repellents against different Anopheles species: a systematic review,” *Malaria Journal*, vol. 18, no. 1, pp. 436–520, 2019.
- [33] M. B. Isman, “Botanical insecticides, deterrents, and repellents in modern agriculture and an increasingly regulated world,” *Annual Review of Entomology*, vol. 51, no. 1, pp. 45–66, 2006.
- [34] A. Ghosh, N. Chowdhury, and G. Chandra, “Plant extracts as potential mosquito larvicides,” *Indian Journal of Medical Research*, vol. 135, no. 5, pp. 581–98, 2012.
- [35] J.-M. Chantraine, D. Laurent, C. Ballivian, G. Saavedra, R. Ibañez, and L. A. Vilaseca, “Insecticidal activity of essential oils on Aedes aegypti larvae,” *Phytotherapy Research*, vol. 12, no. 5, pp. 350–354, 1998.
- [36] L. A. Magalhães, M. P. Lima, M. O. Marques, R. Facanali, A. C. Pinto, and W. P. Tadei, “Chemical composition and larvicidal activity against Aedes aegypti larvae of essential oils from four Guarea species,” *Molecules*, vol. 15, no. 8, pp. 5734–5741, 2010.
- [37] N. Komalamisra, Y. Trongtokit, Y. Rongsriyam, and C. Apiwathnasorn, “Screening for larvicidal activity in some Thai plants against four mosquito vector species,” *The Southeast Asian journal of tropical medicine and public health*, vol. 36, no. 6, pp. 1412–22, 2005.
- [38] S. Ravi Kiran, K. Bhavani, P. Sita Devi, B. R. Rajeswara Rao, and K. Janardhan Reddy, “Composition and larvicidal activity of leaves and stem essential oils of Chloroxylon swietenia DC against Aedes aegypti and Anopheles stephensi,” *Bioresource Technology*, vol. 97, no. 18, pp. 2481–2484, 2006.
- [39] C. N. Dias, L. P. Alves, K. A. Rodrigues et al., “Chemical composition and larvicidal activity of essential oils extracted from Brazilian legal Amazon plants against Aedes aegypti L.(Diptera: Culicidae),” *Evidence-based Complementary and Alternative Medicine*, vol. 2015, Article ID 490765, 2015.
- [40] R. Cauich-Kumul and M. R. Segura Campos, “Bee propolis: properties, chemical composition, applications, and potential health effects,” *Bioactive Compounds*, Woodhead Publishing, vol. 12, pp. 227–243, 2019.
- [41] S. El-Guendouz, B. Lyoussi, and M. G. Miguel, “Insight on propolis from mediterranean countries: chemical composition, biological activities and application fields,” *Chemistry and Biodiversity*, vol. 16, no. 7, Article ID e1900094, 2019.
- [42] F. Nainu, A. Masyita, M. A. Bahar et al., “Pharmaceutical prospects of bee products: special focus on anticancer, antibacterial, antiviral, and antiparasitic properties,” *Antibiotics*, vol. 10, no. 7, p. 822, 2021.
- [43] R. P. Dutra, J. L. Bezerra, M. C. P. d. Silva et al., “Anti-leishmanial activity and chemical composition from Brazilian geopropolis produced by stingless bee Melipona fasciculata,” *Revista Brasileira de Farmacognosia*, vol. 29, no. 3, pp. 287–293, 2019.
- [44] A. N. P. Gomes, C. A. Camara, A. dos Santos Sousa et al., “Chemical composition of bee pollen and leishmanicidal activity of rhusflavone,” *Revista Brasileira de Farmacognosia*, vol. 31, no. 2, pp. 176–183, 2021.
- [45] O. Cuesta-Rubio, M. Campo Fernández, I. Márquez Hernández et al., “Chemical profile and anti-leishmanial activity of three Ecuadorian propolis samples from Quito, Guayaquil and Cotacachi regions,” *Fitoterapia*, vol. 120, pp. 177–183, 2017.
- [46] B. C. Cunha, M. B. De Miranda, L. C. C. Afonso et al., “Brazilian green propolis hydroalcoholic extract as a therapeutic adjuvant to treat cutaneous leishmaniasis,” *Journal of Applied Pharmaceutical Science*, vol. 10, pp. 124–132, 2020.
- [47] A. P. F. dos Santos Thomazelli, F. Tomiotto-Pellissier, S. S. da Silva et al., “Brazilian propolis promotes immunomodulation on human cells from American Tegumentar Leishmaniasis patients and healthy donors infected with L. braziliensis,” *Cellular Immunology*, vol. 311, pp. 22–27, 2017.
- [48] S. Yesmin, A. Paul, T. Naz et al., “Membrane stabilization as a mechanism of the anti-inflammatory activity of ethanolic root extract of Choi (Piper chaba),” *Clinical Phytoscience*, vol. 6, no. 1, p. 59, 2020.
- [49] A. G. Hegazi, F. M. Al Guthami, A. F. Al Gethami, and H. A. El Fadaly, “Beneficial effects of Capparis spinosa honey on the immune response of rats infected with toxoplasma gondii,” *Journal of Pharmacopuncture*, vol. 20, pp. 112–118, 2017.
- [50] R. F. S. Menna-Barreto, K. Salomão, A. P. Dantas et al., “Different cell death pathways induced by drugs in Trypanosoma cruzi: an ultrastructural study,” *Micron*, vol. 40, no. 2, pp. 157–168, 2009.
- [51] A. P. Desbois and V. J. Smith, “Antibacterial free fatty acids: activities, mechanisms of action and biotechnological potential,” *Applied Microbiology and Biotechnology*, vol. 85, no. 6, pp. 1629–1642, 2010.
- [52] G. Casillas-Vargas, C. Ocasio-Malavé, S. Medina et al., “Antibacterial fatty acids: an update of possible mechanisms of action and implications in the development of the next-generation of antibacterial agents,” *Progress in Lipid Research*, vol. 82, Article ID 101093, 2021.
- [53] P. Holzmuller, D. Sereno, M. Cavaleyra et al., “Nitric oxide-mediated proteasome-dependent oligonucleosomal DNA fragmentation in Leishmania amazonensis amastigotes,” *Infection and Immunity*, vol. 70, no. 7, pp. 3727–3735, 2002.



## Research Article

# Phytochemical Analysis, $\alpha$ -Glucosidase and Amylase Inhibitory, and Molecular Docking Studies on *Persicaria hydropiper* L. Leaves Essential Oils

Mater H. Mahnashi <sup>1</sup>, Yahya S. Alqahtani <sup>1</sup>, Bandar A. Alyami <sup>1</sup>, Ali O. Alqarni,<sup>1</sup>  
Muhammad Ayaz <sup>2</sup>, Mehreen Ghufuran <sup>3</sup>, Farhat Ullah <sup>2</sup>, Abdul Sadiq <sup>2</sup>,  
Ihsan Ullah <sup>4</sup>, Ikram Ul Haq <sup>5</sup>, Mohammad Khalid <sup>6</sup>, and H. C. Ananda Murthy <sup>7</sup>

<sup>1</sup>Department of Pharmaceutical Chemistry, College of Pharmacy, Najran University, Najran, Saudi Arabia

<sup>2</sup>Department of Pharmacy, Faculty of Biological Sciences, University of Malakand, Chakdara, 18000 Dir (L), KP, Pakistan

<sup>3</sup>Department of Biochemistry, UCS, Shankar, Abdul Wali Khan University, Mardan 23200, Pakistan

<sup>4</sup>Department of Pharmacy, University of Swabi, Swabi, Pakistan

<sup>5</sup>National Institute of Health, Islamabad, Pakistan

<sup>6</sup>Department of Pharmacognosy, College of Pharmacy, Prince Sattam Bin Abdulaziz University, Al-Kharj 11942, Saudi Arabia

<sup>7</sup>Department of Applied Chemistry, School of Applied Natural Science, Adama Science and Technology University, P O Box 1888, Adama, Ethiopia

Correspondence should be addressed to H. C. Ananda Murthy; [anandkps350@gmail.com](mailto:anandkps350@gmail.com)

Received 10 December 2021; Accepted 27 December 2021; Published 19 January 2022

Academic Editor: Ruchika Garg

Copyright © 2022 Mater H. Mahnashi et al. This is an open access article distributed under the Creative Commons Attribution License, which permits unrestricted use, distribution, and reproduction in any medium, provided the original work is properly cited.

**Objective.** Medicinal plants and essential oils are well known for diverse biological activities including antidiabetic potential. This study was designed to isolate essential oils from the leaves of *Persicaria hydropiper* L. (*P. hydropiper*), perform its phytochemical analysis, and explore its in vitro antidiabetic effects. **Materials and Methods.** *P. hydropiper* leaves essential oils (Ph.Los) were extracted using a hydrodistillation apparatus and were subjected to phytochemical analysis using the gas chromatography mass spectrometry (GC-MS) technique. Ph.Lo was tested against two vital enzymes including  $\alpha$ -glucosidase and  $\alpha$ -amylase which are important targets in type-2 diabetes. The identified compounds were tested using *in silico* approaches for their binding affinities against the enzyme targets using MOE-Dock software. **Results.** GC-MS analysis revealed the presence of 141 compounds among which dihydro-alpha-ionone, cis-geranylacetone,  $\alpha$ -bulnesene, nerolidol,  $\beta$ -caryophyllene epoxide, and decahydronaphthalene were the most abundant compounds. Ph.Lo exhibited considerable inhibitory potential against  $\alpha$ -glucosidase enzyme with 70% inhibition at  $1000 \mu\text{g mL}^{-1}$  which was the highest tested concentration. The inhibitory activity of positive control acarbose was  $77.30 \pm 0.61\%$  at the same tested concentration. Ph.Lo and acarbose exhibited  $\text{IC}_{50}$  of 170 and  $18 \mu\text{g mL}^{-1}$  correspondingly. Furthermore, dose-dependent inhibitions were observed for Ph.Lo against  $\alpha$ -amylase enzyme with an  $\text{IC}_{50}$  of  $890 \mu\text{g mL}^{-1}$ . The top-ranked docking conformation was observed for  $\beta$ -caryophyllene epoxide with a docking score of -8.3182 against  $\alpha$ -glucosidase, and it has established seven hydrogen bonds and one H-pi interaction at the active site residues (Phe 177, Glu 276, Arg 312, Asp 349, Gln 350, Asp 408, and Arg 439). Majority of the identified compounds fit well in the binding pocket of Tyr 62, Asp 197, Glu 233, Asp 300, His 305, and Ala 307 active residues of  $\alpha$ -amylase.  $\beta$ -Caryophyllene epoxide was found to be the most active inhibitor with a docking score of -8.3050 and formed five hydrogen bonds at the active site residues of  $\alpha$ -amylase. Asp 197, Glu 233, and Asp 300 active residues were observed to be making polar interactions with the ligand. **Conclusions.** The current study revealed that Ph.Lo is rich in bioactive metabolites which might contribute to its enzyme inhibitory potential. Inhibition of these enzymes is the key target in reducing postprandial hyperglycemia. However, further detailed in vivo studies are required for their biological and therapeutic activities.



## 1. Introduction

Diabetes mellitus (DM) is a metabolic syndrome associated with hyperglycemia due to the body's inability to produce sufficient amount of insulin or abnormalities in its secretion or tissue resistance to its action [1, 2]. Hyperglycemia in DM may also occur due to defects in the metabolic processes involved in processing carbohydrates, proteins, and fats [3, 4]. This results in development of some classical symptoms including polyuria, polydipsia, and polyphagia [5]. These metabolic abnormalities are due to low insulin level or resistance of target tissues (adipose tissue, skeletal muscles, and liver) to insulin at the level of signal transduction, insulin receptors, genes, or effector enzymes [6]. In DM, elevated level of blood glucose for a long time is associated with a number of acute or chronic complications [7]. Globally, it has been estimated that the occurrence of diabetes has increased from 4% in 1995 to 5.4% by the year 2025 [8]. The overall prevalence as reported by the International Diabetes Federation (IDF) in 2011 was increased to 366 million people and is supposed to increase up to 552 million people by the year 2030 [9]. Furthermore, it has also been reported that 450 million people have been suffering from DM globally and the prevalence is expected to rise to 690 million by the year 2044 [10].

Regarding type-2 diabetes, targeting enzymes involved in processing dietary carbohydrates in the intestinal tract is among the vital targets. Among these,  $\alpha$ -amylase and  $\alpha$ -glucosidase enzymes are of high pharmacological interest and are used to control elevated glucose level in T2DM. These enzymes cause metabolic breakdown of complex dietary carbohydrates to simple sugars which are subsequently absorbed [11]. Long-chain carbohydrates are broken down into glucose by alpha-amylase enzyme, whereas  $\alpha$ -glucosidase is responsible for the breakdown of disaccharides and starch into simpler monosaccharide glucose, resulting in hyperglycemia [12].

The use of medicinal plants and natural products is still a major source of therapy in the developing countries [13–15]. The discovery of modern analytical techniques has further eased the process of ethnomedicinal drug discovery to identify, isolate, and characterize target molecules [16–18]. Approximately more than four hundred plants are identified having antidiabetic potential, but only few of these plants have received medical and scientific evaluation [19]. A large number of  $\alpha$ -amylase and  $\alpha$ -glucosidase inhibitors are produced by different microorganisms and plants to regulate the activities of these enzymes [20]. The natural  $\alpha$ -glucosidase inhibitors from plant sources, whose  $\alpha$ -glucosidase inhibitory activities have been reported previously, include alkaloids, flavonoids, anthocyanins, terpenoids, curcuminoids, and phenolic compounds [21]. Miglitol, voglibose, and acarbose are the only three  $\alpha$ -glucosidase inhibitors which are in clinical practice presently for the treatment of patients with T2DM [22].

*Persicaria hydropiper* L. belongs to the family Polygonoaceae (smartweed family) which consists of about fifty

genera and twelve hundred species. It is ethnopharmacologically famous for its use as a diuretic, anti-inflammatory agent, stomachic, central nervous system (CNS) stimulant, and natural remedy in other gastrointestinal disorders [23]. *P. hydropiper* contains flavonoids, chalcone derivatives, phenylpropanoid derivatives, phenolic compounds, anthraquinone, isocoumarin, terpenoids, and steroids [24]. Previously, crude extracts and isolated compounds were reported for neuroprotective [25, 26], cytotoxic [27, 28], antimicrobial [29], gastroprotective [30], and toxicological potential [23, 31]. The current study aimed to isolate essential oils from the leaves of *P. hydropiper* and evaluate its detailed composition via gas chromatography mass spectrometry (GC-MS). Also, the study analyses the essential oils against two important targets of the type-2 diabetes,  $\alpha$ -glucosidase and  $\alpha$ -amylase and dock the identified compounds against these enzymes.

## 2. Materials and Methods

**2.1. Plant Collection and Extraction of Essential Oils from Leaves.** Fresh leaves from the plant were collected in 2014 from the village of Talash (Dir), KP Pakistan, and authenticated via a botanical taxonomist and curator at the botanical garden in the University of Malakand. For preservation, dried compressed leaves were submitted to the herbarium with reference no H.UOM.BG.107. Fresh leaves were then carefully rinsed using distilled water and were processed via a Clevenger apparatus to isolate essential oils [32]. In brief, leaves were macerated followed by hydrodistillation in a Clevenger apparatus coupled with a condenser. Hydrodistillation was continued for three days at 100°C until a sufficient amount of essential oil was collected. Yellowish oil was collected in air-tight glass bottles and was refrigerated before being used for analysis and other assays.

**2.2. GC-MS Analysis.** GC-MS analysis of essential oils was performed via an Agilent USB-393752 gas chromatograph (Agilent Technologies, Palo Alto, CA, USA) having a HHP-5MS 5% phenylmethylsiloxane capillary column (Restek, Bellefonte, PA) with 30 m  $\times$  0.25 mm  $\times$  0.25  $\mu$ m film thickness and coupled with a mass spectrometer. Initially, oven temperature was sustained at 70°C for one minute, gradually increased to 180°C (at 6°C/min increase), and finally maintained at 280°C for twenty minutes. Temperatures of both the injector and detector were set at 220°C and 290°C, respectively. Helium was used as the carrier gas with a flow rate of 1 ml/min, and diluted Ph.Lo samples (1/1000 in *n*-pentane, v/v) were injected in the split-less mode. Components of the Ph.Lo were identified via comparison of their retention time (RT) with already reported spectral data in NIST, NIH, and Wiley libraries [33]. Moreover, comparison of the fragmentation pattern of mass spectra was done with the published literature [34].

2.3.  *$\alpha$ -Glucosidase Inhibitory Studies.* Enzyme inhibitory potential of Ph.Lo was obtained according to the previously reported standard protocol [35]. Baker's yeast alpha-glucosidase, substrate (P-nitrophenyl- $\alpha$ -D-glucopyranoside), and control (acarbose) were acquired from authentic sources of Sigma Aldrich (USA). Enzyme solution (100 mM) was prepared using phosphate buffer of pH 6.8. Ph.Lo solutions were prepared using a small amount of surfactants

(31.25–1000  $\mu\text{g mL}^{-1}$ ) in 320  $\mu\text{l}$  of 100 mM phosphate buffer and were kept for five minutes at 30°C. Subsequently, 3 ml (50 mM) of NaOH solution was mixed with it, and using a spectrophotometer, absorbency rates were recorded at 410 nm. Control solution consisted of all ingredients except the inhibitor (sample). Positive control was acarbose. Percent enzyme inhibitions were derived from the data using the given formula.

$$\text{"\% Inhibition"} = \left[ \frac{\text{Absorbance of Control} - \text{Absorbance of Sample}}{\text{Absorbance of control}} \right] \times 100. \quad (1)$$

2.4.  *$\alpha$ -Amylase Inhibitory Studies.* Likewise,  $\alpha$ -amylase inhibitory studies were performed following the already established procedure [12]. In brief, 20  $\mu\text{l}$  enzyme was mixed in 200  $\mu\text{l}$  of 0.02 M sodium phosphate buffer mixed with the plant extracts (test compounds) of varying concentration ranges of 31.25–1000  $\mu\text{g mL}^{-1}$ . The assay mixtures were then maintained at  $25 \pm 3^\circ\text{C}$  for about ten minutes, and 200  $\mu\text{l}$  of starch was added to it. To terminate the reaction, 400  $\mu\text{l}$  of DNS reagent (dinitrosalicylic acid) was transferred to the mixture. The resultant solution was kept in a boiling water bath for five minutes and cooled. After cooling, 15 ml of distilled water was added to dilute the mixture and the absorbance was noted at 540 nm. Standard drug was acarbose, and enzyme inhibition was determined via the formula.

of triplicate observations. *P* values < 0.05 were considered as statistically significant. GraphPad Prism software (version 5) (USA) was used for the data analysis and figure creation.

### 3. Results and Discussion

2.5. *Molecular Docking Studies.* The identified compounds were docked for their binding capacity in the enzymes protein pocket via MOE-Dock tool in molecular operating environment (MOE) (<http://www.chemcomp.com>) [36, 37]. Due to unavailability of  $\alpha$ -glucosidase crystal structure, a previously reported homology model was used [38], whereas the  $\alpha$ -amylase (4W93) 3D crystal structure was obtained from the Protein Databank (PDB). Before starting the docking process, the water molecules and ions present in crystal structures were removed via MOE. Thereafter, protein structures were added to hydrogen atoms via 3D protonation with subsequent minimization of energy via MOE default parameters including the gradient of 0.05 and Force Field Amber99.

3.1. *GC-MS Analysis.* In the GC-MS study, 141 compounds were recognized (Table S1), among which the most abundant compounds (File S1) were  $\beta$ -elemene (RT: 14.359, height%: 39.24, area%: 17.79, *m/z*: 81.1), dihydro-alpha-ionone (RT: 14.822, height%: 8.68, area%: 3.52, *m/z*: 43.1), cis-geranylacetone (RT: 15.505, height%: 21.89, area%: 9.7, *m/z*: 43.1), alpha-bulnesene (RT: 16.382, height%: 14.39, area%: 6.67, *m/z*: 93.1), bicyclo[4.1.0]heptane,-3-cyclopropyl,-7-hydroxymethyl, trans (RT: 17.722, height%: 12.08, area%: 7.4, *m/z*: 79.1), nerolidol (RT: 17.838, height%: 13.14, area%: 5.17, *m/z*: 69.1), bicyclo[2.2.2]oct-2-ene, 1,2,3,6-tetramethyl (RT: 18.449, height%: 94.65, area%: 94.88, *m/z*: 79.1), (1R,5S,8R,9R)-4,4,8-trimethyltricyclo [6.3.1.0(1,5)] dodeca-2-en-9-ol (RT: 18.482, height%: 17.96, area%: 2.3, *m/z*: 161.1),  $\beta$ -caryophyllene epoxide (RT: 18.663, height%: 16.02, area%: 7.02, *m/z*: 83), and decahydronaphthalene (RT: 18.951, height%: 100, area%: 100, *m/z*: 109.1) (Figure 1).

Target compound structures were generated in MOE, and using the software default parameters, the energy was minimized. The selected enzymes including  $\alpha$ -glucosidase and  $\alpha$ -amylase subjected to docking with the identified compounds via the MOE parameters including Placement: Triangle Matcher, Rescoring: London dG. At least 10 confirmations were generated for every ligand. Subsequently, for each compound, top-ranked confirmations were developed and were subjected to further analysis. Finally, those docking results having comparatively good poses with polar, arene-arene, H- $\pi$ , and  $\pi$ -H interactions were analyzed via Pymol software.

#### 3.2. Enzyme Inhibition Studies

3.2.1. *Ph.Lo Exhibited Concentration-Dependent  $\alpha$ -Glucosidase Inhibition.* In the present study, Ph.Lo was found to be highly active against  $\alpha$ -glucosidase enzyme as shown in Figure 2. Ph.Lo showed inhibition rates of  $70.00 \pm 0.00$ ,  $63.66 \pm 1.20$ ,  $59.16 \pm 0.60$ ,  $53.00 \pm 1.15$ ,  $47.37 \pm 0.65$ , and  $41.33 \pm 1.30\%$  at selected doses of 1000, 500, 250, 125, 62.50, and 31.25  $\mu\text{g mL}^{-1}$  correspondingly. The standard drug acarbose inhibitory activity showed  $77.30 \pm 0.61$ ,  $73.00 \pm 0.00$ ,  $69.00 \pm 0.00$ ,  $55.50 \pm 1.04$ ,  $49.83 \pm 0.44$ , and  $41.00 \pm 0.00\%$  using the abovementioned doses, respectively. For test (Ph.Lo) and control (acarbose),  $\text{IC}_{50}$  of 170 and 18  $\mu\text{g mL}^{-1}$  was calculated.

2.6. *Statistical Analysis.* Statistical analyses were performed using one-way analysis of variance (ANOVA) followed by Dunnett's test. The results are presented as the means  $\pm$  SEM

3.2.2. *Ph.Lo Exhibits Concentration-Dependent Inhibition against  $\alpha$ -Amylase Enzyme.* Results of alpha-amylase inhibitory potential of Ph.Lo are summarized in Figure 3. Enzyme inhibitory activity of the Ph.Lo was 70.36% at 1000  $\mu\text{g mL}^{-1}$ , 51.91% at 500  $\mu\text{g mL}^{-1}$ , 42.66% at 250  $\mu\text{g mL}^{-1}$ , 32.00% at 125  $\mu\text{g mL}^{-1}$ , 24.00% at 62.50  $\mu\text{g mL}^{-1}$ , and 14.50%

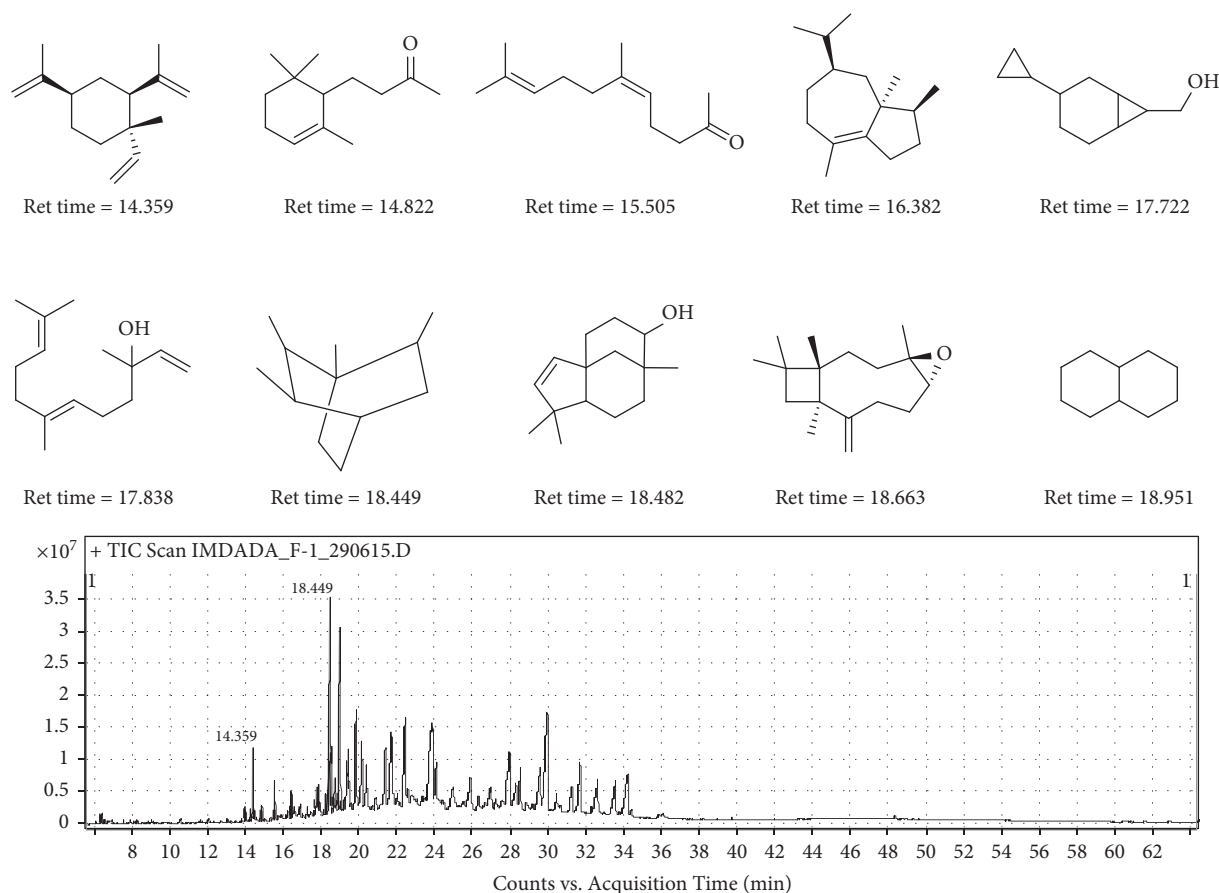


FIGURE 1: Representative image for the most abundant identified compounds.

at  $31.25 \mu\text{g mL}^{-1}$ . Positive control showed inhibition rates of 77.3% at  $1000 \mu\text{g mL}^{-1}$ , 73.00% at  $500 \mu\text{g mL}^{-1}$ , 69.00% at  $250 \mu\text{g mL}^{-1}$ , 55.50% at  $125 \mu\text{g mL}^{-1}$ , 49.83% at  $62.50 \mu\text{g mL}^{-1}$ , and 41.00% at  $31.25 \mu\text{g mL}^{-1}$ . Overall, concentration-dependent amylase inhibitory activities were observed for Ph.Lo as shown in Figure 3 at an  $\text{IC}_{50}$  of  $890 \mu\text{g mL}^{-1}$ .

In GC-MS characterization, 141 phytochemicals were identified, among which dihydro- $\alpha$ -ionone, cis-geranylacetone,  $\alpha$ -bulnesene, nerolidol,  $\beta$ -caryophyllene epoxide, and decahydronaphthalene were the most abundant compounds. It has been suggested by Jabeen et al. that, in a molecule, the presence of lipophilic side chain is responsible for the inhibition of  $\alpha$ -glucosidase enzymes [39]. Inhibitory potential of both glucosidase and amylase enzymes has been reported previously for various volatile oils including *Eruca vesicaria* subsp. *longirostris*. Here, erucin was suggested to inhibit  $\alpha$ -glucosidase. Apart from erucin, it was also reported that  $\beta$ -elemene may inhibit  $\alpha$ -glucosidase activity [40]. In essential oils, the presence of monoterpenes and sesquiterpenes may contribute to inhibition of both selected enzymes [41].  $\alpha$ -pinene, germacrene D, drimenin, and drimane-type sesquiterpene lactone are the compounds in *Hertia cheirifolia* essential oils obtained from its leaves and flowers and were suggested to contribute  $\alpha$ -amylase inhibitory activity [42]. Recently, it has also been reported by Majouli et al. that *H. cheirifolia* volatile

oils possess inhibitory potential against  $\alpha$ -glucosidase enzyme [43]. Apart from this, inhibitory activities against both selected enzymes were reported for *Nepeta curviflora* volatile oils [44]. In these essential oils, the major phytochemical constituents include caryophyllene oxide, 1,6-dimethyl spiro-decane, and  $\beta$ -caryophyllene which are suggested for their anti-amylase and anti-glucosidase activities. These compounds in addition to other bioactive metabolites were identified in Ph.Lo analysis and might contribute to the overall enzyme inhibitory potential.

### 3.2.3. Molecular Docking Studies against $\alpha$ -Amylase Enzyme.

Binding of the selected compounds in the binding pocket was observed (Tyr 62, Asp 197, Glu 233, Asp 300, His 305, and Ala 307 active residues) for the  $\alpha$ -amylase enzyme. Docking studies revealed that the  $\beta$ -caryophyllene epoxide is the most active inhibitor with a docking score of -8.3050 and formed five hydrogen bonds with the active site residues of  $\alpha$ -amylase. Asp 197, Glu 233, and Asp 300 active residues were observed to be making polar interactions with the ligand (Figure 4).

Enzyme inhibition properties of the phytochemicals might be attributed to electron-donating group ( $-\text{CH}_3$ ) on the identified compound. The oxygen atom of the ligand might be implicated in the considerable *in silico* performance of the compound. Interaction reports of the remaining inhibitors are given in Table 1.

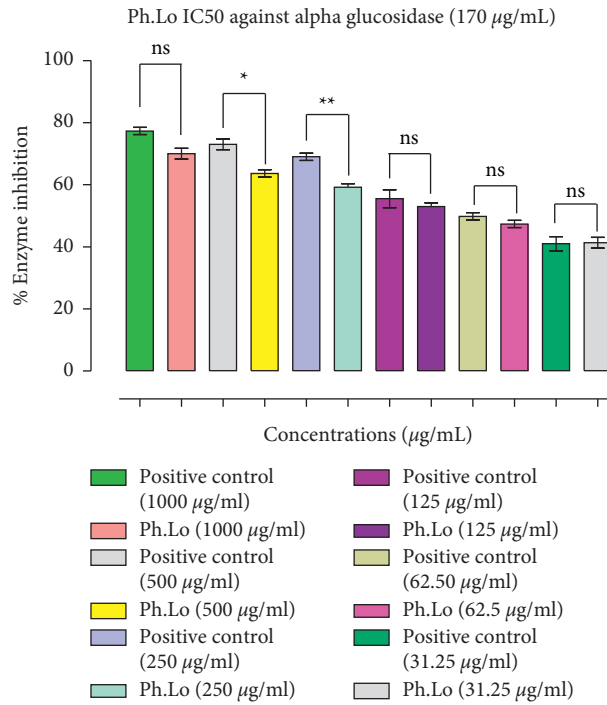


FIGURE 2: Results of  $\alpha$ -glucosidase inhibition study. Data bars represent results from three independent experimental observations. Data are presented as means  $\pm$  SEM. Values are significantly different (\*  $p < 0.05$ , \*\*  $p < 0.01$ ) when compared with positive control at the same tested concentrations. ns represents data groups not significantly different when compared with positive control.

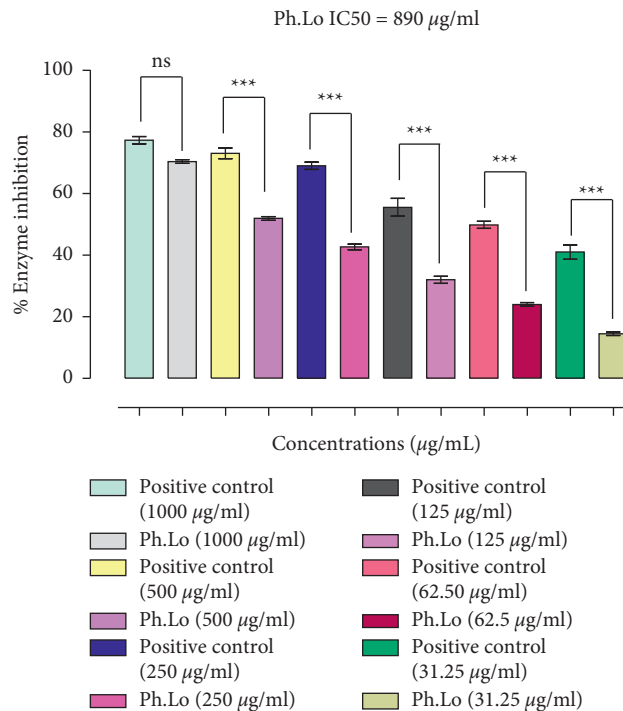
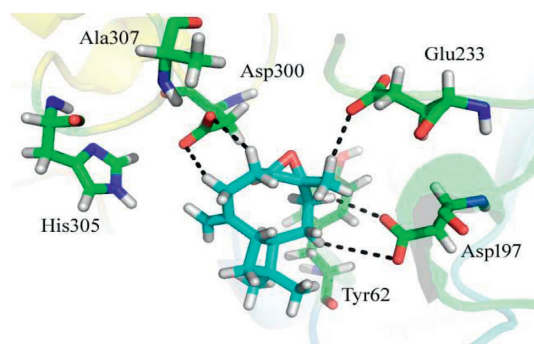


FIGURE 3: Results of  $\alpha$ -amylase inhibition study. Data bars represent results from three independent experimental observations. Data are presented as means  $\pm$  SEM. Values are significantly different (\*\*\*)  $p < 0.001$ ) when compared with positive control at the same tested concentrations. ns represents data groups not significantly different when compared with positive control.

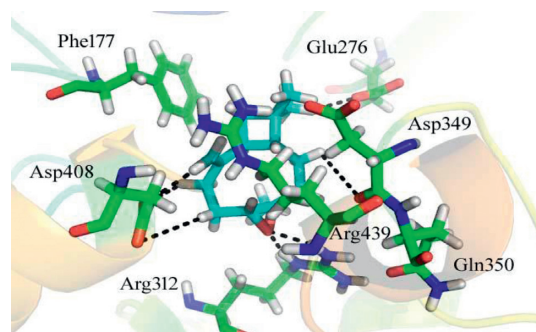
FIGURE 4: Docking conformation of  $\beta$ -caryophyllene epoxide with  $\alpha$ -amylase.TABLE-1: Results of the docking studies against  $\alpha$ -amylase.

Compounds	Ligand	Receptor	Interaction	Distance	E (kcal/mol)	Docking scores
4-Thujanol	O 28	O TYR 62 (A)	Hydrogen-donor	2.98	-1.3	-7.1947
	O 28	NE2 HIS 101 (A)	Hydrogen-acceptor	3.01	-1.5	
Alpha-bulnesene	C 3	OD1 ASP 197 (A)	Hydrogen-donor	3.93	-0.1	-7.3019
	C 14	OE1 GLU 233 (A)	Hydrogen-donor	3.63	-0.1	
Alpha-muurolene	C 33	OD1 ASP 300 (A)	Hydrogen-donor	3.79	-0.1	-6.7334
	C 32	5-ring HIS 101 (A)	Hydrogen-pi	4.77	-0.4	
Beta-elemene	C 36	5-ring HIS 299 (A)	Hydrogen-pi	4.59	-0.3	-6.0798
	C 24	OD2 ASP 300 (A)	Hydrogen-donor	3.91	-0.1	
Beta-ocimene	C 24	5-ring HIS 305 (A)	Hydrogen-pi	4.74	-0.1	-6.5892
	C 11	O TYR 62 (A)	Hydrogen-donor	3.75	-0.1	
Bornyl acetate	C 11	5-ring HIS 101 (A)	Hydrogen-pi	4.03	-0.1	-8.0205
	C 19	5-ring TRP 59 (A)	Hydrogen-pi	4.66	-0.3	
Campherenone	C 6	O TYR 62 (A)	Hydrogen-donor	3.61	-0.1	-5.9272
	C 6	OD2 ASP 197 (A)	Hydrogen-donor	3.3	-0.1	
Caprylic acid	C 25	OD1 ASP 300 (A)	Hydrogen-donor	3.75	-0.1	-7.5270
	C 25	OD2 ASP 300 (A)	Hydrogen-donor	4.12	-0.1	
Fenchol	O 35	NE2 HIS 299 (A)	Hydrogen-acceptor	2.96	-1.1	-6.4744
	C 1	5-ring HIS 101 (A)	Hydrogen-pi	4.52	-0.2	
Fixol	C 16	6-ring TYR 62 (A)	Hydrogen-pi	4.75	-0.1	-6.3792
	C 1	OD1 ASP 197 (A)	Hydrogen-donor	3.86	-0.1	
Isocaryophyllene	O 23	CZ3 TRP 58 (A)	Hydrogen-acceptor	3.69	-0.1	-7.2755
	O 23	NE2 HIS 299 (A)	Hydrogen-acceptor	3.3	-1.9	
Limonene	C 16	6-ring TRP 58 (A)	Hydrogen-pi	4.87	-0.2	-6.7494
	O 1	OD1 ASP 197 (A)	Hydrogen-donor	3.04	-4.5	
Myrcene	O 1	OD2 ASP 197 (A)	Hydrogen-donor	2.95	-1.1	-6.1922
	C 16	OD2 ASP 300 (A)	Hydrogen-donor	3.51	-0.1	
Myrcene	C 19	OD1 ASP 300 (A)	Hydrogen-donor	3.85	-0.1	-6.3792
	C 21	OD1 ASP 197 (A)	Hydrogen-donor	3.71	-0.1	
Myrcene	C 25	OD2 ASP 300 (A)	Hydrogen-donor	3.7	-0.1	-6.3792
	O 29	CZ3 TRP 58 (A)	Hydrogen-acceptor	3.42	-0.1	
Myrcene	C 23	OD1 ASP 197 (A)	Hydrogen-donor	3.66	-0.1	-6.3792
	O 1	NE2 GLN 63 (A)	Hydrogen-acceptor	3.08	-0.4	
Myrcene	O 1	5-ring TRP 59 (A)	Hydrogen-pi	3.62	-0.1	-6.3792
	C 13	OD1 ASP 300 (A)	Hydrogen-donor	3.74	-0.1	
Myrcene	C 13	OD2 ASP 300 (A)	Hydrogen-donor	3.48	-0.1	-6.3792
	C 18	OD2 ASP 300 (A)	Hydrogen-donor	3.5	-0.1	
Myrcene	C 29	OE1 GLU 233 (A)	Hydrogen-donor	3.34	-0.1	-6.3792
	C 5	6-ring TYR 62 (A)	Hydrogen-pi	4.63	-0.4	
Myrcene	C 15	5-ring HIS 299 (A)	Hydrogen-pi	4.56	-0.3	-6.3792
	C 1	OE1 GLU 233 (A)	Hydrogen-donor	3.46	-0.1	
Myrcene	C 1	OD2 ASP 300 (A)	Hydrogen-donor	3.85	-0.1	-6.3792



TABLE : Continued.

Compounds	Ligand	Receptor	Interaction	Distance	E (kcal/mol)	Docking scores
Nerolidol	C 17	OD2 ASP 300 (A)	Hydrogen-donor	3.68	-0.1	-7.0590
	C 20	OD2 ASP 300 (A)	Hydrogen-donor	3.82	-0.1	
	C 27	OD1 ASP 197 (A)	Hydrogen-donor	3.47	-0.1	
Octylcyclopropane	C 20	5-ring HIS 299 (A)	Hydrogen-pi	4.64	-0.2	-6.9528
	C 15	OD2 ASP 197 (A)	Hydrogen-donor	4.11	-0.1	
	C 24	OE1 GLU 233 (A)	Hydrogen-donor	3.93	-0.1	
Sativene	C 3	O TYR 62 (A)	Hydrogen-donor	3.57	-0.1	-6.9528
	C 6	O TYR 62 (A)	Hydrogen-donor	3.45	-0.1	
	C 9	OD2 ASP 300 (A)	Hydrogen-donor	3.65	-0.1	
$\beta$ -Caryophyllene epoxide	C 12	OD1 ASP 197 (A)	Hydrogen-donor	3.57	-0.1	-8.3050
	C 21	OD1 ASP 197 (A)	Hydrogen-donor	3.67	-0.1	
	C 21	OE1 GLU 233 (A)	Hydrogen-donor	3.61	-0.1	
	C 38	OD1 ASP 300 (A)	Hydrogen-donor	3.88	-0.1	
	C 9	OD1 ASP 197 (A)	Hydrogen-donor	3.76	-0.1	
Terpineol	C 12	O TYR 62 (A)	Hydrogen-donor	3.6	-0.1	-7.4857
	C 20	OE1 GLU 233 (A)	Hydrogen-donor	4.15	-0.1	
	C 24	OD1 ASP 197 (A)	Hydrogen-donor	3.58	-0.1	
	O 28	NH2 ARG 195 (A)	Hydrogen-acceptor	3	-0.4	
	O 28	NE2 HIS 299 (A)	Hydrogen-acceptor	3.17	-1.9	
	O 28	6-ring TYR 62 (A)	Hydrogen-pi	3.87	-0.1	

FIGURE 5: Docking conformation of  $\beta$ -caryophyllene epoxide in the active site of  $\alpha$ -glucosidase.TABLE 2: Results of the docking study against  $\alpha$ -glucosidase.

Compounds	Ligand	Receptor	Interaction	Distance	E (kcal/mol)	Docking scores
4-Thujanol	C 1	OD2 ASP 68	Hydrogen-donor	3.26	-0.1	-8.0694
	C 1	OD2 ASP 349	Hydrogen-donor	3.76	-0.2	
	C 18	OD1 ASP 214	Hydrogen-donor	3.48	-0.1	
	O 28	OD2 ASP 68	Hydrogen-donor	2.91	-1.8	
	O 28	NH1 ARG 439	Hydrogen-acceptor	3.06	-3.4	
	C 1	O ASP 349	Hydrogen-donor	3.67	-0.1	
Alpha-bulnesene	C 17	O ASP 349	Hydrogen-donor	3.57	-0.1	-7.6718
	C 21	OE1 GLU 276	Hydrogen-donor	3.84	-0.1	
	C 21	OE2 GLU 276	Hydrogen-donor	3.5	-0.1	
	C 25	OD2 ASP 408	Hydrogen-donor	3.76	-0.1	
	C 3	6-ring PHE 300	Hydrogen-pi	4.61	-0.1	
Alpha-muurolene	C 30	6-ring PHE 177	Hydrogen-pi	4.23	-0.1	-7.5763
	C 22	OD2 ASP 349	Hydrogen-donor	4.14	-0.1	
	C 28	OE1 GLU 276	Hydrogen-donor	3.56	-0.1	
	C 28	OE2 GLU 276	Hydrogen-donor	3.62	-0.1	
	C 32	OD1 ASN 347	Hydrogen-donor	3.79	-0.1	
	C 14	6-ring PHE 300	Hydrogen-pi	4.55	-0.1	
	C 32	6-ring PHE 300	Hydrogen-pi	4.04	-0.3	



TABLE 2: Continued.

Compounds	Ligand	Receptor	Interaction	Distance	E (kcal/mol)	Docking scores
Beta-elemene	C 21	OE1 GLN 350	Hydrogen-donor	3.57	-0.1	
	C 33	OE2 GLU 276	Hydrogen-donor	3.38	-0.1	
	C 36	OD2 ASP 349	Hydrogen-donor	3.81	-0.1	-7.7074
	C 33	5-ring HIS 348	Hydrogen-pi	4.26	-0.1	
	C 7	OD2 ASP 408	Hydrogen-donor	3.76	-0.1	
Beta-ocimene	C 13	O ASP 349	Hydrogen-donor	3.94	-0.1	
	C 19	OE1 GLN 350	Hydrogen-donor	3.86	-0.1	
	C 23	OD1 ASN 347	Hydrogen-donor	3.55	-0.1	-7.1334
	C 23	O ASP 349	Hydrogen-donor	3.41	-0.1	
	C 19	6-ring PHE 300	Hydrogen-pi	3.53	-0.3	
Bornyl acetate	C 23	6-ring PHE 300	Hydrogen-pi	4.55	-0.1	
	C 1	6-ring PHE 177	Hydrogen-pi	4.06	-0.7	-7.2826
Campherenone	O 23	NH1 ARG 439	Hydrogen-acceptor	2.95	-1	-6.5621
	O 1	O ASP 349	Hydrogen-donor	2.97	-1.8	
Caprylic acid	C 19	OD2 ASP 349	Hydrogen-donor	3.48	-0.1	
	O 26	NE ARG 312	Hydrogen-acceptor	3.02	-0.2	-8.0814
	O 26	CE1 TYR 313	Hydrogen-acceptor	3.37	-0.1	
Fenchol	C 6	OD2 ASP 408	Hydrogen-donor	3.67	-0.1	
	O 29	O ASP 349	Hydrogen-donor	2.99	-1.3	
	C 21	6-ring PHE 300	Hydrogen-pi	4.5	-0.1	-7.3643
	C 25	6-ring PHE 300	Hydrogen-pi	4.31	-0.4	
	O 1	OD2 ASP 68	Hydrogen-donor	2.94	-2.3	
Fixol	C 4	OD1 ASP 214	Hydrogen-donor	3.87	-0.1	
	C 8	OD2 ASP 349	Hydrogen-donor	3.58	-0.1	
	C 21	OD2 ASP 408	Hydrogen-donor	3.98	-0.1	-7.6468
	O 1	NH1 ARG 439	Hydrogen-acceptor	3.11	-3.2	
	C 12	6-ring PHE 177	Hydrogen-pi	3.98	-0.2	
Isocaryophyllene	C 1	OD2 ASP 349	Hydrogen-donor	3.75	-0.1	
	C 4	O ASP 349	Hydrogen-donor	3.41	-0.1	
	C 25	OD2 ASP 349	Hydrogen-donor	3.83	-0.1	-7.0742
	C 33	OD1 ASP 214	Hydrogen-donor	4.11	-0.1	
	C 33	OE1 GLU 276	Hydrogen-donor	3.3	-0.1	
Limonene	C 25	5-ring HIS 348	Hydrogen-pi	4.65	-0.1	
	C 2	OE1 GLN 350	Hydrogen-donor	3.96	-0.1	
	C 5	O ASP 349	Hydrogen-donor	3.51	-0.1	
	C 15	O VAL 303	Hydrogen-donor	3.82	-0.1	-7.1971
	C 15	OE1 GLN 350	Hydrogen-donor	3.77	-0.1	
Myrcene	C 24	OD2 ASP 408	Hydrogen-donor	3.75	-0.1	
	C 23	O VAL 303	Hydrogen-donor	3.35	-0.1	
	C 23	OE1 GLN 350	Hydrogen-donor	3.4	-0.1	-7.8979
	C 2	OE1 GLN 350	Hydrogen-donor	3.7	-0.1	
	C 6	O ASP 349	Hydrogen-donor	3.53	-0.1	
Nerolidol	C 33	OD2 ASP 68	Hydrogen-donor	3.31	-0.1	
	C 37	OD2 ASP 68	Hydrogen-donor	3.8	-0.1	
	C 37	OD2 ASP 349	Hydrogen-donor	3.59	-0.1	-8.2988
	C 24	6-ring PHE 177	Hydrogen-pi	4.78	-0.2	
	C 30	6-ring PHE 177	Hydrogen-pi	4	-0.8	
Octylcyclopropane	C 33	6-ring PHE 177	Hydrogen-pi	4.57	-0.3	
	O 41	6-ring PHE 300	Hydrogen-pi	3.96	-0.1	
	C 9	OD1 ASP 214	Hydrogen-donor	3.69	-0.1	
	C 12	OE2 GLU 276	Hydrogen-donor	4.17	-0.1	
	C 15	OD2 ASP 349	Hydrogen-donor	3.51	-0.1	
Sativene	C 21	O ASP 349	Hydrogen-donor	3.96	-0.1	-7.5104
	C 27	O ASP 349	Hydrogen-donor	4.04	-0.1	
	C 30	OE1 GLN 350	Hydrogen-donor	3.72	-0.1	
	C 27	6-ring PHE 300	Hydrogen-pi	3.88	-0.1	
Sativene	C 3	OE1 GLN 350	Hydrogen-donor	3.81	-0.1	
	C 35	OD1 ASP 214	Hydrogen-donor	3.78	-0.1	-7.6121

TABLE 2: Continued.

Compounds	Ligand	Receptor	Interaction	Distance	E (kcal/mol)	Docking scores
β-Caryophyllene epoxide	C 9	OD2 ASP 408	Hydrogen-donor	3.75	-0.1	-8.3182
	C 12	O ASP 349	Hydrogen-donor	3.52	-0.1	
	C 16	OD2 ASP 408	Hydrogen-donor	3.66	-0.1	
	C 30	OE1 GLU 276	Hydrogen-donor	3.6	-0.1	
	C 38	OD2 ASP 408	Hydrogen-donor	3.66	-0.1	
	O 25	NE ARG 312	Hydrogen-acceptor	2.83	-3.7	
	O 25	NH2 ARG 312	Hydrogen-acceptor	2.98	-2.8	
	C 27	6-ring PHE 177	Hydrogen-pi	3.97	-0.2	
	C 7	OD1 ASP 214	Hydrogen-donor	3.91	-0.1	
	C 20	OD1 ASP 214	Hydrogen-donor	3.68	-0.1	
Terpineol	C 24	OE1 GLN 181	Hydrogen-donor	4.12	-0.1	-7.8178
	O 28	OD2 ASP 68	Hydrogen-donor	2.93	-2.2	
	O 28	NH1 ARG 439	Hydrogen-acceptor	3.35	-1.6	
	C 4	6-ring PHE 177	Hydrogen-pi	4.62	-0.5	
	C 24	6-ring PHE 177	Hydrogen-pi	3.49	-0.1	

3.2.4. *Docking with α-Glucosidase Enzyme.* Our simulation studies revealed that the selected phytochemicals preferentially bind with the α-glucosidase receptor active sites. Considerable docking conformations were observed for β-caryophyllene epoxide with a docking score of -8.3182 which indicates that the compound established seven hydrogen bonds and one H-pi interaction with the residues of active sites (Glu 276, Phe 177, Arg 312, Asp349, Arg 439, Gln 350, and Asp 408) (Figure 5).

A considerably high inhibitory potential of the identified metabolite might be attributed to the existence of the two methyl moieties and oxygen atom attached to the (S)-2-methyloxirane moiety of the ligand (Table 2).

## 4. Conclusions

In summary, findings of this study showed that Ph.Lo is rich in bioactive phytochemicals which might contribute to the antidiabetic and health-promoting potentials of the oils. The test samples exhibited concentration-dependent inhibition of the vital enzymes implicated in the gastrointestinal absorption of postprandial glucose and thus might help in reducing the hyperglycemia in type-2 diabetes. The binding mode and energies of the identified phytochemicals against the target enzymes using the molecular docking approach further supported our claim regarding the antidiabetic potential of our test samples. Nevertheless, we suggest that, in future, in vivo studies be performed for the therapeutic and beneficial effects of these compounds in metabolism-associated disorders.

## Data Availability

The experimental data used to support the findings of this study are available from the corresponding author upon request.

## Conflicts of Interest

The authors declare no conflicts of interest.

## Authors' Contributions

All authors contributed equally towards the project design, experimental work, and manuscript writeup. All authors read and approved the manuscript for publication.

## Acknowledgments

The authors would like to acknowledge the support of the Deputy for Research and Innovation, Ministry of Education, Kingdom of Saudi Arabia, for this research through a grant (NU-IF/INT/01/006) under the Institutional Funding Committee at Najran University, Kingdom of Saudi Arabia.

## Supplementary Materials

Supplementary file S1: data related to identified compounds re provided as File S1 and Table S1 containing the list of identified compounds and their details. (*Supplementary Materials*)

## References




- [1] M. Ovais, M. Ayaz, A. T. Khalil et al., "HPLC-DAD finger printing, antioxidant, cholinesterase, and α-glucosidase inhibitory potentials of a novel plant *Oxalis nana*," *BMC Complementary and Alternative Medicine*, vol. 18, no. 1, pp. 1–13, 2018.
- [2] M. H. Mahnashi, Y. S. Alqahtani, A. O. Alqarni et al., "Crude extract and isolated bioactive compounds from *Notolirion thomsonianum* (Royale) Stapf as multitargets antidiabetic agents: in-vitro and molecular docking approaches," *BMC Complementary Medicine and Therapies*, vol. 21, no. 1, pp. 270–313, 2021.
- [3] R. Arky, *Clinical Correlates of Metabolic Derangements of Diabetes Mellitus*, pp. 16–20, Complications of Diabetes Mellitus WB Saunders, Philadelphia, PA, USA, 1982.
- [4] G. Booth, L. Lipscombe, S. Butalia et al., "Pharmacologic management of type 2 diabetes: 2016 interim update," *Canadian Journal of Diabetes*, vol. 40, no. 6, pp. 484–486, 2016.
- [5] F. Ahmed and A. Urooj, "Antihyperglycemic activity of *Ficus glomerata* stem bark in streptozotocin-induced diabetic rats," *Global Journal of Pharmacology*, vol. 2, no. 3, pp. 41–45, 2008.

- [6] A. T. Kharroubi and H. M. Darwish, "Diabetes mellitus: the epidemic of the century," *World Journal of Diabetes*, vol. 6, no. 6, p. 850, 2015.
- [7] H. Løe, "Periodontal disease. The sixth complication of diabetes mellitus," *Diabetes Care*, vol. 16, no. 1, pp. 329–334, 1993.
- [8] A. Kumar, R. Ilavarasan, T. Jayach et al., "Anti-diabetic activity of *Syzygium cumini* and its isolated compound against streptozotocin-induced diabetic rats," *Journal of Medicinal Plants Research*, vol. 2, no. 9, pp. 246–249, 2013.
- [9] D. R. Whiting, L. Guariguata, C. Weil, and J. Shaw, "IDF diabetes atlas: global estimates of the prevalence of diabetes for 2011 and 2030," *Diabetes Research and Clinical Practice*, vol. 94, no. 3, pp. 311–321, 2011.
- [10] N. H. Cho, J. E. Shaw, S. Karuranga et al., "IDF Diabetes Atlas: global estimates of diabetes prevalence for 2017 and projections for 2045," *Diabetes Research and Clinical Practice*, vol. 138, pp. 271–281, 2018.
- [11] H. Gin and V. Rigalleau, "Post-prandial hyperglycemia. post-prandial hyperglycemia and diabetes," *Diabetes & Metabolism*, vol. 26, no. 4, pp. 265–272, 2000.
- [12] S. S. Nair, V. Kavrekar, and A. Mishra, "In vitro studies on alpha amylase and alpha glucosidase inhibitory activities of selected plant extracts," *European Journal of Experimental Biology*, vol. 3, no. 1, pp. 128–132, 2013.
- [13] M. Ayaz, F. Ullah, A. Sadiq, M. O. Kim, and T. Ali, "Editorial: natural products-based drugs: potential therapeutics against alzheimer's disease and other neurological disorders," *Frontiers in Pharmacology*, vol. 10, p. 1417, 2019.
- [14] I. Ullah, F. Subhan, J. Alam, M. Shahid, and M. Ayaz, "Suppression of cisplatin-induced vomiting by cannabis sativa in pigeons: neurochemical evidences," *Frontiers in Pharmacology*, vol. 9, p. 231, 2018.
- [15] U. Saleem, R. Akhtar, F. Anwar et al., "Neuroprotective potential of *Malva neglecta* is mediated via down-regulation of cholinesterase and modulation of oxidative stress markers," *Metabolic Brain Disease*, vol. 36, no. 5, pp. 1–12, 2021.
- [16] B. Petrovska, "Historical review of medicinal plants' usage," *Pharmacognosy Reviews*, vol. 6, no. 11, p. 1, 2012.
- [17] A. T. Khalil, M. Ovais, J. Iqbal et al., "Microbes-mediated synthesis strategies of metal nanoparticles and their potential role in cancer therapeutics," in *Seminars in Cancer Biology* Elsevier, Amsterdam, Netherlands, 2021.
- [18] U. Saleem, S. Khalid, S. Zaib et al., "Phytochemical analysis and wound healing studies on ethnomedicinally important plant *Malva neglecta* Wallr.," *Journal of Ethnopharmacology*, vol. 249, Article ID 112401, 2020.
- [19] C. J. Bailey and C. Day, "Traditional plant medicines as treatments for diabetes," *Diabetes Care*, vol. 12, no. 8, pp. 553–564, 1989.
- [20] A. Choudhury, K. Maeda, R. Murayama, and E. DiMagno, "Character of a wheat amylase inhibitor preparation and effects on fasting human pancreaticobiliary secretions and hormones," *Gastroenterology*, vol. 111, no. 5, pp. 1313–1320, 1996.
- [21] V. Kumar, O. Prakash, S. Kumar, and S. Narwal, " $\alpha$ -glucosidase inhibitors from plants: a natural approach to treat diabetes," *Pharmacognosy Reviews*, vol. 5, no. 9, p. 19, 2011.
- [22] A. M. Dirir, M. Daou, A. F. Yousef, and L. F. Yousef, "A review of alpha-glucosidase inhibitors from plants as potential candidates for the treatment of type-2 diabetes," *Phytochemistry Reviews*, 2021.
- [23] M. Ayaz, M. Junaid, F. Subhan et al., "Heavy metals analysis, phytochemical, phytotoxic and anthelmintic investigations of crude methanolic extract, subsequent fractions and crude saponins from *Polygonum hydropiper* L.," *BMC Complementary and Alternative Medicine*, vol. 14, no. 1, p. 465, 2014.
- [24] M. Ayaz, I. Ahmad, A. Sadiq et al., "*Persicaria hydropiper* (L.) Delarbre: a review on traditional uses, bioactive chemical constituents and pharmacological and toxicological activities," *Journal of Ethnopharmacology*, vol. 251, Article ID 112516, 2020.
- [25] X. Tong, X. Li, M. Ayaz et al., "Neuroprotective studies on *Polygonum hydropiper* L. essential oils using transgenic animal models," *Frontiers in Pharmacology*, vol. 11, Article ID 580069, 2021.
- [26] M. Ayaz, M. Junaid, F. Ullah et al., "Anti-alzheimer's studies on  $\beta$ -sitosterol isolated from *Polygonum hydropiper* L.," *Frontiers in Pharmacology*, vol. 8, p. 697, 2017.
- [27] M. Ayaz, A. Sadiq, A. Wadood, M. Junaid, F. Ullah, and N. Zaman Khan, "Cytotoxicity and molecular docking studies on phytosterols isolated from *Polygonum hydropiper* L.," *Steroids*, vol. 141, pp. 30–35, 2019.
- [28] M. H. Mahnashi, Y. S. Alqahtani, B. A. Alyami et al., "Cytotoxicity, anti-angiogenic, anti-tumor and molecular docking studies on phytochemicals isolated from *Polygonum hydropiper* L.," *BMC Complementary Medicine and Therapies*, vol. 21, no. 1, pp. 1–14, 2021.
- [29] M. Ayaz, M. Junaid, F. Ullah et al., "Chemical profiling, antimicrobial and insecticidal evaluations of *Polygonum hydropiper* L.," *BMC Complementary and Alternative Medicine*, vol. 16, no. 1, pp. 502–514, 2016.
- [30] M. Ayaz, M. Junaid, F. Ullah et al., "GC-MS analysis and gastroprotective evaluations of crude extracts, isolated saponins, and essential oil from *Polygonum hydropiper* L.," *Frontiers of Chemistry*, vol. 5, p. 58, 2017.
- [31] M. Ayaz, M. Junaid, F. Ullah et al., "Molecularly characterized solvent extracts and saponins from *Polygonum hydropiper* L. show high anti-angiogenic, anti-tumor, brine shrimp, and fibroblast NIH/3T3 cell line cytotoxicity," *Frontiers in Pharmacology*, vol. 7, p. 74, 2016.
- [32] M. Ayaz, M. Junaid, F. Ullah et al., "Comparative chemical profiling, cholinesterase inhibitions and anti-radicals properties of essential oils from *Polygonum hydropiper* L: a preliminary anti-alzheimer's study," *Lipids in Health and Disease*, vol. 14, no. 1, pp. 1–12, 2015.
- [33] S. Stein, D. Mirokhin, D. Tchekhovskoi et al., *The NIST Mass Spectral Search Program for the NIST/EPA/NIH Mass Spectra Library*, Standard Reference Data Program of the National Institute of Standards and Technology Gaithersburg, Gaithersburg, MD, USA, 2002.
- [34] Adams RP, *Identification of Essential Oil Components by Gas Chromatography/Mass Spectrometry*, Vol. 456, Allured Publishing Corporation, , Carol Stream, IL, USA, 2007.
- [35] P. McCue, Y.-I. Kwon, and K. Shetty, "Anti-amylase, anti-glucosidase and anti-angiotensin I-converting enzyme potential of selected foods," *Journal of Food Biochemistry*, vol. 29, no. 3, pp. 278–294, 2005.
- [36] M. Ghufuran, A. U. Rehman, M. Shah, M. Ayaz, H. L. Ng, and A. Wadood, "In-silico design of peptide inhibitors of K-Ras target in cancer disease," *Journal of Biomolecular Structure and Dynamics*, vol. 38, no. 18, pp. 5488–5499, 2020.
- [37] M. Ayaz, A. Wadood, A. Sadiq, F. Ullah, O. Anichkina, and M. Ghufuran, "In-silico evaluations of the isolated phytosterols from *Polygonum hydropiper* L against BACE1 and MAO drug targets," *Journal of Biomolecular Structure and Dynamics*, pp. 1–9, 2021.

- [38] M. Liu, W. Zhang, J. Wei, and X. Lin, "Synthesis and  $\alpha$ -glucosidase inhibitory mechanisms of bis(2,3-dibromo-4,5-dihydroxybenzyl) ether, a potential marine bromophenol  $\alpha$ -glucosidase inhibitor," *Marine Drugs*, vol. 9, no. 9, pp. 1554–1565, 2011.
- [39] F. Jabeen, P. V. Oliferenko, A. A. Oliferenko et al., "Dual inhibition of the  $\alpha$ -glucosidase and butyrylcholinesterase studied by molecular field topology analysis," *European Journal of Medicinal Chemistry*, vol. 80, pp. 228–242, 2014.
- [40] F. Hichri, A. Omri, A. S. M. Hossan, and H. Ben Jannet, "Alpha-glucosidase and amylase inhibitory effects of *Eruca vesicaria* subsp. *longirostris* essential oils: synthesis of new 1,2,4-triazole-thiol derivatives and 1,3,4-thiadiazole with potential inhibitory activity," *Pharmaceutical Biology*, vol. 57, no. 1, pp. 564–570, 2019.
- [41] G. Oboh, I. A. Akinbola, A. O. Ademosun et al., "Essential oil from clove bud (*Eugenia aromatica* Kuntze) inhibit key enzymes relevant to the management of type-2 diabetes and some pro-oxidant induced lipid peroxidation in rats pancreas in vitro," *Journal of Oleo Science*, vol. 64, no. 7, pp. 775–782, 2015.
- [42] N. Rahali, S. Mehdi, F. Younsi, M. Boussaid, and C. Messaoud, "Antioxidant,  $\alpha$ -amylase, and acetylcholinesterase inhibitory activities of *Hertia cheirifolia* essential oils: influence of plant organs and seasonal variation," *International Journal of Food Properties*, vol. 20, no. 2, pp. 1637–1651, 2017.
- [43] K. Majouli, M. Besbes Hlila, A. Hamdi, G. Flamini, H. Ben Jannet, and A. Kenani, "Antioxidant activity and  $\alpha$ -glucosidase inhibition by essential oils from *Hertia cheirifolia* (L.)," *Industrial Crops and Products*, vol. 82, pp. 23–28, 2016.
- [44] N. Jaradat, N. Al-Maharik, S. Abdallah, R. Shawahna, A. Mousa, and A. Qtishat, "Nepeta curviflora essential oil: phytochemical composition, antioxidant, anti-proliferative and anti-migratory efficacy against cervical cancer cells, and  $\alpha$ -glucosidase,  $\alpha$ -amylase and porcine pancreatic lipase inhibitory activities," *Industrial Crops and Products*, vol. 158, Article ID 112946, 2020.

## Review Article

# *Allium cepa*: A Treasure of Bioactive Phytochemicals with Prospective Health Benefits

Arka Jyoti Chakraborty,<sup>1</sup> Tanvir Mahtab Uddin,<sup>1</sup> B. M. Redwan Matin Zidan,<sup>1</sup> Saikat Mitra,<sup>1</sup> Rajib Das,<sup>1</sup> Firzan Nainu,<sup>2</sup> Kuldeep Dhama,<sup>3</sup> Arpita Roy ,<sup>4</sup> Md. Jamal Hossain ,<sup>5</sup> Ameer Khusro,<sup>6</sup> and Talha Bin Emran <sup>7</sup>

<sup>1</sup>Department of Pharmacy, Faculty of Pharmacy, University of Dhaka, Dhaka 1000, Bangladesh

<sup>2</sup>Faculty of Pharmacy, Hasanuddin University, Tamalanrea, Kota Makassar, Sulawesi Selatan 90245, Indonesia

<sup>3</sup>Division of Pathology, ICAR-Indian Veterinary Research Institute, Izatnagar, Bareilly 243122, Uttar Pradesh, India

<sup>4</sup>Department of Biotechnology, School of Engineering & Technology, Sharda University, Greater Noida 201310, India

<sup>5</sup>Department of Pharmacy, State University of Bangladesh, 77 Satmasjid Road, Dhanmondi, Dhaka 1205, Bangladesh

<sup>6</sup>Research Department of Plant Biology and Biotechnology, Loyola College, Chennai 34, Tamil Nadu, India

<sup>7</sup>Department of Pharmacy, BGC Trust University Bangladesh, Chittagong 4381, Bangladesh

Correspondence should be addressed to Arpita Roy; [arbt2014@gmail.com](mailto:arbt2014@gmail.com) and Talha Bin Emran; [talhabmb@gmail.com](mailto:talhabmb@gmail.com)

Received 19 December 2021; Revised 28 December 2021; Accepted 31 December 2021; Published 18 January 2022

Academic Editor: Ruchika Garg

Copyright © 2022 Arka Jyoti Chakraborty et al. This is an open access article distributed under the Creative Commons Attribution License, which permits unrestricted use, distribution, and reproduction in any medium, provided the original work is properly cited.

As *Allium cepa* is one of the most important condiment plants grown and consumed all over the world, various therapeutic and pharmacological effects of *A. cepa* were reviewed. Onion (*Allium cepa*) is a high dietary fiber-rich perennial herb that is placed under the family Amaryllidaceae. It contains high concentration of folic acid, vitamin B6, magnesium, calcium, potassium, and phosphorus as well as vitamins and minerals. It is widely used as an antimicrobial agent, but it showed anticancer, antidiabetic, antioxidant, antiplatelet, antihypertensive, and antidepressant effects and neuroprotective, anti-inflammatory, and antiparasitic effects and so on. It is said to have beneficial effects on the digestive, circulatory, and respiratory systems, as well as on the immune system. This review article was devoted to discussing many health benefits and traditional uses of onions in pharmacological perspectives, as well as the safety/toxicological profile. If more detailed research on this perennial herb is conducted, it will open the door to an infinite number of possibilities.

## 1. Introduction

*Allium cepa* (also known as onion) is a perennial herb with the stem in the underground bulb. Onions belong to the Liliaceae family, while some authors mention them as Alliaceae. Common onion has one or two leafless flower stalks reaching 75–180 cm (2.5–6 feet) in height. Most commercially cultivated onions are cultivated from the thin, dark seeds of the plant. Onion is highly regarded and stored as pickles for its flavor and nutritious values. Onions are thought to have originated in Afghanistan/Iran/USSR and are now produced in more than 175 countries [1]. Onion has a high dietary fiber and sugar content of about 90 percent

water. Onion has a high dietary fiber and sugar content of about 90 percent water. A diet rich in vegetables has been identified as providing a number of health benefits to preventing two of the more prevalent and relevant diseases nowadays [2]. Onions contain a number of vitamins (B2, C, and B1), selenium, and potassium. They can cure diabetes mellitus, CVDs, and stomach cancer. Onion peel reveals biological effective hypertrophic scar and keloid prevention. Studies demonstrate that onion extract is capable of removing hypertrophic wounds too [3]. Regular intake of onions lowers the risk of colorectal, lung, liver, brain, stomach, ovarian, prostate, and breast cancer [4]. The function of antiplatelets is significantly influenced by



genotype, climate, and vegetable storage period. *A. cepa* (onions) have antioxidant potential due to the presence of high amounts of organosulfur compounds, polyphenols, and flavonoids which are natural antioxidants. Garlic and onion extract effectively destroys all parasites and suppresses the irreversible reductase *Trypanosoma brucei* trypanothione. Studies demonstrated that onion shows an antidepressant effect too. *A. cepa* and its constituents, especially quercetin, are possible immunomodulatory therapeutic candidates for the treatment of immune dysregulation disorders. The anti-inflammatory and protective impact of *A. cepa* on tracheal tolerance and lung inflammation in asthmatic animals means that it may be used to treat airway disorders like asthma [5–9]. In the presence of liver-damaging or liver-harmful ethanol, *A. cepa* extracts were found to have hepatoprotective effects. Aqueous extract of *A. cepa* bulb has essential antioxidant and hepatoprotective function against ethanol-induced hepatotoxicity [10]. However, researchers found some toxicity reports on onion too. Researches show that OE has an antioxidant potential that protects it from oxidative harm. Onion toxicity induces hemolytic anemia in puppies, according to the researchers [11]. As a result, the goal of this study is to conduct a thorough analysis of the existing literature on *A. cepa*'s chemical and morphological features, pharmacological properties, and therapeutic actions, as well as clinical and preclinical research.

## 2. Morphological Characteristics of *Allium cepa*

*A. cepa* is placed under the family Amaryllidaceae. It is perennial herb with a stem in underground bulb. The root system is fibrous adventitious. The underground bulb, cylindrical and flesh, with sheathy leaf foundation with a parallel venation appears from a cluster of progressive leaves. Pedicels are of the same length, derived from the peduncle apex that equals all flowers. Flowers are ebracteolate, bracteate, and hypogynous, tiny, complete, blonde, trimorous, actinomorphic, and protandrous. There are 6 tepals, arranged, white in two whorls of three each, syntepalous showing aestivation of valvate. There are 6 stamens, arranged in two whorls of three each, apostamenous, epitepalous, and opposite to tepals. Introse, basifixed, anthers dithecous, and dehiscing longitudinally. The gynoecium is syncarpous and tricarpellary. Ovary trilocular, superior with two ovules in each locule on axile placentation. The style of gynoecium is simple with slender stigma. Fruit is loculicidal capsule. Its seed is endospermous. In Asia, about 660 allium species are found. But in Central America, Africa, and South America, some species are found. Onions are thought to have originated in Afghanistan/Iran/USSR and are now produced in more than 175 countries around the world. Onions belong to the Liliaceae family, while some authors mention them as Alliaceae. Onions are a perennial crop that can be red, white, or yellow and eaten raw, mature, pickled, or powder in its tender condition. The plants are normally white or purple with tiny flowers. Onion is highly regarded and stored as pickles for its flavor and nutritious values. Its leaves are also used in soups and salads [1]. The common onion has one or two leafless flower stalks reaching 75–180 cm (2.5–6 feet) in

height and ending in a sphere of flat, greenish, white flowers. The concentric leaf bases of the plant grow swell to form a food bulb in the underground. Most commercially cultivated onions are cultivated from the thin, dark seeds of the plant which are planted directly in the ground, but often from small bulbs or transplants. The onions can thrive under a variety of growing conditions and are very hardy. The bulbs differ in size, form, color, and pungency, while warmer temperatures are usually more mild and sweeter than other climates [12].

### 2.1. Specific Classification of *Allium cepa* [13]

- (1) Kingdom: Plantae
- (2) Division: Magnoliophyta
- (3) Class: Liliopsida
- (4) Order: Asparagales
- (5) Family: Alliaceae
- (6) Genus: *Allium*
- (7) Species: *A. cepa*
- (8) Edible parts: leaves, flowers, seed, root.

## 3. Chemical Characteristics of *Allium cepa*

Onion has a high dietary fiber and sugar content of about 90 percent water. The onion is low in sodium and has a high concentration of folic acid, vitamin B6, magnesium, calcium, potassium, and phosphorus as far as vitamins and minerals are concerned. Onion has a low lipid level, and only glutamic acid and arginine are exceptional in the amino acid content [1]. There have been many phytochemical analysis of *A. cepa*, and several compounds that are responsible for its unique aroma and medicinal properties have been discovered. Phenolic compounds have gained considerable interest from the various groups of phytochemicals as they are contributing to medicinal plants' biological properties. A research on four *A. cepa* variants (violet, red, green, and white) for their compliance with the high-performance liquid chromatography (HPLC) was performed [14]. Kaempferol, ferulic acid, quercetin, gallic acid, and protocatechuic acid were also identified. The number of phenolic compounds found in each variety varied significantly, e.g., gallic acid (9.3–354 lg/g), ferulic acid (13.5–116 lg/g), quercetin (14.5–5110 lg/g), protocatechuic acid (3.1–138 lg/g), and kaempferol (3.2–481 lg/g). In addition, a variety of flavonoids were discovered in various onion varieties: quercetin-40-monoglucoside [15], isorhamnetin 3,40-diglucoside, quercetin-3,40-diglucoside, quercetin aglycon, quercetin-3-monoglucoside, delphinidin 3,5-diglycosides, quercetin 3-glycosides [16], quercetin 7,40-diglucoside, quercetin 3,7,40-triglucoside, quercetin 3,40-diglucoside [17], and many others. When compared to apples (50 mg/kg), broccoli (100 mg/kg), and blueberries (40 mg/kg), *A. cepa* has 5 to 10 times higher quercetin content (300 mg/kg) [18]. Moreover, various experiments have found various onion anthocyanins: cyanidin 7-O-(300-O- $\beta$ -glucopyranosyl)-600-O-malonyl- $\beta$ -glucopyranoside)-40-O- $\beta$ -glucopyranoside,



cyanidin 3-O-(300-O- $\beta$ -glucopyranosyl-600-O-malonyl- $\beta$ -glucopyranoside)-40-O- $\beta$ -glucopyranoside, cyanidin 40-O- $\beta$ -glucoside, cyanidin 3,40-di-O- $\beta$ -glucopyranoside, peonidin 3-O-(600-O-malonyl- $\beta$ -glucopyranoside), and peonidin 3-O-(600-O-malonyl- $\beta$ -glucopyranoside)-5-O- $\beta$ -glucopyranoside were present in minute amounts from parts which are pigmented of red onion [17]. In addition, methanolic extracts of red onion yielded four anthocyanins with the same novel 4-substituted aglycone, carboxypyranocyanidin, 5-carboxypyranocyanidin 3-O- $\beta$ -glucopyranoside, and 5-carboxypyranocyanidin 3-O-(6''-O-malonyl- $\beta$ -glucopyranoside) were known as two of their structures [19]. Furthermore, Fredotovic et al. successfully established malvidin 3'-glucoside and peonidin 3'-glucoside petunidin 3'-glucoside acetate [20]. A study conducted by Vazquez-Armenta et al. demonstrated dipropyl trisulfide and dipropyl disulfide as onion oil main constituents [21]. S-alk(en)yl-L-cysteine sulfoxides (such as c-glutamylcysteine and alliin) is a class of biologically active organo-sulfuric compounds. As the plant materials are crushed, the aroma and the taste of fresh onions is caused by releases of méthiine, alliin, isoalliin, propin, and lipid-soluble sulfur compounds (for example, diallyl-disulfide and diallyl sulfide). It has been assumed that the annoying lachrymatic factor released from cut onion is created spontaneously following the effect of alliinase enzyme [22]. Another compound of thiopropanal S-oxide, the sulfide volatile, is a lachrymal element present exclusively in onions, which ultimately transforms it into methylpentanols [23]. In the red onion varieties, a thin-layer chromatography with dichloromethane extraction was also observed to have many disulfide radicals (methyl, allyl, and propyl) [24]. Quantitative analyzes have shown tri- and disulfides, for example, trans- and cis-methyl-1-propenyl disulfides, dipropyl disulfides, methyl-2-propenyl disulfides, trans- and cis-propenyl propyl disulfides, dipropyl trisulfides, and methyl propyl trisulfides, are approximately 60% sulfur compound in abundance. Additionally, Dhumal et al. detected some organic acids in the bulb extracts. They were citric, tartaric malic, oxalic, ascorbic, and succinic acids. Moreover, in the onion land races of Bianca di Pompei cv., grown in the area Campania, Liguori et al. have found several aldehydes and ketones (Italy) [25]. Of all tests, furfuraldehyde was the most frequent and strongest in Aprilatica. Different in landraces were samples of 2-methyl-2-pentenal material and propionaldehyde. The 1,2-cyclo concentration of pentanedione was greater than that yielded in winter during the spared months of Maggiaiola, Aprilatica, and Giugnese onions (Marzatica and Febbrare). Only onions harvested in spring (Maggiaiola, Aprilatica, and Giugnese) were included in the butyrolactone formula. Allicepin, an antifungal peptide, was isolated by ion exchange chromatography, aqueous extraction on DEAE-cellulose affinity chromatography on FPLC-gel filtration and Affi-gel blue gel on Superdex 75 [26]. Zwiebelane A (cis-2, 3-dimethyl-5, 6-dithiabicyclohexane 5-oxide), another compound isolated from bulbs, was found to improve the possible fungicidal efficacy of the traditional bactericidal antibiotic polymyxin B [27]. Zwiebelane A is the taste compound that is produced during frying. Tversky et al.

isolated two additional phytoalexins from the bulbs. They are 5-octyl-cyclopenta-1,3-dione and 5-hexyl-cyclopenta-1,3-dione [2].

#### 4. Bioactive Compounds

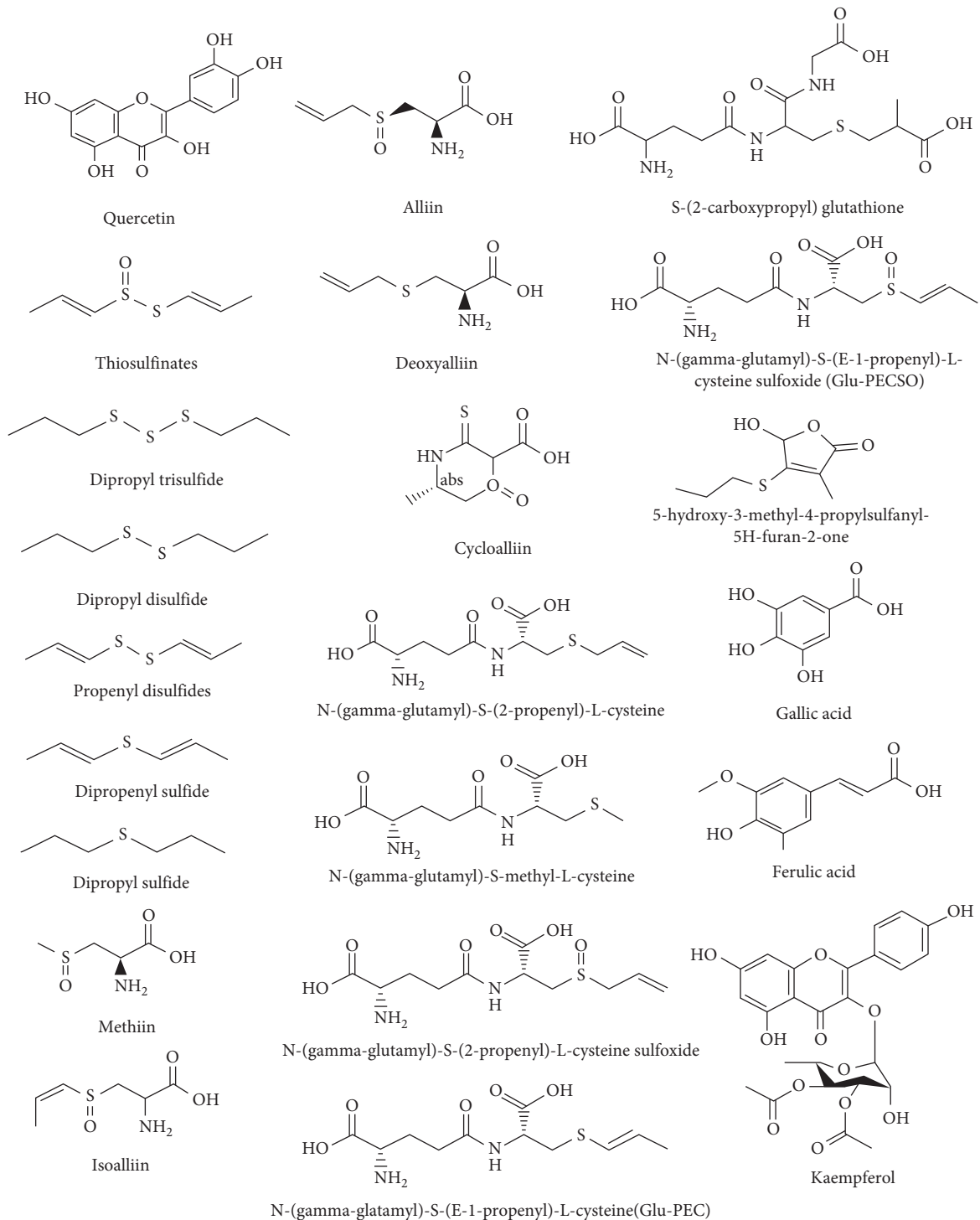
The pungence of onion is caused by the large number of sulfur compounds that make the back of mouth and throat feel burning. Analysis of pyruvic acid, produced in stoichiometric amounts by thiosulfins, is a handy tool for measuring onion pungency. The correlations of pyruvic acid with flavor perception have been observed. The balance of sweetness in an onion is determined by the pungency and sugar levels. Strong pungentness will disguise a high sugar level to avoid the onion being considered sweet. Low-pungent and low-sugar onions may also be considered as bland. Ideally, high sugars and low pungence will be a sweet onion [28]. Thiosulfinates, particularly in heat, are unstable and divided into a complex combination of compounds that dominate mono-, di-, tri- and tetrasulfides [29,30]. The main constituents of onion volatiles are dipropyl trisulfide, dipropyl disulfide, and propenyl disulfides, while several other compounds including dipropenyl sulfide and dipropyl sulfide have been known among them [31]. Recently Yamazaki et al. determined 11 sulfur-containing flavor precursors in onion including methiin, S-alk(en)yl-L-cysteine derivatives, isoalliin, alliin, deoxyalliin, cycloalliin, N-(gamma-glutamyl)-S-(2-propenyl)-L-cysteine, N-(gamma-glutamyl)-S-methyl-L-cysteine, N-(gamma-glutamyl)-S-(2-propenyl)-L-cysteine sulfoxide, N-(gamma-glutamyl)-S-(E-1-propenyl)-L-cysteine(Glu-PEC), S-(2-carboxypropyl) glutathione, and N-(gamma-glutamyl)-S-(E-1-propenyl)-L-cysteine sulfoxide (Glu-PECSO) [32]. Recent literature reports on the isolation of many interesting novel compounds from onion. Saponin and peptides, with their theoretically beneficial health insights, have been isolated and researched. Several distinct saponins in *Allium* species have been found, and processing has caused various saponins again [33,34]. 5-Hydroxy-3-methyl-4-propylsulfanyl-5H-furan-2-one and four other compounds were isolated and reported as in vitro inducers of quinone reductase and glutathione S-transferase [35]. Several research reported antitumor, antifungal, blood coagulability, cytotoxicity, cholesterol-lowering, and antispasmodic effects of saponins isolated from onion and garlic [33]. The seeds of *A. cepa* were isolated from four furostanol saponins, two of which were novel compounds, called cepeoside A and cepeoside B [36]. Corea et al. have also discovered new saponins that have indicated antispasmodic action in the isolated ileum of the guinea pig, an effect that may further justify the traditional use of ointment in the treatment of gastrointestinal disorder [34]. Gamma-glutamyl onion peptide has also been reported to inhibit the growth and function of in vitro osteoclasts [37,38]. The contents of dry matter bulbs represent an essential quality parameter of onion as they contribute directly to the energy required for drying, which is also important in an onion dehydration industry [39,40]. About 65 to 80% of the dry bulb is made of nonstructural carbohydrates. The main nonstructural carbohydrates in onions are glucose,

fructose, and sucrose, although low molecular fructans are absent. FOS are polyfructoses of different molecular sizes which form a major carbohydrate reserve of onions. Fructans are called fructooligosaccharides (FOS). Fructans accumulate during bulbing and catabolism when the bulbs are growing and sprouting [39]. FOS is commonly used only as a name for fructose oligomers that are primarily made of nystose (GF3), ketose (GF2), and fructofuranosyl nystose (GF4) and in which fructosyl units (F) are connected by  $\beta$ -linkage to sucrose position (GF + fructose). Ketoses (GF2) are clearly prevalent in every onion tissue and strongly polymerized fructans are not present. The most fruitful tissues are fleshy layers, such that the external two fleshy layers are the greatest byproduct of onion, a potential source of fructan [41,42]. The fructan degree of polymerization (DP) level in onion is mostly in between 3 and 15. Short chain fructans are theoretically used as natural sweeteners with less than 5 polymerization rates. Onion bulbs with strong DP fructans may be used for lipid substitution with consequential health benefits [40]. Onion shows a higher soluble/insoluble nutritional fiber ratio (SDF:IDF) than other vegetables linked to various physiologic and metabolic effects. SDF increases stomach viscosity causing nutrients to be reduced and absorbed, while IDF decreases intestinal transit and increases food mass for the majority of people [43]. Numerous in vitro, in vivo, and ex vivo trials confirmed the health properties of allium vegetables. In particular, the onions with anticarcinogenic, antioxidant, hypoglycemic, hypolipidemic, and antiaggregatory effects have been identified. From a dietary and medical point of view, it can be observed that the onions used in many dishes as a vegetable or a food ingredient is often very useful in their medicines. A diet rich in vegetables, including onion, has been identified as providing a number of health benefits to preventing two of the more prevalent and relevant diseases nowadays such as cancer insurgences and CVD [1]. The major bioactive compounds from *A. cepa* are shown in Figures 1(a) and 1(b).

## 5. Therapeutic Potential of *Allium cepa*

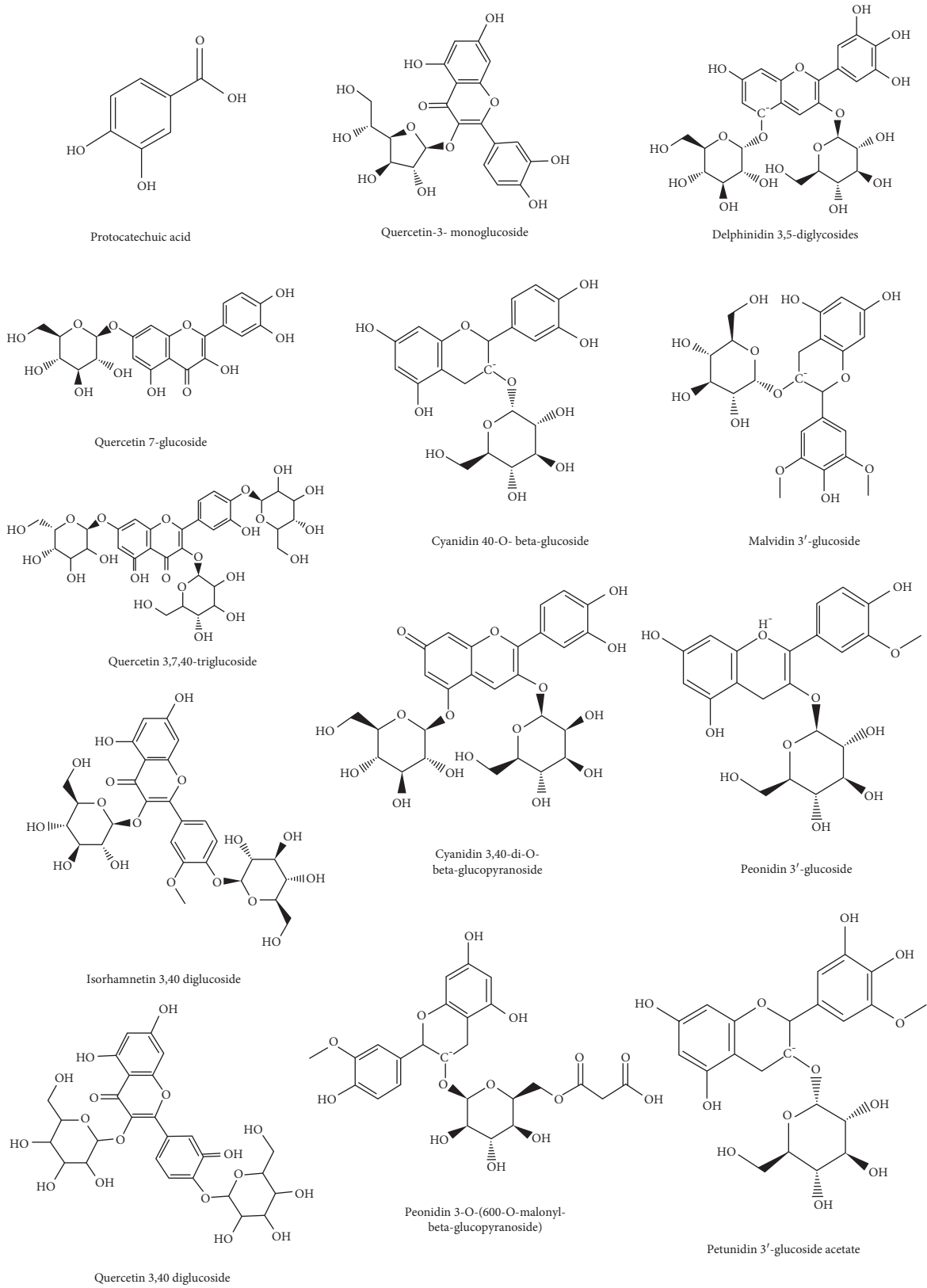
**5.1. Antimicrobial Effect.** *A. cepa* has been identified in the treatment of infectious diseases as an effective antimicrobial agent. Many fungi, bacteria, and viruses have been found vulnerable to various *A. cepa* solvent extracts [2]. The effect of compound organosulfur on growth of microorganisms has been reconsidered by a study by Liguori et al. [25]. The effectiveness of quercetin in inhibiting the growth of *L. monocytogenes*, *B. cereus*, and *P. aeruginosa* was not as high as that of kaempferol, but it was as successful as quercetin in inhibiting the growth of *M. luteus* and *S. aureus* [44]. Another study observed that essential oil of three types of onion (red, green, and yellow) displayed marked antimicrobial efficacy against specific pathogens, including *Salmonella enteritidis*, *Fusarium oxysporum*, *Penicillium cyclopium*, *Staphylococcus aureus*, and *Aspergillus Niger* [39]. The red *A. cepa* extract has been shown to possess more antibacterial properties relative to the yellow and white varieties [45]. Another study showed that *A. cepa* was

successful against *P. aeruginosa* extracted from patients with urinary tract infections, suggesting that it may be useful in the treatment of those infections [46]. A study by has shown how onion synthesized nanoparticles have a beneficial effect on *Klebsiella* spp. inhibition [47]. Saxena et al. published synthesis of silver nanoparticles by onion extract and showed the full antibacterial action against *E. coli* and *Salmonella typhimurium* at 50  $\mu\text{g}/\text{mL}$  concentration [48]. In addition, onion extracts are powerful against fungal species, and their essential oils inhibit dermatophyte fungal products [49]. *Fusarium oxysporum* and *Aspergillus Niger* (MFC/minimum fungicidal concentration = 75 and 100 mg/mL) were strongly inhibited by dehydrated onion ethyl alcohol extract [50, 51]. The growth of airborne pathogens (*B. cereus*, *A. alternata*, *Phomopsis* spp, and *Mucor* spp), soilborne pathogens (*R. solani*), and antagonistic fungi (*T. harzianum* and *T. atroviride*) were inhibited by anti-fungal saponins (ceposide C and A) [52]. High inhibitory effect against *C. albicans* (minimum inhibitory concentration, MIC = 4.522 mg/mL) and *M. furfur* (MIC) = 8.062 mg/mL) were reported [53]. Researches have shown that *A. cepa* essential oil has a total inhibition of 2 yeast development at a concentration of 7% (*S. cerevisiae* and *C. tropicalis*) [54,55]. The growth of molds (*P. griseofulvum* and *A. tamarii*) was also affected by high concentrations of the essential oil, and full inhibition for *E. astelodami* was observed [2]. In vivo study of Ur Rahman et al. observed onion powder effect on the intestinal histomorphology and selected gut microflora in 320 days old broiler and a decrease in *E. coli* population and a substantial rise in *Lactobacillus* spp. were found who were fed onions at a rate of 2.5 g/kg of food [56]. The results of that study were similar to that of Goodarzi et al., whereby 10–30 g onion/kg was given to broilers with diets [57]. An in vitro study by Golestani et al. investigated the effect of *A. cepa* essential oil extract against *Escherichia coli* bacterial strains. The strain studied had a minimum inhibitory concentration (MIC) of  $93.8 \pm 44.2 \text{ g}/\text{mL}$  and a minimum bacterial concentration (MBC) of  $312.5 \pm 265 \text{ g}/\text{mL}$ , indicating that *A. cepa* had certain antibacterial activity. Bag and Chattopadhyay discovered related findings in which both bacteria predicted an inhibition region, but *S. aureus* had a larger inhibitory impact (IZD =  $6.90 \pm 1.26$ ) [58]. Also, methanolic extract of onion inhibit *E. coli* and *S. aureus*. The highest inhibition zone for *S. aureus* was observed to be  $13.5 \pm 0.9 \text{ mm}$  for the extract of red onion, whereas for the extract of yellow onion was  $11.3 \pm 0.7 \text{ mm}$  [45]. The ethanolic, aqueous, petroleum ether, and chloroform extracts of bulb of fresh onion against some fungi by disc diffusion method was investigated by Singh et al. In its aqueous and ethanol production, the onion has shown substantial fungal growth inhibition. Onion is the most efficient chloroform extract, whereas petroleum ether extract is the least effective. The chloroform extract of onion showed highest zone of inhibition with *A. fumigatus* (IZD =  $31 \pm 1.3 \text{ mm}$ ), *A. niger* (IZD =  $28 \pm 1.4 \text{ mm}$ ), and *C. albicans* (IZD =  $32 \pm 1.5 \text{ mm}$ ) but less in case of *A. flavus* (IZD =  $24 \pm 1.1$ ) [59]. In another study, maximum bacterial kill was displayed by 100% aqueous extracts of green onion bulbs, and positive control for *E. aerogenes* was slightly lower than its kill rate [60].



(a)

FIGURE 1: Continued.

FIGURE 1: (a, b) Bioactive compounds of *Allium cepa*.



Shakurfow et al. carried out another trial with the effectiveness of white onion bulb extracts on *Listeria monocytogenes* with respect to boiling water and herbal solvents (mixture of cyclohexane, chloroform, and methanol). He observed the organic solvents were well suited to boiling or cold water extracts [61].

**5.2. Cardiovascular Diseases.** CVD involves hypertension, peripheral artery disease, cerebral disease, pulmonary inflammation, rheumatic heart disease, congenital cardiovascular disease, and heart insufficiency [1]. According to World Health Organization (WHO), by 2030, almost 23.6 million people, primarily cardiac disease and stroke, will die from CVDs. These are projected to remain the single leading causes of death. Therefore, dietary changes and new developments in prevention and treatment of CVD in previous decades have had significant impacts on the death and quality of the lives of humans world-wide [62]. CVD risk factors are mainly determined by lifestyle-related causes (physical inactivity, smoking, unhealthy diet, and stress) and uncontrollable causes (gender, heredity, and age), which can be modified [1]. In coronary disease prevention, bioactive compounds of onions play a significant role. Onions contain flavonoids which are used for treatment and prevention of heartburn [63] and cardiovascular diseases [64]. Quercetin reduces blood pressure in hypertensive subjects, activates platelets, and shows cardiovascular benefits. Onion includes several compounds of sulfur including thiosulphine, thio-sulfone, S-oxide, cepain, and S-dioxide as well as mono-, di-, and trisulfide. Onions contain a number of vitamins (B2, C, and B1), selenium, and potassium. Onions can cure diabetes mellitus, CVDs, and stomach cancer. Atherosclerosis or inflammation of the vascular system, leading to coronary heart disease, hypertension, and stroke is commonly associated with elevated cholesterol level. The start of oxidized LDL-C superoxide formation induces endothelial dysfunction. Excessive synthesis of reactive oxygen species often results in oxidative stress (ROS) and formation of reactive LDL-C. Lots of studies have shown that dietary flavonoids such as quercetin can minimize oxidative stress by mopping free radicals and thereby reduce the risk of heart disease and stroke. Therefore, some scientists focused on lipid reduction in plant nutraceuticals that can be safe to minimize the risk of metabolic syndrome and CVD. Synthetic lipid lowering drugs may have an adverse effect [65]. In doxorubicin-induced cardiotoxicity, onion (*A. cepa*) leaves showed antioxidant and cardioprotective activity in rats [66,67]. In another pilot study, 24 healthy people, 35–55 years of age, were identified and divided into two groups of 12, each having 5 males and 7 females, with moderate hypercholesterolemia ( $>200$  mg/dL). For 8 weeks, a participant received 100 mL of onion or placebo every day. The onion juice contained 52 grams of onion extract double the prescribed dosage of nutraceuticals. This analysis of 11 weeks has been split into three phases. Phase I of one week was called the adaptation stage, followed by phase II of the trial period of eight weeks, and then phase III of the follow-up period, of two weeks. After 8 weeks of care, waist circumference, total

cholesterol, and LDL-C reduced substantially ( $p < 0.05$ ). In addition, onion juice improved overall ability to antioxidant and extended LDL oxidation lag time. The high antioxidant potential was found to be useful in the fight against CVD [68].

**5.3. Wound Healing.** Prostaglandins,  $\beta$ -sitosterol, kaempferol, myricital acid, and ferulic acid are contained in the *A. cepa* bulb. Bulb extract in rats has an ecobolistic influence. The bulb extract of *A. cepa* has traditionally been used as an abortifacient herb containing these constituents and has shown an ecobolic effect in rats and mice. The group treated with *A. cepa* showed extensive granulation growth begun on its surface. The treated unit of wound displayed complete healing of wounds with almost normal architecture of the reticulin and collagen. The increasing tensile strength of the treated community wound may be attributed to the rise in collagen levels, and the increase in collagen synthesis is performed by the alcoholic extract of *A. cepa* [69]. A few drops of onion juice can potentially be extremely useful for people who have acute earaches. The tone of the ringing in the ear may be cured by using cotton wool onion juice [13]. Onion is commonly used to make Ayurvedic wound curing formulations. It also demonstrates biological effectiveness in pediatric patients in prevention of median sternotomy wound [70,71]. The extract of the fibroblast cell line showed the therapeutic impact on human skin and is used in keloid therapy [72]. Extract onion peel reveals biological effective hypertrophic scar and keloid prevention [73]. In addition, ointment extract gel reveals hypertrophic presternal scar defense [74]. It is often used in topical methods for care and mitigation of postoperative hypertrophic scars [3,4] and keloid surgery [75]. *A. cepa*-allantoinpentaglycan gel also cures hypertrophic skin skins [76] and enhances the aesthetic appearance of postoperative scars [77] and burning cells [78]. Tattoos are removed with onion extract, heparin, and allantoin spray. Prevention of postsurgical scars is a topical use of onion extract [79]. Scars and keloids during burning can also be removed by using onion extracts [80]. The elasticity of postburning scares is increased by ointment [78]. Cepan cream is used in burn wounds care [78] and in rabbit ears hypertrophic burns [81]. An in vivo study demonstrates that onion extract is capable of removing hypertrophic scars and keloids at 10% concentration. The research was performed on 7 patients with keloids (five males, two females; mean age  $37 \pm 11.5$  years) and 39 Caucasians with single or multiple HTS (19 females and 20 males; mean age  $36 \pm 12.5$  years) [82].

**5.4. Antiplatelet Activity.** The effect of quercetin extracted from onion peel extract, through upregulation of cAMP levels and the reduction of TXA<sub>2</sub>, Ca<sup>2+</sup>, cyclooxygenase-1 (COX-1), as well as synthase activities of TXA<sub>2</sub>, may be attributed to the antiplatelet effect. It has also been shown that AA release diminution; synthase-blocking TXA<sub>2</sub>; and receptor blockage TXA<sub>2</sub>/PGH<sub>2</sub> may be associated with the antiplatelet system of the onion extract. The antiplatelet activities of onion, namely, allicin, adenosine, and paraffinic

polysulphides, are also due to the components that are sulfur-based [83]. Platelet aggregation reduction has a protective impact on some cardiac diseases, for instance atherosclerosis. Furthermore, the effect of onion extracts is lipid-reducing. Bordia et al. first assessed their antithrombotic ability for water extracts from onion and garlic [84]. Orally and intraperitoneally extracts were administered to rats. A comparatively low dosage (50 mg/kg body weight) of aqueous garlic extract has greatly reduced thromboxane B<sub>2</sub>, independent of how the extract is administered. Onion extracts at higher concentrations were successful (500 mg/kg body weight). Until operation, the boiling of extracts resulted in almost total operation failure. The cooking of powerful antithrombotic components in alliums can then induce decomposition. Allicin and adenosine, each of which appears more often in garlic without influencing cyclooxygenase and lipoxygenase inhibitors of arachidonic acid, have both blocked platelet addition. The trisulphides investigated inhibited platelet aggregation, as well as thromboxane synthesis, along with the induction of lipoxygenase metabolites. The *in vivo* antiplatelet results found seem to have been more adenosine due than onion polysulphides of allicin and alk(en)yl. Several experiments have shown that onion antiplatelet behavior is considered a feature of organosulphur compounds. Antithrombotic activity has been shown in particular by a sulphinyldisulphide class (cepaene) present in onion extracts [85]. Some nonsulfur substances including  $\beta$ -chlorogenine and quercetin have also been shown to suppress the aggregation of platelets [86]. The function of antiplatelet is significantly influenced by genotype, climate, and vegetable storage period [1]. Ko et al. carried out an experiment regarding the efficacy of *A. cepa* in inhibiting platelet aggregation. Sprague Dawley rats were given *A. cepa* extracts at different dosages (0.5, 2, 5, and 6  $\mu\text{g}/\text{mL}$ ). At 6  $\mu\text{g}/\text{mL}$  dose, it showed maximum inhibition of platelets aggregation. From the findings, the activity of quercetin was found to be considerably greater than that of its glucosides. The antiaggregation process of flavonoids was examined *in vitro*, revealing that flavonoid aglycones generally, and the examined flavonoid derivatives did not affect the role of the platelet. In addition, the aggregation of platelet was blocked by flavones such as apigenin, chrysenes, and phloretin. Quercetin and myricetin have had strong anti-aggregating efficacy against amino acids, but the aggregation systems caused by collagen have considered these compounds nearly inactive [87]. The results of onion peel extract (OPE) in the collagen aggregation of washed rat platelet stimulated (5  $\mu\text{g}/\text{mL}$ ) were examined by Ro et al. By blocking dose-dependending TXA<sub>2</sub> synthase (TXAS) and cyclooxygenase-1 (COX-1), OPE prevented platelet aggregation by inhibiting the stimulating enzymes, intracellular Ca<sup>2+</sup>, and thromboxane A<sub>2</sub> (TXA<sub>2</sub>). OPE also raised the formation, but not cyclic guanosine monophosphate, of cyclic adenosine monophosphate (cAMP), the aggregation inhibitory molecule (cGMP). OPE study of the high-level fluid chromatography (HPLC) showed that OPE is composed of quercetin, one of the key antiplatelet flavonoids. The data show that OPES is an important inhibitor of the *in vitro* aggregation of collagen-stimulated platelet. This may

therefore be a promising and effective anticardiovascular approach.

**5.5. Anticancer Effects.** Cancer can be described as the uncontrolled proliferation of abnormal cells in almost every organ or tissue of the body [88]. According to WHO, cancer was the second leading cause of death in 2018, and globally around 10 million people died from cancer in 2020 [89]. The present anticancer drugs have low pharmaceutical indexes which means that, at higher doses, they can cause adverse side effects such as cardiopathy, neuropathy, bone marrow depression, kidney damage, liver damage, and anemia [89]. Again, resistance to anticancer medications has often been a challenge in the modern therapeutic period [90], which is why several studies have been performed in recent years to promote the use of natural products such as herbs and plants as cancer therapy substitutes, as well as their use as dietary supplements to minimize the progression of cancer [91]. Studies suggest that *A. cepa* (onions) have anticancer and similar biological properties, which are thought to be attributed to the presence of different organosulfur derivatives, flavonoids, polyphenols, quercetin, and its glycosides [92]. Many cellular experiments and *in vivo* studies showed that the organosulfur compounds present in onions are powerful anticarcinogens which are due to their function in the activation of detoxifying enzymes that significantly eliminate cancer-causing substances [1]. An MTT assay was performed by Zamri and his colleagues to analyze the antiproliferative effect of various concentrations (10, 50, and 100  $\mu\text{g}/\text{mL}$ ) of crude extracts (ethanol, methanol, and water extracts) of onion on cultured MCF-7 human breast cancer cell for 1, 2, and 3 days of incubation, the results showed that the methanol extract of onion with concentration of 50  $\mu\text{g}/\text{mL}$  generated the lowest percentage of cell viability after three days of incubation. It was reported that the methanol extract of onion contained various organosulfur compounds, and these compounds decrease cancer cell viability in a dose- and time-dependent fashion [91]. Similarly, Pan et al. conducted another MTT assay look at the effects of methanol extracts of onions on cancer cell lines HepG2, HT 29, and PC 3. The results showed that quercetin glucosides present in onion extract inhibited the growth of cancer cell lines, and the report also suggested that quercetin glucosides have antioxidant and antiproliferative activities against the cancer cell line [93]. A group of researchers showed that polyphenols isolated from lyophilized *A. cepa* inhibit the development of human AGS cells (a human gastric adenocarcinoma cell-line) by inhibiting the PI3K/Akt signaling cascade, which leads to apoptosis [94]. Furthermore, a study was performed by Nohara et al. to evaluate the anticancer properties of Allium sulfides on rat models, and the findings revealed that onion in A1, a thiolane-type sulfide extracted from onions, blocks the activation of M2 macrophages, thus restricting tumor cell growth in both mouse osteosarcoma (LM-8) bearing mice model and mouse ovarian cancer (iMOC) bearing mouse model [95]. In addition, Allium vegetables such as onion and garlic contain diallyl trisulfide (DATS) which has anticancer properties [9,14], and studies showed



that DATS triggers cancer cell cycle arrest at the G2/M phase by increasing the release of reactive oxygen species, which induces apoptosis and restricts tumor cell formation [96]. In recent years, many researches have been done to determine the cancer-preventive properties of *A. cepa*, and the outcomes have indicated that regular intake of onions lowers the risk of colorectal, lung, liver, brain, stomach, ovarian, prostate, and breast cancer [1,92]. The notable therapeutic effects of *A. cepa* are shown in Figure 2.

**5.6. Antidiabetic Effects.** Diabetes is a progressive metabolic disorder that affects the heart, blood vessels, skin, kidneys, and nerves and may lead to serious medical conditions such as heart attack, kidney failure, blindness, and stroke [97]. According to WHO datasheet, globally around 422 million people are diagnosed with diabetes, and it is solely responsible for 1.6 million deaths per year. Although the current conventional antidiabetic medicines are able to mitigate diabetes symptoms, they may also show some serious side effects such as hypoglycemia, edema, heart and liver abnormalities, and gastric and respiratory problems [98]. For this reason, scientists are looking at natural resources such as medicinal plants as alternative therapeutic agents against diabetes, as they are less harmful and have a lot of pharmacological value [98,99]. At present, many studies [97,98,100] are being performed on *A. cepa* to investigate its antidiabetic activities, and one of the experiments which was tested on diabetic rats showed that the aqueous extract of onions reduced blood glucose level in the same manner as that of glibenclamide, a conventional antidiabetic drug. The results also reported that the onion extracts contained kaempferol-3-O- $\beta$ -D-6 (*P*-coumaroyl) glucopyranoside which is responsible for the antidiabetic effect by promoting glucose uptake in rat soleus muscle [101]. Likewise, Gautam et al. conducted a research on STZ-induced diabetic rats found that ethanol extracts of *A. cepa* reduced blood glucose levels significantly after 24 hours of oral administration, and the explanation for this effect was proposed to be that the onion extract stimulated pancreatic  $\beta$ -cell regeneration, which induced the synthesis and secretion of insulin, subsequently regulating blood glucose level [102]. In addition, another experiment which was also conducted by Airaodion et al. using the ethanol extract of onions found that the extract contained quercetin and rutin which stimulated glucose uptake in rat skeletal L6 myotubes by increasing GLUT-4 protein synthesis and its mobilization from the cytoplasm to the plasma membrane, as well as triggering the PI-3-K/Akt signaling pathway to regulate glucose transport [103]. Furthermore, in a study of six groups of alloxan-induced diabetic rats, three groups were treated with varying doses of *A. cepa* juice for 14 days, and the results found that the rats treated with onion juice had a markedly decreased blood glucose level than the rats who were not [100]. Jini and his group synthesized silver nanoparticles from *A. cepa* and an in vitro study was designed to evaluate those silver nanoparticles activity against diabetes. The study report revealed that those silver nanoparticles were inhibitors of carbohydrate-hydrolyzing

enzymes such as  $\alpha$ -amylase and  $\alpha$ -glucosidase, and inhibition of these enzymes decreases carbohydrate absorption by the body which consequently leads to the reduction of blood glucose level [104]. Further many studies were conducted on *A. cepa*, and the findings suggested that the antidiabetic properties of onion are attributed to the presence of bioactive compounds such as quercetin, s-methylcysteine sulfoxide, allyl propyl disulfide, and polyphenols which promote glucose uptake in peripheral tissues increasing NADP<sup>+</sup> and NADPH behavior and increasing the sensitivity and secretion for insulin [99].

**5.7. Antihypercholesterolemic Effects.** Hypercholesterolemia can be characterized as the presence of excess levels of cholesterol in the blood than normal, and this elevated level of cholesterol can lead to atherosclerosis, which is the forming of fatty plaques in the arteries' walls [105]. These plaques causes narrowing and/or blocking of the blood vessels which disrupts blood flow in vital organs of the body such as heart and brain and thereby raising the risk of heart attack and stroke. A study performed by Wenyi Li et al. to assess the antihypercholesterolemic activities of *A. cepa* on six groups of hyperlipidemic rats showed that there was a substantial decrease in total cholesterol (TC), triglyceride (TG), low density lipoprotein cholesterol (LDL-c) levels, and a raise in high density lipoprotein cholesterol (HDL-c) levels in both plasma and liver following 4 weeks of oral administration of *A. cepa* extract at different concentration for each group of rats [106]. Ming and his group of researchers performed a clinical trial on twenty-four mildly hypercholesterolemic adults to determine the effectiveness of onion juice against this condition, and the results showed that, after eight weeks of daily administration, the blood plasma TC, LDL-c, and LDL-c/HDL-c ratio levels were significantly lowered in onion juice treated subjects. According to the report, quercetin increased LDL receptor mRNA expression, which resulted in a decrease in serum LDL-c levels, and flavonoids (quercetin and rutin) increased fecal cholesterol excretion, which led to a reduction of serum TC levels [68]. Further studies have revealed that *A. cepa* due to its hypocholesterolemic activity, it is effective against cholesterol gallstone (CGS), i.e., it can reduce the risk of CGS development as well as diminish the preexisting CGS. According to a study evaluating the anticholelithogenic potential of *A. cepa* on mice with lithogenic high cholesterol diet after 10 weeks of daily ingestion of raw or heat processed onions, the likelihood of CGS development was decreased by 15–40%. The reports suggested that onions reduced cholesterol secretion in the bile and enhanced bile acid excretion, which reduced the production of lithogenic bile acids and, as a result, inhibited CGS development [107].

**5.8. Antioxidant Effects.** Our body uses oxygen for metabolism, and this process generates reactive oxygen species (ROS) or free radicals as a byproduct [108]. Free radicals are also produced in our body from alcohol consumption, smoking cigarettes, and long time exposure to sunlight, as products of inflammatory reactions in our body [109].

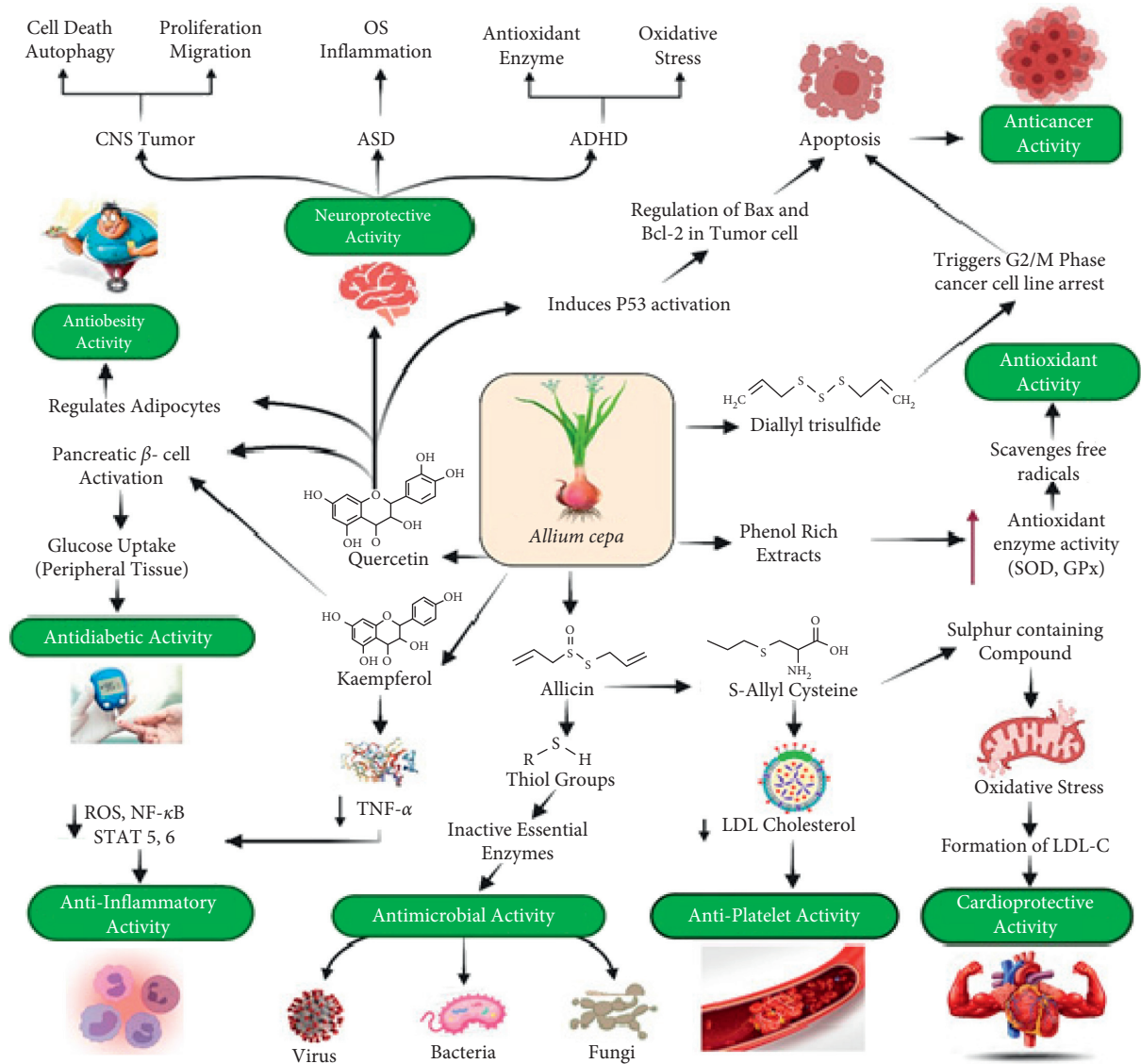


FIGURE 2: Major therapeutic effects of *Allium cepa*.

Though free radicals are essential for our bodies' signaling mechanisms [110], but excessive development of these oxidative free radicals can cause oxidative stress; a situation in which the balance of oxidants and antioxidants in our body is disrupted [111]. Long-term oxidative stress causes damage to body cells, nucleic acids, proteins, and lipids, resulting in severe diseases such as cancer, diabetes mellitus, Alzheimer's disease, and cardiac and liver diseases. Antioxidants, also known as free radical scavengers [112], neutralize free radicals, preventing or reducing cell damage, DNA mutations [112,113], and subsequently lowering the risks of severe diseases like cancer [114]. Studies [108,115,116] have indicated that *A. cepa* have antioxidant potential due to presence to high amounts of organosulfur compounds, polyphenols, and flavonoids which are natural antioxidants [117,118]. An in vitro study was conducted by Antonella Lisanti and her colleagues on three cultivars (*Dorata di Parma*, *Rossa di Toscana*, and *Borettana di Rovato*) of *A. cepa*

to identify their total phenolic content using Folin–Ciocalteu method and total antioxidant activity using the FRAP (ferric reducing antioxidant power), TEAC (trolox equivalent antioxidant capacity), and DPPH (1,1-diphenyl-2-picrylhydrazyl) spectrophotometric methods, with FRAP method based on electron transfer mechanisms and the other two based on radical neutralization mechanisms. According to the findings, all three onion cultivars have antioxidant potential, with *Rossa di Toscana* having the highest antioxidant activity in all three methods [115]. Again, another group of researchers performed an experiment to evaluate the antioxidant potential of onion peel extracts (hot water, ethanol, and subcritical water extracts) using DPPH, lipid peroxidation inhibition method, and ferric thiocyanate (FTC) method with the DPPH method showing the highest antioxidant activity even much higher than BHT at 0.02 mg/mL concentrations. The FTC method showed minimal antioxidant potential, while the inhibition of lipid peroxide

method revealed no antioxidant effect of the extracts, implying that onion peel extracts neutralize radicals by donating hydrogens or electrons instead of inhibiting lipid peroxidation [119]. Additionally, Sunyoung Kim and his colleagues conducted an analysis to define a relationship between the organosulfur compounds and their antioxidant potential using ORAC (oxygen radical absorbance capacity), DPPH, and ABTS (2,2'-azino-bis-3-ethylbenzthiazoline-6-sulphonic acid) testing methods on three separate Allium plants (*Allium Sativum* L., *Allium ampeloprasum* L., and *Allium cepa* L.). The study reports revealed that organosulfur compounds were positively associated with antioxidant activities, and *Allium sativum* L. showed higher antioxidant potential than the other two plants as it contains higher amount of organosulfur compounds, while *A. cepa* showed substantial antioxidant activity despite having the lowest organosulfur content [120]. A study was performed by Yi-Long Ma and his colleagues on the cell wall polysaccharides of *A. cepa* to investigate their antioxidant activity; the polysaccharides were named for their extraction methods such as hot buffer soluble solids (HBSS), chelating agent soluble solids (CHSS), dilute alkaline soluble solids (DASS), concentrate alkaline soluble solids (CASS), and their antioxidant activities were measured using DPPH, ABTS, iron chelation, superoxide anion radical scavenging, hydroxyl radical scavenging, and lipid peroxidation inhibition method. According to the findings, CHSS exhibited the highest antioxidant potential on ABTS (97.52%), iron chelation (98.24%), and superoxide anion scavenging (76.97%), while HBSS had the highest antioxidant potential using the DPPH system (93.68%) and CASS had the best results using the lipid peroxidation inhibition method (86.43%) [121]. Furthermore, an in vivo study was conducted on 400 broiler chickens to assess the effects of phenol-rich *A. cepa* on their development, digestion, antioxidant activity, and immune response. The phenol-rich onion extracts (PROE) were administered at different concentrations to each group (100/group) of subjects for 35 days, and the results revealed that PROE increased antioxidant enzyme activities (catalase, superoxide dismutase, and glutathione peroxidase) which was expected to be due to the presence of high amount of phenol and flavonoids in the onion extract [122].

**5.9. Antiobesity Effects.** Obesity is a metabolic disorder characterized by the buildup of excess fat in the body which occurs as a result of an energy intake and expenditure imbalance [123]. Obesity increases the risk of multiple diseases such as cardiovascular disease, liver disease, stroke, diabetes, cancer, hypertension, polycystic ovarian syndrome, osteoarthritis, and sleep apnea [123,124], and a recent study states that obesity also raises the risk of serious COVID-19 complications in infected patients [125]. According to WHO database, globally more than 650 million adults were found obese (BMI >30 kg/m<sup>2</sup>) in 2016, and over 4 million people died due to the obesity related diseases in 2017 [126]. An in vivo experiment was performed by Ji-Sook Lee and his colleagues on 72 overweight and obese people to assess the

antiobesity effects of onion peel extracts (OPE) rich in quercetin, and the results showed that, after 12 weeks of regular administration of 100 mg of OPE capsules, there was a significant reduction in the body weight (from 70.0 ± 11.4 to 69.2 ± 11.4 kg), BMI (from 26.6 ± 3.3 to 26.3 ± 3.2 kg/m<sup>2</sup>), and waist circumference (from 91.9 ± 7.6 to 89.9 ± 7.7 cm). According to the report, the antioxidant effects of quercetin are responsible for these suppressive effects [127]. Oxidative stress inhibits the cellular respiration process which reduces the energy expenditure in adipocytes ultimately increasing fat accumulation in the adipose tissue. Quercetin as an antioxidant neutralizes free radicals, decreases oxidative damage, and recovers cellular functions. In human adipocytes, quercetin can substantially reduce the levels of adipokines including, adiponectin, ANGPTL4, and PAI-1 and also glycolysis-related enzymes ENO2, PFKFB3, and PFKFB4, all linked with obesity [128]. Likewise, another in vivo study on high fat induced rats found that, after eight weeks of regular consumption of quercetin rich supplements, there was a significant decrease in body weight (from 490 ± 11 to 441 ± 11 g), total body fat levels (from 112.9 ± 4.5 to 86.6 ± 5.7 g), and TG levels (from 102.5 ± 7.3 to 90.7 ± 6.5 mg/dL), and it was suggested that quercetin decreases the expression of SREBP-1c. And, *PPAR-γ* genes in the adipocytes which subsequently attenuates lipogenesis and promotes lipolysis [129]. In addition, Chao Yang and his colleagues performed research on high fat diet induced rats (HFD) to test the antiobesity effects of onion oil, and the study found that, after 60 days of daily administration of onion oil (92.6 mg/kg bw/d), the weight gain in the onion oil administered HFD rats (6.7 ± 0.3 g/d) was lower than the weight gain in the rats who were only fed a high fat diet (8.2 ± 0.8 g/d) suggesting that onion oil has antiobesity properties [130]. An ATP-based assay was performed by D. Torres-Villarreal and his colleagues to assess the antiobesity effects of kaempferol, a bioactive compound that can be isolated from *A. cepa* [101], on cultured 3T3-L1 cells (adipocytes), and the reports suggested that kaempferol shows antiobesity properties by inhibiting adipogenesis by downregulating the expression of *Cebpa* mRNA which is positively related with adipocyte differentiation and also by promoting lipolysis by raising the expression of lipolysis *Pnpla2* and *Lipe* genes which are linked with lipolysis [131]. Furthermore, studies showed that S-propyl-L-cysteine sulfoxide, cycloalliin, S-methyl-L-cysteine, and dimethyl trisulfide present in onion extracts may prevent the formation of oil drop in cells, implying that these compounds may be involved in obesity suppression [132].

**5.10. Antihypertensive Effects.** Researchers found antihypertensive effects of *A. cepa*. Brul et al. described polyphenol quercetin is the cause of its antihypertensive and vasorelaxant properties to prevent cardiovascular disease (CVD). This research examined the efficacy of quercetin in patients with overweight to obese prehypertension and stage I hypertension after daily intake on blood pressure (BP). Furthermore, the possible pathways for the proposed impact of quercetin on BP have been discussed. Subjects (*n* = 70) were



randomized in a two-blinded, placebo-controlled combination experiment with 6-week duration of therapy split by a 6 week washout period to obtain 162 mg/d quercetin from the ointment extract powder or placebo. Ambulatory blood pressure (ABP) and workplace BP are measured before and during the intervention; urine and blood tests were collected; and EndoPAT technology assessed the endothelial activity. Quercetin did not influence 24-hour ABP parameters and BP office substantially in the whole population. In the hypertensive section, quercetin reduced systolic BP by 24 hours by  $-3.6$  mmHg compared with placebo (mean gap,  $-3.9$  mmHg;  $p = 0.049$ ). As compared to the placebo, quercetin decreased. In addition, quercetin greatly reduced systolic BP in hypertensive agents during day and night but without any major intergroup influence. Vasoactive biomarkers including soluble endothelial-originated adherence molecules, endothelin-1, enzyme activity of angiotensin converting, asymmetric dimethylarginine, oxidation parameters, endothelial structure, lipid, inflammation, and glucose metabolism were not impaired by the quercetin in the whole population and not in the hypertensive subgroup. The results show that the 162 mg/d quercetin supplementation from the onion skin extract reduces ABP in hypertensive patients, indicating a cardioprotective function of quercetin. The BP-reducing pathways are still unclarified [133].

**5.11. Gallstones Treatment.** The function of dietary intakes in the nonalcoholic steatohepatitis (NASH)/nonalcoholic fatty liver (NAFLD) pathogenesis was stated by Emamat et al. (2018), but the role of every dietary constituent was not yet clear. The goal was to assess the impact of onion intake on NAFLD/NASH avoidance. Sprague Dawley rats have either been fed high weight, dietary high sugar (model group) or fat, dietary heavy sugar plus onion powder at 7 percent (model + onion), or chow diet ad libitum for 7 weeks. Serum concentrations were determined for fasting glucose, triglyceride, liver enzymes, cholesterol, insulin, and gene expression of hepatic tumor factor-alpha necrosis (TNF- $\alpha$ ). H&E stain has been tested for hepatic histology. The data showed that NAFLD may prevent onion consumption even with other factors of risk, such as obesity, high-energy hypercholesterolemia, fat, and sugar intakes [134]. Enamat et al. have also assessed the impact of onion powder use on NAFLD care in an experimental disease model. Sprague Dawley rats had been fed high fat (HF) diets to cause NAFLD for seven weeks. The rats were then fed either a high-food diet plus 7% onion powder (HF + onion) or, the same diet (HF), or the chow diet (control), or onion powder plus 7% onion powder (control + onion) ad libitum for 4 weeks. Fasting triglyceride, leptin, liver enzymes, cholesterol, insulin, and hepatic tumor necrosis factor-alpha (TNF- $\alpha$ ) concentrations were measured throughout the blood. Eosin and hematoxylin stain have been studied for hepatic histology [135]. Dietary intakes and weight gain in animals feeding control + onion diet were substantially greater in

comparison with other categories. In terms of the plasma levels of lipid profiles, liver enzymes, hepatic TNF- $\alpha$  gene expression, and glycemic indicators, fed control or control diet + onion diet was slightly lower relative to the HF diet groups fed; nevertheless, there was no substantial variation in NAFLD histopathology across groups. The findings show that onion intake may be beneficial when paired with a balanced diet in NAFLD management [136].

**5.12. Antiparasitic Effects.** Krstin et al. reported that since ancient time, garlic and onions have been used to cure parasite and microbial diseases. In several areas of the world, particularly in poor countries, trypanosomiasis and leishmaniasis are a problem. The antiparasite effects of *A. cepa* (onion) and *A. sativum* (garlic) bulbs dichloromethane extracts were investigated with *Trypanosoma brucei* and *Leishmania tarentolae*. A number of G-positive bacteria, G-negative bacteria, and two fungi were tested to validate the documented antimicrobial activity. Ionizing spectrometry (LC-ESI-MS/MS) and high-performance liquid chromatogram (HPLC) were carried out for chemical analysis. Chemical analyzes were conducted. The concentration of a number of secondary sulfur metabolites in the garlic and one (zwibelanes) in the onion extract was supported by chemical tests. The two extracts effectively destroy all parasites and suppress the irreversible reductase *Trypanosoma brucei* trypanothione. In addition, the mitochondrial membrane potential in trypanosomes was reduced with garlic extract. In 50% of the cases, a synergistic or additive effect was obtained with combination of garlic and onion with the popular trypanocidal and leishmanicidal medicines. The biological activity function of garlic and onion seems to be linked to the amounts and profiles of the compounds that produce sulfur. The most frequent disulfide production of important recycled cell substances, such as trypanothione reductase between SH groups and sulfur-containing secondary metabolites, is that essential substances in the parasite cell are blocked [137].

**5.13. Bone Disorder Treatment.** *A. cepa* is used to increase bone resorption activity (osteopenia) [138] and bone density [139] and cure osteoclastogenesis [140]. A recent research investigated the efficacy of *A. cepa* in treating osteoporosis. Law et al. studied the persistent inflammatory disease osteoporosis characterized by bone mineral density loss (BMD). The thesis was carried out to determine the influence from the ingestion of onion juice on the BMD and bone degradation in human (in vivo) corroboration and inhibitory effects of osteoclastic differentiation of the cell line (in vitro). The antiosteoclastogenic impact of onion is investigated using RAW 264.7 (osteoclasts progenitor) cells in in vitro experiments. For in vivo trials, 24 participants were split into two categories, and 100 mL of the onion juice or placebo was recommended to be taken over eight weeks. At an original, 2(nd), 6(th), 8(th) and 10(th) week, anthropometric measurements and blood samples were taken. In vitro experiments show that osteoclastogenesis and its separation

are effectively inhibited by onion extract. In the onion-administered subjects, significant differences were observed in concentrations of alkaline phosphatase (ALP), free radicals, overall antioxidant potential (TEAC), and a variety of antioxidants. Three postmenopausal women have increased their BMD size somewhat in onion juice supplementation. The bone loss and BMD have been shown to be beneficially modulated by improving the antioxidant activity and thus can be advised in the management of multiple osteoporosis-based disorders [141].

**5.14. Antidepressant Effects.** Studies demonstrated that onion shows antidepressant effect too [142]. Samad et al. pointed out that different studies assessed the useful impact on the single immobilization of biochemical and behavioral stress-induced improvements, given the anxiolytic, antidepressant, and memory of the enhancement of the properties of *A. cepa* (AC; onion) bulbs. AC powder (200 mg/kg/day) was given to mice in the research group, dissolved in water when 14 days of drinking water were obtained in the control group. After 14 days of checking, AC-treated mice were split into stressed classes again. Two hours of immobilization tension was imposed on animals in the stressed community. Behavioral events were tracked 24 hours after immobilization tension. In the mouse subject to elevated plus maze test (EPM) and light dark movement test, real-time tension caused anxiety behavior stress (LDA). Two hours of stress-induced immobilization of depressed animal behavior, measuring forced swim (FST). The administration of AC reduced clinical deficits due to immobilization discomfort. In anxious mice pretreated with AC in the Morris labyrinth, highest recollection output was observed (MWM). Estimated processes include brain butchery, antioxidant enzymes (SOD, CAT, and GPx) and acetylcholinesterase (AChE) [143]. This research indicates the importance of antioxidant enzymes in alleviating anxiety and depression caused by stress for 2 hours, as well as enhancing the cognitive function of AC. Therefore, the results show that additional AC could be useful for the treatment of anxiety, depression and memory control [144].

**5.15. Anti-Inflammatory Effect.** Inflammation is considered a dynamic biological process, controlled mostly by tissue homeostasis disruption [145]. It is an intricate biological reaction mechanism [146]. Factors including pathogenic bacteria, environmental irritation, and cell and tissue damage usually lead to it. Many models in animals have been tested to evaluate the effect of flavonoids against inflammation, and quercetin and kaempferol have been confirmed to play an important role in preventing inflammation [147]. Quercetin was found to play a role in inhibiting various immunoglobulin isotypes including IgM, IgG, and IgA; all are activated by mitogenes [148]. Quercetin reduces inflammation and allergy [149], while alfrutamide and typheramide found in *Allium* species affect lipoygenases and COXs activity [146,150]. The freeze-dried onion sprouts steam distillate demonstrates anti-inflammatory and antioxidant properties (*A. cepa*) [151].

Cepaenes and thiosulfinates in onions suppress the chemotaxis of human polymorphonuclear leukocytes [152]. Anti-inflammatory effects have been discovered in Ajoene, a natural component isolated from *Allium* [153]. An aqueous extract of the red onion bulb (EAC: 150 and 300 mg/kg) decreased lymphocyte and eosinophil counts in the blood and bronchoalveolar lavage fluid (BALF) in a rat model of asthma [154]. Another study found that *A. cepa* methanol extract (50, 250, and 500 mg/mL) decreased proinflammatory cytokines IL-1- $\beta$ , TNF- $\alpha$ , and IL-6 in lipopolysaccharide (LPS) treated BV-2 microglial cells, guarding against neuroinflammation [155]. The bulb extract from *A. cepa* (35, 70, and 140 mg/kg/day, 21 days) greatly decreased the overall WBC and pulmonary inflammatory cells, such as eosinophil, neutrophil, and monocyte numbers, however contributed to substantial increases in the number and the extract in the asthmatic Wistar rats [156]. *A. cepa* contains a number of flavonoids that may aid in the treatment of oxidative stress-related disorders, asthma, and mechanical and thermal hyperalgesia [157]. The overview of in vivo and in vitro studies of *A. cepa* based on its therapeutic efficacy is shown in Table 1.

**5.16. Neuroprotective Effects.** The nervous system, its cells, composition, and work can be salvaged, recovered, or regenerated as a consequence of neuroprotection. Many neurochemical modulators of nervous system harm are believed to exist [170]. *A. cepa* is considered to exhibit neuroprotective effects. An in vivo study conducted by Singh et al. demonstrates that *A. cepa* shows neuroprotective potential in aluminium chloride-induced neurotoxicity. Swiss albino male mice were administered 50–200 mg/kg/day of onion and 50 mg/kg/day of aluminium chloride, thus reducing lipid peroxidation and nitrate/nitrite ratios, as well as increasing GSH and catalase activities. The amount of AChE in the body was also decreased. Quercetin, kaempferol, cycloartenol, and phytoosterols such as lophenol, 24-ethyl cycloartenol, and 24-methyl lophenol have been found to inhibit transcription of genes like FAS, S14, transferrin, and apolipoprotein CIII which in turn exhibits neuroprotective effect [161]. Another study indicated that changing the expression of neurotrophic factor protects mice from neuronal harm in I/R-induced retinal injury [162].

**5.17. Insecticidal Effects.** The *Lycoriella ingenua* and Japanese termite (*Reticulitermes speratus* Kolbe) have been shown to be immune to the essential oils and components of onion and garlic plants [171,172]. These essential oils contain significant sulfur compounds such as diallyl disulfide, DATS, diallyl sulfide, eugenol, and  $\beta$ -caryophyllene, of which DATS are found to be the most harmful. Nevertheless, certain substances used in essential oils were found to have fumigant efficacy and had a 100% mortality rate against termites after just two days of treatment reference [171]. Crushed wild onion leaves repel *Diaphorina citri* adults due to the presence of sulfur volatiles from *Allium* spp. These factors also influence the

TABLE 1: An overview of recent in vivo and in vitro studies of *Allium cepa* based on its therapeutic efficacy.

Field of Study	Subject	Dosage	Outcome	Mechanism of Action	References
Antimicrobial effect (in vivo)	Broiler chicks	1.5–2.5 g	Population of <i>E. coli</i> in ileum was decreased at a rate of 2.5 g/kg feed, while the amount of <i>Lactobacillus</i> was increased	Onion may alter a microflora intestinal, which improves digestion and absorption of nutrients in the intestines	[56]
	<i>Escherichia coli</i> bacterial strains	Powdered bulb onion	The strain tested had MIC = $93.8 \pm 44.2$ $\mu\text{g}/\text{mL}$ and MBC = $312.5 \pm 265$ $\mu\text{g}/\text{mL}$ showing that <i>A. cepa</i> had antibacterial effect to a certain extent	Destroys bacteria by using their most active extract forms, or combining them to achieve latent synergistic effects	[158]
	Food-borne bacterial strains	15.6–1000 $\mu\text{g}/\text{mL}$	All bacteria projected inhibition zone, but a greater inhibitory effect was observed for <i>S. aureus</i> (IZD = $6.90 \pm 1.26$ )	n.m.	[58]
Antimicrobial effect (in vitro)	Gram-positive and Gram-negative bacteria	n.m.	Methanolic extract of onion inhibits <i>E. coli</i> and <i>S. aureus</i> .	Flavonoids, phenolic compounds, quercetin inhibited the growth of Gram positive and Gram-negative bacteria	[45]
	Gastrointestinal tract pathogens	n.m.	100% aqueous extracts of green onion bulbs displayed maximum bacterial kill, and its kill rate is slightly higher than the kill rate by positive control for <i>E. aerogenes</i>	Flavonoids and phenolic compounds of green onion bulb destroy bacterial membrane and shows antibacterial activity	[60]
	Sprague Dawley rats	6 $\mu\text{g}/\text{mL}$	Significant inhibition of aggregation of platelets	Flavones such as apigenin, chrysin, and phloretin inhibited aggregation of platelets	[87]
Antiplatelet activity (in vivo)	Rats	5 $\mu\text{g}/\text{mL}$	Platelet aggregation was inhibited	Inhibition of aggregation-inducing molecules, thromboxane A <sub>2</sub> (TXA <sub>2</sub> ), and intracellular Ca <sup>2+</sup> by blocking TXA <sub>2</sub> synthase (TXAS) and cyclooxygenase-1 (COX-1) activities	[159]
Antiplatelet activity (in vitro)	Two healthy nonsmoker donors	n.m.	The dose-response curves developed using different dosages of allium juice vs. the percentage of inhibition of aggregation are calculated for juice levels needed to reduce platelet aggregation by 50% (IC <sub>50</sub> )	Aglycone part did not take part in inhibiting platelet aggregation. The flavone part of flavonoids of <i>A. cepa</i> played the major role	[160]
Gallstone treatment (in vivo)	Sprague Dawley rats	7% (w/w) onion powder	Lowered ballooning, hepatic steatosis, and lobular inflammation	Quercetin decreases the levels of hepatic enzymes, serum lipids, steatosis, and inflammation through regulating the expressions of NF-kB, p65, Sirt1, and iNOS	[134]



TABLE 1: Continued.

Field of Study	Subject	Dosage	Outcome	Mechanism of Action	References
Antiparasitic activity (in vitro)	<i>Leishmania tarentolae</i> and <i>Trypanosoma brucei brucei</i>	3–5 µg/mL	Zwiebelane in the onion extract killed both types of parasites efficiently	The forming of disulfide bonds between SH classes of essential redox compounds and secondary metabolites containing sulfur are inhibiting trypanothion reductases	[137]
Antidepressant activity (in vivo)	Albino Wistar mice	200 mg/kg/day	Immobilization stress substantially reduced	Reduce stress by its potential antioxidant mechanism	[144]
	Wistar rats	35–140 mg/kg/day	Reduced the pulmonary inflammatory cells, such as eosinophil, neutrophil, and monocyte and overall WBC	Inhibited NF-κB cells which induce inflammation	[156]
Anti-inflammatory (in vivo)	BV-2 microglial cells	50–500 mg/mL	Attenuated neuroinflammation	Onion increases iNOS expression at the protein levels and mRNA in LPS-stimulated BV-2 microglial cells, thus reducing proinflammatory cytokines IL-1-b, TNF-a, and IL-6	[155]
	Wistar rats	150 and 300 mg/kg	Reduced lymphocyte and eosinophil count in the blood and bronchoalveolar lavage fluid (BALF)	n.m.	[154]
Inflammatory responses (in vitro)	RAW 264.7 cells	100 mg/mL	LPS-induced inflammation	Dose-dependent reduction in IL-6, TNF-a, and IL-1-b secretion, as well as NO production Quercetin, kaempferol, cycloartenol, phyosterols like lophenol, 24-ethyl cycloartenol, and 24-methyl lophenol have been found to inhibit transcription of genes like FAS, S14, transferrin, apolipoprotein CIII	[4]
Neuroprotective activity (In vivo)	Swiss albino male mice	200 mg/kg/day	Reduced lipid peroxidation and nitrate/nitrite ratios, as well as increased GSH and catalase activities. The amount of AChE in the body was also decreased.		[161]
	Mice	300 mg/kg	Protects mice from neuronal harm in I/R induced retinal injury.	Changes the expression of neurotrophic factor	[162]
Asthma (in vivo)	<i>Blomia tropicalis</i> (a type of mite)	100–1000 mg/kg	Induced asthma	Reduced IL-4, IL-5, IL-13, and IgE levels	[163]
Inhibitory and stimulatory activity (in vivo)	Mice	10–200 g	Inhibitory effect on Th2 activity and stimulatory effect on Th1	Th2 cytokines, IL-4, IL-5, and IL-13, as well as IgE, were inhibited at 1000 µg/mL Cepa inhibited the development of IL-6 and IL-1a while increasing the production of IL-3 and IL-4 and inhibiting the NF- κB pathway	[164]
Osteoclastogenesis (in vitro)	RAW264.7 cells	100–1000 µg/mL	Induced inflammatory conditions		[165]

TABLE 1: Continued.

Field of Study	Subject	Dosage	Outcome	Mechanism of Action	References
In breast cancer (in vivo)	Female BALB/c mice	0.1 mL/100 g bw	Stimulatory effects on Th1 but inhibitory effects on Th2 activity	Induced decreases in IL-4 and rises in IFN- $\gamma$ levels and IFN- $\gamma$ /IL4 ratio (Th1/Th2 balance)	[166]
Allergic rhinitis (In vivo)	BALB/c mice	20–40 mL	Decreased allergic symptoms, Reduced eosinophil penetration of nasal turbinate mucosa, and OVA-specific IgE levels	Levels of IL-4, IL-5, IL-10, IL-13, and IFN- $\gamma$ decreased in groups treated with onion extract	[167]
Immunomodulatory property (in vitro)	BALB/c mice	3.5–15 $\mu$ g/mL	Showed immunomodulatory properties	Inhibited the development of Th2 cytokines such as IL-4, IL-5, IL-13, and IgE	[164]
Immunoprotective effects (in vivo)	Wistar rats	1–100 intraperitoneal	Natural and cyclophosphamide-induced immunosuppression	TNF- $\alpha$ , IL-10, COX-2, IgG and IgA levels in serum were increased by and immune parameters such as myeloid cells (RBC, WBC, and hb), body weight, splenic index, and thymic index in the spleen and thymus were enhanced	[168]
Lung disorder (in vivo)	Wistar rats	0.175–0.7 mg/mL	WBC count were improved, but their lymphocytes were reduced ( $p < 0.05$ to $p < 0.001$ ).	A significant decrease in tracheal tolerance, neutrophil and eosinophil counts, but a significant increase in lymphocyte count ( $p < 0.05$ to $p < 0.001$ )	[169]
Hepatoprotective (in vivo)	Adult male albino rats	200–450 mg/kg	Decreased alanine aminotransferase and overall serum bilirubin levels in a dose-dependent way	Decrease in alanine aminotransferase (ALT), aspartate aminotransferase (AST), alkaline phosphatase (ALP), lactate dehydrogenase (LDH), and complete serum bilirubin (TSB).	[23]
Anti-cancer effect (in vitro)	Murine ovarian cancer model	20 mg/kg	Blocks tumor cell growth	Blocks the activation of M2 macrophages	[95]
Antidiabetic effect (in vivo)	Diabetic rats	Aqueous extract of onions (25 mg/kg) for 21 days	Reduced blood glucose level	Increased glucose uptake into soleus muscle	[101]
	Rats	200 mg/kg	Decrease in blood glucose level	Stimulate the formation of pancreatic $\beta$ cells	[102]
Antihypercholesterolemic effect (in vivo)	Rats	3 mL/100 g	Decrease in blood glucose level	n.m.	[100]
	Sprague Dawley rats	4.5 g/kg body weight	Inhibited the formation of atherosclerosis	n.m.	[106]
	Mice	2% raw or heat processed onions with high cholesterol diet	Reduced the risk of CGS	Decrease cholesterol secretion in bile and increase bile acid excretion	[107]
Antioxidant effects (in vivo)	Broiler chicken	3 g/kg diet	Increased antioxidant enzyme activities	n.m.	[122]

TABLE 1: Continued.

Field of Study	Subject	Dosage	Outcome	Mechanism of Action	References
Antiobesity effects (in vivo)	Rats	92.6 mg/kg bw/ days	Weight gain reduced significantly compared to the rats who were only fed high fat diet	n.m.	[130]

MIC = minimum inhibitory concentration, MBC = minimum bactericidal concentration, IZD = inhibition zone diameter, n.m. = not mentioned, HDL = high density lipoprotein, LDL = low density lipoprotein, ACA = *Allium cepa* agglutinin, PROE = phenol-rich onion extract, CGS = cholesterol gallstone.

reaction of the Asian citrus psyllid, *D. citri* Kuwayama (Hemiptera: Psyllidae), to citrus volatiles. The use of a 1:1 mixture of dimethyl disulfide and dimethyl trisulfide to suppress *D. citri*'s reaction to citrus volatiles has an additive impact [173]. Similarly, *A. cepa* dry powder played an important role in minimizing egg deposition. *Phthorimaea operculella* is repelled by it as an ovipositor [174]. *Allium porrum* (L.) produces alk(en)yl-cysteine sulfoxides, which are precursors to reactive thiosulfonates and disulfides, which are nonprotein sulfur amino acids extracted from cysteine. These protect a wide range of insects, including the leek moth *Acrolepiopsisassectella*. The release of sulfur volatiles increases as the sulfur precursor propyl-cysteine sulfoxide sulfur compounds rise, providing an important buffer against the plant's greatest natural enemy. Evaporating solvents from a volatile microemulsion from oil-in-water may produce essential olive oil nanostructures. Domestic, agriculture, and medicinal pests may all be used to measure the effectiveness of the nanoformulations. Nontarget organism toxicity should be assessed on the formulated nanoformulations [175].

**5.18. Immunomodulatory Effects.** The immune system is a complex defense mechanism that protects vertebrates from foreign invaders. The immune system produces a large number of cells and molecules that detect foreign and unwanted agents and destroy them. Any alteration in the immune response, including expression, activation, suppression, or enhancement of any part or stage of the immune response, is referred to as immune system modulation. Immunomodulators, as a result, are molecules that influence the immune system. Immunomodulators are known as either immunostimulators or immunosuppressors, depending on their impact [9]. These immunomodulators either activate or protect the immune system from viruses or tumors. Immunomodulators are chemicals that alter the immune system's response to an infection. Immunomodulators prepare the immune system for any attack by potentiating and modulating it [176]. The immunomodulatory effects of *A. cepa* and its constituents have been studied in a number of studies. BALB/c pokeweed has been sensitized to *Blomia tropicalis* (PWM). *A. cepa* has been shown to be selective in mice, with methanol extracts of *A. cepa* (10, 200, and 100 g) inhibiting IL-4, IL-13, and IL-5, as well as IgE, at 1000 µg/mL and Th2 cytokines. Oral administration of *A. cepa* methanol extract was also tried by a group of scientists (100 and 1000 mg/kg) reduced IL-4, IgE, IL-5, and IL-13 levels in a murine model of *Blomia tropicalis*-induced asthma [163].

Zinc oxide nanoparticles (ZnO-NPs) extracted from extract of *A. cepa* have been discovered in another study. *A. cepa* (15 mg/mL) decreased the levels of IL-10, IL-6, and TNF- $\alpha$  in human UVB-induced inflammation in epidermal keratinocytes (HaCaT cells) [177]. An ethanol extract of *A. cepa* (1, 0.1, 50, 10, and 100 µg/mL) inhibited the secretion of IL-1b, TNF- $\alpha$ , and IL-6, as well as the formation of iNOS, COX-2, MAPKs, and NF- $\kappa$ B in RAW264.7 cells, in a dose-dependent manner [178]. The effects of *A. cepa* (500, 100, and 1000 µg/mL) on osteoclastogenesis in RAW264.7 cells under LPS-induced inflammatory conditions were investigated using the results of *A. cepa* ethanol extract. *A. cepa* also inhibited the synthesis of IL-1a and IL-6, while increasing IL-4 and IL-3 production and inhibiting the NF- $\kappa$ B pathway. In addition, the researchers also found that the topical application of two outer shells (A 20 and 40 mL), 5 days a week, from day 21 to 41 with BALB/c mice with allergic rhinitis, reduces the allergic effects, eosinophil penetration of nasal turbinine mucosa and OVA-specific IgE volumes, five days a week, from day 21 to day 41. Furthermore, amounts in groups treated with onion extract IL-5, IL-4, IL-13, IL-10, and IFN-c were lower [167]. Scientists showed the effects of an ethanol extract of *A. cepa* (100 mg/mL) on LPS-induced inflammation. Inflammatory responses were studied in RAW 264.7 cells, and the findings revealed a dose-dependent reduction in IL-6, TNF- $\alpha$ , and IL-1- $\beta$  secretion, as well as NO production [178]. In LPS-induced BV2 microglial cells (N27A cells), *A. cepa* methanol extract (50, 250, and 500 mg/mL) reduced proinflammatory cytokines TNF- $\alpha$ , IL-6, and IL-1- $\beta$  [155]. In LPS-induced BV-2 microglial cells (N27-A cells), *A. cepa* methanol extract (50, 250, and 500 mg/mL) reduced proinflammatory cytokines IL-6, TNF- $\alpha$ , and IL-1- $\beta$  [163]. Scientists showed the effects of *A. cepa* constituents in a variety of studies. Quercetin (7.5, 3.5, and 15 µg/mL) inhibited the synthesis of Th2 cytokines such as IL-5, IL-4, IgE, and IL-13 in cultured spleen cells stimulated with PWM from *Blomia tropicalis*-sensitized BALB/c mice [163]. In both normal and cyclophosphamide-induced immunosuppression, *A. cepa* agglutinin (Romneycare) has immunoprotective properties. ACA (1, 10, and 100 µg, intraperitoneal) increased serum levels of IL-10, TNF- $\alpha$ , COX-2, IgA, and IgG as well as immune parameters such as myeloid cells (RBC, WBC, and Hb), body weight, splenic index, and thymic index in the spleen and thymus [179]. The immunomodulatory activity of ACA (0.1, 0.01, 10, and 1 µg/well) was tested in RAW264.7 cells and rat peritoneal macrophages. ACA increased the proliferation of murine thymocytes and the expression of IFN-c and IL-2, as well as mediated proinflammatory cytokines including TNF- $\alpha$  and

IL-12 [168]. Additionally, ACA had little effect on the proliferation of B-cell enriched rat splenocytes. Fructooligosaccharides (FOS; 0.5, 5, 50, and 250 mg/mL) from onions increased phagocytic activity in Wistar rats and cell proliferation or mitogenicity in BALB/c mouse's splenocytes and thymocytes. Lectin, a key component of *A. cepa*, has been shown to increase proinflammatory COX-2 and nitric oxide levels, as well as the expression of immunoregulatory cytokines TNF- $\alpha$ , IL-12, IL-2, and IFN- $\gamma$  [179,180]. Immune cells such as cytotoxic T lymphocytes (CD8 cells), T-helper cells (CD4 cells), natural killer cells/monocytes, and T-regulatory cells (CD25<sup>high</sup> CD4 cells) were tested using TLC of Toscana (red onion) bulb extract (CD16 cells). TLC increased the frequency of antitumor/anti-infection NK CD16 immune cells. *A. cepa* and its constituents have immunomodulatory effects in a number of immune dysregulatory disorders, according to the checked in vitro and in vivo studies. The plant and its components, especially quercetin, reduced Th2 cytokines such as IL-5, IL-4, and IL-13, as well as IL-8, IL-6, IL-1 $\beta$ , IL-10, TNF- $\alpha$ , and IgE levels, while increasing IFN- $\gamma$  levels, CD4 cells, and the IFN- $\gamma$ /IL4 ratio (Th1/Th2 balance), implying a stimulatory effect on Th1 but an inhibitory effect on Th2. *A. cepa* and quercetin, on the other hand, decreased IL-6 and IL-1 $\alpha$  synthesis while increasing IL-3 and IL-4 levels in inflammatory conditions including LPS-induced osteoclastogenesis in RAW264.7 cells. In animal models of allergic rhinitis, the plant reduced allergic symptoms, eosinophil penetration of nasal turbinates mucosa, and OVA-specific IgE levels, as well as IL-5, IL-4, IL-13, IL-10, and IFN- $\gamma$  levels. As a consequence, multiple immune dysregulation disorders have been linked to different types of immunomodulatory effects of *A. cepa* and its constituents. *A. cepa* and its constituents, especially quercetin, have previously been shown to be potential immunomodulatory therapeutic candidates for the treatment of immune dysregulation disorders [4,181].

**5.19. Effects in Lung Disorder.** Lung disease encompasses a wide range of conditions involving the lungs, including influenza, tuberculosis, COPD, viruses such as influenza, and measles, lung cancer, and a variety of other respiratory issues. Respiratory failure may occur as a result of certain lung diseases. *A. cepa* plays a great role in reducing different types of lung disorders [182]. Several experiments have been done by researchers showing the effects of *A. cepa* regarding this subject. The researchers randomly assigned Wistar rats to one of three groups: control (C), asthmatic (A), and asthmatic (A), and the asthmatic (A) treated them with dexamethasone (D, 1.25 g/mL) and *A. cepa* extract (AC, 0.35, 0.7, and 0.175 mg/mL). During the sensitization process [183], the scientists applied dexamethasone and *A. cepa* extract to the animals' drinking water. The group of researchers measured the resistance of the trachea to methacholine and ovalbumin, inflammatory cells' numbers in the lung, and the amount of PLA2 in the BALF. When the scientists compared the asthmatic animals to group C, though their tracheal susceptibility to ovalbumin and methacholine, PLA2 standard, overall and most differential

WBC count were improved, but their lymphocytes were reduced ( $p < 0.05$  to  $p$ ). The researchers treated the sensitized rats with dexamethasone and both doses of *A. cepa*, which resulted in a substantial reduction in overall WBC and PLA2 levels when opposed to the asthmatic population ( $p < 0.001$ ) [184]. In comparison to the asthmatic population, the two higher amounts of *A. cepa* resulted in a significant decrease in tracheal tolerance, eosinophil and neutrophil counts [163,184], but significant lymphocyte count raise ( $p < 0.05$  to  $p < 0.001$ ). In comparison with the asthmatic community, treatment with the maximum *A. cepa* concentration substantially decreased the count of monocytes ( $p < 0.001$ ). The protective and anti-inflammatory impact of *A. cepa* on tracheal tolerance and inflammation of lung in asthmatic animals means that it may be used to treat airway disorders like asthma [169]. In sensitized rats, the scientists observed that *A. cepa* extract substantially decreased the levels of IgE, IL-4 and oxidant markers while increasing the levels of IFN- $\gamma$ , the IFN- $\gamma$ /IL-4 ratio, and antioxidant markers. As a result, the plant extract may have therapeutic value by immunomodulatory and antioxidant therapy in the treatment of asthma [169].

**5.20. Hepatoprotective Effects.** Liver harm caused by paracetamol hepatotoxicity is a significant public health concern around the globe [21]. The researchers used methanolic extracts of *A. cepa* to treat paracetamol-induced hepatotoxicity in rats. This study used 54 adult male albino rats, nine of which were mild and 45 were paracetamol hepatotoxic. In this research, the three-by-three Latin square pattern was used as the experimental design. On the first day, the scientists administered 750 mg/kg IP of paracetamol, which resulted in the induction of paracetamol hepatotoxicity. The researchers measured various biochemical parameters before beginning the study and then annually for the remainder of the analysis [22]. Furthermore, they also took monthly blood samples from the rat's eye for examination and obtained the serum by centrifugation (5000 rpm for 10 minutes) and processed at  $-20^{\circ}\text{C}$  prior to processing. Time effects and increased dosages of *A. cepa* methanol extract (200, 300, and 450 mg/kg) [23] resulted in a duration-based major decrease in alanine levels. Paracetamol hepatotoxic rats' aspartate aminotransferase (AST), aminotransferase (ALT), lactate dehydrogenase (LDH), alkaline phosphatase (ALP), and complete serum bilirubin (TSB) after the period when the researchers compared to those of paracetamol, regular, and silymarin control rats *A. cepa* decreased alanine aminotransferase and overall serum bilirubin levels in a dose-dependent way, but not aspartate aminotransferase, alkaline phosphatase, or lactate dehydrogenase levels. *A. cepa* extracts tested positive for hepatoprotective properties [23]. Some researchers wanted to test the antioxidant properties of the onions they took two forms of onions so in both forms of onion samples, the largest concentration of antioxidant compounds was found in the outermost layers of the bulb, with a clear decreasing tendency towards the innermost layers [185]. The scientists analyzed the carbohydrate content of the onion samples



varied (glucose, fructose, and sucrose) [186], which may have a significant impact on the taste (sweetness and pungency) and processing suitability of these onions. The distribution of antioxidant compounds in the onions' outer layers is higher than in their middle and inner layers, which is a significant finding. Unfortunately, customers often remove the exterior layers, depriving them of an essential health-promoting phytochemical [186]. The researchers tested the (in vivo) hepatoprotective effects and the (in vitro) antioxidant activity in male rats [187]. They measured the antioxidant function of *A. cepa* and contrasted it to that of a standard antioxidant, ascorbic acid. It was a 25 day oral administration of 40% ethanol (3.76 g/kg BW) which caused liver damage. The researchers administered *A. cepa* extracts (100, 300, and 600 mg/kg BW) and silymarin (100 mg/kg BW) orally in preventive and therapeutic models in two separate sets of studies. Moreover, they elevated alanine aminotransferase (ALT), serum aspartate aminotransferase (AST), total bilirubin levels, and alkaline phosphatase (ALP), after ethanol administration, indicating significant hepatic harm. The toxic effects of ethanol on the serum parameters above is blocked in preventative and curative models both through the use of silymarin and *A. cepa*. The study results show the important hepatoprotective and antioxidant role of an aqueous extract of *A. cepa* bulb against hepatotoxicity due to ethanol [188].

## 6. Commercial Uses

For its remedial characteristics, *A. cepa* has traditionally been used to treat different conditions. In ancient Greece, *A. cepa*'s nature has increased to purifying blood for athletes. Gladiators rubbed the onion juice to strengthen the muscles after the conquest of Rome. To avoid scurvy, the Greek and Phoenicians sailors ate it. Hippocrates, a Greek physician, also prescribed onion as a wound reliever, diuretic fighter, and pneumonia fighter. The onion was mentioned as one of the essential plants or spices or medicine of India in the 6th century [189]. In the present day, researchers found that Asian nations, namely, India and Pakistan, were among the most widely used in treating diverse ailments with onion. Overall, *A. cepa* has been found to be used in low-developed countries more often. The shortage of medical services and the convenient availability of alternative medicines, including onions, may have contributed to this. *A. cepa* is also taken raw or decoctions to cure infectious diseases. It is also used in a wide range of indoor and outdoor treatments to alleviate various illnesses, including skin conditions, stomach disorders, insect dents, metabolic diseases, and others.

References [45, 190–194], *A. cepa* is intended for use in all food-producing animals. The use incorporates the concepts of homeopathic treatment, in which animals have their diagnostic pattern. The maximum dosage of 10 mL/animal is prescribed. Treatment may be replicated, but homeopathy does not usually have a set dosage schedule. *A. cepa* is also used as a mother tincture in human homeopathy, lower levels, and human phytotherapy. It is used in gastrointestinal, asthma, and bronchitis therapy. The average oral

dosage prescribed per day is 50 g or 20 g of dried onion. In addition, fresh bulbs or extracts are used to cure insect stings and warts. *A. cepa* is a natural human dietary component. There are no literature reviews on human or animal intoxications [189].

## 7. Side Effects and Toxicity

The cytotoxicity of fractioned extract (ethyl acetate, methanolic, and aqueous), extract of blunt onion (OE), and other onion compounds was studied in the Lucena MDR human erythroleukemic cell line and its parental cell line, K562 (quercetin and propyl disulfide) [193]. The researchers investigated OE's ability to trigger apoptosis and/or necrosis in these cells [194] as well as the potential involvement of oxidative stress [10] and DNA injury [10]. Furthermore, the researchers discovered that both tumoral cells have identical sensitivities, but only OE had a noticeable impact on the cells. In the other side, researchers discovered that K562 cells had an increase in apoptosis, whereas Lucena cells had an increase in necrosis. Researchers discovered that OE has an antioxidant potential that protects it from oxidative harm. OE, on the other hand, caused major DNA harm on both cell lines. As a result, OE's ability to defeat the MDR phenotype means that it has anti-MDR properties [10]. In another research, the researchers investigated the cause of onion poisoning-induced hemolysis in dogs. The researchers fed cooked onions to six clinically normal and adult dogs at a pace of 30 grams per kilogram of body weight a day for two days. They took blood tests on days one, three, five, eight, twelve, eighteen, and twenty-four after onion administration, as well as urine the day after bleeding. In comparison to white blood cell counts, red blood cell volumes, hemoglobin, and hematocrit both decreased from day 1 to day 5, with a significant drop on day 5 ( $P = 0.01$ ). On days 3 ( $P = 0.01$ ) and 4, plasma bilirubin and urobilinogen levels both increased ( $P = 0.01$ ). From day one ( $P = 0.01$ ) to day three ( $P = 0.01$ ), the Heinz body counts rose marginally ( $P = 0.01$ ). The number of reticulocytes in the blood increased from day 1 to day 8, with the highest value ( $P = 0.01$ ) on day 8. In addition to anemia, the following erythrocyte parameters are altered: reduced nicotinamide adenine dinucleotide phosphate was reduced on day 1 ( $P = 0.01$ ); glutathione was reduced ( $P = 0.01$ ), with the lowest value on day 3 ( $P = 0.01$ ); glutathione peroxidase was raised on day 1, but slightly decreased on day 5 ( $P = 0.01$ ); erythrocyte membrane deformity decreased on days 1–12, while fluorescence polarization ( $P = 0.01$ ). MDA and  $g$  and  $q$  had significant correlations, with correlation coefficients of 0.922 and 0.908, respectively ( $P = 0.01$ ), but MDA and deformity index had a poor correlation, with a correlation coefficient of 0.887 ( $P = 0.01$ ). According to the experts, onion toxicity causes hemolytic anemia in puppies [11].

## 8. Clinical Studies

Several tests on human were also conducted to understand the pharmacological effect of *A. cepa* (Table 2).

TABLE 2: Clinical studies of *Allium cepa* based on its pharmacological effects.

Field of Study	Subject	Dosage	Outcome	Mechanism of Action	References
Cardioprotective effect	24 healthy pilot	100 mL onion juice/day	Total cholesterol, waist circumference, and LDL-C reduced substantially	Onion juice contains quercetin which markedly attenuated LDL-c, serum total cholesterol, and HDL-c levels in healthy mild hypercholesterolemic subjects	[68]
Wound healing	39 patients	Onion extract ( <i>Allium cepa</i> ) 10%	Hypertrophic scars and keloids were attenuated properly	Onion extracts inhibit vascular endothelial growth factor (VEGF) production which is the prime cause of HTS and keloids	[82]
Antihypertensive effects	70 people	162 mg/day	Systolic BP was reduced by -3.6 mmHg	Mechanisms remain unclear	[133]
Anti-inflammatory effects	In human epidermal keratinocytes	15 mg/mL extract	Stimulatory effect on Th1 and inhibitory effect on Th2 activity	Reduced amounts of IL-6, IL-10, and TNF- $\alpha$	[4]
	Human	10 g/day	Reduced risk of prostate cancer	Activation of detoxifying enzymes by organosulfur compounds	[1]
Anticancer effects	Human	Taking a combination of 200 mg synthetic DATS and 100 $\mu$ g selenium per month/year for 3 years	Gastric cancer risk is reduced	DATS triggers cancer cell cycle arrest at the G2/M phase	[96]
Antihypercholesterolemic effect	24 hypercholesterolemic patients	100 mL onion juice for 8 weeks	Reduction in serum TC, LDL-c, LDL-c/HDL-c levels	Increase LDL receptor mRNA expression and increase bile acid synthesis	[68]
Antiobesity effects	72 overweight and obese humans	50 mg	Reduction in body weight, BMI, waist circumference	As an anti-oxidant, quercetin scavenges free radicals and restores the respiration process in the adipocytes	[127,128]

BW = body weight; n.m. = not mentioned; DATS = diallyl trisulfide; TC = total cholesterol; LDL-c = low density lipoprotein cholesterol; HDL-c = high density lipoprotein cholesterol; HTS = hypertrophic scars; BP = blood pressure; OPE = onion peel extract; ZnO-NPs = zinc oxide nanoparticles.

## 9. Conclusion and Future Perspectives

Inflammation, cancer, diabetes, extreme wounds, gallstones, neurological disorders, and various microorganisms all respond well to onion, making it a high-value food in the therapeutics sector. Onion can be used as a natural and nontoxic substitute for a variety of nutraceutical ingredients. It owns high-food values, i.e., calcium, moisture, phosphorus, protein, iron, fat, vitamin C, minerals, carbohydrates, and fiber. Mass awareness should be created about the importance of this potential food as it has a low toxicity and only moderate side effects. In the field of pharmacology, *A. cepa* has multi-action capabilities, and researchers can continue to investigate its mode of action so that health practitioners can learn from it. Several potential prospects are there in onion research for various areas such as the creation of

resistance types and hybrids to biotic and abiotic factors, higher quality standards, and antidotes for various ailments.

### Data Availability

All the data are available within the article.

### Conflicts of Interest

The authors declare no conflicts of interest.

### Authors' Contributions

A.J.C., T.M.U., and B.M.R.M.Z. conceived and designed the study; A.J.C., T.M.U., S.M., A.R., and T.B.E. wrote the original draft; R.D., F.N., K.D., A.R., M.J.H., and A.K. edited,



critically reviewed, and revised the manuscript; B.M.R.M.Z. and S.M. collected data. All authors have contributed, read, and approved the final manuscript.

## References

- [1] H. A. R. Suleria, M. S. Butt, F. M. Anjum, F. Saeed, and N. Khalid, "Onion: nature protection against physiological threats," *Critical Reviews in Food Science and Nutrition*, vol. 55, no. 1, pp. 50–66, 2015.
- [2] J. D. Teshika, A. M. Zakariyyah, T. Zaynab et al., "Traditional and modern uses of onion bulb (*Allium cepa*L.): a systematic review," *Critical Reviews in Food Science and Nutrition*, vol. 59, no. sup1, pp. S39–S70, 2019.
- [3] C. W. Foo and P. Tristani-Firouzi, "Topical modalities for treatment and prevention of postsurgical hypertrophic scars," *Facial Plastic Surgery Clinics of North America*, vol. 19, no. 3, pp. 551–557, 2011.
- [4] N. Marefati, V. Ghorani, F. Shakeri et al., "A review of anti-inflammatory, antioxidant, and immunomodulatory effects of *Allium cepa* and its main constituents," *Pharmaceutical Biology*, vol. 59, no. 1, pp. 287–302, 2021.
- [5] A. J. Chakraborty, S. Mitra, and T. E. Tallei, "Bromelain a potential bioactive compound: a comprehensive overview from a pharmacological perspective," *Life*, vol. 11, no. 4, 2021.
- [6] S. Mitra, A. Rauf, and A. M. Tareq, "Potential health benefits of carotenoid lutein: an updated review," *Food and Chemical Toxicology*, vol. 154, 2021.
- [7] E. I. Bahbah, S. Ghozy, and M. S. Attia, "Molecular mechanisms of astaxanthin as a potential neurotherapeutic agent," *Marine Drugs*, vol. 19, no. 4, 2021.
- [8] A. Rauf, A. Olatunde, M. Imran et al., "Honokiol: a review of its pharmacological potential and therapeutic insights," *Phytomedicine: International Journal of Phytotherapy and Phytopharmacology*, vol. 90, Article ID 153647, 2021.
- [9] P. Saroj, M. Verma, K. K. Jha, and M. Pal, "An overview on immunomodulation," *Journal of Advanced Scientific Research*, vol. 3, no. 1, pp. 7–12, 2012.
- [10] L. L. Amado, M. L. Garcia, and P. B. Ramos, "A method to measure total antioxidant capacity against peroxy radicals in aquatic organisms: application to evaluate microcystins toxicity," *The Science of the Total Environment*, vol. 407, no. 6, pp. 2115–2123, 2009.
- [11] X. Tang, Z. Xia, and J. Yu, "An experimental study of hemolysis induced by onion (*Allium cepa*) poisoning in dogs," *Journal of Veterinary Pharmacology and Therapeutics*, vol. 31, no. 2, pp. 143–149, 2008.
- [12] M. Marrelli, V. Amodeo, G. Statti, and F. Conforti, "Biological properties and bioactive components of *Allium cepa* L.: focus on potential benefits in the treatment of obesity and related comorbidities," *Molecules*, vol. 24, no. 1, p. 119, 2019.
- [13] K. P. Sampath Kumar, D. Bhowmik, and P. Tiwari, "*Allium cepa*: a traditional medicinal herb and its health benefits," *Journal of Chemical and Pharmaceutical Research*, vol. 2, no. 21, pp. 283–291, 2010.
- [14] D. Prakash, B. N. Singh, and G. Upadhyay, "Antioxidant and free radical scavenging activities of phenols from onion (*Allium cepa*)," *Food Chemistry*, vol. 102, no. 4, pp. 1389–1393, 2007.
- [15] Z. E. Huma, M. A. Vian, A.-S. Fabiano-Tixier, M. Elmaataoui, O. Dangles, and F. Chemat, "A remarkable influence of microwave extraction: enhancement of antioxidant activity of extracted onion varieties," *Food Chemistry*, vol. 127, no. 4, pp. 1472–1480, 2011.
- [16] S.-l. Zhang, P. Deng, Y.-c. Xu, S.-w. Lü, and J.-j. Wang, "Quantification and analysis of anthocyanin and flavonoids compositions, and antioxidant activities in onions with three different colors," *Journal of Integrative Agriculture*, vol. 15, no. 9, pp. 2175–2181, 2016.
- [17] R. M. Pérez-Gregorio, M. S. García-Falcón, J. Simal-Gándara, A. S. Rodrigues, and D. P. F. Almeida, "Identification and quantification of flavonoids in traditional cultivars of red and white onions at harvest," *Journal of Food Composition and Analysis*, vol. 23, no. 6, pp. 592–598, 2010.
- [18] C. H. H. Peter and C. W. Arts, "Flavonols, flavones and flavanols—nature, occurrence and dietary burden," *Journal of the Science of Food and Agriculture*, vol. 80, pp. 1081–1093, 2000.
- [19] T. Fossen and Ø. M. Andersen, "Anthocyanins from red onion, *Allium cepa*, with novel aglycone," *Phytochemistry*, vol. 62, no. 8, pp. 1217–1220, 2003.
- [20] Ž. Fredotović, M. Šprung, and B. Soldo, "Chemical composition and biological activity of *allium cepa* L. and *Allium × cornutum* (Clementi ex Visiani 1842) methanolic extracts," *Molecules*, vol. 22, no. 3, 2017.
- [21] F. J. Vazquez-Armenta, J. F. Ayala-Zavala, G. I. Olivares, F. J. Molina-Corral, and B. A. Silva-Espinoza, "Antibrowning and antimicrobial effects of onion essential oil to preserve the quality of cut potatoes," *Acta Alimentaria*, vol. 43, no. 4, pp. 640–649, 2014.
- [22] S. Imai, N. Tsuge, M. Tomotake et al., "An onion enzyme that makes the eyes water," *Nature*, vol. 419, no. 6908, Article ID 685, 2002.
- [23] D. J. Thomas and K. L. Parkin, "Quantification of Alk(en)yl-cysteine Sulfoxides and Related Amino Acids in Alliums by High-Performance Liquid Chromatography," *Journal of Agricultural and Food Chemistry*, vol. 42, no. 8, pp. 1632–1638, 1994.
- [24] G. Griffiths, L. Trueman, T. Crowther, B. Thomas, and B. Smith, "Onions - a global benefit to health," *Phytotherapy Research*, vol. 16, no. 7, pp. 603–615, 2002.
- [25] L. Liguori, R. Califano, and D. Albanese, "Chemical composition and antioxidant properties of five white onion (*Allium cepa* L.) landraces," *Journal of Food Quality*, vol. 2017, 2017.
- [26] H. X. Wang and T. B. Ng, "Isolation of allicepin, a novel antifungal peptide from onion (*Allium cepa*) bulbs," *Journal of Peptide Science*, vol. 10, no. 3, pp. 173–177, 2004.
- [27] B. Borjihan, A. Ogita, K.-i. Fujita, M. Doe, and T. Tanaka, "The cyclic organosulfur compound zwiebelene a from onion (*Allium cepa*) functions as an enhancer of polymyxin B in fungal vacuole disruption," *Planta Medica*, vol. 76, no. 16, pp. 1864–1866, 2010.
- [28] I. M. Vågen and R. Slimestad, "Amount of characteristic compounds in 15 cultivars of onion (*Allium cepa* L.) in controlled field trials," *Journal of the Science of Food and Agriculture*, vol. 88, no. 3, pp. 404–411, 2008.
- [29] P. Rose, M. Whiteman, P. K. Moore, and Y. Z. Zhu, "Bioactive S-alk(en)yl cysteine sulfoxide metabolites in the genus *Allium*: the chemistry of potential therapeutic agents," *Natural Product Reports*, vol. 22, no. 3, pp. 351–368, 2005.
- [30] R. Munday and C. M. Munday, "Induction of phase II enzymes by aliphatic sulfides derived from garlic and onions: an overview," *Methods in Enzymology*, vol. 382, pp. 449–456, 2004.

- [31] R. Munday and C. M. Munday, "Relative activities of organosulfur compounds derived from onions and garlic in increasing tissue activities of quinone reductase and glutathione transferase in rat tissues," *Nutrition and Cancer*, vol. 40, no. 2, pp. 205–210, 2001.
- [32] Y. Yamazaki, K. Iwasaki, M. Mikami, and A. Yagihashi, "Distribution of eleven flavor precursors, S-Alk(en)yl-L-cysteine derivatives, in seven allium vegetables," *Food Science and Technology Research*, vol. 17, no. 1, pp. 55–62, 2011.
- [33] V. Lanzotti, "The analysis of onion and garlic," *Journal of Chromatography A*, vol. 1112, no. 1–2, pp. 3–22, 2006.
- [34] G. Corea, E. Fattorusso, V. Lanzotti, R. Capasso, and A. A. Izzo, "Antispasmodic saponins from bulbs of red onion, *Allium cepa* L. var. Tropea," *Journal of Agricultural and Food Chemistry*, vol. 53, no. 4, pp. 935–940, 2005.
- [35] H. Xiao and K. L. Parkin, "Isolation and identification of potential cancer chemopreventive agents from methanolic extracts of green onion (*Allium cepa*)," *Phytochemistry*, vol. 68, no. 7, pp. 1059–1067, 2007.
- [36] L. Yuan, T. F. Ji, A. G. Wang, J. B. Yang, and Y. L. Su, "Two new furostanol saponins from the seeds of *Allium cepa* L.," *Chinese Chemical Letters*, vol. 19, no. 4, pp. 461–464, 2008.
- [37] H. A. Wetli, R. Brenneisen, and I. Tschudi, "Gamma-glutamyl-peptide isolated from onion by bioassay guided fractionation inhibits resorption activity of osteoclasts," *Journal of Bone and Mineral Research*, vol. 19, p. S314, 2004.
- [38] M. Langos, W. Hofstetter, and S. Dolder, "A gamma-glutamyl peptide from onion inhibits the development and activity of osteoclasts in vitro," *Planta Medica*, vol. 73, no. 09, 2007.
- [39] N. Benkeblia, "Antimicrobial activity of essential oil extracts of various onions (*Allium cepa*) and garlic (*Allium sativum*)," *Lebensmittel-Wissenschaft und -Technologie- Food Science and Technology*, vol. 37, no. 2, pp. 263–268, 2004.
- [40] R. Kahane, E. Vialle-Guérin, I. Boukema et al., "Changes in non-structural carbohydrate composition during bulbing in sweet and high-solid onions in field experiments," *Environmental and Experimental Botany*, vol. 45, no. 1, pp. 73–83, 2001.
- [41] L. Jaime, F. Martinez, M. A. Martín-Cabrejas et al., "Study of total fructan and fructooligosaccharide content in different onion tissues," *Journal of the Science of Food and Agriculture*, vol. 81, no. 2, pp. 177–182, 2001.
- [42] L. Jaime, M. A. Martín-Cabrejas, E. Mollá, F. J. López-Andréu, and R. M. Esteban, "Effect of storage on fructan and fructooligosaccharide of onion (*Allium cepa* L.)," *Journal of Agricultural and Food Chemistry*, vol. 49, no. 2, pp. 982–988, 2001.
- [43] L. Jaime, E. Mollá, A. Fernández, M. A. Martín-Cabrejas, F. J. López-Andréu, and R. M. Esteban, "Structural carbohydrate differences and potential source of dietary fiber of onion (*Allium cepa* L.) tissues," *Journal of Agricultural and Food Chemistry*, vol. 50, no. 1, pp. 122–128, 2002.
- [44] J. Santas, M. P. Almajano, and R. Carbó, "Antimicrobial and antioxidant activity of crude onion (*Allium cepa*, L.) extracts," *International Journal of Food Science and Technology*, vol. 45, no. 2, pp. 403–409, 2010.
- [45] K. Sharma, N. Mahato, and Y. R. Lee, "Systematic study on active compounds as antibacterial and antibiofilm agent in aging onions," *Journal of Food and Drug Analysis*, vol. 26, no. 2, pp. 518–528, 2018.
- [46] N. Azu, R. Onyeagba, O. Nworie, and J. Kalu, "Antibacterial activity of *Allium cepa* (onions) and *Zingiber officinale* (ginger) on *Staphylococcus aureus* and *Pseudomonas aeruginosa* isolated from high vaginal swab," *The Internet Journal of Tropical Medicine*, vol. 3, no. 2, pp. 1–7, 2006.
- [47] P. Lekshmi, "Antibacterial activity of nanoparticles from *Allium sp* Antibacterial activity of nanoparticles from *Allium sp*," *Journal of Microbiology and Biotechnology Research*, vol. 2, pp. 115–119, 2015.
- [48] A. Saxena, R. M. Tripathi, and R. P. Singh, "Biological synthesis of silver nanoparticles by using onion (*Allium cepa*) extract and their antibacterial activity," *Digest Journal of Nanomaterials and Biostructures*, vol. 5, no. 2, pp. 427–432, 2010.
- [49] A.-N. Zohri, K. Abdel-Gawad, and S. Saber, "Antibacterial, antidermatophytic and antitoxigenic activities of onion (*Allium cepa* L.) oil," *Microbiological Research*, vol. 150, no. 2, pp. 167–172, 1995.
- [50] R. Irkin and M. Korukluoglu, "Control of some filamentous fungi and yeasts by dehydrated *Allium* extracts," *Journal für Verbraucherschutz und Lebensmittelsicherheit*, vol. 4, no. 1, pp. 3–6, 2009.
- [51] R. Irkin and M. Korukluoglu, "Control of *Aspergillus Niger* with garlic, onion and leek extracts," *African Journal of Biotechnology*, vol. 6, no. 4, pp. 384–387, 2007.
- [52] V. Lanzotti, A. Romano, S. Lanzuise, G. Bonanomi, and F. Scala, "Antifungal saponins from bulbs of white onion, *Allium cepa* L.," *Phytochemistry*, vol. 74, pp. 133–139, 2012.
- [53] M. Shams-Ghahfarokhi, M.-R. Shokoohamiri, N. Amirrajab et al., "In vitro antifungal activities of *Allium cepa*, *Allium sativum* and ketoconazole against some pathogenic yeasts and dermatophytes," *Fitoterapia*, vol. 77, no. 4, pp. 321–323, 2006.
- [54] M. Kivanç, "Antimicrobial activity of fresh plant juice on the growth of bacteria and yeasts," *Journal of Qafqaz University*, vol. 1, no. 1, pp. 27–35, 1997.
- [55] S. Kocic-Tanackov, G. Dimic, A. Tepic, and B. Vujcic, "Influence of *Allium ampeloprasum* L. and *Allium cepa* L. essential oils on the growth of some yeasts and moulds," *Zbornik Matice srpske za prirodne nauke*, vol. 116, no. 116, pp. 121–130, 2009.
- [56] S. ur Rahman, S. Khan, N. Chand, U. Sadique, and R. U. Khan, "In vivo effects of *Allium cepa* L. on the selected gut microflora and intestinal histomorphology in broiler," *Acta Histochemica*, vol. 119, no. 5, pp. 446–450, 2017.
- [57] M. Goodarzi, S. Nanekarani, and N. Landy, "Effect of dietary supplementation with onion (*Allium cepa* L.) on performance, carcass traits and intestinal microflora composition in broiler chickens," *Asian Pacific Journal of Tropical Disease*, vol. 4, no. S1, 2014.
- [58] A. Bag and R. R. Chattopadhyay, "Evaluation of synergistic antibacterial and antioxidant efficacy of essential oils of spices and herbs in combination," *PLoS One*, vol. 10, no. 7, 2015.
- [59] B. K. Singh and R. H. S. P. G. C. Singramau, "Assessment of antifungal activity of onion (*Allium cepa* L.) bulb extracts," *International Education And Research Journal*, vol. 3, no. 9, 2017.
- [60] N. Thampi and V. S. Jeyadoss, "In vitro time-kill and anti-radical assays on green onion and garlic against specific diarrheagenic pathogens," *The Scitech Journal*, vol. 02, no. 03, pp. 28–38, 2015.
- [61] F. A. Shakurfow, M. M. Buazzi, and M. A. Gamal, "Assessment of antimicrobial activity of onion (*Allium cepa*) and garlic (*Allium Sativum*) extracts on *Listeria monocytogenes*; in vitro study," vol. 1, no. 1, 2015.
- [62] M. Wensing, S. Ludt, S. Campbell, J. van Lieshout, E. Volbracht, and R. Grol, "European Practice Assessment of

- Cardiovascular risk management (EPA Cardio): protocol of an international observational study in primary care," *Implementation Science: Iscus*, vol. 4, no. 1, pp. 1–8, 2009.
- [63] E. Block, P. F. Purcell, and S. R. Yolen, "Onions and heartburn," *American Journal of Gastroenterology*, vol. 87, no. 5, pp. 679–680, 1992.
- [64] M. Majewska-Wierzbicka and H. Czczot, "[Flavonoids in the prevention and treatment of cardiovascular diseases]," *Polski merkuriusz lekarski*, vol. 32, no. 187, pp. 50–54, 2012.
- [65] S. Jain, H. S. Buttar, M. Chintamneni, and G. Kaur, "Prevention of cardiovascular diseases with anti-inflammatory and anti-oxidant nutraceuticals and herbal products: an overview of pre-clinical and clinical studies," *Recent Patents on Inflammation & Allergy Drug Discovery*, vol. 12, no. 2, pp. 145–157, 2018.
- [66] J. Y. Toh, V. M. Tan, P. C. Lim, S. T. Lim, and M. F. Chong, "Flavonoids from fruit and vegetables: a focus on cardiovascular risk factors," *Current Atherosclerosis Reports*, vol. 15, no. 12, 368 pages, 2013.
- [67] S. Alpsy, C. Aktas, R. Uygur et al., "Antioxidant and anti-apoptotic effects of onion (*Allium cepa*) extract on doxorubicin-induced cardiotoxicity in rats," *Journal of Applied Toxicology*, vol. 33, no. 3, pp. 202–208, 2013.
- [68] L. TsongMing, C. HuiFang, and S. YouCheng, "Hypocholesterolemic efficacy of quercetin rich onion juice in healthy mild hypercholesterolemic adults: a pilot study," *Plant Foods for Human Nutrition*, vol. 70, no. 4, pp. 395–400, 2015.
- [69] C. Shenoy, M. B. Patil, R. Kumar, and S. Patil, "Preliminary phytochemical investigation and wound healing activity of *Allium cepa* linn (*Liliaceae*)," *International Journal of Pharmacy and Pharmaceutical Sciences*, vol. 2, pp. 167–175, 2009.
- [70] S. Wananukul, S. Chatpreodprai, D. Peongsujarit, and P. Lertsapcharoen, "A prospective placebo-controlled study on the efficacy of onion extract in silicone derivative gel for the prevention of hypertrophic scar and keloid in median sternotomy wound in pediatric patients," *Journal of the Medical Association of Thailand = Chotmai het thangphaet*, vol. 96, no. 11, pp. 1428–1433, 2013.
- [71] O. A. Perez, M. H. Viera, J. K. Patel et al., "A comparative study evaluating the tolerability and efficacy of two topical therapies for the treatment of keloids and hypertrophic scars," *Journal of Drugs in Dermatology: Journal of Drugs in Dermatology*, vol. 9, no. 5, pp. 514–518, 2010.
- [72] M. Piķula, M. E. Źebrowska, L. Poblocka-Olech, M. Krauze-Baranowska, M. Sznitowska, and P. Trzonkowski, "Effect of enoxaparin and onion extract on human skin fibroblast cell line - therapeutic implications for the treatment of keloids," *Pharmaceutical Biology*, vol. 52, no. 2, pp. 262–267, 2014.
- [73] J. M. Zurada, D. Kriegel, and I. C. Davis, "Topical treatments for hypertrophic scars," *Journal of the American Academy of Dermatology*, vol. 55, no. 6, pp. 1024–1031, 2006.
- [74] K. S. Gangopadhyay, M. Khan, S. Pandit, S. Chakrabarti, T. K. Mondal, and T. K. Biswas, "Pharmacological evaluation and chemical standardization of an ayurvedic formulation for wound healing activity," *The International Journal of Lower Extremity Wounds*, vol. 13, no. 1, pp. 41–49, 2014.
- [75] S. Shockman, K. V. Paghdal, and G. Cohen, "Medical and surgical management of keloids: a review," *Journal of Drugs in Dermatology: Journal of Drugs in Dermatology*, vol. 9, no. 10, pp. 1249–1257, 2010.
- [76] C. Tianna, S. Andrea, and S. Lucia, "Effect of allium cepa-allantoin-pentaglycan gel on skin hypertrophic scars: clinical and video-capillaroscopic results of an open-label, controlled, nonrandomized clinical trial," *Dermatologic Surgery*, vol. 36, no. 9, pp. 1439–1444, 2010.
- [77] Z. D. Draelos, "The ability of onion extract gel to improve the cosmetic appearance of postsurgical scars," *Journal of Cosmetic Dermatology*, vol. 7, no. 2, pp. 101–104, 2008.
- [78] S. H. Wai, Y. Y. Shun, C. C. Pik, and H. H. Chan, "Use of onion extract, heparin, allantoin gel in prevention of scarring in Chinese patients having laser removal of tattoos: a prospective randomized controlled trial," *Dermatologic Surgery*, vol. 32, no. 7, pp. 891–896, 2006.
- [79] O. Khadzhiiski, R. Diakov, and M. Petrova, "Contractubex used in the treatment of postburn scars and keloids," *Khirurgiia*, vol. 57, no. 3–4, pp. 44–48, 2001.
- [80] W. Stozkowska, S. Janicki, J. Jařkowski, A. Kasprzak, and W. Kondrat, "Technology and preliminary evaluation of ointments that increase the elasticity of post-burn scars," *Wiadomosci Lekarskie*, vol. 37, no. 22, pp. 1770–2176, 1984.
- [81] A. S. Saulis, J. H. Mogford, T. A. Mustoe, E. E. Tredget, and A. Anzarut, "Effect of Mederma on hypertrophic scarring in the rabbit ear model," *Plastic and Reconstructive Surgery*, vol. 110, no. 1, pp. 177–186, 2002.
- [82] A. Campanati, G. Ceccarelli, and V. Brisigotti, "Effects of in vivo application of an overnight patch containing *Allium cepa*, allantoin, and pentaglycan on hypertrophic scars and keloids: clinical, videocapillaroscopic, and ultrasonographic study," *Dermatologic Therapy*, vol. 34, no. 1, 2021.
- [83] S. Dwivedi and Amrita, "Medicinal plants with antiplatelet activity," *Indian Drugs*, vol. 30, no. 11, pp. 539–548, 1993.
- [84] T. Bordia, N. Mohammed, M. Thomson, and M. Ali, "An evaluation of garlic and onion as antithrombotic agents," *Prostaglandins, Leukotrienes and Essential Fatty Acids*, vol. 54, no. 3, pp. 183–186, 1996.
- [85] E. Block, H. Gulati, D. Putman, D. Sha, N. You, and S.-H. Zhao, "Allium Chemistry: synthesis of 1-[Alk(en)ylsulfanyl]propyl Alk(en)yl Disulfides (Cepaenes), Antithrombotic Flavorants from Homogenates of Onion (*Allium cepa*)," *Journal of Agricultural and Food Chemistry*, vol. 45, no. 11, pp. 4414–4422, 1997.
- [86] K. Rahman and G. M. Lowe, "Garlic and cardiovascular disease: a critical review," *Journal of Nutrition*, vol. 136, no. 3, pp. 736S–740S, 2006.
- [87] E. Y. Ko, S. H. Nile, Y. S. Jung, and Y. S. Keum, "Antioxidant and antiplatelet potential of different methanol fractions and flavonols extracted from onion (*Allium cepa* L.)," *3 Biotech*, vol. 8, no. 3, Article ID 155, 2018.
- [88] D. M. Hausman, "What is cancer?" *Perspectives in Biology and Medicine*, vol. 62, no. 4, pp. 778–784, 2019.
- [89] R. C. Maranhão, C. G. Vital, T. M. Tavoni, and S. R. Graziani, "Clinical experience with drug delivery systems as tools to decrease the toxicity of anticancer chemotherapeutic agents," *Expert Opinion on Drug Delivery*, vol. 14, no. 10, pp. 1217–1226, 2017.
- [90] T. Hu, Z. Li, C.-Y. Gao, and C. H. Cho, "Mechanisms of drug resistance in colon cancer and its therapeutic strategies," *World Journal of Gastroenterology*, vol. 22, no. 30, pp. 6876–6889, 2016.
- [91] N. Zamri and H. A. Hamid, "Comparative study of onion (*Allium cepa*) and leek (*allium ampeloprasum*): identification of organosulphur compounds by UPLC-QTOF/MS and anticancer effect on MCF-7 cells," *Plant Foods for Human Nutrition*, vol. 74, no. 4, pp. 525–530, 2019.



- [92] Y. Asemani, N. Zamani, M. Bayat, and Z. Amirghofran, "Allium vegetables for possible future of cancer treatment," *Phytotherapy Research*, vol. 33, no. 12, pp. 3019–3039, 2019.
- [93] Y. Pan, Y. M. Zheng, and W. S. Ho, "Effect of quercetin glucosides from allium extracts on hepG2, PC-3 AND HT-29 cancer cell lines," *Oncology Letters*, vol. 15, no. 4, pp. 4657–4661, 2018.
- [94] W. S. Lee, S. M. Yi, and J. W. Yun, "Polyphenols isolated from *Allium cepa* L. Induces apoptosis by induction of p53 and suppression of bcl-2 through inhibiting PI3K/akt signaling pathway in AGS human cancer cells," *European Journal of Cancer Prevention*, vol. 19, no. 1, pp. 14–22, 2014.
- [95] T. Nohara, Y. Fujiwara, M. El-Aasr et al., "Antitumor allium sulfides," *Chemical and Pharmaceutical Bulletin*, vol. 65, no. 3, pp. 209–217, 2017.
- [96] M. T. Puccinelli and S. D. Stan, "Dietary bioactive diallyl trisulfide in cancer prevention and treatment," *International Journal of Molecular Sciences*, vol. 18, no. 8, 2017.
- [97] N. K. Vu, C. S. Kim, M. T. Ha et al., "Antioxidant and antidiabetic activities of flavonoid derivatives from the outer skins of *Allium cepa* L.," *Journal of Agricultural and Food Chemistry*, vol. 68, no. 33, pp. 8797–8811, 2020.
- [98] M. Sajid Hamid Akash and S. Chen, "Spice plant *Allium cepa*: dietary supplement for treatment of type 2 diabetes mellitus," *Nutrition*, vol. 30, no. 10, pp. 1128–1137, 2014.
- [99] S. Sabiu, M. Madende, A. A.-n. Ajao, R. A. Aladodo, I. O. Nurain, and J. B. Ahmad, "The genus allium (amarillidaceae: alloideae): features, phytoconstituents, and mechanisms of antidiabetic potential of *Allium cepa* and *allium sativum*," *Bioactive Food as Dietary Interventions for Diabetes*, pp. 137–154, 2019.
- [100] A. I. Airaodion, I. U. Akaninyene, K. O. Ngwogu, J. A. Ekenjoku, and A. C. Ngwogu, "Hypolipidaemic and antidiabetic potency of *Allium cepa* (onions) bulb in alloxan-induced diabetic rats," *Acta Scientific Nutritional Health*, vol. 4, no. 3, pp. 01–08, 2020.
- [101] O. S. Ifeanyi, "The antidiabetic effects of the bioactive flavonoid (Kaempferol-3-O-?-D-6{P- coumaroyl} glucopyranoside) isolated from *Allium cepa*," *Recent Patents on Anti-infective Drug Discovery*, vol. 11, no. 1, pp. 44–52, 2016.
- [102] M. Marrelli, V. Amodeo, G. Statti, and F. Conforti, "Biological properties and bioactive components of *allium cepa* L.: focus on potential benefits in the treatment of obesity and related comorbidities," *Molecules*, vol. 24, no. 1, 2019.
- [103] S. Gautam, S. Pal, R. Maurya, and A. K. Srivastava, "Ethanol extract of *Allium cepa* stimulates glucose transporter typ 4-mediated glucose uptake by the activation of insulin signaling," *Planta Medica*, vol. 81, no. 3, pp. 208–214, 2015.
- [104] D. Jini and S. Sharmila, "Green synthesis of silver nanoparticles from *Allium cepa* and its in vitro antidiabetic activity," *Materials Today Proceedings*, vol. 22, pp. 432–438, 2020.
- [105] S. Adam, J. B. Mohammad, and J. H. Ho, "Hypercholesterolaemia - practical information for non-specialists," *Archives of Medical Science*, vol. 14, no. 1, pp. 1–21, 2018.
- [106] W. Li, C. Yang, and X. Mei, "Effect of the polyphenol-rich extract from *Allium cepa* on hyperlipidemic sprague-dawley rats," *Journal of Food Biochemistry*, vol. 45, no. 1, 2021.
- [107] K. Srinivasan, "Anti-cholelethrogenic potential of dietary spices and their bioactives," *Critical Reviews in Food Science and Nutrition*, vol. 57, no. 8, pp. 1749–1758, 2017.
- [108] V. C. Soto, R. E. González, M. M. Sance, and C. R. Galmarini, "*Organosulfur and phenolic content of garlic (Allium sativum*L.) and onion (*Allium cepa*L.) and its relationship with antioxidant activity," *Acta Horticulturae*, vol. 1143, no. 1143, pp. 277–290, 2016.
- [109] K. Jakubczyk, K. Dec, J. Kałduńska, D. Kawczuga, J. Kochman, and K. Janda, "Reactive oxygen species - sources, functions, oxidative damage," *Polski Merkuriusz Lekarski: Organ Polskiego Towarzystwa Lekarskiego*, vol. 48, no. 284, pp. 124–127, 2020.
- [110] S. Di Meo and P. Venditti, "Evolution of the knowledge of free radicals and other oxidants," *Oxidative Medicine and Cellular Longevity*, vol. 2020, 2020.
- [111] V. Rani, G. Deep, R. K. Singh, K. Palle, and U. C. S. Yadav, "Oxidative stress and metabolic disorders: pathogenesis and therapeutic strategies," *Life Sciences*, vol. 148, pp. 183–193, 2016.
- [112] K. Neha, M. R. Haider, A. Pathak, and M. S. Yar, "Medicinal prospects of antioxidants: a review," *European Journal of Medicinal Chemistry*, vol. 178, pp. 687–704, 2019.
- [113] A. M. Pisoschi and P. Aneta, "The role of antioxidants in the chemistry of oxidative stress: a review," *European Journal of Medicinal Chemistry*, vol. 97, pp. 55–74, 2015.
- [114] K. Athreya and M. F. Xavier, "Antioxidants in the treatment of cancer," *Nutrition and Cancer*, vol. 69, no. 8, pp. 1099–1104, 2017.
- [115] A. Lisanti, V. Formica, F. Ianni et al., "Antioxidant activity of phenolic extracts from different cultivars of Italian onion (*Allium cepa*) and relative human immune cell proliferative induction," *Pharmaceutical Biology*, vol. 54, no. 5, pp. 799–806, 2016.
- [116] A. V. González-de-peredo, M. Vázquez-espinoza, and E. Espada-bellido, "Flavonol composition and antioxidant activity of onions (*Allium cepa* L.) based on the development of new analytical ultrasound-assisted extraction methods," *Antioxidants*, vol. 10, no. 2, pp. 1–22, 2021.
- [117] D. P. Xu, Y. Li, X. Meng et al., "Natural antioxidants in foods and medicinal plants: extraction, assessment and resources," *International Journal of Molecular Sciences*, vol. 18, no. 1, 2017.
- [118] D. J. Cherubim, C. V. Martins, L. Fariña, and R. A. Lucca, "Polyphenols as natural antioxidants in cosmetics applications," *Journal of Cosmetic Dermatology*, vol. 19, no. 1, pp. 33–37, 2020.
- [119] K. A. Lee, K.-T. Kim, H. J. Kim et al., "Antioxidant activities of onion (*Allium cepa* L.) peel extracts produced by ethanol, hot water, and subcritical water extraction," *Food Science and Biotechnology*, vol. 23, no. 2, pp. 615–621, 2014.
- [120] S. Kim, D.-B. Kim, W. Jin et al., "Comparative studies of bioactive organosulphur compounds and antioxidant activities in garlic (*Allium sativum* L.), elephant garlic (*Allium ampeloprasum* L.) and onion (*Allium cepa* L.)," *Natural Product Research*, vol. 32, no. 10, pp. 1193–1197, 2018.
- [121] Y.-L. Ma, D.-Y. Zhu, K. Thakur et al., "Antioxidant and antibacterial evaluation of polysaccharides sequentially extracted from onion (*Allium cepa* L.)," *International Journal of Biological Macromolecules*, vol. 111, pp. 92–101, 2018.
- [122] A. E. Omar, H. S. Al-Khalafah, W. A. M. Mohamed et al., "Effects of phenolic-rich onion (*Allium cepa* L.) extract on the growth performance, behavior, intestinal histology, amino acid digestibility, antioxidant activity, and the immune status of broiler chickens," *Frontiers in veterinary science*, vol. 7, Article ID 582612, 2020.
- [123] M. Blüher, "Obesity: global epidemiology and pathogenesis," *Nature Reviews Endocrinology*, vol. 15, no. 5, pp. 288–298, 2019.

- [124] K. B. Smith and M. S. Smith, "Obesity statistics," *Primary Care: Clinics in Office Practice*, vol. 43, no. 1, pp. 121–135, 2016.
- [125] N. Stefan, A. L. Birkenfeld, M. B. Schulze, and D. S. Ludwig, "Obesity and impaired metabolic health in patients with COVID-19," *Nature Reviews Endocrinology*, vol. 16, no. 7, pp. 341–342, 2020.
- [126] Obesity.
- [127] C. L. Haase, K. T. Eriksen, S. Lopes, A. Satylganova, V. Schneck, and P. McEwan, "Body mass index and risk of obesity-related conditions in a cohort of 2.9 million people: Evidence from a UK primary care database," *Obesity Science & Practice*, vol. 7, no. 2, pp. 137–147, 2021.
- [128] Y. Zhao, B. Chen, J. Shen et al., "The beneficial effects of quercetin, curcumin, and resveratrol in obesity," *Oxidative Medicine and Cellular Longevity*, vol. 2017, Article ID 1459497, 2017.
- [129] Y. Ting, W.-T. Chang, D.-K. Shiau, P.-H. Chou, M.-F. Wu, and C.-L. Hsu, "Antiobesity efficacy of quercetin-rich supplement on diet-induced obese rats: effects on body composition, serum lipid profile, and gene expression," *Journal of Agricultural and Food Chemistry*, vol. 66, no. 1, pp. 70–80, 2018.
- [130] C. Yang, L. Li, L. Yang, H. Lü, S. Wang, and G. Sun, "Anti-obesity and Hypolipidemic effects of garlic oil and onion oil in rats fed a high-fat diet," *Nutrition and Metabolism*, vol. 15, no. 1, 43 pages, 2018.
- [131] D. Torres-Villarreal, A. Camacho, H. Castro, R. Ortiz-Lopez, and A. L. de la Garza, "Anti-obesity effects of kaempferol by inhibiting adipogenesis and increasing lipolysis in 3T3-L1 cells," *Journal of Physiology & Biochemistry*, vol. 75, no. 1, pp. 83–88, 2019.
- [132] M. Lu, Y. Cao, J. Xiao, M. Song, and C.-T. Ho, "Molecular mechanisms of the anti-obesity effect of bioactive ingredients in common spices: a review," *Food & Function*, vol. 9, no. 9, pp. 4569–4581, 2018.
- [133] V. Brüll, C. Burak, B. Stoffel-Wagner et al., "Effects of a quercetin-rich onion skin extract on 24 h ambulatory blood pressure and endothelial function in overweight-to-obese patients with (pre)-hypertension: a randomised double-blinded placebo-controlled cross-over trial," *British Journal of Nutrition*, vol. 114, no. 8, pp. 1263–1277, 2015.
- [134] H. Emamat, F. Foroughi, H. Eini-Zinab, and A. Hekmatdoost, "The effects of onion consumption on prevention of nonalcoholic fatty liver disease," *Indian Journal of Clinical Biochemistry*, vol. 33, no. 1, pp. 75–80, 2018.
- [135] R. Das, S. Mitra, and A. M. Tareq, "Medicinal plants used against hepatic disorders in Bangladesh: a comprehensive review," *Journal of Ethnopharmacology*, vol. 282, 2021.
- [136] H. Emamat, F. Foroughi, and H. Eini-Zinab, "The effects of onion consumption on treatment of metabolic, histologic, and inflammatory features of nonalcoholic fatty liver disease," *Journal of Diabetes and Metabolic Disorders*, vol. 15, no. 1, 2016.
- [137] S. Krstin, M. Sobeh, M. Braun, and M. Wink, "Anti-parasitic activities of allium sativum and Allium cepa against trypanosoma b. brucei and Leishmania tarentolae," *Medicine*, vol. 5, no. 2, 37 pages, 2018.
- [138] T.-H. Huang, R. C. Mühlbauer, C.-H. Tang et al., "Onion decreases the ovariectomy-induced osteopenia in young adult rats," *Bone*, vol. 42, no. 6, pp. 1154–1163, 2008.
- [139] E. M. Matheson, A. G. Mainous, and M. A. Carnemolla, "The association between onion consumption and bone density in perimenopausal and postmenopausal non-Hispanic white women 50 years and older," *Menopause*, vol. 16, no. 4, pp. 756–759, 2009.
- [140] C.-H. Tang, T.-H. Huang, C.-S. Chang, W.-M. Fu, and R.-S. Yang, "Water solution of onion crude powder inhibits RANKL-induced osteoclastogenesis through ERK, p38 and NF- $\kappa$ B pathways," *Osteoporosis International*, vol. 20, no. 1, pp. 93–103, 2009.
- [141] Y.-Y. Law, H.-F. Chiu, H.-H. Lee, Y.-C. Shen, K. Venkatakrishnan, and C.-K. Wang, "Consumption of onion juice modulates oxidative stress and attenuates the risk of bone disorders in middle-aged and post-menopausal healthy subjects," *Food & Function*, vol. 7, no. 2, pp. 902–912, 2016.
- [142] H. Sakakibara, S. Yoshino, Y. Kawai, and J. Terao, "Anti-depressant-like effect of onion (allium cepa L.) powder in a rat behavioral model of depression," *Bioscience Biotechnology and Biochemistry*, vol. 72, no. 1, pp. 94–100, 2008.
- [143] M. N. Islam, A. Rauf, and F. I. Fahad, "Superoxide dismutase: an updated review on its health benefits and industrial applications," *Critical Reviews in Food Science and Nutrition*, 2021.
- [144] N. Samad and A. Saleem, "Administration of Allium cepa L. bulb attenuates stress-produced anxiety and depression and improves memory in male mice," *Metabolic Brain Disease*, vol. 33, no. 1, pp. 271–281, 2018.
- [145] A. J. Chakraborty, S. Mitra, T. E. Tallei et al., "Bromelain a potential bioactive compound: a comprehensive overview from a pharmacological perspective," *Life*, vol. 11, no. 4, Article ID 317, 2021.
- [146] M. M. Rahaman, A. Rakib, and S. Mitra, "The genus curcuma and inflammation: overview of the pharmacological perspectives," *Plants*, vol. 10, no. 1, pp. 1–19, 2021.
- [147] H. P. Kim, I. Mani, L. Iversen, and V. A. Ziboh, "Effects of naturally-occurring flavonoids and biflavonoids on epidermal cyclooxygenase and lipoxygenase from Guinea-pigs," *Prostaglandins, Leukotrienes and Essential Fatty Acids*, vol. 58, no. 1, pp. 17–24, 1998.
- [148] J. C. Cumella, H. Faden, and F. Middleton, "Selective activity of plant flavonoids on neutrophil chemiluminescence (CL)," *The Journal of Allergy and Clinical Immunology*, vol. 79, no. 1, Article ID 157, 1987.
- [149] Y. B. Shaik, M. L. Castellani, A. Perrella et al., "Role of quercetin (a natural herbal compound) in allergy and inflammation," *Journal of Biological Regulators and Homeostatic Agents*, vol. 20, no. 3–4, pp. 47–52, 2006.
- [150] J. B. Park, "Effects of typheramide and alfrutamide found in Allium species on cyclooxygenases and lipoxygenases," *Journal of Medicinal Food*, vol. 14, no. 3, pp. 226–231, 2011.
- [151] M. Takahashi and T. Shibamoto, "Chemical compositions and antioxidant/anti-inflammatory activities of steam distillate from freeze-dried onion (Allium cepa L.) sprout," *Journal of Agricultural and Food Chemistry*, vol. 56, no. 22, pp. 10462–10467, 2008.
- [152] M. K. Naseri, M. Arabian, M. Badavi, and A. Ahangarpour, "Vasorelaxant and hypotensive effects of Allium cepa peel hydroalcoholic extract in rat," *Pakistan Journal of Biological Sciences: PJBs*, vol. 11, no. 12, pp. 1569–1575, 2008.
- [153] V. M. Dirsch and A. M. Vollmar, "Ajoene, a natural product with non-steroidal anti-inflammatory drug (NSAID)-like properties?" *Biochemical Pharmacology*, vol. 61, no. 5, pp. 587–593, 2001.
- [154] F. A. Dawud, A. B. Dubo, N. W. Yusuf, and I. A. Umar, "Effects of aqueous extract of Allium cepa (red onion) on



- ovalbumin-induced allergic asthma in wistar rats," *Bayero Journal of Pure and Applied Sciences*, vol. 9, no. 2, 95 pages, 2016.
- [155] M. Jakaria, S. Azam, D. Y. Cho, M. E. Haque, I. S. Kim, and D. K. Choi, "The methanol extract of *Allium cepa* L. Protects inflammatory markers in LPS-induced BV-2 microglial cells and upregulates the antiapoptotic gene and antioxidant enzymes in N27-A cells," *Antioxidants*, vol. 8, no. 9, 2019.
- [156] V. Ghorani, N. Marefati, F. Shakeri, R. Rezaee, M. Boskabady, and M. H. Boskabady, "The effects of allium cepa extract on tracheal responsiveness, lung inflammatory cells and phospholipase A2 level in asthmatic rats," *Iranian Journal of Allergy, Asthma, and Immunology*, vol. 17, no. 3, pp. 221–231, 2018.
- [157] C. G. Vazhappilly, S. A. Ansari, R. Al-Jaleeli et al., "Role of flavonoids in thrombotic, cardiovascular, and inflammatory diseases," *Inflammopharmacology*, vol. 27, no. 5, pp. 863–869, 2019.
- [158] M. Rezaei Golestani, M. Rad, and A. Afkhami Goli, "Analysis and evaluation of antibacterial effects of new herbal formulas, AP-001 and AP-002, against *Escherichia coli* O157:H7," *Life Sciences*, vol. 135, pp. 22–26, 2015.
- [159] J.-Y. Ro, J.-H. Ryu, H.-J. Park, and H.-J. Cho, "Onion (*Allium cepa* L.) peel extract has anti-platelet effects in rat platelets," *SpringerPlus*, vol. 4, no. 1, 17 pages, 2015.
- [160] H. V. Beretta, F. Bannoud, M. Insani et al., "Relationships between bioactive compound content and the antiplatelet and antioxidant activities of six *Allium* vegetable species," *Food Technology and Biotechnology*, vol. 55, no. 2, pp. 266–275, 2017.
- [161] T. Singh and R. K. Goel, "Neuroprotective effect of *Allium cepa* L. in aluminium chloride induced neurotoxicity," *Neurotoxicology*, vol. 49, pp. 1–7, 2015.
- [162] S. Kumar, S. Modgil, S. Bammidi et al., "Allium cepa exerts neuroprotective effect on retinal ganglion cells of pterygopalatine artery (PPA) ligated mice," *Journal of Ayurveda and Integrative Medicine*, vol. 11, no. 4, pp. 489–494, 2020.
- [163] T. T. Oliveira, K. M. Campos, A. T. Cerqueira-Lima et al., "Potential therapeutic effect of *Allium cepa* L. and quercetin in a murine model of *Blomia tropicalis* induced asthma," *Daru Journal of Pharmaceutical Sciences: Journal of Faculty of Pharmacy, Tehran University of Medical Sciences*, vol. 2318 pages, 2015.
- [164] T. Oliveira, C. A. Figueiredo, and C. Brito, "Allium cepa L. and quercetin inhibit RANKL/*porphyromonas gingivalis* LPS-induced osteoclastogenesis by downregulating NF- B signaling pathway," *Evidence-based Complement Alternative Medicine*, vol. 2015, 2015.
- [165] Evidence Based Complementary and Alternative Medicine, "Retracted: Allium cepa L. and Quercetin Inhibit RANKL/*Porphyromonas gingivalis* LPS-Induced Osteoclastogenesis by Downregulating NF-B Signaling Pathway," *Evidence-based Complement Alternative Medicine*, vol. 2019, Article ID 7906103, 2019.
- [166] K. K. Parisa and B. Sayeh, "Study OF allium cepa effect to inhibit the growth OF tumor cells IN BALB/C mice breast cancer model," *Journal Of Sabzevar University Of Medical Sciences*, vol. 25, no. 2, pp. 63–71, 2018.
- [167] M. Y. Seo, K. R. Kim, and J. J. Lee, "Therapeutic effect of topical administration of red onion extract in a murine model of allergic rhinitis," pp. 9–17, 2019.
- [168] V. K. Prasanna and Y. P. Venkatesh, "Characterization of onion lectin (*Allium cepa* agglutinin) as an immunomodulatory protein inducing Th1-type immune response in vitro," *International Immunopharmacology*, vol. 26, pp. 1–10, 2015.
- [169] N. Marefati, N. Eftekhari, M. Kaveh, J. Boskabadi, F. Beheshti, and M. H. Boskabady, "The effect of Allium cepa extract on lung oxidant, antioxidant, and immunological biomarkers in ovalbumin-sensitized rats," *Medical Principles and Practice*, vol. 27, no. 2, pp. 122–128, 2018.
- [170] F. J. E. Vajda, "Neuroprotection and neurodegenerative disease," *Journal of Clinical Neuroscience*, vol. 9, no. 1, pp. 4–8, 2002.
- [171] I.-K. Park and S.-C. Shin, "Fumigant activity of plant essential oils and components from garlic (*allium sativum*) and clove bud (*eugenia caryophyllata*) oils against the Japanese termite (*reticulitermes speratus kolbe*)," *Journal of Agricultural and Food Chemistry*, vol. 53, no. 11, pp. 4388–4392, 2005.
- [172] I.-K. Park, L.-S. Kim, I.-H. Choi, Y.-S. Lee, and S.-C. Shin, "Fumigant activity of plant essential oils and components from *Schizonepeta tenuifolia* against *Lycoriella ingenua* (Diptera: sciaridae)," *Journal of Economic Entomology*, vol. 99, no. 5, pp. 1717–1721, 2006.
- [173] R. S. Mann, R. L. Rouseff, J. M. Smoot, W. S. Castle, and L. L. Stelinski, "Sulfur volatiles from *Allium* spp. affect Asian citrus psyllid, *Diaphorina citri* Kuwayama (Hemiptera: Psyllidae), response to citrus volatiles," *Bulletin of Entomological Research*, vol. 101, no. 1, pp. 89–97, 2011.
- [174] A. Sharaby, H. Abdel-Rahman, and S. Moawad, "Biological effects of some natural and chemical compounds on the potato tuber moth, *Phthorimaea operculella* Zell. (Lepidoptera:Gelechiidae)," *Saudi Journal of Biological Sciences*, vol. 16, no. 1, pp. 1–9, 2009.
- [175] R. K. Upadhyay, "Nutraceutical, pharmaceutical and therapeutic uses of *Allium cepa*: a review," *International Journal of Green Pharmacy*, vol. 10, no. 1, pp. S46–S64, 2016.
- [176] K. P. Mishra, L. Ganju, M. Sairam, P. K. Banerjee, and R. C. Sawhney, "A review of high throughput technology for the screening of natural products," *Biomedicine & Pharmacotherapy*, vol. 62, no. 2, pp. 94–98, 2008.
- [177] F. Wu, Y. Chen, G. Li, D. Zhu, L. Wang, and J. Wang, "Zinc oxide nanoparticles synthesized from *Allium cepa* prevents UVB radiation mediated inflammation in human epidermal keratinocytes (HaCaT cells)," *Artificial Cells, Nanomedicine, and Biotechnology*, vol. 47, no. 1, pp. 3548–3558, 2019.
- [178] N. Ahn, B. Kang, and K. Kim, "Anti-Inflammatory Effect of Ethanol Extract from Onion (*Allium cepa* L.) Peel on Lipopolysaccharide-Induced Inflammatory Responses in RAW 264.7 Cells and Mice Ears," *Journal of the Korean Society of Food Science and Nutrition*, vol. 44, no. 11, pp. 1612–1620, 2015.
- [179] V. P. Kumar and Y. P. Venkatesh, "Alleviation of cyclophosphamide-induced immunosuppression in Wistar rats by onion lectin (*Allium cepa* agglutinin)," *Journal of Ethnopharmacology*, vol. 186, pp. 280–288, 2016.
- [180] V. P. Kumar, K. V. H. Prashanth, and Y. P. Venkatesh, "Structural analyses and immunomodulatory properties of fructo-oligosaccharides from onion (*Allium cepa*)," *Carbohydrate Polymers*, vol. 117, pp. 115–122, 2015.
- [181] A. Lisanti, V. Formica, and F. Ianni, "Antioxidant activity of phenolic extracts from different cultivars of Italian onion (*Allium cepa*) and relative human immune cell proliferative induction," *Pharmaceutical Biology*, vol. 0209, 2016.

- [182] S. Mitra, S. R. Prova, and S. A. Sultana, "Therapeutic potential of indole alkaloids in respiratory diseases: a comprehensive review," *Phytomedicine*, vol. 90, 2021.
- [183] M. Kaveh, A. Eidi, A. Nemati, and M. H. Boskabady, "The Extract of *Portulaca Oleracea* and its Constituent, Alpha Linolenic Acid Affects Serum Oxidant Levels and Inflammatory Cells in Sensitized Rats," *Iranian Journal of Allergy, Asthma and Immunology*, vol. 16, no. 3, pp. 256–270, 2017.
- [184] A. P. Rogerio, A. Kanashiro, C. Fontanari et al., "Anti-inflammatory activity of quercetin and isoquercitrin in experimental murine allergic asthma," *Inflammation Research*, vol. 56, no. 10, pp. 402–408, 2007.
- [185] B. N. Singh, B. R. Singh, R. L. Singh et al., "Polyphenolics from various extracts/fractions of red onion (*Allium cepa*) peel with potent antioxidant and antimutagenic activities," *Food and Chemical Toxicology*, vol. 47, no. 6, pp. 1161–1167, 2009.
- [186] G. J. Hudson, P. M. V. John, B. S. Bailey, and D. A. T. Southgate, "The automated determination of carbohydrate. Development of a method for available carbohydrates and its application to foodstuffs," *Journal of the Science of Food and Agriculture*, vol. 27, no. 7, pp. 681–687, 1976.
- [187] U. E. Obioha, S. M. Suru, K. F. Ola-Mudathir, and T. Y. Faremi, "Hepatoprotective potentials of onion and garlic extracts on cadmium-induced oxidative damage in rats," *Biological Trace Element Research*, vol. 129, no. 1–3, pp. 143–156, 2009.
- [188] J. S. Sidhu, M. Ali, A. Al-Rashdan, and N. Ahmed, "Onion (*Allium cepa* L.) is potentially a good source of important antioxidants," *Journal of Food Science & Technology*, vol. 56, no. 4, pp. 1811–1819, 2019.
- [189] A. Kabrah, *The Antibacterial Activity of Onion on MSSA and MRSA Isolates of Staphylococcus aureus* ProQuest Dissertation & Theses, 2015.
- [190] N. A. Jaradat, O. I. Ayesh, and C. Anderson, "Ethnopharmacological survey about medicinal plants utilized by herbalists and traditional practitioner healers for treatments of diarrhea in the West Bank/Palestine," *Journal of Ethnopharmacology*, vol. 182, pp. 57–66, 2016.
- [191] M. Kılıç, K. Yıldız, and F. M. Kılıç, "Traditional uses of medicinal plants in artuklu, Turkey," *Human Ecology*, vol. 48, no. 5, pp. 619–632, 2020.
- [192] J. D. Teshika, A. M. Zakariyyah, T. Zaynab et al., "Traditional and modern uses of onion bulb (*Allium cepa* L.): a systematic review," *Critical Reviews in Food Science and Nutrition*, vol. 59, no. sup1, pp. S39–S70, 2019.
- [193] G. S. Trindade, M. A. M. Capella, L. S. Capella, O. R. Affonso-Mitidieri, and V. M. Rumjanek, "Differences in sensitivity to UVC, UVB and UVA radiation of a multidrug-resistant cell line overexpressing P-glycoprotein," *Photochemistry and Photobiology*, vol. 69, no. 6, pp. 694–699, 1999.
- [194] A. Lankoff, A. Banasik, G. Obe et al., "Effect of microcystin-LR and cyanobacterial extract from Polish reservoir of drinking water on cell cycle progression, mitotic spindle, and apoptosis in CHO-K1 cells," *Toxicology and Applied Pharmacology*, vol. 189, no. 3, pp. 204–213, 2003.

## Research Article

# Caffeic Acid Prevents Vascular Oxidative Stress and Atherosclerosis against Atherogenic Diet in Rats

Ying Wang <sup>1</sup>, Gurpreet Kaur <sup>2</sup>, Manish Kumar <sup>3</sup>, Ajay Singh Kushwah <sup>2</sup>,  
Atul Kabra <sup>4</sup> and Ritu Kainth <sup>2</sup>

<sup>1</sup>Department of Ophthalmology and Otorhinolaryngology, Xi'an No. 3 Hospital, The Affiliated Hospital of Northwest University, Xi'an, Shaanxi 710018, China

<sup>2</sup>Department of Pharmacology, Amar Shaheed Baba Ajit Singh Jujhar Singh Memorial College of Pharmacy, Bela, Ropar, Punjab, India

<sup>3</sup>Chitkara College of Pharmacy, Chitkara University, Rajpura, Punjab, India

<sup>4</sup>University Institute of Pharma Sciences, Chandigarh University, Gharuan, Mohali, Punjab, India

Correspondence should be addressed to Manish Kumar; [mkpharmacology@gmail.com](mailto:mkpharmacology@gmail.com) and Ajay Singh Kushwah; [kushwah\\_ph05@yahoo.co.in](mailto:kushwah_ph05@yahoo.co.in)

Received 13 November 2021; Accepted 16 December 2021; Published 13 January 2022

Academic Editor: Ruchika Garg

Copyright © 2022 Ying Wang et al. This is an open access article distributed under the Creative Commons Attribution License, which permits unrestricted use, distribution, and reproduction in any medium, provided the original work is properly cited.

Diet and lifestyle play a crucial role in the progress of some cardiovascular disorders (CVDs). Rising interest in natural products and their pharmacological investigations witnessed therapeutic potential against CVDs. Caffeic acid (CA) is an organic composite hydroxycinnamic acid derivative classified among phenolics. It is a secondary metabolite biosynthesized in all plant species in the form of ester conjugates. The reported pharmacological activities of CA are neuroprotective, cardioprotective, hypoglycemic, antioxidant, and immunomodulatory properties. This work is aimed to examine the outcome of CA in atherogenic diet- (Ath-) induced rat model on lipid profile changes and endothelium function. The method involves a study duration of 35 days utilizing ( $n = 6$ ) male Wistar rats (180–200 g) that were fed either normal chow or Ath. Study groups are given (i) normal chow diet, (ii) Ath, (iii) Ath + CA (25 or 50 mg/kg, *p.o.*), (iv) normal chow diet + CA (50 mg/kg, *p.o.*), and (v) Ath + Atorvastatin (ATORVA) (5 mg/kg, *p.o.*). Blood samples were collected at the end of the study to measure serum lipid profile, alanine aminotransferase, aspartate aminotransferase, lactate dehydrogenase, and tissue oxidative stress level. Hemodynamic parameters and aorta staining were performed. CA treatment ameliorated lipid profile and significantly reduced the oxidative stress level. Aorta staining examination revealed a marked reduction of the atherosclerotic lesions. These findings suggested that CA is an effective treatment approach for preventing atherosclerotic lesion progression attributed to protection against oxidative stress and various enzymatic activities in the Ath model.

## 1. Introduction

At present, cardiovascular origin disorders such as atherosclerotic cardiovascular disease (ASCVD) are the chief reason of illness and death across the globe [1]. In addition to well-established risk factors (e.g., hypertension, dyslipidemia, and smoking), some other factors such as choice of lifestyle, food habits, occupation, and physical inactivity complicate body homeostasis that greatly enhances the risk of ASCVD and other cardiometabolic disorders that may

lead to life-threatening situations [2]. Obesity itself jeopardizes health with diminished quality of life [3]. According to an estimate by the WHO (World Health Organization), India spent \$200–250 billion on healthcare (particularly CVDs) over a period of 10 years. Several reasons attributed for the higher affliction rate of CVD, fatal outcomes, and mortality are inherent pathobiological mechanisms, social factors, lifestyle, alcohol abuse (smoking), and their interactions [4]. Amongst various factors, hypercholesterolemia is directly linked with obesity and is the primary trigger of

underlying inflammation, insulin resistance, and oxidative stress [5]. Higher total cholesterol (TC) levels and low-density lipoprotein cholesterol (LDL-C) help immensely foster an atherosclerotic plaque in the coronary artery. Intake of diets with high content of cholesterol and saturated fats (i.e., Western-type diets) for chronic periods are associated with the amplification of risk of CVDs. One of the most common causes of CVDs is hypercholesterolemia, and an increase in serum LDL-C and TC are the most important risk factors for the development of inflammatory insult, damage to the vessel wall, platelet activation, and subsequent progression of atherosclerosis [6]. Gathering of lipids within arterial walls is the hallmark feature in atherosclerosis that leads to fatty streak and formation of lipid-foam cells in the intima of an artery, which ultimately gets hardened and forms plaque, thereby causing artery constriction and hardening resulting in full blockage in later stages [7]. Plaque buildup in the blood vessels of the heart is responsible for the coronary artery disease, which further leads to a heart attack. Similarly, blockage in brain vessels can lead to ischemic stroke that has widespread implications associated with the death of the patient [8].

Atherosclerosis can be healed by altering lifestyle and eating habits. The treatment of atherosclerosis is centered on either lowering cholesterol synthesis or lowering the synthesis of low-density lipoproteins. At present, statins and peroxisome proliferator-activated receptor (PPAR) agonists are the most widely used medications to combat hyperlipidemia and associated cardiovascular ailments [9]. The main mode of action of statins is in the hepatic cells, where they hinder the 3-hydroxy-3-methyl-glutaryl-coenzyme A reductase (HMG-CoA reductase) enzyme, which catalyzes the rate-limiting stage in the metabolic pathway that gives rise to cholesterol and isoprenoids [10, 11]. A few other drugs such as niacin and fibrates are also used across the globe in hypercholesterolemia conditions that target the reduction of LDL-C formation [12]. However, long-term use of statins (e.g., simvastatin and rosuvastatin) has been associated with adverse effects such as dizziness, gastrointestinal complications, muscle pain, sleep problems, decrease in platelet count, hair loss, hepatitis, pancreatitis, and loss of libido (erectile dysfunction) [13]. These adverse effects along with low patient compliance to the existing hypocholesterolemia drugs propelled seeking alternative treatment approaches, which can not only ameliorate the cholesterol profile but also reduce the risk of developing cardiovascular disorders.

Recently, rejuvenated inquisitiveness in medicinal herbs and biological active dietary products have convinced preventive approaches in the therapeutics of CVDs. Considerable attention on plant phenolic compounds suggested potential evidence against many disorders such as cancer, neurodegenerative disorders, and heart diseases. Antioxidant potency and ubiquitous presence in nature render these phenolic compounds easily available, devoid of major adverse effects when consumed in the long term that enhance patient compliance many-fold [14]. Hydroxycinnamic acids are phenolic compounds with many biological effects such as anti-inflammatory [15], antiviral, antibacterial, anti-atherogenic [16], and anticarcinogenic [17]. Although

several derivatives of hydroxycinnamic acid are found in many plants, however, pharmacologically the most essential and common prototype of hydroxycinnamic acids is caffeic acid (CA) (3, 4-dihydroxycinnamic acid). CA occurs in fruits, olives, coffee beans, grains, propolis, and many dietary supplements [18]. Furthermore, CA has free-radical-scavenging and metal ion-chelating properties and can also fortify endogenous antioxidants that form the basis of detoxifying mechanisms in the body [19]. CA targets several signaling pathways (e.g., p38 MAPK, transcription factor and signal transduction 3, metalloproteinase, nuclear factor kappa B, and adhesion molecules) and molecular mechanisms (e.g., nitric oxide, 5-lipoxygenase, calcium, potassium channels, and adrenergic receptors) associated with oxidative stress, inflammation, and immunomodulation that may modify the pathogenesis of hypercholesterolemia and CVDs [17, 20]. As CA is an antioxidant, it may shield cell components against oxidative mutilation and consequently impede the peril of numerous degenerative ailments linked with pro-oxidative sequences [21].

## 2. Methods and Materials

**2.1. Experimental Animal and Study Protocol.** Albino Wistar rats of either sex (6–8 weeks old having  $180 \pm 20$  g body weight) were arbitrarily selected from the departmental animal facility. Standard size polypropylene cages with husk as bedding were used to house the animals under regulated temperature ( $23 \pm 2^\circ\text{C}$ ), humidity ( $40 \pm 10\%$ ), and a 12:12 h dark/light cycle environment using artificial lights. As per CPCSEA guiding principles, typical diet and reverse osmosis purified water was offered to the rats *ad libitum*. The research protocol had been permitted by the Institutional Animal Ethics Committee (IAEC) of Amar Shaheed Baba Ajit Singh Jujhar Singh Memorial College of Pharmacy, Bela, Ropar, Punjab (Approval no. ASCB/IAEC/08/15/101). Five rats per cage were allowed to acclimatize for one week before the experiments. Figure 1 illustrates a schematic demonstration of the experimental design and treatment timeline. The atherosclerogenic diet (Ath) model was used to induce atherosclerosis in rats. The composition of the diet (for 1 kg) was as follows: normal chow diet (945 g), cholesterol (10 g), pig lard (25 g), multivitamins (10 g), and minerals (10 g) [22]. Thirty animals were randomly divided into six groups ( $n = 6$  in each group) in a single-blind pattern: (i) control group, (ii) Ath control (atherogenic diet), (iii) Ath + CA (25 mg/kg), (iv) Ath + CA (50 mg/kg), (v) control + CA (50 mg/kg), and (vi) Ath + Atorvastatin (ATORVA) (5 mg/kg). Both test drugs, CA (25 and 50 mg/kg) [23–25], and standard drugs, Atorvastatin (5 mg/kg) [26], were administered once a day daily for 30 days *via* the intraperitoneal (*i.p.*) route. In previous studies, no major adverse effects of CA were reported at dose range (5–200 mg/kg) in rats; however, some minor side effects were apparent in pregnant female mice [27, 28]. Control and Ath control groups received an equivalent volume of drug vehicle (normal saline with dose-volume 5 ml/kg) alone for 30 consecutive days. Control and control + CA (50 mg/kg) groups were given a normal chow diet. The mean body weight of rats was analyzed on the first



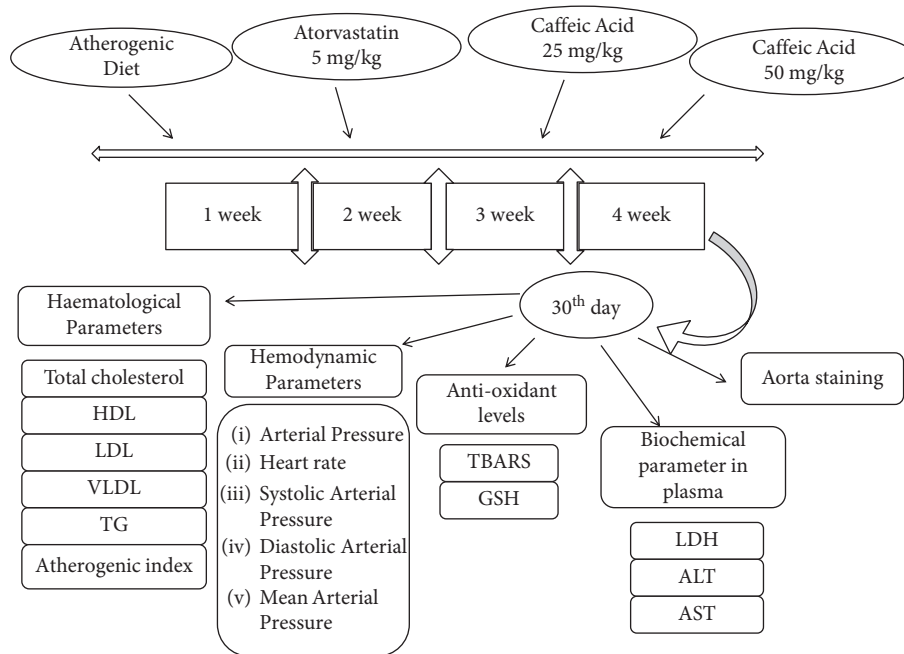


FIGURE 1: Experimental design.

day and subsequently weekly monitored. Blood samples were taken on day 30, and the cervical dislocation technique under anesthesia (sodium pentobarbitone, 150 mg/kg, *i.p.*) was used to euthanize all the animals.

**2.2. Estimation of Hemodynamic Functions.** Rats were subjected to anesthesia using 25% urethane (1.5 g/kg, *i.p.*). During whole investigational procedures, body temperature of the animals was sustained at  $37 \pm 0.5^\circ\text{C}$  using a heating pad. To perform a tracheotomy, the neck region was cut open with a ventral midline incision. The left carotid artery was cannulated using a polyethylene tube (external diameter 0.40 mm; internal diameter 0.30 mm) fastened to a 3-way cannula. The cannula was heparinized (heparin 300 IU/ml), and for the measurement of heart rate (HR), systolic (SAP), diastolic (DAP), and mean arterial pressures (MAPs), it was attached to POWER LAB 4/30 (AD Instruments, NSW, Australia) arrangement using a pressure transducer.

**2.3. Assessment of Biomarkers in Blood Samples.** After the completion of drug treatment duration, the blood samples (1.5–2 ml) were taken by piercing retro-orbital plexus of rats. Serum was isolated from blood by centrifuging (REMI, Mumbai) the samples for 10 min at room temperature with 1000  $\times$ g force to execute biochemical tests. Separated serum diverse enzyme markers such as alanine aminotransferase (ALT/SGPT) (IU/L), aspartate aminotransferase (AST/SGOT) (IU/L), and lactate dehydrogenase (LDH) (IU/L) were quantified. Lipid profile was evaluated by quantifying total cholesterol (TC; mg/dL), HDL (high-density lipoprotein; mg/dL), LDL (low-density lipoprotein; mg/dL), VLDL (very-low-density lipoprotein; mg/dL), and triglycerides (mg/dL) levels in the blood samples [29]. Atherogenic index

in plasma (AIP) was quantified using the formula  $\text{AIP} = (\text{TC} - \text{HDL})/\text{HDL}$ . Standard techniques were followed for quantification of the enzyme activities and lipid profile as per the instructions booklet given in the kits procured from Arkray Healthcare Pvt., Ltd., Mumbai (India) (AutoSpan®) and Reckon Diagnostics P. Ltd., Vadodara (India).

**2.4. Evaluation of Oxidative Stress Biomarkers.** Immediately after blood sample collection, the rats were humanely euthanized using a cervical dislocation technique under anesthesia. The entire heart was surgically removed, pulverized to minor parts (1 cm<sup>3</sup>), and prepared for the preparation of 10% w/v homogenate. Subsequently, the heart sections were homogenized (REMI, Mumbai) in ice-cold phosphate-buffered saline (0.05 M PBS) and centrifuged (3000  $\times$ g, 10 min, 4°C) to obtain the supernatant that was skimmed off for assessment of biomarkers of oxidative stress [29]. Thiobarbituric acid reactive substances (TBARS) were estimated to determine malondialdehyde levels ( $\mu\text{mol/ml}$ ), which is a key lipid peroxidation product [30]. Reduced glutathione (GSH) (nmol/ml) level was estimated to assess endogenous antioxidant levels [31]. Standard protocols were followed for estimating the biomarkers of oxidative stress.

**2.5. Aorta Staining Method.** The external wall of the aorta was organized for amputation of perivascular fat, and the aorta was stained using dye Oil Red O (ORO) as defined in previous reports [32]. After euthanasia of all the animals, the aorta was harvested and rinsed swiftly in cold water to get rid of surplus blood and tissues. The aortic section was positioned in 10% formalin solution for 10 min duration. Afterward, it was rinsed using phosphate buffer solution (pH



7.4 PBS) two or three times as required. Each section was dipped in the ORO solution for 15 min duration at room temperature. Oil Red O-stained regions were quantified using the Image Pro Plus image analysis system.

**2.6. Statistical Analysis.** Data were gathered and subsequently analyzed by an experienced researcher using a one-way ANOVA followed by Tukey's multiple comparison tests. Data were stated as mean  $\pm$  standard error of the mean (S.E.M.) in this study. A value of  $p < 0.05$  was deemed to be significant.

### 3. Results

**3.1. CA Prevents Body Weight Gain in Rats Maintained on Ath.** The Ath control group exhibited a significant ( $p < 0.001$ ) increase in mean body weight (g) when juxtaposed to the saline control group. Ath+CA 25 mg/kg rats showed a significant decline in the mean body weight ( $p < 0.001$ ) relative to the Ath control group. The higher dose of CA (50 mg/kg) and standard drug (ATORVA 5 mg/kg) showed a significant ( $p < 0.001$ ) reduction in the mean body weight of rats that were given Ath diet in comparison to rats in the Ath control group (Figure 2).

**3.2. CA Prevents Ath-Triggered Derangement of Serum Biomarkers.** Ath substantially ( $p < 0.001$ ) augmented the serum levels of ALT, AST, VLDL, LDL, TC triglycerides, LDH activity, and AIP (atherogenic index in plasma) and lowered HDL level when juxtaposed to control treatment. Intraperitoneal injections (for 30 days daily) of CA 25 mg/kg exhibited marked decline in the plasma ALT ( $p < 0.001$ ), AST ( $p < 0.01$ ), VLDL ( $p < 0.001$ ), LDL ( $p < 0.001$ ), TC ( $p < 0.001$ ), triglycerides ( $p < 0.001$ ), LDH ( $p < 0.001$ ) activity, AIP ( $p < 0.001$ ), and enhancement in HDL ( $p < 0.001$ ) relative to Ath control. Ath+CA 50 mg/kg and Ath+ATORVA (5 mg/kg) groups displayed a decrease in the serum ALT ( $p < 0.001$ ), AST ( $p < 0.001$ ), VLDL ( $p < 0.001$ ), LDL ( $p < 0.001$ ), TC ( $p < 0.001$ ), triglycerides ( $p < 0.001$ ), LDH ( $p < 0.01$ ), and AIP ( $p < 0.001$ ) and an increase in HDL ( $p < 0.001$ ) content in relation with Ath control group (Table 1).

**3.3. CA Improves Hemodynamic Parameters in Rats against Ath.** Ath administration substantially ( $p < 0.001$ ) amplified the SAP (systolic arterial pressure), HR (heart rate), DAP (diastolic arterial pressure), and decreased AP (arterial pressure) and MAP (mean arterial pressure) levels when juxtaposed to control treatment. Daily CA (25 mg/kg) treatments for 30 days significantly attenuated Ath caused upsurge in SAP ( $p < 0.05$ ), HR ( $p < 0.001$ ), DAP ( $p < 0.05$ ) and also averted the reduction in AP ( $p < 0.05$ ) and MAP ( $p < 0.05$ ) in comparison with Ath control. The Ath+CA 50 mg/kg group exhibited a significant diminution in the levels of SAP ( $p < 0.001$ ), HR ( $p < 0.001$ ), and DAP ( $p < 0.01$ ) and also displayed a significant upsurge in AP ( $p < 0.01$ ) and MAP ( $p < 0.01$ ) relative to the Ath control

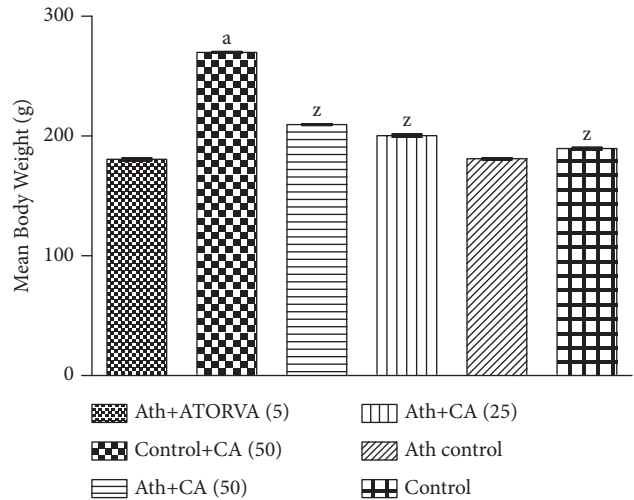


FIGURE 2: Caffeic acid (CA, 25 and 50 mg/kg) prevents body weight gain in rats exposed to atherosclerogenic diet (Ath). Values are expressed as mean  $\pm$  S.E.M. <sup>a</sup> $p < 0.001$  vs. the control group; <sup>z</sup> $p < 0.001$  vs. the Ath control group.

group. The standard group Ath+ATORVA (5 mg/kg) exhibited a significant diminution in the levels of SAP ( $p < 0.001$ ), HR ( $p < 0.001$ ), and DAP ( $p < 0.001$ ) and also a significant growth in AP ( $p < 0.001$ ) and MAP ( $p < 0.001$ ) as compared to the Ath control group (Table 2).

**3.4. CA Prevents Ath-Induced Increase in Oxidative Stress.** Atherosclerogenic diet instigated a significant ( $p < 0.001$ ) intensification in the levels of thiobarbituric acid reactive substances (TBARS) and diminution ( $p < 0.001$ ) in the levels of GSH in the whole heart when juxtaposed to vehicle treatment. CA (25 mg/kg, 50 mg/kg) or ATORVA (5 mg/kg) long-term treatment in Wistar rats significantly ( $p < 0.001$ ) diminished the cardiac TBARS level against Ath in relation with rats that were given Ath and vehicle only. The Ath-induced decline in GSH levels was conspicuously averted by CA *i.p.* injections (25 mg/kg,  $p < 0.01$ ; 5 mg/kg,  $p < 0.001$ ) relative to rats treated with Ath and vehicle (Table 3). ATORVA (5 mg/kg)-treated rats also showed substantially ( $p < 0.001$ ) enhanced GSH content relative to vehicle-treated Ath control rats. CA 50 mg/kg produced an antioxidative effect at par with the standard drug ATORVA against Ath diet in this study.

**3.5. Effects of CA on the Staining of the Aorta.** The aortic lesion percentage was found high in the Ath control group relative to normal chow diet groups (Figure 3). The aortic lesion percentage was decreased by atorvastatin (5 mg/kg) and moderately decreased by caffeic acid (25 and 50 mg/kg, *i.p.*) treatments relative to the Ath control group (Table 4).

### 4. Discussion

Approximately a century has witnessed considerable research and efforts in the field of cardiovascular disorders, particularly coronary heart disease biology and

TABLE 1: Effects of caffeic acid (CA) against atherogenic diet- (Ath-) induced alteration(s) in blood biochemistry.

Group	Cholesterol (mg/dL)	HDL (mg/dL)	LDL (mg/dL)	VLDL (mg/dL)	TG (mg/dL)	LDH (IU/L)	ALT (IU/L)	AST (IU/L)	AIP
Control	157.2 ± 1.515	65.17 ± 0.307	74.16 ± 0.477	30.17 ± 0.477	120.1 ± 0.167	130.1 ± 0.307	80.5 ± 0.428	9 ± 0.365	1.6 ± 1.141
Ath control	321.5 ± 2.861 <sup>a</sup>	25.17 ± 0.307 <sup>a</sup>	212.3 ± 0.615 <sup>a</sup>	62.5 ± 0.563 <sup>a</sup>	346 ± 0.365 <sup>a</sup>	345.3 ± 0.307 <sup>a</sup>	131 ± 0.365 <sup>a</sup>	51.33 ± 0.365 <sup>a</sup>	10.7 ± 0.23 <sup>a</sup>
Ath + CA (25 mg/kg)	238.5 ± 3.442 <sup>z</sup>	35.0 ± 0.3651 <sup>z</sup>	139.8 ± 0.477 <sup>z</sup>	42.5 ± 0.428 <sup>z</sup>	250.83 ± 0.307 <sup>z</sup>	236.5 ± 0.31 <sup>z</sup>	119.16 ± 0.494 <sup>z</sup>	31 ± 0.516 <sup>z</sup>	5.4 ± 1.374 <sup>z</sup>
Ath + CA (50 mg/kg)	187.2 ± 2.926 <sup>z</sup>	48.5 ± 0.2236 <sup>z</sup>	109.6 ± 0.558 <sup>z</sup>	37 ± 0.447 <sup>z</sup>	160.8 ± 0.401 <sup>z</sup>	191.8 ± 0.308 <sup>z</sup>	97.83 ± 0.365 <sup>z</sup>	22 ± 0.364 <sup>z</sup>	3.13 ± 1.137 <sup>z</sup>
Control + CA (50 mg/kg)	157.8 ± 2.428	67.0 ± 0.333	70.8 ± 0.428	28.5 ± 0.429	119.6 ± 0.494	128 ± 0.365	78 ± 0.365	7 ± 0.966	1.4 ± 1.031
Ath + ATORVA (5)	131.7 ± 2.076 <sup>z</sup>	48.0 ± 0.365 <sup>z</sup>	92.5 ± 0.5 <sup>z</sup>	33.6 ± 0.333 <sup>z</sup>	131.1 ± 0.307 <sup>z</sup>	161 ± 0.365 <sup>z</sup>	88.3 ± 0.364 <sup>z</sup>	18.1 ± 0.477 <sup>z</sup>	2.5 ± 0.118 <sup>z</sup>

Values are expressed as mean ± S.E.M. <sup>a</sup>  $p < 0.001$  vs. the control group, <sup>z</sup>  $p < 0.001$  vs. the Ath control group. Data are analyzed using one-way ANOVA followed by Tukey's HSD *post hoc* test. HDL: high-density lipoprotein, LDL: low-density lipoprotein, VLDL: very-low-density lipoprotein, TG: triglyceride, AIP: atherogenic index in plasma.

TABLE 2: Effects of caffeic acid (CA) against atherogenic diet- (Ath-) induced alteration(s) in hemodynamic parameters.

Group	AP (mmHg)	HR (BPM)	MAP (mmHg)	SAP (mmHg)	DAP (mmHg)
Control	120.1 ± 2.913	374.2 ± 8.171	120.06 ± 3.28	121.13 ± 4.248	85.5 ± 2.32
Ath control	96.33 ± 2.883 <sup>a</sup>	449.2 ± 7.977 <sup>a</sup>	93.36 ± 4.222 <sup>a</sup>	144.15 ± 4.19 <sup>a</sup>	99.83 ± 2.822 <sup>a</sup>
Ath + CA (25 mg/kg)	104.8 ± 2.315 <sup>x</sup>	403.8 ± 4.512 <sup>z</sup>	110 ± 3.235 <sup>x</sup>	134.3 ± 4.006 <sup>x</sup>	97.5 ± 3.334 <sup>x</sup>
Ath + CA (50 mg/kg)	112.8 ± 2.496 <sup>y</sup>	386.7 ± 6.168 <sup>z</sup>	114.7 ± 3.63 <sup>y</sup>	129.5 ± 2.754 <sup>z</sup>	95.17 ± 3.229 <sup>y</sup>
Control + CA (50 mg/kg)	118.2 ± 5.029	372 ± 3.715	108.2 ± 4.672	121.3 ± 3.989	81.67 ± 1.054 <sup>z</sup>
Ath + ATORVA (5)	114.67 ± 4.167 <sup>z</sup>	380.2 ± 4.665 <sup>z</sup>	119.2 ± 3.26 <sup>z</sup>	125.3 ± 2.499 <sup>z</sup>	83.17 ± 1.797 <sup>z</sup>

Values are expressed as mean ± S.E.M. <sup>a</sup> $p < 0.001$  vs. the control group, <sup>x</sup> $p < 0.05$ , <sup>y</sup> $p < 0.01$ , and <sup>z</sup> $p < 0.001$  vs. the Ath control group. Data are analyzed using one-way ANOVA followed by Tukey's HSD *post hoc* test. AP: arterial pressure, BPM: beats per minute, HR: heart rate, MAP: mean arterial pressure, SAP: systolic arterial pressure, DAP: diastolic arterial pressure.

TABLE 3: Effects of caffeic acid against atherogenic diet- (Ath-) induced alteration(s) in oxidative stress markers.

Group	MDA ( $\mu$ mol/ml)	GSH (nmol/ml)
Control	0.499 ± 0.003	0.468 ± 0.024
Ath control	0.859 ± 0.004 <sup>a</sup>	0.133 ± 0.017 <sup>a</sup>
Ath + CA (25 mg/kg)	0.738 ± 0.012 <sup>z</sup>	0.229 ± 0.013 <sup>y</sup>
Ath + CA (50 mg/kg)	0.62 ± 0.006 <sup>z</sup>	0.387 ± 0.042 <sup>z</sup>
Control + CA (50 mg/kg)	0.503 ± 0.0004	0.438 ± 0.02
Ath + ATORVA (5)	0.515 ± 0.002 <sup>z</sup>	0.433 ± 0.004 <sup>z</sup>

Values are expressed as mean ± S.E.M. <sup>a</sup> $p < 0.001$  vs. the control group, <sup>y</sup> $p < 0.01$ , <sup>z</sup> $p < 0.001$  vs. the Ath control group. Data are analyzed using one-way ANOVA followed by Tukey's HSD *post hoc* test. MDA: malondialdehyde, GSH: glutathione.

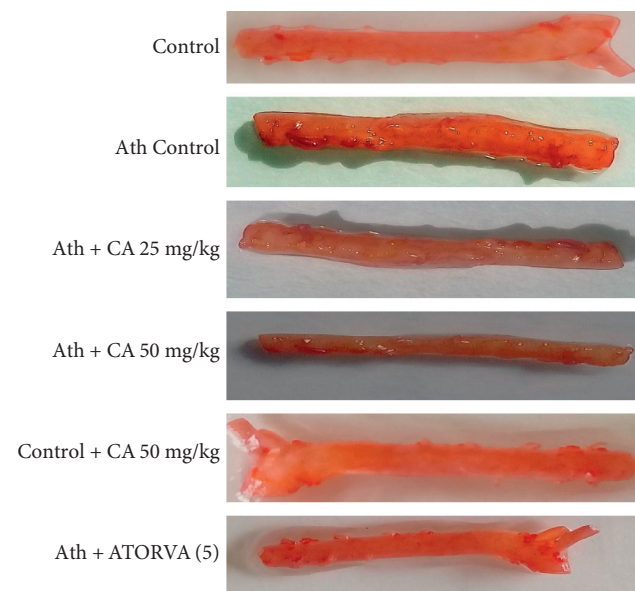


FIGURE 3: Caffeic acid (CA, 25 and 50 mg/kg) prevents aortic lesions in rats exposed to atherosclerogenic diet (Ath).

pathogenesis. Evidence substantiates the intricate involvement of dietary habits, tobacco, alcohol abuse, and physical inactivity in the initiation of coronary heart diseases [33]. Right from the initial stages, it is well recognized that higher consumption of dietary fats is an important inducer of coronary heart disease. Complex interactions between diet, lifestyle, and lipoprotein metabolism govern the progress of atherosclerosis and its associated complications. Various high-fat diet-induced experimental atherosclerosis animal models are available to assess the pathogenesis of atherosclerosis. A rise in body mass/weight and aggregation of fat is

TABLE 4: Effect of caffeic acid on aortic lesions (%).

Group	Aortic lesion (%)
Control	1.34
Ath control	11.8
Ath + CA (25 mg/kg)	10.07
Ath + CA (50 mg/kg)	8.4
Control + CA (50 mg/kg)	1.3
Ath + ATORVA (5)	7.5

the leading pointers for the steady advancement of obesity [34]. Hyperlipidemia is the foremost hazard aspect for atherosclerosis that triggers inflammation and activates platelets and angiotensin-II leading to vascular smooth muscle proliferation and plaque formation. Epidemiological examination exposed a positive relationship between the degree of severity of atherosclerosis and the concentrations of blood cholesterol including LDL [35]. Ath augments lipid levels in the body and predisposes towards atherosclerosis [36].

In this study, supplementation of Ath resulted in a rise in the content of diverse lipids, namely, TC, LDL, VLDL, and triglycerides, in the bloodstream and a decline in HDL levels. Ath might damage endothelial cell function and integrity by augmenting free radicals and peroxidation of lipids, proteins, and genetic material. Estimation of biomarkers of oxidative insult disclosed that Ath supplementation caused an increase in MDA and a decrease in GSH in the heart homogenates. Atherosclerosis is a result of oxidative damage of the endothelial (or intimal) lining of vessels due to free radicals or lipid-free radical interaction toxins such as malondialdehyde or 4-hydroxy 2-nonenal [5]. An enhancement in the concentration of serum cholesterol and triglycerides of atherosclerosis rats may be a result of lipid peroxidation evoked by a high-fat diet [6]. GSH protects

against oxidative damage by the removal of surplus free radicals and associated toxic adducts. GSH is an important tripeptide that acts as a major source of -SH (thiol) antioxidant [37]. Lipid peroxidation with pathogenic protein and DNA modifications helps immensely in the progression of atherosclerosis [21]. Experimental evidence substantiates that endothelial injury amplifies reactive oxygen species that trigger the peroxidation of cellular PUFAs (polyunsaturated fatty acids) that corroborates both functional losses of the myocardium and structural injury [8]. However, Ath-induced increase in TC, LDL, VLDL, and triglycerides in the bloodstream and a decline in HDL levels were attenuated by CA and the standard drug (ATORVA) in the existing study. Furthermore, AIP was decreased by CA and AORVA against Ath in rats. Data from previous studies also indicated that antioxidants impart reduction in atherosclerogenic factors [38]. In preclinical and clinical studies, data suggested that hypocholesterolemia agents can reduce clinical complications of atherosclerosis and prolong the life of a person by lowering the cardiovascular risk.

As a result of endothelial and intimal damage, cytosolic enzymes such as ALT and AST are released into the bloodstream with an increase in LDH activity and assist as the diagnostic indicators of myocardial tissue mutilation [39]. Ath is a well-known causative factor in myocardial tissue necrosis and heart dysfunctions marked by amplified end-diastolic volume, end-diastolic pressure, and left ventricular wall thickness. Long-term treatment with CA averted the escalation of ALT, AST, and LDH activities in the blood of animals that were given Ath for 30 days daily.

Triglycerides and lipids can be stained by Oil Red O that is a lysochrome (fat-soluble) diazo dye. This dye selectively stains fatty aggregates on the tissue surface [32]. Current experimental data suggest an 88.6% upsurge in aortic lesions in the Ath control group that was reduced to 36% in ATORVA (5 mg/kg)- and 15.3% and 27.2% in CA (25, 50 mg/kg)-treated groups, respectively. These findings indicate that CA has the potential to restrict the aortic lesions against Ath and this reduction in the aortic lesion is at par relative to ATORVA (standard drug).

## 5. Conclusions

The findings of the existing study indicate that caffeic acid (CA) might be used as an antiatherosclerogenic drug that lowers oxidative stress, ameliorate lipid levels, and reduce aortic injury. However, a deep insight is required to explore its exact antiatherosclerogenic mechanism by using different agonists and antagonists and molecular techniques to assess the role of signaling pathways. Furthermore, derivatives of CA can also enhance the bioavailability and efficacy against atherosclerosis. Further clinical investigations are required to substantiate the therapeutic use of CA in cardiovascular disorders such as atherosclerosis.

## Data Availability

Data of this study are available upon suitable request from the corresponding author.

## Ethical Approval

All the animal experiments were approved by the IAEC (Approval no. ASCB/IAEC/08/15/101) and were performed as per the ethical guidelines on animal experimentations provided by the Committee for the Purpose of Control and Supervision of Experiments on Animals (CPCSEA), GOI, New Delhi.

## Conflicts of Interest

The authors declare no conflicts of interest.

## Acknowledgments

The authors are appreciative to the Amar Shaheed Baba Ajit Singh Jujhar Singh Memorial College of Pharmacy, BELA (Ropar), for facilitation of the essential research amenities.

## References

- [1] A. B. Reiss, D. S. Glass, I. Voloshyna, A. D. Glass, L. J. Kasselmann, and J. De Leon, "Obesity and atherosclerosis: the exosome link," *Vessel Plus*, vol. 4, p. 19, 2020.
- [2] J. H. Park, S. J. Yoon, H. Lee et al., "Burden of disease attributable to obesity and overweight in Korea," *International Journal of Obesity*, vol. 30, pp. 1661-1669, 2006.
- [3] R. S. Pelman and D. S. Elterman, "Lifestyle and disease, male health and risks," *Revista Médica Clínica Las Condes*, vol. 25, pp. 25-29, 2014.
- [4] H. Thomas, J. Diamond, A. Vieco et al., "Global atlas of cardiovascular disease 2000-2016," *Global Heart*, vol. 13, pp. 143-163, 2018.
- [5] A. N. Hamlin, S. Chinnarasu, Y. Ding, and X. Xian, "Low density lipoprotein receptor-related protein-1 dysfunction synergizes with dietary cholesterol to accelerate steatohepatitis progression," *Journal of Biological Chemistry*, vol. 293, pp. 9674-9684, 2018.
- [6] P. J. Gallagher, R. F. Grimble, P. C. Calder, and C. P. Shearman, "Managing hypercholesterolemia and its correlation with carotid plaque morphology in patients undergoing carotid endarterectomy," *Vascular Health and Risk Management*, vol. 4, pp. 1259-1264, 2008.
- [7] Y. Gu and J. Yin, "Saturated fatty acids promote cholesterol biosynthesis: effects and mechanisms," *Obesity Medicine*, vol. 18, Article ID 100201, 2020.
- [8] F. R. Maxfield and G. V. Meer, "Cholesterol, the central lipid of mammalian cells," *Current Opinion in Cell Biology*, vol. 22, pp. 422-429, 2010.
- [9] S. C. Berghuanu, M. C. Bodde, and J. W. Jukema, "Pathophysiology and treatment of atherosclerosis," *Netherlands Heart Journal*, vol. 25, no. 4, pp. 231-242, 2017.
- [10] M. Gupta and A. Kumar, "Comparison of minimum inhibitory concentration (mic) value of statin drugs: a systematic review," *Antiinfective Agents*, vol. 17, pp. 4-19, 2019.
- [11] R. Rana, R. Sharma, and A. Kumar, "Repurposing of existing statin drugs for treatment of microbial infections: how much promising?" *Infectious Disorders - Drug Targets*, vol. 19, pp. 224-237, 2019.
- [12] T. N. Nguyen, "New standards for intracranial atherosclerotic disease treatment," *Frontiers in Neurology*, vol. 2, p. 3389, 2011.



- [13] S. Ramkumar, A. Raghunath, and S. Raghunath, "Statin therapy: review of safety and potential side effects," *Acta Cardiologica Sinica*, vol. 32, pp. 631–639, 2016.
- [14] G. S. Četković, S. M. Djilas, J. M. Čanadanović-Brunet, and V. T. Tumbas, "Antioxidant properties of marigold extracts," *Food Research International*, vol. 37, pp. 643–650, 2004.
- [15] K. S. Kumaran and P. S. M. Prince, "Protective effect of caffeic acid on cardiac markers and lipid peroxide metabolism in cardiotoxic rats: an in vivo and in vitro study," *Metabolism*, vol. 59, pp. 1172–1180, 2010.
- [16] I. Gülçin, "Antioxidant activity of caffeic acid (3,4-dihydroxycinnamic acid)," *Toxicology*, vol. 217, pp. 213–220, 2006.
- [17] K. M. M. Espíndola, R. G. Ferreira, L. E. M. Narvaez et al., "Chemical and pharmacological aspects of caffeic acid and its activity in hepatocarcinoma," *Frontiers in Oncology*, vol. 9, p. 541, 2019.
- [18] L. d. L. d. Oliveira, M. V. d. Carvalho, and L. Melo, "Health promoting and sensory properties of phenolic compounds in food," *Revista Ceres*, vol. 61, no. suppl, pp. 764–779, 2014.
- [19] B. Shao, L. Mao, M. Tang et al., "Caffeic acid phenyl ester (CAPE) protects against iron-mediated cellular dna damage through its strong iron-binding ability and high lipophilicity," *Antioxidants*, vol. 10, 2021.
- [20] H. Silva and N. M. F. Lopes, "Cardiovascular effects of caffeic acid and its derivatives: a comprehensive review," *Frontiers in Physiology*, vol. 11, Article ID 595516, 2020.
- [21] Ü. Görkem, C. Togrul, I. Sahin et al., "Protective effect of caffeic acid phenethyl ester (CAPE) on ischemia-reperfusion injury in rat ovary," *International Journal of Morphology*, vol. 35, pp. 141–147, 2017.
- [22] S. Leite Matos, H. de Paula, M. Lúcia Pedrosa et al., "Dietary models for inducing hypercholesterolemia in rats," *Brazilian Archives of Biology and Technology*, vol. 48, pp. 203–209, 2005.
- [23] J. Anwar, R. M. Spanevello, G. Thomé et al., "Effects of caffeic acid on behavioral parameters and on the activity of acetylcholinesterase in different tissues from adult rats," *Pharmacology Biochemistry and Behavior*, vol. 103, no. 2, pp. 386–394, 2012.
- [24] G. Liang, B. Shi, W. Luo, and J. Yang, "The protective effect of caffeic acid on global cerebral ischemia-reperfusion injury in rats," *Behavioral and Brain Functions*, vol. 11, p. 18, 2015.
- [25] W. Xu, Q. Luo, X. Wen, M. Xiao, and Q. Mei, "Antioxidant and anti-diabetic effects of caffeic acid in a rat model of diabetes," *Tropical Journal of Pharmaceutical Research*, vol. 19, pp. 1227–1232, 2020.
- [26] T. J. Khan, Y. M. Ahmed, M. A. Zamzami et al., "Effect of atorvastatin on the gut microbiota of high fat diet-induced hypercholesterolemic rats," *Scientific Reports*, vol. 8, p. 662, 2018.
- [27] A. Hagiwara, M. Hirose, S. Takahashi, K. Ogawa, T. Shirai, and N. Ito, "Forestomach and kidney carcinogenicity of caffeic acid in F344 rats and C57BL/6N x C3H/HeN F1 mice," *Cancer Research*, vol. 51, pp. 5655–5660, 1991.
- [28] Y. Liu, S. Qiu, L. Wang et al., "Reproductive and developmental toxicity study of caffeic acid in mice," *Food and Chemical Toxicology*, vol. 123, pp. 106–112, 2019.
- [29] G. Kaur, T. B. Shivanandappa, M. Kumar, and A. S. Kushwah, "Fumaric acid protect the cadmium-induced hepatotoxicity in rats: owing to its antioxidant, anti-inflammatory action and aid in recast the liver function," *Naunyn-Schmiedeberg's Archives of Pharmacology*, vol. 393, pp. 1911–1920, 2020.
- [30] H. Ohkawa, N. Ohishi, and K. Yagi, "Assay for lipid peroxides in animal tissues by thiobarbituric acid reaction," *Analytical Biochemistry*, vol. 95, pp. 351–358, 1979.
- [31] G. L. Ellman, "Tissue sulfhydryl groups," *Archives of Biochemistry and Biophysics*, vol. 82, no. 1, pp. 70–77, 1959.
- [32] J. J. Nunnari, T. Zand, I. Joris, and G. Majno, "Quantitation of oil red O staining of the aorta in hypercholesterolemic rats," *Experimental and Molecular Pathology*, vol. 51, pp. 1–8, 1989.
- [33] D. Prabhakaran, P. Jeemon, and A. Roy, "Cardiovascular diseases in India: current epidemiology and future directions," *Circulation*, vol. 133, pp. 1605–1620, 2016.
- [34] S. S. Shah, G. B. Shah, S. D. Singh et al., "Effect of piperine in the regulation of obesity-induced dyslipidemia in high-fat diet rats," *Indian Journal of Pharmacology*, vol. 43, pp. 296–299, 2011.
- [35] M. Haberka, M. Skilton, M. Biedroń et al., "Obesity, visceral adiposity and carotid atherosclerosis," *Journal of Diabetic Complications*, vol. 33, pp. 302–306.
- [36] A. M. Okafor, E. K. Ngwu, and R. N. B. Ayogu, "Prevalence and associated factors of dyslipidaemia among university workers in Southeast Nigeria: a cross-sectional study," *Archives of Public Health*, vol. 79, pp. 1–9, 2021.
- [37] L. M. LeBlanc, A. F. Paré, J. Jean-Francois, M. J. G. Hébert, M. E. Surette, and M. Touaibia, "Synthesis and antiradical/antioxidant activities of caffeic acid phenethyl ester and its related propionic, acetic, and benzoic acid analogues," *Molecules*, vol. 17, pp. 14637–14650, 2012.
- [38] X. Yang, Y. Li, Y. Li et al., "Oxidative stress-mediated atherosclerosis: mechanisms and therapies," *Frontiers in Physiology*, vol. 8, p. 600, 2017.
- [39] S. S. Ali, W. A. N. W. Ahmad, S. B. Budin, and S. Zainalabidin, "Implication of dietary phenolic acids on inflammation in cardiovascular disease," *Reviews in Cardiovascular Medicine*, vol. 21, pp. 225–240, 2020.



## Research Article

# Distribution of Therapeutic Efficacy of Ranunculales Plants Used by Ethnic Minorities on the Phylogenetic Tree of Chinese Species

Da-Cheng Hao <sup>1,2</sup>, Yulu Zhang <sup>1</sup>, Chun-Nian He <sup>3</sup>, and Pei-Gen Xiao <sup>3</sup>

<sup>1</sup>Biotechnology Institute, School of Environment and Chemical Engineering, Dalian Jiaotong University, Dalian 116028, China

<sup>2</sup>Institute of Molecular Plant Science, University of Edinburgh, Edinburgh EH9 3BF, UK

<sup>3</sup>Institute of Medicinal Plant Development, Chinese Academy of Medical Sciences, Beijing 100193, China

Correspondence should be addressed to Da-Cheng Hao; haodc@126.com and Pei-Gen Xiao; pgxiao@implad.ac.cn

Received 6 November 2021; Revised 3 December 2021; Accepted 9 December 2021; Published 12 January 2022

Academic Editor: Jelena Zivkovic

Copyright © 2022 Da-Cheng Hao et al. This is an open access article distributed under the Creative Commons Attribution License, which permits unrestricted use, distribution, and reproduction in any medium, provided the original work is properly cited.

The medicinal properties of plants can be evolutionarily predicted by phylogeny-based methods, which, however, have not been used to explore the regularity of therapeutic effects of Chinese plants utilized by ethnic minorities. This study aims at exploring the distribution law of therapeutic efficacy of Ranunculales plants on the phylogenetic tree of Chinese species. We collected therapeutic efficacy data of 551 ethnomedicinal species belonging to five species-rich families of Ranunculales; these therapeutic data were divided into 15 categories according to the impacted tissues and organs. The phylogenetic tree of angiosperm species was used to analyze the phylogenetic signals of ethnomedicinal plants by calculating the net relatedness index (NRI) and nearest taxon index (NTI) in R language. The NRI results revealed a clustered structure for eight medicinal categories (poisoning/intoxication, circulatory, gastrointestinal, eyesight, oral, pediatric, skin, and urinary disorders) and overdispersion for the remaining seven (neurological, general, hepatobiliary, musculoskeletal, otolaryngologic, reproductive, and respiratory disorders), while the NTI metric identified the clustered structure for all. Statistically, NRI and NTI values were significant in 5 and 11 categories, respectively. It was found that *Mahonia eurybracteata* has therapeutic effects on all categories. iTOL was used to visualize the distribution of treatment efficacy on species phylogenetic trees. By figuring out the distribution of therapeutic effects of Ranunculales medicinal plants, the importance of phylogenetic methods in finding potential medicinal resources is highlighted; NRI, NTI, and similar indices can be calculated to help find taxonomic groups with medicinal efficacy based on the phylogenetic tree of flora in different geographic regions.

## 1. Introduction

The vascular plants, thriving in diverse environments, include mosses, liverworts, ferns, gymnosperms (conifers), and angiosperms (flowering plants) [1]. Among these taxonomic groups, angiosperms are the latest in evolution, but have the most species; in accordance with their strong environmental adaptability, a majority of phytometabolites with known/potential services to humankind is from angiosperms [2]. There are more than 10,000 extant genera and more than 200,000 species of angiosperms in our planet, accounting for more than half of all plant species. There are more than 2,700 genera and more than 30,000 known species

of angiosperms in China, which represents one of the most species-rich areas of the world. The survival and health of human beings are closely related to angiosperms; more than 50 ethnic minorities in China have accumulated rich experiences in collecting and applying botanical drugs [3], especially those from angiosperms. In China, there are 10,027 kinds of medicinal angiosperms (including the infraspecies taxonomic units) [4], accounting for 90% of Chinese medicinal species. Most of the traditional Chinese medicine (TCM) and ethnomedicine/folk medicine are from angiosperms, but the quantitative study exploring the association between Chinese angiosperm phylogeny and various therapeutic effects of phytomedicine is rare [5, 6], and the

traditional medicinal knowledge of China ethnic minorities has not been elaborated within the context of plant phylogeny. The continued globalization of herbal medicine, badly controlled exploitative practices, and inadequate conservation efforts are pushing many precious medicinal plants to the edge of extinction. Meanwhile, traditional therapeutic knowledge is being eroded due to changing lifestyles, awareness, social transformations, and acculturation [7]. Phylogenetic methods constantly reveal the predictive ability of traditional medical knowledge in bioprospecting and pharmaceutical resource discovery [8–11], which, however, has not been systematically utilized in scrutinizing and expanding Chinese ethnomedicinal resources. We hypothesize that the traditionally used ethnomedicinal plants in China can be quantitatively and phylogenetically explored, which afford generally applicable clues for bio-screening medicinal flora and discovering alternative/complementary medicine.

The medicinal value of plants is an essential part of ecosystem services. The botanical chemo diversity, based on plant biodiversity [6], is the cornerstone of pharmacotherapy diversity of plants and plant-based products. In many areas, medicinal herbs were the main approaches of traditional therapies, which were considered the main lifeline and recurrently were the first and/or only choice [7]. About 80% of plant species used globally as drug sources have an ethnomedicinal use identical or related to the current use of active elements of the plant [12]. Therefore, ecosystem services are closely related to human well-being. The rapid growth of population and public health crisis faced by many regions, especially in developing countries, make it imperative to find alternative and complementary phytomedicine resources [13]. Due to the lack of awareness of environmental protection, human activities have caused severe damage to the ecological environment, in which numerous factors play an important role in the formation and accumulation of effective components of medicinal plants [14]. In view of the importance of ethnomedicinal plants in combating diseases and improving primary healthcare, it is a must to strengthen the protection of medicinal plant resources, and the most fundamental is to protect the ecological environment.

Phylogenetic approaches may help in finding resources for natural and eco-friendly therapy [15]. China is an ideal country to analyze the phylogenetic model of medicinal plants, because of the diversity and good regional phylogeny of Chinese traditional medicinal plants [16–18]. Many secondary metabolites of ethnomedicinal plants of Ranunculales, for example, alkaloids, terpenoids, and flavonoids, have unique functions and biological activities, providing a probability premise for appropriately targeting the dysfunctional organs of the human body [19, 20]. For example, berberine extracted from *Coptis* of Ranunculaceae had a synergistic anticancer effect by inducing apoptosis and inhibiting cell proliferation of esophageal cancer cells [21]. Five benzyloquinoline alkaloids (columbamine, palmatine, dauricine, jatrorrhizine, and berberine; BIAs) from *Dichocarpum* of Ranunculaceae had the *in vitro* inhibitory activity against acetylcholinesterase [22, 23].

Therefore, taking the order Ranunculales as a representative, we aim at studying the distribution pattern of Chinese ethnomedicinal plants on the phylogenetic tree by combining the species phylogenetic tree of Chinese angiosperms and therapeutic data of ethnomedicinal plants at the species level.

## 2. Materials and Methods

**2.1. Efficacy Arrangement of Ethnomedicinal Plants.** In the Chinese Dictionary of Ethnic Medicine [3], 180 ethnomedicine books and 1,118 journal papers published by various ethnic groups in the past 40 years were cited. It is confirmed that there are 7,736 kinds of drugs used by 53 ethnic minorities in China, including 7,022 phytomedicines, 551 animal drugs, and 163 mineral drugs, among which 656 are also recorded in Chinese Pharmacopoeia. The data of skin efficacy were also searched in NCBI PubMed and China National Knowledge Infrastructure (<https://cnki.net/>). The therapeutic effects of 551 medicinal species, including 104 varieties, in five species-rich families were collected and summarized (Table S1), which involve 300 Ranunculaceae species (54.4% of all species), 69 Berberidaceae species (12.5%), 42 Menispermaceae species (7.6%), 14 Lardizabalaceae species (2.5%), and 126 Papaveraceae species (22.9%). All curative effects were divided into 15 categories: poisoning/intoxication, circulatory diseases, gastrointestinal diseases, nervous system diseases, eye diseases, other/general diseases, hepatobiliary diseases, musculoskeletal diseases, oral diseases, ear/nose/throat diseases, pediatric diseases, reproductive system diseases, respiratory diseases, skin diseases, and urinary diseases. The therapeutic efficacy of ethnomedicinal plants was coded with binary characters: when a species has the efficacy of treating specific diseases, it is 1; otherwise, it is 0.

**2.2. Phylogenetic Tree of Ranunculales.** The phylogenetic tree used in this study is full\_tree\_461.tre (<http://www.darwintree.cn/resource/Nature2018/>), which is the overall phylogenetic diversity model of China angiosperms constructed by Lu et al. [17] at the species level. The phylogenetic data of 92% angiosperms in Chinese flora are utilized in this large tree, which is a nearly complete species-level phylogenetic tree including 26,978 species. The Ranunculales subtree was extracted from the above large tree, including Ranunculaceae, Berberidaceae, Menispermaceae, Lardizabalaceae, Circaeasteraceae, Papaveraceae, and Eupteleaceae; the scientific names of species are mainly based on the Flora of China (<http://www.iplant.cn/frps>). The R packages Picante [24] and Ape (<https://cran.r-project.org/web/packages/ape/>) were used to generate the subtree with the following commands: `sample <- read.csv("species.csv," header = T), tree <- read.tree("full_tree_461.tre"), tip.all <- tree$tip.label, tip.not <- tip.all[!tip.all%in%(sample[,1])], length(tip.not), tr.new <- drop.tip(tree,tip.not), write.tree(tr.new, "phylo_zhang_MGM.tree"), read.tree("phylo_zhang_MGM.tree"). iTOL v6 (https://itol.embl.de/) was used to draw and visualize the phylogenetic tree of Ranunculales.`

### 2.3. Statistics and Calculation of Phylogenetic Distribution.

The NRI (net relatedness index) was used to quantify the mean pairwise phylogenetic distance (MPD) of ethnomedicinal plants [10], which designates the dispersion of medicinal uses toward the root of phylogeny. The NTI (nearest taxon index) is a standardized index to measure the average phylogenetic distance between each sample and its nearest taxon, which can be used to calculate the mean nearest taxon distance (MNTD); NTI describes the dispersion of medicinal uses toward the tips of phylogeny [9]. The positive values of these two indicators suggest the phylogenetic aggregation of medicinal species, whereas negative values indicate that species with the same therapeutic use are dispersed in the phylogenetic tree [9]. The observed patterns of species distribution were compared with the expected patterns to quantitatively assess whether the values of NRI and NTI were statistically significant ( $p < 0.05$ ). The calculation formula is as follows:

$$\text{NRI} = -1 \times \frac{\text{MPD}_{\text{obs}} - \text{MPD}_{\text{null}}}{\text{sd}(\text{MPD}_{\text{null}})}, \quad (1)$$

where  $\text{MPD}_{\text{obs}}$  is the observed MPD,  $\text{MPD}_{\text{null}}$  is the expected MPD of the randomized group, and  $\text{sd}(\text{MPD}_{\text{null}})$  is the standard deviation of  $\text{MPD}_{\text{null}}$ . The NTI is given as

$$\text{NTI} = -1 \times \frac{\text{MNTD}_{\text{obs}} - \text{MNTD}_{\text{null}}}{\text{sd}(\text{MNTD}_{\text{null}})}, \quad (2)$$

where  $\text{MNTD}_{\text{obs}}$  denotes the observed MNTD, whereas  $\text{MNTD}_{\text{null}}$  denotes the expected MNTD of the randomized group, and  $\text{sd}(\text{MNTD}_{\text{null}})$  denotes the standard deviation of  $\text{MNTD}_{\text{null}}$  [25].

The functions `ses.mpd` and `ses.mntd` of Picante package [24] were used to calculate the NRI and NTI, respectively. The “`taxa.labels`” was used as the null model, which shuffles the distance matrix labels across all taxa included in the distance matrix with 999 runs; “`mpd.obs.p`” is the  $p$  value of observed MPD vs. null communities (=  $\text{mpd.obs.rank}/(\text{runs} + 1)$ ). R language codes for the construction of tree as well as calculation of the NRI and NTI are shown in the Supplementary text and are available from the authors upon request.

## 3. Results

**3.1. Distribution of Therapeutic Efficacy in the Order Ranunculales.** In Chinese ethnomedicinal plants of Ranunculales (Figure 1), the highest number of species (435, 78.9% of all medicinal species) is used for the treatment of general/other diseases, followed by musculoskeletal disease (389), skin disease (348), and gastrointestinal disease (343). The least species are used to treat pediatric diseases (73, 13.2% of species). The NRI designates the dispersion of medicinal uses toward the root of phylogeny [9]. A clustered structure was suggested by NRI values ( $>0$ ) for eight categories, that is, poisoning/intoxication (e.g., *Anemone*, Ranunculaceae; Tables S1 and S2), circulatory disease (*Corydalis*, Papaveraceae), gastrointestinal disease (*Aconitum*, Ranunculaceae), eye disease (*Thalictrum*, Ranunculaceae),

oral disease (*Aconitum*), pediatric disease (*Thalictrum*), skin disease (*Aconitum*), and urinary disease (*Clematis*, Ranunculaceae). The other seven categories were of overdispersion ( $\text{NRI} < 0$ ), although it still can be seen that there are more therapeutic species against nervous system diseases, other/general diseases, hepatobiliary diseases, musculoskeletal diseases, and respiratory diseases in *Corydalis* (Table S1), and species against ear/nose/throat diseases and reproductive system diseases are concentrated in *Berberis* (Berberidaceae) and *Clematis*, respectively. The NTI describes the dispersion of medicinal uses toward the tips of phylogeny [9], and the clustered structure was suggested for all 15 categories ( $\text{NTI} > 0$ ). In a statistical test, the NRI suggested that five categories, that is, eye diseases, oral diseases, ear/nose/throat diseases, skin diseases, and urinary diseases, are of cluster with statistical significance ( $p < 0.05$ ; Table 1), whereas the NTI suggested 11 categories with statistically significant cluster ( $p < 0.05$ ). Both the NRI and the NTI suggest eye diseases, oral diseases, skin diseases, and urinary diseases as statistically significant clustered.

It is found that 66 Ranunculales species, accounting for 12% of species, have therapeutic effects on no less than ten categories of diseases (Table 2). For example, *Mahonia eurybracteata* of Berberidaceae showed medicinal utilities against all 15 categories. In Dong medicine, the whole plant is used against rheumatic pain, bruise and swelling pain, stomach cold pain, snake/centipede bite, and the like [3]; in Tu Jia medicine, its efficacy is the same as that of *M. bealei*. Three multipurpose species covering 14 therapeutic categories are *M. bealei*, *M. fortunei*, and *M. gracilipes*; no wonder the Chinese name of the genus *Mahonia* literally means “the top ten credits.” Three *Tinospora* species, two *Berberis* species, and two *Aconitum* species have 13 therapeutic categories (Table 2).

### 3.2. Distribution of Therapeutic Efficacy in Five Major Families of Ranunculales.

Among Chinese ethnomedicinal plants of Ranunculaceae (buttercup family), the highest number of species (233, 77.7% of species; Table S2) is used for the treatment of general/other diseases, followed by musculoskeletal diseases (199), skin diseases (199), and gastrointestinal diseases (188). The least species are used to treat circulatory diseases (27, 9% of species). A clustered structure was suggested by NRI values ( $>0$ ) for 10 categories, whereas the other five categories were of overdispersion ( $\text{NRI} < 0$ ). The clustered structure was suggested by  $\text{NTI} > 0$  for 13 categories. In the statistical test, the NRI suggested that six categories, that is, circulatory disease, nervous system diseases, eye diseases, pediatric diseases, reproductive system diseases, and urinary diseases, are of cluster with statistical significance ( $p < 0.05$ ; Table S2), whereas the NTI suggested six categories with statistically significant cluster ( $p < 0.05$ ). Both the NRI and the NTI suggest eye diseases, reproductive system diseases, and urinary diseases as significantly clustered.

In Chinese ethnomedicinal plants of Berberidaceae (barberry family), the highest number of species (56, 81.1% of species; Table S2) is used for the treatment of general/

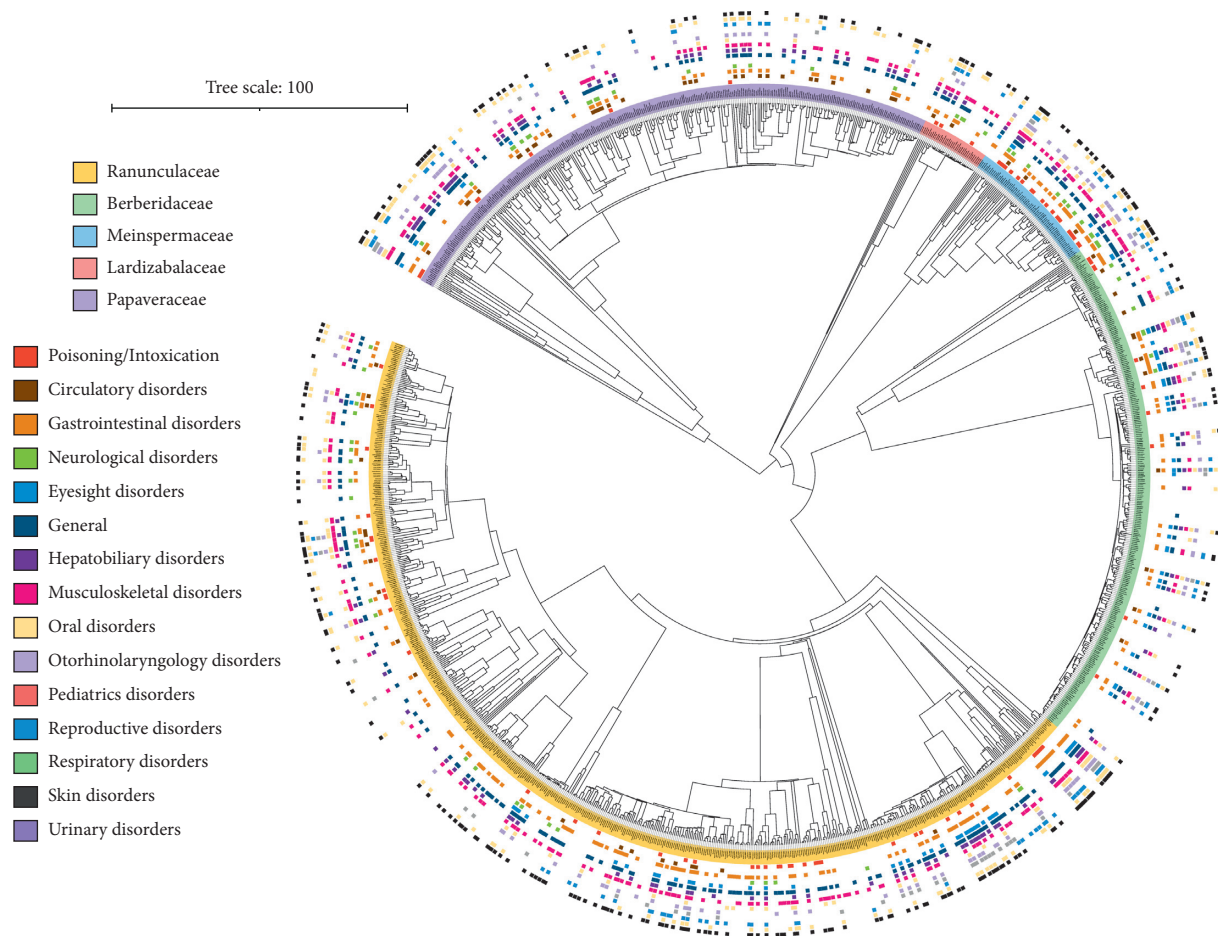


FIGURE 1: Distribution of 15 therapeutic efficacies of Chinese ethnomedicinal species on the phylogenetic tree of Chinese angiosperms. There are 1,519 Chinese Ranunculales species in this large tree, including 725 Ranunculaceae species (yellow in the inner circle), 306 Berberidaceae species (green), 78 Menispermaceae species (blue), 44 Lardizabalaceae species (red), 364 Papaveraceae species (purple), one Eupteleaceae species, and one Circaeasteraceae species. From the inside to the outside of the outer circle are poisoning, circulatory diseases, gastrointestinal diseases, nervous system diseases, eye diseases, other/general diseases, hepatobiliary diseases, musculoskeletal diseases, oral diseases, ear/nose/throat diseases, pediatric diseases, reproductive system diseases, respiratory diseases, skin diseases, and urinary diseases.

TABLE 1: Phylogenetic clustering of Chinese ethnomedicinal plants of Ranunculales used for 15 diseases.

Disease category	NRI	<i>p</i> value	NTI	<i>p</i> value	No. of species
Poisoning/intoxication	0.2827673	0.382	2.5808124	0.001*	105
Circulatory disease	0.3276161	0.357	0.9576053	0.176	80
Gastrointestinal disease	0.8993280	0.178	2.3439243	0.012*	<b>343</b>
Nervous system disease	-1.2169750	0.900	1.6407281	0.046*	78
Eye disease	5.3230108	0.001*	3.1022603	0.001*	110
Other/general disease	-0.4234927	0.644	2.9096083	0.005*	<b>435</b>
Hepatobiliary disease	-2.0673037	0.987	1.1511975	0.134	183
Musculoskeletal disease	-1.8124459	0.978	2.0655373	0.024*	<b>389</b>
Oral disease	2.9318791	0.006*	2.3750417	0.009*	132
Ear/nose/throat disease	-1.3491137	0.922	2.5423622	0.007*	181
Pediatric disease	3.0196803	0.006*	1.2504461	0.108	73
Reproductive system disease	-1.9141517	0.985	2.3016542	0.011*	144
Respiratory disease	-3.7510929	1.000	0.4516397	0.340	239
Skin disease	2.0247475	0.025*	2.1795913	0.023*	<b>348</b>
Urinary disease	1.8995941	0.048*	2.3121644	0.012*	124

Note: NRI, net relatedness index; NTI, nearest taxon index; \*  $p < 0.05$ , statistically significant; four categories with the largest number of species are shown in bold.

TABLE 2: Chinese ethnomedicinal species with no less than 10 categories of therapeutic efficacy.

Species	No. of therapeutic categories
Ranunculaceae: <i>Aconitum carmichaelii</i>	13
<i>Aconitum flavum</i>	10
<i>Aconitum kusnezoffii</i>	10
<i>Aconitum naviculare</i>	11
<i>Aconitum scaposum</i>	13
<i>Anemone hupehensis</i>	10
<i>Anemone rivularis</i>	12
<i>Anemone rivularis var. flore-minore</i>	10
<i>Anemone vitifolia</i>	11
<i>Clematis armandii</i>	12
<i>Clematis chinensis</i>	12
<i>Clematis hexapetala</i>	12
<i>Clematis manshurica</i>	12
<i>Coptis chinensis</i>	12
<i>Coptis chinensis var. brevisepala</i>	12
<i>Coptis deltoidea</i>	12
<i>Coptis omeiensis</i>	12
<i>Coptis quinquesecta</i>	12
<i>Coptis teeta</i>	12
<i>Nigella glandulifera</i>	10
<i>Nigella glandulifera</i>	10
<i>Ranunculus japonicus</i>	10
<i>Semiaquilegia adoxoides</i>	12
<i>Thalictrum acutifolium</i>	10
<i>Thalictrum alpinum var. elatum</i>	12
<i>Thalictrum cultratum</i>	11
<i>Thalictrum delavayi</i>	11
<i>Thalictrum foliolosum</i>	11
<i>Thalictrum ramosum</i>	11
<i>Thalictrum reticulatum</i>	11
<i>Thalictrum trichopus</i>	11
Berberidaceae: <i>Berberis amurensis</i>	12
<i>Berberis dasystachya</i>	10
<i>Berberis diaphana</i>	12
<i>Berberis heteropoda</i>	10
<i>Berberis jamesiana</i>	10
<i>Berberis julianae</i>	11
<i>Berberis poiretii</i>	13
<i>Berberis pruinosa</i>	10
<i>Berberis verna</i>	13
<i>Berberis vulgaris</i>	11
<i>Berberis wilsoniae</i>	12
<i>Epimedium acuminatum</i>	10
<i>Epimedium sagittatum</i>	10
<i>Mahonia bealei</i>	14
<i>Mahonia eurybracteata</i>	15
<i>Mahonia fortune</i>	14
<i>Mahonia gracilipes</i>	14
Menispermaceae: <i>Arcangelisia gusanlung</i>	11
<i>Cyclea hypoglauca</i>	10
<i>Stephania cepharantha</i>	11
<i>Stephania hernandiifolia</i>	10
<i>Stephania kuinanensis</i>	10
<i>Stephania kwangsiensis</i>	11
<i>Stephania kwangsiensis</i>	11
<i>Stephania micrantha</i>	10
<i>Stephania tetrandra</i>	10
<i>Tinospora capillipes</i>	13

TABLE 2: Continued.

Species	No. of therapeutic categories
<i>Tinospora crispa</i>	10
<i>Tinospora sagittata</i>	13
<i>Tinospora sinensis</i>	13
Lardizabalaceae: <i>Akebia trifoliata</i>	10
<i>Akebia trifoliata var. australis</i>	11
<i>Sargentodoxa cuneata</i>	10
Papaveraceae: <i>Corydalis edulis</i>	10
<i>Eomecon chionantha</i>	10
<i>Macleaya cordata</i>	10
<i>Macleaya microcarpa</i>	10

other diseases, followed by gastrointestinal diseases (55), musculoskeletal diseases (51), and skin diseases (48). The least species are used to treat nervous system diseases (9, 13.0% of species). A clustered structure was suggested by NRI values ( $>0$ ) for seven categories, while the other eight categories were of overdispersion ( $\text{NRI} < 0$ ). The clustered structure was suggested by  $\text{NTI} > 0$  for 12 categories. In the statistical test, the NRI suggested that four categories, that is, gastrointestinal diseases, eye disease, hepatobiliary diseases, and ear/nose/throat diseases, are of cluster with statistical significance ( $p < 0.05$ ; Table S2), whereas the NTI suggested no category with statistically significant cluster ( $p > 0.05$ ).

Among Chinese ethnomedicinal plants of Menispermaceae, the highest number of species (34, 80.9% of species; Table S2) is used for the treatment of gastrointestinal/musculoskeletal diseases, followed by general/other diseases (33) and skin diseases (27). Only two species are used to treat pediatric diseases. A clustered structure was suggested by NRI values ( $>0$ ) for 13 categories, whereas the other two categories were of overdispersion ( $\text{NRI} < 0$ ). The clustered structure was suggested by  $\text{NTI} > 0$  for 13 categories. In the statistical test, the NRI suggested that two categories, that is, other/general diseases and pediatric diseases, are of cluster with statistical significance ( $p < 0.05$ ; Table S2), whereas the NTI suggested seven categories with statistically significant cluster ( $p < 0.05$ ). Both the NRI and the NTI suggest other/general diseases and pediatric diseases as significantly clustered.

In Chinese ethnomedicinal plants of Lardizabalaceae, the highest number of species (14, 100% species; Table S2) is used for the treatment of musculoskeletal diseases, followed by other/general diseases (12) and skin/respiratory/urinary diseases (10 of each). No species is used to treat eye/oral diseases. A clustered structure was suggested by NRI values ( $>0$ ) for four categories, that is, poisoning/intoxication, nervous system disease, ear/nose/throat disease, and urinary disease, whereas the other seven categories were of overdispersion ( $\text{NRI} < 0$ ). The clustered structure was suggested by  $\text{NTI} > 0$  for four categories. In the statistical test, the NRI suggested that nervous system disease is of cluster with statistical significance ( $p < 0.05$ ), whereas the NTI suggested no statistically significant category.



Among Chinese ethnomedicinal plants of Papaveraceae (poppy family), the highest number of species (101, 80.1% of species) is used for the treatment of general/other diseases, followed by musculoskeletal diseases (91), respiratory diseases (83), and skin diseases (64). The least species are used to treat eye/pediatric diseases (eight of each). A clustered structure was suggested by NRI values ( $>0$ ) for two categories, that is, circulatory and nervous system diseases, whereas the other 13 categories were of overdispersion ( $\text{NRI} < 0$ ; Table S2). The clustered structure was suggested by  $\text{NTI} > 0$  for 14 categories. In the statistical test, the NRI suggested that circulatory and nervous system diseases are of cluster with statistical significance ( $p < 0.05$ ), whereas the NTI suggested circulatory and hepatobiliary diseases with statistically significant cluster ( $p < 0.05$ ). Both the NRI and the NTI suggest circulatory disease as significantly clustered.

#### 4. Discussion

By utilizing NRI and NTI in R language, this study presents the first quantitative evidence of the association between angiosperm phylogeny and therapeutic efficacy of Chinese ethnomedicinal species. These indices were calculated for 14 categories of diseases to examine the phylogenetic clustering of TCM plants in China [5]. However, this study focused on legal medicinal plants of China, and it is unknown how many medicinal plants used by ethnic minorities were included. China is a multi-ethnic country, in which the Han population is the largest, accounting for about 92% of the total population. The total population of the other 55 ethnic groups is ~115,145,902, accounting for about 8% of the total population, so they are called ethnic minorities. At least 7,022 botanical species are used medicinally by China ethnic minorities [3], representing an enormous space for bio-prospecting and drug development. Here, the order Ranunculales is chosen for the case study of traditional medicinal knowledge of China ethnic minorities, which belongs to the basal eudicots and is evolutionarily older than other eudicots [26, 27]. Basal eudicots radiate for maximum disorders [5]; accordingly, various Ranunculales species have been employed in TCM, traditional oriental medicine, and Western folk medicine for diverse ailments [19, 28]. Widely known Ranunculales members, for example, blue cohosh, black seed, poppies, barberries, and buttercups, are being studied for their pharmacological activities via integrative omics techniques and from the systems perspective. Ranunculales contributes plenty of botanical extracts with therapeutic efficacy and/or health-promoting effects. As there are more than 4,000 and more than 1,500 Ranunculales species in the world and China, respectively, and novel Ranunculales taxa, that is, *Dichocarpum lobatipetalum* and *D. malipoense* [29], are being discovered, there are still vast biological and chemical space to be prospected in this well-known medicinal order.

**4.1. Ranunculaceae.** At the order level, the NRI and NTI revealed eight and 15 therapeutic categories with clustered structure, respectively, but scrutinizing each family could

help gain deeper understanding of the therapeutic values of genera/species and narrow down bio-screening. Ranunculaceae could be the most important medicinal family in Ranunculales and even in basal eudicots; in TCM, up to 63% of Ranunculaceae medicinal species have utilities in musculoskeletal disorders [5], followed by hepatic disorders (56%) and circulatory disorders (42.2%). In the present study, 199 out of 300 Ranunculaceae medicinal species are used by China ethnic minorities against musculoskeletal diseases and skin diseases (Table S2), followed by 188 for gastrointestinal disease and 84 for hepatobiliary disease. Berberidaceae is the second important medicinal family in Ranunculales. In TCM, 81.5% of Berberidaceae medicinal species are used against eyesight disorders [5], followed by hepatic disorders (80.8%) and digestive disorders (78.6%). In contrast, 55 and 51 out of 69 Berberidaceae medicinal species are used by China ethnic minorities against gastrointestinal and musculoskeletal diseases, respectively (Table S2), followed by 48 for skin disease and 42 for eye disease. These results illustrate the significant difference of disease spectrum and medication experience between TCM and traditional medicine of ethnic minorities; the latter is a precious intangible cultural heritage. In order to avoid rapid loss, its protection, sorting, and inheritance should be vigorously strengthened.

Ranunculaceae, mostly herbs and some of which are small shrubs or woody vines, includes about 60 genera and 2,200 species [30]. Plants of this family are distributed worldwide, mainly in the temperate region of the northern hemisphere. Forty-two genera and around 720 species are distributed throughout China, most of which are in the southwest mountainous region. In this study, up to nine therapeutic categories showed a clustered structure in Ranunculaceae (Tables S1 and S2, Figure 1). Some species of genera *Clematis*, *Coptis*, and *Ranunculus* are commonly used by some ethnic minority groups in China to combat against ocular inflammation, infection, keratopathy, and cataract, among others [3]. *Cimicifuga*, *Clematis*, and *Coptis* are often used to treat reproductive system diseases, especially gynecological and obstetric ones. *Clematis*, *Nigella*, and *Thalictrum* are salient in the treatment of urinary inflammation, infection, and calculi. The therapeutic species against skin/gastrointestinal diseases are relatively concentrated in *Aconitum*, *Clematis*, and *Delphinium*; the circulatory disease targeting species are concentrated in *Aconitum* and *Clematis*. Thirty-four Ranunculaceae species are used ethnomedicinally against nervous system disease (Tables S1 and S2). We also noted the folk medicine use of *Dichocarpum auriculatum* (Ranunculaceae) in Sichuan Province against sow mania (epilepsy of sow) [23], which is not recorded in the Dictionary of Chinese Ethnic Medicine [3], as this book mainly reflects the traditional medicine knowledge of Chinese ethnic minorities. Accordingly, five BIAs of *D. auriculatum* had the *in vitro* inhibitory activity against acetylcholinesterase [22].

Chemical components of Ranunculaceae include several representative groups: BIA, ranunculin, triterpenoid saponin, and diterpene alkaloid, [30]. Ranunculin and magnoflorine coexist in some genera. Our early

ethnopharmacological investigation showed that the most frequent ethnopharmacological uses, mainly in Han Nationality, are heat-clearing and detoxification, ulcer disease and sore, anti-microbe, and anti-inflammation [31]; the most studied bioactivities are anticancer/cytotoxic, antimicrobial, and anti-inflammatory activities. These results cross-validate the utility of traditional medicinal knowledge in bioprospecting and contemporary phytotherapy research.

**4.2. Berberidaceae.** In other four species-rich families of Ranunculales, hot nodes/clades for drug discovery and development are also identified by NRI/NTI (Tables S1 and S2, Figure 1). In Berberidaceae (17 genera, 650 species), four therapeutic categories showed a clustered structure (Tables S1 and S2, Figure 1). Some species of genera *Berberis*, *Dysosma*, and *Mahonia* are especially useful in the treatment of gastrointestinal, eye, and ear/nose/throat diseases [3]. The therapeutic species against eye and hepatobiliary diseases are relatively concentrated in *Berberis* and *Mahonia*, which are close to each other phylogenetically. Twenty-six *Berberis* species and 11 *Mahonia* species are used by China ethnic minorities against various eye diseases. For example, in Mongolian medicine, *B. amurensis* and *B. verna* are used for sore red swollen eyes, acute conjunctivitis, and ocular leukoplakia; in Tibetan medicine, the flower juice of *B. verna* is used to drop eyes to treat eye diseases. *Mahonia bealei* is used by Bu Yi, Mao Nan, Miao, Mu Lao, and Yi Nationality against acute conjunctivitis. In Ge Lao medicine, the water decoction of *M. bealei* root is used to wash eyes for treating ocular itching and lacrimation. It happens that *Berberis* is similarly used in other traditional medicine systems. For example, in far-west Nepal, *B. asiatica* is frequently used for eye problems [32]; in Islamic traditional medicine, different parts of *B. vulgaris* and *B. integririma* are prescribed for skin, liver, stomach, kidney, and eye problems [33]. In the Indian and European systems of traditional medicine, *Berberis* is used for curing eye disease, fever, jaundice, rheumatism, vomiting during pregnancy, kidney and gall bladder stone, and such like [34]. Interestingly, the utility of *Mahonia* in eye disease is not salient in these traditional medicine systems except in TCM and traditional medicine of China ethnic minorities. There are about 100 species in the genus *Mahonia*, which are distributed in Central/North America and Asia. The unique ethnopharmacological uses in China ethnic minorities might contribute much in the search for new sources of pharmaceuticals.

*Berberis* and *Mahonia* contain mainly BIAs, for example, berberine, palmatine, jatrorrhizine, columbamine (Protoberberine type), magnoflorine (aporphine type), particularly a higher content of bisbenzylisoquinoline (BBI) alkaloids berbamine [35], isotetrandrine, and oxyacanthine. Phenolics, flavonoids, and tannins are abundant in *Berberis* [36]. These compounds constitute the material basis of traditional/modern therapeutic efficacy. Berberine is the principal component of many medicinal plants, for example, *Coptis chinensis*, *Hydrastis canadensis* [37], *Berberis vulgaris* [38], *B. aristate* [39], and *Mahonia bealei*, which could

partially explain the shared therapeutic efficacy between Ranunculaceae and Berberidaceae. It should be noted that although the genus *Epimedium* was not suggested by the NRI and NTI, eight *Epimedium* species are ethnomedicinally used for various diseases [3], especially reproductive disorders, musculoskeletal disorders, and pediatrics disorders. This illustrates the complementarity, rather than substitutability, of the phylogenetic approach in bioprospecting.

**4.3. Menispermaceae, Lardizabalaceae, and Papaveraceae.** In Menispermaceae (65 genera, >350 species), seven categories showed a clustered structure. Two *Tinospora* species are ethnomedicinally used for pediatric diseases, whereas *Cocculus*, *Cyclea*, and *Stephania* species are traditionally used for various general/difficult-to-classify diseases. BBI alkaloids are abundant in Berberidaceae and Menispermaceae [28]. BBI alkaloids, morphine alkaloids, aporphine alkaloids, syringaresinol, and aristolochic acid I could be marker compounds of Menispermaceae and could be responsible for the efficacy of *Stephania* and *Tinospora* against poisoning, ear/nose/throat diseases, and skin diseases, among others (Tables S1 and S2). In TCM, the root of *Stephania tetrandra* is used to treat arthralgia caused by rheumatism, wet beriberi, dysuria, eczema, and inflamed sores [40], which is similar to the usage of ethnic minorities. In Southeast Asia, the stems, leaves, and tubers of *Stephania rotunda* are used in the Cambodian, Lao, Indian, and Vietnamese folk medicine systems for years to treat a wide range of ailments [41], including asthma, headache, fever, and diarrhea. *Tinospora cordifolia* is used in folk and Ayurvedic medicines throughout India [42]. This plant contains many pharmaceutical compounds such as alkaloids, diterpenoid lactones, glycosides, steroids, sesquiterpenoid, and phenolics, which make it antidiabetic, antipyretic, anti-inflammatory, antioxidant, hepatoprotective, and immuno-modulatory. The phytochemistry and pharmacology of *T. cordifolia* are analogous to that of *Tinospora* species used by China ethnic minorities [3].

The small family Lardizabalaceae has nine genera and 50 species; only species against nervous system disease showed a cluster, that is, the genus *Stauntonia* [3], *Stauntonia brachyanthera*, *S. chinensis*, *S. obovatifoliola*, and *S. yaoshanensis* are ethnomedicinally used to alleviate trigeminal neuralgia. Recent pharmacological investigations revealed the anti-inflammatory activity of *S. hexaphylla* [43] and *S. brachyanthera* [44], but not nervous system effects; thus, our results could be valuable for future research direction. Ten out of 14 Lardizabalaceae species are used by China ethnic minorities against urinary diseases (Table S2). For example, in Dong medicine, the rattan stems of *Akebia quinata* are used against edema, adverse urination, blennorrhagia, and urinary stone [3]; in Mongolian medicine and Miao medicine, the fruit of *A. quinata* is used for adverse urination; in Tu Jia medicine, the fruit of *A. quinata* is used for rough voidings of reddish urine, and its pericarp and seeds benefit the kidney and reduce swelling. *A. trifoliata* and *A. trifoliata* var. *australis* are similarly used by ethnic minorities. It is found that akebia saponin D ameliorated

kidney injury and exerted anti-inflammatory and anti-apoptotic effects in diabetic nephropathy by activating NRF2/HO-1 and inhibiting NF- $\kappa$ B pathway [45]. More pharmacological explorations of Lardizabalaceae components are warranted, so as to validate the ethnopharmacological uses and expand new application space.

The BIA biosynthetic pathway underwent the parallel evolution between two basal eudicot orders Ranunculales and Proteales [46], which diverged 122 million years ago (MYA). Berberine, belonging to the protoberberine class of BIAs, is present in species of each Ranunculales family, while the benzophenanthridine class, including the antimicrobial sanguinarine, is specific to the Papaveraceae family, and biosynthetic genes emerged after the split with the Ranunculaceae family 110 MYA but before the split of Papaveraceae species at 77 MYA. The phthalideisoquinoline noscapine and morphinan class of BIAs are exclusive to the opium poppy lineage. The morphine biosynthesis evolved more recently than 18 MYA in the genus *Papaver*. The major differences of medicinal BIAs between Papaveraceae and related families partially explain the uniqueness of its ethnomedicinal uses, and the material basis of therapeutic efficacies of different Papaveraceae genera also varies greatly [28]. In Papaveraceae (38 genera, >700 species), three categories showed a clustered structure. Thirty-two and seventeen *Corydalis* ethnomedicinal species are used for circulatory and nervous system diseases, respectively [3]. Accordingly, *Corydalis* components showed vascular relaxation effect [47] and neuroprotective effect [48] *in vitro* and/or *ex vivo*. Analgesia is one of the most important effects of *Corydalis* components, which are relatively nonaddictive and of low tolerance as compared to other analgesics [49]. Fifty-three out of 126 Papaveraceae species are used by China ethnic minorities against hepatobiliary diseases (Table S2), and *Corydalis* and *Meconopsis* species are salient in this treatment [20]. For instance, in Tibetan medicine, the whole plant of *Corydalis adunca* is used against liver-gallbladder sthenic heat [3], the root tuber is used against cholelithiasis, and the aboveground part is effective against biliary anorexia. In Tibetan medicine, the whole plant and flower of *Meconopsis quintuplinervia* are used against hepatitis, liver heat, and cholecystitis; in Qiang medicine, its whole plant and flower are used against jaundice. It should be pointed out that the overdispersion therapeutic categories are not trivial, as they may show a clustered structure at the subfamily, tribe, and/or genus level, or possibly because the relevant therapeutic compounds are ubiquitous throughout the whole family.

## 5. Conclusion

In conclusion, we compiled traditional ethnomedicinal uses of 551 Chinese species belonging to five families of Ranunculales from the Dictionary of Chinese Ethnic Medicine and recent literature, and the species-level phylogeny of angiosperms was used to analyze the phylogenetic signals of ethnomedicinal plants by calculating NRI and

NTI. At the order level, the NRI results disclosed a clustered structure for eight therapeutic categories, that is, poisoning/intoxication, circulatory, gastrointestinal, eyesight, oral, pediatric, skin and urinary disorders, and the overdispersion for other seven categories; the NTI metric identified the clustered structure for all 15 categories. The NRI and NTI values were statistically significant in five and 11 categories, respectively. *Mahonia eurybracteata* of Berberidaceae has therapeutic effects on all categories. The most studied phytometabolites of Ranunculales include BIA, flavonoid, terpenoid, saponin, and lignan. [28]. The compound basis corresponding to the traditional efficacy is the focus of future exploration. By figuring out the phylogenetic distribution of therapeutic effects of Ranunculales ethnomedicinal plants, we illustrate the importance of quantitative phylogenetic methods in mining potential phytomedicine. The traditional medicinal knowledge could/should be scrutinized within the phylogenetic framework, making them not only important to local health and livelihoods, but also beneficial to the global health and sustainability. The protection of medicinal plant resources must be strengthened for better ecosystem service; protecting ecological environment is a basic national/global policy and is indispensable for human survival and welfare. To discover lead compounds with versatile bioactivities, in the near future, the ethnobotanical resources can be evaluated expansively by correlating large-scale phylogeny, spatial/geographic data, phytochemistry, and ethnopharmacology cues.

## Abbreviations

BBI:	Bisbenzylisoquinoline
BIA:	Benzylisoquinoline alkaloid
MNTD:	Mean nearest taxon distance
MPD:	Mean pairwise phylogenetic distance
NRI:	Net relatedness index
NTI:	Nearest taxon index
TCM:	Traditional Chinese medicine.

## Data Availability

The data generated or analyzed during this study are included within the article.

## Conflicts of Interest

The authors declare that they have no conflicts of interest.

## Acknowledgments

The authors thank Prof. Yi Zhang (Chengdu University of TCM) for providing the database Dictionary of Chinese Ethnic Medicine and Zhang-Jian Shan (Institute of Botany, Chinese Academy of Sciences) for his suggestions in subtree analyses. This study was supported by the Scientific Research Funds Project of Liaoning Education Department (JDL2019012) and the Innovation Team and Talents Cultivation Program of National Administration of Traditional Chinese Medicine (ZYYCXTD-D-202005).

## Supplementary Materials

Table S1: detailed efficacy matrix of Ranunculales ethnomedicinal plants. Table S2: phylogenetic clustering of Chinese ethnomedicinal plants of five major Ranunculales families used for 15 diseases. R language codes for the construction of the tree as well as calculation of the NRI and NTI. (*Supplementary Materials*)

## References

- [1] L. Li, B. Zhang, P. Xiao et al., "Patterns and environmental determinants of medicinal plant: vascular plant ratios in Xinjiang, Northwest China," *PLoS One*, vol. 11, no. 7, Article ID e0158405, 2016.
- [2] E. Defosse, C. Pitteloud, P. Descombes et al., "Spatial and evolutionary predictability of phytochemical diversity," *Proceedings of the National Academy of Sciences*, vol. 118, no. 3, Article ID e2013344118, 2021.
- [3] M. R. Jia and Y. Zhang, *Dictionary of Chinese Ethnic Medicine*, China Medical Science Press, Beijing, China, 2016.
- [4] W. H. Wang and X. L. Guan, *Botany*, China Forestry Press, Beijing, China, 2015.
- [5] W. Zaman, J. Ye, S. Saqib et al., "Predicting potential medicinal plants with phylogenetic topology: inspiration from the research of traditional Chinese medicine," *Journal of Ethnopharmacology*, vol. 281, Article ID 114515, 2021.
- [6] W. Zaman, J. F. Ye, M. Ahmad, S. Saqib, Z. K. Shinwari, and Z. Chen, "Phylogenetic exploration of traditional Chinese medicinal plants: a case study on Lamiaceae (angiosperms)," *Pakistan Journal of Botany*, vol. 54, no. 3, 2022.
- [7] W. Zaman, M. Ahmad, M. Zafar et al., "The quest for some novel antifertility herbals used as male contraceptives in district Shangla, Pakistan," *Acta Ecologica Sinica*, vol. 40, no. 1, pp. 102–112, 2020.
- [8] C. H. Saslis-Lagoudakis, V. Savolainen, E. M. Williamson et al., "Phylogenies reveal predictive power of traditional medicine in bioprospecting," *Proceedings of the National Academy of Sciences*, vol. 109, no. 39, pp. 15835–15840, 2012.
- [9] K. Yessoufou, B. H. Daru, and A. M. Muasya, "Phylogenetic exploration of commonly used medicinal plants in South Africa," *Molecular Ecology Resources*, vol. 15, no. 2, pp. 405–413, 2015.
- [10] E. N. F. Souza, E. M. Williamson, and J. A. Hawkins, "Which plants used in ethnomedicine are characterized? Phylogenetic patterns in traditional use related to research effort," *Frontiers of Plant Science*, vol. 9, p. 834, 2018.
- [11] R. K. Wati, E. F. de Graaf, and D. Bogarín, "Antimicrobial activity of necklace orchids is phylogenetically clustered and can be predicted with a biological response method," *Frontiers in Pharmacology*, vol. 11, Article ID 586345, 2020.
- [12] D. S. Fabricant and N. R. Farnsworth, "The value of plants used in traditional medicine for drug discovery," *Environmental Health Perspectives*, vol. 109, no. S1, pp. 69–75, 2001.
- [13] H. A. Jan, S. Jan, R. W. Bussmann, S. Wali, F. Sisto, and L. Ahmad, "Complementary and alternative medicine research, prospects and limitations in Pakistan: a literature review," *Acta Ecologica Sinica*, vol. 40, no. 6, pp. 451–463, 2020.
- [14] Y. Li, D. Kong, Y. Fu, M. R. Sussman, and H. Wu, "The effect of developmental and environmental factors on secondary metabolites in medicinal plants," *Plant Physiology and Biochemistry*, vol. 148, pp. 80–89, 2020.
- [15] W. Zaman, S. Saqib, F. Ullah, A. Ayaz, and J. Ye, "COVID-19: Phylogenetic approaches may help in finding resources for natural cure," *Phytotherapy Research*, vol. 34, no. 11, pp. 2783–2785, 2020.
- [16] Z.-D. Chen, T. Yang, L. Lin et al., "Tree of life for the genera of Chinese vascular plants," *Journal of Systematics and Evolution*, vol. 54, no. 4, pp. 277–306, 2016.
- [17] L.-M. Lu, L.-F. Mao, T. Yang et al., "Evolutionary history of the angiosperm flora of China," *Nature*, vol. 554, no. 7691, pp. 234–238, 2018.
- [18] H. H. Hu, B. Liu, Y. S. Liang et al., "An updated Chinese vascular plant tree of life: phylogenetic diversity hotspots revisited," *Journal of Systematics and Evolution*, vol. 58, no. 5, pp. 663–672, 2020.
- [19] D. C. Hao and L. Yang, "Drug metabolism and disposition diversity of *Ranunculales* phytometabolites: a systems perspective," *Expert Opinion on Drug Metabolism & Toxicology*, vol. 12, no. 9, pp. 1047–1065, 2016.
- [20] D.-C. Hao, P.-G. Xiao, and C. Liu, "Traditional Tibetan medicinal plants: a highlighted resource for novel therapeutic compounds," *Future Medicinal Chemistry*, vol. 10, no. 21, pp. 2537–2555, 2018.
- [21] K. Ren, W. Zhang, G. Wu et al., "Synergistic anti-cancer effects of galangin and berberine through apoptosis induction and proliferation inhibition in oesophageal carcinoma cells," *Biomedicine & Pharmacotherapy*, vol. 84, pp. 1748–1759, 2016.
- [22] P. Li, S. Liu, and Q. Liu, "Screening of acetylcholinesterase inhibitors and characterizing of phytochemical constituents from *Dichocarpum auriculatum* (Franch.) WT Wang and P. K. Hsiao through UPLC-MS combined with an acetylcholinesterase inhibition assay *in vitro*," *Journal of Ethnopharmacology*, vol. 245, Article ID 112185, 2019.
- [23] D.-C. Hao, P. Li, P.-G. Xiao, and C.-N. He, "Dissection of full-length transcriptome and metabolome of *Dichocarpum* (Ranunculaceae): implications in evolution of specialized metabolism of Ranunculales medicinal plants," *PeerJ*, vol. 9, Article ID e12428, 2021.
- [24] S. W. Kembel, P. D. Cowan, M. R. Helmus et al., "Picante: R tools for integrating phylogenies and ecology," *Bioinformatics*, vol. 26, no. 11, pp. 1463–1464, 2010.
- [25] C. O. Webb, D. D. Ackerly, M. A. McPeck, and M. J. Donoghue, "Phylogenies and community ecology," *Annual Review of Ecology and Systematics*, vol. 33, no. 1, pp. 475–505, 2002.
- [26] A. M. Lu and Y. C. Tang, *The Origin and Evolution of Primitive Angiosperms*, Science Press, Beijing, China, 2020.
- [27] Z. D. Chen, A. M. Lu, B. Liu, and J. F. Ye, *Tree of Life for Chinese Vascular Plants*, Science Press, Beijing, China, 2020.
- [28] D. C. Hao, *Ranunculales Medicinal Plants: Biodiversity, Chemodiversity and Pharmacotherapy*, Elsevier/Academic Press, London, UK, 2018.
- [29] S.-N. Xie, Q. Yuan, and Q.-E. Yang, "*Dichocarpum lobatipetalum* and *D. malipoense* (Ranunculaceae) are both merged with *D. hypoglaucum*," *Phytotaxa*, vol. 298, no. 2, pp. 181–186, 2017.
- [30] D.-C. Hao, P.-G. Xiao, H.-Y. Ma, Y. Peng, and C.-N. He, "Mining chemodiversity from biodiversity: pharmacophylogeny of medicinal plants of Ranunculaceae," *Chinese Journal of Natural Medicines*, vol. 13, no. 7, pp. 507–520, 2015.
- [31] P. G. Xiao, L. W. Wang, and S. J. Lv, "Statistical analysis of the ethnopharmacologic data based on Chinese medicinal plants by electronic computer I. Magnoliidae," *Chinese Journal of*

- Integrated Traditional and Western Medicine*, vol. 6, no. 4, pp. 253–256, 1986.
- [32] R. M. Kunwar, L. Mahat, R. P. Acharya, and R. W. Bussmann, “Medicinal plants, traditional medicine, markets and management in far-west Nepal,” *Journal of Ethnobiology and Ethnomedicine*, vol. 9, p. 24, 2013.
- [33] Z. Sobhani, M. Akaberi, M. S. Amiri, M. Ramezani, S. A. Emami, and A. Sahebkar, “Medicinal species of the genus *Berberis*: a review of their traditional and ethnomedicinal uses, phytochemistry and pharmacology,” *Pharmacological Properties of Plant-Derived Natural Products and Implications for Human Health*, vol. 1308, pp. 547–577, 2021.
- [34] S. Srivastava, M. Srivastava, A. Misra, G. Pandey, and A. Rawat, “A review on biological and chemical diversity in *Berberis* (Berberidaceae),” *EXCLI Journal*, vol. 14, pp. 247–67, 2015.
- [35] X.-J. Jia, X. Li, F. Wang, H.-Q. Liu, and D.-J. Zhang, “Berbamine exerts anti-inflammatory effects via inhibition of NF- $\kappa$ B and MAPK signaling pathways,” *Cellular Physiology and Biochemistry*, vol. 41, no. 6, pp. 2307–2318, 2017.
- [36] T. Belwal, L. Giri, I. D. Bhatt, R. S. Rawal, and V. Pande, “An improved method for extraction of nutraceutically important polyphenolics from *Berberis jaeschkeana* C.K. Schneid. fruits,” *Food Chemistry*, vol. 230, pp. 657–666, 2017.
- [37] C. F. Chignell, R. H. Sik, M. A. Watson, and A. R. Wielgus, “Photochemistry and photocytotoxicity of alkaloids from goldenseal (*Hydrastis canadensis* L.) 3: effect on human lens and retinal pigment epithelial cells,” *Photochemistry and Photobiology*, vol. 83, no. 4, pp. 938–943, 2007.
- [38] M. Imenshahidi and H. Hosseinzadeh, “Berberine and barberry (*Berberis vulgaris*): a clinical review,” *Phytotherapy Research*, vol. 33, no. 3, pp. 504–523, 2019.
- [39] B. Malhotra, G. T. Kulkarni, N. Dhiman et al., “Recent advances on *Berberis aristata* emphasizing berberine alkaloid including phytochemistry, pharmacology and drug delivery system,” *Journal of Herbal Medicine*, vol. 27, Article ID 100433, 2021.
- [40] Y. Jiang, M. Liu, H. Liu, and S. Liu, “A critical review: traditional uses, phytochemistry, pharmacology and toxicology of *Stephania tetrandra* S. Moore (Fen Fang Ji),” *Phytochemistry Reviews*, vol. 19, no. 2, 2020.
- [41] C. Desgrouas, N. Taudon, S.-S. Bun et al., “Ethnobotany, phytochemistry and pharmacology of *Stephania rotunda* Lour,” *Journal of Ethnopharmacology*, vol. 154, no. 3, pp. 537–563, 2014.
- [42] P. Kumar, M. Kamle, D. K. Mahato et al., “*Tinospora cordifolia* (Giloy): phytochemistry, ethnopharmacology, clinical application and conservation strategies,” *Current Pharmaceutical Biotechnology*, vol. 21, no. 12, pp. 1165–1175, 2020.
- [43] L. B. Vinh, S. J. Jo, P. Nguyen Viet et al., “The chemical constituents of ethanolic extract from *Stauntonia hexaphylla* leaves and their anti-inflammatory effects,” *Natural Product Research*, vol. 35, no. 11, pp. 1852–1855, 2021.
- [44] J. Li, K. Du, D. Liu, and D. Meng, “New nor-oleanane triterpenoids from the fruits of *Stauntonia brachyanthera* with potential anti-inflammation activity,” *Natural Product Research*, vol. 34, no. 7, pp. 915–922, 2020.
- [45] C. Lu, G. Fan, and D. Wang, “Akebia Saponin D ameliorated kidney injury and exerted anti-inflammatory and anti-apoptotic effects in diabetic nephropathy by activation of NRF2/HO-1 and inhibition of NF- $\kappa$ B pathway,” *International Immunopharmacology*, vol. 84, Article ID 106467, 2020.
- [46] Y. Li, T. Winzer, Z. He, and I. A. Graham, “Over 100 million years of enzyme evolution underpinning the production of morphine in the Papaveraceae family of flowering plants,” *Plant Communications*, vol. 1, no. 2, Article ID 100029, 2020.
- [47] Z. Y. Zhou, W. R. Zhao, and W. T. Shi, “Endothelial-dependent and independent vascular relaxation effect of tetrahydropalmatine on rat aorta,” *Frontiers in Pharmacology*, vol. 10, p. 336, 2019.
- [48] Y. J. Kim, H.-S. Lim, Y. Kim, J. Lee, B.-Y. Kim, and S.-J. Jeong, “Neuroprotective effect of *Corydalis ternata* extract and its phytochemical quantitative analysis,” *Chemical and Pharmaceutical Bulletin*, vol. 65, no. 9, pp. 826–832, 2017.
- [49] A.-P. Deng, Y. Zhang, L. Zhou et al., “Systematic review of the alkaloid constituents in several important medicinal plants of the genus *Corydalis*,” *Phytochemistry*, vol. 183, Article ID 112644, 2021.



## Research Article

# Quanzhenyiqitang Reverses LPS-Induced Inflammation via Inhibiting PYK2/p38MAPK/HDAC2/CK2 Signaling Pathway in Rat Alveolar Macrophage

Ke-Qiang Chen, Da-zhi Li, Zhi-bin Chen, Chuan-lin Zhang, Bin-can Wang, and Chun-e Wang 

Department of Respiratory and Critical Care Medicine,  
The Second Affiliated Hospital of Fujian Traditional Chinese Medical University, Fuzhou, China

Correspondence should be addressed to Chun-e Wang; wangchunesci@163.com

Received 29 November 2021; Revised 20 December 2021; Accepted 21 December 2021; Published 10 January 2022

Academic Editor: Ruchika Garg

Copyright © 2022 Ke-Qiang Chen et al. This is an open access article distributed under the Creative Commons Attribution License, which permits unrestricted use, distribution, and reproduction in any medium, provided the original work is properly cited.

Chronic obstructive pulmonary disease (COPD) is a common chronic pulmonary disease with multiple etiologies and pathological changes. PYK2 expression is significantly increased in lipopolysaccharide-induced lung injury, but it mediates chronic lung inflammation. The mechanism of its occurrence remains unclear. Quanzhenyiqitang is often used in clinical treatment of COPD, so this study explored the mechanism of its treatment of lipopolysaccharide-induced lung injury. In this study, transfection, flow cytometry, QRT-PCR, and Western blotting methods were used to study the mechanism of Quanzhenyiqitang lipopolysaccharide-induced lung injury. The results showed that the mechanism of occurrence remains unclear. Our novel observations imply that the PYK2/p38MAPK/HDAC2/CK2 pathway is one of the fundamental underlying mechanisms that mediate the pathogenic progression of COPD, and Quanzhenyiqitang may be the therapeutic drug to prevent chronic inflammation and delay the progression of COPD by inhibiting PYK2 signaling pathways.

## 1. Introduction

Macrophages are an important component of the human body's innate immunity. It was originated in the yolk sac and liver precursor cells during embryonic development and then entered into the lungs and settled to form alveolar macrophages [1]. Alveolar macrophages are mostly distributed in the alveolar cavity, accounting for 80% of the alveolar resident cells. It is the only inner cell group that contacts with air in the human body in the first line of defense against pollutants and pathogenic bacteria [2]. It can secrete more than one hundred types of inflammatory mediators. These substances further trigger an innate immune response in the normal lung tissues. According to the activation pathway, alveolar macrophages have two phenotypes: classic activated macrophages (M1 macrophages) activated classically and alternately activated macrophages

(M2 macrophages) activated in a selective pathway [3]. During the inflammatory response, M1 and M2 are involved in mediating the innate immune response and various inflammatory responses. M1 macrophages respond to microbial factors and Th1 proinflammatory cytokines, exhibit glycolysis, and are associated with the release of inflammatory cytokine, enhancing bacterial killing, and recruitment of immune cell into the lung parenchyma and alveoli [4]. In contrast, M2 macrophages exposed to Th2 cytokines induce the oxidative metabolism, which is related to the release of anti-inflammatory cytokines, phagocytosis (apoptosis) of apoptotic cells, and collagen deposition, thus contributing to the resolution and damage of inflammation [5]. Being highly plastic and highly responsive to environmental signals, alveolar macrophages can rapidly mediate inflammatory phenotypes, and the changes of alveolar macrophages are reversible. In the process of lung

inflammation, macrophages continue to interact with epithelial cells, microvascular endothelial cells, neutrophils, lymphocytes, fibroblasts, and stem cells or tissue progenitor cells to regulate the stability of the lung environment and the pathogens [5]. The polarized states of alveolar macrophages are not mutually exclusive, and cells can simultaneously display two subtypes of M1 and M2 macrophages according to environmental signals.

There have been a series of published articles, reviews, and research reports that emphasize the role of alveolar macrophages in lung inflammation. Feller et al. found that continuous smoking activated the atypical Wnt5a-PPAR $\gamma$  signaling, leading to macrophage polarization from M2 to M1, lung inflammation, and eventually chronic obstructive pulmonary disease [6]. In rats exposed to endotoxin, alveolar macrophages, and interleukin-6, toll-like receptor 4 was significantly upregulated in vivo. Lee et al. discovered that alveolar macrophages interact with lung epithelial cells via extracellular vesicles and intracellular vesicles [7]. Through extracellular vesicle-mediated signal transduction, the bidirectional paracrine interaction between macrophages and epithelial cells may trigger an inflammatory cascade in the lung. In a mouse model of bleomycin-induced pulmonary fibrosis, Elewa et al. reported an increase in the CD80<sup>+</sup> M1 macrophage subpopulations, and the number of macrophage infiltration in the lung and mediastinal fat-related lymphoid clusters was significantly positively correlated [8]. This study suggests that macrophage infiltration of the lung and mediastinal fat-associated lymphoid clusters may be profoundly involved in the progression of pulmonary inflammatory diseases.

As a nonreceptor protein tyrosine kinase, proline-rich tyrosine kinase-2 (PYK2) can sense a variety of extracellular signaling molecules and participate in intracellular signaling pathway transmission. The activation of its downstream pathway plays an important role in the pathogenesis of airway stenosis and fibrosis, lung parenchyma destruction, and mucus hypersecretion in chronic lung inflammation [9]. PYK2 and its downstream pathways play a crucial role in the pathogenesis of airway stenosis and fibrosis, lung parenchyma destruction, and mucus hypersecretion in chronic lung inflammation. At present, there are few studies concerning the downstream mechanism of PYK2. It has not been shown how the PYK2 signal transduction pathway could be involved in the pulmonary inflammatory response associated with alveolar macrophages. We speculate that the PYK2/p38MAPK/HDAC2/CK2 pathway might be one of the fundamental mechanisms of LPS-induced lung injury and is the key to the development of new strategies for the prevention and treatment of chronic lung inflammatory diseases.

To scrutinize the role of the PYK2-mediated p38MAPK/HDAC2/CK2 signaling pathway in LPS-induced inflammation of alveolar macrophages, we directly investigated the expression levels of PYK2 and downstream signaling pathways in alveolar macrophages stimulated by LPS. In rat alveolar macrophages stimulated by LPS, PYK2 was phosphorylated, resulting in changes in the downstream p38MAPK/HDAC2/CK2 signaling pathway, which

ultimately affects the function and inflammation of alveolar macrophages. Quanzhenyiqitang is widely used in the treatment of various senile diseases with deficiency, such as chronic heart failure, chronic obstructive pulmonary disease, and lung cancer [10]. Targeting PYK2 by lentiviral transfection technology or Quanzhenyiqitang-treated serum, we found that the PYK2/p38MAPK/HDAC2/CK2 signaling pathway significantly contributed to the inflammatory response of alveolar macrophages induced by LPS stimulation. In conclusion, our results indicate that PYK2 mediates the p38MAPK/HDAC2/CK2 signaling pathway in LPS-induced alveolar macrophage inflammation and Quanzhenyiqitang may be the potential drug that could reverse this immune response.

## 2. Materials and Methods

**2.1. Cell Culture.** Rat alveolar macrophages NR8383 were obtained from the Cell Bank of the Chinese Academy of Sciences (Shanghai, China) and contained 10% fetal bovine serum, 100 U/mL penicillin, and 100 mg/L streptomycin in a humidified incubator at 37°C and 5% CO<sub>2</sub> DMEM medium.

**2.2. Acquisition of Quanzhenyiqitang-Treated Serum Acquisition.** Sixty SPF male SD rats were 4–6 weeks old and weighed 180–220 g, drink and eat freely for 7 days to acclimate to the environment. 15 g ginseng, 15 g red peony, 15 g *Rehmannia glutinosa*, 6 g aconite, 6 g *Atractylodes*, 15 g *Achyranthes*, and 6 g *Schisandra* had been decocted for 20 minutes. Each rat was given by gavage twice a day, 5 ml each time with Quanzhenyiqitang, for 7 days. On day 7, after 12 hours of fasting, the rats were gavaged twice with a complete daily dose [10]. For Quanzhenyiqitang-untreated group, each rat was lavaged with 5 ml saline solution at the same time. One hour after the administration, the rats were anesthetized by intraperitoneal injection of pentobarbital sodium (0.2 ml/100 g). After routine sterilization, we collect abdominal aortic blood (approximately 6 ml) and transfer it into a negative pressure container using a puncture needle under sterile conditions. The blood sample was then placed in a 37°C waterbath for 15 minutes and centrifuged at 400xg for 15 minutes. The serum was filtered through a 0.22  $\mu$ m filter and transferred into new Eppendorf tubes and stored at -20°C.

**2.3. Design and Transfection of Pyk2 siRNAs.** siRNAs were obtained from RiboBio and transfected according to the manufactures' instructions. To put it simply, siRNA was diluted with 200  $\mu$ L Opti-MEM. After gently inverting and mixing the transfection reagents, 4  $\mu$ L Lipofectamine<sup>TM</sup> 2000 was also diluted with 200  $\mu$ L Opti-MEM. Transfection reagent and siRNA diluent were then mixed and placed in a 6-well cell plate. siRNA sequences are given in Table 1.

**2.4. Apoptosis Assay.** After performing corresponding stimulation, cells were centrifuged at 1000g for 5 minutes. The supernatant was discarded, and the cells were then

TABLE 1: siRNA sequences for rPtk2b-siRNA.

rPtk2b-siRNA-1 sense	GCUAUUUGCCAGAAGACUUTT
rPtk2b-siRNA-1 antisense	AAGUCUUCUGGCAAAUAGCGG
rPtk2b-siRNA-2 sense	GCAUAGAGUCAGACAUUCUATT
rPtk2b-siRNA-2 antisense	UAGAUGUCUGACUCUAUGCTA
rPtk2b-siRNA-3 sense	CCGUGAAGAUGUAGUUCUUTT
rPtk2b-siRNA-3 antisense	AAGAACUACAUCUUCACGGGC
rPtk2b-siRNA-4 sense	GCAGCCUUCUUCUGGCUUTT
rPtk2b-siRNA-4 antisense	AAGCCAGAAGAAAGGCUGCTT
rPtk2b-siRNA-5 sense	GCAGUCUCAGUGACAUUUUATT
rPtk2b-siRNA-5 antisense	UAAAUGUCACUGAGACUGCAC
rPtk2b-siRNA-6 sense	GCUUGGACCCGAUGGUUUUATT
rPtk2b-siRNA-6 antisense	UAAACCAUCGGGUCCAAGCAT

resuspended gently with PBS and counted. After adding Annexin V-FITC binding solution and propidium iodide staining solution, the cells were incubated at room temperature (20–25°C) in the dark for 10–20 minutes and then transferred onto the board for testing.

**2.5. ELISA Detection.** After cell supernatants were centrifuged and collected, a series of performances including antigen coating, primary antibody reaction, secondary antibody binding, substrate preparation, and microplate reader were completed according to the manufacturer's instructions. The process was repeated three times for all samples.

**2.6. Real-Time Quantitative PCR.** RNA samples were extracted with quality tests meeting the onboard standards. The extended reverse transcription products were amplified and quantified by the SYBR Green master mixes detection kit. Primer sequences are given in Table 2.

**2.7. Western Blotting.** Cell samples were washed twice with PBS, lysed with lysis buffer for 10–15 min, and then sonicated in 200 W for 4 times, 5 sec each time, at 2 s intervals. Being centrifuged in 12000xg for 15 min, the protein concentrations of each sample were determined by the BCA method. Following sample loading, transferring, milk blocking, primary antibody incubation, and secondary antibody incubation, the exposed band showed the expression of the protein of interest. The detailed information of antibodies is given in Table 3.

**2.8. Statistical Analysis.** Statistical analysis was performed using SPSS17.0. Student's *t*-test was employed to compare the result between two groups, and one-way ANOVA was used to assess the difference among more than two groups. The data are presented in the form of mean  $\pm$  SEM. *P* value <0.05 was considered significant.

### 3. Results

**3.1. Quanzhenyiqitang-Treated Serum Inhibits LPS-Stimulated PYK2 Signaling Pathways in Rat NR8383 Cell.** Western blotting and qRT-PCR were performed to scrutinize the effect of Quanzhenyiqitang-treated serum on the

TABLE 2: Primer sequences.

Name	Sequence (5'-3')
rPtk2b-qF	CTGGAGAGCATCAACTGTGTGC
rPtk2b-qR	GATGGGTAGACGTGTACAGAG
rHDAC-qF	CAACCTAACTGTCAAAGGTCACGC
rHDAC-qR	TGAAGTCTGGTCCAAAATACTCGA
rGAPDH-qF	TGATTCTACCCACGGCAAGTT
rGAPDH-qR	TGATGGGTTTCCCATTGATGA

LPS-stimulated Pyk2/p38MAPK/HDAC2/CK2 signaling pathway in rat alveolar macrophage. The results showed that the expression of p-Pyk2, p-p38MAPK, and CK2 was activated, while HDAC2 was downregulated after LPS stimulation of rat alveolar macrophages, and Quanzhenyiqitang-treated serum significantly inhibited this progression (Figure 1(a)). The same result was also obtained in the expression levels of HDAC2 and CK2 mRNA (Figure 1(b)).

**3.2. Verification of Pyk2 siRNA Interference Efficiency.** To verify the potential role of Pyk2 in macrophage, we designed six Pyk2 siRNA fragments, and by the method of qRT-PCR, found that siRNA-5 and siRNA-6 had a better effect than others, but the efficiency was still not satisfactory (Figure 2(a)). So, we chose a combination of siRNA-5 and siRNA-6 to treat rat alveolar macrophage. The qRT-PCR result showed that the inhibitory rate was up to 80%. Western blot also showed that the expression levels of Pyk2 and p-Pyk2 were both significantly decreased (Figure 2(b)).

**3.3. Pyk2 siRNA Silencing or Quanzhenyiqitang-Treated Serum Enhancing the Function of Rat Alveolar Macrophage.** After LPS stimulation, the apoptosis rate of rat alveolar macrophage NR8383 cell was significantly increased, compared with the LPS Ctrl group (Figure 3(a)). While, cotransfection of rat alveolar macrophages with Pyk2 siRNA-5 and Pyk2 siRNA-6 or Quanzhenyiqitang-treated serum alleviates the apoptosis effect significantly (Figure 3(b)). ELISA results showed that after LPS stimulation, the secretion of inflammatory mediator IL-8 in rat alveolar macrophage was significantly increased. However, after Pyk2 siRNA transfection or Quanzhenyiqitang-treated serum stimulation, IL-8 secretion in rat alveolar macrophage was inhibited to a certain extent. The results indicate that targeting Pyk2 expression could inhibit alveolar macrophages from producing inflammatory mediator IL-8 (Figure 3(c)). After LPS stimulated rat alveolar macrophages, the expression of p-Pyk2, p-p38MAPK, and CK2 upregulated, while HDAC expression was downregulated significantly, and the expression trends of HDAC2 and CK2 mRNA levels were also similar to the previous result. Nevertheless, after Pyk2 siRNA transfection or Quanzhenyiqitang-treated serum stimulation, this process was blocked (Figure 3(d)).

**3.4. Quanzhenyiqitang-Treated Serum Alleviates the Side Effect of Pyk2 OE on Rat Alveolar Macrophage.** After cotransfection of rat alveolar macrophages with Pyk2 OE,

TABLE 3: The detailed information of antibodies.

Actin	PYK2	p-PYK2	P38	p-P38	CK2	HDAC2
Abcam	Abcam	Abcam	Abcam	Abcam	R&D	Abcam
ab179467	ab32571	ab4800	ab170099	ab4822	MAB7957	ab32117
1 : 3000	1 : 2000	1 : 1000	1 : 3000	1 : 1000	1 : 2000	1 : 2000

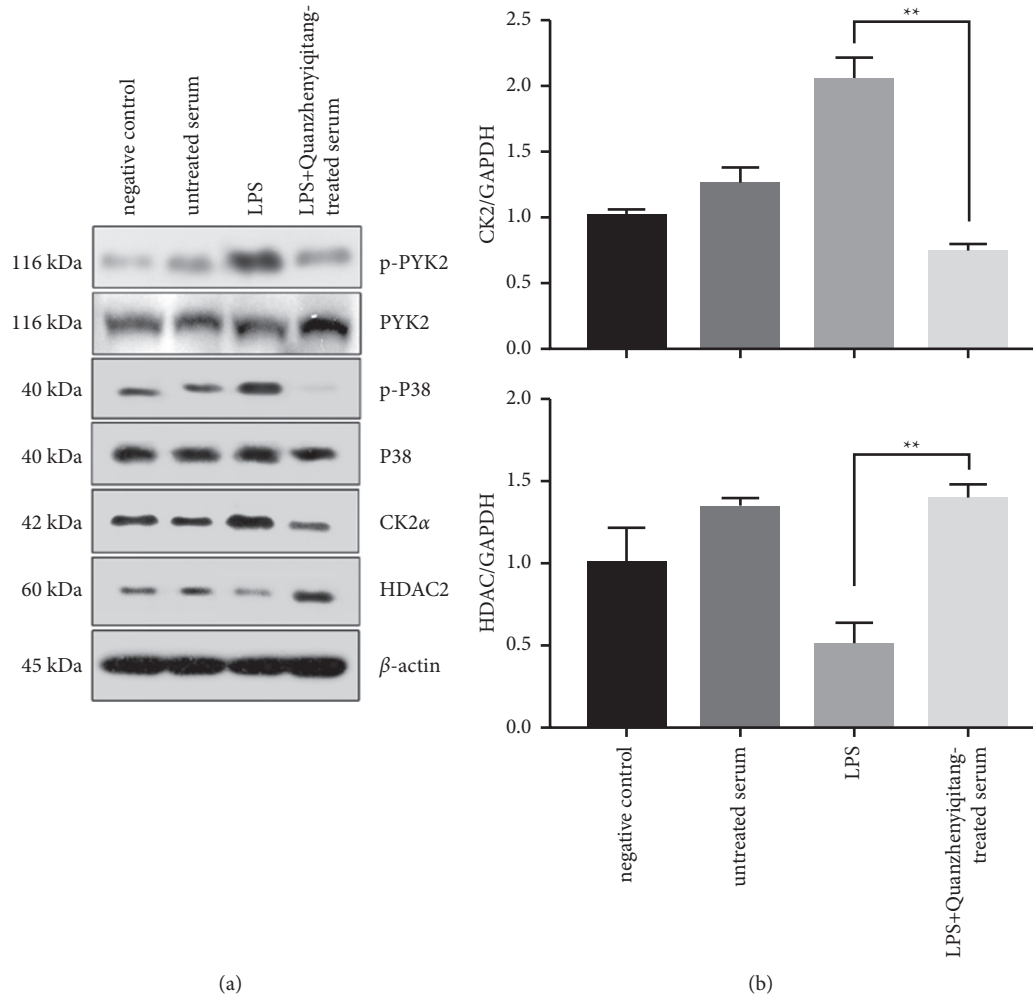


FIGURE 1: Expression of p-Pyk2, p-p38MAPK, HDAC2, and CK2 after LPS induction. (a) The gel figure of p-Pyk2, p-p38MAPK, HDAC2, and CK2 after LPS induction. (b) The expression of p-Pyk2, p-p38MAPK, HDAC2, and CK2 after LPS induction.

the apoptosis process was exacerbated significantly (Figure 4(a)). However, after Quanzhenyiqitang-treated serum stimulation, the apoptosis rate was decreased significantly compared with the Pyk2 OE group (Figure 4(b)); ELISA results also showed that after Quanzhenyiqitang-treated serum stimulation, the secretion level of inflammatory mediator IL-8 in rat alveolar macrophage was downregulated significantly compared with the Pyk2 OE group. Meanwhile, after Pyk2 siRNA transfection or Quanzhenyiqitang-treated serum stimulation, IL-8 secretion in rat alveolar macrophage was inhibited to a certain extent. This indicates that targeting Pyk2 expression could inhibit alveolar macrophages from producing inflammatory mediator IL-8 (Figure 4(c)). Western blot results also showed that after Pyk2 OE transfection, the expression of p-Pyk2,

p-p38MAPK, and CK2 upregulated while HDAC2 was downregulated, as well as the expression levels of HDAC2 and CK2 mRNA levels and Quanzhenyiqitang-treated serum stimulation inhibited this signaling pathway cascade (Figure 4(d)).

#### 4. Discussion

In this study, we investigated the role of the Pyk2-mediated p38MAPK/HDAC2/CK2 signaling pathway in LPS-induced inflammation of rat alveolar macrophages and focused on the effect of potential therapeutic drug Quanzhenyiqitang on this signaling pathway. The results showed that LPS could induce apoptosis of alveolar macrophages. In addition, LPS stimulated the phosphorylation of Pyk2 in rat alveolar



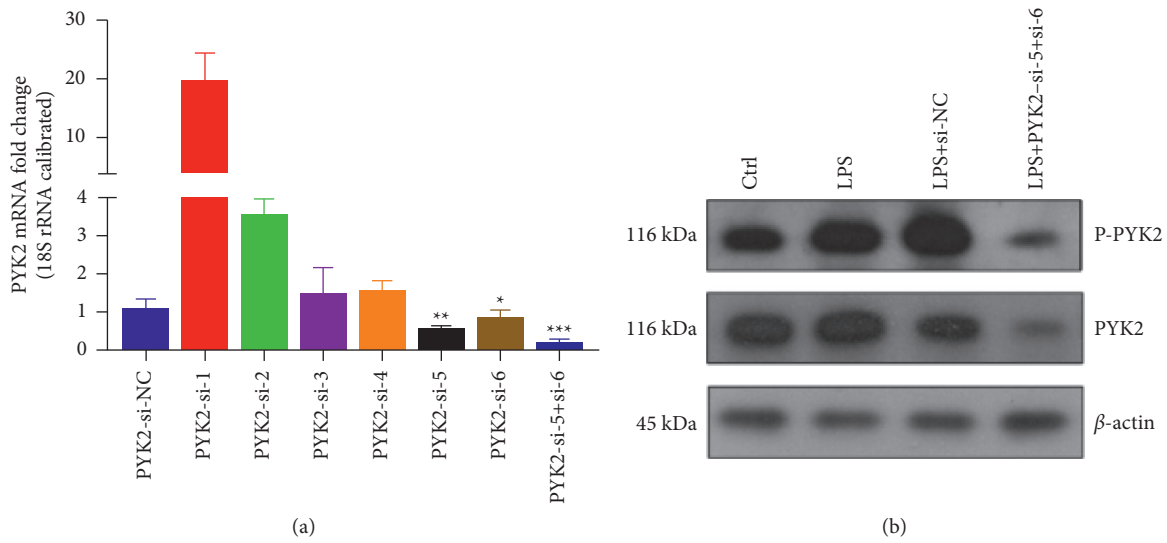


FIGURE 2: Verification of Pyk2 siRNA interference efficiency by qRT-PCR and Western blotting. (a) The verification of Pyk2 siRNA interference efficiency by qRT-PCR. (b) The verification of Pyk2 siRNA interference efficiency by Western blotting.

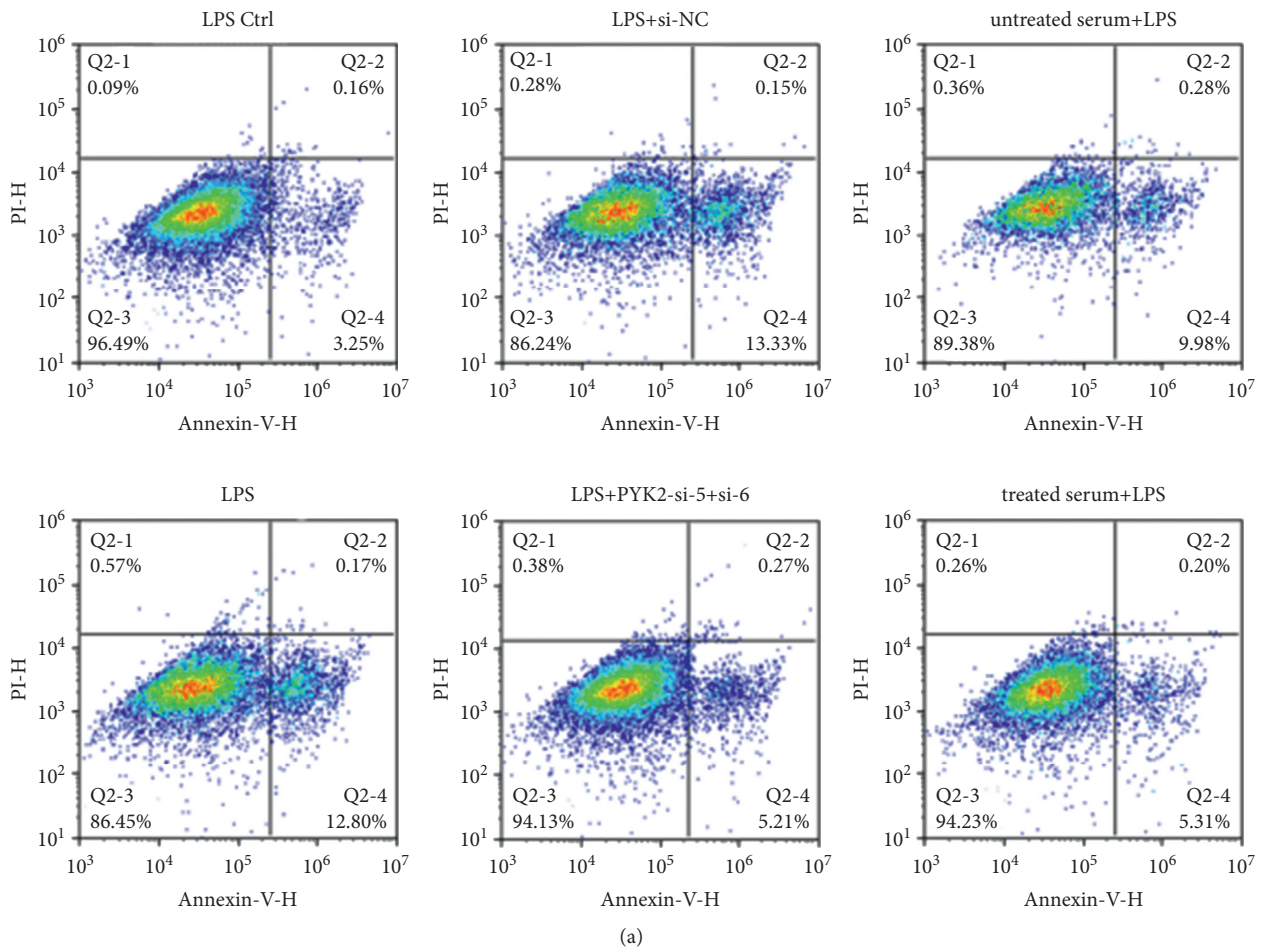
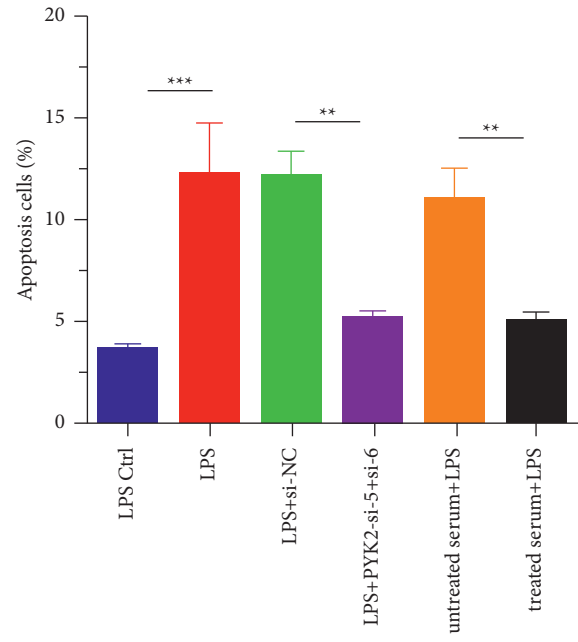
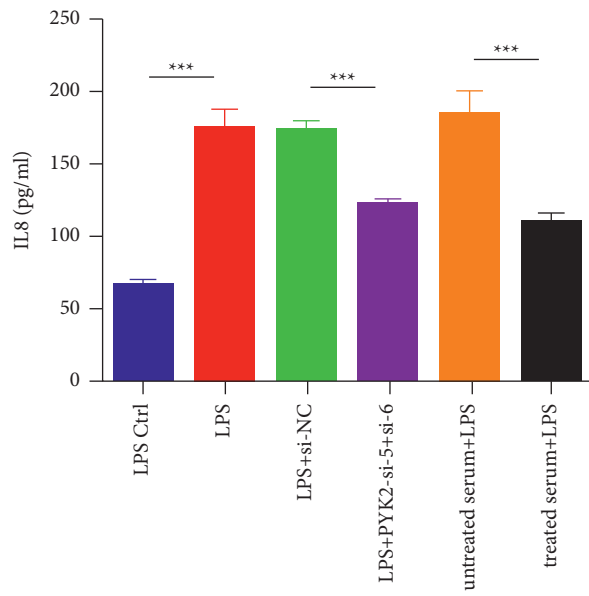


FIGURE 3: Continued.





(b)



(c)

FIGURE 3: Continued.

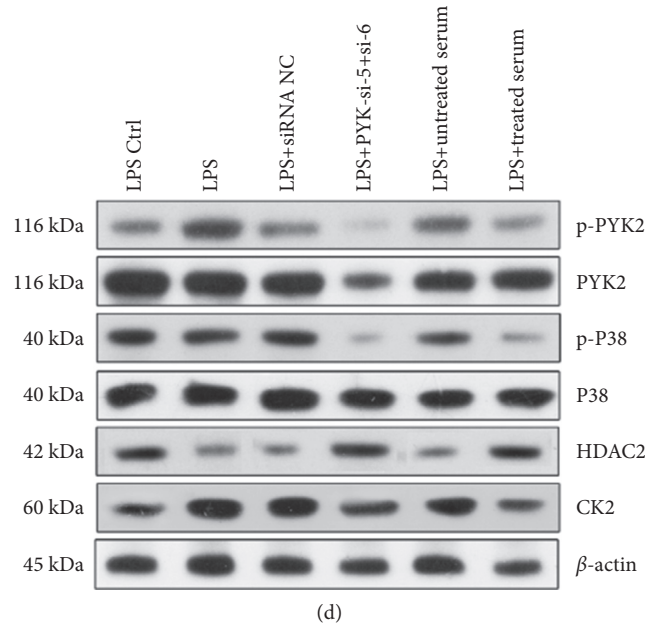


FIGURE 3: The function of the rat alveolar macrophage and signaling pathway after Pyk2 siRNA silencing or Quanzhenyiqitang-treated serum stimulation. (a) Cell apoptosis detected by flow cytometry after Pyk2 siRNA silencing or Quanzhenyiqitang-treated serum stimulation. (b) Apoptosis rate after Pyk2 siRNA silencing or Quanzhenyiqitang-treated serum stimulation. (c) IL-8 level after Pyk2 siRNA silencing or Quanzhenyiqitang-treated serum stimulation. (d) The gel figure of proteins after Pyk2 siRNA silencing or Quanzhenyiqitang-treated serum stimulation.

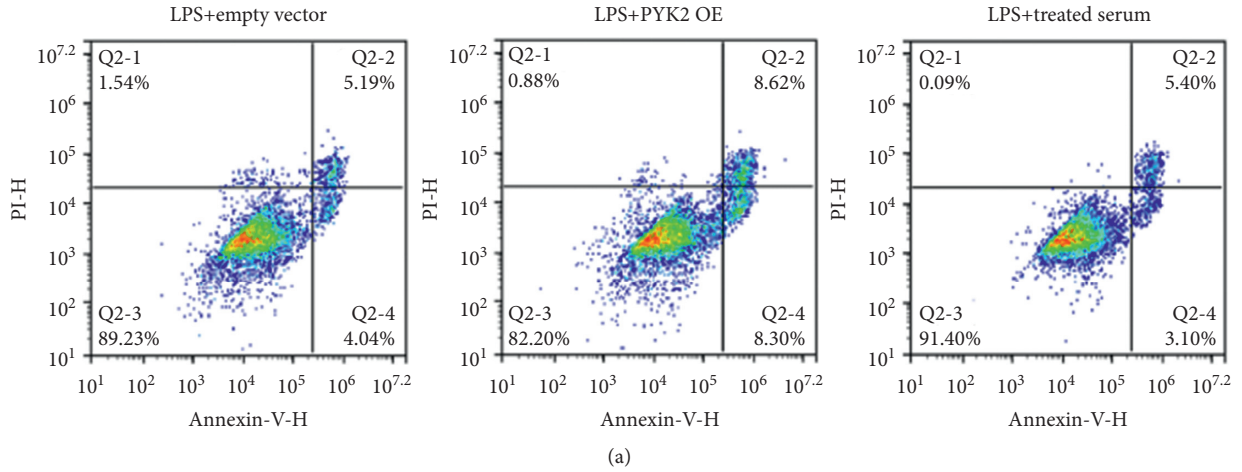
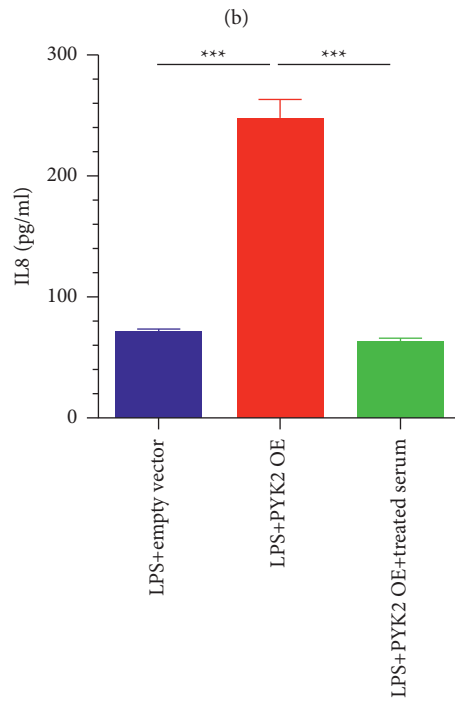
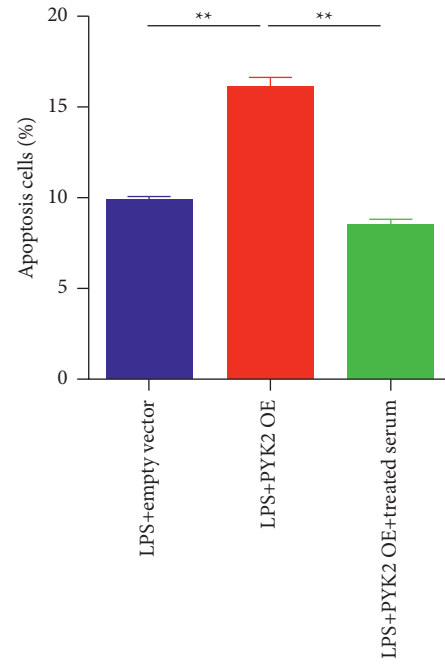


FIGURE 4: Continued.



(c)  
FIGURE 4: Continued.

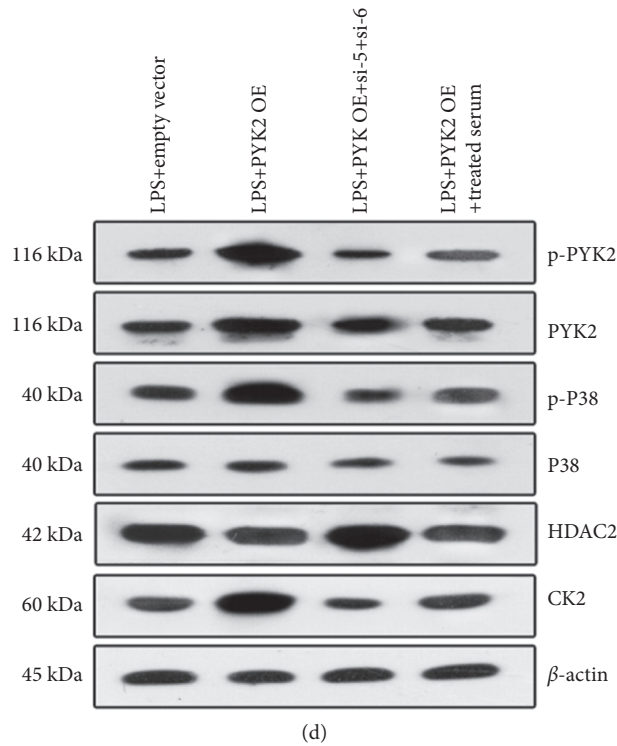


FIGURE 4: Quanzhenyiqitang-treated serum alleviates the side effect of Pyk2 OE on rat alveolar macrophage (a) Cell apoptosis detected by flow cytometry after Quanzhenyiqitang-treated serum alleviates the side effect of Pyk2 OE on rat alveolar macrophage. (b) Apoptosis rate after Quanzhenyiqitang-treated serum alleviates the side effect of Pyk2 OE on rat alveolar macrophage. (c) IL-8 level after Quanzhenyiqitang-treated serum alleviates the side effect of Pyk2 OE on rat alveolar macrophage. (d) The gel figure of proteins after Quanzhenyiqitang-treated serum alleviates the side effect of Pyk2 OE on rat alveolar macrophage.

macrophages through LPS, thus activating downstream factors p38MAPK, HDAC2, and CK2, which in return induced the secretion of the inflammatory mediator IL-8. We also found that transfection of alveolar macrophages with Pyk2 siRNA-5/-6 or Quanzhenyiqitang-treated serum stimulation could effectively inhibit the LPS-induced apoptosis process of rat alveolar macrophages and decrease the secretion of the inflammatory mediator IL-8.

Alveolar macrophages are known as the first line of defense for the lungs against pathogenic microorganisms and lung damage. They are the dominant inflammatory cells in the lungs and can be directly activated by tobacco extracts to release inflammatory regulators [10]. The number of alveolar macrophages is increased in chronic inflammation environments such as COPD airway, lung, and bronchoalveolar lavage fluid, and sputum of patients with sexual lung disease increased. Previous studies have shown that LPS pretreatment can accelerate the inflammatory response and mimic the pathological process of COPD [11]. It is a prevalent method to create a COPD-like mouse model within a short exposure period and expose mice to CS and LPS for 3 consecutive months [12]. Therefore, this study used LPS to induce an inflammatory response in rat alveolar macrophages and to explore the effects and potential mechanisms of Pyk2 in LPS-stimulated inflammatory response. We know that IL-8 was synthesized and secreted by monocytes, macrophages, endothelial cells, fibroblasts, and

epidermal cells under the activation of stimulating factors [13]. As far as known, IL-8 was the strongest neutrophil-activating factor and chemokine, which can effectively dilate blood vessels and promote the proliferation of blood vessels. Neutrophils are the target cells for the activation of IL-8 [14]. IL-8 can specifically chemoattract neutrophils into inflammatory tissues, promoting their degranulation and producing superoxide anions, finally causing respiratory outbreaks, and activating inflammatory cells. Aband AR et al. found in vitro experiments that inhibiting the activity of Pyk2 by transfection in endothelial cells can prevent the process of LPS-induced IL-8 production [15]. Our results indicated that LPS could cause apoptosis of rat alveolar macrophages and stimulated cells to secrete IL-8 inflammatory mediators. These results demonstrated that LPS indeed induced cellular inflammation. Interestingly, we observed that after LPS-induced alveolar macrophages, apoptosis and IL-8 secretion levels were significantly reduced after Pyk2 siRNA-5 and Pyk2 siRNA-6 transfection or Quanzhenyiqitang-treated serum stimulation. Therefore, our study novelly confirmed that this inhibition of Pyk2 phosphorylation alleviated the apoptosis of alveolar macrophages and the release of inflammatory mediator IL-8.

Proline-rich tyrosine kinase (proline-rich tyrosine kinase-2, Pyk2) participates in intracellular signaling pathways, regulates cell movement, regulates cell proliferation and migration, apoptosis, and other processes. Previous

studies have shown that Pyk2 regulated the chemotaxis of macrophages [16]. In Pyk2-knockout mice, the capability of stimulating factors to promote macrophage infiltration into tissues was significantly reduced [17]. The latest research showed that Pyk2 played an important role in acute lung injury. Duan Y et al. confirmed that inhibition of Pyk2 protein in serious LPS-induced acute lung injury mice was the key to inhibiting acute lung inflammation and edema formation [18]. In macrophages chemoattracted by LPS, Pyk2 is also closely associated with the secretion of cytokines. Under the condition that a chemical inducer was added to the lung tissue, as long as the activity of Pyk2 was inhibited, the process of LPS-induced neutrophil exudation could also be blocked. The results of our study showed that LPS induced a high expression of Pyk2 and p-Pyk2 in rat alveolar macrophages. At the same time, we determined the impact of LPS on p38 MAPK and CK2 in alveolar macrophages. Pyk2-mediated p38MAPK/HDAC2/CK2 was the key to LPS-induced inflammation of alveolar macrophages. We conducted Pyk2 functional experiments using Pyk2 siRNA transfection and Quanzhenyiqitang-treated serum stimulation.

Protein kinase CK2, also known as casein kinase-2 (casein kinase II), is a highly conserved second messenger-independent protein kinase that plays a crucial role in cell growth, proliferation, and apoptosis. Therefore, CK2 has become a promising therapeutic target. CK2a expression and activity levels increase in many inflammatory pathologies [19]. Many proteins involved in inflammatory signaling pathways can interact with CK2a, such as NF- $\kappa$ B, CREB, CREM, c-Jun, c-Fos, c-Myc, and Max. The p38MAPK inhibition by applying the p38MAPK inhibitor SB203580 also inhibited the activation of CK2a [20], which implied that CK2a was downstream of the p38MAPK pathway. Our results showed that CK2 was highly expressed in LPS-stimulated rat alveolar macrophages, and its trend was consistent with Pyk2. Inhibiting Pyk2 expression by Pyk2 siRNA transfection and Quanzhenyiqitang-treated serum stimulation inhibited Pyk2 expression; the phosphorylation level of p38MAPK was also consistent with Pyk2 which verified that CK2 was the downstream factor of Pyk2 and p38MAPK.

Histone deacetylase (HDAC) is the key component in the modification of chromosome structure and the regulation of gene expression. In the nucleus, the process of histone acetylation and histone deacetylation is in a dynamic balance and is jointly regulated by HDAC [21]. The function of HDAC is to transfer the acetyl group on the lysine residue of the chromosomal core histone, resulting in the condensation of DNA, and reducing the binding of transcription factors to their binding sites, thereby inhibiting the transcription of genes. HDAC2 is the major histone deacetylase subtype involved in the pathogenesis of COPD. The phosphorylation level of HDAC2 depends on the level of CK2a protein kinase. During the phosphorylation of HDAC2, it is mainly regulated by CK2a. Being knocked out of the CK2a gene can effectively reduce the phosphorylation of HDAC2 [22]. CK2a can promote the phosphorylation of HDAC2, thereby losing the ability to acetylate. The activity

and expression of HDAC2 in the alveolar cells, airways, and lung parenchyma of COPD patients and normal smokers are reduced, thereby activating the expression of IL-8 and other inflammatory factors. Studies have shown that in patients with COPD, with the increase of the inflammation indicators, C-reactive protein (CRP) and procalcitonin (PCT) increase, and HDAC2 levels gradually decrease. In COPD patients treated with hormones, the expression of HDAC2 was upregulated, and NF- $\kappa$ B inhibited, leading to inhibition of the expression of IL-8 and other inflammatory factors, and finally, the patient's airway inflammation was alleviated. Our research showed that HDAC2 was highly expressed in LPS-stimulated rat alveolar macrophages, and Pyk2 siRNA transfection and Quanzhenyiqitang-treated serum stimulation inhibited Pyk2 expression and downregulated the expression of HDAC2 which indicated that HDAC2 is profoundly involved and played an important role in the inflammatory response mediated by Pyk2 in alveolar macrophages.

## 5. Conclusion

In summary, we have demonstrated that LPS induced the apoptosis process of rat alveolar macrophages and secrete the inflammatory mediator IL-8 by upregulating the levels of Pyk2 and downstream factors p38MAPK, HDAC2, and CK2. Pyk2 siRNA transfection and Quanzhenyiqitang-treated serum stimulation could reverse these trends, which may provide a new strategy for the treatment of COPD patients.

## Data Availability

The data used to support the findings of this study are available from the corresponding author upon request.

## Conflicts of Interest

The authors declare that they have no conflicts of interest.

## Acknowledgments

The authors thank the support provided by the National Natural Science Foundation of China (81774097) and the Education Department of Fujian Province (JAT190279).

## References

- [1] S. Gordon and L. Martinez-Pomares, "Physiological roles of macrophages," *Pfluegers Archiv European Journal of Physiology*, vol. 469, no. 3-4, pp. 365-374, 2017.
- [2] K. Hu, Y. Jin, Z. Chroneos, X. Han, H. Liu, and L. Lin, "Macrophage functions and regulation: roles in diseases and implications in therapeutics," *Journal of immunology research*, vol. 2018, Article ID 7590350, 13 pages, 2018.
- [3] F. O. Martinez and S. Gordon, "The M1 and M2 paradigm of macrophage activation: time for reassessment," *F1000prime reports*, vol. 6, p. 13, 2014.
- [4] C. Atri, F. Z. Guerfali, and D. Laouini, "Role of human macrophage polarization in inflammation during infectious



- diseases," *International Journal of Molecular Sciences*, vol. 19, no. 6, 2018.
- [5] B. Allard, A. Panariti, and J. G. Martin, "Alveolar macrophages in the resolution of inflammation, tissue repair, and tolerance to infection," *Frontiers in Immunology*, vol. 9, p. 1777, 2018.
- [6] N. Vij, P. Chandramani-Shivalingappa, C. Van Westphal, R. Hole, and M. Bodas, "Cigarette smoke-induced autophagy impairment accelerates lung aging, COPD-emphysema exacerbations and pathogenesis," *American Journal of Physiology-Cell Physiology*, vol. 314, no. 1, pp. C73–C87, 2018.
- [7] H. Lee, E. Abston, D. Zhang, A. Rai, and Y. Jin, "Extracellular vesicle: an emerging mediator of intercellular crosstalk in lung inflammation and injury," *Frontiers in Immunology*, vol. 9, p. 924, 2018.
- [8] Y. H. A. Elewa, O. Ichii, K. Takada, T. Nakamura, M. A. Masum, and Y. Kon, "Histopathological correlations between mediastinal fat-associated lymphoid clusters and the development of lung inflammation and fibrosis following bleomycin administration in mice," *Frontiers in Immunology*, vol. 9, p. 271, 2018.
- [9] X. Zhu, Y. Bao, Y. Guo, and W. Yang, "Proline-rich protein tyrosine kinase 2 in inflammation and cancer," *Cancers*, vol. 10, no. 5, 2018.
- [10] L. I. Da-zhi, R. U. A. N. Shi-wei, and L. I. Xi, "Effect of Quanzhen Yiqi Decoction on IgM and Cystatin C in blood serum from COPDrats with syndrome of kidney Qi deficiency failing to control respiring Qi," *China Journal of Traditional Chinese Medicine and Pharmacy*, vol. 27, no. 3, 2012.
- [11] E. Hardaker, M. Freeman, N. Dale et al., "Exposing rodents to a combination of tobacco smoke and lipopolysaccharide results in an exaggerated inflammatory response in the lung," *British Journal of Pharmacology*, vol. 160, no. 8, pp. 1985–1996, 2010.
- [12] V. Ghorani, M. H. Boskabady, M. R. Khazdair, and M. Kianmeher, "Experimental animal models for COPD: a methodological review," *Tobacco Induced Diseases*, vol. 15, no. 1, p. 25, 2017.
- [13] I. Bosch, K. Khaja, L. Estevez et al., "Increased production of interleukin-8 in primary human monocytes and in human epithelial and endothelial cell lines after dengue virus challenge," *Journal of Virology*, vol. 76, no. 11, pp. 5588–5597, 2002.
- [14] H. U. Zeilhofer and W. Schorr, "Role of interleukin-8 in neutrophil signaling," *Current Opinion in Hematology*, vol. 7, no. 3, pp. 178–182, 2000.
- [15] A. R. Anand, M. Cucchiari, E. F. Terwilliger, and R. K. Ganju, "The tyrosine kinase Pyk2 mediates lipopolysaccharide-induced IL-8 expression in human endothelial cells," *The Journal of Immunology*, vol. 180, no. 8, pp. 5636–5644, 2008.
- [16] H. Park, D. Ishihara, and D. Cox, "Regulation of tyrosine phosphorylation in macrophage phagocytosis and chemotaxis," *Archives of Biochemistry and Biophysics*, vol. 510, no. 2, pp. 101–111, 2011.
- [17] M. Okigaki, C. Davis, M. Falasca et al., "Pyk2 regulates multiple signaling events crucial for macrophage morphology and migration," *Proceedings of the National Academy of Sciences*, vol. 100, no. 19, pp. 10740–10745, 2003.
- [18] Y. Duan, J. Learoyd, A. Y. Meliton, A. R. Leff, and X. Zhu, "Inhibition of Pyk2 blocks lung inflammation and injury in a mouse model of acute lung injury," *Respiratory Research*, vol. 13, no. 1, p. 4, 2012.
- [19] S. A. Gibson and E. N. Benveniste, "Protein kinase CK2: an emerging regulator of immunity," *Trends in Immunology*, vol. 39, no. 2, pp. 82–85, 2018.
- [20] M. Sayed, S. O. Kim, B. S. Salh, O.-G. Issinger, and S. L. Pelech, "Stress-induced activation of protein kinase CK2 by direct interaction with p38 mitogen-activated protein kinase," *Journal of Biological Chemistry*, vol. 275, no. 22, pp. 16569–16573, 2000.
- [21] E. Seto and M. Yoshida, "Erasers of histone acetylation: the histone deacetylase enzymes," *Cold Spring Harbor Perspectives in Biology*, vol. 6, no. 4, Article ID a018713, 2014.
- [22] D. Adenuga and I. Rahman, "Protein kinase CK2-mediated phosphorylation of HDAC2 regulates co-repressor formation, deacetylase activity and acetylation of HDAC2 by cigarette smoke and aldehydes," *Archives of Biochemistry and Biophysics*, vol. 498, no. 1, pp. 62–73, 2010.

## Research Article

# Structure-Based In Silico Investigation of Agonists for Proteins Involved in Breast Cancer

Arpita Roy <sup>1</sup>, Ashutosh Anand,<sup>2</sup> Saksham Garg <sup>2</sup>, Mohd Shahnawaz Khan,<sup>3</sup> Sidharth Bhasin <sup>4</sup>, Muhammad Nadeem Asghar,<sup>5</sup> and Talha Bin Emran <sup>6</sup>

<sup>1</sup>Department of Biotechnology, School of Engineering & Technology, Sharda University, Greater Noida, India

<sup>2</sup>Delhi Technological University, Rohini, New Delhi, India

<sup>3</sup>Department of Biochemistry, College of Sciences, King Saud University, Riyadh, Saudi Arabia

<sup>4</sup>Indian Institute of Technology Delhi, Delhi, India

<sup>5</sup>Department of Medical Biology, University of Québec at Trois-Rivières, Trois-Rivières, Québec G9A 5H7, Canada

<sup>6</sup>Department of Pharmacy, BGC Trust University Bangladesh, Chittagong 4381, Bangladesh

Correspondence should be addressed to Arpita Roy; [arbt2014@gmail.com](mailto:arbt2014@gmail.com) and Talha Bin Emran; [talhabmb@gmail.com](mailto:talhabmb@gmail.com)

Received 13 December 2021; Revised 21 December 2021; Accepted 23 December 2021; Published 6 January 2022

Academic Editor: Ruchika Garg

Copyright © 2022 Arpita Roy et al. This is an open access article distributed under the Creative Commons Attribution License, which permits unrestricted use, distribution, and reproduction in any medium, provided the original work is properly cited.

Cancer is recognized as one of the main causes of mortality worldwide by the World Health Organization. The high cost of currently available cancer therapy and certain limitations of current treatment make it necessary to search for novel, cost-effective, and efficient methods of cancer treatment. Therefore, in the current investigation, sixty-two compounds from five medicinal plants (*Tinospora cordifolia*, *Ocimum tenuiflorum*, *Podophyllum hexandrum*, *Andrographis paniculata*, and *Beta vulgaris*) and two proteins that are associated with breast cancer, i.e., HER4/ErbB4 kinase and ER $\alpha$  were selected. Selected compounds were screened using Lipinski's rule, which resulted in eighteen molecules being ruled out. The remaining forty-four compounds were then taken forward for docking studies followed by molecular dynamics studies of the best screened complexes. Results showed that isocolumbin, isopropylideneandrographolide, and 14-acetylandrographolide were potential lead compounds against the selected breast cancer receptors. Furthermore, *in vitro* studies are required to confirm the efficacy of the lead compounds.

## 1. Introduction

Breast cancer is a heterogeneous group of diseases that originate in the breast tissue and result in the formation of a lump or a mass in the breast. Breast cancer mostly originates from the epithelial cells lining the milk duct [1, 2]. When the tumor is small and easily treatable, no concrete symptoms are observed, therefore making early screening important. However, a major symptom is the presence of a painless lump/mass in the breast. In some cases, cancer spreads to the lymph nodes present in the underarms and can cause swelling or lumps, even though the tumor itself is not large enough to be felt by the patient. Pain in the breast, a feeling of heaviness, swelling, or redness of the skin, and spontaneous discharge from the nipples are some of the rare symptoms experienced by some patients [3]. It is the most frequent cause of cancer and cancer-related death among

women worldwide. It impacts more than 2.1 million women each year. According to the World Health Organization, in 2018, more than 620 thousand women died from breast cancer worldwide. This constitutes about 15% of all cancer-related deaths among women [4]. A total of 6.9% of cancer deaths are attributed to breast cancer with 684,996 deaths in 2020.

Estrogen receptor (ER)  $\alpha$ , an ER subtype, plays a major role in the physiological development of the body [5]. The reproductive, central nervous system, skeletal, and cardiovascular systems are some of the organ systems where ER $\alpha$  plays an important role in the development and functioning [5]. As shown in [5–7], ER $\alpha$  is widely expressed throughout the body such as in the uterus, mammary glands, male reproductive system, ovaries, spleen, kidney, and lungs among other organs. ER $\alpha$  is responsible for human breast cancer progression [6, 8]. Approximately 75% of breast

tumors have ER $\alpha$  at the time of diagnosis (ER-positive breast cancer). Therefore, it has been selected as a marker for prognosis during the course of therapy that a patient receives. ER-positive markers have been found to have a better prognosis than ER-negative tumors. Tamoxifen is the most widely used drug for treating cases of ER-positive breast cancer when the patient requires endocrine therapy [9]. Other selective ER modulatory drugs are toremifene and raloxifene. Aminoglutethimide and exemestane are potent aromatase inhibitors for ER [10].

HER4/ErbB4 is a member protein of the epidermal growth factor receptor (EGFR) family. Each member of the EGFR family is essential for normal development [11] in animals and humans. They are necessary for the healthy development of the heart, nervous system, and mammary gland [11]. HER4 is known for its crucial role in carcinogenesis [12]. However, unlike other members of EGFR, HER4 signaling is less understood. It is known to play a positive role in cancer progression, especially breast cancer in humans [13, 14]. As reported by Zhu et al. [15], HER4, alone, could moderate the estrogen-induced growth of breast cancer cells. And, as observed *in vitro*, overexpression of HER4 influences cell cycle arrest and apoptosis significantly in breast cancer [15, 16]. Canertinib, developed by Pfizer, inhibits HER2 and HER4, but due to its limited effect, as shown in phases I and II, this drug was discontinued [17]. Afatinib, an irreversible tyrosine kinase inhibitor, simultaneously targets HER2 and HER4 [18]. It also suppresses HER3-mediated signaling [19].

Natural compounds are one of the potential sources of bioactive compounds [20]. Plant-derived compounds possess a wide range of therapeutic actions, which include anticancer, antidiabetic, antibacterial, and antifungal activities [21–23]. The anticancer activity of various plant-derived compounds has been reported in various studies [24–28]. This study elucidates the molecular docking and dynamic results between biochemical compounds taken from five different plants, namely, *Tinospora cordifolia*, *Ocimum tenuiflorum*, *Podophyllum hexandrum*, *Andrographis paniculata*, and *Beta vulgaris*, and two proteins, namely, human ER $\alpha$  (PDB Id: 2IOG) and HER4/ErbB4 (PDB Id: 3BBT), to propose a natural phytochemical compound which could potentially treat breast cancer.

## 2. Materials and Methods

**2.1. Protein and Ligand.** The 3D crystal structures of the proteins considered in this study were imported from the Protein Data Bank (RCSB PDB) Web server [28]. For the following study, two proteins were taken for the search of their antagonists, HER4/ErbB4 kinase (PDB ID: 3BBT) and human estrogen receptor  $\alpha$  (PDB ID: 2IOG).

**2.2. Ligands.** For the analysis and prediction of the potential ligand, a data set of 62 phytocompounds from *Tinospora cordifolia*, *Podophyllum hexandrum*, *Andrographis paniculata*, *Beet vulgaris*, and *Ocimum sanctum* was selected (Table 1). The structures obtained from the PubChem

database [27, 29] of all compounds were converted from .sdf format to .pdb format using the Discovery Studio Visualizer by BIOVIA.

**2.3. ADME Testing.** The SwissADME tool [30] by ExPASy tools was used to determine the values of parameters proposed in the Lipinski Rule of Five [31]. In addition to lipophilicity, the number of hydrogen bond donors and acceptors, and molecular weight, one parameter, molar refractivity (Ghose rule), was also taken into account to test the drug-likeness of all the 62 compounds [32].

**2.4. Molecular Docking.** Interaction studies of receptor structure with selected ligands were performed using the AutoDock v4.2.6 interface. The protocol started with the preparation of a receptor/protein in which surrounding water was removed from the vicinity of the protein, Kollman charges were added, and polar hydrogens were added, merging nonpolar at the same time. All the rotatable bonds of the ligand were allowed to rotate, and the Gasteiger charges were computed. Grid coordinates were selected using the existing inhibitor in the receptor after which the bound inhibitor was also removed to vacate the active site. The Lamarckian GA output was used to obtain the docking results using a genetic algorithm. Of the 10 conformations obtained, the one with the least binding energy was selected, and 2D binding interactions between active site residues and the ligand were generated using the BIOVIA Discovery Studio Visualizer v19.1.0.18287.

**2.5. Molecular Dynamics.** 100 ns simulations of the docked receptor-ligand complex were carried out. Molecular simulations were carried out on the Desmond–Maestro module 2020. All the parameters and algorithms were kept as default. Desmond by itself uses the most efficient algorithms for generating precise output data. The TIP3P model system of water was provided to the docked complex to provide a medium. 0.15 M Na<sup>+</sup> ions were added to neutralize the whole system with OPLS-AA 2005 as the assigned force field. The SHAKE/RATTLE algorithm restricted the covalent bond movement. NVT ensemble with 300K as temperature and 1 bar as pressure, and all inputs were combined using the RESPA integrator. 100 ns simulations were allowed to be subdivided into 1000 frames for dynamic analysis of protein-ligand interaction [33, 34].

**2.6. PASS Webserver.** Based on the structures using multi-level neighbors of atoms description, the PASS webserver can be used to predict the biological activity of the compound. The SMILES of the compound are taken as the input, and the probability of a biological activity can be obtained as the output.

## 3. Result and Discussion

**3.1. ADME Testing.** A preliminary structure-based analysis was conducted on the selected 62 phytocompounds which

TABLE 1: Molecular docking analysis with 2IOG.

Compounds	Binding energy	Ligand efficiency	Inhibition constant ( $\mu\text{M}$ )	Intermolecular energy	Vdw H bond desolvation energy
Isopropylideneandrographolide	-10.3	-0.37	0.02811	-11.2	-11.05
14-Acetylandrographolide	-9.26	-0.33	0.16439	-11.34	-11.37
(8S,12R)-Isoandrographolide	-9.2	-0.37	0.18169	-10.39	-10.07
Dehydroandrographolide	-9.07	-0.38	0.22425	-10.56	-10.15
Isocolumbin	-9.05	-0.35	0.23209	-9.65	-9.58
Andrographolide	-8.87	-0.35	0.31251	-10.66	-10.38
Palmarin	-8.79	-0.33	0.36334	-9.38	-9.45
19-O-Acetyl-14-deoxy-11,12-didehydroandrographolide	-8.72	-0.32	0.40811	-10.51	-10.46
14-Deoxy-11,12-didehydroandrographolide	-8.48	-0.35	0.60911	-9.97	-9.87
Azatoxin	-8.41	-0.3	0.68172	-9.61	-9.61
Podophyllotoxin	-8.38	-0.28	0.72584	-9.87	-9.77
4-Demethylpodophyllotoxin	-8.35	-0.29	0.76082	-9.84	-9.86
Tinosporin	-8.28	-0.29	0.85158	-9.77	-9.79
Palmatine	-8.26	-0.32	0.88102	-9.45	-9.44
Tetrahydropalmatine	-8.26	-0.32	0.87684	-9.46	-9.25
Luteolin	-8.1	-0.39	1.16	-9.59	-9.04
Tembetarine	-8.05	-0.32	1.26	-9.84	-9.61
Cirsilineol	-7.89	-0.32	1.42	-9.77	-9.71
Cirsimaritin	-7.81	-0.34	1.9	-9.3	-9.04
Apigenin	-7.76	-0.39	2.06	-8.95	-8.57
Jatrorrhizine	-7.75	-0.31	2.08	-8.95	-9
Rhamnetin	-7.64	-0.33	2.5	-9.43	-8.93
Magnoflorine	-7.62	-0.3	2.59	-8.81	-8.43
Aporphine	-7.61	-0.42	2.63	-7.61	-7.25
Quercetin	-7.61	-0.35	2.65	-9.4	-8.87
Isothymusin	-7.41	-0.31	3.67	-9.2	-8.95
Kaempferol	-7.39	-0.35	3.85	-8.88	-8.53
Moslosooflavone	-7.17	-0.33	5.57	-8.36	-8.3
Rosmarinic acid	-7.16	-0.28	5.63	-10.74	-10.42
Rhamnocitrin	-7.12	-0.32	6.06	-8.61	-8.34
$\alpha$ -Elemene	-6.89	-0.46	8.9	-7.49	-7.49
Betaxanthin	-6.88	-0.26	9.06	-9.27	-9.61
Myrtenal	-6.44	-0.59	19.15	-6.73	-6.46
Bornyl acetate	-6.25	-0.45	26.32	-6.84	-6.82
Eugenol	-5.49	-0.46	94.23	-6.69	-6.61
Methyl eugenol	-5.26	-0.4	138.4	-6.46	-6.27
Berberin	-5.25	-0.21	141.76	-5.85	-5.83
Ferulic acid	-5.24	-0.37	144.6	-6.73	-5.47
Neral	-5.19	-0.47	157.53	-6.38	-6.24
p-Coumaric acid	-5.09	-0.42	186.95	-6.28	-4.94
Caffeic acid	-5.08	-0.39	190.47	-6.57	-6.19
Syringic acid	-4.86	-0.35	274.22	-6.35	-5.78
Betaine	-3.6	-0.45	2310	-4.19	-2.83
Choline	-3.16	-0.45	4810	-4.06	-3.63

were reported in our earlier study [35]. Compounds were subjected to a total of 5 parameters: logP/lipophilicity (<5), molar refractivity (40–130), molecular weight (<500 Da), hydrogen bond acceptor (<10), and hydrogen bond donors (<5) [36, 37]. 18 small molecules showed two or more violations of parameters which resulted in their omission from further analysis.

**3.2. Molecular Docking.** The minimum binding energy among all 3BBT-isopropylideneandrographolide complexes was  $-9.41$  kcal/mol. A total of 16 residues interacted with the

ligand molecule. THR835 and PHE837 formed strong hydrogen bonds. Another type of interaction was alkyl and van der Waals. CYS778, LEU825, ALA724, VAL707, LEU769, and LYS726 formed an alkyl bond with isopropylideneandrographolide (Figure 1) (Table 2).

Out of the 10 conformations obtained for the 3BBT-isocolumbin complex,  $-9.06$  kcal/mol was the best binding energy. Four different types of bond formation took place. THR835 and LEU 825 interacted with the five membered ring with pi-sigma interaction. ASP836 formed a conventional carbon-hydrogen bond. LYS726, VAL756, LEU758, LEU769, LEU839, and MET747 interacted by forming alkyl

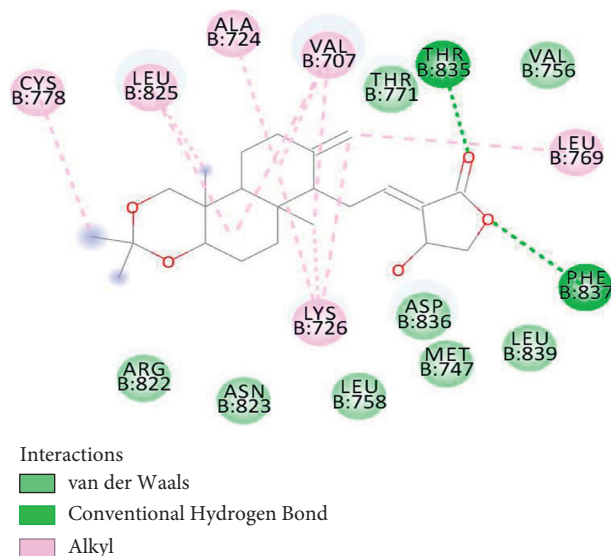


FIGURE 1: 3BBT residues interacting with isopropylideneandrographolide.

TABLE 2: Molecular docking analysis with 3BBT.

Compounds	Binding energy	Ligand efficiency	Inhibition constant ( $\mu\text{M}$ )	Intermolecular energy	Vdw H bond desolvation energy
Isopropylideneandrographolide	-9.41	-0.34	0.12718	-10.3	-10.2
Isocolumbin	-9.06	-0.35	0.22848	-9.66	-9.46
Azatoxin	-8.9	-0.32	0.30049	-10.09	-9.87
19-O-Acetyl-14-deoxy-11,12-didehydroandrographolide	-8.84	-0.33	0.329	-10.63	-10.48
Kaempferol	-8.18	-0.39	1	-9.68	-9.41
(8S,12 R)-Isoandrographolide	-8.11	-0.32	1.13	-9.31	-9.27
14-Acetylandrographolide	-8.1	-0.29	1.16	-10.19	-10.04
14-Deoxy-11,12-didehydroandrographolide	-7.97	-0.33	1.43	-9.46	-9.31
Cirsilineol	-7.95	-0.32	1.49	-9.74	-9.38
Apigenin	-7.95	-0.4	1.49	-9.14	-9.06
Betaxanthin	-7.93	-0.31	1.53	-10.32	-8.98
Rhamnetin	-7.88	-0.34	1.68	-9.67	-9.57
Andrographolide	-7.87	-0.31	1.69	-9.66	-9.39
4-Demethylpodophyllotoxin	-7.76	-0.27	2.06	-9.25	-8.96
Luteolin	-7.68	-0.37	2.35	-9.17	-8.82
Berberin	-7.6	-0.3	2.69	-8.2	-8.13
Palmatine	-7.6	-0.29	2.67	-8.8	-8.7
<i>alpha</i> -Elemene	-7.57	-0.5	2.82	-8.17	-8.18
Dehydroandrographolide	-7.56	-0.32	2.86	-9.06	-8.7
Rhamnocitrin	-7.54	-0.34	2.95	-9.04	-8.99
Palmarin	-7.5	-0.28	3.19	-8.09	-8
Quercetin	-7.48	-0.34	3.3	-9.27	-9.18
Moslosooflavone	-7.47	-0.34	3.33	-8.67	-8.93
Cirsimaritin	-7.33	-0.32	4.21	-8.83	-8.53
Podophyllotoxin	-7.32	-0.24	4.31	-8.81	-8.83
Rosmarinic acid	-7.2	-0.28	5.26	-10.78	-10.09
Magnoflorine	-7.09	-0.28	6.4	-8.28	-8.32
Tetrahydropalmatine	-6.99	-0.27	7.47	-8.19	-8.48
Jatrorrhizine	-6.96	-0.28	7.86	-8.16	-8.2
Isothymusin	-6.91	-0.29	8.64	-8.7	-8.42
Bornyl acetate	-6.88	-0.49	9.09	-7.47	-7.36
Myrtenal	-6.52	-0.59	16.71	-6.82	-6.84
Tembetarine	-6.48	-0.26	17.84	-8.27	-8.35



TABLE 2: Continued.

Compounds	Binding energy	Ligand efficiency	Inhibition constant ( $\mu\text{M}$ )	Intermolecular energy	Vdw H bond desolvation energy
Tinosporin	-6.19	-0.21	28.94	-7.68	-7.65
Caffeic acid	-6.11	-0.47	33.16	-7.6	-6.32
Ferulic acid	-5.85	-0.42	51.48	-7.34	-6.23
Neral	-5.8	-0.53	56.3	-6.99	-6.88
p-Coumaric acid	-5.79	-0.48	57.24	-6.98	-5.72
Methyl eugenol	-5.73	-0.44	63.14	-6.92	-6.79
Syringic acid	-5.41	-0.39	107.55	-6.91	-6.22
Eugenol	-5.28	-0.44	134.03	-6.48	-6.46
Aporphine	-5	-0.28	216.99	-5	-5.44
Betaine	-3.69	-0.46	1980	-4.28	-2.67
Choline	-2.91	-0.42	7360	-3.81	-3.93

bonds with the ligand. The other six residues complemented these interactions with van der Waal forces (Figure 2).

Figure 3 represents the best docked conformation of the 2IOG-isopropylideneandrographolide complex having a binding energy of  $-10.3\text{ kcal/mol}$ . 18 residues in total interacted with the present ligand. CYS530 and THR347 formed conventional hydrogen bonds. ASP351 was the only residue forming a carbon-hydrogen bond. 4 residues interacted with weak van der Waals forces. All the other residues either interacted with either the alkyl or pi-alkyl bond formation.

The best complex with 14-acetylandrographolide showed a binding energy of  $-9.26\text{ kcal/mol}$ ; cumulatively, 21 residues around the ligand interacted with it. CYS530 and MET343 acted as anchors forming strong conventional hydrogen bonds. MET421, LEU384, MET388, LEU387, PHE404, LEU525, and LEY346 formed either alkyl or pi-alkyl bonds. 11 residues showed weak van der Waals interactions. THR347 formed an unfavorable donor-donor bond (Figure 4) (Table 1).

**3.3. Molecular Dynamics.** Simulation studies were carried out on the two best docked complexes for each receptor taken into account. Each dock was allowed to simulate in the dynamic environment for 100 ns seconds to yield the potential energy and total energy (Table 3).

**3.4. Structural Deviation and Compactness.** Using four parameters, the conformational stability of the protein and ligand can be analyzed. The root mean square deviation (RMSD), root mean square fluctuations (RMSF), radius of gyration (rGyr), and solvent accessible surface area (SASA) plots can be insightful for defining the compactness of protein and ligand complexes.

**3.4.1. HER4/ErbB4 Kinase (3BBT).** A stabilized RMSD plot can be observed with isocolumbin as the ligand molecule. The graph can be observed to fluctuate a little but around a fixed average value only, i.e.,  $2.5\text{ \AA}$ . Although during 20–40 ns a few small peaks are visible of magnitude  $1\text{ \AA}$  for backbone atoms and C $\alpha$  atoms, this sudden peak can be

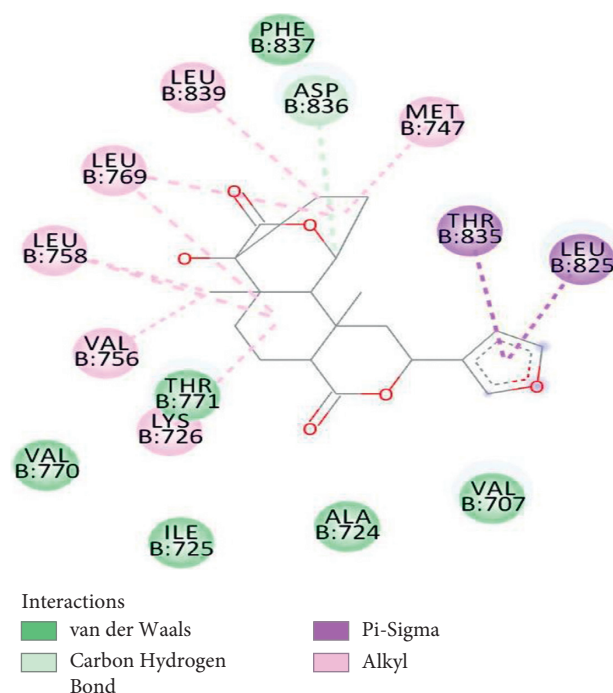


FIGURE 2: 3BBT residues interacting with isocolumbin.

regarded to the internal vibrations of the atoms. After 40 ns, a stable plateau is attained, lasting throughout the simulation. With isopropylideneandrographolide as a ligand molecule, a significant deviation ( $>3$ ) can be seen ( $>3\text{ \AA}$ ) suggesting large conformational changes in the protein, which is not preferable. After 40 ns the graph stabilizes to the end around a value of 5 which is still higher compared to the RMSD of the 3BBT-isocolumbin complex (Figure 5(a)).

RMSF graphs for both the ligand complexes can be observed as they should be. Secondary structures like the alpha-helix and beta-sheets are more rigid portions of the protein and therefore should fluctuate less, which is exactly what the RMSF plot showed. The unstructured part, including loops and straight chains of amino acids, fluctuated relatively more (Figure 5(b)).

The rGyr plot for the isocolumbin complex yielded a value of  $3.66 \pm 0.12\text{ \AA}$ . The probability distribution graph revealed

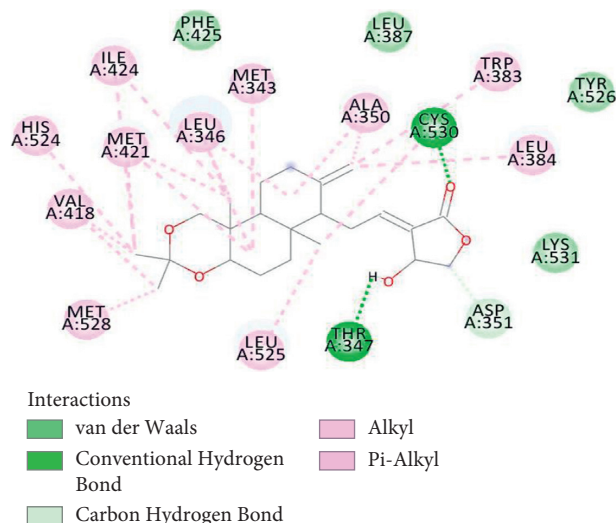


FIGURE 3: 2IOG residues interacting with isopropylideneandrographolide.

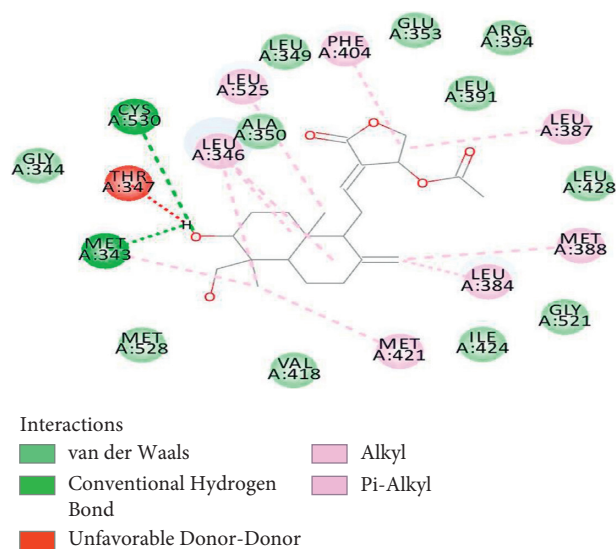


FIGURE 4: 2IOG residues interacting with 14-acetylandrographolide.

TABLE 3: Potential and total energies (kcal/mol) of systems obtained after 100 ns simulation.

S. no.	Complex	Potential energy (kcal/mol)	Total energy (kcal/mol)
1.	3BBT-Isopropylideneandrographolide	-166930.943	-205596.718
2.	3BBT-Isocolumbin	-166941.883	-205610.056
3.	2IOG-Isopropylideneandrographolide	-85478.448	-105151.438
4.	2IOG-14-Acetylandrographolide	-85481.496	-105151.587

that in most frames, the 3.66 Å was achieved with little or no fluctuation overall. The isopropylideneandrographolide complex showed a higher rGyr value of 4.40 Å with a very nominal crest and troughs. Both the graphs suggest the compactness of the complex; however, the lower value of isocolumbin gives it an edge suggesting a more compact structure during the simulation course (Figure 5(c)).

Isocolumbin again provides a lower SASA value than the isopropylideneandrographolide; an average of 30 Å SASA is observed with the isocolumbin ligand, whereas this number

goes up to 100 Å with the other ligand, with more variations in the overall graph. The binding of isocolumbin with the protein is fairly more stable and the core residues are not exposed to the surrounding water, suggesting a good binding of the ligand with the 3BBT receptor (Figure 5(d)).

**3.4.2. Human Estrogen Receptor  $\alpha$  (2IOG).** Toward the later stages of the dynamics, the RMSD plot with 14-acetylandrographolide stabilized almost at 3.2 without any

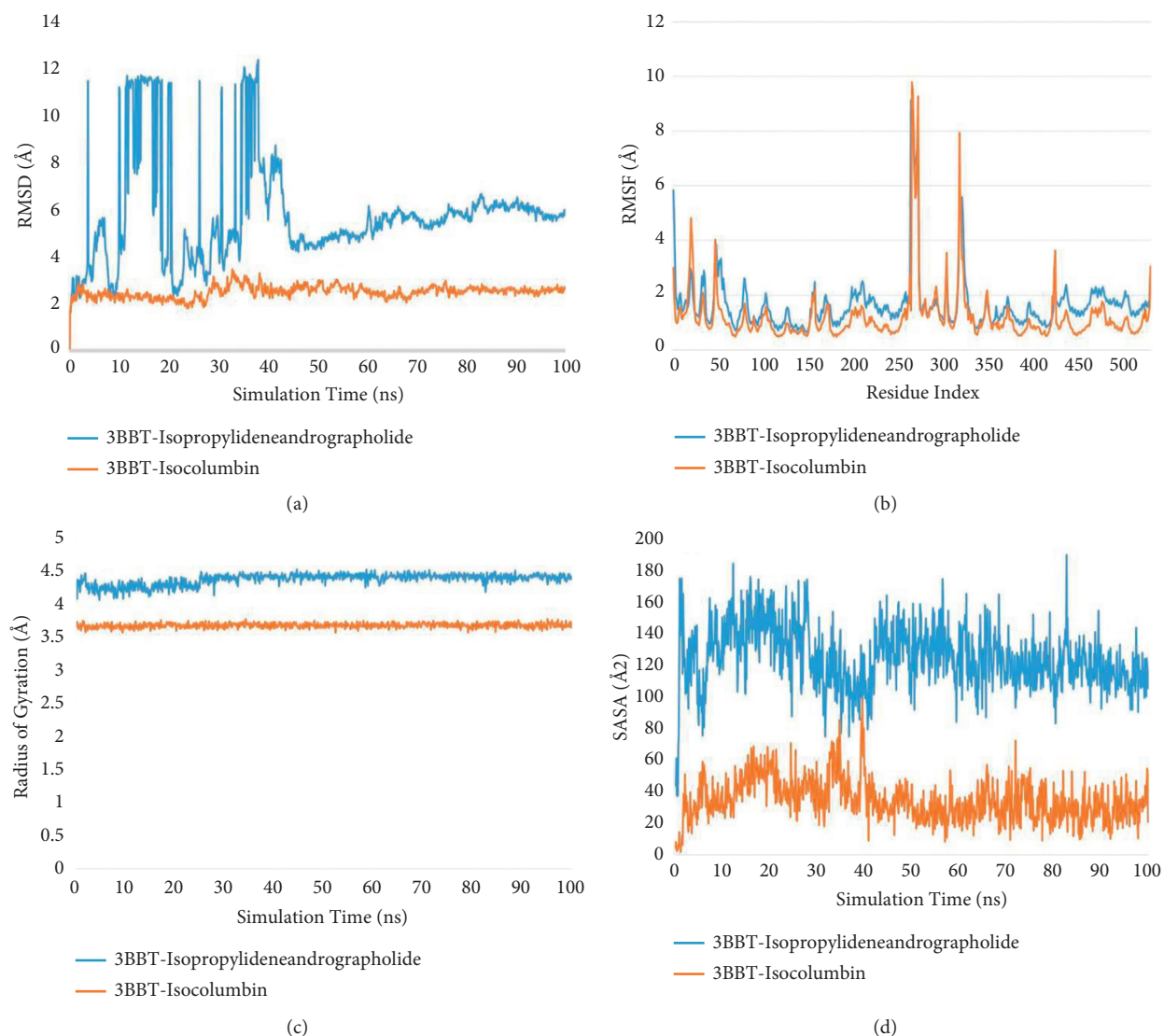


FIGURE 5: Structural and compactness analysis. (a) Root mean square deviation (RMSD) plot. (b) Root mean square fluctuation (RMSF) plot. (c) Radius of gyration (rGyr) plot. (d) Solvent accessible surface area (SASA) plot of isopropylideneandrographolide (blue) and isocolumbin (orange) with 3BBT.

considerable fluctuations. With the second ligand molecule, i.e., isopropylideneandrographolide, the graph can be observed averaging at about 3.5 Å. At the beginning, from 10 to 20 ns, a relatively higher peak can be observed, but after 20 ns, the plateau is attained. Toward the end, there was a dip in the graph as well. The observations are suggestive of protein stability with both the ligand molecules (Figure 6(a)).

Fluctuations considering residues as the basic entity were measured using the RMSF plot. The general convention of amino acids forming secondary structures deviating less as compared to free amino acids such as loops and straight chains was quite visibly followed by both ligand complexes. The binding pocket can be said to lie somewhere in the

middle of being flexible and rigid as residues of both natures interacted with the ligand (Figure 6(b)).

The rGyr plot is suggestive of the compactness of the protein structure. At 100 ns, a value of 3.8 Å was obtained with the protein-14-acetylandrographolide complex, while with isopropylideneandrographolide a value of 4.2 Å was obtained. The smaller value of 2IOG-14-acetylandrographolide suggests a more compact protein (Figure 6(c)).

Both the complexes averaged 10 Å<sup>2</sup> in the SASA plot which is also confirmed by the probability distribution plot. The exposure of core residues to the surrounding solvent is minimal which is an additive property to protein stability. The formation of a hydrophobic pocket around both

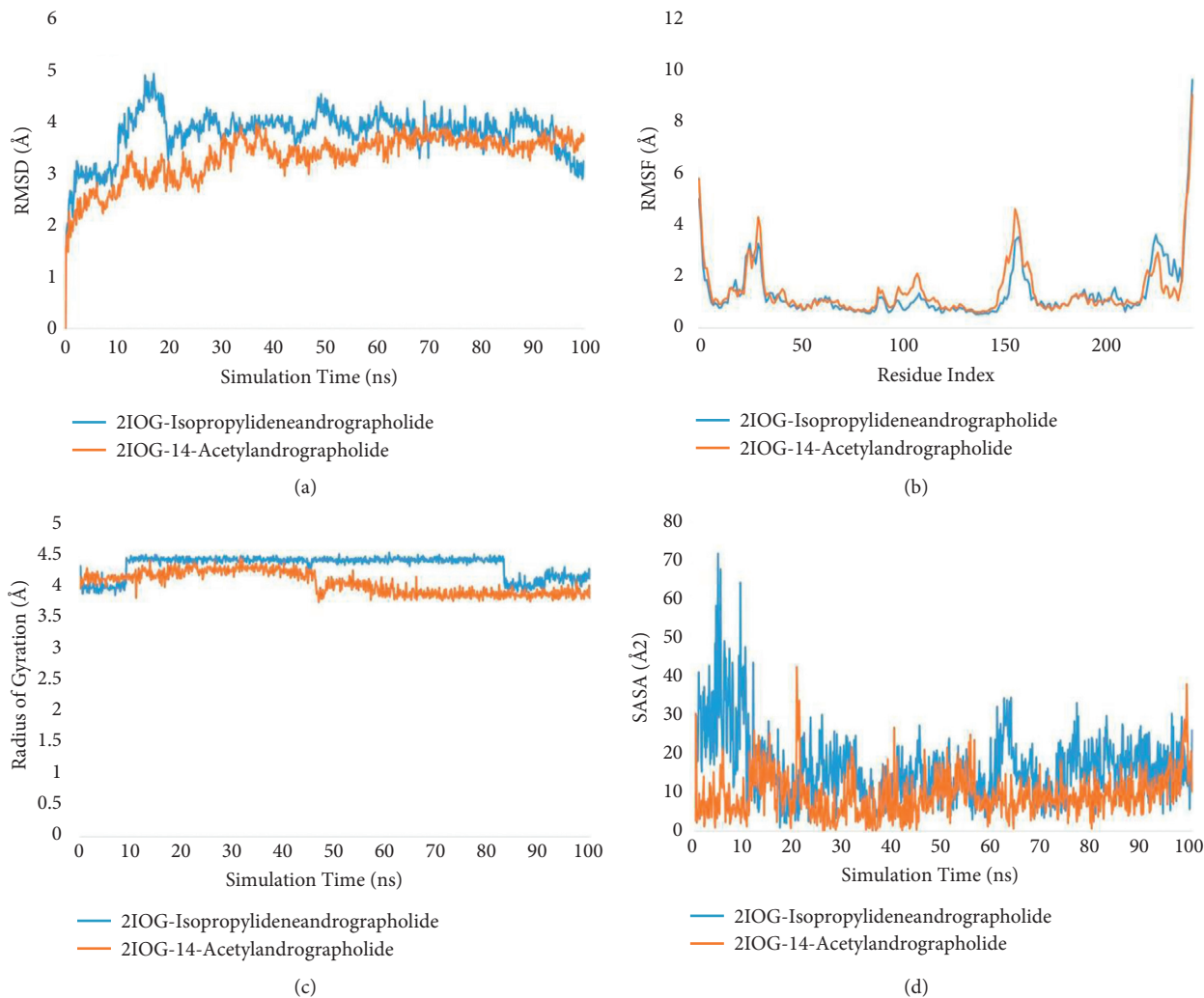


FIGURE 6: Structural and compactness analysis. (a) Root mean square deviation (RMSD) plot. (b) Root mean square fluctuation (RMSF) plot. (c) Radius of gyration (rGyr) plot. (d) Solvent accessible surface area (SASA) plot of isopropylideneandrographolide (blue) and 14-acetylandrographolide (orange) with 2IOG.

residues also provides confirmation for the lower SASA value (Figure 6(d)).

**3.5. Secondary Structure Count and Interaction Dynamics.** 44.39% of amino acids of 3BBT when bound to isocolumbin took part in secondary structure formation, while with isopropylideneandrographolide the percentage reduced to 41.03% which can be targeted toward the increased SASA value.

A difference of 1% can be observed in the 2IOG protein with two different ligands. With 14-acetylandrographolide, a total of 58.08% of residues formed secondary structures, while the number decreased to 57.07% with isopropylideneandrographolide (Table 4).

To assess the binding of protein-ligand complexes, protein-ligand contact estimation and analysis become crucial.

TABLE 4: Protein secondary structure estimation.

Complex	Helix (%)	Strand (%)	Total (%)
3BBT-Isopropylideneandrographolide	27.54	13.49	41.03
3BBT-Isocolumbin	31.00	13.39	44.39
2IOG-14-Acetylandrographolide	55.23	2.86	58.08
2IOG-Isopropylideneandrographolide	54.08	2.99	57.07

Considering the 3BBT-isocolumbin complex (Figure 7(b)), ASP836 and GLY838 anchored the ligand molecules with multiple contacts, and both formed significant string hydrogen bonds. They are assisted by the VAL756 residue, which forms the major water bridges. A total of 25 residues interacted with the ligand at different instances. LYS726, PHE837, LEU758, and VAL756 formed multiple types of bonds. The timeline



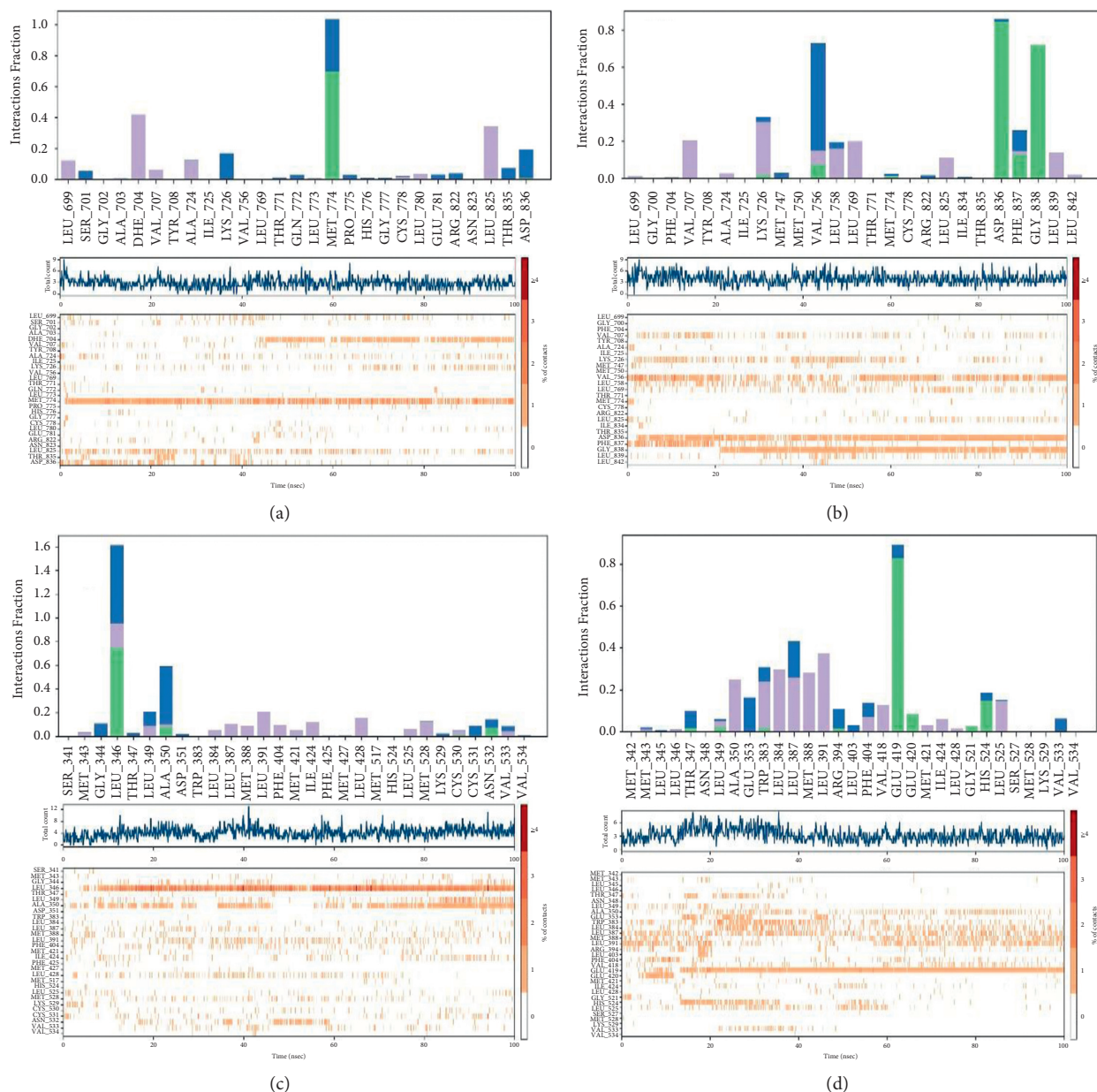


FIGURE 7: Interaction analysis of (a) 3BBT- isopropylideneandrographolide, (b) 3BBT-isocolumbin, (c) 2IOG-isopropylideneandrographolide, and (d) 2IOG-14-acetylandrographolide.

graph showed a well-complemented scattered binding with only 1 instant of no binding. The other complex with isopropylideneandrographolide (Figure 7(a)) interacts with 27 amino acids, but only MET774 acts as the anchor to the ligand. The remaining amino acids interacted with the ligand in a scattered and faded manner with a lot more instances of zero contact with the ligand.

Two 2IOG complexes showed quite significant interactions in their own sense. The complex with 14-acetylandrographolide had 31 total residues that interacted with it. GLU419 forms a strong hydrogen bond along with HIS524 and a few more residues. ALA350, TRP383, LEU387, MET388, LEU391, PHE404, VAL418, and LEU525 (Figure 7(c)) stabilized the protein-ligand complex using

hydrophobic interactions and contributed to the retention of the ligand in the binding pocket. On the other hand, with isopropylideneandrographolide, LEU346 formed major interactions by showing 3 types of binding, i.e., hydrogen bonds, hydrophobic bonds, and water bridges. The LEU346 interaction is briefly assisted by various residues such as ALA350, LEU383, LEU391, LEU428, MET525, MET421, PHE404, and MET388 (Figure 7(d)). In the beginning, a lot of instances can be observed having no contact with the ligand which may explain the higher RMSD in the beginning.

In the last decade or so, virtual screening of ligand libraries has proven to be a quite effective methodology for aiding research in the therapy of various ailments. Breast



TABLE 5: Biological activity prediction of the selected three ligands.

Compound	Pa	Pi	Biological activity prediction
Isocolumbin	0.882	0.005	Antineoplastic
Isopropylideneandrographolide	0.954	0.004	Antineoplastic
14-Acetylandrographolide	0.959	0.004	Antineoplastic

Pa = probability to be active; Pi = probability to be inactive.

cancer is one such ailment which predominantly affects women. Developing a lead molecule for breast cancer is important and also interesting, considering the complex molecular nature. In this investigation, the computational-based screening defines the initial steps toward the development of a lead compound. Numerous other studies have shown the essentiality of the protein molecules taken in this study, i.e., the estrogen receptor and HER4 protein. Recently, phytochemicals have been an area of interest for all drug formulation experts, and a similar interest drove us to explore the compounds known from five plants which are under investigation for their anticancer effects. *Beet vulgaris* has been of interest to many researchers, and they have successfully shown its cytotoxic activities [38] against various tumors such as liver, skin, and lung tumors [38–41]. Similar activity is shown by *Ocimum sanctum* extract against leukemic cell lines [42], while *Tinospora cordifolia* is being extensively studied. It modulated multiple pathways in colon cancer to prevent its proliferation and growth [43]. Some investigations regard *Andrographis paniculata* as a miracle folk plant for treating cancer. Studies have concluded its extract puts a stopper to cell growth and reduces the chromosomal aberrations [44]. In certain cell lines, the extract also influenced the inflammatory pathways by inactivating NF- $\kappa$ B pathways [45]. Our study, coincidentally, concluded to find two potential compounds extracted from *Andrographis paniculata* alone and the other from *Tinospora cordifolia*. Our study highlights the particular compounds present in the extracts which can specifically target the breast cancer proteins. The results are even suggestive of a multitarget drug molecule, i.e., isopropylideneandrographolide.

#### 4. PASS Webserver Prediction

The webserver can be used to predict the biological activity based on the ligand's structure. The three shortlisted compounds in the study were subjected to the prediction. All of the compounds led to the same biological activity. The probability of the ligands acting as antineoplastics, i.e., drugs having tumor restrictive property, ranged between 0.882 and 0.959 when  $P_a > P_i$  (Table 5).

#### 5. Conclusion

The aim of this study was to identify natural compounds that can prove effective against different proteins associated with breast cancer with few or no side effects. Sixty-two compounds from five selected plants were shortlisted for this study, out of which eighteen compounds were ruled out in violation with Lipinski's rule of five. The least binding

affinities and corresponding binding poses for the remaining forty-four compounds were determined. Thereafter, MD simulation studies were carried out on the two best docked complexes for each receptor taken into account, followed by prediction of biological activity of the lead compounds. The results revealed that isocolumbin, isopropylideneandrographolide, and 14-acetylandrographolide are lead compounds against selected breast cancer proteins. All these compounds have antineoplastic effects. Further research should be encouraged to determine the in vitro efficacy of the lead compounds and their exact mechanism of action.

#### Data Availability

The data used to support the findings of this study are included within the article.

#### Conflicts of Interest

The authors declare that they have no conflicts of interest.

#### Acknowledgments

MSK acknowledges the generous support from the Research Supporting Project (RSP-2021/352) by King Saud University, Riyadh, Kingdom of Saudi Arabia.

#### References

- [1] K. Polyak, "Heterogeneity in breast cancer," *Journal of Clinical Investigation*, vol. 121, no. 10, pp. 3786–3788, 2011.
- [2] S. Datta and A. Roy, "Antimicrobial peptides as potential therapeutic agents: a review," *International Journal of Peptide Research and Therapeutics*, vol. 27, no. 1, pp. 555–577, 2021.
- [3] D. A. Shumway, A. Sabolch, and R. Jagsi, "Breast cancer, Med. Radiol," pp. 1–43, 2020.
- [4] "Preventing cancer," April 2021, <https://www.who.int/activities/preventing-cancer>.
- [5] S. S. Mohanty, C. R. Sahoo, and R. N. Padhy, "Role of hormone receptors and HER2 as prospective molecular markers for breast cancer: an update. Genes & Diseases," 2020.
- [6] M. Bondesson, R. Hao, C.-Y. Lin, C. Williams, and J.-A. Gustafsson, "Estrogen receptor signaling during vertebrate development," *Biochimica et Biophysica Acta (BBA) - Gene Regulatory Mechanisms*, vol. 1849, no. 2, pp. 142–151, 2015.
- [7] S. C. Hewitt, J. F. Couse, and K. S. Korach, "Estrogen receptor transcription and transactivation Estrogen receptor knockout mice: what their phenotypes reveal about mechanisms of estrogen action," *Breast Cancer Research*, vol. 2, no. 5, p. 345, 2000.
- [8] I. Paterni, C. Granchi, J. A. Katzenellenbogen, and F. Minutolo, "Estrogen receptors alpha (ER $\alpha$ ) and beta (ER $\beta$ ):

- subtype-selective ligands and clinical potential,” *Steroids*, vol. 90, pp. 13–29, 2014.
- [9] M. Warner, S. Nilsson, and J.-A. Gustafsson, “The estrogen receptor family,” *Current Opinion in Obstetrics and Gynaecology*, vol. 11, no. 3, pp. 249–254, 1999.
- [10] F. Lumachi, A. Brunello, M. Maruzzo, U. Basso, and S. Basso, “Treatment of estrogen receptor-positive breast cancer,” *Current Medicinal Chemistry*, vol. 20, no. 5, pp. 596–604, 2013.
- [11] F. Lumachi, “Current medical treatment of estrogen receptor-positive breast cancer,” *World Journal of Biological Chemistry*, vol. 6, no. 3, p. 231, 2015.
- [12] M. A. Olayioye, “NEW EMBO MEMBERS’ REVIEW: the ErbB signaling network: receptor heterodimerization in development and cancer,” *The EMBO Journal*, vol. 19, no. 13, pp. 3159–3167, 2000.
- [13] J. Wang, J. Yin, Q. Yang et al., “Human epidermal growth factor receptor 4 (HER4) is a favorable prognostic marker of breast cancer: a systematic review and meta-analysis,” *Oncotarget*, vol. 7, no. 47, pp. 76693–76703, 2016.
- [14] J. A. Määttä, M. Sundvall, T. T. Junttila et al., “Proteolytic cleavage and phosphorylation of a tumor-associated ErbB4 isoform promote ligand-independent survival and cancer cell growth,” *Molecular Biology of the Cell*, vol. 17, no. 1, pp. 67–79, 2006.
- [15] T. T. Junttila, M. Sundvall, M. Lundin et al., “Cleavable ErbB4 isoform in estrogen receptor-regulated growth of breast cancer cells,” *Cancer Research*, vol. 65, no. 4, pp. 1384–1393, 2005.
- [16] Y. Zhu, L. L. Sullivan, S. S. Nair et al., “Coregulation of estrogen receptor by ERBB4/HER4 establishes a growth-promoting autocrine signal in breast tumor cells,” *Cancer Research*, vol. 66, no. 16, pp. 7991–7998, 2006.
- [17] R. S. Muraoka-Cook, L. S. Caskey, M. A. Sandahl et al., “Heregulin-dependent delay in mitotic progression requires HER4 and BRCA1,” *Molecular and Cellular Biology*, vol. 26, no. 17, pp. 6412–6424, 2006.
- [18] J. B. Smail, G. W. Rewcastle, J. A. Loo et al., “Tyrosine kinase inhibitors. 17. Irreversible inhibitors of the epidermal growth factor receptor: 4-(phenylamino)quinazoline- and 4-(Phenylamino)pyrido[3,2-d]pyrimidine-6-acrylamides bearing additional solubilizing functions,” *Journal of Medicinal Chemistry*, vol. 43, no. 7, pp. 1380–1397, 2000.
- [19] I. De Pauw, A. Wouters, J. Van den Bossche et al., “Preclinical and clinical studies on afatinib in monotherapy and in combination regimens: potential impact in colorectal cancer,” *Pharmacology & Therapeutics*, vol. 166, pp. 71–83, 2016.
- [20] A. Roy and N. Bharadvaja, “Venom-derived bioactive compounds as potential anticancer agents: a review,” *International Journal of Peptide Research and Therapeutics*, vol. 27, no. 1, pp. 129–147, 2021.
- [21] S. Garg, A. Anand, Y. Lamba, and A. Roy, “Molecular docking analysis of selected phytochemicals against SARS-CoV-2 Mpro receptor,” *Vegetos*, vol. 33, no. 4, pp. 766–781, 2020.
- [22] A. Roy, N. Jauhari, and N. Bharadvaja, “Medicinal plants as a potential source of chemopreventive agents,” in *Anticancer Plants: Natural Products and Biotechnological Implements*, pp. 109–139, Springer, Singapore, 2018.
- [23] A. Roy and N. Bharadvaja, “Medicinal plants in the management of cancer: a review,” *International Journal of Complementary & Alternative Medicine*, vol. 9, no. 2, p. 00291, 2017.
- [24] A. Roy, “Plumbagin: a potential anti-cancer compound,” *Mini Reviews in Medicinal Chemistry*, 2020.
- [25] A. Roy, S. Ahuja, and N. Bharadvaja, “A review on medicinal plants against cancer,” *Journal of Plant Sciences and Agricultural Research*, vol. 2, p. 1008, 2017.
- [26] A. Roy, T. Attre, N. Bharadvaja, A. Tiezzi, and T. M. Karpiński, “Anticancer agent from medicinal plants: a review,” *New aspects in medicinal plants and pharmacognosy*, vol. 1, p. 54, 2017.
- [27] A. Roy and N. Bharadvaja, “A review on pharmaceutically important medical plant: plumbago zeylanica,” *Journal of Ayurveda and Holistic Medicine*, vol. 3, no. 4, pp. 225–228, 2017.
- [28] A. Roy and N. Bharadvaja, “Centella asiatica: a pharmaceutically important medicinal plant,” *Current Trends in Biomedical Engineering & Biosciences*, vol. 5, no. 3, pp. 1–5, 2017.
- [29] H. M. Berman, J. Westbrook, Z. Feng et al., “The protein data bank,” *Nucleic Acids Research*, vol. 28, no. 1, pp. 235–242, 2000.
- [30] S. Kim, P. A. Thiessen, E. E. Bolton et al., “PubChem substance and compound databases,” *Nucleic Acids Research*, vol. 44, no. D1, pp. D1202–D1213, 2016.
- [31] C. R. Sahoo, S. K. Paidesetty, and R. N. Padhy, “Nostocine A derivatives as human DNA topoisomerase II- $\alpha$  inhibitor,” *Indian Journal of Pharmaceutical Education and Research*, vol. 54, no. 3, pp. 669–675, 2020.
- [32] A. Daina, O. Michielin, and V. Zoete, “SwissADME: a free web tool to evaluate pharmacokinetics, drug-likeness and medicinal chemistry friendliness of small molecules,” *Scientific Reports*, vol. 7, no. 1, p. 42717, 2017.
- [33] C. A. Lipinski, “Lead- and drug-like compounds: the rule-of-five revolution,” *Drug Discovery Today: Technologies*, vol. 1, no. 4, pp. 337–341, 2004.
- [34] C. R. Sahoo, S. K. Paidesetty, S. Sarathbabu, B. Dehury, N. Senthil Kumar, and R. N. Padhy, “Molecular dynamics simulation, synthesis and topoisomerase inhibitory actions of vanillin derivatives: a systematic computational structural integument,” *Journal of Biomolecular Structure and Dynamics*, pp. 1–11, 2021.
- [35] *User Manual, Impact 6.7, Schrödinger*, 2015.
- [36] K. S. Bhatia, S. Garg, A. Anand, and A. Roy, “Evaluation of different phytochemicals against BRCA2 receptor,” *Bio-interface Research in Applied Chemistry*, vol. 2022, no. 12, pp. 1670–1681, 2021.
- [37] S. Garg and A. Roy, “In silico analysis of selected alkaloids against main protease (Mpro) of SARS-CoV-2,” *Chemico-Biological Interactions*, vol. 332, p. 109309, 2020.
- [38] S. Garg, A. Anand, Y. Lamba, and A. Roy, “Molecular docking analysis of selected phytochemicals against SARS-CoV-2 Mpro receptor,” *Vegetos*, vol. 33, no. 4, pp. 766–781, 2020.
- [39] G. J. Kapadia, M. A. Azuine, G. Subba Rao, T. Arai, A. Iida, and H. Tokuda, “Cytotoxic effect of the red beetroot (*Beta vulgaris* L.) extract compared to doxorubicin (adriamycin) in the human prostate (PC-3) and breast (MCF-7) cancer cell lines,” *Anti-Cancer Agents in Medicinal Chemistry*, vol. 11, no. 3, pp. 280–284, 2011.
- [40] J. F. Lechner, L.-S. Wang, C. M. Rocha et al., “Drinking water with red beetroot food color antagonizes esophageal carcinogenesis in N-Nitrosomethylbenzylamine-Treated rats,” *Journal of Medicinal Food*, vol. 13, no. 3, pp. 733–739, 2010.
- [41] G. Kapadia, “Chemoprevention of DMBA-induced UV-B promoted, NOR-1-induced TPA promoted skin carcinogenesis, and DEN-induced phenobarbital promoted liver tumors in mice by extract of beetroot,” *Pharmacological Research*, vol. 47, no. 2, pp. 141–148, 2003.

- [42] M. Harsha, K. Mohan Kumar, S. Kagathur, and V. Amberkar, "Effect of *Ocimum sanctum* extract on leukemic cell lines: a preliminary in-vitro study," *Journal of Oral and Maxillofacial Forest Pathology*, vol. 24, p. 93, 2020.
- [43] A. Palmieri, L. Scapoli, A. Iapichino et al., "Berberine and *Tinospora cordifolia* exert a potential anticancer effect on colon cancer cells by acting on specific pathways," *International Journal of Immunopathology & Pharmacology*, vol. 33, 2019.
- [44] M. S. Ahmad, S. Ahmad, M. Arshad, and M. Afzal, "Andrographia paniculata a Miracle Herbs for cancer treatment: in vivo and in vitro studies against Aflatoxin B1 Toxicity," *Egyptian Journal of Medical Human Genetics*, vol. 15, no. 2, pp. 163–171, 2014.
- [45] S. Singh, A. Mehta, S. Baweja, L. Ahirwal, and P. Mehta, "Anticancer activity of *Andrographis paniculata* and *Silybum marianum* on five human cancer cell lines," *Journal of Pharmacology and Toxicology*, vol. 8, no. 1, pp. 42–48, 2012.

## Research Article

# Hepatoprotective Effects of (–) Epicatechin in CCl<sub>4</sub>-Induced Toxicity Model Are Mediated via Modulation of Oxidative Stress Markers in Rats

Khadijah B. Alkinani <sup>1</sup>, Ehab M. M. Ali <sup>2,3</sup>, Turki M. Al-Shaikh <sup>4</sup>,  
Jalaluddin A. Awlia Khan <sup>2</sup>, Tahani M. Al-naomasi <sup>5</sup>, Soad S. Ali <sup>6,7</sup>,  
Asaad A. Abduljawad <sup>1</sup>, Osama F. Mosa <sup>1,8</sup> and Tariq A. Zafar <sup>1</sup>

<sup>1</sup>Public Health Department, Health Sciences College at Leith, Umm Al Qura University, Makkah, Saudi Arabia

<sup>2</sup>Department of Biochemistry, Faculty of Science, King Abdulaziz University, Jeddah, Saudi Arabia

<sup>3</sup>Division of Biochemistry, Chemistry Department, Faculty of Science, Tanta University, 31527 Tanta, Egypt

<sup>4</sup>Department of Biology, College of Science and Arts at Khulis, University of Jeddah, Jeddah, Saudi Arabia

<sup>5</sup>Chemistry Department, Faculty of Science, Hail University, Hail, Saudi Arabia

<sup>6</sup>Faculty of Medicine, Assiut University, Assiut, Egypt

<sup>7</sup>Yousef Abdul Latif Jameel Chair of Prophetic Medicine Application, King Abdulaziz University, Jeddah, Saudi Arabia

<sup>8</sup>Biochemistry Department, Bukhara State Medical Institute Named after Abu Ali Ibn Sino, Bukhara, Uzbekistan

Correspondence should be addressed to Osama F. Mosa; ofmosa@uqu.edu.sa

Received 18 November 2021; Accepted 8 December 2021; Published 22 December 2021

Academic Editor: Ruchika Garg

Copyright © 2021 Khadijah B. Alkinani et al. This is an open access article distributed under the Creative Commons Attribution License, which permits unrestricted use, distribution, and reproduction in any medium, provided the original work is properly cited.

**Objective.** (–) Epicatechin (EP) is a naturally occurring antioxidant flavonoid found in some green plants. The current study was designed to evaluate the potential role of antioxidant mechanisms in the hepatoprotective properties of EP using the carbon tetrachloride (CCl<sub>4</sub>)-induced acute liver injury model. **Materials and Methods.** Rats ( $n = 7$  per group) were divided into five groups including control group, (–) epicatechin group (20 mg·kg<sup>-1</sup> body weight), CCl<sub>4</sub> group (1 mL<sup>-1</sup> body weight), CCl<sub>4</sub>-EP treatment group, and CCl<sub>4</sub>-silymarin (SILY) group. The levels of enzymes including hepatic malondialdehyde (MDA), glutathione (GSH), catalase (CAT), glutathione S-transferase (GST), nitric oxide synthase (NOS), glutathione peroxidase (GPx), and cytochrome P450 (CYP450) were analyzed via enzyme-linked immunosorbent assay (ELISA). Histological studies were performed on all groups to assess the regenerative effects of test sample and compare it with the control group. **Results.** Test compound EP and standard drug silymarin (SILY) considerably reduced liver function enzyme levels in the blood, which were raised by CCl<sub>4</sub> administration, and increased serum albumin and total protein (TP) concentrations. The hepatic malondialdehyde (MDA) level was considerably declined, whereas glutathione (GSH), catalase (CAT), glutathione S-transferase (GST), nitric oxide synthase (NOS), glutathione peroxidase (GPx), and cytochrome P450 (CYP450) levels were upregulated in the EC-treated groups. The hepatoprotective results of the study were further confirmed via the histological assessments, which indicated a regeneration of the damaged hepatic tissue in treated rats. **Conclusions.** The results of this study revealed a significant protective efficacy of EP against CCl<sub>4</sub>-induced liver injury, which was potentially mediated via upregulation of antioxidant enzymes and direct scavenging effects of the compound against free radicals.

## 1. Introduction

The liver plays a key role in metabolism, storage, and secretion and in the detoxification of harmful chemicals [1].

Carbohydrates, proteins, and fats are mainly metabolized in the liver [2]. The liver function can be negatively affected by oxidative stress resulting from exposure to various xenobiotics (naturally occurring harmful compounds such as free



radicals and hydroperoxides) [3, 4]. The liver can also be damaged by certain chemicals including paracetamol,  $\text{CCl}_4$ , and polycyclic aromatic hydrocarbons. Hepatic injury caused by chronic exposure to these chemicals and via infectious agents may lead to progressive liver fibrosis with ultimate cirrhosis and liver failure [3]. Hepatic diseases represent the fifth most prevalent cause of death according to a statistical study done in the United Kingdom [5, 6]. In 2010, the “New Global Burden of Disease” estimated more than one million deaths due to liver cirrhosis [7]. Although liver issues can be life-threatening and are known to have a high mortality rate, there is no complete treatment or prevention. Alternatively, herbal products and pure compounds are under consideration for the preventive and therapeutic outcomes in liver diseases [8].

(–) Epicatechin (EP), an antioxidant flavonoid, belongs to the catechin group and has numerous health benefits [9]. It is found in fruits, vegetables, and beverages. It can also be obtained from green tea, tannins, grape seeds, and strawberries in very high amounts [10]. The previous studies revealed that the protective effects of EP are mediated through oxidizing and reducing glutathione, protecting tissues from any oxidative stress [11]. The studies have also shown that flavonoid-rich diets can reduce the risk of oxidative stress caused by excessive free radicals [3, 9]. The effect of prostacyclin (also known as prostaglandin I<sub>2</sub> or PGI<sub>2</sub>) in relation to  $\text{CCl}_4$ -induced liver injury was previously reported [8] and found that after *in vitro* poisoning with  $\text{CCl}_4$ , amino acid incorporation could be partially restored by PGI<sub>2</sub>. PGI<sub>2</sub> can reduce accumulated triglyceride and serum glutamic oxaloacetic transaminase also known as SGOT in the liver. Importantly, it can also increase liver glycogen content 24 hours after  $\text{CCl}_4$ -induced injury [12]. In 2002, a study demonstrated the efficacy of EP in rat liver epithelial cells. It was noted at the end of the study that the transport of connexin 43 between cellular compartments was affected by tetradecanoylphorbol acetate (TPA), and it was also noted that this effect could be neutralized by EP or genistein [13]. Cui and his colleagues in 2014 conducted a study on liver protection with an extract rich in polyphenols (HMTP) against carbon tetrachloride-induced liver injury in mice. The protection of HMTP (extracted from Huangshan Maofeng) against changes in the liver caused by  $\text{CCl}_4$  was confirmed after a pathological study. As a result, it has been suggested that hepatoprotection can be achieved from extracts containing polyphenols [14]. In 2019, a study proved that hepatic veno-occlusive disease (VOD) can be reduced by EP by stopping hepatic oxidation through nuclear factor erythroid 2-related factor 2 (Nrf2). EP may prevent hepatitis by terminating the signaling pathway nuclear factor-kappa B (NF- $\kappa$ B) activated by protein 60 [15]. Another study determined the efficacy of EP protection in rats concerning the alteration of oxidative stress factors and inflammation following the treatment with cypermethrin (CYP). Furthermore, the levels of pro-inflammatory cytokines, nucleic acid marker, interleukin 6 (IL-6), nitroguanidine, and tumor necrosis factor-alpha (TNF- $\alpha$ ) were increased due to CYP. EP administration reduced the pro-inflammatory and antioxidative effects in rats exposed to CYP [16].

Based on the protective potentials of EP, this study was designed to evaluate its hepatoprotective potentials in  $\text{CCl}_4$ -induced toxicity models. The effect of EC on liver enzymes, MDA level, reduced glutathione (GSH), glutathione peroxidase activity (GPx), catalase activity (CAT), nitric oxide synthase (NOS), glutathione S-transferase (GST), and cytochrome P450 was evaluated. Further, the histological and histopathological examinations were performed for various treated groups to validate the protective and regenerative effects of EC.

## 2. Materials and Methods

**2.1. Animals.** Adult male Wistar rats weighing  $238.5 \pm 38.5$  g were used in this study. The animals were purchased from the Central Animal House, King Fahd Medical Research Center at KAU, Jeddah, KSA. The rats were fed standard rat pellets and water *ad libitum*. The protocol for animal care and handling used in this study was approved by the Animal Care and Use Committee, KAU, with Reference No: 520-18.

**2.2. Chemicals and Drugs.** Silymarin (SILY) and EP were purchased from Sigma-Aldrich (St. Louis, Missouri, USA; MDL numbers MFCD00075648 and MFCD01776359), respectively. Carbon tetrachloride ( $\text{CCl}_4$ ) was purchased from the Laboratory of Faculty of Sciences, KAU. Dimethyl sulfoxide (DMSO) and other consumables were purchased from authentic distributors. (–) Epicatechin was dispersed in DMSO and distilled water, whereas silymarin solutions were prepared in distilled water.

**2.3. Experimental Design.** The rats were randomly divided into five groups with each group containing seven animals ( $n = 7$ ) as follows. The following groups were devised for the study:

Group I (control/placebo group): the animals of this group were maintained on normal diet and were used as the placebo control group.

Group II (EC group): the animals received (–) epicatechin orally ( $20 \text{ mg} \cdot \text{kg}^{-1}$  body weight for 3 weeks) [11].

Group III ( $\text{CCl}_4$  group): this is the disease control group. The animals of this group received  $\text{CCl}_4$  (mixed with olive oil 50%) [17] intraperitoneally ( $1 \text{ ml} \cdot \text{kg}^{-1}$  body weight two times/week continued for 3 weeks).

Group IV ( $\text{CCl}_4$  and EP group): the animals of this group received  $\text{CCl}_4$  intraperitoneally ( $1 \text{ ml} \cdot \text{kg}^{-1}$  body weight twice/week continued for 3 weeks) and (–) epicatechin orally ( $20 \text{ mg} \cdot \text{kg}^{-1}$  body weight for 3 weeks).

Group V ( $\text{CCl}_4$  and SILY group): the animals of this group received  $\text{CCl}_4$  intraperitoneally ( $1 \text{ ml} \cdot \text{kg}^{-1}$  body weight twice/week for 3 weeks) and standard hepatoprotective drug silymarin orally ( $50 \text{ mg} \cdot \text{kg}^{-1}$  body weight of for 21 days) [18].



The rats were fasted for 12 hours, euthanized, and blood samples were collected. Blood was set for coagulation at the room temperature. After that, centrifugation was done at 2500 rpm for 15 minutes to separate the serum. For the biochemical assessment of liver function, the serum was kept at  $-20^{\circ}\text{C}$ . The animals' livers were dissected and cut into small pieces; some pieces were immediately frozen under  $-80^{\circ}\text{C}$  for ELISA examination and antioxidant enzyme detection, and other pieces were fixed in 10% neutral buffered formalin for histopathological studies.

**2.4. Liver Function Assessment.** Alanine amino transaminase (ALT), aspartate amino transaminase (AST), and alkaline phosphatase (ALP) [19] were measured by an automated analyzer (FLEXOR EL200, France), and several different liver markers were measured, including total protein (TP) and albumin following previously reported standard procedures [20].

**2.5. Biochemical Analysis of Antioxidant Enzymes.** The liver sections were homogenized in 50 mM  $\text{K}_3\text{PO}_4$  at pH of 7.5 and 1 mM EDTA for the measurements of CAT, NO, GPx, and GSH. Sonication was performed twice on homogenized tissues with interval of 30 s at  $4^{\circ}\text{C}$ . After that, centrifugation was applied for 10 minutes at  $4000\text{ rpm}\cdot\text{min}^{-1}$ . The concentrations of the enzymes were estimated following previously reported protocols [20–22].

**2.6. Measurement of Malondialdehyde (MDA) Level.** The determination of MDA level in the hepatic homogenates was performed using kits from Biodiagnostic, Egypt. The adducts were produced when thiobarbituric acid reacted with homogenate in a water bath and were separated by *n*-butanol. Malondialdehyde was calculated by the difference in optical densities (ODs), which were produced at different wavelengths of 535 nm and 525 nm. The results were expressed as  $\text{nmol}\cdot\text{g}^{-1}$  tissue [23].

**2.7. Reduced Glutathione (GSH) Analysis.** GSH is the most important antioxidant synthesized in cells. It is a reducing molecule, which can react with oxygen species by neutralizing the unpaired electrons that make them highly reactive and dangerous. GSH level in liver cell homogenate was determined following previously reported standard protocol [24] using biodiagnostic assay kits. Briefly, glutathione was added into GSH monoclonal precoated wells and then incubated. Biotin-labeled anti-GSH antibodies were added to combine with HRP-conjugated streptavidin, which forms an antigen-antibody complex. After incubation, the enzymes that remained unbound were washed and removed. Substrates A and B were added to the solution, and the change in color was observed. There is a positive correlation between the concentration of rat GSH and the shades of the solution. The concentration of GSH was expressed as  $\text{mmol}\cdot\text{g}^{-1}$  tissue.

**2.8. Estimation of Glutathione Peroxidase Activity (GPx).** Kits provided by Biodiagnostic, Egypt, were used to determine the GPx of the liver homogenates. This was calculated in a coupled enzyme assay with glutathione reductase by calculating the oxidation of nicotinamide adenine dinucleotide phosphate keeping hydrogen peroxide ( $\text{H}_2\text{O}_2$ ) as the substrate at 340 nm [25]. It was demonstrated in  $\text{nmol}/\text{min}/\text{mg}$  protein.

**2.9. Estimation of Tissue Catalase Activity (CAT).** The determination of CAT in the hepatic homogenates was performed using kits from Biodiagnostic, Egypt, and was calculated according to Aebi [26]. Hydrogen peroxide reacts with CAT enzyme of known amount. The reaction was stopped after the addition of catalase inhibitor after exactly one minute. The rest of the hydrogen peroxide forms a chromophore by reacting with DHBS and AAP. This chromophore has a color intensity inversely related to the quantity of CAT present in the original sample. The absorbance of samples was observed at 510 nm. It was demonstrated in  $\mu\text{mol}/\text{min}/\text{mg}$  [23].

**2.10. Analysis of Nitric Oxide Synthase (NOS).** The level of NOS in homogenized hepatic tissues was measured using specific enzyme-linked immunosorbent assay (ELISA) kits, provided by Bioassay Technology. Nitric oxide synthase in liver cell lysates was calculated by the procedure reported previously [24]. NOS was added to the precoated NOS monoclonal antibody wells and then incubated. Anti-NOS biotin-labeled antibodies combined with streptavidin-HRP were added, forming an immune complex. The enzymes remained unbound after the incubation was removed and washed. Two substrates A and B were added, which turned the color of the solution into blue, which then changed into yellow due to the acid. There is a positive correlation between the solution shades and the concentration of NOS [27]. The concentration of NO was expressed as  $\text{pg}\cdot\text{mg}^{-1}$  protein.

**2.11. Determination of Glutathione S-Transferases (GST).** The level of GST in homogenized liver tissues was measured using ELISA kits. Kits were provided by Biodiagnostic, Egypt, and GST was calculated via previously reported procedure [28]. The procedure relied upon the conjugation of GSH with CDNB. This occurs when GST forms adduct of 2,4-dinitrophenyl-S-glutathione. This adduct was calculated via a beam spectrophotometer at 340 nm.

**2.12. Assessments of Cytochrome P450.** Cytochrome P450 in hepatic homogenates was determined utilizing kits given by Bioassay Technology. For the analysis of the cytochrome P450 1A2 (CYP1A2), these kits use biotin double-antibody sandwich technology-based ELISA. CYP1A2 in cell lysates was calculated by the procedure given by [24]. CYP1A2 was added to the CYP1A2 precoated monoclonal antibody wells, which were later set for incubation. After the incubation of these cells, the immune complex was formed by the addition

of anti-CYP1A2 biotin-labeled antibodies and was combined with streptavidin-HRP. Those enzymes that were not bound were removed and washed. Then, we added two substrates A and B. As a result, the color of the solution changed to blue, which then changed to yellow. There is a positive correlation between the concentration of (CYP1A2) and the shades of the solution.

**2.13. Histological and Histopathological Studies.** The rats were dissected via an abdominal incision after anesthesia. The livers of the rats were extracted for microscopic histopathological examinations. The liver was cut into slices, fixed in 10% formalin, washed, dehydrated in the ascending graded series of alcohol cleared in xylene, and embedded in paraffin. The sections of 5  $\mu$ m thickness were stained with hematoxylin and eosin (H&E), and other sections were stained with Masson's trichrome. These sections were examined under the light microscope (Olympus BX61, USA) with a digital camera (Olympus DP72, USA). The photographs with different magnifications were then screened to study the liver injury and the protection efficiency.

**2.14. Statistical Study.** All results were expressed as mean  $\pm$  SD. The data were analyzed utilizing GraphPad Prism 3.0 Software. The differences among the experimental groups were detected by *t*-test. The values of  $p \leq 0.05$  were considered statistically significant.

### 3. Results

**3.1. (-) Epicatechin Positively Modulates Liver Function Parameters.** The concentrations of ALT, AST, ALP, TP, and albumin were measured in samples to assess liver function. It was observed that the activity of ALT, AST, and ALP was significantly increased ( $p < 0.001$ ), while TP and serum albumin levels were noticeably decreased ( $p < 0.001$ ) in CCl<sub>4</sub>-injected rats compared with the control group. There was a decrease in AST, ALP, and ALT levels in group IV (CCl<sub>4</sub> and EP) and group V (CCl<sub>4</sub> and SILY), whereas TP and albumin levels were increased when compared with group III (CCl<sub>4</sub>) ( $p < 0.001$ ). Furthermore, the level of AST, ALP, and ALT was decreased in the SILY and CCl<sub>4</sub> groups compared with group I ( $p < 0.01$ , 0.01, and 0.05). The deficiency was improved by EP treatment ( $p < 0.001$ ) and SILY treatment ( $p < 0.01$ ) (Table 1).

**3.2. (-) Epicatechin Modulates MDA and GSH in the CCl<sub>4</sub> Toxicity Model.** The results of the oxidative stress changes are summarized in Figure 1. An increase in the level of MDA was observed after CCl<sub>4</sub> administration compared with the control group ( $p < 0.001$ ). The animals in group V (CCl<sub>4</sub> and SILY) also showed an increase in MDA in comparison with the control group ( $p < 0.01$ ) (Figure 1). The rats with CCl<sub>4</sub>-induced hepatic injury and treated with EP showed a decrease in MDA level compared with group III (CCl<sub>4</sub>) ( $p < 0.001$ ). Similar results were observed in group V when compared with group III ( $p < 0.01$ ). The injection of CCl<sub>4</sub>

decreased the liver GSH level in group III compared with the control group ( $p < 0.001$ ). The treatment with EP and SILY in groups IV and V increased the level of GSH compared with that in group III (Figure 1).

**3.3. Effect of (-) Epicatechin on Liver GPx and CAT Caused by CCl<sub>4</sub>.** The activities of GPx and CAT decreased in group III (CCl<sub>4</sub>) compared with the control group ( $p < 0.001$ ). The decrease in CAT level was also noted in group V (CCl<sub>4</sub> and SILY) compared with the control group ( $p < 0.01$ ). The rats in groups IV and V showed an increased level of GPx ( $p < 0.001$ ) and ( $p < 0.001$ ), respectively, compared with the CCl<sub>4</sub> group (Figure 2). The treatment of CCl<sub>4</sub>-injected rats with either EP or SILY increased CAT activity in the liver ( $p < 0.001$  and  $p < 0.001$ , respectively) compared with the CCl<sub>4</sub> group (Figure 2).

**3.4. (-) Epicatechin and Silymarin's Effects on Liver NOS Activities.** In the NOS study, it was found that the NOS level in group III ( $34.8 \pm 10.37$ ) was significantly reduced when compared to the control group ( $72.77 \pm 14.88$ ) ( $p < 0.001$ ). The treatment of CCl<sub>4</sub>-injected rats with either EP or SILY increased NOS activity at  $p < 0.001$  (Figure 3).

**3.5. Effect of (-) Epicatechin on Liver GST and CYP450.** As shown in Figures 4 and 5, GST and CYP450 activities were decreased ( $p < 0.001$ ) in group III (CCl<sub>4</sub>) compared with the control group. SILY treatment resulted in a significant increase ( $p < 0.001$ ) in GST activity compared with the control group. The decline in GST and CYP450 levels after CCl<sub>4</sub> treatment was significantly ( $p < 0.001$ ) reversed by EP treatment. Similar results were observed in the SILY-treated groups, whereby GST and CYP450 were significantly improved ( $p < 0.001$  and  $p < 0.001$ , respectively) when compared with group III (CCl<sub>4</sub>). Moreover, the increase in the GST activity of EP-treated group (group IV) was very comparable with the SILY-treated group (group V). The MDA level was significantly reduced, whereas proteins were increased as shown in Figures 6 and 7.

**3.6. Effect of EP and SILY Treatment on Histopathological Changes in the Liver Induced by CCl<sub>4</sub>.** To evaluate the effect of EP or SILY in the liver of CCl<sub>4</sub>-injected rats, we performed hematoxylin and eosin (H&E) and Masson's trichrome staining.

**3.6.1. Hematoxylin and Eosin (H&E) Stain.** The sections from groups I and II showed a normal histological structure of hepatic tissue (Figure 8), while liver sections from the CCl<sub>4</sub>-treated group showed narrowing of the sinusoidal lumen and irregularity in the liver parenchyma. A large number of inflammatory cells surrounded the central vein (CV), which replaced the degenerated necrotic cells. Inflammatory cells were also present in the portal area (PA), which showed thickening of blood vessel walls. After treatment with either EP or SILY, the hepatic tissue retained

TABLE 1: Effect of (-) epicatechin on ALT, AST, ALP, total protein, and albumin concentrations.

Samples	Control	EP	CCl <sub>4</sub>	CCl <sub>4</sub> -EP	CCl <sub>4</sub> -SILY	Samples	Control	EP	CCl <sub>4</sub>	CCl <sub>4</sub> -EP	CCl <sub>4</sub> -SILY
Serum ALT activity (U·L <sup>-1</sup> )						Serum AST activity (U·L <sup>-1</sup> )					
1	15.23	9.84	80.15	19.2	13.33	1	36.31	24.12	118.09	25.07	35.54
2	11.42	11.11	41.74	10.79	18.57	2	30.28	30.45	129.83	35.87	55.22
3	14.6	10.15	37.45	12.06	13.33	3	25.07	21.9	124.12	30.15	28.24
4	13.33	14.6	26.66	18.25	19.84	4	24.75	22.85	143.16	29.83	48.72
5	12.69	8.89	55.23	17.93	21.74	5	25.07	19.67	125.39	26.34	53.17
6	10.15	8.57	66.32	12.06	25.98	6	28.24	26.34	95.07	26.97	30.46
7	11.74	13.33	72.38	18.25	30.74	7	18.72	26.97	121.9	39.67	27.29
8	9.2	9.84	82.38	22.45	35.40	8	23.17	19.67	84.12	35.8	52.99
9	10.79	12.06	27.5	18.22	19.00	9	25.07	15.87	130.15	26.7	22.21
10	7.93	8.25	73.65	17.00	25.00	10	36.87	30.15	93.17	36.2	50.34
Mean	<b>11.70</b>	<b>10.66</b>	<b>56.34***</b>	<b>16.62###</b>	<b>22.29###**</b>	Mean	<b>27.35</b>	<b>23.79</b>	<b>116.5***</b>	<b>31.26###</b>	<b>40.418###,**</b>
* <i>p</i> vs. control		<b>0.82</b>	<b>4.04</b>	<b>0.22</b>	<b>0.027</b>	* <i>p</i> vs. control		<b>0.14</b>	<b>8.03</b>	<b>0.53</b>	<b>0.011</b>
# <i>p</i> vs. CCl <sub>4</sub> group				<b>5.50</b>	<b>3.30</b>	# <i>p</i> vs. CCl <sub>4</sub> group				<b>3.14</b>	<b>6.68</b>
# <i>p</i> vs. SILY group				<b>0.078</b>		# <i>p</i> vs. SILY group				<b>0.07</b>	
Serum ALP activity (U·L <sup>-1</sup> )						Serum albumin level (g %)					
1	58.81	49.62	165.46	64.11	111.19	1	3.064	2.74	2.78	3.12	2.59
2	102.92	49.62	168	79.95	128.76	2	3.206	3.46	2.50	2.77	2.55
3	101.01	68.92	162.66	45.03	73.52	3	3.149	3.70	2.86	2.76	3.03
4	85.46	85.46	110.54	36.76	67.08	4	2.809	3.50	2.67	3.59	3.18
5	102.44	94.65	107.52	48.70	55.95	5	3.20	3.01	2.22	3.12	3.18
6	44.70	45.03	175.35	61.57	110.28	6	3.45	3.26	2.11	3.03	3.39
7	38.57	36.76	91.46	38.59	116.71	7	3.21	3.64	2.10	3.26	3.39
8	38.59	88.46	151.46	97.23	67.30	8	3.45	2.95	2.81	3.21	3.18
9	40.11	98.00	162.49	100.3	143.47	9	3.33	3.54	2.25	3.4	3.43
10	52.95	51.46	172.60	103.2	55.35	10	2.95	3.21	2.56	3.56	2.11
Mean	<b>66.56</b>	<b>66.80</b>	<b>146.75***</b>	<b>67.54###</b>	<b>92.96###,**</b>	Mean	<b>3.18</b>	<b>3.30</b>	<b>2.49***</b>	<b>3.18###</b>	<b>3.00###</b>
* <i>p</i> vs. control		<b>0.983</b>	<b>1.03</b>	<b>0.93</b>	<b>0.01</b>	* <i>p</i> vs. control		<b>0.327</b>	<b>9.90</b>	<b>0.97</b>	<b>0.27</b>
# <i>p</i> vs. CCl <sub>4</sub> group				<b>7.83</b>	<b>1.10</b>	# <i>p</i> vs. CCl <sub>4</sub> group				<b>4.62</b>	<b>0.00075</b>
# <i>p</i> vs. SILY group				<b>0.06</b>		# <i>p</i> vs. SILY group				<b>0.30</b>	

The data are presented as the mean ± SD ( $n = 7$ ).  $p^* \leq 0.05$  vs. control group and  $p^\# \leq 0.05$  vs. CCl<sub>4</sub> group. Control: placebo group; EP: (-) epicatechin group; CCl<sub>4</sub>-EP: CCl<sub>4</sub> and (-) epicatechin group; SILY: silymarin group.

its normal architecture. The severity of hepatic fibrosis decreased except for some hepatocytes that showed necrosis around the CV. These results demonstrated that EP and SILY have a vital role in improving liver fibrosis.

**3.6.2. Masson's Trichrome.** Collagen deposition and hepatic fibrosis were detected by Masson's trichrome stain. Collagen appeared distributed in few amounts around the central vein and portal area in the control and EP groups (Figure 9). The deposition of blue collagen and red fibers increased in the CCl<sub>4</sub>-treated group in CV and PA by a somewhat greater amount. After treatment with EP and SILY, the amount of collagen decreased compared with group III.

#### 4. Discussion

Hepatic injury may lead to inflammation, fibrosis, and necrosis causing liver failure [29]. Phytochemicals from several plants have been used for medicinal purposes in

many regions of the world [30–33]. Silymarin, a highly potent phytochemical, is used against hepatic diseases [34]. Since EP belongs to polyphenols, which are potent antioxidants against ROS-induced oxidative stress, it is used to control liver diseases [35]. CCl<sub>4</sub> is commonly used in hepatotoxicity studies using experimental animal models because it causes lipid peroxidation due to the production of free radicals [36]. CCl<sub>4</sub> is the best animal model characterized by free radical-induced hepatotoxicity by xenobiotics [37]. In this analysis, CCl<sub>4</sub> caused significant hepatic damage and oxidative stress in animals as evidenced by altered liver function tests and antioxidant enzymes [36, 38].

This study revealed the attenuating effects of EP and SILY against CCl<sub>4</sub>-induced liver injury in rats. As indicated by our findings, EP administration significantly improved liver functions by decreasing blood ALT, AST, and ALP levels and increasing the levels of TP and serum albumin. EP treatment, especially in combination with SILY, declined MDA levels and ROS production, whereas NOS and CYP450

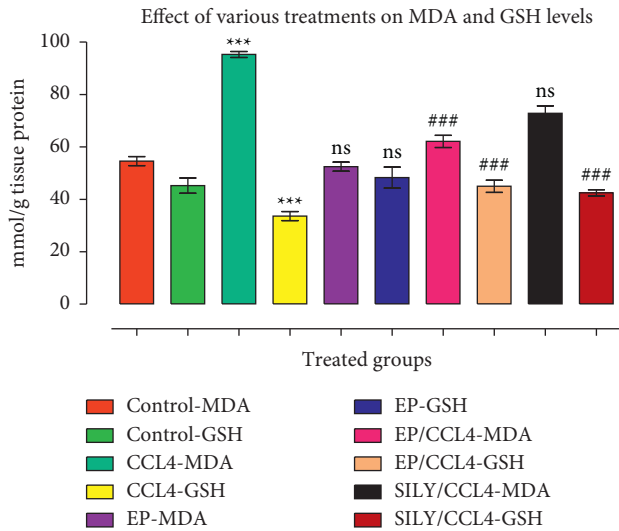


FIGURE 1: (–) Epicatechin and silymarin's effect on liver MDA and GSH activities caused by carbon tetrachloride. The data are presented as the mean  $\pm$  SD ( $n=7$ ). ns: values not significantly different when compared with the CCl<sub>4</sub>-treated group. \*\* $p < 0.01$  and \*\*\* $p < 0.001$  vs. CCl<sub>4</sub> group (GSH group); ## $p < 0.01$  and ### $p < 0.001$  values vs. CCl<sub>4</sub> group (MDA group).

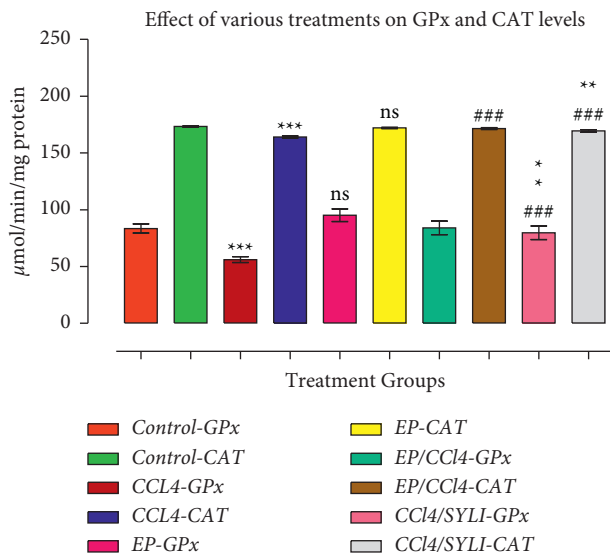


FIGURE 2: (–) Epicatechin and silymarin's effect on liver GPx and CAT activities caused by carbon tetrachloride. The data are presented as the mean  $\pm$  SD ( $n=7$ ). ns: values not significantly different when compared with the CCl<sub>4</sub>-treated group. \*\* $p < 0.01$  and \*\*\* $p < 0.001$  vs. CCl<sub>4</sub> group (GPx group); ### $p < 0.001$  values vs. CCl<sub>4</sub> group (CAT group) and † $p < 0.05$  vs. SILY group.

levels were upregulated. Moreover, EP and SILY have improved the hepatic histopathological changes caused by CCl<sub>4</sub> administration.

This study showed that EP and SILY can protect against CCl<sub>4</sub>-induced liver injury. These results were in accordance with previously reported studies [39, 40], where the findings suggested that EP or SILY could be important potential protective supplements against liver injury induced by CCl<sub>4</sub>

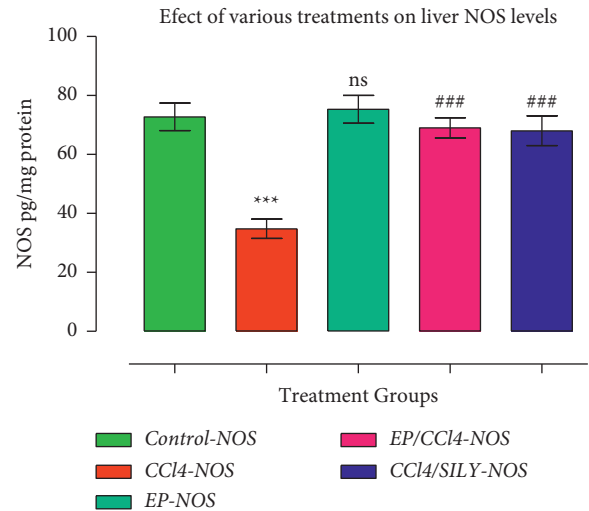


FIGURE 3: (–) Epicatechin and silymarin's effect on liver NOS activities caused by carbon tetrachloride. The data are presented as the mean  $\pm$  SD ( $n=7$ ). \*\*\* $p < 0.001$  vs. control group and ### $p < 0.001$  values vs. CCl<sub>4</sub> group.

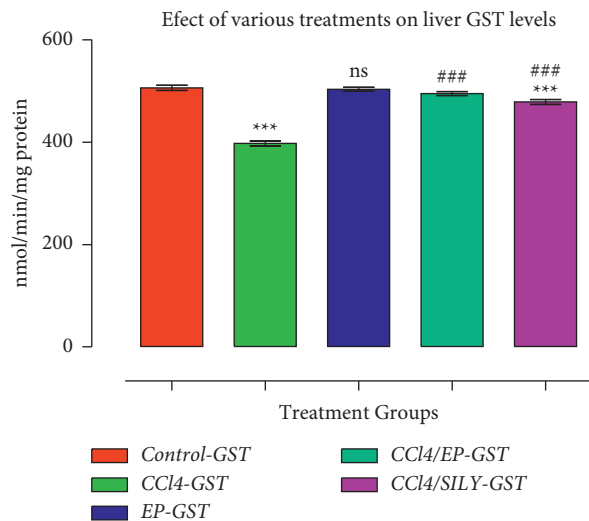


FIGURE 4: (–) Epicatechin and silymarin's effect on liver GST activity caused. The data are presented as the mean  $\pm$  SD ( $n=7$ ). \*\*\* $p < 0.001$  vs. control group; ### $p < 0.001$  values vs. CCl<sub>4</sub> group; † $p < 0.05$  vs. SILY group.

in rats. It should be noted that the most common marker enzymes in the liver are AST, ALT, and ALP, whereas MDA, GSH, GPx, and CAT are vital oxidants and antioxidant balance biomarkers [41]. The toxic effects of CCl<sub>4</sub> are mediated via free radicals leading to an increase in lipid peroxide, which is a major cause of CCl<sub>4</sub>-induced hepatic injury [42]. An increase in serum MDA was observed in this study, while the CCl<sub>4</sub>-treated group, in comparison with the first group, showed a significant decrease in hepatic GSH, GPx, and CAT activities. The level of MDA in the liver has been used to assess the extent of liver damage [30].

During (–) epicatechin and silymarin treatments, the level of enzymatic antioxidants showed a significant



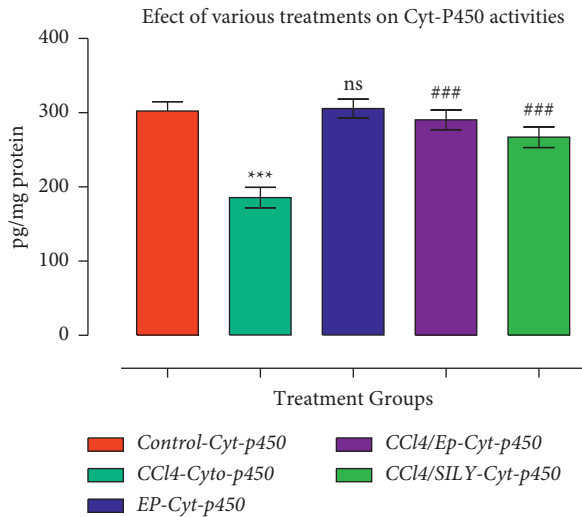


FIGURE 5: (–) Epicatechin and silymarin's effect on liver CYP450. The data are presented as the mean  $\pm$  SD ( $n = 7$ ). \*\*\* $p < 0.001$  vs. control group; ### $p < 0.001$  values vs. CCl<sub>4</sub> group.

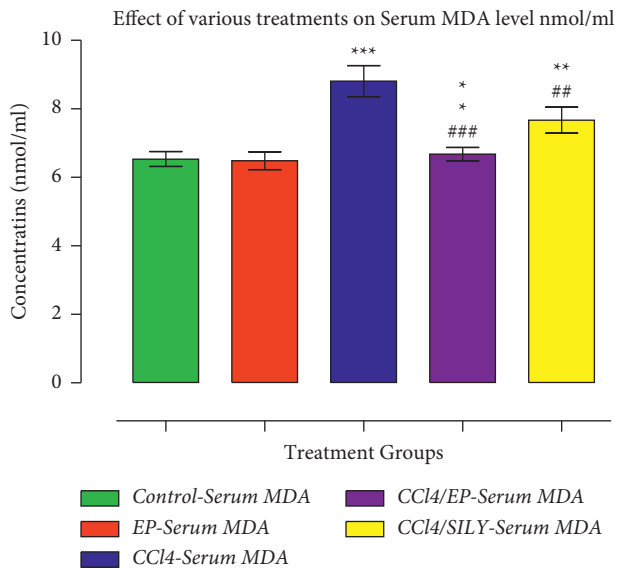


FIGURE 6: (–) Epicatechin and silymarin's effect on serum MDA. The data are presented as the mean  $\pm$  SD ( $n = 7$ ). \*\*\* $p < 0.001$  vs. control group; ### $p < 0.001$  values vs. CCl<sub>4</sub> group.

increase. This demonstrated that hepatic antioxidant activity could be maintained and restored using these compounds. Thus, oxidative damage of the liver could be treated by neutralizing it with antioxidants [43], increasing the activity of the antioxidant enzymes and inhibiting the production of MDA and lipid peroxidation [39].

GSH has an anti-hepatotoxic effect against oxidative stress [44]. H<sub>2</sub>O<sub>2</sub> is degraded into water and oxygen by CAT, which protects hepatocytes from oxidative damage caused by H<sub>2</sub>O<sub>2</sub> [45]. A wide range of xenobiotics and carcinogens are metabolized by the GST [46]. It has been proven from many studies that carbon tetrachloride alters GST activities [36, 47]. It was observed in this study that the level of GST

was decreased in the liver of rats with CCl<sub>4</sub>-induced injury compared with the control group, which indicated that GST in the liver could cause tumorigenesis during chronic liver damage [38]. GST can be restored in the liver through the use of EP and SILY as they detoxify CCl<sub>4</sub> and protect the liver from damage.

Oxidation of foreign chemicals occurs via cytochrome P450 enzyme [39, 48]. It also metabolizes CCl<sub>4</sub> to trichloromethyl radicals leading to some harmful effects when they interact with proteins and lipids [49]. A decrease in hepatic CYP450 was also observed in this study on rats with CCl<sub>4</sub>-induced injury when compared to the control group. However, an increase in CYP450 activity was observed in the EP- and SILY-treated groups when compared to the CCl<sub>4</sub> group. Other studies have also shown that liver cytochrome is affected by it [50]. This study showed that EP and SILY can be used to protect the liver as they have antioxidant properties. Nitric oxide synthase can also be considered as an anti-inflammatory agent [27]. NOS may play a critical role in the prevention of hepatic injury and fibrosis [51]. In the results of this work, it was observed that NOS level in the CCl<sub>4</sub> group was decreased compared with the control group. Hepatic injury can be mitigated by the production of nitric oxide [17]. The treatment with EP and SILY restored the level of NOS, and reference [52] found that (–) epicatechin prevents oxidative stress and regulates nitric oxide bio-availability. Reference [53] also reported that HIF-1 $\alpha$  expression was reduced with silymarin and with iNOS.

The histological study was applied to confirm the biochemical findings. Microscopic observation showed that the EP and SILY groups showed the best histopathological results compared with the CCl<sub>4</sub> group. They may reduce liver fibrosis and infiltration of inflammatory cells. These protective effects against several toxins have been reported in the literature; Wang et al. demonstrated the protective activity of catechin derivative epigallocatechin gallate (EGCG) on hepatic injury caused by paracetamol. Their research showed that EGCG can reduce the occurrence of necrosis around the CV in the liver [54]. A different study indicated that catechin derivative EGCG (a beneficial plant compound called polyphenol) can improve edema, steatosis, and degeneration of the hepatocytes [55]. Cao et al. showed that green tea protects liver tissue from alcohol-induced injury by reducing lipid accumulation and preventing tissue damage due to the presence of polyphenols and their antioxidant effects [48].

It was confirmed by this study that carbon tetrachloride changes the biochemical functions of the liver through histological alteration. Necrosis of hepatocytes and their replacement with other inflammatory cells in the third group injected with carbon tetrachloride explained the fluctuation of the enzymes of the liver and other sera possibly due to the production of free radicals. The same findings were also discussed by [56] who reported that injuries caused by CCl<sub>4</sub> in the liver caused inflammatory cell infiltration, fibrous bridge formation, and perivenular cell necrosis. CCl<sub>4</sub> depicts its hepatotoxic effects through several pathways: dilation and congestion of blood vessels, abnormal mitosis, hemosiderin deposition, bile duct proliferation, and hepatocyte necrosis



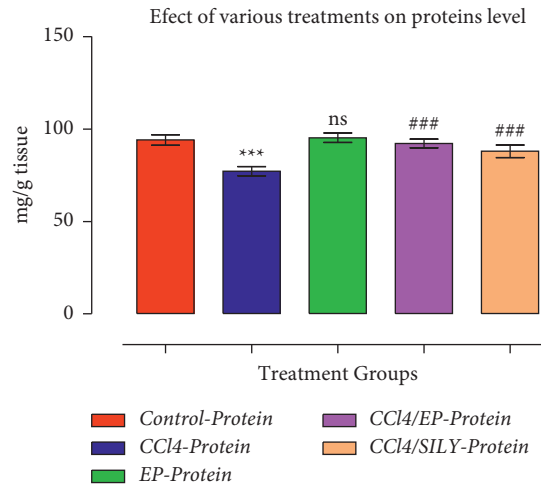


FIGURE 7: (–) Epicatechin and silymarin's effect on proteins. The data are presented as the mean  $\pm$  SD ( $n = 7$ ). \*\*\* $p < 0.001$  vs. control group; ###  $p < 0.001$  values vs. CCl<sub>4</sub> group.

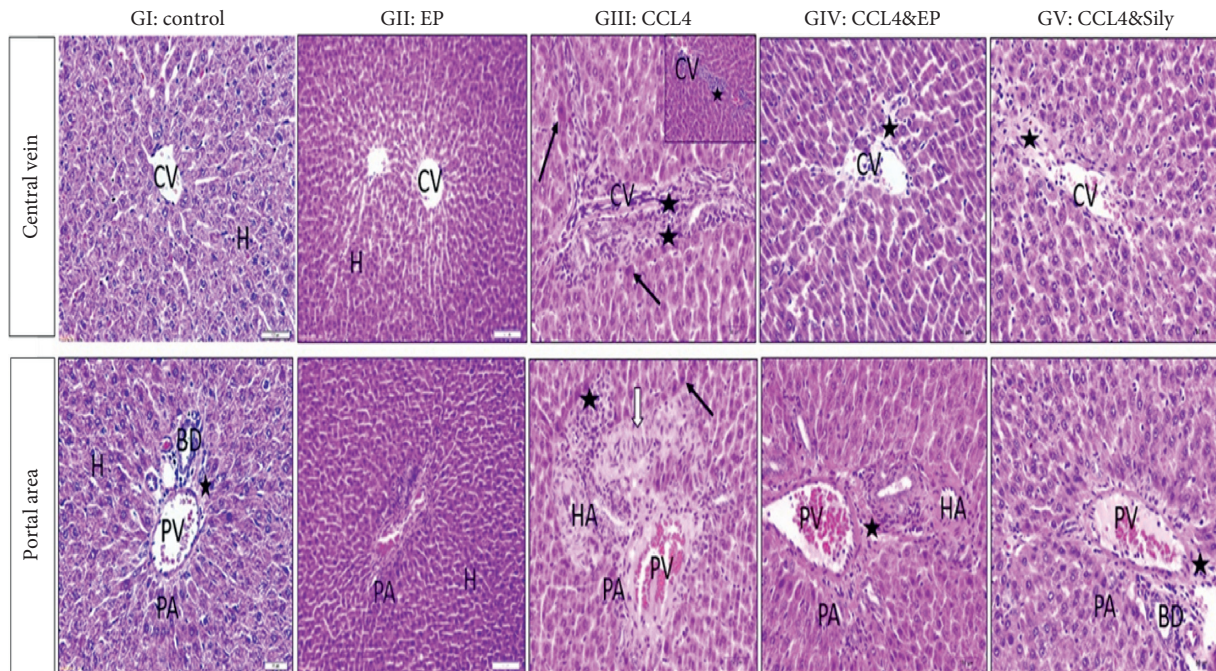


FIGURE 8: (–) Epicatechin and silymarin's effect on the liver's histopathological changes in both central vein (CV) and portal area (PA) regions caused by carbon tetrachloride. GI: control normal hepatocytes (H) in both central vein (CV) and portal area (PA) with few connective tissue cells (asterisk). BD: bile duct. GII: EP showing the normal cytoarchitecture of the lobule. The central vein is surrounded by hepatic cells separated by blood sinusoids. GIII: CCl<sub>4</sub> showing cell necrosis around CV with inflammatory cells and fibroblasts (black asterisks), vascular wall (HA) thickening (white arrow) with inflammatory cells (black asterisks), and degenerating hepatocytes (black arrow) in the portal area. GIV: CCl<sub>4</sub> and EP showing only a few fibrotic and inflammatory cells (black asterisks) around CV and thickening of artery (HA). Absence of fibrotic and inflammatory cells in PA (asterisks). GV: CCl<sub>4</sub> and SILY. Absence of fibrotic and inflammatory cells except for a small area (asterisks) around CV and PA.

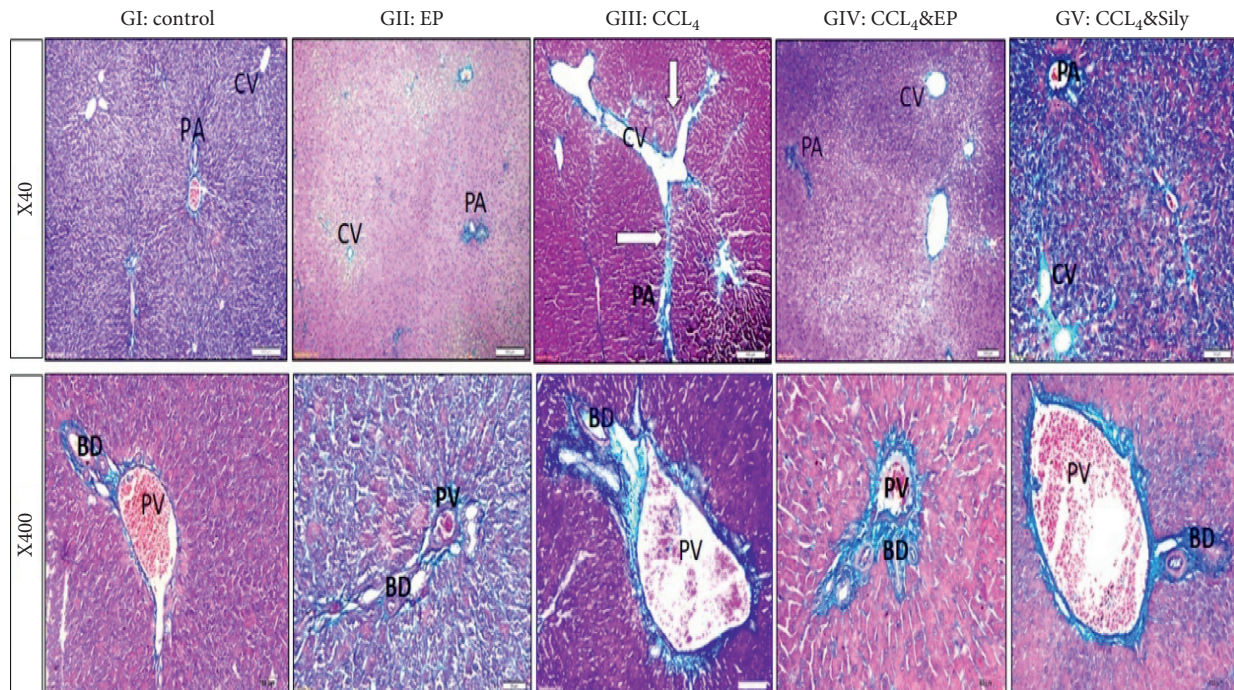


FIGURE 9: Effect of (–) epicatechin and silymarin on histopathological changes in  $\text{CCl}_4$ -induced toxicity study. The collagen components are stained blue, and the cytoplasm appears in varying degrees of red. GI: showing few amounts of collagen fibers around the portal area (PA), portal vein (PV), and bile duct (BD). GII: no change in collagen density. GIII: collagen is increased in the portal region forming bridges between the lobules (white arrows). High-power X400 showed dilated portal vein (PV) and marked fibrosis around bile duct (BD). GIV: moderate deposition in collagen in CV, PA, and PV areas. GV: mild collagen deposition.

[57]. EP coupled with SILY exhibited considerable hepatoprotective effects in the liver of rats treated by  $\text{CCl}_4$ . Among these two, EP proved to be more effective [58]. As discussed, EP is a very strong antioxidant [35] and it can be used to protect the liver from many toxins.

## 5. Conclusion

The findings of this study revealed that EP ameliorates  $\text{CCl}_4$ -induced hepatotoxicity and oxidative stress in rats. The intraperitoneal injection of  $\text{CCl}_4$  increases the activity of ALT, AST, and ALP, decreases the levels of TP and serum albumin, increases the level of MDA and ROS production, and decreases the level of NOS and CYP450. Oral administration of EP and SILY mitigates all of these harmful effects in the livers of rats. They reduce oxidative stress, suppress inflammatory cell infiltration, increase the regenerative capacity of damaged tissues, and reduce liver apoptosis. Thus, we believe that the use of natural products such as EP and SILY can aid in reducing the toxic effects resulting from exposure to xenobiotics such as  $\text{CCl}_4$  and other various toxic substances.

## Abbreviations

EP:	(–) Epicatechin
$\text{CCl}_4$ :	Carbon tetrachloride
SILY:	Silymarin
MDA:	Malondialdehyde
GSH:	Glutathione
CAT:	Catalase
GST:	Glutathione S-transferase
NOS:	Nitric oxide synthase
GPx:	Glutathione peroxidase
CYP450:	Cytochrome P450
TPA:	Tetradecanoylphorbol acetate
VOD:	Veno-occlusive disease
Nrf2:	Nuclear factor erythroid 2-related factor 2
NF- $\kappa$ B:	Nuclear factor-kappa B
CYP:	Cypermethrin
TNF- $\alpha$ :	Tumor necrosis factor-alpha
DMSO:	Dimethyl sulfoxide
ALT:	Alanine amino transaminase
AST:	Aspartate amino transaminase
ALP:	Alkaline phosphatase
TP:	Total protein



ODs: Optical densities  
 H<sub>2</sub>O<sub>2</sub>: Hydrogen peroxide  
 ELISA: Enzyme-linked immunosorbent assay  
 CYP1A2: Cytochrome P450 1A2  
 H&E: Hematoxylin and Eosin.

## Data Availability

The data in the manuscript belong to the research work of Khadijah B. Alkinani and will be provided to researchers upon request.

## Conflicts of Interest

The authors declare no conflicts of interest.

## Authors' Contributions

K. B. A. and E. M. M. A. conceptualized the data; K. A. A., T. M. A., and J. A. A. K. designed methodology; K. B. A. curated the data; K. B. A., E. M. M. A., T. M. A., J. A. K., T. M. A., S. S. A., A. A., O. F. M., and T. Z. wrote the original manuscript and prepared the draft; and K. B. A., E. M. M. A., T. M. A., J. A. K., T. M. A., S. S. A., A. A., O. F. M., and T. Z. wrote, reviewed, and edited the manuscript. All authors have read and agreed to the published version of the manuscript.

## Acknowledgments

The authors are grateful to Mrs. Sharifah, Mr. Basheer Alkinani, and Dr. Khalid Balbaid for their financial and moral support. The authors also thank all those who participated in this study patiently.

## References

- [1] S. Hussain, F. Ullah, A. Sadiq et al., "Cytotoxicity of *Anchusa arvensis* against HepG-2 cell lines: Mechanistic and computational approaches," *Current Topics in Medicinal Chemistry*, vol. 19, no. 30, pp. 2805–2813, 2019.
- [2] H. Nishikawa and Y. Osaki, "Liver cirrhosis: evaluation, nutritional status, and prognosis," *Mediators of Inflammation*, vol. 2015, Article ID 872152, 9 pages, 2015.
- [3] N. O. Al-Harbi, F. Imam, A. Nadeem, M. M. Al-Harbi, M. Iqbal, and S. F. Ahmad, "Carbon tetrachloride-induced hepatotoxicity in rat is reversed by treatment with riboflavin," *International Immunopharmacology*, vol. 21, no. 2, pp. 383–388, 2014.
- [4] S. Hussain, F. Ullah, M. Ayaz et al., "In silico, cytotoxic and antioxidant potential of novel ester, 3-hydroxyoctyl -5- transdocosenoate isolated from *anchusa arvensis* (L.) M. Bieb. against HepG-2 cancer cells," *Drug Design, Development and Therapy*, vol. 13, pp. 4195–4205, 2019.
- [5] Y.-J. Zhou, Y.-Y. Li, Y.-Q. Nie et al., "Prevalence of fatty liver disease and its risk factors in the population of south China," *World Journal of Gastroenterology*, vol. 13, no. 47, pp. 6419–6424, 2007.
- [6] S. Ratib, J. West, C. J. Crooks, and K. M. Fleming, "Diagnosis of liver cirrhosis in England, a cohort study, 1998–2009: a comparison with cancer," *American Journal of Gastroenterology*, vol. 109, no. 2, pp. 190–198, 2014.
- [7] I. M. Jacobson, G. L. Davis, H. El-Serag, F. Negro, and C. Trépo, "Prevalence and challenges of liver diseases in patients with chronic hepatitis C virus infection," *Clinical Gastroenterology and Hepatology*, vol. 8, no. 11, pp. 924–933, 2010.
- [8] P. V. Kumar, A. Sivaraj, E. Elumalai, and B. S. Kumar, "Carbon tetrachloride-induced hepatotoxicity in rats-protective role of aqueous leaf extracts of *Coccinia grandis*," *International Journal of PharmTech Research*, vol. 1, no. 4, pp. 1612–1615, 2009.
- [9] P. S. M. Prince, "A biochemical, electrocardiographic, electrophoretic, histopathological and in vitro study on the protective effects of (-) epicatechin in isoproterenol-induced myocardial infarcted rats," *European Journal of Pharmacology*, vol. 671, no. 1, pp. 95–101, 2011.
- [10] M. Rubio-Osornio, E. Gorostieta-Salas, S. Montes et al., "Epicatechin reduces striatal MPP (+) -induced damage in rats through slight increases in SOD-Cu, Zn activity," *Oxidative Medicine and Cellular Longevity*, vol. 2015, Article ID 276039, 6 pages, 2015.
- [11] P. S. M. Prince, "(-) Epicatechin attenuates mitochondrial damage by enhancing mitochondrial multi-marker enzymes, adenosine triphosphate and lowering calcium in isoproterenol induced myocardial infarcted rats," *Food and Chemical Toxicology: An International Journal Published for the British Industrial Biological Research Association*, vol. 53, pp. 409–416, 2013.
- [12] E. Ujhelyi, A. Divald, G. Vajta, A. Jeney, and K. Lapis, "Effect of PGI2 in carbon tetrachloride-induced liver injury," *Acta Physiologica Hungarica*, vol. 64, no. 3-4, pp. 425–430, 1984.
- [13] N. Ale-Agha, W. Stahl, and H. Sies, "(-) Epicatechin effects in rat liver epithelial cells: stimulation of gap junctional communication and counteraction of its loss due to the tumor promoter 12-O-tetradecanoylphorbol-13-acetate," *Biochemical Pharmacology*, vol. 63, no. 12, pp. 2145–2149, 2002.
- [14] Y. Cui, X. Yang, X. Lu, J. Chen, and Y. Zhao, "Protective effects of polyphenols-enriched extract from Huangshan Maofeng green tea against CCl<sub>4</sub>-induced liver injury in mice," *Chemico-Biological Interactions*, vol. 220, pp. 75–83, 2014.
- [15] Z. Huang, X. Jing, Y. Sheng et al., "(-)-Epicatechin attenuates hepatic sinusoidal obstruction syndrome by inhibiting liver oxidative and inflammatory injury," *Redox Biology*, vol. 22, Article ID 101117, 2019.
- [16] O. K. Afolabi, F. A. Aderibigbe, D. T. Folarin, A. Arinola, and A. D. Wusu, "Oxidative stress and inflammation following sub-lethal oral exposure of cypermethrin in rats: mitigating potential of epicatechin," *Heliyon*, vol. 5, no. 8, Article ID e02274, 2019.
- [17] M. Fathy, E. M. M. A. Khalifa, and M. A. Fawzy, "Modulation of inducible nitric oxide synthase pathway by eugenol and telmisartan in carbon tetrachloride-induced liver injury in rats," *Life Sciences*, vol. 216, pp. 207–214, 2019.
- [18] S. M. Eraky, M. El-Mesery, A. El-Karef, L. A. Eissa, and A. M. El-Gayar, "Silymarin and caffeine combination ameliorates experimentally-induced hepatic fibrosis through down-regulation of LPAR1 expression," *Biomedicine & Pharmacotherapy*, vol. 101, pp. 49–57, 2018.
- [19] G. Ozdemir, M. Ozden, H. Maral, S. Kuskay, P. Cetinalp, and I. Tarkun, "Malondialdehyde, glutathione, glutathione peroxidase and homocysteine levels in type 2 diabetic patients with and without microalbuminuria," *Annals of Clinical Biochemistry*, vol. 42, no. 2, pp. 99–104, 2005.
- [20] S. Uraz, V. Tahan, C. Aygun et al., "Role of ursodeoxycholic acid in prevention of methotrexate-induced liver toxicity,"

- Digestive Diseases and Sciences*, vol. 53, no. 4, pp. 1071–1077, 2008.
- [21] U. Saleem, R. Akhtar, F. Anwar et al., “Neuroprotective potential of *Malva neglecta* is mediated via down-regulation of cholinesterase and modulation of oxidative stress markers,” *Metabolic Brain Disease*, vol. 36, no. 5, pp. 889–900, 2021.
- [22] N. T. Mir, U. Saleem, F. Anwar et al., “*Lawsonia inermis* markedly improves cognitive functions in animal models and modulate oxidative stress markers in the brain,” *Medicina*, vol. 55, no. 5, p. 192, 2019.
- [23] T. Yoshioka, K. Kawada, T. Shimada, and M. Mori, “Lipid peroxidation in maternal and cord blood and protective mechanism against activated-oxygen toxicity in the blood,” *American Journal of Obstetrics and Gynecology*, vol. 135, no. 3, pp. 372–376, 1979.
- [24] M. Moron, J. Depierre, and B. Mannervik, “Levels of glutathione, glutathione reductase and glutathione S-transferase activities in rat lung and liver,” *Biochimica et Biophysica Acta (BBA)—General Subjects*, vol. 582, no. 1, pp. 67–78, 1979.
- [25] D. T. Y. Chiu, F. H. Stults, and A. L. Tappel, “Purification and properties of rat lung soluble glutathione peroxidase,” *Biochimica et Biophysica Acta (BBA)—Enzymology*, vol. 445, no. 3, pp. 558–566, 1976.
- [26] H. Aebi, “[13] Catalase in vitro,” in *Methods in Enzymology*, vol. 105, pp. 121–126, Academic Press, 1984.
- [27] A. Garcia-Angueta, A. Kakourou, and K. K. Tsilidis, “Biomarkers of inflammation and immune function and risk of colorectal cancer,” *Current Colorectal Cancer Reports*, vol. 11, no. 5, pp. 250–258, 2015.
- [28] W. H. Habig, M. J. Pabst, and W. B. Jakoby, “Glutathione S-transferases. The first enzymatic step in mercapturic acid formation,” *Journal of Biological Chemistry*, vol. 249, no. 22, pp. 7130–7139, 1974.
- [29] D. Schuppan and N. H. Afdhal, “Liver cirrhosis,” *The Lancet*, vol. 371, no. 9615, pp. 838–851, 2008.
- [30] M. F. Akhtar, M. O. Mehal, A. Saleem et al., “Attenuating effect of *Prosopis cineraria* against paraquat-induced toxicity in prepubertal mice, *Mus musculus*,” *Environmental Science and Pollution Research International*, pp. 1–17, 2021.
- [31] A. T. Khalil, M. Ovais, J. Iqbal et al., “Microbes-mediated synthesis strategies of metal nanoparticles and their potential role in cancer therapeutics,” in *Seminars in Cancer Biology*, Elsevier, Amsterdam, Netherlands, 2021.
- [32] M. Ayaz, A. Wadood, A. Sadiq, F. Ullah, O. Anichkina, and M. Ghufuran, “In-silico evaluations of the isolated phytosterols from *Polygonum hydropiper* L against BACE1 and MAO drug targets,” *Journal of Biomolecular Structure and Dynamics*, pp. 1–9, 2021.
- [33] M. Ghufuran, A. U. Rehman, M. Shah, M. Ayaz, H. L. Ng, and A. Wadood, “In-silico design of peptide inhibitors of K-Ras target in cancer disease,” *Journal of Biomolecular Structure and Dynamics*, vol. 38, no. 18, pp. 5488–5499, 2020.
- [34] G. Karimi, M. Vahabzadeh, P. Lari, M. Rashedinia, and M. Moshiri, “Silymarin”, a promising pharmacological agent for treatment of diseases,” *Iranian Journal of Basic Medical Sciences*, vol. 14, no. 4, pp. 308–317, 2011.
- [35] M. L. Salem, A. A.-H. Khamis, A.-H. A.-H. Mostafa, and E. M. Ali, “Antitumor potential of some selective medicinal plants on experimental tumor ascites,” *Journal of Investigational Biochemistry*, vol. 6, 2017.
- [36] K. R. Ritesh, A. Suganya, H. V. Dileepkumar, Y. Rajashekar, and T. Shivanandappa, “A single acute hepatotoxic dose of  $\text{CCl}_4$  causes oxidative stress in the rat brain,” *Toxicology Reports*, vol. 2, pp. 891–895, 2015.
- [37] R. A. R. Elgawish, H. G. A. Rahman, and H. M. A. Abdelrazek, “Green tea extract attenuates  $\text{CCl}_4$ -induced hepatic injury in male hamsters via inhibition of lipid peroxidation and p53-mediated apoptosis,” *Toxicology Reports*, vol. 2, pp. 1149–1156, 2015.
- [38] H.-M. Lin, H.-C. Tseng, C.-J. Wang, J.-J. Lin, C.-W. Lo, and F.-P. Chou, “Hepatoprotective effects of *Solanum nigrum* Linn extract against  $\text{CCl}_4$ -induced oxidative damage in rats,” *Chemico-Biological Interactions*, vol. 171, no. 3, pp. 283–293, 2008.
- [39] J. Liu, J.-f. Lu, X.-y. Wen, J. Kan, and C.-h. Jin, “Antioxidant and protective effect of inulin and catechin grafted inulin against  $\text{CCl}_4$ -induced liver injury,” *International Journal of Biological Macromolecules*, vol. 72, pp. 1479–1484, 2015.
- [40] B. Shanmugam, K. R. Shanmugam, S. Ravi et al., “Exploratory studies of (–)-epicatechin, a bioactive compound of *Phyllanthus niruri*, on the antioxidant enzymes and oxidative stress markers in D-galactosamine-induced hepatitis in rats: a study with reference to clinical prospective,” *Pharmacognosy Magazine*, vol. 13, no. 1, pp. S56–S62, 2017.
- [41] T. A. Gheita and S. A. Kenawy, “Measurement of malondialdehyde, glutathione, and glutathione peroxidase in SLE patients,” in *Methods in Molecular Biology*, vol. 1134, pp. 193–199, Springer, 2014.
- [42] Z.-W. Zhao, J.-C. Chang, L.-W. Lin, F.-H. Tsai, H.-C. Chang, and C.-R. Wu, “Comparison of the hepatoprotective effects of four endemic *Cirsium* species extracts from Taiwan on  $\text{CCl}_4$ -induced acute liver damage in C57BL/6 mice,” *International Journal of Molecular Sciences*, vol. 19, no. 5, p. 1329, 2018.
- [43] O. M. Ighodaro and O. A. Akinloye, “First line defence antioxidants-superoxide dismutase (SOD), catalase (CAT) and glutathione peroxidase (GPX): their fundamental role in the entire antioxidant defence grid,” *Alexandria Journal of Medicine*, vol. 54, no. 4, pp. 287–293, 2018.
- [44] C. Zhang, N. Wang, Y. Xu, H.-Y. Tan, S. Li, and Y. Feng, “Molecular mechanisms involved in oxidative stress-associated liver injury induced by Chinese herbal medicine: an experimental evidence-based literature review and network pharmacology study,” *International Journal of Molecular Sciences*, vol. 19, no. 9, p. 2745, 2018.
- [45] A. A. Abolfathi, D. Mohajeri, A. Rezaie, and M. Nazeri, “Protective effects of green tea extract against hepatic tissue injury in streptozotocin-induced diabetic rats,” *Evidence-Based Complementary and Alternative Medicine*, vol. 2012, Article ID 740671, 10 pages, 2012.
- [46] W. M. Haschek, C. G. Rousseaux, M. A. Wallig, B. Bolon, and R. Ochoa, *Haschek and Rousseaux’s Handbook of Toxicologic Pathology*, Academic Press, Cambridge, MA, USA, 2013.
- [47] O. B. Adewale, A. Adekeye, C. Akintayo, A. Onikanni, and S. Sabiu, “Carbon tetrachloride ( $\text{CCl}_4$ )-induced hepatic damage in experimental Sprague Dawley rats: antioxidant potential of *Xylopiya aethiopica*,” *Journal of Pharmacology*, vol. 3, no. 2, 2014.
- [48] S. M. Shah, M. Ayaz, A.-u. Khan et al., “1,1-Diphenyl, 2-picrylhydrazyl free radical scavenging, bactericidal, fungicidal and leishmanicidal properties of *Teucrium stocksianum*,” *Toxicology and Industrial Health*, vol. 31, no. 11, pp. 1037–1043, 2015.
- [49] J. E. Manautou, S. N. Campion, and L. M. Aleksunes, “Regulation of hepatobiliary transporters during liver injury,” in *Comprehensive Toxicology*, C. A. McQueen, Ed., pp. 175–220, Elsevier, Amsterdam, Netherlands, 2nd edition, 2010.
- [50] A. M. Abdel-Moneim, M. A. Al-Kahtani, M. A. El-Kersh, and M. A. Al-Omar, “Free radical-scavenging, anti-

- inflammatory/anti-fibrotic and hepatoprotective actions of taurine and silymarin against CCl<sub>4</sub> induced rat liver damage,” *PLoS One*, vol. 10, no. 12, Article ID e0144509, 2015.
- [51] M. C. Litterio, G. Jagers, G. Sagdicoglu Celep et al., “Blood pressure-lowering effect of dietary (-)-epicatechin administration in L-NAME-treated rats is associated with restored nitric oxide levels,” *Free Radical Biology and Medicine*, vol. 53, no. 10, pp. 1894–1902, 2012.
- [52] N. Al-Rasheed, L. Faddah, I. A. Sharaf, A. M. Mohamed, N. Al-Rasheed, and N. Abdelbaky, “Assessment of the potential role of silymarin alone or in combination with vitamin E and/or curcumin on the carbon tetrachloride induced liver injury in rat,” *Brazilian Archives of Biology and Technology*, vol. 58, no. 6, pp. 833–842, 2015.
- [53] D. Bhatia, M. Bansal, S. Bhangu, and G. Singh, “Hepatoprotective effects of epigallocatechin gallate via mitochondrial permeability transition pore in paracetamol induced hepatotoxicity,” *Plant Archives*, vol. 19, no. 2, pp. 2162–2167, 2019.
- [54] D. Wang, Q. Gao, T. Wang et al., “Green tea polyphenols and epigallocatechin-3-gallate protect against perfluorodecanoic acid induced liver damage and inflammation in mice by inhibiting NLRP3 inflammasome activation,” *Food Research International (Ottawa, Ont.)*, vol. 127, Article ID 108628, 2020.
- [55] A. T. Abbas, N. A. El-Shitany, L. A. Shaala et al., “Red sea *Suberea mollis* sponge extract protects against CCl<sub>4</sub>-induced acute liver injury in rats via an antioxidant mechanism,” *Evidence-Based Complementary and Alternative Medicine*, vol. 2014, Article ID 745606, 9 pages, 2014.
- [56] S. Sangi, S. A. El-feky, S. S. Ali, E. I. Ahmedani, and M. Tashtoush, “Hepatoprotective effects of oleuropein, thymoquinone and fruit of *Phoenix dactylifera* on CCl<sub>4</sub> induced hepatotoxicity in rats,” *World Journal of Pharmacy and Pharmaceutical Sciences*, vol. 3, Article ID 3475e3486, 2014.
- [57] N. A. Schwarz, Z. J. Blahnik, S. Prahadeeswaran, S. K. McKinley-Barnard, S. L. Holden, and A. Waldhelm, “(-)-Epicatechin supplementation inhibits aerobic adaptations to cycling exercise in humans,” *Frontiers in Nutrition*, vol. 5, no. 132, 2018.
- [58] M. Prakash, B. V. Basavaraj, and K. N. Chidambara Murthy, “Biological functions of epicatechin: plant cell to human cell health,” *Journal of Functional Foods*, vol. 52, pp. 14–24, 2019.
- [59] S. A. Sheweita, M. Abd El-Gabar, and M. Bastawy, “Carbon tetrachloride changes the activity of cytochrome P450 system in the liver of male rats: role of antioxidants,” *Toxicology*, vol. 169, no. 2, pp. 83–92, 2001.



## Review Article

# The Effect of Terpenoid Natural Chinese Medicine Molecular Compound on Lung Cancer Treatment

Heng Sun <sup>1,2</sup>, Lijia Zhang <sup>3</sup>, Bowen Sui <sup>4</sup>, Yu Li <sup>1</sup>, Jun Yan,<sup>1</sup> Peng Wang,<sup>1</sup> Ye Wang,<sup>5</sup> and Songjiang Liu <sup>1</sup>

<sup>1</sup>The First Affiliated Hospital of Heilongjiang University of Chinese Medicine, Department of Oncology, Harbin, China

<sup>2</sup>Heilongjiang University of Chinese Medicine, Harbin, China

<sup>3</sup>The First Affiliated Hospital of Heilongjiang University of Chinese Medicine, Department of Oncology Ethics Office, Harbin, China

<sup>4</sup>The First Affiliated Hospital of Heilongjiang University of Chinese Medicine, Department of Oncology Respiratory, Harbin, China

<sup>5</sup>The First Affiliated Hospital of Heilongjiang University of Chinese Medicine, Academic Affairs Section, Harbin, China

Correspondence should be addressed to Songjiang Liu; liusongjiang@hljucm.net

Received 3 November 2021; Revised 18 November 2021; Accepted 1 December 2021; Published 16 December 2021

Academic Editor: Ruchika Garg

Copyright © 2021 Heng Sun et al. This is an open access article distributed under the Creative Commons Attribution License, which permits unrestricted use, distribution, and reproduction in any medium, provided the original work is properly cited.

Among all malignant tumors in the whole universe, the incidence and mortality of lung cancer disease rank first. Especially in the past few years, the occurrence of lung cancer in the urban population has continued to increase, which seriously threatens the lives and health of people. Among the many treatments for lung cancer, chemotherapy is the best one, but traditional chemotherapy has low specificity and drug resistance. To address the above issue, this study reviews the five biological pathways that common terpenoid compounds in medicinal plants interfere with the occurrence and development of lung cancer: cell proliferation, cell apoptosis, cell autophagy, cell invasion, metastasis, and immune mechanism regulation. In addition, the mechanism of the terpenoid natural traditional Chinese medicine monomer compound combined with Western medicine in the multipathway antilung cancer is summarized.

## 1. Introduction

The latest research has shown that lung cancer is the most common form of the malignant tumor whose morbidity and mortality have increased year by year in recent years. It has become the major cause of death due to cancer around the globe [1, 2]. According to the latest report, in 2018, approximately 18.1 million people worldwide were affected by different types of cancer. Among them, the number of deaths caused by lung cancer is about 2.1 million [3]. There has been advanced technology operated to treat lung cancer named as targeted therapy. The earliest targeted drugs used in clinics are mainly targeted at the epidermal growth factor and its receptor (EGF-EGFR) pathway, tyrosine kinase inhibitor, anti-VEGF monoclonal antibody, and VEGFR tyrosine kinase inhibitor (VEGFR-TKI) [4]. Since the beginning of 2000, multitarget drugs have rapidly developed [5].

Crizotinib is an ALK inhibitor, but it also targets LTK, CHEK2, FLT3, PHKG2, and RET. Nintedanib and sorafenib are multiple tyrosine kinase inhibitors targeting FGFR, PDGFR, and VEGFR [6]. Among them, gefitinib (Iressa) and erlotinib (trocet) are the most commonly used inhibitors. They are epidermal growth factor receptor inhibitors. Still, because of their selectivity for patients with gene mutations and the ease of medication, the occurrence of drug resistance has become the bottleneck of its widespread application [7, 8]. In the year 2020, there are a total of 89 small molecule targeted antitumor drugs that were approved by the American FDA and China's NMPA. These small molecule targeted anticancer drugs are still at the challenging phase where they face drug resistance and low response rates [9].

Many active ingredients derived from herbal medicines of China have anticancer properties that include anti-proliferative, proapoptotic, antimetastatic, and

antiangiogenic effects [10]. These active ingredients can target the gene targets of the malignant proliferation of tumor cells, selectively induce tumor cell apoptosis without affecting normal cells, provide new research strategies for tumor treatment, and improve the treatment results of patients with NSCLC. New research emerges, including terpenoids, flavonoids, polyphenols, polysaccharides, and alkaloids. [11]. Among them, terpenoids are natural products derived from mevalonic acid (mevalonic acid, MVA). Terpenoids are composed of multiple isoprene (isoprene, C5) structural units, and the general formula is (C<sub>5</sub>H<sub>8</sub>)<sub>*n*</sub>, which is also the most common compound among natural products. It is present in a large quantity in the plant kingdom and has a large variety of styles. It has the potential to be a lead compound to develop efficient and new and safe antitumor drugs. At present, terpenoids with antitumor activity are classified into monoterpenes, sesquiterpenes, diterpenes, and triterpenes (Table 1).

In recent years, people have gradually realized that there are major effects of natural products on NSCLC, especially when it comes to improving anticancer activity and drug sensitivity. On the basis of this fact, the anticancer mechanism of natural small molecule compounds of terpenoid Chinese medicine on lung cancer has been summarized.

## 2. Cell Cycle Regulation and Inhibition of Tumor Cell Proliferation

An important feature of tumor cells is uncontrolled growth. The occurrence of tumors stems from changes in genetic material DNA (or genes), and this change is a multistep cellular process of multiple genetic changes. As mentioned above, cell cycle regulation is a delicate balance process, and any defects in this process may lead to changes in genetic information. The different phases of the cell cycle are highly accurately coordinated to ensure strict timing. For example, cyclins, CDK inhibitors, and other regulatory molecules need to be activated or degraded in time to ensure the regular operation of the cell cycle [12, 13]. In the course of normal cells into tumor cells, there may be cell cycle disorders, tumor cell invasion and metastasis, and drug insensitivity phenomenon [14]. Almost all tumors destroy the cell cycle regulation mechanism, leading to the characteristics of uncontrolled cell growth, blocked differentiation, and abnormal apoptosis [15]. In short, the destruction of the molecular regulation mechanism of the cell cycle, or the disorder of its upstream agent, will lead to an abnormal cell cycle. The following content is introduced, that is, the molecular mechanism of terpenoid natural TCM small molecules in treating lung cancer by inhibiting cell proliferation (Table 2).

Andrographolide (Andro) is the main active compound that is wholly spread in *Andrographis paniculata*, a kind of herb that is used as a natural remedy for various diseases [23, 24]. Studies have shown that Andro treatment can increase DNA fragmentation and reduce Na<sup>+</sup>-K<sup>+</sup>-ATPase activity, indicating  $\alpha$ -subunit dysfunction and/or mitochondrial membrane damage, and also indicating mitochondrial dysfunction caused by AD, and reducing TGF- $\beta$ 1

and VEGF expression levels inhibits tumor cell proliferation and downregulates PCK to promote lung cancer cell apoptosis [16, 17].

The small molecule active substance of licorice is mainly glycyrrhizic acid with different chemical structure. Among them, there are many related types of research on glycyrrhizic acid [25, 26]. Glycyrrhizic acid has various medicinal activities just like retinoic acid and steroids. Relevant studies have shown that 18 $\beta$ -GA can inhibit cell proliferation and induce NSCLC cell apoptosis at least in part [18, 19].

Glycyrrhetic acid (GA) can inhibit cell lines of humans (A549 and NCI-H460), of which A549 is more sensitive than NCI-H460. Glycyrrhetic acid activates p18/p16 to inactivate the CDK4/6-cyclin-D1/D3 complex. Glycyrrhetic acid can activate p27/p21 to inactivate the CDK2-cyclin-E2 complex, thereby causing cell arrest in the G1 period. This condition can lead to the dephosphorylation of pRb in both cell types to regulate cell cycle progression and the inactivation of transcription factor 1 (E2F-1), a critical apoptotic transcription factor. GA is upregulated, and it has the ability to inhibit the proliferation of NSCLC cells via the emergency pathway of the endoplasmic reticulum. GA induces chaperones of ER, which reduces the synthesis of proteins [27].

Carnosic acid has various biological functions, which majorly include antibacterial, antioxidant, and anti-proliferative activities [20]. Different treatment concentrations of CA can inhibit the proliferation/G one and G 2/M phases of IMR-90 and NCI-H460 cells [28].

There are two subclasses of ginsenosides, namely, protopanaxadiol (PPD) and protopanaxatriol (PPT) [21]. Related research has synthesized 13 kinds of ginseng diol derivatives through amino acids. Compared with PD, ginseng diol derivatives 3, 12, and 13 have a significant effect of inhibition on the cell proliferation of cancer cells. Among them, ginseng diol has the IC<sub>50</sub> value for A549 (IC<sub>50</sub> = 18.91  $\pm$  1.03 microns) [19].

Astragaloside is the main active component of *Astragalus*, which is composed of many triterpene saponins, including astragaloside I-IV [29]. The study found that astragaloside IV if given in high dose can inhibit the growth of NSCLC cells (A549, HCC827, and NCI-H1299); while if it is present in low concentration, there will be no apparent cytotoxicity to the viability of the cell. In addition, astragaloside IV combined with medication majorly enhances the chemosensitivity of NSCLC cells [22].

## 3. Mechanisms of Inducing Apoptosis of Lung Cancer Cells

The process of apoptosis is a highly conservative suicide program of the cell. The body clears excess cells and dangerous cells through apoptosis to maintain homeostasis [30]. Inactivation of the apoptosis program can lead to the occurrence of autoimmune diseases and tumors. In cell cycle-monitoring point function inactivation, the obstruction of cell apoptosis can cause DNA damage to be carried into daughter cells, thereby increasing genome instability and causing cell malignancy [31]. Tumor cells can usually resist

TABLE 1: Part of terpenoids and category of traditional Chinese medicine (TCM) for lung cancer treatment.

Category	For example
Terpenoid natural TCM molecular compound	Monoterpene, sesquiterpene, diterpene, and triterpene
A single TCM	Andrographis, licorice, carnosic, ginseng, astragalus, atractylodes, aucklandia, pachymic, rhizoma bolbostemmae, curcumol, tripterygium wilfordii, and bupleurum
TCM monomer	Andro, glycyrrhizic acid, glycyrrhetic acid, carnosic acid, ginsenosides, astragaloside, atractylodes macrocephala, costunolide, pachymic acid, polypropenic acid, tubeimoside, ivy saponins, curcumol, oridonin, triptolide, lupeol, betulinic acid, saikosaponin, and cucurbitacin

TABLE 2: Molecular mechanism of terpenoid natural TCM small molecules in treating lung cancer by inhibiting cell proliferation.

Terpenoid natural TCM small molecules	Experimental model	Dose/concentration	Mechanism of action	Ref.
Andrographolide (AD)	H3255 NSCLC cells	AD (1.0, 2.5, or 5.0 $\mu\text{M}$ ) for 24 h	Decreased in the na (+)-k (+)-ATPase activities; decreased VEGF and TGF- $\beta$ 1 level; inhibited protein kinase C activities in H3255 cells. Released lactate dehydrogenase. Increased DNA fragmentation level.	[16]
Andrographolide (AD)	H3255 NSCLC cells	AD (1, 5, or 10 $\mu\text{M}$ ) for 24, 48, or 72 h	Inhibited proliferation of H3255 cell; decrease in MMP-9 expression and activity. Decrease in cell proliferation induced by transfection with TxAS small-interfering RNA (siRNA);	[17]
18 $\beta$ -glycyrrhetic acid (18 $\beta$ -GA)	A549, NCI-H460, and NCI-H23 NSCLC cells	18 $\beta$ -GA (80, 160, or 320 $\mu\text{M}$ ) for 24 h	Inhibited TxAS and its initiated ERK/CREB signaling. Arrested cell cycle in G0/G1.; Inhibited (CKIs) (p18, p16, p27, and p21);	[18]
Glycyrrhetic acid (GA)	A549 and NCI-H460 NSCLC cells	GA (50, 25, 12.5, 6.25 or 3.125 $\mu\text{mol/l}$ ) 24, 48, or 72 h	Inhibited cyclins (cyclin-D1, cyclin-D3, and cyclin-E); Inhibited cyclin-dependent kinases (CDKs) (CDK4, CDK6, and CDK2).	[19]
Carnosic acid (CA)	IMR-90 (human fetal lung fibroblasts) and NCI-H460 NSCLC cells	CA (40, 80, 160, 240, or 320 $\mu\text{M}$ ) 24 h	Arrest at G0/G1 and G2/M phases.	[20]
13 panaxadiol (PD)	HepG-2 (human hepatoma cells), A549 NSCLC cells, MCF-7 (human breast cancer cells), or HCT-116 (human colon cancer cells)	PD ( $\text{IC}_{50} = 8.62 \pm 0.23 \mu\text{M}$ )	Inhibited cellular proliferation.	[21]
Astragaloside IV	A549, HCC827, NCI-H1299 NSCLC cells	Astragaloside IV high doses (10, 20, and 40 ng/ml) and low doses (1, 2.5, and 5 ng/ml)	Inhibited the mRNA and protein levels of B7-H3.	[22]

apoptosis [32]. At present, the primary strategies for targeted tumor therapy include the following: (1) the expression of the proapoptotic gene p53 is restored [33]; (2) the anti-apoptotic gene Bcl-2 is inactivated [34]; (3) the sensitivity of tumor cell apoptosis is increased by regulating metabolism (Bax and Bak) [35]; and (4) biological therapy is related (antibody-directed therapy, immunotherapy, virus-based introduction of apoptosis-inducing factor p53, and

proapoptotic miRNA) [36–38]. The following is introduced, that is, the molecular mechanism of terpenoid natural Chinese medicine small molecules to promote apoptosis of cancerous cells in the treatment of lung cancer (Table 3).

Atractylodes macrocephala I and III (ATL-I, III) are sesquiterpenoids derived from Atractylodes macrocephala. In *in vitro* studies, Bcl-2 and Bcl-XL in the expression of A549 cells treated with ATL-I decreased. *In vivo* studies have shown

TABLE 3: The molecular mechanism of terpenoid natural Chinese medicine small molecules to promote tumor cell apoptosis in the treatment of lung cancer.

Terpenoid natural TCM small molecules	Experimental model	Dose/concentration	Mechanism of action	Ref.
Atractylodes macrocephala I (ATL-I)	A549 and HCC827 NSCLC cells	ATL-I (10, 20, and 40 $\mu$ M) for 48 h	Upregulation of caspase-3, caspase-9, and Bax; Downregulation of Bcl-2 and Bcl-XL Increased lactate dehydrogenase release;	[39]
Atractylodes macrocephala III (ATL-III)	A549 NSCLC cells	ATL-II I (1–100 $\mu$ M) for 24 h	Modulated cell cycle on A549 cells; Induced the release of cytochrome c; Upregulation of Bax expression	[40]
Costunolide	A549 NSCLC cells	Costunolide (0, 5, 10, 15, 25, or 30 $\mu$ M) for 24 h	Upregulation of GRP78 and IRE1 $\alpha$ and the activation of ASK1 and JNK; Induced ROS generation;	[41]
Costunolide	SK-MES-1 human lung squamous carcinoma cells	Costunolide (40 and 80 $\mu$ M) for 24 h	Changed the antiapoptotic function of Bcl-2; Induced cell cycle arrest at G1/S phase; Upregulation in the expression of p53 and Bax;	[42]
Pachymic acid (PA)	NCI-H23 and NCI-H460 lung cancer cells	PA (20, 40, or 80 $\mu$ M) for 24 h	Downregulation in the expression of Bcl-2 and activation of caspase-3; Induced cell cycle arrest at G2/M phase; Induced ROS generation;	[43]
Pachymic acid (PA)	A549 NSCLC cells	PA (0, 3, 10, 30, 60, 100, and 200 $\mu$ M) for 24 or 48 h	Activation of both c-Jun N-terminal kinase (JNK) and endoplasmic reticulum (ER) stress apoptotic pathways. Inhibited anchorage-dependent and anchorage-independent A549 growth; Induced apoptosis of A549 cells;	[44]
Pachymic acid (PA)	A549 NSCLC cells	PA (0, 3, 10, 30, 60, 100, and 200 $\mu$ M) for 24 or 48 h	Decreased IL-1 beta-induced activation of cPLA (2) and COX-2; Suppressed IL-1 beta-induced activation of MAPKs;	[44]
Polyporenic acid C (PPAC)	A549 NSCLC cells	PPAC (0, 2, 6, 20, 60, or 200 $\mu$ M) for 24, 48, or 72 h	Inhibited IL-1 beta-stimulated nuclear factor kappa B of NF-kB; Suppressed PI3-kinase/Akt signal pathway; Enhanced p53 activation.	[45]
Tubeimoside I (TBMS1)	NCI-H1299 and NCI-H1975 lung cancer cells	TBMS1 (0, 10, 20, and 30 $\mu$ M) for 24 h	Induction of DRP1-mediated mitochondrial fragmentation; Inhibited V-ATPase and blocked late-stage autophagic flux via; Blocked the removal of dysfunctional mitochondria; Induced ROS generation.	[46]

that ATL-I can effectively inhibit tumor growth in xenograft of mice by upregulating caspase-3 and caspase-9 [40].

Costunolide is known to be present in the germacranolide series. It was first extracted from the roots of *Saussurea lappa* Clarke [47]. Costus lactone is mediated by stress, and exposure activates the (UPR) signaling pathway. In addition, costus lactone induces ROS production, while the antioxidant N-acetylcysteine (NAC) is effective. It blocked ER stress and apoptosis activation, induced A549 cell apoptosis, and showed antitumor activity [41]. Costus lactone involves in the activation of caspase-3 and induces SK-MES-1 cell apoptosis [42].

Pachydermic acid (PA) can simultaneously induce apoptosis of NCI-H23 and NCI-H460 lung cancer. In addition, PA inhibits the NCI-H23 growth and xenograft cancers with an inability to cause toxicity in the host cell, inhibits proliferation of cells in tumor xenograft tissues, induces tumor

cell apoptosis, and can also induce A549 cell apoptosis and destroy mitochondrial membrane potential [43, 44].

Polyphonic acid C (PPAC) is a triterpene compound derived from *Poria cocos*. PPAC induces cell apoptosis via the death receptor. In addition, the inhibition of the PI3-kinase/Akt signaling pathway and the enhancement of p53 activation indicate that this is an extra process to induce apoptosis [45].

Tubeimoside I (TBMS1), also known as tubeimoside A, is a triterpenoid isolated from the *Bolbostemma paniculatum* plant [48]. Tubeimoside I also has the ability to initiate apoptosis of lung cancer cells and destruct lysosome and mitochondrial pathways. One of its mechanisms is to induce DRP1-mediated mitochondrial breakage. It also disrupts lysosomal acidification by inhibiting V-ATPase, thereby blocking late-stage autophagic flux; this leads to the accumulation of reactive oxygen species (ROS). Cathepsin B

upregulates Bax-mediated mitochondrial outer membrane permeability [46].

#### 4. Autophagy and the Treatment of Lung Cancer

Cisplatin is an alkylating agent that has been approved for the treatment of ovarian, bladder, and lung cancers. However, accumulated evidence reveals the resistance to this platinum-containing drug, especially in lung cancer. The modulation of apoptosis-regulating proteins is widely accepted as a major molecular mechanism associated with chemoresistance. Cisplatin-induced DNA damage generally results in the activation of p53 and, depending on the extent of damage and induces a variety of cellular responses including autophagy, apoptosis, and senescence. In this study, cisplatin induced autophagy to similar extents in H460 cells where p53 activity had been nullified by CRISPR/Cas9 (H460 crp53) as in the parental p53 wt H460 (H460wt) NSCLC cells and confirmed that cisplatin induced two different functional forms of autophagy, protective autophagy in the H460crp53 cells, and nonprotective autophagy in the H460wt cells. This autophagic switch was associated with greater sensitivity to cisplatin in the p53 wt cells. Of particular relevance, with pharmacologic or genetic inhibition of the cytoprotective autophagy in the p53 crp cells, the temporal decline in cell viability in response to cisplatin became virtually identical to that in the p53 wt cells through increased susceptibility to the promotion of apoptosis.

Andrographolide (Andro) is an active compound dispersed in *Andrographis paniculata*. *Andrographis paniculata* is a kind of herbal medicinal drug being utilized in Asia as a traditional medicine to treat many diseases [23, 24]. At present, cisplatin is used as first-line treatments for lung cancer. But, the effectiveness of this chemotherapy has the limitation that it is drug resistant. At the same time, the Andrographolide drug can inhibit cisplatin-induced autophagy and enhance cisplatin-mediated apoptosis [49]. In addition, Andro promotes the activation of Akt/mTOR signal by downregulating PTEN and inhibiting autophagy, resensitizing drug-resistant cells. Combination therapy with cisplatin and andrographolide can significantly prevent the growth of drug-resistant cells [50]. Therefore, Andro provides an ideal autophagy inhibitor candidate for clinical applications.

The inhibition of autophagy was found to improve the chemotherapy and its efficacy [51] GA-induced inhibition of cell proliferation and apoptosis are enhanced by inhibiting autophagy of the JNK pathway [52]. Ivy saponins are triterpenoids, and the inducible accumulation of ROS enhances cisplatin cytotoxicity by blocking autophagic flux. The proliferation of ROS promotes the proapoptotic effects of cisplatin and paclitaxel, and the ROS scavenger can eliminate the synergistic impact of N-acetyl-L-cysteine [53]. The above contents are described, that is, the molecular mechanism of terpenoid natural Chinese medicine small molecules to intervene in tumor cell autophagy in the treatment of lung cancer (Table 4).

#### 5. Metastasis and Inhibition of Tumor Invasion

Metastasis linked with tumor invasion is a very complex phenomenon; multiple molecules affect tumor invasion-metastasis behavior from different aspects. Cell adhesion molecules are the key molecules to maintain the tissue structure, and they are also the main molecules that affect cell adhesion and motility [54]. The extracellular matrix is the tissue barrier for cancer cell invasion and metastasis. The enzymes responsible for degrading the extracellular matrix and their inhibitors are closely related to tumor metastasis [55]. Hepatocyte growth factor (HGF) and chemotactic factors are critical driving forces for tumor cell movement [56]. Promoting and inhibiting the balance between VEGF, PDGF, and TGF- $\beta$  also directly affect the blood supply of tumors, which further affect metastasis [57–59]. An in-depth analysis of these various factors will help us more deeply understand the mechanism of tumor metastasis.

Curcumin is a kind of sesquiterpenoids with pharmacological activity, and it is an essential bioactive component mainly from plants of the genus *Curcuma* [60, 61]. Studies have been conducted to extract zedoary turmeric essential oil (EO-CZ) by steam distillation and to test the growth of cancerous metastasis in mice. The experimental results show that EO-CZ has effects of antiproliferation on B16BL6 and SMMC-7721 cells. MMP-7 is the smallest member of the matrix metalloproteinase. Extracellular matrix and substrate together constitute the first barrier in tumor metastasis, and its degradation is tumor invasion, and it is the critical link of transfer [62].

Tumor cells can induce tumor lymphatic endothelial cell (LEC) proliferation and lymphangiogenesis by expressing VEGF-C and VEGF-D to increase the number of lymphatic vessels and promote tumors. Lymphatic metastasis of cells can also increase the permeability of lymphatic vessels and the pressure of tumor interstitium, which facilitates the entry of tumor cells into blood vessels [63, 64]. At the same time, LEC can express chemokines and interact with surrounding microenvironmental mediators [65]. It can attract tumor cells expressing the corresponding receptor and promote tumor lymph node metastasis [66]. Some studies have extracted ten compounds, including costanolactone, by chromatography using bioassay-guided fractionation methods, which can inhibit TR-LE cells [67].

Oridonin is a natural compound that derives from entkarate tetracyclic diterpene. It is first extracted from *Isodon* as a species [68]. It has the ability to inhibit the proliferation of H1688 cells and induce their apoptosis under high-dose treatment (20  $\mu$ mol/L). At the same time, oridonin (5 and 10  $\mu$ mol/L) inhibits the FAK-ERK1/2 signaling pathway without affecting cell proliferation and apoptosis [69].

Triptolide (TP) is a natural compound that has been isolated from the root of TP. Triptolide can change the expression of microRNA being utilized in cell movement and reduce the invasion of lung cancer cells. Triptolide reduces the expression of cell adhesion molecules, which leads to impaired downstream signal transduction and inhibits the formation of metastatic tumors in lung cancer mice injected with H358 cells [70]. In addition, TP combined



TABLE 4: The molecular mechanism of terpenoid natural Chinese medicine small molecules to intervene in tumor cell autophagy in the treatment of lung cancer.

Terpenoid natural TCM small molecules	Experimental model	Dose/concentration	Mechanism of action	Ref.
Andrographolide (Andro)	A549 and Lewis lung cancer (LLC) cells	Andro (0, 7.5, 15, or $\mu\text{M}$ ) for 0, 6, 12, or 24 h	Suppressed autophagy; Enhanced cisplatin-mediated apoptosis; Promoted the activation of the Akt/mTOR signaling by downregulating PTEN and suppressed autophagy;	[49]
Andrographolide (Andro)	A549 NSCLC cells	Andro (0, 7.5, 15, or $\mu\text{M}$ ) for 0, 6, 12, or 24 h	Resensitized the resistant cells to cisplatin-mediated apoptosis;	[50]
Glycyrrhetic acid (GA)	A549 and NCI-H1299 cells	GA (0, 40, and 60 $\mu\text{M}$ ) for 24 h	Induced cytoprotective autophagy; Activated the IRE1 $\alpha$ -JNK/c-Jun pathway;	[52]
Hederagenin	NCI-H1299 and NCI-H1975 cells	Hederagenin (0, 25, 50, and 75 $\mu\text{M}$ ) for 0, 2, 6, 12, or 24 h	Induced the increased autophagosomes; Upregulation of LC3-II and p62; Indicated the impairment of autophagic flux	[53]

with gefitinib can increase E-cadherin levels and inhibit cell proliferation. Therefore, a synergistic effect is produced to increase the resistance of A549 lung cancer cells to gefitinib and reverse the epithelial-mesenchymal transition (EMT) [71].

Astragaloside IV is the compound that has been extracted from *Astragalus membranaceus* [72]. AS-IV can inhibit the migration and invasion of A549, MMP-2, MMP-9, and integrin  $\beta$ 1 and significantly reduce the level of E-cadherin. In addition, AS-IV can also considerably decrease the TGF- $\beta$ 1, TNF- $\alpha$ , and IL-6 levels [73] (Table 5).

## 6. Tumor-Immune Mechanism and Immunotherapy

The immune system is directly connected with the occurrence and formation of tumors in the body. The cancer antigens abnormally expressed by cells in the process of carcinogenesis are the core of tumor immunodiagnosis, and the body's various antitumor immune mechanisms are the theoretical basis for tumor immunotherapy. The body's antitumor mechanism is mainly based on cellular immune mechanisms. Different immune cells play an essential role in antitumor immunity. Antibodies' complements and cytokines are also effective molecules of tumor immunity [74]. Although the body has an antitumor immune mechanism, tumor cells can also evade immune attack through various mechanisms, eventually causing tumors to occur and develop in the body and even inhibit the body's immune function. Researchers, through the in-depth understanding of the body's antitumor immune mechanism, immune intervention on tumor patients, used various methods to reverse the body's immune status and activate the body's antitumor immune effect to achieve the purpose of treating tumors and prolonging survival [75].

Atractylenolide III (ATL-III) has been shown to inhibit the Jak3/Stat3 pathway-dependent IDO activation triggered by IFN- $\gamma$ , and it is achieved by direct binding to the Jak3 protein [76]. IDO is also known to act as a checkpoint molecule that combines with cytotoxic T-lymphocyte antigen-4 and programmed cell death-1 to cause T-cell

suppression after tumor transformation, in order to be prevented by the immune system from initiating the attack on cancer [77]. Experiments prove that Astragaloside IV (AS-IV) inhibits tumor growth in vivo experiments [78]. Studies have found that lupeol inhibits the growth of THP-1 by inhibiting the production of plasminogen activator inhibitor-1 (PAI-1) in H1299 cells. In addition, lupeol can inhibit the polarization of M2 macrophages and lead to the reduction in Lewis lung carcinoma (LLC) cell migration [79] (Figure 1).

## 7. Combination Medication and MultiChannel antitumor

The use of multiple combinations as combined drugs to selectively target cancer cells has brought hope to a new generation of therapies (Figure 2).

**7.1. Betulinic Acid.** Betulinic acid (BA) can be considered ideal in treating lung cancer, and it provides a new treatment strategy for combination therapy. Studies have shown that the combination of 3 drugs (BA, ERKi, and HCQ) has a better therapeutic effect than a single treatment or therapy in xenotransplantation mouse models. Among them, betulinic acid, a natural compound, can inhibit cell proliferation and induce NSCLC cell apoptosis [80–84]. At the same time, the autophagy inhibition of hydroxychloroquine (HCQ) increased the response of lung cancer cells to the combination of BA and ERKi [80]. In addition, studies have proposed that betulinic acid (BA) and dichloroacetic acid (DCA) are chemically modified to synthesize a new combination drug Bet-CA, and its in vitro studies revealed that Bet-CA has apparent synergistic cytotoxicity to a broad spectrum of cancer cells, increased the production of reactive oxygen species (ROS), and promoted cells to undergo mitochondrial-mediated apoptosis; in vivo studies of Bet-CA showed tumor inhibition potential, and the clinically achievable dose will not produce any apparent toxicity [85].

Studies have suggested that BA treatment can induce apoptosis of paclitaxel-resistant human lung cancer H460 cells. In addition, BA can downregulate the expression of

TABLE 5: The molecular mechanism of terpenoid natural Chinese medicine small molecules to inhibit invasion and metastasis in the treatment of lung cancer.

Terpenoid natural TCM small molecules	Experimental model	Dose/concentration	Mechanism of action	Ref.
Essential oil of curcuma zedoaria (EO-CZ)	B16BL6 and SMMC-7721 cells; HUVEC (human umbilical vein endothelial cells); Sprout vessels of Sprague-Dawley male rat aortic ring;	EO-CZ (0, 5, 10, 20, 40, 80, and 120 $\mu\text{M}/\text{ml}$ ) for 48 h	Inhibit B16BL6 and SMMC-7721 cell proliferation; Inhibited CD34, MMP-2, and MMP-9;	[62]
Andrographis (Andro)	A549 NSCLC cells;	Andro (0, 1.0, 2.5, and 5.0 $\mu\text{M}$ ) for 24 h	Inhibited the migration and invasion of A549 cells; Inhibited MMP-7 but not MMP-2 or MMP-9; Suppressed on PI3K/Akt/AP-1 signaling pathway;	[63]
Dehydrocostus lactone (DL)	Temperature-sensitive rat lymphatic endothelial (TR-LE) cells;	DL (0.01, 0.1, and 0.5 $\mu\text{M}$ ) for 0, 6, 12, 24, or 48 h	Inhibition of the proliferation of TR-LE cells;	[67]
Oridonin	H1688 SCLC cells; BEAS-2B and HBE cells;	Oridonin (0, 2.5, 5, 10, 20, and 40 $\mu\text{M}$ ) for 24 or 48 h	Inhibited cell migration; Not-affected cell proliferation and apoptosis;	[69]
Triptolide (TP)	A549 NSCLC cells; H460 and H358 cells;	TP 10 nM for 48 h	Decreased migration and invasion of lung cancer cells; Inhibited the migration and invasion of A549;	[70]
Triptolide (TP)	A549 NSCLC cells;	TP (1, 2, 4, 8, 16, and 32 ng/ml) for 24, 36, or 48 h	Upregulated E-cadherin protein expression; Downregulated the MMP9, Snail, and vimentin expression levels; Inhibited the migration and invasion of A549;	[71]
Astagaloside IV (AS-IV)	A549 NSCLC cells.	AS-IV (0, 5, 10, and 20 $\mu\text{M}$ ) for 24 h	Decreased the levels of MMP-2, MMP-9, integrin $\beta$ 1, TGF- $\beta$ 1, TNF- $\alpha$ , and IL-6 levels; Related to the PKC- $\alpha$ -ERK1/2-NF- $\kappa$ B pathway.	[73]

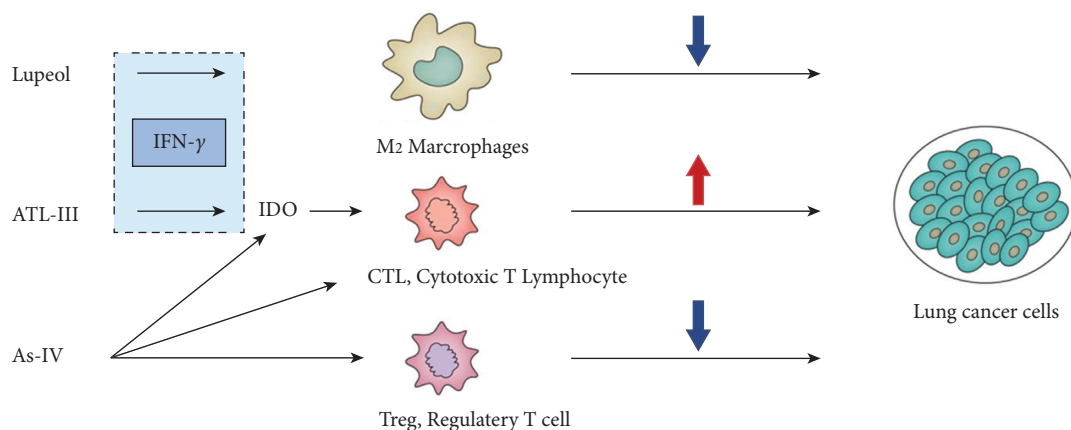


FIGURE 1: The influence of ATL-III, AS-IV, and lupeol on the immune mechanism of lung cancer.

Bcl-2 and upregulate the expression of Bcl-2-related X (Bax) [86]. Studies have also suggested that sorafenib combined with betulinic acid strongly induces apoptosis of different NSCLC cells. In addition, this combination is not toxic to human peripheral blood lymphocytes. Compared with using

two compounds alone, sorafenib combined with betulinic acid can induce apoptosis on different NSCLC cells (A549, H358, and A427) and eliminate the clonogenic activity [87, 88]. In vitro studies have shown that if, honokiol, ginsenoside Rh2, and betulinic acid are present in

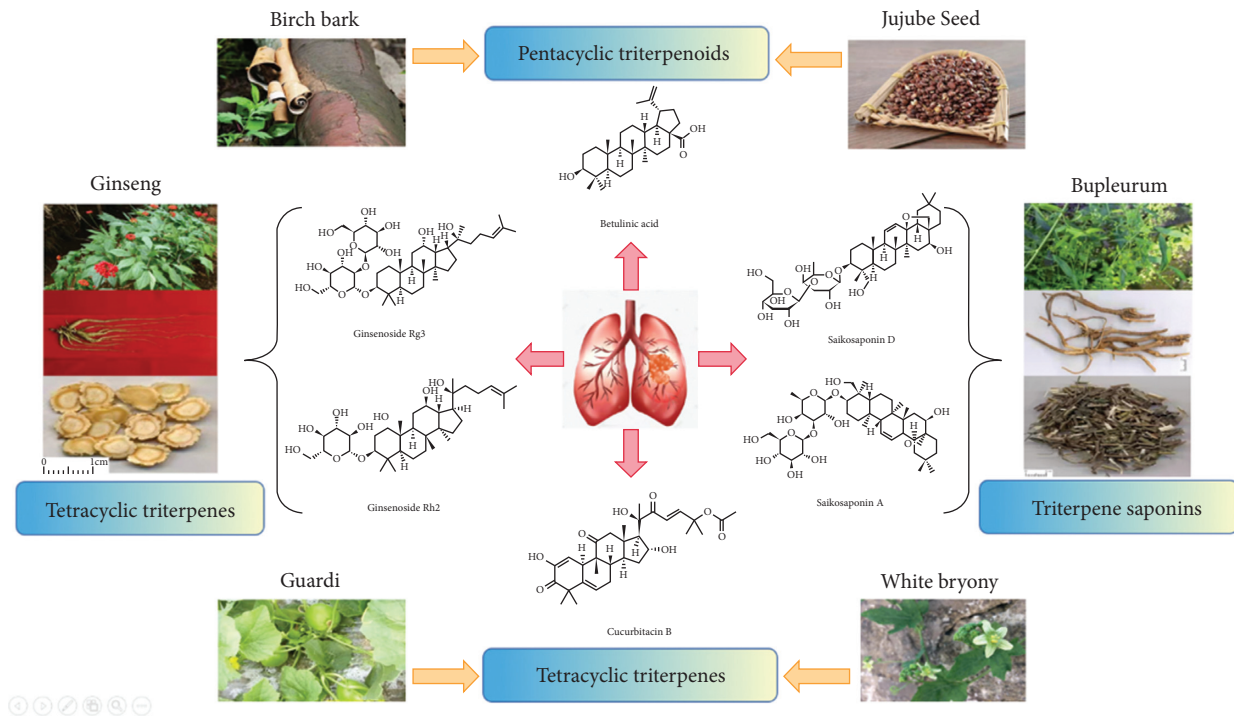


FIGURE 2: Herbal sources of terpenoid herbal compounds.

combination, they exhibit synergistic effects. Compared with the combination therapy group, the cisplatin group has obvious renal damage, and the combination therapy and the combination drug liposome therapy are safer [89].

**7.2. Saikosaponin D.** Saikosaponin D is a saponin extract extracted from *Bupleurum* (Umbelliferae), which can induce apoptosis to inhibit the proliferation of A549 [90]. Studies suggest that saikosaponin D inhibits the proliferation of lung cancer cells A549 (IC 50, 3.57  $\mu\text{M}$ ) and H1299 (IC 50, 8.46  $\mu\text{M}$ ) [91].

Saikosaponin A and saikosaponin D are two natural compounds derived from *Bupleurum*. At present, the combined application of natural small molecule compounds and chemotherapeutic drugs has become a research hotspot. Relevant studies have explored whether saikosaponins can sensitize the cytotoxicity of tumor cells induced by cisplatin. The results show that saikosaponin can make tumor cells [92].

In addition, studies have shown that saikosaponin D (SSD) and (EGFR-TKIs) gefitinib have an enhanced anti-tumor effect on NSCLC cells. It is related to the inhibition of the STAT3/Bcl-2 signaling pathway [93].

**7.3. Cucurbitacin B.** Cucurbitacin is a natural plant triterpenoid that belongs to the Cucurbitaceae. Cucurbitacin B (CuB) has antimetastatic, antiangiogenic, and antitumor immunity potential for NSCLC in vitro and in vivo [94, 95]. The expression of TPG and TSG can inhibit cell proliferation and induce apoptosis in NSCLC [96]. CUCs lead to the induction of programmed cell death, the inhibition of cell

migration, and cell invasion. It can also regulate the expression of cyclin B1 to induce apoptosis and G2/M cell cycle arrest, thereby interfering with lung cancer metastasis [97, 98].

In the combined application of CuB and chemotherapeutics, the new semisynthetic derivatives of CuB (DACE) and three chemotherapeutic drugs, namely, cisplatin (CIS), irinotecan (IRI), and paclitaxel (PAC), can induce apoptosis in A549 cells. It regulates the cell cycle, has a synergistic antiproliferative effect, and does not reduce the proliferation of nontumor lung cells (MRC-5) [99]. In addition, the semisynthetic derivative of CuB, DACE (2-deoxy-2-aminecucurbitacin E), and paclitaxel (PTX) showed potential in vitro synergistic antiproliferative effects in A549 cells [99]. In addition, CuB can reduce the proliferation of gefitinib-resistant (GR) PC9 cell lines by regulating the miR-17-5p/STAT3 axis [100].

**7.4. Ginsenoside.** Ginsenosides are one of the main components of ginseng and belong to typical terpenoids. Ginsenoside Rg3 reduces vascular endothelial growth factor expression and increases the ratio of CD4/CD8 T cells [101, 102]. We found that ginsenoside metabolite K (CK) can significantly enhance the expression and activity of p53 in the two lung cancer cell lines H460 and A549 induced by cisplatin and cooperate with cisplatin to inhibit tumor cell proliferation and induce apoptosis [103]. It decreased the antiapoptotic protein Bcl-2, which significantly increased the cells of NSCLC cell lines. Apoptosis substantially reduces the migration of NSCLC cells [104]. The combination therapy of ginsenoside Rg3 and gemcitabine can dramatically reduce the expression of VEGF and

MVD, blood flow, and PSV signals in tumors, inhibit tumor growth, and prolong survival [105]. In addition, ginsenoside Rg18 can inhibit tumor cell proliferation by mediating G1 phase block and intracellular ROS production in A549 human NSCLC cells, and p38, JNK, and NF- $\kappa$ B/p65 [106, 107].

## 8. Discussion

In recent years, the application of small molecular compounds of natural Chinese medicine in antitumor research has gradually become a new focus of international cancer research. With the continuous in-depth analysis of the anticancer activity of natural Chinese medicines, many biologically active compounds derived from traditional Chinese medicines can be used to treat NSCLC. The role is gradually recognized. At present, plant-derived anticancer drugs account for about 32% of the total anticancer drugs, of which terpenoids account for a large proportion. Researchers use small molecular compounds of traditional Chinese medicine to influence the cell cycle, induce cell apoptosis, promote autophagy, inhibit tumor cell invasion and metastasis, improve tumor-immune microenvironment, and other ways to achieve tumor treatment and prolong patient survival. Even the combination of natural products and traditional drugs shows more vigorous anticancer activity and lower toxic and side effects than single chemotherapeutic drugs and targeted drug treatments. The application of Chinese herbal medicine with permanent history and economic benefits to cancer treatment, including lung cancer, may also bring new opportunities and challenges to cancer treatment. If traditional Chinese medicine can effectively reduce the cost of cancer treatment, improve the effect of cancer treatment, and apply it to the clinic, the cancer cure rate in China and even the world may be effectively controlled.

The multicomponent, multitarget, and multipathway characteristics of the active ingredients of traditional Chinese medicine also cast a veil of mystery on the study of the biological activity of conventional Chinese medicine monomers. In the future, we need to separate and extract effective small molecule compounds from traditional Chinese medicine by different scientific means so as to apply them to the treatment of tumors. There are still many challenges to overcome in clinical treatment. However, it is undeniable that in exploring new anticancer drugs, the combination of natural anticancer active ingredients of traditional Chinese medicine combined with chemotherapy and targeted therapy may become a unique choice for the treatment of patients with NSCLC.

## Data Availability

The data used to support this study are available from the corresponding author upon request.

## Conflicts of Interest

The authors declare that they have no conflicts of interest.

## Authors' Contributions

Heng Sun and Lijia Zhang contributed equally.

## Acknowledgments

This paper was funded by the Heilongjiang Applied Technology Research and Development Plan Project named "Based on the academic thought of Professor Duan Fujin, a master of Chinese medicine, on the treatment of gastrointestinal toxic and side effects after radiotherapy and chemotherapy for lung cancer with spleen deficiency" (no. GA19C109), Exploration on the operation mode of "one body and two wings" of provincial TCM tumor diagnosis and treatment center (no. 2020GSP07), Clinical observation of Zhen wu decoction plus dilong combined with cisplatin in the treatment of malignant pleural effusion (no. 2019MS07), and Effect of Zhen wu decoction plus dilong combined with cisplatin on the levels of IL-17 and VEGF in the treatment of malignant pleural effusion (no. ZHY2020-109).

## References

- [1] F. Nasim, B. F. Sabath, and G. A. Eapen, "Lung cancer," *Medical Clinics of North America*, vol. 103, no. 3, pp. 463–473, 2019.
- [2] W. Wu, X. Wang, C. Shan, Y. Li, and F. Li, "Minichromosome maintenance protein 2 correlates with the malignant status and regulates proliferation and cell cycle in lung squamous cell carcinoma," *OncoTargets and Therapy*, vol. 11, pp. 5025–5034, 2018.
- [3] I. Naz, S. Ramchandani, M. R. Khan, M. H. Yang, and K. S. Ahn, "Anticancer potential of raddeanin A, a natural triterpenoid isolated from anemone raddeana regel," *Molecules*, vol. 25, no. 5, p. 1035, 2020.
- [4] M. Liu, X. Wang, H. Li et al., "The effect of apatinib combined with chemotherapy or targeted therapy on non-small cell lung cancer in vitro and vivo," *Thoracic Cancer*, vol. 10, no. 10, pp. 1868–1878, 2019.
- [5] R. R. Ramsay, M. R. Popovic-Nikolic, K. Nikolic, E. Uliassi, and M. L. Bolognesi, "A perspective on multi-target drug discovery and design for complex diseases," *Clinical and Translational Medicine*, vol. 7, no. 1, p. 3, 2018.
- [6] M. Yumura, T. Nagano, and Y. Nishimura, "Novel multi-target therapies for lung cancer and respiratory disease," *Molecules*, vol. 25, no. 17, p. 3987, 2020.
- [7] C. Wen, G. Xu, S. He et al., "Screening circular RNAs related to acquired gefitinib resistance in non-small cell lung cancer cell lines," *Journal of Cancer*, vol. 11, no. 13, pp. 3816–3826, 2020.
- [8] K. Wu, C. Guo, and R. Li, "Clinical characterization of icotinib-induced chemoresistance in erlotinib-treated lung adenocarcinoma patient with EGFR mutations," *Medicine*, vol. 98, no. 18, p. e15489, 2019.
- [9] L. Zhong, Y. Li, L. Xiong et al., "Small molecules in targeted cancer therapy: advances, challenges, and future perspectives," *Signal Transduction and Targeted Therapy*, vol. 6, no. 1, p. 201, 2021.
- [10] H. Luo, C. T. Vong, H. Chen et al., "Naturally occurring anticancer compounds: shining from Chinese herbal medicine," *Chinese Medicine*, vol. 14, no. 1, p. 48, 2019.
- [11] L.-Q. Wan, Y. Tan, M. Jiang, and Q. Hua, "The prognostic impact of traditional Chinese medicine monomers on

- tumor-associated macrophages in non-small cell lung cancer,” *Chinese Journal of Natural Medicines*, vol. 17, no. 10, pp. 729–737, 2019.
- [12] P. Gutiérrez-Escribano and P. Nurse, “A single cyclin-CDK complex is sufficient for both mitotic and meiotic progression in fission yeast,” *Nature Communications*, vol. 6, no. 1, p. 6871, 2015.
  - [13] D. Lane, “Development of CDK inhibitors as cancer therapeutics,” *Breast Cancer Research*, vol. 7, no. S2, p. 38, 2005.
  - [14] S. Zhao, X.-f. Yang, D.-f. Shen et al., “The down-regulated ING5 expression in lung cancer: a potential target of gene therapy,” *Oncotarget*, vol. 7, no. 34, pp. 54596–54615, 2016.
  - [15] Y.-H. Zhong, H.-Z. Cheng, H. Peng, S.-C. Tang, and P. Wang, “Heat shock factor 2 is associated with the occurrence of lung cancer by enhancing the expression of heat shock proteins,” *Oncology Letters*, vol. 12, no. 6, pp. 5106–5112, 2016.
  - [16] X. Luo, W. Luo, C. Lin, L. Zhang, and Y. Li, “Andrographolide inhibits proliferation of human lung cancer cells and the related mechanisms,” *International Journal of Clinical and Experimental Medicine*, vol. 7, no. 11, pp. 4220–4225, 2014.
  - [17] W. Luo, Y. Liu, J. Zhang, X. Luo, C. Lin, and J. Guo, “Andrographolide inhibits the activation of NF- $\kappa$ B and MMP-9 activity in H3255 lung cancer cells,” *Experimental and therapeutic medicine*, vol. 6, no. 3, pp. 743–746, 2013.
  - [18] R.-Y. Huang, Y.-L. Chu, Q.-C. Huang et al., “18 $\beta$ -Glycyrrhetic acid suppresses cell proliferation through inhibiting thromboxane synthase in non-small cell lung cancer,” *PLoS One*, vol. 9, no. 4, p. e93690, 2014.
  - [19] J. Zhu, M. Chen, N. Chen et al., “Glycyrrhetic acid induces G1-phase cell cycle arrest in human non-small cell lung cancer cells through endoplasmic reticulum stress pathway,” *International Journal of Oncology*, vol. 46, no. 3, pp. 981–988, 2015.
  - [20] A. C. Corveloni, S. C. Semprebon, A. Baranoski, B. I. Biazzi, T. A. Zanetti, and M. S. Mantovani, “Carnosic acid exhibits antiproliferative and proapoptotic effects in tumoral NCI-H460 and nontumoral IMR-90 lung cells,” *Journal of Toxicology and Environmental Health. Part A*, vol. 83, no. 10, pp. 412–421, 2020.
  - [21] S. Xiao, Z. Lin, X. Wang, J. Lu, and Y. Zhao, “Synthesis and cytotoxicity evaluation of panaxadiol derivatives,” *Chemistry and Biodiversity*, vol. 17, no. 1, p. e1900516, 2020.
  - [22] C.-S. He, Y.-C. Liu, Z.-P. Xu, P.-C. Dai, X.-W. Chen, and D.-H. Jin, “Astragaloside IV enhances cisplatin chemosensitivity in non-small cell lung cancer cells through inhibition of B7-H3,” *Cellular Physiology and Biochemistry*, vol. 40, no. 5, pp. 1221–1229, 2016.
  - [23] J.-J. Zhang, T.-T. Gao, Y. Wang et al., “Andrographolide exerts significant antidepressant-like effects involving the hippocampal BDNF system in mice,” *International Journal of Neuropsychopharmacology*, vol. 22, no. 9, pp. 585–600, 2019.
  - [24] A. Banerjee, V. Banerjee, S. Czinn, and T. Blanchard, “Increased reactive oxygen species levels cause ER stress and cytotoxicity in andrographolide treated colon cancer cells,” *Oncotarget*, vol. 8, no. 16, pp. 26142–26153, 2017.
  - [25] F. Rauchensteiner, Y. Matsumura, Y. Yamamoto, S. Yamaji, and T. Tani, “Analysis and comparison of Radix Glycyrrhizae (licorice) from Europe and China by capillary-zone electrophoresis (CZE),” *Journal of Pharmaceutical and Biomedical Analysis*, vol. 38, no. 4, pp. 594–600, 2005.
  - [26] Z. Lin, S. Qiu, A. Wufuer, and L. Shum, “Simultaneous determination of glycyrrhizin, a marker component in Radix Glycyrrhizae, and its major metabolite glycyrrhetic acid in human plasma by LC-MS/MS,” *Journal of Chromatography B*, vol. 814, no. 2, pp. 201–207, 2005.
  - [27] M. V. Barni, M. J. Carlini, E. G. Cafferata, L. Puricelli, and S. Moreno, “Carnosic acid inhibits the proliferation and migration capacity of human colorectal cancer cells,” *Oncology Reports*, vol. 27, no. 4, pp. 1041–1048, 2012.
  - [28] K. Dhuna, M. Felgate, S. M. Bidula et al., “Ginsenosides act as positive modulators of P2X4 receptors,” *Molecular Pharmacology*, vol. 95, no. 2, pp. 210–221, 2019.
  - [29] Q. Mao, C. Chen, H. Liang, S. Zhong, X. Cheng, and L. Li, “Astragaloside IV inhibits excessive mesangial cell proliferation and renal fibrosis caused by diabetic nephropathy via modulation of the TGF- $\beta$ 1/Smad/miR-192 signaling pathway,” *Experimental and therapeutic medicine*, vol. 18, pp. 3053–3061, 2019.
  - [30] H. Schenker, M. Büttner-Herold, R. Fietkau, and L. V. Distel, “Cell-in-cell structures are more potent predictors of outcome than senescence or apoptosis in head and neck squamous cell carcinomas,” *Radiation Oncology*, vol. 12, no. 1, 2017.
  - [31] X. Yan, F. Li, I. Dozmorov et al., “External Qi of Yan Xin Qigong induces cell death and gene expression alterations promoting apoptosis and inhibiting proliferation, migration and glucose metabolism in small-cell lung cancer cells,” *Molecular and Cellular Biochemistry*, vol. 363, no. 1–2, pp. 245–255, 2012.
  - [32] Y. Cui, L. Li, Z. Li et al., “Dual effects of targeting S100A11 on suppressing cellular metastatic properties and sensitizing drug response in gastric cancer,” *Cancer Cell International*, vol. 21, no. 1, 2021.
  - [33] P. Shi, C. Chen, X. Li, Z. Wei, Z. Liu, and Y. Liu, “MicroRNA-124 suppresses cell proliferation and invasion of triple negative breast cancer cells by targeting STAT3,” *Molecular Medicine Reports*, vol. 19, no. 5, pp. 3667–3675, 2019.
  - [34] L. F. Al-Alem, A. T. Baker, U. M. Pandya, E. L. Eisenhauer, and B. R. Rueda, “Understanding and targeting apoptotic pathways in ovarian cancer,” *Cancers*, vol. 11, no. 11, p. 1631, 2019.
  - [35] F. Liu, H. A. Kalpage, D. Wang et al., “Cotargeting of mitochondrial complex I and bcl-2 shows antileukemic activity against acute myeloid leukemia cells reliant on oxidative phosphorylation,” *Cancers*, vol. 12, no. 9, p. 2400, 2020.
  - [36] X. Hu, J. Moisan, K. Majchrzak et al., “RORgamma agonists enhance survival and memory of type 17 T cells and improve anti-tumor activity,” *Journal for Immunotherapy of Cancer*, vol. 3, no. S2, 2015.
  - [37] S. Forster and R. Radpour, “Molecular immunotherapy: promising approach to treat metastatic colorectal cancer by targeting resistant cancer cells or cancer stem cells,” *Frontiers in oncology*, vol. 10, p. 569017, 2020.
  - [38] A. Guha, D. Ahuja, S. Das Mandal et al., “Integrated regulation of HuR by translation repression and protein degradation determines pulsatile expression of p53 under DNA damage,” *iScience*, vol. 15, pp. 342–359, 2019.
  - [39] H. Liu, Y. Zhu, T. Zhang et al., “Anti-tumor effects of atractylenolide I isolated from *Atractylodes macrocephala* in human lung carcinoma cell lines,” *Molecules*, vol. 18, no. 11, pp. 13357–13368, 2013.
  - [40] T.-H. Kang, J.-Y. Bang, M.-H. Kim, I.-C. Kang, H.-M. Kim, and H.-J. Jeong, “Atractylenolide III, a sesquiterpenoid, induces apoptosis in human lung carcinoma A549 cells via mitochondria-mediated death pathway,” *Food and Chemical Toxicology*, vol. 49, no. 2, pp. 514–519, 2011.



- [41] Z. Wang, X. Zhao, and X. Gong, "Costunolide induces lung adenocarcinoma cell line A549 cells apoptosis through ROS (reactive oxygen species)-mediated endoplasmic reticulum stress," *Cell Biology International*, vol. 40, no. 3, pp. 289–297, 2016.
- [42] P. Hua, G. Zhang, Y. Zhang et al., "Costunolide induces G1/S phase arrest and activates mitochondrial-mediated apoptotic pathways in SK-MES 1 human lung squamous carcinoma cells," *Oncology Letters*, vol. 11, no. 4, pp. 2780–2786, 2016.
- [43] J. Ma, J. Liu, C. Lu, and D. Cai, "Pachymic acid induces apoptosis via activating ROS-dependent JNK and ER stress pathways in lung cancer cells," *Cancer Cell International*, vol. 15, no. 1, p. 78, 2015.
- [44] H. Ling, X. Jia, Y. Zhang et al., "Pachymic acid inhibits cell growth and modulates arachidonic acid metabolism in nonsmall cell lung cancer A549 cells," *Molecular Carcinogenesis*, vol. 49, 2010.
- [45] H. Ling, L. Zhou, X. Jia, L. A. Gapter, R. Agarwal, and K.-y. Ng, "Polyporenic acid C induces caspase-8-mediated apoptosis in human lung cancer A549 cells," *Molecular Carcinogenesis*, vol. 48, no. 6, pp. 498–507, 2009.
- [46] K. Wang, Y. Zhan, B. Chen et al., "Tubeimoside I-induced lung cancer cell death and the underlying crosstalk between lysosomes and mitochondria," *Cell Death & Disease*, vol. 11, no. 8, p. 708, 2020.
- [47] D. Y. Kim and B. Y. Choi, "Costunolide-A bioactive sesquiterpene lactone with diverse therapeutic potential," *International Journal of Molecular Sciences*, vol. 20, no. 12, p. 2926, 2019.
- [48] J. Du, Z. Dong, L. Tan et al., "Tubeimoside I inhibits cell proliferation and induces a partly disrupted and cytoprotective autophagy through rapidly hyperactivation of MEK1/2-ERK1/2 cascade via promoting PTP1B in melanoma," *Frontiers in cell and developmental biology*, vol. 8, p. 607757, 2020.
- [49] D. Yuwen, S. Mi, Y. Ma et al., "Andrographolide enhances cisplatin-mediated anticancer effects in lung cancer cells through blockade of autophagy," *Anti-Cancer Drugs*, vol. 28, no. 9, pp. 967–976, 2017.
- [50] S. Mi, G. Xiang, D. Yuwen et al., "Inhibition of autophagy by andrographolide resensitizes cisplatin-resistant non-small cell lung carcinoma cells via activation of the Akt/mTOR pathway," *Toxicology and Applied Pharmacology*, vol. 310, pp. 78–86, 2016.
- [51] M. R. Alotaibi, H. M. As Sobeai, F. A. Alaqil et al., "A newly synthesized platinum-based compound (PBC-II) increases chemosensitivity of HeLa ovarian cancer cells via inhibition of autophagy," *Saudi Pharmaceutical Journal: The Official Publication of the Saudi Pharmaceutical Society*, vol. 27, no. 8, pp. 1203–1209, 2019.
- [52] Z.-H. Tang, L.-L. Zhang, T. Li et al., "Glycyrrhetic acid induces cytoprotective autophagy via the inositol-requiring enzyme 1 $\alpha$ -c-Jun N-terminal kinase cascade in non-small cell lung cancer cells," *Oncotarget*, vol. 6, no. 41, pp. 43911–43926, 2015.
- [53] K. Wang, X. Liu, Q. Liu et al., "Hederagenin potentiated cisplatin- and paclitaxel-mediated cytotoxicity by impairing autophagy in lung cancer cells," *Cell Death & Disease*, vol. 11, no. 8, p. 611, 2020.
- [54] H.-H. Chuang, P.-H. Wang, S.-W. Niu et al., "Inhibition of FAK signaling elicits lamin A/C-associated nuclear deformity and cellular senescence," *Frontiers in oncology*, vol. 9, 2019.
- [55] H. Liu, T. Lu, G.-J. Kremers, A. L. B. Seynhaeve, and T. L. M. Ten Hagen, "A microcarrier-based spheroid 3D invasion assay to monitor dynamic cell movement in extracellular matrix," *Biological Procedures Online*, vol. 22, 2020.
- [56] E. Q. X. Mulcahy, R. R. Colón, and R. Abounader, "HGF/MET signaling in malignant brain tumors," *International Journal of Molecular Sciences*, vol. 21, no. 20, p. 7546, 2020.
- [57] M. Labelle, S. Begum, and R. O. Hynes, "Direct signaling between platelets and cancer cells induces an epithelial-mesenchymal-like transition and promotes metastasis," *Cancer Cell*, vol. 20, no. 5, pp. 576–590, 2011.
- [58] D. Schumacher, B. Strilic, K. K. Sivaraj, N. Wettschreck, and S. Offermanns, "Platelet-derived nucleotides promote tumor-cell transendothelial migration and metastasis via P2Y2 receptor," *Cancer Cell*, vol. 24, no. 1, pp. 130–137, 2013.
- [59] S. Takagi, A. Takemoto, M. Takami, T. Oh-hara, and N. Fujita, "Platelets promote osteosarcoma cell growth through activation of the platelet-derived growth factor receptor-Akt signaling axis," *Cancer Science*, vol. 105, no. 8, pp. 983–988, 2014.
- [60] A. Takemoto, M. Okitaka, S. Takagi et al., "A critical role of platelet TGF- $\beta$  release in podoplanin-mediated tumour invasion and metastasis," *Scientific Reports*, vol. 7, no. 1, p. 42186, 2017.
- [61] W. Wei, A. Rasul, A. Sadiqa et al., "Curcumol: from plant roots to cancer roots," *International Journal of Biological Sciences*, vol. 15, no. 8, pp. 1600–1609, 2019.
- [62] W. Chen, Y. Lu, M. Gao, J. Wu, A. Wang, and R. Shi, "Anti-angiogenesis effect of essential oil from *Curcuma zedoaria* in vitro and in vivo," *Journal of Ethnopharmacology*, vol. 133, no. 1, pp. 220–226, 2011.
- [63] Y.-C. Lee, H.-H. Lin, C.-H. Hsu, C.-J. Wang, T.-A. Chiang, and J.-H. Chen, "Inhibitory effects of andrographolide on migration and invasion in human non-small cell lung cancer A549 cells via down-regulation of PI3K/Akt signaling pathway," *European Journal of Pharmacology*, vol. 632, no. 1–3, pp. 23–32, 2010.
- [64] B. Sitohy, S. Chang, T. E. Sciuto et al., "Early actions of anti-vascular endothelial growth factor/vascular endothelial growth factor receptor drugs on angiogenic blood vessels," *American Journal of Pathology*, vol. 187, no. 10, pp. 2337–2347, 2017.
- [65] J.-Y. Chen, Y.-S. Lai, P.-Y. Chu, S.-H. Chan, L.-H. Wang, and W.-C. Hung, "Cancer-derived VEGF-C increases chemokine production in lymphatic endothelial cells to promote CXCR2-dependent cancer invasion and MDSC recruitment," *Cancers*, vol. 11, no. 8, p. 1120, 2019.
- [66] T. Iwasaki, Y. Takeda, K. Maruyama et al., "Deletion of tetraspanin CD9 diminishes lymphangiogenesis in vivo and in vitro," *Journal of Biological Chemistry*, vol. 288, no. 4, pp. 2118–2131, 2013.
- [67] D. Jeong, K. Watari, T. Shirouzu et al., "Studies on lymphangiogenesis inhibitors from Korean and Japanese crude drugs," *Biological and Pharmaceutical Bulletin*, vol. 36, no. 1, pp. 152–157, 2013.
- [68] D. Li, T. Han, J. Liao et al., "Oridonin, a promising ent-kaurane diterpenoid lead compound," *International Journal of Molecular Sciences*, vol. 17, no. 9, p. 1395, 2016.
- [69] L. Xu, Y. Bi, Y. Xu et al., "Oridonin inhibits the migration and epithelial-to-mesenchymal transition of small cell lung cancer cells by suppressing FAK-ERK1/2 signalling pathway," *Journal of Cellular and Molecular Medicine*, vol. 24, no. 8, pp. 4480–4493, 2020.

- [70] T. A. Reno, J. Y. Kim, and D. J. Raz, "Triptolide inhibits lung cancer cell migration, invasion, and metastasis," *The Annals of Thoracic Surgery*, vol. 100, no. 5, pp. 1817–1825, 2015.
- [71] F. Li, H. Cui, X. Jin, X. Gong, W. Wang, and J. Wang, "Triptolide inhibits epithelial-mesenchymal transition and induces apoptosis in gefitinib-resistant lung cancer cells," *Oncology Reports*, vol. 43, no. 5, pp. 1569–1579, 2020.
- [72] J. Zhang, C. Wu, L. Gao, G. Du, and X. Qin, "Astragaloside IV derived from *Astragalus membranaceus*: a research review on the pharmacological effects," *Pharmacological Advances in Natural Product Drug Discovery*, vol. 87, pp. 89–112, 2020.
- [73] X. Cheng, J. Gu, M. Zhang et al., "Astragaloside IV inhibits migration and invasion in human lung cancer A549 cells via regulating PKC- $\alpha$ -ERK1/2-NF- $\kappa$ B pathway," *International Immunopharmacology*, vol. 23, no. 1, pp. 304–313, 2014.
- [74] R. Thibaut, P. Bost, I. Milo et al., "Bystander IFN- $\gamma$  activity promotes widespread and sustained cytokine signaling altering the tumor microenvironment," *Nature cancer*, vol. 1, no. 3, pp. 302–314, 2020.
- [75] A. Anichini, V. E. Perotti, F. Sgambelluri, and R. Mortarini, "Immune escape mechanisms in non small cell lung cancer," *Cancers*, vol. 12, p. 3605, 2020.
- [76] J.-b. Liu, D. Chen, T.-t. Bao, F.-t. Fan, and C. Yu, "The anticancer effects of atractylenolide III associate with the downregulation of jak3/stat3-dependent Ido expression," *Frontiers in Pharmacology*, vol. 10, p. 1505, 2020.
- [77] D. H. Munn and A. L. Mellor, "Indoleamine 2,3 dioxygenase and metabolic control of immune responses," *Trends Immunology*, vol. 34, no. 3, pp. 137–143, 2013.
- [78] A. Zhang, Y. Zheng, Z. Que et al., "Astragaloside IV inhibits progression of lung cancer by mediating immune function of Tregs and CTLs by interfering with Ido," *Journal of Cancer Research and Clinical Oncology*, vol. 140, no. 11, pp. 1883–1890, 2014.
- [79] H.-J. Park, G.-Y. Chi, Y.-H. Choi, and S.-H. Park, "Lupeol suppresses plasminogen activator inhibitor-1-mediated macrophage recruitment and attenuates M2 macrophage polarization," *Biochemical and Biophysical Research Communications*, vol. 527, no. 4, pp. 889–895, 2020.
- [80] C.-Y. Sun, D. Cao, Q.-N. Ren et al., "Combination treatment with inhibitors of ERK and autophagy enhances antitumor activity of betulinic acid in non-small-cell lung cancer in vivo and in vitro," *Frontiers in Pharmacology*, vol. 12, p. 684243, 2021.
- [81] H. Kommera, G. N. Kaluderović, S. Dittrich et al., "Carbamate derivatives of betulinic acid and betulin with selective cytotoxic activity," *Bioorganic & Medicinal Chemistry Letters*, vol. 20, no. 11, pp. 3409–3412, 2010.
- [82] W. Rzeski, A. Stepulak, M. Szymański et al., "Betulinic acid decreases expression of bcl-2 and cyclin D1, inhibits proliferation, migration and induces apoptosis in cancer cells," *Naunyn-Schmiedeberg's Archives of Pharmacology*, vol. 374, no. 1, pp. 11–20, 2006.
- [83] T.-I. Hsu, M.-C. Wang, S.-Y. Chen et al., "Betulinic acid decreases specificity protein 1 (Sp1) level via increasing the sumoylation of sp1 to inhibit lung cancer growth," *Molecular Pharmacology*, vol. 82, no. 6, pp. 1115–1128, 2012.
- [84] J. H. Kessler, F. B. Mullauer, G. M. de Roo, and J. P. Medema, "Broad in vitro efficacy of plant-derived betulinic acid against cell lines derived from the most prevalent human cancer types," *Cancer Letters*, vol. 251, no. 1, pp. 132–145, 2007.
- [85] S. Saha, M. Ghosh, and S. K. Dutta, "A potent tumoricidal co-drug "Bet-CA"—an ester derivative of betulinic acid and dichloroacetate selectively and synergistically kills cancer cells," *Scientific Reports*, vol. 5, no. 1, p. 7762, 2015.
- [86] X. K. Zhan, J. L. Li, S. Zhang, P. Y. Xing, and M. F. Xia, "Betulinic acid exerts potent antitumor effects on paclitaxel-resistant human lung carcinoma cells (H460) via G2/M phase cell cycle arrest and induction of mitochondrial apoptosis," *Oncology letters*, vol. 16, no. 3, pp. 3628–3634, 2018.
- [87] Q. Li, Y. Li, X. Wang et al., "Co-treatment with ginsenoside Rh2 and betulinic acid synergistically induces apoptosis in human cancer cells in association with enhanced caspase-8 activation, bax translocation, and cytochrome c release," *Molecular Carcinogenesis*, vol. 50, no. 10, pp. 760–769, 2011.
- [88] X. Jin, Q. Yang, N. Cai, and Z. Zhang, "A cocktail of betulinic acid, parthenolide, honokiol and ginsenoside Rh2 in liposome systems for lung cancer treatment," *Nanomedicine*, vol. 15, no. 1, pp. 41–54, 2020.
- [89] Y.-L. Hsu, P.-L. Kuo, and C.-C. Lin, "The proliferative inhibition and apoptotic mechanism of Saikosaponin D in human non-small cell lung cancer A549 cells," *Life Sciences*, vol. 75, no. 10, pp. 1231–1242, 2004.
- [90] S. Wu, W. Chen, K. Liu et al., "Saikosaponin D inhibits proliferation and induces apoptosis of non-small cell lung cancer cells by inhibiting the STAT3 pathway," *Journal of International Medical Research*, vol. 48, no. 9, p. 030006052093716, 2020.
- [91] X. Chen, C. Liu, R. Zhao et al., "Synergetic and antagonistic molecular effects mediated by the feedback loop of p53 and JNK between saikosaponin D and SP600125 on lung cancer A549 cells," *Molecular Pharmaceutics*, vol. 15, no. 11, pp. 4974–4984, 2018.
- [92] Q. Wang, X.-l. Zheng, L. Yang et al., "Reactive oxygen species-mediated apoptosis contributes to chemosensitization effect of saikosaponins on cisplatin-induced cytotoxicity in cancer cells," *Journal of Experimental & Clinical Cancer Research*, vol. 29, no. 1, p. 159, 2010.
- [93] J.-c. Tang, F. Long, J. Zhao et al., "The effects and mechanisms by which saikosaponin-D enhances the sensitivity of human non-small cell lung cancer cells to gefitinib," *Journal of Cancer*, vol. 10, no. 26, pp. 6666–6672, 2019.
- [94] S. Shukla, S. Sinha, S. Khan et al., "Cucurbitacin B inhibits the stemness and metastatic abilities of NSCLC via down-regulation of canonical Wnt/ $\beta$ -catenin signaling axis," *Scientific Reports*, vol. 6, no. 1, p. 21860, 2016.
- [95] P. Lu, B. Yu, and J. Xu, "Cucurbitacin B regulates immature myeloid cell differentiation and enhances antitumor immunity in patients with lung cancer," *Cancer Biotherapy and Radiopharmaceutics*, vol. 27, no. 8, pp. 495–503, 2012.
- [96] S. Shukla, S. Khan, S. Kumar et al., "Cucurbitacin B alters the expression of tumor-related genes by epigenetic modifications in NSCLC and inhibits NNK-induced lung tumorigenesis," *Cancer Prevention Research*, vol. 8, no. 6, pp. 552–562, 2015.
- [97] I. T. Silva, F. C. Geller, L. Persich et al., "Cytotoxic effects of natural and semisynthetic cucurbitacins on lung cancer cell line A549," *Investigational New Drugs*, vol. 34, no. 2, pp. 139–148, 2016.
- [98] J. Guo, G. Wu, J. Bao, W. Hao, J. Lu, and X. Chen, "Cucurbitacin B induced ATM-mediated DNA damage causes G2/M cell cycle arrest in a ROS-dependent manner," *PLoS One*, vol. 9, no. 2, p. e88140, 2014.
- [99] L. L. Marostica, I. T. Silva, J. M. Kratz et al., "Synergistic antiproliferative effects of a new cucurbitacin B derivative

- and chemotherapy drugs on lung cancer cell line A549,” *Chemical Research in Toxicology*, vol. 28, no. 10, pp. 1949–1960, 2015.
- [100] B. Yu, L. Zheng, H. Tang, W. Wang, and Y. Lin, “Cucurbitacin B enhances apoptosis in gefitinib resistant non-small cell lung cancer by modulating the miR-17-5p/STAT3 axis,” *Molecular Medicine Reports*, vol. 24, no. 4, p. 710, 2021.
- [101] T. Xu, Z. Jin, Y. Yuan et al., “Ginsenoside Rg3 serves as an adjuvant chemotherapeutic agent and VEGF inhibitor in the treatment of non-small cell lung cancer: a meta-analysis and systematic review,” *Evidence-based Complementary and Alternative Medicine*, vol. 2016, Article ID 7826753, 14 pages, 2016.
- [102] Z. Peng, W. W. Wu, and P. Yi, “The efficacy of ginsenoside Rg3 combined with first-line chemotherapy in the treatment of advanced non-small cell lung cancer in China: a systematic review and meta-analysis of randomized clinical trials,” *Frontiers in Pharmacology*, vol. 11, p. 630825, 2021.
- [103] Y. Li, T. Zhou, C. Ma, W. Song, J. Zhang, and Z. Yu, “Ginsenoside metabolite compound K enhances the efficacy of cisplatin in lung cancer cells,” *Journal of Thoracic Disease*, vol. 7, no. 3, pp. 400–406, 2015.
- [104] Y. Dai, W. Wang, Q. Sun, and J. Tuohayi, “Ginsenoside Rg3 promotes the antitumor activity of gefitinib in lung cancer cell lines,” *Experimental and Therapeutic Medicine*, vol. 17, no. 1, pp. 953–959, 2019.
- [105] T.-G. Liu, Y. Huang, D.-D. Cui et al., “Inhibitory effect of ginsenoside Rg3 combined with gemcitabine on angiogenesis and growth of lung cancer in mice,” *BMC Cancer*, vol. 9, no. 1, p. 250, 2009.
- [106] D. G. Leem, J. S. Shin, K. T. Kim, S. Choi, M. H. Lee, and K. T. Lee, “Dammarane-type triterpene ginsenoside-Rg18 inhibits human non-small cell lung cancer A549 cell proliferation via G1 phase arrest,” *Oncology Letters*, vol. 15, no. 4, pp. 6043–6049, 2018.
- [107] H. Li, N. Huang, W. Zhu et al., “Modulation the crosstalk between tumor-associated macrophages and non-small cell lung cancer to inhibit tumor migration and invasion by ginsenoside Rh2,” *BMC Cancer*, vol. 18, no. 1, p. 579, 2018.